Copyrighted Materials
Copyright © 2008 American Society of Civil Engineers (ASCE)
Retrieved from www.knovel.com

ASCE Manuals and Reports on Engineering Practice No. 110

Sedimentation Engineering

Processes, Measurements, Modeling, and Practice

Edited by Marcelo H. García, Ph.D., P.Eng.

Prepared by
the ASCE Task Committee to Expand and Update Manual 54
of the Sedimentation Committee of
the Environmental and Water Resources Institute

ASCE

Published by the American Society of Civil Engineers

Library of Congress Cataloging-in-Publication Data

American Society of Civil Engineers. Task Committee for the Preparation of the Manual on Sedimentation.
Sedimentation engineering : processes, management, modeling, and practice / edited by Marcelo H. Garcia ; prepared by the ASCE Task Committee for the Preparation of the Manual on Sedimentation of the Sedimentation Committee of the Hydraulics Division
p. cm. — (ASCE manuals and reports on engineering practice ; no. 110).
Completary to Sedimentary engineering, edited by Vito A. Vanoni.
Includes bibliographical references and index.
ISBN–13: 978–0–7844–0814–8 (alk. paper)
ISBN–10: 0–7844–0814–9 (alk. paper)
1. Sediment transport. 2. Soil conservation. I. García, Marcelo H., 1959– II. Title.

TC175.2 .A432 2007
627' . 042—dc22

2006027517

Published by American Society of Civil Engineers
1801 Alexander Bell Drive
Reston, Virginia 20191
www.pubs.asce.org

Any statements expressed in these materials are those of the individual authors and do not necessarily represent the views of ASCE, which takes no responsibility for any statement made herein. No reference made in this publication to any specific method, product, process or service constitutes or implies an endorsement, recommendation, or warranty thereof by ASCE. The materials are for general information only and do not represent a standard of ASCE, nor are they intended as a reference in purchase specifications, contracts, regulations, statutes, or any other legal document.

ASCE makes no representation or warranty of any kind, whether express or implied, concerning the accuracy, completeness, suitability, or utility of any information, apparatus, product, or process discussed in this publication, and assumes no liability therefore. This information should not be used without first securing competent advice with respect to its suitability for any general or specific application. Anyone utilizing this information assumes all liability arising from such use, including but not limited to infringement of any patent or patents.

ASCE and American Society of Civil Engineers—Registered in U.S. Patent and Trademark Office.

Photocopies and reprints. You can obtain instant permission to photocopy ASCE publications by using ASCE's online permission service (http://pubs.asce.org/permissions/requests/). Requests for 100 copies or more should be submitted to the Reprints Department, Publications Division, ASCE (address above); email: permissions@asce.org. A reprint order form can be found at http://pubs.asce.org/support/reprints/

Copyright © 2008 by the American Society of Civil Engineers.
All Rights Reserved.
ISBN 13: 978–0–7844–0814–8
ISBN 10: 0–7844–0814–9

Manufactured in the United States of America.

About the cover: River dunes in the Rio Paraná near Paso de la Patria, Argentina. Bed morphology measurements were made with a multibeam echo sounder in May 2004. Note the ubiquitous superimposition of smaller bedforms on the stoss side of the larger dunes. Image courtesy of Dan Parsons and Jim Best, University of Leeds, U.K.

Copyrighted Materials
Copyright © 2008 American Society of Civil Engineers (ASCE)
Retrieved from www.knovel.com

CONTENTS

Foreword xvii

Dedication xxi

CHAPTER 1 OVERVIEW OF SEDIMENTATION ENGINEERING 1
Robert C. MacArthur, Charles R. Neill, Brad R. Hall, Vic J. Galay, and Andrey B. Shvidchenko

1.1 Introduction 1
1.2 Overview of Erosion 4
1.3 Overview of Sediment Transport 8
1.4 Overview of Sediment Deposition 11
1.5 Management and Treatment of Sedimentation Problems 14
References 17

CHAPTER 2 SEDIMENT TRANSPORT AND MORPHODYNAMICS 21
Marcelo H. García

2.1 Sediment Transport Mechanics and Related Phenomena 21
2.2 Fluid Mechanics and Hydraulics for Sediment Transport 24
2.3 Sediment Properties 34
2.4 Threshold Condition for Sediment Movement 44
2.5 Sediment Transport 60
2.6 Bed Load Transport 66
2.7 Bed Forms 77
2.8 Bed Forms, Flow Resistance, and Sediment Transport 99
2.9 Suspended Load 107
2.10 Dimensionless Relations for Total Bed-Material Load in Sand-Bed Streams 123
2.11 Morphodynamics of Rivers and Turbidity Currents 129
2.12 Morphodynamics of Lake and Reservoir Sedimentation 133
References 146

CHAPTER 3 TRANSPORT OF GRAVEL AND SEDIMENT MIXTURES 165
Gary Parker

3.1 Fluvial Phenomena Associated with Sediment Mixtures 165
3.2 Engineering Relevance 171
3.3 Grain-Size Distributions 175

3.4 Dimensionless Bank-Full Relations for Gravel-Bed and Sand-Bed Streams 178
3.5 The Active Layer Concept 183
3.6 General Formulation for Bed-Load Transport of Mixtures 186
3.7 Relations for Hiding and Bed-Load Transport in Mixtures 191
3.8 Field Data 209
3.9 Abrasion 210
3.10 Numerical Modeling of Bed Level Variation with Sorting 213
3.11 Static and Mobile Armoring: Observations, Experiments, and Modeling 216
3.12 Downstream Fining: Observations, Experiments, and Modeling 223
3.13 Morphodynamics of Local Planform Sorting 227
3.14 The Case of Suspension-Dominated Sand-Bed Rivers 229
3.15 Tracers and Vertical Sorting 237
Notation 239
References 243

CHAPTER 4 FINE-GRAINED SEDIMENT TRANSPORT 253
Ashish J. Mehta and William H. McAnally

4.1 Introduction 253
4.2 Sediment Characterization 254
4.3 Sediment Transport Processes 259
4.4 Aggregation 261
4.5 Settling Velocity 266
4.6 Deposition Under Flow 270
4.7 Consolidation and Gelling 272
4.8 Erosion 275
4.9 Wave-Induced Erosion 283
4.10 Diffusion 291
4.11 Applications 293
References 297

CHAPTER 5 SEDIMENT TRANSPORT MEASUREMENTS 307

5.1 General 307
P. Diplas, R. Kuhnle, J. Gray, and D. Glysson
5.2 Bed-Material Measurement Techniques 309
P. Diplas
5.3 Suspended-Sediment Samplers and Sampling Methods 320
J. Gray, D. Glysson, and T. Edwards
5.4 Bed Load Samplers 339
R. Kuhnle
References 346

CHAPTER 6 FUNDAMENTALS OF FLUVIAL GEOMORPHOLOGY 355
D. S. Biedenharn, C. C. Watson, and C. R. Thorne

6.1 Basic Concepts 355
6.2 Channel Morphology 359

6.3 Sediment Transport 363
6.4 Channel-Forming Discharge 364
6.5 Relationships in Rivers 367
6.6 Channel Stability and Instability 371
6.7 Channel Classification 375
6.8 Channel Evolution Models 379
6.9 Geomorphic Assessment 381
6.10 Closure 382
Notation 382
References 383

CHAPTER 7 STREAMBANK EROSION AND RIVER WIDTH ADJUSTMENT 387
James E. Pizzuto and the ASCE Task Committee on Hydraulics, Bank Mechanics, and Modeling of River Width Adjustment

7.1 Introduction 387
7.2 Geomorphic Context of River Width Adjustment 387
7.3 Factors Influencing Bank Erosion and Width Adjustment 391
7.4 Methods for Evaluating Bank Erosion and Width Adjustment 408
7.5 Procedure for Approaching Width-Adjustment Problems 426
7.6 Conclusions 428
Appendix. Data Sources 429
Acknowledgments 430
References 430

CHAPTER 8 RIVER MEANDERING AND CHANNEL STABILITY 439
A. Jacob Odgaard and Jorge D. Abad

8.1 Introduction 439
8.2 Meandering Process 439
8.3 Flow and Bed Topography in Meanders 443
8.4 Channel Stability 445
8.5 Applications of Flow and Stability Relations 449
8.6 Simulation of Meander Evolution 450
8.7 Channel Stabilization 451
References 454

CHAPTER 9 STREAM RESTORATION 461
F. Douglas Shields, Jr., Ronald R. Copeland, Peter C. Klingeman, Martin W. Doyle, and Andrew Simon

9.1 Introduction 461
9.2 Preparation of Sediment Studies Plan 466
9.3 Selecting Values for Design Discharge and Bed Material Size 469
9.4 Stability Assessment 474

9.5 River Restoration Design 485
9.6 Stability Checks 494
9.7 Implementation and Construction 496
9.8 Monitoring and Postconstruction Adjustment 496
9.9 Conclusions 497
Acknowledgments 497
References 497

CHAPTER 10 BRIDGE SCOUR EVALUATION 505
J. R. Richardson and E.V. Richardson

10.1 Introduction 505
10.2 Total Scour 506
10.3 Clear-Water and Live-Bed Scour 507
10.4 Long-Term Bed Elevation Changes 507
10.5 General Scour 508
10.6 Critical Velocity for Movement of Bed Material 510
10.7 Local Scour 511
10.8 Local Scour at Piers 512
10.9 HEC 18 Pier Scour Equation 513
10.10 Scour Depths with Debris on Piers 523
10.11 Jain and Fisher's Equation 523
10.12 Melville's Equation 524
10.13 Other Pier Scour Equations 525
10.14 Top Width of Pier Scour Holes 525
10.15 Local Scour at Abutments 525
10.16 Chang and Davis Abutment Scour Equation 527
10.17 Sturm Abutment Scour Equation 528
10.18 Richardson and Trivino Abutment Scour Equation 529
10.19 Richardson et al. Equation for $\boldsymbol{L/y} > 25$ 530
10.20 Computer Models 530
10.21 Stream Instability 530
10.22 Scour in Tide-Affected Waterways 531
10.23 Scour Calculations for Tidal Waterways 532
10.24 Overview of Tidal Processes 533
10.25 Preliminary Analysis 534
10.26 Determination of Hydraulic Variables 536
References 539

CHAPTER 11 BRIDGE-SCOUR PREVENTION AND COUNTERMEASURES 543
Bruce W. Melville, Arthur C. Parola, and Stephen E. Coleman

11.1 Introduction 543
11.2 Scour Processes 543
11.3 Protection against General Scour and Contraction Scour 549
11.4 Countermeasures for Local Scour at Bridge Piers 557
11.5 Abutment Protection 568
11.6 Environmental Considerations 574
References 574

CHAPTER 12 RESERVOIR SEDIMENTATION 579
Gregory L. Morris, George Annandale, and Rollin Hotchkiss

12.1 Introduction 579
12.2 Sedimentation Rates 580
12.3 Sustainability 582
12.4 Sedimentation Impacts 585
12.5 Sediment Delivery to Reservoirs 587
12.6 Quantifying Sediment Yield 590
12.7 Sediment Deposition in Reservoirs 595
12.8 Sediment Management in Reservoirs 598
12.9 Dam Removal 607
12.10 Concluding Remarks 608
References 609

CHAPTER 13 ICE EFFECTS ON SEDIMENT TRANSPORT IN RIVERS 613
Robert Ettema

13.1 Introduction 613
13.2 Ice Formation 615
13.3 Ice-Cover Effects on Flow Distribution 619
13.4 Ice-Cover Breakup 623
13.5 Sediment Transport by Ice 625
13.6 Ice-Cover Effects on Sediment Transport by Flow 627
13.7 River-Ice Effects on Alluvial-Channel Morphology 635
Acknowledgments 645
References 645

CHAPTER 14 COMPUTATIONAL MODELING OF SEDIMENTATION PROCESSES 649
William A. Thomas and Howard Chang

14.1 Introduction 649
14.2 Local Scour and Deposition 650
14.3 General Equations for Flow in Mobile Boundary Channels 650
14.4 Similarity between Computational Model Studies and Physical Model Studies 654
14.5 Data Types and Resolution 656
14.6 Model Calibration 667
14.7 Base Test 670
14.8 Plan Test 671
14.9 Interpretation of Results 671
14.10 Examples to Illustrate Model Applicability 671
14.11 An Example Application 672
14.12 Available Computational Models 679
References 680

CHAPTER 15 TWO- AND THREE-DIMENSIONAL NUMERICAL SIMULATION OF MOBILE-BED HYDRODYNAMICS AND SEDIMENTATION 683
Miodrag Spasojevic and Forrest M. Holly, Jr.

15.1 Introduction 683
15.2 Problem Types and Available Techniques and Modeling Systems—A Survey 685
15.3 Mathematical Basis for Hydrodynamics in Two and Three Dimensions 690
15.4 Overview of Models of Sediment Transport and Bed Evolution 695
15.5 Bed and Near-Bed Processes 701
15.6 Suspended-Material Processes 705
15.7 Sediment-Exchange Processes 707
15.8 System Closure and Auxiliary Relations 708
15.9 Mobile-Bed Numerical Solution Considerations 712
15.10 Field Data Needs for Model Construction, Calibration, and Verification 714
15.11 Examples 720
15.12 Critical Assessment of State of the Art and Future Perspectives 755
References 759

CHAPTER 16 TURBULENCE MODELS FOR SEDIMENT TRANSPORT ENGINEERING 763
D. A. Lyn

16.1 Introduction 763
16.2 Turbulence, Models, and Particulate Flows 763
16.3 The Reynolds-Averaged Equations 766
16.4 Turbulence Closure Models 771
16.5 Applications of Turbulence Models to Problems Related to Sediment Transport 794
16.6 Discussion 812
Appendix I. Cartesian Tensor Notation 815
Appendix II. Spatially Averaged Models 817
References 820

CHAPTER 17 WATERSHED SEDIMENT YIELD 827
Deva K. Borah, Edward C. Krug, and Daniel Yoder

17.1 Introduction 827
17.2 Upland Soil Erosion 829
17.3 Gully Erosion 837
17.4 Streambed and Bank Erosion 839
17.5 Gross Erosion, Delivery Ratio, and Sediment Yield 839
17.6 Watershed Models 840
References 854

CHAPTER 18 ENGINEERING GEOMORPHOLOGY 859
S. A. Schumm and M. D. Harvey

18.1 Introduction 859
18.2 History 861
18.3 Systems Approach 865
18.4 Geomorphic Hazards 873
18.5 The Engineering Geomorphic Approach 878
18.6 Conclusions 880
References 880

CHAPTER 19 SEDIMENTATION HAZARDS 885
Marcelo H. García, Robert C. MacArthur, Richard French, and Julianne Miller

19.1 Introduction 885
19.2 Sedimentation Hazards—History and Magnitude 887
19.3 Mechanics of Mudflows, Debris-Flows, and Mud-Floods 889
19.4 Alluvial Fan Flooding and Sedimentation 900
19.5 Methods to Mitigate the Consequences of Sedimentation Hazards 905
19.6 Mathematical Modeling of Mudflows and Debris-Flows 909
References 917

APPENDIX CHAPTER 19 CASE STUDY MOUNT ST. HELENS—20 YEARS LATER 923
Jeffrey Bradley, Tom Grindeland, and Hans Hadley

Introduction and Chronology 923
Watershed Recovery 927
Sediment Sources 930
Sediment Yield 933
Conclusions 934
References 936

CHAPTER 20 AMERICAN SEDIMENTATION LAW AND PHYSICAL PROCESSES 937
James E. Slosson, Douglas Hamilton, and Gerry Shuirman

20.1 Introduction 937
20.2 Manual 54: Sedimentation Engineering (Vanoni 1975) 937
20.3 Recent Trends in American Sedimentation Law 939
20.4 Key Trend-Setting Court Decisions 939
20.5 Public Liability and Natural Hazards: Common Law and Regulatory "Takings"—Future Directions 940

20.6 Various Defenses 946
20.7 Sovereign Immunity 946
20.8 Statutes of Limitations 948
20.9 Hazard Mitigation Measures Based upon Tort Theories 948
20.10 More on the Takings Issue: Expanded Status and Trends in Tort and Takings Laws 949
20.11 Upstream versus Downstream Legal Issues 949
20.12 Act of God Defense 950
20.13 Forensic Geology 952
20.14 Future Directions 952
20.15 Summary and Recent Developments 954
20.16 Conclusion 956
Acknowledgments 956
References 956
Court Citations and Other References 957

CHAPTER 21 CONTAMINANT PROCESSES IN SEDIMENTS 959
Danny D. Reible

21.1 Introduction 959
21.2 Contaminants of Concern 960
21.3 Contaminant Release and Exposure Pathways 962
21.4 Water-Side Mass Transfer Processes 968
21.5 Analysis of Sediment Bed Fate and Transport Mechanisms 969
21.6 Engineering Management of Contaminated Sediments 974
21.7 Summary 979
References 979

CHAPTER 22 SEDIMENT OXYGEN DEMAND (SOD) IN RIVERS, LAKES, AND ESTUARIES 983
Miki Hondzo and Nancy Steinberger

22.1 Introduction 983
22.2 Diffusive Sublayer Thickness 984
22.3 Mass-Transfer Coefficient 987
Appendix: Developed Flow Concepts 989
References 990

CHAPTER 23 DEVELOPMENT AND APPLICATION OF NUMERICAL MODELS OF SEDIMENT TRANSPORT ASSOCIATED WITH DAM REMOVAL 995
Yantao Cui and Andrew Wilcox

23.1 Introduction 995
23.2 Dam Removal and Sediment-Transport Modeling 995
23.3 Numerical Simulation of Sediment Transport Following the Removal of Marmot Dam, Sandy River, Oregon 1000
Acknowledgments 1019
References 1019

APPENDIX A ROCK SCOUR 1021
George W. Annandale and Erik F. R. Bollaert

Introduction 1021
Overview of Rock Scour 1021
Combined Application of Methods 1024
The EIM 1024
The CSM 1026
Summary 1035
References 1035

APPENDIX B RIPRAP DESIGN 1037
Steve Maynord and Charles Neill

B.1 Introduction 1037
B.2 Riprap Structure Types 1037
B.3 Physical Characteristics of Riprap Stone 1039
B.4 Significance of Hydraulic Loading 1041
B.5 Geotechnical Requirements for Riprap 1044
B.6 Environmental Requirements for Riprap 1045
B.7 Scour Protection Requirements for Bank Revetments 1046
B.8 Size Requirements for Riprap 1048
B.9 Construction and Maintenance 1053
References 1054

APPENDIX C SEDIMENT TRANSPORT SCALING FOR PHYSICAL MODELS 1057
Clifford A. Pugh

C.1 Introduction 1057
C.2 Modeling Considerations 1057
C.3 Nomenclature 1064
References 1065

APPENDIX D ESTIMATING SEDIMENT DISCHARGE 1067
John R. Gray and Francisco J. M. Simões

D.1 Introduction 1067
D.2 Suspended-Sediment Concentration Interpolation Method 1067
D.3 Transport-Curve Method for Suspended Sediment Load, Bed Load, and Total Load 1069
D.4 Equations for Estimating Bed Load and Bed-Material Load 1073
D.5 Toward Collection of Consistent, Reliable Fluvial-Sediment Data 1083
References 1084

APPENDIX E LIMITED GLOSSARY OF SELECTED TERMS 1089
Robert C. MacArthur and Brad R. Hall

APPENDIX F CONVERSION OF UNITS 1103

Vito A. Vanoni (1904 – 1999) 1107
Norman H. Brooks

Index 1115

Copyrighted Materials
Copyright © 2008 American Society of Civil Engineers (ASCE)
Retrieved from www.knovel.com

CHAPTER 1

Overview of Sedimentation Engineering

Robert C. MacArthur, Charles R. Neill, Brad R. Hall, Vic J. Galay, and Andrey B. Shvidchenko

1.1 INTRODUCTION

1.1.1 General

Sedimentation engineering embraces the identification, planning, analysis, and remediation, principally in the context of civil and hydraulic engineering practice, of projects or technical investigations to avoid and/or mitigate problems caused by sedimentation processes. These processes include erosion, entrainment, transport, deposition, and compaction of sediment. External agents and forces driving these processes may include water, wind, gravity, and ice. Human activities also affect sedimentation processes. This volume of *Sedimentation Engineering*, referred to herein as Manual 110, focuses primarily on physical processes, measurements, modeling, and the practice of sedimentation engineering, mainly in the context of rivers and inland water bodies. (Chapter 4, however, addresses fine sediments topics, including those found in coastal and estuarine environments.)

The original ASCE Manual 54 *Sedimentation Engineering,* edited by Vito A. Vanoni (1975), represents a 10-year effort by the Task Committee for the Preparation of a Manual on Sedimentation under the coordination of the Sedimentation Committee of the Hydraulics Division of ASCE. Professor Vanoni and the Task Committee assembled and organized state-of-the-art information on sediment mechanics and sedimentation engineering available at the time. Since then, awareness of the importance, scope, and potential consequences of sedimentation processes in relation to civil engineering works, human activities, and the environment has greatly increased. Also greatly expanded are the scientific and engineering understanding and knowledge of underlying processes related to sedimentation engineering. Manual 110 is designed to update selected topics in the original manual and to present recent advances and new topics in sedimentation engineering as a complement to the original Manual 54. Manual 110 is intended to supplement rather than replace the original manual, which contains a wealth of fundamental information that has not lost its validity. Together, both manuals document the evolution of the specialized field of sedimentation engineering over a 50-year period.

1.1.2 Global Aspects and Changing Roles

As awareness of sedimentation processes and the consequences of poor sediment-management practices has increased among civil engineers and other water resources professionals, it has increasingly been realized that a multidisciplinary approach to problem identification, quantification, and management is often required to deal with the interrelated effects of geomorphologic, environmental, and engineering issues. This type of comprehensive systems approach is also demanded by more stringent legal and regulatory requirements regarding sediment and hydraulic processes in water bodies.

Factors that have resulted in increased public awareness and greater potential impacts to water resources and the environment include the following:

- Growing global populations place increasing pressures on land and water resources. As forest and farmlands become subject to increased soil erosion (Fig. 1-1), reservoirs designed for centuries of useful life may fill with sediment in a few decades, and water supply, irrigation systems, and critical aquatic habitat areas may become clogged with sediment deposits, while poorly managed forests and farmlands decline in function and productivity.
- Human settlements have increasingly occupied areas more vulnerable to erosion and sedimentation, thus aggravating runoff, soil erosion, and gullying (Fig. 1-2). Poor land use planning, management, and maintenance

Fig. 1-1. Severe soil erosion resulting from annual burning of underbrush in teak forests on hillsides in Java, Indonesia. *Photograph by B. J. Evans.*

Fig. 1-2. Accelerated land erosion and gullying: active gullying resulting in severe soil loss and high sediment yields on the upper plateau of Rio Calicanto, Bolivia. This fertile cropland was abandoned by local farmers because of their migration to coca producing areas. Because of neglect and lack of annual maintenance, the altered lands are no longer managed or stabilized, resulting in rapid erosion and headcutting of gullies during rainstorms. Irrigation reservoirs downstream are now filled with sediment eroded from this area, resulting in significant impacts to water supply and flood control. *Photograph by V. J. Galay.*

practices often lead to dramatic consequences. Severe natural events such as floods, hurricanes, earthquakes, landslides, and volcanic eruptions can produce more dramatic geomorphic changes and sedimentation effects in highly altered settings that can last for decades.

- One of the most significant factors affecting global management and delivery of sediment has been the construction of dams on rivers. Approximately 80,000 dams have been built in the United States of America during the past century (Graf 2001). Morris and Fan (1997) summarize how construction of dams provides many benefits but may alter a river's natural balance of sediment inflow and outflow. They emphasize the urgent need to improve global planning, operation, maintenance, and management of dams and reservoirs with respect to sediment-related problems. An example is the Davis Dam on the Colorado River near Las Vegas (Fig. 1-3), which, along with the Hoover, the Glen Canyon, the Parker, the Headgate Rock, the Palo Verde, the Imperial, and the Laguna dams, have fragmented the river into a series of pools and sediment sinks that alter the nature and movement of sediment along the Colorado River.
- Scientific experts and governments worldwide acknowledge strong scientific evidence demonstrating that human activities are changing the Earth's climate and that further change is inevitable. Expected results include an increasing likelihood worldwide for more frequent occurrences of extreme storms and flood events (National Research Council 1989; Hasselmann et al. 2003; Watson 2003). Such events are often responsible for a major part of long-term morphologic changes and sedimentation activity, while the occurrence of severe hydrologic events on highly altered, destabilized landscapes may result in more dramatic consequences than previously anticipated. This may become one of the most important engineering and environmental issues facing societies worldwide.

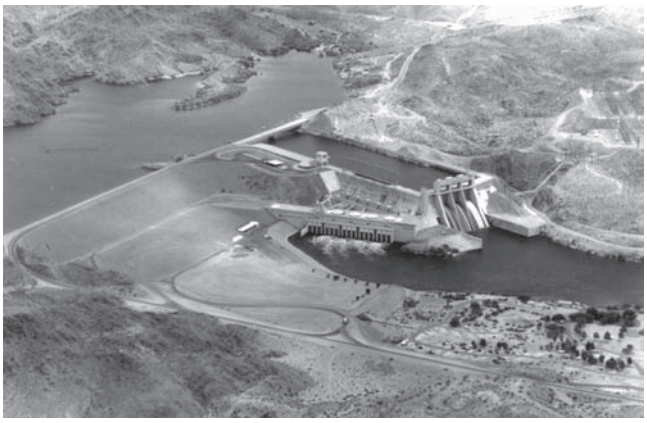

Fig. 1-3. Photo of Davis Dam on the Colorado River. Watershed sediments are trapped behind a series of eight dams and reservoirs resulting in approximately 20 feet of riverbed lowering in places along the Colorado River. *Photograph by V. J. Galay.*

The following excerpts from a volume devoted to reservoir sedimentation by Morris and Fan (1997) raise difficult issues related to water resources and sedimentation engineering:

> In a number of countries population growth seems to be rapidly outstripping the available water resources base. . . . Water resource engineers and development planners have a responsibility to study, understand and communicate the capacity and limits of the earth's resources. . . . Is it a legitimate or ethical function of the engineering profession to destroy entire ecosystems to feed a runaway human population?

With increasing awareness of the importance, scope, and potential consequences of sedimentation processes in relation to civil engineering works, human activities, and the environment, sedimentation engineering studies require consideration of basinwide processes associated with sediment sources, transport routes, and depositional sinks, as well as the potential future effects on the environment and on upstream and downstream interests. Forecasting may be required of incremental and cumulative impacts from a sequence of past and future projects—for example, possible impacts of a series of road and bridge crossings on the hydraulics and morphology of a river floodplain should be assessed prior to project construction. Sedimentation issues often embrace water quality, contaminant transport (e.g., heavy metals, pesticides, and petroleum by-products that attach to sediments), and impacts on natural habitat, health, and amenities, requiring that sedimentation engineers participate in multidisciplinary teams to plan and design effective projects. In the United States and other countries, legislation increasingly calls for detailed quantification of sedimentation processes as well as other impacts from water resources projects.

1.1.3 Additional Comments

Some general observations on the state of sedimentation engineering in the early years of the twenty-first century are as follows:

- Sedimentation processes are not always adverse or undesirable as some writings suggest. To the contrary, sedimentation processes are essential for the maintenance of morphologic balance and are critical components of aquatic ecosystems. For example, fertile agricultural lands and wildlife areas may benefit from periodic flooding and silt deposition, and fish may rely on continual renewal of bed sediment (gravels) in spawning areas. Sedimentation processes are key components of most fluvial systems.
- Project planners and designers are presented with so much information on environmental and biological issues that the importance of hydraulic and sedimentation processes are sometimes overlooked or underestimated. Given the need for reliable field data, however, it is important to address sedimentation issues at an early stage. Where there are clearly significant problems or impacts, sediment data collection should receive as much attention as hydrometeorologic and environmental data. It is as important to develop uninterrupted long-term sedimentation data sets as it is to monitor hydrologic and biologic changes and trends.
- Field studies providing full-scale confirmation of theoretical and laboratory results are relatively scarce, compared to the large number of theoretical and small-scale experimental studies proposing methods for the computation of sediment transport rates, scour depths at bridge foundations, and so on. This is not surprising given their difficulty and cost, but the limitations of theoretical formulations and scaled-up laboratory results are sometimes overlooked.
- Sediment management issues and morphological changes may arise from reduction of sediment inputs as well as from increases in sediment production. Poor project planning, poor land use management, or the occurrence of significant natural hazards (fires, earthquakes, and floods) may result in short- or long-term sediment imbalances. For example, construction of storage reservoirs that trap fluvial sediment or excessive mining (extraction) of fluvial sediments may have adverse effects on channel morphology and the biological habitat in downstream river reaches and cause undermining of structure foundations and alter coastal morphology and stability.
- Addressing real-world problems in water resources and sedimentation engineering is often challenging because of the extreme complexities related to large spatiotemporal heterogeneities, sparsity of reliable data, and knowledge gaps that limit our ability to predict morphologic changes during individual storm events or during longer, decadal periods of time. Perhaps even more challenging to hydraulic and sediment engineering scientists is understanding and quantifying the interaction between flow and sediment dynamics, and the short- and long-term effects of these processes on aquatic ecosystems (modified from Lyn, 2006). Solutions to this class of challenging issues will require a multidisciplinary approach from engineers and scientists. This need is "driving the development of a predictive science of Earth surface dynamics that integrates many disciplines and approaches, including hydrology, geomorphology, ocean and atmospheric science, sedimentary and structural geology, geochemistry, and ecology" (Paola et al. 2006).

1.1.4 Scope of Subsequent Chapters and Appendices

Chapters 2 through 23 and Appendices A through D address a wide range of sedimentation topics. To a considerable extent, the topics covered reflect the expertise and interests of individual authors and are intended to present recent

advances and new topics in sedimentation engineering. Primary topics include:

- Sediment sources, erosion, and hazards: Chapters 6, 17–19.
- Sediment transport mechanics and measurement: Chapters 2–5.
- Computational modeling of sediment transport: Chapters 14, 15, 19, and 23.
- Lateral stability of river channels: Chapters 7 and 8.
- Assessment and remediation of selected sedimentation problems: Chapters 9–12 and 23.
- Environmental issues: Chapters 9, 21, and 22.
- Ice effects on sediment transport: Chapter 13.
- Turbulence modeling: Chapter 16.
- Sedimentation law: Chapter 20.

Appendices A through D provide summaries on additional topics including rock erosion, riprap design, the use of physical models for assessing sediment engineering problems, and methods for estimating sediment discharge. Appendices E and F provide a glossary of terms and unit conversions.

1.2 OVERVIEW OF EROSION

1.2.1 General

ASCE's original Manual 54 (Vanoni 1975) distinguished between geological (or natural) erosion and accelerated (or human-induced) erosion, viewing the latter as a mainly local phenomenon. In the twenty-first century, such a view is outdated. Hooke (1994) estimated annual global volumes of erosion due to various agents and concluded that "humans are arguably the most important geomorphic agent currently shaping the surface of the Earth." However, others (Valdiya 1998) have shown that geological erosion through mountain ranges, such as the Himalayas, continues to produce immense volumes of sediment.

It is often difficult to determine whether an observed erosional process is natural or whether it results wholly or partly from human influences. For example, gullying and landslides that appear natural may have been triggered or aggravated by overgrazing, significant land use modifications such as urbanization, infiltration of irrigation water, or deforestation. Overviews of erosion, sediment transport, and deposition are presented in Sections 1.2, 1.3, and 1.4, respectively.

1.2.2 Geologic or Natural Erosion

Geological erosion results from tectonic uplift, earthquakes, weathering, and chemical decomposition and the long-term action of water, wind, gravity, and ice (see Chapters 6, 17, and 18). Over long periods, such processes have produced some enormous erosional scars—for example, the Grand Canyon in Arizona (Fig. 1-4). In some regions, the bulk of natural erosion may result from severe episodic events like earthquakes, landslides, volcanic eruptions, and extreme floods.

Fig. 1-4. Grand Canyon, Arizona: spectacular example of geologic erosion by flowing water through layers of sedimentary deposits. Note sites where active erosion provides sediment directly into the river from small, steep drainages. *Photograph by V. J. Galay.*

Rates of geologic erosion vary widely both among and within regions. Summerfield and Hutton (1994) list average rates of natural erosion estimated for major world drainage basins. Rates tend to be slow in terms of a human lifetime but may be significant enough to require consideration in some projects. Control is often difficult or impractical because the erosion is distributed over large areas divided among multiple owners and resource management jurisdictions. Poorly designed and implemented land or water use projects can dramatically accelerate prior erosion rates.

Geologic erosion rates have varied widely over time, primarily as a result of climatic variations. Rapid climate change in the form of global warming has led to unprecedented erosion in sensitive areas like the Arctic coast of North America (McCarthy et al. 2001).

1.2.3 Accelerated or Human-Induced Erosion

Accelerated erosion may be wholly or partly caused by human activities. The impacts of individual or cumulative human activities may be subtle and may commence slowly but can result in dramatic rapid changes in morphology, sediment production, and deposition with time once critical geomorphic stability thresholds are exceeded. Hatheway (2005) explains that prior to the nineteenth century, humans possessed a relatively limited ability to alter the geologic landscape. However, anthropogenic effects on global landscapes and the environment dramatically accelerated during the nineteenth and twentieth centuries. Besides causing sedimentation problems and impacting constructed facilities, poorly planned human activities often lead to environmental degradation and damage to habitat. Simply to address accelerated erosion as a local engineering problem without regard to basinwide sources and responses is generally inadvisable. The potential for erosion should be considered in the context of a multidisciplinary and participatory approach to a range of associated problems. In the face of growing populations and associated pressures placed on land and natural resources, the basic problems associated with sedimentation processes may not be fully solvable, but at least they should be recognized and faced by authorities and the public.

1.2.4 Sources of Accelerated Erosion

Extensive discussions on a number of sources of accelerated erosion are contained in the original Manual 54. Some important sources are discussed briefly below and in Chapters 6 and 17 through 19.

1.2.4.1 Agricultural Activities Manual 54 cited an estimated annual soil loss from croplands in the United States of 4×10^9 tons/year, of which about 25% was estimated to reach the oceans. In the United States, severe soil erosion in the 1930s was followed by intensive conservation efforts, which substantially reduced rates of soil loss by about 40% in vulnerable regions, between 1982 and 1997 (Uri and Lewis 1998).

Global population increases, on the order of 80 million people per year between 1975 and 2000, have placed severe pressures on agricultural and water resources on several continents. It has been estimated that toward the end of the twentieth century, from 5 to 7 million hectares of arable land worldwide were lost annually because of soil degradation and erosion (Hauck 1985; Jalees 1985; Brown 1991). Although improvements have occurred and continue to take place in the United States, Canada, and some other parts of the world, soil loss has substantially increased in other regions, leading to a net increase in worldwide annual soil loss (Barrow 1991; Food and Agricultural Organization of the United Nations [FAO] 2001).

1.2.4.2 Forest Activities World timber demand, extended agriculture, and use of wood for fuel in many regions have caused extensive destruction of forest land by cutting or burning, especially in parts of Africa, Asia, and South America (Bryant et al. 1997). In a single decade between 1990 and 1999, the global forest area declined by nearly 20% (FAO 2001). It has been claimed that conversion of forestland to agriculture generally increases soil erosion by a factor ranging from several times to as much as 25 times (Golubev 1982).

Where forests are managed for sustainable timber yield, extraction activities are not necessarily erosional, but accelerated erosion often results from cutting on steep slopes or close to streambanks and from construction of access roads and skid trails. In steep terrain, alteration of streams and drainage patterns can trigger destructive debris flows containing boulders, gravel, fine sediment, and woody debris (Costa 1988; Slaymaker 1988). Poorly planned, irresponsible conversion of forestlands has led to dramatic long-term environmental impacts and loss of stable forest areas in Asia, Africa, and in the Amazon River basin in South America. Stabilization and rehabilitation of such channels and river systems may require large-scale and expensive engineering measures (Wieczorek and Naeser 2000).

1.2.4.3 Urbanization Rapid growth of cities and suburban areas in the later twentieth century, especially in less developed countries, contributed to increases in erosion due to accelerated runoff from developed areas, especially where steep hillsides are used for unregulated low-cost shelter (Ismail 1997). In some cases, disastrous landslides and mud flows following severe rainfall have caused large-scale property destruction and loss of life (Quinones and Johnson 1987).

In well-planned urban developments, on the other hand, local erosion tends to be important only during construction. Accelerated runoff from developed areas has customarily been directed into storm drains or hard-lined flood-control channels, but this may cause adverse changes in downstream rivers and water bodies. In some jurisdictions, there is pressure to replace hard-lined channels with restored natural stream systems (see Chapter 9). Restoring natural streams to a semistable condition where they receive substantial urban runoff requires multidisciplinary planning and careful engineering design, generally involving storage facilities or the maintenance of large undeveloped floodplain areas to reduce flow peaks and trap sediment. Once confined, realigned, and affected by increased urban runoff, former natural channel processes are forever altered. This often results in regular, long-term management and maintenance requirements (including annual monitoring, permitting, and funding to support these activities) that may have been unanticipated by project proponents.

1.2.4.4 Roads, Railways, Bridges, and Levees The main sedimentation impacts of these facilities, apart from temporary construction effects, are (1) alteration of natural drainage patterns by redirecting and concentrating dispersed

cross-flows into bridge and culvert openings (which may have serious effects in steep terrain) and (2) interference with natural river migration and overbank flow patterns by construction of permanent bridge crossings, approach embankments, and levees running alongside rivers (Figs. 1-5 and 1-6). Chapters 8, 10, and 11 present materials relevant to these topics.

1.2.4.5 Mining Activities Attention is given in technically advanced countries to controlling erosion from open-pit mining operations, but operations in less developed countries have often proceeded with insufficient planning and oversight. Uncontrolled excessive in-channel and floodplain mining can result in geomorphic alteration of river form and processes (Collins and Dunne 1990; Kondolf 1994, 1998a, 1998b; Brown et al. 1998; Church 2001). Poorly managed mining can lower water surface elevations and disrupt the balance between sediment supply and a stream's transporting capacity, which can result in channel incision, bed degradation, diversion of flow through disturbed sediment removal sites, increase of channel instability, and changes in overall channel morphology and sediment transport processes (Fig. 1-7).

1.2.4.6 Dams and River Regulation The primary sedimentation effect of a dam is usually to trap riverborne sediment in the reservoir and thereby reduce the availability of sediment load for downstream sediment transport, often leading to local "sediment starvation" and channel incision downstream of the reservoir. Sediment deposition

Fig. 1-5. Jacalitos Creek, California: the creek is attempting to outflank a highway bridge because the narrow bridge constriction and approach embankment prevent natural down-valley migration of meanders. Flow is from right to left. *Photograph by V. J. Galay.*

Fig. 1-6. Lower Guadalupe River below the City of San Jose, California: an example of a channelized urban river. The formerly meandering river was significantly straightened and leveed, restricting floodwaters to the main river channel. Formerly an agricultural area, the floodplain is now mainly occupied by urban and industrial development. View downstream. *Photograph by R. C. MacArthur.*

Fig. 1-7. Natural (top photo) and mined (bottom photo) reaches of Cache Creek, California, in 1986. Historically, excessive aggregate mining significantly altered the channel's morphology, causing channel degradation and thalweg lowering (incision). Implementation of comprehensive mining regulations in 1996 has improved conditions. *Photographs by R. C. MacArthur.*

in reservoirs is addressed in Chapters 2 and 12. Chapters 6 and 18 discuss other beneficial aspects of reservoirs as well as their potential impacts on river systems.

Erosional effects associated with dams and reservoirs may include the following:

- Slope flattening and headcutting of the downstream river and consequent destabilization of tributary streams due to sediment starvation, increased flow duration, and/or magnitude of flows (Fig. 1-8).
- Wave erosion around the shorelines.
- In circumpolar regions, collapse of shorelines by thawing of permafrost.

Engineering works such as flood protection levees, which do not generally produce increased sediment inputs, may nevertheless have significant erosional effects because they increase in-channel flows and as well as average channel velocities. The downstream channel gradient may flatten by channel incision and headcutting, resulting in undercutting of channel banks and undermining of engineering works such as bridge and pipeline crossings (U.S. Army Corps of Engineers [USACE] 1994).

River channel alterations designed to augment hydraulic capacity for drainage purposes can cause serious erosion, particularly when meandering channels are straightened and cleared of vegetation without introducing resistant linings or grade control structures (Schumm et al. 1984; USACE 1994). Chapters 6 through 9 present relevant information regarding these topics.

Fig. 1-8. Severe erosion and headcutting in former natural channel below Grapevine Dam Spillway, Texas, resulting mainly from greatly increased maximum outflows from collected urban flood runoff. *Photograph by C. R. Neill.*

1.2.4.7 Warfare and Population Migrations The main potential erosional effect of these activities results from construction of defense works and the neglect or abandonment of traditional agricultural methods, water conveyance systems, or engineering works that previously protected land and streams against erosion. Heavy armored transport, shelling, bombing, and fires can also cause significant destruction of forests and erosion protection and land conservation systems. Rose (2005) discusses how historical military activities have impacted local and regional geological conditions by changing the nature and rate of erosion and deposition processes.

1.2.4.8 Multiple Causes Accelerated erosion in many world regions may arise from a combination of causes. For example, a publication edited by Walling et al. (1992) presents a regional approach for evaluating basin-wide changes and deals with interrelated problems of erosion, debris flows, and the environment in mountain regions, with particular attention to the Pacific Rim.

1.2.5 Estimation of Erosion Rates and Quantities

Estimation of erosion rates and sediment yield from river basins can involve large uncertainties due to the sparsity of reliable data. The problem can be approached indirectly by considering source quantities of erosion or soil loss, or more directly by considering sediment yield—that is, the quantity delivered to the river system—which is usually much less than the source erosion. The first approach tends to be favored by geographers, soil scientists, and agriculturists and the second by urban planners and water resource engineers. Extensive literature exists for both approaches (see, e.g., Barfield et al. 1981; Simons and Senturk 1992; Haan et al. 1994; Reid and Dunne 1996; de Boer et al. 2003). In many basins, a significant proportion of the material eroded from the land surface does not reach the river system because of intermediate topographic features that act as sediment sinks (traps or temporary storage areas).

Erosion from land surfaces can be considered on a large scale in the context of typical rates per unit area from specific regions or specific types of terrain, or at small scale in the context of experimental plots that measure erosion from different types of soil under different vegetation covers and land uses. Experimental plots often tend to overpredict effective sediment production and delivery rates from larger areas. On the other hand, estimates based only on land surface erosion may overlook erosion from valley slopes, gullies, and stream channels. In the case of migrating stream channels, reliable determination of net erosion quantities is difficult because erosion at one location is often compensated by deposition at another.

Sediment yield can be considered globally in the form of typical rates per unit area from various regions or terrain types,

or more locally from measured deposition quantities in lakes and reservoirs or measured rates of sediment transport in rivers. Uninterrupted, long-term sediment delivery data from monitored basins produce the most reliable sediment yield estimates. Unfortunately, very few basins have such data, so sediment yield estimates must usually be developed from empirical relationships. For specific regions, empirical correlations are available relating sediment "delivery ratio" (the ratio of net sediment yield to gross erosion) to drainage area or other physiographic parameters. There are also methods (Barfield et al. 1981; Haan et al. 1994; Reid and Dunne 1996) for estimating sediment yield in unmonitored basins from regional soil erosion and yield maps, empirical yield estimation relationships, or simplified soil loss and delivery models, as well as methods for translating measured sediment yield values from a monitored basin to an unmonitored basin of similar character. Sediment yield is addressed in Chapter 17.

1.2.6 Local Erosion and Scour Associated with Engineering Works

Many types of engineering works in water bodies with erodible beds cause local erosion, usually referred to as scour when it proceeds downward into a channel bed (Fig. 1-9). This problem is an important consideration in the design of bridge foundations, dams, culverts, weirs, riverbank protection, and other works. Scour associated with bridges is treated in Chapters 10 and 11; references include Melville and Coleman (2000), Richardson and Davis (2001), and Transportation Association of Canada (2001). Rock scour is addressed in Appendix A. Other publications covering a broader range of local scour and erosion problems include USACE (1994), Julien (2002), and May et al. (2002). Thompson (2005) discusses the history of the use and effectiveness of in-stream structures on river processes in the United States. Appendix B discusses erosion countermeasures.

Fig. 1-9. 1995 photo of bed scour and bank erosion under Highway 162 Bridge on Sacramento River, California. Long lengths of formerly buried piles are exposed by bank recession associated with toe scour. *Photograph by R. C. MacArthur.*

1.3 OVERVIEW OF SEDIMENT TRANSPORT

1.3.1 General

Sediment transport is treated extensively in several chapters of Manual 54 (Vanoni 1975). That earlier treatment includes transport by wind and transport in pipes, neither of which is addressed in the present volume. Substantial parts of the material in the original Manual 54 are of a fundamental nature and retain their validity. Chapters 2 through 5 of Manual 110 mainly update selected aspects of the topic. Chapters 14 through 16 and 23 cover numerical modeling, a topic that has developed rapidly since 1975 and was not covered in the original Manual 54. Appendix D discusses methods for estimating sediment discharge.

1.3.2 Modes of Sediment Transport

The term *sediment* covers a wide range of grain sizes transported by flowing water, ranging from fine clay particles to large boulders. These are often viewed in specific size classes, such as fine sand, coarse gravel, and so on, using one of several alternative classification systems (ASCE 1962). Depending on grain sizes and sediment material density, fluid density and viscosity, and the strength and turbulence of the flow, sediment transport may occur in a variety of modes involving different size classes at the same time or the same classes at different times.

In rivers and channels with moderate gradients, there are two overlapping systems of classifying transport modes: (1) as *bed load* plus *suspended load* or (2) as *bed-material load* plus *wash load* (see Chapter 2). Under the first system, *suspended load* consists of the finer sediment maintained in suspension by turbulence, whereas *bed load* consists of the coarser particles transported along the bed intermittently by rolling, sliding, or saltating. Under the second system, *bed-material load* comprises all sizes normally found in the bed, whether transported as bed load or in suspension, whereas *wash load* consists of fine sizes that always travel in suspension and are not found in significant quantities in the bed.

Bed-load transport may take place similarly to a "conveyor belt" (or "moving layers") or by evolution and migration of various bed and channel forms (dunes, bars, bends, and so on). In some environments, unusual and rare forms of bed-load transport may occur, such as the development and movement of "armored mud balls" (Fig. 1-10).

Suspended load is generally transported within and at the same velocity as the water, whereas *bed-load* transport may occur only occasionally during high-flow events. The boundary between suspended sediment and bed-load transport is not precise and may vary with the flow strength. The higher the flow, the coarser the sediment that can be suspended by turbulence. Suspended load plus bed load, or wash load plus bed-material load, together compose the *total sediment load* (see Table 2-4 in Chapter 2).

Fig. 1-10. Mud ball train in ephemeral Arroyo Hondo, western San Joaquin Valley, California. These rare bed-load features, up to 1 meter in diameter, formed and were transported during an intense flood in March 1997. Flow direction is from right to left. Such ball-like sediment agglomerations are found in some ephemeral streams in California with high loads of clay, silt, and sand. *Photograph by R. Leclerc.*

Particles that can move either as suspended load or as bed load and that periodically exchange with the nonmoving bed constitute the bed-material load. At least in theory, this part of the total sediment load can be calculated from hydraulic parameters and the composition of the bed material. On the other hand, wash load consists of the finer particles (usually silt and clay) in the suspended load that are continuously maintained in suspension by the flow turbulence and that are not found in significant quantities in the bed. This part of the total load is usually related to watershed supply and cannot be determined theoretically in most cases.

Another form of transport that occurs only in limited settings and steep channels is referred to as *hyperconcentrated flow,* where water and very high concentrations of sediment move as an integrated mass having properties somewhere between those of a Newtonian and a non-Newtonian fluid. Flows of this type, which include mud flows, debris flows, lahars, and rock and boulder torrents, form a special group of sediment hazards with unique fluid properties, high energy, and very destructive capabilities. Snow avalanches and ocean density currents represent somewhat analogous phenomena in other environments. Chapter 19 addresses this class of fluids and associated sediment hazards.

1.3.3 Sediment Transport Mechanics

Sediment transport mechanics as used herein (Chapters 2 through 5) refers to theories and experiments concerning physical factors that determine sediment displacement and transport and methods of estimating quantities transported. Although the fundamentals were fairly well established before 1975, the output of publications treating the subject has continued. Significant references since 1975 include Raudkivi (1976), Garde and Ranga Raju (1977), Yalin (1977), Parker (1978), Graf (1984), Thorne et al. (1987), Chang (1988), Ikeda and Parker (1989), Parker (1990), Simons and Senturk (1992), van Rijn (1993), Yang (1996), Chien and Wan (1999), and Julien (2002).

When estimating sediment transport rates for given hydraulic conditions, the engineer may select from a wide range of transport formulas, algorithms, or procedures, many of which are offered as options in computer programs for sediment transport modeling. Most of those have a partially theoretical background but depend importantly on laboratory experimental data for their quantitative aspects. A considerable degree of experience and judgment may be required to select those most appropriate for the particular circumstances. It is usually advisable to compare results from several methods because results may vary over a wide range. Wherever practicable, some degree of calibration against field measurements is highly desirable. Comparisons of sediment transport calculation procedures were summarized by Vanoni (1975) and more recently by Chang (1988), Gomez and Church (1989), Simons and Senturk (1992), Yang (1996), Chien and Wan (1999), and Julien (2002), among others. This topic is covered further in Chapters 2 through 5.

Published procedures may deal with one or more components of total sediment transport. In general, hydraulic-based relationships cannot predict wash load, which is usually supply limited and may constitute a significant portion of the total load. The wash load portion of the total load is generally determined from field measurements. Some hydraulic relationships predict bed load only and are limited mainly to gravel and coarser sediment. Others predict total bed-material load and are more appropriate where sand is an important size class. Although theoretical relationships cannot predict wash load in quantitative terms, they can predict the competence of the flow to transport given sizes in suspension and their distribution with depth. This can greatly assist interpretation and extrapolation of suspended sediment data obtained from field measurements.

Basic issues in sediment transport mechanics are the definition of hydraulic conditions required to (1) initiate movement of a given sediment grain size on the bed of a channel and (2) lift it into suspension. These issues which are closely linked to sediment transport calculations and in the first case to the determination of stable sizes for erosion protection, have been addressed both theoretically and experimentally since the early days of hydraulic engineering and form the subject of numerous studies and publications. Chapters 2 through 5 address these topics in considerable detail.

1.3.4 Sediment Transport Measurements

Sediment measurement techniques are discussed in detail in Chapter 5 and Appendix D. Edwards and Glysson (1999) also

provide a thorough summary of sediment measurement methods according to USGS-approved protocols. Field data are often needed to develop reliable sediment budgets and are essential for proper calibration and validation of numerical models used to predict sediment dynamics in rivers and reservoirs. Borgen et al. (2003) report advances in these techniques.

Suspended load concentrations are often reported routinely along with stream-flow data at certain river gauging stations. Limited data on grain size distributions in suspended loads and in the bed may also be reported. Suspended load data reports are usually based on sampling the water column down to a short distance above the bed. Measured suspended-load data include virtually all the wash load and, especially in the case of sand transport, part of the bed-material load. Where routine data are not available, special measurements may be undertaken over a limited time period.

For estimation of sedimentation in reservoirs and related problems, measured suspended-load data over a period of years are generally correlated with flow data to develop a sediment rating curve. Total sediment delivery over a period is then determined by applying the sediment rating curve to a flow-duration relationship. An allowance on the order of 10% is often added to account for bed load or other unmeasured load. However, the percentage of bed load can be substantially greater than 10% in steep rivers and streams with large supplies of gravel and coarse materials.

Sediment rating curves usually show wide scatter because the transport-flow relationship may vary widely with season, basin cover conditions, and other factors. Where the available data do not include much information on high flows, extrapolation of the curve to flood flows—which may account for a large proportion of the transport—may introduce a high degree of uncertainty. Testing and validation of extrapolated values is always recommended.

Bed load is difficult to measure and is not normally measured on a routine basis. For project purposes, special field measurements may be undertaken using techniques described in Chapter 5 and Appendix D.

1.3.5 Sediment Modeling

After the publication of Manual 54 in 1975, the use of integrated computer programs for numerical modeling of sediment erosion, transport, and deposition in time and space became increasingly common (see Chapters 14 and 15). Some are one-dimensional, typically applied for evaluation of sedimentation processes along rivers and channels. Others are two- or three-dimensional, typically applied for evaluation of sedimentation processes in broad floodplains, estuaries, coastal regions, and stratified water bodies. Numerical models are particularly valuable for examining the effects of historical or proposed changes and of alternative project proposals. Chapter 23 presents methods for modeling the effects of sediment transport associated with dam removal, while Chapter 16 discusses turbulence modeling associated with sedimentation processes.

Modeling programs generally contain default values of various parameters that are meant to be adjusted by calibration against real data, typically consisting of observed morphological changes (erosion or deposition) or observed sediment transport rates. In the absence of model calibration, results may differ widely from reality. There is also a danger of redefining the actual problem to suit the limitations of the model being used. In modeling future conditions, past data may not provide reliable guidance because of shifts in trends or changes in controlling factors. Experience and insight are often needed to select a reasonable range for key variables and hydrologic conditions. It may also be necessary to consider the potential for catastrophic events that are not represented in the historical record (see Chapter 19).

Physical modeling of sediment displacement and transport for proposed civil engineering projects or facilities can provide an alternative means for assessing project performance and testing project alternatives. This is accomplished in a hydraulic laboratory with a mobile-boundary modeling facility. The reproduction on a small scale of both bed-load and suspended-load behavior may present severe difficulties, and modeling compromises are often necessary with concentration on key aspects for the problem in hand. Where the prototype setting involves sand beds, it is usually advisable to use low-density granular material in the model in order to achieve sufficient mobility and transport. Sediment transport scaling for physical models is addressed in Appendix C.

Numerical sedimentation models are sometimes referred to as morphological models because the processes being simulated involve the interaction and feedback between the flow structure and the movable channel boundaries. Typically, sediment erosion, transport, and deposition are simulated along the long profile (i.e., down-channel) through a one-dimensional formulation. The St. Venant equations for open channel flow (or some simplification of these equations) are typically coupled to a solution of the conservation of sediment mass—often referred to as the Exner equation (USACE 1993a). The simulation progresses forward in time, with user-specified boundary conditions defining the hydrologic events of interest. Numerical model results typically consist of the time history of river stage, discharge, channel bed elevation, bed material gradation, and quantity and gradation of sediment transport, all at specified locations along the long profile axis. Additional details on the formulation, assumptions, and typical applications of one-dimensional numerical models can be found in Chapter 14.

As of 2006, application of multidimensional (two- and three-dimensional) numerical models is becoming more common, given the relative economy of powerful computers, the continued development and testing of efficient numerical approximation schemes, and the ongoing training and experience gained by practitioners as the tools become more widely available and affordable (Gessler et al. 1999). Chapter 15 provides extensive information on issues associated with the theoretical formulation and application of these computational tools. Graphical user interfaces (GUIs) are usually

applied for the setup, execution, and evaluation of the extensive databases typically generated by the time-variant solution of multidimensional equations of hydrodynamics and conservation of sediment mass. On the other hand, the convenience of GUIs enables inexperienced users to unknowingly set up poorly formulated or erroneous simulations. (This dilemma is not unique to multidimensional sedimentation modeling.) It is, therefore, highly recommended that modelers seek thorough independent review of their problem formulations and results.

Additional subsets of computational numerical models presented in Chapter 8 were developed specifically to depict and quantify the response of channel cross-sectional geometry and planform to changes in water and sediment inputs. Although not as extensively applied in engineering practice as the one-dimensional and multidimensional models described in Chapters 14 and 15, these models utilize advances in understanding of complex morphological processes and provide a means of assessing erosion risk for infrastructure located in the vicinity of active fluvial systems. (Chapter 7 summarizes the extensive research and analysis on stream-bank erosion and channel width adjustment conducted since publication of Manual 54.) Recent models address the effects of human-induced influences such as flow regulation by reservoirs, land use changes and associated changes in runoff and sediment yield, and alteration of floodplain boundaries due to levee construction (Parker 1978; Paola et al. 2006). Chapter 8 discusses the physical processes and numerical modeling of river meandering and channel planform adjustment. Planform response models are based on linkages between channel curvature, velocity redistribution, and bank erodibility (Ikeda and Parker 1989). Chapter 19 addresses the computational modeling of sediment hazards such as mud and debris flows and flooding in alluvial fans.

1.4 OVERVIEW OF SEDIMENT DEPOSITION

1.4.1 General

As in the case of erosion, sediment deposition can be categorized into geological (or natural) and accelerated (or human-induced) deposition. Geologic deposition occurs because of natural processes of tectonic uplift, volcanic eruptions, earthquakes, climate warming, glacial movements, and so on. This category of processes usually occurs over long periods but may also result from severe episodic events. On the other hand, human-induced deposition resulting from various human activities usually results in relatively rapid changes in river morphology and sedimentation.

Products of erosion may be transported and deposited over a wide range of distances from their source. Where there are long distances to the ultimate sink of the oceans, only a minor fraction of the source load may arrive there. It has been estimated that in the United States, only about 10% of the material eroded from upland basins reaches the oceans, the remainder being stored in lakes, reservoirs, channels, and land surfaces (Curtis et al. 1973; Holeman 1981).

Deposited sediment may be harmful or beneficial according to circumstances and viewpoints. Although sediment may fill reservoirs and eliminate their storage capacity or aggrade riverbeds and lead to increased flooding, silt deposits on floodplains may eventually form valuable agricultural soils, and gravel deposits in rivers may provide valuable fish habitat and a source for building materials. Where deposition in downstream reaches of rivers poses problems, settlement basins are sometimes provided to store deposited sediment at upstream locations. These may offer only temporary relief unless the deposits can be removed at regular intervals. Construction of dams and other flow control structures that encourage sediment deposition can reduce sediment delivery downstream to coastal areas and may lead to long-term beach erosion and shoreline retreat.

Problems and studies involving sediment deposition have greatly expanded beyond concerns over engineering works (structures) into environmental concerns such as effects on fish habitat and benthic communities and the role of sediment in storing and releasing toxic contaminants. Chapters 21 through 23 address these topics further. Acute problems of sediment deposition may follow catastrophic events such as earthquakes, volcanic eruptions, dam failures, massive landslides, and debris flows (see MacArthur et al. 1985, 1990; Costa and Wieczorek 1987; Committee on Alluvial Fan Flooding (CAFF) 1996; Chen 1997; Wieczorek and Naeser 2000). Chapter 19 discusses these topics further.

1.4.2 Causes of Sediment Deposition

1.4.2.1 Upland River Deposits Deposits at the base of eroding slopes are discussed in Manual 54. Some other forms of near-source deposits are described briefly below.

Debris flows in steep streams produce run-out deposits containing large woody debris mixed with finer organic material and sediment of a wide range of sizes up to large boulders (Fig. 1-11). Such deposits may block roads and

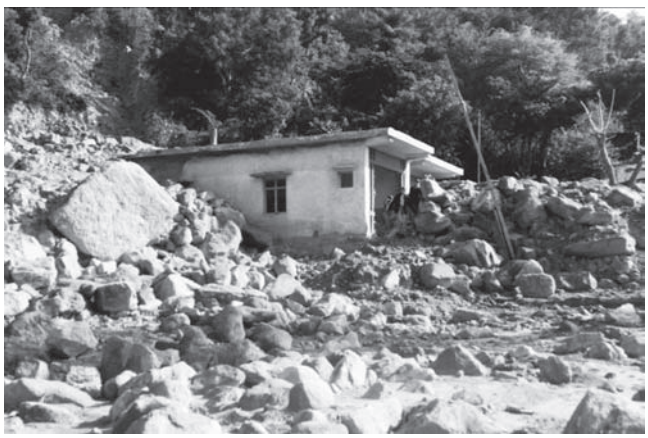

Fig. 1-11. Debris flow deposit from small tributary of Tinau River in Nepal. *Photograph by V. J. Galay.*

railroads, redirect the course of streams, or destroy buildings and properties. Debris flows may have natural causes but may also be initiated or aggravated by logging and road construction on steep forest slopes.

Alluvial fans (or inland deltas) generally form where a stream emerges from a mountain zone, becomes laterally unconfined, and undergoes an abrupt reduction in gradient. Fans, which may be of any size, may contain sand, gravel, and boulders and are characterized by multiple shifting stream channels with sudden "avulsions" during floods. Fans may exist in an aggrading, degrading, or stable state. The morphology and hydraulics of fans are discussed by French (1987), Rachocki and Church (1990), and CAFF (1996).

Braided river deposits (or outwash valley trains) somewhat resemble narrow elongated fans, with multiple shifting channels (Fig. 1-12). They may be found downstream of eroding mountain ranges or glaciers. Gravel deposits are most common in braided river systems; however, braided sand or boulder rivers also occur (Ikeda and Parker 1989; Best and Bristow 1993).

1.4.2.2 Intermediate and Lowland River Deposits Channel and floodplain deposits are discussed in Manual 54. Other forms are discussed briefly below.

Deposits of riverborne sediment often cause problems in engineered conduits such as canals, tunnels, culverts, and pipelines that divert river water for irrigation, hydropower, and so on (Fig. 1-13). The sediment may deposit at shallow depths over a long length and may not be noticed until hydraulic capacities are severely reduced by loss of area, increased roughness, and weed growth.

Meandering rivers with their adjacent floodplains generally represent large volumes of stored sediment that gradually work downstream through a process of meander migration, eroding sediment from one place and depositing it farther downstream (Fig. 1-14). A section through the floodplain generally exhibits coarser riverbed sediments up to a certain level and fine overbank deposits above. Installation of dikes, levees, and bank protection may disrupt natural processes and cause unforeseen problems, such as channel aggradation or degradation or accelerated erosion of unprotected banks.

1.4.2.3 Sedimentation Due to Mining Activities Mining activities in river basins and failures of mine tailings dams can produce disastrous sedimentation and contamination of downstream rivers/water bodies (Figs. 1-15 and 1-16). The design, construction, and maintenance of such facilities have often been inadequate (see, e.g., United Nations Environment Program and International Commission on Large Dams [UNEP/ICOLD] 2001). Once constructed, mines and tailings dams often result in long-term hazards that may culminate in costly mitigation having to be performed by future generations of landowners and governments. When mines and tailing ponds are eventually abandoned, extensive engineering measures may be needed to prevent future erosion or release of contaminated sediments.

1.4.2.4 Deposits in Lakes and Reservoirs Deposits in larger lakes and reservoirs that receive riverborne sediment generally consist of coarser sediment (sand and gravel) forming a delta at the inlet end and finer sediment (silt and clay)

Fig. 1-12. Braided river system located on the Rio Maule, Chile, comprised primarily of cobble and boulder materials. *Photograph by C. R. Neill.*

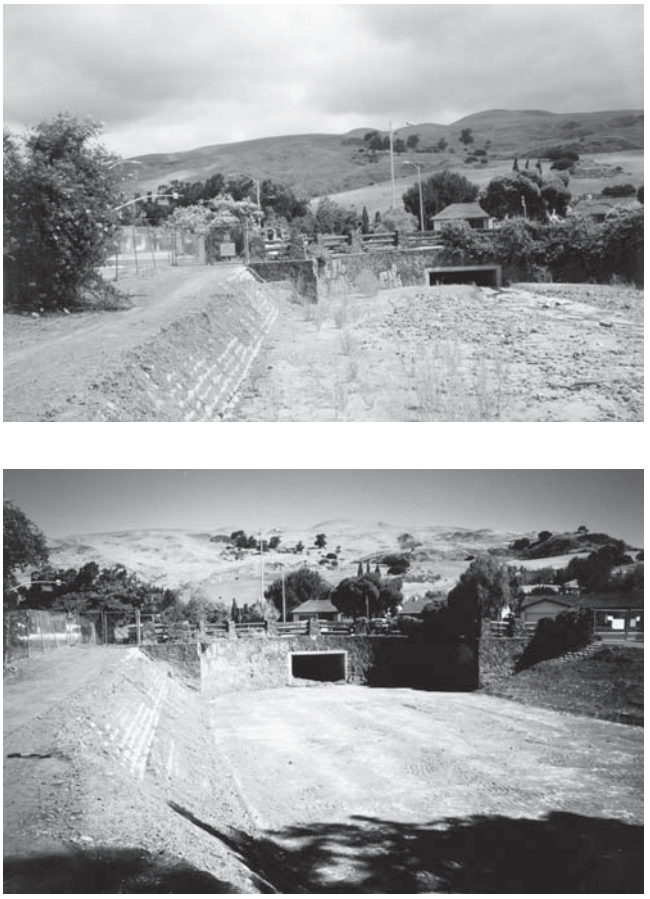

Fig. 1-13. Box culvert and sediment detention basin on urbanized reach of Upper Berryessa Creek in Milpitas, California. Basin filled with gravel is shown in top photo and after cleaning in bottom photo. View is upstream. *Photographs by R. C. MacArthur.*

Fig. 1-14. Meandering reach of Walker River, California. *Photograph by E. Wallace.*

Fig. 1-15. Copper and gold mine on Mount Fubilan in Papua New Guinea. Since the mid-1980s, the mine has discharged 70 million tons per year of contaminated rock and tailings into the Ok Tedi and Fly rivers. *Photograph by B. Hall.*

Fig. 1-16. Fly River in Papua New Guinea: an example of man-induced ecological disaster. Sediment deposition from the Ok Tedi mine continues to aggrade riverbeds and amplifies flooding and sedimentation of forest areas, killing fish, forcing animals to migrate, and destroying vegetation over vast areas. *Photograph by B. Hall.*

spread out over all or a substantial part of the bottom area (Figs. 1-17 and 1-18). In smaller water bodies, the delta may eventually extend to occupy most of the volume. Lake-bottom sediments in some regions exhibit annual layers ("varves") that reflect different conditions of deposition between seasons. These can sometimes be used to determine the variation of deposition rates over long periods of time. Deposition patterns of finer sediment may be affected by weak currents, wind, and density currents arising from the different densities of sediment-bearing inflows and clear lake water.

During the middle part of the twentieth century, when large numbers of dams and reservoirs were constructed worldwide in regions of unstable physiography for purposes such as hydropower, irrigation, and water supply, the problem of reservoir sedimentation tended to receive insufficient attention in many preproject planning studies. Sediment deposition severely affects operations and

Fig. 1-17. High sediment concentration turbidity currents from Frosst Creek, British Columbia, Canada, plunging through delta into Cultus Lake. *Photograph by V. J. Galay.*

Fig. 1-18. Lake Solano, California: example of significant reservoir siltation. *Photograph by R. C. MacArthur.*

the useful life of the facility. A related problem is how to manage reservoir sediment deposits to avoid adverse downstream consequences when a dam is removed or decommissioned because of disuse, structural deterioration, and so on. Chapter 23 discusses how numerical models can be used to assess potential changes in sediment transport associated with dam removal.

Morris and Fan (1997) provide extensive information regarding deposition in reservoirs and lakes, including dam removal, and cite numerous case studies. They provide an overview that emphasizes sustainable development and the need for long-term viewpoints in planning and design. White (2001) presents information devoted to removal of sediment from reservoirs. The morphodynamics of reservoir sedimentation is addressed in Chapter 2. Chapter 12 provides an additional overview of reservoir sedimentation issues.

1.4.3 Environmental and Habitat Effects of Sediment Deposition

Sediment deposition may have major effects on zoological habitat, particularly for salmonid and other non-warmwater fish species in streams. Problems tend to occur whenever the natural hydrologic and sediment regime is disrupted in such a way that changes occur in quantities and gradation of delivered sediment or in the physical characteristics of the riverbed. In many jurisdictions, regulations regarding both short- and long-term disturbances have become increasingly stringent.

Where sediment is trapped in new reservoirs, downstream fishery effects may be beneficial or harmful. If the stream formerly carried high suspended loads of fine sediment, trapping may be beneficial to aquatic species. On the other hand, if sand and gravel is trapped from a relatively clear stream, downstream reaches may downcut to a flatter gradient and become paved with large stones that offer poor habitat and biological environment for a variety of benthic and pelagic species. Reduction of flood peaks by reservoir regulation may adversely affect annual flushing of fine sediment from spawning areas. Chapter 3 contains material useful to addressing these topics.

Where land use changes increase inputs of fine sediment to a river, its deposition downstream may clog spawning beds (Huang and Garcia 2000). Construction operations for bridge and pipeline crossings may temporarily increase fine sediment inputs, with similar results.

Many toxic substances and contaminants in water become preferentially attached to sediment (particularly to fine sediments) and accumulate within deposition zones. Contaminated sediments may become buried if the source is discontinued but may be exposed later by erosion and channel shifting. Concentration by bioaccumulation, especially of heavy metals and pesticides, is often a major concern. Deposits behind mine tailings dams are often highly contaminated, requiring massive cleanup operations in cases of failures of such structures (UNEP/ICOLD 2001). These topics are discussed further in Chapters 21 and 22.

1.4.4 Estimation of Deposition Rates and Quantities

Estimation of past rates and quantities of deposition in static water bodies is usually based on periodic bathymetric surveys aided by core sampling and dating. Reservoirs subject to significant sediment deposition should be surveyed and sampled at regular intervals. Statistics on reservoir deposition are often available from owners, operators, and regulating agencies.

Estimation of future deposition rates for new reservoirs, flood control facilities, and sediment basins may be based empirically on data from other water bodies in similar environments with regard to dimensions and trap efficiency or semiempirically on studies of sediment yield and delivery with regard to grain size distributions and settlement rates or based on comprehensive numerical modeling that accounts for currents, wind, and turbulence. Depending on the dimensions of the water body, one- or two-dimensional modeling may be appropriate and beneficial during project evaluations.

1.5 MANAGEMENT AND TREATMENT OF SEDIMENTATION PROBLEMS

1.5.1 General

In general, management and treatment of sedimentation engineering problems can be addressed upstream at the sources of the sediment production, downstream at the site of the problem, or at intermediate locations. However, the efficacy of sediment management can be enhanced by addressing and managing sediment problems at a whole-watershed level rather through a series of disconnected locally independent projects. Obviously, the best solution is to avoid problems through good planning and design. More important, restoration of process is more likely to address the causes of river degradation, whereas restoration toward a fixed endpoint addresses only the symptoms (Wohl et al. 2005). Some problems, such as scour at bridge foundations, are clearly local and require only local treatment. Others, such as deposition in reservoirs, often derive from an extensive drainage basin and might be addressed either on a local or on a basinwide basis. In many sedimentation problems, a complete "solution" is not possible, and the best that can be achieved is a reliable system for management and monitoring. Attention should generally be given to the feasibility of nonengineering as well as engineering approaches.

Treatment of erosion at the source would often be the most satisfactory solution in the long term, but in many cases it may not be physically, economically, or socially feasible because the sources are too widely distributed and are associated with natural geological processes or human activities regarded as inviolable. The engineer must then design works

and develop methods for handling sediment at or nearer to the site of interest to ensure that the performance and life of the works are not unreasonably affected. In the case of a storage reservoir liable to fill too rapidly with sediment, consideration could be given to land reclamation in the basin, to the provision of intermediate sediment detention basins upstream of the site, or to methods of bypassing sediment past the reservoir or flushing it out at intervals to minimize downstream impacts. The relative advantages of alternative approaches may depend on the planned life of the facility and on environmental concerns upstream or downstream.

Sediment control methods are treated extensively in Manual 54. As of 2005, much of the material contained therein is still valid. In the present volume, coverage and updating are limited. Chapter 9 addresses the restoration of streams adversely affected by human activities or extreme natural events, Chapter 11 addresses prevention of scour around bridge foundations, Chapter 12 addresses reservoir sedimentation, Chapter 19 discusses "sediment hazards," Chapter 23 discusses the use of modeling to determine changes in sediment transport associated with dam removal, and Appendix B addresses the design of riprap erosion protection.

1.5.2 Problem Identification and Definition

During planning and design of new projects and before attempting to devise alternative solutions to existing sedimentation engineering problems, it is important to develop a clear definition of existing and potential problems, which may be complex and may ultimately involve other interdisciplinary concerns. To do this, each important component of a problem (or potential problems) must be identified and quantified to some level of certainty. Thorough project planning and evaluation of future project performance can greatly increase project reliability while reducing maintenance and possible future sediment-related problems. Chapter 3 in the Corps of Engineer's EM 1110-2-1416, *River Hydraulics* (USACE 1993b), outlines procedures for conducting hydraulic engineering studies so as to avoid unforeseen sediment or project performance problems. Questions to consider during plan formulation and problem identification and definition phases may include the following:

- Where are the sources of erosion and sediment, and what are their relative significances?
- Is the problem ascribable mainly to fine wash-load sediment such as silt and clay; to coarser bed-material sediment such as sand, gravel, and boulders; or to both? In what modes will the material be transported under various stream-flow conditions?
- Is the problem associated mainly with river flood conditions or with a wide range of stream flows?
- Is the problem new or has it been developing for a long period of time? Is the problem periodic or chronic? What is the history of the sources of erosion?
- Is the problem localized or more regional in nature? Is its scale small or large?
- Is the problem associated with scour, deposition of materials, or both?
- What information is available on rates and quantities and grain sizes of sediment in transport?
- Have rates and quantities been increasing, and, if so, why? Have there been significant changes in land use or river works and management, or have extreme events occurred recently?
- If sediment will be stored in reservoirs or detentionbasins, how fast will this occur, and what will happen when these are filled? What are the downstream engineering and environmental implications of periodic storage and release of materials from the reservoir in the future?
- What are the degrees of uncertainty in quantitative estimates, and what are the project implications of under- or overestimating future quantities? What allowances should be made for land use change and climate change?
- What essential data are needed to better define potential problems and solutions?
- What alternative solutions are there, and how sustainable are alternative solutions in both engineering and environmental terms?

Many of these important questions are addressed in the following chapters and appendices of this manual. The key to successful problem avoidance and solution is to achieve objective, credible problem identification early in project planning. This will facilitate more effective field and office investigations and the development of feasible alternatives. Careful attention to this step can produce economies in investigations and avoid the formulation of inappropriate solutions. Chapter 20, "American Sedimentation Law and Physical Processes," discusses changes in legal requirements and liabilities associated with standards of care, responsible project planning, and design.

Since the printing of Manual 54 in 1975, the focus of sedimentation engineering has greatly expanded from the identification and solution of individual problems (however complex they may be) to much broader involvement in multidisciplinary planning, analysis, and design of multipurpose projects. This role often requires careful balancing of engineering science, environmental concerns, public interests, and affordability.

1.5.3 Engineering Treatment

Engineering (or engineered) treatment embraces the planning and design of civil engineering works and operational systems to deal with and manage sedimentation processes so as to avoid serious problems. The chapter on sediment control methods in Manual 54 is devoted mainly to this type of treatment. Engineering treatments and erosion countermeasures are usually associated with more traditional structural "hardscape" solutions (see Chapters 11 and 19 and Appendices A and B).

Examples of works and projects most amenable to engineering treatment include (1) intakes from rivers into pipelines and canals for purposes of hydropower, irrigation, or water supply, where the aim is to reduce or eliminate the inflow of specific size classes of sediment that would clog or deposit in diversion conduits and facilities; (2) bank protection and channel maintenance in large or fast-flowing rivers and streams (Fig. 1-19); (3) protection of river-crossing facilities against bank erosion and bed scour; (4) dams and reservoirs, where it is infeasible to deal with upstream basin conditions and sediment inflows must be accepted as delivered to the site; and (5) flood control facilities to provide public safety during severe flood events.

The design of intakes to reduce the entry of sediment is addressed, among others, by Bouvard (1992), Raudkivi (1993), and ASCE (1995). Riverbank protection is addressed by Appendix B and USACE (1991, 1994), CUR (1995), Thorne et al. (1995), and Escarameia (1998). Scour at bridges is addressed in Chapters 10 and 11 herein, and reservoir sedimentation is addressed in Chapter 12.

In formulating and presenting engineering solutions, it is important to identify limitations in knowledge and uncertainties as to future outcomes and to provide flexibility for future changes if quantitative estimates and performance of works prove to be less favorable than expected. The limitations and uncertainties inherent in quantitative sediment estimates and sediment modeling are not always fully understood by project planners, environmentalists, and structure designers. Legal aspects and responsibilities of sediment engineers are discussed in Chapter 20.

1.5.4 Nonengineering (Nonstructural) Treatment

In the latter part of the twentieth century, a trend developed to replace engineering treatment of sedimentation problems by nonengineering, or nonstructural, treatment with apparently greater environmental benefits; fewer hardscape-type structures; more bioengineering features; and more environmental acceptability. Project planning and design specifications began to seek opportunities and requirements for enhancing and restoring natural aspects of water resource systems and to discourage engineered "hardscaping." Examples of nonengineering treatments include the following: (1) for reservoirs, upstream improvements in soil conservation and land use, such as reforestation, reduction of grazing pressure, or restriction of urban development; (2) for shifting streams, bank stabilization and restoration using vegetation and bioengineering techniques instead of rock or concrete erosion protection (Figs. 1-20 and 1-21); and (3) for flood control projects, restoring wetlands and natural water and sediment storages instead of constructing artificial sediment detention basins or excavating larger

Fig. 1-20. Planting vegetation to reduce flow velocities, capture debris, and encourage sediment deposition to provide protection along an eroding bank of the Russian River, California. *Photograph by D. Ripple.*

Fig. 1-19. Bank protection works in urban setting consisting of riprap toe armor and bank revetment materials with horizontal rows of willow pole plantings, as installed on Soquel Creek, California. *Photograph by S. Seville.*

Fig. 1-21. Bioengineered logjams being installed to protect eroding river banks, to increase habitat complexity, and to provide deep pools for fish on the Mahatta River, British Columbia, Canada. *Photograph by B. Walsh.*

flood conveyance channels. Chapter 9 presents detailed discussions of the benefits and methods for restoring river systems using a variety of bioengineering techniques.

Some publications and guidelines prepared by nonengineers have tended to recommend the application of nonengineering and bioengineering measures in circumstances where they are unlikely to be successful—for example, vegetation plantings for bank protection in steep streams with high velocities and turbulence. It is therefore an unfortunate misrepresentation associated with recent movement toward nonengineered or bioengineered methods to imply that less engineering analyses and judgment is required in order to achieve better results. To the contrary, significant hydraulic, river, and sedimentation engineering experience and analyses are required with input from other biological and ecological disciplines to ensure successful project planning and design. Also of importance is the movement toward "restoration of function" as opposed to piecemeal treatment of site-specific problems. In general, a holistic view should be taken of sedimentation management to utilize both engineering and nonengineering measures where appropriate and feasible (Petts and Calow 1996; Federal Interagency Stream Restoration Working Group 1998; Copeland et al. 2001). In locations that have been severely damaged by poor land use practices and neglect, the benefits of such an approach may extend far beyond the project under consideration (see Natural Resource Conservation Service 1992, 1996; Gray and Sotir 1996).

1.5.5 Fish Habitat and Environmental Issues

Since publication of Manual 54 in 1975, many jurisdictions in technically advanced countries have enacted strict requirements for the design and construction of works in water bodies to avoid or mitigate erosion and sedimentation effects on fish habitat and aquatic resources. Engineers and planners have sometimes considered certain regulatory controls to be excessive—for example, when placement of small areas of rock riprap around river bridge piers is prohibited or made conditional on the provision of artificially constructed "habitat" elsewhere. In general, however, recognition by engineers of the necessity for tough legal requirements for environmental protection (see Chapter 20) has improved significantly since the mid-1980s (Bass and Herson 1993a, 1993b).

Stream restoration projects are often designed to improve or restore fish habitat (Fig. 1-21) or improve fish passage (Fig. 1-22) (Clay 1995) and to support ecosystems in streams that have been adversely affected by logging or other human activities (Committee on Restoration of Aquatic Ecosystems 1992; Cooke et al. 1993; Wohl et al. 2005). As of 2006, the success of such projects in terms of biological productivity was not universally accepted. Kellerhals and Miles (1996) stated that the scientific basis linking morphological change, habitat, and fish productivity was weak in terms of prediction and that some stream restoration projects had been undertaken without a proper understanding of biological limiting factors or a sound basis for predicting the results of habitat manipulations. In some cases, long periods of many years may be needed to re-establish a viable habitat, and the effort may be largely nullified by overexploitation of the fish resource. This complex topic is discussed further in Chapter 9.

Fig. 1-22. Photos show barrier to fish passage through bridge culvert before (top) and after (bottom) construction of log step weirs and gravel-bottom pool and step approach aprons on Little Salmon Creek, Toledo, Washington. View is upstream. *Photographs by J. Johnson.*

REFERENCES

ASCE. (1962). "Nomenclature for hydraulics." *Manual 43,* ASCE, New York, 501 p.

ASCE. (1995). *Guidelines for design of intakes for hydroelectric plants,* Committee on Hydropower Intakes of the Energy Division, ASCE, Reston, Va., 475 p.

Barfield, B. J., Warner, R. C., and Haan, C. T. (1981). *Applied hydrology and sedimentology for disturbed areas,* Oklahoma Technical Press, Stillwater, Okla.

Barrow, C. J. (1991). *Land degradation: Development and breakdown of terrestrial environments,* Cambridge University Press, Cambridge, 295 p.

Bass, R. E., and Herson, A. I. (1993a). *Mastering NEPA: A step-by-step approach,* Solano Press Books, Point Arena, Calif.

Bass, R. E., and Herson, A. I. (1993b). *Successful CEQA compliance: A step-by-step approach,* Solano Press Books, Point Arena, Calif.

Best, J. L., and Bristow, C. S. (1993). *Braided rivers*. Geological Society Special Publication 75, London, 419 p.

Borgen, J., Fergus, T., and Walling, D. E., eds. (2003). *Erosion and sediment transport measurement in rivers: Technological and methodological advances.* Publication 283, IAHS Press (Intern. Assoc. of Hydrological Sciences), Wallingford, United Kingdom.

Bouvard, M. (1992). *Mobile barrages and intakes on sediment transporting rivers*. IAHR Monograph Series, A. A. Balkema, Rotterdam, 320 p.

Brown, A. V., Lyttle, M. M., and Brown, K. B. (1998). "Impacts of gravel mining on gravel bed streams." *Trans. Am. Fish. Soc.,* 127, 979–994.

Brown, L. (1991). "The global competition for land." *J. Sci. Water Conserv.,* 46(6), 394–397.

Bryant, D., Nielsen, D., and Tangley, L. (1997). *The last frontier forests: Ecosystems and economics on the edge*. Research Report, World Resources Institute, Washington, D.C., 42 p.

Chang, H. H. (1988). *Fluvial processes in river engineering,* John Wiley & Sons, New York, 432 p.

Chen, C., ed. (1997). *Debris-flow hazards mitigation: Mechanics, prediction and assessment,* Proceedings of the First International Conference, ASCE, Reston, Va., 830 p.

Chien, N., and Wan, Z. (1999). *Mechanics of sediment transport,* ASCE Press, Reston, Va., 913 p.

Church, M. (2001). *River science and Fraser River: Who controls the river?,* Gravel-Bed Rivers V, New Zealand Hydrological Society Inc., Wellington, New Zealand, 607–632.

Clay, C. H. (1995). *Design of fishways and other fish facilities,* 2nd ed., Lewis Publishers, Boca Raton, Fla.

Collins, B., and Dunne, T. (1990). *Fluvial geomorphology and river-gravel mining: A guideline for planners, case studies included,* California Department of Conservation, Division of Mines and Geology, Sacramento, Calif., 29 p.

Committee on Alluvial Fan Flooding. (1996). *Alluvial fan flooding,* Water Science and Technology Board, Commission on Geosciences, Environment, and Resources, National Research Council, National Academy Press, Washington, D.C., 182 p.

Committee on Restoration of Aquatic Ecosystems. (1992). *Restoration of aquatic ecosystems,* Water Science and Technology Board, Commission on Geosciences, Environment, and Resources, National Research Council, National Academy Press, Washington, D.C., 576 p.

Cooke, G. D., Welch, E. B., Peterson, S. A., and Newroth, P. R. (1993). *Restoration and management of lakes and reservoirs,* 2nd ed., Lewis Publishers, Boca Raton, Fla.

Copeland, R. R., McComas, D. N., Thorne, C. R., Soar, P. J., Jonas, M. M., and Fripp, J. B. (2001). *Hydraulic design of stream restoration projects*. Report ERDC/CHL TR-01-28, U.S. Army Corps of Engineers, Vicksburg, Miss., 172 p.

Costa, J. E. (1988). "Rheologic, geomorphic, and sedimentologic differentiation of water floods, hyperconcentrated flows, and debris flows." *Flood geomorphology,* V. R. Baker, R. C. Kochel, and P. C. Patton, eds., John Wiley & Sons, New York, 113–122.

Costa, J. E., and Wieczorek, G. F., eds. (1987). *Debris flows/avalanches: Process, recognition, and mitigation*. Reviews in Engineering Geology 7, Geological Society of America, Boulder, Colo.

CUR. (1995). "Manual on the use of rock in hydraulic engineering." *CUR/RWS Report 169,* Centre for Civil Engineering Research and Codes, A. A. Balkema, Rotterdam.

Curtis, W., Culbertson, J., and Chase, E. (1973). *Fluvial-sediment discharge to the oceans from the conterminous United States,* U.S. Geological Survey Circular 670, U.S. Geological Survey, Reston, Va.

de Boer, D. H., Froehlich, W., Mizuyama, T., and Pietroniro, A., eds. (2003). *Erosion prediction in ungauged basins (PUBs): Integrating methods and techniques.* Publication 279, IAHS Press (Int. Assoc. of Hydrological Sciences), Wallingford, United Kingdom.

Edwards, T. K., and Glysson, G. D. (1999). *Field methods for measurement of fluvial sediment*. U.S. Geological Survey, Techniques of Water Resources Investigations, Book 3, Chapter C2, 89 p., Reston, Va.

Escarameia, M. (1998). *River and channel revetments: A design manual,* Thomas Telford Publications, London, 245 p.

Food and Agriculture Organization of the United Nations. (2001). "Comparison of forest area and forest area change estimates derived from FRA 1990 and FRA 2000." *Working Paper 59,* Forest Resources Assessment Programme, Rome, 69 p.

Federal Interagency Stream Restoration Working Group. (1998). *Stream corridor restoration: Principles, processes and practices,* U.S. Department of Agriculture, Washington, D.C.

French, R. H. (1987). *Hydraulic processes on alluvial fans,* Elsevier Scientific Publishing, Amsterdam.

Garde, R. J., and Ranga Raju, K. G. (1977). *Mechanics of sediment transportation and alluvial stream problems,* Wiley Eastern Ltd, New Delhi, 483 p.

Gessler, D., Hall, B., Spasojevic, M., Holly, F., Pourtaheri, H., and Raphelt, N. (1999). "Application of 3D mobile bed hydrodynamic model." *J. Hydr. Engrg.,* 125(7), 737–749.

Golubev, G. N. (1982). "Soil erosion and agriculture in the world: An assessment and hydrological implications." *Proceedings, Recent developments in the explanation and prediction of erosion and sediment yield,* Proc. of the Exeter Symp., July 1982, Publication 137, IAHS, Wallingford, United Kingdom, 261–268.

Gomez, B., and Church, M. (1989). "An assessment of bed load sediment transport formulae for gravel bed rivers." *Water Resour. Res.,* 25(6), 1161–1186.

Graf, W. H. (1984). *Hydraulics of sediment transport,* Water Resources Publications, Littleton, Colo.

Graf, W. H. (2001). "Damage control: Restoring the physical integrity of America's rivers." *Annals of the Association of American Geographers,* 91(1), 1–27.

Gray, D. H., and Sotir, R. B. (1996). *Biotechnical and soil bioengineering slope stabilization: A practical guide for erosion control,* John Wiley & Sons, New York.

Haan, C. T., Barfield, B. J., and Hayes, J. C. (1994). *Design hydrology and sedimentology for small catchments,* Academic Press, New York, 588 p.

Hasselmann, K., Latif, M., Hooss, G., Azar, C., Edenhofer, O., Jaeger, C. C., et al. (2003). "The challenge of long-term climate change." *Science,* 302, 1923–1925.

Hatheway, A. (2005). "George A. Kiersch: Engineering geology applied to anthropogenic problems." *Reviews in Engineering Geology,* 16, 1–6.

Hauck, F. W. (1985). *Soil erosion and its control in developing countries,* Soil Erosion and Conservation, Soil Conservation Society of America, Ankeny, Iowa, p. 718–728.

Holeman, J. N. (1981). "The national erosion inventory of the Soil Conservation Service, U.S. Department of Agriculture, 1977–1979." *Erosion and sediment transport measurement,* Publication 133, IAHS, Wallingford, United Kingdom, 315–319.

Hooke, R. L. (1994). "On the efficacy of humans as geomorphic agents." *GSA Today,* 4(9), 217, 224–225.

Huang, X., and Garcia, M. H. (2000). "Pollution of gravel spawning grounds by deposition of suspended sediment." *J. of Env. Eng.*, 126(10), 963–967.

Ikeda, S., and Parker, G., eds. (1989). *River meandering*. Water Resources Monograph 12, American Geophysical Union, Washington, D.C.

Ismail, W. R. (1997). "The impact of hill land clearance and urbanization on runoff and sediment yield of small catchments in Pulau Pinang, Malaysia." *Proceedings, Human Impact on Erosion and Sedimentation,* Publication 245, D. E. Walling and J. L. Probst, eds., IAHS, Wallingford, United Kingdom.

Jalees, K. (1985). "Loss of productive soil in India." *Int. J. Environ. Stud.,* 24(3/4), 245–250.

Julien, P. Y. (2002). *River mechanics,* Cambridge University Press, Cambridge, 454 p.

Kellerhals, R., and Miles, M. (1996). *Fluvial geomorphology and fish habitat: Implications for river restoration*. *Proc., Second Int. Symp. on Habitat Hydraulics,* M. Leclerc et al., eds., INRS-Eau, Quebec, A261–A279.

Kondolf, G. M. (1994). "Geomorphic and environmental effects of instream gravel mining." *Landscape Urban Planning,* 28, 225–243.

Kondolf, G. M. (1998a). "Environmental effects of aggregate extraction from river channels and floodplains." *Aggregate resources: A global perspective,* P. T. Bobrowsky, ed., A. A. Balkema, Rotterdam, 113–129.

Kondolf, G. M. (1998b). "Large-scale extraction of alluvial deposits from rivers in California: Geomorphic effects and regulatory strategies." *Gravel-bed rivers and the environment,* P. C. Klingeman, R. L. Beschta, P. D. Komar, and J. B. Bradley, eds., Water Resources Publications, Littleton, Colo., 455–470.

Lyn, D. A. (2006). "The idea of a hydraulic engineering journal." *J. Hydr. Engrg.,* 132(5), 439.

MacArthur, R. C., Brunner, G., and Hamilton, D. L. (1990). *Numerical simulation of mudflows from hypothetical failures of the Castle Lake debris blockage near Mount St. Helens, WA*. Special Projects Report 90-05, U.S. Army Corps of Engineers, Hydrologic Engineering Center, Davis, Calif.

MacArthur, R. C., Hamilton, D. L., and Schamber, D. R. (1985). *Toutle River mudflow investigation*. Special Projects Report 85-3, U.S. Army Corps of Engineers, Hydrologic Engineering Center, Davis, Calif.

May, R., Ackers, J., and Kirby, A. (2002). *Manual on scour at bridges and other hydraulic structures*. CIRIA Report C551, Construction Industry Research and Information Association, London, 225 p.

McCarthy, J. J., Canziani, O. F., Leary, N. A., Dokken, D. J., and White, K. S., eds. (2001). *Climate change 2001: Impacts, adaptation and vulnerability*. Contribution of Working Group II to Third Assessment Report of Intergovernmental Panel on Climate Change (IPCC), Cambridge University Press, Cambridge, 1,000 p.

Melville, B. W., and Coleman, S. E. (2000). *Bridge scour,* Water Resources Publications, Littleton, Colo., 550 p.

Morris, G. L., and Fan, J. (1997). *Reservoir sedimentation handbook,* McGraw-Hill, New York, 848 p.

National Research Council. (1989). *Reducing disasters' toll: The United States decade for natural disaster reduction,* National Academy Press, Washington, D.C., 40 p.

Natural Resource Conservation Service. (1992). *Soil bioengineering for upland slope protection and erosion reduction*. Engineering Field Handbook, Part 650, Chapter 18, U.S. Department of Agriculture, Washington, D.C.

Natural Resource Conservation Service. (1996). *Streambank and shoreline protection*. Engineering Field Handbook, Part 650, Chapter 16, U.S. Department of Agriculture, Washington, D.C.

Paola, C., Foufoula-Georgiou, E., Dietrich, W., Hondzo, M., Mohrig, D., Parker, G., et al. (2006). "Toward a unified science of the Earth's surface: Opportunities for synthesis among hydrology, geomorphology, geochemistry, and ecology." *Water Resour. Res.,* 42, W03S10, 10.1029/2005WR004336, 6 p.

Parker, G. (1978). "Self-formed straight rivers with equilibrium banks and mobile bed, part 2: The gravel river." *J. Fluid Mech.,* 89, 127–146.

Parker, G. (1990). "Surface based bedload transport relation for gravel rivers." *J. Hydr. Res.,* 28(4), 417–436.

Petts, G., and Calow, P., eds. (1996). *River restoration,* Blackwell Science, Oxford, 231 p.

Quinones, F., and Johnson, K. G. (1987). *Floods of May 17–18, 1985 and October 6–7, 1985 in Puerto Rico*. Open File Report 87-123, U.S. Geological Survey, Reston, Va., 22 p.

Rachocki, A. H., and Church M. (1990) *Alluvial fans,* John Wiley & Sons., New York.

Raudkivi, A. J. (1976). *Loose boundary hydraulics,* Pergamon Press., Oxford.

Raudkivi, A. J. (1993). *Sedimentation: Exclusion and removal of sediment from diverted water*. Hydraulic Structures Design Manual 6, A. A. Balkema, Rotterdam, 164 p.

Reid, L., and Dunne, T. (1996). *Rapid evaluation of sediment budgets*. GeoEcology paperback, CATENA VERLAG, Reiskerchen, Germany, 164 p.

Richardson, E. V., and Davis, S. R. (2001). *Evaluating scour at bridges*. Hydraulic Engineering Circular 18, U.S. Department of Transportation, Federal Highway Administration, Washington, D.C.

Rose, E. (2005). "Impact of military activities on local and regional geologic conditions." *Reviews in Engineering Geology,* 16, 51–66.

Schumm, S. A., Harvey, M. D., and Watson, C. C. (1984). *Incised channels: Morphology, dynamics and control,* Water Resources Publications, Littleton, Colo., 200 p.

Simons, D. B., and Senturk, F. (1992). *Sediment transport technology: Water and sediment dynamics,* Water Resources Publications, Littleton, Colo., 897 p.

Slaymaker, O. (1988). "Distinctive attributes of debris torrents." *Hydrological Sciences Journal,* 33(6), 567–573.

Summerfield, M. A., and Hutton, N. J. (1994). "Natural controls of fluvial denudation rates in major world drainage basins." *J. Geophys. Res.,* 99(B7), 13,871–13,883.

Thompson, D. (2005). "The history of the use and effectiveness of instream structures in the United States." *Reviews in Engineering Geology,* 16, 35–50.

Thorne, C. R., Abt, S. R., Barends, F.B.J., Maynord, S. T., and Pilarczyk, K. W., eds. (1995). *River, coastal and shoreline protection: Erosion control using riprap and armourstone,* John Wiley & Sons, Hoboken, N. J., 784 p.

Thorne, C. R., Bathurst, J. C., and Hey, R. D., eds. (1987). *Sediment transport in gravel-bed rivers,* John Wiley & Sons, New York, 1,012 p.

Transportation Association of Canada. (2001). *Guide to bridge hydraulics,* 2nd ed., Transportation Association of Canada, Ottawa, 181 p.

United Nations Environment Program International Commission on Large Dams. (2001). *Tailings dams: Risk of dangerous occurrences, lessons learnt from practical experiences*. ICOLD Bulletin 121, United Nations Environment Program, Paris, 144 p.

Uri, N. D., and Lewis, J. A. (1998). "Agriculture and the dynamics of soil erosion in the United States." *Journal of Sustainable Agriculture,* 14(2–3), 63–82.

U.S. Army Corps of Engineers. (1991). *Hydraulic design of flood control channels*. Engineer Manual 1110-2-1601, Washington, D.C.

U.S. Army Corps of Engineers. (1993a). *HEC-6, Scour and deposition in rivers and reservoirs*. User's Manual, Hydrologic Engineering Center, Davis, Calif.

U.S. Army Corps of Engineers. (1993b). *River hydraulics.* Engineering Manual 1110-2-1416, Washington, D.C.

U.S. Army Corps of Engineers. (1994). *Channel stability assessment for flood control projects*. Engineer Manual 1110-2-1418, Washington, D.C.

Valdiya, K. S. (1998). *Dynamic Himalaya,* Universities Press, Hyderabad, India.

Vanoni, V. A., ed. (1975). *Sedimentation engineering*. Manual 54, American Society of Civil Engineers, New York, 745 p.

Van Rijn, L. C. (1993). *Principles of sediment transport in rivers, estuaries and coastal seas,* Aqua Publications, Amsterdam, 715 p.

Walling, D. E., Davies, T. R. and Hasholt, B., eds. (1992). *Erosion, debris flows and environment in mountain regions.* Publication 209, IAHS Press, Wallingford, United Kingdom.

Watson, R. T. (2003). "Climate change: The political situation." *Science,* 302, 1925–1926.

White, R. (2001). *Evacuation of sediments from reservoirs,* Thomas Telford Publishing, London, 260 p.

Wieczorek, G. F., and Naeser, N. D., eds. (2000). *Debris-flow hazards mitigation: Mechanics, prediction, and assessment*. Proc., Second Int. Conference on Debris-Flow Hazards Mitigation, Taipei. Balkema, Rotterdam, 608 p.

Wohl, E., Angermeier, P., Bledsoe, B., Kondolf, G., MacDonnell, L., Merritt, D., et al. (2005). "River restoration." *Water Resour. Res.,* 41, W0301, 10.1029/2005WR003985, 1–12.

Yalin, M. S. (1977). *Mechanics of sediment transport,* 2nd ed., Pergamon Press, Oxford, 298 p.

Yang, C. T. (1996). *Sediment transport: Theory and practice,* McGraw-Hill, New York, 396 p.

Copyrighted Materials
Copyright © 2008 American Society of Civil Engineers (ASCE)
Retrieved from www.knovel.com

CHAPTER 2

Sediment Transport and Morphodynamics

Marcelo H. García

ASCE Manual 54, *Sedimentation Engineering*, prepared under the leadership of Professor Vito A. Vanoni, has provided guidance to theoreticians and practitioners' world wide on the primary topic of sediment problems involved in the development, use, and conservation of water and land resources. First published in 1975, Manual 54 gives an understanding of the nature and scope of sedimentation problems, of the methods for their investigation, and of practical approaches to their solution. It is essentially a textbook on sedimentation engineering, as its title accurately reflects. Manual 54 was the first and most comprehensive text of its kind and has been circulated throughout the world for the past 30 years as the most complete reference on sedimentation engineering in the world. It has recently been published again as the *Classic Edition* (Vanoni 2006). In the spirit of its predecessor, this chapter of Manual of Practice 110, *Sedimentation Engineering,* aims at presenting the state of the art concerning the hydraulics of sediment transport in fluvial systems based on the knowledge gained in the last three decades. A concerted effort is made to relate the mechanics of sediment transport in rivers and by turbidity currents to the morphodynamics of lake and reservoir sedimentation, including the formation of fluvial deltas.

2.1 SEDIMENT TRANSPORT MECHANICS AND RELATED PHENOMENA

The field of sediment transport might just as well be called "transport of granular particles by fluids." As such, it embodies a type of two-phase flow, in which one phase is fluid and the other phase is solid. The prototype for the field is the river. Here, the fluid phase is river water, and the solid phase is sediment grains, e.g., quartz sand. The most common modes of sediment transport in rivers are those of bed load and suspended load. In bed load, particles roll, slide, or saltate over each other, never rising too far above the bed. In suspended load, fluid turbulence comes into play, carrying the particles well up into the water column. In both cases, the driving force for sediment transport is the action of gravity on the fluid phase; this force is transmitted to the particles via drag. Whether the mode of transport is saltation or suspension, the volume concentration of solids anywhere in the water column tends to be rather dilute in rivers. As a result, it is generally possible to treat the two phases separately.

In the geophysical domain, the field is much broader than rivers alone. The same phenomena of bed load and suspended load transport occur in a variety of other geophysical contexts. Sediment transport is accomplished in the nearshore of lakes and oceans by wave action. Turbidity currents act to carry suspended sediment into lakes, reservoirs, and the deep sea. Landslides, debris flows and mud flows provide mass transport mechanisms for the delivery of sediment from highlands to lowlands.

The solid phase can vary greatly in size, ranging from clay particles to silt, sand, gravel, cobbles, and boulders. Rock types can include quartz, feldspar, limestone, granite, basalt, and other less common types such as magnetite. The fluid phase can, in principle, be almost anything that constitutes a fluid. In the geophysical sense, however, the two fluids of major importance are water and air.

The phenomenon of sediment transport can sometimes be disguised as rather esoteric phenomena. When water is supercooled, large quantities of particulate frazil ice can form. As the water moves under a frozen ice cover, one has the phenomenon of sediment transport in rivers stood on its head. The frazil ice particles float rather than sink, and thus tend to accumulate on the bottom side of the ice cover rather than on the riverbed. Turbulence tends to suspend the particles downward rather than upward.

In the case of a powder snow avalanche, the fluid phase is air and the solid phase consists of snow particles. The dominant mode of transport is suspension. These flows are close analogues of turbidity currents, insofar as the driving

force for the flow is the action of gravity on the solid phase rather than the fluid phase. That is, if all the particles drop out of suspension, the flow ceases. In the case of sediment transport in rivers, it is accurate to say that the fluid phase drags the solid phase along. In the cases of turbidity currents and powder snow avalanches, the solid phase drags the fluid phase along.

Desert sand dunes provide an example for which the fluid phase is air, but the dominant mode of transport is saltation rather than suspension. Because air is so much lighter than water, quartz sand particles saltate in long, high trajectories, relatively unaffected by the direct action of turbulent fluctuations. The dunes themselves are created by the effect of the fluid phase acting on the solid phase. They, in turn, affect the fluid phase by changing the resistance.

In the limiting case of vanishing solids, the field reduces to pure fluid mechanics. As a result, sediment transport must be considered to be a subfield of fluid mechanics. In the limiting case of vanishing fluid, the problem reduces to that of the flow of a granular substance in a vacuum. The driving force now typically, but not always, becomes gravity. This problem, as well, can be treated with the techniques of fluid mechanics, as long as one is willing to move far afield of traditional Newtonian fluid mechanics. Martian rock avalanches constitute a geophysical realization of grain flows in a near vacuum, and it is likely that the fluid phase plays only a subsidiary role in many terrestrial rock avalanches. Another example of grain flow is a slab avalanche of snow. If they attain sufficient speed, slab avalanches tend to devolve into more dilute powder snow avalanches in which the fluid phase plays a greater role.

Among the more interesting intermediate cases are debris flows, mud flows, and hyperconcentrated flows. In all of these cases, the solid and fluid phases are present in similar quantities. A debris flow typically carries a heterogeneous mixture of grain sizes ranging from boulders to clay. Mud flows and hyperconcentrated flows are generally restricted to finer grain sizes. In most cases, it proves useful to think of such flows as consisting of a single phase, the mechanics of which is highly non-Newtonian.

The study of the movement of grains under the influence of fluid drag and gravity constitutes a fascinating field in its own right. The subject becomes even more interesting when one considers the link between sediment transport and morphology. In the laboratory, the phenomenon can be studied in the context of a variety of containers, such as flumes and wave tanks, specified by the experimentalist. In the field, however, the fluid-sediment mixture constructs its own container: the river. This new degree of freedom opens up a variety of intriguing possibilities for river and coastal morphodynamics (Parker and Garcia 2006).

Consider a river. Depending on the existence or lack thereof of a viscous sublayer and the relative importance of bed load and suspended load, a variety of rhythmic structures can form on the riverbed. These include ripples, dunes, antidunes, and alternate bars. The first three of these can have a profound effect on the resistance to flow offered by the riverbed. Thus, they act to control river depth. Riverbanks themselves can also be considered to be a self-formed morphological feature, thus specifying the entire container.

The container itself can deform in plan. Alternate bars cause rivers to erode their banks in a rhythmic pattern, thus allowing the onset of meandering. Fully developed river meandering implies an intricate balance between sediment erosion and deposition. If a stream is sufficiently wide, it will braid rather than meander, dividing into several intertwining channels. Braided rivers are an important component of the Earth's surface. The deposits of ancient braided rivers may contain significant reserves of water and hydrocarbon.

Rivers create morphological structures on much larger scales as well. These include canyons, alluvial fans, and deltas. Turbidity currents act to create similar structures in the oceanic environment. In the coastal environment, the beach profile itself is created by the interaction of water and sediment. On a larger scale, offshore bars, spits, and capes constitute rhythmic features created by wave-current-sediment interaction. The boulder levees often created by debris flows provide another example of a morphological structure created by a sediment-bearing flow.

This chapter is an introduction to the mechanics of sediment transport and river morphodynamics. Rivers evolve over time in accordance with the interaction between the flow and sediment-transport fields over an erodible bed (which changes the bed) and the changing morphology of the bed (which changes the flow and sediment-transport fields). This co-evolution is termed morphodynamics. Sediment transport by turbidity currents and the mechanics of lake and reservoir sedimentation are also considered in this chapter. The approach is intended to be as mechanistic and deductive as possible so that readers will be able to gain a firm foundation in the mechanics of sediment transport. This should be beneficial both for understanding the rest of the material presented in the manual as well as for sedimentation engineering and teaching purposes.

2.1.1 The Sediment Cycle in the Environment

The sediment cycle starts with the process of erosion, whereby particles or fragments are weathered from rock material. Action by water, wind, and glaciers as well as plant and animal activities, contributes to the erosion of the earth's surface. Fluvial sediment is the term used to describe the case where water is the key agent for erosion. Natural, or geological, erosion takes place slowly, over centuries or millennia. Erosion that occurs as a result of human activity may take place much faster. It is important to understand the role of each when studying sediment transport.

The dynamics of sediment in the environment and its morphological consequences are schematized in Fig. 2-1. Any material that can be dislodged is ready to be transported. The

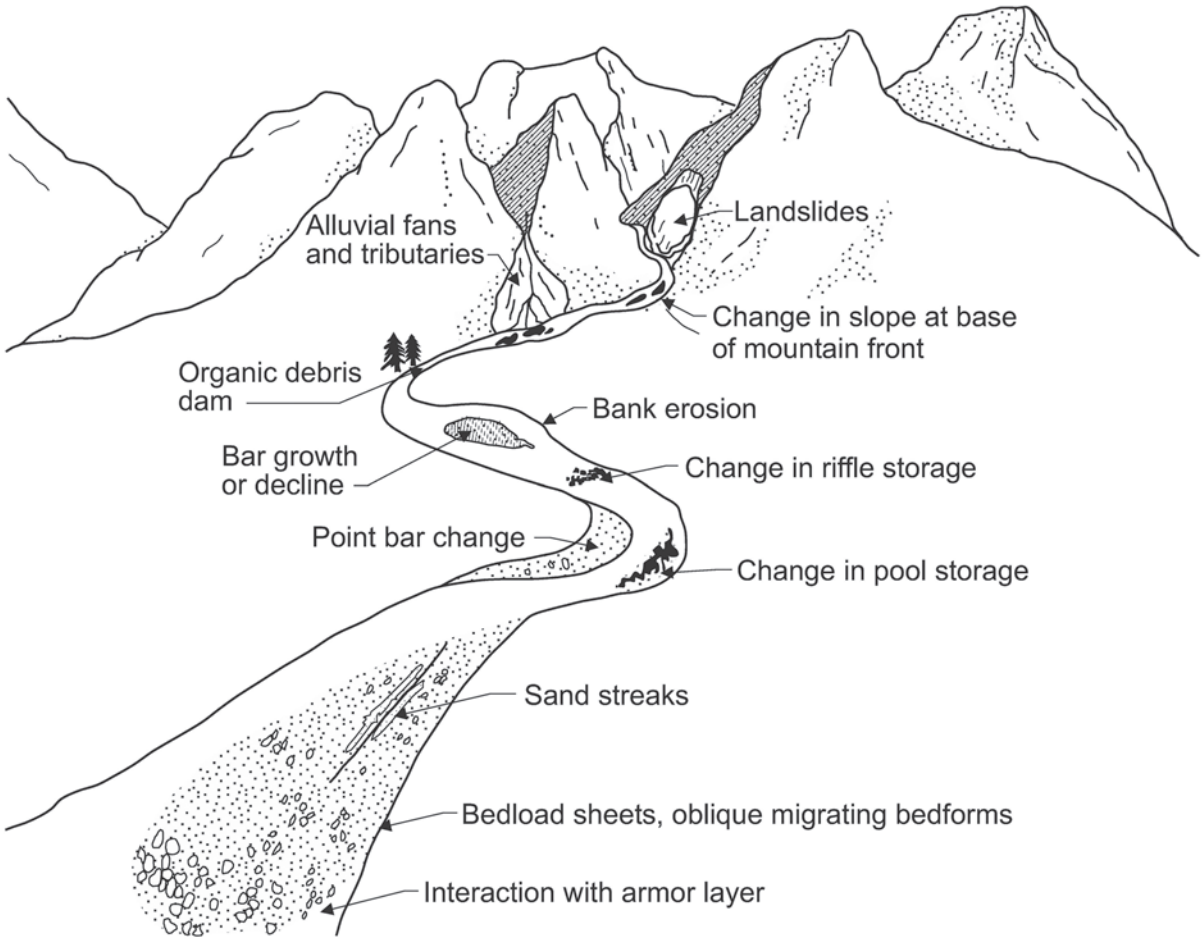

Fig. 2-1. Sedimentation processes and associated morphological changes in a Watershed (adapted from Dietrich and Gallinatti 1991).

transportation process is initiated on the land surface when raindrops result in sheet erosion. Rills, gullies, streams, and rivers then act as conduits for sediment movement. The greater the discharge, or rate of flow, the higher the capacity for sediment transport. Mass sediment transport can also occur through landslides, debris flows, and mudflows. Hyperconcentrated flows have also a tremendous capacity to transport vast amounts of sediment as observed after the release of large amounts of sediment following the eruption of Mt. St. Helens in Washington State, USA (Chapter 19).

The final process in the sediment transport cycle is deposition. When there is not enough energy to transport the sediment, it comes to rest. Sinks, or depositional areas, can be visible as newly deposited material on a floodplain, bars and islands in a channel, and deltas. Considerable deposition occurs that may not be apparent, as on lake and river beds. Alluvial fans are depositional environments typically encountered at the base of a mountain front. Flooding processes occurring on alluvial fans are considerably different from those occurring along single-thread rivers with well-defined floodplains (French 1987; Bridge 2003). Active erosion, rapid deposition, and uncertainty in flow path make the prediction of flood evolution and extent rather difficult (NRC 1996).

2.1.2 Scope of this Chapter

This chapter presents fundamental aspects of the erosion, entrainment into suspension, transport, and deposition of sediment in fluvial systems. The emphasis is on providing an introduction to the fluid mechanics of sediment transport in rivers and the morphodynamics of lake and reservoir sedimentation by turbidity currents, with the objective of establishing the background needed for sedimentation engineering and management. Emphasis is placed on the transport of noncohesive sediment, where the material involved is in granular form and ranges in size from fine silt to coarse sand. The transport of gravel and sediment mixtures is treated in Chapter 3, whereas the transport of fine-grained, cohesive sediment is considered in Chapter 4. Fluvial processes are addressed in Chapter 6 while engineering aspects of geomorphology are covered in Chapter 16. Sediment

transport in ice-covered rivers is the subject of Chapter 13. Hyperconcentrated flows, including mud flows and debris flows as well as sediment hazards related to flows in alluvial fans, are treated in Chapter 19. This chapter is intended to provide the foundation for the rest of the manual.

2.2 FLUID MECHANICS AND HYDRAULICS FOR SEDIMENT TRANSPORT

In this section, basic fluid mechanics and hydraulics concepts needed for the analysis of sedimentation processes are presented.

2.2.1 Flow Velocity Distribution: Law of the Wall

Consider a steady, turbulent, uniform, open-channel flow having a mean depth H and a mean flow velocity U (Fig. 2-2). The channel has a mean width B that is much greater than the mean flow depth H, and its bottom has a mean slope S and a surface roughness that can be characterized by the effective height k_s (Brownlie 1981). For very wide channels (i.e. $B/H \gg 1$), the hydraulic radius of the channel, R_h (cross-sectional area over wetted perimeter), can be approximated by the mean flow depth H. When the bottom of the channel is covered with sediment having a mean size or diameter D, the roughness height k_s will be proportional to this diameter. Due to the weight of the water, the flow exerts on the bottom a tangential force per unit bed area known as the bed shear stress τ_b, which in the case of steady, uniform flow can be expressed as:

$$\tau_b = \rho g H S \tag{2-1}$$

where

ρ = water density and
g = gravitational acceleration.

This equation is simply the one-dimensional momentum conservation equation for the channel reach under consideration. With the help of the boundary shear stress, it is possible to define the shear velocity u_* as

$$u_* = \sqrt{\tau_b/\rho} \tag{2-2}$$

The shear velocity, and thus the boundary shear stress, provides a direct measure of the flow intensity and its ability to entrain and transport sediment particles. The size of the sediment particles on the bottom determines the surface roughness, which in turn affects the flow velocity distribution and its sediment transport capacity. Because flow resistance and sediment transport rates are interrelated, it is important to be able to determine the role played by the bottom roughness.

In the case of steady, uniform flow the shear stress varies linearly in the vertical direction as shown in Fig. 2-2 and is given by the following expression:

$$\tau = \tau_b \left(1 - \frac{z}{H}\right) \tag{2-3}$$

It is well established, both experimentally and from dimensional arguments (Schlichting 1979; Nezu and Rodi 1986) that the flow velocity distribution is well represented by:

$$\frac{u}{u_*} = \frac{1}{\kappa} ln\left(\frac{z}{z_0}\right) \tag{2-4}$$

Here

u = time-averaged flow velocity at a distance z above the bed;
z_0 = bed roughness length (i.e., distance above the bed where the flow velocity goes to zero); and
κ is known as von Karman's constant and has a value of approximately 0.41 (Nezu and Rodi 1986; Long et al. 1993). The above law is known as the "law of the wall." It strictly applies only in a relatively thin layer ($z/H < 0.2$) near the bed (Nezu and Nakagawa 1993). It is commonly used as a reasonable approximation throughout most of the flow in many streams and rivers.

If the bottom boundary is sufficiently smooth, a condition rarely satisfied in rivers, turbulence will be drastically suppressed in an extremely thin layer near the bed, known as the viscous sublayer. In this region, a linear velocity profile holds (O'Connor 1995):

$$\frac{u}{u_*} = \frac{u_* z}{v} \tag{2-5}$$

where v is the kinematic viscosity of water. This law merges with the logarithmic law near $z = \delta_v$, where

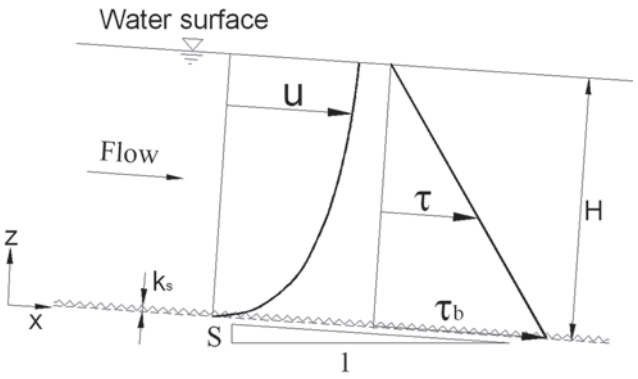

Fig. 2-2. Definition diagram for open-channel flow over a sediment bed.

$$\delta_v = 11.6\frac{v}{u_*} \tag{2-6}$$

denotes the height of the viscous sublayer. In the logarithmic region, the constant of integration introduced above has been evaluated from data to yield

$$\frac{u}{u_*} = \frac{1}{\kappa} ln\left(\frac{u_* z}{v}\right) + 5.5 \tag{2-7}$$

Comparing Eqs. (2-7) and (2-4), it follows that $z_o = v/9u_*$ for a hydraulically smooth flow.

Understanding the physics of the flow in the viscous sublayer is of relevance in benthic boundary layer flows (e.g., Boudreau and Jorgensen 2001). For example, sediment oxygen demand is affected by viscous effects as well as near-bed turbulence levels, as is shown in Chapter 22 of this manual. Also, the existence of a viscous sublayer seems to be a necessary condition for the development of ripples in unidirectional flows (e.g., Raudkivi 1997; Coleman and Melville 1994, 1996).

Most boundaries in alluvial rivers are hydraulically rough. Let k_s denote an effective roughness height. If $k_s/\delta_v > 1$, then no viscous sublayer will exist, because the roughness elements will protrude through such layer. In this case the corresponding logarithmic velocity profile is given by

$$\frac{u}{u_*} = \frac{1}{\kappa} ln\left(\frac{z}{k_s}\right) + 8.5 = \frac{1}{\kappa} ln\left(30\frac{z}{k_s}\right) \tag{2-8}$$

It follows that $z_o = k_s/30$ for a hydraulically rough flow. As noted above, the logarithmic velocity distribution often holds as a first approximation throughout the flow depth in a river. It is by no means exact since wake effects near the free surface can be important (Coleman 1981; Lyn 1991). Sediment-induced stratification as well as the presence of bed forms can also influence the flow velocity distribution. For many years, the effect of suspended sediment was understood to be in a change of von Karman's constant k (Einstein and Chien 1955; Vanoni 1975). However, there is now conclusive evidence that von Karman's constant is not affected by the presence of suspended sediment as previously believed, and its clear-water value ($k \approx 0.41$) can be considered to be a universal one (Smith and McLean 1977; Coleman 1981, 1986; Lyn 1991; Soulsby and Wainright 1987; Wright and Parker 2004a).

As is to be shown, it is not uncommon under field conditions to find that the flow regime is neither hydraulically smooth nor hydraulically rough. The conditions $k_s/\delta_v \gg 1$ for hydraulically rough flow and $k_s/\delta_v \ll 1$ for hydraulically smooth flow can be rewritten to indicate that the roughness Reynolds number, given by $u_* k_s/v$, should be much larger than 11.6 for turbulent rough flow, and much smaller than 11.6 for turbulent smooth flow. A composite form that represents both ranges, as well as the transitional range between them, can be written as (Yalin 1992)

$$\frac{u}{u_*} = \frac{1}{\kappa} ln\left(\frac{z}{k_s}\right) + B_s \tag{2-9a}$$

with B_s as a function of $Re_* = u_* k_s/v$ which can be estimated with the following empirical fit

$$B_s = 8.5 + \left[2.5\ ln\left(Re_*\right) - 3\right] e^{-0.121\left[ln\left(Re_*\right)\right]^{2.42}} \tag{2-9b}$$

A plot of this function can be seen in Fig. 2-3.

An alternative way of writing Eq. (2-9a) is

$$\frac{u}{u_*} = \frac{1}{\kappa} ln\left(A_s\frac{z}{k_s}\right) \tag{2-9c}$$

It follows then that A_s and B_s are related by

$$A_s = e^{\kappa B_s} \tag{2-9d}$$

Another useful fit to the vertical velocity distribution in open-channel flows, which also covers the entire range from hydraulically smooth to hydraulically rough as well as the transition, was proposed by Swamee (1993),

$$\frac{u}{u_*} = \left\{\left(\frac{v}{u_* z}\right)^{10/3} + \left[\kappa^{-1} ln\left(1 + \frac{9(u_* z/v)}{1 + 0.3(u_* k_s/v)}\right)\right]^{-10/3}\right\}^{-0.3} \tag{2-10}$$

Typically, muddy bottoms as well as beds covered with silt and fine sand are hydraulically smooth, whereas the presence of coarse sands and gravel leads, in general, to hydraulically rough conditions.

2.2.2 Flow Velocity Distribution: Velocity-Defect and Log-Wake Laws

The flow velocity distribution given by the law of the wall, Eq. (2-4), requires some knowledge of the bed roughness characteristics. An alternative formulation can be obtained if the flow depth H is introduced as the relevant length scale. Assuming that the maximum flow velocity u_{max} takes place at the water surface, $z = H$, Eq. (2-4) can be manipulated to obtain the so-called velocity-defect law, also known as the outer form of the law of the wall (Schlichting 1979)

$$\frac{u_{max} - u}{u_*} = -\frac{1}{\kappa} ln\frac{z}{H} \tag{2-11}$$

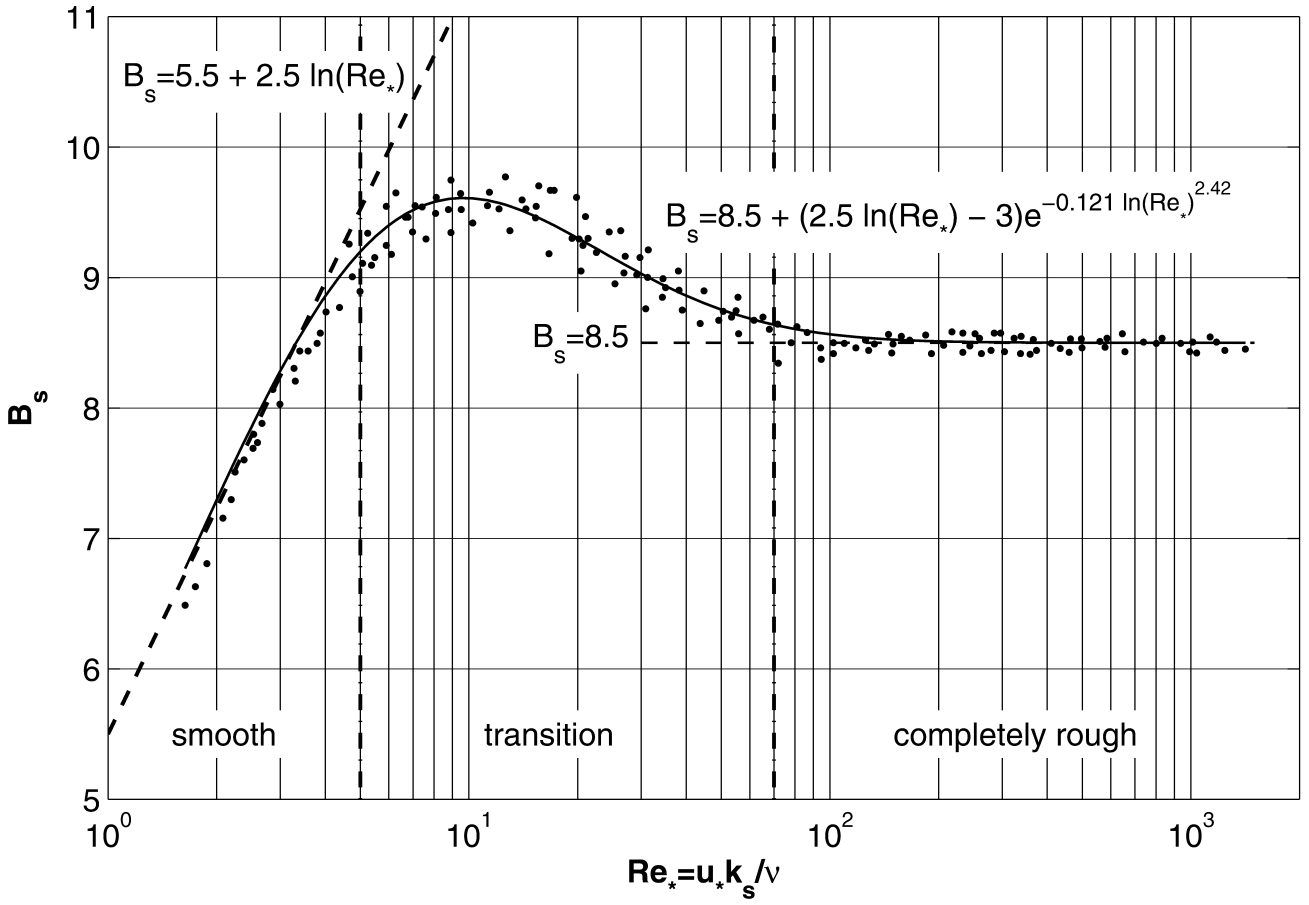

Fig. 2-3. Plot of Bs function in log-law velocity distribution.

A number of researchers have argued that the logarithmic behavior of the velocity distribution, either in the inner form given by Eq. (2-4) or in the outer form given by Eq. (2-11), can be justified only for a restricted region near the bed ($z/H < 0.2$), and that, for $z/H > 0.2$, a correction of the logarithmic function is necessary (Coleman and Alonso 1983; Sarma et al. 1983).

Nezu and Nakagawa (1993) added a wake function to the standard log law given by Eq. (2-7), calling it the "log-wake law," as follows,

$$\frac{u}{u_*} = \frac{1}{\kappa} ln\left(\frac{u_* z}{\nu}\right) + 5.5 + w\left(\frac{z}{H}\right) \qquad (2\text{-}12a)$$

where $w(z/H)$ is the wake function first proposed by Coles (1956) for turbulent boundary-layer flows, which takes the form

$$w\left(\frac{z}{H}\right) = \frac{2W_0}{\kappa} sin^2\left(\frac{\pi}{2}\frac{z}{H}\right) \qquad (2\text{-}12b)$$

In this relation W_0 is known as the Coles wake parameter, expressing the strength of the wake function. Through trigonometric substitution, Eq. (2-11) can also be written in log-wake form (Coleman 1981; Coleman and Alonso 1983).

$$\frac{u_{max} - u}{u_*} = -\frac{1}{\kappa} ln\left(\frac{z}{H}\right) + \frac{2W_0}{\kappa} cos^2\left(\frac{\pi z}{2H}\right) \qquad (2\text{-}13)$$

A procedure to estimate the Coles wake parameter from flow velocity measurements, originally proposed by Coleman (1981), can be found in Julien (1995 p. 103). Nezu and Rodi (1986), in experiments on flat-bed, smooth-bed, turbulent flows, found W_0 to vary from 0 to 0.253, with a mean value of $W_0 \approx 0.2$. This result was confirmed independently by Lyn (1991). Coleman (1981) and Parker and Coleman (1986) demonstrated that for the case of sediment-laden flows over flat beds, W_0 increases with increasing sediment concentration, ranging from 0.191 to 0.861. Lyn (1993) found that for flow over artificial bed forms, W_0 ranged from –0.05 to 0.1, and suggested that negative values of W_0 are the result of

strong, favorable pressure gradients. Lyn (1993) also found good results in replicating measured velocity profiles over bed forms with the log-wake law.

Most knowledge of flow velocity distribution in turbulent, free-surface flows stems from laboratory studies (e.g., Nezu and Rodi 1986; Nelson et al. 1993; Song et al. 1994; Bennett and Best 1995; 1996; Best et al. 2001; Lemmin and Rolland 1997; Muste and Patel 1997; Graf and Cellino 2002). In the past few years, however, new acoustic technology for flow measurement has made possible the observation of velocity profiles in streams and rivers as well (Kostaschuk et al. 2004; Dinehart and Burau 2005). With the help of observations made in the Missouri river, Holmes (2003) has found that the velocity-defect law, Eq. (2-13), works well for field conditions and the Coles wake parameter takes values ranging from -0.035 to 0.36. In all cases, dune-like bed forms were present, suggesting that such features might be responsible for the deviations from the logarithmic velocity distribution, observed away from the bottom. More field observations need to be made to quantify the effect of bed forms on the velocity distribution in alluvial rivers as well as the role played by stratification induced by suspended sediments. A recent review of mean flow, turbulence and bed form dynamics in alluvial rivers can be found in Best (2005).

2.2.3 Relations for Channel Flow Resistance

Most river flows are commonly considered to be hydraulically rough. Neglecting wake effects, Eq. (2-8) can be used to obtain an approximate expression for depth-averaged velocity U that is reasonably accurate for most flows. Integrating the mean flow velocity distribution given by Eq. (2-8) and dividing by the mean flow depth yields

$$U = \frac{1}{H}\int_0^H u\,dz \tag{2-14}$$

Now by slightly changing the lower limit of integration to avoid the fact that the logarithmic law is singular at $z = 0$, the following result is obtained:

$$\frac{U}{u_*} = \frac{1}{H}\int_{k_s}^{H}\left[\frac{1}{\kappa} ln\left(\frac{z}{k_s}\right) + 8.5\right]dz \tag{2-15}$$

or after the integration is performed

$$\frac{U}{u_*} = \frac{1}{\kappa} ln\left(\frac{H}{k_s}\right) + 6 = \frac{1}{\kappa} ln\left(11\frac{H}{k_s}\right) \tag{2-16}$$

This relation is known as Keulegan's resistance law for rough flow (Keulegan 1938) and it has been extensively used to estimate grain-induced resistance in gravel-bed streams (e.g. Bray 1979; Parker 1990).

It can be shown that the logarithmic form of Eqs. (2-8) and (2-16) can be approximated by power laws of the Manning-Strickler form, as follows:

$$\frac{u}{u_*} = \frac{1}{\kappa} ln\left(30\frac{z}{k_s}\right) \cong 9.34\left(\frac{z}{k_s}\right)^{1/6} \tag{2-17a}$$

$$\frac{U}{u_*} = \frac{1}{\kappa} ln\left(11\frac{H}{k_s}\right) \cong 8.1\left(\frac{H}{k_s}\right)^{1/6} \tag{2-17b}$$

To facilitate their comparison, a plot of Eqs. (2-17a) and (2-17b) is shown in Fig. 2-4. It is similar to the one presented by Brownlie (1983). The relative error between the log law and the power law is less than 4.2% in Eq. (2-17a) and less than 3% in the case of Eq. (2-17b). Keulegan (1938) was the first to point out the equivalence between the log-law and the power-law, given by Eq. (2-17b), in the context of open-channel flows. Chen (1991) provides a rigorous discussion of logarithmic and power-law velocity distributions, including a comparison of the associated flow resistance relations for both hydraulically smooth flows and fully rough flows.

Now, between Eqs. (2-2) and (2-16), a resistance relation can be found for the bed shear stress:

$$\tau_b = \rho C_f U^2 \tag{2-18}$$

where the friction coefficient C_f is given by

$$C_f = \left[\frac{1}{\kappa} ln\left(11\frac{H}{k_s}\right)\right]^{-2} \tag{2-19}$$

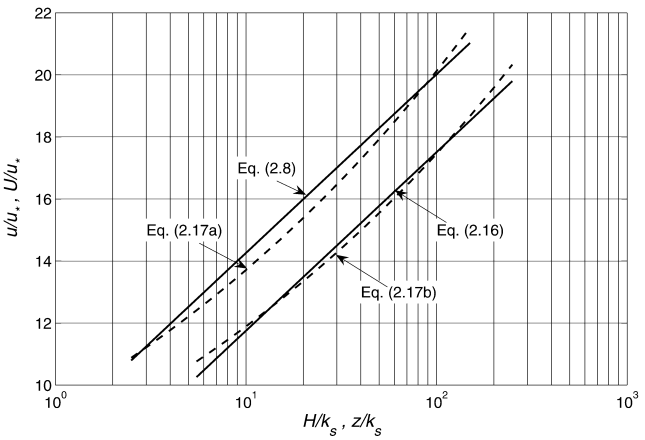

Fig. 2-4. Comparison of logarithmic laws versus power laws for velocity distribution and flow resistance.

If Eq. (2-17b) is used instead of Eq. (2-16), the friction coefficient takes the form:

$$C_f = \left[8.1 \left(\frac{H}{k_s} \right)^{1/6} \right]^{-2} \tag{2-20}$$

It is important to emphasize that Eq. (2-18) provides a local point estimate of bed shear stress, while Eq. (2-1) gives a reach-averaged value of the bed shear stress (Yen 2002).

It is useful to show the relationship between the friction coefficient C_f and the roughness parameters in open-channel flow relations commonly used in practice. Between Eqs. (2-1) and (2-18), a form of Chezy's law can be derived (Chow 1959):

$$U = C_z H^{1/2} S^{1/2} \tag{2-21}$$

where the Chezy coefficient Cz is given by the relation

$$C_Z = \left(\frac{g}{C_f} \right)^{1/2} \tag{2-22}$$

A specific evaluation of Chezy's coefficient can be obtained by substituting Eq. (2-19) into Eq. (2-22). It is seen that the coefficient is not constant, but varies as the logarithm of the relative roughness H/k_s. A logarithmic dependence is typically a weak one, partially justifying the common assumption that Chezy's coefficient in Eq. (2-21) is roughly a constant. By substituting Eq. (2-20) into Eq. (2-21) and Eq. (2-22), Manning's equation in metric units is obtained

$$U = \frac{1}{n} H^{2/3} S^{1/2} \tag{2-23a}$$

Here Manning's n is given by

$$n = \frac{k_s^{1/6}}{8.1\, g^{1/2}} \tag{2-23b}$$

This relation is often called the *Manning-Strickler* form of Manning's n (Brownlie 1983). It is deceptively simple but it also contains important information. Even for large increases in roughness height k_s, Manning's n does not change much. The opposite behavior is seen if large values of Manning's n are considered, and the corresponding value of k_s is estimated with the help of Eq. (2-23b). Often the back-calculated values of k_s turn out to be larger than the mean flow depth H, suggesting that the value of Manning's n being used is not a realistic one. From the analysis above, it should also be apparent that Manning's equation can only be applied to uniform, hydraulically rough, fully turbulent flows. Extensive tables of Manning's n values for different channel characteristics are given in Chow (1959) and Yen (1991).

It is also important to notice that according to Eq. (2-23b), Manning's n is not a dimensionless parameter. Yen (1992, 2002) and Dooge (1991), as well as Mostafa and McDermid (1971), have proposed dimensionally homogeneous forms of Manning's equation. Such dimensionless equation can be readily obtained from Eqs. (2-23a) and (2-23b) as follows:

$$U = M \left(\frac{H}{k_s} \right)^{1/6} \sqrt{gHS} \tag{2-24a}$$

Where the dimensionless constant $M = 8.1$ in this case and is valid for very wide channels. Different values for M can be found in the literature depending on the Strickler (1923) coefficient used in Eq. (2-23b). Yen (1993) reports values of M between 6.71 and 12.82, while Julien (2002) fits a value of $M = 5$ to field observations. With the help of Eq. (2-23b), it is possible to define a dimensionless Strickler number

$$St = \frac{n\sqrt{g}}{k_s^{1/6}} = \frac{1}{8.1} = 0.12 \tag{2-24b}$$

It follows that the constant M in Eq. (2-24a) is the inverse of the Strickler number St. An alternative way to express the Strickler number is with Keulegan's equation and power-law equivalent. Assuming that $k_s = D$, the identity given in Eq. (2-17b) can also be used to estimate the Strickler number

$$St = \frac{(H/D)^{1/6}}{(1/\kappa) ln(11 H/D)} \tag{2-24c}$$

This relation gives values of St close to 0.12, as obtained from Eq. (2-24b) in the range of relative flow depth H/D from 10 to 1,000 (Niño 2002). For values H/D lower than about 10, a sharp increase of St has been reported (e.g., Limerinos 1970), due to form resistance added to the grain (skin) friction, associated with flow separation in the wake of large bed elements relative to the flow depth. For instance, Ayala and Oyarce (1993) calibrated the following relation from field data obtained in the Mapocho River in the Chilean side of the Andean mountains, for values of H/D lower than 10 and taking $D = D_{90}$,

$$St = 0.30 \left(\frac{H}{D_{90}} \right)^{-0.40} \tag{2-24d}$$

This implies that M in the relation to estimate the mean flow velocity (Eq. 2-24a) would no longer be constant but would change as a function of flow depth for $H/D < 10$.

There is no accepted standard equation for predicting flow velocities in channels with large relative roughnes, i.e. where channel bed material is large relative to water depth. This is typical of mountain streams (Jarrett 1984; Aguirre-Pe and Fuentes 1990). Smart et al. (2002) conducted an analysis of existing flow resistance equations which points to the difficulties associated with the definition of depth and hydraulic radius when the bed roughness is large relative to the flow depth. They found that the log law, or the equivalent power law, is only applicable when the roughness is of sufficiently small scale, and recommended the use of a square-root power law to estimate flow velocity in the presence of large-scale roughness.

In the case of sand-bed streams, flow resistance is influenced by both grain or skin friction as well as form drag induced by the development of bed forms such as ripples, dunes and bars, so any estimate of Manning's n, or any other roughness coefficient, has to account for the possibility of different flow regimes (i.e., lower and upper regimes). Bruschin (1985), Camacho and Yen (1991), Wu and Wang (1999), and Hager and Del Giudice (2001) have proposed equations to estimate Manning's n for the case of sand-bed rivers. A modified Manning-Strickler formula for flow in alluvial channels with sand beds has also been advanced by Yu and Lim (2003). Flow resistance predictors for sand-bed streams are discussed later in the chapter.

2.2.4 Fixed-Bed (Skin or Grain) Roughness

It is clear that to use these relations for channel flow resistance, a criterion for evaluating the equivalent roughness height k_s is necessary. Friction factors for turbulent flow in pipes and in fixed-bed channels have their roots in the classic sand-roughened pipe experiments conducted by Nikuradse (1933). He conducted a set of pioneer experiments and proposed the following criterion. Suppose a rough surface is subjected to a flow. Then the equivalent roughness height k_s of the surface would be equal to the diameter of sand grains that, when glued uniformly to a completely smooth wall, and then subjected to the same external conditions, yields the same velocity profile. Nikuradse used sand glued to the inside of pipes to conduct this evaluation.

To analyze the work of Nikuradse, it is convenient to introduce another relation that can be used to estimate mean flow velocity in open-channel flows, known as the Darcy-Weisbach equation

$$U = \sqrt{\frac{8}{f}}\sqrt{gR_hS} = \sqrt{\frac{8}{f}}u_* \qquad (2\text{-}26)$$

In this equation
g = gravitational acceleration;
u_* = shear velocity;
R_h is the hydraulic radius (approximately equal to the flow depth H for very wide channels); and f is the dimensionless Darcy-Weisbach friction coefficient, which, for a pipe with diameter D is known to be a function of the flow Reynolds number $R_e = UD/\nu$ and the relative roughness D/k_s.

Brownlie (1981) re-examined Nikuradse's data and proposed the friction factor diagram shown in Fig 2-5. The diagram provides the values of the friction factor f, introduced in Eq. (2-26), as a function of the Reynolds number $R_e = UD/\nu$ and the relative roughness D/k_s. This diagram is equivalent to the well known Moody diagram shown in Fig. C-2 of Appendix C, and can be used for sidewall corrections in laboratory experiments (Vanoni and Brooks 1957) as well as for separating total resistance into grain resistance and form resistance in alluvial streams with dunes (Brownlie 1981; Fedele and García 2001). For open-channel flow calculations, the pipe diameter D should be replaced by $4R_h$, in which R_h is the hydraulic radius. Again, for a very wide channel, the hydraulic radius can be replaced by the mean flow depth. The sidewall correction procedure is explained in detail both in Brownlie (1981) as well as in *ASCE Manual 54* (Vanoni 2006) and therefore is not repeated here.

In the late 1930s, Zegzhda conducted a set of experiments in straight rectangular flumes of varying roughness, using an experimental method (gluing sand to the walls) similar to the one used by Nikuradse for flow in pipes (see Novak and Cabelka 1981, p. 124). Because this work was not published in English, it is not as well known as Nikuradse's work on pipes. However, this experimental study was conducted for a set of relative-roughness (R_h/k_s) values more representative of the conditions observed in the field for the case of sand-bed streams with plane beds. In fact, the relation obtained by Zegzhda for fully-rough hydraulic conditions is very similar to the expression advanced independenly at about the same time by Keulegan (Eq. 2-16).

A fit to the experimental results of Nikuradse that can be used to estimate the roughness length parameter z_0 in Eq. (2-4) as a function of k_s was proposed by Christofferson and Jonsson (1985)

$$z_0 = \frac{k_s}{30}\left[1 - exp\left(\frac{-u_*k_s}{27\nu}\right)\right] + \frac{\nu}{9u_*} \qquad (2\text{-}27)$$

Smith (1977) seems to have been the first to plot Nikuradse's data in a way useful to estimate the roughness length. Similar empirical relations have been proposed by Fuentes and Carrasquel (1981) and Dade et al. (2001). For $u_*k_s/\nu < 3$, the flow is hydraulically smooth and $z_0 = 0.11\nu/u_*$; whereas for $u_*k_s/\nu > 100$ the flow is hydraulically rough and $z_0 = 0.033k_s$. In many interesting sediment transport situations the flow is hydraulically transitional and an equation such as Eq. (2-27) has to be used to estimate the roughness length in Eq. (2-4) associated with grain-induced roughness (Kamphuis 1974). Typically, muds and flat fine sands are

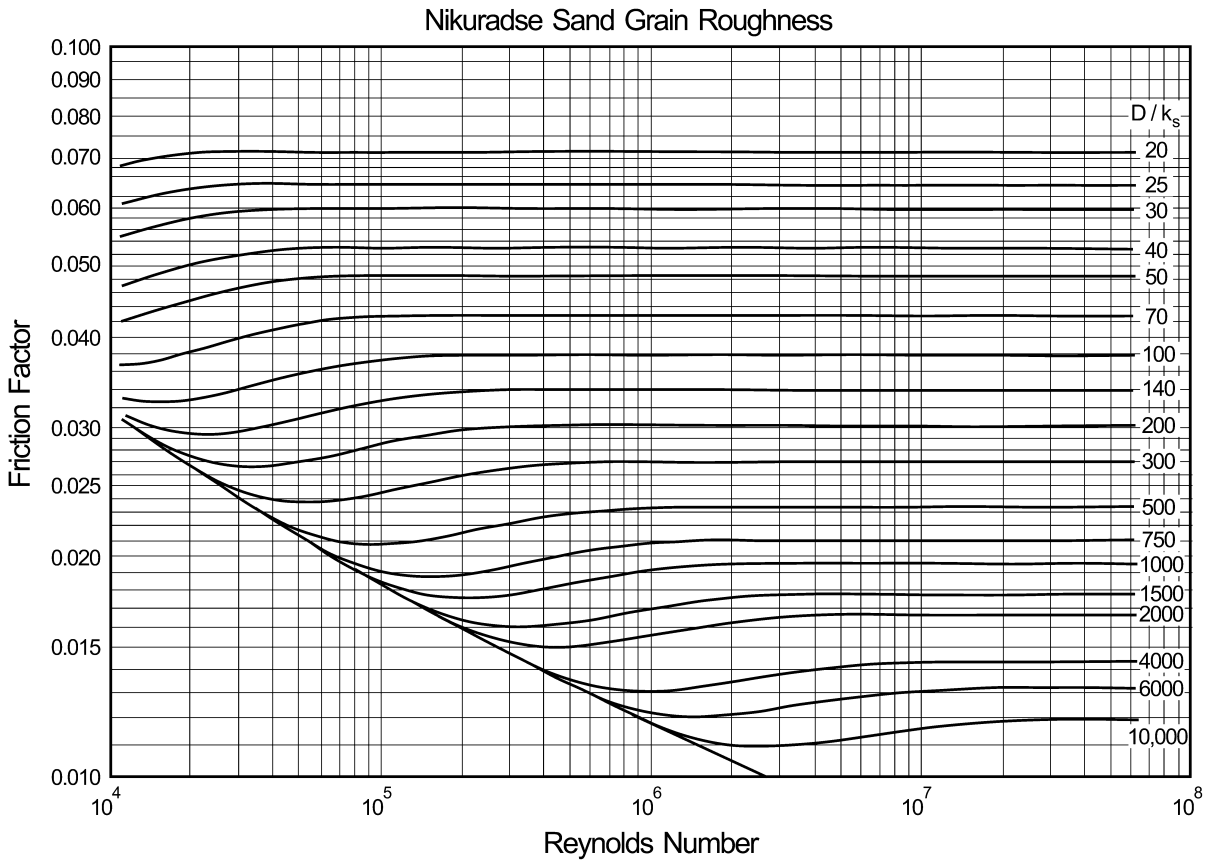

Fig. 2-5. Revised Nikuradse friction factor diagram for flow in pipes of diameter D or open-channel flows with hydraulic radius R_h = D/4 (after Brownlie, 1981).

hydraulically smooth or transitional, and coarse sands and gravels are hydraulically rough (Soulsby, 1997). It is common practice to treat all flows over sands as being hydrodynamically rough since this simplifies the analysis. This simplifying approximation makes less than 10% error in the estimation of the shear velocity u_*, for all values u_* above the threshold of motion (see Section 2.4.2) of grains larger than 60 μm.

Although it is clear that the sediment size distribution in most rivers is not as uniform as the material used in his experiments, Nikuradse's concept of grain-induced roughness for pipe flows has been extended to estimate friction factors in streams and rivers as well (Yen 1992). Nikuradse's equivalent sand-grain roughness, k_s, is commonly taken to be proportional to a representative sediment size D_x,

$$k_s = \alpha_s D_x \tag{2-28}$$

Suggested values of α_s which have appeared in the literature are listed in Table 2-1, originally compiled by Yen (1992; 2002) and updated for this manual. Different sediment sizes have been suggested for D_x in Eq. (2-28). Statistically, D_{50} (the grain size for which 50% of the bed material is finer) is most readily available. Physically, a representative size larger than D_{50} is more meaningful to estimate flow resistance because of the dominant effect of large sediment particles. The range of α_s values and the diverse representative sediment size used for D_x indicate that further research on this concept is necessary.

In a study of flow resistance associated with rip-rapped surfaces, Maynord (1991) reviewed a number of formulations commonly used to estimate the Darcy-Weisbach friction coefficient and found that a power-law equation can be used for most riprap (i.e., fixed-bed) problems in very wide open-channel flows, as follows:

$$\left(\frac{8}{f}\right)^{1/2} = 6.89\left(\frac{H}{D_{50}}\right)^{1/6} \tag{2-29}$$

Notice the similarity with the power-law equations for flow resistance presented earlier. Maynord (1991) also found a logarithmic expression for flow resistance, based on his own experiments as well as on data from other sources, given by

$$\left(\frac{8}{f}\right)^{1/2} = 3.92\log\left(\frac{H}{D_{50}}\right) + 6.86 \tag{2-30}$$

Table 2-1 Ratio of Nikuradse Equivalent Roughness Size and Sediment Size for Rivers

Investigator	Measure of sediment size, D_x	$\alpha_s = k_s/D_x$
Ackers andWhite (1973)	D_{35}	1.23
Aguirre-Pe and Fuentes (1990)	D_{84}	1.6
Strickler (1923)	D_{50}	3.3
Katul et al (2002)	D_{84}	3.5
Keulegan (1938)	D_{50}	1
Meyer-Peter and Muller (1948)	D_{50}	1
Thompson and Campbell (1979)	D_{50}	2.0
Hammond et al. (1984)	D_{50}	6.6
Einstein and Barbarossa (1952)	D_{65}	1
Irmay (1949)	D_{65}	1.5
Engelund and Hansen (1967)	D_{65}	2.0
Lane and Carlson (1953)	D_{75}	3.2
Gladki (1979)	D_{80}	2.5
Leopold et al. (1964)	D_{84}	3.9
Limerinos (1970)	D_{84}	2.8
Mahmood (1971)	D_{84}	5.1
Hey (1979), Bray (1979)	D_{84}	3.5
Ikeda (1983)	D_{84}	1.5
Colosimo et al. (1986)	D_{84}	3.6
Whiting and Dietrich (1990)	D_{84}	2.95
Simons and Richardson (1966)	D_{85}	1
Kamphuis (1974)	D_{90}	2.0
Van Rijn (1982)	D_{90}	3.0

which applies in the range $2.2 < H/D_{50} < 23$. Similar empirical relations have been advanced by Hey (1979), Thompson and Campbell (1979), Grifiths (1981), Pyle and Novak (1981), and Bathurst (1985).

From these equations, it follows that for wide, open channel flows the Darcy-Weisbach friction coefficient and Manning's roughness coefficient are related by

$$\left(\frac{8}{f}\right)^{1/2} = \frac{K_n H^{1/6}}{n g^{1/2}} = \frac{U}{\sqrt{gHS}} \tag{2-31}$$

in which K_n is a constant equal to 1 in metric units and equal to 1.486 in English units (Yen 2002). The velocity distribution in high-gradient streams with relatively low values of relative submergence H/D_{50} is no longer logarithmic near the bed due to the wake effect produced by large roughness elements. Wiberg and Smith (1991) have developed a model for the velocity field in steep streams with coarse gravel beds that is capable of reproducing the field observations made by Marchand et al. (1984). At about the same time, Aguirre-Pe and Fuentes (1990) proposed a theory for flow resistance in steep, rough streams that takes into account the existence of the highly turbulent wake zone near a very rough bed. Their model predictions compare favorably against field observations by several authors. As shown by Smart (1999; 2002), most of the uncertainty when dealing with coarse gravel and cobbles in shallow channels is in the determination of the mean bed location so that the origin of the flow velocity profile can be ascertained. In relation to the difficulties associated with defining the mean bed elevation, Nikora et al. (2001) show the importance of spatial averaging when dealing with shallow flows over gravel bed streams. In the absence of a logarithmic velocity distribution, Katul et al. (2002) developed a velocity distribution equation based on mixing-length theory capable of reproducing flow resistance characteristics observed in shallow streams with large relative roughness. More recently, Buffington et al. (2004) studied the effects of channel type and associated hydraulic roughness on salmonid spawning-gravel availability in mountain catchments.

2.2.5 Movable Flat-Bed Roughness

In flows over geometrically smooth, fixed boundaries, the apparent roughness of the bed k_s can be computed using Nikuradse's approach, as shown above. However, once the transport of bed material has been instigated, the characteristic grain diameter and the viscous sublayer thickness no longer provide the relevant length scales. The characteristic length scale in this situation is the thickness of the layer where the sediment particles are being transported by the flow, usually referred to as the bed-load layer height (Wiberg and Rubin 1989). As the grains start to roll and saltate along the bed, they take momentum away from the mean flow via drag, resulting in an increase in flow resistance that translates into an increase in bed roughness.

Once the bed shear stress τ_b exceeds the critical shear stress for particle motion τ_c, the roughness length can be estimated with an expression inspired by the work of Owen (1964) for wind-induced sediment transport, and first proposed by Smith (1977) for sediment transport by water currents,

$$z_0 = \alpha_0 \frac{(\tau_b - \tau_c)}{(\rho_s - \rho) g} + z_{0N} \tag{2-32a}$$

where

α_0 = 26.3;
$z_{0N} = 0.033 k_s$ and k_s = Nikuradse roughness length; and
ρ_s = bed sediment density.

This approach is particularly suitable for sand-bed rivers and has been widely used in coastal sedimentation (e.g., Smith and McLean 1977).

The roughness parameter also can be estimated with a scheme proposed by Dietrich and Whiting (1989),

$$z_0 = \alpha_1 \delta_b + z_{0N} \tag{2-32b}$$

where

α_1 = empirical constant equal to 0.077;
$z_{0N} = 0.033 k_s$ and k_s = Nikuradse roughness length; and
δ_b = bedload-layer height,

which is computed as

$$\delta_b = \frac{1.2 D (1 - \cos\phi)\left[\tau_b / \tau_c\right]}{1 + 0.2\left[\tau_b / \tau_c\right]} \tag{2-32c}$$

where

ϕ = angle of friction, and
D = mean diameter of the bed material.

Since both estimators depend on the flow intensity as given by the bed shear stress, Eqs. (2-32a) and (2-32b) provide an estimate of a variable roughness appropriate for movable beds without the presence of bed forms.

Wiberg and Rubin (1989) evaluated several expressions for characterizing bed roughness produced by a layer of saltating sediment grains; they proposed with the help of a formulation for the vertical eddy diffusivity coefficient (Gelfenbaum and Smith 1986; Long et al. 1993) a formulation which makes use of a vertical flow velocity distribution given by the following expression

$$u(z) = \frac{u_*}{\kappa} \int_{z_0}^{z} \frac{1 - (z/H)}{z \exp\left[-(z/H) - 3.3(z/H)^2 + 2.2(z/H)^3\right]} dz \tag{2-33}$$

where

z = distance from the bed;
H = flow depth; and
κ = 0.41 = von Karman's constant.

Seven upper plane-bed experiments of Guy et al. (1966) were used to obtain best fit values for the shear velocity u_* and bed roughness length z_0 with the help of Eq. (2-33). The analysis of Wiberg and Rubin (1989) shows that the bed roughness associated with sediment transport can reach values about an order of magnitude larger than the Nikuradse grain roughness in plane-bed flows, but this roughness will in general be significantly smaller than the roughness associated with ripples and dunes when they are present on the bed surface.

At high bed shear stresses and sediment transport intensities in sand-bed streams, dunes are washed out and the bed becomes plane. In this regime, sediment is transported near the bed in a layer with a thickness that is much larger than the grain size. Collisions between grains are intense in this layer, resulting in a grain flow or granular fluid flow. This regime is known as sheet flow and measurements taken by researchers (Wilson 1987, 1989; Nnadi and Wilson 1992) have shown that flow resistance increases drastically with flow intensity in this regime. Sumer et al (1996) found that flow resistance induced by the sheet-flow layer can be expressed in terms of the ratio of Nikuradse's equivalent sand roughness to the grain diameter (k_s/D). This ratio was found to behave differently whether of not the grains became suspended near the bed. In the absence of suspension mode, k_s/D depends only on the Shields parameter (τ^*) defined by Eq. (2-56). In the suspension mode, k_s/D depends not only on τ^* but also on a dimensionless sediment fall velocity parameter R_f defined by Eq. (2-46b). There is also evidence that sediment transport in the sheet-flow layer is influenced by the turbulent bursting process (e.g., Sumer et al. 2003).

2.2.6 Equivalent Roughness of Bed Forms

As the flow intensity increases, bed forms such as ripples and dunes can develop (e.g., Raudkivi 1997). In this situation, the bed roughness also will be influenced by form drag due to the presence of bed forms. The fundamental problem is that the bed form characteristics and, hence, the bed roughness depend on the main flow characteristics (e.g., mean velocity, depth) and sediment characteristics (e.g., grain size, density). Thus, the hydraulic roughness in the presence of bed forms is a dynamic parameter that depends strongly on flow conditions as well as on the bed sediment properties. The equivalent roughness of alluvial beds in the presence of ripples and dunes was addressed with the Nikuradse hydraulic roughness approach by Brownlie (1981) and van Rijn (1982, 1984c). In van Rijn's approach, the height due to grain-induced roughness (Eq. 2-28) was added to an estimate of the equivalent roughness height produced by ripples and dunes obtained from field and laboratory observations, to obtain a measure of the total (grain plus form resistance) effective roughness,

$$k_s = \alpha_s D_{90} + \gamma_{sf} 1.1 \Delta (1 - e^{-25\Delta/\lambda}) \qquad (2\text{-}34a)$$

where

α_s = 3 (see Eq. 2-28);
D_{90} = grain size for which 90% of the bed material is finer;
γ_{sf} = dune shape factor = 1.
Δ and λ = bed form height and length, respectively; and
Δ / λ = bedform steepness.

The effective roughness height was then used to estimate the Chezy friction coefficient (Eq. 2-22),

$$C_Z = \left(\frac{g}{C_f} \right)^{1/2} = 18 \log \left(\frac{12 R_{hb}}{k_s} \right) \qquad (2\text{-}34b)$$

In this equation, R_{hb} = hydraulic radius of the river bed (i.e., substracting streambank effects on flow resistance) according to Vanoni-Brooks (1957) (see Vanoni 2006, p. 91). Notice that the Chezy coefficient is not dimensionless. A dimensionless expression of the Chezy coefficient applicable to bank-full sand bed and gravel bed streams can be found in Chapter 3.

Application of Eq. (2-34a) to field conditions resulted in considerable overestimation of the hydraulic roughness (van Rijn 1996). Further analysis showed that the lee-side slopes of natural sand dunes in rivers were less steep than those of dunes in the laboratory and a shape factor $\gamma_{sf} = 0.7$ was recommended for application to natural river dunes.

A different approach based on boundary-layer theory and measured velocity profiles was proposed by Fedele and García (2001). When spatially-averaged velocity profiles of flow (Nikora et al. 2001) over dunes are available, this method can be used to estimate a spatially-averaged composite roughness k_c due to the combined effect of both grain friction and form drag due to bed forms in large sand-bed rivers. Boundary layer studies have shown that an alternative to Eq. (2-9a) for describing the vertical flow velocity distribution in flows where the geometry and size of the roughness elements is such that skin friction and form drag are present, is given by the following equation

$$\frac{u}{u_*} = \frac{1}{\kappa} ln \left(\frac{z u_*}{\nu} \right) + A - \frac{\Delta u}{u_*} \left[\frac{u_* k_c}{\nu} \right] \qquad (2\text{-}35a)$$

In Eq. (2-35a), $\kappa = 0.41$ and $A = 5.5$ are universal constants previously introduced, and $\Delta u/u_*$ is a roughness function which is equal to zero for smooth walls (square brackets indicate functional relationship). When plotting u/u_* versus $\ln(u_* z/\nu)$, this equation represents a family of parallel lines, each being displaced downwards from the smooth-wall velocity profile by an amount $\Delta u/u_*$ (Schlichting 1979).

The roughness function for alluvial streams with dunes is shown in Fig. 2-6. It shows $\Delta u/u_*$ as a function of the parameter $k_c u_*/\nu$ for laboratory and field streams with fully-developed dunes (Fedele and García 2001). It is observed that for values of the roughness Reynolds number $k_c u_{*T}/\nu$ larger than 100-200, most of the data collapse along a straight line, along the fully-rough hydraulic regime, which is well represented by the following fit,

$$\frac{\Delta u}{u_*} = 2.43 \, ln \left(\frac{u_* k_c}{\nu} \right) - 3.24 \qquad (2\text{-}35b)$$

An application of the alluvial roughness function is its potential use to assess the effect of temperature changes on flow structure and bed morphology. It is observed in Fig. 2-6 that even though the flows are under fully-rough hydraulic conditions, temperature variations will affect the viscosity of the water and this in turn will cause variations in the roughness Reynolds number and the flow structure.

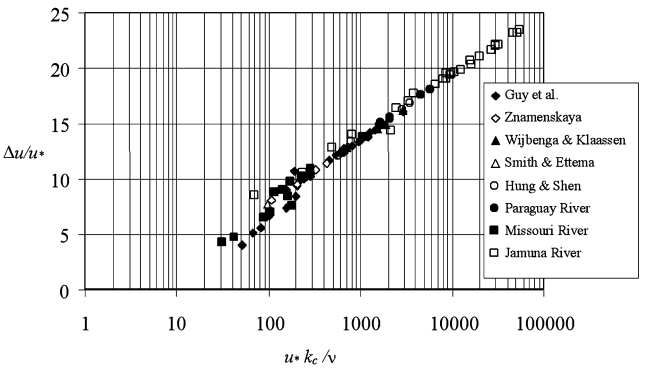

Fig. 2-6. Roughness function for alluvial streams with dunes (after Fedele and García 2001).

Fedele and García (2001) also found that the composite roughness k_c could be approximated with

$$\frac{k_c}{D} = 1.45 \times \tau^{*3/2} R_{ep} \left(\frac{H}{D} \right)^{1/3} \qquad (2\text{-}35c)$$

which is valid for $(H/D) > 10^3$ and $R_{ep} < 30$, which are commonly found conditions for large alluvial rivers with sand dunes.

Here,

τ^* = dimensionless bed shear stress (i.e., Shields parameter) for uniform flow = $(HS)/(RD)$;
H = flow depth;
S = channel slope;
R = $\rho_s/\rho - 1$ = submerged specific gravity of sediment;
D = sediment size;
R_{ep} = $\sqrt{gRD}D/\nu$ = particle Reynolds number; and
H/D = relative flow depth.

A simple method to estimate the composite roughness k_c has been proposed by Wright and Parker (2004b) and can be found in Section 2.8.3.3 below.

The total friction coefficient for flow in an alluvial channel in the presence of dunes can be estimated with the help of Keulegan's Eq. (2-16), Eq. (2-19), and Eq. (2-35c),

$$C_f^{-1/2} = \frac{U}{u_*} = \frac{1}{\kappa} ln \left[\frac{(H/D)^{3/2}}{\tau^{*3/2} R_{ep}} \right] + 5.1 \qquad (2\text{-}35d)$$

The data used to by Fedele and García (2001) to obtain this fit are shown in Fig. 2-7. This expression provides only a crude approximation for the friction factor, but clearly indicates that the roughness in alluvial streams with dunes is a dynamic parameter that depends nonlinearly on the flow intensity given by the Shields stress parameter (τ^*), the relative flow depth (H/D), and the particle Reynolds number (R_{ep}).

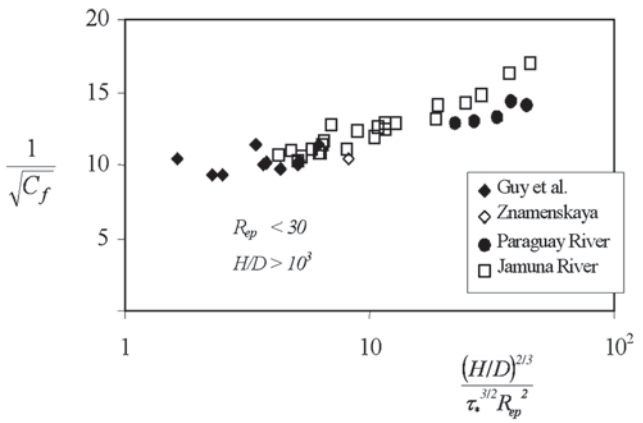

Fig. 2-7. Total friction coefficient for alluvial flows with sand dunes (after Fedele and García 2001).

2.3 SEDIMENT PROPERTIES

In this section, rock types, as well as fundamental characteristics of sediment particles such as size, size distribution, density, and fall velocity are considered. The role of sediment size on stream morphology is analyzed also, with the goal of understanding the behavior of sand-bed and gravel-bed streams.

2.3.1 Rock Types

The solid phase in sediment transport can be any granular substance. In terms of engineering applications, however, the granular substance in question typically consists of fragments ultimately derived from rocks—hence the name "sediment" transport. The properties of these rock-derived fragments, taken singly or in groups of many particles, all play a role in determining the transportability of the grains under fluid action. The important properties of groups of particles include porosity and size distribution. The most common rock type one is likely to encounter in the river or coastal environment is quartz. Quartz is a highly resistant rock and can travel long distances or remain in place for long periods of time without losing its integrity. Another highly resistant rock type that is often found together with quartz is feldspar. Other common rock types include limestone, basalt, granite, and more esoteric types such as magnetite. Limestone is not a resistant rock; it tends to abrade to silt rather easily. Silt-sized limestone particles are susceptible to solution unless the water is sufficiently buffered. As a result, limestone is not typically found to be a major component of sediments at locations distant from its source. On the other hand, it can often be the dominant rock type in mountain environments.

Basaltic rocks tend to be heavier than most rocks composing the crust of the earth. They are typically brought to the surface by volcanic activity. Basaltic gravels are relatively common in rivers that derive their sediment supply from areas subjected to volcanism in recent geologic history. Basaltic sands are much less common. Regions of weathered granite often provide copious supplies of sediment. The particles produced by weathering are often in the granule size but often quickly break down to sand sizes.

Sediments in the fluvial or coastal environment in the size range of silt, or coarser, are generally produced by mechanical means, including fracture or abrasion. The clay minerals, on the other hand, are produced by chemical action. As a result, they are fundamentally different from other sediments in many ways. Their ability to absorb water means that the porosity of clay deposits can vary greatly over time. Clays also display cohesiveness, which renders them more resistant to erosion.

2.3.2 Specific Gravity

Sediment specific gravity is defined as the ratio between the sediment density ρ_s and the density of water ρ. Some typical

specific gravities for various natural and artificial sediments are listed in Table 2-2.

2.3.3 Model Laboratory Sediments

In the laboratory, it is often of value to employ light weight model sediment (Shen 1990). To see the utility of this, it is useful to consider a movable-bed scale model of an actual river. Consider a reach of the Minnesota River, Minnesota, with a bank-full width of 90 m, a bank-full depth of 4 m, a streamwise slope of 0.0002, and a median sediment size D_{50} of 0.5 mm. The reach is scaled down by a factor of 100 to fit into a typical laboratory model basin, resulting in a bank-full width of 90 cm and a bank-full depth of 4 cm. In an undistorted model, slope remains constant at 0.0002.

If the sediment employed in the model were to be the same as in the field, it would most likely not move at all in the scale model. Carrying the analogy to its logical conclusion, it would be as if the sediment in the field Minnesota River had a median size of 0.5 mm $\times$ 100 = 0.5 m, i.e., boulders. It should be clear that, in this case, the field sediment cannot be employed directly in the model. The obvious alternative is to scale down sediment size by the same factor as all other lengths, i.e., by a factor of 100. This would yield a size of 5 μm, which is so close to the clay range that it can be expected to display some kind of pseudocohesiveness. In addition, viscous effects are expected to be greatly exaggerated due to the small size. The net result is model sediment that is much less mobile than it ought to be and, in addition, behaves in ways radically different from the prototype sediment.

There are several ways out of this dilemma. One of them involves using artificial sediment with a low specific gravity. Let ρ denote the density of water, and ρ_s denote the specific gravity of the material in question. The weight W of a particle of volume V_p is given by

$$W = \rho_S g V_P \tag{2-36a}$$

Table 2-2 Specific Gravity of Rock Types and Artificial Materials

Rock type or material	Specific gravity ρ_s/ρ
Quartz	2.60–2.70
Limestone	2.60–2.80
Basalt	2.70–2.90
Magnetite	3.20–3.50
Bakelite	1.30–1.45
Coal	1.30–1.50
Ground walnut shells	1.30–1.40
PVC	1.14–1.25

where

g = acceleration of gravity.

Quartz, for example, is a mineral with a specific gravity ρ_s/ρ near 2.65. If a grain of the same volume were modeled in the laboratory using crushed coal with a specific gravity of 1.3, it would follow from Eq. (2-36a) that the coal grain would be only 1.3/2.65 or 0.49 times the weight of the quartz grain. Rephrasing, the coal grain is 2.04 times lighter than the quartz grain, and thus, in some sense, twice as mobile.

In fact, the benefit of using lightweight material is much greater than this, because the effective weight determining the mobility of a grain is the submerged weight W_s, i.e., the actual weight minus the buoyancy force associated with the hydrostatic pressure distribution about the particle. That is,

$$W_S = (\rho_S - \rho) g V_P = \rho R g V_P \tag{2-36b}$$

where

$$R = \left(\frac{\rho_S}{\rho} - 1 \right) \tag{2-36c}$$

denotes the submerged specific gravity of the sediment. Comparing coal and quartz again in terms of submerged weight, it is seen that

$$\frac{(W_S)_{coal}}{(W_S)_{quartz}} = \frac{(R)_{coal}}{(R)_{quartz}} = \frac{0.30}{1.65} = 0.18 \tag{2-36d}$$

It follows that under water, the coal grain is 1/0.18 = 5.5 times lighter than a quartz grain of the same size. Lightweight model sediments are thus a very effective way of increasing mobility in laboratory experiments (Zwamborn 1981; ASCE 2000, p. 105). More material on physical modeling of sedimentation processes can be found in Appendix C.

2.3.4 Size

The notation D will be used to denote sediment size, the typical units of which are millimeters (mm—sand and coarser material) or micrometers (μm–clay and silt). Another standard way of classifying grain sizes is the sedimentological Φ scale, according to which

$$D = 2^{-\Phi} \tag{2-37a}$$

Taking the logarithm of both sides, it is seen that

$$\Phi = -\log_2(D) = -\frac{\ln(D)}{\ln(2)} \tag{2-37b}$$

Note that the size $\Phi = 0$ corresponds to $D = 1$ mm. The utility of the Φ scale will become apparent upon a consideration of grain size distributions. The minus sign has been

inserted into Eq. (2-37b) simply as a matter of convenience to sedimentologists, who are more accustomed to working with material finer than 1 mm rather than coarser material. The reader should always recall that larger Φ implies finer material.

The Φ scale provides a very simple way of classifying grain sizes into the following size ranges in descending order: boulders, cobbles, gravel, sand, silt, and clay. This is illustrated in Table 2-3.

It should be noted that the definition of clay according to size ($D < 2$ μm) does not always correspond to the definition of clay according to mineral. That is, some clay mineral particles can be coarser than this limit, and some silt particles produced by grinding can be finer than this. In general, however, the effect of viscosity makes it quite difficult to grind up particles in water to sizes finer than 2 μm.

In practical terms, there are several ways to determine grain size. The most popular way for grains ranging from $\Phi = 4$ to $\Phi = -4$ (0.0625 to 16 mm) is with sieves. Each sieve has a square mesh, the gap size of which corresponds to the diameter of the largest sphere that would fit through. The grain size D thus measured exactly corresponds to diameter only in the case of a sphere. In general, the sieve size D corresponds to the smallest sieve gap size through which a given grain can be fitted.

For coarser grain sizes, it is customary to approximate the grain as an ellipsoid. Three lengths can be defined. The length along the major (longest) axis is denoted as a, that along the intermediate axis is denoted as b, and that along the minor (smallest) axis is denoted as c. These lengths are typically measured with a caliper. The value b is then equated to grain size D.

Table 2-3 Sediment Grade Scale

		Size range			Approximate sieve mesh openings per inch	
Class Name	Millimeters	F	Microns	Inches	Tyler	U.S. standard
Very large boulders	4096 ~ 2048			160 ~ 80		
Large boulders	2048 ~ 1024			80 ~ 40		
Medium boulders	1024 ~ 512			40 ~ 20		
Small boulders	512 ~ 256	−9 ~ −8		20 ~ 10		
Large cobbles	256 ~ 128	−8 ~ −7		10 ~ 5		
Small cobbles	128 ~ 64	−7 ~ −6		5 ~ 2.5		
Very coarse gravel	64 ~ 32	−6 ~ −5		2.5 ~ 1.3		
Coarse gravel	32 ~ 16	−5 ~ −4		1.3 ~ 0.6	2 ~ 1/2	
Medium gravel	16 ~ 8	−4 ~ −3		0.6 ~ 0.3	5	5
Fine gravel	8 ~ 4	−3 ~ −2		0.3 ~ 0.16	9	10
Very fine gravel	4 ~ 2	−2 ~ −1		0.16 ~ 0.08	16	18
Very coarse sand	2.000 ~ 1.000	−1 ~ 0	2000 ~ 1000		32	35
Coarse sand	1.000 ~ 0.500	0 ~ 1	1000 ~ 500		60	60
Medium sand	0.500 ~ 0.250	1 ~ 2	500 ~ 250		115	120
Fine sand	0.250 ~ 0.125	2 ~ 3	250 ~ 125		250	230
Very fine sand	0.125 ~ 0.062	3 ~ 4	125 ~ 62			
Coarse silt	0.062 ~ 0.031	4 ~ 5	62 ~ 31			
Medium silt	0.031 ~ 0.016	5 ~ 6	31 ~ 16			
Fine silt	0.016 ~ 0.008	6 ~ 7	16 ~ 8			
Very fine silt	0.008 ~ 0.004	7 ~ 8	8 ~ 4			
Coarse clay	0.004 ~ 0.002	8 ~ 9	4 ~ 2			
Medium clay	0.002 ~ 0.001		2 ~ 1			
Fine clay	0.001 ~ 0.0005		1 ~ 0.5			
Very fine clay	0.0005 ~ 0.00024		0.5 ~ 0.24			

For grains in the silt and clay sizes, many methods (hydrometer, sedigraph, etc.) are based on the concept of equivalent fall diameter. That is, the terminal fall velocity v_s of a grain in water at a standard temperature is measured. The equivalent fall diameter D is the diameter of the sphere having exactly the same fall velocity under the same conditions. Sediment fall velocity is discussed in more detail below.

A variety of other more recent methods for sizing fine particles rely on blockage of light beams. The area blocked can be used to determine the diameter of the equivalent circle, i.e., the projection of the equivalent sphere. It can be seen that all of these methods can be expected to operate consistently as long as grain shape does not deviate too greatly from that of a sphere. In general, this turns out to be the case. There are some important exceptions, however. At the fine end of the spectrum, mica particles tend to be platelike; the same is true of shale grains at the coarser end. Comparison with a sphere is not necessarily a particularly useful way to characterize grain size for such materials. More recently, techniques employing light-scattering are becoming more popular for both particle-size analysis and settling velocity measurements (e.g., Pedocchi and García 2006). More material can be found in Chapter 5.

2.3.5 Size Distribution

Any sediment sample normally contains a range of sizes. An appropriate way to characterize these samples is in terms of a grain size distribution. Consider a large bulk sample of sediment of given weight. Let $p_f(D)$—or $p_f(\Phi)$—denote the fraction by weight of material in the sample of material finer than size $D(\Phi)$. The customary engineering representation of the grain size distribution consists of a plot of $p_f \times 100$ (percent finer) versus $\log_{10}(D)$—that is, a semilogarithmic plot is employed. The plot, then, would look like the one in Fig. 2-8(a).

The same size distribution plotted in sedimentological form would involve plotting $p_f \times 100$ versus Φ on a linear plot, like shown in Fig. 2-8(b).

Note that Φ on a linear axis is completely equivalent to D on a logarithmic axis because Φ is related linearly to $\log_{10}(D)$:

$$\Phi = -\frac{1}{log_{10}(2)} log_{10}(D) \tag{2-38}$$

The utility of a logarithmic scale for grain size now becomes apparent. Consider a sediment sample in which one-third of the material lies in the range 0.1–1.0 mm, one-third lies in the range 1.0–10 mm, and one-third lies in the range 10–100 mm. In Fig. 2-8(c) $p_f \times 100$ is plotted versus D on a linear scale, and in Fig. 2-8(d) $p_f \times 100$ is plotted versus D on a logarithmic scale—$p_f \times 100$ is plotted against $\log_{10}(D)$. Plot (c) is virtually unreadable, as the finest two ranges are crowded off the scale. Plot (d) provides a useful and consistent characterization of the distribution. It can be concluded that for the purposes of statistics, the relevant grain size should be on a logarithmic scale, e.g., Φ rather than D itself.

The size distribution $p_f(\Phi)$ and size density $p(\Phi)$ by weight (Fig. 2-8(e)) can be used to extract useful statistics concerning the sediment in question. Let x denote some percentage, say 50%; the grain size Φ_x denotes the size such that x% of the weight of the sample is composed of finer grains. That is, Φ_x is defined such that

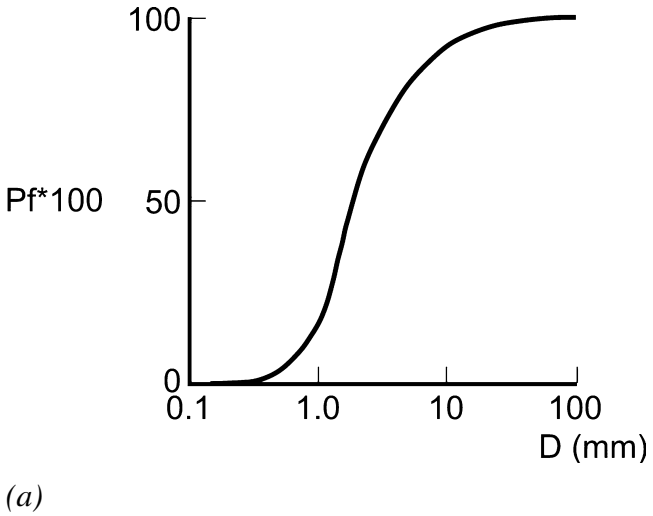

(a)

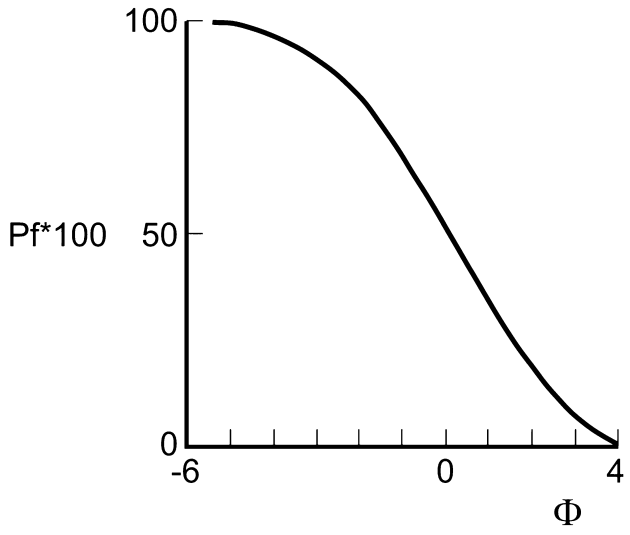

(b)

Fig. 2-8. Sediment grain size distribution in (a) semilog scale, (b) sedimentological scale Φ, (c) linear scale, (d) log scale, (e) size distribution and size density, and (f) discretization of grain size distribution.

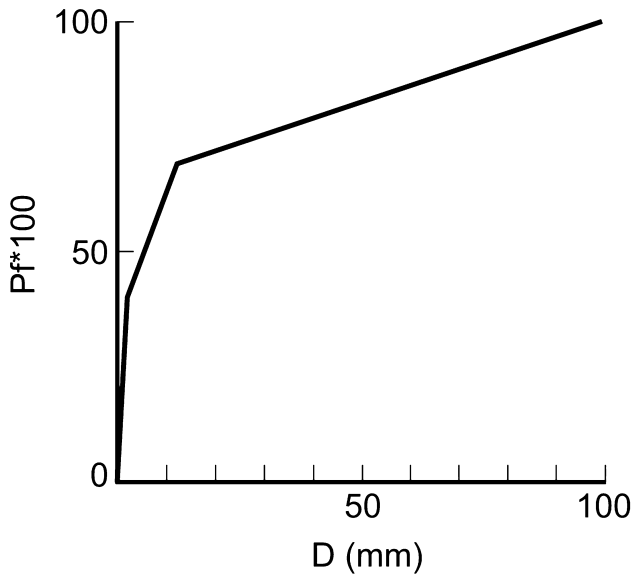

(c)

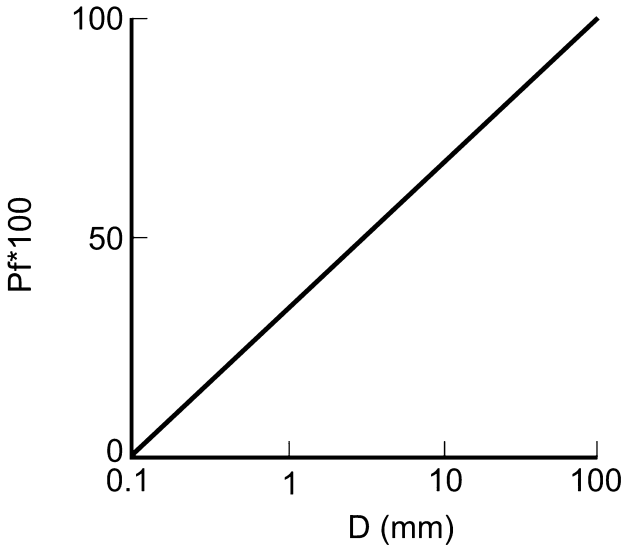

(d)

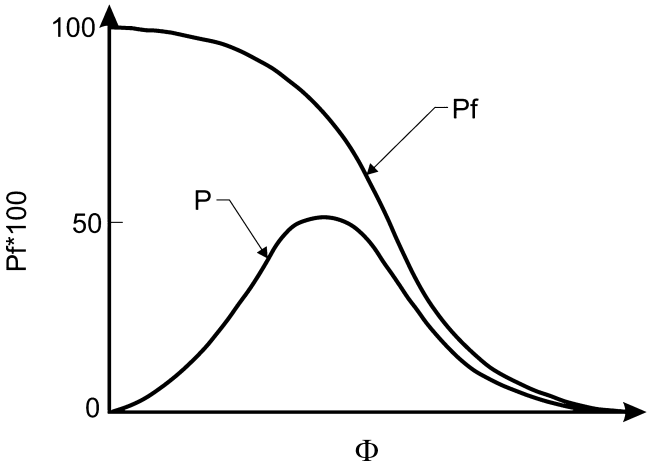

(e)

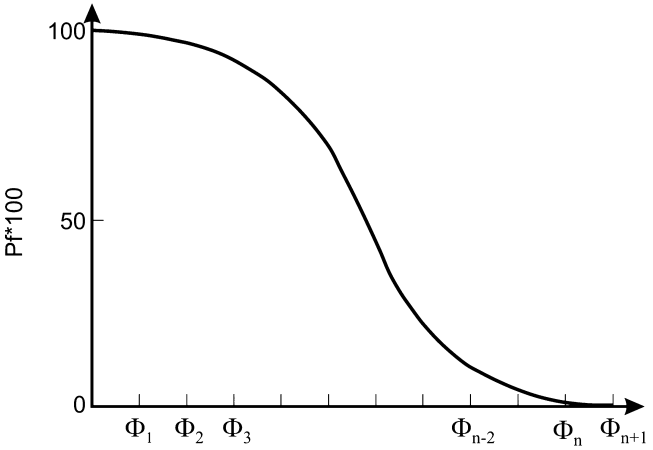

(f)

Fig. 2-8. Sediment grain size distribution in (a) semilog scale, (b) sedimentological scale Φ, (c) linear scale, (d) log scale, (e) size distribution and size density, and (f) discretization of grain size distribution. *(Continued)*

$$p_f(\Phi_x) = \frac{x}{100} \tag{2-39a}$$

It follows that the corresponding grain size in terms of equivalent diameter is given by D_x, where

$$D_x = 2^{-\Phi_x} \tag{2-39b}$$

The most commonly used grain sizes of this type are the median size D_{50} and the size D_{90} such that 90% of the sample by weight consists of finer grains. The latter size is particularly useful for characterizing bed roughness, as discussed previously.

The density $p(\Phi)$ can be used to extract statistical moments. Of these, the most useful are the mean size Φ_m and the standard deviation σ. These are given by the relations

$$\Phi_m = \int \Phi \, p(\Phi) \, d\Phi \tag{2-40a}$$

$$\sigma^2 = \int (\Phi - \Phi_m)^2 \, p(\Phi) \, d\Phi \tag{2-40b}$$

The corresponding geometric mean diameter D_g and geometric standard deviation σ_g are given as

$$D_g = 2^{\Phi_m} \tag{2-41a}$$

$$\sigma_g = 2^{\sigma} \tag{2-41b}$$

Note that for a perfectly uniform material, $\sigma = 0$ and $\sigma_g = 1$. As a practical matter, a sediment mixture with a value of σ_g of less than 1.3 is often termed well-sorted and can be treated as a uniform material. When the geometric standard deviation exceeds 1.6, the material can be said to be poorly-sorted.

In point of fact, one never has the continuous function $p(\Phi)$ with which to compute the moments of Eqs. (2-40a) and (2-40b). One must rather rely on a discretization. To this end, the size range covered by a given sediment sample is discretized in terms of n intervals bounded by $n + 1$ grain sizes Φ, Φ_2, . . ., Φ_{n+1} in ascending order of Φ, as illustrated in Fig. 2-8(f). The following definitions are made from $i = 1$ to n:

$$\overline{\Phi}_i = \frac{1}{2}\left(\Phi_i + \Phi_{i+1}\right) \tag{2-42a}$$

$$p_i = p_f\left(\Phi_i\right) - p_f\left(\Phi_{i+1}\right) \tag{2-42b}$$

Relations (2-40a) and (2-40b) now discretize to

$$\Phi_m = \sum_{i=1}^{n} \overline{\Phi}_i \, p_i \tag{2-43a}$$

$$\sigma^2 = \sum_{i=1}^{n} \left(\overline{\Phi}_i - \Phi_m\right)^2 p_i \tag{2-43b}$$

In some cases, especially when the material in question is sand, the size distribution can be approximated as Gaussian on the Φ scale (i.e., log-normal in D). For a perfectly Gaussian distribution, the mean and median sizes coincide:

$$\Phi_m = \Phi_{50} = \frac{1}{2}\left(\Phi_{84} + \Phi_{16}\right) \tag{2-43c}$$

Furthermore, it can be demonstrated from a standard table that in the case of the Gauss distribution the size Φ displaced one standard deviation larger that Φ_m is accurately given by Φ_{84}; by symmetry, the corresponding size one standard deviation smaller than Φ_{84} is Φ_{16}. The following relations thus hold:

$$\sigma = \frac{1}{2}\left(\Phi_{84} + \Phi_{16}\right) \tag{2-44a}$$

$$\Phi_m = \frac{1}{2}\left(\Phi_{84} + \Phi_{16}\right) \tag{2-44b}$$

Rearranging the relations with the aid of Eqs. (2-40a), (2-40b) and (2-43) and (2-44a), it is found that

$$\sigma_g = \left(\frac{D_{84}}{D_{16}}\right)^{1/2} \tag{2-45a}$$

$$D_g = \left(D_{84}\, D_{16}\right)^{1/2} \tag{2-45b}$$

It must be emphasized that the relations are exact only for a Gaussian distribution in Φ. This is often not the case in nature. As a result, it is strongly recommended that D_g and σ_g be computed from the full size distribution via Eqs. (2-43a), (2-43b), (2-41a), and (2-41b) rather than the approximate form embodied in the above relations.

2.3.6 Porosity

The porosity λ_p quantifies the fraction of a given volume of sediment that is composed of void space. That is,

$$\lambda_p = \frac{volume\ of\ voids}{volume\ of\ total\ space}$$

If a given mass of sediment of known density is deposited, the volume of the deposit must be computed assuming that at least part of it will consist of voids. In the case of well-sorted sand, the porosity can often take values between 0.3 and 0.4. Gravels tend to be more poorly-sorted. In this case, finer particles can occupy the spaces between coarser particles, reducing the void ratio to as low as 0.2. So-called open work gravels are essentially devoid of sand and finer material in their interstices; these may have porosities similar to that of sand. Freshly deposited clays are notorious for having high porosities. As time passes, clay deposits tend to consolidate under its own weight so that porosity slowly decreases. Wu and Wang (2006) proposed an empirical relation to estimate the initial porosity of sediments, which have bed deposited within a year or less, as a function of the median diameter D_{50} of the sediment mixture. In situ measurements of porosity indicate that biological activity can have an important effect on the porosity of sediments (Wheatcroft 2002).

The issue of porosity becomes of practical importance as regards, for example, salmon spawning grounds in gravel-bed rivers (Alonso and Mendoza 1992; Huang and García 2000). The percentage of sand and silt contained in the

sediment is often referred to the percentage of "fines" in the gravel deposit. When this fraction rises above 20–26 % by weight, the deposit is often rendered unsuitable for spawning. Salmon bury their eggs within the gravel, and high fines content implies low porosity and thus reduced permeability. The flow of groundwater necessary to carry oxygen to the eggs and remove metabolic waste products is impeded. In addition, newly hatched fry may encounter difficulty in finding pore space through which to emerge to the surface. All of the above factors dictate lowered survival rates. An empirical relationship between percent embryo survival and the geometric mean diameter of the substrate in gravel-bed rivers is shown in Fig. 2-9 (Shirazi and Seim 1981). It is clear that as the material becomes coarser, the substrate porosity can be expected to increase accordingly, augmenting the embryo survival rates. Chief causes of elevated fines in gravel-bed rivers include road building and clear-cutting of timber in the watershed.

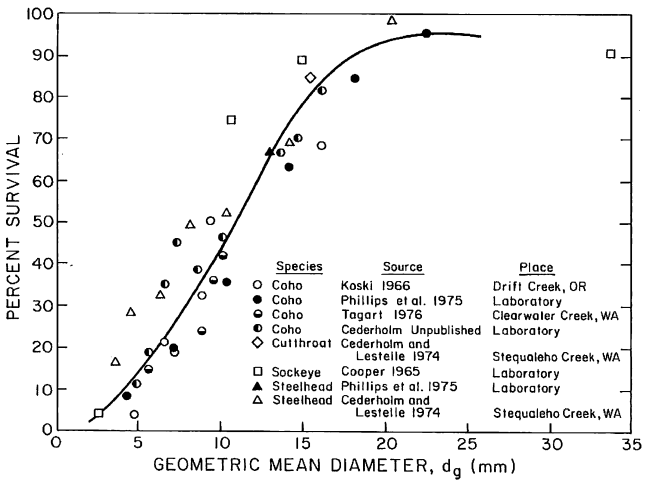

Fig. 2-9. Relationship between percent embryo survival and the geometric mean diameter of the substrate (after Shirazi and Seim, 1981).

2.3.7 Shape

There are a number of ways in which to classify grain shape (Vanoni 2006). One of these, the Zingg classification scheme, is illustrated here. According to the definitions introduced earlier, a simple way to characterize the shape of an irregular clast (stone) is in terms of the lengths a, b, and c of the major, intermediate, and minor axes, respectively. If these three are all equal, the grain can be said to be close to a sphere in shape. If a and b are equal but c is much smaller, the grain is rodlike. Finally, if c is much smaller than b, which is, in turn, much smaller than a, the resulting shape should be bladelike. This is illustrated in terms of the Zingg diagram in Fig. 2-10.

In studies of the fall velocity of geometric shapes and sand grains by McNown, Albertson and others, the shape of the particles has been expressed by the Corey shape factor SF, which makes use of the characteristic lengths, defined above, and is given by (Vanoni 2006, p. 14)

$$SF = \frac{c}{\sqrt{ab}}$$

It follows that a spherical particle will have a $SF = 1$. For natural sands $SF = 0.7$. The shape factor has been used in

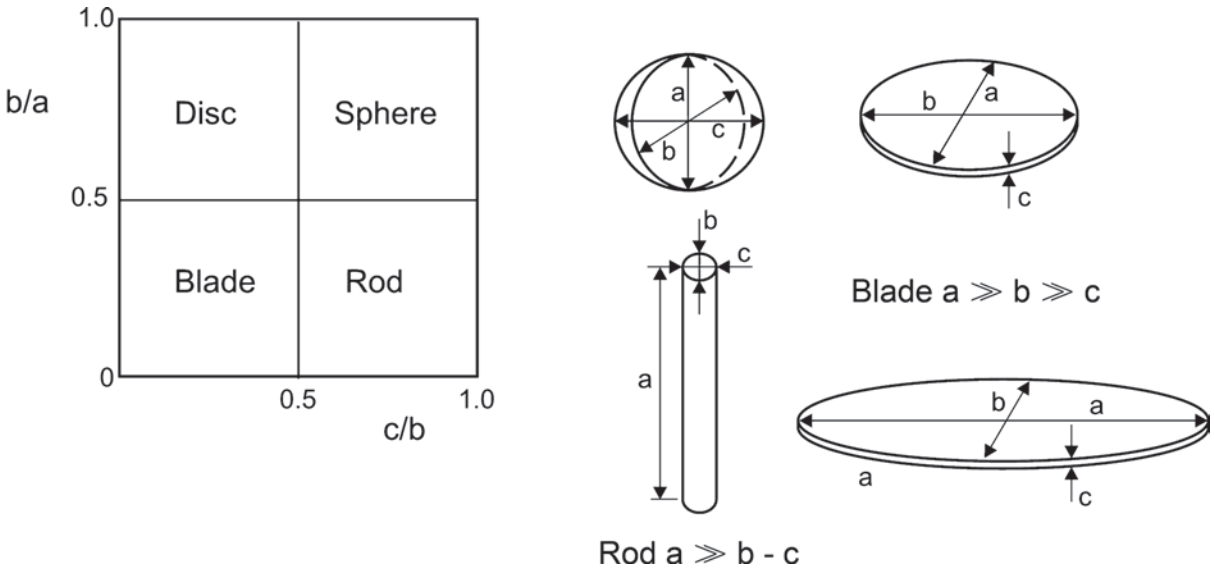

Fig. 2-10. Definition of Zingg diagram.

studies of particle fall velocity (Dietrich 1982; Jimenez and Madsen 2003; Wu and Wang 2006). More material on sediment particle shape and its effect on particle fall velocity can be found in Vanoni (2006, p. 14).

2.3.8 Fall Velocity

A fundamental property of sediment particles is their fall or settling velocity. The fall velocity of sediment grains in water is determined by their diameter and density and by the viscosity of the water. Falling under the action of gravity, a particle will reach a constant, terminal velocity once the drag equals the submerged weight of the particle. The relation for terminal fall velocity for a spherical particle in quiescent fluid v_s can be presented as

$$R_f = \left[\frac{4}{3} \frac{1}{C_D \left(R_p \right)} \right]^{1/2} \tag{2-46a}$$

where

$$R_f = \frac{\nu_s}{\sqrt{gRD}} \tag{2-46b}$$

$$R_p = \frac{\nu_s D}{\nu} \tag{2-46c}$$

and the functional relation $C_D = f(R_p)$ denotes the drag coefficient for spheres (García 1999). Here g is the acceleration of gravity, $R = (\rho_s - \rho)/\rho$ is the submerged specific gravity of the sediment, and ν is the kinematic viscosity of water. This relation is not very useful because it is not explicit in ν_s; one must compute fall velocity by trial and error. One can use the following equation for the drag coefficient C_D

$$C_D = \frac{24}{R_p}\left(1 + 0.152\, R_p^{1/2} + 0.0151\, R_p\right) \tag{2-46d}$$

and the definition

$$R_{ep} = \frac{\sqrt{gRD}\, D}{\nu} \tag{2-46e}$$

to obtain an explicit relation for fall velocity in the form of R_f versus R_{ep}. Such a diagram is presented in Fig. 2-11, where the ranges for silt, sand, and gravel are plotted for a kinematic viscosity $\nu = 0.01$ cm^2/s (clear water at 20°C) and a submerged specific gravity $R = 1.65$ (quartz). An equivalent diagram to estimate fall velocity of particles was proposed earlier by Parker (1978).

Notice that for fine silts, R_p is smaller than one and the drag coefficient given by Eq. (2-46d) reduces to

$$C_D = \frac{24}{R_p} \tag{2-46f}$$

Substitution of (2-46f) into (2-46a) yields the well-known Stokes law for settling velocity of fine particles,

$$v_s = \frac{gRD^2}{18\nu} \tag{2-46g}$$

A useful empirical relation to estimate the kinematic viscosity of clear water is:

$$\nu = \frac{1.79\ 10^{-6}}{1 + 0.03368\,T + 0.00021\,T^2} (m^2/s) \tag{2-46h}$$

where

T = temperature of the water in degrees centigrade (°C).

A number of relations for terminal fall velocity for the case of nonspherical (natural) particles can be found in the literature. Dietrich (1982) analyzed fall velocity data for natural particles and used dimensional analysis to obtain the useful fit

$$\begin{aligned} R_f = exp\Big\{ &- b_1 + b_2\, ln\left(R_{ep}\right) - b_3\left[ln\left(R_{ep}\right)\right]^2 \\ &- b_4\left[ln\left(R_{ep}\right)\right]^3 + b_5\left[ln\left(R_{ep}\right)\right]^4 \Big\} \end{aligned} \tag{2-47a}$$

where

$$b_1 = 2.891394,\ b_2 = 0.95296,\ b_3 = 0.056835,$$
$$b_4 = 0.002892,\ b_5 = 0.000245 \tag{2-47b}$$

In an attempt to obtain a more practical relation, Jimenez and Madsen (2003) fitted the formula of Dietrich (1982) to the expression

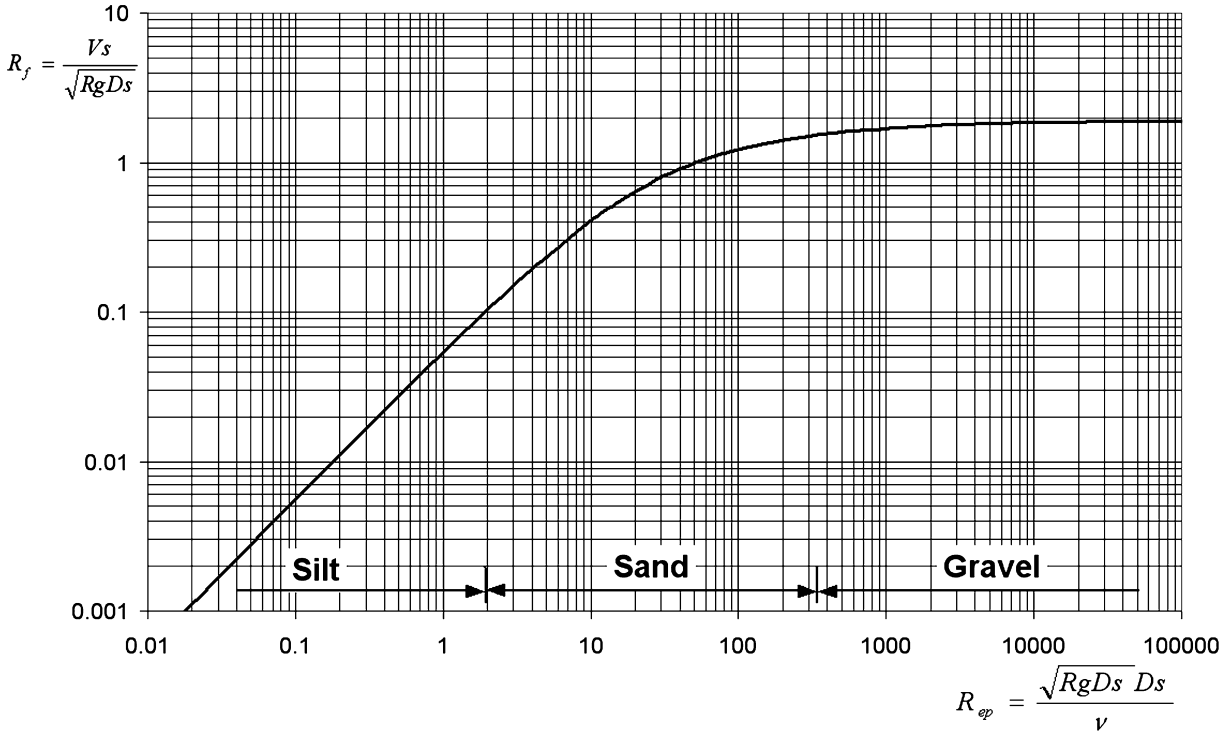

Fig. 2-11. Diagram of R_f versus R_{ep} calculated from the drag coefficient for spheres.

$$W_* = \frac{v_s}{\sqrt{g\,R\,D_N}} = \left(A + \frac{B}{S_*}\right)^{-1} \qquad (2\text{-}48a)$$

in which

$$S_* = \frac{D_N}{4\nu}\sqrt{gRD_N} \qquad (2\text{-}48b)$$

Here, D_N= nominal particle diameter. The coefficients A and B in Eq. (2-48a) are functions of Corey shape factor and particle roundness and are expressed graphically by Jimenez and Madsen (2003). In many practical applications, the sediment is naturally worn quartz sands characterized by their sieve diameter D_s. For this typical application, $D_N = D_s/0.9$, A = 0.954 and B = 5.12, are recommended. With these values incorporated in to it, Eq. (2-48a) was found to provide reliable predictions of fall velocity for natural quartz sediment with sieving diameters ranging from 0.063 mm up to 2 mm (Jimenez and Madsen 2003).

Another simple relation to estimate the fall velocity of natural sand particles has been proposed by Soulsby (1997) for use in the marine environment,

$$v_s = \frac{\nu}{D}\left[(10.36^2 + 1.049\,D_*^3)^{1/2} - 10.36\right] \qquad (2\text{-}49a)$$

where

$$D_* = \left[\frac{gR}{\nu^2}\right]^{1/3} D \qquad (2\text{-}49b)$$

Here

- g = acceleration of gravity;
- ν = kinematic viscosity of water;
- D = mean sieve diameter of grains; and
- $R = (\rho_s - \rho)/\rho$ is the submerged specific gravity of the grains.

Equations very similar to (2-49a) have been proposed independently by Zanke (1977) and van Rijn (1984).

At high concentrations the flows around adjacent settling grains interact resulting in a larger drag than for the same grain in isolation. This phenomenon is known as hindered settling and results in the hindered settling velocity v_{sC} for high sediment concentrations to be smaller that the fall velocity v_s at low sediment concentrations (less than 0.05). Applying reasoning similar to the one that led to Eq. (2-49a),

Soulsby (1997) proposed the following relation for the hindered fall velocity v_{sc} of grains in a dense suspension having a volumetric sediment concentration C:

$$v_{sC} = \frac{\nu}{D}\left[(10.36^2 + 1.049(1-C)^{4.7} D_*^3)^{1/2} - 10.36\right] \quad \text{(2-49c)}$$

which is valid for all values of D_* and C. When $C = 0$, Eq. (2-49c) reduces to Eq. (2-49a).

The subject of sediment fall velocity is far from being resolved. However, the empirical fits presented here should suffice for engineering purposes. Other useful relations to estimate sediment fall velocity can be found in Swamee and Ojha (1991), Cheng (1997), Ahrens (2000), and Ahrens (2003). Recently, Wu and Wang (2006) compared different formulations and developed another empirical fit to estimate fall velocity which accounts for the effect of particle shape through the Corey shape factor $\left(SF = c/\sqrt{ab}\right)$.

Material on particle settling for the case of fine-grained cohesive sediment is presented in Chapter 4.

2.3.9 Relation between Size Distribution and Stream Morphology

The study of sediment properties, and in particular size distribution, is most relevant in the context of stream morphology. The material that follows is intended to point out some of the more interesting issues, and in particular, morphological differences between sand-bed and gravel-bed streams. More discussion on the subject can be found in Chapters 3 and 6.

In Fig. 2-12, several size distributions from the sand-bed Kankakee River, Illinois, are shown (Bhowmik et al. 1980). The characteristic *S*-shape suggests that these distributions might be approximated by a Gaussian curve. The median size D_{50} falls near 0.3–0.4 mm. The distributions are very tight with a near-absence of either gravel or silt. For practical purposes, the material can be approximated as uniform.

In Fig. 2-13, several size distributions pertaining to the gravel-bed Oak Creek, Oregon, are shown (Milhous 1973). In gravel-bed streams, the surface layer ("armor" or "pavement") tends to be coarser than the substrate (identified as "subpavement" in the figure). Whether the surface or substrate is

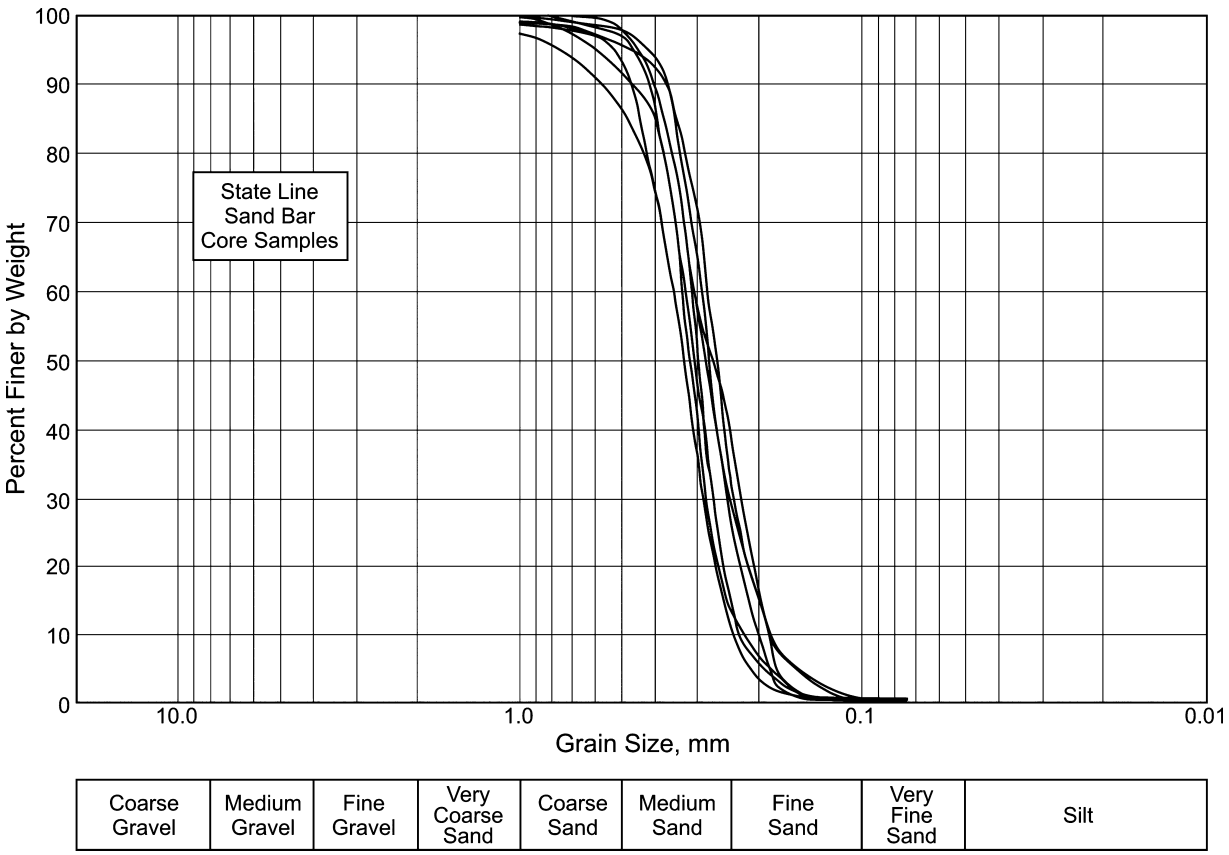

Fig. 2-12. Particle size distributions of bed materials in Kankakee River, Illinois (after Bhowmik et al. 1980).

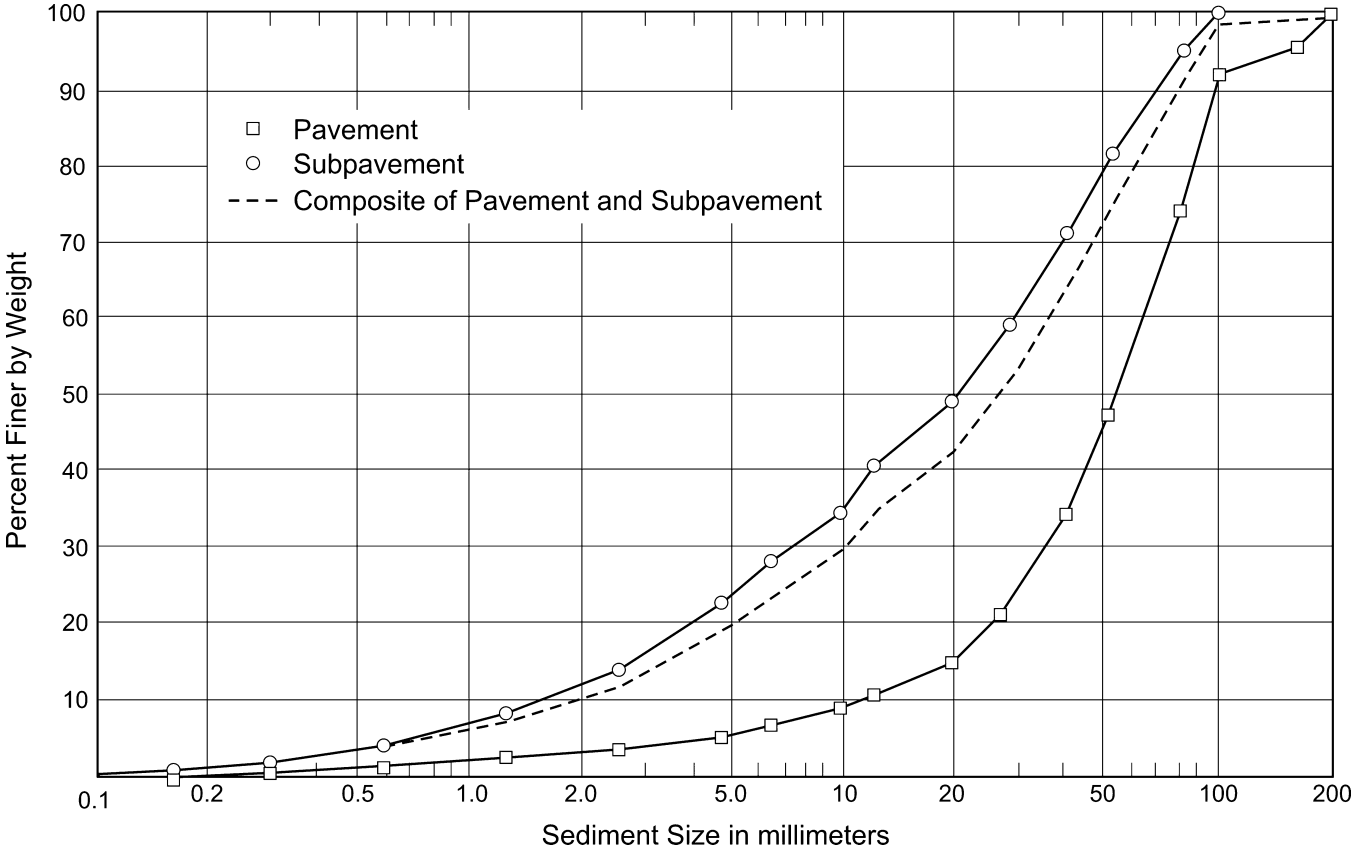

Fig. 2-13. Size distribution of bed material samples in Oak Creek, Oregon (after Milhous 1973).

considered, it is apparent that the distribution ranges over a much wider range of grain sizes than in the case of Fig. 2-12. More specifically, in the distributions of the sand-bed Kankakee River, Φ varies from about 0 to about 3, whereas in Oak Creek, Φ varies from about -8 to about 3. In addition, the distribution of Fig. 2-13 is upward concave almost everywhere, and thus deviates strongly from the Gaussian distribution.

These two examples provide a window toward generalization. A river may loosely be classified as sand-bed or gravel-bed according to whether the median size D_{50} of the surface material or substrate is less or greater than 2 mm. The size distributions of sand-bed streams tend to be relatively narrow and also tend to be S-shaped. The size distributions of gravel-bed streams tend to be much broader and to display an upward-concave shape. There are, of course, many exceptions to this behavior, but it is sufficiently general to warrant emphasis.

More evidence for this behavior is provided in Fig. 2.14. Here, the grain size distributions for a variety of stream reaches have been normalized using the median sediment size D_{50}. Four sand-bed reaches are included with three gravel-bed reaches. All of the sand-bed distributions are *S*-shaped, and all have a lower spread than the gravel-bed distributions. The figure indicates that the standard deviation of the grain size distribution can be expected to increase systematically with increasing sediment size (White et al. 1973). The three gravel-bed size distributions differ systematically from the sand-bed distributions in a fashion that accurately reflects Oak Creek (Fig. 2-13). The standard deviation is, in all cases, markedly larger than for any of the sand-bed distributions, and the distributions are upward concave except perhaps near the coarsest sizes.

2.4 THRESHOLD CONDITION FOR SEDIMENT MOVEMENT

In this section the threshold conditions for initiation of motion are analyzed. A mechanistic model for initiation of motion is presented. The Shields diagram and other methods for assessing initiation of motion are introduced. The analysis is limited to noncohesive granular sediments such as silt, sand and gravel.

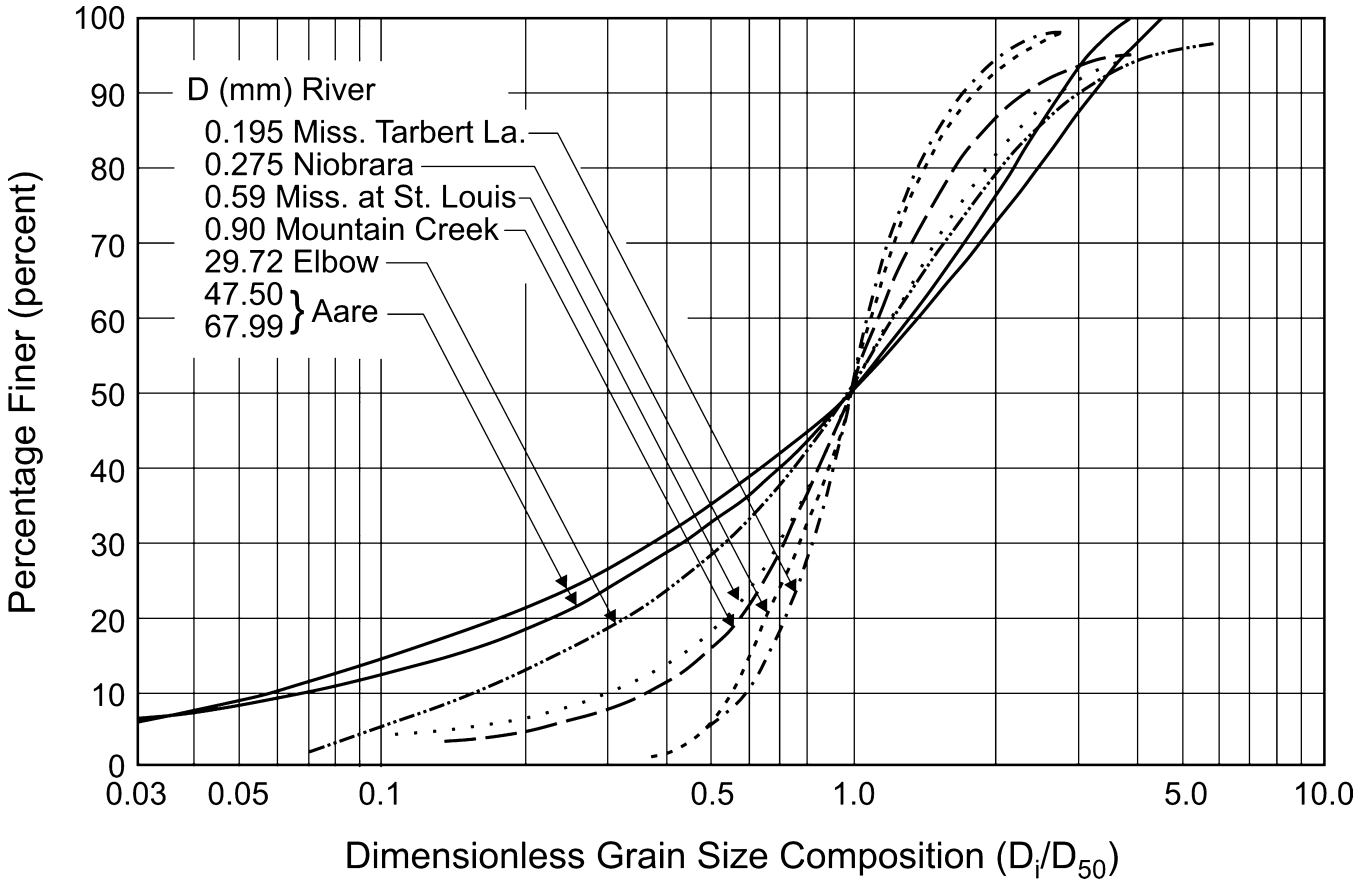

Fig. 2-14. Dimensionless grain-size distribution for different rivers (after White et al. 1973).

2.4.1 Submerged Angle of Repose

If granular particles are allowed to pile up while submerged in a fluid, there is a specific slope angle ϕ beyond which spontaneous failure of the slope occurs. This angle is termed the angle of repose, or alternatively, the friction angle. To study this in more detail, consider a typical grain resting on the surface of such a slope as shown in Fig. 2-15.

The coefficient of Coulomb friction is defined to be μ, where

$$\mu = \frac{tangential\ resistive\ force}{downward\ normal\ force} \tag{2-50a}$$

The forces acting on the particle along the slope are the submerged force of gravity (gravitational force minus buoyancy force), which has a downslope component F_{gt} and a normal component F_{gn}, and a tangential resistive force F_r due to Coulomb friction. These are given by

$$F_{gt} = (\rho_s - \rho) g V_p \sin\phi \tag{2-50b}$$

$$F_{gn} = (\rho_s - \rho) g V_p \cos\phi \tag{2-50c}$$

$$F_r = \mu F_{gn} \tag{2-50d}$$

The condition for incipient motion is given by

$$F_{gt} = F_r \tag{2-50e}$$

That is, the downslope impelling force of gravity should just balance with the Coulomb resistive force. From the above four relations, it is found that

$$\mu = \tan\phi \tag{2-50f}$$

The angle of repose is an empirical quantity. Tests with well-sorted material indicate that ϕ is near 30° for sand, gradually increasing to 40° for gravel. Poorly sorted, angular material tends to interlock, giving greater resistance to failure, and as a result, a higher friction angle ϕ. Such material is thus often chosen for riprap (see Appendix B).

Friction angle measurements obtained in gravel-bed streams, including implications for critical shear stress estimations, can be found in Kirchner et al. (1990) and Buffington et al. (1992).

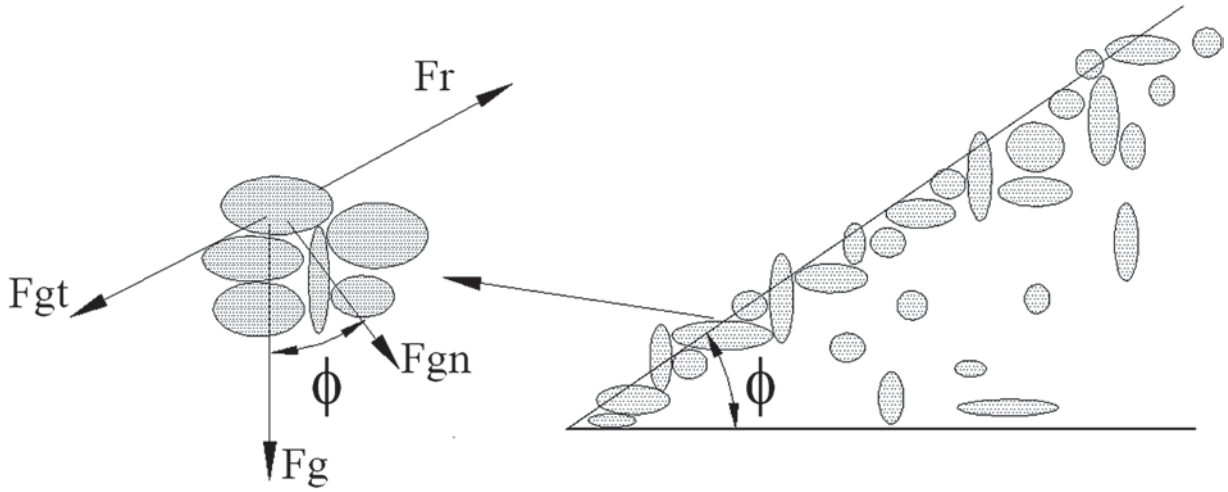

Fig. 2-15. Definition diagram for angle of repose.

2.4.2 Critical Stress for Flow over a Granular Bed

When a granular bed is subjected to a turbulent flow, it is found that virtually no motion of the grains is observed at some flows, but that the bed is noticeably mobilized at other flows (Cheng and Chiew 1998; Papanicolau et al. 2002; Niño et al. 2003). Literature reviews on incipient motion can be found in Miller et al. (1977); Lavelle and Mofjeld (1987); and Buffington and Montgomery (1997).

Factors that affect the mobility of grains subjected to a flow are summarized as follows,

- Randomness
  - Grain placement
  - Turbulence
- Forces on grains
  - Fluid (Mean & turbulent)
    - Lift
    - Drag
  - Gravity

In the presence of turbulent flow, random fluctuations typically prevent the clear definition of a critical or threshold condition for motion: the probability of grain movement is never precisely zero (Paintal 1971; Graf and Paziz 1977; Lopez and García 2001; Zanke 2003). It is, nevertheless, possible to define a condition below which movement can be neglected for many practical purposes.

The following analysis is a slightly generalized version of the derivation of the full Shields curve for the threshold of motion presented by Ikeda (1982), which is based on the work of Iwagaki (1956) and Coleman (1967). A similar analysis was presented by Wiberg and Smith (1987) for the case of nonuniform sediment size. Consider the granular bed of Fig. 2-16. The flow forces on a dangerously placed spherical sediment particle protruding upward from the mean bed are considered in order to analyze the threshold of motion.

Certain assumptions enter into the Ikeda-Coleman-Iwagaki analysis. The flow is taken to follow the logarithmic law near the boundary (Eq. 2-4). The origin of the z-coordinate for evaluating the logarithmic law is taken to be the base of the dangerously exposed particle. Turbulent forces on the particle are neglected. Drag and lift forces act through the particle center (in general, they do not, giving rise to torque as well as forces). The value of the drag coefficient c_D can be approximated by the free-stream value (Coleman 1967). The coordinate z is taken to be vertically upward, corresponding to very low streamwise slopes S. The roughness height k_s is equated to the particle diameter D.

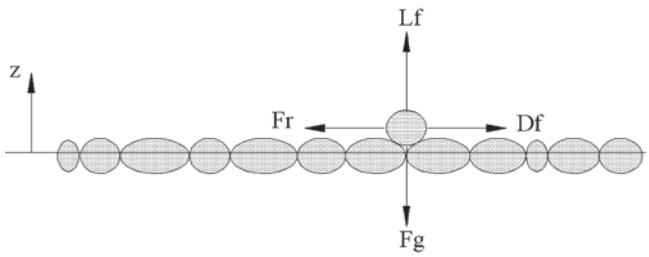

Fig. 2-16. Forces acting on a "dangerously" placed particle.

It is seen from the above assumptions that the particle center is located at $z = D/2$. It is necessary to use some information about turbulent boundary layers to define the effective fluid velocity u_f acting on the particle in order to facilitate computation of the fluid forces. A viscous sublayer exists (see Eq. 2-6) when D/δ_v is less than about 0.5, or $(u_* D/\nu) < 5$. In this case, the effective fluid velocity u_f acting on the particle is estimated with Eq. (2-5) as

$$\frac{u_f}{u_*} = \frac{1}{2}\frac{u_* D}{\nu} \tag{2-51a}$$

On the other hand, if $D/\delta_v > 2$, no viscous sublayer exists, and the logarithmic law applies near (but not at) the bed. So the flow velocity acting on the particle can be estimated by

$$\frac{u_f}{u_*} = 2.5 ln\left(30\frac{z}{D}\right)\Big|_{z=\frac{1}{2}D} = 6.77 \tag{2-51b}$$

It follows then that Eqs. (2-51a) and (2-51b) can be written in the more general form

$$\frac{u_f}{u_*} = F\left(\frac{u_* D}{\nu}\right) \tag{2-51c}$$

where

$$F = \frac{1}{2}\frac{u_* D}{\nu} \text{ for } \frac{u_* D}{\nu} < 13.5 \tag{2-51d}$$

and

$$F = 6.77 \text{ for } \frac{u_* D}{\nu} > 13.5 \tag{2-51e}$$

However, it would be more convenient to have a continuous function F, so that the transition between hydraulically smooth and fully rough condition, is smooth. The fit proposed by Swamee (1993) can be used to evaluate F in Eq. (2-51c) by setting $z = D/2$ and $k_s = D$ in Eq. (2-10),

$$F = \left\{\left(\frac{2\nu}{u_* D}\right)^{10/3} + \left[\kappa^{-1} ln\left(1 + \frac{\frac{9}{2}\frac{u_* D}{\nu}}{1 + 0.3\frac{u_* D}{\nu}}\right)\right]^{-10/3}\right\}^{-0.3} \tag{2-51f}$$

Now the forces acting on the particle can be considered. The streamwise fluid drag force D_f, upward normal (vertical in this case) fluid lift force L_f, and downward vertical submerged gravitational force F_g acting on the particle of the previous figure are thus

$$D_f = \rho\frac{1}{2}\pi\left(\frac{D}{2}\right)^2 c_D u_f^2 \tag{2-52a}$$

$$L_f = \rho\frac{1}{2}\pi\left(\frac{D}{2}\right)^2 c_L u_f^2 \tag{2-52b}$$

$$F_g = \rho R g\frac{4}{3}\pi\left(\frac{D}{2}\right)^3 \tag{2-52c}$$

From Eq. (2-50d), it is seen that the Coulomb resistive force F_r is given by

$$F_r = \mu\left(F_g - L_f\right) \tag{2-52d}$$

The critical condition for incipient motion of the particle is that the impelling drag force is just balanced by the resisting Coulomb frictional force:

$$D_f = F_r \tag{2-53}$$

That is, if $D_f < F_r$, the particle will not move, and if $D_f > F_r$, it will move. Between Eqs. (2-52a), (2-52b), (2-52c), (2-52d), and (2-53), the following relation is obtained for critical fluid velocity u_f at $z = D/2$:

$$\frac{u_f^2}{RgD} = \frac{4}{3}\frac{\mu}{c_D + \mu c_L} \tag{2-54}$$

This relation is now converted to a relation in terms of boundary shear stress. It may be recalled that by definition $\rho u^2{}_* = \tau_b$, where τ_b denotes the boundary shear stress. In this case, the shear stress in question is the critical one for the onset of motion and is denoted by τ_{bc}. Between Eqs. (2-51c) and (2-54), the Ikeda-Coleman-Iwagaki relation is obtained for the critical shear stress:

$$\tau_c^* = \frac{4}{3}\frac{\mu}{\left(c_D + \mu c_L\right)}\frac{1}{F^2(u_{*c} D/\nu)} \tag{2-55a}$$

The equation is valid for nearly horizontal beds but the effect of channel slope can be readily incorporated. For a channel with a downstream slope angle α, the downslope

effect of gravity has to be included in the force balance presented earlier, resulting in the following expression for the critical shear stress

$$\tau_c^* = \frac{4}{3}\frac{(\mu\, cos\,\alpha - sin\,\alpha)}{(c_D + \mu\, c_L)}\frac{1}{F^2(u_{*_c}D/\nu)} \qquad (2\text{-}55b)$$

Notice that for $\alpha = 0$, Eq. (2-55b) reduces to Eq. (2-55a).

A predecessor of all these equations was advanced by Egiazaroff (1965). It can be found in Vanoni (2006, p. 58) and is used for sediment mixtures in Chapter 3. Similar relations were also obtained by Fredsøe and Deigaard (1992, p. 203) and can also be found, albeit without derivation, in Chien and Wan (1999, p. 319).

In the above relation, τ_c^* is a dimensionless measure of boundary shear stress known as the Shields parameter and given by the definition

$$\tau_c^* = \frac{\tau_{bc}}{\rho g R D} \qquad (2\text{-}56)$$

where

$\tau_{bc} = \rho u^2_{*_c}$ = critical bed shear stress for initiation of motion;
u_{*_c} = critical shear velocity;
ρ = water density;
$R = (\rho_s - \rho)/\rho$ is the submerged specific gravity of the sediment;
g = acceleration of gravity; and
D = sediment particle diameter.

The most relevant fact about the mechanistic approach to this problem of initiation of motion relates to the possibility of obtaining an explicit formulation of the relation explored by Shields with dimensional analysis and experiments. Eq. (2-55a) can be evaluated with the aid of Eq. (2-51f) and certain realistic assumptions about the internal angle of friction ϕ, and the drag c_D and lift c_L coefficients. As an example, two internal friction angles are considered, $\phi = 40°$ ($\mu = 0.84$) and $\phi = 60°$ ($\mu = 1.73$), and the following assumptions are made: $k_s = 2D$, and $c_L = 0.85\, c_D$. It is furthermore assumed that c_D is given as a function of u_*D/ν according to the standard drag curve for spheres (i.e., Eq. 2-46d). A plot of Eq. (2-55a) is shown in Fig. 2-17, together with the data of Shields (1936). Considering all the assumptions made for developing the threoretical model, the agreement is quite reasonable. The best agreement between the Ikeda-Coleman-Iwagaki model and Shields observations is found for $\phi = 60°$ ($\mu = 1.73$). Such friction angle is rather high but is not possible to know the exact value of this parameter for the sediment used by Shields in his experiments, and whether or not incipient transport conditions were present

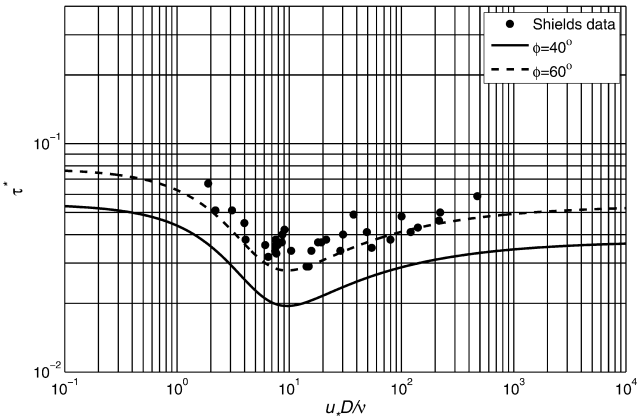

Fig. 2-17. Comparison of Ikeda-Coleman-Iwagaki model for initiation of motion with Shields data.

(Buffington 1999). The theoretical model developed here is for idealized spherical particles for which the friction angle can be expected to be lower than for natural sediments. For the case of $\phi = 40°$ ($\mu = 0.84$), the curve predicted with Eq. (2-55a), follows the trend of Shields data but predicts values of critical shear stress that are smaller by a factor of about 1.6. It is interesting that several researchers have found that Shields crtical shear stress values are indeed higher than those observed. More discussion on the internal friction angle is given below when the model of Wiberg and Smith (1987) is presented.

Although there are a number of assumptions made in its derivation, the mechanistic Ikeda-Coleman-Iwagaki model (Eq. 2.55a) makes it possible to visualize the sources of uncertainty (i.e., angle of repose, drag and lift coefficients, particle location, etc.) and helps to understand why it is so difficult to characterize the threshold condition with a deterministic model (e.g., Bettess 1984; Lavelle and Mojfeld 1987; Komar 1996; Papanicolau et al. 2001; Shvidchenko and Pender 2001; Niño et al. 2001; Dancey et al. 2002). Recently the role played by turbulence on initiation of motion has been examined by Zanke (2003), who found that turbulence-induced fluctuations in the lift force make particles "lighter" and easier to move.

2.4.3 Shields Diagram

Shields (1936) conducted his set of pioneering experiments to elucidate the conditions for which sediment grains would be at the verge of moving. While doing this, Shields introduced the fundamental concepts of similarity and dimensional analysis and made a set of observations that have become legendary in the field of sediment transport (Kennedy 1995). Shields deduced from dimensional analysis and fluid mechanics considerations that τ_c^* should be a function of shear Reynolds number $u_{*_c}D/\nu$, as implied by Eq. (2-55a). The Shields diagram is expressed by dimensionless

combinations of critical shear stress τ_{bc}, sediment and water specific weights γ_s and γ, respectively, sediment size D, critical shear velocity $u_{*c} = \sqrt{\tau_{bc}/\rho}$, and kinematic viscosity of water ν. These quantities can be expressed in any consistent set of units. The Shields dimensionless parameters are related by a simple expression,

$$\tau_c^* = \frac{\tau_{bc}}{\rho\, g\, R\, D} = F_* \left(\frac{u_{*c}\, D}{\nu} \right) \qquad (2\text{-}57)$$

The Shields diagram shown in Fig. 2-18 was originally prepared by Vanoni (1964). This diagram is the predecessor of the one that finally appeared when Manual 54 was first published in 1975 (Vanoni 2006, p. 57). A modern account of the Shields diagram and its history can be found in Kennedy (1995). Critical Shields values τ_c^* are commonly used to denote conditions under which bed sediment particles are stable but on the verge of being entrained. The curve in the Shields diagram was originally introduced by Rouse (1939), whereas the auxiliary scale was proposed by Vanoni (1964) to facilitate the determination of the critical shear stress τ_{bc} once the submerged specific gravity, the particle diameter D and the kinematic viscosity of water ν are specified. It is known that the values obtained from the Shields diagram (Fig. 2-18) for initiation of motion are indeed larger than those observed by other researchers, in particular for coarse material. For example, Neill (1968) gives $\tau_c^* = 0.03$ instead of 0.06 for the dimensionless critical shear stress for values of $Re_* = u_* D/\nu$ in excess of 500, while Gessler (1971) suggests using a value of $\tau_c^* = 0.046$ for such condition.

The value of τ_c^* to be used in design depends on the particular case at hand. If the situation is such that grains that are moved can be replaced by others moving from upstream, some motion can be tolerated, and the values from the Shields curve may be used. On the other hand, if grains removed cannot be replaced as on a stream bank, the Shields value of τ_c^* are too large and should be reduced. As already mentioned it is well known from observations by Neill and Yalin (1969) and Gessler (1970) that Shields original values for initiation of motion of coarse material are too high and should be divided by a factor of 2 for engineering purposes.

As first noticed by Vanoni (1964), the Shields diagram is not practical in the form of Fig. 2-18, because in order to find the critical shear stress for incipient motion τ_{bc}, one must know the critical shear velocity $u_{*c} = \sqrt{\tau_{bc}/\rho}$. The relation can be cast in explicit form by plotting τ_c^* versus R_{ep}, noting the internal relation

$$\frac{u_*\, D}{\nu} = \frac{u_*}{\sqrt{g\, R\, D}} \frac{\sqrt{g\, R\, D}\; D}{\nu} = \left(\tau^*\right)^{1/2} R_{ep} \qquad (2\text{-}58)$$

where $R = \dfrac{\rho_s - \rho}{\rho}$ is the submerged specific gravity of the sediment.

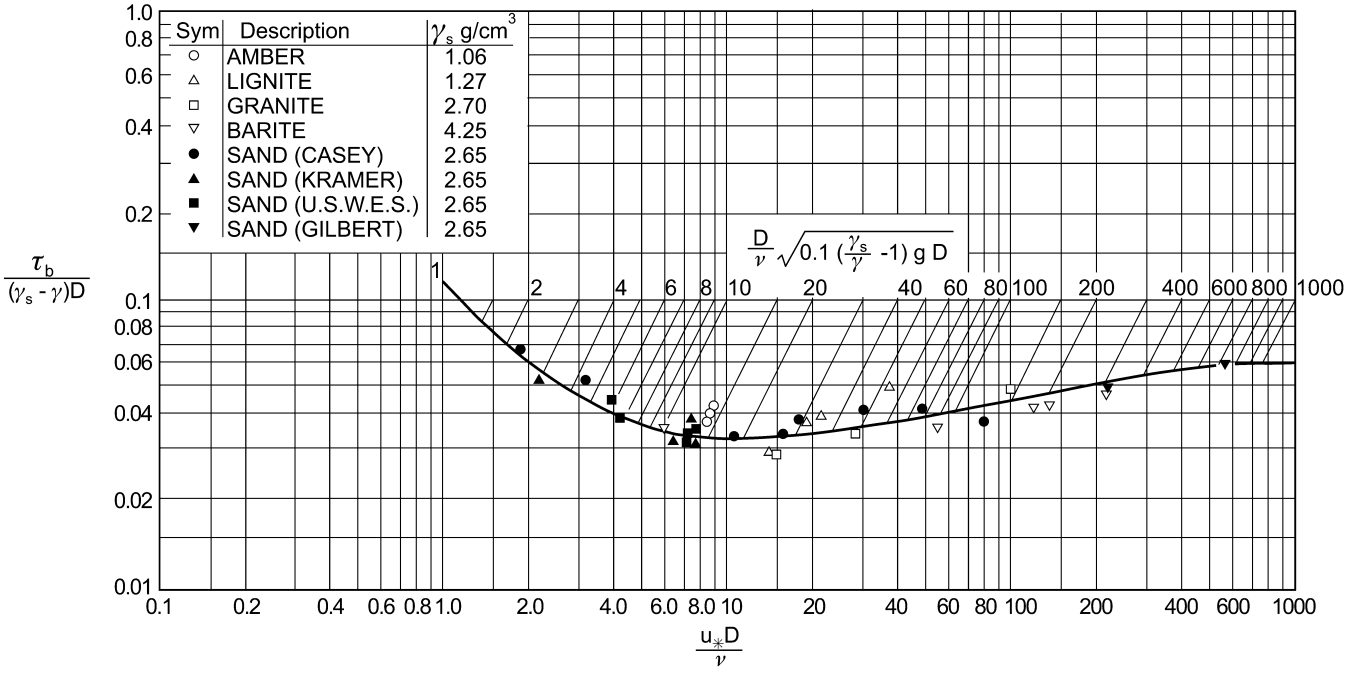

Fig. 2.18. Shields diagram for initiation of motion (source Vanoni, 1964).

Brownlie (1981) used this relation to convert the original Shields diagram into one with τ_c^* versus R_{ep}. Similar diagrams using D^* (see Eq. 2-49b) instead of R_{ep} have been advanced among others by Bonnefille (1963), Smith (1977), van Rijn (1984a), García and Maza (1997), and Soulsby and Whitehouse (1997). A useful fit to the Shields data was proposed by Brownlie (1981, p.161):

$$\tau_c^* = 0.22\, R_{ep}^{-0.6} + 0.06\ exp\left(-17.77\, R_{ep}^{-0.6}\right) \quad \text{(2-59a)}$$

With this relation, the value of τ_c^* can be readily computed when the properties of the water and the sediment are given. As already mentioned, to be on the safe side the values given by Eq. (2-59a) should be divided by 2 for engineering purposes, resulting in the following expression

$$\tau_c^* = \frac{1}{2}\left[0.22\, R_{ep}^{-0.6} + 0.06\, exp\left(-17.77\ R_{ep}^{-0.6}\right)\right] \quad \text{(2-59b)}$$

This equation is plotted in the modified Shields diagram shown in Fig. 2-19, where the size ranges for silt, sand and gravel are also shown.

For fine-grained sediments (silt and finer), the Shields diagram does not provide realistic results. Mantz (1977) conducted a series of experiments and observed that for fine-grained, noncohesive sediments the critical shear stresses can be estimated with the following relation

$$\tau_c^* = 0.135 R_{ep}^{-0.261} \quad \text{(2-59c)}$$

which is valid for the range $0.056 < R_{ep} < 3.16$. Equations (2-59a) and (2-59c) merge for $R_{ep} = 4.22$.

Lavelle and Mofjeld (1987) used the pioneering bed-stability observations made by Grass (1970) to question the existance of a deterministic value of critical stress for incipient motion as foreseen by Shieds and to promote a probabilistic approach to address threshold conditions for initiation of motion and entrainment into suspension. Along the same line of thought, Lopez and García (2001) have proposed a risk-based approach showing that the Shields diagram can be interpreted in a probabilistic way. At the same time, there is also evidence that the Shields diagram is quite useful for field application. For instance, Fisher et al. (1983) experimentally investigated incipient motion of organic detritus and inorganic sediment particles on sand and gravel beds and found that their observations followed the characteristics of the Shields diagram. Recently, Marsh et al (2004) tested the Shields approach together with three other methods available in the literature and showed that it is still one of the best methods available for sand-bed streams. More

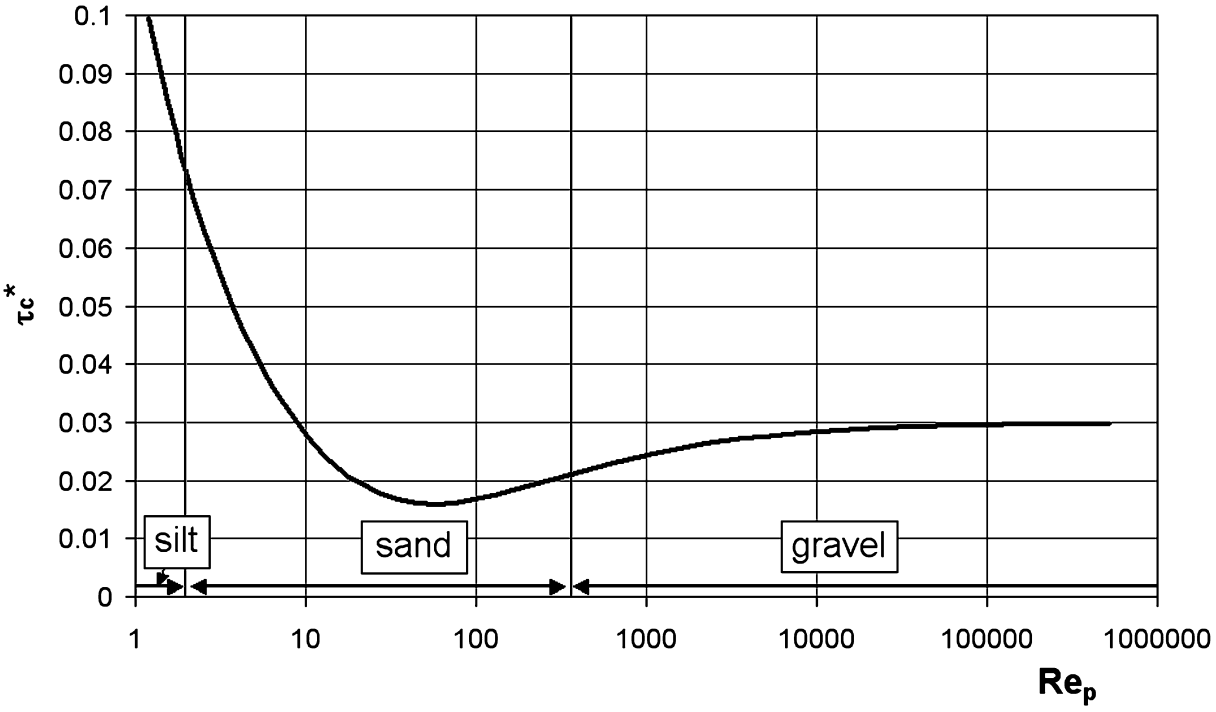

Fig. 2-19. Modified Shields diagram (after Parker 2005).

recently, Sarmiento and Falcon (2006) introduced the novel idea of using spatially-averaged (over many particles) shear stresses to define incipient conditions for particle motion at low transport rates.

Buffington (1999) thoroughly reanalyzed Shields' work, pointing out some inconsistencies in the way Shields observations had been interpreted and used by others. This motivated a discussion that analyzed the universality of the Shields diagram in the context of sand- and gravel-bed rivers (García 2000), resulting in the river sedimentation diagram presented below (Fig. 2-29).

2.4.3.1 Application to Riprap Sizing and Flow Competence It is worthwhile to show how knowledge about velocity distribution and initiation of motion can be used for a practical problem. Consider the design of a riprap cap to protect contaminated river-bed sediment against erosion. A geotextile or a filter layer can be used to cover the contaminated river-bed portion and then this layer can be protected with riprap material having a size D_{RR}. The riprap size has to be determined to ensure the stability of the cap design.

As introduced earlier, the Manning-Strickler relation for flow resistance is

$$\text{(i)} \qquad \frac{U}{u_*} = 8.1\left(\frac{H}{k_s}\right)^{1/6}$$

Here

$$\text{(ii)} \qquad k_s = \alpha_s D_{RR}$$

Typical values for the coefficient α_s can be found in Table 2-1.

The critical condition for motion of the coarse material making up the riprap can be written as

$$\text{(iii)} \qquad \tau_c^* = \frac{u_{*c}^2}{R\,g\,D_{RR}}$$

Where τ_c^* should be between 0.02 and 0.03 depending upon how broadly the bed is covered with riprap (see Fig. 2-19). Combining the above relations yields

$$\text{(iv)} \qquad \frac{U}{\sqrt{R\,g\,D_{RR}}} = 8.1\left(\tau_c^*\right)^{1/2}\,\alpha_s^{-1/6}\left(\frac{H}{D_{RR}}\right)^{1/6}$$

For example, if $\tau_c^* = 0.03$ and $\alpha_s = 2.5$, this relation reduces to:

$$\text{(v)} \qquad \frac{U}{\sqrt{R\,g\,D_{RR}}} = 1.204\left(\frac{H}{D_{RR}}\right)^{1/6}$$

This equation is very similar to the many empirical equations that have been determined for riprap design (see Eq. B.5 in Appendix B). In particular, this relation is very similar to the one proposed by Neill (1968) for initiation of motion of coarse material

$$\text{(vi)} \qquad \frac{U}{\sqrt{R\,g\,D_{RR}}} = 1.204\left(\frac{H}{D_{RR}}\right)^{1/6}$$

Suppose that the riprap is to be designed to be able to withstand a 10-year flood, at which the mean flow velocity U is estimated to be 3 m/s and the flow depth H is estimated to be 2.5 m. Using a submerged specific gravity $R = 1.65$, Eq. (v) gives a riprap size $D_{RR} = 15.2$ cm (6 inches), and Neill's relation yields $D_{RR} = 9.3$ cm (3.65 inches). A safety factor should be built into the design and if the material is poorly-sorted, the riprap size should be selected so that $D_{RR} = D_{90}$. The reader is referred to Appendix B for a full treatment of this topic.

A similar analysis can be used to estimate the flow competence to move coarse river-bed material of a given size. In this case, the question would be what mean flow velocity and depth are needed to move coarse material of a certain size? This is a typical problem when analyzing salmonid spawning gravel streams (e.g., Buffington et al. 2004).

2.4.4 Yalin and Karahan Diagram

In a study of temperature effects on initiation of motion, Taylor and Vanoni (1972) reported that small but finite amounts of fine-grained sediment were transported in flows with values of τ_c^* well below those given by the Shields curve. They found that as the size of sediment grains decreases, the dimensionless critical shear stress increases more slowly than one would infer by extrapolating the Shields curve. Similar observations were made by Mantz (1977; 1980) but the most conclusive evidence for such behavior was provided by Yalin and Karahan (1979) through carefully conducted experiments.

Yalin and Karahan (1979) compiled a substantial number of data while conducting their own set of experiments with sand sizes ranging from 0.10 to 2.86 mm for both laminar and turbulent flow conditions. In this diagram, $Y_{cr} = \tau_c^*$ and $X_{cr} = Re_*$. They used glycerine in some of the experiments to increase the thickness of the viscous sublayer, thus making it possible to observe initiation of motion under laminar and turbulent flow conditions. As shown in Fig. 2-20, Yalin and Karahan were able to elucidate the nature of transport inception conditions for a wide range of grain Reynolds number $Re_* = u_{*c}D/\nu$. For $Re_* > 70$, hydraulically rough conditions, τ_c^* takes a value of about 0.045. For values of $Re_* < 10$, the relation between τ_c^* and Re_* depends on the flow regime, i.e., whether the flow is laminar or turbulent.

Like the original Shields diagram, the Yalin-Karahan diagram can only be used in an iterative way since τ_c^* appears

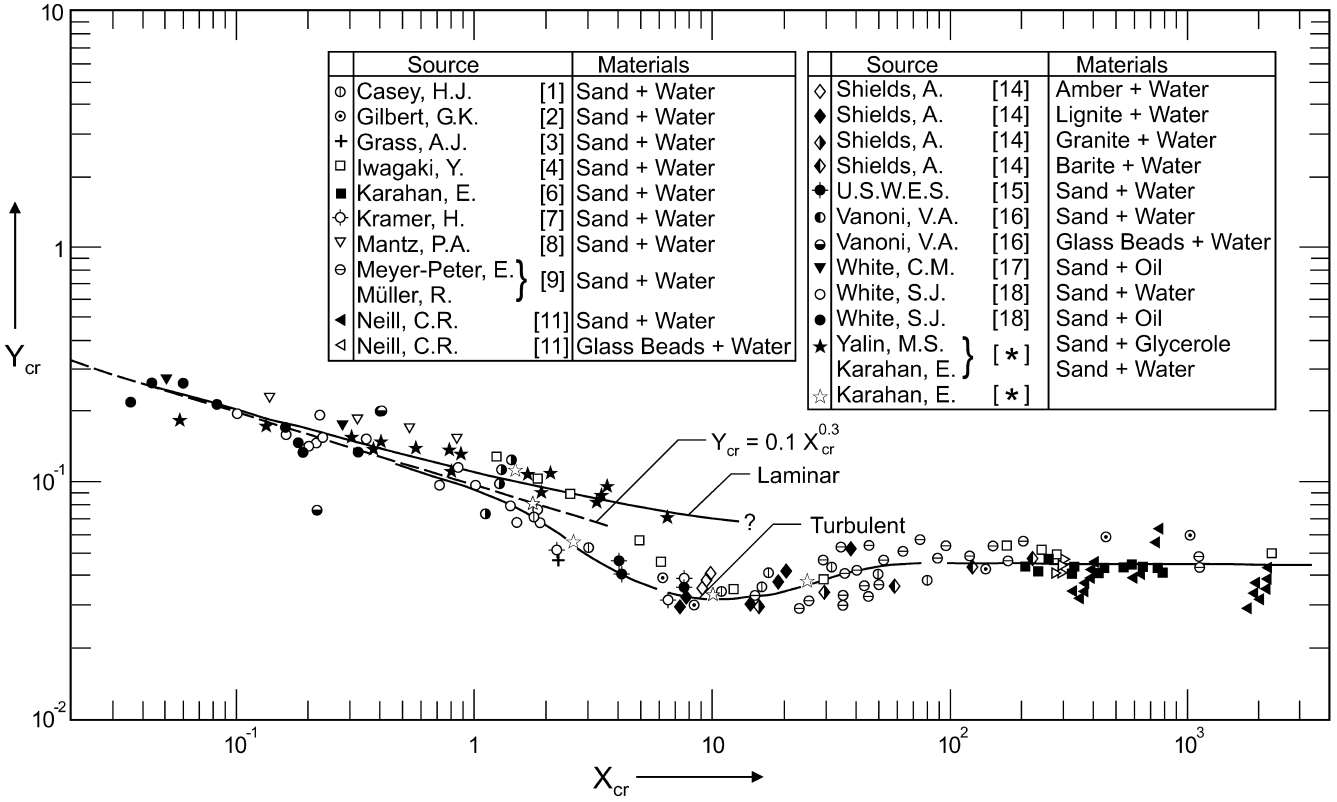

Fig. 2-20. Diagram for Initiation of Motion, Yalin and Karahan (1979).

both in the abscissas and in the ordinates. To obtain an explicit set of curves, a transformation similar to Eq. (2-58) can be introduced, as follows

$$D_{*c} = \left(\frac{Re_{*c}^2}{\tau_c^*}\right)^{1/3} = D\left(\frac{(\gamma_s - \gamma)}{\gamma}\frac{g}{\nu^2}\right)^{1/3} \qquad (2\text{-}60)$$

Here γ and γ_s = specific weight of water and sediment, respectively. García and Maza (1997) have proposed the following useful fit to the Yalin-Karahan data:

For turbulent flow conditions,

$$\tau_{*c} = 0.137\, D_{*c}^{-0.377}; \qquad 0.1074 < D_{*c} < 2.084 \qquad (2\text{-}61a)$$

$$\tau_c^* = \frac{0.178}{D_{*c}^{0.7303}} + 0.0437\, exp - \left[\frac{31.954}{D_{*c} + 10}\right]^{2.453} \qquad 2.084 < D_{*c} < 47.75 \qquad (2\text{-}61b)$$

$$\tau_c^* = 0.045; \qquad D_{*c} > 47.75 \qquad (2\text{-}61c)$$

For laminar flow conditions,

$$\tau_{*c} = \frac{0.1439}{D_{*c}^{0.352}} + 0.0084\, exp - \left[\frac{5.6243}{D_{*c}}\right]^{9.21}; \qquad 0.2164 < D_{*c} < 11.252 \qquad (2\text{-}61d)$$

These relations can be used to estimate critical shear stress for a wide range of sediment sizes and flow conditions. Dey (1999) has also proposed a rather simple model for threshold conditions that captures the behavior displayed by the Yalin and Karahan (1979) laboratory observations.

2.4.5 Wiberg and Smith Diagram for Heterogeneous Sediments

Most of the work on initiation of motion has been done for uniform size sediment. One exception is the model advanced by Wiberg and Smith (1987). They derived an expression for the critical shear stress of noncohesive sediment using a balance of forces on individual particles very similar to the one shown previously. For a given grain size and density, the resulting equation depends on the near-bed drag force, lift force to drag force ratio, and particle angle

of repose. They were able to reproduce the observations of Shields for uniform size sediments as well as initiation of motion in the case of sediment mixtures. They found that for mixed grain sizes the initiation of motion also depends on the relative protrusion of the grains into the flows and the particle angle of repose. The relation obtained by Wiberg and Smith (1987) for natural sediment is practically identical to the Ikeda-Coleman-Iwagaki relation (Eq. 2-55b) presented earlier for nearly spherical particles, and can be written as

$$\tau_c^* = \frac{4}{3}\frac{\left(tan\,\phi_0\,cos\,\alpha - sin\,\alpha\right)}{\left(c_D + tan\,\phi_0\,c_L\right)}\frac{1}{F^2(z/z_o)} \qquad (2\text{-}62a)$$

where

α = bed slope angle;
ϕ_0 = angle of repose of the grains; c_D and c_L drag and lift coefficients, respectively;

and the function $F = u(z)/u_*$ is the logarithmic function (i.e. Eq. 2-4) that relates the effective fluid velocity acting on the particle to the shear velocity. Wiberg and Smith (1987) evaluate the logarithmic function with an equation for the velocity distribution first proposed by Reichardt in the early 1950s, which provides a smooth transition between the viscous sublayer and the outer portion of the velocity profile (Schlichting 1979, p. 601). Critical shear velocities computed with Eq. (2-62a) as a function of nominal grain diameter for quartz density sediment are shown in Fig. 2-21. The agreement with observations made by a number of authors is excellent.

To evaluate the angle of repose ϕ_0 of natural particles in mixed-size beds, the observations made by Miller and Byrne (1966) with naturally sorted sediments were used. The following geometric relationship was found to represent the data well,

$$\phi_0 = \cos^{-1}\left[\frac{D/k_s + z_*}{D/k_s + 1}\right] \qquad (2\text{-}62b)$$

where $z_* = -0.02$ is the average level of the bottom of an "almost moving" grain and depends on particle sphericity and roundness. Here k_s is the equivalent Nikuradse roughness length. Equation (2-62b) was found to represent the data of Miller and Byrne (1966) well for $D/k_s > 0.5$. Computed curves for nondimensional critical shear stress for a range of ratios of particle diameter to bed roughness, $D/k_s = 0.5 - 5.0$, are shown in Fig. 2-22a. A large ratio of D/k_s indicates a larger particle on a smaller bed, and vice versa. In this plot, the critical roughness Reynolds number $(R_*)_{cr} = (u_*)_{cr}\,k_s/\nu$ is a characteristic of the bed. Thus, for any bed roughness, the intersections of a vertical line through some $(R_*)_{cr}$ and the $(\tau_*)_{cr}$ curves for the appropriate D/k_s values determine the critical shear stress for the sizes of material present in the bed.

Wiberg and Smith (1987) found that their model (i.e., Eqs. (2-62a) and (2-62b)) reproduced such observations. As in the case of the original Shields diagram, Wiberg and

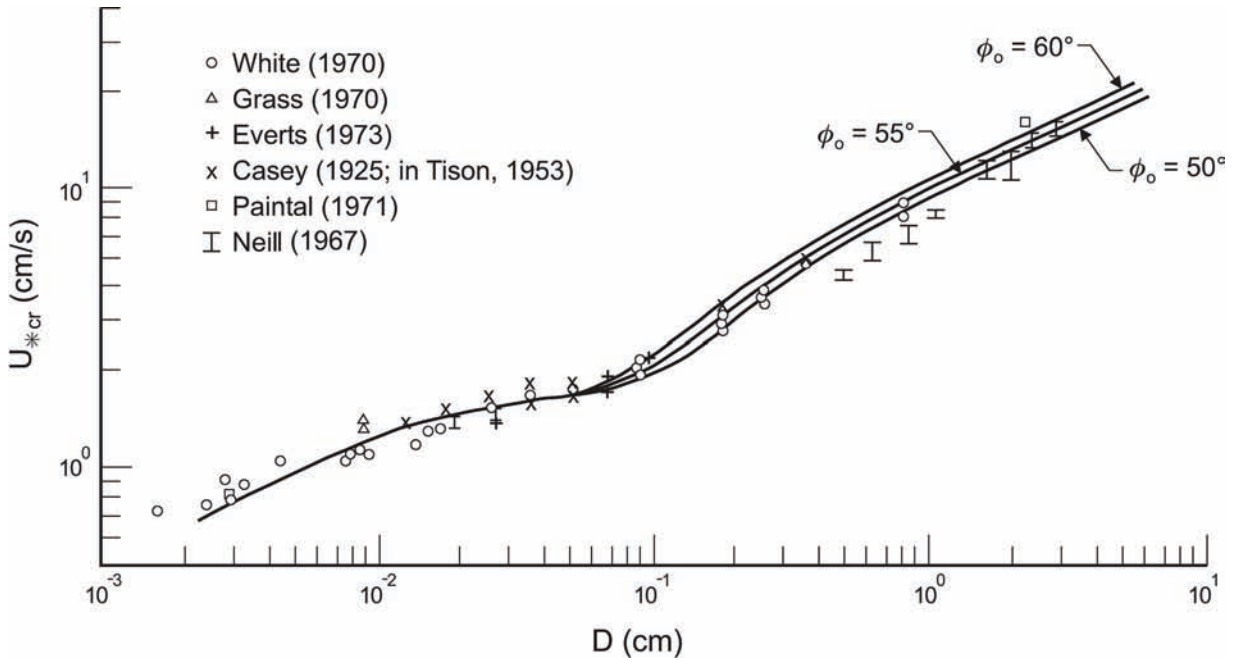

Fig. 2-21. Calculated critical shear velocity as a function of grain diameter (after Wiberg and Smith 1987).

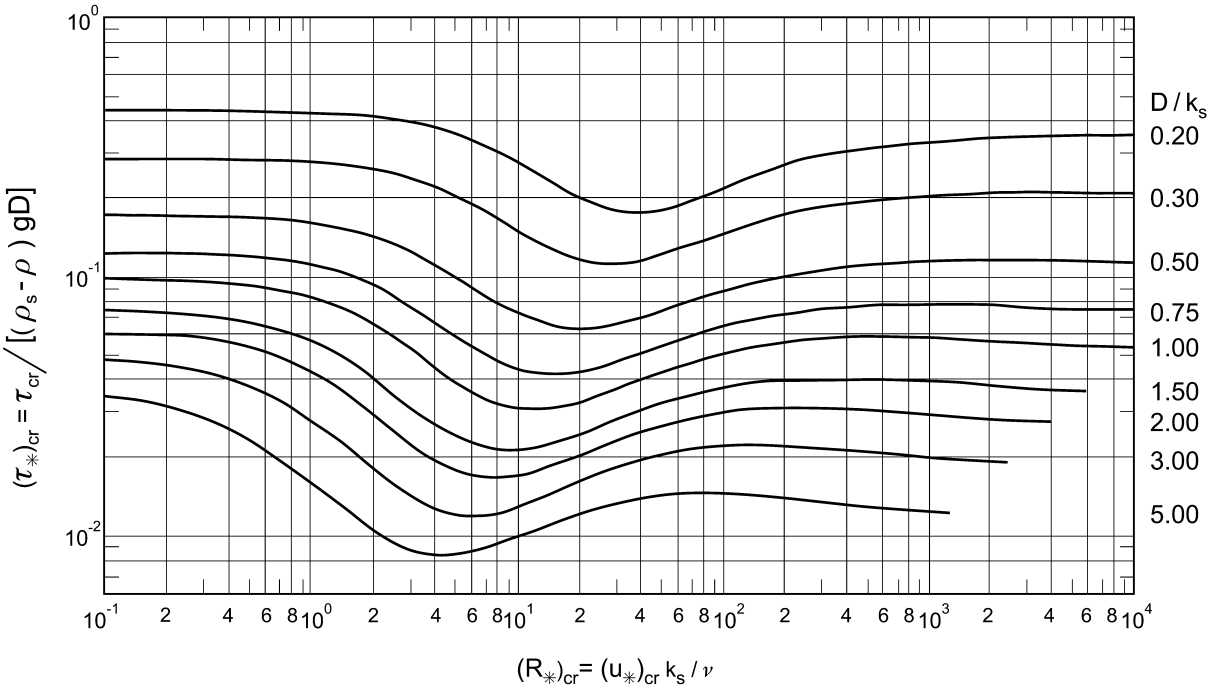

(a)

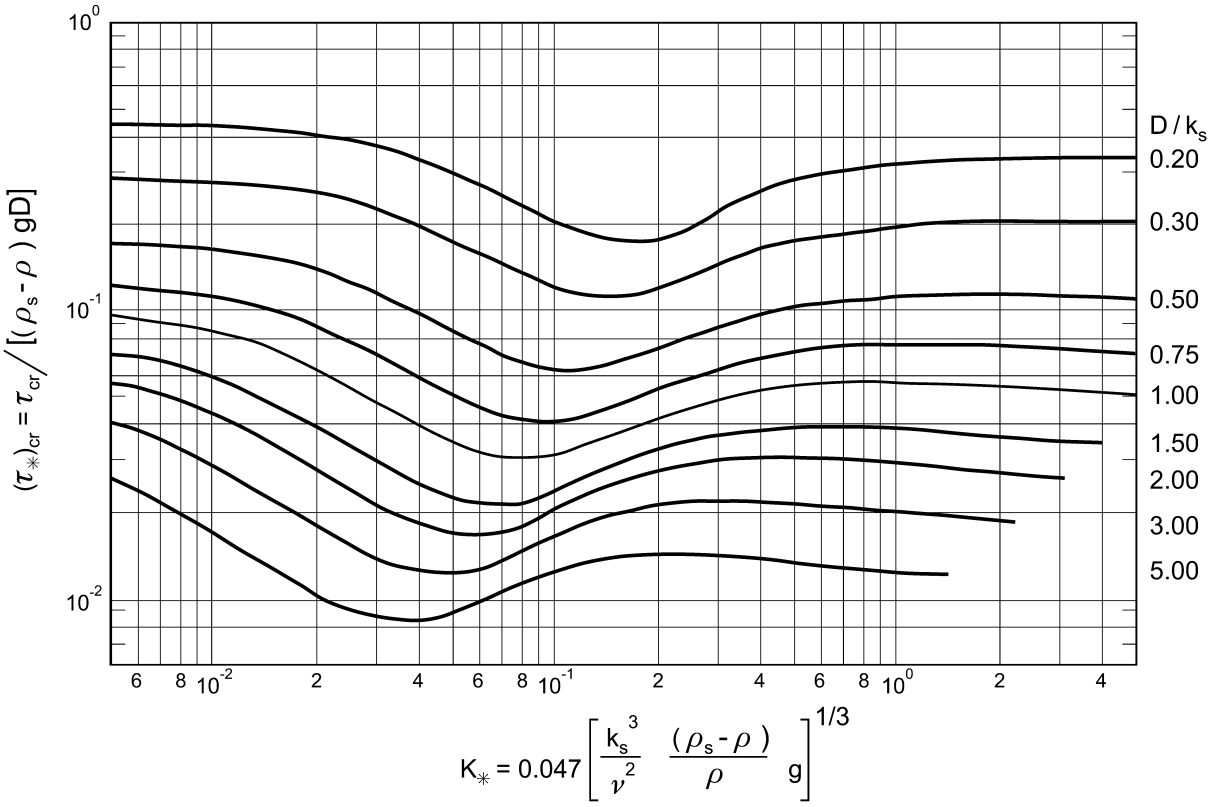

(b)

Fig. 2-22. (a) Calculated nondimensional critical shear stress as a function of critical roughness Reynolds number for values of particle diameter to bed roughness scale. (b) Calculated nondimensional critical shear stress as a function of nondimensional particle diameter for values of particle diameter to bed roughness scale ratio (after Wiberg and Smith, 1987).

Smith found it more useful to express the critical shear stress in terms of a parameter that depends only on grain size and density and on fluid density and viscosity. As shown in Fig. 2-22b, the abscissa in the critical shear stress diagram is given by a variable $K_* = 0.0047(\zeta_*)^{1/3}$ where

$$\zeta_* = \frac{D^3}{\nu^2}\frac{\rho_s - \rho}{\rho} g = \frac{\left[(R_*)_{cr} D/k_s\right]^2}{(\tau_*)_{cr}} \qquad (2\text{-}62c)$$

In this fashion, iteration is not needed to find the critical shear stress for a particle of diameter D in a bed with characteristic roughness length k_s.

A systematic analysis of eight decades of incipient motion studies, with special reference to gravel-bed rivers was conducted by Buffington and Montgomery (1997). Different models available in the literature to estimate entrainment into motion of sediments having mixed grain sizes and densities are reviewed by Komar (1996). The work of James (1990) with spheres and Carling et al (1992) employing regularly shaped particles (rods, cylinders, discs and cubes) illustrates that grain-shape variability and grain orientation are important to entrainment, resulting in a range of stresses for particles that have otherwise the same weight. Bridge and Bennett (1992) have developed a mathematical model for entrainment and transport, which accounts for different grain sizes, shapes and densities. Niño et al (2003) were able to measure the effect of grain-size variability on sediment entrainment into suspension with the help of laboratoty experiments. More information about initiation of motion and transport of gravel and sediment mixtures can be found in Chapter 3.

2.4.6 Lischtvan-Lebediev Diagram for Maximum Permissible Flow Velocity

In practice, it is often convenient to estimate the flow velocity necessary for initiation of motion and sediment erosion. A number of researchers have conducted flume experiments to collect data relating grain sizes and densities to flow velocities, discharges and mean stresses needed to initiate particle movement (e.g. Miller et al. 1977). In the early 1920s, Fortier and Scobey first introduced the concept of maximum permissible flow velocity (Chow 1959, p. 165). The maximum permissible flow velocity, or the nonerosible flow, is the greatest mean velocity that will not cause erosion of the channel bed. Lischtvan and Lebediev used observations made in Russian channels (Lebediev 1959) for wide ranges of quartz sediment sizes (0.005 mm $< D <$ 500 mm) and flow depths (0.40 m $< H <$ 10 m) to obtain values of the maximum permissible flow velocity U_c as a function of the relative flow depth H/D (Garcia and Maza 1997). The Lischtvan-Lebediev data are plotted in dimensionless form in Fig. 2-23. Two curves have been found to fit the data by García and Maza (1997).

For $H/D \leq 744.2$

$$\frac{U_c}{\sqrt{RgD}} = 1.630\left(\frac{H}{D}\right)^{0.1283} \qquad (2\text{-}63a)$$

For $H/D > 744.2$

$$\frac{U_c}{\sqrt{RgD}} = 1.453\left(\frac{H}{D}\right)^{0.3221} \qquad (2\text{-}63b)$$

An inspection of Fig. 2-23 suggests that Eq. (2-63a) corresponds to flow conditions representative of gravel-bed and cobble-bed streams (i.e., low relative flow depth), while Eq. (2.63b) corresponds conditions commonly found in sand-bed streams (i.e., large relative flow depth). Notice that the general form of these relations is very similar to the one obtained in Section 2.4.3.1. The Lischtvan-Lebediev relations are widely used in Latin America for the design of stable channels and to estimate potential sediment erosion conditions in sand-bed rivers (e.g. Schreider et al. 2001).

2.4.7 Effect of Bed Slope on Incipient Motion

2.4.7.1 Granular Sediment on a Sloping Bed The work of Shields and others on initiation of motion applies only to the case of nearly horizontal slopes. Most streams, particularly in mountain areas, have steep gradients, creating a need to account for the effect of the downslope component of gravity on the initiation of motion. In fact, the model of Wiberg and Smith (1987) as given by Eq. (2-62a) does account for the effect of streamwise channel slope.

As shown for the case of negligible longitudinal slope, the effect of the streamwise bed slope on incipient sediment motion can be illustrated by considering the forces (lift, drag, buoyancy, and gravity) acting on a particle lying in a bed consisting of similar particles over which water flows. Such analysis yields the equation (Chiew and Parker 1994)

$$\frac{\tau^*_{c\alpha}}{\tau^*_{co}} = cos\,\alpha\left(1 - \frac{tan\,\alpha}{tan\,\phi}\right) \qquad (2\text{-}65a)$$

where

ϕ = angle of repose;
$\tau^*_{c\alpha}$ = critical shear stress for sediment on a bed with a longitudinal slope angle α; and
τ^*_{co} = critical shear stress for a bed with very small slope.

The value of τ^*_{co} can be found from the Shields diagram with Eq. (2-59), or with Eq. (2-61). Eq. (2-65a) is for positive α, which applies for downward sloping beds. For beds with adverse slope, α is negative and the term tan α/tanφ in

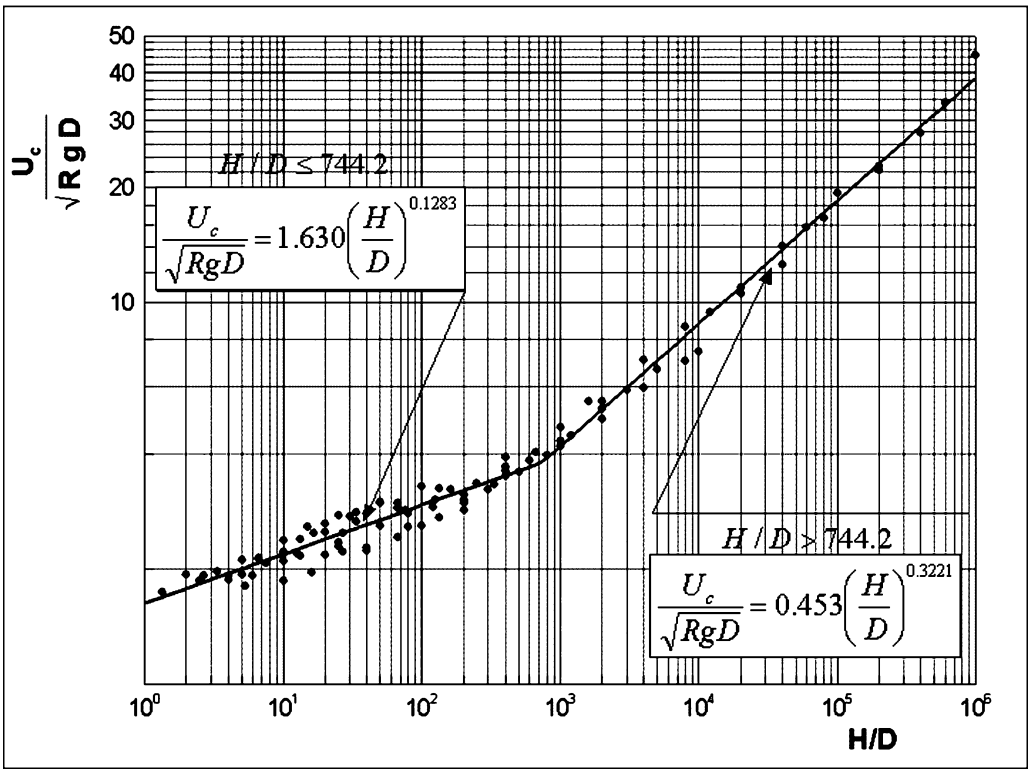

Fig. 2-23. Lischtvan-Lebediev diagram for maximum permissible flow velocity.

Eq. (2-65a) is positive. In terms of shear velocities the relation takes the form

$$\frac{u_{*_c}}{u_{*_o}} = \sqrt{\cos\alpha\left(1 - \frac{\tan\alpha}{\tan\phi}\right)} \qquad (2\text{-}65b)$$

An expression similar to Eq. (2-65a) was derived by Lysne (1969), who also performed a set of experiments on the effect of the bed slope on the incipient motion of sand in a closed channel. Lysne's results agree very well with the curve given by equation (2-65a) for a value of $\phi = 47°$. A similar result was found by Fernandez-Luque and Van Beek (1976), who also fitted a relationship similar to Eq. (2-65a) to their results for the incipient motion of sand, gravel, and magnetite in open channel flow on sloping beds.

Chiew and Parker (1994) conducted a set of laboratory experiments with a closed duct, to test the validity of Eq. (2-65b) for both positive and adverse slopes. The results are plotted in Fig. 2-24. In general, good agreement is observed between the experimental observations and the values predicted with Eq. (2-65b).

Lau and Engel (1999) used dimensional analysis coupled with the observations made by Fernandez-Luque and Van Beek (1976) and Chiew and Parker (1994) to obtain an equation mathematically equivalent to Eq. (2-65a) of the form

$$\frac{\tau^*_{c\alpha}}{\tau^*_{co}} = \frac{sin(\phi - \alpha)}{sin\,\phi} \qquad (2\text{-}65c)$$

They found that the condition for inception of motion depends on the slope angle as well as on the Reynolds number of the flow. Their recommendation is that Eq. (2-65c) can be used for slope angles all the way up to the angle of repose togther with Shields criteria to estimate τ^*_{co}. Whitehouse et al. (2000) tested Eq. (2-65c), finding good agreement with experimental observations. This relation has been rediscovered many times since Armin Schoklitsch introduced it for the first time in the early 1900s.

Several investigators, such as Stevens et al. (1976), Fernandez Luque and van Beek (1976), Howard (1977), Allen (1982), Smart (1984), Dyer (1986), Whitehouse and Hardisty (1988); Chiew and Parker (1994), Iversen and Rasmussen (1994), Dey (1999), and Dey and Debnath (2000), have used relationships similar to either Eq. (2-65a), Eq. (2-65b), Eq. (2-65c) to determine the critical shear stress for sediment lying on a nonhorizontal slopes. Stevens et al. (1976) used such relationship to investigate the factor of safety

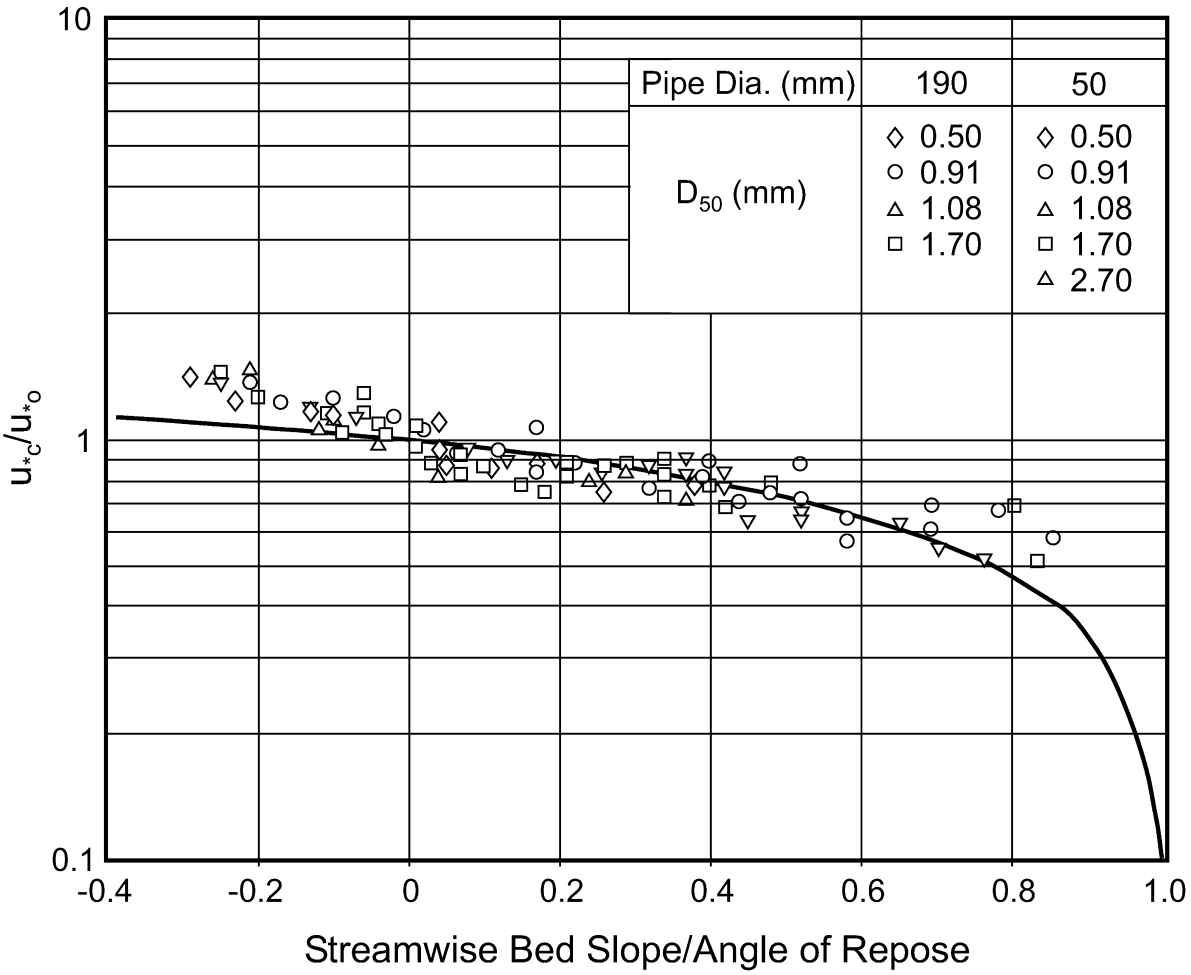

Fig. 2-24. Effect of streamwise bedslope on critical shear velocity. Curve correspond to Eq. 2.65b (modified from Chiew and Parker 1994).

for riprap protection, whereas Smart (1984) used them to evaluate sediment transport rates in a steep channel. Kostic et al. (2002) used Eq. (2-65a) to study the foreset slope of prograding deltas in lakes and reservoirs. Whitehouse and Hardisty (1988), Graf et al. (2000), and Damgaard et al. (2003) used similar concepts to study the inception of bed load transport on steep slopes. The effect of seepage on inita-tion of motion has been analyzed by Oldenziel and Brink (1974), Cheng and Chiew (1999), and Dey and Zanke (2004).

2.4.7.2 Threshold Condition on Side Slopes The analyses presented above apply strictly to the case of flow on a nearly horizontal or sloping bed in the streamwise direction that is horizontal in the transverse direction (i.e., negligible transverse bed slope). An important problem in engineering applications is the case of sediment particles on a side slope (Simons and Senturk 1992). This problem is of particular relevance to the design of riprap protection and stable channels in coarse material (see Appendix B). Thus it is worthwhile to present a more detailed analysis.

In the present simplified analysis, the flow velocity profile is again taken to be logarithmic upward normal from the bed. A force balance is done for a particle located on a side slope, as shown in Fig. 2-25. The flow is taken to be in the streamwise direction, parallel to the side slope. The vectorial fluid drag force D_f acting on a particle is thus given as

$$D_f = \rho \frac{1}{2} \pi \left(\frac{D}{2} \right)^2 c_D u_f^2 \vec{e}_1 \tag{2-66a}$$

The gravitational force F_g has a transverse as well as a downward normal component:

$$F_g = F_{g2} \vec{e}_2 + F_{g3} \vec{e}_3 \tag{2-66b}$$

where $\vec{e}_1$, $\vec{e}_2$, and $\vec{e}_3$ are unit vectors in the streamwise, transverse, and downward normal to the side directions, respectively.

$$\left(F_{g2},\, F_{g3}\right) = -\rho R g \frac{4}{3}\pi\left(\frac{D}{2}\right)^3 \left(\sin\theta,\, \cos\theta\right) \qquad (2\text{-}66c)$$

and θ denotes the local transverse angle of the side slope, as illustrated in Fig. 2-25.

The lift force is given as

$$L_f = \rho\frac{1}{2}\pi\left(\frac{D}{2}\right)^2 c_L u_f^2 \vec{e}_3 \qquad (2\text{-}67)$$

The Coulomb resistive force acting on a grain has a magnitude given by $\mu\left|F_{g3}\vec{e}_3\right| + L_f$. As shown in the diagram, under critical conditions, it must precisely balance the vectorial sum of the impelling forces due to flow (D_f) and due to the transverse downslope pull of gravity ($F_{g2}\vec{e}_2$).

These conditions on magnitude and direction lead to the following result for threshold conditions:

$$\mu^2\left|F_{g3}\vec{e}_3 + L_f\right|^2 = \left|D_f\right|^2 + \left|F_{g2}\vec{e}_2\right|^2 \qquad (2\text{-}68)$$

Substituting Eqs. (2-66a), (2-66b), (2-66c) and (2-67) into Eq. (2-68) and reducing, the following relation is obtained:

$$\left[\left(\frac{u_f^2}{RgD}\right)^2 + \left(\frac{4}{3c_D}\sin\theta\right)^2\right]^{1/2} = \mu\left(\frac{4}{3c_D}\cos\theta - \frac{c_L}{c_D}\frac{u_f^2}{RgD}\right) \qquad (2\text{-}69a)$$

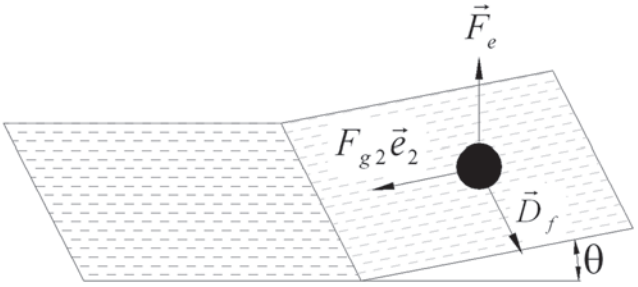

Fig. 2-25. Definition diagram for particle located on a side slope.

Further reducing with the aid of Eqs. (2-54) and (2-55), it is found that

$$\left[\left(\tau_c^*\right)^2 + \left(\frac{4}{3c_D F^2}\sin\theta\right)^2\right]^{1/2} = \frac{4\mu}{3c_D F^2}\cos\theta - \mu\frac{c_L}{c_D}\tau_c^* \qquad (2\text{-}69b)$$

The case of a transversely horizontal bed is recovered by setting $\theta = 0$. The critical Shields stress is found to be given by Eq. (2-55a) for this case. This value is denoted as τ_{co}^*, the subscript o denoting that the bed is horizontal in the transverse direction. Using this value to normalize the value τ_c^* obtained on a side slope of angle θ, Eq. (2-69b) reduces to

$$\left\{\left(\frac{\tau_c^*}{\tau_{co}^*}\right)^2 + \left[\frac{\left(1 + \mu c_L/c_D\right)}{\mu}\sin\theta\right]^2\right\}^{1/2} = \left(1 + \mu c_L/c_D\right)\cos\theta - \mu\frac{c_L}{c_D}\left(\frac{\tau_c^*}{\tau_{co}^*}\right) \qquad (2\text{-}69c)$$

Equation (2-69c) is a quadratic polynomial in τ_c^*/τ_{co}^*, and as such is easily solved. A solution is shown in Fig. 2-26, which has been evaluated for the case $\mu = 0.84$ ($\phi = 40°$) and $c_L = 0.85c_D$. It is also assumed that c_D is given as a function of $u_f D/\nu$ according to the standard drag curve for spheres (i.e. Eq. 2-46d). As can be seen there, the Shields stress takes the value τ_{co}^* on a horizontal bed ($\theta = 0$). It progressively decreases as the side slope angle θ increases, reaching a value of 0 at the angle of repose.

Many methods for stable channel design, starting with the classic work of Glover and Florey in the early 1950s, make use of Eq. (2-69c) to design a channel in coarse alluvium that is at the threshold for sediment motion but is stable (e.g., Li et al. 1976; Diplas and Vigilar 1992). Parker (1978) also used this approach to analyze flow in self-formed straight rivers with mobile beds and stable banks. More material on stable movable-bed channels can be found in Chapter 7.

If the lift force is neglected (i.e., $c_L = 0$), Eq. (2-69c) reduces to the well-known Lane (1955) relation,

$$\frac{\tau_c^*}{\tau_{co}^*} = \cos\theta\sqrt{1 - \left(\frac{\tan\theta}{\tan\phi}\right)^2} \qquad (2\text{-}70)$$

Equation (2-70) has also been derived for application to coastal sediment transport problems by Fredsøe and Deigaard (1992, p. 204). Whitehouse et al (2000) tested

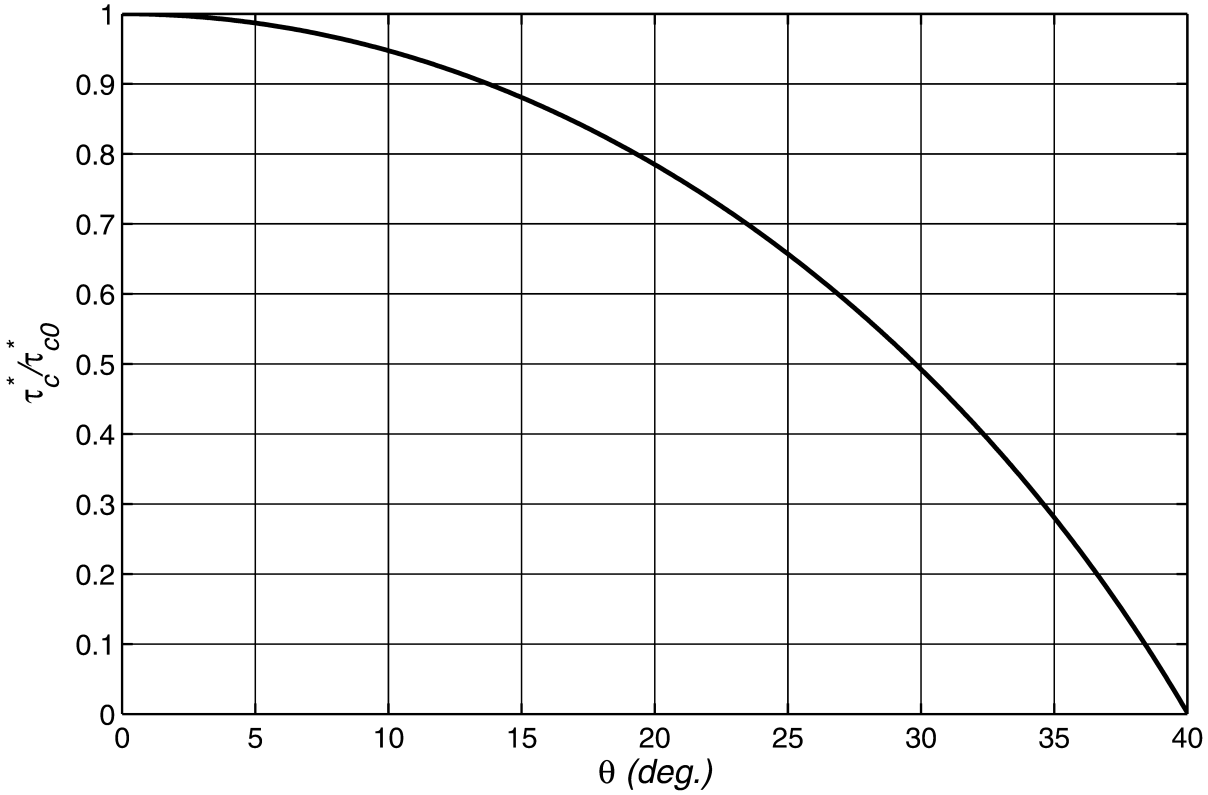

Fig. 2-26. Variation of normalizedcritical Shields stress for initiation of motion as a function of side slope angle as predicted by Eq. 2.69c.

the values predicted by Eq. (2-70) with the observations made by Ikeda (1982) and found reasonable agreement. Christensen (1972) found out that the critical shear stresses estimated with Eq. (2-70) have a tendency to be too conservative and proposed an alternative method that takes into account the ratio between the bed roughness and the grain size. As this ratio increases, Lane's Eq. (2-70) and Christensen's method give identical results. The method of Wiberg and Smith (1987) presented above also takes into account the effect of the relative roughness D/k_s on the evaluation of critical shear stress condition for motion. James (1990) has also provided useful information on the effect of such parameter on initiation of motion. Similar approaches, which follow the so-called grain pivoting model, have been suggested by Slingerland (1977) and Komar and Li (1988) among others (Komar, 1996). Bridge and Bennett (1992) have also advanced a model that accounts for bedslope effects on initiation of motion.

2.4.7.3 Threshold Condition for Motion on an Arbitrarily Sloping Bed The general case of an arbitrarily sloping bed was first treated analytically by Kovacs and Parker (1994), who developed a vectorial equation for sediment threshold on a combined transverse and longitudinal sloping bed. Their analysis was extended by Seminara et al. (2002) to include the effect of lift force. While studying coastal sediment transport, Calantoni (2002, p. 77) generalized the analysis of Fredsøe and Deigaard (1992) and obtained a quadratic equation for the threshold condition for motion, similar to Eq. (2-69c), which shows promise for practical use. The positive root of the equation gives an equation that can be used to estimate the critical shear stress for motion of a particle located on a bed surface having a longitudinal (parallel the flow direction) slope angle α and a transverse (perpendicular to flow direction) slope angle θ,

$$\frac{\tau_c^*}{\tau_{co}^*} = \cos\alpha\left(\cos\theta\sqrt{1-\left(\frac{\tan\theta}{\tan\phi}\right)^2} - \frac{\tan\alpha}{\tan\phi}\right) \quad \text{(2-71a)}$$

Notice that when $\alpha = 0$, Eq. (2-71a) reduces to Eq. (2-70) and when $\theta = 0$, Eq. (2-71a) reduces to Eq. (2-65a). Calantoni and Drake (1999) used Eq. (2-71) to develop a discrete-particle model for bed load transport in the surf zone that accounts for variations in bottom slope.

Duan et al. (2001) and Duan and Julien (2005) have used the following formulation for sediment transport modeling in meandering channels,

$$\frac{\tau_c^*}{\tau_{co}^*} = cos\theta\left[1 - \left(\frac{tan\theta}{tan\phi}\right)^2\right]^{1/2}\left(\frac{sin(\phi - \alpha)}{sin\phi}\right) \quad (2\text{-}71b)$$

Notice that when $\theta = 0$, Eq. (2-71b) reduces Eq. (2-65c) which is also equivalent to Eq. (2-65a). When $\alpha = 0$, Eq. (2-71b) reduces to Eq. (2-65a). It should be clear that Eqs. (2-71a) and (2-71b) are mathematically equivalent. In the early 1960s, Norman Brooks provided an excellent theoretical analysis of this problem in the context of river bends. It can be found in Vanoni (2006, p.64).

Other efforts to estimate critical shear stress values for sediments on arbitrarily sloping beds include the work of Dey (1999, 2003). More research, including experiments over a wide range of conditions that can be used to test and improve different formulations, is needed on this important topic. Stream channel stability, bank erosion, and meandering channels are topics where the material covered previously plays a crucial role. This will become apparent in Chapter 7, Chapter 8, and in Appendix B "RipRap design."

2.5 SEDIMENT TRANSPORT

Sediment load in this manual refers to the sediment that is in motion in a river. There are two common ways of classifying the sediment load as shown in Table 2-4. The first divides the sediment load according to the mechanism for transport into bed load and suspended load. The second classifies the load based on particle size into wash load and bed sediment load. The suspended load, as the term denotes, moves in suspension and is that part of the load which is not bed load. Wash load is fine sediment moving in suspension which makes up a very small part, usually a few percent, of the sediment on the bed. Wash load is commonly taken as the silt and clay fraction of the bed sediment, i.e., that fraction with grain sizes finer than 0.062 mm. The bed sediment load consists of particles that are coarser than the wash load. The transport rate or discharge of wash load tends not to be correlated with water discharge while discharge of bed sediment, both in suspension and as bed load, is usually correlated with water discharge. The total sediment load is made up of wash load, suspended (bed-material) load and bed load. Methods and technologies for measuring sediment transport are covered in Chapter 5.

In some rivers the different components of the sediment load can be clearly differentiated. This is the case of the Niger River, Nigeria, depicted in Fig. 2-27, where the different components of the sediment load were measured in cubic meters per year by NEDECO (1959). In this particular example the wash load is many times larger than the load of bed material transported as suspended and bed load. Notice also that there are two peaks for the wash load associated with sediment grain sizes of about 0.001 mm and 0.025 mm. These might be related to the watershed activities taking place at the time the observations were made.

Table 2-4 Sediment Load Classification

	Classification system	
Total sediment load	Based on mechanism of transport	Based on particle size
Wash load	Suspended load	Wash load
Suspended bed-material load	Suspended load	Bed-material load
Bed load	Bed load	Bed-material load

2.5.1 Sediment Transport Modes: Bed-Material Load and Wash Load

The sediment transport processes that can be characterized with fluid and sediment dynamics principles are those of bed load and suspended load. In the former case, the particles roll, slide, or saltate along the bed, never deviating too far above the bed. In the latter case, the fluid turbulence comes into play carrying the particles well up into the water column. In both cases, the driving force for sediment transport is the action of gravity on the fluid phase; this force is transmitted to the particles via drag. While it is possible to quantify the mechanics of bed-material transport as suspended load and bed load, a similar analysis to assess the wash load has proved rather elusive. Before considering bed-material transport in more detail, the wash load will be considered next. Important questions are what is role of sediment in the flow energy balance and how the division between wash load and bed-material load in sand-bed streams can be made?

The floodplains of most sand-bed rivers often contain copious amounts of silt and clay finer than about 0.062 mm. This material is known as wash load because it often moves through the river system in suspension without being present in the bed in significant quantities (Colby 1957). Increased wash load does not cause deposition on the bed, and decreased wash load does not cause erosion, because it is transported at well below capacity. This is not meant to imply that the wash load does not interact with the river system. Wash load in the water column exchanges with the banks and the floodplain rather than the bed. Greatly increased washload, for example, can lead to thickened floodplain deposits with a consequent increase in bank-full channel depth. Soil fertility depends

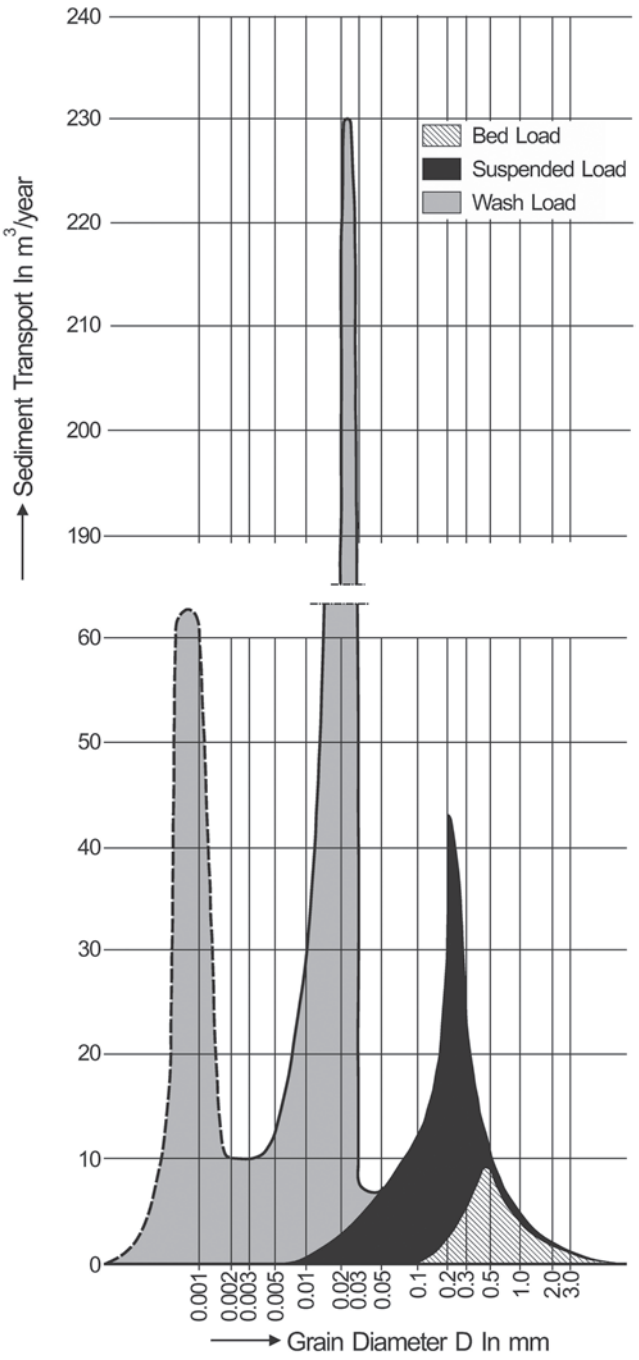

Fig. 2-27. Total Sediment Load in the upper Niger River, Nigeria (adapted from Jansen et al. 1979). Ordinates are in hundreds of thousands of cubic meters per year for each sediment size fraction.

largely on the amount of wash load deposited by floods on a given floodplain over the years. This fact was well known by the Egyptians, who practice agriculture in the floodplains of the Nile River. Also of relevance, is the fact that contaminants such as PCBs and heavy metals are often attached to the fine-grained sediments that constitute the wash load. The wash load is controlled by land surface erosion (rainfall, vegetation, land use) and not by channel-bed erosion. However, cohesive stream banks can contribute to the wash load during bank full flow events. Mining activities can also contribute substantially to the wash load of river systems, with potential environmental effects on estuarine and coastal areas (e.g., coral reefs). Despite its importance, a physical characterization of the wash load is not an easy task.

By definition, the wash load is not determined by the hydraulic characteristics of a given river reach; hence it can not be computed (Einstein and Chien 1953). At the same time, sediment transport formulae apply only to bed-material transport and do not account for wash load. De Vries (1993) argues that there are at least two reasons why a quantitative distinction between bed-material load and wash load is necessary.

(i) For comparison of sediment transport predictions with values measured in the field it is necessary to substract the wash load component.
(ii) A reduction of the flow velocity in the direction of the current will make a fraction of the wash load become bed-material load (e.g., reservoir sedimentation).

Vlugter (1962) discriminated between *sinking* material and *floating* material. He argued that fine sediment particles (i.e., floating material) being moved downstream in a river add part of their potential energy to the flow and can be transported in suspension indefinitely as long as the flow conditions do not change. On the other hand, coarse grains (i.e., sinking material) require kinetic energy from the mean flow to remain in suspension. Bagnold (1962) arrived to a similar conclusion while studying turbidity currents, and called this condition "autosuspension." Interestingly, both Vlugter and Bagnold ideas were very similar to those articulated a few years earlier by Knapp (1938) while looking at the energy balance in streams carrying suspended sediment. As pointed out by Jansen et al (1979) in their river engineering book, the energy balance concept underlying the Vlugter and Bagnold arguments has not yet been accepted by everyone (e.g., Parker 1982). In order to better understand some of these ideas it is useful to consider the energy balance in sediment-laden flows.

Consider a steady, uniform sediment-laden open-channel flow in a channel with a bed slope S, as described in Fig. 2-31. The role of fine sediment in the energy balance can be observed by considering the average rate of work P_g (i.e., dot product of momentum and velocity) done by gravity on the flow which can be approximated as follows,

$$P_g \cong \underset{(1)}{\rho g S U H} + \underset{(2)}{\rho R g S C U H} - \underset{(3)}{\rho R g H C v_s} \qquad (2\text{-}72a)$$

In this simplified energy balance relation, U = mean flow velocity, H = flow depth, C = mean volumetric concentration of suspended sediment, $R = (\rho_s/\rho - 1)$ = submerged

specific gravity of the sediment, ρ_s = sediment density, ρ = water density, v_s = sediment fall velocity, and g = gravitational acceleration.

The physical significance of the terms in Eq. (2-72a) can be identified as follows:

(1) Mean rate of energy input to the fluid phase (i.e., water).
(2) Mean rate of energy input to the mean flow through the solid phase (i.e. sediment).
(3) Mean rate of energy loss by mean flow through turbulent mixing required for maintaining sediment in suspension.

The main input of energy to the mean flow through the sediment phase can thus be positive or negative, depending on whether or not term (2) is greater than term (3). If term (2) is larger than (3), it means that the suspended sediment contributes energy to the flow. On the other hand, if (3) is larger than (2) it means that the flow is expenging energy to keep the sediment in suspension. However for a dilute open-channel suspension ($C \ll 1$), terms (2) and (3) are very small compared to term (1). Thus the flow energetics is to a first approximation independent of sediment concentration. It follows that whether or not term (2) is greater than term (3) has essentially nothing to do with whether the flow has enough energy to sustain itself, since almost all the energy enters through the water via term (1).

In the case of a turbid underflow or turbidity current overlain by clear, still, nonstratified water and flowing down a submarine channel with a slope S (Fig. 2-59), the situation is drastically changed. Clear water will not flow down a submarine channel or canyon due to gravity in the absence of suspended sediment. An analysis of the equations of motion (see Section 2.11.3) shows that the work done by the hydrostatic pressure gradient of the fluid phase just cancels term (1), so that in fact there is no positive energy input to the fluid phase. In the case of turbidity currents, gravity acts on the solid phase which in turn drags the fluid phase downslope forming an underflow. The net mean energy input through the solid phase P_{gs} is simply

$$P_{gs} = \underset{(2)}{\rho R g S C U H} - \underset{(3)}{\rho R g H C v_s} \qquad (2\text{-}72b)$$

Thus the only positive energy input into the turbidity current is via term (2). It follows that term (2) must exceed term (3) for a self-sustaining turbidity current,

$$\rho R g S C U H > \rho R g H C v_s \qquad (2\text{-}72c)$$

This relation can be reduced to

$$\frac{U S}{v_s} > 1 \qquad (2\text{-}72d)$$

This is the classical Bagnold criterion for turbidity currents (Bagnold 1962). It ensures that the sediment supplies more energy than it consumes. The Bagnold criterion must be satisfied if a self-sustaining turbidity current is to occur. This is a necessary condition but is not sufficient as described by Parker et al (1986) since the flow has to be capable of entraining sediment into suspension to sustain itself.

The analogous energy constraint for a self-sustaining, dilute ($RC \leq 0.1$), open-channel suspension is found to be from Eq. (2-72a),

$$\frac{U S}{v_s} > \frac{R C}{I + R C} \cong R C \qquad (2\text{-}72e)$$

This condition was first articulated by Knapp (1938) and expressed mathematically by Vlugter (1942, 1962). An open-channel suspension can guarantee that the Knapp-Vlugter criterion is satisfied, by lowering the suspended sediment concentration C, and thus its excess fractional density RC, via sediment deposition. Vlugter (1962) used the above criterion to design stable irrigation channels in Indonesia. According to Vlugter, sediment with a fall velocity v_s that satisfies the above condition constitutes the *floating* material that does not require energy from the flow to be transported. The *floating* material is equivalent to the wash load. On the other hand, sediment with fall velocities that do not satisfy the Knapp-Vlugter condition and that take energy away from the flow to be transported is dubbed the *sinking* material. The *sinking* material can be regarded as the bed-material load. Vlugter states that in practice, when the mean flow velocity $U > 0.5$ m/s, all silt particles smaller than 0.07 mm appear to behave as *floating material* (i.e., wash load). This is close to the grain diameter of 0.062 mm commonly used to define the wash load (e.g., Colby 1957).

De Vries (1993) has suggested that the Knapp-Vlugter criterion (Eq. 2-72e) could be used to find a tentative division between wash load and bed-material load in sand-bed streams. There have also been attempts to use Bagnold's ideas, which are applicable only to turbidity currents as previously shown, for the analysis of self-sustaining suspensions in open-channels flows (e.g., Southard and Mackintosh 1981; Wang 1984). As could be expected, this has generated a substantial amount of discussion in the literature (e.g., Parker 1982; Paola and Southard 1983; Nordin 1985a; Brush 1989). It should be clear that Bagnold's criterion does not correspond to an energy constraint on open-channel suspensions. The fundamental differences and similarities between sediment transport by rivers and turbidity currents are addressed in Section 2.11.

While conducting sedimentation studies in the Orinoco River in Venezuela, Nordin and Perez-Hernandez (1985) defined the wash load as the material that can be suspended (i.e., $u_*/v_s \geq 1.25$) as soon as its motion at the bed is initiated

(i.e., $\tau_b = \tau_{bc}$). Mathematically, this condition can be defined in dimensionless form by the relations

$$\tau^* \geq 1.11\ R_f^2 \text{ when } \tau^* = \tau_c^* \qquad (2\text{-}72f)$$

where

τ^* = dimensionless Shields stress parameter defined by Eq. (2-73a);

τ_c^* = dimensionless critical Shields stress for incipient motion (Fig. 2-19);

$R_f = \dfrac{v_s}{\sqrt{gRD}}$ = dimensionless fall velocity (Eq. 2-46b) which is a function of

$R_{ep} = \dfrac{\sqrt{gRD}D}{\nu}$ and can be evaluated, for example, with Dietrich's relation (Eq. 2-47).

Nordin (1985b) suggests that the most practical way to apply this criterion in the field is to plot the largest particle size that can be suspended and the largest particle size that can be moved at the bed, as functions of the shear velocity (u_*). The sediment diameter at which the two curves intersect defines the upper limiting size of the wash load, and particles finer than this would not be found in appreciable quantities in the bed because they would go into suspension as soon as their motion is initiated. In the case of the Orinoco River, Nordin (1985b) found that the upper limiting size for the wash load is 0.095 mm for a water temperature of 25°C. A limiting size for the wash load in dimensionless form which implicitly includes the effect of temperature, can be found from the dimensionless particle Reynolds number (R_{ep}) where the curves for initiation of motion and suspension intersect, as shown in Fig. 2-28 below. However, the relations proposed by Mantz (Eq. 2-59c) or Yalin and Karahan (Eq. 2-61a) for incipient motion of fine-grained sediment should be used instead of the Shields criterion (Eq. 2-59b) which does not work for the grain sizes found in the wash-load.

While Nordin's approach can provide an idea of the size of the particles making up the wash load, because this fine-grained material is transported well below capacity what ultimately determines how much sediment is transported as wash load is the supply of fine sediment to a given river from its watershed and not the transport capacity of the river itself. Watershed sediment yield is addressed in Chapter 17.

In what follows, the emphasis is placed on understanding the mechanics of bed load and suspended load transport in open-channel flows, including morphological changes in rivers, lakes and reservoirs, with the goal of providing the knowledge needed for sedimentation engineering. The mechanics of transport by turbidity currents is also considered, and used to analyze delta formation and reservoir sedimentation.

2.5.2 Shields-Parker River Sedimentation Diagram

Alluvial rivers that are free to scour and fill during floods can broadly be divided into two types: sand bed streams and gravel bed streams. Sand bed streams typically have values of median bed sediment size between 0.1 mm and 1 mm (Fig. 2-12). The sediment tends to be relatively well sorted, with values of geometric standard deviation of the bed sediment size varying from 1.1 to 1.5. Gravel bed streams typically have values of median size of the bed sediment exposed on the surface of 15 mm to 200 mm or larger; the substrate is usually finer by a factor of 1.5 to 3 (Fig. 2-13). The geometric standard deviation of the substrate sediment size is typically quite large, with values in excess 3 being quite common. Although gravel and coarser material constitute the dominant sizes, there is usually a substantial amount of sand stored in the interstices of the gravel substrate (Chapter 3).

Two dimensionless parameters provide an effective delineator of rivers into the above two types (García 2000). The first of these parameters is the dimensionless Shields stress for uniform flow conditions, defined as:

$$\tau^* = \frac{\tau_b}{\rho g R D} = \frac{HS}{RD} \qquad (2\text{-}73a)$$

where

τ_b = bed shear stress;

g = gravitational acceleration

ρ and ρ_s water and sediment density, respectively;

$R = (\rho_s - \rho)/\rho$ = submerged specific gravity of the sediment;

D = mean sediment diameter;

H is the flow depth; and

S is the stream slope which for steady, uniform flow is the same as the energy gradient.

The second of these parameters is the particle Reynolds number R_{ep} defined as:

$$R_{ep} = \frac{\sqrt{gRD}D}{\nu} \qquad (2\text{-}73b)$$

where ν is the kinematic viscosity of water. This second parameter can be considered as a dimensionless surrogate for grain size.

Rivers were first introduced into the Shields diagram by Gary Parker in the early-1980s. Parker used these two parameters but his diagram, shown in Fig. 2-28, did not include field data (García 1999). Parker's diagram, however, gave an indication of the areas in the modified Shields diagram corresponding to sand-bed and gravel-bed streams.

Motivated by a thorough review of the Shields diagram done by Buffington (1999), García (2000) used field and laboratoty data to confirm the early ideas of Parker, resulting in Fig. 2-29. This figure shows a plot of the values of the Shields stress (Eq. 2-73a) evaluated at bankfull flow versus particle Reynolds number (Eq. 2-73b) for six sets of field

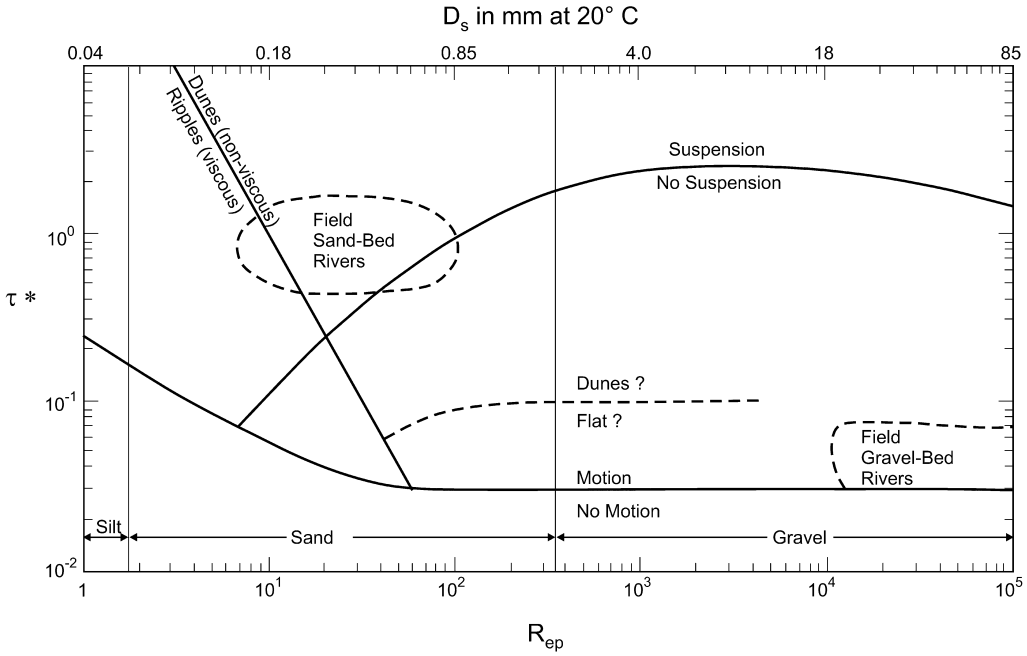

Fig. 2-28. Parker's River Sedimentation Diagram (García 1999).

data: a) gravel bed rivers in Wales, UK (Wales); b) gravel bed rivers in Alberta, Canada (Canada); c) gravel bed rivers in the Pacific Northwest, USA (Pacific); d) single-thread sand streams (Sand sing); e) multiple-thread sand streams (Sand mult); f) large sand-bed rivers (Parana, Missouri, etc.); and g) large-scale laboratory experiments on bridge-pier scour conducted at St Anthony Falls Laboratory (SAFL), University of Minnesota.

There are three curves in the Shields-Parker river sedimentation diagram of Fig. 2-29 that make it possible to know, for different values of (τ^*, R_{ep}), if a given bed sediment grain will go into motion, and if this is the case, whether or not the prevailing mode of transport will be suspended load or bed load. The diagram can also be used to estimate what kind of bed forms can be expected for different flow conditions and sediment characteristics. For example, ripples will develop in the presence of a viscous sublayer and fine-grained sediment. If the viscous sublayer is disrupted by coarse sediment particles, then dunes will be the most common type of bed form.

As could be expected, the Shields-Parker diagram (Fig. 2-29) also shows that in gravel-bed rivers, bed material is transported mainly as bed load. On the other hand, in sand-bed rivers, suspension and bed load transport of bed material coexist, particularly at high flows. The diagram is valid for steady, uniform flow conditions, where the bed shear stress can be estimated with $\tau_b = \rho g H S$ (Eq. 2-1). The ranges for silt, sand, and gravel are also included. In this diagram, the critical Shields stress for motion was plotted with Eq. (2-59a). The critical condition for suspension is given by the ratio (Niño and García 1998; Lopez and García 2001)

$$\frac{u_*}{v_s} = 1 \tag{2-74}$$

where u_* is the shear velocity; and v_s is the sediment fall velocity. Eq. (2-74) can be transformed into:

$$\tau_s^* = R_f^2 \tag{2-75}$$

where:

$$\tau_s^* = \frac{u_*^2}{gRD} \tag{2-76}$$

denotes a threshold Shields number for suspension and R_f is given to be Eq. (2-46b), and can be computed for different values of R_{ep} with the help of Dietrich's fall velocity relation given by Eq. (2-47a).

Finally, the critical condition for viscous effects (ripples) was obtained with the help of the definition for the viscous sublayer thickness (Eq. 2-6) as follows,

$$11.6\ \frac{\nu}{u_* D} = 1 \tag{2-77}$$

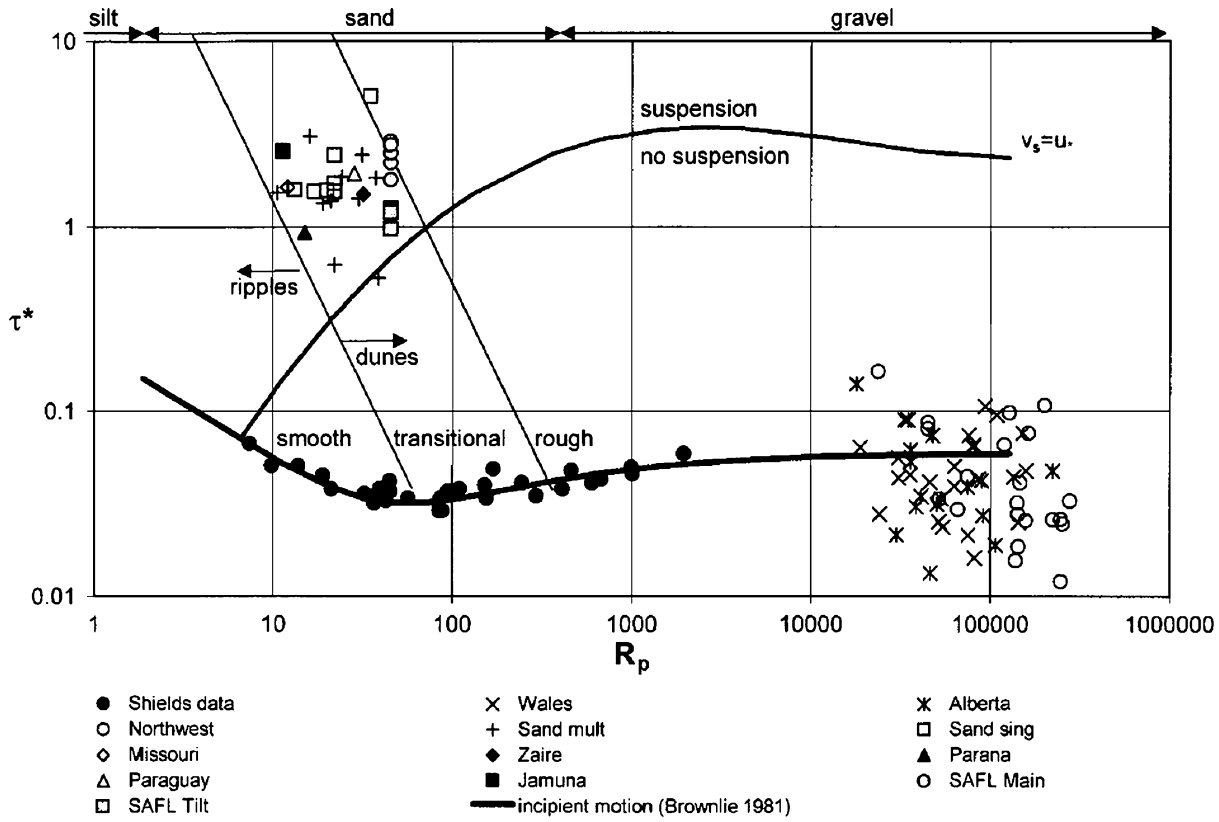

Fig. 2-29. Shields-Parker River Sedimentation Diagram (after García 2000).

which in dimensionless form can be written as

$$\tau_v^* = \left(\frac{11.6}{R_{ep}} \right)^2 \tag{2-78}$$

In this equation, τ_v^* denotes the threshold Shields number below which ripples can be expected.

Relations (2-59a), (2-75), and (2-78) are the ones plotted in Fig. 2-29. The Shields-Parker diagram should be useful for studies concerning stream restoration and naturalization (Chapter 9), for it provides the range of dimensionless shear stresses corresponding to bankfull flow conditions for gravel-bed streams ($0.01 < \tau^* < 0.2$) and for sand-bed streams ($0.6 < \tau^* < 6$). Notice that the bank-full dimensionless Shields shear stress is in general, an order of magnitude larger for sand-bed streams than for gravel-bed streams.

An interesting observation is that sand-bed streams are in the transition between smooth and hydraulically rough conditions, while gravel-bed streams are always hydraulically rough. This has implications, for instance, for the use of Manning's relation (Eq. 2-23a) which applies only to fully rough and turbulent hydraulic conditions (Yen 2002).

The Shields-Parker diagram also shows a very clear distinction between the conditions observed in sand-bed and gravel-bed rivers at bank-full stage, which has implications for movable-bed physical modeling. If one wanted to model in the laboratory sediment transport in rivers, the experimental conditions would be quite different depending on the river type in question. In order to satisfy similarity in a small-scale, river model, it would be necessary to satisfy the identities (García 2000)

$$\tau^*\big|_{model} = \tau^*\big|_{prototype} \tag{2-79a}$$

$$R_{ep}\big|_{model} = R_{ep}\big|_{prototype} \tag{2-79b}$$

for bank-full flow conditions. In most movable-bed models, Froude similarity is enforced and Eq. (2-79a) is used to achieve sediment transport similarity. However, sediment transport conditions and the associated bed morphology in a model, seldom precisely reproduce prototype conditions because the second condition given by Eq. (2-79b) is rarely satisfied. This leads to the common practice of using light-weight material (Table 2-2) to reproduce prototype conditions in small-scale models (e.g., Shen 1990). However, this does not imply that the bedforms observed in the model will be the same as those in the prototype. The river sedimentation

diagram provides a tool to quickly determine potential scale effects in movable-bed model studies by simply plotting the values of (τ^*; R_{ep}) for model and prototype conditions in Fig. 2-29. As discussed in Henderson (1966, p. 504), the condition given by Eq. (2-79b) can be relaxed for sufficiently large values of R_{ep} (i.e. hydraulically rough flow) in both model and prototype. It is clear from Fig. 2-29, that this would be possible only for the case of gravel-bed streams. More information on movable-bed physical models can be found in Appendix C.

2.6 BED LOAD TRANSPORT

Since the publication of ASCE Manual 54 (Vanoni 1975), a significant amount of work has been done to understand the mechanics of bed load transport. Two schools of thought can be clearly identified and they bear the name of two giants in the field of sedimentation, Brigadier Ralph Alger Bagnold and Professor Hans Albert Einstein.

Bagnold (1956) defined the bed load transport as that in which the successive contacts of the particles with the bed are strictly limited by the effect of gravity, whereas the suspended load transport is defined as that in which the excess weight of the particles is supported by random successions of upward impulses imported by turbulent eddies. Einstein (1942, 1950), however, presented a somewhat different view of the phenomenon. Einstein defined bed load transport as the transport of sediment particles in a thin layer about two particle diameters thick just above the bed by sliding, rolling, and making jumps with a longitudinal distance of a few particle diameters. The bed load layer is considered to be a layer in which mixing due to turbulence is so small that it cannot directly influence the sediment particles, and therefore suspension of particles is impossible in the bed load layer. Further, Einstein assumed that the average distance traveled by any bed load particle (as a series of successive movements) is a constant distance of about 100 particle diameters, independent of the flow condition, transport rate, and bed composition. In Einstein's view, saltating particles belong to the suspension mode of transport, because the jump heights and lengths of saltating particles are greater than a few grain diameters. On the other hand, Bagnold (1956, 1973) regards saltation as the main mechanism responsible for bed load transport.

Most research works that provide a mechanistic description of bed load transport under uniform equilibrium conditions have fallen into one or the other school of thought. The centerpiece of the Einsteinean formulation is the specification of an entrainment rate of particles into bed load transport (pick-up function) as a function of boundary shear stress and other parameters. The work of Nakagawa and Tsujimoto (1980), van Rijn (1984a) and Tsujimoto (1991), for example, represent formulations of this type.

In the Bagnoldean formulation, however, a relation for the areal concentration of bedload particles as a function of boundary shear stress derives automatically from the imposition of a dynamic condition at the bed, according to which the fluid shear stress drops to the critical value for the onset of sediment motion. The physical implication is that moving grains will extract enough momentum from the fluid in the bed load layer, such that the fluid stress at the bed remains at the critical shear stress for motion. This dynamic condition is referred to as the Bagnold hypothesis or Bagnold constraint. The hypothesis was used by Owen (1964) to calculate sediment transport by saltation for the case of wind-blown sand. It is implicit in the bedload formulations of Ashida and Michiue (1972) and Engelund and Fredsøe (1976) for nearly horizontal beds. Wiberg and Smith (1989), Sekine and Kikkawa (1992) and Niño and García (1994; 1998), for example, have used the hypothesis to derive models of bed load transport on nearly horizontal beds based on an explicit calculation of grain saltation. Sekine and Parker (1992) used the Bagnold hypothesis to develop a saltation model for bed load on a surface with a mild transverse slope, and Kovacs and Parker (1994) extended the analysis of Ashida and Michiue (1972) to the case of arbitrarily sloping beds. Bridge and Bennett (1992) have employed the Bagnold hypothesis to study the bedload transport of sediment mixtures.

Based on the most recently published formulations of bed load transport, then, it is possible to say that the field as a whole has tended away from the Einsteinean and toward the Bagnoldean formulation. This notwithstanding, doubts have been expressed from time to time concerning the Bagnold hypothesis. For example, the experimental work of Fernandez-Luque and van Beek (1976) does not support the Bagnold hypothesis. A re-analysis of the data and formulation presented in Niño et al. (1994) and Niño and García (1994) caused Niño and García (1998) to cast further doubts on the hypothesis. Kovacs and Parker (1994) were forced to modify the hypothesis in order to obtain a well-behaved theory of bed load transport on arbitrarily sloping beds. With the help of numerical experiments, McEwan et al. (1999) have found that only in the case of high sediment availability does the fluid shear stress at the bed equal the critical stress for intiation of motion. Seminara et al. (2002) and Parker et al. (2003) have shown that Bagnold's hypothesis breaks down when applied to equilibrium bedload transport on beds with transverse slopes above a relatively modest value that is well below the angle of repose. All of the above suggests that formulae that make use of Bagnold's hypothesis might only be able to predict bed load transport for certain conditions (Niño and García 1998). This notwithstanding the ideas of Bagnold have nevertheless contributed substantially to the understanding the physics of the sediment transport problem. A collection of hallmark papers by R.A. Bagnold has been published by ASCE (Thorne et al 1988).

2.6.1 Bed Load Transport Analysis

Sediment can be transported in several ways. A grain will begin to move when the boundary shear stress just exceeds a critical value. At the lowest transport stages, particles move by sliding and rolling over the surface of the bed, but with a small increase in boundary shear stress these grains will hop up from the bed and follow ballistic-type trajectories. This latter mode of bed load transport is known as saltation. Gilbert (1914) seems to have been the first to use the term saltation, derived fom the Latin verb *saltare*, which means to leap or dance, to describe the motion of sand particles in water.

Saltation is described as the unsuspended transport of particles over a granular bed by a fluid flow, in the form of consecutive hops within the near-bed region. It is governed mainly by the action of hydrodynamic forces that carry the particles through the flow, the downward pull of gravity and the collision of the particles with the bed, which transfers their streamwise momentum into upward momentum, thus sustaining the saltation motion (Niño and García 1998). This differs from an earlier definition given by Bagnold (1973) who assumed that the only upward impulses exerted on the saltating particles were those resulting from the impact of particles with the bed. Thus, Bagnold neglected the effect of hydrodynamic lift and vertical impulses owing to flow turbulence, which have been shown to play an essential role in the saltation phenomenon (e.g. Leeder 1979a; Bridge and Dominic 1984; Bridge and Bennett 1992; Niño et al., 1994; Niño and García 1994). Experimental studies on saltation of gravel and sand by Niño et al. (1994) and Niño and García (1998b) have given detailed information on the physics of particle saltation. In particular, they have provided a description of the particle collision with the bed, allowing calibration of a stochastic model for this phenomenon, and have also provided statistics for the geometric and kinematic properties of the saltation trajectories.

In addition to its significance for the flux of sediment moving as bed load, the bed load layer serves as an exchange zone between the bed and sediment transported in suspension; the upward flux of sediment at the top of the bed load layer provides the boundary condition for suspended sediment transport calculations. Once sediment starts moving and sliding along the bed, the prevalent mode for bed load transport will most likely be saltation for a range of bed shear stresses. At higher values of boundary shear stress, the surface layer of the bed may deform and move as a grain flow or granular fluid flow (Wilson 1987, 1989). Grain flow is also known as sheet flow (Fredsøe and Deigaard 1992; Sumer et al 1996). Collision of the moving particles with the bed exerts both a tangential and a normal stress on the bed surface. The work of Bagnold (1954), Hanes and Inman (1985), and Jenkins and Hanes (1998) on high-concentration, granular shear flows have shown that if the ratio of the applied tangential to normal shear stresses exceeds the critical yield criterion, the frictional resistance of the bed will be overcome, and a grain flow will be initiated in the surface layer of the bed (Fredsøe and Deigaard 1992). So it is important to be able to discriminate between different modes of sediment transport so that the domain of applicability of bed load transport models can be determined (Sumer et al 1996).

In an attempt to interpret different transport modes following initiation of motion, Wiberg (1987) used a mechanistic model of bed load transport (Wiberg and Smith 1985) to produce a diagram (Fig. 2-30) of transport stage ($T_* = \tau_b / \tau_{bc}$) or bed shear stress (τ_b) versus quartz grain diameter(D), depicting the range of conditions over which sediment moves strictly as bed load and a saltation-based model can be used to describe the phenomenon. Conditions for the initiation of motion, the transition to suspension and the transition to grain flow, are also included.

As shown in Fig. 2-30(a), at transport stages $T_* < 1$ no sediment moves in a uniform bed of a given grain size. For grain sizes $D < 0.08$ cm (coarse sand and finer), the conditions for incipient motion occur at transport stages lower than those at which the applied stresses at the bed are sufficient to overcome the bed's frictional resistance. For sizes $D > 0.08$ cm, this situation is reversed, and the conditions for potential grain flow (sheet flow) at the bed surface are reached before the particles are significantly affected by the vertical turbulent velocity fluctuations that could entrain the grains into suspension (Niño and García 1996). Wiberg (1987, p. 94) indicates that the advent of either of these processes does not preclude the possibility of the other, but changes in the bed load dynamics produced by these processes are certain to influence the transport stage at which the other could occur. This is supported by the observations made by Wilson (2005), which show that when the ratio between the shear velocity (u_*) and the sediment fall velocity (v_s) increases over a critical value ($u_* / v_s > 6.5$), a rapid increase in both flow resistance and sediment entrainment into suspension is observed.

For all sediment sizes, Fig. 2-30(a) suggests that a transport stage of about 20 is an upper limit for saltation-based bed load transport. A saltation model might still provide reasonable transport predictions for incipient grain-flow conditions beyond this limit, but the physics of the phenomenon becomes more complicated as grain-grain interaction becomes more intense (e.g., Kobayashi and Seung 1985).

Fig. 2-30(b) presents the same results as shown in Fig. 2-30(a), but in terms of dimensional boundary shear stress, τ_b (dy/cm^2), to give a better sense of when the transition to these transport modes are actually likely to occur. For sediment sizes $D < 0.018$ cm (fine sand and finer) at initial motion, the moving particles go directly into suspension following intiation of motion. The corresponding critical shear stress $\tau_b < 2$ dy/cm^2, is quite low, and material of these sizes is frequently mobilized, provided cohesive effects are not large (see Chapter 4). Fine to coarse sand (D = 0.018–0.08 cm) moves initially as bed load, with particles starting to go into suspension at higher shears stresses. For example, medium

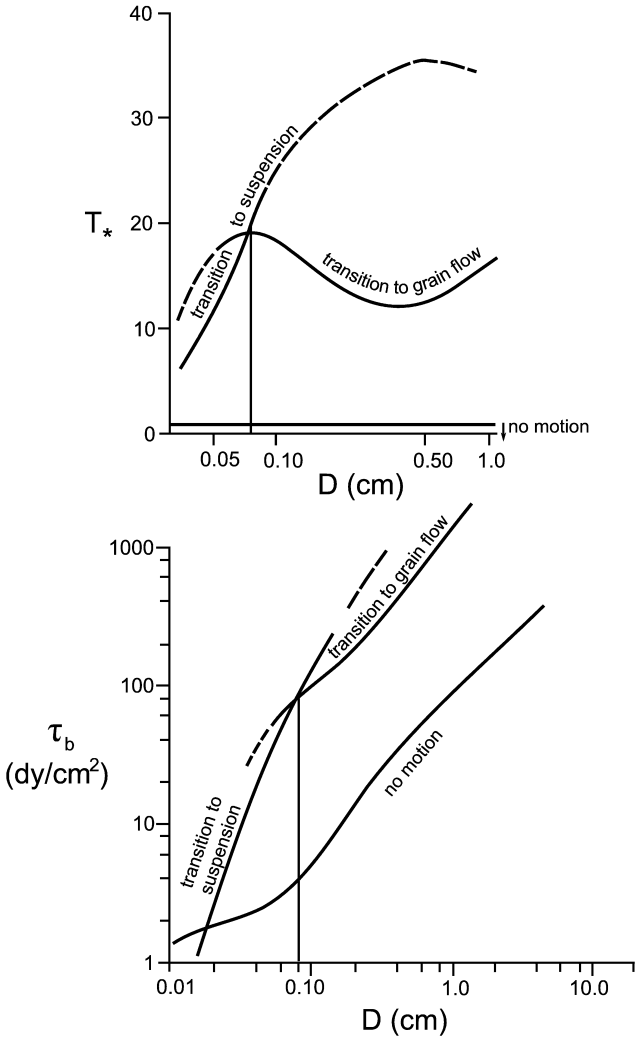

Fig. 2-30. Tentative ranges of conditions over which sediment moves strictly as bed load. (a) Initiation of motion, the transition to suspension and the transition to grain flow plotted in terms of transport stage versus grain size. (b) The same curves plotted in terms of dimensional boundary shear stress (in dy/cm^2), versus gran size. The vertical line marks the particle size at the intersection of the incipient suspension and incipient grain flow curves, $D \cong 0.08$ cm (adapted from Wiberg 1987).

sand begins to move at $\tau_b = 2$ to 3 dy/cm^2 and incipient suspension begins at $\tau_b = 10$ to 30 dy/cm^2 Shear stresses of such magnitude can be reached during moderate river flows and during storms on continental shelves.

In very energetic environments, such as the surf zone in coastal areas or during large river floods, it may also be possible for a grain flow (sheet flow) to develop (Wilson 1987, 1989; Sumer et al 1996). For coarse sand and gravel ($D =$ 0.08–6 cm), a relatively large boundary shear stress is required just to initiate the motion of the sediment. For example, for $D = 0.5$ cm (fine gravel), the critical shear stress is $\tau_{bc} = 45$ dy/cm^2) and a grain flow is possible at a shear stress $\tau_b >$ 550 dy/cm^2; these conditions are only likely to occur in very large sand-bed rivers or in high-gradient mountain streams. Thus for the grain sizes commonly encountered, suspended-load transport is an important mode of transport for fine sediment, whereas high-concentration grain flows are probably relatively uncommon except in a few specific environments. For a large range of sediment sizes in the medium to coarse sand range and above, if the sediment is moving at all, it is certainly moving as bed load.

2.6.2 Bed Load Transport Definition

Bed load particles roll, slide, or saltate along the bed. The transport thus is tangential to the bed. When all of the transport is directed in the streamwise, or s direction, the volume bed load transport rate per unit width (n-direction) is given by q_b; the units are length^3/length/time, or length^2/time. In general, q_b is a function of boundary shear stress τ_b and other sediment parameters; that is,

$$q_b = q_b\left(\tau_b, other\ parameters\right) \tag{2-80}$$

In general, bed load transport is vectorial, with components q_{bs} and q_{bn} in the s (streamwise) and n (lateral) directions, respectively. Basically the bed load transport rate can be defined as the product of particle concentration, particle velocity, and bed load layer thickness,

$$q_b = u_b c_b \delta_b \tag{2-81}$$

in which q_b is the volumetric bed load transport rate (m^2 / s), c_b is the volumetric sediment concentration (i.e. volume of sediment/volume of water-sediment mixture), u_b is particle velocity (m / s), and δ_b is the thickness of the bed load layer (m). Bagnoldean bed load transport models use this definition of the bedload transport rate (Ashida and Michiue 1972; Engelund and Fredsøe 1976; Van Rijn 1984a; Wiberg and Smith 1987; Sekine and Kikkawa 1992; Niño and García 1994; Lee and Hsu 1994; Niño and García 1998; Lee et al., 2000).

The bed load transport rate can also be defined as the product of the number of moving particles per unit area, the particle volume and the particle velocity (García 2000),

$$q_b = N_b V_b u_b \tag{2-82}$$

in which N_b is the number of particles per unit bed area (m^{-2}), V_b is the particle volume (m^3), and u_b is the particle velocity (m/s). If the particle velocity is defined as the ratio of the saltation or step length λ and the saltation or movement period T (*i.e.* $u_b = \lambda / T$), then

$$q_b = N_b V_b \lambda / T = E_p \lambda = D_p \lambda \tag{2-83}$$

Here, E_p and D_p = eroded and deposited volume of particles per unit bed area per unit time (m/s), respectively. Equilibrium bed load transport conditions imply that $E_p = D_p$.

The idea of a pick-up rate and a step length was first proposed by Einstein (1942; 1950) and constitutes the basis of Einsteinian bedload transport models (Nakagawa and Tsujimoto, 1980; Tsujimoto, 1992). A comparison of several pick-up rate functions and their applications can be found in Van Rijn (1984b; 1986). Einstein defined the particle step length as the particle travel distance from entrainment to deposition (i.e., when the particle stops moving and comes to rest) and estimated it to be equal to about 100 times the particle diameter. Einstein's particle length can be expected to be several times the saltation length λ previously defined. This assumption will be considered below in light of the experimental observations made by Wong and Parker (2006a).

2.6.3 Conservation of Sediment Mass: The Exner Equation and Morphodynamics

Before considering bed load transport relations in more detail, it is useful to formulate the interaction between bed sediment and the water column through erosion and deposition, so that the sediment mass conservation can be formulated. Consider the definition diagram for a sediment-laden, uniform, open-channel flow shown in Fig. 2-31. The volume rate of erosion of bed material into suspension per unit time per unit bed area is denoted as E_r. The units of E_r are length^3/length^2/time, or velocity. A dimensionless sediment entrainment rate E_s can thus be defined in terms of the sediment fall velocity v_s:

$$E_r = v_s E_s \tag{2-84}$$

In general, E_s can be expected to be a function of boundary shear stress τ_b and sediment related parameters (García and Parker 1991; Niño et al. 2003). Erosion into suspension can be taken to be directed upward normal, i.e., in the positive z direction.

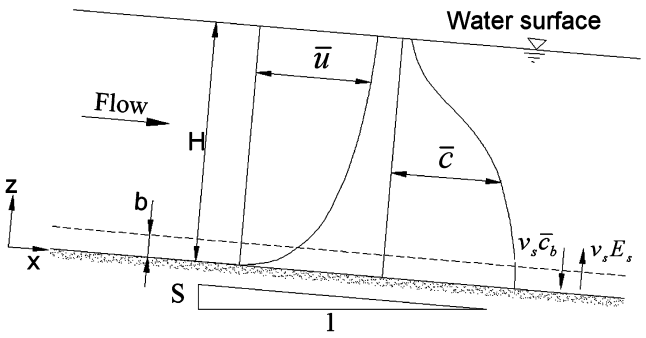

Fig. 2-31. Definition diagram for sediment-laden open channel flow.

Let $\overline{u}$ denote the mean flow velocity (m/s) at a point located at a distance z normal to the bed, and $\overline{c}$ denote the mean volumetric concentration of suspended sediment (m^3 of sediment/m^3 of sediment-water mixture), averaged over turbulence. The streamwise volume transport rate of suspended sediment per unit width is given by

$$q_S = \int_0^H \overline{u}\,\overline{c}\; dz \tag{2-85}$$

Let s denote the streamwise direction and n denote the lateral direction in a two-dimensional case; then two components, q_{Ss} and q_{Sn} result, where

$$q_{Ss} = \int_0^H \overline{u}\,\overline{c}\;\; dz \tag{2-86a}$$

$$q_{Sn} = \int_0^H \overline{v}\,\overline{c}\; dz \tag{2-86b}$$

where $\overline{v}$ is the mean lateral (n-direction) velocity at a distance z above the bed.

Deposition onto the bed is by means of settling. The rate at which material is fluxed vertically downward onto the bed (volume/area/time) is given by $v_s\overline{c}_b$, where $\overline{c}_b$ is a near-bed value of the volumetric sediment concentration $\overline{c}$. Some authors assume that the value of the near-bed concentration is the same as the sediment concentration in the bed load layer defined previously (Einstein 1950; Engelund and Fredsøe 1976; Zyserman and Fredsøe 1994). The deposition rate D_r realized at the bed is obtained by computing the component of this flux that is actually directed normal to the bed as

$$D_r = v_s\overline{c}_b \tag{2-87}$$

which gives the volume of sediment deposited per unit bed area per unit time (García 2001).

Now it is possible to formulate the sediment mass conservation for bed material taking into account both bed load transport and sediment erosion into and from suspension. Consider a portion of river bottom (Fig. 2-32), where the bed material is taken to have a constant porosity λ_p. Mass balance of sediment requires that the following equation be satisfied:

$$\frac{\partial}{\partial t}\left[\textit{mass of bed material}\right] = \textit{net mass bedload inflow rate} + \textit{net mass rate of deposition from suspension}$$

A datum of constant elevation is located well below the bed level, and the elevation of the bed with respect to

Copyrighted Materials
Copyright © 2008 American Society of Civil Engineers (ASCE)
Retrieved from www.knovel.com

CHAPTER 3

Transport of Gravel and Sediment Mixtures

Gary Parker

3.1 FLUVIAL PHENOMENA ASSOCIATED WITH SEDIMENT MIXTURES

When *ASCE Manual No. 54*, "Sedimentation Engineering," was first published in 1975, the subject of the transport and sorting of heterogeneous sediments with wide grain-size distributions was still in its infancy. This was particularly true in the case of bed-load transport. At the time, the method of Einstein (1950) was one of the few available that were capable of computing the entire grain-size distribution of particles in bed-load transport. However, this capability had not been extensively tested against either laboratory or field data. Since that time there has been a steady increase in research on the subject of the selective (or nonselective) transport of sediment mixtures. A brief attempt to summarize this research in a useful form is provided in this chapter.

A river that is supplied with a wide range of grain sizes has the opportunity to sort them. Although the grain-size distribution found on river beds is never uniform, the range of sizes tends to be particularly broad in the case of rivers with beds that consist of mixtures of gravel and sand. These streams are termed "gravel-bed streams" if the mean or median size of the bed material is in the gravel range; otherwise they are termed "sand-bed streams." The river can sort its gravel and sand in the streamwise, lateral, and vertical directions, resulting in each case in a characteristic morphology. Summaries of these morphologies are given in Whiting (1996) and Powell (1998); Parker (1992) provides a mechanistic basis for their study.

Sorting phenomena range from very small scale to very large scale. In many gravel-bed rivers, the bed is vertically stratified, with a coarse armor layer on the surface. This coarse layer limits the supply of fine material from the subsurface to the bed load at high flow. Some gravel-bed streams, however, show no vertical stratification. An example of each type of stream is shown in Fig. 3-1, which illustrates the difference between a perennial stream with low sediment supply and moderate floods (left) and an ephemeral stream with a high sediment supply and violent floods (right).

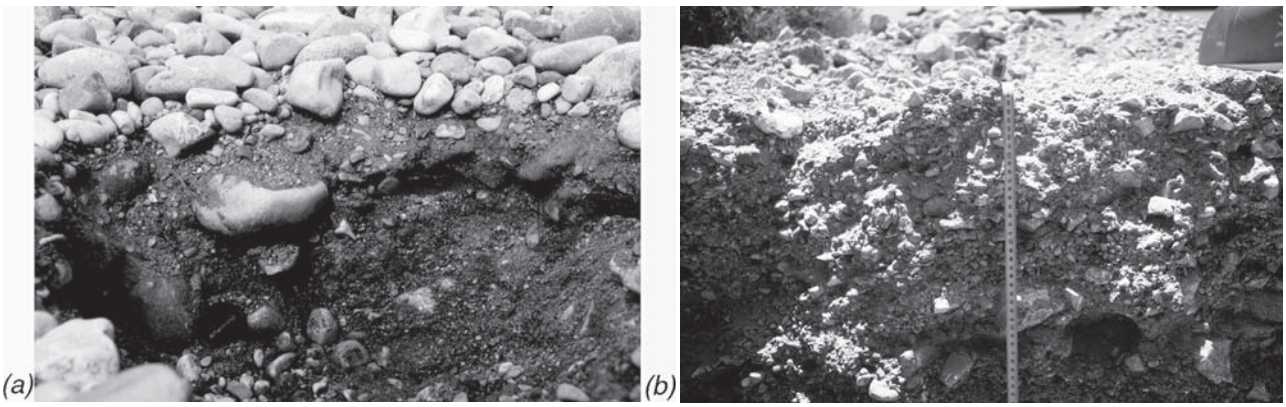

Fig. 3-1. Contrasts in surface armoring between (a) the River Wharfe, UK, a perennial stream with a low sediment supply (left) and (b) the Nahal Yatir, Israel, an ephemeral stream with a high rate of sediment supply (right). Images courtesy of J. Laronne and I. Reid; see also Powell (1998).

If the flow is of sufficient strength, bed forms such as dunes can form in gravel-bed streams (Dinehart 1992). Dunes are the most common bed form in sand-bed streams. Depending on the strength of the flow, the parent grain-size distribution can interact with the bed forms to induce strong vertical and streamwise sorting, with coarser material accumulating preferentially in dune troughs. This is illustrated in Fig. 3-2. Note that the transition from lower-regime plane bed to dunes, which is illustrated in Fig. 2-28, thus engenders a reversal of vertical sorting, with a coarse layer at the top of the bed in the former case and near the base of the dunes in the latter case.

Under conditions of weak transport, the dunes devolve into bed-load sheets, which are rhythmic waves expressing downstream variation predominantly in terms of alternating zones of fine and coarse sediment rather than elevation variation (Fig. 3-3). Both dunes and bed-load sheets result in

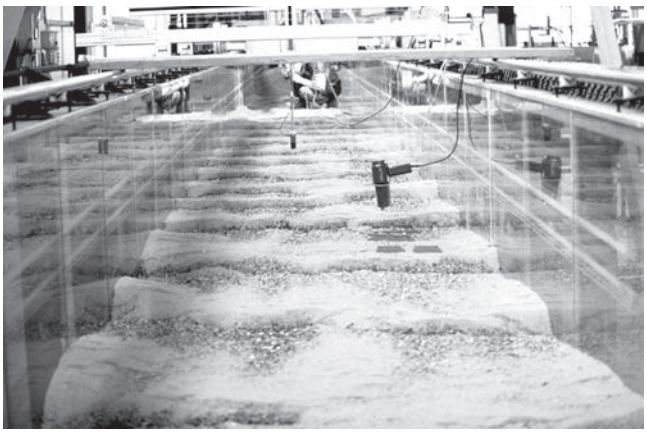

Fig. 3-2. Sediment sorting in the presence of a dune field. Flow was from top to bottom. Image courtesy A. Blom.

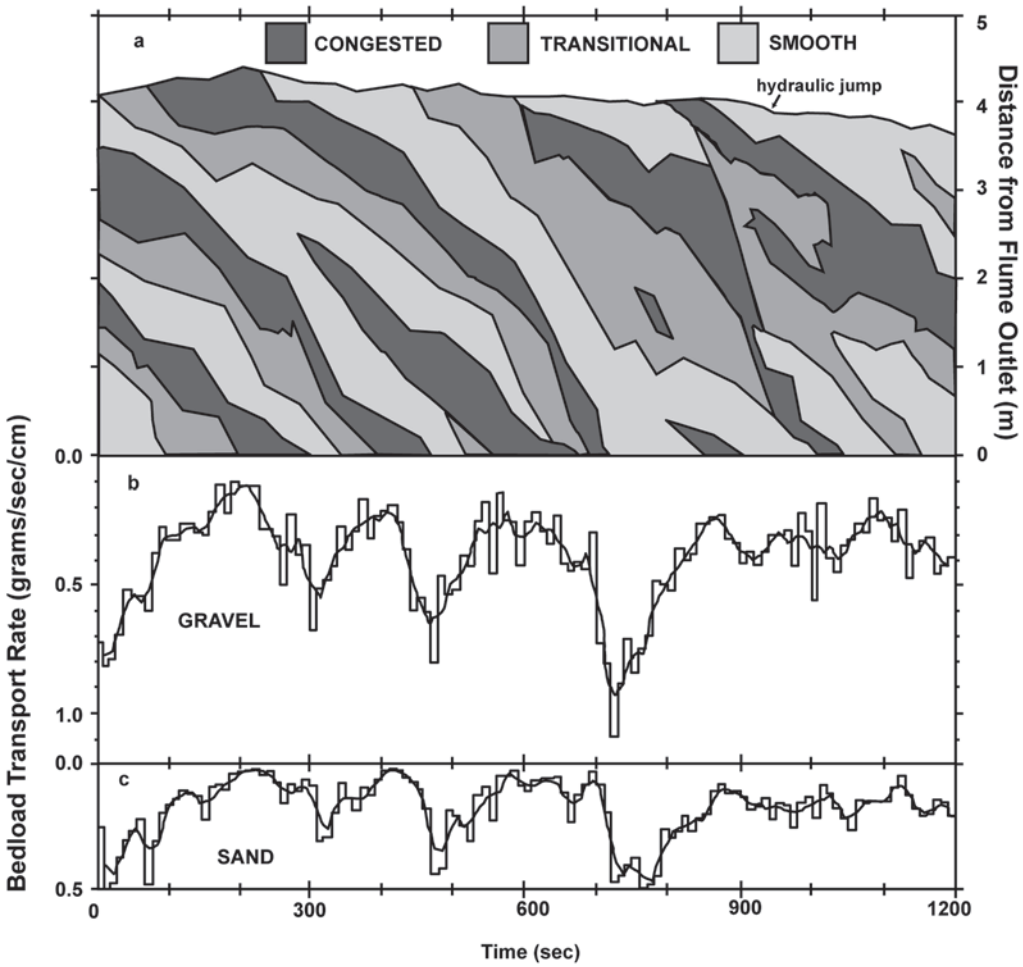

Fig. 3-3. Pulsations associated with experimental bedload sheets composed of a mixture of sand and gravel. (a) Alternating arrangement of three bed states. (b) Fluctuation in gravel transport rate. (c) Fluctuation in sand transport rate. From Iseya and Ikeda (1987), with permission of Blackwell Publishing.

Fig. 3-4. View of the Ooi River, Japan, showing sorting of gravel and sand on bars. From Ikeda (2001), with permission of Hiroshi Ikeda. The direction of flow is from the bottom to the top of the image.

a bed-load transport that strongly pulsates in terms of both total rate and characteristic grain size.

Bars and bends that form in rivers interact with sediment to produce sorting morphologies at a larger scale. Figure 3-4 shows a mildly sinuous reach of the Ooi River, Japan. It is readily apparent that bar heads tend to be coarser, whereas bar tails tend to be finer. Similar patterns can be observed in the bars of braided streams.

At sufficiently steep slopes, bars give way to pool-riffle sequences, which are barlike undulations in bed elevation and grain size that, for the most part, are expressed in the streamwise rather than the lateral direction. As opposed to dunes and some bars, pool-riffle patterns usually show little tendency to migrate downstream. At even steeper slopes, which support flow that is supercritical in the Froude sense during floods, the bed devolves into a well-defined step-pool pattern. Each step is defined by what can be described as a boulder jam, as seen in Fig. 3-5; the pools between steps contain much finer material.

Fig. 3-5. Step-pool topography in the Hiyamizu River, Japan. Image courtesy K. Hasegawa.

A lake or reservoir interrupts the downstream transport of sediment. As a result, the riverbed often aggrades upstream of the dam and degrades downstream. Figure 3-6 shows the aggradational deposit upstream of a sediment retention dam on the North Fork Toutle River, Washington. Over the 10 km upstream of the dam, the characteristic bed-sediment size shows a pronounced pattern of downstream fining, declining from about 7.4 to 0.4 mm. This downstream fining appears to be abetted by the tendency of the bed to devolve into local patches or lanes of finer and coarser sediment. Figure 3-7 illustrates two such patches on the North Fork Toutle River. An extreme limiting case of such local segregation is the formation of roughness "streaks," "stripes," or "ribbons," which consist of vertical lanes of alternating coarse and fine material, with a high transport rate of the latter relative to the former. These streaks are shown in Fig. 3-8.

Downstream of a dam, on the other hand, the bed often both degrades and coarsens in response to the cutoff of sediment, eventually forming static or nearly static armor that inhibits further bed erosion. An image of the static armor downstream of the Lewiston Dam on the Trinity River, California is shown in Fig. 3-9. The static armor is partially covered by mobile, pea-sized gravel from a tributary entering downstream of the dam.

Sorting appears at the largest scale in terms of the tendency for characteristic grain size to become finer over tens or hundreds of kilometers. This large-scale downstream fining is typically associated with a long profile of the river that is concave upward. A famous example, the Kinu River, Japan, is shown in Fig. 3-10. This river displays not only downstream fining, but also a relatively abrupt transition from gravel bed to sand bed. Strong downstream fining is

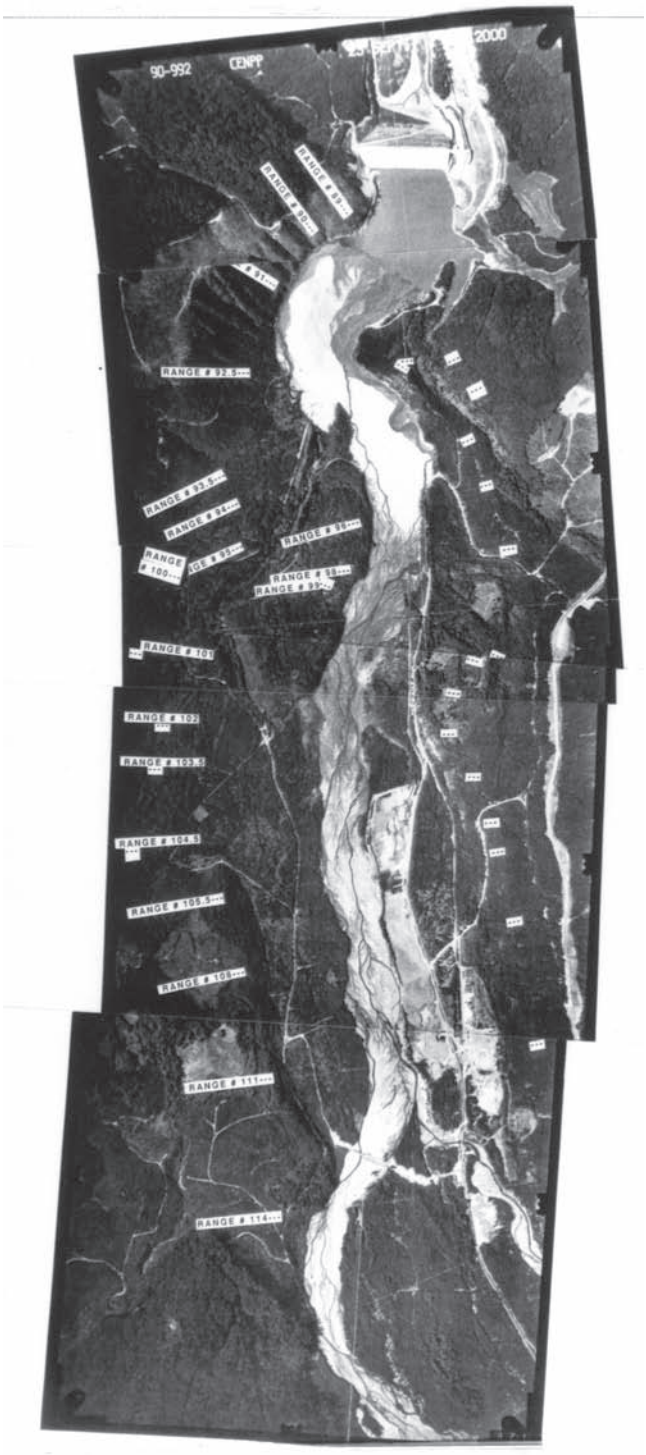

Fig. 3-6. View of sedimentation upstream of a sediment retention dam on the North Fork Toutle River, Wash. Flow is from bottom to top. From Seal and Paola (1995). (Copyright 1995 American Geophysical Union. Reproduced by permission of American Geophysical Union.)

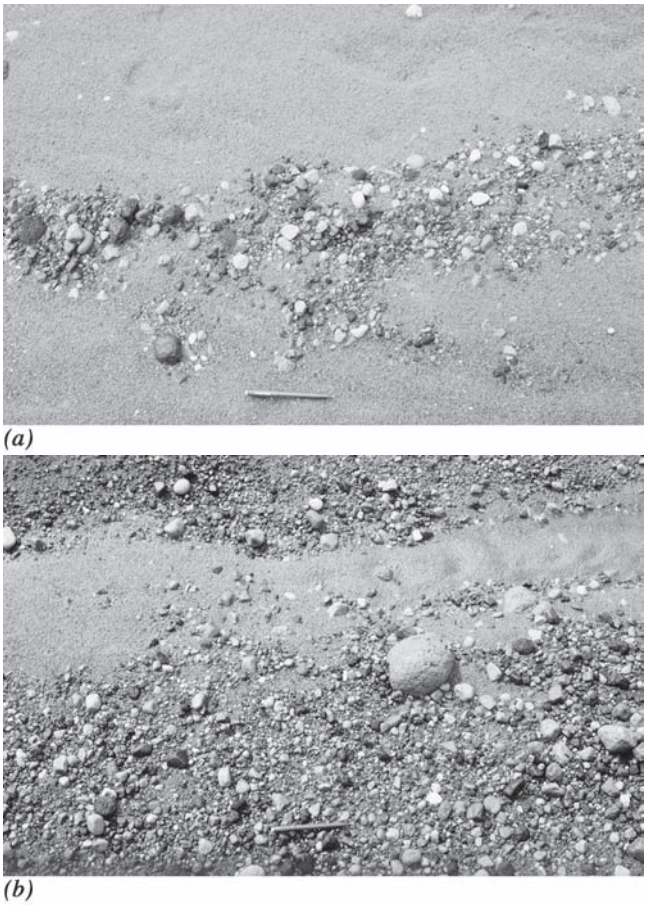

Fig. 3-7. Sorted sediment patches on the North Fork Toutle River, Wash.: (a) coarse patch on fine sediment; (b) fine patch on coarse sediment. From Paola and Seal (1995). (Copyright 1995 American Geophysical Union. Reproduced by permission of American Geophysical Union.)

observed along the gravel-bed reach, and weaker downstream fining along the sand-bed reach.

Abrupt gravel-sand transitions are quite common in the field and are associated with the tendency for grain sizes in the range of pea gravel to be relatively scarce in rivers. This tendency is common, but by no means universal. An example of this tendency is shown in Fig. 3-11, which shows bed-material grain-size distributions of 174 river reaches in Alberta, Canada (Shaw and Kellerhals 1982). Note that the sand-bed streams (i.e., median size in the sand range) contain very little gravel. The gravel-bed streams (i.e., median size in the gravel range) often contain a substantial amount of sand, but very little material between 1 and 8 mm.

Transient sorting can be induced by a pulse of sediment introduced into a river from a debris flow or landslide. An example illustrating a landslide that flowed into and blocked the Navarro River, California is shown in Fig. 3-12. Such inflows often contain copious amounts of material that is much finer than the ambient bed material. They can also contain some material that

(a)

(b)

Fig. 3-8. Streaks of sorted sediment in (a) a laboratory flume (from Günter, 1971; courtesy A. Günter) and (b) a river (image courtesy T. Tsujimoto).

(a)

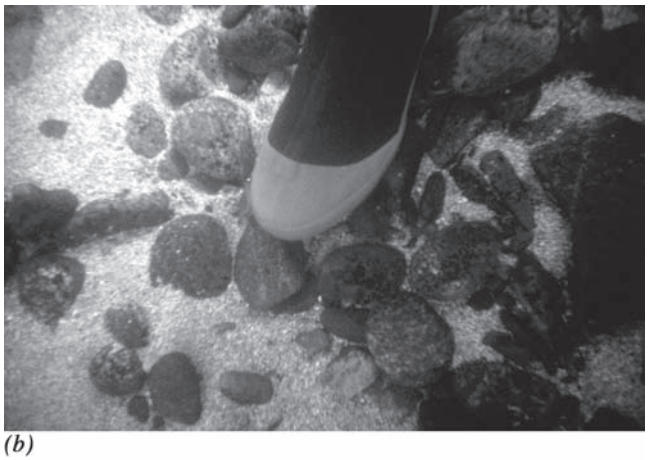

(b)

Fig. 3-9. Coarse static armor (dark grains) with a partial coverage of finer, mobile sediment (light grains) on the bed of the Trinity River, Calif. The coarse grains are rendered immobile by the presence of the Lewiston Dam upstream. (a) View of the river. (b) Closeup of the bed. Images courtesy Peter Wilcock.

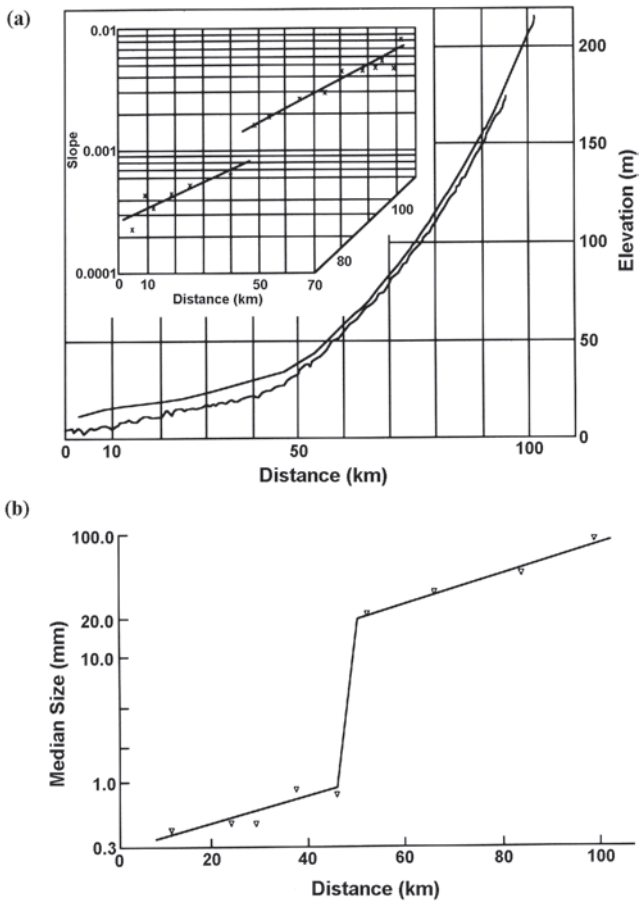

Fig. 3-10. (a) Long profile and (b) downstream change in grain size of the Kinu River, Japan, illustrating downstream fining and a gravel-sand transition. Redrafted from an original in Yatsu (1955). (Copyright 1955 American Geophysical Union. Reproduced by permission of American Geophysical Union.)

is much coarser than the ambient bed material. Grain size sorting plays a key role in the process by which rivers digest such sediment inputs.

Most sediment sorting in rivers is accomplished by the differential transport of different sizes. In the case of heavy minerals (placers), however, increased specific gravity replaces increased size in this role. The issue is of some interest with regard to the extraction of placer gold from rivers. That finer grains are more mobile than coarser grains of the same specific density may appear to be intuitively obvious. However, this is usually but not always the case.

In addition to selective transport, rivers have the opportunity to create finer grains from coarser grains. This is sometimes accomplished by shattering of grains, but is more commonly associated with gradual abrasion and rounding of stones, yielding silt and some sand as a result. Abrasion can thus be a contributor to downstream fining. Figure 3.13 illustrates the effect of abrasion in gradually rounding grains downstream from their source.

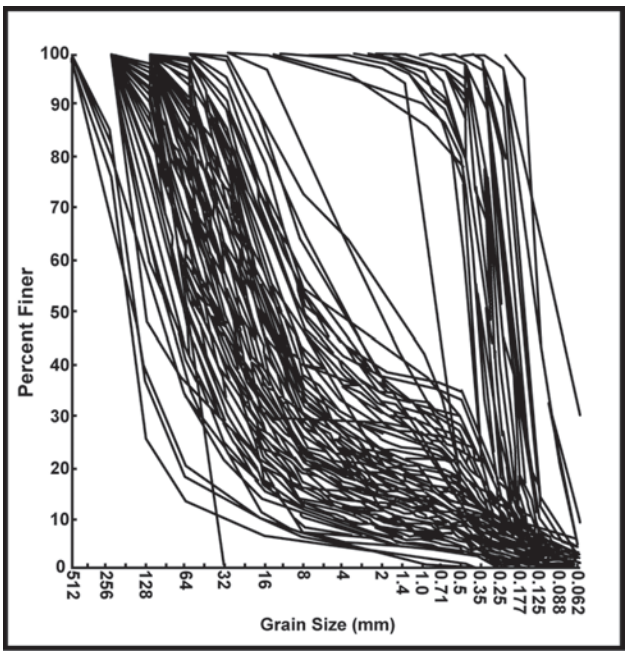

Fig. 3-11. Grain size distributions of 174 samples of bed sediment from rivers in Alberta, Canada. From Shaw and Kellerhals (1982).

Fig. 3-12. View of a landslide that blocked the Navarro River, Calif. in 1995. Image courtesy of T. Lisle.

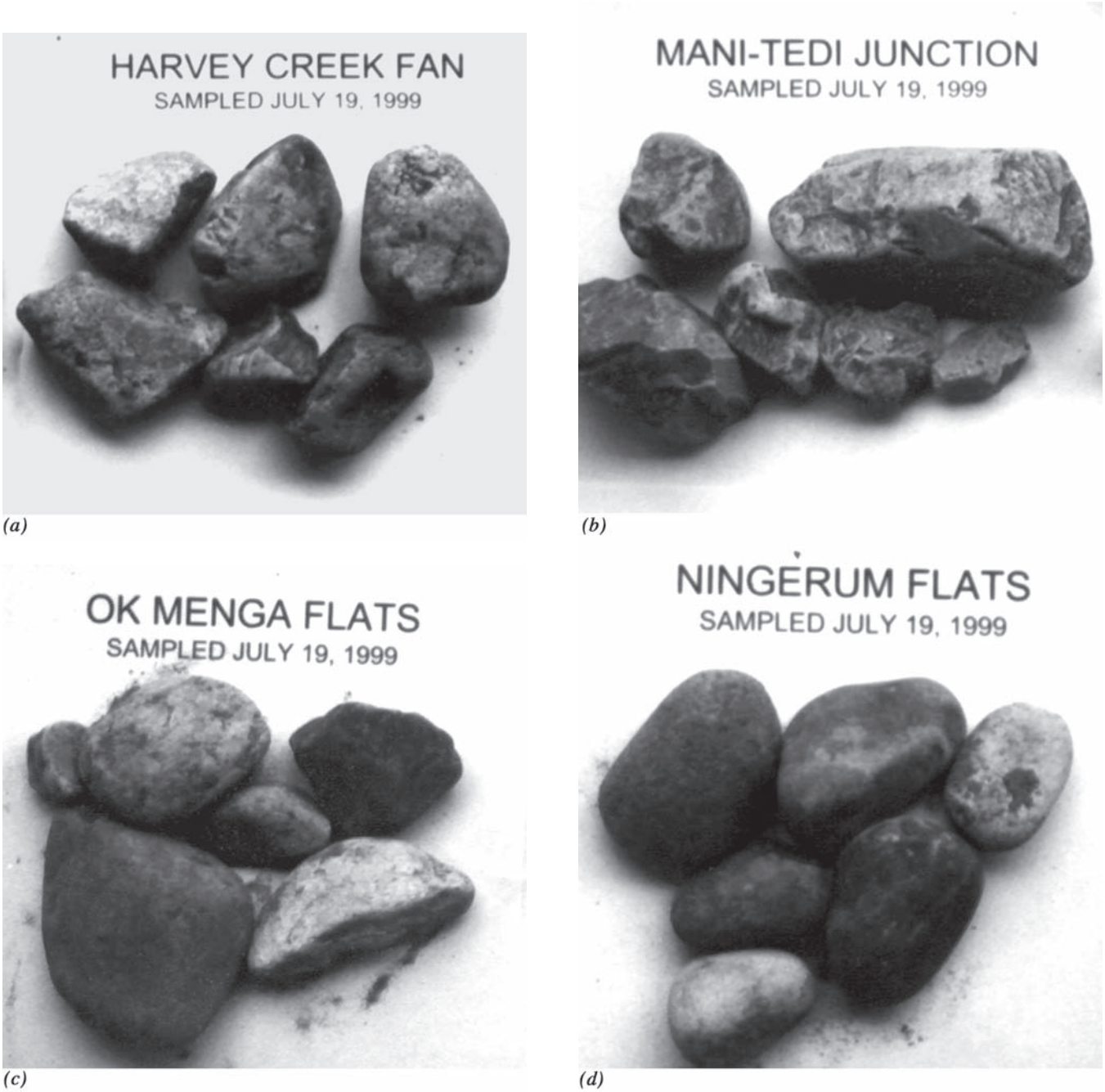

Fig. 3-13. Four sediment samples from the Ok Tedi River system, Papua New Guinea: (a) 1 km downstream of the Southern Dumps of the Ok Tedi Mine, after passage over a high waterfall, in the Harvey Creek debris flow fan as it enters the Ok Mani; (b) 8 km downstream, at the fluvial fan of the Ok Mani where it enters the Ok Tedi; (c) 27 km downstream on the Ok Tedi near the junction with the Ok Menga; and (d) 90 km downstream on the Ok Tedi at Ningerum Flats. Note that the grains become progressively rounder as the distance from the source increases.

The main focus of this chapter is on transport of mixed sizes and concomitant sorting in bed-load-dominated rivers. In the field, this usually refers to gravel-bed rivers. Some (typically small) sand-bed streams, such as Muddy Creek (Dietrich and Whiting 1999) also satisfy this criterion. Near the end of the chapter, however, suspension-dominated rivers, i.e., most sand-bed streams, are considered as well.

3.2 ENGINEERING RELEVANCE

Various aspects of grain sorting are relevant to river engineering design, habitat maintenance, and restoration of river ecosystems. First and foremost among these is gravel extraction, or mining from rivers for concrete aggregate and other construction purposes. The word "gravel" is used loosely with

regard to gravel mining and includes sand as well. The mining of fluvial gravels is particularly common in the western part of the United States. Gravel mining without appropriate constraints can lead to severe bed degradation downstream, with resulting failure of bridges and exposure of buried pipelines (Galay 1983). The Mad River, California, has been heavily utilized for gravel extraction. The effect on bed elevation at the bridge piers where Highway 101 crosses the river is readily apparent in Fig. 3-14. Gravel extraction was taking place on the day the photo was taken. Engineering models of the erosion, transport, and deposition of heterogeneous gravels have an important role to play in determining how much gravel can be safely extracted without adverse effects.

A common practice in many western rivers is "bar scalping," by which high-quality material is locally stripped from the surface of bars. This is done on the supposition that the river will eventually replace the mined gravel with material of similar competence. Anadromous fish such as salmon, however, are rather particular about the gravels in which they choose to build redds (egg nests) (Reiser 1998). If the bed material is too coarse the fish cannot excavate a redd. If the bed is too fine, and in particular if it contains too much sand and silt, the fish will avoid it, instinctively knowing that eggs will be suffocated and poisoned by the inability of groundwater flow to carry away excreta. The Ooi river of Fig. 3-4 might be a good candidate for bar scalping in the United States, but in Japan, gravel extraction from most rivers has been banned in order to control bed degradation. The degradation of Japan's rivers is not only a product of gravel mining in previous times, but also a result of intensive sediment control works (e.g., sabou dams) in the upstream reaches of Japanese rivers that have dramatically reduced the sediment supply.

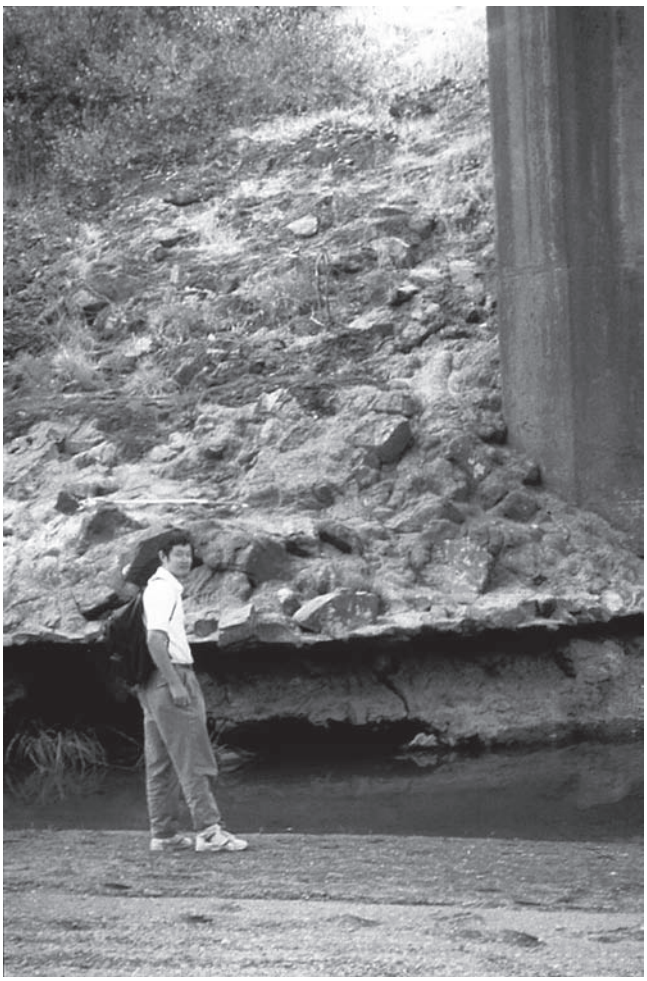

Fig. 3-14. Evidence of channel degradation on the Mad River, California under the Highway 101 bridge.

Spawning grounds can also be damaged or destroyed by agriculture or forestry. Road building for forest harvesting, if not done properly, can cause massive inputs of sand and finer material to a stream that is intrinsically gravel-bed. This finer material is usually transient, being washed downstream by successive floods. If the bed happens to be buried in fines, however, just before spawning, fish recruitment can drop drastically (e.g., Reiser 1998).

The installation of a dam on a river typically blocks the downstream delivery of all but the finest sediment, creating a pattern of bed aggradation upstream. The dam raises base level (i.e., the downstream water surface elevation to which the river upstream must adjust), forcing upstream-migrating deposition. This deposition is most intense near the delta at the upstream end of the reservoir. As a result, the effect is to intensify the upward concavity of the long profile of the bed upstream of the dam. The more sharply declining bed slope intensifies selective transport of fine material, setting up strong local downstream fining. This is what has taken place in the reservoir of the North Fork Toutle River, Washington, as illustrated in Fig. 3-6.

Downstream fining has a beneficial effect in terms of engineering that should be taken into consideration in designing dams. Aggradation induced by dams can require the leveeing of towns upstream of the dam. Sorting, however, tends to concentrate the aggradation toward the downstream end of the reach in question. Indeed, Leopold et al. (1964) observed that upstream aggradation driven by a dam never extends infinitely far upstream, no matter how much time has passed. Part of the reason for this is the tendency for the main stem and tributaries farther upstream in the drainage basin to absorb the effect of the dam. Sediment sizes that deposit in the backwater zone of the dam can be carried without deposition by the steeper main stem and tributaries upstream.

An extreme case of this tendency for sorting to damp upstream effects is often seen in gravel-bed streams, many of which carry loads of sand far in excess of the corresponding loads of gravel. However, the bed surface consists largely of gravel, with sand partially or completely filling the interstices. Analogously to the mud washload of sand-bed rivers, this sand load on a gravel-bed stream is called "throughput

load" if it interacts only passively with the bed (i.e., simply filling the pores of a gravel deposit). Sand can be carried as throughput load over a gravel bed when the rate of sand input necessary to drown the bed in sand is higher than the prevailing sand input. In gravel-bed rivers, the disparity between the two becomes increasingly large with increasing bed slope. The threshold for major sand deposition is crossed as bed slope declines. As a result, the sandy deposit caused by a dam migrates upstream only until the stream becomes sufficiently steep to prevent it from covering the bed completely.

The dam in Fig. 3-6 was installed as a debris-control measure in the wake of the Mount St. Helens eruption in 1980. Such dams play an important role in disaster mitigation. In Fig. 3-6 the dam is nearly full. Understanding the process of filling requires an understanding of the transport of sediment mixtures.

The cutoff of sediment at a dam often induces bed degradation, as the river mines itself to replace the lost load. Bed degradation rarely continues unabated. Even small amounts of coarse, erosion-resistant material in the substrate tend to concentrate on the bed surface as the bed degrades, eventually limiting the process through the formation of static armor. Figure 3-15 gives an example of the time evolution of bed armoring of the Colorado River downstream of Hoover Dam (Williams and Wolman 1984).

It would be a mistake, however, to believe that the installation of a dam universally causes bed degradation downstream. As illustrated in Fig. 2-29, bank-full flows in gravel-bed rivers often correspond to conditions that do not much exceed those needed to mobilize the gravel. When dams are operated for flood control, cutting off the flood peaks needed to mobilize the gravel can cause a river to lose most of its capacity to move gravel. As a result, downstream of the first tributary the riverbed aggrades, as the sediment from the tributaries reaches a main stem that is no longer competent to transport it. This process has been documented in the Peace River, Canada, downstream of the W. A. C. Bennett Dam (Kellerhals and Gill 1973).

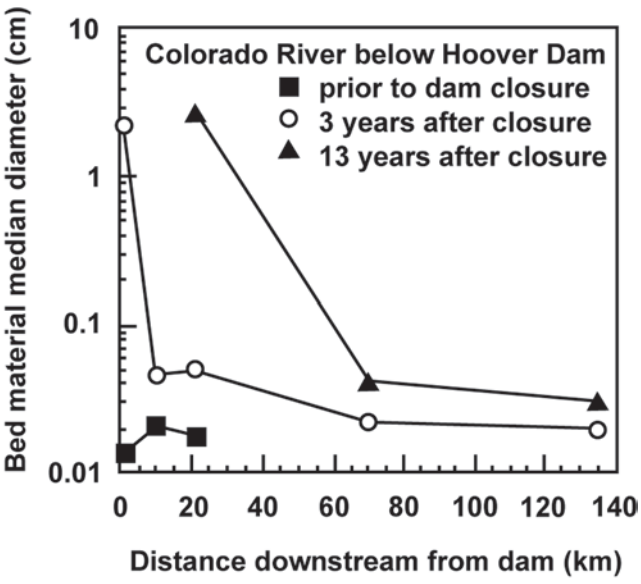

Fig. 3-15. Bed surface median grain size downstream of Hoover Dam on the Colorado River before and after closure. From Williams and Wolman (1984).

The Trinity River, California, downstream of the Lewiston Dam, provides a type example of the downstream effects of a dam (Kondolf and Wilcock 1996). This dam not only cuts off the sediment, but also maintains a constant flow that is well below bank-full flow. From the dam to the first major tributary downstream, not only is the gravel not replenished, but also the lack of the flows necessary to mobilize it has allowed the interstices of the gravel to become filled with debris that is not cleaned out by floods (Fig. 3-9). This lack of renewal not only degrades the gravel bars as a spawning habitat, but also leads to general decline in the ecological productivity of the system. The first tributary brings in a substantial quantity of corn-sized grains of weathered granite that partially fill the pores of the gravel and further degrade habitat. Loss of flood flows has also caused channel narrowing, which is associated with the encroachment of alders as well as humans, the latter being lulled by the lack of flood flows. The renewal of such a stream requires at the least controlled flood releases from the dam. How much and how long must be determined at least partially in terms of the mobility of the various sizes of sediment in the bed (Wilcock et al. 1996).

Dam removal has become quite popular in recent years, the main motivating factors being habitat improvement and stream restoration. Lack of understanding of the transport mechanics of heterogeneous sediments has often led to complete excavation of the deposit behind dams, even when the sediment is uncontaminated. The techniques necessary to evaluate the fate of both coarse and fine sediments released from a dam, and thus whether or not removal is necessary, are available, but have not usually been put into practice. Fortunately, however, a description of one version of the technology is provided as Chapter 23 of this manual. Developments in the area of river restoration can be found in Hay (1998) and Hotchkiss and Glade (2000).

Disposal of mine waste into a river can lead to massive bed aggradation. This aggradation is almost invariably associated with a pattern of downstream fining. The Ok Tedi copper/gold mine in Papua New Guinea is a case in point (Parker et al. 1996; Dietrich et al. 1999). Throughout much of the latter 1990s the mine disposed of some 40 Mtn/year of waste rock and 30 Mtn/year of tailings into a river system characterized by a steep gravel-bed reach with a fairly sharp transition to a sand-bed reach (Fig. 3-16). The extreme overloading of the system has caused massive channel and floodplain deposition, as well as major modification in the pattern of downstream fining. Input sizes range from boul-

(a)

(b)

(c)

Fig. 3-16. (a) View of waste rock dump site at the Ok Tedi Mine, Papua New Guinea. (b) View of the Ok Tedi gravel-bed downstream of the mine. The channel bed has aggraded and widened in response to disposal of mine sediment. (c) View of the Fly River sand-bed downstream of its confluence with the Ok Tedi. Aggradation of bed sediment has exacerbated both flooding and the overbank deposition of fine sediment, resulting in the loss of riparian forest.

ders to silt. The coarse material contains several mineral types, some of which are highly subject to abrasion. The effect of wear on the coarser grains is illustrated in Fig. 3-13; the degree of overloading makes it highly likely that all grains in the image originated from the mine. Any numerical model designed to track the fate of the sediment, the evolution of the river profile, and the design of countermeasures must account for downstream fining, abrasion of several rock types, and overbank deposition of finer material. Cui and Parker (1999) describe such a model. Part of the model was adapted to study the effects of dam removal (Appendix A, this volume).

These examples represent a subset of the engineering problems requiring a description of the selective transport of heterogeneous sediments. Other examples include woody debris in rivers, flow augmentation by diversion, the effect of extreme floods, the fate of contaminated sediments from mines and industrial sites, avulsion on alluvial fans, and the competence of riprap placed on or in an alluvial bed to resist scour.

3.3 GRAIN-SIZE DISTRIBUTIONS

3.3.1 Definitions and Continuous Formulation

The sedimentological phi (ϕ) scale introduced in Chapter 2 has the disadvantage that grain size decreases as the value of ϕ increases. With this in mind, the alternative ψ scale is introduced (Parker and Andrews 1985); where D denotes grain size in mm,

$$\psi = \frac{\ln(D)}{\ln(2)} \tag{3-1a}$$

$$D = 2^{\psi} \tag{3-1b}$$

Thus $\psi = -\phi$. Let $p(\psi)$ denote the probability density by weight of a sample associated with size ψ, and let $p_f(\psi)$ denote the associated probability distribution. Then by definition,

$$\int_{-\infty}^{\infty} p(\psi)d\psi = 1 \tag{3-2a}$$

$$p_f(\psi) = \int_{-\infty}^{\psi} p(\psi)d\psi \tag{3-2b}$$

Thus $p_f(\psi)$ denotes the fraction of the sample that is finer than size ψ. Let x denote some percentage, say 50%, and let ψ_x denote the grain size on the ψ scale such that x% of the sample is finer. It then follows that

$$p_f(\psi_x) = \frac{x}{100} \tag{3-3}$$

The corresponding grain size in mm D_x is given from (3-1b) as

$$D_x = 2^{\psi_x} \tag{3-4}$$

A value of $x = 50$ yields the median grain size D_{50}; the value $x = 90$ yields the value D_{90} such that 90% of the sample is finer, a value commonly used in the computation of the roughness associated with skin friction (grain roughness).

The arithmetic mean ψ_m and arithmetic standard deviation σ_m of the grain-size distribution are given as

$$\psi_m = \int \psi p(\psi)d\psi \tag{3-5a}$$

$$\sigma^2 = \int (\psi - \psi_m)^2 p(\psi)d\psi \tag{3-5b}$$

The corresponding geometric mean D_g and geometric standard deviation σ_g are then given as

$$D_g = 2^{\psi_m} \tag{3-6a}$$

$$\sigma_g = 2^{\sigma} \tag{3-6b}$$

Sediment samples with values of σ_g in excess of 1.6 are said to be poorly sorted (Chapter 5, this volume). Poorly sorted sediment provides grist for the mill of the river as it sorts it spatially over the planform and in the vertical.

A grain-size distribution is said to be unimodal if the density $p(\psi)$ displays a single peak and bimodal if it displays two peaks. The grain-size densities and distributions associated with unimodal and bimodal distributions are illustrated in Figs. 3-17a and 3-17b. When Fig. 3-11 is compared with Figs. 3-17a and 3-17b, it is seen that the sediment samples from the sand-bed streams of the former diagram, those for which D_{50} is in the sand size range, are unimodal, and those from the gravel-bed streams of the former diagram, those for which D_{50} is in the gravel range, are bimodal, with peaks in the sand and gravel range and a paucity in the pea gravel range (2–8 mm). It is not accurate to say that the sediment in all sand-bed streams is unimodal and the sediment in all gravel-bed streams is bimodal, but this general tendency is observed.

The simplest realistic analytical form for the probability density and distribution of grain sizes is the lognormal form (normal distribution of the logarithm of grain size),

$$p(\psi) = \frac{1}{\sqrt{2\pi}\,\sigma}\exp\left(-\frac{(\psi - \psi_m)^2}{2\sigma^2}\right) \tag{3-7a}$$

$$p_f(\psi) = \frac{1}{\sqrt{2\pi}\,\sigma}\int_{-\infty}^{\psi}\exp\left(-\frac{(\psi' - \psi_m)^2}{2\sigma^2}\right)d\psi' \tag{3-7b}$$

Equation (3-7a) describes a symmetric, unimodal probability density that often provides a reasonable fit for samples from sand-bed streams, but rarely does so in the case of gravel-bed streams. (The size densities of gravel-bed streams with a bimodal mix of sand and gravel can sometimes be approximated as weighted sums of two lognormal densities.)

In the case of a sediment sample that is lognormally distributed, it can be shown that the mean size ψ_m and the standard deviation σ are given by the relations

$$\psi_m = \frac{1}{2}(\psi_{84} + \Psi_{16}) \tag{3-8a}$$

$$\sigma = \frac{1}{2}(\psi_{84} - \Psi_{16}) \tag{3-8b}$$

The corresponding geometric mean and geometric standard deviation are

$$D_g = \sqrt{D_{84}\, D_{16}} \tag{3-9a}$$

$$\sigma_g = \sqrt{\frac{D_{84}}{D_{16}}} \tag{3-9b}$$

It should be emphasized, however, that Eqs. (3-9a) and (3-9b) are not generally accurate when the distribution cannot be approximated as lognormal, in which case D_g and σ_g must be computed from Eqs. (3-5) and (3-6).

The necessity of using a logarithmic scale to treat the grain-size distributions of poorly sorted river sediments cannot be overemphasized. Consider a size distribution that is half sand (0.0625–2 mm) and half gravel (2–64 mm), uniformly distributed over all sizes. A plot of the distribution versus the logarithmic scale ψ (equivalent to a logarithmic scale for D) is given in Fig. 3-17c; the corresponding plot

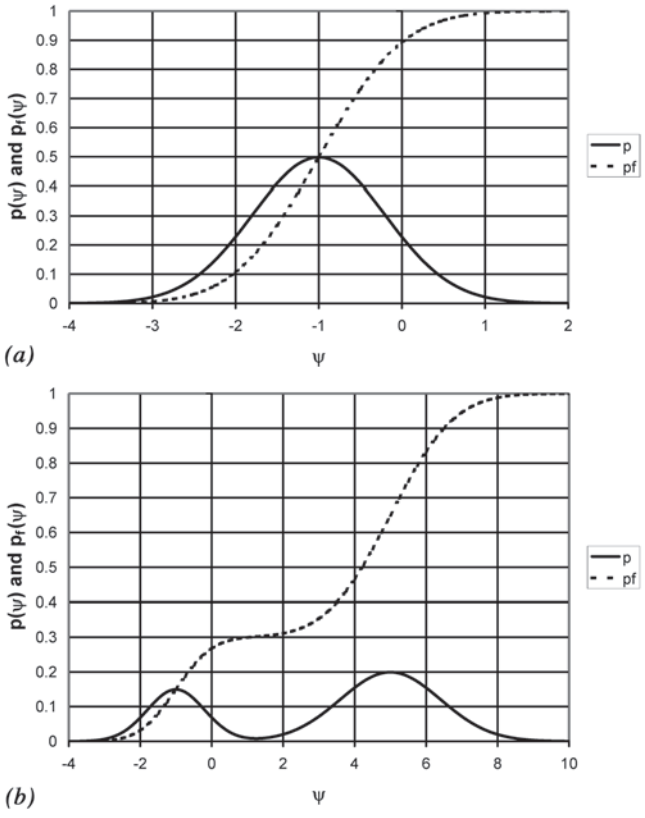

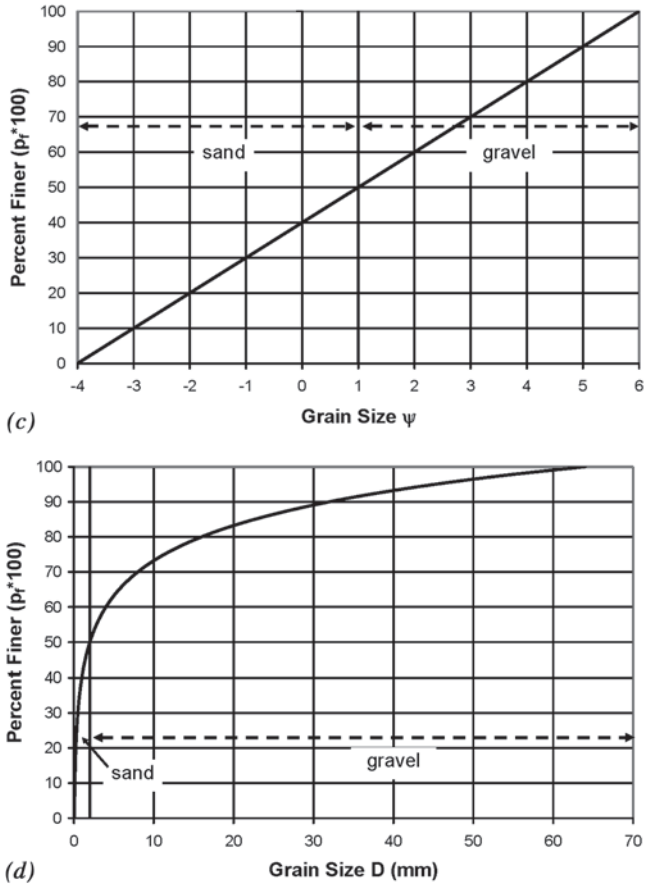

Fig. 3-17. (a) Diagram illustrating the probability density and distribution functions of a unimodal sediment sample. (b) Diagram illustrating the probability density and distribution functions of a bimodal sediment sample. (c) Plot of probability distribution function for a sand-gravel mix with constant content density as percent finer versus logarithmic grain size ψ. (d) Plot of the same probability distribution function versus D in mm on a linear scale.

using a linear scale for D is given in Fig. 3-17d. Figure 3-17c clearly reflects the fact that half of the sample is sand and half is gravel, whereas in the case of Fig. 3-17d the sand is squeezed into a tiny range on the left-hand size of the graph. The use of statistics based on D rather than any logarithmic scale for D (such as ψ) implies the computation of an arithmetic mean grain size D_m, given as

$$D_m = \int Dp(D)dD \tag{3-10}$$

rather than the geometric mean grain size D_g given from Eqs. (3-5a) and (3-6a). In the case of the distribution of Figs. 3.17c and 3.17d, the two differ substantially; D_g is equal to 2 mm, reflecting the fact that the sample is half sand and half gravel, whereas D_m is 9.25 mm, reflecting a strong bias toward the coarse material.

These comments notwithstanding, at least three bed-load transport relations for mixtures discussed in Section 3.7, proposed by Ashida and Michiue (1972), Tsujimoto (1991;

Copyrighted Materials
Copyright © 2008 American Society of Civil Engineers (ASCE)
Retrieved from www.knovel.com

CHAPTER 4

Fine-Grained Sediment Transport

Ashish J. Mehta and
William H. McAnally

4.1 INTRODUCTION

The origin of fine-grained sediment transport engineering as a component of hydraulics in the United States must be credited to the work of Hans Albert Einstein and his students at the University of California, Berkeley. Berkeley became a center of sediment transport research with Carl Gustav Gilbert of the U.S. Geological Survey, who, during the early part of the twentieth century, carried out sediment transport studies in a flume located within the Berkeley campus. These studies were conducted in response to a major sedimentation problem in the Sacramento-San Joaquin River delta and the San Francisco Bay due to the significant hydraulic mining activity in the Sierra Nevada mountains starting around the mid-nineteenth century. The bottom of the San Francisco Bay is dominated by fine sediment that is highly cohesive, and much of the early experimental work and its phenomenological interpretation for the development of transport formulas is derived from studies on that sediment.

Fine-grained sediment is generally characterized by size, composition, and plasticity. For fine-grained sediment transport, the first two are especially important and are briefly described here. For definitions related to plasticity, including the Atterberg limits see, for example, Lambe and Whitman (1969). With regard to size, Table 4-1 identifies coarse-grained versus fine-grained sediment and the degree of cohesion. Cohesion is due to electrochemical forces acting on the particle surface. Hence the degree of cohesion depends on the ratio of particle surface area to particle weight, that is, the specific surface area. Clay mineral particles, which occur in sizes less than 2 μm, and many of which are platelike, have a high specific surface area and are cohesive. In contrast, small but less platy particles with comparatively low specific surface areas do not exhibit significant cohesion. Mantz (1977), for example, showed that, with respect to incipient motion, sediment consisting of crushed silica particles in the coarse silt range showed little cohesion and behaved like sand.

In Table 4-1, observe that cohesion increases as particle size decreases (and the associated specific surface area increases). As a result, the tendency for particles to cohere and form aggregates or flocs also increases with decreasing size. An indirect and very approximate measure of the relationship between particle size and cohesion was demonstrated by Migniot (1968), who tested several natural muds and clays in a settling column and plotted the ratio of floc settling velocity to (individual) particle settling velocity against particle size (in micro-meters). He showed that this ratio increased from a little over unity at 40 μm to 300–400 at 1 μm, because with decreasing particle size and increasing cohesion the floc size increased.

With regard to fine-grained sediment composition, two properties are important to transport, namely, the inorganic mineral content and the organic content, including biochemicals. The inorganic constituent can be a clay mineral or a nonclay mineral. Clays are crystalline chemicals composed of silica (SiO_2), alumina (Al_2O_3), and water, frequently along with appreciable quantities of iron, alkalis (Na^+, K^+), and alkaline earths (Ca^{++}, Mg^{++}). Clay minerals have the property of sorbing certain anions (e.g., NO_3^-) and cations (e.g., K^+), and retaining them in an exchangeable state; i.e., these anions and cations can be removed by other anions and cations by treatment with such ions in water solution (Grim 1968).

A characteristic gauge of clay mineral cohesion is the cation exchange capacity (CEC), expressed as milliequivalents of exchangeable ion (e.g., Na^+ in terms of Na_2O, whose equivalent weight is 31 g) per 100 g of clay (Grim 1968). The higher the CEC the greater the cohesion, which causes micro-meter-sized individual clay particles to coagulate, or flocculate, in water to form much larger aggregates, or flocs, when water salinity exceeds a critical value, which depends on the clay mineral. Even though flocs are particle-formed units, they contain mostly water. For example, a floc having a density of 1,090 kg/m^3 and composed of clay particles

Table 4-1 Sediment Size and its Relation to Cohesion

Size range (μm)	Classification	Degree of cohesion
>62	Coarse-grained	Cohesionless
40–62	Fine-grained: coarse silt	Practically cohesionless
20–40	Fine-grained: coarse silt	Cohesion increasingly important with decreasing size
2–20	Fine-grained: medium and fine silt	Cohesion important
<2	Fine-grained: coarse, medium, and fine clay	Cohesion very important

of density 2,650 kg/m^3 will contain nearly 95% water by volume, locked within the interstitial particulate fabric. For descriptions of floc properties, including size, density, and strength, see for example Krone (1963), Dyer (1989), Lick and Huang (1993), and Partheniades (1993).

The (individual) particle size in terms of nominal particle diameter, CEC, and critical salinity for the three most commonly found clays—kaolinite, illite, and smectite (or montmorillonite)—are given in Table 4-2. Also given is information on chlorite, which is rarer but is found in some large estuaries, e.g., San Francisco Bay (Krone 1962). Kaolinite has the lowest CEC and exhibits the lowest degree of cohesion, whereas smectite has the highest CEC and is the most cohesive of the four, with illite and chlorite in between. As salinity increases above the critical value, floc size, density, and strength vary. However, above a salinity of about 10 ppt, its effect on floc properties is comparatively minor (Krone 1962; 1986).

Two commonly found nonclay minerals in coastal and estuarine sediments are quartz and calcium carbonate, the latter being the dominant bottom material in many biogenically active temperate waters (Bentley and Nittrouer 1997). Numerous other nonclay materials can occur; for example, sediment in San Francisco Bay contains iron flocs and organic matter (Krone 1962). Organic matter can measurably influence the electrochemical flocculation process and the composition of flocs (Dennett et al. 1998). This influence depends on the type of organic matter. Thus, for example, biopolymers can modulate floc properties through adhesive bridge formations (Wells and Goldberg 1993). Mucous filaments formed by bacteria can coat flocs and also reinforce the physicochemical bonds holding particles together (Kranck 1986; Luettich et al. 1993). McCave (1984) showed that active contributions to marine flocculation by zooplankton filtering can be significant compared to those by inorganic processes alone, and Kranck and Milligan (1980) reported that a mixture of 50% organic and 50% inorganic sediments settled an order of magnitude faster than an equivalent concentration of 100% inorganic sediment. In areas of high biodeposition, large suspended aggregates have been recorded *in situ* using a focused-beam laser (Law and Bale 1998).

Several measures of the influence of biochemicals on the erodibility of fine-grained sediment have been examined. Examples include the effects of chlorophyll-*a* (Montague et al. 1993) and colloidal carbohydrate (Amos et al. 1998; Sutherland et al. 1998) on the critical shear stress for erosion. Brief overviews of the interaction between physical and biological parameters in governing erodibility have been provided by, among others, Dade and Nowell (1991), Patterson (1997), and Black et al. (1998). Such interaction has also been examined in Couette flocculators (Drapeau and Dam 1994).

4.2 SEDIMENT CHARACTERIZATION

4.2.1 Characterization Tests

To make possible intercomparisons of transport-related data from different sites or studies, it is helpful to report values of basic sedimentary parameters that influence floc properties. Table 4-3 lists selected parameters, all of which can be determined through relatively simple and mostly

Table 4-2 Clay Minerals, CEC, and Critical Salinity for Flocculation

Clay mineral	Nominal diameter[a] (μm)	Cation exchange capacity (meq/100 g)	Critical salinity (ppt)
Kaolinite	0.36	3–15	0.6
Illite	0.062	10–40	1.1
Chlorite	0.062	24–35	—[b]
Smectite (or montmorillonite)	0.011	80–150	2.4

[a]Defined here as the diameter of a circle with the same surface area as platelike clay particles.
[b]Not reported.
Sources: Ariathurai et al. (1977); McAnally (1999).

documented laboratory test procedures. They include particle size, fall or settling velocity, sediment mineral composition, organic content, clay cation exchange capacity, and fluid salinity. These parameters are considered to be minimally essential; a much larger list has been compiled by Berlamont et al. (1993). There are, however, practical reasons for limiting the number of parameters used to identify a sediment sample. First, the actual number of parameters that determine the behavior of fine sediment in water is so large that it is currently unrealistic to come up with accurate predictive correlations between such parameters and transport-related quantities, e.g., the critical shear stress for erosion (Lee and Mehta 1994). Second, the cost of evaluating a large number of parameters is usually prohibitive for most technical studies. Finally, the six parameters chosen in Table 4-3 are considered to be adequate for a gross characterization of sediment for situations in which the transport is not overwhelmingly influenced by biochemical factors.

An early summary of work related to the erodibility of irrigation channels and agricultural lands is based on a different set of erosion-governing soil parameters including the dispersion ratio, plasticity index, and moisture content (TCECM 1968).

4.2.2 Mud Definition and Rheology

Interpretation of the information contained in Table 4-1, according to which the degree of cohesion increases with decreasing particle size, becomes complex in the natural environment, in which mixtures of sizes commonly occur. Such mixtures, or muds, are typically (although not always) cohesive due to the presence of clay minerals. Several definitions of mud are found in the literature. Most are based on the *state* of mud. However, since the *transport* of mud is of present interest, mud is best characterized by its response to an applied stress, based on its rheology. Accordingly, the following definition of mud can be useful (Mehta 2002):

> Mud is a sediment-water mixture of grains that are predominantly less than 63 μm in size, exhibits a rheological behavior that is poroelastic or viscoelastic when the mixture is particle-supported, and is highly viscous and non-Newtonian when it is in a fluid-like state.

Other noteworthy parameters are fluid temperature and pH. Temperature affects floc behavior; however, over the normal range of temperature in temperate coastal and estuarine waters

Table 4-3 Parameters for Characterization of Fine-Grained Sediment Transport

Parameters	Comments
Particle size	Use standard procedure, e.g., the hydrometer test (ASTM 1993d) or the settling column bottom withdrawal test, preferably using sediment in native water. The exception to the standard procedure is that naturally wet samples should not be air-dried initially, i.e., before the test, because of the difficulty that may occur in completely dispersing the rewetted dry sample (Krone 1962). In this case, to obtain the total weight of the sample necessary for calculations, sediment accumulated at the bottom in the cylinder or column should be collected after the test by filtration and then air-dried. If the sample contains material larger than 75 mm, use the wet-sieving method to separate the coarse fraction (ASTM 1993d). If the organic content is greater than about 10%, this test should not be performed, because, as the organic matter will not deflocculate on addition of floc dispersing agent, the resulting size distribution will not correlate with transport behavior. Instead measure the settling velocity of the untreated, i.e., nondispersed sample.
Fall or settling velocity	Obtain the characteristic relationship between settling velocity and sediment concentration or dry density of the untreated, i.e., nondispersed, sample from measurements in a multiport settling column. See McLaughlin (1959) for test procedure.
Mineral composition	Obtain types and relative quantities of the principal clay and non-clay minerals using standard X-ray diffraction tests (Whittig and Allardice 1986; Rich and Barnhisel 1977).
Organic content	Loss of sample mass on ignition is often measured for this purpose through a standard test (ASTM 1993b). Sometimes this method yields an approximate value due to the loss of structural water from the sample. An alternative is to measure total organic carbon (Walkley and Black 1934).
Cation exchange capacity	Follow standard procedure for clay minerals (ASTM 1993c; SCS 1992). If the organic content is greater than about 10%, the CEC may be excessively high, not representative of the clay constituent.
Salinity	Report salinity if less than about 10 ppt. At higher salinities the influence of salinity on floc structure is comparatively minor (Krone 1962).

the effect is usually considered small and can instead be dominated by biogenic effects. Slightly acidic waters likewise appear to increase aggregation (Tsai and Hu 1997), but pH is not highly variable in estuarine waters and thus is usually ignored (CTH 1960; Partheniades 1971). On the other hand changing soil pH can alter bed stability to a significant extent (Ravisangar et al. 2001).

Inasmuch as the above definition of mud does not depend on whether the sediment is inorganic or organic, or on such factors as the degree of cohesion or biochemical binding, it encompasses most natural muds. Muds largely composed of silt-sized material have been found to be poroelastic; that is, the internal loss of energy is characterized by Coulomb damping arising from friction between grains. For such muds Darcy's equation for water seepage through the pores is used to determine the pore pressure (Yamamoto and Takahashi 1985; Foda 1987). Most muds also include significant clay-sized fractions, and these are usually considered to be viscoelastic; in such muds internal loss is due to grain-fluid contact (Dade and Nowell 1991).

Figure 4-1 compares four rheological models of materials (continua) in terms of the rate of strain, $\dot{\gamma}$, as a function of applied shear, τ. Curve *A* is the Newtonian model, in which the dynamic viscosity, $\mu = \tau / \dot{\gamma}$, is independent of $\dot{\gamma}$. Curve *B* represents a pseudoplastic, which shows a shear-thinning behavior; i.e., μ decreases with increasing $\dot{\gamma}$. Curve *C* is the Bingham model, which represents a viscoplastic material that shows a purely Newtonian response, once τ exceeds the Bingham yield strength, τ_B. Otherwise it remains a solid. A pseudoplastic can be approximated as a Bingham plastic by extrapolation as shown, which defines what can be called the apparent Bingham yield strength, τ_y. Last, curve *D* represents a dilatant or shear-thickening response, in which μ increases with $\dot{\gamma}$. Most natural, soft muds are shear-thinning, although some seemingly show shear-thickening behavior over certain ranges of shear rate specific to the material (Faas 1995). True Bingham plastic sediments are rare in the coastal and estuarine environment, inasmuch as most soft muds creep even at very low rates of strain. However, many muds have been approximated as Bingham plastics for simplicity of treatment of their flow behavior (Krone 1963; Williams 1986; Mei and Liu 1987; Toorman 1995; Huang and Garcia 1996; 1998; 1999). On a slope over which gravity-induced bottom stress exceeds yield stress, fluid mud can creep and accumulate in downstream depressions in navigation channels and reservoirs (Ali and Georgiadis 1991; Einstein 1941).

A simple model representing the shear-thinning or shear-thickening behavior of mud is the Sisko (1958) power-law relation for the dynamic viscosity,

$$\mu = c_r \dot{\gamma}^{n_r - 1} + \mu_\infty \tag{4-1}$$

in which

c_r = consistency of the non-Newtonian fluid, and
n_r = coefficient characterizing flow behavior.

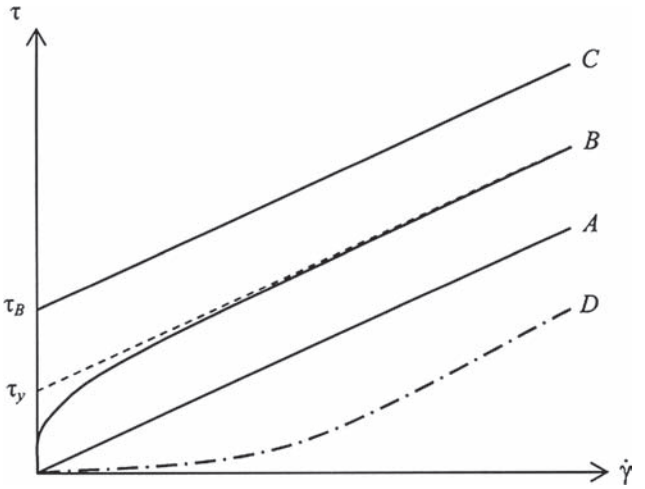

Fig. 4-1. Schematic drawing of models for the relationship between applied stress and rate of strain.

In (4-1), $n_r < 1$ corresponds to shear-thinning flow behavior, and $n_r > 1$ represents shear-thickening flow. When $n_r = 1$ the flow is Newtonian with a constant viscosity μ_∞, since in that case the consistency, c_r, is nil. At high, theoretically infinite shear rate a shear-thinning material also becomes Newtonian with a viscosity μ_∞.

Ross (1988) summarized a few studies in which μ_∞ was, empirically related to the suspension concentration, *C* (dry sediment mass divided by volume of sediment plus water), according to

$$\mu_\infty = \mu_w \left(1 + \alpha_r C^{\beta_r}\right) \tag{4-2}$$

where

μ_w = viscosity of water.

For example, for a kaolinite in fresh water, the rheometric data of Engelund and Zhaohui (1984) are commensurate with values of the coefficients $\alpha_r = 1.68$ and $\beta_r = 0.346$, when *C* is measured in kg/m^3. In general, the range of *C* over which (4-2) applies varies with the sediment, from a low 5–10 kg/m^3 to a high 400–500 kg/m^3.

Following Odd et al. (1993) and based on sediment from the Amazon and (4-1), Vinzon (1998) explicitly included the effect of concentration, *C* (kg/m^3), and the shear rate, $\dot{\gamma}$ (Hz), in the following Sisko-type relations for the kinematic viscosity, $\nu = \mu/\rho$ (m^2/s), where ρ is the fluid (nominally water) density:

$$\nu = C \exp(-0.78\dot{\gamma} - 10.24) \quad \text{for } \dot{\gamma} < 3.9 \text{ Hz} \tag{4-3a}$$

$$\nu = C \exp(-0.017\dot{\gamma} - 12.95) \quad \text{for } \dot{\gamma} \geq 3.9 \text{ Hz} \tag{4-3b}$$

Jinchai (1998) conducted rheometric tests on clayey mixtures of a kaolinite (*K*), an attapulgite (*A*), and a bentonite (which is a montmorillonite) (*B*) in fresh water and found the following relations applicable to (4-1): $\mu_\infty = 0.05\text{CEC}_s + 0.001$, $n_r = -0.033 CEC_s + 0.28$,

and $\log c_r = 0.13 CEC_s + 0.22$. The mixture cation exchange capacity, CEC_s, was defined as

$$CEC_s = f_K CEC_K + f_A CEC_A + f_B CEC_B \tag{4-4}$$

where

f = weight fraction of subscripted sediment, and
CEC = cation exchange capacity corresponding to subscript

Note that given the water content (weight of water divided by weight of sediment) f_W, we have $f_K + f_A + f_B + f_W = 1$. The selected cation exchange capacities (in milliequivalents per 100 g of sediment) were 6 for *K*, 28 for *A,* and 105 for *B*. The water content (in percent) in the tests ranged from 86 to 423, and the range of CEC_s was 1.9 to 10.4 meq/100 g.

Mud viscosity typically decreases with increasing temperature. A simple rheological model can be used to explain this trend based on the theory of momentum exchange between molecules (Krone 1983). According to this theory and data on fluids, the logarithm of μ varies linearly with the inverse of the absolute temperature.

At this point it is useful to introduce the relationship between (dry mass) concentration, *C*, and (wet) bulk density of mud, ρ. From mass balance,

$$C = \frac{\rho - \rho_w}{\rho_s - \rho_w}\rho_s \tag{4-5}$$

where

ρ_w = water density,
ρ_s = grain or particle density, and
$\phi = C/\rho_s$ = solids volume fraction (volume of solids divided by sum of the volumes of solids and water).

The three measures of sediment concentration in water, namely *C*, ρ, and φ, are frequently used in this chapter.

Starting with pure water, with increasing mud density, ρ, the state of a sediment-water mixture changes from fluid to soft solid to solid with rigidity increasing with increasing density. The transition from a fluid (mud) to a solid (bed) with an interconnected particulate matrix depends on mud composition and stress history. As a rule of thumb, the transition density ranges from about 1,150 to 1,250 kg/m^3. Since bed rigidity increases rapidly beyond about 1,250 kg/m^3, it must be included explicitly in the rheological description of mud, especially because flow curves such as those shown in Fig. 4-1 are not easily obtained for dense muds, e.g., with density exceeding, say, 1,300 to 1,400 kg/m^3 (James et al. 1988). Thus, while for a fluid mud (4-1) is a reasonable descriptor of rheology, for dense muds linear viscoelastic models are used as simplified indicators of a characteristically very complex mud rheology. Two noteworthy constitutive models are the standard solid model in Fig. 4-2a and the Kelvin or Voigt model in Fig. 4-2b (Keedwell 1984). The respective constitutive equations are as follows:

Standard solid:

$$\tau + \frac{\mu}{G_1 + G_2}\dot{\tau} = \frac{G_1 G_2}{G_1 + G_2}\gamma + \frac{\mu G_1}{G_1 + G_2}\dot{\gamma} \tag{4-6}$$

Voigt:

$$\tau = G\gamma + \mu\dot{\gamma} \tag{4-7}$$

where

μ = viscosity,
G_1, G_2, and G = shear moduli of elasticity,
τ = shear stress,
γ = strain, and the dot over γ signifies the time derivative.

Thus we note that the standard solid model is a combination of a Hookean solid element (i.e., an elastic spring of rigidity, or storage modulus, G_2) and a Newtonian fluid element in parallel, with an additional Hookean element of rigidity G_1 in series. Setting $G_1 \to \infty$ and $G_2 = G$ results in the Voigt model, a special case of the standard solid. If now *G* is set equal to zero, a Newtonian fluid element ensues. For fluid

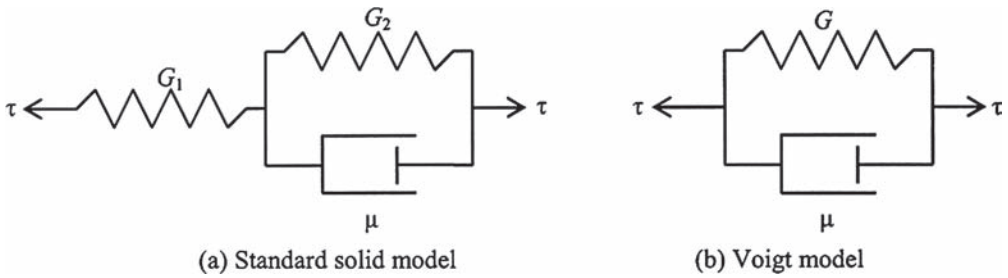

Fig. 4-2. Two linear viscoelastic models: (a) standard solid model; (b) Voigt model.

muds, viscoelasticity has been represented by the Maxwell (fluid) element, which includes a Hookean element and a Newtonian element in series (Li 1996).

Cyclic loading by the action of water waves on mud beds is a means by which loss of structure and rigidity occur, which in turn can lead to the generation of fluid mud. By embedding a miniature rheometer capable of measuring the speed of a high-frequency shear wave through the material, the change in rigidity with time following the inception of water wave motion can be determined. Thus, for example, for a Voigt solid it can be shown that G is approximately equal to ρV^2 where ρ is the material density and V is the shear-wave velocity (Mehta et al. 1995). Hence, by tracking the change in V in a constant density mud, the corresponding change in G can be estimated. In Fig. 4-3, the ratio $V(t)/V(0)$ is plotted against time, t; $V(0)$ being the initial value of the shear-wave velocity $V(t)$ at the onset of wave action. This laboratory result is for a clayey bed composed of an aqueous mixture of a kaolinite and an attapulgite of equal weight (AK in Table 4-4). The bed density was 1,170 kg / m, the mean water depth over the bed was 19 cm, and the monochromatic water wave amplitude was 2 cm at a frequency of 1 Hz. The initial rigidity $G(0)$ was 4,680 Pa; however, in association with a drop in V, within the first half hour the rigidity decreased by 44%.

Determination of the coefficients in viscoelastic models, e.g., (4-6) and (4-7), requires a combination of creep and dynamic shear tests, ideally in a controlled-stress rheometer, in which mud response to stress can be measured directly (James et al. 1987, 1988; Jones 1997). Thus, for example, Jiang and Mehta (1995) found that all the muds they tested in this way and fit to (4-6) showed the coefficients μ, G_1 and G_2 to vary with the frequency of the forcing (small-amplitude) stress wave. This dependence suggests that (4-6) did not truly represent the rheology, since in that case the coefficients would be independent of frequency. Equation (4-6) therefore must be treated as an operational (rather than theoretically correct) model. The coefficients were found to be related to frequency f (Hz) according to

$$G_1,\ G_2,\ \mu = \exp(\alpha_{rh}) f^{\beta_{rh}} \tag{4-8}$$

For muds characterized by particle size and constituents in Table 4-4, values of coefficients α_{rh} and β_{rh} are given in Table 4-5. The range of frequency, f, was 0.02 to 40 Hz. Over such a wide frequency range mud response to dynamic loading may be further complicated by thermodynamic effects, inasmuch as while at low frequency the energy dissipation process is thought to occur isothermally, with increasing frequency the process becomes increasingly adiabatic (Krizek 1971).

In general, given the inherent limitations of the standard solid model and its application through (4-6) and (4-8), it has been found reasonable to simplify the rheological description of mud by treating it as a Voigt solid. In this case, characterization of the coefficients in rheometric tests is less cumbersome (Chou 1989; Maa and Mehta 1988).

In Tables 4-4 and 4-5, the effect of sediment composition on the viscoelastic parameters can be qualitatively gaged from the observed variability in the coefficients values. Also, for the Mobile Bay mud (MB), the effect of density can be evaluated. This is shown in Table 4-6, in which μ and G_2 are calculated for a representative frequency, $f = 0.1$ Hz. For comparative purposes, the additional contribution from G_1 to the constitutive behavior may be ignored. Observe the rapid increase in the values of μ and G_2 with an increase in ϕ from 0.07 to 0.17.

The description of rheology provided thus far is limited to the effect of shearing the material by the application of a tangential stress. Under wave action, mud also undergoes cycles of compression and tension, for which models representing what is called extensional or elongational rheology are essential (Barnes et al. 1989). In simple dynamical systems, e.g., a viscoelastic element undergoing forcing by

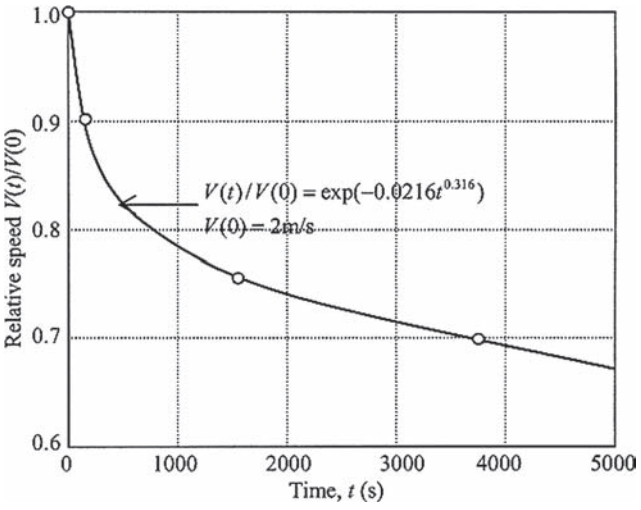

Fig. 4-3. Time variation of relative shearwave velocity (adapted from Mehta et al. 1995).

Table 4-4 Properties of Mud used in Rheometry

Mud type	Median size(μm)	Principal constituents
Kerala, India (KI)	2	Montmorillonite, kaolinite, illite, gibbsite, organic matter (5%)
Okeechobee, Florida (OK)	9	Kaolinite, sepiolite, montmorillonite, 40% organic matter
Mobile Bay, Alabama (MB)	15	Clayey silt of undetermined composition, sand
Attapulgite + kaolinite (AK)	1	Attapulgite (50%) + kaolinite (50%)

Source of data: Jiang (1993); Jiang and Mehta (1993).

Table 4-5 Values of Coefficients in (4-8) for Muds of Table 4-4

Mud	Solids weight fraction, ϕ	G_1 (Pa)		G_2 (Pa)		μ (Pa.s)	
		α_{rh}	β_{rh}	α_{rh}	β_{rh}	α_{rh}	β_{rh}
KI	0.12	9.160	0.257	3.843	−0.405	9.292	−0.405
OK	0.11	5.548	0.127	0.318	−0.687	5.290	−0.687
MB	0.07	3.659	0.030	−1.439	−0.975	3.165	−0.975
MB	0.11	6.352	0.075	2.139	−0.745	6.695	−0.745
MB	0.17	8.274	0.108	3.864	−0.696	8.374	−0.696
AK	0.12	8.049	0.114	2.604	−0.490	8.222	−0.490

Source of data: Jiang (1993); Jiang and Mehta (1993).

Table 4-6 Parameters μ and G_2 for Muds of Table 4-4 at Frequency $f = 0.1$ Hz

Mud	ϕ	μ (Pa s)	G_2 (Pa)
KI	0.12	2.76×10^4	1.19×10^2
OK	0.11	9.65×10^2	6.68×10^0
MB	0.07	2.24×10^2	2.24×10^0
MB	0.11	4.49×10^3	4.72×10^1
MB	0.17	2.15×10^4	2.37×10^2
AK	0.12	1.15×10^4	4.18×10^1

Source of data: Jiang (1993); Jiang and Mehta (1993).

normal stress with strain assumed to be important only in the direction of applied stress, it can be shown that the extensional viscosity and elastic modulus are related to their shear counterparts defined by (4-7). Given such relations, shear rheometry can be used to determine the extensional coefficients. Such a model has for example been used to calculate the thickness of the fluid mud layer generated by water waves (Li and Mehta 2001).

4.3 SEDIMENT TRANSPORT PROCESSES

4.3.1 Concentration Profile

The classification of fine-grained sediment transport processes is facilitated by a qualitative description of the vertical profile of the sediment-water mixture concentration or density, as shown in Fig. 4-4. In this description, the term "mobile" means moving horizontally. In contrast, "stationary" implies not moving horizontally. Starting from the water surface, in the top layer the sediment is well-mixed and mobile. In this layer the concentration is so low that fluid rheology is practically Newtonian; i.e., the viscosity is independent of the concentration and the rate of flow shear. The flocs settle independent of each other in the *free settling* mode, with a fall or settling velocity that is independent of concentration, because the frequency of interparticle collisions is so low that collision outcomes leading to agglomeration or aggregation of particles and flocs are sparse (Krone 1962). The concentration profile is relatively smooth, and turbulent mass diffusion is practically neutral; i.e., upward diffusion of sediment is not significantly influenced by buoyancy stabilization due to the concentration gradient.

Below the mixed layer the suspension is initially nearly Newtonian and has been called concentrated benthic suspension (CBS) (Toorman 2001). With increasing depth the suspension becomes increasingly non-Newtonian as the concentration increases, and concurrently the frequency of interparticle collisions increases. The settling velocity usually increases with increasing concentration as the flocs become larger in the *flocculation settling* mode. Upward mass diffusion due to turbulence is retarded by the concentration gradient due to the negative buoyancy of the suspension. Coupling between concentration-dependent settling velocity and concentration-gradient-dependent diffusion leads to the formation of a stratified structure of the concentration

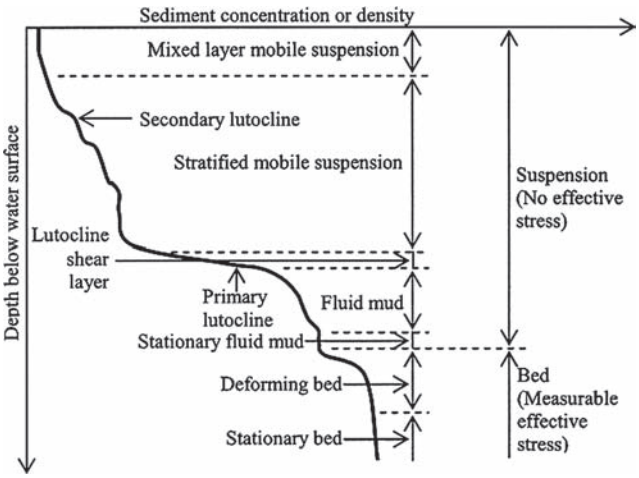

Fig. 4-4. Classification of the vertical profile of sediment concentration (or density).

profile with vertical gradients called secondary lutoclines, which occur above what is called the primary lutocline. A lutocline is a sediment-induced pycnocline (Kirby and Parker 1977; Parker 1987). Its occurrence manifests as a steplike structure of the concentration profile. The primary lutocline occurs near the base of the stratified mobile suspension. This concentration gradient encompasses a shear layer that resembles the boundary layer above a rigid bed, with high shear production and energy dissipation. However, unlike a rigid bed, the "bottom" below the primary lutocline tends to have fluidlike consistency and is dragged by the flow above. Thus the flow velocity does not become zero at the lutocline, but at some depth below it. An important feature of the primary lutocline, in contrast to the usually less stable secondary lutoclines, is that it can persist even under significant flow-induced forcing. This persistence is due to the inability of the turbulent flow to dissipate the lutocline easily by mixing, as a result of the high degree of buoyancy stabilization from the sharp concentration gradient and the inability of the material below the lutocline to fall rapidly due to *hindered settling*. In this mode the settling flux decreases as the concentration increases with depth. Hindered settling is due to the low permeability coupled with increased buoyancy and viscosity of the sediment-water mixture, hence the inability of the interstitial water to easily escape upward.

The layer below the lutocline shear layer is commonly called fluid mud, which is mobile because it tends to move horizontally due to forcing by the flow above. Within fluid mud turbulence is heavily damped and may even collapse completely when a certain threshold concentration is exceeded (Winterwerp 1999), and the base of this layer is defined by the zero mean velocity plane. Below this plane, mud, having a low permeability, may still occur in a fluidlike state but remains stationary; i.e., within it there is practically no horizontal movement. The thickness of the fluid mud layer depends on the type, magnitude, and duration of forcing by tides and waves, on the availability of sediment, and to some extent on its composition. Whereas in low-suspended-sediment-concentration (e.g., a few tens of milligrams per liter at the most) and low-energy (e.g., microtidal sea and calm weather) environments fluid mud is often absent or forms thin layers, in highly energetic environments such as the Amazon estuary it can be several meters thick. In low-energy areas it is often generated episodically when storm waves and surges occur.

A fine-grained sediment bed, which has a very low permeability in comparison with that of a silty or sandy bed, can be differentiated from the suspension above by the effective normal stress, which is practically nil above the bed surface and increases below it with increasing concentration. This stress is the result of interparticle contact within the structured matrix of the bed. The upper part of the bed may undergo time-dependent deformations due to oscillatory water motion by waves for example, whereas the bed below remains stationary.

4.3.2 Unit Transport Processes

The description presented in Fig. 4-4 is an instantaneous one, because the concentration profile, along with the elevations and thicknesses of the various layers, changes continuously as the forcing changes. Thus, for example, due to continued deformation the bed particulate matrix can break up and generate fluid mud. Fluid mud can entrain sediment and raise the turbidity of the upper water column. Upon cessation of forcing by a current or waves, the water column will be clarified, and if the system remains disturbed, clear water and a hardened bed will eventually result. Such changes can be predicted provided we specify all relevant vertical and horizontal sediment transport fluxes. Since the horizontal transport load strongly depends on the vertical sediment transport mechanisms, we will identify the vertical *unit transport processes* (in qualitative analogy with the terminology once coined at MIT for chemical engineering processes) and fluxes that must be modeled to calculate the horizontal sediment load.

Consider the simplified concentration (or density) profile description shown in Fig. 4-5. Also shown is the horizontal velocity profile. At the boundary between (mobile) fluid mud and (mobile) suspension, sediment entrainment and settling fluxes must be specified. Entrainment of fluid mud depends on turbulent energy resulting from eddy generation in the boundary layer. In this process, the lutocline interface becomes destabilized, interfacial wave generation and breaking occur, and the lower fluid, with its higher sediment content, is ejected into the upper fluid, where sediment concentration increases. The entrained material is then carried above the lutocline by turbulent diffusion. At the bed surface marking the lower level of the fluid mud layer, the bed can undergo erosion, its rate depending on the magnitude of the flow-induced bed shear stress. Bed erosion occurs either by a gradual dislodgement and entrainment of the flocs at the bed surface, or by a more traumatic Mohr-Coulomb type failure of a sizeable thickness of the bed (Lambe and Whitman 1969) and subsequent, relatively rapid entrainment of the failed material. The former process is called surface erosion and the latter mass erosion. Once the material is entrained it can fall by gravitational settling, the settling flux depending on the settling velocity and sediment concentration. For a given settling velocity and concentration, the sediment deposition flux onto the lutocline or the bed is the highest when there is no flow, and decreases as the flow-induced bed shear stress increases. Deposition involves a sorting process by which heavier and stickier particles/flocs that arrive close to the bed by settling become attached to the bed, whereas the remaining material stays in suspension, or elastically rebounds upward from the bed surface (McAnally 1999). The fraction of depositable material decreases with increasing bed

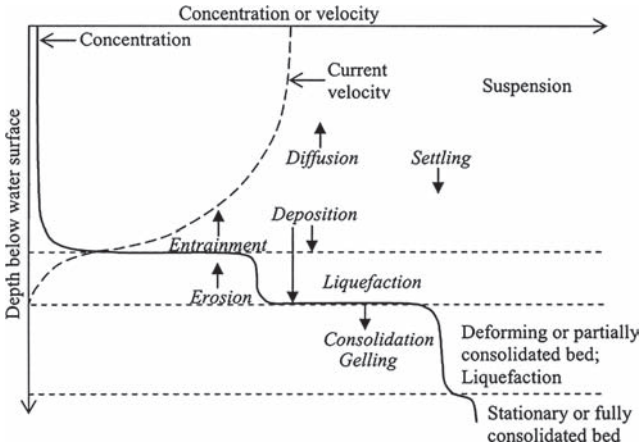

Fig. 4-5. Unit transport processes governing sediment concentration (or density) profile dynamics.

shear stress, and above a certain shear stress practically no deposition occurs. When the rate of deposition is high, fluid mud can form because settling is hindered. At low rates of deposition, in case no fluid mud initially exists between the water column and the bed, the settling sediment may deposit to form a bed without generating fluid mud inasmuch as the rate of consolidation is greater than the rate of deposition.

Waves can loosen the bed and generate fluid mud. Technically, liquefaction is considered to occur due to breakup of the soil matrix by shear stresses, while the process of breakup due to excess pore pressure buildup is called fluidization (Toorman 2001). For simplicity, the term liquefaction will be used here, and will be considered to occur by stresses due to pore pressure gradients and associated flows within the bed, which weaken and eventually disrupt the soil matrix. This process manifests itself as a gradual disappearance of the effective normal stress, which becomes practically nil when fluid mud is generated. Once wave action ceases, fluid mud starts to dewater and reform as bed. Dewatering of fluid mud or a partially consolidated bed is described by hindered settling and consolidation. Consolidation is also accompanied by gelling due to rearrangement of water molecules within the pores.

In the above description, the identifiable unit transport processes include settling and deposition, consolidation and gelling, erosion and entrainment, and upward diffusion of eroded/entrained sediment. These processes are considered further in this chapter following a brief description of the particle and floc aggregation processes that govern particle/floc size, density, and strength.

4.4 AGGREGATION

4.4.1 Floc Transport

Figure 4-6 illustrates the concept of a fine sediment particle or a floc undergoing the process of aggregation, defined as the set of mechanisms by which floc size, density, and strength change due to flow-particle (or flow-floc) and particle-particle (or floc-floc) interactions. A particle, either an individual grain or a floc of many grains, may originate in the water column or in the bed. Once in suspension, it is subjected to forces due to gravity, inertia, mean flow, turbulent fluctuations, and collisions with other particles in suspension. It may undergo aggregation in the water column, bonding with other particles and breaking apart from them. If the floc grows large enough, it settles toward the bed and can be considered to enter a notional "stirred layer" of high sediment concentration and high shear (Mehta 1991). There it may be deposited on the soft mud layer and eventually become part of the bed, or it may be broken into smaller particulate units and be picked up by the flow and begin the process anew (McDowell and O'Connor 1977).

Aggregation of individual grains into larger, multiple particle units occurs when a collision brings two particles close enough together for mutually attractive forces to overcome repulsive forces, and the two particles bond as a result of those attractive forces. Similarly, fluid forces and collisions exceeding floc strength will break flocs apart. The forces acting on waterborne fine particles include the following fluid and particle forces (Krishnappan 1990; McAnally 1999).

Fluid forces:

1. Brownian motion: Thermal motion of fluid molecules causes collisions between the molecules and individual particles, imparting "kicks" that move the particles in random directions.
2. Normal stresses: Small-scale turbulent eddies cause pressure forces that, like Brownian motion, impart random motion to particles of size similar to the eddies.
3. Shear stresses: Both laminar and turbulent shear flows impose tangential stresses on particles that are of the

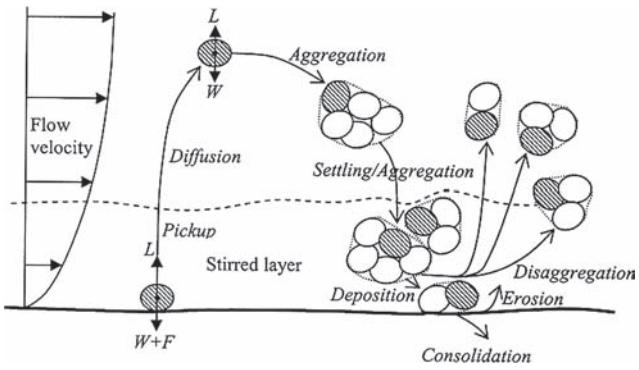

Fig. 4-6. Schematic drawing showing transport and aggregation of cohesive sediment particles or flocs. L = lift force, W = particle submerged weight, and F = cohesion (adapted from McAnally 1999).

same size order as the distance over which the velocity changes significantly.

4. Mean flow drag: Any difference between the mean flow velocity and the particle mean velocity will result in a drag force due to pressure and frictional forces.

Particle forces:

5. Van der Waals attraction: Generated by mutual influence of electron motion within the particles, van der Waals forces act between all matter and are extremely strong, but decay very rapidly (from the 3rd to the 7th power) with distance, so particles must be very close together before the forces exert a significant influence.
6. Electric surface attractions and repulsions; The surface electrical charges of fine particles induce both attractive and repulsive forces between two similar particles.
7. Collisions; Colliding particles impart forces and torques on one another.

Other forces:

Once two or more sediment particles bond together, additional forces may act on them, including chemical and biochemical cementation and biopolymeric binding, and forces due to pore fluid motion at extremely small scales. Such forces require explicit consideration in theories meant to simulate natural aggregation (Hill 1992; Hill et al. 1992; Hill and Nowell 1995).

The electrical forces include predominantly negative surface charges of most fine sediment grains (exceptions are some metal hydroxides that have positive face charges and negative edge charges), which give most fine sediment grains a net negative charge. This charge induces a repulsive force between two similar grains. If the overall repulsive force is reduced and the positive edge of one grain approaches the negative face of another, the two grains may bond in a T-formation. The overall charge of a grain attracts a cloud of opposite-charge ions if they are available in the surrounding fluid. The cloud of ions, called the Gouy double layer, balances the grain's net charge and represents an equilibrium in the ion field between electrical attraction toward the grain and diffusion away from it. The double layer exerts a repulsive force on other like-charged grains and their double layer, just as the net charge does, and also extends outward some distance to keep grains farther apart. These electrical forces are weaker than the van der Waals force, but decay more slowly with distance, so they dominate the net force between grains unless other processes come into play as discussed below. In a fluid with abundant free ions the double-layer thickness is suppressed, reducing the distance over which the repulsive forces act and permitting grains to approach more closely. The electrically neutral unit consisting of a mineral grain and its double layer is called a clay micelle (van Olphen 1977).

In nearly ion-free water the net grain charge keeps the clay micelles, and hence the cohesive grains, apart, and only those collisions bringing an edge (typically positive) directly to an oppositely charged face can bring the two close enough together to allow the van der Waals forces to bind them in an edge-to-face configuration. Adding only a few free ions (for example, by dissolving salt in the fluid) creates large ionic double layers and retards aggregation by repelling grains at larger spacings, but at some higher ionic concentration the double layer's diffusion is suppressed and it shrinks, permitting closer approach between grains and collisions that overcome the faces' electrical repulsion so that the short-range van der Waals forces can bind them face-to-face.

Under low ionic concentrations, floc structures can be likened to houses of playing cards with large pore spaces, low density, and low strength, because the edge-to-face connection puts only a few molecules within the range of the attractive forces. Such flocs commonly occur in freshwater lakes. At the higher dissolved-ion concentrations of upper estuaries and some rivers, the orientation of aggregated grains tends toward face-to-face contacts and most often resembles a deck of cards that has been messily stacked. With larger contact areas and shorter moment arms, such structures are significantly stronger than those formed by edge-to-face orientation (Burban et al. 1989; Parchure 1984).

4.4.2 Order of Aggregation

Based on tests on estuarine sediments, Krone (1963) inferred a conceptual model of floc structure. In this model, initial aggregation creates small, compact flocs of primary grains with strong bonds, referred to as "zero order aggregates," designated *p*0*a* in Fig. 4-7. Subsequent collisions between zero order aggregates create slightly weaker bonds between two or more of these aggregates, leading to an assemblage of *p*0*a*'s, a particle aggregate-aggregate, or first order aggregate, *p*1*a*.

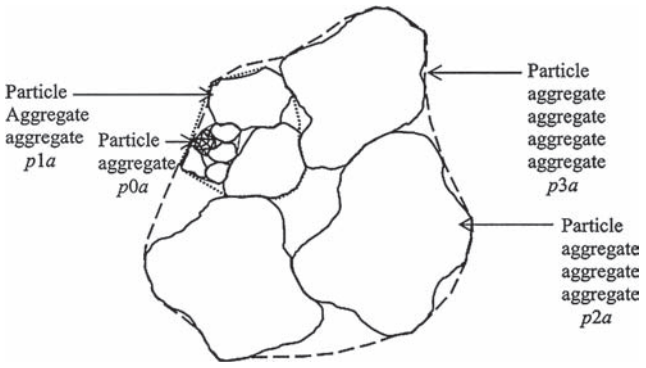

Fig. 4-7 Idealized floc structure depicting orders of aggregation.

Successive levels (orders) of aggregation lead to particle aggregate-aggregate-aggregates *p2a*, then *p3a*, and so on.

Based on rheometric experiments with sediments from five locations covering the U.S. Atlantic, Gulf of Mexico, and Pacific coasts, plus one inland river, Krone (1963) calculated up to 6 orders of aggregation with corresponding densities and strengths for each. As an example, results for San Francisco Bay sediment are given in Table 4-7. These properties refer to sediment in suspension. When the material deposits, overburden, gelling, and consolidation alter floc properties. As a result, there is only a remote connection between the density and strength of the suspended flocs and the erodibility of flocs at the bed surface, especially after the bed has aged following its formation by sediment deposition.

4.4.3 Fractal Description

The floc model of Krone (1963), which assigns discrete structures to flocs, is notionally compatible with models of floc structure based on the fractal principle (e.g., Meakin 1988; Kranenburg 1994a; Winterwerp 1998; 1999). The basic model, which has long been used in wastewater treatment research, assumes that floc structure approximately conforms to the fractal property of geometric self-similarity. Self-similar structure leads to a power-law relationship between floc size and properties such as density and surface area. Thus, for example, the relationship between diameter and density for a three-dimensional floc can be expressed as

$$d_f = \sigma_f \rho_f^{1/(n_f-3)} \tag{4-9}$$

where

d_f = floc diameter,
ρ_f = floc density, and
n_f = fractal dimension.

Table 4-7 Characteristics of Aggregate Orders of San Francisco Bay Sediment

Order of aggregation	Floc density[a] (kg/m^3)	Floc strength (Pa)
0	1,269	2.2
1	1,179	0.39
2	1,137	0.14
3	1,113	0.14
4	1,098	0.082
5	1,087	0.036
6	1,079	0.020

[a]In sea water of density 1,025 kg/m^3.
Source: Krone (1963).

The proportionality constant σ_f depends on the sediment and fluid properties. For example, Tambo and Watanabe (1979) report a range of 0.0002 to 0.0012, when d_f is measured in cm and ρ_f in g/cm^3.

For bodies in three-dimensional (Cartesian) space, $1 \leqslant n_f \leqslant 3$. For a nonfractal solid sphere, n_f has a value of 3. Wiesner (1992) showed that for aggregation due to Brownian motion, an irreversible process, n_f should be about 1.78. For reversible processes such as flow shear-induced collisions, it should be about 1.9 to 2.1. He noted, however, that for distinct scales of structure, such as Krone's order-of-aggregation model, each scale may be characterized by a different fractal dimension and the overall apparent dimension will be larger, perhaps 2.1 to 2.6 for a second order aggregate (*p2a*) structure. Kranenburg (1994a) noted that it would be inappropriate to assume that the complex, multicomponent structure of real muds possesses completely self-similar geometry. He concluded that muds are probably only approximately self-similar, but that the concept seems useful in interpreting experimental results. These observations have been supported by experimental evidence (Winterwerp 1999); however, from field data Manning and Dyer (1999) reported that there was more variation in floc density for the same floc size than suggested by the fractal model.

4.4.4 Floc Strength

Floc strength, i.e., resistance to breakup or disaggregation, is a function of cohesion, size, and orientation of particles within the floc and organic content (Partheniades 1971; Wolanski and Gibbs 1995), and to a lesser extent depends on salinity and pH (Raveendran and Amirtharajah 1995). Experimental results (e.g., Krone 1963; Hunt 1986; Mehta and Parchure 2000) show that as floc size and organic content increase, floc density and strength decrease. Partheniades (1993) reported that Krone's (1963) data for floc strength fit the expression

$$\tau_f = \alpha_c \Delta\rho_f^{\beta_c} \tag{4-10}$$

where

τ_f = floc strength (in Pa),
$\Delta\rho_f = \rho_f - \rho_w$ (in kg/m^3),
ρ_w = water density, and
α_c, β_c = empirical coefficients, e.g., 1.524×10^{-7} and 3, respectively, for San Francisco Bay sediment.

The fractal model of Kranenburg (1994a) results in a floc strength that follows Eq. (4-10), with $\beta_c = 2/(3\text{-}n_f)$. Kranenburg noted that his expression brackets Krone's (1963) data for $n_f = 2.1$ and 2.3.

Logically, for given sediment, floc density should be a function of the shearing intensity, sediment concentration and salinity. In practice, it is usually inferred from measured floc size and settling velocity, assuming free settling

and Stokes' law. Empirically, the relation $\Delta\rho_f = \alpha_{cd} d_f^{-\beta_{cd}}$ is found to hold on a very approximate basis. For San Francisco Bay sediment, Kranck and Milligan (1992) and Kranck et al. (1993) reported $\alpha_{cd} = 35{,}000$ and $\beta_{cd} = 1.09$, when d_f is measured in μm. These coefficients hold in the range of d_f approximately between 100 and 1,000 μm. For Chesapeake Bay sediment Gibbs (1985) found $\beta_{cd} = 0.97$, which is close to the value of Kranck et al.

4.4.5 Floc Size, Concentration, Turbulence, and Shear Stress

In Eq. (4-9), d_f may be considered to be the mean floc diameter. In addition, other statistical measures of size and their relationships with other parameters have been proposed. For example, Kranck (1986) and Kranck and Milligan (1992) noted that despite the dramatic shift in the particle size spectra due to coagulation of individual (i.e., dispersed) particles into flocs, a relationship was found between the modal floc size and the corresponding modal (individual) grain size. This was the case because the following equation could be fit to both individual particle spectra and floc spectra, with suitable adjustments of the coefficients:

$$C_v = C_{v0} d_f^{\xi} \exp\left(-\kappa_f \zeta d_f^2\right) \tag{4-11}$$

where

C_v = volume concentration of sediment in any one size class, i.e., volume of sediment divided by volume of suspension,
C_{v0}, ξ, κ_f = sediment-specific coefficients,
$\zeta = g(\rho_f - \rho_w)/8\nu\rho_w$,
g = acceleration due to gravity, and
ν = kinematic viscosity of fluid.

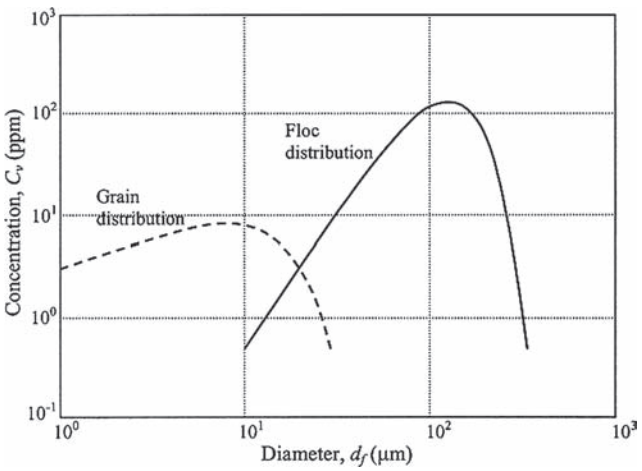

Fig. 4-8. Examples of Eq. (4-11). Dashed curve shows dispersed grain size distribution and continuous curve is for flocs (based on (Kranck 1986; Kranck and Milligan 1992).

Note that ζd_f^2 is the Stokes settling velocity. Examples of the fit of (4-11) are shown in Fig. 4-8 for (dispersed) grain size distribution and floc size distribution. Values of C_{v0}, ξ, κ_f, ν, ρ_f, and ρ_w are based on the work of Kranck (1986) and Kranck and Milligan (1992). The respective set of values are 3.123 ppm, 0.608, 0.0055 s/μm, 10^{-6} m^2/s, 2,650 kg/m^3, and 1,000 kg/m^3 for dispersed grain distribution, and 0.001 ppm, 2.72, 0.00081 s/μm, 10^{-6} m^2/s, 1,200 kg/m^3, and 1,000 kg/m^3 for floc distribution. From settling tests using a flocculated marine glacial mud, Kranck (1986) reported wide-ranging values of C_{v0}, ξ_f, and κ_f.

It is feasible to obtain a simple formula relating the median floc size to sediment concentration and turbulence (Galani et al. 1991; Lick et al. 1992): Winterwerp (1998) derived expressions for the equilibrium floc size resulting from a balance between floc formation and breakup, and also the maximum or limiting floc size in a given flow-sediment field. In the latter context, Krone (1963) proposed the following relation for the limiting size:

$$d_{flim} = \frac{2\tau_f \Delta R}{\mu_w \dot{\gamma}} \tag{4-12}$$

where

τ_f = floc strength,
μ_w = viscosity of water,
$\dot{\gamma}$ = local flow shear rate, and
ΔR = interpenetration distance for two colliding flocs.

Assume a moderate flow shearing rate (i.e., the vertical gradient of the horizontal flow velocity) of 10 Hz and a first order aggregate of San Francisco Bay sediment with a strength of 0.39 Pa (Table 4-7). Krone (1962) suggested 2 μm to be a

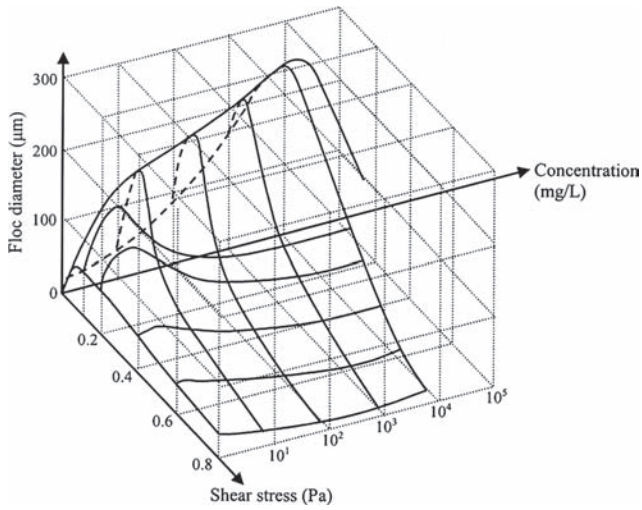

Fig. 4-9. Diagram showing the relationship between floc diameter, suspended sediment concentration and shear stress (after Dyer 1989).

reasonable value of ΔR. Substituting these values into Eq. (4-12) along with $\mu = 0.001$ Pa s gives $d_{flim} = 156$ μm.

On a graphical basis, from an analysis of data on modal floc sizes from a variety of experiments Dyer (1989) developed the plot of Fig. 4-9 relating the modal (equilibrium) floc size to suspended sediment concentration and shear stress. From a statistical mechanical representation of two- and three-body collision mechanisms between particles and flocs sorted out by size classes for sediment from the San Francisco Bay, McAnally (1999) developed a plot relating the equilibrium diameter (actually diameter at time equal to the 99.9% of the time required to reach full equilibrium), the suspended sediment concentration, and the local rate of energy dissipation in the fluid. The plot showed a qualitative resemblance to Fig. 4-9.

4.4.6 Modes of Transport

Referring to Fig. 4-6 we note that the pickup and deposition of particles or flocs must inherently follow a transport regime somewhat different from that for cohesionless grains. Let us represent cohesion simply by a representative force F, which binds the cohesive particle to the bed. Also, let us assume that the entraining force is represented solely by the hydrodynamic lift L, i.e., excluding any contribution from drag. Accordingly, the condition for incipient entrainment will be $L / (W + F) \geq 1$, where W is the buoyant weight of the particle. On the other hand, the condition for deposition of a suspended particle will be $L / W < 1$.

Following the classical derivation of the bed load function by Einstein (1950), in which bed load is obtained under the condition of equality of number flux (i.e., number of particles per unit bed area per unit time) of entraining and depositing cohesionless particles, Partheniades (1977) examined the transport of cohesive particles. He showed that, under the assumption of L fluctuating (due to turbulence) between an upper and a lower bound (as opposed to Einstein's boundless Gaussian distribution), cohesion (F) precludes, in general, the development of a bed load function, and hence bed load transport. This is so because under this scenario, for instance, deposition can occur exclusively, i.e., without corresponding erosion of bed. In other words, he showed that cohesive sediment is characteristically transported in suspension, rather than as bed load. This transport can occur either as bed material load or as wash load. As for the latter mode, lightweight organic detritus is often transported as wash load through rivers and tidal waters where currents are strong. In quiescent basins where currents become weak this material may be deposited and if so, would be reclassified as bed material load. It is essential to point out, however, that cohesive materials often form balls or pebbles (e.g., Jacinto and Le Hir 2001), and these comparatively hard particles have distinct and durable forms that can be transported as bed load; i.e., their transport can be represented in a large measure by a bed load function derived for coarse sediment transport, when such "particles" occur in sufficiently large numbers per unit bed area.

To support his argument regarding the mode of transport of cohesive sediment, Partheniades (1977) used evidence from steady flow experiments on the deposition of initially suspended kaolinite in a flume. He showed that the variation of suspension concentration with time during deposition could be explained only if it was assumed that no erosion of the deposited material occurred during the depositional process. The main observation that supported this inference was that up to a fairly high suspension concentration, on the order of 25 kg/m^3, the sediment-carrying capacity of the flow was found to be independent of flow velocity; being dependent, instead, on how much sediment was externally introduced into the suspension. Later, Parchure (1984) showed that his steady-flow experimental results on the erosion of a variety of cohesive beds could be explained provided it was assumed that no deposition of the eroded sediment occurred. This inference was mainly based on the observation that at steady state, if the suspension was replaced by clear water without stopping the flow, no significant erosion subsequently occurred. Lick (1982), however, based his erosion rate expression on the assumption of continuous exchange, citing his own experimental evidence for simultaneous deposition and erosion.

Notwithstanding the analysis of Partheniades (1977), which relies on the single grain size analysis of Einstein (1950), the issue of whether erosion and deposition are "mutually exclusive" does not appear to have been fully resolved. The difficulty seems to be due largely to the nature of the experiments that have been conducted thus far; almost all based on relatively simple laboratory setups in which it has not been possible to "observe" particle transport close to the bed. In every case the behavior of particles with regard to near-bed entrainment and deposition has had to be inferred from essentially indirect evidence. For example, by tagging part of the initially suspended sediment with radioactive gold and comparing the rate of deposition of tagged sediment with that of untagged sediment sampled at mid-depth (rather than close to the bed surface, which is typically ill-defined and unidentifiable during deposition), Krone (1962) indirectly inferred that some of the deposited material had seemingly reentrained during the predominantly depositional process.

The question of bed sediment exchange becomes especially important in modeling sediment transport under oscillatory flows, due both to tides and to waves. Whereas in his modeling of tide-induced transport Hayter (1983) assumed mutually exclusive erosion and deposition, Jiang (1999) considered continuous exchange. Similarly, in wave-induced transport modeling, Maa (1986) assumed continuous exchange. Sanford and Halka (1993) showed that in situ measurement of resuspension of fine sediment in the Chesapeake Bay could be better modeled by assuming continuous exchange than by assuming nonsimultaneous erosion/deposition. On the other hand, Teeter (2001b) argued for nonsimultaneous exchange, citing the need to model sediment sorting

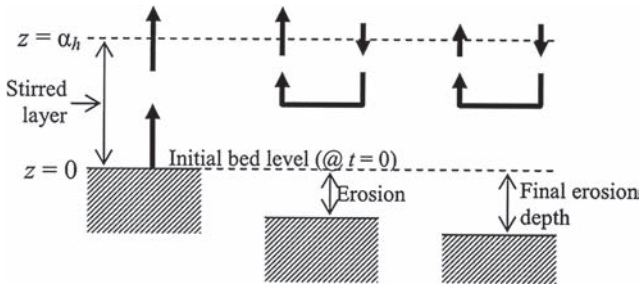

Fig. 4-10. Schematic description of vertical sediment fluxes (arrows) in the stirred layer actuated by bed erosion (adapted from Cervantes et al. 1995). Reproduced with permission of PIANC-COPEDEC.

during erosion/deposition, rather than continuous exchange, for an explanation of bed response to unsteady forcing in the prototype environment.

In order to conceptually bridge the knowledge gap between laboratory observed mutually exclusive erosion/deposition and the commonly encountered need to render these processes simultaneous in modeling resuspension in field applications, the schematic drawing of near-bed sediment exchange shown in Fig. 4-10 can be helpful (Cervantes et al. 1995; Mehta 1991). The layer extending from the bed (at $z = 0$) to some suitable notional height a_h may be idealized as a stirred layer mentioned earlier, within which entrainment of sediment from the bed starting at $t = 0$ sets up a convective cell of upward diffusive flux of sediment and, as a result, gravity-induced settling flux. Under constant fluid stress-induced forcing at the bed these fluxes will eventually approach equality, erosion of the stratified bed will practically cease at some final depth where the applied shear stress equals the erosion shear strength, and a steady-state concentration of sediment in the water column will occur. Thus, by applying, at $z = a_h$, laboratory expressions for erosion and deposition evaluated at $z = 0$, formulas compatible with mutually exclusive erosion/deposition can be used in simulating resuspension on a simultaneous basis. Even though this is merely a "convenient" interpretation of two unresolved concepts, it appears that the "insertion" of the stirred layer may be useful in explaining some flume experimental results meant to study deposition, but in which two-way exchange between bed and suspended sediment may actually have occurred (McAnally 1999).

4.5 SETTLING VELOCITY

4.5.1 Aggregation and Settling

The rate at which suspended flocs settle depends on their weight, diameter, and shape, which in turn are related to their order of aggregation, the latter being governed by the frequency of interparticle collisions. Three mechanisms that have been explicitly shown to influence aggregation in estuarine and coastal waters are Brownian motion, flow-induced shear, and differential settling (Krone 1962). By way of the last mechanism, particles/flocs of different settling velocities collide as they fall. For these three mechanisms, the frequency functions of collision between two particles of sizes i and j β_c are given as (McAnally 1999; Burban et al. 1989; Delichatsios and Probestein 1975; Saffman and Turner 1956)

$$\beta_c \begin{cases} \dfrac{2}{3}\dfrac{\kappa T F_c}{\mu}\dfrac{\left(d_i + d_j\right)^2}{d_i d_j} & \text{Brownian motion} \\ \left[\dfrac{\pi F_c^2}{4}\sqrt{\dfrac{2}{15\,\pi}}\right] G_s \left(d_i + d_j\right)^3 & \text{fluid shear} \\ \left[\dfrac{\pi F_c^2}{4}\right]\left(d_i + d_j\right)^2 \left|w_{si} - w_{sj}\right| & \text{differential settling} \end{cases} \tag{14-13}$$

where

κ = Boltzmann constant;
T = absolute temperature;
μ = dynamic viscosity of fluid;
F_c = collision diameter correction factor (which varies between 0 and 1);
d_i, d_j = sizes of colliding particles from i and j size classes, respectively;
w_{si}, w_{sj} = corresponding settling velocities;
G_s = measure of flow shear given by $G_s = (\epsilon/\nu)^{1/2} = \nu/\lambda^2$;
ϵ = flow energy dissipation per unit mass of fluid per unit time;
$\nu = \mu/\rho_w$ = kinematic viscosity of fluid (nominally water) and
λ = Kolmogorov turbulence microscale.

The settling velocities can be simply related to the corresponding diameters through Stokes' law: $w_{si} = \Delta\rho_i d_i^2/18\mu$ and $w_{sj} = \Delta\rho_j d_j^2/18\mu$

where

$\Delta\rho_i = \rho_{si} - \rho_w$;
$\Delta\rho_j = \rho_{sj} - \rho_w$;
ρ_i, ρ_j = densities of i and j particles and
ρ_w = water density.

Among others, Hunt (1982), Lick et al. (1992), and McAnally (1999) have described the manner in which the relative importance of the above three collision mechanisms changes as aggregation of particles proceeds. In Fig. 4-11 a comparison is made of these mechanisms based on Eq. (4-13) and typical water column conditions. Observe that as aggregation proceeds and the second particle size increases, fluid shear takes over as the dominant mechanism, while the influence of Brownian motion becomes negligible. Note also that when the two particles are of the same size, in this case 1 μm, there is no contribution from differential settling because the two particles settle at the same rate, and therefore do not collide by that mechanism.

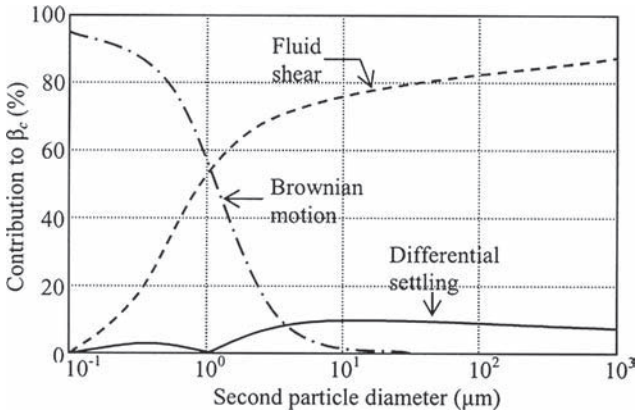

Fig. 4-11. Simulated relative contributions to the collision frequency for typical water column conditions in the estuary. First particle diameter is 1 μm (after McAnally 1999).

In general, fluid shear is the most important of the three collision mechanisms, because it produces relatively tightly packed, durable flocs in comparison with the other two mechanisms (Krone 1963; 1986). Differential settling is important during and close to times of slack water. At very low flow shear Brownian motion becomes responsible for aggregation; however, the flocs thus produced tend to be weakly bonded.

4.5.2 Settling Velocity and Concentration

Floc settling velocities typically range from 1×10^{-5} to 1×10^{-1} m/s for particles of size 10 to 1,000 μm (Dyer 1989; van Leussen 1994; Moudgil and Vasudevan 1989). The settling velocity depends on the floc properties, especially size, density, and shape, which in turn are governed by the interparticle collision frequency and the outcome of collisions. Inasmuch as collisions depend on particle concentration in the suspension, suspended sediment concentration can be used as an approximate lumped parameter for estimating the settling velocity of flocs (Krone 1962). As a result, and given the convenience with which concentration can be measured, formulas relating the settling velocity to concentration have been proposed.

Following Wolanski et al. (1989), a general expression for the mean settling velocity divides the settling range into four zones—free settling, flocculation settling, hindered settling, and negligible settling. The settling velocity, w_s, in each zone can be expressed as (Hwang 1989)

$$w_s = \begin{cases} w_{sf} & C < C_1 \\ a_w \dfrac{C^{n_w}}{\left(C^2 + b_w^2\right)^{m_w}} & C_1 < C < C_3 \\ \sim negligible & C_3 < C \end{cases} \qquad (4\text{-}14)$$

where

w_{sf} = free settling velocity;
C = suspension concentration;
a_w = velocity scaling coefficient;
n_w = flocculation settling exponent;
b_w = hindered settling coefficient;
m_w = hindered settling exponent and
C_1, C_3 = zone concentration limits defined in Fig. 4-12.

Free settling occurs at low suspension concentrations when w_s is independent of C, and can be calculated from Stokes' law, especially when settling occurs under quiescent conditions. Between C_1 and C_2, w_s increases with concentration due to the formation of stronger, denser and larger flocs. In the hindered settling zone between C_2 and C_3, the occurrence of an aggregated particulate network inhibits, or hinders, the upward transport of interstitial water in the deposit. As a result, w_s decreases with increasing C in this zone. At concentrations above C_3, settling becomes comparatively small as consolidation takes over.

Values of coefficients a_w, b_w, m_w, and n_w along with C_1 are given in Table 4-8 based on the application of Eq. (4-14) to measured variations of the settling velocity (m/s) with concentration (kg/m^3). In general, C_1 ranges between 0.1 and 0.3 kg/m^3, in agreement with the original observations of Krone (1962). In reality, the transition between free and flocculation settling is gradual and may occur over a wider concentration range, e.g., on the order on 0.01 to 0.3 kg/m^3 (Krone 1962; Ozturgut and Lavelle 1986). For computational purposes, it is convenient to select w_{sf} as the value of the settling velocity corresponding to the intersection of the curve for flocculation settling obtained from (4-14) with the vertical line corresponding to C_1=0.1 kg/m^3.

The concentration C_2, corresponding to the peak settling velocity w_{sm}, can vary between 1 and 15 kg/m^3. Odd and Cooper (1989) reported C_3 to be on the order of 75 kg/m^3 in their measurements of settling rates of mud from the Severn

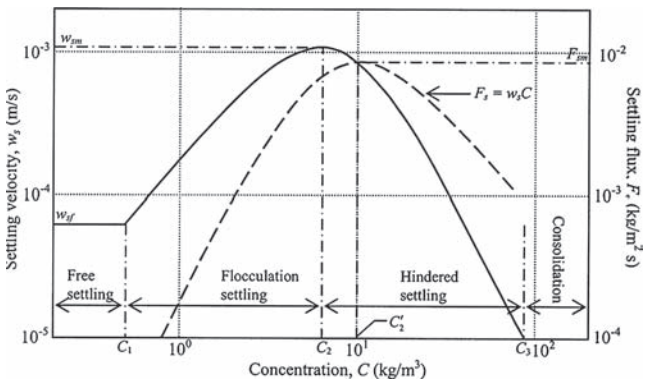

Fig. 4-12. A representative plot of settling velocity and associated settling flux variation with suspension concentration.

Table 4-8 Values of Coefficients in (4-14) Derived from Several Studies

Investigator(s)	Sediment source	a_w	b_w	m_w	n_w	C_1 (kg/m^3)
Krone (1962)	San Francisco Bay, California	0.048	25.0	1.00	0.40	0.30
Owen (1970)	Severn River, U.K., salinity 2 g/L	0.140	17.0	1.40	1.10	0.20
Owen (1970)	Severn River, U.K., 8 g/L	0.110	11.0	1.53	1.50	0.20
Owen (1970)	Severn River, U.K., 17 g/L	0.160	15.0	1.15	0.50	0.20
Owen (1970)	Severn River, U.K., 32 g/L	0.100	10.0	1.30	1.00	0.20
Owen (1970)	Severn River, U.K., 48 g/L	0.080	9.50	1.34	1.00	0.20
Huang et al. (1980)	Yangtze River, China	0.012	1.70	2.80	2.20	0.20
Thorn (1981)	Severn River, U.K.	0.010	2.00	1.46	2.10	0.20
Burt and Stevenson (1983)	Thames River, U.K., 1981 sample	0.170	3.00	1.90	1.65	0.15
Burt and Stevenson (1983)	Thames River, U.K., 1982 sample	0.060	2.00	1.90	1.50	0.20
Nichols (1984/85)	James River, Va.	0.039	3.80	1.32	1.52	0.20
Odd and Rodger (1986)	Severn River, U.K.	0.080	6.50	1.35	1.42	0.10
Lott (1986)	Commercial kaolinite	0.010	3.00	1.60	1.30	0.20
Ross (1988)	Tampa Bay, Fla.	0.001	1.80	1.40	2.10	0.30
Hwang (1989)	Lake Okeechobee, Fla., 40% organic, particle size 10 μm	0.080	3.50	1.88	1.65	0.15
Hwang (1989)	Lake Okeechobee, Fla., 40% organic, particle size 15 μm	0.027	5.50	1.60	1.00	0.20
Hwang (1989)	Lake Okeechobee, Fla., 40% organic, particle size 7 μm	0.090	4.50	1.85	1.80	0.30
Costa (1989)	Hangzhou Bay, China	0.100	6.20	1.60	1.20	0.20
Wolanski et al. (1991)	Cleveland Bay, Australia, field test	0.200	1.40	2.25	2.45	0.10
Wolanski et al. (1991)	Cleveland Bay, Australia, laboratory tests	0.07	1.30	2.5	2.80	0.20
Jiang (1999)	Jiaojiang, China, neap tide	0.045	6.00	1.51	1.50	0.20
Jiang (1999)	Jiaojiang, China, spring tide	0.230	10.00	1.80	1.50	0.20
Marván (2001)	Ortega River, Fla.	0.160	4.50	1.95	1.70	0.20
Ganju (2001)	Loxahatchee River, Fla.	0.190	5.80	1.80	1.80	0.20

River estuary in United Kingdom. This value is in approximate agreement with the concentration at which a suspension changes to a bed due to the development of effective normal stress (Sills and Elder 1986).

From Eq. (4-14) we find that when $C << b_w$, i.e., the "low" concentration condition,

$$w_s = a_w b_w^{-2m_w} C^{n_w} \tag{4-15}$$

Equation (4-15), which describes flocculation settling, was derived by Krone (1962), who also provided a phenomenological explanation for the form of the equation. Using the data of Overbeek (1952) on the aggregation of initially dispersed particles, Krone determined the value $n_w = 4/3$ and showed that it agreed with his data on settling of San Francisco Bay sediment in a flume as well as in a settling column.

When $C >> b_w$, i.e., the "high" concentration condition, Eq.(4-14) reduces to

$$w_s = a_w C^{n_w - 2m_w} \tag{4-16}$$

where $n_w - 2m_w$ must be less than zero, because hindered settling causes the settling velocity to decrease with increasing concentration. The form of Eq. (4-16) agrees with the experimental data of Richardson and Zaki (1954), who also derived it theoretically based on idealized geometric arrays of particles falling in the hindered settling mode.

From Eq. (4-14) the following useful quantities related to settling velocity and associated settling flux $F_s = w_s C$ (Fig. 4-12) are obtained:

Peak velocity, w_{sm}:

$$w_{sm} = a_w b_w^{n_w - 2m_w} \frac{\left(\dfrac{2m_w}{n_w} - 1\right)^{m_w - n_w/2}}{\left(\dfrac{2m_w}{n_w}\right)^{m_w}} \tag{4-17}$$

Concentration, C_2:

$$C_2 = \frac{b_w}{\left(\dfrac{2m_w}{n_w} - 1\right)^{1/2}} \tag{4-18}$$

Settling flux, F_s ($=w_s C$):

$$F_s = a_w \frac{C^{n_w+1}}{\left(C^2 + b_w^2\right)^{m_w}} \tag{4-19}$$

Maximum settling flux, F_{sm}:

$$F_{sw} = a_w b_w^{n_w - 2m_w + 1} \frac{\left(\dfrac{2m_w}{n_w + 1} - 1\right)^{m_w - \frac{n_w+1}{2}}}{\left(\dfrac{2m_w}{n_w + 1}\right)^{m_w}} \tag{4-20}$$

Concentration at maximum flux, C_2':

$$C_2' = \frac{b_w}{\left(\dfrac{2m_w}{n_w + 1} - 1\right)^{1/2}} \tag{4-21}$$

Inasmuch as C_2' is obtained from Eq. (4-18) by replacing n_w by $n_w + 1$, it is characteristically greater than C_2. Physically this is so because of the dependence of settling velocity on concentration, which means that the settling flux is a nonlinear function of concentration. Thus, for example, from the data of Nichols (1984/1985) in Table 4-8 we find that C_2 = 4.4 kg/m^3 and $C_2' = 17.4$ kg/m^3. In a depositional environment, i.e., in the absence of significant reentrainment of sediment, C_2' marks the level of the lutocline. Consequently, in Fig. 4-4 this concentration corresponds to the upper level of the fluid mud layer. Likewise, C_3 very approximately marks the transition between the fluid mud layer and the bed. The concentration C_1 defines the transition between the mixed suspension layer and the stratified suspension layer. When entrainment is significant these concentration limits and the elevations at which they occur in the concentration profile tend to change, depending on the importance of entrainment in relation to settling.

An example of settling velocity data from the Jiaojiang estuary in China and data fit using Eq. (4-14) is shown in Fig. 4-13a. An illustration of settling flux variation with

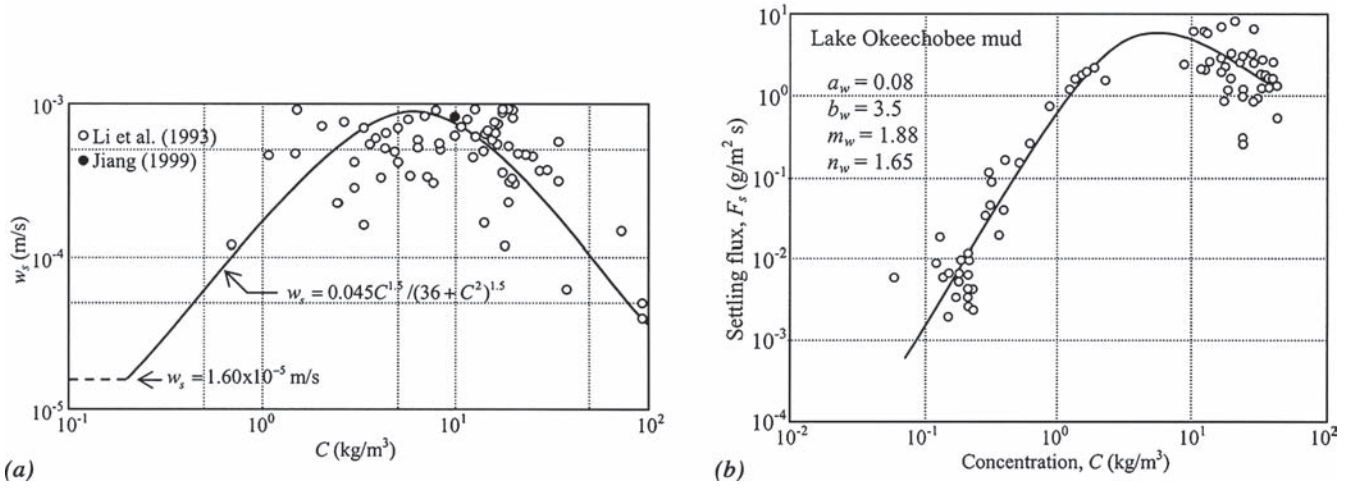

Fig. 4-13. Settling velocity as a function of (a) suspension concentration during a neap tide in the Jiaojiang estuary, China (after Jiang 1999) and (b) suspended sediment concentration for Lake Okeechobee, Fla. mud (data from Hwang 1989; the curve is based on Eq. (4-19)).

concentration is shown in Fig. 4-13b, based on the data of Hwang (1989) from Lake Okeechobee in Florida. The curve is obtained from Eq. (4-19).

4.5.3 Other Effects on Settling

Jiang (1999) found that deposition data from the flume experiments of Lau (1994) using a kaolinite under controlled conditions of fluid temperature showed a well-defined temperature dependence of the form

$$w_{s50}(C,T_c)=\Phi w_{s50}(C,15) \tag{4-22a}$$

where

$w_{s50}(C,15)$ = concentration-dependent median settling velocity as defined by Eq. (4-14) at temperature $T_c = 15°\text{C}$, and

$$\Phi=1.776(1-0.875T') \tag{4-22b}$$

where

$T' = T_c / 15.$

This finding suggests that the mean floc size decreases with increasing temperature, which is a reasonable conclusion because thermal activity of the clay micelle ions tend to increase the repulsive effect between grains, reducing the number of collisions available to pump sediment mass up the size distribution in an environment in which continued aggregation occurs.

In order to account for the effect of flow shear on the settling velocity, van Leussen (1994) and Teeter (2001a) proposed equations relating w_s to the flow shear rate, whereas Burban et al. (1990) relate w_s to shear stress. Winterwerp (1998) used Kranenburg's (1994) fractal model as a framework to formulate settling velocity relationships based directly on grain and floc sizes. Following van Leussen (1994), Malcherek and Zielke (1996) and Teisson (1997), Teeter (2001a), used the expression:

$$\frac{w_s}{w_{s|\dot\gamma=0}}=\frac{(1+\lambda_1\dot\gamma)}{1+\lambda_2\dot\gamma^2} \tag{4-23}$$

in which $w_{s|\dot\gamma=0}$ is obtained from a concentration dependent settling velocity function such as (4-14), G is the shear rate (Hz or s^{-1}), and λ_1 and λ_2 are sediment-specific coefficients. From laboratory work on mud from San Francisco Bay, the values of these two coefficients are found to be 266 and 9, respectively.

Sheng (1986) showed that submerged vegetative canopies offer considerable resistance to settling and deposition. Ganju (2001) found that for Florida sediments the coefficient a_w in (4-14) depends on the organic content OC(%/100) according to $a_w = a_{w0} + a_1 OC + a_2 OC^2 + a_3 OC^3 + a_4 OC^4$, with $a_{w0} = 0.2$, $a_1 = 6.6.7 \times 10^{-4}$, $a_2 = -1.7 \times 10^{-4}$, $a_3 = 7.1 \times 10^{-6}$, and $a_4 = -1.3 \times 10^{-7}$. Note that a_{w0} is the value of a_w when $OC = 0$. This relationship amounts to the trend of decreasing aggregate diameter and settling velocity with increasing organic content, because the aggregates become both smaller and lighter as the density and cohesion of the composite material decrease with increasing organic fraction.

4.6 DEPOSITION UNDER FLOW

4.6.1 Rate of Deposition

Referring to Fig. 4-6, if a settling floc approaches a bed where concentration, collision frequency, and shearing rate are high, it will either break apart and be reentrained or bond with particles at the bed surface and be deposited. Deposition can be characterized as the outcome of interaction between two stochastic processes occurring just above the bed—interfloc collisions causing both floc breakup and growth that creates a distribution of floc sizes and strengths, and the probability that a floc of a given strength and size will be deposited (Stolzenbach et al. 1992). Thus, the deposition rate is a function of floc settling velocity, concentration, and the near-bed shearing rate. The shearing rate is conveniently characterized by the bed shear stress.

A widely used expression for the sediment mass deposition rate Ψ, when only one size class is considered, is

$$\Psi=\frac{d\overline{C}}{dt}=-\frac{w_s\overline{C}}{h}\left(1-\frac{\tau_b}{\tau_d}\right);\quad \tau_b<\tau_d \tag{4-24}$$

where

$\overline{C}$ = depth-averaged suspended sediment concentration;
h = water depth;
τ_b = bed shear stress; and
τ_d = critical stress for deposition.

When $\tau_b \leqslant \tau_d$ all initially suspended sediment deposits and, conversely, no sediment deposits when $\tau_b > \tau_d$. Thus, in the free settling range (w_s = constant), an exponential law of concentration decay is obtained from (4-24) by integration;

$$\frac{C}{C_0}=\exp\left[-\left(1-\frac{\tau_b}{\tau_d}\right)\frac{w_s}{h}t\right];\quad \tau_b<\tau_d \tag{4-25}$$

where

C_0 = initial suspension concentration;
t = time;
and the bar over C is omitted for convenience of further treatment.

In the flocculation settling range, in which the settling velocity increases with increasing concentration, e.g., according to Eq. (4-15), the concentration-time relationship becomes logarithmic; i.e., log C decreases linearly with log t (Krone 1993; Shrestha and Orlob 1996). However, Eq. (4-25) has been found to hold reasonably well up to concentrations on the order of 1 kg/m^3 (Mehta and Lott 1987).

4.6.2 Multiclass Deposition

Among others, Ockenden (1993) and Teeter (2001a; 200b) extended Eq. (4-24) to multiple grain sizes using

$$\Psi_i = \frac{dC_i}{dt} = -\frac{w_{si}C_i}{h}\left(1-\frac{\tau_b}{\tau_{di}}\right);\ \tau_b < \tau_{di} \qquad (4\text{-}26)$$

where for each size class i,

Ψ_i = mass deposition rate;
C_i = depth-mean concentration;
w_{si} = settling velocity; and
τ_{di} = critical shear stress for deposition.

Assumed τ_d to vary between a minimum value τ_{d1} for the finest sediment size class and a maximum τ_{dM} for the coarsest class M, the concentration-time variation during deposition can be shown to depend on the magnitude of τ_b in relation to τ_{d1} and τ_{dM}. The three types of curves that can result are shown schematically in Fig. 4-14. In this plot, C_f is the final, steady-state suspension concentration attained at the end of the transient period, during which the concentration decreases from its initial value. For further illustration, flume data on the deposition of a kaolinite and curves based on the multiclass relation of Mehta and Lott (1987) are shown in Fig. 4-15. The simulations are based on the equation

$$\frac{C}{C_0} = \frac{1}{C_0}\sum_{i=l}^{M} C_i = \sum_{i=1}^{M}\phi\left(w_{st}\right)$$

$$\times \exp\left\{-\left[1-\frac{\tau_b}{\tau_{d1}}\left(\frac{w_{sl}}{w_{si}}\right)^{\frac{\left[\ln\left(\tau_{dM}/\tau_{d1}\right)\right]}{\ln\left(w_{sM}/w_{s1}\right)}}\right]\frac{w_{sl}}{h}t\right\} \qquad (4\text{-}27)$$

which is subject to the condition $C_i = C_{0i}$, the initial concentration for each class i, for all $\tau_b \geq \tau_{di}$, also for each class i. For a single-size sediment $M=1$, and Eq. (4-27) reduces to Eq. (4-25). It must be pointed out that Eq. (4-27) is based on multiclass distribution of floc settling velocity, rather than size. Given the histogram of w_{si} values obtained from settling velocity tests, $\phi(w_{si})$ is the frequency of the ith class and w_{s1} is the smallest value of the settling velocity in the histogram. For simulation of the curves in Fig. 4-15, the range τ_{d1} to τ_{dM} was 0.04 to 1 Pa, which is typical in laboratory flumes. The histogram of settling velocity was derived from settling tests conducted with flocculated kaolinite in a settling column (Yeh 1979) and assumed to be applicable to flume conditions. A limitation of this approach is that the settling velocity is assumed to be unaffected by ongoing aggregation. Therefore, in those water bodies in which the flocs are composed of highly cohesive sediment and floc

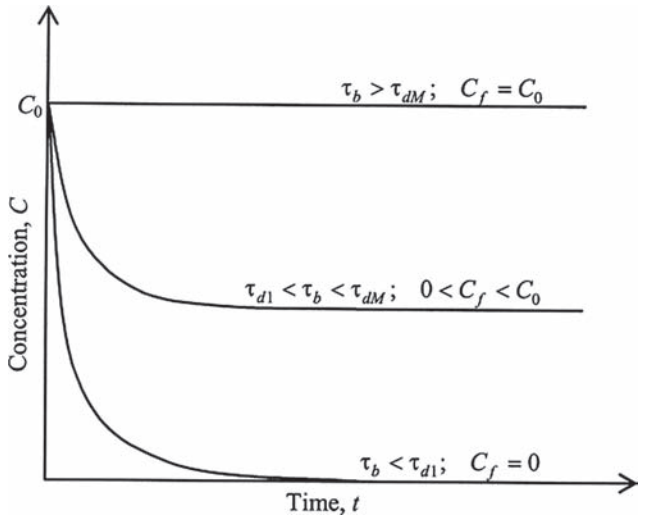

Fig. 4-14. Schematic drawing of concentration-time relationships during multiclass sediment deposition.

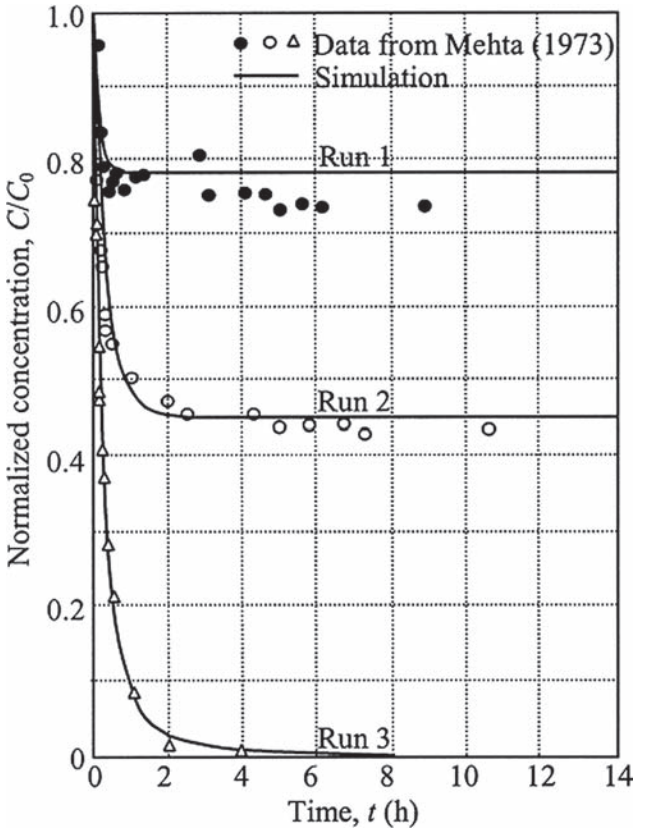

Fig. 4-15. Concentration-time relationships for kaolinite deposition in a flume (after Mehta and Lott 1987).

growth/breakup is strongly influenced by flow shear, Eq. (4-27) as used may lead to errors in the prediction of the time-concentration history. Thus for example, whereas kaolinite, which is weakly cohesive, may be appropriate for (4-27), answers obtained using cohesive mud from the San Francisco Bay must be interpreted carefully (McAnally and Mehta 2000; 2002).

In a depositional environment such as a dead-end or finger canal, or wherever deposition is the dominant process, multiclass simulation enables the prediction of sorting by size (Lau and Krishnappan 1992), which typically manifests as a decrease in grain size with distance from the initial point of deposition (Lin 1986; Lin and Mehta 1997; McAnally 1999). However, in cases where resuspension cannot be ignored, the use of either Eq. (4-24) or (4-26) effectively amounts to a simulation of nonsimultaneous bed sediment exchange when the bed shear stress exceeds the critical stress for deposition. Size sorting also occurs during resuspension, particularly when the sediment is only weakly cohesive, such as a kaolinite, and this leads to a bed armoring effect because larger, especially unaggregated, grains erode less easily than the finer fractions (Teeter et al. 1997). However, since this selective resuspension process is less well understood than multiclass deposition, tracking particles, especially in the presence of ongoing aggregation of suspended matter, becomes cumbersome. To obviate this complexity in process modeling, it is convenient to assume a single size class only and to further consider τ_d to be equal to the maximum value of τ_b expected to be encountered in the simulation process (Jiang 1999). Then Eq. (4-24) reduces to $\Psi = -w_s \overline{C}/h$, which allows deposition to occur at all prevailing shear stresses.

It should be emphasized that (4-24) and (4-26) are based on laboratory data. Their applicability to the field requires a careful interpretation of the relationship between vertical gradients of concentration and their role in influencing the deposition rate. Also, when the total water depth is large, deposition is found to correlate with sediment concentration in the near-bed suspension layer, in contrast to depth-mean concentration, used in Eq. (4-24) and (4-26). Scale effects associated with the structure of turbulence also play a role (Sanford and Chang 1997).

4.7 CONSOLIDATION AND GELLING

4.7.1 Settling and Consolidation

If a clay mixture in water is allowed to settle, three stages of the settlement process can be identified, as shown schematically in Fig. 4-16 (Schiffman et al. 1985). In the first, flocculation stage, aggregation is important but no significant settling occurs. For some slurries, e.g., those of kaolinite, this stage may be only tens of seconds long, but for a bentonite slurry it may last effectively up to tens of minutes. In the second stage, flocs gradually settle and form a bed layer, which undergoes what is called primary consolidation and associated dewatering. The initial settling process is complicated by a significant change in the structure of the newly deposited flocs. Krone (1963) conceptualized this change in terms of the aggregate order—when aggregates of order n deposit they form an initial "fluffier" and weaker layer of aggregates of order $n + 1$. When this layer exceeds a thickness on the order of 2.5 cm, overburden crushes the $n + 1$ order aggregates to n order aggregates, which are then crushed further by overburden to result in aggregates of order $n-1$, $n-2$, and so on.

The upper boundary of the settling zone in the second stage, which can generally be defined as a lutocline, drops with time until it meets the rising bed boundary at the onset of the third stage. In this stage, settling is terminated and bed consolidation continues. Accordingly, the bed surface gradually drops until no further consolidation takes place. Whereas the second stage may last from minutes to hours, the third stage can range between hours to days or months. In some case it may take years for full consolidation. During this stage, even after dewatering ends, internal rearrangements of particles may occur under secondary consolidation. It should be noted however, that in a large number of cases involving fresh estuarine deposits, consolidation is practically over in one to two weeks. Because this time scale coincides with the synodic spring-neap tidal cycle, consolidation plays an important role in governing estuarine sediment transport and budget.

The rate of settling, which is typically in the hindered mode, and consolidation are both governed by the rate at which interstitial or pore water escapes the particle matrix. Within the settling zone there is no significant effective normal stress; i.e., the pore water pressure is practically equal to the total hydrostatic pressure. Within the consolidation zone, because a part of the total weight

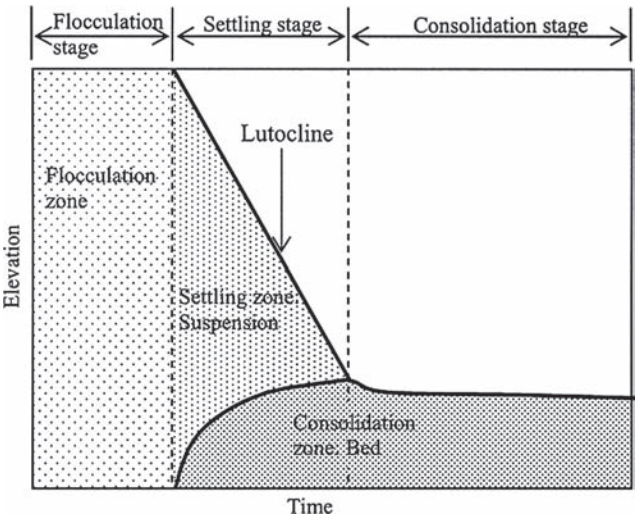

Fig. 4-16. Flocculation, settling, and consolidation zones (adapted from Schiffman et al. 1985).

of the slurry is supported by the particle matrix, the pore pressure is less than the total pressure, with the difference, equal to the effective stress, representing the particle-supported load. Figure 4-17a shows an instantaneous density profile within a settling silty clay in an experimental column, 4.75 h after test initiation starting with a uniformly mixed suspension having a density of 1,090 kg/m^3 (Sills and Elder 1986). The corresponding measured profiles of total pressure (i.e., normal stress) and pore pressure are shown in Fig. 4-17b. The elevation separating the settling suspension (without effective stress) from the consolidating bed (with effective stress) is practically at 60 cm, close to the level of the lutocline at that point in time.

The settling behavior can be analyzed through the sediment continuity equation in the vertical direction, which yields the time-variation of the lutocline as it settles, and also the associated density profile within the suspension. Consolidation of soils in general has been simulated with non-linear, finite strain models (Gibson et al. 1967; 1981). For the estuarine environment, models for self-weight consolidation, i.e., settling due to the weight of the deposit itself, have been developed through linearized analytic solutions (e.g., Been and Sills 1981; Govindaraju et al. 1999) and nonlinear numerical solutions (e.g., Papanicolaou and Diplas 1999). Interest with respect to fine sediment transport is in tracking the change in the density of deposit, because both the bed shear strength and the mass of material eroded per unit time depend on density. Change in bottom elevation due to consolidation is usually of lesser interest, inasmuch as generally it is only a small fraction of the total water depth.

With regard to density determination during consolidation, the commonly used correlations between density and bed shear strength are empirical and inherently approximate. As a result the calculation of rate of erosion, which depends on the shear strength, is also approximate. Thus it often suffices to calculate the density to first-order accuracy. For this requirement, it is useful to consider simple approaches to track density though (hindered) settling and consolidation combined. Such approaches rely on the physical similarities between these two processes (e.g., Schiffman et al. 1985).

Following the continuity approach of Kynch (1952), and accounting for the accumulation or depletion of bed deposit by deposition or erosion, respectively, the sediment continuity equation can be written as

$$\frac{\partial h' C}{\partial t} = \frac{\partial w_{sc} C}{\partial z'} + q \tag{4-28}$$

where

h' = thickness of the consolidating layer;
w_{sc} = velocity or rate of consolidation;
$z' = z / h'$;
z = vertical coordinate originating at the bottom and positive upward; and
q = net settling flux (i.e., deposition less erosion) of sediment mass at the top of the consolidating layer (Jiang 1999).

In general, two modes of consolidation can be recognized from the plot of consolidation rate against concentration,

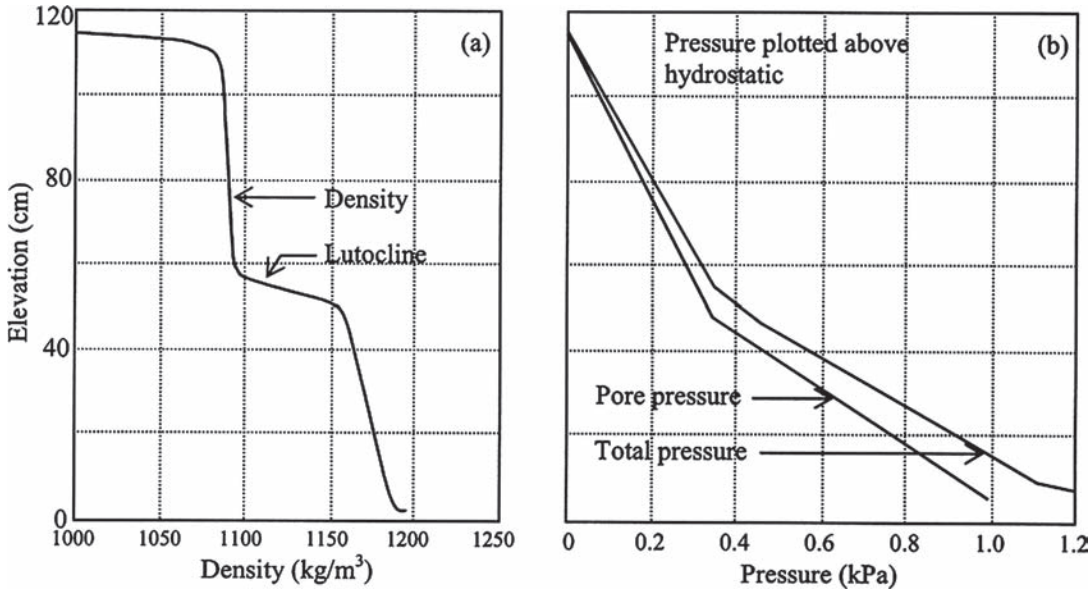

Fig. 4-17. (a) Instantaneous density profile during settling of a silty clay in tap water; (b) corresponding total and pore pressure profiles (adapted from Sills and Elder 1986).

Table 4-9 Compilation of Parameters for (4-29)

Reference(s)	Sediment source	w_{sc1} (m/s)	C_{s1}(kg/m^3)	w_{sc2} (m/s)	C_{s2} (kg/m^3)	C_t (kg/m3)	m_t	n_t
Burt and Parker (1984); Jiang (1999)	Estuarine mud, UK	—[a]	—[a]	4.2×10^{-6}	680	15	6.0	15
Toorman and Berlamont (1993)	Doel Dock, Belgium	5.0×10^{-4}	20	7.0×10^{-6}	205	160	3.0	13
Jiang (1999)	Jiaojiang estuary, China	1.0×10^{-4}	31	6.0×10^{-6}	350	210	4.5	15
Marván (2001)	Ortega River, Florida	6.0×10^{-5}	15	3.0×10^{-6}	1000	83	5.5	18

[a]First mode absent.

namely loose soil consolidation and compact soil consolidation. For these two modes, Toorman and Berlamont (1993) developed a combined relationship of the form

$$w_{sc} = w_{sc1} \exp\left(-\frac{C}{C_{s1}}\right) F_t + w_{sc2}\left(1-\frac{C}{C_{s2}}\right)^{m_t}(1-F_t); \qquad F_t = \exp\left[-\left(\frac{C}{C_t}\right)^{n_t}\right] \tag{4-29}$$

where

F_t = characteristic mode transition (from loose soil to compact soil) function with $n_t > 10$;
m_t = sediment-dependent constant;
C_t = mode transition concentration;

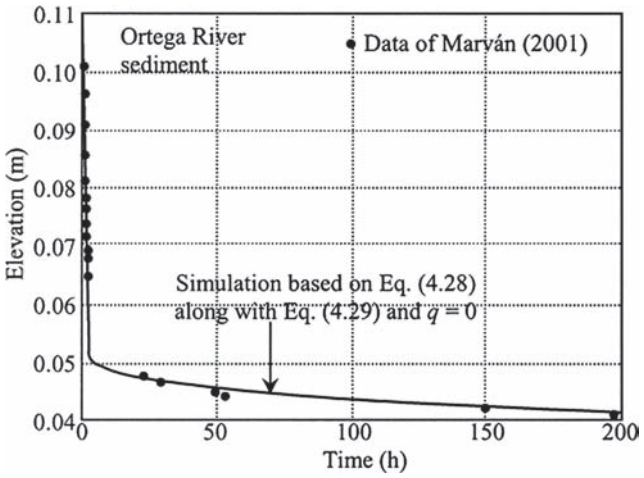

Fig. 4-18. Settling consolidation of sediment from the Ortega River, Florida.

w_{sc1}, w_{sc2} = rates of consolidation for the first and the second modes, respectively;
C_{s1} = concentration corresponding to the maximum settling flux; and
C_{s2} = saturation concentration, i.e., maximum attainable compaction concentration.

Table 4-9 gives representative values of these coefficients. Data points for sediment from the Ortega River in Florida (Marván 2001) are shown in Fig. 4-18 along with a comparison with Eq. (4-28) assuming $q = 0$, Eq. (4-29), and the corresponding coefficients from Table 4-9. Note that in addition to Eq. (4-28) the equation of conservation of total mass is needed to solve for h' and C (Jiang 1999). In Fig. 4-18 both the data and computations start with a uniformly mixed suspension of constant concentration (38.7 kg/m^3). Observe the two identifiable (initially rapid, then slow) trends in the rate of fall of the bed deposit elevation. It can be shown that whereas the initial consolidation time is inversely proportional to the thickness of the deposit, subsequently this time becomes inversely proportional to the square of the bed thickness (Toorman 1996; Winterwerp 1999).

4.7.2 Gelling

Clayey muds exhibit various degrees of thixotropy depending on composition. Thixotropy is an isothermal, reversible, time-dependent process occurring under conditions of constant composition and volume, whereby a material stiffens, or gels, while at rest and softens or liquefies upon remolding (Mitchell 1993). Once mud gels it is harder to erode than when it is remolded.

Day and Ripple (1966) showed that a bed of kaolinite in water practically lost its strength upon shearing, but the strength was recovered in about a day. This process is schematized in Fig. 4-19, in which S_P is the peak undisturbed strength and S_R is the remolded strength. These values can be determined from the unconfined compression test, or

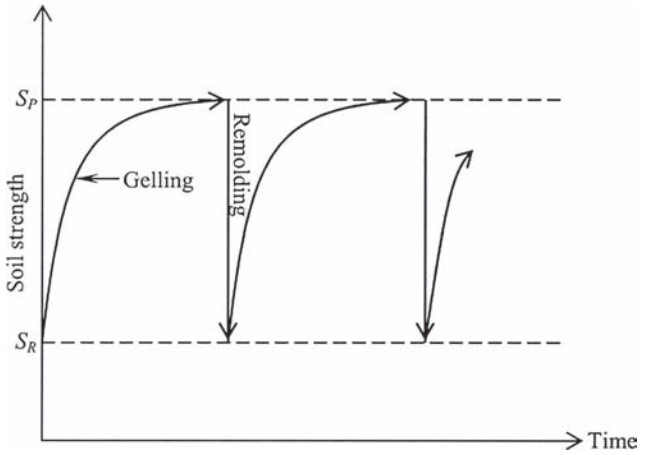

Fig. 4-19. Schematic drawing of changes in soil strength due to repeated cycles of gelling and remolding (based on Mitchell, 1976).

vane shear test, for low strength soils (Lambe and Whitman 1969). A measure of the gelling effect is the sensitivity, $S_t = S_P/S_R$. Accordingly, $S_t = 1$ implies no sensitivity, and 4 to 5 is considered very sensitive (Mitchell 1976). Gelling occurs because water molecules within the pore fluid and close to the clay surface form a "solid" layered structure through hydrogen bonding. When the sample is disturbed this structure collapses and water molecules are randomized. Gelling therefore can be detected through changes in the pore water pressure. Starting with a disturbed sample, as the material gels the pore water pressure drops with increasing ordering of water molecules. A tensiometer is commonly employed to record these changes (Kirkham and Powers 1972).

4.8 EROSION

4.8.1 Modes of Erosion

The four modes of erosion mentioned in Section 4.3.2 are surface erosion, mass erosion, fluid mud generation, and fluid mud entrainment. Note that generation of fluid mud is considered to be erosion because in this process there is a phase change from a bed to a suspension. This fourfold classification of erosion is meant mainly to understand and treat a very complex set of mechanisms through simplified analytic and empirical treatments. These treatments are considered in what follows.

4.8.2 Surface Erosion

Modeling surface erosion continues to pose problems, largely due to a lack of basic understanding of the way in which the bed-water interface responds to flow-induced stress. For steady or quasi-steady (e.g., tidal) flows, numerous formulas relating the rate of bed surface erosion to the bed shear stress have been proposed. In this mode of erosion, particles or flocs at the bed surface are detached and entrained, thus causing bed scour. Some of the early formulas have been summarized by Mehta et al. (1982). Subsequent developments may be found in, among others, Jepsen et al. (1997); Piedra-Cueva and Mory (2001); and Taki (2001). These formulas are generally applicable to cases of low to moderate suspended sediment concentrations, up to about C_2 in Fig. 4-12. At high concentrations settling of eroded sediment is hindered, and a layer of fluid mud is formed over the bed. The mechanism by which this layer erodes is not modeled well by simple, stress-based formulations used for surface erosion. Furthermore, damping of turbulence within fluid mud alters the bed shear stress from its value under clear or nearly clear water conditions. In that regard, Bedford et al. (1987) showed that, at least in the context of their experiments in Long Island Sound, the turbulent kinetic energy proved to be better correlated with resuspension than the Reynolds stress.

Following the stochastic theory of Einstein (1950) for coarse grain transport, and considering erosion to occur in the absence of deposition, Partheniades (1962; 1965) developed a phenomenological formula relating the rate of erosion to the bed shear stress. This formula and the flume data on mud erosion with which the formula was compared showed a nonlinear relationship between erosion rate and bed shear stress. Subsequently, Ariathurai (1974) assumed a straight line approximating the nonlinear relation, and attributed the resulting linearized formula to Partheniades (1962). This linear "Ariathurai-Partheniades" formula, which was essentially empirical, led to the expression, investigated extensively by Kandiah (1974),

$$\epsilon = \epsilon_M \left(\frac{\tau_b - \tau_s}{\tau_s} \right) \tag{4-30}$$

in which

ϵ = erosion rate or mass flux (mass eroded per unit bed area per unit time);
τ_b = bed shear stress;
τ_s = bed shear strength with respect to erosion; and
ϵ_M = the erosion rate constant, the value of ϵ when $\tau_b = 2\tau_s$.

Equation (4-30) is characteristically applicable to homogenous beds of uniform (i.e., nonstratified) density and indicates that ϵ varies with the excess shear stress $\tau_b - \tau_s$. Thus, a plot of ε versus $\tau_b - \tau_s$ ideally appears as a straight line as illustrated in Fig. 4-20, in which the erosion rate and the shear strength (determined by the intercept of a given line with the horizontal axis) are seen to depend on the percentage (by weight) of montmorillonite in a mixture of this clay with Yolo loam from California. Also observe that the effect of the highly cohesive montmorillonite was to decrease the

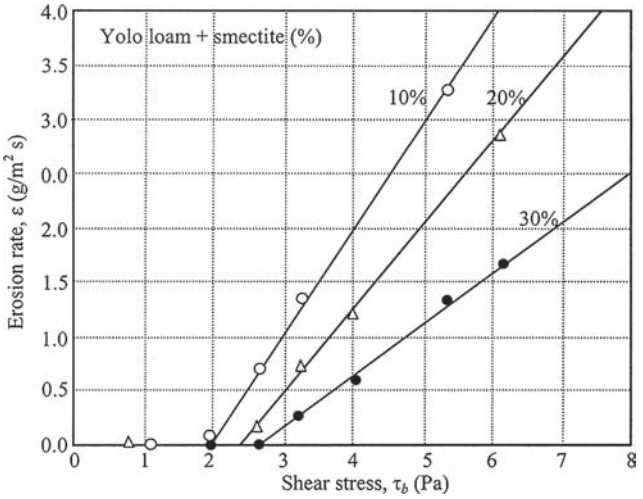

Fig. 4-20. Erosion rate versus bed shear stress for mixtures of Yolo loam and montmorillonite. Percent indicates montmorillonite by weight (adapted from Kandiah 1974).

line slope due to an increase in the shear strength of the mixture.

For beds that are stratified with respect to density and shear strength, formulas that account for the variation in τ_s with depth have been developed, e.g., by Parchure (1984) and Piedra-Cueva and Mory (2001). Although such formulas differ from (4-30), in most of them the erosion rate varies with the excess shear stress. This similarity, as well as experience from modeling applications, suggests that (4-30) can also be used for stratified beds with a reasonable degree of accuracy by allowing τ_s to vary with depth, i.e., by replacing τ_s by $\tau_s(z)$, where z denotes the vertical coordinate (Ariathurai et al. 1977; Hayter 1983).

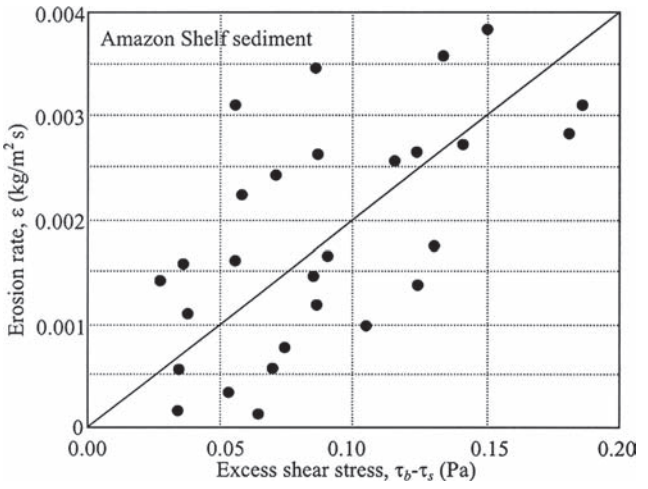

Fig. 4-21. Erosion rate versus excess shear stress based on the analysis of Vinzon (1998) using data from Kineke (1993).

Vinzon (1998) used measured time series of near-bed velocities and suspended sediment concentrations at sites on the Amazon shelf off Brazil reported by Kineke (1993) to develop the linear plot shown in Fig. 4-21. The observed relationship is akin to the lines in Fig. 4-20 and therefore conforms to Eq. (4-30), but with a considerably greater degree of data scatter. Similar plots have been developed by, among others, Sanford et al. (1991) and Sanford and Halka (1993) using data from the Chesapeake Bay.

4.8.3 Shear Strength

Although bed shear strength and bed density are neither uniquely interrelated nor are dimensionally homogeneous, efforts have been made to correlate these two parameters empirically, recognizing that, in general, the denser the soil the harder it is to erode. Thus, given τ_{sh} as a measure of soil shear strength, relationships have been developed of the general form (Table 4-10)

$$\tau_{sh} = \zeta_s \left(\phi - \phi_\ell\right)^{\xi_s} \tag{4-31}$$

where

ϕ = solids volume fraction;
ϕ_ℓ = limiting or minimum value of ϕ below which $\tau_{sh}=0$; and
ζ_s, ξ_s = sediment-specific coefficients.

Thus, according to Eq. (4-31), τ_{sh} depends on the excess solids volume fraction, $\phi-\phi_\ell$. Measures of shear strength in general include the apparent Bingham yield strength (τ_y), the vane shear strength (τ_v) and the surface erosion shear strength (τ_s). Among these, τ_y and τ_v are representative of the bulk physical properties of the soil. As noted in Section 4.2.2, τ_y is associated with soil rheology, and has been used, for example, to determine the bottom slope required to generate mud underflows (Mei and Liu 1987). Wotherspoon and Ashley (1992) correlated τ_y to the liquid content of sewer sediment deposit. The quantity τ_y is a measure of the bulk strength of the soil and has been used in geotechnical evaluations of cohesive soil consistency. Thus, for example, Annandale (1995) has suggested the classification given in Table 4-11.

Most studies on the erosion of submerged soils in the estuarine and marine environments are limited to "very soft" to "soft" cohesive materials identified in Table 4-11. This is because wave- and current-induced bed shear stresses in these environments are usually not large enough to erode stiffer soils. On the other hand, in rivers with high flow velocities, even firm soils can erode significantly over months and years (Jiang 1999). Thus, the vane shear strength is a convenient parameter commonly used to assess the erosion potential of cohesive soils in a given flow environment, even though it is not a highly accurate measure (Lee 1985).

Table 4-10 Expressions Relating Shear Strength to Solid Volume Fraction

Investigator(s)	Sediment	Shear strength, τ_{sh}(Pa)	ϕ_ℓ^a	ζ_s	ξ_s	ϕ range[a]
Krone (1963)	Estuary muds	Apparent Bingham yield (τ_y)	—[b]	466	2.55	0.008–0.57
Migniot (1968)	Marine muds	Apparent Bingham yield (τ_y)	—	Variable	4.00	0.094–0.19
Owen (1970)	Estuary mud	Apparent Bingham yield (τ_y)	—	1110	2.33	0.042–0.11
Vinzon (1998)	Shelf mud	Apparent Bingham yield (τ_y)	—	2024	2.62	0.021–0.19
Hwang (1989)	Lake mud	Vane (τ_y)	0.06	22.6	1.00	0.060–0.26
Thorn and Parsons (1980)	Estuary muds	Surface erosion (τ_s)	—	37.5	2.28	0.014–0.12
Kusuda et al. (1984)	Estuary mud	Surface erosion (τ_s)	—	6.50	1.60	0.032–0.11
Villaret and Paulic (1986)	Bay mud	Surface erosion (τ_s)	—	1.65	1.00	0.10–0.38
Black (1991)	Estuary mud	Surface erosion (τ_s)	—	1.88	2.30	0.13–0.25
Berlamont et al. (1993)	Marine muds	Surface erosion (τ_s)	—	5.41	0.90	0.02–0.07

[a]Use ρ_s = 2,650 kg/m^3 to convert ϕ ($=C/\rho_s$) to dry density or concentration C, except for the relationship of Hwang (1989) for which ρ_s = 2,140 kg/m^3.

[b]Not determined.

Source: Mehta and Parchure (2000).

Table 4-11 Soil Consistency Classification Based on Vane Shear Strength

Soil consistency	Identification	Vane shear strength (kPa)
Very soft	Easily molded by fingers	0–80
Soft	Molded by fingers with some pressure	80–140
Firm	Very difficult to mold; can be penetrated by a hand-spade	140–210
Stiff	Requires a hand pick for excavation	210–350
Very stiff	Requires a power tool for excavation	350–750

Source: Annandale (1995).

In contrast to τ_y and τ_v, the parameter τ_s, which occurs in Eq. (4-30), is related to the strength of surface flocs. Referring to the results in Table 4-10, the characteristic difference between τ_y and τ_s is reflected in the value of the proportionality coefficient ζ_s, which is considerably higher for τ_y (mean $\zeta_s = 1{,}200$, excluding the data of Migniot 1968) than for τ_s (mean $\zeta_s = 10.6$). Likewise, the exponent ξ_s is higher for τ_y (mean value 2.88) than for τ_s (mean value 1.62). With respect to the sole correlation for τ_v, observe that $\xi_s = 1$. It should be noted that this relationship of Hwang (1989) was developed for a lacustrine mud that contained a high amount (40% by weight) of organic material.

Conceptually the minimum value of ϕ, namely ϕ_ℓ, is analogous to the space-filling volume fraction at which the particle matrix begins to exhibit a measurable shear modulus of elasticity, which increases with increasing ϕ ($> \phi_\ell$) (James et al. 1988). The same threshold condition, sometimes referred to as the "gelling point," may apply to the development of

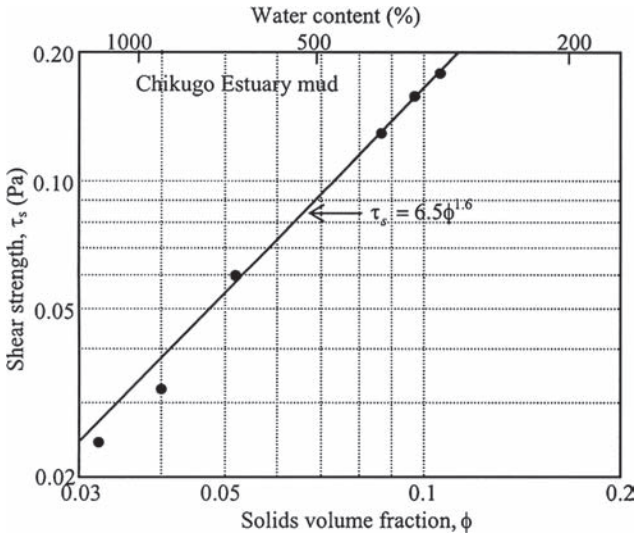

Fig. 4-22. Bed shear stress versus solids volume fraction and water content for Chikugo estuary (Japan) mud (after Kusuda et al. 1985).

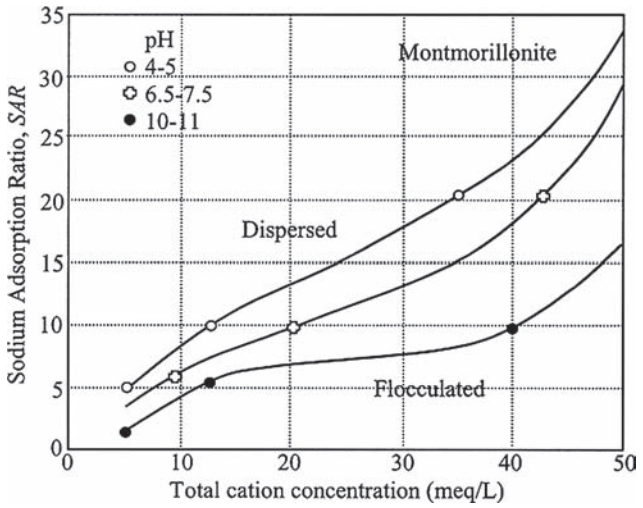

Fig. 4-23. Flocculation-dispersion boundary curves for a montmorillonite at three pH ranges (adapted from Kandiah 1974).

normal effective stress in the soil (Ross 1988). Hwang (1989) determined that $\phi_\ell = 0.06$ from a plot of measured τ_y versus ϕ by extrapolating the linear relationship ($\xi_s = 1$) to $\tau_y = 0$ when $\phi = \phi_\ell$. He further showed that this value of ϕ_ℓ ($= 0.06$) was commensurate with the density below which the mud was in a fluid-like state, and was therefore devoid of measurable strength. As seen from Table 4-10, other investigators did not report ϕ_ℓ, and therefore only limited use can be made of this parameter at present. An example of data conforming to (4-31) but without a knowledge of ϕ_ℓ is shown in Fig. 4-22, based on the work of Kusuda et al. (1985) on mud from the Chikugo River estuary in Japan.

Two factors on which ζ_s, ξ_s, and ϕ_ℓ can be expected to depend are bed sediment composition and fluid chemistry. This dependence is reflected in the variability in the values of ζ_s and ξ_s associated with τ_s in Table 4-10. The relative importance of composition and chemistry cannot be separated easily in these cases, because the shear strength of a given soil can be significantly influenced by even minor changes in the chemical composition of pore water (Ravisangar et al. 2001). Furthermore, even though salinity is reported in many investigations on estuarine and marine muds, other chemical factors can also affect the soil fabric, thereby influencing soil erodibility. For example, Fig. 4-23 shows the results of Kandiah (1974) for a montmorillonite based on measurements of the sodium adsorption ratio (SAR). This ratio of sodium ions (Na^+) to the sum of calcium (Ca^{++}) and magnesium ions (Mg^{++}) in the bed pore fluid is defined as

$$\mathrm{SAR} = \frac{\mathrm{Na}^+}{\left[0.5\left(\mathrm{Ca}^{++} + \mathrm{Mg}^{++}\right)\right]^{1/2}} \qquad (4\text{-}32)$$

where the ionic concentrations are measured in milliequivalents per liter. Figure 4-23 shows that this montmorillonite could be altered between dispersed (i.e., nonflocculated) and flocculated states merely by changing the pH of the pore fluid, either holding SAR constant or holding constant the total cation concentration in the pore fluid. Since a dispersed clay bed can erode with considerably greater ease than a flocculated bed of the same clay, Fig. 4-23 demonstrates that sediment composition alone cannot be a unique, or even dominant, determinant of bed erosion potential. This consideration underscores the need to use native water in laboratory erosion tests, or to reconstitute the eroding fluid based on an analysis of the native water with regard to its ionic composition. It is also a reason for in situ testing of bed erodibility in the prototype environment (Maa et al. 1993).

Inasmuch as τ_s is a measure of the strength of flocs at the bed surface, it reflects the order of aggregation of these surface flocs. In a bed prepared by allowing suspended sediment to deposit, the bed density characteristically increases with depth due to sorting and consolidation. The rate of increase is usually the highest just below the surface and gradually decreases with depth until the overburden is no longer sufficient to cause further consolidation. In the estuarine environment, beds formed by deposition in this way tend to increase in density until they reach ~1,300 to ~1,400 kg/m^3 at depths on the order of 20–60 cm. Increasing density with depth decreases the order of aggregation and increases the shear strength.

The trend of increasing shear strength with depth is seen in Fig. 4-24, in which shear strength profiles are given for the same bed of flocculated kaolinite in salt water, but after different periods of consolidation (Parchure 1984). The shear strength at a given consolidation period T_{dc} was determined by eroding the bed layer by layer. This procedure,

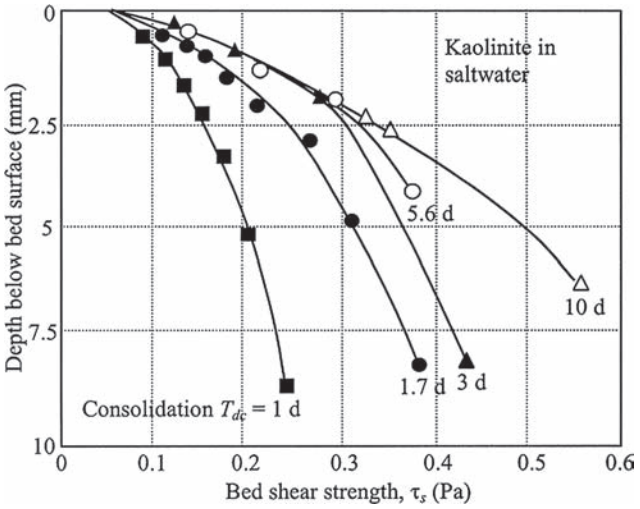

Fig. 4-24. Bed shear strength profiles for a bed of kaolinite in salt water (adapted from Parchure 1984).

credited to Thorn and Parsons (1980), was accomplished by increasing the flow-induced bed shear stress in steps, allowing the test to run at each step for a sufficiently long duration to cause bed scour to proceed to a depth at which no further erosion took place, because the shear stress at that depth was equal to the shear strength. In this way, the profile of strength variation with depth was constructed by knowing the applied stress at each depth. In Fig. 4-24 observe that because the aggregate order did not change at the surface due to the absence of overburden, the shear strength remained independent of the period of consolidation. Such a finding was also reported previously by Partheniades (1965), who correctly pointed out that this independence means that erosion occurs by breakup of inter particle bonds, and hence that this breakup process cannot be parameterized by such bulk soil indices as the Atterberg indices. Beneath the surface however, increasing shear strength reflects increasing floc strength with decreasing aggregate order. Recognizing that the time-variation of erosion rate depends on the shear strength profile, which in turn depends on the density profile, Jepsen et al. (1997) correlated the erosion rate directly with bed density.

When inorganic fine sediment is mixed with other materials, the effect on shear strength can be significant (Ashley and Verbanck 1996). Two common cases of interest are mixtures of mineral particles with organic material and with sand. In Table 4-12, shear strength parameters of Eq. (4-31) from three studies are summarized (Mehta and Parchure 2000; Marván et al. 2002). In all cases the experiments were conducted in the laboratory using muds from water bodies in Florida. These bodies receive organic sediments from a variety of terrigenous and aqueous sources. Observe that the exponent ξ_s is 0.83 for sediment from the Ortega River with 28% (by weight) organic matter. This value may be compared with the mean value of 1.62 from Table 4-10 for largely inorganic sediment beds. The organic-rich samples from the Rodman Reservoir (45% organic content) and the Lower Kissimmee River basin (50% organic content) showed practically no dependence ($\xi_s = 0$) of shear strength on density. Furthermore, these samples had very low shear strengths, on the order of 0.1 Pa.

The usually (but not always; see, e.g., Dennett et al. 1998) high erosion potential of organic-rich sediments is due to the comparatively light and weakly bound nature of the flocs or floccules. The lack of significant dependence of erosion on bed density may be explained as follows. Unlike clayey beds whose interface with water can be reasonably well defined, especially for dense beds, the organic-rich bed-water interface tends to develop a layer of "fluff' consisting of flocs released by way of elastic rebound from the bed with a thickness of a few floc diameters. Due to its low excess density, this fluff layer does not consolidate easily. Thus when fluid stress is applied, it is this layer of weakly interconnected particles,

Table 4-12 Shear Strength Parameters for Organic-Rich Sediments

Location	Organic fraction by weight (%)	Mixture granular density, ρ_s (kg/m^3)	ϕ_ℓ	ζ_s	ξ_s	ϕ range
Ortega River, Florida	28	2,032	NN. D.[a]	1.1	0.83	0.06 – 0.07
Lake Okeechobee, Florida	40	2,140	00.06	1.0	0.2	0.06 – 0.17
Rodman Reservoir, Florida	45	1,914	NN. D.	0.105	0	0.02 – 0.28
Lower Kissimmee River basin, Florida	50	1,586	NN. D.	0.099	0	0.08 – 0.38

[a]Not determined.
Sources: Mehta and Parchure (2000); Marván et al. (2002).

with a low negative buoyancy, that is entrained. Further, as the layer erodes it is replenished by continual "release" of flocs from within the bed that is disturbed by flow-induced deformations. As a result, since the density of the fluff layer is determined by the released flocs rather than the bed, the shear strength is largely unaffected by bed density.

4.8.4 Shear Strength of Fine/Coarse Sediment Mixtures

Fine sediment and sand can occur as interbedded layers alternating between fine- and coarse-grain layers (Jaeger and Nittrouer 1995), or as more homogenous mixtures. In general, bed stratigraphy reflects the depositional history of the accumulated sediment, and any subsequent changes brought about by physicochemical transformations and biogenic effects. Among the latter, bioturbation usually enhances homogeneity and causes the bed to become less resistant to erosion (Jaeger and Nittrouer 1999). In turn, coring data that show intact laminated structures may imply the absence of bioturbation (Kirby et al. 1994).

In a nonstratified bed composed of a mixture of sand and fine sediment, the shear strength may vary in a nonlinear way with the proportion of fine fraction. In order to demonstrate this effect, Torfs et al. (2001) derived the following expression for the critical shear stress of the homogeneous mixture:

$$\tau_{cm} = \left[\frac{\alpha_{3cg} \tan \Phi_{cg}}{\left(\alpha_{1cg} + \alpha_{2cg} \tan \Phi_{cg}\right)} + \frac{K' \zeta_s \left(\Phi_v - \Phi_{vc}\right)^{\xi_s}}{g\left(\rho_{sm} - \rho\right) d_m} \right] \times g\left(\rho_{sm} - \rho\right) d_m \quad (4\text{-}33)$$

where α_{1cg}, α_{2cg}, α_{3cg}, ϕ_{cg}, and K' are sediment-specific constants, ζ_s and ξ_s are defined per (4-31), and

ρ_{sm} = representative granular density of the mixture;
ρ = fluid density;
ϕ_v = solids volume fraction of the fine sediment-water mixture before it is mixed with sand;
ϕ_{vc} = value of ϕ below which the bed has practically no shear strength;
g = acceleration due to gravity; and
d_m = representative mixture diameter.

Torfs et al. have provided the necessary equations for the selection and calculation of these parameters.

In Fig. 4-25, τ_{cm} is plotted against the fine sediment weight fraction of the mixture, ψ. The dependence of τ_{cm} on ψ is embodied in the empirical relations $K' = 60|\psi - 0.018|^{1.9} - 0.029$ for $\psi \le 0.018$ and $K' = 0.88 - (1-\psi)^{3.5}$ for $\psi > 0.018$. The comparison between (4−33) and the data of Torfs (1995) is wholly diagnostic, because these relations, as well as parameters in (4−33), were derived from the experimental data included in the figure. These data, obtained in a laboratory flume, were on the erodibility of mixtures of a kaolinite with 0.23 mm diameter sand and, also, mixtures of a natural mud with the same sand. Starting with $\psi = 0$ corresponding to pure sand (at a nominal bulk density of 1,850 kg/m^3), the fine fraction was increased without changing the mixture bulk density, up to a maximum value of $\psi = 0.38$. The variation of τ_{cm} with ψ is observed to be nonmonotonic and seemingly passes through a minimum, yielding values of τ_{cm} that may at first be lower than those for sand (0.35 Pa), then increase to values larger than for sand, and increase further with increasing ψ. Notwithstanding the fact that this description is constrained by the paucity of data, and by possible albeit unquantified uncertainties in the estimates of the bed shear stress (Torfs 1995), it can be elaborated upon as follows.

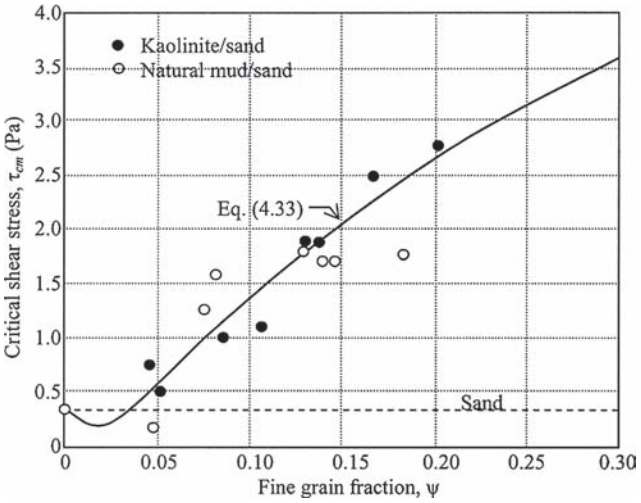

Fig. 4-25. Critical shear stress for erosion of kaolinite/sand and natural mud/sand mixtures versus fine-grain weight fraction: data points of Torfs (1995) and curve based on (4-33) (after Torfs et al. 2001).

Referring to Fig. 4-26, when a small quantity of fines is added to sand, a reduction in the intergranular friction between sand particles due to partial filling of pore spaces by the fines causes sand grains to erode with greater ease than in the absence of fines, thus lowering the critical stress for erosion below that for pure sand. This effect increases with increasing fine fraction until an interconnected, "space-filling" network of fines is established, when the threshold of motion becomes minimum. Given this condition, any further increase in the fine fraction causes the bed surface to be increasingly influenced by the fines. This is so because as clayey particles increasingly surround sand grains, sand-sand contacts decrease and also, the number of sand grains per unit surface area of bed decreases. Finally, as the fine fraction approaches unity, one can expect τ_{cm} to approach τ_s, the bed shear strength of the fine sediment (Panagiotopoulos et al. 1997).

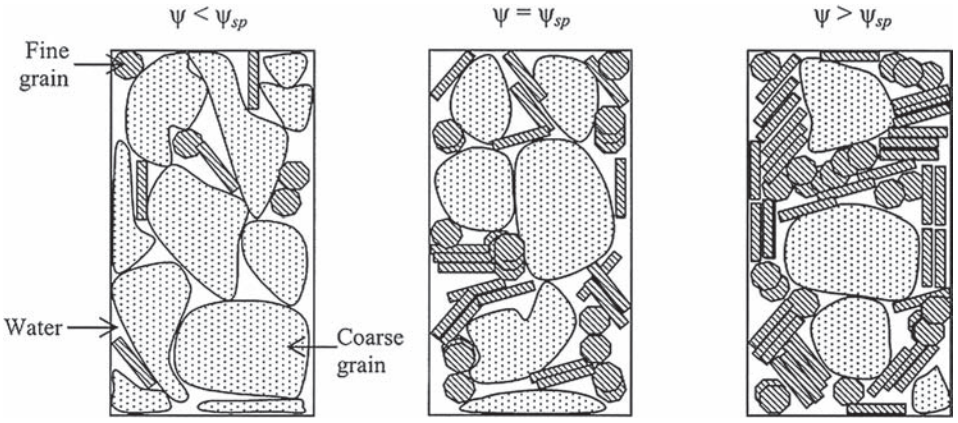

Fig. 4-26. Schematic drawings of a saturated bed composed of large and small grain populations. Left: small grain fraction is less than space-filling; center: small grain fraction is space-filling; right: small grain fraction exceeds space-filling value (after Torfs et al. 2001).

4.8.5 Erosion Rate Constant

The erosion rate constant ϵ_M in (4-30) generally depends on the same factors that influence τ_s. A noteworthy effect studied in the laboratory is the variation of ϵ_M with fluid temperature. In that regard, surface erosion of cohesive beds has been treated as a mechanism that is phenomenologically akin to the rate process theory for chemical reactions (Paaswell 1973). Conceptually, erosion occurs when a threshold "energy of activation" is exceeded, and interparticle electrochemical bonds are broken. Following this concept it can be shown that ϵ_M, and hence the rate of erosion ϵ, increases with increasing temperature in such a way that $\log(\epsilon/T)$ varies linearly with $1/T$, where T is the absolute temperature. This behavior can be represented by

$$\frac{\epsilon}{T} = \exp\left(\Delta - \frac{\Lambda}{T}\right) \tag{4-34}$$

Equation (4-34) was shown by Kelly and Gularte (1981) to hold for the erosion of a bed of grundite, with $\Delta = 34.7$ and $\Lambda = 10{,}145$. These coefficients are specific to the sediment-fluid mixture used and were obtained at a constant eroding flow velocity of 0.18 m/s. Their magnitudes conform to the units of ϵ in g/m^2 s and T in K. In general, these coefficients can be expected to depend on the physicochemical properties of the sediment and fluid, on the solids weight fraction ϕ and, especially with respect to Δ, on the applied bed shear stress. As Lau (1994) indicated, an increase in temperature only marginally affects the van der Waals attractive force at the particle surface, but the interparticle repulsive force increases significantly. As a result, particle-particle bonds rupture more easily at higher temperatures, thereby leading to enhanced erosion.

Based on the observation that the rate of erosion decreases as the shear strength increases, Arulanandan et al. (1980) defined another erosion rate constant $\epsilon_N = \epsilon_M/\tau_s$, and plotted it against τ_s derived from erosion tests on a large number of soil samples. Introducing this modified rate constant conveniently redefines (4-30) in terms of ϵ_N and τ_s as

$$\epsilon = \epsilon_N \left(\tau_b - \tau_s\right) \tag{4-35}$$

It was found that, notwithstanding data scatter, in the mean ϵ_N decreased monotonically and exponentially with increasing τ_s. Compilation of laboratory data from numerous studies in addition to those of Arulanandan et al. (1980), when examined collectively, suggests that the empirical relationship between ϵ_N and τ_s may be extended to include data grouped by sediment and fluid composition. Despite the evidently approximate nature of the resulting curves relating ϵ_N to τ_s, this approach affords a crude means to calculate the erosion rate from (4-30) knowing the bed density, inasmuch as the shear strength in related to density via (4-31). Accordingly, the plot shown in Fig. 4-27 was prepared based on the relationship

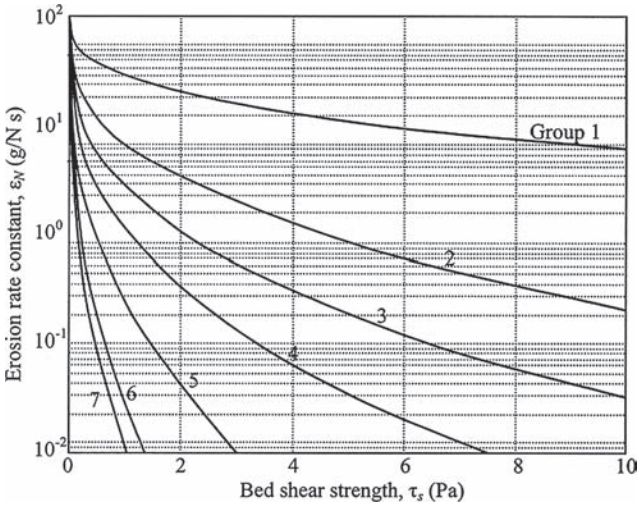

Fig. 4-27. Erosion rate constant ϵ_N versus bed shear strength τ_s for different bed groups identified in Table 4-13. (after Mehta and Parchure 2000).

Table 4-13 Coefficients for (4-36) and Properties of Groups 1–7

Group no.	Coefficients in (4-36)[a]		Clay content (%)	Cation exchange capacity (meq/100 g)
	χ_s	λ_s		
1	1.345	0.368	24	13
2	2.892	0.372	27	18
3	3.905	0.356	28	15
4	4.938	0.355	23	15
5	6.594	0.382	27	15
6	9.011	0.386	33	16
7	10.582	0.252	19	23

[a]These values of χ_s and λ_s apply when τ_s is in Pa and ϵ_N is in g/N s.

Source: Mehta and Parchure (2000).

$$\epsilon_N = \epsilon_{N0} \exp\left(-\chi_s \tau_s^{\lambda_s}\right) \tag{4-36}$$

for which the value of ϵ_{N0} was conveniently chosen as 200 g/N s. Mehta and Parchure (2000) provide actual fits of (4-36) with data within each of seven groups. These groups and the coefficients χ_s and λ_s for each group are given in Table 4-13. As observed therein, χ_s and λ_s show a weak correlation with the cation exchange capacity of the sediment, although evidently the exchange capacity is by no means the sole determinant of soil erodibility. Observe also that while λ_s varies within a narrow range (0.252 to 0.386), χ_s varies over an order of magnitude (1.345 to 10.582), which implies that this parameter is sensitive to soil composition. The curves in Fig. 4-27 highlight the wide range of ϵ_N values that can occur for a given τ_s. The form of (4-36) is consistent with the observation of, among others, Galani et al. (1991), who showed that ϵ_N decreases with increasing duration of consolidation of the bed, which essentially increases the bed shear strength.

Using Eq. (4-35) along with (4-31), (4-34), and (4-36), the following erosion rate expression is obtained:

$$\epsilon = \epsilon_{N0}\, T \exp\left(\Delta - \frac{\Lambda}{T}\right) \exp\left(-\chi_s \left[\zeta_s \left(\phi - \phi_l\right)^{\xi_s}\right]^{\lambda_s}\right) \times \left[\tau_b - \zeta_s \left(\phi - \phi_l\right)^{\xi_s}\right] \tag{4-37}$$

The application of (4-37) can be illustrated by the following example of erosion in a channel. Consider values of the coefficients ϵ_{N0}=200 g/N s, χ_s=2.892; λ_s=0.372, ζ_s=1.65, ξ_s=1.00, ϕ_ℓ=0, Δ=27.0, and Λ= 10,145. Now consider a bed of density ρ=1,545 kg/m^3 subject to a flow-induced bed shear stress τ_b=1 Pa at a water temperature T=27° C (300° K). With ρ_w=1,000 kg/m^3 and ρ_s=2,650 kg/m^3, we obtain ϕ=0.33 from Eq. (4-5). Equation (4-37) then yields ϵ=2.98 g/m^2 s.

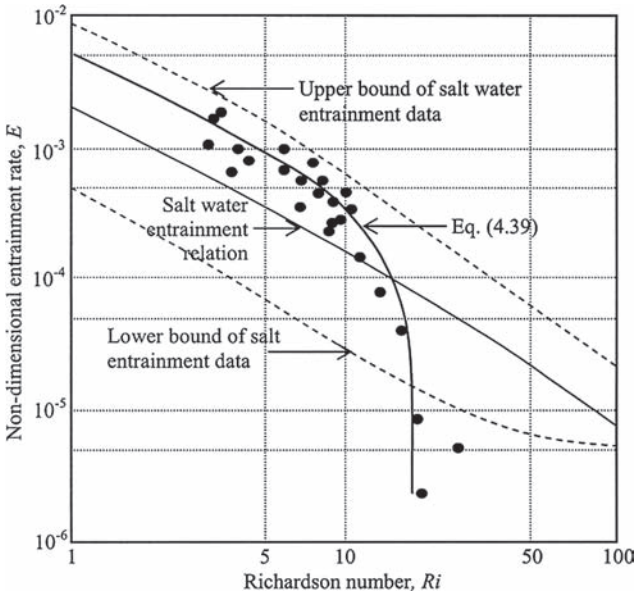

Fig. 4-28. Nondimensional entrainment rate against Richardson number. Comparison between data on fluid mud entrainment (dark circles), corresponding curve based on (4-39), salt entrainment data (upper and lower bounds) reported by Christodoulou (1986) and salt entrainment relation obtained from (4-39) (after Mehta and Srinivas, 1993).

4.8.6 Mass Erosion

Mass erosion, in which the bed fails and releases chunks or clasts of material, has been modeled on Eq. (4-30), even though this relation was derived for surface erosion (Mehta and Lee 1994). This approach, although very approximate, is convenient because one merely has to calibrate for ϵ_M and τ_s. Mass erosion is often considered to occur when stiff beds are subjected to high stresses (Ariathurai et al. 1977). However, even weak beds can mass erode at comparatively low stresses. In flume tests, Hwang (1989) reported mass erosion of beds of organic-rich sediment from Lake Okeechobee in Florida (Table 4-4). Starting with no flow and increasing the bed shear stress in steps, resuspension initially occurred by surface erosion, and at high stresses (but low compared to those for stiff clays, for example) the 3- to 4-cm-thick bed failed almost entirely. A feature of the erosion process was that in some cases ϵ_M and τ_s were considerably higher for mass erosion than for surface erosion of the same bed. Thus, for example, for a bed of density 1,200 kg/m^3, ϵ_M and τ_s for surface erosion were 5.6×10^{-6} kg/m^2 s and 0.65 Pa, respectively, whereas the corresponding values for mass erosion were 5.6×10^{-4} kg/m^2 s and 1.8 Pa.

Recognizing the rapidity with which mass erosion occurs, Ariathurai et al. (1977) introduced a simple model, which

essentially amounts to instantaneous erosion of a bed layer of thickness Δz_b in time Δt,

$$\epsilon = \rho_b \frac{\Delta z_b}{\Delta t} \tag{4-38}$$

where ϵ is the mass rate of erosion (or erosion flux) and ρ_b is the bed density. Equation (4-38) applies when the bed shear stress exceeds the shear strength for mass erosion. The thickness Δz_b was determined by calibration against data on the time-variation of the suspended sediment concentration in the Savannah River estuary, Georgia.

When a water jet impinges on a fine-grained soil a hole develops when the jet momentum exceeds the requisite critical value. In this mass erosion process, the rate of erosion is usually measured as the time-rate of change of the cube-root of the hole volume. Traditionally, this rate is expressed as a function of the erosion-governing parameters through dimensional analysis (Hanson 1990; Hollick 1976; Moore and Masch 1962).

4.8.7 Fluid Mud Entrainment

Sediment entrainment can occur due to hydrodynamic instabilities at the interface between very soft mud and water, resulting in the generation and breakup of the interfacial billows by shear flow. This process has been described in terms of a balance between production of turbulent kinetic energy, buoyancy work in entraining the sediment, and viscous energy dissipation (Uittenbogaard 1995; Kranenburg 1994b; Scarlatos and Mehta 1993; Winterwerp et al. 1993; Winterwerp and Kranenburg 1997a). Bottom response in this case is distinct from surface erosion of sediment flocs, which occurs over typically harder cohesive beds (Taki 1990). In the prototype environment, interfacial undulations can occur at the frequency of surface wave forcing, i.e., in the forced mode, and also in the free mode. In the forced mode, additional, low-frequency oscillations can occur as a result of interactions among the forcing wave frequencies (Jiang 1993). In the free mode the interface tends to oscillate at the buoyancy (Brunt-Väisälä) frequency (Jiang 1999; Wright et al. 1988).

Based on laboratory tests in a flume, Mehta and Srinivas (1993) proposed the relation for the rate of sediment entrainment

$$E = \frac{dz_b/dt}{U} = A\ Ri^{-1} - D\ Ri \tag{4-39}$$

where

E = dimensionless entrainment rate, i.e., the rate of change of bottom height, dz_b/dt, divided by U, the characteristic flow velocity above the water-mud interface;

A and D = sediment dependent coefficients; and

Ri = the global Richardson number, defined as

$$Ri = \frac{hg\left(\rho - \rho_w\right)/\ \rho_w}{U^2} \tag{4-40}$$

In Eq. (4-40), h is a characteristic water depth above the interface, ρ is the suspension density, and ρ_w is water density. In Fig. 4-28, E is plotted against Ri and compared with data on the entrainment of a clayey fluid mud in a laboratory flume. Values of the coefficients are $A = 5.2 \times 10^{-3}$ and $D = 1.6 \times 10^{-5}$. Since the second term on the right hand side of (4-39) arises from the effect of settling, D depends on the settling velocity. Setting $D = 0$ leads to the inverse dependence of E on Ri, as in salt entrainment. In Fig. 4-28, the resulting expression is compared with data on the entrainment of salt water into fresh water compiled by Christodoulou (1986). Observe that due to the settling effect, at relatively high values of Ri sediment entrains much less efficiently than salt. Several factors are responsible for the drop in the entrainment rate at high Ri, including the viscous effect and wall friction. In addition, increased resistance to entrainment due to density stratification plays a role. When these and related effects can be explicitly included in the entrainment rate formulation, the final equation is found to be similar in form to Eq. (4-30) (Kranenburg and Winterwerp 1997; Winterwerp and Kranenburg 1997b). Referring to Eq. (4-40), one may define a critical value Ri_c of the Richardson number above which sediment entrainment can be assumed to be zero, as suggested by Odd and Cooper (1989). In Fig. 4-28 Ri_c is seen to be close to 20.

When fluid mud is mobile, i.e., has been set in motion by flow above the interface, U must be replaced by ΔU, the characteristic difference between the velocity above and below the interface. It is common to find layers of fluid mud set in motion by tidal flows, as shown in Fig. 4-29 from measurements in the Avon River, U.K. (Kendrick and Derbyshire 1985). Ross (1988) examined fluid mud layer motion as a simple Rayleigh flow problem (Phan-Thien 1983) in which the layer is set in motion by the downward diffusion of momentum. Trowbridge and Kineke (1994) provided a fuller treatment, both datawise and from the perspective of non-Newtonian flow modeling of fluid mud driven by flow over the Amazon Shelf.

4.9 WAVE-INDUCED EROSION

4.9.1 Nearshore Zone

In shallow nearshore waters the mode of erosion of bottom mud depends on waves and on the bottom condition. As schematized in Fig. 4-30, the sediment-active zone is bounded by the shoreline and the terminal depth, defined as that depth seaward of which wave action is unable to reach the bottom to cause significant changes in the bed profile. The nearshore profile is subdivided by the wave breakerline

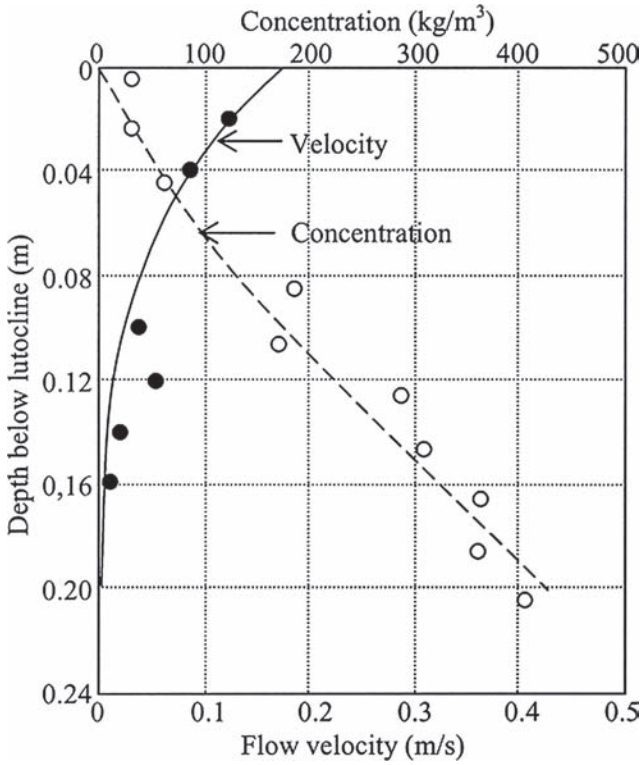

Fig. 4-29. Flow velocity and concentration profiles below lutocline in the Avon River, UK (adapted from Kendrick and Derbyshire, 1985).

into the surf zone and the offshore zone between this line and the terminal depth.

Although the terminal depth has been shown to be a reasonably well-defined parameter (depth of closure) characterizing the active sand profile, for fine sediment profiles laden with fluid mud it is a notional depth that requires quantitative assessment. Fluid mud generation has been examined in laboratory flumes and in the lacustrine environment where wave forcing dominates (e.g., Lindenberg et al. 1989; Li 1996), and it appears that rough estimates of the thickness of the fluid mud layer formed under sustained wave action can be obtained by calculating the depth, i.e., the lower level of the fluid mud layer, at which the wave-induced (maximum) lift on a unit sediment mass balances

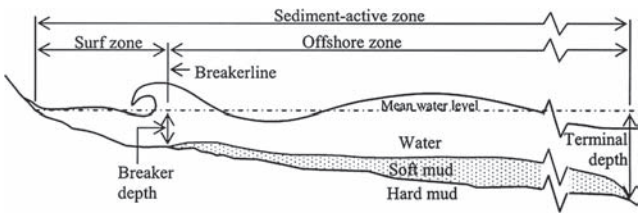

Fig. 4-30. Definitions related to the sediment-active nearshore zone (after Rodriguez 2000).

the resistance to liquefaction due to gravity and cohesion (Li and Mehta 2001). Hence the terminal depth, h_c, corresponds to the critical condition when the layer thickness reduces to nil. Accordingly, it can be shown that this depth can be estimated from $h_s = \alpha_d \log(\beta_d H_s)$, where H_s is a characteristic maximum wave height, and α_d, β_d are coefficients that depend on the bed properties and also on the wave period (Rodriguez 2000). This equation is applicable to areas where the terminal depth is on the order of 1 m or higher. Very little prototype information on α_d, β_d is available, inasmuch as the distance from the shoreline up to which the muddy bottom is regularly or episodically turned over by waves has not been explored in any systematic way. From data on waves, water depths, and fluid mud thickness in Lake Okeechobee in Florida, $\alpha_d = 20.4$ and $\beta_d = 0.73$ have been obtained, with the wave height and water depth measured in meters (Rodriguez 2000; Li 1996).

The position of the breakerline, and hence the breaker (water) depth below mean water level, depends on the shape of the profile and the degree of wave damping. Profile shape, in turn, depends on the composition of bottom material and also on whether it is molded by waves or tide (Friedrichs 1993; Roberts et al. 2000). Wave breaking in the surf zone tends to erode and rapidly disperse the eroded material over the water column. In the comparatively less energetic zone seaward of the breakerline mud liquefaction by waves can occur, and transport of the resulting soft mud is often the main reason for profile changes. It appears that apart from gravity slide, which is typically seaward, fluid mud transport can occur landward due to streaming, a second-order hydrodynamic effect associated with wave propagation at the water surface and at the interface between water and fluid mud, and the associated fluid velocities. Depending on the direction of wave incidence, streaming can be in the cross-shore direction or both cross-shore and alongshore directions (Shibayama et al. 1986; Sakakiyama and Bijker 1989; Jiang and Mehta 1996; Rodriguez and Mehta 1998).

Depending on tide and wave conditions, bottom sediment properties and sediment sources and sinks, muddy coast profile shapes can be "convex-upward" or "concave-upward," the latter being qualitatively akin to sandy beach profiles (Kirby 1992; Friedrichs 1993; Lee 1995). By assuming wave height to decrease with distance by damping due to viscous dissipation within bottom mud, and wave breaking in the surf zone, Lee (1995) obtained the following expression for the profile depth, $h(y)$, below mean water level

$$h = h_0 e^{4k_i(y_0 - y)} \left(\frac{y}{y_0}\right)^2 + F_0 y e^{-\beta_0 y} \tag{4-41}$$

where

y = distance from shoreline;

h_0, y_0 = coordinates of the offshore end of the profile;
k_i = wave damping coefficient;
F_0 = bottom slope at $y = 0$;

and the coefficient β_0 accounts for the offshore extent of the combined influence of bottom slope at the shoreline and scour due to wave breaking at the shoreline.

Relatively few measurements of the wave-damping coefficient applicable to muddy coast profile dynamics seem to have been made. From two nearshore wave gages that were 3.4 km apart in the Gulf of Mexico off Louisiana, Tubman and Suhayda (1976) recorded a 48% reduction in wave energy corresponding to $k_i = 0.00020$ 1/m. Near Triangular Marsh in Corte Madera Bay, California, Liang and Williams (1993) also reported $k_i = 0.00020$ 1/m based on wave data. An example of fitting Eq. (4-41) to a convex-upward profile measured along the coast of Louisiana (Kemp 1986) is shown in Fig. 4-31 (Lee 1995). A similar comparison for a concave-upward profile is shown in Fig. 4-32. When the profile is molded by tide, the shape is different from (4-41) and is strongly influenced by the tidal range (Kirby 1992; Friedrichs 1993; Roberts and Whitehouse 2001).

The coefficient k_i is particularly sensitive to mud density. Lee and Mehta (1997) for instance showed that in the muddy bottom environment of the Gulf of Mexico off Mobile Bay in Alabama, k_i increased from 0.0005 1/m to 0.023 1/m as the

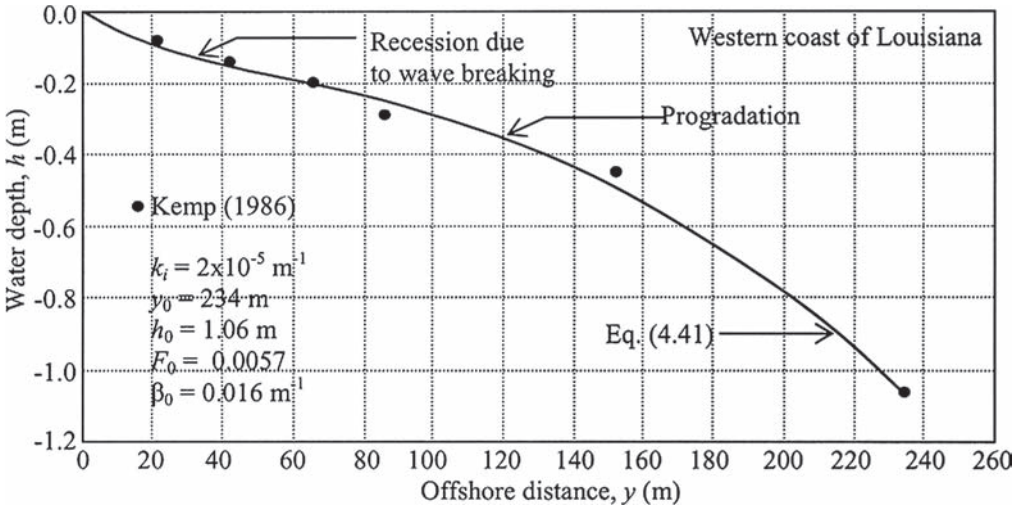

Fig. 4-31. Comparison of (4-41) with profile data from Louisiana coast obtained by Kemp (1986).

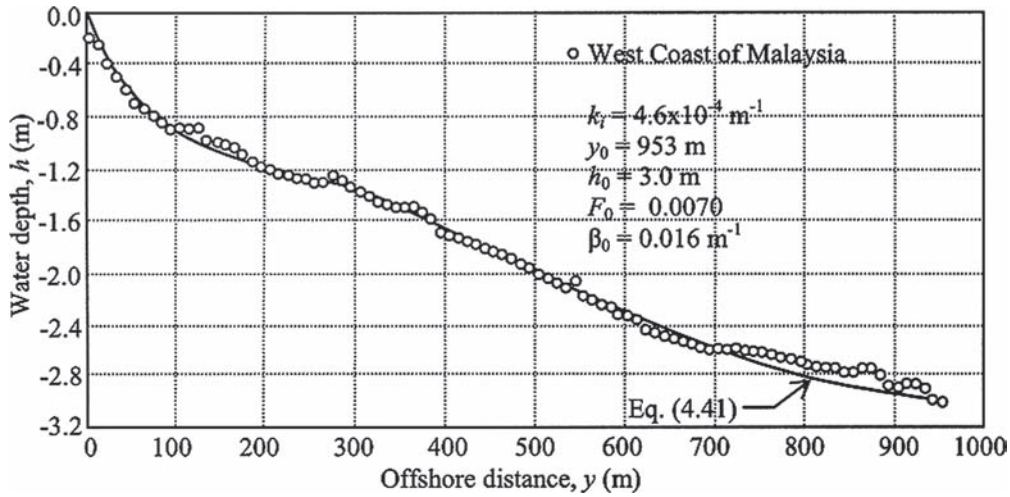

Fig. 4-32. Comparison of Eq. (4-41) with profile from the west coast of Malaysia (after Lee and Mehta, 1997).

Table 4-14 Coefficients in (4-41) for Concave and Convex Profile Configurations

Location (source)	Profilestate	F_0		β_0 (1/m)		k_i (1/m)	
		Mean	Std. dev.	Mean	Std. dev.	Mean	Std. dev.
Malaysia, China, U.S. (Lee and Mehta 1997)	Concave (81 profiles)	0.059	0.083	0.046	0.054	0.42	0.13
	Convex (15 profiles)	0.026	0.019	0.015	0.0084	0.016	0.027

mud density decreased from 1,302 to 1,139 kg/m^3. In general, the wave attenuation coefficient, k_i, is related to wave amplitude according to $k_i = -(1/\ell)\ln(a_1/a_0)$, where a_0 is the wave amplitude at $y = y_0$ and a_1 is the amplitude at a shoreward distance ℓ. Based on 96 profiles, F_0, β_0, and k_i were correlated with the state of the profile (Lee 1995), considering concave-upward profiles to be "erosional" and convex-upward profiles to be "accretionary." The resulting values (means and standard deviations) of these three parameters are given in Table 4-14.

4.9.2 Profile Stability Factor

Profile stability, i.e., whether a given profile will accrete, will remain as it is, or will erode, can be characterized by the ratio of an overall shore stabilizing factor, F_S, to an overall shore destabilizing factor, F_D. A profile stability number, S, can then be defined (Mehta and Kirby 1996) as

$$S = 1 - \frac{F_S}{F_D} \tag{4-42}$$

With respect to Eq. (4-42) the three cases that can arise are (1) $F_D = F_S$ or $S = 0$, signifying marginal stability; (2) $F_D > F_S$ or $S > 0$, for destabilizing or eroding conditions; and (3) $F_D < F_S$ or $S < 0$, for stable or accretionary conditions. Summing the corresponding individual stabilizing and destabilizing factors, f_{Di} and f_{si}, respectively, F_D and F_S, are obtained from $F_D = \sum \alpha_{Di} f_{Di}$ and $F_S = \sum \alpha_{Si} f_{Si}$, where α_{Di} and α_{Si} are weighting coefficients, subscript i represents a particular factor, and $\sum$ denotes summation. By definition, the weighting coefficients must satisfy the conditions: $\sum \alpha_{Di} = 1$; $\sum \alpha_{Si} = 1$. Equation (4-42) can now be stated as

$$S = 1 - \frac{\sum \alpha_{Si} f_{Si}}{\sum \alpha_{Di} f_{Di}} \tag{4-43}$$

To calculate S from Eq. (4-43) for a given shoreline, all relevant factors and the corresponding weighting coefficients must be evaluated. For a broad categorization stability, the effectiveness of individual factors contributing to S can be considered to assume the following values and associated effects on stability: 0 = no or low effect, ± 1 = moderate effect, ± 2 = significant effect, and ± 3 = very significant effect. Further, one may conveniently consider that "moderate" effect for any particular factor corresponds to marginal stability ($S = 0$), i.e., a nonerroding, nonaccreting profile. Thus, in Eq. (4-43), setting $S = 0$ and each f_{Di} and f_{Si} to unity yields $0 = 1 - (\Sigma \alpha_{Si} / \sum \alpha_{Di})$, which is consistent with the definition of the weighting coefficients. It follows from this qualitative assignment of parametric values that the weighting coefficients represent the relative magnitudes of the various factors when they individually have moderate effects.

Although numerous shore destabilizing factors actually contribute to profile stability, noteworthy factors include waves and storm surge, structures, tides, and biophysicochemical processes. The corresponding stabilizing factors are sediment supply, bottom hardness, structures, morphologic control, sediment composition, vegetative cover, and biophysicochemical processes.

Waves, storm surge, and intrusive structures often contribute significantly to erosion, as do tides (and associated currents) when they are strong. Because storm surge data are not commonly available, one may consider waves as surrogates for the storm surge effect, even though wave and storm surge statistics are often not entirely interdependent. Also, an influence not easily quantified is the sediment transporting role of a storm surge and the ensuing change in the profile.

Among biological processes, bioturbation is probably the most important destabilizing factor, although biochemical production of gas, e.g., methane, can also destabilize the bottom. Such factors as air and water temperature, salinity and water quality parameters, and the various positive and negative feedbacks linking physical and biophysicochemical processes further complicate biologically driven systems, which tend to play an important role, at times even a dominant one, in areas where waves and tides are comparatively weak.

Sediment supply is a characteristically significant factor governing shore stability because, irrespective of the magnitude of the erosive forces, a profile can hold fast or accrete as long as the rate of sediment supply equals or exceeds the rate of depletion. Conversely, if sediment supply becomes

insufficient, the likelihood of a shoreline remaining static is low, especially in the long run, except perhaps through hardening by structural means. Bottom hardness, as defined by standard measures of soil strength, can be quite important in distinguishing between overconsolidated and weakly consolidated beds.

Some structures can promote stability by sheltering a coast from erosive forces, and their role can be as noteworthy as that of bottom hardness. Other structures can have the opposite effect, namely, one of shoreline destabilization by reduction or elimination of sediment supply. In a similar vein, morphologic control can be exerted by offshore bathymetry on wave action and associated alongshore water and sediment transport. Shoreline configuration can be equally significant, for instance by promontories in sequestering sediment and thereby enhancing stability. Sediment composition partly determines hardness, although hardness also depends on consolidation and gelling. On the other hand, given two sediment beds of the same density, the less cohesive material is likely to erode more easily than the other.

Vegetative canopies tend to impart stability, as do certain benthic biological processes, e.g., surficial mats produced by secretions including mucopolysaccharides. Finally, tide and tidal currents can also influence stability through intertidal wetting and drying, because desiccation can measurably enhance profile hardness by soil encrustation.

From an inspection of the effects of the various factors at several muddy coasts, the following expression for S can be defined:

$$S = 1 - \frac{0.25f_{S\text{sed}} + 0.20f_{S\text{bh}} + 0.15f_{S\text{st}} + 0.15f_{S\text{mor}} + 0.10f_{S\text{com}} + 0.10f_{S\text{veg}} + 0.05f_{S\text{bio}}}{0.40f_{D\text{wv}} + 0.30f_{D\text{st}} + 0.25f_{D\text{tc}} + 0.05f_{D\text{bio}}} \tag{4-44}$$

where subscripts are wv for waves, st for structures, tc for tide and tidal currents, sed for sediment supply, bh for bottom hardness, mor for morphology, com for sediment composition, veg for vegetation, and bio for biophysicochemical effects.

To fully assess the applicability of Eq. (4-44) in predicting shore stability, extensive data sets for evaluating the coefficients and factors are required. Here we will illustrate how this might be accomplished by considering some diagnostic examples, giving consideration only to the most important factors contributing to stability.

The Gulf of Mexico shoreline of Louisiana near Cheniere au Tigre undergoes seasonal fluctuations due to a variable wave climate, and its mean position is stabilized by mud supply derived ultimately from the Mississippi River (Kemp 1986). In this moderate coastal environment, the mean astronomical tidal range is on the order of 0.5 m, which is modulated by frequency contributions from frontal-wind-induced oscillations, especially in winter. The shore, backed by marsh vegetation, has a biogenically active mud flat morphology with sediment diameter in the range 1 to 5 μm and is dominated by fluid mud. On the basis of a scale for effects ranging from 0 to ±3 the following values will be assigned: $f_{D\text{wv}}$, $f_{S\text{sed}}$, $f_{S\text{bh}}$, $f_{S\text{veg}}$, and $f_{S\text{bio}}$ all equal to unity, and the remainder equal to zero. Equation (4-44) then yields $S = -0.50$, which is less than zero, and correlates with the observed seasonal mean stability of the shoreline, notwithstanding longer term changes due to the relative rise in sea level experienced in this region.

The value of S for Louisiana and other sites including India (Mathew and Baba 1995), Indonesia (Tarigan et al. 1996), and Suriname (Eisma et al. 1991; Wells 1983), are given in Table 4-15. Along the coast of Kerala in India, mudbanks are believed to be enhanced in part by the inclement monsoonal waves but are less active in fair weather, because the high monsoonal waves are able to transport quantities of mud from an offshore pool to the shore by streaming. At the end of the monsoon, in the absence of significant streaming, the nearshore-transported mud is thought to slide offshore and to not return until the onset of the following monsoon (Mathew and Baba 1995).

The shorelines of Indonesia at Teluk Waru, Madura, and Surabaya are partly sheltered against waves by neighboring islands, and in conjunction with the absence of significant sediment supply they exhibit marginal stability. In general, notwithstanding the example from India, which is unique in

Table 4-15 Calculated Stability Numbers versus Observed Shore Stability

Location	Stability number, S	Observed profile stability
Louisiana	−0.50	Generally stable, with seasonal variability
Kerala (monsoon), India	~0	Shore-attached mudbanks occur at specific locations
Kerala (fair weather), India	0.75	Mudbanks are absent
Teluk Waru, Indonesia	~0	Marginally stable environment
Surinam	~0	Mudbanks are stable over short term; translate alongshore over a decadal time scale
Selangor, Malaysia	0.67	Eroding coast
Madura, Indonesia	~0	Marginally stable environment
Surabaya, Indonesia	~0	Marginally stable environment

terms of the historically transient nature of the mudbanks, if a long-established muddy coast is currently eroding, it is natural to look for possible anthropogenic causes of the altered state of the shoreline. Thus, for example, at the Selangor coast of Malaysia where $S = 0.67$, this once-stable mangrove-fringed coast has been eroding in recent decades due to reduced detrital supply from rivers as a result of diversion of river waters for agricultural usage (Midun and Lee 1989).

4.9.3 Erosion by Breaking Waves

Referring to the surf zone in Fig. 4-30, among others, Azam (1998) and Yamanishi et al. (1998) have shown that the erosion of mud bed is caused by the impact force as the wave breaks. An expression for the mass flux or the rate of bed erosion, ϵ_b, can be introduced as (Rodriguez 2000)

$$\epsilon_b = \epsilon_{bw}\left(\frac{H_b - H_{bc}}{H_{bc}}\right)^{\delta_b} \tag{4-45}$$

where H_b is the breaker height, H_{bc} is the critical value of H_b below which there is no measurable erosion, ϵ_{bw} is the value of ϵ_b when $H_b = 2H_{bc}$ and $\delta_b = 1$, and δ_b is a sediment-specific coefficient. In (4-45) ϵ_b is conveniently considered to depend on the breaker height, i.e., the wave height at the seaward end of the surf zone, rather than the local wave height within the surf zone, and thus represents a mean value applicable over the entire surf zone. This is often a reasonable approximation because, as a result of wave damping by bottom mud, the surf zone over a muddy bottom tends to be considerably narrower than that over a rigid or sandy bottom. However, in general, with increasing surf zone width the applicability of Eq. (4-45) becomes increasingly qualitative, unless H_b is replaced by the corresponding local wave height and the equation is locally calibrated for ϵ_{bw}, H_{bc}, and δ_b.

Coefficients in Eq. (4-45) from some studies are given in Table 4-16. In each case the rate of erosion was determined by comparing nearshore bottom profiles at different times, calculating the associated volumetric changes, and from these the corresponding mass changes, given the bottom density. Illustrative plots of Eq. (4-45) are shown in Fig. 4-33. The data are for a consolidated glacial till from the northern shore of Lake Ontario in Canada (Gelinas and Quigley 1973). With regard to Eq. (4-45) it is observed that, although both a linear regression fit ($\delta_b = 1$) and a power-law fit ($\delta_b = 0.5$) appear to be reasonable, the power-law fit is better (regression coefficient $r^2 = 0.80$) than the linear fit ($r^2 = 0.71$). In all other cases given in Table 4-16, $\delta_b = 1$ was found to be reasonable, contingent upon the typically sparse data sets used to fit Eq. (4-45) (Rodriguez 2000).

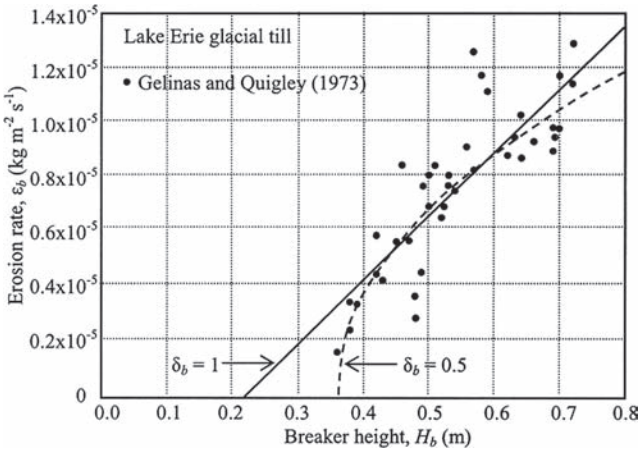

Fig. 4-33. Erosion rate within the surf zone as a function of breaking wave height for the northern shore of Lake Erie using data of Gelinas and Quigley (1973). Curves are based on Eq. (4-45) (after Rodriguez 2000).

4.9.4 Erosion by Nonbreaking Waves

Here we will consider the offshore zone (Fig. 4-30), i.e., the zone seaward of the surf zone up to the depth of closure, under nonbreaking waves and when the bed is not liquefied, i.e., no significant layer of fluid mud is present. In this case,

Table 4-16 Coefficient Values for Eq. (4-45) for Breaking Wave-Induced Erosion

Sediment source and investigator(s)	ϵ_{bw} (kg/m^2 s)	H_{bc} (m)	δ_b
50/50 (by weight) mixture of a kaolinite and an attapulgite: laboratory tests (Lee 1995; Tarigan 1996)	7.56×10^{-6}	0.027	1
Louisiana coast mud (Kemp 1986)	2.37×10^{-6}	0.087	1
Lake Erie glacial till: laboratory tests (Bishop and Skafel 1992; Bishop et al. 1992; Skafel and Bishop 1994)	1.39×10^{-3}	0.083	1
Lake Ontario glacial till (Nairn 1992)	4.18×10^{-5}	0.57	1
Lake Erie glacial till (Kamphuis 1986)	7.34×10^{-6}	0.29	1
Lake Erie glacial till (Gelinas and Quigley 1973)	5.48×10^{-6}	0.23	1
Lake Erie glacial till (Gelinas and Quigley 1973)	1.07×10^{-5}	0.36	0.5

Source: Rodriguez (2000).

erosion rate formulas determined for wind-generated as well as mechanically produced waves in flumes tend to support the validity of the functional form of Eq. (4-30), i.e., the erosion rate expression developed for steady flows. Relevant information is summarized in Table 4-17, in which characteristic parameters are given for the expression

$$\epsilon = \epsilon_W \left(\frac{\tau_b - \tau_s}{\tau_s} \right)^{\delta_W} \tag{4-46}$$

For $\delta_W = 1$, Eq. (4-46) reduces to Eq. (4-30). In fact, as seen from Table 4-17, experimental data at times have yielded values of δ_W close to unity. In Eq. (4-46), τ_b is the peak value of the bed shear stress during the wave cycle, and the shear strength τ_s can differ from that associated with current-induced erosion due to the effect of cyclic loading on the soil matrix (Maa 1986; Mimura 1993). An example of (4-46) is shown in Fig. 4-34 based on the work of Maa (1986) in a flume in which a kaolinite, as well as mud from Cedar Key in Florida, was eroded by waves. The associated wave characteristics are given in Table 4-17.

4.9.5 Fluid Mud Entrainment by Waves

Laboratory flume tests show that when wave action above a threshold value necessary for bed liquefaction continues for a sufficient length of time, an equilibrium thickness of the fluid mud layer occurs. This threshold depends on bottom mud density and rheology, and fluid layer thickness increases with increasing wave height (Li 1996). Results from some laboratory tests are given in Table 4-18. On the prototype scale, in Lake Okeechobee, Florida, fluid mud thickness ranges between 0.05 and 0.20 m, depending on the water depth (Li and Mehta 2001). Thicker layers of fluid mud are found off the coast of Louisiana (Kemp 1986); the coast of Suriname/Guayana (Augustinus 1987; Eisma et al. 1991); the Amazon shelf (Kineke and Sternberg 1995); and the southwestern coast of India (Mathew and Baba 1995).

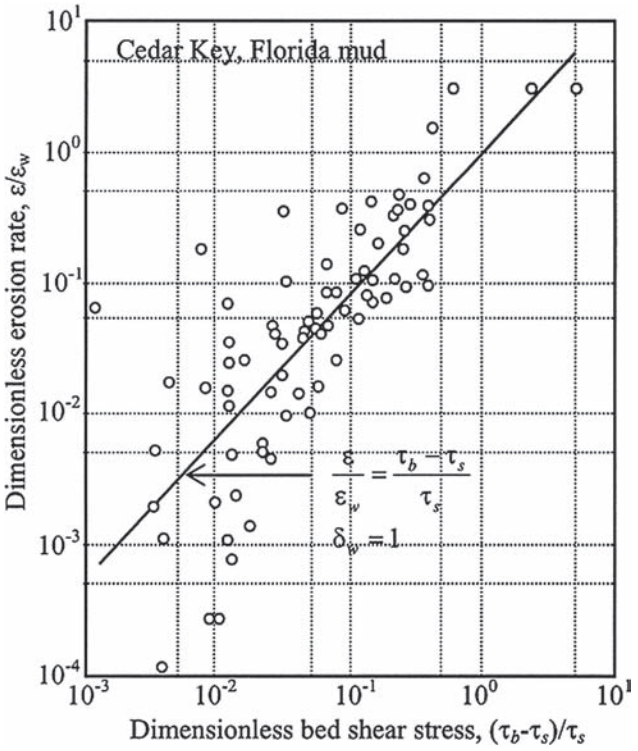

Fig. 4-34. Erosion rate relationship for nonbreaking waves obtained by Maa (1986).

In the offshore zone (Fig. 4-30), when the surficial layer at the bottom occurs as very soft or fluid mud, its entrainment can be described by an expression paralleling that used to quantify fluid entrainment from a stratified flow interface, e.g., Eq. (4-39). Li (1996) developed the following relation for the net rate entrainment by waves over fluid mud, ϵ_f (mass per unit bottom area per unit time), in which the first

Table 4-17 Parameters for Eq. (4-46) for NonBreaking Wave-Induced Erosion

Investigator(s)	Mode of wave generation	Sediment	Parameter ranges [a] a (cm); ω (rad/s); k (1/cm)	Parameter values in Eq. (4-46)		
				ϵ_w(g /m^2 s)	τ_s(Pa)	δ_W
Alishahi and Krone (1964)	Wind	Bay mud	$0.9 \leq a \leq 3.4$	Test 1: 0.48 Test 2: 11.2	0.29 0.39	1.72 1.15
Thimakorn (1984)	Mechanical	River mud	$3.1 \leq \omega \leq 12.6$ $0.16 \leq ak \leq 1.60$	$= \mu_b \delta_{bl} / 2\tau_s^b$	Variable	1.00
Maa (1986)	Mechanical	Kaolinite; bay mud	$1.4 \leq a \leq 3.7$ $3.3 \leq \omega \leq 6.3$	Kaolinite: 131 Mud: 30	Depth-varying Depth-varying	1.15 0.95
Mimura (1993)	Mechanical	Clays; bay mud	$0.6 \leq a \leq 6.9$ $4.8 \leq \omega \leq 8.2$	0.27	0.15	1.82

[a] a = wave amplitude = $H/2$, H = wave height, ω = wave angular frequency ($=2\pi f$); k = wave number.

[b] u_b = amplitude of bottom (or near-bottom) orbital velocity; δ_{bl} = wave boundary layer thickness = $(\nu/f)^{1/2}$ and ν = kinematic viscosity of water.

Source: Mehta (1996).

Table 4.18 Summary of Selected Fluid Mud Generation Experiments in Flumes

Source	Mud	Water depth (cm)	Bed thickness (cm)	Mud density (kg/m^3)	Wave amplitude (cm)	Wave frequency (Hz)	Mud viscosity (Pa.s)	Mud rigidity (Pa)	Fluid mud thickness (cm)
Ross (1988)	Tampa Bay, Florida	31.4–31.7	11.8–13.0	1,080	3.1–3.6	1.0–1.1	25.0	100	5.0–6.3
Lindenberg et al. (1989)	Kaolin	25	4.8–4.9	1,300	2.4–3.6	0.4–0.7	3.0	5	1.0–2.5
Feng (1992)	AK[a]	18.4–20.2	14.7–16.6	1,170	1.9–4.0	1.0	6.1	295	2.0–3.5

[a]A 50/50 (by weight) clayey mixture of an attapulgite and a kaolinite; see Table 4-4.
Source: Li (1996).

term represents upward entrainment and the second embodies entrained sediment settling onto the fluid mud:

$$\epsilon_f = \begin{cases} \alpha_w \rho u_b \left(\dfrac{R_c^2}{R_g} - R_g \right) - w_s C_a & R_g < R_c \\ 0 & R_g \geq R_c \end{cases} \quad (4\text{-}47)$$

In Eq. (4-47),

ρ = density of the fluid mud;
u_b = near-bottom velocity amplitude;
α_w = sediment-dependent coefficient;
C_a = near-bottom sediment concentration; and
R_g = Richardson number, given by:

$$R_g = \frac{(\rho_m - \rho_w) g \delta_{bl}^2}{\rho_w \Delta u_i^2} \quad (4\text{-}48)$$

In Eq. (4-48), δ_{bl} = wave boundary layer thickness (see footnote of Table 4-17) and Δu_i = absolute value of the maximum (horizontal) wave velocity difference across the interface. In Eq. (4-47) R_c is the critical value of R_g below which no entrainment is assumed to occur. This equation is plotted in Fig. 4-35 using the laboratory data of Maa (1986) and Li (1996) on the entrainment of natural and clayey sediments by waves in a flume. The coefficients $\alpha_w = 2 \times 10^{-6}$ and $R_c = 0.043$ were selected for both sets of data. In general, when direct measurements are not available, the calculation of the velocities u_b and Δu_i can be carried out as follows.

When bottom mud is soft, wave-induced orbital motion tends to penetrate the water-mud interface and, in turn, due to the high viscosity of mud (Table 4-6), wave damping often becomes significant. Several models have been used to determine the velocity field in two-layered (water and mud) flows in which energy dissipation is significant in the lower (mud) layer. An early model is due to Gade (1958), who assumed the lower layer to be a viscous fluid and the water layer above to be inviscid. He further limited his solution for the velocity field to waves in shallow water. Dalrymple and Liu (1978) considered both layers to be viscid and did not restrict the water depth. MacPherson (1980) assumed the lower layer to be viscoelastic and water to be inviscid. Piedra-Cueva (1993) extended the work of MacPherson by introducing a boundary layer at the water-mud interface. Jiang (1993) expanded on the solution of Dalrymple and Liu by including second order effects. The velocities u_b and Δu_i for the plot of Eq. (4-44) in Fig. 4-34 were derived by Li (1996) using the solutions of Jiang. A brief review of these and other models is provided in Rodriguez (2000).

A case of a simple flow field is one in which damped oscillation of the fluid mud layer is ignored in comparison with the orbital velocity above the interface. Then one has $\Delta u_i \approx u_b$, which can be easily calculated assuming the applicability of, for instance, the Airy wave theory (e.g., Dean and Dalrymple 1991) by ignoring the boundary layer effect in the water layer. In the simplest case of a shallow water wave the bottom velocity can be obtained from

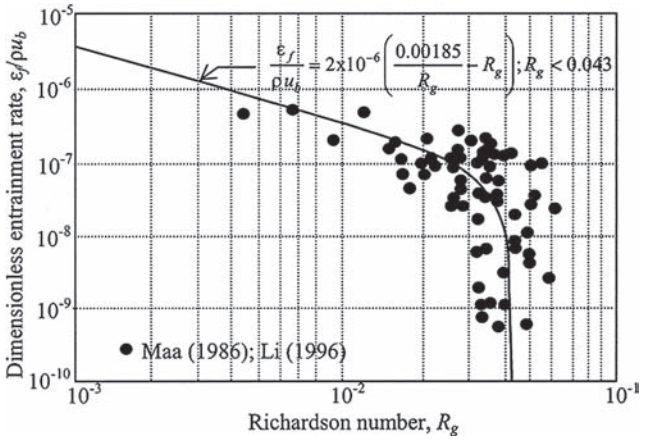

Fig. 4-35. Dimensionless wave-induced entrainment flux as a function of Richardson number (after Li and Parchure 1998).

$$u_b = \frac{H}{2}\left(\frac{g}{h}\right)^{1/2} \tag{4-49}$$

where H is the local wave height and h is the water depth.

4.10 DIFFUSION

4.10.1 Diffusion and Stratification

The (negative) buoyancy effect due to sediment-induced stratification tends to restore fluid lumps moved upward by turbulent diffusion back to their original positions, and thereby restricts the vertical transfer of momentum and sediment mass. This effect can be simply characterized by the way in which the momentum and mass mixing lengths vary with sediment concentration. In general, as the concentration increases the mixing length decreases, and below the lutocline almost complete turbulent collapse may occur, essentially leading to viscous flow (Jiang 1999; Winterwerp 1999; Jiang and Mehta 2000).

The Fickian flux due to vertical diffusion is

$$F_d = K_v \frac{\partial C}{\partial z} \tag{4-50}$$

where

K_v = diffusion coefficient.

From the analogy between sediment-induced density stratification and that induced by salinity and thermal gradients, along with the so-called Reynolds analogy between momentum and mass transport (Bird et al. 1960), expressions relating K_v to turbulence-mean flow and sedimentary parameters have been derived. Thus, for example, based on the phenomenological development of Rossby and Montgomery (1935), Munk and Anderson (1948) proposed the semiempirical formula

$$K_v = K_{v0}\left(1+\beta_v Ri_g\right)^{\gamma_v} \tag{4-51}$$

where

K_{v0} = "neutral" diffusivity in homogenous flow
and β_v and γ_v are sediment-dependent coefficients.

In Eq. (4-51), in which the second term within parentheses represents buoyancy correction to neutral diffusion, the gradient Richardson number Ri_g is defined as

$$Ri_g = \frac{g}{-\rho}\frac{\partial\rho/\partial z}{\left(\partial u/\partial z\right)^2} \tag{4-52}$$

where

u = local horizontal velocity.

With reference to the well-known mixing length concept of Prandtl and von Karman, K_{v0} can be stated as

$$K_{v0} = \kappa u_* z\left(\frac{(h-z)}{h}\right) \tag{4-53}$$

where

κ = Karman constant and
$u_*\ [=(\tau_b/\rho_w)^{1/2}]$ = friction velocity (Guo and Wood, 1995).

The use of (4-53) (with a nominal value of $\kappa = 0.4$) is contingent on the assumption of a logarithmic boundary layer velocity profile in the nonstratified water column. In reality, a Monin-Obukhov correction to the boundary layer velocity profile must be applied when stratification is significant (Friedrichs et al. 2000).

Jobson and Sayre (1970) noted that vertical mixing of suspended sediment in open-channel flow occurs as a result of two diffusion processes that can be shown to be additive. These processes include diffusion due to tangential components of turbulent velocity fluctuations and the centrifugal force arising from the curvature of fluid particle path lines. Based on these observations, they derived the following expressions for K_{v0}:

$$K_{v0} = \alpha_j \kappa u_* z\left(1-\frac{z}{h}\right) + \beta_j u_* h\left(\frac{1-z/h}{0.9}\right)^3 \quad \text{for } \frac{z}{h} \geq 0.1$$

$$K_{v0} = \alpha_j \kappa u_* z\left(1-\frac{z}{h}\right) + \beta_j u_* h\left(\frac{z/h}{0.1}\right)^3 \quad \text{for } \frac{z}{h} \leq 0.1 \tag{4-54}$$

Coefficients values from flume tests were reported to be $\alpha_j = 0.038$ and $\beta_j = 0.98$.

Values of the coefficients in Eq. (4-51) for forcing by current and applicable to fine sediment transport are given from some sources in Table 4-19. In general, fewer sets of values of these coefficients are available than for momentum transfer (Ross 1988; Jiang 1999). Momentum diffusivity can be converted to mass diffusivity if the turbulent Schmidt number S_c, i.e., the ratio of momentum to mass diffusivity, is known from measurement. From estuarine measurements, Oduyemi

Table 4-19 Parameters for (4-48) for Stratification Correction

Source/forcing	β_v	γ_v
Ross (1988)/ current	4.2	−2.0
Ross (1988)/waves	2.0	−0.5
Costa (1989)/ current	1.0–8.0	−2.0
Hwang (1989)/waves	0.5	−0.5
Jiang (1999)/ current	10	−0.5

(1986) found that the behavior of these two diffusivities over a tidal cycle was not self-similar, meaning that the S_c varied over the tide. Costa (1989) also reported that S_c varied with tide in Hangzhou Bay in China, in the range of 0.94 to 2.45.

Starting with a homogeneous suspension, the behavior of the diffusive flux F_d according to Eq. (4-50) along with Eq. (4-51) and (4-52) can be examined as a function of the concentration gradient, $\partial C/\partial z$. The resulting trend is illustrated in Fig. 4-36. It is assumed that ρ in the denominator of Eq. (4-51) is equal to water density ρ_w. Furthermore, the velocity gradient $\partial U/\partial z = u_*/\kappa z$ is based on the logarithmic velocity profile, and $\partial\rho/\partial z = [1 - (\rho_w/\rho_s)]\,\partial C/\partial z$. Relevant values are $h = 3$ m, $u_* = 0.1$ m/s, $z = 0.1$ m, $\kappa = 0.4$, $\rho_w = 1{,}000$ kg/m^3, $\rho_s = 2{,}650$ kg/m^3, $\beta_v = 4$, and $\gamma_v = -2$. Observe the effect of increasing negative buoyancy in limiting upward diffusion.

Glenn and Grant (1987) developed a correction factor for sediment-induced stratification due to the effects of waves superimposed on current. In general, the use of higher order turbulence closure schemes for modeling diffusion partially obviates the empirical limitations of Fickian closure described here (Nunes Vaz and Simpson 1994). Among others, Sheng and Villaret (1989) modeled resuspension using a second-order closure model for turbulence, which also yielded a better measure of the bottom stress than from the usual assumption of a constant bottom drag coefficient and wave-induced velocity unaffected by suspended sediment. In fact, turbulence damping due to suspended sediment was shown to measurably reduce bottom drag, hence resuspension. The same trend was found by Adams and Weatherly (1981) using a similar modeling approach.

4.10.2 Wave Effect

To model diffusion according to Eq. (4-50) for wave-induced processes, appropriate formulations for K_{v0} must be used.

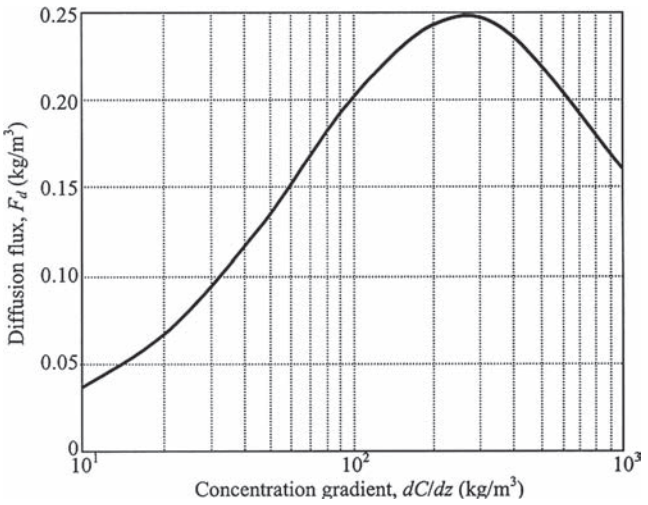

Fig. 4-36. Dependence of vertical mass diffusive flux on suspended sediment concentration gradient.

Several formulas have been proposed (e.g., Homma et al. 1965; Bhattacharya 1971; Kennedy and Locher 1972). A brief review of the subject is found in Dyer (1986). Focusing on the ambient water column rather than the near-bottom wave boundary layer, Hwang and Wang (1982) proposed the expression

$$K_{v0} = \alpha_{wd}\frac{H^2}{2}\frac{\sinh^2 k(h+z)}{\sinh^2 kh} \tag{4-55}$$

in which

H = wave height,
h = water depth,
k = wave number,
and the diffusion scaling coefficient α_{wd} for a given sediment depends on the flow field.

In Eq. (4-55), the vertical coordinate z is measured positive upward from the mean water level, so at the bottom $z = -h$. Based on wave energy dissipation in the water column and experimental data, Thimakorn (1984) arrived at an expression for K_{v0} that is akin to Eq. (4-55), with $\alpha_{wd} = 1.77/\sinh kh$. In Lake Erie, Lick (1982) reported a mass diffusivity, value K_{v0}, of 25 cm^2/s. For calculation of K_v from K_{v0} using Eq. (4-51), Table 4-19 provides values of the coefficients β_v and γ_v from wave-induced resuspension studies by Ross (1988) and Hwang (1989).

Under wave action, vertical diffusion of sediment tends to be considerably less efficient than in a current in the sense that whereas, under waves, the sediment tends to remain sequestered within a comparatively thin bottom boundary layer, under a current-induced thicker boundary layer the material is swept upward much more easily, thus resulting in a greater suspension height (Li and Parchure 1998). Furthermore, release of bed pore water and associated chemical constituents appears to be influenced by a diffusive sublayer close to the bed, which seemingly restricts upward entrainment. On the other hand, heaving motion of mud, especially when it is soft, enhances upward transport (Li et al. 1997). When heaving and relative motion between water and mud at the interface become significant, the calculation of bed shear stress must also account for the "slippage" between the two layers (Maa 1986). In addition, there seems to be an effect on bottom drag associated with the flocs at the bed. Typically, the drag coefficient for a cohesive bed, especially one composed of soft mud, tends to be low. For example, from flume experiments Dixit (1982) reported values of the Manning's bed resistance coefficient, n, to be on the order of 0.011. As postulated by Gust (1976), such a low value may in part be due to an elastic deformation of flocs induced by flow at the bed surface. Bed resistance is also mitigated by the effect of sediment-induced buoyancy. Li and Gust (2000) further ascribe the reduction effect to severe damping of turbulence in the wall boundary layer.

4.11 APPLICATIONS

The description of fine sediment behavior given in the preceding sections is used in engineering studies to predict sediment movement and deposition and to design sediment management measures (Zeigler and Nisbet 1994; 1995). A few examples will illustrate how they are used.

4.11.1 Measurement

Measurement of fine sediment transport rate and bed changes is accomplished by several methods, none of which provides a complete picture of the important processes. The greatest difficulty lies in measuring near the active bed-water interface and at lutoclines, where intrusive instruments may disrupt the processes to be measured.

The depth-mean suspended sediment mass transport rate is obtained from

$$\boldsymbol{q}(x,y,t) = \int_0^{h(x,y,t)} C(x,y,z,t)\boldsymbol{u}_s(x,y,z,t)\,dz \qquad (4\text{-}56)$$

in which

x and y = the longitudinal and transverse coordinates, respectively;
z = the vertical coordinate;
$h(x,y,t)$ = the instantaneous water depth; and
$\boldsymbol{u}_s$ = the sediment velocity vector.

Because it is currently unrealistic to deal with the sediment velocity, which is difficult to quantify, especially for flocculated sediments, $\boldsymbol{u}_s$ is characteristically replaced by the corresponding fluid velocity, $\boldsymbol{u}$. Thus, assuming isokinetic motion of water and sediment, we restate Eq. (4-56) as

$$\boldsymbol{q}(x,y,t) = \int_0^{h(x,y,t)} C(x,y,z,t)\boldsymbol{u}(x,y,z,t)\,dz \qquad (4\text{-}57)$$

Suspended sediment load in the water column away from the bed is obtained by direct or indirect methods. Direct sampling involves collecting water samples at several depths while simultaneously measuring the flow velocity profile, and repeating these measurements at several locations along a cross section. The water samples may be taken by submerged bottle-type samplers or by pumping to a bottle on a vessel or platform. Samples are then analyzed for sediment concentration, usually by filtration and drying. Integration of the product of sediment concentration, flow velocity, and cross-sectional area over the profile yields an estimate of sediment discharge. Flow velocities can be measured by devices using vanes or propellers held at the sampling point, but the preferred method is now an acoustic Doppler current profiler (ADCP), either sitting on the bed or held just below the water surface, which emits multiple sound pulses and measures the time and frequency of reflected sound waves to compute three-dimensional velocities. Analysis of the reflected wave intensity can also be used to estimate suspended sediment concentration, but requires careful, site-specific calibration of the signal against standard methods (Teeter et al. 1996; Land et al. 1997).

Other methods of measuring the sediment load include optical backscatter sensors (OBS), which emit a beam of light, measure the intensity of reflected light, and convert that reading to a sediment concentration. Such devices must be calibrated to the sediment in transport at each site, because the particle's reflectance is a function of shape, color, size, and surface coating (Downing and Beach 1989). Optical transmissometers are used in both low-concentration (Bocuniewicz et al. 1991) and high-concentration (Costa 1989) environments.

Measuring the location of the bed is commercially important for navigable waterways because it defines the depth available for navigation (Parker 1994), and scientifically important for defining rates of erosion and deposition. Despite its importance, the process is fraught with uncertainty in definition of what the bed surface is and where it is. Acoustic depth-sounding equipment is standard in most waterways and works well when the bed is composed of sand-size or larger sediment. For muddy beds the technique may or may not yield accurate results, because the acoustic signal is reflected by sharp density gradients, not by specific densities; thus the acoustic record may suggest that the bed occurs at the first fluid density inflection, such as is shown in Fig. 4-4, producing a bed elevation estimate that is one to several meters above the actual firm bed. In the presence of fluid mud, multiple density inflection points may produce multiple false bed locations (Parker and Kirby 1982). More accurate and reliable methods for locating the bed include nuclear density meters (Parker and Kirby 1982) and towed devices that respond to both suspension density and viscosity (Alexander et al. 1997).

4.11.2 Modeling

For many years physical models based on scaling principles were the primary engineering tool of choice for fine sediment studies (Herrmann and Letter 1990; Letter and McAnally 1977), but have now been largely replaced by numerical models which solve the equations of transport and bed change using computational methods.

In some situations involving steady or periodic flows, Eq. (4-57) can be solved through simple modeling techniques (e.g., McAnally 1999; Krone 1985). In steady and also quasi-steady flows such as those due to tides, and when the suspended concentration does not exceed a few tens of milligrams per liter, the classical Rouse (1937) profile of suspended sediment (Dyer 1986; Hill et al. 1988) is often found to be adequate to describe the variation of concentration C with depth. In this development the settling velocity is assumed to be independent of C and vertical diffusion is assumed to be neutral. Depth variation of C is obtained under the assumption of the equality of upward

diffusion and settling fluxes. The resulting profile of C along with the well-known logarithmic variation of flow velocity $\bar{u}'$ with depth (Dyer 1986) can be used to calculate the sediment load via (4-57).

Introduction of time-dependence of C in the Rouse formulation leads to a one-dimensional (vertical) model that has been used extensively in modeling the time-variation of the vertical profile of C due to tide as well as waves (e.g., Adams and Weatherly 1981; Maa and Mehta 1988; Sheng and Villaret 1989; Le Hir et al. 2001; Teeter 2001a, 2001b).

In most cases, it becomes essential to use complex two- or three-dimensional time-dependent numerical models to calculate $\boldsymbol{u}$ and C, incorporating the described unit transport processes, i.e., settling and deposition of suspended material, consolidation of the fresh deposit, and erosion and entrainment of the fresh as well as of the consolidated deposit (Zeigler and Nisbet 1994; Cardenas et al. 1995; Costa 1995; Zeigler and Nisbet 1995; Jiang 1999).

The solved governing equations for transport of suspended sediment load, either cohesive or noncohesive, are usually the general advection-diffusion equations,

$$\frac{D}{Dt} = \frac{\partial}{\partial x}\left(K_x \frac{\partial}{\partial y}\right) + \frac{\partial}{\partial y}\left(K_y \frac{\partial C}{\partial y}\right) + \frac{\partial}{\partial y}\left(K_z \frac{\partial C}{\partial z}\right) + \sum_{\text{sources}} - \sum_{\text{sinl}} \tag{4-58}$$

where the left hand side is the total derivative and

C = suspended sediment concentration;
t = time,
x, y, and z = spatial coordinates, and
K_x, K_y, and K_z = directional diffusion coefficients.

The source term as represented in (4-58) denotes external sediment that enters the system being modeled, such as that due to shoreline or bluff erosion and river or slough runoff. Organic sediments can both be internally produced, e.g., by photosynthesis, and arrive from external sources. Sediments that leave the system are represented in the sink term. Erosion and deposition of sediment within the system is handled through the bottom boundary condition when the model includes the variation of flow and sediment properties in the vertical (z) direction. In depth-averaged models, erosion and deposition become (external) source and sink, respectively.

A bed model, which describes the density, resistance to erosion, and other characteristics of the sediment bed, keeps track of the net deposition/erosion and thus the elevation of the bed and the variation of properties with depth into the bed (see, for example, McAnally and Thomas 1989). One of the first models in which the bed was discretized into horizontal layers, with density and erodibility indices changing from layer to layer, is due to Ariathurai et al. (1977), who applied the model to simulate tidally driven fine sediment deposition in the dredged channel leading to the port of Savannah, Georgia. Maa (1986) extended this concept to wave modeling, in which the bottom density, erodibility, and rheological parameters were varied with depth. It is now recognized that an eventual goal of modeling should be to simulate the solid and fluid phases on a continuous rather than discretized basis (Teisson 1997; Toorman, 2001). Simulation of phase changes between the bed and suspension due to erosion/deposition must be integral to such a development, as opposed to the present piecemeal approach based on unit transport processes. It is certain that considerable additional experimental work will be required to fully evolve such a modeling approach.

Two aspects of modeling that are essential for simulating cohesive bottom related processes include fluid mud transport and bed stratification. In estuaries with large tidal ranges such as the Severn in the UK (Kirby 1986; Smith and Kirby 1989), the Loire in France (Le Hir et al. 2001), and the Amazon in Brazil (Kineke 1993; Geyer 1995; Vinzon and Mehta 2001), fluid mud tends to persist through the entire tidal cycle and plays a major role in determining the sediment budget. In the microtidal to mesotidal environment, such as along much of the U.S. coastal zone, thick layers of fluid mud are less common in fair weather, but can become significant in terms of their contribution to the total sediment load when, for example, storm waves occur (Kemp and Wells 1987).

The technology of sediment modeling has evolved rapidly in recent decades, and any description of the state of the art will quickly become obsolete. The one-dimensional numerical model HEC-6 and its variations are widely used for rivers and occasionally estuaries (e.g., Thomas et al. 1988). The TABS-MD and other systems of models have been extensively used for estuarine sediment transport (Donnell et al. 1991; McAnally 1989; Willis and Crookshank 1997), and the 2DV model LAEM-SED has been used in a few estuaries (Smith et al. 1987; Johnson et al. 1989). Three-dimensional models constitute the state of the art in fine sediment modeling, and are exemplified by applications reported by, among others, Teeter and Callegan (2000).

4.11.3 Case Studies

Indian River Inlet, Delaware, connects Indian River Bay and Rehoboth Bay to the Atlantic Ocean on the U.S. East Coast. In 1938–1940 the previously ephemeral inlet was stabilized by parallel jetties 150 m apart with a maximum inlet depth of about 6 m below mean low water. Almost immediately the sandy inlet bed began to scour, and by 1991 nearly all of the inlet was deeper than 12 m and some holes exceeded 30 m in depth. Scour had uncovered lagoonal cohesive clay deposits at depths of about 11 m and the deepest holes had eroded through the clay layer, exposing consolidated Pleistocene sand and gravel (CTH 1994). Concern over the

possibility of further erosion undermining the jetties and a state highway bridge over the inlet prompted an analysis of the inlet's stability, a question usually associated with cohesionless sediments, but in this case one in which the erodibility of cohesive sediments was a controlling factor. The Corps of Engineers CTH (1994) analyzed the inlet's stability, employing a mix of field, laboratory, and desktop calculations as summarized below.

The average depth of the bays is 1.5 m below mean low water. Mean tide range is approximately 1 m in the offshore area, 0.6 m in Indian River Bay and 0.3 m in Rehoboth Bay. Small freshwater inflows (usually less than 100 m^3/s) create a longitudinal salinity gradient in the bays, with minor to no vertical stratification occurring under normal conditions. In 1992 the inlet had an average cross-sectional area of about 2,100 m^2. Tidal flow speeds through the inlet exceeded 2 m/s under spring tides.

A vessel-mounted 1,200-KHz ADCP was used to measure current speed and direction profiles along 12 ranges. Each range was profiled during peak ebb and peak flood flows for two tidal cycles. The ADCP measured three-dimensional velocity vectors, averaging within zones, or bins, approximately 50 cm deep. Sediment samples were taken to characterize the erodibility of the cohesive sediments and to obtain grain size distributions of the exposed bed sands. Clam-shell samples, drag bucket samples, and cores were taken at 10 locations throughout the inlet. Laboratory erosion tests were conducted to define the two characteristic parameters of Eq. (4-30) for the cohesive sediment samples. Tests were conducted in a particle entrainment simulator (PES) (Tsai and Lick 1986), a vertical loop sediment tunnel (VOST) (Teeter and Pankow 1989), and a rotating cylinder erosion device (see, e.g., Chapuis and Gatien 1986). Lee and Mehta (1994) have reviewed these and several other types of erosion-measuring devices reported in the literature. The PES induced bed stresses up to 0.7 Pa by means of a vertically oscillating grid, whereas the VOST generated horizontal flow stresses up to 3 Pa and the rotating cylinder generated stresses up to 16 Pa. The value of the erosion shear strength τ_s developed from those experiments was 4 Pa for an intact sample and 5.8 Pa for a remolded sample. The erosion rate constant for the tested sediments ranged from 5.8×10^{-4} to 1×10^{-3} kg/m^2 s.

Typical mean flow velocities for the inlet were obtained by smoothing measured values and then adjusting them to an appropriate tide range and inlet cross-sectional area by means of the Keulegan (1967) tidal inlet method. Half-hourly shear stresses on the bed were estimated via Manning's flow velocity equation. These stresses were used to compute erosion rates for neap, mean, and spring tides using Eq. (4-30) and then composited to create annual erosion rates. Comparison with observed historical rates led to adjustment of the laboratory-derived erosion rate coefficients to make the bed somewhat more erodible, which was probably caused by sand abrasion of the clay bed leading to more rapid erosion than by water flow alone.

The calculations showed that the clay bed would stop eroding at an inlet size of about 2,800 m^2, or about 30% larger than the then existing inlet size. Based on these and other, sand-based calculations, it was decided to do nothing other than continue monitoring the inlet to ensure that the predicted size stability would occur.

Hayter and Gu (2001) applied a two-dimensional numerical model (HSCTM-2D) to the problem of contaminated sediment transport in the Maurice River-Union Lake, New Jersey, system in order to predict the effects of dredging on sediment and arsenic distribution in the system. Union Lake is a 4-km-long impoundment on the Maurice River about 40 km upstream of Delaware Bay. Its average width is 1.6 km. Bed sediments were contaminated with arsenic concentrations above 0.05 mg/l, and the model was used to compare natural flushing of arsenic from the system to a proposed remedial plan that would remove some contaminated sediments by dredging. Data collected for the modeling effort included daily stages and discharges; suspended sediment concentrations and arsenic concentrations in the river, tributaries, and lake during storms and normal conditions; cross-sectional hydrographic surveys; sediment cores that were analyzed for grain size distribution, mineral composition, density, organic content, and arsenic concentration; and bed pore water samples that were analyzed for arsenic, pH, and conductivity. Sedimentation traps were deployed in the system to accurately measure deposition rates; however, the traps were lost during high flow events and provided no data.

The model solved the depth-averaged form of Eq. (4-58) for three sediment size classes, plus selected dissolved and suspended contaminants, using the finite element method. Depth-averaged water velocities and water surface elevations were computed by a companion module that solved the Reynolds form of the Navier-Stokes equations. The cohesive sediment source-sink terms in Eq. (4-58) employed Eq. (4-26) for deposition rate to the bed and a form of Eq. (4-37) for bed erosion rate. The bed sediment density structure and thickness were computed by a one-dimensional finite strain model developed by Cargill (1982).

The model was validated by adjustment to, and comparison with, 3-year-long data as described above. As is the case in most engineering studies, the data were less complete and comprehensive than in the ideal case, and the results were interpreted in light of those limitations. Numerical experiments were then performed, using a synthetic typical year's flows that included four storm events. Model results showed that arsenic flushing times (time required for arsenic concentrations to decline to less than 120 mg/kg throughout the system) ranged from 15 years for the no-action alternative to 4 years for dredging contaminated sediments out of the river and lake. The estimated error in flushing times was ± 1.2 years, based on the model validation and a sensitivity analysis of arsenic desorption rates.

Rodriguez (2000) examined the problem of assessing the fate of mud placed off the beach, from where it may be carried away mainly by wave-induced currents. Referring to the elemental control volume in Fig. 4-37, and considering the cross-shore distance coordinate y to be the dependent variable and water depth h to be the independent one, the sediment continuity equation can be conveniently stated as

$$\frac{\partial y}{\partial t} = -\frac{1}{m\rho_D}\frac{\partial q_x}{\partial x} - \frac{1}{\rho_D}\frac{\partial q_y}{\partial h} \tag{4-59}$$

where

q_x and q_y = the components of mass sediment fluxes per unit length in the x and y directions, respectively;
ρ_D = the dry density of the deposit; and
$m = \partial h/\partial y$ = the local bottom slope.

Equation (4-59) makes possible tracking changes in the bottom contour position with time, as opposed to tracking water depth. The output at every time step is therefore a bottom contour "map" dependent on the fluxes q_x and q_y (Perlin and Dean 1983).

In Eq. (4-59), q_x must be determined in accordance with Eq. (4-57) from the product of the cross-shore distributions of suspension concentration and water velocity (Rodriguez and Mehta 2000). The corresponding cross-shore flux q_y can be related to the difference in the instantaneous rate of wave energy dissipation and the corresponding dissipation rate over an "equilibrium" or "target" profile (Lee and Mehta 1997).

The simplest application of Eq. (4-59) is to waves normally incident on a coast with shore-parallel contours (Coakley et al. 1988). In this case the alongshore transport mode is switched off in the model, so that profile change, either accretion or erosion, is due to sediment moving landward or seaward. The erosion of a beach consisting of overconsolidated till along Lake Ontario in Canada was reported by Davidson-Arnott (1986), who also noted that as the profile translated landward the eroded material was carried away beyond the sediment-active profile, leaving practically no sediment deposit within this zone. Profile evolution over the period 1980–1984 is simulated in Fig. 4-38 (Rodriguez 2000).

When obliquely incident waves and alongshore current occur, simulation of profile evolution becomes considerably more complicated, due to the effects of alongshore as well as cross-shore forcing on shore processes. At the Mahin coast in Nigeria, waves are dominated by swell originating at storm centers in the southern Atlantic region. The tide is semidiurnal with a mean range of 1.5 m, and the beach and nearshore material consist mainly of poorly sorted silt with mean size ranging from 20 to 50 μm. Due to submarine canyons that act as sinks of littoral drift, this region is starved of sediment supply. In the 1970s a navigation cut was dredged perpendicular to the coast near the village of Awoye about 20 km west of the Benin River (Fig. 4-39) to connect inland creeks and canals with the ocean. This cut apparently enabled larger waves to penetrate inland, exacerbating the erosion of the shoreline in the vicinity. In addition, salt water intrusion occurred, which in turn affected vegetation sensitive to brackish water. The ensuing die-back exposed bottom sediment otherwise protected by rooting and considerably increased land loss (Eedy et al. 1994).

Shoreline erosion adjacent to the cut was in response to a combination of wave-induced and tidal forcing, consistent with sediment transport associated with the typical flood and ebb flow distributions that develop near a tidal inlet or cut. Accordingly, sediment eroded by wave action along the shoreline was drawn toward the cut by flood flow. During ebb flow, the material that had accumulated near the entrance was jetted offshore. Since the lost nearshore sediment was not replenished by alongshore drift, shoreline recession occurred. As observed from Fig. 4-39,

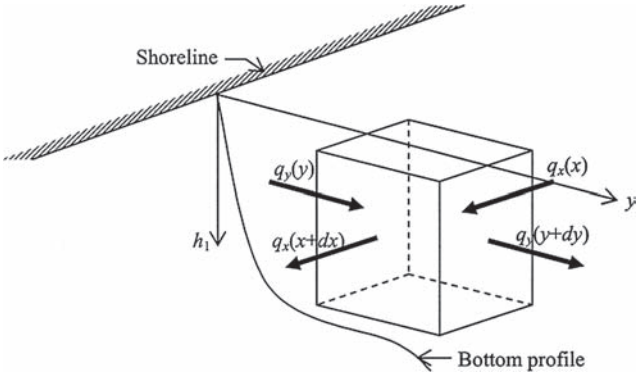

Fig. 4-37. Elemental control volume and suspended sediment fluxes in open coast waters.

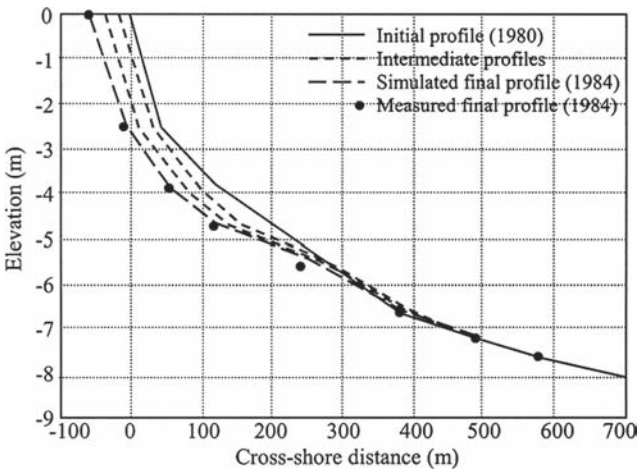

Fig. 4-38. Glacial till profiles at Grimsby, Lake Ontario, Canada measured by Davidson-Arnott (1986) and comparison with simulated profiles (after Rodriguez 2000).

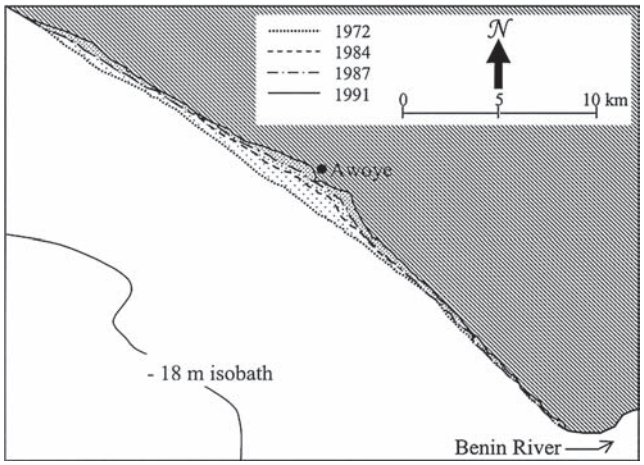

Fig. 4-39. Shoreline recession in the vicinity of Awoye (after Redriguez 2000).

erosion was rapid in the first few years, and a recession on the order of 1.5 to 2.0 km occurred near Awoye between 1972 and 1991.

It is instructive to examine the bathymetric change near Awoye by considering it to be due to an equivalent effect of shore-normal waves over a bottom with shore-parallel contours disturbed by a cut acting as a sediment sink. The resulting change in the bottom, in this case due to increasing deviation from the initial "target" profile, is shown in Fig. 4-40 (Rodriguez and Mehta 2001). In order to mimic the observed (Fig. 4-39) pattern of bottom change, sediment was withdrawn through the cut at a rate of 800 kg/s. This exceptionally high rate merely reflects the rapid rate of erosion that actually occurred. At the end of the initial period of 7 years covered in the simulation the shoreline was recessed by about 1 km.

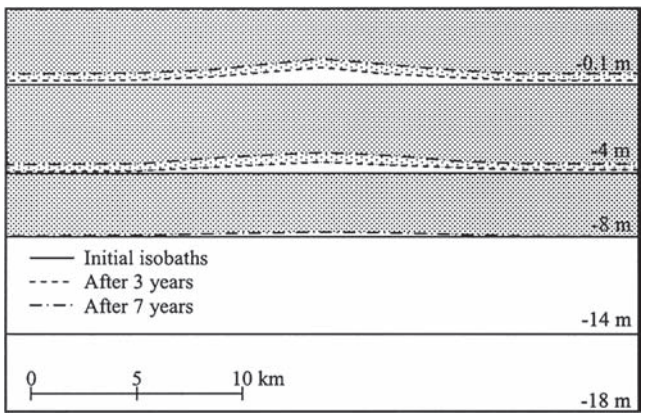

Fig. 4-40. Simulated contour recession due to the effect of a dredged channel (after Rodriguez and Mehta 2001).

REFERENCES

Adams, C. E., Jr., and Weatherly, G. L. (1981). "Some effects of suspended sediment stratification on an oceanic boundary layer." *Journal of Geophysical Research*, 86(C5), 4,161–4,172.

Alexander, M. P., Teeter, A. M., and Banks, G. E. (1997). "Development and verification of an intrusive hydrographic survey system for fluid mud in channels." *Technical Rep. DRP-97-1,* U. S. Army Engineer Waterways Experiment Station, Vicksburg, Miss.

Ali, K. H. M., and Georgiadis, K. (1991). "Laminar motion of fluid mud." *Proceedings of the Institution of Civil Engineers, Part 2, Research and Theory*, 91, 795–821.

Alishahi, M. R., and Krone, R. B. (1964). "Suspension of cohesive sediments by wind-generated waves. *Technical Rep. HEL-2-9*, Hydraulic Engineering Laboratory, University of California, Berkeley, Calif.

Amos, C. L., Brylinsky, M., Sutherland, T. F., O'Brien, D., Lee, S., and Cramp, A. (1998). "The stability of a mudflat in the Humber estuary, South Yorkshire, UK." *Sedimentary processes in the intertidal zone*, K. S. Black, D. M. Paterson, and A. Camp, eds., The Geological Society, London, 25–44.

Annandale, G. W. (1995). "Erodibility." *Journal of Hydraulic Research*, 33(4), 471–493.

Ariathurai, R. (1974). "A finite element model for sediment transport in estuaries." PhD, thesis, University of California, Davis, Calif.

Ariathurai, R., MacArthur, R. C., and Krone, R. B. (1977). "Mathematical model of estuarial sediment transport." *Technical Rep. D-77-12*, U.S. Army Engineer Waterways Experiment Station, Vicksburg, Miss.

Arulanandan, K., Gillogly, E., and Tully, R. (1980). "Development of a quantitative method to predict critical shear stress and rate of erosion of natural undisturbed cohesive soils." *Technical Rep. GL-805*, U.S. Army Engineer Waterways Experiment Station, Vicksburg, Miss.

Ashley, R. M., and Verbanck, M. A. (1996). "Mechanics of sewer sediment erosion and transport." *Journal of Hydraulic Engineering*, 34(6), 753–769.

ASTM (1993a). "Standard test method for amount of material in soils finer than the no. 200 (75-μm) sieve." *Annual Book of ASTM Standards*, Section 4, Vol. 04.08, American Society for Testing and Materials, Philadelphia, 191–193.

ASTM (1993b). "Standard test methods for moisture, ash, and organic matter of peat and other organic soils." In: *Annual Book of ASTM Standards*, Section 4, Vol. 04.08, American Society for Testing and Materials, Philadelphia, 400–402.

ASTM (1993c). "Standard test methods for operating performance of particulate cation-exchange materials." *Annual Book of ASTM Standards*, Section 11, Vol. 11.02, American Society for Testing and Materials, Philadelphia, 772–776.

ASTM (1993d). "Standard test for particle-size analysis of soils." *Annual Book of ASTM Standards*, Section 4, Vol. 04.08, American Society for Testing and Materials, Philadelphia, 93–99.

Augustinus, P. G. E. F. (1987). "The geomorphologic development of the coast of Guyana between the Corentyne River and the Essequibo River." *International Geomorphology 1986 Part I*, V. Gardener, ed., Wiley, London, 1,281–1,292.

Azam, M. H. (1998). "Breaking wave over mud flats." PhD thesis, Universiti Teknologi Malaysia, Kuala Lumpur, Malaysia.

Barnes, H. A., Hutton, J. F., and Walters, K. (1989). *An introduction to rheology*. Elsevier, Amsterdam.

Bedford, K. W., Onyx, W., Libicki, C. M., and Van Evra, R. (1987). "Sediment entrainment and deposition measurements in Long Island Sound." *Journal of Hydraulic Engineering*, 113(10), 1,325–1,342.

Been, K., and Sills, G. C. (1981). "Self-weight consolidation of soft soils: An experimental and theoretical study." *Geotechnique*, 31(4), 519–535.

Bentley, S. J., and Nittrouer, C. A. (1997). "Environmental influences on the formation of sedimentary fabric in the fine-grained carbonate-shelf environment: Dry Tortugas, Florida Keys." *Geo-Marine Letters*, 17, 268–275.

Berlamont, J., Ockenden, M., Toorman, E., and Winterwerp, J. (1993). "The characterisation of cohesive sediment properties." *Coastal Engineering*, 21(1–3), 105–128.

Bhattacharya, P. (1971). "Sediment suspension in shoaling waves." PhD thesis, University of Iowa, Iowa City, Iowa.

Bird, R. B., Stewart, W. E., and Lightfoot, E. N. (1960). *Transport Phenomena*. Wiley, New York.

Bishop, C. T., and Skafel, M. G. (1992). "Detailed description of laboratory tests on the erosion by waves of till profiles." *NWRI Contribution No. 92-26,* National Water Research Institute, Burlington, Ont., Canada.

Bishop, C. T., Skafel, M. G., and Nairn, R. (1992). "Cohesive profile erosion by waves." *Proceedings of the 23rd Coastal Engineering Conference,* B. L. Edge, ed., ASCE, New York, 2,976–2,989.

Black, K. S. (1991). "The erosion characteristics of cohesive estuarine sediments: Some in situ experiments and observations." PhD thesis, University of Wales, Menai Bridge, UK.

Black, K. S., Paterson, D. M., and Cramp, A. (1998). Preface. In: *Sedimentary processes in the intertidal zone*, K. S. Black, D. M. Paterson, and A. Camp, eds., The Geological Society, London, vii–ix.

Bocuniewicz, H., McTiernan, L., and Davis, W. (1991). "Measurement of sediment resuspension rates in Long Island Sound." *Geo-Marine Letters*, 11(3/4), 159–161.

Burban, P. Y., Lick, W., and Lick, J. (1989). The flocculation of fine-grained sediments in estuarine waters. *Journal of Geophysical Research*, 94(C6), 8,323–8,330.

Burban, P. Y., Xu, Y. J., McNeil, J., and Lick, W. (1990). Settling speeds of flocs in fresh water and seawater. *Journal of Geophysical Research*, 95(C10), 18,213–18,220.

Burt, T. N., and Parker, W. R. (1984). "Settling and density in beds of natural mud during successive sedimentation." *Rep. No. IT 262*, HR Wallingford, Wallingford, UK.

Burt, T. N., and Stevenson, J. R. (1983). "Field settling velocity of Thames mud." *Rep. No. IT 251*, HR Wallingford, Wallingford, UK.

Cardenas, M., Galiani, J., Zeigler, C. K. and Lick, W. (1995). "Sediment transport in Lower Saginaw River." *Marine and Freshwater Research*, 46(1), 337–347.

Cargill, K. W. (1982). "Consolidation of soft layers by finite strain analysis." *Miscellaneous Paper GL-82-3*, U.S. Army Engineer Waterways Experiment Station, Vicksburg, Miss.

Cervantes, E., Mehta, A. J. and Li, Y. (1995). "A laboratory-based examination of 'episodic' resuspension of fine-grained sediments by waves and current." *Proceedings of the International Conference on Coastal and Port Engineering in Developing Countries*, Rio de Janeiro, Brazil, 1–13.

Chapuis, R. P., and Gatien, T. (1986). "An improved rotating cylinder technique for quantitative measurement of the scour resistance of clays." *Canadian Geotechnical Journal*, 23(1), 83–87.

Chou, H. T. (1989). "Rheological response of cohesive sediments to water waves." PhD thesis, University of California, Berkeley, Calif.

Christodoulou, G. G. (1986). "Interfacial mixing in stratified flows." *Journal of Hydraulic Research*, 24(2), 77–92.

Coakley, J. P., Skafel, M. G., Davidson-Arnott, R. G. D., Zeman, A. J., and Rukavina, N. A. (1988). "Computer simulation of nearshore profile evolution in cohesive material." *Proceedings of the IAHR Symposium on Mathematical Modeling of Sediment transport*, Copenhagen, Denmark, 290–299.

Committee on Tidal Hydraulics (CTH). (1960). "Soil as a factor in shoaling processes: A literature review." *Technical Bulletin No. 4*, U.S. Army Engineer Waterways Experiment Station, Vicksburg, Miss.

Committee on Tidal Hydraulics (CTH). (1994). "Indian River Inlet: An evaluation by the Committee on Tidal Hydraulics." *Unpublished Rep.*, U.S. Army Engineer Committee on Tidal Hydraulics, Vicksburg, Miss.

Costa, R. C. F. G. (1989). "Flow-fine sediment hysteresis in sediment-stratified coastal waters." *MS thesis*, University of Florida, Gainesville, Fla.

Costa, R. C. F. G. (1995). "Three-dimensional modeling of cohesive sediment transport in estuarine environments." PhD thesis, University of Liverpool, Liverpool, UK.

Dade, W. B., and Nowell, A. R. M. (1991). Moving muds in the marine environment. *Proceedings of Coastal Sediments'91*, N. C. Kraus, K. J. Ginerich, and D. L. Kriebel, eds., ASCE, New York, 54–71.

Dalrymple, R.A., and Liu, P. L.-F. (1978). "Waves over soft muds: A two-layer fluid model." *Journal of Physical Oceanography,* 8(6)*,* 1,121–1,131.

Davidson-Arnott, R. G. D. (1986). "Erosion of the nearshore profile in till: Rates, controls, and implications for shore protection." *Proceedings of the Symposium on Cohesive Shores*, Burlington, Ont., Canada, 137–149.

Day, P. R., and Ripple, C. D. (1966). Effect of shear on suction in saturated clays. *Soil Science Society of America Proceedings*, 30, 675–690.

Dean, R. G., and Dalrymple, R. A. (1991). *Water wave mechanics for engineers and scientists.* World Scientific, Singapore.

Delichatsios, M. A., and Probestein, R. F. (1975). "Coagulation in turbulent flow: Theory and experiment." *Journal of Colloid and Interface Science*, 51(3), 394–405.

Dennett, K. E., Sturm, T. W., Amrithrajah, A., and Mahmood, T. (1998). "Effects of adsorbed organic matter on the erosion of kaolinite sediments." *Water Environment Research*, 70(3), 268–275.

Dixit, J. G. (1982). "Resuspension potential of deposited kaolinite beds." M S thesis, University of Florida, Gainesville, Fla.

Donnell, B. P., Letter, J. V., and Teeter, A. M. (1991). "The Atchafalaya River delta, report 11: Two-dimensional modeling." *Technical Rep. HL-82-15*, U. S. Army Engineer Waterways Experiment Station, Vicksburg, Miss.

Downing, J. P., and Beach, R. A. (1989). "A laboratory apparatus for calibrating optical suspended solids sensors." *Marine Geology*, 86, 243–249.

Drapeau, D. T., Dam, H. G. (1994). "An improved flocculator design for use in particle aggregation experiments." *Limnology and Oceanography*, 39(3), 723–729.

Dyer, K. R. (1986). *Coastal and estuarine sediment dynamics*. Wiley, Chichester, UK.

Dyer, K. R. (1989). "Sediment processes in estuaries: Future research requirements." *Journal of Geophysical Research*, 94(C10), 14,327–14,339.

Eedy, W., Rodgers, B., Saunders, K. E., and Akindunni, F. (1994). "Application of satellite remote sensing to coastal recession in Nigeria." *Proceedings of Coast. Zone Management Conference*, Halifax, Nova Scotia, Canada, 1–4.

Einstein, H. A. (1941). "The viscosity of highly concentrated underflows and its influence on mixing." *Transactions of the 22nd Annual Meeting of the American Geophysical Union*, Part I, Hydrology Papers, National Research Council, Washington, D.C., 597–603.

Einstein, H. A. (1950). "The bed-load function for sediment transportation in open channel flows." *Technical Bulletin No. 1026*, U.S. Department of Agriculture, Washington, D.C.

Eisma, D., Augustinus, P. G. E. F., and Alexander, C. (1991). "Recent and subrecent changes in the dispersal of Amazon mud." *Netherlands Journal of Sea Research*, 28, 181–192.

Engelund, F., and Zhaohui, W. (1984). "Instability of hyperconcentrated flow." *Journal of Hydraulic Engineering*, 101(3), 219–233.

Faas, R. W. (1995). "Mudbanks of the southwest coast of India. III: Role of non-Newtonian flow properties in the generation and maintenance of mudbanks." *Journal of Coastal Research*, 11(3), 911–917.

Feng, J. (1992). "Laboratory experiments on cohesive soil bed fluidization by water waves." MS thesis, University of Florida, Gainesville, Fla.

Foda, M. A. (1987). "Internal dissipative waves in poro-elastic media." *Proceedings of the Royal Society of London*, *Series A* 413, 383–405.

Friedrichs, C. T. (1993). "Hydrodynamics and morphodynamics of shallow tidal channels and intertidal flats." PhD thesis, Woods Hole Oceanographic Institution, Woods Hole, Mass.

Friedrichs, C. T., Wright, D., Hepworth, D. A., and Kim, S. C. (2000). "Bottom-boundary-layer processes associated with fine sediment accumulation in coastal seas and bays." *Continental Shelf Research*, 20, 807–841.

Gade, H.G. (1958). "Effects of a non-rigid, impermeable bottom on plane surface waves in shallow water." *Journal of Marine Research,* 16(2)*,* 61–82.

Galani, J., Zeigler, C. K., and Lick, W. (1991). "Transport of suspended solids in the lower Fox River." *Journal of Great Lakes Research*, 17(4), 479–494.

Ganju, N. K. (2001). "Trapping organic-rich fine sediment in an estuary." MS Thesis*,* University of Florida, Gainesville, Fla.

Gelinas, P. J., and Quigley, R. M. (1973). "The influence of geology on erosion rates along the north shore of Lake Erie." *Proceedings of the 16th Conference on Great Lakes Research,* International Association for Great Lakes Research, Ann Arbor, Mich., 421–430.

Geyer, W. (1995). "Tide-induced mixing in the Amazon frontal zone." *Journal of Geophysical Research*, 100(C10),2,341–2,353.

Gibbs, R. J. (1985). "Estuarine flocs: Their size, settling velocity and density." *Journal of Geophysical Research*, 90(C2), 3, 249–3,251.

Gibson, R. E., England, G. L., and Hussey, M. J. L. (1967). "The theory of one-dimensional consolidation of saturated clays. I: Finite nonlinear consolidation of thin homogeneous layers." *Geotechnique*, 17, 261–273.

Gibson, R. E., Schiffman, R. L., and Cargill, K. W. (1981). "The theory of one-dimensional consolidation of saturated clays. II: Finite nonlinear consolidation of thick homogeneous layers." *Canadian Geotechnical Journal*, 18(2), 280–293.

Glenn, S. M., and Grant, W. D. (1987). "A suspended sediment stratification for combined wave and current flows." *Journal of Geophysical Research*, 84(C4), 1,797–1,808.

Govindaraju, R. S., Ramireddygari, S. R., Shrestha, P. L., and Roig, L. C. (1999). "Continuum bed model for estuarine sediments based on nonlinear consolidation theory." *Journal of Hydraulic Engineering*, 125(3), 300–304.

Grim, R. E. (1968). *Clay mineralogy*. McGraw–Hill, New York.

Guo, J., and Wood, W. L. (1995). "Fine suspended sediment transport rates." *Journal of Hydraulic Engineering*, 121(12), 919–922.

Gust, G. (1976). "Observations of turbulent drag reduction in a dilute suspension of clay in seawater." *Journal of Fluid Mechanics*, 75(May–June), 29–47.

Hanson, G. J. (1990). "Surface erodibility of earthen channels at high stresses. Part I Developing an in situ testing device." *Transactions of the American Society of Agricultural Engineers*, 33(1), 132–137.

Hayter, E. J. (1983). "Prediction of cohesive sediment transport in estuarial waters." PhD thesis, University of Florida, Gainesville, Fla.

Hayter, E. J., and Gu, R. (2001). "Predictions of contaminated sediment transport in the Maurice River-Union Lake, New Jersey, USA." *Coastal and estuarine fine sediment transport: Processes and applications,* W. H. McAnally and A. J. Mehta, eds., Elsevier, Amsterdam, 439–458.

Herrmann, F. A., and Letter, J. V. (1990). "Advancements in tidal hydraulics." *50th Anniversary of the Hydraulics Division, American Society of Civil Engineers*, A. M. Alsaffar, ed., ASCE, New York, 36–80.

Hill, P. S. (1992). "Reconciling aggregation theory with observed vertical fluxes following phytoplankton blooms." *Journal of Geophysical Research*, 97(C2), 2295–2308.

Hill, P. S., and Nowell, A. R. M. (1995). "Comparison of two models of aggregation in the continental-shelf boundary layers." *Journal of Geophysical Research*, 100(C11), 22,749–22,763.

Hill, P. S., Nowell, A. R. M., and Jumars, P. A. (1988). "Flume evaluation of the relationship between suspended sediment concentration and excess boundary shear stress." *Journal of Geophysical Research*, 93(C10), 12,499–12,509.

Hill, P. S., Nowell, A. R. M., and Jumars, P. A. (1992). "Encounter rate by turbulent shear of particles similar in diameter to the Kolmogorov scale." *Journal of Marine Research*, 50(4), 643–667.

Hollick, M. (1976). "Towards a routine assessment of the critical tractive forces cohesive soils." *Transactions of the American Society of Agricultural Engineers*, 19(6), 1076–1081.

Homma, M., Horikawa, K., and Kajima, R. (1965). "A study of suspended sediment due to wave action." *Coastal Engineering in Japan*, 8, 85–103.

Huang, S., Han, N., and Zhong, X. (1980). "Analysis of siltation at mouth bar of the Yangtze River estuary." *Proceedings of the International Symposium on River Sedimentation*, Paper C6, Chinese Society of Hydraulic Engineering, Beijing, China (in Chinese).

Huang, X., and Garcia, M. H. (1996). "A perturbation solution for Bingham-plastic mudflows." *Journal of Hydraulic Engineering*, 123(11), 986–994.

Huang, X., and Garcia, M. H. (1998). "A Herschel-Bulkley model for mud flow down a slope." *Journal of Fluid Mechanics*, 374, 305–333.

Huang, X., and Garcia, M. H. (1999). "Modeling of non-hydroplaning mudflows on continental slopes." *Marine Geology*, 154, 131–142.

Hunt, J. R. (1982). "Self-similar particle-size distributions during coagulation: Theory and experimental verification." *Journal of Fluid Mechanics*, 122(Sep.), 169–185.

Hunt, J. R. (1986). "Particle aggregate breakup by fluid shear." *Estuarine cohesive sediment dynamics*, A. J. Mehta, ed., Springer-Verlag, Berlin, 85–109.

Hwang, K.-N. (1989). "Erodibility of fine sediment in wave dominated environments." MS thesis, University of Florida, Gainesville, Fla.

Hwang, P. A., and Wang, H. (1982). "Wave kinematics and sediment suspension at wave breaking point." *Technical Rep. No. 13*, Department of Civil Engineering, University of Delaware, Newark, Del.

Jacinto, R. S., and Le Hir, P. (2001). "Response of stratified muddy beds to water waves." *Coastal and estuarine fine sediment transport processes*, W. H. McAnally and A. J. Mehta, eds., Elsevier, Amsterdam, 95–108.

Jaeger, J. M., and Nittrouer, C. A. (1995). "Tidal controls on the formation of fine-scale sedimentary strata near the Amazon mouth." *Marine Geology*, 125, 259–281.

James, A. E., Williams, D. J. A., and Williams, P. R. (1987). "Direct measurement of static yield properties of cohesive suspensions." *Rheologica Acta*, 26, 437–446.

James, A. E., Williams, D. J. A., and Williams, P. R. (1988). "Small strain, low shear rate rheometry of cohesive sediments." *Physical processes in estuaries*, J. Dronkers and W. van Leussen, eds., Springer-Verlag, Berlin, 488–500.

Jepsen, R., Roberts, J., and Lick, W. (1997). "Effects of bulk density on sediment erosion rates." *Water, Air and Soil Pollution*, 99(1–4), 21–31.

Jiang, F. (1993). "Bottom mud transport due to water waves." PhD thesis, University of Florida, Gainesville, Fla.

Jiang, F., and Mehta, A. J. (1993). "Some observations on water wave attenuation over nearshore underwater mudbanks and mud berms." *Rep. No. UFL/COEL/MP-93/01*, Coastal and Oceanographic Engineering Department, University of Florida, Gainesville, Fla.

Jiang, F., and Mehta, A. J. (1995). "Mudbanks of the southwest coast of India. IV: Mud viscoelastic properties." *Journal of Coastal Research*, 11(3), 918–926.

Jiang, F., and Mehta, A. J. (1996). "Mudbanks of the southwest coast of India. V: Wave attenuation." *Journal of Coastal Research*, 12(4), 890–897.

Jiang, J. (1999). "An examination of estuarine lutocline dynamics." PhD thesis, University of Florida, Gainesville, Fla.

Jiang, J., and Mehta, A. J. (2000). "Lutocline behavior in a high-concentration estuary." *Journal of Waterway, Port, Coastal and Ocean Engineering*, 126(6), 324–328.

Jobson, H. E., and Sayre, W. W. (1970). "Vertical transfer in open channel flow." *Journal of the Hydraulics Division of ASCE*, 96(3), 7,148–7,152.

Johnson, B. H., Trawle, M. J., and Kee, P. G. (1989). "A numerical model study of the effect of channel deepening in shoaling and salinity intrusion in the Savannah estuary." *Technical Rep. HL-89-26,* U.S. Army Engineer Waterways Experiment Station, Vicksburg, Miss.

Jones, T. E. R. (1997). "A review of rheometric methods for use with fine sediments." *Cohesive sediments*, N. Burt, R. Parker, and J. Watts, eds., Wiley, Chichester, UK., 317–329.

Kamphuis, J. W. (1986). "Erosion of cohesive bluffs, a model and a formula." *Proceedings of the Symposium on Cohesive Shores,* M. G. Skafel, ed., National Research Council Canada, Ottawa, Canada, 226–245.

Kandiah, A. (1974). "Fundamental aspects of surface erosion of cohesive soils." PhD thesis, University of California, Davis, Calif.

Keedwell, M. J. (1984). *Rheology and soil mechanics,* Elsevier, London, 339p.

Kelly, W. E., and Gularte, R. C. (1981). "Erosion resistance of cohesive soils." *Journal of the Hydraulics Division of ASCE*, 107(10), 1,211–1,224.

Kemp, G.P. (1986). "Mud deposition at the shoreface: Wave and sediment dynamics on the chenier plain of Louisiana." PhD thesis, Louisiana State University, Baton Rouge, La.

Kemp, G. P., and Wells, J. T. (1987). "Observations of shallow-water waves over a fluid mud bottom: Implications to sediment transport." *Proceedings of Coastal Sediments'87*, N. C. Kraus, ed., ASCE, New York, 363–378.

Kendrick, M. P., and Derbyshire, B. V. (1985). "Monitoring of a near-bed turbid layer." *Rep. No. SR44*, HR Wallingford, Wallingford, UK.

Kennedy, J. F., Locher, F. A. (1972). "Sediment suspension by waves." *Waves on beaches and resulting sediment transport*, R. E. Meyer, ed., Academic Press, New York, 249–296.

Keulegan, G. H. (1967). "Tidal flow in entrances: Water level fluctuations of basins in communication with seas." *Technical Bulletin No. 14*, Committee on Tidal Hydraulics, U.S. Army Corps of Engineers, Vicksburg, Miss.

Kineke, G. C. (1993). "Fluid muds on the Amazon continental shelf." PhD thesis, University of Washington, Seattle.

Kineke, G. C., and Sternberg, R. W. (1995). "Distribution of fluid muds on the Amazon Continental Shelf." *Marine Geology*, 125, 193–223.

Kirby, R. (1986). "Suspended fine cohesive sediment in the Severn estuary and Inner Bristol Channel." *Rep. No. ESTU-STP-4042*, Department of Atomic Energy, Harwell, UK.

Kirby, R. (1992). "Effect of sea-level rise on muddy coastal margins." *Dynamics and exchanges in estuaries and the coastal zone*, D. Prandle, ed., American Geophysical Union, Washington, D.C., 313–334.

Kirby, R., Hobbs, C. H., and Mehta, A. J. (1994). "Shallow stratigraphy of Lake Okeechobee, Florida: A preliminary reconnaissance." *Journal of Coastal Research*, 10(2), 339–350.

Kirby, R., and Parker, W. R. (1977). "The physical characteristics and environmental significance fine sediment suspensions in estuaries." *Estuaries, geophysics and the environment*, National Research Council, National Academy Press, Washington, D.C., 110–120.

Kirkham, D., and Powers, W. L. (1972). *Advanced soil physics,* Wiley, New York.

Kranck, K. (1986). "Settling behavior of cohesive sediment." *Estuarine cohesive sediment dynamics*, A. J. Mehta, ed., Springer-Verlag, Berlin, 151–169.

Kranck, K., and Milligan, T. G. (1980). "Macroflocs: Production of marine snow in the laboratory." *Marine Ecology Progress Series*, 3(July), 19–24.

Kranck, K., and Milligan, T. G. (1992). "Characteristics of suspended particles at an 11-hour anchor station in San Francisco Bay, California." *Journal of Geophysical Research*, 97(C7), 11,373–11,382.

Kranck, K., Petticrew, E., Milligan, T. G., and Droppo, I. G. (1993). "In situ particle size distributions resulting from flocculation of suspended sediment." *Nearshore and estuarine cohesive sediment transport*, A. J. Mehta, ed., American Geophysical Union, Washington, D.C., 60–74.

Kranenburg, C. (1994a). "The fractal structure of cohesive sediment aggregates." *Estuarine, Coastal and Shelf Science*, 39(5), 451–460.

Kranenburg C. (1994b). "An entrainment model for fluid mud." *Rep. No. 93-10*, Faculty of Civil Engineering, Delft University of Technology, Delft, The Netherlands.

Kranenburg, C., and Winterwerp, J. C. (1997). "Erosion of fluid mud layers. I: Entrainment model. *Journal of Hydraulic Engineering*, 123(6), 504–511.

Krishnappan, B. G. (1990). "Modeling settling and flocculation of fine sediments in still water." *Canadian Journal of Civil Engineering*, 17, 763–770.

Krizek, R. J. (1971). Rheological behavior of clay soils subjected to dynamic loads. *Transactions of the Society of Rheology*, 15(3), 433-489.

Krone, R. B. (1962). "Flume studies of the transport of sediment in estuarial shoaling processes." *Final Rep.*, Hydraulic Engineering Laboratory and Sanitary Engineering Research Laboratory, University of California, Berkeley, Calif.

Krone, R. B. (1963). "A study of rheological properties of estuarial sediments." *Technical Bulletin No. 7*, Committee on Tidal Hydraulics, U.S. Army Engineer Waterways Experiment Station, Vicksburg, Miss.

Krone, R. B. (1983). "A viscosity-temperature relation for Newtonian liquids." *Chemical Engineering Communications*, 22(3–4), 161–180.

Krone, R. B. (1985). "Simulation of marsh growth under rising sea levels." *Proceedings of the Conference on Hydraulics and Hydrology in the Small Computer Age*, W. R. Waldrop, ed., ASCE, New York, 106–115.

Krone, R. B. (1986). "The significance of aggregate properties to transport processes." *Estuarine cohesive sediment dynamics*, A. J. Mehta, ed., Springer-Verlag, Berlin, 66–84.

Krone, R. B. (1993). "Sedimentation revisited." *Nearshore and estuarine cohesive sediment transport*, A. J. Mehta, ed., American Geophysical Union, Washington, D.C., 108–125.

Kusuda, T., Umita, T., Koga, T., Futawatari, T. and Awaya, Y. (1985). "Erosional process of cohesive sediments." *Water Science and Technology*, 17(6–7), 891–901.

Kynch, G. J. (1952). "A theory of sedimentation." *Transactions of Faraday Society*, 48, 166–176.

Lambe, T. W., and Whitman, R. V. (1969). *Soil mechanics.* Wiley, New York.

Land, J. M., Kirby, R., and Massey, J. B. (1997). "Developments in the combined use of acoustic doppler current profilers and profiling siltmeters for suspended solids monitoring." *Cohesive sediments*, N. Burt, R. Parker, and J. Watts, eds., Wiley, Chichester, UK., 187–196.

Lau, Y. L. (1994). "Temperature effect on settling velocity and deposition of cohesive sediments." *Journal of Hydraulic Research*, 32(1), 41–51.

Lau, Y. L., and Krishnappan, B. G. (1992). "Size distribution and settling velocity of cohesive sediments during settling." *Journal of Hydraulic Research*, 30(5), 673–683.

Law, D. J., and Bale, A. J. (1998). "*In situ* characterization of suspended particles using focused-beam, laser reflectance particle sizing." *Sedimentary processes in the intertidal zone*, K. S. Black, D. M. Patterson, and A. Cramp, eds., Geological Society, London, 57–68.

Lee, H. J. (1985). "State of the art: Laboratory determination of the strength of marine soils." *Strength testing of marine sediments and in-situ measurements,* R. C. Chaney and K. R. Demars, eds., ASTM STP 883, American Society of Testing and Materials, Philadelphia, 181–250.

Lee, S.-C. (1995). "Response of mud shore profiles to waves." PhD thesis, University of Florida, Gainesville, Fla.

Lee, S.-C., and Mehta, A. J. (1994). "Cohesive sediment erosion." *Rep. No. DRP-94-6*, U.S. Army Engineer Waterways Experiment Station, Vicksburg, Miss.

Lee, S-C., and Mehta, A. J. (1997). "Problems in characterizing dynamics of mud shore profiles." *Journal of Hydraulic Engineering*, 123(4), 351–361.

Le Hir, P., Bassoullet, P., and Jestin, H. (2001). "Application of the continuous modeling concept to simulate high-concentration suspended sediment in a macrotidal estuary." *Coastal and estuarine fine sediment transport processes*, W. H. McAnally and A. J. Mehta, eds., Elsevier, Amsterdam, 229–247.

Letter, J. V., and McAnally, W. H. (1977). "Physical hydraulic models: Assessment of predictive capabilities," Report 2, Galveston entrance movable bed model. *Research Rep. HL-75-3,* U.S. Army Engineer Waterways Experiment Station, Vicksburg, Miss.

Li, M. Z., and Gust, G. (2000). "Boundary layer dynamics and drag reduction in flows of high cohesive sediment suspensions." *Sedimentology*, 47(1), 71–86.

Li, Y. (1996). "Sediment-associated constituent release at the mud-water interface due to monochromatic waves." PhD thesis, University of Florida, Gainesville, Fla.

Li, Y., Mehta, A. J., Hatfield, K., and Dortch, M. S. (1997). "Modulation of constituent release across the mud-water interface by water waves." *Water Resources Research*, 33(6), 1,409–1,418.

Li, Y., and Parchure, T. M. (1998). "Mudbanks of the southwest coast of India. VI: Suspended sediment profiles." *Journal of Coastal Research*, 14(4), 1363–1372.

Li, Y., and Mehta, A. J. (2001). "Fluid mud in the wave-dominated environment revisited." *Coastal and estuarine fine sediment transport processes*, W. H. McAnally and A. J. Mehta, eds., Elsevier, Amsterdam, 79–93.

Liang, H.-B., and Williams, P. (1993). "An assessment of the impact of the operation of an additional ferry on shoreline erosion in Corte Madera Bay." *Rep. No. 847/877*, Philip Williams, San Francisco.

Lick, W. (1982). "Entrainment, deposition and transport of fine-grained sediment in lakes." *Hydrobiologia*, 91(2), 31–40.

Lick, W., Lick, J., and Zeigler, C. K. (1992). "Flocculation and its effect on the vertical transport of fine-grained sediments." *Hydrobiologia*, 235(July), 1–16.

Lick, W., and Huang, H. (1993). "Flocculation and the physical properties of flocs." *Nearshore and estuarine cohesive sediment transport*, A. J. Mehta, ed., American Geophysical Union, Washington, D.C., 21–39.

Lin, C.-P. (1986). "Turbidity currents and sedimentation in closed-end channels." PhD thesis, University of Florida, Gainesville, Fla.

Lin, P. C.-P., and Mehta, A. J. (1997). "A study of fine sedimentation in an elongated laboratory basin." *Journal of Coastal Research*, SI25, 19–30.

Lindenberg, J., van Rijn, L. C. and Winterwerp, J. C. (1989). "Some experiments on wave-induced liquefaction of soft cohesive soils." *Journal of Coastal Research*, SI 5, 127–137.

Luettich, R. A., Jr., Wells, J. T., and Kim, S.-Y. (1993). "*In situ* variability of large aggregates: Preliminary results on the effect of shear." *Nearshore and estuarine cohesive sediment transport*, A. J. Mehta, ed., American Geophysical Union, Washington, D.C., 447–466.

Maa, P.-Y. (1986). "Erosion of soft mud by waves." PhD thesis, University of Florida, Gainesville, Fla.

Maa, P.-Y., and Mehta, A. J. (1988). "Soft mud properties: Voigt model." *Journal of Waterway, Port, Coastal and Ocean Engineering*, 114(6), 765–770.

Maa, J. P.-Y., Wright, L. D., Lee, C.-H., and Shannon, T. W. (1993). "VIMS Sea Carousel: A field instrument for studying sediment transport." *Marine Geology*, 115, 271–287.

MacPherson, H. (1980). "The attenuation of water waves over a non-rigid bed." *Journal of Fluid Mechanics,* 97(April), 721–742.

Manning, A. J., and Dyer, K. R. (1999). "A laboratory examination of floc characteristics with regard to turbulent shearing." *Marine Geology*, 160(1/2), 147–170.

Mantz, P. A. (1977). "Incipient transport of fine grains and flakes by fluids—extended Shields diagram." *Journal of the Hydraulics Division of ASCE*, 103(6), 601–615.

Marván, F. G. (2001). "A two-dimensional numerical transport model for organic-rich cohesive sediments in estuarine waters." PhD thesis, Heriot-Watt University, Edinburgh, UK.

Marván, F. G., Wallis, S. G., and Mehta, A. J. (2002). "Episodic transport of organic-rich sediments in a microtidal estuarine systems." *Fine sediment dynamics in the marine environment*, J. C. Winterwerp and C. Kranenburg, eds., Elsevier, Amsterdam, 611–626.

Mathew, J., and Baba, M. (1995). "Mudbanks of the southwest coast of India. II: Wave mud interactions." *Journal of Coastal Research*, 11(1), 179–187.

McAnally, W. H. (1989). "Lessons from 10 years experience in 2D sediment modeling." *Proceedings of the International Symposium on Sediment Transport Modeling,* S. S. Y. Wang, ed., ASCE, New York, 350–355.

McAnally, W. H. (1999). "Aggregation and deposition of estuarial fine sediment." PhD thesis, University of Florida, Gainesville, Fla, 383p.

McAnally, W. H., and Mehta, A. J. (2000). "Aggregation rate of fine sediment." *Journal of Hydraulic Engineering*, 126(12), 883–892.

McAnally, W. H., and Mehta, A. J. (2002). "Significance of aggregation of fine sediment particles in their deposition." *Estuarine, Coast and Shelf Science*, 54, 643–653.

McAnally, W. H. and Thomas, W. A. (1989). "STUDH: A two-dimensional numerical model for sediment transport." *Sediment Transport Modeling*, S. Y. Wang, ed., ASCE, New York, 659–664.

McCave, I. N. (1984). "Size spectra and aggregation of suspended particles in the deep ocean." *Deep Sea Research*, 31(4), 329–352.

McDowell, D. M., and O'Connor, B. A. (1977). *Hydraulic behavior of estuaries*. Wiley, New York.

McLaughlin, R. T. (1959). "The settling properties of suspensions." *Journal of the Hydraulics Division, of ASCE*, 85 (12), 9–41.

Meakin, P. (1988). "Fractal aggregates." *Advances in Colloid and Interface Science*, 28, 249–331.

Mehta, A. J. (1991). "Review notes on cohesive sediment erosion." *Proceedings of Coastal Sediments'91*, N. C. Kraus, K. J. Ginerich, and D. L. Kriebel, eds., ASCE, New York, 40–53.

Mehta, A. J. (1996). "Interaction between fluid mud and water waves." *Environmental hydraulics*, V. P. Singh and W. H. Hager, eds., Kluwer, Dordrecht, The Netherlands, 153–187.

Mehta, A. J. (2002). "Mudshore dynamics and controls." *Muddy coasts of the world: Processes, deposits and function*, T.Healy, Y. Wang, and J.-A. Healy, eds., Elsevier, Amsterdam, 19–60.

Mehta, A. J., and Kirby, R. (1996). "Mitigation measures for eroding muddy shores." *Proceedings of North American Water & Environment Congress*, Session W-17, ASCE, New York.

Mehta, A. J., and Lee, S.-C. (1994). "Problems in linking the threshold condition for the transport of cohesionless and cohesive sediment grains." *Journal of Coastal Research*, 10(1), 170–177.

Mehta, A. J., and Lott, J. W. (1987). "Sorting of fine sediment during deposition." *Proceedings of Coastal Sediments'87*, N. C. Kraus, ed., ASCE, New York, 348–362.

Mehta, A. J., and Parchure, T. M. (2000). "Surface erosion of fine-grained sediment revisited." *Muddy coast dynamics and resource management*, B. W. Flemming, M. T. Delafontaine, and G. Liebezeit, eds., Elsevier, Oxford, UK, 55–74.

Mehta, A. J., Parchure, T. M., Dixit, J. G. and Ariathurai, R. (1982). "Resuspension potential of deposited cohesive sediment beds." *Estuarine comparisons*, V. S. Kennedy, ed., Academic Press, New York, 591–609.

Mehta, A. J., and Srinivas, R. (1993). "Observations on the entrainment of fluid mud by shear flow." *Nearshore and estuarine cohesive sediment transport*, A. J. Mehta, ed., American Geophysical Union, Washington, D.C., 224–246.

Mehta, A. J, Williams, D. J. A., Williams, P. R. and Feng, J. (1995). "Tracking dynamic changes in mud bed due to waves." *Journal of Hydraulic Engineering*, 121(5), 504–506.

Mei, C. C., and Liu, K. F. (1987). "A Bingham-plastic model for a muddy seabed under long waves." *Journal of Geophysical Research*, 92(C13), 14,581–14,594.

Midun, Z. B., and Lee, S.-C. (1989). "Mud coast protection—The Malaysian experience." *Proceedings of Sixth Symposium on Coastal and Ocean Management*, ASCE, New York, 806–820.

Migniot, P. C. (1968). "A study of the physical properties of different very fine sediments and their behavior under hydrodynamic

action." *La Houille Blanche*, 7, 591–620 (in French, with abstract in English).

Mimura, N. (1993). "Rates of erosion and deposition of cohesive sediments under wave action." *Nearshore and estuarine cohesive sediment transport*, A. J. Mehta, ed., American Geophysical Union, Washington, D.C., 247–264.

Mitchell, J. K. (1976). *Fundamentals of soil behavior,* Wiley, New York.

Montague, C. L., Paulic M., and Parchure, T. M. (1993). "The stability of sediments containing microbial communities: Initial experiments with varying light intensity." *Nearshore and estuarine cohesive sediment transport*, A. J. Mehta, ed., American Geophysical Union, Washington, D.C., 348–359.

Moore, W. L., and Masch, F. D., Jr. (1962). "Experiments on the scour resistance of cohesive sediments." *Journal of Geophysical Research*, 67(4), 1437–1449.

Moudgil, B. M., and Vasudevan, T. V. (1989). "Evaluation of floc properties for dewatering fine particle suspensions." *Minerals and Metallurgical Processing*, 6(3), 142–145.

Munk, W. H., and Anderson, E. A. (1948). "Notes on a theory of the thermocline." *Journal of Marine Research*, 7, 276–295.

Nairn, R. B. (1992). "Erosion processes evaluation paper." *Final Report for International Joint Commission Great Lakes–St. Lawrence River Reference Study Board*, submitted by W. F. Baird and Associates to Water Planning and Management Branch, Environment Canada, Burlington, Ont., Canada.

Nichols, M. (1984/1985). "Fluid mud accumulation processes in an estuary." *Geo-Marine Letters*, 4–5, 192–198.

Nunes Vaz, R. A., and Simpson, J. H. (1994). "Turbulence closure modeling of estuarine stratification." *Journal of Geophysical Research*, 99(C8), 16,143–16,160.

Ockenden, M. C. (1993). "A model for the settling of non-uniform cohesive sediment in a laboratory flume and a field setting." *Journal of Coastal Research*, 9(4), 1,094–1,105.

Odd, N. M. V., Bentley, M. A., and Waters, C. B. (1993). "Observations and analysis of the movement of fluid mud in an estuary." *Nearshore and estuarine cohesive sediment transport*, A. J. Mehta, ed., American Geophysical Union, Washington, D.C., 430–446.

Odd, N. M. V., and Cooper, A. J. (1989). "A two-dimensional model of the movement of fluid mud in a high energy turbid estuary." *Journal of Coastal Research*, SI5, 185–193.

Odd, N. V. M., and Rodger, J. G. (1986). "An analysis of the behaviour of fluid mud in estuaries." *Report No. SR 84*, HR Wallingford, Wallingford, UK.

Oduyemi, K. O. K. (1986). "Turbulent transport of sediment in estuaries." PhD thesis, University of Birmingham, Birmingham, UK.

Overbeek, J. Th. G. (1952). "Kinetics of flocculation." *Colloid science*, Vol. 1, H. R. Kruyt, ed., Elsevier, Amsterdam, 278–301.

Owen, M. W. (1970). "A detailed study of the settling velocity of an estuary mud." *Rep. No. IT 78*, HR Wallingford, Wallingford, UK.

Ozturgut, E., and Lavelle, J. W. (1986). "Settling analysis of fine sediment in salt water at concentrations low enough to preclude flocculation." *Marine Geology*, 69(3–4), 353–362.

Paaswell, R. E. (1973). "Causes and mechanisms of cohesive soil erosion: The state of the art." *Soil erosion: Causes and mechanisms; Prevention and control*, D. H. Gray, ed., Special Report 135, Highway Research Board, Washington, D.C., 52–74.

Panagiotopoulos, I., Voulgaris, G., and Collins, M. B. (1997). "The influence of clay on the threshold of movement of fine sandy beds." *Coastal Engineering*, 32, 19–43.

Papanicolaou, A. N., and Diplas, P. (1999). "Numerical solution of a non-linear model for self-weight settlement." *Applied Mathematical Modelling*, 23(5), 345–362.

Parchure, T. M. (1984). "Erosional behavior of deposited cohesive sediments." PhD thesis, University of Florida, Gainesville, Fla.

Parker, W. R. (1987). "Observations on fine sediment transport phenomena in turbid coastal environments." *Continental Shelf Research*, 7(11/12), 1,285–1,293.

Parker, W. R. (1994). "Determining depth and navigability in fine sediment areas." *Coastal, estuarial and harbour engineer's reference book*, M. B. Abbott and W. A. Price, eds., Chapman & Hall, London, 611–614.

Parker, W. R., and Kirby, R. (1982). "Time dependent properties of cohesive sediment relevant to sedimentation management—European experience." *Estuarine comparisons,* V. S. Kennedy, ed., Academic Press, New York, 573–589.

Partheniades, E. (1962). "A study of erosion and deposition of cohesive soils in salt water." PhD thesis, University of California, Berkeley, Calif.

Partheniades, E. (1965). "Erosion and deposition of cohesive soils." *Journal of the Hydraulics Division, ASCE*, 91(1), 105–138.

Partheniades, E. (1971). "Erosion and deposition of cohesive materials." *River mechanics*, H. W. Shen, ed., H. W. Shen, Fort Collins, Colo., 25-1–25-91.

Partheniades, E. (1977). "Unified view of wash load and bed material load." *Journal of the Hydraulics Division of ASCE*, 103(9), 1,037–1,057.

Partheniades, E. (1993). "Turbulence, flocculation and cohesive sediment dynamics." *Nearshore and estuarine cohesive sediment transport*, A. J. Mehta, ed., American Geophysical Union, Washington, D.C., 40–59.

Patterson, D. M. (1997). "Biological mediation of sediment erodibility: Ecology and physical dynamics." *Cohesive sediments*, N. Burt, R. Parker, and J. Watts, Eds., Wiley, Chichester, UK, 215–229.

Perlin, M., and Dean, R. G. (1983). "A numerical model to simulate sediment transport in the vicinity of coastal structures." *Miscellaneous Rep. 83-10*, Coastal Engineering Research Center, U.S. Army Corps of Engineers, Fort Belvoir, Va., 117.

Phan-Thien, N. (1983). "A similarity solution for Rayleigh flow of a Bingham fluid." *Journal of Applied Mechanics*, 50(1), 229.

Piedra-Cueva, I. (1993). "On the response of muddy bottom to surface water waves." *Journal of Hydraulic Research*, 31(5), 681–696.

Piedra-Cueva, I., and Mory, M. (2001). "Erosion of a deposited layer of cohesive sediment." *Coastal and estuarine fine sediment transport processes*, W. H. McAnally and A. J. Mehta, eds., Elsevier, Amsterdam, 41–51.

Raveendran, P., and Amritharajah, A. (1995). "Role of short-range forces in particle detachment during filter backwashing." *Journal of Environmental Engineering*, 121(13), 860–868.

Ravisangar, V., Dennett, K. E., Sturm, T. W., and Amrithrajah, A. (2001). "Effect of sediment pH on resuspension of kaolinite sediments." *Journal of Environmental Engineering*, 127(6), 531–538.

Rich, C. I., and Barnhisel, R. I. (1977). "Preparations of clay samples for X-ray diffraction analysis." *Minerals in soil environments*,

J. B. Dixon and S. B. Weed, eds., Soil Science Society of America, American Society of Agronomy, Madison, Wisc., 797–809.

Richardson, J. F., and Zaki, W. N. (1954). "The sedimentation of a suspension of uniform spheres under conditions of viscous flow." *Chemical Engineering Science*, 3, 65–73.

Roberts, W., Le Hir, P., and Whitehouse, R. J. S. (2000). "Investigation using simple mathematical models of the effects of tidal currents and waves on the profile shape of intertidal mudflats." *Continental Shelf Research*, 20(11/12), 1079–1097.

Roberts, W., and Whitehouse, R. J. S. (2001). "Predicting the profile of intertidal mudflats formed by cross-shore tidal currents." *Coastal and estuarine fine sediment transport processes*, W. H. McAnally and A. J. Mehta, eds., Elsevier, Oxford, UK, 263–285.

Rodriguez, H. N. (2000). "Mud bottom evolution at open coasts." PhD thesis, University of Florida, Gainesville, Fla.

Rodriguez, H. N., and Mehta, A. J. (1998). "Considerations on wave-induced fluid mud streaming at open coasts." *Sedimentary processes in the intertidal zone*, K. S. Black, D. M. Patterson, and A. Cramp, eds., Geological Society, London, 177–186.

Rodriguez, H. N., and Mehta, A. J. (2000). "Longshore transport of fine-grained sediment." *Continental Shelf Research*, 20(11/12), 1–14.

Rodriguez, H. N., and Mehta, A. J. (2001). "Modeling muddy coast response to waves." *Journal of Coastal Research*, SI 27, 137–148.

Ross, M. A. (1988). "Vertical structure of estuarine fine sediment suspensions." PhD thesis, University of Florida, Gainesville, Fla.

Rossby, C. G., and Montgomery, R. B. (1935). "The layer of functional influence in wind and ocean currents." *Papers in Physical Oceanography*, 3(3), 1–101.

Rouse, H. (1937). "Modern conceptions of the mechanics of fluid turbulence." *Transactions of the ASCE*, 102, 436–451.

Sakakiyama, T., and Bijker, E. W. (1989). "Mass transport velocity in mud layer due to progressive waves." *Journal of the Waterway Port, Coastal and Ocean Engineering*, 115(5), 614–633.

Sanford, L. P., and Chang, M.-L. (1997). "The bottom boundary condition for suspended sediment deposition." *Journal of Coastal Research*, SI5, 3–17.

Sanford, L. P., and Halka, J. P. (1993). "Assessing the paradigm of mutually exclusive erosion and deposition of mud, with examples from upper Chesapeake Bay." *Marine Geology*, 114(1–2), 35–37.

Sanford, L. P., Panageotou, W., and Halka, J. P. (1991). "Tidal resuspension of sediments in northern Chesapeake Bay." *Marine Geology*, 97(1/2), 87–103.

Scarlatos P. D., and Mehta A. J. (1993). "Instability and entrainment mechanisms at the stratified fluid mud-water interface." *Nearshore and estuarine cohesive sediment transport*, A. J. Mehta, ed., American Geophysical Union, Washington, D.C., 205–223.

Schiffman, R. L., Pane, V., and Sunara, V. (1985). "Sedimentation and consolidation." *Flocculation, sedimentation and consolidation*, B. M. Moudgil and P. Somasundaran, eds., Engineering Foundation, New York, 57–121.

Sheng, Y. P. (1986). Modeling bottom boundary layer and cohesive sediment dynamics in estuarine and coastal waters. In: *Estuarine Cohesive Sediment Dynamics*, A. J. Mehta, ed., Springer-Verlag, Berlin, 360-400.

Sheng, Y. P., and Villaret, C. (1989). "Modeling the effect of suspended sediment stratification on bottom exchange processes." *Journal of Geophysical Research*, 94(C10), 14,429–14,444.

Shibayama, T., Takikawa, H., and Horikawa, K. (1986). "Mud mass transport due to waves." *Coastal Engineering in Japan*, 29, 151–161.

Shrestha, P. L., and Orlob, G. T. (1996). "Multiphase distribution of cohesive sediments and heavy metals in estuarine systems." *Journal of Environmental Engineering*, 122(8), 730–740.

Sills, G. C., and Elder, D. McG. (1986). "The transition from sediment suspension to settling bed." *Estuarine cohesive sediment dynamics*, A. J. Mehta, ed., Springer-Verlag, Berlin, 192–205.

Sisko, A. W. (1958). "The flow of lubricating greases." *Industrial Engineering Chemistry*, 50(1), 1,789–1,792.

Skafel, M.G., and Bishop, C. T. (1994). "Flume experiments on the erosion of till shores by waves." *Coastal Engineering,* 23(3–4)*,* 329–348.

Smith, T. J., and Kirby, R. (1989). "Generation, stabilization and dissipation of layered fine sediment suspensions." *Journal of Coastal Research*, SI5, 63–73.

Smith, T. M., McAnally, W. H., and Teeter, A. M. (1987). "Corpus Christi inner harbor shoaling investigation." *Technical Rep. HL-87-13*, U. S. Army Engineer Waterways Experiment Station, Vicksburg, Miss.

Soil Conservation Service (SCS). (1992). "Ion exchange analysis." *Soil survey laboratory methods manual*, U.S. Department of Agriculture, Washington, D.C., 145.

Stolzenbach, K. D., Newman, K. A., and Wang, C. S. (1992). "Aggregation of fine particles at the sediment-water interface." *Journal of Geophysical Research*, 97(C11), 17,889–17,898.

Sutherland, T. F., Grant, J., and Amos, C. L. (1998). "The effect of carbohydrate production by the diatom *Nitzschia curvilineata* on the erodibility of sediment." *Limnology and Oceanography*, 43(1), 65–72.

Taki, K. (1990). "Hydraulic study on the rate of resuspension of mud due to free surface water flow." PhD thesis, Chuo University, Tokyo (in Japanese).

Taki, K. (2001). "Critical shear stress for cohesive sediment transport." *Coastal and estuarine fine sediment transport processes*, W. H. McAnally and A. J. Mehta, eds., Elsevier, Amsterdam, 53–61.

Tambo, N., and Watanabe, Y. (1979). "Physical characteristics of flocs. I: The floc density function and aluminum floc." *Water Resources Research*, 13(5), 409–419.

Tarigan, A. P. M. (1996). "An examination of the dependence of mud shore profiles on the nearshore environment." MS thesis, University of Florida, Gainesville, Fla.

Tarigan, A.M., Lee, S.-C., and Mehta, A. J. (1996). "Recession of the muddy coast: A departure from the Bruun Rule?" *Proceedings of the 10th Congress of the Asia and Pacific Division of IAHR*, S.-C. Lee, K.-L. Hiew, and S.-H. Ong, eds., National Hydraulics Research Institute of Malaysia, Kuala Lumpur, 468–477.

Task Committee on Erosion of Cohesive Materials (TCECM). (1968). "Erosion of cohesive sediments." *Journal of the Hydraulics Division of ASCE*, 94(4), 1017–1049.

Teeter, A. M. (2001a). "Clay-silt sediment modeling using multiple grain classes. I: Settling and deposition." *Coastal and estuarine fine sediment transport processes*, W. H. McAnally and A. J. Mehta, eds., Elsevier, Amsterdam, 157–171.

Teeter, A. M. (2001b). "Clay-silt sediment modeling using multiple grain classes. II: Application to shallow-water resuspension and deposition." In: *Coastal and estuarine fine sediment transport processes*, W. H. McAnally and A. J. Mehta, eds., Elsevier, Amsterdam, 173–187.

Teeter, A. M., and Callegan, C. (2000). "Effects of channel modifications on currents, salinity, and sedimentation near Daniel Island, Charleston Harbor, SC." *Technical Rep.*, U.S. Army Engineer Waterways Experiment Station, Vicksburg, Miss.

Teeter, A. M., Letter, J. V., Pratt, T. C., Coleman, C. J., and Boyt, W. L. (1996). "San Francisco Bay long-term management strategy (LTMS) for dredging and dredged material disposal, report 2, baywide suspended sediment transport modeling." *Technical Rep. HL-96-8*. U. S. Army Engineer Waterways Experiment Station, Vicksburg, Miss.

Teeter, A. M., and Pankow, W. (1989). "Deposition and erosion testing on the composite dredged material sediment sample from New Bedford Harbor, Massachusetts." *Technical Rep. Hl-89-11*, U.S. Army Engineer Waterways Experiment Station, Vicksburg, Miss.

Teeter, A. M., Parchure, T. M., and McAnally, Jr. (1997). "Size-dependent erosion of two silty-clay sediment mixtures." *Cohesive sediments*, N. Burt, R. Parker, and J. Watts, eds., Wiley, Chichester, UK, 253–262.

Teisson, C. (1997). "A review of cohesive sediment transport models." *Cohesive sediments*, N. Burt, R. Parker, and J. Watts, eds., Wiley, Chichester, UK, 367–381.

Thimakorn, P. (1984). "Resuspension of clays under waves." *Seabed mechanics*, B. Denness, ed., Graham and Trotman, London, 191–196.

Thomas, W. A., Heath, R. E., Stewart, J. P., and Clark, D. G. (1988). "The Atchafalaya River delta, Report 5: Quasi-two-dimensional model of delta growth and impacts on river stages." *Technical Rep. HL-82-15*, U. S. Army Engineer Waterways Experiment Station, Vicksburg, Miss.

Thorn, M. F. C. (1981). "Physical processes of siltation in tidal channels." *Proceedings of the Conference on Hydraulic Modeling Applied to Maritime Engineering Problems*, Institution of Civil Engineers, London, 47–55.

Thorn, M. F. C., and Parsons, J. G. (1980). "Erosion of cohesive sediments in estuaries: an engineering guide." *Proceedings of the 3rd International Symposium on Dredging Technology*, British Hydraulics Research Association, Cranfield, UK, 349–358.

Toorman, E. A. (1995). "Controlled rate concentric cylinder rheometry of estuarine suspensions." *Report HYD148*, Hydraulics Laboratory, Civil Engineering Department, Catholic University of Leuven, Leuven, Belgium.

Toorman, E. A. (1996). "Sedimentation and self-weight consolidation: general unifying theory." *Geotechnique*, 46(1), 103–133.

Toorman, E. A. (2001). "Cohesive sediment transport modeling: European perspective." *Coastal and estuarine fine sediment transport processes*, W. H. McAnally and A. J. Mehta, eds., Elsevier, Amsterdam, 1–18.

Toorman, E. A., and Berlamont, J. E. (1993). "Mathematical modeling of cohesive sediment settling and consolidation." *Nearshore and estuarine cohesive sediment transport*, A. J. Mehta, ed., American Geophysical Union, Washington, D.C., 148–184.

Torfs, H. (1995). "Erosion of mud/sand mixtures." PhD thesis, Catholic University of Leuven, Leuven, Belgium.

Torfs, H., Jiang, J., and Mehta, A. J. (2001). "Assessment of erodibility of fine/coarse sediment mixtures." *Coastal and estuarine fine sediment transport processes*, W. H. McAnally and A. J. Mehta, eds., Elsevier, Amsterdam, 109–123.

Trowbridge, J. H., and Kineke, G. C. (1994). "Structure and dynamics of fluid muds on the Amazon continental shelf." *Journal of Geophysical Research*, 99(C1), 865–874.

Tsai, C. H., and Hu, J. Q. (1997). "Flocculation of particles by fluid shear in buffered suspensions." *Proceedings of the 7th Symposium on Interactions Between Sediments and Water*, Kluwer, Dordrecht, The Netherlands, 55–62.

Tsai, C. H., and Lick, W. (1986). "A portable device for measuring sediment resuspension." *Journal of Great Lakes Research*, 12(4), 314–321.

Tubman, M. W., and Suhayda, J. N. (1976). "Wave action and bottom movements in fine sediments." *Proceedings of the 15th Conference on Coastal Engineering*, ASCE, New York, 1, 168–1,183.

Uittenbogaard, R. E. (1995). "The importance of internal waves for mixing in a stratified estuarine tidal flow." PhD thesis, Technical University of Delft, Delft, The Netherlands.

Van Leussen, W. (1994). "Estuarine macroflocs and their role in fine-grained sediment transport." PhD thesis, Utrecht University, Utrecht, The Netherlands.

Van Olphen, H. (1977). *Clay colloid chemistry,* 2nd Ed., Wiley, New York.

Villaret, C. and Paulic, M. (1986). "Experiments on the erosion of deposited and placed cohesive sediments in an annular flume and a rocking flume." *Rep. No. UFL/COEL-86/07*, Coastal and Oceanographic Engineering Department, University of Florida, Gainesville, Fla.

Vinzon, S. B. (1998). "A preliminary examination of Amazon shelf sediment dynamics." Engineer Degree thesis, University of Florida, Gainesville, Fla.

Vinzon, S. B., and Mehta, A. J. (2001). "Boundary effects due to suspended sediment in the Amazon River estuary." *Coastal and estuarine fine sediment transport processes*, W. H. McAnally and A. J. Mehta, eds., Elsevier, Amsterdam, 359–372.

Walkley, A. and Black, I. A. (1934). "An examination of the Degtjareff method for determining soil organic matter and a proposed modification of the chromic acid titration method." *Soil Science*, 37, 29–38.

Wells, J. T. (1983). "Dynamics of coastal fluid muds in low-, moderate-, and high-tide-range environments." *Canadian Journal of Fisheries and Aquatic Sciences*, 40 (Supplement 1), 130–142.

Wells, M. L., and Goldberg, E. D. (1993). "Colloid aggregation in seawater." *Marine Chemistry*, 41, 353–358.

Whittig, L. D., and Allardice, W. R. (1986). "X-ray diffraction techniques." *Methods of soil analysis, Part 1*, A. Klute, ed., Soil Science Society of America, American Society of Agronomy, Madison, Wisc., 331–362.

Wiesner, M. R. (1992). "Kinetics of aggregate formation in rapid mix." *Water Resources Research*, 26(3), 379–387.

Williams, D. J. A. (1986). "Rheology of cohesive suspensions." *Estuarine cohesive sediment dynamics*, A. J. Mehta, ed., Springer-Verlag, Berlin, 110–125.

Willis, D. H., and Crookshank, N. L. (1997). "Modelling multiphase sediment transport in estuaries." *Cohesive sediments*, N. Burt, R. Parker, and J. Watts, eds., Wiley, Chichester, UK, 383–394.

Winterwerp, J. C. (1998). "A simple model for turbulence induced flocculation of cohesive sediment." *Journal of Hydraulic Research*, 36(3), 309–326.

Winterwerp, J. C. (1999). "On the dynamics of high-concentrated mud suspensions." PhD thesis, Technical University of Delft, Delft, The Netherlands.

Winterwerp, J. C., Cornelisse, J. M., and Kuijper, C. (1993). "A laboratory study on the behavior of mud from the Western Scheldt under tidal conditions." *Nearshore and estuarine cohesive sediment transport*, A. J. Mehta, ed., American Geophysical Union, Washington, D.C., 295–313.

Winterwerp, J. C., and Kranenburg, C. (1997a). "Erosion of fluid mud by entrainment." *Cohesive sediments*, N. Burt, R. Parker, and J. Watts, eds., Wiley, Chichester, UK, 263–277.

Winterwerp, J. C., and Kranenburg, C. (1997b). "Erosion of fluid mud layers.II: Experiments and model validation." *Journal of Hydraulic Engineering*, 123(6), 512–519.

Wolanski, E., Asaeda, T., and Imberger, J. (1989). "Mixing across a lutocline." *Limnology and Oceanography*, 34(5), 931–938.

Wolanski, E., and Gibbs, R. J. (1995). "Flocculation of suspended sediment in the Fly River estuary, Papua New Guinea." *Journal of Coastal Research*, 11(3), 754–762.

Wolanski, E., Gibbs, R., Ridd, P., King, B., Hwang, K. Y., and Mehta, A. (1991). "Fate of dredge spoil, Cleveland Bay, Townsville." *Proceedings of the 10th Austalasian Conference on Coastal and Ocean Engineering*, Institution of Engineers Australia, Canberra, Australia, 63–66.

Wotherspoon, D. J. J., and Ashley, R. M. (1992). "Rheological measurement of the yield strength of combined sewer deposits." *Water Science & Technology*, 25(8), 165–170.

Wright, L. D., Wiseman, W. J., Bornhold, B. D., Prior, P. B., Suhayda, J. N., Keller, G. H., Yang, Z. S., and Fan, Y. B. (1988). "Marine dispersal and deposition of Yellow River Silts by gravity driven underflows." *Nature*, 332(6164), 629–632.

Yamamoto, T., and Takahashi, S. (1985). "Wave damping by soil motion." *Journal of the Waterway, Port, Coastal and Ocean Engineering*, 111(1), 62–77.

Yamanishi, H., Higashi, O., Kusuda, T., Watanabe, R. (1998). "Scouring of cohesive sediment on a slope under breaking wave action." *Journal of the Waterway, Port, Coastal and Ocean Engineering*, 111(1), 62–77.

Yeh, H.-Y. (1979). "Resuspension properties of flow deposited cohesive sediment beds." MS thesis, University of Florida, Gainesville, Fla.

Ziegler, C. K., and Nisbet, B. S. (1994). "Fine-grained sediment transport in Pawtuxet River, Rhode Island." *Journal of Hydraulic Engineering*, 120(5), 561–576.

Ziegler, C. K., and Nisbet, B. S. (1995). "Long-term simulation of fine-grained sediment transport in large reservoir." *Journal of Hydraulic Engineering*, 121(11), 773–781

Copyrighted Materials
Copyright © 2008 American Society of Civil Engineers (ASCE)
Retrieved from www.knovel.com

CHAPTER 5

Sediment Transport Measurements

P. Diplas, R. Kuhnle, J. Gray, D. Glysson, and T. Edwards

5.1 GENERAL

P. Diplas, R. Kuhnle, J. Gray, and D. Glysson

Sediment erosion, transport, and deposition in fluvial systems are complex processes that are treated in detail in other sections of this book. Development of methods suitable for the collection of data that contribute to understanding these processes is a still-evolving science. Sediment and ancillary data are fundamental requirements for the proper management of river systems, including the design of structures, the determination of aspects of stream behavior, ascertaining the probable effect of removing an existing structure, estimation of bulk erosion, transport, and sediment delivery to the oceans, ascertaining the long-term usefulness of reservoirs and other public works, tracking movement of solid-phase contaminants, restoration of degraded or otherwise modified streams, and assistance in the calibration and validation of numerical models.

This chapter presents techniques for measuring bed-material properties and suspended and bed-load discharges. Well-established and relatively recent, yet adequately tested, sampling equipment and methodologies, with designs that are guided by sound physical and statistical principles, are described. Where appropriate, the theory behind the development of the equipment and guidelines for its use are presented.

The theory and statistical methods described in the bed-material section represent the developments that have taken place mainly since the 1970s. Research on bed-material sampling techniques commenced later than research in the other two areas discussed in this chapter, and the relevant work is available almost exclusively in journals and conference proceedings. Therefore, emphasis has been placed on several key aspects of the concepts and development of bed-material sampling techniques. Improving and validating existing sediment-sampling techniques remains an active area of research today. It is worth mentioning that the methods discussed in this section can be used to estimate the necessary size of suspended or bed-load samples in order to determine their sediment size characteristics at a desirable level of accuracy.

Many of the concepts described in the section on suspended-sediment sampling were developed in the mid-twentieth century, although several new sampler types and modifications to traditional sampling methods have been developed. The collection of accurate bed-load samples has always been a challenge, because of the spatial and temporal variability associated with its transport. Several studies have successfully sampled bed load on small streams with semipermanent installations. For many projects, however, sampling programs using manually operated portable samplers continue to be the method of choice. The most common types of manually operated samplers, along with several new analyses that define improved techniques for measuring and calculating the accuracy of manually collected bed-load samples, have been reviewed. These new analyses provide needed information on the expected errors associated with bed-load data collected using a given sampling design.

Bed-material sampling is usually conducted during low flows. Bed-load and suspended-sediment sampling can be conducted over the entire hydrograph, although emphasis is usually directed toward higher flows and particularly floodflows.

5.1.1 Terminology

Bed material, suspended sediment, and bed load can be defined by their origin, or operationally by their method of collection (Fig. 5-1). Bed material is the sediment mixture of which the streambed is composed (ASTM International 1998). However, bed-material data will necessarily reflect the attributes of the sampler and its means of deployment. Hence, bed material collected by a US BM-54 would represent the topmost 5 cm of a bed composed of material finer than medium-sized pebbles.

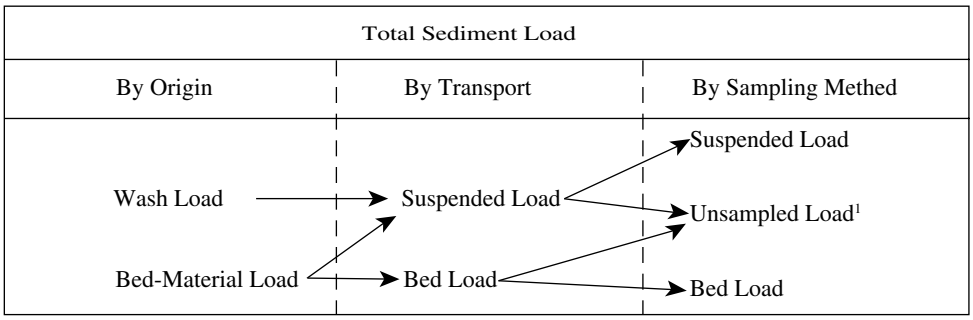

[1]That part of the sediment load that is not collected by the depth-integrating suspended-sediment and pressure-difference bedload samplers used, depending on the type and size of the sampler(s). Unsampled-load sediment can occur in one or more of the following categories: a) sediment that passes under the nozzle of the suspended-sediment sampler when the sampler is touching the streambed and no bedload sampler is used; b) sediment small enough to pass through the bedload sampler's mesh bag; c) sediment in transport above the bedload sampler that is too large to be sampled reliably by the suspended-sediment sampler; and d) material too large to enter the bedload-sampler nozzle.

Fig. 5-1. Components of total sediment load considered by origin, by transport, and by sampling method.

The total amount of sediment in transport can be described by its origin as being composed of bed-material load plus wash load. Bed-material load is that part of the total load that is composed of particle sizes present in appreciable quantities in the shifting portions of the streambed (ASTM International 1998). Wash load is that part of the total load composed of particles, usually finer than 0.062 mm in diameter, that are found, if at all, only in relatively small quantities in the bed (ASTM International 1998). Again, the operational definition of sediment in transport is in part a function of the types of samplers used to obtain the data. Suspended-sediment and bed load discharge are the quantities of suspended sediment and bed load passing through a stream cross section per unit time, respectively. Suspended-sediment discharge can include some of the bed-material load component and includes all of the wash load component. Bed load discharge includes some of the bed-material load component. Data from physical samples of suspended sediment and bedload, necessarily obtained by use of samplers, may not equal the sum of bed-material load plus washload (Fig. 5-1). This is a result of one or more factors associated with the range in size of sediments in transport, and the characteristics and deployment methods of the suspended-sediment and bedload samplers.

5.1.2 History of Development of Sediment-Sampling Equipment

The initial attempts to develop sediment-sampling equipment were made by independent investigators. The equipment lacked calibration and was deployed using widely different operating techniques. Most instruments were designed with limited attention to, or knowledge of, sediment transport concepts or the influence of the equipment on the local flow pattern (Glysson 1989a). As a result, data obtained by different investigators before the 1940s were not comparable, nor could their accuracy be evaluated. It became apparent that reliable sediment data could not be obtained unless equipment, data collection, and analytical methods were standardized.

In 1939, various agencies of the U.S. government organized an interagency program to study methods and equipment used in measuring the sediment discharge of streams and to improve and standardize equipment and methods where practicable (FISP 1941). The Federal Interagency Sedimentation Project (FISP) (Skinner 1989; Glysson and Gray 1997) was created under the sponsorship of the Committee on Sedimentation of the Federal Water Resources Council. The comprehensive study of sampling equipment included suspended-sediment, bed-load, and bed-material samplers. As a result of research conducted by the FISP and others, an integrated system of sediment samplers, sampling, and analytical techniques has been developed and is widely used around the world.

Progress is being made in improving available or devising new technologies to measure selected characteristics of fluvial sediment. Instruments that operate on acoustic, differential density, pump, focused beam reflectance, laser diffraction, nuclear, optical backscatter, optical transmission, and spectral reflectance principles have been developed (Wren et al. 2000). Ideally, a surrogate parameter that varied as a function of the sedimentary property of interest (such as concentration, particle-size distribution, or particle or bed form movement) would be available, which could be automatically monitored and recorded.

The literature is full of descriptions of emerging technologies for measuring selected characteristics of fluvial sediment; for example, see Lee (1990); Mertes et al. (1993); Lodhi et al. (1997); Gray and Schmidt (1998); Agrawal and Pottsmith (2001); Byrne and Patiño (2001); Christiansen et al. (2001); Gartner and Cheng (2001); Land and Jones (2001); Larsen et al. (2001); Rubin et al. (2001); Schoellhamer (2001); Gray

et al. (2005). Although some techniques show considerable promise, none is yet commonly accepted nor extensively used. Isokinetic samplers—primarily those developed by the FISP and described by Edwards and Glysson (1999)—generally are considered the standard against which other types of samplers are calibrated (Morris and Fan 1997; Wren et al. 2000). Adoption of any sediment surrogate technology for large-scale sediment-monitoring programs should be predicated on favorable comparisons between an adequate number of comparative data from the surrogate technology and data from isokinetic samplers collected for a sufficient time period over a broad range of flow and sedimentary conditions. Hence, the following sections focus primarily on methods for obtaining bed-material, suspended-sediment and bed-load data available at the advent of the twenty first century.

5.2 BED-MATERIAL MEASUREMENT TECHNIQUES

P. Diplas

5.2.1 Introduction

Many hydraulic, geomorphic, and ecological aspects of river behavior are closely linked to the characteristics of the material composing a river's streambed. Flood levels, sediment transport rates, and streambed stability, for example, depend on the grain-size distribution of the bed material. Similarly, the quality and quantity of stream habitats are greatly influenced by the amount of fine particles present in the streambed. Recent surveys undertaken by the U.S. Environmental Protection Agency (USEPA 1994) and the U.S. Fish and Wildlife Service (USDA 1994) concluded that stream siltation was the most important factor causing water quality impairment and adversely affecting fishery habitats in streams. Various best management practices, such as reforestation and slope stabilization, are typically employed to reduce sediment input into streams and thus minimize the adverse effects of fine sediment on stream ecology. To effectively gauge the success of these practices, the bed-material size distribution within streams must be monitored. It is therefore evident that there is a need to use accurate and efficient techniques for collecting, analyzing, and interpreting results obtained from bed-material samples.

5.2.2 Sediment-sampling Issues

For certain phenomena, and the feasibility study phases of some engineering projects, knowledge of the median grain size, D_{50}, or some other single sediment parameter might be adequate. However, for other cases, knowledge of the entire size distribution, and especially of its tails, might be essential. For example, channel grain roughness is typically associated with the coarser sizes of the bed material, e.g., D_{90}, whereas for spawning habitat studies the size of the finer portions, e.g., D_{10}, is more critical (Waters 1995). An appropriate method should sample the correct bed-material population and collect the entire range of particle sizes available within it in a way that consistently and accurately represents the parent material distribution. The analysis of the sampled material should render an unbiased grain-size distribution, such as that typically provided from a volumetric sample analyzed in terms of weight through the use of a series of sieves. Furthermore, it is desirable to estimate the effort, or sample size, required to determine various sediment sizes with a certain accuracy or degree of precision.

The requirements stated here are rather difficult to meet in the field, especially for the case of gravel-bed streams. The difficulties stem from three ubiquitous characteristics of sediment deposits in gravel streams: the presence of a wide range of sediment sizes, from clay to gravel or coarser particles, which at times may span up to five orders of magnitude; the vertical stratification in terms of particle size (Church et al. 1987; Diplas and Sutherland 1988); and the considerable spatial variability, or patchiness, of bed surface sediments (Mosley and Tindale 1985).

Three distinct horizontal layers are typically present in gravel-bed streams. The top layer, or pavement, is in direct contact with the flow and thus dictates the grain roughness of the channel boundary and the stability of the channel bed. The makeup of the second layer, or subpavement, affects the quality of spawning grounds (Diplas and Parker 1992). The third, or bottom, layer represents the bulk of the subsurface material. Although all three layers seem to contain the same range of particle sizes, the top layer is usually the coarsest and the subpavement has the highest proportion of finer particles. Each of the top two layers is usually as thick as the coarsest particle size present and all three represent different sample populations. In some cases, for example when there is no excess infeed of fine sediment into a river reach due to human activities within the surrounding basin, the second layer is absent. It is this condition that is most frequently mentioned in the literature.

Not only does a gravel bed's composition change vertically, but also it varies laterally and longitudinally. On the stream reach scale, this inhomogeneity can easily be seen on a depositional bar, which contains several distinct areas each having a different particle composition (Bluck 1982; Diplas 1994), and in the contrast between the grain sizes found in pools and in riffles (Sear 1996). On larger scales, the fining of the bed material in the downstream direction has been well documented (Church and Kellerhals 1978; Parker 1991).

The results of extensive sediment sampling undertaken by numerous researchers indicate that there is not a single grain-size distribution type capable of describing the material in different fluvial deposits. Although the lognormal has been proposed in many textbooks as the distribution representing most fluvial sediments, in reality things are more complicated. For example, it has been suggested that in about 50% of the cases, samples obtained from gravel streams possess bimodal

distributions (Kondolf and Wolman 1993), whereas there is no convincing evidence to support the use of a single distribution even for materials located within the same stream.

The need to use proper procedures for collecting and analyzing bed-material samples, which take into consideration some of the features observed in natural streams, has only recently been recognized. Such procedures are necessary for field and laboratory studies as well as for calibrating and validating numerical models dealing with stream behavior. Considerable effort has been devoted to this subject during the past two decades.

5.2.3 Sample Collection and Analysis Methods

Some of the methods commonly used for sediment sampling include volumetric, grid, areal, transect, and photographic methods. The analysis of a sample may vary depending on the method used for collecting it.

Volumetric or bulk sampling is the method most commonly used in obtaining the size distribution of the grains in a sediment deposit. The extracted sample consists of a predetermined volume that is large enough so that its dimensions are independent of the dimensions of individual grains (Kellerhals and Bray 1971). The sample is then sieved, and the results are plotted in terms of grain (sieve) size versus percentage by weight passing that sieve size. One tonne of material is considered a practical limit for hand sieving (Church et al. 1987). Dry sieving is usually limited to particles having diameter equal to or coarser than 0.0625 mm. For particles smaller than this size, hydraulic settling methods are typically employed. These two methods may not provide equivalent measures of particle size. Bulk sampling procedures are appropriate for deposits that are isotropic with respect to grain size and other sediment properties (e.g., particle shape and density), such as sandy streams and the bottom layers of gravel streams. Bulk sampling is desirable because it provides unbiased estimates of the size distribution of the sediments available in the deposit. Strictly speaking, for the volumetric sample to be unbiased it should be analyzed in terms of the volumes occupied by the various grain sizes. However, when the specific weight of all the particles in the sample is the same, a condition that is typically met in most samples, this is equivalent to analyzing the sample in terms of weight through the use of the sieves. A question that arises is with respect to the minimum excavation depth necessary to render a sample volumetric. Experiments have indicated that the minimum depth required for a sample to be volumetric is about twice the size of the largest particle present in the sampled deposit (Diplas and Fripp 1992).

The pavement and subpavement layers, though, each having thickness roughly equal to the size of the coarsest particle present, have volumes that are dependent upon the size of the sediments and thus cannot be sampled volumetrically (Kellerhals and Bray 1971). A volumetric sample of a gravel bed would combine the different sample populations found in the pavement, subpavement, and bottom layers. The resulting grain-size distribution would not accurately describe any of these layers. Therefore, in the presence of vertical size (or any other sediment property) stratification, it is necessary to devise surface-oriented methods that would be able to collect sediment from each stratum separately. Such methods should be able to infer three-dimensional information about the makeup of the sediment deposit from things represented on a two-dimensional surface.

Wolman (1954) was the first to introduce the use of the grid method for sampling fluvial sediments. This method is suitable for collecting sediment from a single layer of bed material such as the pavement. The sample consists of only the particles that lie directly below an established grid covering the area of interest. The grid may be established in several ways. A wire mesh may overlie the sampled area or for larger areas a pacing procedure may be used (Kellerhals and Bray 1971). A method used widely in the field is a variant known as Wolman's walk method. In this method an operator paces off at regular intervals and picks up the particle below his toe. Systematic sampling on a predefined, regular grid gives the highest accuracy for a given number of collected stones (Underwood 1970). Random sampling is not as efficient.

The particle's size is usually measured with a gravelometer (Hey and Thorne 1983). Gravelometers, shown in Fig. 5-2, are templates that contain square holes consistent with sieve openings. The smallest aperture that a particle can fit through is recorded as the grain size. Gravelometers are convenient for measuring particles that can be handled with one hand, up to about 216 mm (Church et al. 1987). However, some particles, even smaller than 216 mm, might be buried within the channel bed and thus it might be difficult to remove and measure them (Marcus et al. 1995). A gravelometer, together with waterproof paper or a tape recorder, makes it possible

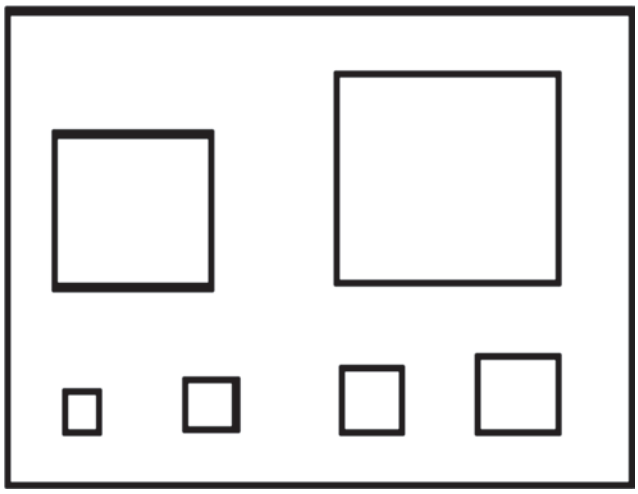

Fig. 5-2. A gravelometer.

for a single operator to sample an area and record the number, size, and possibly location of stones with the help of a GPS apparatus or a well-defined grid, without retaining any of the material (Fripp and Diplas 1993). Larger or embedded stones, however, may have to be measured with a tape. In this case, the intermediate axis is the closest to a sieve diameter. The distribution is obtained by plotting the grain size versus the percentage of stones in the sample that are finer than this size. This method is a type of grid-by-number sampling. In the presence of very large, exposed boulders, areal photos might be necessary to account for their contribution to the overall grain-size distribution.

To reduce the effort spent in the field, an adaptation of the grid-by-number approach has been proposed, using photographs of a sediment deposit, together with a grid of known spacing (Ritter and Helley 1969; Adams 1979). Determining the actual dimensions of the particles from the photographs is the main difficulty encountered in this case. The results seem to be biased, typically smaller than the real particle sizes measured in the field (Kellerhals and Bray 1971; Church et al. 1987). This bias is attributed to imbrication angle, grain packing, shadow effects, and scale distortion, factors that tend to be variable from site to site. To overcome the limitations of the photographic method, Ibbeken and Schleyer (1986), among others, have proposed digitizing the particle outline from an enlarged print and then measuring its dimensions. The use of the photographic method is deemed to be adequate for estimating the median size of a sediment deposit, containing gravel and larger particles, with moderate accuracy (Church et al. 1987). Recent developments in image analysis hold promise for further improvements in the use of the photographic method (Russ and Dehoff 2000).

In the absence of any structural features within a riverbed, the grid spacing does not affect the outcome of a sampling exercise. The only requirement in this case is that if two or more grid points fall on the same particle, the particle must be counted as many times. However, in natural streams, particle clusters and other features tend to dominate the bed morphology (Church et al. 1987; Hassan and Church 2000). To avoid serially correlated results it is therefore recommended that the spacing between grid points be at least $2D_{max}$, where D_{max} is the largest particle size present in the sampled deposit (Rice and Church 1998). About 1,500 particles per day can be measured and recorded in an exposed area by a team of two operators using a gravelometer (Rice and Church 1996). The corresponding time for the case of a submerged deposit will be longer and will depend on the depth and temperature of the water.

An areal sample consists of all the grains that are exposed on the surface of a specified area. One can use wax, clay, or other adhesives, paint, and photographs to sample an area (Kellerhals and Bray 1971; Adams 1979; Diplas and Sutherland 1988; McEwan et al. 2000). If an area is spray-painted, the painted particles can later be picked by hand. Wax poured onto the surface of a sample will harden and remove all of the surface particles and possibly some below that. The wax sample is melted and poured away, leaving the grains to be sieved. Moist pottery clay may also be used to obtain a surface sample; however, unlike wax, it can be used underwater as well as on dry surfaces, making it more suitable for field sampling (Diplas and Fripp 1992). A pistonlike apparatus, shown in Fig. 5-3, contains a round flat plate that is covered with a layer of clay. Surrounding the piston is a plastic shield, which protects the sample from the river's current. The piston is pushed against the surface material and retrieves the gravel sample. Finally, the sample is placed into a sieve with openings smaller than the smallest particle of interest and wet sieved to remove the clay (Fripp and Diplas 1993). The size distribution is obtained by plotting size versus percent weight in total sample. A sample recorded in this manner is known as an area-by-weight sample.

5.2.4 Bias of Sampling Methods

5.2.4.1 Equivalence of Samples Grid and areal sampling techniques allow collecting a sample from a specific population, such as the pavement and subpavement, but cannot be compared to one another because surface-oriented

Fig. 5-3. The device used to collect areal samples. A thin layer of clay has been applied on the flat plate inside the piston.

samples, like all nonvolumetric samples, are biased (Kellerhals and Bray 1971).

In general, for a sampling procedure to be unbiased, the exponent of the removed sample, expressed as D^y, minus the exponent of the method used for analysis, expressed as D^z, should be zero. This renders the sampling procedure dimensionless (Underwood 1970). For example, a bulk sample is unbiased because $y = z = 3$. Similarly, a grid sample analyzed by number is unbiased and equivalent to a volumetric sample because $y = z = 0$. The zero-dimensionality of these sampling and analysis methods allows the presentation of the results as a fraction or percent. Delesse (1848) was the first to show that the volume fraction of solids is equal to their area fraction captured in a planar section ($y = z = 2$). The equivalency of the point count fraction and the volume fraction of solids was demonstrated for the first time by Thomson (1930). An areal sample, though analyzed in terms of weight, is biased. To convert such an areal sample into its volumetric equivalent, Kellerhals and Bray (1971) suggested the formula

$$p(V-W)_i = Cp_i(A)\, D_i^x \tag{5-1}$$

where

$p(V-W)_i$ = percentage of material retained on sieve size i based on a volumetric sample;
$p(A)_i$ = percentage of material retained on sieve size i by an areal sampling method;
$D_i = \sqrt{D_i\, D_{i+1}}$ = geometric mean of two consecutive sieve sizes i and $i+1$; and
C = a constant that is used to adjust the sum of the converted volumetric equivalent percentiles to 100.

The exponent x is equal to $y - z$, and as such it depends on the type of adhesive used in collecting the sample. For example, when an adhesive that removes only the rocks found at the very top of the sampled surface was used ($y = 2$ and $z = 3$), as with clay or adhesive tape, laboratory tests indicated that $x = -1$, in agreement with the theory (Diplas and Sutherland 1988). However, when wax was used as the adhesive, x attained an average value of -0.47 (Diplas and Fripp 1992). Furthermore, the exponent for all the clay samples remained relatively constant, whereas the exponent for the wax samples varied significantly depending on the wax temperature and the makeup of the bed material. Wax penetrates the pores of the surface material and picks up subsurface grains, rendering the sample partly volumetric rather than strictly areal ($2 \leq y \leq 3$) (Church et al. 1987; Diplas and Fripp 1992). As a result, the value of the exponent x for wax samples can vary between -1 and 0 (Diplas and Sutherland 1988). Therefore, wax does not consistently remove the same material and should be avoided as an adhesive for sampling. Fig. 5-4 shows a clay sample analyzed by weight and a volumetric sample, both obtained from the same deposit. Whereas the areal sample significantly overestimates the grain-size characteristics of the sediment deposit, the converted size distribution (using Eq. 5-1 with $x = -1$) is close to the distribution obtained from the volumetric approach. As explained earlier, a grid-by-number sample is unbiased and thus the exponent x becomes zero. This is demonstrated in Fig. 5-5 for a sample of known volumetric size distribution. A complete list of the values of the exponent x necessary to convert a sample collected and analyzed with one method to that of another is shown in Table 5-1.

An approach to sampling a sediment deposit that has been suggested in the literature is to remove all the material up to the depth of the largest particle present and analyze it by weight. Such a sample provides a volumetric representation of the smallest grains, an areal representation of the coarsest grains, and in between for the intermediate sizes. In this case $2 \leq y \leq 3$ and $z = 3$. A more accurate statement, though, would be that $y = 3$ for the smallest grains, $y = 2$ for the coarsest ones, and $2 < y < 3$ for the

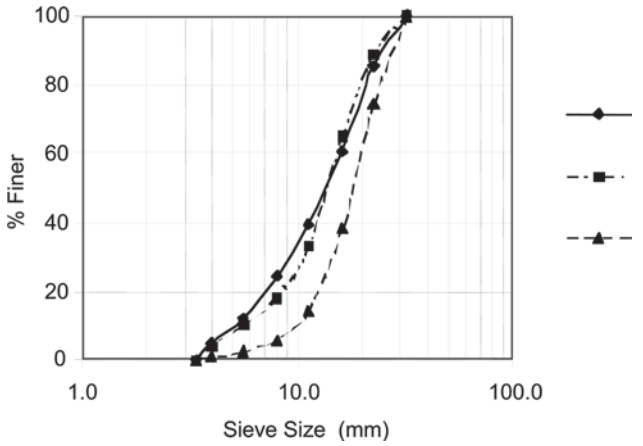

Fig. 5-4. A clay sample analyzed by weight (triangles) and converted using Eq. 5-1 with $x = -1$ (squares). Diamonds represent the results of a volumetric sample of the same deposit analyzed by weight.

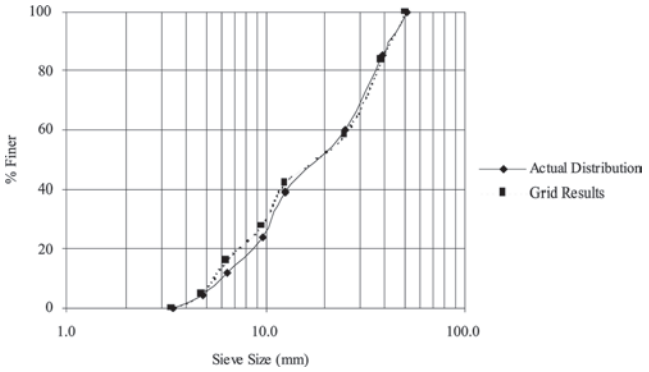

Fig. 5-5. Results of a 400-stone grid sample performed on a natural sediment deposit with the actual grain-size distribution curve.

Table 5-1 Conversions Based on the Recommendations of Kellerhals and Bray (1971)

	Conversion to								
Conversion From	Volume-by-weight	Volume-by-area	Volume-by-number	Grid-by-weight	Grid-by-area	Grid-by-number	Area-by-weight	Area-by-area	Area-by-number
Volume-by-weight	1	$1/D$	$1/D^3$	D^3	D^2	1	D	1	$1/D^2$
Volume-by-area	D	1	$1/D^2$	D^4	D^3	D	D^2	D	$1/D$
Volume-by-number	D^3	D^2	1	D^6	D^5	D^3	D^4	D^3	D
Grid-by-weight	$1/D^3$	$1/D^4$	$1/D^6$	1	$1/D$	$1/D^3$	$1/D^2$	$1/D^3$	$1/D^5$
Grid-by-area	$1/D^2$	$1/D^3$	$1/D^5$	D	1	$1/D^2$	$1/D$	$1/D^2$	$1/D^4$
Grid-by-number	1	$1/D$	$1/D^3$	D^3	D^2	1	D	1	$1/D^2$
Area-by-weight	$1/D$	$1/D^2$	$1/D^4$	D^2	D	$1/D$	1	$1/D$	$1/D^3$
Area-by-area	1	$1/D$	$1/D^3$	D^3	D^2	1	D	1	$1/D^2$
Area-by-number	D^2	D	$1/D$	D^5	D^4	D^2	D^3	D^2	1

intermediate sizes. Therefore, this procedure is biased, resulting in a sample that overestimates the degree of coarseness of the material. To render this sample unbiased, it is necessary to use different values for the exponent x in Eq. (5-1) for the different parts of the sampled material, with $x = 0$ for the smallest particles and $x = -1$ for the coarsest (see Fig. 5-4 in Diplas and Fripp 1992). An average value of x is typically employed in Eq. (5-1) to obtain the approximately equivalent volumetric distribution. Although this value depends on the makeup of the particular deposit, a limited number of tests have indicated that $x \approx -0.4$ for samples having a depth of about D_{90} (Diplas and Fripp 1992).

In most cases, the exponent in Eq. (5-1) assumes values different from unity. This suggests that nonvolumetric samples are nonlinearly biased. Therefore, samples that are not volumetric equivalents cannot be compared directly with each other, even if the samples are collected and analyzed by the same method (Diplas 1992; Diplas and Fripp 1992). In other words, each nonvolumetric sample has its own bias, which depends on the sampling method used and the actual size distribution of the sampled deposit, and must be converted to a volumetric (unbiased) equivalent before comparing it to a sample taken by the same or another method. This is demonstrated in Fig. 5-6, which shows the size distributions of two samples obtained by the use of clay from two different deposits and analyzed by weight through the use of sieves. These deposits have volumetric grain-size distributions with identical median values (8 mm) but different standard deviations. The corresponding median values of the areal samples analyzed by weight, however, are 14.5 and 22.8 mm. Thus, an appropriate method must first sample the correct population, and second convert it to a volumetric equivalent.

5.2.4.2 Truncation of Sample Populations Sediment size distributions also become biased when the technique employed cannot sample the entire range of grain sizes in a representative way, thus resulting in a truncated sample.

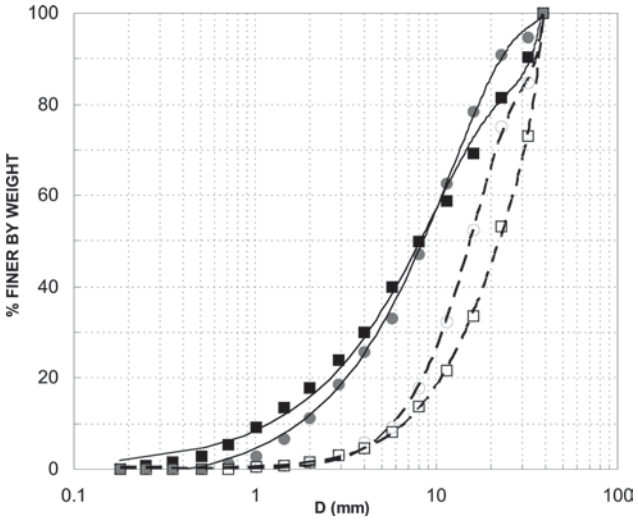

Fig. 5-6. Clay samples (open symbols) of two sediment deposits and the corresponding volumetric samples (solid symbols).

Truncation can occur at either the lower or upper end of a size range. When material smaller or larger than a specific size is truncated from the sample, it changes the frequency distribution of the particles and all its statistical measures (Fripp and Diplas 1993). It is difficult to determine the degree of change because the percentage of the bed material that belongs to the truncated portion of the sample is unknown. Truncation, besides its effect on determining D_{50} and other statistical parameters, may severely affect the estimates for D_{90} and D_{10}.

Truncation of the smaller size particles occurs in the Wolman's walk method and similar grid-sampling techniques. The reason for this is the inability of an operator whose eyes are averted from the sampled location to distinguish among

particles smaller than about 15 mm, approximately the width of the index finger, in an unbiased way (Fripp and Diplas 1993). Other researchers suggest that, for a properly trained person, truncation for grid samples starts between 2 and 8 mm (Wolman 1954; Kellerhals and Bray 1971). The more conservative values would be appropriate for sampling under water, where the problem becomes even more difficult because of low water temperature and the use of gloves by operators. One way to partially remedy the problem when the operator is unable to choose between two or more small particles is to designate that the outcome of the trial resulted in a particle smaller than a predetermined size, say 10 mm. Although the shape of the grain-size distribution below this size is not known, the proportion of these particles is estimated, thus avoiding a truncated sample (Petrie and Diplas 2000).

Truncation of the larger particle sizes may occur when clay, or some other adhesive, is used to obtain an areal sample in the presence of very coarse particles. For example, clay is only capable of consistently removing particles less than about 40 mm (Diplas and Fripp 1992).

5.2.4.3 Operator Error The accuracy of a grid sample is influenced by random and systematic errors. The former are due to the natural variability of the grain sizes present within the sediment deposit and their significance is reduced as the sample size increases, according to some statistical criteria. The latter are associated with biases exhibited by the operator and are not affected by the sample size (Hey and Thorne 1983). As a result, as the sample size increases, differences between samples obtained by different operators become more pronounced. Unless special precautions are taken, Hey and Thorne (1983) concluded that systematic, operator-related errors become the dominant type for grid samples exceeding 100 particles. There are two major sources of operator bias: (1) inappropriate selection of particles, and (2) erroneous measurement of their size (Hey and Thorne 1983; Marcus et al. 1995). The first can be rectified by using well-defined grid points that unambiguously identify the particle to be chosen. This is more difficult to accomplish under submerged conditions. Selection and measurement of particles below a size that operators cannot distinguish (e.g., 10 mm) should also be avoided. Much larger errors are exhibited within this smaller size range when samples obtained by different operators are compared (Marcus et al. 1995). The second operator bias can be corrected by using a consistent and repeatable means of measuring the particle size, such as the gravelometer. The best strategy for curtailing systematic sampling errors is to provide the operators with thorough training in the field. It has been suggested that, when possible, a single, carefully trained operator be employed to monitor changes in a sediment deposit over space or time (Hey and Thorne 1983; Marcus et al. 1995; Wohl et al. 1996). Although such an approach does not necessarily preclude the occurrence of bias, it has the potential for providing more consistent results.

5.2.5 Sample Size and Accuracy

5.2.5.1 Determining Sample Size If truncation is not a problem, and a sample is converted to a volumetric equivalent, an unbiased sample has been obtained. However, one important issue remains, and that is its accuracy. How accurate a sample needs to be can vary depending on what the results are being used for. The accuracy with which a sample describes the true statistical parameters of the bed material depends a great deal on its size, the shape of its size distribution, and its standard deviation. Typically, the larger the sample size, the higher the accuracy. Unfortunately, sampling large amounts of material is often physically or economically impractical. Considerable effort has been spent on calculating the minimum sample size needed to obtain a desired level of accuracy. Normally, the sample size is determined either by weight or by the number of stones.

5.2.5.2 Sample Size Determined by Number The size of grid sample necessary to provide consistent estimates of the mean grain size of a sediment deposit has been discussed frequently in the literature. Originally, Wolman (1954) suggested that 100 stones constituted an adequate sample size. Bray (1972) and Church and Kellerhals (1978) found that samples of 50 stones were sufficient. Hey and Thorne (1983) stated that samples as small as 40 stones provide repeatable estimates of the mean grain size, whereas Mosley and Tindale (1985) suggested 70 particles, and Edwards and Glysson (1999) indicated that at least 100 pebbles should be collected. Based on these results and the experience of others (e.g., Yuzyk 1986; Kondolf 1997), it is proposed that 100-stone grid samples be used to provide routine estimates of the sediment mean grain size.

Even more important to consider, though, is the development of methods that specify the sample size necessary to determine a certain sample characteristic, e.g., the median particle diameter, with a desired level of accuracy after the collected material has been analyzed. The level of accuracy may be considered in absolute terms, e.g., mm or ϕ (phi) units, or in relative terms, e.g., percent error. The results of a grid-by-number procedure are presented in terms of frequency by number, a process that is well suited to statistical treatment. Statistical methods can be used in a variety of ways. If the distribution type describing the particle sizes available in a deposit, together with an estimate of its mean and standard deviation values, is known beforehand, well-established methods that are easily accessible from books can be employed (e.g., Gilbert 1987). If such information is not available, as is typically the case, either a two-stage sampling approach or methods that do not require prior knowledge of the distribution should be used.

The first step in a two-stage sampling scheme is to undertake a preliminary or pilot sampling program that will provide an advance estimate of the variation that a particle size of interest, e.g., D_{84}, exhibits (Durand 1971). These

results can be used to guide the extent of the sampling effort required to determine this size with a desired degree of accuracy and confidence level. Student's *t*-distribution can be used for that purpose (Gilbert 1987; Durand 1971). This approach is recommended by the International Organization of Standards (ISO 1992).

The bootstrap (Rice and Church 1996) and the binomial (Fripp and Diplas 1993) are two methods that can be used to estimate the sample size necessary to determine the confidence intervals around a *specific* grain-size percentile without knowing or making any assumptions about the grain-size distribution type of the sampled deposit (Petrie and Diplas 2000). The bootstrap is a numerically intensive method that requires a grid sample that is sufficiently large, possibly in excess of 1,000 or even 2,000 stones (Sprent 1998), to accurately represent the population grain-size distribution of the parent material. The sizes of all these stones are recorded and subsequently stored in a computer. The standard error for a given percentile is determined by considering its variation obtained from a great number of subsamples, all drawn from the large grid sample in a random fashion through the use of a computer program. Each subsample has the same number of particles and represents a replicate sample that could have been made in the field. To obtain stable error estimates, it is recommended that more than 100, and preferably closer to 200, sub/replicate samples be considered (Efron and Tibshirani 1991; Rice and Church 1996). The largest subsample size considered with the bootstrap method should not exceed one-third the size of the actual grid sample collected in the field.

The use of binomial distribution for grid sampling was initially suggested by Fripp and Diplas (1993) and modified by Petrie and Diplas (2000) for estimating grid sample errors at specified percentiles. The binomial distribution considers only two possibilities for each particle sampled: (1) it is within a specified size class (e.g., smaller than a certain size) or (2) it is outside the specified size class (Ott 1988). Fig. 5-7 shows the way that the results of this approach can be used when the percentiles of interest are D_{50}, D_{16}, and D_{84}. Based on the accuracy level required, 95% in this case, the necessary sample size that will allow an acceptable error band is determined. For example, a grid sample of 100 stones is necessary to keep the confidence intervals around the median size D_{50} within $\pm 10\%$ (D_{40} and D_{60} of the grain-size distribution). The error around D_{50} in absolute terms, e.g., mm or ϕ (phi) units, is determined after the sample has been collected, analyzed, and plotted in terms of a frequency-by-number distribution so that D_{40} and D_{60} can be determined. It is through this last step that the standard deviation of the grain-size distribution is factored in the error estimate. Fig. 5-8 provides a graph for determining the error bands for D_{10}, D_{30}, D_{70}, and D_{90} at 95% accuracy levels, or confidence coefficient, α, of 0.05. The validity of this approach has been verified through extensive laboratory tests and computer simulations (Diplas and Crowder 1997; Petrie and Diplas 2000).

Except for the case of median size, the confidence intervals obtained through the use of the exact binomial

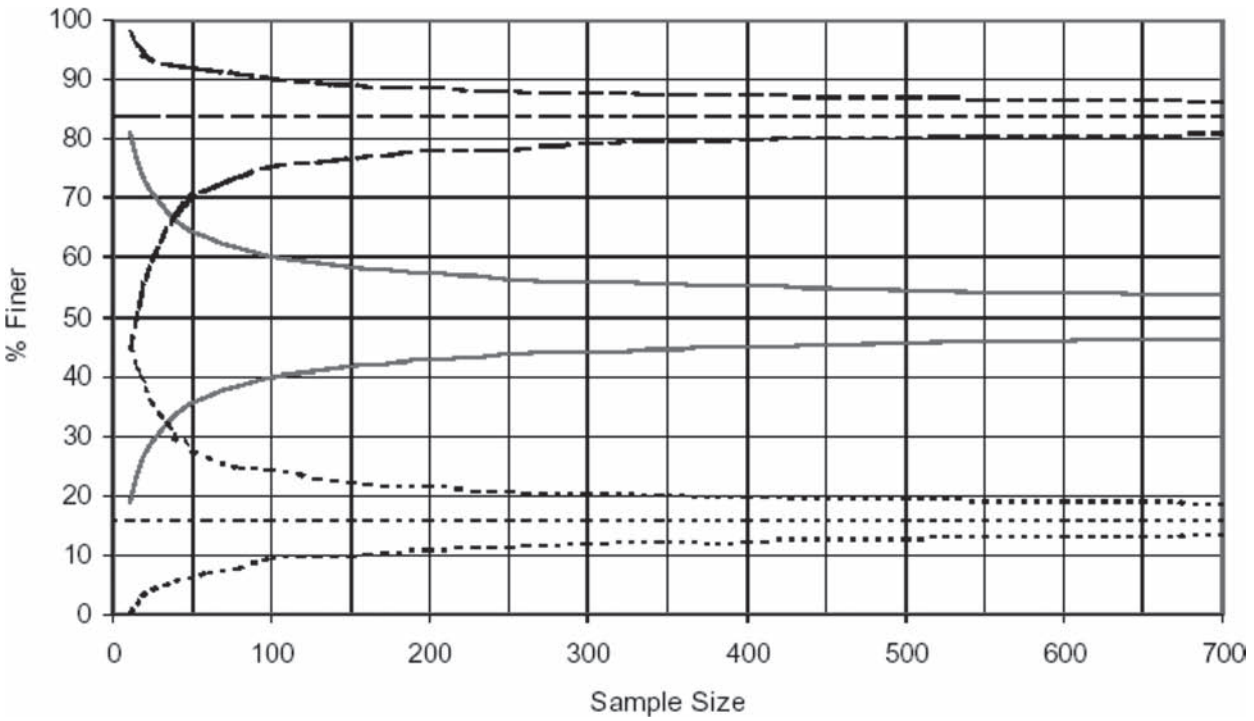

Fig. 5-7. Binomial sample size determination graph for D_{16}, D_{50}, and D_{84} for $\alpha = 0.05$.

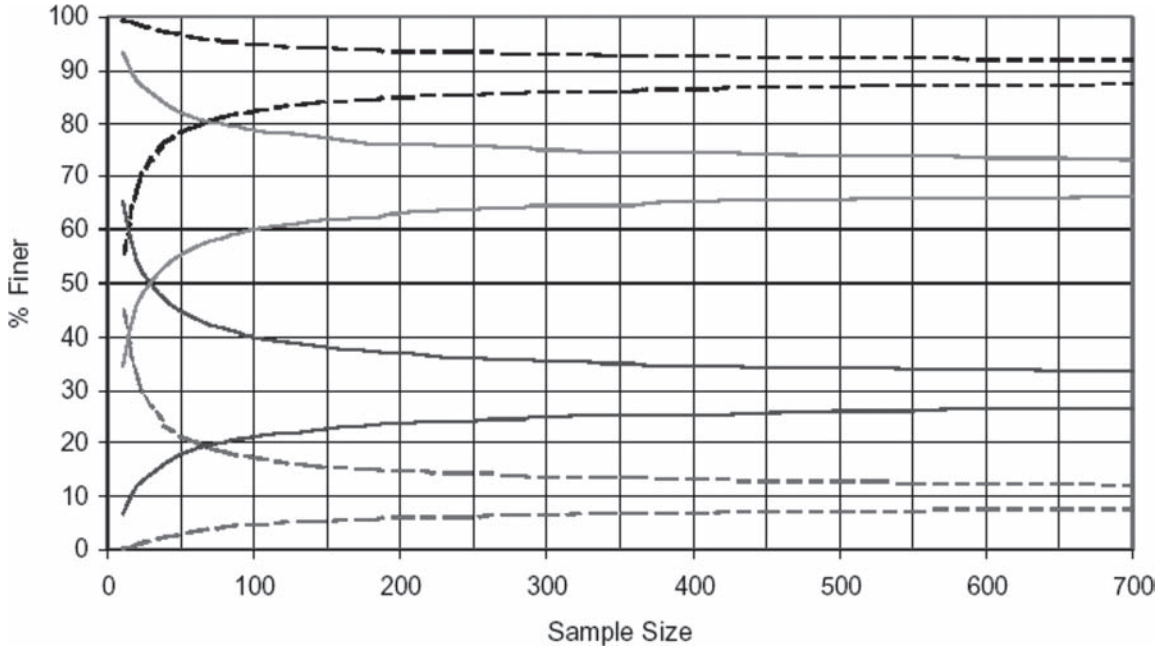

Fig. 5-8. Binomial size determination graph for D_{10}, D_{30}, D_{70}, and D_{90} for $\alpha = 0.05$.

distribution are not symmetric around a specified percentile (Figs. 5-7 and 5-8). As can be seen from Figs. 5-7 and 5-8, the largest percentile error for a given sample size is always that for the median grain size. This does not necessarily mean that D_{50} suffers the largest error in absolute terms. As a matter of fact, because the part of the cumulative distribution around D_{50} tends to have the steepest slope, the median size will typically have the smallest absolute error. Similarly, the fact that two percentiles equidistant from the median size, e.g., D_{10} and D_{90}, have the same relative percent error (Fig. 5-8) does not mean that these sizes will have the same absolute error in mm or ϕ units as well, except for the case of a symmetric distribution. The absolute error depends on the shape of the distribution surrounding the percentile of interest. Thus, the binomial approach supports the well-accepted notion that for a distribution that is skewed toward the coarser grains, a given sample size will result in better estimates of the coarser particles, e.g., D_{90}, than the finer particles, e.g., D_{10}. Furthermore, for two distributions having the same numerical value for a certain percentile, e.g., D_{50}, but different overall ranges of particle sizes, or different standard deviations, the relative percent error will be the same but the absolute error will be larger for the distribution having the larger standard deviation (Fripp and Diplas 1993).

The curves describing the confidence intervals in Figs. 5-7 and 5-8 approximately follow the expression $1/\sqrt{n}$, where n is the number of stones in the sample. This suggests that if a sample is quadrupled in size, a 50% reduction of the percentage error results. For example, Fig. 5-7 indicates that a 400-stone sample provides confidence intervals at a distance of $\pm 5\%$ around the median diameter, compared to $\pm 10\%$ for a sample of 100 stones. It is therefore suggested that for $\alpha = 0.05$, sample sizes larger than 400 stones are not warranted for most studies, because significantly greater effort is required to achieve relatively modest gains in accuracy (Fripp and Diplas 1993; Rice and Church 1996).

The use of the exact binomial distribution in calculating the required sample size, n, given the particle size value of interest (p_i in percent, e.g., D_{84}), the desirable accuracy level, α, and the maximum allowable error, E, requires a rather tedious iterative procedure. Nowadays, though, computer programs are available for these types of calculations. Another, much simpler approach would be to employ the normal approximation of the binomial distribution. This approximation is valid when both $n p_i$ and $n(1-p_i)$ are larger than 20, whereas for values between 5 and 20 it can still be employed, especially if the continuity correction is implemented (Ott 1988). Experience has shown that, except for the case of small sample size and the case of the particle size of interest being very fine or very coarse, the estimates obtained by the normal distribution approximate those obtained through the exact binomial fairly well. The required sample size, n, based on the binomial approximation is estimated by the expression

$$n = \frac{z^2_{(\alpha/2)}\, p_i\,(1-p_i)}{E^2} \tag{5-2}$$

where

$z_{(\alpha/2)}$ = a value obtained from tables prepared for the normal distribution curve for a given confidence interval of $100(1-\alpha)$.

As can be seen from Eq. (5-2), in contrast to the results provided by the exact binomial, the normal approximation of the binomial distribution results in symmetric confidence intervals, with the upper confidence limit for p_i given by $\tilde{p}_{iu} = p_i + E$ and the lower limit by $\tilde{p}_{il} = p_i - E$.

Whenever it is desirable to generate confidence intervals about the entire grain-size distribution, the multinomial distribution needs to be employed to account for all possible outcomes of sieve analysis dictated by the number of particle size classes considered (Burdick and Graybill 1992; Petrie and Diplas 2000). Whereas the binomial and bootstrap methods deal with a single size or percentile, one confidence interval at a time, the multinomial approach deals with all size classes at the same time, simultaneous confidence intervals. Therefore, a simultaneous confidence interval with a confidence level of α around a grain-size curve states that there is a probability of $(1-\alpha)$ that the population grain-size curve is within the confidence interval at each size class. As a result, simultaneous confidence intervals are wider than one-at-a-time intervals. The additional parameter that needs to be considered in the multinomial case is the number of sieves or size classes. Even though this number is not known before the sample is collected, it can be estimated by surveying the site and making a visual approximation of the largest and smallest particles present in the deposit. The range of sizes between these two particles, together with the estimated number of particles that need to be removed, will dictate the number of sieves necessary for the analysis of the sample (Emerson and Hoaglin 1983; Russ and Dehoff 2000). Fig. 5-9 shows the error bands around the median size diameter, with $\alpha = 0.05$, calculated using the multinomial distribution for different numbers of sieves k (Petrie and Diplas 2000). The binomial distribution is a special case when $k = 2$. The Goodman (1965) method, one of several techniques that have been proposed for calculating simultaneous confidence intervals for multinomial proportions, has been used to draw these curves. This method is relatively easy to use and consistently meets the required confidence coefficient (May and Johnson 1997). The formula proposed by Goodman is as follows,

$$n(p_i - \hat{p}_i)^2 = \chi^2_{\alpha/k,1}\,\hat{p}_i(1-\hat{p}_i) \quad i = 1, 2, \ldots, k \qquad (5\text{-}3)$$

where

n = sample size;
p_i = sample estimate for proportion of size class i;
$\tilde{p}_i$ = confidence interval proportions for size class i; and
$\chi^2_{\alpha/k,1}$ = upper $100(1-\alpha/k)$ percentage point of the χ^2 distribution with one degree of freedom.

Equation (5-3) provides two p_i values for each size class considered, one corresponding to the proportion for the upper confidence interval ($\tilde{p}_{iu} = p_i + E_{iu}$) and another for the lower confidence interval ($\tilde{p}_{il} = p_i - E_{il}$). For the median size

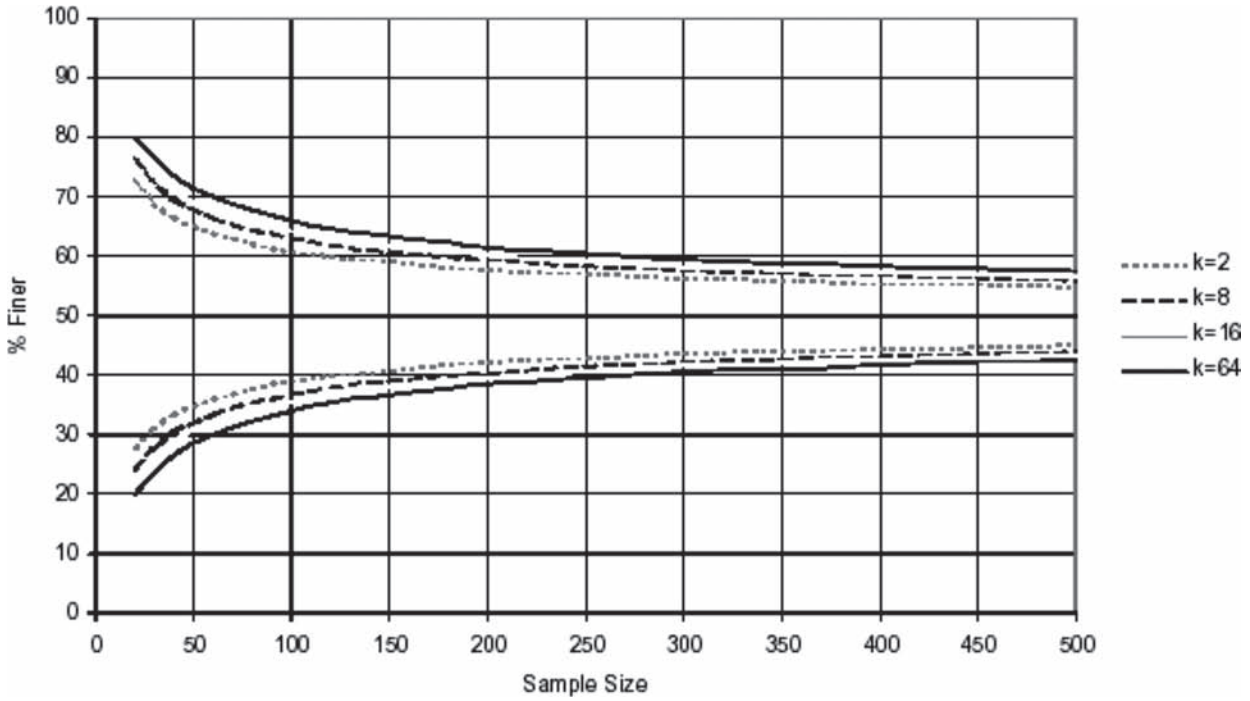

Fig. 5-9. Error bands around D_{50} for different grid sample sizes and numbers of sieves k obtained using the multinomial distribution ($\alpha = 0.05$).

($p_i = D_{50}$), $E_{50u} = E_{50l}$, whereas for every other percentile the upper and lower errors are different.

Fig. 5-9 indicates that a 180-stone grid sample is necessary for estimation of the median size within ±10% when eight sieves are used to analyze it. This is 80% larger than the binomial results for the same error bands (Fig. 5-7). Another way of presenting the multinomial results is shown in Figs. 5-10 to 5-12. In all these cases, the number of stones that need to be collected is determined when the maximum acceptable error, E, the confidence level, α (= 0.05 in all these plots), and the number of sieves that will be used for the analysis are known. Because for the case of the median size the error bands are symmetric, one figure is sufficient (Fig. 5-10). For any other percentile, two figures are necessary, one for the upper and another for the lower confidence limits. Figs. 5-11 and 5-12 represent the respective figures for D_{84}. The expression in Eq. (5-3) dictates that for two grain sizes D_i and D_j with $i + j = 100$, $E_{iu} = E_{jl}$ and $E_{il} = E_{ju}$ Therefore, Figs. 5-12 and 5-11 can be used to determine the upper and lower confidence limits, respectively, for D_{16}. An example showing the entire grain-size distribution obtained from a 50-stone grid sample together with the confidence intervals determined from the multinomial distribution for $\alpha = 0.05$ and $k = 10$ is drawn in Fig. 5-13. For comparison purposes, the exact binomial confidence intervals for the same sample are also included in this figure.

The binomial/multinomial approaches estimate the sample size based on a desirable/acceptable error presented in terms of percentage points. This might be preferable to error estimates in terms of absolute units because in the former case the error scales with the properties of the unknown distribution and its particle sizes. For an appropriate choice of error in terms of absolute units it is necessary to have prior knowledge of the grain size to be considered.

Grid-by-number is the most efficient technique for sampling sediment. It requires the smallest sample size for achieving a given degree of accuracy (Petrie and Diplas 2000; Russ and Dehoff 2000). For nonuniform deposits exhibiting spatial variation in the bed-material size, use a grid of constant size. This approach will sample the various patches proportionally (make grid size sufficiently small to capture the contribution of the patches). Reporting the data in an array form can reveal the spatial characteristics exhibited by the bed material. The method developed by Crowder and Diplas (1997) can be used to identify boundaries of sediment patches and other variations in terms of grain size.

5.2.5.3 Sample Size Determined by Weight The volumetric method is the approach most commonly used for sampling and analyzing mineral aggregates. It is not surprising, therefore, that a large number of recommendations regarding appropriate sample size have been put forth by various researchers and organizations (De Vries 1970; Mosley and Tindale 1985; Church et al. 1987; Fripp and Diplas 1993; Ferguson and Paola 1997; Bunte and Abt 2001). It is worth mentioning that the methods described here can also be used to calculate the weight of material that needs to be collected with bed or suspended-load sampling devices to determine their size distribution or just a representative grain size.

The most widely quoted criteria for sample volumes of fluvial sediments are those proposed by De Vries (1970)

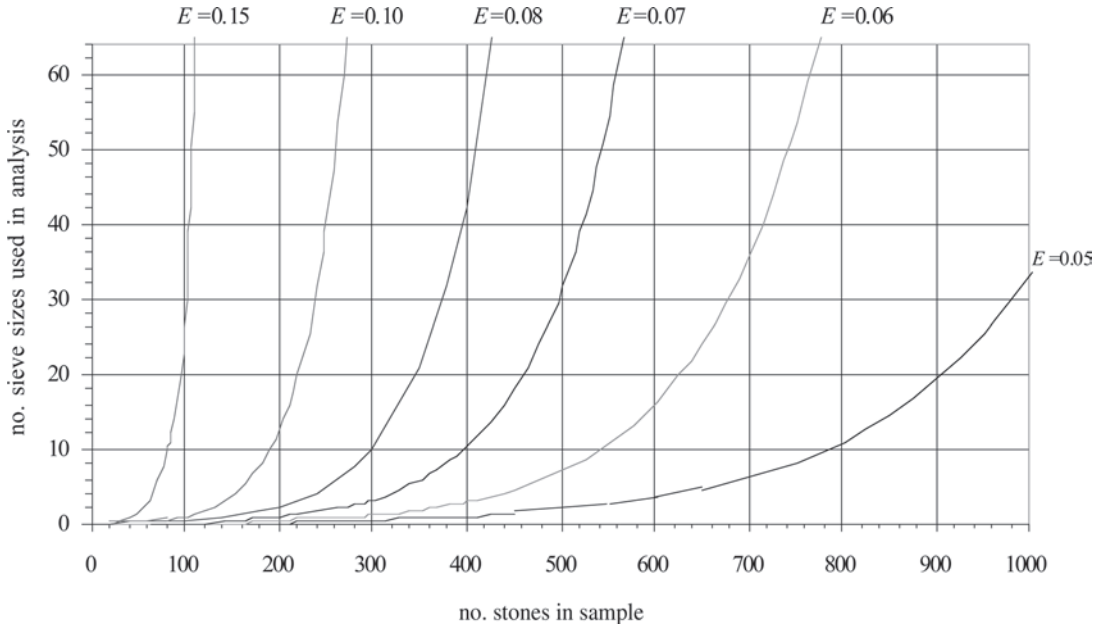

Fig. 5-10. Multinomial sample size determination graph for D_{50} with $\alpha = 0.05$. Petrie and Diplas (2000). Copyright 2000 American Geophysical Union. Reproduced by permission of American Geophysical Union.

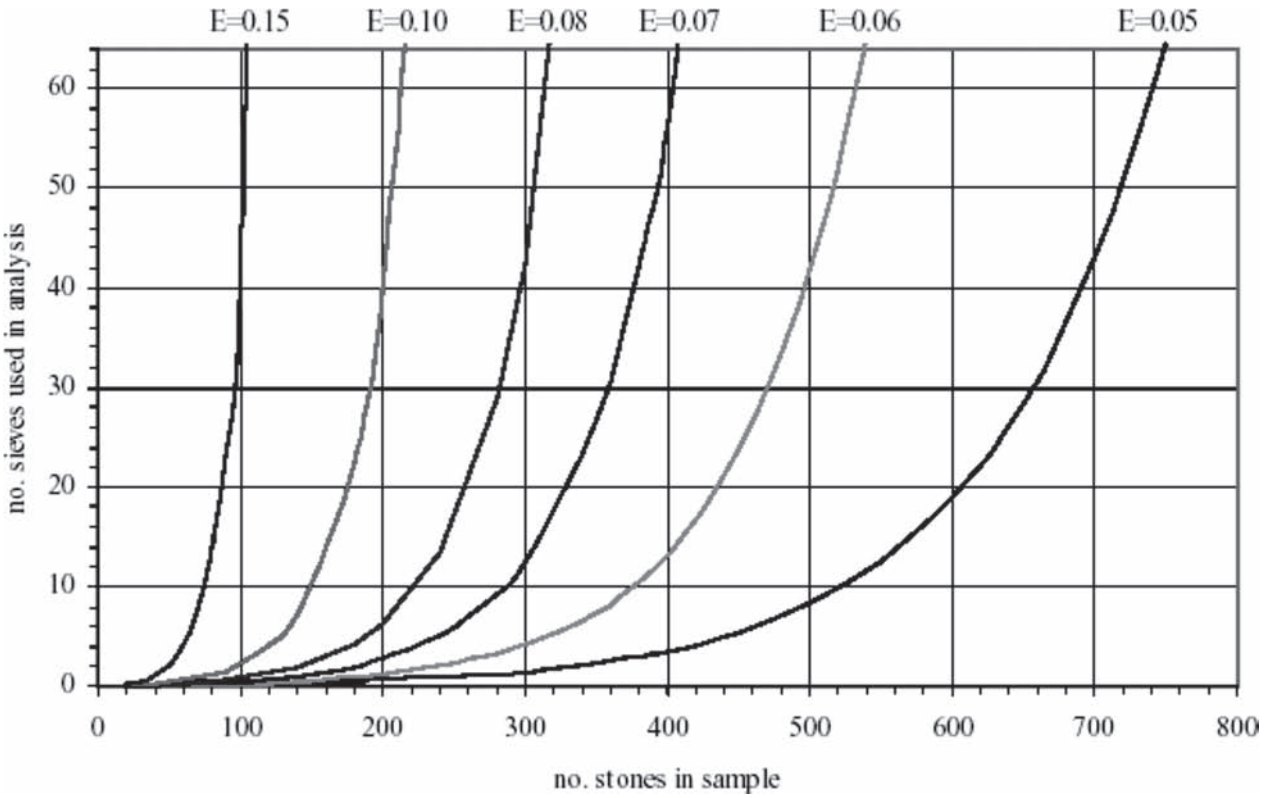

Fig. 5-11. Multinomial sample size determination graph for D_{16} (upper confidence limit) and D_{84} (lower confidence limit) with $\alpha = 0.05$.

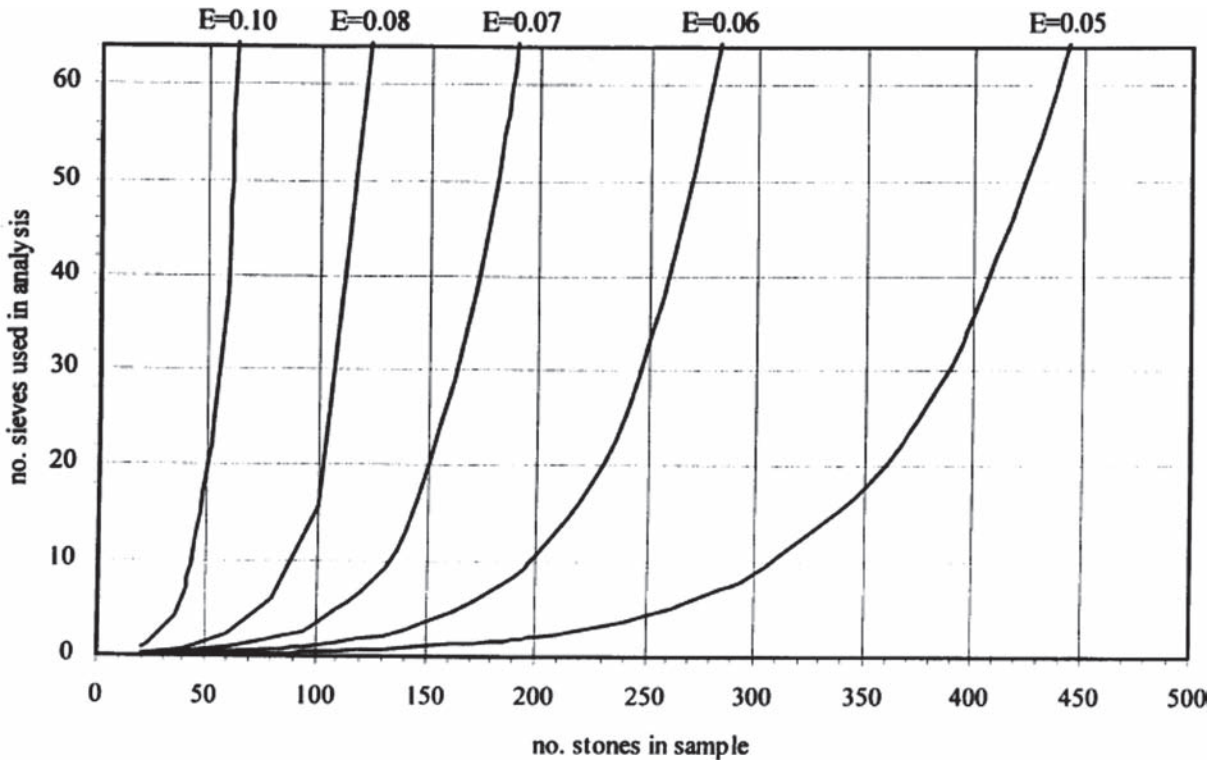

Fig. 5-12. Multinomial sample size determination graph for D_{16} (lower confidence limit) and D_{84} (upper confidence limit) with $\alpha = 0.05$.

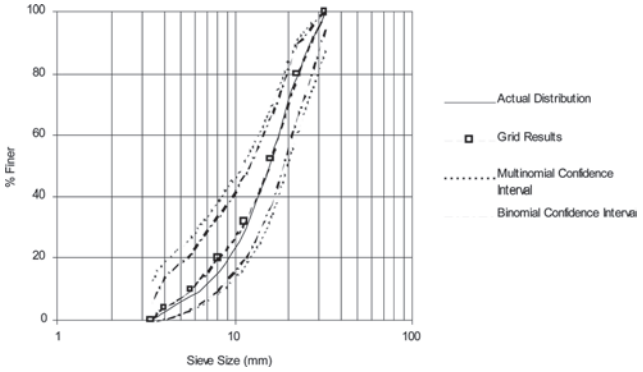

Fig. 5-13. Fifty-stone grid sample results and actual grain-size distribution with 95% multinomial ($k = 10$) and binomial confidence intervals.

and Church et al. (1987). De Vries suggested bulk samples expressed in terms of mass, m, to satisfy three accuracy levels, high, normal, and low. The required total sample mass is obtained as a function of the mass of the D_{84} grain size and can be expressed as follows (Bunte and Abt 2001):

$$m = 0.8 \times 10^{\beta} \rho_s D_{84}^{3} \tag{5-4}$$

where meters and kilograms are the units of all the terms. The coefficient of 0.8 is based on empirical results obtained from laboratory experiments with sand and fine gravel ($D < 14$ mm); its value might be different for sizes and shapes other than those used by De Vries. The exponent β takes the value of 5 for high, 4 for normal, and 3 for low level of accuracy. Prior knowledge, or estimation, of D_{84} is necessary to determine the sample mass. Because 1 t of material is typically considered the practical limit for hand sieving, excessive amounts of material are required to meet the high-accuracy criterion for sediments coarser than fine gravel. This is a typical requirement of the various methods that have been suggested for volumetric sampling. Although this appears to be a major limitation, the fact is that grain-size stratification in gravel streams precludes the use of the volumetric method in streams that do not possess predominantly sandy or fine gravel sediment deposits.

To provide guidance for obtaining accurate, yet manageable volumetric samples, Church et al. (1987) suggested a sliding method that provides the necessary sample mass based on the D_{max} particle size present in the deposit. For bed material with $D_{max} < 32$ mm, $32 \text{ mm} < D_{max} < 128$ mm, and $D_{max} > 128$ mm they suggested that the sample mass, m, be 1,000, 100, and 20 times the mass of D_{max}, respectively. One problem with this approach is that the resulting expression is not a monotonic function of the mass of D_{max}. More specifically, deposits having D_{max} values near the beginning of one of the larger two size ranges require smaller sample masses than deposits having D_{max} values near the end of the previous size range. To remedy this problem and unite the three sample-mass criteria, Yuzyk (1986) proposed a staircase approach, whereas Bunte and Abt (2001) fitted the following regression equation through the corner points of the staircase function,

$$m = 2{,}882\, D_{max} - 47.6 \tag{5-5}$$

with m in kilograms and D_{max} in meters. Equation (5-5) should be used for $D_{max} > 32$ mm, whereas the Church et al. criterion should be employed for $D_{max} < 32$ mm. It is evident that the Church et al. method and its variations do not maintain consistent accuracy levels for the various size ranges. Furthermore, these methods do not account for the effect of standard deviation (e.g., Gale and Hoare 1994).

To obtain consistent results and volumes that are determined on the basis of a desirable degree of accuracy, two-stage sampling methods need to be employed (Hogan et al. 1993; Ferguson and Paola 1997; Petrie and Diplas 2000). During the first stage, a sample is obtained to approximate the size distribution of the parent material or some of its main characteristics, such as D_{50} and standard deviation. Hogan et al. proposed computer-generated replicate samples, whereas Petrie and Diplas suggested nonlinear transformations of grid-by-number plots and their confidence intervals for determining the necessary volumetric sample size. Though both of these methods are nontrivial to carry out, they are valid for any grain-size distribution. Ferguson and Paola have provided simpler expressions for calculating the sample volume; however, their results are limited to deposits having lognormally distributed particle sizes.

5.3 SUSPENDED-SEDIMENT SAMPLERS AND SAMPLING METHODS

J. Gray, D. Glysson, and T. Edwards

5.3.1 Introduction

This section focuses on collection of suspended-sediment data. It includes criteria for a sediment data set; descriptions of manual suspended-sediment samplers and methods for their deployment; description, installation, and operation of automatic samplers; and a summary of equipment used for obtaining water-sediment subsamples.

The origins of suspended-sediment sampling and transport measurements go back at least to 1808, when Gorsse and Subuors collected samples of the Rhone River at Arles, France. Baumgarten's samples collected in the River Garonne at Marmande, France, from 1839 to 1846 resulted in what were probably the first sediment discharge computations. Sediment discharge measurements in the United States began in 1838 when Captain Talcott sampled the Mississippi River. The fluvial sediment measurements made in the Rio

Grande at Embudo, New Mexico, beginning January 15, 1889 represent the beginning of the U.S. Geological Survey's sediment program (Glysson 1989a). Fluvial sediment measurements have been made regularly in the Rio Grande since 1897; the lower Colorado River since 1909; and the upper Colorado River basin since 1925. A detailed investigation of sediment loads starting in 1942 as part of the Missouri River Project included determination of the feasibility of storage reservoirs on streams transporting heavy sediment loads. Beginning in about 1930, extensive sediment surveys have been made in many other streams of the United States (FISP 1940; Nelson and Benedict 1950; Glysson 1989a; Turcios et al. 2000; USGS 2000b; Turcios and Gray 2001). After the end of World War II, the number of sites at which the USGS collected daily suspended-sediment data increased rapidly, peaking at 360 in 1982 (Glysson 1989a; Osterkamp and Parker 1991). By 2003, only 120 daily-record sediment sites were being operated in the 50 states, although suspended-sediment and bed-load data were being collected periodically at 615 and 49 sites, respectively (USGS 2004).

The earliest suspended-sediment samples were collected using instantaneous samplers, such as the open container or pail used by Riddell in the lower Mississippi River at New Orleans from 1843 to 1848 (Nelson and Benedict 1950). Subsequently developed samplers included those that could be filled at a selected depth below the water surface and horizontal trap-type samplers that aligned in the direction of flow (FISP 1940). After 1900, and particularly during the period from 1925 to 1940, many new sediment samplers were developed. By 1939, at least nine different types of sediment samplers were being used by U.S. Federal agencies (Glysson 1989a). Most of the samplers had been developed by independent investigators, lacked calibration, and were deployed using various operating techniques. A survey of sediment-sampling equipment used in the United States indicated that the 30 instantaneous samplers studied had very limited applicability, either because of poor intake-velocity characteristics or because of the short filament of water-sediment mixture sampled (FISP 1940; 1941; Nelson and Benedict 1950). As a consequence, data reliability and comparability suffered. For example, a consistent decrease in suspended-sediment discharges measured at gauges in the Colorado River Basin—originally attributed to changes in climatic, land use, or other factors—was probably the result of bulk oversampling of sediment by the Colorado sampler, a weighted bottle-type sampler (FISP 1940) used in the southwest United States from the 1920s to the 1940s. Tests of the Colorado sampler by Topping et al. (1996) found that the Colorado sampler preferentially oversampled coarser material, resulting in overestimation of the mass of suspended-phase material by a factor of about 3. This conclusion is consistent with mid-1940s changes in slope in the relations between water discharge and suspended-sediment discharge for three Colorado River Basin stream gauging sites (Thompson 1982; 1984; 1985), although comparative tests at the San Juan River near Bluff, Utah, indicate that the Colorado River Sampler collected an average of 82% of the sediment mass obtained by the US D-43 suspended-sediment sampler (Nelson and Benedict 1950). The US D-43 sampler, which replaced the Colorado River Sampler in the mid-1940s, and subsequently developed isokinetic samplers sample the water-sediment mixture isokinetically, that is, collecting a filament of water at the ambient stream velocity, thereby providing an unbiased sample for subsequent sedimentary analysis.

Paul C. Benedict, the principal U.S. Geological Survey (USGS) engineer involved in the midcentury development of sediment-sampling equipment, once remarked in relation to sampler development during the 1920s and 1930s that "all this development work was being done with no knowledge of the physical laws governing the transport of sediment or of the intake characteristics of the samplers themselves" (Glysson 1989a). The data obtained by the different investigators during this period were not comparable, nor could their accuracy be evaluated. It became apparent that consistent and comparable sediment data could not be obtained unless equipment and data-collection and analytical methods were standardized.

In 1939, various agencies of the U.S. government organized an interagency program to study methods and equipment used in measuring the sediment discharge of streams, and to improve and standardize equipment and methods where practicable (FISP 1941). The Federal Interagency Sedimentation Project (FISP) (Skinner 1989; Glysson and Gray 1997) was created under the sponsorship of the Committee on Sedimentation of the Federal Water Resources Council. The comprehensive study of sampling equipment included suspended-sediment, bed-load, and bed-material samplers. As a result of research conducted by the FISP and others, an integrated system of sediment samplers, sampling, and analytical techniques has been developed and is widely used around the world.

5.3.2 Criteria for a Sediment Data Set

Collection of data to enable reliable sediment-transport estimates is often difficult, time-consuming, and expensive. It is frustrating to obtain data for a location and set of conditions of interest, only to subsequently discover that not all of the requisite parameters were quantified (Glysson 1989b), or that the collected data were inappropriate for the analysis at hand.

The types of data required depend on the goals of the assessment and the intended storage medium for the data. For example, sediment-concentration and water-discharge data are needed to compute continuous records of suspended-sediment discharge (Porterfield 1972; Koltun et al. 1994; McKallip et al. 2001). Other relevant data include particle-size distributions of suspended sediment and bottom material. The integrity of large-scale, long-term monitoring programs, such as the Vigil Network (Osterkamp and Emmett 1992),

or that proposed for North America (Osterkamp et al. 1998; 2004), the United States (Osterkamp and Parker 1991), and Canada (Day 1991), is particularly dependent on the reliability and comparability of the data collected.

The most reliable databases accept only selected data types representing sediment and ancillary variables obtained using a consistent set of protocols. For example, sediment data stored by the USGS as part of the National Water Information System—World Wide Web (NWISWeb) and other databases (Turcios et al. 2000; USGS 2000a; 2000b; Turcios and Gray 2001) are collected by techniques described by Edwards and Glysson (1999) and analyzed in a USGS-approved laboratory by techniques described by Guy (1969); Matthes et al. (1991); Knott et al. (1992; 1993); and the USGS (1998a; 1999).

One commonly used analogue for suspended-sediment concentration—total suspended solids (TSS)—is not comparable to suspended-sediment concentration data under some circumstances, and fundamentally is unreliable when applied to open-channel flows (Gray et al. 2000; USGS 2001). TSS data tend to underestimate suspended solid-phase concentrations, by a proportionate amount of 25% to 34% (Gray et al. 2000). This tendency has important ramifications for computing sediment discharges. Instantaneous sediment discharges computed from TSS data may differ substantially from those computed from suspended-sediment concentrations and the same water-discharge time series, with the TSS-generated loads usually biased low (Glysson et al. 2001). This result is of particular concern for sites where the percentage of sand-size material in water samples can exceed about a quarter of the sediment mass percent and where concentrations of sand-size material in transport increase with flow. No broadly applicable and reliable means of adjusting TSS data to estimate suspended-sediment concentration data in open-channel flow has been identified (Glysson et al. 2000).

Glysson (1989b) divided data-set requirements for computing sediment transport using the more common sediment-transport equations for noncohesive sediments into three categories: sediment, hydraulic, and others. Required sediment parameters include suspended-sediment concentration, bed-material particle-size distributions, particle specific gravity, and bed load discharge and particle-size distributions when bed load is the target parameter. Additional sediment parameters are specific diameters, sample method of collection, sampler and nozzle type, the analyzing laboratory, and the method that is used to analyze the samples.

Water discharge, watercourse stage, cross-sectional geometry, width, depth, area, hydraulic radius, and a slope parameter are required hydraulic parameters. Water temperatures should always be measured. Other parameters to be measured include a roughness coefficient, particle shape, bed-form information, and dissolved-solids concentrations. A site description that may include a channel classification based on one or more channel classification schemes should be included.

5.3.3 Units of Measurement

The concentration of suspended sediment is reported in milligrams of sediment per liter of water-sediment mixture (mg/L). However, as a matter of convenience, it is determined in the laboratory in parts per million (ppm), which is the dry weight of suspended material per million equal weights of water-sediment mixture (Porterfield 1972). The units of mg/L and ppm are equivalent at concentrations less than 8,000 mg/L. The equivalent value for mg/L at concentrations ≥8,000 ppm can be calculated using the equation

$$C_{mg/L} = C_{ppm}/(1 - C_{ppm}(6.22 \times 10^{-7}))$$

where

$C_{mg/L}$ = sediment concentration, in mg/L; and
C_{ppm} = sediment concentration, in ppm.

5.3.4 Samplers and Sampling Methods

The purpose of a suspended-sediment sampler is to obtain a representative sample of the water-sediment mixture moving in the stream in the vicinity of the sampler intake. There are two categories of suspended-sediment samplers: manually operated samplers and automatic samplers. Manually operated samplers include instantaneous and isokinetic samplers. Isokinetic samplers include those with rigid sample bottles (bottle samplers) and with flexible bags (bag samplers). Additional information on samplers for sediment and other water-borne constituents can be obtained from the Federal Interagency Sedimentation Project (FISP 2000; Davis 2005).

5.3.4.1 Manually Operated Samplers

5.3.4.1.1 Instantaneous Samplers Instantaneous samplers are applicable for sampling flows that do not meet the following criteria for deployment of an isokinetic sampler: sampling depths of greater than about 0.3 m and mean velocities greater than approximately 0.5 m/s. At small depths, the part of the stream from the streambed to the isokinetic sampler nozzle, referred to as the unsampled zone, becomes unacceptably large with respect to the total depth. At small velocities, only silt- and clay-size material typically is in suspension, and these finer size fractions tend to be fairly uniformly distributed with depth (Colby 1963; Guy 1970). Under these circumstances, an instantaneous sample from the water column may provide a reasonably accurate estimate of the concentration at the sampled point, or in the sampled vertical. Instantaneous samplers may also be deployed at flow velocities too high to submerge an isokinetic sampler, or when the presence of debris makes normal sample collection dangerous or impossible.

Although nonisokinetic samplers may provide acceptable results under certain sediment-transport conditions, such as when fine material constitutes all or nearly all of the

sediment load, conditions for which nonisokinetic sampling is appropriate are often not apparent at the time of collection. The most reliable suspended-sediment samples are obtained using isokinetic samplers.

The simplest instantaneous sampler is an open bottle used to obtain a surface, or dip, sample. The WBH-96 weighted bottle sampler (FISP 2000) is deployed with a hand line in still or slow-moving water. The Van Dorn sampler and Kemmerer sampler are thief-type samplers that are typically used for still-water sampling, such as in lakes and reservoirs, but that may be useful in slow-moving streamflows (Webb and Radtke 1998).

5.3.4.1.2 Isokinetic Samplers Isokinetic samplers are designed to collect a representative velocity-weighted sample of the water-sediment mixture. Water approaching the nozzle of an isokinetic sampler undergoes essentially no change in speed or direction as it enters the nozzle orifice (Fig. 5-14). When deployed using prescribed methods at strategic locations in a cross section, an isokinetic sampler integrates a sample proportionally by velocity and area, resulting in a

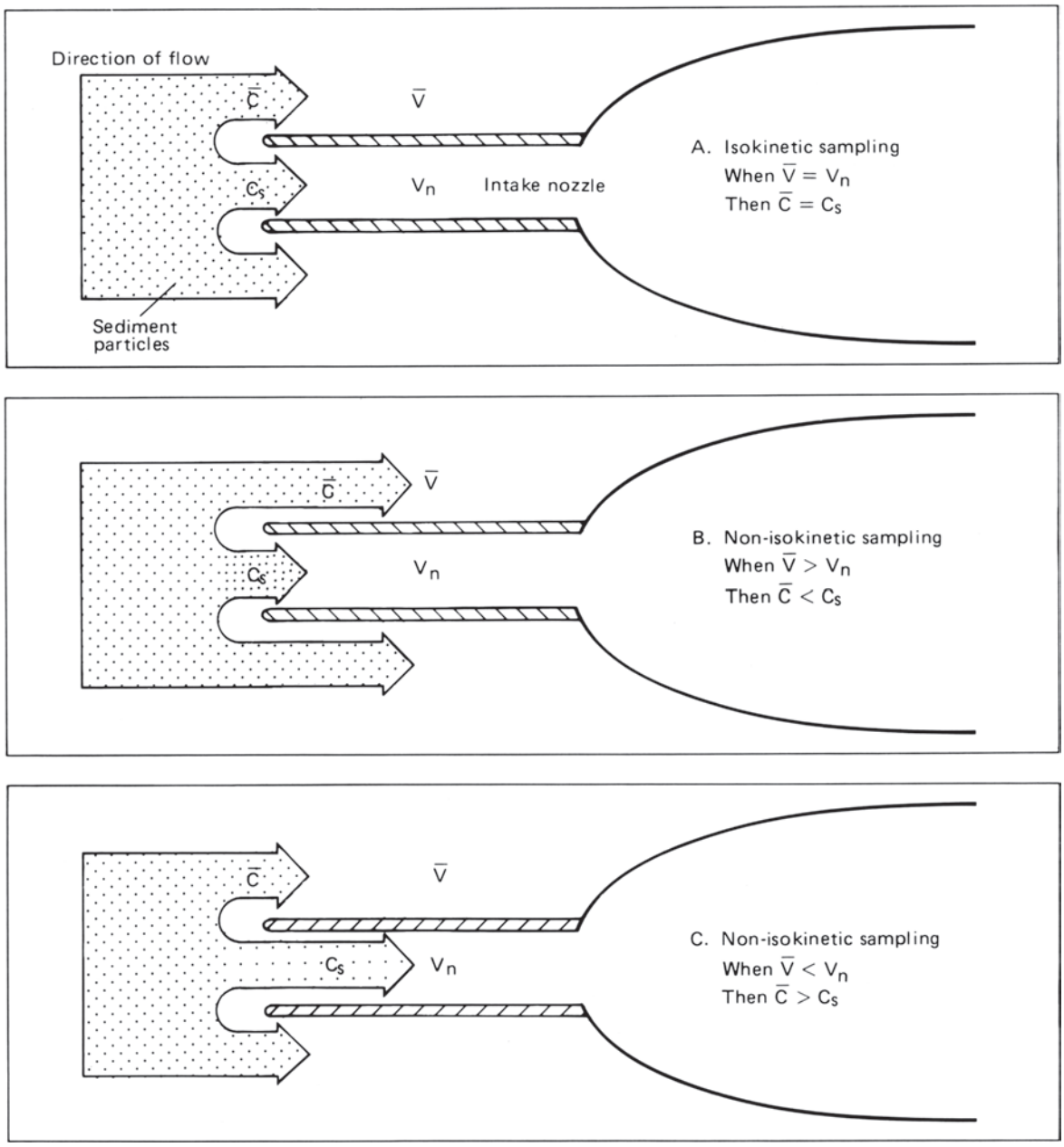

Fig. 5-14. Relation between intake velocity and sample concentration for (A) isokinetic and (B, C) non-isokinetic sample collection of particles larger than 0.062 mm. $\bar{V}$ = mean stream velocity, V_n = velocity in the sampler nozzle, $\bar{C}$ = mean sediment concentration in the stream, and C_s = sample sediment concentration.

discharge-weighted sample. A discharge-weighted sample contains a concentration and size distribution representative of the material in transport at the time the sample was collected.

A list of isokinetic samplers available from the FISP is shown in Table 5-2. FISP isokinetic samplers are designed to sample at a relative sampling rate—a dimensionless value defined as the velocity through the nozzle divided by the approaching stream velocity—of 1.0 at a 1.2 m/s (3.9 ft/s) flow velocity. In practice, FISP isokinetic samplers are designed to ensure that the water velocity entering the nozzle is within 10% of the ambient stream velocity throughout the samplers' operating velocity range (Broderick Davis, Federal Interagency Sedimentation Project, 2001, written communication).

Concentration errors in samples collected with isokinetic-type samplers may stem from a combination of the size of suspended material and the relative sampling rate. The relation between percent error in concentration and relative sampling rate for sediments with a density of 2.65 and median diameters of 0.45, 0.15, 0.06, and 0.01 mm in flows of 1.5 m/s is shown in Fig. 5-15 (adapted from FISP 1941). Under these test conditions, relative sampling rates for 0.45-mm-size sediments can range from 0.75 to 1.3 without introducing more than about a 10% error in sample concentration values. Conversely, at relative sampling rates less than 0.25, resultant concentration errors can exceed 100%. The range of errors tends to decrease with decreasing sediment size. For example, 0.01-mm-size sediments have less than a 5% error for relative sampling rates ranging from about 0.2 to almost 5 (Fig. 5-15). In each case, relative sampling rates less than about 1.0 result in positive concentration bias, and those larger than about 1.0 result in zero or negative concentration bias.

The FISP's suite of depth-integrating samplers and point-integrating samplers (Davis 2005) are isokinetic samplers. A depth-integrating sampler is designed to isokinetically and continuously accumulate a representative sample from a stream vertical while transiting the vertical at a uniform rate (FISP 1952). A depth-integrating sampler collects and accumulates a velocity or discharge-weighted sample as it descends and ascends at a constant rate through the sampling vertical provided that the appropriate transit rate is not exceeded and the sample container does not overfill.

The point-integrating sampler uses an electrically activated valve, enabling the operator to isokinetically sample points in, parts of, or the entire vertical. For stream cross sections less than 9 m deep (30 ft), the full depth can be traversed in one direction at a time by opening the valve and depth integrating either from surface to bottom or vice versa. Stream cross sections deeper than 9 m (30 ft) can be integrated in segments of 9 m (30 ft) or less by collecting integrated-sample pairs consisting of a downward integration and a corresponding upward integration in separate containers.

The FISP (1963) provides the following summary of point-integrating sampler characteristics that make them useful in conditions beyond the limits of the simpler depth-integrating samplers:

> Point-integrating samplers are more versatile than the simpler depth-integrating types. They can be used to collect a suspended-sediment sample representing the mean sediment concentration at any point from the surface of a stream to within several centimeters of the bed, as well as to integrate over a range in depth. These samplers were designed for depth integration of streams too deep (or too swift) to be sampled in a continuous round-trip integration. When depth integrating, sampling can begin at any depth and proceed either upward or downward from that initial point through a maximum vertical distance of 9 m (30 ft).

5.3.4.1.3 Rigid-Bottle Samplers When a rigid-bottle suspended-sediment sampler is submerged with the nozzle pointing directly into flow of sufficient velocity, a part of the streamflow enters the sampler container via the nozzle and air in the container exhausts under the combined effect of three forces:

1. A positive dynamic head at the nozzle entrance due to the flow;
2. A negative head at the end of the air-exhaust tube due to flow separation;
3. A positive pressure due to difference in elevation between the nozzle entrance and the air-exhaust tube.

Under these conditions, a calibrated isokinetic sampler will collect a sample with a sediment concentration and size distribution essentially unchanged from those at the sampling point in the stream, and a representative sample will result. However, when the sample in the container reaches the level of the air exhaust, the intake flow-rate drops, and circulation of the streamflow into the nozzle and out of the air-exhaust tube occurs. Because the velocity of the water flowing through the bottle is less than the stream velocity, coarser particles in transport tend to settle in the sample bottle, causing the sample to become enriched in sediment. Additionally, the resulting subefficient sampling rate may increase the positive concentration bias. Substantial errors in sediment concentration and particle-size distribution can result from samples collected using an incorrect or uncontrolled sample rate. The magnitude of errors tends to increase concomitant with increases in the percentage and size of suspended sand-size material (FISP 1941; Fig. 5-15). Edwards and Glysson (1999) and the USGS (1998b) provide more information on ranges in transit rates required to sample isokinetically.

5.3.4.1.4 Handheld and Handline Samplers: US DH-81, US DH-48, US DH-59, US DH-76, and US DH-95 Where streams are wadable or access can be obtained from a culvert, low bridge span, or cableway, any of six lightweight samplers can be used to obtain suspended-sediment samples via a wading rod or handline. The US

Table 5-2 Designations and Characteristics for Federal Interagency Sedimentation Project (FISP) Manually Operated Isokinetic Samplers (Davis 2005)

Sampler Designation[1]	Nozzle Inner Diameter, cm (in)	Container Type and Capacity	Mode of Suspension	Maximum Depth, m (ft)	Minimum Isokinetic Velocity, m/s (ft/s)	Maximum Recommended Velocity[2], m/s (ft/s)	Unsampled Zone, cm (in)	Mass, kg (weight, lbs)
US DH-48	0.48 (3/16)[3], 0.64 (¼)	Rigid 0.47 L (pint)	Rod	2.7 (9)	0.5 (1.5)	2.7 (8.9)	8.9 (3.5)	2 (4)
US DH-59	0.48 (3/16)		Handline or Cable Reel	4.6 (15)		1.5 (5.0)	11 (4.5)	10 (22)
US DH-59	0.64 (¼)			2.7 (9)				
US DH-76	0.48 (3/16), 0.64 (¼)	Rigid 0.95 L (quart)		4.6 (15)		2.0 (6.6)	8.1 (3.2)	11 (25)
US DH-81	0.48 (3/16)	Rigid 1 L (1.1 quart)	Rod	2.7 (9)	0.6 (2.0)	1.9 (6.2)	10 (4.0)	0.5 (1)
US DH-81	0.64 (¼)					2.3 (7.6)		
US DH-81	0.79 (5/16)					2.1 (7.0)		
US DH-95	0.48 (3/16)		Handline or Cable Reel	4.6 (15)	0.6 (2.1)	1.9 (6.2)	12 (4.8)	13 (29)
US DH-95	0.64 (¼)				0.5 (1.7)	2.1 (7.0)		
US DH-95	0.79 (5/16)				0.6 (2.1)	2.3 (7.4)		
US DH-2	0.48 (3/16)	Flexible 1 L (1.1 quart) bag		11 (35)	0.6 (2.0)	1.8 (6.0)	8.9 (3.5)	14 (30)
US DH-2	0.64 (¼)			6.1 (20)				
US DH-2	0.79 (5/16)			4.0 (13)				
US D-74	0.48 (3/16)	Rigid 0.47 L (pint) or 0.95 L (quart)	Cable Reel	4.6 (15)	0.5 (1.5)	2.0 (6.6)	10 (4.1)	28 (62)
US D-74	0.64 (¼)			2.7 (9) pint 4.6 (15) quart				
US D-74AL	0.48 (3/16)			4.6 (15)		1.8 (5.9)		19 (42)
US D-74AL	0.64 (¼)			2.7 (9) pint 4.6 (15), quart				
US D-95	0.48 (3/16)	Rigid 1 L (1.1 quart)		4.6 (15)	0.5 (1.7)	1.9 (6.2)	12 (4.8)	29 (64)
US D-95	0.64 (¼)					2.0 (6.7)		
US D-95	0.79 (5/16)				0.6 (2.0)			
US D-96	0.48 (3/16)	Flexible 3-L (3.2-quart) bag		34 (110)		3.8 (12.5)	10 (4.0)	60 (132)
US D-96	0.64 (¼)			18 (60)				
US D-96	0.79 (5/16)			12 (39)				
US D-96-A1	0.48 (3/16)			34 (110)		1.8 (6.0)		36 (80)
US D-96-A1	0.64 (¼)			18 (60)				
US D-96-A1	0.79 (5/16)			12 (39)				
US D-99	0.48 (3/16)	Flexible 6-L (6.3-quart) bag		67 (220)	1.1 (3.5)	4.6 (15.0)	24 (9.5)	125 (275)
US D-99	0.64 (¼)	Flexible 6-[4] or 3-L (6.3- or 3.2-quart) bag[5]		37 (120)	1.1 (3.5)[4] or 0.6 (2.0)[5]			
US D-99	0.79 (5/16)			24 (78)				
US P-61-A1	0.48 (3/16)	Rigid 0.47 L (pint) or 0.95 L (quart)		55 (180), pint 37 (120), quart	0.5 (1.5)	3.0 (10.0)	11 (4.3)	48 (105)
US P-63	0.48 (3/16)					4.6 (15.0)	15 (5.9)	91 (200)
US P-72	0.48 (3/16)			22 (72), pint 16 (51), quart		1.6 (5.3)	11 (4.3)	19 (41)

[1]Samplers designated in *italics* may also be used for water-quality sampling as described in the *U.S. Geological Survey National Field Manual for the Collection of Water Quality-Data* (variously dated).

[2]For rigid-bottle samplers, the maximum recommended velocity for sampler deployment is based either on measured isokinetic limitations or, for prototypes of samplers tested at Anthony Falls Hydraulic Laboratory flume, on the maximum velocities used in tests. Bag samplers were determined to retain isokinetic characteristics at the highest velocities tested. Their maximum recommended velocity was selected to correspond with the velocity at which the angle of the suspension cable was drawn back just shy of "excessive" by testing personnel—25 to 30 degrees—and upon safety considerations.

[3]The 0.48-mm (3/16-in) internal diameter nozzle is designated for use in high-velocity flows.

[4]A minimum isokinetic velocity of 1.1 m/s (3.5 ft/s) applies to the D-99 sampler using a 6-L (6.3-quart) flexible bag and a 0.48-mm (3/16-in) internal diameter nozzle.

[5]A minimum isokinetic velocity of 0.61 m/s (2 ft/s) applies to the D-99 sampler using a 3-L (3.2-quart) flexible bag and a 0.64-mm (¼-in) or 0.79-mm (5/16-in) internal diameter nozzle.

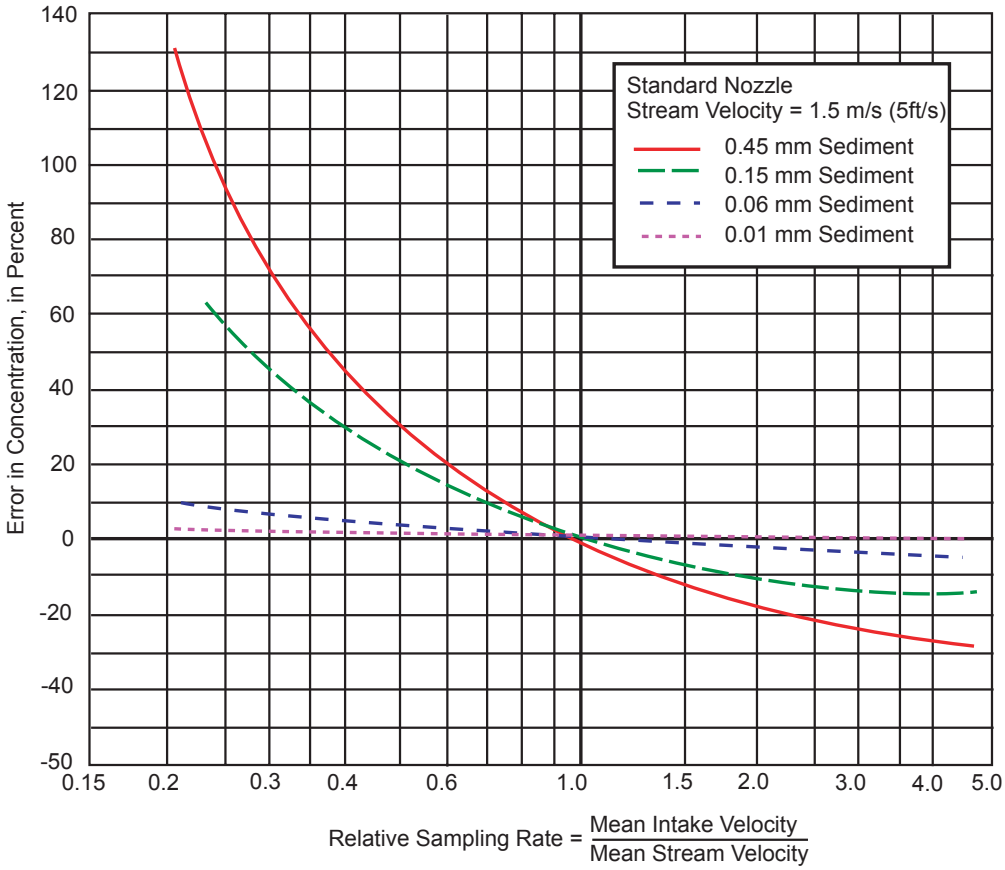

Fig. 5-15. Effect of sampling rate on measured sediment concentration for four sediment size distributions, adapted from Federal Interagency Sedimentation Project (1941).

DH-81 sampler (Fig. 5-16A; Table 5-2), which is deployed by a wading rod, consists of a US DH-81A adapter and US D-77 cap and nozzle (Webb and Radtke 1998; Edwards and Glysson 1999). All parts are autoclavable, enabling the collection of a depth-integrated sample for bacterial analysis. Any bottle having standard mason jar threads can be used with the US DH-81 sampler. The unsampled zone—the distance from the centerline of the nozzle to the streambed when the sampler contacts a flat bed—varies depending on the size of bottle used. The US DH-81 is particularly useful for sampling in cold weather because the plastic sampler head and nozzle attach directly to the bottle, eliminating a metal body. Under subfreezing conditions, a metal sampler body conducts heat away from the nozzle, air exhaust, and bottle more rapidly, resulting in increased potential for ice blockage of the nozzle and/or the exhaust port.

The rod-suspended US DH-48 sampler (Fig. 5-16B; Table 5-2) features a streamlined aluminum casting that partially encloses the sample container (FISP 1952; Edwards and Glysson 1999). The container, usually a 0.45-L glass milk bottle, is sealed against a gasket recessed in the head cavity of the sampler by a hand-operated, spring-tensioned pull-rod assembly at the tail of the sampler.

The US DH-59 and US DH-76 samplers (Figs. 5-16C and D, respectively; Table 5-2) are designed for use in unwadable streams with maximum depths less than 4.6 m and flow velocities up to about 1.5 m/s. The fundamental difference between the samplers is that the US DH-59 accommodates a 0.45-L sample bottle, whereas the US DH-76 uses a 0.9-L container. The tailfin assembly for each sampler ensures sampler alignment parallel to the flow direction with the intake nozzle entrance oriented upstream.

The US DH-95 sampler (Fig. 5-16E) is designed to make possible collection of unbiased samples for trace-element analyses in addition to samples collected for suspended-sediment analyses (McGregor 2000a) in depths less than 4.6 m at flow velocities up to about 2.4 m/s. The sampler is designed to use a 1-L Teflon or plastic bottle, a US D-95 Teflon cap, and a US D-77 sampler cap and nozzle. The bottle cavity is machined from a low-lead bronze casting and is plastic-coated. The tail section is constructed from plastic.

5.3.4.1.5 Cable-and-Reel Samplers: US D-74, US D-95, US P-61A1 US P-63, US P-72 The US D-74 (Figs. 5-17A and B), US D-74AL, and US D-95 (Fig. 5-17C) depth-integrating samplers can be used to obtain suspended-

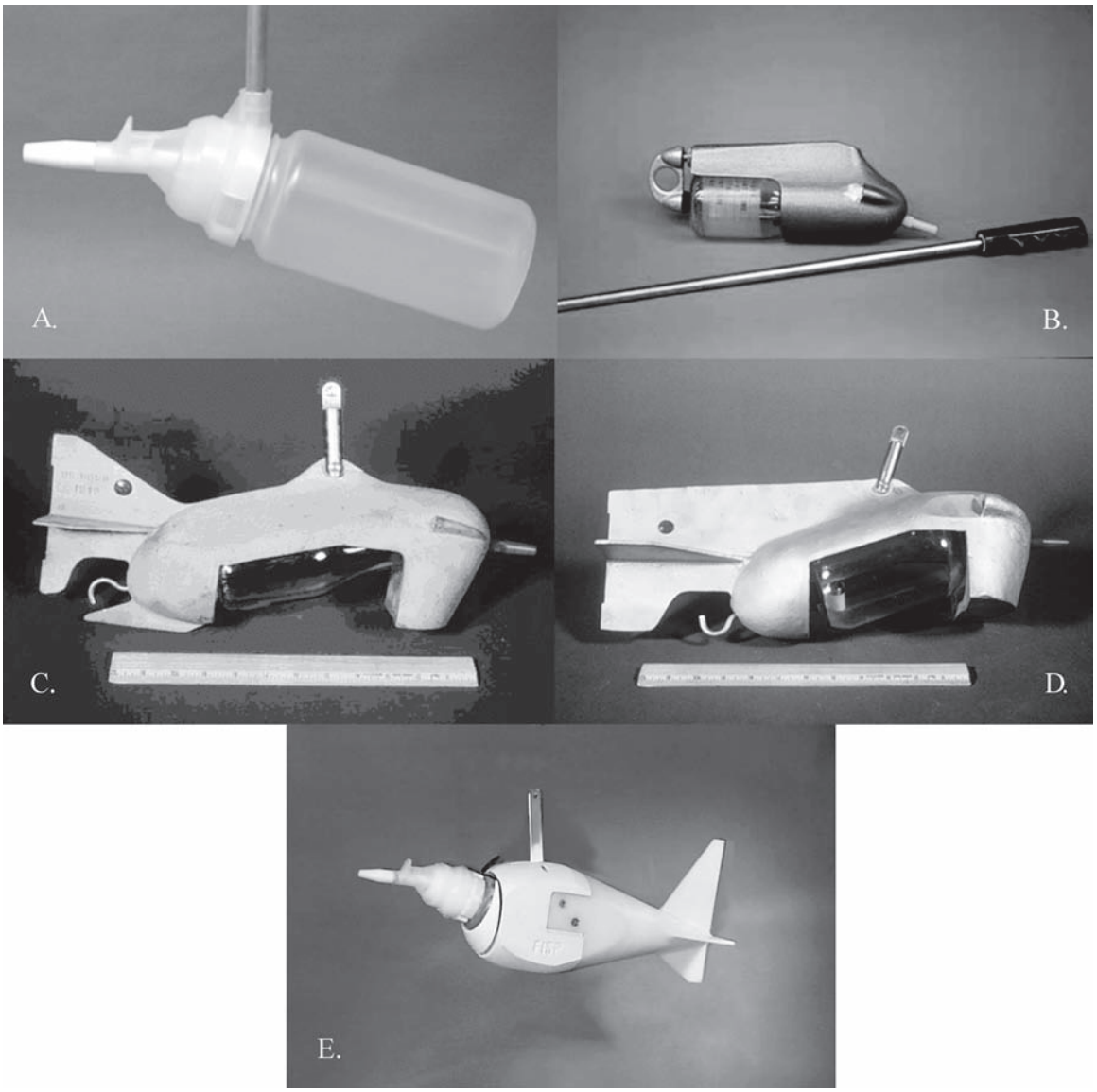

Fig. 5-16. Handheld and hand-line samplers. (A) The US DH-81 suspended sampler with an attached wading rod. (B) The US DH-48 suspended-sediment sampler with an unattached wading rod. (C) The US DH-59 suspended-sediment sampler with hanger bar. (D) The US DH-76 suspended-sediment sampler with hanger bar. (E) The US DH-95 suspended-sediment sampler with hanger bar.

sediment samples in unwadable streams less than 4.6 m deep (Table 5-2). A third cable-and-reel sampler, the US D-77, is being phased out by the USGS and is also no longer being manufactured by the FISP (USGS 2002), although the US D-77 cap and nozzles will continue to be manufactured for use with other FISP samplers.

The bronze US D-74 and aluminum US D-74AL are designed to be suspended from a bridge, cableway, or boat. These samplers replaced the US D-49, which in turn replaced the US D-43 for general use. The US D-74 sampler completely encloses a 0.9-L sample container or a standard 0.45-L milk bottle when an adapter is used. The sampler head is hinged at the bottom and swings downward to provide access to the sample-container chamber. The body includes tail vanes that serve to align the sampler and the intake nozzle with the flow.

The US D-95 sampler, like the US DH-95 (Fig. 5-16E), is designed to make possible collection of unbiased samples for trace-element analyses in streams not exceeding 4.6 m in depth (McGregor 2000b) at stream velocities ranging from 0.5 to 2.3 m/s. The bronze body casting is coated with plastic and the tail section is constructed from plastic to help avoid metal contamination during water-quality sampling.

Point-integrating suspended-sediment samplers in wide use are the US P-61A1 (Fig. 5-17D), US P-63, and US P-72

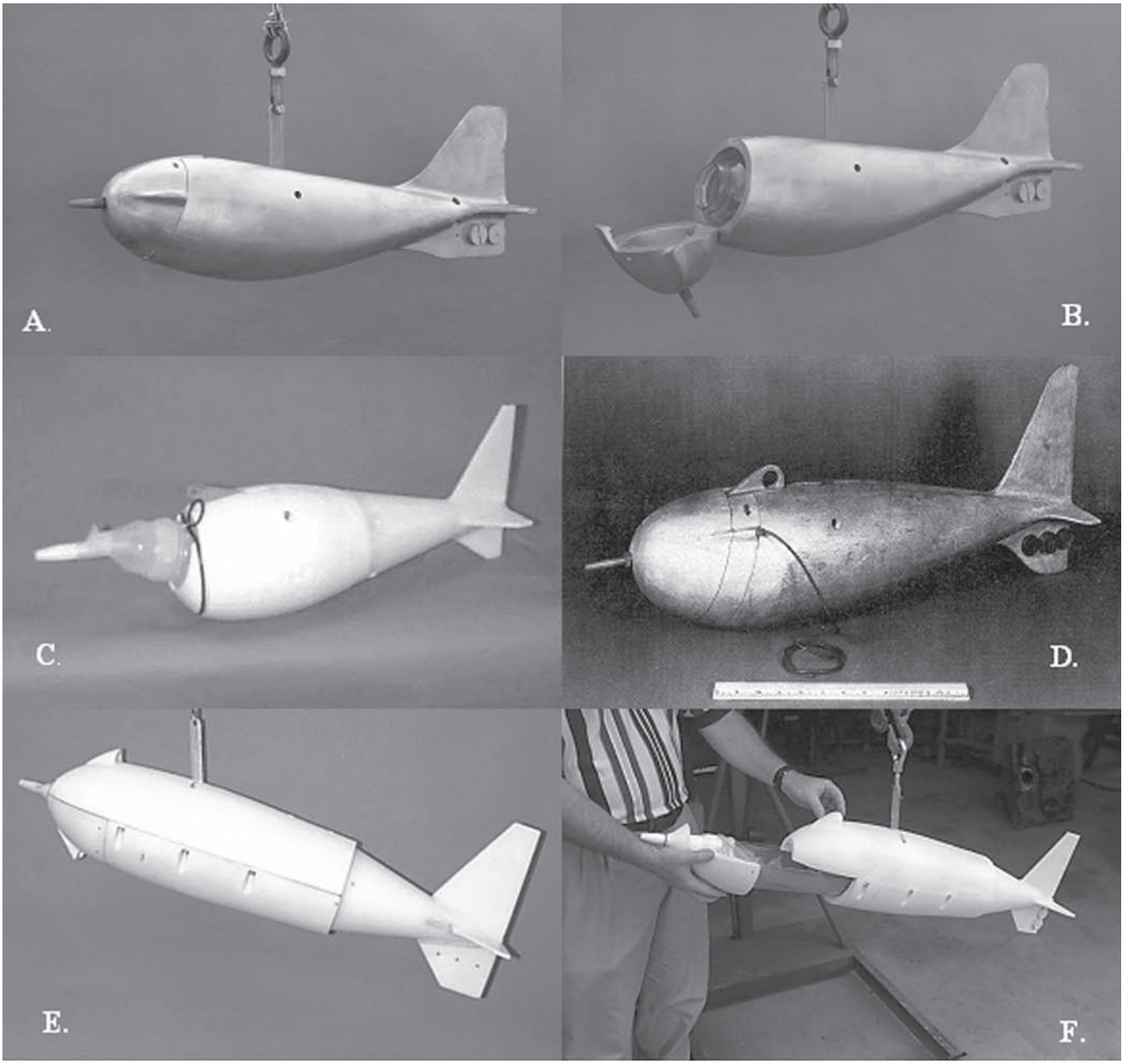

Fig. 5-17. (A) The US D-74 suspended-sediment sampler. (B) The US D-74 suspended-sediment sampler open. (C) The US D-95 suspended-sediment sampler. (D) The US P-61A1 point-integrating suspended-sediment sampler. (E) The US D-96 suspended-sediment sampler. (F) The US D-96 suspended-sediment sampler with tray extended.

(Table 5-2). These samplers also can be used in depth-integration mode.

An operator-controlled sampler solenoid valve powered by a nonsubmersible battery pack makes possible collection of a sample at a discrete depth, or can start and stop depth-integrated sample collection. Automatic pressure equalization at depth precludes a sudden inrush of sample due to a static-head differential when the valve is opened.

The US P-61A1 (Fig. 5-17D; Table 5-2) is calibrated for use in velocities up to 2 m/s, but there is evidence to suggest that it can collect samples isokinetically at velocities of at least 3 m/s (Wayne O'Neal, FISP, 2000, written communication). The US P-63 and US P-72 are lighter and heavier

versions and have higher and lower flow-velocity limits, respectively, but otherwise are functionally similar to the US P-61A1.

Because of the comparatively complex nature of point-integrating samplers, the user may find it useful to seek additional information given in FISP reports (1952; 1963; Davis 2005) or to obtain information directly from the FISP (FISP 2000).

5.3.4.1.6 Bag Samplers Samplers using collapsible bags as the sample container have been used since the 1970s (Stevens et al. 1980). Nordin et al. (1983) tested a large-volume bag sampler in the Rio Orinoco and Rio Amazonas, South America. Moody and Meade (1994) deployed a bag sampler of the type devised by Stevens et al. (1980) in the Mississippi River and selected tributaries.

As with rigid-bottle isokinetic samplers, water enters the bag sampler through a nozzle. However, bag samplers have no exhaust port, and the sample container is a collapsible bag. Air is manually expelled from the bag before submersion of the sampler. The transit rate for a bag sampler is constrained by the intake-nozzle and the bag volume, in addition to the maximum rate of 0.4 times the mean flow velocity in the vertical that applies to all depth-integrating samplers. When a Teflon bag is used, they are capable of collecting unbiased samples for trace-element analyses in addition to those collected for suspended-sediment analyses.

The US D-96 collapsible bag sampler (Fig. 5-17E and F; Table 5-2) was the first such sampler developed in part to address the limitations and disadvantages associated with bottle samplers and experimental bag samplers (Davis 2000; Webb and Radtke 1998). This cable-suspended sampler can provide up to 3 L of sample for subsequent unbiased trace-element analyses in addition to physical-sediment analyses. It is fabricated from bronze and aluminum castings with a high-density polyethylene tail. All metal parts are plastic-coated with commercially available "PlastiDip." A sliding tray (Fig. 5-17F) in the sampler holds the nozzle holder with nozzle in place and supports a perfluoroalkoxy bag.

The US D-96 sampler will collect velocity-weighted samples in streams with velocities from 0.6 to 3.8 m/s. At a maximum transit rate of 0.4 times the mean flow velocity in the vertical, the US D-96 sampler is capable of sampling to a depth of 12 m (39 ft) with a 7.9-mm (5/16-in.) nozzle, 18 m (60 ft) with a 6.4-mm (¼-in.) nozzle, and 34 m (110 ft) with a 4.8-mm (3/16-in.) nozzle (Davis 2000). Bag samplers with smaller and larger capacities than the US D-96 sampler are also available. The 13-kg (29-lb) US DH-2 is a hand-line sampler capable of collecting a 1-L sample. The 125-kg (275-lb) US D-99 is a cable-suspended sampler capable of collecting a 6-L sample.

5.3.4.2 Manual Sampling Methods The most common purpose of sediment sampling is to determine the instantaneous mean discharge-weighted suspended-sediment concentration at a cross section. Derived concentration values are combined with water discharge to compute the measured suspended-sediment discharge. A discharge-weighted suspended-sediment concentration representative of the mean value in the cross section is desired for this purpose and for the development of coefficients to adjust data collected by observers and automatic samplers.

Ideally, the best method for sampling any stream to determine sediment discharge would be to collect the entire flow of the stream over a given time period, remove the water, and weigh the sediment. This method is rarely feasible. Instead, the sediment concentration in the flow is determined by collecting depth-integrated suspended-sediment samples that define the mean discharge-weighted concentration in the sample vertical, and collecting sufficient verticals to define the mean discharge-weighted concentration in the cross section (Edwards and Glysson 1999).

5.3.4.2.1 Single-Vertical Sampling The objective of collecting a single-vertical sample is to obtain a concentration value representative of the mean discharge-weighted suspended-sediment concentration in the vertical being sampled at the time the sample was collected. An isokinetic sampler deployed at a constant rate in a downward and upward transit will collect a sample weighted for the variations in velocity and concentration in the vertical from the surface to the top of the unsampled zone. The following equation demonstrates this concept:

$$C_i = \frac{\int_{B_i+UZ}^{D_i} c_i(s)\,v_i(s)\,ds}{\int_{B_i+UZ}^{D_i} v_i(s)\,ds} \qquad (5\text{-}6)$$

where

C_i = mean suspended-sediment concentration in vertical i;
Bi = elevation of the streambed in vertical i;
UZ = distance from the bed to the nozzle of a sampler resting on the bed (unsampled zone);
D_i = elevation of the water surface in vertical i;
$c_i(s)$ = concentration at depth s in vertical i;
s = depth in the vertical; and
v_i = velocity at depth s in vertical i.

The method used to obtain the mean concentration of suspended sediment in a vertical thus depends on the flow conditions and particle-size distribution of the sediment in transport. These conditions can be generalized to four types of situations:

1. Low velocity ($v < 0.6$ m/s) when little or no sand is being transported in suspension;

2. High velocity ($0.6 \leq v \leq 3.7$ m/s) when depths are less than 5.6 m;
3. High velocity ($0.6 \leq v \leq 3.7$ m/s) when depths are greater than 5.6 m; and
4. Very high velocity ($v > 3.7$ m/s).

First case. In the first case, where $v < 0.6$ m/s, barring extremely shallow depths, the velocity is low enough so that little if any sand is in suspension. The distribution of any silt- and clay-size material (<0.062 mm in diameter; Folk 1974) in transport is relatively uniform from stream surface to bed (Guy 1970). The sampling error for this case is 10% or less with relative sampling rates in a range from about 0.2 to at least 5.0 (Fig. 5-15). Consequently, it is less important to collect the sample isokinetically with fines in suspension than it is when sand-size particles (≥0.062 mm in diameter; Folk 1974) are in suspension. In shallow streams, a sample may be collected by manually submerging an open-mouthed bottle into the stream. The mouth should be pointed upstream and the bottle held tilted upward at approximately a 45° angle from the streambed. The bottle should be filled by moving it from the surface to the streambed and back. An unsampled zone of about 8 cm should be maintained in order to obtain samples that are compatible with depth-integrated samples collected at higher velocities and to avoid collecting streambed material. If the stream is not wadable, a weighted-bottle type sampler, such as the US WBH-96, may be used (Webb and Radtke 1998). Samples collected in this manner are not discharge-weighted.

Second case. In the second case, when $0.6 \leq v \leq 3.7$ m/s and the depth is less than 4.6 m, a depth-integrating sampler described in Table 5-2 that is suitable for the ambient streamflow condition should be used. The method of sample collection basically is the same for all these samplers, whether used while wading or deployed from a bridge, cableway, or boat. Insert a clean sample container into the sampler and ensure that the air-exhaust tube and/or nozzle is unobstructed. Then lower the sampler to the water surface so that the nozzle is above the water, and the lower tail vane or back of the sampler is in the water to orient it parallel to the flow. The sampler then is lowered at a constant rate until it touches the bottom. It is immediately retrieved at a constant rate until it clears the water surface. Although the ascending transit rate need not be equal to the descending rate, in practice it is simpler to maintain a constant rate in both directions. However, both rates must be constant to obtain a velocity- or discharge-weighted sample. The rates should be such that the bottle fills to near its optimum level (Johnson 1997; Edwards and Glysson 1999).

For streams that transport heavy loads of sand, and perhaps for some other streams, at least two complete depth integrations of the sample vertical should be made as close together in time as possible, one bottle for each integration. Each bottle then constitutes a sample and can be analyzed separately or, for the purposes of computing the sediment record (a time series of sediment discharges often reported as daily values), concentration values representing two or more bottles can be averaged as a set and tagged with a single time of collection. This set is used as a single sediment-concentration value for computing the sediment record. Analytical results from two or more individual bottles for a given observation are useful for checking sediment variations among bottles, which is advantageous in the event that sediment concentrations in samples collected consecutively from the same vertical differ markedly. Immediately after collection, the sample should be inspected by briefly swirling or agitating the container and then observing the quantity of sand particles that collect in the bottom of the container. If there is an unusually large estimated mass of sand among bottles with similar sample volumes, or the mass of sand inexplicably differs among the bottles, at least one more sample from the same vertical should be taken immediately. The sample container suspected of having too much sand should be marked as having "excess sand," or, if it is likely to be contaminated, the sample should be discarded. If a container is overfilled or if water is ejected from the nozzle when the sampler is raised past the water surface, the sample should be discarded. A clean container must be used to resample the vertical.

Third case. In the third case, where $0.6 \leq v \leq 3.7$ m/s and the depth is greater than 4.6 m, rigid-bottle depth-integrating samplers cannot be used because the depth exceeds the maximum allowable depth for these samplers. In this case, one of the point-integrating or bag-type samplers must be used. The method for collection of a sample using the bag-type sampler is similar to that used with the depth-integrating samplers.

The point samplers may be used to collect depth-integrated samples in verticals where the depth is greater than 4.6 m. For streams with depths of 4.6 to 9.1 m, a procedure for sampling modified from that described by Edwards and Glysson (1999) is as follows:

1. Insert a clean bottle in the sampler and close the sampler head.
2. Lower the sampler to the streambed, keeping the solenoid valve closed; note the depth to the bed.
3. Start raising the sampler to the surface, using a constant transit rate. Open the valve at the same time the sampler begins the upward transit.
4. Keep the valve open until after the sampler has cleared the water surface. Close the valve.
5. Remove the bottle containing the sample, check the volume of the sample, and mark the appropriate information on the bottle. (If the sample volume exceeds allowable limits, discard the sample and repeat depth integration using a higher transit rate.)
6. Insert another clean bottle into the sampler and close the sampler head.
7. Lower the sampler until the lower tail vane is touching the water, allowing the sampler to align parallel to the flow.

8. Open the valve and lower the sampler at a constant transit rate until the sampler touches the bed.
9. Close the valve the instant the sampler touches the bed (by noting the depth to the streambed in step 2 above, the operator will know when the sampler is approaching the bed).

If the stream depth is greater than 9.1 m, the process is similar, except that the descending and ascending integrations are broken into segments no larger than 9.1 m. Samples collected by this technique may be composited for each vertical if the same transit rate is used. Otherwise, samples should be analyzed separately. A single mean concentration is computed for the vertical.

Fourth case. In the fourth case, where $v > 3.7$ m/s, the velocities are too large to deploy depth- or point-integrating samplers safely. In this case, and when the presence of debris, ice in flow, or other factors makes normal sample collection dangerous or impossible, surface or dip samples may be collected.

A surface sample is one taken on or near the surface of the water, with or without an isokinetic sampler. At some locations, stream velocities can be so large that even the heaviest, most streamlined samplers will not reach the streambed in one or more sampled verticals. Under such conditions, it can be expected that all but perhaps the largest sediment particles in suspension will be well mixed within the flow; and, therefore, a sample from near the surface, non-depth-integrated, may contain a concentration and size distribution representative of the entire vertical. However, results from these samples should be correlated with those from depth-integrated samples collected under more normal flow conditions as soon as possible after the large velocities diminish. Along with the depth-integrated sample, a sample should be collected in a manner duplicating the sampling procedure used to collect the surface or dip sample. Analytical results from these samples will be used to adjust those from the surface or dip sample collected during the higher flow, if necessary, to facilitate the use of these data in sediment-discharge computations and data analyses.

5.3.4.2.2 Multivertical Sampling A depth-integrated sample collected using the procedures outlined in the previous section will accurately represent the discharge-weighted suspended-sediment concentration in a vertical at the time of the sample collection. Samples collected at appropriately spaced verticals can be used to calculate the instantaneous sediment concentration at a cross section. The International Standards Organization (ISO 1993) lists three methods for suspended-sediment data collection in a cross section: the equal-discharge-increment, equal-width-increment, and equal-area-increment methods. The equal-area-increment method is rarely used in the United States. The first two methods are described in the following sections (Edwards and Glysson 1999).

5.3.4.2.3 The Equal-Discharge-Increment Method With the equal-discharge-increment (EDI) method, samples are obtained from the locations representing equal increments of discharge. The EDI method requires that three criteria be met:

1. Samples are collected isokinetically;
2. The vertical represents the mean concentration and particle-size distribution for the subsection sampled;
3. The discharges on both sides of the sampling vertical are predetermined proportions of the total discharge, which requires information on the lateral distribution of discharge in the cross section.

The mean discharge-weighted suspended-sediment concentration in a cross section using the EDI method is calculated from the mean concentrations from individual verticals (see "Single Vertical Sampling") as follows:

$$C_{xs} = \frac{1}{n}\sum_{i=1}^{n} C_i \tag{5-7}$$

where

C_{xs} = mean discharge-weighted suspended-sediment concentration in the cross section;
n = number of verticals used in the EDI measurement; and
C_i = mean concentration in the vertical i (see Eq. (5-6)).

The distribution of discharge can be derived from a discharge measurement made immediately prior to selecting sampling verticals (Rantz 1982), or, if the channel is relatively stable, on an analysis of the lateral distribution of discharges measured over a range of historical flows. If such knowledge can be obtained, the EDI method can save time and labor (compared to the equal-width-increment method, discussed in the next section), especially on larger streams, because fewer verticals are required (Hubbell et al. 1956).

The inverse of the number of verticals, n, to be sampled by the EDI method is multiplied by 100% to derive q_{percent}, the percentage of discharge to be represented in samples collected in each vertical. The location of a vertical nearest the left bank is selected at a point at which the cumulative discharge to the left of the vertical is one-half of the total discharge times q_{percent}. The location of a vertical nearest the right bank is selected at a point at which the cumulative discharge to the right of the vertical is one-half of the total discharge times q_{percent}. All other verticals are selected at points where the cumulative discharge between adjacent verticals is equal to the total discharge times q_{percent}.

For example, from the discussion in the previous paragraph, samples are to be collected from five increments of equal discharge from a 100-m-wide cross section of a river flowing at 500 m^3/s. The percentage of the total discharge to be represented in samples collected from each vertical is 1/5 times 100%, or 20%. The location of the vertical nearest the left bank is selected at the point at which the cumulative discharge to the left of that vertical is 0.5 times 500 m^3/s

times 20%, or at the point in the cross section where 50 m^3/s of discharge occurs between the vertical and the left bank. Likewise, the vertical nearest the right bank is selected at the point at which 50 m^3/s occurs between that vertical and the right bank. The other three verticals are located at points separating adjacent verticals by discharges of 100 m^3/s, the product of the total river discharge of 500 m^3/s, times $q_{percent}$, 20%. The location of each vertical represents the centroid of the discharge in its respective subarea, with each subarea containing equal increments of discharge.

Samples are collected from each EDI method vertical as described previously in the "single-vertical" section. The descending and ascending transit rates in any one vertical need not be equal, nor do the rates need to be equal from vertical to vertical. Although different diameter nozzles for the isokinetic sampler can be used from vertical to vertical, it complicates the data-collection procedure and hence the practice is discouraged.

The EDI method requires a minimum of four verticals; rarely are more than nine verticals necessary. The greater the potential heterogeneity in the distribution of suspended-sediment concentrations and particle-size distributions in the cross section, the more verticals should be selected.

If an equal amount of sample is collected at each vertical, the samples can be composited and analyzed as a single sample. In most cases, the samples are analyzed separately and the results of the analyses are added and then divided by the number of subsections to derive a mean discharge-weighted sediment concentration. One advantage of this method is that data describing the cross-sectional variation in concentrations are produced. Additionally, a bottle containing an abnormally large sediment concentration compared to others in the set (because of recirculation or to punching the nozzle into the bed) can be identified and excluded from the calculated mean cross-sectional suspended-sediment concentration to preclude a biased result.

The bed of a sand channel can shift substantially, at single points and across segments of the width, over a period ranging from weeks to fractions of an hour. This not only makes it difficult at best to establish a relation between stage and the cross-sectional discharge distribution from one visit to the next, but also makes it impossible to be certain the discharge distribution does not change between the time of the water-discharge measurement and sample collection (see Guy 1970). Under conditions where the lateral distribution of flow changes rapidly, the EDI method may yield unreliable results.

5.3.4.2.4 The Equal-Width-Increment Method A cross-sectional suspended-sediment sample obtained by the equal-width-increment (EWI) method requires a sample volume proportional to the amount of flow at each of 10 or more equally spaced verticals in the cross-section (Edwards and Glysson 1999). Equal spacing between EWI verticals across the stream and sampling at an equal transit rate at all verticals yields a cumulative sample volume proportional to the total discharge. This method first was used by Colby in 1946 (FISP 1963) and is used most often in relatively shallow, wadable streams and/or sand-bed streams where the distribution of water discharge in the cross section is unstable. It also is useful where suspended-sediment concentrations in the cross section are substantially heterogeneous, such as in streams where tributary flow has not completely mixed with the flow.

The mean discharge-weighted suspended-sediment concentration in a cross section using the EWI method is calculated from the mean concentrations from individual verticals (see "Single Vertical Sampling") as follows:

$$C_{xs} = \frac{\sum_{j=1}^{J} \mathrm{Vol}_j C_j}{\sum_{j=1}^{J} \mathrm{Vol}_j} \tag{5-8}$$

where

C_{xs} = mean discharge-weighted suspended-sediment concentration in the cross section;
J = number of sample bottles used in the EWI measurement;
C_j = concentration in the sample bottles j; and
Vol_j = the total volume of water collected in sample bottle j.

The number of verticals required for an EWI sediment-discharge measurement depends on the distribution of concentrations and flow in the cross section at the time of sampling, as well as on the a relative assessment of the desired accuracy of the result. For many streams, statistical approaches and experience are needed to determine the desirable number of verticals. Until such experience is gained, the number of verticals used should be larger than that deemed to be minimally necessary. In all cases, a minimum of 10 verticals should be used for streams exceeding 1.5 m wide. For streams less than 1.5 m wide, as many verticals as possible should be used, as long as they are spaced a minimum of 7.6 cm apart, to allow discrete sampling of each vertical and to avoid overlaps. Through general experience with similar streams, field personnel can estimate the required minimum number of verticals to yield a desired level of accuracy. For all but the widest and shallowest streams, 20 verticals usually are ample.

The width of the increments to be sampled, or the distance between verticals, is determined by dividing the stream width by the number of verticals, n, necessary to collect a discharge-weighted suspended-sediment sample representative of the sediment concentration of the flow in the cross section. The locations of the two verticals nearest to the banks are at a distance of one-half of the total width divided by n. The locations of the other verticals are separated from adjacent verticals by a distance of the total width divided by n. The locations of these verticals represent the centroid of subareas with boundaries one-half the distance to adjacent verticals. Hence, only the widths of the subareas necessarily are equal.

The EWI sampling method requires use of the same size nozzle for a given measurement, and all verticals must be traversed using a transit rate that will not result in overfilling the sample bottle at the deepest and fastest vertical in the cross section. The descending and ascending transit rates must be equal for all verticals and during the sampling traverse of each vertical. By using this equal-transit-rate technique with a standard depth- or point-integrating sampler at each vertical, a volume of water proportional to the flow in the vertical will be collected.

For example, from the previous paragraphs, samples from 12 verticals are to be collected from a stream with a surface width of 120 m with zero width referenced to the left bank. The location of the leftmost vertical is at a distance of one-half of 120 m divided by 12, or 5 m from the left bank. The 12 verticals are located 10 m apart with the rightmost vertical 5 m from the right bank. The second vertical from the left bank is located at 15 m, and the 12th vertical from the left bank is located at 115 m.

Because the maximum transit rate must not exceed $0.1\ v_m$, $0.2\ v_m$, or $0.4\ v_m$ (a $0.4\ v_m$, transit rate applies to all bag samplers) depending on the nozzle size and bottle volume (v_m equals the mean ambient velocity in the sampled vertical), and because the minimum rate must be sufficiently fast to keep from overfilling any of the sample bottles, the transit rate to be used for all verticals is limited by conditions at the vertical containing the largest discharge per unit width, or, in operational terms, the largest product of depth times mean velocity. A discharge measurement can be made to determine the location of this vertical. In practice, this location often is estimated by sounding for depth and acquiring a feel for the relative velocity with a sampler or wading rod. The transit rate required at the maximum discharge vertical then must be used at all other verticals in the cross section and usually is set to provide the maximum sample volume in a round-trip transit. It is permissible to sample at multiple verticals using the same bottle as long as the bottle is not overfilled. If a bottle is overfilled, the contents must be discarded, and all verticals previously sampled using that bottle must be resampled, using a sufficient number of bottles to avoid overfilling.

5.3.4.2.5 Advantages of the Equal-Discharge-Increment and Equal-Width-Increment Methods Some advantages and disadvantages of both the EDI and EWI methods have been noted in the previous discussion. It must be remembered, however, that both methods, if properly used, will yield similar cross-sectionally averaged results.

The advantages of the EDI method are as follows:

1. Fewer requisite verticals typically result in a reduced collection time, which is particularly advantageous during periods of rapidly changing discharge;
2. Bottles composing a sample set may be composited for single laboratory analysis when equal volumes of sample are collected from each vertical;
3. The cross-sectional variation in concentration can be determined if samples are analyzed individually;
4. Duplicate cross-sectional samples can be collected during the measurement;
5. A variable transit rate can be used among verticals.

The advantages of the EWI method are as follows:

1. No antecedent knowledge of flow distribution in the cross section is required;
2. Variations in the distribution of concentration in the cross section may be better integrated in the composite cross section sample due to the larger number of verticals sampled;
3. Analytical time and costs are minimized as sample bottles are composited for single laboratory analysis;
4. This method is easily learned and used due to the straightforward spacing of sample verticals based on stream width, rather than on the cross-sectional distribution of discharge;
5. Generally, less total time is required on site if no discharge measurement is deemed necessary and the cross section is relatively stable during the measurement.

The advantages of one method are, in many cases, the disadvantages of the other. The USGS (1998b) considers the EDI method the most universally applicable and useful discharge-weighted sampling method.

5.3.4.2.6 Transit Rates for Suspended-Sediment Sampling A sample obtained with an isokinetic sampler using depth integration is quantitatively weighted according to the velocities through which it passes. Therefore, if the sampling vertical represents a specific width of flow, the sample is considered to be discharge weighted because, with a uniform transit rate, the suspended sediment conveyed at varying velocities throughout the sampled vertical is given equal time to enter the sampler.

The transit rate used with any depth-integrating sampler must be regulated to make possible the collection of representative samples (i.e., isokinetically collected). An insufficient transit rate can result in an unacceptable sample due to overfilling of the sample container. An excessive transit rate can result in intake velocities less than the stream velocity due to a large entrance angle between the nozzle and streamflow lines caused by the vertical movement of the sampler in the flow (FISP 1952). Transit rates should never exceed the product of 0.4 and the mean velocity ($0.4\ v_m$) in a vertical with any isokinetic sampler.

Additional limitations may be imposed on maximum transit rates for rigid-bottle depth-integrating samplers due to changes in hydrostatic pressure during deployment. The maximum allowable transit rate is attained when the rate of change in the internal pressure due to filling equals the rate of change of hydrostatic pressure. If the sampler is lowered too fast in the vertical, inflow through the nozzle is insufficient to

increase the pressure in the container at the same rate; consequently, hydrostatic pressure increases at a greater rate than pressure in the container. The resulting pressure imbalance causes the sample to enter the nozzle at a velocity greater than the ambient stream velocity. Stream water can also enter the exhaust port under these circumstances. Both potential outcomes result in violation of isokinetic sampling principles (Stevens et al. 1980). Likewise, if the sampler is raised too rapidly, the hydrostatic pressure will decrease at a greater rate than the pressure inside the container. This pressure imbalance will result in reduced flow of sample into the container with respect to the ambient stream velocity. Either outcome—larger or smaller intake velocities with respect to the ambient stream velocity—can result in collection of a sample that contains neither a representative concentration nor particle-size distribution of suspended sediment.

The maximum allowable transit rate for rigid-bottle samplers can be determined with knowledge about (1) the depth of the sample vertical, (2) the mean velocity of the vertical, (3) the nozzle size being used, and (4) the sample bottle size used in the sampler. Different combinations of nozzle diameters and bottle volumes result in maximum transit rates ranging from about $0.1v_m$ to $0.4v_m$. Tables providing isokinetic transit rates as a function of nozzle diameters and bottle volumes are provided by the USGS (1998b). Graphs delineating permissible and optimal transit rates for a combination of sample container and nozzle sizes as a function of stream depth and mean velocity are provided by Edwards and Glysson (1999). A vertical transit pacer is available to assist in quantifying the transit rate for a reel-deployed sampler (FISP 2001).

5.3.4.2.7 Point-Integrated Sampling A point-integrated sample is a sample of the water-sediment mixture collected isokinetically from a single point in the cross section. Point-integrated samples are collected using one of the point-integrating samplers previously presented. Multiple point samples may be used to define the distribution of sediment in a vertical, the vertical and horizontal distributions of sediment in a cross section, and the mean cross-sectional sediment concentration.

The purpose for which point samples are to be collected determines the collection method to be used. If samples are collected for the purpose of defining the horizontal and vertical distribution of concentration and/or particle-size distributions, samples collected at numerous points in the cross section with any of the "P" type samplers will be sufficient. Normally, 5 to 10 verticals are sufficient for horizontal definition of suspended-sediment concentrations. Vertical distributions can be adequately defined by obtaining samples from a number of points in each sample vertical. Specifically, samples should be taken with the sampler lightly touching the bed, 0.3 m off the bed, at from 6 to 10 additional points in the vertical above that point, and from near the surface. Each point sample should be analyzed separately.

If point samples are collected to define the mean concentration in a vertical, 5 to 10 samples should be collected from the vertical. The sampling time for each sample (the elapsed time that the nozzle is open) must be equal. This result will ensure that sample volumes collected are proportional to the flow at the point of collection. These samples may be composited for a single laboratory analysis. If the EDI method is used to define the stationing of the verticals, the sampling time may be varied among verticals. If the EWI method is used, a constant time for collecting samples from all verticals must be used.

The mean discharge-weighted suspended-sediment concentration in a cross section using the point-integration and EDI sampling methods is calculated from the mean concentrations from individual sampling points as follows:

$$C_{xs} = \frac{1}{n}\sum_{i=1}^{n}\left\{\frac{\sum_{d=1}^{D_i}\mathrm{Vol}_{id}C_{id}}{\sum_{d=1}^{D_i}\mathrm{Vol}_{id}}\right\} \tag{5-9}$$

where

C_{xs} = mean discharge-weighted suspended-sediment concentration in the cross section;
D_i = total number of points sampled in vertical i;
n = number of verticals in which point samples are collected;
C_{id} = suspended-sediment concentration in a sample from point d of vertical i; and
Vol_{id} = volume of sample collected from point d of vertical i.

If multiple points are sampled with a single bottle, computation of the mean sample concentration is accomplished by treating the contents of the bottle as if collected at a single point.

5.3.5 Automatic Samplers

Some sediment-monitoring programs and studies include sites where collection of sediment samples is required at a frequency, at a time, and/or under a set of conditions that cannot be accommodated through manual sampling. Safety considerations, remoteness or inaccessibility of site location, flow conditions, operational costs, and other factors may render manual collection of sediment and flow data at a site impractical or impossible. In lieu of manual sampling, automatic samplers may be deployed to accommodate sediment data-collection needs at some sites.

Automatic samplers are useful for collecting suspended-sediment samples during periods of rapid discharge changes from storm-runoff and in reducing the need for manual measurements associated with intensive sediment-collection programs (FISP 1981). However, under some circumstances, use of automatic samplers to collect data can actually result in costs greater than those for an observer at the same site. Automatic samplers, and particularly pumping samplers,

often require more frequent site visits by the field personnel than would be required at the conventional observer station, owing to their mechanical complexity, power requirements, and limited sample capacity. Use of automatic samplers does not preclude the need for collecting medium- and high-flow cross-sectional samples. Additionally, use of automatic samplers typically results in reduced data quality. This result is particularly true for automatic sample collection from streams conveying high percentages of suspended sand-size material.

As noted previously, emerging technologies for monitoring suspended sediment show great promise, although none is commonly accepted nor extensively used. The most commonly used automatic samplers are automatic pumping samplers, which require power to obtain water samples. Single-stage samplers, which rely on changes in stream stage and/or velocity to collect water-sediment samples on the rising phase of a hydrograph, are also available.

5.3.5.1 Automatic Pumping Samplers Automatic pumping samplers generally consist of a pump, bottle-container unit, and sample distribution, activation, and intake systems. Ideally, this combination of components should be designed to meet the following criteria (Bent et al. 2001; Edwards and Glysson 1999):

1. Stream velocity and sampler intake velocity should be equal to allow for isokinetic sample collection if the intake is aligned into the approaching flow;
2. A suspended-sediment sample should be delivered from stream to sample container without a change in sediment concentration or particle-size distribution;
3. Cross contamination of samples caused by residual sediment in the sampler plumbing between sample-collection periods should be prevented;
4. The sampler should be capable of sampling over the full range of suspended-sediment concentrations and particle sizes;
5. Sample container volumes should meet minimum sample analysis volume requirements;
6. The inside diameter of the intake should be at least three times the diameter of the largest particles sampled, although small enough to maintain a mean sample velocity that will substantially exceed the fall velocity of those particles;
7. The sampler should be capable of vertical pumping lift elevations of about 10 m from intake to sample container for clear water;
8. The sampler should be capable of collecting a reasonable number of samples—usually at least 24—dependent upon the purpose of sample collection and the flow conditions;
9. Some provision should be made for protection against freezing, evaporation, and dust contamination of collected samples;
10. The sample container unit should be constructed to facilitate removal and transport as a unit;
11. The sampling cycle should be initiated in response to a timing device, flow change, or external signal based on a set of criteria that maximizes the potential for collecting samples at desired points over one or more hydrographs;
12. The capability of recording the sample-collection date and time should be present;
13. The provision for operation using ac power or dc battery power should be present.

Nearly all of the automatic pumping samplers in use today are available commercially. The PS-69, CS-77, and PS-82 pumping samplers are no longer manufactured.

The ISCO 6700 and American Sigma 900 automatic pumping samplers, for example, share various features for collecting water samples. Both are computer-controlled portable samplers capable of collecting up to 24 1-L samples based on time, flow, and/or other user-selected criteria. They use built-in peristaltic pumps and operate on ac power or dc battery power. Both samplers feature a back-flush cycle to reduce cross contamination between consecutively collected samples.

Neither sampler is capable of sampling clear freshwater if the peristaltic pump is at an elevation of about 9.7 m or more above that of the water surface. Cavitation can occur at smaller heads with larger specific gravities associated with increasing suspended-sediment concentrations and/or lower barometric pressures. Where lift requirements potentially exceed the capacity of a sampler, an auxiliary pump may be used to pump water to the sampler under a positive pressure. Gray and Fisk (1992) describe an automatic pumping sampling system used to collect samples of highly concentrated streamflow in Arizona and New Mexico. An auxiliary pump in a diving bell affixed at an elevation of a meter or two above that of the water surface at low flow pumps stream water to a gauging station. In the gauging station, a commercial sampler modified to collect 9-L samples periodically draws an aliquot of the pumpage from the auxiliary pump via a Y connector in the intake line. A data-collection platform controls collection of up to 24 samples based on time, stage, and rate-of-stage-change criteria. The data-collection platform records hydrologic information and data related to the number and times of samples collected and periodically updates a USGS database via satellite.

5.3.5.1.1 Installation and Use Criteria The decision to use a pumping sampler for collection of sediment samples usually is based on physical and fiscal criteria. Installation of an automatic pumping sampler requires careful planning before installation, including selection of the sampler site location and an evaluation of available or newly collected data to maximize the potential to collect useful pumping sampler data.

Before installation of an automatic pumping sampler, many of the problems associated with installing stream-gauging equipment must be addressed. In addition, specific data concerning the sediment-transport characteristics at the proposed sampling site must be obtained and evaluated prior to emplacement of the sampler and location of the intake within the streamflow. Logistically, the sample site must be evaluated as to accessibility, availability of electrical power, location of a bridge, cableway, or other means to safely obtain manual measurements at the site, and normal range of ambient air temperatures inherent in local weather conditions. The availability of a local observer to collect periodic reference samples also should be considered. The sediment-transport characteristics should include detailed information on the distribution of concentrations and particle sizes throughout the sampled cross section over a range of discharges. Glysson (1989b) describes other information requirements associated with collection of sediment data.

5.3.5.1.2 Placement and Orientation of Sampler Intake The primary concept to consider when placing a sampler intake in the streamflow at a sample cross section is that only one point in the flow is being sampled. Therefore, to yield the most reliable and representative data, the intake should be placed at the point where the concentration and particle-size distribution are most representative of the mean sediment concentration for the cross section over the full range of flows. This idealistic concept has great merit, but the mean cross section concentration almost never exists at the same point under varying streamflow conditions. It is even less likely that specific guidelines for locating an intake under given stream conditions at one stage would produce the same intake location relative to the flow conditions at a different stage. These guidelines would have even less transfer value from cross section to cross section and stream to stream. For these reasons, some generalized guidelines are outlined here and should be considered on a case-by-case basis in placing a sampler intake in the streamflow at any given cross section (Edwards and Glysson 1999):

1. Select a stable cross section in a reach with reasonably uniform depths and widths to maximize the stability of the relation between sediment concentration at a point and the mean sediment concentration in the cross section. This guideline is of primary importance in the decision to use a pumping sampler in a given situation; if a reasonably stable relation between the sample-point concentration and mean cross section concentration cannot be attained by the following outlined steps, an alternate location for the installation should be considered.
2. Consider only the part of the vertical that could be sampled using a standard US depth- or point-integrating suspended-sediment sampler, excluding the unsampled zone, because data collected with a depth- or point-integrating sampler will be used to calibrate the pumping sampler.
3. Determine, if possible, the depth of the point of mean sediment concentration in each vertical for each size class of particles finer than 0.25 mm from a series of carefully collected point-integrated samples.
4. Determine, if possible, the mean depth of occurrence of the mean sediment concentration in each vertical for all particles finer than 0.25 mm.
5. Use the mean depth of occurrence of the mean sediment concentration in the cross section as a reference depth for placement of the intake.
6. Identify or install a means to fix the intake at the desired location in flow. The attachment feature and intake should have a high probability of remaining in place at high flows and should be not be prone to collecting debris.
7. Adjust the depth location of the intake to avoid interference by dune migration or contamination by bed material.
8. Adjust the depth location of the intake to ensure submergence at all times.
9. Locate the intake in the flow at a distance far enough from the bank to eliminate any possible bank effects. Avoid placing the intake in an eddy.
10. Place the intake in a zone of high velocity and turbulence to improve sediment distribution by mixing, reduce possible deposition on or near the intake, and provide for rapid removal of any particles disturbed during a purge cycle.

Because of the generalized nature of these guidelines and because selected guidelines may prove to be mutually exclusive, it will often be impossible to satisfy them all when situating a pumping sampler intake into streamflows. The investigator is encouraged, however, to try to satisfy these guidelines or, at the very least, to satisfy as many as possible and to minimize the effects of those not satisfied.

The orientation of the pumping sampler intake nozzle can drastically affect sampling efficiency. There are five ways in which an intake could be oriented to the flow (see Fig. 5-18): (1) normal and pointing directly upstream (Fig. 5-18A), (2) normal and horizontal to the flow (Fig. 5-18B), (3) normal and vertical with the orifice up (Fig. 5-18C), (4) normal and vertical with the orifice down (Fig. 5-18D), and (5) normal and pointing directly downstream (Fig. 5-18E). Of these five orientations, A, C, and D should be avoided because of high sampling errors and trash-collection problems. Orientation B, with the nozzle positioned normal and horizontal to the flow, is the most common alternative used. The major problem with this orientation is that sand-size particles may not be adequately sampled (see the following section on pumped-sample data analysis). Orientation E, pointing directly downstream, may be advantageous over orientation B (Winterstein and Stefan 1986). When the

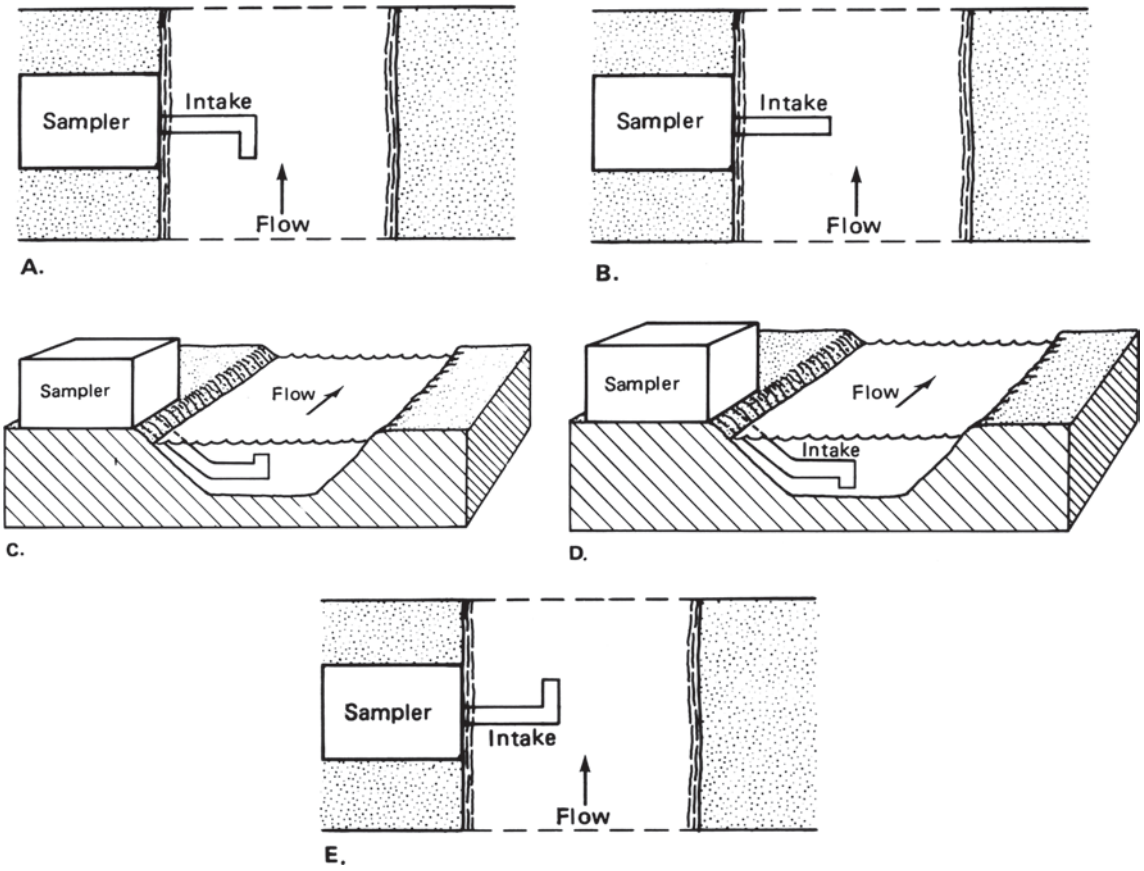

Fig. 5-18. Examples of pumping-sampler intake orientations. (A) Normal and pointing directly upstream. (B) Normal and horizontal to flow. (C) Normal and vertical with the orifice up. (D) Normal and vertical with the orifice down. (E) Normal and pointing directly downstream.

intake is pointing downstream, a small eddy is formed at the intake, which envelops the sand particles and thus allows the sampler to collect a more representative sample of the coarse load. Regardless of the intake orientation selected, the ratios of concentrations representative of the mean cross-sectional concentration and those from pumped samples are needed to define the sampling efficiency over a broad range of flows.

5.3.5.1.3 Activation The advent of the microprocessor as an integral part of the sampler, or as an external controller, provides many options for controlling pumping samplers that can be tailored to data-collection requirements on-hand. Gray and Fisk (1992) describe a method for controlling an automatic water sampler based on time, stage, and rate-of-stage-change criteria. Their technique is designed to provide adequate definition of the flood hydrograph to make possible reliable computations of daily sediment and associated solid-phase radionuclide discharges. Lewis (1996) describes a means for controlling an automatic sediment sampler based on real-time turbidity measurements. A technique for controlling an automatic water sampler that provides unbiased estimates of suspended-sediment discharges, based on time-stratified sampling and selection at list time, is described by Thomas (1985; 1991), and Thomas and Lewis (1993a).

5.3.5.2 Single-Stage Samplers Single-stage samplers were developed to meet the urgent needs for instruments useful in obtaining sediment data on streams where remoteness of site location and/or rapid changes in stage make it impractical to use a conventional depth-integrating sampler. They are generally less reliable, both in operation and in data accuracy, than depth-integrating samplers. However, even approximate information on the concentration of sediment between visits to the stream can be important if nothing better is available (FISP 1961; Edwards and Glysson 1999).

The US U-59 series single-stage samplers designed and tested by the FISP consist of a 0.45-L milk bottle or other sample container, a 4.7-mm inside diameter air exhaust, and a 4.7- or 6.4-mm inside diameter intake constructed of copper tubing. Each tube is bent to an appropriate shape and inserted through a stopper sized to fit and seal the mouth of the sample container. There are four models of US U-59 samplers. That designated US U-59A is designed for collection of silt- and clay-size sediments in low (less than about 0.7

m/s stream velocities. Those designated US U-59B, US U-59C, and US U-59D are for collection of sand-size and finer material in stream velocities less than 1, 1.6, and 2.1 m/s, respectively. A US U-59D single-stage suspended-sediment sampler is shown in Fig. 5-19A.

The US U-59 series of samplers obtains a sample on the rising phase of the hydrograph from a point near the water surface when the water level inside the intake tube reaches the weir elevation. As the sample siphons from the intake orifice into the sample bottle, air from the sample bottle vents out of the exhaust tube. The sampler is designed to cease filling when the sample elevation reaches the inner exhaust tube orifice. The sample velocity in the intake tube is a function of various factors, including stream velocity, intake orifice orientation, turbulence, and the presence of obstructions in the intake or exhaust tube.

The sampling operation just described is somewhat idealistic because, in reality, the operation is affected by various factors including flow velocity and turbulence. These factors alter the effective pressure at the nozzle entrance, which in turn alters the sampler's intake velocity.

The US U-59 sampler has many limitations with respect to good sampling objectives. It is a type of point sampler because it samples a single point in the stream at whatever stage the intake nozzle is positioned when immersed in flow. Its primary purpose is to collect a sample automatically, and it is used at stations on flashy streams or other locations that are difficult to visit in time to manually collect samples. Besides being automatic, the US U-59 is simple and inexpensive compared to automatic pumping samplers; a bank of them can be used to obtain a sample at various elevations during the rising hydrograph. However, despite these seemingly important advantages, the US U-59 sampler has many limitations. Following are the most important of these limitations:

1. Samples are collected at or near the stream surface, so that, in the analysis of the data, theoretical adjustments for vertical distribution of sediment concentration or size are necessary.
2. Samples usually are obtained near the edge of the stream or near a pier or abutment; therefore, theoretical adjustments for lateral variations in sediment distribution are required.
3. Even though combinations of size, shape, and orientation of intake and air-exhaust tubes are available, the installed system may not result in intake ratios sufficiently close to unity to sample sands accurately at parts of the runoff hydrograph.
4. Covers or other protection from trash, drift, and vandalism often create unnatural flow lines at the point of sampling.
5. Water from condensation may accumulate in the sample container prior to sampling.
6. Sometimes the sediment content of the sample changes during subsequent submergence.
7. The device is not adapted to sampling on falling stages or on secondary rises.
8. No specific sampler design is best for all stream conditions.
9. The time and gauge height at which a sample was taken may be uncertain.
10. At high velocities, flow can circulate into the intake nozzle and out the air exhaust. This can result in an

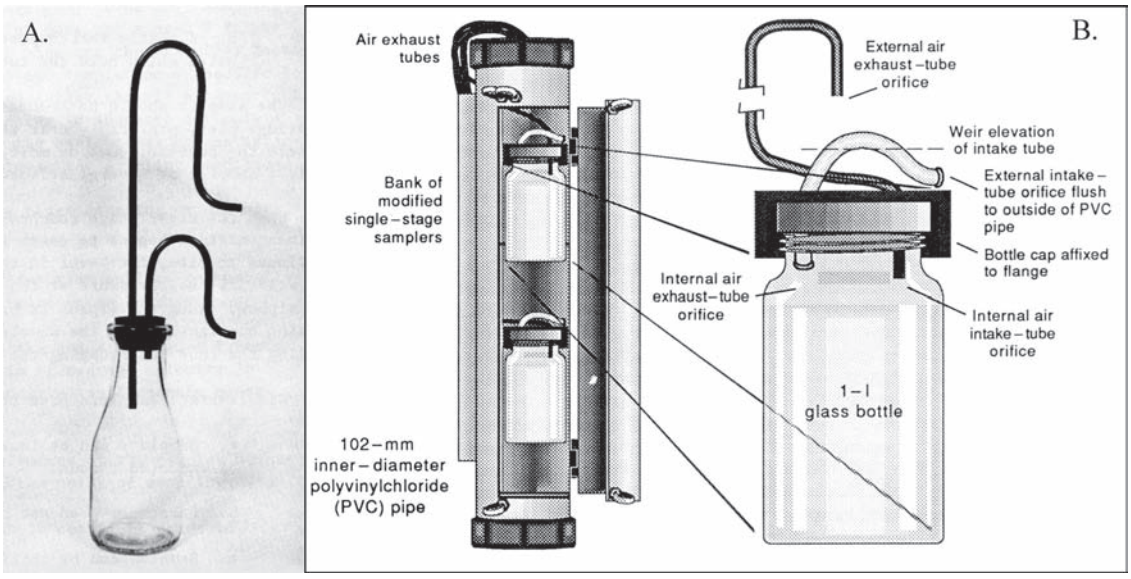

Fig. 5-19. (A) US U-59D single-stage suspended-sediment sampler and (B) Modified single-stage sampler. Reprinted from Gray and Fisk (1992) with permission.

increase in the concentration of coarse material in the sample by at least an order of magnitude.

Gray and Fisk (1992) developed a modified single-stage sampler that provides a measure of protection against vandalism and flood damage while minimizing the potential for water circulation (Fig. 5-19B). Various single-stage samplers are arranged vertically inside a protective polyvinyl chloride (PVC) pipe capped at both ends. Screw-cap 0.9-L bottles are used to provide a larger sample volume and a more positive seal. External air-exhaust orifices extend through the top cap to the highest elevation feasible for the site, reducing the potential for its inundation. External intake orifices are set flush with the exterior PVC pipe so that debris cannot snag on them. A hinged lockable door provides access to the 0.9-L sample bottles.

The US U-73 single-stage sampler is more sophisticated than the previously described single-stage samplers. It can be used to obtain samples on the rising and falling phases of a hydrograph. Additionally, it features an exterior design that allows for a degree of protection from trash or drift without additional covers or deflection shields. Aside from these advantages, the US U-73 has the same limitations and should be used under the same conditions as the US U-59 sampler. Although the US U-73 sampler is no longer stocked by the FISP, plans are available for its construction (FISP 2000).

The investigator using single-stage samplers may find protective measures necessary to avoid blockage of intakes or air exhausts due to nesting insects. In freezing temperatures, precautions against sample-container breakage due to expansion of a freezing sample are advised.

The percent sand-size material should be analyzed for all samples collected by single-stage samplers. This analysis will help identify instances of bias in concentrations resulting from sample recirculation.

5.3.6 Subsampling Equipment

Samples of water-sediment mixtures are sometimes subsampled, or split into multiple parts to make possible different analytical determinations on the subsamples. The validity of data obtained from subsamples depends on their comparability of selected constituent concentrations to those in the original sample. Subsamples tend to have larger constituent variances than the original, and also may be biased. Subsampling should be avoided unless it is necessary to achieve the ends of the sampling program.

Before 1976, USGS guidelines on manual sample splitting required compositing the water sample into a large, clean jug or bottle, shaking it for uniform mixing, and then withdrawing the required number of samples (USGS 1976). In 1976, the 14-L churn splitter was introduced to facilitate the withdrawal of a representative subsample of a water sediment mixture (Capel and Larson 1996; Lane et al. 2003). A fluoropolymer version of the churn splitter for trace-element subsampling is also available (FISP 2002). The cone splitter, a device developed to split water samples for suspended sediment and other water-quality constituents into up to 10 equal and representative aliquots, was introduced for wide-scale use in 1980 (Capel and Nacionales 1995; Capel and Larsen 1996).

Based on test results on the sediment-splitting efficiency of the churn and cone splitters (USGS 1997), the USGS has approved the use of the churn splitter for providing subsampling when the original sample's sediment concentration is less than 1,000 mg/L at mean particle sizes less than 0.25 mm. The cone splitter is approved for providing subsamples at sediment concentrations up to 10,000 mg/L at mean particle sizes less than 0.25 mm. The test data suggests that the cone splitter's acceptable concentration range exceeds 10,000 mg/L, and may be as large as 100,000 mg/L.

5.4 BED LOAD SAMPLERS

R. Kuhnle

The part of the total sediment load that is transported by traction or saltation on or immediately above the streambed is termed the bed load. Sediment transported as bed load can range in size from fine sands to coarse gravel depending on the flow strength. The separation of sediment in transport into bed load and suspended load is artificial, as there is often no clear-cut break between the two groups. The distinction is convenient, however, because most suspended sediment samplers currently in use have an unsampled zone that extends from the bed to several centimeters up into the flow. The sediment in transport in this zone near the bed is often referred to as the unmeasured load and consists of the bed load plus the lowermost fraction of the suspended load.

Knowledge of the rate of bed load transport is important for several reasons. The bed load is part of the total sediment load that represents net erosion from upstream areas of the watershed. Sediment conveyed downstream may fill reservoirs and channels, which impedes navigation, may increase the likelihood of flooding, and may degrade water quality and aquatic habitats. Local erosion and deposition of the bed material may also cause instability of the channel banks. Any long-term program of channel stabilization or rectification must take into account the transport of bed load and ensure that sediment is not accumulating or eroding.

The rate and size of sediment in transport as bed load varies dramatically with time at a point, and spatially at a given time over a cross section of a channel (Figs. 5-20A and B), even when the flow is steady (Ehrenberger 1932; Leopold and Emmett 1976; Carey 1985; Hubbell et al. 1985; Iseya and Ikeda 1987; Kuhnle and Southard 1988; Whiting et al. 1988; Kuhnle et al. 1989; Gray et al. 1991). This creates the challenge of designing a sampler that will sample with equal efficiency over widely varying transport rates, and collect

enough samples at a point and across the cross section to adequately define the mean rate for a given flow strength.

The determination of bed load has relied on three general methods (Hubbell 1964): direct measurement, using bed load transport relations, or measuring the erosion or deposition of bed-material sediment in a confined area. None of these techniques is suitable for a wide range of uses. Direct measurements suffer from the difficulty of deploying the samplers and collecting a sufficient number of samples, whereas no one bed load transport relation has been shown to have general applicability (e.g., Gomez and Church 1989; Vanoni 1975, pp. 221–222), and many areas do not have a convenient area to carry out erosion or deposition measurements. Therefore, no general empirical or theoretical technique is completely adequate for determining the discharge of bed load in natural streams and rivers.

The placement of any type of bed load sampler onto a bed must alter the local flow pattern and movement of sediment to some extent. The degree of disturbance a sampler will cause in local conditions is dependent on many things; among them are the shape and size of the sampler, the local flow velocity, the characteristics of the bed-material sediment, and the presence or absence of bed forms. The degree to which the sampler affects the local flow conditions will be reflected in the efficiency of the sampler in collecting samples of the bed load. To estimate the relation between the sampled rate and the true rate, the sampler will need to be calibrated. The calibration of a sampler is plagued by the problem of comparing the amount of sediment collected by the sampler to the undisturbed bed load movement that would have occurred if the sampler had not been in place (Einstein 1937). Due to the extreme variability of bed load transport processes this is an extremely difficult problem to solve and persists to this day.

5.4.1 Types of Bed Load Samplers

Over the past 100 years, several types of bed load samplers have been developed by researchers at a variety of locations. These samplers may be generalized into three types: samplers installed into the bed of a channel (pit and trough samplers), manually operated portable samplers, and noninvasive samplers. Each of these sampler types has its use in the sampling of bed load. Perhaps the most accurate of these three types are the pit or trough samplers; however, the difficulty and high cost of their installation and servicing preclude their use in many studies. Portable samplers have the advantage of low setup costs, but personnel must be on site continuously during sample collection, sampler deployment may be difficult, and the number of samples needed to characterize temporal and spatial variability is usually large. Also, no generally accepted method has been developed for calibrating portable samplers. Samplers that use noninvasive techniques show much promise, but have not been developed to the point where they can be widely useful for the measurement of bed load transport.

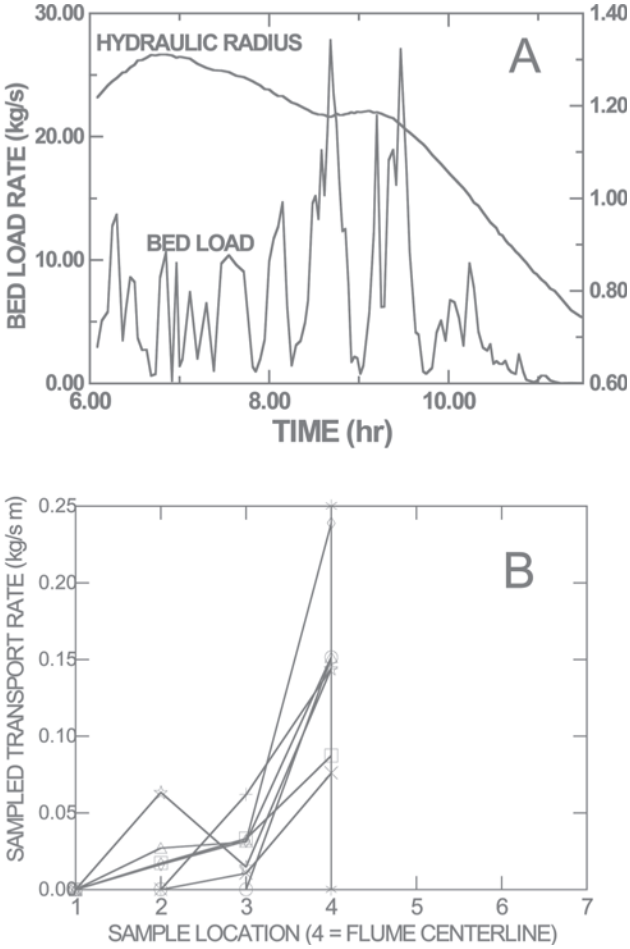

Fig. 5-20. (A) Bed load transport rate and flow changes with time, Goodwin Creek, station 2. Samples were collected in the center of the structure during runoff event on 11/08/86 (Kuhnle et al. 1989). (B) Plots of lateral sets of samples collected at Goodwin Creek, station 2, during 02/27/87 transport event. The distance between sample locations is 1.5 m. Lateral samples were collected on one side of the structure centerline (Kuhnle 1992b).

5.4.1.1 Manually Operated Portable Samplers Bed load samplers of this type have been developed and used in many countries to determine rates of bed load movement for sediment varying in size from 1 to 300 mm (FIARBC 1940; Hubbell 1964). The development of bed load samplers has often been associated with individual project studies. These samplers have been classified as to their type of construction and principle of operation, mainly as basket samplers, pan or tray samplers, and pressure-difference samplers (Hubbell 1964). Basket and pan samplers cause an increased resistance to flow through the sampler and water velocity in the sampler is therefore lower than in the free stream. This reduction in flow velocity in the sampler reduces the shear stress and the rate of bed load transport in the vicinity of the sampler, with the result that some particles accumulate at the entrance to

the sampler and others are diverted away. The pressure-difference type samplers are designed to eliminate the reduction in water velocity in the sampler, and thus any reduction in the rate of bed load movement at the entrance to the sampler. The velocity in the sampler is made equal to that of the flow by creating a decrease in pressure at the exit of the sampler nozzle by having a gradual increase in area. Pressure-difference samplers generally have a hydraulic efficiency (ratio of flow velocity in sampler to flow velocity for same location without sampler) of about one or greater (Hubbell et al. 1985). One key parameter in the design of pressure-difference samplers is to make the hydraulic efficiency large enough to prevent sediment from depositing in front of the sampler, but not so large as to cause scouring of the bed and oversampling.

For a bed load sampler to operate correctly, it should be used within the range of conditions for which it was designed. The most restrictive of these design elements include bed load particle sizes as compared to the inlet opening of the sampler; bed load rates as compared to the size of the catchment volume; water depth according to whether the sampler was designed for wading or cable suspension; and flow velocities as related to resistance of the sampler in the flow and range of calibration velocities. Only a few of these types of samplers have been calibrated and there is no widespread agreement on the methodology to use to calibrate a bed load sampler (Engel and Lau 1980; Hubbell et al. 1985; Thomas and Lewis 1993b). Calibrations of these samplers indicate a mean efficiency of about 45% for basket or pan type and vary from 80% to 180% for pressure-difference types. These efficiencies may vary with transport rate, sediment size, and sediment gradation.

Descriptions of some pressure-difference bed load samplers that are in current use are presented in Table 5-3. These include the Federal Interagency Sedimentation Project BL-84 (Fig. 5-21) (Davis 2005); the 7.62-cm-square Helley-Smith (Helley and Smith 1971); the 15.24-cm-square Helley-Smith; the Toutle River-2 (Childers 1992); the Elwha River (Childers et al. 2000); the Delft-Nile sampler (Van Rijn and Gaweesh 1992); and the BTMA-2 (Duizendstra 1999). Typical problems with operation of pressure-difference samplers include the following (Van Rijn and Gaweesh 1992):

1. The initial effect: Sand particles of the bed may be stirred up and trapped when the instrument is placed on the bed (oversampling).
2. The gap effect: A gap between the bed and the sampler mouth may be present initially or generated at a later stage under the mouth of the sampler due to migrating ripples or erosion processes (undersampling).
3. The blocking effect: Blocking of the bag material by sand, silt, clay particles, and organic materials will reduce the hydraulic coefficient and thus the sampling efficiency (undersampling).
4. The scooping effect: The instrument may drift downstream during lowering to the bed, and may be pulled forward (scoop) over the bed when raised again so that it acts as a grab sampler (oversampling).

Five types of conditions occurring during collection of bed load samples with the Delft-Nile sampler were recognized by Gaweesh and Van Rijn (1994) using a video camera mounted near the sampler on the Nile and Rhine Rivers. Two of these types of conditions (the gap effect and scooping effect) were found to result in either significant under- or oversampling by the Delft-Nile sampler. Gaweesh and Van Rijn (1994) recommended removing the highest and lowest 10% of the collected samples based on the fact that these two types each occurred approximately 10% of the time. This technique was found to improve the results of their field bed load sampling.

Table 5-3 Portable Bed Load Samplers

Sampler name	Sediment sizes (mm)	Entrance width (m)	Entrance height (m)	Type of sampler	Hydraulic efficiency (%)	Sampling efficiency (%)	Capacity ofs ampler (kg)
FISP BL-84[a]	1–38	0.076	0.076	c, w	135[b]	100–140[b–e]	10
Helley-Smith[f]	1–38	0.076	0.076	c, w	154[g]	100–180[d,e,h,i]	10
Helley-Smith[f]	1–76	0.152	0.152	c, w	154[g]	100–180[d,e,h,i]	10
Toutle River-2[e]	1–150	0.305	0.152	c	140[b]	80–116[b,c,e]	60
Elwha River[j]	1–100	0.203	0.102	c, w	140[b]	80–116[b,c,e]	30
Delft-Nile[k]	0.25–0.85	0.096	0.055	c	100[k]	120–140[k]	24
BTMA-2[l]	0.5–150	0.30	0.30	c	100[est]	unknown	300

Note: est, estimated.

[a]Hubbell et al. 1985; [b]Hubbell et al. 1987; [c]Hubbell and Stevens 1986; [d]Childers 1991; [e]Childers 1992; [f]Helley and Smith 1971; [g]Druffel et al. 1976; [h]Emmett 1980; [i]Huanjin 1991; [j]Childers et al. 2000; [k]Van Rijn and Gaweesh 1992; [l]Duizendstra in press.

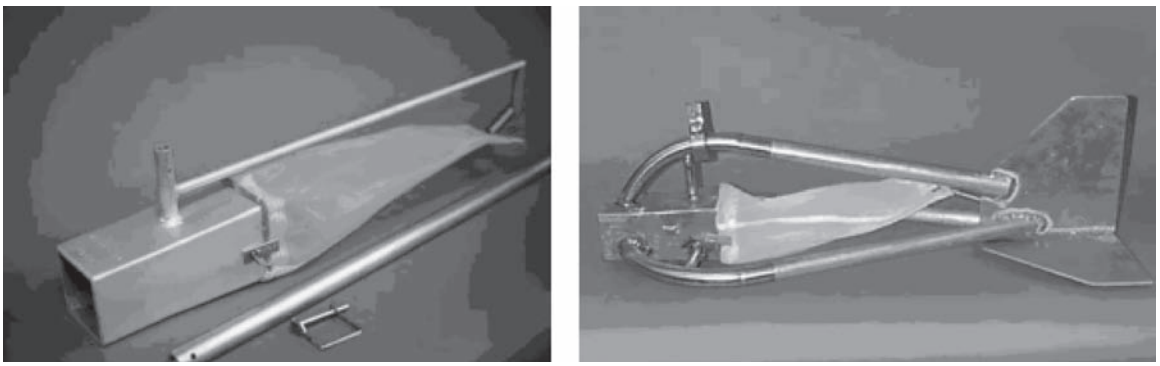

Fig. 5-21. Photograph of Federal Interagency Sedimentation Project BL-84 samplers. (A) Hand version: BLH-84. (B) Cable-mounted version: BL-84. The ratio of the inlet area to the outlet area is 1.40 on this sampler.

The orientation of the Helley-Smith sampler with respect to the mean flow velocity vector has also been found by Gaudet et al. (1994) to affect the efficiency of sediment sampling. If the sampler was misaligned as little as 10° from the mean flow velocity vector, significant decreases in sediment sampler efficiency were found by Gaudet et al. (1994). Although misalignment may not be a problem in many situations, sampling in complex flow fields could be affected by this problem.

These potential problems with pressure-difference samplers have been recognized by researchers over the years and design and sampling procedure changes have been made to correct for these problems. Stay lines have been used successfully by several researchers to aid in controlling the sampler in high-velocity conditions (Childers 1992). Samplers with flexible bottoms, guide fins, larger collection bags (Bunte et al. 2001), bottom sensors, and underwater video cameras (Dixon and Ryan 2001) have been designed to solve these problems. The BTMA-2 sampler (Duizendstra 1999) is perhaps the most advanced system in use to date to avoid the problems outlined above that occur with pressure-difference samplers.

5.4.1.1.1 Manually Operated Portable Sampler Calibrations Most types of portable samplers cause some degree of disruption to the flow and some degree of disruption to the transport of bed material as well. Unless steps are taken in portable sampler design to increase the flow through the sampler, sediment will tend to be deposited in front of or inside the sampler orifice and low and erratic sampling efficiencies will result. To improve the sediment-sampling efficiency of portable samplers, pressure difference nozzles were designed (Helley and Smith 1971) to increase the flow of water through the sampler. Thus hydraulic efficiency in pressure difference samplers is designed to be equal to or greater than 100% (Druffel et al. 1976). Hydraulic efficiencies are readily measured in laboratory flumes, however, sediment-sampling efficiencies are much more difficult to measure.

Unless a sampler works perfectly and collects an unbiased sample of the sediment in transport, a calibration coefficient is needed to correct the sampled rate to the actual rate.

$$q_b = \alpha c_s \tag{5-10}$$

where

q_b = actual bed load transport rate;
c_s = sampled transport rate; and
α = calibration coefficient.

Equation (5-10) assumes that the actual bed load rate is a linear function of the sampled rate. In general,

$$q_b = f(c_s) \tag{5-11}$$

where q_b is an unknown function of c_s. If q_b is not a linear function of c_s, their mean values will not satisfy equation (5-10) and the use of means will lead to erroneous results (de Vries 1973). This complicates considerably the calibration of bed load samplers. One proposed solution to this problem is to compare the actual and sampled bed load transport rates that occur for the same probability (Einstein 1937; de Vries 1973; Hubbell et al. 1985). This procedure was termed "probability matching" by Hubbell et al. (1985) and was used to define composite calibration curves for several portable samplers. The results from the probability matching procedure were disputed by Thomas and Lewis (1993b). As an alternate method of analysis, Thomas and Lewis (1993b) transformed the sampler and bed load trap data from Hubbell et al. (1985) to obtain a linear relation between the two variables. Their results from this transformed data indicated that pressure-difference samplers with higher nozzle ratios (3.22) collected more sediment than the ones with lower ratios (1.4), and that samplers with smaller orifices performed more uniformly than ones with larger orifices (0.076 m square versus 0.152 m square).

Other researchers have worked on the problem of portable bed load sampler calibration (Emmett 1980; Engel and Lau 1980; Ryan and Porth 1999). Engel and Lau (1980) developed a dimensional analysis technique and used it with data collected from a scale model of a basket sampler to calculate a calibration curve for the full-sized basket sampler used by the Water Survey of Canada. The efficiency of the

basket sampler was found to vary from about 50% at low trap numbers (low transport rates) to about 25% at high trap numbers. Emmett (1980) calculated calibration curves for the original version of the Helley-Smith sampler (Helley and Smith 1971), using data collected on the East Fork River. Bed load transport data collected using the trough conveyor-belt sampler on the East Fork River, when compared to data collected with the Helley-Smith sampler, yielded efficiencies near 100% for grain sizes from 0.5 to 16 mm. Ryan and Porth (1999) compared data collected from three pressure difference samplers, the original Helley-Smith sampler, the BL-84, and an original design Helley-Smith sampler constructed of sheet metal. The data from the three samplers were compared to data on bed load obtained from surveying sediment accumulation in a weir pond. Calculations of annual bed load for all three samplers (Ryan and Porth 1999) were well within an order of magnitude of the accumulations measured in the weir pond. Studies comparing different portable samplers to each other have been made by Childers et al. (1989); Childers (1991; 1992); Gray et al. (1991); and Pitlick (1988). These studies demonstrate that relatively minor differences in sampler design can cause large differences in the size of the collected samples. The original version of the Helley-Smith sampler has been shown in one study to have an sediment efficiency of nearly 100% (Emmett 1980) for one set of conditions and to oversample for another set of conditions (Hubbell et al. 1985). Gray et al. (1991) found that the original Helley-Smith sampler tended to collect more material at high sediment transport rates and collect less material at lower rates than an early version of the BL-84 bed load sampler. The sometimes conflicting results, however, serve to underline the complexity of the transport of bed load by streams and rivers and to highlight the importance of the conditions of the streams in which the measurements are collected.

5.4.1.2 Pit and Trough Samplers One of the most accurate ways to sample bed load is through the use of carefully designed and installed pit or trough samplers (Hubbell 1964; Poreh et al. 1970). These samplers are installed in the bed of the channel by burying the sampler so that the top is flush with the surface of the bed. Pit and trough samplers range from simple containers to complicated weighing and recording instruments. Basic ones consist of small containers that catch and retain all bed load sediment that is transported to the sampler (e.g., Waslenchuk 1976; Murphy and Amin 1979; Church et al. 1991; Wilcock et al. 1996). Samplers of this type capture the total or minimum amount (if the sampler is filled in an unknown time) of sediment transported as bed load during the measurement period. For studies in which information on the beginning of bed load transport and the rates of transport during the measurement periods are needed, recording pit samplers (Fig. 5-22) have been designed and used successfully (Reid et al. 1980; Lewis 1991; Kuhnle 1992; Laronne et al. 1992).

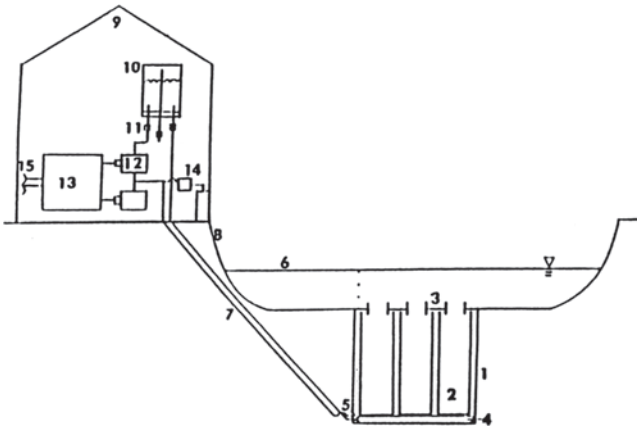

Fig. 5-22. Schematic cross section of box sampler: (1) outer box, (2) inner box, (3) slotted cover, (4) pressure pillow, (5) bubble tube outlet, (6) water surface, (7) tubes from bubbler and pillow, (8) stream bank, (9) instrument house, (10) air trap, (11) valves, (12) pressure transducer, (13) power supply, (14) bubble gauge, and (15) wires to remote telemetry system (Kuhnle 1991).

For sand-bedded channels, experiments have shown that samplers having slot widths of 100 to 200 grain diameters collect nearly 100% of the bed load (Einstein 1944). Sand particles often move by making brief excursions into the flowing water and then falling back to the bed. The specification of slot widths for sand grains was determined from the probable lengths of these excursions. As particle sizes increase into the gravel size range, transport occurs with grains spending progressively more time in contact with the bed (gravel-size grains usually slide or roll along the bed) and the parameter for slot widths from Einstein is no longer applicable. Poreh et al. (1970) have shown in a laboratory flume that when the ratio of the stream parallel slot length to the sediment grain diameter is about 35 for grain sizes between 1.88 and 4.5 mm, the efficiency of a channel-wide pit sampler approaches 100%. Poreh et al. (1970) also recommend using an unerodable apron upstream of the sampler to reduce the effect of bed forms on sampler performance. Slot lengths parallel to flow should not be made too much larger than necessary as secondary flows in the trap increase with slot length (Ethembabaogla 1978) and may cause smaller grains moving as bed load to be excluded from the trap (Wilcock et al. 1996). Some pit samplers (Kuhnle 1992) have incorporated flow transverse vanes to break up secondary flows in the sampler. Another potential problem with pit traps with widths narrower than the channel width is the lateral entry of sediment into the slot. Emmett (1980) calculated that when only part of the slot was used to sample on the East Fork River, bed load transport was consistently overestimated by a factor of 1.3 compared to using the whole width of the slot. Lewis (1991) described the use of low-profile fences along the top of the sampler cover to minimize the possibility of lateral entry of sediment into the sampler.

Most pit samplers have been designed to be installed permanently at one location. Installation of pit samplers requires access to the streambed. After sediment transport events, pit samplers usually must be emptied manually or with a slurry pump. These requirements favor installations on streams that either are ephemeral or drop to very low base flows between sediment transport events (Reid et al. 1980; Lewis 1991; Kuhnle 1992; Laronne et al. 1992). More complicated pit-type bed load samplers with systems to continuously remove the accumulated bed load sediment have been constructed on larger streams; however, the cost of the installation and servicing rises considerably (Enoree River, FIARBC 1940; East Fork River, Leopold and Emmett 1976; Emmett 1980).

Einstein (1944) and Hubbell (1964) have described a semiportable pit sampler for use in sand-bedded streams that automatically dredges a place in the bed of the stream for the sediment trap. Following installation of the sediment trap, a valve is thrown and the dredging pump is used to continuously remove the sediment as it accumulates in the trap. The sediment and water slurry is then routed to a weighing tank and then returned to the stream. Some preliminary investigations have been conducted with a sampler of this type by Einstein (1944) and Hubbell (1964). The sampler would be restricted to streams with sand beds and low flow velocities. For most streams, several of these samplers would need to be used simultaneously to assure adequate coverage of the cross section.

5.4.1.3 Vortex Tube Bed Load Samplers Vortex tubes have been used to sample bed load successfully at several locations (Milhous 1973; Hayward and Sutherland 1974; O'Leary and Beschta 1981; Tacconi and Billi 1987). The design of these samplers was based on a vortex tube sand trap that was designed for excluding unwanted bed load sediment from irrigation and other canals (Robinson 1962). These samplers consist of a 45º diagonal slot in a concrete broad crested weir constructed across the channel at the measurement site (Fig. 5-23). A vortex is generated in the diagonal slot and from 5% to 15% of the flow carries the bed load sediment to a trap on the side of the channel. The sediment is then weighed and sampled and returned to the stream downstream of the weir. Robinson (1962) reports that when designed correctly, such samplers remove approximately 80% of the sediment with size greater than 0.5 mm from the stream. The efficiency of these samplers for smaller and larger grain sizes would be expected to be lesser and greater respectively. Milhous (1973) estimates that the overall efficiency of the vortex tube sampler on Oak Creek to range from 85% for low transport rates to 95% for higher sediment transport rates with all grains larger than 4.76 mm trapped.

Vortex tube samplers have been shown to be effective bed load samplers on small gravel-bed streams. These samplers have many of the same disadvantages, however, as pit samplers. They are not portable and the initial construction cost is high. One important advantage that vortex tube samplers have over pit samplers is that the sediment is delivered to the side of the stream and does not need to be removed from the sampler after the transport event. Therefore, the sampler will not fill before the transport event is completed.

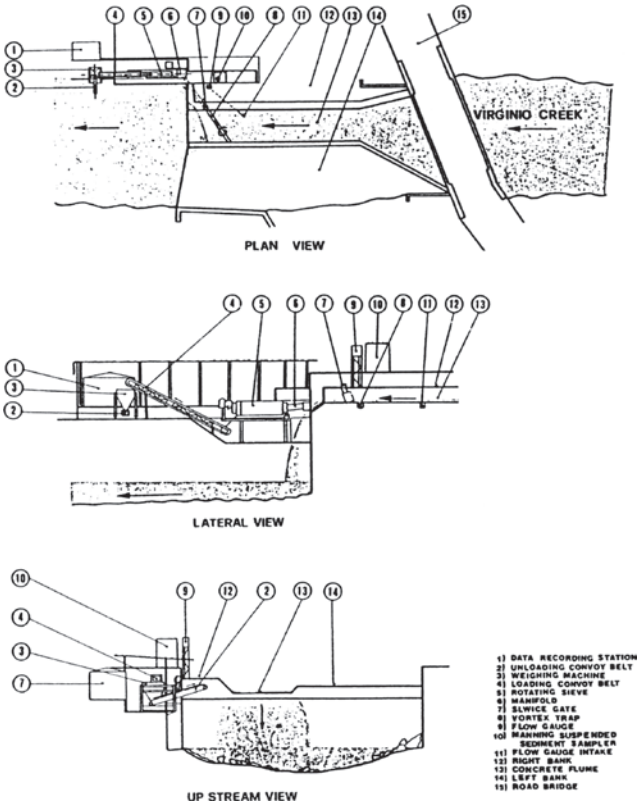

Fig. 5-23. Sketch of bed load measuring station using a vortex-tube trap on Virginio Creek (from Tacconi and Billi 1987, p. 586). Copyright 1987, John Wiley and Sons Ltd. Reproduced with permission.

5.4.1.4 Other Methods Several other methods have been used experimentally to measure the rate of bed load transport. These methods include particle imaging (Drake et al. 1988), bed form tracking (Simons et al. 1965; Willis 1968; Willis and Kennedy 1977; Engel and Lau 1980; Kuhnle and Derrow 1994; Garcia 1998; Tate and Rubin 1998; Dinehart 2001; Rubin et al. 2001), magnetic tracking (Reid et al. 1984; Carling et al. 1993), and acoustic techniques (Thorne et al. 1989). Although these methods show varying degrees of promise for improved samplers, none has been developed to the extent that it can be considered a standard technique for sampling bed load in streams and rivers. Such things as the necessity of clear water, bed forms, magnetic bed material, or the calibration of sediment generated noise all currently combine to limit the extent that the above techniques will be usable.

5.4.1.5 Summary A variety of sampler types are available to sample the bed loads of streams and rivers. It is clear that no one sampler type is generally superior to the others for the collection of bed load data. All of the types reviewed above have advantages and disadvantages in different situations. Pit

and trough samplers have been shown to operate reliably on relatively small gravel-bed streams; however, their use on larger streams and rivers would be very difficult. Portable samplers are generally inexpensive to acquire, but may be expensive to operate and suffer from uncertain calibrations. Bed load samplers that use acoustic, optical, magnetic, bed form tracking, or other emerging technologies have shown a great deal of promise, but have not been proven to be reliable to date except under controlled laboratory conditions.

5.4.2 Bed Load Discharge Measurements

Measurement of bed load is difficult because it is highly variable in both space and time (Ehrenberger 1932; Hubbell 1964; Leopold and Emmett 1976; Carey 1985; Hubbell 1987; Whiting et al. 1988; Dinehart 1989; Kuhnle et al. 1989; Wathen et al. 1995; Powell et al. 1998). Bed load generally varies greatly both longitudinally along the channel and transversely across a cross section. These variations are caused by several factors and are difficult to predict. Causes of the variations include the presence of dunes or other bed forms; locally varying shear stress due to bed topography, secondary flow, or turbulence changes; varying supply of bed material from upstream sources; and changes in bed surface grain sizes. The design of bed load sampling needs to account for the spatial and temporal variability inherent in the processes of bed load transport. Pit, vortex-tube, or other samplers that sample for long periods of time and encompass a significant portion of the width of a stream cross section integrate the fluctuations in bed load transport rate in a cross section. In many instances time, monetary constraints, or logistics precludes the use of these types of samplers, however. The use of portable samplers that essentially only collect samples at a point for short periods of time is often the only practical way to collect samples of bed load. To effectively use portable samplers, the number and location of the samples collected must be carefully designed to assure sufficient information about the temporal and spatial variability is collected. To accomplish this task, information on the scales of spatial and temporal variability is needed.

Several studies have concentrated on the temporal variability of bed load transport. Carey (1985) and Carey and Hubbell (1986) have shown that a series of 120 bed load samples collected at a point in a sand-bed stream yielded a distribution very similar to that proposed by Hamamori (1962). Hubbell and Stevens (1986) showed that bed load data collected in a large flume at the Saint Anthony Falls Hydraulic Laboratory, as well as bed load data from other researchers, were reasonably well approximated by the Hamamori distribution. Kuhnle (1996) showed that sample durations of several minutes to tens of minutes were required to obtain an adequate estimate of the mean bed load transport rate in laboratory flume experiments. Gomez et al. (1990), using the flume data collected by Hubbell et al. (1987), determined that at-a-point bed load transport samples should cover the movement of at least one primary bed form past the sampling location. Preferably, more than one primary bed form should be covered by the sampling period. Gaweesh and Van Rijn (1994) found that 25 samples should be taken distributed along the bed form length to adequately represent the variability of bed load transport in sand-bed rivers.

Only a limited number of studies have documented spatial variability by collecting bed load samples simultaneously at several locations across a channel (Leopold and Emmett 1976; Hubbell et al. 1987; Powell et al. 1998). Emmett (1980) tested the Helley-Smith sampler using the bed load rates calculated from the East Fork River trough sampler. This study yielded a calibration of the Helley-Smith sampler on the East Fork River and a test of the sampling technique used with the Helley-Smith sampler to arrive at a mean cross-sectional bed load rate. Emmett found that sometimes all or most of the bed load transport occurred in a narrow part of the channel. The location of this high-transport zone was stable on short time scales (hours), but not necessarily for longer periods of time. Emmett (1980) recommended that two sampling traverses should be conducted, each of which should consist of at least 20 equally spaced cross-channel locations, to describe the spatial variation across the channel. It was recommended that spacings between samples range from 0.5 to 15 m apart.

Hubbell and Stevens (1986; Hubbell 1987) generated simulated bed load data that varied in time according to the Hamamori (1962) distribution and assumed several different patterns of lateral variation in bed load transport. The generated bed load record was "sampled" using traverses of 4 and 20 equal positions across the cross section. In cross sections in which the lateral variability was moderately nonuniform, the numbers of samples needed to predict the mean transport rate to within 30% were comparable for sampling designs that collected samples at 4 and 20 positions in each transect. For nonuniform lateral distributions the number of samples required for the 4-position transect was approximately double that required for the 20-position.

Gaweesh and Van Rijn (1994) determined the number of positions required to obtain relative errors in bed load transport rates less than 20% over the width of the Nile River at several cross sections. This analysis was based on measured flow velocities on the cross sections and applying the transport formula of Engelund and Hansen (1967) at each potential sampled position. Gaweesh and Van Rijn (1994) concluded that irregular cross sections should be divided into seven subsections and 25 samples should be collected distributed equally along the bed form length at each subsection to obtain an overall relative error of 20%.

Gomez and Troutman (1997) conducted a study in which process errors due to different sampling techniques were evaluated for simulated bed load records that represented the temporal and lateral variations that would be expected for dune beds. Gomez and Troutman found that four or five sampling traverses, and collection of 20 to 40 samples at a rate of five

or six samples per hour, were necessary to adequately sample the bed load of a hypothetical stream. These samples would be collected over a period of 3 to 8 h, which would allow a number of bed forms to pass through the sampling section.

The accuracy associated with the collection of bed load transport on a large sand-gravel-bed river was calculated by Kleinhans and Ten Brinke (2001). They evaluated the uncertainty of the integrated transport for bed load by assuming the transport samples were normally distributed without measurement and prediction errors. This evaluation was applied to sediment transport data collected using modified Helley-Smith samplers on the Waal River in the Netherlands. Their calculations yielded an uncertainty of 10% to 20% in integrated bed load transport, using five subsections and 30 samples/subsection. A major problem identified in this study was the long periods of time required for the collection of these samples (3.5 days) and the changes in discharge that occurred over that time.

Studies that yield guidance on the numbers of traverses and samples that are required to reliably calculate the mean bed load rate are useful, but suffer from several shortcomings. Perhaps most critical of these shortcomings is the fact that the time and length scales of temporal and lateral variability in streams are poorly known and generally vary with time at a given location and from stream to stream. To design an adequate sampling strategy these time and length scales must be known at least approximately before the sampling procedure is defined. In the recommendations previously reviewed above (Emmett 1980; Hubbell and Stevens 1986; Gaweesh and Van Rijn 1994; Gomez and Troutman 1997; Kleinhans and Ten Brinke 2001), the amount of time required to collect the recommended number of samples is too long for many streams. Flow in many streams and rivers is not steady for periods of hours to days. For streams in which variable flow is the norm, portable samplers will not be practical unless many flow events can be sampled. Edwards and Glysson (1999) concluded that no one sampling protocol can be used at all stations. They recommend that to the extent possible, a sampling protocol should be derived for each site where bed load is to be sampled. Initial samples collected can provide information to serve as a basis for developing the sampling plan.

REFERENCES

Adams, J. (1979). "Gravel Size Analysis from Photographs." *J. Hydr. Div., ASCE*, 105(10), 1247–1255.

Agrawal, Y. C., and Pottsmith, H. C. (2001). "Laser sensors for monitoring sediments: Capabilities and limitations, a survey." *Proceedings of the 7th Federal Interagency Sedimentation Conference,* March 25–29, 2001, Reno, Nevada, Vol. I, pp. III-144–III-151.

ASTM International (1997). *Terminology for fluvial sediment:* Active standard *D4410-98,* ASTM International West Consho hocken, Pa.

Bent, G. C., Gray, J. R., Smith, K. P., and Glysson, G. D. (2001). "A synopsis of technical issues for monitoring sediment in highway and urban runoff." *U.S. Geological Survey Open-File Report 00-497*, U.S. Geological Survey, Reston, Va.; also <http://ma.water.usgs.gov/FHWA/NDAMSP1.html>.

Bluck, B. J. (1982). "Texture of gravel bars in braided streams." *Gravel bed rivers. Fluvial processes, engineering and management*, R. D. Hey, J. C. Bathurst, and C. R. Thorne, eds., Wiley, London, 339–355.

Bray, D. I. (1972). "Generalized regime-type analysis of Alberta rivers." PhD thesis, Department of Civil Engineering, University of Alberta, Edmonton, Alta., Canada.

Bunte, K., and Abt, S. R. (2001). "Sampling surface and subsurface particle-size distributions in wadable gravel- and cobble-bed streams for analyses in sediment transport, hydraulics, and streambed monitoring." *General Technical Report RMRS-GTR-74,* USDA Forest Service, Fort Collins, Colo.

Bunte, K. I., Abt, S. R., Potyondy, J. P. (2001). "Portable bedload traps with high sampling intensity for representative sampling of gravel transport in wadable mountain streams." *Proceedings of the Seventh Federal Interagency Sedimentation Conference,* Reno, Nev., III-24–III-31.

Burdick, R. K., and Graybill, F. A. (1992). *Confidence intervals on variance components,* Marcel Dekker, New York.

Byrne, M. J., and Patiño, E. (2001). "Feasibility of using acoustic and optical backscatter instruments for estimating total suspended solids concentration in estuarine environments." *Proceedings of the 7th Federal Interagency Sedimentation Conference, March* 25–29, 2001, Reno, Nevada, Vol. I, pp. III-135–III-138.

Capel, P. D., and Larsen, S. J. (1996). "Evaluation of selected information on splitting devices for water samples." *U.S. Geological Survey Water-Resources Investigations Report 95-4141*, U.S. Geological Survey, Reston, Va.

Capel, P. D., and Nacionales, F. (1995). "Precision of a splitting device for water samples." *U.S. Geological Survey Open-File Report 95-293*, U.S. Geological Survey, Reston, Va.

Carey, W. P. (1985). "Variability in measured bedload-transport rates." *Water Resources Bulletin,* 21(1), 39–48.

Carey, W. P., and Hubbell, D. W. (1986). "Probability distributions for bedload transport." *Proceedings of the 4th Federal Interagency Sedimentation Conference,* Subcommittee on Sedimentation, Interagency Advisory Committee on Water Data, Las Vegas, Nev., 4-131–4-140.

Carling, P. A., Williams, J. J., Glaister, M. G., and Orr, H. G. (1993). "Particle dynamics and gravel-bed adjustments." *Final Technical Report DAJA45-90-C-0006*, European Research Office of the Army, London.

Childers, D. (1991). "Sampling differences between the Helley-Smith and BL-84 bedload samplers." *Fifth Federal Interagency Sedimentation Conference,* Subcommittee on Sedimentation, Interagency Advisory Committee on Water Data, Las Vegas, Nev., 6-31–6-38.

Childers, D. (1992). "Field comparisons of six pressure-difference bedload samplers in high-energy flow." *Report 92-4068,* U.S. Geological Survey Water Resources Investigations, Reston, Va.

Childers, D., Hanjin, G., and Gangyan, Z. (1989). "Field comparisons of bedload samplers from the United States of America and People's Republic of China." *Fourth International Symposium on River Sedimentation,* Science Press, Beijing, China, 1309–1316.

Childers, D., Kresch, D. L., Gustafson, S. A., Randle, T. J., Melena, J. T., Cluer, B. (2000). "Hydrologic data collected during the 1994 Lake Mills drawdown experiment, Elwha River, Washington." *Water Resources Investigation Report 99-4215,* U.S. Geological Survey, Reston, Va.

Christiansen, V. G., Ziegler, A. C., and Xiaodong, J. (2001). "Continuous turbidity monitoring and regression analysis to estimate total suspended solids and fecal coliform bacteria loads in real time." *Proceedings of the 7th Federal Interagency Sedimentation Conference,* March 25–29, 2001, Reno, Nevada, Vol. I, pp. III-94–III-101.

Church, M., and Kellerhals, R. (1978). "On the statistics of grain size variation along a gravel river." *Can. J. Earth Sci.,* 15, 1151–1160.

Church, M. A., McLean, D. G., and Wolcott, J. F. (1987). "River bed gravels: Sampling and analysis." *Sediment transport in gravel bed rivers,* C. R. Thorne, J. C. Bathurst, and R. D. Hey, eds., Wiley, London, 43–88.

Church, M., Wolcott, J. F., and Fletcher, W. K. (1991). "A test of equal mobility in fluvial sediment transport: behavior of the sand fraction." *Water Resources Research,* 27(11), 2941–2951.

Colby, B. R. (1963). "Fluvial sediments—A summary of source, transportation, deposition, and measurement of sediment transport." *U.S. Geological Survey Bulletin 1181-A*, U.S. Geological Survey, Reston, Va. <http://pubs.er.usgs.gov/usgspubs/b/b1181A>

Crowder, D. W., and Diplas, P. (1997). "Sampling heterogeneous deposits in gravel-bed streams." *J. Hydr. Eng., ASCE,* 123(12), 1106–1117.

Davis, B. E. (2000). "The US D-96: An isokinetic suspended-sediment/water-quality collapsible bag sampler." *Federal Interagency Sedimentation Project Report PP*, Federal Interagency Sedimentation Project, Vicksburg, Miss., USACE Engineer, and Research Development Center; also <http://fisp.wes.army.mil/>.

Davis, B. E. (2005). *A guide to the proper selection and use of federally approved sediment and water-quality samplers.* U.S. Geological Survey Open-File Report 2005-1087, U.S. Geological Survey, Reston, Va. (also published as *Federal Interagency Sedimentation Project Report QQ),* <http://fisp.wes.army.mil/Report%20QQ-Users%20Guide.pdf>(Aug. 12, 2005).

Day, T. J. (1991). "Sediment monitoring in Canada." *Proceedings of the Fifth Federal Interagency Conference,* Subcommittee on Sedimentation of the Interagency Advisory Committee on Water Data, Las Vegas, Nev., Vol. I, pp. 1-24–1-29.

Delesse, A. (1848). "Pour determiner la composition des roches." *Ann. Des Mines*, 13, fourth series, 379.

De Vries, M. (1970). "On accuracy of bed-material sampling." *J. of Hydr. Research,* 8(4), 523–533.

De Vries, M. (1973). "On measuring discharge and sediment transport in rivers." *Publication No. 106,* Delft Hydraulics Laboratory, Delft, the Netherlands.

Dinehart, R. L. (1989). "Dune migration in a steep coarse-bedded stream." *Water Resources Research*, 25(5), 911–923.

Dinehart, R. L. (2001). "Bedform mapping in the Sacramento River." *Proceedings of the Seventh Federal Interagency Sedimentation Conference,* Subcommittee on Sedimentation, Reno, Nev., III-55–III-62.

Diplas, P. (1992). "Discussion of 'Experimental investigation of the effect of mixture properties on transport dynamics.'" *Dynamics of gravel bed rivers,* P. Billi, R. D. Hey, C. R. Thorne, and P. Tacconi, eds., Wiley, Chichester, U.K., 131–135.

Diplas, P. (1994). "Modeling of fine and coarse sediment interaction over alternate bars." *J. of Hydrol.*, 159, 335–351.

Diplas, P., and Crowder, D. (1997). Discussion of "Statistical approach to bed-material surface sampling." *J. Hydr. Eng., ASCE,* 123(9), 823–824.

Diplas, P., and Fripp, J. B. (1992). "Properties of various sediment sampling procedures." *J. Hydr. Eng. ASCE,* 118(7), 955–970.

Diplas, P., and Parker, G. (1992). "Deposition and removal of fines in gravel-bed streams." *Dynamics of gravel-bed rivers,* P. Billi, R. D. Hey, C. R. Thorne, and P. Tacconi, eds., Wiley, Chichester, U.K., 313–329.

Diplas, P., and Sutherland, A. J. (1988). "Sampling techniques of gravel sized sediments." *J. Hydr. Eng., ASCE,* 114(5), 484–501.

Dixon, M., and Ryan, S. (2001). "Using an underwater video camera for observing bed load transport in mountain streams." *Proceedings of the Seventh Federal Interagency Sedimentation Conference,* Subcommittee on Sedimentation, Reno, Nev., P-70–P-73.

Drake, T. G., Dietrich, W. E., Whiting, P. J., Leopold, L. B., and Shreve, R. L. (1988). "Bed load transport of fine gravel observed by motion-picture photography." *Journal of Fluid Mechanics,* 192, 193–217.

Druffel, L., Emmett, W. W., Schneider, V. R., and Skinner, J. V. (1976). "Laboratory hydraulic calibration of the Helley-Smith bedload sediment sampler." *Open File Report, 76–752*, U.S. Geological Survey, Reston, Va.

Duizendstra, H. D. (1999). "Measuring, observing and pattern recognition of sediment transport in an armoured river." *Physics and Chemistry of the Earth,* in press.

Durand, D. (1971). *Stable chaos, an introduction to statistical control,* General Learning Press, Morristown, N.J.

Edwards, T. K., and Glysson, G. D. (1999). "Field methods for measurement of fluvial sediment." *Techniques of water-resources investigations of the U.S. Geological Survey,* Book 3, Applications of Hydraulics, C2, U.S. Geological Survey, Washington, D.C.

Efron, B., and Tibshirani, R. (1991). "Statistical data analysis in the computer age." *Science*, 253, 390–395.

Ehrenberger, R. (1932). "Geschiebemessungen an flüssen mittels auffanggeräten und modellversuche mit letzteren [Detritus measurements in rivers by means of gripping instruments and model experiments with the latter]." Die Wasserwirtschaft, Vienna, Vols. 33, 36 (in German). Translation Minnesota University.

Einstein, A. H. (1937). "Die Eichung des im Rhein verwendeten Geschiebefängers [Calibrating the bed load trap as used in the Rhein]." *Bauzeitung 110(12),* Switzerland. Translation Soil Conservation Service, California Institute of Technology, Pasadena, Calif.

Einstein, A. H. (1944). "Bed-load transportation in Mountain Creek." *Technical Bulletin 55,* Soil Conservation Service, U.S. Department of Agriculture, Washington, D.C.

Emerson, J. D., and Hoaglin, D. C. (1983). "Stem-and-leaf displays." in *Understanding robust and exploratory data analysis,*

D. C. Hoaglin, F. Mosteller, and J. W. Tuckey, eds., Wiley, New York, 7–31.

Emmett, W. W. (1980). "A field calibration of the sediment-trapping characteristics of the Helley-Smith bedload sampler." U.S. Geological Survey Professional Paper 1139, 44 pp, Reston, Va.

Engel, P., and Lau, Y. L. (1980). "Calibration of bed-load samplers." *Journal of the Hydraulics Division*, 106(HY10), 1679–1685.

Engelund, F., and Hansen, E. (1967). *A monograph on sediment transport in alluvial streams.* Teknisk Vorlag, Copenhagen, Denmark.

Ethembabaogla, S. (1978). "Some characteristics of unstable flow past slots." *Journal of the Hydraulics Division,* 104(HY5), 649–666.

Federal Inter-Agency River Basin Committee (FIARBC). (1940). "Equipment used for sampling bed load and bed material." *A Study of Methods Used in Measurement and Analysis of Sediment Loads in Streams*, Report 2, Federal Inter-Agency River Basin Committee, University of Iowa, Iowa City.

Federal Interagency Sedimentation Project (FISP). (1940). "Field practice and equipment used in sampling suspended sediment." *Interagency Report No. 1*, Iowa University Hydraulics Laboratory, Iowa City, Iowa.

Federal Interagency Sedimentation Project (FISP). (1941). "Laboratory investigation of suspended-sediment samplers." *Interagency Report No. 5*, Iowa University Hydraulics Laboratory, Iowa City, Iowa.

Federal Interagency Sedimentation Project (FISP). (1952). "The design of improved types of suspended-sediment samplers." *Interagency Report No. 6*, St. Anthony Falls Hydraulics Laboratory, Minneapolis, Minn.

Federal Interagency Sedimentation Project (FISP). (1961). "The single-stage sampler for suspended sediment." *Interagency Report No. 13*, St. Anthony Falls Hydraulics Laboratory, Minneapolis, Minn.

Federal Interagency Sedimentation Project (FISP). (1963). "Determination of fluvial sediment discharge." *Interagency Report No. 14*, St. Anthony Falls Hydraulics Laboratory, Minneapolis, Minn.

Federal Interagency Sedimentation Project (FISP). (1981). "Test and design of automatic fluvial suspended-sediment samplers." *Interagency Report W*, St. Anthony Falls Hydraulics Laboratory, Minneapolis, Minn.

Federal Interagency Sedimentation Project (FISP). (2000). "Federal Interagency Sedimentation Project home page." <http://fisp.wes.army.mil/>(June 28, 2000).

Federal Interagency Sedimentation Project (FISP). (2001). "US VTP-99 vertical transit pacer." <http://fisp.wes.army.mil/Catalog%20Page%20US%20VTP-99.htm>(December 28, 2001).

Federal Interagency Sedimentation Project (FISP). (2002). "US SS-1 Fluoropolymer churn sample splitter." <http://fisp.wes.army.mil/Catalog%20Page%20US%20SS-1.htm> (March 26, 2002).

Ferguson, R. I., and Paola, C. (1997). "Bias and precision of percentiles of bulk grain size distributions." *Earth Surface Processes and Landforms,* 22, 1061–1077.

Folk, R. L. (1974). *Petrology of sedimentary rocks,* Hemphill Publishing Company, Austin, Tex.; also <http://www.lib.utexas.edu/geo/FolkReady/>.

Fripp, J. B., and Diplas, P. (1993). "Surface sampling in gravel streams." *J. Hydr. Eng. ASCE*, 119(4), 473–490.

Gale, S. J., and Hoare, P. G. (1994). "Reply: Bulk sampling of coarse clastic sediments for particle size analysis." *Earth Surface Processes and Landforms,* 19, 263–268.

Garcia, M. H. (1998). "Bed-image velocimetry: A technique for measuring bedload transport in large alluvial rivers." *Proceedings of the Federal Interagency Workshop, Sediment Technology for the 21st Century,* U.S. Geological Survey, St. Petersburg, Fla.

Gartner, J. W., and Cheng, R. T. (2001). "The promises and pitfalls of estimating total suspended solids based on backscatter intensity from acoustic Doppler current profile." *Proceedings of the 7th Federal Interagency Sedimentation Conference,* March 25–29, 2001, Reno, Nevada, Vol. I, pp. III-119–III-126.

Gaudet, J. M., Roy, A. G., and Best, J. L. (1994). "Effect of orientation and size of Helley-Smith sampler on its efficiency." *Journal of Hydraulic Engineering*, 120(6), 758–766.

Gaweesh, M. T. K., and Van Rijn, L. C. (1994). "Bed-load sampling in sand-bed rivers." *Journal of Hydraulic Engineering,* 120(12), 1364–1384.

Gilbert, R. O. (1987). *Statistical methods for environmental pollution monitoring,* Wiley, New York.

Glysson, G. D. (1989a). "100 years of sedimentation study by the USGS." *Proceedings of the International Symposium, Sediment Transport Modeling,* Sam S. Y. Wang, ed., ASCE, Reston, Va., 260–265.

Glysson, G. D. (1989b). "Criteria for a sediment data set." *Proceedings of the International Symposium on Sediment Transport Modeling*, Hydraulics Division, ASCE, Reston, Va., pp. 1–7.

Glysson, G. D., and Gray, J. R. (1997). "Coordination and standardization of federal sedimentation activities." *Proceedings of the U.S. Geological Survey Sediment Workshop, "Expanding Sediment Research Capabilities in Today's USGS,"* Reston, Virginia, and Harpers Ferry, West Virginia, February 4–7, 1997, <http://water.usgs.gov/osw/techniques/workshop/glysson.html>.

Glysson, G. D., Gray, J. R., and Conge, L. M. (2000). "Adjustment of total suspended solids data for use in sediment studies." *Proceedings of the ASCE's 2000 Joint Conference on Water Resources Engineering and Water Resources Planning and Management,* ASCE, Reston, Va., <http://water.usgs.gov/osw/pubs/ASCEGlysson.pdf>(Aug. 16, 2005).

Glysson, G. D., Gray, J. R., and Schwarz, G. E. (2001). "A comparison of load estimates using total suspended solids and suspended-sediment concentration data." *Proceedings of the ASCE World Water & Environmental Resources Congress,* ASCE, Reston, Va., <http://water.usgs.gov/osw/pubs/TSS_Orlando.pdf>(Aug. 16, 2005).

Gomez, B., and Church, M. (1989). "An assessment of bed load sediment transport formulae for gravel bed rivers." *Water Resources Research,* 25(6), 1161–1186.

Gomez, B., Hubbell, D. W., and Stevens, H. H., Jr. (1990). "At-a-point bed load sampling in the presence of dunes." *Water Resources Research,* 26(11), 2717–2731.

Gomez, B., and Troutman, B. M. (1997). "Evaluation of process errors in bed load sampling using a dune model." *Water Resources Research,* 33(10), 2387–2398.

Goodman, L. A. (1965). "On simultaneous confidence intervals for multinomial proportions." *Technometrics,* 7(2), 247–254.

Gray, J. R., and Fisk, G. G. (1992). "Monitoring radionuclide and suspended-sediment transport in the Little Colorado River basin, Arizona and New Mexico, USA." *Erosion and sediment transport monitoring programmes in river basins.* IAHS Publication No. 210. International Association of Hydrological Sciences, Wallingford, U.K. 505–516.

Gray, J. R., and Schmidt, L. (1998). *Sediment technology for the 21st century.* U.S. Geological Survey <http://water.usgs.gov/osw/techniques/sedtech21/index.html>.

Gray, J. R., Glysson, G. D., Turcios, L. M., and Schwarz, G. E. (2000). "Comparability of total suspended solids and suspended-sediment concentration data." *U.S. Geological Survey Water-Resources Investigations Report 00-4191,* U.S. Geological Survey, Reston, Va.; also <http://water.usgs.gov/osw/pubs/WRIR00-4191.pdf>.

Gray, J. R., Mellis, T. S., Patiño, E., Gooding, D. J., Topping, D. J., Larsen, M. C., and Rasmussen, P. P. (2005). "U.S. Geological Survey suspended-sediment surrogate research on optic, acoustic, and pressure-difference technologies." *Proceedings of the Federal Interagency Sediment Monitoring Instrument and Analysis Workshop, September 9–11, 2003, Flagstaff, Arizona,* J. R. Gray, ed., U.S. Geological Survey Circular 1272, <http://water.usgs.gov/osw/techniques/sediment/sedsurrogate-2003workshop/list of papers.html>(Aug. 4, 2005).

Gray, J. R., Webb, R. H., and Hyndman, D. W. (1991). "Low-flow sediment transport in the Colorado River." *Fifth Federal Interagency Sedimentation Conference*, Subcommittee on Sedimentation, Interagency Advisory Committee on Water Data, Las Vegas, Nev., 4-63–4-71.

Guy, H. P. (1969). "Laboratory theory and methods for sediment analysis." *U.S. Geological Survey Techniques of Water-Resources Investigations, book 3, chapter C1*, U.S. Geological Survey, Reston, Va.

Guy, H. P. (1970). "Fluvial sediment concepts." *U.S. Geological Survey Techniques of Water-Resources Investigations, book 3, chapter C1*, U.S. Geological Survey, Reston, Va. <http://pubs.er.usgs.gov/usgspubs/twri/twri03C1>

Hamamori, A. (1962). "A theoretical investigation on the fluctuation of bedload transport." Delft Hydraulics Laboratory Report R4, Delft, the Netherlands.

Hassan, M. A., and Church, M. (2000). "Experiments on surface structure and partial sediment transport on a gravel bed." *Water Resour. Res.*, 36(7), 1885–1895.

Hayward, J. A., and Sutherland, A. J. (1974). "The Torlesse Stream vortex-tube sediment trap." *J. Hydrol.,* 13(1), 41–53.

Helley, E. J., and Smith, W. (1971). "Development and calibration of a pressure-difference bedload sampler." *Open File Report,* U.S. Geological Survey, Reston, Va.

Hey, R. D., and Thorne, C. R. (1983). "Accuracy of surface samples from gravel bed material." *J. Hydr. Eng. ASCE*, 109(6), 842–851.

Hogan, S. A., Abt, S. R., and Watson, C. C. (1993). "Development and testing of a bed material sampling method for gravel and cobble bed streams." Civil Engineering Department Report, Colorado State University, Fort Collins, Colo.

Huanjin, Gao (1991). "The comparison tests of the gravel bed load samplers." *Fifth Federal Interagency Sedimentation Conference,* Las Vegas, Nev., 6-55–6-62.

Hubbell, D. W. (1964). "Apparatus and techniques for measuring bedload." *Water-Supply Paper 1748,* U.S. Geological Survey, Reston, Va.

Hubbell, D. W. (1987). "Bed load sampling and analysis." *Sediment transport in gravel-bed rivers*, C. R. Thorne, J. C. Bathurst, and R. D. Hey, eds., Wiley, Chichester, U.K., 89–118.

Hubbell, D. W., et al. (1956). "Investigations of some sedimentation characteristics of a sand-bed stream." *Progress Report No. 1,U.S. Geological Survey Open-File Report,* U.S. Geological Survey, Reston, Va.

Hubbell, D. W., and Stevens, H. H., Jr. (1986). "Factors affecting accuracy of bedload sampling." *Proceedings of the 4th Federal Interagency Sedimentation Conference,* Subcommittee on Sedimentation, Interagency Advisory Committee on Water Data, Las Vegas, Nev., 4-20–4-29.

Hubbell, D. W., Stevens, H. H., Jr., Skinner, J. V., and Beverage, J. P. (1985). "New approach to calibrating bedload samplers." *Journal of the Hydraulics Division*, 111(4), 677–694.

Hubbell, D. W., Stevens, H. H., Jr., Skinner, J. V., and Beverage, J. P. (1987). "Laboratory data on coarse-sediment transport for bedload-sampler calibrations." *Water-Supply Paper 2299,* U.S. Geological Survey, Reston, Va.

Ibbeken, K., and Schleyer, R. (1986). "Photo sieving: A method for grain-size analysis of coarse-grained, unconsolidated bedding surfaces." *Earth Surface Processes and Landforms,* 11, 59–77.

International Standards Organization (ISO). (1992). "Liquid flow measurement in open channels—Sampling and analysis of gravel-bed material." *9195:1992(E),* International Standards Organization, Geneva.

International Standards Organization (ISO). (1993). "Measurement of liquid flow in open channels—methods for measurement of suspended sediment." *ISO 4363*, 2nd Ed., International Standards Organization, Geneva.

Iseya, F., and Ikeda, H. (1987). "Pulsations in bedload transport rates induced by a longitudinal sediment sorting: a flume study using sand and gravel mixtures." *Geografiska Annaler,* 69A, 15–27.

Johnson, G. P. (1997). "Instruction manual for U.S. Geological Survey sediment observers." *U.S. Geological Survey Open-File Report 96-431*, U.S. Geological Survey, Reston, Va.

Kellerhals, R., and Bray, D. I. (1971). "Sampling procedures for coarse fluvial sediments." *J. Hydr. Eng. Div. ASCE*, 103(HYB), 1165–1180.

Kleinhans, M. G., and Ten Brinke, W. B. M. (2001). "Accuracy of cross-channel sampled sediment transport in large sand-gravel-bed rivers." *Journal of Hydraulic Engineering*, 127(4), 258–269.

Knott, J. M., Glysson, G. D., Malo, B. A., and Schroder, L. J. (1993). "Quality assurance plan for the collection and processing of sediment data by the U.S. Geological Survey, Water Resources Division." *U.S. Geological Survey Open-File Report 92-499*, U.S. Geological Survey, Reston, Va.

Knott, J. M., Sholar, C. J., and Matthes, W. J. (1992). "Quality assurance guidelines for the analysis of sediment concentration by U.S. Geological Survey sediment laboratories." *U.S. Geological Survey Open-File Report 92-33*, U.S. Geological Survey, Reston, Va.

Koltun, G. F., Gray, J. R., and McElhone, T. J. (1994). "User's manual for SEDCALC, a computer program for computation of suspended-sediment discharge." *U.S. Geological Survey Open-File Report 94-459*, U.S. Geological Survey, Reston, Va.

Kondolf, G. M. (1997). "Application of the pebble count: Notes on purpose, method, and variants." *Water Resources Bulletin,* 33(1), 79–87.

Kondolf, G. M., and Wolman, M. G. (1993). "The sizes of salmonid spawning gravels." *Water Resour. Res.*, 29(7), 2275–2285.

Kuhnle, R. A. (1992). "Bed load transport during rising and falling stages on two small streams." *Earth Surface Processes and Landforms,* 17, 191–197.

Kuhnle, R. A. (1996). "Unsteady transport of sand and gravel mixtures." *Advances in fluvial dynamics and stratigraphy*, P. A. Carling, M. R. Dawson, eds., Wiley, Chichester, U.K., 183–201.

Kuhnle, R. A., and Derrow, R. W., II (1994). "Using the SedBed monitor to measure bed load." *Proceedings of the Symposium, Fundamentals and Advancements in Hydraulic Measurements and Experimentation,* C. A. Pugh, ed., ASCE, Reston, Va., pp. 129–139.

Kuhnle, R. A., and Southard, J. B. (1988). "Bed load transport fluctuations in a gravel bed laboratory channel." *Water Resources Research,* 24(2), 247–260.

Kuhnle, R. A., Willis, J. C., Bowie, A. J. (1989). "Variations in the transport of bed load sediment in a gravel-bed stream, Goodwin Creek, northern Mississippi, U.S.A." *Proceedings of the Fourth International Symposium on River Sedimentation,* Science Press, Beijing, China, 539–546.

Land, J. M., and Jones P. D. (2001). "Acoustic measurement of sediment flux in rivers and near-shore waters." *Proceedings of the 7th Federal Interagency Sedimentation Conference,* March 25–29, 2001, Reno, Nevada, Vol. I, pp. III-127–III-134.

Lane, S. L., Flanagan, S., and Wilde, F. D. (2003). "Selection of equipment for water sampling (ver. 2.0)." *U.S. Geological Survey Techniques of Water-Resources Investigations,* vol. 9, chap. A2, Reston, Va., <http://pubs.water.usgs.gov/twri9A2/> (Aug. 12, 2005).

Laronne, J. B., Reid, I., Yitshak, Y., and Frostick, L. E. (1992). "Recording bedload discharge in a semiarid channel, Nahal Yatir, Israel." *Proceedings of Erosion and Sediment Transport Monitoring Programmes in River Basins,* Publication No. 210, IAHS, Oslo, Norway, 79–86.

Larsen, M. C., Alamo, C. F., Gray, J. R., and Fletcher, W. (2001). "Continuous automated sensing of streamflow density as a surrogate for suspended-sediment concentration sampling." *Proceedings of the 7th Federal Interagency Sedimentation Conference,* March 25–29, 2001, Reno, Nevada, Vol. I, pp. III-102–III-109.

Lee, T. L. (1990). The use of multispectral video remote sensing to monitor suspended sediment concentrations. University of Arizona PhD dissertation, Tucson, Arizona, 167 p.

Leopold, L. B., and Emmett, W. W. (1976). "Bedload measurements, East Fork River, Wyoming." *Proceedings National Academy of Sciences,* 73, 1000–1004.

Lewis, J. (1991). "An improved bedload sampler." *Proceedings of the 5th Federal Interagency Sedimentation Conference,* Subcommittee on Sedimentation, Interagency Advisory Committee on Water Data, Las Vegas, Nev., 6-1–6-8.

Lewis, J. (1996). "Turbidity-controlled suspended sediment sampling for runoff-event load estimation." *Water Resources Research,* 32(7), 2299–2310.

Lodhi, M. A., Rundquist, D. C., Han, L., and Kuzila, M. S. (1997). "The potential for remote sensing of loess soils suspended in surface waters." *Journal of the American Water Resources Association* 33(1): 111–117.

Marcus, W. A., Ladd, S., and Stoughton, J. (1995). "Pebble counts and the role of user-dependent bias in documenting sediment size distributions." *Water Resour. Res.,* 31(10), 2625–2631.

Matthes, W. J., Sholar, C. J., and George, J. R. (1991). "Quality assurance plan for analysis of fluvial sediment by laboratories of the U.S. Geological Survey." *U.S. Geological Survey Open-File Report 91-469,* U.S. Geological Survey, Reston, Va.

May, W. L., and Johnson, W. D. (1997). "Properties of simultaneous confidence intervals for multinomial proportions." *Commun. Stat. Simul. Comput.,* 26(2), 495–518.

McEwan, I. K., Sheen, T. M., Cunningham, G. J., and Allen, A. R. (2000). "Estimating the size composition of sediment surfaces through image analysis." *Proc. of the Institution of Civil Engineers—Water Maritime and Energy,* 142(4), 189–195.

McGregor, J. (2000a). "Development of the US D-95 Suspended-Sediment Sampler." *Report LL*, Federal Interagency Sedimentation Project, Vicksburg, Miss.; also <http://fisp.wes.army.mil/>.

McGregor, J. (2000b). "Development of the US DH-95 Suspended-Sediment Sampler." *Report MM*, Federal Interagency Sedimentation Project, Vicksburg, Miss.; also <http://fisp.wes.army.mil/>.

McKallip, T. E., Koltun, G. F., Gray, J. R., and Glysson, G. D. (2001). "GCLAS—A graphical constituent loading analysis system." *Proceedings of the 7th Federal Interagency Sedimentation Conference,* Vol. II, VI-49–VI-52, U.S. Geological Survey, Reston, Va.

Mertes, L. A. K., Smith, M. O., and Adams, J. B. (1993). "Estimating suspended sediment concentrations in surface waters of the Amazon River wetlands from Landsat Images." *Remote Sensing of Environment* 43: 281–301.

Milhous, R. T. (1973). "Sediment transport in a gravel-bottomed stream." PhD thesis, Oregon State University.

Moody, J. A., and Meade, R. H. (1994). "Evaluation of the method of collecting suspended sediment from large rivers by discharge-weighted pumping and separation by continuous-flow centrifugation." *Hydrological Processes*, 8, 513–530.

Morris, G. L., and Fan, J. (1997). *Reservoir sedimentation handbook.* McGraw-Hill, New York.

Mosley, M. P., and Tindale, D. S. (1985). "Sediment variability and bed material sampling in gravel-bed rivers." *Earth Surface Processes,* 10(5), 465–482.

Murphy, P. J., and Amin, M. I. (1979). "Compartmented sediment trap." *Journal of the Hydraulics Division,* 105(HY5), 489–500.

Nelson, M. E., and Benedict, P. C. (1950). "Measurement and analysis of suspended sediment loads in streams." *American Society of Civil Engineers, Transactions,* Paper No. 2450, 891–918.

Nordin, C. F., Cranston, C. C., and Mejia-B, A. (1983). "New technology for measuring water and suspended-sediment discharge of large rivers." *Proceedings of the Second International Symposium on River Sedimentation,* Water Resources and Electric Power Press, Beijing, 1145–1158.

O'Leary, S. J., and Beschta, R. L. (1981). "Bed load transport in an Oregon Coast Range stream." *Water Resources Bulletin,* 17(5), 886–894.

Osterkamp, W. R., and Emmett, W. W. (1992). "The Vigil network." *Erosion and Sediment Transport Monitoring Programmes in River Basins: Proceedings of the Oslo Symposium,* Publication

No. 210, International Association of Hydrological Sciences, Oslo, Norway, 397–404.

Osterkamp, W. R., Heilman, P. N., Gray, J. R., et al. (2004). "An invitation to participate in a North American sediment-monitoring network." *American Geophysical Union, EOS,* 84(40), 386–389.

Osterkamp, W. R., Heilman, P. N., and Lane, J. (1998). "Economic considerations of a continental sediment-monitoring program." *International Journal of Sediment Research,* 13(4), 12–24.

Osterkamp, W. R., and Parker, R. S. (1991). "Sediment monitoring in the United States." *Proceedings of the Fifth Federal Interagency Conference,* Subcommittee on Sedimentation of the Interagency Advisory Committee on Water Data, Las Vegas, Nev., I, 1-15–1-23.

Ott, L. (1988). *An introduction to statistical methods and data analysis,* 3rd Ed., PWS-Kent Publishing Co., Boston, Mass.

Parker, G. (1991). "Selective sorting and abrasion of river gravel. I: Theory." *J. Hydr. Engrg., ASCE,* 117(2), 131–149.

Petrie, J., and Diplas, P. (2000). "Statistical approach to sediment sampling accuracy." *Water Resour. Res.*, 36(2), 597–605.

Pitlick, J. (1988). "Variability of bed load measurement." *Water Resources Research,* 24(1), 173–177.

Poreh, M., Sagiv, A., and Seginer, I. (1970). "Sediment sampling efficiency of slots." *Journal of the Hydraulics Division,* 96(HY10), 2065–2078.

Porterfield, G. (1972). "Computation of fluvial-sediment discharge." *Techniques of Water Resources Investigations,* U.S. Geological Survey, Reston, Va., Book 3, C3.

Powell, D. M., Reid, I., Laronne, J. B., and Frostick, L. E. (1998). "Cross-stream variability of bedload flux in narrow and wide ephemeral channels during desert flash floods." *Gravel-Bed Rivers in the Environment*, P. C. Klingeman, R. L. Beschta, P. D. Komar, and J. B. Bradley, eds., Water Resources Publications, Highlands Ranch, Colo., 177–196.

Rantz, S. E. (1982). "Measurement and computation of streamflow." *Water-Supply Paper 2175*, U.S. Geological Survey, Reston, Va., Vols. 1 and 2, <http://water.usgs.gov/pubs/wsp/wsp2175>(Aug. 16, 2005).

Reid, I., Brayshaw, A. C., and Frostick, L. E. (1984). "An electromagnetic device for automatic detection of bedload motion and its field applications." *Sedimentology,* 31, 269–276.

Reid, I., Layman, J. T., Frostick, L. E. (1980). "The continuous measurement of bedload discharge." *Journal of Hydraulic Research*, 18, 243–249.

Rice, S., and Church, M. (1996). "Sampling surficial fluvial gravels: The precision of size distribution percentile estimates." *J. Sedimentary Research,* 66(3), 654–665.

Rice, S., and Church, M. (1998). "Grain size along two gravel-bed rivers: Statistical variation, spatial pattern and sedimentary links," *Earth Surface Processes and Landforms,* 23, 345–363.

Ritter, J. R., and Helley, E. J. (1969). "An optical method for determining particle sizes of coarse sediment." *Techniques of Water-Resources Investigations, Book 5,* U.S. Geological Survey, Washington, D.C.

Robinson, A. R. (1962). "Vortex tube sand trap." *ASCE Transactions,* 127(III), 391–424.

Rubin, D. M., Tate, G. B., Topping, D. J., Anima, R. A. (2001). "Use of rotating side-scan sonar to measure bedload." *Proceedings of the 7th Federal Interagency Sedimentation Conference,* March 25–29, 2001, Reno, Nevada, Vol. I, pp. III-139–III-143.

Russ, J. C., and Dehoff, R. T. (2000). *Practical stereology*, 2nd Ed., Kluwer Academic/Plenum, New York, 381.

Ryan, S. E., and Porth, L. S. (1999). "A field comparison of three pressure-difference bedload samplers." *Geomorphology* 30: 307–322.

Schoellhamer, D. H. (2001). "Continuous monitoring of suspended sediment in rivers by use of optical sensors." *Proceedings of the 7th Federal Interagency Sedimentation Conference,* March 25–29, 2001, Reno, Nevada, Vol. I, pp. III-160–III-167.

Sear, D. A. (1996). "Sediment transport processes in pool-riffle sequences." *Earth Surface Processes and Landforms,* 21, 241–262.

Simons, D. B., Richardson, E. V., and Nordin, C. F., Jr. (1965). "Bedload equation for ripples and dunes." *Professional Paper 462-H,* U. S. Geological Survey, Reston, Va.

Skinner, J. V. (1989). "History of the Federal Interagency Sedimentation Project." *Proceedings of the International Symposium, Sediment Transport Modeling,* S. S. Y. Wang, ed., ASCE, Reston, Va., 266–271.

Sprent, P. (1998). *Data driven statistical methods*, Chapman & Hall, London, U.K.

Stevens, H. H., Jr., Lutz, G. A., and Hubbell, D. W. (1980). "Collapsible-bag suspended-sediment sampler." *Am. Soc. Civ. Engin. Proc.*, 106(HY4), 11–16.

Tacconi, P., and Billi, P. (1987). "Bed load transport measurements by the vortex-tube trap on Virginio Creek, Italy." *Sediment transport in gravel-bed rivers*, C. R. Thorne, J. C. Bathurst, and R. D. Hey, eds., Wiley, Chichester, U.K., 583–616.

Tate, G., and Rubin, D. (1998). "Interferometric rotary scanning sonar for bed load transport investigations." *Proceedings of the Federal Interagency Workshop, Sediment Technology for the 21st Century,* U.S. Geological Survey, St. Petersburg, Fla., <http://water.usgs.gov/osw/techniques/sedtech21/index.html>(Aug. 15, 2005).

Thomas, R. B. (1985). "Estimating total suspended sediment yield with probability sampling." *Water Resources Research*, 21(9), 1381–1388.

Thomas, R. B. (1991). "Systematic sampling for suspended sediment." *Proceedings of the Fifth Federal Interagency Sedimentation Conference,* Subcommittee on Sedimentation of the Interagency Advisory Committee on Water Data, Las Vegas, Nev., 1, 2-17–2-24.

Thomas, R. B., and Lewis, J. (1993a). "A comparison of selection at list time and time stratified sampling for estimating suspended sediment loads." *Water Resources Research,* 29(4), 1247–1256.

Thomas, R. B., and Lewis, J. (1993b). "A new model for bed load sampler calibration to replace the probability-matching method." *Water Resources Research*, 29(3), 583–597.

Thompson, K. R. (1982). "Characteristics of suspended sediment in the San Juan River near Bluff, Utah." *Water-Resources Investigations Report 82-4104,* U.S. Geological Survey, Reston, Va.

Thompson, K. R. (1984). "Annual suspended-sediment loads in the Colorado River at Green River, Utah, 1930–82." *Water-Resources Investigations Report 84-4169,* U.S. Geological Survey, Reston, Va.

Thompson, K. R. (1985). "Annual suspended-sediment loads in the Colorado River near Cisco, Utah, 1930–82." *Water-Resources Investigations Report 85-4011*, U.S. Geological Survey, Reston, Va.

Thomson, E. (1930). "Quantitative microscopic analysis." *J. Geol.*, 38(3), 193–222 .

Thorne, P. D., Williams, J. J., and Heathershaw, A. D. (1989). "In situ acoustic measurements of marine gravel threshold and transport." *Sedimentology*, 36, 61–74.

Topping, D. J., Parker, R. S., Nelson, J. M., and Bennett, J. P. (1996). "The apparent mid-20th century sediment load decrease in the Colorado River basin—an investigation of the mechanics of the Colorado River." *Sampler, Geological Society of America Abstracts and Program,* Geological Society of America, Denver, Colo., 28(7,) A-261.

Turcios, L. M., and Gray, J. R. (2001). "U.S. Geological Survey sediment and ancillary data on the World Wide Web." *Proceedings of the 7th Federal Interagency Sedimentation Conference,* Subcommittee on Sedimentation, Reno, Nev., Poster 31-36.

Turcios, L. M., Gray, J. R., and Ledford, A. L. (2000). "Summary of U.S. Geological Survey on-line instantaneous fluvial sediment and ancillary data." <http://water.usgs.gov/osw/sediment>(June 26, 2001).

Underwood, E. E. (1970). *Quantitative stereology,* Addison-Wesley, Reading, Mass.

U.S. Department of Agriculture (USDA). (1994). "Evaluating the effectiveness of forestry best management practices in meeting water quality goals or standards." *Miscellaneous Publication 1520*, USDA Forest Service, Washington, D.C.

U.S. Environmental Protection Agency (USEPA). (1994). "National water quality inventory—1992 report to Congress." *EPA 841-R-94-001*, Washington, D.C.

U.S. Geological Survey (USGS). (1976). "Sampling mixtures of water and suspended sediment in streams." *Technical memorandum 76.17,* U.S. Geological Survey Office of Water Quality, <http://wwwroper.er.usgs.gov/memos/qw/qw76.17.html>(July 17, 2000).

U.S. Geological Survey (USGS). (1997). "Comparison of the suspended-sediment splitting capabilities of the churn and cone splitters." *Technical Memorandum 97.06*, U.S. Geological Survey Office of Water Quality, <http://wwwoper.er.usgs.gov/memos/qw/qw97.06.html>(June 28, 2000).

U.S. Geological Survey (USGS). (1998a). "A national quality assurance program for sediment laboratories operated or used by the Water Resources Division." *Technical Memorandum No. 99.01,* U.S. Geological Survey, Office of Surface Water, <http://water.usgs.gov/admin/memo/SW/sw99.01.html>(July 19, 2001).

U.S. Geological Survey (USGS). (1998b). "Guidance for collecting discharge-weighted samples in surface water using an isokinetic sampler." *Technical Memorandum 99.01*, U.S. Geological Survey Office of Surface Water, <http://wwwoper.er.usgs.gov/memos/sw/sw99.01.html>(June 9, 2000).

U.S. Geological Survey (USGS). (1999). "Guidelines from the 1998 Sediment Laboratory Chiefs Workshop." *Technical Memorandum 99.04,* U.S. Geological Survey Office of Surface Water<http://wwwoper.er.usgs.gov/memos/99/sw99.04.txt>(July 6, 1999).

U.S. Geological Survey (USGS). (2000a). "Water-quality samples for USA." U.S. Geological Survey, <http://water.usgs.gov/nwis/qwdata>(July 13, 2000).

U.S. Geological Survey (USGS). (2000b). "Suspended-sediment database, daily values of suspended-sediment and ancillary data." U.S. Geological Survey, <http://webserver.cr.usgs.gov/sediment/>(July 13, 2000).

U.S. Geological Survey (USGS). (2001). "Collection and use of total suspended solids data." Offices of Water Quality and Surface Water Technical Memorandum 2001.03, November 27, 2000, Reston, Va. <http://water.usgs.gov/admin/memo/SW/sw01.03.html>(Aug. 12, 2005).

U.S. Geological Survey (USGS). (2002). "Water-quality field methods phaseout of US D-77 and frame-type samplers." U.S. Geological Survey, <http://wwwoper.er.usgs.gov/memos/qw/qw02.09.html>(March 25, 2002).

U.S. Geological Survey (USGS). (2004). "Statistics for hydrologic data-collection stations operated by the USGS in fiscal year 2003, <http://1stop.usgs.gov/StationCounts/sc2004/rpts/view_SW_rpt.cfm?state=tr>(Aug 4, 2005).

U.S. Geological Survey (USGS). (Variously dated). *National field manual for the collection of water-quality data: U.S. Geological Survey techniques of water-resources investigations,* book 9, chaps. A1–A9, <http://pubs.water.usgs.gov/twri9A>(Aug. 16, 2005).

U.S. Geological Survey Techniques of Water-Resources Investigations, book 5, chapter C1, U.S. Geological Survey, Reston, Va.

Vanoni, V. A. (1975). "Sedimentation Engineering." *ASCE Manuals and Reports on Engineering Practice, No. 54,* ASCE, Reston, Va.

Van Rijn, L. C., and Gaweesh, M. T. K. (1992). "New total sediment-load sampler." *Journal of Hydraulic Engineering,* 118(12), 1686–1691.

Waslenchuk, D. G. (1976). "New diver-operated bed load sampler." *Journal of the Hydraulics Division,* 102(HY6), 747–757.

Waters, T. F. (1995). "Sediment in streams—Sources, biological effects, and control." *American Fisheries Society Monograph 7*, American Fisheries Society, Bethesda, Md.

Wathen, S. J., Ferguson, R. I., Hoey, T. B., and Werritty, A. (1995). "Unequal mobility of gravel and sand in weakly bimodal river sediments." *Water Resources Research,* 31(8), 2087–2096.

Webb, W. W., and Radtke, D. B. (1998). "Surface-water sampling equipment: National field manual for the collection of water-quality data—Surface-water sampling equipment." U.S. Geological Survey Techniques of Water-Resources Investigations, Book 9, A2, variously paged, <http://water.usgs.gov/owq/FieldManual/Chapter2/2.1.html#2.1.1>(September 26, 2001).

Whiting, P. J., Dietrich, W. E., Leopold, L. B., Drake, T. G., and Shreve, R. L. (1988). "Bedload sheets in heterogeneous sediment." *Geology,* 16, 105–108.

Wilcock, P. R., Barta, A. F., Shea, C. C., Kondolf, G. M., Mathews, W. V. G., and Pitlick, J. C. (1996). "Observations of flow and sediment entrainment on a large gravel-bed river." *Water Resources Research,* 32(9), 2897–2909.

Willis, J. C. (1968). "A lag-deviation method for analyzing channel bed forms." *Water Resources Research*, 4(6), 1329–1334.

Willis, J. C., and Kennedy, J. F. (1977). "Sediment discharge of alluvial streams calculated from bed-form statistics." *Report No. 202,* Iowa Institute of Hydraulic Research, Iowa City.

Winterstein, T. A., and Stefan, H. E. (1986). "Effects of nozzle orientation on sediment sampling." *Proceedings of the Fourth Federal Interagency Sedimentation Conference,* Subcommittee on Sedimentation of the Advisory Committee on Water Data, Las Vegas, Nev., 1, 1-20–1-28.

Wohl, E. E., Anthony, D. J., Madsen, S.W., and Thompson, D. M. (1996). "A comparison of surface sampling methods for coarse fluvial sediments." *Water Resources Res.*, 32(10), 3219–3226.

Wolman, M. G. (1954). "A method of sampling coarse river-bed material." *Transactions of the American Geophysical Union*, 35 (6), 951–956.

Wren, D. G., Barkdoll, B. D., Kuhnle, R. A., and Derrow, R. W. (2000). "Field techniques for suspended-sediment measurement." *Journal of Hydraulic Engineering* (ASCE) 126(2): 97–104.

Yuzyk, T. R. (1986). "Bed material sampling in gravel-bed streams." *Report IWD-HQ-WRB-SS-86-8,* Water Survey of Canada, Water Resources Branch, Inland Waters Directorate, Conservation and Protection Environment Canada, Winnipeg, Man.

Copyrighted Materials
Copyright © 2008 American Society of Civil Engineers (ASCE)
Retrieved from www.knovel.com

CHAPTER 6

Fundamentals of Fluvial Geomorphology

D. S. Biedenharn, C. C. Watson, and C. R. Thorne

Geomorphology is the study of landforms and the processes responsible for making and modifying them. Fluvial geomorphology is the study of landforms whose genesis and evolution are affected by flowing water. A river or stream constitutes a geomorphic system and in working on a natural watercourse the complete system must be considered because, even though a project may directly involve only a small portion of the system, it has the potential to trigger morphological responses in any part of the system. It is impossible to predict the types and locations of morphological responses without a good understanding of the fluvial system, and this demands thorough knowledge of the water and sediment regimes of the river, because the water discharge and associated sediment load drive morphological processes in the system. Water and sediment regimes in rivers derive from the natural climatic, geologic, topographic, and biologic characteristics of the watershed, together with land use and water resource management effects in developed watersheds. It is these watershed attributes and activities that control runoff and sediment sources, the magnitude and distribution of flows, the caliber and type of sediment, and the manner in which water and sediment are supplied to the channel network. In turn, interaction of the flow and sediment load with the materials forming the bed and banks of the channel dictate the three-dimensional morphology of the alluvial channel and its propensity for stability or change (Schumm 1977).

The purpose of this chapter is to present an overview of some basic concepts of fluvial geomorphology and river mechanics, with an emphasis on their application to engineering design of channel rehabilitation projects. In this chapter, "channel rehabilitation" is used in a broad sense that encompasses all aspects of channel modification to achieve a desired channel improvement, whether for river restoration, flood control, navigation, water supply, channel stability, sediment control, or other beneficial use. Regardless of the goals of the rehabilitation project, sound understanding of geomorphic processes and forms in fluvial systems is essential to successful performance of channel rehabilitation projects.

6.1 BASIC CONCEPTS

The six fundamental concepts that should be considered in designing engineering works in rivers and watersheds are:

1. The channel in the project reach is only part of the broader fluvial system;
2. The fluvial system is dynamic;
3. The fluvial system behaves with complexity;
4. Adjustment and response in the system are nonlinear, and abrupt changes can be triggered by relatively small external perturbations or the crossing of geomorphic thresholds;
5. System evolution and response are time-scale-dependent and engineering geomorphic analyses must include a historical perspective; and
6. System evolution and response are space-scale-dependent and the physical size of the system or subsystem must be considered in engineering geomorphic analyses.

6.1.1 The Fluvial System

Schumm (1977) provides an idealized sketch of a fluvial system (Fig. 6-1). Zone 1 is the upper portion of the system, that is, the watershed or drainage basin; this portion of the system functions as the zone of sediment supply. Zone 2 is the middle portion of the system, that is, the river; this portion of the system functions as the sediment exchange and transfer zone. Zone 3 is the lower portion of the system, which may be an estuary, delta, lake, floodplain, wetland, or reservoir; this portion of the system functions as the zone of sediment deposition. These three zones are idealized, because in real

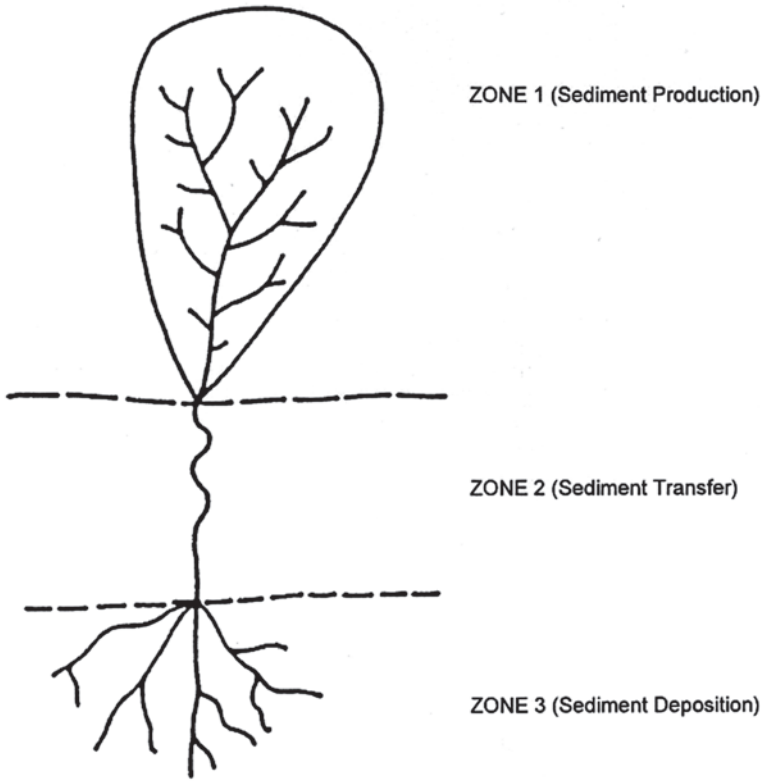

Fig. 6-1. The fluvial system (Schumm 1977, with permission from S. Schumm).

systems sediments can be eroded, transported, and stored in any of the zones. However, within each zone one process is usually dominant, and Schumm's idealized schematization illustrates graphically how sediment processes throughout the system are connected.

In planning any type of engineering alteration to a stream, the potential impacts of disrupting or breaking sediment connectivity in the fluvial system must be considered. For instance, if a channel rehabilitation project is planned for a specific reach of stream in Zone 2, the design engineer must ensure, from a system viewpoint, that the scheme does not interfere unduly with the transfer of sediment from the source zone upstream (Zone 1) to the storage zone downstream (Zone 3).

The fundamental concept that a stream is part of a larger, complex system was eloquently encapsulated by Hans Albert Einstein (1972):

> If we change a river we usually do some good somewhere and "good" in quotation marks. That means we achieve some kind of a result that we are aiming at but sometimes forget that the same change, which we are introducing, may have widespread influences somewhere else. I think if, out of today's emphasis of the environment, anything results for us it is that it emphasizes the fact that we must look at a river or a drainage basin or whatever we are talking about as a big unit with many facets. We should not concentrate only on a little piece of that river unless we have some good reason to decide that we can do that.

6.1.2 The System Is Dynamic

Fluvial processes in each of Schumm's idealized zones are dominated by activity. Zone 1 is the sediment source zone, implying that erosion dominates, driving channel change through net incision or valley widening. Zone 2 is the exchange and transfer zone, implying that as runoff and sediment yield from the watershed increase, the transport capacity of the stream is able to keep pace, exchanging sediment between transport and storage while maintaining dynamic equilibrium in channel form and reworking the floodplain. Zone 3 is the zone of sediment accumulation, implying that deposition dominates, with channel change and long-term storage increasing as sediment accrues in this zone. The functioning of each zone indicates that the system is dynamic and that change in the fluvial system is not only natural, but also essential to its operation.

From an engineering viewpoint the impacts of these dynamics and channel changes may be very significant. For example, loss of 100 ft of stream bank due to channel migration may endanger a home or destroy valuable agricultural land. From a geomorphic viewpoint, channel migration is to be expected and channel shifting represents a natural

manifestation of the fluvial system. Indeed, it may not even signal a departure from conditions of natural, dynamic equilibrium. In planning channel rehabilitation measures, engineers must realize that when faced with having to work on a dynamic fluvial system we must try to understand the fluvial system and avoid disrupting it unduly while we are accomplishing our design task. Where disruption, for example, through perturbing the balance between sediment supply and transport capacity, is inevitable, we must predict the system response and take appropriate steps to prevent or at least mitigate adverse responses.

6.1.3 Complexity

Landscape changes are usually complex (Schumm and Parker 1973). The stream and its watershed are a landscape system; change to one portion of the system may result in complex changes, both locally and throughout the remainder of the system.

During complex response, the system responds through the activation of different processes at different locations and times in response to one triggering event or intervention. Consequently, when a fluvial system is subjected to an engineering intervention, changes should be expected to occur throughout the system and over a prolonged period. For example, channelization of a reach of the stream usually accelerates stream velocities, disrupting the sediment-transfer system by increasing sediment transport capacity and allowing the stream to carry away more sediment than is being supplied from upstream. This sediment imbalance results in bed erosion that can migrate upstream through the headcutting process and in increased sediment output that can migrate downstream as a wave of deposition. Through time, headcutting migrates upstream, increasing sediment supply to the channelized reach and eventually causing aggradation there. Thus, in response to a single external intervention, channelization, the affected reach can experience an initial degradational response followed by a secondary aggradational response. This type of complex response not only is theoretically possible, but also has been observed in nature. For example, several Yazoo Basin streams in north Mississippi that were channelized in the 1960s responded initially through degradation, but later exhibited aggradation (Harvey and Watson 1986; Watson et al. 1997). Over the 40 years since the initial perturbation, repeated waves of degradation, temporary stability, and aggradation have occurred, but dynamic equilibrium has still not yet been reestablished.

6.1.4 Thresholds

Rivers and watersheds are described theoretically as nonlinear, complex systems (Richards and Lane 1997) in that they display discontinuous responses to progressive and incremental change in control variables. In the context of fluvial geomorphology, threshold behavior is characterized by progressive change in one variable that eventually results in abrupt change in the system. In engineering terms, the crossing of a geomorphic threshold may be evidenced either by an abrupt change in the rate, direction, or type of change in a naturally evolving fluvial system, or by a disproportionately strong response to a perturbation by an engineering intervention. Bank collapse due to channel incision has been cited as an example of threshold behavior (Thorne and Osman 1988) and may be used to illustrate the phenomenon and related consequences. As an alluvial river accumulates sediment on its bed, morphological evolution occurs through progressive channel aggradation. As aggradation continues, the channel slope gradually increases until, eventually, a limiting condition for bed slope with respect to sediment transport is reached. At this moment the trend of morphological evolution switches from aggradation to degradation as a geomorphic threshold (critical channel slope) is crossed.

Schumm (1973) argued that drainage basins exhibit both *extrinsic* thresholds and *intrinsic* thresholds. In the preceding example, channel change was driven by gradual accumulation of sediment on the bed, which could occur as part of sediment storage in Zone 3 in the natural system. This would be characteristic of an intrinsic threshold. Extrinsic thresholds are crossed when the system is perturbed by an external factor that triggers a disproportionate morphological response. The design engineer must be aware of the existing geomorphic thresholds, the possibility that a natural system may be close to an intrinsic threshold, and the widespread adverse effect that an ill-planned channel stabilization project may have if it causes the system to cross a threshold.

Alluvial channels have a measure of resilience that enables perturbations and imposed changes to be absorbed by morphological adjustments without widespread disequilibrium in the system. Greater resilience implies that the system is a greater distance from a geomorphic threshold than a less resilient system. Systems of greater resilience are less sensitive to change, and those of low resilience are highly sensitive to perturbation.

Threshold theory is often expressed in terms of apparently simple examples, such as the transition between meandering and braiding. This is often quoted as representing a geomorphic threshold, even though Leopold and Wolman recognized as long ago as 1957 that there is actually a continuum of planforms (Leopold and Wolman 1957). Bledsoe (1999) demonstrated that whereas a meandering stream may respond to an increase in bed-material mobility by braiding, it may also respond by incising. In fact, for a given sediment size (D_x), increasing energy (expressed as a mobility index) can result in either a braided or an incised channel, depending on the relative erosion resistance of the bed and bank materials. Also, the threshold mobility index is not single-valued, but is better characterized by a stochastically determined range of values (Fig. 6-2). These findings illustrate that in practice, the geomorphic threshold behavior of alluvial streams may be complex.

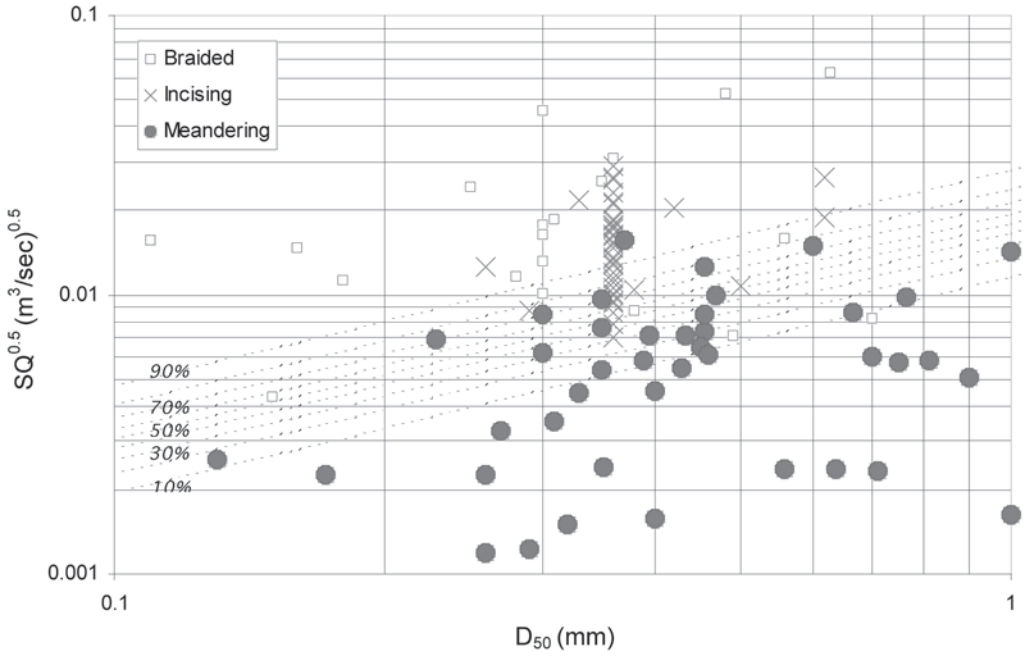

Fig. 6-2. Probability (%) of incising or braiding (dashed lines) is shown as a function of SQ (vertical axis) and D_{50} (horizontal axis) for sand beds. Discharge is represented by annual flood as first priority and then by bank-full flow (reprinted from Bledsoe and Watson 2001, with permission from Elsevier).

6.1.5 Time

Geomorphologists usually refer to three time scales when analyzing rivers:

1. Geologic time,
2. Modern time, and
3. Present time.

Geologic time is expressed in thousands or millions of years, and in this time frame the river is affected by major geologic and climatic changes such as formation of mountain ranges, changes in sea level, and climate change. Equilibrium is not possible over geologic time because, inevitably, the system evolves as material is washed from the mountains to the plains and responds to external changes. The modern time scale describes a period of tens of years to several hundred years, and has also been called the graded time scale (Schumm and Lichty 1965). During this period, a river may adjust to a balanced condition; that is, it may be fully adjusted to prevailing watershed water and sediment regimes and largely retain the same form as it operates in dynamic equilibrium. Present time is considered to be an even shorter period, perhaps 1 year to 10 years. Within this very short time frame, equilibrium may be static—that is, change in the system may be insignificant. Although the duration of these time scales is suggested, no fixed rules govern these definitions. The design of a major project may require less than 10 years, and numerous minor projects are designed and built within the limited scope of observations made during present time. However, project life often extends into graded time, when static equilibrium cannot be assumed to apply. From a geomorphological viewpoint, engineers build major projects in an instant of time, and base their design on an instantaneous snapshot of the river, but still expect these projects to operate successfully and last for a significant period in a dynamically changing system.

Recognition of the importance of time is especially important in considering the postconstruction performance of a project. Society demands a quick return on its investments and projects are expected to produce positive results almost instantaneously. Often, success or failure of a project is judged within one or two years, regardless of whether formative events have occurred to drive geomorphic recovery from construction impacts, or design events have occurred to test whether the project works as intended. With respect to the morphological impacts of a river engineering project, it must be remembered that short-term channel stability or adjustment is not necessarily indicative of long-term behavior. For this reason, the morphological performance of channel projects should be monitored and appraised over a period longer than a few years before a project is declared to have been successful.

6.1.6 Scale

The size or scale of the fluvial system has a bearing on the way in which it evolves toward a natural equilibrium, adjusts to catchment and climate change, and responds to engineering interventions. The time taken for the system to evolve,

adjust, or respond increases with the scale of the system. As a general rule, a small stream will react more rapidly to engineering works than a large stream. For instance, channel adjustments in the Mississippi River are still occurring in response to artificial meander cutoffs constructed in the 1930s, and it may require over 100 years before morphological changes triggered by the cutoffs are completed (Biedenharn 1995; Biedenharn and Watson 1997). Conversely, some small bluff line streams in north Mississippi that were channelized in the 1960s have adjusted through initial degradation, secondary aggradation, and dynamic stability within a period of less than 25 years (Watson et al. 2002).

The physical size of a stream also conditions and may limit the type of engineering works that are appropriate and feasible. Although the materials involved in alluvial stream mechanics (basically water, sediment, and vegetation) are scale-independent, the ways that they interact are not. For example, the morphological impact and significance of a large tree on the bank of a small stream is quite different from that of a similar tree on the bank of a large river. From an engineering perspective, it is particularly important to recognize that analyses, techniques, and solutions designed for one scale of stream may not be directly transferable to another. Deciding whether an analytical tool, stabilization technique, or channel enhancement solution developed for streams of a particular size is transferable to streams at other scales demands a thorough understanding of the underpinning science and engineering principles involved. It is not enough to have demonstrated repeatedly that a given approach *works* when applied to streams of a particular scale. Before tools, techniques, or solutions developed for one scale of system are promulgated for wider application, it must be established *how* and *why* they work. Principles, such as stabilizing a retreating bankline by increasing bank erosion resistance and mass stability or by retarding near bank velocities, are transferable across different scales of river; however, the hydraulic models, bank stability analyses, and structural measures appropriate to control bank retreat successfully may not be.

6.2 CHANNEL MORPHOLOGY

Alluvial rivers and streams are dynamic and continuously change position, shape, and other morphological characteristics in response to variations in discharge, sediment load, and boundary conditions. It is therefore important to study not only the existing morphology of the river but also possible variations during the lifetime of the project. The river morphology is determined by the water discharge, quantity and character of the sediment load, characteristics of the bed and bank materials (including vegetation), geologic controls, and valley topography. Morphological changes and adjustments take place in response to variations in any of these parameters through time or human activities. To predict the behavior of a river in a natural state or as affected by human activities, we must understand how fluvial and geotechnical processes operate on the boundary materials to form and adjust the morphological features of the channel through time.

A schematic diagram defining the morphological features associated with straight and meandering channels is shown in Fig. 6-3. The *thalweg* is the trace of the deepest point of the channel. The thalweg and associated line of maximum velocity cross from side to side within the channel, and this pattern of flow affects the overall cross-sectional geometry of the stream. At a bend, there is a concentration of flow in the outer half of the channel due to secondary flow. This causes the scour depth to increase at the outside of the bend, to produce a *pool*. As the thalweg crosses the channel downstream of a bend, the velocity distribution and cross-sectional shape become more symmetrical, and scour depths decrease

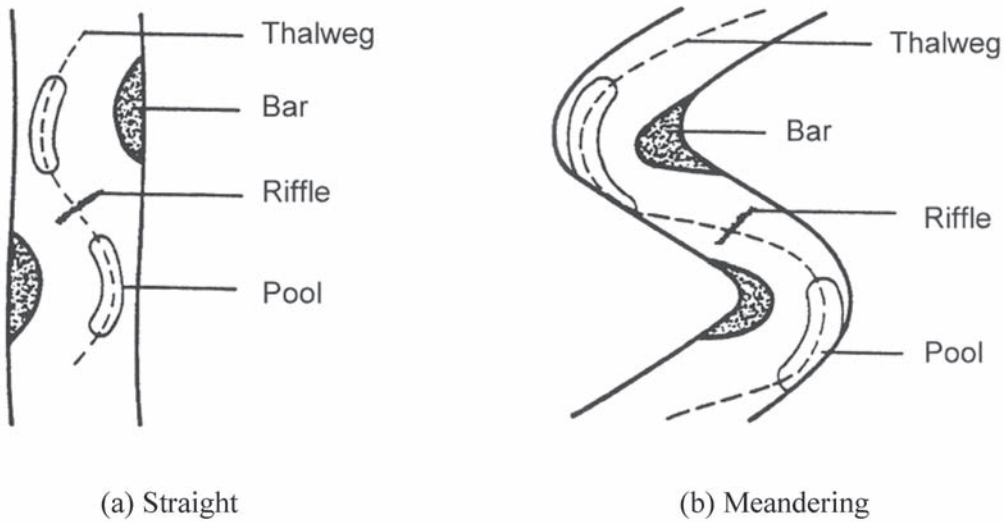

Fig. 6-3. Features associated with (a) straight and (b) meandering rivers.

because of deposition of sediment eroded from the pool upstream. This area is known as the *riffle* or *crossing*.

Pool-riffle sequences are characteristic of cobble, gravel, and mixed load rivers of moderate gradient ($S < 5\%$) (Sear 1996). Riffles are topographic high points in an undulating bed profile and pools are low points. Typically, sediment grain size is coarser on riffles than in pools. A sorting mechanism was proposed by Keller (1971) to explain this variation. According to Keller, fine sediment is removed from riffles during low flows and deposited in pools because velocities and bed shear stresses are higher at riffles (Keller 1971). As discharge rises, velocity and shear stress in the pool increase quickly, with little, if any, increase over the riffle. Consequently, the formative flow velocities and shear stresses in pools are higher than at riffles, resulting in scour of large sediment from the pools and deposition on the next riffle downstream. However, field evidence for this conceptual explanation is equivocal. Ashworth (1987), Petit (1987), and Clifford (1990) have measured the shear stress reversal hypothesized by Keller, but other studies have suggested that pool and riffle velocities equalize at bank-full flow, but do not reverse (Lisle 1979; Carling 1991).

Yalin (1971) suggests that pools and riffles may be explained by macro-turbulent eddies generated at the boundaries of a straight, uniform channel, which produce alternate acceleration and deceleration of flow. Yalin showed theoretically that the longitudinal spacing of faster and slower zones would average πw (w = channel width) for macro-turbulent eddies with diameters similar to the channel width. This is about half the riffle spacing of five to seven times

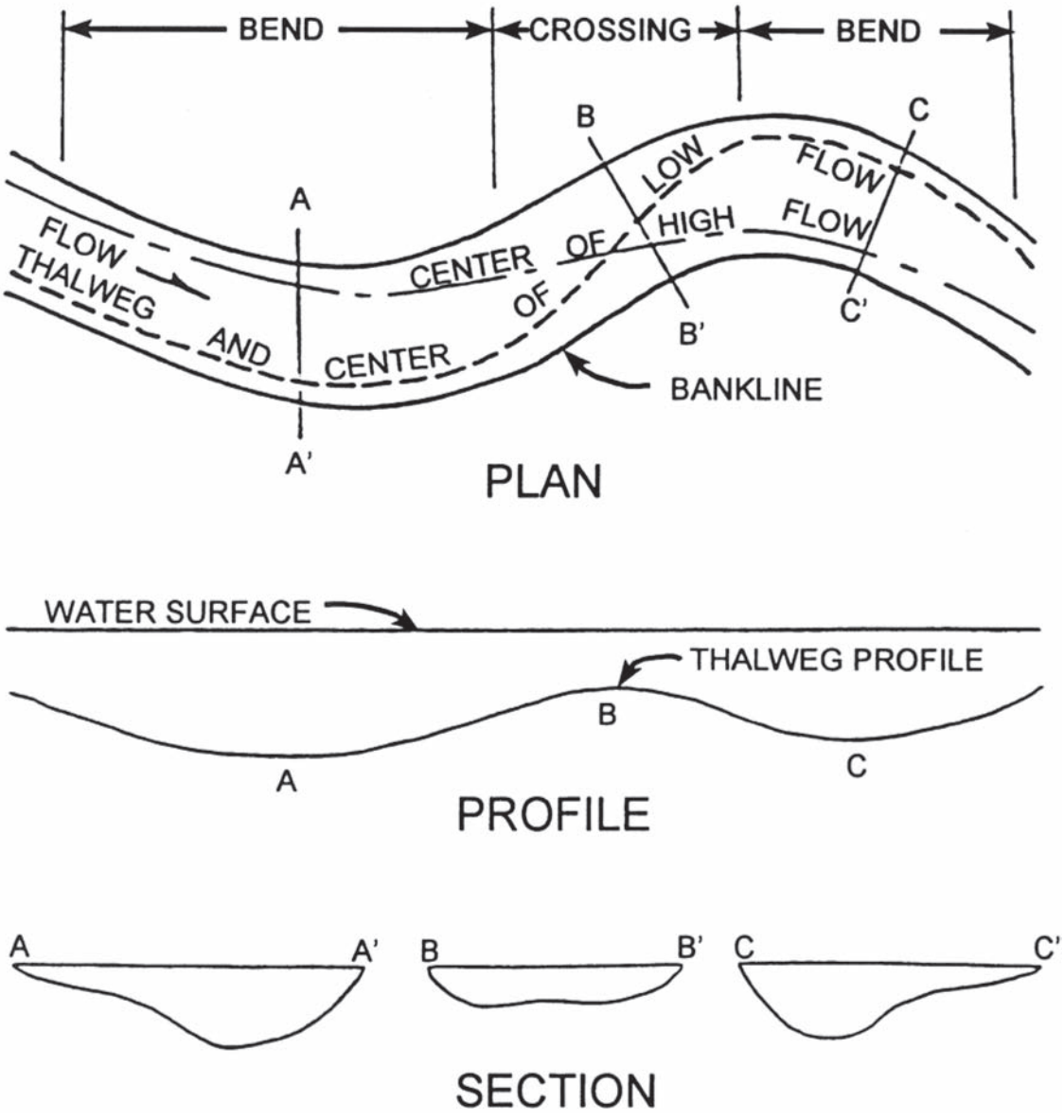

Fig. 6-4. Typical plan, profile, and cross-sectional views of pools and crossings.

the channel width observed in nature (Keller and Melhorn 1973). Hey (1976) proposed a resolution to this difference between theory and observation by proposing that the largest eddies in a stream do not scale on the width, but the half-width, with the centerline of the channel acting as a line of symmetry. According to Hey's hypothesis, riffles would be spaced at $2\pi w$, which better accords with observations.

The cross-sectional shape of a stream varies systematically with distance along the channel in relation to the plan geometry, the type of channel, and the characteristics of the sediment that is formed and transported within the channel. The cross section at a bend is typically deeper at the *concave* (outer bank) side, with a nearly vertical bank, and has a sloping bank formed by the point bar at the *convex* side. The cross section is more trapezoidal or rectangular at a crossing (Fig. 6-4). Cross-sectional dimensions and shape are described by a number of variables. Some of these, such as the *area (A), width (w)*, and *maximum depth (dm)*, are self-explanatory. Other commonly used parameters warrant explanation. *Wetted perimeter (P)* refers to the length of the wetted cross section measured normal to the direction of flow. *Average depth (d)* is calculated by dividing the cross-sectional area by the channel width. *Width-depth ratio (w/d)* is the channel width divided by the average depth. *Hydraulic radius (R)*, which is important in hydraulic computations, is defined as the cross-sectional area divided by the wetted perimeter. In wide channels, with *w/d* greater than about 20, the hydraulic radius and the mean depth are approximately equal. The *conveyance*, or capacity, of a channel is related to the area and hydraulic radius and is defined as $AR^{2/3}$.

Bars are depositional features that occur within a channel. The types, sizes, frequency of occurrence, and locations of bars are related to the quantity and caliber of the sediment load, local sediment transport capacity, and the morphology of the reach. The most common types of bars are point bars, middle bars, and alternate bars.

Point bars form at the inside (convex) bank of bends in a meandering stream (Fig. 6-5). The size and profile of the point bar are influenced by the characteristics of the flow, the degree of sinuosity, and the quantity and caliber of the sediment deposited at the bend. The development of a point bar is driven by reduction in the sediment transport capacity at the inner bank and sediment sorting due to the action of transverse flows and secondary currents (Dietrich et al. 1984), often coupled with flow separation at the inside of the bend downstream of the apex (Leeder and Bridges 1975). *Middle bar* is the term given to areas of deposition lying within, but not connected to, the banks. Middle bars in meandering rivers may form at riffles, especially where the crossing reaches between consecutive bends are long, and in bends, due to the development of a chute channel that separates part of the point bar from the inner bankline. Figure 6-6 shows a typical middle bar on the Mississippi River formed by this process. *Alternate bars* are regularly spaced depositional features positioned on opposite sides of a straight or slightly sinuous channel (Fig. 6-7a) and may be precursors to meander initiation or braiding. *Braid bars* are sediment features found between the subchannels of multithread, braided rivers (Fig. 7b). Braid bars are highly mobile, and deflection of flow due to bar movement is responsible for the shifting pattern of anabranches and the frequent bank attack that characterize braided river morphology.

Sinuosity (P) is a commonly used parameter to describe the degree of meandering in a stream. Sinuosity is defined as the ratio of distance measured along the channel (channel length) to distance measured along the valley axis (valley length). A perfectly straight channel has a sinuosity of unity, whereas a channel with a sinuosity of 3 or more would have tortuous meanders. *Meander wavelength (L)* is the straight-line repeating distance for the meander waveform, as depicted in Fig. 6-8, and is twice the inflection point spacing. The *meander path length* is the channel length between inflection points. *Meander amplitude (A)* is the width of the meander bends measured perpendicular to the valley or straight-line axis (Fig. 6-8). The ratio of amplitude to meander wavelength is generally within the range from 0.5 to 1.5.

Fig. 6-5. Typical meandering channel with point bars.

Fig. 6-6. Typical middle bar.

(a) Alternate

(b) Braided

Fig. 6-7. Typical bar patterns: (a) alternate, (b) braided.

Meander wavelength and amplitude are primarily dependent on water and sediment discharge, but are usually locally modified by spatial variation in the erodibility of the material in which the channel is formed. The effects of different bank materials are responsible for the irregularities found in the alignment of natural channels. In rare cases where the material forming the banks is practically homogeneous, meanders take a form that may be approximated by a sine-generated curve with a uniform meander wavelength. The *meander belt* is formed by and includes all the locations historically held by a stream due to meander development and migration. It should be noted that the width of the meander belt is usually greater than the meander amplitude and, in many cases, may include all of the active floodplain.

The *radius of curvature* (r_c) is the radius of the circle defining the centerline curvature of an individual bend, measured between the bend entrance and the bend exit (Fig. 6-8). The *arc angle* (θ) is the angle swept out by the radius of curvature. The ratio of radius of curvature to width (r_c/w) is a very useful parameter in the description and comparison of meander behavior and, in particular, bank erosion rates. The radius of curvature is dependent on the same factors as the meander wavelength and width. Meander bends generally develop a radius-of-curvature-to-width ratio (r_c/w) of 1.5 to 4.5, with the majority of bends falling in the range from 2 to 3. Nanson and Hickin (1986) examined the influence of r_c/w on bend migration rate and reported that maximum bank erosion rates occurred when the channel acquired an r_c/w between 2 and 3. This finding has been supported by many empirical studies, for example, Thorne (1991). Plots of erosion rate versus r_c/w do, however, display wide scatter and Biedenharn et al. (1989) showed that part of this scatter could be explained by variations in the erodibility of the outer bank material (Fig. 6-9).

River slope is one of the best indicators of the ability of a river to do morphological work. In general, rivers with steep slopes are much more active with respect to channel changes achieved through sediment movement, bed scour, bar building, and bank erosion. Slope can be defined in a number of

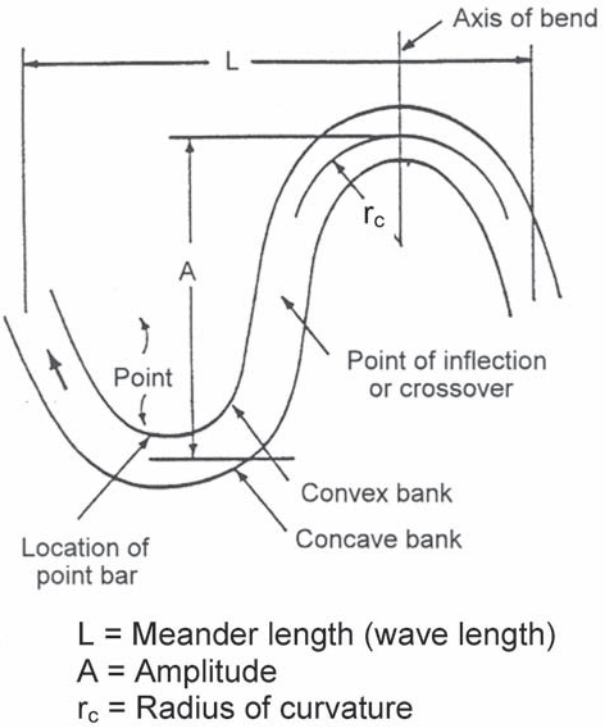

Fig. 6-8. Definition sketch for channel geometry (FISRWG 1998, with permission from the USDA).

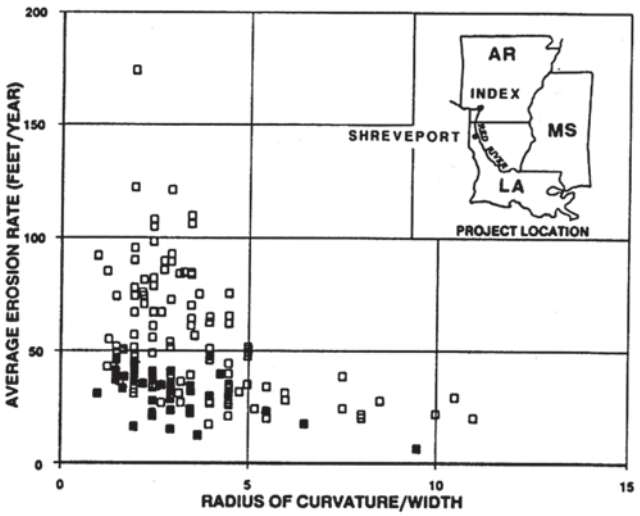

Fig. 6-9. Average annual erosion rate versus *r/w* for meander bends of the Red River. Open symbols represent free, alluvial bends and closed symbols, constrained bends (Biedenharn et al. 1989, with permission of ASCE Publications).

ways, however, leading to inconsistency in the way slope is used to represent the ability of a river to do morphological work. Ideally, energy slope should be used to calculate stream power, but the data required are seldom available. In gauged streams, water surface slope may be calculated using stage readings at consecutive gauging stations along the channel. However, many small streams are ungauged. In ungauged streams, thalweg slope is often used to calculate stream power. The thalweg profile not only provides a reasonable basis for calculation of stream power, but also may aid in locating bed controls due to geologic outcrops, other nonerodible materials, or inputs of relatively immobile sediments from steep tributaries. Repeat thalweg profiles are particularly useful in identifying bed-level adjustments through aggradation, degradation, local scour, and fill. When different slopes are used to calculate stream power, it must be kept in mind that the thalweg, water surface, and energy slopes are not necessarily equal.

6.3 SEDIMENT TRANSPORT

One aspect of river engineering that causes considerable confusion and misunderstanding is the terminology associated with sediment transport. In discussing the sediment transport, it is important to be familiar with the terminology adopted and the nature of the load being discussed. Over an extended period, a common terminology has emerged, and although it is not universally agreed upon or applied, it provides the basis for at least reducing inconsistency.

Total sediment load is the mass of granular sediment transported by a stream. It can be broken down by source, transport mechanism, or measurement status (Table 6-1). *Bed load* is a component of total sediment load made up of particles moving in continuous or frequent contact with the bed. Transport occurs at or near the bed, with the submerged weight of particles supported by solid-solid contact with the bed. Bed load movement takes place by processes of rolling, sliding, and saltation. *Suspended load* is a component of the total sediment load made up of sediment particles moving in continuous or semicontinuous suspension within the water column. Transport occurs above the bed, with the submerged weight of particles supported by anisotropic turbulence within the body of the flowing water. *Bed-material load* is the portion of total sediment load composed of grain sizes that are found in appreciable quantities in the streambed. The bed-material load is the bed load plus the coarser portion of the suspended load, that is, particles of a size that are found in significant quantity in the bed. *Wash load* is the portion of the total sediment load composed of grain sizes finer than those found in appreciable quantities in the streambed. *Measured load* is the portion of total sediment load that is sampled by conventional suspended load samplers. The sediment sampled in

Table 6-1 Classification of the Sediment Load

Measurement method	Transport mechanism	Sediment source
Unmeasured load	*Bed load*	*Material load*
Measured load	*Suspended load*	*Wash load*

deriving the measured load includes a large proportion of the suspended load, but excludes that portion of the suspended load moving very near the bed (that is, below the sample nozzle) and all of the bed load. *Unmeasured load* is that portion of the total sediment load that passes beneath the nozzle of a conventional suspended load sampler, moving in near-bed suspension and as bed load.

6.4 CHANNEL-FORMING DISCHARGE

Morphological studies have revealed that channel form depends on a delicate balance between the flows of water and sediment that shape the channel, the processes by which channel form is changed, and the ability of the boundary materials to resist change. Variability of water and sediment discharges is a characteristic of the watershed and, over a sufficiently long period, the morphology of the channel will adjust to accommodate the range of flow events responsible for regulating the balance between the erosive and resistive forces that mold the channel. Consequently, the shape and dimensions of an alluvial river channel are adjusted to and reflect the wide range of flows that entrain, transport, and deposit boundary sediments (Lane 1955). The concept that there is a single discharge that, if it prevailed all the time, would produce the same width, depth, slope, hydraulic roughness, and planform as those produced by the actual range of discharges is attractive, but viewed in this context it is clearly a gross simplification. The single discharge best able to represent the actual spectrum of sediment-transport events to yield the same bank-full morphology as that shaped by the natural sequence of flows is referred to as the channel-forming flow or the dominant discharge. Dunne and Leopold (1978) define channel maintenance flow as the most effective discharge for moving sediment, forming or removing bars, forming or changing bends and meanders, and generally doing work that results in the average morphological characteristics of channels. Their definition of channel maintenance flow is very similar to the concept of channel-forming discharge.

In a regulated canal system, the dimensions of the channel can appropriately be based on a single design discharge. Empirical analysis of the relationship between that discharge and the dimensions for a stable, unlined canal formed in alluvial materials produced the regime theory. Early work on regime theory stems from design of straight canals in the Indian subcontinent (Inglis 1941; 1947; 1949), and North America (Blench 1952; 1957). Later, flume experiments extended the regime approach to channels with meandering planforms (Ackers and Charlton 1970a; 1970b). However, for widely varying flows emanating from a natural watershed, the problem of identifying the single channel-forming discharge is both challenging and critical.

Soar (2000) recently reviewed the huge literature pertaining to the concept of channel-forming flow. This concept is closely related to the theory of dynamic equilibrium, which is characterized by fluctuations of channel form around an average condition that persists through time. In perennial rivers, recovery of equilibrium following a major event occurs relatively quickly, partly because rapid vegetation growth encourages sedimentation (Hack and Goodlett 1960; Gupta and Fox 1974). Hence, the long-term time-averaged condition is a valid representation of the channel form. Recovery in the ephemeral channels of semiarid regions tends to take longer, reflecting the influence of relatively wet and dry periods on vegetation growth (Schumm and Lichty 1965; Burkham 1972). In arid areas, infrequent floods impart long-lasting imprints on channels because more frequent flows do not have the power to restore a regime condition (Schick 1974). It has been concluded that the channel-forming flow concept may be inapplicable to ephemeral rivers that exhibit highly variable flow regimes, because there may not be a single discharge that can explain channel form (Stevens et al. 1975; Baker 1977). This is because channel morphology is likely to be perpetually in disequilibrium with the prevailing flows rather than fluctuating around an average state.

Channel-forming flow or dominant discharge is actually a geomorphological concept and not strictly a measurable parameter. However, a number of discharges that may be taken to represent the channel-forming flow can be defined and calculated using prescribed methodologies. The first approach is to identify a candidate flow based on channel morphology, such as the bank-full discharge. A second approach is to select a discharge based on a specified recurrence interval discharge, typically between the 1- and 3-year events in the annual maximum series. The third approach is analytical and involves calculating the effective discharge.

6.4.1 Bank-Full Discharge

Based on both theoretical and empirical arguments, bank-full discharge is generally recognized as being the moderate flow that best fits Wolman and Miller's (1960) dominant discharge concept for rivers in dynamic equilibrium. Leopold et al. (1964) proposed that the bank-full discharge was responsible for channel maintenance and form, and therefore that it was equivalent to the channel-forming discharge. Dury (1961) also suggested that the channel-forming discharge is approximately equal to the bank-full discharge and Dunne and Leopold (1978) concluded that their maintenance discharge corresponded to the bank-full stage. Field identification of bank-full discharge is, however, problematic (Williams 1978). It is usually based on identification of the minimum width-to-depth ratio (Wolman 1955; Pickup and Warner 1976), together with the recognition of some discontinuity in the nature of the channel, such as a change in sedimentary or vegetative characteristics. Nixon (1959) defined the bank-full state as the highest flood of a river that can be contained within its channel without spilling water on the river floodplain. Wolman and Leopold (1957) defined

the bank-full stage as the elevation of the active floodplain. Woodyer (1968) suggested that bank-full discharge corresponds to the elevation of the middle bench of rivers having several overflow surfaces. Schumm (1960) defined bank-full stage as the height of the lower limit of perennial vegetation, primarily trees. Similarly, Leopold (1994) states that bank-full stage is indicated by a change in vegetation, such as herbs, grasses, and shrubs. Finally, the bank-full stage is also defined as the average elevation of the highest surface of the channel bars (Wolman and Leopold 1957). Harrelson et al. (1994) provide explanations of field methods for determining bank-full discharge using vegetation, gradation of bank materials, and elevation of sedimentary features. Although several criteria have been identified to assist in field identification of bank-full stage, ranging from vegetation boundaries to morphological breaks in bank profiles, considerable experience is required to apply these in practice, especially on rivers that have in the past undergone aggradation or degradation.

Table 6-2 Recommended Frequencies for Bank-Full Discharge (after Soar 2000)

Discharge frequency	Recommended by
1 to 5 years	Wolman and Leopold (1957)
1.5 years	Leopold et al. (1964); Hey (1975); Leopold (1994)
1.58 years	Dury (1973, 1976); Riley (1976)
1.02 to 2.69 years	Woodyer (1968)
1.01 to 32 years	Williams (1978)
1.18 to 3.26 years	Andrews (1980)
1 to 10 years, 2 years	USACE (1994)
2 years	Bray (1973, 1982)

6.4.2 Specified Recurrence Interval Discharge

Problems and subjectivity in the field identification of bank-full elevation and discharge make it attractive to use an objectively defined discharge such as a specific recurrence interval flow. This recurrence interval flow can, in turn, be related to the bank-full elevation (Table 6-2). Wolman and Leopold (1957) suggested that the bank-full frequency has a recurrence interval of 1 to 2 years. The most often quoted recurrence interval is 1.5 years. Dury (1973) concluded that the bank-full discharge is approximately 97% of the 1.58-year discharge, or the most probable annual flood. Hey (1975) showed that for three British gravel-bed rivers, the 1.5-year flow in an annual maximum series passed through the scatter of bank-full discharges measured along the course of the rivers. Richards (1982) suggests that, in a partial duration series, bank-full discharge equals the most probable annual flood, which has a 1-year return period. Leopold (1994) concludes that most investigations have found that the recurrence interval for bank-full discharge ranges from 1.0 to 2.5 years. However, there are many instances where the bank-full discharge does not fall within this range. For example, Williams (1978) showed that for 35 floodplains in the United States the recurrence interval of bank-full discharge varied between 1.01 and 32 years, and found that only about one-third of those streams had a bank-full discharge with a recurrence interval between 1 and 5 years. In a similar study, Pickup and Warner (1976) determined that bank-full recurrence intervals ranged from 4 to 10 years on the annual series.

If a specified recurrence interval flow is used to estimate the channel-forming discharge, a range of 1 to 3 years should be used. However, because of the uncertainties discussed above, it is recommended that discharges in this range be compared to the bank-full stage in the field to verify that they do have morphological significance.

6.4.3 Effective Discharge

The effective discharge is defined as the increment of discharge that transports the largest fraction of the annual sediment load over a period of years (Andrews 1980). The effective discharge incorporates the principle prescribed by Wolman and Miller (1960) that the channel-forming or dominant discharge is a function of both the magnitude of sediment-transporting events and their frequency of occurrence. An advantage of using the effective discharge is that it is a calculated value that integrates the discharge and sediment-transport regimes of the stream.

Equivalence between bank-full and effective discharges for natural alluvial channels that are in regime has been demonstrated for a range of river types (sand, gravel, cobble, and boulder-bed rivers) and in different hydrological environments, if the flow regime is adequately defined and the appropriate component of the sediment load is correctly identified (Andrews 1980; Carling 1988; Hey 1997). However, Benson and Thomas (1966), Pickup and Warner (1976), Webb and Walling (1982), Nolan et al. (1987), and Lyons et al. (1992) report that the effective and bank-full discharges are not always equivalent. This suggests that the effective discharge may not always be a direct surrogate for the channel-forming flow or the bank-full discharge.

Although the effective discharge is straightforward conceptually, and has been used for many years, many engineers have expressed concerns that the effective discharge calculations do not yield reasonable results in some instances. These problems may be attributable to data limitations, insufficient understanding of the morphology of the stream, or improper calculation procedure. To minimize these uncertainties a standardized procedure for the determination of the effective discharge has been developed and is outlined

in the following paragraphs. This procedure is intended to help investigators avoid many of the potential problems that the authors have experienced in the calculation of effective discharge. Interested readers are referred to Biedenharn et al. (2000a) for a more detailed discussion of effective discharge calculation.

The method most commonly adopted for determining the effective discharge is to calculate the total load (tons) transported by the range of flows over a period of time by multiplying the frequency of occurrence of selected discharge classes (number of days) by the median magnitude of the sediment load (tons/day) transported by that class of flows. Although this approach has the merit of simplicity, the accuracy of the estimate of the effective discharge is clearly dependent on the calculation procedure adopted. The basic inputs required for calculation of effective discharge are (1) flow-duration data and (2) sediment transport as a function of stream discharge.

The first step in an effective discharge calculation is to group the discharge data into classes and determine the number of events occurring in each class during the period of record. This is usually accomplished from a flow-duration curve, which is a cumulative distribution function of measured discharges. A flow-duration curve shows the percentage of time a specific discharge is equaled or exceeded during the period of record, for which the curve was developed. From the flow-duration curve, the number of days that discharges within the specified class interval occurred can be calculated. The three critical components that must be considered in developing a flow-duration curve are the time base, the number of class intervals, and the period of record.

Conventionally, values of mean daily discharge are used to compute the flow-duration curve. Although this is convenient and uses readily available mean daily flow data that are published by the U.S. Geological Survey (USGS), it can, in some cases, introduce bias into the calculations. Mean daily values underestimate the influence of the high flows that occur within the averaging period and overestimate the significance of the low flows. On large streams such as the Mississippi River, the use of mean daily values is acceptable because differences between mean daily and daily peak discharges are negligible. However, on flashy streams, the time from the flood peak to base flow may be only a few hours, so mean daily flow cannot adequately describe the hydrograph. Missing flood peaks and associated high sediment loads can result in the effective discharge being underestimated. Rivers with a high flashiness index, defined as the ratio of the instantaneous peak flow to the associated daily mean flow, are most affected.

To avoid this problem it may be necessary to increase the temporal density from 24 h (mean daily) to 1 h, or even 15 min, especially on flashy streams. This will ensure that the hydrograph is adequately described, enabling a more representative effective discharge to be determined.

Class intervals should be arithmetic and must be of equal width. It has been demonstrated that the use of logarithmic or non-equal-width arithmetic classes introduces systematic bias into the calculation of effective discharge (Soar 2000; Soar and Thorne 2001). However, interested readers should review Holmquist-Johnson (2002) for guidance in calculating effective discharge for conditions under which equal-width class intervals are not usable. The selection of class interval may influence the calculated effective discharge. There are no definitive rules for selecting the most appropriate interval and number of classes. Yevjevich (1972) stated that the class interval should not be larger than $s/4$, where s is an estimate of the standard deviation of the sample. For hydrological applications he suggested that the number of classes should be between 10 and 25, depending on the sample size. Hey (1997) found that 25 classes with equal, arithmetic intervals produced a relatively continuous flow-frequency distribution and a smooth sediment-load histogram with a well-defined peak, indicating an effective discharge that corresponded exactly with bank-full flow. However, in the authors' experience, 25 classes may not always produce satisfactory results. It is recommended that in difficult cases the number of intervals be increased, but not to the extent that individual classes have zero events or only one event.

The period of record must be sufficiently long to include a wide range of morphologically significant flows, but not so long that changes in the climate, land use, or runoff characteristics of the watershed produce significant changes with time in the data. If the period of record is too short, there is a significant risk that the effective discharge will be inaccurate because of the occurrence of unrepresentative flows. A reasonable minimum period of record for an effective discharge calculation is about 10 years, with 20 years of record providing more certainty that the range of morphologically significant flows is fully represented in the data. Records longer than 30 years should be examined carefully for evidence of temporal changes in flow and/or sediment regimes.

The next step in the determination of the effective discharge is to develop a sediment-rating curve that relates the sediment transport and discharge. The sediment-rating curve can be developed from observed, measured sediment loads or using a computational procedure. Effective discharge is very sensitive to the slope of the sediment-discharge relationship.

The sediment load that is responsible for shaping the channel should be used in the calculation of the effective discharge. The suspended sediment load reported by USGS publications usually includes a portion of the bed-material load and most of the wash load. If measured suspended-sediment data are used for the effective-discharge calculation, then the fine sediment load, consisting of particles not found in appreciable quantities in the bed, should be omitted. If the bed load in the stream is only a small percentage of the total bed-material load, it may be acceptable to use only the measured suspended bed-material load in the

effective discharge calculations. However, if the bed load is a significant portion of the load, it should be calculated using an appropriate sediment-transport function and then added to the suspended bed-material load to provide an estimate of the total bed-material load. If bed-load measurements are available, which seldom is the case, observed data may be used.

Once the fines have been removed from the data set, a sediment-rating curve is developed from the concentration data by plotting sediment load (concentration times discharge) against discharge, and then calculating a best-fit regression curve through the data, or, as required in some cases, multiple segments of best-fit regression.

The discharges used to generate the bed-material load histogram are the arithmetic mean discharges in each class of the flow-frequency distribution. The bed-material transport rate for each discharge class is found from the rating curve equation. This load is multiplied by the frequency of occurrence of that discharge class to find the total amount of bed material transported by that discharge class during the period of record. Care should be taken to ensure that the time units in the bed-material load rating equation are consistent with the frequency units for the distribution of flows. The results are plotted as a histogram. The bed-material load histogram should display a continuous distribution with a single mode (peak). If this is the case, the effective discharge corresponds to the mean discharge for the modal class (that is, the peak of the histogram). If the modal class cannot be identified readily, the peak of a smooth curve drawn through the tops of the histogram bars can be used to estimate the effective discharge by interpolation.

6.4.4 Overview

All three approaches to estimating the channel-forming flow or dominant discharge (bank-full estimate, discharge of a selected return period, and effective discharge) present challenges. The selection of the appropriate method will be based on data availability, the physical characteristics of the study stream, the level of study, and time and funding constraints. It is recommended that all three methods be used and the results cross-checked to reduce the uncertainty in the final estimate of the channel-forming flow. If the effective discharge method is used, then it is recommended that the standardized procedure presented here be followed.

6.5 RELATIONSHIPS IN RIVERS

Given the evident complexity of fluvial processes and their interactions with channel morphology, it is perhaps surprising that the characteristic forms adopted by alluvial rivers are limited in number and frequent in occurrence. For example, the planforms of meandering rivers display clear similarity in their proportions. Brice (1984) suggested that the similarity of meanders accounts for the fact that, if scale is ignored, all meandering rivers tend to look alike in plan view. It is the familiar and almost ubiquitous nature of the forms and features displayed by alluvial streams of different sizes, in widely varying landscapes, that makes these complex systems amenable to description by relatively simple empirical relationships. For example, relationships developed by Williams (1986) illustrate how Brice's recognition of the similarity of meanders may be expressed quantitatively through empirical relationships relating the geometric properties of channel meander to one another (Table 6-3).

Similarly, in regime theory the concept that the width, depth, slope, and planform of a river are adjusted to a channel-forming discharge is expressed numerically in simple power-law equations. The *Stream Corridor Restoration Manual* (FISRWG 1998) provides the selected summary of regime equations reproduced in Table 6-4.

Independent of regime theory, Leopold and Maddock (1953) compiled important statistical equations linking various channel dimensions to discharge using USGS gauging records. These equations, termed *hydraulic geometry relationships*, describe how width, depth, velocity, and other hydraulic characteristics vary both with stage at a station and with changing bank-full discharge downstream for some streams in the United States. The hydraulic geometry relationships are of the same general form as the regime equations of Kennedy (1895):

$$W = \mathrm{a}\, Q^{\mathrm{b}}$$
$$D = \mathrm{c}\, Q^{\mathrm{f}}$$
$$V = \mathrm{k}\, Q^{\mathrm{m}}$$

where W = channel width, Q = discharge, D = depth, and V = velocity. Later versions of these hydraulic geometry relationships (listed in Table 6-5) add the median bed sediment size (D_{50}) to improve the predictive power of the equations, and appear in the following format:

$$W = k_1\, Q^{k2}\, D_{50}{}^{k3}$$
$$D = k_4\, Q^{k5}\, D_{50}{}^{k6}$$
$$S = k_7\, Q^{k8}\, D_{50}{}^{k9}$$

The relationships presented here are only a small sample of those available in the literature. Regime relationships are empirical, which means that the relationships are derived from observed physical correlations and are strictly only applicable to the data sets from which they were derived. In this regard, Rinaldi and Johnson (1997) are correct to point out the inappropriateness of using simple regression equations in the design of meander restorations when fluvial processes and channel morphology in the project stream differ manifestly from conditions in the rivers used to develop the equations. In practice, hydraulic geometry and other empirical relationships may be widely and usefully applied, provided that conditions in the study watershed are similar to those in the watersheds for which the equations were developed. However, even under ideal conditions these equations remain incomplete representations of the factors that actually

Table 6-3 Derived Empirical Equations for River Meander and Channel Size (FISRWG 1998, with permission from USDA)

Equation number	Equation	Applicable range (meters)
	Interrelations between meander features	
2	$L_m = 1.25\ L_b$	$5.49 < L_b < 13{,}293$
3	$L_m = 1.63\ B$	$3.69 < B < 13{,}689$
4	$L_m = 4.53\ R_c$	$2.59 < R_c < 3{,}598$
5	$L_b = 0.8\ L_m$	$7.93 < L_m < 16{,}494$
6	$L_b = 1.29\ B$	$3.69 < B < 10{,}000$
7	$L_b = 3.77\ R_c$	$2.59 < R_c < 3{,}598$
8	$B = 0.61\ L_m$	$7.93 < L_m < 23{,}201$
9	$B = 0.78\ L_b$	$5.49 < L_b < 13{,}293$
10	$B = 2.88\ R_c$	$2.59 < R_c < 3{,}598$
11	$R_c = 0.22\ L_m$	$10.06 < L_m < 16{,}494$
12	$R_c = 0.26\ L_b$	$6.80 < L_b < 13{,}293$
13	$R_c = 0.35\ B$	$4.88 < B < 10{,}000$
	Relations of channel size to meander features	
14	$A = 0.0054\ L_m^{1.53}$	$10.06 < L_m < 23{,}201$
15	$A = 0.0085\ L_d^{1.53}$	$6.10 < L_d < 13{,}293$
16	$A = 0.0103\ B^{1.53}$	$4.88 < B < 11{,}616$
17	$A = 0.0669\ R_c^{1.53}$	$2.13 < R_c < 3{,}598$
18	$W = 0.0167\ L_m^{0.89}$	$7.93 < L_m < 23{,}201$
19	$W = 0.0228\ L_b^{0.89}$	$4.88 < L_b < 13{,}293$
20	$W = 0.0279\ B^{0.89}$	$3.05 < B < 13{,}689$
21	$W = 0.7108\ R_c^{0.89}$	$2.59 < R_c < 3{,}598$
22	$D = 0.0267 L_m^{0.66}$	$10.06 < L_m < 23{,}201$
23	$D = 0.0361 L_b^{0.66}$	$7.01 < L_b < 13{,}293$
24	$D = 0.0367 B^{0.66}$	$4.88 < B < 11{,}616$
25	$D = 0.0848\ R_c^{0.66}$	$2.59 < R_c < 3{,}598$
	Relations of meander features to channel size	
26	$L_m = 29.99\ A^{0.65}$	$0.04 < A < 20{,}914$
27	$L_b = 21.42\ A^{0.65}$	$0.04 < A < 20{,}914$
28	$B = 18.57\ A^{0.65}$	$0.04 < A < 20{,}914$
29	$R_c = 5.86\ A^{0.65}$	$0.04 < A < 20{,}914$
30	$L_m = 7.50\ W^{1.12}$	$1.49 < W < 3{,}963$
31	$L_b = 5.07\ W^{1.12}$	$1.49 < W < 2{,}134$
32	$B = 4.27\ W^{1.12}$	$1.49 < W < 3{,}963$
33	$R_c = 1.50\ W^{1.12}$	$1.49 < W < 2{,}134$
34	$L_m = 239.25\ D^{1.52}$	$0.03 < D < 18$
35	$L_b = 159.50\ D^{1.52}$	$0.03 < D < 18$
36	$B = 148.37\ D^{1.52}$	$0.03 < D < 18$
37	$R_c = 42.66\ D^{1.52}$	$0.03 < D < 18$
	Relations between channel width, channel depth, and channel sinuosity	
38	$W = 21.33\ D^{1.45}$	$0.03 < D < 18$
39	$D = 0.1492\ W^{0.89}$	$1.50 < W < 3{,}963$

(Continued)

Table 6-3 Derived Empirical Equations for River Meander and Channel Size (FISRWG 1998, with permission from USDA) *(Continued)*

Equation number	Equation	Applicable range (meters)
40	$W = 95.93\ D^{1.23}\ K^{-2.35}$	$0.03 < D < 17.99$ And $1.2 < K < 2.6$
41	$D = 0.08\ W^{0.05}\ K^{1.48}$	$1.49 < W < 3963$ And $1.2 < K < 2.6$

Note: A = bank-full cross-sectional area; B = meander belt width; D = bank-full mean depth; K = channel sinuosity; L_b = along-channel bend length; L_m = meander wavelength; R_c = loop radius of curvature; W = bank-full width. 1 ft = 0.3048 m.

Table 6-4 Limits of Data Sets used to Derive Regime Formulas (FISRWG 1998, with permission from the USDA)

Reference	Data source	Median bed-material size (mm)	Banks	Discharge (m^3/s)	Sediment concentration (ppm)	Slope	Bedforms
Lacey (1958)	Indian canals	0.1 to 0.4	Cohesive to slightly cohesive	2.37 to 237.3	< 500		
Blench (1969)	Indian canals	0.1 to 0.6	Cohesive	0.02 to 2,372.8	< 30[a]	Not specified	Ripples to dunes
Simons and Albertson (1963)	U.S. and Indian canals	0.318 to 0.465	Sand	2.37 to 9.5	< 500	0.000135 to 0.000388	Ripples to dunes
		0.06 to 0.46	Cohesive	0.12 to 2,095.2	< 500	0.000059 to 0.00034	Ripples to dunes
		Cohesive, 0.029 to 0.36	Cohesive	3.25 to 12.1	< 500	0.000063 to 0.000114	Plane
Nixon (1959)	U.K. rivers	Gravel		16.61 to 428.3	Not measured		
Kellerhals (1967)	U.S., Canadian, and Swiss rivers of low sinuosity, and lab	7 to 265	Noncohesive	0.03 to 1,675.2	Negligible	0.00017 to 0.0131	Plane
Bray (1982)	Sinuous Canadian rivers	1.9 to 145		4.60 to 3,284.0	"Mobile" bed	0.00022 to 0.015	
Parker (1982)	Single-channel Canadian rivers		Little cohesion	8.38 to 5,028.0			
Hey and Thorne (1986)	Meandering U.K. rivers	14 to 176		3.27 to 355.2	*Qs* computed to range up to 114	0.0011 to 0.021	

[a] Blench (1969) provides adjustment factors for sediment concentrations between 30 and 100 ppm. 1 ft^3/s = 0.0283 m^3/s.

influence channel form. For example, many popular hydraulic geometry equations express the stable width solely as a function of bank-full discharge. Intuitively, it would be expected that the width of a channel with sandy banks would be greater than that of an equivalent stream with clay banks. Indeed, Schumm's relationship between width-to-depth ratio (F) and the silt-clay weighted percentage in the channel perimeter (M) confirms this expectation empirically. If Schumm's relationship is valid, a width equation based only on discharge cannot fully account for observed width variability. Clearly, the generation of reliable results through application of simple and imperfect morphological relations

Table 6-5 Coefficients for Selected Hydraulic Geometry Formulas (FISRWG 1998, with permission from the USDA)

References	Data	Domain	k_1	k_2	k_3	k_4	k_5	k_6	k_7	k_8	k_9
Nixon (1969)	U.K. rivers	Gravel-bed rivers		0.5		0.545	0.33		$1.258n^{2b}$	−0.11	
Leopold et al. (1964)	Midwestern U.S.		1.65	0.5			0.4			−0.49	
	Ephemeral streams in semiarid U.S.			0.5			0.3			−0.95	
Kellerhals (1967)	Field (U.S., Canada, and Switzerland) and laboratory	Gravel-bed rivers with paved beds and small bed material concentration	1.8	0.5		0.33	0.4	−0.12[a]	0.00062	−0.4	0.92[a]
Schumm (1977)	U.S. (Great Plains) and Australia (Riverine Plains of New South Wales)	Sand-bed rivers	$37k_1^*$	0.38		$0.6k_4^*$	0.29	−0.12[a]	$0.01136k_7^*$	−0.32	
Bray (1982)	Canadian rivers	Gravel-bed rivers	3.1	0.53	−0.07	0.304	0.33	−0.03	0.00033	−0.33	0.59
Parker (1982)	Single-channel Alberta rivers	Gravel-bed rivers, banks with little cohesion	6.06	0.444	−0.11	0.161	0.401	−0.0025	0.00127	−0.394	0.985
Hey and Thorne (1986)	U.K. rivers	Gravel-bed rivers with									
		Grassy banks with no trees or shrubs	2.39	0.5		0.41	0.37	−0.11	$0.00296k_7^{**}$	−0.43	−0.09
		1-5% tree/shrub cover	1.84	0.5		0.41	0.37	−0.11	$0.00296k_7^{**}$	−0.43	−0.09
		Greater than 5-50% tree/ shrub cover	1.51	0.5		0.41	0.37	−0.11	$0.00296k_7^{**}$	−0.43	−0.09
		Greater than 50% shrub cover or incised floodplain	1.29	0.5		0.41	0.37	−0.11	$0.00296k_7^{**}$	−0.43	−0.09

Notes: b_n = Manning n.
$k_1^* = M^{-0.39}$, where M is the percent of bank materials finer than 0.074 mm. The discharge used in this equation is mean annual rather than bank-full.
$k_4^* = M^{0.432}$, where M is the percent of bank materials finer than 0.074 mm. The discharge used in this equation is mean annual rather than bank-full.
$k_7^* = M^{-0.36}$, where M is the percent of bank materials finer than 0.074 mm. The discharge used in this equation is mean annual rather than bank-full.
$k_7^{**} = D_{54}^{0.84} Q_x^{0.10}$, where Q_x = bed material transport rate in kg s^{-1} at water discharge Q, and D_{54} refers to bed material and is in mm.
[a] Bed material size in Kellerhals' equation is D_{90}.

relies heavily on good insight and sound judgment on the part of the individual responsible for their application.

A misapplication of empirical relationships was lampooned by Mark Twain (1944) in *Life on the Mississippi.* Describing the Mississippi River cutoffs of which he had knowledge, he conceived a simple empirical relationship between river shortening and time, and then used it to predict the historical and future lengths of the Mississippi River, concluding that:

> Geology never had such a chance, nor such exact data to argue from! In the space of 176 years, the Lower Mississippi has shortened itself 242 miles. That is an average of a trifle over one mile and a third per year. Therefore, any calm person, who is not blind or idiotic, can see that in the Old Oölitic Silurian Period, just a million years ago next November, the Lower Mississippi River was upwards of 1,300,000 miles long, and stuck out over the Gulf of Mexico like a fishing rod. And by the same token, any person can see that 742 years from now the Lower Mississippi will be only a mile and three-quarters long, and Cairo and New Orleans will have joined their streets together, and be plodding comfortably along under a single mayor and a mutual board of aldermen. There is something fascinating about science. One gets such wholesale returns of conjecture out of such a trifling investment of fact.

The primary points of this passage are that, no matter what their basis in fact and observation, empirical relationships cannot be extrapolated either backward or forward in time, and engineers must avoid falling into the trap of designing a project based solely on "…wholesale returns of conjecture out of a trifling investment of fact."

6.6 CHANNEL STABILITY AND INSTABILITY

In designing river enhancement and channel rehabilitation projects the design engineer must recognize that rivers are dynamic systems, and must consider both the existing and possible future channel morphologies in the design. The problem is compounded when engineering interventions are planned, because the future morphology of the channel depends not only on the natural, or autonomous, evolution of the system, but also on channel response to construction, operation, and maintenance of the project. For this reason, it is important for the design engineer to acquire a broad understanding of the current stability status of the project reach and the extended channel network and to use this understanding to predict the type and extent of adjustments to the fluvial system likely to be triggered by the project. The capability to predict system response to the proposed works is vital to ensure that the selected enhancement or rehabilitation measures will work in harmony with both existing and future river conditions. The concept of channel stability status (which incorporates instability) builds on the basic geomorphic principles introduced previously and may be applied to the river at system and local scales.

6.6.1 System Stability

The geomorphic concept underpinning stability assessment in rivers is that over time the cross-sectional dimensions and longitudinal slope of the channel of an alluvial stream adjust so that the channel is able to convey the discharges of water and sediment supplied from upstream with no net change in hydraulic geometry or planform. On this basis, a stream may be classified as either *stable* or *unstable*, depending on whether the channel has adjusted or is still adjusting to the flow and sediment regimes. Mackin (1948) expressed the stability concept in his definition of the *graded stream*:

> A graded stream is one in which, over a period of years, slope is delicately adjusted to provide, with available discharge and with prevailing channel characteristics, just the velocity required for the transportation of the load supplied from the drainage basin. The graded stream is a system in equilibrium.

By definition, a graded stream does not have to have a channel that is static or fixed, and it may exhibit temporary morphological changes in response to the impacts of extreme events. Alluvial channel morphology is certain to be affected by major floods or protracted periods of low water, but provided that the time for moderate events to restore the graded morphology (termed the *recovery time*) is shorter than the return period for the extreme event (*recurrence interval*), the channel may be considered to be dynamically stable. The key attribute of a graded stream is that fluvial processes operating under formative flows tend to restore channel morphology to the graded condition following disturbance, rather than perpetuating or amplifying the changes imposed by the extreme event. A term commonly used for this type of stability is *dynamic equilibrium*.

The concept of dynamic equilibrium is inherent in a widely applied (and often misapplied), qualitative relationship for adjustment in alluvial streams proposed by Lane (1955):

$$QS \sim Q_s D_{50}$$

where Q = water discharge, S = slope, Q_s = bed-material load, and D_{50} = median size of the bed material. This relationship is commonly visualized as *Lane's balance* (Fig. 6-10). Mackin's explanation of how a graded stream responds to changes in the controlling variables is easily illustrated by Lane's balance, which shows how a change in any of the four driving variables will tend to produce a response in the others such that equilibrium is restored. When a channel is in dynamic equilibrium, it has adjusted these four variables so that the sediment transported into the reach is also transported out, without aggradation or degradation.

It should be noted that the map coordinates of a graded stream may change through time as the river reworks the

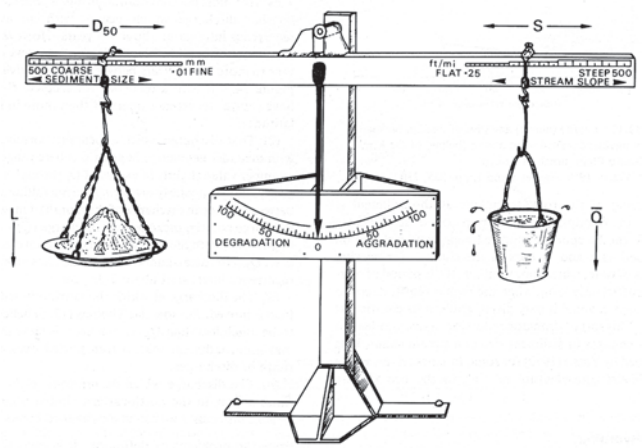

Fig. 6-10. Lane's balance (Rosgen 1996, with permission from Wildland Hydrology).

floodplain through meandering or braiding, provided that the reach-averaged values of width, depth, slope, and planform geometry are time-invariant. Indeed, meandering provides an important mechanism for an alluvial stream to adjust the slope relatively quickly and without transferring the large amounts of (relatively coarse) bed sediment necessary to alter slope materially through aggradation and degradation. Viewed in this context, changes in channel length achieved through meander extension and cutoff represent a natural adjustment mechanism, and planform changes do not necessary indicate disequilibrium. When natural cutoffs occur, the river may be obtaining additional length elsewhere through meander growth, with the net result being that the overall reach length, and therefore slope, remains unchanged.

In nature, few rivers actually attain a graded condition because the driving variables change through time. The concept still has value, however, because it provides an indication of the likely trend of channel evolution over engineering time scales, which are generally less than about 50 years. Although it is a mistake to assume that a river will be stable or unchanging over this period, the concept of dynamic equilibrium gives useful clues regarding the rates and types of adjustment that may be expected as the channel evolves toward a graded condition. Also, the proximity of the system to a graded condition gives an indication of how the river will respond to engineering interventions and, particularly, how sensitive it is to being destabilized. Finally, the geomorphic concept of the stable channel is valuable in that it establishes a reference point for the definition and treatment of morphological instability on a variety of scales.

6.6.2 Channel Instability

Channel instability is defined as temporal change in the hydraulic geometry, long profile, or planform pattern of a channel because of inequality between the supply and removal of sediment. Instability is, in a broad sense, inherent in the natural action of rivers in changing the landscape by eroding, transporting, and depositing sediment. In fact, the situation where sediment input exactly matches sediment output (dynamic stability) is actually a special case that can strictly occur only in subreaches of a fluvial system and that cannot persist for long periods.

Instability may result when the flow of water and transfer of sediment through a drainage network is disrupted or significantly perturbed. The fluvial system initially responds to disequilibrium by adjusting channel morphology in ways that tend to restore the previous equilibrium or graded condition. If stability is restored through a process-response that returns channel morphology to the predisturbance configuration (or something essentially similar), then the adjustments involved are restricted to the immediate vicinity of the disruption and, by definition, constitute *local instability*. However, if the magnitude of the change in driving variables is large, or the river is sensitive to destabilization because of channel characteristics (high stream power, easy availability of sediment, high erodibility of bed and bank materials, or absence of geologic or artificial controls) or proximity to a geomorphic threshold, then morphological adjustments can take the channel toward a new equilibrium configuration different from the predisturbance morphology. Under these circumstances, *system instability* propagates throughout the channel network and may spread into the watershed or even into neighboring systems.

6.6.3 Local Instability

Local instability refers to channel changes that result from adjustments to a fluvial system inherent in the maintenance of a dynamically stable configuration. There are three common causes of local instability. The first is channel response to temporary variations in discharge or sediment flux. Typically, discharge variations occur seasonally, or result from longer periods of above-average or below-average precipitation, whereas sediment input varies because of pulsing of sediment between storage and transport reaches or shifts in upstream channel alignment. The second cause is the series of adjustments that occur when channel morphology is altered by, and subsequently recovers from, the impact of a rare event such as a flood, drought, wildfire, or earthquake. The third cause is disruption of fluvial forms or processes associated with human activity or construction of infrastructure in or around a channel that triggers the channel changes necessary to accommodate the impacts of that disturbance within the existing, dynamically stable condition. Local instability is not symptomatic of significant disequilibrium in the system, but this does not mean that the processes of bed scour, bar deposition, and bank erosion associated with local instability are limited to a single location or that their consequences are negligible.

A good example of local instability is bankline movement due to planform evolution in a meandering river. Whereas the reach-averaged dynamically stable parameters of hydraulic geometry and slope remain steady, individual bends in a meandering river grow, migrate, and are abandoned. On average, channel lengthening through bank erosion along the concave bank in growing meander bends is offset by cutoffs at other bends as part of the natural meandering process. Under these circumstances, problems associated with bank erosion at a bend are amenable to local bank protection works, provided that the hydraulic geometry and slope of the reach are not significantly altered. However, it should be kept in mind that the channel may respond to stabilization of one bend through accelerated morphological activity in adjacent free bends. Hence, care must be taken to ensure that management of local instability at one location does not transfer or concentrate this natural process elsewhere in a way that is detrimental to the dynamic stability of the system.

The causes of local instability are not limited to the channel. This type of instability can also be triggered by activities in surrounding riparian and floodplain areas. For example, a reach of stream may display local channel widening due to trampling and overgrazing by cattle, while upstream and downstream reaches are not directly affected and are able to remain dynamically stable. In this situation, a local management solution, based on restriction of access by fencing, construction of suitably reinforced access ramps at water points, and reinstatement of the regime width, is all that is needed to alleviate a site-specific problem. Site-specific instability problems may respond satisfactorily to design alternatives developed using reference reach techniques.

In practice, however, it is not always easy to establish whether a local instability problem results from and is amenable to a local solution or is symptomatic of more serious, system-scale impacts and adjustments. Even if the engineer suspects that local instability results from adjustments of the fluvial system to channel instability, human activities, or catchment land-use changes, they may lack the authority or resources to address off-site and nonpoint causes. Under these circumstances, the engineer may have to modify the adopted solution by constructing a local structure with the capability to continue functioning successfully even when system-driven channel adjustments have significantly altered local conditions. For example, local bank stabilization may be required at the outside of a migrating bend on a river that is predicted to degrade in the future because of system instability downstream. Ideally, the system-scale problem (degradation) should be addressed directly using one or more grade control structures, but this may be institutionally or financially unfeasible. Recognition that the problem is not entirely local is nonetheless still valuable, as it allows the engineer to determine the degree of additional toe scour protection necessary to ensure that the bank protection measures can withstand the additional bed lowering associated with degradation during the design life of the project.

6.6.4 System Instability

Adjustments involved in system instability typically involve *aggradation* (increasing bed elevation), *degradation* (decreasing bed elevation), or *planform metamorphosis* (abrupt alteration from one planform pattern to another). The response of an alluvial stream to an episode of system instability is, in detail, unique to that stream and the circumstances and timing of the events responsible for destabilization. Although channel evolution models (discussed later in the section on stream classification) have been developed to characterize commonly observed styles and sequences of adjustment in unstable systems, there is no generally applicable model for process-response to system instability.

Serious engineering and river-management problems often result from channel instability and may include endangerment of bridges, buildings, roads, and other infrastructure, undermining of pipeline and utility crossings, accelerated bed and bank erosion, loss of valuable environmental habitat, and increased sediment loads that adversely impact flood control and navigation channels, water quality, reservoir areas, and wetlands. Figure 6-11 illustrates some common consequences of system instability.

The causes of system instability can be grouped into three categories: downstream factors, upstream factors, and basin-wide factors.

6.6.4.1 Downstream Factors The stability of a fluvial system can be affected significantly by changes to downstream base level. *Base level* refers to the downstream limit of the channel network, the elevation of which defines the datum for measurement of potential energy in the system upstream. In subcritical flow, the water surface elevation at the downstream limit of the channel controls the longitudinal water surface profile for a stream. Similarly, the bed elevation at the downstream limit of the system represents the origin of the thalweg profile. It follows from these facts that changes in base level have strong potential to trigger system instability.

Base-level lowering, due to engineering interventions such as meander cutoffs or channelization (Fig. 6-12), triggers process-response by locally steepening the slope and increasing bed-material transport capacity. As capacity exceeds supply, the bed scours to make up the supply deficit as the channel adjusts through degradation. This adjustment may generate only local instability if armoring stabilizes the bed or a geological control prevents significant bed lowering. However, if unchecked by a local channel response or control, a wave of degradation migrates upstream through the system as a headcut or knickpoint. If degradation triggers bank instability, then a wave of channel widening may follow the headcut, generating further morphological adjustments and additional sediment input

(a) Bed and Bank Instability

(c) Damage to Infrastructure

(b) Formation of Gullies in Floodplain

(d) Excessive Sediment Deposition in Lower Reaches of Watershed

Fig. 6-11. Consequences of system instability: (a) bed and bank instability, (b) formation of gullies in floodplain, (c) damage to infrastructure, and (d) excessive sediment deposition in lower reaches of watershed.

Fig. 6-12. Channelized stream and abandoned old channel.

to the channel. As the degradational wave moves upstream, the zone of increased slope and additional sediment production moves with it. Sediment supply to the downstream reaches, coupled with local slope reduction due to upstream bed lowering, then triggers aggradation, which also migrates upstream through the system. Subsequently, sediment output and bed elevation at the downstream limit of the system display damped oscillation until, following a number of cycles of degradation/aggradation, the long profile is adjusted to the new base level and stability is restored.

6.6.4.2 Upstream Factors The stability of a fluvial system can also be significantly affected by changes to upstream reaches that alter the downstream discharge or sediment supply. The flow regime and sediment load together constitute the two main driving variables responsible for forming and maintaining the channel, and it is no surprise that the stability of an alluvial river may well be disturbed by changes in one or both of these factors. Upstream factors are often affected by engineering and river-management projects. River regulation by a dam or diversion structure is a common cause of downstream channel adjustment that serves to illustrate the types and complexity of system response that may result from such changes.

Channel response downstream of a dam or diversion structure depends on the way the works are constructed and operated. When the structure is built, sediment supply downstream may be elevated by disruption of the channel and floodplain during construction. This may increase supply over transport capacity, inducing an initial adjustment through aggradation. However, this response will be absent if appropriate sediment-control measures are applied on site. Once the works are complete, process-response downstream will depend on the balance of changes in the water and sediment regimes. Following closure of the dam or diversion, sediment is trapped in the pool upstream from the structure. Sediment-free water released from the structure then scours the bed downstream, generating degradation in the first few kilometers below the dam. Initially, the flush of sediment produced drives aggradation further downstream, but as the channel slope immediately downstream of the dam flattens, sediment output decreases, and the leading edge of the zone of degradation migrates downstream to re-erode recently deposited sediment and sends it further downstream as an aggradational wave. This river response to closure of a dam has been observed in many rivers, and yet this pattern of adjustment is by no means universal. To explain why, it is necessary to consider the other morphological responses that may dominate adjustment of the fluvial system. For example, if the bed downstream of the dam includes a widely graded, coarse-grained fraction, bed armoring may limit degradation and stabilize the bed at a slope *steeper* than that prior to dam construction. The same effect may result from the presence of a geological control, whereas widening with limited reduction in bed level may be triggered if the channel banks downstream of the dam are close to the critical height for mass instability (Thorne and Osman 1988). If regulation by the dam significantly reduces the magnitude or frequency of sediment-transporting flows, degradation may be limited or negligible, and if a reduction in the competence of the main stream is coupled with the input of a substantial sediment load from unregulated tributaries, aggradation may occur downstream of the dam, where degradation was expected (Biedenharn 1984). The point of citing these examples is to demonstrate that morphological response to change in one or more upstream factors is complex and difficult to predict. The specific attributes of system instability and channel response depend not only on the magnitude of changes imposed on the flow regime and sediment loads, but also on the sensitivity and boundary conditions of the downstream channel network.

6.6.4.3 Basin-Wide Factors In morphological studies, flow regime and sediment load are often cited as the independent variables controlling channel form and process. In reality, these variables are not truly independent, but depend in turn on the characteristics of the watershed, including factors such as climate, rainfall-runoff relationship, natural vegetation, land use, and resource management. Even if upstream and downstream factors remain constant, changes in the watershed may trigger instability in the fluvial system that leads to widespread morphological adjustments. For example, urbanization can increase peak flows and reduce sediment delivery to the channel network. These changes would reinforce one another (see Lane's balance in Fig. 6-10) to drive marked degradation in the channel draining the urbanized area, with morphological impacts migrating upstream and downstream through the system by slope adjustment and sediment transmission, respectively. Afforestation of the headwaters of a stream could produce very different morphological adjustments, depending on whether fluvial processes respond more strongly to decreases in runoff (due to increased consumptive use in the watershed) or elevated sediment delivery (due to erosion along forestry roads and ditches). In practice it is even more difficult to predict the morphological response of a fluvial system to basin changes than to upstream changes. In attempting to develop the capability to predict channel response to basinwide changes, engineers and river managers should make every effort to familiarize themselves with the geography of the basin, processes operating in the fluvial system, sedimentary features, and channel morphology. This knowledge, together with application of conventional hydrologic, hydraulic, and sediment-transport analyses, represents the best current option for regional sediment management and channel stabilization in a changing watershed.

6.7 CHANNEL CLASSIFICATION

The existence of a few distinctive channel forms provides the rationale for morphological classification of channels. The relationships linking channel form to fluvial process suggest that the morphological classification of a channel may allow the morphologist to infer process from classified channel form. The first step in classification is to identify whether the channel is either alluvial or nonalluvial. An *alluvial* channel is "self-formed" in that the bed and banks are composed of material transported by the river under present flow conditions. The channel is therefore free to adjust dimensions and location in response to changes in flow and sediment load. Conversely, a *nonalluvial river* is neither self-formed nor free to adjust. Examples of nonalluvial rivers include bedrock-controlled channels and streams flowing over very coarse glacial deposits.

Many classification schemes rest on channel planform pattern and stem from Leopold and Wolman's (1957) classification of channel planforms as straight, meandering, or braided. In this respect, the diagram produced by Brice (1975) is notable because it builds on earlier schemes to cover a wide range of commonly observed planforms and has proved useful in engineering geomorphic studies (Fig. 6-13). Schumm (1981; 1985) recognized an even broader range of channel patterns, although the basic straight, meandering, and braided patterns are still recognized within his classification of 14 basic patterns (Fig. 6-14).

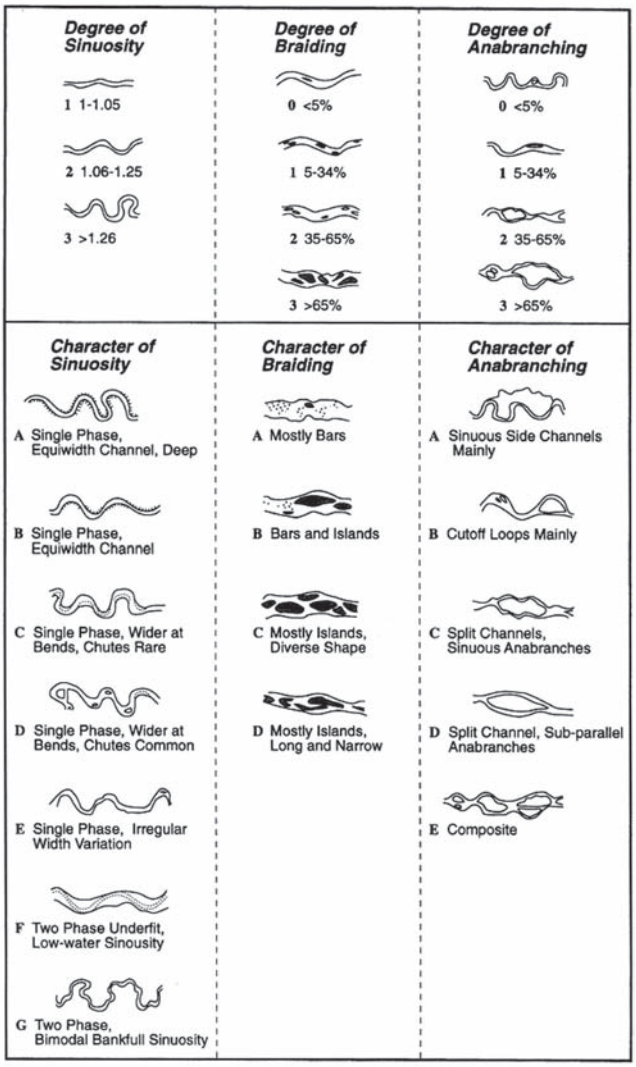

Fig. 6-13. Channel Pattern classification devised by Brice (after Brice 1975).

Knighton (1998) related Schumm's 14 patterns to investigations by Carson (1984a; 1984b); Knighton and Nanson (1993); and Nanson and Knighton (1996). Knighton (1998) noted that the patterns in Fig. 6-14 are related to the classification by the type of sediment load (Schumm 1976): bed load, mixed load, and suspended load. Types 1 through 5 are bed load streams, Types 6 through 10 are mixed load streams, and Types 11 through 14 are suspended load streams. Carson (1984a; 1984b) specified two types of wandering, gravel-bed rivers. The first is characterized by very rapid bend migration and frequent chute cutoffs of point bars, similarly to Type 3. A second wandering type is similar to Type 14, with vegetated islands separating most of the channels. Knighton and Nanson (1993) point out that coarse-grain, anastomosing channels do exist. Therefore, despite the variety of channel patterns that have been investigated and discussed, a continuum of channel patterns does exist and these patterns are controlled by the interaction of a series of continuous variables. Figure 6-14 suggests some of the variables that should be considered, such as sediment size and transport mechanism, whereas Bledsoe's (1999) logistic threshold approach indicates that specific stream power and sediment size are also important (Fig. 6-2).

In parallel with the development of his morphological classification, Schumm (1977) considered of the type of sediment load being transported by the stream, the percentage of silt and clay in the channel bed and banks, and the stability of the channel to describe the morphology associated with stable conditions and the morphological changes expected in response to instability through aggradation or degradation (Table 6-6). For purposes of this classification system, a stable channel complies with Mackin's definition of a graded stream in that slope is adjusted to supply just the sediment transport capacity necessary to convey the sediment load supplied from upstream. An unstable stream may be either *degrading* (eroding) or *aggrading* (depositing). It is very important to remember that the work on which this classification was based was conducted in the Midwestern United States during the second half of the 20th century. Extrapolation or transfer of the classification or related implications to other times and places should, therefore, be done cautiously.

Other, more ambitious stream classifications have been developed by Neill and Galay (1967); Rundquist (1975); and Rosgen (1994). These classifications go well beyond a description of channel form to include description of land use and vegetation in the basin, geology of the watershed, hydrology, channel bed and bank materials, sediment concentration, channel pattern, and channel stability.

Rosgen (1994) presented a stream classification system similar to the earlier Rundquist (1975) system. Rosgen (1996) included classification of valley type and introduced an entrenchment ratio, defined as the ratio of the width of the flood-prone area to the surface width of the bank-full channel. Table 6-7 is a summary of delineative criteria for broad-level classification from Rosgen (1994). Each of the stream types can be associated with dominant bed material types as follows: bedrock—1, boulder—2, cobble—3, gravel—4, sand—5, and silt/clay—6.

Through modification of Fig. 6-14, Fig. 6-15 attempts to combine some of the concepts of Schumm and Rosgen. Schumm's classification system depends heavily on his Midwestern experience, whereas Rosgen's experience began in steep mountain streams. In addition, Schumm's (1977) classification does not specifically include incised channels, which are included in Rosgen's (1994) F and G classes. Figure 6-15 includes Rosgen's C, D, DA, and E classes, and could be expanded to include all of Rosgen's (1994) classes. The point of Fig. 6-15 is to demonstrate that moving from class to class is a somewhat predictable morphological response that manages energy, materials, and channel planform to reestablish the balance between the local capacity of

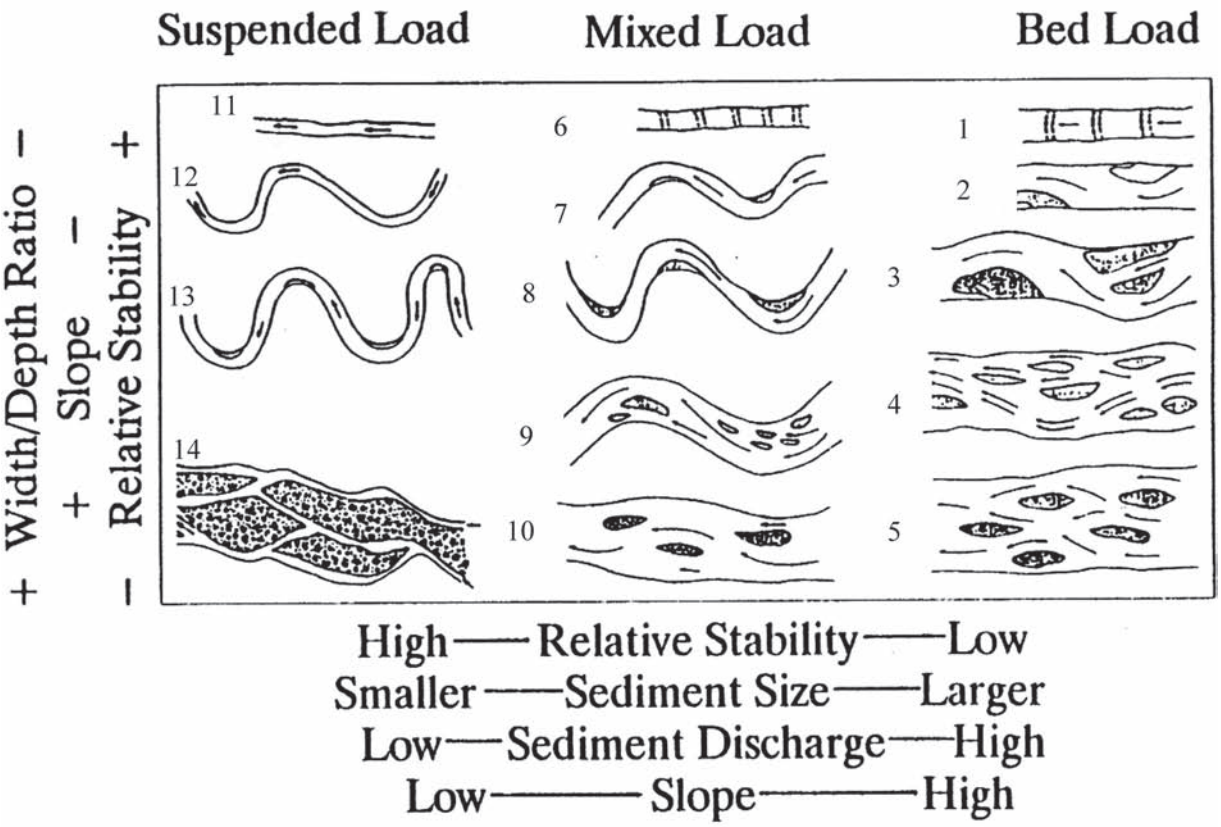

Fig. 6-14. Channel classification based on pattern and type of sediment load (Schumm 1981, with permission from SEPM [Society for Sedimentary Geology]).

Table 6-6 Classification of Alluvial Channels (Schumm 1977, with permission from S. Schumm)

Mode of sediment transport and type of channel	Channel sediment (*M*) (%)	Bedload (percentage of total load)	Channel stability		
			Stable (graded stream)	Aggrading (excess sediment discharge)	Degrading (deficiency of sediment discharge)
Suspended load	>20	<3	Stable suspended-load channel. Width/depth ratio <10; sinuosity usually >2.0; gradient, relatively gentle	Depositing suspended load channel. Major deposition on banks cause narrowing of channel; initial streambed deposition minor	Eroding suspended-load channel. Streambed erosion predominant; initial channel widening minor
Mixed load	5-20	3-11	Stable mixed-load channel. Width/depth ratio >10, <40; sinuosity usually <2.0, >1.3; gradient moderate	Depositing mixed-load channel. Initial major deposition on banks followed by streambed deposition	Eroding mixed-load channel. Initial streambed erosion followed by channel widening
Bed load	<5	>11	Stable bed-load channel. Width/depth ratio >40; sinuosity usually <1.3; gradient, relatively steep	Depositing bed-load channel. Streambed deposition and island formation	Eroding bed-load channel. Little streambed erosion; channel widening predominant

Table 6-7 Summary of Delineative Criteria for Broad-Level Classification (Rosgen 1994, with permission from Wildland Hydrology)

Stream type	Entrench. ratio	*w/d* ratio	Sinuosity	Slope	Meander belt/ bank-full width	Dominant bed material[a]
Aa+	<1.4	<12	1.0–1.1	> 0.10	1.0–3.0	1,2,3,4,5,6
A	<1.4	<12	1.0–1.2	0.04–0.10	1.0–3.0	1,2,3,4,5,6
B	1.4–2.2	>12	>1.2	0.02–0.039	2.0–8.0	1,2,3,4,5,6
C	>2.2	>12	>1.2	< 0.02	4.0–20	1,2,3,4,5,6
D	na	>40	na	< 0.04	1.0–2.0	3,4,5,6
DA	>2.2	variable	variable	< 0.005	na	4,5,6
E	>2.2	<12	>1.5	< 0.02	20–40	3,4,5,6
F	<1.4	>12	>1.2	< 0.02	2.0–10	1,2,3,4,5,6
G	<1.4	<12	>1.2	< 0.039	2.0–8.0	1,2,3,4,5,6

[a] Dominant bed material key: 1, bedrock; 2, boulders; 3, cobble; 4, gravel; 5, sand; 6, silt/clay.

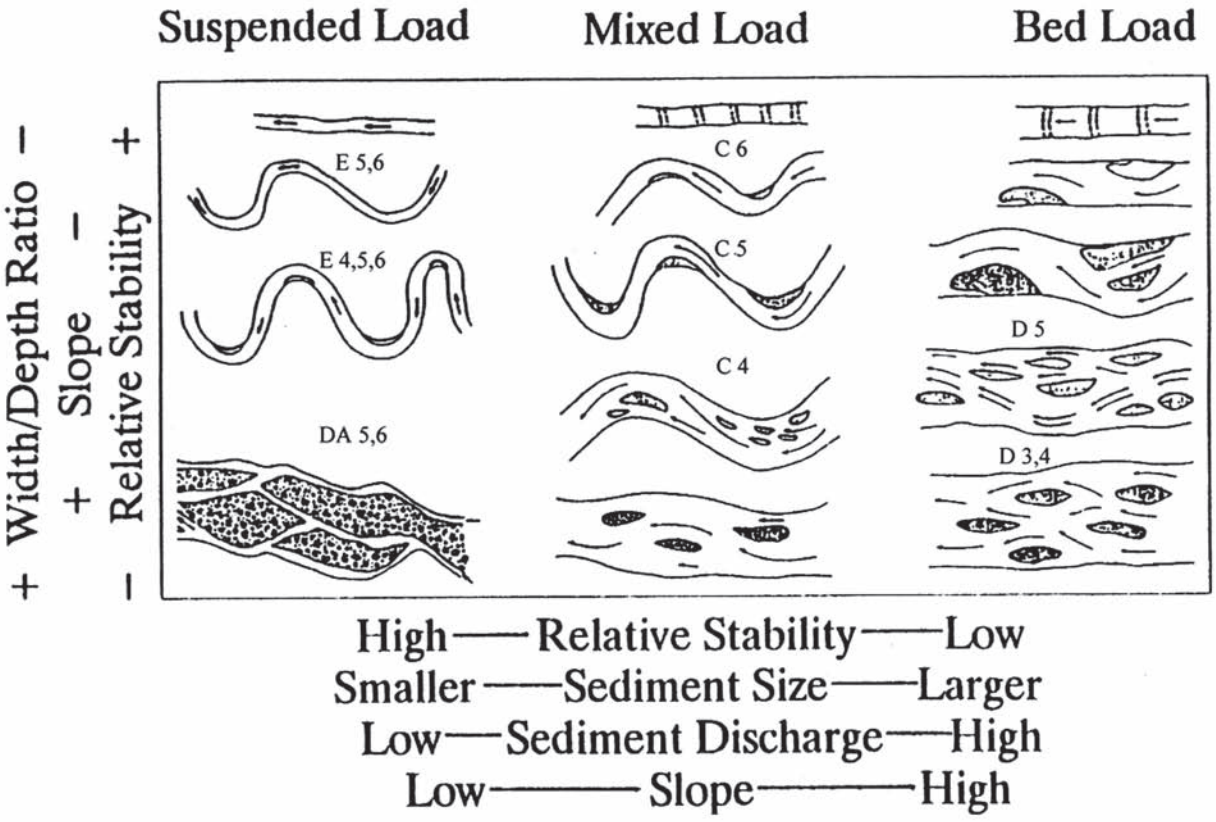

Fig. 6-15. Channel classification combining aspects of Schumm (1981) and Rosgen (1994) (Schumm 1981 and Rosgen 1994, with permission from SEPM [Society for Sedimentary Geology]).

the channel to convey water and sediment and the discharge and supply of sediment from upstream.

Thorne et al. (1997) point out that many classification systems fail to account for dynamic adjustment or evolution of the fluvial system. Downs (1995) developed a comprehensive system that incorporates the classifications of Brice (1975) and Brookes (1981) and builds on their earlier work by linking observed trends and patterns of adjustment to the fluvial and sediment processes responsible for driving channel change (Fig. 6-16). Adjustment-based classifications such

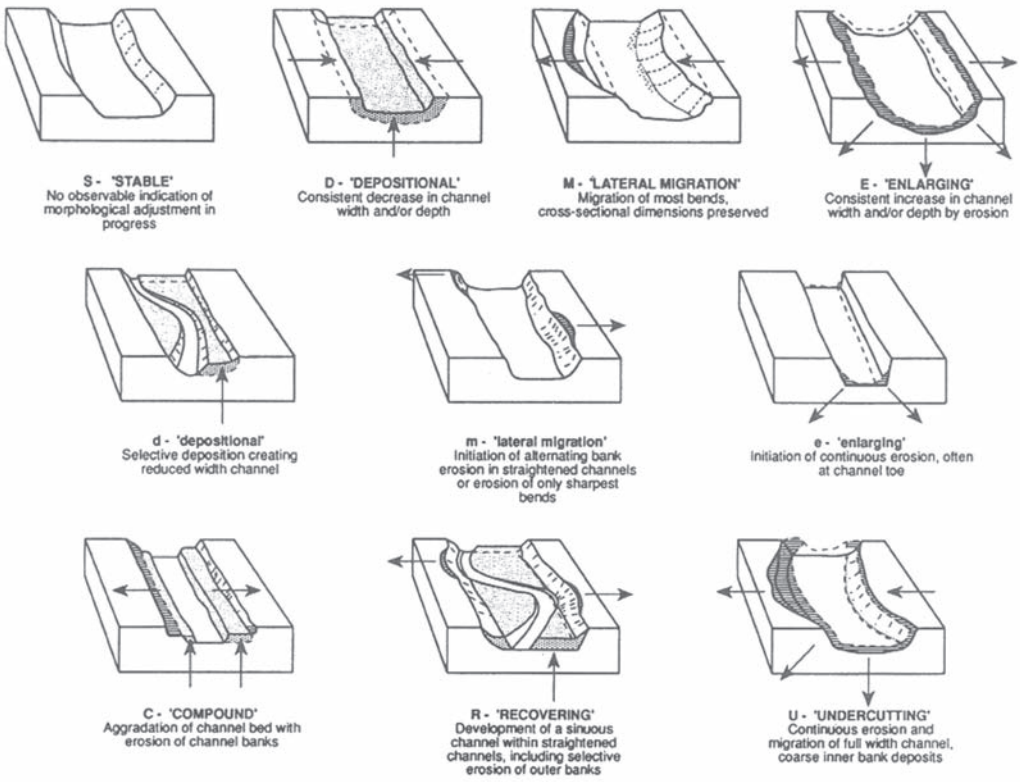

Fig. 6-16. Downs's channel classification, based on trends and types of morphological change (modified from Downs 1995).

as that of Downs differ fundamentally from morphology-based schemes in that each system requires the observer to determine the current stability status of the channel and the nature of channel adjustment processes. Because data may not be available to document change, these schemes require sound judgment on the part of the engineer, who must infer processes and trend of adjustment from channel form.

Although any conceivable morphological channel classification will oversimplify the variability of channel patterns in nature, the underlying concept of a continuum of channel patterns that is related to a limited number of controlling variables remains valid. The opportunity and challenge for the river engineer is to develop and refine associations between channel pattern characteristics and controlling variables and to use these relationships with care and caution to predict the manner in which pattern will change in response to alteration of controlling variables. Schumm (1976) points out that major alterations in pattern change, which he terms channel metamorphosis, may be triggered by a relatively minor change in a controlling variable, if the existing pattern is near a geomorphic threshold.

6.8 CHANNEL EVOLUTION MODELS

Numerous geomorphological studies have used data developed from different locations to infer landform development through time, commonly employing a technique termed location-for-time substitution. This technique assumes that by observing channel form as one moves downstream along a channel, the effect of physical processes at one location through time can be predicted; that is, changing location is substituted for changing time. This technique was used to develop a channel evolution model (CEM) for Oaklimeter Creek, an incised stream in northern Mississippi (Schumm et al. 1984). Simon and Hupp (1987) later developed a similar model of channel evolution based on their observations of incised streams in western Tennessee.

The CEM (Fig. 6-17) consists of five channel-reach types, which describe the evolutionary phases typically encountered in an incised channel. These evolutionary phases range from strong disequilibrium to a new state of quasi-equilibrium. Quasi-equilibrium implies that the system is not static and changes through time, but over a period of years the average condition is one of stability. The model is based on the assumption that moving downstream through the system is equivalent to remaining in place and monitoring changes due to the passage of time. The response at any given location in the channel can then be predicted from the morphology of downstream channel locations.

The channel reach types in the CEM are labeled I through V and are assumed to occur consecutively in the downstream direction. The CEM assumes that each channel type will occur in turn at a given location as the channel evolves. The CEM

channel types are shown in Fig. 6-17. Type I reaches are located upstream of the actively degrading reach and have not yet experienced significant bed or bank instabilities. These reaches are generally characterized by U-shaped cross sections with little or no recently deposited sediment stored in the channel bed.

Type II reaches are encountered immediately downstream of Type I reaches. Bed degradation is the dominant process in the Type II reach. Type II channels are over steepened reaches where the sediment transport capacity exceeds the sediment supply. Although the channel is actively degrading in a Type II reach, the bank heights (h) do not exceed the critical bank height (h_c), and therefore, reach-scale geotechnical bank instability is not encountered.

As bed degradation continues, the bank heights and angles continue to increase. When the bank heights exceed the critical bank height for stability in the Type III reaches, mass failures (geotechnical instability) begin. The dominant process in the Type III reach is channel widening. In places, the Type III reach may continue to be slightly degradational.

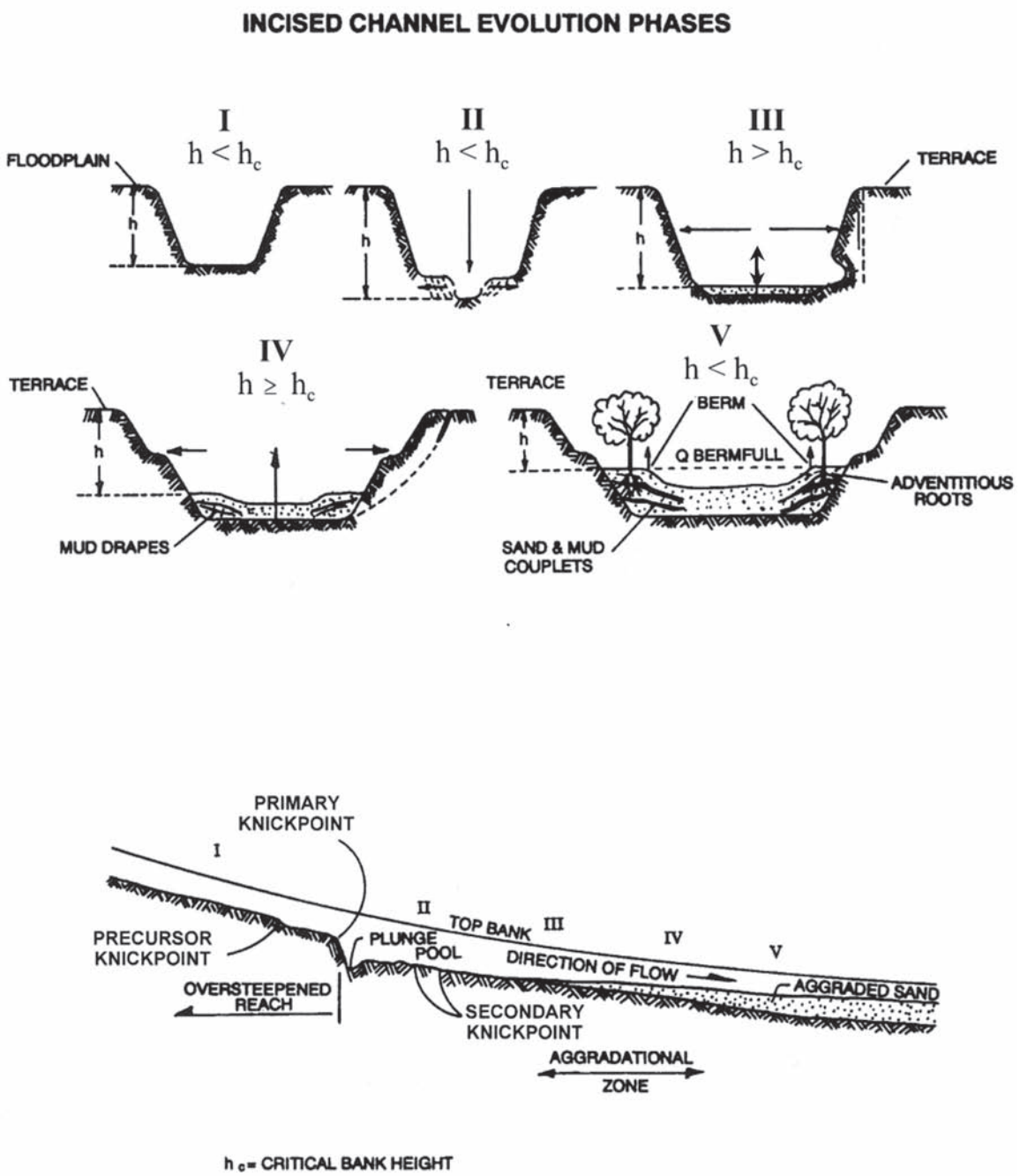

Fig. 6-17. Incised channel evolution sequence (after Schumm et al. 1984).

However, the reduced sediment transport capacity resulting from longitudinal channel slope decrease combined with increased sediment supply from upstream due to instability and from bank failures within the reach often results in the initiation of sediment deposition on the channel bed.

Type IV reaches are downstream of the Type III reaches and represent the first manifestation of the incising channel returning to a new state of dynamic equilibrium. In the Type IV reach, geotechnical bank instabilities and channel widening may continue, but at a much reduced rate. The sediment supply from upstream (Type III) exceeds the sediment transport capacity, resulting in aggradation of the Type IV channel bed. The Type IV reach is also characterized by the development of *berms*, which are depositional features along margins of the overwidened channel. These berms represent the beginning of a new inner channel with dimensions adjusted to the flow and sediment regime.

Type V reaches represent a state of dynamic equilibrium, with a balance between sediment transport capacity and sediment supply. Bank heights in the Type V channel are generally less than the critical bank height, and therefore, reach-scale geotechnical bank instability ceases. However, local bank failures can still exist as part of the meander process, or as the results of constrictions, obstructions, or other local factors. The berms that were initiated in the Type IV reach have now become colonized by riparian vegetation, forming a compound channel within the larger incised channel. The equilibrium channel of Type V is of a compound shape, with a smaller inner channel bounded by a narrow floodplain. The original floodplain of the Type I channel is now a terrace.

The channel evolution model addresses the channel stability status within a system context. Dynamic equilibrium in a Type V reach simply implies that system stability has been attained. A Type V reach may exhibit considerable erosion that is part of the natural meander process or some other local process, yet still be classified as being in dynamic equilibrium.

The primary value of the CEM sequence is to underpin identification of the evolutionary state of the channel from field reconnaissance. The morphometric characteristics of the channel reach types can also be correlated with hydraulic, geotechnical, and sediment-transport parameters (Harvey and Watson 1986; Watson et al. 1988). The evolution sequence provides an understanding that although reaches of a stream may differ markedly in appearance, the channel form in one reach is associated with those in adjacent and remote reaches by an evolutionary process. Form, process, and time relate dissimilar reaches of the stream linked to complex response and connectivity in the water and sediment-transfer systems.

6.9 GEOMORPHIC ASSESSMENT

Given the significance of fluvial geomorphology to engineering and management of rivers, the problem remains of gathering the data and qualitative information necessary to characterize and define channel form, process, and stability status in the project river. A thorough geomorphic assessment of the river and watershed is required. Unfortunately, many engineers charged with the design of river projects either fail to fully appreciate the importance of geomorphic assessments, or lack the education or training background to perform them adequately.

Geomorphic assessment is an essential part of the design process for schemes ranging from local bank protection through reach-scale habitat enhancement to master planning for water resource management in an entire watershed. The aims of geomorphic assessment are to provide the baseline information necessary to characterize process-form interactions in the river, identify control points and problem reaches, and support division of the system into geomorphically distinct subreaches that may be individually classified with respect to morphology. Once the system has been characterized and classified, the engineer may assess the stability status on a reach-by-reach basis and predict the medium- and long-term autonomous evolution under a do-nothing scenario. This provides a baseline against which to assess the morphological responses of the project reach and wider system to the proposed engineering, rehabilitation, or water resources project.

Perhaps the most important step in any geomorphic assessment is ensuring that the scope and content match the project goals, authority, channel and watershed characteristics, and available resources. There is no standardized or "cookbook" approach, but over the past two decades a number of assessment schemes have been developed, and these provide valuable guidance based on direct experience (Simons et al. 1982; Schumm et al. 1984; Richardson and Huber 1991; Schall and Lagasse 1991; Shirole and Holt 1991; Robinson and Thompson 1993; Biedenharn et al. 2000b). Typically, existing geomorphic assessment techniques may be subdivided into procedural steps dealing with

1. Assembly of existing and archived data/information in a desk study;
2. Establishment of current channel forms and sediment features through stream reconnaissance and field surveys;
3. Geomorphic analysis and interpretation of historical and contemporary information;
4. Stream classification and assessment of stability status at reach scale;
5. Prediction of past and future morphological evolution and response to proposed project; and
6. Integration of results into engineering design to optimize performance.

For more detailed reviews of practical and procedural issues in geomorphic studies and assessment, the reader is referred to articles by Thorne (1998; 2002).

The results of geomorphic assessment are rarely clear-cut. More often the individual elements of the assessment produce outcomes that are equivocal or even contradictory.

For example, the specific gauge record for a hydrological station may indicate that stages for a given discharge have decreased significantly, whereas the few available repeat cross sections from the same period show variations in bed topography but no evidence for discernible change, and stream reconnaissance indicates that the channel is hydraulically connected to its floodplain. The specific gauge record may suggest that the channel has degraded, but there may be a lack of supporting evidence from resurveyed cross sections and stream reconnaissance that the channel bed and floodplain levels are mutually-adjusted. In these situations, a level of confidence must be assigned to morphological conclusions based on different components of the assessment, based on the quantity, quality, and reliability of the data and the assessor's experience in applying the techniques involved. It may then be possible to reconcile apparently contradictory results by weighing the levels of confidence associated with each one. It is emphasized that sound judgment, based on insight and experience, is essential for accurate geomorphic assessment.

Obviously, geomorphic assessment alone can never provide a proper basis for engineering analysis or design. It is, however, of value when combined with computational and analytical methods for stable channel design. The wider contribution provided by geomorphic assessment is to establish the system context and framework within which the designer may

1. Select hydrodynamic and sediment transport equations appropriate to the stream and conditions;
2. Design stable channel dimensions that mimic natural channel forms and diversity while meeting project goals;
3. Use computer models matched to the alluvial setting and incorporating existing geologic and artificial controls to predict morphological response of the channel system to proposed rehabilitation measures;
4. Integrate environmental features effectively into morphological and engineering aspects of the project;
5. Anticipate maintenance requirements and optimize the design to ensure that the benefits are sustainable; and
6. Consider and propose the scope of post-project appraisal (PPA) and monitoring regime necessary to establish the strengths and weaknesses of project performance.

Geomorphic assessment alone is not sufficient to guarantee that a project will perform adequately with regard to morphological and environmental goals, but it is a valuable and necessary component of the integrated channel design process that is essential to ensure long-term sustainability in river engineering and management projects.

6.10 CLOSURE

Fluvial geomorphology, analytical river mechanics, and sound engineering judgment together provide the foundations for sound river engineering, rehabilitation, and management. Insights and understanding provided by geomorphic principles and identification of causal links between channel form, fluvial processes, and connectivity of the river system can be invaluable in the design of river projects and management strategies. This is the case not only because the engineering geomorphic approach is consistent with environmental goals such as minimizing negative impacts and maximizing biodiversity, but also because solutions that recognize and deal with the causes rather than the symptoms of channel problems represent better engineering. Many engineering stabilization and rehabilitation projects have failed not as the result of deficient hydraulic or structural design, but rather because the significance of geomorphology to the project and the project to geomorphology has not been identified and accounted for in the design. Experience is accumulating that engineering designs guided by knowledge of the fluvial system are able to avoid having to attempt to "tame the river," instead working with the river to produce schemes that have lower long-term maintenance requirements. Engineering-geomorphology thereby opens the door to cost-effective, sustainable solutions that do not commit future generations to heavy and expensive maintenance.

NOTATION

The following symbols are used in this paper:

A	=	area;
A	=	meander amplitude (Leopold et al. 1964);
A	=	bank-full cross-sectional area (in Table 6-3, from FISRWG 1998);
$AR^{2/3}$	=	conveyance;
a	=	coefficient;
B	=	meander belt width (in Table 6-3, from FISRWG 1998);
b	=	exponent;
b_n	=	Manning n (in Table 6-5, from FISRWG 1998);
c	=	coefficient;
D	=	depth (from Kennedy 1895);
D	=	bank-full mean depth (in Table 6-3, from FISRWG 1998);
D_x	=	given sediment size;
D_{50}	=	median size of the bed material (from Lane 1955);
D_{54}	=	bed material (in Table 6-5, from FISRWG 1998);
d	=	average depth of the channel;
dm	=	maximum depth;
F	=	width-to-depth ratio (from Schumm 1977);
f	=	exponent;
h	=	bank height;
h_c	=	critical bank height;

K = channel sinuosity (in Table 6-3, from FISRWG 1998);
k = coefficient;
L = meander wavelength (Leopold et al. 1964);
L_b = along-channel bend length (in Table 6-3, from FISRWG 1998);
L_m = meander wavelength (in Table 6-3, from FISRWG 1998);
M = channel sediment;
M = weighted percentage silt-clay in the channel perimeter (from Schumm 1977);
M = percentage of bank materials finer than 0.074 mm (Table 6-5, from FISRWG 1998);
m = exponent;
n = number;
P = wetted perimeter;
P = sinuosity;
Q = discharge (from Kennedy 1895);
Q = water discharge (from Lane 1955);
Q_s = bed-material load (from Lane 1955);
Q_x = bed-material transport rate in kg s^{1} at water discharge Q (Table 6-5, from FISRWG 1998);
R = hydraulic radius;
R_c = loop radius of curvature (in Table 6-3, from FISRWG 1998);
r_c = radius of curvature;
r_c/w = radius of curvature to width ratio;
S = slope (from Lane 1955);
S = estimate of the standard deviation of the sample (from Yevjevich 1972);
V = velocity (from Kennedy 1895);
W = width (from Schumm 1977);
W = channel width (from Kennedy 1895); and
W = bank-full width (in Table 6-3, from FISRWG 1998):
w = width;
w/d = width-depth ratio;
θ = arc angle;
π = pi.

REFERENCES

Ackers, P., and Charlton, F. G. (1970a). "Meander geometry arising from varying flows." *J. Hydrology*, 11, 230–252.

Ackers, P., and Charlton, F. G. (1970b). "The geometry of small meandering streams." *Proc., Institution of Civil Engineers*, Supplements, Paper 7328S, 289–317.

Andrews, E. D. (1980). "Effective and bank-full discharges of streams in the Yampa River Basin, Colorado and Wyoming," *J. Hydrology*, 46, 311–333.

Ashworth, P. J. (1987). "Bedload transport and channel changes in gravel-bed streams." Ph.D. thesis, University of Stirling, Stirling, Scotland.

Baker, V. R. (1977). "Stream-channel response to floods, with examples from Central Texas." *Bulletin, Geological Society of America*, 88, 1057–1071.

Benson, M. A., and Thomas, D. M. (1966). "A definition of dominant discharge." *Bulletin, International Association of Scientific Hydrology*, 11, 76–80.

Biedenharn, D. S. (1984). "Channel response on the Little Tallahatchie River downstream of Sardis Dam." *Meandering Rivers*, C. M. Elliott, C. M. ed., ASCE, New York, 500–509.

Biedenharn, D. S. (1995). "Lower Mississippi River channel response: Past, present, and future." Ph.D. dissertation, Department of Civil Engineering, Colorado State University, Fort Collins, Colo.

Biedenharn, D. S., Combs, P. G., Hill, G. J., Pinkard, C. F., and Pinkstone, C. B. (1989). "Relationship between channel migration and radius of curvature of the Red River." *Proc., International Symposium, Sediment Transport Modeling*, ASCE, New York, 536–641.

Biedenharn, D. S., and Watson, C. C. (1997). "Stage adjustment in the lower Mississippi River, USA." *Regulated Rivers: Research & Management*, 13, 517–536.

Biedenharn, D. S., Copeland, R. C., Thorne, C. R., Soar, P. J., Hey, R. C., and Watson, C. C. (2000a). "Effective discharge calculation: A practical guide." Technical Report ERDC/CHL TR-00-15, U.S. Army Corps of Engineers, Engineer Research Development Center, Vicksburg, Miss.

Biedenharn, D. S., Thorne, C. R., and Watson, C. C. (2000b). "Recent morphological evolution of the lower Mississippi River." *Geomorphology*, 34, 227–249.

Bledsoe, B. P. (1999). "Specific stream power as an indicator of channel pattern, stability, and response to urbanization." Ph.D. dissertation, Department of Civil Engineering, Colorado State University, Fort Collins, Colo.

Bledsoe, B. P., and Watson, C. C. (2001). "Logistic analysis of channel pattern thresholds: Meandering, braiding, and incising." *Geomorphology*, 38, 281–300.

Blench, T. (1952). "Regime theory for self-formed sediment bearing channels." *Transactions American Society of Civil Engineers*, Paper 2499, 117, 383–400.

Blench, T. (1957). *Regime behaviour of canals and rivers*. Butterworth's, London.

Blench, T. (1969). "Coordination in mobile-bed hydraulics." *J. Hydraulics Div., ASCE*, 95(HY6), 1871–1898.

Bray, D. I. (1973). "Regime relations for Alberta gravel bed rivers." *Fluvial Processes and Sedimentation*, *Proc.*, *Hydrology Symposium*, National Research Council of Canada, Ottawa, 440–452.

Bray, D. I. (1982). "Regime equations for gravel-bed rivers." *Gravel-Bed Rivers*, R. D. Hey, J. C. Bathurst, and C. R. Thorne, eds., Wiley, Chichester, UK, 517–542.

Brice, J. C. (1975). "Airphoto interpretation of the form and behavior of alluvial rivers." Final Report to the U.S. Army Research Office, Durham, Washington University, St. Louis, Mo.

Brice, J. C. (1984). "Planform properties of meandering rivers." *River Meandering*, S. Y. Wang, ed., ASCE, New York, 1–15.

Brookes, A. (1981). "Channelization in England and Wales." *Discussion Paper No. 11*, Department of Geography, University of Southampton, Southampton, UK.

Burkham, D. E. (1972). "Channel changes of the Gila River in Safford Valley, Arizona, 1946–1970." *Professional Paper 655G*, U.S. Geological Survey, Washington, DC.

Carling, P. A. (1991). "An appraisal of the velocity reversal hypothesis for stable pool/riffle sequences in the River

Severn, England." *Earth Surface Processes and Landforms*, 8, 1–18.

Carling, P. A. (1988). "The concept of dominant discharge applied to two gravel-bed streams in relation to channel stability thresholds." *Earth Surface Processes and Landforms*, 13, 355–367.

Carson, M. A. (1984a). "Observations on the meandering-braided transition, Canterbury Plains, New Zealand." *New Zealand Geographer*, 40, 89–99.

Carson, M. A. (1984b). "The meandering-braided river threshold: A reappraisal." *J. Hydrology*, 113, 1402–1421.

Chorley, R. J., Schumm, S. A., and Sugden, D. E. (1985). *Geomorphology*. Methuen, New York.

Clifford, N. J. (1990). "The formation, nature and maintenance of riffle-pool sequences in gravel-bed rivers." Ph.D. Thesis, University of Cambridge, Cambridge, UK.

Dietrich, W. E., Smith, J. D., and Dunne, T. (1984). "Boundary shear stress, sediment transport and bed morphology in a sand-bedded river during high and low flow." *Meandering Rivers*, C. M. Elliott, ed., ASCE, New York, 632–639.

Downs, P. W. (1995). "Estimating the probability of river channel adjustment." *Earth Surface Processes and Landforms*, 20, 687–705.

Dunne, T., and Leopold, L. B. (1978). *Water in Environmental Planning*. Freeman, New York, San Francisco.

Dury, G. H. (1961). "Bank-full discharge: An example of the statistical relationships." *Bulletin, International Association of Scientific Hydrology,* 6(3), 48–55.

Dury, G. H. (1973). "Magnitude-frequency analysis and channel morphology." *Fluvial Geomorphology*, M. Morisawa, ed., Allen and Unwin, London, 91–121.

Dury, G. H. (1976). "Discharge prediction, present and former, from channel dimensions." *J. Hydrology*, 30, 219–245.

Einstein, H. A. (1972). "Final remarks." *Sedimentation*, Symposium to Honor Professor H. A. Einstein, H. W. Shen, ed., Sedimentation Symposium, Berkeley, Calif., 27-7.

Federal Interagency Stream Restoration Working Group (FISRWG). (1998). "Stream corridor restoration: Principles, processes, and practice." FISRWG, October, <http://www.nrcs.usda.gov/technical/stream_restoration/>.

Gupta, A., and Fox, H. (1974). "Effects of high magnitude floods on channel form: A case study in Maryland piedmont." *Water Resources Research*, 10(3), 499–509.

Hack, J. T., and Goodlett, J. C. (1960). "Geomorphology and forest ecology of a mountain region in the central Appalachian." *Professional Paper 347*, U.S. Geological Survey, Washington, DC.

Harrelson, C. C., Rawlins, C. L., and Potyondy, J. P. (1994). "Stream channel reference sites: An illustrated guide to field technique." *General Report No. RM-245*, U. S. Department of Agriculture, Forest Service, Fort Collins, Colo.

Harvey, M. D., and Watson, C. C. (1986). "Fluvial processes and morphological thresholds in incised channel restoration." *Water Research Bulletin*, 3(3), 359–368.

Hey, R. D. (1975). "Design discharge for natural channels." *Science, Technology and Environmental Management*, R. D. Hey and T. D. Davies, eds., Saxon House, Farnborough, 73–88.

Hey, R. D. (1976). "Geometry of river meanders." *Nature*, 262, 482–484.

Hey, R. D. (1988). "Mathematical models of channel morphology." *Modeling Geomorphological Systems*, M. G. Anderson, ed., Wiley, Chichester, 99–126.

Hey, R. D. (1990). "Design of flood alleviation schemes: Engineering and the environment." School of Environmental Sciences, University of East Anglia, Norwich, UK.

Hey, R. D. (1997). "Channel response and channel forming discharge." *Final Report*, *Contract No. R&D 6871-EN-01,* U.S. Army Research Office (London), University of East Anglia, Norwich, UK.

Hey, R. D., and Thorne, C. R. (1986). "Stable channels with mobile gravel beds." *J. Hydraulic Engineering*, 112(8), 671–689.

Holmquist-Johnson, C. (2002). "Computational methods for determining effective discharge in the Yazoo River Basin, Mississippi." MS thesis, Department of Civil Engineering, Colorado State University, Fort Collins, Colo.

Inglis, C. C. (1941). "Digest of answers to the Central Board of Irrigation questionnaire on meandering of rivers with comments on factors controlling meandering and suggestions for future actions." *Central Board of Irrigation Annual Report (Technical), 1939–1940 Session*, A. R. B. Edgecombe, ed., Publication 24, Chanakyapuri, New Delhi, India, 100–114.

Inglis, C. C. (1947). "Meanders and their bearing on river training." *Paper No. 7*, Institution of Civil Engineers, Maritime and Waterways Engineering Division, London.

Inglis, C. C. (1949). "The behavior and control of rivers and canals." *Research Publication 13*, Central Water Power, Irrigation and Navigation Research Station, Poona, India.

Keller, E. A. (1971). "Areal sorting of bed material: The hypothesis of velocity reversal." *Geological Society of America Bulletin*, 83, 915–918.

Keller, E. A., and Melhorn, W. (1973). "Bedforms and fluvial processes in alluvial stream channels: Selected observations." *Fluvial Geomorphology*, M. Morisawa, ed., Publications in Geomorphology, SUNY Binghampton, 253–283.

Kellerhals, R. (1967). "Stable channels with gravel-paved beds." *J. Waterways Div., Proc., ASCE*, 93(1), 63–84.

Kennedy, R. G. (1895). "The prevention of silting in irrigation canals." *Proc., Institution of Civil Engineers*, 119, 281–290.

Knighton, A. D. (1998). *Fluvial Forms and Processes: A New Perspective*. Arnold, London.

Knighton, A. D., and Nanson, G. C. (1993). "Anastomosis and the continuum of channel pattern." *Earth Surface Processes and Landforms*, 18, 613–625.

Lacey, G. (1958). "Flow in alluvial channels with mobile sandy beds." *Proc., Institution of Civil Engineers*, 9, 145–164.

Lane, E. W. (1955). "The importance of fluvial morphology in hydraulic engineering." *Proc., ASCE*, 81(745), 1–17.

Leeder, M. R., and Bridges, P. H. (1975). "Flow separation in meander bends." *Nature*, 253, 338–339.

Leopold, L. B. (1994). *A View of the River.* Harvard University Press, Cambridge, Mass.

Leopold, L. B., and Maddock, T., Jr. (1953). "The hydraulic geometry of stream channels and some physiographic implications." *Professional Paper 242*, U.S. Geological Survey, Washington, DC.

Leopold, L. B., and Wolman, M. G. (1957). "River channel patterns: Braided, meandering and straight." *Professional Paper 282-B*, U.S. Geological Survey, Washington, DC.

Leopold, L. B., Wolman, M. G., and Miller, J. P. (1964). *Fluvial Processes in Geomorphology*. Freeman, New York, San Francisco.

Lisle, T. E. (1979). "A sorting mechanism for a riffle-pool sequence." *Geological Society of America Bulletin*, 90, 1142–1157.

Lyons, J. K., Pucherelli, M. J., and Clark, R. C. (1992). "Sediment transport and channel characteristics of a sand-bed portion of the Green River below Flaming Gorge Dam, Utah, USA." *Regulated Rivers: Research and Management*, 7, 219–232.

Mackin, J. H. (1948). "Concept of the graded river." *Geological Society of America Bulletin*, 59, 463–512.

Nanson, G. C., and Hickin, E. J. (1986). "A statistical analysis of bank erosion and channel migration in western Canada." *Geological Society of America Bulletin*, 97(4), 497–504.

Nanson, G. C., and Knighton, A. D. (1996). "Anabranching rivers: Their cause, character and classification." *Earth Surface Processes and Landforms*, 21, 217–239.

Neill, C. R., and Galay, V. J. (1967). "Systematic evaluation of river regime." *ASCE, J. Waterways and Harbors Division*, 93(WW1), 25–51.

Nixon, M. (1959). "A study of bank-full discharges of rivers in England and Wales." *Proc., Institution of Civil Engineers,* 12, 157–175.

Nolan, K. M., Lisle, T. E., and Kelsey, H. M. (1987). "Bank-full discharge and sediment transport in northwestern California." *Proc., Corvallis Symposium, Erosion and Sedimentation in the Pacific Rim*, IAHS Publication 165, IAHS, Washington, DC.

Parker, G. (1982). "Discussion of Chapter 19: Regime equations for gravel-bed rivers." *Gravel-bed Rivers: Fluvial Processes, Engineering and Management*, R. D. Hey, J. C. Bathurst, and C. R. Thorne, eds., Wiley, Chichester, UK, 542–552.

Petit, F. (1987). "The relationship between shear stress and the shaping of the bed of a pebble-loaded river, La Rulles, Ardennes." *Catena*, 14 (5), 453–468.

Pickup, G., and Warner, R. F. (1976). "Effects of hydrologic regime on the magnitude and frequency of dominant discharge." *J. Hydrology*, 29, 51–75.

Richards, K. S. (1982). *Rivers: Form and Process in Alluvial Channels.* Methuen, London.

Richards, K. S., and Lane, S. N. (1997). "Prediction of morphological changes in unstable channels." *Applied Fluvial Geomorphology for River Engineering and Management*, C. R. Thorne, R. D. Hey, and M. D. Newsom, eds., Wiley, Chichester, UK, 269–292.

Richardson, E. V., and Huber, F. W. (1991). "Evaluation of bridge vulnerability to hydraulic forces, stream instability and scour." *Report No. 1290*, Vol. 1, U.S. Transportation Research Board, Washington DC, 25–38.

Riley, S. J. (1976). "Aspects of bank-full geometry in a distributary system of eastern Australia." *Hydrological Sciences J*., 21, 545–560.

Rinaldi, M., and Johnson, P. A. (1997). "Characterization of stream meanders for stream restoration." *J. Hydraulic Engineering, ASCE*, 123(6), 567–570.

Robinson, B. A., and Thompson, R. E. (1993). "An efficient method for assessing channel instability near bridges." *Hydraulic Engineering '93*, H. W. Shen, S. T. Su, and F. Wen, eds., ASCE, New York, 513–518.

Rosgen, D. L. (1994). "A classification of natural rivers." *Catena*, 22, 169–199.

Rosgen, D. L. (1996). *Applied River Morphology*. Wildland Hydrology, Pagosa Springs, Colo. (8 sections plus bibliography).

Rundquist, L. A. (1975). "A classification and analysis of natural rivers." Ph.D. dissertation, Department of Civil Engineering, Colorado State University, Fort Collins, Colo.

Schall, J. D., and Lagasse, P. F. (1991). "Stepwise procedure for evaluating stream stability." *Report No. 1290*, Vol. 2, U.S. Transportation Research Board, Washington, DC, 254–267.

Schick, A. P. (1974). "Formation and obliteration of desert stream terraces—A conceptual analysis." *Zeitschrift für Geomorphologie*, Supplement, 21, 88–105.

Schumm, S. A. (1960). "The shape of alluvial channels in relation to sediment type." *Professional Paper No. 352B,* U.S. Geological Survey, Washington, DC.

Schumm, S. A. (1973). "Geomorphic thresholds and the complex response of drainage systems." *Fluvial Geomorphology,* M. Morisawa, ed., Publications in Geomorphology, State University of New York, Binghamton, N.Y., 299–310.

Schumm, S. A. (1976). "Episodic erosion, a modification of the Davis cycle." *Theories of Landform Development,* W. N. Melhorn, and R. C. Flemal, R. C. eds., Publications in Geomorphology, State University of New York, Binghamton, N.Y. 69–85.

Schumm, S. A. (1977). *The Fluvial System*, Wiley, New York.

Schumm, S. A. (1981). "Evolution and response of the fluvial system, sedimentologic implications." *Special Publ. No. 31*, Society of Economic Paleontologists and Mineralogists, Tulsa, Okla., 19–29.

Schumm, S. A. (1985). "Patterns of alluvial rivers." *Annual Review of Earth and Planetary Sciences*, 13, 5–27.

Schumm, S. A., Harvey, M. D., and Watson, C. C. (1984). *Incised Channels: Morphology, Dynamics and Control*. Water Resources Publications, Littleton, Colo.

Schumm, S. A., and Lichty, R. W. (1965). "Time, space and causality in geomorphology." *Am. J. Sci.*, 263, 110–119.

Schumm, S. A., and Parker, R. S. (1973). "Implications of complex response of drainage systems for Quaternary alluvial stratigraphy." *Nat. Phys. Sci.*, 243, 99–100.

Sear, D. A. (1996). "Sediment transport processes in pool-riffle sequences." *Earth Surface Processes and Landforms*, 12, 241–262.

Shirole, A. M., and Holt, R. C. (1991). "Planning for a comprehensive bridge safety assurance program." *Report No. 1290*, Vol. 1, U.S. Transportation Research Board, Washington, DC, 39–50.

Simon, A., and Hupp, C. R. (1987). "Channel evolution in modified alluvial streams." U.S. Geological Survey, Washington, DC.

Simons, D. B., and Albertson, M. L. (1963). "Uniform water conveyance channels in alluvial material." *Trans Am. Soc. Civil Eng., ASCE*, 128(1), 65–167.

Simons, D. B., Li, R.-M., and Associates (1982). *Engineering Analysis of Fluvial Systems*. Simons, Li and Associates, Fort Collins, Colo.

Soar, P. J. (2000). "Channel restoration design for meandering rivers." Ph.D. thesis, University of Nottingham, Nottingham, UK.

Soar, P. J., and Thorne, C. R. (2001). "Channel restoration design for meandering rivers." *Report ERDC/CHL CR-01-1*, Coastal and Hydraulics Laboratory, Engineer Research and Development Center, U.S. Army Corps of Engineers, Vicksburg, Miss.

Stevens, M. A., Simons, D. B., and Richardson, E. V. (1975). "Nonequilibrium river form." *J. Hydraulics Division, ASCE,* 101(HY5), 557–567.

Thorne, C. R. (1991). "Bank erosion and meander migration of the Red and Mississippi Rivers, USA." *Hydrology for the Water Management of Large River Basins*, *Proc*., *Vienna Symposium*, IAHS Publ. No. 201, IAHS, Wallingford, UK, 301–313.

Thorne, C. R. (1998). *Stream Reconnaissance Handbook*. Wiley, Chichester, UK.

Thorne, C. R. (2002). "Geomorphic analysis of large alluvial rivers." *Geomorphology*, 44, 3–4, 203–220.

Thorne, C. R., Hey, R. D., and Newson, M. D. (1997). *Applied Fluvial Geomorphology for River Engineering and Management*. Wiley, Chichester, UK.

Thorne, C. R., and Osman, A. M. (1988). "Riverbank stability analysis. II: Applications." *J. Hydraulic Engineering*, ASCE, 114, 2, 151–172.

Twain, M. (1944). *Life on the Mississippi.* The Heritage Press, New York.

U.S. Army Corps of Engineers (USACE). (1994). "Channel stability assessment for flood control projects." *Report EM1110-2-1418*, USACE, Washington, DC, <http://www.usace.army.mil/inet/usace-docs/eng-manuals/em1110-2-1418/>.

Watson, C. C., Biedenharn, D. S., and Bledsoe, B. P. (2002). "Use of incised channel evolution models in understanding rehabilitation alternatives." *J. American Water Resources Association,* 38(1), 151–160.

Watson, C. C., Harvey, M. D., Biedenharn, D. S., and Combs, P. G. (1988). "Geotechnical and hydraulic stability numbers for channel rehabilitation. I: The approach." *Proc., ASCE Hyd. Div. 1988 National Conf.*, S. R. Abt and J. Gessler, eds., 120–125.

Watson, C. C., Raphelt, N. K., and Biedenharn, D. S. (1997). "Historical background of erosion problems in the Yazoo Basin." *Proc. of the Conf. on Management of Landscapes Disturbed by Channel Incision*, S. S. Y. Wang, E. J. Langendoen, and F. D. Shields, Jr., F. D. eds., The University of Mississippi, University, Miss., 115–119.

Webb, B. W., and Walling, D. E. (1982). "The magnitude and frequency characteristics of fluvial transport in the Devon drainage basin and some geomorphological implications." *Catena*, 9, 9–23.

Williams, G. P. (1978). "Bank-full discharge of rivers." *Water Resources Res.,* 14, 1141–1154.

Williams, G. P. (1986). "River meanders and channel size." *J. Hydrology*, 88, 147–164.

Wolman, M. G. (1955). "The natural channel of Brandywine Creek, Pennsylvania." *Professional Paper No. 271*, U.S. Geological Survey, Washington, DC.

Wolman, M. G., and Leopold, L. B. (1957). "River flood plains: Some observations on their formation." *Professional Paper* 282C, U.S. Geological Survey, Washington, DC, 87–107.

Wolman, M. G., and Miller, J. P. (1960). "Magnitude and frequency of forces in geomorphic processes." *J. Geol.,* 68, 54–74.

Woodyer, K. D. (1968). "Bank-full frequency in rivers." *J. Hydrology,* 6, 114–142.

Yalin, M. S. (1971). "On the formation of dunes and meanders: Hydraulic research and its impact on the environment." *Proc., 14th Congress of the International Association for Hydraulic Research,* Société Hydrotechnique de France, Paris, 3, C 13, 101–108.

Yevjevich, V. (1972). "Structural analysis of hydrologic time series." *Hydrology Paper 56*, Colorado State University, Fort Collins, Colo.

Copyrighted Materials
Copyright © 2008 American Society of Civil Engineers (ASCE)
Retrieved from www.knovel.com

CHAPTER 7

Streambank Erosion and River Width Adjustment

James E. Pizzuto and the ASCE Task Committee on Hydraulics, Bank Mechanics, and Modeling of River Width Adjustment

7.1 INTRODUCTION

Many different methods are available to describe river channel morphology and morphological adjustments for river engineering purposes. Available approaches range from equations that predict the regime or graded morphology of equilibrium channels to mathematical models that simulate channel changes in time and space. Most mathematical models, however, neglect time-dependent channel-width adjustments and do not simulate processes of bank erosion or deposition. Although changes in channel depth caused by aggradation or degradation of the riverbed can be simulated, changes in width cannot. For prediction of the behavior of natural streams, this is a significant limitation, because channel morphology usually changes with time, and adjustment of both width and depth (in addition to changes in planform, roughness, and other variables) is the rule rather than the exception (Leopold et al. 1964; Simon and Thorne 1996). As a result, our ability to model and predict changes in river morphology and their engineering impacts is limited. This is unfortunate, because width adjustments can seriously impact floodplain dwellers, riparian ecosystems, and bridge crossings, bank protection works, and other riverside structures through bank erosion, bank accretion, or bankline abandonment of the active river channel.

In this chapter, methods for assessing processes of bank erosion and river width adjustment are reviewed. Most of this chapter was originally written by the ASCE Task Committee on Hydraulics, Bank Mechanics, and Modeling of River Width Adjustment (1998a; 1998b), which was chaired by Dr. Colin R. Thorne.

7.2 GEOMORPHIC CONTEXT OF RIVER WIDTH ADJUSTMENT

River width adjustments have varied causes and occur in different geomorphic settings (Figs. 7-1 and 7-2). Widening can occur by erosion of one or both banks without substantial incision (Fig. 7-1a) (Everitt 1968; Burkham 1972; Hereford 1984; Pizzuto 1994). Widening in sinuous channels may occur when outer bank retreat exceeds the rate of advance of the opposite bank (Fig. 7-1b) (Nanson and Hickin 1983; Pizzuto 1994). In braided rivers, bank erosion by flows deflected around growing braid bars is a primary cause of widening (Fig. 7-1c) (Leopold and Wolman 1957; Best and Bristow 1993; Thorne et al. 1993). In degrading streams, widening often follows incision of the channel when the increased height and steepness of the banks cause them to become unstable (Fig. 7-1d). Bank failures can cause very rapid widening under these circumstances (Thorne et al. 1981a,b; Little et al. 1982; Harvey and Watson 1986; Simon 1989). Widening in coarse-grained, aggrading channels can occur when flow acceleration due to a decreasing cross-sectional area, coupled with current deflection around growing bars, generates bank erosion (Fig. 7-1e) (Simon and Thorne 1996).

Processes of channel narrowing are equally diverse (Fig. 7-2). Rivers may narrow through the formation of in-channel berms, or benches at the margins (Fig. 7-2a) (Pizzuto 1994; Moody et al. 1999) (Fig. 7-3). The growth of berms or benches often occurs when bed levels stabilize following a period of degradation and can eventually lead to the creation of a new, low-elevation floodplain and establishment of a narrower, quasi-equilibrium channel (Woodyer 1975; Harvey and Watson 1986; Simon 1989). Encroachment of riparian vegetation into the channel often contributes to the growth, stability and, in some cases, to the initiation of berm or bench features (Hadley 1961; Schumm and Lichty 1963; Harvey and Watson 1986; Simon 1989). Narrowing in sinuous channels occurs when the rate of alternate or point bar growth exceeds the rate of retreat of the cut bank (Fig. 7-2b) (Nanson and Hickin 1983; Pizzuto 1994). In braided channels, narrowing may result when a marginal anabranch is abandoned (Fig. 7-2c) (Schumm and Lichty 1963). Sediment is deposited in the abandoned channel until it merges into the

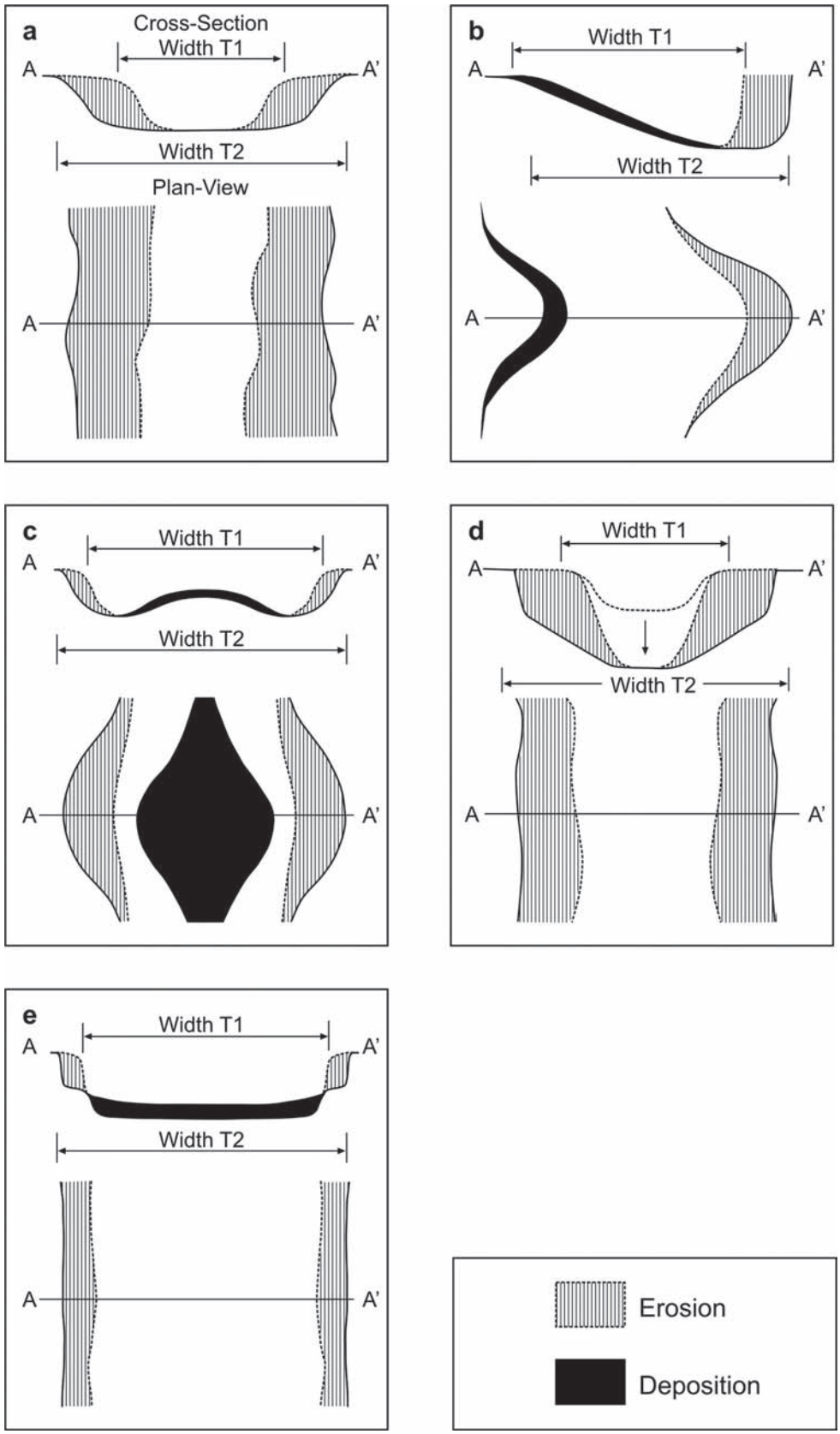

Fig. 7-1. Geomorphology of channel widening: (a) channel enlargement by bank erosion without incision; (b) erosion of outer bank in sinuous channel at faster rate than accretion on bar opposite; (c) deflection of flows by growing braid bar; (d) bank failure and retreat due to mass instability following channel incision; (e) bank erosion due to flow acceleration and deflection in aggrading channel (ASCE Task Committee on Hydraulics, Bank Mechanisms and Modeling of River Width Adjustment 1998a, with permission from ASCE).

floodplain. Also, braid bars or islands may become attached to the floodplain, especially following a reduction in discharge (Fig. 7-2d). Island tops are already at about floodplain elevation and attached bars are built up to floodplain elevation by sediment deposition on the surface of the bar, often in association with the establishment of riparian vegetation. Attached islands and bars may, in time, become part of the floodplain bordering a much narrower, often single-threaded channel (Williams 1978; Nadler and Schumm 1981).

If the flow regime and sediment supply are quasi-steady over periods of decades or centuries, then a river may adjust its morphology to create a metastable equilibrium form (Schumm and Lichty 1965). Such rivers are described as being graded or in regime (Mackin 1948; Leopold and Maddock 1953; Wolman 1955; Leopold et al. 1964; Ackers 1992). Although the width of an equilibrium stream may change due to the impact of a large flood or some other extreme event, the stable width is often eventually recovered following such perturbations (Costa 1974; Gupta and Fox 1974; Wolman and Gerson 1978). Unfortunately, predicting the time-averaged morphology of equilibrium channels remains a difficult problem, despite years of effort

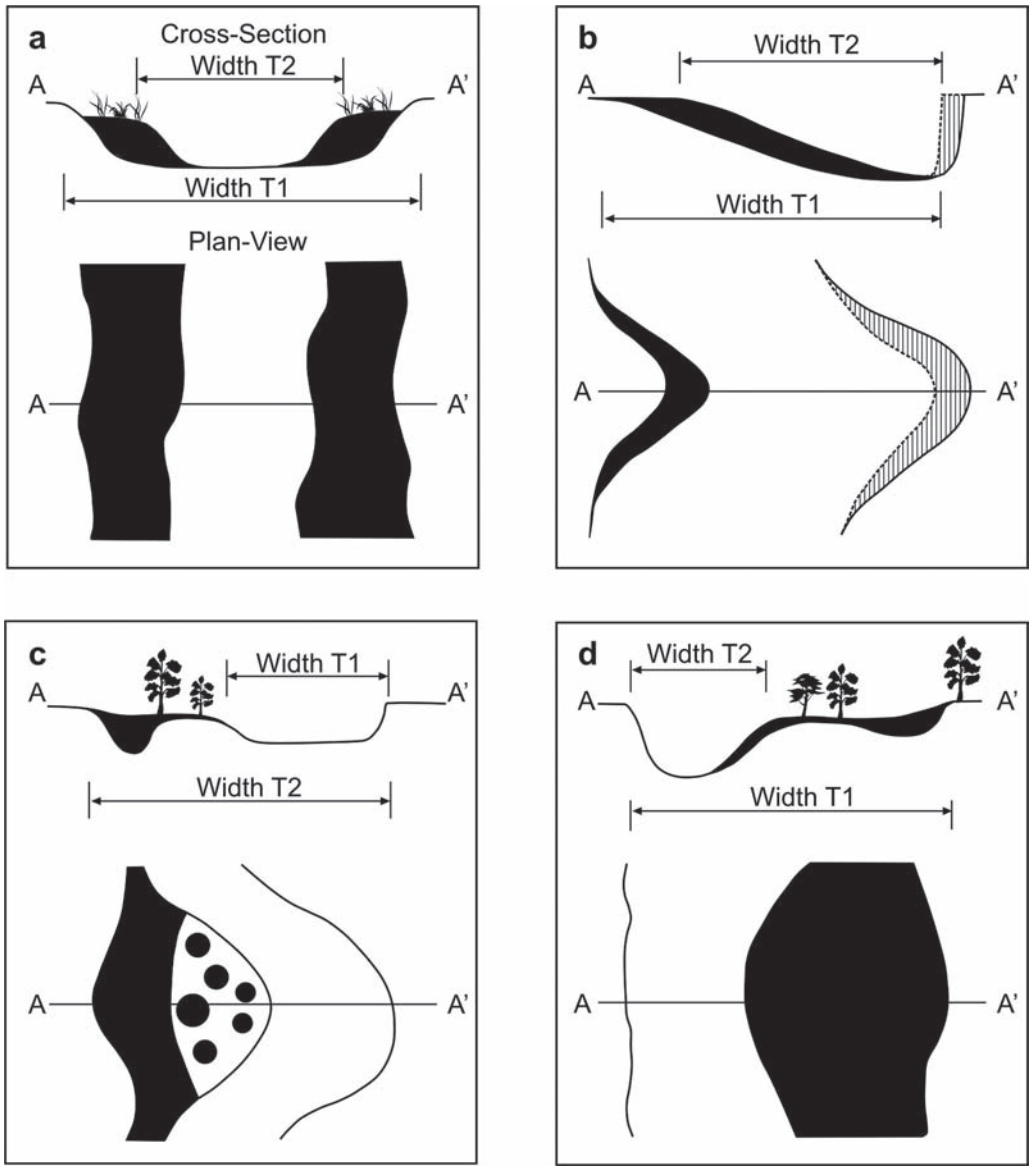

Fig. 7-2. Geomorphology of channel narrowing: (a) channel reduction by berm or bench formation; (b) accretion on advancing bar at faster rate than erosion of bank opposite; (c) abandonment of marginal anabranch in braided channel; (d) closure of marginal channel when braid bars or island becomes attached to floodplain (ASCE Task Committee on Hydraulics, Bank Mechanisms and Modeling of River Width Adjustment 1998a, with permission from ASCE).

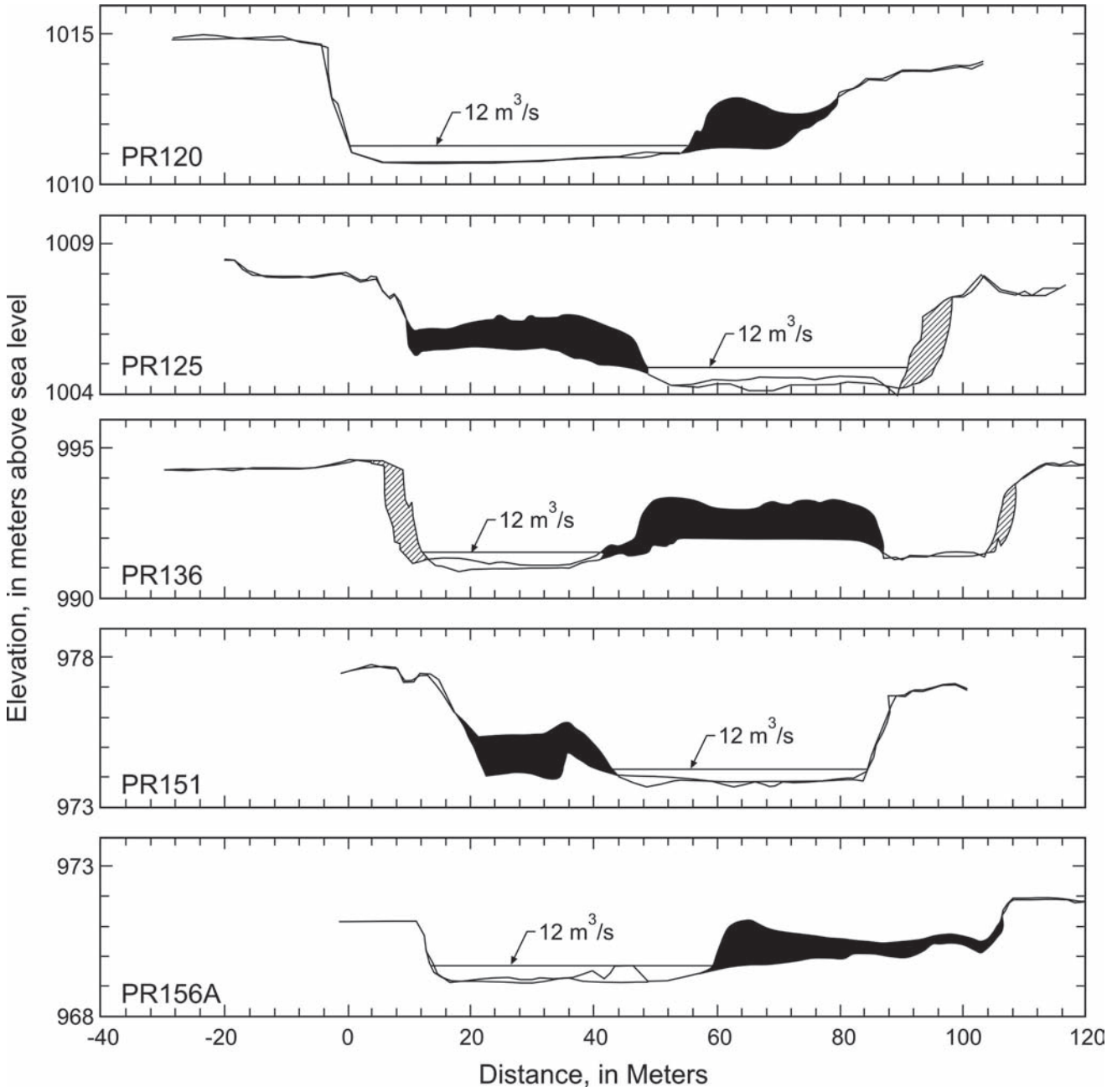

Fig. 7-3. Five examples of channel narrowing by floodplain formation along Powder River in southeastern Montana based on surveyed cross sections in 1978 and 1996 (solid lines). Surveys in 1978 were done after a 25–50-year flood that widened the channel. The hachured areas represent net erosion, and the solid black areas represent net deposition (from Moody et al. 1999).

(Ackers 1992; White et al. 1982; Ferguson 1986; Bettess and White 1987).

Many rivers, however, cannot be considered to have equilibrium channels, even as an engineering approximation. These rivers display significant morphological changes, including width adjustments, when viewed over decades or centuries. For example, some rivers in arid and semiarid regions of the American West change their morphologies drastically as the volume of annual precipitation, frequency of flood events, and other factors vary stochastically (Schumm and Lichty 1963; Everitt 1968; Burkham 1972; Osterkamp and Costa 1987). Because these streams vary so dramatically, they cannot be considered as graded or regime channels (Stevens et al. 1975) but are perpetually enlarging rapidly in response to a period of relatively high discharges, or contracting during periods of less than

average runoff (Schumm and Lichty 1963; Stevens et al. 1975; Pizzuto 1994).

Other nonequilibrium rivers may be actively adjusting to changes in flow regime and sediment supply (Andrews 1986; Madej 1977; Smith and Smith 1984), changing valley slope (Patton and Schumm 1975), succession of riparian vegetation (Hadley 1961; Graf 1978), climate change (Schumm 1968; Knox 1983; Hereford 1984), watershed land-use change (Hammer 1972), neotectonic valley floor tilting (Burnet and Schumm 1983; Schumm and Winkley 1994), or sea-level rise (Brammer et al. 1993). The resulting width adjustments can occur at various rates and in different temporal sequences. For example, Hammer (1972) suggested that rivers of southeastern Pennsylvania adjust to the impacts of urbanization in less than 5 years, but Andrews (1986), Jacobson and Coleman (1986), and other researchers have documented disruptions in river morphology that persisted for more than a century.

Width adjustments not only encompass a variety of time scales; they are also accomplished by a wide range of fluvial processes and geotechnical mechanisms associated with varying discharge, climatic, and environmental conditions. Bank erosion processes provide a useful example. Wolman (1959) noted that significant bank erosion on Watts Branch in the Maryland Piedmont occurred more than 10 times per year during relatively small but frequent flow events. However, scientists working elsewhere report that significant bank erosion has been caused mostly by large floods with recurrence intervals of decades or centuries (Williams and Guy 1973; Costa 1974; Gupta and Fox 1974; Gardner 1977; Osterkamp and Costa 1987). In other cases, bank retreat has been found to be almost entirely unrelated to flow stage and intensity but correlated with precipitation events and ground-water levels that generate erosion through sapping or piping (Brunsden and Kesel 1973; Ullrich et al. 1986; Hagerty 1991). Thus, identifying the dominant erosion processes and failure mechanisms and selecting the appropriate discharge or climate events to be included in either conceptual or mathematical models of width adjustment remain very difficult tasks.

These examples indicate that channel changes involving width adjustment occur in a wide variety of geomorphic contexts, that width adjustment will usually be accompanied by changes in other morphological parameters such as channel depth, roughness, bed-material composition, riparian vegetation, energy slope, and channel planform, and that the processes responsible for width adjustments are diverse. Furthermore, adjustment processes display a variety of spatial patterns and operate over a wide variety of time scales. Because of this diversity, it is unlikely that a single method can be developed to predict the trends and rates of width adjustment for all rivers. Therefore, engineers must establish the morphological context of width adjustment and identify the major processes and mechanisms involved before selecting appropriate methods for analysis, modeling, and solution of width adjustment problems. This is best achieved through systematic field observation and monitoring.

7.3 FACTORS INFLUENCING BANK EROSION AND WIDTH ADJUSTMENT

7.3.1 Cause and Effect: The Influence of Scale

Causes of bank erosion and width adjustments can be viewed at several different spatial scales. Bank erosion, for example, may occur because high discharges cause increased shear forces on the banks. However, the high discharges themselves may be a result of changes in land use or climatic changes that are controlled by processes external to a particular river reach. Channel enlargement caused by urbanization provides a useful example (Hammer 1972). Impervious surfaces throughout the watershed generate increased runoff (Leopold 1968), which in turn causes bank erosion and increases in channel width and cross-sectional area.

It is important for engineers to understand both local and larger-scale causes of bank erosion and width adjustment. In some cases, bank protection or other small-scale engineering structures may provide the best solution to a bank erosion problem. In other cases, however, trying to mitigate erosion at a particular reach may be futile and wasteful because the problem is ultimately caused by land use practices throughout a watershed.

The following discussion of factors influencing bank erosion and width adjustment focuses on local processes that may affect individual river cross sections. However, the broader context of the entire watershed should always be considered in trying to understand and solve bank erosion and width adjustment problems.

7.3.2 Fluvial Hydraulics

7.3.2.1 Introduction The flow of water and sediment in rivers is described by Newton's laws, which are straightforward until turbulence is encountered. The simplified, one-dimensional (1D) St. Venant equation is commonly applied in river engineering because the flow can be considered to occur predominantly in the downstream direction. An appropriate rigid boundary resistance law is then usually adopted to relate the conveyance capacity to the geometry (see, for example, Keulegan 1938; ASCE Task Committee on Friction Factors in Open Channels 1963; Chow 1959; Cunge et al. 1980; and Yen 1993). For alluvial channels the resistance law must also take into account the additional energy losses arising from bed forms and sediment transport (Engelund 1966; Alam and Kennedy 1969; Garde and Ranga-Raju 1977; White et al. 1982; van Rijn 1984). For meandering channels, additional resistance terms are required for form drag due to channel curvature (Nelson and Smith 1989a).

A 1D representation is simple but is inadequate to define the processes and the mechanics of river width adjustment.

A three-dimensional (3D) formulation is better, but 3D models are so complex to solve that they are of little value except in the most well-funded of projects. A two-dimensional (2D) representation (depth integration of 3D equations) can be solved more readily, but it is still limited because it is not strictly applicable in the near-bank zone and does not give any motion in the vertical direction. Vertical motion is particularly important at river bends, where most bank erosion and bar deposition occur. However, a 2D formulation is still frequently used because it yields useful information about the lateral variation of most of the important hydraulic parameters that impact bank erosion and accretion. A detailed review of aspects of channel hydraulics that directly influence width adjustment is given here. A broader river of river and floodplain hydraulics is given elsewhere by Knight and Shiono (1995).

7.3.3.2 Cross-Sectional Shape The shape of a river cross section influences the isovel, secondary flow, and boundary shear stress distributions in a number of ways. A typical example (Fig. 7-4) is a rectangular cross section in a straight river with vertical banks. The data are from a rectangular duct experiment with an equivalent open-channel width/depth ratio of 20. Even in this relatively wide case the isovels and boundary shear stress distribution indicate the presence of secondary flow cells and 3D effects in the near-bank zone, which in this case is 15% of the channel width. Fig. 7-5 shows isovels and boundary shear stresses for flow in a narrow trapezoidal channel with an aspect ratio of 1.5. In this case the narrowness

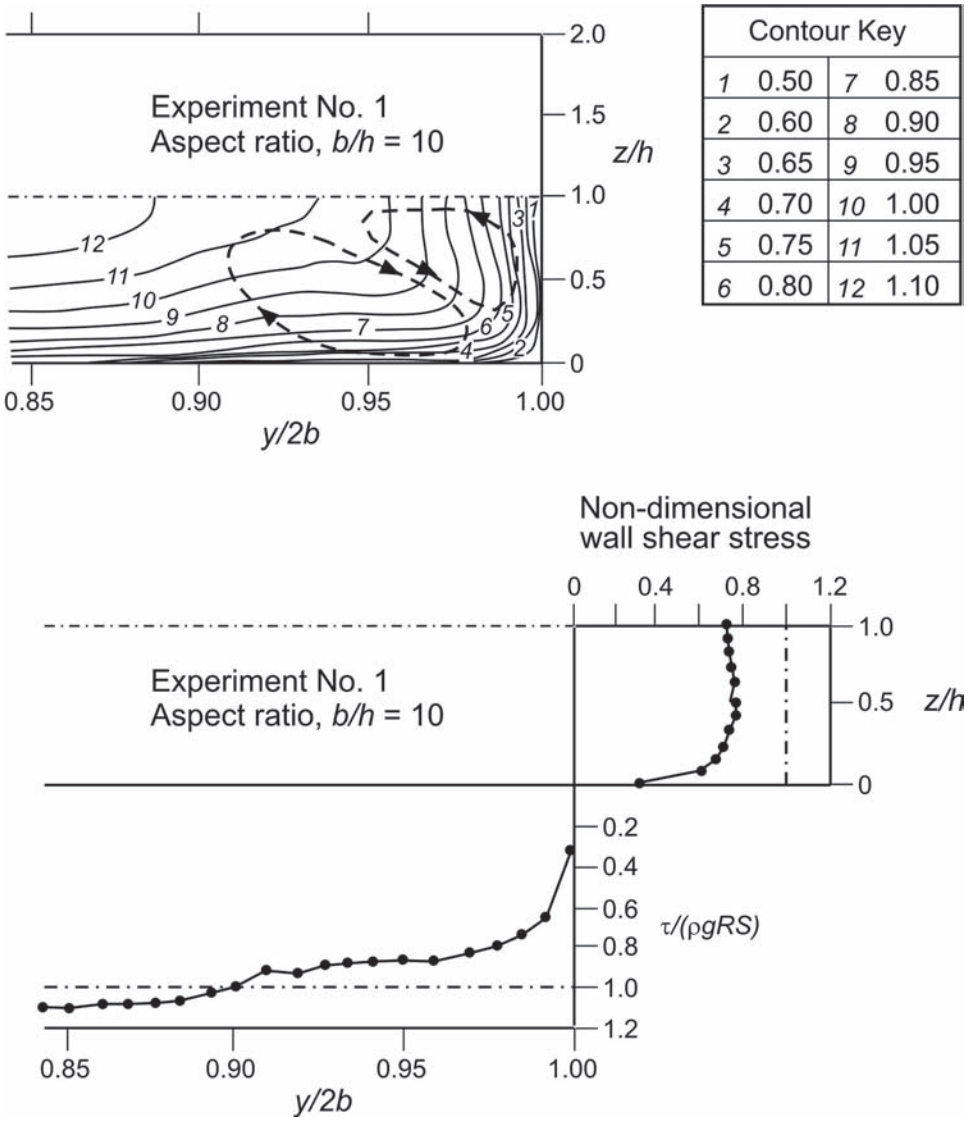

Fig. 7-4. Typical influence of vertical riverbank on velocity and boundary shear stress in wide rectangular channel (Rhodes and Knight 1994, with permission from ASCE).

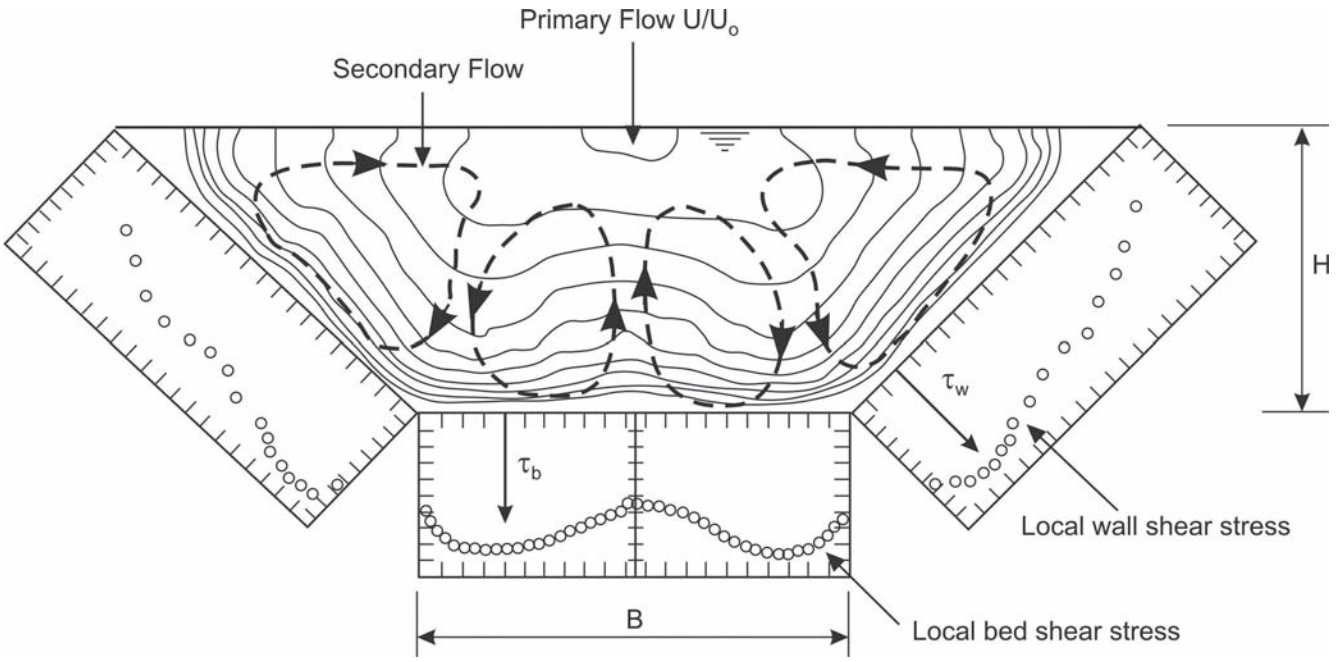

Fig. 7-5. Typical relationship between boundary shear stress distribution, secondary currents, and primary velocities in trapezoidal channel. The Froude number F = 3.24, width/depth = 1.52. (Adapted from Knight et al. 1994. Copyright John Wiley & Sons Limited. Reproduced with permission.)

of the channel causes the flow in the entire cross section to be influenced by 3D flow structures, unlike the case shown in Fig. 7-4. In the wide-channel case, flow in the central region is almost 2D, provided that $y/2b < 0.85$, and for this condition standard boundary layer distributions may be assumed for velocity and Reynolds stress. However, even in a wide ($B/H > 20$) channel, although it may be acceptable to ignore bank effects for many hydraulic and geomorphic analyses, the bank still influences the flow in the near-bank zones sufficiently to require that the resulting 3D flow structures be accounted for in models of width adjustment.

Secondary flow cells may be generated by anisotropic turbulence (stress-induced secondary currents) or streamwise curvature (skew-induced secondary currents) and are always present in any turbulent flow along a channel with a noncircular cross section, such as a natural river channel (Einstein and Li 1958; Liggett et al. 1965; Tracy 1965; Perkins 1970; Melling and Whitelaw 1976; Chiu and Hsiung 1981; Naot and Rodi 1982; Nezu 1993; Meyer and Rehme 1994). In straight channels, stress-induced secondary velocities are usually small, typically being 1 to 2% of the primary velocity. Modeling these weak motions is especially difficult in complex cross sections such as those of natural rivers. In meandering channels, skew-induced secondary velocities may be as great as 10 to 20% of the primary flow, and they are known to affect the distributions of primary velocity and bed-shear stress significantly (Bathurst et al. 1979; Ikeda and Parker 1989; Nelson and Smith 1989a; 1989b; Shiono and Muto 1993; Knight and Shiono 1995).

River engineers are often concerned with the parameters at the channel boundary. A depth-averaged form of the streamwise equation of motion of flow in a straight channel is given by Shiono and Knight (1988; 1991) as

$$\rho g H S_0 - \frac{1}{8}\rho f U_d^2\left(1+\frac{1}{s^2}\right)^{1/2} + \frac{\partial}{\partial y}\left(\rho\lambda H^2\left(\frac{f}{8}\right)^{1/2} U_d \frac{\partial U_d}{\partial y}\right) = \frac{\partial}{\partial y}[H(\rho UV)_d] \tag{7-1}$$

where

ρ = water density;
g = acceleration due to gravity;
H = water depth;
U = streamwise velocity;
V = cross-stream velocity;
y = lateral distance across the channel;
S_0 = streamwise channel slope;
s = local channel side slope of the banks; and
U_d = depth-averaged mean velocity, defined by

$$U_d = \frac{1}{H}\int_0^H U dz \tag{7-2}$$

Three coefficients, f, λ, and Γ are introduced to deal with the local friction factor, dimensionless eddy viscosity, and secondary flow parameter, defined respectively by

$$\tau_b = \frac{f}{8}\rho U_d^2 \tag{7-3a}$$

$$\overline{\tau}_{yx} = \rho\overline{\varepsilon}_{yx}\frac{\partial U_d}{\partial y} \tag{7-3b}$$

$$\overline{\varepsilon}_{yx} = \lambda U_* H \tag{7-3c}$$

$$\frac{\partial H(\rho UV)_d}{\partial y} = \Gamma \tag{7-3d}$$

where

$\overline{\varepsilon}_{yx}$ = depth-averaged eddy viscosity; and
τ_b = local boundary shear stress.

Equation (7-1) governs lateral distributions of U_d or τ_b across the channel width, provided that appropriate values of f, λ, and Γ are specified for each boundary element. Applications of this model to both in-bank and over-bank flow are described in Shiono and Knight (1990) and Abril (1995).

The depth-mean apparent shear stress τ_a acting on a vertical plane in the streamwise direction of a river cross section may be determined by laterally integrating (7-1) to give

$$\tau_a = -\frac{1}{H}\int_0^y \left[\rho g H S_0 - \tau_b\left(1+\frac{1}{s^2}\right)^{1/2}\right]dy \tag{7-4}$$

A comparison between (7-1) and (7-4) illustrates that the depth-averaged apparent shear stress has two distinct components, one arising from depth-averaged secondary flow motion and the other from turbulent Reynolds stresses. It is this apparent shear stress that is often required in sediment transport models, because it links the local boundary shear stress at a point on the wetted perimeter with the streamwise resolved weight force and the resultant net stress. Some values of τa are shown in Fig. 7-6 for trapezoidal channels with roughened banks and width/depth ratios between 4 and 10.

Significantly, the right-hand side of (7-1) contains a depth-averaged secondary flow term. This term is often ignored in stream-tube models and in some eddy viscosity/width-adjustment models (Wark et al. 1990; Darby and Thorne 1992; James and Wark 1994; Kovacs and Parker 1994). However, this term is, in fact, important, as is well illustrated by the examples of Knight and Abril (unpublished paper 1996) using benchmarked experimental data from the U.K. Flood Channel Facility (Knight and Sellin 1987; HR Wallingford 1992).

From the point of view of sediment transport, although it is known that the entrainment and motion of grains may be correlated with turbulent bursts and sweeps (Jackson 1976b; Raudkivi 1995), inclusion of burst and sweep phenomena in a practical model of width adjustment is at this stage premature, owing to our lack of knowledge concerning all the details of coherent structures in the boundary layer close to the bed (Tehrani 1992; Ashworth et al. 1996). As a result, one of the flow parameters still most closely associated with sediment motion is the local time-averaged boundary shear

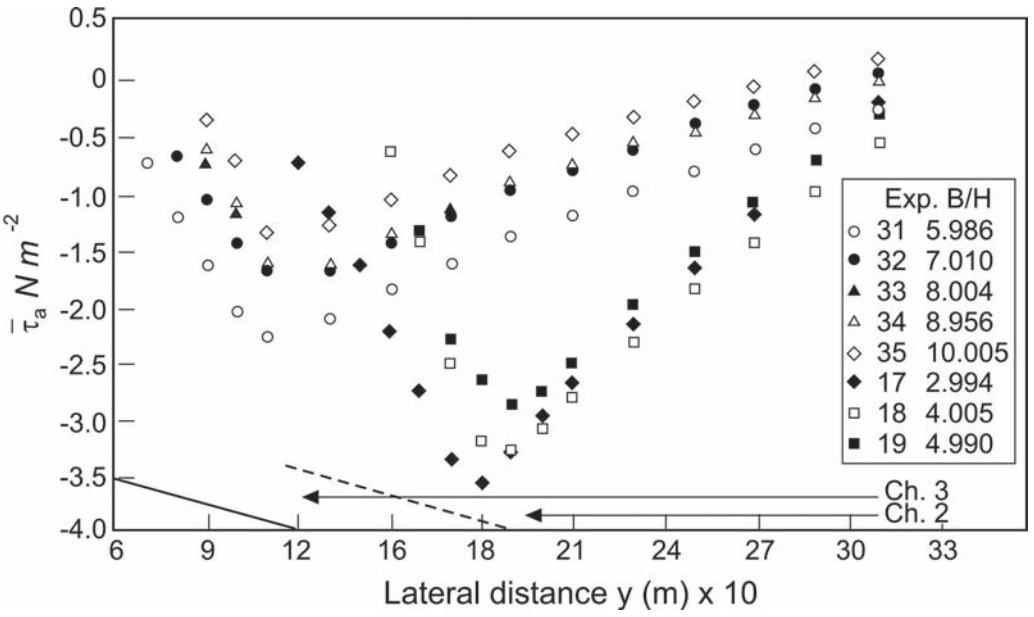

Fig. 7-6. Lateral variation of depth-averaged apparent shear stress τ_a for trapezoidal channels with roughened walls and smooth bed (ASCE Task Committee on Hydraulics, Bank Mechanisms and Modeling of River Width Adjustment 1998a, with permission from ASCE).

stress. Many researchers have attempted either to predict or to measure the lateral distribution of local time-averaged boundary shear stress around the wetted perimeters of channels of various shapes and the longitudinal distribution of local boundary shear stress over sand dunes or in channel reaches. These studies have usually been conducted at laboratory scale using, for convenience, rectangular, trapezoidal, or lenticular cross sections (Engelund 1964; Lundgren and Jonsson 1964; Knight et al. 1994; Rhodes and Knight 1994), and only a few studies have been undertaken in the field at full scale (Bathurst et al. 1979; Dietrich and Whiting 1989; Nece and Smith 1970).

Although the applicability of laboratory-based work to field situations is limited, most previous studies of the relevant hydraulic processes have been carried out under carefully controlled laboratory conditions. Figures 7-7 and 7-8 illustrate how the average wall or bank stress τ_w and bed shear stress τ_b vary for uniformly roughened trapezoidal channels (side slope angles of 45º, 68º, and 90°) and how they compare with simple exponential equations. These data

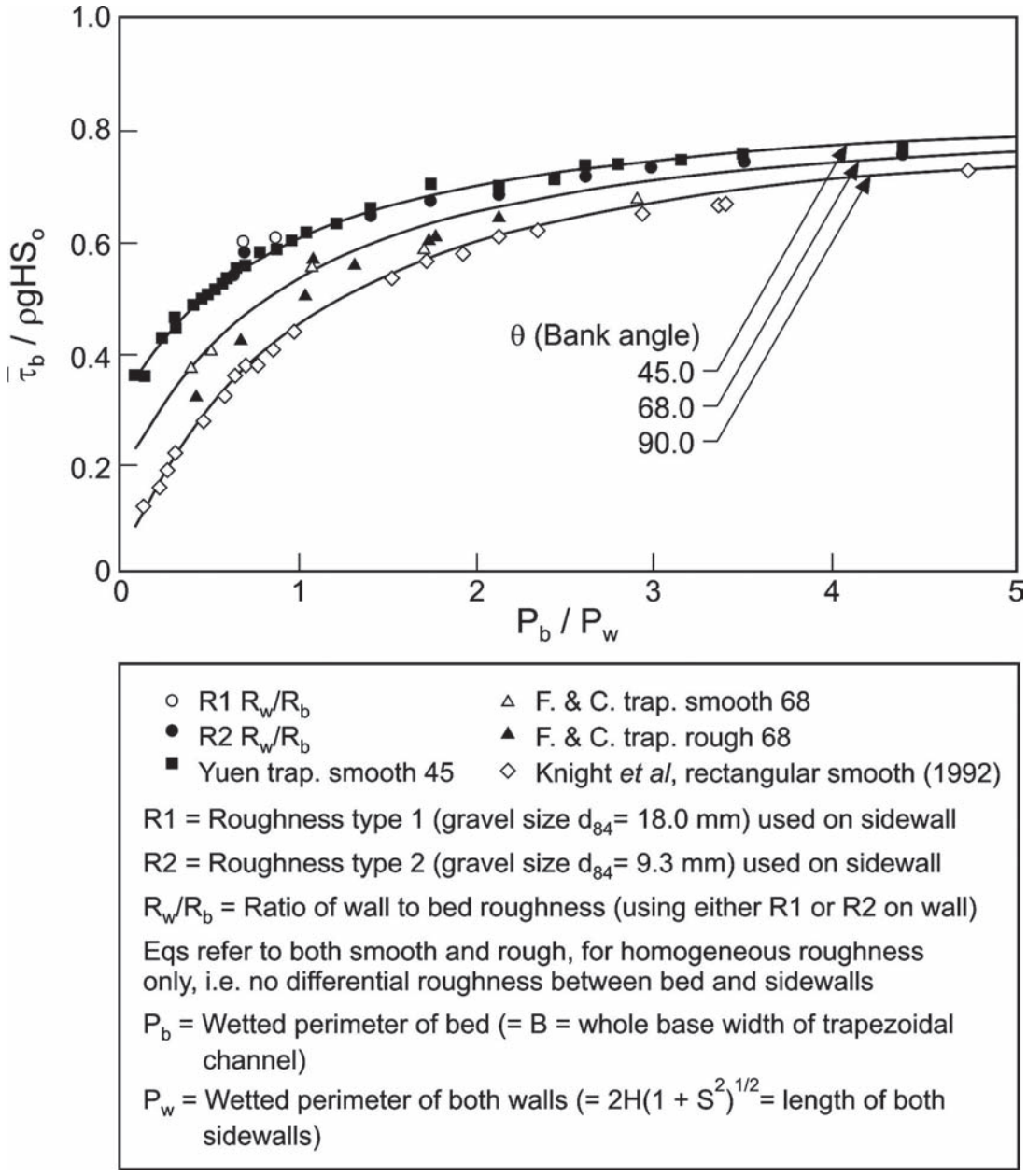

Fig. 7-7. Average wall shear stress $\tau_b/\rho g H S_o$ for smooth and rough trapezoidal channels with different side-slope angles (ASCE Task Committee on Hydraulics, Bank Mechanisms and Modeling of River Width Adjustment 1998a, with permission from ASCE).

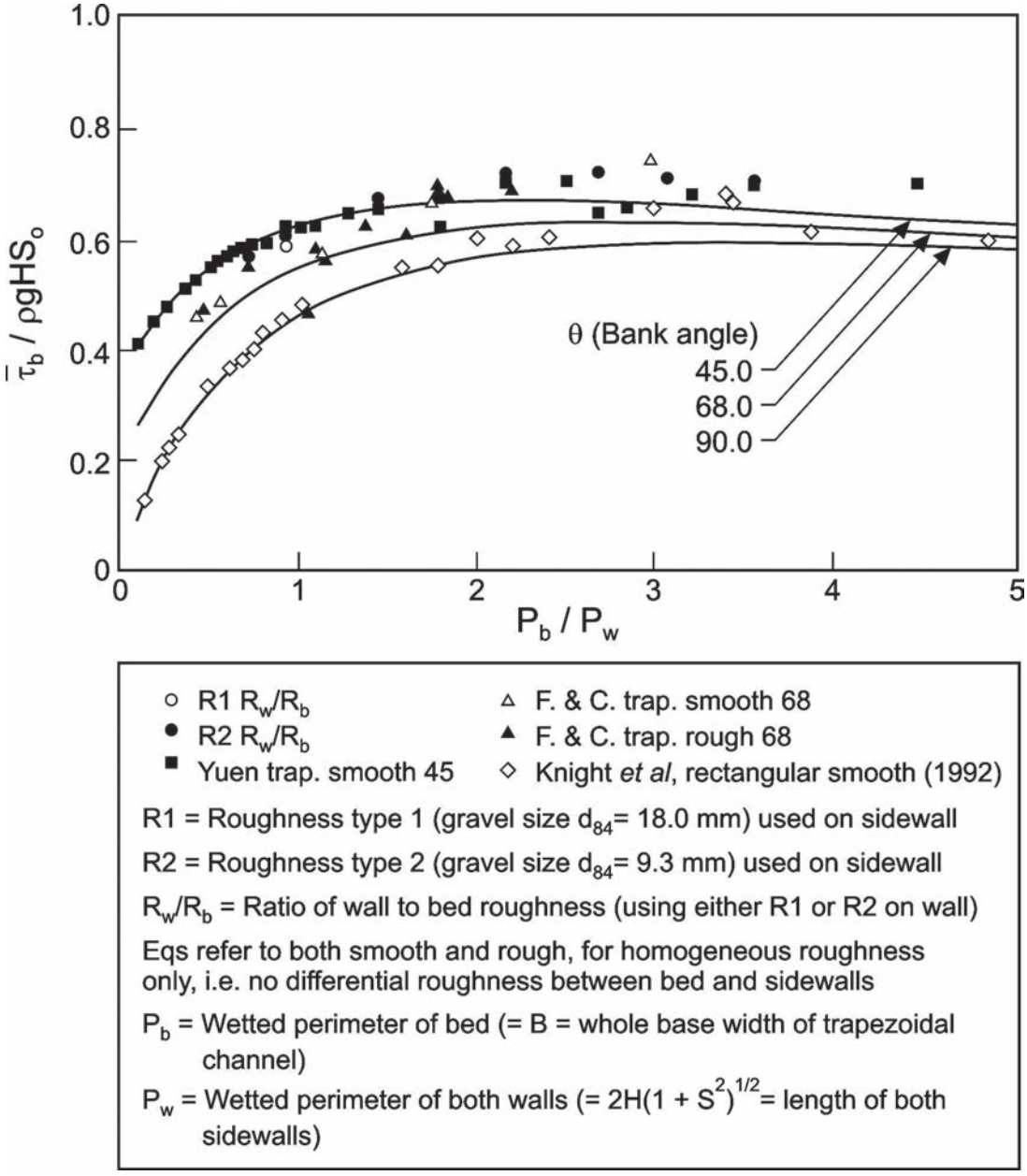

Fig. 7-8. Average wall shear stress $\tau_b/\rho g H S_o$ for smooth and rough trapezoidal channels with different side-slope angles (ASCE Task Committee on Hydraulics, Bank Mechanisms and Modeling of River Width Adjustment 1998a, with permission from ASCE).

all relate to in-bank flows. Similar plots and equations are available for the maximum stresses on the bed and banks, together with their locations, for both uniformly and non-uniformly roughened channels. High differential roughness may occur in engineered channels (with portions of the wetted perimeter especially rough due to riprap) or in natural channels (with banks that are significantly rougher than the bed due to dense riparian vegetation).

Because lenticular shapes more closely approximate the shape of natural alluvial channels they have often been the focus of river studies (Lundgren and Jonsson 1964; Ikeda 1981; Kovacs and Parker 1994). Five methods for determining the local boundary shear stress were reviewed by Lundgren and Jonsson (1964), with the area method being found to be most suitable for general use. Distributions of boundary shear stress based on a particular lenticular shape (Fig. 7-9) are shown for all five methods in Fig. 7-10. The way in which a noncohesive riverbank might be eroded into an equilibrium shape under the action of these distributions of applied shear stress is illustrated in Figs. 7-11 to 7-13 (Kovacs and

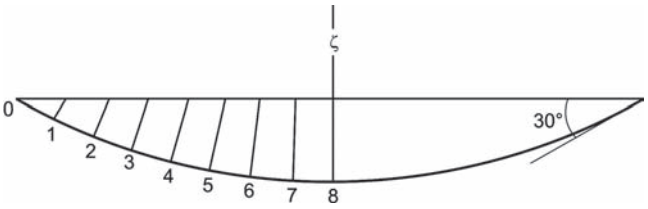

Fig. 7-9. Cross section used in numerical example (circular) (ASCE Task Committee on Hydraulics, Bank Mechanisms and Modeling of River Width Adjustment 1998a, with permission from ASCE).

Parker 1994). In these sketches the lateral distribution of streamwise boundary shear stress is of special significance because those regions of the cross section in which the stress is above the transport threshold will become active with regard to bed-material transport and will form the active width. The resulting cross-sectional shapes for straight alluvial channels under both threshold and mobile bed conditions have also been the subject of much investigation. However, it should be noted that, because the discharge and sediment supply in natural rivers are highly variable, the actual channel cross-sectional shape is constantly responding to changing stage bed forms and flow resistance. Hence, it is only possible to predict medium-term (5–10 years) time-averaged, cross-sectional shapes.

For over-bank flows in straight and meandering channels, considerably fewer experimental data are found with regard to both velocity and boundary shear stress (Knight and Demetriou 1983; Knight et al. 1989, 1990; Tominaga and Nezu 1991; Ackers 1992; Knight et al. 1992; Ackers 1993; Sellin et al. 1993; Tominaga and Nezu 1993). In general terms, for straight channels with floodplains the boundary shear stresses under over-bank flows vary in a more complex way than those for in-bank flows, with stresses in the main river channel decreasing because of the influence of the slower floodplain flows. Conversely, the floodplain boundary shear stresses rise above their expected 2D values because of the effect of the faster flowing, main river flow. Interaction between channel and floodplain flows results in some localized and complex effects in the vicinity of the

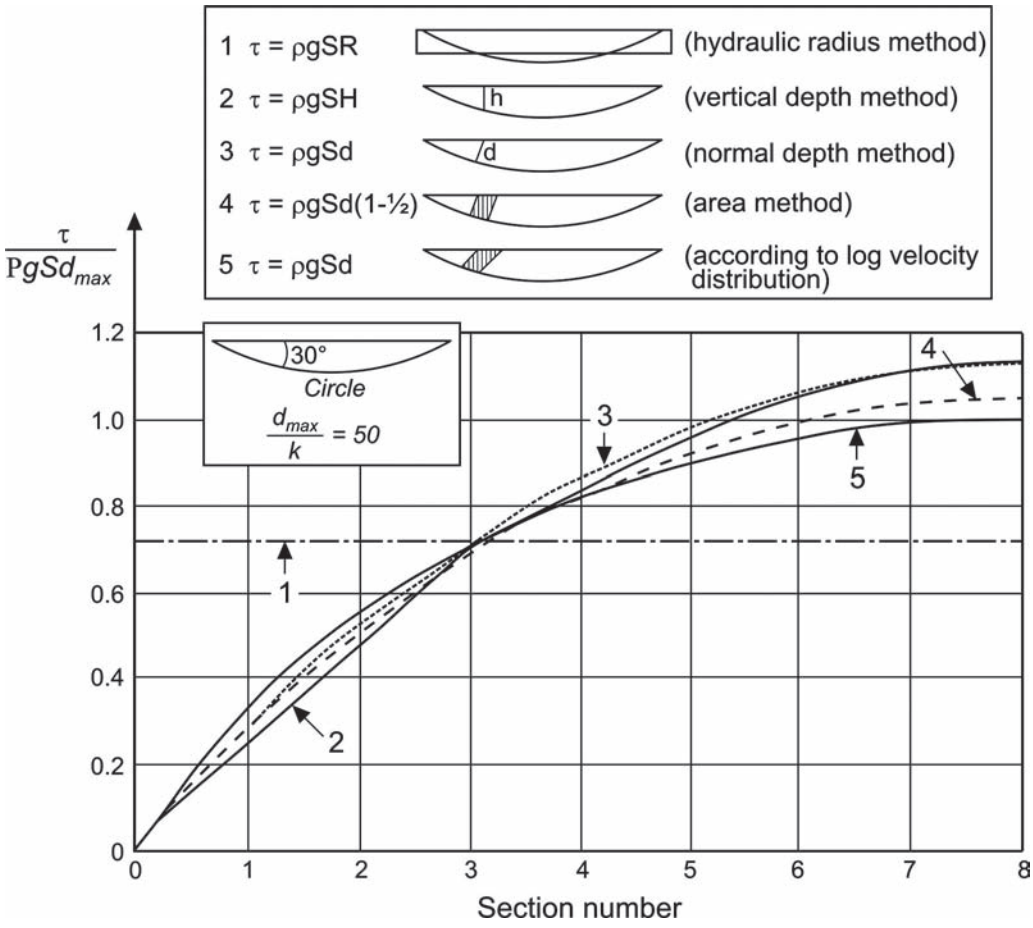

Fig. 7-10. Comparison between five different methods of determining shear stress distribution (ASCE Task Committee on Hydraulics, Bank Mechanisms and Modeling of River Width Adjustment 1998a, with permission from ASCE).

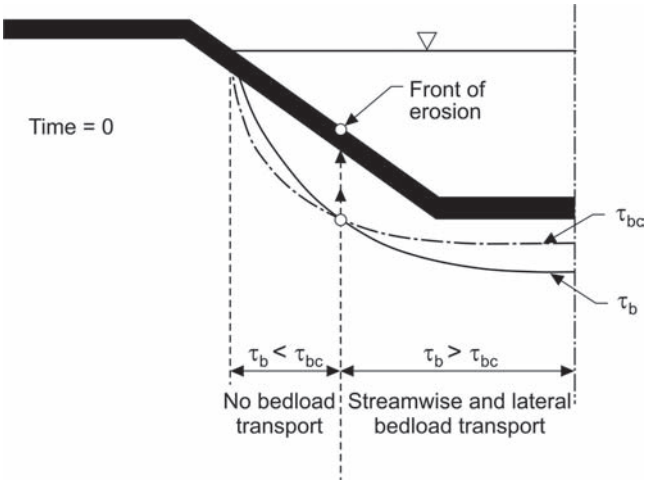

Fig. 7-11. Definition of front of erosion for initially straight trapezoidal cross section at time 0 (ASCE Task Committee on Hydraulics, Bank Mechanisms and Modeling of River Width Adjustment 1998a, with permission from ASCE).

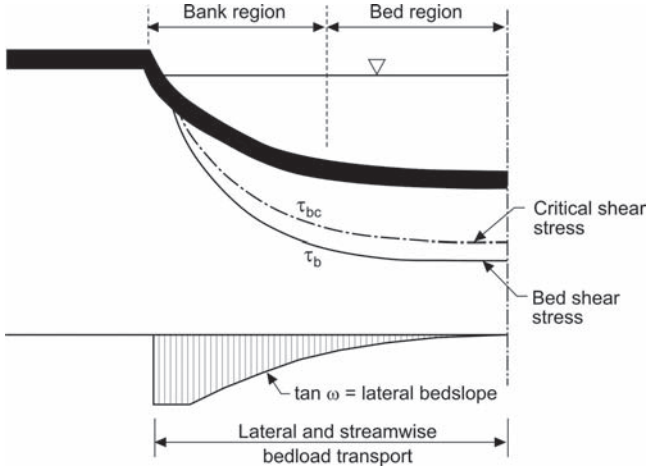

Fig. 7-12. Sketch of distribution of shear stress τ_b and lateral bed slope tan ω along perimeter of straight channel cross section during development of stable profile (ASCE Task Committee on Hydraulics, Bank Mechanisms and Modeling of River Width Adjustment 1998a, with permission from ASCE).

main channel riverbanks. These features are discussed by Knight and Cao (1994) in relation to large-scale experimental studies and by Knight and Shiono (1995) in relation to the relative importance of the three terms in (7-1).

The redistribution of boundary shear stress within the cross section during over-bank flow also has a profound effect upon sediment transport rate, as shown by Ackers (1992) and Abril (1995). It will consequently also have an effect on bank adjustments that occur when the river overflows its bank.

7.3.2.3 Longitudinal Changes Unlike artificially constructed channels, river channel cross sections are not generally uniform trapezoids. Consequently, width, depth, slope, and planform change significantly in the streamwise direction. Some schematization of the natural river is therefore necessary before a numerical model is constructed (Samuels 1990), and inevitably some streamwise averaging of cross-sectional area, hydraulic radius, energy gradient, mean boundary shear stress, etc. must be performed. This is potentially a source of error in any representation of the channel hydraulics and

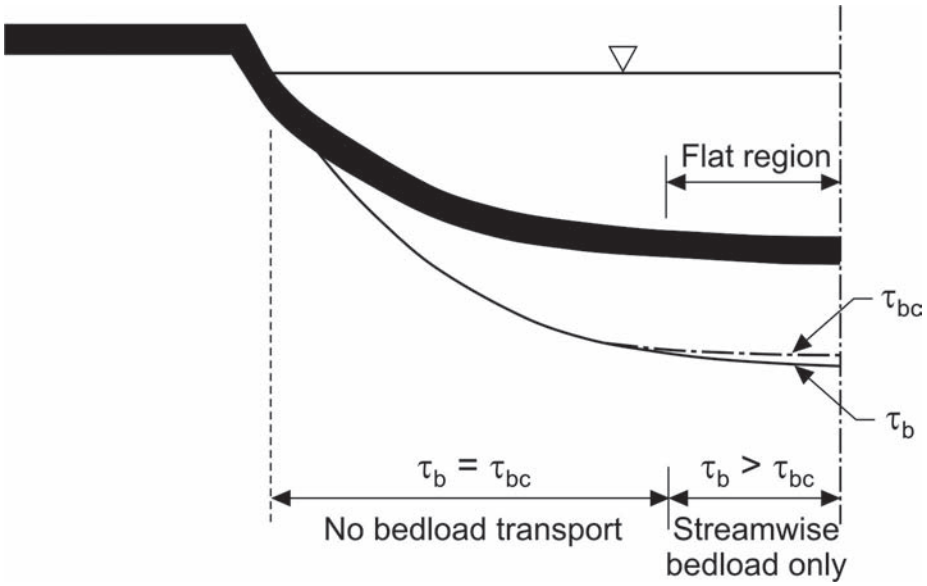

Fig. 7-13. Shear stress distribution in state of dynamic equilibrium (ASCE Task Committee on Hydraulics, Bank Mechanisms and Modeling of River Width Adjustment 1998a, with permission from ASCE).

must be treated with appropriate care (McBean and Perkins 1975; Cunge et al. 1980; Laurenson 1986). Samuels (1989; 1990) used perturbation analysis of the steady-flow equation to show that weighting the friction slope toward the upstream section gives considerably improved accuracy. For example, the longitudinal spacing between channel cross sections may be doubled if weighting coefficients are used rather than the arithmetic mean, with the same accuracy in water levels being achieved. However, the correct representation of the energy gradient or water-surface slope is difficult to achieve in natural channels where width, pool-riffle sequences (especially in gravel-bed rivers), and pool-crossing geometry (in sinuous rivers) introduce marked channel variability. In these cases, channel schematization, even using a weighting technique, may be inadequate. Further work is needed on the derivation of representative reach-averaged parameters and their significance in 1D models.

In meandering alluvial rivers, the boundary shear stress distribution, bed topography, bed load transport rate, and channel cross-sectional shape all vary considerably over the meander wavelength due to flow curvature effects. Field data (Dietrich and Smith, 1983, 1984, and many others) indicate that the near-bed flow and bed load transport along the outside bank of a meander bend are directed toward the inside bank (Fig. 7-14), leading to the development of a deep pool along the outside of the bend. On the inside bank, shoaling of the flow over the point bar causes the near-bank velocity to be directed toward the outside bank. Because the development of the pool can increase the effective height of the outside bank, scour on the outside of meander bends is an important hydraulic process that promotes bank erosion. Smith and McLean (1984) and Nelson and Smith (1989a; 1989b) have developed effective numerical models for computing flow and transport processes in meander bends, although these models are not accurate close to the bank itself because lateral momentum diffusion terms in the governing equations are neglected.

In overbank flows on meandering rivers, hydraulic processes are extremely complex and difficult to predict. Laboratory studies (Tominaga and Neza 1991; Sellin et al. 1993; Tominaga and Neza 1993; Wark et al. 1994; Knight and Shiono 1995) show that new flow structures are introduced during over-bank flow, and field studies (Fukuoka 1993; 1994; Lawler 1993a; 1993b) indicate that over-bank flows are strongly influenced by local morphological features.

7.3.2.4 Near-Bank Zone Knowledge of the velocity, boundary shear stress, secondary flows, and turbulence structure close to a riverbank is required before fluvial processes can be linked to channel-width adjustment. The preceding sections have highlighted current difficulties in predicting the details of near-bank hydraulics, even for relatively simple prismatic channels, whether flowing in-bank or over-bank. The 3D nature of near-bank flow leads to nonlinear distributions of Reynolds stresses normal to the boundary and velocity profiles that are not logarithmic (Knight and Shiono 1990; Shiono and Knight 1991; Meyer and Rehme 1994; Knight and Shiono 1995). The effect of these flow complexities on boundary shear stress distributions in the vicinity of riverbanks has been illustrated by Knight and Cao (1994).

At present, no simple formulas exist to characterize the lateral distribution of local time-averaged boundary shear stress around the wetted perimeter of a natural channel, although Figs. 7-7 and 7-8 give some guidance, and experimental data, such as those shown in Figs. 7-4 and 7-5, indicate how local values may vary about the cross-sectional mean. Consequently, boundary shear stresses in the near-bank zone either have been estimated from trends established experimentally, such as those shown in Figs. 7-4 to 7-10, or else have been obtained from turbulence models, of which the nonlinear k-ε (k is the turbulent kinetic energy and ε is the turbulent dissipation rate) and large-eddy simulation models are probably the most appropriate (Rodi 1980; Nezu and Nakagawa 1993; Thomas and Williams 1995; Younis 1996). Assuming that these local values are known, Figs. 7-11 to 7-13 show how the boundary shear stress and bed load region are often conceptualized in a typical width adjustment model (Ikeda and Izumi 1991; Kovacs and Parker 1994; Knight and Yu 1995). It should be remembered, however, that although the boundary shear stress is arguably one of the more important connecting links between the flow field and the distributions of erosion (or scour), deposition, and channel change (Breusers and Raudkivi 1991), it is not necessarily the dominant parameter responsible for bank erosion or width adjustment. Process dominance also depends on the geomorphic context within which width adjustment is taking place, the channel type (Fukuoka et al. 1993), and location within the watershed (Lawler 1992).

7.3.2.5 Adjustment of Channel Boundaries in Near-Bank Zone The adjustment of alluvial channel boundaries is usually related to spatially averaged hydraulic parameters, such as boundary shear stress, streamwise stream power, and energy gradient, together with data defining the net sediment supply to the system and the bank material properties (Molinas and Yang 1986; Hasegawa and Mochizuki 1987; Chang 1988a, 1988b; Hasegawa 1989; Wiele and Paola 1989; Pizzuto 1990; Lawler 1993a; Parker 1995). The variability of channel morphology and complexity of the turbulent flows described earlier might suggest that a probabilistic approach is more suitable than the deterministic treatments described previously. Whichever approach is selected, the same key hydraulic parameters are still likely to be included in process equations or functions and should be represented as faithfully as possible, despite some implicit longitudinal smoothing of localized flow structures or morphological features. The appropriate inclusion of 3D phenomena in either a 1D model or a depth-averaged model is still awaited and is likely to be derived from detailed 3D numerical simulations (ASCE Task Committee on Turbulence Models in Hydraulic Computation 1988; Li and Wang 1994a,b; Thomas and Williams 1995; Younis 1996). However, even allowing for future advances in representing the 3D flow,

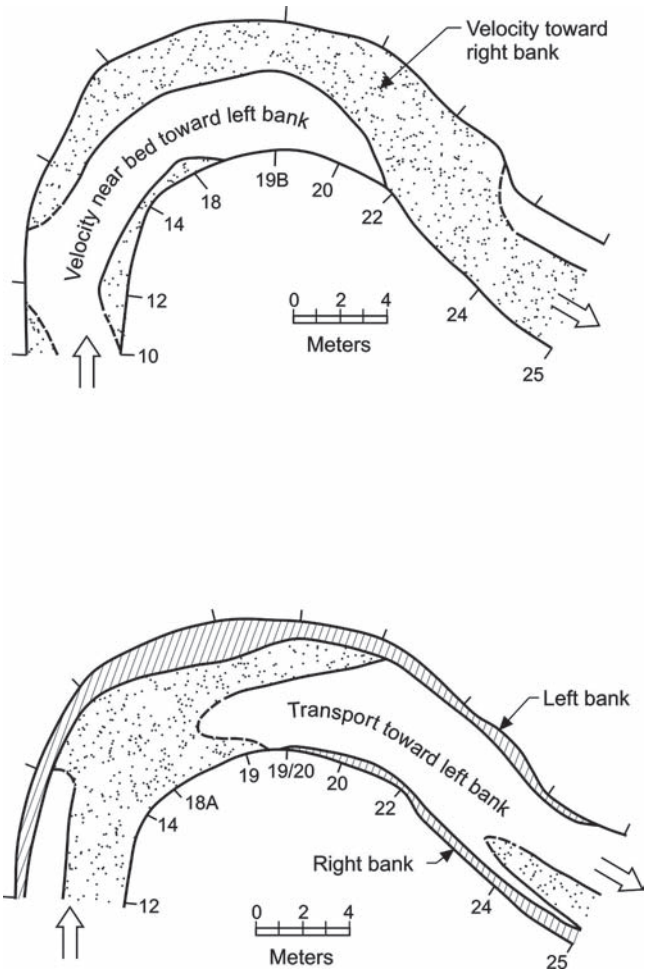

Fig. 7-14. Top: direction of flow near the bed in a meander bend determined using current meter data (Dietrich and Smith 1983). Bottom: direction of bed load transport in a meander bend. The shaded area represents bed load transport toward the right bank, whereas the clear area denotes bed load transport toward the left bank. The dashed lines indicate uncertainty as to correct position of the boundary between fields. Diagonal lines define the area occupied by submerged bank and immobile gravel (Dietrich and Smith 1984).

a comprehensive theoretical framework for determining the equilibrium form of stable alluvial channels still needs to be developed before attempting to simulate changes from the equilibrium profile.

Identification of the junction point between active (eroding) and inactive (noneroding) elements of the bank, together with characterization of the erosion front that moves this point, appears to be crucial to quantifying width adjustment. Hydraulic conditions at the active-inactive junction are especially difficult to determine with precision, even for in-bank flows. Near-bank hydraulic conditions for over-bank flows are strongly influenced by secondary flow structures close to the banks and must be represented carefully through the correct use of local friction factors, eddy viscosities, and depth-averaged secondary flow values. For this purpose, the depth-averaged approach described earlier is worthy of further study. Although this approach still has major drawbacks, a need still exists for calibration of specific channel shapes, and no details of vertical motion are available from the process equations.

It is also important to know the rates at which width, depth, slope, and local morphological adjustments are made, so that errors can be assessed when an incremental series of quasi-steady-state discharges are used to simulate a hydrograph. The dominant or effective discharge responsible for forming channel morphology, although easy to define in theory, is still poorly understood and, except for work by Ackers (1992), very little attention has been paid to the influence of over-bank flows on dominant discharge. The hypothesis that in an equilibrium channel the bank-full stage corresponds to the dominant or effective discharge has some theoretical basis, but it may be a special case within a variety of associations between important features of channel morphology and a range of effective flows (Hey 1975; Thorne et al. 1993; Biedenharn and Thorne 1994). Further experimental work on equilibrium and nonequilibrium alluvial channels is required before linkages between dominant discharge, the range of effective flows, and channel morphology can be substantiated.

7.3.3 Bank Mechanics

The fundamental processes responsible for channel-width adjustment are fluvial erosion, fluvial deposition, and mass bank failure. The following seven topics concerned with the mechanics of bankline movement are addressed in this section: (1) bank erosion; (2) weakening of resistance to erosion; (3) bank stability with respect to mass failure; (4) basal endpoint control; (5) effects of vegetation; (6) seepage effects; and (7) bank advance.

7.3.3.1 Bank Erosion Water flowing in an alluvial channel exerts forces of drag and lift on the boundaries that tend to detach and entrain surface particles. To remain in place, the boundary sediment must be able to supply an internally derived force capable of resisting the erosive forces applied by the flow. The origin of these resisting forces varies according to the grain size, the size distribution, and the nature of electrochemical bonding that may exist between particles. Alluvial bank materials are formed primarily by fluvial deposition and are often stratified, with a general fining-upward sequence. Therefore, the engineering characteristics and erodibility of the bank may vary with elevation. Also, floodplain deposits typically include alluvial sands and gravels, clay plugs, and strongly cohesive backswamp deposits, so that bank material properties vary spatially over relatively short distances. Although the distribution of sustained bank retreat along the course of a river depends primarily on the distribution of boundary shear stress in the near-bank zones, outcrops of particularly resistant material may act to slow the local bank retreat rate and

to distort the fluvially driven pattern of channel planform evolution (Sun et al. 1996).

In the case of noncohesive sands and gravels, the forces resisting erosion are generated mainly by the immersed weight of the particles, although close packing of grains in imbricated patterns can also wedge particles in place, greatly increasing the critical boundary shear stress necessary for entrainment. Generally, the mobility of noncohesive bank materials can be predicted using a Shields-type entrainment function, but this must be modified to take into account the destabilizing effect of channel side slope. Also, the critical value of the dimensionless shear stress must be adjusted to allow for excessive tightness or looseness in packing of bank material particles (Thorne 1982).

Fine-grained bank materials, containing significant amounts of silt and clay, are to some degree cohesive and resist entrainment primarily through interparticle electrochemical bonding rather than through the immersed weight of the particles. When cohesive bank materials are entrained by the flow, it is aggregates of grains (such as soil crumbs or peds that have been produced by soil-forming processes) that are detached. Fluvial entrainment, therefore, requires that the local boundary shear stresses exceed the critical value to initiate motion of crumbs or peds rather than that related to the primary soil particles. Ped size and stability and interped bonding strength are not conservative soil properties, because they depend to some degree on the local history of soil development, in general, and recent antecedent conditions of wetting and drying, in particular. It follows that the conditions of incipient motion for cohesive bank materials are complex, time-dependent, and difficult to define.

A task committee (ASCE Task Committee on Erosion of Cohesive Sediments 1968) summarized early studies into the mechanics of cohesive bank erosion. The task committee recorded the results of noteworthy contributions by, among others, Smerdon and Beasley (1961) and Flaxman (1963) on channel stability in cohesive materials and Grissinger and Asmussen (1963) and Grissinger (1966) on the erodibility of cohesive soils. For example, Grissinger and Asmussen (1963) found that erosion resistance of clayey soils increased with the time that the materials were wetted. They postulated that when clay is initially wetted, the free water releases bonds between particles, but that, as free water is absorbed, the clay minerals hydrate and interparticle bonds are strengthened. This illustrates how the chemical bonding of clay particles may vary with time and the history of soil moisture changes.

A wealth of subsequent work has further addressed fundamental aspects of cohesive soil behavior, leading to important papers by Parthenaides and Passwell (1970); Kandiah and Arulanandan (1974); Arulanandan (1975); Arulanandan et al. (1975); Ariathurai and Krone (1976); Ariathurai and Arulanandan (1978); Abt (1980); Grissinger (1982)—who presents an excellent review of progress achieved up to the early 1980s; Kamphuis and Hall (1983); Parchure and Mehta (1985); Springer et al. (1985); Shaikh et al. (1988a; 1988b); and, more recently, Annadale and Parkhill (1995) and Kranenburg and Winterwerp (1997). Space limitations preclude an in-depth review of the findings of these papers here. However, in summary it can be concluded that although critical boundary shear stresses for cohesive bank soils are extremely difficult to predict accurately (Grissinger 1982), they tend to be higher than those for noncohesive bank materials. As a result, erosion rates for cohesive banks are generally lower than those for noncohesive materials (Vanoni 1975; Thorne and Tovey 1981).

Once entrained, crumbs and peds disintegrate rapidly due to corrasion at the channel boundaries and turbulent buffeting in the flow, so that most silt- and clay-sized sediment derived from bank erosion is transported in suspension and is conventionally classified as wash load.

7.3.3.2 Weakening of Resistance to Erosion The erodibility of bank soils can be increased markedly by processes of weakening and weathering. The processes responsible for loosening and detaching grains and aggregates are closely associated with soil moisture conditions at and beneath the bank surface. In poorly drained soils, positive pore-water pressures act to reduce bank stability, which can lead to bank failure, particularly during rapid drawdown of the channel stage following a high flow. Conversely, rapid immersion of a dry bank can lead to slaking, which is the detachment of aggregates by positive pore pressures due to compression of trapped air.

Changes in moisture content and freezing and thawing can significantly influence the erodibility of a riverbank. Swelling and shrinkage of soils during repeated cycles of wetting and drying can contribute to cracking that significantly increases erodibility and reduces soil shear strength. Shrinkage is especially damaging to the strength of the bank when intense drying of the soil leads to desiccation cracking. Heaving due to the 9% increase in water volume on freezing (Ritter 1978) and the growth of needle ice crystals at the bank surface, followed by collapse of ice wedges and needles during thawing of soil moisture, are highly effective in increasing the susceptibility of cohesive bank materials to flow erosion (Lawler 1993b).

Temporal variability in the erodibility of bank soils due to the operation of weakening processes means that the effectiveness of a given flow event in eroding a bank depends not only on the magnitude and duration of a particular event but also on antecedent conditions (Wolman 1959).

7.3.3.3 Bank Stability with Respect to Mass Failure Fluvial erosion drives bank retreat directly by removing material from the bank face, but it often also causes bank retreat by triggering mass instability. The stability of a bank with regard to mass failure depends on the balance between gravitational forces, which tend to move soil downslope, and forces of friction and cohesion, which resist movement. Failure of the bank occurs when scour of the bed next to the bank toe increases the bank height, or when undercutting increases the bank angle, to the point that motivating

forces exceed restoring forces on the most critical potential failure surface, and the bank collapses in a gravity-induced mass failure.

The analysis of slope stability with respect to mass failure has been the topic of considerable research, primarily by geotechnical engineers but also by geomorphologists and geophysicists. Engineering research has concentrated on development of engineering designs for artificial slopes and embankments, but rather little of this work is applicable to the very steep slopes, undisturbed soils, complex sedimentary layering, and unspecified drainage conditions found in eroding natural riverbanks. Also, application of most geotechnical analyses requires detailed site investigation to provide the necessary data on profile geometry, soil properties, bank stratigraphy, and ground-water flow net. Although it is possible to collect such detailed information for a specific construction site or key location, the data obtained cannot easily be generalized to represent bank conditions along a reach of a river, due to inherent variability in the properties of natural alluvium and uncertainty concerning the local bank environment.

In fact, relatively little research specifically concerned with streambank stability has been undertaken, and the following brief review of slope stability literature concentrates on more recent work that is directly relevant to mass failure of riverbanks. However, it is acknowledged that treatment of riverbank stability shares a common origin with that of engineered slopes and embankments in the fundamental work of researchers, such as Bishop (1955); Peck and Deere (1958); Bishop and Morgenstern (1960); Morgenstern and Price (1965); Spencer (1967); Terzaghi and Peck (1967); Vaughan and Walbancke (1973); Fredlund and Krahn (1977); and Poulos et al. (1985).

There is a clear contrast in failure mechanics between noncohesive and cohesive materials because of significant differences in their soil properties. In a noncohesive bank, shear strength increases more rapidly with depth than does shear stress, so that critical conditions are more likely to occur at shallow depths. In a cohesive bank, shear stress increases more quickly than shear strength with increasing depth, so that critical surfaces tend to be located deep within the bank (Terzaghi and Peck 1967).

Noncohesive materials usually fail by dislodgement and avalanching of individual particles or by shear failure along shallow, very slightly curved slip surfaces. Deep-seated failures occur in cohesive materials with a block of disturbed, but more or less intact, bank material sliding into the channel along a curved failure surface. In high banks with shallow slope angles ($\theta < 60°$), the failure surface is curved and the block tends to rotate back toward the bank as it slides in a rotational slip (Fig. 7-15). Steep banks characteristically fail along almost planar surfaces, with the detached block of soil sliding downward and outward into the channel in either a planar slip or a toppling failure (Fig. 7-16) (Thorne 1982).

Rotational slips may be defined as base, toe, or slope failures depending on where the failure arc intercepts the ground surface (Fig. 7-15(a) and are analyzed using conventional geotechnical procedures (Bishop 1955; Fredlund 1987). The risk of failure is usually expressed by a factor of safety, defined as the ratio of restoring to disturbing moments about the center of the failure circle. In the method of slices (Fig. 7-15(b), the soil body within the failure arc is divided into vertical slices with forces acting as shown. To obtain a determinate solution for the factor of safety, it is necessary to make an assumption regarding interslice forces. For example, these forces are often assumed to act horizontally. The critical slip failure circle cannot be located simply, and usually a computer program is used to explore the large number of possible solutions to determine the position of the most critical arc.

Many eroding riverbanks are very steep, and near-vertical banks often occur at the outer margins of meander bends and along severely incised channels. Such steep slopes formed in friable soils are rarely encountered in hillslope and embankment studies, and consequently, stability analyses for planar slip have received relatively little attention in the geotechnical literature. Approaches that have been developed stem from the Culmann method, in which forces acting on the potential failure block are resolved normal to and along

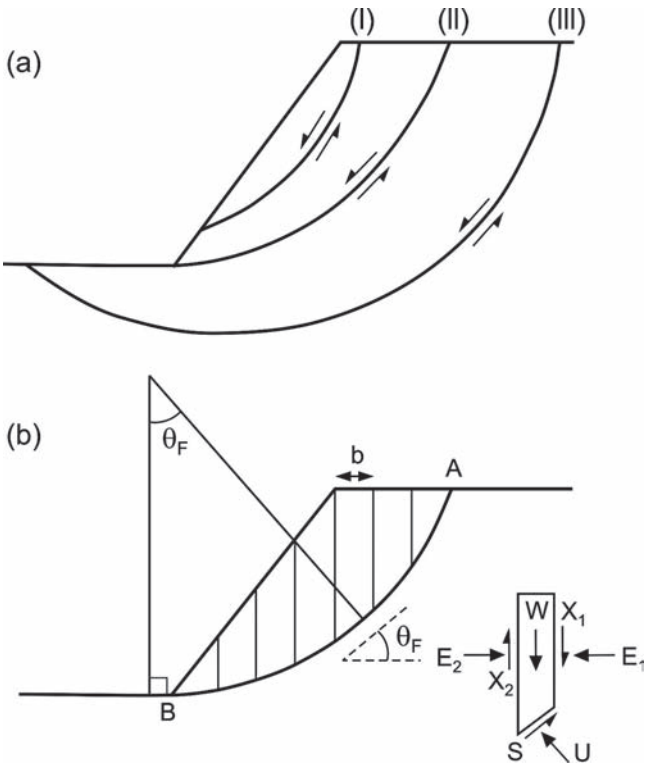

Fig. 7-15. (a) Rotational slip failures in cohesive bank: (i) slope failure, (ii) toe failure, (iii) base failure. (b) Stability analysis of slip circle by methods of slices. (After Thorne 1982. Copyright John Wiley & Sons Limited. Reproduced with permission.)

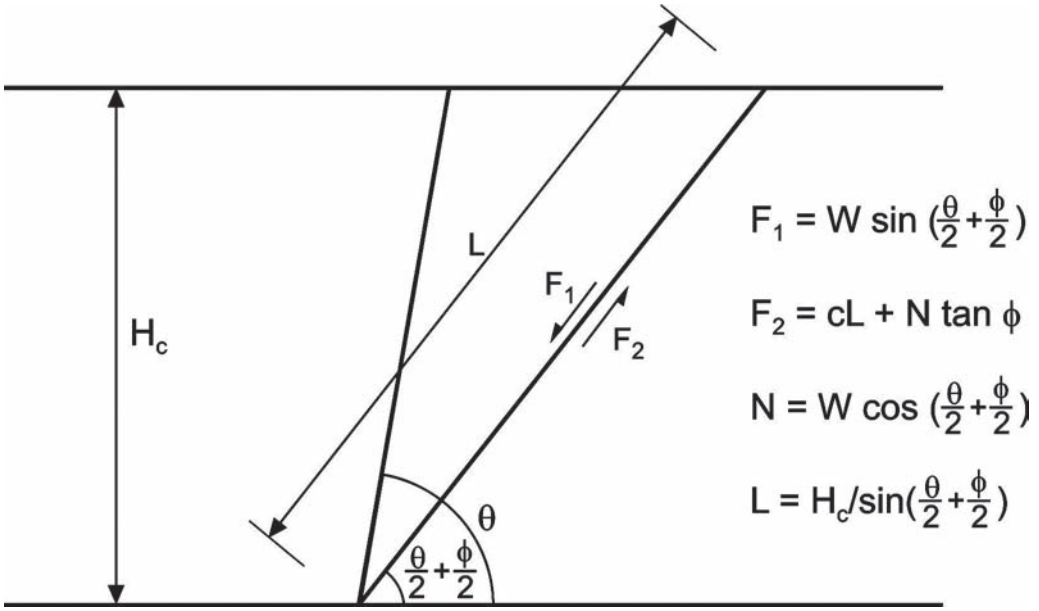

Fig. 7-16. Culmann analysis for plane slip failure. (After Thorne 1982. Copyright John Wiley & Sons Limited. Reproduced with permission.)

the failure plane, leading to the following equation to define the critical height for mass failure:

$$H_c = 4c(\sin\theta\cos\phi)/\gamma[1-\cos(\theta-\phi)] \qquad (7\text{-}5)$$

where

H_c = critical bank height;
c = cohesion;
θ = bank angle;
γ = bank material unit weight; and
ϕ = friction angle.

Tension cracks often develop downward from the ground surface, parallel to the bankline, behind steep banks because of horizontal tensile stress in the soil at this location (Terzaghi and Peck 1967). Tension cracks truncate the effective length of the potential failure surface, tending to destabilize the bank and reducing its stability relative to that predicted from a Culmann analysis. Cracks may occupy as much as half of the bank height, isolating a column or slab of soil, which then slides and topples forward into the channel in a toppling failure (Fig. 7-17).

Stability analyses applicable to the very steep (almost vertical), deeply cracked river cliffs associated with eroding, unstable streambanks have been undertaken by researchers in hydraulic engineering and fluvial geomorphology, but much more testing and validation is required before these models can be adopted for routine application as engineering design tools (Osman and Thorne 1988; Darby and Thorne 1996a; Millar and Quick 1997).

Cantilevered or overhanging banks are generated when erosion of an erodible layer in a stratified or composite bank leads to undermining of overlying, erosion-resistant layers. Thorne and Tovey (1981) pointed out that cantilevered banks may fail by shear, beam, or tensile collapse (Fig. 7-18). Shear failure (Fig. 7-18(a) occurs when the weight of the cantilever block exceeds the soil shear strength, causing the overhanging block to slip downward along a vertical plane. In a beam failure, a block rotates forward about a horizontal axis within the block (Fig. 7-18(b)) when disturbing moments about the neutral axis exceed restoring moments. Tensile failure (Fig. 7-18(c)) occurs when the tensile stress exceeds the soil tensile strength and the lower part of the overhanging block falls away. Frequently, the strength of cantilever blocks is significantly increased by root reinforcement due to riparian and floodplain vegetation. Flow erosion and tensile failure occurs below the root mat, leaving root-bound cantilevers that fail subsequently by either the beam or shear mechanism.

Whether bank failure occurs by rotational slip, toppling, or cantilever collapse, the primary force tending to move the failure block is the tangential component of the weight of the block. Fluvial erosion can increase the motivating force by increasing the bank height (through bed scour next to the bank toe) or by increasing the bank slope angle (through lateral erosion of the toe and lower bank). The weight of bank material also increases with the moisture content of the soil, and failure often follows the change from submerged to saturated conditions that occurs when drawdown occurs in the channel (Rinaldi and Casagli, 1999; Simon et al. 2000).

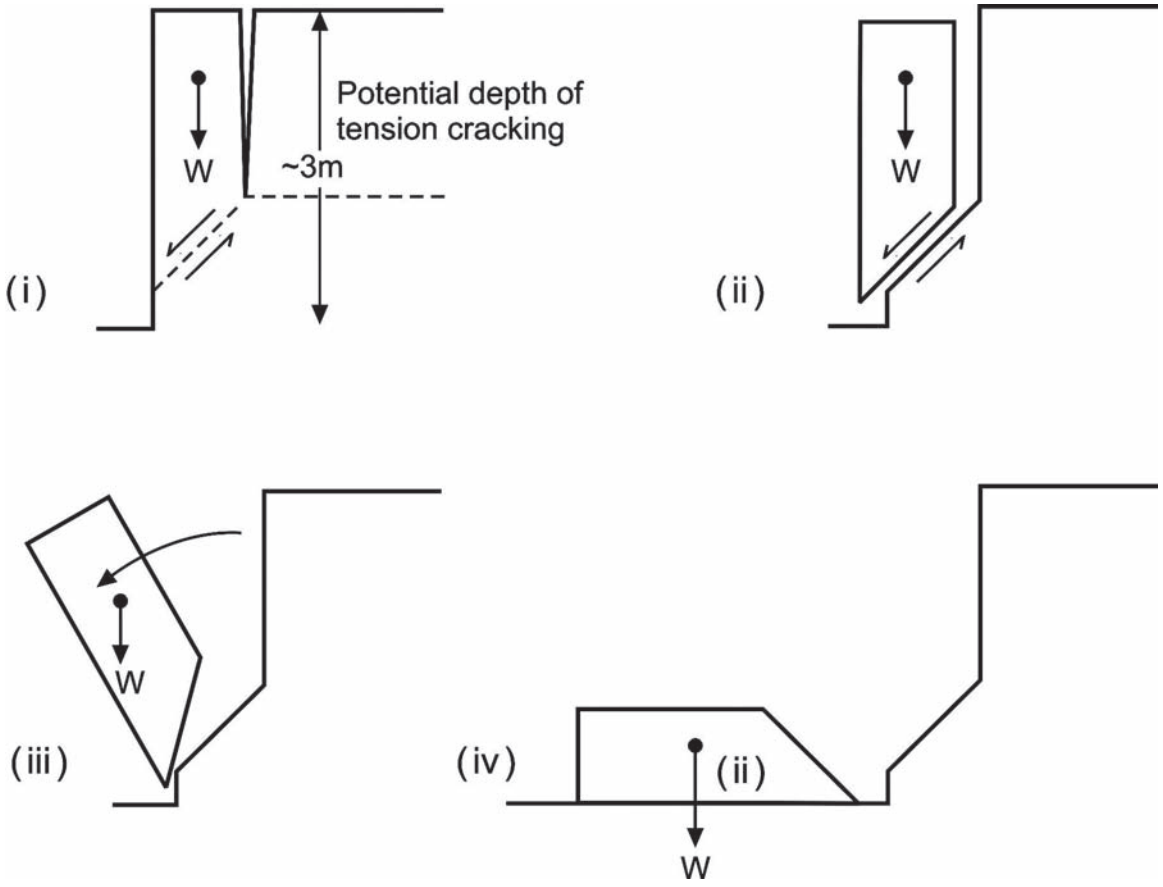

Fig. 7-17. Sequence (i–iv) of toppling failure on low steep stream bank. (After Thorne and Tovey 1981. Copyright John Wiley & Sons Limited. Reproduced with permission.)

Ample field evidence exists that bank failure may be triggered by any of these changes in motivating force. For example, Abam (1993) noted that bank failure in the Niger Delta, Nigeria, could often be attributed to increases in bank height and bank angle due to fluvial erosion and bed scour at the riverbanks. Abam (1993) also documented decreased bank stability due to rapidly falling water levels that led to (1) the loss of the confining pressure provided by the channel water level; (2) positive pore pressures due to poor drainage resulting from the low permeability of the soil; and (3) increases in the effective unit weight of the soil due to saturation.

7.3.3.4 Basal Endpoint Control Although fluvial erosion processes and geotechnical failures are controlled by different aspects of bank geomorphology, they are actually linked. The key to characterizing this link lies in recognizing that mass wasting delivers the failed material to the toe of the slope, or basal area, but does not entirely remove it from the bank profile. The removal of failed material from the basal area depends primarily on its entrainment by current and wave action, following by fluvial transport downstream. The concept of basal endpoint control explains how the medium- to long-term retreat rate of the bank is controlled by the rate of sediment entrainment and removal from the toe.

The concept of basal endpoint control was first developed by Carson and Kirkby (1972) to explain variations in hillslope profiles. Thorne (1982) applied the concept to riverbanks, proposing that bank retreat can only be sustained when the near-bank flow is able to remove failure debris and to continue to scour the basal area. In contrast, where the flow is unable to remove all the debris, basal accumulation occurs and a berm or bench of failed material develops. This tends to protect the bank from fluvial erosion and, by acting as a buttress against gravity failures, increases bank stability. On this basis, the balance of basal supply and removal of sediment can be defined by one of the following three states of basal endpoint control:

1. *Impeded removal*—Bank failures supply debris to the base at a higher rate than it is removed. Basal accumulation results, decreasing the bank angle and height and therefore increasing stability with respect to mass failure. The rate of debris supply decreases, favoring the second state.
2. *Unimpeded removal*—Processes delivering debris to the base and removing it are in balance. No changes in basal elevation or slope angle occur. The bankline

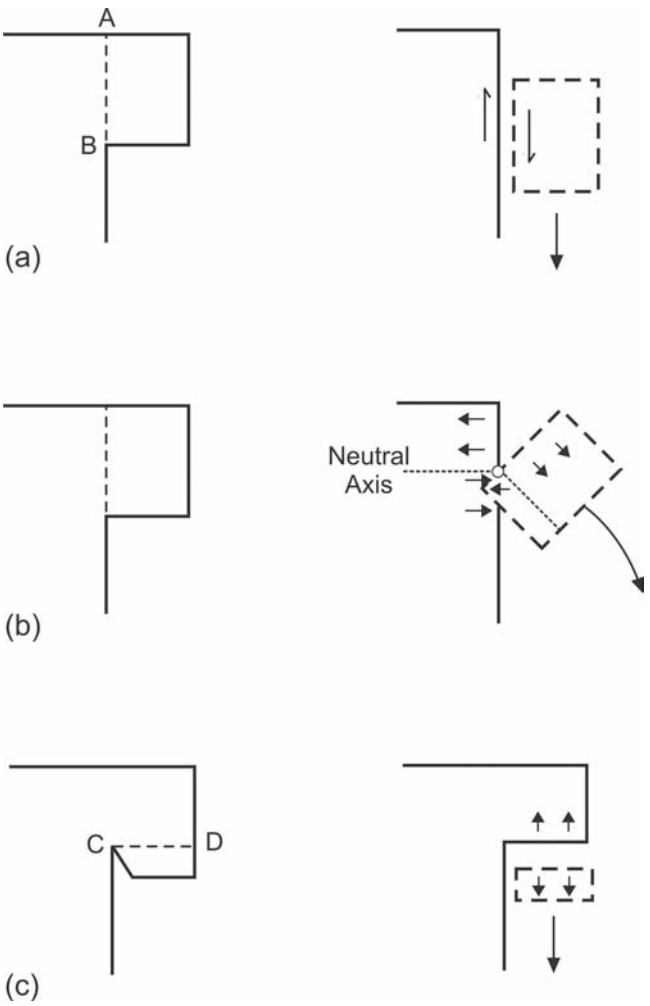

Fig. 7-18. Mechanisms of cantilever failure: (a) shear failure along AB; (b) beam failure about neutral axis; (c) tensile failure across (CD). (After Thorne and Tovey 1981. Copyright John Wiley & Sons Limited. Reproduced with permission.)

recedes by parallel retreat at a rate determined by the degree of fluvial activity at the base.

3. *Excess basal capacity*—Basal scour has excess capacity over the debris supply from bank failures. Basal lowering occurs, increasing bank angle and height, and therefore, decreasing stability with respect to mass failure. The rate of debris supply increases, favoring the second state.

The state of basal endpoint control is useful in explaining the medium- to long-term rates of riverbank retreat of advance. It also highlights the importance of considering the response of near-bank morphology to bank stabilization. The concept indicates that a reduction in debris supply that is due to bank stabilization may induce a state of excess basal capacity that generates very deep toe scour (Thorne et al. 1995). As pointed out by Maynord (1996), this additional scour must be properly accounted for in the design of the stabilization works if failure due to undermining is to be avoided.

Hagerty (1991) proposed that not all sustained bank retreat depends on the state of basal endpoint control. This proposal was based on the fact that piping is a widespread cause of sustained bank retreat along the Ohio River, which is apparently independent of the state of basal endpoint control. Even though the bank toe is stable, upper bank retreat has continued unabated for many years. However, closer inspection of the relevant bank profiles indicates that the reason that the toe has been stable is that, in this regulated river, the toe is well below pool level and is thus morphologically inactive. Piping in sand layers at about the elevation of the stranded low water plane has produced a bench that represents the toe of the morphologically active bank. At this elevation, bank retreat may still be considered to be covered by the concept of basal endpoint control, with the bank profile above pool elevation almost continually in a state of unimpeded removal, due to the ability of current and wave action to remove the fine debris supplied by piping. Creation of the bench and control of the profile thus depend on the piping process in supplying debris that can easily be removed by waves and currents that would not otherwise be able to erode intact bank material.

Hagerty et al.'s (1995) detailed treatment highlights the subtlety of interactions between fluvial and mechanical processes responsible for bank retreat, and it illustrates that great care must be taken in interpreting bank processes from bank form, especially in regulated rivers.

7.3.3.5 Vegetation Effects The role of vegetation in affecting bank erosion and width adjustment is complex and poorly understood. Although vegetation generally reduces soil erodibility, its impact on bank stability with respect to mass failure may be either positive or negative. Hence, depending on the geomorphic context and dominance of either fluvial processes or mass failure, vegetation may product either a net increase or a decrease in the rate of bankline shifting.

Vegetation can play an important role in limiting the effectiveness of bank erosion by detachment and entrainment of individual grains or aggregates of bank material. Compared to unvegetated banks, erosion of well-vegetated banks is reduced by one to two orders of magnitude (Carson and Kirkby 1972; Smith 1976; Kirkby and Morgan 1980). Gray and Leiser (1982) have reviewed the effects of herbaceous and, to a lesser extent, woody vegetation in reducing flow erosivity and bank erodibility and concluded that major effects include the following:

—Foliage and plant residues intercept and absorb rainfall energy and prevent soil compaction by raindrop impact.
—Root systems physically restrain soil particles.
—Near-bank velocities are retarded by increased roughness.
—Plant stems dampen turbulence to reduce instantaneous peak shear stresses.

—Roots and humus increase permeability and reduce excess pore water pressures.
—Depletion of soil moisture reduces water-logging.

Gray and Leiser (1982) also reviewed the ways that woody vegetation may affect the balance of forces promoting and resisting mass failure. Roots mechanically reinforce soil by transferring shear stresses in the soil to tensile stresses in the roots, which root strength is able to resist. However, this effect operates only to the rooting depth of the vegetation, and it does not reinforce potential failure planes that pass beneath the plant rootballs. Hence, root reinforcement is negated when bank height significantly exceeds rooting depth.

Soil moisture levels are decreased by interception on the canopy and evapotranspiration from the foliage, reducing the frequency of occurrence of the saturated conditions conducive to bank collapse. Anchored and embedded stems can act as buttress piles or arch abutments in a slope, counteracting downslope shear stresses and increasing bank stability. However, roots may also invade cracks and fissures in a soil or rock mass and thereby cause local instability by their wedging or prying action. The surcharge weight of vegetation may significantly increase motivating forces, causing destabilization of the bank, and wind loading of tall vegetation may exert an additional and potentially critical destabilizing moment on the bank.

These few examples illustrate the complexity of vegetation impacts on flow erosivity, soil erodibility, and mass stability. A recent scoping study on bank vegetation and bank protection reached the conclusion that vegetation may be either a positive or negative influence on bankline stability and retreat rate (Thorne et al. 1997). This may explain the apparently contradictory conclusions regarding the effect of bank vegetation on equilibrium channel width of, for example, Hey and Thorne (1986), who reported that stable channel width decreases as the density and stiffness of bank vegetation increase, and Murgertroyd and Ternan (1983), who found the opposite in a study of the effects of afforestation on channel form. Also, they may explain why the notable increases in the shear strength of root-permeated soils found in laboratory test soils by Waldron (1977) are not always replicated in strength measurements made in real riverbanks (Amarasinghe 1992).

As pointed out by Thorne and Osman (1988a), Darby and Thorne (1996a), and most recently, Thorne et al. (1997), a great deal of further research is necessary before vegetation effects can be properly understood and incorporated into the technical description of bank material characteristics under conditions representative of the range of environments encountered along natural streams and waterways.

7.3.3.6 Seepage Effects In addition to fluvial activity causing scour at the toe of the slope, grain-by-grain detachment, and mass wasting, Parola and Hagerty (1993) have identified a general class of failure mechanisms that is often very important to bank stability. This class of mechanisms is driven by seepage within the bank.

Pore-water movement within a bank is most vigorous during and following a high-flow event. As flood waters rise in a stream, the increased hydraulic head drives seepage into the bed and banks, resulting in groundwater recharge. As the flood stage recedes, hydraulic gradients reverse, driving seepage into the stream from the banks. The distribution of inflow, movement, and outflow through the bank is seldom uniform but is, in fact, strongly influenced by the layered stratigraphy that is characteristic of alluvial banks.

Alluvial banks consisting of sand, silt, and clay layers typically have hydraulic conductivity that is much greater in the horizontal direction than the vertical. Consequently, groundwater flow occurs principally by horizontal seepage into and out of sandy layers. During bank drainage, outflowing water may entrain and remove grains from a sand layer—a process termed piping by Hagerty (1991). Piping erosion leads to undermining of overlying, less pervious layers causing those layers to deflect and distort. The most common result of this undermining is the formation of cracks in the undermined layer, where the soil is unable to support the tensile stresses created by deflection (Parola and Hagerty 1993). Mass wasting then occurs as cracking reduces the operational strength of the bank.

Another type of bank failure associated with strong seepage is gully development. Although gully development is usually regarded as resulting from surface erosion, subsurface erosion by piping may lead to subsequent collapse of the pipes to form gullies along streambanks (Harvey et al. 1985). This mode of gully formation is particularly likely in loess deposits.

Bank weakening and erosion by seepage are often overlooked by river engineers. Failure to identify subsurface piping erosion can lead to misclassification of the erosion problem and subsequent problems with bank stabilization works that are adequate to armor the bank against fluvial attack but that are likely to fail due to internal erosion driven by piping.

7.3.3.7 Bank Advance Bank advance occurs through sediment deposition, a process that tends to narrow the channel. Bank advance occurs in a variety of different geomorphic settings (Figs. 7-1 and 7-2), and sediment may be deposited from bed load, suspended bed-material load, wash load, or a combination of all three transport processes. Despite this diversity, however, processes of bank advance have a common result: new floodplain deposits are created as the bank advances. This suggests that bank advance should be more broadly viewed as one of several processes that create new floodplains.

In a meandering stream, bank advance may occur on point bars on the insides of the channel bends (Figs. 7-1b and 7-2b) (Sundborg 1956; Leopold and Wolman 1957; Leopold et al. 1964; Jackson 1976a, 1976b) or on concave bank benches on the outsides of channel bends. Point bars are initiated by

the creation of a point bar platform deposited primarily from bed load transport (Nanson 1980). The platform is the base on which develops a scroll bar of fine traction and suspended load. As the scroll bar grows, vegetation may be established, further enhancing deposition. When the scroll bar is fully developed, approximately half of the new floodplain sediment is deposited from suspension, and the other half from bed load (Nanson 1980).

Bank advance and channel narrowing can also occur by deposition of berms or benches at the margins of the channel (Fig. 7-2a). Pizzuto (1994) and Moody et al. (1999) describe the formation of new floodplain "benches" along the Powder River in southeastern Montana (Fig. 7-19). These new floodplains were formed primarily by deposition from suspension in a widened channel created by a 25 to 50 year flood in 1978. Schumm et al. (1984) and Simon (1989) described the formation of "berms" as part of the evolution of incised channels. These authors note that as incised channels recover, the bed aggrades and berms develop on the channel margins. Harvey and Watson (1988) propose that the berms are formed from dunes left as remnant bed forms following high flows. The remnant dunes are then draped with fine-grained silts and clays from the suspended load as the flow diminishes, stabilizing the deposits. Repetition of this process eventually produces a stable berm, permanently advancing the bankline.

Bank advance may also occur as sediment is draped onto riverbanks from suspension. Taylor and Woodyer (1978) describe sand-mud couplets that increase in thickness and grain size with depth that are formed by deposition of suspended sediment on riverbanks. Taylor and Woodyer (1978) note that the bank advance process may be accelerated through sediment trapping in pioneer vegetation.

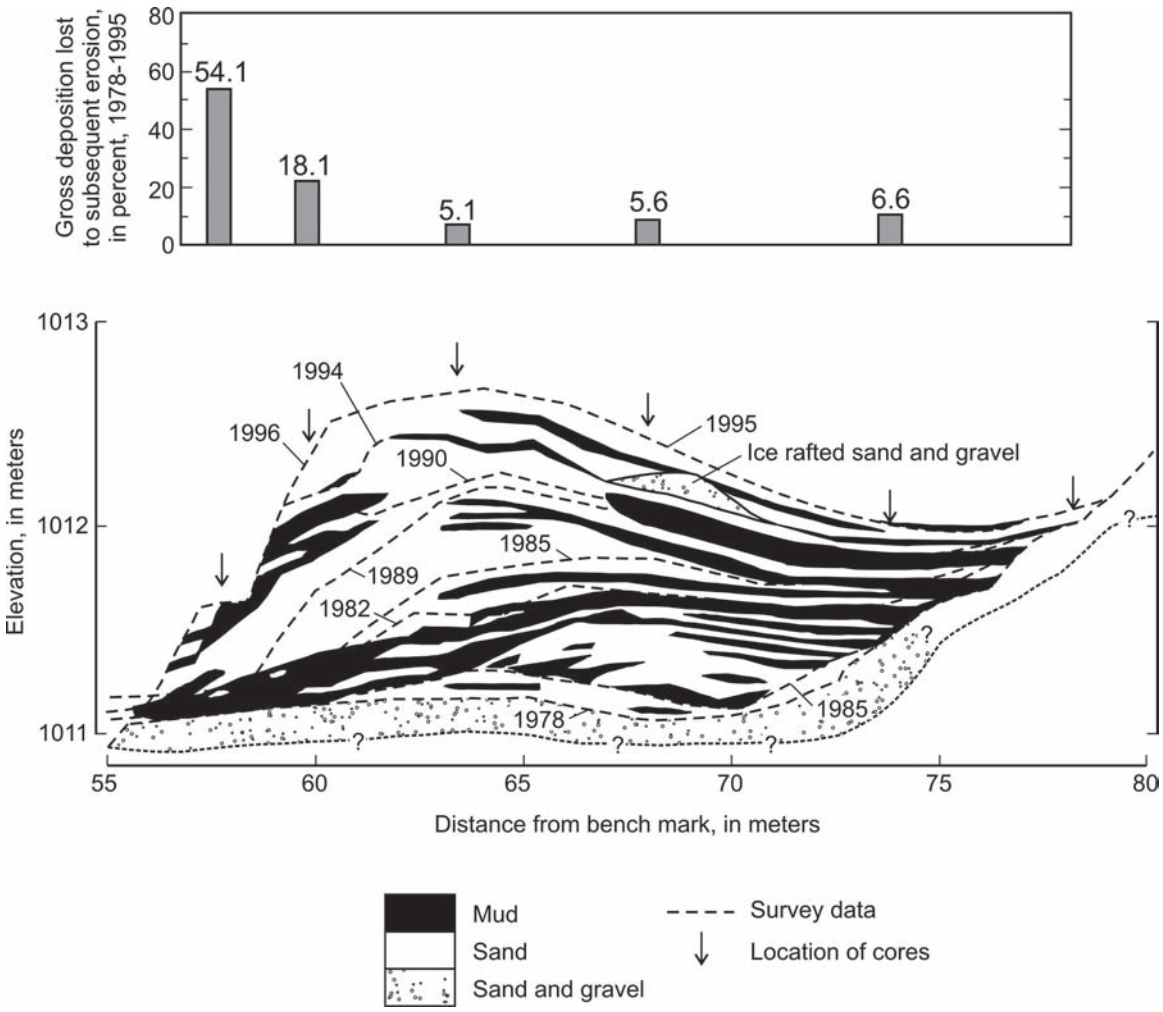

Fig. 7-19. Stratigraphic cross section of the flood plain at Section PR120 across Powder River near Moorhead, Montana, showing the history of bank advance from 1978 to 1996. The mud is shown as solid black areas and the sand as white areas. Some of the annual and biennial surveyed surfaces are labeled and the arrows indicate the locations of cores. Complete topographic cross sections of this site in 1978 and 1996 are presented in Fig. 7-3 (uppermost sections).

7.4 METHODS FOR EVALUATING BANK EROSION AND WIDTH ADJUSTMENT

7.4.1 Introduction

In this section, methods for evaluating bank erosion and width adjustment are described. The first method involves the development of qualitative conceptual models. The remaining methods are quantitative, involving either empirical equations or equations developed theoretically by specifying quantitative models of selected physical processes.

It is important to recognize that none of these methods apply to all rivers, and that all of the methods greatly simplify field conditions. Furthermore, the variety of different approaches available in the literature suggests that scientists who study rivers rarely agree on the best method for predicting the extent of bank erosion or deposition. As a result, the scientific knowledge required to solve practical engineering problems of bank erosion and width adjustment may not always be available. Each problem, then, will require careful study before an engineering solution can be proposed.

7.4.2 Conceptual Models of Channel Evolution and Processes

For a problem to be solved, it must be clearly defined. For problems of bank erosion and width adjustment, this implies understanding the processes that are acting at a particular site and their temporal and spatial context. This understanding may be developed as a "conceptual model," which could be summarized as a series of diagrams, or as a verbal description of how bank erosion and width adjustment occur at a particular site. In a very few selected cases, the conceptual model could actually be quantified and summarized by one or more equations.

The first part of this chapter summarized processes that control bank erosion and width adjustment, and some conceptual models of channel evolution were presented in Figs. 7-1 and 7-2. Here, a detailed example of a conceptual model of incised channel evolution is presented.

7.4.2.1 A Conceptual Model for Incised Channel Evolution Although applicable only to incised channels, the six-stage conceptual channel evolution model of Harvey and Watson (1986) has been of value in developing an understanding of watershed and channel dynamics and in characterizing whether or not a reach is stable (Fig. 7-20). The model was originally based on observations of the channel evolution of Oaklimiter Creek, a tributary of Tippah River in northern Mississippi (Schumm et al. 1984). The Oaklimiter sequence describes the systematic response of a channel to base level lowering and encompasses conditions that range from disequilibrium (Type I) to a new state of dynamic equilibrium (Type VI). It should be recognized that these categories are only conceptual and variation may be encountered in the field. Similar conceptual models have been proposed by Thorne and Osman (1988a; 1988b) and Simon and Hupp (1992).

Type I reaches are characterized by sediment transport capacity that exceeds sediment supply, bank height that is less than the critical bank height, a U-shaped cross section, and small precursor knickpoints in the bed of the channel (provided that the bed material is sufficiently cohesive and little or no bed material is deposited). Width/depth ratios at bank-full stage are highly variable.

Type II reaches are located immediately downstream of the primary knickpoint and are characterized by sediment transport capacity that exceeds sediment supply, bank height that is less than the critical bank height ($h < h_c$), little or no bed sediment deposits, a lower bed slope than the Type I reach, and a lower width/depth ratio than the Type I reach because the depth has increased, but the banks are not yet unstable.

Type III reaches are located downstream of Type II reaches and are characterized by sediment transport capacity that is highly variable with respect to the sediment supply, bank height that is greater than the critical bank height ($h > h_c$), bank erosion that is due primarily to slab failure (Bradford and Piest 1980), bank loss rates that are at a maximum, bed sediment accumulation that is generally <0.6 m but can be greater locally due to local erosion sources, and channel depth that is somewhat less than in Type II reaches.

Type IV reaches are downstream of Type III reaches and are characterized by sediment supply that exceeds sediment transport capacity, resulting in aggradation of the channel bed, bank height that approaches the critical bank height with a rate of bank failure lower than for Type III reaches, nearly trapezoidal cross-sectional shape, and width/depth ratio higher than the Type II reaches. The Type IV reach is aggradational and has a reduced bank height. Bank failure has increased channel width, and in some reaches, the beginnings of berms along the margins of an effective discharge channel can be observed. These berms are the beginning of natural levee deposits that form in aggraded reaches that were overwidened during earlier degradational phases.

Type V and VI reaches are located downstream of Type IV reaches and are characterized by dynamic balance between sediment transport capacity and sediment supply for the effective discharge channel, abank height that is less than the critical bank height for the existing bank angle, colonization by riparian vegetation, accumulated bed sediment depth that generally exceeds 1.0 m, width/depth ratio that exceeds the Type IV reach, and generally a compound channel formed within a new floodplain. The channel is in dynamic equilibrium. Bank angles have been reduced by accumulation of berm materials. Types V and VI reaches are distinguished primarily by the possible occurrence of overbank deposition in Type VI reaches.

The primary value of the sequence is that it enables the evolutionary state of the channel to be determined from field observations that record the characteristic channel forms

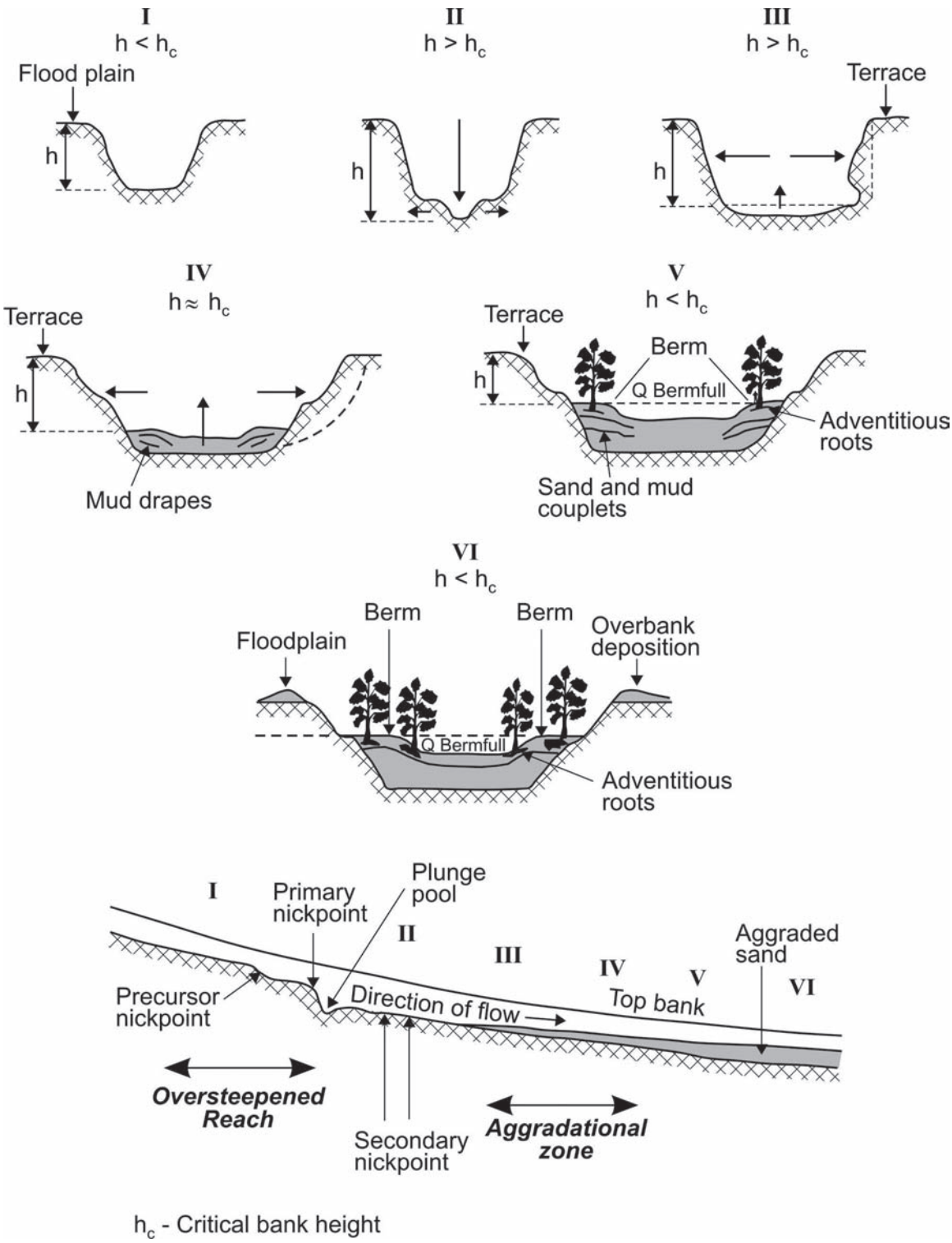

Fig. 7-20. Six-stage sequence of incised-channel evolution originally used to describe the evolution of Oaklimiter Creek (ASCE Task Committee on Hydraulics, Bank Mechanisms and Modeling of River Width Adjustment 1998b, with permission from ASCE).

associated with each stage of evolution. The morphometric characteristics of the channel reach types can also be correlated with hydraulic, geotechnical, and sediment transport parameters (Harvey and Watson 1986; Watson et al. 1988a; 1988b).

7.4.2.2 Channel Stability Diagram The channel evolution sequence of Schumm et al. (1984) and Harvey and Watson (1986) can be viewed in terms of two dimensionless stability numbers: (1) N_g is a measure of bank stability, and (2) N_h is a measure of fluvial stability. For a channel to be stable, fluvial stability and bank stability are both essential conditions. The desirable range for long-term channel stability is for N_g to be <1, and for N_h to be ~1, as shown in Fig. 7-21 (Watson et al. 1988a; 1988b). Quantifying the channel evolution sequence through the use of the dimensionless parameters N_g and N_h allows stability conditions along channel reaches to be ranked during rapid assessment and reconnaissance studies.

N_g is defined as any reasonable measure of bank stability expressed in terms of a factor of safety. The factor of safety represents the ratio between resisting and driving forces, such that banks are unstable for $N_g < 1$ and stable for $N_g > 1$. To allow flexibility, the operational definition of N_g is tailored according to the data available during a specific study (Watson et al. 1988a, 1988b). For example, in an initial reconnaissance of a site, the field investigator may note that banks over 3 m in height are generally unstable. In that circumstance, N_g could be the ratio of the bank height at a site divided by 3 m, which would yield $N_g \leq 1$ for stable bank heights. With better data and analyses, N_g could be the geotechnical bank safety factor computed with full knowledge of geotechnical properties, bank angle, and materials.

Similar flexibility is built into the operational definition of N_h, which was first defined as the ratio between the desired sediment supply and the actual sediment transport capacity (Watson et al. 1988a; 1988b). However, N_h could be any reasonable ratio of parameters that could be used as surrogates for sediment transport, such as the ratio of computed (or measured) sediment transport rates for the upstream supply reach and the stream reach of interest. In an initial reconnaissance, the thalweg slope of a stable channel may be surveyed and compared with the thalweg slope of the reach of interest. N_h would equal the ratio of the slope of the reach of interest divided by the stable slope. N_h is >1 for degradational reaches and is <1 for aggradational reaches.

The dimensionless stability numbers, N_g and N_h, can be related to the Oaklimiter sequence, as shown in Fig. 7-21. As the channel evolves from a state of disequilibrium to a state

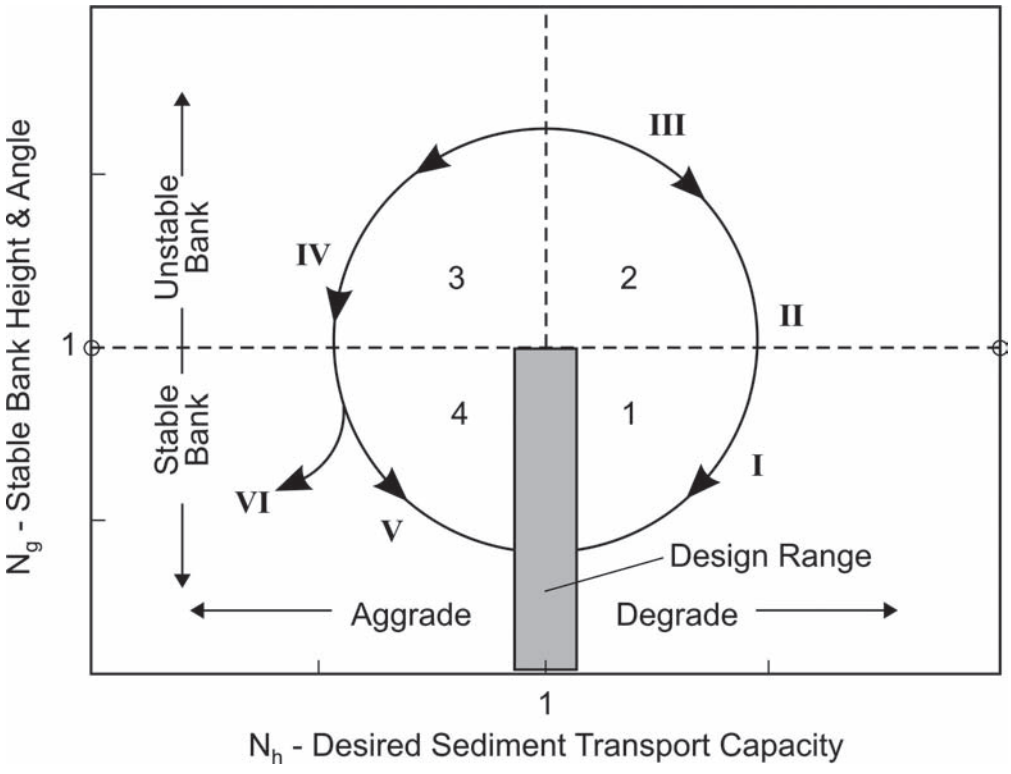

Fig. 7-21. Comparison of Oaklimiter Creek channel evolution sequence and channel stability parameters (ASCE Task Committee on Hydraulics, Bank Mechanisms and Modeling of River Width Adjustment 1998b, with permission from ASCE).

of dynamic equilibrium through the six reach types of the Oaklimiter sequence, the channel progresses through the four stability diagram quadrants in a counterclockwise direction. Rehabilitation of the channel should attempt to avoid as many of the quadrants as possible to reduce the amount of channel deepening and widening.

Each quadrant of the stability diagram is characterized by geotechnical and hydraulic stability number pairs, and stream reaches that plot in each quadrant have common characteristics with respect to stability, flood control, and measures that may be implemented to achieve a project goal.

In Quadrant 1 ($N_g < 1$, $N_h > 1$), the channel bed may be degrading or may be incipiently degradational; however, the channel banks are not geotechnically unstable. Bank erosion is occurring only locally, and bank stabilization measures, such as riprap or bioengineered stabilization, could be applied. However, local bank stabilization would not be successful if bed degradation continued and destabilized the stabilization measures; therefore, bed stabilization measures should be considered for long-term effectiveness of bank stabilization measures. If flood control is a project goal, almost any channelization or levee construction would increase N_h and shift the value to the right. Flow control using a reservoir can address flood control capacity, which may cause other changes in channel dynamics. The designer must be aware of the channel response to imposed conditions relating to the stability factors.

Quadrant 2 ($N_g > 1$, $N_h > 1$) streams are unstable. The channel bed is degrading and channel banks are geotechnically unstable. Grade control must be used to reduce bed slope, transport capacity and N_h. Bank stabilization measures will fail in this quadrant because the bed is continuing to degrade, which will destabilize the foundation of the bank stabilization. Both flood control and bank stability must be considered when determining the height to which grade control should be constructed. A series of grade control structures can reduce bank height sufficiently to stabilize the banks, but a combination of lower grade control and bank stabilization may meet flood control, ecological, and stability objectives. Emplaced habitat features are subject to failure caused by degradation of the bed, bank failure, and lowering of water-surface elevations.

Quadrant 3 ($N_g > 1$, $N_h > 1$) is characterized by gravity-driven bank failure but without continued bed degradation. Bank stabilization could be effective without grade control emplacement, but both measures should be considered. Flow control in these two quadrants could be beneficial. Emplaced habitat features may be inundated by channel aggradation or affected by adjacent bank failure.

Quadrant 4 ($N_g < 1$, $N_h < 1$) is characterized by general stability. Local bank stabilization measures will be effective. As N_h decreases in this quadrant, the potential for channel aggradation-related flood control problems or inundation of habitat features will increase.

7.4.3 Equilibrium Approaches

7.4.3.1 The Engineering Significance of Geomorphic Equilibrium In section 7.2, streams that are "graded" or "in regime" are defined as those whose morphology does not change "significantly" with time due to quasi-steady supplies of water and sediment. In section 7.4.3, quantitative models of graded streams are discussed. Before these models are presented, however, it is important to understand how graded streams are defined and how they may be recognized. Streams that are "graded" are not static, and they may change their morphologies during floods or other short-term perturbations. These changes may be large enough to have important engineering consequences.

A useful conceptual model of the temporal evolution of graded streams has been proposed by Schumm and Lichty (1965), who explained how streams can change progressively with time and yet still be considered "graded." To resolve this paradox, Schumm and Lichty (1965) defined three timescales for viewing river channels. Figure 7-22 presents these timescales using channel gradient to illustrate morphologic change, though any morphologic feature (e.g., width, depth) could be used. It is also important to recognize that the time axis of Fig. 7-22 is imprecise, and may be shorter or longer depending on the morphologic variable plotted on the y axis and the particular river system that is being investigated.

Over short periods, referred to by Schumm and Lichty (1965) as "steady time," the channel morphology is constant, because flows large enough to change the slope are not likely to occur. Over longer periods, defined as "graded time" by Schumm and Lichty (1965), the channel morphology oscillates about a temporally steady average value. This is the classic behavior associated with graded streams. It is important to note that the morphology is not constant, but changes tend to average to zero when viewed over sufficient time. Over the longest time scale, defined by Schumm and Lichty (1965) as "cyclic time," a drift in the morphology may be observed.

Schumm and Lichty's (1965) conceptual model suggests that field observations over graded timescales could be used to determine if a stream is graded or not. However, because decades of measurements are typically required, such data are rarely available. As an alternative, geomorphologists and engineers often use regression equations to determine if a river's morphology can be explained by variables such as discharge or bank sediment type that do not involve time (the power-law approach presented in section 7.4.3.2 is a typical example) (Fig. 7-23). If these regression equations explain a significant amount of the variance in the observations, streams are often considered to be graded or in a quasi-equilibrium state (Leopold and Maddock 1953; Wolman 1955; Leopold et al. 1964).

Figure 7-22 implies, however, that significant morphologic variation may still occur even if stream morphology

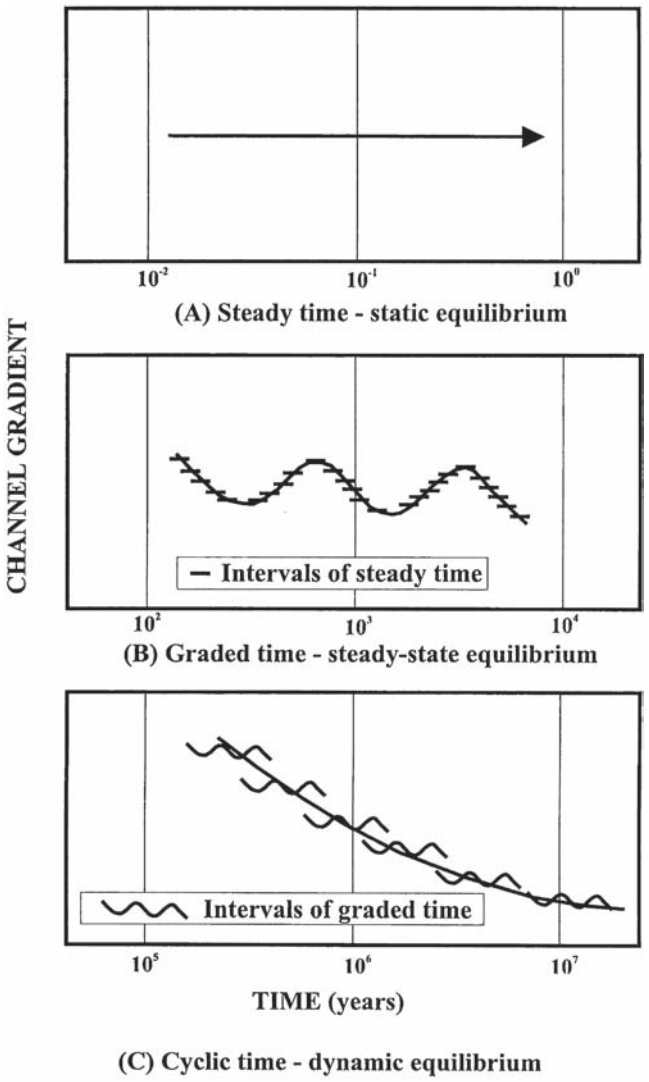

Fig. 7-22. Different time intervals and associated equilibrium in geomorphic analyses. (A) Steady time (static equilibrium). No change in channel gradient over short periods. (B) Graded time (steady-state equilibrium). Constant average channel gradient with periodic fluctuations above and below the average condition. Measurements made during intervals of steady time within the graded time period may show no change in channel gradient. (C) Cyclic time (dynamic equilibrium). Gradual lowering of the average channel gradient over long time intervals. Intervals of graded time and steady-state equilibrium exist within the cyclic time scale (Ritter 1978).

can be explained by discharge or any other variable that does not include time. Data from the Powder River watershed (Figs. 7-3, 7-19, and 7-22) present a useful example. Figure 7-23 demonstrates that the width is highly correlated with mean annual discharge in the Powder River basin. However, observations of the channel morphology of the Powder River between Moorhead and Broadus, Montana, from 1975 to 1998 demonstrate that a 25 to 50 year flood increased the channel area by an average of 62% (Pizzuto 1994). Subsequent deposition caused a substantial decrease in channel area (Moody et al. 1999). These oscillations are not large enough to invalidate Fig. 7-23, and thus the channel is in some sense graded or in regime. However, the observed temporal changes in channel form could greatly influence engineering structures, suggesting that equilibrium approaches should be used with considerable caution as design tools.

7.4.3.2 Regime Theory: A Power-law Approach The initial approach to predicting equilibrium channel form was based on empirical methods developed from field observations and regression equations and applied to the design of stable canals. The first regime relation was proposed by Kennedy (1885) over a century ago. Several regime relations followed, and these have been repeatedly refined and enhanced. The regime equations attributed to Lindley (1919), Lacey (1920), Simons and Albertson (1963), and Blench (1969) are probably the most widely known.

Although regime equations are extensively used by engineers, with successful outcomes, they suffer several shortcomings, including the facts that they are not dimensionally homogeneous and that their validity is limited to the basins and data from which they were derived. More sophisticated regime relations have been proposed by employing computers to obtain regression equations based on much larger data sets (Brownlie 1981a; 1981b). Most work, including that previously cited, pertains to sand-bed streams, but equivalent regime relations have also been proposed for gravel-bed streams; reviews are presented by Bray (1982) and Hey and Thorne (1986). More recently, semianalytical work by Julien and Wargadalam (1995) has attempted to refine the regime approach within a framework based on the governing principles of open channel flow.

Geomorphologists have used data from natural steams and laboratory flumes to develop power-law hydraulic geometry relations between channel top width, average depth, average velocity, and bank-full discharge (Leopold and Maddock 1953); Fig. 7-23 is an example. The exponents in these relations exhibit surprising universality, particularly the one for channel width, which has been found to be ~0.5 for rivers with widely varying flow regimes and sediment characteristics located in different physiographic regions of the world. However, the regression coefficients are found to vary significantly from one locality to another, which renders power-law hydraulic geometry relations inappropriate as tools for general design purposes.

The relevant empirical formulas developed in these approaches, as well as others that are not mentioned here due to lack of space, are described in detail in standard river mechanics books (e.g., Garde and Ranga-Raju (1977) and Simons and Senturk (1992)) and earlier review papers (e.g., Ferguson (1986)).

7.4.3.3 Extremal Hypothesis Approach The last two decades have seen the proliferation of approaches that employ an extremal hypothesis as part of their formulation for predicting channel morphology. Equations for sediment

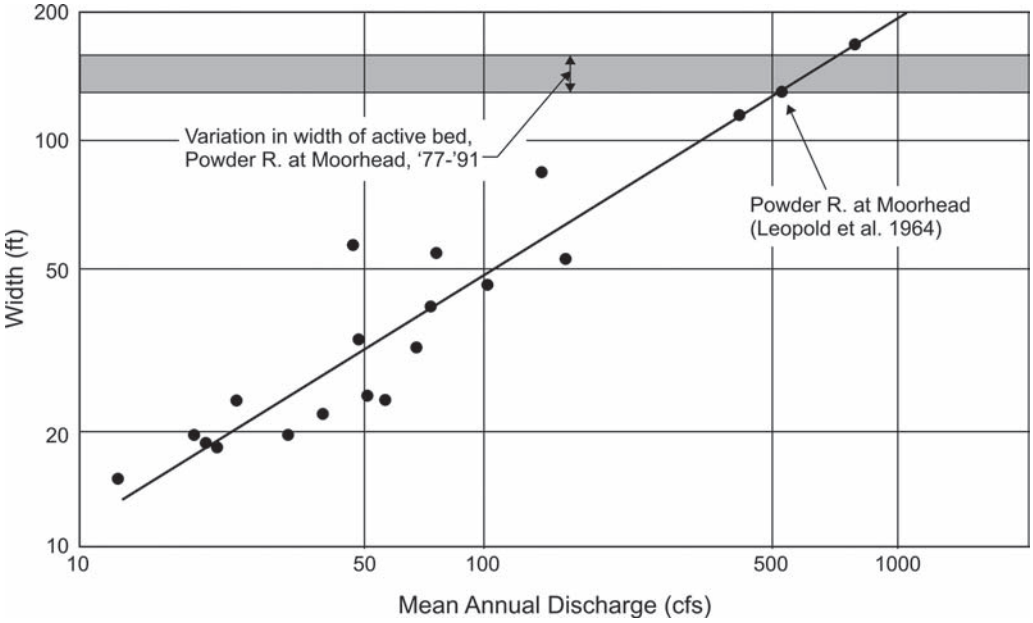

Fig. 7-23. Relationship between mean annual discharge and width for the Powder River watershed in Wyoming and Montana (Leopold et al. 1964). The shaded region represents the variation in width documented by cross sections from 1977 to 1991 (Pizzuto 1994).

transport and alluvial friction are combined with a third relationship to determine channel width and to predict regime or equilibrium conditions. This third relationship has frequently been expressed in terms of the maximization or minimization of a parameter, such as stream power, energy dissipation rate, or sediment concentration. Extremal hypotheses have been introduced by Chang (1980); Yang et al. (1981); Yang and Song (1986); Bettess and White (1987); Chang (1988a); Yang (1992); Chiu and Abidin (1995); and Millar and Quick (1997), among others. An extremal hypothesis, based on stream power, also forms the basis of the analytical approach of White et al. (1981) to the river regime and the Wallingford tables for the design of stable channels (White et al. 1981).

The theoretical justification for such hypotheses and the relationships between them are still not entirely clear. Also, when extremal hypotheses are applied, a clear understanding is required of the physical constraints presented by geological or other boundary conditions on the evolution of a channel toward a form that minimizes its rate of energy expenditure. The predictions based on such methods, however, provide global, if not exacting, agreement with a wide range of observations.

7.4.3.4 Tractive Force Methods Tractive force methods employ the basic laws of mechanics to obtain expressions that specify the geometry of stable channel cross sections. This approach was initiated in the late 1940s by the U.S. Bureau of Reclamation, and it resulted in the threshold channel theory (Glover and Florey 1951; Lane 1955). The theory is based on a fluid momentum balance that is used to obtain the local boundary shear stress and a stability criterion for the sediment particles that make up the channel perimeter. It assumes that the channel is straight, that secondary flow is negligible, and that sediment is noncohesive and does not vary within the channel. Most importantly, the tractive force approach assumes that the channel morphology is adjusted so that sediment across the perimeter of the cross section is at the threshold of motion. Under these conditions, sediment is neither eroded nor deposited at any point on the cross section. When these assumptions are satisfied, a cosine profile is predicted for the stable cross section (Fig. 7-24).

A threshold channel does not allow for bed-load transport. Diplas (1990) and Parker (1979) showed that the Glover and Florey method cannot be extended to generate channels capable of transporting sediment while they maintain threshold banks. This result is contrary to numerous observations from natural streams and flume experiments, which attest to the possible coexistence of a mobile bed and

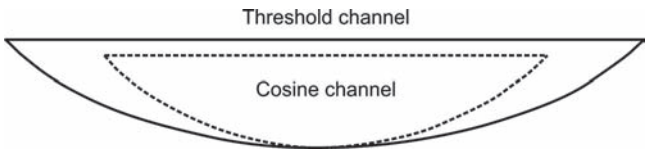

Fig. 7-24. Comparison between threshold channel profile obtained from momentum-diffusion model and cosine profile (adapted from Vigilar and Diplas 1997, with permission from ASCE).

stable banks. Parker (1978b) overcame this inconsistency by employing the momentum balance of Lundgren and Jonsson (1964), which accounts for lateral turbulent diffusion of downstream momentum. Due to the complexity of the corresponding differential equation, his solution was limited to the flatbed region, whereas the bank geometry was solved as a first-order solution, yielding a cosine profile. Thus, Parker (1978b) was able to reconcile the existence of sediment movement within a stable channel. Ikeda et al. (1988) extended the results of Parker (1978b) to include sediment heterogeneity, and Ikeda and Izumi (1990) considered the effect of bank vegetation, whereas Parker (1978a) and Ikeda and Izumi (1991) examined the influence of suspended load on channel dimensions.

The tractive force model, in the form proposed by Parker, was recently refined by Diplas and Vigilar (1992). The main differences from the previous work were that the governing equations were solved numerically and the bank geometry was not assumed, but became part of the solution. As a result, the threshold channel shape turned out to be different from a cosine curve, having a greater top width and center depth (Diplas and Vigilar 1992; Vigilar and Diplas 1994; 1997; 1998). For the example shown in Fig. 7-24, the longitudinal slope is 0.00081, the value of the critical Shields parameter is 0.056, and the sediment is semiangular, with $D_{50} = 45$ mm and $D_{90} = 75$ mm. The cross-sectional area of the threshold channel and the water discharge that it conveys are more than twice those for a cosine channel under the same conditions. This is attributed to the role of momentum diffusion, which results in decreased stresses in the central region of the channel (thus allowing a deeper flow) and increased stresses in the upper bank regions (forcing banks to assume gentler slopes to prevent erosion). Knowledge of the local topography, the sediment size and shape, and the value of the critical Shields parameter uniquely determine the dimensions of a threshold channel and its discharge.

In the case of a channel with stable banks and a mobile bed, the bank profiles change with the width of the flatbed section (Fig. 7-25) (Vigilar and Diplas 1997; 1998). However, beyond an aspect ratio of 12, which is typical of natural streams, the bank profile remains constant, and the channel is termed "wide." The stable channel dimensions and bed load transport capacity can be determined for known local bed slope, sediment size and shape, value of the critical Shields parameter, and water discharge. If the bed load discharge is specified, the channel bed slope becomes part of the solution.

It is important to recognize, however, that tractive force methods do not accurately represent channels where sediment is deposited on the banks or eroded from the banks. For these conditions (which represent the majority of natural channels), only a few preliminary mechanistic models of equilibrium channels are available (Parker 1978b; Pizzuto 1984).

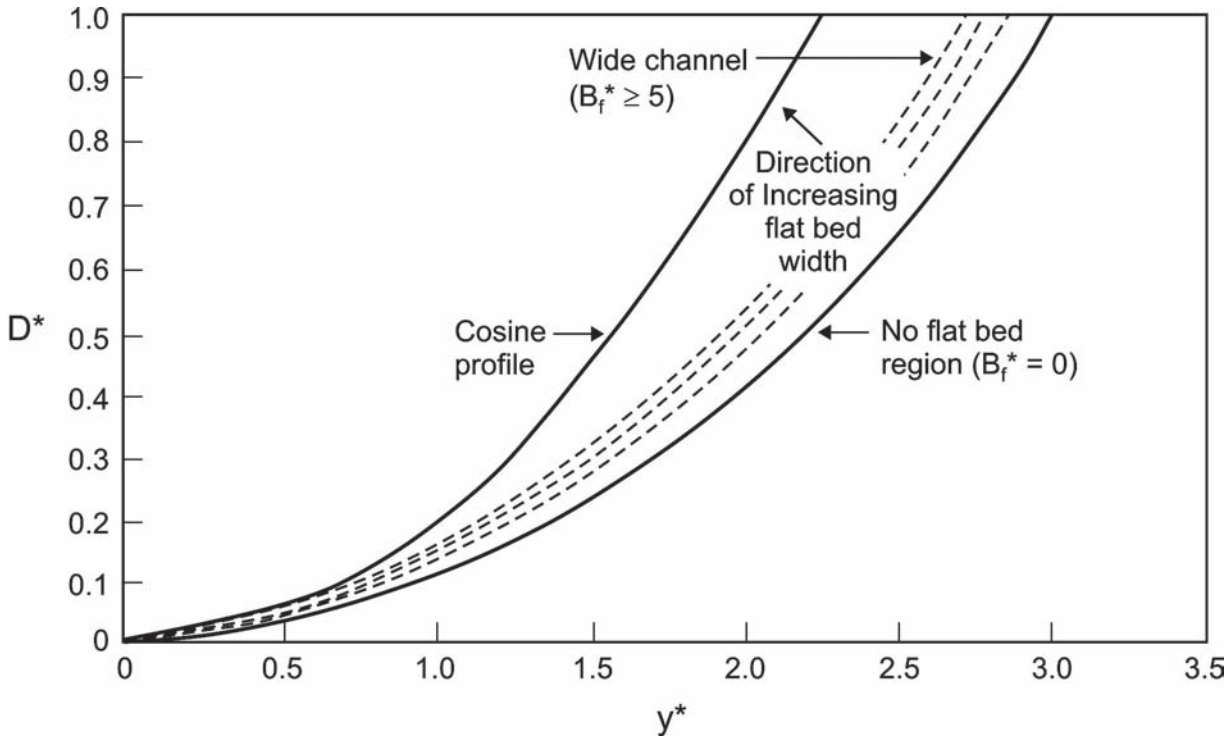

Fig. 7-25. Bank profiles generated by momentum-diffusion model for different values of flatbed width of channel (ASCE Task Committee on Hydraulics, Bank Mechanisms and Modeling of River Width Adjustment 1998a, with permission from ASCE).

7.4.4 Empirical Methods Based on Field Observations

In many cases, an existing theory or model may not be available to predict rates of bank erosion, deposition, or width adjustment at a particular site. However, field observations may be used to develop empirical equations that may be used for prediction. Although such empirical equations typically have little or no generality, they may provide useful short-term predictions if future conditions are similar to those used to develop the empirical equations.

Rates of bank retreat are predicted by two different methods. One involves using maps, aerial photographs, or historical surveys to determine past rates of bank erosion. For prediction, these rates may simply be extrapolated into the future to provide an estimate of the future position of the eroding bank. Another method involves developing an empirical equation that includes one or more physical parameters that control rates of bank erosion. Figure 7-26 illustrates a correlation between rates of bank retreat and velocity near the bank (Pizzuto and Meckelnburg 1989) based on field observations of bank retreat from the Brandywine Creek in southeastern Pennsylvania (the values of the near-bank velocity were obtained using the flow model of Ikeda et al. 1981). The regression equation represented by the best-fit line, although only valid at the study site, could provide accurate predictions of the future positions of the retreating bank.

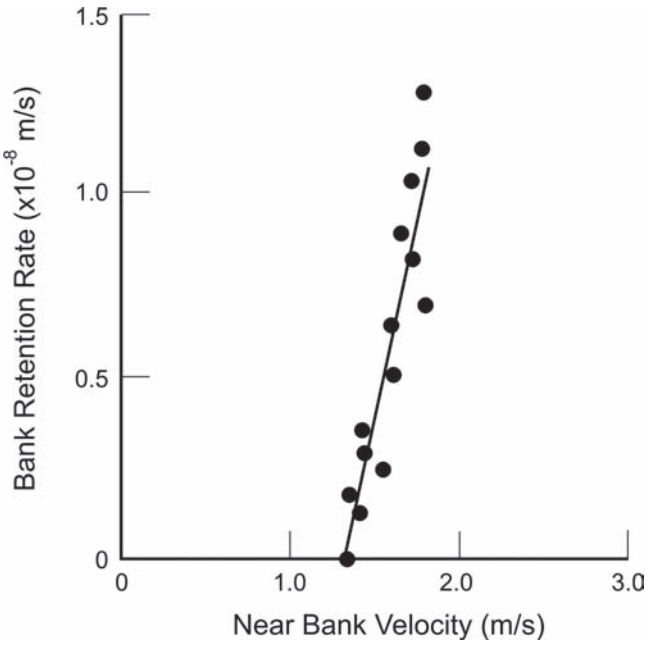

Fig. 7-26. Relationship between rate of bank retreat and near-bank velocity for a meander bend of the Brandywine Creek in southeastern Pennsylvania (after Pizzuto and Meckelnburg 1989).

7.4.5 Numerical Width Adjustment Models

Fixed-width numerical morphological models are now commonly used in engineering practice to obtain predictions of the extent of scour and fill of a bed in response to changes in the independent variables of flow and sediment discharge. The status of fixed-width numerical morphological modeling has been reviewed by Fan (1988).

Fixed-width numerical models are limited in applicability to cases where width adjustments in the prototype channel are not significant. To address this deficiency, a number of attempts to account for time-dependent width adjustments in numerical morphological models have been made. It should be recognized at the outset that each of these models is in some way limited. Twelve numerical width adjustment models based on various approaches to representing the governing processes of flow, flow resistance, sediment transport, and bank mechanics are reviewed in Table 7-1. A promising numerical width adjustment model described by Nagata et al. (2000) was published after the following analysis was completed.

7.4.5.1 Fluvial Hydraulics and Hydrodynamics A number of approaches have been used to estimate the flow field in the computational domains of the various numerical models (Table 7-2). Despite their undoubted significance, over-bank flows are excluded from all of these approaches. The approaches are based on simplifications of the governing flow momentum and continuity equations and are therefore limited in validity to the particular conditions defined in making the simplifying approximations. Additionally, each approach requires an estimate of the friction factor, which is usually either specified by the user or calculated using an empirically calibrated roughness equation. The friction factor estimate may or may not be allowed to vary through space and time (Table 7-2). Each of the flow resistance equations in Table 7-2 is, strictly speaking, valid only for the physical conditions corresponding to the data originally used to derive it. None of the reviewed models account for the effects of vegetation on flow.

The water-routing submodel of the FLUVIAL-12 model (Chang 1988a; 1988b) computes the water-surface elevation and energy gradient at each cross section by solving 1D versions of the flow momentum and continuity equations. For steady flow, the standard step method is employed, whereas solution procedures suggested by Fread (1971; 1974) and Chow (1973) are followed for unsteady-flow routing. A correction for flow resistance due to secondary flow effects in curved channels is made (Chang 1988a). Osman (1985), Alonso and Combs (1986), and Borah and Bordoloi (1989) developed similar approaches to flow routing in their morphological models. Unlike FLUVIAL-12, these methods also neglect secondary flows and are applicable to steady flows only, though unsteady flows are approximated through the use of a stepped hydrograph with discharge constant in any one time step. The 1D flow-routing methods provide estimates of cross-sectionally averaged flow parameters

Table 7-1 List of Reviewed Models

Model (1)	Category (2)	Additional references (3)
Darby and Thorne (1996a)	Geofluvial, cohesive bank	Darby and Thorne (1996b); Darby et al. (1996)
CCHEBank (Li and Wang 1993)	Geofluvial, noncohesive bank	Li and Wang (1994a, b)
Kovacs and Parker (1994)	Geofluvial, noncohesive bank	Kovacs (1992)
Wiele (1992)	Geofluvial, noncohesive bank	Wiele and Paola (1989)
RIPA (Mosselman 1992)	Geofluvial, cohesive bank	Struiksma et al. (1985); Olesen (1987); Mosselman (1991); Talmon (1992)
Simon et al. (1991)	Geofluvial, cohesive bank	
Pizzuto (1990)	Geofluvial, noncohesive bank	
STREAM2 (Borah and Bordoloi 1989)	Geofluvial, cohesive bank	Borah and Dashputre (1994)
GSTARS (Yang et al. 1988)	Extremal hypothesis	
FLUVIAL-12 (Chang 1988b)	Extremal hypothesis	
Alonso and Combs (1986)	Geofluvial, cohesive bank	
WIDTH (Osman 1985)	Geofluvial, cohesive bank	

Table 7-2 Features of Flow Routing Submodels of Reviewed Models

Model (1)	Dimension (2)	Discharge variation over time (3)	Secondary flow (4)	Lateral shear (5)	Friction factor (6)	Flow resistance formulas[a] (7)
Darby-Thorne	Quasi2D[b]	Stepped hydrograph	No	Yes	Time and space variable	Strickler
CCCHEBank	3D	Unsteady flow	Yes	Yes	Constant	Keulegan
Kovacs-Parker	2D	Steady flow	No	Yes	Constant	Keulegan
Wiele	2D	Steady flow	No	Yes	Constant	Keulegan
RIPA	2D	Stepped hydrograph	Yes	No	Constant	Specified
Simon et al.	Quasi2D[b]	Stepped hydrograph	No	No	Time and space variable	Strickler, Darcy, and Chezy
Pizzuto	2D	Steady flow	No	Yes	Constant	Einstein
STREAM2	1D	Stepped hydrograph	No	No	Constant	Specified
GSTARS	Quasi2D[b]	Stepped hydrograph	No	No	Time and space variable	Strickler, Darcy, and Chezy
Fluvial-12	1D	Unsteady flow	Yes	No	Time and space variable	Strickler and Brownlie
Alonso-Combs	1D	Stepped hydrograph	No	No	Constant	Specified
WIDTH	1D	Stepped hydrograph	No	No	Time and space variable	Strickler

Note: Strickler = Strickler (1923); Keulegan = Keulegan (1938); Einstein = Einstein (1950); Brownlie = Brownlie (1983).
[a]None of these formulas account for the effects of bed forms.
[b]Quasi2D models refer to those models that simulate lateral variation of bed topography through use of multiple 1D stream tubes.

and are unable to resolve near-bank boundary shear stresses sufficiently accurately to estimate fluvial erosion of bank materials.

Various attempts to account for the lateral variation of flow fields in natural channels have been made. Both the GSTARS (Molinas and Yang 1986; Yang et al. 1988) and modified BRI-STARS (Simon et al. 1991) models employ quasi-two-dimensional (quasi-2D) flow-routing procedures based on the stream tube approach. Stream-tube-based approaches are limited because they normally exclude lateral momentum exchange processes due to secondary flows and lateral shear induced by bank friction, and they are limited to steady flows. These approaches are also expected, therefore, to have low predictive ability for near-bank-zone applications.

Darby and Thorne (1996c) adopted a quasi-2D method in which lateral distributions of flow velocity and boundary shear stress were estimated at each cross section via numerical solution of a version of the flow momentum and continuity equations in which lateral shear stress terms were retained (Wark et al. 1990). The method is valid for steady, uniform flow but was applied in conjunction with a gradually varied 1D flow-routing model solved using the standard step method (Chow 1973) to estimate longitudinal variations in water-surface elevations and energy gradients at each of the modeled sections. The flow submodel employed by Darby and Thorne provides an improved representation of the flow field compared to 1D and stream-tube flow-routing methods. However, the validity of this method is limited because secondary flows are neglected (the approach was intended for straight channels only).

The 2D depth-averaged flow submodel of RIPA (Mosselman 1992) is based on differential equations expressing the conservation of mass and momentum of water. This model includes a correction for the deformation of the flow field due to secondary flow, but the influence of lateral shear on near-bank flows is neglected. Wiele (1992) included both terms in his flow submodel.

The flow submodels employed by Pizzuto (1990) and Kovacs and Parker (1994) model the distribution of fluid-induced boundary shear stress on gently curved riverbanks in straight channels. The methods are valid for steady, uniform flows; they include lateral shear stress terms but ignore momentum transfer by secondary currents. Both methods are only valid where bed and bank curvature is small.

In the CCHEBank model (Li and Wang 1993; 1994a,b), the flow field is computed using CCHE3D (Wang and Hu 1990), an advanced 3D hydrodynamic model, which can simulate unsteady free surface turbulent 3D flow fields in open channels. Secondary flows and lateral shear stress terms are also included in the model. This 3D flow model has the fewest simplifying approximations of the models reviewed here and, therefore, has the greatest potential for successfully modeling near-bank flows. However, simplifying assumptions are still required in the eddy viscosity closure model, and the flow model is also subject to the limitations of the method used to specify the friction factor.

7.4.5.2 Sediment Transport and Continuity Methods of sediment routing in each of the 12 models reviewed here are summarized in Table 7-3. Sediment routing is accomplished by relating sediment transport at each computational node to the flow field and physical properties of the bed material there. An empirically calibrated sediment transport equation is used to estimate the sediment flux field. Some models offer users the choice of specifying a particular equation from a menu. Spatial differences in sediment flux so estimated determine the evolution of the bed topography through solution of the sediment continuity equation.

The models are uniformly limited in validity to conditions corresponding to those originally used to calibrate the available sediment transport equation. Even within these constraints, and optimistically assuming that the flow field has been predicted accurately, sediment flux predictions are prone to order-of-magnitude errors (Gomez and Church 1989; Yang and Wan 1991).

A particular limitation of width adjustment modeling applications is that most sediment transport equations are valid only for bed surfaces inclined at low angles ($\sin\theta < 0.1$), though in noncohesive channels such equations are applied in bank regions that are often inclined at angles close to the angle of repose (typically 35°). The vertical bed load transport equation developed by Kovacs and Parker (1994), and included in their bank erosion model, is the only model reviewed here that accounts for the effects of large bed slopes ($\sin\theta > 0.1$).

In some models, sediment sorting is handled through the use of mixed (active) layer theory. Accurate prediction of the bed-material grain-size distribution throughout the model simulation is important if the flow resistance and sediment transport submodels are to have any chance of continuing to predict the flow and sediment-transport fields with acceptable accuracy throughout the simulation. Research has indicated that bed-material grain-size adjustments in unstable rivers are as important as adjustments in gradient, depth, or width (Hoey and Ferguson 1994). Ability to account for the transport of heterogeneous sediment mixtures is particularly important in the context of width-adjustment models, because the grain-size distribution of eroded bank materials is often quite different from that of the original bed material. Summary information regarding the mixed layer scheme employed in each of the models is provided in Table 7-3.

The wide ranges of potential grain sizes frequently involved in the width-adjustment process also dictate that both bed load and suspended-sediment fluxes must be accounted for in width-adjustment modeling. Table 7-3 summarizes the capabilities of the various sediment-routing submodels with respect to this issue.

Table 7-3 Features of Sediment-Routing Submodels of Reviewed Models

Model (1)	Routing methods (2)	Streamwise flux difference (3)	Transverse flux difference (4)	Bed load (5)	Suspended load (6)	Transport equations (7)	Sorting (8)	Bed material (9)
Darby-Thorne	Quasi2D	Yes	Yes	Yes	Yes	Engelund and Hansen (1967)	Yes	Sand
CCCHEBank	2D	Yes	Yes	Yes	No	Meyer-Peter and Muller (1948)	No	Gravel
Kovacs-Parker	2D	No	Yes	Yes	No	Kovacs and Parker (1994)	No	Gravel
Wiele	2D	No	Yes	Yes	No	Parker (1979) and Meyer-Peter and Muller (1948)	No	Sand and gravel
RIPA	2D	Yes	Yes	Yes	No	Engelund and Hansen (1967) and Meyer-Peter and Muller (1948)	No	Sand and gravel
Simon et al.	Quasi2D	Yes	No	Yes	Yes	Yang (1973; 1984); Ackers and White (1973); and Engelund and Hansen (1967)	Yes	Sand and gravel
Pizzuto	2D	No	Yes	Yes	No	Parker (1983)	No	Sand
STREAM2	1D	Yes	No	Yes	Yes	Yang (1973); Graf (1971); and Meyer-Peter and Muller (1948)	Yes	Sand and gravel
GSTARS	Quasi2D	Yes	No	Yes	Yes	Yang (1973; 1984); Ackers and White (1973); and Engelund and Hansen (1967)	Yes	Sand and gravel
FLUVIA L-12	1D	Yes	No	Yes	Yes	Yang (1973); Parker et al. (1982); Ackers and White (1973); Engelund and Hansen (1967); and Graf (1971)	Yes	Sand and gravel
Alonso-Combs	1D	Yes	No	Yes	Yes	Alonso et al. (1981)	Yes	Sand and gravel
WIDTH	1D	Yes	No	Yes	Yes	Engelund and Hansen (1967)	No	Sand

In each model, changes in bed elevation resulting from spatial differences in the predicted sediment flux field are computed through numerical solution of the sediment continuity equation. The sediment continuity equation is usually simplified by neglecting either the longitudinal or transverse sediment-flux difference terms (Table 7-3). These simplifications limit the validity of these models; it can be shown that both streamwise and transverse sediment-flux differences are, in fact, equally significant in controlling near-bank bed topography changes (Darby and Thorne 1992).

One-dimensional sediment-routing procedures (Table 7-3) neglect transverse sediment fluxes and require various assumptions concerning the distribution of predicted changes in bed elevation across the channel cross section. In this context, the most important areas are the near-bank zones, because predicted changes in bed elevation directly influence the stability of the banks and, hence, the predicted widening or narrowing rates. For example, Osman (1985) assumed that the bed level change is distributed evenly over the entire cross section. In contrast, Alonso and Combs (1986) and Borah and Bordoloi (1989) utilized various assumptions to distribute the scour and fill more realistically across the section. Alonso and Combs (1986) accounted for nonuniform sediment deposition across the channel cross section using relations describing the lateral flux of suspended sediments proposed by Parker (1978a). No method of accounting for nonuniform distribution of erosion is described.

To address this issue, quasi-2D approaches have been proposed (Table 7-3). Simon et al. (1991) proposed a quasi-2D sediment-routing model based on the stream-tubes concepts employed in the GSTARS model. Darby and Thorne (1996c) divided each modeled cross section into three (one central and two near-bank) segments. This was done to provide more refined estimates of bed topography evolution in the near-bank zones. Each near-bank segment extended a distance of two bank heights from the base of the bank. In contrast to the quasi-2D approaches, fully 2D solutions of the sediment continuity equation (Table 7-3) provide higher definition, though not necessarily more accurate, estimates of bed topography changes in the near-bank zones.

7.4.5.3 Riverbank Mechanics A summary of methods of modeling bank mechanics in each of the reviewed models is provided in Table 7-4. None of these methods accounts for the impacts of riparian vegetation.

7.4.5.3.1 Retreat and Advance Processes Processes of bank retreat and advance may occur together or separately at different locations and times along the same reach of a river. Modeled rates of bank advance and retreat on both banks at a single section determine the rate of width adjustment. Bank advance processes, that is, processes of bank deposition and channel narrowing, are excluded by most of the modeling approaches reviewed here.

Fluvially controlled processes of bank retreat are essentially twofold. Fluvial shear erosion of bank materials results in progressive incremental bank retreat. Additionally, increases in bank height due to near-bank bed degradation or increase in bank steepness due to fluvial erosion of the lower bank may act alone or together to decrease the stability of the bank with respect to mass failure. Bank collapse may lead to rapid, episodic retreat of the bankline. Depending on the constraints of the bank material properties and the geometry of the bank profile, banks may fail by any one of several possible mechanisms Thorne 1982), including planar (e.g., Lohnes and Handy (1968)-, rotational (e.g., Bishop (1955)-, and cantilever (e.g., Thorne and Tovey (1981)-type failures. A separate analysis is required for analysis of bank stability with respect to each type of failure.

Nonfluvially controlled mechanisms of bank retreat include the effects of wave wash, trampling and grazing by livestock, and piping- and sapping-type failures (e.g., Hagerty 1991; Ullrich et al. 1986) associated with stratified banks and adverse groundwater conditions. Nonfluvial processes leading to bank retreat are excluded from all of the models reviewed here.

7.4.5.3.2 Fluvial Entrainment of Bank Materials For models of noncohesive bank erosion, hydraulic shear erosion of the banks is implicitly simulated through application of the sediment-transport submodel in the near-bank zone. Comparatively little is known about the mechanics of cohesive-bank fluvial entrainment. Excess-shear-stress formulations are difficult to apply because the value of shear stress required to entrain the bank particles varies widely and is influenced by diverse processes (Grissinger 1982). For example, processes such as frost heave or desiccation, which result in weakening of the intact material, may exert a more dominant control on observed rates of fluvial erosion than the intensity of the near-bank flow (Lawler 1986).

It is important to include a method of predicting the hydraulic shear erosion of cohesive bank materials in width-adjustment modeling because erosion directly influences the rate of retreat of the banks, and it also steepens the bank profiles and promotes retreat due to mass bank instability. Approaches that exclude analysis of fluvial erosion of bank materials (Table 7-4) are therefore somewhat limited. Widening models that attempt to account for fluvial erosion of cohesive bank materials (Table 7-4) utilize empirically based methods, such as that of Arulanandan et al. (1980), which was reviewed extensively by Osman and Thorne (1988). Borah and Dashputre (1994) and Darby and Thorne (1996b) have, however, suggested that these methods are subject to serious shortcomings.

7.4.5.3.3 Cohesive- and Noncohesive-Bank Stability Analyses Despite the fact that natural riverbanks are liable to failure by a number of specific mechanisms of bank collapse, most cohesive bank-width-adjustment modeling approaches (Table 7-4) have been based solely on analysis of planar failures.

The mass-wasting algorithms developed by Osman (1985) and reported in Osman and Thorne (1988) account for the bank profile geometry associated with natural, eroding

Table 7-4 Features of Bank Mechanics Submodels of Reviewed Models

Model (1)	Bank Process				Bank Material			
	Deposition (2)	Fluvial Entrainment (3)	Types of bank failure (4)	Longitudinal extent of failure included (5)	Cohesive (6)	Noncohesive[a] (7)	Layered (8)	Heterogenous (9)
Darby-Thorne	No	Yes	Planar curved	Yes	Yes	No	No	No
CCCHEBank	Yes	Yes	None	No	No	Yes	No	No
Kovacs-Parker	No	Yes	None	No	No	Yes	No	No
Wiele	No	Yes	None	No	No	Yes	No	No
RIPA	No	Yes	Planar	No	Yes	No	No	No
Simon et al.	No	No	Planar	No	Yes	No	No	No
Pizzuto	No	Yes	None	No	No	Yes	No	No
STREAM2	No	Yes	Planar	No	Yes	No	No	No
GSTARS	—[b]	—[b]	—[b]	—[b]	—[b]	—[b]	—[b]	—[b]
FLUVIA L-12	—[b]	—[b]	—[b]	—[b]	—[b]	—[b]	—[b]	—[b]
Alonso-Combs	No	No	Planar	No	Yes	No	No	No
WIDTH	No	Yes	Planar Curved	No	Yes	No	No	No

[a]Noncohesive bank sediments are assumed uniform in size.

[b]Bank mechanics submodels are not included in these models, which are instead based on extremal hypotheses.

riverbanks that are destabilized through a combination of lateral erosion and bed degradation. These algorithms are employed in most of the cohesive bank approaches listed in Table 7-4. Previous stability analyses were restricted to a simple bank geometry and excluded the effects of lateral fluvial erosion on the bank profile (Lohnes and Handy 1968; Little et al. 1982).

The Osman-Thorne stability analysis is, however, subject to two main limitations (Simon et al. 1991). First, it does not include the effects of pore-water pressure and hydrostatic confining pressures. Second, the analysis constrains the failure plane to pass through the toe of the bank, excluding the possibility of secondary, upper-bank failures. Such failures are fairly common (Thorne et al. 1981a,b; Simon and Hupp 1992).

Simon et al. (1991) employed a bank stability analysis designed to account explicitly for hydrostatic and pore-water pressure effects on bank stability, while relaxing the assumption that the failure plane must pass through the toe of the bank. This enables bankline adjustments in response to secondary, upper-bank failures to be simulated. Conversely, Simon et al. (1991) excluded the effects of fluvial erosion on the bank profile that were accounted for in the Osman-Thorne (1988) stability analysis.

Darby and Thorne (1996a) accounted for two specific mechanisms of bank erosion and retreat, using the stability analyses proposed by Osman (1985) for rotational failure mechanisms and Osman and Thorne (1988) for planar failure mechanisms. Consideration of both rotational and planar failures, the failure mechanisms being discriminated on the basis of lower predicted factor of safety, represents the first attempt to account for the possibility of multiple failure mechanisms. This is important, because the shape of the failure surface is largely determined by the failure mechanism, and the failure surface forms the new bank profile following mass failure. Because stability of the bank is sensitive to the shape of the bank profile, predicting the correct failure surface is important in ensuring that predictions of bank stability and retreat continue to be accurate throughout a model simulation that includes several consecutive bank failures. However, the range of specific mechanisms of bank collapse included by Darby and Thorne (1996c) is still small compared to the number of potential failure mechanisms that may occur in nature.

For noncohesive riverbanks, models of widening have been proposed by Wiele and Paola (1989); Pizzuto (1990); Kovacs (1992); Wiele (1992); Li and Wang (1993; 1994a,b); and Kovacs and Parker (1994). These approaches can be subdivided into two categories. First, Pizzuto (1990) and Li and Wang (1993; 1994a,b) simulate the bank erosion mechanism using a heuristic procedure (a similar approach is also adopted by Nagata et al. [2000]). When bank slope exceeds the angle of repose of the boundary materials, a slumping model is employed such that a failure surface inclined at the angle of repose is projected to the flood-plain surface. Sediment above the failure plane is moved downslope, forming a deposit with a linear upper surface.

The second approach is characterized by the work of Kovacs and Parker (1994). Their vectorial bed load equation and bank erosion models represented considerable advances in modeling noncohesive sediment transport. Kovacs and Parker (1994) realized that the fundamental problem of previous analyses was that the bed-load formulations employed were valid only at angles much less than the angle of repose, but it is the entrainment and transport of noncohesive sediment particles on steep slopes that is precisely the problem of interest. To avoid this problem, Kovacs and Parker (1994) formulated a vectorial bed load transport equation (Parker and Kovacs 1993) for coarse-sediment transport that was applicable to slopes up to the angle of repose in both the streamwise and transverse directions. Kovacs and Parker (1994) applied the vectorial bed load transport equation to simulate the widening observed by Ikeda (1981) in his laboratory experiments. According to their approach, widening is initiated when bank erosion along the lower part of the bank causes the local slope of the upper bank to exceed the angle of repose of the sediments. A discontinuity in slope is created between the over-steepened upper bank and the lower part of the bank; this discontinuity migrates up the bank with a characteristic velocity, widening the channel as it propagates. Using their bed load transport equation and an integral form of the sediment continuity equation, Kovacs and Parker (1994) derived a rigorous expression for the propagation velocity of the discontinuity in slope, allowing them to reproduce the widening rates observed by Ikeda (1981).

Further development of their methods is needed before they can become a practical design and simulation tool. In particular, the bank erosion and transport models need to be coupled with a sophisticated 2D or 3D flow model to account for complex hydraulics found in natural rivers. Furthermore, the method should also be extended to account for mixtures of varying grain sizes before it can be widely applied to field conditions.

7.4.5.3.4 Homogenous and Heterogenous Bank Structures The physical properties of natural riverbanks are frequently characterized by great spatial variability in their vertical structure and distribution. Many banks are composed of multiple sediment horizons, often featuring a fine-grained cohesive layer above a noncohesive granular layer. Despite this, all of the bank stability analyses employed in the models reviewed here assume that banks are characterized by a homogeneous vertical structure. Additionally, some models (Table 7-4) do not represent spatial variation in the physical properties of bank materials, either along the banks in the streamwise direction, or extending into the flood plain.

7.4.5.3.5 Longitudinal Extent of Mass Failure Most of the reviewed analyses assume that the volume of bank sediments delivered to the channel per unit reach length, required as a source term in the sediment continuity

equation, is equal to the product of the unit failure volume of bank material and the reach length. Application of bank stability analyses without consideration of the actual longitudinal extent of the failure can result in serious overestimation of this source term in the sediment continuity equation, propagating errors in estimated bed and bank adjustments throughout the entire simulation. Darby and Thorne (1996b) attempted to account for the longitudinal extent of mass failures within modeled reaches. Darby and Thorne suggested that the volume of sediment supplied within a modeled reach should be equal to the unit volume (per unit channel length) supplied by mass-wasting processes multiplied by the product of the length of the modeled reach and the probability of failure occurring at the computational node. Darby and Thorne suggested that the measurable statistical variations in bank material properties along the reach (Simon 1989) could be substituted into the deterministic Osman-Thorne bank stability equations to obtain the probability of failure using the procedure of Huang (1983). Darby and Thorne's approach is a tentative first step toward solving this important problem.

7.4.5.4 Interaction of Fluvial Hydraulics and Bank Mechanics

7.4.5.4.1 Approaches Based on Extremal Hypotheses Two numerical models that use extremal hypotheses to simulate width and other channel adjustments are the FLUVIAL-12 (Chang 1988a,b) and GSTARS codes (Molinas and Yang 1986; Yang et al. 1988). FLUVIAL-12 and GSTARS assume that changes in cross-sectional area determined from the sediment-routing module represent an overall change in area that may be applied to both the bed and the banks. The total area is distributed over the cross section by first calculating the magnitude of width adjustment, and then distributing the computed area over the bed and banks. Width corrections at each cross section are computed assuming that the stream power for the reach moves toward uniformity (FLUVIAL-12) or toward a minimization of energy dissipation rate (GSTARS), in accordance with the extremal hypothesis that forms the basis for each of these approaches. However, banks composed of cohesive sediments are not accounted for in any of the (noncohesive) sediment-transport equations used in the sediment-routing module. This procedure is not obviously applicable, therefore, to channels with banks composed of cohesive sediments.

FLUVIAL-12 and GSTARS also add entrained bank materials into the bed-material transport scheme simplistically: The bank-material size distribution is transferred instantaneously to the bed-material active layer. Although this is reasonable for noncohesive sediments, the processes of cohesive bank-material breakdown are not yet known. The authors of the two models provided no information on how both cohesive and noncohesive bank sediments were distributed across the channel section following mass failure.

Independent of their capability to predict changes in channel width, FLUVIAL-12 and GSTARS are both characterized by another limitation. Only an overall estimate of the total change in channel width in any time step is made by the extremal hypothesis, and therefore the extent of advance and/or retreat of the left and right banks individually is unknown. Distributions of changes in total width between left and right banks are specified by the user.

7.4.5.4.2 Geofluvial Approaches In contrast to approaches based on extremal hypotheses, other methods have been developed that are based on coupling flow- and sediment-routing models with bank-erosion and mass-wasting algorithms. Such approaches are here termed "geofluvial" and focus on treating bankline adjustments mechanistically. Critical issues concern the need to

1. Predict accurately, in channels with the complex topography characteristic of natural rivers, the boundary shear stress distribution in each of the near-bank zones;
2. Determine the corresponding sediment flux field over the entire channel width;
3. Use the boundary shear stress distribution to determine the rate of fluvial particle-by-particle erosion on both banks, whether composed of cohesive or noncohesive materials;
4. Estimate the stability of the updated bank geometries and determine the volume (if any) of bank sediments delivered to the channel;
5. Characterize the exchanges of sediment between the banks and the bed material to satisfy conservation of sediment mass in channels that either are undergoing width adjustments, or are laterally migrating with stable width.

Topic 5 is the main focus of concern in this section. In geofluvial approaches, interactions between fluvial hydraulic and bank processes are modeled based on a solution of the sediment continuity equation. A given bed topography describes the geometry of the bank profile. Estimates of the sediment flux field and stability of the banks with respect to mass failure are then obtained. If a bank is unstable, then the width of the simulated failure block(s) determines the magnitude of bankline retreat during a time step. The volume of material involved in the failure, determined by the geometry of the failure surface, controls the bank-material input term in the sediment continuity equation, which is solved to determine the bed topography in the subsequent time step.

To couple the flow- and sediment-routing and bank-mechanics submodels in this way, an overall estimate of the failure-block volume is, in itself, insufficient. Precise details of the mechanics by which the failed bank materials are transferred down the failure surface are needed, because the lateral distribution of failure products determines the magnitude of the bank-material inflow term at each computational node. In addition, information regarding the physical properties (size, density, and cohesion) of the disturbed bank material at each

node is required so that the fluvial transport of these materials can be calculated in subsequent time steps.

No empirical information regarding the processes of, and controls on, the lateral distribution and physical status of bank material following fluvial entrainment or mass failure is currently available, either for laboratory or natural channels. Empirical information is not available regarding the fluvial transport of heterogeneous mixtures of disturbed bank and bed material. Conceptually, the lateral distributions and physical status of failed bank materials are determined by the geometry of the failure surface and channel-bed topography, the physical characteristics of the undisturbed bank materials, and the hydraulics of the flow.

In light of these difficulties, a distinction can be made between mechanistic widening models applicable to cohesive and noncohesive bank materials. For noncohesive banks, at least the physical status (size, density, and cohesion) of disturbed noncohesive bank materials is known, because these values are identical to those of the undisturbed bank materials. In contrast, disturbed cohesive bank materials may have physical properties distinct from those of intact bank materials, particularly if the failure products become immersed in the flow.

For noncohesive banks, two main approaches to estimating the lateral distribution of bank failure products can be identified. Pizzuto (1990) and Li and Wang (1993; 1994a,b) employed schemes such that, when the bank slope exceeded the angle of repose, a heuristic slumping model was employed in which a failure surface inclined at the angle of repose was projected to the floodplain surface. Sediment above the failure plane was translated downslope, forming a deposit with a linear upper surface. The highest point of the deposit was the lowest point of the failure plane. The deposit extended downslope until its value equaled the volume eroded. Wiele (1992) and Kovacs and Parker (1994) employed an approach in which the sediment continuity equation was manipulated to treat the bank erosion products as a transverse sediment flux. This approach is more consistent with a grain-by-grain noncohesive bank erosion mechanism, whereas the former approach is more consistent with slumping or toppling mechanisms of bank failure (Wiele 1992).

For cohesive banks, geofluvial approaches assume that failed bank materials are instantaneously deposited close to the toe of the bank. Failure products are distributed uniformly across the near-bank flow segments defined by Simon et al. (1991) and Darby and Thorne (1996c). Mosselman (1992) stated that failure products were distributed evenly across the near-bank computational cells. Borah and Bordoloi (1989) used a linear distribution function based on local sediment transport capacity. Osman (1985) and Alonso and Combs (1986) did not specify exactly how bank failure products were distributed in their models, other than stating that they were deposited close to the toe.

Some mechanistic approaches (Osman 1985; Alonso and Combs 1986; Borah and Bordoloi 1989; Mosselman 1992) assume that the banks are composed of a fraction of cohesive material (ω) that becomes wash load after being eroded and a fraction of noncohesive materials ($1-\omega$) with the same properties as the bed material. The sediment-transport submodels employed in these approaches are then directly applied to compute transport rates for noncohesive sediment.

Simon et al. (1991) proposed a conceptual model where failed bank materials are considered to represent bank material, bed material, bed-material load, or wash load, according to the physical properties of the failed materials and the hydraulic properties of the flow. The approach they present is perhaps best regarded as a conceptual framework from which to proceed. Application of the existing approach is currently hindered by two limitations. First, Simon et al. (1991) did not allow the possibility of bed-material load being deposited on the banks, thus excluding the possibility of fluvially controlled bank-accretion and channel-narrowing mechanisms. Second, no information is yet available on how to predict the physical properties of the failed bank materials that are significant with respect to fluvial transport processes.

Darby and Thorne (1996c) assumed that undisturbed cohesive bank material failure blocks tended to disaggregate into disturbed aggregates of some measurable size range during mass failure. Darby and Thorne noted that these disturbed aggregates, though composed of cohesive particles, were themselves large enough to behave as noncohesive sediment particles. Darby and Thorne went on to suggest a criterion to discriminate whether or not the failure block would disaggregate, based on energy dissipated during mass failure and internal resistance of the failure block. Darby and Thorne used the criterion to hypothesize that steep planar failures would tend to result in disaggregated blocks delivered to the basal region of the bank as noncohesive sediment clasts, whereas shallower rotational failures would tend to remain as intact blocks of bank materials. Knowledge of the size and density of deposited sediment assumed to behave as noncohesive sediment particles allowed standard sediment-transport analyses for heterogeneous sediment (Rahuel et al. 1989) to be applied to the failed bank material aggregates deposited as bed material in the near-bank sediment-routing segments. No means of predicting the size of the disturbed bank material aggregates was suggested by Darby and Thorne.

7.4.5.5 Testing and Application of Numerical Models The capabilities, predictive abilities, scope, limitations, and usefulness of the various numerical models are now summarized. Tables 7-2 to 7-5 indicate that the reviewed models are limited in terms of the range of conditions to which they may be applied, as determined by the limitations of the assumptions in the hydraulic, flow-resistance, sediment-transport, and bank-erosion modules used in each model.

7.4.5.5.1 Tests with Laboratory Data The reviewed models applicable to noncohesive bank materials (Pizzuto

Table 7-5 Summary of Approaches, Testing Status, and User Documentation of Reviewed Models

Model (1)	Approach (2)	Planform (3)	Test case run (4)	Laboratory data test (5)	Field data test (6)	User's Manual (7)
Darby-Thorne	Geofluvial	Straight	Yes	No	Yes	No
CCHEBank	Geofluvial	Straight	Yes	Yes	No	No
Kovacs-Parker	Geofluvial	Straight	Yes	Yes	No	Yes
Wiele	Geofluvial	Straight	Yes	Yes	Yes[a]	No
RIPA	Geofluvial	Arbitrary single-thread	Yes	No	Yes[a]	No
Simon et al.	Geofluvial	Straight	No	No	No	No
Pizzuto	Geofluvial	Straight	No	Yes	No	No
STREAM2	Geofluvial	Straight	Yes	No	Yes[a]	No
GSTARS	Extremal	Arbitrary	Yes	No	Yes[a]	Yes
FLUVIAL-12	Extremal	Arbitrary	Yes	No	Yes[a]	Yes
Alonso-Combs	Geofluvial	Straight	Yes	No	No	No
WIDTH	Geofluvial	Straight	Yes	No	No	No

[a]Denotes calibrated field test.

1990; Wiele 1992; Li and Wang 1993; 1994a,b; Kovacs and Parker 1994) have been tested with a common data set obtained from a laboratory study (Ikeda 1981). Results from these studies are shown in Fig. 7-27. However, assessment of the relative performance of these models is not attempted here because some small, but significant, differences are found in the numerical values of coefficients used by each of the aforementioned authors. Specifically, the critical dimensionless Shields stress is assumed to be 0.03 by Li and Wang (1993; 1994a,b) and Pizzuto (1990), 0.035 by Kovacs and Parker (1994), and 0.038 by Wiele (1992), respectively. The value of the internal angle of friction of the boundary material (which also influences the dynamic Coulomb friction coefficient) was assumed to be 33° by Pizzuto (1990) and 40° by the other authors.

Although a direct comparison of the relative performance of each model is not appropriate, Fig. 7-27 can be used to provide some insight into the capabilities of each of the individual models. The Kovacs and Parker model (Fig. 7-27(a)) resulted in predicted cross sections with cross-sectional areas larger than those measured in reality. Pizzuto's (1990) (Fig. 7-27(b)) model provided close agreement between simulated and measured channel shapes throughout the extent of the simulation. Wiele's (1992) model (Fig. 7-27(b)) underpredicted measured widening rates, presumably reflecting the relatively high Shields stress and friction-angle values selected by that author. Finally, Li and Wang (1993; 1994a,b) obtained overpredictions of widening compared to the observed channel changes (Fig. 7-27(d)).

7.4.5.5.2 Field Testing Those authors who have attempted to test their models with field data have tended to calibrate the adjustable model parameters to improve agreement between predicted and observed data. Authors also tend to characterize their results using qualitative terminology such as "reasonable agreement" and "acceptable results." In these circumstances, it is futile to attempt to summarize and compare the accuracy of those models, particularly because the same source data set has not been used to test each analysis. For calibrated testing analyses, the reader is referred to the source material. Borah et al. (1982) and Borah and Dashputre (1994) tested components of the Borah and Bordoloi (1989) model, whereas Chang (1988a,b), Yang et al. (1988), Mosselman (1992), and Wiele (1992) fully reported both the development and testing of their codes.

One model (Darby and Thorne 1996c) has been applied with unadjusted calibration parameters (Darby et al. 1996) (Fig. 7-28.). Model calibration parameters were not adjusted from the values set during the course of the model development. Although the model appeared to be able to replicate the observed sequence of channel adjustment, and the magnitudes of simulated and observed widths and depths agreed within ±10% of each other overall, simulated widening rates were underpredicted by a factor of 3 (Darby et al. 1996). Darby et al. (1996) attributed this poor result to limitations of the Osman and Thorne (1988) mass-wasting algorithm.

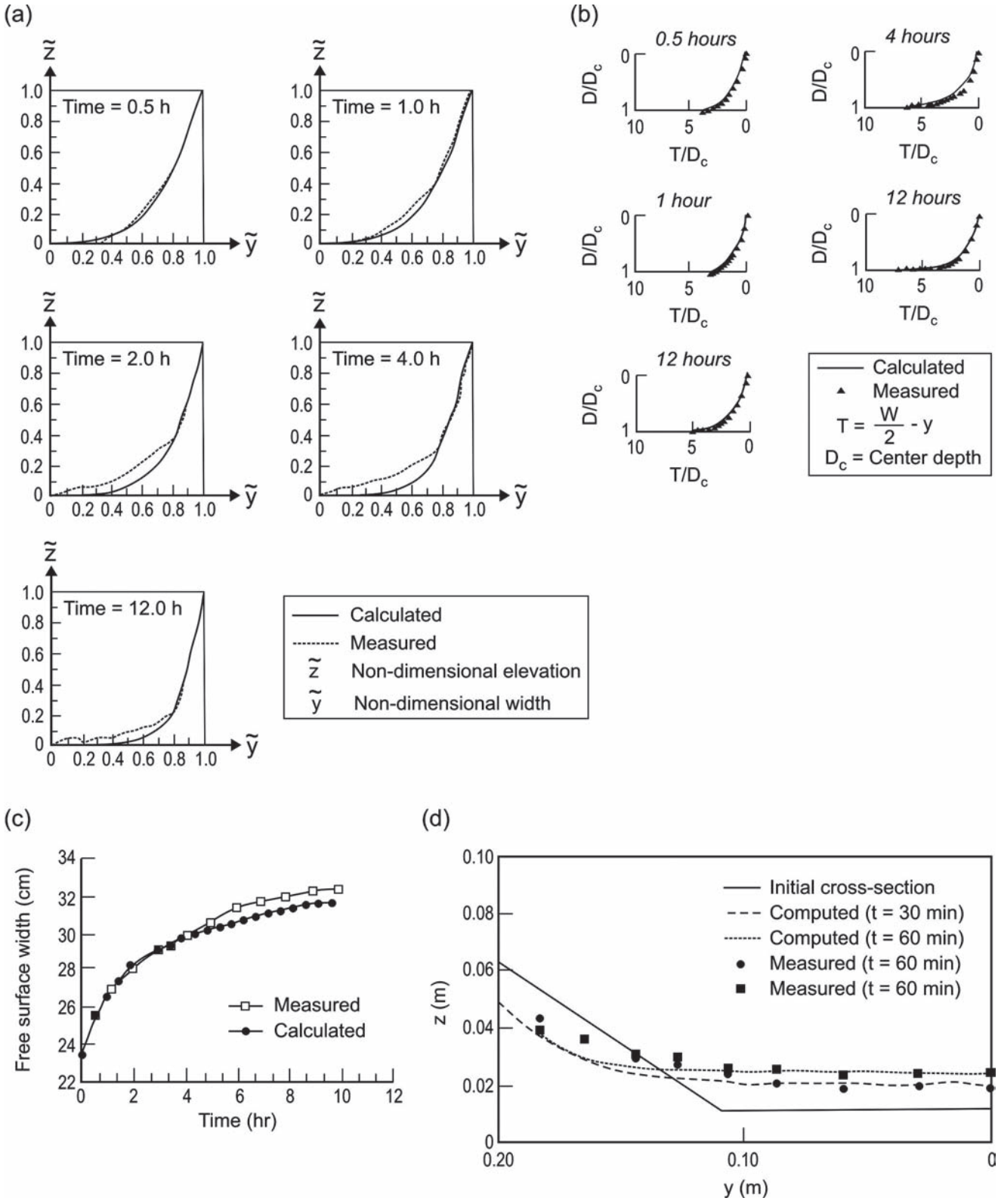

Fig. 7-27. Comparison of simulated output and Ikeda (1981) flume data for models by (a) Kovacs and Parker (1994); (b) Pizzuto (1990); (c) Wiele (1992); (d) Li and Wang (1993; 1994a,b) (ASCE Task Committee on Hydraulics, Bank Mechanisms and Modeling of River Width Adjustment 1998b, with permission from ASCE).

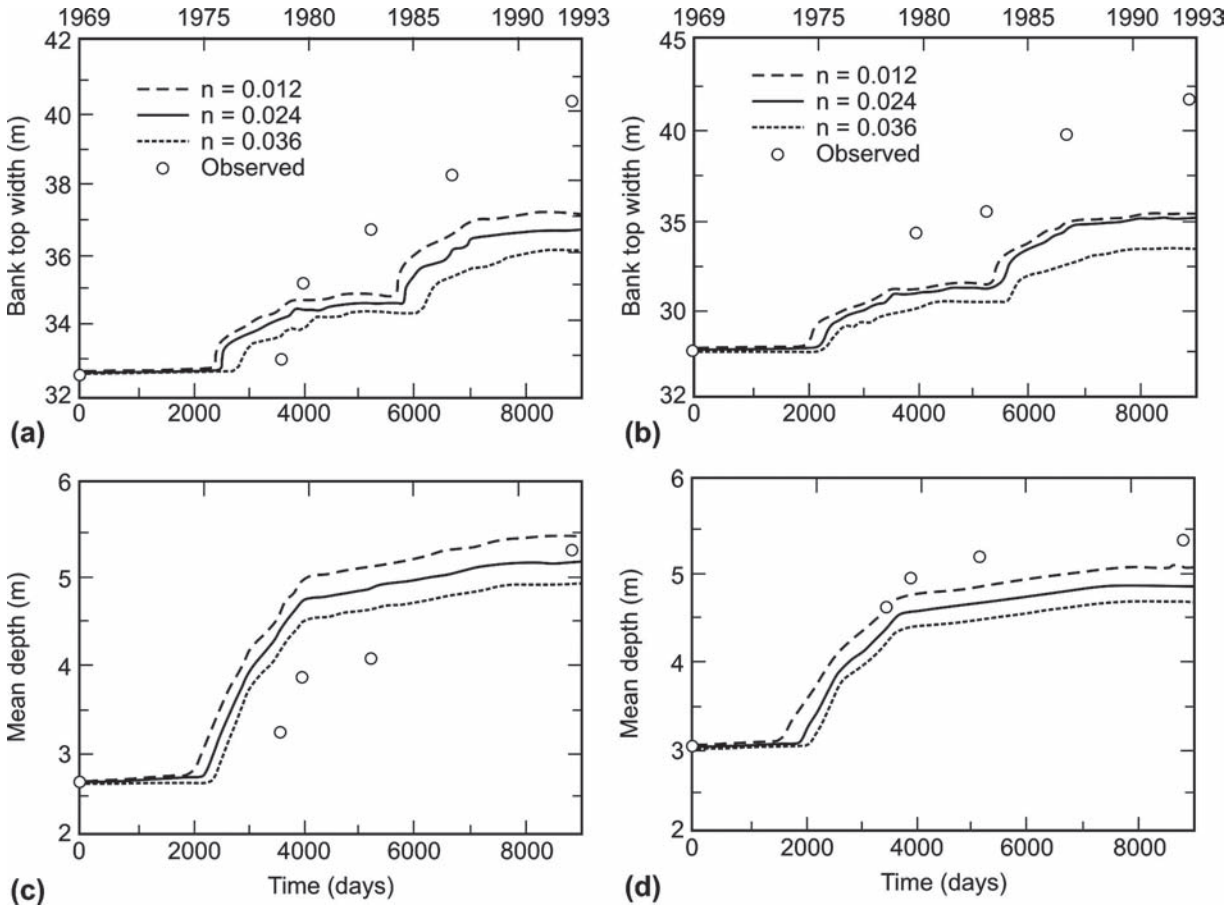

Fig. 7-28. Comparison of simulated versus observed channel morphology parameters for Darby-Thorne model at two study sites in West Tennessee: (a) bank-top widths at Chestnut Bluff; (b) bank-top widths at Crossroads; (c) mean depths at Chestnut Bluff; (d) mean depths at Crossroads (from Darby et al. 1996, with permission from ASCE).

7.5 PROCEDURE FOR APPROACHING WIDTH-ADJUSTMENT PROBLEMS

The wide range of geomorphic and engineering contexts associated with width adjustment makes it essential that practicing engineers adopt a broad and rational approach to such problems. Such an approach can be used to analyze the majority of problems that arise with the assurance that important factors are not overlooked, appropriate analytic techniques are applied, and effective engineering solutions are selected. The procedure proposed here (Fig. 7-29) is based on amassing and utilizing a wide range of information. Although each case is unique, the proposed procedure should have a number of elements that are relevant for the majority of situations.

7.5.1 Step 1: Problem Identification

Width-adjustment problems may be associated with a range of river engineering and societal activities. Questions to consider are the following:

1. Does the problem arise from a natural response?
2. Does it involve channel response to existing engineering works?
3. Does it require the prediction of channel response to proposed engineering works?

In all cases, it is necessary to formulate the problem in terms of whether it is existing or predicted, who or what is affected, and what level of analysis and response is appropriate. The aim of successful problem identification is to select a cost-effective engineering approach that will solve the problem.

7.5.2 Step 2: Field Data Collection

In all cases, visits to the site and river reaches upstream and downstream are essential. Particular attention should be paid to identifying channel characteristics, bank conditions, bank materials, the extent of existing or expected bank problems, the nature of the flow, the nature of the bed materials, the presence and nature of any vegetation, and the presence and

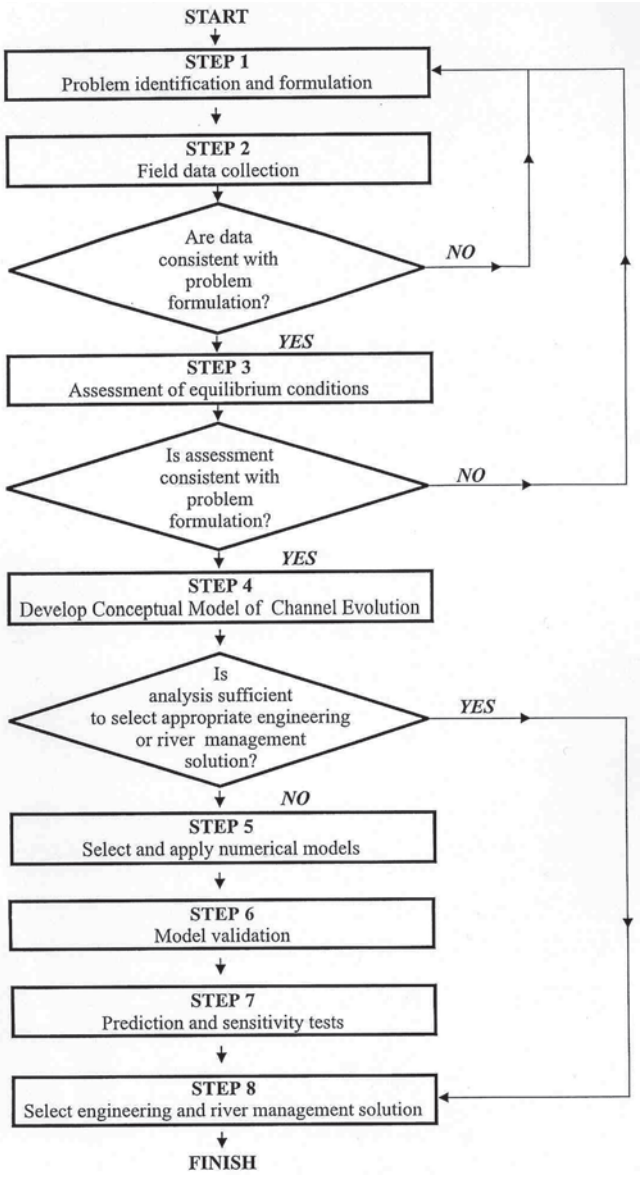

Fig. 7-29. Proposed procedure for identifying, analyzing, and modeling width-adjustment problems.

condition of any engineering structures. Stream reconnaissance techniques are described by, among others, Kellerhals et al. (1976); Thorne (1992); and Downs and Brookes (1994).

In all cases, it is necessary to identify the nature and extent of the width-adjustment problem that may arise. Where there have been width changes in the past, both reaches that have been subject to change and reaches that are stable should be examined.

Depending on the number of existing data available, it may be necessary to mount a specific data-gathering campaign. Data are needed to assess the equilibrium morphology of the channel and, in some cases, to understand the nature of the problem. If the use of numerical models is warranted, field measurements will always be needed. Data requirements for numerical modeling studies are discussed further in Appendix I.

7.5.3 Step 3: Assessment of Equilibrium Morphology

As a first step, the equilibrium morphology of the channel should be estimated using methods described in section 7.4.3. Of the methods discussed in section 7.4.3, regime theory is probably the most reliable, but field data near the particular field site will be needed to determine the necessary empirical coefficients and exponents.

Once predictions of the equilibrium morphology are available, the predicted morphology should be compared with the existing morphology to provide an assessment of the current morphological status of the channel; for example, whether it is overwide, of equilibrium width, or underwide. Where the impact of proposed engineering works is being considered, the equilibrium conditions should also be compared to the proposed channel conditions.

7.5.4 Step 4: Developing Conceptual Models of Channel Evolution

If the channel is actively evolving under natural conditions, or is responding to engineering intervention or regulation, then simple empirical channel response or dynamic models, such as those described in section 7.4.2, should be developed and applied in an attempt to explain both existing and, if appropriate, proposed conditions. Application of such models should aid in identifying the dominant processes and trends of channel change and can form a framework for subsequent, more detailed modeling.

7.5.5 Step 5: Application of Numerical Models

If the complexity and severity of the width adjustment problem merit numerical modeling, a hierarchical modeling approach will usually be appropriate. Initially a 1D model should be applied to the study reach to provide the overall setting of any additional detailed modeling. If appropriate, to provide a more detailed assessment of width adjustment, it may be necessary to apply 2D or 3D models to the whole or part of the study reach. Selection of numerical models appropriate for this purpose may be guided by the comments provided in this paper. At present, models of width adjustment are still undergoing active development, so selecting a useful model is not a simple task.

7.5.6 Step 6: Model Validation

The numerical model results should be validated. This will nearly always require an extensive program of field observations.

7.5.7 Step 7: Model Prediction

The numerical models should be applied to existing conditions and also used to assess the impacts of any proposed works. Model predictions should include a sensitivity analysis of the results to the various parameters specified in the model. Particular attention should be paid to parameters that either are difficult to determine or exhibit significant spatial or temporal variation.

7.5.8 Step 8: Selection of Engineering or River Management Solution

On the basis of the previous steps, an appropriate plan of action should be formulated and implemented. One example of a management approach is provided by Simon and Downs (1995). They describe an interdisciplinary approach to evaluating stream-channel instability conditions on the regional or statewide scale. The regionwide studies were motivated primarily by the desire of some state transportation departments in the United States to inventory the potential for channel instability to damage bridge crossings and other transportation infrastructure. A modular procedure was developed based on (1) initial site evaluations; (2) geographic-information-system-based data input and management; (3) ranking of relative channel stability conditions; (4) identification of spatial trends; (5) ranking of socioeconomic impacts and identification of problem sites; and (6) collection of additional field data for enhanced desktop and modeling analyses of future conditions at the problem sites (Simon and Downs 1995). Based on this approach, the state transportation departments were provided with a product that enabled them to optimize repair and maintenance schedules for damaged infrastructure or infrastructure at risk from channel adjustment.

7.6 CONCLUSIONS

1. Width adjustments take place within a wide range of geomorphic contexts. Adjustments may occur as part of the natural evolution of the channel morphology, or they may be caused by river engineering structures, river management policies, or changes in land use in the watershed or riparian zone.
2. To understand, predict, and manage changing channel width, it is essential that civil engineers understand the geomorphic context within which width adjustment is occurring.
3. The time- and space-averaged boundary shear stress is an important parameter in predicting both equilibrium width and width adjustment. However, the lateral distribution of local values of boundary shear stress is poorly understood, especially for channels with nonuniform cross sections.
4. Improved understanding of the effects of over-bank flows on river-width adjustment processes is needed.
5. A variety of mass-failure mechanisms may be involved in bankline retreat. Care must be taken to match the slope stability analysis used to check bank stability to the critical failure mechanisms observed in the field. It is essential that engineers identify actual and potential instability mechanisms prior to selecting an engineering or management strategy for dealing with bank retreat and width adjustment.
6. The long-term rate of bank retreat or advance of the bank toe can be explained using the concept of basal endpoint control. However, seepage-driven procedures operating within a bank can lead to serious bank instability due to piping even when wave and current action at the toe is not excessive.
7. Bank advance takes place through sediment accumulation as a berm or bench in the channel and by the development of floodplains on migrating point bars. Bank advance is often accelerated by invasion of pioneer riparian vegetation.
8. Current knowledge of bank processes and flow modeling is sufficient to allow some tentative *predictions* of width adjustment to be made.
9. Analysis of equilibrium width in stable channels can be approached using (1) empirical regime methods; (2) extremal hypotheses; and (3) rational tractive force methods. These approaches are strictly limited to prediction of time-invariant width in graded or regime channels. They can be used with care to predict asymptotic values of width following disturbance of the graded or regime condition, but they cannot predict either the rate of change or intermediate width attained during dynamic adjustment of channel morphology. Tractive force methods are limited to straight channels with noncohesive banks. Despite these limitations, these methods have many useful engineering applications.
10. To date, models of river width adjustment can be divided into two broad approaches: (1) those based on extremal hypotheses, and (2) those based on the geofluvial approach. The former have been used in engineering practice more frequently than the latter, which are at present used essentially as research tools. However, geofluvial approaches have the potential to become adopted as standard engineering tools.
11. Currently, very few appropriate laboratory and field data sets are suitable for testing width-adjustment models. This has resulted in a lack of comprehensive testing and verification analyses of existing models on benchmark field and laboratory data sets.
12. At present, no single model or method exists that is applicable to all the circumstances under which width adjustments may occur.

APPENDIX. DATA SOURCES

1 Equilibrium Channels

Equilibrium channel geometry measurements have been reported for at least a century. A summary of published data sources was presented by Julien and Wargadalam (1995), based on a compilation of available data by Wargadalam (1993). The data encompass measurements from 835 field channels and 45 laboratory channels that were used to test semitheoretical downstream hydraulic geometry relationships.

Brownlie (1981a,b; 1983) published an extensive compilation of laboratory and field data. Khan (1971) reported 45 laboratory measurements of hydraulic geometry for straight, meandering, and braided reaches. Griffiths (1981) reported 136 gravel-bed river geometry measurements collected from 46 rivers in New Zealand. Of these, 84 were conducted under rigid bed conditions, whereas 52 are for mobile bed conditions. Church and Rood (1983) published a compendium of river regime data that lists 496 hydraulic geometry measurements reported in the technical literature. This data set includes measurements from rivers in Canada and the United States, which were carefully selected from 25 references published between 1955 and 1983. Hey and Thorne (1986) reported data from 62 river measurement sites from stable gravel-bed rivers in the United Kingdom. Higginson and Johnston (1988) published data from 68 sites under bank-full flow conditions from rivers in Northern Ireland. Colosimo et al. (1988) published 42 gravel-bed river measurements from streams in Calabria, Southern Italy. The range of flow parameters covered by all these data is summarized in Table 7-7.

Table 7-7 Range of Flow Parameters Covered in Equilibrium Channel Data Set of Julien and Wargadalam (1995)

Parameter (1)	Range (2)
Discharge	0.00018–26,600 m^3/s
Channel width	0.16–1,100 m
Average flow depth	0.003–15.7 m
Mean flow depth	0.09–4.7 m/s
Channel slope	0.00004–0.08
Median grain size	0.12–400 mm
Width/depth ratio	4.2–507
Relative submergence	1.4–70,400
Froude number	0.017–4
Shields number	0.001–8.5
Grain shear Reynolds number	1.6–156,000

2 Nonequilibrium Channels

For nonequilibrium channels, data sets that include all the parameters required to apply width adjustment models (Table 7-6) are comparatively rare. Laboratory experiments involving width adjustments in straight channels formed in sand were conducted by Ikeda (1981). Ikeda et al. (1988) performed similar experiments in a gravel channel. Data on width adjustment in rivers can be found in Brice (1982); Nanson and Hickin (1983); Richardson et al. (1990); and the USACE (1981). However, these reports do not contain all of the required data listed in Table 7-6. Data sets that include many of the parameters listed in Table 7-6 are generally not available in the literature. However, three data sets have been identified that are suitable for use with numerical models of width adjustment. Data for the Toutle River, Washington, are described by Simon (1992). Similarly, data from the South Fork Forked Deer River, West Tennessee, were used by Darby et al. (1996) to test the Darby and Thorne (1996c) numerical

Table 7-6 Minimum Data Required to Apply Geofluvial-Based Numerical Width Adjustment Models

Data Item (1)	Notes (2)
(*a*) Time-independent data (initial conditions)	
Cross-sectional surveys	Required to define initial channel morphology. Surveys are required at several sites along the prototype reach.
Bed material size distribution	Required to define the initial bed material characteristics. Data is required at each cross section.
Bank material characteristics	Measurements of cohesion, friction angle, unit weight, and particle size distribution at left and right banks of each cross section are required to define the bank-material characteristics.
(*b*) Time-dependent data (boundary conditions)	
Discharge	Value of discharge to be used in each discrete time step of the simulation
Sediment supply	Value of sediment load at the upstream boundary of the prototype reach during each discrete time step of the simulation.

model. Further information about these two data sets may be obtained through contact with the authors of these reports. Finally, data from Goodwin Creek, Mississippi, are available through contact with personnel at the USDA-ARS National Sedimentation Laboratory, Oxford, Mississippi.

ACKNOWLEDGMENTS

Most of the text of this chapter was prepared by the ASCE Task Committee in River Width Adjustment and published in the Journal of Hydraulic Engineering (reprinted with permission from ASCE). The Task Committee was chaired by Colin R. Thorne of the University of Nottingham, U.K. The members of the Task Committee were Carlos Alonso, USDA-ARS National Sedimentation Library; Roger Bettess, HR Wallingford, U.K.; Deva Borah, Illinois State Water Survey; Stephen Darby, University of Southampton, U.K.; Panos Diplas, Virginia Polytechnic University; Pierre Julien, Colorado State University; Donald Knight, University of Birmingham, U.K.; Lingeng Li, University of Mississippi; Jim Pizzuto, University of Delaware; Michael Quick, University of British Columbia; Andrew Simon, USDA-ARS National Sedimentation Laboratory; Michael Stevens, Stevens and Associates; Sam Wang, University of Mississippi; and Chester Watson, Colorado State University. Agnes Kovacs, Erik Mosselman, Leonardo Schippa, and Steven Wiele provided materials and discussions that aided in the preparation of the original Task Committee review papers published in the Journal of Hydraulic Engineering.

REFERENCES

Jose Rodriguez helped with the completion of this chapter by updation some of the references.

Abam, T. K. (1993). "Factors affecting distribution of instability of river banks in the Niger delta." *Engineering Geology*, 35, 123–133.

Abril, B. (1995). "Numerical modeling of turbulent flow in compound channels by the finite element method." *Hydra 2000, Proc., 26th IAHR Congress International Association for Hydraulic Research,* London.

Abt, S. R. (1980). "Scour at culvert outlet in cohesive bed materials." PhD thesis, Department of Civil Engineering, Colorado State University, Fort Collins, Colo.

Ackers, P. (1992). "1992 Gerald Lacey memorial lecture—Canal and river regime in theory and practice: 1929–92." *Proc., Inst. Civ. Engrs. Wat., Marit. and Energy*, Institution of Civil Engineers, London, 167–178.

Ackers, P. (1993). "Stage-discharge functions for two-stage channels: The impact of new research." *Journal of the Institution of Water and Environmental Management*, 7(1), 52–61.

Ackers, P., and White, W. R. (1973). "Sediment transport: New approach and analysis." *Journal of the Hydraulic Division, ASCE*, 99(11), 2041–2060.

Alam, Z. U., and Kennedy, J. F. (1969). "Fraction factors for flat bed flows in sand bed channels." *Journal of the Hydraulics Division, ASCE*, 95(4), 1973–1992.

Alonso, C. V., Borah, D. K., and Prasad, S. N. (1981). "Numerical model for routing graded sediments in alluvial streams." *Appendix J, Rep. Prepared for the U.S. Army Corps of Engrs., Vicksburg District*, USDA Sedimentation Lab., Oxford, Miss.

Alonso, C. V., and Combs, S. T. (1986). "Channel width adjustment in straight alluvial streams." *Proc., 4th Fed. Interagency Sedimentation Conf.*, U.S. Government Printing Office, Washington, D.C., 5-31–5-40.

Amarasinghe, I. (1992). "Effects of root reinforcement on soil strength and bank stability." PhD thesis, Open University, Milton Keynes, U.K.

Andrews, E. D. (1986). "Downstream effects of Flaming Gorge Reservoir on the Green River, Colorado and Utah." *Geological Society of America Bulletin*, 97, 1012–1023.

Annadale, G. W., and Parkhill, D. L. (1995). "Stream ban erosion: Application of the erodibility index model." *Proc., 1st Int. Conf. on Water Resour. Engrg.*, ASCE, New York, N.Y., 2, 1570–1574.

Ariathurai, R., and Arulanandan, K. (1978). "Erosion rates of cohesive soils." *Journal of the Hydraulic Division, ASCE*, 104(3), 279–283.

Ariathurai, R., and Krone, R. B. (1976). "Finite element model for cohesive sediment transport." *Journal of the Hydraulic Division, ASCE*, 102(3), 323–338.

Arulanandan, K. (1975). "Fundamental aspects of erosion of cohesive soils." *Journal of the Hydraulics Division, ASCE*, 101(5), 635–639.

Arulanandan, K., Gillogley, E., and Tully, R. (1980). "Development of a quantitative method to predict critical shear stress and rate of erosion of naturally undisturbed cohesive soils." *Rep. G1-80-5*, U.S. Army Waterway Experiment Station, Vicksburg, Miss.

Arulanandan, K., Loganathan, P., and Krone, R. B. (1975). "Pore and eroding fluid influences on the surface erosion of a soil." *Journal of the Geotechnology Engineering Division, ASCE*, 101(1), 51–66.

ASCE Task Committee on Erosion of Cohesive Sediments. (1968). "Erosion of cohesive sediments." *Journal of the Hydraulic Division, ASCE*, 94(4), 1017–1050.

ASCE Task Committee on Friction Factors in Open Channels. (1963). "Friction factors in open channels." *Journal of the Hydraulic Division, ASCE*, 89(2), 97–143.

ASCE Task Committee on Hydraulics, Bank Mechanics and Modeling of River Width Adjustment. (1998a). "River width adjustment. I: Processes and mechanisms." *Journal of Hydraulic Engineering, ASCE*, 124(9): 881–902.

ASCE Task Committee on Hydraulics, Bank Mechanics and Modeling of River Width Adjustment. (1998b). "River width adjustment. II: Modeling." *Journal of Hydraulic Engineering, ASCE*, 124(9), 903–917.

ASCE Task Committee on Turbulence Models in Hydraulic Computation. (1988). "Turbulence modeling of surface water flow and transport. Parts I–IV." *Journal of Hydraulic Engineering, ASCE*, 114(9), 970–1073.

Ashworth, P. J., Bennett, S. J., Best, J. L., and McLelland, S. J. (1996). *Coherent flow structures in open channels*. Wiley, Chichester, U.K.

Bathurst, J. C., Thorne, C. R., and Hey, R. D. (1979). "Secondary flow and shear stress at river bends." *Journal of the Hydraulic Division, ASCE*, 105(10), 1277–1295.

Best, J. L., and Bristow, C. S. (1993). "Braided rivers." Geological Soc. of London Spec. Publ. No. 75.

Bettess, R., and White, W. R. (1987). "Extremal hypotheses applied to river regime." Sediment transport in gravel-bed rivers, C. R. Thorne, J. C. Bathurst, and R. D. Hey, eds., Wiley, Chichester, U.K., 767–791.

Biedenharn, D. S., and Thorne, C. R. (1994). "Magnitude-frequency analysis of sediment transport in the lower Mississippi River." *Regulated Rivers Research and Management*, 9, 237–251.

Bishop, A. W. (1955). "The use of the slip circle in the stability analysis of slopes." *Géotechnique*, 5, 7–17.

Bishop, A. W., and Morgenstern, N. R. (1960). "Stability coefficients for earth slopes." *Géotechnique*, 19(3), 129–150.

Blench, T. (1969). Mobile-bed fluviology: A regime treatment of canals and rivers. University of Alberta Press, Edmonton, Alberta, Canada, 168.

Borah, D. K., Alonso, C. V., and Prasad, S. N. (1982). "Routing graded sediments in streams: Applications." *Journal of the Hydraulic Division, ASCE*, 108, 1504–1517.

Borah, D. K., and Bordoloi, P. K. (1989). "Stream bank erosion and bed evolution model." *Sediment transport modeling*, S. Wang, ed., ASCE, New York, 612–619.

Borah, D. K., and Dashputre, M. S. (1994). "Field evaluation of the sediment transport model 'STREAM' with a bank erosion component." *Proc., Hydr. Engrg. '94*, G. V. Cotroneo and R. R. Rumer, eds., ASCE, New York, 979–983.

Bradford, M. J., and Piest, R. F. (1980). "Erosional development in valley-bottom gullies in the upper midwestern United States." *Thresholds in geomorphology*, D. R. Coates and J. D. Vitak, eds., Allen and Unwin, Boston, 75–101.

Brammer, H., Asaduzzaman, M., and Sultana, P. (1993). "Effects of climate and sea-level changes on the natural resources of Bangladesh, briefing document 3." *Bangladesh: Greenhouse effect and climate change*, Bangladesh Unnayan Parishad, Dhaka, Bangladesh, 31.

Bray, D. I. (1982). "Regime equations for gravel-bed rivers." *Gravel-bed rivers: Fluvial processes, engineering and management*, R. D. Hey, J. C. Bathurst, and C. R. Thorne, eds., Wiley, Chichester, U.K., 517–552.

Breusers, H. N. C., and Raudkivi, A. J. (1991). "Scouring." *Hydr. Struct. Des. Manual No. 2*, IAHR, Balkema, Rotterdam, The Netherlands.

Brice, H. (1982). "Stream channel stability assessment." *Rep. FHWA/RD/82/02*, Ofc. of Res. and Development, Dept. of Transportation, Washington, D.C.

Brownlie, W. R. (1981a). "Prediction of flow depth and sediment discharge in open channels." PhD dissertation, California Institute of Technology, Pasadena, Calif.

Brownlie, W. R. (1981b). "Prediction of flow depth and sediment discharge in open channels." *Rep. KH-R-43*, W. M. Keck Lab. of Hydr. and Water Resour., Pasadena, California Institute of Technology, available at http://caltechkhr.library.caltech.edu/7/.

Brownlie, W. R. (1983). "Flow depth in sand-bed channels." *Journal of Hydraulic Engineering, ASCE*, 109(7), 959–990.

Brunsden, D., and Kesel, R. H. (1973). "Slope development on a Mississippi bluff in historic time." *Journal of Geology*, 81, 570–598.

Burkham, D. E. (1972). "Channel changes of the Gila River in Safford Valley, Arizona—1846–1970." *Professional Paper 655-G*, U.S. Geological Survey, ASCE, Reston, Va., 24.

Burnet, A. W., and Schumm, S. A. (1983). "Alluvial river response to neotectonic deformation in Louisiana and Mississippi." *Science*, 222, 49.

Carson, M. A., and Kirkby, M. J. (1972). *Hillslope form and process*. Cambridge University Press, Cambridge, U.K., 475.

Chang, H. H. (1980). "Geometry of gravel streams." *Journal of Hydraulic Engineering, ASCE*, 106(9), 1443–1456.

Chang, H. H. (1988a). *Fluvial processes in river engineering*. Wiley-Interscience, New York, 429.

Chang, H. H. (1988b). "Introduction to FLUVIAL-12 mathematical model for erodible channels." *Twelve selected computer stream sedimentation models developed in the United States,* S. Fan, ed., Federal Energy Regulatory Commission, Washington, D.C.

Chiu, C. L., and Abidin, C. A. (1995). "Maximum and mean velocities and entropy in open channel flow." *Journal of Hydraulic Engineering, ASCE*, 121(1), 26–35.

Chiu, C. L., and Hsiung, D. E. (1981). "Secondary flow, shear stress and sediment transport." *Journal of theHydraulic Division, ASCE*, 107(7), 879–898.

Chow, V. T. (1959). *Open channel hydraulics*. McGraw-Hill, London, 680.

Chow, V. T. (1973). *Open-channel hydraulics*. McGraw-Hill, Singapore.

Church, M., and Rood, R. (1983). "Catalogue of alluvial river channel regime data." University of British Columbia, Vancouver, Canada.

Colosimo, C., Coppertino, V. A., and Veltri, M. (1988). "Friction factor evaluation in gravel-bed rivers." *Journal of Hydraulic Engineering, ASCE*, 114(8), 861–876.

Costa, J. E. (1974). "Response and recovery of a piedmont watershed from tropical storm Agnes, June 1972." *Water Resources Research*, 10, 106–112.

Cunge, J. A., Holly, F. M., and Verwey, A. (1980). *Practical aspects of computational river hydraulics.* Pitman, London, and Iowa State University Press, Ames, Iowa.

Darby, S. E., and Thorne, C. R. (1992). "Simulation of near bank aggradation and degradation for width adjustment modeling." Proc., 2nd Int. Conf. on *Hydraulic and Environmental Modeling of Coast, Estuarine and River Waters*, R. A. Falconer, K. Shiono, and R. G. S. Matthews, eds., Ashgate, Aldershot, U.K., 431–442.

Darby, S. E., and Thorne, C. R. (1996a). "Development and testing of a riverbank-stability analysis." *Journal of Hydraulic Engineering, ASCE*, 122(8), 443–455.

Darby, S. E., and Thorne, C. R. (1996b). "Numerical simulation of widening and bed deformation of straight sand-bed rivers. I: Model development." *Journal of Hydraulic Engineering, ASCE*, 122(4), 184–193.

Darby, S. E., and Thorne, C. R. (1996c). "Modeling the sensitivity of channel adjustments in destabilized sand-bed rivers." *Earth Surface Processes and Landforms*, 21, 1109–1125.

Darby, S. E., Thorne, C. R., and Simon, A. (1996). "Numerical simulation of widening and bed deformation of straight sand-bed rivers. II: Model evaluation."*Journal of Hydraulic Engineering, ASCE*, 122(4), 194–202.

Dietrich, W. E., and Smith, J. D. (1983). "Influence of the point bar on flow through curved channels." *Water Resources Research* 19, 1173–1192.

Dietrich, W. E., and Smith, J. D. (1984). "Bed load transport in a river meander." *Water Resources Research* 20, 1355–1380.

Dietrich, W. E., and Whiting, P. (1989). "Boundary shear stress and sediment transport in river meanders of sand and gravel." *River meandering*, S. Ikeda and G. Parker, eds., Water Resources

Monograph No. 12, American Geophysical Union, Washington, D.C., 1–50.

Diplas, P. (1990). "Characteristics of self formed straight channels." *Journal of Hydraulic Engineering, ASCE*, 116(5), 707–728.

Diplas, P., and Vigilar, G. G. (1992). "Hydraulic geometry of threshold channels." *Journal of Hydraulic Engineering, ASCE*, 118(4), 597–614.

Downs, P. W., and Brookes, A. (1994). "Developing a standard geomorphological approach for the appraisal of river projects." *Integrated river basin development*, C. Kirby and W. R. White, eds., Wiley, Chichester, U.K., 299–310.

Einstein, H. A. (1950). "The bed-load function for sediment transportation in open channel flows." *Tech. Bull. 1026*, Soil Conservation Service, U.S. Dept. of Agriculture, Washington, D.C.

Einstein, H. A., and Li, H. (1958). "Secondary currents in straight channels." *Transactions of the American Geophysical Union*, 39, 1085–1088.

Engelund, F. (1964). "Flow resistance and hydraulic radius." *Acta Polytechnica Scandinavia, Civ. and Engrg. Series, Ci 24*, 1–23.

Engelund, F. (1966). "Hydraulic resistance of alluvial streams." *Journal of the Hydraulic Division, ASCE*, 92(2), 315–327.

Engelund, F., and Hansen, E. (1967). "A monograph on sediment transport in alluvial streams." TekniskForlag, Copenhagen, Denmark.

Everitt, B. L. (1968). "Use of cottonwood in an investigation of the recent history of a floodplain." *American Journal of Science*, 266, 417–439.

Fan, S., ed. (1988). *Twelve selected computer stream sedimentation models developed in the United States*. Federal Energy Regulatory Commission, Washington, D.C.

Ferguson, R. I. (1986). "Hydraulics and hydraulic geometry." *Progress in Physical Geography*, 10, 1–31.

Flaxman, E. M. (1963). "Channel stability in undisturbed cohesive soils." *Journal of the Hydraulic Division, ASCE*, 89(2), 87–96.

Fread, D. L. (1971). "Discussion on 'Implicit flood routing in natural channels'' by M. Amein and C. S. Fang." *Journal of the Hydraulic Division, ASCE*, 97(7), 1156–1159.

Fread, D. L. (1974). "Numerical properties of implicit four-point finite difference equations of unsteady flow." *Tech. Memo. NWS Hydro-18*, National Weather Service, NOAA, Washington, D.C.

Fredlund, D. G. (1987). *Slope stability analysis using PC-slope*. Geo-Slope Programming Ltd., Calgary, Alta., Canada.

Fredlund, D. G., and Krahn, J. (1977). "Comparison of slope stability methods of analysis." *Canadian Geotechnical Journal*, 14, 429–439.

Fukuoka, S. (1993). "Flood control measures that utilize natural functions of rivers." *Proc., XXV Congr., Int. Assn. for Hydr. Res.*, International Association for Hydraulic Research, Madrid, 71–78.

Fukuoka, S. (1994). "Erosion processes of natural river bank." *Proc., 1st Int. Conf. on Flow Measurement*, Vol. 2, 222–229.

Fukuoka, S., Kogure, Y., Sato, K., and Daito, M. (1993). "Erosion processes of river bank with strata." *Annual Journal of Hydraulic Engineering*, 37, 643–648 (in Japanese).

Garde, R. J., and Ranga-Raju, K. G. (1977). *Mechanics of sediment transportation and alluvial stream problems*. Wiley Eastern, New Delhi, India.

Gardner, J. S. (1977). "Some geomorphic effects of a catastrophic flood in the Grand River, Ontario." *Canadian Journal of the Earth Sciences*, 14, 2294–2300.

Glover, R. E., and Florey, Q. L. (1951). "Stable channel profiles." *Vol. 235,* U.S. Bureau of Reclamation, Denver.

Gomez, B., and Church, M. (1989). "As assessment of bed load sediment transport formulae for gravel bed rivers." *Water Resources Research*, 25(6), 1161–1186.

Graf, W. H. (1971). *Hydraulics of sediment transport*. McGraw-Hill, New York.

Graf, W. L. (1978). "Fluvial adjustments to the spread of tamarisk in the Colorado Plateau region." *Geological Society of America Bulletin*, 89, 1491–1501.

Gray, D. H., and Leiser, A. T. (1982). Biotechnical slope protection and erosion control. Krieger, Malabar, Fla.

Griffiths, G. A. (1981). "Stable channels with mobile gravel beds." *Journal of Hydrology*, 52, 291–305.

Grissinger, E. H. (1982). "Bank erosion of cohesive materials." *Gravel-bed rivers*, R. D. Hey, J. C. Bathurst, and C. R. Thorne, eds., Wiley, Chichester, U.K., 273–287.

Grissinger, E. H. (1966). "Resistance of selected clay systems to erosion by water." *Water Resources Research*, 2(1), 131–138.

Grissinger, E. H., and Asmussen, L. E. (1963). "Channel stability in undisturbed cohesive soils." *Journal of the Hydraulic Division, ASCE*, 89(6), 259–264.

Gupta, A., and Fox, H. (1974). "Effects of high-magnitude floods on channel form: A case study in Maryland Piedmont." *Water Resources Research*, 10, 499–509.

Hadley, R. F. (1961). "Influence of riparian vegetation on channel shape, northeastern Arizona." *Professional Paper 424-C*, U.S. Geological Survey, Reston, Va., C30–C31.

Hagerty, D. J. (1991). "Piping/sapping erosion. II: Identification-diagnosis." *Journal of Hydraulic Engineering, ASCE*, 117(8), 1009–1025.

Hagerty, D. J., Spoor, M. F., and Parola, A. C. (1995). "Near bank impacts of river stage control." *Journal of Hydraulic Engineering, ASCE*, 121(2), 196–207.

Hammer, T. R. (1972). "Stream channel enlargement due to urbanization." *Water Resources Research*, 8, 1530–1540.

Harvey, M. D., and Watson, C. C. (1986). "Fluvial processes and morphological thresholds in incised channel restoration." *Water Resources Bulletin*, 3(3), 359–368.

Harvey, M. D., and Watson, C. C. (1988). "Channel response to grade-control structures on Muddy Creek, Mississippi." *Regulated Rivers: Research and Management*, 2, 79–92.

Harvey, M. D., Watson, C. C., and Schumm, S. A. (1985). "Gully erosion." *Rep.*, U.S. Bureau of Land Mgmt., Dept. of the Interior.

Hasegawa, K. (1989). "Universal bank erosion coefficient for meandering rivers." *Journal of Hydraulic Engineering, ASCE*, 115(4), 744–765.

Hasegawa, K., and Mochizuki, A. (1987). "Erosion process of silt fine sand banks." *Proc., 31st Japanese Conf. on Hydr.*, 725–730 (in Japanese).

Hereford, R. (1984). "Climate and ephemeral-stream processes: Twentieth-century geomorphology and alluvial stratigraphy of the Little Colorado River, Arizona." *Geological Society of America Bulletin*, 95, 654–668.

Hey, R. D. (1975). "Design discharge for natural channels." *Science, technology and environmental management*, R. D.

Hey and T. D. Davies, eds., Saxon House, Farnborough, U.K., 73–88.

Hey, R. D., and Thorne, C. R. (1986). "Stable channels with mobile gravel beds." *Journal of Hydraulic Engineering, ASCE*, 112(6), 671–689.

Higginson, N. N. J., and Johnston, H. T. (1988). "Estimation of friction factors in natural streams." *River regime*, W. R. White, ed., Wiley, Chichester, U.K., 251–266.

Hoey, T. B., and Ferguson, R. (1994). "Numerical simulation of downstream fining in gravel bed rivers: Model development and illustration." *Water Resources Research*, 30(7), 2251–2260.

HR Wallingford. (1992). "Flood channel facility data." *Rep. No. 314*, Vols. 1–15, HR Wallingford, Wallingford, U.K.

Huang, Y. H. (1983). *Stability analysis of earth slopes*, Van Nostrand Reinhold, New York.

Ikeda, S. (1981). "Self formed straight channel in sand beds." *Journal of the Hydraulic Division, ASCE*, 108(1), 95–114.

Ikeda, S., and Izumi, N. (1990). "Width and depth of self-formed straight gravel rivers with bank vegetation." *Water Resources Research*, 26(10), 2353–2364.

Ikeda, S., and Izumi, N. (1991). "Stable channel cross section of straight sand rivers." *Water Resources Research*, 27(9), 2429–2438.

Ikeda, S., and Parker, G. (1989). "River meandering." *Water Resources Monograph No. 12*, American Geophysical Union, Washington, D.C., 485.

Ikeda, S., Parker, G., and Kimura, Y. (1988). "Stable width and depth of straight gravel rivers with heterogeneous bank materials." *Water Resources Research*, 24, 713–722.

Ikeda, S., Parker, G., and Sawai, K. (1981) "Bend theory of river meanders. Part 1. Linear development." *Journal of Fluid Mechanics*, 112, 363–377.

Jackson, R. G. (1976a) "Depositional model of point bars in the lower Wabash River." *Journal of Sedimentary Petrology*, 46, 574–594.

Jackson, R. G. (1976b). "Sedimentological and fluid-dynamic implications of the turbulent bursting phenomenon in geophysical flows." *Journal of Fluid Mechanics, ASCE*, 77, 531–560.

Jacobson, R. B., and Coleman, D. J. (1986). "Stratigraphy and recent evolution of Maryland Piedmont floodplains." *American Journal of Science*, 286, 617–637.

James, C. S., and Wark, J. B. (1994). "Conveyance estimation for meandering channels." *Rep. SR 329*, HR Wallingford, Wallingford, U.K., 86.

Julien, P. Y., and Wargadalam, J. (1995). "Alluvial channel geometry: Theory and applications." *Journal of Hydraulic Engineering, ASCE*, 121(4), 312–325.

Kamphuis, J. W., and Hall, K. R. (1983). "Cohesive material erosion by unidirectional current." *Journal of Hydraulic Engineering, ASCE*, 109(1), 49–61.

Kandiah, A., and Arulanandan, K. (1974). "Hydraulic erosion of cohesive soils." *Transp. Res. Rec. No. 497*, Transp. Res. Bd, National Research Council, Washington, D.C., 60–68.

Kellerhals, R., Church, M., and Bray, D. I. (1976). "Classification and analysis of river processes." *Journal of theHydraulic Division, ASCE*, 102, 813–829.

Kennedy, R. G. (1885). "The prevention of silting in irrigation canals." *Proceedings, Institute of Civil Engineers*, 119, 281.

Keulegan, G. H. (1938). "Laws of turbulent flow in open channels." *Journal of Research of the National Bureau of Standards*, Res. Paper 1151, 21(6), 707–741.

Khan, H. R. (1971). "Laboratory study of alluvial river morphology." PhD dissertation, Colorado State University, Fort Collins, Colo.

Kirkby, M. J., and Morgan, R. P. C. (1980). *Soil erosion*. Wiley-Interscience, New York, 312.

Knight, D. W., Alhamid, A. A. I., and Yuen, K. W. H. (1992). "Boundary shear in differentially roughened trapezoidal channels." *Proc., Int. Conf. on Hydr. and Envir. Modeling of Coast., Estuarine and River Waters*, R. A. Falconer, ed., Ashgate, Aldershot, U.K., 419–428.

Knight, D. W., and Cao, S. (1994). "Boundary shear in the vicinity of river banks." *Proc., Hydr. Engrg. '94*, G. V. Cotreano and R. R. Rumer, eds., ASCE, New York, 954–958.

Knight, D. W., and Demetriou, J. D. (1983). "Flood plain and main channel flow interaction." *Journal of Hydraulic Engineering, ASCE*, 109(8), 1073–1092.

Knight, D. W., Samuels, P. G., and Shiono, K. (1990). "River flow simulation: Research and developments." *Journal of the Institution of Water and Environmental Management*, 4(2), 163–175.

Knight, D. W., and Sellin, R. H. J. (1987). "The SERC Flood Channel Facility." *Journal of the Institution of Water and Environmental Management*, 1(2), 198–204.

Knight, D. W., and Shiono, K. (1990). "Turbulence measurements in a shear layer region of a compound channel." *Journal of Hydraulic Research*, 28(2), 175–196.

Knight, D. W., and Shiono, K. (1995). "River channel and floodplain hydraulics." *Floodplain processes*, M. Anderson, D. Walling, and J. Bates, eds., Wiley, Chichester, U.K.

Knight, D. W., Shiono, K., and Pirt, J. (1989). "Prediction of depth mean velocity and discharge in natural rivers with overbank flow." *Proc., Int. Conf. on Hydr. and Envir. Modeling of Coast., Estuarine and River Waters*, R. A. Falconer, ed., Gower Technical Press, Hampshire, U.K., 419–428.

Knight, D. W., and Yu, G. (1995). "A geometric model for self formed channels in uniform sand." *Hydra 2000, Proc., 26th IAHR Congr.*, Vol. 1, International Association of Hydraulic Research, Madrid, 345–359.

Knight, D. W., Yuen, K. W. H., and Alhamid, A. A. I. (1994). "Boundary shear stress distributions in open channel flow." *Mixing and transport in the environment*, K. Beven, P. Chatwin, and J. Millbank, eds., Wiley, Chichester, U.K., 51–87.

Knox, J. C. (1983). "Responses of river systems to Holocene climates." *Last quaternary environments of the United States*, H. E. Wright, ed., Univ. of Minnesota Press, Minneapolis, Minn., 26–41.

Kovacs, A. E. (1992). "Time development of straight self-formed channels in non-cohesive material." PhD thesis, Univ. of Minnesota, Minneapolis.

Kovacs, A., and Parker, G. (1994). "A new vectorial bedload formulation and its application to the time evolution of straight river channels." *Journal of Fluid Mechanics*, 267, 153–183.

Kranenburg, J. C., and Winterwerp, C. (1997). "Erosion of fluid mud layers. I: Entrainment model." *Journal of Hydraulic Engineering, ASCE*, 123(6), 504–511.

Lacey, G. (1920). "Stable channels in alluvium." *Proceedings, Institute of Civil Engineers*, 229, 259–292.

Lane, E. W. (1955). "Design of stable channels." *Transactions of the ASCE*, 120, 1234–1260.

Laurenson, E. M. (1986). "Friction slope averaging." *Journal of Hydraulic Engineering, ASCE*, 112(12), 1151–1163.

Lawler, D. M. (1986). "River bank erosion and the influence of frost: A statistical analysis." *Transactions of the Institute of British Geographers*, NS11, 227–242.

Lawler, D. M. (1992). "Process dominance in bank erosion systems." *Lowland floodplain rivers: Geomorphological perspectives*, P. A. Carling and G. E. Petts, eds., Wiley, Chichester, U.K., 117–143.

Lawler, D. M. (1993a). "The measurement of river bank erosion and lateral channel change: A review." *Earth Surface Processes and Landforms*, 18, 777–821.

Lawler, D. M. (1993b). "Needle ice processes and sediment mobilization on river banks: the River Ilston, West Glamorgan, U.K." *Journal of Hydrology*, 150, 81–114.

Leopold, L. B. (1968). "Hydrology for urban land planning: A guidebook on the hydrologic effects of urban land use." *Circular 554*, U.S. Geological Survey, Washington, D.C., 18.

Leopold, L. B., and Maddock, T., Jr. (1953). "The hydraulic geometry of stream channels and some physiographic implications." *Professional Paper 252*, U.S. Geological Survey, 57.

Leopold, L. B., and Wolman, M. G. (1957). "River channel patterns—Braided, meandering and straight." *Professional Paper 282B*, U.S. Geological Survey, Reston, Va.

Leopold, L. B., Wolman, M. G., and Miller, J. P. (1964). *Fluvial processes in geomorphology*. Freeman, San Francisco, 522.

Li, L., and Wang, S. S. Y. (1993). "Numerical modeling of alluvial stream bank erosion." *Advances in hydro-science and engineering*, S. S. Y. Wang, ed., University of Mississippi, Oxford, Miss., 1, 2085–2090.

Li, L., and Wang, S. S. Y. (1994a). "Computational simulation of channel bank erosion and retreat." *Tech. Rep.*, CCHE, Univ. of Mississippi, Oxford, Miss.

Li, L., and Wang, S. S. Y. (1994b). "Numerical modeling of alluvial stream bank erosion." *Advances in hydro-science and engineering*, S. S. Y. Wang, ed., University of Mississippi, Oxford, Miss., 1, 2085–2090.

Liggett, J. A., Chiu, C. L., and Miao, L. S. (1965). "Secondary currents in a corner." *Journal of the Hydraulics Division, ASCE*, 91(6), 99–117.

Lindley, E. S. (1919). "Regime channels." *Proc., Punjab Engrg. Congr.*, Vol. 7.

Little, W. C., Thorne, C. R., and Murphey, J. B. (1982). "Mass bank failure analysis of selected Yazoo basin streams." *Transactions, ASAE*, 25(5), 1321–1328.

Lohnes, R., and Handy, R. L. (1968). "Slope angles in friable loess." *Journal of Geology*, 76, 247–258.

Lundgren, H., and Jonsson, I. G. (1964). "Shear and velocity distribution in shallow channels." *Journal of the Hydraulics Division, ASCE*, 90(1), 1–21.

Mackin, J. H. (1948). "Concept of the graded river." *Geological Society of America Bulletin*, 59, 463–512.

Madej, M. A. (1977). "Changes of a stream channel in response to an increase in sediment load." *Geological Society of America Abstracts with Programs*, 9, 1081.

Maynord, S. T. (1996). "Toe scour estimation in stabilized bendways." *Journal of Hydraulic Engineering, ASCE*, 122(8), 460–464.

McBean, E., and Perkins, F. (1975). "Numerical errors in water profile computation." *Journal of the Hydraulics Division, ASCE*, 101(11), 1389–1403.

Melling, A., and Whitelaw, J. H. (1976). "Turbulent flow in a rectangular duct." *Journal of Fluid Mechanics*, 78(2), 289–315.

Meyer, L., and Rehme, K. (1994). "Large scale turbulence phenomena in compound rectangular channels." *Experimental Thermal and Fluid Science*, 8, 286–304.

Meyer-Peter, E., and Muller, R. (1948). "Formulas for bed load transport." *Proc., 2nd Congr. of the Int. Assn. for Hydr. Res.*, 39–64.

Millar, R. G., and Quick, M. C. (1997). "Discussion of 'Development and testing of a riverbank-stability analysis,' by S. E. Darby, and C. R. Thorne." *Journal of Hydraulic Engineering, ASCE*, 123(11), 1051.

Molinas, A., and Yang, C. T. (1986). *Computer program user's manual for GSTARS (generalized stream tube model for alluvial river simulation)*, U.S. Dept. Interior, Bureau of Reclamation, Engrg. and Res. Ctr., Denver.

Moody, J.A., Pizzuto, J. E., and Meade, R. H. (1999) "Ontogeny of a flood plain." *Geological Society of America Bulletin*, 111: 291–303.

Morgenstern, N., and Price, V. E. (1965). "The analysis of the stability of general slip surfaces." *Géotechnique*, 15, 79–93.

Mosselman, E. (1991). "Modeling of river morphology with non-orthogonal horizontal curvilinear coordinates." *Communications on Hydr. and Geotech. Engrg., No. 89-3*, Delft Univ. of Technol., Delft, The Netherlands.

Mosselman, E. (1992). "Mathematical Modeling of Morphological Processes in Rivers with Erodible Cohesive Banks." PhD thesis, Delft University of Technology, Delft, The Netherlands.

Murgertroyd, A. L., and Ternan, J. L. (1983). "The impact of afforestation on stream bank erosion and channel form." *Earth Surface Processes and Landforms*, 8, 357–370.

Nadler, C. T., and Schumm, S. A. (1981). "Metamorphosis of South Platte and Arkansas Rivers, eastern Colorado." *Physical Geography*, 2, 95–115.

Nagata, N., Hosoda, T., and Muramoto, Y. (2000). "Numerical analysis of river channel processes with bank erosion." *Journal of Hydraulic Engineering*, 126: 243–252.

Nanson, G. C. (1980) "Point bar and floodplain formation of the meandering Beatton River, northeastern British Columbia, Canada." *Sedimentology*, 27: 3–29.

Nanson, G. C., and Hickin, E. J. (1983). "Channel migration and incision on the Beatton River." *Journal of Hydraulic Engineering, ASCE*, 109, 327–337.

Naot, D., and Rodi, W. (1982). "Calculation of secondary currents in channel flow." *Journal of the Hydraulics Division, ASCE*, 108(8), 948–968.

Nece, R. E., and Smith, J. D. (1970). "Boundary shear stress in rivers and estuaries." *Journal of the Waterway, Harbor and Coast Division, ASCE*, 96(2), 335–358.

Nelson, J. M., and Smith, J. D. (1989a). "Flow in meandering channels with natural topography." *Water Res. Monograph No. 12*, American Geophysical Union, Washington, D.C., 69–102.

Nelson, J. M., and Smith, J. D., (1989b). "Evolution and stability of erodible channel beds." *Water Resources Monograph No. 12*, American Geophysical Union, Washington, D.C., 321–378.

Nezu, I. (1993). "Turbulent structures and the related environment in various water flows." *Scientific research activities, Dept. of Civ. and Global Envir. Engrg.*, Kyoto Univ., Kyoto, Japan, 1–140.

Nezu, I., and Nakagawa, H. (1993). *Turbulence in open-channel flow*. IAHR Monograph, Balkema, Rotterdam, The Netherlands, 1–281.

Olesen, K. W. (1987). "Bed topography in shallow river bends." *Communications on Hydr. and Geotech. Engrg., No. 87-1*, Delft Univ. of Technol., Delft, The Netherlands.

Osman, A. M. (1985). "Channel width response to changes in flow hydraulics and sediment load." PhD thesis, Colorado State University, Fort Collins, Colo.

Osman, A. M., and Thorne, C. R. (1988). "Riverbank stability analysis. I: Theory." *Journal of Hydraulic Engineering, ASCE*, 114, 134–150.

Osterkamp, W. R., and Costa, J. E. (1987). "Changes accompanying an extraordinary flood on a sand-bed stream." *Catastrophic flooding*, L. Mayer and D. Nash, eds., Allen and Unwin, Boston, 201–224.

Parchure, T. M., and Mehta, A. J. (1985). "Erosion of soft cohesive sediment deposits." *Journal of Hydraulic Engineering, ASCE*, 111(10), 1308–1326.

Parker, G. (1978a). "Self-formed straight rivers with equilibrium banks and mobile bed. 1: The sand-silt river." *Journal of Fluid Mechanics*, 89(1), 109–125.

Parker, G. (1978b) "Self-formed straight rivers with equilibrium banks and mobile bed: 2, The gravel river." *Journal of Fluid Mechanics*, 89: 127–146.

Parker, G. (1979). "Hydraulic geometry of active gravel rivers." *Journal of the Hydraulics Division, ASCE*, 105(9), 1185–1201.

Parker, G. (1983). "Discussion of 'Lateral bed load transport on side slopes' by S. Ikeda." *Journal of Hydraulic Engineering, ASCE*, 109, 197–199.

Parker, G. (1995). "Gravel-bed channel instability." *Issues and directions in hydr: An Iowa Hydr. Colloquium in honor of Prof. John F. Kennedy*, R. Ettema and I. Nakato, eds., Iowa Inst. of Hydr. Res., Iowa City, Iowa.

Parker, G., Klingeman, P. C., and McLean, D. G. (1982). "Bedload and size distribution in paved gravel-bed streams." *Journal of the Hydraulics Division, ASCE*, 108(4), 544–571.

Parker, G., and Kovacs, A. (1993). "MYNORCA: A Pascal program for implementing the Kovacs-Parker vectorial bedload transport relation on arbitrarily sloping beds." *Tech. Memo. No. M-233*, St. Anthony Falls Hydr. Lab., Minneapolis.

Parola, A. C., and Hagerty, D. J. (1993). "Highway bridge failure due to foundation scour and instability." *Proc., 42nd Annu. Hwy. Geol. Symp.*, R. H. Fickies, ed, Highway Geology Symposium, 151–168, available at http://www.highwaygeologysymposium.org/uploads/pastmeetings/hgs%2042.pdf.

Partheniades, E., and Passwell, R. E. (1970). "Erodibility of channels with cohesive boundaries." *Journal of the Hydraulics Division, ASCE*, 96(3), 755–771.

Patton, P. C., and Schumm, S. A. (1975). "Gully erosion in northern Colorado: A threshold phenomenon." *Geology*, 3, 88–90.

Peck, R. B., and Deere, D. U. (1958). "Stability of cuts in fine sands and varved clays." *Proceedings, American Railway Engineers' Association*, 59, 807–815.

Perkins, H. J. (1970). "The formation of streamwise vorticity in turbulent flow." *Journal of Fluid Mechanics*, 44(4), 721–740.

Pizzuto, J. E. (1984) "Equilibrium bank geometry and the width of shallow sand-bed streams." *Earth Surface Processes and Landforms*, 9, 199–207.

Pizzuto, J. E. (1990). "Numerical simulation of gravel river widening." *Water Resources Research*, 26, 1971–1980.

Pizzuto, J. E. (1994). "Channel adjustments to changing discharges, Powder River, Montana." *Geological Society of America Bulletin*, 106, 1494–1501.

Pizzuto, J. E., and Meckelnburg, T. S. (1989) "Evaluation of a linear bank erosion equation." *Water Resources Research*, 25, 1005–1013.

Poulos, S. J., Castro, G., and France, J. W. (1985). "Liquefaction evaluation procedures." *Journal of Geotechnical Engineering, ASCE*, 111(6), 772–792.

Rahuel, J. L., Holly, F. M., Belleudy, P. J., and Yang, G. (1989). "Modeling of riverbed evolution for bedload sediment mixtures." *Journal of Hydraulic Engineering, ASCE*, 115, 1521–1542.

Raudkivi, A. J. (1995). "Fundamentals of sediment transport." *Issues and directions in hydr.: An Iowa Hydr. Colloquium in honor of Prof. John F. Kennedy*, R. Ettema and I. Nakato, eds., Iowa Inst. of Hydr. Res., Iowa City, Iowa, 1–9.

Rhodes, D. G., and Knight, D. W. (1994). "Distribution of shear force on boundary of smooth rectangular duct." *Journal of Hydraulic Engineering*, 120(7), 787–807.

Richardson, E. V., Simons, D. B., and Julien, P. Y. (1990). "Highways in the river environment." *Rep. No. FHWA-HI-90-016*, Dept. of Transp., Nat. Tech. Information Service, Springfield, Va.

Rinaldi, M., and Casagli, N. (1999) "Stability of streambanks formed in partially saturated soils and effects of negative pore water pressures: the Sieve River (Italy)." *Geomorphology* 26: 253–277.

Ritter, D. F. (1978). *Process geomorphology*. Wm. C. Brown, Dubuque, Iowa.

Rodi, W. (1980). *Turbulence models and their application in hydraulics*. Int. Assn. for Hydr. Res. (IAHR), Delft, The Netherlands, 1–104.

Samuels, P. G. (1989). "Backwater length in rivers." *Proceedings, Institute of Civil Engineers, Part 2, Research and theory*, 87, 571–582.

Samuels, P. G. (1990). "Cross section location in 1-d models." *River flood hydraulics*, W. R. White, ed., Wiley, Chichester, U.K., 339–348.

Schumm, S. A. (1968). "River adjustment to altered hydrologic regime, Murrumbidgee River and paleochannels, Australia." *Professional Paper 598*, U.S. Geological Survey, Reston, Va., 65.

Schumm, S. A., Harvey, M. D., and Watson, C. C. (1984). *Incised channels: Morphology, dynamics, and control*. Water Resources Publications, Littleton, Colo., 200.

Schumm, S. A., and Lichty, R. W. (1963). "Channel widening and floodplain construction along Cimmaron River in southwestern Kansas." *Professional Paper 598*, U.S. Geological Survey, 65.

Schumm, S. A., and Lichty, R. W. (1965). "Time, space and causality, in geomorphology." *American Journal of Science*, 263, 110–119.

Schumm, S. A., and Winkley, B. R. (1994). *The variability of large alluvial rivers*, ASCE, New York, 467.

Sellin, R. H. J., Ervine, D. A., and Willetts, B. B. (1993). "Behavior of meandering two-stage channels." *Proc., Instn. Civ. Engrs. Water Maritime and Energy*, 101, 99–111.

Shaikh, A., Ruff, J. F., and Abt, S. R. (1988a). "Erosion rates of compacted montmorillonite soils." *Journal of Geotechnical Engineering, ASCE*, 114(3), 296–305.

Shaikh, A., Ruff, J. F., Charlie, W. A., and Abt, S. R. (1988b). "Erosion rates of dispursive and non-dispursive clays." *Journal of Geotechnical Engineering, ASCE*, 114(5), 589–600.

Shiono, K., and Knight, D. W. (1988). "Two dimensional analytical solution for a compound channel." *Proc., 3rd Int. Symp. on Refined Flow Modeling and Turbulence Measurements*, 503–510.

Shiono, K., and Knight, D. W. (1990). "Mathematical models of flow in two or multi-stage straight channels." *River flood hydraulics*, W. R. White, ed., Wiley, Chichester, U.K., 229–238.

Shiono, K., and Knight, D. W. (1991). "Turbulent open channel flows with variable depth across the channel." *Journal of Fluid Mechanics*, 222, 617–646.

Shiono, K., and Muto, Y. (1993). "Secondary flow structure for in-bank and over-bank flows in trapezoidal meandering compound channel." *Proc., 5th Int. Symp. on Refined Flow Modeling and Turbulence Measurements*, 645–652.

Simon, A. (1989). "A model of channel response in disturbed alluvial channels." *Earth Surface Processes and Landforms,* 14, 11–26.

Simon, A. (1992). "Energy, time, and channel evolution in catastrophically disturbed fluvial systems." *Geomorphology*, 5, 345–372.

Simon, A., Curini, A., Darby, S. E., and Langendoen, E. J. (2000) "Bank and near-bank processes in an incised channel." *Geomorphology*, 35: 193–217.

Simon, A., and Downs, P. W. (1995). "An interdisciplinary approach to evaluation of potential instability in alluvial channels." *Geomorphology*, 12(3), 215–232.

Simon, A., and Hupp, C. R. (1992). "Geomorphic and vegetative recovery processes along modified stream channels of West Tennessee." *Open File Rep. No. 91-502*, U.S. Geological Survey, Washington, D.C.

Simon, A., and Thorne, C. R. (1996). "Channel adjustment of an unstable coarse-grained stream: Opposing trends of boundary and critical shear stress, and the applicability of extremal hypotheses." *Earth Surface Processes and Landforms*, 21, 155–180.

Simon, A., Wolfe, W. J., and Molinas, A. (1991). "Mass wasting algorithms in an alluvial channel model." *Proc., 5th Fed. Interagency Sedimentation Conf.*, U.S. Government Printing Office, Washington, D.C., 8-22–8-29.

Simons, D. B., and Albertson, M. (1963). "Uniform water conveyance channels in alluvial material." *Transactions of the ASCE*, 128(1), 65–167.

Simons, D. B., and Senturk, F. (1992). *Sediment transport technology*. Water Resources Publications, Littleton, Colo., 919.

Smerdon, E. T., and Beasley, R. P. (1961). "Critical tractive forces in cohesive soils." *Agricultural Engineering*, 42, 26–29.

Smith, D. G. (1976). "Effects of vegetation on lateral migration of anastomosed channels of a glacial meltwater." *Geological Society of America Bulletin*, 87, 857–869.

Smith, J. D., and McLean, S. R. (1984) "A model for flow in meandering streams." *Water Resources Research*, 20, 1301–1315.

Smith, N. D., and Smith, D. G. (1984). "William River: An outstanding example of channel widening and braiding caused by bed-load addition." *Geology*, 12, 78–82.

Spencer, E. (1967). "A method of analysis of the stability of embankments assuming parallel inter-slice forces." *Géotechnique*, 15, 11–26.

Springer, F. M., Jr., Ullrich, C. R., and Hagerty, D. J. (1985). "An analysis of streambank stability." *Journal of Geotechnical Engineering, ASCE*, 111(5), 624–640.

Stevens, M. A., Simons, D. B., and Richardson, E. V. (1975). "Nonequilibrium river form." *Journal of the Hydraulics Division, ASCE*, 101, 557–566.

Strickler, A. (1923). "Beitrage zur frage der geschwindigheits-formel und der rauhigkeitszahlen fur strome, kanale und geschlossene leitungen." *Mitteilungen des eidgenossicher amtes fur wasserwirtschaft*, Bern, Switzerland, 16g (in German).

Struiksma, N., Olesen, K. W., Flokstra, C., and de Vriend, H. J. (1985). "Bed deformation in curved alluvial channels." *Journal of Hydraulic Research*, 23, 57–79.

Sun, T., Meakin, P., Jossang, T., and Schwarz, K. (1996) "A simulation model for meandering rivers." *Water Resources Research*, 32, 2937–2954.

Sundborg, A. (1956) "The River Klaralven, a study of fluvial processes." *Geographiska Annaler*, 38, 127–316.

Talmon, A. M. (1992). "Bed topography of river bends with suspended sediment transport." *Communications on Hydr. and Geotech. Engrg., No. 92-5*, Delft Univ. of Technol., Delft, The Netherlands.

Taylor, G., and Woodyer, K. D. (1978). "Bank deposition in suspended-load streams." *Fluvial sedimentology*, A. D. Miall, ed., Can. Soc. Petroleum Geologists, Calgary, Alta., Canada, 257–275.

Tehrani, M. M. (1992). "Spatial distribution and scaling of bursting events in boundary layer turbulence over smooth and rough surfaces." PhD thesis, Dept. of Civ. and Envir. Engrg., University College, London.

Terzaghi, K., and Peck, R. B. (1967). *Soil mechanics and engineering practice*, Wiley, New York, 729.

Thomas, T. G., and Williams, J. J. R. (1995). "Large eddy simulation of turbulent flow in an asymmetric compound open channel." *Journal of Hydraulic Research, ASCE*, 33(1), 27–41.

Thorne, C. R. (1982). "Processes and mechanisms of river bank erosion." *Gravel-bed rivers*, R. D. Hey, J. C. Bathurst, and C. R. Thorne, eds., Wiley, Chichester, U.K., 227–271.

Thorne, C. R. (1992). "Field assessment techniques for bank erosion modelling." *Final Rep., to U.S. Army Eur. Res. Ofc., Contract No. R&D 6560-EN-09*, Dept. of Geography, Univ. of Nottingham, Nottingham, England.

Thorne, C. R., Amarasinghe, I., Gardiner, J. L., Gardiner, C., and Sellin, R. (1997). "Bank protection using vegetation with special reference to the use of willows." *Rep.*, Engrg. and Phys. Sci. Res. Council, Univ. of Nottingham, Nottingham, U.K., 85.

Thorne, C. R., Maynord, S. T., and Abt, S. R. (1995). "Prediction of near-bank velocity and scour depth in meander bends for design of riprap revetments." *River, coastal and shoreline protection: Erosion control using riprap and armourstone*, C. R. Thorne, S. R. Abt, S. T. Maynord, K. Pilarcyzk, and F. Barends, eds., Wiley, Chichester, U.K., 115–136.

Thorne, C. R., Murphey, J. B., and Little, W. C. (1981a). "Stream channel stability Appendix D: Bank stability and bank material properties in the bluffline streams of north-west Mississippi." *Rep. to U.S. Army Corps of Engrs.*, Vicksburg District, Vicksburg, Miss.

Thorne, C. R., Murphy, J. B., and Little, W. C. (1981b). "Bank stability and bank material properties in the bluffline streams of North-west Mississippi." *Appendix D, Rep. to the U.S. Army Corps of Engrs.*, Vicksburg Dist. under Sect. 32 Program, Work Unit 7, USDA-ARS Sedimentation Lab., Oxford, Miss., 258.

Thorne, C. R., and Osman, A. M. (1988a). "Riverbank stability analysis. II: Applications." *Journal of Hydraulic Engineering*, 114(2), 151–172.

Thorne, C. R., and Osman, A. M. (1988b). "The influence of bank stability on regime geometry of natural channels." *River regime*, W. R. White, ed., Wiley, Chichester, U.K., 135–147.

Thorne, C. R., Russell, A. P. G., and Alam, M. K. (1993). "Planform pattern and channel evolution of the Brahmaputra River, Bangladesh." *Braided rivers*, J. L. Best and C. S. Bristow, eds., Spec. Publ. No. 75, Geological Society of London, 257–276.

Thorne, C. R., and Tovey, N. K. (1981). "Stability of composite river banks." *Earth Surface Processes and Landforms*, 6, 469–484.

Tominaga, A., and Nezu, I. (1991). "Turbulent structure in compound open channel flows." *Journal of Hydraulic Engineering, ASCE*, 117(1), 21-41.

Tominaga, A., and Nezu, I. (1993). "Flows in compound channels." *Journal of Hydroscience and Hydraulic Engineering*, JSCE Special Issue S1-2, Fluvial hydraulics, 121–140.

Tracy, H. J. (1965). "Turbulent flow in a three-dimensional channel." *Journal of the Hydraulics Division, ASCE*, 91(6), 9–35.

Ullrich, C. R., Hagerty, D. J., and Holmberg, R. W. (1986). "Surficial failures of alluvial stream banks." *Canadian Geotechnical Journal*, Ottowa, Canada, 23, 304–316.

U.S. Army Corps of Engineers (USACE). (1981). " Missouri River degradation, Volume IV." *Supporting technical report,* Omaha Dist., Dept. of the Army, Omaha, Nebr.

Vanoni, V. A. (1975). "Sedimentation engineering." *Manuals and Rep. on Engrg. Practice No. 54*, ASCE, New York, 745.

Van Rijn, L. C. (1984). "Sediment transport. Part III: Bed forms and alluvial roughness." *Journal of Hydraulic Engineering, ASCE*, 110(12), 1733–1754.

Vaughan, P. R., and Walbancke, H. J. (1973). "Pore pressure changes and the delayed failure of cutting slopes in overconsolidated clay." *Géotechnique*, 23(4), 531–539.

Vigilar, G. G., and Diplas, P. (1994). "Determination of geometry and stress distribution of an optimal channel." *Proc., Hydr. Engrg. '94*, G. V. Cotreano and R. R. Rumer, eds., ASCE, New York, 959–968.

Vigilar, G. G., and Diplas, P. (1997). "Stable channels with mobile bed: Formulation and numerical solution." *Journal of Hydraulic Engineering, ASCE*, 123(3), 189–199.

Vigilar, G. G., and Diplas, P. (1998) "Stable channels with mobile bed: model verification and graphical solution." *Journal of Hydraulic Engineering*, 124, 1097–1108.

Waldron, L. J. (1977). "Shear resistance of root permeated homogeneous and stratified soil." *Soil Science Society of America Journal*, 41, 843–849.

Wang, S. S. Y., and Hu, K. K. (1990). "Improved methodology for formulating finite element hydrodynamic models." *Finite Elements in Fluids*, 8.

Wargadalam, J. (1993). "Hydraulic geometry equations of alluvial channels." PhD dissertation, Colorado State University, Fort Collins, Colo.

Wark, J. B., James, C. S., and Ackers, P. (1994). "Design of straight and meandering channels." *R&D Rep. No. 13*, Nat. Rivers Authority, Bristol, U.K., 86.

Wark, J. B., Samuels, P. G., and Ervine, D. A. (1990). "A practical method of estimating velocity and discharge in a compound channel." *River flood hydraulics*, W. R. White, ed., Wiley, Chichester, U.K., 163–172.

Watson, C. C., Harvey, M. D., Biedenharn, D. S., and Combs, P. G. (1988a). "Geotechnical and hydraulic stability numbers channel rehabilitation. I. The approach." *Proc., ASCE Hydr. Div. 1988 Nat. Conf.*, S. R. Abt and J. Gessler, eds., ASCE, New York, 20–125.

Watson, C. C., Harvey, M. D., Biedenharn, D. S., and Combs, P. G. (1988b). "Geotechnical and hydraulic stability numbers for channel rehabilitation: Part II. Application." *Proc., ASCE Hydr. Div. 1988 Nat. Conf.*, S. R. Abt and J. Gessler, eds., ASCE, New York, 126–131.

White, W. R., Bettess, R., and Paris, E. (1982). "Analytical approach to river regime." *Journal of the Hydraulics Division, ASCE*, 108(10), 1179–1193.

White, W. R., Paris, E., and Bettess, R. (1981). "Tables for the design of stable alluvial channels." *Rep. No. IT 208*, HR Wallingford, Wallingford, U.K., 30.

Wiele, S. M. (1992). "A computational investigation of bank erosion and midchannel bar formation in gravel-bed rivers." PhD thesis, University of Minnesota, Minneapolis.

Wiele, S. M., and Paola, C. (1989). "Calculation of bed stress and bank erosion in a straight channel." *Eos: Transactions of the American Geophysical Union*, 70, 329–339.

Williams, G. P. (1978). "The case of the shrinking channels—The North Platte and Platte Rivers in Nebraska." *Circular 781*, Washington, D.C., U.S. Geological Survey.

Williams, G. P., and Guy, H. P. (1973). "Erosional and depositional aspects of Hurricane Camille in Virginia, 1969." *Professional Paper 804*, Washington, D.C., U.S. Geological Survey, 80.

Wolman, M. G. (1955). "The natural channel of Brandywine Creek." *Professional Paper 271*, U.S. Geological Survey, Reston, Va., 56.

Wolman, M. G. (1959). "Factors influencing erosion of cohesive river banks." *American Journal of Science*, 257, 204–216.

Wolman, M. G., and Gerson, R. (1978). "Relative scales of time and effectiveness of climate in watershed geomorphology." *Earth Surface Processes and Landforms*, 3, 189–208.

Woodyer, K. D. (1975). "Concave-bank benches on the Barwon River, New South Wales." *Australian Geographer*, 13, 36–40.

Yang, C. T. (1973). "Incipient motion and sediment transport." *Journal of the Hydraulics Division, ASCE*, 99(10), 1679–1704.

Yang, C. T. (1984). "Unit stream power equation for gravel." *Journal of Hydraulic Engineering, ASCE*, 110, 1783–1797.

Yang, C. T. (1992). "Force, energy, entropy and energy dissipation rate." *Entropy and energy dissipation in water resources*, V. P. Singh and M. J. Fiorention, eds., Kluwer Academic, Dordrecht, The Netherlands, 63–89.

Yang, C. T., Molinas, A., and Song, C. S. (1988). "GSTARS—Generalized stream tube model for alluvial river simulation." *Twelve selected computer stream sedimentation models developed in the United States*, S. Fan, ed., Federal Energy Regulatory Commission, Washington, D.C.

Yang, C. T., and Song, C. C. S. (1986). "Theory of minimum energy and energy dissipation rate." *Encyclopedia of fluid mechanics*, Gulf Publishing, Houston, 353–399.

Yang, C. T., Song, C. C. S., and Woldenberg, M. J. (1981). "Hydraulic geometry and minimum rate of energy dissipation." *Water Resources Research*, 17(4), 1014–1018.

Yang, C. T., and Wan, S. (1991). "Comparison of selected bed-material formulas." *Journal of Hydraulic Engineering, ASCE*, 117, 973–989.

Yen, B. C. (1993). *Channel flow resistance: Centennial of Manning's formula*. Water Resources Publications, Littleton, Colo.

Younis, B. A. (1996). "Modeling over-bank flow." *Floodplain processes*, M. G. Anderson, D. E. Walling, and P. D. Bates, eds., Wiley, Chichester, U.K., 299–332.

Copyrighted Materials
Copyright © 2008 American Society of Civil Engineers (ASCE)
Retrieved from www.knovel.com

CHAPTER 8

River Meandering and Channel Stability

A. Jacob Odgaard and Jorge D. Abad

8.1 INTRODUCTION

River meandering is a planform process that generates a series of bends of alternate curvature connected by straight reaches. The outer banks of the bends tend to erode, causing the channel planform to gradually shift or migrate (Fig. 1). The rate of shift depends on the properties of the surrounding material, which can vary from alluvium to rock. Depending on the surrounding material, the channel is termed either *freely meandering* or *rock incised*. Most rock-incised channels are formed by down-cutting over long periods of time (Leopold et al. 1964; Dury 1966). This chapter deals with freely meandering channels.

The planforms of freely meandering channels migrate by down-valley translation, lateral expansion, or a combination of both. Down-valley translation is essentially a longitudinal shift of the meander pattern, whereas lateral expansion is a widening of the meander pattern. This chapter presents a summary of analytical approaches to the description of this process.

The chapter starts with a brief review of historical relationships, which is then followed by a summary of recent approaches to the calculation of flow and bed topography in rivers, migration rates, and dominant meander wavelength. The chapter concludes with a brief review of technologies for channel stabilization.

The review is not inclusive. It is focused on concepts and findings that have direct bearing on river engineering practice more than on scientific discourse. As such, important contributions may have been omitted. For a more inclusive review, readers are referred to Callander (1978); Richards (1982); and Howard (1992; 1996).

8.2 MEANDERING PROCESS

It is generally assumed that meandering is the result of channel instability. This assumption implies that a straight channel is unstable and that a slight perturbation in any of its flow or boundary characteristics causes an increase in shear stress along one bank, resulting in erosion, and a decrease in shear stress along the opposite bank, promoting deposition. The result is gradual increase in channel sinuosity (ratio of channel length to valley length) with time. As the length of the channel increases, the channel slope decreases and becomes less than the valley slope.

The process of erosion and deposition results in sideways migration of the channel, which, as indicated previously, may or may not be combined with down-valley translation. Sideways migration may eventually result in a cut-off, after which the process starts over again.

Field observations have been described by, among others, Leopold and Wolman (1957); Wolman and Leopold (1957); Schumm (1963); Kondrat'yev (1968); Konditerova and Ivanov (1969); Schumn and Khan (1971, 1972); Brice (1973); Kulemina (1973); Brice (1974); Hickin (1974); Hickin and Nanson (1975); Lewin (1976); Allen (1977); Hooke (1977); Lewin and Brindle (1977); Dort (1978); Lewin (1978); Nanson (1980); Allen (1982); Beck et al. (1983b); Lewis and Lewin (1983); Nanson and Hickin (1983), Schumm (1983); Hooke (1984); Schumm (1985); Carson and Lapointe (1986); Lapointe and Carson (1986); Nanson and Hickin (1986).

The meandering process has also been demonstrated in numerous laboratory studies. An early demonstration was by Friedkin (1945). By studying the evolution of a laboratory channel from straight to meandering (Fig. 8-2), Friedkin defined some of the key variables of the process. He also made a first attempt to establish qualitative relationships between the variables.

8.2.1 Meandering Criteria

A significant amount of literature suggests that this process takes place only when certain combinations of variables are in place. Data suggest that as the channel slope becomes

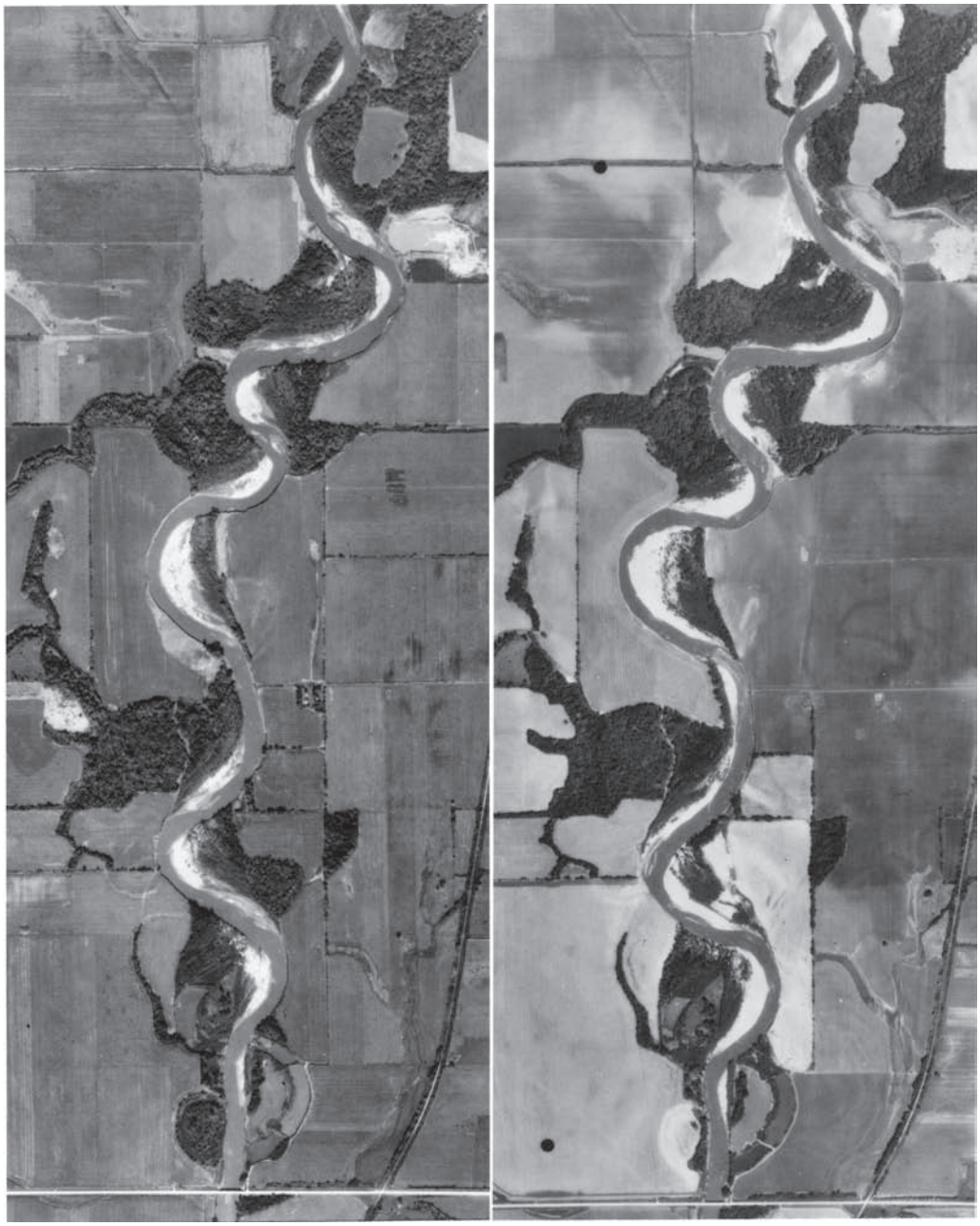

Fig. 8-1. Aerial photos of the East Nishnabotna River just south of Red Oak, Iowa: (left) October 5, 1973; (right) May 25, 1979.

steeper, there is a tendency for the river to become braided, that is, split into several channels. Leopold and Wolman (1957) analyzed data from a large number of rivers in the United States and in India and found that the threshold between the two classifications (meandering and braided) for these rivers is a function of channel slope S and bank-full discharge $Q(\mathrm{m}^3/\mathrm{s})$,

$$S = 0.012Q^{-0.44} \tag{8-1}$$

For a braided river, S is greater, and for a meandering river, it is less than the value given by Eq. (8-1). As indicated in Fig. 8-3, the data suggest that one and the same river can have both braided and meandering reaches.

Henderson (1963) attempted to refine Eq. (8-1) by accounting for the effect of size of bed material and proposed the relation

$$S = 0.0002\, D^{1.14}Q^{-0.44} \tag{8-2}$$

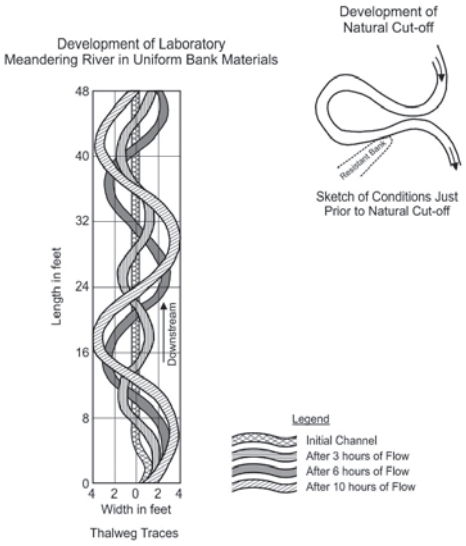

Fig. 8-2. Meandering process demonstration by Friedkin (1945).

in which D = median-particle diameter in millimeters and Q = discharge in m³/s.

Based on observations of sand-bed rivers in the United States, Lane (1957) proposed a slightly different criterion for braided and meandering rivers,

$$S = KQ^{-0.25} \tag{8-3}$$

in which K = constant. Figure 8-4 summarizes Lane's plots and shows that when $K \leq 0.0017$ English units ($K \leq 0.0007$ metric units), a sand-bed river will tend toward a meandering pattern, and when $K \geq 0.01$ (0.004 metric units), it will tend toward a braided pattern. It is noted that channel slopes for these two extremes differ by a factor of nearly 6. It is also noted that many U.S. rivers fall in between these extremes.

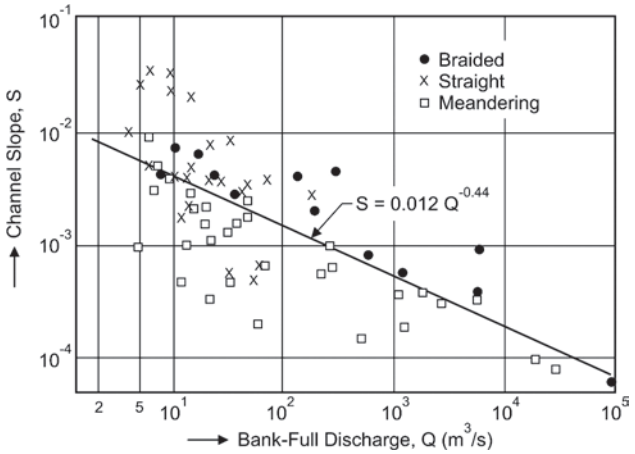

Fig. 8-3. Threshold between meandering and braided channels (Leopold and Wolman 1957).

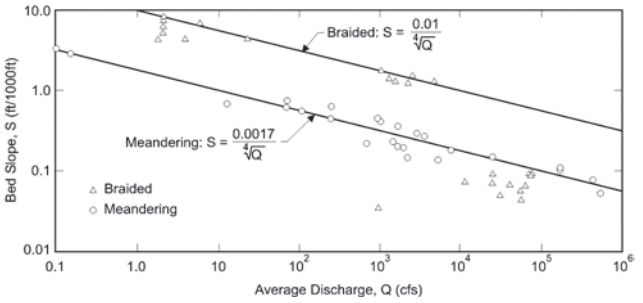

Fig. 8-4. Slope-discharge relationships in meandering and braided sand-bed streams (after Lane 1957).

Recently Millar (2000) showed that bank vegetation influences channel patterns and that the meandering-braiding transition slope increases with the erosional resistance of the banks. Millar's relation, which is based on theoretical analysis and curve fitting, using data from 137 rivers, reads as

$$S = 0.0002\, D^{0.61}\, \phi^{1.75}\, Q^{-0.25} \tag{8-4}$$

where

D = median sediment diameter for the banks and bed surface (meters);
ϕ = bank sediment friction angle (degrees); and
Q = bank-full discharge ($m^3 s^{-1}$).

With no vegetation on the bank, ϕ is the angle of repose for noncohesive bank sediment, which for coarse gravel is up to 40°. As vegetation increases, ϕ increases. Millar states that ϕ represents a lumped calibration parameter that probably accounts for several different processes, including reduction of near-bank velocity and shear stress, binding of the bank sediment by root networks, packing and imbrication, and cementing of the gravel clasts by interstitial fines.

These relations are just a few of the many criteria for meandering that have been proposed over the years (for a more complete summary, see Bridge 1993). Although they have been, and are still being, challenged by engineers and scientists, the relations offer some guidance to river engineers.

8.2.2 Meander Planform

Measurements of the dimensions of meander patterns suggest that there are relations between certain planform characteristics that are relatively consistent for a wide range of stream sizes. The planform characteristics, defined in Fig. 8-5, are wavelength λ, amplitude A, bank-full channel width b, and minimum radius of curvature r_c. Leopold and Wolman (1960) have suggested the following relationships between these variables:

$$\mathrm{L} = 11.0 b^{1.01} \tag{8-5}$$

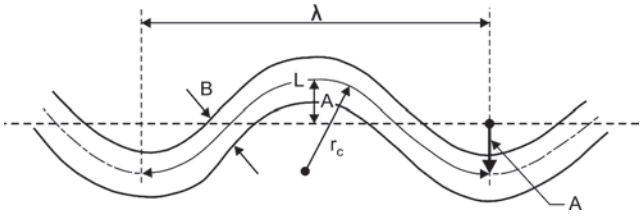

Fig. 8-5. Meander planform characteristics.

$$A = 3.0b^{1.1} \tag{8-6}$$

$$\lambda = 4.6 r_c^{0.98} \tag{8-7}$$

All dimensions are in meters. These relationships imply that $r_c \approx 2.4\ b$. Leopold et al. (1964) and Zeller (1967) later confirmed these relationships in a comprehensive data analysis that included furrow meanders, meanders in glacier ice, and meanders of the Gulf Stream.

A number of theories have been proposed to explain the observed regularity of plan form. They include theories based on optimization concepts such as minimum energy dissipation and minimum variance (Langbein and Leopold 1966; Chang 1979; 1984; 1988b). For a review of these theories, readers are referred to Chang (1988a).

The consistency of these relations may suggest that the meandering process, as described in Section 8.2, is a transitional (transient) process that, as sinuosity increases, tends toward some form of planform equilibrium or order, which is disrupted only during extreme events when cutoffs occur.

The notion of a time-limited equilibrium or order has been promoted in recent studies that attempt to simulate meandering through chaotic dynamics and self-organization. These simulations show the meandering process as oscillating in space and time between a state in which the river planform is ordered and one in which it is chaotic (Stølum 1996; 1997; 1998).

8.2.3 Meander Migration—Bank Erosion

As indicated in the Introduction, the planforms of meanders tend to migrate. The aforementioned relations do not predict rate and direction of migration. Specific migration relations have been developed by, among others, Hickin (1974); Hickin and Nanson (1975); Hooke (1980); Brice (1982); Nanson and Hickin (1983). Their relations are in the form of measured correlations between rates of bank retreat and width or width-radius ratio.

Brice demonstrated that the rate of bank retreat increases with increasing channel width. His data consist of 43 data points from four different stream types (equiwidth, wide bend, braided point bar, braided) with rates ranging from 0.1 m/year on a 10-m-wide channel to about 9 m/year on a 600-m-wide channel. The approximate relationship is mean erosion rate in meters per year = 0.01 times channel width in meters.

An increase in erosion rate with channel width is also indicated indirectly in Hooke's (1980) data. Her plot of erosion rates versus drainage area for 11 streams in Devon, England, and 43 streams compiled from the literature covers rates from 0.05 m/year for a drainage area of 3 km to 800 m/year for a drainage area of 1 million km^2. The approximate relationship is mean erosion rate in meters per year = 0.05 times square root of drainage area in square kilometers.

Hickin and Nanson (1975) and Nanson and Hickin (1983) demonstrated that channel curvature plays an important role in determining the rate of bank retreat. They used the technique of dendrochronology to determine the relative ages of scroll bars on the floodplain of the Beatton River, Canada, and they correlated local migration rate with local radius-width ratio. Their data (Nanson and Hickin 1983) conform, approximately, to the relation

$$\begin{aligned} v_e\ (m/\text{year}) &= 2.0\ b/r_c \quad b/r_c \le 0.3 \\ v_e\ (m/\text{year}) &= 0.2\ r_c/b \quad b/r_c \ge 0.3 \end{aligned} \tag{8-8}$$

in which *ve* is the erosion rate, b is the channel width, and r_c is the radius of curvature of the channel.

Ikeda et al. (1981), in their theory of river meanders, assume that the rate of bank retreat v_e is proportional to the difference between near-bank depth-averaged mean velocity u_b and the reach-averaged mean velocity u at bank-full discharge,

$$v = E\left(u_b - u\right) = Eu_b' \tag{8-9}$$

in which E = parameter describing the erodibility of the bank material and u_b' = near-bank velocity increment. This relationship is based on the assumption that soil particles on the bank are eroded and removed by the flow whenever the near-bank velocity exceeds the reach-averaged velocity. Field data support the assumption of a linear relationship between erosion rate and near-bank velocity increment (Odgaard 1987; Hasagawa 1989; Pizzuto and Meckelnburg 1989).

By determining u_b using Engelund's (1974) second approximation, Parker (1983) and Parker and Andrews (1986) developed a convolutional relation between migration rate and curvature. For developed bend flow in a constant-radius curve, their relation reduces to

$$\frac{v_e}{r} = EA\frac{u}{b} \tag{8-10}$$

in which A is "an order-one scour factor parameterizing the role of secondary currents" (Parker 1983, p. 727). Equation (8-10) supports Hickin and Nanson's (1975) notion that the rate of channel migration is a function of width-radius ratio. Odgaard (1987) used Eq. (8-10) for analysis of stream bank erosion along rivers in Iowa.

A convolutional relationship between migration rate and curvature has also been suggested by Howard and Knutson (1984) and Furbish (1988; 1991) and has been used in several simulation models. A convolutional relationship is often

appropriate because it allows the migration rate at a given point to depend not only on the local channel curvature but also on the upstream curvatures. The merits of a convolutional model have been discussed and demonstrated by Furbish (1991), among others.

Odgaard (1989a) has suggested that erosion rate may also be related to increase in scour depth at the bank,

$$\frac{v_e}{u} = E' \frac{d_b'}{d} \tag{8-11}$$

in which $d_b' = d_b - d$ = near-bank depth increment. The rationale behind this relation is that as the height of the outer bank increases, the stability of the bank decreases, which is indicated by the analyses of Osman and Thorne (1988) and Thorne and Osman (1988). Hasegawa also includes near-bank depth increment as a factor in determining the rate of bank migration; however, in his equation, the effect is negative under certain conditions. Howard (1992) has suggested that the migration rate may be related to both u_b' and d_b' Such a relationship may read

$$\frac{v_e}{u} = E'' \left(C_1 \frac{u_b'}{u} + C_2 \frac{d_b'}{d} \right) \tag{8-12}$$

in which C_1 and C_2 are weighting factors. The value of C_1 is positive, whereas C_2 may be positive, negative, or zero.

The mechanism of bank failure varies from river to river and there are cases where none of the aforementioned relationships come even close to a description of it. For example, bank failure by piping and sapping (Hagerty 1991a; 1991b), which occurs along many rivers in the midwestern states of the United States, may have little or no relationship to stream-flow variables. The same applies to bank failure triggered by vegetative growth or climate-influenced deterioration (weathering) of the bank material. A more extended description of these mechanisms can be found in ASCE (1998); Langendoen (2000); and in chapter 7 of this volume. Lawler et al. also describe bank erosion measurement techniques that are under development, including a photo-electronic erosion pin (PEEP) automatic erosion and deposition monitoring system.

8.3 FLOW AND BED TOPOGRAPHY IN MEANDERS

It is the dynamics of the flow in the river, in particular in bends, that determines whether the bends migrate sideways or down-valley or both.

As the flow enters a bend, the centrifugal acceleration drives the faster-moving surface current toward the outer bank and the flow near the bed toward the inner bank (secondary current). The result is a spiraling flow that produces greater depths and higher velocities near the outer bank. The channel-deepening undermines the bank, and the higher velocity and shear stress attack it, setting the stage for bank erosion. Near the inner bank a point bar tends to form. Thomson (1876) may have been the first to suggest that this is the process that causes rivers to meander. His qualitative description of the bend flow has remained unchallenged.

There are other features of flow and bed topography in meander curves that also must be recognized. As a result of the secondary current, pressure builds along the outer bank, causing the water surface to rise or superelevate (Thomson 1876; Ippen and Drinker 1962; Yen 1965; Yen and Yen 1971). In sharp curves of the river there is a tendency for flow to separate at the point bar (Dietrich and Whiting 1989; Kawai and Julien 1996; Hodskinson and Ferguson 1998; Ferguson et al. 2003). In fact, the sharper the curve the more complex are the secondary currents and boundary shear stresses (Hey and Thorne 1975; Bathurst et al. 1979; Cheng and Shen 1983; Allen 1985; Thorne et al. 1985; Hey and Rainbird 1996; Blanckaert and Graf 2001; Blanckaert 2003). The complexity of flow is also reflected in the sediment transport. A sorting of bed sediment often occurs (Parker and Andrews 1985; Ikeda 1989; Bridge 1992; Yen and Lee 1995; Julien and Anthony 2002). Readers are referred to Chapter 3 for more details about sediment transport of mixtures.

Because, as indicated in the previous section, the rate of bank erosion may be closely related to near-bank depth and velocity, many attempts have been made over the years to relate these variables to mean-flow properties (Thomson 1879; van Bendegom 1947; Rozovskii 1957; Yen1965; Yen 1970; Yen and Yen 1971; Apmann 1972; Yen 1972; Engelund 1974; Ikeda 1974; Engelund 1975; Hooke 1975; Ikeda 1975; Yen 1975; Bridge 1976; Bridge and Jarvis 1976; Gottlieb 1976; Kikkawa et al. 1976; Bridge 1977; Bridge and Jarvis 1977; DeVriend 1977; Allen 1978; Zimmermann and Kennedy 1978; Dietrichet al. 1979; Begin 1981; Odgaard 1981; Bridge and Jarvis 1982; DeVriend and Geldof 1983; Dietrich and Smith 1983; Falcon and Kennedy 1983; Geldof and DeVriend 1983; Parker et al. 1983; Thorne et al. 1983; Bridge 1984; Chang 1984; Dietrich and Smith 1984; Kitanidis and Kennedy 1984; Odgaard 1984; Smith and McLean 1984; Ikeda and Nishimura 1985; Parker and Andrews 1985; Struiksma et al. 1985; Odgaard 1986a; 1986b; Parker and Andrews 1986; Dietrich 1987; Odgaard 1987; Furbish 1988; Odgaard and Bergs 1988; Dietrich and Whiting 1989; Ikeda 1989; Nelson and Smith 1989; Odgaard 1989a; 1989b; Parker and Johannesson 1989; Shimizu and Itakuru 1989; Bridge 1992; Mosselman 1995; 1998; Seminara et al. 2001; Zolezzi and Seminara 2001). Summaries have been given by, among others, Odgaard (1984) and Chang (1988a).

8.3.1 Governing Equations and Sample Solution

Several attempts to relate near-bank depth and velocity to mean-flow properties are based on solving the equations for conservation of mass (water and sediment) and momentum and using a stability criterion for sediment particles on the

streambed. The attempts differ in the way the equations are reduced. As an example, Odgaard (1989a; 1989b) employs an order-of-magnitude consideration and linearization and reduces the equations to those of a damped oscillating system. He utilizes the observation, from both laboratory and field, that both u and d are essentially constant along the river channel's centerline, and that their variation in transverse direction is nearly linear over the central portion of the cross section (Fig. 8-6). Consequently, the following description is deemed appropriate:

$$\frac{\bar{u}}{\bar{u}_c} = 1 + \frac{n}{d_c} U_{tc} \tag{8-13}$$

$$\frac{d}{d_c} = 1 + \frac{n}{d_c} S_{tc} \tag{8-14}$$

in which S_{tc} = transverse bed slope at the centerline = $(\partial d/\partial n)_c$ and U_{tc} = normalized transverse velocity gradient at thecenterline = $d_c[\partial/\partial n(\bar{u}/\bar{u}_c)]_c$, in which subscript c = the centerline values, and overbars denote the depth-averaged values. In Fig. 8-6 the s-axis is along the channel centerline, and positive in the streamwise direction, the n-axis is perpendicular to the s-axis and positive toward the concave bank, and the z-axis is vertically upward. The velocity components (time-averaged) in the s-, n-, and z-directions are denoted u, v, and w, respectively.

Odgaard assumes a transverse distribution of sediment transport q_s described by a power law,

$$q_s = q_{sc}\left(\frac{\bar{u}}{\bar{u}_c}\right)^M \tag{8-15}$$

in which exponent M is a function of sediment characteristics and q_s is the volumetric rate per unit width. Such a power law is often used for description of bed load transport in straight alluvial channels, where the value of M is generally between 2 and 4 (Simons and Sentürk 1977).

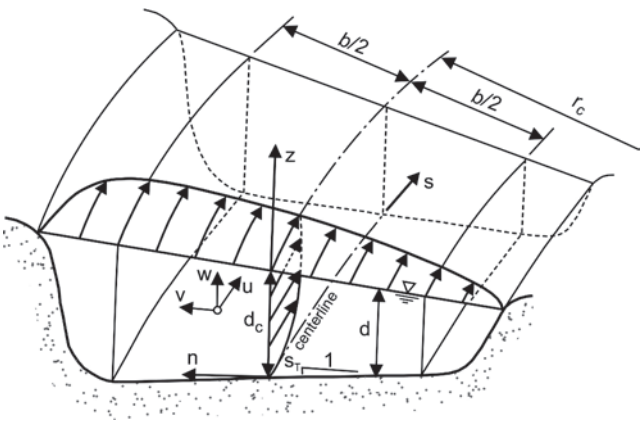

Fig. 8-6. Definition sketch for sinusoidal channel flow.

Odgaard is then able to reduce the equations to two ordinary differential equations,

$$\frac{dU_{tc}}{d\sigma} + a_1 U_{tc} = \frac{1}{2} a_1 S_{tc} \tag{8-16}$$

$$\frac{d^2S_{tc}}{d\sigma^2} + a_2\frac{d^2U_{tc}}{d\sigma^2} + a_3\frac{dS_{tc}}{d\sigma} + a_4\frac{dU_{tc}}{d\sigma} + a_5 S_{tc} = a_6 \tag{8-17}$$

in which $\sigma = s/b$ and

$$a_1 = \frac{2k^2}{m^2}\frac{b}{d_c} \tag{8-18}$$

$$c_2 = 1 - \frac{o+1}{m+2} M \tag{8-19}$$

$$a_3 = \frac{8 B \sqrt{\theta}}{\alpha \kappa F_{Dc}} \frac{m(m+1)}{m+2}\frac{d_c}{b} + \frac{2\kappa^2 m}{(m+1)(m+2)}\frac{b}{d_c} \tag{8-20}$$

$$a_4 = \frac{2\kappa^2 m}{(m+1)(m+2)}\left[1 - M\left(1 + \frac{1}{2m} + \frac{1}{2m^2}\right)\right]\frac{b}{d_c} \tag{8-21}$$

$$a_5 = \frac{8 B \kappa \sqrt{\theta}}{\alpha(m+2)\ F_{Dc}}\left(1 + \frac{2m^2}{m+1}\right) \tag{8-22}$$

$$a_6 = \frac{8}{\alpha}\frac{2m+1}{m(m+2)}\frac{d_c}{r_c} \tag{8-23}$$

in which factor F_{Dc} = particle densimetric Froude number, defined as $F_{Dc} = \bar{u}_c/\sqrt{\Delta g D}$. m = friction parameter, whose relationship to shear velocity u_*, Darcy-Weisbach's friction factor f, and Chezy's coefficient C is $m = \kappa\bar{u}/u_* = \kappa\sqrt{8/f} = \kappa C/\sqrt{g}$ is in which κ = von Karman's constant (≈0.4), and $u_* = \sqrt{\tau_{bs}/\rho}$, τ_{bs} = bed shear stress in the s-direction, ρ =density of water, Δ = specific weight of submerged sediment = $(\rho_s - \rho)/\rho_s$; ρ_s = density of sediment (for quartz sand, Δ = 1.65), B = transverse bed-slope factor (see Odgaard 1989a), α = transverse-mass flux factor (Odgaard 1989a), θ = dimensionless critical bed shear stress (Shield's parameter), and g = acceleration due to gravity. Typical values of α, B, and θ are 0.4, 6, and 0.03, respectively.

By eliminating S_{tc}, using Eq. (8-16), Eq. (8-17) is reduced to

$$\frac{d^3U_{tc}}{d\sigma^3} + h_1\frac{d^2U_{tc}}{d\sigma^2} + h_2\frac{dU_{tc}}{d\sigma} + h_3U_{tc} = h_4 \qquad (8\text{-}24)$$

in which $h_1 = a_1 + (\frac{1}{2})a_1a_2 + a_3$; $h_2 = a_1a_3 + (\frac{1}{2})a_1a_4 + a_5$; $h_3 = a_1a_5$; and $h_4 = (\frac{1}{2})a_1a_6$. The system ($U_{tc}$ and S_{tc}) described by these equations is a damped oscillation forced by curvature (h_4). With given boundary conditions, the solution is readily obtained.

In fully developed bend flow, where $d/d\sigma = 0$, Eqs. (8-16) and (8-17) yield

$$\frac{\bar{u}}{\bar{u}_c} = \sqrt{\frac{d}{d_c}} \qquad (8\text{-}25)$$

and

$$S_{tc} = HF_{Dc}\frac{d_c}{r_c} \qquad (8\text{-}26)$$

in which $H = (2m + 1)(m + 1)/[B\kappa\sqrt{\theta}\, m(m + 1 + 2m^2)]$. These equations are well supported by both laboratory and field data (Kikkawa et al. 1976; Falcon and Kennedy 1983; Ikeda and Nishimura 1985; Odgaard and Bergs 1988). The composition of factor H, however, varies somewhat from author to author.

8.3.2 Sample Simulation of Bed Topography in Laboratory Channel

The oscillatory behavior of the flow system is illustrated by a simulation of S_{tc} in a recirculating 180° constant-radius alluvial-bend model at IIHR Hydroscience and Engineering. This model has width 2.44 m and centerline radius $r_c = 13.11$ m. At a discharge of 0.153 m^3/s, centerline values of depth, velocity, particle Froude number, and water surface slope are $d_c = 0.15$ m, $u_c = 0.45$ m/s, $F_{Dc} = 6.5$, and $S_c = 0.00116$, respectively; resistance parameters are $m = 5.3$ and $\kappa = 0.52$; and bed load transport $q_s \cong 4$ g/cm/min. Flow and sediment conditions were described earlier by Odgaard and Bergs (1988) and Bergs (1989). The bend is preceded by a 20-m-long straight reach. Under such conditions, $d^2U_{tc}/d\sigma^2$ is negligibly small, and Eqs. (8-16) and (8-17) yield

$$\frac{d^2S_{tc}}{d\sigma^2} + \left(a_3 + \frac{1}{2}a_4\right)\frac{dS_{tc}}{d\sigma} + a_5S_{tc} = a_6 \qquad (8\text{-}27)$$

With S_{tc} and $dS_{tc}/d\sigma$ being zero at the beginning of the bend at $\sigma = 0$, the solution is

$$S_{tc} = S_{tco} - S_{tco}\sqrt{1 + \left(\frac{a'}{2\omega}\right)^2}\cos\left(\omega\sigma - \psi\right)\exp\left(-\frac{1}{2}a'\sigma\right) \qquad (8\text{-}28)$$

in which $\omega = (1/2)\sqrt{4a_5 - a'^2}$; $a' = a_3 + (\frac{1}{2})a_4$; $\psi = \arctan[a'/(2\omega)]$; and S_{tco} = fully developed value of S_{tc} (Eq. (8-26)). The simulation (using values $B = 3$, $\alpha = 1$, $\theta = 0.03$, and $M = 2.7$) is shown in Fig. 8-7 with measured data. The oscillation of S_{tc} is very distinct in this flow situation. The transverse bed slope is seen to overshoot its equilibrium (fully developed) value by a factor of about 1.5. A similar overshoot was measured in Struiksma et al.'s (1985) experiments and also predicted by their model. The overshoot is associated with redistribution of flow and sediment transport in the beginning of the bend, where both q_n and $\partial u/\partial n$ are greater than zero (q_n = volumetric bed load transport per unit width in the n-direction). A positive value of q_n is necessary there to provide the increase of sediment transport associated with the increase in velocity along the outer bank. It is apparent that the system generates such a transverse transport of sediment by locally increasing transverse bed slope beyond that of fully developed bend flow (to make the downslope gravity force component larger than the upslope drag force component). The magnitude of the overshoot is dependent on the value of M. Overshoot of "overdeepening" is also discussed by Zolezzi and Seminara (2001). Using a linear, depth-averaged flow model coupled with the Exner equation, they simulate, and obtain good agreement with, the overshoot measured by Struiksma et al. (1985).

8.4 CHANNEL STABILITY

One of the critical questions from a river-engineering point of view is the extent to which a given channel alignment is prone to future changes. There is an obvious need for answers to this question. The problem is one of stability of river channel alignment.

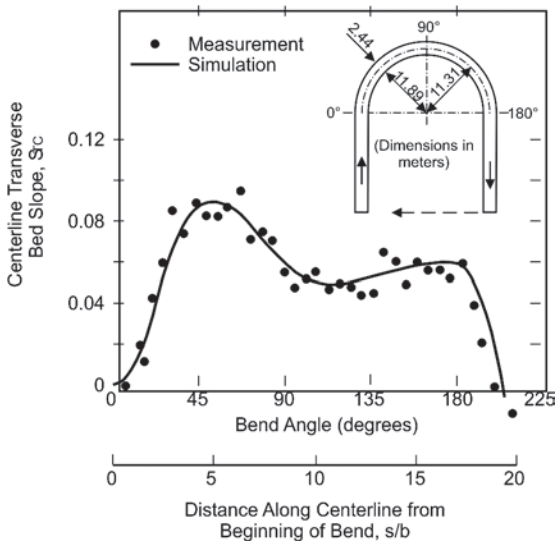

Fig. 8-7. Measured and computed transverse bed slopes in IIHR bend model experiment.

8.4.1 Regime Theories

Many attempts have been made in the past to establish guidelines for assessment of channel stability. Among the guidelines are the so-called regime theories (Kennedy 1895; Lacey 1930; Blench 1952; Kellerhals 1967; Charlton et al. 1978), which are empirical techniques, used primarily for the design of stable, straight channels. These theories generally predict that channel width must be less than 6 to 10 times depth for the channel to remain stable.

Most natural channels have a width-depth ratio larger than 6 to 10, and their planforms are unstable. They consist of meanders that, as mentioned above, usually migrate by both downstream translation and lateral expansion.

8.4.2 Perturbation Stability Analyses

As indicated earlier, it is generally believed that meandering is the result of channel instability. Building on this assumption, many researchers have attempted to simulate the initiation of the meandering process by a perturbation stability analysis. Early attempts were made by, among others, Callander 1969; Hansen 1967; Engelund and Skovgaard 1973; Fredsoe 1978; and Parker 1976. As they progressed in sophistication, the perturbation stability analyses were also used to evaluate the stability of given channel alignments. That is, if a given channel alignment had characteristics similar to those calculated by the stability analysis, the alignment was considered "relatively stable" or "minimally destructive" in terms of bank erosion. Early alternate approaches are reviewed by Yang (1971), Chitale (1973), and Callander (1978) among others. The theory of minimum variance has also been offered as a possible cause of meandering (von Schelling 1951; Langbein and Leopold 1966; and Chang 1988a).

In a perturbation stability analysis, small traveling perturbations are introduced into the system of equations governing river flow, and their effect on channel planform is determined by calculating the rate of growth of the perturbations. The primary advantage of the perturbation stability analysis is that it allows channel planform stability to be described as a feature of the basic flow equations. Whereas the regime formulas and empirically based meander relations correlate flow and meander variables using data and simple, one-dimensional, straight-channel resistance formulas (Manning, Chezy, etc.), the perturbation analyses generally employ models that are based on the complete set of governing equations, including those of sediment transport, and describe flow and depth distributions in the channel in at least two dimensions.

Two categories of stability theories exist: (1) bar theories, which examine conditions for formation of alternating bars in straight channels, and (2) bend theories, which examine migration features of weakly meandering flows. It is the latter category that is addressed in this section. It should be noted that the two categories may in fact be related. Theoretical analyses by Blondeaux and Seminara (1983; 1985), Seminara and Tubino (1989), Parker and Johannesson (1989), and Tubino and Seminara (1990) suggest that alternating bars may under certain circumstances trigger bend instability and lead to meandering.

Representative bend theories are those of Ikeda et al. (1981); Kitanidis and Kennedy (1984); Blondeaux and Seminara (1985); and Odgaard (1989a). These theories differ in their treatment of bank erosion and of centrifugally induced secondary flow and its effect on bed topography and primary flow. Kitanidis and Kennedy assume that the rate of bank retreat is proportional to and in phase with the secondary current, whereas the other authors assume that the rate is proportional to and in phase with the difference between near-bank and section-average velocity. Kitanidis and Kennedy account for effects of secondary current and assume that transverse bed slope has negligible effect on stability. Ikeda et al., on the other hand, consider effects of transverse bed slope and neglect effects of secondary current. Blondeaux and Seminara (1983; 1985) and Odgaard (1989a) include effects of both secondary current and transverse bed slope. In Blondeaux and Seminara's model, the secondary current is controlled by an external stress relation, whereas in Odgaard's model it is controlled by the basic flow equations. Odgaard's approach allows for phase lag between channel curvature and secondary current and thus calculates the direction of migration. None of these analyses account for convective transport of primary flow momentum by the secondary current. One reason for this is that depth averaging of the governing flow equations eliminates it; in addition, in mildly curved channels, the effect is minor.

In Odgaard's stability analysis, the bed topography is calculated based on a coupling between flow field and sediment transport. This was done in response to the findings of Struiksma et al. (1985) and Johanneson (1988) that redistribution of sediment transport can have a significant effect on bed topography. In most other stability analyses, sediment redistribution is not considered.

8.4.3 Example of a Perturbation Stability Analysis

The following example illustrates the principles of stability analysis (Odgaard 1989a) based on the equations of a damped oscillating system. The stability of the system is tested by subjecting it to a channel alignment perturbation in the form of a traveling sinusoid,

$$\eta(x,t) = A(t)\ \sin\left[k\left(x - ct\right)\right] \tag{8-29}$$

in which x = coordinate distance along the unperturbed channel axis; $k = 2\pi/\lambda$ is the wave number; A = amplitude; λ = meander wavelength; t = time; and c = celerity of sinusoid. The channel-centerline displacement $\eta(t)$ is limited to values much smaller than the meander wavelength. The centerline curvature is then

$$\frac{1}{r_c} = -\frac{d^2\eta}{dx^2} = k^2\, A(t)\ \sin\left[k\left(x - ct\right)\right] \tag{8-30}$$

The differential equation for U_{tc} is obtained by substituting Eq. (8-30) into Eq. (8-24). The solution, which is periodic and independent of the initial condition, is

$$U_{tc} = \frac{N b k^2 A}{\sqrt{e_1^2 + e_2^2}} \sin\left[k(x - ct) - \gamma\right] \tag{8-31}$$

in which $N = 8\kappa^2(2m + 1)/[\alpha m^3(m + 2)]$; $e_1 = h_3 - 2h_1k^2b^2$; and $e_2 = h_2kb - k^3b^3$. The phase shift between U_{tc} and the channel-axis displacement is $\gamma = \arctan(e_2/e_1)(0 \le \gamma \le \pi/2)$. The corresponding transverse bed slope is obtained by substituting Eq. (8-31) into Eq. (8-16),

$$S_{tc} = \frac{2 N b k^2 A}{\sqrt{e_1^2 + e_2^2}} \sqrt{1 + \left(\frac{bk}{a_1}\right)^2} \sin\left[k(x - ct) - \phi\right] \tag{8-32}$$

in which $\phi = \gamma - \arctan(bk/a_1)$.

To determine $A(t)$, an equation is introduced that describes the rate of lateral shifting of the channel axis due to erosion of the concave bank and deposition on the convex bank. In this example, two alternatives are used. One is the relation proposed by Ikeda et al. (1981), which assumes that the rate of bank retreat is proportional to the difference between near-bank depth-averaged velocity u_{bank} and the section-averaged velocity $\bar{u}_0$. By using the depth-averaged centerline velocity $\bar{u}_c$ for $\bar{u}_0$, the relation reads

$$v_e = E\bar{u}_c\left(\frac{\bar{u}_{\text{bank}}}{\bar{u}_c} - 1\right) \tag{8-33}$$

in which v_e = rate of bank retreat and E = parameter describing the erodibility of the bank material. This model is labeled IKD. The other relation, which is proposed by Odgaard (1989) and labeled ODG, assumes that rate of bank retreat is linearly related to increase in scour depth at the bank,

$$v_e = E'\bar{u}_c\left(\frac{d_{\text{bank}}}{d_c} - 1\right) \tag{8-34}$$

in which E' = erosion parameter. It follows that $E' \cong (\frac{1}{2})E$. Because of the assumed mild curvature of the channel, v_e may be equal to the rate of change of channel alignment, $\partial\eta/\partial t$. The parenthetical expressions in Eqs. (8-33) and (8-34) equal $bU_{tc}/2d_c$ and $bS_{tc}/2d_c$, respectively. The closing of the problem is achieved by substituting Eq. (8-29) into the left-hand sides of Eqs. (8-33) and (8-34), and Eqs. (8-31) and (8-32) into the right-hand sides of Eqs. (8-33) and (8-34), respectively. After some reduction, relationships for amplitude growth rate, $\partial A/\partial t$, and celerity, c, are obtained. Using the IKD bank erosion model (Eq. (8-33)), the relations are

$$\frac{1}{A}\frac{\partial A}{\partial t} = \frac{E\bar{u}_c}{b} K b k \cos\gamma \tag{8-35}$$

$$c = E\bar{u}_c K \sin\gamma \tag{8-36}$$

in which

$$K = \frac{1}{2} N \frac{b}{d_c} \frac{kb}{\sqrt{e_1^2 + e_2^2}} \tag{8-37}$$

The ODG bank erosion model [Eq. (8-34)] yields

$$\frac{1}{a}\frac{\partial A}{\partial t} = 2\frac{E'\bar{u}_c}{b} Kbk\sqrt{1 + \left(\frac{bk}{a_1}\right)^2}\cos\phi \tag{8-38}$$

$$c = 2E'\bar{u}_c K\sqrt{1 + \left(\frac{bk}{a_1}\right)^2}\sin\phi \tag{8-39}$$

8.4.4 Dominant Wavelength

It is generally assumed that the dominant wavelength is the wavelength that is associated with the conditions that yield maximum growth rate of alignment amplitude. The wave number at which the maximum amplitude growth rate occurs is termed the dominant wave number, and it is determined from the equation

$$\partial^2 A/\partial t\,\partial k = 0. \tag{8-40}$$

Sample calculations are shown in Fig. 8-8, which shows dominant wavelengths λ_d and corresponding phase shifts φ_d and γ_d as a function of width-depth ratio for different friction factors, densimetric Froude numbers, and transverse bed slope factor. A value of $M = 3$ is used. It is seen that the calculations based on the IKD bank erosion model yield a stronger dependence of wavelength on width-depth ratio than do calculations based on the ODG bank erosion model. The typical bank-full range for F_{Dc} and m are $5 \le F_{Dc} \le 15$ and $3 \le m \le 5$. For width-depth ratios between 10 and 60 (the typical range), the ODG model then yields dominant wavelengths between 9 and 24 times the width, which is in agreement with data presented by Zeller (1967) and Leopold and Wolman (1957; 1960). For the same width-depth ratios, the IKD model yields wavelengths between 9 and 57 times the width, somewhat larger than those indicated by data.

The calculations based on the IKD bank erosion model yield dominant-wavelength relationships ranging from $\lambda_d \sim d_c$ at small width-depth ratios to $\lambda_d \sim \sqrt{bd_c}$ at large width-depth ratios. This range covers that represented by the theories of Ikeda et al. and Kitanidis and Kennedy. The IKD model yields a nearly linear dependence of λ_d on m, or the inverse of $\sqrt{f}$, which is also predicted by Ikeda et al. and Kitanidis and Kennedy. The ODG model yields a roughly linear dependence on m only at large width-depth ratios; the dependence on m is weaker at smaller width-depth ratios. For large width-depth ratios, the two analyses yield essentially the same results. The two analyses also differ in their prediction

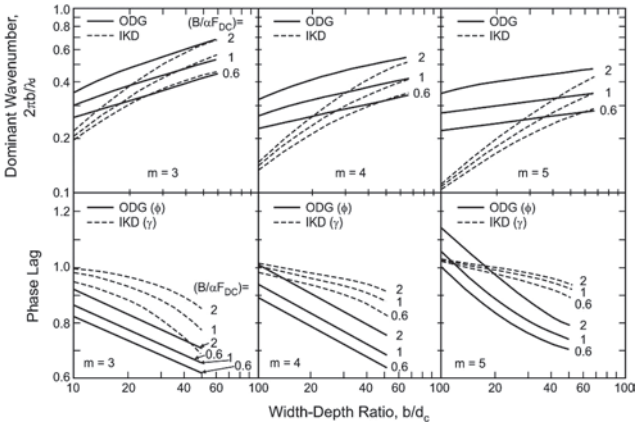

Fig. 8-8. Results of sample stability analysis: dominant wavelengths and phase shifts as functions of width-depth ratio.

of dominant phase lag, and thus of distance from crossover to first outer-bank erosion occurrence. The phase lags predicted based on the ODG model are generally smaller than those predicted when the IKD bank erosion model is used. Computed data points, obtained using the ODG model and $M = 3$, conform roughly to the following curve-fitted relations:

$$\frac{2\pi b}{\lambda_d} = 0.11 m^{1/4} \left(\frac{B}{\alpha F_{Dc}} \right)^{0.41} \left(\frac{b}{d_c} \right)^{1/m} \tag{8-41}$$

and

$$\phi_d = 0.16(m+5) \left(\frac{B}{\alpha F_{Dc}} \right)^{0.1} \left(\frac{d}{b} \right)^{0.125 m^{0.27}} \tag{8-42}$$

Within the range $2 \leq M \leq 4$, dominant meander wavelength and phase shift are relatively insensitive to M. For width-depth ratios between 10 and 40, a 50% increase (decrease) of M causes λ_d to decrease (increase) by less than 10%.

8.4.5 Finite-Amplitude Meanders

In the analysis presented, it is assumed that curvature is small and that the meander wavelength is the same whether it is measured along the down-valley axis or along the channel centerline. As the process of meandering progresses, the wavelength measured along the centerline, L, becomes larger than that measured along the down-valley axis, λ. The ratio L/λ is often termed the sinuosity of the channel. Stochastic analysis, as well as field data (Langbein and Leopold 1966), indicates that a sine-generated alignment persists during the migration of many meanders. The curvature may then be written

$$\frac{1}{r_c} = \frac{1}{R_c} \sin\left(\frac{2\pi s}{L} \right) \tag{8-43}$$

in which R_c = minimum value of r_c at apex; and transverse bed slope and velocity may be obtained from the aforementioned equations with x replaced by s, k by $2\pi/L$, and $k^2A(t)$ by $1/R_c$. It easily can be shown (Langbein and Leopold 1966) that L and R_c are related as

$$L = 4.4\pi R_c \sqrt{1 - \frac{\lambda}{L}} \tag{8-44}$$

8.4.6 Prediction Uncertainties

This sample stability analysis shows that the description of meander migration is very sensitive to the manner in which bank erosion is related to primary flow variables. The rates of bank retreat are, of course, particularly sensitive to the values of E and E'. The direction of channel migration (lateral expansion versus downstream translation) is different depending on the bank erosion model used. There are not enough data available to determine which of the models, ODG or IKD, performs better. In fact, it is still an open question whether any of them comes even close to complete description of the relationship between flow variables and bank erosion.

In the sample analysis, the transverse bed slope factor B and the transverse-mass flux factor α play significant roles. Factor B represents the bed sediment's motion-resistive properties. Its value has been reported to range from 3 to 6, possibly depending on sediment gradation. For the field cases analyzed by Odgaard (1989b), its value is about 6, which is in agreement with findings of Kikkawa et al. (1976). The transverse-mass flux factor α corrects the cross-channel flows of water and sediment when these are calculated based on linear distributions of u and d in the cross-channel direction. Its value is defined by comparing the calculation (with the continuity equation) of transverse flow of water using linear u and d distributions with that computed with measured u and d distributions. A value of $\alpha = 0.4$ is found to be reasonable for field cases.

The sediment transport relation is another uncertain element in the analysis. By using a simple power law (Eq. (8-15)), as is done in the preceding example, all sediment properties are embodied in the exponent M. Consequently, M varies from river to river. The value of M has a significant influence on transverse bed slope in accelerating bend flow, although not as dominant as that of B. In Odgaard's analysis of field data, a value of $M = 3$ is used.

It must be kept in mind that the formulas presented in the previous example are based on linear analysis; they cannot be expected to apply to river channels with large curvature. The studies by Nelson (1988), Blanckaert and Graf (2001) and Blanckaert (2003) show that in channels with large curvature,

nonlinear terms in the flow equations can have a significant effect on the description of flow. Blanckaert (2003) demonstrates that in a large-curvature channel bend, an additional secondary flow cell develops near the outer bank. There is even a tendency for stacking of cells. Moreover, multiple point bars may develop as has been demonstrated by Whiting and Dietrich (1993a; 1993b; 1993c).

8.5 APPLICATIONS OF FLOW AND STABILITY RELATIONS

The flow and stability analysis in the preceding sections provides formulas and graphs for calculation of (1) rate and direction of channel migration; (2) dominant meander wavelength and phase shift; and (3) velocity and depth distributions in meandering channels.

Input consists of primary channel characteristics: slope S, width b, centerline depth d_c, median grain size D, friction factor f, and bank-erosion constants E and E'. Lateral and down-valley migration rates are then calculated by Eqs. (8-35) to (8-39), velocity and depth distributions by Eqs. (8-13), (8-14), (8-31), and (8-32), and dominant wavelength and phase lag by Eqs. (8-40) and (8-41) or Fig. 8-8.

Velocity and depth distribution in channels with arbitrary curvature are obtained by solving Eqs. (8-16) and (8-17) (or (8-24)) with appropriate boundary conditions, and by using Eqs. (8-13) and (8-14). In a constant-radius channel with a long straight approach reach, velocity and depth distributions may be calculated by Eqs. (8-28) and (8-16) together with Eqs. (8-13) and (8-14).

Two alternative bank-erosion models have been tested, the Ikeda et al. model (1981), denoted by IKD, which assumes that the rate of bank retreat is proportional to and in phase with the difference between near-bank and section-averaged velocity (Eq. (8-33)), and a model proposed by Odgaard (1989), denoted by ODG, which relates the rate of bank retreat to increase in near-bank scour depth (Eq. (8-34)).

The principal quantities and concepts are shown in Figs. 8-9(a) and 8-9(b). The figures show the paths of maximum velocity and flow depth through two consecutive meander bends. As indicated, the velocity and depth distributions respond to the change in curvature with a certain lag, which equals $\gamma L/2\pi$ for velocity and $\varphi L/2\pi$ for depth. In the IKD bank-erosion model, it is assumed that bank erosion occurs with the same lag as velocity, whereas the ODG model assumes that bank erosion occurs with the same lag as depth. A basic assumption is that λ is nearly equal to L.

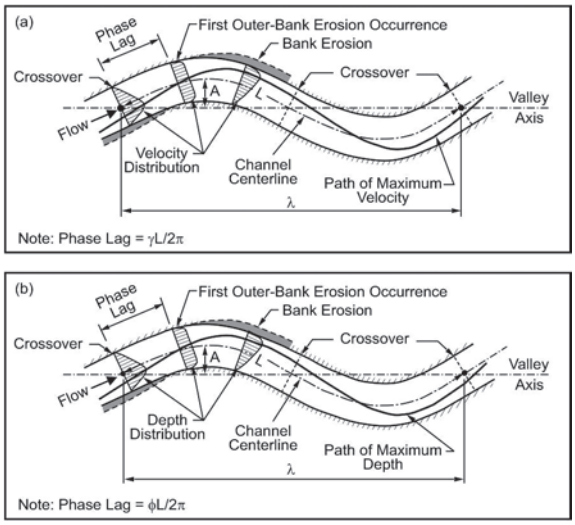

Fig. 8-9. Applications of flow and stability relations. Definition sketch for principal quantities and concepts: (a) utilizing IKD bank erosion model; (b) utilizing ODG bank erosion model.

8.5.1 Numerical Example

The application of the previously given formulas is best illustrated by an example with data from a hypothetical river (Odgaard 1989b). The bank-full characteristics of the river channel are taken to be $S = 0.0005$; $b = 150$ m; $d_c = 6$ m; $f = 0.08$ (i.e., $m = \kappa\sqrt{8/f} = 4$); $D = 1$ mm; $\bar{u}_c = 1.72$ m/s ($\simeq\sqrt{8gSd_c/f}$); $M = 3$; $\theta = 0.06$; and $F_{Dc} = \bar{u}_c/\sqrt{\Delta g D} = 13.5$. Transverse bed slope and mass flux factors are $B = 6$ and $\alpha = 0.4$, and erosion constants are $E = 3 \times 10^{-7}$ and $E' = 1.5 \times 10^{-7}$, values typical of rivers in the Midwest (Odgaard 1987).

To estimate dominant wavelength and phase lag, the graphs in Fig. 8-8 (or Eqs. (8-40) and (8-41)) are used. With $B/\alpha F_{Dc} = 1.1$, $m = 4$, and $b/d_c = 25$, the ODG curve yields $\lambda_d = 2{,}700$ m and $\varphi = 0.8$, and the IKD curve $\lambda_d = 3{,}500$ m and $\gamma = 0.95$. The phase shifts indicate that the first outer-bank erosion occurrence may occur at a distance from crossover of 0.12 to 0.15 times meander length, or slightly more. Lateral and down-valley migration rates are estimated by Eqs. (8-35), (8-36), or (8-38) and (8-39). The values of pertinent variables are listed in Table 8-1. If $A = 200$ m, then $\partial A/\partial t$ (ODG) = 5 m/year; and $\partial A/\partial t$ (IKD) = 2 m/year. The variation of transverse bed slope through the meander is obtained from Eq. (8-32) with $A = 200$ m (or, if L is given instead of A, with $k^2A = 1/R_c$, and R_c obtained from Eq. (8-43))

$$S_{tc}\,(\text{ODG}) = 0.071 \sin\left(\frac{2\pi s}{L} - 0.8\right) \qquad (8\text{-}45)$$

$$S_{tc}\,(\text{IKD}) = 0.039 \sin\left(\frac{2\pi s}{L} - 0.8\right) \qquad (8\text{-}46)$$

and near-bank depth by Eq. (8-14) with $n = 75$ m and $d_c = 6$ m (or by Eq. 49 in Odgaard (1986a)). Maximum depth of scour is estimated to be 11.3 m based on ODG and 8.9 m based on IKD, and to occur at $s/L = 0.38$ (downstream from bend apex). Migration rates of and flow and bed topography

Table 8-1 Computation of Lateral and Down-Valley Migration Rates for Hypothetical River

	Bank erosion model	
Variable	ODG	IKD
kb	0.35	0.27
a_1	0.50	0.50
a_2	−1.50	−1.50
a_3	1.793	1.793
a_4	−2.633	−2.633
a_5	1.074	1.074
h_1	1.918	1.918
h_2	1.312	1.312
h_3	0.537	0.537
e_1	0.067	0.257
e_2	0.416	0.335
N	0.075	0.075
K	0.778	0.600
$(1/A)\partial A/\partial t$	8.0×10^{-10} s^{-1}	3.2×10^{-10} s^{-1}
c	11 m/year	8 m/year

in channels with planform different from that of the dominant wave are computed in the same manner with k = actual wave number. Note that if L is significantly larger than λ, the calculations should be performed with $k = 2\pi/L$ instead of $2\pi/\lambda$.

8.6 SIMULATION OF MEANDER EVOLUTION

Many attempts have been made over the years to develop models that can simulate the evolution or long-term behavior of a meandering river. They range from purely stochastic models to more rigorous process models.

The stochastic models include models based on the "most probable path" assumption with various degrees of simulated randomness (von Schelling 1951; Langbein and Leopold 1966; Thakur and Scheidegger 1968; Surkan and van Kan 1969; Thakur and Scheidegger 1970; Ferguson 1973; 1976; 1977; Stølum 1996; 1997; 1998). These models generally attempt to reproduce the evolution of meander patterns on a large scale with no or little consideration of local flood-plain characteristics and local sedimentary processes.

The process models attempt to reproduce the relationship between rates of migration and flow and channel variables quantitatively. The relationship is typically one of the equations listed in Section 8.2.3 or a convolutional relation between migration and curvature. The process models attempt to predict the long-term evolution of rivers, taking into consideration flood-plain characteristics that modulate, in both time and space, the channel parameters and erosion coefficient (Parker 1982; Beck et al. 1983a; 1983b; Howard 1983; Beck 1984; Beck et al. 1984; Howard and Knutson 1984; Johannesson and Parker 1985; Parker and Andrews 1986; Parker et al. 1988; Crosato 1989; Furbish 1991; Howard 1992; Garcia et al. 1994; Mosselman 1995; Meakin et al. 1996; Sun et al. 1996; Mosselman 1998; Sun et al. 2001a; 2001b; 2001c; Lancaster and Bras 2002). A few process models are developed in which bank erosion is calculated by a separate process model that accounts for near-bank scour, bank collapse, and deposition and removal of bank material (Nagata et al. 2000; Duan et al. 2001; Darby 2002; Darby and Delbono 2002).

The simulations by Stølum (1996; 1997; and 1998) are examples of a combination of process and stochastic modeling. Stølum assumes that meander evolution is the result of two opposing processes: lateral migration, which acts to increase sinuosity, and cutoffs, which act to decrease it. Lateral migration results form bend erosion and deposition, whereas cutoffs result from local geometry. According to Stølum, these opposing processes self-organize the sinuosity into a steady state around a mean value of 3.14, the sinuosity of a circle π.

Recently, several attempts have been made to overcome the limitations of using a calibrated bank erosion coefficient. They include two-dimensional flow-field (mass and momentum), sediment-transport and bank erosion models (Nagata et al. 2000; Duan et al. 2001; Darby 2002; Darby and Delbono 2002).

8.6.1 Sample Simulations

Figure 8-10 shows a simulation by Johannesson and Parker (1985) of the evolution of Red Lake River, Minnesota. The evolution of the channel is obtained by tracking the channel migration over time. Channel width is assumed constant. It is also assumed that the channel centerline is displaced at the same rate as the bank. The migration is described by a Hickin mapping (so called in recognition of the original work of Hickin (1974)), according to which the centerline displacement is described as

$$\frac{dx_p}{dt} = v_e \sin\theta \tag{8-47}$$

$$\frac{dy_p}{dt} = -v_e \cos\theta \tag{8-48}$$

in which x_p and y_p are the coordinates of point P of the channel centerline, and θ = local angle of centerline with x-axis. See Fig. 8-11.

A slightly modified Johannesson and Parker model was used by Garcia et al. (1994) to simulate the evolution of rivers in Illinois. In order to better determine the magnitude

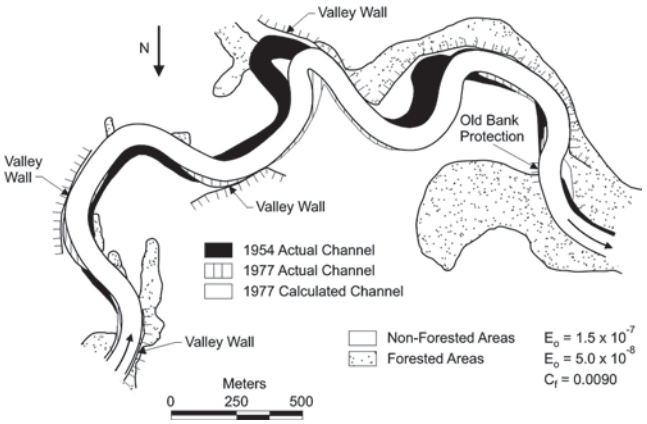

Fig. 8-10. Simulation of the evolution of the Red Lake River, Minnesota, from 1954 to 1977 (from Johannesson and Parker 1985).

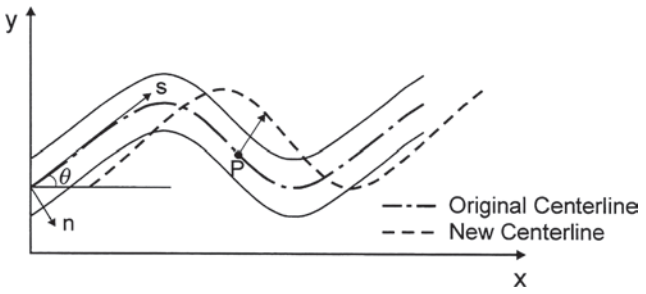

Fig. 8-11. Schematic showing migration of Point P on channel centerline.

and characteristics of channel shifts, Garcia et al. used the computer program MEANDER, developed by MacDonald et al. (1992). MEANDER measures various components of channel shift, the most important of which is the average normal shift. It also measures sinuosity, time rate of change of sinuosity, and average rate of curvature. Figure 8-12a shows the simulation of the evolution of the Big Muddy River in Illinois (Garcia et al. 1994). Abad and Garcia (2004) have also presented a methodology for simulating the evolution of meandering streams in restoration and naturalization processes. The remeandering of Poplar Creek, Illinois, was analyzed. In this application, Kinoshita curves (Kinoshita 1961; Kinoshita and Miwa 1974; Parker et al. 1982; Parker et al. 1983; Parker and Andrews 1986; Seminara et al. 2001) were used to delineate the new channel. Figure 8-12b shows the planform migration of Poplar Creek at bank-full flow over a period of 100 years. Recently, Abad and Garcia (2006) developed a Windows-based and geographical information system-based interface for the analysis and modeling of planform migration (this program contains the models of Garcia et al. (1994) and MacDonald et al. (1992)).

8.7 CHANNEL STABILIZATION

Channel stabilization is an important part of floodplain management. Channels are stabilized to enhance the utility of floodplains, whether for business or recreation. Specific objectives are to (1) prevent bank erosion and loss of property, including bridges and other infrastructure; (2) enhance conveyance, in particular for floods; (3) facilitate traffic (commercial navigation and recreation); and (4) facilitate water usage (utilities, irrigation, diversion, etc.).

8.7.1 Strategy

The basic strategy is to stabilize the channel alignment and the channel cross section. The river should maintain a natural alignment (a path of easy bends of reverse curvature) and have a cross section that can accommodate the river's water and sediment regime. A good practice is to find a relatively stable reach of the river, determine channel and alignment characteristics for that reach and then apply those characteristics to the reach to be stabilized.

A complementary or supplementary approach is to calculate alignment characteristics using stability theory. This approach is described in detail in the previous sections of this chapter. The approach is based on (1) equations for conservation of mass (water and sediment) and momentum and (2) a stability criterion for sediment particles on the bed. The equations are reduced to those of a damped oscillating system, which is then subjected to a traveling small-amplitude channel alignment wave. It is the growth characteristics of this wave that defines the natural alignment. This approach results in (1) planform development in terms of lateral and downstream migration rates; (2) flow and bed topography in terms of transverse gradients of depth and depth-averaged velocity; and (3) formulas for estimates of dominant meander wavelength and phase shift.

8.7.2 Technologies

Several technologies are available for stabilizing a channel. Reviews are given by Biedenharn et al. (1997) and Petersen (1986). The techniques range from the construction of revetments and dikes, vanes or weirs, to dredging. They function by adjusting bank resistance and/or bank erodibility and/or flow and bed topography.

8.7.2.1 Revetments Revetments are structures that are aligned parallel to the current. They are used most often to protect eroding banks and to form a smooth bank line. Petersen 1986 classifies revetments into the following types: (1) standard revetment with mattresses (e.g., gabions); (2) woven wooden mattresses; (3) articulated concrete mattresses; (4) standard trench-fill revetments; (5) pile revetments; and (6) stone-fill revetments. Biomattresses are also used to promote vegetation on banks.

8.7.2.2 Dikes, Submerged Vanes, Bendway Weirs Dikes, submerged vanes, and bendway weirs are structures placed at

an angle to a current. They are typically used for (1) fairing out sharp bends to a larger radius of curvature to provide a more desirable channel alignment (and thus stabilize concave banks); (2) closing off secondary channels and old bend ways; (3) redistributing flow within a channel cross section (for example, to constrict a channel to increase depth in certain areas or to concentrate a braided river into a single channel); and (4) protecting bridges, utility crossings, and structures along the bank.

Most dikes are made with stone fill, but other materials are used. Petersen (1986) provides a comprehensive review of standard techniques. The submerged vane technique has received less coverage in the literature and will be described in more detail in a subsequent section. The technique for bendway weirs also has received little coverage so far. Made of rocks, they function like dikes. They are oriented upstream, at an angle with the bank of, typically, 60º to 80º. Reference is made to Pokrefke (1993) and U.S. Army Corps of Engineers (2002).

8.7.2.3 Dredging Dredging is the process of moving material from one part of a channel to another or to a disposal site on land. It is used most often for deepening or widening navigation channels or for land reclamation. This technique is also described in detail in Petersen (1986).

8.7.3 Submerged Vanes

Submerged vanes are small flow-training structures (foils) designed to modify the near-bed flow pattern and redistribute flow and sediment transport within the channel cross section. The structures are installed at an angle of attack 15º to 25 with the flow, and their initial height is 0.2 to 0.4 times local water depth at the design stage. The vanes function by generating secondary circulation in the flow (Fig. 8-14). The circulation alters the magnitude and direction of the bed shear stresses and causes a change in the distribution of velocity, depth, and sediment transport in the area affected by the vanes. As a result, the riverbed aggrades in one portion of the channel cross section and degrades in another (Fig. 8-15).

Vanes or panels for flow training have been discussed previously by Potapov and Pyshkin (1947); Potapov (1950, 1951); Chabert et al. (1961); and Jansen et al. (1979). However, it is only recently that efforts have been made to optimize vane design and document performance. The first known attempts to develop a theoretical design basis were those of Odgaard and Kennedy (1983) and Odgaard and Spoljaric (1986). Odgaard and Kennedy's efforts are aimed at designing a system of vanes to stop or reduce bank erosion in river curves. In such an application, the vanes are laid out so that the vane-generated secondary current eliminates the centrifugally induced secondary current, which is the root cause of bank undermining. Centrifugally induced secondary current in river bends results from the difference in centrifugal acceleration along a vertical line in the flow because of the nonuniform vertical profile of the velocity. The secondary current forces high-velocity surface current outward and low-velocity near-bed current inward. The increase in velocity at the outer bank increases the erosive attack on the bank, causing it to fail. By directing the near-bed current toward the outer bank, the submerged vanes counter the centrifugally induced secondary current and thereby inhibit bank erosion. The vanes can be laid out to make the water and sediment move through a river curve as if it were straight. Figure 8-15 shows a typical layout, and Fig. 8-16 indicates the primary design variables. Field tests with this application have been conducted by Odgaard and Mosconi (1987); Fukuoka and Watanabe (1989); and others. Figure 8-17(a) shows vanes being installed in a bend of the Wapsipicon River, Iowa, in the summer of 1988 during low flow. Figure 8-17(b) shows the same bend 2 years later.

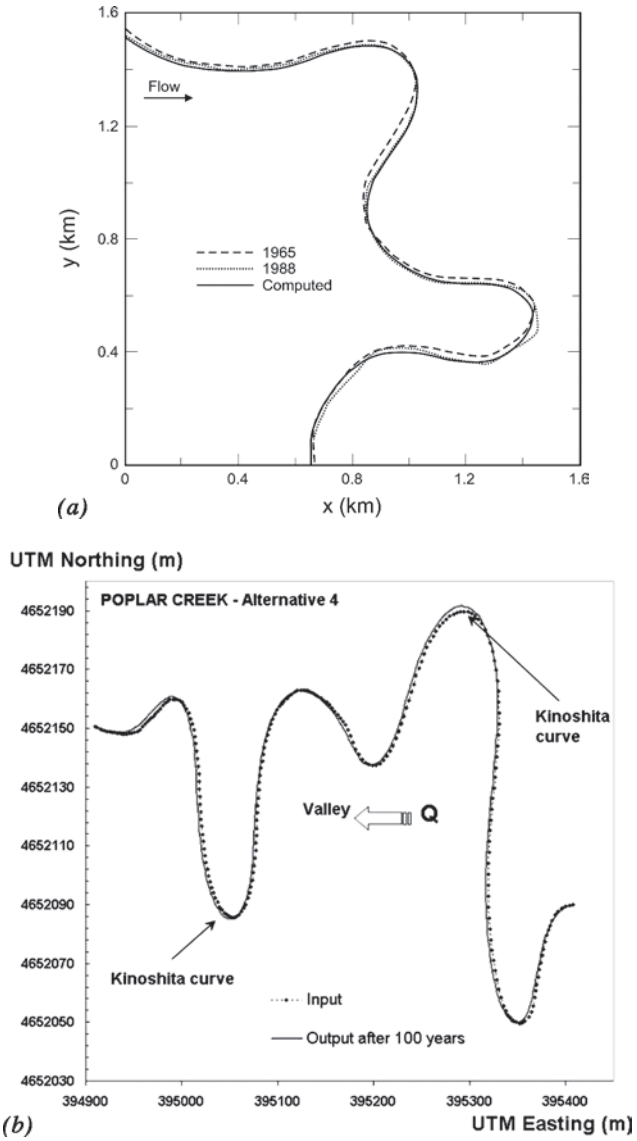

Fig. 8-12. (a) Simulation of the evolution of the Big Muddy River, Illinois (from Garcia et al. (1994)); (b) prediction of planform migration for Poplar Creek, Illinois (from Abad and Garcia (2006)).

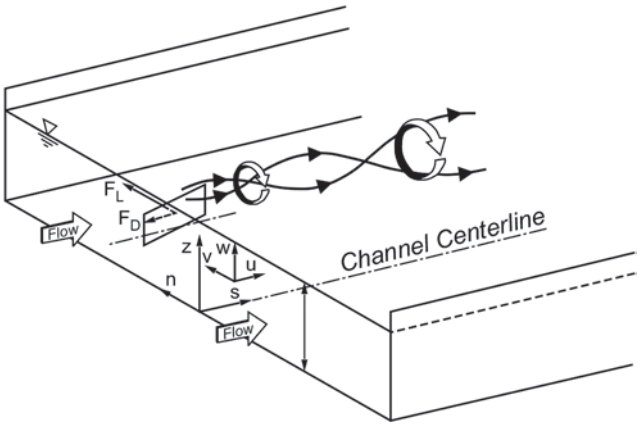

Fig. 8-13. Schematic of flow situation showing vane-induced circulation.

Fig. 8-14. Schematic showing vane-induced circulation.

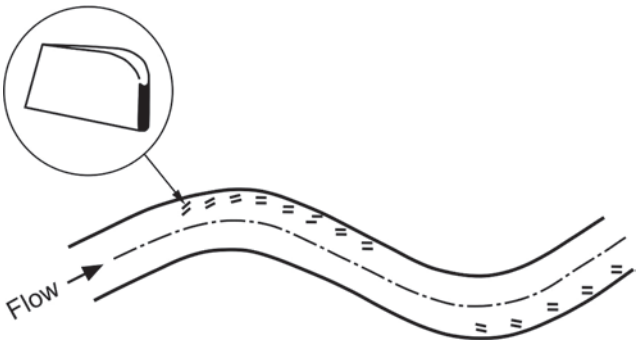

Fig. 8-15. Layout of vane systems in a curved channel.

The technique has been further developed to ameliorate shoaling problems in rivers. This application is suggested by laboratory tests by Odgaard and Spoljaric (1986), in which vanes were laid out to change the cross-sectional profile of the bed in a straight channel. The tests showed that significant changes in depth could be achieved without causing significant changes in cross-sectional area, energy slope, or downstream sediment transport. The changes in cross-sectional average parameters are small because the vane-induced secondary current changes the direction of the bed shear stresses by only a small amount.

Further field and laboratory studies (Odgaard and Wang 1991a; 1991b; Pokrefke 1993; Wang et al. 1996; Sinha and Marelius 2000; Zijlstra 2003; Van Zwol 2004) and three-dimensional numerical modeling of the flow around vanes

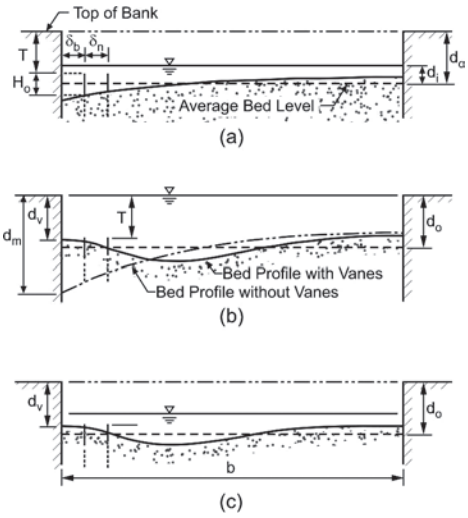

Fig. 8-16. Schematic showing primary design variables and flow sections at (a) installation, (b) subsequent bank-full (design) flow, and (c) subsequent low flow.

Fig. 8-17. (a) Installation of Iowa vanes in the Wapsipinicon River bend, 1988; (b) Iowa vanes 2 years after installation, 1990.

(Marelius and Sinha 1998; Marelius 2001; Flokstra et al. 2003; Abad et al. 2004) have resulted in an improved understanding of the functioning of vanes and an improved design basis.

REFERENCES

Abad, J. D., and Garcia, M. H. (2004). "Conceptual and mathematical model for evolution of meandering rivers in naturalization processes." *Proceedings of Joint Conference on Water Resources Engineering and Water Resources Planning and Management,* EWRI/ASCE, June 27–July 1, Salt Lake City, Utah.

Abad, J. D., and Garcia, M. H. (2006). "RVR meander: A toolbox for re-meandering of channelized streams." *Computers & Geosciences,* 32, 92–101.

Allen, J. R. L. (1977). "Changeable rivers: Some aspects of their mechanics and sedimentation." *River channel changes*, K. J. Gregory, ed., Wiley, New York, 15–45.

Allen, J. R. L. (1978). "L. van Bendegom: A neglected innovation in meander studies." *Fluvial sedimentology,* A. D. Miall, ed., Memoir No. 5, Canadian Society of Petroleum Geologists, Calgary, Alta., 199–209.

Allen, J. R. L. (1982). "Free meandering channels and lateral deposits." *Sedimentary structures: Their character and physical basis*, Vol. 2, Elsevier Science, Amsterdam, New York, 53–100.

Allen, J. R. L. (1985). *Principles of physical sedimentology*. Cambridge University Press, Cambridge, U.K.

Apmann, R. P. (1972). "Flow processes in open channel bends." *Journal of the Hydraulics Division, American Society of Civil Engineers*, 98, 795–809.

ASCE Task Committee on Hydraulics, Bank Mechanics, and Modelling of River Width Adjustments. (1998). "River width adjustments. I: Processes and mechanisms." *Journal of Hydraulic Engineering*, 124(9), 881–902.

Bathurst, J. C., Thorne, C. R., and Hey, R. D., (1979). "Secondary flow and shear stress at river bends." *Journal of the Hydraulics Division, American Society of Civil Engineers*, 105(HY10), 1277–1295.

Beck, S. (1984). "Mathematical modeling of meander interaction." *River meandering*, *Proceedings of the conference Rivers 1983*, C. M. Elliott, ed., ASCE, New York, 932–941.

Beck, S., Harrington, R. A., and Andres, D. D. (1983a). *Lateral channel stability of the Pembina River near Rossington, Alberta*, Alberta Research Council, Edmonton, Alta.

Beck, S., Melfi, D. A., and Yalamanchili, K. (1983b). "Later migration of the Genesee River, New York." *River meandering, Proceedings of the conference Rivers 1983*, C. M. Elliott, ed., ASCE, New York, 510–517.

Begin, Z. B., (1981). "Stream curvature and bank erosion: A model based on the momentum equation." *Journal of Geology*, 89, 497–504.

Bergs, M. A. (1989). "Flow processes in a curved alluvial channel." Ph.D. thesis, University of Iowa, Iowa City, Iowa.

Biedenharn, D. S., Elliot, C. M., and Watson, C. C. (1997). *The WES stream investigation and streambank stabilization handbook*. U.S. Army Corps of Engineers, Vicksburg, Miss.

Blanckaert, K. (2003). "Flow and turbulence in sharp open-channel bends." Ph.D. diss., École Polytechnique Fédérale de Lausanne, Lausanne, Switzerland.

Blanckaert, K., and Graf, W. H. (2001). "Mean flow and turbulence in open-channel bend." *Journal of Hydraulic Engineering, ASCE,* 127(10), 835–847.

Blench, T. (1952). "Regime theory for self-formed sediment-bearing channels." *Transactions, ASCE*, 117, 383–400.

Blondeaux, P., and Seminara, G. (1983). "Bed topography and instabilities in sinuous channels." *River meandering*, *Proceedings of the conference Rivers 1983*, C. M. Elliott, ed., ASCE, New York, 747–758.

Blondeaux, P., and Seminara, G. (1985). "A unified bar-bend theory of river meanders." *Journal of Fluid Mechanics*, 157, 449–470.

Brice, J. C. (1973). "Meandering pattern of the White River in Indiana: An analysis." *Fluvial geomorphology*, M. Morisawa, ed., Allen & Unwin, London, 178–200.

Brice, J. C. (1974). "Evolution of meander loops." *Geological Society of America Bulletin*, 85, 581–586.

Brice. J. C. (1982). "Stream channel stability assessment." *Rep. FHWA/RD-82/021*, Federal Highway Administration, U.S. Department of Transportation, Washington, D.C.

Bridge, J. S. (1976). "Bed topography and grain size in open channel bends." *Sedimentology*, 23, 407–414.

Bridge, J. S. (1977. "Flow, bed topography, grain size and sedimentary structure in open channel bends: A three-dimensional approach." *Earth Surface Processes*, 2, 401–416.

Bridge, J. S. (1984). "Flow and sedimentary processes in river bends: Comparison of field observations and theory." *River meandering*, *Proceedings of the conference Rivers 1983*, C. M. Elliott, ed., ASCE, New York, 857–872.

Bridge, J. S. (1992). "A revised model for water flow, sediment transport, bed topography, and grain size sorting in natural river bends." *Water Resources Research*, 28, 999–1013.

Bridge, J. S. (1993). "The interaction between channel geometry, water flow, sediment transport and deposition in braided rivers." *Braided rivers*, J. L. Best and C. S. Bristow, eds., Spec. Pub. 75, London Geological Society, 13–71.

Bridge, J. S., and Jarvis, J. (1976). "Flow and sedimentary processes in the meandering river South Esk, Glen Clova, Scotland." *Earth Surface Processes*, 1, 303–336.

Bridge, J. S., and Jarvis, J. (1977). "Velocity profiles and bed shear stress over various bed configurations in a river bend." *Earth Surface Processes*, 2, 281–294.

Bridge, J. S., and Jarvis, J. (1982). "The dynamics of a river bend: A study in flow and sedimentary processes." *Sedimentology*, 29, 499–541.

Callander, R. A. (1969). "Instability and river channels." *Journal of Fluid Mechanics*, 36, 465–480.

Callander, R. A. (1978). "River meandering." *Annual Review of Fluid Mechanics*, 10, 129–158.

Carson, M. A., and Lapointe, M. F. (1983). "The inherent asymmetry of river meanders." *Journal of Geology*, 91, 41–55.

Chabert, J., Remillieux, M., and Spitz, I. (1961). "Application de la circulation transversale à la correction des rivieres et à la protection des prises d'eau." *Proc. of the Ninth Convention, Int. Assoc. for Hydraulic Research*, International Association for Hydraulic Research, Dubrounik, Yugoslavia, 1216–1223 (in French).

Chang, H. H. (1979). "Minimum stream power and river channel patterns." *Journal of Hydrology*, 41, 303–327.

Chang, H. H. (1984). "Analysis of river meanders." *Journal of Hydraulic. Engineering, ASCE*, 110(1), 37–50.

Chang, H. H. (1988a). *Fluvial processes in river engineering*, Wiley, New York.

Chang, H. H. (1988b). "On the cause of river meandering." *Proceedings of International Conference on River Regime*, W. R. White, ed., Wiley, New York, 83–94.

Charlton, F. W., Brown, P. M., and Benson, R. W., (1978). "The hydraulic geometry of some gravel rivers in Britain." *Rep. IT180*, Hydraulic Research Station, Wallingford, England.

Cheng, G., and Shen, H. W. (1983). "River curvature-width ratio effect on shear stress." *River meandering*, *Proceedings of the conference Rivers 1983*, C. M. Elliott, ed., ASCE, New York, 687–699.

Chitale, S. V. (1973). "Theories and relationships of river channel patterns." *Journal of Hydrology*, 19, 285–308.

Crosato, A. (1989). *Meander migration prediction,* Vol. 4, Excerpta, G.N.I., Libreria Progetto, Padova, Italy, 169–198.

Darby, S. E. (2002). "Numerical simulation of bank erosion and channel migration in meandering rivers." *Water Resources Research*, 38(9), 1163.

Darby, S. E., and Delbono, I. (2002). "A model of equilibrium bed topography for meander bends with erodible banks." *Earth Surface Processes and Landforms*, 27, 1057–1085.

DeVriend, H. J. (1977). "A mathematical model of steady flow in curved shallow channels." *Journal of Hydraulic Research*, 15(1), 37–54.

DeVriend, H. J., and Geldof, H. J. (1983). "Main flow velocity in short and sharply curved river bends." *Communications of Hydraulics, Rep. 83-6*, Dept. of Civ. Engrg., Delft University of Technology, Delft, The Netherlands.

Dietrich, W. E. (1987). "Mechanics of flow and sediment transport in river bends." *River channels: Environment and process*, K. S. Richards, ed., Blackwell Science, Oxford, U.K., 179–227.

Dietrich, W. E., and Smith, J. D. (1983). "Influence of the point bar on flow through curved channels." *Water Resources Research*, 19(5), 1173–1192.

Dietrich, W. E., and Smith, J. D. (1984). "Bed load transport in a river meander." *Water Resources Research*, 20, 1355–1380.

Dietrich, W. E., Smith, J. D., and Dunne, T. (1979). "Flow and sediment transport in a sand bedded meander." *Journal of Geology*, 87, 305–314.

Dietrich, W. E., and Whiting, P. (1989). "Boundary shear stress and sediment transport in river meanders of sand and gravel." *River meandering*, S. Ikeda and G. Parker, eds., Water Resources Monograph 12, American Geophysical Union, Washington, D.C., 1–50.

Dort, W., Jr. (1978). "Channel migration investigation: Historic channel change maps." Kansas City District, U.S. Army Corps of Engineers, 50.

Duan, J. G., Wang, S. Y., and Jia, Y. (2001). "The applications of the enhanced CCHE2D model to study the alluvial channel migration processes." *Journal of Hydraulic Research*, 39(5).

Dury, G. H. (1966). *The face of the earth*, Penguin, Baltimore, 238.

Engelund, F. (1974). "Flow and bed topography in channel bends." *Journal of the Hydraulic Division, ASCE*, 100, 1631–1648.

Engelund, F. (1975). "Instability of flow in a curved alluvial channel." *Journal of Fluid Mechanics*, 72(1), 145–160.

Engelund, F., and Skovgaard, O. (1973). "On the origin of meandering and braiding in alluvial streams." *Journal of Fluid Mechanics*, 57, 289–302.

Falcon, M. A., and Kennedy, J. F. (1983). "Flow in alluvial-river curves." *Journal of Fluid Mechanics*, 133, 1–16.

Ferguson, R. I. (1973). "Regular meander path models." *Water Resources Research*, 9, 1079–1086.

Ferguson, R. I. (1976). "Disturbed periodic model for river meanders." *Earth Surface Processes*, 1, 337–347.

Ferguson, R. I. (1977). "Meander migration: Equilibrium and change." *River channel changes*, K. J. Gregory, ed., Wiley, New York, 235–263.

Ferguson, R. I., Parsons, D. R., Lane, S. N., and Hardy, R. J. (2003). "Flow in meander bends with recirculation at the inner bank." *Water Resources Research*, 39(11).

Flokstra, C., Jagers, H. R. A., Wiersma, F. E., Mosselman, E., and Jongeling, T. H. G. (2003). "Numerical modeling of vanes and screens." *Technical rep. DC1-331-3*, WL | Delft Hydraulics.

Fredsoe, J. (1978). "Meandering and braiding of rivers." *Journal of Fluid Mechanics*, 84, 609–624.

Friedkin, J. F. (1945). "A laboratory study of the meandering of alluvial rivers." Mississippi River Commission, Waterways Experiment Station, U.S. Army Corps of Engineers, 40.

Fukuoka, S., and Watanabe, A. (1989). "New bank protection methods against erosion in the river." *Proc. of the Japan-China Joint Seminar on Natural Hazard Mitigation*, July 16–20, Kyoto, Japan, 439–448.

Furbish, D. J. (1988). "River-bed curvature and migration: How are they related?" *Geology*, 16, 752–755.

Furbish, D. J. (1991). "Spatial autoregressive structure in meander evolution." *Geological Society of America Bulletin*, 103, 1576–1589.

Garcia, M. H., Bittner, L., and Nino, Y. (1994). "Mathematical modeling of meandering streams in Illinois: A tool for stream management and engineering." *Hydraulic Engineering Series No. 43*, Department of Civil Engineering, University of Illinois at Urbana-Champaign.

Geldof, H. J., and deVriend, H. J. (1983). "Distribution of main flow velocity in alternating river bends." Special Publication 6, International Association of Sedimentologists, U.K., 85–95.

Gottlieb, L. (1976). "Three-dimensional flow pattern and bed topography in meandering channels." *Series Paper 11*, Institute of Hydrodynamics and Hydraulic Engineering, Technical University of Denmark.

Hagerty, D. J. (1991a). "Piping/sapping erosion. I: Basic considerations." *Journal of Hydraulic Engineering*, 117(8), 991–1008.

Hagerty, D. J. (1991b). "Piping/sapping erosion. II: Identification-diagnosis." *Journal of Hydraulic Engineering*, 117(8), 1009–1025.

Hansen, E. (1967). "On the formation of meanders as a stability problem." *Basic Research Progress Rep. 13*, Hydraul. Lab., Technical University of Denmark, 9–13.

Hasegawa, K. (1989). "Universal bank erosion coefficient for meandering rivers." *Journal of Hydraulic Engineering*, 115(6), 744–765.

Henderson, F. M. (1963). "Stability of alluvial channels." *Transactions, ASCE*, 128(I), 657.

Hey, R. D., and Rainbird, P. C. B., (1996). "Three-dimensional flow in straight and curved reaches." *Advances in fluvial dynamics and stratigraphy*, P. A. Carling and M. R. Dawson, eds., Chichester, U.K., Wiley, 33–66.

Hey, R. D., and Thorne, C. R., (1975). "Secondary flows in river channels." *Area* (7), 191–195.

Hickin, E. J. (1974). "The development of meanders in natural river channels." *American Journal of Science*, 274, 414–442.

Hickin, E. J., and Nanson, G. C. (1975). "The character of channel migration on the Beaton River, Northeast British Columbia, Canada." *Geological Society of America Bulletin*, 86, 487–494.

Hodskinson, A., and Ferguson, R. I. (1998). "Numerical modeling of separated flow in river bends: Model testing and experimental investigation of geometric controls on the extent of flow separation at the concave bank." *Hydrological Processes*, 12, 1323–1338.

Hooke, J. M. (1977). "The distribution and nature of changes in river channel patterns: The example of Devon." *River channel changes*, K. J. Gregory, ed., Wiley, New York, 265–280.

Hooke, J. M. (1980). "Magnitude and distribution of rates of river bank erosion." *Earth Surface Processes*, 5, 143–157.

Hooke, J. M. (1984). "Meander behavior in relation to slope characteristics." *River meandering*, *Proceedings of the conference Rivers 1983*, C. M. Elliott, ed., ASCE, New York, 67–76.

Hooke, R. B. (1975). Distribution of sediment transport and shear stress in a meander bend. *Journal of Geology*, 83, 543–565.

Howard, A. D. (1983). "Simulation model of meandering." *River meandering*, *Proceedings of the conference Rivers 1983*, C. M. Elliott, ed., ASCE, New York, 952–963.

Howard, A. D. (1992). "Modeling channel migration and floodplain sedimentation in meandering streams." *Lowland floodplain rivers*, P.A. Carling and G. E. Petts, eds., Wiley, New York, 1–41.

Howard, A. D. (1996). "Modelling channel evolution and floodplain morphology." *Floodplain processes*, M. A. Anderson, D. E. Walling, and P. D. Bates, eds., Wiley, Chichester, U.K., 15–62.

Howard, A. D., and Knutson, T. R. (1984). "Sufficient conditions for river meandering: A simulation approach." *Water Resources Research*, 20, 1659–1667.

Ikeda, S. (1974). "On secondary flow and dynamic equilibrium of transverse bed profile in alluvial curved open channel." *Proceedings of the Japanese Society of Civil Engineers*, 229, 55–65.

Ikeda, S. (1975). "On secondary flow and bed profile in alluvial curved open channel." *Proceedings, 16th Congress, IAHR*, 2, 105–112.

Ikeda, S. (1989). "Sediment transport and sorting in bends." *River meandering*, S. Ikeda and G. Parker, eds., Water Resources Monograph 12, American Geophysical Union, Washington, D.C., 103–126.

Ikeda, S., and Nishimura, T. (1985). "Bed topography in bends of sand-silt rivers." *Journal of Hydraulic Engineering, ASCE*, 111(11), 1397–1411.

Ikeda, S., Parker, G., and Sawai, K. (1981). "Bend theory of river meanders. I: Linear development." Journal of Fluid Mechanics, 112, 363–377.

Ippen, A. T., and Drinker, P. A. (1962). "Boundary shear stresses in curved trapezoidal channels." *Journal of the Hydraulics Division, ASCE,* 88(HY5), 143–179.

Jansen, P. Ph., van Bendegom, L., van den Berg, J., de Vries, M., and Zanen, A. (1979). *Principles of river engineering*, Pitman, London.

Johannesson, H. (1988). "Theory of river meanders." Ph.D. thesis, University of Minnesota, Minneapolis.

Johannesson, H., and Parker, G. (1985). "Computer simulated migration of meandering rivers in Minnesota." *Project Rep. 242*, St. Anthony Falls Hydraulic Laboratory, University of Minnesota.

Julien, P. Y., and Anthony, D. J. (2002). "Bed load motion and grain sorting in a meandering stream." *Journal of Hydraulic Research*, 40(2), 125–133.

Kawai, S., and Julien, P. Y. (1996). "Point bar deposits in narrow sharp bends." *Journal of Hydraulic Research*, 34(2), 205–218.

Kellerhals, R. (1967). "Stable channels with gravel-paved beds." *Journal of the Waterways and Harbors Division, ASCE*, 93(1), 63–84.

Kennedy, R. G. (1895). "The prevention of silting in irrigation canals." *Proceedings, Institution of Civil Engineers,* 119, 281–290.

Kikkawa, H., Ikeda, S., and Kitagawa, A. (1976). "Flow and bed topography in curved open channels." *Journal of the Hydraulics Division, ASCE*, 102(9), 1317–1342.

Kinoshita, R. (1961). "Investigation of channel deformation in Ishikari River." *Report of the Bureau of Resources,* Department of Science and Technology, Japan, 1–174.

Kinoshita, R., and Miwa, H. (1974). "River channel formation which prevents downstream translation of transverse bars." *ShinSabo*, (94), 12–17 (in Japanese).

Kitanidis, P. K., and Kennedy, J. F. (1984). "Secondary current and river-meander formation." *Journal of Fluid Mechanics*, 114, 217–229.

Konditerova, E. A., and Ivanov, I. V. (1969). "Pattern of variation of the length of freely meandering rivers." *Soviet Hydrology: Selected Papers*, 4, 356–364.

Kondrat'yev, N. Ye. (1968). "Hydromorphological principles of computations of free meandering. 1: Signs and indices of free meandering." *Soviet Hydrology: Selected Papers*, 4, 309–335.

Kulemina, N. M. (1973). "Some characteristics of the process of incomplete meandering of the channel of the upper Ob' River." *Soviet Hydrology: Selected Papers*, 6, 518–534.

Lacey, G. (1930). "Stable channels in alluvium." *Proceedings, Institution of Civil Engineers,* 229, 259–292.

Lancaster, S. T., and Bras, R. L. (2002). "A simple model of river meandering and its comparison to natural channels." *Hydrological Processes*, 16, 1–26.

Lane, E. W. (1957). "A study of the shape of channels formed by natural streams flowing in erodible material." U.S. Army Engineer Division, Missouri River.

Langbein, W. B., and Leopold, L. B. (1966). "River meanders—Theory of minimum variance." *Professional Paper 422-H*, U.S. Geological Survey, Washington, D.C.

Langendoen, E. L. (2000). "CONCEPTS—Conservational channel evolution and pollutant transport system." *Research Rep. 16*, USDA-ARS National Sedimentation Laboratory, Oxford, Miss.

Lapointe, M. F.., and Carson, M. A. (1986). "Migration patterns of an asymmetric meandering river: The Rouge River, Quebec." *Water Resources Research*, 22, 731–743.

Lawler, D. M. (2005). "The importance of high-resolution monitoring in erosion and deposition dynamics studies: Examples from estuarine and fluvial systems." *Geomorphology*, 64, 1–23.

Leopold, L. B., and Wolman, M. G. (1957). "River channel patterns—Braided, meandering and *Professional Paper 282B*, U.S. Geological Survey, Washington, D.C.

Leopold, L. B., and Wolman, M. G. (1960). "River meanders." *Geological Society of America Bulletin,* 71, 769–794.

Leopold, L. B., Wolman, M. G., and Miller, J. P. (1964). *Fluvial processes in geomorphology*. Freeman, San Francisco, London.

Lewin, J. (1976). "Initiation of bed forms and meanders in coarse-grained sediment." *Geological Society of America Bulletin*, 87, 281–285.

Lewin, J. (1978). "Meander development and floodplain sedimentation: A case study from mid-Wales." *Geological Journal*, 13, 25–36.

Lewin, J., and Brindle, B. J. (1977). "Confined meanders." *River channel changes*, K. J. Gregory, ed., Wiley, New York, 221–233.

Lewis, G. W., and Lewin, J. (1983). "Alluvial cut-offs in Wales and the Borderlands." *Modern and ancient fluvial systems*, Blackwell Science, Oxford, U.K., 145–154.

MacDonald, T., Parker, G., and Leuthe, D. (1992). "Inventory and analysis of stream meander problems in Minnesota." Project Report. St. Anthony Falls Hydraulic Laboratory, University of Minnesota.

Marelius, F. (2001). "Experimental investigation of vanes as means of beach protection." *Coastal Engineering*, 42 (1), 1–16.

Marelius, F., and Sinha, S., (1998). "Experimental investigation of flow past submerged vanes." *Journal of Hydraulic Engineering*, 124(5), 542–545.

Meakin, P., Sun, T., Jossang, T., and Schwarz, K. (1996). "A simulation model for meandering rivers and their associated sedimentary environments." *Physica A*, 233, 606–618.

Millar, R. G. (2000). "Influence of bank vegetation on alluvial channel patterns." W*ater Resources Research*, 36(4), 1109–1118.

Mosselman, E. (1995). "A review of mathematical models of river planform changes." *Earth Surface and Landforms*, 20, 661–670.

Mosselman E. (1998). "Morphological modeling of rivers with erodible banks." *Hydrological Processes*, 12, 1357–1370.

Nagata, N., Hosoda, T., and Muramoto, Y. (2000). "Numerical analysis of river channel processes with bank erosion." *Journal of Hydraulic Engineering*, 126(4), 243–252.

Nanson, G. C. (1980). "Point bar and floodplain formation of the meandering Beatton River, northeastern British Columbia, Canada." *Sedimentology*, 27, 3–29.

Nanson, G. C., and Hickin, E. J. (1983). "Channel migration and incision on the Beatton River." *Journal of Hydraulic Engineering, ASCE*, 109(3), 327–337.

Nanson, G. C., and Hickin, E. J. (1986). "A statistical analysis of bank erosion and channel migration in western Canada." *Geological Society of America Bulletin*, 97, 497–504.

Nelson, J. M. (1988). "Mechanics of flow and sediment transport over nonuniform erodible beds." Ph.D. thesis, University of Washington, Seattle.

Nelson, J. M., and Smith, J. D. (1989). "Flow in meandering channels with natural topography," *River meandering*, S. Ikeda and G. Parker, eds., Water Resources Monograph 12, American Geophysical Union, Washington, D.C., 69–102.

Odgaard, A. J. (1981). "Transverse bed slope in alluvial channel bends." *Journal of the Hydraulics Division, ASCE*, 107(12), 1677–1694.

Odgaard, A. J. (1984). "Flow and bed topography in alluvial channel bend." *Journal of Hydraulic Engineering, ASCE*, 110(4), 521–536.

Odgaard, A. J. (1986a). "Meander flow model. I: Development." *Journal of Hydraulic Engineering, ASCE*, 112(12), 1117–1136.

Odgaard, A. J. (1986b). "Meander flow model. I: Applications." *Journal of Hydraulic Engineering, ASCE*, 112(12), 1137–1150.

Odgaard, A. J. (1987). "Streambank erosion along two rivers in Iowa." *Water Resources Research*, 23(7), 1225–1236.

Odgaard, A. J. (1989a). "River-meander model. I: Development." *Journal of Hydraulic Engineering, ASCE*, 115(11), 1433–1450.

Odgaard, A. J. (1989b). "River-meander model. II: Applications." *Journal of Hydraulic Engineering, ASCE*, 115(11), 1431–1464.

Odgaard, A. J., and Bergs, M. A. (1988). "Flow processes in a curved alluvial channel." *Water Resources Research*, 24(1), 45–56.

Odgaard, A. J., and Kennedy, J. F. (1983). "River-bend bank protection by submerged vanes." *Journal of Hydraulic Engineering, ASCE*, 109(8), 1161–1173.

Odgaard, A. J., and Mosconi, C. E. (1987). "Streambank protection by submerged vanes." *Journal of Hydraulic Engineering, ASCE*, 113(4), 520–536.

Odgaard, A. J., and Spoljaric, A. (1986). "Sediment control by submerged vanes." *Journal of Hydraulic Engineering, ASCE*, 112(12), 1164–1181.

Odgaard, A. J., and Wang, Y. (1991a). "Sediment management with submerged vanes. I: Theory." *Journal of Hydraulic Engineering, ASCE*, 117(3), 267–283.

Odgaard, A. J., and Wang, Y. (1991b). "Sediment management with submerged vanes. II: Applications." *Journal of Hydraulic Engineering, ASCE*, 117(3), 284–302.

Osman, A. M., and Thorne, C. R. (1988). "Riverbank stability analysis. I: Theory." *Journal of Hydraulic Engineering, ASCE*, 114(2), 134–150.

Parker, G. (1976). "On the cause and characteristic scales of meandering and braiding in rivers." *Journal of Fluid Mechanics*, 76, 457–480.

Parker, G. (1982). "Stability of the channel of the Minnesota River near the State Bridge 93, Minnesota." *Project Rep. 205*, St. Anthony Falls Hydraulic Laboratory, University of Minnesota, Minneapolis.

Parker, G. (1983). "Theory of meander bend deformation." *River meandering*, *Proceedings of the conference Rivers 1983*, C. M. Elliott, ed., ASCE, New York, pp. 722–732.

Parker, G., and Andrews, E. D. (1985). "Sorting of bed load sediment by flow in meander bends." *Water Resources Research*, 21(9), 1361–1373.

Parker, G., and Andrews, E. D. (1986). "On the time development of meander bends." *Journal of Fluid Mechanics*, 162, 139–156.

Parker, G., and Johannesson, H. (1989). "Observations on several recent theories of resonance and over deepening in meandering channels." *River meandering*, S. Ikeda and G. Parker, eds., Water Resources Monograph No. 12, American Geophysical Union, Washington, D.C., 379–415.

Parker, G., Johannesson, H., Garcia, M., and Okabe, K. (1988). "Diagnostic study of the siltation problem at the Wilmarth Power Plant Cooling Water Intake on the Minnesota River." *Project*

Rep. 277, St. Anthony Falls Hydraulic Laboratory, University of Minnesota, Minneapolis.

Parker, G., Panayiotis, P., and Akiyama, J. (1983). "Meander bends of high amplitude." *Journal of the Hydraulics Division, ASCE*, 109, 1323–1337.

Parker, G., Sawai, K., and Ikeda, S., (1982). "Theory of river meanders. 2: Nonlinear deformation of finite-amplitude bends." *Journal of Fluid Mechanics*, 115, 303–314.

Petersen, M. S. (1986). *River engineering*, Prentice-Hall, Englewood Cliffs, N.J.

Pizzuto, J. E., and Meckelnburg, T. S. (1989). "Evaluation of a linear bank erosion equation." *Water Resources Research*, 25, 1005–1013.

Pokrefke, T. J. (1993). "Demonstration erosion control project monitoring program." *Technical Rep. HL-93-3*, Waterways Experiment Station, U.S. Army Corps of Engineers, Vicksburg, TN.

Potapov, M. V. (1950). *Sochineniya v trekh' tomakh—I*. Gos Izd. Sel'sko-khozyaistvennoi Lit., Moscow (in Russian).

Potapov, M. V. (1951). "Sochineniya v trekh tomakh—II." Gos. Izd. Sel'sko-khozyaistvennoi Lit., Moscow, the Soviet Union (in Russian).

Potapov, M. V., and Pyshkin, B. A. (1947). *Metod poperechnoy tsirkulyatsii. I: Ego primenenie v. gidrotekhnike*. Izd. Ak. Nauk SSSR, Moscow, Leningrad (in Russian).

Richards, K. S. (1982). *Rivers: Form and process in alluvial channels*. Methuen, London.

Rozovskii, I. L. (1957). *Flow of water in bends of open channels*. Academy of Sciences of the Ukrainian SSR, Kiev, USSR (in Russian); English translation, Israel Program for Scientific Translation, Jerusalem, Israel, 1961.

Schumm, S. A. (1963). "Sinuosity of alluvial rivers on the Great Plains." *Geological Society of America Bulletin*, 74, 1089–1100.

Schumm, S. A. (1983). "River morphology and behavior: Problems of extrapolation." *River meandering*, *Proceedings of the conference Rivers 1983*, C. M. Elliott, ed., ASCE, New York, 16–29.

Schumm, S. A. (1985). "Patterns of alluvial rivers." *Annual Review of Earth and Planetary Science*, 13, 5–27.

Schumm, S. A., and Khan, H. R. (1971)."Experimental study of channel patterns." *Nature*, 233, 407–409.

Schumm, S. A., and Khan, H. R. (1972). "Variability of river patterns." *Nature Physical Science*, 237, 75–76.

Seminara, G., and Tubino, M. (1989). "Alternate bars and meandering: Free, forced and mixed interactions." *River meandering*, S. Ikeda and G. Parker, eds., Water Resources Monograph No. 12, American Geophysical Union, Washington, D.C., 267–320.

Seminara, G., Zolezzi, G., Tubino, M., and Zardi, D. (2001). "Downstream and upstream influence in river meandering. 2: Planimetric development." *Journal of Fluid Mechanics*, 438, 213–230.

Shimizu, Y., and Itakura, T. (1989). "Calculation of bed variation in alluvial channels." *Journal of Hydraulic Engineering*, 115, 367–384.

Simons, D. B., and Sentürk, F. (1977). *Sediment transport technology*. Water Resources Publications, Fort Collins, Colo.

Sinha, S. K., and Marelius, F., (2000). "Analysis of flow past submerged vanes." *Journal of Hydraulic Research*, 38(1), 65–72.

Smith, J. D., and McLean, S. R. (1984). "A model for flow in meandering streams." *Water Resources Research*, 20, 1301–1315.

Stølum, H.-H. (1996). "River meandering as a self-organization process." *Science*, 271(5256), 1710–1713.

Stølum, H.-H. (1997). "Fluctuations at the self-organized critical state." *Physical Review E*, 56(6), 6710–6718.

Stølum, H.-H. (1998). "Planform geometry and dynamics of meandering rivers." *Geological Society of America Bulletin*, 110(11), 1485–1498.

Struiksma, N., Olesen, K. W., Flokstra, C., and DeVriend, H. J. (1985). "Bed deformation in curved alluvial channels." *Journal of Hydraulic Research*, 23, 57–79.

Sun Tao, Meakin, P., and Jossang, T. (2001a). "Meander migration and the lateral tilting of floodplains." *Water Resources Research*, 37(5), 1485–1502.

Sun Tao, Meakin, P., and Jossang, T. (2001b). "A computer model for meandering rivers with multiple bed load sediment sizes. 1: Theory." *Water Resources Research*, 37(8), 2227–2241.

Sun Tao, Meakin, P., and Jossang, T. (2001c). "A computer model for meandering rivers with multiple bed load sediment sizes. 2: Computer simulations." *Water Resources Research*, 37(8), 2243–2258.

Sun Tao, Meakin, P., Jossang, T., and Schwarz, K. (1996). "A simulation model for meandering." *Water Resources Research*, 32(9), 2937–2954.

Surkan, A. J., and van Kan, J. (1969). "Constrained random walk meander generation." *Water Resources Research*, 5, 1343–1352.

Thakur, T. R., and Scheidegger, A. E. (1968). A test of the statistical theory of meander formation. *Water Resources Research*, 4, 317–329.

Thakur, T. R., and Scheidegger, A. E. (1970). Chain model of river meanders. *Journal of Hydrology*, 12, 25–47.

Thomson, J., (1876). "On the origin of windings of rivers in alluvial plains, with remarks on the flow of water round bends in pipes." *Proceedings of the Royal Society of London*, 25, 5–8.

Thomson, J. (1879). "Flow round river bends." *Proceedings, Institute of Mechanical Engineers,* 6, 456–460.

Thorne, C. R., et al. (1983). Measurements of bend flow hydraulics on the Fall River at low stage. *WRFSL Rep. 83-9P*, National Park Service, 107C Natural Resources, Colorado State University, Fort Collins, Colo.

Thorne, C. R., and Osman, A. M. (1988). "Riverbank stability analysis. II: applications." *Journal of Hydraulic Engineering, ASCE*, 114(2), 151–172.

Thorne, C. R., Zevenbergen, L. W., Pitlick, J. C., Rais, S., Bradley, J. B., and Julien, P. Y. (1985). "Direct measurements of secondary currents in a meandering sand-bed river." *Nature*, 316(6022), 746–747.

Tubino, M., and Seminara, G. (1990). "Free-forced interactions in developing meanders and suppression of free bars." *Journal of Fluid Mechanics*, 214, 131–159.

U.S. Army Corps of Engineers. (2002). "Physical model test for bend way weir design criteria." *Technical Report ERDC/CHL TR-02-28*, Coastal and Hydraulics Laboratory, Vicksburg, TN.

Van Bendegom, L. (1947). "Eenige beschouwingen ovrriviermorphologie en rivierverbetering." *De Ingenieur*, 59(4),1–11.

Van Zwol, J. A. (2004). "Design aspects of submerged vanes." M.Sc. thesis, Faculty of Civil Engineering and Geosciences, Delft University of Technology, Delft, The Netherlands.

Von Schelling, H. (1951). "Most frequent particle paths in a plane." *American Geophysical Union Transactions*, 32, 222–226.

Wang, Y., Odgaard, A. J., Melville, B. W., and Jain, S. C. (1996). "Sediment control at water intakes." *Journal of Hydraulic Engineering, ASCE*, 122(6), 353–356.

Whiting, P. J., and Dietrich, W. E. (1993a). "Experimental studies of bed topography and flow patterns in large-amplitude meanders 1: Observations." *Water Resources Research*, 29(11).

Whiting, P. J., and Dietrich, W. E. (1993b). "Experimental studies of bed topography and flow patterns in large-amplitude meanders. 2: Mechanisms." *Water Resources Research*, 29(11).

Whiting, P. J., and Dietrich, W. E. (1993c). "Experimental constraints on bar migration trough bends: Implications for meander wavelength selection." *Water Resources Research*, 29(4).

Wolman, M. G., and Leopold, L. B. (1957). "River floodplains: Some observations on their formation." *Professional Paper 282-G*, U.S. Geological Survey, Washington, D.C., 183–210.

Yang, C. T. (1971). "On river meanders." *Journal of Hydrology*, 13, 231–253.

Yen, B. C. (1965). "Characteristics of subcritical flow in a meandering channel." *Technical paper*, Institute of Hydraulic Research. The University of Iowa, Iowa City.

Yen, B. C. (1972). "Spiral motion of developed flow in wide curved open channels." *Sedimentation*, H.W. Shen, ed., Fort Collins, Colo., 22.

Yen, B. C. (1975). "Spiral motion and erosion in meanders." *Proceedings of the 16th Congress, International Association for Hydraulic Research*, 338–346.

Yen, C., and Yen, B. C. (1971). "Water surface configuration in channel bends." *Journal of Hydraulics Division, ASCE*, 97, 303–321.

Yen, C-L. (1970). "Bed topography effect on flow in a meander." *Journal of the Hydraulics Division, ASCE*, 96 (HY1), 57–73.

Yen, C-L., and Lee, K. T. (1995). Bed topography and sediment sorting in channel bend with unsteady flow. *Journal of Hydraulic Engineering*, vol. 121, No. 8.

Zeller, J. (1967). "Meandering channels in Switzerland." *International Association of Scientific Hydrology, Symp. On River Morphology*, Bern, 75, 174–186.

Zimmermann, C., and Kennedy, J. F. (1978). "Transverse bed slopes in curved alluvial streams." *Journal of the Hydraulics Division, ASCE*, 104(1), 33–48.

Zijlstra, R. (2003). "The morphological effect of bottom vanes." M.Sc. thesis, Faculty of Civil Engineering and Geosciences, Delft University of Technology, Delft, The Netherlands.

Zolezzi, G., and Seminara, G. (2001). "Downstream and upstream influence in river meandering. 1: General theory and application to overdeepening." *Journal of Fluid Mechanics*, 438, 183–211.

Copyrighted Materials
Copyright © 2008 American Society of Civil Engineers (ASCE)
Retrieved from www.knovel.com

CHAPTER 9

Stream Restoration

F. Douglas Shields, Jr., Ronald R. Copeland, Peter C. Klingeman, Martin W. Doyle, and Andrew Simon

9.1 INTRODUCTION

9.1.1 Scope

This chapter describes the application of the principles described elsewhere in this manual to a special class of engineering problems: stream restoration. Basic concepts are presented first in a qualitative discussion of "big ideas" rather than technical "how-to" guidance. This is followed by a description of how to prepare and execute a sediment studies plan for a stream restoration project. The generic approach described here may be too elaborate for small-scale, simple projects, but is less complex than needed for systemic types of restoration that aim to promote fundamental shifts in fluvial characteristics. However, some sedimentation analysis is needed for all stream restoration projects. Analytical tools useful for restoration analysis range from empirical relationships many decades old to recently developed science. References are provided in lieu of a full description of some of the analytical tools.

9.1.2 Basic Concepts

9.1.2.1 Definitions The term "river restoration" is used to refer to a wide spectrum of activities (Table 9-1). Definition of terms is an essential starting point, because the engineer must be able to communicate clearly with project stakeholders to create realistic expectations for project outcomes. Stakeholders may prefer to call a project "restoration," when in fact it is something else (e.g., an effort to improve aesthetics). No harm is done if everyone understands that the project will not restore a preexisting ecosystem. Whereas restoration aims to return an ecosystem to a former condition, rehabilitation and reclamation imply putting a landscape to a new or altered use to serve a particular human purpose. Restoration is not preservation, which keeps conditions in their current state, nor is it naturalization, which targets socially desirable improvement, but not a preexisting state. True restoration may be thought of as an attempt to return an ecosystem to its historic (predegradation) trajectory (SER 2002). Although this "trajectory" may be impossible to determine with accuracy, the general direction and boundaries may be established through a combination of information about the system's previous state, studies on comparable intact ecosystems, information about regional environmental conditions, and analysis of other ecological, cultural, and historical reference information (SER 2002). In this chapter, "restoration" refers to restoration, rehabilitation, and components of the other activities listed in Table 9-1 that lead to partial recovery of predisturbance ecosystem functions and attributes.

- In practice, river restoration projects are either targeted at entire watersheds or at reaches of channel 20 to 100 channel widths long, or more local measures to control erosion of gullies, zero-order tributaries, or single bends (Shields et al. 1999). Smaller-scale local measures are nested within reach-scale projects, whereas watershed restoration projects include reach-scale efforts and/or activities and programs designed to fundamentally impact land use and management (Williams et al. 1997). Watershed-scale actions are generally preferred from an engineering and ecological perspective because they have the greatest potential to influence fundamental causes of degradation. Fluvial processes operating at landscape or watershed scale can govern system response at smaller scales. However, economic and political factors usually dictate smaller-scale strategies for restoration projects. Local measures often used for restoration include erosion control structures (e.g., bank protection measures or grade control structures), floodplain and streambank revegetation, and habitat

Table 9-1 Definitions for Terms often Associated with River Restoration (NRC 1992; Brookes and Shields 1996; FISRWG 1998)

Term	Definition	Remarks
Restoration	Reestablishment of the structure and function of ecosystems. Ecological restoration is the process of returning an ecosystem as closely as possible to predisturbance conditions and functions. In the United States "predisturbance" usually refers to pre-European settlement. Because ecosystems are dynamic, perfect replication of a previous condition is impossible.	The restoration process re-establishes the general structure, function, and dynamic but self-sustaining behavior of the ecosystem. It is a holistic process not achieved through the isolated manipulation of individual elements.
Rehabilitation	Partial recovery of ecosystem functions and processes. Rehabilitation projects include structural measures and "assisted recovery." Assisted recovery refers to removal of a basic perturbation or disturbance (e.g., excluding grazing livestock from a riparian zone) and allowing natural processes (e.g., regrowth of vegetation, fluvial processes) to operate, leading to recovery of ecosystem function.	Rehabilitation does not necessarily re-establish the predisturbance structure, but does establish geological and hydrologically stable landscapes that support the natural ecosystem mosaic.
Preservation	Activities to maintain current functions and characteristics of an ecosystem or to protect it from future damage or losses.	
Mitigation	An activity to compensate for or alleviate environmental damage. Mitigation may occur at the damaged site or elsewhere. It may restore a site to a socially acceptable condition, but not necessarily to a natural condition.	Mitigation is often a permit requirement as part of some nonrestoration type of action; it thus may form the basis for a restoration project.
Naturalization	Management aimed at establishing hydraulically and morphologically varied, yet dynamically stable fluvial systems that are capable of supporting healthy, biologically diverse aquatic ecosystems. Does not require reference to a certain preexisting state.	The naturalization concept (Rhoads and Herricks 1996; Rhoads et al. 1999) recognizes that naturalization strategies are socially determined and place-specific. In human-dominated environments recurring human management and manipulation may be a desired and even necessary ingredient in the dynamics of the "naturalized" system.
Creation	Forming a new system where one did not formerly exist (e.g., constructing a wetland).	Concepts similar to those used in restoration or rehabilitation are often applied to produce ecosystems consistent with contemporary hydrology and morphology.
Enhancement	Subjective term for activities undertaken to improve existing environmental quality.	Stream enhancement projects of the past often emphasized changing one or two physical attributes in expectation that biological populations would respond favorably. But monitoring data were typically limited.
Reclamation	A series of activities intended to change the biophysical capacity of an ecosystem. The resulting ecosystem is different from the ecosystem existing prior to recovery.	Historically used to refer to adapting wild or natural resources to serve a utilitarian purpose, such as draining wetlands for agriculture.

structures (Section 9.5.2). Reach-scale measures include local measures applied over long reaches plus fencing to exclude livestock from stream corridors, channel reconstruction (Section 9.5.1.1.2), floodplain reconnection, dam removal, and revision of reservoir release strategies. Watershed-scale efforts include widespread application of these local and reach strategies plus programs that address exotic species, land use management, best management practices for forestry and agriculture, and storm water management. Strategies for restoration projects often include activities to promote higher levels of physical dynamism (e.g., flooding, avulsion, island formation, braiding, channel migration) in streams that have been dammed, leveed, or channelized.

On the other hand, many stream systems have been so disturbed by human activities or natural events that they have levels of physical instability that far exceed natural levels to which plants and animals are adapted. Restoration activities in these systems involve recovering stability through flow regulation, revegetation, and building erosion control structures (Shields et al. 1999). A tension exists between restoring the dynamic character of fluvial systems and providing socially acceptable levels of channel stability. During the last 50 years, most efforts at stream manipulation have emphasized stabilization. The shift toward allowing dynamic behavior may be difficult for many stakeholders to accept—given their lack of experience with such approaches. This concept is explored further in Section 9.5.

9.1.2.2 River Dynamism Because restoration implies at least a partial return to naturally dynamic structure, processes, and functions, it is useful to consider the characteristics of unmodified or lightly impacted rivers. When viewed over several decades, natural fluvial systems appear to be complex physically and ecologically; well connectedw vertically between water and substrate, longitudinally between upstream and downstream zones, and laterally between channels and floodplains; and infrequently disturbed by large natural events that keep the system in a long-term state of adaptation to seek balance and stability (Vannote et al. 1980; Williamson et al. 1995a; Bella et al. 1996; Klingeman et al. 1998). The movement of water and the transport of sediment and large woody debris cause the physical features of rivers to change continually. Although channel slope, sinuosity, and floodplain elevation evolve gradually, smaller-scale features such as individual bends, bars, and short bank segments may change rapidly during high flows. Large flows cause extensive interactions between river channels and floodplains. Infrequent disruptive events such as floods, earthquakes, volcanic eruptions, and landslides often trigger systemwide fluvial response. Severe droughts also constitute a type of natural disturbance.

The response of a fluvial system to natural or manmade disturbance varies with the geomorphic context. For example, lightly altered stream systems in regions of mild relief and humid climate (e.g., the United Kingdom or the eastern coastal plain of the United States) approach a conceptual ideal referred to as dynamic equilibrium (Schumm 1977). Bank erosion and bank-line migration typically occur in such a stream, but over a period of, say, several decades, the reach-average channel width, depth, and slope do not change, and sediment outflow is equal to sediment inflow (Thorne et al. 1996a). Furthermore, the average dimensions of such stream channels appear to be power functions of discharge of a certain frequency (see Section 9.3.1). When perturbed, such systems tend to respond in a way that returns the channel dimensions to the equilibrium status or to a new set of equilibrium dimensions. In contrast, systems with high-variance flood-frequency regimes are governed by extreme floods and exhibit transient behavior without the development of "characteristic" geometries typical of systems in dynamic equilibrium. Such fluvial systems are common in arid, semiarid, and proglacial environments. Flood-dominated streams pose an especially difficult challenge for restoration because system dynamics are pulsed, episodic, and often catastrophic in nature. A single flood can radically reconfigure stream morphology for years, decades, or centuries (Baker et al. 1988).

Stream ecosystems are resilient and well adapted to natural disturbances (Pickett and White 1985). Removal of moderate disturbances causes progressive physical changes (e.g., infilling of pools by sediment) and reduces the ability of biological populations to recover from severe disturbances. Biological changes follow removal of disturbances. For example, the plant community in a large fresh-water marsh in an arid hydrologically closed basin was found to require significant interannual flow variation (Klingeman et al. 1971). In another case, an intermediate frequency of bed-mobilizing events was associated with maximum species richness in a gravel-bed stream (Townsend et al. 1997). Evidently a greater frequency of bed disturbance reduced richness by excluding taxa that could not quickly recolonize in the intervals between disturbances, whereas less frequent disturbance allowed competitive exclusion of species that were capable colonists but poor competitors.

9.1.3 Role of Sedimentation Engineering in Stream Restoration Projects

9.1.3.1 The Engineer as Part of a Team Comprehensive restoration activities influence the entire fluvial system—including the channel, banks, riparian zone, and floodplain—and address biological processes and functions as well as physical conditions and river flows. Thus, hydrology, hydraulics, sediment transport, and channel morphology must be evaluated for the restoration site and for other potentially impacted areas. Frequently the same engineer or engineering team assumes responsibility for hydrologic, hydraulic, and sedimentation analyses. For example, the same person may perform hydrologic simulation to generate design discharges; backwater computations to predict water surface elevation, depths, velocities, and shear stresses at design discharge; and sediment transport computations to assess potential for erosion and sedimentation. Regardless of the division of labor, the persons charged with sedimentation engineering analyses should be involved in project planning, design, construction, and postconstruction activities (monitoring, operation, maintenance, and management).

Stream channel restoration projects can succeed as engineering exercises but fail dismally as ecological resource recovery efforts. As noted above, the definitions for restoration-type activities imply that the bottom-line objective for these efforts is ecological. It is imperative, therefore, that the engineer obtain guidance and input from

a multidisciplinary team including earth and natural scientists. Communication within such a team is often difficult, because each discipline has its own values, tacit assumptions, and jargon. FISRWG (1998) can be very helpful in cross training among disciplines and facilitating team communication. Successful team function depends upon members working within the confines of their areas of expertise but understanding and interacting with other team members. A hydraulic engineer with a short course in ecology is not qualified to set habitat objectives, whereas a fisheries biologist with a short course in fluvial geomorphology is similarly not qualified to perform geomorphic assessment or channel design. Although many hydraulic engineers have broad experience in river erosion and sedimentation, team participation by geomorphologists (persons with regional experience and advanced degrees) is often necessary if the project locale is characterized by dynamic landforms and channels.

9.1.3.2 Setting Objectives Restoration project objectives should be defined early and clearly by stakeholders. Support for a restoration project is usually related to broad social, political, and institutional goals (Smith and Klingeman 1998). For implementation, such goals require rephrasing in terms of achievable objectives with measurable outcomes. Thus, although project goals may be general, project objectives must be specific and quantified to allow clear communication and postproject appraisal. Facilitation by the project manager and by technical experts such as the sedimentation engineer may be needed to convert general goals into achievable objectives, as well as to build consensus among diverse stakeholder groups and to ensure that objectives are clearly stated and not contradictory. For example, some projects may inadvertently adopt mutually exclusive objectives such as (1) the elimination of stream bank erosion and (2) the restoration of riparian plant communities that depend on erosion and deposition. Setting objectives for restoring physical habitat value to degraded river corridors requires an assessment of current habitat quality and a description of the factors contributing to degradation. As planning and design proceed, additional social or natural constraints may become apparent, and the original objectives may need to be modified accordingly.

9.1.3.2.1 Habitat Assessment and Setting Objectives Restoration project objectives often are phrased in terms of habitat manipulation. River corridors are often a rich complex of plant and animal habitats. Each life stage of each species has its own habitat requirements, and these are often expressed as ranges of physical variables. However, because stream corridors contain many species, and because habitat requirements are normally not known with precision, assessing the current status of habitat quantity or quality is inexact and involves professional judgment. Many natural events and human activities degrade habitat (Table 9-2), but the nature and magnitude of the degradation is hard to quantify. The engineer must work closely with biologists or ecologists to obtain an adequate assessment of the current status of habitat quality and to define critical elements that should be addressed in the restoration project. A geomorphologist can assist by identifying the factors responsible for physical habitat characteristics. The engineer may provide expertise in obtaining and interpreting data and model simulations describing physical aspects of habitat such as discharge, bed material characteristics, flow width and depth, current velocity, temperature, turbidity, and dissolved oxygen concentration.

An introduction to quantitative habitat assessment tools including the instream flow incremental methodology and the habitat evaluation procedure is provided by Federal Interagency Stream Restoration Working Group (FISRWG

Table 9-2 Typical Forms of River Corridor Degradation (FISRWG 1998; SRSRT 1994)

Basic cause	Typical examples	Types of degradation
Natural events	Floods, landslides, earthquakes, other tectonic events	Alteration of habitat, blockage of access to habitat, change in water quality or quantity
Land use changes	Urbanization, logging, animal grazing, mining, road building	Direct: Damage to banks and bed from animals and machines, pollution. Indirect: Increase in sediment production, water pollution, reduction in shade and organic inputs (leaves and twigs) from riparian zone, perturbation of hydrologic patterns
Flow regulation, withdrawal, or diversion	Dams, irrigation withdrawals, interbasin transfers	Depletion of aquatic habitat, inundation of stream habitat, replacement of natural flow patterns with regulated flow, perturbation of sediment transport patterns
Channel modifications	Channelization, bank protection, clearing, and snagging	Replacement of natural boundaries and geometries, overall simplification of physical complexity and heterogeneity.

1998). Additional tools for evaluating stage, discharge, and other time series variables relative to a reference or undegraded condition are described by Richter et al. (1996; 1998).

9.1.3.2.2 Effects of Project Scale on Objectives Project scale is a major consideration for stakeholders and the design team in setting objectives (Smith and Klingeman 1998). Project scope and scale control the breadth of restoration options (Klingeman 1998; Smith and Klingeman 1998) as well as the role of sedimentation engineering. Early stream restoration projects were usually small-scale efforts to manipulate physical habitat (e.g., Thompson (2002b)). Similar efforts remain common today. These projects typically focus on local scour and deposition but often do not consider sediment transport beyond the immediate site. Initial successes and failures showed the need to develop approaches that would operate at watershed and ecosystem scales using concepts from physical and biological sciences. A larger-scale project may address major system processes such as channel meandering, ecosystem diversity, and ecosystem complexity.

9.1.3.2.3 Opportunities Offered by Large-Scale Projects A broad, integrated approach is usually needed to rehabilitate severely degraded streams. Project planning that addresses habitat collectively rather than for individual species is usually preferred. Such a collective approach ("whole system restoration") may necessitate actions that address riparian zones, floodplains, and watersheds. General objectives have been suggested for restoring large-scale natural riverine functions (NRC 1992; Williamson et al. 1995a; 1995b; Bella et al. 1996), including the following:

- Restore dynamic ecosystem processes and functions in channels, riparian zones, and floodplains, including flooding, erosion, deposition, and exchange of sediment and organic material between channels and floodplains.
- Restore habitat diversity and complexity, system connectivity, and natural disturbance regimes.
- Provide a means whereby natural processes will function with little human intervention.

As an example of large-scale restoration, consider a channelized stream with extremely degraded aquatic habitat. One restoration strategy might feature the reinstatement of the meandering planform that existed before channelization. Meanders could be restored using strategies that either limited or expanded natural processes. The new channel alignment could be (1) designed and constructed, (2) designed and then allowed to develop through fluvial processes with structural constraints at key points, or (3) allowed to develop without intervention or structural constraint. Comparing these alternatives may require extensive sedimentation engineering analysis. Clearly, option (1) could have the greatest initial cost and create the greatest disturbance of existing conditions but also pose the least risk of subsequent changes, whereas option (3) would tend to be just the opposite—having the least cost and least immediate disturbance but the highest uncertainty regarding the predictability of subsequent changes. The latter option would require the most challenging sedimentation analyses.

9.1.3.3 Specific Habitat Restoration Objectives Habitat goals should be based on the attributes of relatively unaltered aquatic ecosystems or the causes of habitat degradation. General goals (e.g., improve water quality for aquatic organisms) must be supported by more specific objectives (e.g., reduce mean daily maximum water temperature below 17°C) (SRSRT 1994; Williamson et al. 1995a). Specific objectives are often phrased in terms of the same quantities used for habitat evaluation, including the following:

- Streamflow quantity. For example, provide adequate streamflow to meet seasonal needs for particular life stages or particular species or to mirror patterns in a lightly degraded reference system (Richter et al. 1996).
- Water quality. For example, maintain dry-season pool depths to meet temperature criteria.
- Channel dimensions for spawning, rearing, or refuge. For example, modify riffle frequency, increase channel pool volume and maximum depth, or increase the availability of steep or undercut banks.
- Longitudinal channel conditions for movement of organisms. For example, remove barriers or eliminate dewatered reaches.
- Streambank conditions. For example, reduce soil exposure and erosion; increase shade, cover, and refuge; or improve general condition, maturity, and successional opportunities for riparian vegetation.
- Influx and movement of sediment. For example, allow sediment to enter reach from upstream or local sources, provide flows for periodic sediment transport and flushing of substrate, or allow lateral bar formation along channel margins.
- Conditions in spawning gravel. For example, maintain intra-gravel flows when gravel-spawning species are important, such as salmonids.
- Input of organic matter and nutrients. For example, provide healthy riparian zones to ensure direct sources for organic matter and insects or maintain longitudinal continuum of organic matter from upstream sources and to downstream zones.

9.1.3.4 Scope of Sedimentation Analysis Stream restoration projects often change channel characteristics that impact sediment transport, including width, depth, slope, planform, bank erosion potential, hydraulic roughness, and bed material gradation. The sedimentation engineer may provide expertise in obtaining and interpreting data and model simulations describing physical aspects of habitat such as discharge, bed material characteristics, flow width and depth, current velocity, temperature, turbidity, and dissolved oxygen concentration. The engineer should also ensure that designs have acceptable outcomes with respect to erosion and sedimentation. Table 9-3 catalogs instability problems associated with various types of channel changes that are often key components of restoration projects.

Table 9-3 Potential Stability Problems Associated with Stream Restoration Projects

Modification	Potential stability problems		
	Project reach	Upstream	Downstream
Increase vegetation, woody debris, boulders, and other types of large-roughness elements	Aggradation	Aggradation	Degradation
Increase channel complexity (adding sinuosity or increasing the irregularity of cross-sectional shape and size)	Bank erosion, aggradation	Aggradation	Degradation
Remove of dams or weirs	Degradation upstream from structure, aggradation downstream.	Degradation	Aggradation or degradation, depending on impacts on flow and sediment discharge
Increase number of channel structures (e.g., weirs, spurs, bank covers, etc.)	Localized scour, bank erosion, aggradation	Aggradation	Degradation
Decrease bed slope	Aggradation	Aggradation	Degradation
Increase bed slope	Degradation	Degradation	Aggradation
Enlarge channel	Bank erosion, aggradation	Headcutting	Aggradation

Sedimentation analysis to support restoration design should predict the fluvial response to the project. For example, increasing channel width, increasing hydraulic roughness with vegetation or habitat structures, or decreasing channel slope by adding sinuosity will decrease sediment transport capacity and may lead to channel aggradation. On the other hand, if the restored channel is too steep, bed degradation may occur. Secondary responses may follow. For example, bank erosion may be triggered by bed aggradation or degradation. Even processes such as natural revegetation of a stream corridor can generate adjustments to the channel. Vegetation and in-channel woody debris can influence morphology of channels including the pool and riffle sequence, channel roughness, bank stability, locations of cutoffs, routing peak discharges, sediment routing and discharge, and the distribution of erosion. It follows that formulation of a sediment budget (Section 9.6.2) for the project reach using with- and without-project scenarios is one of the most basic sedimentation engineering tasks to support stream restoration.

9.1.3.5 Risk Evaluation Stream restoration projects that experience a significant imbalance between sediment supply and transport capacity either fail (do not deliver the desired benefits) or are not sustainable (have prohibitive maintenance requirements) (Brookes and Shields 1996). Because sediment transport analyses feature high levels of uncertainty, there are no standard approaches for determining what level of sediment transport imbalance is "significant." The designer must integrate knowledge gained from the stability assessment, preliminary design, and detailed design. The designer is responsible for making the client and other stakeholders aware of projected performance under various scenarios. For example, the project may experience unacceptable levels of erosion or sedimentation if discharges exceed a specified maximum peak or maximum average over some time period. Critical discharge levels may be lower during and shortly after project implementation. Nevertheless, sediment transport analyses are useful in reducing uncertainty (Johnson and Rinaldi 1998).

Restoration projects also experience failure when they do not generate the desired benefits. Even if the project performs perfectly with respect to water and sediment transport, the target species or communities may respond only weakly or may even decline. Biotic factors such as competition or predation, rather than physical habitat, may govern ecological response. In other cases, the linkages between habitat and ecological response may not be well understood enough to support reliable analysis. Biotic responses are heavily influenced by water quality, channel-floodplain interactions, and hydrologic variations. Some or all of these factors may not be altered by the restoration project. Inclusion of biotic factors into risk analysis must often be simply qualitative.

9.2 PREPARATION OF SEDIMENT STUDIES PLAN

A sediment studies plan (Fig. 9-1) is a critical early component of a stream restoration project. A good plan will ensure that significant sediment problems are identified and that analysis of alternatives is satisfactory. The schematic

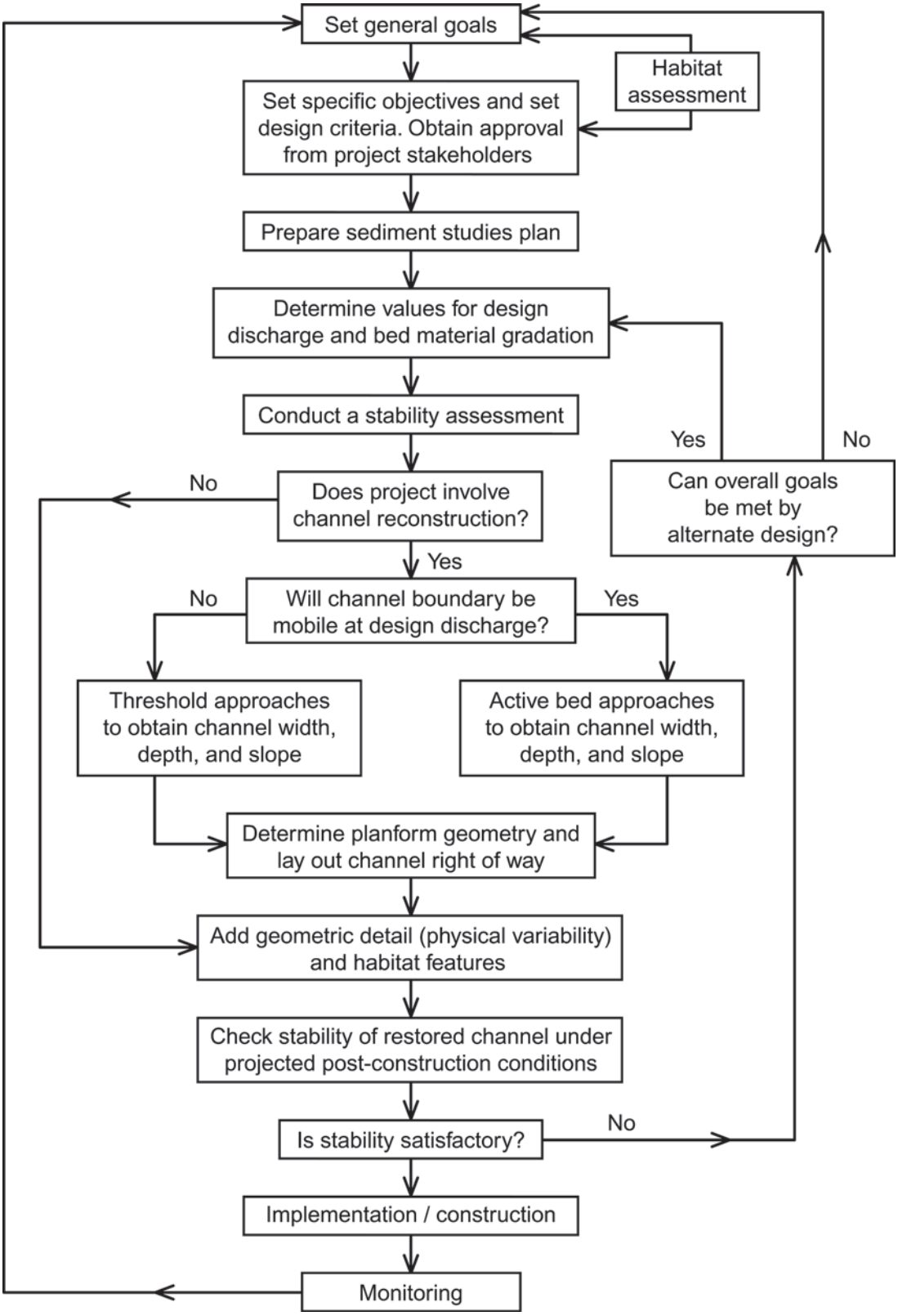

Fig. 9-1. Flow chart for sedimentation engineering aspects of stream restoration projects.

plan (Fig. 9-1) may be adjusted to fit a wide range of situations. For example, the stability assessment may be mainly qualitative for a simple project, but highly quantitative with multiple approaches to investigate the applicable variables for a complex project. As another example, the channel boundary may be constrained in urban areas, and therefore planform geometry will require little analysis.

9.2.1 Boundary of Study Area

The sediment studies plan should delineate the boundaries of the study area. Project impacts usually extend upstream and downstream beyond the project boundary. The region included in the assessment ideally should extend to major geomorphic boundaries such as watershed divides, reservoirs, or major confluences. However, resource limitations often dictate a smaller study area, and the engineer must exercise judgment in making tradeoffs between study quality and resource investment.

9.2.2 Stability Assessment

The sediment studies plan should include an assessment of historic and current system stability as described in Section 9.4.

9.2.3 Identification of Potential Problem Areas

The sediment studies plan should identify the potential problems in the study area. Sediment problems are most likely to occur in conjunction with the following project features:

- Expansions
- Bridge crossings or other constrictions
- Abrupt changes in channel slope
- Cutoffs and changes in channel alignment
- The upstream approach to the project reach
- The transition from the project reach to the existing channel downstream
- Appurtenant structures in the channel such as dikes and weirs
- Tributary junctions
- Lower reaches of tributaries
- Water diversions
- Upstream from reservoirs and grade control structures
- Downstream from dams and grade control structures.

9.2.4 Data Inventory

The plan should include a catalog of available geometric, hydrologic, hydraulic, sedimentary, and land use data. Potential future watershed land use changes should be identified using zoning maps, GIS, study of sequential air photographs, and other approaches. The previously established boundaries and problem area identification will guide selection of gauge sites and justify data requirements. Watershed history and project life may be used to select time periods for trend evaluation.

9.2.5 Determination of Study Approach

The sediment studies plan should document the basis for the selection of methodology, such as time, cost, and data availability, as well as geomorphic factors. The current dynamism of the project reach and watershed should be considered, because the magnitude of sediment problems related to the restoration project will be in direct proportion to the scale of changes made to the channel geometry, boundary roughness, or discharge of a currently stable system. The level of study detail should ensure that major decisions about the project remain sound as more data become available during planning and design.

Sediment studies often include sediment budgets (Section 9.6.2) generated using various approaches. Because sediment budgets usually require extensive data sets (channel thalweg profile and cross sections, bed material gradations, flow duration curve, sediment inflows from upstream) and may involve substantial effort, an assessment based on the risk and consequences of project failure should be performed before a sediment budget analysis is launched. Many projects may require less elaborate analyses, but levels of uncertainty regarding project outcomes will be higher.

9.2.6 Data Collection

A data collection plan should be established and scheduled in the sediment studies plan if required data are not available. Standardized methods and equipment should be used to develop detailed and reliable sediment databases (e.g., Federal Interagency Sedimentation Project 2005). Chapter 5 in this volume and Edwards and Glysson (1988) describe approved samplers, standard sampling procedures, and laboratory analysis. Careful reduction and interpretation of the data is required in addition to the use of standardized data collection techniques. This is especially true when the data are collected over a relatively short time and at a relatively few sites within a large system. The engineer should advise the client regarding data collection needs and the levels of uncertainty that result from a lack of data.

9.2.7 Other Elements

The sediment studies plan should provide a reliable time and cost estimate for completion. A schedule of activities including preparation and review of end products should also be included. There should be a clear understanding among all participants in the planning and design processes about the scope of end products. An outline of the proposed final report may be helpful in this regard. A list of topics that may be included in such a report is provided in

Table 9-4 Topics to Include in a Sediment Studies Report

Topic	Remarks
Geography	Project and study area boundaries, current and projected future watershed land use
Data	Available data and sources Recommendations for data collection
History	Historic land use in the contributing watershed Hydrologic record Stream behavior in the study reach including aggrading and/or degrading trends, behavior of the system during flood events, and historical changes to and by the river system.
Bed and banks	Bed controls, bed material, bank heights, angles, vegetation, and stability
Channel stability	Existing channel and problems upstream and downstream from the proposed project area Knickpoints (headcuts) and knickzones
Physical habitat	Physical features that should be preserved or modified by a project
Project effects	Water-surface elevations and sediment transport capacity upstream of, within, and downstream of the project Tributaries (e.g., headcutting or induced deposition)
Recommendations	Project alternatives Future data collection and analyses to support design

Table 9-4. It should be clear how results of sediment studies will be used to affect decisions about overall project safety, efficiency, reliability, first cost, maintenance cost, environmental factors, social factors, and mitigation of adverse impacts resulting from sediment problems. Finally, the sediment studies plan and end products should be reviewed by scientists or engineers with expertise in sedimentation engineering and geomorphology to guard against costly oversights.

9.3 SELECTING VALUES FOR DESIGN DISCHARGE AND BED MATERIAL SIZE

9.3.1 Discharge

A representative discharge or discharge range is needed for many stability assessment tools (Section 9.4) and channel design (Section 9.5.1). The "channel-forming" or "dominant" discharge is often used as this representative value. The channel-forming discharge concept is based on the idea that for a given alluvial channel geometry, there exists a single steady discharge that, given enough time, would produce width, depth, and slope equivalent to those produced by the natural hydrograph. Although the channel-forming discharge concept is not universally accepted, most river engineers and scientists agree that the concept has merit, at least for perennial nonincised streams, particularly coarse-bed snowmelt-dominated streams in the montane west. See Soar and Thorne (2001) and Biedenharn et al. (2000) for a review of relevant literature. Producing a single value for channel-forming discharge, Q_{cf}, has proven difficult in many cases. In attempts to provide quantitative expressions for discharge values that are believed to approximate Q_{cf}, the following terms have been suggested:

- The effective discharge, or the discharge that, over time, transports the most sediment (Q_{eff}),
- The bank-full discharge (Q_{bf}), and
- A discharge based on statistical return intervals (Q_{ri}).

Of the three quantitative approaches to Q_{cf}, Q_{eff} generally requires the most data and effort (Table 9-5). Some workers have used sediment-discharge rating curves coupled with detailed geomorphic analysis to find Q_{eff} when historical hydrologic data were unavailable (Boyd et al. 1999). Additional comments dealing with ungauged sites are provided in Section 9.3.1.4.

9.3.1.1 Effective Discharge, Q_{eff}

9.3.1.1.1 Concept and Cautions Although discharge varies continuously, it is usually represented by a time series of discrete values measured at daily or shorter intervals. These data may be used to construct a frequency histogram by breaking the observed range into a finite number of increments. The mass of sediment transported by each discharge increment may be computed using a sediment rating curve or sediment transport formula if hydraulic and bed-material parameters are available. The effective discharge, Q_{eff}, is the increment of discharge that transports the largest sediment load over a period of years (Andrews 1980) (Fig. 9-2). Thus Q_{eff} integrates the magnitude and frequency of flow events (Wolman and Miller 1960) and is the best basis for channel restoration design. However, there are several problems associated with Q_{eff}:

- Computed values of Q_{eff} are sensitive to the number of increments used to build the discharge histogram.
- Computation of Q_{eff} has the same drawback as other methods in identifying one flow rather than a range of flows for channel formation (see Section 9.3.1.1.2 for details).
- Care must be exercised in applying the effective discharge procedure, particularly in unstable channels and those that have experienced catastrophic events during the period of record, because flow-frequency and sediment-transport relations may have changed or be changing with time as the channel adjusts. Results

Table 9-5 Quantitative Representations of Channel-Forming Discharge (Q_{cf})

Quantitative estimate of Q_{dom}	Data requirements	Recommended for	Limitations
Effective discharge (Q_{eff})	Historical hydrology for flow duration curve (10 years or more recommended) or synthetic flow duration curve; channel survey; hydraulic analysis; sediment gradation; sediment transport analysis and model calibration (if possible)	Channel design	Requires large data set
Bank-full discharge (Q_{bf})	Channel survey; hydraulic analysis and model calibration (if possible); identification of field indicators in a stable, alluvial reach.	Stability assessment; estimation of Q_{eff} in stable channels	Can be very dynamic in unstable channels/watersheds; field indicators can be misleading
Return interval discharge (Q_{ri})	Historical hydrology for flood frequency analysis, regional regression equations, or hydrologic model	First approximation of Q_{eff} and/or Q_{bf} in stable channels	No physical basis; relations to Q_{eff} and Q_{bf} inconsistent in literature

may therefore represent a transient average condition that does not accurately depict either the present flow and sediment-transport conditions or those prior to the event or disturbance.

The effective discharge is useful in comparing various channel geometries for competence to transport the incoming sediment load, facilitating study of project alternatives. Results of the effective discharge analysis are also useful when predicting the impact of alteration of watershed sediment loads (e.g., upstream dam removal) or hydrology (e.g., urbanization) on channel stability.

9.3.1.1.2 Determining Effective Discharge A three-phase process is involved in determining Q_{eff}:

1. Construct a frequency distribution (histogram) for discharge;
2. Construct a sediment-transport rating from either bed-material transport data or an analytical sediment transport relationship and reach hydraulics; and
3. Integrate the two relations by multiplying the sediment-transport rate for a specific discharge class by that discharge, with the maximum product being the effective discharge.

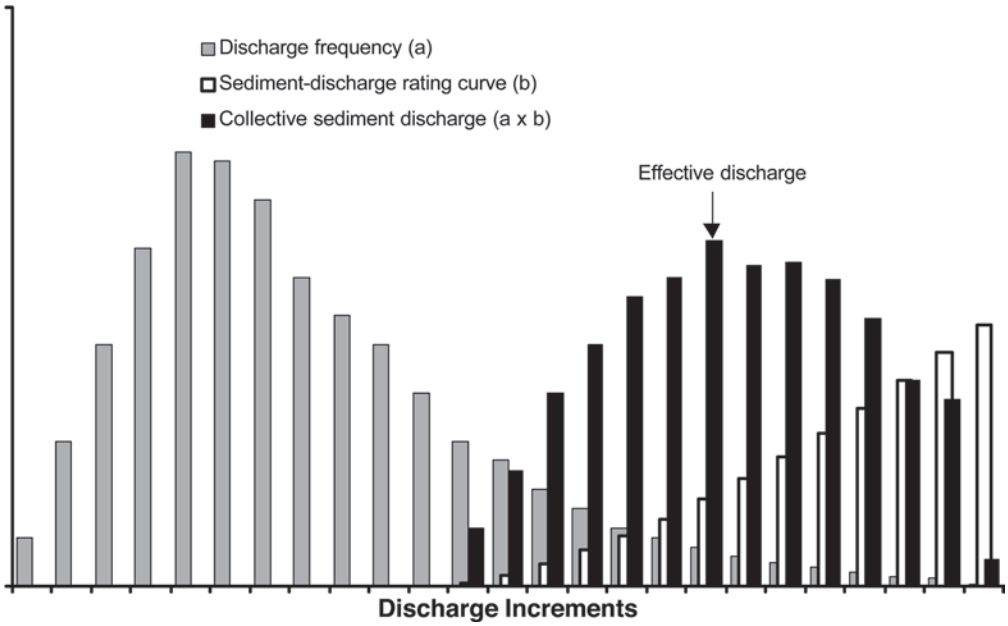

Fig. 9-2. Derivation of effective discharge by multiplying the discharge frequency histogram and the sediment rating curve to produce a collective sediment discharge histogram. Vertical axis represents frequency (percent of time), sediment discharge (mass per time), and collective sediment discharge (mass) for grey, white, and black bars, respectively.

The first phase involves selecting the type of discharge data to be used and a method for subdividing the observed range of discharge into classes to produce a frequency histogram. The period of record should be at least 10 to 15 years. In many cases, mean daily discharges are used because these data are readily available from the USGS and others. However, except for large rivers, mean daily flows tend to be underestimators of sediment transport because they mask the effects of short-duration peak flows. Discharges representing time periods shorter than a day, such as the 15-min data collected by the USGS, provide a more accurate means of establishing a sediment-transport rating relation. These data, although superior for a broader size range of streams and rivers, are not readily available, but may sometimes be obtained via special request.

There are no definite rules for selecting the most appropriate interval and number of classes (Thorne et al. 1998). The reader should note that the outcome of an effective discharge analysis is sensitive to the method used to derive the flow histogram. Yevjevich (1972) stated that the class interval should not be larger than 25% of the standard deviation of the sample. Hey (1997) found that 25 classes with equal arithmetic intervals produced a relatively continuous flow-frequency distribution and a smooth sediment load histogram with a well-defined peak, indicating an effective discharge that corresponded exactly with bank-full flow. Biedenharn et al. (2000) recommend setting the interval size equal to the discharge range (maximum observed discharge minus the minimum observed discharge) divided by 25. The first interval should begin at zero for suspended-load channels and at the critical discharge for initiation of bed load movement for gravel-bed rivers. Experience has shown that in some cases 25 classes produce unsatisfactory results, and a larger number of classes may be required. However, class size should be large enough so that some discharges occur in each class. In cases where the hydrologic response is extremely flashy, use of constant increments for the flow histogram may result in an extremely high relative frequency for the lowest interval, biasing Q_{eff} downward (Fig. 9-3). Soar and Thorne (2001) advocate using a continuous probability density function based on very small discharge intervals to avoid the problems associated with histogram development. If the frequency distribution is based on real data, it will exhibit a "noisy" appearance, but this may be addressed by using a moving average approach in phase 3, described below.

The second phase of the procedure involves developing a rating curve showing sediment concentration as a function of water discharge. Only sediment size classes that form the channel boundary should be used in the rating curve (Kuhnle et al. 2000). Typically, this range corresponds to the bed material sediment, but it may include finer sizes if significant material is being deposited on top of the banks (e.g., to form natural levees). The use of total-load transport data separated into suspended-, wash-, and bed-load components is ideal, but data in such detail are usually not available. Suspended sediment data are generally most readily available, and these data represent the sum of wash load and bed-material load moving

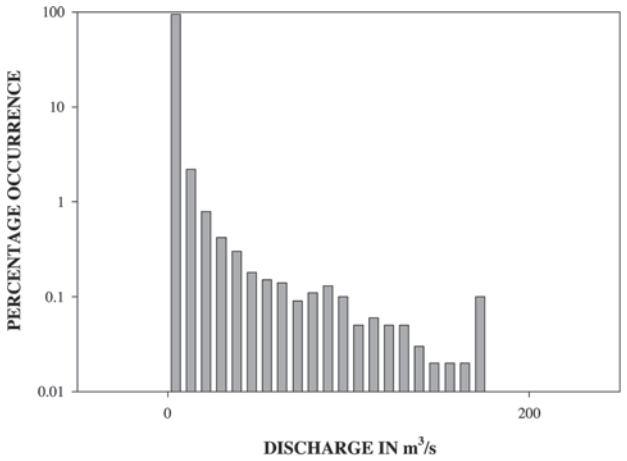

Figure 9.3a. 25 Equal arithmetic class intervals.

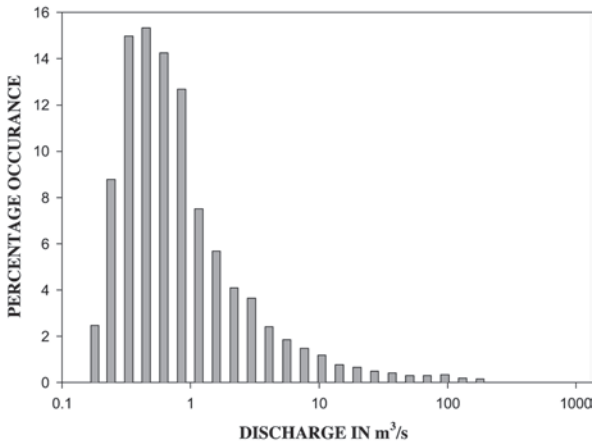

Figure 9.3b. 25 Logarithmic classes

Fig. 9-3. Effects of using (a) 25 equal ("arithmetic") class intervals and (b) 25 "logarithmic" class intervals for developing the flow-frequency histogram. The large number of discharges in the first class interval may bias the resulting value of Q_{eff} downward.

in suspension. Bed material moving as bed load is usually not measured. The transport of bed material load can be classified as bed-load-dominant, mixed-load-dominant, or suspended-load-dominant on the basis of the ratio of shear velocity to fall velocity (Julien 1995). If sediment data are not available, bed-material load transport rates can be derived from a variety of transport functions, as described in Chapter 2 and elsewhere (Stevens and Yang 1989; Andrews and Nankervis 1995). Generally, sediment concentrations are plotted against discharge in log-log space and regressed to create a simple rating relation (Fig. 9-4a). However, power functions derived in this way are often inadequate to define the transport relation because they overestimate transport at high flows. In addition, transport can also be overestimated at low discharges because

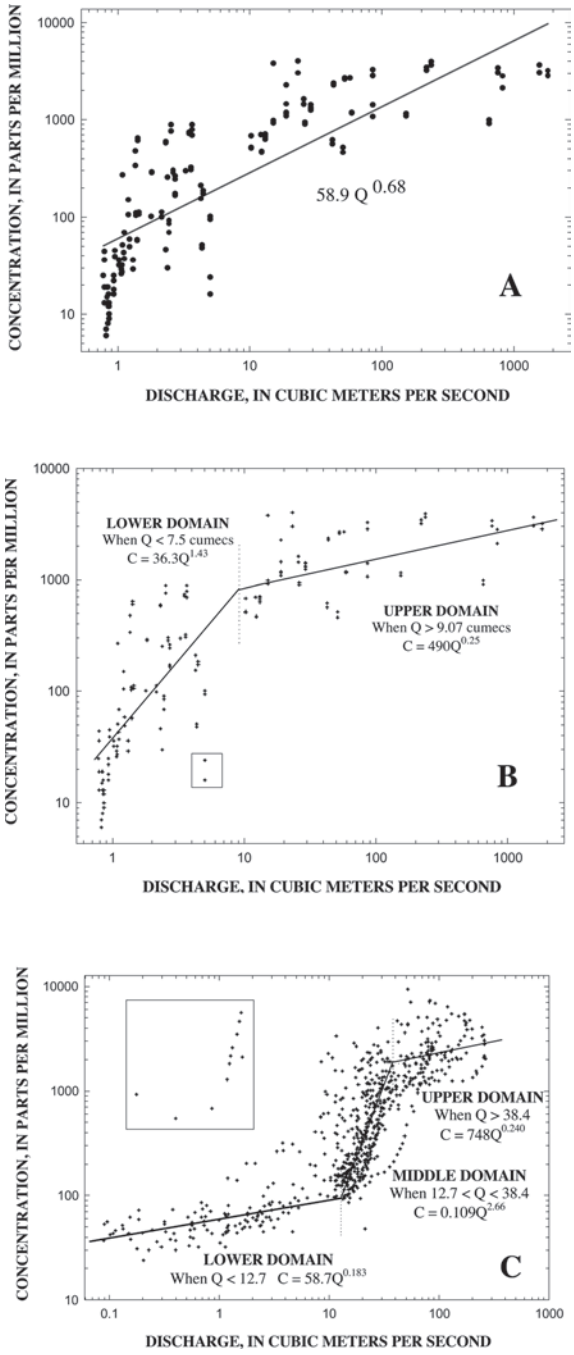

Fig. 9-4. Sediment rating curve derivation. (A) Use of simple power function relation. (B) Use of two linear segments. Points inside rectangular box were regarded as anomalies and were not included in regression. (C) Use of three linear segments. Points inside rectangular box were regarded as anomalies and were not included in regression.

of the sensitivity of transport relations to bed-material gradations, which sometimes vary with discharge. This necessitates using two or three linear segments or a curved rating (Glysson 1987; Simon et al. 2004; Fig. 9-4b and c). In gravel-bed rivers, surface armoring and incipient motion flow requirements (Parker and Klingeman 1982) also suggest the use of more than one segment for the bed load relation.

Phase three of the procedure is accomplished by multiplying the frequency (in percent) of each discharge class by the sediment load corresponding to the discharge at the center of the class interval. The resulting values represent the average transport rate for each discharge class. The center of the class interval with the greatest transport rate is Q_{eff} (Andrews 1980) (see Fig. 9-2). In some cases, however, there may not be a single class interval representing a maximum. Instead, the peak average transport rate may spread across a range of classes, indicating that there is no single effective discharge but that significant geomorphic work is performed by a wide range of flows (e.g., Biedenharn and Thorne 1994). There is considerable support for this concept in the literature, and such a situation calls for considerable professional judgment in selecting design discharge capacity for the restored channel.

9.3.1.2 Bank-Full Discharge, Q_{bf} The bank-full discharge is the maximum discharge that a channel can convey without overflow. Theoretically, Q_{bf} and Q_{eff} are generally equivalent in channels that have remained stable for a period of time, thus allowing the channel morphology to adjust to the current hydrologic and sediment regime of the watershed (e.g., Andrews 1980). However, in an unstable channel that is adjusting its morphology to changes in the hydrologic or sediment regime, Q_{bf} can vary markedly from Q_{eff}. Therefore, the expression "bank-full discharge" should never be used to refer to Q_{ri} or Q_{eff}. The relationship of Q_{bf} to Q_{ri} and Q_{eff} is useful as an indicator of channel stability and sheds light on morphologic changes to be expected locally as well as up- and downstream (Schumm et al. 1984; Simon 1989; Thorne et al. 1996a). The Q_{bf} from "template" or "reference" reaches (stable reaches from similar reaches/watersheds) has been used as a guideline for relevant dimensions of the restored channel (Rosgen 1996). Three problems should be noted in regard to Q_{bf}:

- Identifying the relevant features in the field that define the stage associated with Q_{bf} can be problematic. Many field indicators have been proposed, but none appear to be universally applicable or free from subjectivity (Williams 1978). Similar statements hold for the methods developed for selecting appropriate ranges of Q_{bf} values based on these indicators (Johnson and Heil 1996). Field methods presented by Harrelson et al. (1994) should be considered in Q_{bf} determination.
- Channel restoration is most often (if not always) practiced in unstable channels (instability is often the reason for restoration), and hence, unstable watersheds. Other candidates for restoration include channels that have stable boundaries but that have been greatly enlarged for flood control. In such cases Q_{bf} can be highly dynamic and very different from Q_{cf} (Doyle et al. 1999) and should not be assumed to be the same as Q_{cf}.

- In certain instances, the current Q_{bf} may be a poor choice for future channel performance. For example, an apparently stable channel may overflow frequently due to upstream urbanization. Urbanization typically increases the amount of impervious area, decreasing infiltration and increasing runoff peaks and quantities. Urbanization has the greatest impact on small, frequent events (Hollis 1975), and there may be a threshold level of watershed imperviousness (approximately 15%) beyond which effects significantly increase (Moscrip and Montgomery 1997). As another example, streams in arid landscapes may adjust to large, infrequent events and have very large values for Q_{bf}. Additional discussion is provided in numerous references, including FISRWG (1998).

9.3.1.3 Discharge for a Specific Return Interval, Q_{ri} If gauge data are available, the discharge equivalent to the event with a given return interval is often assumed to be the channel-forming discharge; for example, $Q_{cf} = Q_2$ (where Q_2 is the two-year event). Similarities exist between certain recurrence interval discharges, Q_{eff}, and Q_{bf}. In general, Q_{bf} in stable channels corresponds to a flood recurrence interval of approximately 1 to 2.5 years in the partial duration series (Simon et al. 2004), although intervals outside this range are not uncommon. Recurrence interval relations for channels with flashy hydrology are intrinsically different from those for channels with less variable flows. Because of such discrepancies, many studies have concluded that recurrence interval approaches tend to generate poor estimates of Q_{bf} (Williams 1978) and of Q_{eff} (Pickup 1976; Doyle et al. 1999). Hence, assuming a priori that Q_{ri} is related to either Q_{bf} or Q_{eff} should be avoided in channel design, although it may be useful at times to take Q_{ri} as a first estimate of Q_{eff} and/or Q_{bf} in stable channels, particularly those with snowmelt hydrology (Doyle et al. 1999). Watershed urbanization typically causes greater runoff amounts and larger peak discharges for similar storms, increasing the frequency of higher discharges. Channel enlargement may result. This makes the recurrence interval approach tenuous, because it is commonly based on events that have occurred over the full historical record.

9.3.1.4 Ungauged Sites When gauge records are not available, estimates of Q_{ri} can be based on similar gauged watersheds or on regression formulas (Wharton et al. 1989; Jennings et al. 1994; Ries and Crouse 2002) developed using appropriate regional data sets. Calculation of Q_{eff} will require synthesis of a flow duration curve. Two methods are described by Biedenharn et al. (2000; 2001): the drainage area-flow duration curve method (Hey 1975) and the regionalized duration curve method. It should be noted that both methods simply provide an approximation to the true flow duration curve for the site because perfect hydrologic similarity never occurs. Accordingly, caution is advised.

9.3.1.4.1 Drainage Area-Flow Duration Curve Graphs of Q_{ri} versus drainage area are developed for a number of sites on the same river or within hydrologically similar portions of the same drainage basin as the ungauged location. If data are reasonably homogenous, power functions may be fit using regression and used to generate a flow duration curve for the ungauged location.

9.3.1.4.2 Regionalized Duration Curve A nondimensional flow duration curve is developed for a hydrologically similar gauged site by dividing discharge by Q_{bf} or Q_2. Then Q_2 is computed for the ungauged site using the aforementioned regression equations. Finally the flow duration curve for the ungauged site is derived by multiplying the dimensionless flows (Q/Q_2) from the nondimensional curve by the site Q_2.

9.3.1.5 Checking Computed and Estimated Channel-Forming Discharges The quantities Q_{eff}, Q_{bf}, and Q_{ri} are all hypothetical estimates of Q_{cf}. Their equivalence to the theoretical single discharge that would produce the same channel geometry as the natural runoff sequence is based on observations and judgment. For this reason it is important that more than one estimator for the channel-forming discharge be considered. Computed effective and bank-full discharges outside the range between the 1- and 3-year recurrence intervals should be questioned. The computed effective and recurrence interval discharges should be compared with field evidence to ascertain if these discharges have geomorphic significance.

9.3.1.6 A Range of Discharges The quantities Q_{eff}, Q_{bf}, and Q_{ri} provide single values for a design discharge. However, inspection of a natural channel reveals the inherent variability present in natural fluvial systems. Hence, in designing channels that are intended to replicate natural channel features, but also remain stable over long periods of time, it is important to establish an acceptable range of design discharges. In addition, channel flow resistance may change appreciably with discharge, producing major effects on stage, sediment transport, and channel stability. Acceptable discharge capacity ranges may also be needed to guide channel sizing. For example, to incorporate natural variability, specifications could allow a range of channel widths and depths. If Q_{bf} is used for design discharge, then an appropriate range of discharges should be selected based on the range of Q_{bf} observed in the reference reaches. If Q_{eff} is used as the design tool, then the range of discharges should correspond to the effective discharge increment.

After a preliminary design is prepared, channel stability checks (Fig. 9-1 and Section 9.6) may include simulation of sediment transport either for selected hydrologic events or a flow duration curve. This type of analysis will indicate if the channel will experience unacceptable levels of scour or deposition during discharges above and below the design flow.

The discussion above deals with selection of discharges for channel design. Other types of stream restoration design problems may require selection of different discharges. For example, structural or vegetative bank treatments may be

designed to withstand events with a certain probability of annual occurrence. Riparian vegetation may require limited periods of inundation during certain seasons. Riffles and other zones with coarse bed material may be designed to allow disturbance for removal of fines ("flushing") at a certain frequency (see Section 9.5.4).

9.3.2 Bed Material Size Distribution

A description of the bed material size distribution that is planned or anticipated under project conditions is needed for stability assessment and restoration design. Supplemental information will also be needed on bank material characteristics, particularly if banks are noncohesive. Information about the streambed and banks may be gathered at the same time using suitable sampling methods (cores, bulk samples, or layer samples, as appropriate) and sample processing techniques (sieving or sedimentation tests, as appropriate) for the sizes of material present. Although the bed material and bank material sizes may be visually estimated for rough preliminary estimates, careful sampling is required for quantitative analyses.

Bed material is characteristically heterogeneous. Bed material sampling techniques should vary with the bed type and the purpose for sampling. For example, floodplain boring may be needed to determine bed sediment size when a new channel is to be excavated. In other cases, bed material may be sampled from the existing channel or from a reference reach that serves as a restoration template. The resulting data may be used for sediment transport and channel stability computations, habitat assessment, or design of habitat features (e.g., flow regimes for periodically flushing coarse beds; stability of aquatic habitat structures).

Bed material sampling should provide estimates of representative sizes as well as information regarding spatial variability in the channel. Coarse beds pose greater difficulties than sand beds. Techniques applicable to coarse-bed rivers have been described by Bunte and Abt (2001), whereas techniques for sands and smaller materials are described by USACE (1995), and Ferguson and Paola (1997). If a coarse bed is rarely mobilized, then a surface hand-sampling technique (e.g., a Wolman (1954) pebble-count procedure) may be sufficient. If sediment transport is expected at a coarse bed, then sieve analysis of bulk sample is needed to include smaller subsurface particles. Relationships between gradations of bulk samples representing surface and subsurface sediments are presented by Parker (1990).

The median particle size, D_{50} (the size for which 50% of the bed material by weight is smaller), is the parameter most commonly used in sediment transport calculations. Less common descriptors include D_{90}, D_{84}, D_{75}, D_{65}, D_{35}, and D_{16} (for use in bed load, incipient motion, and flow resistance equations) and D_{60}, D_{25} and D_{10} (e.g., to describe particle sorting). For some types of aquatic habitat work (e.g., habitats for fish that spawn in gravel) it is also important to know the proportion of particles finer than gravel (<2 mm) found within the coarse matrix. Some streams have beds composed of mixtures of sand and larger sediments that have bimodal particle size distributions. Bimodality can also have a major impact on incipient motion and sediment transport (Chapter 2 of this volume and Wilcock 1998). Specific gravity of bed material can be quite important if it departs from standard values between 2.6 and 2.7.

Streamwise and lateral variations in bed material sizes occur along point bars, at lateral bars, and between pools and riffles, as well as for straight reaches with little thalweg variability. Bed particles near an eroding bank containing gravel or coarser materials are likely to be similar in size to the coarse component of bank material, rather than to upriver bed material. Therefore, if a restoration project for a coarse-bed stream emphasizes benthic habitats, it will be necessary to consider the spatial variability of bed material in detail. But if the restoration project emphasizes sediment transport and continuity of sediment supply from upstream to downstream reaches, the bed material size available for transport is of greatest interest.

Clearly, site-specific factors should be considered. Bed material along a mid-channel bar or other obvious depositional surface indicates the size of sediment transported by recent events. However, care should be taken that long-term stable morphologic features are not assumed to be representative of short-term channel dynamics. For example, channels with relict glacial outwash material often have riffles that are not mobilized by any but extreme events. Material in such features is not representative of normal bed material load.

9.4 STABILITY ASSESSMENT

9.4.1 Purpose and Scope

Stability assessment and analysis are a key aspect of planning and design for restoration of dynamic stream corridors. River channels are often perturbed by imbalances in watershed sediment supply, transport, or storage (Sear 1996) triggered by large floods (Stevens et al. 1975), channelization (Schumm et al. 1984; Simon 1989), upstream reservoirs (Simons and Senturk 1976), urbanization (Hammer 1972; Moscrip and Montgomery 1997), or other watershed land use changes. Using results of a system stability assessment, the project manager can select an appropriate level of effort for sedimentation engineering aspects of predesign assessment, design, and postproject monitoring. In addition, because habitat degradation is often related to erosion or sedimentation, stability assessment is needed to develop restoration alternatives. Furthermore, the restoration project may itself affect channel stability (Table 9-3), and this possibility must be evaluated during design. More detailed guidance for performing stream channel stability assessments is provided by the U.S. Army Corps of Engineers (USACE 1994) and by Lagasse et al. (2001). A template for geomorphic investigations is provided in Chapter 6 of this volume.

A stability assessment consists of examination of a selected part of the fluvial system encompassing the restoration project to determine the direction and speed of morphologic changes. The assessment provides a foundation for design and predictions of how the system will respond to the restoration project. Inadequate assessment may result in a restoration design that is obliterated by erosion or deposition within a short period of time, or one that degrades stream corridor resources or endangers floodplain assets. If possible, the dominant geomorphic processes influencing the channel and their root causes should be identified. Relative magnitudes are emphasized rather than quantification during assessment. The nature of the existing hydrologic response and the likelihood of future shifts in discharge and sediment load due to land use changes (e.g., urbanization or afforestation) should be considered. Existing instabilities in the channel system should be identified (Kondolf and Sale 1985; Kondolf 1990).

If significant sedimentation problems are identified, more detailed engineering analysis will be required during design. Stream channel performance includes both conveyance and geometric stability, especially as they relate to long-term maintenance. Stability impacts are generally determined by comparing bed-material sediment transport for existing and anticipated project conditions. The stability assessment also provides an inventory of available data and may include recommendations for additional data collection programs and more detailed studies.

The first step in conducting the stability assessment is to determine the spatial domain for the investigation. Usually, this area will coincide with the project boundaries identified in the sediment studies plan (Section 9.2).

The second step is to formulate a statement describing acceptable rates of morphologic change. Current and projected channel stability may be assessed relative to these levels. From a strictly pragmatic standpoint, a reach is unstable when morphologic change (i.e., erosion or deposition) is rapid enough to generate public concern (Brice 1982). From a more scientific perspective, a stream is unstable only if it exhibits abrupt, episodic, or progressive changes in location, geometry, gradient, or pattern because of changes in water or sediment inputs or outputs (Rhoads 1995; Thorne et al. 1996b). In other words, a stream may be highly dynamic but considered geomorphically stable (i.e., in a state of dynamic equilibrium, Section 9.1.2.2) if its long-term temporal average properties (channel width and sediment input and output) are stationary. Such a stream may have relatively rapid rates of lateral migration and thus bank retreat. Thus the statement defining acceptable rates of change should provide a clear rationale.

The scale of observed instabilities should also be considered in setting criteria. Short segments of channels may be locally stable or unstable due to structures, vegetation, or geological conditions, but the reach or watershed that surrounds them may exhibit different patterns. For example, reaches upstream of headcuts in incising channel networks are often quite stable, but downstream zones are extremely disturbed (Simon 1989). If headcuts migrate upstream, stable reaches may quickly shift to unstable. Local flow constrictions (e.g., bridge crossings) may produce serious local scour in an otherwise stable stream. An assessment should differentiate between local, reach, and systemwide instabilities. Clearly, systemic instability is most serious and is usually not amenable to purely local treatment. Spatial patterns of channel form and process are best understood when stability assessment results are placed on a watershed map or within a geographic information system.

9.4.2 Types of Stability Assessments

9.4.2.1 Qualitative Stability Assessments Qualitative assessments are simple efforts requiring less than 1 week of effort for one person, and consist mostly of visual inspection. This type of assessment can be powerful when performed by someone with a high level of expertise. Large areas can be inspected from low-flying aircraft, with follow-up on the ground. On-the-ground reconnaissance should include the project reach and adjoining upstream and downstream reaches. Spatial trends in channel conditions should be examined. If the downstream reach is degrading, it is possible that disturbance could move upstream into the project reach in the form of a headcut or knickzone. Instability upstream could increased sediment supply to the project reach.

Qualitative assessments should also include a review of the available information regarding the geological and physiographic setting for the project, as well as its temporal context. The engineer should develop a timeline or table showing major disturbances (e.g., large floods, avulsions, dam closure, channelization, deforestation) affecting the project reach. Review of historic maps and air photo coverage can be a powerful tool (Rhoads and Urban 1997). Sear (1996) provides an excellent overview of factors to be considered in qualitative stability assessments for river restoration projects. Additional guides are provided by Biedenharn et al. (1998) and USACE (1995, Appendix E).

9.4.2.2 Quantitative Stability Assessments Quantitative assessments vary in methodology, but have in common the collation of numerical data about the study area from a variety of sources to describe channel geometry, bed sediments, hydrology, and land use in the past and present. Five types of tools are commonly used in stability assessment: (1) Lane relations, (2) channel classification, (3) hydraulic geometry relationships, (4) relationships between sediment transport and hydraulic variables, and (5) bank stability. All five are easily misused, so professional judgment is required. These tools are discussed in the following section, and comments are made regarding tool selection.

9.4.3 Tools for Stability Assessment

9.4.3.1 Lane Relations The first group of tools is based on the Lane (1955a) relationship (also due to Gilbert 1914), which states that stream power is proportional to the product of sediment discharge (Q_s) and bed material size (D_s) in an alluvial stream in a state of dynamic equilibrium:

$$Q_w S \sim Q_s D_s$$

Note that $Q_w S$, the product of water discharge (Q_w) and stream gradient (S) is a reduced form of stream power, dimensionally corresponding to power per unit weight of fluid per unit length of channel. In this relationship and the others that follow the water discharge of interest is a fluvially significant (e.g., channel-forming) discharge. Other investigators have combined the original proportionality with others (e.g., H = flow depth, B = channel width) to form a set of relationships useful for characterizing fluvial behavior:

$$S \sim B D_{50} / Q_w \tag{9-1}$$

$$B/H \sim Q_w Q_s \tag{9-2}$$

$$\text{Channel sinuosity} \sim 1/Q_s \tag{9-3}$$

Many other workers (e.g., Schumm 1969; Nunnally 1985; Sear 1996; Hooke 1997) have extended these relationships to predict fluvial response to disturbance. In the following relations, a superscript of + indicates increase, 0 indicates no change, − indicates decrease, and ± indicates unpredictable shifts.

Increase of water discharge, for example, diversion of water into a reach:

$$Q_s^{\,0}\ Q_w^{+} \sim S^{-},\ D_{50}^{+},\ H^{+},\ B^{+} \tag{9-4}$$

Decrease of water discharge, for example, extraction of water from a reach resulting in a narrower channel:

$$Q_s^{\,0}\ Q_w^{-} \sim S^{+},\ D_{50}^{-},\ H^{-},\ B^{-} \tag{9-5}$$

Increased sediment supply, for example due to hydraulic mining:

$$Q_s^{+}\ Q_w^{0} \sim S^{+},\ D_{50}^{-},\ H^{-},\ B^{-} \tag{9-6}$$

Decrease in bed material load as water discharge increases, for example in later stages of urbanization as paved area increases:

$$Q_s^{-}\ Q_w^{+} \sim S^{-},\ D_{50}^{+},\ H^{+},\ B^{\pm} \tag{9-7}$$

Decrease in bed material load and water discharge, following dam construction, for example:

$$Q_s^{-}\ Q_w^{-} \sim S^{\pm},\ D_{50}^{\pm},\ H^{\pm},\ B^{-} \tag{9-8}$$

Bed material and water discharge both increase, but water discharge increases more. For example, in long-term urbanization, the frequency and magnitude of discharge increase, triggering channel erosion (increasing width and depth):

$$Q_s^{+}\ Q_w^{++} - S^{-}\ D_{50}^{+},\ H^{+},\ B^{+} \tag{9-9}$$

Sediment supply and water discharge both increase, but sediment supply increases more. For example, when forest is converted to row crop production, gravel beds tend to change to sand, and channels become wider and shallower:

$$Q_s^{++}\ Q_w^{+} \sim S^{+},\ D_{50}^{-},\ H^{-},\ B^{+} \tag{9-10}$$

Use of these and similar relations for stability assessment is discussed in standard texts (e.g., Chang 1988; USACE 1995, Appendix D). The engineer should be aware of important limitations:

- Anticipated adjustments may not occur because the system is currently responding to prior disturbance. Accordingly, a review of watershed history for events creating channel system disturbance is an important part of stability assessment.
- The channel system may not comply with the relation because it is not free to adjust. For example, the bed may contain bedrock controls that limit changes in slope, or bed material may not become coarser because gravel and cobble are not available for transport or because fine sediment contributions from eroding banks and tributaries overwhelm main channel processes. Slope is governed by channel pattern (straight, braided, meandering, etc.), but channel pattern changes are very difficult to predict and may be governed by discontinuous (threshold) relations rather than continuous relationships.
- Lane-type relations do not explicitly allow for complex response (Schumm 1977), in which fluvial systems exhibit unsteady, complex behaviors (e.g., a period of channel scour followed by aggradation or long lags in system response) in response to a single external influence.
- Lane-type relations allow prediction of the direction of a change, but not its magnitude.

Despite these limitations, the Lane-relation approach may be quite powerful when the history of disturbance is known. For example, a straightened stream experiencing accelerated bed and bank erosion may be responding to the increased

slope by increasing sediment load (e.g., Parker and Andres 1976).

The discharge-slope product QS that forms the left side of the Lane relation is one representation of stream power. Various workers have noted that stream channel pattern (straight, meandering, or braided) is reflective of the balance between stream power and sediment grain size. A review of the numerous resultant equations for planform prediction is provided by Thorne (1997). These relations may be useful in stability assessment, because systems that are near the threshold between meandering and braided may respond strongly to restoration actions. Further, the engineer should avoid designing a channel with a slope that is too small or too great for the selected planform. One of the more recent contributions is by van den Berg (1995), who proposes a relationship based on "potential" stream power, which is computed using the valley slope rather than the channel slope. A data set representing observations from 228 streams was used to produce a formula defining the threshold between single-thread meandering rivers with sinuosities greater than 1.5 and less-sinuous braided rivers:

$$\omega_{vt} = 843\, D_{50}^{0.41} \tag{9-11}$$

where

ω_{vt} = the specific stream power at the transition between meandering and braided planforms in W m^{-2}.

Specific stream power, or stream power per unit bed area, is defined by

$$\omega_v = CS_v Q_{bf}^{0.5} \tag{9-12}$$

where

C = 2.1 for sand-bed rivers and 3.3 for gravel-bed rivers, and
S_v = valley (not channel) slope.

Channel width, which appears in the conventional definition of unit stream power ($\omega = \gamma Q S/B$, power per unit bed area), does not appear in the relationship because it is assumed to be a function of Q_{bf}. Streams with values of specific stream power greater than the threshold will braid, whereas those with lower values will meander, as shown in Fig. 9-5. Limits for the function are $Q_{bf} > 10$ m^3 s^{-1} and 0.1 mm $< D_{50} <$ 100 mm. Dade (2000) produced a more qualitative planform discriminator based on channel slope, median bed material size, and discharge.

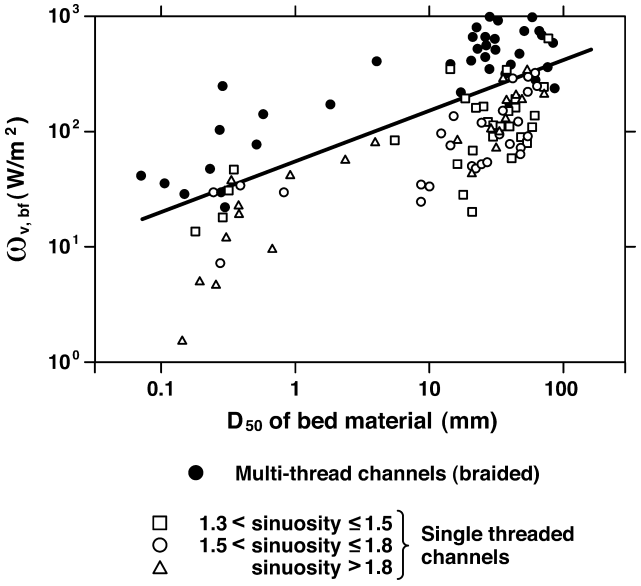

Fig. 9-5. Planform prediction diagram developed by van den Berg (1995) after Thorne (1997).

9.4.3.2 Channel Classification Channel classification is a primarily qualitative approach for stability analysis in which the engineer divides the channel network in the study area into reaches and assigns each channel reach to a class or type based on visual inspection or measurement of key variables (Chapter 6). The quantity and quality of regional experience of the engineer is the key determinant of the quality of channel stability assessment based upon qualitative reconnaissance. Ideally, results from reconnaissance should be verified using tools that examine recent trends such as specific gauge analyses, comparison of thalweg profiles, and comparison of channel width, depth, and bed elevation depicted on successive surveys of several cross sections through time (USACE 1994; Biedenharn et al. 1998). Examination of historical photographs (aerial and ground) and maps and interviews with landowners and other observers can also be particularly valuable.

Results of inspection and salient data can be recorded on a form for each reach and entered into a GIS or mapping software for synoptic visualization of ongoing processes throughout the system. It is critical to view results of classifications within the context of the entire watershed, because changes and modifications within a reach may be propagated through the system. Systemwide trends should be clearly identified. Presentation of classification results in map format can be extremely useful for communication with funding agencies or local landowners involved with or impacted by channel modifications.

Classification schemes generally fall into two broad groups, descriptive and process-based. Among the former is the scheme proposed by Rosgen (1994, 1996). Using this scheme, a reach can be assigned an alphanumeric taxonomic code based on its appearance and rough estimates of channel dimensions. For instance, a channel classified as "C4" is a single-thread meandering gravel-bed channel with a width-to-depth ratio greater than 1.4 and a slope less than 0.02, whereas a "D3" channel is a braided cobble-bed channel with a width-to-depth ratio greater than 40 and a slope less

than 0.02. Codes in this classification scheme range from A1 to G6 and ostensibly cover all river conditions. The widespread adoption of the Rosgen method is an indicator of its ease of use. However, simple descriptive classifications do not allow the user to infer what processes control channel form and future response. The Rosgen method has drawn severe criticism for its use beyond description and communication (Miller and Ritter 1996; Doyle and Harbor 2000).

In contrast to descriptive schemes, process-based classifications can be used as preliminary indicators of channel stability. However, because these schemes describe processes in addition to form, they require more expertise to use. In particular, process-based schemes require the user to relate processes occurring at the watershed scale to the reach of interest. For example, Schumm (1977) proposed placing of components of a fluvial system in one of three classes based on their current dominant geomorphic function: sediment sources, sediment transportation zones, or sediment sinks, and a similar approach was proposed by Montgomery (1999). Thorne et al. (1996b) suggested that all channels are either unstable (active morphological changes), dynamically stable (no characteristic change over engineering time scales), or "moribund" (unable to alter morphology due to the presence of geologic or engineering controls on geometry or discharge).

A specific example of application of the Schumm approach to disturbed fluvial systems involves the use of conceptual channel evolution models (CEMs) (Harvey and Watson 1986; Simon 1989). Though essentially qualitative, CEMs are powerful tools because they link channel forms to key geomorphic processes in a rational way that allows post- and prediction. However, their use is limited to channel systems experiencing adjustment by channel incision. Typically real-world watersheds do not follow the CEM models perfectly, but the absence of a distinct longitudinal progression in channel stages indicates that instabilities are the result of local phenomena rather than systemwide instability. In other words, classification systems can be used to indicate channel stability either directly or indirectly.

Simon and Downs (1995) and Thorne et al. (1996b) provide rough guidelines on inspecting key sites throughout a channel network in a given watershed to assess channel stability via reach classification. Inspection includes visually assessing key parameters such as bed material types, channel morphology, and bank stability. Measurements such as channel width and depth, thickness of sediment deposits, and bank height and angle may also be collected. Inspection of a single reach (6–12 channel widths long) can be done by an experienced person in 1 to 1.5 h (Simon and Downs 1995). These inspections should be conducted at key sites throughout the watershed. Selection of reaches to inspect is critical—sites must form a sufficiently dense network, and additional attention must be paid to the most dynamic reaches. Local influence of bridge crossings should be avoided by inspecting reaches several hundred meters upstream from, rather than at, bridges.

Johnson et al. (1999) reviewed and synthesized rapid stream channel stability assessment tools developed by Pfankuch (1978), the Federal Highway Administration (FHA 1995), and the previously noted work of Simon and Downs (1995) and Thorne et al. (1996b). A key component of the Johnson procedure is computation of the ratio of average boundary shear stress to critical shear stress. In gravel-bed rivers, as a rule of thumb, bed motion begins when this shear stress ratio exceeds 1. When the ratio exceeds about 2, most of the bed is in motion, and when it exceeds 3, the entire bed is in motion. However, Parker and Klingeman (1982) noted that bed shear stresses in gravel-bed streams rarely exceed more than two or three times the critical value even during severe floods. The Johnson procedure is not limited to use in watersheds experiencing incision, and it results in a qualitative stability rating (excellent, good, fair, or poor) rather than a CEM stage. The effort and experience required to use this assessment method are similar to that for the other methods. However, estimates of average boundary shear stress and critical shear stress are required, and the effort required to generate these estimates varies widely based upon the availability of existing data, the size of bed sediments, and the confidence level required. Average boundary shear stress should be computed for a range of discharges bounding the effective or design discharge. Johnson et al. (1999) suggest computing critical shear stress using the Shields (1936) equation,

$$\tau_c = \theta(\gamma_s - \gamma_w) D_{\text{critical}} \tag{9–13}$$

where

θ = dimensionless critical shear stress (Shields constant);
τ_c = critical shear stress for movement of material of size D_{critical}; and
γ_s and γ_w = specific weights for water and sediment.

Modification of τ_c for the effects of sediment mixtures when bed sediments are mixtures of sand and gravel may be in order. Critical shear τ_c may also be modified for the effect of gravity on bank slopes, if banks are comprised of granular, noncohesive sediments. See Chapter 2 in this volume for a full discussion of the Shields constant. A useful compilation of reported values for θ is provided by Buffington and Montgomery (1997). A compilation of data from natural rivers showed that θ exhibits modal values of approximately 10, 1, and 0.04 for rivers characterized by suspended-load, mixed-load, and bed-load regimes (Dade and Friend 1998).

In using this (Johnson et al. 1999) method, as well as other assessment methods, the user should bear in mind the conditions and purposes of the original tool. The Johnson method was developed specifically for road crossing stability and may require some modification for reach stability assessment. In particular, some of the indicators do not necessarily distinguish between local instability and natural channel processes

(Doyle et al. 2000). Both Johnson et al. (1999) and Pfankuch (1978) equate channel stability with channel uniformity, associating local erosion caused by flow obstructions like woody debris with channel instability. Although such features may be causes of instability at road crossings, they are common in natural channels and are critical for maintaining aquatic habitat and overall fluvial system stability. Hence, the method provides an estimate of stability, but each case should be treated individually due to local effects and inherent variability between sites.

9.4.3.3 Hydraulic Geometry Relationships The third type of stability assessment tool involves application of hydraulic geometry relations, which are empirical formulas that predict channel width, depth, slope, etc. as a function of a characteristic discharge, Q_{cf}, Q_{bf}, Q_{eff}, or Q_{ri}. Use of hydraulic geometry relations for restoration planning (Allen et al. 1994) and channel design (e.g., Shields 1996) is discussed elsewhere; here we focus on their use for stability assessment. These relationships are sometimes referred to as "downstream" hydraulic geometry formulas to differentiate them from formulas that describe how flow width and depth change at a given location as discharge increases ("at-a-station" formulas) (Leopold and Maddock 1953; Dunne and Leopold 1978). Surrogates for discharge, such as contributing drainage area, have been used in modified versions of these formulas, although this may introduce additional error. Hydraulic geometry relationships have also been applied to other dependent variables such as depth, slope, and velocity. Hydraulic geometry relations are sometimes stratified according to bed material size or other factors.

Hydraulic geometry relations can be developed for a specific river or watershed, or for streams with similar physiographic characteristics. River reaches that are judged to be in a state of dynamic equilibrium are selected for data collection. Use of field indicators rather than gauge data to determine channel-forming discharge is usually unwise (Williams 1978). Data scatter about the developed curves is expected even in the same river reach. The more dissimilar the stream and watershed characteristics are, the greater the expected data scatter. So-called "regional curves" would be expected to have data scatter across a full log cycle. It is important to recognize that this scatter represents a valid range of stable channel configurations due to variables such as geology, vegetation, land use, sediment load and gradation, and runoff characteristics. The composition of banks is very important in the determination of stable channel width. It has been shown that the percentage of cohesive material (Schumm 1977) and the type and amount of bank vegetation (Hey and Thorne 1986; Trimble 1997) significantly affect channel width.

The departure of a reach from a relationship based on data from adjacent lightly disturbed watersheds may be diagnostic of instability. For example, in their assessment of the Blackwater River in England, Thorne et al. (1996b) found that mean width and depth were 47% and 42% larger, and mean velocity 233% smaller, respectively, than values predicted using applicable hydraulic geometry relationships (Hey and Thorne 1986). Although the computed stream power was 57% greater than predicted using the Hey and Thorne (1986) relationship, it remained low (~13 W m^{-2}) relative to unstable, eroding channels in the United Kingdom and Denmark ($\geq$ ~35 W m^{-2}) (Brookes 1990). In contrast, meander wavelength and arc length were only 12% and 20% larger, respectively, than predicted. Using this information and the results of a qualitative reconnaissance of a larger area, they concluded that the reach in question had been enlarged, but not straightened. The reach was assessed to be geomorphically active, but recovering its natural size only slowly due to low stream power and limited sediment availability. This case study highlights the importance of professional judgment and field observations in interpreting results of stability analysis.

Hydraulic geometry formulas are easily and widely misused in river restoration. Like all empirical regressions, they are limited in their predictive capacity to the domain of independent variables used in their derivation. Extrapolation of formulas developed using data from England to the western United States or from the Rocky Mountains to the eastern seaboard leads to erroneous results. For example, Rinaldi and Johnson (1997) found that meander geometry equations developed by Leopold and Wolman (1960) overpredicted meander dimensions for small streams in central Maryland by average factors of 2.67, 2.22, and 2.48 for meander wavelength, amplitude, and radius of curvature, respectively. Because hydraulic geometry formulas are continuous, deterministic functions free of time dependence, they overlook threshold behaviors, indeterminacy (equifinality), and long-term dynamism, which are common in many fluvial systems (Schumm 1977). Analytical tools (discussed below) coupled with modern geomorphic analyses are required for more reliable assessments.

9.4.3.4 Relationships between Sediment Transport and Hydraulic Variables The fourth and largest suite of tools used in stability assessment are various types of relationships between sediment transport and hydraulic variables. These may be applied at the watershed level, or at a particular cross section.

9.4.3.4.1 Slope-Drainage Area Relations Data from reconnaissance surveys (described above) may be used to develop relationships between channel slope and channel-forming discharge for channel reaches 1 to 10 km long. Discharge is plotted against slope for each reach, and points are classified as representatives of stable or unstable reaches. Stability classification is based on subjective interpretation of field indicators of stability (Thorne et al. 1996a; 1996b), successive surveys and aerial photos, and specific gauge analyses. If discharge information is lacking, channel slope is plotted against contributing drainage area, and specific gauge analyses are omitted. For example, field reconnaissance and evaluation of the Yalobusha River Watershed, Mississippi, indicated that stable reaches could be plotted close to a line defined by

$$S = 0.0028A^{-0.433} \tag{9.14}$$

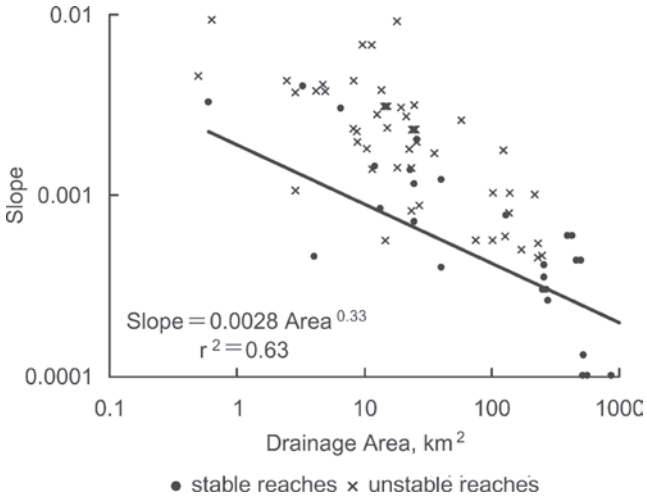

Fig. 9-6. Example of channel bed slope-drainage area relation used for reach stability assessment. Solid line represents the power function shown on the plot, which was obtained from regression of data from stable reaches (Simon and Thomas 2002). Unstable reaches generally plot above the line.

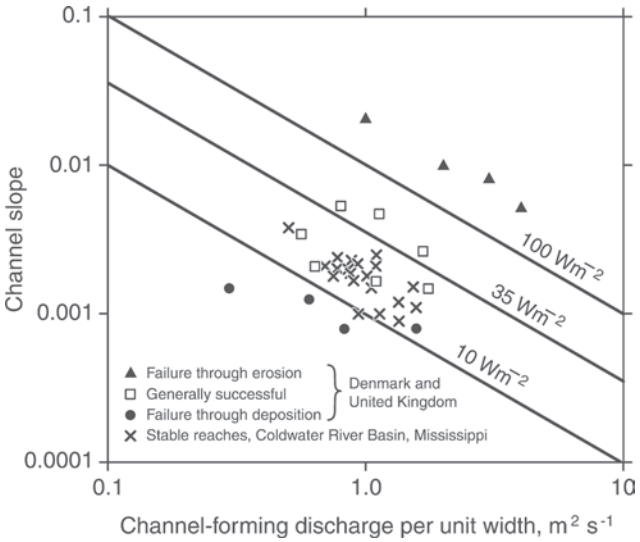

Fig. 9-7. Stream power stability criteria (Brookes 1990). Squares, triangles, and circles represent straightened, re-meandered channels in Denmark and the United Kingdom with sandy banks and beds of glacial outwash sands. Stars represent stable reaches in the Coldwater River watershed of northwestern Mississippi. This watershed is characterized by incised, straight (channelized) sand-bed channels with cohesive banks. Slopes for stable reaches shown were measured in the field, and channel-forming discharges were assumed equal to Q_{2yr}, computed using a watershed model (HEC-1) (USACE 1993).

where

S = slope of the energy gradient and
A = upstream drainage area in km^2

(Simon and Thomas 2002, Fig. 9-6). Steeper reaches tended to be unstable.

9.4.3.4.2 Stream Power Outputs from one-dimensional hydraulic models may be used to compute stream power or average boundary shear stress, and these values may be compared to those developed for nearby stable reaches. For example, the product of mean velocity and shear stress at channel-forming discharge, which is one form of the stream power per unit bed area, may be used as a criterion for stability in stream restoration projects (Brookes 1990). Unit stream power data are plotted as squares, triangles, and circles for initially straightened channels that were restored by meander reconstruction in Fig. 9-7. Based on experience with several restoration projects in Denmark and the United Kingdom with sandy banks, beds of glacial outwash sands, and a rather limited range of Q_{bf} (~0.4−2 m^3 s^{-1}); a unit stream power value of 35 W m^{-2} discriminated well between stable and unstable re-meandered channels. Projects with unit stream powers less than about 15 W m^{-2} failed through deposition, whereas those with unit stream powers greater than about 50 W m^{-2} failed through erosion.

Because these criteria are based on observation of a limited number of sites in specific geographical areas and with small bed sediment sizes, application to different situations (e.g., cobble-bed rivers) should be avoided. However, similar criteria may be developed for basins of interest. For example, data points representing stable reaches in the Coldwater River watershed of northwestern Mississippi are shown in Fig. 9-7 as x's. This watershed is characterized by incised straight (channelized) sand-bed channels with cohesive banks. Slopes for stable reaches shown were measured in the field, and 2-year discharges were computed using a watershed model (HEC-1) (USACE 1993). Downs (1995) developed stability criteria for channel reaches in the Thames Basin of the United Kingdom based entirely on slope: channels straightened during the twentieth century were depositional if slopes were less than 0.005, and erosional if slopes were greater.

9.4.3.4.3 Incipient Motion Fundamental principles regarding incipient motion of sediments on channel bed and banks are presented in Chapter 2 in this volume. Incipient motion analyses offer a quick check of bed stability in channels with beds coarser than sand (Pemberton and Lara 1984). These approaches indicate whether or not the bed will move when subjected to certain hydraulic conditions, but do not directly tell anything about channel stability. For example, shear stress may exceed the level needed to move a representative particle size, but because there is a supply of sediments from upstream, bed elevation may remain stable or even aggrade. Use of incipient motion relationships is further complicated by the fact that there is no true threshold condition where all the particles of a given size begin to move. Most critical shear stress relationships were developed by extrapolation of sediment transport rate versus shear stress curves to zero transport. This process results in critical shear stresses

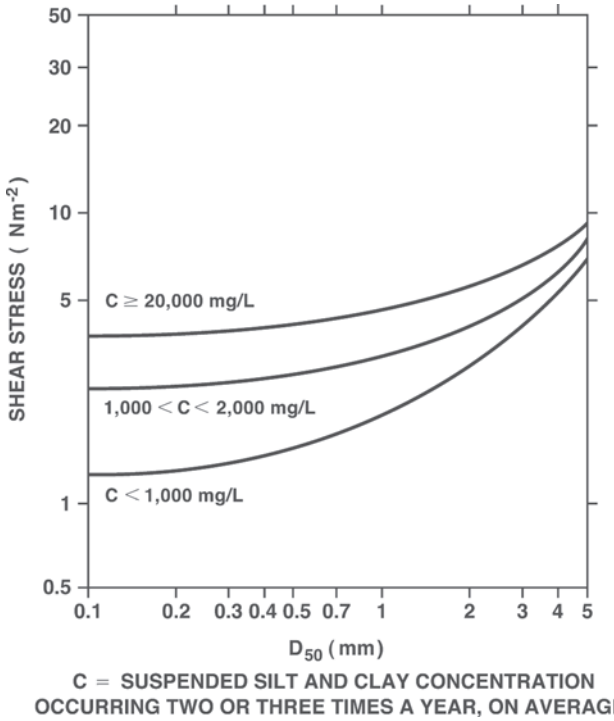

Fig. 9-8. Allowable mean shear stress for channels with boundaries of noncohesive material smaller than 5 mm carrying negligible bed-material load (after Lane 1955b in USDA 1977). "Allowable" stresses may be tolerated without causing serious erosion or endangering channel stability. Average shear stress may be adjusted for trapezoidal channel side slopes and width-depth ratio. Details are provided by Chang (1988) and USDA (1977). Values are for straight channels, and should be reduced approximately 10%, 25%, and 40% for slightly, moderately, and very sinuous channels, respectively.

that may be significantly higher than those at which sediment actually begins to move (Gessler 1971; Paintal 1971).

Some incipient motion relations indicate that critical bed size in mm is about 20 times the average velocity in m s^{-1} or about 10,000 times the product of depth in meters and slope. Typically, the median grain size, D_{50}, is used for the critical bed size in assessing the stability of a particular slope-width-depth-discharge combination (Pemberton and Lara 1984). A guideline used by the U.S. Department of Agriculture (USDA 1977) is shown in Fig. 9-8. It should be noted that the curves in Fig. 9-8 were drawn based on observations from straight canals, which have much more steady, uniform flows than most natural streams. In addition, the original source (Lane 1955b) for these curves states that "where much sand is carried, this method of analysis is not applicable," and "for crooked canals, lower values [of critical shear stress] must be used."

A list of five procedures useful for gravel or cobble beds is presented in Table 9-6. These five relationships predict a critical sediment size of 20 to 31 mm for a hypothetical example where Q = 14.2 m^3 s^{-1}, channel width = 18.3 m, mean depth = 1.2 m, mean velocity = 1.0 m s^{-1}, slope = 0.0021, D_{90} = 34 mm, and Manning n based on bed material size = 0.03 (Pemberton and Lara 1984). Typically, the engineer computes the bed material sizes that are at the threshold of motion for the upper and lower bounds of the discharge range of interest, but the relationships in Table 9-6 may also be solved for slope or discharge given the other variables.

The relationships in Table 9-6 involve varying amounts of theory and empiricism, and the engineer should be familiar with the underlying assumptions before interpreting their results. However, for ease of use we have omitted the details and simply reduced the equations to simplest form to yield

Table 9-6 Incipient Motion Stability Checks for Coarse, Noncohesive Beds Solved for Critical Bed Material Size, $D_{critical}$ (from Pemberton and Lara 1984)

Basic relationship	$D_{critical}$ (mm)	Remarks	Source
$D_{critical} = 20.2\ V_m^2$	$20.2\ V_m^2$	Based on assumption that velocity near bed is 0.7 V_m.	Mavis and Laushey (1949)
$V_m / V_f = 2.05$	$21.6\ V_m^2$ ($D_{critical} > 2$ mm)	V_f is the terminal fall velocity, approximated by the settling velocity formula of Rubey (1933)	Yang (1973)
$\tau_c = \gamma_w HS$	$13{,}000\ HS$ ($D_{critical} > 6$ mm)	Fig. 9-8 gives range of values for τ_c	Lane (1955b)
$\theta = \tau_c / [(\gamma_s - \gamma_w) D_{crit}]$	$10{,}000\ HS$ ($D_{critical} > 1$ mm)	Assumes Shields constant = 0.06	Shields (1936)
$D_{crit} = HS / [0.058 (n_s / D_{90}^{1/6})^{3/2}]$	$17.2\ HS\ D_{90}^{0.25}\ n_s^{-1.5}$	Reduces to form similar to Lane and Shields when Strickler equation is used for n_s	Meyer-Peter and Muller (1948)

Note: V_m = mean velocity, V_f = terminal fall velocity.

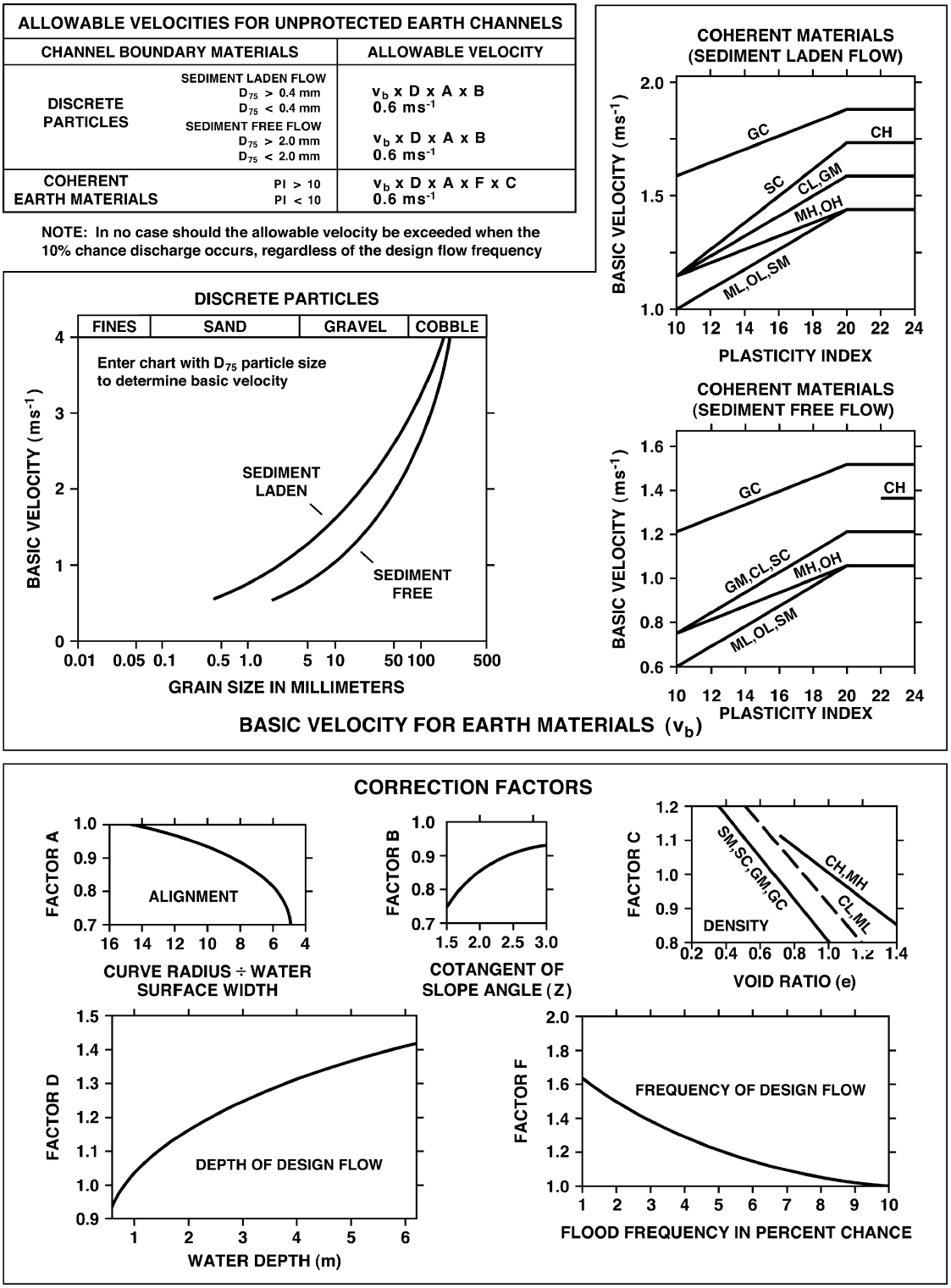

Fig. 9-9. USDA (1977) allowable-velocity charts for "unprotected earth channels." "Allowable velocities" are the maximum cross-sectional average flow velocities that do not cause serious boundary erosion. Allowable velocity for a given channel is determined using the formula in the box at the top left. The basic velocity, v_b, is given by one of the group of three plots at the top of the figure, whereas correction factors A, B, C, D, and F are obtained from the five plots in the bottom group. The letters PI = plasticity index, and the abbreviations GC, SC, CH, CL, GM, MH, OH, ML, OL, SM, etc. refer to the type of boundary as classified using the Unified Soil Classification System.

Table 9-7 Suggested Maximum Permissible Mean Channel Velocities (after USACE 1991)

Channel material	Mean channel velocity m s^{-1}
Fine sand	0.6
Coarse sand	1.0
Fine gravel[a]	2.0
Earth	
Sandy silt	0.6
Silt clay	1.0
Clay	2.0
Grass-lined earth[b]	
Bermuda grass	
Sandy silt	2.0
Silt clay	2.0
Kentucky blue grass	
Sandy silt	2.0
Silt clay	2.0
Poor rock (usually sedimentary)	3.0
Soft sandstone	2.0
Soft shale	1.0
Good rock (usually igneous or hard metamorphic)	6.0

[a]For particles larger than about 20 mm.

[b]For slopes less than 5%. Keep velocities less than 1.5 m s^{-1} unless good cover and proper maintenance can be obtained.

bed material size in mm. It is important to note that incipient motion analyses are invalid for sand channels or gravel beds in motion at the discharge of interest because they presume zero transport of the critical bed size at the selected discharge.

Incipient motion approaches based on velocity rather than shear stress are also available. Because channels with identical average velocities can experience different bed shear stresses, correction factors for variation in flow depth, sediment load, channel curvature, and so forth have been developed (USDA 1977). A series of charts for determining allowable velocity is presented in Fig. 9-9, and a commonly used set of values based on experience is presented in Table 9-7. The allowable-velocity approach is not recommended for channels transporting a significant load of material larger than 1 mm.

9.4.3.4.4 Silt and Clay Beds For beds finer than sand, few tools exist and much uncertainty arises due to the complexity of cohesive bed erosion. However, the preceding discussion regarding critical values of stream power and slope offers some guidance. Erosion of cohesive materials is affected by water quality, by material history (weathering and saturation), and by macroscale phenomena (e.g., zones of weakness between cohesive blocks). A review is provided in Chapter 4 of this volume. Current research emphasizes the importance of positive and negative pore water pressure in cohesive beds (Simon and Collison 2001) and banks (Simon et al. 2000). A field test for measuring cohesive bed erodibility is available, but many replications are required to characterize a channel reach, because of local variations (Hanson and Simon 2001).

At present, most guidance for stability of cohesive material is based on scattered observations. Neill (1973, in Pemberton and Lara 1984) published competent velocities for erosion of cohesive materials ranging from 0.6 to 1.8 m s^{-1} for flow depth of 1.5 m, and 0.8 to 2.6 m s^{-1} for flow depth of 15 m. Fortier and Scobey (1926, in French 1985) suggested a maximum permissible mean velocity of 1.1 m s^{-1} for alluvial silts and stiff clay and a value of 1.8 m s^{-1} for shales and hardpans. These values correspond to mean bed shear stresses of 12 and 32 N m^{-2}, respectively. Values are

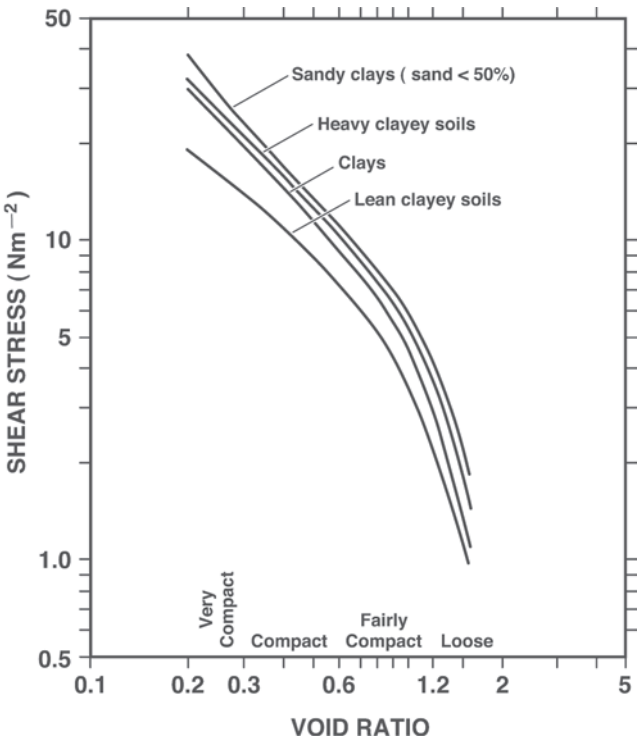

Fig. 9-10. Allowable shear stresses for cohesive materials based on conversion by Chow (1959) of permissible velocities published by "The maximum"(1936) to boundary shear stresses. "Allowable" stresses may be tolerated without causing serious erosion or endangering channel stability. Curves represent the maximum allowable boundary shear stress for cohesive soils with void ratios as given on the x-axis and soil properties shown on the curve labels. Values are for straight channels, and should be reduced approximately 10%, 25%, and 40% for slightly, moderately, and very sinuous channels, respectively.

for "straight channels of small slope after aging" and depths of flow less than 0.9 m. The Fortier and Scobey values should be reduced 25% for sinuous channels, increased by 0.15 m s^{-1} when depth exceeds 0.9 m, and increased 0.3 to 0.6 m s^{-1} for streams carrying high sediment loads (French 1985). Data presented by Chow (1959) regarding allowable shear stresses for cohesive materials are shown in Fig. 9-10, and additional empirical data are presented by Julien (1995). Empirical data such as those shown in Fig. 9-10 should be used with extreme caution, because they represent a limited data set and do not allow for inclusion of macroscale phenomena that may be most important.

9.4.3.4.5 Sediment Budgets Sediment budgets for channel reaches are at the upper end of a continuous scale of complexity and effort for stability assessments, and at the lower end of the scale for design. The purpose of a sediment budget analysis is to determine if a specific channel reach has the capacity to transport the sediment load delivered to it by upstream channels. If significant differences are found between the inflowing sediment rating curve and a rating curve for the specific channel reach, then a condition of channel instability has been identified. Detailed computations must necessarily be postponed until the design stage, because project dimensions and boundaries may not yet be known. Nevertheless, assumed channel properties may be used to good effect within the bounds of normal sediment transport relationship accuracy. Sediment budgets are discussed in greater detail in Section 9.6.2.2.

9.4.3.5 Bank Stability Streambank erosion may be classified as fluvial erosion of material from a bank face (generally analyzed using incipient motion approaches described above) or collapse of large masses of bank material. These masses are removed from the bank toe ("basal cleanout"), resteepening the bank profile and creating conditions conducive to another failure. Mass failure of steep, cohesive banks is related to bank height, bank angle, and soil properties (Simon et al. 2000). If bank heights are greater than about 3 m and angles greater than about 45º, a stability analysis may allow assessment of the severity of bank instability and the need for remedial measures. A stability chart may be prepared for a given set of bank soil properties, as described by Thorne (1999). Software packages may prove helpful in simulating effects of stage and groundwater table fluctuations on banks of various height and angle (e.g., Simon et al. 2000; 2003). If bank soil properties are not known, a tabulation of stable and unstable bank heights derived from the watershed qualitative reconnaissance may prove helpful, particularly when coupled with forecasts of future channel degradation or aggradation.

9.4.4 Assessment Tool Selection

Normally a stability assessment proceeds by dividing the channel network into reaches displaying consistent fluvial properties and applying a set of assessment tools to each reach. A greatly simplified example is provided in Table 9-8.

Table 9-8 Summary of Simplified Hypothetical Stability Assessment

Assessment tool	Reach 1	Reach 2	Reach 3	Reach 4	Value required for stability	Reference
Bed slope from a slope-drainage area relationship[a]	0.002	0.00018	0.0022	0.0024	0.0006–0.0008	Simon and Thomas (2002)
Unit stream power, W m^{-2}	29	43	33	52	<35	Brookes (1990)
Potential specific unit stream power, W m^{-2}[b]	24	32	38	45	≤ 30 for meandering planform	Van den Berg (1995)
Channel evolution model	Stage V	Stage V	Stage IV	Stage II	Stage V or VI	Simon (1989), reconnaissance per Thorne et al. (1996b)
Average bed shear stress, N m^{-2}	24	26	30	29	20–25[c]	Regional observations
Height of near-vertical banks, m	5.1	4.7	4.3	2.2	3.8	Bank stability analysis per Thorne (1999) and Simon et al. (2003)

Note: Consensus of assessment indicates incision (and instability) is proceeding upstream through reach 3 to reach 4. Reaches 1 and 2 are slightly aggradational, but accelerated lateral channel migration likely continues there.

[a] $S = 0.0028\ A^{-0.33}$.

[b] $2.1\ S_v\ Q_{bf}^{0.5} < 843\ D_{50}^{0.41}$.

[c] Larger than value based on incipient motion (12 N m^{-2}) due to significant bed material load.

Selection of a suite of tools for a particular project involves considerable judgment and is strongly influenced by the availability of existing data sets, the experience of responsible personnel, and economic factors. However, some generalizations can be made. Lane-type relations are good for quick preliminary assessments, particularly where system disturbance is dominated by a shift in one of the main variables. Process-based classification schemes are most highly developed for fluvial systems disturbed by influences leading to rapid incision or aggradation. Hydraulic geometry approaches are limited to projects located in regions with lightly perturbed alluvial channels in dynamic equilibrium for which extensive data sets are available. Incipient motion type analyses including Shields parameters are usually limited to channels with beds dominated by material coarser than sand, whereas sediment budgets are best for sand-bed streams prone to aggradation. Cohesive boundary channels are most difficult to analyze, and empirical tools such as slope-area relations, regional stream power indices, or shear stress thresholds are often applied. Channels with cohesive banks higher than about 3 m usually call for some type of bank stability analysis.

9.5 RIVER RESTORATION DESIGN

Following stability assessment, the restoration project enters the design phase (Fig. 9-1). Although not shown in Fig. 9-1, preliminary analyses may be performed for several alternatives, and detailed design may be reserved for subsequent iterations using the selected alternative. The complexity of design studies should be related to project scale, but an understanding of likely impacts on sediment transport and channel morphology is needed for all restoration projects. Techniques used for design borrow principles from the engineering topics of stable channel design and channel stability analyses and the science of fluvial geomorphology (Chapter 6).

The adaptive, dynamic quality of river systems gives them a certain capacity for recovery (self-restoration). Some stream ecosystems may respond more favorably to assisted recovery (e.g., creating conditions that allow natural revegetation of riparian zones) than strategies featuring aggressive intervention. Generally, strategies that involve the greatest structural modification hold potential for the greatest project-induced adverse environmental impacts, but may prove most beneficial in the long run. Reconstruction of a meandering or braided channel with appropriate width, depth, bed texture, and sinuosity may be necessary to restore a drastically altered stream.

9.5.1 Channel Design

9.5.1.1 Channel Design for Restoration Projects If the existing stream is stable (Thorne et al. 1996b), a good rule of thumb is to modify the channel as little as possible. However, in some cases it may be necessary to modify a stable channel to meet overall project objectives (e.g., restoring some of the functional attributes of the ecosystem). When the existing stream is unstable, significant intervention may be necessary for restoration. In reach-scale projects consideration should be given to isolating the restored reach from the disturbed channel (e.g., through the use of grade controls or sediment traps).

Analytical equations are preferred for design over empirical formulas. Many empirical relations (e.g., hydraulic geometry formulas) are based on limited, regional data sets, and the influence of variables that become important in application may be hidden. For example, a relationship between discharge and velocity based only on data from streams with engineered bank protection would not be applicable to a natural stream with unprotected banks. When design variables are related to a single independent variable such as discharge, the reliability of the relationship is limited.

9.5.1.1.1 Acceptable Levels of Dynamism Conventional flood control, navigation, and channel stabilization projects have focused on increasing the stability of channel position, geometry, and flow conditions. A premium has been placed on high levels of certainty regarding performance and fluvial response. In contrast, restoration projects often seek to enhance the dynamic behavior of fluvial systems, often by relaxing constraints when past activities have led to highly regulated flows or uniform, fixed boundaries. System restoration may involve restoration of processes such as flooding, meander migration, channel avulsion, formation and destruction of large woody debris jams, and backwater sedimentation. For example, high flows may be ecologically beneficial in a number of ways: flushing fine sediments from coarse deposits and thus maintaining conditions that allow intra-gravel movement of water and oxygen, recharging floodplain water tables, depositing nutrient-laden silt on floodplain lands, and temporarily creating extensive "lakes" and feeding areas for migratory waterfowl, fish, and other organisms. Removing or changing the operational strategy for flood control structures may restore high-flow regimes. Experiments by the U.S. Bureau of Reclamation in 1996 and 2004 that produced artificial floods of preset magnitude and duration on the Colorado River in the Grand Canyon downstream from Glen Canyon Dam provide an example of flood restoration. The artificial floods were designed to restore beaches, bars, and wildlife habitat impacted by decades of reservoir operation. Immediate results of the 1996 event showed that morphologic response occurred rapidly—changes were observed after only a few days of high flow (Vaselaar 1997; Schmidt et al. 1998), but longer-term outcomes were less satisfactory, driving plans for the second experiment (Pennisi 2004).

Restoring natural fluvial processes present challenges to engineers because it requires changing streams from

an understood present condition to an uncertain, more dynamic future situation. Human systems tend to call for stability, reliability, and predictability; natural systems tend to be dynamic and unpredictable. The reluctance to venture into unknown outcomes may be addressed in at least three ways:

- Incorporating new physical controls into project design. For example, if meandering processes are to be restored or enhanced, then meander belt boundaries could be established. These may be geologic controls, existing structural controls, or new structural controls installed either during project construction or at a later date if and when needed. Similarly, longitudinal limits for re-meandering (e.g., at bridges) might be established at existing or constructed controls such as drop structures.
- Developing the restoration project in stages. If each stage is well conceived and fits into the ultimate restoration condition, this allows the uncertainties to be reduced with each stage and the dynamism and instabilities to be somewhat restricted.
- Providing sediment sinks or sources as needed to maintain sediment continuity and channel stability. These measures will generally require costly operation or maintenance programs.

Restoring a channel to a state of dynamic equilibrium may not be a socially acceptable outcome if the resulting situation poses threats to riparian resources or infrastructure. The need for a relatively high level of channel stability is often a driving factor in urban settings, where tolerance for channel adjustments is low. Clearly, human factors may force design tradeoffs that lead to less than full restoration of channel dynamics and dependent ecosystem attributes. Although these tradeoffs were common in historical river engineering projects, they usually reduce the value of restoration projects. Regardless of strategy, the consequences for channel stability of design alternatives under various scenarios may be evaluated using approaches described in Section 9.6.

9.5.1.1.2 Channel Reconstruction Design analyses should attempt to ensure that the reconstructed channel is not rapidly damaged or destroyed by erosion or sedimentation. The approaches described in Sections 9.5.1.2 and 9.5.1.3 may be used to select the channel width, depth, and slope required for an acceptable level of stability given water and sediment inflows anticipated for the future with-project condition. However, it should be noted that the analytical approaches described in these sections are applicable only to fluvial systems that, given enough time, develop characteristic forms (equilibrium morphologies) in response to an unchanging hydrologic regime. Usually these are perennial, moderate-to-low-energy, single-thread, meandering streams. In these systems, channel width, depth, slope, and bed material grain size eventually adjust to the channel-forming discharge and the input bed-material sediment load. The restoration designer seeks to assist this adjustment by computing and selecting appropriate values for channel geometry. When the computed channel geometry is not feasible due to site or project constraints, the resulting maintenance requirements (erosion controls or sediment removal requirements) may be computed. However, it is important to understand that many fluvial systems are not responsive to a channel-forming discharge of a given average frequency (see Section 9.3.1). Special analyses (Section 9.5.2) may be appropriate when hydraulic structures or habitat enhancement features will be used within the channel, in adjacent backwaters, or on the floodplain.

9.5.1.1.3 Design Variables and Approaches The engineer must select average channel width, depth, slope, and hydraulic roughness and lay out a planform so that the channel will pass the incoming sediment load without significant degradation or aggradation. These design variables are functions of the independent variables of water discharge, sediment inflow, and streambed and stream bank characteristics. In some cases, channel dimensions may be based on a preexisting condition, but this set of dimensions may not be stable if watershed land use or climate has changed. The design process is most challenging when the project reach is unstable due to straightening, channelization, or changing hydrologic or sediment inflow conditions, as is the case in most urban areas. The effects of urbanization on hydrologic response (e.g., increasing flow quantities and peaks) can trigger rapid bed and bank erosion, particularly when these effects are coupled with declining watershed sediment yield as development proceeds.

Channel design approaches may be classified as threshold or active-bed methods. These approaches are discussed in the following sections. The engineer should select an approach based on boundary mobility at design discharge conditions (Fig. 9-1).

9.5.1.2 Design Procedure for Threshold Channels

9.5.1.2.1 When to Use the Threshold Approach Threshold methods are appropriate in cases where bed-material inflow is negligible and the channel boundary is immobile even at high flows. For example, streambeds that are composed of very coarse material or that contain numerous bedrock controls may be immobile even during bank-full flows. Channels with bed material derived from events or processes not currently operative, such as glaciation, may also be candidates for threshold analyses. It should be noted, however, that unmodified channels generally transport significant quantities of material composing their boundaries. Because restoration projects usually are intended to promote natural processes and functions, use of threshold approaches is rarely appropriate. An example of an appropriate use of threshold methods is provided by Newbury and Gaboury (1993), who used tractive-force analysis to size stone used to construct permanent artificial spawning riffles in a channelized stream.

Threshold channels are designed so that a selected fraction of the bed material will be at the threshold of motion (see Section 2.4) at design discharge. Clearly, selection of the design bed material size is crucial. Guidance for sampling bed material is provided in Section 9.3.2. If fine material is moved as throughput over a pavement of coarser sediment, the pavement material should be used to determine the sediment size for design. However, an active-bed analysis may be necessary to ensure that the throughput transport rate is maintained. Threshold methods do not provide unique solutions for channel geometry, and geomorphic principles may be used to finalize selection of reasonable design variables.

9.5.1.2.2 Allowable Velocity and Tractive Force Threshold-of-motion channel design procedures have been widely used for many years (e.g., Lane 1955b). The allowable-velocity approach of USDA (1977) is reviewed in Section 9.4.3.4.3, and graphs are provided in Fig. 9-9. Allowable velocity values are based on experience and various observations. The tractive-force approach (also known as the tractive-stress approach) is a more scientific method based on an analysis of the forces acting on sediment particles on channel boundaries. The basic derivation of equations used in the tractive-force approach assumes that channel cross sections and slopes are uniform, beds are flat, and bed-material transport is negligible. These conditions are rarely found in nature, particularly in lightly degraded streams. Therefore this approach has limited applicability to restoration design.

9.5.1.2.3 Step-by-Step Approach Although design should include reiteration to refine values based on preliminary estimates, a threshold approach may proceed as follows:

- Determine design bed material gradation and water discharge as described above. Note that the use of Q_{eff} is inappropriate for most cases of threshold channel design, because the boundary of the channel will be immobile under design discharge conditions. The discharge selected for sizing a threshold channel should be less than the channel-forming discharge, which, by definition, "does the most work on the channel." Accordingly, the discharge used for design will usually be Q_{ri} or Q_{bf} and will be smaller than Q_{eff}, unless Q_{eff} is determined based on transport of sediments finer than the boundary materials.
- Use hydraulic geometry or regime formulas (see above) to compute a preliminary average flow width.
- Using the design bed material size gradation, estimate critical bed shear stress. The compilation of data presented by Buffington and Montgomery (1997) may prove helpful, because it includes many values from natural streams (as opposed to laboratory flumes) and extensive information regarding the collection and derivation of each value of dimensionless critical shear stress.
- Use bed material size, estimated channel sinuosity, bank vegetation, and flow depth to estimate a flow resistance coefficient. Normally resistance due to bars and bed forms will not be important in threshold channels flowing full, so formulas such as those proposed by Limerinos (1970) or Hey (1979) may be used to compute resistance coefficients. Bathurst (1997) provides a review of flow resistance equations and their proper application.
- Using the continuity equation and a uniform flow equation (e.g., Manning or Chezy), compute the average depth and bed slope needed to pass the design discharge. Sinuosity may be computed by dividing the valley slope by the bed slope. Adjustment of the flow resistance coefficient for sinuosity and reiteration may be required.

9.5.1.2.4 Example An example of a preliminary design developed using the above step-by-step process is provided in Table 9-9. The hydraulic geometry formula chosen for flow width corresponds to bank-full discharge in gravel-bed streams with armor layers and "5 to 50% tree and shrub cover" on the banks. A Shields constant of 0.042 was computed and used to define threshold conditions, but other approaches such as maximum permissible velocity or tractive stress could also be used. The value of the flow resistance coefficient (Darcy-Weisbach f) computed using the formula by Hey (1979) was not modified to account for head losses due to bends, because bend losses would be a relatively small fraction of total loss in such a channel (Onishi et al. 1976). Bend losses are more important for channels with finer bed material and more pronounced bars and bed forms. Channel sinuosity, planform, and alignment were designed as described in Section 9.5.1.4.

9.5.1.2.5 Refinements Additional refinements to shear-stress-based threshold design approaches to allow for the effects of the angle of repose of noncohesive materials, channel side slopes, and bend flow are explained in textbooks (e.g., French 1985; Chang 1988; Julien 1995). For channels with bottom widths greater than twice the flow depth and with side slopes steeper than 1V:2H, the maximum boundary shear stress at a point on the bed or banks may be approximated by $1.5\ \gamma_w HS$ (Chang 1988). Information on the cross-sectional distribution of velocity and shear stress in bends is provided by the USACE (1991).

9.5.1.3 Design Procedure for Active-Bed Channels Active-bed approaches should be used for channels with beds that are mobilized during all high-flow events (at least several times a year). These systems are much more sensitive to relationships between channel geometry and sediment inflow than threshold channels, and design requires more attention. The method described here is applicable for hydraulic design of channels for single-thread streams with mobile beds. Design of braided channel networks is beyond the scope of this chapter. The active-bed design procedure is intended to produce a channel that will transport the sediment supplied to the reach from upstream. Selecting

Table 9-9 Example of Preliminary Channel Design Using Threshold Approach

Quantity	Relationship	Source	Value
Valley slope		Survey or topographic map	0.007
Downvalley distance, km		Survey or topographic map	1.5
D_{50} of bed material, mm		Samples and sieve analysis	45
D_{84} of bed material, mm		Samples and sieve analysis	60
Design discharge, $m^3\ s^{-1}$	$Q_{1.5\ yr}$	Flood-frequency curve	6.7
Width, B, m	$2.73\ Q^{0.5}$	Hey and Thorne (1986)	7.1
Shields constant, θ	Appropriate value or relationship[a]	Buffington and Montgomery (1997)	0.042
Depth-slope product, RS, m[b]	$1.65\ D_s\theta$		0.0031
Variation in depth at a section	R/H_{max}	Assumed based on reference reach	0.75
Channel shape coefficient, a	$11.1\ [R/H_{max}]^{-0.314}$	Hey (1979)	12.15
Darcy-Weisbach flow resistance coefficient, f[c]	$\frac{8}{\left[5.75\log\left(\frac{aR}{3.5D_{84}}\right)\right]^2}$	Hey (1979)	0.10
Hydraulic radius, R, m[d]	$\sqrt{\frac{fQ^2}{8gP^2(RS)}}$	Simultaneous solution of continuity and uniform flow equations for depth.	0.6
Bed slope, S	RS/R		0.005
Sinuosity	Valley slope/channel slope		1.3
Channel length, km	Sinuosity × downvalley distance		2.0

[a]Many of the relations tabulated by Buffington and Montgomery (1997) require an entire gradation curve for both surface (armor) and subsurface bed sediments.

[b]Assumes that average flow depth = hydraulic radius.

[c]Assume a trial value for R. Numerous other relationships are available. For example, the equation due to Limerinos (1970) leads to a Manning n of 0.032, which is equivalent to a Darcy-Weisbach f of 0.10.

[d]Assume wetted perimeter P = width, B. Check R computed with this formula against trial value assumed for computation of Darcy f. Iterate as needed.

channel geometry based on preexisting conditions or threshold approaches without regard to sediment continuity can produce channels that are competent to transport only a fraction of the supplied sediment (Shields 1997). Rapid sedimentation, instability, and high maintenance requirements may result.

The reader should note that the approach described below is based on one-dimensional models, and the highly three-dimensional nature of fluid motion in meanders, which is closely coupled with complex bed topography, is poorly represented. In most cases, two- and three-dimensional effects (e.g., bends) must be incorporated into design computations by professional judgment. The overall approach described could be used with more sophisticated numerical models of flow and sediment movement, but input requirements are often prohibitive for application to smaller projects. Future advances in the state of the art of hydrodynamic modeling may address these issues.

9.5.1.3.1 Width Determination When channel width is not constrained by right-of-way limitations, design width may be determined using the analogy method, hydraulic geometry formulas, and analytical methods (in order of preference). Each is discussed briefly here.

Analogy Method The width may be set equal to the average of measured widths from a reference reach. The reference

reach must be in a state of dynamic equilibrium and have the same channel-forming discharge as the project reach. The reference reach may be in the project reach itself, upstream and/or downstream from the project reach, or in a physiographically similar watershed. Streambanks and streambeds in the project and reference reaches must be composed of similar material, and there should be no significant hydrologic, hydraulic, or sediment differences in the reaches.

Hydraulic Geometry Hydraulic geometry formulas (described in Section 9.4.3.3) for width generally display less scatter (residual error) than those for depth or slope. Appropriate formulas, wisely applied, can therefore be used to generate initial values for reach-average channel width.

Analytical Methods If a reliable width versus channel-forming discharge relationship cannot be determined from field data, or if there is significant sediment transport, analytical methods may be employed to obtain a range of feasible solutions, as described below.

9.5.1.3.2 Average Slope and Depth Depth and slope should be calculated using analytical techniques. Analytical techniques are based on physical laws and limited empiricism, and therefore are preferred to empirical hydraulic geometry relationships. In addition to depth and slope, analytical methods may also be used to calculate width in lieu of an empirical method. The design variables of width, slope, and depth may be calculated from the independent variables of water discharge, sediment inflow, and bed-material composition. Three equations are required for a unique solution of the three dependent variables. Flow resistance and sediment transport equations are readily available. Several investigators propose using the extremal hypothesis to supply the third equation (Chang 1980; White et al. 1982; Millar and Quick 1993). However, extensive field experience demonstrates that channels can be stable with widths, depths, and slopes different from extremal conditions.

The stable-channel design routine in the hydraulic design software SAM (Copeland 1994; Thomas et al. 1995; "SAM Hydraulic" 2005) and also found within HEC-RAS 3.1 and higher may be used to determine channel depth and slope. This method is based on a typical trapezoidal cross section and assumes steady uniform flow. The method is especially applicable to small streams because it accounts for sediment transport, bed form and grain roughness, and bank roughness. The first step in using an analytical method for channel dimensions is to determine the sediment inflow into the project reach. SAM requires that the user either provide the bed material discharge input to the design reach or specify the discharge, channel geometry, and bed sediment size for a "supply reach" upstream from the design reach. SAM computes sediment discharge for the supply reach assuming that it is transporting bed material at full capacity. Supply reach computations are important in restoration projects, because restoration almost never extends to the upper limits of disturbance. Therefore the designer must develop features (such as sediment traps) that allow a transition from the sediment supply typical of the disturbance regime to the regime provided by the restored reach. Many urban areas are built on alluvial fans or other aggradational features with channels supplied by relatively steep headwaters. Historically, the downstream reaches maintained equilibrium by periodically avulsing. However, once floodplains are developed, such channel changes are typically prevented, thus exacerbating channel aggradation (personal communication, D. Simons).

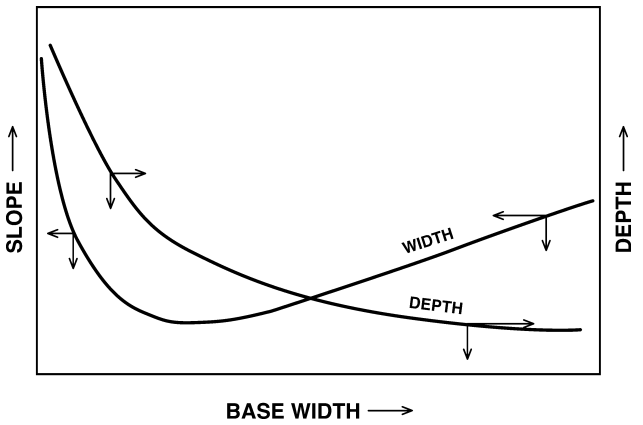

Fig. 9-11. Stable channel design chart showing family of solutions yielding a stable channel for a given design discharge.

The second step in active-bed analytical channel design is to develop a family of slope-width solutions that satisfy the resistance and sediment transport equations. For each combination of slope and base width, a unique value of depth is calculated. The engineer may select any appropriate flow resistance and sediment transport relations to generate the family of slope-width solutions. Shiono et al. (1999) present a simple equation useful for computing flow resistance of a two-stage channel with a meandering low-flow channel, but the equation is based on data from a physical model with uniformly smooth floodplains and main channel. The stable channel design routine in SAM uses either resistance and sediment transport equations by Brownlie (1981; 1983) or a combination of the Meyer-Peter and Muller (1948) sediment transport equation and the Limerinos (1970) resistance equation to calculate bed resistance and sediment transport. The routine may also be used to assess the stability of an existing channel.

An example stability curve is shown in Fig. 9-11. Any combination of slope and base width from this curve will be stable for the prescribed stable channel design discharge. Using the width from a hydraulic geometry predictor or from a reference reach, a unique slope and depth are determined. Width could also be obtained from the minimum slope. Other possible stable channel width and slope combinations can be found from the stability curve. Depth is specified by

a given slope and width (or width by a given slope and depth). Constraints on this wide range of solutions may result from a maximum possible slope or a width constraint due to right-of-way. Maximum allowable depth could also be a constraint. With constraints, the range of solutions is reduced. Combinations of width, depth, and slope above the stability curve will result in degradation, and combinations below the curve will result in aggradation. The greater the distance from the curve, the more severe the instability will be. The relationship between sediment transport in the restoration project reach and in downstream reaches must also be investigated. The same general discussion applies, except that the restoration reach becomes the sediment supply reach and the downstream reach is evaluated for an imbalance between bed material transport capacity and sediment supply.

9.5.1.3.3 Example A preliminary design for a hypothetical channel reconstruction for rehabilitation of a sand-bed stream in an urban area with actively eroding banks was developed using the process described above (Table 9-10). Reaches upstream and downstream from the project are relatively stable, except for a few bend locations where bank failure is occurring.

The effective discharge was found by developing a flow-duration curve using data from a downstream gauge. The flow-duration curve was then integrated with a sediment-discharge-rating curve calculated using the Brownlie (1981) equation and channel geometry upstream from the project reach. An hydraulic geometry formula was developed for flow width using appropriate regional data (Table 9-10). Use of the inflowing sediment load to solve for depth and slope ensures that the restoration design will be competent to transport the supplied load.

9.5.1.4 Design of Channel Alignment and Geometric Detail Designing the reconstructed channel alignment involves selecting a channel right-of-way that produces appropriate bed slope and, for single-thread meandering channels, meander geometry. Procedures are similar for threshold and active-bed channel designs. In some cases, preexisting channel alignments determined from maps, aerial photos, or soil surveys may be used if the resulting channel slope is adequate. Channel alignment may be designed by arranging a curve of fixed length (=channel length) on a map of the site. The channel length is simply the down-valley distance times the reach sinuosity, which is the ratio of valley slope to channel slope. Reach sinuosity may be

Table 9-10 Example of Preliminary Channel Design Using Active-Bed Approach

Quantity	Relationship	Source	Value
Valley slope		Survey or topographic map	0.001
Downvalley distance, km		Survey or topographic map	10
Median bed material size, mm		Samples and sieve analysis	0.6
D_{84} of bed material, mm		Samples and sieve analysis	1.0
Design discharge, $m^3\ s^{-1}$		Effective discharge analysis	68
Sediment load at design discharge, $kg\ s^{-1}$	Sediment transport equation and channel geometry from upstream reach	Brownlie (1981)	25
Channel side slope		Assumed	1V:1.5H
Manning n value for side slopes		Estimated	0.05
Top width B, m	$3.6Q^{0.5}$	Developed from stable reaches within watershed	30
Depth, m and bed slope	Simultaneous solution of sediment transport and uniform flow equations	Brownlie (1983) for bed resistance	2.4 (depth) 0.00061 (slope)
	Bed resistance composited with assumed Manning n-value for side slopes	Equal-velocity approach (Chow 1959) for compositing	
Sinuosity	Valley slope/channel slope		1.6
Channel length, km	Sinuosity × downvalley distance		16

checked against values for reference reaches in nearby, similar watersheds.

Meander wavelengths resulting from channel right-of-way layout may be checked against values obtained from hydraulic geometry formulas (e.g., Leopold et al. 1964; Ackers and Charlton 1970) or analytical functions (Langbein and Leopold 1966), but care should be taken to ensure that the data sets used to generate the formulas are from geomorphically similar regions and streams (Rinaldi and Johnson 1997). In general, hydraulic geometry formulas that give wavelength as a function of width are preferred. Uniform geometries (e.g., constant bend length and radius) should not be used. Values derived from formulas may be taken as averages, but bend-to-bend variation should occur. Constant dimensions for channel width, depth, slope, and meander radius and wavelength should not be used for design. Instead, design should capture the spatial variability typical of lightly degraded systems. For example, meandering channels tend to be wider and shallower at riffles, which are often found at meander inflection points, and narrower and deeper at bend apices (Richards 1978; Hey and Thorne 1986). The dimensions computed as described in Sections 9.5.12 and 9.5.1.3 should be used only as averages. Excavation and fill are generally less effective than flow constriction and expansion in producing and maintaining bed features such as pools and riffles. Well-designed projects will develop higher levels of physical heterogeneity with time as vegetation develops, bed material is sorted, large woody debris is trapped, and patterns of local scour and deposition replace uniform dimensions with those typical of natural, lightly degraded streams. Physical response tends to be most favorable for sinuous channels.

As an example, the design outlined in Table 9-10 has a valley slope of 0.001 and a channel slope of 0.00061. Thus a channel sinuosity of 1.6 is feasible. Using a hydraulic geometry formula ($L = 61.21\ Q_{bf}^{0.467}$) curve for meander wavelength (Ackers and Charlton 1970), an approximate meander wavelength of 439 m was selected. Using GIS or mapping software, a mildly sinuous planform channel of fixed length was laid out on a digital topographic map of the project reach.

9.5.2 Habitat Structures

In addition to varying channel geometry, additional physical heterogeneity may be introduced into a reconstructed channel by constructing various types of in-channel habitat structures. Many river restoration projects consist entirely of placing habitat structures and planting riparian vegetation. In some cases, structures are intended to control erosion and enhance habitat (e.g., Shields et al. 1995a). Some workers have questioned the philosophy of using structures to restore habitat, reasoning that if natural fluvial forms and processes are restored, artificial structural elements will be unnecessary or even detrimental. In all types of aquatic habitat planning and design, it is best to let natural processes guide choices for actions. Wherever natural conditions can be used to advantage, the actions are likely to become most compatible with the habitat needs in the ecosystem. Structures not in harmony with the geomorphic processes controlling channel form and physical aquatic habitat are at best a waste of resources, and may damage the stream corridor ecosystem. Conversely, when watershed and riparian conditions are restored to predisturbance status, there is generally little need for habitat structure (except to produce rapid change, which may be desired by stakeholders).

Many types of structural measures have been used for in-channel aquatic habitat improvement, but most fall into four categories (Shields 1983): sills, deflectors, random rocks, and covers. An overview of these categories is provided in Table 9-11. Some structures are essentially erosion control structures (e.g., irregularly shaped revetments and intermittently spaced spur dikes), whereas others are designed to cause bed or bank erosion. Materials used for construction may be natural or artificial, but materials occurring naturally in the stream corridor prior to degradation are preferred.

9.5.2.1 Design of Habitat Structures The design of aquatic habitat structures is a combination of hydraulic engineering concepts and experience. Care should be used to ensure that structures do not induce unwanted erosion or sedimentation that adversely impacts riparian structures. Shields (1983) provides a review of several habitat structure design case studies. Additional case studies of use of deflectors (Shields et al. 1995a) and sills (Shields et al. 1995b) in small sand- and gravel-bed streams are also available. Long-term case studies are provided by Thompson (2002b). Unfortunately, there have been many failures (Table 9-11). Gabion structures often fail because of poor anchorage or because abrasion from cobbles transported by large flows causes breaks in wire meshes and loss of fill material. Various structures have been damaged during floods by debris or by being moved out of position. Other structures have succeeded in providing the intended physical effects, but have not produced measurable biological responses. Given these difficulties, the designer must proceed with caution. A step-by-step approach is provided by Shields (1983) and FISRWG (1998). In addition to the design guides referenced in Table 9-11, information useful for designing large woody debris structures is given by Shields and Gippel (1995), Hilderbrand et al. (1998), D'Aoust and Millar (2000), and Shields et al. (2004).

9.5.2.2 Spawning Gravel and Fish Passage Habitat structures are used to provide pool habitat, cover, and overall physical heterogeneity in many types of stream ecosystems, but additional issues arise in streams that support gravel-spawners and migratory species.

9.5.2.2.1 Spawning Gravel Design of habitat measures to trap and hold gravel for fish spawning beds involves competing constraints: bed sediment stability is needed to protect eggs while incubating, but periodic sediment transport

Table 9-11 Typical Characteristics of In-Channel Habitat Structures

Structure type	Intended effects	Typical location	Materials	Common problems	Design guidance
Sills	Increase scour away from banks	Extending across channel from bank to bank	Stone, gabion, or log weirs with uniform, sloping, or notched crests	Flanking. Fish passage. Undermined by downstream scour hole. Erosion of crest. Abrasion and failure of gabion wire.	Klingeman et al. (1984). "Simple bed control structures," in Biedenharn et al. (1998). Artificial riffles described by Newbury and Gaboury (1993)
Deflectors	Increase surface flow disturbance along banks; deflect flow away from banks	Along banks	Irregularly shaped revetments, intermittently spaced short spurs or groins, boulders, or root wads	Erosion of crest. Structure subsidence in fine-bed channels. Erosion of opposite bank. Scour holes too small. Covered by deposition. Flanking.	Klingeman et al. (1984). "Dikes and retards," in Biedenharn et al. (1998). Kuhnle et al. (1999b; 2002), Thompson (2002a)
		Extending out from river bank	Cabled (anchored) trees; longer spur dikes, groins, or jetties		
Random rocks	Induce scour, create zones of low velocity in wake	Isolated midchannel flow obstructions	Boulders, boulder clusters (groups), root wads, vanes, or sills detached from banks	Fall or roll into downstream scour hole.	
Covers	Little impact on flow or sediment; primarily intended to provide shade and hiding places	Along undercut banks	Lumber piers, trees, brush, rafts, and features that cause local turbulence and thus reduce water transparency	Habitat protected by cover may be eliminated by sedimentation.	

is needed to prevent fine sediment from depositing in the upper portions of the gravel matrix. Hydraulic analysis is required to select appropriate bed material gradations and flow regimes (Reiser et al. 1989; Reiser 1998; Wu and Chou 2003).

9.5.2.2.2 Migratory Barrier Removal Removal of passage blockages has been undertaken in many tributary streams in order to expand the range of habitat use for migratory fish. Blockages have also been removed on larger rivers, usually older dams or weirs or landslides that have blocked channels that once allowed fish to pass. A full discussion of the subject of dam removal is beyond the scope of this chapter (see HCSEE 2002), but recent studies have begun to document the physical (Doyle et al. 2003) and ecological (Stanley et al. 2002) changes associated with removing dams, and other studies provide specific guidance for dam decommissioning and removal (ASCE Task Committee 1997). Bedrock outcrops have been modified by drilling or blasting to carve steps or pools. Artificial structures have also been built to bypass blockages and older dams and weirs have been removed or rebuilt to provide passage. Large hydraulic structures have been constructed to allow fish passage past hydroelectric dams, and voluminous literature is available (e.g., Bell 1986; Jungwirth et al. 1998). Information is also available regarding fish passage over simple rock ramps or weirs (Harris et al. 1998).

9.5.3 Channel-Floodplain Connectivity

Past engineering activities have included placing streambank protection to control channel migration and constructing levees to eliminate floodplain inundation. These actions have often altered and degraded ecosystems. Because hydrologic interaction between the floodplain and channel is so ecologically important, reestablishment of floodplain functions is often a goal of river restoration projects.

9.5.3.1 Floodplain Reconnection Issues Floodplain reconnection may simply involve levee breaching to allow pastures or gravel pits to flood during high-water periods. More generally, reconnection is a major undertaking, particularly where extensive floodplain development has occurred. It involves full or partial restoration of large-scale flow and sediment transport conditions. It may be necessary to limit floodplain reconnection projects to elementary bank-line alterations that result in most of the water and all of the bed load remaining in the prerestoration channel and only minor diversions of water and suspended sediments. In other cases it may be possible to introduce major alterations that allow limited re-meandering between set-back levees or within a low-elevation floodplain.

Channel stability and flooding are primary concerns when floodplain reconnections are considered. Breaching or removing dikes and revetments may trigger channel destabilization. Hence, economic, physical, and environmental impacts of various levels of confinement of flow, sediment load, and meandering processes must be assessed. Hydrologic conditions (river flows, floods, droughts) and physical space (channels, riparian zones, floodplains) are key elements for working with these concepts (Williamson et al. 1995a; 1995b; Bella et al. 1996).

9.5.3.2 Longitudinal Variation in Floodplain Confinement In projects where there is significant longitudinal variation in floodplain confinement, sediment transport continuity during high flows should be carefully considered. For example, when the project reach is located in a relatively broad valley just downstream from the mouth of a steep-walled canyon, deposition is likely in the project reach during flows that exceed bank-full in the project channel but remain confined to the upstream channel. A similar situation may occur in developed areas where the upstream floodplain has been encroached upon by levees. In such a situation, simulation of sediment transport for large single events or long-term flow records including such events will allow determination of the magnitude of the sediment transport imbalance. It may be necessary to increase the channel capacity in the project reach. Designs featuring excavation to lower berms or terraces, in order to increase the frequency of overbank flooding, may be especially vulnerable to aggradation in this type of situation (Fullerton and Baird 1999).

A contrasting situation occurs when the proposed restoration reach has incised, but upstream reaches have not. Because the incised channel is larger, high flows are generally confined to the channel, and sediment transport rates and erosive forces are elevated relative to the upstream reaches. Reestablishment of the hydraulic connectivity between the channel and floodplain is often desirable in such a situation. Two approaches are possible: the incised channel may be filled to preincision elevations, or a berm (an artificial floodplain) may be excavated along and adjacent to the incised channel (Shields et al. 1999). Filling may be done during construction or gradually by sedimentation in response to low weirs or roughness elements placed in the incised reach, thus accelerating natural incised channel evolution. Hydraulic and sediment transport analysis can assist in determining the most feasible approach and the appropriate geometry for the restored channel cross section. Impacts of incised channel filling on flooding may be important in some situations.

9.5.4 Channel Bottom Habitats

Sediment size and gradation are key aspects of riverine aquatic habitats. The ASCE Task Committee (1992) developed a bed-material-based stream-reach classification (Table 9-12) and reviewed literature dealing with biological functions of bed sediments within each stream type. Interstitial voids are an important component of habitat in gravel and cobble beds for some fish (e.g., salmonid reproduction) and many invertebrates. Some cobble- or gravel-bed streams are impaired due to deposition of fine sediments within the coarse matrix as a result of flow stabilization by

Table 9-12 Bed-Material-Based Stream Reach Classification (after ASCE Task Committee 1992)

Bed type	Particle size (mm)	Relative frequency of bed movement	Typical benthic macroinvertebrate density/diversity	Fish use of bed sediments
Boulder-cobble	≥64	Rare	High/high	Cover, spawning, feeding
Cobble-gravel	2–256	Rare to periodic	Moderate/moderate	Spawning, feeding
Sand	0.062–2	Continual	Low/low	Silt and clay bed deposits in off-channel backwaters are used for feeding
Fine material	<0.062	Continual or rare	High/low	Feeding

upstream dams or sediment-producing watershed activities (Reiser 1998). Rehabilitation activities include control of sediment sources and techniques to mobilize the fine sediment trapped in the bed using mechanical flushing, scour-producing structures, and the release of "flushing flows" from upstream reservoirs. Design of a flushing flow regime requires considerable analysis (Reiser et al. 1989; Reiser 1998) to define flows adequate to winnow fines away from the matrix without destroying it.

9.5.5 Backwater Protection

River development activities have routinely led to closing secondary channels, sloughs, and other backwater zones (Gore and Shields 1995; Klingeman et al. 1998). They have been used for disposal of dredged or excavated material. In other cases they have been deepened to provide dock access or storage of vessels. Unaltered backwaters (e.g., secondary channels, sloughs, and floodplain lakes) support local ecosystems directly connected to the main channel on a continuous, perennial, or seasonal basis. For example, backwaters sustain organisms that would not otherwise survive or thrive in the stream because they provide low-velocity habitats and critical refuge zones, especially during floods. Because backwater areas are depositional zones, they are relatively transient features. Because many rivers have been stabilized, the creation of new backwaters by channel migration, avulsion and other processes has been slowed or eliminated. As a result, backwater habitats are declining along many rivers (ASCE Task Committee 1992). Backwater zones primarily receive suspended sediment through connecting channels that introduce flow from the mainstem or by flooding. During floods, coarse material may be swept into backwater channels from the tops of intervening bars. The mouths of connecting channels are susceptible to bed load deposition and eventual closure, thus degrading ecological and recreational values (Shields and Abt 1989).

True restoration would involve restoration of processes responsible for backwater creation (e.g., avulsions). Although this strategy is preferred, it is often not feasible, particularly along larger rivers. Instead, strategies intended to reverse or retard sedimentation in existing backwaters and to create new backwaters (e.g., dredging or excavation) are often pursued. Backwater projects include development of connecting channels and protection of existing backwaters using weirs, blocks, or river training structures. Effects of these measures may be short-lived without maintenance. Sedimentation in zones adjacent to river training dikes is complex, but appears to be inversely related to dike crest elevation relative to annual flood stage (Shields 1984 and 1995). Typical sediment transport calculations (e.g., one-dimensional models) may not replicate phenomena in the vicinity of channel margins where backwaters connect to the main channel. Backwater protection may require more elaborate sedimentation analyses (e.g., Barkdoll et al. 1999).

9.6 STABILITY CHECKS

Because of the uncertainties involved in channel design, a series of stability checks should be performed. Stability checks include simple approaches such as those discussed in Section 9.4 as well as more detailed analyses of bank stability and sediment transport capacity.

9.6.1 Bed and Bank Stability

Bank erosion is difficult to predict and simulate, and thus the outer banks of bends and other locations subjected to potentially erosive flows should be protected if the consequences of bank erosion are unacceptable. Mass failure of steep, cohesive banks is related to bank height, bank angle, and soil properties. Stability assessment analyses that incorporate

these variables are described in Thorne (1999) and numerical models (e.g., Simon et al. 2000; 2003) are available. In general, cohesive banks over 3 m high should be analyzed for slope stability. Because bank stability is sensitive to bank height, impacts of channel aggradation and degradation on bank stability should be considered. Bank protection of any type (vegetation or structure) is usually ineffective if bed erosion (degradation) is occurring. If the aim of the project is a partial return to a less disturbed stream condition, then usually some bank erosion is desirable because many ecosystems have key species that depend on habitats created by lateral channel migration.

Restoration projects often feature the use of vegetation to protect banks. A full discussion of vegetation for streambank protection is beyond the scope of this chapter, but engineers should bear in mind that bank erosion is often governed by erosion of the toe of the bank, which cannot be stabilized by vegetation in channels with perennial flow. With adequate structural toe protection, woody vegetation has been used to stabilize banks along channels experiencing mean velocities as great as 2 to 3 m s^{-1} (Nunnally and Sotir 1997). Limited information is available regarding critical levels of hydraulic loading for plant materials (e.g., Hoitsma and Payson 1998; Fischenich 2001). Newly constructed banks are more readily eroded than those that have become well vegetated, and may require protection with temporary measures such as biodegradable fabric during the period of plant establishment. The rate of the fabric degradation should be analyzed in tandem with the expected growth rate of the planted vegetation in order to ensure that the protection is not compromised through time. Miller and Skidmore (1998) describe a bank protection design featuring vegetation on the upper bank and toe protection with cobbles wrapped in a biodegradable fabric (coir). The fabric decays as plants become established, gradually leading to a well-vegetated, but deformable bank. Additional useful information regarding bed and bank stabilization is provided by Biedenharn et al. (1998), FISRWG (1998), and Gray and Sotir (1996), and science underpinning interactions between channels and vegetation is reviewed in Bennett and Simon (2004).

9.6.2 Sediment Budgets

A sediment budget is a tool for assessing the long-term stability of a restored reach and estimating maintenance requirements. Average annual bed-material yields of the design channel and either the existing channel (if it is stable) or the upstream reach (if the existing channel is unstable) are compared. Large differences in bed-material yields indicate potential channel instability. The level of confidence that can be assigned to the sediment budget is a function of the reliability of the available data. In many restoration projects, the absence of relevant flow data will require the use of synthetic or extrapolated flow data, greatly reducing the confidence level.

9.6.2.1 Tools Effects of alternative designs with different reach-average widths, depths, and slopes on sediment continuity may be analyzed using spreadsheets, but the most reliable way to determine the long-term effects of changes in a complex mobile-bed channel system is to use a numerical model such as HEC-6 (e.g., Copeland 1986) or HEC-RAS, one-dimensional models based on a series of channel cross sections, which may vary in shape and are available at Hydrologic Engineering Center (2005). A simpler treatment is provided by SAM, which simulates steady, uniform flow at a single cross section. SAM is described in Section 9.5.1.3.2. The SAM approach is appropriate if longitudinal changes in cross-sectional shape and bed-material gradation are small, because it does not account for hydraulic sorting or bed armoring.

It should be noted that most numerical models suitable for design work do not simulate bank erosion, and few simulate washload transport or effects of unsteady flows. In addition, one- and two-dimensional models do not simulate flow phenomena that are three-dimensional. A full discussion of sediment transport models is provided in Chapters 14 and 15.

9.6.2.2 Step-by-Step Approach The following steps are recommended for conducting a sediment budget analysis:

- Calculate hydraulic parameters for a typical or average reach for a range of discharges. This range should extend from the average annual low flow to the peak of the design discharge. If restoration channel design is based on a single discharge value (e.g., the channel-forming discharge), sediment budget analysis for the entire range of discharges that will affect the stability of the project should be performed as a check on design.
- Select an appropriate sediment transport function for the study reach. This can be done by comparing calculated sediment transport to measured data, taking care to ensure that bed-material load is being compared. When no data are available, one may rely on experience with similar streams in choosing an equation.
- Calculate bed-material sediment transport rating curves for the existing channel in the project reach and upstream and downstream from the project reach. Sediment transport curves should also be calculated for the alternative project design channels. Pre- and post-project sediment transport rating curves should also be determined for tributaries that might be affected by the proposed design.
- Calculate bed-material yield for the existing and project channels using the flow duration sediment discharge rating curve method as described by USACE (1995, pp. 3-4 through 3-10). Average annual bed-material yield should be calculated using the flow duration curve. This provides an estimate of average annual deposition

or degradation. Performance of the project during a design flood event should be evaluated using the design flood hydrograph. If the project will affect the flow duration curve or the flood hydrograph, then this should be reflected in the analysis.

- Calculate trap efficiency by comparing the pre- and postproject bed-material yields. The reach trap efficiency, E, in percent is expressed by the equation

$$E = \frac{100\,(Y_{s_{in}} - Y_{s_{out}})}{Y_{s_{in}}} \tag{9-15}$$

where

Y_s = annual bed-material yield,

and subscripts "in" and "out" refer to inflow and outflow, respectively. Negative trap efficiency implies that bed material sediment will be eroded from the project reach. A positive value means that bed material sediment will be deposited in the project reach. Forecast stability is highest for trap efficiency of zero.

9.6.2.3 Interpretation Consider a reach that contains three-dimensional features and longitudinal differences that require repeated basic sediment transport calculations at successive cross sections along the length of the channel. Assuming that a reliable formula is used or that accurate field measurements are made, it is quite likely that bed-material yield at adjacent cross sections may be unequal. The engineer must resist the temptation to quickly dismiss differences in sediment transport at opposite ends of a reach as the product of formula limitations or measurement errors (or to immediately accept agreement in sediment transport at opposite ends of the reach). Local hydraulic conditions may well lead to local deposition or erosion. Hence the analysis must include consideration of spatial and temporal sources and sinks for sediment within the reach. Otherwise, a situation where sediment is placed into or removed from local storage may be treated as one where sediment merely passes through a reach. Given enough time or a large enough sediment transport event, the consequences could be surprising and damaging.

9.6.2.4 Example Using the example channel geometry described in Section 9.5.1.3.3 and Table 9-10, a new sediment-rating curve was developed and integrated with the flow duration curve to determine the effect of the new geometry on the sediment budget. By comparing the calculated annual design channel sediment transport with the bed-material yield from the supply reach, it was found that about 83% of the annual bed-material load would be transported through the reach. Higher levels of bed-material transport could be obtained by increasing the channel slope, but it was determined that decreasing sinuosity would adversely affect habitat quality. In order to retain sinuosity, the preliminary design planform was adopted for the final design, and plans for periodic sediment removal were included in the operation and maintenance plan.

9.7 IMPLEMENTATION AND CONSTRUCTION

In general, disturbance of a river and its riparian corridor should be minimized during construction. Standard practices for sediment and erosion control should be employed. These require design, careful installation, and repeated inspection and maintenance. Complicated projects may require sequenced measures, including site dewatering. Unexpected site conditions may require fit-in-field adjustments. Contingency plans should include scenarios involving extreme floods or droughts during and shortly after construction. Features involving live vegetation require special considerations for selecting, handling, installing, and caring for plant materials. FISRWG (1998) provides an introduction to these topics.

Projects involving only minor changes to channel systems with negligible sedimentation problems are good candidates for design-build contracts. In simple low-cost projects for which consequences of failure are acceptable, a low-level or conceptual design may be used with a higher-than-normal level of on-site construction oversight. With such conceptual designs, it is relatively easy to incorporate habitat variability and diversity, as adherence to specified dimensions may be relaxed. Detailed plans and specifications, which are necessary for complex projects, often feature strict adherence to design criteria, and the resulting habitat is too uniform. When possible, contract specifications should be written in terms of maximum and minimum values for key parameters (e.g., "channel top width shall be no less than 16 m and no greater than 18 m"), and because contractors will tend to employ the limit of tolerance to achieve lowest cost (e.g., a constant width = 16 m), construction oversight must be employed to provide suitable physical irregularity. Personnel assigned to oversee construction must have an understanding of fluvial systems and project objectives to effectively translate the design into reality.

9.8 MONITORING AND POSTCONSTRUCTION ADJUSTMENT

Fluvial system response to restoration projects cannot be precisely predicted, and dynamic watershed land use, extreme weather events, and changing project objectives add more uncertainty. Accordingly, project plans should provide for adaptive management after initial construction. Information from monitoring project performance is required for adaptive management decisions. Monitoring efforts are normally tightly constrained by economic factors. A standard suite of variables for monitoring includes stage, discharge, and sediment concentration and periodic determinations of bed material size and channel geometry. Evaluation of hydraulic performance may include determination of changes in flow resistance due to changes in bank and floodplain vegetation, bed material size, and channel planform. Because project objectives usually focus on

ecosystem response, it may be important to monitor water quality, biological populations, or social variables. Clearly, it is not possible to monitor every project fully. Even projects that have monitoring programs may produce little useful information if monitoring data are not combined into well-defined metrics reflective of overall system response. In addition, monitoring results must be disseminated so that future restoration projects are responsive to new knowledge gained. Feedback should be provided to project designers and to those charged with program management. Restoration projects should be viewed within a landscape context. Individual restoration projects should be viewed as staged components of overall, long-term ecosystem management schemes for the larger river system and watershed (Seal et al. 1999).

No simple rules exist for setting the length of a monitoring program, but several seasonal cycles should be included. Monitoring intensity may be greatest during the first two or three years, when greatest response is anticipated, and less frequent in subsequent years except after extreme events. The life cycles for key species should also be considered. The impact of physical habitat improvements on plant and animal communities may not become apparent rapidly. Vegetative growth and fluvial response take time. For example, it may take many years for riparian zone revegetation to supply large woody debris for instream recruitment. Furthermore, the physical recovery of degraded stream banks requires more time than is needed only for the recovery of plant community composition (Clary and Webster 1989). Similarly, structures may require high flows to produce the intended effects.

9.9 CONCLUSIONS

Stream restoration is a term often used to refer to stream corridor manipulation. True restoration, however, seeks to return the status of an ecosystem to a former, less degraded state with recovery of function and processes. Large-scale projects, though not always economically or socially feasible, offer the greatest potential for true restoration. All stream restoration projects require some level of sedimentation engineering to reduce the risk of undesirable outcomes. Often the basic task for the engineer is to formulate a sediment budget for the project and to determine how alternatives and various sequences of hydrologic events will impact the quantity and size of sediments within the reach. The outcome of this analysis provides a foundation for a projection of the sustainability of the project. Due to the unorthodox nature and relatively high level of uncertainty surrounding stream restoration projects, involvement of the sedimentation engineer should continue through the implementation phase, and a monitoring program should be included in project plans.

ACKNOWLEDGMENTS

Meg Jonas, Bruce Rhoads, Peter Downs, and Darryl Simons read an earlier version of this paper and made many helpful comments, leading to substantial improvement. Chester Watson, Colin Thorne, Philip Soar, and David Biedenharn provided useful insights in the discussion of channel-forming discharge. The authors also acknowledge contributions by other control and corresponding members of the Task Committee on River Restoration in the form of conference papers and oral discussions at committee meetings. Among these members are Rebecca Soileau, William Fullerton, Richard Hey, and Drew Baird.

REFERENCES

Ackers, P., and Charlton, F. G. (1970). "Meander geometry arising for varying flows." Journal of Hydrology, 11(3), 230–252.

Allen, P. M., Arnold, J. G., and Byars, B. W. (1994). "Downstream channel geometry for use in planning-level models." Water Resources Bulletin, 30(4), 663–670.

Andrews, E. D. (1980). "Effective and bankfull discharges of streams in the Yampa River basin, Colorado and Wyoming." Journal of Hydrology, 46, 311–330.

Andrews, E. D., and Nankervis, J. M. (1995). "Effective discharge and the design of channel maintenance flows for gravel-bed rivers." Natural and Anthropogenic Influences in Fluvial Geomorphology, J. E. Costa, A. J. Millar, K. W. Potter, and P. R. Wilcock, eds., Geophysical Monograph 89, American Geophysical Union, Washington, D.C., 151–164.

ASCE Task Committee on Guidelines for Retirement of Dams and Hydroelectric Facilities of the Hydropower Committee of the Energy Division of the American Society of Civil Engineers. (1997). Guidelines for retirement of dams and hydroelectric facilities. ASCE, Reston, Va.

ASCE Task Committee on Sediment Transport and Aquatic Habitat. (1992). "Sediment and aquatic habitat in river systems." Journal of Hydraulic Engineering, 118(5), 669–687.

Baker, V. R., Kochel, R. C., and Patton, P. C., eds. (1988). Flood geomorphology, Wiley, New York.

Barkdoll, B. D., Ettema, R., and Odgaard, A. J. (1999). "Sediment control at lateral diversions: Limits and enhancements to vane use." Journal of Hydraulic Engineering, 125(8), 862–870.

Bathurst, J. C. (1997). "Chapter 4: Environmental river flow hydraulics." Applied fluvial geomorphology for river engineering and management, C. R. Thorne, R. D. Hey, and M. D. Newson, eds., Wiley, Chichester, U.K., 69–93.

Bell, M. C. (1986). "Fisheries handbook of engineering requirements and biological criteria." Rep., U.S. Army Corps of Engineers, Office of the Chief of Engineers, Washington, D.C.

Bella, D. A., Klingeman, P. C., and Li, H. W. (1996). "River meander zones and floodplain reconnection." Proceedings of the 1996 North American Water and Environment Congress (CD-ROM), C. Bathala, ed., ASCE, Reston, Va.

Bennett, S. J., and Simon, A., eds. (2004). Riparian vegetation and fluvial geomorphology. American Geophysical Union, Washington, D.C.

Biedenharn, D. S., Copeland, R. R., Thorne, C. R., Soar, P. J., Hey, R. D., and Watson, C. C. (2000). "Effective discharge calculation: A practical guide." ERDC/CHL TR-00-15, U.S. Army Corps of Engineers, Engineer Research and Development Center, Vicksburg, Miss.

Biedenharn, D. S., Elliot, C. M., Watson, C. C., Maynord, S. T., Leech, J., and Allen, H. H. (1998). Streambank stabilization handbook, Version 1.0 (CD-ROM), Veri-Tech, Inc., Vicksburg, Miss.

Biedenharn, D. S., and Thorne, C. R. (1994). "Magnitude-frequency analysis of sediment transport in the Lower Mississippi River." Regulated Rivers: Research and Management, 9, 237–251.

Biedenharn, D. S., Thorne, C. R., Soar, P. J., Hey, R. D., and Watson, C. C. (2001). "Effective discharge calculation guide." International Journal of Sediment Research, 16(4), 445–459.

Boyd, K. F., Doyle, M., and Rotar, M. (1999). "Estimation of dominant discharge in an unstable channel environment." Proceedings of the 1999 Water Resources Engineering Conference (CD-ROM), C. T. Bathala, ed., ASCE, Reston, Va.

Brice, J. C. (1982). "Stream channel stability assessment." Rep. FHWA/RC-821021, U.S. Department of Transportation, Washington, D.C.

Brookes, A. (1990). "Restoration and enhancement of engineered river channels, some European experiences." Regulated Rivers: Research and Management, 5(1), 45–56.

Brookes, A., and Shields, F. D., Jr., eds. (1996). River channel restoration. Wiley, Chichester, U.K.

Brownlie, W. R. (1981). "Prediction of flow depth and sediment discharge in open channels." Rep. No. KH-R-43A, W. M. Keck Laboratory of Hydraulics and Water Resources, California Institute of Technology, Pasadena, Calif.

Brownlie, W. R. (1983). "Flow depth in sand bed channels." Journal of Hydraulic Engineering, ASCE, 111(4), 625–643.

Buffington, J. M., and Montgomery, D. R. (1997). "A systematic analysis of eight decades of incipient motion studies, with special reference to gravel-bedded rivers." Water Resources Research, 33(8), 1993–2029.

Bunte, K., and Abt, S. R. (2001). "Sampling surface and subsurface particle-size distributions in wadable gravel- and cobble-bed streams for analyses in sediment transport, hydraulics, and streambed monitoring." General Technical Rep. RMRS-GTR-74, U.S. Department of Agriculture Forest Service, Fort Collins, Colo.

Chang, H. H. (1980). "Stable alluvial canal design." Journal of the Hydraulics Division, ASCE, 106(HY5), 873–891.

Chang, H. H. (1988). Fluvial processes in river engineering. Wiley, New York.

Chow, V. T. (1959). Open channel hydraulics. McGraw-Hill, New York.

Clary, W. P., and Webster, B. F. (1989). "Managing grazing and riparian areas in the intermountain region." General Technical Rep. INT-263. USDA Forest Service, Intermountain Research Station, Ogden, Utah.

Copeland, R. R. (1986). "San Lorenzo River sedimentation study, numerical model investigation." Technical Rep. HL-86-10, Waterways Experiment Station, Vicksburg, Miss.

Copeland, R. R. (1994). "Application of channel stability methods-case studies." Technical Rep. HL-94-11, U.S. Army Engineer Waterways Experiment Station, Vicksburg, Miss.

Dade, W. B. (2000). "Grain size, sediment transport and alluvial channel pattern." Geomorphology, 35, 119–126.

Dade, W. B., and Friend, P. F. (1998). "Grain size, sediment-transport regime and channel slope in alluvial rivers." Journal of Geology, 106, 661–675.

D'Aoust, S. G., and Millar, R. G. (2000). "Stability of ballasted woody debris habitat structures." Journal of Hydraulic Engineering, 126(11), 810–817.

Downs, P. W. (1995). "Estimating the probability of river channel adjustment." Earth Surface Processes and Landforms, 20, 687–705.

Doyle, M. W., Boyd, K. F., and Skidmore, P. B. (1999). "River restoration channel design: Back to the basics of dominant discharge." Proc., Second International Conference on Natural Channel Systems: Stream Corridors: Adoptive Management and Design, Watershed Science Centre, Trent University, Peterborough, Ont.

Doyle, M. W., and Harbor, J. M. (2000). "Discussion of 'Evaluation of Rosgen's streambank erosion potential assessment in northeast Oklahoma.'" Journal of the American Water Resources Association, 36(5), 1191–1192.

Doyle, M. W., Rich, C., Harbor, J. M., and Spacie, A. (2000). "Examining effects of urbanization on streams using indicators of geomorphic stability," Physical Geography 21(2), 155–181.

Doyle, M. W., Stanley, E. H., and Harbor, J. M. (2003). "Channel adjustments following two dam removals in Wisconsin." Water Resources Research, 39(1), 1011 (doi:10.1029/2002WR001714).

Dunne, T., and Leopold, L. B. (1978). Water in environmental planning. Freeman, New York, San Francisco.

Edwards, T. K., and Glysson, G. D. (1988). "Field methods for measurement of fluvial sediment." Open-File Report 86-531, U.S. Geological Survey, Reston, Va.

Federal Highway Administration (FHA). (1995). "Stream stability at highway structures." Hydraulic Engineering Circular No. 20, FHWA-IP-90-014, 2nd Ed., Office of Engineering, Bridge Division Federal Highway Administration, Washington, D.C.

Federal Interagency Sedimentation Project. (2005). FISP Home Page <http://fisp.wes.army.mil>(Aug. 1, 2005).

Federal Interagency Stream Restoration Working Group (FISRWG). (1998). Stream corridor restoration: Principles, processes and practices. National Technical Information Service, U.S. Department of Commerce, Springfield, Va.

Ferguson, R. T., and Paola, C. (1997). "Bias and precision of percentiles of bulk grain size distributions." Earth Surface Processes and Landforms, 22, 1061–1077.

Fischenich, C. (2001). "Stability thresholds for stream restoration materials." EMRRP Technical Notes Collection (ERDC TN EMRRP-SR-29), U.S. Army Engineer Research and Development Center, Vicksburg, Miss.

Fortier, S., and Scobey, F. C. (1926). "Permissible canal velocities." Transactions of the ASCE, 89, 940–984.

French, R. H. (1985). Open-Channel Hydraulics. McGraw-Hill, New York.

Fullerton, W. T., and Baird, D. C. (1999). "Sedimentation engineering design in river restoration: sediment transport aspects of design." Proceedings of the 1999 International Water Resources Engineering Conference (CD-ROM), C. T. Bathala, ed., ASCE, Reston, Va.

Gessler, J. (1971). "Chapter 7: Beginning and ceasing of sediment motion." River mechanics, H. W. Shen, ed., Vol. I, H. W. Shen, Fort Collins, Colo.

Gilbert, G. K. (1914). "The transportation of debris by running water." Professional Paper No. 86, U.S. Geological Survey, Washington, D.C.

Glysson, G. D. (1987). "Sediment-transport curves." Open-File Report 87-218 , U.S. Geological Survey, Washington, D.C.

Gore, J. A., and Shields, F. D., Jr. (1995). "Can large rivers be restored? A focus on rehabilitation." Bioscience, 45(3), 142–152.

Gray, D. H., and Sotir, R. B. (1996). Biotechnical and soil bioengineering slope stabilization: A practical guide for erosion control, Wiley, Chichester, U.K.

Hammer, T. R. (1972). "Stream channel enlargement due to urbanization." Water Resources Research, 8, 1530–1540.

Hanson, G. J. and Simon, A. (2001). "Erodibility of cohesive streambeds in the loess area of the midwestern USA." Hydrological Processes, 15(1), 23–38.

Harrelson, C. G., Rawlins, C. L., and Potyondy, J. P. (1994). "Stream channel reference sites: An illustrated guide to field technique." General technical report RM-245, U.S. Department of Agriculture, Forest Service, Rocky Mountain Forest and Range Experiment Station, Fort Collins, Colo.

Harris, J. H., Thorncraft, G., Wem, P. (1998). "Evaluation of rock-ramp fishways in Australia." Fish migration and fish bypasses, M. Jungwirth, S. Schmutz, and S. Weiss, eds., Marston Book Services, Abingdon, U.K., 331–347.

Harvey, M. D., and Watson, C. C. (1986). "Fluvial processes and morphological thresholds in incised channel restoration." Water Resources Bulletin: American Water Resources Association, 22(3), 359–368.

Heinz Center for Science, Economics and the Environment (HCSEE). (2002). "Dam removal: Science and decision making." Heinz Center for Science, Economics and the Environment. Washington, D.C.

Hey, R. D. (1975). "Design discharge for natural channels." Science, technology and environmental management, R. D. Hey and T. D. Davies, eds., Saxon House, 73–88.

Hey, R. D. (1979). "Flow resistance in gravel-bed rivers." Journal of the Hydraulics Division, ASCE, 105(HY4), 365–379.

Hey, R. D. (1997). "Channel response and channel forming discharge: Literature review and interpretation." US Army Contract No. R&D 6871-EN-01, U.S. Army Engineer Waterways Experiment Station, Vicksburg, MS.

Hey, R. D., and Thorne, C. R. (1986). "Stable channels with mobile gravel beds." Journal of Hydraulic Engineering, 112(8), 671–689.

Hilderbrand, R. H., Lemly, A. D., Dolloff, C. A., and Harpster, K. L. (1998). "Design considerations for large woody debris placement in stream enhancement projects." North American Journal of Fisheries Management, 18, 161–167.

Hoitsma, T. R., and Payson, E. M. (1998). "The use of vegetation in bioengineered streambanks: Shear stress resistance of vegetal treatments." Engineering Approaches to Ecosystem Restoration, Proceedings of the 1998 Wetlands Engineering and River Restoration Conference (CD-ROM), D. F. Hayes, ed., ASCE, New York.

Hollis, G. E. (1975). "The effect of urbanization on floods of different recurrence interval." Water Resources Research, 11, 431–435.

Hooke, J. M. (1997). "Chapter 9: Styles of channel change." Applied fluvial geomorphology for river engineering and management, C. R. Thorne, R. D. Hey, and M. D. Newson, eds., Wiley, Chichester, U.K.

Hydrologic Engineering Center. (2005). <http://www.hec.asace.army.mil/>(Aug. 2, 2005).

Jennings, M. E., Thomas, W. O., Jr., and Riggs, H. C. (1994). "Nationwide summary of U.S. geological survey regional regression equations for estimating magnitude and frequency of floods for ungaged sites." 1993: U.S. Geological Survey Water-Resources Investigations Report 94-4002, U.S. Geological Survey, Washington, D.C.

Johnson, P., and Heil, T. (1996). "Uncertainty in estimating bankfull conditions." Water Resources Bulletin, 32(6), 1283–1291.

Johnson, P. A., and Brown, E. R. (2001). "Incorporating uncertainty in the design of stream channel modifications." Journal of the American Water Resources Association, 37(5), 1225–1236.

Johnson, P. A., Gleason, G. L., and Hey, R. D. (1999). "Rapid assessment of channel stability in vicinity of road crossing." Journal of Hydraulic Engineering, 125(6), 645–651.

Johnson, P. A., and Rinaldi, M. (1998). "Uncertainty in stream channel restoration." Uncertainty Modeling and Analysis in Civil Engineering, B. M. Ayyub, ed., CRC Press, Boston, 425–437.

Julien, P. Y. (1995). Erosion and sedimentation. Cambridge University Press, New York.

Jungwirth, M., Schmutz, S., and Weiss, S., eds. (1998). Fish migration and fish bypasses. Marston Book Services, Abingdon, U.K.

Klingeman, P. C. (1998). "Conceptualization for long-reach river restoration." Engineering Approaches to Ecosystem Restoration, Proceedings of the 1998 Wetlands Engineering and River Restoration Conference (CD-ROM), D. F. Hayes, ed., ASCE, Reston, Va.

Klingeman, P. C., et al. (1971). "Environmental considerations and the water resources of the Silvies basin." Report WRRI-6. Oregon State University, Water Resources Research Institute, Corvallis, Ore.

Klingeman, P. C., Bravard, J. P., Guiliani, Y., Olivier, J. M., and Paytou, G. (1998). "Chapter 15: Hydropower reach by-passing and dewatering impacts in gravel-bed rivers." Gravel-bed rivers in the environment, P. C. Klingeman, R. L. Beschta, P. D. Komar, and J. B. Bradley, eds., Water Resources Publications, Highlands Ranch, Colo.

Klingeman, P. C., Kehe, S. M., and Owusu, Y. A. (1984). "Streambank erosion protection and channel scour manipulation using rockfill dikes and gabions." Report WRRI-98. Oregon State University, Water Resources Research Institute, Corvallis, Ore.

Kondolf, G. M. (1990). "Hydrologic and channel stability considerations in stream habitat restoration." In Environmental Restoration: Science and Strategies for Restoring the Earth, Berger, J., ed., Island Press, Covelo, CA, 214–227.

Kondolf, G. M., and Sale, M. J. (1985). "Application of historical channel stability analysis to instream flow studies." Publication No. 2527, Environmental Sciences Division, Oak Ridge National Laboratory. Proceedings of the Symposium on Small Hydropower and Fisheries, American Fisheries Society, Bethesda, Md., 184–194.

Kuhnle, R. A., Alonso, C. V., and Shields, F. D. (2002). "Local scour associated with angled spur dikes." Journal of Hydraulic Engineering, 128(12), 1087–1093.

Kuhnle, R. A., Alonso, C. V., and Shields, F. D., Jr. (1999). "Volume of scour holes associated with 90-degree spur dikes." Journal of Hydraulic Engineering, 125(9), 972–978.

Kuhnle, R. A., Simon, A., and Bingner, R. L. (2000). "Dominant discharge of the incised channels of Goodwin Creek." In Proceedings of the 1999 International Water Resources Engineering Conference (CD-ROM), C. T. Bathala, ed., ASCE, Reston, Va.

Kuhnle, R. A., Simon, A., and Bingner, R. L. (2000). "Dominant discharge of the incised channels of Goodwin Creek. "In Proceedings of the 1999 Institutional Water Resources Engineering Conference, Walton, R., and Nece, R. E., eds., Environmental and Water Resources Institute, ASCE, Reston, VA, CD-ROM.

Lagasse, P. F., Schall, J. D., and Richardson, E. V. (2001). "Stream stability at highway structures." Hydraulic Engineering Circular No. 20, 3rd Ed., NHI-01-002, U.S. Department of Transportation, Federal Highway Administration, Washington, D.C.

Lane, E. W. (1955a). "The importance of fluvial morphology in hydraulic engineering." Proceedings, ASCE, 81(745), 1–17.

Lane, E. W. (1955b). "Design of stable channels." Transactions, ASCE, 120, 1234–1279.

Langbein, W. B., and Leopold, L. B. (1966). "River meanders theory of minimum variance." USGS Professional Paper 422-H, U.S. Government Printing Office, Washington D.C.

Leopold, L. B., and Maddock, T., Jr. (1953). "The hydraulic geometry of stream channels and some physiographic implications." U.S. Geological Survey Professional Paper 252, U.S. Government Printing Office, Washington, D.C.

Leopold, L. B., and Wolman, M. G. (1960). "River meanders." Bulletin of the Geological Society of America, 71, 769–794.

Leopold, L. B., Wolman, M. G., and Miller, J. P. (1964). Fluvial processes in geomorphology. Freeman, New York, San Francisco.

Limerinos, J. T. (1970). "Determination of the Manning coefficient from measured bed roughness in natural channels." U.S. Geological Survey Water-Supply Paper 1989-B, U.S. Government Printing Office, Washington, D.C.

Mavis, F. T., and Laushey, L. M. (1949). "Formula for velocity at beginning of bed-load movement is reappraised." Civil Engineering, ASCE, 19(1), 38–39, 72.

Meyer-Peter, E., and Muller, R. (1948). "Formulas for bed-load transport." Proc. Second Meeting of the International Association for Hydraulic Research, IAHR, Stockholm, Sweden, 39–64.

Millar, R. G., and Quick, M. C. (1993). "Effect of bank stability on geometry of gravel rivers." Journal of Hydraulic Engineering, ASCE, 119(12), 1343–1363.

Miller, D. E., and Skidmore, P. B. (1998). "Application of deformable stream bank concepts to natural channel design." Proceedings of the International Conference on Water Resources Engineering, S. R. Abt, P. J. Young, and C. C. Watson, eds., ASCE, Reston, Va., 441–446.

Miller, J. R., and Ritter, J. B. (1996). "An examination of the Rosgen classification of natural rivers." Catena, 27, 295–299.

Montgomery, D. R. (1999). "Process domains and the river continuum." The Journal of the American Water Resources Association, 35(2), 397–410.

Moscrip, A. L., and Montgomery, D. R. (1997). "Urbanization, flood frequency, and salmon abundance in Puget Sound lowland streams." Journal of the American Water Resources Association, 33, 1289–1297.

National Research Council (NRC) (1992). Restoration of aquatic ecosystems. National Academy Press, Washington, D.C.

Neill, C. R. (1973). Guide to bridge hydraulics. University of Toronto Press, Toronto, Ont.

Newbury, R., and Gaboury, M. (1993). "Exploration and rehabilitation of hydraulic habitats in streams using principles of fluvial behavior." Freshwater Biology, 29, 195–210.

Nunnally, N. R. (1985). "Application of fluvial relationships to planning and design of channel modifications." Environmental Management, 9(5), 417–426.

Nunnally, N. R., and Sotir, R. B. (1997). "Criteria for selection and placement of woody vegetation in streambank protection." Management of Landscapes Disturbed by Channel Incision, Stabilization, Rehabilitation, and Restoration, S. Y. Wang, E. Langendoen, and F. D. Shields, Jr., eds., Center for Computational Hydroscience and Engineering, University of Mississippi, University, Miss., 816–821.

Onishi, Y., Jain, S. C., and Kennedy, J. F. (1976). "Effects of meandering in alluvial streams." Journal of the Hydraulics Division, ASCE, 102(HY7), 899–917.

Paintal, A. S. (1971). "Concept of critical shear stress in loose boundary open channels." Journal of Hydraulic Research, 1, 90–113.

Parker, G. (1990). "Surface-based bedload transport relation for gravel rivers." Journal of Hydraulic Research, 28(4), 417–436.

Parker, G., and Andres, D. (1976). "Detrimental effects of river channelization." Proceedings of the Symposium on Inland Waters for Navigation, Flood Control & Water Diversions, ASCE, New York, 1248–1266.

Parker, G., and Klingeman, P. C. (1982). "On why gravel bed streams are paved." Water Resources Research, 18(5), 1409–1423.

Pemberton, E. L., and Lara, J. M. (1984). "Computing degradation and local scour." Technical Guideline, Sedimentation and River Hydraulics Section, Hydrology Branch, Division of Planning Technical Services, Engineering and Research Center, Bureau of Reclamation, Denver, Colo.

Pennisi, E. (2004). "The Grand (Canyon) experiment." Science, 306(5703), 1884–1886.

Pfankuch, D. J. (1978). "Stream reach inventory and channel stability evaluation: A watershed management procedure." Rep. 797-059/31, U.S. Department of Agriculture, Forest Service, Northern Region, U.S. Government Printing Office, Region 10.

Pickett, S. T. A., and White, P. S., eds. (1985). The ecology of natural disturbance and patch dynamics, Academic Press, Orlando, Fla.

Pickup, G. (1976). "Adjustment of stream-channel shape to hydrologic regime." Journal of Hydrology, 30, 365–373.

Reiser, D. W. (1998). "Chapter 10: Sediment in gravel bed rivers: Ecological and biological considerations." Gravel-bed rivers in the environment, P. C. Klingeman, R. L. Beschta, P. D. Komar, and J. B. Bradley, eds., Water Resources Publications, Highlands Ranch, Colo.

Reiser, D. W., Ramey, M. P., Beek, S., Lambert, T. R., and Geary, R. E. (1989). "Flushing flow recommendations for maintenance of salmonid spawning gravels in a steep, regulated stream." Regulated Rivers: Research and Management, 3(1–4), 267–275.

Rhoads, B. L. (1995). "Stream power: A unifying theme for urban fluvial geomorphology." Stormwater runoff and receiving systems, E. E. Herricks, ed., Lewis Publishers, Boca Raton, Fla., 65–75.

Rhoads, B. L., and Herricks, E. E. (1996). "Chapter 12: Naturalization of headwater streams in Illinois: Challenges and possibilities." River channel restoration, A. Brookes and F. D. Shields, Jr., eds., Wiley, Chichester, U.K., 331–368.

Rhoads, B. L., and Urban, M. A. (1997). "Human-induced geomorphic change in low-energy agricultural streams: An example

from east-central Illinois." Management of landscapes disturbed by channel incision, stabilization, rehabilitation, and restoration, S. Y. Wang, E. Langendoen, and F. D. Shields, Jr., eds., Center for Computational Hydroscience and Engineering, University of Mississippi, University, Miss., 968–973.

Rhoads, B. L., Wilson, D., Urban, M., and Herricks, E. E. (1999). "Interactions between scientists and nonscientists in community-based watershed management: Emergence of the concept of stream naturalization." Environmental Management, 24(3), 297–308.

Richards, K. S. (1978). "Channel geometry in the riffle-pool sequence." Geografiska Annaler, 60A, 23–27.

Richter, B. D., Baumgartner, J. V., Braun, D. P., and Powell, J. (1996). "A method for assessing hydrologic alteration within ecosystems." Conservation Biology, 10(4), 1163–1174.

Richter, B. D., Baumgartner, J. V., Braun, D. P., and Powell, J. (1998). "A spatial assessment of hydrologic alteration within a river network." Regulated Rivers: Research and Management, 14, 329–340.

Ries, K. G., III, and Crouse, M. Y. (2002). "The National Flood Frequency Program, version 3. A computer program for estimating magnitude and frequency of floods for ungaged sites." Water Resources Investigations Report 02-4168, U.S. Geological Survey, Reston, VA.

Rinaldi, M., and Johnson, P. A. (1997). "Characterization of stream meanders for stream restoration." Journal of Hydraulic Engineering, 123(6), 567–570.

Rosgen, D. L. (1994). "A classification of natural rivers." Catena, 22, 169–199.

Rosgen, D. L. (1996). Applied river morphology. Wildland Hydrology Publications, Pagosa Springs, Colo.

Rubey, W. W. (1933). "Settling velocities of gravel, sand, and silt particles." American Journal of Science, Fifth Series, 25(148), 325–338.

"SAM Hydraulic Design Package for Channels." (2005). <http://www.erdc.usace.army.mil/pls/erdcpub/www_welcome.navigation_page?tmp_next_page=18758>(Aug. 2, 2005).

Schmidt, J. C., Webb, R. H., Valdez, R. A., Marzolf, G. R., and Stevens, L. E. (1998). "Science and values in river restoration in the Grand Canyon." Bioscience, 48(9), 735–747.

Schumm, S. A. (1969). "River metamorphosis." Journal of the Hydraulics Division, ASCE, 95(HY1), 255–274.

Schumm, S. A. (1977). The fluvial system. Wiley, New York.

Schumm, S. A., Harvey, M. D., and Watson, C. C. (1984). Incised channels: Morphology, dynamics and control. Water Resources Publications, Littleton, Colo.

Seal, R. B., Copeland, R. R., and Hall, B. R. (1999). "Sedimentation engineering design in river restoration: The role of sedimentation engineering design." Proceedings of the 1999 Water Resources Engineering Conference, ASCE, Reston, Va.

Sear, D. A. (1996). "Chapter 6: The sediment system and channel stability." River channel restoration: Guiding principles for sustainable projects, A. Brookes and F. D. Shields, Jr., eds., Wiley, Chichester, U.K., 149–199.

Shields, A. (1936). "Anwendung der aenlichkeitsmechanik und der turbulenzforschung auf die geschiebebewegung." Mitteilungen der Preussischen Versuchsanstalt fur Wasserbau und Schiffbau, Berlin, Germany, by W. P. Ott and J. C. van Uchelen, California Institute of Technology, Pasadena, Calif.

Shields, F. D., Jr. (1983). "Design of habitat structures for open channels." Journal of Water Resources Planning and Management, 109(4), 331–344.

Shields, F. D., Jr. (1984). "Environmental guidelines for dike fields." River Meandering, Proceedings of the conference Rivers '83, C. M. Elliott, ed., ASCE, New York, 430–442.

Shields, F. D., Jr. (1995). "Fate of Lower Mississippi River habitats associated with river training dikes." Aquatic Conservation: Marine and Freshwater Systems, 5, 97–108.

Shields, F. D., Jr. (1996). "Chapter 2: Hydraulic and hydrologic stability." River channel restoration, A. Brooks and F. D. Shields, Jr., eds., Wiley, Chichester, U.K., 24–74.

Shields, F. D., Jr. (1997). "Reach-average dimensions for channel reconstruction." Environmental and coastal hydraulics: Protecting the aquatic habitat. Proceedings Theme B, Vol. 1, XXVII Congress of the International Association for Hydraulic Research, S. Y. Wang and T. Carstens, eds., IAHR, Madrid, Spain, and ASCE, Reston, Va., 388–393.

Shields, F. D., Jr., and Abt, S. R. (1989). "Sediment deposition in cutoff meander bends and implications for effective management." Regulated Rivers: Research and Management, 4, 381–396.

Shields, F. D., Jr., Brookes, A., and Haltiner, J. (1999). "Chapter 14: Geomorphological approaches to incised stream channel restoration in the United States and Europe." Incised river channels: Processes, forms, engineering and management, S. E. Darby and A. Simon, eds., Wiley, Chichester, U.K., 371–394.

Shields, F. D., Jr., Cooper, C. M., and Knight, S. S. (1995a). "Experiment in stream restoration." Journal of Hydraulic Engineering, 121(6), 494–502.

Shields, F. D., Jr., and Gippel, C. J. (1995). "Prediction of effects of woody debris removal on flow resistance." Journal of Hydraulic Engineering, 121(4), 341–354.

Shields, F. D., Jr., Knight, S. S., and Cooper, C. M. (1995b). "Incised stream physical habitat restoration with stone weirs." Regulated Rivers: Research and Management, 10, 181–198.

Shields, F. D., Jr., Morin, N., and Cooper, C. M. (2004). "Large woody debris structures for sand bed channels." Journal of Hydraulic Engineering, 130(3), 208–217.

Shiono, K., Al-Romaih, J. S., and Knight, D. W. (1999). "Stage-discharge assessment in compound meandering channels." Journal of Hydraulic Engineering, 125(1), 66–77.

Simon, A. (1989). "The discharge of sediment in channelized alluvial streams." Water Resources Bulletin, 25(6), 1177–1188.

Simon, A., and Collison, A. J. C. (2001). "Pore-water pressure effects on the detachment of cohesive streambeds: Seepage forces and matric suction." Earth Surface Processes and Landforms, 26(13), 1421–1442.

Simon, A., Curini, A., Darby, S. E., and Langendoen, E. J. (2000). "Bank and near-bank processes in an incised channel." Geomorphology, 35, 193–217.

Simon, A., Dickerson, W., and Heins, A. (2004). "Suspended-sediment transport rates at the 1.5-year recurrence interval for ecoregions of the United States: Transport conditions at the bankfull and effective discharge?" Geomorphology, 58, 243–262.

Simon, A., and Downs, P. W. (1995). "An interdisciplinary approach to evaluation of potential instability in alluvial channels." Geomorphology, 12, 215–232.

Simon, A., Langendoen, E. J., and Thomas, R. E. (2003). "Incorporating bank-toe erosion by hydraulic shear into a bank-stability model: Missouri River, eastern Montana." Proc., First Interagency Conference on Research in the Watersheds, October 27–30, Benson, Ariz., K. G. Renard, S. A. McElroy, W. J. Gburek,

H. E. Canfield, and R. L. Russell, eds., U.S. Department of Agriculture, Agricultural Research Service, Beltsville, Md., 70–76.

Simon, A., and Thomas, R. E. (2002). "Processes and forms of an unstable alluvial system with resistant, cohesive streambeds." Earth Surface Processes and Landforms, 27, 699–718.

Simons, D. B., and Senturk, F. (1976). Sediment transport technology. Water Resources Publications, Littleton, Colo.

Smith, C. L., and Klingeman, P. C. (1998). "Institutional structures for river restoration." Proceedings of the International Conference on Water Resources Engineering, S. R. Abt, J. Young-Pezeshk, and C. C. Watson, eds., ASCE, Reston, Va., 654–659.

Snake River Salmon Recovery Team (SRSRT). (1994). "Snake River Salmon Recovery Team: Final recommendations to the National Marine Fisheries Service." Summary Report, National Marine Fisheries Service, National Oceanic and Atmospheric Administration, Portland, Ore.

Soar, P. J., and Thorne, C. R. (2001). "Channel restoration design for meandering rivers." ERDC/CHL CR-01-1, U.S. Army Corps of Engineers, Engineer Research and Development Center, Vicksburg, Miss.

Society for Ecological Restoration Science & Policy Working Group (SER). (2002). "The SER primer on ecological restoration." <www.ser.org/Primer.pdf>(July 10, 2002).

Stanley, E. H., Luebke, M. A., Doyle, M. W., and Marshall, D. W. (2002). "Short-term changes in channel form and macroinvertebrate communities following low-head dam removal in the Baraboo River, Wisconsin." Journal of the North American Benthological Society, 21, 172–187.

Stevens, H. H., and Yang, C. T. (1989). "Summary and use of selected fluvial sediment-discharge formulas." Water Resources Investigations Report 89-4026, U.S. Geological Survey, Washington, D.C.

Stevens, M. A., Simons, D. B., and Richardson, E. V. (1975). "Nonequilibrium river form." Journal of the Hydraulics Division, ASCE, 101(HY5), 557–566.

"The maximum permissible mean velocity in open channels." (1936). Gidrotekhnicheskoie Stroitel'stvo (Hydrotechnical construction), 5(May), 5–7.

Thomas, W. A., Copeland, R. R., Raphelt, N. K., and McComas, D. N. (1995). "Hydraulic design package for flood control channel: (SAM) User's manual." U.S. Army Engineer Waterways Experiment Station, Vicksburg, Miss.

Thompson, D. M. (2002a). "Channel-bed scour with high versus low deflectors." Journal of Hydraulic Engineering, ASCE, 128(6), 640–643.

Thompson, D. M. (2002b). "Long-term effect of instream habitat-improvement structures on channel morphology along the Blackledge and Salmon Rivers, Connecticut." Environmental Management, 29(1), 250–265.

Thorne, C. R. (1997). "Chapter 7: Channel types and morphological classification." Applied fluvial geomorphology for river engineering and management, C. R. Thorne, R. D. Hey, and M. D. Newson, eds., Wiley, Chichester, U.K., 175–222.

Thorne, C. R. (1999). "Chapter 5: Bank processes and channel evolution in the incised rivers of north-central Mississippi." Incised river channels, S. E. Darby and A. Simon, eds., Wiley, Chichester, U.K., 97–122.

Thorne, C. R., Allen, R. G., and Simon, A. (1996a). "Geomorphological river channel reconnaissance for river analysis, engineering and management." Transactions, Institute of British Geography, 21, 469–483.

Thorne, C. R., Reed, S., and Doornkamp, J. C. (1996b). "A procedure for assessing river bank erosion problems and solutions." Rep., National Rivers Authority, Almondsbury, U.K.

Thorne, C. R., Soar, P. J., Hey, R. D., and Watson, C. C. (1998). "Dominant discharge calculation: A practical guide." Rep., submitted to the U.S. Army Research, Development and Standardisation Group–U.K., London, under Contract No. N68171-97-M-5757, Project No. R&D8399-EN-01, Department of Geography, University of Nottingham, U.K.

Townsend, C. R., Scarsbrook, M. R., and Doledec, S. (1997). "The intermediate disturbance hypothesis, refugia, and biodiversity in streams." Limnology and Oceanography, 42, 938–939.

Trimble, S. W. (1997). "Stream channel erosion and change resulting from riparian forests." Geology, 25(5), 467–469.

U.S. Army Corps of Engineers (USACE). (1991). "Hydraulic design of flood control channels." EM 1110-2-1601. U.S. Army Corps of Engineers, Washington, D.C.

U.S. Army Corps of Engineers (USACE). (1993). "Coldwater River watershed." Supplement I to General Design Memorandum No. 54, Yazoo Basin, Mississippi, Demonstration Erosion Control Project, U.S. Army Corps of Engineers, Vicksburg, Miss.

U.S. Army Corps of Engineers (USACE). (1994). "Engineering and design—Channel stability assessment for flood control projects." EM 1110-2-1418. U.S. Army Corps of Engineers, Washington, D.C.

U.S. Army Corps of Engineers (USACE). (1995). "Sedimentation investigation of rivers and reservoirs." EM-1110-2-4000. U.S. Army Corps of Engineers, Washington, D.C.

U.S. Department of Agriculture (USDA). (1977). "Design of open channels." Technical Release No. 25, Soil Conservation Service, Washington, D.C.

Van den Berg, J. J. H. (1995). "Prediction of channel pattern of alluvial rivers." Geomorphology, 12(1995), 259–279.

Vannote, R. L., Minshall, G. W., Cummins, K. W., Sedell, J. R., and Cushing, C. E. (1980). "The river continuum concept." Canadian Journal of Fisheries and Aquatic Sciences, 37, 103–137.

Vaselaar, R. T. (1997). "Opening the flood gates: The 1996 Glen Canyon Dam experiment." Restoration and Management Notes, 15(2), 119–125.

Wharton, G., Arnell, N. W., Gregory, K. J., and Gurnell, A. M. (1989). "River discharge estimated from channel dimensions." Journal of Hydrology, 106, 365–376.

White, W. R., Bettess, R., and Paris, E. (1982). "Analytical approach to river regime." Journal of the Hydraulics Division, ASCE, 108(HY10), 1179–1193.

Wilcock, P. R. (1998). "Two-fraction model of initial sediment motion in gravel-bed rivers." Science, 280, 410–412.

Williams, G. P. (1978). "Bankfull discharge of rivers." Water Resources Research, 14(6), 1141–1480.

Williams, J. E., Wood, C. A., and Dombeck, M. P., eds. (1997). Watershed restoration: Principles and practices. American Fisheries Society, Bethesda, Md.

Williamson, K. J., et al. (1995a). Gravel disturbance impacts on salmon habitat and stream health. Volume I: Summary report, Oregon State University, Water Resources Research Institute, Corvallis, Ore.

Williamson, K. J., et al. (1995b). Gravel disturbance impacts on salmon habitat and stream health. Volume II: Technical background report. Oregon State University, Water Resources Research Institute, Corvallis, Ore.

Wolman, M. G. (1954). "A method of sampling coarse river bed material." Transactions of the American Geophysical Union, 35(6), 951–956.

Wolman, M. G., and Miller, J. P. (1960). "Magnitude and frequency of forces in geomorphic processes." Journal of Geology, 68, 54–74.

Wu, F. C., and Chou, Y. J. (2003). "Simulation of gravel-sand bed response to flushing flows using a two-fraction entrainment approach: Model development and flume experiment." Water Resources Research, 39(8) 1211 (doi:10.1029/2003WR002184,2003).

Yang, C. T. (1973). "Incipient motion and sediment transport." Journal of the Hydraulics Division, ASCE, 99(HY10), 1679–1704.

Yevjevich, V. (1972). Probability and statistics in hydrology. Water Resources Publications, Fort Collins, Colo.

Copyrighted Materials
Copyright © 2008 American Society of Civil Engineers (ASCE)
Retrieved from www.knovel.com

CHAPTER 10

Bridge Scour Evaluation

J. R. Richardson
and E. V. Richardson

10.1 INTRODUCTION

Scour at highway bridges is the result of the erosive action of flowing water removing bed material from around the abutments and piers that support the bridge and erosion of stream bed and bank material which the bridge crosses. The latter results from stream migration and degradation. Both stream migration and degradation (stream instability) and scour at highway bridges can cause bridge failure.

Bridge failures cost millions of dollars each year as a result of both direct costs necessary to replace and restore bridges, and indirect costs related to disruption of transportation facilities. However, of even greater consequence is loss of life from bridge failures (Richardson et al. 1989). In the United States there are over 575,000 bridges in the National Bridge Inventory. These numbers include federal highway system, state, county, and city bridges. Approximately 84% of these bridges are over water. Erosion of the foundations of the bridges resulting from stream instability, long-term degradation, contraction scour, and local scour cause 60% of bridge failures. There have been 25 fatalities from bridge failures in the United States since 1987 (Richardson and Lagasse 1999).

Chang's study for the Federal Highway Administration (Chang 1973) indicated that about $75 million was expended annually to repair flood damage to roads and bridges. Rhodes and Trent (1993) document that $1.2 billion was expended for restoration of flood damaged highway facilities during the 1980s. They state that this amount is conservative because (1) they only include the amount funded by the U.S. government, which ranges from 75 to 100% of the total restoration costs, and (2) the funds were only for disasters that are very large and do not include the hundreds of smaller events that occur every year. These costs do not include the additional indirect costs to highway users for fuel and operating costs resulting from temporary closures and detours and to the public for costs associated with higher tariffs, freight rates, additional labor costs, and time. Rhodes and Trent (1993) also demonstrate that the indirect cost (operating a vehicle over a detour and time lost traveling when a bridge fails) exceed by several times the direct cost of bridge replacement or repair.

Research efforts have developed a large body of knowledge on bridge scour, mostly from laboratory studies. This bridge scour research started in the early 1950s through Carl Izzard's efforts to have the U.S. Bureau of Public Roads (predecessor agency to the Federal Highway Administration) and the Iowa State Highway Department fund Emmett Laursen's research on bridge scour (Laursen and Toch 1956; Laursen 1958; 1960; 1963). However, field data and measurements of scour at bridges, which are necessary to better understand the problem of stream instability and scour and to evaluate analytical methods for scour prediction, are extremely limited. In addition, many of the problems of stream instability and bridge scour have not been studied in depth. Many analytical techniques are recommended for use simply because they are the best currently available, and are overly conservative. For example, many equations for determining local scour depths at bridge abutments use abutment and roadway approach length as a variable instead of the flow they intercept (Richardson and Richardson 1993; Richardson and Davis 2001). In the field case, this is a spurious correlation.

All material on the stream bed and banks at a bridge crossing will erode. It is just a matter of time. Some material, such as granite, may take hundreds of years, Whereas sand-bed streams will erode to the maximum depth of scour in hours. Sandstones, shales, and other sedimentary bed rock material do not erode in hours or days but will, over time, if subjected to the erosive force of water, erode to the extent that a bridge will be in danger unless the substructure is founded deep enough. Cohesive bed and bank material such as clays, silty clays, silts, and silty sand or material such as

glacial tills, which are cemented by chemical action or compression, will erode. The erosion of these materials is slower than that of sand-bed material, may take the erosive action of several major floods, but ultimately the scour hole will be equal to the depth with a noncohesive sand-bed material (Jackson et al. 1991; Briaud et al. 1999).

Scour at bridge crossings is a sediment transport process. Long-term degradation, contraction scour, and local scour at piers and abutments result from the fact that more sediment is removed from these areas than is transported into them. If there is no transport of bed material into the bridge crossing, *clear-water* scour exists. Transport of appreciable bed material into the crossing results in *live-bed* scour. In this latter case the transport of the bed material may limit scour depth. With clear-water scour the scour depths are limited by the critical velocity or critical shear stress of a dominant size in the bed material at the crossing.

Major floods tend to scour the material at a bridge crossing during the rising limb of the flood and refill the scour holes during the recession limb. Often the redeposited material in the scour hole is more easily eroded by subsequent floods. Postflood inspection of the bridge crossing may indicate that the material around the foundations is adequate when, in fact, the bridge is in jeopardy of failing during the next flood. This infilling also makes it difficult to obtain field measurements of scour depths because the measurements have to be made during a flood.

The magnitude of the scour depth depends on the flow variables of the stream (discharge, flow velocity and depth, angle of the flow to the bridge, etc.), bed and bank material characteristics (bed rock, alluvial or nonalluvial, cohesive or noncohesive, size distribution, etc.), and bridge characteristics (size and shape of the pier and abutments, elevation of the deck, etc).

The magnitude of the flow variable depends on the selection of a design discharge. The design discharge selected for a bridge is based on the design life of the bridge, bridge importance, consequences of failure, etc. The design discharge for a divided highway with large average daily traffic (ADT) (interstate highway, autobahns, etc.) would be larger than that for a farm-to-market or logging road. Some engineers advocate a maximum possible flood for important bridges (Laursen 1998); others recommend risk analysis. Important bridges are those with large ADT, interstate highways, school bus and ambulance routs, etc.

For important highways the Federal Highway Administration in HEC 18 (Richardson and Davis 2001) recommends that bridges should be designed to resist the flood event(s) that are expected to produce the most severe scour conditions. HEC 18 recommends the 100-year flood or the overtopping flood when it is less than the 100-year flood. Overtopping refers to flow over the approach embankment(s), the bridge itself, or both. Also, investigate other flood events if there is evidence that such events would create deeper scour than the 100-year or overtopping floods. In addition, HEC 18 states, "Bridges should be designed to withstand the effects of scour from a super-flood (a flood exceeding the 100-year flood) with little risk of failing. This requires careful evaluation of the hydraulic, structural, and geotechnical aspects of bridge foundation design. It is recommended that this super-flood or check flood be on the order of a 500-year event. "The bridge design for the 100 year or overtopping flood should be designed with the normal safety factors but checking the design for the super flood is made with safety factors of 1.0." Also, "The foundation should be designed by an interdisciplinary team of engineers with expertise in hydraulic, geotechnical, and structural design."

10.2 TOTAL SCOUR

Total scour at a highway crossing is composed of long-term degradation, general scour (contraction and other general scour), and local scour. The components are assumed to be additive. In addition, lateral shifting of a stream can cause or increase the scour of bridge foundations. Each of the three types of scour and stream instability are introduced separately below.

10.2.1 Long-Term Aggradation and Degradation

Aggradation is the deposition of sediment in the bridge reach of a stream, whereas, degradation is the erosion of the sediment in the bridge reach. The former causes the bed elevation to increase and the latter causes the bed elevation to decrease. These riverbed elevation changes are over long lengths and times due to natural or man-made changes. These changes can be in controls, such as dams or bed rock, in sediment discharge, and in river form, such as from a meandering to a braided stream. Long-term degradation is defined as long-term scour and is added to the other scour components to obtain total scour, but long-term aggradation is not usually considered because over time it could stop or change to degradation.

10.2.2 General Scour

General scour is a uniform or nonuniform lowering of the waterway bed as a result of the passage of high flow. It may result from contraction of the flow (contraction scour) or flow around a bend (other general scour).

- *Contraction scour* is erosion of the stream bed under a bridge that results from the acceleration of the flow due to either a natural oraman-made contraction. It may occur during the passage of a flood, scouring during the rising stage and refilling on the falling limb of the runoff.
- *Other general scour* may result from flow around a bend, variable downstream control, or other stream changes that decrease the bed elevation.

- *General scour* is different from *long-term degradation* in that it may be cyclic and/or related to the passage of a flood.

10.2.3 Local Scour

Erosion of the stream bed around a pier or abutment as the result of the pier or abutment obstructing the flow is *local scour*. These obstructions accelerate the flow and create vortexes that remove bed material around them.

10.2.4 Lateral Shifting of the Stream

In addition to the above, lateral shifting of a stream (stream instability) may erode the approach roadway and abutments of a bridge and/or change the angle of the flow to the piers and abutments (angle of attack). This latter can increase local scour at the piers or abutments.

10.3 CLEAR-WATER AND LIVE-BED SCOUR

There are two conditions for contraction and local scour. These are clear-water and live-bed scour. Clear-water scour occurs when there is no transport of bed material in the flow upstream of the bridge. Live-bed scour occurs when there is transport of bed material from upstream of and into the bridge cross-section. However, clear-water scour may occur if the material being transported in the upstream reach or floodplain is transported in suspension through the bridge cross-section.

Typical clear-water scour situations include (1) coarse bed material streams, (2) flat gradient streams during low flow, (3) local deposits of bed materials that are larger than the biggest fraction being transported by the flow (rock riprap is a special case of this situation), (4) armored stream beds where the only locations with tractive forces adequate to penetrate the armor layer are at piers and/or abutments, and (5) vegetated channels where, again, the only locations where, cover is penetrated are at piers and/or abutments.

During a flood event, bridges over streams with coarse bed material are often subjected to clear-water scour at low discharges, live-bed scour at the higher discharges, and then clear-water scour in the falling stages. Clear-water scour reaches its maximum over a longer period of time than live-bed scour (see Fig. 10-1). In fact, local clear-water scour may not reach a maximum until after several floods.

Equations given later for determining the velocity or shear stress associated with initiation of motion can be used as indicators for clear-water or live-bed scour. If the mean velocity (V) or average shear stress (τ_0) in the upstream reach is less than the critical velocity (V_c) or critical shear stress (τ_c) of the median diameter (D_{50}) of the bed material, then contraction and local scour will be clear-water scour.

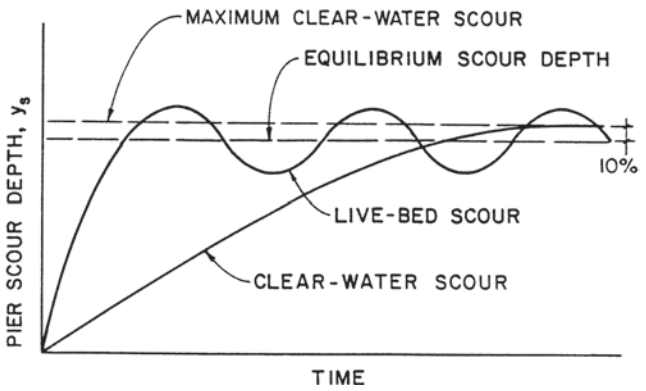

Fig. 10-1. Illustrative pier scour depth in a sand-bed stream as a function of time (not to scale) (Richardson and Davis 2001).

10.4 LONG-TERM BED ELEVATION CHANGES

Long-term bed elevation changes (aggradation or degradation) may be the natural trend of a stream or may be the result of some modification to the watershed condition of the stream. The stream bed may be aggrading, degrading, or not changing in the bridge crossing reach. When the bed of the stream is neither aggrading or degrading, it is considered to be in equilibrium with the sediment discharge supplied to the bridge reach. It is the long-term trends, not the cutting and filling of the bed of the stream that might occur with contraction scour, that must be determined. The engineer must assess the present state of the stream and watershed and determine future changes in the river system, and from this, determine the long-term stream bed elevation changes.

Factors that affect long-term bed elevation changes are dams and reservoirs upstream and downstream of a bridge, changes in watershed land use (urbanization, deforestation, etc.), channelization, cutoff of meander bends (natural or man-made), changes in the downstream base level (control) of the bridge reach, gravel mining from the stream bed, diversion of water into or out of the stream, natural lowering of the total system, movement of a bend, bridge location in reference to stream plan form, and stream movement in relation to the crossing (Keefer et al., 1980). Richardson et al. (1990; 2001) provide examples of long-term bed elevation changes.

Analysis of long-term stream bed elevation changes must be made using the principles of river mechanics in the context of a fluvial system analysis. Such an analysis of a fluvial system requires consideration of all influences upon the bridge crossing, i.e., runoff from the watershed to the channel (hydrology), sediment delivery to the channel (erosion), sediment transport capacity of the channel (hydraulics), and response of the channel to these factors (geomorphology and river mechanics). Many of the stream impacts are

from human activities, in either the past, present, or future. Analysis requires a study of the past history of the river and human activities on it; a study of present water and land use and stream control activities; and finally contacting all agencies involved with the river to determine future changes to the river system.

A method for organizing such an analysis is to use a three-level fluvial system approach. This method provides three levels of detail in an analysis, (1) qualitative determination based on general geomorphic and river mechanics relationships, (2) engineering geomorphic analysis using established qualitative and quantitative relationships to establish the probable behavior of the stream system in various scenarios of future conditions, and (3) quantifying the changes in bed elevation using available physical process mathematical models such as BRI-STARS (Molinas 1993), HEC-6 (USACE 1993), or SAMwin (Ayres Associates 2003), extrapolation of present trends, and engineering judgment to assess the result of the changes in the stream and watershed. Recent FHWA reports, such as "Stream Channel Degradation and Aggradation: Analysis of Impacts to Highway Crossings" (Brown et al. 1980), "Stream Stability at Highway Structures" (Lagasse et al. 2001a), and "River Engineering for Highway Encroachments—Highways in the River Environment" (Richardson et al. 2001) discuss methodologies to determine long-term elevation trends. Vanoni (1975) discusses degradation and aggradation in Section 21, pp. 64 and 65. The general discussion of sediment transport in Vanoni (1975) is also very useful in understanding and determining long-term degradation.

10.5 GENERAL SCOUR

10.5.1 Contraction Scour

Contraction scour occurs when the flow area of a stream at flood stage is reduced, either by a natural contraction or by a bridge and/or its approach embankments. From continuity, a decrease in flow area results in an increase in average velocity and bed shear stress through the contraction. Hence, there is an increase in erosive forces in the contraction and more bed material is removed from the contracted reach than is transported into the reach. This increase in transport of bed material from the reach lowers the bed elevation. As the bed elevation is lowered, the flow area increases and, in the riverine situation, the velocity and shear stress decrease until relative equilibrium is reached. That is, either the quantity of bed material that is transported into the contraction is equal to that removed from the reach, *live-bed scour***,** or the mean velocity (V) or average shear stress (τ_0) in the contraction is less than the critical velocity (V_c) or critical stress (τ_c) of the median diameter (D_{50}) of the bed material, *clear-water scour***.**

In coastal streams that are affected by tides, as the cross-sectional area increases the discharge from the ocean may increase and thus the velocity and shear stress may not decrease. Consequently, relative equilibrium may not be reached. Thus, at tidal inlets that experience clear-water or live-bed scour, contraction scour may result in continual lowering of the bed (long-term degradation) (Richardson et al 1993; 1995; Richardson and Davis 2001).

Live-bed contraction scour is typically cyclic. That is, the bed scours during the rising stage of a runoff event and fills in the falling stage. The contraction of flow due to a bridge can be caused either by a natural decrease in the flow area of the stream channel or by abutments projecting into the channel and/or the piers blocking a large portion of the flow area. Contraction can also be caused by the approaches to a bridge cutting off floodplain flow. This can cause clear-water scour on a setback portion of a bridge section and/or a relief bridge because the floodplain flow does not normally transport significant concentrations of bed material sediments.

Other factors that can cause contraction scour are (1) ice formation or jams, (2) natural berms along the banks due to sediment deposits, (3) island or bar formations upstream or downstream of the bridge opening, (4) debris, and (5) growth of vegetation in the channel or floodplain.

10.5.2 Other General Scour

In a natural channel, the depth of flow and the velocity are always greater on the outside of a bend. In fact there may well be deposition on the inner portion of the bend at the point bar. Other general scour at a bridge located on or close to a bend will be concentrated on the outer part of the bend. Also, in bends, the thalweg (the part of the stream where the flow is deepest and, typically, the velocity is the greatest) may shift toward the center of the stream as the flow increases. This can increase scour and the nonuniform distribution of the scour in the bridge opening (chute channel).

10.5.3 Contraction Scour Equations

Contraction scour equations are based on the principle of conservation of sediment transport. In the case of live-bed scour, this simply means that the fully developed scour in the bridge cross-section reaches equilibrium when sediment transported into the contracted section equals sediment transported out and the conditions for sediment continuity are in balance. For clear-water scour, the transport into the contracted section is essentially zero and maximum scour occurs when the shear stress reduces to the critical shear stress of the bed material.

To determine if the contraction scour at a bridge is *clear-water* or *live-bed,* determine if the critical velocity (V_c) or critical shear stress (τ_c) of the median diameter (D_{50}) of the bed material in the channel upstream from the bridge opening is greater than the average velocity or shear stress (clear-water scour) or smaller (live-bed scour). Or calculate the contraction scour using both equations and take the smaller scour depth (Richardson and Davis 2001).

10.5.4 Live-Bed Contraction Scour Equation

Laursen (1958,1962) derived the following equation for live-bed contraction scour. It is based on a simplified transport function (Laursen and Toch 1956) to obtain equilibrium sediment transport in a long contraction. In short contractions, such as at a bridge, it slightly overestimates the scour depth,

$$\frac{y_2}{y_1} = \left(\frac{Q_2}{Q_1}\right)^{6/7}\left(\frac{W_1}{W_2}\right)^{k_1}\left(\frac{n_2}{n_1}\right)^{k_2} \qquad (10\text{-}1)$$

$$y_s = y_2 - y_0 = \text{(average scour depth, m, ft)}$$

where

y_1 = average depth in the upstream main channel, m, ft;
y_2 = average depth in the contracted section, m, ft;
y_0 = average depth in the contracted section before contraction scour, m, ft;
W_1 = bottom width of the upstream main channel, m, ft;
W_2 = bottom width of main channel in the contracted section, m, ft;
Q_1 = flow in the upstream channel transporting sediment, m^3 s, cms, cfs;
Q_2 = flow in the contracted channel, m^3/s, cfs (often this is equal to the total discharge unless the total flood flow is reduced by relief bridges or water overtopping the approach roadway);
n_2 = Mannings n for contracted section;
n_1 = Mannings n for upstream main channel;
k_1,k_2 = exponents determined depending on the mode of bed material transport;
V_* = $(gy_1S_1)^{1/2}$ shear velocity in the upstream section, m/s, ft/s;
ω = median fall velocity of the bed material based on the D_{50} (see Fig. 10-2);
g = acceleration of gravity (9.81 m/s^2, 32.2 ft/s^2);
S_1 = slope of energy grade line of main channel, m/m, ft/ft;
D_{50} = median diameter of the bed material, m, ft.

V_*/w	k_1	k_2	Mode of Bed Material Transport
<0.50	0.59	0.066	Mostly contact bed material
0.50–2.0	0.64	0.21	Some suspended bed material discharge
>2.0	0.69	0.37	Mostly suspended bed material discharge

The value of y_0 may be difficult to determine because of residual contraction scour from previous floods or other factors. Nevertheless, y_0 must be determined. A reasonable value can be determined by a study of the channel using cross sections and longitudinal profiles from upstream, through the bridge, and downstream.

Richardson and Davis (2001) recommend that the Manning n ratio in Eq. (10-1) be eliminated. The Manning n ratio can be significant for a condition of dune bed in the main channel and a corresponding plane bed, washed out dunes or antidunes in the contracted channel. However, Laursen's equation does not correctly account for the increase in transport that will occur as the result of the bed planing out (which decreases resistance to flow and increases the velocity and the transport of bed material at the bridge). That is, Laursen's equation indicates a decrease in scour for this case, whereas in reality, there would be an increase in scour depth. In addition, in flood flows, a plane bedform will usually exist upstream and through the contracted waterway, and the values of Manning's n will be equal.

10.5.5 Clear-Water Contraction Scour Equations

Clear-water contraction scour occurs in a long contraction when (1) there is no significant bed material transport in the upstream reach into the downstream bridge reach or (2) the material being transported in the upstream reach is transported through the downstream bridge reach mostly in suspension. With clear-water contraction scour, the area of the contracted section increases until, in the limit, the velocity of the flow (V) or the shear stress (τ_0) on the bed is equal to the critical velocity (V_c) or the critical shear stress (τ_c) of a certain large size (D) in the bed material. The width (W) of the contracted section is constrained and the depth (y) increases until the limiting conditions are reached.

Following a development proposed by Laursen (1963), Richardson and Davis (2001) developed the following equation for determining the clear-water contraction scour in a long contraction:

$$\tau_0 = \tau_c \qquad (10\text{-}2)$$

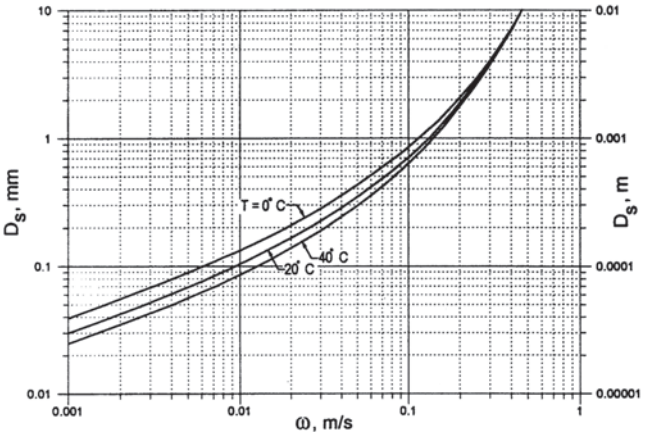

Fig. 10-2. Fall velocity of sand-sized particles.

where

τ_0 = average bed shear stress, contracted section, N/m^2, lb/ft^2
τ_c = critical bed shear stress at incipient motion, N/m^2, lb/ft^2.

The average bed shear stress using y for the hydraulic radius (R) and the Manning equation to determine the slope (S_f) can be expressed as

$$\tau_0 = \gamma y S_f = \frac{\rho g V^2 n^2}{y^{1/3}} \tag{10-3}$$

For noncohesive bed materials and for fully developed clear-water contraction scour, the critical shear stress can be determined using the Shields (Vanoni 1975) relation,

$$\tau_c = K_s (\rho_s - \rho) g D \tag{10-4}$$

The bed in a long contraction scours until $\tau_0 = \tau_c$, resulting in

$$\frac{\rho g n^2 V^2}{y^{1/3}} = K_s (\rho_s - \rho) g D \tag{10-5}$$

Solving for the depth (y) in the contracted section gives

$$y = \left[\frac{n^2 V^2}{K_s (S_s - 1) D} \right]^3 \tag{10-6}$$

In terms of discharge (Q) the depth (y) is

$$y = \left[\frac{n^2 Q^2}{K_s (S_s - 1) D W^2} \right]^{3/7} \tag{10-7}$$

where

V = average velocity in the contracted section, m/s, ft/s;
Q = discharge, m^3/s or cms, *c*fs;
D = diameter of smallest nontransportable bed material particle, m, ft;
γ = the unit weight of water (9,800 N/m^3 62.4 lb/ft^3);
n = Manning roughness coefficient;
K_s = Shield's coefficient;
S_s = specific gravity (2.65 for quartz);
ρ = density of water (999 kg/m^3, 1.94 slugs/ft^3);
ρ_s = density of sediment (quartz-2,647 kg/m^3, 5.14 slugs/ft^3);
g = acceleration of gravity (9.81 m/s^2, ft/s^2).

Equation (10-7) is the basic equation for the clear-water scoured depth (y) in a long contraction. Laursen (1963), in English units, used a value of 4 for $K_s (S_s - 1)\gamma$ in Eq. (10-4); D_{50} for the size (D) of the smallest nonmoving particle in the bed material, and Strickler's approximation for Manning's n ($n = 0.034\ D_{50}^{1/6}$). Laursen's value for Shield's coefficient, K_s is 0.039. Froehlich (1995) gives equations for Manning's n and Shield's coefficient, taking into account size distribution of the bed material and the fact that the bed material increases in size as the section scours.

Shield's coefficient for initiation of motion ranges from 0.03 to 0.1 (Vanoni 1975). Strickler's equation for n given by Laursen, in metric units, is $n = 0.041\ D^{1/6}$. Research discussed in Richardson et al. (1990; 2001) recommends the use of the effective mean bed material size (D_m) in place of the D_{50} size. The use of D_m would also be in accordance with the work of Froehlich (1995). D_m is approximately 1.25 D_{50}. Using Laursen's value for Shield's coefficient K_s of 0.039, $n = 0.04\ Dm^{1/6}$, and $S_s = 2.65$ in Eq. (10.7) results in

$$y = \left[\frac{0.025 Q^2}{D_m^{2/3} W^2} \right]^{3/7} \tag{10-8}$$

$$y_s = y - y_0 \text{ (average scour depth)} \tag{10-9}$$

where

D_m = effective mean diameter of the bed material (1.25 D_{50}) in the contracted section, m;
y_s = depth of scour in the contracted section, m;
y_0 = original depth in the contracted section before scour, m;

other variables are as previously defined.

Clear-water contraction scour equations assume homogeneous bed materials. However, with clear-water scour in stratified materials, assuming the layer with the finest D_{50} would result in the most conservative estimate of contraction scour. Alternatively, the clear-water contraction scour equations could be used sequentially for stratified bed materials.

Both the live-bed and clear-water contraction scour equations are the best that are available and should be regarded as a first level of analysis. If a more detailed analysis is warranted, a sediment transport model such as BRI-STARS (Molinas 1993) or HEC 6 (USACE 1993) could be used.

10.6 CRITICAL VELOCITY FOR MOVEMENT OF BED MATERIAL

The velocity and depth given in Eq. (10-6) are associated with initiation of motion of the indicated size (D). Rearranging Eq. (10-6) to give the critical velocity for the beginning of motion of bed material of size D results in

$$V_c = \frac{K_s^{1/2} (S_s - 1)^{1/2} D^{1/2} y^{1/6}}{n} \tag{10-10}$$

Using $K_s = 0.039$, $S_s = 1.65$, and $n = 0.041\ D^{1/6}$,

$$V_c = K u y^{1/6} D^{1/3} \tag{10-11}$$

where

V_c = critical velocity above which bed material of size D and smaller will be transported, m/s, ft/s;

K_s = Shield's parameter;
S_s = specific gravity of the bed material;
D = size of bed material, m, ft;
y = depth of flow, m, ft;
n = Manning's roughness coefficient;
Ku = 6.19 SI units and 11.17 English units.

Additional discussion of beginning of motion is given in Vanoni (1975, pp. 91–107 for noncohesive sediments and 107–114 for cohesive sediments).

10.7 LOCAL SCOUR

The basic mechanism causing local scour at piers or abutments is the formation of vortices at their bases (known as the horseshoe vortex at a pier, Fig. 10-3, and horizontal vortex at an abutment, Fig. 10-4). The horseshoe vortex results from the pileup of water on the upstream surface of the obstruction and subsequent acceleration of the flow around the nose of the pier or embankment. The action of the vortex removes bed material from around the base of the obstruction. The transport rate of sediment away from the base region is greater than the transport rate into the region, and, consequently, a scour hole develops. As the depth of scour increases, the strength of the horseshoe vortex is reduced, thereby reducing the transport rate from the base region. Eventually, for live-bed local scour, equilibrium is reestablished and scouring ceases. For clear-water scour, scouring ceases when the shear stress caused by the horseshoe vortex equals the critical shear stress of the sediment particles at the bottom of the scour hole.

In addition to the horseshoe vortex around the base of a pier, there are vertical vortices downstream of the pier, called the wake vortex (Fig. 10-3). Both the horseshoe and wake vortices remove material from the pier base region. However, the intensity of wake vortices diminishes rapidly as the distance downstream of the pier increases. Therefore, immediately downstream of a long pier there is often deposition of material.

At abutments, in addition to the horizontal vortex that forms around and erodes their bases there is a vertical vortex that results from flow separation at the downstream side of the abutment (Fig. 10-4). This vortex erodes the approach embankment and the abutment foundations on the downstream corner and side. Thus, there are two scour problems at abutments, (1) a scour hole at the abutment base resulting from the horizontal vortex and (2) erosion of the downstream approach embankment and abutment foundation by the vertical vortex caused by the flow separation.

Factors that affect the magnitude of local scour at piers are (1) width of the pier; (2) length of the pier if skewed to flow; (3) depth and (4) velocity of the approach flow upstream of the pier; (5) size and gradation of bed material; (6) angle of attack of the approach flow; (7) shape; (8) bed configuration; (9) ice formation or jams; and (10) debris. The scour results from free surface flow unless the bridge is submerged or overtopped; then the scour results from pressure flow. The shape of many piers is complex. The piers may rest on footings or pile caps on piles. The footings or pile caps may be in the flow or at the mean water elevation by design or erosion.

Factors that affect the magnitude of local scour at abutments are (1) discharge intercepted by the abutment and returned to the main channel at the abutment (in laboratory flumes this discharge is a function of projected length of an abutment and approach roadway into the flow); (2) depth of flow; (3) velocity of flow at the upstream and downstream ends of the abutment; (4) size and gradation of bed material; (5) angle of attack of the approach flow; (6) shape;

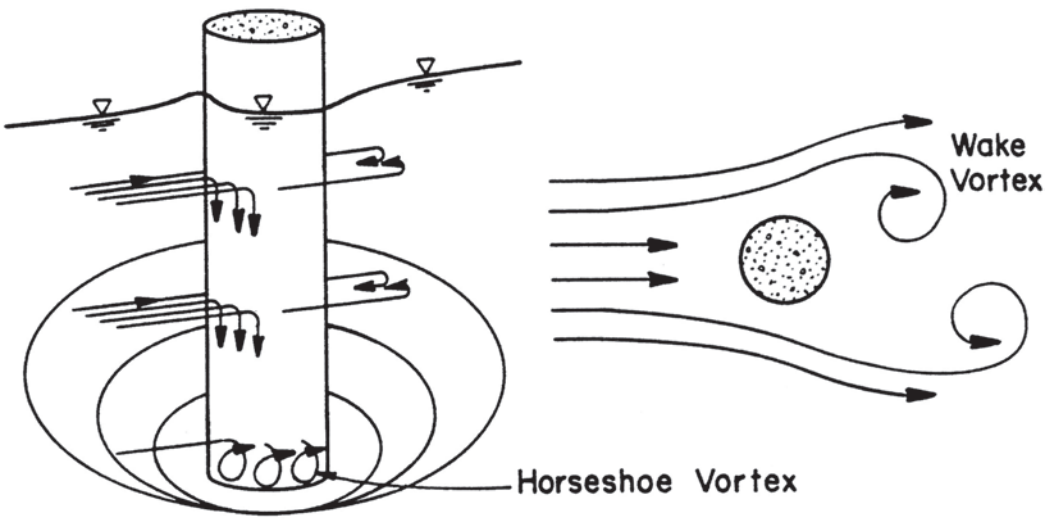

Fig. 10-3. Schematic representation of scour at a cylindrical pier (Richardson and Davis 2001).

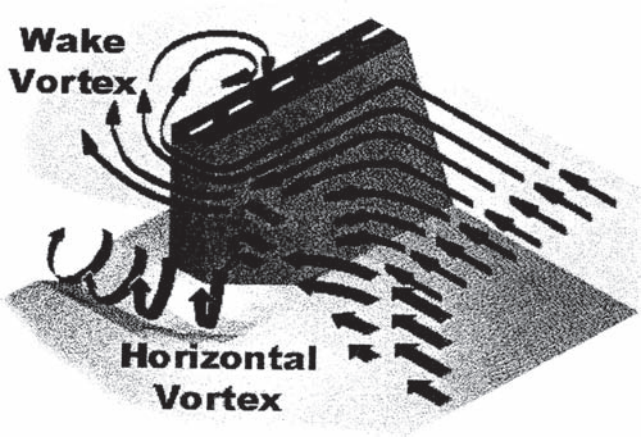

Fig. 10-4. Schematic representation of scour at an abutment.

(7) bed configuration; (8) ice formation or jams; and (9) debris. The scour results from free surface flow unless the bridge is submerged or overtopped. Then the scour results from pressure flow. As with piers, abutments may have complex shape.

10.8 LOCAL SCOUR AT PIERS

Local scour at piers has been studied extensively since the late 1940s (Loungen and Toch 1956; Laursen 1958; 1960; 1963; Richardson and Lagasse 1999). As a result of the many studies there are many equations. In general the equations are for ultimate (maximum) scour in sand beds. Jones (1983) compared the more common equations, Fig. 10-5. An equation developed by Melville and Sutherland in 1988 has been added to the figure. Many of the equations have velocity of the flow just upstream of the pier as a variable, normally in the form of a Froude number. However, some equations, such as Laursen's do not include velocity. As can be seen from Fig. 10-5, the Colorado State University (CSU) (Richardson et al. 1990) equation envelops all the points, but gives lower values of scour than Laursen's (1960), Jain and Fischer's (1979), Melville and Sutherland's (1988), and Neill's (Blench 1989) equations. Fred Chang (Richardson and Davis 2001) pointed out that Laursen's 1960 equation is essentially a special case of the CSU equation with the $F = 0.4$.

In Fig. 10-6, from flume studies in sand bed material, the ratio of scour depth to pier width (y_s / a) as a function of the ratio of approach velocity to critical velocity (V / V_c) for different-sized bed material is given. Nondimensional scour (y_s / a) starts when the mean approach velocity is approximately half of V_c the critical velocity for the beginning of motion of the bed material ($V / V_c = 0.5$) and reaches a maximum when this ratio equals 1.0. This maximum value of the nondimensional scour depth decreases with decreased bed material size. The scour that takes place from $V / V_c = 0.5$ to 1.0 is clear-water scour. For values of $V / V_c > 1.0$ the scour is live-bed. As can be seen from Fig. 10-6 after $V / V_c = 1.0$, the nondimensional scour depth decreases and then increases. The bed configuration after $V / V_c = 1.0$ in the flumes is either ripples or dunes. When the live-bed scour nondimensional depth starts to increase with an increase in V / V_c the bed configuration changes to plain bed and antidunes. The increase in nondimensional scour depth results because

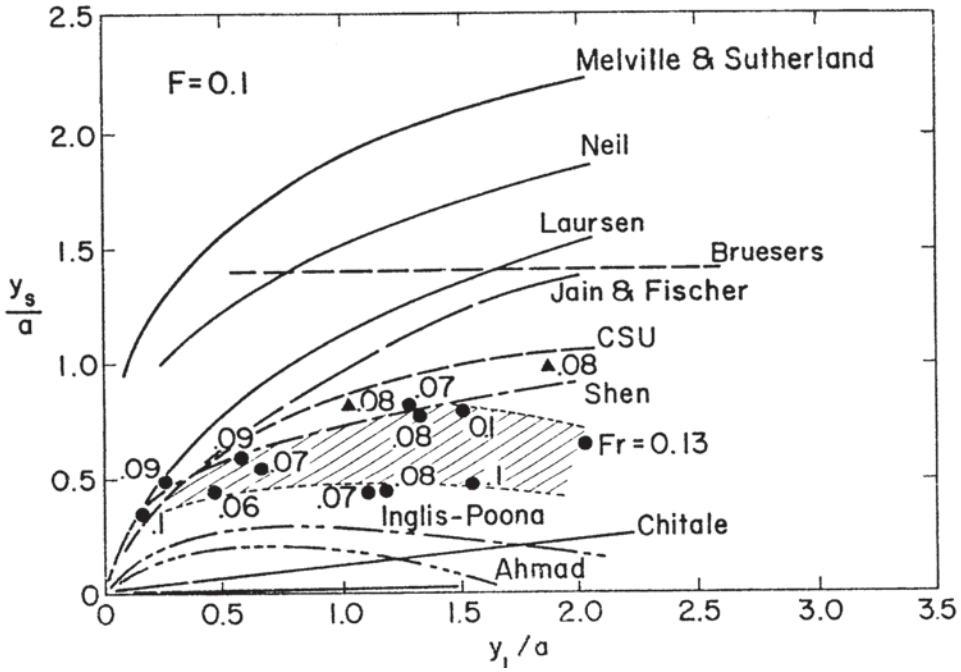

Fig. 10-5. Comparison of scour formulas for variable depth ratios (y/a) after Jones (1983).

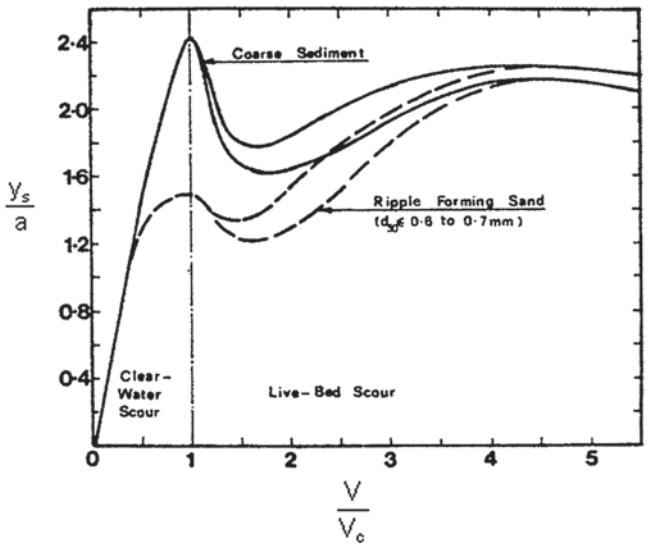

Fig. 10-6. Nondimensional local scour depth as a function of nondimensional velocity and bed material size (Melville 1984).

during plain bed and antidune flow conditions some of the sediment in transport washes through the scour hole. At high values of V / V_c the scour condition is similar to clear-water scour. That is, the bed material that is being transported upstream of the pier is swept through the scour hole and takes no part in the scouring process.

Chang (Richardson and Davis 2001) noted that in all the data he studied, there were no values of the ratio of scour depth to pier width (y_s / a) larger than 2.3. Melville and Sutherland (1988) reported 2.4 as an upper limit ratio for cylindrical piers. In these studies, the Froude number was less than 1.0. Values of y_s / a around 3.0 were obtained by Jain and Fischer (1979) for chute-and-pool flows with Froude numbers as high as 1.5. Their largest value of y_s / a for antidune flow was 2.5 with a Froude number of 1.2. These upper limits were derived for circular piers and were uncorrected for pier shape and for skew. Also, pressure flow or debris can increase the ratio.

From the above discussion, the ratio of y_s / a can be as large as 3 at large Froude numbers. Therefore, Richardson and Davis (2001) recommended that the maximum value of the ratio be taken as 2.4 for Froude numbers less than or equal to 0.8 and as 3.0 for larger Froude numbers. These limiting ratio values apply only to round nose piers that are aligned with the flow.

Over 30 equations have been developed for pier scour (Jones 1983; McIntosh 1989; Landers and Mueller 1996). In the following, three of the equations given in the literature are presented.

10.9 HEC 18 PIER SCOUR EQUATION

To determine pier scour, an equation based on the CSU equation (Richardson et al. 1990; 2001) was recommended by the Federal Highway Administration in HEC 18 (Richardson and Davis 2001) for both live-bed and clear-water pier scour. A study of 22 scour equations using field data presented by Landers et al. (1996) indicated that the HEC 18 equation was good for design because it rarely underpredicted measured scour depth, but frequently grossly overpredicted the observed scour (Mueller 1996). The data contained 384 measurements of scour at 56 bridges. The Landers and Mueller data are also given by Richardson and Lagasse (1999). The HEC 18 equation slightly underpredicted 6 of the 384 scour measurements. The maximum deviation was 3 ft when the scour depth was 25 ft (7.62m). The HEC 18 equation overestimated scour in coarse bed streams because of restrictions placed on a correction factor K_4 for coarse bed material. A K_4 factor for coarse bed material developed by Mueller (1996) decreased the overprediction without altering the underprediction.

The HEC 18 pier scour equation is

$$\frac{y_s}{y_1} = 2.0\, K_1\, K_2\, K_3\, K_4\, K_w \left(\frac{a}{y_1}\right)^{0.65} \mathsf{F}_1^{0.43} \qquad (10\text{-}12)$$

In terms of y_s / a, Eq. (10-12) is

$$\frac{y_s}{a} = 2.0\, K_1\, K_2\, K_3\, K_4\, K_w \left(\frac{y_1}{a}\right)^{0.35} \mathsf{F}_1^{0.43} \qquad (10\text{-}13)$$

$$\begin{aligned} y_s &\le 2.4\, a \qquad \mathsf{F} < 0.8 \\ y_s &\le 3.0\, a \qquad \mathsf{F} > 0.8 \end{aligned} \qquad (10\text{-}14)$$

where

y_s = scour depth, m, ft;
y_1 = flow depth directly upstream of the pier, m, ft;
K_1 = correction factor for pier nose shape from Fig. 10-7 and Table 10-1;
K_2 = correction factor for angle of attack of flow from Eq. (10-15) or Table 10-2;
K_3 = correction factor for bed condition from Table 10-3;
K_4 = correction factor for size of bed material;
K_w = correction factor for very wide, piers;
a = pier width, m, ft;
L = length of pier, m, ft;
F_1 = Froude number = $V_1 / (g y_1)^{1/2}$;
V_1 = mean velocity of flow directly upstream of the pier, m/s, ft/s.

The correction factor for angle of attack of the flow K_2 given in table 10-2 can be calculated using the equation:

$$K_2 = (\cos\theta + L/a \sin\theta)^{0.65} \qquad (10\text{-}15)$$

If L / a is larger than 12, use $L / a = 12$ as a maximum in Eq. (10-15).

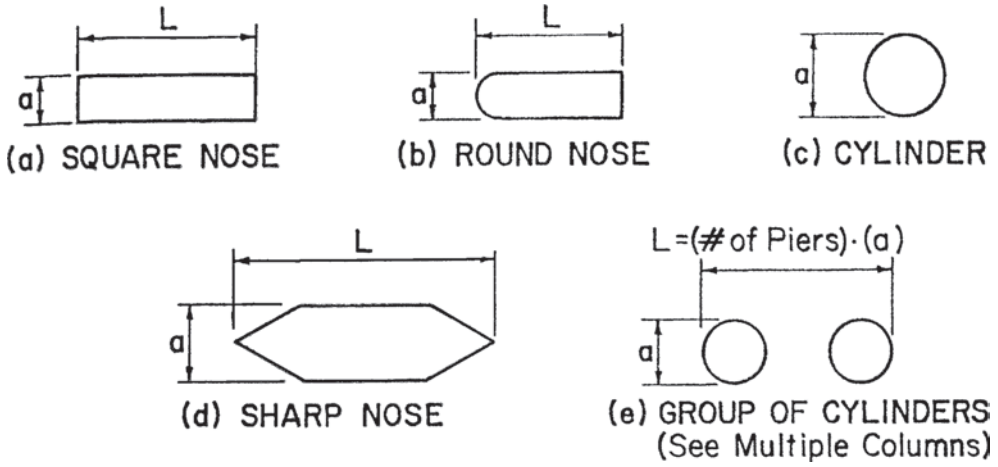

Fig 10-7. Common pier shapes (Richardson, and Davis 2001).

10.9.1 Mueller (1996) K_4 Correction Coefficient

Mueller (1996) developed a K_4 correction coefficient from a study of 384 field measurements of scour at 56 bridges. It is as follows:

$$\begin{aligned} &M_4 = 1 \text{ if } F_{50} < 2 \text{ mm or } F_{95} < 20 \text{ mm} \\ &\mathrm{K}_4 = 0.4\left(M_5\right)^{0.15} \text{ if} \\ &F_{50} \geq 2 \text{ mm and } F_{95} \geq 20 \text{ mm} \end{aligned} \tag{10-16}$$

where

$$K_5 = \frac{V_1 - V_{icD_{50}}}{V_{cD_{50}} - V_{icD_{95}}} > 0 \tag{10-17}$$

V_{icDx} = the approach velocity corresponding to critical velocity for incipient scour in the accelerated flow region at the pier for the grain size D_x, m/s;

$$V_{icD_x} = 0.645\left(\frac{D_x}{a}\right)^{0.053} V_{cD_x} \tag{10-18}$$

V_{cDx} = the critical velocity for incipient motion for the grain size D_x, m/s, ft/s.

Mueller (1996) used a variable Shield's parameter to define the critical velocity for incipient motion. However, for the coarser size of bed material to which K_4 is applicable, it can be determined using Eq. (10-11). It is as follows:

$$V_{cDx} = Ku\, y_1^{1/6} D_x^{1/3} \tag{10-19}$$

y_1 = depth of flow just upstream of the pier, excluding local scour, m, ft;
V_1 = velocity of the approach flow just upstream of the pier, m/s, ft/s;
D_x = grain size for which x% of the bed material is finer, m, ft;
Ku = 6.19 SI units and 11.17 English units.

Although this K_4 provides a good fit to the field data the velocity ratio terms are so formed that if D_{50} is held constant and D_{95} increases the value of K_4 increases rather than decreases (Mueller and Jones 1999). For field data an increase in D_{95} was always accompanied by an increase in D_{50}. A minimum value for K_4 is 0.4.

10.9.2 Correction Factor for Very Wide Piers

Field and flume studies of scour depths at wide piers in shallow flows indicate that existing scour equations over estimate scour depths. Johnson and Torrico (1994) suggest the following equations for a K_w to correct for wide piers in shallow flows.

The correction factor should be used when the ratio of depth of flow to pier width is less than 0.8; the ratio of the pier width to the median diameter of the bed material is greater than 50; and the Froude number of the flow is subcritical:

$$K_w = 2.58\,(y/a)^{0.34}\,\mathrm{F}^{0.65} \quad \text{for} \quad V/V_c < 1 \tag{10-20}$$

$$K_w = 1.0\,(y/a)^{0.13}\,\mathrm{F}^{0.25} \quad \text{for} \quad V/V_c \geq 1 \tag{10-21}$$

Engineering judgment should be used in applying K_w because it is based on limited data.

10.9.3 Scour for Complex Pier Foundations

10.9.3.1 Introduction The piers of many bridges may not be solid single shafts as shown in Figs. 10-3 and 10-7 but may be composed of a combination of elements. In the general case, the flow could be obstructed by three

Table 10-1 Correction Factor K_1 for Pier Nose Shape

Shape of pier nose	K_1
(a) Square nose	1.1
(b) Round nose	1.0
(c) Circular cylinder	1.0
(d) Sharp nose	0.9
(e) Group of cylinders	1.0

Table 10-2 Correction for Angle of Attack θ of the Flow

Angle	$L/a=4$	$L/a=8$	$L/a=12$
0	1.0	1.0	1.0
15	1.5	2.0	2.5
30	2.0	2.75	3.5
45	2.3	3.3	4.3
90	2.5	3.9	5.0

Note: = Angle = skew angle of flow; L = length of pier, m, ft.

Table 10-3 Increase in Equilibrium Pier Scour Depths (K_3) for Bed Condition

Bed condition	Dune height, m	K_3
Clear-water scour	N/A	1.1
Plane bed and antidune flow	N/A	1.1
Small dunes	$3 > H < 0.6$	1.1
Medium dunes	$9 > H > 3$	1.1 to 1.2
Large dunes	$H > 9$	1.3

Note: The correction factor K_1 for pier nose shape should be determined using Table 9-2 for angles of attack up to 5°. For greater angles, K_2 dominates and K_1 should be considered as 1.0. If L/a is larger than 12, use the values L/a = 12 as a maximum. The correction factor K_3 results from the fact that for plane-bed conditions, which are typical of most bridge sites for the flood frequencies employed in scour design, the maximum scour may be 10% greater than computed with the CSU equation (Richardson et al. 1990). In the unusual situation where a dune bed configuration with large dunes exists at a site during flood flow, the maximum pier scour may be 30% greater than the predicted value. This may occur on very large rivers, such as the Mississippi. For smaller streams that have a dune bed configuration at flood flow, the dunes will be smaller and the maximum scour may be only 10 to 20%, greater than equilibrium scour. For antidune bed configuration the maximum scour depth may be 10% greater than the computed equilibrium pier scour depth.

substructural elements, which include the pier stem, the pile cap or footing, and the pile group. The three types of exposure to the flow may be by design or by scour (long-term degradation, general (contraction) scour, and local scour, in addition to stream migration).

Ongoing research has determined methods and equations to determine scour depths for complex pier foundations (Jones 1989; Salim and Jones 1995; 1996; 1999; Jones and Sheppard 2000). The results of this research are given in HEC 18 (Richardson and Davis 2001) and are given in the following sections. Physical model studies are still recommended for complex piers with unusual features such as staggered or unevenly spaced piles or for major bridges where conservative scour estimates are not economically acceptable (Richardson et al. 1987). However, the methods presented in this section provide a good estimate of scour for a variety of complex pier situations.

The following steps are recommended for determining the depth of scour for any combination of the three substructural elements exposed to the flow. However, engineering judgment is an essential element in applying the design graphs and equations presented in this section, as well as in deciding when a more rigorous level of evaluation is warranted. Engineering judgment should take into consideration the volume of traffic, type of traffic (school bus, ambulance, fire trucks, local road, interstate, etc.), importance of the highway, cost of a failure (potential loss of life and dollars), and increase in cost that would occur if the most conservative scour depth were used. The stability of the foundation should be checked for the following:

Determine the scour depths for the 100-year flood or smaller discharge if it causes deeper scour and the superflood, i.e., the 500-year flood, as recommended in this manual.

If needed, use computer programs such as HEC-RAS (USACE 2001), FESWMS (Froehlich 1996), or RMA2 (USACE 1997) to compute the hydraulic variables.

Determine total scour depth by separating the scour-producing components, determining the scour depth for each component and adding the results. The method is called "superposition of the scour components."

Analyze the complex pile configuration to determine the components of the pier that are exposed to the flow or will be exposed to the flow, which will cause scour.

Determine the scour depths for each component exposed to the flow using the equations and methods presented in the following sections.

Add the components to determine the total scour depths.

Plot the scour depths and analyze the results using an interdisciplinary team to determine their reliability and adequacy for the bridge, flow and site conditions, and safety and costs.

Conduct a physical model study if engineering judgment determines that it will reduce uncertainly, increase the safety of the design, and/or reduce cost.

10.9.3.2 Superposition of Scour Components Method of Analysis The components of a complex pier are illustrated in Fig. 10-8. Note that the pile cap can be above the water surface, at the water surface, in the water, or on the bed. The location of the pile cap may result from design or from long-term degradation and/or contraction scour. The pile group, as illustrated, is in uniform (lined up) rows and columns. This may not always be the case. The support for the bridge in many flow fields and designs may require a more complex arrangement of the pile group. In more complex pile group arrangements, this methods of analysis may give smaller or larger scour depths.

The variables illustrated in Fig. 10-8 and others used in computations are as follows:

f = distance between front edge of pile cap or footing and pier, m (ft);
h_0 = height of the pile cap above bed at beginning of computation, m (ft);
$h_1 = h_0 + T$ = height of the pier stem above the bed before scour, m (ft);
$h_2 = h_0 + y_{s\ pier} / 2$ = height of pile cap after pier stem scour component has been computed, m (ft);
$h_3 = h_0 + y_{s\ pier} / 2 + y_{s\ pc} / 2$ = height of pile group after the pier stem and pile cap scour components have been computed, m (ft);
S = spacing between columns of piles, pile center to pile center, m (ft);
T = thickness of pile cap or footing, m (ft);
V_1 = approach velocity used at the beginning of computations, m/s (ft/s);
$V_2 = V_1(y_1 / y_2)$ = adjusted velocity for pile cap computations, m/s (ft/s);
$V_3 = V_1(y_1 / y_3)$ = adjusted velocity for pile group computations, m/s (ft/s).
y_1 = approach flow depth at the beginning of computations, m (ft);
$y_2 = y_1 + y_{s\ pier} / 2$ = adjusted flow depth for pile cap computations, m (ft);
$y_3 = y_1 + y_{s\ pier} / 2 + y_{s\ pc} / 2$ = adjusted flow depth for pile group computations, m ;(ft)

Total scour from superposition of components is given by

$$y_s = y_{s\,\text{pier}} + y_{s\,\text{pc}} + y_{s\,\text{pg}} \tag{10-22}$$

where

y_s = total complex pier scour depth, m (ft);
$y_{s\ pier}$ = scour component for the pier stem in the flow, m (ft);
$y_{s\ pc}$ = scour component for the pier cap or footing in the flow, m (ft);
$y_{s\ pg}$ = scour component for the piles exposed to the flow, m (ft).

Each of the scour components is computed from the basic pier scour by Eq. (10.12) using an equivalent-sized pier to represent the irregular pier components, adjusted flow depths, and velocities as described in the list of variables for Fig. 10-8 and height adjustments for the pier stem and pile group. The height adjustment is included in the equivalent pier size for the pile cap. In the following sections, guidance for calculating each of the components is given.

10.9.3.3. Determination of the Pier Stem Scour Depth Component The need to compute the pier stem scour depth component occurs when the pier cap or the footing is in the flow and the pier stem is subjected to sufficient flow depth and velocity to cause scour. The first computation is the scour estimate, $y_{s\ pier}$, for a full-depth pier that has the width and length of the pier stem using the basic pier equation

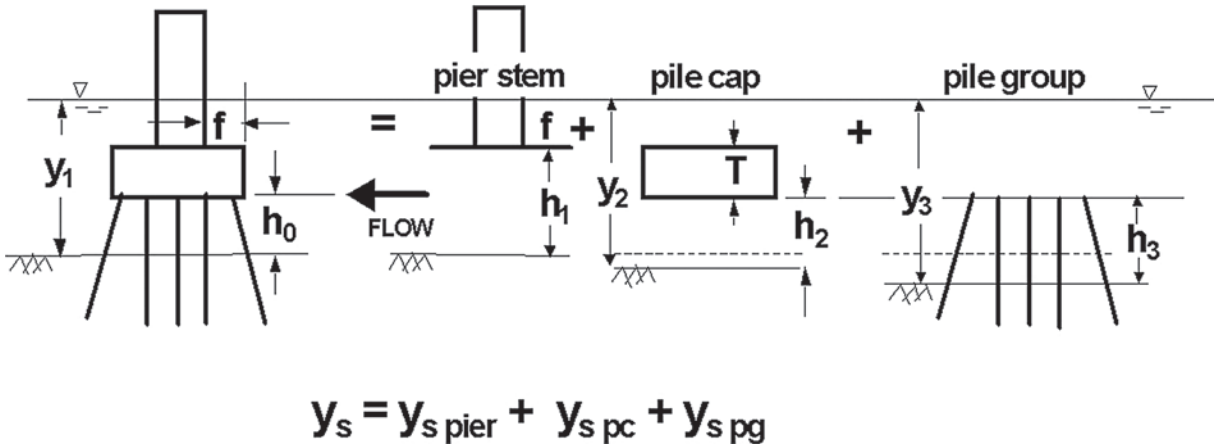

Fig. 10-8. Definition sketch for scour components for a complex pier (Richardson and Davis 2001).

(Eq. (10-12)). In Eq. (10-12), a_{pier} is the pier width and other variables in the equation are as defined previously. This base scour estimate is multiplied by $K_{h\ \text{pier}}$, given in Fig. 10-9 as a function of h_1/a_{pier} and f/a_{pier}, to yield the pier stem scour component

$$\frac{y_{s\text{pier}}}{y_1} = K_{h\ \text{pier}}\left[2.0\ K_1\ K_2\ K_3\ K_4\ K_w \times \left(\frac{a_{\text{pier}}}{y_1}\right)^{0.65}\left(\frac{V_1}{\sqrt{gy_1}}\right)^{0.43}\right] \quad (10\text{-}23)$$

where

$K_{\text{h pier}}$ = coefficient to account for the height of the pier stem above the bed and the shielding effect by the pile cap overhang distance f in front of the pier stem (from Fig. 10-9).

The quantity in the square brackets in Eq. (10-23) is the basic pier scour ratio as if the pier stem were full depth and extended below the scour.

10.9.3.4 Determination of the Pile Cap (Footing) Scour Depth Component The need to compute the pile cap or footing scour depth component occurs when the pile cap is in the flow by design, or as the result of long-term degradation, contraction scour, and/or by local scour attributed to the pier stem above it. As described below, there are two cases to consider in estimating the scour caused by the pile cap (or footing). Eq. (10-12) is used to estimate the scour component in both cases, but the conceptual strategy for determining the variables to be used in the equation is different (partly due to limitations in the research that has been done to date). In both cases the wide pier factor, K_w, may be applicable for this computation.

Case 1: The bottom of the pile cap is above the bed and in the flow, either by design or after the bed has been lowered by scour caused by the pier stem component. The strategy is to reduce the pile cap width, a_{pc}, to an equivalent full depth solid pier width, a^*_{pc}, using Fig. 10-10. The equivalent pier width, an adjusted flow depth, y_2, and an adjusted flow velocity, V_2, are then used in Eq. (10-12) to estimate the scour component.

Case 2: The bottom of the pile cap or footing is on or below the bed. The strategy is to treat the pile cap or exposed footing like a short pier in a shallow stream of depth equal to the height to the top of the footing above the bed. The portion of the flow that goes over the top of the pile cap or footing is ignored. Then, the full pile cap width, a_{pc}, is used in the computations, but the exposed footing height, y_f (in lieu of the flow depth), and the average velocity, V_f, in the portion of the profile approaching the footing are used in Eq. (10-12) to estimate the scour component.

An inherent assumption in this second case is that the footing is deeper than the scour depth, so it is *not necessary*

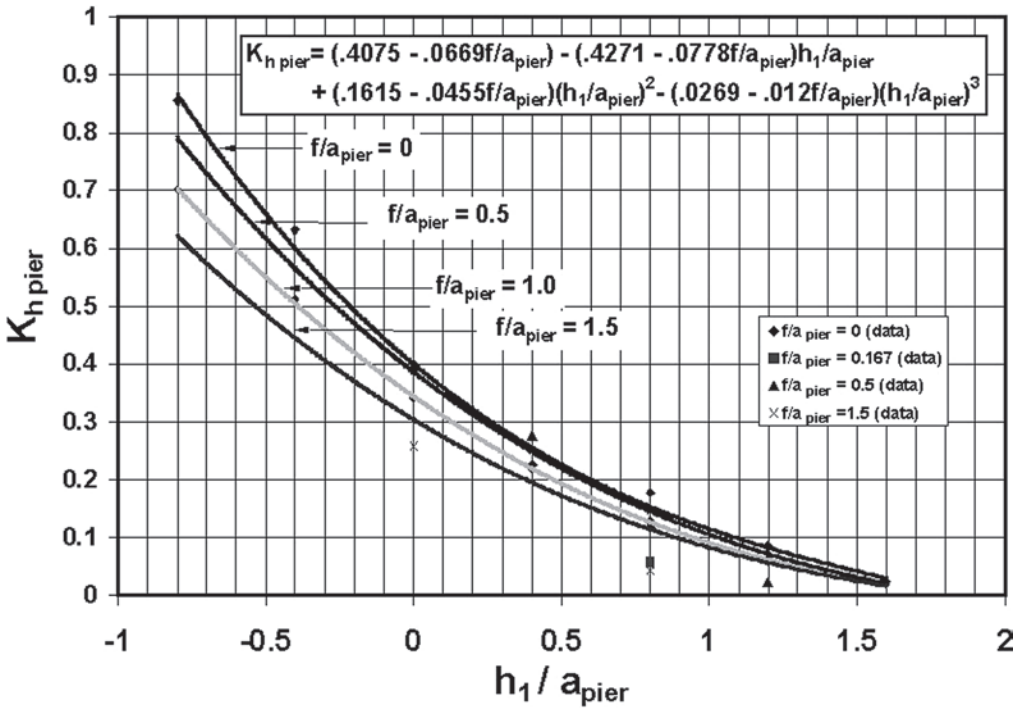

Fig. 10-9. Suspended pier scour ratio (Jones and Sheppard 2000; Richardson and Davis 2001).

to add the pile group scour as a third component in this case. If the bottom of the pile cap happened to be right on the bed, either the case 1 or case 2 method could be applied, but they would not necessarily give the same answers. If both methods are tried, then engineering judgment should dictate which one to accept.

Details for determining the pile cap or footing scour component for these two cases are described in the following paragraphs.

10.9.3.4.1 Case 1. Bottom of the Pile Cap (Footing) in the Flow above the Bed

T = thickness of the pile cap exposed to the flow, m (ft);
$h_2 = h_0 + y_{s\,pier}/2$, m (ft);
$y_2 = y_1 + y_{s\,pier}/2$, = adjusted flow depth, m (ft);
$V_2 = V_1(y_1 / y_2)$ = adjusted flow velocity, m/s (ft/s),

where

h_0 = original height of the pile cap above the bed, m (ft);
y_1 = original flow depth at the beginning of the computations before scour, m (ft);
$y_{s\,pier}$ = pier stem scour depth component, m (ft);
V_1 = original approach velocity at the beginning of the computations, m/s (ft/s).

Determine a^*_{pc} / a_{pc} from Fig. 10-10 as a function of h_2 / y_2 and T / y_2 (note that the maximum value of $y_2 = 3.5\, a_{pc}$).

Compute $a^*_{pc} = (a^*_{pc} / a_{pc})\, a_{pc}$ where a^*_{pc} is the width of the equivalent pier to be used in Eq. (10-12) and a_{pc} is the width of the original pile cap. Compute the pile cap scour component, $y_{s\,pc}$, from Eq. (10-12) using a^*_{pc}, y_2, and V_2 as the pier width, flow depth, and velocity parameters, respectively. The rationale for using the adjusted velocity for this computation is that the near-bottom velocities are the primary currents that produce scour and they tend to be reduced in the local scour hole from the overlying component. For skewed flow use the L/a for the original pile cap as the L/a for the equivalent pier to determine K_2. Apply the wide pier correction factor, K_w, if (1) the total depth $y_2 < 0.8\, a^*_{pc}$, (2) the Froude number $V_2 / (g\, y_2)^{1/2} < 1$, and (3) $a^*_{pc} > 50\, D_{50}$. The scour component equation for the case 1 pile cap can then be written

$$\frac{y_{s\,pc}}{y_2} = 2.0\, K_1\, K_2\, K_3\, K_4\, K_w \left(\frac{a^*_{pc}}{y_2}\right)^{0.65} \left(\frac{V_2}{\sqrt{g y_2}}\right)^{0.43} . \quad (10\text{-}24)$$

Next, the pile group scour component should be computed. This is discussed later.

10.9.3.4.2 Case 2. Bottom of the Pile Cap (Footing) Located on or below the Bed One limitation of the procedure described above is that the design chart in Fig. 10-10 has not been developed for the case of the bottom of the pile cap or footing being below the bed (i.e., negative values of h_2).

As for case 1,

$y_2 = y_1 + y_{s\,pier}/2$, m (ft);
$V_2 = V_1(y_1 / y_2)$, m/s (ft/s).

The average velocity of flow at the exposed footing (V_f) is determined using the following equation

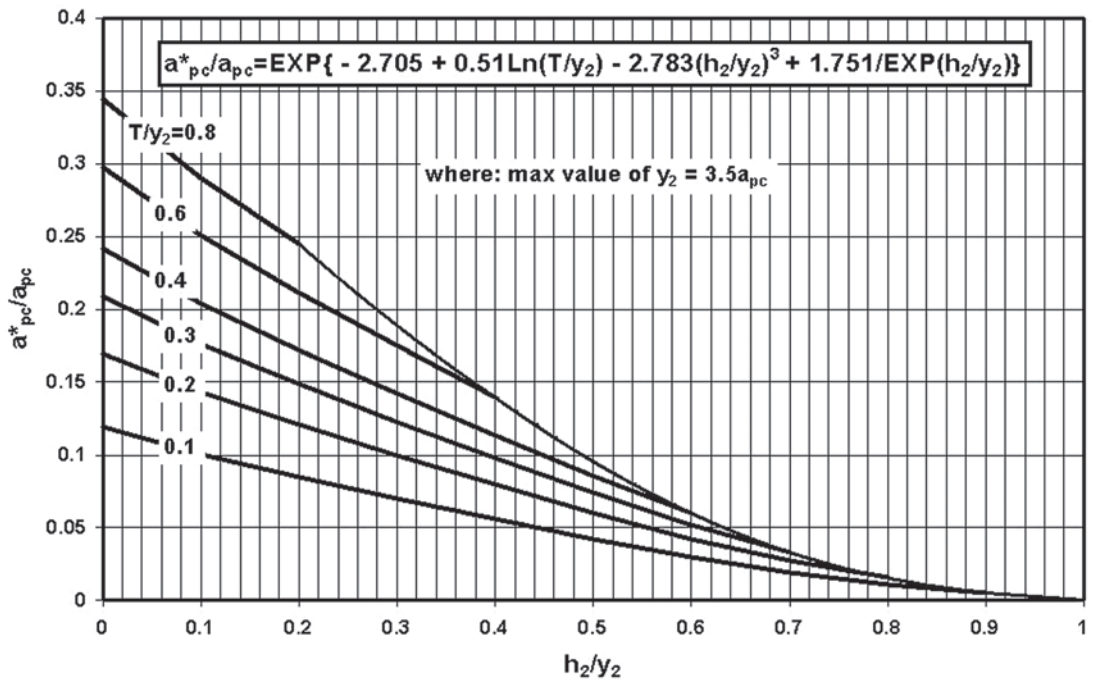

Fig. 10-10. Pile cap (footing) equivalent width (Jones and Sheppard 2000; Richardson and Davis 2001).

$$\frac{V_f}{V_f} = \frac{\ln\left(10.93\frac{y_f}{k_s} + 1\right)}{\ln\left(10.93\frac{y_2}{k_s} + 1\right)} \qquad (10\text{-}25)$$

where

V_f = average velocity in the flow zone below the top of the footing, m/s (ft/s);
V_2 = average adjusted velocity in the vertical of flow approaching the pier, m/s (ft/s);
In = log to the base *e* (natural log);
y_f = $h_1 + y_{s\,\text{pier}}/2$ = distance from the bed (after degradation, contraction scour, and pier stem scour) to the top of the footing, m (ft);
k_s = grain roughness of the bed (normally taken as D_{84} for sand-size bed material and 3.5 D_{84} for gravel and coarser bed material), m (ft);
y_2 = adjusted depth of flow upstream of the pier, including degradation, contraction scour, and half the pier stem scour, m (ft).

See Fig. 10-11 for an illustration of variables.

Compute the pile cap scour depth component $y_{s\,\text{pc}}$ from Eq. (10-12) using the full pile cap width a_{pc}, y_f, and V_f as the width, flow depth, and velocity parameters, respectively. The wide pier factor K_w should be used in this computation if (1) the total depth $y_2 < 0.8\ a_{\text{pc}}$, (2) the Froude, number $V_2 / (gy_2)^{1/2} < 1$, and (3) $a_{\text{pc}} > 50\ D_{50}$. Use y_2 / a_{pc} to compute the K_w factor if it is applicable. The scour component equation for the case 2 pile cap or footing can then be written

$$\frac{y_{s\,\text{pc}}}{y_f} = 2.0K_1K_2K_3K_4K_w\left(\frac{a_{\text{pc}}}{y_f}\right)^{0.65}\left(\frac{V_f}{\sqrt{gy_f}}\right)^{0.43} \qquad (10\text{-}26)$$

In this case assume the pile cap scour component includes the pile group scour and compute the total scour depth as

$$y_s = y_{s\,\text{pier}} + y_{s\,\text{pc}} \text{ (for case 2 only)} \qquad (10\text{-}27)$$

10.9.3.5 Determination of the Pile Group Scour Depth Component Research by Salim and Jones (1995; 1996; 1999) and by Smith (1999) has provided a basis for determining pile group scour depth by taking into consideration the spacing between piles, the number of pile rows, and a height factor to account for the pile length exposed to the flow. Guidelines are given for analyzing the following typical cases:

Piles aligned with each other and with the flow. No angle of attack.
Pile group skewed to the flow, with an angle of attack, or pile groups with staggered rows of piles.

The strategy for estimating the pile group scour component is the same for both cases, but the technique for determining the projected width of piles is simpler for the special case of aligned piles. The strategy is as follows:

Project the width of the piles onto a plane normal to the flow.

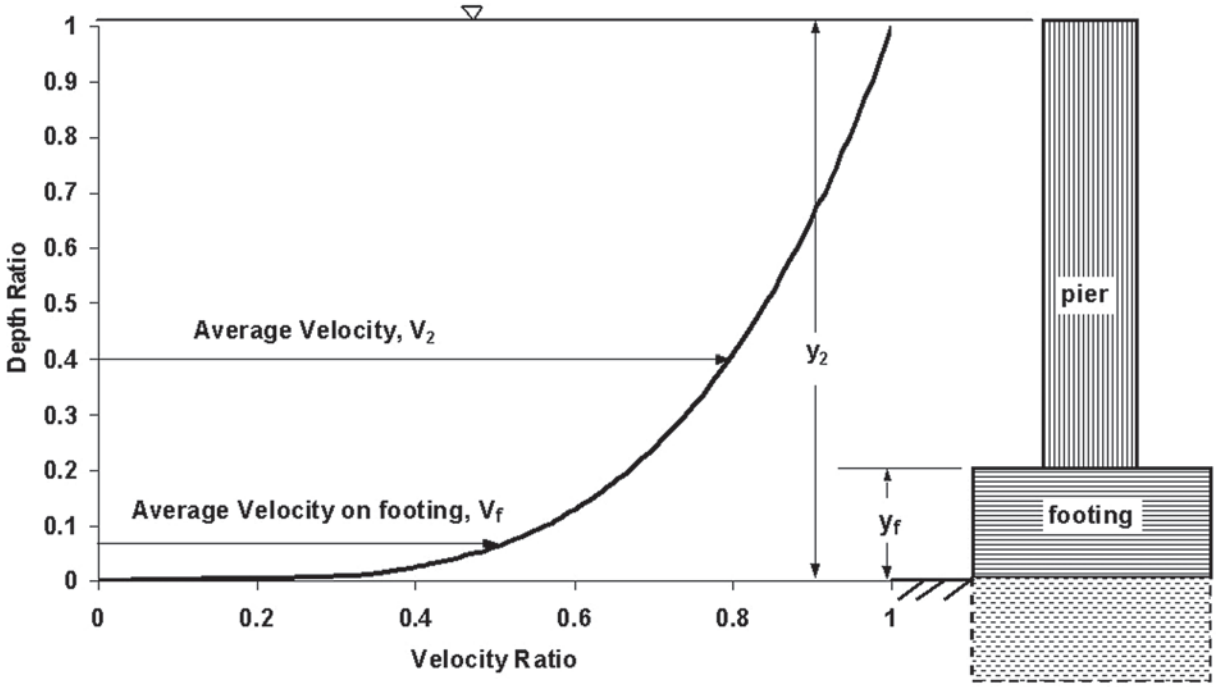

Fig. 10-11. Definition sketch for velocity and depth on exposed footing (Richardson and Davis 2001).

Determine the effective width of an equivalent pier that would produce the same scour if the pile group penetrated the water surface.

Adjust the flow depth, velocity, and exposed height of the pile group to account for the pier stem and pile cap scour components previously calculated.

Determine the pile group height factor based on the exposed height of the pile group above the bed.

Compute the pile group scour component using a modified version of Eq. (10-12).

10.9.3.5.1 Projected Width of Piles For piles aligned with the flow, the projected width, a_{proj}, onto a plane normal to the flow is simply the width of the collapsed pile group as illustrated in Fig. 10-12.

Pile groups not aligned to the flow are represented by an equivalent solid pier that has an effective width, a^*_{pg}, equal to a spacing factor multiplied by the sum of the nonoverlapping projected widths of the piles onto a plane normal to the flow direction (Smith 1999). The projected width can be determined by sketching the pile group to scale and projecting the outside edges of each pile onto a projection plane as illustrated in Fig. 10-13 or by systematically calculating coordinates of the edges of each pile along the projection plane. The coordinates are sorted in ascending order to facilitate inspection to eliminate double counting of overlapping areas. Additional experiments are being conducted at the FHWA hydraulics laboratory to test simpler techniques for estimating the effective width, but currently Smith's summation technique is a logical choice.

Smith attempted to derive weighting factors to adjust the impact of piles according to their distance from the projection plane, but concluded that there were not enough data and the procedure would become very cumbersome with weighting factors. A reasonable alternative to using weighting factors is to exclude piles other than the two rows and one column closest to the plane of projection, as illustrated in Fig 10-13.

10.9.3.5.2 Effective Width of an Equivalent Full Depth Pier The effective width for an equivalent full depth pier is the product of the projected width of piles multiplied by a spacing factor and a number of aligned rows factor (used for the special case of aligned piles only),

$$a^*_{pg} = a_{proj} K_{sp} K_m \qquad (10\text{-}28)$$

where

a_{proj} = sum of nonoverlapping projected widths of piles (see Figs 10-12 and 10-13);
K_{sp} = coefficient for pile spacing (Fig 10-14)
K_m = coefficient for number of aligned rows, m, (Figure 10-15 — note that K_m is constant for all S/a values when there are more than six rows of piles)
K_m = 1.0 for skewed or staggered pile groups.

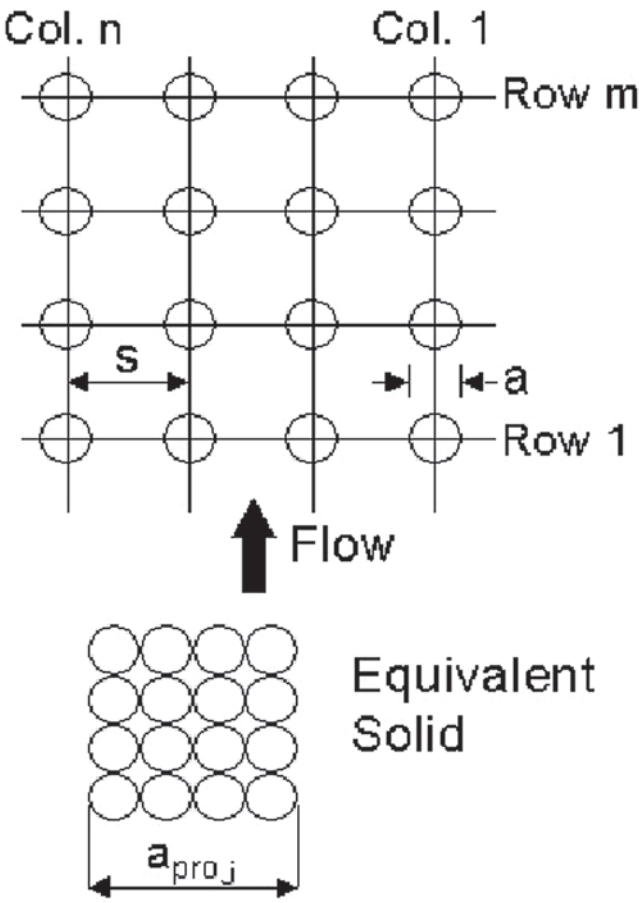

Fig. 10-12. Projected width of piles for flow aligned with the piles (Richardson and Davis 2001).

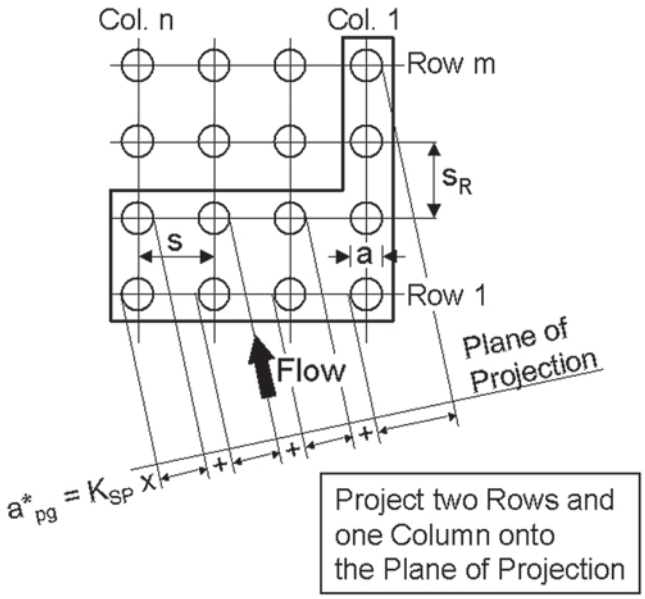

Fig. 10-13. Projected width of piles for skewed flow (Richardson and Davis 2001).

The number of rows factor, K_m, is 1.0 for the general case of skewed or staggered rows of piles because the projection technique for skewed flow accounts for the number of rows and is already conservative for staggered rows.

10.9.3.5.3 Adjusted Flow Depth and Velocity The adjusted flow depth and velocity to be used in the pier scour equation are as follows:

$$y_3 = y_1 + y_{s\,\text{pier}} / 2 + y_{s\,\text{pc}} / 2, \text{ m (ft)} \quad (10\text{-}29)$$

$$V_3 = V_1 (y_1/y_3), \text{ m/s (ft/s)} \quad (10\text{-}30)$$

The scour equation for a pile group can then be written as

$$\frac{y_{s\,\text{pg}}}{y_3} = K_{h\,\text{pg}} \left[2.0 K_{10} K_3 K_4 K_w \left(\frac{a^*_{\text{pg}}}{y_3} \right)^{0.65} \left(\frac{V_3}{\sqrt{g y_3}} \right)^{0.43} \right] \quad (10\text{-}31)$$

where

$K_{h\,\text{pg}}$ = pile group height factor given in Fig 10-16 as a function of h_3 / y_3 (note that the maximum value of $y_3 = 3.5\ a^*_{\text{pg}}$);

$h_3 = h_0 + y_{s\,\text{pier}} / 2 + y_{s\,\text{pc}} / 2$ = height of pile group above the lowered stream bed after pier and pile cap scour components have been computed, m (ft).

K_2 from Eq. (10-12) has been omitted because pile widths are projected onto a plane that is normal to the flow. The quantity in the square brackets is the scour ratio for a solid pier of width a^*_{pg}, if it extended to the water surface. This is the scour ratio for a full depth pile group.

In many complex piers, the pile groups have different numbers of piles in rows or columns, the spacing between piles is not uniform, and the widths of the piles may not all be the same. An estimate of the scour depth can be obtained using the methods and equations in this section. However, again it is recommended that a physical model study be conducted to arrive at the final design and to determine the scour depths.

Engineering judgment must be used if debris is considered a factor, in which case it would be logical to treat the pile group and debris as a vertical extension of the pile cap and to compute scour using the case 2 pile cap procedure described previously.

In cases of complex pile configurations where costs are a major concern or where significant savings are anticipated, and/or for major bridge crossings, physical model studies are still the best guide. Nevertheless, the equations and methods described in this section provide a good calculation of the scour depth.

10.9.4 Multiple Columns Skewed to the Flow

Scour depth for multiple columns skewed to the flow (as illustrated as a group of cylinders in Fig. 10–7) depends on the spacing between the columns. The correction factor for angle of attack would be smaller than that for a solid pier. How much smaller is not known. Raudkivi (1986), in discussing effects of alignment, states that "the use of cylindrical

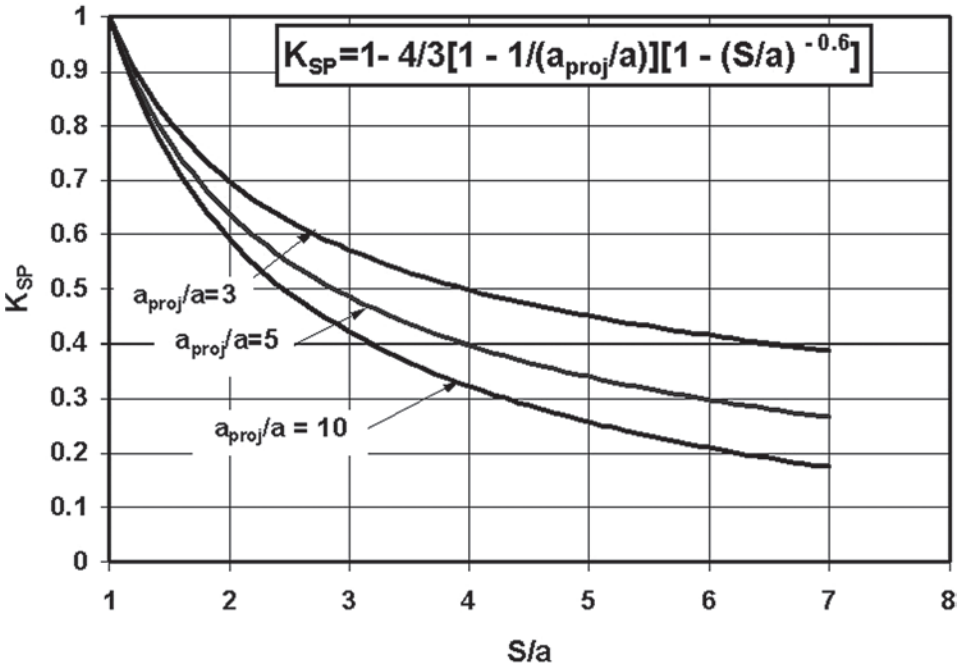

Fig. 10-14. Pile spacing factor (D.M. Sheppard, unpublished design procedure, University of Florida, 2001).

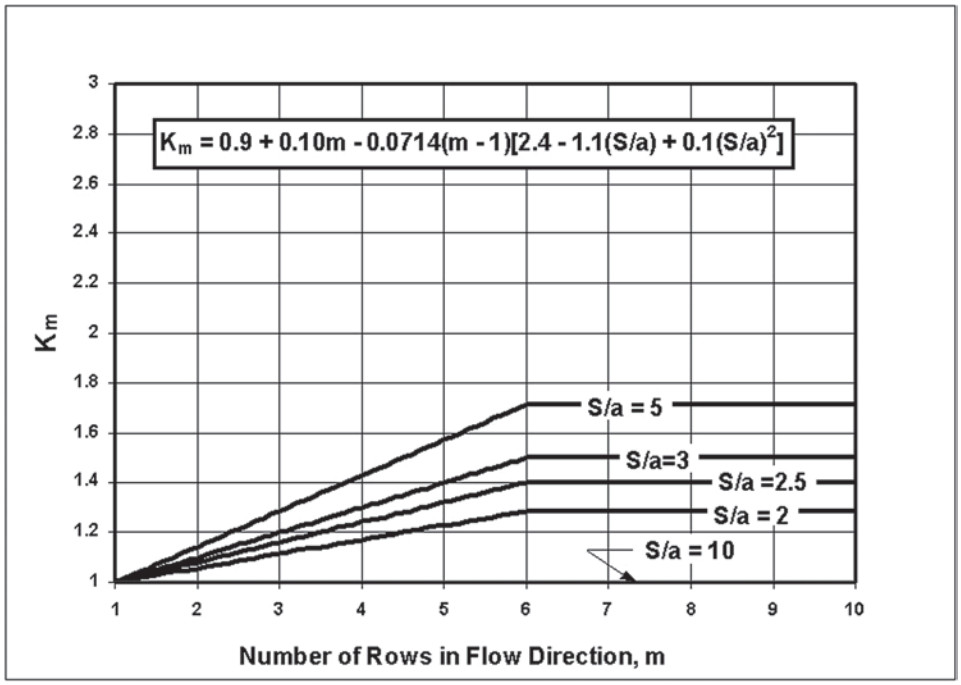

Fig. 10-15. Adjustment factor for number of aligned rows of piles (D.M. Sheppard, unpublished design procedure, university of Florida, 2001).

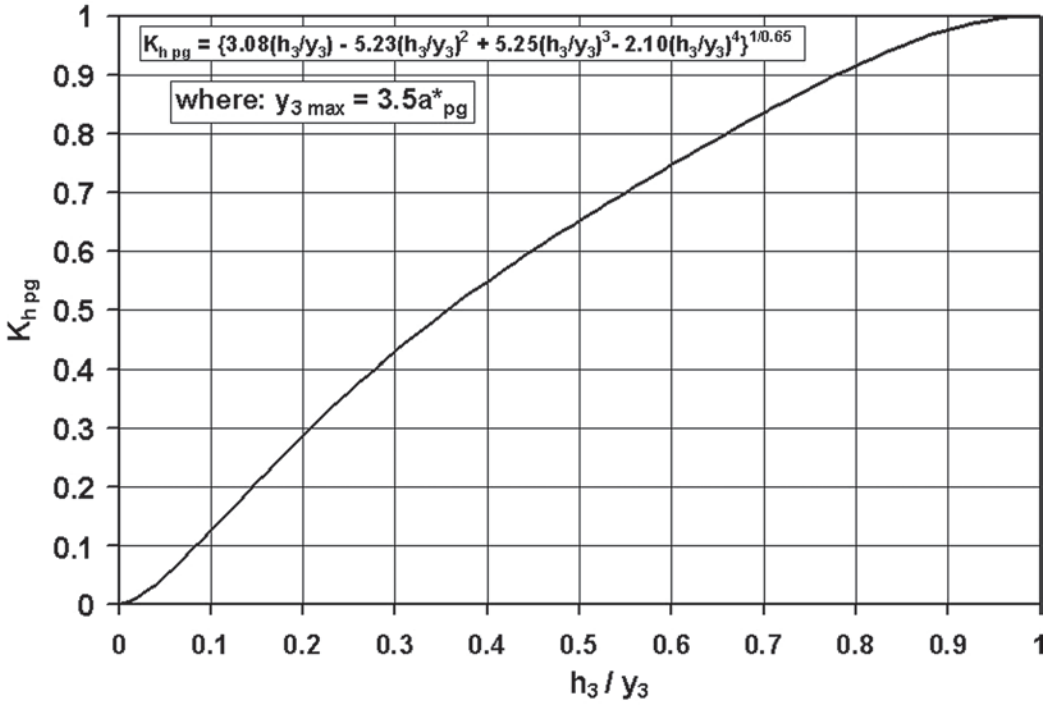

Fig. 10-16. Pile group height adjustment factor (D.M. Sheppard, unpublished design procedure, University of Florida, 2001).

columns would produce a shallower scour; for example, with five-diameter spacing between columns the local scour can be limited to about 1.2 times the local scour at a single cylinder." Thus for multiple columns spaced five diameters or more apart and at an angle, Richardson and Davis (2001) recommend that the local scour depth can be taken as 1.2 times the local scour depth at a single column.

For multiple columns spaced less than five pier diameters apart, the pier width "a" is the total projected width of all the columns in a single row, normal to the flow angle of attack. This composite pier width would be used in Eq. (10-12) to determine depth of pier scour. The correction factor K_1 would be 1.0 regardless of column shape. The coefficient K_2 would also be equal to 1.0 because the effect of skew would be accounted for by the projected area of the piers normal to the flow (Richardson and Davis 2001).

The depth of scour for a multiple column bent will be analyzed in this manner except in addressing the effect of debris lodged between columns. If debris is evaluated, it would be logical to consider the multiple columns and debris as a solid elongated pier.

Additional laboratory studies are necessary to provide guidance on the limiting flow angles of attack for a given distance between multiple columns, beyond which multiple columns can be expected to function as solitary members with minimal influence from adjacent columns.

10.9.5 Pressure Flow Scour

Pressure flow, which is also denoted as orifice flow, occurs when the water surface at the upstream face of the bridge is greater than or equal to the low chord of the bridge superstructure and the water is in significant contact with the bridge deck. At higher approach flow depths, the bridge can be entirely submerged, with the resulting flow being a complex combination of plunging flow under the bridge (orifice flow) and flow over the bridge (weir flow). In many cases, when a bridge is submerged, flow will also overtop adjacent approach embankments. Hence, for any overtopping situation, the total weir flow can be subdivided into weir flow over the bridge and weir flow over the approach. Weir flow over approach embankments and the bridge reduces the discharge that passes under the bridge.

With pressure flow, the local scour depths at a pier or abutment may be larger than those for free surface flow with similar depths and approach velocities. The increase in local scour at a pier subjected to pressure flow results from vertical contraction scour and local pier scour caused by the horseshoe vortex (Jones et al. 1993). However, sometimes when a bridge becomes submerged, the average velocity under the bridge is reduced due to a combination of additional backwater caused by the bridge superstructure impeding the flow, and a reduction of the discharge that passes under the bridge due to weir flow over the bridge and approach embankments. As a consequence scour depths are reduced.

Abed (Abed 1991; Abed et al. 1991), from a limited clear-water flume study at Colorado State University, stated that pressure flow could increase pier scour depths by 2.3 to 10 times. These results were obtained by comparison of scour depths for free surface and pressure flow simulations with similar hydraulic characteristics.

Jones (Jones et al. 1993; 1996; Richardson and Lagasse 1999, p. 288), in clear-water pressure flow studies at FHWA's Turner-Fairbank Research Center, found that (1) local pier scour with pressure flow has two components; (2) one component is vertical contraction scour caused by the bridge superstructure and the other is local pier scour caused by the pier obstructing the flow; (3) the magnitude of the local pier scour with pressure flow is approximately the same as for free surface flow; and (4) the two components are additive.

Arneson (1997; Arneson and Abt 1998), in a comprehensive live-bed flume study of pressure flow scour sponsored by the FHWA, verified Jones's findings. Equation (10-12) is used to determine the local pier scour component caused by the pier obstructing the flow. For the vertical contraction pier scour component additional research is needed.

10.10 SCOUR DEPTHS WITH DEBRIS ON PIERS

Debris lodged on a pier usually increases local scour at the pier. The debris may increase pier width, and local velocity and deflect the flow downward. This increases the transport of sediment out of the scour hole. When floating debris is lodged on the pier, the scour depth is estimated by assuming that the pier width is larger than the actual width. The problem is in determining the increase in pier width to use in the pier scour equation. Furthermore, at large depths, the effect of the debris on the scour depths should diminish. Also, debris lodged on piers and abutments can deflect the flow against another pier or abutment, resulting in very large angles of attack and larger velocities. This may be worse than the scour at the pier or abutment with the debris.

As with estimating local scour depths with pressure flow, only limited research has been done on local scour with debris. Melville and Dongol (1992) have conducted a limited quantitative study of the effect of debris on local pier scour and have made some recommendations. However, additional laboratory studies will be necessary to better define the influence of debris on local scour.

10.11 JAIN AND FISHER'S EQUATION

Jain and Fisher (1979) studied local pier scour at large Froude numbers in the laboratory. They found that live-bed scour at a circular pier first slightly decreased and then increased with the increase in the Froude number. Live-bed scour depths at

high Froude numbers are larger than the maximum clear-water scour. The contribution of bed-form scour to the total scour depth in the upper flow regime becomes significant with higher flow velocities. They developed the following two equations:

For live-bed scour $(\mathsf{F} - \mathsf{F}_c) > 0.2$,

$$y_s/a = 2.0(\mathsf{F}-\mathsf{F}_c)^{0.25}\left(y_1/a\right)^{0.5}. \tag{10-32}$$

For clear-water scour, $(\mathsf{F} - \mathsf{F}_c) \le 0.2$,

$$y_s/a = 1.84(\mathsf{F}_c)^{0.25}(y_1/a)^{0.3} \tag{10-33}$$

where

F_c = Froude number for beginning of motion, $V_c/(gy_1)^{½}$) of the D_{50} size of the bed material.

The other variables are as defined previously.

They determined the critical velocity for the beginning of motion using a procedure based on Einstein's (1950) logarithmic velocity equations. His equations are given by Richardson et al, (1990) as follows:

1. Determine the median diameter, D_{50}, of the bed material, m, ft;
2. Determine τ_c from Shield's relation, N/m^2, lb/ft^2;
3. Compute $U_*c = (\tau_c/p)^{0.5}$, m/s, ft/s;
4. Compute $V_c = U_* c\,[(2.5 \ln (12.27\, y\, X/D_{65})]$, m/s, ft/s;
5. Assume χ is 1.0, i.e., hydraulically rough flow;
6. Compute $\mathsf{F}_c = V_c / (gy_1)^{0.5}$.

The equation given in Section 10.6 can also be used to determine the critical velocity.

They also recommended that the scour depth for $0 < (\mathsf{F} - \mathsf{F}_c) < 0.2$ can be assumed equal to the larger of the two values of scour obtained from Eqs. 10-29 and 10-30. For shapes different from circular piers and pier alignment other than parallel with the flow direction, multiply the results given by Jain and Fisher's equations by the coefficients given in Tables 10-1 and 10-2.

10.12 MELVILLE'S EQUATION

Mellville (1997) gave the following equation for computing local scour depths at piers

$$y_s = K_1\, K_2\, K_{ya}\, K_i\, K_D \tag{10-34}$$

where

y_s = depth of scour, m;
K_1 = correction for pier nose shape from Figure 10-7 and Table 10-1;
K_2 = correction for flow angle of attack from Eq. (10-15);
K_{ya} = flow depth-pier size expression

$$K_{ya} = 2.4a, \text{ if } y/a < 0.7$$
$$K_{ya} = 2\sqrt{y_1 a},\ 0.7 < \frac{a}{y_1} < 5 \tag{10-35}$$
$$K_{ya} = 4.5y_1, \frac{a}{y_1} > 5$$

K_i = flow intensity factor

$$K_i = \frac{V_1 - (V_a - V_c)}{V_c}, \text{ if } \frac{V_1(V_a - V_c)}{V_c} < 1$$
$$K_i = 1, \text{ if } \frac{V_1 - (V_a - V_c)}{V_c} \ge 1 \tag{10-36}$$

K_D = sediment size factor

$$K_D = 1.0, \quad \text{if } a/D_{50} > 25$$
$$K_D = 0.57\log\left(2.24a/D_{50}\right), \quad \text{if } a/D_{50} \le 25 \tag{10-37}$$

V_1 = mean approach velocity, m/s;
V_a = mean approach velocity at the armor peak = 0.8 V_{ca}, m/s;
V_c = critical velocity at beginning of motion, m/s.

Melville gives the equation

$$\frac{V_c}{V_{*c}} = 57.5\ \log\left(5.53\frac{y_1}{D_{50}}\right) \tag{10-38}$$

where

V_{ca} = maximum mean approach velocity for armoring of the channel bed to occur, m/s.

Mellville gives the equation

$$\frac{V_{ca}}{V_{*ca}} = 57.5\log\left(5.53\frac{y_1}{D_{50a}}\right) \tag{10-39}$$

where

V_{*c} = critical shear velocity for the D_{50} defined by the Shield's relation, m/s;
V_{*ca} = critical shear velocity for the D_{50a} defined by the Shield's relation, m/s;
D_{50a} = median armor size, m, where $D_{50a} = D_{max}/1.8$;
D_{max} = maximum bed material size, m.

Melville gives as an approximation to the Shield's diagram for quartz sediment in water at 20ºC the following,

$$V_{*c} = 0.0115 + 0.0125D^{1.4}, 1\text{mm} < D < \phi.0.1\text{mm}$$
$$V_{*c} = 0.305D^{0.5} - 0.0065D^{-1},\ 1\text{mm} < D < 100\text{mm} \quad (10\text{-}40)$$

where V_{*c} or (V_{*ca}) is in m/s and $D = D_{50}$ or D_{50a} in mm.

10.13 OTHER PIER SCOUR EQUATIONS

Other pier scour equations and data sets are given by Jones (1983); Froehlich (1988); Johnson and Torrico (1994); Landers and Mueller (1996); Landers, et al. (1996); Mueller (1996); and Richardson and Lagasse (1999). Vanoni (1975) discusses pier scour and gives Laursen's equation.

10.14 TOP WIDTH OF PIER SCOUR HOLES

The top width of a scour hole in cohesionless bed material from one side of a pier or footing can be estimated from the equation (Richardson and Abed 1993; Richardson and Lagasse 1999; Richardson and Davis 2001)

$$W = y_s\left(K + \cot\theta\right) \quad (10\text{-}41)$$

where

- W = top width of the scour hole from each side of the pier or footing, m, ft;
- y_s = scour depth, m, ft;
- K = bottom width of the scour hole as a fraction of scour depth;
- θ = angle of repose of the bed material which ranges from about 30° to 44°.

If the bottom width of the scour hole is equal to the depth of scour y_s ($K = 1$), the top width in cohesionless sand will vary from 2.07 to 2.80 y_s. At the other extreme, if $K = 0$, the top width will vary from 1.07 to 1.8 y_s. Thus, the top width could range from 1.0 to 2.8 y_s and would depend on the bottom width of the scour hole and the composition of the bed material. In general, the deeper the scour hole, the smaller the bottom width. A top width of 2.0 y_s is suggested for practical application.

10.15 LOCAL SCOUR AT ABUTMENTS

Local scour at abutments has two components (see Fig. 10-4). One component is caused by a horizontal vortex that forms at the upstream end of the abutment and runs along the abutment toe. The other component is a vertical vortex that forms at the downstream end of the abutment when the flow separates and starts to expand. This vertical vortex erodes the downstream corner of the abutment and the downstream approach roadway. There are no equations available to determine the erosion caused by this downstream vortex. The abutment is protected from erosion caused by this vertical vortex by riprap or a short guidebank (Lagasse et al. 2001). The available equations are for the scour caused by the horizontal vortex.

Equations for predicting local scour depths at abutments are almost all based entirely on laboratory data. For example, equations by Laursen and Toch (1956), Liu et al. (1961), Laursen (1980), Froehlich (1989; 1989b), and Melville (1992; 1997) are based entirely on laboratory data. The problem is that few field data on abutment scour exist. Liu et al.'s equations were developed by dimensional analysis of the variables with a best-fit line drawn through the laboratory data. Laursen's equations are based on inductive reasoning on the change in transport relations due to the acceleration of the flow caused by the abutment. Froehlich's equation was derived from dimensional analysis and regression analysis of the available laboratory data. Melville's equations were derived from dimensional analysis and development of relations between dimensionless parameters using best-fit lines through laboratory data.

All equations in the literature, prior to 1993, were developed using the abutment and roadway approach length (L) as one of the variables and result in excessively conservative estimates of scour depth. As Richardson and Richardson (1992) and Richardson and Richardson (1998) point out in a discussion of Melville's (1992; 1997) papers and in a 1993 paper, the reason the equations in the literature predict excessively conservative abutment scour depths for the field situation is that, in the laboratory flume, the discharge intercepted by the abutment is directly related to the abutment length; whereas, in the field, this is rarely the case.

Figure 10-17 illustrates the difference. Thus, using the abutment length in the equations instead of the discharge returning to the main channel at the abutment results in a spurious correlation between abutment lengths and scour depth at the abutment end.

Abutment scour depends on the interaction of the flow obstructed by the abutment and roadway approach and the flow in the main channel at the abutment. Also, abutment scour depth depends on abutment shape, sediment characteristics, cross-sectional shape of the main channel at the abutment (especially the depth of flow in the main channel and the depth of the overbank flow at the abutment), velocity in the main channel and in the flow returning to the main channel at the abutment, and alignment. In addition, field conditions may have tree-lined or vegetated banks, low velocities, and shallow depths upstream of the abutment. Much of the research up to 1993 failed to replicate these field conditions. However, since 1993, research by Sturm et al., Young et al., Kouchakzadeh and Townsend, Chang and Davis, and Molinas et al. (Richardson and Lagasse

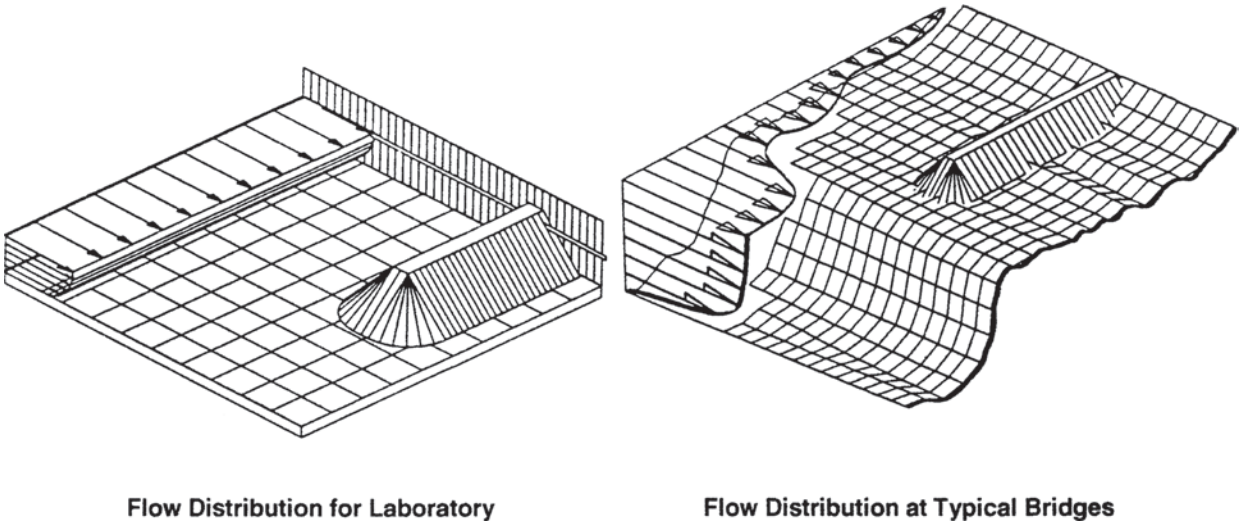

Fig. 10-17. Comparison of laboratory flow characteristics to field conditions (Richardson and Richardson 1998).

1999) has addressed the problem of using abutment length as the primary variable for the discharge intercepted by the abutment.

Therefore, engineering judgment is required in designing foundations for abutments. In many cases, foundations can be designed with shallower depths than predicted by the equations when the foundations are protected with rock riprap placed below the streambed and/or a guide bank placed upstream of the abutment (Richardson and Davis 2001). The design of guide banks is given by Lagasse et al. (2001).

10.15.1 Abutment Site Conditions

Abutments can be at the channel bank, be set back from the natural stream bank, or project into the channel. They can have various shapes and can be set at varying angles to the flow. Scour at abutments can be live-bed or clear-water scour. Finally, there can be varying amounts of overbank flow intercepted by the approaches to the bridge and returned to the stream at the abutment. More severe abutment scour will occur when the majority of overbank flow returns to the bridge opening directly upstream of the bridge crossing. Less severe abutment scour will occur when overbank flows gradually return to the main channel upstream of the bridge crossing.

10.15.2 Abutment Shape

There are three general shapes for abutments: (1) spill-through abutments, (2) vertical-wall abutments with wing walls, and (3) vertical walls without wing walls (Fig. 10-18). Depth of scour is approximately double for vertical-wall abutments as compared with spill-through abutments. In Table 10-4 coefficients for correcting scour equations for abutment shape (Froehlich, 1989) is given. However, recent research by Sturm (1999) on abutment scour in compound channels demonstrated that abutment shape is important for shorter abutments but detected no abutment shape effects as abutments increased in length and caused more contraction with encroachment on the main channel.

10.15.3 Skew Adjustment of Abutment Scour Depths

Figure 10-19 shows the effect of flow angle of attack on abutment scour (Ahmad 1953). As shown, an abutment or spur angled downstream decreases scour depth, whereas an abutment angled upstream into the flow increases scour depth.

10.15.4 Design for Scour at Abutments

The lack of adequate abutment scour equations (some equations are fundamentally wrong and/or overconservative) lead the Federal Highway Administration to recommend that in setting abutment foundation depths the potential for lateral migration, long-term degradation, and contraction scour should be considered. It is recommended that foundation depths for abutments be set at least 1.8 m below the stream bed, including long-term degradation and contraction scour, and rock riprap and/or guide banks should be used to protect the abutment. As a check on the potential scour depth they gave two equations to aid in design and placement of rock riprap (Richardson and Davis 2001).

In the following sections four equations are given. These equations are the result of recent research that properly uses the discharge obstructed by the abutment rather than abutment length. These are

- The Chang and Davis equation (Richardson and Lagasse 1999), which is based on the Laursen live-bed contraction scour equation.
- The Sturm (1999) equation for abutments in compound channels with variable setbacks from the main channel.

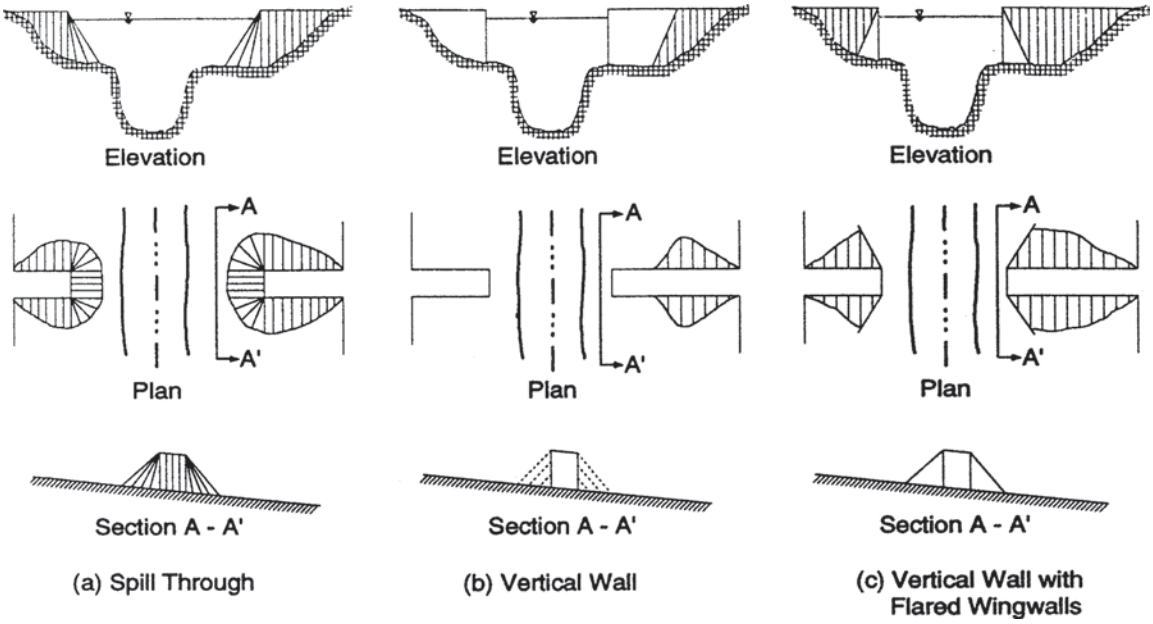

Fig. 10-18. Abutment shape.

- The Richardson and Trivino (1999) equation, based on momentum exchange.
- The Richardson et al. (1990) equation, based on Corps of Engineers data on scour at the end of spur dikes in the Mississippi River. It is recommended for use when abutment length divide by flow depth is greater than 25 ($L / y > 25$).

10.16 CHANG AND DAVIS ABUTMENT SCOUR EQUATION

Chang and Davis (Richardson and Davis 2001) present methods for computing local scour at abutments, developed for the Maryland Department of Transportation. Different equations and methods are given for live-bed and clear-water scour. The equations are adjustments to live-bed and clear-water contraction scour for the increase in local scour caused by the horizontal vortex at the abutment. Both equations are nondimensional and can be used for either English or SI units. In the process a computer program titled ABSCOUR was developed. Their equations are given in the following.

10.16.1 Live-Bed Abutment Scour

The equation is

$$\frac{y_{2a}}{y_1} = k_f \left(\frac{k_v \, q_2}{q_1} \right)^{K_2} \tag{10-42}$$

where

y_{2a} = total flow depth in the abutment scour hole after scour has occurred, measured from the water surface to the bottom of the scour hole, m (ft);
y_1 = approach flow depth, m (ft);

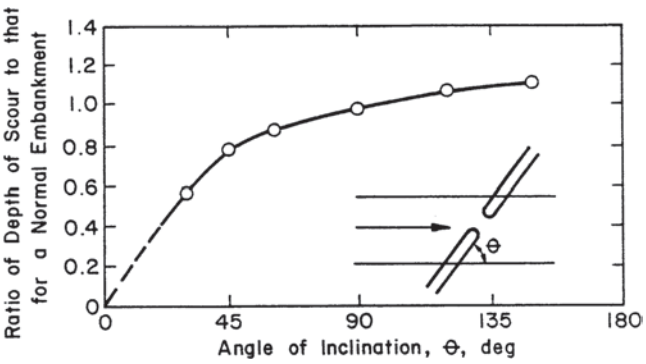

Fig. 10-19. Adjustment of abutment scour estimate for skew (Ahmad 1953).

Table 10-4 Abutment Shape Coefficients (Froehlich 1989)

Description	K_1
Vertical-wall abutment	1.00
Vertical-wall abutment with wing walls	0.82
Spill-through abutment	0.55

q_1 = flow rate per unit width in the approach section, $m^3/s/m$ ($ft^3/s/ft$);
q_2 = flow rate per unit width in contracted section, $m^3/s/m$($ft^3/s/ft$) (determination of q_1 and q_2 is explained in a section);
k_v = $0.8\ (q_1 / q_2)^{1.5} + 1$;
k_f = $0.1 + 4.5\ F_1$ for clear-water scour;
k_f = $0.35 + 3.2\ F_1$ for live-bed scour.

Equation (10-42) applies to live-bed scour. It can be used for clear-water scour only for the condition where the shear stress in the approach section (Section 1) is at the critical value.

Values of k_v should range from 1.0 to 1.8. If the calculated value is smaller or larger than this range, use the limiting value.

Values of k_f should range from 1.0 to 3.3. If the calculated value is smaller or larger than this range, use the limiting value.

The Froude number in the approach section, Section 1, $F_1 = V_1/(gy_1)^{0.5}$, where V_1 = average flow velocity in the approach floodplain or channel section (m/s or ft/s) and y_1 = average flow depth in the approach floodplain or channel section (m or ft).

Laursen's sediment transport function for K_2 is

$$K_2 = 0.11\ (\tau_c/\tau_1 + 0.4)^{2.2} + 0.623 \qquad (10\text{-}43)$$

where

τ_c = critical shear stress of soil, N/m^2 (lb/ft^2);
τ_1 = shear stress at approach section, Section 1, N/m^2 (lb/ft^2), $\tau_1 < \tau_c$. The value of K_2 varies from 0.637 to 0.857. $\tau_c \geqslant \tau_1$, select a value of K_2 equal to 0.857.

Chang (personal communication 2000) determined that, although K_2 in Eq. (10-35) is based on a concept similar to K_1 in the table accompanying the live-bed contraction scour equation, (10-1), the values of these coefficients are derived in different ways and cannot be mathematically correlated.

10.16.2 Clear-Water Abutment Scour

Clear-water scour occurs if the shear stress in the approach section, Section 1, is less than critical, or if the approach section is armored. The clear-water abutment scour equation is

$$y_{2a} = k_f\ (k_v)^{0.857}\ y_{2c} \qquad (10\text{-}44)$$

where

y_{2a} = total depth of flow at the abutment, measured from the water surface down to the bottom of the abutment scour hole, m (ft);
y_{2c} = clear-water contraction scour depth in the channel or on the floodplain (beyond the abutment scour hole) at critical velocity $y_{2c} = q_2 / V_c$, m (ft) (Eq. 10-11) or similar equations can be used to compute V_c. Another approach would be to compute y_{2c}, the clear-water contraction scour, from Eq. (10-7) or (10-8);
k_f and k_v = dimensionless coefficients as defined in the discussion of live-bed scour.

10.17 STURM ABUTMENT SCOUR EQUATION

Sturm (1999) evaluated abutment scour using a flume with a compound channel. He determined that a discharge distribution factor (M) is a better measure of the effect of abutment length on the flow redistribution and abutment scour. His resurch resulted in an equation for clear-water scour around setback and bankline abutments and for live-bed scour around bankline abutments. His equations are given in the following discussions.

10.17.1 Clear-Water Scour

Sturm's clear-water abutment scour equation is

$$y_s / y_{fo} = 8.14\ K_{st}\ (q_{fl} / MV_{xc}\ y_{fo} - 0.47) + \mathrm{FS} \qquad (10\text{-}45)$$

where

y_s = depth of scour at the abutment, m;
y_{fo} = average depth of flow on the floodplain at the approach section for existing conditions based on normal flow conditions in the river without backwater from the proposed bridge, m;
K_{st} = abutment shape factor given below;
q_{fl} = unit flow rate on the approach floodplain section that will be blocked by the embankment at Section 2 (The conditions are based on the proposed structure in place and creating backwater effects at the approach section), m^3/s /m;
M = discharge distribution factor $= (Q_{1/2\ \text{channel}} + Q_{\text{floodplain}} - Q_{\text{blocked flow}}) / (Q_{1/2\,\text{channel}} + Q_{\text{floodplain}})$— $Q_{1/2\ \text{channel}}$ is the discharge from the centerline to the bank of the main channel in the approach section, $Q_{\text{floodplain}}$ is the floodplain discharge in the approach section, and $Q_{\text{blocked flow}}$ is the floodplain discharge blocked by the embankment in the approach section;
V_{xc} = critical velocity at the approach floodplain section for existing conditions based on normal flow conditions in the river without backwater from the

proposed bridge, m/s (use Eq. (10-10) or (10-11) and the D_{50} of the bed material);
FS = factor of safety, with a recommended value of 1.0;
K_{st} = 1.0 for vertical wall abutments.

For spillthrough abutments K_{st} is as follows:

$K_{st} = 1.52\,(K_a - 0.67)/(K_a - 0.40)$ where $0.67 \leq K_a \leq 1.2$
1.0 where $K_a > 1.2$
0.0 where $K_a < 0.67$

$$K_a = q_{fl} / (M \times V_{xc} \times y_{f0}) \quad (10\text{-}46)$$

10.17.2 Live-Bed Scour around Bankline Abutments

Sturm's live-bed abutment scour equation around bankline abutments is

$$y_s / y_{f0} = 2.0 K_{st} [q_{ml} / (M V_{m0c}\, y_{f0}) - 0.47] + \text{FS} \quad (10\text{-}47)$$

where

y_s = depth of scour at the abutment, m (ft);
y_{f0} = average depth of flow on the floodplain (Step 5), m (ft);
K_{st} = 1.0;
q_{ml} = unit flow rate in the main channel at the approach section 1 for the approach critical velocity, i.e., $(V_{m1c} \times y_{m1})$, m^3/s/m (cfs/ft);
M = discharge distribution factor as defined above;
V_{m0c} = critical velocity in the main channel for unconstricted flow at depth y_{m0}, m/s (ft/s);
FS = factor of safety, with a recommended value of 1.0.

Note that Eq. (10-47) is based on experimental results for clear-water scour around bankline abutments. Its extension to the live-bed case by assuming threshold live-bed scour is tentative at this time.

10.18 RICHARDSON AND TRIVINO ABUTMENT SCOUR EQUATION

Using a regression technique developed by Box and Tidwell (1962), Richardson and Trivino (1999) regressed approximately 160 clear-water scour data compiled by Froehlich (1989); Lim (1993; 1997); and a field measurement of abutment scour obtained during the 1993 Missouri–Mississippi River flood. The last was an 18.3-m (60-ft)-deep abutment scour hole near the right abutment of the 1-70 Bridge over the Missouri River, near Columbia, MO (Brian Hefner, Hydraulic Section, Missouri Department of Transportation, Bridge Inspection File for Interstate 70 near Rocheport; Missouri, personal communication, 1999). A hydraulic study by Greble (1999) noted that the 2,060-m (6,760-ft)-long approach embankment cut off nearly 80% of the estimated 9,900 m^3/s (349,700 cfs) floodplain discharge. The equation is

$$\frac{y_s}{y_1} = 0.02K_1^{-6.81} + 7.47\mathsf{F}^{1.60} + 1.68\left(\frac{L}{y_1}\right)^{0.41} - 3.32\left(\frac{M_1}{M_2}\right)^{2.46} - 335\left(\frac{D_{50}}{y_1}\right)^{1.66} - 1.41 \quad (10\text{-}48)$$

where

y_s = the depth of abutment scour, m (ft);
y_1 = the unscoured average flow depth on the overbank (near the abutment end), m (ft);
K_1 = the coefficient for abutment shape (as previously defined), m (ft);
F = the Froude number of the approach flow unobstructed by the abutment;
L = the length the approach embankment projects into the floodplain, m (ft);
D_{50} = the median grain size of the bed material, m (ft);
M_1 = the momentum of the flow intercepted by the abutment and approach (Eq. (10-48));
M_2 = the momentum of the flow in the bridge opening (Eq. (10-49)).

M_1/M_2 is the momentum ratio of the flow that is mixed near the abutment end, which causes the horizontal vortex and abutment scour:

$$M_1 = \rho\, Q_1\, V_1 \quad (10\text{-}49)$$

$$M_2 = \rho\, Q_2\, V_2 \quad (10\text{-}50)$$

Where

ρ = mass density of water;
Q_1 = overbank discharge cutoff by the abutment and approach one bridge length upstream, m^3/s (cfs);
Q_2 = discharge in the constricted section (bridge section), m^3/s (cfs)—for an abutment set back from the main channel it is the discharge between the end of the abutment and the channel bank, whereas for abutments at the channel bank or projecting into the main channel it is the total discharge in the bridge section;
V_1 = average overbank velocity of the flow cutoff by the abutment and approach embankment one bridge length upstream of the bridge (corresponding to Q_1), m/s (ft/s);
V_2 = average velocity of the flow in the constricted (bridge section corresponding to Q_2), m/s (ft/s).

Equation (10-48), for Froehlich's and Lim's data set, has a computed R^2 equal to 0.895. The standard error, S_e, of estimating d_s/d_1 was 0.48. In comparison, the S_e was computed to be 1.12 and 1.98 for Froehlich's and Lim's equation when applied to the same data set. It accurately predicted the actual y_s/y_1 of 3.9 for the I-70 scour hole. This contrasts with y_s/y_1 values of 6.4 and 17.8 using Froehlich's and Lim's equation respectively. When Eq. (10-47) was applied to a set of 37 complex laboratory channel data documented by Sturm (1998) and Sturm and Janjua (1994), the standard error of estimate (S_e) was 0.89. S_e was likely greater due to the relatively small sample size. Considering all of the data, the S_e was only slightly higher ($S_e = 0.56$).

A separate Box-Tidwell regression without the L/d_1 term produced good agreement with the Missouri River data, but the correlation with the flume data was poor. This was not surprising because the flume experiments were performed using the approach and abutment length as the primary variable, not the momentum or discharge ratios. Also, at small laboratory scales the momentum ratio is small and has a minimal influence on the resulting dependent variable. At larger scales, the influence of the momentum ratio, M_1 / M_2 is more important than the L / y_1. Because of its importance in the data set, the L / y_1 was retained in the formulation. The sensitivity of the dependent variable (y_s / y_1) to L / y_1 is significantly less than for other formulations involving the ratio of abutment length to flow depth.

Due to the manner in which the equation was formulated, Eq. (10-48) is applicable to conditions in which the abutment is set back from the main channel. All of the data used to develop the equation was for approach embankments normal to the average flow direction, and therefore no correction for abutments angled to the flow is incorporated into the equation. However, for abutments at an angle to the flow, the length L should be adjusted to its normal length and Fig. 10-19 used to correct the scour depths. As with all other existing abutment scour equations, the equation has not been thoroughly verified for field conditions.

10.19 RICHARDSON ET AL. EQUATION FOR $L/y > 25$

Richardson et al. (1990, 2001) give an equation developed using Corps of Engineers field data on scour at the end of spurs in the Mississippi River. This field situation closely resembles the laboratory experiments for abutment scour in that the discharge intercepted by the spurs was a function of the spur length. This is recommended when the ratio of projected abutment length (L) to flow depth (y_1) is greater than 25. This equation can be used to estimate scour depth (y_1) at an abutment where conditions are similar to the field conditions from which the equation was derived,

$$\frac{y_s}{y_1} = 4F_1^{0.33}\frac{K_1}{0.55} \qquad (10\text{-}51)$$

where

y_s = scour depth, m, ft;
y_1 = depth of flow at the abutment, on the overbank or in the main channel, m, ft;
F_1 = Froude number based on the velocity and depth adjacent to and upstream of the abutment;
K_1 = abutment shape coefficient, from Table 10-6.

To correct Eq. (10-51) for abutments skewed to the stream use Fig. 10-19.

10.20 COMPUTER MODELS

The hydraulic routines of computer models WSPRO (Shearman 1987) or HEC-RAS (USACE 2001), can determine the one-dimensional flow variable for use in the determination of scour depths at a bridge. These models determine average flow depths and velocities over a roadway and bridge, as well as average velocities and depths approaching and under the bridge.

10.21 STREAM INSTABILITY

Streams are dynamic. Areas of flow concentration continually shift bank lines. In meandering streams having an S-shaped planform, the channel moves both laterally and downstream. A braided stream has numerous channels that are continually changing. In a braided stream, the deepest natural scour occurs when two channels come together or when the flow comes together downstream of an island or bar. This scour depth has been observed to be one to two times the average flow depth (Northwest Hydraulic Consultants Ltd., personal communication, 1973; Richardson and Davis 2001).

A bridge is static. It fixes a stream at one place in time and space. A meandering stream whose channel moves laterally and downstream into the bridge reach can erode the approach embankment and affect contraction and local scour because of changes in flow direction. A braided stream can shift under a bridge and have two channels come together at a pier or abutment, increasing scour. Descriptions of stream morphology are given by Schumm (1977), Lagasse et al., (2001), and Richardson et al. (2001), among others.

Factors that affect lateral shifting of a stream and the stability of a bridge are the geology and geomorphology of the stream, the location of the crossing on the stream, flood characteristics, the characteristics of the bed and bank material, and wash load.

It is difficult to anticipate when a change in planform may occur. It may be gradual with time or the result of a major flood. Also, the direction and magnitude of the movement of the stream are not easily determined. It is difficult to evaluate the vulnerability of a bridge properly due to changes in

planform. It is important to incorporate potential planform changes into the design of new bridges and design of countermeasures for existing bridges.

Countermeasures for lateral shifting and instability of a stream may include changes in the bridge design, construction of river control works, protection of the foundations with riprap, or careful monitoring of the river in a bridge inspection program. Richardson and Davis (2001) recommend that foundations of piers and abutments located on floodplains be placed at elevations approximating those for piers located in the main channel.

To control lateral shifting requires river training works, bank stabilization by riprap, and/or guide banks. Design methods are given in publications of the Federal Highway Administration, U.S. Army Corps of Engineers, and American Association of State Highway and Transportation Officials (AASHTO). Of particular importance are "Spurs and Guide Banks" (Richardson and Simons 1974); "The Design of Spurs for River Training" (Richardson et al. 1975); "The Streambank Erosion Control Evaluation and Demonstration Act of 1974" (USACE 1981); "Streambank Protection Guidelines for Landowners and Local Governments" (USACE 1983); "Use of Spurs and Guidebanks for Highway Crossings" (Richardson and Simons, 1984); "Streambank Stabilization Measures for Highway Stream Crossings" (Brown 1985); "Highways in the River Environment" (Richardson et al. 1990); "Hydraulic Analysis for the Location and Design of Bridges," Volume VII, Highway Drainage Guidelines (AASHTO 1992); "Bridge Scour and Stream Instability Countermeasures" (Lagasse et al. 2001a); "Stream Stability at Highway Structures" (Lagasse et al. 2001b); "River Engineering for Highway Encroachments" (Richardson et al. 2001).

10.22 SCOUR IN TIDE-AFFECTED WATERWAYS

Scour (erosion) of the foundations of bridges over tidal waterways in the coastal region that are subjected to the effects of astronomical tides and storm surges is a combination of long-term degradation, contraction scour, local scour, and waterway instability (Richardson et al. 1993; 1995; Richardson and Lagasse 1999; Richardson and Davis 2001). These are the same scour mechanisms that affect nontidal (riverine) streams. Although many of the flow conditions are different in tidal waterways, the equations used to determine riverine scour are applicable if the hydraulic forces are carefully evaluated.

Bridge scour in the coastal region results from the unsteady diurnal and semidiurnal flows resulting from astronomical tides, large flows that can result from storm surges (hurricanes, nor'easters, and tsunami), and the combination of riverine and tidal flows. Also, the small size of the bed material (normally fine sand) as well as silts and clays with cohesion and littoral drift (transport of beach sand along the coast resulting from wave action) affect the magnitude of bridge scour. In addition, tidal flows are subject to mass density stratification and water salinity, but these have only a minor effect on bridge scour. The hydraulic variables (discharge, velocity, and depth) and bridge scour in the coastal region can be determined with as much precision as riverine flows. These determinations are conservative and research is needed to improve scour determinations in both cases. Determining the magnitude of the combined flows can be accomplished by simply adding riverine flood flow to the maximum tidal flow or routing the design riverine flows to the crossing and adding them to the storm surge flows.

Some of the similarities and differences between tidal and riverine flows are as follow:

- Tidal flows are unsteady with short-duration peak flows. Riverine flows are also unsteady and many have short-duration peak flows. Existing scour equations predict scour depths for these short-duration peak riverine flows. Also, waterways in the coastal zone are composed of fine sand that erodes easily. Therefore, riverine scour equations will predict scour depths in short-duration tidal flows.
- Astronomical tides, with their daily or twice-daily in- and outflows, can and do cause long-term degradation if there is no source of sediment except at the crossing. This has resulted in long-term degradation of several feet per year with no indication of stopping (Butler and Lillycrop 1993; Vincent et al. 1993). Existing scour equations can predict the magnitude of this scour, but not the time history (Richardson et al. 1993).
- Mass density stratification (saltwater wedges), which can result when denser, more saline ocean water enters an estuary or tidal inlet with significant freshwater inflow, can result in larger velocities near the bottom than the average velocity in the vertical (Sheppard 1993). However, with careful evaluation, the correct velocity for use in the scour equations can be determined. With storm surges, mass density stratification will not normally occur. The density difference between salt and fresh water, except when it causes saltwater wedges, is not significant enough to affect scour equations. Density and viscosity differences between fresh and sediment-laden water can be much larger in riverine flows than the differences between salt and fresh water. Salinity can affect the transport of silts and clays by causing them to flocculate and possibly deposit, which may affect stream stability and must be evaluated. Salinity may affect the erodibility of cohesive sediments, but this will only affect the rate of scour, not ultimate scour.
- Littoral drift is a source of sediment to a tidal waterway (Sheppard 1993) and its availability can decrease contraction and possible local scour and may result in a stable or aggrading waterway. The lack of sediment

from littoral drift can increase long-term degradation, contraction scour, and local scour. Evaluating the effect of littoral drift is a sediment transport problem involving historical information, future plans (dredging, jetties, etc.) for the waterway and/or the coast, sources of sediment, and other factors.

- *There is one major difference between riverine scour at highway structures and scour resulting from tidal forces*. In determining scour depths for riverine conditions, a design discharge is used (discharge associated with a 50-, 100-, or 500-year return period). For tidal conditions, a design storm surge elevation is used (elevation for the 50-, 100-, or 500-year storm surge return period), and from the storm surge elevation, the discharge is determined. That is, for the riverine case, the discharge is fixed, whereas, for the tidal case, the discharge may not be. In the riverine case, as the area of the stream increases, the velocity and shear stress on the bed decrease because of the fixed discharge. In the tidal case, as the area of the waterway increases, the discharge may also increase and the velocity and shear stress on the bed may not decrease appreciably. Thus, long-term degradation and contraction scour can continue until sediment inflow equals sediment outflow or the discharge driving force (difference in elevation across a highway crossing an inlet, estuary, or channel between islands or islands and the mainland) reduces to a value that the discharge no longer increases (Richardson et al. 1993; Richardson and Davis 2001).

The reason the design discharge for the same return periods for tidal waterways may increase is that the discharge is dependent on the design storm surge elevation, the volume of water in the tidal prism upstream of the bridge, and the area of the waterway under the bridge at mean tide. If there is erosion of the waterway from the constant daily flow from the astronomical tides or from the storm surge, the discharge may increase as the waterway area increases.

10.22.1 Design Discharge

The design discharge for tidal waterways is determined from the 50-, 100-, and 500-year storm surge return period elevation. From this elevation, tidal prism volume, and waterway area, the design discharge is determined. If the waterway area increases the design discharge may increase. This is a major difference between the tidal and riverine design discharge (see discussion above) (Richardson et al. 1993; Richardson and Davis 2001). Models are available to generate synthetic storm surge hydrographs combined with different periods of the daily tides (Zevenbergen et al. 1997a, b).

Determination of the design discharge for scour analysis for bridges in tidal waterways consists of a three-level approach. First is preliminary qualitative evaluation of the stability of a tidal waterway, estimation of the magnitude of the tides, storm surges, littoral drift, and flow in the tidal waterway, and determination of whether the hydraulic analysis depends on tidal or river conditions or both. Next an engineering analysis is used to obtain the velocity, depths, and discharge for tidal waterways to be used in determining long-term aggradation or degradation, contraction scour, and local scour using existing scour equations. Finally, if necessary for complex tidal situations, one- or two-dimensional computer models or even physical models must be used.

10.23 SCOUR CALCULATIONS FOR TIDAL WATERWAYS

Long-term degradation, contraction scour, and local scour can be determined in tidally affected waterways using methods and equations given previously for riverine flows (Richardson and Davis 2001). A brief summary for long-term degradation and contraction scour follows.

10.23.1 Long-Term Degradation

To determine if long-term degradation is occurring, site conditions, fluvial geomorphology, historical data on changes in waterway bed elevation, and potential future changes in the tidal waterway or coastal conditions must be studied to determine if the waterway is aggrading or degrading. If the waterway is degrading, an estimate of the amount of degradation that will occur in the future is made and added to the other scour components. Historical data sources could be maps, soundings, tide gauge records, and bridge inspection reports for the site and in the area. Determine if there are plans to construct jetties or breakwaters, dredge the channel, construct piers, etc., which could affect waterway stability. Also, determine changes in the riverine environment, such as dams, which could change flow conditions.

In tidal conditions long-term degradation can occur from the daily tides if there is little or no sediment supply to an inlet or estuary or it is decreased (Butler and Lillycrop 1993; Richardson et al. 1993; Vincent 1993). The potential magnitude but not the time of this long-term degradation can be determined using the clear-water contraction scour equation given previously. Richardson and Davis (2001) present an example of the use of the clear-water contraction scour equation to estimate potential long-term degradation.

10.23.2 Contraction Scour

Contraction scour can occur at a tidal inlet, estuary, or passage between islands or islands and the mainland. It may be live-bed or clear-water scour. It would be considered live-bed scour if there were a substantial quantity of bed material transport in contact with the bed. Equations given previously can be used to determine contraction scour from the daily

tidal or storm surge flows. Because the discharge in a contracted tidal waterway depends on the area of the waterway for a given tidal or storm surge amplitude and tidal prism, the discharge will need to be recalculated after the area has increased from contraction scour.

10.23.3 Local Scour

The equations and method given previously for local scour at piers and abutments are used for tidal waterways.

10.24 OVERVIEW OF TIDAL PROCESSES

10.24.1 Glossary of Terms

Bay: A body of water connected to the ocean by an inlet.
Estuary: Tidal reach at the mouth of a river.
Flood or flood tide: Flow of water from the ocean into the bay or estuary.
Ebb or ebb tide: Flow of water from the bay or estuary to the ocean.
Littoral drift: Transport of beach material along a shoreline by wave action.
Run-up: Height to which water rises above still-water level when waves meet a beach or wall.
Storm surge: Tidelike phenomenon resulting from wind and barometric pressure changes. Hurricane surge, storm tide.
Tidal amplitude: Generally, half of tidal range.
Tidal cycle: One complete rise and fall of the tide.
Tidal inlet: A channel connecting a bay or estuary to the ocean.
Tidal passage: A tidal channel connected with the ocean at both ends.
Tidal period: Duration of one complete tidal cycle.
Tidal prism: Volume of water contained in a tidal bay, inlet, or estuary between low and high tide levels.
Tidal range: Vertical distance between specified low and high tide levels.
Tidal waterways: A generic term that includes tidal inlets, estuaries, bridge crossings to islands or between islands, crossings between bays, tidally affected streams, etc.
Tides, astronomical: Rhythmic diurnal or semidiurnal variations in sea level that result from gravitational attraction of the moon and sun and other astronomical bodies acting on the rotating earth.
Tsunami: Long-period ocean wave resulting from an earthquake, or other seismic disturbance, or a submarine landslide.
Waterway opening: Width or area of bridge opening at a specific elevation, measured normal to principal direction of flow.
Wave period: Time interval between arrivals of successive wave crests at a point.

10.24.2 Definition of Tidal and Coastal Processes

Typical bridge crossings of tidal waterways are diagramed in Fig. 10-20. Tidal flows are defined as being between the ocean and a bay (or lagoon), from the ocean into an estuary, or through passages between islands or between islands and the mainland. Idealized astronomical tidal conditions and tidal terms are illustrated in Fig. 10-21.

The forces that drive tidal fluctuations are, primarily, the result of the gravitational attraction of the sun and moon on the rotating earth (astronomical tides), wind and storm setup or seiching (storm surges), and geologic disturbances (tsunami). As illustrated in Fig. 10-21, the maximum discharge (Q_{max}) at the flood or ebb tide occurs often (but not always) at the crossing from high to low or low to high tide. The continuous rise and fall of astronomical tides will usually influence long-term trends of aggradation and degradation. Conversely, when storm surges or tsunami occur, the short-term contraction and local scour can be significant. Storm surges and tsunami are single-event phenomena that, due to their magnitude, can cause significant scour at a bridge crossing.

Although the hydraulics of flow for tidal waterways is complicated by the presence of two-directional flow, the basic concept of sediment continuity is valid. Consequently, a clear understanding of the principle of sediment continuity is essential for evaluating scour at bridges spanning waterways influenced by tidal fluctuations. The sediment continuity concept states that the sediment inflow minus the sediment outflow equals the time rate of change of sediment volume in a given reach.

In addition to sediments from upland areas, littoral drift (Figs. 10-20 and 10-22) is a source of sediment supply to an inlet, bay estuary, or tidal passage. During flood tide, sediments can be transported and deposited into the bay or estuary. During ebb tide, sediments can be remobilized and transported out of the inlet or estuary and either deposited on shoals or moved further down the coast as littoral drift.

Sediment transported to a bay or estuary from an upland river system can also be deposited in the bay or estuary during flood tide and remobilized and transported through the inlet or estuary during the ebb tide. However, if the bay or estuary is large, sediments derived from the upland river system can be deposited in the bay or estuary in areas where the velocities are low and may not contribute to the supply of sediment to the bridge crossing. The result is clear-water scour unless sediment transported on the flood tide (ocean shoals, littoral drift) is available on the ebb. Sediments transported from upland rivers into an estuary may be stored there on the floor and transported out during ebb tide. This would produce live-bed scour conditions unless the sediment source in the estuary were disrupted. Dredging, jetties, or other coastal engineering activities can limit sediment supply to a reach and influence live-bed and clear-water scour conditions.

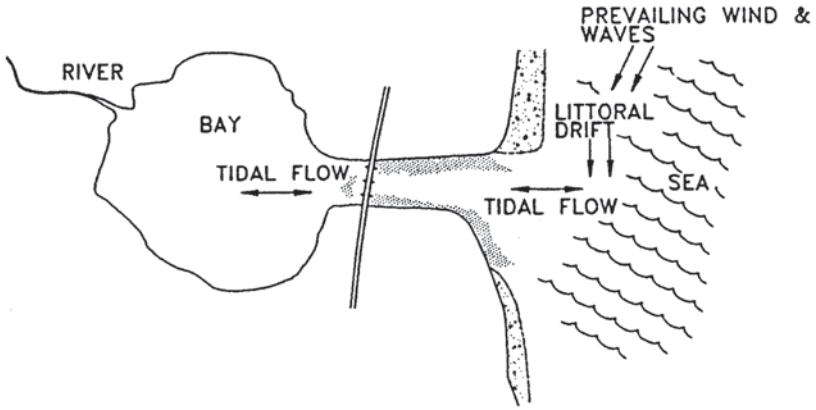

1. Inlets between the open sea and an enclosed lagoon or bay, where most of the discharge results from tidal flows. Tidal inlet fed by littoral drift.

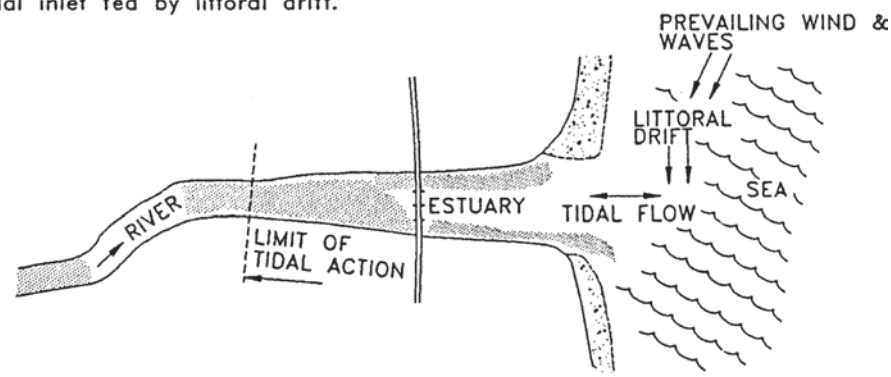

2. River estuaries where the net discharge comprises river flow as well as tidal flow components

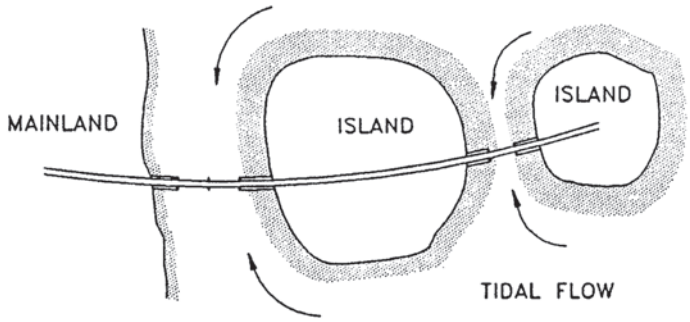

3. Passages between islands, or between an island and the mainland, where a route to the open sea exists in both directions.

Fig.10-20. Types of tidal waterway crossings (after Neill 1973).

10.25 PRELIMINARY ANALYSIS

As a preliminary analysis it is necessary to determine (1) classification of the tidal crossing, (2) tidal characteristics, (3) lateral, vertical, and overall stability of the waterway and bridge foundations, and (4) characteristics of the riverine and tidal flows. In such a design, plans, boring logs, inspection and maintenance reports, fluvial geomorphology, historical flood, scour and tidal information, 100- and 500-year return period storm surge elevations, riverine flows, etc. are collected and analyzed. In addition, field reconnaissance and contact with agencies such as the Federal Emergency Management Agency (FEMA), National Oceanic and Atmospheric Administration (NOAA), U.S. Geological Survey (USGS), U.S. Coast Guard (USCG), U.S. Corps of Engineers (USCOE), state agencies, etc. are used.

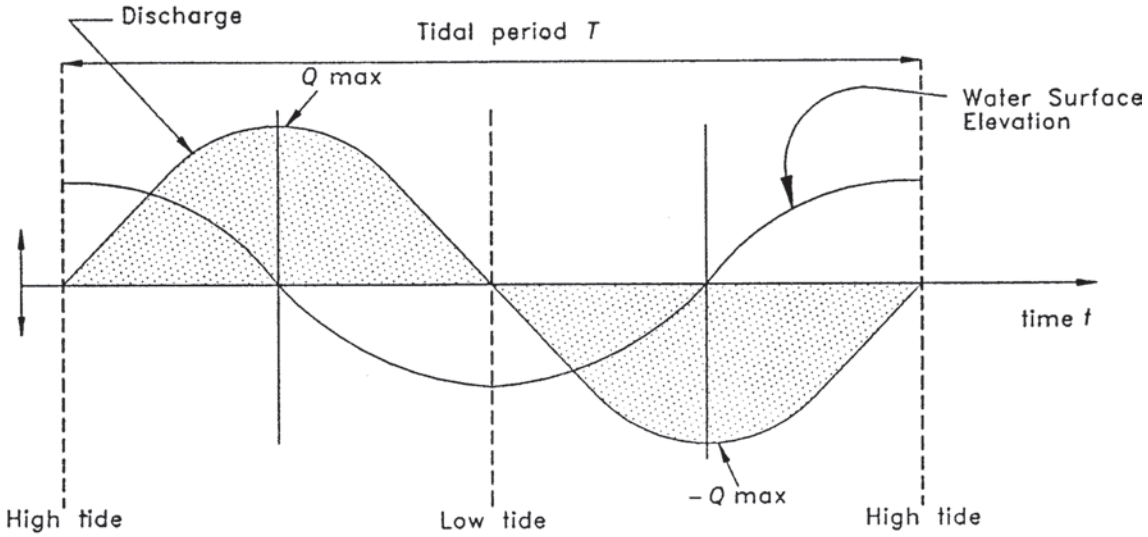

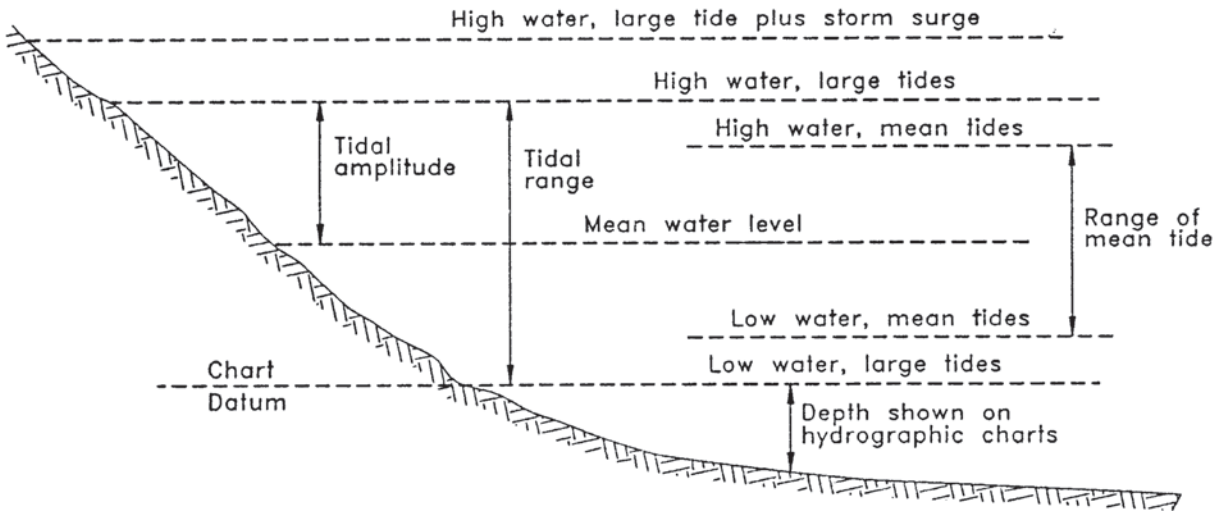

Fig. 10-21. Principal tidal terms (after Neill 1973).

The crossing is classified as an inlet, bay, estuary, or passage between islands or islands and the mainland (Fig. 10-20). The crossing may be tidally affected or tidally controlled. Tidally affected crossings do not have flow reversal, but the tides act as a downstream control. Tidally controlled crossings have flow reversal. The limiting case for a tidally affected crossing is when the magnitude of the tide is large enough to reduce the discharge through the bridge to zero.

The objectives of the preliminary analysis are to determine the magnitude of the tidal effects on the crossing, the overall long-term vertical and lateral stability of the waterway and bridge crossing, and the potential for waterway and crossing to change.

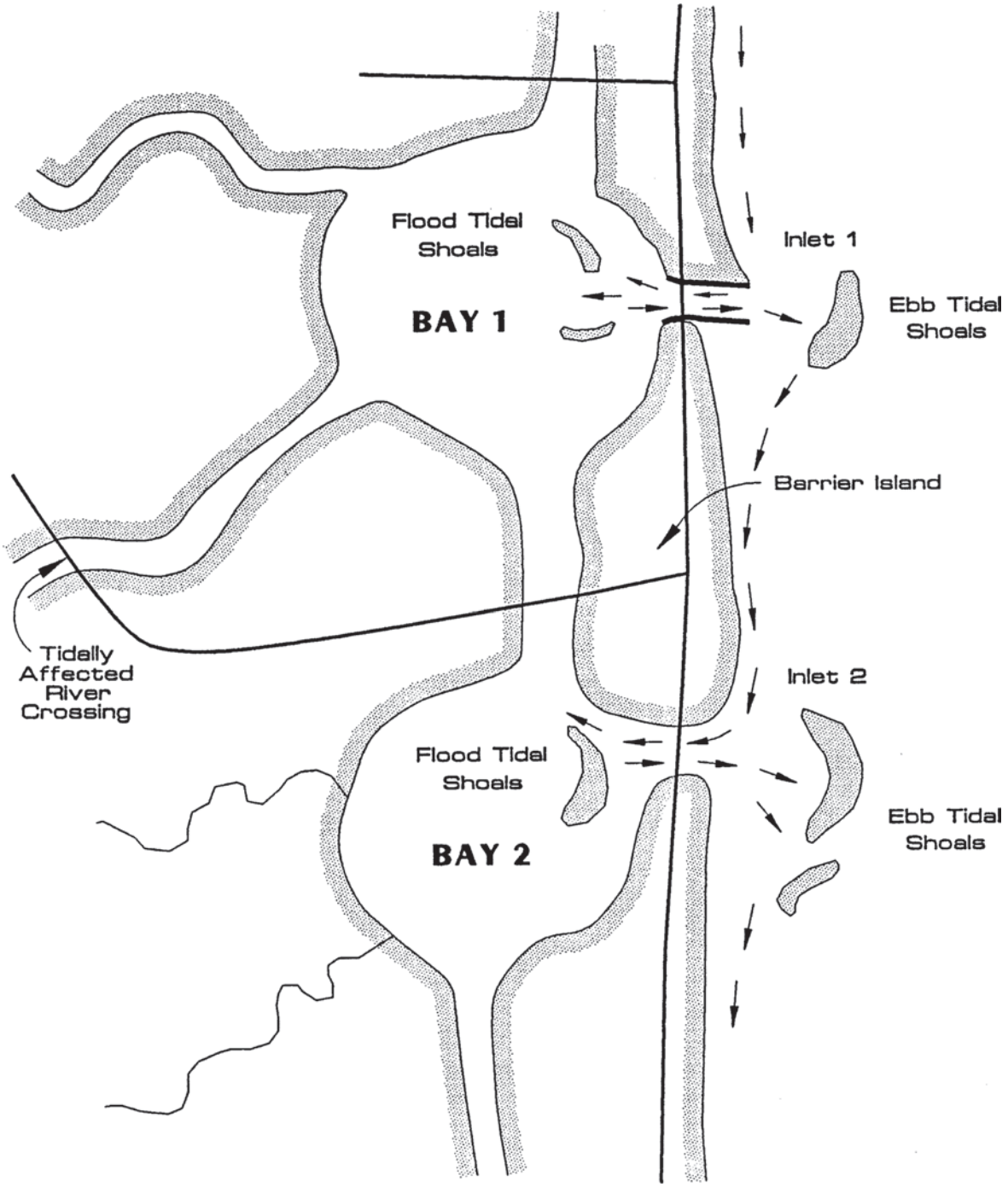

Fig. 10-22. Sediment transport in tidal inlets (after Sheppard 1993).

10.26 DETERMINATION OF HYDRAULIC VARIABLES

The general procedure is to determine (1) design flows (100- and 500-year storm tides and riverine floods), and (2) hydraulic variables of discharge, velocity, and depths. These variables are then used to determine the scour components (depths of degradation, contraction scour, pier scour, and abutment scour) using the equations and methods given previously, followed by (3) evaluation of the results.

10.26.1 Design Flows and Hydraulic Variables

The riverine 100- and 500-year return period storm discharge is determined by standard hydrology frequency analysis procedures. The magnitude of the 100- and 500-year return

period discharges for a tidal surge depends on the elevation of the surge at the crossing, the volume of water in the tidal prism above the crossing, the area of the bridge waterway at the water surface elevation between high and low tide (ebb) or low and high tide (flood), and the tidal period (time between successive high or low tides).

The elevation of the 100- and 500-year storm surge, tidal period, and surge hydrographs for storm surges can be obtained from FEMA, NOAA, and USCOE. From this information, the volume of the tidal prism above the crossing, the area of the waterway at the bridge and the elevation of the crossing between high and low tide, the design storm surge discharges, and hydraulic variables for use in the scour equations can be determined for an unconstricted waterway by a method given by Neill (1973) and for a constricted waterway by a method given by Chang et al. (1994).

10.27.2 Hydraulic Variables for Unconstricted Waterways

Richardson and Davis (2001) present Neill's (1973) method as follows:

1. Determine and plot the net waterway area at the crossing as a function of elevation. Net area is the gross waterway area between abutments minus area of the piers.
2. Determine and plot tidal prism volumes as a function of elevation. The tidal prism is the volume of water between low and high tide levels or between the high tide elevation and the bottom of the tidal waterway.
3. Determine the elevation versus time relation for the 100- and 500-year storm tides. The relation can be approximated by a sine curve, which starts at mean water level or a cosine curve which starts at the maximum tide level. The cosine equation is

$$y = A\cos\theta + Z \tag{10-52}$$

where

y = amplitude or elevation of the tide above mean water level, time t;
A = maximum amplitude of the tide or storm surge, m, ft, defined as half the tidal range or half the height of the storm surge;
θ = angle in degrees subdividing the tidal cycle where one tidal cycle is equal to 360°,

$$\theta = 360\left(\frac{t}{T}\right) \tag{10-53}$$

t = time in minutes from beginning of total cycle;
T = total time for one complete tidal cycle, min;
Z = vertical offset to datum, m, ft.

To determine the elevation versus time relation for the 100- and 500-year storm tides, the tidal range and period must be known. The FEMA, USCOE, NOAA, and other federal or state agencies compile records that can be used to estimate the 100- and 500-year storm surge elevation, mean sea level elevation, low tide elevation, and time period.

Tides, and in particular storm tides, may have different periods than astronomical semidiurnal and diurnal tides, which have periods of approximately 12.5 and 25 h, respectively. This is because storm tides are influenced by factors other than the gravitational forces of the sun, moon, and other celestial bodies. Factors such as the wind, path of the hurricane or storm creating the storm tide, freshwater inflow, shape of the bay or estuary, etc. influence the storm tide amplitude and period.

4. Determine the discharge, velocities, and depth. The maximum discharge, in an ideal tidal estuary, may be approximated by the equation (Neill 1975)

$$Q_{max} = \frac{3.14\,\mathrm{VOL}}{T} \tag{10-54}$$

where

Q_{max} = maximum discharge in the tidal cycle, cms, cfs;
VOL = volume of water in the tidal prism between high and low tide levels, m^3, ft^3;
T = tidal period between successive high or low tides, s.

In the idealized case, Q_{max} occurs in the estuary or bay at mean water elevation and at a time midway between high and low tides when the slope of the tidal energy gradient is steepest (Fig. 10-21). In many field cases, Q_{max} occurs 1 or 2 h before or after the crossing, but any error caused by this is diminutive.

The corresponding maximum average velocity in the waterway is

$$V_{max} = \frac{Q_{max}}{A'} \tag{10-55}$$

where

V_{max} = maximum average velocity in the cross section at Q_{max}, m/s, ft/s;
A' = cross-sectional area of the waterway at mean tide elevation, halfway between high and low tide, m^2, ft^3.

The average velocity must be adjusted to determine velocities at individual piers to account for nonuniformity of velocity in the cross section. As for inland rivers, local velocities can range from 0.9 to approximately 1.7 times the average velocity depending on whether the location in the cross section is near the bank or near the flow thalweg. The calculated velocities should be compared with any measured

velocities for the bridge site or adjacent tidal waterways to evaluate the reasonableness of the results.

The discharge at any time t in the tidal cycle, (Q_t) is given by:

$$Q_t = Q_{\max} \sin\left(360\frac{t}{T}\right) \tag{10-56}$$

5. Include any riverine flows. This may range from simply neglecting the riverine flow into a bay (which is so large that the riverine flow is insignificant in comparison to the tidal flows), to routing the riverine flow through the crossing.
6. Evaluate the discharge, velocities and depths that were determined in Steps 4 and 5.
7. Determine scour depths for the bridge using the values of the discharge, velocity and depths determined from the above analysis.

10.26.3 Hydraulic Variables for Constricted Waterways

To determine the hydraulic variables at a constricted waterway (constricted either by the bridge or the channel), the tidal flow may be treated as orifice flow and the following equation taken from van de Kreeke (1967) and Bruun (1990) reported by Richardson and Davis (2001) can be used:

$$V_{\max} = C_d\left(2g\Delta H\right)^{1/2} \tag{10-57}$$

$$Q_{\max} = A'V \tag{10-58}$$

where

$V_{\max}$ = maximum velocity in the inlet, m/s, ft/s;
$Q_{\max}$ = maximum discharge in the inlet, cms, csf;
C_d = coefficient of discharge ($C_d < 1.0$);
g = acceleration due to gravity, 9.81 m/s^2, 32.2 ft/s^2;
ΔH = difference in water surface elevation between the up- and downstream sides of a crossing or channel for the 100- and 500-return period storm surges as well as for the normal astronomical average tides. —this latter is used to determine the average normal discharge on a daily basis to determine potential long-term degradation at the crossing of a tidal waterway if it becomes unstable (*3*), m, ft;
A' = net cross-sectional area at the crossing, at mean water surface elevation, m^2, ft^2.

The coefficient of discharge (C_d) is:

$$C_d = \left(\frac{1}{R}\right)^{1/2} \tag{10-59}$$

where

$$R = K_u + K_d + \frac{2g\ n^2\ L_c}{1.49^2\ h_c^{4/3}} \tag{10-60}$$

and

R = coefficient of resistance;
K_d = velocity head loss coefficient on downstream side of the waterway;
K_u = velocity head loss coefficient on upstream side of the waterway;
n = Manning's roughness coefficient;
L_c = length of the waterway or bridge opening, m, ft;
h_c = average depth of flow at the bridge at mean water elevation, m, ft.

If ΔH is not known, the following method, developed by Chang et al. (1994), which combines the orifice equation with the continuity equation, can be used. The total flow approaching the bridge crossing at any time (t) is the sum of the riverine flow (Q) and tidal flow. The tidal flow is calculated by multiplying the surface area of the upstream tidal basin (A_s) by the drop in elevation (H_s) over the specified time ($Q_{\text{tide}} = A_s\ dH_s/dt$). This total flow approaching the bridge is set equal to the flow calculated from the orifice equation,

$$Q + A_s\frac{dH_s}{dt} = C_d A_c\sqrt{2g\Delta H} \tag{10-61}$$

where

A_c = bridge waterway cross-sectional area, m^2, ft^2.

The other variables have been defined previously.

Equation (10-52) may be rearranged into the form of Eq. (10-53) for the time interva, $\Delta t = t_2 - t_1$, subscripts 2 and 1 representing the end and beginning of the time interval, respectively. Then

$$\frac{Q_1+Q_2}{2} + \frac{A_{s1}+A_{s2}}{2}\frac{H_{s1}-H_{s2}}{\Delta t} = C_d\left(\frac{A_{c1}+A_{c2}}{2}\right)\sqrt{2g\left(\frac{H_{s1}+H_{s2}}{2}-\frac{H_{t1}+H_{t2}}{2}\right)} \tag{10-62}$$

For a given initial condition, t_1, all terms with subscript 1 are known. For $t = t_2$, the downstream tidal elevation (H_{t2}), riverine discharge (Q_2), and waterway cross-sectional area (A_{c2}) are also known or can be calculated from the tidal elevation. Only the water-surface elevation (H_{s2}) and the surface area (A_{s2}) of the upstream tidal basin remain to be determined. Because surface area of the tidal basin is a function of the water-surface elevation, the elevation of the tidal basin at time t_2 (H_{s2}) is the only unknown term in Eq. (10-62), which can be determined by trial and error to balance the values on the right and left sides.

Chang et al. (1994) suggest the following for computing the discharge:

1. Determine the period and amplitude of the design tide(s) to establish the time rate of change of the water surface on the downstream side of the bridge.

2. Determine the surface area of the tidal basin upstream of the bridge as a function of elevation by planimetering successive contour intervals and plotting the surface area versus elevation.
3. Plot bridge waterway area versus elevation.
4. Determine the quantity of riverine flow that is expected to occur during passage of the storm tide through the bridge.
5. Route the flows through the contracted waterway using Eq. 10-62 and determine the maximum velocity of flow.

Chang et al. (1994) give an example problem using a spreadsheet and have developed a computer program to aid in using this method. Richardson and Davis (1995) also give the sample problem and list the computer progress.

10.26.4 Hydraulic Variables Using Computer Programs

A Federal Highway Administration Pooled Fund study funded by the Connecticut, Florida, Georgia, Louisiana, Maine, Maryland, Mississippi, New Jersey, New York, North Carolina, South Carolina, and Virginia Departments of Transportation of computer models to analyze tidal stream hydraulic conditions at highway structures recommended a one-dimensional unsteady flow model entitled UNET (Burkau 1993; USACE 1996) and a two-dimensional unsteady flow model entitled FESWMS (Froehlich 1996). The studies were carried out by Ayres Associates, Inc., and Edge & Associates, Inc, with William H. Hulbert, North Carolina DOT, as project manager (Ayres Associates 1994; Zevenbergen et al. 1997a; 1997b). The use of FESWMS was enhanced by the FHWA-supported development of a graphical user interface called the Surface Water Modeling System (SMS) (Brigham Young University 1997). The interface develops two-dimensional model networks, run control, variable assignment, and output analysis for FESWMS. Both models proved themselves under a wide range of field tidal conditions.

Methods for predicting storm surge hydrographs using peak storm surge elevation and hurricane characteristics (radius of maximum winds and forward speed) for the 50-, 100-, and 500-year hurricanes are included. Zevenbergen et al. (1997a, b) contain methods and procedures for using UNET, FESWMS, and SMS and developing of storm surge hydrographs.

REFERENCES

Abed, L. M. (1991). "Local scour around bridge piers in pressure flow." PhD dissertation, Colorado State University, Fort Collins, Colo.

Abed, L. M. Richardson, E. V., and Richardson, J. R. (1991). "Bridges and structures." *Transportation Research Record 1290*, Vol. 2, Third Bridge Engineering Conference, Transportation Research Board, Washington, D.C.

Ahmad, M. (1953). "Experiments on design and behavior of spur dikes." Proceedings IAHR, ASCE Joint Meeting, University of Minnesote.

American Association of State Highway and Transportation Officials (AASHTO) (1992). *Hydraulic analysis for the location and design of bridges*, Vol. VII, Highway Drainage Guidelines, American Association of State Highway and Transportation Officials, Washington, D.C.

Arneson, L. A. (1997). "The effects of pressure flow on local scour in bridge openings," PhD dissertation, Colorado State Univ., Fort Collins, Colo.

Arneson, L.A., and Abt, S.R. (1998). "Vertical contraction scour at bridges with water flowing under pressure conditions." *Stream Stability and Scour at Highway Bridges, Compendium of Stream Stability and Scour Papers*, E.V. Richardson and P.F. Lagasse, eds., ASCE, Reston, Va., 189-204.

Ayres Associates, (1994). "Development of hydraulic computer models to analyze tidal and coastal stream hydraulic conditions at highway structures." *Final Report, Phase I,* South Carolina Department of Transportation, Columbia, S.C.

Ayres Associates. (2003). "SAMwin-Hydraulic Design Package for Channels." Users Guide to Windows Based Program, Ayres Associates, Ft. Collins, Co.

Box, G. E. P., and Tidwell, P. W.(1961). "Transformation of the independent variables." *Technometrics*, 4(4), 531–550.

Briaud, J. L., Ting, F. C., Chen, H. C., Gudavalli, R., Perugu, S., and Wei, G.(1999). "SRICOS: Prediction of scour rate in cohesive soils at bridge piers." *ASCE Journal of Geotechnical and Geoenvironmental Engineering,* 125(4), 237–246.

Brigham Young University (1997). "SMS surface water modeling system." *Reference manual; version 5.0, Engineering Computer Graphics Laboratory, (1980)*. Provo, Utah.

Brown, S. A. (1985). "Stream bank stabilization measures for highway engineers." *FHWA/RD-84.100*, Federal Highway Administration, Washington, D.C.

Brown, S. A., McQuivey, R. S., and Keefer, T. N. (1980). "Stream channel degradation and aggradation: Analysis of impacts to highway crossings." Rep. *FHWA/RD-80/159,* Federal Highway Administration, U.S. Department of Transportation, Washington, D.C., 202.

Bruun, P. (1990). "Chapter 9. Tidal inlets on salluvial shores." *Port engineering,* 4th Ed., Vol. 2, Gulf Publishing, Houston, Tex.

Burkau, R. L. (1993). "UNET—One dimensional unsteady flow through a full network of open channels." *Report CPD-66*. U.S. Army Corps of Engineers, Hydrologic Engineering Center, Davis, Calif.

Butler, H. L., and Lillycrop. J. (1993). "Indian River inlet: Is there a solution?" *Hydraulic Engineering, Proc. of the 1993 National Conference*, Vol. 2, ASCE, New York, 1218–1224.

Chang, F., Davis, S.R., and Veeramanchaneni, R. (1994). "Tidal flow through contracted bridge openings." *Miscellaneous Report, Names Bridge Section, Maryland Department of Transportation*, Baltimore, Md.

Chang, F. F. M. (1973). *A statistical summary of the cause and cost of bridge failures*, Federal Highway Administration, U.S. Department of Transportation, Washington, D.C.

Einstein, H. A. (1950). "The bed load function for sediment transportation in open channel flows." *Tech. Bull. 1026*, U.S. Department of Agriculture Washington, D.C.

Froehlich, D. C, (1988). "Analysis of onsite measurements of scour at piers." Hydraulic Engineering, Proc. of the 1988 Nat Conf. ASCE, Reston, Va., 534-539.

Froehlich, D. C. (1989). "Local scour at bridge abutments." *Proc., Nat. Hydr. Conf.,* ASCE, New York, 13-18.

Froehlich, D. C. (1995). "Contracted Scour at Bridges: Clear-water conditions with Armoring." Hydraulic Engineering, ASCE, Reston, Va., 1995.

Froehlich, D. C., "Finite element surface-water modeling system: Two-dimensional flow in a horizontal plane." *FESWMS-2DH, Version 2, User's Manual*, Federal Highway Administration, Turner-Fairbank Highway Research Center, McLean, Va.

Greble, D. F. (1999)., "Clear water abutment scour at the I-70 bridge near Rocheport, Missouri." Master's study, Department of Civil and Environmental Engineering, University of Missouri at Kansas City.

Jackson, L. E., Thompson, P. D., Richardson, E. R. (1991). "Hatchie River and Schoharie Creek bridge failures." *Hydraulic Engineering Proc., 1991 National Conf. Nashville, TN,* ASCE, New York.

Jain, S. C., and Fisher, E. E. (1979). "Scour around circular bridge piers at high Froude numbers." *Rep. FHWA-RD-79-104*, NTIS, Springfield, Va.

Johnson, P. A., Torrico, E. F. (1994). "Scour around wide piers in shallow water." *Transportation Research Board Record 1471,* Washington, D.C.

Jones, J. S. (1983). "Comparison of prediction equations for bridge pier and abutment scour." *Transportation Research Record 950*, TRB, National Research Council, Washington, D.C., 202-209.

Jones, J. S. (1989). "Laboratory studies of the effects of footings and pile groups on bridge pier scour." U.S. Interagency Sedimentation Committee Bridge Scour Symposium, Turner-Fairbank Highway Research Center, Federal Highway Administration, U.S. Department of Transportation, Mclean, Va.

Jones, J. S., Bertoldi, D. A., and Umbrell, E. R. (1995). "Preliminary studies of pressure flow scour." *Hydraulic Engineering, ASCE*., V1, 916–921.

Jones, J. S., Bertoldi, D. A., and Umbrell, E. R. (1996). "Interim procedures for pressure flow scour." *North American Water and Environment Congress*, (CD-ROM), ASCE, Reston, Va.

Jones, J. S., and Sheppard, D. M. (2000). "Local scour at complex pier geometries." *Proc., Joint Conference on Water Resources Engineering and Water Resources Planning and Management,* ASCE, Reston, Va.

Keefer, T. N., McQuivey, R. S., and Simons, D. B. (1980). "Stream channel degradation and aggradation: Causes and consequences to highways." *FHWA Rep. FHWA/RD-80/038*, Federal Highway Administration. Washington, D.C.

Lagasse, P. F., Byars, M. S., Zevenbergen, L. W., and Clopper, P. (2001a). "Bridge scour and stream instability countermeasures," HEC 23. *Publ. No. FHWA NHI 01-003*, Federal Highway Administration, Washington, D.C.

Lagasse, P. F., Schall, J. D., Johnson, F., Richardson, E. V., and Chang, F. (2001b). "*Stream stability at highway structure,"* 3rd Ed., HEC 20. *Publ. No. FHWA NHI 01-002*., Federal Highway Administration, Washington D.C.

Landers, M. N., and Mueller, D. S. (1998). "Channel scour at bridges in the United States." *FHWA Rep. FHWA-RA-95-184,* Federal Highway Administration, Washington D.C.

Landers, M. N., Mueller, D. S., and Marten, G. R. (1996). Bridge-scour data management system user's manual." *U. S. Geological Survey Open File Report 95-754*, Reston, Va.

Laursen, E. M. (1958). "Scour at bridge crossings." *Bulletin No. 8,* Iowa Highway Research Board, Ames, Iowa.

Laursen, E. M. (1962). "Scour at bridge crossings." *ASCE,* Transaction, 127, 166-179.

Laursen, E. M. "An analysis of relief bridge scour." *Journal of the Hydraulics Division, ASCE*, 92, HY3, 93–118.

Laursen, E. M. (1980). "Predicting scour at bridge piers and abutments," *General Report No*. 3, Arizona Department of Transportation, Phoenix, Ariz.

Laursen, E. M. (1998). "Discussion of B. W. Melville, 1997 paper 'Pier and abutment scour: Integrated approach." *Journal of the Hydraulics Division, ASCE*, 124 (HY7), 769–771.

Laursen, E. M., and Toch, A. (1956). "Scour around bridge piers and abutments." *Bulletin No. 4*, Iowa Highway Research Board, Ames, Iowa..

Lee, J. K., and Froehlich D. C. (1989). "Two dimensional finite element modeling of bridge crossings." *Report FHWA-RD-88-149.* Federal Highway Administration, Washington. D.C.

Lim, S. Y. (1993). "Clear water scour in long contractions." *Proceedings, Institution of Civil Engineers, Maritime and Energy*, 101, 93–98.

Lim, S. Y. (1997). "Equilibrium clear-water scour around an abutment." *Journal of the Hydraulics Divisions, ASCE*, 123 (3). 237–243.

Liu, M. K., Chang, F. M., and Skinner, M. M. (1961). "Effect of bridge construction on scour and backwater." *Dept. of Civil Engineering, Colorado State University. Rep. CER60-HKL22,* Ft. Collins, Colo.

McIntosh, J. L. (1989) "Use of scour prediction formulae." *FHWA Report FHWA-RD-90-035*, Federal Highway Administration, Washington, D.C.

Melville, B. W. (1984). "Live-bed acour at bridge piers." *ASCE Journal. of Hydraulic Engineering,* Hydraulic Division, Vol. 110, No. 9, 1234–1247.

Melville, B. W. (1992). "Local scour at bridge abutments." *Journal. of Hydraulic Engineering, Hydraulic Division, ASCE*, 118(4), 615–631.

Melville, B. W., (1997). "Pier and abutment scour: Integrated approach," *Journal of the Hydraulic Division, ASCE*, 123(2), 125–136.

Melville, B. W., and Dongol, D. M. (1992). "Bridge pier scour with debris accumulation." *Journal of the Hydraulic Division, ASCE*, 118(9), 1306–1310.

Melville, B. W., and Sutherland, A. J. (1988). "Design method for local scour at bridge piers." *Journal of the Hydraulic Division, ASCE*, 114(10), 1210–1226.

Molinas, A. (1993). "Bri-stars model for alluvial river simulation." *Hydraulic Engineering, ASCE*, 2, 1726-1731.

Mueller, D. S. (1996). "Local scour at bridge piers in nonuniform sediment under dynamic conditions." Ph.D, dissertation, Colorado State University, Ft. Collins, Colo.

Mueller, D. S., and Jones, J. S. (1999). "Evaluation of recent field and laboratory research on scour at bridges in coarse bed materials." *Stream Stability and Scour at Highway Bridges, Compendium of Stream Stability and Scour Papers*, E.V. Richardson and P.F. Lagasse, eds., ASCE, Reston, Va., 298-310.

Neill, C. R., ed. (1973). *Guide to bridge hydraulics,* Roads and Transportation Association of Canada, University of Toronto Press, Toronto.

Raudkivi, A. J. (1986). "Functional trends of scour at bridge piers." *Journal of the Hydraulic Division, ASCE,* 112(1), 1–13.

Rhodes, J., and Trent, R. (1993). "Economics of floods, scour, and bridge failures." *Hydraulic Engineering, ASCE*, 1 (1974), 928–933.

Richardson, E. V., and Abed, L. (1993). "The top width of pier scour holes in free and pressure flow." *Hydraulic Engineering, ASCE*, V1, 911–915.

Richardson, E. V., and Davis, S. R. (1995). "Evaluating scour at bridges," 3rd Ed., HEC 18, Publ. FHWA-IP-90-017, Federal Highway Administration, U.S. Department of Transportation, Washington, D.C.

Richardson, E. V., and Lagasse, P. F., eds. (1999). *Stream stability and scour at highway bridges, compendium of papers, ASCE Water Resources Engineering Conferences, 1991 to 1998,* ASCE, Reston, Va.

Richardson, E. V., Lagasse, P. F., Schall, J.D., Ruff, J. F., Brisbane, T. E., and Frick, D. M. (1987). "Hydraulic, erosion and channel stability analysis of the Schoharie Creek Bridge failure, New York," Resources Consultants, Inc. and Colorado State University, Fort Collins, Colo.

Richardson, E. V., and Richardson, J. R. (1998). Discussion of B. W. Melville, 1997 paper 'Pier and Abutment Scour: Integrated Approach,' *Journal of the Hydraulics Division, ASCE*, 124 (HY7) 771–772.

Richardson, E. V., Richardson, J. R., and Edge, B. E. (1993). "Scour at highway structures in tidal waters." *Hydraulic Engineering, ASCE*, 2, 1206 –1212.

Richardson, E. V., and Simons, D. B. (1974). "Spurs and guide banks." *Open File Report,* Colorado State University Engineering Research Center, Fort Collins, Colo.

Richardson, E. V., and Simons, D. B. (1984). "Use of spurs and guidebanks for highway crossings." *Proc. Second Bridge Eng. Conf., Tran. Research Board Report 950*, Washington, D.C.

Richardson, E. V., Simons, D. B., and Julien, P. (1990). "Highways in the river environment." *FHWA-HI-90-016*, Federal Highway Administration, U.S. Department of Transportation, Washington, D.C. Revision of Richardson, E. V., D. B. Simons, S. Karaki, K. Mahmood and M. A Stevens, 1975 "Highways in the river environment." *Hydraulic and environmental design considerations training and design manual*.

Richardson, E. V., Simons, D. B., and Lagasse, P. F. (2001). "River engineering for highway encroachments—Highways in the river environment." *Hydraulic Design Series 6 (HDS 6) Publ, No FHWA NHI 01-004*, Federal Highway Administration, U.S. Department of Transportation, Washington, D.C.

Richardson, E. V., Stevens, M. A., and Simons, D. B. (1975). "The design of spurs for river IAHR, training." *Proc., XVIth IAHR Congress*, Sao Paulo, Brazil.

Richardson, J. R., and Richardson, E. V. (1992). "Discussion of B. W. Melville, 1992 paper 'Local Scour at Bridge Abutments.'" *Journal of the Hydraulics Division, ASCE*, 119 (HY9), 1069–1071.

Richardson, J. R., and Richardson, E. V. (1993). "The fallacy of local abutment scour equations." *Hydraulic Engineering, ASCE*, 1, 749–755.

Richardson, J. R., Richardson, E. V., and Edge, L. (1995). "Bridge scour in the coastal region." *Proc*. of the *Fourth International Bridge Engineering Conference*, TRB, National Research Council, Washington, D.C.

Richardson, J. R. and Trivino, R. (1999) "Estimating clear water abutment scour," *Report*, Department of Civil and Environmental Engineering, University of Missouri–Kansas City.

Salim, M., and Jones, J. S. (1995). "Effects of exposed pile foundations on local pier scour." Water Resources Engineering Proc. of the 1995 Nat. Water Resources Conf., ASCE, Reston, Va. v2, 1814–1818.

Salim, M., and Jones, J. S. (1996). "Scour around esposed pile foundations." *ASCE Compendium, Stream Stability and Scour at Highway Bridges*, Richardson and P. B. Lagasse, ASCE, eds., Reston, Va., 349–364.

Schumm, S. A. (1977). *The fluvial system*, Wiley, New York.

Shearman, J. O. (1987). "Bridge waterways analysis model for mainframe and microcomputers." *WSPRO/HY-7*, Federal Highway Administration, U.S. Department of Transportation, Washington, D.C.

Sheppard, D. M. (1993). "Bridge scour in tidal waters." *Transportation Research Record 1420,* Washington, D.C., 1–6.

Sheppard, D. M. (2001). "A methodology for predicting local scour depths near bridges piers with complex geometries." unpublished design procedure, University of Florida, Gainesville, Fla.

Smith, W. L. (1999) "Local structure-induced sediment scour at pile groups." M.S. thesis University of Florida, Gainesville, Fla.

Sturm, T. W. (1998). "Abutment scour in compound channels." *Stream Stability and Scour at Highway Bridges, Compendium of Stream Stability and Scour Papers*, E.V. Richardson and P.F. Lagasse, eds., ASCE, Reston, Va.

Sturm, T. W. (1999). "Abutment scour studies for compound channels." *FHWA Report FHWA-RD-99-156,* Federal Highway Administration, U.S. Department. of Transportation, McLean, Va.

Sturm, T. W., and Janjua, N. S. (1994) "Clear-water scour around abutments in floodplains." *Journal of Hydraulic Engineering,* 120(8), 956–972.

U.S. Army Corps of Engineers (USACE). (1981). "The Streambank Erosion Control Evaluation and Demonstration Act of 1974." Final Report to Congress, Executive Summary and Conclusions, Washington, D.C.

U.S. Army Corps of Engineers (USACE). (1983). "Streambank protection guidelines for landowners and local governments." M. P., Keown, Waterways Experiment Station, Vicksburg, Miss. p. 1983.

U.S. Army Corps of Engineers (USACE). (1983). "HEC-6 scour and deposition in rivers and reservoirs, computer program." User's Manual. Hydrologic Engineering Center, Davis, Calif.

U.S. Army Corps of Engineers (USACE). (1996). "UNET—One-dimensional unsteady flow through a full network of open channels," User's Manual, CPD-66, Version 3.1, Hydrologic Engineering Center, Davis, Calif.

U.S. Army Corps of Engineers (USACE). (1997). "User's guide to RMA2 WES Version 4.3," Barbara Donnell, ed., Waterways Experiment Station, Vicksburg, Miss.

U.S. Army Corps of Engineers (USACE). (2001). "HEC-RAS river analysis," Hydrologic Engineering Center, Davis, Calif.

Van de Kreeke, J. (1967). "Water-level fluctuations and flow in tidal inlets." *Journal of the Hydraulics Division, ASCE*, 93 (HY4), 97–106.

Vanoni, V. A., ed. (1975). "Sedimentation engineering." *ASCE Manual 54*, New York.

Vincent, M. S., Ross, M. A., and Ross, B. E. (1993). "Tidal inlet bridge scour assessment model." *Transport Research Record 1420,* Washington, D.C., 7–13.

Zevenbergen, L. W., Hunt, J. H., Byars, M. S., Edge, B. L., Richardson, E. V., and Lagasse, P. F. (1997a). "Tidal hydraulic modeling for bridges; Users manual." *Pooled Fund Study SPR-3(22)*, Ayres Associates, Ft. Collins, Colo.

Zevenbergen, L. W., Richardson, E. V., Edge, B. L., Lagasse, J. S., and Fisher, J. S. (1997b). "Development of hydraulic computer models to analyze tidal and coastal stream hydraulic conditions at highway structures." *Final Report*, Phase II. South Carolina Department of Transportation, Columbia, S.C.

Copyrighted Materials
Copyright © 2008 American Society of Civil Engineers (ASCE)
Retrieved from www.knovel.com

CHAPTER 11

Bridge-Scour Prevention and Countermeasures

Bruce W. Melville, Arthur C. Parola, and Stephen E. Coleman

11.1 INTRODUCTION

Bridge-scour countermeasures are methods to protect bridges from scour and channel instability. Countermeasures include specific protection for piers and abutments, such as riprap, gabions, and other alternatives to riprap, the construction of guide banks at the ends of approach embankments encroaching on wide floodplains, grade control structures such as rock weirs, channel bank protection such as groins, and channel improvements such as channel straightening at the bridge site. The various bridge-scour countermeasures are described and categorized by scour type in Table 11-1. Design information for rock riprap is included in Appendix B.

The need for countermeasures can be avoided or reduced by appropriate bridge design. Good design practice comprises both the selection of a crossing site to reduce the likelihood of excessive scour and the design of the foundations and bridge superstructure to minimize the total depth of scour at the chosen site.

The results of a survey of bridge authorities in the United States conducted in 1995 (Parker et al. 1998) are shown in Table 11-2. The survey included more than 220,000 bridges and revealed that scour countermeasures were employed at 36,432 sites. Monitoring of scour depths was included as a form of countermeasure. Excluding monitoring, rock riprap is the most common countermeasure. Other commonly used countermeasures are rock gabions, extended footings, concrete pavement, grout-filled bags, and spurs. Table 11-2 lists a number of nonstructural countermeasures, including monitoring of scour depths, bridge closure, use of alarms, and imposing restrictions on vehicle use.

This chapter principally addresses countermeasures for local scour at bridge abutments and bridge piers, as well as countermeasures for general scour or channel degradation. The discussion is focused on commonly encountered countermeasures, especially riprap.

11.2 SCOUR PROCESSES

11.2.1 Mechanisms of Local Scour around Piers

The mechanics of flow at bridge piers is driven by strong pressure gradients caused by the stagnation of the flow on the upstream side of the pier, coupled with the nonuniform velocity distribution of the approaching flow, edge effects on the sides of piers, and flow expansion on the downstream side of the pier. The nonuniform velocities and pressures create flow separations and several three-dimensional vortex systems, which are scour-producing features that can fluctuate dramatically in size and intensity. Figure 11-1 shows a schematic representation of the dominant flow features at a rectangular pier.

The strong pressure gradient induced by the pier and the vertical velocity gradient causes a three-dimensional boundary-layer separation upstream and a system of three-dimensional vortices known as the horseshoe vortex system (Dargahi 1987; 1989). The nonuniform stagnation pressure zone on the upstream side of the pier forces high-velocity surface flow downward, where it impinges on the streambed at the base of the pier and rolls up into a horseshoe vortex system that is eventually carried to the pier sides. Under many flow conditions, the deepest scour has been observed to form under the area of flow impingement beneath the horseshoe vortex system (Melville and Coleman 2000).

A feature similar to the horseshoe vortex forms on the water surface upstream of the pier. The momentum gradient caused by the reduction in density at the air/water interface, in combination with the adverse pressure gradient of the pier, forms a flow reversal near the water surface. The general rotation in the surface roller is opposite to the rotation of the horseshoe vortex system. In addition, the deformation of the free surface by the roller instigates a wave that emanates from the pier nose. For relatively shallow flows, a weakening of the horseshoe vortex at the base of the pier has been attributed to the interaction of the surface roller.

Table 11-1 Bridge-Scour Countermeasures

Scour type	Measures	Purposes	Examples	Description
Channel instability – bank erosion	Armoring devices (revetment)	Prevention of erosion to the channel bank in the vicinity of the bridge; stabilization of channel alignment	Rock riprap	Dumped or placed broken rock
			Artificial riprap	Alternatives to rock riprap, including tetrapods, toskanes, akmons, and dolos
			Gabions and Reno mattresses	Wire-mesh baskets and mattresses filled with loose stone
			Precast concrete blocks	Concrete blocks of a cellular shape, possibly interlocking
			Cable-tied blocks	Concrete blocks or slabs interconnected with steel cables
			Grout-filled bags	Fabric bags filled with concrete
			Vegetation	Trees, shrubs, grasses
			Used tires	Used tires placed as a mattress or stacked against a bank
			Grouted riprap, concrete apron, grout-filled mats	Rigid revetments, grout-filled mats (fabric bags filled with concrete), and grouted riprap
	Flow-retarding devices	Reduction of flow velocity near the channel bank and inducement of deposition of sediment	Timber piles, sheet piles, Jack or tetrahedron fields	Permeable structures in a channel, generally placed parallel to the bank
			Vegetation planting	Trees planted to control bank erosion
	Flow-training devices	Reduction of flow velocity near the channel bank and inducement of deposition of sediment; stabilization of channel alignment	Groins (also known as spurs, dikes, jetties, wing dams, or deflectors)	Permeable or impermeable structures, projecting into the flow
			Hardpoints	Small spur-like structure of stone fill spaced along an eroding bank line
			Bendway weirs	Small spur-like structures, typically submerged at normal water levels, spaced along an eroding bank line
			Iowa vanes	Vertical plates installed in a streambed designed to break up secondary flow and mitigate the tendency to lateral migration of banks
Degradation and contraction scour	Check dams	Control of channel grade	Low dams or rock weirs	Constructed across the channel width
	Channel lining	Control of vertical erosion	Concrete or bituminous-concrete pavement	Reinforced-concrete or bituminous-concrete pavement covering channel bed and banks
			Boundary-armoring measures above	For contraction scour and not degradation

(Continued)

Table 11-1 Bridge-Scour Countermeasures *(Continued)*

Degradation and contraction scour	Bridge waterway area	Increase of bridge opening size or efficiency	Channel widening, relief bridges, or guide banks	
Aggradation	Channel improvement	Increased sediment transport to reduce sediment deposition at bridge crossing	Dredging, clearing of channel	
			Formation of a cutoff	
			Flow-control structures	
	Controlled mining	Reduction in sediment input at bridge site	Mining of bed sediment	
			Bar mining	
	Debris basin	Reduction in sediment input at bridge site	Debris basin	Constructed to trap sediment
Local scour	Armoring devices	Reduced local scour	Rock riprap	Dumped or placed broken rock
			Artificial riprap	Alternatives to rock, including tetrapods, toskanes, and akmons
			Gabions and Reno mattresses	Wire mesh baskets and mattresses filled with loose stone
			Cable-tied blocks	Concrete blocks or slabs interconnected with steel cables
			Grout-filled bags	Fabric bags filled with concrete
			Grouted riprap, concrete apron, grout-filled mats	Rigid revetments
	Flow-altering devices	Reduced local scour at piers	Sacrificial piles	Piles or vanes placed upstream of bridge pier(s) to deflect flow away from the piers
			Iowa vanes	
			Horizontal collars	Thin horizontal plates attached to the base of the pier, to deflect flow away from the sediment bed
	Foundation modification	Reduced local scour	Underpinning	Extending bridge foundations to lower levels
			Extended footing	Slab footing to piers, which can inhibit local scour
	Guide banks	Improved flow alignment at bridge crossing; reduction in local scour at abutments		Straight or outward-curving structure, extending upstream from the end(s) of the approach embankment

Table 11-2 Distribution of Types of Scour Countermeasure in a 1995 U.S. Survey (after Parker et al. 1998)

Countermeasure	Number	Percentage
Dumped riprap	5,913	16.23
Self-launching riprap	72	0.20
Rock gabions	567	1.56
Other flexible revetment	37	0.10
Pavement	253	0.69
Grout-filled bags	97	0.27
Concrete-grouted riprap	27	0.07
Concrete-filled mat	51	0.14
Tetrapods	1	0.003
Extended footings	778	2.14
Cable-tied blocks	6	0.02
Vanes (pier or bed)	1	0.003
Sacrificial piles	22	0.06
Flow-direction plates	6	0.02
Jetties	43	0.12
Spurs	420	1.15
Retards	35	0.10
Check dams	83	0.23
Rock bank protection	79	0.22
Soil cement	7	0.02
Increase bridge span	2	0.005
Brace piles in transverse direction	5	0.01
Monitoring	27,770	76.22
Alarms	22	0.06
Bridge closure	111	0.30
Vehicle restriction	0	0.00
Other	24	0.07
Total	36,432	100.0

Three-dimensional spiral-edge vortices form downstream of flow separation lines on the corners of rectangular piers, on the sides of cylindrical piers, and at the upstream and downstream edges of round-nosed piers skewed to the flow direction. The vertically oriented vortices remain attached to the streambed just downstream of the separation from pier corners. These tornado-like flow structures transfer flow and sediment from the streambed upward and may be a primary mechanism of removal of dislodged sediment from scour holes. For clear-water scour conditions, Hjorth (1975), Parola (1993), and others reported that the primary mechanism of initial failure of armor protection was related to the flow at the edge separation points on rectangular piers, where conditions have been reported to be as much as an order of magnitude higher than those of the approaching flow.

Wake vortices form in response to the adverse pressure gradient of flow expansion, along with the highly nonuniform flow that is created along the shear flow zone on the pier sides. These vortices dominate the flow structure downstream of piers.

The pressure gradient that causes formation of the horseshoe vortex also deflects flow to the pier sides. The vertical nonuniformity of the boundary-layer flow approaching the pier in the presence of the stagnation pressure gradient causes a secondary flow throughout the flow depth as flow passes around the sides of the pier. Where the stagnation pressure gradient is relatively weak (wide piers in shallow flows), the vortical flow developed from flow curvature may be the most important feature in the formation of scour holes.

These large-scale vortical flow structures combine to increase the sediment entrainment and transport capacity by increasing near-bed flow velocity, turbulence levels, vorticity, and seepage gradients. In locations where surface water impinges on the streambed, near-bed streamlines and the sediment carried along them are deflected away from the region of the pier. Protection placed in this environment must resist the forces generated by these mechanisms and undermining by seepage and winnowing.

11.2.2 Mechanisms of Local Scour around Abutments

Although conceptually the pressure gradients and vertical nonuniformity that create the vortical flow at piers are also present at abutments, many factors associated with the generally large lateral extent of the flow field disturbed by abutments become important. In particular, the lateral extent of the flow disturbance is typically much larger than the flow depth. In contrast to the relatively uniform approach flow at piers, floodplain and main-channel geometry and roughness cause flow nonuniformity. The nonuniform lateral velocity distribution and extensive upstream adverse pressure gradients create upstream horizontal flow separation and recirculation zones. In laboratory experiments, where relatively low-roughness floodplains have typically been simulated, large separation regions called dead-water zones have been reported to form. Although the extent of the pressure gradients is larger, they are general much weaker than at piers. As a consequence, the dominant large-scale vortical structures include

- the flow curvature upstream that causes the primary vortex (see below) to form,
- the spiral edge vortices that form at flow separation from the edges, and
- the wake vortex systems.

Where abutments extend into the main channel or where bends force high-velocity flows against abutments, strong pressure gradients similar to those at piers may develop.

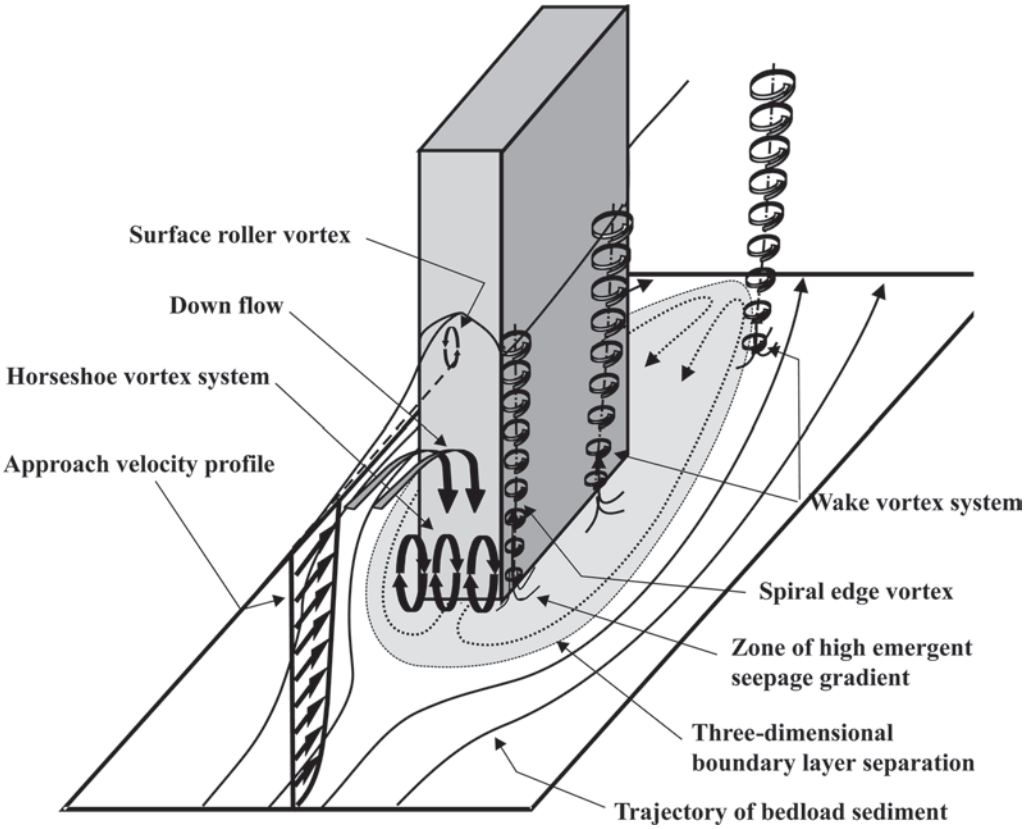

Fig. 11-1. Flow structures at a rectangular pier (modified from Parola 1995).

The pressure gradients caused by the flow at abutments force flow to contract toward the bridge opening. For short abutments that project into high-velocity flow, strong pressure gradients, similar to those at piers, cause a vortex to form that is similar to the horseshoe vortex. For relatively long abutments in relatively shallow flows, pressure gradients may be weaker; therefore, long vortices with their axes in the streamwise direction develop. The strongest of these vortices has been called the primary vortex (Kwan 1984). Although the pressure gradients induced by abutments are typically not as severe as those at piers, the effects of the pressure gradients are more extensive, causing flow curvature that extends far upstream of a bridge crossing. The flow curvature causes the formation of longitudinal vortex systems. Spiral-edge vortices, similar to those created at piers, form along the vertical edges of vertical-wall abutments and along spillthrough abutments at the point of flow separation. Initial scour-hole formation frequently is initiated at these locations. The initial movement of rock protection has been reported to occur at these locations in model studies by Pagan-Ortiz (1991).

11.2.3 Effects of River Morphology Development and Channel Contraction on Bridge Scour

Bridge-scour processes occur over a range of scales, from the local-scour scale around individual foundations described above, to the catchment scale extending to the limits of the catchment of the flow through the bridge section. In addition to local scour arising directly from the presence of individual bridge foundations, scour at a bridge site can arise due to contraction of flow width for the waterway section associated with the bridge structure (contraction scour), and also general river processes (general scour), including the respective processes of aggradation; degradation; scour in channel bends and channel confluences; scour due to the movement of both the channel thalweg and waves in the channel bed sediments; and lateral erosion arising from general bank erosion, channel widening, and channel migration processes. The total scour at a bridge site is given by the combination of the relevant components of general, contraction, and local scour.

Contraction scour can occur wherever the waterway section is laterally contracted by either natural channel morphology, such as a narrow neck in the river (a common bridge location), or imposed structures such as bridge foundations and associated road approach embankments. The width reduction causes increased flow velocities and bed shear stresses through the section, potentially increasing scour across the site as a whole. Analogously to local scour occurring at a bridge abutment, additional localized scour also typically occurs along boundaries at the entrance to a contraction where the flow is nonuniform. In practice,

contraction scour and local scour can occur together and it may be difficult to distinguish between them.

Aggradation, involving the building up of bed levels, can be ascribed to sediment supply generally exceeding sediment transport capacity or to a raising of the base level. Degradation, the lowering of bed levels over a region larger than the immediate vicinity of the bridge site, is conversely the result of sediment transport capacity generally exceeding sediment supply or a lowering of the channel base level. With sediment supply for a reach provided by erosion of the catchment and waterway, and sediment transport capacity a function of sediment size, channel size and discharge, degradation and aggradation are strongly influenced by changes in hydraulic regimes, geomorphic channel controls, and also catchment land uses, including changes in mining, deforestation, agricultural, urbanization, and river management practices within the catchment. Both aggradation and degradation can proceed in upstream or downstream directions, and both can induce associated lateral channel instability. It is important to recognize that cyclic aggradation and degradation responses of bed levels can follow from a disturbance to a channel system.

For most flows inducing general sediment motion at a bridge site, sediment waves will be migrating through the site. Waves in sand beds are commonly classified as ripples, dunes, antidunes, or chutes, and pools. In gravel-bed rivers, waves occur mostly as gravel bars moving down the river. With heights of migrating dunes and bars in natural alluvial channels potentially up to the order of the mean flow depth (Melville and Coleman 2000), the passage of these waves can potentially influence bridge scour significantly with wave troughs temporally and locally lowering bed elevations as the waves propagate through a site. Bed roughnesses determined by these waves also significantly affect stage-discharge relationships during the passage of floods.

Lateral movement of the channel thalweg (the line of lowest bed elevation along the channel) is a natural process that alters local bed elevations, inducing scour, and can change the point and/or angle of attack for a flow at a bridge site. Bridges need therefore to be designed for the potential influence of the thalweg occurring in the vicinity of each foundation.

At a confluence of river channels, the individual streams typically meet toward the centerline of the confluence, plunge to the channel bed, and then return to the water surface along the sides of the confluence. The induced helicoidal secondary currents, similar to such currents formed in river bends, result in a deep scour hole with steep sides. Channel confluences can form randomly in time and space for braided reaches, with the resulting scour holes potentially reaching depths below the surrounding bed of up to five times the mean flow depth in the converging channels. Such scour holes have been noted to be contributing factors in a number of bridge failures (Coleman et al. 2000; Coleman and Melville 2001).

For flow around a curved reach or bend, the interaction between the vertical gradient of streamwise velocity and the curvature of the primary flow generally produces secondary currents leading to greater flow depths, velocities, and shear stresses at the outside of the bend. These result in channel deepening at the outside of the bend (bend scour) and, in conjunction with concurrent undermining of the outside stream bank, increased lateral erosion at the outside of the bend.

Lateral erosion, reflecting the dynamic nature of channel planform, can have significant consequences if not allowed for in the design of static bridge structures. In addition to being associated with bend scour, lateral erosion can be in the form of general channel-bank erosion, channel widening, or channel shift for meandering and braided rivers. The relative importance of lateral erosion processes is reflected by the conclusion of Simon (1994; 1995) that width adjustment processes may represent the dominant mode of morphology adjustment for rivers. Certainly, Parola et al. (1996) indicate lateral channel instability to be one of the most common factors underlying excessive bridge and abutment scour and approach endangerment.

General channel-bank erosion can result from weathering mechanisms such as freeze-thaw and desiccation, seepage effects, surface runoff, erosion by current flow, the action of waves, the sediment-transport capacities of flows exceeding the potential supply of sediment from the channel bed, and mass failure mechanisms for banks, including sliding along a deep failure surface, shallow slips, and block failures.

Channel widening can accompany aggradation as flows seek to increase in width when the bed aggrades and flow depths decrease. Degradation can also result in channel widening, owing to the removal of toe support for the river banks, or resulting from increased excess pore pressures on the declining limbs of flood hydrographs causing bank failure.

For meandering and braided (including anabranched) rivers, incremental channel shift is inherent. Meander migration is typically directed outward and downstream and is typically a relatively slow and somewhat methodical process. For braided reaches, dramatic channel avulsion can occur in the course of a single flood, particularly for rivers with little vegetation within the floodplain. Incremental channel shift can be exacerbated by human activities such as land-use practices, gravel mining (Coleman and Melville 2001), and the removal of riparian vegetation.

Where bank erosion is a significant source of floating debris, lateral erosion can also lead to increased floating debris loading on bridges in the river, exacerbating any local scour at bridge foundations.

In regard to the overall assessment of potential scour magnitudes for a bridge, analyses of case studies of scour-induced bridge failure (Coleman and Melville 2001) indicate that ranges of combinations of potential scour components need to be considered—for example, solely pier scour, or pier scour combined with bend and contraction scours. Floods on the order of bank-full flows should be considered to assess

channel lateral migration and the influence of countermeasures on long-term lateral and vertical stream stability. Countermeasures should be designed to provide transport of sediment and debris through the bridge during bank-full events that is similar to that of the upstream and downstream reaches to prevent degradation or aggradation and lateral shift within the bridge opening. Case studies of scour-induced bridge failure (Coleman and Melville 2001) highlight, however, that both bridge-scour vulnerability and countermeasure design also need to be assessed for the occurrence of minor floods made more critical by present or potential river morphology at the bridge site.

11.3 PROTECTION AGAINST GENERAL SCOUR AND CONTRACTION SCOUR

11.3.1 Site Selection

The characteristics of a river can change considerably over short distances. Where multiple choices of bridge site are available, the following factors should be considered, although economic considerations may dictate selection of the shortest crossing point. Generally, sites exhibiting evidence of channel instability including degradation and aggradation, lateral movement and bank erosion, and hydraulic problems at other bridges in the area need to be assessed carefully.

11.3.1.1 Catchment Influences In bridge site selection, the potential influence on the site of changes within the catchment should be assessed, including history and patterns of water levels, flood magnitudes, earth flows, landslides, volcanic or earthquake activity, channel bars, channel confluence location, channel morphological controls, bank erosion, degradation, aggradation, and lateral channel instability. In particular, changes in human activities within a catchment can potentially influence vertical and lateral channel stability for the catchment. Such activities include agriculture, vegetation clearing, forestation, strip mining, urbanization, dam construction or removal, stream-bed mining or dredging, channel clearing, and channel realignment or containment.

11.3.1.2 Alluvial Fans Alluvial fans are inherently unstable, channels on the fan being potentially subject to rapid aggradation, degradation, and shift in channel location. Thus, bridges located on alluvial fans may be subject to continual problems due to channel instability. It is normally better to select a location at the apex of the fan where the channel is relatively more stable.

11.3.1.3 Influence of Channel Curvature Potential variation in river planform needs to be allowed for in the design of bridge foundations. Bridge locations on stable straight reaches or gentle bends, or at positions of geologically stabilized morphology, are often preferable. In meandering rivers, the choice is between a location at a bend or at a crossover point, although in some cases, the ideal location of a nodal point may exist, where the river has been flowing permanently irrespective of past river alignment changes. At a crossover the channel is wider, but may be more stable laterally than at a bend, where the channel is typically narrower and deeper. Bridge locations at stable bends necessitate designing the piers on the outside of the bend for the deepest channel scour, whereas the piers on the inside of the bend can be designed for less scour. If the bend can migrate, then all foundations need to be designed for the maximum scour in the bend. In straight reaches, the point of deepest scour can shift from side to side so that all piers need to be designed for the maximum scour. Foundations in the floodplain of a river need to be placed at the same level as those in the main channel if analyses indicate that the main channel can potentially move across the present floodplain.

11.3.2 Bridge Waterway Area

Wide, unimpeded bridge waterways are preferable. Constricted waterways induce contraction scour. The constriction can be lateral, due to the bridge foundations, or vertical, due to the bridge superstructure becoming submerged. It is important to ensure that the bridge is designed with adequate clearance between the maximum water level and the lowest level of the superstructure (including allowance for potential debris accumulations) to avoid superstructure submergence. In addition, it may be desirable to have the approach roadways at a lower level than the underside of the bridge superstructure, this allowing floodwater to overtop the approaches without intercepting the superstructure. The consequences of flow contraction can also be relieved by the construction of auxiliary (relief) bridges for floodplain flow.

In the design of new and replacement bridges where river morphology or existing structures severely contract flow, additional floodplain spans and relief structures should be considered. In the design of a replacement for a bridge structure that may be providing grade control, any increase in the bank-full flow capacity of the bridge opening may initiate degradation upstream and may thereby warrant the installation of appropriate grade control structures at the site to prevent such progressive degradation.

11.3.3 River Training Works

The cost of river training works at bridge sites can be significant. Training works are not normally required in relatively straight and stable reaches, where sites having the narrowest main channels and the smallest proportion of floodplain flow are preferable. In less stable rivers, sites requiring a minimum of river training are often preferable. For example, sites may be found where rock outcrops or other controls effectively limit lateral movement of the river channel.

11.3.4 Bank Protection

Lateral instability through general channel-bank erosion, bend scour, channel widening, or channel shift can result in

erosion of abutments, breaching of bridge approaches leading to the bridge being outflanked, and scour of bridge foundations located outside of the main channel. Where bank failure is by rotational slip, lateral pressures on bridge foundations within the slip zone can further result in displacement or cracking of the foundations.

Lagasse et al. (2001) indicate that impermeable longitudinal stone dikes parallel to the bank line, or smaller rock toe-dikes, provide the most effective toe protection of all bank stabilization measures studied for very dynamic and/or actively degrading channels, the authors presenting design procedures for these dikes. Aside from such bank stabilization measures, measures to counter lateral erosion act to armor the boundary or retard or train the flow. Flow training measures include groins, hardpoints, bendway weirs, and Iowa vanes. The following focuses on countermeasures that are more commonly encountered or that hold potential.

11.3.4.1 General Comments on Armoring Measures Armoring measures, also known as revetments, are channel linings used to provide erosion-resistant surfaces. They can be flexible or rigid. Flexible revetments include rock riprap, artificial riprap (including akmons, dolos, and tetrapods), broken concrete, used tires, grout-filled bags, precast blocks, cable-tied blocks, gabions and Reno mattresses, and vegetation. Rigid revetments used include concrete pavement, grouted riprap, concrete-filled fabric mat, and cement-stabilized soil. Flexible revetments have the advantage of being able to adjust to local displacement of underlying materials without complete failure of the installation, although such deformations tend to be limited for mattresses of used tires or precast blocks. All revetment types must be designed to protect against

- slumping due to over-steepened slopes,
- undermining due to inadequate toe protection, and
- outflanking due to inadequate lateral coverage.

Any hardening of the outer bank of a bend to counter lateral erosion can potentially exacerbate vertical erosion in the bend by preventing the supply of sediment from bank erosion. There is evidence, however (Harvey and Sing 1989; Thorne et al. 1995), that hardening of the outer bank has no effect on maximum flow depth in the bend.

11.3.4.2 Rock Riprap and Broken Concrete Rock riprap is the measure most commonly used to protect banks from erosion. Guidelines and principles for the use of riprap as bank protection are given in Appendix B. Broken concrete has been used as an alternative to rock riprap in emergencies where rock of suitable sizes and quality has not been readily available.

11.3.4.3 Artificial Riprap, Grout-Filled Bags, Precast (including Cable-Tied) Blocks, and Used Tires Artificial riprap, typically fabricated of reinforced concrete in the form of standard units, may become cost-effective where rock riprap of a required size and quality is not readily available. Prefabricated units such as dolos, tetrapods, tetrahedrons, and toskanes (Fig. 11-2) are designed to give maximum interlocking, and thereby maximum protection of the underlying surface, using a minimum amount of material. Artificial riprap is widely used in the coastal environment and for riverbank protection. The most common mode of failure of these armor units is edge failure. Each form of armor unit will have unique design criteria, and reference should be made to the unit manufacturer. Specifications for tetrapods and toskanes are given in USACE (1984). Filter layers or bedding material may be required to achieve the desired hydraulic performance.

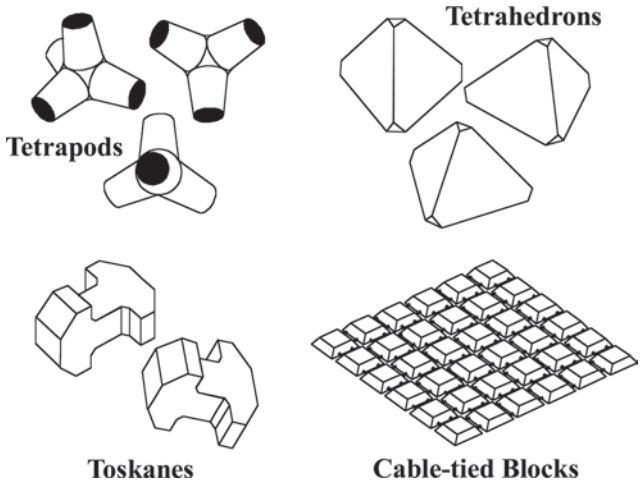

Fig. 11-2. Example of flexible armoring measures.

Stacked grout-filled bags form a flexible armoring countermeasure. These bags, however, provide little interlocking, with or without a geotextile, and are thereby subject to sliding and dispersion, leading to failure of the armoring measure, in the presence of degradation or a dune field. Lagasse et al. (2001) observe that grout-filled bags are installed only where rock of suitable size and quality has not been readily available. They comment that engineering judgment is typically used to select a bag size that will not be moved by channel flows. Installation practices critical to the success of grout-filled bag systems are discussed in Lagasse et al. (2001). Bags filled with sand instead of grout may offer additional advantages, including increased countermeasure flexibility, and possibly better interlocking.

Cable-tied blocks are flexible mats of interconnected smaller units (Fig. 11-2), typically concrete blocks or slabs interconnected with steel cables. The flexibility of the mat enables settlement of the mat edges, facilitating self-anchoring of mats in sand-bed streams. The blocks can be constructed in units with a preattached geotextile. The interconnected nature of the blocks allows stable scour protection to consist of smaller block units than for loose riprap. Failure modes for cable-tied blocks are found to include overturning and rolling up of unsecured leading edges and uplift of inner mats at higher velocities.

Lagasse et al. (2001) cite favorable reports of the performance of precast concrete blocks, where vegetation growing between the blocks can improve the appearance and stability of the countermeasure. They observe that each form of preformed block unit, including those that interlock and those held together by steel rods or cables, will have unique design criteria that should be available from the block manufacturer, these criteria having been formulated to ensure that intimate contact between the revetment and the protected subgrade is maintained under the desired hydraulic conditions. Lagasse et al. (2001) note that the significant influence of block protrusion into the flow on block stability necessitates construction inspection to ensure that blocks are installed within design tolerances.

Revetments of used tires in lieu of rock riprap have been successfully used for flow velocities up to 3 m/s on mild bends. These revetments can accommodate minor bank subsidence, but are somewhat unsightly and vandalism-prone and are typically expensive, owing to construction being labor-intensive. To aid revetment stability, tires should typically be tied together, with the revetment edges tied to the bank. They can also be packed with rock. In addition, the tires should fit together well; they can be assisted by vegetation planted in the tires (also aiding aesthetics); and they should resist uplift by being anchored to the bank at intervals and by having the sidewalls pierced to prevent flotation.

11.3.4.4 Concrete-Grouted Riprap, Concrete Pavement, and Grout-Filled Mats Concrete-grouted riprap is relatively cost-effective, making possible the use of rock of smaller sizes and wider gradings, although it scores poorly in terms of aesthetics and environmental acceptability. The decreased countermeasure flexibility negates the natural benefit of riprap being able to deform and armor developing scour, caused by toe undermining or bank settlement, for example. The reduced permeability of the armor layer arising from the grouting, although decreasing the need for filter layers beneath the countermeasure, is disadvantageous in that uplift from turbulence and confined groundwater can lead to failure of the rigid riprap layer in entirety.

Concrete pavement is similarly subject to problems of aesthetics, environmental acceptability, and susceptibility to uplift pressures. Weep holes can be used for relief of hydrostatic pressures for both concrete-grouted riprap and concrete pavement. Partially grouted riprap (in conjunction with underlying filter layers) can be used as a compromise measure, the grout acting to increase the stability of riprap installations without sacrificing all of the flexibility or pore-pressure-drainage advantages of loose riprap.

Grout-filled mats are continuous layers of fabric with pockets or cells that are filled with concrete. These mats, typically strengthened with cables, form a monolithic armoring countermeasure that is taken to be rigid in action. Grout-filled mats face the same problems as concrete-grouted riprap and concrete pavements, although porous mats may act to relieve hydrostatic pressures. Lagasse et al. (2001) present analyses of the hydraulic stability of these mats that make possible determination of mat thickness for a desired factor of safety against sliding of the unanchored mat.

In addition to potential failure due to uplift, these rigid revetments are subject to undermining by both hydraulic action (at the toe, the upstream and downstream edges, and also the upper edge if overtopped) and channel degradation. Grout-filled mats can also fail by overturning and rolling up of an unsecured leading edge, or uplift of the inner mat at higher velocities.

11.3.4.5 Gabions and Reno Mattresses Rock-and-wire gabions and mattresses comprise wire-mesh baskets and mattresses filled with loose stone, often connected together and often anchored to the channel boundary.

In comparison to more solid countermeasures, gabions are less susceptible to uplift forces, owing to the porous nature of the loose-rock fill material. In addition, should the countermeasure installation become unstable, the flexibility of the wire mesh enables gabions to mould themselves somewhat to restore stability of the installation. Gabions and Reno mattresses further allow the use of smaller rock than used for standard riprap protection (Simons et al. 1984), and can be used to protect steeper slopes, although gabions and mattresses are more expensive.

Damage to the wire mesh is a major reliability problem for gabions and Reno mattresses, potentially resulting in failure of individual gabions or even complete failure of the countermeasure installation as a whole. Wire damage may be from long-term corrosion or from abrasion due to the movement of either contained rock in highly turbulent flows or passing sediments in floods.

Design criteria for gabions can be determined from the unified formula (Table 11-3) of Pilarczyk (1995); this formula combines various design formulae for armoring countermeasure options. Alternatively, for stream slopes less than 2%, Maynord (1995) proposes use of the U.S. Army Corps of Engineers equation of B.11, where riprap size of which 30% by weight is finer, D_{30}, is replaced with the average filling rock diameter, D_m, which in turn is taken to be equivalent to half of a minimum gabion-basket thickness, $D_{n\min}$; that is, $D_{30} \rightarrow D_m = D_{n\min}/2$. For this procedure, a blanket thickness coefficient of $C_T = 1$ is adopted, and the stability coefficient C_s is taken to be $C_s = 0.1$. For additional detailed guidelines in regard to the materials and construction of gabions and Reno mattresses, the reader is referred to Parker et al. (1998).

11.3.4.6 Vegetation Through root action, dissipation of flow energy, and encouragement of sediment deposition, grasses and woody plants (trees and shrubs) act to armor surfaces to counter erosion and stabilize banks. Grasses can be used to protect upper banks that are subject to erosion due to rainfall, overland flow, and minor wave action. Woody plants offer better erosion protection owing to more extensive root systems. The U.S. Department of Agriculture (USDA 1996) provides U.S. guidelines for the use of vegetation as a method

Table 11-3 Unified Formula for Armoring Countermeasure Options (after Pilarczyk, 1995)

Factor		Relation
Unified formula	$\Delta D_n = \phi_c K_t \frac{0.035}{\theta_c} \frac{K_h}{K_{sl}} \frac{V^2}{2g}$ (11-6)	
	V = depth-averaged mean velocity	
Relative density, Δ	$\Delta = (S_s - 1)$	Rock riprap, Blocks, Blockmats
	$\Delta = (1-n)(S_s - 1)$	Gabions, Mattresses
	n = porosity of stones	
	S_s = specific gravity of stones	
Unit size, D_n	$D_n = 0.84 D_{r50}$	Rock riprap
	D_n = block thickness	Blocks
	D_n = basket thickness	Gabions, Mattresses
	D_{r50} = median size of riprap	
Stability factor, ϕ_c	$\phi_c = 1.0 \rightarrow 1.5$	Exposed edges
	$\phi_c = 0.50 \rightarrow 0.75$	Continuous protection
	$\phi_c = 0.75$	Common value for rock
Turbulence factor, K_t	$K_t = 1.0$	Normal turbulence (rivers)
	$K_t = 1.5$	Nonuniform flow with increased turbulence, Outer bends ($r/W > 2$)
	$K_t = 2.0$	High turbulence, e.g. sharp outer bends, ($r/W \leq 2$)
	r = bend radius	
	W = channel width	
Critical shear stress, θ_c	$\theta_c = 0.035$	Rock
	$\theta_c = 0.05$	Free blocks
	$\theta_c = 0.05 \rightarrow 0.07$	Blockmats, Mattresses
	$\theta_c \leq 0.10$	Rock-fill in gabions, Mattresses
Velocity profile factor, K_h	$K_h = \frac{2}{\log^2\left(1 + 12\frac{H}{D_n}\right)}$	For a fully-developed log velocity profile
	$K_h = \left(1 + \frac{H}{D_n}\right)^{-0.2}$	For a not-fully-developed velocity profile
	H = flow depth	
Bank slope factor, K_{sl}	$K_{sl} = \left(1 - \frac{\sin^2\alpha}{\sin^2\theta}\right)^{0.5}$	
	α = slope angle	
	θ = angle of repose	
Roughness height, k_s	$k_s = D_n$	Smooth units, e.g., concrete blocks
	$k_s = 1 \rightarrow 3D_n$	Rough units, i.e., rock

of streambank protection, including descriptions of principles, practice characteristics, design, construction materials, and appropriate techniques for streams, lakes, and estuaries. Willow trees have been successfully used in New Zealand (Acheson 1968) for protection of lower banks, where they establish quickly, withstand inundation, and are sufficiently dense to promote deposition of sediment. In terms of using vegetation as a countermeasure for bridge scour, care must be taken to ensure that any introduced vegetation does not adversely reduce channel capacity. In addition, Lagasse et al. (2001) recommend that vegetation not be seriously considered as a countermeasure against severe bank erosion where a highway facility is at risk.

11.3.4.7 Flow-Retarding Measures Flow-retarding measures (retards) are typically permeable structures, generally installed parallel to the bank and placed at the toe of the bank. They are thus best suited to protecting low banks or the lower portions of stream banks. They are designed to reduce flow velocity and control flow alignment, and thereby induce sediment deposition and prevent lateral erosion, creating an environment suitable for the establishment of vegetation. Retards include piles (typically timber or steel), fences, vegetation planting, and fields of jacks or tetrahedrons (with individual units possibly tied together using cables).

Key factors in the design of these measures include the availability of adequate floating debris and bed material to facilitate development of flow resistance and sediment deposition and the potential for bank revegetation to aid bank stability. The required permeability of retards is inversely proportional to the radius of curvature of the bend being protected, sharper bends requiring less permeable retards. Retards must be designed to withstand local scour processes and the potential impact of debris on structural loads and local-scour magnitudes.

Brown et al. (1981) conclude that retards are most successful for channels of widths less than about 100 m, flow velocities not frequently exceeding 1.5 to 1.8 m/s, and beds of sands with relatively large bed and suspended loads.

11.3.4.8 Groins and Bendway Weirs Groins (also referred to as spurs, dikes, wing dams, jetties, or deflectors) are structures that project from the bank into the channel (Fig. 11-3). Commonly constructed using rock, they may be permeable or impermeable and submerged or unsubmerged. They are designed to control flow alignment and reduce flow velocities near scour-threatened boundaries, thereby preventing lateral erosion, and possibly also inducing sediment deposition in the scour-threatened zone. They act through a combination of diverting flow around the structure, reducing flow along the bank as it passes through the structure, and redirecting flow passing over the weir. Groins are typically used to control meander migration. They can also be used to align wide, poorly defined streams into well-defined channels, reducing required lengths for any planned bridge crossings.

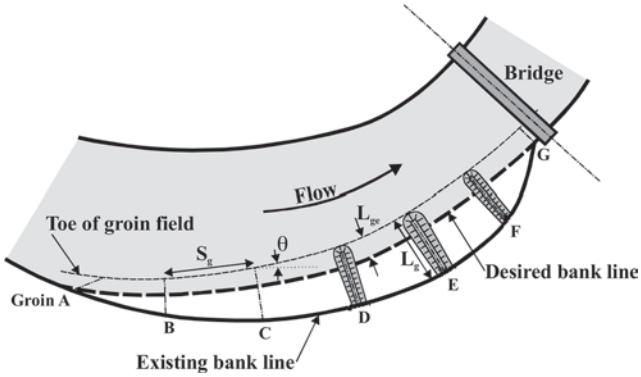

Fig. 11-3. Aspects of the design of a field of 7 groins.

The specification of standardized procedures for the design of groin fields is inappropriate owing to any given design being inherently site-specific. Some general principles, including published guidelines for groin spacing, are summarized in Table 11-4. Bendway weirs, also referred to as stream barbs, bank barbs, and reverse sills, essentially act as upstream-pointing submerged groins. Alternative guidelines (in terms of lengths, orientations, spacings, locations and numbers, heights, cross-sections, and construction) for these structures, particularly for larger structures or larger rivers, are given in Lagasse et al. (2001).

11.3.4.9 Hardpoints Hardpoints are small groin-like structures of stone fill placed along an eroding bank line. They are distinguished from groins because they protrude only short distances into the channel, typically acting individually to provide localized protection against scour. Lagasse et al. (2001) indicate that hardpoints are most effective where streamlines and bank lines are approximately parallel and velocities within 15 m of the bank line are less than approximately 3 m/s. These structures can be effective where bank erosion is mainly caused by a wandering thalweg, but close spacings required by the short lengths typically render these structures uneconomic for protection of meander bends.

11.3.4.10 Submerged (Iowa) Vanes Iowa vanes are submerged vertical plates installed in the streambed to deflect flow and control sediment deposition and erosion (Odgaard and Wang 1987). These vanes have been successfully used to control erosion in river bends (Odgaard and Kennedy 1983), ameliorate shoaling problems in rivers (Odgaard and Spoljaric 1986), and control sediment at lateral diversions (Barkdoll et al. 1999). The reader is referred to these papers, and particularly Odgaard and Wang (1991a; 1991b), for design guidelines and principles for the use of Iowa vanes in these situations.

11.3.5 Degradation, Contraction, Thalweg, and Sediment-Wave Effects

Each process of degradation, contraction scour, thalweg effects, or sediment-wave effects can lead to undermining

Table 11-4 Principles and Guidelines for the Design of Groin Fields (see Fig. 11-3)

Factor	Design criteria
Groin length, L_g (normal to flow or bank)	Where the bank is irregular, groin length should be adjusted to provide even curvature of the thalweg Generally, $L_{ge} < 0.15W$ (W = channel width) for impermeable groins, and $L_{ge} < 0.25W$ for permeable groins, where L_{ge} = effective groin length = distance between arcs describing the toe of the groin field and the desired bank line
Groin orientation	Orientation affects groin spacing, scour depth at the tip of the groin, and degree of flow control achieved Groins oriented normal to the flow are most economical because they provide maximum protrusion for a given groin length The first (upstream) groin should be angled downstream
Groin spacing, S_g	$S_g = L_{ge}\cot\theta$; where θ is the flow expansion angle downstream of the groin tips ($\approx 17°$ for impermeable groins, and increasing with permeability greater than 35%, Lagasse et al. 2001)

Reference	S_g/L_g	*Applicability*
Acheson (1968)	3–4	Depends on curvature and channel slope
Ahmad (1951)	4.3	Straight channels
	5	Curved channels
Copeland (1983)	2–3	Concave banks
Grant (1948)	3	Concave banks
Maza Alvarez (1989)	5.1–6.3	Straight channels
	2.5–4	Curved channels
Neill (1973)	4	General practice
Richardson et al. (1988)	2–6	Depends on flow and groin characteristics
Strom (1962)	3–5	General practice
Suzuki et al. (1987)	<4	Straight channels
United Nations (1953)	1	Concave banks
	2–2.5	Convex banks

Groin plan shape	Straight groins are preferred Top widths of impermeable groins should be at least 1 m
Longitudinal extent of groin field	Field and aerial surveys of the extent of scour are a good basis for determination of the necessary extent of a groin field Protection downstream of a bend is especially important because meander bends propagate downstream
Groin height	To avoid bank overtopping, impermeable groins generally do not exceed bank height Similarly, a sloping crest height (downward away from the bank line) is advantageous for impermeable groins Permeable groins should allow floating debris to pass over, unless the design requires trapping of light debris
Groin side slopes	Side slopes should be 2:1 (H:V) or flatter
Groin permeability	Permeability up to about 35% does not affect the length of channel bank protected Impermeable groins give better flow control, but induce greater end scour and, if submerged, can induce bank erosion High-permeability groins are preferred for mild bends and regions requiring small flow velocity reductions
Bed and bank contact	Adequate bed contact is necessary to avoid undermining of the groin, especially at the toe, where a launching apron is advantageous Adequate bank contact is necessary to avoid outflanking of the groin
Erosion protection	Riprap protection to the upstream and downstream faces and the end of the groin is recommended (possibly aided by filter layers)

of flow- and grade-control structures and bank protection, a need for bridge relocation, and bridge failure due to undermining of the foundations. Successful protection of piers and abutments involves providing adequate foundation depths, by underpinning of existing foundations if necessary, and allowing adequate setback of abutments from slumping banks where appropriate. Aside from such considerations of foundation design or modification, the countermeasures for these vertical-erosion processes act either to maintain stable bed levels through the bridge site or to ease the passage of flows past the bridge.

11.3.5.1 Check Dams Check dams are low dams or weirs constructed across the entire width of a channel. These dams act to establish a fixed grade point, maintaining bed levels at the bridge site and controlling any upstream migration of degradation. The structures are usually constructed of rock riprap (rock weirs), timber piles, gabions, concrete, or sheet piles, the first two materials being more for lower dams and channel widths less than 30 m. Typically, check dams are installed immediately downstream of the bridge they protect, although they can extend through the bridge site. For severe cases of degradation, two or more check dams in succession can be used, where a single higher dam may inhibit fish movement or cause severe scour downstream. Figure 11-4 shows the degradation protection for the Oreti River road bridge in New Zealand, the protection consisting of a rock weir downstream of the bridge and rock mattresses installed through the bridge site. Check dams are widely used in New Zealand to maintain bed levels through a bridge site, although increased focus on possible adverse ecosystem impacts is hindering the ready use of this countermeasure at present.

The dam height (relative to the bridge foundations) required to protect a bridge will depend on the identified causes of degradation and the morphology and hydrology of the river at both bridge and catchment scales. To be successful, check dams must not be undermined by piping or seepage around or beneath the dam or erosion upstream or downstream of the structure. In this regard, Parker et al. (1998) observe that the degree of degradation that such structures can withstand before they fail (Fig. 11-5) remains to be determined. Check dams can also initiate erosion of the banks and bed downstream of the structure. Such erosion, which can potentially undermine the dam, or lead to the river outflanking the dam, can be countered by energy dissipation measures for flows over the dam, including stilling basins (Lagasse et al. 2001). Alternatively, several lower weirs, a constructed artificial rapid, or an armored riverbed can be used. Any bank erosion caused by check dams can be controlled by the bank protection measures discussed above. Means of calculating potential scour depths downstream of check dams are discussed in Melville and Coleman (2000) and Lagasse et al. (2001). Breusers and Raudkivi (1991) recommend, however, that predictions of scour downstream of low weirs be derived from specific model tests, owing to possibly significant variations in the predictions of currently available analytical expressions.

11.3.5.2 Channel Lining (Paving) Parker et al. (1998) note that pavements and asphalt paving are limited in application to ephemeral rivers in arid environments. In general, riprap or concrete channel lining (paving) in the vicinity of a bridge has proved unsuccessful at stopping degradation, the lining being subject to undermining. A check dam may be used to protect such a lining, in which case the lining essentially becomes redundant. Channel-lining armoring measures for contraction, thalweg, and sediment-wave effects are discussed further in Sections 11.3.4.1 to 11.3.4.6.

11.3.5.3 Channel Widening, Relief Bridges, and Guide Banks Relief flow paths and widening of the bridge opening and the channel in the vicinity of a bridge can act to alleviate contraction-scour lowering of bed levels at the bridge site (Section 11.3.2). Guide banks (Section 11.5.4) and measures acting to retard flows along upstream floodplains (Section 11.3.4.7) can also be used to reduce flow contraction effects and resulting scour by improving the alignment and efficiency of flows through the bridge opening (Lagasse et al. 2001). Where appropriate, use of streamlined and solid

Fig. 11-4. The rock weir and rock mattresses protecting the Oreti River road bridge (looking downstream).

Fig. 11-5. An undermined and failed concrete check dam designed to control degradation on a Taiwanese river (looking upstream).

foundations can also ease potential debris accumulations and contraction effects.

11.3.6 Aggradation

Potential consequences of aggradation range from bridges being buried by sediment, to a need for bridge relocation, to increased loading on bridge structures (particularly during flooding), to increased likelihood of bridge overtopping and flooding of surrounding areas (with possible associated erosion) owing to a reduced waterway. Associated channel widening and lateral instability can also lead to bridge failure or erosion of bridge approaches, and can result in greater volumes of in-stream floating debris, increasing the potential for blocked waterways and for increased hydraulic loads and scour at bridges downstream.

If aggradation threatening a site is a temporary phenomenon, which in time will dissipate or pass downstream, then the sediment pulse can be dredged or simply allowed to migrate through the site if it is judged that the pulse will not endanger the infrastructure.

For longer-term aggradation, ideally the cause of the aggradation can be remedied, although typically the required measures prove to be complex, extensive, and very costly. Alternatively, and in lieu of diverting the river to accommodate or redesigning the bridge and bridge approaches, the river morphology resulting from the aggradation, active countermeasures are adopted. These countermeasures aim to increase sediment-transport capacity in the vicinity of the bridge site through the use of bridge or channel modifications, or reduce the volume of sediment supplied to the site through the use of structures to trap sediment upstream of the bridge, channel-bed mining or bar removal to control the bed level at the bridge, or general channel maintenance. Any countermeasure method adopted needs to be appropriate to the cause of the associated problem; otherwise it may not be successful.

Ongoing in-channel dredging and removal of channel vegetation can be used to increase flow capacity and consequent sediment-transport capacity. The frequency of such measures will be dictated by comparison of monitored rates of aggradation with tolerable rates determined for the bridge site. Any such measures will require assessments of possible associated pollution and ecosystem impacts.

Alternative control structures reducing the width of the channel can give increased flow velocities and sediment-transport rates.

Construction of a cutoff downstream of a bridge will increase channel slope, inducing higher sediment-transport rates upstream of the cutoff, thereby moderating aggradation at the bridge while the river adjusts to the changed alignment. Cutoffs must be designed with considerable study to correctly assess the magnitudes and locations of potential degradation, aggradation, and lateral erosion. The viability of such a channel realignment solution essentially depends upon the volume of the source aggradation material and the hydraulics and sediment-storage potential of possible alternative channel realignments.

Sediment traps and dams in the catchment upstream of the bridge can be used to reduce the supply of sediment to the bridge site, thereby moderating aggradation at the site. The performance of any in-channel trap must ensure that potential degradation downstream of the trap does not endanger the bridge structure. Sediment traps and dams can be expected to require some degree of ongoing maintenance. Johnson et al. (2001) observe that design of any sediment trap must consider

- appropriate width and depth to enable sediment to settle out of the flow and deposit,
- location facilitating ease of access for sediment-removal equipment,
- location enabling collection of sediments otherwise causing aggradation at the bridge site, and
- environmental impacts, including possible pollution and ecosystem impacts caused by trap maintenance procedures.

Channel-bed mining and bar removal provide very effective means of controlling aggradation or even inducing degradation at a bridge site, although such measures must continue as long as aggradation is occurring. The rate of sediment removal must be monitored to ensure that adverse degradation does not result at the bridge site.

In terms of a general channel-maintenance solution, equipment retained at the bridge site can be used to train the aggrading channel, pushing deposited material across to form terraced riverbanks. This maintenance process must continue as long as aggradation is occurring, and can result in the potentially dangerous situation of large channel levees of ungraded material containing flows over a channel bed elevated above the surrounding countryside. Such a scenario in the South Island of New Zealand has resulted in the Franz Josef community being threatened by the potential of flows being released by flood-induced breaching of the levees elevated above the township. Other measures must then be considered to alleviate the aggradation problem.

In general, any potentially adverse influence of the hydraulic and morphologic impacts of these countermeasure solutions on the bridge site and the general river system must be considered before the countermeasure can be adopted. A useful reference analysis of the potential benefits, disadvantages and costs of aggradation countermeasure options for a bridge in northern Pennsylvania, is presented by Johnson et al. (2001).

11.3.7 Bend and Confluence Scour

Vertical erosion arising from either bend scour or confluence scour can lead to undermining of flow- and grade-control

structures and bank protection, a need for bridge relocation, and bridge failure due to undermining of the foundations.

Channel lining (paving) at the outside of the bend using armoring measures discussed above (Sections 11.3.4.1–11.3.4.6) can be used as a countermeasure for vertical erosion arising from bend scour. Flow training measures discussed above (Sections 11.3.4.8–11.3.4.10) can alternatively be used to redirect flow through the bend, although it must be ensured that such measures do not simply relocate any adverse scour to a foundation away from the outside of the bend.

In the absence of foundation designs allowing for confluence scour magnitudes (Melville and Coleman 2000), foundations can be protected by maintenance of bed levels using check dams running through the bridge site and encompassing the foundations. Use of check dams extending across the entire width of the channel reflects the variable nature of confluence locations for braided rivers. Where constructing a check dam would prove prohibitively expensive for a wide braided river, monitoring of river planform development could alternatively be adopted as a form of countermeasure (Coleman et al. 2000). Protection measures at an individual foundation would then only be instigated when observed patterns of channel development indicate the possibility of a confluence scour hole impacting the foundation. Protection measures adopted for individual foundations could include armoring or flow training measures discussed above (Section 11.3.4).

11.3.8 Debris and Ice Jams

The accumulation of debris at bridge foundations typically increases the scour. Streamlined pier shapes are less likely to cause debris to accumulate, whereas pile bents are particularly prone to debris accumulation. Similarly, ice jams can exacerbate scour. At locations where ice jams and debris accumulations are expected, relief structures and roadway overtopping can be used effectively to reduce flooding as well as scour.

Piers and low-elevation superstructure may disrupt the flow of debris and ice through bridge openings. Velocities near the bridge may be significantly higher than those estimated when ice or debris accumulates on piers and superstructures blocking large areas of flow. Consequently, estimates of the potential impact of debris and ice blockage and their effect on flow direction and velocity should be considered when determining the type and size of countermeasures necessary to protect a bridge. Diehl (1997) provides a method for assessing the potential for debris accumulation on bridge elements that may be adapted for design of countermeasures at locations where debris is likely to be a problem. Bridges located on actively incising or widening streams are highly susceptible to blockage by debris because of the high input and transport of trees delivered through bank erosion (Diehl 1997; Parola et al. 1998).

11.4 COUNTERMEASURES FOR LOCAL SCOUR AT BRIDGE PIERS

11.4.1 Introduction

There are two categories of methods of protection of bridge piers against scour: armoring devices, such as riprap and alternatives to riprap, and flow-altering devices, such as sacrificial piles, horizontal collars, and deflector vanes. Alternatives to riprap include artificial riprap, such as toskanes and dolos, cable-tied blocks, grout-filled bags, and foundation extensions such as extended footings. The last can be effective in reducing local scour if the top level of the footing is at or below the undisturbed bed level, but can increase scour if the footing is at a higher level.

11.4.2 Pier Shape Design

The local scour at circular bridge piers is unaffected by changes in flow direction, rendering circular piers preferable to all other shapes where changes in flow alignment are likely. For piled foundations, the scour increases with the number and closeness of the piles. Therefore, it is better to develop bearing capacity using fewer and deeper piles. The local scour at piers with slab footings, pile bents, and piers founded on caissons may be exacerbated if the footing, pile cap, or caisson is at or above the undisturbed bed level. For piled foundations, it is preferable to construct pile caps above normal water level to minimize their influence on scouring.

11.4.3 Riprap Protection at Piers

The most commonly employed method of protecting bridge piers against scour is the use of a layer of riprap around the piers. Figure 11-6 shows riprap protection at a model-scale bridge pier (diameter 200 mm) prior to testing. The model riprap is crushed rock with median diameter 50 mm. The principle behind this technique is that large stones that are heavier than the bed sediment are able to withstand the higher shear stresses that occur around a bridge pier. A number of studies and reports dealing with riprap protection at bridge piers have been published, including Engels (1929); Gales (1938); Sousa Pinto (1959); Maza Alvarez (1968); Bonasoundas (1973); Neill (1973); Quazi and Peterson (1973); Posey (1974); Hjorth (1975); Breusers et al. (1977); Dargahi (1982); Farraday and Charlton (1983); Worman (1987); CBIP (1989); Parola and Jones (1989); Worman (1989); Breusers and Raudkivi (1991); Parola (1991, 1993); Austroads (1994); Chiew (1995); Parola (1995); Richardson and Davis (1995); Croad (1997); Lim and Chiew (1997); Parker et al. (1998); Lauchlan (1999); and Melville and Coleman (2000).

11.4.3.1 Failure Mechanisms for Riprap Placed at Bridge Piers The following four failure mechanisms of riprap layers at bridge piers were observed during laboratory

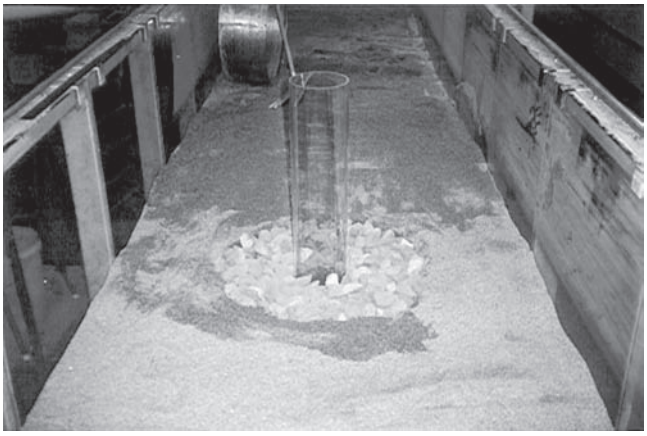

Fig. 11-6. Riprap protection at a model-scale bridge pier prior to testing (after Lauchlan 1999).

studies, including those of Parola (1993), Chiew (1995), and Lauchlan (1999):

- *Shear failure*. Shear failure occurs where the riprap stones are entrained by the flow, because they are unable to resist the hydrodynamic forces induced by the flow.
- *Winnowing failure*. The action of turbulence and seepage flows erodes the underlying bed material through voids between the riprap stones, a process that is more likely to occur in sand-bed rivers than in coarser bed materials. A filter is often recommended to resist winnowing failure.
- *Edge failure*. Scouring at the periphery of the riprap layer undermines the riprap stones. Riprap is vulnerable to edge failure in conditions where there is insufficient lateral extent of the protective layer.
- *Bed-form undermining*. The migration past the pier of the troughs of large dunes undermines the riprap layer, which settles as a consequence. Bed-form undermining is the controlling failure mechanism at bridge piers founded in riverbeds subject to migration of dunes, especially sand-bed rivers, according to Lim and Chiew (1997), Parker et al. (1998), and Lauchlan (1999). Figure 11-7 is a schematic diagram showing the failure mechanisms for a dune bed for riprap placed at the bed surface and riprap placed below the bed surface, respectively.

11.4.3.2 Riprap Design for Pier Protection Riprap design for pier protection against scour involves consideration of the following characteristics of the riprap layer, as illustrated in Fig. 11-8:

- Median size (D_{r50}) and gradation of the riprap material;
- Vertical thickness (t_r) of the riprap layer;
- Plan layout and horizontal coverage of the riprap layer, B_r and L_r;

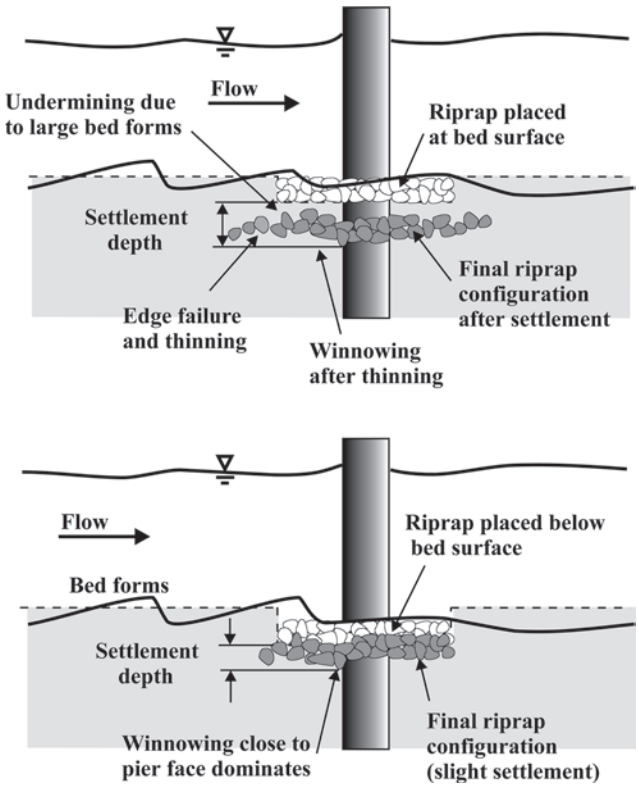

Fig. 11-7. Failure mechanisms for riprap protection at bridge piers (after Melville and Coleman 2000).

- Placement depth (Y_r) of the surface of the riprap layer below the sediment bed level; and
- Need for, and design of, a filter layer beneath the riprap.

11.4.3.3 Riprap Size Some of the equations that have been suggested for sizing riprap at bridge piers are given in Table 11-5. Most of these equations can be expressed in the form

$$\frac{D_{r50}}{H} = \frac{C}{(S_s - 1)^x} \mathrm{F}^y \qquad (11\text{-}1)$$

where

F = $U/(gH)^{0.5}$;
H = flow depth;
U = mean flow velocity;

and C, x, and y are coefficients, y typically varying between 2 and 3. It is apparent that riprap stone size depends strongly on flow velocity, but is less dependent on flow depth. In using these equations, U and H can be taken to be the depth-averaged velocity and the depth of the flow approaching the pier under consideration.

Melville and Coleman (2000) show that the riprap size equations predict widely varying stone sizes. Several of the

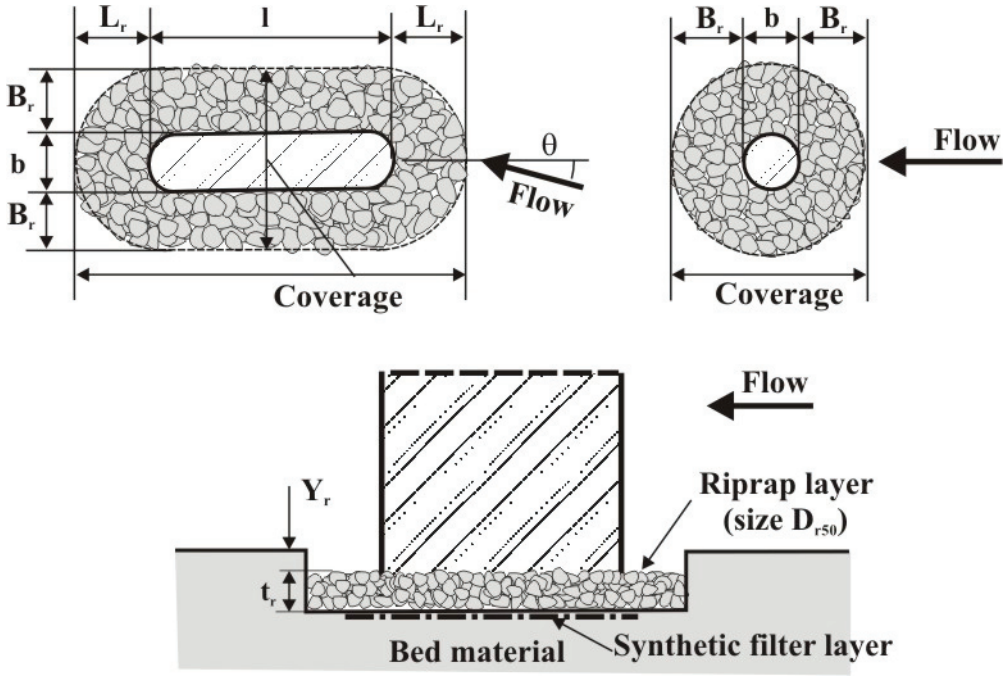

Fig. 11-8. Definition diagram for placement of riprap protection at bridge piers.

equations are based on laboratory data, whereas others have not been validated with data. Significant among the former group are the equations derived from the laboratory studies of Parola (1990)—see Parola and Jones (1989); Parola (1993; 1995); and Richardson and Davis (1995)—and those of Quazi and Peterson (1973) and Lauchlan (1999). Parola (1990) investigated the stability of riprap layers around circular and rectangular piers under clear-water conditions. The riprap was either placed flush with the bed or mounded above the bed. The failure criterion was related to the exposure of any part of the second layer of a three-stone thick layer. Parola (1993) presented an equation for cylindrical piers ($N_{sc} = 1.4$) and three equations for rectangular piers, depending on the riprap size relative to the pier width. Comparison of the former equation with standard riprap size relations (see Appendix B) indicates that riprap placed at a bridge pier needs to be about 2 to 3.6 times larger than the size required for stability in uniform undisturbed flow for the same flow conditions (Parola et al. 1995). Lauchlan (1999) examined the stability of riprap layers at circular and rectangular piers under live-bed conditions, finding no significant difference in riprap stability for the two pier shapes. The riprap was adjudged to have failed if the scour depth exceeded 20% of that at an unprotected pier under the same conditions. Lauchlan (1999) also investigated the effect of placing riprap below the sediment bed surface as a means of counteracting the influence of bed-form undermining. Quazi and Peterson (1973) formed a sediment bed of riprap stones and determined the flow velocity at which the stones were just stable for a round-nosed pier. Richardson and Davis (1995) recommend the Parola and Jones (1989) equation with an additional factor (f_2) for pier location in the channel. This equation is also suggested for use by Parker et al. (1998). The equations based on laboratory data, discussed above, are compared in Fig. 11-9 over the range F = 0 to 0.6 and for specific gravity of riprap $S_s = 2.65$.

Given the different experimental methods and, in particular, diverse failure criteria among these methods, the riprap size predictions of these equations are acceptably consistent and give reasonable estimates of stone size for design. A conservative combination of the rock size estimates given by the plotted equations is obtained by using the upper envelope generated by the Lauchlan (1999) relation together with the appropriate Parola relation.

11.4.3.4 Riprap Gradation Although the exact size distribution of riprap is not critical, it is important that the riprap should be well graded. Richardson and Davis (1995) state that the maximum rock size should not exceed twice the median size of the riprap; that is, $D_{r\max} \leq 2D_{r50}$. Croad (1997) gives an additional criterion, $D_{r50} \leq 2D_{r15}$. The grading curve envelope (upper and lower limits) shown in Fig. 11-10 encompasses most of the recommended gradings (Gregorius 1985).

11.4.3.5 Lateral Extent Recommendations for the areal extent of riprap protection at bridge piers, based on

Table 11-5 Equations for Sizing Riprap at Bridge Piers

Reference	Equation		Symbols
Bonasoundas (1973)	$D_{r50}\,(\mathrm{cm}) = 6 - 3.3U + 4U^2$	(11-7)	D_{r50} = riprap stone size for which 50% are finer by weight The equation applies to stones with $S_s = 2.65$ U = mean approach flow velocity (m/s)
Quazi and Peterson (1973)	$N_{sc} = 1.14\left(\frac{D_{r50}}{H}\right)^{-0.2}$	(11-8)	N_{sc} = Critical Stability Number = $U^2/[g(S_s\text{-}1)D_{r50}]$ F = Froude number of the approach flow = $U/(gH)^{0.5}$ H = mean approach flow depth
Breusers et al. (1977)	$U5\ 0.42[2g(S_s 2\ 1)D_{r50}]^{0.5}$	(11-9)	S_s = specific gravity of riprap stones
Farraday and Charlton (1983)	$\frac{D_{r50}}{H} = 0.547\,\mathrm{F}^3$	(11-10)	
Parola and Jones (1989)	$\frac{D_{r50}}{H} = \frac{0.346\,f_1^{\,2}}{(S_s - 1)}\mathrm{F}^2$	(11-11)	f_1 = factor for pier shape: $f_1 = 1.5$ (round-nose), 1.7 (rectangular)
Breusers and Raudkivi (1991)	$U = 4.8(S_s - 1)^{0.5}\ D_{r50}^{1/3} H^{1/6}$	(11-12)	
Austroads (1994)	$\frac{D_{r50}}{H} = \frac{0.58\,K_p\,K_v}{(S_s - 1)}\mathrm{F}^2$	(11-13)	K_p = factor for pier shape: $K_p = 2.25$ (round-nose), 2.89 (rectangular) K_v = velocity factor, varying from 0.81 for a pier near the bank of a straight channel to 2.89 for a pier at the outside of a bend in the main channel
Richardson and Davis (1995)	$D_{r50} = \frac{0.692\,(f_1 f_2 V)^2}{(S_s - 1)\,2g}$	(11-14)	f_2 = factor ranging from 0.9 for a pier near the bank in a straight reach to 1.7 for a pier in the main current at a bend
Chiew (1995)	$D_{r50} = \frac{0.168}{\sqrt{H}}\left(\frac{U}{U_*\sqrt{(S_s - 1)g}}\right)^3$ $U_* = \frac{0.3}{K_D\ K_H}$	(11-15)	K_H = flow depth factor $K_H = 0.783\left(\frac{H}{b}\right)^{0.322} - 0.106 \quad 0 \le \left(\frac{H}{b}\right) < 3$ $K_H = 1 \quad \left(\frac{H}{b}\right) \ge 3$ K_D = sediment size factor $K_D = 0.398\ln\left(\frac{b}{D_{r50}}\right) - 0.034\left[\ln\left(\frac{b}{D_{r50}}\right)\right]^2 \quad 1 \le \left(\frac{b}{D_{r50}}\right) < 50$ $K_D = 1 \quad \left(\frac{b}{D_{r50}}\right) \ge 50$
Parola (1993; 1995)	Rectangular: $N_{sc} = 0.8 \quad 20 < (b_p / D_{r50}) < 33$ $N_{sc} = 1.0 \quad 7 < (b_p / D_{r50}) < 14$ $N_{sc} = 1.2 \quad 4 < (b_p / D_{r50}) < 7$ Aligned Round-nose: $N_{sc} = 1.4$	(11-16)	b_p = projected width of pier
Croad (1997)	$\frac{U}{A\sqrt{(S_s - 1)gD_{r50}}} = 1.16\left(\frac{H}{D_{r50}} - 2\right)^{1/6}$ $D_{r50} = 17\,D_{b50}$	(11-17)	A = acceleration factor: $A = 0.45$ (circular and slab piers), $A = 0.35$ (square and sharp-edged piers) D_{b50} = median size of bed material Equation given for factor of safety = 1.25, as recommended by Croad (1997)
Lauchlan (1999)	$\frac{D_{r50}}{H} = 0.3S_f\left(1 - \frac{Y_r}{H}\right)^{2.75}\mathrm{F}^{1.2}$	(11-18)	S_f = safety factor, with a minimum recommended value = 1.1 Y_r = placement depth below bed level

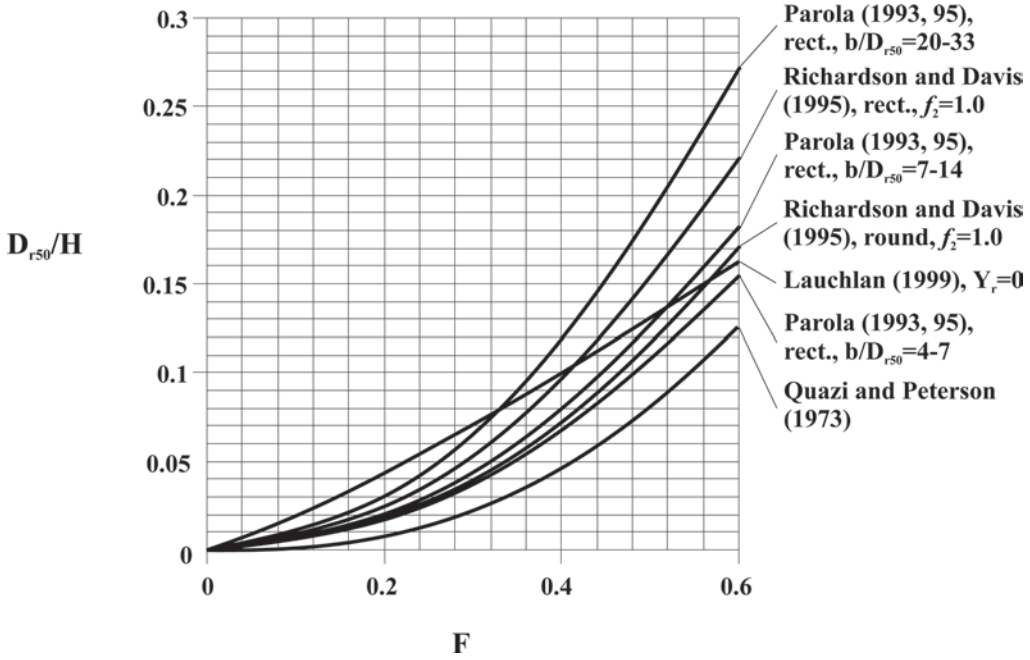

Fig. 11-9. Comparison of equations for sizing riprap at bridge piers.

laboratory testing, have been made by Sousa Pinto (1959); Maza Alvarez (1968); Bonasoundas (1973); Ruff and Nickelson (1993); Chiew (1995); Parola (1995); Croad (1997); Parker et al. (1998); and Lauchlan (1999), among others. These recommendations range from placing riprap only at the nose of the pier to completely surrounding the pier with a riprap layer extending up to 3*b* (where *b* is pier width) from the pier face in all directions. For rectangular piers, Parker et al. (1998) suggest the equation

$$B_r = L_r = \frac{1.5b}{\cos\theta} \tag{11-2}$$

where:

θ = angle of attack of the flow (see Fig. 11-8).

Oblong-shaped piers can be treated similarly. An equivalent coverage for a circular pier is to use a circular stone mat of diameter 4*b*, where *b* is the pier diameter.

11.4.3.6 Layer Thickness A range of recommendations for riprap layer thickness (t_r), typically from $t_r = 2D_{r50}$ to $3D_{r50}$, have been made. Thicker riprap layers impede the winnowing process and are able to resist disintegration through rearmoring. Chiew (1995) showed that thicker layers resist higher flow velocities, whereas laboratory testing by Lauchlan (1999) indicated an approximate 70% reduction in local scour pertaining to an increase in thickness from $1D_{r50}$ to $3D_{r50}$.

11.4.3.7 Placement Level Richardson and Davis (1995) and others propose that the surface of the riprap layer be placed at the streambed level. Neill (1973) and Breusers et al. (1977) recommend placing the riprap below the expected general scour level. Lauchlan (1999) found that placing riprap at some depth within the bed significantly improved the performance of the layer under live-bed conditions in sand-bed streams. The term $(1\text{-}Y_r/H)^{2.75}$ in her equation (Table 11-5) reflects this advantage, as shown in Fig. 11-11. Riprap placed deeper is inherently more stable, especially in sand-bed rivers, because the stones

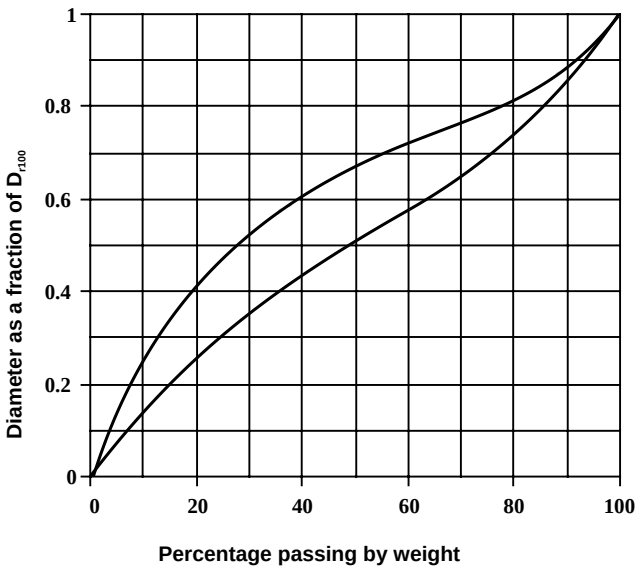

Fig. 11-10. Riprap grading curve envelope (after Gregorius 1985).

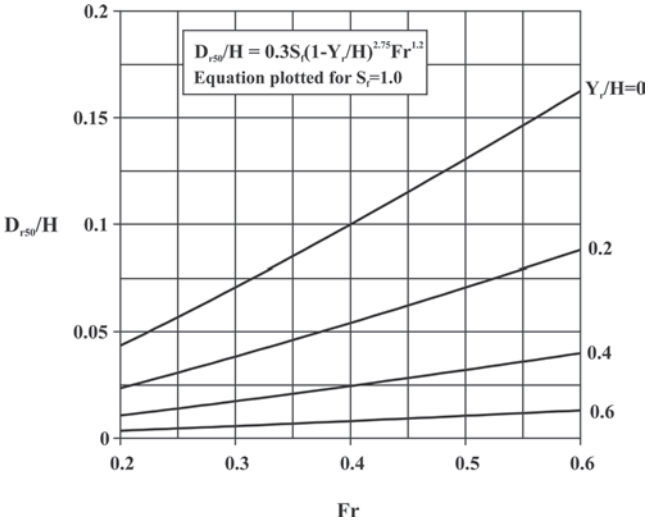

Fig. 11-11. Pier riprap size according to Lauchlan (1999) (modified from Melville and Coleman 2000).

are more resistant to bed-form undermining; see Fig. 11-8. Conversely, Parola (1991; 1993) observed enhanced stability for riprap mounded around the pier under clear-water conditions compared to that for riprap placed in preformed scour holes. Mounded riprap has construction advantages, and the mound may provide a source for replenishment of riprap material in the event of loss of riprap stones during a flood. Richardson and Davis (1995) warn that "it is a disadvantage to bury riprap so that the top of the mat is below the streambed because inspectors have difficulty determining if some or all of the riprap has been removed." Also, Parker et al. (1998) found that riprap dumped over a geotextile placed on an unexcavated bed performed almost as well as riprap placed with prior excavation.

11.4.3.8 Filters To combat winnowing effects at the pier face and to improve general stability of riprap layers, the use of a filter layer beneath the riprap stones has been proposed. Filters can be either granular filters, which make use of the filtering effect of graded sediments, or synthetic filters, commonly known as geotextiles. Filters must prevent the passage of the finer bed sediment, but also have adequate permeability to prevent build-up of water pressure in the underlying sediment. The well-known Terzaghi and Peck filter criteria (see Appendix B) have been proposed to select suitable granular filter media, although Posey (1974) found that a single filter layer was sufficient and Worman (1989) found that a thick single layer of riprap was an adequate alternative to the conventional Swedish practice of using multilayered riprap (incorporating a granular filter layer). The use of granular filters in the highly turbulent flow region at the base of a bridge pier is questionable. For example, Escarameia and May (1992) concluded from an experimental study that sand complying with the Terzaghi-based requirements performs poorly in highly turbulent environments.

An advantage of using geotextiles is fabric flexibility, which allows the geotextile to deform and remain intact, as well as to be reasonably resistant to tension and tearing. Important parameters in geotextile selection are appropriate pore size to retain finer sediments without clogging, adequate permeability to release pore pressures without causing uplift of the fabric under flood conditions, ultraviolet light resistance, puncture resistance, and shear strength. The lateral extent of the synthetic filter should be limited to about 75% of the lateral extent of the riprap. The reduced coverage of the synthetic filter ensures that edge stones in the riprap layer are able to protect the synthetic filter from being rolled up by the flow (Parker et al. 1998). It is important that the geotextile be adequately sealed to the pier face to prevent sediment from leaching at the pier/geotextile interface. Parker et al. (1998) offer suggestions for underwater installation of geotextiles at bridge piers.

On the basis of a detailed, large-scale laboratory study of riprap protection at bridge piers, with and without geotextiles, Parker et al. (1998) found "that under flood conditions in sand-bed streams with developed bed forms, the leaching of sand from the interstices of any armoring countermeasure may ultimately result in failure of the countermeasure. With this in mind, and in light of the positive results of experimental testing, it is suggested that such an armoring countermeasure be underlain by an appropriately selected geotextile." They also suggest that geotextiles not be used for gravel bed streams, due to the abrasive nature of gravel and its low potential for leaching. In addition, geotextiles should not be used at sites where significant degradation is likely, because the scour may leave the geotextile and riprap perched during floods, possibly leading to the loss of both (see below). At bridge piers on the floodplain where clear-water scour conditions typically pertain, this potential disadvantage of the use of geotextiles is less likely to exist.

11.4.3.9 Riprap Tolerance to Degradation Degradation occurs in rivers when the outflow of sediment exceeds the inflow, leading to a net loss of sediment in the reach. Lauchlan (1999) investigated the effect of a degrading bed on riprap protective layers at bridge piers. Laboratory experiments indicated that riprap layers are capable of providing a reasonably high degree of protection for bridge piers for high rates of degradation and high flow rates. However, the results also imply that in a degrading bed situation, riprap protective layers would eventually fail. As the bed surrounding the riprap degrades, the stones subside and can move outward. Long-term degradation causes the majority of the stones to move outward from the pier, which reduces the thickness of the riprap layer and its ability to protect the pier. However, if lack of sediment input is merely a short-term problem, the layer is likely to be able to withstand the attack.

Because subsidence of the riprap layer with the degrading bed is important in maintaining stability of the layer, filters should not be employed where significant degradation is anticipated. A geotextile or granular filter would prevent

winnowing from occurring at the pier face, and winnowing is essential if the riprap is to subside. The implication is that the riprap would not subside if coupled with a filter, leading to increased exposure of the stones, disintegration of the riprap, and loss of protection against scour. At sites where degradation is anticipated, it is preferable to increase riprap layer thickness rather than use a filter.

11.4.4 Alternatives to Riprap

Alternatives to rock riprap include other armoring measures, overviewed in Section 11.3.4, and flow-altering measures. Aside from these active countermeasures to prevent scour, bridges can also be structurally modified through underpinning or foundation extension. Examples of flow-altering measures that have been used or suggested to protect piers against local scour include sacrificial piles placed upstream of the pier, Iowa vanes, and flow deflectors attached to the pier such as collars. Field experience of flow-altering devices is limited.

11.4.4.1 Artificial Riprap Each form of artificial armor unit (Section 11.3.4.3) will have unique design criteria that should be available from the unit manufacturer. In terms of common forms of artificial riprap, Parker et al. (1998) consider guidelines for implementation at bridge piers to be complete, the work of Ruff and Fotherby (1995) being noteworthy.

Despite the detailed design criteria available, there are few examples of the use of artificial riprap as a scour countermeasure at bridge piers. Studies to date indicate that artificial riprap does not offer significant advantages over rock riprap for scour protection at piers. Ruff and Fotherby (1995) conclude this in terms of toskanes. Fotherby (1992) and Bertoldi et al. (1996) both suggest that the use of tetrapods at bridge piers offers little advantage over riprap in terms of stability of the armoring units. An additional disadvantage of artificial riprap in comparison to rock riprap is a possible lengthy installation time to achieve the required interlocking nature of the units.

If artificial riprap is to be utilized at a bridge pier, the reader is referred to Fotherby and Ruff (1996) and Parker et al. (1998) for design guidelines and principles, along with comments on construction and maintenance for this scour countermeasure. In addition, Lagasse et al. (2001) provide summaries of design procedures and present design examples for bridge-pier protection using toskanes (Fotherby and Ruff, 1996) and modules of A-Jacks (Armortec Inc., Bowling Green, Kentucky).

11.4.4.2 Cable-Tied Blocks A few examples of the use of cable-tied blocks (Section 11.3.4.3) currently exist at piers in the United States. More such installations may follow; cable-tied blocks have recently been shown (Jones et al. 1995; Bertoldi et al. 1996; University of Minnesota 1996; 1997; Parker et al. 1998) to provide a useful alternative to riprap at bridge piers over a wide range of conditions and over successive flow events. The performance of this countermeasure is aided by the blocks being underlain by an appropriately sized geotextile filter, and also by the geotextile being sealed to the pier. Design guidelines given by Parker et al. (1998) are summarized in Table 11-6.

11.4.4.3 Gabions and Reno Mattresses Gabions (Section 11.3.4.5) have experienced significant use in the field as a countermeasure for bridge scour, although a recent evaluation of their field use in New York State is rather pessimistic, following the failure of many installations. Design guidelines given by Parker et al. (1998) for the use of gabions and Reno mattresses (Section 11.3.4.5) at bridge piers are summarized in Table 11-7. Additional detailed guidelines for the materials and construction of gabions and Reno mattresses are also given in Parker et al. (1998).

11.4.4.4 Grout-Filled Bags or Mats Grout-filled bags (sacks) or mats constitute fabric shells filled with concrete. These measures can be deployed rapidly and provide an economical alternative to rock riprap where this is not readily available. A particular advantage is that shells filled with dry concrete can be placed directly at bridge foundations, with hydration occurring naturally.

With regard to their potential to slide and disperse (Section 11.3.4.3), Parker et al. (1998) recommend avoiding grout-filled bags, concluding that riprap and cable-tied blocks are generally more effective as countermeasures for pier scour. In the event that grout-filled bags are nevertheless to be utilized, design guidelines given by Parker et al. (1998) are summarized in Table 11-8. Installation practices at bridge foundations, critical to the success of grout-filled bag systems, are also discussed in Lagasse et al. (2001).

Fotherby (1992), Jones et al. (1995), and Bertoldi et al. (1996) report studies of the use of concrete-filled mats (Section 11.3.4.4) for pier protection. These studies show that mats need to be bound to and sealed with the pier (although they recognize potential increased pier loadings) and recommend that mats be installed with their top surfaces flush with the bed, this reducing or eliminating the need for any anchoring to prevent uplift failure. Failure likely involves replacement of the entire unit; failure modes include undermining, overturning and rolling up of an unsecured leading edge, and uplift of the inner mat at higher velocities. Guidelines for mattress areal extent, thickness, and anchoring remain to be determined, including a lift criterion to size grout mattresses to prevent failure by rollup.

11.4.4.5 Concrete Apron and Grouted Riprap Concrete pavements and asphalt paving are best suited to applications in ephemeral rivers in arid environments (Parker et al. 1998). In general, bridge designers doubt the durability of in-stream pavements and anticipate turbulence-induced and confined-groundwater uplift stresses generated during flood events to cause failure of the impermeable pavement. Pavement edges are also prone to undermining, possibly leading to destabilization of the pavement.

Table 11-6 Principles and Guidelines for the Design of Cable-Tied Blocks (Fig. 11-2) for Pier-scour Protection

Factor	Design criteria
Feasibility	Suitable for sand-bed and gravel-bed rivers Not suitable for pile bents or complex pier shapes Not suitable for rivers with large cobbles or rocks Not suitable for corrosive water quality, such as saline (including estuarine) or acidic environments Favorable characteristics for ephemeral, flashy, and moderate hydrograph streams, as well as floodplain installations May become cost-effective where rock riprap of a required size and quality is not readily available
Block shape, spacing, and size	Block shape to facilitate mat flexibility Spacing between blocks to facilitate mat flexibility $\varsigma = a_{cb}\left(\frac{\rho_{cb}}{\rho_{cb}-\rho}\right)\rho U^2$ and $\varsigma = \rho_{cb}\, gH_{cb}\,(1-p)$ where: ζ = weight per unit mat area (N/m^2) (required for mat stability) H_{cb} = block height (m) p = volume fraction pore space of the mat ρ = water density = 1000 kg/m^3 ρ_{cb} = density of the block material for the mat (kg/m^3) a_{cb} = 0.20 U = depth-averaged flow velocity (m/s)
Mat installation	Preexcavation of the upstream edge is required, and for gravel-bed streams, all edges must be anchored (requiring preexcavation) General prior excavation is not required unless $4H_{cb} >$ design approach flow depth Mat (centered on the pier) is to be of width ($4D/\cos\beta$) and length in the direction of flow [L + ($3D/\cos\beta$)] where: β = angle of flow attack ($\beta = 0^\circ$ giving the flow aligned with the pier) D = pier diameter for cylindrical pier, and pier width for rectangular pier L = pier length (= D for cylindrical pier)
Cable location and quality	Cables to be located near the center of each block to allow maximum mat flexibility Cables to be sufficiently flexible to allow mat deformation, but sufficiently durable to survive at least 20 years in situ Stainless steel to be used for harsh environments
Geotextile filter	Resists leaching of bed material from between blocks To be fastened firmly to the base of a mat for a sand-bed river Not to be used for a gravel-bed river Not to extend to the mat edges, but (approximately extending 2/3 of the distance from each pier face to the mat edge) to be of width ($3D/\cos\beta$) and length in the direction of flow [$L + (2D/\cos\beta)$] Not to be replaced with a granular filter layer In some cases, local grouting is recommended wherever there is danger of abrasion of the geotextile
Pier seal	Mat (and geotextile filter) to be fastened and sealed to the pier (recognizing potential increased pier loadings), aided by a granular filter zone if required

Table 11-7 Principles and Guidelines for the Design of Gabions and Reno Mattresses for Pier-scour Protection

Factor	Design criteria
Feasibility	Potential abrasion of casing materials by passing sediments of sand-size and larger needs to be recognized and addressed where possible by material selection Gabions are not recommended for gravel-bed streams owing to bed-load abrasion wearing out the casing causing gabion rupture Well suited to ephemeral streams, but potentially difficult to place in deeper channels Not suitable for corrosive water quality, such as saline or acidic environments Potentially difficult to implement for nonuniform riverbed or pier geometries Useful where rock riprap of a large required size is not readily available
Basket size and shape	$V_{\min} = 0.069\left[\frac{U^6 K^6}{(S_{sr}-1)^3 g^3}\right]$, where: $V_{\min}$ = minimum basket volume for individual unconnected baskets (m^3) U = depth-averaged flow velocity (m/s) K = pier-shape factor (round-nosed piers, $K=1.5$; square-nosed piers, $K=1.7$) $S_{sr} = \rho_r/\rho$ = rock specific gravity ρ_r = rock density (kg/m^3) ρ = water density = 1000 kg/m^3 g = gravitational acceleration, g = 9.81 m/s^2 Basket volumes larger than $V_{\min}$ may be appropriate Baskets to be kept relatively low in height to reduce cross-sectional blockage and resist uplift, with basket heights to exceed a minimum of 0.15 m Standard gabions are of nominal heights of 0.3, 0.45, or 0.9 m; nominal lengths of 1.8, 2.7, or 3.6 m; and a nominal width of 0.9 m Standard Reno mattresses are of nominal heights of 0.15 or 0.225 m; nominal lengths of 2.7 or 3.6 m; and a nominal width of 1.8 m
Gabion-field installation	Riverbed to be smoothed and existing scour holes filled with stones before gabions are installed, preexcavation to give the top of the gabion installation flush with the bed being advantageous The gabion-field coverage (centered on the pier) is to be of width ($5D/\cos\beta$) and length in the direction of flow [$L+(4D/\cos\beta)$], where: β = angle of flow attack ($\beta = 0^\circ$ giving the flow aligned with the pier) D = pier diameter for cylindrical pier, and pier width for rectangular pier L = pier length (= D for cylindrical pier) Gabions are readily stacked in stable configurations and mould themselves in response to instabilities Adjacent baskets to be joined using the same wire used to lace the baskets Completed gabions lifted into place, or empty baskets joined to gabions already in position, then stretched and correctly aligned before being filled Hand work helps to minimize the percentage of voids in baskets
Basket materials	Minimum rock size to be at least 25% larger than the minimum basket opening Maximum rock size not to exceed 2/3 of the minimum basket dimension Casing materials must be durable and also facilitate basket flexibility, ideally single-strand galvanized or PVC-coated wiring that resists corrosion (and with the wire recommended to be like a chain-link fence, i.e., formed with a double twist to prevent unraveling) Basket sidewalls to be reinforced with wires of diameter larger than that used for the basket mesh in order to provide sidewall stiffness
Geotextile filter	Resists leaching of bed material from beneath the gabions To be used underneath the gabion field for a sand-bed river Not to extend to the edges of the basket field Can be replaced with a granular filter layer if the geotextile is not available
Pier seal	Geotextile filter to be fastened and sealed to the pier (in recognition of potential increased pier loadings), aided by a granular filter zone if required

Table 11-8 Principles and Guidelines for the Design of Grout-Filled Bags for Pier-scour Protection

Factor	Design criteria
Feasibility	Potentially applicable only to small streams, or where bag width (~1 m) > pier width (bags then being large relative to any local scour hole) Not suitable for gravel-bed streams, or sand-bed streams with developed dunes Can be aesthetically unacceptable Useful where rock riprap of a required size and quality is not readily available
Bag size and shape	Design as for riprap, with D_{r50} = bag height, and with the following amendments: In calculations, use the material density ρ_r pertaining to the grout Increasing the bag size D_{r50} by a factor of 1.2 is recommended to aid bag stability Bags are not to be of sizes or shapes that hinder flexibility of the installed countermeasure Shorter bags heights are desirable An example bag size is 3 × 0.9 × 0.3m
Bag-field installation	The bag-field coverage (centered on the pier) is to be of width ($5D/\cos\beta$) and length in the direction of flow [$L + (4D/\cos\beta)$], where β = angle of flow attack ($\beta = 0^\circ$ giving the flow aligned with the pier) D = pier diameter for cylindrical pier, and pier width for rectangular pier L = pier length (= D for cylindrical pier) Upstream bags are to overlap downstream bags to aid stability Fotherby (1992) indicates that properly sized bags are more effective if used to extend a single layer of protection laterally, rather than if they are stacked Imbricated (shingled) stacking can potentially enhance interlocking and aid stability
Bag materials	If possible, the surface of the bag should be rendered angular and rough Grout quality should ensure that the grout does not degrade and break or crumble
Geotextile filter	Resists leaching of bed material from between bags To be used underneath the bag field for a sand-bed river Not to be used for a gravel-bed river Not to extend to the edges of the bag field, but to be of width ($3D/\cos\beta$) and length in the direction of flow [$L + (2D/\cos\beta)$] Can be replaced with a granular filter layer if the geotextile is not available
Pier seal	Geotextile filter to be fastened and sealed to the pier (recognizing potential increased pier loadings), aided by a granular filter zone if required

Parker et al. (1998) indicate concrete-grouted riprap to be relatively cost-effective, although it scores poorly in terms of aesthetics and environmental acceptability, as well as on feasibility for use with finer sediments such as silt. The reduced permeability arising from the grouting is disadvantageous because uplift can cause failure of the riprap layer in entirety. The decreased countermeasure flexibility also negates the natural benefit of riprap being able to deform and armor a developing scour hole.

11.4.4.6 Sacrificial Piles Sacrificial piles are piles placed upstream of a pier to deflect high-velocity flow from impacting the pier, with the pier located in the wake region behind the piles (Fig. 11-12). The piles can be arranged in a variety of plan configurations, with varying pile sizes and numbers, and with the piles submerged or extending over the full depth of flow. A triangular pile configuration, with the apex pointing upstream, has been shown to be one of the better configurations in terms of protecting the pier (Fig. 11-12). Sacrificial piles have the benefit of being relatively quick to implement. They are, however, not suited to riverbeds of bedrock or boulders, and they can be unacceptable on aesthetic grounds. Chang and Karim (1972) and Paice and Hey (1993) report laboratory studies and field experience of the use of sacrificial piles for pier-scour protection. Further laboratory studies are reported by Chabert and Engeldinger (1956); Levi and Luna (1961); Shen et al. (1966); Wang (1994); Singh et al. (1995); and Melville and Hadfield (1999).

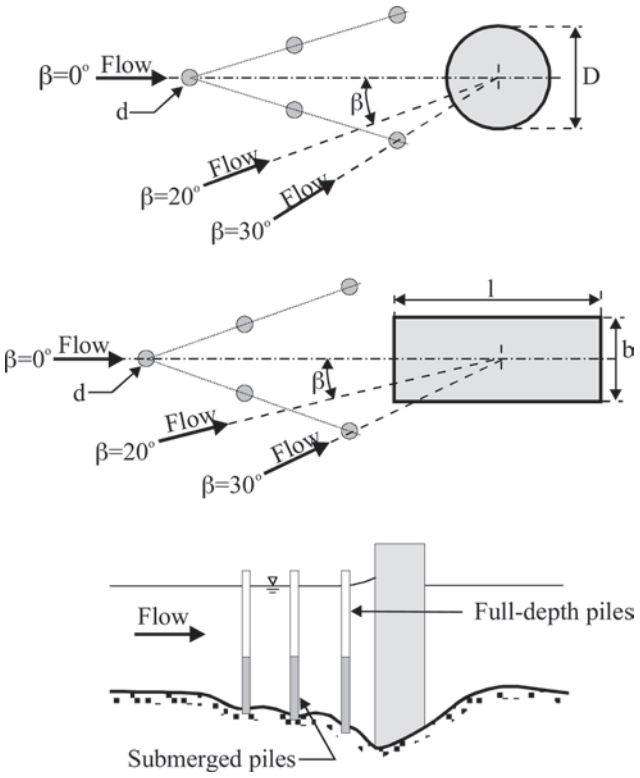

Fig. 11-12. Example configurations of five sacrificial piles.

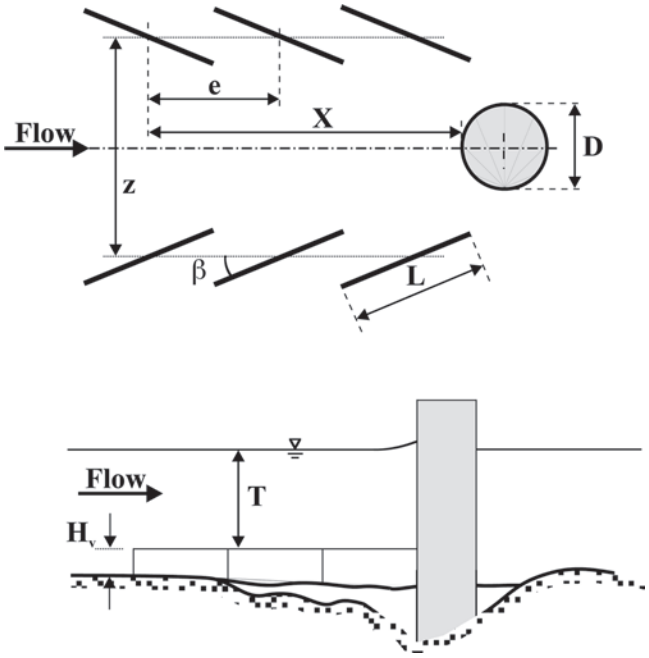

Fig. 11-13. The use of Iowa vanes as a pier-scour countermeasure.

The effectiveness of sacrificial piles for pier-scour protection is found to be particularly dependent on the approach flow angle β (Fig. 11-12) and flow intensity V/V_c, where V is depth-averaged flow velocity, and V_c is this velocity at the threshold condition for sediment movement. For aligned ($\beta = 0^o$) clear-water ($V/V_c < 1$) flows, sacrificial pile configurations can give up to 40 to 50% reduction in scour at the protected pier, with reduced effectiveness under live-bed conditions of $V/V_c > 1$ (Melville and Hadfield 1999) due to the passage of bed forms. Parker et al. (1998) conclude that sacrificial piles are an ineffective way to suppress scour under mobile-bed conditions. A significant consideration is that variation in flow alignment β typically reduces the effectiveness of the pile configuration in protecting the pier. Large flow skewness ($\beta > 20^o$) may result in the piles actually exacerbating scour at the pier.

In general, sacrificial piles are not recommended unless the flow remains aligned ($\beta = 0^o$) and the flow intensity is relatively low. Under such conditions, submerged and full-depth piles give similar reductions in scour. If sacrificial piles are to be utilized for such conditions, model testing to determine the optimum pile configuration is recommended, with the piles themselves needing to be designed against scour undermining. The effects of debris contamination on the performance of the piles also need to be considered, as do any effects of the piles on navigation.

11.4.4.7 Iowa Vanes As a countermeasure for pier scour, Iowa vanes (Section 11.3.4.10) are installed just upstream of the pier and angled inward, looking downstream (Fig. 11-13), with the vane configuration designed both to induce secondary currents that interfere with the horseshoe vortex and also to encourage sediment deposition in the region of local scour at the pier. Potential disadvantages of a field of vanes include the potential to collect debris, the potential for damage by sediment in motion, and possible decreased performance for skewed flows. Parker et al. (1998) conclude, however, that of flow-altering countermeasures, only Iowa vanes show enough promise to warrant further study. Comments on construction and maintenance of Iowa vanes are given in Parker et al. (1998).

By varying vane height H_v (and thereby submergence T for constant flow depth), vane angle of attack β, vane spacings z and e, vane length L, and longitudinal extent of vane field X for two flow velocities (Fig. 11-13), Lauchlan (1999) investigated the performance of vane configurations in terms of countering clear-water and live-bed scour at a cylindrical pier. The results of the tests indicate the angle of attack β and the streamwise spacing e to be principal parameters affecting the performance of vane configurations. The testing, although indicating potential scour reductions through use of the vanes, is not comprehensive, and further tests remain to

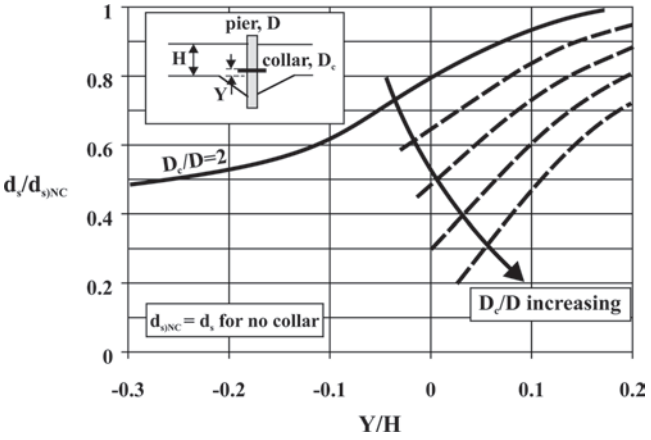

Fig. 11-14. The influence of horizontal-collar location and size on equilibrium scour depth d_s for a cylindrical pier (modified from Melville and Coleman 2000).

determine the degree of usefulness of Iowa vanes for control of pier scour.

11.4.4.8 Horizontal Collars Horizontal collars (Fig. 11-14) are designed to protect piers against scour by shielding the sediment bed from the downflow and horseshoe-vortex flow structures (Fig. 11-1) in the vicinity of the pier. These collars are thin in vertical section in order not to exacerbate scour. They have the potential disadvantage, however, of encouraging debris accumulation. The concept of using collars as scour countermeasures has been investigated by Schneible (1951); Chabert and Engeldinger (1956); Tanaka and Yano (1967); Thomas (1967); Ettema (1980); Dargahi (1990); Chiew (1992); and Fotherby (1992).

To date, collars have not been tested under live-bed conditions, and so they should not be considered for use other than in low sediment-transport conditions, such as may exist on floodplains or in vegetated channels.

For clear-water conditions, Fig. 11-14 summarizes the trends of available data on the influence of collar diameter D_c and location Y above the surrounding bed on scour reduction. The data indicate that a collar can reduce scour depth significantly. For maximum scour protection, the collar should be placed beneath the surrounding bed level. Scour depth for a circular pier can thereby be halved for a collar diameter twice that of the pier. Despite these encouraging results, Parker et al. (1998) do not consider horizontal collars to warrant further study or the development of user guidelines.

11.5 ABUTMENT PROTECTION

11.5.1 Introduction

Protection of bridge abutments from scour includes countermeasures that alter flow and scour patterns and those that armor the bed, bank, floodplain, and embankment slopes. Armor protection frequently includes the coverage of susceptible portions of embankment slopes. Many design guidance documents recommend that an apron be constructed around the toe of the embankment slope. Armor aprons can protect vertical-wall abutments founded on spread footings. Filters have been recommended below the protection to prevent piping of soils through the armor layers. The filters also may be beneficial to prevent winnowing of soils from beneath aprons, especially where the armor layer is used to protect embankments under live-bed conditions. There is evidence that fabric filters may be detrimental to the performance of armor protection where settlement and movement of the armor layer is necessary for the armor layer to conform to general bed degradation or scour hole formation.

Based on extensive field observations of flood-damaged bridges, Parola et al. (1998) suggest that under many circumstances where abutments are founded on piles of sufficient depth, prevention of progressive failure of spillthrough embankments may be detrimental to the protection of the bridge from scour. At many locations, failures of the approach embankments increase flow area substantially, reducing flow velocity and preventing the formation of deep abutment scour holes. This relief mechanism may greatly reduce the depth of scour at piers and the location of the abutment pile bents. This method may be acceptable at locations where such failures would pose no risk to bridge users and would have limited effect on the transportation network.

11.5.2 Failure Mechanisms

Lewis (1972), Macky (1986), Kwan (1988), Croad (1989), Kandasamy (1989), and Eve (1999) ran exploratory experiments on bridge abutments that showed the primary failure mechanism of spillthrough embankments to be the formation of scour holes along the toe of the embankment with subsequent mass failure of the embankment into the scour hole. Progressive failure of the abutment slope into the scour holes eventually leads to failure of the embankment and supported roadway. Observations of flood-damaged bridges confirm the laboratory observations (Parola et al. 1998). Bridge abutments supported on piles frequently are not damaged although sections of approach embankments and portions of roadway may be destroyed.

In a laboratory study of abutment scour protection methods typically used in practice, Macky (1986) found that scour and undermining of the slope protection was initiated at the upstream toe of the embankment. Pagan-Ortiz (1991) observed a critical zone where riprap failure was initiated on the apron at the point of flow separation from the upstream edge for vertical-wall abutments and along a separation line downstream of the spillthrough abutments. Both reports present observations that show a critical point for apron failure and initial undermining of the slope protection at or near the slope toe. Both experiments showed

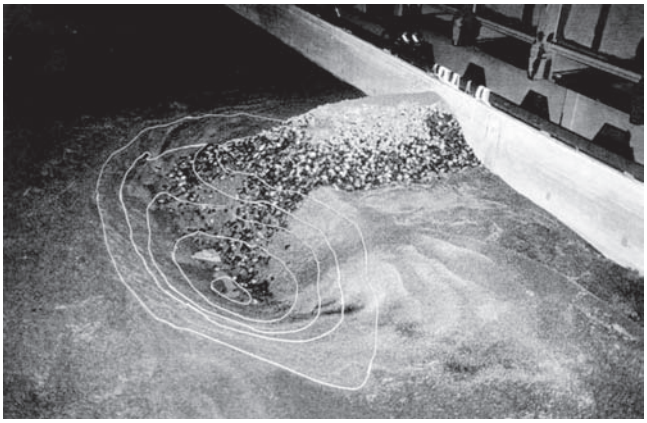

Fig. 11-15. Photograph showing laboratory study of riprap protection at an abutment (after Eve 1999).

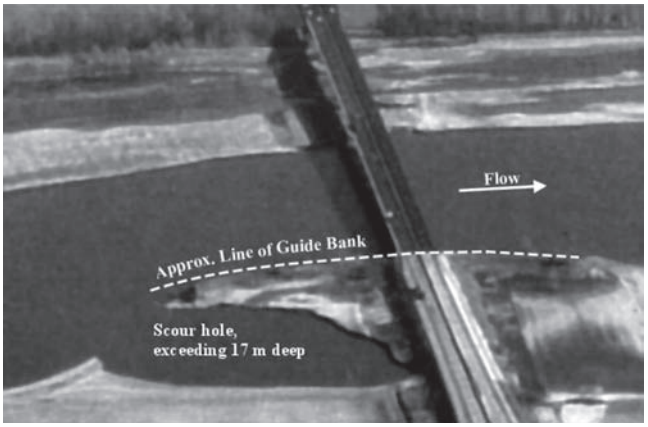

Fig. 11-16. Guide banks at Interstate 70 highway bridge embankment, bridge over Missouri River near Rocheport, Missouri, after 1993 flood.

subsequent failure of the embankment to be governed by mass movements such as translational slides of the granular fill materials used. Eve (1999) conducted clear-water scour experiments and a limited number of live-bed experiments on the failure conditions of slope and toe protection that included filters beneath the riprap. She found that failure under clear-water conditions was progressive, with failure of the protection being initiated at three different locations. These initial failure mechanisms were failure of the edge of the protection where the protection rolled into a scour hole, entrainment of pieces of riprap along the toe of the abutment, and entrainment on the upstream edge of the embankment slope. Undermining of the protection occurred as slope materials mass-failed toward the slope toe. Fig. 11-15 shows a downstream scour hole and the dispersal of riprap within the scour hole. Under live-bed conditions without a filter, winnowing of the particles beneath the riprap caused rapid failure of the protection.

11.5.3 Abutment Shape Design

For abutments that are sited near the edge of a channel, considerable reductions in local scour depth are associated with streamlined abutment shapes. The local scour at spillthrough abutments can be as much as 50% less than that at the same-sized vertical-wall abutment, for example. On the other hand, waterway contraction effects for a given bridge span are greater at a bridge founded on spillthrough abutments.

11.5.4 Guide Banks

Guide banks are curved embankments that extend upstream and, in some cases, downstream from and perpendicular to the abutment end. The use of guide banks was first introduced in 1888 for the construction of a bridge on the Chenab River, Pakistan (CBIP 1989). Guide banks extending upstream from the end of bridge embankments have been used to

- confine flow in braided rivers to the bridge opening;
- improve flow distribution and alignment through bridge openings;
- alter flow in bends that impinge on abutments; and
- transfer the point of highest flow curvature and deepest scour upstream of the bridge away from the abutment.

An illustration of the benefits of guide banks is presented in Fig. 11-16, which shows the Interstate 70 highway bridge embankment after the 1993 Midwestern U.S. flooding of the Missouri River near Rocheport, Missouri. Guide banks upstream and downstream of the Interstate 70 embankment transferred the formation of a deep scour hole upstream of the bridge. Although this scour hole was in excess of 17 m deep and caused the failure of the tip of the guide bank, the embankment slopes, including the toe of the highway embankments, were not damaged. The scour hole extended beneath the structure; however, the maximum scour depth under the structure was less than 8 m.

Guidance for the design of guide banks is presented in Neill (1973); Bradley (1978); Ministry of Works and Development (MWD 1979); CBIP (1989); and Lagasse et al. (1995). Lagasse et al. (1995) present detailed guidance that is based on the laboratory research of Karaki (1959; 1961), procedures developed by Bradley (1978), and experience of many U.S. state highway agencies. The main features of guide banks are their orientation with respect to the abutment face and embankment, plan view shape, upstream and downstream length, cross-section shape, and crest elevation. The recommended shape is a quarter of an ellipse with upstream length (L_s) equal to 2.5 times the offset length; see Fig. 11-17. The alignment of the guide bank should be parallel to the face of the abutment in the

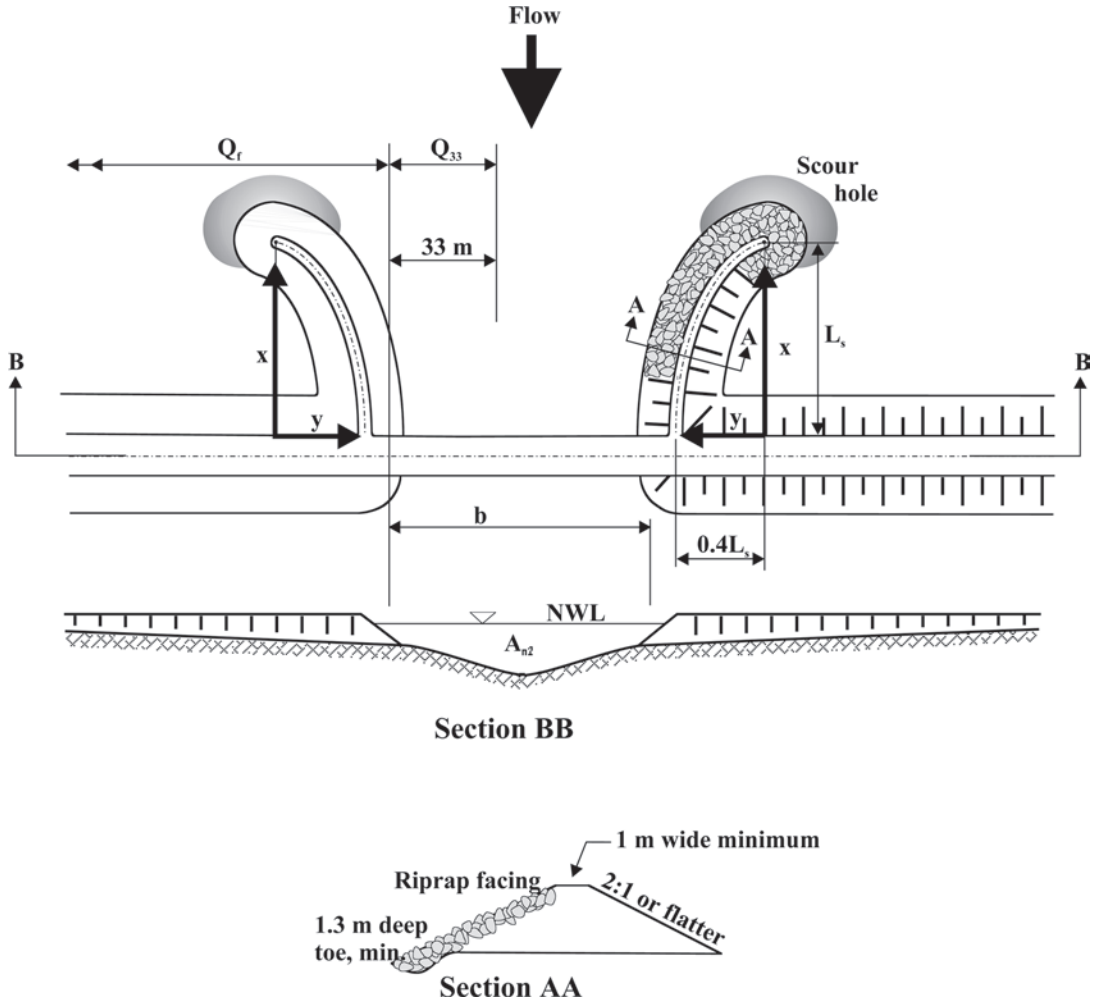

Fig. 11-17. Typical guide bank details (modified from Lagasse et al. 1995).

bridge opening. The plan view coordinates for the crest can be determined from

$$\frac{x^2}{L_s^2} + \frac{y^2}{(0.4L_s)^2} = 1 \qquad (11\text{-}3)$$

The length, L_s, is determined from the nomograph in Fig. 11-18 developed from the studies of Karaki (1959; 1961) and Neeley (unpublished report, U.S. Geological Survey, 1966). In the nomograph, Q is total discharge of the stream; Q_f is lateral or floodplain discharge of either floodplain; Q_{33} is discharge in a 33-m width of stream adjacent to the abutment; A_{n2} is cross-sectional flow area at the bridge opening during normal stage; $V_{n2} = Q / A_{n2}$ is average velocity through the bridge opening (m/s); Q_f / Q_{33} is guide bank discharge ratio; and L_s is projected length of guide bank (m).

The use of the nomograph should be limited to a minimum length of 16 m and a maximum length of 82 m. Lagasse et al. (1995) recommend that guide banks should not be shorter than 16 m or longer than 250 m. Experience indicates that a standard length of 50 m has performed well. Shorter lengths have been used successfully when the upstream end of the guide bank was extended to a tree line where the roughness of the trees reduced velocities at the tip of the guide bank.

The crest of the guide bank should be placed at least 0.6 m above the design flood elevation to prevent flows over the guide banks that may be damaging to the bridge. A downstream guide bank of length 16 m is used to prevent rapid expansion of flow in some U.S. states. Riprap protection is recommended for the channel side of the protection and the upstream tip of the guide bank. Rock protection may not be necessary at locations where vegetation will reliably protect guide banks.

11.5.5 Design Criteria for Riprap Protection

Model studies have shown and field observations have confirmed that failure of spillthrough abutments is progressive, in contrast to piers, which can fail catastrophically. The

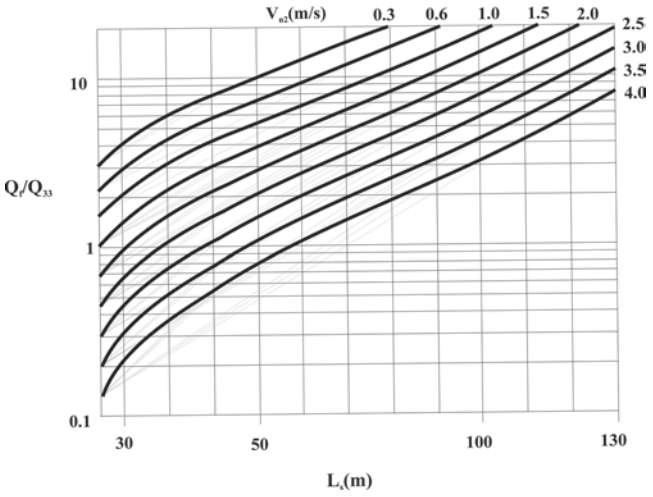

Fig. 11-18. Nomograph for selecting the length of guide banks at bridge crossings (modified from Lagasse et al. 1995).

design of countermeasures may require that partial failure of the armor protection be acceptable. For extreme event design and where abutment foundations are supported on piled foundations, complete erosion and failure of the embankment and supported roadway may be acceptable as long as the piles have sufficient depth to resist failure of the embankment.

Research on the performance of riprap protection on abutment slopes and aprons was conducted by a number of researchers including Simons and Lewis (1971); Lewis (1972); Macky (1986); Croad (1989); Simons et al. (1989); Pagan-Ortiz (1991); and Eve (1999). These laboratory studies were conducted under clear-water conditions. Design guidance is presented by the Ministry of Works and Development (MWD 1979); Gregorius (1985); Harris (1988); Richardson et al. (1988); Brown and Clyde (1989); Central Board of Irrigation and Power (1989); Austroads (1994); Richardson and Davis (1995); and Lagasse et al. (1997).

11.5.5.1 Riprap Size Simons and Lewis (1971), using the research of Lewis (1972), developed a method for predicting the stability of rock based on detailed velocity measurements around and on the slopes of spillthrough abutments. The method requires the use of a two-dimensional numerical model and the determination of the velocity one rock diameter above the streambed. Croad (1989), based on a limited number of small-scale model tests and velocity measurements, developed an equation to predict the critical conditions for initial failure of riprap protection at the toe of the spillthrough abutment. Croad's method requires a depth-averaged velocity measured over the critical failure point at the abutment toe. He recommended that the depth-averaged velocity over the critical failure point be estimated as 1.5 times the average approach flow velocity.

Pagan-Ortiz (1991) conducted fixed-bed small-scale experiments on the stability of riprap on a spillthrough abutment with side slopes of 2H:1V and on vertical-wall abutments. Flow conditions were adjusted until failure conditions were observed near the abutment. Critical failure zones were found on the streambed protection at or near points of flow separation from the upstream end of the rectangular abutments and downstream of the flow separation point on the spillthrough abutment. Prediction equations for the critical conditions were developed based on the average contracted flow velocity measured in the experiments.

A. T. Atayee (Unpublished TRB paper No. 931021, 1993) extended the research of Pagan-Ortiz (1991) to include compound channel geometry. Critical failure zones similar to those described in Pagan-Ortiz (1991) were observed. The data of both Pagan-Ortiz (1991) and Atayee were used to develop two equations that are based on the contracted flow velocity on the floodplain portion of the bridge opening (Atayee et al. 1993). They recommend that a two-dimensional depth-averaged numerical model be used for determining the average contracted flow velocity on the floodplain. The method presented in Atayee et al. (1993) is recommended as design guidance by Richardson and Davis (1995), although ad hoc recommendations were added to allow for prediction of contracted flow velocity on the floodplain based on cross-section averaged contracted flow velocity and the width of the floodplain in the contracted bridge opening.

A list of the riprap sizing equations for abutment protection is provided in Table 11-9. The equations of Simons and Lewis (1971), Croad (1989), and Atayee et al. (1993) for $\mathsf{F} < 0.8$ can be arranged into the form

$$\frac{D_r}{H} = \frac{C}{(S_s - 1)}\mathsf{F}^2 \tag{11-4}$$

where C is a coefficient. For $\mathsf{F} < 0.8$ and flat-bed conditions, the Simons and Lewis (1971) relation at the critical location of failure can be considered identical to that of Atayee et al. (1993) if the local velocity one rock diameter over the bed is 1.15 times the average contracted flow velocity on the floodplain. For the same flow range and conditions, the Croad (1989) equation can be considered identical to that of Atayee et al. (1993) if the depth-averaged velocity at the critical point of failure is 1.48 times the average contracted flow velocity on the floodplain.

Simon and Lewis (1971) and Croad (1989) both recommend that down-slope gravitational force should be considered in determining the size of rock on the abutment slope. They recommend increasing the rock size according to the relation provided by Lane (1955). The studies by Ulrich (1987) and Maynord (1995; 1996), as described in Appendix B, indicate that the theoretical slope adjustment factors used by Lane (1955) may be as much as 35% larger

Table 11-9 Equations for Sizing Riprap at Abutments

Reference	Applicability	Equation		Symbols
Simons and Lewis (1971)	Spillthrough abutments	$\eta = \dfrac{0.4U_r^2}{(S_s-1)gD_r}$	(11-19)	D_r = riprap stone size U_r = velocity at a level of one rock diameter above the bed H = approach flow depth S_s = specific gravity of rock η = stability factor = 0.595, for flow over a horizontal bed
Croad (1989)	Spillthrough abutments	$D_{r50} = 0.025\,U_b^2\,K_{sl}^{-1}$ $K_{sl} = \sqrt{1 - \dfrac{\sin^2\phi}{\sin^2\theta}}$	(11-20)	U_b = velocity at abutment end K_{sl} = embankment slope factor ϕ = slope angle θ = angle of repose F = Froude number of approach flow = $U/(gH)^{0.5}$
Brown and Clyde (1989)		$D_{r50} = \dfrac{0.006\,U^3}{H^{0.5}K_{sl}^{1.5}}\left(\dfrac{S_f}{1.2}\right)^{1.5}$	(11-21)	S_f = stability factor varying from 1.6 to 2.0 for abutment protection
Pagan-Ortiz (1991)	Vertical-wall abutment	$D_{r50} = \left(\dfrac{1.064\,U_2^2\,H_2^{0.23}}{(S_s-1)g}\right)^{0.81}$	(11-22)	U_2 = mean velocity in contracted (bridge) section H_2 = flow depth in contracted section
	Spillthrough abutment	$D_{r50} = \dfrac{0.535\,U_2^2}{(S_s-1)g}$	(11-23)	
Austroads (1994)		$\dfrac{D_{r50}}{H} = \dfrac{1.026}{(S_s-1)}\mathrm{F}^2$	(11-24)	
Atayee et al. (1993) and Richardson and Davis (1995)	$F_2 \le 0.8$	$\dfrac{D_{r50}}{H_2} = \dfrac{K_s}{(S_s-1)}\mathrm{F}_2^2$	(11-25)	K_s = shape factor = 0.89 for spillthrough abutments = 1.02 for vertical-wall abutments
	$F_2 > 0.8$	$\dfrac{D_{r50}}{H_2} = \dfrac{K_s}{(S_s-1)}\mathrm{F}_2^{0.14}$	(11-26)	F_2 = Froude number in the contracted section K_s = 0.61 for spillthrough abutments = 0.69 for vertical-wall abutments

than data would indicate. If the rock protection on the slope is sized according to Atayee et al. (1993), then consideration should be given to use of slope correction factors by Ulrich (1987) and Maynord (1995; 1996).

11.5.5.2 Extent of Rock Protection Under clear-water conditions, Pagan-Ortiz (1991) found that an apron that extended along the toe of the abutment from the point of tangency on the upstream side of the abutment to the point of tangency on the downstream side of the abutment and extended a distance equal to two times the flow depth away from the toe of the abutment was adequate. Atayee et al. (1993) recommended that the width of the apron not exceed 7.5 m.

Eve (1999) conducted riprap tests with approach flow conditions at 90% of the approach shear stress required to mobilize the approach sand bed. Based on her observations of progressive failure of the abutment embankments, she developed the following relation for determining the extent of protection,

$$\frac{W}{H}\left(\frac{0.5W+r}{H+r}\right) = \left(0.5 - 1.82\frac{D_{r50}}{H}\right)\left(\frac{B}{B-L}\right)\left(\frac{180}{180-(\theta+\phi)}\right) \tag{11-5}$$

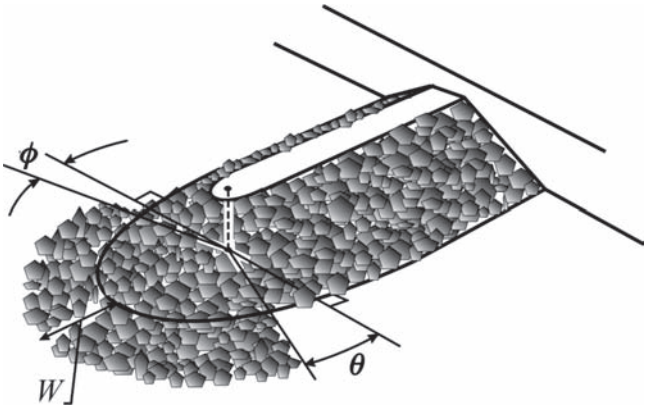

Fig. 11-19. Definition diagram for placement of a riprap launching apron at a spillthrough abutment (after Eve 1999).

where

H = approach flow depth;
B = upstream width of the flume;
L = abutment length;
r is the radius of the spillthrough abutment toe;
and W, θ, and ϕ are defined in Fig. 11-19.

Macky (1986) examined typical New Zealand practice, rather than recommended practices, in small-scale model studies in which the protection on the slope was extended only slightly below the previously existing bed level and no apron was provided. He reported that riprap failed into scour holes that formed around the abutment; however, the slumped riprap armored part of the scour hole. Additionally, the remaining slope angle decreased and was armored by riprap that translated down slope. The tested abutment was substantially undamaged. Macky also found that for aligned flows, the downstream side of the abutment required only nominal protection.

Riparian and floodplain vegetation may provide adequate protection where shading beneath the structure does not prevent its growth. Although insufficient data are available for reliance on vegetation at the critical failure points, vegetation may provide reliable protection on the upper slope areas and at locations upstream and downstream of the bridge. Substantial reduction in the extent of armor protection may be possible. In practice, sufficient protection has been provided to bridges by armoring the area beneath the bridge superstructure. Unfortunately, laboratory studies have not modeled the effects of vegetation under similar conditions. Armor protection should be considered at all critical locations where unraveling of the vegetal cover may be initiated, such as on the toe of the abutment and around piers located within the high-velocity flow of the abutment and any areas where shading may prevent the growth of erosion-resistant vegetal covers. Use of two-dimensional numerical models to determine the extent of armor protection required and the appropriate locations for vegetation should be considered.

11.5.5.3 Thickness of Riprap Although specific tests on the thickness of riprap protection on abutment slopes and aprons have not been conducted, information on the thickness of riprap revetments for stream banks and streambeds is provided by Maynord (1995; 1996) and is given in Appendix B. Where riprap is placed in water, on fine-grained sediment without a filter, or where extensive scour holes are anticipated at the edges of the protection, increased riprap thickness may be warranted. Lagasse et al. (1997) suggest that the thickness should not be less than the larger of either 1.5 D_{r50} or D_{r100} and should be increased by 50% when it is placed underwater to provide for uncertainties associated with underwater placement methods.

11.5.5.4 Filter Requirements An exploratory study by Eve (1999) showed the need for filters at abutments under live-bed conditions. In a very limited number of live-bed experiments, complete failure of approach embankments, initiated by bed-form undermining and winnowing of the bed material beneath the riprap, was observed on the apron as well as on the slope. On the other hand, Macky (1986) and Eve (1999) reported stable riprap configurations in several clear-water experiments in which filters were not used. Other factors such as groundwater flows from such sources as surface runoff may necessitate the use of filters on slopes. Additional research is needed to determine the benefit of placing riprap under the apron and on the slope, especially where riprap is designed to conform to adjacent scour holes or bed-form undermining.

11.5.6 Alternatives for Protection of Abutments

Where riprap of adequate size is unavailable or where environmental or geometric constraints preclude use of riprap, alternatives to riprap are necessary. Lagasse et al. (1997) describe several armoring alternatives for abutment slopes, including articulated concrete block (Section 11.3.4.3), articulated grout-filled mattresses (Section 11.3.4.4), soil cement, wire-enclosed mattresses, interlocking armor units (toskanes, Section 11.3.4.3), and cement-filled bags (Section 11.3.4.3).

As part of the study was completed to evaluate the performance of typical rather than recommended methods of protecting spillthrough abutments, Macky (1986) examined the performance of several alternatives to riprap including: interlocking concrete armor units (akmons), concrete mattresses (Section 11.3.4.4), gabions (Section 11.3.4.5) laid on the embankment slopes, gabions stacked horizontally and staggered up the slope, and boulder-filled wire baskets laid on the bed beneath the stacked gabions. Although a very limited number of tests were conducted, several important aspects of abutment protection were revealed. Although the interlocking armor units behaved similarly to riprap, their interlocking capabilities appeared to hinder dispersal on the slope after toe scour undermined the protection. Tests on riprap showed that dispersal of the rock is a key factor in the

ability of the protection to adjust and conform to scour holes and subsequent slope failures. Consequently, large areas of the slope were left unprotected after slope failures occurred. Macky (1986) recommended that noninterlocking shapes be considered. Concrete mattresses, gabions, and wire-filled baskets generally performed poorly, because of their inability to adjust and conform to scour holes and slope failures. As the experience of U.S. state highway agencies has shown, use of rigid concrete pavements (Section 11.3.4.4) on abutment slopes suffers from the same problems. Preexcavation of the scour hole at the toe of the slope and extension of the slope protection to the depth of scour were recommended as a possible way to improve the performance of mattress- and gabion-type countermeasures. An apron using these techniques may also improve the performance of these techniques.

The work on riprap protection on abutments, coupled with the work by Macky (1986), clearly shows that design of spillthrough abutment protection should either extend to a depth near to the scour depth, provide an extensive apron, or conform to progressive scour hole formation and slope failure.

11.6 ENVIRONMENTAL CONSIDERATIONS

Countermeasures for bridges should be constructed so that they enhance aquatic habitat and bridge-crossing aesthetics rather than degrading them. Selection of the size distribution of rock for armor protection should satisfy requirements for stream stability and habitat. Grade control structure drops should be selected to provide for fish migration. Consideration should also be given to countermeasure placement methods and their impact on aquatic habitat.

Although the full spectrum of potential flows at bridges should be considered, the countermeasure should be designed to protect the bridge for design flood events (500, 100, and/or overtopping event), maintain channel stability at bank-full levels, and enhance stream habitat at average annual and lower flow levels. Stream restoration concepts and habitat objectives given in Chapter 9 should be incorporated into the countermeasure designs at the bridge; however, highway right-of-way limits and cost may be apparent barriers to extensive modification of stream channels as part of bridge-scour countermeasures. Use of structures such as spur dikes, barbs, and bendway weirs provide nonuniformity to flow and topography through the bridge opening, which generally improve habitat: conversely, use of uniform rock revetments and other uniform topography and material configurations will tend to degrade habitat. Vegetation, especially riparian trees, should be used to protect streambanks where safety of the bridge is not compromised.

REFERENCES

Acheson, A. R. (1968). "River control and drainage in New Zealand and some comparisons with overseas practices." Ministry of Works, Wellington, New Zealand.

Ahmad, M. (1951). "Spacing and projection of spurs for bank protection." *Civil Engineering and Public Work Review*, 172–174, April, 256–258.

Atayee, A. T., Pagan-Ortiz, J. E., Jones, J. S., and Kilgore, R. T. (1993). "A Study of Riprap as a Scour Protection for Spill-Through Abutments." ASCE Hydraulic Conference, San Francisco, Calif., 973–978.

Austroads. (1994). *Waterway design—A guide to the hydraulic design of bridges, culverts and floodways*, Austroads, Sydney, Australia.

Barkdoll, B. D., Ettema, R., and Odgaard, A. J. (1999). "Sediment control at lateral diversions: Limits and enhancements to vane use." *Journal of Hydraulic Engineering, ASCE*, 125(8), 862–870.

Bertoldi, D. A., Jones, J. S., Stein, S. M., Kilgore, R. T., and Atayee, A. T. (1996). "An experimental study of scour protection alternatives at bridge piers." *Rep. No. FHWA-RD-95-187*, Turner-Fairbank Highway Research Center, Federal Highway Administration, U.S. Department of Transportation, Washington, D.C.

Bonasoundas, M. (1973). "Strömungsvorgang und kolkproblem." *Report No. 28,* Oskar v. Miller Institut, Tech. Univ. Munich, Germany.

Bradley, J. N. (1978). "Hydraulics of bridge waterways." *Hydraulic Design Series No. 1*, Federal Highway Administration, U.S. Department of Transportation, Washington, D.C.

Breusers, H. N. C., Nicollet, G., and Shen, H. W. (1977). "Local scour around cylindrical piers." *Journal of Hydraulic Research*, 15(3), 211–252.

Breusers, H. N. C., and Raudkivi, A. J. (1991). "Scouring." *Hydraulic Structures Design Manual No. 2*, IAHR, Balkema., Rotterdam, The Netherlands.

Brown, S. A., and Clyde, E. S. (1989). "Design of riprap revetment." *Hydraulic Engineering Circular 11 (HEC-11)*, Report No. FHWA-IP-89-016, Federal Highway Administration, U.S. Department of Transportation, Washington, D.C.

Brown, S. A., McQuivey, R. S., and Keefer, T. N. (1981). "Stream channel degradation and aggradation analysis of impacts to highway crossings." *Final Rep. No. FHWA-RD-80-159*, Federal Highway Administration, U. S. Department of Transportation, Washington, D. C.

Central Board of Irrigation and Power (CBIP). (1989). "River behaviour management and training." *Publication No. 204, Vol. 1,* C. V. J. Sharma, K. R. Saxema, and M.K. Rao, eds., Central Board of Irrigation and Power, New Delhi, India.

Chabert, J., and Engeldinger, P. (1956). *Etude des affouillements autour des piles des ponts*, Laboratoire d'Hydraulique, Chatou, France (in French).

Chang, F. F. M., and Karim, M. (1972). "An experimental study of reducing scour around bridge piers using piles." *Report*, South Dakota Department of Highways, Pierre, S.D.

Chiew, Y. M. (1992). "Scour protection at bridge piers." *Journal of Hydraulic Engineering, ASCE*, 118(9), 1260–1269.

Chiew, Y. M. (1995). "Mechanics of riprap failure at bridge piers." *Journal of Hydraulic Engineering, ASCE*, 121(9), 635–643.

Coleman, S. E., and Melville, B. W. (2001). "Case study: New Zealand bridge scour experiences." *Journal of Hydraulic Engineering, ASCE*, 127(7), 535–546.

Coleman, S. E., Melville, B. W., and Lauchlan, C. S. (2000). "Bealey Bridge scour failure." *Scour of Foundations, Proc., Int.*

Symp., J. Briaud (ed.), Department of Civil Engineering, Texas A & M University, College Station, Tex., 387–393.

Copeland, R. R. (1983). *Bank protection techniques using spur dikes*. Hydraulics Laboratory, U.S. Army Engineer Waterways Experiment Station, Vicksburg, Miss.

Croad, R. N. (1989). "Investigation of the pre-excavation of the abutment scour hole at bridge abutments." *Rep. 89-A9303*, Central Laboratories, Works and Development Services Corporation (NZ), Lower Hutt, New Zealand.

Croad, R. N. (1997). "Protection from scour of bridge piers using riprap." *Transit New Zealand Research Rep. No. PR3-0071*, Works Consultancy Services Ltd., Central Laboratories, Lower Hutt, New Zealand.

Dargahi, B. (1982). "Local scour at bridge piers—A review of theory and practice." *Bulletin No. TRITA-VBI-114,* Hydraulics Laboratory, Royal Institute of Technology, Stockholm, Sweden.

Dargahi, B. (1987). "Flow field and local scouring around a cylinder." *Bulletin No. 137,* Royal Institute of Technology Hydraulics Laboratory, Stockholm, Sweden.

Dargahi, B. (1989). "The turbulent flow field around a circular cylinder." *Experiments in Fluids,* 8, 1–12.

Dargahi, B. (1990). "Controlling mechanism of local scouring." *Journal of Hydraulic Engineering, ASCE*, 116(10), 1197–1214.

Diehl, T. H. (!997). "Potential drift accumulation at bridges." *Rep. No. FHWA-RD-97-28*, Federal Highway Administration, Washington, D.C.

Engels, H. (1929). "Chapter V: Experiments pertaining to the protection of bridge piers against undermining." *Hydraulic Laboratory Practice*, ASME, New York.

Escarameia, M., and May, R. W. P. (1992). "Channel protection—Turbulence downstream of structures." *Rep. SR 313*, HR Wallingford, Howbery Park, Wallingford, U.K.

Ettema, R. (1980). "Scour at bridge piers." *Rep. No. 216*, School of Engineering, The University of Auckland, Auckland, New Zealand.

Eve, N. (1999). "Riprap protection at bridge abutments." ME thesis, The University of Auckland, Auckland, New Zealand.

Farraday, R. V., and Charlton, F. G. (1983). *Hydraulic factors in bridge design*. Hydraulics Research Station, Wallingford, U.K.

Fotherby, L. M. (1992). "Footings, mats, grout bags, and tetrapods: Protection methods against local scour at bridge piers." MS thesis, Colorado State University, Fort Collins, Colo.

Fotherby, L. M., and Ruff, J. F. (1996). "Riprap and concrete armor to prevent pier scour." *Proc., North American Water and Environment Congress*, ASCE, Reston, Va.

Gales, R. R. (1938). "The principles of river-training for railway bridges, and their application to the case of the Harding Bridge over the Lower Ganges at Sara." *Journal of the Institution of Civil Engineers*, 10(2), 136–224.

Grant, R. J. (1948). "Channel improvements in alluvial streams." *Proceedings, New Zealand Institution of Engineers*, 34, 231–279.

Gregorius, B. H. (1985). "Waterway design procedures—Guidelines." *Civil Division Publication*, Ministry of Works and Development, Hamilton, New Zealand.

Harris, J. D. (1988). "Chapter I: Hydraulic design of bridges." *MTC Drainage Manual*, Drainage and Hydrology Section, Ontario Ministry of Transportation, Downsview, Ont.

Harvey, M. D., and Sing, E. F. (1989). "The effects of bank protection on river morphology." *Proc., National Conference on Hydraulic Engineering*, M. A. Ports, ed., ASCE, New York, 212–217.

Hjorth, P. (1975). "Studies on the nature of local scour." *Bulletin, Series A, No. 46,* Institutionen for teknisk vattenresurslara, Lund, Sweden.

Johnson, P. A., Hey, R. D., Horst, M. W., and Hess, A. J. (2001). "Aggradation at bridges." *Journal of Hydraulic Engineering, ASCE*, 127(2), 154–157.

Jones, J. S., Bertoldi, D. A., and Stein, S. (1995). "Alternative scour countermeasures." *Proc., Hydraulic Engineering '95,* W. H. Espey Jr. and P. S. Combs, eds., ASCE, New York, 1819–1823.

Kandasamy, J. K. (1989). "Abutment scour." *Rep. No. 458*, School of Engineering, The University of Auckland, Auckland, New Zealand.

Karaki, S. S. (1959). "Hydraulic model study of spur dikes for highway bridge openings." *Rep. CER59SSK36*, Civil Engineering section, Colorado State University, Fort Collins, Colo.

Karaki, S. S. (1961). "Laboratory study of spur dikes for highway bridge protection." *Bulletin 286*, Highway Research Board, Washington, D.C.

Kwan, T. F. (1984). "Study of abutment scour." *Rep. No. 328*, School of Engineering, The University of Auckland, Auckland, New Zealand.

Kwan, T. F. (1988). "A study of abutment scour." *Rep. No. 451*, School of Engineering, The University of Auckland, Auckland, New Zealand.

Lagasse, P. F., Schall, J. D., Johnson, F. M., Richardson, E. V., and Chang, F. (1995). "Stream stability at highway structures." *Hydraulic Engineering Circular No. 20 (HEC-20), Rep. No. FHWA-IP-90-014*, Federal Highway Administration, U.S. Department of Transportation, Washington, D.C.

Lagasse, P. F., Schumm, S. A., and Zevenbergen, L. W. (1997). "Quantitative techniques for stream stability analysis." *Proc., 27th Congress of the International Association for Hydraulic Research*, A147–A153.

Lagasse, P. F., Zevenbergen, L. W., Schall, J. D., and Clopper, P. E. (2001). "Bridge scour and stream instability countermeasures: Experience, selection, and design guidance." *Hydraulic Engineering Circular No. 23 (HEC-23), Report No. FHWA-NHI-01-003*, 2nd ed., Federal Highway Administration, U.S. Department of Transportation, Washington, D.C.

Lane, E. W. (1955). "Design of stable channels." *Transactions, ASCE*, 120, Paper No. 2776, 1234–1279.

Lauchlan, C. S. (1999). "Countermeasures for pier scour." PhD thesis, The University of Auckland, Auckland, New Zealand.

Levi, E., and Luna, H. (1961). "Dispositifs pour reduire l'affouillement au pied des piles de pont." *Proc., 9th I.A.H.R. Congress*, IAHR, Madrid, Spain, 1061–1069.

Lewis, G. L. (1972). "Riprap protection of bridge footings." PhD thesis, Colorado State University, Fort Collins, Colo.

Lim, F. H., and Chiew, Y.M. (1997). "Stability of riprap layer under live-bed conditions." Conference on Management of Landscapes disturbed by Channel Incision, S. Y. Wang, E. J. Langendoen, and F. D. Shields Jr., eds., Center for the Computational Hydroscience and Engineering, University of Mississippi, Oxford, Mississippi, 277–287.

Macky, G.,H. (1986). "Model testing of bridge abutment scour protection." *Rep. 3-86/12*, Central Laboratories, Ministry of Works and Development, Lower Hutt, New Zealand.

Maynord, S.,T. (1995). "Gabion-mattress channel-protection design." *Journal of Hydraulic Engineering, ASCE*, 121(7), 519–522.

Maynord, S.,T. (1996). "Toe-scour estimation in stabilised bendways." *Journal of Hydraulic Engineering*, 122(8), 460–464.

Maza Alvarez, J. A. (1968). "Scour in natural channels." *Rep. No. 114*, A. J. Miguel-Rodriguez, translator, School of Engineering, The University of Auckland, Auckland, New Zealand.

Maza Alvarez, J. A. (1989). "Design of groynes and spur dikes." *Proc., 1989 National Conference on Hydraulic Engineering*, 296–301.

Melville, B. W., and Coleman, S. E. (2000). *Bridge scour*. Water Resources Publications, Highlands Ranch, Colo.

Melville, B. W., and Hadfield, A. C. (1999). "Use of sacrificial piles as pier scour countermeasures." *Journal of Hydraulic Engineering, ASCE*, 125(11), 1221–1224.

Ministry of Works and Development (MWD). (1979). "Code of practice for the design of bridge waterways." *Civil Division Publication CDP 705/C*, Ministry of Works and Development, Wellington, New Zealand.

Neill, C. R., ed. (1973). *Guide to bridge hydraulics*. Roads and Transportation Assoc. of Canada, University of Toronto Press, Toronto.

Odgaard, A. J., and Kennedy, J. F. (1983). "River bend bank protection by submerged vanes." *Journal of Hydraulic Engineering, ASCE*, 109(8), 1161–1173.

Odgaard, A. J., and Spoljaric, A. (1986). "Sediment control by submerged vanes." *Journal of Hydraulic Engineering, ASCE*, 112(12), 1164–1181.

Odgaard, A. J., and Wang, Y. (1987). "Scour prevention at bridge piers." *Proc., National Conference on Hydraulic Engineering*, ASCE, New York, 523–527.

Odgaard, A. J., and Wang, Y. (1991a). "Sediment management with submerged vanes. I: Theory." *Journal of Hydraulic Engineering, ASCE*, 117(3), 267–283.

Odgaard, A. J., and Wang, Y. (1991b). "Sediment management with submerged vanes. II: Applications." *Journal of Hydraulic Engineering, ASCE*, 117(3), 284–302.

Pagan-Ortiz, J. E. (1991). "Stability of rock riprap for protection at the toe of abutments located at the flood plain." *Rep. No. FHWA-RD-91-057*, Federal Highway Administration, U.S. Department of Transportation, Washington, D.C.

Paice, C., and Hey, R. (1993). "The control and monitoring of local scour at bridge piers." *Proc., Hydraulic Engineering Conference*, ASCE, New York, 1061–1066.

Parker, G., Toro-Escobar, C., and Voigt, R. L., Jr. (1998). "Countermeasures to protect bridge piers from scour." *Draft Final Report (Project NCHRP 24-7)* prepared for National Co-operative Highway Research Program, University of Minnesota, Minneapolis.

Parola, A. C. (1990). "The stability of riprap used to protect bridge piers." PhD thesis, Pennsylvania State University, University Park, Pa.

Parola, A. C. (1991). "The stability of riprap used to protect bridge piers." *Rep. No. FHWA-RD-91-063*, Federal Highway Administration, U.S. Department of Transportation, Washington, D.C.

Parola, A. C. (1993). "Stability of riprap at bridge piers." *Journal of Hydraulic Engineering, ASCE*, 119(10), 1080–1093.

Parola, A. C. (1995). "Boundary stress and stability of riprap at bridge piers." *River, coastal and shoreline protection: Erosion control using riprap and armorstone*, C. R. Thorne et al., eds., Wiley, New York.

Parola, A. C., Hagerty, D. J., and Kamojjala, S. (1998). "NCHRP 12-39: Highway infrastructure damage caused by the 1993 Upper Mississippi River Basin flooding." *Transportation Research Board 1483*, National Research Council, Washington, D.C.

Parola, A. C., Hagerty, D. J., Mueller, D. S., Melville, B. W., Parker, G., and Usher, J. S. (1996). "Scour at bridge foundations: Research needs." *NCHRP Project 24-8, Preliminary Draft Strategic Plan*, National Co-operative Highway Research Program, Washington, D.C.

Parola, A. C., and Jones, J. S. (1989). "Sizing riprap to protect bridge piers from scour." *Transportation Research Record*, 2(1290), 276–279.

Pilarczyk, K. W. (1995). "Simplified unification of stability formulae for revetment." *River, coastal and shoreline protection*, C. R. Thorne, S. R. Abt, F. B. J. Barends, S. T. Maynord, and K. W. Pilarczyk, eds., Wiley, New York.

Posey, C. J. (1974). "Tests of scour protection at bridge piers." *Journal of the Hydraulics Division, ASCE*, 100(HY12), 1773–1783.

Quazi, M. E., and Peterson, A. W. (1973). "A method for bridge pier riprap design." *Proc., First Canadian Hydraulics Conference*, 96–106.

Richardson, E. V., and Davis, S. R. (1995). "Evaluating scour at bridges." *Rep. No. FHWA-IP-90-017, Hydraulic Engineering Circular No. 18 (HEC-18)*, 3rd Ed., Office of Technology Applications, HTA-22, Federal Highway Administration, U.S. Department of Transportation, Washington, D.C.

Richardson, E. V., Simons, D. B., and Julien, P. Y. (1988). *Highways in the river environment*. Federal Highway Administration, U.S. Department of Transportation, Washington, D.C.

Ruff, J. F., and Fotherby, L. M. (1995). "Bridge scour protection systems using toskanes." *Final Report, Project 91-02*, Engineering Research Center, Colorado State University, Fort Collins, Colo.

Ruff, J. F., and Nickelson, J. R. (1993). "Riprap coverage around bridge piers." *Proc., National Hydraulic Engineering Conference*, ASCE, New York, 1540–1545.

Schneible, D. E. (1951). "An investigation of the effect of bridge-pier shape on the relative depth of scour." MS thesis, University of Iowa, Iowa City, Iowa.

Shen, H. W., Schneider, V. R., and Karaki, S. S. (1966). Mechanics of local scour, Institute for Applied Technology, National Bureau of Standards, U.S. Department of Commerce, Washington, D.C.

Simon, A. (1994). "Width adjustment: relative dominance in unstable alluvial streams." *Proc., ASCE National Hydraulics Conference*, ASCE, New York, G. V. Cotroneo and R. R. Ramer, eds., 974–978.

Simon, A. (1995). "Adjustment and recovery of unstable alluvial channels: Identification and approaches for engineering management." *Earth Surface Processes and Landforms*, 20, 611–628.

Simons, D. B., Chen, Y. H., and Swenson, L. J. (1984). "Hydraulic test to develop design criteria for the use of Reno mattresses." *Report*, Colorado State University, Fort Collins, Colo.

Simons, D. B., and Lewis, G. L. (1971). "Report—flood protection at bridge crossings." *Rep. No. CER71-72DBS-GL10*, C.S.U. Civil Engineering Report, prepared for the Wyoming State Highway Department in conjunction with the U.S. Department of Transportation.

Simons, D. B., Li, R. M., and Associates (1989). "Sizing riprap for the protection of approach embankments and spur dykes

and limiting the depth of scour at bridge piers and abutments." *Report No. FHWA-AZ-89-260*, Vol. 1, Arizona Department of Transportation, Phoenix.

Singh, K. K., Verma, D. V. S., and Tiwari, N. K. (1995). "Scour protection at circular bridge piers." Sixth International Symposium on River Sedimentation, New Delhi, India.

Sousa Pinto, N. L. de (1959). "Riprap protection against scour around bridge piers." Master's thesis, University of Iowa, Iowa City, Iowa.

Strom, H. G. (1962). *River improvement and drainage in New Zealand and Australia*. State Rivers and Water Supply Commission, Victoria, Australia.

Suzuki, K., Michiue, M., and Hinokidani, O. (1987). "Local bed form around a series of spur-dikes in alluvial channel." *Proc., 22nd. Congress, I.A.H.R.*, 316–321.

Tanaka, S., and Yano, M. (1967). "Local scour around a circular cylinder." *Proc., 12th. Congress, IAHR*., Vol. 3, IAHR, Delft, The Netherlands, 193–201.

Thomas, Z. (1967). "An interesting hydraulic effect occurring at local scour." *Proc., 12th. Congress, IAHR*, Vol. 3, IAHR, Delft, The Netherlands, 125–134.

Thorne, C. R., Abt, S. R., and Maynord, S. T. (1995). "Prediction of near-bank velocity and scour depth in meander bends for design of riprap revetments." *River, coastal and shoreline protection: Erosion control using riprap and armorstone*, C. R. Thorne, S. R. Abt, F. B. J. Barends, S. T. Maynord, K. W. Pilarczyk, Wiley, New York.

Ulrich, T. (1987). "Stability of rock protection on slopes." *Journal of Hydraulic Engineering, ASCE*, 113(7), 879–891.

United Nations Economic Commission for Asia and the Far East (United Nations). (1953). "River training and bank protection." *Flood Control Series No. 4*, Bangkok, Thailand.

University of Minnesota (1996). "Countermeasures to protect bridge piers from scour." *Second Interim Report, NCHRP Project No. 24-7*, St. Anthony Falls Laboratory, University of Minnesota, Minneapolis.

University of Minnesota (1997). "Countermeasures to protect bridge piers from scour." *Quarterly Progress Report for period April 1997 to June 1997, NCHRP Project No. 24-7*, St. Anthony Falls Laboratory, University of Minnesota, Minneapolis.

U.S. Army Corps of Engineers (USACE). (1984). *Shore protection manual*,Vol. II. U.S. Army Coastal Engineering Research Center, Vicksburg, Miss.

U.S. Department of Agriculture (USDA). (1996). "Chapter 16: Streambank and shoreline protection." *Natural Resources Conservation Service (NRCS) Engineering Field Handbook*, U.S. Department of Agriculture, Washington, D.C.

Wang, T. W. (1994). "A study of pier scouring and scour reduction." *Proc., 9th Congress, Asia Pacific Division, IAHR*, IAHR, Delft, The Netherlands, 18–28.

Worman, A. (1987). "Erosion mechanisms in a riprap protection around a pier." *Bulletin No. TRITA-VBI-I36*, Hydraulics Laboratory, Royal Institute of Technology, Stockholm, Sweden.

Worman, A. (1989). "Riprap protection without filter layers." *Journal of Hydraulic Engineering, ASCE*, 115(12), 1615–1630.

Copyrighted Materials
Copyright © 2008 American Society of Civil Engineers (ASCE)
Retrieved from www.knovel.com

CHAPTER 12

Reservoir Sedimentation

Gregory L. Morris, George Annandale, and Rollin Hotchkiss

12.1 INTRODUCTION

Manual 54 was originally published in 1975, toward the end of a period of intensive dam building worldwide. Sedimentation investigations at that time focused primarily on computing rates of sediment inflow, predicting sediment-induced shifts in the stage–storage curve over time, sizing dead pools typically equivalent to 50 or 100 years of sediment storage, and determining the "life of the reservoir." Today an increasing number of dams are reaching the end of their "design life," and their operation is increasingly affected by long-term sedimentation issues ignored at the time of construction.

Dams represent a unique category of engineered infrastructure because their eventual obsolescence is determined by the geologic processes of erosion and sedimentation rather than by engineered works themselves, which can be continually rehabilitated. When sedimentation is controlled, dams can have useful lives greatly exceeding any other type of engineered infrastructure. For example, Schnitter (1994) lists 12 ancient dams that had operational periods exceeding 2,000 years. Four of these are still in operation, five have been rehabilitated and are operating again, and only three are no longer operational. However, absent sediment control, today's dams represent an unsustainable pattern of water resource development.

There are over 75,000 dams in the United States, of which over 7,000 are classified as large dams having a height of at least 15 m. Most U.S. rivers have been essentially fully developed with respect to dams, and the rate of dam construction in the U.S. and worldwide has decreased dramatically since the 1970s (Fig. 12-1).

Dam sites are limited, and the best sites, which were developed first, are accumulating sediment. New dams can replace silted reservoirs in some cases but not others, with the largest and most important reservoirs being virtually irreplaceable. Siting obstacles to new reservoirs are formidable, and even when technically feasible alternative dam sites exist, they may not be feasible from the economic, social, political, or environmental standpoint. This leaves today's owners and engineers facing long-term sedimentation issues ignored in the original project concept.

In 1946, Brown recognized that major reservoirs are irreplaceable, and at the brink of the most active period of dam construction in U.S. history, he wrote,

> If the contemplated public and private reservoir construction programs are carried out, we shall have utilized by the end of this generation a very substantial portion of all the major reservoir sites. . . . We cannot discover new reserves, as we will of oil. Nor can we grow new resources, as we can of forests. To whatever degree we conserve the capacity of the reservoirs built on these sites, to just that degree shall we conserve this indispensable base of our national strength and prosperity.

Whereas the twentieth century focused on dam construction, the twenty-first will focus on sustaining the function of existing infrastructure as it becomes increasingly affected by sedimentation.

Most natural river reaches are approximately balanced with respect to sediment inflow and outflow. Dam construction dramatically upsets this balance by creating a quiescent reach that accumulates sediment until the balance between sediment inflow and outflow is again reestablished. The objective of sediment management is to manipulate the river–reservoir system to achieve sediment balance while retaining as much beneficial storage as possible and minimizing environmental impacts and socioeconomic costs.

In addition to determining the rate of storage loss, sedimentation issues today are becoming increasingly focused on issues such as (1) continuation of reservoir operation beyond the original design life despite sediment accumulation,

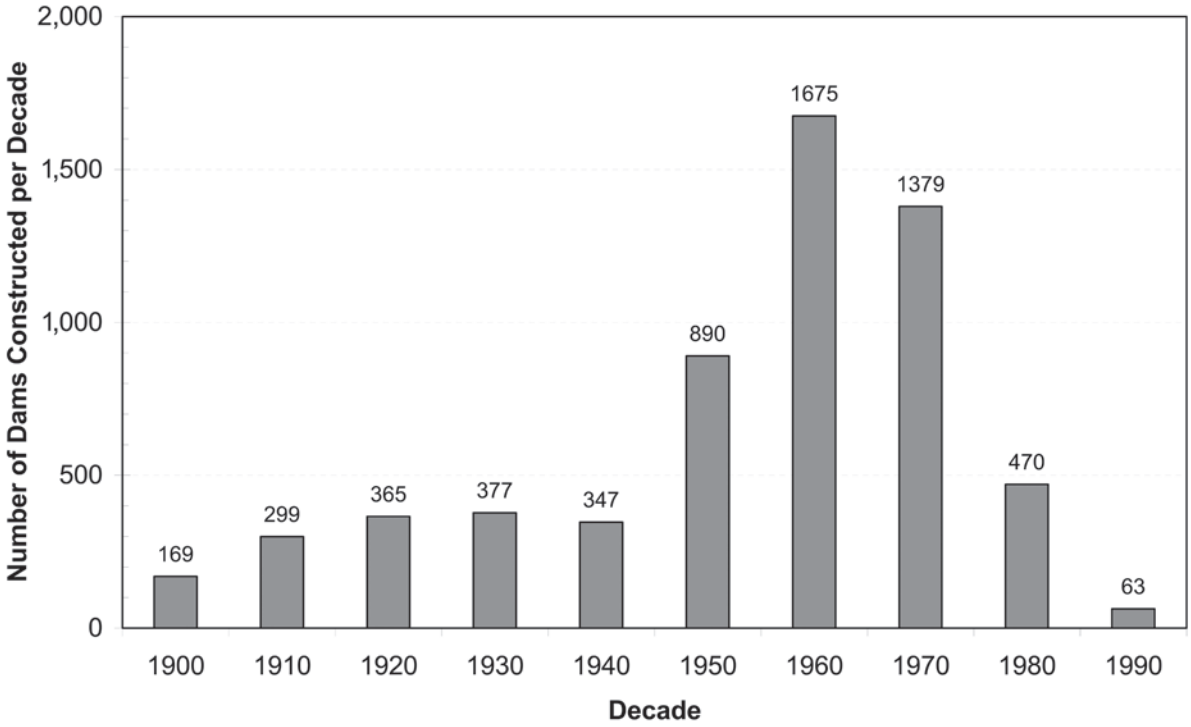

Fig. 12-1. Rate of large dam construction in the United States (data from USCOLD 1994).

(2) modification of existing structures and operating rules to minimize sedimentation impacts, (3) design and management of new reservoirs to minimize sediment accumulation, (4) dredging and other sediment removal techniques, (5) sediment impacts associated with dam decommissioning and removal, and (6) sediment management to minimize or mitigate environmental impacts. Environmental issues associated with reservoir sedimentation include the consequences of altered sediment supply and regulated flows on the morphology and ecology of downstream channels. Sediment management is also a primary environmental issue associated with the decommissioning of dams because dam removal will expose deposits to scour and can potentially release large volumes of sediment and any included contaminants to the downstream channel.

There are three basic themes in this chapter. First, basic sustainable use concepts pertinent to dams and reservoirs are introduced. Second, concepts of sediment delivery processes and sampling are introduced. This topic is presented because sediment management for sustainable use requires a more detailed understanding of sediment delivery processes than the traditional approach of simply determining long-term yield to compute the rate of sediment accumulation. The third theme describes basic sediment management strategies applicable to reservoirs.

This chapter presents only a summary introduction to this complex topic, and additional resources should be consulted. The following references represent a useful starting point. Morris and Fan (1998) provide a comprehensive treatise on sediment management in reservoirs and regulated river systems, including background descriptions of measurement, monitoring and modeling techniques, case studies, and an extensive bibliography. The World Bank's emerging approach to Reservoir Conservation (RESCON) is described by Palmieri et al. (2003) and Kawashima et al. (2003). An overview of reservoir-flushing techniques is provided by Atkinson (1996) and White (2001). Strand and Pemberton (1987) present a summary of reservoir sedimentation techniques used by the U.S. Bureau of Reclamation, and Corps of Engineers procedures are outlined by the U.S. Army Corps of Engineers (1989). Additional information is provided by Annandale (1987).

12.2 SEDIMENTATION RATES

12.2.1 Sedimentation Rates Worldwide

Sedimentation rate may be expressed as of the percentage of total original reservoir volume lost each year. Crowder (1987) estimated the rate of storage loss in the coterminous 48 states in the United States at 0.22% per year. Data on U.S. reservoirs compiled by Dendy et al. (1973) showed that storage loss tends to be more rapid in smaller reservoirs than in larger ones due to generally higher capacity: inflow ratios and lower specific sediment yields in the latter. The rate of storage loss in other parts of the world is generally higher than in the United States, and Mahmood (1987) estimated that storage capacity worldwide is being lost at an annual rate of 1%,

Table 12-1 Worldwide Rates of Reservoir Sedimentation

Region	Inventoried large dams	Storage (km^3)	Annual percent storage loss by sedimentation
China	22,000	510	2.3
Asia excluding China	7,230	861	0.3–1.0
North America	7,205	1,845	0.2
Europe	5,497	1,083	0.17–0.2
South and Central America	1,498	1,039	0.1
North Africa	280	188	0.08–1.5
Sub-Sahara Africa	966	575	0.23
Middle East	895	224	1.5
Worldwide	45,571	6,325	0.5–1.0

Source: Adapted from White (2001).

and estimates compiled by White (2001) are summarized in Table 12-1. The world is now losing reservoir capacity much faster than new capacity is being constructed.

Within a given geographic region, there are wide variations in the rate of storage loss. For example, Gogus and Yalcinkaya (1992) examined data from 16 reservoirs in Turkey and computed a mean annual rate of storage loss of 1.2%, but the rates for individual reservoirs ranged from 0.2% to 2.4%. In India, Morris (1995) estimated an annual rate of storage loss of 0.5%, meaning that about half of India's total reservoir capacity will be lost during the twenty-first century. However, the least affected 20% of the reservoirs will not lose half their capacity until after the year 2500. Thus, the problem is highly site specific, and new reservoir construction at a geographically distant location will not solve a local water supply problem stemming from sedimentation. Only in the case of hydropower can a distant new site offset local problems because, unlike water, electricity can be transported for long distances at low cost.

12.2.2 Reservoir Half-Life

Common practice has been to compute "reservoir life" by dividing total reservoir volume by annual sedimentation volume during the early years of impoundment, thereby estimating the number of years to completely fill the reservoir. However, in most reservoirs, sediment will seriously interfere with design functions by the time half the storage pool is lost (Dendy et al. 1973; Murthy 1977). *Reservoir half-life,* the time required to lose half the original capacity to sedimentation, is thus a much better approximation of when sedimentation problems will become truly serious. At many sites, sediments will seriously interfere with reservoir function when much less than half the original capacity has been lost. For example, Loehlein (1999) describes problems including hindered floodgate operation and clogging of hydropower and water supply intakes due to sedimentation at several Corps of Engineers flood control reservoirs in Pennsylvania, with only 6% storage loss.

12.2.3 Reservoir Life

Reservoir life has traditionally been conceptualized based on the continuous filling of the usable storage pool, presumably followed by abandonment of the structure. However, the "life" of a reservoir is better described based on the three distinct stages:

Stage 1: *Continuous sediment trapping*. During the first stage of reservoir life, continuous sediment trapping occurs during all inflowing flood events. A cross section perpendicular to the axis of the reservoir in continuously impounded areas will reveal a depositional sequence that fills the deepest part of the cross section first, eventually producing sediment deposits that are essentially flat (Fig. 12-2).

Stage 2: *Partial sediment balance*. During the second stage, the reservoir transitions from a continuously depositional environment to a mixed regime of deposition and removal. If sedimentation is allowed to proceed uninterrupted, the reservoir at this stage will become largely filled with sediment, and a channel–floodplain configuration will develop in the former pool area. The inflow and discharge of fine sediment may be nearly balanced, but coarse bed material continues to accumulate. Sediment management techniques, such as drawdown to pass sediment-laden flood flows through the impounded reach or periodic flushing, can produce a partial sediment balance to help preserve useful reservoir capacity.

Stage 3: *Full sediment balance*. A long-term balance between sediment inflow and outflow is achieved when both the fine and the coarse portions of the inflowing load can be transported beyond the dam or artificially removed on a sustainable basis. However, sediment movement through the impounded reach is not necessarily the same as the preimpoundment condition because sediment may accumulate during smaller events and be washed out during large floods or may be removed at intervals by dredging or flushing.

Most reservoirs worldwide are in Stage 1, continuously trapping sediment. Only a handful of reservoirs worldwide have been designed to achieve sediment balance. A notable example is the large (more than 600 km long) Three Gorges reservoir on China's Yangtze River, designed to reach full sediment balance after about 100 years.

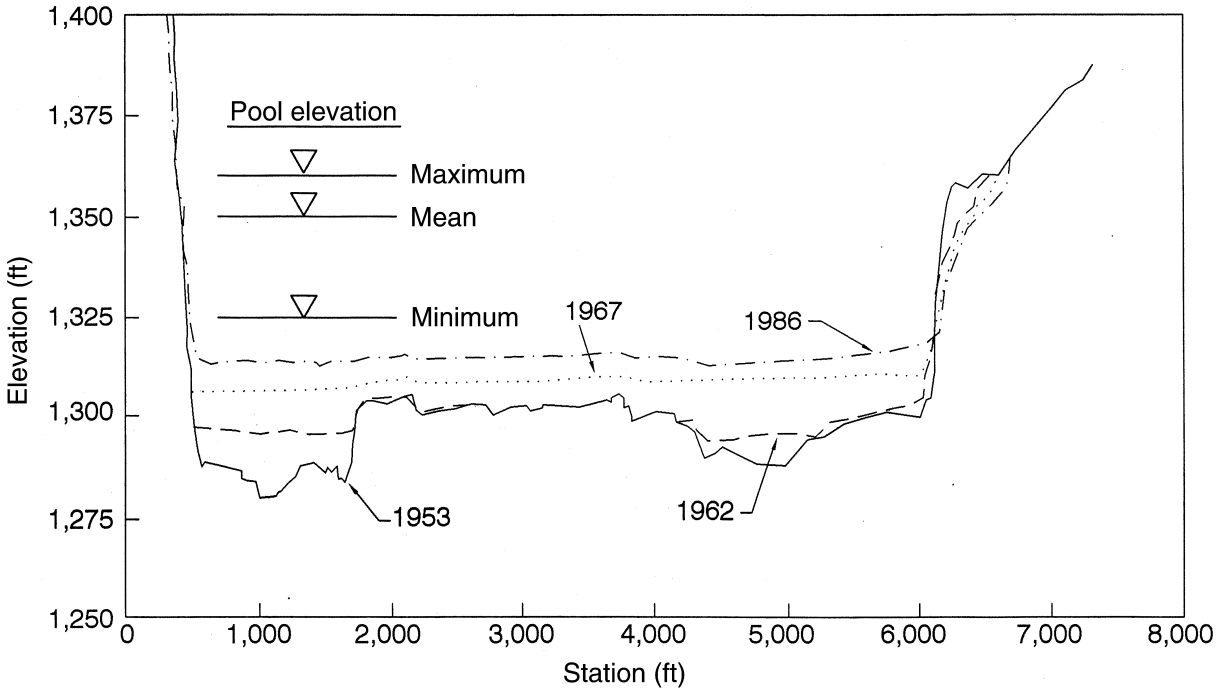

Fig. 12-2. Successive cross sections of Lake Francis Case on Missouri River above Ft. Randall Dam, showing the deposition of sediment in flat beds (Stanley Consultants 1989).

12.2.4 Capacity–History Curves

Reservoir volumetric capacity will steadily diminish in a reservoir that is continuously impounded, although the rate of storage loss will tend to decrease as the reservoir's hydrologic size and trap efficiency diminish (Brune 1953). Sediment management can retard or reverse this trend, and storage capacity can increase over time as sediment is removed. Capacity–history curves may be drawn to illustrate historical and anticipated changes in usable storage volume under different management options.

Illustrative capacity–history curves are given in Fig. 12-3, illustrating the case where sediment management is initiated when half the reservoir capacity has been lost. This example compares dredging alone versus dredging in combination with pass-through routing of major sediment-producing floods. The rate of sediment accumulation eventually decreases under the do-nothing alternative because of the declining capacity to inflow ratio (Brune, 1953). Similar curves may be constructed for other types of sediment management operations and can be useful in visualizing the impacts of alternative strategies on the long-term evolution of the reservoir.

12.3 SUSTAINABILITY

12.3.1 Sustainability and Economic Analysis

The underlying concept of sustainable development is that the welfare of future generations (including our own children and grandchildren) should logically figure into the project decision-making process. This concept arose from the recognition that many development and resource utilization patterns could not be sustained in the long term, coupled with the failure of conventional economic analysis to formally consider impacts over periods as short as a single human life span. Reservoirs arguably represent today's most important class of nonsustainable infrastructure.

Definitions of sustainable development have proliferated, but the following basic concepts are most relevant from the standpoint of water resource infrastructure: (1) Today's patterns of infrastructure development should not compromise the ability of future generations to access these same resources. (2) Maintain biological diversity and environmental integrity. (3) Minimize the potential for catastrophic disasters resulting from infrastructure failure or obsolescence. (4) Avoid activities that create a legacy of environmental restoration or infrastructure rehabilitation obligations that fall disproportionately on future generations.

Hotchkiss and Bollman (1996) have emphasized the need to assess project configurations on the basis of long-term parameters rather than relying solely on limited-horizon economic performance. Project economic analysis is based on benefit-cost techniques in which the future streams of benefits and costs are time discounted. Using a discount rate of 7%, for example, the present value of a $100 benefit 50 years in the future is only $5.83, and end-of-project decommissioning costs are typically ignored. Traditional discounting procedures discourage additional construction costs aimed at sustaining long-term function, such as large low-level flushing outlets that do not produce quantifiable

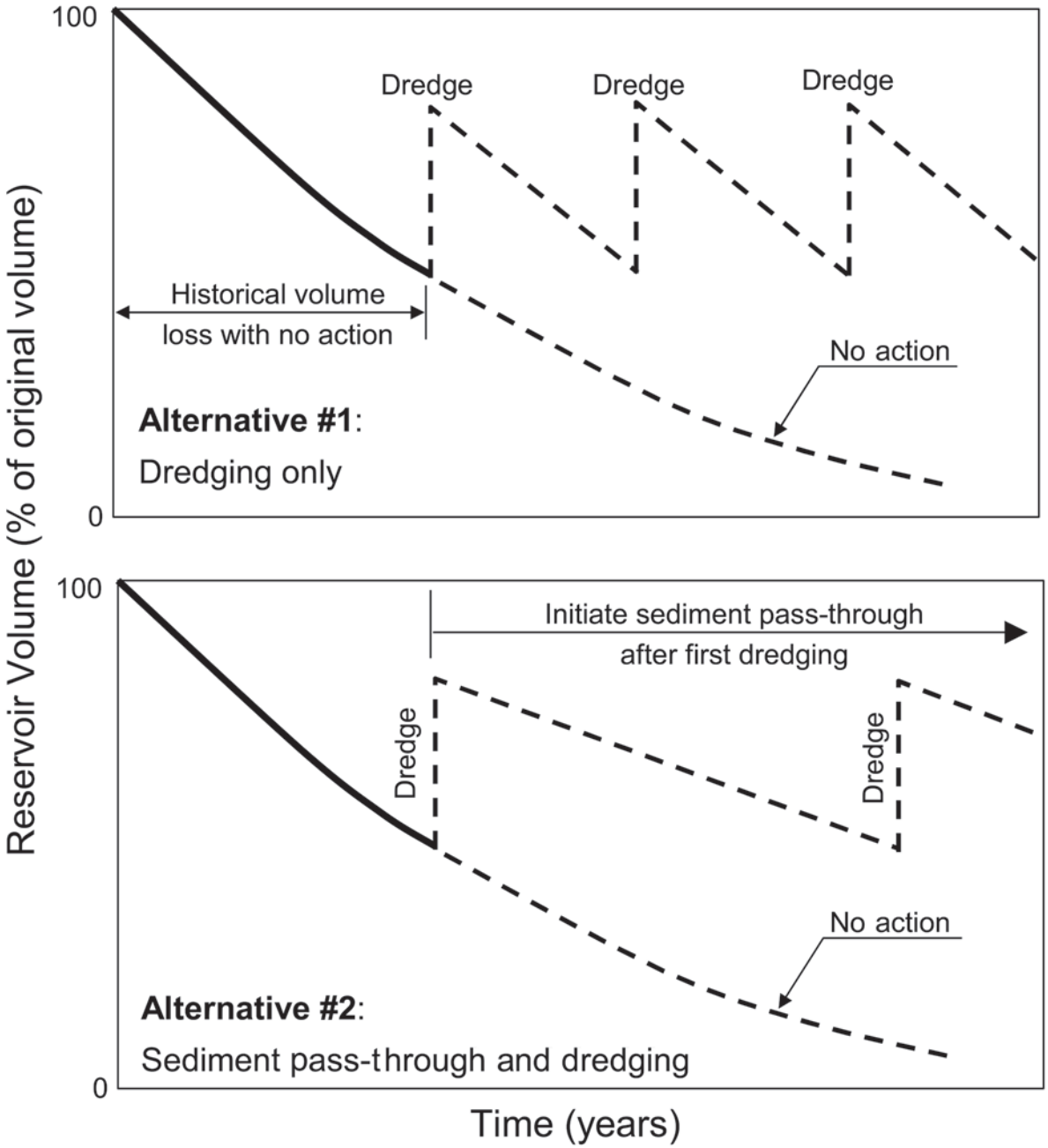

Fig. 12-3. Alternative storage history curves to conceptually illustrate sediment management alternatives, dredging only versus sediment-pass through with less frequent dredging.

economic benefits during the initial decades of reservoir life. Despite the logic behind sustainability considerations and the technical feasibility of a variety of preventive sediment management options, there is usually little economic incentive for an owner to invest today in strategies that reduce future sedimentation problems.

Cairns (1993) concluded that short-term economic gain overrides long-term sustainability or ecological considerations. He observed that historical development in the United States has followed this policy and that the same policy is definitely being pursued in developing countries. Weiss (1993) points out that market conditions also tend to be evaluated within the context of the present generation, and the needs of future generations are not explicitly represented. In addition to the problem posed by limited planning horizons, the benefit-cost analysis is not always appropriate for two other reasons: (1) incomplete information and improper valuation of impacts and (2) uncertainties in future markets. Most secondary impacts of reservoir sedimentation are not included in benefit-cost analysis. O'Neil

(1997) concluded that uncertain futures, both economic and technological, make the use of benefit-cost analysis for far-distant project impacts questionable.

Requiring a reservoir life measured in terms of generations instead of decades will demand new methods of analyzing costs and benefits. Palmieri et al. (1998) demonstrate that "for a very wide range of realistic parameter values, sustainable management of reservoirs is economically more desirable than the prevailing practice of forcing a finite reservoir life through excessive sediment accumulation." They reach such a conclusion after comparing the salvage value of projects to the cost of continuing dam operation. They suggest than an annual contribution to a "retirement fund" or to an "insurance policy" will affect future salvage value and may extend the economic life of a reservoir indefinitely.

12.3.2 The RESCON Approach

The RESCON (REServoir CONservation) approach to sustainable reservoir management developed under the auspices of the World Bank is described by Palmieri et al. (2003), and its technical details are outlined by Kawashima et al. (2003). The methodology proceeds in three stages: (1) determine which methods of sediment management are technically feasible; (2) determine which alternatives are more desirable based on an economic analysis; and (3) incorporate environmental and social factors to select the best course of action for sediment management.

The RESCON methodology can be applied to proposed or existing dams and reservoirs to make a preliminary assessment of sustainable management alternatives, and to compare them to the nonsustainable alternative of allowing the reservoir to silt up and implement decommissioning procedures at the end of a dam's physical life. Should the latter choice be identified as the only feasible alternative, a sinking fund to pay for decommissioning should be established to ensure intergenerational equity?

The RESCON approach accounts for all major benefits and costs over the complete project life-cycle and, in particular, acknowledges the need for intergenerational equity. This is achieved by maximizing the algebraic sum of net benefits, capital cost, and salvage value, that is,

$$Maximize \sum_{t=0}^{T} NB_t \cdot d^t - C2 + V \cdot d^T,$$

subject to

$$S_{t+1} = S_t - M + X_t,$$

given the initial capacity S_0 and other physical and technical constraints, and where: NB_t = net benefit in year t; d = discount rate factor defined as $1/(1 + r)$, where r = discount rate; $C2$ = initial capital cost of construction (= 0 for existing facilities); V = salvage value; T = terminal year; S_t = remaining reservoir capacity (volume) in year t; M = trapped annual incoming sediment; and X_t = sediment removed in year t.

In the case of reservoirs, the salvage value V is usually negative as it represents the cost of decommissioning at terminal year T, should this prove the most economical solution. Allowance for intergenerational equity is made by creating a sinking fund that will create a large enough retirement fund to decommission the facility, if required. The annual investment, k, into the sinking fund is calculated as

$$k = -m \cdot V / \left[(1+r)^T - 1 \right]$$

where m = interest rate (which can differ from the discount rate r). When assessing the economic feasibility of a decommissioning option, k is subtracted from the net benefits on an annual basis.

12.3.3 Regulatory and Legal Aspects

Important sustainability criteria are already established by regulation or law rather than economic analysis, such as the requirements for environmental protection and dam safety. From the owner's standpoint, these may be viewed as onerous and uneconomic measures, and it is precisely this difference in perception between the owner and society in general that has given rise to socially protective regulations and engineering standards. From this standpoint, it may be logical for the engineering community to develop minimum standards for considering long-term sustainability in future design and management activity related to reservoir sedimentation.

A logical starting point would be to formally evaluate and incorporate to the extent possible measures to sustain long-term capacity in all designs for new reservoirs, or significant modifications to existing ones. These measures are not necessarily costly. For example, in a new reservoir having crest gates and where sediment passthrough may eventually be feasible, this future option is facilitated by the specification of bottom-opening gates, as opposed to bascule gates which are unsuited to passing sediment. Similarly, outlets for river diversion during construction might be closed, but not filled with concrete, to facilitate the installation of bottom gates at some point in the future.

Legal and liability considerations will also have impacts on sediment management activities. In addressing this issue, Thimmes et al. (2005) have pointed out that the dam owner may be liable for the accumulation of sediment within

the reservoir that causes upstream flooding, as well as for impacts of sediment release downstream.

12.4 SEDIMENTATION IMPACTS

Sedimentation impacts not only the impoundment but also areas extending far downstream and short distances upstream of the design pool. Typical impacts are outlined in Table 12-2. Fig. 12-4 presents a highly simplified longitudinal profile along a reservoir, illustrating the various patterns of sediment deposition and associated impacts.

The primary sedimentation impact within a reservoir is storage loss that impairs water supply, hydropower, flood control, and both commercial and recreational navigation. The impacts of storage loss on water supply yield may be quantified as a gradual reduction in firm yield based on the storage–yield relationship for the site or as the increased risk (increased frequency) of water shortage with time when attempting to maintain a stated rate of withdrawal.

Coarse sediments (>0.6 mm diameter) can abrade hydromechanical equipment, and sediment deposits against the dam may increase the static loading on the structure. The presence of contaminants in sediments (Chapter 21) can greatly hinder any procedure that would release these sediments, such as dredging, flushing, or dam removal (Chapter 23).

Deltas can form where the main or side tributaries discharge into a reservoir, and these deltas will create backwater and bed aggradation above the normal pool level (Chapter 2). This deposition can create problems such as increased frequency and depth of flooding, decreased navigational clearance at bridge crossings, and sedimentation of upstream water intakes. Streambed aggradation will increase groundwater levels, which in turn can saturate vegetative root zones and waterlog riparian agricultural soils, increase soil salinity, and alter ecological habitats.

Below a dam, the river will adjust to both reduced sediment inputs and the altered stream flows produced by reservoir releases. Dams are highly efficient bed-load traps, and even reservoirs operated for sediment release may trap most of the inflowing bed material. Reservoir trapping of bed material encourages channel incision along the river reach below the dam, lowering the base level of the river. This can trigger processes much the opposite of those upstream: degradation of tributaries, destabilization and undercutting of streambanks, undermining of bridge piers and river training works, and sediment starvation of river bars and beaches important for both environmental and recreational benefits. Sediment starvation will also reduce aggregate supplies in the stream channel and contribute to coastal erosion.

Also, as the base level in the river incises in response to sediment trapping by the reservoir, channel degradation

Table 12-2 Sedimentation Impacts

Impact location and type	Impact description
Within-reservoir impacts:	
Storage loss	Reduced firm yield, hydropower, and flood-control benefits.
Reservoir operations	Sediment can clog intakes, interfere with gate operation, and abrade hydromechanical equipment.
Organic sediments	Oxygen demand can make bottom waters anaerobic.
Turbidity	Reduced euphotic zone and decreased primary productivity. Aesthetically unpleasant for recreation.
Navigation	Sedimentation of marinas and navigation channels. Interferes with recreational use and sport fisheries.
Air pollution	During drawdown, fine sediment exposed to air can dry out and be carried by wind.
Above-reservoir impacts:	
Delta deposition	Higher river levels flooding and reduce navigational clearance beneath bridges. Groundwater levels can rise causing soil waterlogging, salinization, and increased evaporation from vegetated deltas.
Below-reservoir impacts:	
Reduced bed-material load	Streambed incision and accelerated bank erosion. Bed may become too coarse for spawning. Structures such as bridges, intakes, and training works may be undermined. Cutoff of sand supply contributes to coastal erosion. Reduced supply of aggregate materials.
Reduced fine sediment load	Reduced nutrient delivery to downstream ecosystems. Increased water clarity will alter ecological conditions and benefit recreational use.

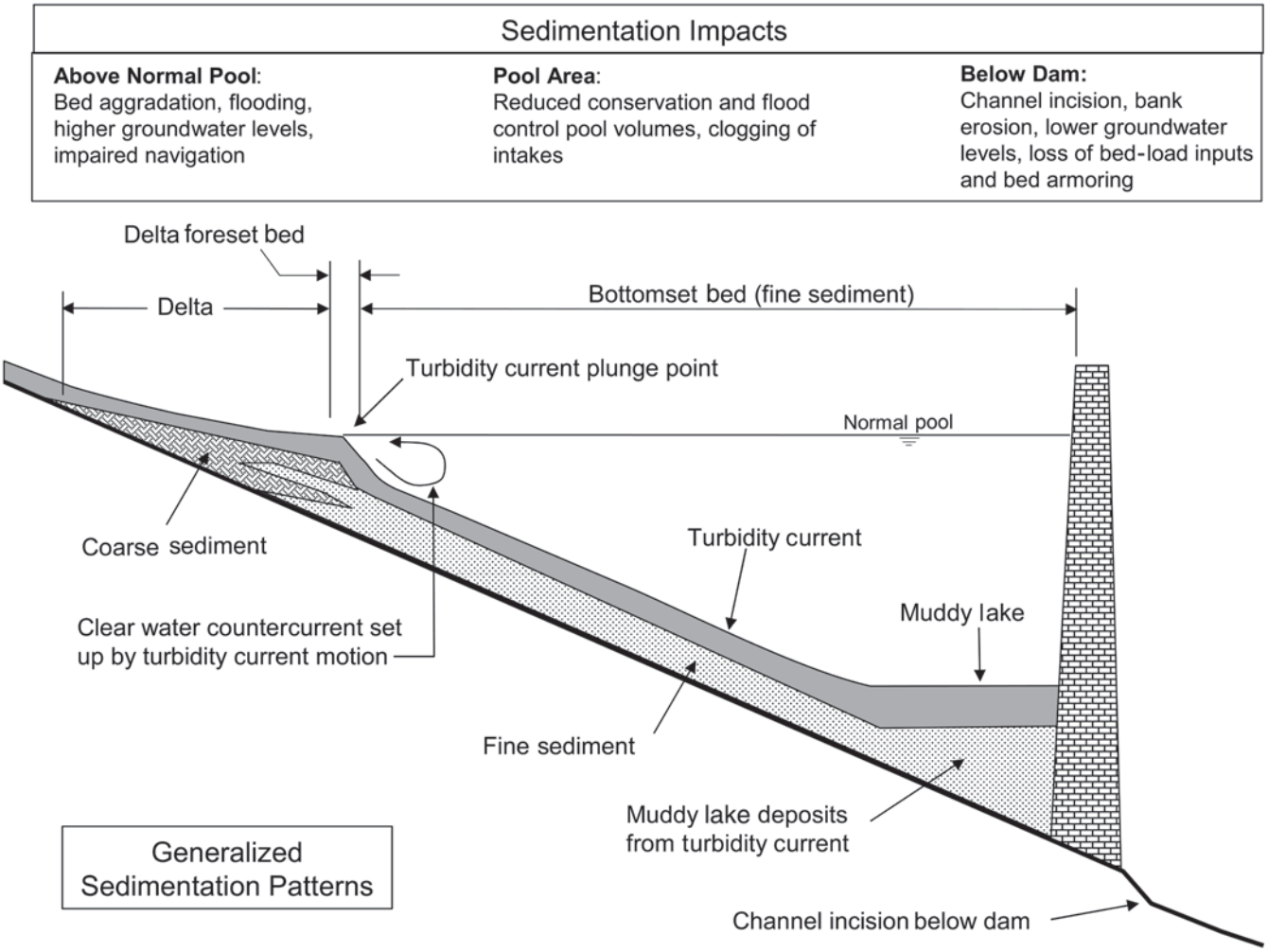

Fig. 12-4. Deposition patterns in reservoirs and classes of sediment-related impacts imposed by the dam.

can proceed upstream along tributaries and thereby affect stream reaches not themselves directly below the dam and thus unaffected by reservoir hydrology. Lower groundwater levels can result in loss of riparian vegetation and dewatering of wetlands. Fish habitats may degrade as a smaller fraction of the bed material is washed downstream, leaving behind an armored bed too coarse for fish spawning.

Dams reduce downstream flood peaks even in reservoirs not operated for flood control. This reduces the energy available to mobilize bed material, allowing an armor layer to form with smaller material than in the predam river channel (Chapter 3). This peak flow reduction and armoring will limit channel degradation below the dam, but without periodic mobilization of the armor layer and flushing of fines from the riverbed sediment, the immobilized bed can become useless for spawning and habitat. Although streambed degradation and bed-material coarsening below dams tend to occur in the first decades after construction, the process occurs erratically rather than as a uniform progression (Williams and Wolman 1984).

Channels below dams do not always degrade. When the dam significantly reduces downstream flows and sediment transport capacity yet below-dam tributaries continue to deliver large sediment loads to the river, the channel may aggrade, as in the case of Río Grande at Presidio, Texas, below Elephant Butte reservoir (Collier et al. 1995).

There is growing appreciation that the long-term impacts of dams on river systems have often been underestimated or even ignored, that dams can cause unnecessary environmental damage, and that the wise development and utilization of environmental resources is incompatible with the destruction of biological habitats. However, with proper management, these impacts can be greatly diminished. Environmental and related impacts of dams have been reviewed by Goldsmith and Hildyard (1984, 1985), McCully (1996), and Petts (1984).

River channels are maintained by periodic flood events, and the channel-forming event typically has a return interval of about 1.5 years (Leopold et al. 1964; Simon and Heins 2005). When downstream flood releases are reduced,

the channel can no longer maintain its original size and is encroached on by vegetation, as shown in the example pictured in Fig. 12-5. Ligon et al. (1995) described impacts on the McKenzie River in Oregon by flow regulation in two Corps of Engineer dams that reduced peak discharges by over 50%. Reduced flows allowed channel simplification, channel stabilization, and vegetative encroachment, substantially reducing the areas of gravel suitable for salmon spawning. They also reduced the area of sloughs, backwaters, and traces of former channels created by meander cutoffs, habitat required for rearing juveniles.

The increased resistance of public and environmental organizations to new reservoir construction is a logical reaction to the extensive reservoir building that has already occurred and to the impacts of dams on free-flowing rivers, including impacts not necessarily understood by their original designers. By 1990, a total of 965,000 km of rivers had been submerged by dams in the United States, versus only 15,000 km protected under the Wild and Scenic Rivers Act (Graf 1993). Much of the "wild and scenic" river mileage is itself downstream of or sandwiched between dams.

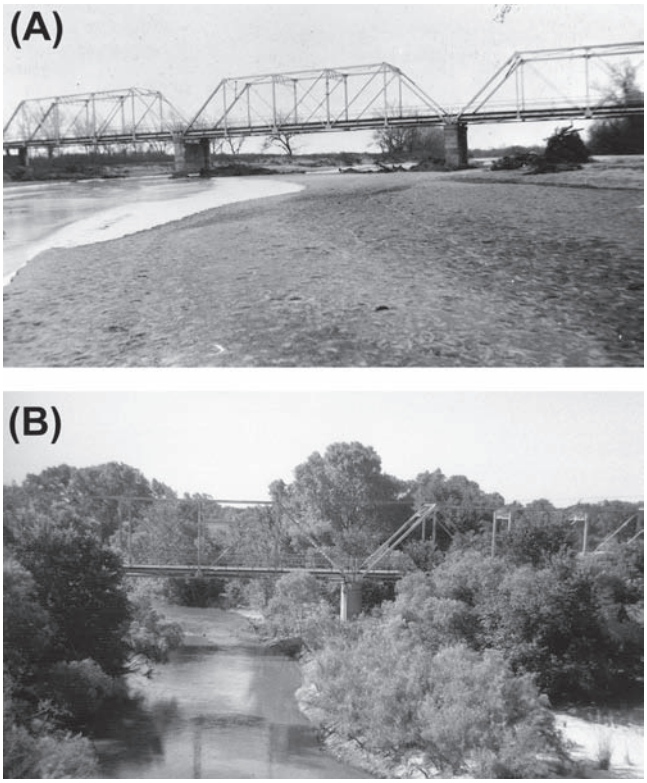

Fig. 12-5. Encroachment of vegetation into channels of North Canadian River 0.8 km below Canton Dam, Oklahoma, due to reduction in channel-maintaining flows. Photos taken in (A) 1938 and (B) 1980 (Williams and Wolman 1984).

12.5 SEDIMENT DELIVERY TO RESERVOIRS

Sediment yields vary remarkably over time and space, and this variability must be understood to properly interpret data, to predict sediment yields, and to successfully implement strategies for reducing sediment inflow or passing sediment-laden flows around or through the storage pool. This section outlines basic concepts of variability in sediment yield and delivery to reservoirs. The discussion focuses on suspended load because it is responsible for most sediment discharge worldwide, but basic concepts are generally applicable to the bed load as well.

12.5.1 Erosion and Sediment Yield

Erosion is the process of detaching particles from the soil matrix and initiating their transport away from the point of detachment. Erosion rates are measured using small plots, and the distance that a particle must travel before being counted as having been "eroded" may be a few meters or less. Erosion rates from farms and watersheds are computed by empirical models, such as the Universal Soil Loss Equation (USLE) and its variants (MUSLE, RUSLE), or the more complex physically based detachment and transport models, such as AGNPS, ANSWERS, CREAMS, SEDIMONT, and WEPP.

Sediment yield is the amount of sediment transported beyond or delivered to a specified point in the drainage network over a specified time period. It is always less than and typically much less than the amount of sediment eroded within a watershed due to redeposition prior to reaching stream channels or reservoirs. Watershed sediment yield is also addressed in Chapter 17.

Sediment delivery ratio is ratio of eroded sediment to delivered sediment. Because erosion rates are computed rather than measured, the sediment delivery ratio is actually the ratio of computed erosion to measured yield. Sediment yield estimates derived from erosion estimates are typically more sensitive to errors in estimating the sediment delivery ratio than to errors in erosion rate. For example, with a sediment delivery ratio equal to 10% of erosion, a 1% error in estimating sediment delivery ratio would have the same impact on computed sediment yields as a 10% error in the erosion estimate. For a good review of the problems associated with estimating sediment delivery ratio, see Walling (1983).

12.5.2 Spatial Variation in Sediment Yield

Sediment yield is highly variable over space, and a small part of the landscape unit will contribute a disproportionate amount of the total sediment yield. Dividing total sediment discharge by total basin area to obtain the average yield can be grossly misleading by masking the underlying variability in sediment yield (Campbell 1985). Variations in specific sediment yield, the sediment yield per unit of land area, can be particularly

Table 12-3 Sediment Yield from Gauge Stations Worldwide

Yield Class (tn/km^2/year)	Number of Gauge Stations	Gauged Land Area (%)	Total Gauged Sediment Load (%)
0–10	230	21.3	0.3
11–50	285	25.6	1.8
51–100	172	11.9	2.1
101–500	426	25.6	14.7
501–1,000	145	6.9	12.0
>1000	179	8.8	69.1

Source: Jansson (1988).

Table 12-4 Median Suspended Sediment Characteristics of 1.5-year Discharge at USGS Gauge Stations, Selected U.S. Ecoregions

Ecoregion	Number of Stations	Concentration (mg/L)	Specific Yield (tn/d/km^2)
Northern Rockies	13	30.13	0.05
Arizona—New Mexico Plateau	40	4143	6.5
Middle Atlantic Coastal Plain	22	22.1	0.16
Mississippi Valley Loess Plains	33	2175	173

Source: Data from Simon and Heins (2005).

dramatic in watersheds subject to disturbance. For example, Megahan (1975) showed that, compared to natural conditions, logging increased specific sediment yield by a factor of 1.6 on forest soils subjected to tree felling and skidding but by a factor of 550 on logging roads subject to mass erosion. For this reason, erosion control on forestlands focuses foremost on logging roads. On a larger scale, Jansson (1988) analyzed data from 1,358 gauge stations worldwide with tributary watersheds between 350 and 100,000 km^2. These data, summarized in Table 12-3, show that only 9% of the land area accounts for 69% of the sediment load. Effectively targeting erosion-control efforts requires that the landscape units and land use practices responsible for most sediment delivery be identified.

Sediment yield is particularly sensitive to vegetative cover. Thus, in selecting data sets for use in the estimation of sediment yield at an ungauged site or to confirm the reasonableness of an available data set, data should be compared within ecoregion. Background material and GIS mapping products for North American ecoregions can be found on several sites by Internet search. The Holdridge life zone system of ecological classification, more widely used in tropical areas, may represent another suitable landscape classification method.

An example of suspended sediment variability in the United States is presented by Simon and Heins (2005). They examined suspended sediment characteristics of the effective discharge, defined as the discharge or range of discharges that transport the largest proportion of the annual suspended sediment load over the long term (Wolman and Miller 1960). The 1.5-year discharge ($Q_{1.5}$) approximates the effective discharge. The range of median concentration and daily load values corresponding to the $Q_{1.5}$ discharge for representative ecoregions are illustrated in Table 12-4. Although the highest concentrations occur in the semiarid Arizona–New Mexico area, the highest yield occurs in a moist environment with erodible soils.

The size of the area analyzed can have a significant impact on both delivery ratio and sediment yield. The long-term delivery ratio decreases as watershed area increases because the opportunity for sediment trapping increases as a function of the distance from the erosion source. As a result, both delivery ratio and sediment yield tend to vary as a log-log function of drainage area (Fig. 12-6), although this trend may not be evident in all data sets.

12.5.3 Temporal Variation in Sediment Yield

Suspended sediment concentration typically increases as a function of discharge, making sediment yield more concentrated in time than the discharge of water (Chapter 2). In their review of data from stream gauges in the United States, Meade and Parker (1984) found that 50% of the annual sediment load is discharged on 1% of the days. Extreme storms or cycles of wet and dry years can dramatically influence annual yield, and it is not unusual for a single large storm event to deliver more sediment than an entire year of average flows. Uncertainty parameters affecting annual sedimentation rates have been analyzed by Salas and Shin (1999).

That most sediment yield is high focused in time implies that large sediment reduction benefits can be achieved from control methods focused on these highest-discharge days. In hydrologically small reservoirs having a capacity–inflow ratio less than about 0.2, it may not be necessary to capture every runoff event; large but infrequent sediment-producing events may be passed around or through the storage pool.

Sediment yield is also heavily influenced by land use changes such as deforestation or reforestation, changes in grazing intensity, and urbanization and by climatic variation. For example, analysis of sediment cores covering 110 years of impounding at Fairfield Lake, North Carolina, revealed a several-fold increase in the rate of sediment deposition following relatively limited urban development activities in its 7.3-km^2 watershed.

Techniques for evaluating long-term sediment yield have been summarized by Strand and Pemberton (1987) and MacArthur et al. (1995). They are also considered in Chapter 17. Long-term trends can be visualized by constructing a cumulative mass curve for water and sediment,

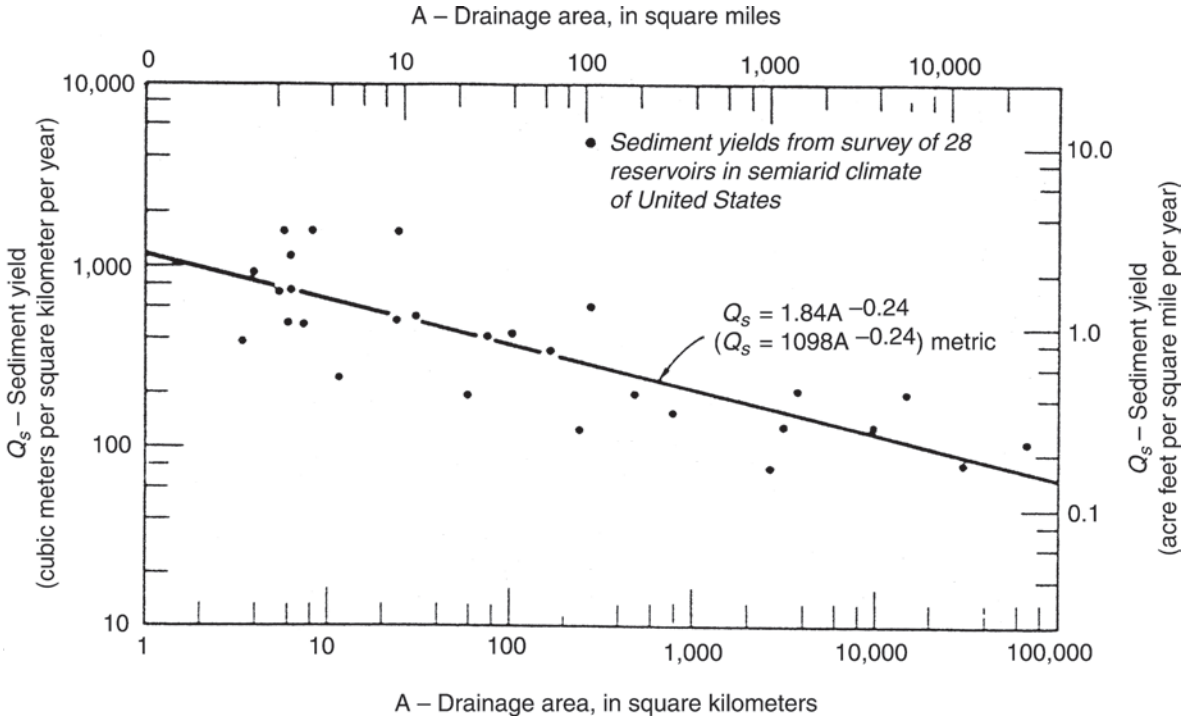

Fig. 12-6. Average annual sediment yield versus drainage area for semiarid areas of the United States (Strand and Pemberton 1987).

as in Fig. 12-7. This format gives a better idea of trends than a timewise plot since it helps compensate for runoff variability. Lacking site-specific data, long-term sediment yield can be estimated by data from similar watersheds within the ecoregion. Sediment yield data from various sources may be plotted on a log-log graph of yield versus drainage area for verification. Plotting yield data from several regional sources (Fig. 12-8) can help arrive at a better sediment yield estimate when site-specific data are sparse or are collected over a short time period (Burns and MacArthur, 1996).

In applying regional curves to a particular study site, take care to consider local features such as upstream reservoirs, a history of fire, and land use, topographic, or geological conditions that may depart from regional norms. Departures from average regional conditions by one or two orders of magnitude may be anticipated in heavily disturbed areas.

With long service lives, reservoirs will be affected by very long-term trends in sediment yield plus the years of lag time that may occur between changed erosion rates in the watershed and sediment delivery to the reservoir. As an example, consider the long-term changes in the erosion rates and sediment yield from the Piedmont area of the eastern United States from 1700 to 1970 documented by Trimble (1974, 1977). Deforestation for agricultural use began in the late 1700s, and the area was completely deforested by

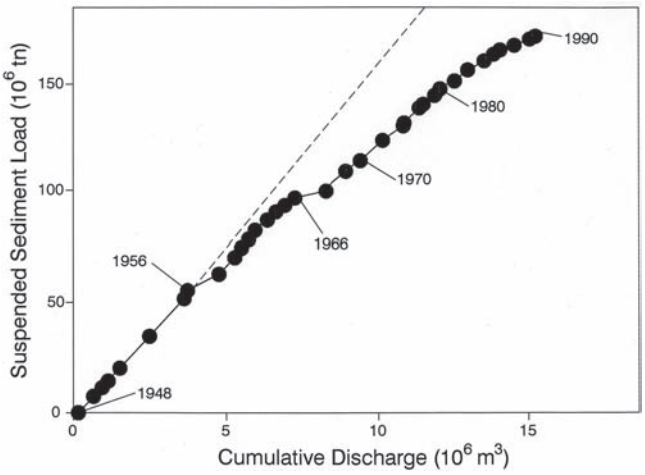

Fig. 12-7. Cumulative mass curve of water and sediment showing a long-term trend of declining sediment yield, Río Puerco, New Mexico (after Gellis 1991).

the mid-1800s, greatly accelerating erosion rates and sediment yield. Erosion rates declined after the 1920s as hillside farms were abandoned and revegetated naturally and soil conservation methods were developed and implemented on the remaining farms. Despite the erosion of 1 mm/year of soil over a 150-year period, export by rivers accounted for less than 0.053 mm/year (a sediment delivery ratio of

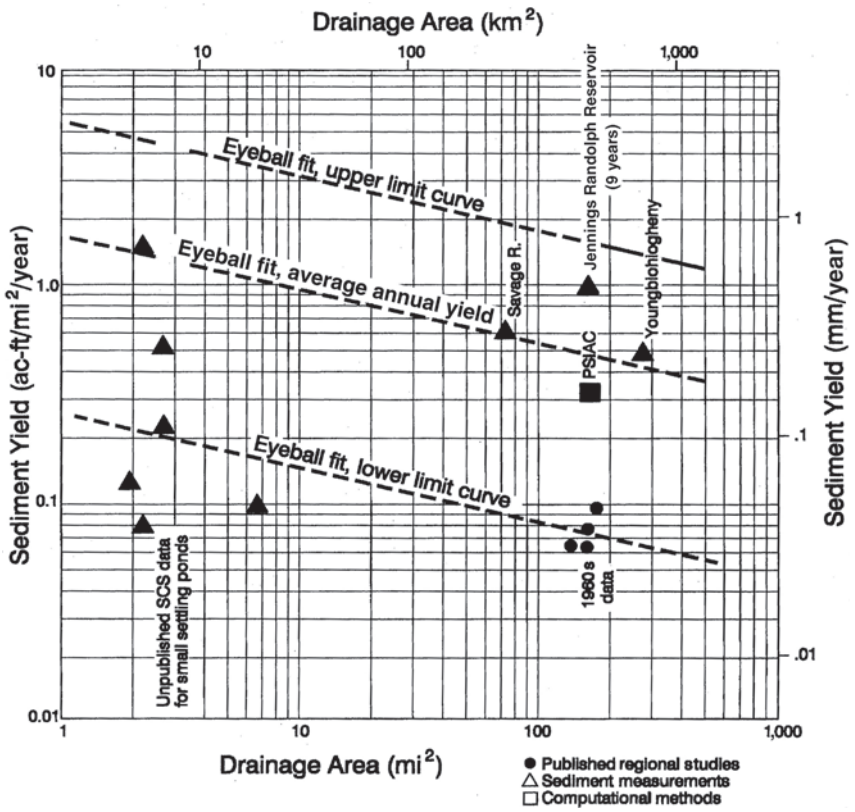

Fig. 12-8. Regional values of sediment yield versus drainage area, Jennings Randolph Reservoir (Burns and MacArthur 1996).

only 5.3%) because eroded sediment was redeposited further downslope in downstream channels and on floodplains. Debris filled streams and covered floodplains, and stream aggradation frequently swamped adjacent bottomlands, making them unfit for agriculture. Today, with low rates of erosion, the aggrading stream reaches are now incising.

Long-term sediment yield may also decline as the watershed degrades and the supply of readily erodible sediment is progressively exhausted (Sutherland and Bryan 1988; Rooseboom 1992). Long-term variations in sediment yield from rivers in the semiarid southwestern United States appear to be cyclic and attributable to a complex interaction of variables including climate (sequence of drought years and floods) and grazing pressure (Gellis et al. 1991). Sediment yield data from Río Puerco exhibits a long-term trend due to these effects (Fig. 12-7). Fire can cause a temporary increase in sediment yield. In areas subject to urban development, sediment yield is typically low in the predevelopment period, increases dramatically during development because of earth movement activity, and declines to lower levels after all soils in the catchment are stabilized with pavement and landscaping (Livesey 1975). Long-term yield can also be reduced by construction a large upstream reservoirs or by thousands of small stock watering ponds across the watershed (Chapter 17).

There has been a tendency to underestimate long-term sediment yield, particularly in developing areas where increasing population pressure results in the deforestation of sloping soils. In a comparison of predicted sedimentation rates with actual performance at 21 reservoirs in India, Tejwani (1984) found that sediment yield was less than predicted at one site, but from 40% to 2,166% higher than predicted at the other 20 sites. Lagwankar et al. (1995) found sediment delivery 1.5 to 3 times higher than predicted in 24 of 27 Indian reservoirs. Major factors contributing to underprediction of sediment inflows are watershed degradation and the lack of accurate long-term records.

12.6 QUANTIFYING SEDIMENT YIELD

12.6.1 Estimating Sediment Yield by Reservoir Survey

There are two basic strategies for measuring sediment yield: (1) by the volume of sediment deposited in reservoirs and (2) continuous monitoring of fluvial sediment discharge. Reservoir resurvey data are generally more accurate because reservoirs collect sediment from all events since their construction, eliminating problems of missed or underreported events at fluvial gauge stations. They also reveal patterns of sediment deposition critical to evaluating remedial actions.

As a disadvantage, reservoir data do not reveal the spatial or temporal patterns of sediment delivery needed to analyze some sediment management alternatives.

12.6.1.1 Bathymetric Survey Bathymetric data from successive reservoir surveys are used to track volume depletion and revise elevation–capacity curves; to predict the type, magnitude, and time horizon for sedimentation problems; to calibrate mathematical models of sedimentation; and to help develop and monitor the effectiveness of sediment management practices. For modeling of sedimentation processes, bathymetric mapping should be complemented with borings to determine the grain size of the deposits and verify estimates of deposit bulk density determined by empirical methods. Mathematical models of sedimentation processes are considered in Chapters 14 and 15.

Reservoir may be generally performed at intervals of about 5 to 20 years, but this can vary substantially depending on budgetary constraints, rate of storage depletion, the type and importance of the uses threatened by sediment accumulation, and management requirements. In reservoirs with very low rates of sedimentation, the intersurvey period may be several decades. Unscheduled surveys may be called for after a major flood delivers a large volume of sediment to the reservoir, and partial surveys may address specific issues such as shoreline erosion, delta advancement, and flood studies in delta and backwater areas. Periodic cross-section surveys should also be made in areas below the dam where the riverbed is expected to adjust because of the reduced sediment supply and changed stream-flow regime.

If the goal is to identify long-term sediment accumulation trends, more than 20 years of survey record encompassing several surveys may be needed before a reliable trend can be established. During the first years of reservoir operation, the apparent rate of storage loss may be higher than the long-term rate because of incomplete sediment compaction. When the intersurvey sedimentation volume is small compared to the total reservoir volume, estimates of deposition rate can be significantly affected by use of different survey techniques or volume computation algorithms.

Reservoir volume computations are performed by either range-line or contour surveys. The original volume of reservoirs is generally computed using the contour method based on preimpoundment topographic mapping. The range-line method uses a system of ranges (cross sections) selected and surveyed after initial impounding. Each range line is tied to the initial elevation–capacity relationship of the reservoir reach corresponding to that range (as determined by preimpoundment contour survey) and provides the base against which all future surveys will be compared. The range lines are resurveyed at intervals, and the elevation–capacity relationship is recomputed for each reach on the basis of the change in the cross-sectional area of each range line. This method has been widely used, as it allows sediment accumulation to be tracked using minimum field data.

The contour method entails the complete survey of the reservoir and preparation of a bathymetric contour map. This method is more accurate than the range-line method and gives a more complete picture of the pattern of sediment deposition. Contour surveys are facilitated by modern GPS and bathymetric measurement equipment and are preferred today.

Every survey method incorporates different types of data collection errors and approximations in the algorithms for volume computation. The same types of field data and computational algorithm must be used for each survey if results are to be strictly comparable. Therefore, when updating from the range method to contour surveying, compute the reservoir volume using both methods to determine how much of the apparent intersurvey volume change is attributable to differences in methodology.

Bathymetric surveys are typically performed using GPS positioning system in combination with a depth sounder, both connected to a portable computer that records the resulting *x, y, z* coordinate data into a file that can be processed subsequently to draw a contour map. Survey systems can also incorporate navigational features that allow the planned tracks to be laid out prior to the survey, giving directional instructions and positional plots to the operator during the survey. An example of this method is provided by Odhiambo and Boss (2004).

Accurate contouring requires that the data be checked and contour lines adjusted during postprocessing to eliminate contouring errors introduced by automated mapping. Because error-correction effort declines as the density of data points increases, the distance between survey lines used for automated contouring should be shorter than the reservoir width, and a much higher data densities should be obtained if possible. The data density will ultimately be limited by data-collection budget since a typical surveying speed is about 2 m/second. An example of survey track lines for construction of a contour map is given in Fig. 12-9.

On large reservoirs, if the pool is drawn down or emptied regularly, the lake surface area can be photographed from aircraft or satellite at different reservoir stages to construct a contour map based on the area of the water surface at each stage.

When computing average specific sediment yield (tn/km^2/year) based on the sediment volume trapped in a reservoir, it is necessary to compensate for sediment trapping by upstream reservoirs constructed over the period covered by the data. The changing area of the watershed effectively contributing sediment can be expressed as *effective watershed-years* by the following expression:

$$\begin{pmatrix}\text{Effective}\\ \text{Watershed}\\ \text{Years}\end{pmatrix} = \left[\begin{pmatrix}\text{Unregulated}\\ \text{Area}\end{pmatrix} + \begin{pmatrix}\text{Regulated}\\ \text{Area}\end{pmatrix} * \begin{pmatrix}\text{Sediment}\\ \text{Release}\\ \text{Efficiency}\end{pmatrix}\right] * \text{Years}$$

where the sediment release efficiency = 1 – trap efficiency for upstream reservoirs. The time period in years should be

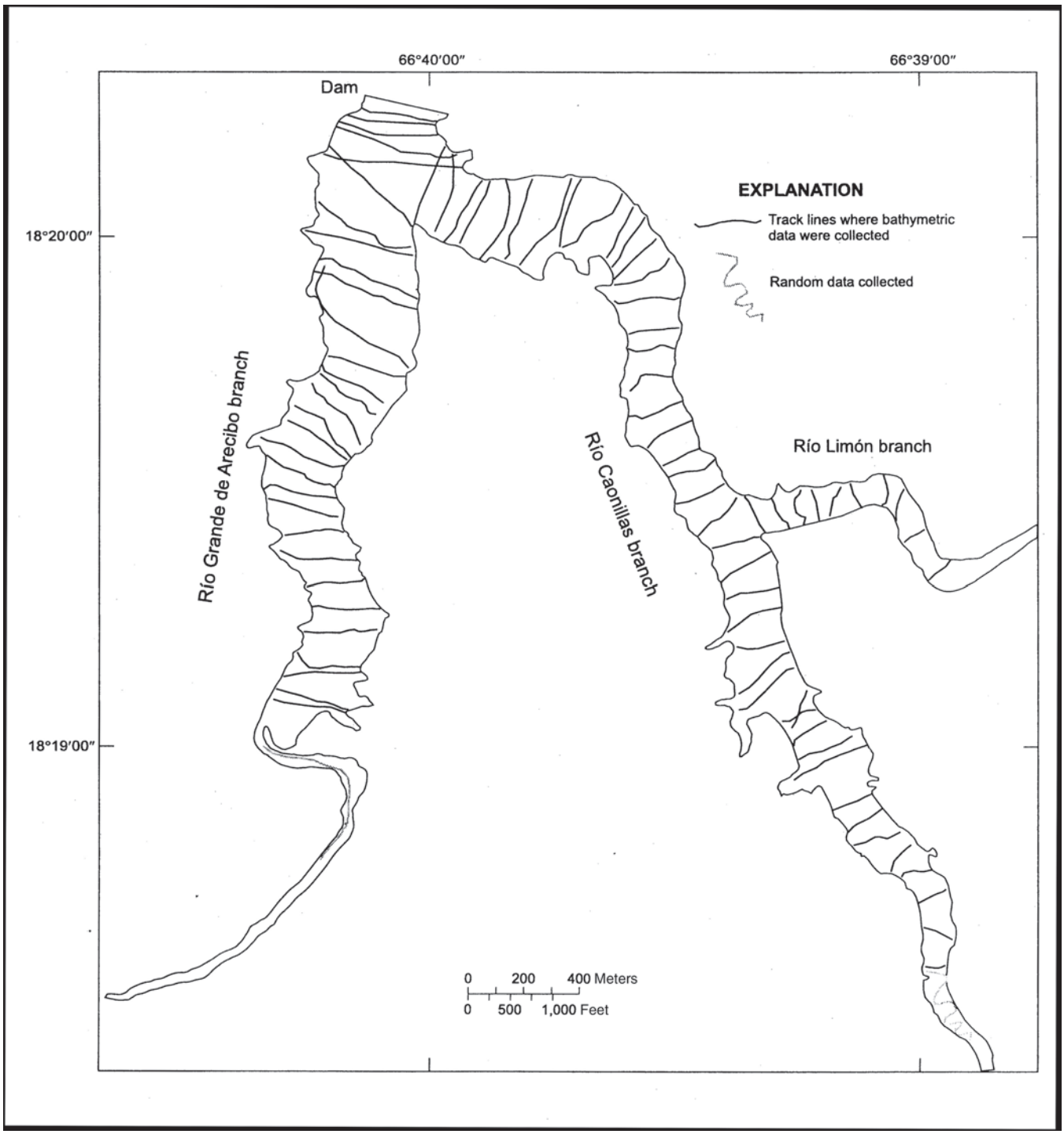

Fig. 12-9. Hydrographic track lines for contour surveying of a reservoir (Soler-López 2001).

computed for each interval of upstream reservoir construction and summed to obtain the effective sediment-contributing area as the basis for computing specific yield.

12.6.1.2 Deposit Thickness over Event Horizons Lacking reliable original bathymetric data, sediment thickness over a datable horizon can also be used to determine sedimentation rate. Cesium 137 is a man-made isotope produced only by the atmospheric testing of thermonuclear devices and dispersed globally. It was first produced in measurable amounts in 1954; its concentration peaked in 1964 and declined rapidly thereafter following signature of the international treaty to ban atmospheric testing. Cs^{137} is tightly sorbed onto clay particles and penetrates only a short distance into clayey soils. As these soils are washed into lakes and reservoirs, they mark

radioactive horizons corresponding to the initiation of significant nuclear weapons testing and the peak weapons testing activity. This marker can be used to determine sedimentation depths overlying this event horizon both in reservoirs and in natural lakes. Cores are obtained, sectioned, and counted in a gamma-ray spectrometer. With a half-life of 30 years, Ce^{137} will be useful as a dating tool into the first decades of the twenty-first century (McHenry and Ritchie 1980). If the watershed has been impacted by a large fire, volcanic eruption, Chernobyl radioactivity, and so on, these events may also leave similar datable horizons within the sediments. An extensive bibliography of erosion and sedimentation studies based on Ce^{137} are located at http://hydrolab.arsusda.gov/cesium137bib.htm (accessed March 12, 2006).

Horizon-dating methods have several important limitations. When a reservoir is drawn down, sediments can be mobilized and reworked, making horizon-dating methods useful only in areas of continuous deposition. Also, the depth of sediment deposition in reservoirs is uneven, making it necessary to core and analyze samples from a number of locations to reliably map deposition thickness.

Sediment depth over the density horizon corresponding to the original bottom can also be determined by a subbottom profiler, which uses a higher-frequency sonar signal (200 MHz) for bathymetric mapping in combination with a lower-frequency signal (4–28 MHz). The lower-frequency signal penetrates finer sediment and is reflected from underlying denser layers corresponding to the original bottom, allowing the sediment thickness to be mapped. For example, a 28-MHz subbottom signal was used by Odhiambo and Boss (2004) in an Arkansas study that penetrated sediment deposits not more than about 1 m thick. Subbottom profiling is limited by several factors: thick sediments cannot be penetrated, coarse sediments that have prograded over previously deposited fines may register as a false preimpoundment bottom, and sonar signals are also strongly reflected by the gas–liquid interface generated by the anaerobic decomposition of organic sediment, which creates methane bubbles.

12.6.2 Sediment Yield Estimation from Fluvial Data

Fluvial sediment data are required to determine variations in sediment yield over time. Techniques and methods for sediment measurements are addressed in Chapter 5. However, the collection of accurate fluvial sediment data has potential sources for error that should be understood by users. For more information on procedures and potential sources of error, consult Guy and Norman (1970), Glysson (1987), Edwards and Glysson (1988), and Walling and Webb (1981, 1988). The USGS suspended sediment database is available at http://co.water.usgs.gov/sediment/.

12.6.2.1 Sediment Rating Curves Fluvial sediment load is determined by the product of stream-flow and discharge-weighted sediment concentration. See Appendix D on estimation of sediment discharge. Sediment load is usually computed from a long-term discharge record and a sediment rating curve that relates concentration to stream flow. The rating curve is constructed from instantaneous discharge–concentration data pairs, but the resulting relationship typically exhibits considerable scatter, and sediment concentration may vary over two log scales at a given discharge. Furthermore, the large floods or hurricane events responsible for much sediment transport may be represented by very few data points, if any at all.

Sediment load is the product of concentration and discharge, and when plotted as a function of discharge, it will exhibit less apparent scatter than a concentration–discharge plot using the same data because the discharge term occurs on both the ordinate and the abscissa. Both Ferguson (1986) and Glysson (1987) have cautioned against use of rating curves of load versus discharge because they can incorporate significant spurious correlation.

A sediment rating curve developed from several years of field data and that includes sampling of flood events can be applied to a longer-term discharge data set to estimate long-term sediment yield. In these computations, the time base for the rating curve must be representative of the discharge data set time base. For example, one would not apply a rating curve derived from instantaneous discharge–concentration data pairs to a hydrological record consisting of average daily flows in a flashy mountain stream, yet this same procedure may be acceptable in a river with a slowly rising and falling hydrograph. Published USGS data typically report total daily load versus average daily discharge.

Recommended procedures for the development of accurate rating curves have been summarized by Cohn (1995). Appendix D also provides guidance on methods currently used by the USGS. Regression techniques commonly used to develop rating curves incorporate a significant undercounting bias and will produce sediment loads significantly lower than observed even when applied to the data set from which the regression was derived. In some cases, this error can undercount sediment discharge by 50%. It is important to back test a rating relationship by applying it to the original stream-flow data set to ensure that it accurately computes the total load. Also, a multiple-slope relationship should be used as necessary to restrict maximum sediment concentration to realistic values at high discharges. Without this precaution, the resulting relationship will ascribe an inordinate amount of sediment yield to the highest discharges, thereby skewing the results of sediment management simulations.

The suspended sediment concentration in streams is determined primarily by watershed processes responsible for delivering fine sediment to channels, but bed material transport is controlled primarily by channel hydraulics. Whereas stream discharge is a consequence of rainfall, suspended-sediment concentration is also influenced by many watershed parameters not directly related to discharge, such as seasonal changes in land use and vegetative cover, variation in rainfall intensity and erodibility, exhaustion

of erodible sediment supply by antecedent events, and variable arrival times of runoff from subbasins having large differences in sediment yield (Chapter 17).

If sediment concentration varies directly as a function of discharge, there will be a single-valued relationship between discharge and concentration (or load). However, sediment concentration and discharge often do not peak simultaneously, creating graphs of concentration versus discharge that are looped rather than single-value functions (Williams 1989). Error-free sampling over multiple events of this type will produce a sediment-rating curve of "average" conditions including both rising and falling limbs of the hydrographs. Additional scatter is produced by seasonal variations in rainfall intensity, rain versus snowmelt events, seasonal or long-term changes in vegetative cover, different antecedent conditions, and so on.

Within a highly scattered discharge–concentration data set may reside seasonal or within-event patterns that can be exploited to reduce reservoir sedimentation. A clockwise loop in the concentration versus discharge graph indicates that most sediment is discharged during the rising limb of the hydrograph, and water in the falling limb has a much lower sediment concentration. This may be caused by declining erosion rates in the latter part of the storm as rainfall intensity diminishes and the readily erodible sediment supply is exhausted. To the extent the sediment-laden portion of the hydrograph is made to bypass or pass through the storage pool, sedimentation will be reduced. Similarly, early-season flows may carry more sediment than subsequent flows because of the seasonal increase in vegetative cover and seasonal exhaustion of readily erodible sediment supply. Frequent sediment sampling is required to determine if the scatter typically inherent in sediment data conceal temporal patterns of sediment transport that may be used for sediment management.

12.6.2.2 Monitoring Sediment Yield by Turbidity Measurements If frequent sediment concentration data are available, sediment load can be computed directly as the product of discharge and concentration at short intervals (e.g., every 15 minutes) instead of relying on a sediment-rating curve (Chapter 5). With this level of detail, the temporal variation in sediment concentration and load will also be apparent, which can be helpful in detecting looped rating curves and in planning sediment-routing strategies.

In rivers with rapidly rising and falling hydrographs, sampling is required at short sampling intervals to accurately track sediment yield. However, short-interval sampling using an automatic pumping sampler produces many samples with high laboratory costs. Also, the sample bottles in an automatic sampler can be filled prior to the end of a prolonged or multiple-peak event, leaving part of the event unsampled. Resultant undercounting errors as high as 50% by conventional sampling and rating curve techniques are discussed by Walling and Webb (1981, 1988) and Olive and Rieger (1988).

The combination of pumped samplers and turbidity measurement has been shown to represent a viable strategy for improving the quality of sediment discharge data. There is no direct relationship between turbidity and suspended-sediment concentration, yet the discharge–sediment relationship is also a poor predictor of sediment loads as evidenced by the order-of-magnitude scatter typical of concentration–discharge graphs. However, turbidity can be recorded every few seconds, averaged, and logged to onboard memory, thereby eliminating the error due to the unreported periods that occur with manual and pumped sediment samplers.

Specific turbidity is the turbidity measured in formazin units divided by the mass particle concentration in mg/L. Because the optical properties of a suspension vary as a function of grain size and other factors, specific turbidity changes over the duration of an event as the grain size distribution varies. Fines have a much higher specific turbidity than sands. Specific turbidity can vary by an order of magnitude as a function of the suspended-sediment particle sizes (Foster et. al. 1992; Gippel 1995).

Time-stratified and flow-stratified turbidity sampling schemes have been compared by Thomas and Lewis (1993). A protocol for suspended-sediment sampling based on turbidity reported by Lewis (1996) uses pumped samples to periodically calibrate the turbidity–concentration relationship to overcome the problem of variations in specific turbidity. This protocol generates more accurate data than a pumped sampler working alone while simultaneously collecting fewer pumped samples for analysis. Because suspended-sediment concentration varies over a cross section, sediment concentration at the fixed sampling point used by automatic samplers or turbidity sensors must be correlated against depth-integrated samples.

12.6.3 Neural Network Models for Sediment Yield

Neural network models have been demonstrated useful for better definition of the relationship between hydrologic parameters and sediment concentration. The neural network model is essentially a nonlinear black box that correlates outputs to inputs by training its internal algorithms and their weighting scheme against a calibration data set. Applications of neural networks in hydrology have been reviewed by the ASCE Task Committee (2000a, 2000b). Unlike the single-parameter sediment rating curve, which relates concentration to discharge, a neural network model can incorporate multiple parameters including both current and antecedent values for stream flow, rainfall, temperature, and other parameters from one or more gauging stations in the watershed.

One approach is to use the neural network to develop rating relationships based on channel hydraulic characteristics. Jain (2001) and Sen et al. (2004) have used this approach to develop a model to predict suspended-sediment concentration in the Mississippi River based on time-series data including using both current and lagged values of discharge and suspended-sediment concentration. Nagy et al. (2002) developed a more generalized sediment transport model correlating suspended-sediment concentration to eight unlagged channel hydraulic characteristics.

An alternative approach is to predict suspended-sediment concentration or discharge based on channel plus watershed hydrologic parameters or watershed parameters alone. For example, Cigizoglu and Alp (2003) accurately predicted suspended sediment in the Juniata River, Pennsylvania, on the basis of both current and lagged values of discharge and rainfall but found that Thiessen-averaged rainfall alone was not an adequate predictor in this 8,690-km^2 watershed. In a smaller 92-km^2 watershed in northeastern India, Raghuwanshi et al. (2006) predicted both runoff and sediment yield for both daily and weekly time steps from temperature and rainfall data alone.

12.6.4 Sediment Yield Estimation by Spatial Modeling

Computationally intensive techniques can significantly improve the ability to predict and manage sediment, particularly when baseline data and good calibration data sets are available (Chapter 17). There are many alternative approaches, but no generally accepted methodology has yet emerged. This is due in part to the wide diversity of questions that can be addressed by these models plus regional differences in data availability, engendering problem-specific model formulations.

Spatially distributed data may be analyzed in a GIS-type framework to compute the yield of both water and sediment from the watershed on the basis of soil, land use, and hydrologic input parameters, and the resulting runoff and its sediment load is then routed to the watershed exit. Empirical soil erosion models have been in use for many decades, and parameter values are widely available, but the sediment delivery process must be simulated by other means. An example of the coupling of empirical erosion prediction models with a sediment delivery module to simulate sediment yield is presented by Kothyari et al. (1996).

Alternatively, physically based models that simulate both sediment detachment and transport processes may be coupled with fluvial routing procedures to simulate sediment yield. An example of the latter is the continuous water and sediment modeling approach demonstrated on watershed scales ranging from 17.7 to 9,000 km^2 by Arnold et al. (1995). This model coupled continuous physically based erosion prediction models with a routing scheme based on reasonably available data and was successfully tested against both annual and monthly sediment discharge data at the largest watershed scale. As an advantage, spatial data can be used to simulate the impact of alternative land use scenarios and identify areas where erosion control would provide the highest benefit, taking into account both erosion rate and the sediment delivery process. Neural network models can also be incorporated into a GIS framework (Doris et al. 2004).

The GIS environment can also be used to organize, interpret, and manipulate massive amounts of spatial data. The ongoing development of a GIS-based sediment assessment and management model incorporating 250 sediment gauging stations and spatial sediment yield data across the 1×10^6-km^2 watershed tributary to the Three Gorges Project has been described by Lu et al. (1999).

12.7 SEDIMENT DEPOSITION IN RESERVOIRS

The understanding and prediction of deposition patterns is important for a variety of reasons. Delta deposition can cause a stream to aggrade upstream of a reservoir and affect flood levels, groundwater levels, bridge clearance, commercial and recreational navigation, and environmentally sensitive areas. The shape of the stage–storage curve will change because of sedimentation, affecting different beneficial pools within the reservoir. Deposition by turbidity currents can interfere with low-level intake at the dam, even with as little as 1% storage loss in the impoundment (Garcia 1999; De Cesare et al. 2001). Observations of deposition patterns can also be helpful in developing strategies for sediment management. Reservoir surveys are undertaken at intervals can document both the volume and the pattern of sediment deposition.

12.7.1 Trapping and Releasing Efficiency

Trap efficiency is the percentage of the total inflowing sediment load that is trapped within a reservoir over a stated period of time. *Release efficiency* is the amount of sediment exiting a reservoir, expressed as a percentage of the inflowing load, and is the complement of trap efficiency:

$$\text{trap efficiency} = \text{sediment trapped/inflowing sediment}$$
$$\text{release efficiency} = \text{released sediment/inflowing sediment} = (1 - \text{trap efficiency})$$

From the standpoint of sediment management, sediment release efficiency is a more useful concept than trap efficiency because it can be used to express events in which sediment discharge exceeds sediment inflow, as occurs during flushing and some sediment-routing events. Sediment trapping or releasing efficiency is not constant but is influenced by factors including detention period, inflowing sediment characteristics, and reservoir operation.

For preliminary screening of sediment trapping or release, two methods have been widely used. Brune (1953) developed an empirical relationship between the *capacity: inflow* (C:I) ratio and long-term trap efficiency (Fig. 12-10). Trap efficiency declines as sedimentation reduces the capacity:inflow ratio. Temporarily lowering the reservoir pool during a flood (pass-through sediment routing) reduces both detention time and sediment trapping. This straightforward method is widely used to make preliminary estimates, as the data required are usually readily available. Another well-known method, that of Churchill (1948), requires information on reservoir capacity, reservoir length, and inflow during the study interval and is better oriented to the analysis of specific events. Strand and Pemberton (1987) recommend use of the Brune curve for large storage

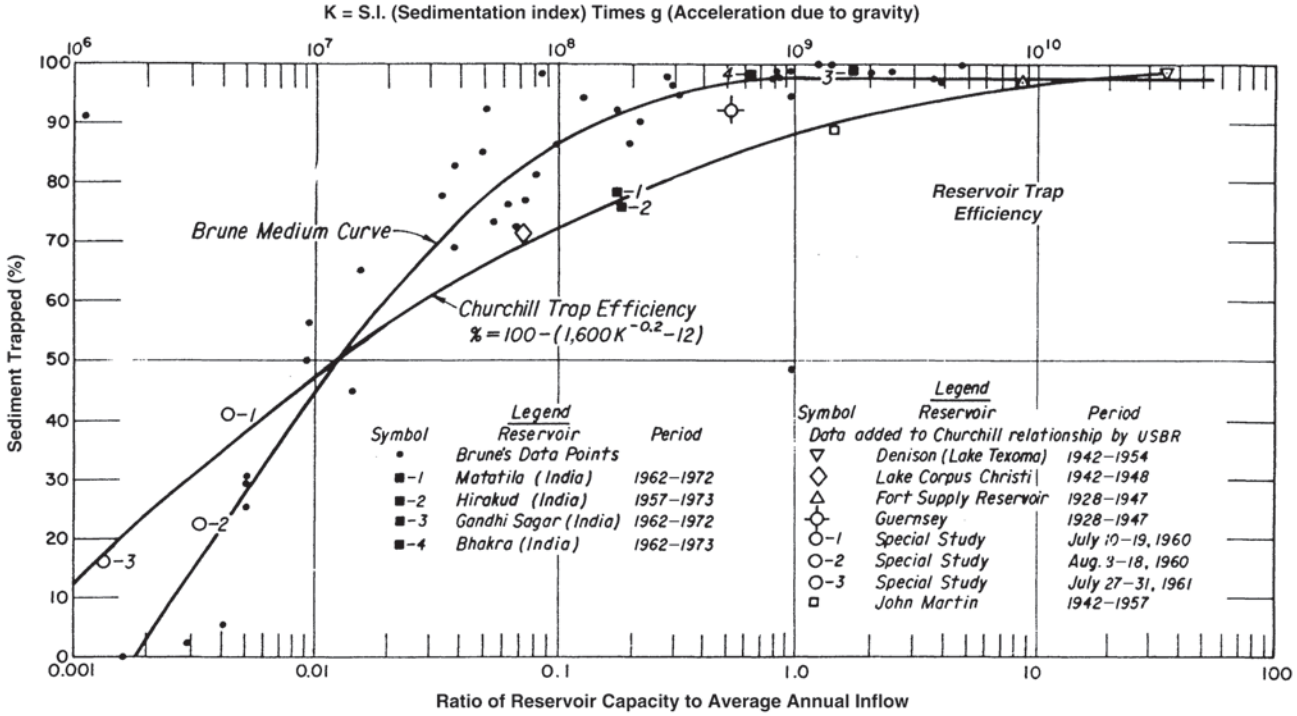

Fig. 12-10. Relationship between reservoir hydrologic size (capacity:inflow ratio) and sediment-trapping efficiency by Brune and the sedimentation index approach by Churchill (Strand and Pemberton 1987).

or normally ponded reservoirs and Churchill's method for settling basins, small reservoirs, and flood-retarding structures.

Churchill's (1948) relationship to predict sediment trapping is based on a reservoir sedimentation index, defined as the ratio of retention period to mean flow velocity through the reservoir. The Churchill curve has been converted to dimensionless form in Fig. 12-10 by multiplying the sedimentation index by the gravitational constant, g. Definitions of the terms required to compute Churchill's sedimentation index are as follows:

Capacity is the mean volume of the operating pool during the analysis period (m^3).

Inflow is the mean daily inflow during the analysis period (m/second).

Retention period is the capacity divided by the inflow (seconds).

Length is reservoir length (m) at the mean operating pool level during the analysis period.

Velocity is the mean velocity (m/second), computed as *inflow* divided by the mean cross-sectional area (m^2) of the pool. The cross-sectional area can be computed as *capacity* divided by *length*.

Sedimentation index is the retention period divided by the velocity.

For more than a preliminary analysis, mathematical modeling is required. Models of lake and reservoir sedimentation model are presented in Chapter 2.

12.7.2 Depositional Geometry

A highly generalized depiction of sedimentation processes was presented in Fig. 12-4. The coarse fraction of the inflowing load creates a delta deposit where the main river or side tributaries enter the reservoir. Depending on the inflowing load, delta deposits can range from silt to cobbles. The delta may be divided into the topslope and foreslope deposits, and the downstream limit of the delta is characterized by a rather abrupt reduction in grain size (Chapter 2). This change in grain size may occur even in reservoirs lacking an obvious delta (Fan and Morris 1992a). Although the delta can often have a slope about one-half of the original river streambed, there can be wide variations in delta topslope. Deltaic deposits not only extend into the reservoir, but they also extend upstream because of backwater effects (Chapter 2). This can be exacerbated by ice jams in reservoir headwater areas that retard flow and produce sedimentation further upstream than might otherwise be predicted. Mathematical modeling is the recommended method for predicting deltaic deposition patterns (U.S. Army Corps of Engineers 1989). The mechanics of deltaic sediment deposition is addressed in Chapter 2.

The depositional sequence within a single cross section illustrated in Fig. 12-2 shows that sediments first fill the deepest part of each cross section and subsequently spread out across the submerged floodplain to create broad flat sediment deposits. However, depositional patterns can also be more complex. Previously deposited sediments can be reworked and moved further downstream during drawdown, and large floods can transport coarse sediment deeper into the pool, prograding over finer sediment and producing layered deposits. Multiple deltas can be formed, each corresponding to a different pool elevation, and side tributaries can discharge coarser materials into an area where only fine sediment would otherwise be encountered. During periods lacking significant flood events, sediment deposits may consist only of fines and organic material, and shallow sediment samples collected during that period may not reveal coarser materials transported and deposited during flood events. The cores presented by Evans et al. (2002) provide a good example of depositional horizons of coarse sediment corresponding to floods in a hydrologically small reservoir.

12.7.3 Turbid Density Currents

Turbid density currents or turbidity currents are sediment-laden density-driven currents that flow along the bottom of the reservoir (Garcia 1993, 1994). These currents are caused primarily by density differences between clear and sediment-laden water, but cold water flowing into a warmer pool can also form temperature-driven density currents carrying suspended solids along the bottom of the reservoir. When significant amounts of suspended solids are present, the density differences imparted by the solids are much more important than temperature-induced density differences.

Turbid density currents occur frequently and are important in explaining sediment deposition patterns. The mechanics of sediment transport and deposition by turbidity currents in lakes and reservoirs is considered in Chapter 2. These currents focus fine sediment transport along the deepest part of the cross section instead of mixing sediments uniformly across the cross section. These currents are the primary reason that sediments in reservoirs fill from the bottom up within each cross section (as in Fig. 12-2) instead of having a more uniform depth of sediment deposits across the cross section.

Under favorable conditions, the turbulence generated by turbidity current motion will maintain a significant amount of sediment in suspension, thereby maintaining the driving force that sustains the motion of the current until it reaches the dam. Prior to the construction of Glen Canyon Dam further upstream, turbid density currents were documented to travel 129 km along Lake Mead to Hoover Dam (Grover and Howard 1938), the longest documented travel distance of turbidity currents in any reservoir. Although turbid density currents commonly occur in reservoirs, they often fail to reach the dam because the suspended sediment settles out of the current. Sediment loss diminishes the gravitational density difference driving the current, causing it to slow down, which in turn allows it to drop more of its sediment load. This cycle continues until the current dissipates. Turbidity currents will also dissipate if the inflow of turbid water at the upstream end of the reservoir stops before the current reaches the dam (Fan and Morris 1992a; DeCesare et al. 2001).

Turbidity currents reaching a dam or other submerged obstruction will create a submerged lake of muddy water, and sedimentation from this muddy lake will leave horizontal deposits of fine sediment extending upstream from the dam, as illustrated in Fig. 12-4. Deposits of this nature indicate that turbidity currents are transporting a significant amount of sediment to the dam. The release of turbid water from low-level outlets while the reservoir surface water is clear also indicates a turbidity current that reaches the dam. Indicators of turbid density currents may also be observed where the turbid water enters the reservoir and plunges beneath the surface. The *plunge point* or *plunge line* is marked by a dramatic change in water color. The conditions for plunging of a muddy turbidity current are discussed in Chapter 2. The plunging flow tends to create a surface countercurrent that flows upstream, and floating debris becomes trapped near the plunge line by the two opposing currents.

Turbidity current movement may be best ascertained by monitoring, from which data required for numerical modeling may be obtained (De Cesare et al. 2001). Modeling of turbidity currents is also addressed in Chapter 2.

12.7.4 Bulk Density of Sediment Deposits

Typical values of bulk density for reservoir sediments are given in Table 12-5. A more accurate empirical method for estimating initial bulk density was developed by Lara and Pemberton (1963). To estimate initial specific weight, reservoir operation should be classified into one of the following categories: (1) sediment always submerged or nearly

Table 12-5 Typical Specific Weights for Reservoir Deposits, t/m^3 or g/cm^3 (Geiger 1963)

Dominant grain size	Always Submerged	Aerated
Clay	0.64–0.96	0.96–1.28
Silt	0.88–1.20	1.20–1.36
Clay-silt mixture	0.64–1.04	1.04–1.36
Sand-silt mixture	1.20–1.52	1.52–1.76
Sand	1.36–1.60	1.36–1.60
Gravel	1.36–2.00	1.36–2.00
Poorly sorted sand and gravel	1.52–2.08	1.52–2.08

Table 12-6 Coefficient Values for Specific Weight Computation by Lara-Pemberton Method

Operational Condition	Initial Weight (kg/m³ [lb/ft³])		
	W_c	W_m	W_s
Continuously submerged	416 (26)	1,120 (70)	1,554 (97)
Periodic drawdown	561 (35)	1,140 (71)	1,554 (97)
Normally empty pool	641 (40)	1,150 (72)	1,554 (97)
Riverbed sediment	961 (60)	1,170 (73)	1,554 (97)

Table 12-7 Coefficient Values for Computing Sediment Consolidation

Operational Condition	Value of Coefficient B (kg/m³ [lb/ft³])		
	Sand	Silt	Clay
Continuously submerged	0	91 (5.7)	256 (16)
Periodic drawdown	0	29 (1.8)	135 (8.4)
Normally empty reservoir	0	0	0

submerged, (2) normally moderate to considerable drawdown, (3) normally empty reservoir, and (4) riverbed sediments. The grain size of the deposit must also be apportioned into sand, silt, and clay fractions by weight percent. Specific weight may be computed from the values in Table 12-6 and the equation

$$W = W_c P_c + W_m P_m + W_s P_s$$

where

W = specific weight of the deposit (kg/m³, lb/ft³);
P_c, P_m, and P_s = weight percentages of clay, silt, and sand, respectively, for deposited sediment; and
W_c, W_m, and W_s = initial weights for deposits of clay, silt, and sand, respectively.

12.7.5 Sediment Consolidation over Time

Sandy sediments attain their ultimate bulk density virtually as soon as they are deposited, but fine sediments may compact and consolidate for decades. If a constant mass of fine sediment accumulates in a reservoir each year, the volumetric rate of sedimentation will be highest in the first year and will appear to decline in subsequent years because the volume occupied by the second year's sediment deposition is decreased by compaction of the first year's deposit. To compensate, all sediment volumes can be adjusted to account for 50 years of compaction, by which time sediments have typically approached their ultimate density.

Sediment compaction over time is described in the equation by Lane and Koelzer (1943):

$$W_t = W_1 + B \log t$$

where

W_t = specific weight of deposit at an age of t initial years,
W_1 = initial weight at the end of the first year of consolidation, and
B = parameter value given in Table 12-7.

For sediment deposits containing mixed grain sizes, determine the value of B as the weighted average of the tabulated values, based on the weight percent of each gain size in the deposit.

12.7.6 Prediction of Sedimentation Patterns

The Bureau of Reclamation developed the empirical area reduction method for predicting the change in the stage–storage relationship due to sedimentation, based on observations at reservoirs in the United States. This method is described by Strand and Pemberton (1987) and by Morris and Fan (1998). In this method, the user determines the reservoir trap efficiency, places the reservoir into one of four geometric classes, and then follows a procedure to apportion the sediment deposition into different depth ranges on the basis of empirical relationships. This is the accepted method for predicting adjustments to the stage–storage curve in the absence of computer modeling. However, it is not suited for use in reservoirs where operating rules are modified to reduce sedimentation. More detailed information on depositional patterns requires computer modeling as described in Chapters 14 and 15.

12.8 SEDIMENT MANAGEMENT IN RESERVOIRS

12.8.1 Sediment Control Strategies

Sediment management strategies in reservoirs may be divided among five basic strategies:

1. *Sediment yield reduction*. Apply erosion-control techniques to reduce sediment yield from tributary watersheds. These techniques will typically focus primarily on soil stabilization and revegetation.
2. *Sediment storage*. Provide sediment storage volume adequate for the anticipated sediment yield over a "long" period of time either in the reservoir itself or in upstream impoundments or debris basins.

3. *Sediment routing*. Pass sediments around or through the storage pool to minimize sediment trapping by employing techniques such as offstream storage, temporary reservoir drawdown for sediment pass-through, and release of turbid density currents.
4. *Sediment removal*. Remove deposited sediment by dredging or hydraulic flushing.
5. *Sediment focusing*. These techniques are designed to tactically rearrange sediments within the impoundment to solve localized problems such as impacts from delta deposition. Any washout of sediment from the reservoir that may occur is incidental to the primary objective.

In reviewing options, a full range of management alternatives should be analyzed. An example of this approach is described by Harrison et al. (2000) for Solano Lake, California. Optimal management may include two or more strategies applied simultaneously or at different points in the reservoir life. The applicability of different strategies varies at different stages of reservoir life, being a function of the reservoir's hydrologic size (capacity:inflow ratio), beneficial uses, and other factors, such as environmental regulations.

Techniques such as sediment routing require significant pool drawdown and use part of the natural inflow to transport sediment beyond the storage pool, making it impossible to capture and regulate 100% of the flow. Consequently, some types of routing techniques will not be feasible at hydrologically large reservoirs. However, sedimentation will eventually convert large reservoirs into small ones, and sediment-routing techniques may become feasible at a future date.

12.8.2 Sediment Yield Reduction

Erosion control to reduce sediment yield is widely recommended to prolong reservoir function but is most difficult to implement successfully. Many reservoirs, particularly in developing areas, have experienced accelerated erosion from intensified land use and deforestation, despite recommendations for erosion control. Even when land use changes to less erosive patterns, many years may be required before significant reduction in sediment yield occurs. For example, 20 years after transition to less erosive land use within the 1,150-km^2 Buffalo River basin in Wisconsin, Faulkner and McIntyre (1996) could not detect any reduction in sediment yield.

Accelerated soil erosion has many negative impacts in addition to reservoir sedimentation. Clark (1985) estimated that storage loss in reservoirs accounted for only 11% of total annual erosion costs of $6.1 billion (1980 dollars) in the United States, where the largest single cost was impairment of water quality for recreational use. Biological impacts were not estimated in that study. In less developed countries, the largest impacts of soil erosion may be borne by small hillside farmers who experience loss of soil fertility and reduced soil moisture–holding capacity and declining yields as topsoil is washed away.

Appropriate land use practices are well known and readily demonstrable on model farms or experimental watersheds. However, implementing and sustaining good land use practices by many thousands of land users across a watershed is highly problematic. A good overview of the socioeconomic barriers to the adoption of soil conservation measures by farmers of all income levels and on every continent is provided by Napier et al. (1994). Land users will not altruistically change their practices to reduce sedimentation of a downstream reservoir, especially if the reservoir benefits accrue to another community. Sustained improvements will not be achieved unless land users understand how they will directly benefit from these practices. For this reason, successful watershed management programs must be developed as a community-level effort with readily identifiable benefits to land users.

Because measures to reduce erosion typically benefit many parties in addition to dam owners, any dam owner attempting to reduce sediment yield from a watershed may have many potentially helpful alliances. For example, in the North Fork Feather River watershed in California, where the Rock Creek and Cresta hydropower dams were experiencing sedimentation problems, the dam owner, PG&E, catalyzed the implementation of a community-based coordinated resource management group to implement watershed management activities. The group eventually expanded to involve 17 different institutions and community groups, all having a vested interest in erosion control and sediment management. Participants included landowners desiring to control streambank erosion; state and federal forestry agencies desiring to stabilize eroding logging roads; federal, state, and local environmental resource agencies; fishermen and other recreational users; environmentalists; and tourist interests (Harrison and Lindquist 1995; Morris and Fan 1998).

The literature on watershed management is extensive; the reader is referred to the following sources for publications and contacts:

- Natural Resources Conservation Service (www.nrcs.usda.gov). This is the lead national agency for erosion control in rural areas, with local offices in communities throughout the nation.
- Environmental Protection Agency (www.epa.gov). Regulates water quality and sediment discharge from construction sites through the NPDES program and has numerous publications.
- Soil and Water Conservation Society (www.swcs.org). Focus on agricultural soil conservation in the United States and worldwide.
- Conservation Technology Information Center (www.ctic.purdue.edu). Focus on mechanized agriculture in the United States. Also contains electronic listing of

watershed management programs and contacts throughout the United States.
- International Erosion Control Association (www.ieca.org). Trade publication focusing on manufacturers of erosion-control equipment and materials with a focus on urban areas.

12.8.3 Provision of Large Storage Volume

Sedimentation has traditionally been "controlled" by providing a storage volume large enough to postpone anticipated sedimentation problems for 50 to 100 years. The "sediment pool" assigned to reservoirs has typically consisted of the dead storage space below the lowest outlet, but sediment deposits are frequently not focused in that zone, and sedimentation problems may be caused by deposits in the delta or other areas prior to filling of the provided sediment storage pool.

An often-used strategy for increasing the storage volume in the face of sedimentation issues is to raise the dam. Garbrecht and Garbrecht (2004) offer an interesting historical example of successive raising of the Marib diversion dam in Yemen between 940 B.C. and its final destruction around A.D. 570 to accommodate both increased sediment upstream of the dam and an increase in land level as much as 15 m in the downstream irrigation area due to silt loads in the diverted irrigation water. Loehlein (1999) described the raising of pool elevations in a flood-control reservoir due to sediment accumulation.

A 500-year horizon should be considered for analysis of the geomorphic evolution of the impounded river reach and its sediment management alternatives. Against the argument that this is an unreasonably long time frame, consider that Schnitter (1994) has documented dams with operational lives exceeding 1,000 years. Among all types of engineered infrastructure, dams are unique in terms of their longevity and their interrelationship to the geomorphic processes along rivers. The time frame for their analysis should consider their potential operational life (including prolongation by sediment management) and the structure's long-term impact on the fluvial sediment balance.

The objective of long-term analysis is to define, on a preliminary basis, the probable time frames and types of sedimentation problems to be anticipated, the potential sediment management strategies potentially feasible as a function of reservoir age, and any long-term sediment management elements that can be incorporated into current design or operational practices. Sedimentation problems are both difficult and costly to cure, and the consideration of long-term consequences can help both the design and regulatory communities to identify effective long-term solutions. For example, it is often assumed that reservoirs will be dredged or alternative reservoir sites developed in the future. However, if the land area required for either of these two options is not acquired or otherwise protected by zoning restrictions, the planned-for alternative may no longer be feasible when it is needed. Similarly, if bank instability due to long-term channel incision below a dam is anticipated, it would be prudent to create no-development buffer zones along the riparian corridor where bank erosion is anticipated.

This long-term analysis is limited to geomorphic and sedimentation issues within and below the impounded reach and does not necessarily imply 500-year computer simulations, and it would not impact the time frame normally used for socioeconomic or similar evaluations. It seeks to extrapolate geomorphic processes along the impounded river reach to their logical conclusion and to identify any feasible present-day actions or design strategies that will help ameliorate long-term negative consequences.

12.8.4 Sediment-Routing Strategies

12.8.4.1 Offstream Reservoir for Sediment Bypass

The ideal way to manage sediment is to prevent it from entering the reservoir. High volumes of sediment-laden floodwaters can be bypassed around a storage pool by placing the pool offstream and diverting only relatively clear water from moderate flows into storage (Fig. 12-11). The key feature of the offstream reservoir is an intake system that has a limited inflow capacity and will therefore exclude most flood flow and its associated sediment because the flood discharge will be much greater than the intake capacity. Additional sediment exclusion can be achieved by closing the intake during floods with high sediment concentration or in anticipation of hurricanes.

As compared to a conventional onstream reservoir, an offstream reservoir can generate many benefits in addition to a reduced rate of storage depletion:

- The dam does not pose a barrier to migratory aquatic species or to navigation.
- Instream water quality (e.g., temperature, dissolved oxygen) is not altered by the reservoir.
- Riparian wetlands and river corridor habitats are not submerged.

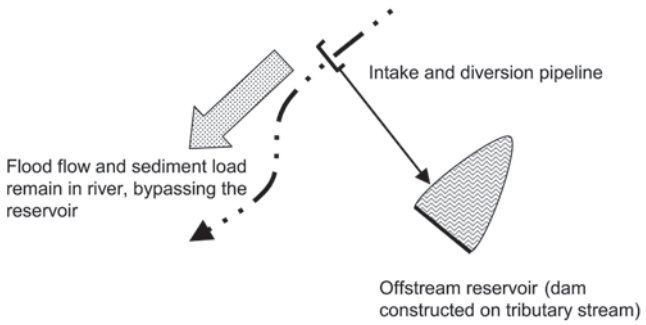

Fig. 12-11. Conceptual representation of sediment exclusion by an offstream reservoir.

- The dam does not impact bed-load transport processes essential to maintain instream sediment transport, river morphology, and the ecological integrity of instream ecosystems.
- The large-capacity onstream spillway is eliminated.
- Low sediment loading and turbidity levels in the reservoir benefit users, such as water filtration plants, by reducing coagulant and sludge handling costs.
- The intake can be closed to exclude contaminants from hazardous waste spills, treatment plant malfunctions, or periodic water quality degradation by fertilizers or other nonpoint runoff.

These environmental advantages can favor offstream reservoirs over conventional structures, independent of sediment-loading considerations. However, offstream reservoirs may not develop the full yield potential of the stream because sediment-laden flood flow is not diverted to storage, especially in hydrologic environments with annual runoff concentrated in a short time period.

An example of this strategy is the offstream reservoir supplied from Río Fajardo, Puerto Rico, which began filling in 2006. Suspended sediment loads in Puerto Rico are high. To achieve a multicentury reservoir life, the impoundment volume for an onstream reservoir becomes controlled by the size of the sediment storage pool rather than the water conservation pool.

Río Fajardo is a flashy mountain stream in a moist tropical environment with a 38-km^2 watershed area. Behavior simulations using 33 years of daily data and a continuously open intake were used to develop the relationship between storage, yield, and sediment loading. At the selected design point, 37% of the long-term stream flow is diverted into the reservoir and thence to municipal use, but less than 10% of the suspended sediment load enters the reservoir and none of the bed load material. Firm yield for the offstream design is only 5% less than for a conventional onstream reservoir having the same conservation pool volume, but with the low sedimentation rate, there is no need to oversize the reservoir to provide a large sediment storage pool.

The half-life of Fajardo offstream reservoir is estimated to exceed 1,000 years, as compared to only 180 years for a larger-volume instream reservoir originally proposed on this same river. To sustain reservoir capacity indefinitely, dredging of volumes less than 0.5 Mm^3 per event are planned at intervals of about 200 years in this 4.5 Mm^3 reservoir. A spoil disposal site adjacent to the reservoir has been reserved for this purpose. Offstream reservoirs have also been used for sediment control at nine sites in Taiwan, two of which are described by Wu (1991).

12.8.4.2 Sediment Bypass of Onstream Reservoirs In some cases, it may be possible to construct a reservoir onstream yet bypass sediment. For the passage of large sediment-discharging events, this would be most readily accomplished by locating the reservoir at the terminus of a meander and diverting flood flows across the meander floodplain (Annandale 1987).

The trapping of bed material by dams is an important environmental issue, and at several sites, processes have been used to move gravels from the delta upstream of the reservoir and deposit it below the dam. Procedures may involve trucking or pipeline, or on a steep channel even a tunnel may be used. The Asahi hydropower dam in Japan is constructed in a narrow gorge on a steep gravel-bed river. A low-head concrete diversion dam constructed immediately upstream of the reservoir intermittently diverts flushing flows and entrained gravels into a tunnel that runs parallel to the reservoir and then discharges below the powerhouse. This costly alternative was implemented to help preserve a popular recreational fishery below the dam.

12.8.4.3 General Characteristics of Pass-Through by Drawdown Sediments are maintained in suspension by high-velocity flows; they become trapped in reservoirs as flow velocity diminishes and hydraulic retention time increases. By opening high-capacity gates to minimize reservoir level, drawing down the pool as much as possible to

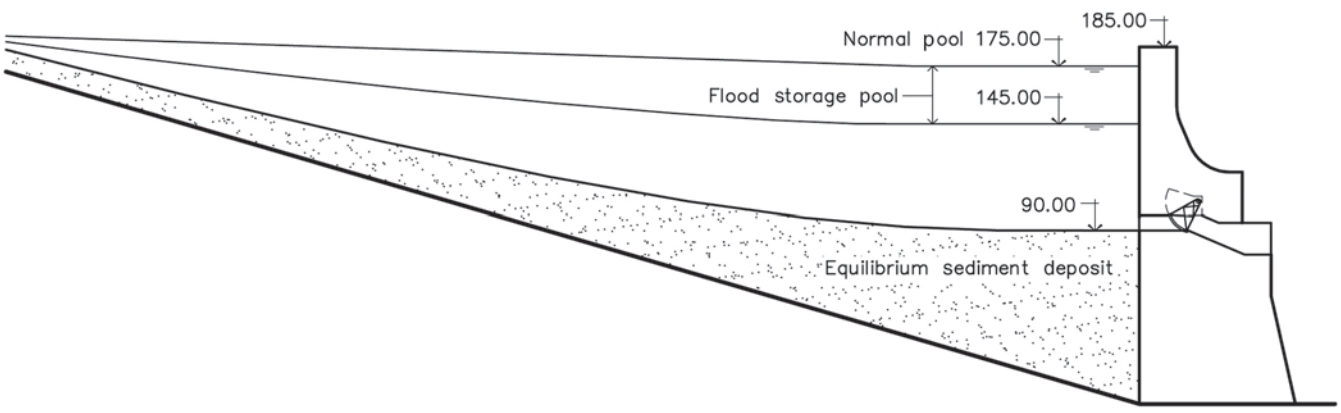

Fig. 12-12. Longitudinal profile of Three Gorges Reservoir, Yangtze River, China (modified from Lin et al. 1993).

pass sediment-laden floods at the highest possible velocity, the opportunity for deposition is minimized. The reservoir pool is refilled at the end of the drawdown period.

Pass-through techniques are based on translating the inflowing flood hydrograph and accompanying sediment through the pool with the least possible attenuation. Although the high flow velocities generated by drawdown may scour some of the previously deposited sediment, the outflowing concentration will be similar to the inflowing concentration. Discharging sediment with a high flow eliminates excessive sediment concentrations and sediment redeposition in the channel below the dam, two serious problems that normally accompany sediment flushing.

Drawdown duration and operating rules will vary depending on hydrologic characteristics and reservoir size. Three distinct procedures are described. First, in large reservoirs such as the Three Gorges Project in China, drawdown is performed on a seasonal basis. Second, in smaller reservoirs, drawdown may be accomplished by the prediction of hydrographs for specific runoff events. Third, in very small reservoirs or diversions with limited storage, gate operation may be performed on the basis of a rule curve that does not require hydrograph prediction.

Techniques to optimize operating rules in multiple reservoirs to achieve specific sediment management objectives in river channels and pool areas has been demonstrated by Nicklow and Mays (2000) and Nicklow and Bringer (2001). These studies used data from the literature to formulate a three-reservoir network to demonstrate the interfacing of the HEC-6 sediment transport model with an optimization scheme. The HEC-6 model solves the hydraulic and sediment transport equations that govern the physical parameters of the system under the overall control of the optimization algorithm (Chapter 14). The control scheme operates within the systemwide constraints imposed by established operating parameters such as storage levels and release rates to optimize the specific sediment-management objectives.

Pass-through will tend to establish and maintain the river channel, but in wide reservoirs the off-channel areas will continue to be depositional during impounding periods, and a channel–floodplain configuration can develop over a number of years, similar to the geometry associated with flushing as discussed in Section 12.8.6. Although routing can substantially reduce the rate of sediment accumulation, the ultimate reservoir volume that can be sustained by this method is limited by the channel dimension.

12.8.4.4 Pass-Through by Seasonal Drawdown Under seasonal drawdown, the pool is seasonally lowered or emptied to pass sediment-laden flows through the reservoir, which is refilled during the late part of the wet season. In areas with strong rainfall seasonality, runoff from initial wet-season rains may transport considerably more sediment than late-season runoff, when vegetation has regrown to protect the soil. Sediment pass-through techniques incorporated into the Three Gorges reservoir in China have been described by Lin et al. (1989, 1993), Chen (1994), and Morris and Fan (1998).

The 39-km^3 Three Gorges reservoir on the Yangtze River has been designed to achieve sediment balance across the impounded reach after approximately 100 years, allowing the project to operate indefinitely while passing 530×10^6 tn/year of sediment and 451 km^3 of water. This is achieved by designing a hydrologically small reservoir (C:I ratio 0.087) with adequate low-level outlet capacity to operate in seasonal drawdown mode. A conventional impounding reservoir of this same capacity on the Yangtze River would have a half-life of less than 100 years.

A conceptual profile of the Three Gorges reservoir is shown in Fig. 12-12. The reservoir is gradually drawn down during the dry season by making releases for hydropower and downstream navigation. Outlets and turbines will be operated during the initial part of the flood season to maintain the reservoir pool at a low level. This empties the flood storage pool and also generates high flow velocities along the reservoir, which is generally not more than 1 km wide along its 600-km length. These high velocities will transport most suspended sediment and sandy bed material through the reservoir and beyond the dam. Once equilibrium conditions have been reached, gravels will continue to be trapped and must be removed by dredging. About 2×10^6 m^3 of sand and silt is also expected to be dredged annually in the vicinity of the navigational locks at the dam.

12.8.4.5 Pass-Through by Hydrograph Prediction At hydrologically small reservoirs on rivers lacking prolonged and predictable periods of high flow, it may be possible to draw down the pool in anticipation of floods, pass the sediment-laden water through the reservoir with the shortest possible detention time, and refill the reservoir with the recession limb of the storm hydrograph. This strategy was analyzed at Puerto Rico's Loíza (Carraízo) reservoir (26.8×10^6 m^3 original volume, 538-km^2 tributary watershed), the primary water supply for San Juan (Morris and Hu 1992; Morris et al. 1992; Morris and Fan 1998).

The spillway crest equipped with high-capacity Tainter gates that control most of the usable storage pool. The reservoir has a capacity:inflow ratio of only about 0.06, and stream-gauge records show that over half of the inflowing sediment is delivered to the reservoir by large storms occurring on the average of only two days per year. This points to significant sediment reduction by passing large flows and their associated sediment through the reservoir.

The total volume of water upstream of the dam can be continuously computed during tropical depressions as the sum of two components: the water already in the reservoir and the water predicted to arrive on the basis of rainfall already received. Reporting rain gauges within the watershed, coupled with hydrologic software, can predict the volume of the recession hydrograph from received rainfall, and a

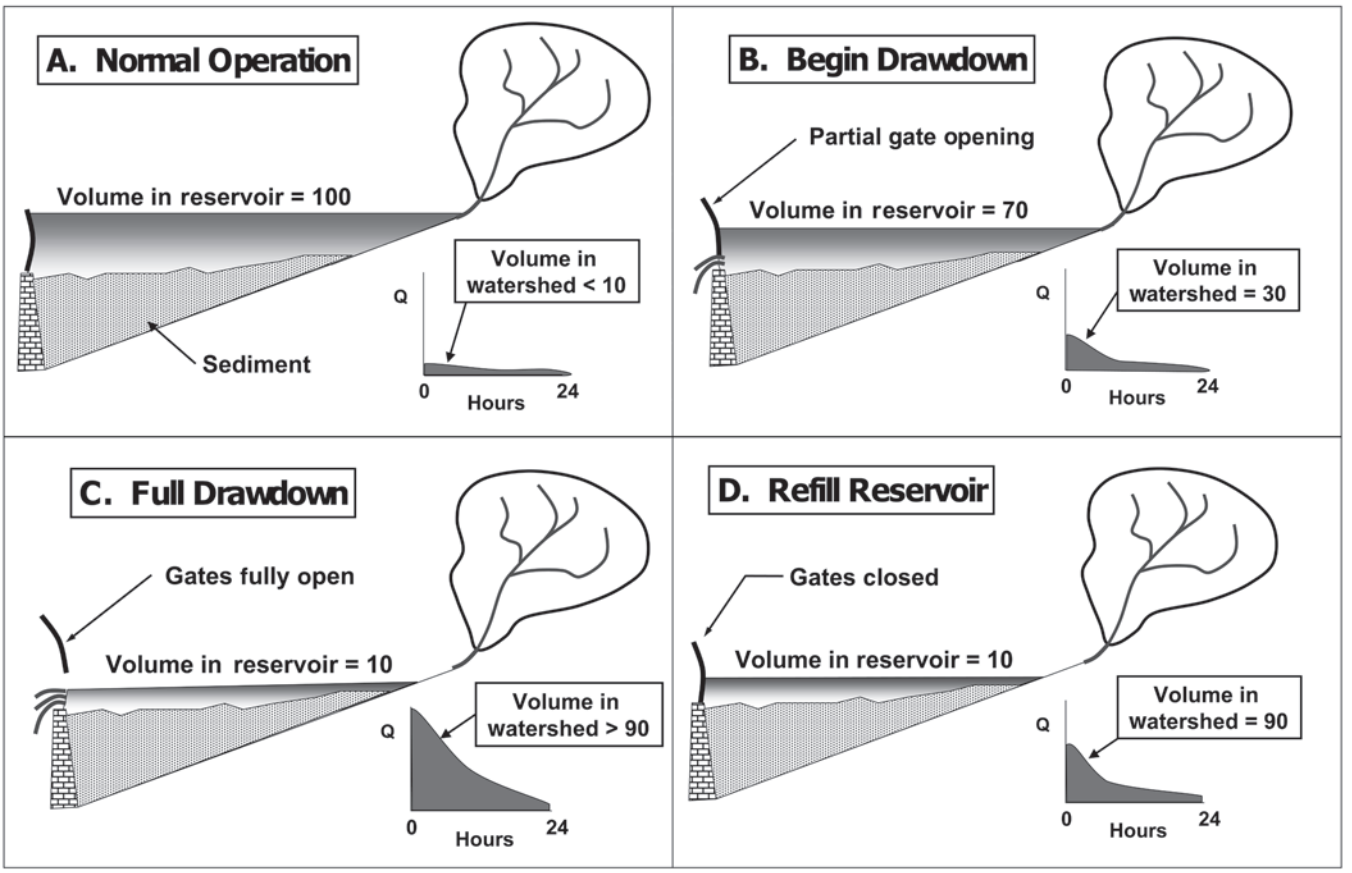

Fig. 12-13. Proposed operational sequence for sediment pass-through at Loíza reservoir, Puerto Rico. See text for description.

combination of stage gauges and hydraulic modeling can compute within-reservoir volume.

The proposed operational sequence is illustrated in Fig. 12-13. (A) When a storm begins, the reservoir's gates are opened to release a volume of water equal to the volume of runoff water accumulating in the watershed as predicted from the recession hydrograph computations but not yet delivered to the reservoir. (B) As the storm continues and more water accumulates in the watershed, gate openings are increased, and the reservoir is progressively lowered until all gates are fully open. (C) The gates remain fully open as long as the total water volume tributary to the dam exceeds the total volumetric capacity of the dam. (D) During the storm recession, the gates are closed as soon as the total tributary water volume drops to the full reservoir volume. Gate closure at this point allows the reservoir to refill completely with water during the next 24 hours (Morris and Hu 1992; Morris et al. 1992).

12.8.4.6 Drawdown by Rule Curve At very small reservoirs, pool drawdown for sediment pass-through during floods may be regulated by a rule curve based only on the rate of inflow. A rule curve of this type was implemented at the Cowlitz Falls dam in Washington State, which impounds a hydrologically small reservoir having a capacity:inflow ratio of only 0.3% (Locher and Wang 1995). This rule curve is shown in Fig. 12-14. A similar rule-curve operation has been studied at the Rock Creek and Cresta hydropower reservoirs on the North Fork Feather River, California (Chang 1996).

12.8.4.7 Routing of Turbid Density Currents Turbid water entering a reservoir typically plunges to the bottom and will flow along the original (but now submerged) riverbed. Under favorable conditions, the turbidity current will be transported to the dam where it can be released through a low-level outlet. Turbidity currents can carry fine sediment into the vicinity of the dam and obstruct low-level outlets even though there is little sediment accumulation elsewhere within the reservoir. When the reservoir profile is viewed longitudinally, the accumulation of a flat bed of sediment deposits extending upstream from the dam is an indication that turbid density currents reach the dam (Fig. 12-4).

Turbid density currents are inherently unsteady and are influenced by the variable discharge of the inflowing hydrograph, varying suspended sediment concentration, and variation in reservoir level over the duration of the event. The forward velocity of the density current is maintained by the continued inflow of turbid water, and when inflow ceases, the turbidity current will stall. In highly favorable situations

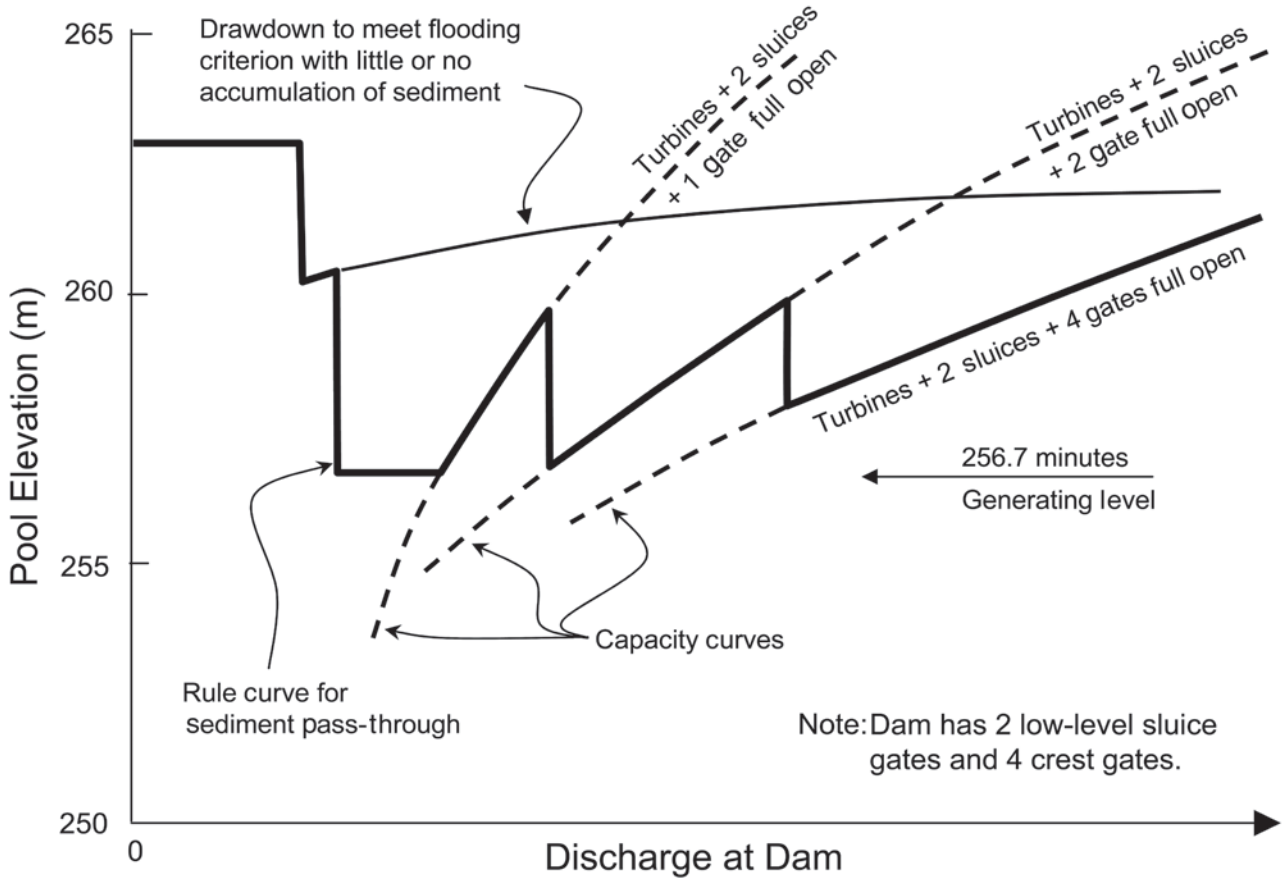

Fig. 12-14. Rule curve for sediment pass-through at Cowlitz Falls Dam, Washington (Locher and Wang 1995).

in China, it has been possible to release as much as 50% of the inflowing sediment as a turbid density current.

Gravity-driven density currents will run along the bottom of the reservoir seeking the lowest part of the cross section. In newly impounded reservoirs, this corresponds to the original river channel. In reservoirs where a channel is maintained by sediment routing or flushing, the turbidity current and its deposits will be focused along this channel, thereby facilitating the removal of turbidity current deposits during subsequent free-flow events. At the Cachí hydropower reservoir in Costa Rica, it was found that 18% of the total inflowing sediment load was accounted for by turbidity currents that ran along the flushing channel and passed through the turbines, and an additional 54% of the total inflowing load was deposited along the length of this channel prior to reaching the hydropower inlet and was removed by subsequent flushing events (Sundborg and Jansson 1992). However, if the submerged channel fills with sediments, the turbidity current will tend to spread across the flat bottom of the reservoir, reducing its velocity and sediment transport capacity, dropping its sediment load, and causing it to stall and dissipate.

De Cesare et al. (2001) undertook monitoring and numerical modeling of turbidity current processes at the Luzzone alpine hydropower reservoir in Switzerland with an average bed slope of about 4%. Turbidity current velocities up to about 0.4 m/second were observed for smaller inflow events. Turbidity currents caused sediment accumulation in front of the dam that required reconstruction of the intakes even though the reservoir had lost only 1% of its capacity to sedimentation. Turbidity currents had focused sediment accumulation beneath only 8% of the reservoir surface area.

Equations needed for the analysis of turbidity current phenomena in lakes and reservoirs are presented in Chapter 2.

12.8.5 Sediment Removal by Hydraulic Dredging

Dredging is any activity involving removal of sediment from underwater. Dredging in reservoirs is generally understood to have the objective of removing sediment to sustain or recover volumetric capacity. However, *tactical dredging* may be focused in a limited area to remove sediments from the vicinity of an intake or a navigation channel, and the dredged sediments are

not necessarily removed from the pool. Information on dredging is presented by the U.S. Army Corps of Engineers (1987), Turner (1996), Herbich (1992), and Morris and Fan (1998).

Dredging is being used increasingly for the removal of sediment deposits from reservoirs. However, dredging can be considered a sustainable method for controlling sedimentation only if it can be repeated indefinitely. If a reservoir is to be dredged once, it will need to be dredged again. Assuming that the first dredging consumes the best available disposal site, sediment disposal for each subsequent dredging will become increasingly problematic and costly.

The two major impediments to large-scale dredging in reservoirs are high cost and limited availability of sediment disposal sites, and the cost of slurry transportation to distant disposal sites can dominate the cost of a dredging project. An example of a large reservoir-dredging job undertaken in the United States is the removal of 6×10^6 m^3 of sediment from the Loíza reservoir in Puerto Rico during 1997 at a cost of about \$10/m^3 including dredging cost, land acquisition and construction of three sediment-disposal sites, engineering, permitting, and environmental protection (Morris and Fan 1998).

Most reservoir dredging employs conventional hydraulic dredges having a cutter head, a submerged "ladder" pump near the cutter head to lift the slurry (if dredging to depths greater than about 10 m), a main pump on the dredge, and a pipeline to convey the slurry to the point of discharge. Booster pumps may also be required along the discharge pipeline. Because of the requirement for portability, dredges in reservoirs typically have discharge lines not larger than about 400 mm (16 in.) in diameter, although transportable dredging equipment up to 760 mm (30 in.) in diameter can be manufactured.

Dredged material is discharged to a diked containment area where it is allowed to settle, with supernatant return to the reservoir or other water body. Because of bulking of fine sediment, the containment area volume must be larger than the volume of sediment removed. The *bulking factor*, the ratio of sediment volume deposited in the containment area to the in situ sediment volume, may range from 1.0 for sands to about 1.5 for clays. The suspended sediment concentration in the supernatant will depend on the hydraulic loading rate in the spoil area plus the layout to prevent short-circuiting.

When dredging is completed and the disposal area dewatered, dredged sediments may be used beneficially. Sediments dredged from Lake Springfield, Illinois, were converted to agricultural use after 3 years. When dredging involves sands and gravels, the coarse material may be separated from the fines and used as construction aggregate.

Siphon dredges eliminate the dredge pump by discharging through the base of the dam and into the downstream channel, using the static head in the reservoir to discharge the dredged slurry. The typical arrangement involves a floating dredge, a submerged suction pipe that may be fitted with a mechanical cutter head, and a submerged line that discharges to the riverbed through the base of the dam. Intermittent reservoir spills scour and carry away the deposited sediment. This system has been used most notably in Algeria and China but has not been applied in the United States because of environmental regulations. The largest system to date is the 700-mm siphon dredge at the Valdesia hydropower dam in the Dominican Republic, no longer operational. Small-scale U.S. experiments with this type of system have been performed by Hotchkiss and Xi (1995). Because the maximum hydraulic head is limited by the available static head, siphon dredge systems typically do not extend more than about 2 km upstream of the dam.

In considering the feasibility of tactical dredging, it is important to consider that it may be simply creating a hole into which sediment inflows will be focused and quickly refill, and as such it may represent a costly and futile effort. For example, Loehlein (1999) noted that 66,000 m^3 of sediment were dredged from the Conemaugh River reservoir in Pennsylvania within 120 m of the dam, yet over a single winter, 38,000 m^3 of sediment had refilled into the dredged area. Plans for additional dredging were abandoned.

12.8.6 Sediment Removal by Hydraulic Flushing

Hydraulic flushing involves the opening of bottom outlets to completely empty the reservoir and allow stream flow to scour sediment deposits. Sediment flushing may be distinguished from pass-through because its principal objective is to scour and remove previously deposited sediment. The flushing flow will erode a "main channel" through the sediments, typically following the original river thalweg, but deposits on the normally submerged "floodplain" will be unaffected by scour (Fig. 12-15). Subsequent flushing events may deepen or widen the main channel to approximately the width of the preimpoundment stream channel, but sediments on the floodplain area will not be removed. The outflowing sediment concentration is typically one or two orders of magnitude higher than the inflowing concentration. Case studies on flushing are reported by Morris and Fan (1998) and White (2001). An overview of the method and empirical methods to evaluate flushing parameters are presented by Atkinson (1996) and White (2001).

For flushing to be effective, the reservoir must be emptied with free flow along its length and through the outlet. In contrast, operation of bottom outlets under partial drawdown, referred to as *pressure flushing*, will redistribute sediment primarily within the reservoir, eroding upstream deposits and redepositing this material closer to the dam where water remains impounded. Similar processes occur as a result of normal changes in the reservoir's operational level. Pressure flushing will develop and maintain a scour cone in sediment deposits upstream of the bottom outlet, but the scour effect does not extend a significant distance either upstream or laterally.

The reservoir volume at each cross section that can be sustained free of sediment by free-flow flushing is determined by the combination of channel width and angle of repose of

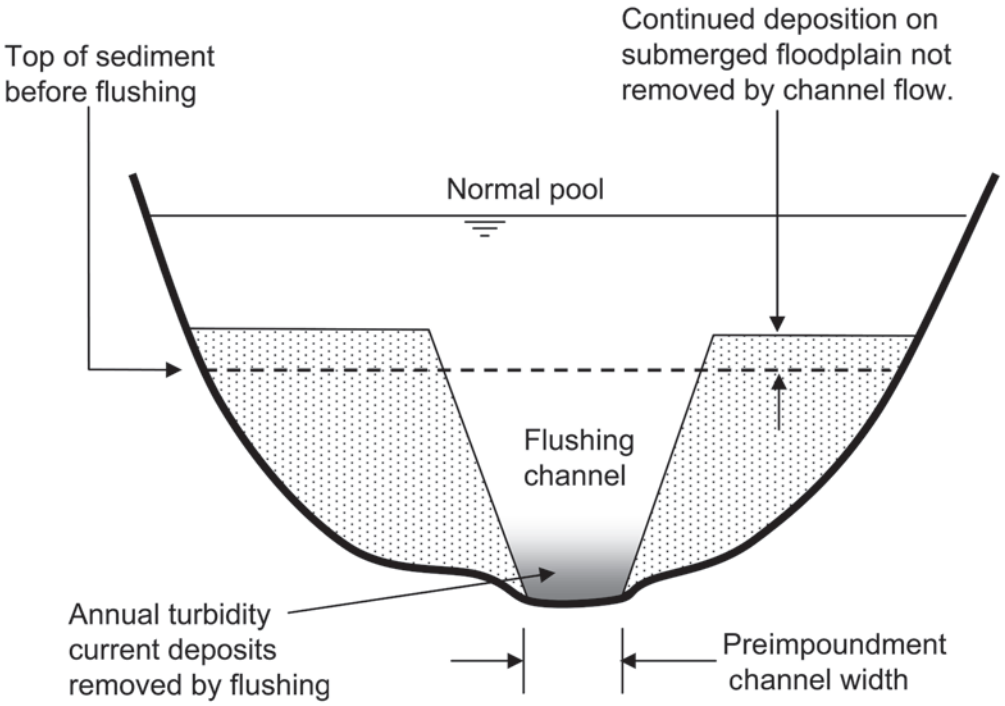

Fig. 12-15. Configuration of deposits in a reservoir subject to drawdown for sediment routing or flushing showing main channel with a stable thalweg profile along which turbidity currents will be focused. The floodplain submerged during normal impounding will continue to accumulate sediment, but the annual deposit thickness on the floodplain during each period will decline as the floodplain level rises. In narrow reaches, the main channel may extend across the entire width of the impoundment, and floodplains may be absent.

the sediment deposits (Fan and Morris, 1992b). On the basis of information reported in the literature, Atkinson (1996) presented an empirical equation to predict the self-formed flushing channel width:

$$W_f = 12.8\, Q_f^{0.5}$$

where Q_f = flushing flow (m^3/second) and W_f = flushing channel width (m). This equation provides a good fit with the available data sets and has the same form as the Lacey regime relation for irrigation canals, but Lacey's multiplier of 4.8 (in SI units) is lower. However, no reasonably reliable general purpose relationship could be found for predicting flushing channel side slopes.

Flushing removes previously deposited sediment using a small percent of the annual discharge water at flow rates low enough to pass through bottom outlets with minimal backwater upstream of the dam. However, the volume of water released by emptying the reservoir will typically exceed the flushing volume itself. This impact is lessened when the released water is used for hydropower production or the reservoir is normally drawn down by annual irrigation deliveries. Flushing durations of several days are typical at hydropower sites, whereas flushing periods of weeks to months durations have been used at larger reservoirs. There is little experience with hydraulic flushing in the United States due to downstream environmental impacts.

The transport of coarse material through a reservoir is the key to achieving long-term equilibrium by flushing. Low discharge rates through low-level outlets may not be adequate to mobilize and transport a significant fraction of the coarse material delivered to the reservoir by floods.

When a main channel is maintained by flushing, density currents during impounding periods will focus fine sediment deposition along the submerged channel to be removed during the next flushing event. Without flushing these sediments would first infill the channel and then spread across and deposit on the submerged floodplain. Well-documented annual flushing at the Cachí hydropower reservoir on Río Reventezón in Costa Rica (Jansson and Rodríguez 1992; Morris and Fan 1998) is illustrative of the procedure. At Cachí, the pool is drawn down at 1 m per day over a 30-day period by turbine operation, followed by a three-day period during which the bottom gate is opened and the river flows freely along the bottom of the reservoir. At the end of the flushing period, the bottom gate is closed, allowing the

reservoir to refill and resume normal operation. Flushing is conducted during the wet season to provide a high flushing flow and allow rapid refilling of the pool.

At the Cachí reservoir, this flushing procedure releases 73% of the inflowing load, as compared to only 18% of the inflowing load when the reservoir was operated at a continuously high water level. Because of the presence of turbid density currents that flow along the flushing channel, most fine sediments are deposited in the main channel and can be flushed out every year. The principal material that continues to be trapped at Cachí is the coarse bed-material load, which is advancing into the reservoir as a delta and is not effectively mobilized by hydraulic flushing.

The generalized sequence of sediment release during flushing events is shown in Fig. 12-16. The release of the greater part of the annual sediment inflow over a period of only a few days and at flow rates limited by bottom outlet capacity produces extremely high peak sediment concentrations. Experience at sites in Costa Rica, Iran, Switzerland, France, and China indicates that peak suspended sediment concentrations exceeding 200,000 mg/L should be expected during flushing. These concentrations will smother or suffocate aquatic organisms in addition to impacts by the release of potentially anoxic bottom water from the reservoir, the oxygen demand exerted by organic sediment, and elevated ammonia concentrations (toxic to fish). Fine sediment released by flushing can also clog coarse-bed river channels, infill natural pools and navigation channels, affect aquifer recharge from stream flow, clog spawning gravels, obstruct intakes and irrigation channels, make the water unfit for municipal or industrial use, and so forth. The releases needed to move flushed sediment through the downstream system will typically exceed the volume required to remove the material from the reservoir. To date there has been little systematic investigation of means of modifying flushing schemes to reduce environmental impacts to more acceptable levels.

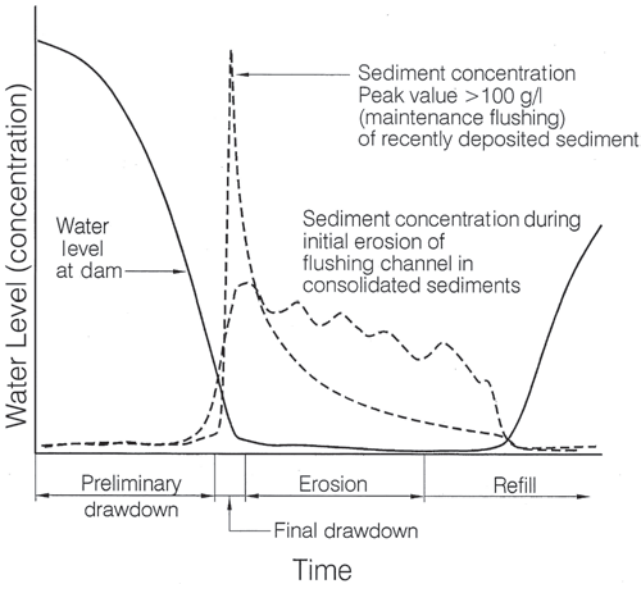

Fig. 12-16. Variation in sediment concentration and other parameters immediately downstream of a dam during reservoir flushing (Morris and Fan 1998).

Liu and Tominaga (2003) have reported on an "environmentally friendly" flushing scheme involving the simultaneous flushing of two reservoirs sequentially located along the Kurobe River in Japan, using high flows to minimize suspended sediment concentration. Environmental impacts were further mitigated by the construction of fish refuges along the downstream channel. However, this site has limited fines and oxygen-depleting organics, and during 10 flushing events over a 9-year period, minimum dissolved oxygen levels never fell below 5.8 mg/L (59% saturation) despite suspended sediment concentrations as high as 161,000 mg/L.

12.8.7 Sediment Focusing

Sediment focusing encompasses hydraulic techniques designed to redistribute sediment within the reservoir. Sediment deposition is naturally focused in deeper parts of the reservoir by turbidity currents, as described in previous sections, and the construction and maintenance of channels or other in-reservoir features can in some cases be used to hydraulically focus sediment deposition in areas where they lessen adverse impacts. Dredging may be used as part of this strategy, principally as a means to alter flow patterns and thereby influence sediment transport and deposition processes. An example is the study of delta deposition processes in Lake Sharpe on the Missouri River (Teal and Remus 2001). Options evaluated were a reduced pool level to move sediment deposits into deeper portions of the reservoir and the construction of dikes.

12.9 DAM REMOVAL

There is an increasing focus on the decommissioning and removal of older dams made obsolete by sedimentation or safety considerations or in the interest of environmental enhancement. To date, most dam removal projects have been limited to smaller structures with limited amounts of sediment accumulation. An ASCE (1997) guideline on the retirement of dams is available. Chapter 23 deals specifically with the numerical modeling of sediment transport following the removal of a dam.

Dam removal is in many ways similar to flushing; riverine flow is re-established along the length of the reservoir, and sediments are released, but following dam removal sediment deposits will continue to be scoured until a new stable geometry has been reached along the formerly impounded

reach. Depending on the volume of sediments and stream flow, this process may occur in a period of weeks to decades. Similar to flushing, the highest concentration of sediment release can be anticipated immediately after free-flowing river conditions are established across the deposits. In the case of staged removal, a new peak in sediment concentration may be anticipated as each successive removal stage exposes a new layer of sediments to scour (Chapter 23).

The release of high sediment concentrations and loads can produce a wide range of environmental and socioeconomic impacts: closure of intakes and requirement to provide alternative water supplies; bed aggradation, which increases flood hazard and groundwater levels; navigation impairment; and conflict with recreation, sport fisheries, and tourism. Environmental impacts can potentially include massive mortality through the entire aquatic food chain. As a mitigating circumstance, these impacts will gradually lessen as the sediment is washed downstream and out of the system.

MacBroom (2005) has characterized the geomorphic process of channel evolution associated with dam removal and noted that sediment release will not necessarily create adverse impacts in the removal of small dams. Several points are important in planning for dam removal. (1) All potentially involved parties should be represented in project planning. (2) It is essential to have a complete inventory of potential impacts, and, to the extent possible, these impacts should be quantified. (3) The goals of impact mitigation should be clearly defined and prioritized, identifying critical species or economic activities for mitigation. (4) Alternatives should be understood, as should the inevitable trade-offs. For example, partial dam removal may reduce downstream sediment loading and environmental impact, but it will not restore the aquatic migration corridor. (5) The planning process should lead to a clear understanding and consensus of the river management approach and procedures to be used during the removal process.

Several strategies may be employed reduce the impact of sediment releases. Dam removal can be performed by lowering the crest in stages to release sediments at a lower and more controlled rate. Alternatively, it may be determined more feasible to simple remove (or notch) the entire structure at once, pushing the sediments through the downstream system as rapidly as possible and then allowing the stream and riparian ecosystems to recover. Dam removal and sediment release may be timed on a seasonal basis to minimize impacts to downstream species of critical concern.

Sediments may be partially or completely removed prior to dam removal. In this case it is important to define the stable geometry of the postdam deposits and focus removal on those areas where the sediments could be expected to be removed by fluvial action as opposed to areas that will remain as terraces following dam removal. In reservoirs where submerged sediment deposits will remain as terrace deposits after dam removal, dredging of the postdam channel and deposition on these terrace areas may be an option for minimizing sediment release to the downstream channel.

If the regime of stream flow and sediment load entering the impounded reach is similar to preimpoundment conditions, the channel scoured through the deposits can be anticipated to resemble the geometry of the original preimpoundment channel. Quantification of this channel width and its progression over time is necessary to compute sediment loads below the dam. A dam removal express assessment model (DREAM) for estimating sediment release has been advanced by Cui et al. (2006a, 2006b). More information about the components of this model can also be found in Chapter 23.

Chang (2005) used the FLUVIAL-12 sediment transport model to analyze the proposed removal of Matilija dam in California on the Ventura River, illustrating the application of an erodible boundary model that adjusts channel dimensions throughout the simulation, as opposed to an erodible bed model in which the bed width must be input as a parameter value. The simulated enlargement of a cross section in the delta portion of the reservoir over a period of years as simulated by modeling is presented as Fig. 12-17.

Definition of channel side slopes is a critical element in determining the amount of sediment that will be released. Rather than to allow channel slopes to naturally come to their stable angle of repose, it may be desirable to cut them back to create a more natural channel and floodplain configuration and a more stable channel reach. This would also eliminate the potential for future slope failures that could deliver large new sediment volumes to the river after it had experienced recovery from the initial perturbation.

Sediment deposits may contain contaminants that constrain removal options. Rathbun et al. (2005) described a general screening framework for possible contaminants, and Bennett et al. (2002) described a detailed sediment assessment program at two reservoirs in Oklahoma. Chapters 21 and 22 address contaminant processes in sediments as well as sediment oxygen demand in lakes and reservoirs, respectively.

12.10 CONCLUDING REMARKS

Sustainable sediment management represents a relatively new area of focus within the engineering community, and attainment of this goal is not impossible. However, it must be recognized that the "sedimentation problem" is ultimately neither about sediment nor about water itself but about the services provided by water. At most sites it will not be economically feasible to indefinitely maintain levels of water utilization corresponding to the original sediment-free reservoir, and work beyond sedimentation engineering will be required. Themes such as water conservation, more efficient irrigation, and alternative energy sources will all eventually come into play to address sedimentation impacts. Legal sedimentation aspects, addressed in Chapter 20, might also play an important role. These broader themes should also be considered as essential components of the sustainability equation.

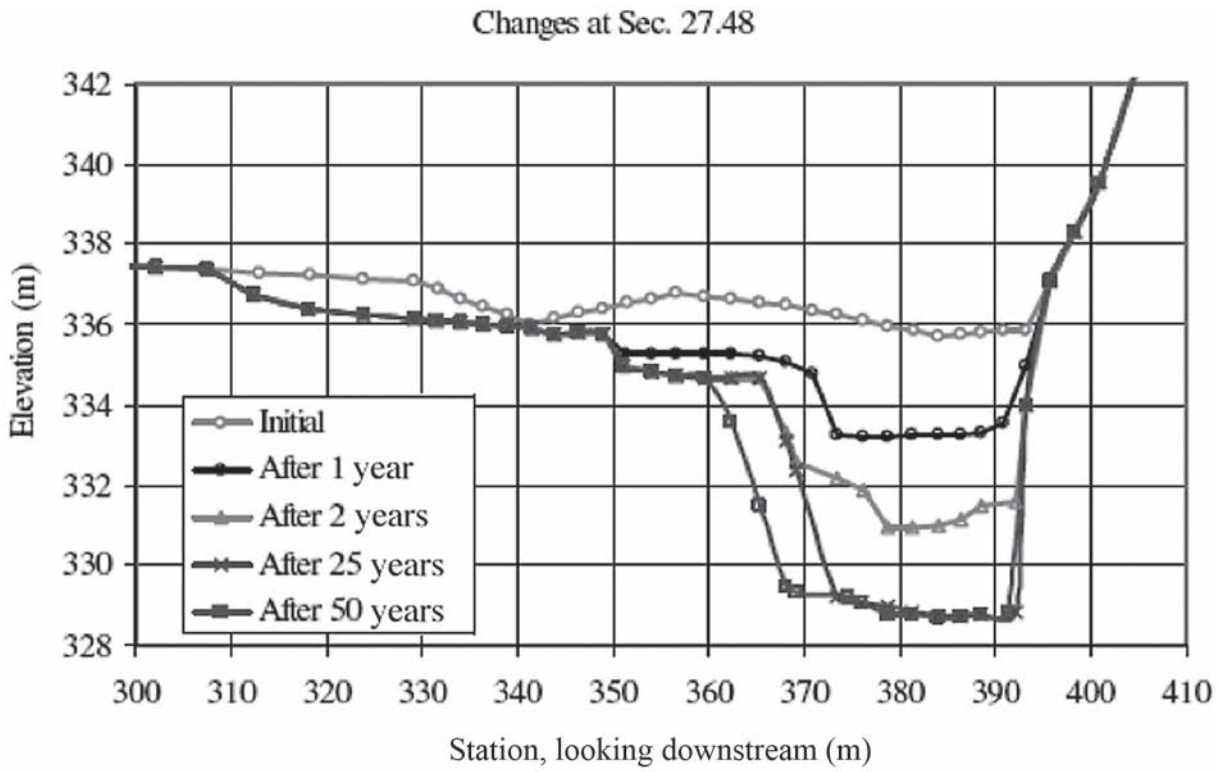

Fig. 12-17. Anticipated morphological changes in the channel as it incises through delta deposits of Matilija dam, California, following proposed dam removal (Chang 2005).

REFERENCES

Annandale, G. W. (1987). *Reservoir sedimentation*. Elsevier Science, New York.

Arnold, J. G., Williams, J. R., and Maidment, D. R. (1995). "Continuous-time water and sediment-routing model for large basins." *J. Hydr. Engrg.,* 121(2), 171–183.

ASCE. (1997). *Guidelines for Retirement of Dams and Hydroelectric Facilities*. ASCE, Reston, Va.

ASCE Task Committee on Application of the Artificial Neural Networks in Hydrology. (2000a). "Artificial neural networks in hydrology I: Preliminary concepts." *J. Hydrol. Engng., ASCE* 5(2), 115–123.

ASCE Task Committee on Application of the Artificial Neural Networks in Hydrology. (2000b). "Artificial neural networks in hydrology II: Hydrologic application." *J. Hydrol. Engng., ASCE* 5(2), 124–137.

Atkinson, E. (1996). "The feasibility of flushing sediment from reservoirs." H. R. Wallingford Report OD 137, Report to Overseas Development Admin., London. 97 pp.

Bennett, S. J., Cooper, C. M., Ritchie, J. C., Dunbar, J. A., Allen, P. E., Caldwell, L. W., and McGee, T. M. (2002). "Assessing sedimentation issues within aging flood control reservoirs in Oklahoma." *J. Am. Water Resour. Assn.,* 38(5), 1307–1322.

Brown, C. B. (1946). "Aspects of protecting storage reservoirs and soil conservation." *J. Soil and Water Conservation*, 1(1), 15–45.

Brune, G. M. (1953). "Trap efficiency of reservoirs." *Trans. Am. Geophys. Union*, 34 (3), 407–418.

Burns, M., and MacArthur, R. (1996). "Sediment deposition in Jennings Randolph Reservoir, Maryland and West Virginia," Proc., 6th *Federal Interagency Sedimentation Conf.,* Las Vegas, 10.16–10.21.

Cairns, J., Jr. (1993). "The economic basis for a partnership between human society and natural ecosystems." *Water Resour. Update*, 93, 18–22.

Campbell, I. A. (1985). "The partial area concept and its application to the problem of sediment source areas," *Soil erosion and conservation*, M. El-Swaify and A. Lo, eds., Soil Conservation Society of America, Ankeny, Iowa, 128–138.

Chang, H. H. (1996). "Reservoir erosion and sedimentation for model calibration." *Proc., 6th Federal Interagency Sedimentation Conf.,* Las Vegas, I-93–I-100.

Chang, H. H. (2005). "Fluvial modeling of Ventura River responses to Matilija Dam removal," *ASCE Conf. Proc.,* 178, 32.

Chen, J. (1994). "Sedimentation studies at Three Gorges." *Int. Water Power and Dam Construction*, August, 54–58.

Churchill, M. A. (1948). "Discussion of 'Analysis and Use of Reservoir Sedimentation Data,' by L. C. Gottschalk." *Proc., Federal Inter-Agency Sedimentation Conf.,* Denver, 139–140.

Cigizoglu, K. H., and Alp, M. (2003). "Suspended sediment forecasting by artificial neural networks using hydro-meteorological data." *ASCE Conf. Proc.,* 118, 173.

Clark, E. H. (1985). "The off-site costs of soil erosion." *J. Soil and Water Conservation*, 40(1), 19–22.

Cohn, T. A. (1995). "Recent advances in statistical methods for the estimation of sediment and nutrient transport in rivers."

Rev. Geophys., 33 (Suppl.), <http://www.agu.org/revgeophys/cohn01/cohn01.html>(Mar. 12, 2006).

Collier, M., Webb, R. H., and Schmidt, J. C. (1995). "Dams and rivers: A primer on the downstream effects of dams." USGS Circular 1126, Denver.

Crowder, B. M. (1987). "Economic cost of reservoir sedimentation: A regional approach to estimating cropland erosion damages." *J. Soil and Water Conservation*, 42(3), 194–197.

Cui, Y., Parker, G., Braudrick, C., Dietrich, W. E., and Cluer, B. (2006a). "Dam removal express assessment models (DREAM), part 1: Model development and validation." *J. Hydr. Res*. 44(3), 291–307.

Cui, Y., Braudrick, C., Dietrich, W. E., Cluer, B., and Parker, G. (2006b). "Dam removal express assessment models (DREAM), part 2: Sample runs/sensitivity tests." J. Hydr. Res. 44(3), 308–323.

De Cesare, G., Schleiss, A., and Herman, F. (2001). "Impact of turbidity currents on reservoir sedimentation." *J. Hydr. Engrg.,* 127, 6–16.

Dendy, F. E., Champion, W. A., and Wilson, R. B. (1973). "Reservoir sedimentation surveys in the United States." *Man-made lakes: Their problems and environmental effects*, W. C. Ackerman, G. F. White, and E. B. Worthington, eds., Geophysical Monograph No. 17, American Geophysical Union, Washington, D.C.

Doris, J. J., Underwood, K. L., and Rizzo, D. M. (2004). "A watershed classification system using hierarchical artificial neural networks for diagnosing watershed impairment at multiple scales." *ASCE Conf. Proc.,* 138, 317.

Edwards, T. K., and Glysson, G. D. (1988). "Field methods for measurement of fluvial sediment." USGS Open-File Report 86-531, Reston, Va.

Evans, J. E., Levine, N. S., Roberts, S. J., Gottgens, J. F., and Newman, D. M. (2002). "Assessment using GIS and sediment routing of the proposed removal of Ballville Dam, Sandusky River, Ohio." *J. Am. Water Res. Assn.,* 30(6), 1549–1565.

Fan, J., and Morris, G. L. (1992a). "Reservoir sedimentation. I: Delta and density current deposits." *J. Hydr. Engrg.,* 118(3), 354–369.

Fan, J., and Morris, G. L. (1992b). "Reservoir sedimentation. II: Reservoir desiltation and long-term storage capacity." *J. Hydr. Engrg.,* 118(3), 370–384.

Faulkner, D., and McIntyre, S. (1996). "Persisting sediment yield and sediment delivery changes." *Water Resour. Bull.,* 31(4), 817–829.

Ferguson, R. I. (1986). "River loads underestimated by rating curves." *Water Resour. Res.,* 22(1), 74–76.

Foster, I.D.L., Millington, R., and Grew, R. G. (1992). "The impact of particle size controls on stream turbidity measurements: Some implications for suspended sediment yield estimation." *Erosion and Sediment Transport Monitoring Programmes in River Basins*, IAHS Publ. 210, Wallingford, U.K., 51–62.

Garbrecht, J. D., and Garbrecht, G.K.N. (2004). "Siltation behind dams in antiquity." *ASCE Conf. Proc.,* 140, 6.

Garcia, M. H. (1993). "Hydraulic jumps in sediment-laden bottom currents." *J. Hydr. Engrg.,* 199, 1094–1117.

Garcia, M. H. (1994). "Depositional turbidity currents laden with poorly-sorted sediment." *J. Hydr. Engrg.,* 120, 1240–1263.

Garcia, M. H. (1999). "Sedimentation and erosion hydraulics." Hydraulic design handbook, Larry Mays, ed., McGraw-Hill, New York, 6.1–6.113.

Geiger, A. F. (1963). "Developing sediment storage requirements for upstream retarding reservoirs." In *Proc. Federal Interagency Sediment Conf.*, USDA-ARS Misc. Pub. 970, USDA, Washington, D.C., 881–885.

Gellis, A. (1991). "Decreasing trends of suspended sediment concentrations at selected streamflow stations in New Mexico." *Proc., 36th Annual New Mexico Water Conf.,* C. T. Ortega-Klett, ed., New Mexico State Univ., Las Cruces.

Gellis, A., Hereford, R., Schumm, S. A., and Hayes, B. R. (1991). "Channel evolution and hydrologic variations in the Colorado River basin: Factors influencing sediment and salt loads." *J. Hydrology,* 124, 317–344.

Gippel, C. J. (1995). "Potential of turbidity monitoring for measuring the transport of suspended solids in streams." *Hydrological Processes*, 9, 83–97.

Gogus, M., and Yalcinkaya, F. (1992). "Reservoir sedimentation in Turkey." *5th Int. Symp. River Sedimentation*, Karlsruhe, 909–918.

Goldsmith, E., and Hildyard, N. (1984). *The social and environmental effects of large dams. Vol. 1: Overviews*, Wadebridge Ecological Centre, Cornwall, United Kingdom.

Goldsmith, E., and Hildyard, N. (1985). *The social and environmental effects of large dams. Vol. 2: Case Studies*, Wadebridge Ecological Centre, Cornwall, U.K.

Glysson, G. D. (1987). "Sediment transport curves." USGS Open-File Report 87-218, Reston, Va.

Graf, W. L. (1993). "Landscapes, commodities, and ecosystems: The relationship between policy and science for American rivers." *Sustaining our water resources*, National Academy Press, Washington, D.C., 11–42.

Grover, N. C., and Howard, C. S. (1938). "The passage of turbid water through Lake Mead." *Trans. ASCE*, 103, 720–790.

Guy, H. P., and Norman, V. W. (1970). "Field methods for measurement of fluvial sediment." *Techniques of water resources investigations of the U.S. Geological Survey*, Book 3, Chap. C2, USGS, Reston, Va.

Harrison, L. L., and Lindquist, D. S. (1995). "Hydropower benefits of cooperative watershed management." *Waterpower '95*, ASCE, New York.

Harrison, L. L., MacArthur, R. C., and Sanfort, R. A. (2000). "Lake Solano sediment management study." *ASCE Conf. Proc*., 105, 167.

Herbich, J. B., ed. (1992). *Handbook of dredging engineering*, McGraw-Hill, New York.

Hotchkiss, R. H., and Bollman, F. (1996). "Socioeconomic analysis of reservoir sedimentation." *Revised Proc., International Conference on Reservoir Sedimentation*, M. Albertson, A. Molinas, and R. Hotchkiss, eds., Ft. Collins, Colo., Sept. 9–13, Vol. 1, 52.39–52.50.

Hotchkiss, R. H., and Xi, H. (1995). "Designing a hydrosuction sediment removal system." *6th Int. Symp. River Sedimentation*, Central Board of Irrigation and Power, New Delhi, 165–174.

Jain, S. K. (2001). "Development of integrated sediment rating curves using ANNs." *J. Hydr. Engrg*., 127, 30–37.

Jansson, M. B. (1988). "A global survey of sediment yield." *Geogr. Ann*., 70, ser. A(1–2), 81–98.

Jansson, M. B., and Rodríguez, A., eds. (1992). "Sedimentological studies on the Cachí Reservoir, Costa Rica." UNGI Report No. 81, Dept. of Physical Geography, Uppsala Univ., Sweden.

Kawashima, S., Johndrow, T. B., Annandale, G. W., and Shah, F. (2003). *Reservoir conservation: The RESCON approach*, Vol. I. The World Bank, Washington, D.C.

Kothyari, U. C., Tiwari, A. K., and Singh, R. (1996). "Temporal variation of sediment yield." *J. Hydr. Engrg*., 1(4), 169–176.

Lagwankar, V. G., Gorde, A. K., Barikar, D. A., and Patil, K. D. (1995). "Trends in reservoir sedimentation in India." *6th Int. Symp. River Sedimentation*, Management of Sediment, Central Board of Irrigation and Power, New Delhi, 91–111.

Lane, E. W., and Koelzer, V. A. (1943). "Density of sediments deposited in reservoirs," Report No. 9, *A study of methods used in measurement and analysis of sediment loads in streams*, Hydraulic Lab, Univ. of Iowa.

Lara, J. M., and Pemberton, E. L. (1963). "Initial unit weight of deposited sediments." *Proc. Federal Interagency Sedimentation Conf*., USDA–ARS Misc. Publ. 970, 818–845.

Leopold, Luna B., Wolman, M. Gordon, and Miller, John P. (1964). *Fluvial processes in geomorphology*, W. H. Freeman, San Francisco.

Lewis, J. (1996). "Turbidity-controlled suspended sediment sampling for runoff-event load estimation." *Water Resour. Res*., 32(7), 2299–2310.

Ligon, F. K., Dietrich, W. E., and Trush, W. J. (1995). "Downstream ecological effects of dams." *Bioscience*, 45(3), 183–192.

Lin, B., Dou, G., Xie, J., Dai, D., Chen, J., Tang, R., and Zhang, R. (1989). "On some key sedimentation problems of Three Gorges Project." *Int. J. Sediment Res*., 4(1), 57–74.

Lin, B., Dou, G., Xie, J., Dai, D., Chen, J., Tang, R., and Zhang, R. (1993). "On some sedimentation problems of Three Gorges Project in the light of recent findings." *Notes of sediment management in reservoirs: National and international perspectives*, S. S. Fan and G. L. Morris, eds., Federal Energy Regulatory Commission, Washington, D.C.

Liu, J., and Tominaga, A. (2003). "New development of sediment flushing technique." *ASCE Conf. Proc*., 118, 52.

Livesey, R. H. (1975). "Corps of Engineers methods for predicting sediment yield." *Present and prospective technologies for predicting sediment yields and sources*, ARS-S-40, USDA Sedimentation Lab, Oxford, Miss.

Locher, F. A., and Wang, J. S. (1995). "Operational procedures for sediment bypassing at Cowlitz Falls Dam." *15th Annual USCOLD Lecture Series*, USCOLD, Denver, 75–90.

Loehlein, W. C. 1999. "The growing reservoir sedimentation problem in the U.S. Army Engineer District, Pittsburgh." *ASCE Conf. Proc*., 111, 313.

Lu, X., Wang, J., and Zhang, Q. (1999). "A GIS-based sediment assessment and management system for the Three Gorges area, China." *Geoinformatics and socioinformatics*, B. Li et al., eds., *Proc. of Geoinformatics '99 Conf*., Ann Arbor, Mich., 1–11.

MacArthur, R. C., Hamilton, D., and Gee, D. M. (1995). "Application of methods and models of prediction of land surface erosion and yield." Training Document No. 36, U.S. Army Corps of Engineers, Hydrologic Engineering Center, Sacramento, Calif.

MacBroom, J. G. (2005). "Evolution of channels upstream of dam removal sites." *ASCE Conf. Proc*., 178, 26.

McCully, P. (1996). *Silenced rivers—The ecology and politics of large dams*, Zed Books, London.

McHenry, J. L., and Ritchie, J. C. (1980). "Dating recent sediments in impoundments." *Surface water impoundments*, ASCE, New York, 1279–1289.

Mahmood, K. (1987). "Reservoir sedimentation: Impacts, extent, mitigation." World Bank Technical Report No. 71, Washington, D.C.

Meade, R. H., and Parker, R. S. (1984). "Sediment in rivers of the U.S." *National water summary*, USGS, Reston, Va.

Megahan, W. F. (1975). "Sedimentation in relation to logging activities in the mountains of central Idaho." *Present and prospective technologies for predicting sediment yields and sources*, ARS-S-40, USDA Sedimentation Lab, Oxford, Miss., 74–82.

Morris, G. L. (1995). "Reservoir Sedimentation and Sustainable Development in India: Problem Scope and Remedial Strategies." *6th Int. Symp. River Sedimentation*, Central Board of Irrigation and Power, New Delhi, 53–61.

Morris, G. L., Colón, R., Laura, R., and Anderson, G. T. (1992). "GRASS modeling of Loíza Reservoir, Puerto Rico, for Sediment Management Operations." *Water Forum* '92, ASCE, New York.

Morris, G. L., and Fan Jiahua. (1998). *Reservoir sedimentation handbook*, McGraw-Hill, New York.

Morris, G. L., and Hu, G. (1992). "HEC-6 modeling of sediment management in Loíza Reservoir, Puerto Rico." *Hydraulic engineering, Water Forum '92*, M. Jennings and N. Bhowmik, eds., ASCE, New York, 630–635.

Murthy, B. N. (1977). *Life of reservoir*, Central Board of Irrigation and Power, New Delhi.

Nagy, H. M., Watanabe, K., and Hirano, M. (2002). "Prediction of sediment load concentration in rivers using artificial neural network model." *J. Hydr. Engrg*., 128, 588–595.

Napier, T. L., Camboni, S. M., and El-Swaify, S. A., eds. (1994). *Adopting conservation on the farm: An International Perspective on the socioeconomics of soil and water conservation*, Soil and Water Conservation Society, Ankeny, Iowa.

Nicklow, J. W., and Bringer, J. A. (2001). "Optimal control of sedimentation in multi-reservoir river systems using genetic algorithms." *ASCE Conf. Proc*., 111, 93.

Nicklow, J. W., and Mays, L. W. (2000). "Optimization of multiple reservoir networks for sedimentation control." *J. Hydr. Engrg*., 126, 232–242.

Odhiambo, B. K., and Boss, S. K. (2004). "Integrated echo sounder, GPS, and GIS for reservoir sedimentation studies: Examples from two Arkansas lakes." *J. Am. Water Resour. Assn.,* 40, 981–997.

Olive, N.R.B., and Rieger, W. A. (1988). "An examination of the role of sampling strategies in the study of suspended sediment transport." *Sediment budgets*, IAHS Publ. 174, Wallingford, United Kingdom, 259–268.

O'Neil, W. B. (1997). "The discipline of imperfect bean counting." *Water Resources Update*, 109, 49–54.

Palmieri, A., Shah, F., and Dinar, A. (1998). "Reservoir sedimentation and the sustainable management of dams." *Proc., World Conf. of Environmental and Resource Economists*, Venice, June 23–27.

Palmieri, A., Farhed, S., Annandale, G. W., and Dinar, A. (2003). "The RESCON approach: Economic and engineering evaluation of alternatives strategies for managing sedimentation in storage reservoirs." The World Bank, Washington, D.C. <http://www.ucc.uconn.edu/~wwware/Sustpub.htm>(Mar. 15, 2006).

Petts, G. E. (1984). *Impounded rivers: Perspectives for ecological management*, Wiley-Interscience, New York.

Raghuwanshi, N. S., Singh, R., and Reddy, L. S. (2006). "Runoff and sediment yield modeling using artificial neural networks: Upper Siwane River, India." *J. Hydr. Engrg*., 11(1), 71–79.

Rathbun, J., Braber, B. E., Pelto, K. I., Turek, J., and Wildman, L. (2005). "A sediment quality assessment and management framework for dam removal projects." In Moglen, G. E., ed., *Proc. Managing Watersheds for Human and Natural Impacts*, July 19–22, ASCE, Williamsburg, Va. (178) 19.

Rooseboom, A. (1992). "Sediment transport in rivers and reservoirs: A South African perspective." Report to Water Research Commission of South Africa by Sigma Beta Consulting Engineers, Stellenbosch.

Salas, J. D., and Shin, H-S. (1999). "Uncertainty analysis of reservoir sedimentation." *J. Hydr. Engrg*., 125, 339–350.

Schnitter, N. J. (1994). *A history of dams, the useful pyramids*, A. A. Balkema, Rotterdam.

Sen, Z., Altunkaynak, A., and Özger, M. (2004). "Sediment concentration and its prediction by perceptron Kalman filtering procedure." *J. Hydr. Engrg*., 130, 816–826.

Simon, A., and Heins, A. (2005). "Suspended-sediment transport rates and recurrence intervals at the effective discharge." ASCE *Conf. Proc*., 173, 605.

Soler-López, L. R. (2001). "Sedimentation survey of Lago Dos Bocas, Puerto Rico, October 1999." USGS Water-Resources Investigations Report 00-4234, San Juan.

Stanley Consultants. (1989). "Lake Francis Case Aggradation Study, 1953–1986." U.S. Army Corps of Engineers, Omaha.

Strand, R. I., and Pemberton, E. L. (1987). "Reservoir sedimentation." *Design of Small Dams*, U.S. Bureau of Reclamation, Denver.

Sundborg, A., and Jansson, M. B. (1992). "Present and future conditions of reservoir sedimentation." *Sedimentological studies on the Cachí Reservoir, Costa Rica*, M. B. Jansson and A. Rodríguez, eds., UNGI Report No. 81, Dept. of Physical Geology, Uppsala Univ., Sweden.

Sutherland, R. A., and Bryan, R. B. (1988). "Estimation of colluvial reservoir life from sediment budgeting, Katiorin Experimental Basin, Kenya." *Sediment budgets*, IAHS Publ. 174, Wallingford, United Kingdom, 549–560.

Teal, M. J., and Remus, J. I. (2001). "Lake Sharpe sediment flushing analyses." *ASCE Conf. Proc*., 111, 140.

Tejwani, K. G. (1984). "Reservoir sedimentation in India: Its causes, control and future course of action." *Water International*, 9(4), 150–154.

Thimmes, A., Huffaker, R., and Hotchkiss, R. (2005). "A law and economics approach to resolving reservoir sediment management conflicts." *J. Am. Water Resour. Assn*., 41, 1449–1456.

Thomas, R. B., and Lewis, J. (1993). "A comparison of selection at list time and time-stratified sampling for estimating suspended sediment loads." *Water Resour. Res*., 29(4), 1247–1256.

Trimble, S. W. (1974). "Man-induced soil erosion on the southern piedmont, 1700–1970," Soil Conservation Society of America, Ankeny, Iowa.

Trimble, S. W. (1977). "The fallacy of stream equilibrium in contemporary denudation studies." *Am. J. Sci*., 277, 876–887.

Turner, T. M. (1996). *Fundamentals of hydraulic dredging*, 2nd ed., ASCE, New York.

U.S. Army Corps of Engineers. (1987). "Confined disposal of dredged materials." EM 1110-2-5027, Washington, D.C.

U.S. Army Corps of Engineers. (1989). "Sedimentation investigations in rivers and reservoirs." EM 1110-2-4000, Washington, D.C.

U.S. Committee on Large Dams (USCOLD). (1994). *Tailings Dam Incidents*, USCOLD, Denver, Colo.

Walling, D. E. (1983). "The sediment delivery problem." *J. Hydrology*, 65, 209–237.

Walling, D. E. and Webb, B. W. (1981). "The reliability of suspended sediment load data." *Erosion and Sediment Transport Measurement Symp*., IAHS Publ. 133, Wallingford, United Kingdom, 177–194.

Walling, D. E., and Webb, B. W. (1988). "The reliability of rating curve estimates of suspended sediment yield: Some further comments." Sediment budgets, IAHS Publ. 174, Wallingford, United Kingdom, 337–350.

Weiss, E. B. (1993). Intergenerational fairness and water resources." *Sustaining our water resources*, Water Science and Technology Board 10th Anniversary Symp., National Academy Press, Washington D.C., 3–10.

White, R. (2001). *Evacuation of sediments from reservoirs*, Thomas Telford Press, London. (Avail. ASCE)

Williams, G. P. (1989). "Sediment concentration versus water discharge during single hydrologic events in rivers." *J. Hydrology*, 111, 89–106.

Williams, G. P., and Wolman, M. G. (1984). "Downstream effects of dams on alluvial rivers." USGS Prof. Paper 1286, Washington, D.C.

Wolman, M. G., and Miller, J. P. (1960). "Magnitude and frequency of forces in geomorphic *processes." J. Geology*, 68, 58–74.

Wu, C. M. (1991). "Reservoir capacity preserving practice in Taiwan." *Proc. 5th Federal Interagency Sedimentation Conf*., Las Vegas, 10.75–10.81.

Copyrighted Materials
Copyright © 2008 American Society of Civil Engineers (ASCE)
Retrieved from www.knovel.com

CHAPTER 13

Ice Effects on Sediment Transport in Rivers

Robert Ettema

13.1 INTRODUCTION

The winter cycle of river-ice formation seasonally grips many rivers in large areas of the Northern hemisphere. The cycle affects river-channel capacity to convey water and sediment, it may aggravate riverbank erosion, and it may perturb the stability of alluvial channels. The severity with which the cycle of river-ice formation affects sediment-transport dynamics for rivers depends on a combination of factors related to the cycle's duration and coldness (usually expressed as accumulated degree-days of freezing). Figure 13-1 indicates the extent of the Northern hemisphere that annually experiences at least 1 month of average air temperature below 0 C.

Of major importance is the seasonal availability of water flow. Under natural conditions in many rivers, the winter cycle of ice is accompanied by a decline in water runoff and channel flow. Rates of sediment supply and channel transport diminish commensurately. Runoff and channel flow subsequently increase during spring thaws, and it is then that ice-cover effects on sediment transport become significant. For many flow-regulated rivers subject to the ice cycle, though, ice effects on sediment transport and alluvial-channel behavior are of special interest. Substantial flows may occur while such rivers are ice-covered in winter.

Also important are the materials composing the bed and bank of a river. Diverse other factors, such as north-south river flow orientation and snowfall, also can exert significant influences. The overall impacts of all these factors on sediment transport and channel morphology vary widely from one river to the next and differ from reach to reach along a river. The impacts may be distinct and clearly observable, for rivers in permafrost or annually subjected to severe ice runs following ice-cover breakup in spring. They may be obvious from stunted riparian vegetation, scarred trees, or gouged channel features. They may be subtle and blurred by the inherent complexities and apparent irregularities of alluvial-channel flow. They also may be intermittent, being significant at one site on one occasion, but not the next. A good deal of the variability in ice impacts is attributable directly to variability in flow conditions.

Ice effects on sediment transport may be noticeable over varying scales of time and channel length. On the scales of months and of miles of channel, for instance, ice alters the relationship between flow rate, flow depth, and sediment transport rates. As it forms, an ice cover usually increases and redistributes a channel's resistance to flow and reduces its overall capacity to move water and sediment. In a sense, because the channel's bed roughness does not actually increase (in fact it may decrease; Smith and Ettema 1997), the effect of ice-cover presence on channel morphology may be likened to the effect produced by a reduction in energy gradient associated with flow along the channel. More precisely, it may be likened to a change in thalweg geometry; the additional flow energy consumed in overcoming the resistance created by the cover offsets a portion of the flow's energy that the channel dissipates by thalweg lengthening or bifurcation. This sort of postulation, though fun and possibly sound theoretically, may be difficult to verify practically, because ice covers vary in length, thickness, and roughness along most rivers. The fact remains that, at present, scant data exist for rivers.

On the local scale, an ice cover over a short reach may redistribute flow laterally across the reach, accentuating erosion in one place and deposition in another place. Such local changes of the bed may develop during the entire cycle of ice formation, presence, and release. They may develop briefly, lasting slightly longer than the ice cover, and disappear shortly after the cover breaks up. Or they may trigger a change that persists for some time. In any event, they should be verifiable from a site investigation.

Ice may dampen or amplify erosion processes locally. Obvious damping effects of ice are reduced water runoff from a watershed, cementing of bank material by frozen

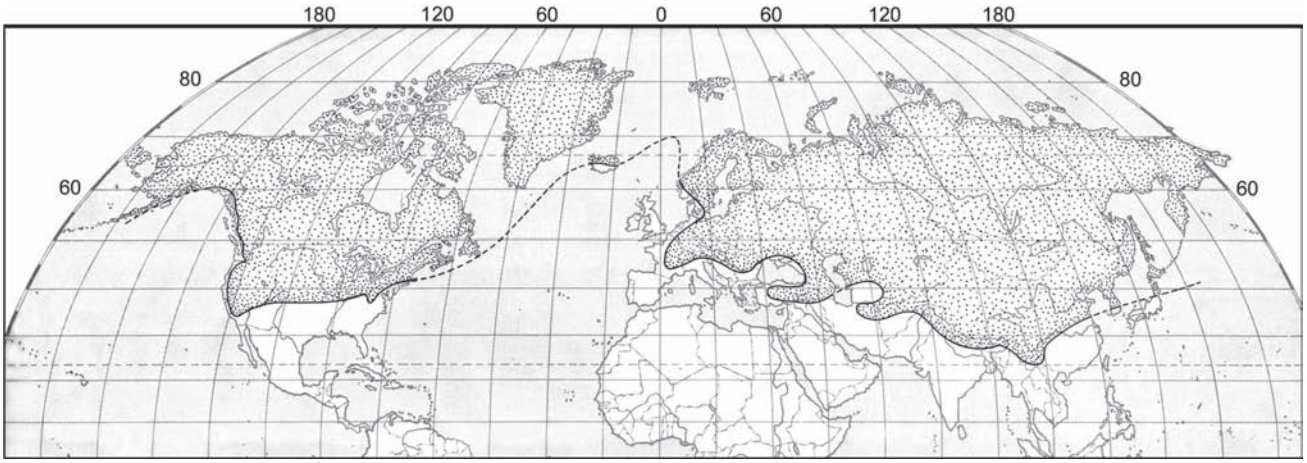

Fig. 13-1. Area of Northern Hemisphere that experiences at least one month per year with average air temperatures less than 0 C.

water, and ice armoring of bars and shorelines by ice-cover setdown with reduction in flow rates. Yet ice may amplify erosion and sediment-transport rates, notably during the surge of water and ice consequent to the collapse of a large ice jam.

In recent years, growing interest in the wintertime management of reservoir-regulated rivers that become ice-covered, especially the winter environments of such rivers, has made it necessary to better understand and model flow and transport processes in ice-covered alluvial channels. The need has become especially acute for river reaches in which flow regulation results in significantly larger wintertime flows than occurred during preregulation conditions. For such situations it is necessary to develop more accurate estimates of flow stage, quantity of sediment conveyed, and possible changes in channel morphology. Even for essentially unregulated or wild rivers, such as the Yellowstone River shown in Fig. 13-2, it has become important to understand channel response to the winter cycle of ice.

The present chapter describes how the ice cycle may affect sediment transport, locally as well as over long reaches. It is necessary to point out that the literature dealing with ice effects on sediment transport and channel morphology is not extensive. Moreover, what exists contains a fair amount of hypothesis and conjecture. Inevitably, therefore, this chapter also contains its share of hypothesis and conjecture. An unavoidable difficulty is that ice can have various and, at times, apparently contradictory effects. General conclusions about the net effects of ice are not at all straightforward to state, except to say that ice effects are closely related to velocity and elevation of flow; i.e., higher flows incur higher impacts under ice-covered conditions than under open-water conditions.

This chapter does not address the influence of permafrost on sediment transport. Permafrost is an important factor affecting riverbank and channel stability of high-latitude rivers. Scott (1978) and Lawson (1983), for example, provide some insights into channel behavior in permafrost. Johnston (1981) and Andersland and Anderson (1990) usefully describe the geotechnical properties of permafrost.

This chapter begins with an introductory description of the typical cycle of ice formation, ice effects on flow distribution, and ice-cover breakup in rivers (names commonly used for the various ice formations are introduced in italics). It then briefly describes how ice can directly entrain and transport sediment from the beds of certain rivers. Subsequently, it goes on to discuss the typical mechanisms whereby ice and cold water influence sediment transport by flow in rivers. The latter portion of the chapter addresses river-ice influences on

Fig. 13-2. The Yellowstone River, Montana, under an ice cover, whose formation, presence, and eventual breakup significantly influences sediment-transport dynamics, channel-thalweg location, and riverbank erosion.

channel stability. Of particular interest, in this regard, are rivers whose inflow is regulated by upstream dams.

13.2 ICE FORMATION

During autumn and into winter, river water cools. In cold regions, such as indicated in Fig. 13-1, it usually cools to the water-freezing temperature, or momentarily to a fraction of a degree below it (supercooling is needed to nucleate or initiate ice growth), whereupon ice rapidly forms. For a river whose inflow is regulated by a large reservoir, water temperature decreases with downstream distance of flow, and initial ice-cover formation develops commensurably at some distance downstream of the reservoir.

Ice-cover formation over a river comprises several main processes, which Fig. 13-3 (from Matousek 1984) usefully summarizes in terms of bulk velocity of flow, U, and heat flux to air, ϕ. The ice terminology in Fig. 13-3 is explained further in the ensuing sections of this chapter. Implied in this figure are the influences of vertical and lateral mixing within the flow, as well as the strength of thin newly formed ice. As water cools below 4 C, it becomes lighter, and thereby more difficult to mix within the body of flow.

One formation process is static or thermal, and could be called the *bankfast-ice* process. It occurs for flows of negligibly small surface velocity and is evident as ice growth outward from riverbanks. *Frazil-ice* formation starts with the supercooling of water over some portion of flow depth. *Skim ice* may form on flows whose surface velocity and turbulence levels are sufficiently low so that only a surface layer of water supercools, resulting in thin sheets of ice. As flow velocity and turbulence levels increase, the initial formation of ice becomes more dynamic. The full depth of water at some reach may supercool, so that frazil-ice crystals form throughout the flow. Frazil-ice formation usually dominates ice formation on alluvial rivers whose flow has sufficient velocity to move bed sediment. A given reach of river may undergo all three forms of ice growth, depending on the distribution of flow velocity upstream of and through the reach.

For river flow in a watershed unregulated by dams, factors related to channel size and air-temperature variation with altitude and latitude determine rate of water cooling and where ice first appears and gradually envelops a channel. Though exceptions exist, ice first forms in the upper reaches of a watershed for most rivers that drain toward the south (e.g., the Mississippi River). For northward draining rivers (e.g., the Red River of the North, the Mackenzie River), or rivers with more or less east-west orientations (e.g., the Yellowstone River, the Yukon River), the sequence of ice formation occurs in a more complicated manner along the length of the river.

An important factor influencing first ice formation in a channel whose flow is regulated by an upstream reservoir is the temperature of the water released into the channel. In most situations, the reservoir changes the temperature of the flow entering the channel; besides storing water volume, a reservoir stores heat. During freeze-up conditions in late fall and winter, the flow entering the channel is warmer than the flow in the channel prior to construction of the reservoir. Consequently, the reservoir likely will cause ice formation to

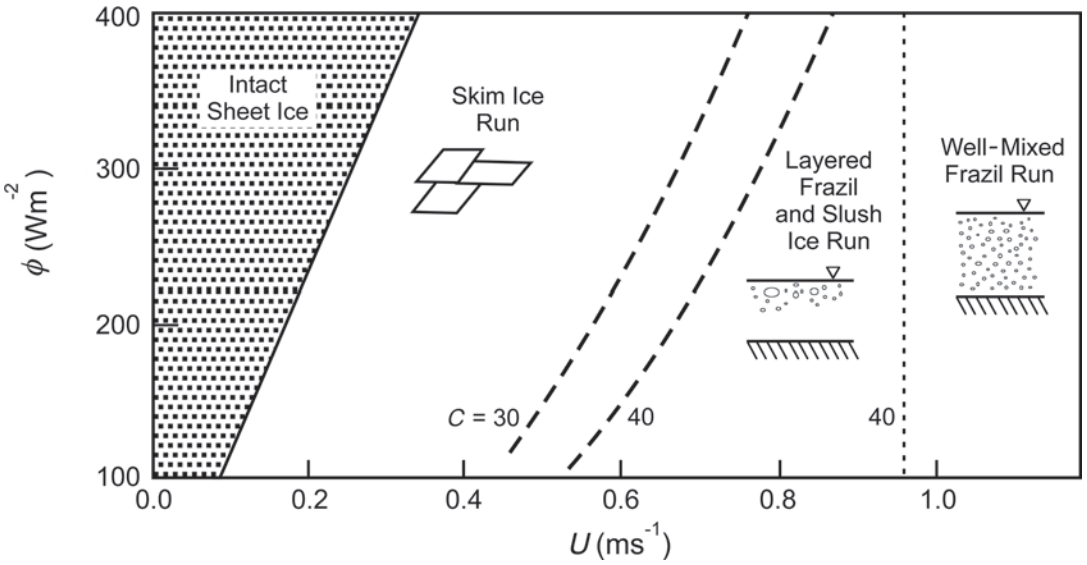

Fig. 13-3. Types of initial river-ice formation as a function of flow velocity and surface heat-loss rate; C is Chezy coefficient, and ϕ is rate of heat loss per unit area of river water surface (Matousek 1984). Larger flow velocity, U, results in greater mixing and cooling of flow over its full depth.

begin further downstream along the channel than it did prior to construction of the reservoir. The thermal influence of a reservoir on ice-cover formation can be demonstrated quite readily. If, prior to construction of the reservoir, the flow entering the channel reach was at the freezing temperature of water (0 C), ice potentially could begin forming throughout the full length of the channel. For example, if a 3-m-deep flow of 4 C water were released with an average velocity of 1 m/s and exposed to −20 C air under representative conditions of heat loss (say, 20 W/m^2 / C), the flow would travel almost 117 km downstream from the reservoir before cooling to 0 C. If the initial temperature of the water leaving the reservoir were 1 C, the distance would be reduced to about 30 km. Therefore, as the water in the reservoir's water cools during winter, the ice cover on the river may progress further upstream. Water density is greatest at 4 C, and therefore water at the elevation of a reservoir's outflow conduit, usually placed low through the dam, is likely to be at this temperature.

Cold, clear, windy nights are especially conducive to ice formation. During such nights, rivers lose heat at maximum rates to the atmosphere by means of long-wave radiation, convection, and evaporation. Consequently, it is common for ice to form, or at least to form at its greatest rate, during the night.

13.2.1 Bankfast Ice

As can be seen from the river view shown in Fig. 13-4, bankfast ice (also called border ice) usually is the first type of ice to appear along a river. It forms in low-velocity zones along banks. The top layer of the water adjacent to the bank mixes minimally with lower layers and soon becomes supercooled in frigid air, while water elsewhere is still above the freezing temperature. Ice fragments in the air and at the riverbank nucleate the supercooled water at the surface. The nucleated water propagates an ice sheet on the water surface outward from the bank. The edge of the ice sheet eventually extends to a zone of turbulent water, whereupon its further progress depends on thermal atmospheric exchange. The growth does not stop just because the water is above the freezing temperature, though it slows. It continues growing by virtue of net heat loss of water fringing the bankfast-ice edge. Bankfast-ice extension accelerates when drifting frazil slush and small pans lodge against it. The slush and pans fuse in rows to the dendrite crystals extending from the bankfast-ice edge, and they may form successive layers in the outward progressing border ice.

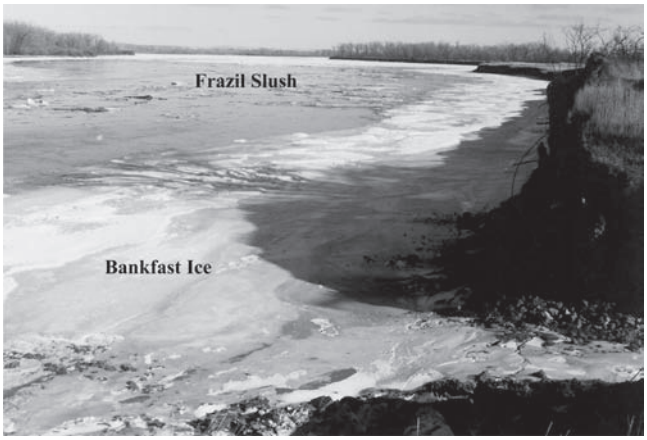

Fig. 13-4. Bankfast ice formed along a bank of the Missouri River. Frazil-ice slush and pans drift in center channel.

Bankfast-ice growth is a prominent ice-formation process in small rivers and streams with mild slopes. Together with skim ice, it is the static type of ice growth that occurs in lakes during calm but frigid weather. In the context of bank-erosion concerns, the effects of border ice on bank-material strength and loading are not well understood. For instance, not much is known about how bankfast-ice growth affects freezing of groundwater within a riverbank.

13.2.2 Skim Ice

When surface velocities are low, the surface layer of flow may become supercooled and spawn frazil ice, which rises and forms fragile, thin sheets of skim ice (e.g., Matousek 1984; Ashton 1986). Marcotte (1984) reports large sheets of skim ice forming when surface velocities of flow along the St Lawrence River were about 0.3 m/s; he reports that, in very cold weather, skim ice may form at surface flows with velocities of about 1.0 m/s. Sheets of skim ice drift until they gently lodge against each other along a river. The river then quickly freezes over completely. Skim ice and bankfast ice are common ice forms on rivers and streams whose slopes are sufficiently mild so that flow velocities are of the magnitude ranges tentatively indicated above.

13.2.3 Frazil Ice

For fully turbulent flow, frazil-ice formation begins with the formation of frazil-ice crystals throughout the depth of flow in an ice-generation zone. It is an especially striking and dominant feature of river behavior in cold regions.

Frazil ice appears quickly in a flow that supercools to a fraction of a degree below the freezing temperature of water, i.e., nominally about −0.01 to −0.1 C. As frazil crystals form, the latent heat of fusion they release gradually raises the water temperature to 0 C. During this period, the frazil is in what is termed the "active" state, in which it fuses readily with solid objects that it contacts (e.g., other frazil ice crystals, sediment on the riverbed, boulders, and some aquatic plants). For a flow-regulated river, the zone of active frazil formation may be fixed and extend only a few hundred feet, producing frazil conveyed downstream by the flow. The continuous variation in weather conditions in nature (notably,

fluctuations in air temperature, wind speed, and net heat loss by means of radiation) causes the zone to shift. Lowering air temperature or water flow rate, for example, causes the zone to move upstream. Supercooling could occur at the same river site for several days, depending on daily fluctuations in weather and flow. As an ice cover forms and progresses downstream along an unregulated river, the zone of frazil-ice production may also move downstream.

Frazil crystals grow rapidly in size, fuse to each other, agglomerate, and (owing to ice buoyancy) rise to the water surface if able to drift for a sufficient distance of flow. When initially in supercooled water, frazil crystals fuse to almost any solid boundary in the flow. For instance, they may fuse to the river bottom, forming an accumulation termed *anchor ice*. As frazil drifts, it rises to the water surface, agglomerates, crusts over, and forms ice pans, which have a hard, flat circular top and an approximately hemispherical accumulation of slush below. At this stage, the water no longer is supercooled and the frazil is termed inactive frazil; it has lost its propensity to fuse readily.

Long reaches of rivers may become covered with drifting *slush*, *pans*, and *floes* formed of fused pans. Figure 13-5 (adapted from Michel 1971) illustrates the genesis of an ice cover formed primarily from frazil ice. In deep sections with relatively low surface velocity, or in other locations with low surface velocities, the ice coverage concentrates. The pans and floes drift with the flow until they become congested (such as in a traffic jam) or lodge against some constriction. Once cover has started, it progresses upstream rapidly as a juxtaposed layer of pans and floes cemented with frazil slush. It is typical for ice covers on large rivers to progress upstream at a rate of about 40 km per day in this manner (e.g., Michel 1971). Alternately, a pile-up of ice may occur and form what is termed a freeze-up jam. *Freeze-up jams* retard flow and raise water levels, possibly causing flooding upstream of the jam toe. Several flow-related variables influence the upstream progression of a level cover comprising juxtaposed pans and floes. However, an approximate rule of thumb (e.g., Michel 1971; 1978; Ashton 1986) is that a level cover may develop when the Froude number for flow at the site is about 0.1 or less; i.e., the Froude number $= U/(gY)^{0.5} < 0.1$, in which U = bulk flow velocity, Y = flow depth, and g = gravitational acceleration. For typical rivers, it is easier to use simple velocity criteria; e.g., frazil slush passes under the front of an ice cover when flow velocity exceeds about 0.6 m/s, and frazil pans will go under when velocity exceed about 2 m/s. The cover still may progress upstream when ice passes under its front if the rate of ice arrival at the cover front exceeds the rate at which ice is subducted beneath the front.

When the upstream front of the cover reaches a high-velocity section of a river, large amounts of slush and pans are forced under the front and conveyed beneath the cover. The slush sometimes forms clusters and *granules* or *pebbles* conveyed long distances under ice covers, being transported as a form of "bed load" of frazil that rumbles along the cover underside (Shen and Wang 1995). The granules, as well as slush and small pans, may come to rest and accumulate in zones of lower velocity beneath the cover. Chacho et al. (1986) describe similar transport of frazil along the underside of the ice cover of the Tanana River, Alaska.

Large accumulations of ice may develop under the cover and be resistant to shoving. In some situations, they may form a feature known as a *hanging dam*. Ice moving under

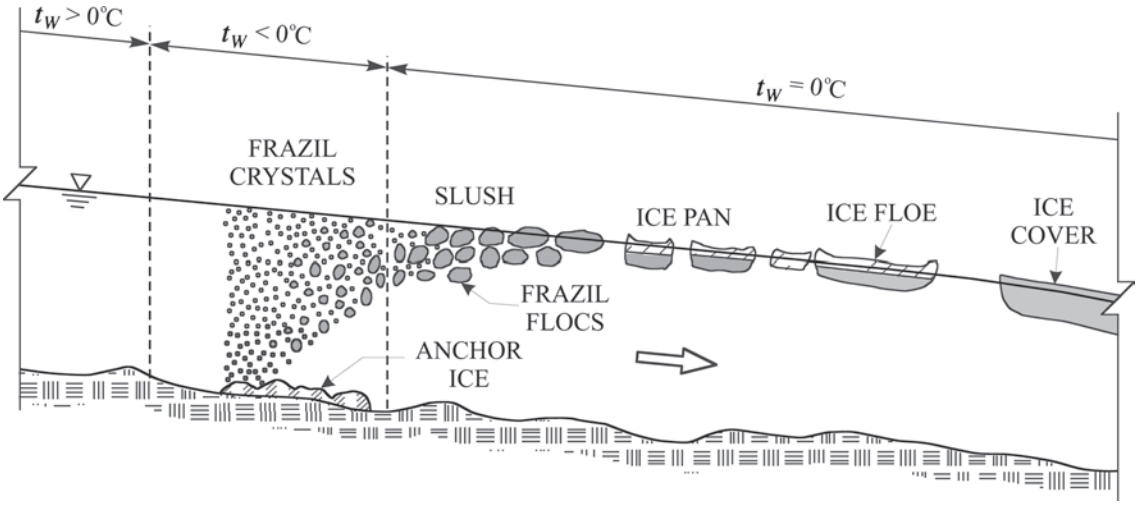

Fig. 13-5. The genesis of frazil ice in a river or stream. The water cools until slightly supercooled, whereupon frazil ice crystals rapidly appear, agglomerate as slush, develop as ice pans, which then may align juxtaposed as an ice cover. t_w = temperature of water.

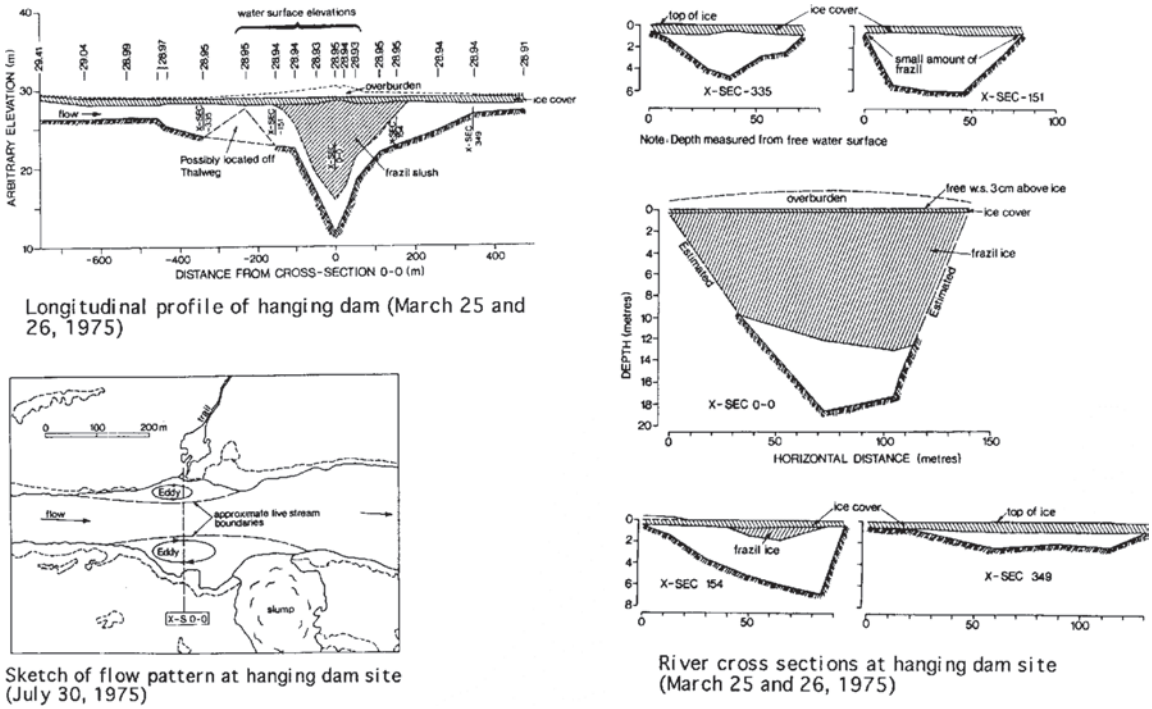

Fig. 13-6. A hanging jam of frazil ice may develop under an ice cover when flow velocities exceed those needed to form an ice cover of juxtaposed pans of ice. This example, taken from Beltaos and Dean (1981), shows a hanging dam in the Smoky River, Alberta.

the cover progressively accumulates in locations of reduced flow velocity, concentrating the flow velocity so that it locally scours the river's bed (a later section of the chapter further discusses this concern) and increases flow area. The hummocking of an ice cover can be a clue to the presence of a hanging dam. As hanging dams and similar accumulations increase in size, they increase flow resistance, raise water level, reduce and possibly redistribute flow velocity, and enable the cover to continue progressing upstream. Figure 13-6, taken from Beltaos and Dean (1981), depicts typical aspects of a hanging dam in the Smoky River, Alberta.

For steep, highly turbulent streams, another form of dam building occurs. Weirs of anchor ice (frazil ice bonded to the bed, not the ice cover) may extend up from the streambed, reducing flow velocity and enabling the cover to progress upstream. The anchor-ice weirs retard the flow and eventually help a cover form over the flow.

In relatively steep, swift-flowing channels, frazil ice may not develop to the level cover of juxtaposed pans or covers with hanging dams. Instead, the higher flow velocities associated with steeper channels, pans, and slush, sometimes mixed with snow, form a jumbled accumulation known as a freeze-up jam. Such jams may be free-floating or partially grounded on the bed. The remnant of such a jam in a gravel-bed reach of the Yellowstone River, Montana, is depicted in Fig. 13-7. The jam clogged much of the reach, especially in shallower, slower current portions to the side of the river's thalweg.

A cover of pans and slush solidifies contiguously between the ice pieces and may thicken thermally. The contiguous solidified cover resists the hydrodynamic drag exerted by the water and the streamwise component of the cover's weight. The cover may locally buckle, shove, hummock, and bummock at weak spots as the cover progresses upstream, the flow rate fluctuates, and/or air temperature changes.

Fig. 13-7. The remnants of a freeze-up jam in the Yellowstone River, Montana. The jam comprised frazil slush and pans mixed with snow and is partially grounded.

13.3 ICE-COVER EFFECTS ON FLOW DISTRIBUTION

An ice cover imposes an additional resistant boundary that decreases a channel's flow capacity and vertically redistributes streamwise velocity of flow in a channel. If the cover is free-floating, it may reduce the erosive force of flow in the channel and thereby reduce rates of sediment transport. However, cover presence also may laterally redistribute flow, usually concentrating it along a thalweg. If the thalweg lies close to one side of a channel, flow concentration may locally increase bank erosion and channel shifting. On the other hand, if the thalweg is more or less centrally located in a channel, the cover may reduce bank erosion and channel shifting. Additionally, if the full cover is fixed to the riverbank, it may increase locally flow velocities and rates of sediment transport.

The variability of flow response to ice cover makes it difficult to draw simple overall conclusions about ice-cover effects on a river's bed and banks. The net effects will vary from site to site.

If the flow rate and channel slope are assumed constant, the main individual effects of a uniformly thick ice cover on a straight uniformly deep alluvial channel are as follows:

1. Raised water level (ice-covered depth exceeds open-water depth for the same flow rate);
2. Reduced bulk velocity of flow (discharge/flow area);
3. Reduced drag on the channel bed;
4. Reduced velocity of secondary currents (i.e., currents associated with transverse circulation of flow in the channel);
5. Reduced rates of bed-sediment transport; and
6. Altered size and shape of bed forms (notably dunes).

The effects are evident in the comparison of Figs. 13-8(a and b) and the ensuing explanation, which considers cover effects on flow distribution in fixed-bed channels. Section 13.6 discusses flow and sediment transport in ice-covered alluvial channels.

13.3.1 Ice-Cover Influence on Vertical Distribution of Flow (Fixed Bed)

The direct effect of imposing a level ice cover on a two-dimensional open-water flow is to increase the wetted perimeter of the flow substantially. For a wide channel, the wetted perimeter is almost twice that for the open channel flow. The usual consequence is increased water depth for constant discharge and bed slope, as indicated in Figs. 13-8(a and b). Because roughness characteristics of the ice-cover and the bed likely differ, the influence of the roughness of the bed and the ice-cover underside on velocity distribution and flow resistance must be taken into account. However, doing so accurately is not straightforward.

For the same uniform two-dimensional flows (one open-water, the other covered, as in Figs. 13-8(a and b)) having

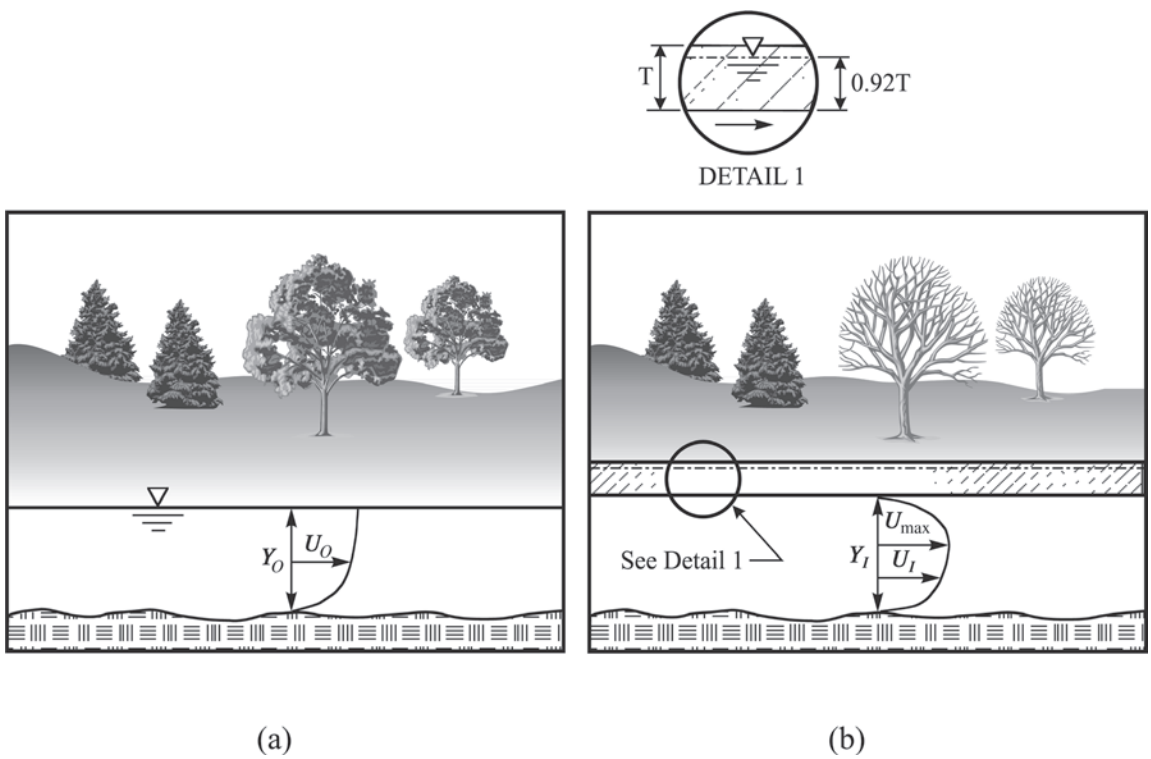

Fig. 13-8. Presence of a free-floating ice cover usually increases flow depth and redistributes flow.

the same unit discharge and energy slope, the ratio of flow depths is

$$\frac{Y_I}{Y_O} = \frac{U_O}{U_I} = \left(2\frac{f_I}{f_O}\right)^{1/3} \tag{13-1}$$

in which Y and U define the flow depth and the bulk velocity, respectively; f is the Darcy-Weisbach resistance factor; and subscripts O and I refer to open-water and ice-covered flows, respectively. Because the overall resistance coefficient for the ice-covered flow, f_I, exceeds 0.5-f_O (where f_O is the resistance coefficient for the same discharge during open-water flow), $Y_I > Y_O$. Typically, flow depth increases by about 10 to 30%; i.e., the covered flow is about 10 to 30% deeper than the open-water flow for the same discharge. Bulk velocity of flow decreases by the same amount. The actual piezometric water level in the channel would be about 0.92 times the ice-cover thickness, T, above the cover underside; the density ratio of solid ice and water is 0.92. The cover floats with a freeboard of about $0.08T$ above the water level. The freeboard can be suppressed or even slightly negative if there is a thick snow layer on top of the ice cover.

The resistance factor for covered flow, f_I, is a composite value expressing the total resistance exerted by the bed and the cover; i.e., for two-dimensional flow,

$$\mathrm{f_I} = \frac{4\tau_{\mathrm{tot}}}{\rho \mathrm{U_I^2}} = \frac{4\left(\tau_b + \tau_i\right)}{\rho \mathrm{U_I^2}} \tag{13-2}$$

in which

τ_{tot} = combined flow resistance exerted by the bed and the ice cover;
ρ = water density;

and subscripts b and i refer to the channel bed and ice-cover underside, respectively. Equation (13-2) implies that a change in resistance at one surface will alter U_I and thereby alter the flow resistance exerted by the opposite surface.

The customary practice (e.g., Michel 1978; Ashton 1986; Beltaos 1995) is to calculate flow resistance in ice-covered channels using what is termed the two-layer hypothesis, whereby flow resistance is taken to be a linear composite of flow resistance attributed to flow drag along the bed and ice-cover underside. In accordance with this hypothesis, each resistance coefficient or drag contribution is assessed independent of the other. The resistance coefficients are related to boundary roughness (bed or ice underside) normalized with the part of the total flow depth extending from the pertinent boundary to the elevation of the velocity maximum. This approach entails use of the Sabaneev equation, a semiempirical approximation proposed by A. A. Sabaneev (Nezhikovskiy 1964),

$$n_I = n_b\left[\frac{1 + \left(n_i/n_b\right)^{3/2}}{2}\right]^{2/3} \tag{13-3}$$

in which

n_b and n_i = values of Manning's resistance coefficient associated with the bed and the ice cover, respectively; and
$n = R^{1/6} f^{0.5}/(8g)^{0.5}$, with
R = hydraulic radius.

The two-layer hypothesis is inadequate for estimating bedform geometry, flow resistance, rates of sediment transport, and dispersion processes. Significant physical inaccuracies arise in partitioning covered flow in accordance with the two-layer hypothesis and applying Manning's equation to estimate flow resistance for each part. Flow resistances, both at the bed and at the ice cover, directly alter distribution of flow velocity. They affect the length scales and intensities of turbulence across the full depth of flow. Flow resistance is not simply the sum of flow drag determined from linear variation for each boundary, independent of the other boundary. In effect, there occurs an interactive "cross-torque" between the ice cover and the bed.

Even when the two roughnesses are identical, strictly speaking it is not physically meaningful to partition the flow at the plane of maximum velocity. Though, in this case, the plane may coincide with the plane of zero shear stress and mid-depth, the upper limit of the turbulence structures in the flow scales with the full flow depth, and turbulence diffuses and interacts across the flow. Differences in ice-cover and bed roughnesses offset the elevations of maximum velocity and zero shear stress. The offset increases when the roughness of one boundary is markedly greater than that of the other boundary.

The wind tunnel experiments carried out by Hanjalic and Launder (1971) and Reynolds (1974), for flow through a duct with top and bottom boundaries of differing roughness, and the flume experiments conducted by Gogus and Tatinclaux (1981) and Muste et al. (2000) are worth mentioning. These studies found, as expected, that the difference in top and bottom roughness shifted the position of the maximum streamwise velocity toward the roughest surface. In addition, the central region of the flow is characterized by strong diffusion of turbulent shear stress and kinetic energy from the rougher wall to the smoother one. The result is an appreciable offset of the plane of maximum velocity and zero-shear-stress plane. For a fully developed asymmetric flow, the noncoincidence of the surfaces of zero shear stress and mean velocity caused the production of turbulent kinetic energy to be negative over the central portion of the flow. In other words, a loss of turbulence energy occurs locally that affects velocity distribution over this portion. This loss of turbulence energy in the region where the smoother- and rougher-wall turbulence structures mix is attributable to the net interaction of Reynolds stresses of opposing sign.

Several recent studies report data on turbulence quantities for flow in ice-covered channels. One study (Muste et al. 2000), conducted with simulated free-floating ice cover

and constant discharge in a laboratory flume, shows that cover presence decreases Reynolds stresses in the near-bed region and that rougher covers further decrease Reynolds stresses in the near-bed region. Turbulence was measured using laser-Doppler velocimetry. For a free-floating cover, such reductions in Reynolds stresses follow from overall reductions in bulk velocity of flow. Cover presence, however, did increase Reynolds stresses near the top of the flow. Martin and Roy (1999) report field measurements of turbulence for the Sainte-Anne River, Quebec. Their measurements, taken using an electromagnetic velocity meter, indicate that a damping of larger-scale turbulence structures occurs. Sukhodolov et al. (1999) used an acoustic-Doppler velocimeter to investigate turbulence structures in an ice-covered sand-bed reach of the River Spree, Germany. They found that the spatial scale of turbulence ejections emanating from bed forms was as large as flow depth, whereas sweeps scaled at about 0.7–0.8 flow depth.

13.3.2 Ice-Cover Influence on Lateral Distribution of Flow (Fixed Bed)

An ice cover imposes an additional flow-retarding boundary that decreases the flow-conveyance capacity of a channel and redistributes flow vertically and laterally. Vertical redistribution of flow is marked by flow depth increase (usually) and by null flow velocity at the cover underside. Lateral redistribution of flow, though, depends on how the ice cover forms, is attached to the channel banks, and thickens. It can be explained using the Darcy-Weisbach flow-resistance equation, written here for open-water flow in a channel of uniform depth,

$$Q_O = Y_O B\left(8gR_O S_O / f_O\right)^{1/2} = K_O S_O^{1/2} \qquad (13\text{-}4)$$

in which

Q_O = flow rate;
B = flow width; and
K_O = unit conveyance.

Cover presence may laterally redistribute or concentrate flow in accordance with lateral variations in flow depth and/or ice-cover thickness. This impact can be illustrated in simple terms using an idealized channel comprising two bottom elevations of equal width, as in Figs. 13-9(a–d). Flow in such a channel may be described approximately in terms of two conveyance components, K_{O1} and K_{O2}, one component (1, 2) associated with each bottom elevation.

For constant flow, a free-floating, uniformly thick ice cover reduces the relative magnitudes of the two conveyance components. It smears flow over the full channel width, as $K_{I1}/K_{I2} < K_{O1}/K_{O2}$ (Fig. 13-9(b)). However, if the ice cover were fixed to the channel banks and thickened, the reverse

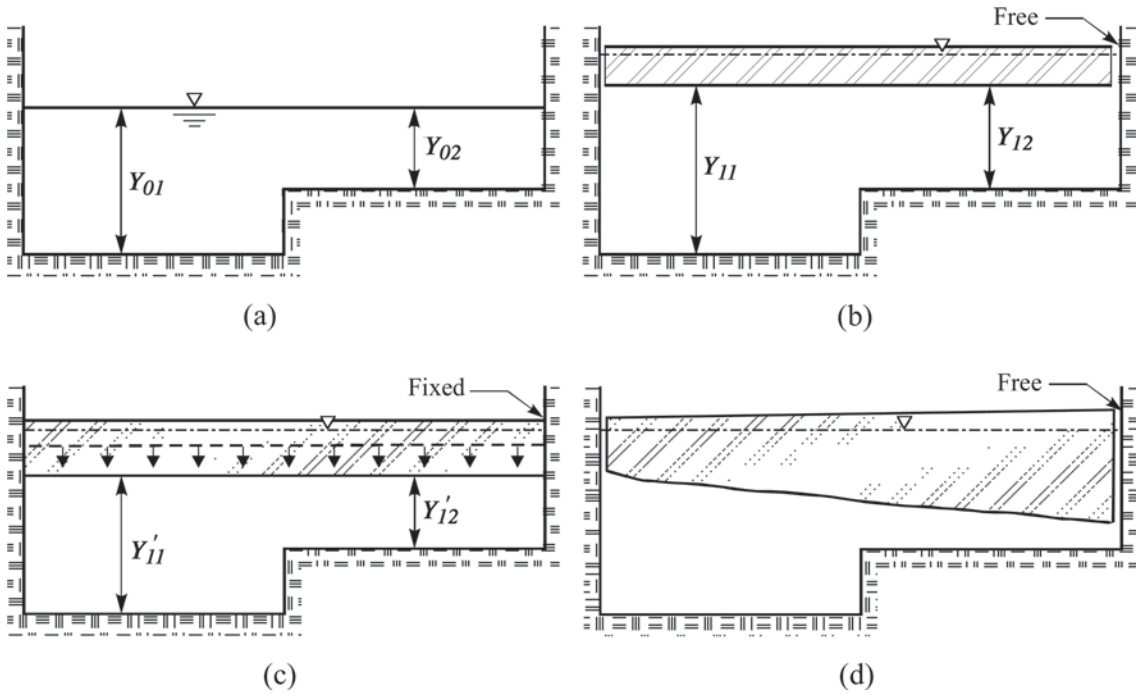

Fig. 13-9. An ice cover may reduce open-water proportions (a) of flow conveyance in lateral segments of a two-part compound channel if the cover is level and free floating (b); increase them if the cover is fixed and thickens (c); or, increase them if the cover is not uniformly thick (d).

would occur: $K_{I1}/K_{I2} > K_{O1}/K_{O2}$ (Fig. 13-9(c)), because flow depth decreases more in the shallower portion. Under this condition, cover squeezes or concentrates flow along a thalweg, where flow is deeper. If the thalweg lies close to one side of a channel (e.g., near the outer bank of a bend), such a concentration of flow may promote thalweg shifting and deepening. On the other hand, if the thalweg is located more or less centrally in a channel, a fixed cover may deepen or entrench the thalweg. An important further point is that the cover, by reducing flow through the shallow portion, may trigger further reductions in conveyance through the shallower portion by promoting ice accumulation (frazil slush or pans) and/or bed-sediment deposition there. Additional flow concentration is possible if the cover is not uniformly thick (Fig. 13-9(d)), if ice is grounded on the channel bed, or if shorefast/accumulated ice develops from one or both banks.

Lateral variations in cover thickness, however, may further concentrate flow in a channel of nonuniform depth and may override the more subtle effects described for a level ice cover. Significant lateral and streamwise variations in cover thickness may occur in channels with significant variations in flow depth and velocity. Because flow velocities decrease with decreasing flow depth, velocities usually are lower in regions of shallower flows and often in the wake of flow obstructions, such as bars. Ice covers whose formation involved substantial amounts of frazil-ice slush may become thicker in regions of shallower flow. Lower values of flow conveyance in those regions also result in relatively faster bankfast-ice formation. Also, because flow velocities are lower, ice (frazil slush and ice pieces) is less readily conveyed through those regions and is prone to accumulate. Figure 13-10 illustrates the accumulation of ice at a cross-section of the Tanana River, Alaska, at two times during winter (Lawson et al. 1986). That river is comparable to the lower Missouri River in flow rates, but is of steeper slope and more braided in channel morphology, and its flow is not regulated.

Further concentration of flow is possible if an ice cover is not free to float upward with increasing flow rate. Hydraulic analyses usually assume (e.g., Michel 1978; Ashton 1986;

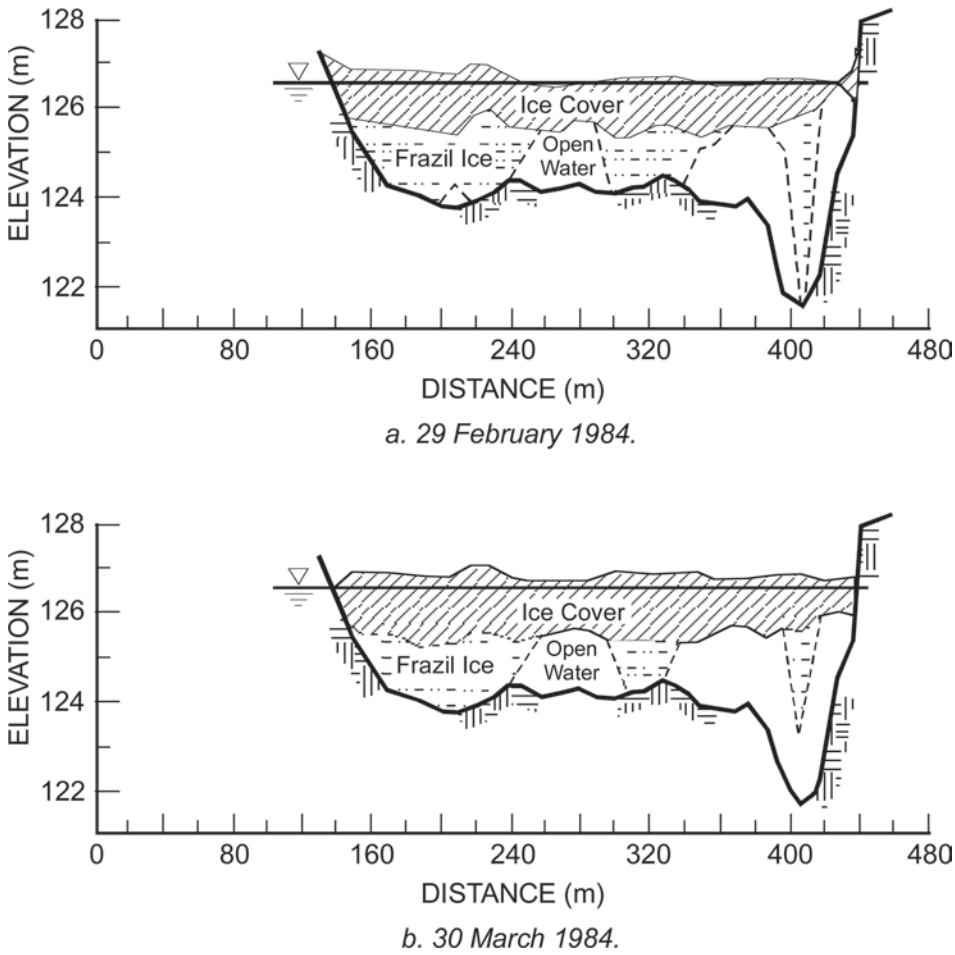

Fig. 13-10. Nonuniform ice accumulation across a section of the Tanana River, Alaska (Lawson et al. 1986).

Beltaos 1995) that ice covers are free-floating; i.e., streamwise cracks separate the floating ice cover from adjoining bank-fast ice. Actually, a cover may not always be free-floating. A stationary cover exposed to very frigid air may fuse to the channel banks. The cover then becomes constrained from freely floating up or down with changes in the flow, at least initially. Therefore, increasing flow discharge is forced partially beneath the ice cover, initially increasing flow velocities before flow erodes the bed beneath the cover. The extent to which a flow may be pressurized beneath a cover apparently has not yet been measured (the usual assumption is that covers are free-floating). An estimate would suggest that the pressure-head increase above the hydrostatic would be approximately equal to the ice thickness, the increment in water depth retained by the upstream end of the cover. Therefore, the thicker the cover the greater the pressurization possible. Eventually, the pressure would force the cover to bow upward. Also, as flow rises at the upstream end of the cover, some of it will pass over the cover. As the flow increases further, the upward pressure causes the cover to develop longitudinal cracks parallel to the banks and to float freely on the water surface. It is conjectured (e.g., Beltaos 1990) that pressure-flow conditions can only exist for a brief time, because small increases in flow suffice to cause longitudinal cracking of ice covers of thickness about 0.3 m or less; pressure flows may be more common under very thick covers. Some evidence (Zabilansky et al. 2000) suggests that scour of the channel bed may relieve the pressurized flow in alluvial channels. Very little information exists on this flow condition, especially with regard to how it may locally affect the channel bed and banks.

13.3.3 Ice-Cover Influence on Secondary Currents

For constant discharge, a free-floating level ice cover reduces bulk flow velocity and alters the vertical distribution of streamwise flow. In doing so, it usually dampens secondary currents.

For instance, it reduces the centrifugal acceleration exerted on flow around a river bend; though only one study has investigated this effect (Tsai and Ettema 1994). That study found that cover presence alters patterns of lateral flow distribution in a channel bend. The two sketches in Figs. 13-11 (a and b) show the main alteration, which is a splitting of the large secondary-flow spiral into two weaker spirals; owing to centrifugal acceleration acting on moving water, a large secondary-flow spiral is typical of many curved channels. The presence of a level ice cover reduces radial components of velocity and lateral bed slope in channel bends, causing the bed level to rise near the outer bank. Tsai and Ettema found a reduction in lateral bed slope of about 10%. This ice-cover effect would tend to retard bank erosion in channel bends, because it may result in reduced flow velocities near the outer bank of a bend. In other words, this effect of cover presence may dampen streamwise oscillations in bed elevation and oscillations in channel position. The dampening effect that an ice cover is calculated to have on the angle of transverse slope of the bed around a 180 bend is evident in Fig. 13-12, taken from Tsai and Ettema (1994).

13.4 ICE-COVER BREAKUP

Ice-cover breakup and clearance from a river typically coincide with substantial increases in water-flow rates in the river. Not coincidentally, these events also are periods of substantial sediment movement in alluvial rivers. For many rivers in cold regions (notably those in permafrost), breakup flows are considered to be the dominant channel-forming flows. The processes attendant to breakup and jamming are reasonably well understood; not so the impacts of breakup and jamming on channel erosion and sediment transport.

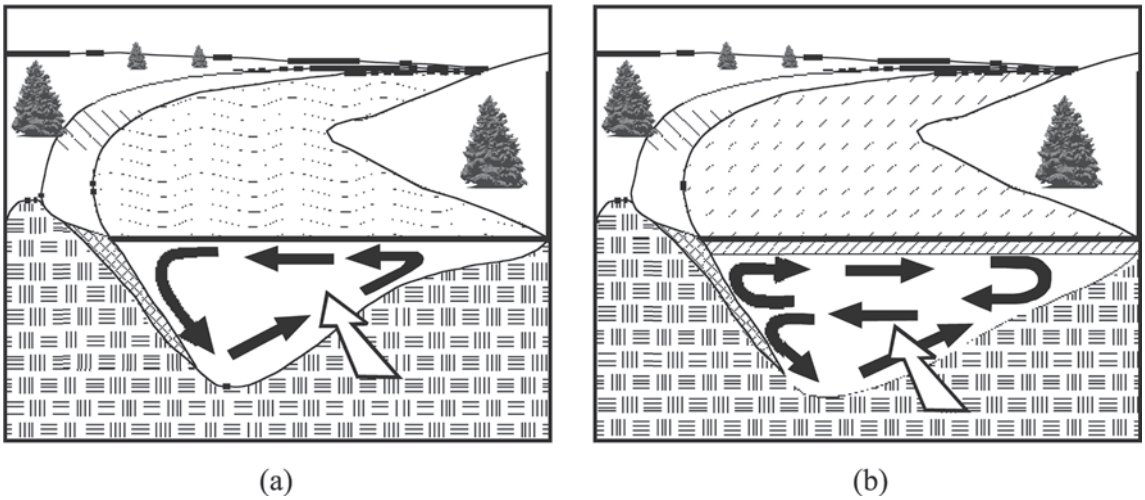

Fig. 13-11. Ice-cover effects on secondary currents in a channel bend (a) open-water flow; (b) ice-covered flow.

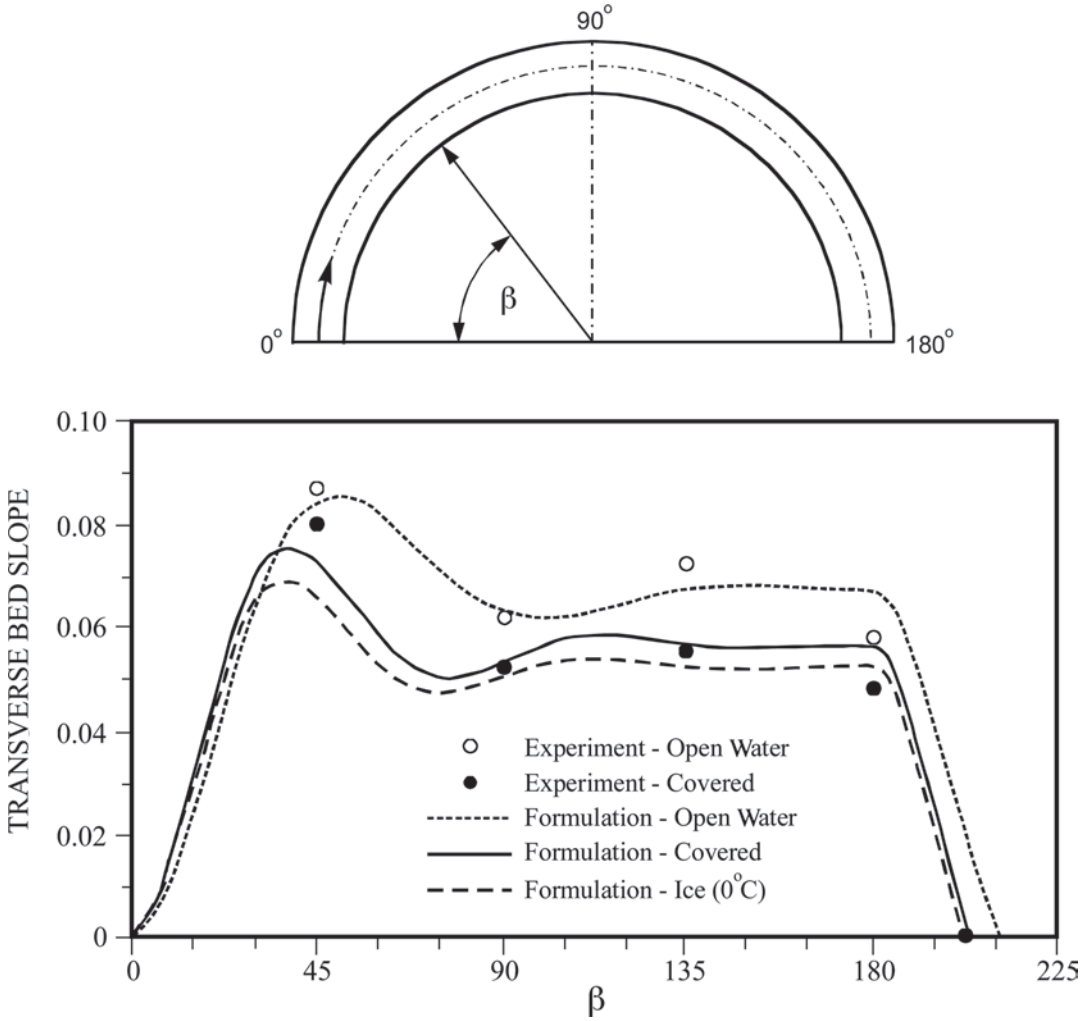

Fig. 13-12. Ice-cover effects on transverse bed slope around an alluvial-channel bend (Tsai and Ettema 1994). The effects, determined from a flume experiment and a numerical simulation, show that cover presence reduces transverse slope.

With the onset of warmer weather, ice-cover strength and thickness decrease. Ice strength usually decreases more significantly than ice thickness (Ashton 1986). In most situations, an ice cover may "rot" or "candle," becoming porous and greatly weakened before thinning. Also, with the onset of warmer weather, flow increases as snow melts, possibly accompanied by rain. Increased flow rate and depth increase the hydraulic load exerted against an ice cover, raising uplift pressure and drag, which results in hinge cracks and transverse cracks, respectively. Additionally, increased water elevation creates more surface area for ice to move.

The breakup of a river ice cover may be considered as occurring in three phases. Not all of them may occur. The phases are the prebreakup weakening of the cover, the breakup and ice run, and the breakup jam. For most river reaches, an ice cover weakens, disintegrates or breaks up, and then its fragments drift downstream. In some rivers, ice-cover breakup is followed by the development of *breakup ice jams*. For one of several reasons, certain reaches in those rivers have insufficient capacity to convey the broken ice.

The prebreakup begins with the start of runoff from the watershed when solar radiation begins to melt the snow cover, even before the average daily air temperature exceeds 0 C. The discharge in the river begins to increase, exerting an uplift pressure on the ice cover, possibly with water flowing over the cover as well as under it. With increasing discharge, the ice cover fractures in several places. For a long reach with low velocities, the break usually occurs first along the banks. The central part of the cover floats freely, but the border ice may be flooded. In areas of high flow velocity, water may rise and flow over the cover through numerous uplift fractures. Several pieces of ice may detach and begin to move downstream on the ice cover. As the discharge increases and

is accompanied by daily fluctuations (responding to daytime variations in air temperature and solar radiation), ice pieces detach themselves at regions of highest flow velocity and accumulate at the front of regions of the stronger ice cover over the low-velocity reaches.

The occurrence of an *ice run* depends on a combination of flow conditions and ice-cover strength. In this regard, the direction of flow can be important. Rivers flowing into warmer regions usually begin cover breakup at the downstream end of the ice cover. The cover then progressively breaks up in an upstream direction, with the ice moving downstream in an orderly manner, provided it does not develop a jam at some congestion location. Rivers flowing into colder regions (e.g., rivers flowing north, in the Northern hemisphere) usually begin breakup near the upstream end. Breakup may also begin for river reaches for which the inflow hydrograph includes a higher peak flow rate than the outflow hydrograph, owing to flow-resistance attenuation of the hydrograph.

13.4.1 Breakup Ice Jams

It is not uncommon for ice to clear a river by means of a series of breakup jams. An initial jam forms from ice first broken over a reach upstream. Increased flow and warming cause the jam to be released, and then to be dislodged and break more ice, forming new jams downstream. Eventually, by means of this stop-go process, the flow shunts ice from the river. In the continental United States, breakup jams may occur at any time once an ice cover has formed on a river. Though spring is the usual time for breakup to occur, mid-winter thaws may cause a river to experience a series of freeze-up and break-up events. At latitudes higher than those of the continental United States, breakup jams usually occur with the onset of spring.

Many aspects of breakup-jam formation and release remain inadequately understood. An inherent difficulty with ice jams is that they radically alter the stage-discharge relationship for a river reach; a moderate flow rate in a jam-covered channel usually produces a flow stage much higher that produced by the same flow under open-water conditions. Jam formation and release may occur in fairly gentle or gradual manners. They also may occur rapidly, especially if they involve a steep hydrograph of flow or a surge. Abrupt jam release creates a surge similar to that obtained with dam-break flow; surges and ice runs have been clocked at speeds in excess of 5 m/s (Beltaos 1995).

The net effects (detrimental and beneficial) of ice-jams on channel morphology and river ecosystems have not been extensively investigated and therefore are not well understood. Of particular and common concern is the formation of ice jams at bridges, such as that shown in Fig. 13-13. Ice jams lodged against bridges not only impose substantial lateral and uplift forces on bridges, but also may aggravate constriction scour of the channel bed at the bridge site.

Fig. 13-13. Ice jam at a bridge across the Iowa River, Iowa.

13.5 SEDIMENT TRANSPORT BY ICE

Sediment-laden ice slush and clumps of ice-bonded sediment may appear during the early stages of ice formation in certain rivers and or streams subject to the winter cycle of ice formation. The ice slush and clumps comprise a mix of frazil ice and anchor ice that once was briefly bonded to the beds of such rivers and streams. The amounts of sediment entrained or rafted with the ice slush and clumps can produce a substantial momentary surge in the overall quantity of sediment moved by some rivers and streams, though at present there are no reliable measurements or estimates of ice-rafted sediment-transport rates. Much of the entrained sediment becomes included in an ice cover, where it remains stored until the cover breaks up. Though ice-rafting of sediment is known to occur (observations are reported by, for example, Barnes 1928; Wigle 1970; Michel 1972; Benson and Osterkamp 1974; Kempema et al. 1993), the implications of its occurrence largely remain unknown.

The short treatment given in this section limits itself to ice transport of sediment in rivers and streams. Shallow coastal (marine and lacustrine) waters in cold regions also are prone to bed-sediment entrainment and ice-rafting by frazil and anchor ice. Barnes et al. (1982), Osterkamp and Gosink (1983), Reimnitz and Kempema (1987), Kempema et al. (1993), Barnes et al. (1994), and Kempema (1993) describe coastal locations where ice entrains significant quantities of sediment. Storms in frigid weather conditions agitate coastal waters and can produce large quantities of frazil ice. The mechanisms whereby anchor ice forms in coastal waters include the same elements that cause anchor ice to form in rivers and streams. The formation mechanisms for coastal anchor ice are complicated, however, by the more complex flow conditions of coastal waters and by salinity considerations in marine systems. Ice can significantly affect sediment erosion and deposition in estuaries and tidal reaches of rivers. Desplanques and Bray (1986)

and Morse et al. (1999) describe the influence of ice accumulation in estuaries of the northeast portion of the Bay of Fundy. The accumulations form as ice walls from stranded ice and included sediment. The ice walls confine flow and can accentuate localized channel scour. Of particular concern in this regard is scour near hydraulic structures such as bridge piers and abutments.

The mechanisms whereby ice entrains and transports sediment are not well understood. Also, the distances over which ice-rafted sediment typically may be transported are not really known. To date the only detailed laboratory investigations of the entrainment mechanisms are the studies reported by Kempema et al. (1986; 1993). A handful of experiments on anchor ice formation have been conducted, though (e.g., Tsang 1982; Kerr et al. 1998). The experiments and field observations indicate that the following two mechanisms contribute to anchor ice formation:

1. The prime mechanism is frazil ice adhesion to bed sediment. Large-scale turbulence in comparatively shallow, swift-flowing rivers and streams can mix suspended ice crystals and flocs of active frazil ice across the full depth of flow, as sketched in Fig. 13-14. When the flow is supercooled, the frazil ice may adhere to bed sediment or individual boulders and accumulate as a porous and spongy mass (Wigle 1970; Arden and Wigle 1972; Tsang 1982; Beltaos 1995). Rapids and riffles are common locations for anchor ice formation (Marcotte 1984; Terada et al. 1997). Altberg (1936) reports the occurrence of anchor ice in river flows as deep as 20 m. The foregoing references report rapid rates of anchor ice growth, such that large volumes of anchor ice form in a short period.
2. A much less significant mechanism for sediment transport is direct ice growth on the bed or on objects protruding from the bed. Together with frazil ice, supercooled water can be mixed across the flow depth. The downdraft of supercooled water chills objects in the flow (e.g., boulders and debris of various types) and enables ice to nucleate and form directly on those objects. The resultant ice crystals are relatively small and develop a fairly smooth and dense ice mass (e.g., Ashton 1986; Kerr et al. 1998).

The diurnal formation of frazil and anchor ice (as mentioned in Section 13.2) may result in repeated ice-rafting events along a river reach, each event potentially entraining substantial quantities of bed sediment. Under conditions of sufficiently frigid weather and substantial flow turbulence, extensive areas of a river's bed can become blanketed by anchor ice. Arden and Wigle (1972), for instance, describe anchor-ice formation along a several-mile reach of the Upper Niagara River, New York; the anchor ice attains sufficient bulk during a single night so that it reduces inflow into the river from Lake Erie by 20 to 30%. Usually, once the surface of a river reach is ice-covered and its water prevented from supercooling, anchor-ice formation and consequent ice rafting cease.

Because the larger sizes of sediment on a river bed protrude more into the flow, they usually are more affected by the thermal condition of the flow than by that of the bed on which they rest. Significant heat flux can occur from a sub-bed zone that is at 1 to 2°C and supercooled flow (typical supercooling is about -0.01 to -0.1 C) essentially over the full flow depth of a river or stream. Consequently, larger amounts of anchor ice typically form on coarser bed sediment. Several factors militate against extensive anchor ice formation on

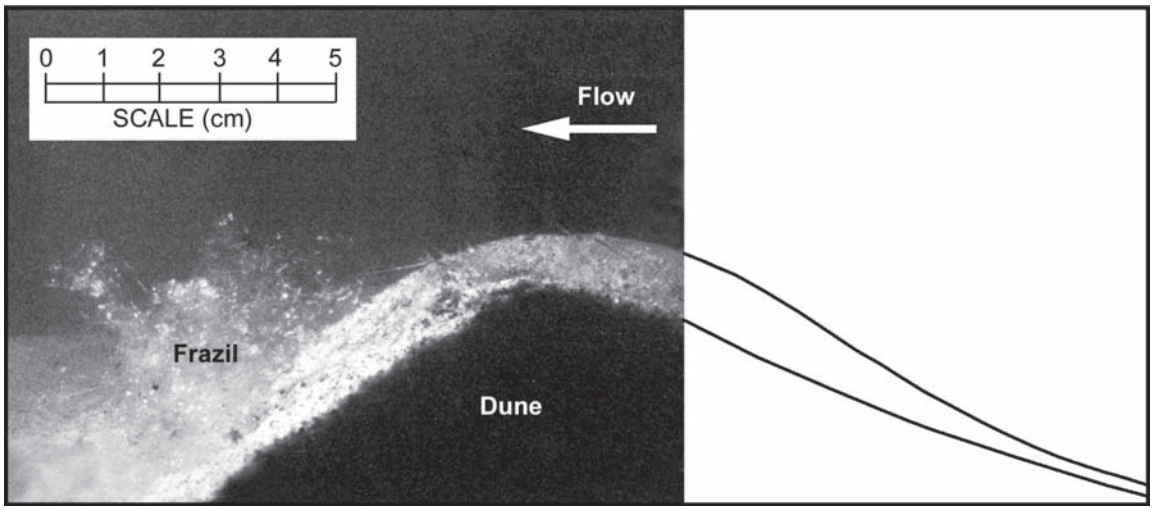

Fig. 13-14. Frazil ice accumulated in the lee of a dune, which migrates and envelops the frazil ice, eventually forming an ice-bonded clump of sand. This photo was taken from a flume experiment described by Kempema et al. (1993). (Photo taken by Ed Kempema, University of Wyoming.)

river beds of fine noncohesive sediment. In particular, such sediments are readily lifted and therefore cannot hold a significant anchor ice accumulation (Arden and Wigle 1972; Marcotte 1984).

The laboratory studies conducted by Kempema and his coworkers provide interesting insights into aspects of anchor-ice formation in the presence of bed forms. Their experiments, which were conducted with a racetrack-shaped flume fitted with sand beds in a ripple regime, show how frazil flocs become sediment-laden and lose their buoyancy as they tumble along the flume's sand bed and eventually become included within an ice-sand clump of anchor ice. As the negatively buoyant flocs of frazil and sediment accumulate in the trough of ripples (as illustrated in Fig. 13-15), they become infiltrated by sand, buried, and compressed. The resulting clumps of bonded ice and sediment may then enlarge as additional frazil flocs fuse to them, or as the clumps grow further amid supercooled water.

Eventually, a clump of anchor ice accumulation may attain sufficient buoyancy to lift sediment from the bed. The resulting concentrations of suspended sediment that the ice conveys can get quite high. Kempema et al. (1986) calculate that a neutrally buoyant clump of ice-bonded sediment may contain up to 122 grams of sediment per liter of ice and sediment. Kempema (1998) measured sediment concentrations in released anchor ice masses in southern Lake Michigan of 1.2 to 102 g/L, with an average concentration of about 26 g/L.

Accumulations of anchor ice also move gravel and cobbles. Martin (1981) mentions an instance where anchor ice entrained and moved boulders up to 30 kg in weight. Such ice rafting can move cobbles and boulders through long reaches of relatively sluggish flow deep pools in rivers.

Kempema et al. (1993) report that interactions of suspended sediment and frazil ice in the water column may directly result in the inclusion of suspended sediment in ice slush. The exact nature of the interactions and the likelihood of their occurrence, require further examination. Nonetheless, Barnes (1928) and Altberg (1936) mention an intriguing observation that frazil-ice formation appears to remove suspended sediment from a flow; after a frazil-ice event, water seems clearer. When frazil and anchor ice form, it is possible that they may diminish bed-sediment entrainment and transport. Initially, accumulating frazil and anchor ice would bind bed sediment, thereby retarding entrainment. Also, by virtue of the ice concentrations involved, frazil ice may dampen flow turbulence, a key factor in suspended-sediment transport. Once anchor ice lifts from a bed, however, it would entrain and convey sediment, although that sediment may become frozen and temporarily stored in a floating ice cover.

13. 6 ICE-COVER EFFECTS ON SEDIMENT TRANSPORT BY FLOW

The extent to which sediment transport by flow responds to ice-cover formation and presence has yet to be fully determined. Some responses are reasonably well understood, some barely recognized; few have been investigated

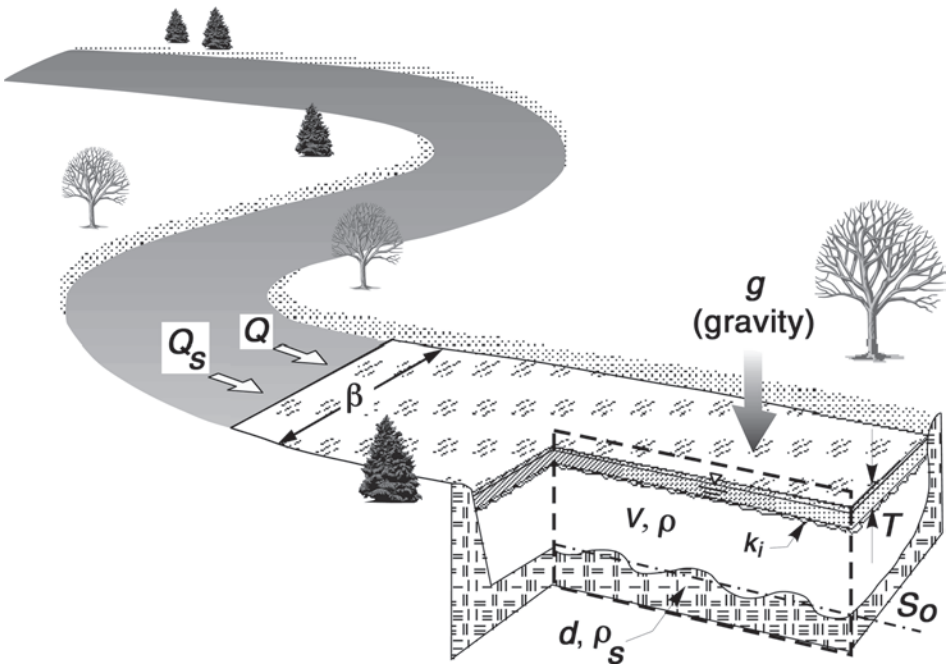

Fig. 13-15. Independent variables usually associated with flow in a loose-bed channel indicated here for an ice-covered reach.

rigorously. The interactions affect the full gamut of relationships between flow discharge and stage, macroturbulence structures, sediment-transport and mixing processes, and channel stability. This section discusses the interactions and raises practical issues stemming from them.

An essential feature of alluvial channels is that their morphology and flow-resistance characteristics alter in response to changing flow and sediment conditions. Simply put, flow and bed interact. During frigid winters, river ice modifies the interaction, over a range of scales in space and time.

The literature on river-ice hydraulics currently contains little information about ice effects on loose-bed hydraulics. Virtually all analyses of ice-covered flows (whether the ice cover is sheet ice or jammed ice) treat the bed as being fixed and thereby of constant hydraulic roughness. By the same token, the extensive literature on loose-bed hydraulics says little about flow resistance and sediment transport in alluvial channels when they are ice-covered.

13.6.1 Parameters

Dimensional analysis of variables associated with flow in a loose-bed channel (Fig. 13-15) provides a useful framework for discussing loose-bed issues in river-ice hydraulics. It quickly and formally identifies most of the interactions between cover, flow, and bed. Typically, a dependent quantity A of a channel may have the following functional dependence for flow in a reach that has a comparatively wide channel comprising a bed of uniform-diameter sediment under a uniformly thick ice cover:

$$A = f_A\left(Q, Q_S, \nu, \rho, \rho_s, d, g, S_0, B, T, k_i\right) \tag{13-5}$$

In Eq. (13.5),

Q_s = sediment discharge into reach;
ν = kinematic viscosity of water;
ρ = water density;
ρ_s = sediment density;
d = median size of bed particles;
g = gravity acceleration;
S_0 = channel slope;
B = reach width;
T = ice-cover thickness; and
k_i = hydraulic roughness of ice-cover underside.>

The dependent quantities of practical concern for the reach are flow depth, hydraulic radius, bulk velocity of flow, flow-energy gradient, sediment-transport capacity of the flow in the reach, and possibly thalweg alignment through the reach.

Though ice-cover properties T and k_i actually may also be dependent variables, especially for ice covers formed from accumulated drifting ice, here they are treated as independent variables. The variable k_i directly affects flow resistance, whereas cover thickness, T, affects flow insofar as it is of use in characterizing cover rigidity and elevation of hydraulic grade line. The present focus is on the ways in which existing ice cover modifies interactions between flow and bed. An interesting broader discussion would consider how flow and bed interaction influence cover formation. That discussion might include thermal variables, such as water temperature.

In terms of nondimensional parameters and, for convenience, considering unit discharges of water, q ($= Q/B$) and sediment q_S ($= Q_S/B$), Eq. (13-5) may be restated as

$$\Pi_A = \varphi_A\left(\frac{q}{\nu}, \frac{q_s}{\nu}, d\left(\frac{g\Delta\rho}{\rho\nu^2}\right)^{1/3}, \frac{\rho_s}{\rho}, S_0, \frac{d}{k_i}, \frac{T}{d}\right) \tag{13-6}$$

in which sediment diameter, d, is used as the scaling or normalizing length. Here, sediment discharge is total sediment discharge. Also, $\Delta\rho = \rho_S - \rho$.

The second and third parameters can be combined to express sediment transport more usefully nondimensionally as

$$\frac{q_s}{\nu}\left[d\left(\frac{g\Delta\rho}{\rho\nu^2}\right)^{1/3}\right]^{-3/2} = \frac{q_s}{\sqrt{g(\Delta\rho/\rho)d^3}} \tag{13-7}$$

For most situations, ρ_S/ρ is more or less constant (about 2.65). Thus Eq. (13-6) reduces to

$$\Pi_A = \varphi_A\left(\frac{q}{\nu}, \frac{q_s}{\sqrt{g\left(\Delta\rho/\rho\right)d^3}}, d\left(\frac{g\Delta\rho}{\rho\nu^2}\right)^{1/3}, S_0, \frac{d}{k_i}, \frac{T}{d}\right) \tag{13-8}$$

In Eqs. (13-6) and (13-8), for example, Froude number, $\mathsf{F} = (q/Y)/(gY)^{0.5}$ is a dependent parameter, because flow depth, Y, is a dependent variable.

For the case of a long, rigid, and uniformly thick, free-floating ice cover, the significance of T/d diminishes, and Eq. (13-8) simplifies to

$$\begin{aligned}\Pi_A &= \varphi_A\left(\frac{q}{\nu}, \frac{q_s}{\sqrt{g\left(\Delta\rho/\rho\right)d^3}}, d\left(\frac{g\Delta\rho}{\rho\nu^2}\right)^{1/3}, S_0, \frac{d}{k_i}\right) \\ &= \varphi_A\left(\mathsf{R}, \frac{q_s}{\sqrt{g\left(\Delta\rho/\rho\right)d^3}}, D_*, S_0, \frac{d}{k_i}\right)\end{aligned} \tag{13-9}$$

in which $D_* = d(g\Delta\rho/[\rho\nu^2])^{1/3}$, and $\mathsf{R} = q/\nu$.

Many relationships in alluvial-channel hydraulics are expressed in terms of particle Reynolds number, $\mathsf{R}_* = u_{*b}d/\nu$,

and Shields parameter, $\theta = \rho u_{*b}^2/(g\Delta\rho d)$; here, u_{*b} = shear velocity associated with bed component of velocity distribution. In this regard, using $D_* = (\mathsf{R}_*)^2/\theta$, Eq. (13-9) can be recast more usefully as

$$\Pi_A = \varphi_A\left(\mathsf{R}, \frac{q_s}{\sqrt{g(\Delta\rho/\rho)d^3}}, D_*, S_0, \frac{d}{k_i}\right) = \varphi'_A\left(\mathsf{R}, \frac{(\mathsf{R}_*)^2}{\theta}, \frac{d}{k_i}, \frac{q_s}{\sqrt{g(\Delta\rho/\rho)d^3}}, S_0\right) \quad (13\text{-}10)$$

Most equations for bed load transport relate transport rate empirically to flow intensity, θ, (e.g., ASCE 1975; Raudkivi 1998). As shown subsequently in this chapter, the combined parameter $\theta d/k_i$ is convenient for indicating how cover roughness moderates θ. To simplify the discussion, the inflow and outflow rates of sediment, q_S, are taken to be equal, thereby relaxing Eq. (13-10) to

$$\Pi_A = \varphi''_A\left(\mathsf{R}, \mathsf{R}_*, \eta\frac{d}{k_i}, S_0\right) \quad (13\text{-}11)$$

which also recasts θ as $\eta = \theta/\theta_c$, thereby expressing θ relative to a critical value, θ_c, for incipient sediment movement. Many relationships for Π_A are expressed in terms of η or excess flow intensity, $\eta - 1$ (ASCE 1975).

The ensuing discussion considers how the parameters in Eq. (13-11) influence flow and sediment movement. It begins with a brief review of the pertinent cold-water properties.

13.6.2 Water-Temperature Effects

Ice is attended by cold water, usually at or slightly above 0 C. Most empirical relationships for alluvial-channel hydraulics are based on data obtained with water in the range from 10 to 20 C. All but one of the independent parameters in Eq. (13-10) directly involve water properties: ν, ρ, and $\Delta\rho$. Reduced water temperature increases kinematic viscosity, ν (it increases 100%, when water cools from 25 to 0 C), and slightly changes ρ (it increases about 0.3%, when water cools from 25 to 0 C, but attains a maximum at 4 C). An increase in ν directly reduces R and R_* values, at constant q. In so doing, it increases flow drag on the bed, decreases particle fall velocity, and thereby increases flow capacity to convey suspended sediment overall. By and large, the effect of low water temperature can be taken into account using R, R_*, and θ (insofar as it scales particle size and fall velocity relative to bed shear velocity, u_{*b}). The quantitative impacts of increased fluid viscosity on macroturbulence are unclear as yet.

A fair number of studies have investigated water-temperature effects on sediment transport or sediment fall velocity. The studies confirm that sediment-transport rate increases with decreasing water temperature. Lane et al. (1949) and Colby and Scott (1965) show such a trend in field data taken from the Missouri, Colorado, and Middle Loup Rivers. Extensive flume experiments are reported by Ho (1939), Straub (1955), Colby and Scott (1965), Taylor and Vanoni (1972), and Hong et al. (1984). Taken together, the flume data confirm that sediment transport rates increase as water temperature decreases, the increases becoming substantial when water temperature drops below about 15 C. The flume data reported by Hong et al. (1984), for instance, show that the mean concentration of bed-sediment transport increased by factors of up to 7 and 10 for a water temperature drop from 30 to 0 C. The increase, obtained with $d = 0.11$ mm, is attributable to increased concentration of sediment transport in a bed layer (layer thickness taken as $d\eta^{0.5}$) and increased uniformity of concentration distribution over the flow depth. The latter effect is largely owing to the reduced fall velocity of suspended particles. Hong et al. (1984) concluded that temperature reduction significantly increases bed-level concentration of sediment movement only if bed-layer Reynolds number, R_B (defined by Hong et al. as $\{u_* d\eta^{0.5}\}/\nu$) exceeds about 20; $\mathsf{R}_B = \mathsf{R}(\eta)^{0.5}$.

Several studies have looked at water-temperature affects on particle fall velocity (e.g., Interagency Committee 1957). No study seems yet to have looked at the settling velocity of cohesive sediments, or cohesive-sediment behavior overall, at water temperatures close to 0 C. For example, Huang (1981) examined water-temperature effects on cohesive-sediment fall velocities for the range from 32 C down only to 6.1 C.

13.6.3 Sediment Movement and Bed Forms

The overall magnitude of the tractive force (drag and lift components) that flow exerts on bed particles, together with the impacts of flow turbulence on all its scales, prescribes bed sediment motion. Ice-cover presence influences water drag on the bed and turbulence generation by redistributing flow and reducing the rate of flow energy expenditure along the bed. In so doing, cover poses three practical issues in using Eq. (13-10).

The first issue concerns estimation of τ_b or u_{*b}, shear stress or velocity associated with the channel bed. These variables are considerably more difficult to estimate than for open-water loose-bed hydraulics. A second issue is that the dependent loose-bed parameters (Π_A) of practical importance for alluvial-bed flows typically are estimated using semiempirical relationships developed for open-water conditions. Simply stated, at issue is the applicability of open-water empirical relationships to ice-covered flow.

A third issue concerns the streamwise variation of the flow and sediment-transport capacity of an ice-covered channel. If the sediment-transport capacity of an ice-covered channel is less than the rate at which sediment load is supplied to the channel, the bed must locally aggrade. If the converse holds, the bed must degrade locally. The former condition usually prevails for free-floating cover, because bulk velocity of flow

decreases. The latter condition may occur when the cover is fixed and/or thick (large *T/d*), because the bulk velocity of flow under the cover increases. The various states of ice-cover condition complicate prediction of flow resistance and sediment transport in ice-covered alluvial channels.

The intrinsically complicated aspect of estimating flow resistance and sediment transport is that the single relevant length scale for ice-covered flow is the total flow depth, *Y*, which itself usually is a dependent variable. For open-water flow, flow drag on the bed can be characterized using R and D_*, because they are not explicitly dependent on flow depth and flow velocity, depending instead on *q* as well as water and particle properties.

Two practical concerns are whether river ice influences bed form geometry and, if so, whether its influence is describable using relationships developed for open-water flow. These issues have implications for estimation of flow resistance and mixing processes. Following from Eq. (13-10), bed form length, *L*, and steepness, δ, can be expressed functionally as

$$L_* = L/d = \varphi_{L_*}\left(\mathsf{R}, \mathsf{R}_*, \eta\frac{d}{k_i}, S_0\right) \qquad (13\text{-}12)$$

and

$$\delta = H/L = \varphi_{\delta}\left(\mathsf{R}, \mathsf{R}_*, \eta\frac{d}{k_i}, S_0\right) \qquad (13\text{-}13)$$

in which H = bed form height. Equations (13-12) and (13-13) indicate that ice-cover presence should influence bed form geometry. The practical concern is accurate estimation of η or u_{*b}. Figures 13-16 and 13-17 show that bed form geometry in ice-covered flow essentially conforms to the same relationships as prevail for open-water flow. Figure 13-17 shows additionally that an ice cover, by reducing excess flow intensity at the bed, $\eta-1$, reduces bed form steepness for the range of values indicated.

However, there is an important cover influence not immediately evident from Eqs. (13-12) and (13-13) and Figs. 13-16 and 13-17. The influence is not adequately described in terms of cover influence on η or u_{*b}. Bed forms generate macroscale turbulence, or coherent turbulence structures. Cover presence, by redistributing flow, influences the development of macroturbulence and its consequences for bed sediment suspension as well as other dispersive processes. Recent experiments by Ettema et al. (2000) suggest that smooth level cover may invigorate macroturbulence generation, mildly increasing the frequency of structures generated from bed forms and enabling them to penetrate the full depth of flow.

13.6.4 Flow Resistance

The issues concerning flow resistance hinge on the issues mentioned above for sediment entrainment, bed forms, and macroturbulence. They entail estimation of resistance coefficients, f_b, associated with the bed and the ice cover, and then estimation of flow depth, *Y*, given *q*. From Eq. (13-11),

$$Y/d = Y_* = \varphi_{Y_*}\left(\mathsf{R}, \mathsf{R}_*, \eta\frac{d}{k_i}, S_0\right) \qquad (13\text{-}14)$$

Eq. (13-14), however, is not immediately useful for predictive purposes, because open-water methods estimate *Y* as a composite of form-drag and skin-friction resistance components. It is more useful to use the Darcy-Weisbach relationship for flow in a wide channel with a free-floating ice cover written in terms of unit discharge, *q*,

$$Y_I = \left(\frac{f_I q^2}{4gS}\right)^{1/3} \qquad (13\text{-}15)$$

with flow hydraulic radius $R_I = Y/2$, $f_I = 0.5 f_b\left(1 + \frac{f_i}{f_b}\right)$, and $f_b = f_b' + f_b''$. The functional relationship for each of these component resistance coefficients can be adjusted in terms of parameters used by existing empirical, estimation relationships; e.g.,

1. for bed-surface resistance

$$f_b' = \varphi_{f_b'}\left(\mathsf{R}, D_*, S_0, \frac{d}{k_i}\right) \qquad (13\text{-}16a)$$

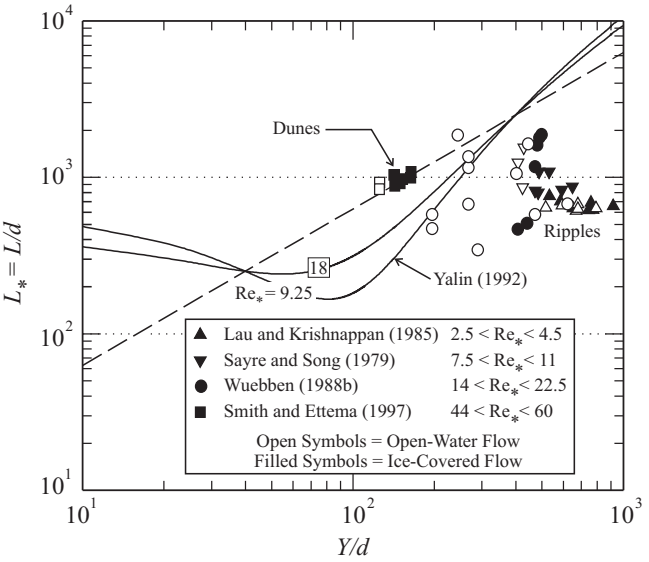

Fig. 13-16. Flume data on bedform length in ice-covered flow conform to empirical open-water curves developed by Yalin (1992).

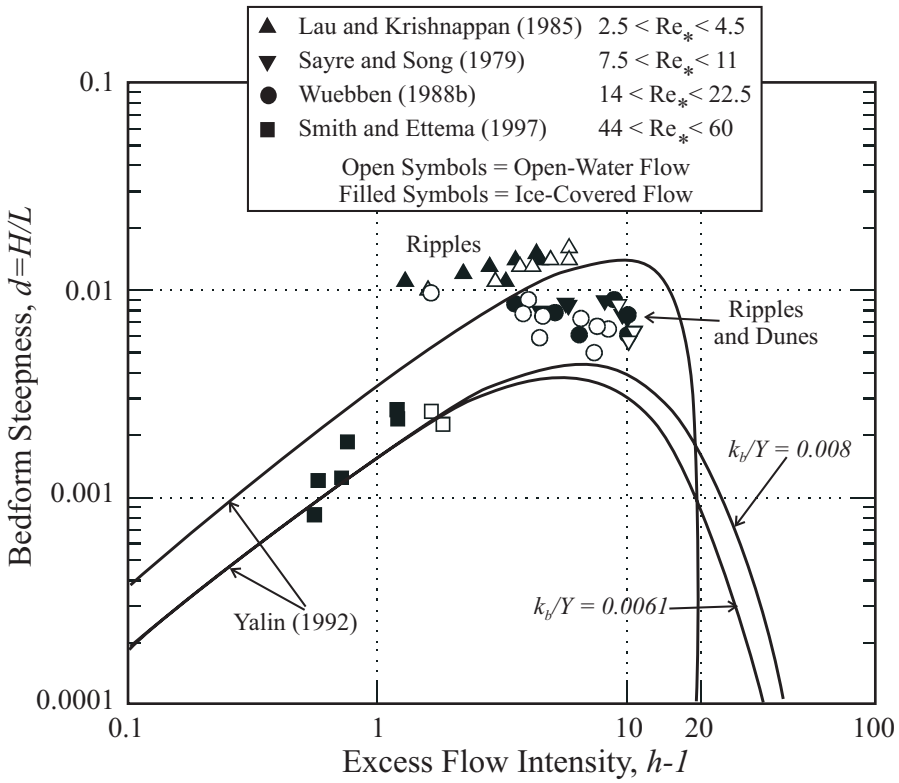

Fig. 13-17. Flume data on bedform heights in ice-covered flow conform to empirical open-water curves developed by Yalin (1992).

2. for form-drag resistance attributable to bed forms, such as dunes,

$$f_b'' = \varphi_{f_b''}\left(\mathsf{R}, D_*, S_0, \frac{d}{k_i}\right) = \varphi_{f_b''}\left(\mathsf{R}, D_*, f_b', \frac{d}{k_i}\right) \quad (13\text{-}16b)$$

3. and for the ratio

$$\begin{aligned} f_i/f_b &= \alpha = \varphi_\alpha\left(\mathsf{R}, D_*, S_0, \frac{d}{k_i}\right) \\ &= \varphi_\alpha'\left(\mathsf{R}, \mathsf{R}_{*b}, S_0, \eta\frac{d}{k_i}\right) \end{aligned} \quad (13\text{-}16c)$$

Again, an immediate practical issue implicit in Eqs. (13-16a–c) is that flow resistance in ice-covered alluvial channels can be estimated using open-water relationships, provided the influence of $\eta d/k_i$ in conjunction with the other parameters can be determined. If its influence can be determined, open-water relationships, such as those given by Einstein and Barbarossa (1952) and Engelund and Hansen (1967), can be used to predict bed resistance in ice-covered loose-bed flow. A semiempirical expression for Eq. (13-16c) is given in Fig. 13-18, which contains data from several flume studies.

Smith and Ettema (1997) developed a method, based on laboratory flume data, for estimating flow resistance in ice-covered alluvial channels. Their method is iterative and uses the following assumptions:

1. The mechanics of bed-form formation essentially is the same for open-water and ice-covered channels.
2. Methods for predicting bed-form drag in open-water flow (e.g., the Einstein-Barbarossa method or the Engelund method) can be used to predict bed form drag in ice-covered flow. This can be done by replacing the bulk drag term, $\rho g Y_1 S$, with an estimate of the actual bed shear stress in an ice-covered flow.
3. The ratio of boundary shear stresses along the bed to those along the cover underside is estimated as

$$\alpha = \tau_i/\tau_b = 0.84(\eta d/k_i)^{-0.20} \quad (13\text{-}17)$$

Equation (13-17) is an equation fitted to the flume data shown in Fig. 13-18. The limits of the equation have yet to be determined for values of η beyond those indicated in Fig. 13-18.

The proposed method requires the following input variables: cover roughness, k_i; median bed-sediment diameter, d; submerged specific gravity of bed sediment, $\Delta\rho/\rho$; unit discharge of water, q; channel slope, S_0; and, an initial guess at flow depth, Y_1 (say, $Y_1 \approx 1.2Y_O$). The procedure uses the Einstein-Barbarossa method for predicting bed form resistance and predicts values of flow depth, Y_1.

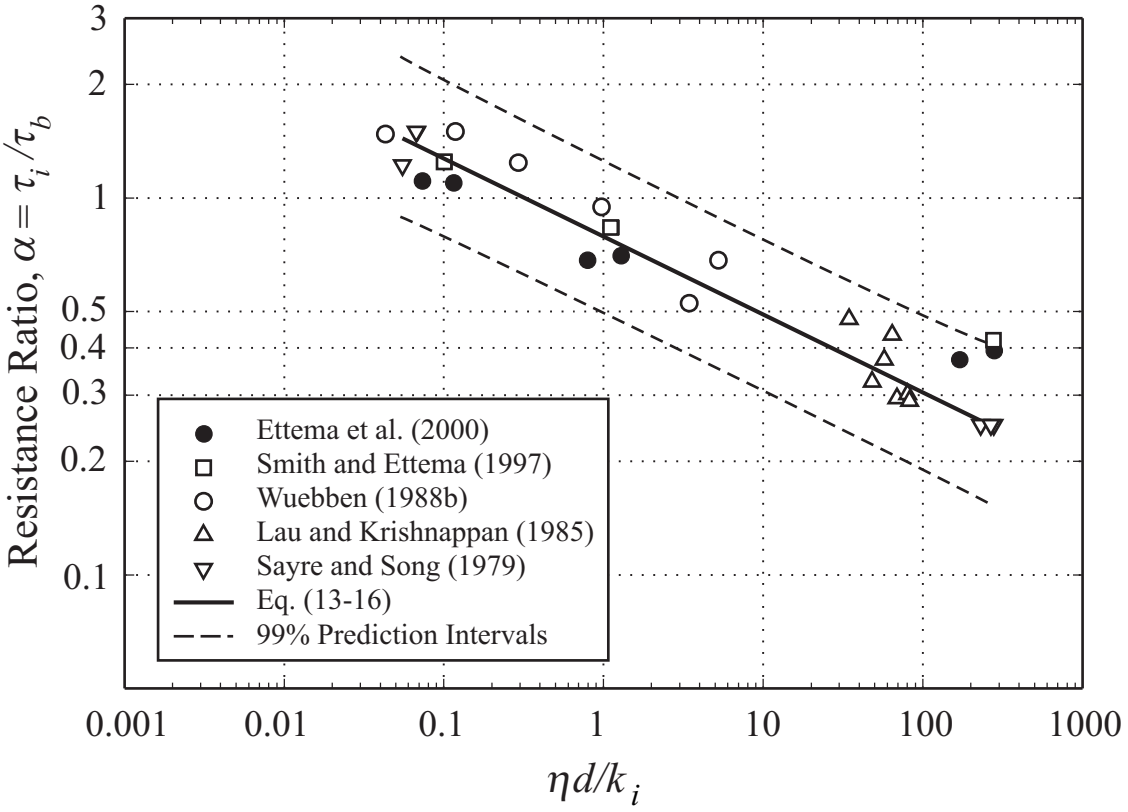

Fig. 13-18. Resistance ratio, α, for an ice-covered flow in an alluvial channel.

13.6.5 Bed-Sediment Transport

A basic issue concerns an imbalance between rate of bed-sediment supply to an ice-covered reach, q_s, and the sediment-transport capacity of that reach, q_{sI}. This issue involves the complex problem of spatially varied flow and sediment transport, with all its repercussions for local channel slope and morphology. The sediment-transport capacity of an ice-covered channel can be expressed functionally as

$$\frac{q_{SI}}{\sqrt{g\left(\Delta\rho/\rho\right)d^3}} = \varphi_{q_{SI}}\left(\mathsf{R}, \mathsf{R}_{*_b}, S_0, \eta\frac{d}{k_i}\right) \qquad (13\text{-}18)$$

This equation functionally characterizes bed-load and suspended-load portions of bed-sediment transport. A fundamental issue relates directly to estimation of η or R_{*_b}. However, cover influence on macroturbulence now becomes especially significant, because macroturbulence affects sediment entrainment and suspension.

13.6.5.1 Laboratory Data When examined in terms of η, or u_{*_b}, data on bed load capacity of ice-covered flow experiments concur well with the open-water trend shown in Fig. 13-19 for Meyer-Peter and Mueller's formulation (1948) and Einstein's method (1950). Essentially, if η can be estimated, bed-load transport in an ice-covered channel can be estimated using an open-water method, such as the two used in Fig. 13-19. The data in Fig. 13-19 encompass the dune-bed and ripple-dune regimes.

Estimation of suspended load in an ice-covered channel is not as straightforward as bed-load estimation. Suspended load depends not only on the bed shear stress, or u_{*_b}, but also on macroturbulence and flow distribution. As mentioned previously, cover presence likely significantly alters these. So far, there is no direct way to account for macroturbulence effects on suspended load.

By virtue of its reduction of bulk velocity of flow, U, and thereby τ_b and η, a free-floating ice cover typically reduces a channel's capacity to transport bed sediment. At certain zones within a channel, where the cover concentrates flow, sediment-transport rates may increase locally, however. Several laboratory studies have investigated cover-presence effects on sediment transport rate (Sayre and Song 1979; Wuebben 1986; Wuebben 1988b; Smith and Ettema 1995; Ettema et al. 2000). They all involved a free-floating cover that rises and subsides with changing flow rates. Their findings confirm that cover presence reduces rates of sediment transport. The rates decline rapidly with cover presence. Bed-load transport rate, for instance, can be almost halved

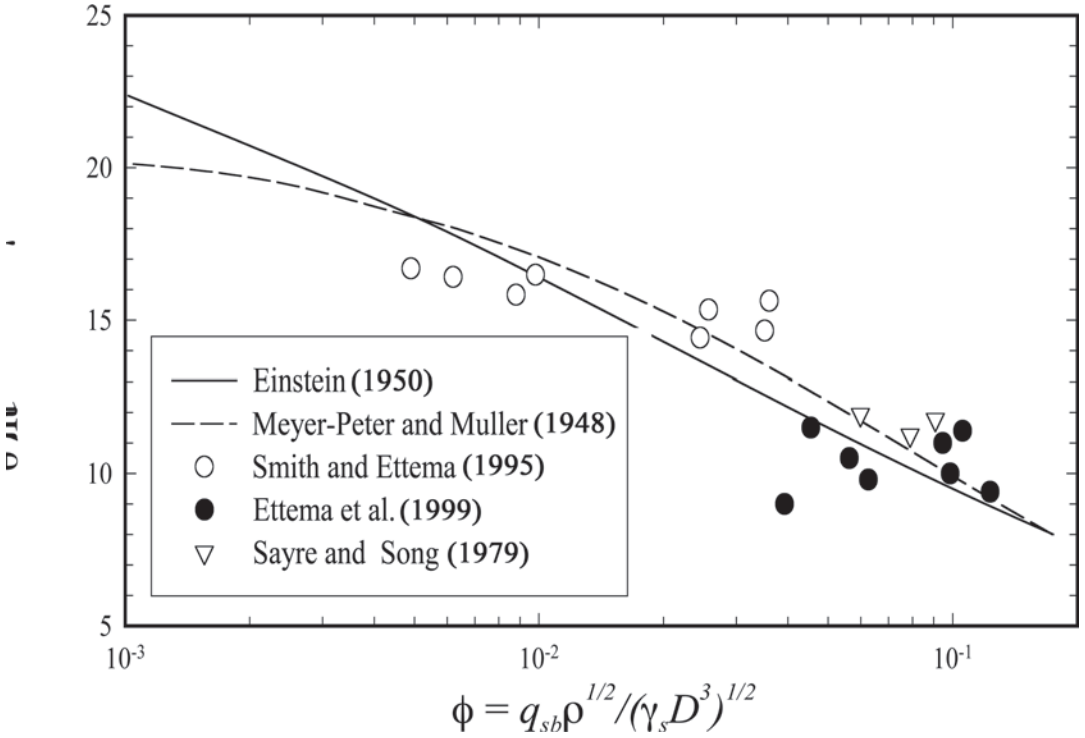

Fig. 13-19. Bedload data compared with curves generated using Einstein's procedure and the Meyer-Peter and Muller formula developed from open-water data. Covered-flow data conform to the same curves developed using open-water data.

by an ice cover that raises flow depth 15%, for a constant flow rate; this estimate assumes, reasonably, that bed-load transport rate $\propto \tau_b^2 \propto U^4$, with U decreasing by 15%; τ_b is shear stress acting on the bed and U is bulk velocity of flow (ice-covered or open water). An important point here is that sediment eroded under an ice cover may not be transported far from the erosion location.

13.6.5.2 Field Data on Bed-Sediment Load Few field studies have been conducted in which rates of sediment transport were measured for ice-covered channels. The studies indicate the inherent difficulty of obtaining such measurements and of interpreting them. Lawson et al. (1986) conducted an extensive study of flow and sediment movement at a reach of the Tanana River, Alaska. They obtained measurements of bed-load and suspended-load rates at one cross section. The rates were comparable in magnitude to rates measured during a survey conducted about a year earlier at two cross sections in close proximity to that used by Lawson et al. Burrows and Harrold (1983) describe the earlier survey. Together, these data sets indicate a great reduction in the ratio suspended load relative to the bed-load from summer to winter. The reduction is attributed tentatively to reduced flow of melt water from glaciers drained by the Tanana River. Laboratory data obtained by Lau and Krishnappan (1985) and Ettema et al. (2000) show the opposite result, which both studies attribute to cover underdamping of turbulence generated by flow over bed forms.

Alterations in flow distribution often complicate evaluation of ice-cover effects on transport rates for. This difficulty is evident in Fig. 13-2, which shows an ice cover over the Yellowstone River, near Fallon, Montana, and from figures such as Fig. 13-10, which shows nonuniform ice accumulation across the Tanana River. The series of shear lines evident in the ice cover on the Yellowstone River (Fig. 13-2) indicate that the flow area has successively narrowed. Flow-width alteration is more difficult to predict than flow depth change due to ice. The formation of subchannels within an ice-covered channel may accentuate narrowing of the flow area, especially if the channel is not prismatic. The subchannels form when accumulations of frazil slush or other ice pieces develop under the ice cover. In effect, they duct the flow in a manner that significantly alters the flow distribution from that attributable to the imposition of a level ice cover.

13.6.5.3 Field Data on Suspended Load The few field studies on sediment transport during ice-covered flow focus on suspended load and do distinguish between bed sediment and washload sediment.

The study carried out by Tywonik and Fowler (1973) focused on the measurement of suspended-sediment load in several rivers in the Canadian prairie (e.g., Assiniboine River and Red River). They report that periods of ice cover

on these rivers coincide with periods of low discharge and, therefore, low rates of suspended-sediment transport. In addition, they experienced considerable difficulty in making the suspended-load measurements, owing to frigid weather conditions and the presence of slush ice.

For most cold-region rivers, the major sediment-transport event each year occurs during the large flows associated with ice runs resulting from the dynamic breakup of an ice-cover or the release of a breakup ice jam, if a jam develops. In addition to the large flow rates usually involved, these events may produce severe gouging and abrasion of banks by moving ice. The resultant sediment transport comprises a mix of bed sediment and fine sediment washed into the river during snowmelt. Bed-load measurements are very difficult to obtain under ice-run conditions.

Two studies, though, have provided some suspended-load data from individual breakup events. Prowse (1993) measured suspended-load concentrations during ice breakup of the Liard River, Northwest Territories. His data show a gradual increase in concentration with increasing water discharge immediately prior to breakup. When breakup occurred, suspended-load concentration increased by an order of magnitude, being comparable to concentrations associated with peak open-water flows of about two to five times the peak flow at breakup. Data obtained by Beltaos and Burrell (2000) during ice breakup on the St John River, N.B., show a similar trend.

13.6.6 Local Scour beneath Ice Jams

The erosive behavior of a flow may increase locally beneath an ice jam if the jam concentrates flow, increasing the magnitude of its velocity and turbulence. Also, an ice jam may deflect flow, altering its direction in a manner that aggravates bank erosion or channel shifting. This mechanism locally increases flow velocity, and it may occur when flow and ice pieces are forced beneath an ice accumulation, such as an ice jam or an ice cover. Localized scour of an alluvial bed or bank of a channel may occur in the vicinity of an ice cover when the flow field at the cover locally increases flow velocities and thereby increases flow capacity to erode bed or bank sediment. There are several conditions under which this mechanism may occur.

The most severe condition typically occurs near the toe of an ice jam (freeze-up or breakup), as illustrated in Fig. 13-20. There, where jam thickness is greatest and flow most constricted, increased flow velocities may locally scour the bed (Neill 1976, Mercer and Cooper 1977, Wuebben 1988a). Channel locations recurrently (nominally every year) subject to ice jams may develop substantial scour holes. Tietze (1961) and Newbury (1982), for example, suggest instances of such scour holes at sites of recurrent freeze-up jams. In most circumstances, the scour hole would have no lasting or adverse effect on channel morphology, because it would gradually fill once the jam was released. It is conceivable that in certain circumstances, nonetheless, the localized scour could have a longer-term effect on channel morphology—e.g., if it promoted bank erosion at the jam site, or led to the washout of the channel feature triggering the jam, such as an island or bar.

To a lesser extent, local scour of bed and bank may also occur when ice pieces collect at the leading edge of an ice cover or at some channel feature (e.g., a set of channel bars) that impedes their drift. These situations are quite marginal in extent, likely occurring more or less randomly along a channel, and are short-lived. However, they potentially may trigger more severe erosion in some situations.

13.6.7 Constriction Scour and Local Scour at Bridge Piers

The consequences of ice-cover presence for constriction scour and local scour depth at bridge piers have yet to be examined. The prime ice-related concern is that a bridge crossing may congest ice passage in a river and, thereby,

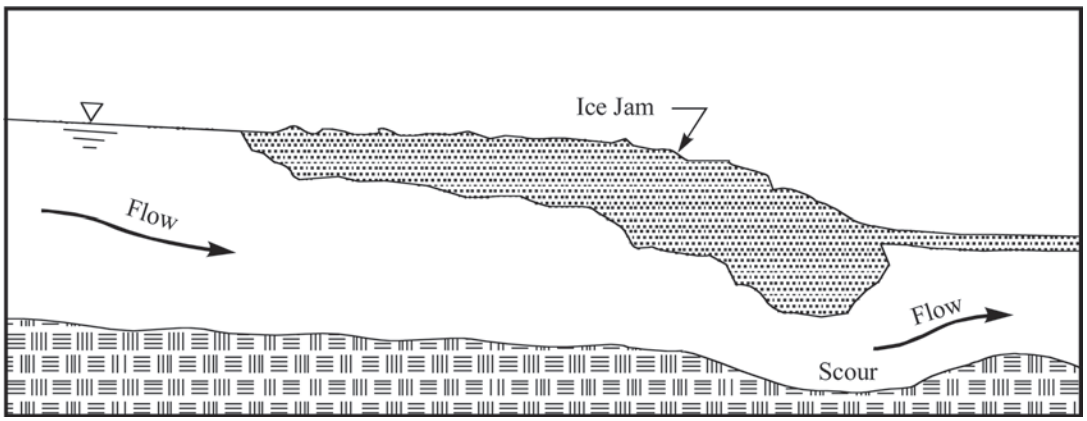

Fig. 13-20. Flow acceleration and local scour beneath an ice jam.

trigger an ice jam, such as illustrated in Fig. 13-13. Should the toe (thickest part, as sketched in Fig. 13-20) of the jam coincide with the bridge site, the jam would constrict flow through the bridge site and consequently aggravate constriction scour, as well as local scour caused by pier or abutment presence. Wuebben (1988a) describes this situation. Some work has gone in to developing instrumentation for monitoring scour depths near bridge piers in ice-covered flow (Zabilansky 1998). In summary, though, ice effects on scour likely are essentially the same as those caused by debris accumulation at bridges.

As mentioned in Section 13.5, the formation of ice walls in tidal channels can constrict flow through bridge openings in such channels (Desplanques and Bray 1986).

13.7 RIVER-ICE EFFECTS ON ALLUVIAL-CHANNEL MORPHOLOGY

An open question is the extent to which the seasonal appearance and disappearance of river ice perturbs the stability of alluvial channels in cold regions. It seems from limited field observations (e.g., Mackay et al. 1974; Zabilansky et al. 2002) that river ice may exert a compound impact of hydraulic and geomechanical impacts that continually destabilize certain planform geometries of channel subject to substantial, reservoir-regulated flow during frigid winters.

The volume of literature dealing with river-ice influences on channel morphology and bank erosion is not large. Moreover, what exists contains a fair amount of hypothesis and conjecture; there is a lack of rigorous investigation into most ice effects. Indeed, the issues of whether ice modifies channel morphology and reduces or amplifies bank erosion are still matters of considerable debate. On one hand, some articles (e.g., Neill 1982; Blench 1986) largely seem to dismiss the influences. On the other hand, there are fairly numerous anecdotal articles (e.g., Marusenko 1956, Lane 1957, Collinson 1971, MacKay et al. 1974, Hamelin 1979, USACE 1983, Doyle 1988, Uunila 1997, Milburn and Prowse 1998) and the odd review article (Ettema 1999) suggesting ways in which river ice perceptibly affects channel morphology. The dismissive articles would seem to draw their conclusions overhastily, basing them on cursory observations of overall planforms of a few rivers. They do not consider the impacts of reservoir regulation of flow during winter, take into account the diversity of channel morphologies, nor consider the important ephemeral impacts of ice that trigger local changes in thalweg, without appearing to alter channel planform appreciably. There is a need for quantitative information documenting and ranking the importance of ice impacts.

Several factors influence alluvial channel stability. Most of them are explainable in terms of the equation

$$\Pi_A = \varphi''_A\left(\mathsf{R}, \mathsf{R}_*, \eta\frac{d}{k_i}, S_0\right) \tag{13-11}$$

Dependent variables of practical interest are average depth of flow, Y, and hydraulic radius, R, as well as channel width, B; sinuosity, ζ, and shape; flow-energy gradient, S; and sediment-transport capacity, q_{sI}. Significant changes in any of the independent variables in Eq. (13-11) may alter R, ζ, or q_{sI} and may destabilize the alluvial reach. The greatest natural disturbances typically result from changes in water and sediment inflow rates q, or q_s. (In some respects, ice influences on channel morphology are discussed more conveniently in terms of total discharge rates Q and Q_S, because of the three-dimensional nature of channel morphology. The present discussion, however, continues in terms of unit discharges.)

A relatively long, level ice cover, for instance, practically doubles the wetted perimeter of flow in a channel, and it thereby significantly increases the boundary resistance exerted on the flow. Ice accumulated as an ice jam increases flow resistance by locally constricting flow. Increased flow resistance typically results in increased flow depth, altered flow distribution, and reduced flow drag on the bed—at least for fixed-bed channels. For a given channel, ice impacts on channel bed and banks increase in significance as unit water discharge, q, increases. Sediment entrainment and transport increase with increased flow in a channel when ice-covered channel as with open-water flow. Increased flow also increases the velocity of moving ice and increases the possibility of over-bank flow. River-ice impacts likely become more significant when water discharge fluctuates appreciably; then the prospects for other adverse ice influences increase, such as ice-cover breakup followed by ice jamming.

13.7.1 Hydraulic Impacts

River ice may exert the following hydraulic impacts on a channel reach:

1. By reducing the sediment-transport capacity of a river reach, ice redistributes bed sediment along the channel. Whatever local effects river ice may exert, overall river ice usually reduces the channel's overall capacity to convey the eroded sediment a significant distance from the erosion location. Consequently, bars may develop in response to flow conditions under river ice and be washed out shortly after the cover breaks up. In situations where a significant load of bed sediment enters a long reach that has a free-floating ice cover, river ice may tend to cause mild aggradation of the channel it covers. In situations where the reach is under a fixed ice cover, local degradation may occur.
2. Through its effects on lateral distribution of flow resistance and, thereby, flow and boundary drag, river ice may modify channel cross-sectional shape developed under open-water flow conditions.

3. Congestion or jamming of river ice at one channel location may divert flow into an adjoining channel, which then enlarges (anabranching/thalweg avulsion), or over a bank, which may result in a channel cutoff (avulsion).
4. Difficulties in ice passage through channel confluences may initiate ice jamming at confluences (Ettema et al. 2000; Ettema and Muste 2001). In turn, an ice jam may modify confluence bathymetry.
5. By imposing additional flow resistance, a free-floating ice cover diminishes the effective gradient of flow energy available for sediment transport and alluvial-channel shaping. It consequently alters channel-thalweg alignment.

Ice jams, especially breakup ice jams, likely exert the greatest ice-hydraulic impact on unregulated alluvial channels. Mackay et al. (1974), for instance, describe the significant impacts that breakup ice jams exert on the Mackenzie River. For channels regulated by reservoirs used for hydropower generation during winter, ice-cover formation and presence can exert significant effects (e.g., Zabilansky et al. 2002). In overall terms, ice impacts have yet to be rigorously investigated or even to be assessed quantitatively. Brief discussions of the impacts ensue.

13.7.1.1 Ice-Cover Influence on Local Elevation of Channel Bed A basic issue concerns an imbalance between unit rate of sediment supply to an ice-covered reach, q_s, and the sediment-transport capacity of that reach, q_{sI}. This issue involves the complex problem of spatially varied flow and sediment transport, with all its repercussions on local channel slope and morphology. If the sediment-transport capacity of an ice-covered channel, q_{sI}, were less than the rate at which sediment load was supplied to the channel, q_s, the bed elevation must rise locally. Conversely, if $q_{sI} > q_s$, the bed elevation must drop locally. The former condition usually would prevail for a floating cover, because bulk velocity of flow decreases. The latter condition may occur when the cover is fixed and/or thick, because the bulk velocity of flow is forced to increase substantially under the ice cover, with some flow spilling over the cover, as indicated in Fig. 13-21. An ice jam, by constricting flow, may scour a riverbed locally, especially at the jam's toe (Neill 1976; Wuebben 1988a), as shown in Figure 13-20.

13.7.1.2 Channel Anabranching, Avulsions, and Cutoffs Channels with tight meander loops or with subchannels around numerous bars or islands are prone to ice-jam formation. Such channels typically have insufficient capacity to convey the incoming amount of ice. Their morphology may be too narrow, shallow, curved, or irregular to enable drifting ice pieces to pass. Jam formation may greatly constrict flow, causing it to discharge along an alternate, less resistant course. Prowse (2001), King and Martini (1984), and Dupre and Thompson (1979) suggest that ice-jam induced avulsion plays a major role in shifting the distributary channels of river deltas. Zabilansky et al. (2002) indicate that ice-induced avulsions of subchannels may occur in sinuous-braided reaches of the Missouri River.

At sites where a river flows in two or more subchannels, ice-cover formation can trigger a switch of the principal thalweg from one subchannel to the other. Figure 13-22 illustrates the processes involved. When a rougher ice cover forms in one subchannel, the cover partially diverts flow from that subchannel to the subchannel with the smoother ice cover. The subchannel with the smoother ice cover then enlarges while the rougher-covered subchannel shrinks. Survey observations from the Fort Peck reach of the Missouri River (Zabilansky et al. 2001) suggest that thalweg switching is a recurrent process and that switches may take several winters to fully occur. Strictly speaking, such switching is a stochastic dynamic process that may be narrow-banded about a dominant period (e.g., a certain number of winters). It also may be broad-banded due to several factors (e.g., variability of flow conditions during a year or during ice-cover formation).

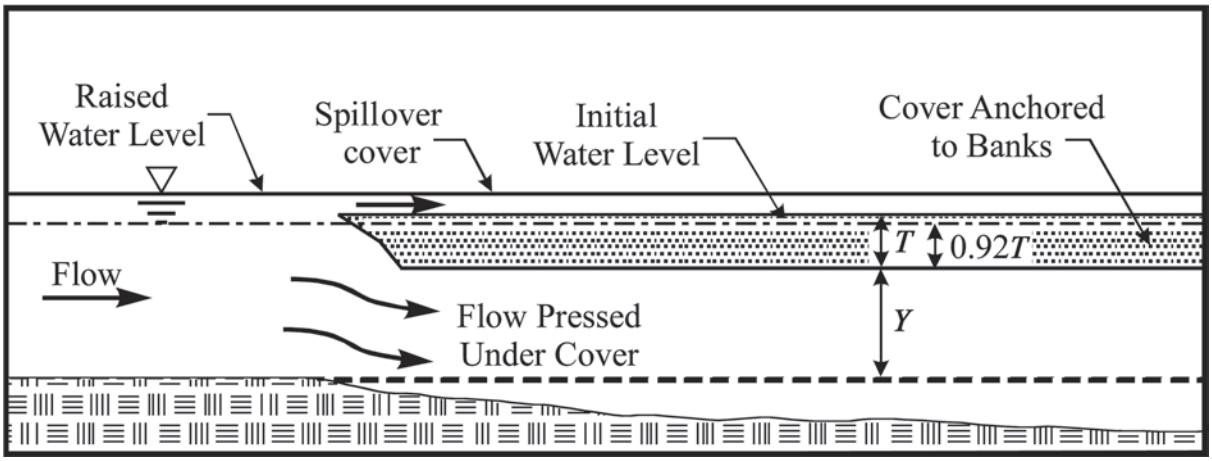

Fig. 13-21. Flow in a channel reach constricted by a fixed ice cover.

When an ice jam forms in a meander loop, upstream water levels may rise to the extent that flow proceeds overbank and across the neck of a meander loop. If the meander neck comprises readily erodible sediment and the flow is of sufficient scouring magnitude, flow diverted by the jam may result in a meander-loop neck cut, whereby a new channel forms through the neck, and the former channel is left largely cut off. A meander cutoff shortens and steepens a channel reach, the consequences of which are felt upstream and downstream of the cutoff reach. The net effect of ice jams, in this regard, is to reduce channel sinuosity. Mackay et al. (1974), for instance, cite examples of such events.

If, on the other hand, the meander loop is wide and not easily eroded, overbank flow resulting from an ice jam may have the reverse effect. Rather than the net consequence being the erosion of channel through the meander loop, overbank flow may deposit sediment, thus raising bank height and reinforcing the meander loop. Eardly (1938) reports that ice jams cause substantial sediment deposition on the flood plain of the Yukon River. A similar event is reported in Simon et al. (1999) for the Fort Peck reach of the Missouri River. Overbank deposition of sediment, together with ice-run gouging and abrasion of sediment erosion from the lower portion of a bank, may oversteepen riverbanks.

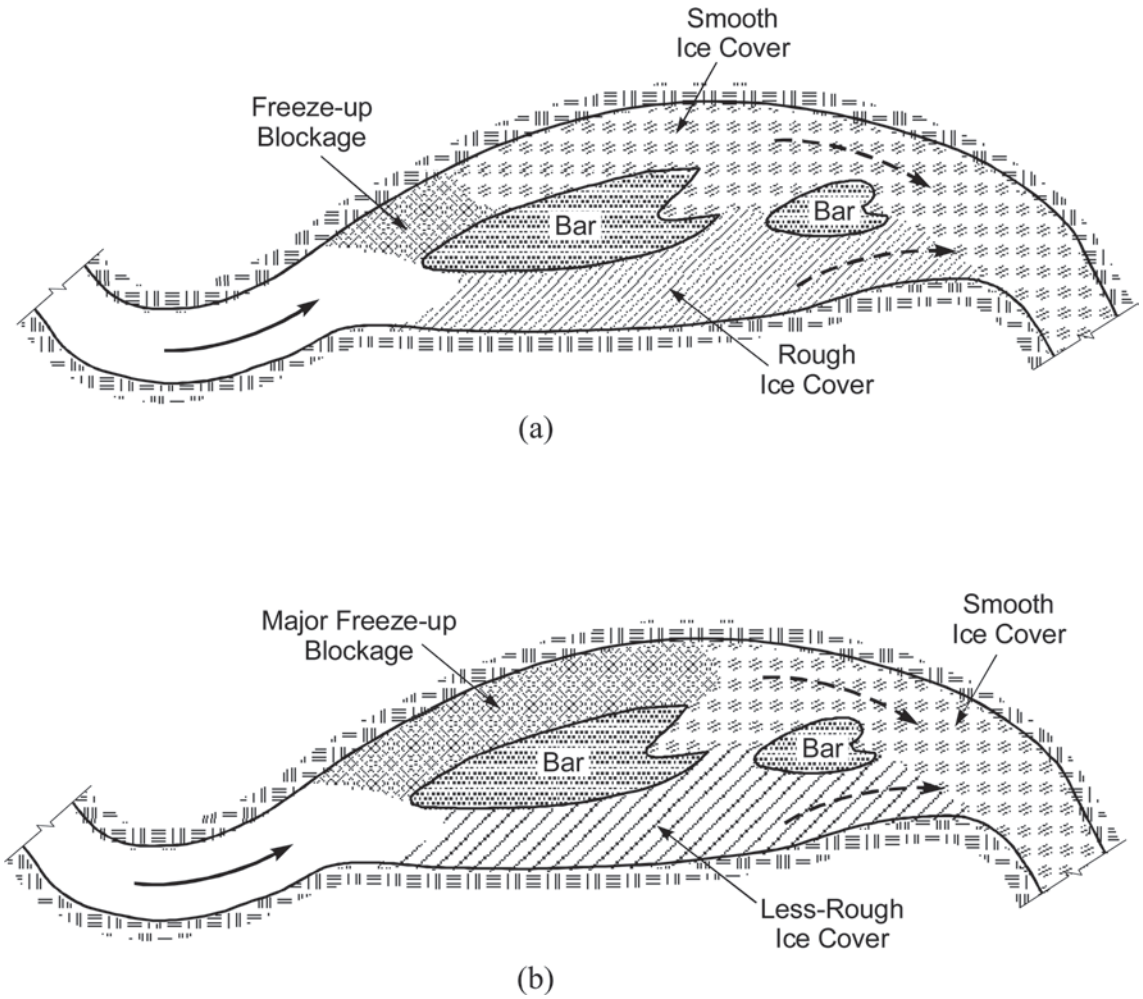

Fig. 13-22. Ice-cover formation in a sinuous-braided channel may alternate the location of the major subchannel. Two scenarios for alternation of major subchannel were identified: (a) A relatively short initial accumulation of drifting ice in subchannel 1 may divert ice into subchannel 2, which then becomes extensively enveloped by a rough ice cover. Meanwhile, subchannel 1 freezes over with a smooth ice cover, or may remain partially open. The greater flow resistance in subchannel 2 causes flow to favor subchannel 1, which then enlarges. (b) A relatively long initial accumulation of drifting ice in subchannel 1 may divert ice and flow into subchannel 2, which then becomes extensively enveloped by a less-rough ice cover. The greater flow resistance in subchannel 1 causes flow to favor subchannel 2, which then enlarges.

13.7.1.3 Channel Confluences By virtue of their role in connecting channels and thereby concentrating ice within a watershed, confluences are perceived as locations especially prone to the occurrence of ice jams. Fairly numerous accounts exist of jams in the vicinity of a confluence (Tuthill and Mamone 1997). Flow and ice concentration in a confluence may cause ice to jam within a confluent channel, within the confluence itself, or at some distance downstream from the confluence. Various mechanisms may trigger jams in the vicinity of confluences. Confluence bathymetry plays a significant role in jam initiation, and in turn jamming can modify confluence bathymetry; see Ettema and Muste (2001).

13.7.1.4 Cover Influence on Thalweg Alignment Ice cover reduces the effective energy gradient of flow (and thereby the stream power) available for sediment transport and channel shaping. Therefore, cover formation may trigger a change in thalweg alignment.

Figures 13-23(a to c) suggest that, in terms of flow drag on the channel bed, a covered flow is effectively equivalent to a deepened and slowed open-water flow. For a constant flow rate, this influence is equivalent to a reduction in channel slope (or reduced stream power). Figure 13-24 tentatively relates thalweg and channel sinuosity to channel slope (in effect, to energy gradient and stream power). It suggests that thalweg sinuosity is relatively sensitive to change in energy gradient, much more sensitive than is overall channel sinuosity. For a given flow rate, sediment provenance, and bed-sediment composition, thalweg sinuosity and channel planform change as channel slope changes. Fig. 13-24 indicates that, for a given flow rate and bed sediment size, channels lengthen or branch into subchannels as channel slope increases. Channel lengthening and branching are mechanisms whereby an alluvial-channel flow increases flow resistance (and thereby rate of energy use) to offset increased flow energy associated with a larger channel slope.

When the channel is ice-covered (Fig. 13-23b) and q is constant, flow resistance imparted by the cover deepens the flow to Y_I. The unit discharge may be written as

$$q_I = q_O = Y_I \left(8gR_I S / f_I\right)^{1/2} \tag{13-19}$$

It is assumed here that the overall reach slope, S_0, and channel width do not change significantly. Cover presence, by reducing flow velocity, reduces the portion of flow energy gradient (or stream power) expended as flow drag along the channel's bed.

For an alluvial channel, a reduction in energy gradient usually implies an adjustment in planform geometry. Because an ice cover deepens and slows flow in a channel, the channel responds as if it were at a flatter slope. In effect, the channel responds as if it were conveying an equivalent open-water flow whose cross-sectional area was as shown in Fig. 13-23(c), but whose energy gradient was reduced. The effective hydraulic radius, resistance coefficient, and energy gradient of the equivalent flow are R_e, f_e, and S_e, respectively; with $R_e \approx 2R_I$ and $S_e < S_0$. For this equivalent open-water flow,

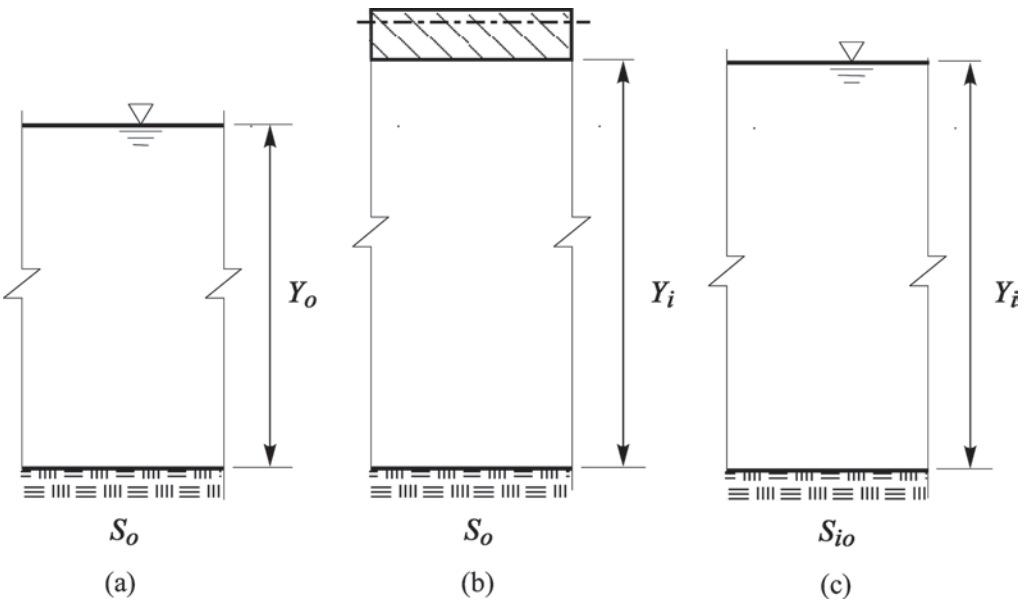

Fig. 13-23. A simplified sketch illustrating flow in an initial open-water flow (a) deepened by an ice cover (b) for the same flow rate. The ice-covered channel essentially experiences flow at a raised depth and reduced average velocity (c) (i.e., at a reduced slope, or energy gradient, S_e).

$$q_I = q_O = Y_e \left(8gR_eS_e/f_e\right)^{1/2} \qquad (13\text{-}20)$$

Equations (13-19) and (13-20) give

$$\frac{S_e}{S_0} = \left(\frac{f_e}{f_O}\right)\left(\frac{Y_O}{Y_e}\right)^2\left(\frac{R_O}{R_e}\right) \approx \left(\frac{f_e}{f_O}\right)\left(\frac{Y_O}{Y_e}\right)^3 \approx \left(\frac{Y_O}{Y_e}\right)^3 \qquad (13\text{-}21)$$

Equation (13-21) assumes the wide-channel approximation $R_O \approx Y_O$ and $R_e \approx Y_e$ and, because the bed sediment does not change and if the ice cover is fairly level, the ratio $f_e/f_O \approx 1$.

Equations (13-19) through (13-21), though entailing simplifying assumptions, lead to a clear result. Because covered flow depth, Y_I, usually exceeds open-water depth, Y_O, the ratio S_e/S_0 is less than 1. Therefore, the energy gradient (and stream power) available for sediment transport and channel formation decreases when a channel becomes ice-covered. For a typical situation, say, $Y_O/Y_I \approx 0.8$, $S_e/S_0 \approx 0.5$; in other words, for a given flow rate in a channel of given length, approximately half the rate of energy expenditure is available for sediment transport and channel forming. The effect of an ice cover, therefore, is to trigger a shift in thalweg sinuosity and alignment so as to balance flow-energy availability and use. However, given the magnitude and duration of flow likely needed to shift the thalweg of a channel, this ice-cover effect likely is significant only for alluvial channels whose flow is regulated by an upstream dam (notably a hydropower dam) that releases substantial flows during winter.

Figure 13-24 suggests, for instance, that halving the slope of a meandering channel (say, from 0.008% to 0.004%) will reduce thalweg sinuosity; i.e., the thalweg attempts to straighten and the meander wavelengths shorten, as sketched in Fig. 13-25.

For sinuous braided channels, as in Fig. 13-26, ice-cover formation and associated decrease in energy gradient may cause flow to concentrate in a single thalweg of greater sinuosity than the open-water thalweg. For braided channels, ice-cover presence may concentrate flow into the larger subchannels.

13.7.1.5 Jam-Collapse Surges The surge created by the collapse of an ice jam usually generates high velocities of flow that entrain considerable amounts of sediment from the channel bed as well as channel banks and possibly flood plains. As noted in Section 13.4, surge speeds up to about 5 m/s have been recorded for break-up ice jams (Beltaos 1995). Such surges can be very erosive. Anecdotal evidence exists of a case where a surge resulted in the complete removal of a small island in a river. Not unexpectedly, concentrations of suspended sediment greatly increase during the passage of a surge, as mentioned in Section 13.6.5.

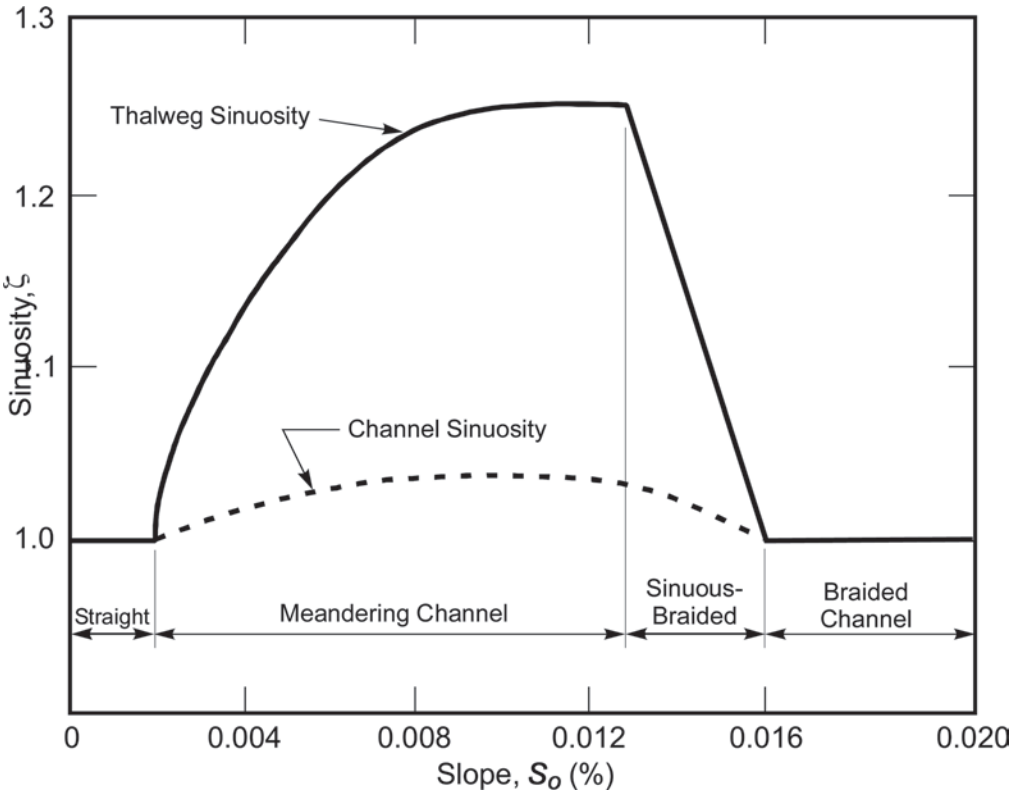

Fig. 13-24. Variation of channel and thalweg sinuosity, ζ, with channel slope, S_0. Figure adapted from Schumm and Khan (1972).

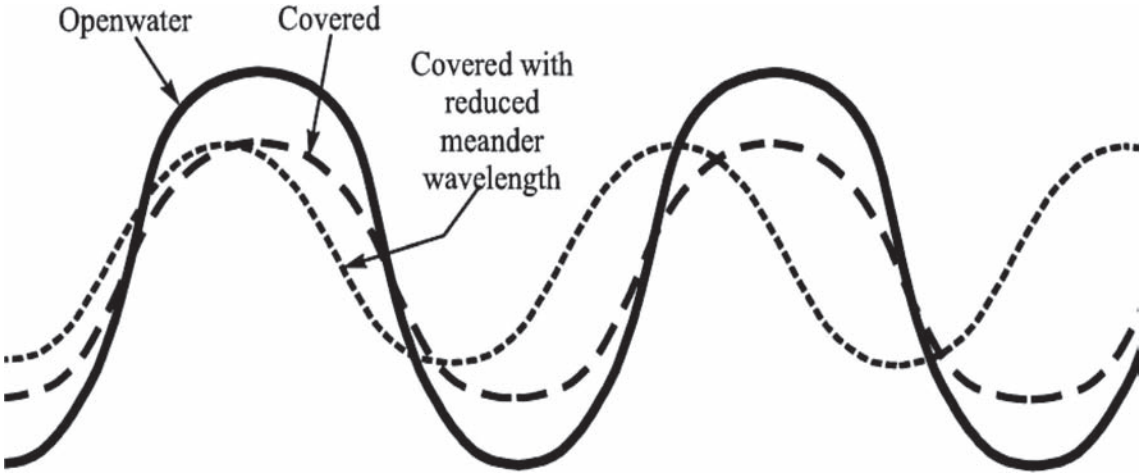

Fig. 13-25. Conceptual influence of an ice cover on a meandering channel of more-or-less uniform flow depth. The cover may cause the thalweg to straighten and meander loops to shorten.

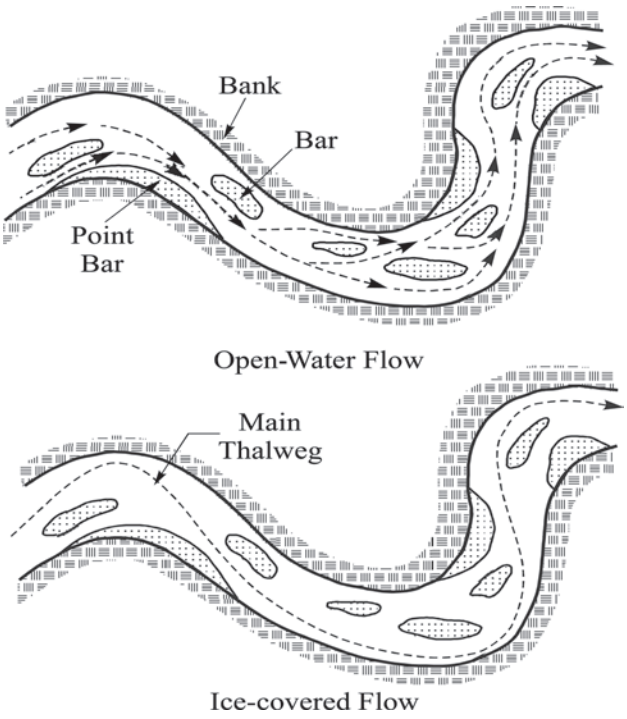

Fig. 13-26. River-ice impact on the thalweg of a sinuous-braided channel. An ice cover causes the main thalweg to become more sinuous.

13.7.2 Impacts on Riverbanks

River ice may influence channel cross-section shape, alignment, and bed elevation through several geomechanical impacts on riverbanks:

1. Reducing riverbank strength by increasing pore-water pressure or by producing rapid drawdown of the bank water table during dynamic ice-cover or ice-jam breakup. This impact is part of the overall consequences of freeze-thaw behavior for riverbanks under frigid conditions.
2. Tearing, battering, and dislodging riverbank material and vegetation during collapse of bankfast ice.
3. Gouging and abrading riverbank material and vegetation during an ice run.

The three impacts reduce riverbank resistance to scour and increase the local supply of sediment to the channel. The first two impacts are not well studied. The third has received some attention, but the extent to which it affects channel shape is unclear. It is normal for river channels and floodplains subject to ice to be denuded of larger vegetation, as is sketched in Fig. 13-27.

Engelhardt and Waren (1991), for instance, briefly describe the consequences of such combined processes for the Missouri River downstream of dams in Montana and North Dakota. Increased rates of ice-covered flow, increased movement up and down riverbanks, bank freezing at higher elevation, and more frequent freeze-thaw cycles exacerbate bank erosion. The consequences become noticeable in early spring, when large portions of riverbanks fail. Similar observations are reported by Zabilansky et al. (2001).

The ensuing subsections briefly discuss these impacts, beginning with a short review of riverbank-strength response to freezing and thawing.

13.7.2.1 Freeze-Thaw Influences on Riverbank Strength It is well known that the freezing and thawing of soil affect the erosion of riverbanks adjoining rivers and lakes. Lawson (1983; 1985) and Gatto (1988; 1995), among others, provide extensive reviews of the subject. In short, because frozen soil is more resistant to erosion

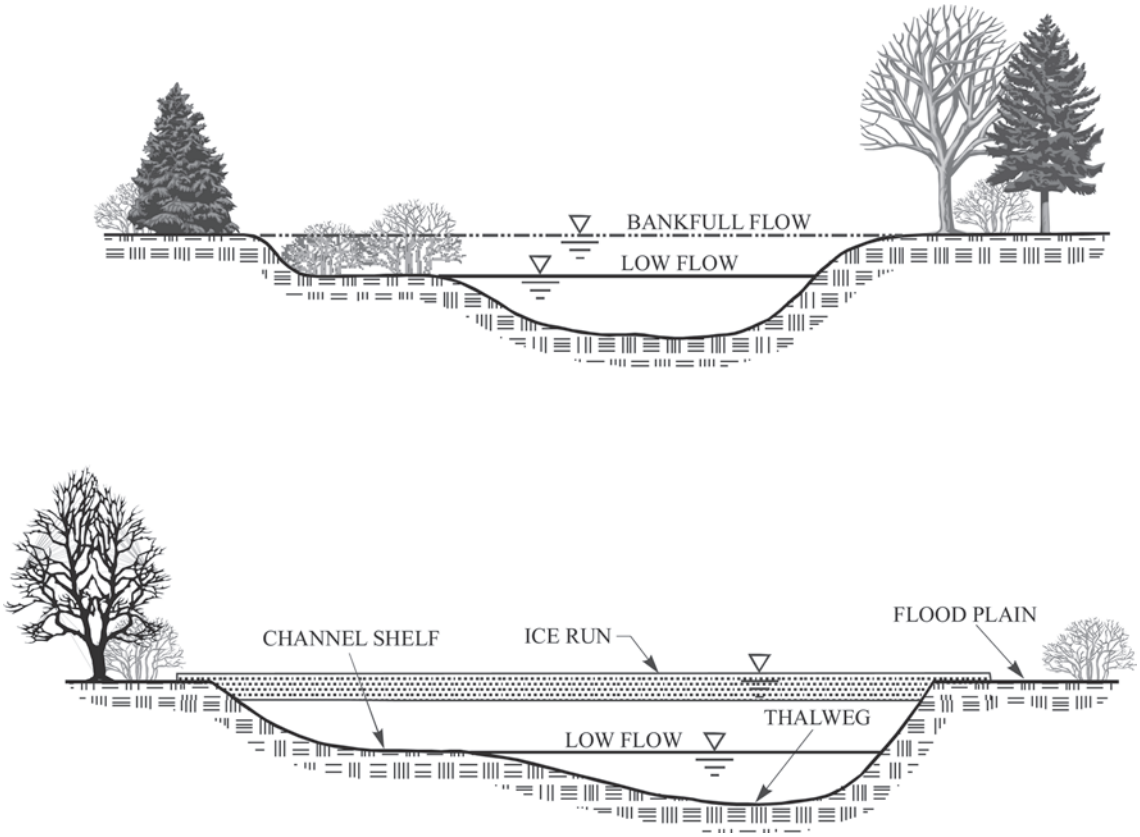

Fig. 13-27. Severe ice runs may inhibit riparian vegetation growth along riverbanks and floodplains.

than is unfrozen soil, riverbanks are less erodible while frozen. Freezing and thawing, however, usually weakens soils, making thawed (or thawing) riverbanks more susceptible to erosion. The net consequences for the overall rate of riverbank erosion, therefore, remain a matter of debate. Most likely, the net consequences vary regionally and from site to site.

Freeze-thaw cycles affect soil structure, porosity, permeability, and density. These changes in soil properties can substantially reduce soil shear strength and bearing capacity; strength reductions of as much as 95% are reported (Andersland and Anderson 1990). Such adverse effects on soil strength depend on soil-particle size and gradation, moisture content, the number and duration of freeze-thaw cycles, and several other factors. Though there is no single, standard test to determine whether a soil is prone to significant weakening due to freeze-thaw (Chamberlain 1981), particle size is commonly used as an approximate indicator of soil sensitivity to freeze-thaw weakening. Soils containing fine sands and silts are especially sensitive, because they are permeable and susceptible to change in soil structure. By virtue of their particle size (about 0.1 to 0.06 mm) and the surface-tension properties of water, fine sandy and silty soils absorb moisture more readily than do coarser or fine sediment. Clayey soils are less sensitive, because of their low permeability. The variability of soil properties along a riverbank and within a specific riverbank location causes the effects of riverbank freezing to differ along a reach.

Gatto (1995) suggests that an eroding riverbank is especially subject to deep penetration of freezing, thereby making more of the riverbank prone to freeze-thaw weakening and erosion. The absence or stunted extent of vegetation that characterizes many eroding riverbanks results in diminished insulation of the riverbank and increased heat loss to air. In addition, the crest region of a riverbank experiences greatest heat loss, owing to the crest's exposure to air on at least two sides. Because of its exposure to wind, the crest may also accumulate less snow. Less snow, in turn, means deeper frost penetration during winter and faster thaw in spring. However, less snowmelt is available to percolate into the riverbank. Questions exist about the exact manner in which border ice is anchored to the riverbank, and other factors (notably, variations in water-table (or piezometric) surface and moisture content of the top zone of the riverbank) would modify the extent of the frozen zone and its connection with river ice. Presumably, if the top portion of the riverbank and upland were dry, the riverbank crest might be the zone of

least heat loss, because the distance between air and water table is greatest there.

As the upper zone of frozen ground thaws, melt water likely drains down, over the surface of the still frozen ground. The riverbank, weakened by thaw expansion of ground and subject to the seepage pressures, is in its least stable, annual condition.

Several studies (e.g., Harlan and Nixon 1978; Reid 1985) have found that south-facing riverbanks (in the northern hemisphere) experience lesser thickness of freezing, all else being equal, than north-facing riverbanks. The explanation for this is that south-facing riverbanks receive more insolation (energy in the form of short-wave radiation from the sun). South-facing riverbanks also may undergo more diurnal frequent freeze-thaw cycles (Gatto 1995). The net effect of riverbank alignment on weakening of riverbank material has yet to be determined.

13.7.2.2 Reduction of Riverbank Strength Flow stage and stage fluctuations influence seepage pressures and the freeze-thaw behavior of riverbanks. Higher flow stage raises water table in a riverbank, and a rapid drop in flow stage may momentarily reduce riverbank stability by increasing seepage pressures and thereby reducing the shearing resistance of the material comprising the riverbank. Ice-cover formation raises flow stage, whereas cover breakup may abruptly lower it. River-ice formation, thereby, may weaken riverbanks.

Riverbank freezing is closely linked to bankfast-ice formation along a channel, though the details of relationship between them are unclear. They depend on riverbank condition (material, vegetation, snow, etc.), the relative elevations of water table and flow stage, and temperatures of groundwater and river water. The strength of bankfast-ice attachment to a bank depends on the relative elevations of the water table and flow stage and on the relative water temperatures. A relatively warm (i.e., several degrees above freezing) flow of groundwater into a river will retard bankfast-ice growth and weaken its hold on the bank. The growth of a thick fringe of bankfast ice, on the other hand, may affect seepage flow through the bank, possibly constricting it and slightly raising the water table. This is especially significant for regulated rivers, for which flows do not diminish during winter.

13.7.2.3 Bankfast-Ice Loading of Bank Bankfast-ice weakening of banks likely is significant for steep banks, typically those banks containing sufficient clay to be termed cohesive. It also likely is significant for banks whose water table declines in elevation away from flow elevation in a channel, because the bankfast ice is less securely anchored into the bank. This erosion mechanism seems not to have been investigated heretofore but was observed, e.g., along the Fort Peck reach of the Missouri River (Zabilansky et al. 2001). When the flow stage in a channel drops, portions of an ice cover attached to a bank during the higher flow stage may be left momentarily cantilevered from the bank. The cantilevered ice soon collapses, weakening and wrenching bank material as it does so.

Figure 13-28 illustrates how bankfast ice might weaken a bank. The ice cover freezes into the bank. The extent of the root is limited by groundwater elevation and temperature and by the nature of the bank material. When the water level in the channel drops and the ice cover breaks up, ice attached to the bank is cantilevered out from the bank, rotates, and tears a portion of the bank as it drops. It is difficult to get direct field observations of this mechanism for bankfast ice attached to vertical banks. For the moment, evidence for

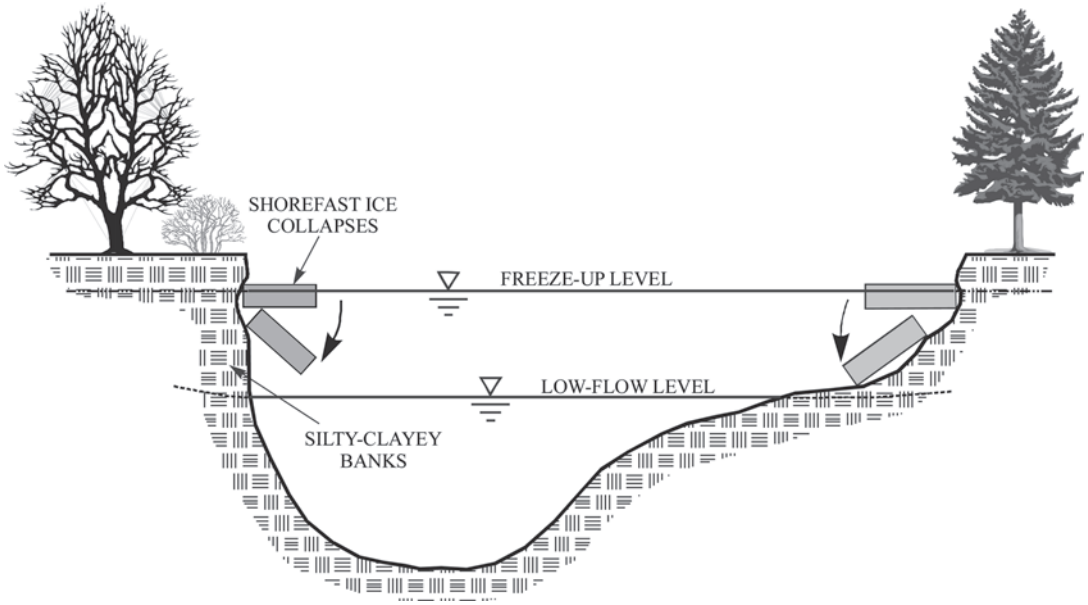

Fig. 13-28. Collapse of shorefast ice may erode banks when flow stage is lowered.

it is circumstantial. There is evidence for a related mechanism commonly termed plucking, which is the loss of riprap stones frozen to an ice sheet. Wuebben (1995), for instance, discusses plucking concerns extensively in the design of riprap for bank protection.

13.7.2.4 Gouging and Abrasion of Banks During heavy ice runs resulting from ice-cover break-up or ice-jam release, large pieces of ice potentially may gouge and abrade channel banks. There exists significant evidence showing that it substantially affects channel-bank morphology subject to dynamic ice runs (Marusenko 1956; Hamelin 1979; Smith 1979; Martinson 1980; Uunila 1997; USACE 1983; Doyle 1988; Brooks 1993; Wuebben 1995; Wuebben and Gagnon 1995). Such channels usually are relatively steep and convey high-velocity flows. Moreover, their ice covers typically break up fairly dramatically in concert with a sudden rise in flow, due, for example, to rapid snowmelt and/or rain. The resultant ice rubble comprises hard, angular blocks of ice.

One study of 24 rivers in Alberta (Smith 1979) led to the intriguing hypothesis that ice runs enlarge channel cross sections at bank-full stage by as much as 2.6 to 3 times those of comparable-flow rivers not subject to ice runs. The hypothesis is based on a comparison of the recurrence interval of bank-full flows in the 24 rivers and an empirical relationship between the cross-section area and flow rate for bank-full flow. The channel-widening effect of ice runs is plausible. However, the extent of widening indicated seems overlarge and requires further confirmation. Kellerhals and Church (1980), in a discussion of Smith (1979), argue against Smith's hypothesis. They suggest that other factors have led to an apparent widening of the channels analyzed by Smith; e.g., recent entrenchment of major rivers in Alberta and ice-jam effects of flow levels. Moreover, it is possible that the banks are somewhat protected by a band of ice forming a shear wall flanking the riverbanks. It is interesting to contrast Smith's hypothesis with a further hypothesis mentioned previously that ice jams may promote channel narrowing by causing overbank flow (e.g., Uunila 1997). For channels whose dominant channel-forming flow coincides with ice-cover breakup, overbank loss of flow reduces the flow rate to one that can be accommodated by the channel.

In many situations, notably those in which an ice run is sluggish, a shear wall of broken ice may fend moving ice from contacting the bank. The shear wall usually becomes smooth-faced, and protects riverbanks from direct ice impact or gouging. Running ice, if sufficiently thick, may still gouge the lower portion of a bank. Significant gouging may occur downstream of the toe of a jam, before the arrival of sufficient ice rubble to form shear walls. A surge front released from the jam may fracture an ice cover into large slabs, which then are set in motion. The surge front typically moves faster than the ice rubble comprising the jam, but gradually attenuates. Typically, ice gouging occurs within a relatively short reach of a river.

Ice gouging and abrasion, though, can be severe for channel features protruding into the flow. In addition, channel locations with a substantial change in channel alignment are especially prone to ice-run gouging and abrasion; e.g., a sharp bend, point bar, and portions of a channel confluence. There is a little information on how ice runs affect the local morphology of these sites. Two features have been observed in gravelly rivers: ice-push ridges and cobble pavements. Ice-push ridges form when a heavy ice run gouges and shoves sediment along the base of banks (e.g., Bird 1974). The gouged sediment piles up as ridges beneath the ice run as it comes to rest as a jam. The finer sediments eventually get washed out, leaving the more resistant gravel and boulders in ridges. The ridges usually develop in the vicinity of locations subject to recurrent ice jams.

Cobble pavements may cover bars and the lower portions of banks subject to ice gouging and abrasion. Essentially, an overriding mix of ice and cobbles removes the finer material from the surface of the bars or banks. The resultant cobble surface comprises cobbles whose major axis is aligned parallel to the channel and whose size gradually decreases downstream (Mackay and Mackay 1977). The resultant cobble pavement may extend for many miles along the banks of large northern rivers, such as the Mackenzie and Yukon Rivers (Kindle 1918; Wentworth 1932).

The gouging and abrasion of the lower portion of banks, in conjunction with overbank sediment deposition during ice-jam flooding, may produce an elevated ridge or bench feature along some northern rivers. These features have been dubbed bechevniks for Siberian rivers (Hamelin 1979). A bechevnik is the marginal strip comprising the lower portion of a riverbank and the exposed portion of the adjoining river bed that, in days gone by, formed a convenient path for towing boats upstream manually or by horse; becheva apparently is Russian for towrope. Figure 13-29 illustrates the main features of a bechevnik, which may form partly from ice abrasion and partly from the deposition of sediment and debris left by the melting of ice rubble stranded after ice runs.

Moving ice also may grind banks formed of soft rock (e.g., sandstones and mudstones) or stiff clay. Danilov (1972) and Dionne (1974), for instance, describe how moving ice has affected rock banks of rivers such as the St Lawrence River. The extent of erosion, though, is less than for banks formed of alluvial sediment.

Ice-run gouging and abrasion have an important, though as yet not quantified, effect on riparian vegetation that, in turn, may affect bank erosion and channel shifting. Where ice runs occur with about annual frequency, riparian vegetation communities have difficulty getting established. Ice abrasion and ice-jam flooding may suppress certain vegetation types along banks, as illustrated in Figs. 13-27 and 13-28 for a bechevnik, possibly exacerbating bank susceptibility to erosion. This aspect of river ice has yet to be further investigated.

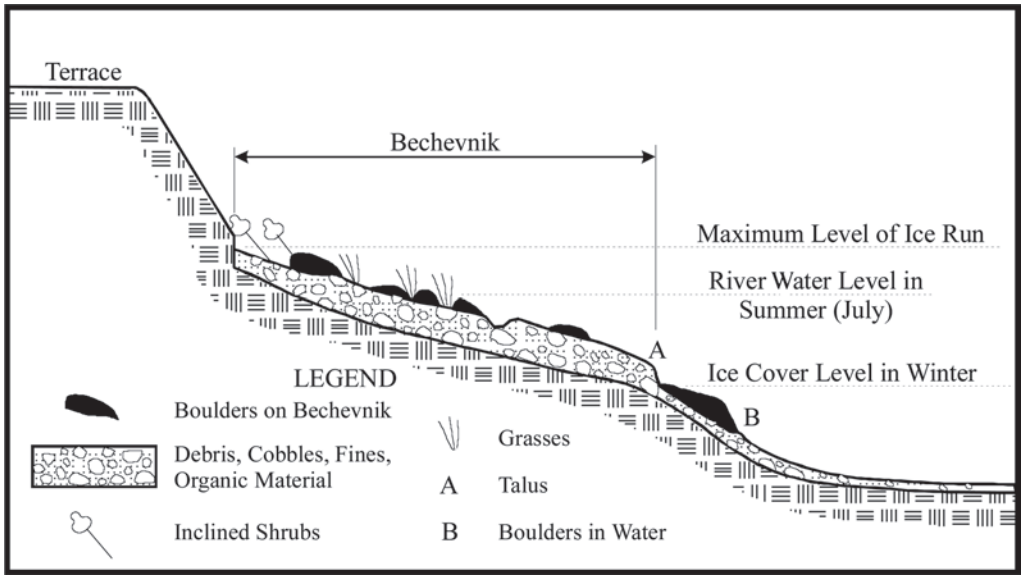

Fig. 13-29. Sketch of a bechevnik. Figure adapted from Hamelin (1979).

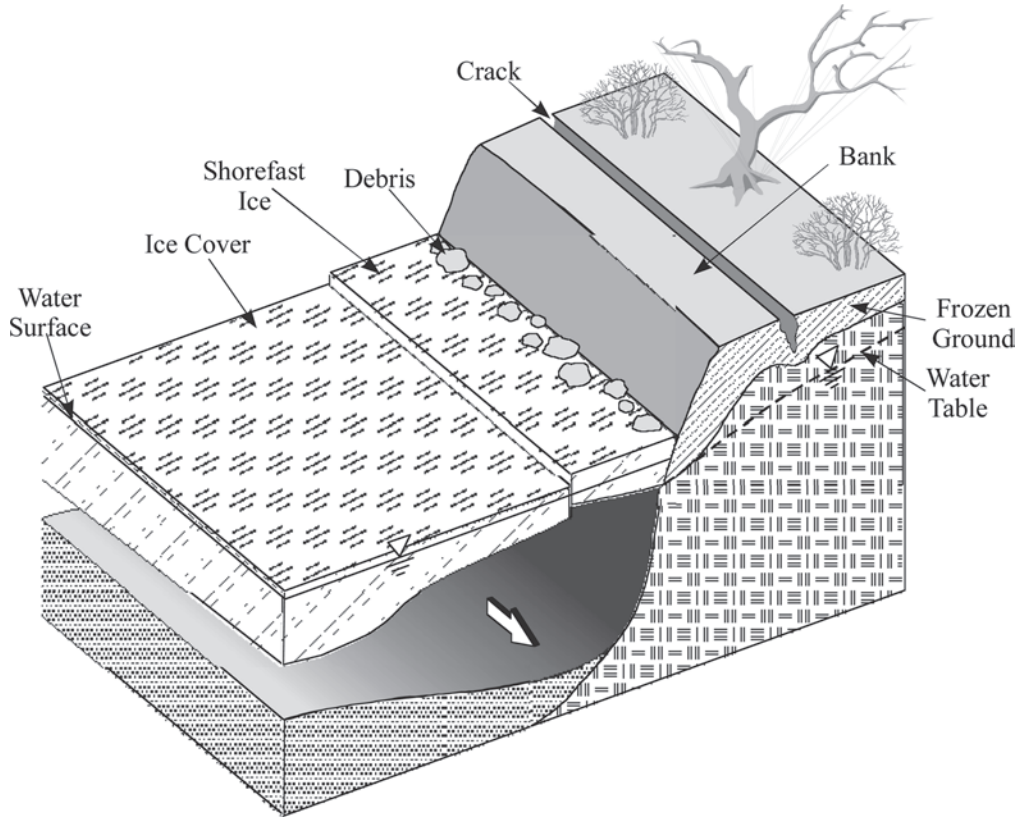

Fig. 13-30. Hydraulic impacts (e.g., thalweg shift and bank-toe erosion), together with geomechanic impacts (e.g., freeze-thaw weakening of bank material, elevated seepage pressures, bankfast-ice loading) may weaken and erode channel banks, especially along channel bends, and results in continual overall channel destabilization.

Scrimgeour et al. (1994) and Prowse (2001) provide useful early reviews.

13.7.3 Combined Hydraulic and Geomechanical Impacts on Channels

A single hydraulic or geomechanical impact of river ice may disturb a channel, but not necessarily destabilize it. A combination of hydraulic and geomechanical impacts, though, may destabilize a channel. A shift in thalweg alignment or a bank failure alone may not destabilize a channel. The channel may adjust back more or less to its stable open-water condition once open-water conditions resume. Besides, a single ice impact may be damped or possibly constrained. For instance, flow concentration along a thalweg may be damped by an increase in bed resistance resulting from an increase in bed-form size, and bank erosion may be damped as bank slope consequently flattens. High banks, which deposit a large mass of sediment into the channel, or scour-resistant strata (e.g., a clay layer or rock outcrop) may constrain thalweg shifting or entrenchment.

It probably is not surprising that channels usually considered less stable under open-water conditions are more likely to be adversely impacted by river ice. Sinuous point-bar, sinuous braided, and braided alluvial channels are especially prone to river ice impact, especially if they have steep banks formed of fine and partially cohesive sediments. The thalwegs of such channels usually lie close to the outer banks of bends, and the banks themselves are prone to bank-fast-ice loading, lack of vegetation cover (typical of eroding banks), and freeze-thaw weakening. Figure 13-30 illustrates this susceptibility. The thalweg lies close to the bank, so that the flow continually erodes the bank-toe, thereby keeping the bank steep and possibly undercutting it. Snow cannot protectively blanket the bank face. Frost penetration potentially is deep, the water table is held relatively high, and the channel shifts, destabilized.

An intriguing question is whether the destabilizing impacts of river ice uniquely modify alluvial-channel morphology. Only a tentative answer can be suggested at this moment. It is likely that the major geometric parameters do not change appreciably (e.g., channel thalweg sinuosity, width, hydraulic radius, meander radius). However, river ice likely increases irregularities in channel planform and the frequencies with which channel cross section and thalweg alignment shift. In a sense, it adds noise to the signal form of an alluvial-channel in dynamic equilibrium.

ACKNOWLEDGMENTS

The author gratefully acknowledges the contributions made to this chapter by Ed Kempema, University of Wyoming; Spyros Beltaos, Inland Waters, Canada; and Hung Tao Shen, Clarkson University.

REFERENCES

Altberg, V. I. (1936). "Twenty years of work in the domain of underwater ice formation (1915–1935)." *Bulletin, International Association for Scientific Hydrology*, 23, 373–407.

Andersland, O., and Anderson, D. M. (Eds.). (1990). *Geotechnical engineering for cold regions*. McGraw-Hill, New York.

Arden, R. S., and Wigle, T. E. (1972). "Dynamics of ice formation in the Upper Niagara River." *The Role of Ice and Snow in Hydrology*. Publication 107, International Association for Scientific Hydrology, Grenoble, France, 1296–1312.

ASCE. (1975). *Sedimentation manual.* ASCE, New York.

Ashton, G. (1986). *River and lake ice engineering*. Water Resources Publications, Littleton, Colo.

Barnes, H. T. (1928). *Ice engineering*. Renouf Publishing Company, Montreal, Que., Canada.

Barnes, P. W., Kempema, E. W., Reimnitz, E., and McCormick, M. (1994). "The influence of ice on southern Lake Michigan coastal erosion." *Journal of Great Lakes Research,* 20, 179–195.

Barnes, P. W., Reimnitz, E., and Fox, D. (1982). "Ice rafting of fine-grained sediment, a sorting and transport mechanism, Beaufort Sea, Alaska." *Journal of Sedimentary Petrology*, 52, 493–502.

Beltaos, S. (1990). "Fracture and breakup of river ice cover." *Canadian Journal of Civil Engineering*, 17(2), 173–183.

Beltaos, S. (1995). *River ice jams*. Water Resources Publications, Highlands Ranch, Colo.

Beltaos, S., and Burrel, B. (2000). "Suspended sediment concentration in the St John River during ice breakup." *Proc. Canadian Society of Civil Engineers Annual Conference*, Canadian Society of Civil Engineers, Toronto, Ont., 235–242.

Beltaos, S., and Dean, A. (1981). "Field Investigations of a hanging ice dam." *Ice Symposium*, Vol. II, International Association of Hydraulic Research, Delft, the Netherlands, 485–449.

Benson, C. S., and Osterkamp, T. E. (1974). "Underwater ice formation in rivers as a vehicle for sediment transport." *Oceanography of the Bering Sea*. Institute of Marine Science, University of Alaska, Fairbanks, Alaska, 401–402.

Bird, J. B. (1974). "Chapter 12: Geomorphic processes in the Arctic." *Arctic and alpine environments*, J. D. Ives and R. G. Barry, eds., Methuen, London, 703–720.

Blench, T. (1986). *Mechanics of plains rivers*. University of Alberta, Edmonton, Alta., Canada.

Bogordskii, V. V., and Gavrola, V. P. (1980). *Ice. Physical properties, modern methods of glaciology* (in Russian). Gidrometeoizdat, St Petersburg, Russia.

Brooks, G. R. (1993). "Characteristics of an ice-scoured river bank near Keele River confluence, Mackenzie Valley, Northwest Territories. Current Research, Part B." *Paper 93-1*, Geological Survey of Canada, Ottawa, Ont., Canada, 21–27.

Burrows, R. L., and Harrold, P. E. (1983). "Sediment transport in the Tanana River near Fairbanks, Alaska (1980–1981)." *Water Resources Investigations Report 83-4064*, U.S. Geological Survey, Reston, Va.

Chacho, E. F., Lawson, D. E., and Brockett, B. E. (1986). "Frazil ice pebbles: Frazil ice aggregates in the Tanana River near Fairbanks, Alaska." *Proc. IAHR Symposium on Ice*, International Association for Hydraulic Research, Delft, the Netherlands, 475–484.

Chamberlain, E. J. (1981). "Frost susceptibility of soil: review of index tests." *Monograph 81-2*, U.S. Army Corps of Engineers, Cold Regions Research and Engineering Laboratory, Hanover, N.H.

Colby, B. R., and Scott, C. H. (1965). "Effects of temperature on discharge of bed material." *Professional Paper 462-G*, U.S. Geological Survey, U.S. Government Printing Office, Washington, D.C.

Collinson, J. D. (1971). "Some effects of ice on a river bed." *Journal of Sedimentary Petrology*, 41(2), 557–564.

Danilov, I. D. (1972). "Ice as a factor of relief formation and sedimentation." *Problemy Krioliltogii*, 2, 137–143.

Desplanqes, C., and Bray, D. I. (1986). "Winter ice regime in tidal estuaries of the northeastern portion of the Bay of Fundy, New Brunswick." *Canadian Journal of Civil Engineering*, 13(2), 130–139.

Dionne, C.-J. (1974). How ice shapes the St Lawrence. *Canadian Geographical Journal*, 88(2), 4–9.

Doyle, P. F. (1988). "Damage from a sudden river ice breakup." *Canadian Journal of Civil Engineering*, 15, 609–615.

Dupre, W. R., and Thompson, R. (1979). The Yukon Delta: a model for deltaic sedimentation in an ice-dominated environment. 11th Annual Offshore Technology Conference, 657–664.

Eardley, A. J. (1938). Yukon channel shifting. Bulletin of the Geological Society of America, Vol. 49, 343–358.

Einstein, H. A. (1950). The bedload function for sediment transport in open channels. Technical Bulletin 1026, U.S. Dept of Agriculture, Washington, D.C.

Einstein, H. A., and Barbarossa, N. (1952). "River channel roughness." *Transactions of the ASCE*, 117(2528).

Engelhardt, B., and Waren, G. (1991). "Upper Missouri River bank erosion." Report prepared by North Dakota and Montana, North Dakota State Water Commission, Bismark, N.D.

Engelund, F., and Hansen, E. (1967). "A monograph on sediment transport in alluvial streams." *Teknisk Forlag*, Technical University of Denmark, Copenhagen.

Ettema, R. (1999). "A review of river-ice impacts on alluvial-channel stability." *Canadian Workshop on River Ice*, Canadian National Research Council, Ottawa, Ont., 125–140.

Ettema, R., Braileanu, F., and Muste, M. (2000). "A method for estimating sediment transport in ice-covered channels." *Journal of Cold Regions Engineering,* 14(2), 130–145.

Ettema, R., and Muste, M. (2001). "Laboratory observations of ice jams in channel confluences." *Journal of Cold Regions Engineering,* 15(1), 41–51.

Ettema, R., Muste, M., and Kruger, A. (1999). "Ice jams at river confluences." *CRREL Report 99-6,* U.S. Army Corps of Engineers, Cold Regions Research and Engineering Laboratory, Hanover, N.H.

Gatto, L. W. (1988). "Techniques for measuring reservoir bank erosion." *Special report 88-3*, U.S. Army Corps of Engineers, Cold Regions Research and Engineering Laboratory, Hanover, N.H.

Gatto, L. W. (1995). "Soil freeze-thaw effects on bank erodibility and stability." *Special Report 95-24*, U.S. Army Corps of Engineers, Cold Regions Research and Engineering Laboratory, Hanover, N.H.

Gogus, M., and Tatinclaux, J-C. (1981). "Mean characteristics of asymmetric flows: application to flow below ice jams." *Canadian Journal of Civil Engineering*, 8(3), 342–350.

Hamelin, L.-E. (1979). "The bechevnik: A river bank feature from Siberia." *The Musk Ox*, 25, 70–72.

Hanjalic, K., and Launder, B. E. (1972). "Fully developed asymmetric flow in a plane channel." *Journal of Fluid Mechanics*, 51, 301–335.

Harlan, R. L., and Nixon, J. F. (1978). "Section 3: Ground thermal regime." *Geotechnical engineering for cold regions*, O. Andersland and D. M. Anderson, eds., McGraw-Hill, New York.

Ho, P. Y. (1939). "Dependence of bedload movement on grain shape and water temperature." *Mitteilungen der Preusssischen Versuchsanstalt fuer Wasser-, Erd-, und Schiffbau*, 39.

Hong, R.-J., Karim, F., and Kennedy, J. F. (1984). "Low-temperature effects on flow in sand-bed streams." *ASCE Journal of Hydraulic Engineering*, 110(2), 109–125.

Huang, J. (1981). "Experimental study of settling properties of cohesive sediment in still water." *Journal of Sediment Research*, (2), 30–42.

Interagency Committee. (1957). "Some fundamentals of particle size analysis, a study of methods used in measurement and analysis of sediment loads in streams." *Report 12*, Subcommittee on Sedimentation, Interagency Committee on Water Resources, St Anthony Falls Hydraulic Laboratory, Minneapolis, Minn.

Johnston, G. H. (Ed.). (1981). *Permafrost: Engineering design and construction*. Wiley, New York.

Kellerhals, R., and Church, M. (1980). "Comment on 'Effects of channel enlargement by river ice processes on bankfull discharge in Alberta, Canada,' by Smith, D. G." *Water Resources Research*, 16(6), 1131–1134.

Kempema, E. W. (1998). "Nearshore ice formation and sediment transport in southern Lake Michigan. Ph.D. thesis, University of Washington, Seattle.

Kempema, E. W., Reimnitz, E., Clayton, J. R., and Payne, J. R. (1993). "Interactions of frazil and anchor ice with sedimentary particles in a flume." *Cold Regions Science and Technology*, 21, 137–149.

Kempema, E. W., Reimnitz, E., and Hunter, R. E. (1986). "Flume studies and field observations of the interaction of frazil ice and anchor ice with sediments." *Open-File Report 86-515*, U.S. Geological Survey, Menlo Park, Calif.

Kerr, D. J., Shen, H.T., and Daly, S. F. (1998). "Evolution and hydraulic resistance of anchor ice on gravel beds." *Proc. of the International Association for Hydraulic Research, 14th Ice Symposium*, International Association for Hydraulic Research, Delft, the Netherlands, 703–710.

Kindle, E. M. (1918). "Notes of sedimentation in the Mackenzie River Basin." *Journal of Geology*, 26, 341–360.

King, W. A. and Martini, I. P. (1984). "Morphology and recent sedimentations of the anastomizing reaches of the Attawapiskat River, James Bay, Ontario, Canada." *Sedimentary Geology*, 37(4), 295–320.

Lane, E. W. (1957). "A study of the shape of channels formed by natural streams flowing in erodible material." *Missouri River Series Report No. 9*, U.S. Army Corps of Engineers, Missouri River Division, Omaha, Neb.

Lane, E. W., Carlson, E. J., and Hanson, O. S. (1949). "Low temperature increase in sediment transportation in Colorado River." *Civil Engineer*, 19, 619–621.

Lau, Y. L., and Krishnappan, B. G. (1985). "Sediment transport under ice cover." *Journal of Hydraulics Division, ASCE*, 111(6), 934–950.

Lawson, D. E. (1983). "Erosion of perennially frozen streambanks." *CRREL Report 83-29*, U.S. Army Corps of Engineers, Cold Regions Research and Engineering Laboratory, Hanover, N.H.

Lawson, D. E. (1985). "Erosion of northern reservoir shores: Analysis and application of pertinent literature." *Monograph 85-1*, U.S. Army Cold Regions Research and Engineering Laboratory, Hanover, N.H.

Lawson, D. E., Chacho, E. F., Brockett, B. E., Wuebben, J. L., Collins, C. M., Arcone, S. A., and Delaney, A. J. (1986). "Morphology, hydraulics and sediment transport of an ice-covered river: Field techniques and initial data." *Report 86-11*, U.S. Army Corps of Engineers, Cold Regions Research and Engineering Laboratory, Hanover, N.H.

Mackay, J. R., and Mackay, D. K. (1977). "The stability of ice-push features, Mackenzie River, Canada." *Canadian Journal of Earth Sciences*, 14(10), 2213–2225.

Mackay, D. K., Sherstone, D. A., and Arnold, K. C. (1974). "Channel ice effects and surface water velocities from aerial photography of Mackenzie River break-up." *Hydrological aspects of northern pipeline development*. Report No. 74-12, Task Force on Northern Oil Development, Environmental-Social Program, Northern Pipelines, Saskatoon, Sask., Canada.

Marcotte, N. (1984). "Anchor ice in Lachine Rapids: Results of observations and analysis." *Proc. IAHR Symposium on Ice*, 1, 151–159.

Martin, N., Roy, A. G., and Bergeron, N. E. (1996). "Structure of turbulent flow in an ice-covered tidal environment." *Proc. 2nd International Symposium on Habitat Hydraulics,* INRS-Eau, Quebec, A435–A445.

Martin, S. (1981). "Frazil ice in rivers and oceans." *Annual Review of Fluid Mechanics*, 13, 379–397.

Martinson, C. (1980). "Sediment displacement in the Ottauquechee River—1975–1978." *CRREL Special Report 80-20*, U.S. Army Corps of Engineers, Cold Regions Research and Engineering Laboratory, Hanover, N.H.

Marusenko, Y. I. (1956). "The action of ice on river banks." *Priroda*, 45(12), 91–93.

Matousek, V. (1984). "Types of ice and conditions for their formation." *Proc. IAHR Ice Symposium*, International Association for Hydraulic Research, Delft, the Netherlands, 1, 315–327.

Mercer, A. G., and Cooper, R. H. (1977). "River bed scour related to the growth of a major ice jam." *Proc. 3rd National Hydrotechnical Conference*, Canadian Society of Civil Engineers, Toronto, Ont., 291–308.

Meyer-Peter, E., and Muller, R. (1948). "Formulas for bedload transport." *Second Congress International Association for Hydraulic Research*, International Association for Hydraulic Research, Delft, the Netherlands, 39–64.

Michel, B. (1971). "Winter regime of rivers and lakes." *CRREL Monograph III-IBa*, U.S. Army Corps of Engineers, Cold Regions Research and Engineering Laboratory, Hanover, N.H.

Michel, B. (1972). "Properties and processes of river and lake ice." *Proc. The Role of Ice and Snow in Hydrology*, Publication No. 107, International Association for Scientific Hydrology, Grenoble, France, 454–481.

Michel, B. (1978). *Ice mechanics*. University of Laval Press, Laval, Que., Canada.

Milburn, D., and Prowse, T. D. (1998). "The role of an ice cover on sediment transport and deposition in a northern delta." *Proc. IAHR Ice Symposium,* International Association for Hydraulic Research, Delft, the Netherlands, 189–196.

Morse, B., Burrell, B., St. Hilaire, A., Bergeron, N., Messier, D., and Quach, T. T. (1999). "River ice processes in tidal rivers: Research needs." *Canadian River Ice Workshop,* University of Manitoba, Winnipeg, 388–399.

Muste, M., Braileanu, F., and Ettema, R. (2000). "Flow and sediment-transport measurements in simulated ice-covered channel." *Water Resources Research*, 36(9), 2711–2720.

Neill, C. R. (1976). "Scour holes in a wandering gravel river." *Proc. Symposium on Inland Waterways for Navigation, Flood Control, and Water Diversions, 3rd Annual Conf. Of ASCE Waterways, Harbors and Coastal Engineering Division*, ASCE, New York, 1301–1317.

Neill, C. R. (1982). "Hydrologic and hydraulic studies for northern pipelines." *Proc. Canadian Society of Civil Engineering Annual Conference,* Canadian Society of Civil Engineers, Toronto, Ont., 247–256.

Newbury, R. W. (1982). *The Nelson River: A study of sub-Arctic processes*. John Hopkins University Press, Baltimore, Md.

Nezhikovskiy, R. A. (1964). "Coefficients of roughness of bottom surface of slush ice cover." *Transactions of the State Hydrologic Institute* (Trudy GGI), (110), 54–82.

Osterkamp, T. E., and Gosink, J. (1983). "Frazil ice formation and ice-cover development in interior Alaska streams." *Cold Regions Science and Technology*, 8, 43–56.

Prowse, T. D. (1993). "Suspended sediment concentration during river ice breakup." *Canadian Journal of Civil Engineering*, 20, 872–875.

Prowse, T. D. (2001). "Rice-ice ecology. I: Hydrologic, geomorphic and water-quality aspects." *ASCE Cold Regions Engineering*, 15(1), 17–33.

Raudkivi, A. J. (1998). *Loose boundary hydraulics.* A. A. Balkema, Rotterdam, the Netherlands.

Reid, J. R. (1985). "Bank-erosion processes in a cool-temperate environment, Orwell Lake, Minnesota." *Geological Society of America Bulletin*, 96(6), 781–792.

Reimnitz, E., and Kempema, E. W. (1987). Field observations of slush ice generated during freeze up in arctic coastal waters. *Marine Geology*, 77, 219–231.

Reynolds, A. J. (1974). *Turbulent flows in engineering*. Wiley, New York.

Sayre, W. W., and Song, G. B. (1979). "Effects of ice covers on alluvial channel flow and sediment transport processes." *IIHR Report No. 218*, Iowa Institute of Hydraulic Research, The University of Iowa, Iowa City, Ia.

Schumm, S. A. and Khan, H. R., (1972). "Experimental Study of Channel Patterns."*Geological Society of America Bulletin,* 83, 1755–1770.

Scott, K. M. (1978). "Effects of permafrost on stream channel behavior in Arctic Alaska." *Professional Paper No. 1068*, U.S. Geological Survey, Washington, D.C.

Scrimgeour, G. J., Prowse, T. D., Culp, J. M., and Chambers, P. A. (1994). "Ecological effects of river ice break-up: A review and perspective." *Freshwater Biology*, 32, 261–275.

Shen, H. T., and Wang, H. Y. (1995). "Under cover transport and accumulation of frazil granules." *Journal of Hydraulic Engineering, ASCE*, 121(2), 184–195.

Simon, A. Shields, F. D., Ettema, R., Alonso, C., Marshall-Garsjo, M., Curini, A., and Steffen, L. (1999). "Channel erosion on the Missouri River, Montana, between Fort Peck Dam and the North Dakota Border." *Technical Report*, USDA-Agricultural

Research Service, National Sedimentation Laboratory, Oxford, Miss.

Smith, B., and Ettema, R. (1997). "Flow resistance in ice-covered alluvial channels." *Journal of Hydraulic Engineering, ASCE*, 123(7), 592–599.

Smith, D. G. (1979). "Effects of channel enlargement by river ice processes on bankfull discharge in Alberta, Canada." *Water Resources Research*, 15(2), 469–475.

Straub, L. G. (1955). "Effect of water temperature on suspended sediment load in an alluvial river." *Proc. 6th General Meeting of IAHR*, International Association for Hydraulic Research, Delft, the Netherlands, D25-1–D25-5.

Sukhodolov, A., Thiele, M., Bungartz, H., and Engelhardt, C. (1999). "Turbulence structure in an ice-covered, sand-bed river." *Water Resources Research*, 35(3), 889–894.

Taylor, B. D., and Vanoni, V. (1972). "Temperature effects in low-transport flat-bed flows." *Journal of Hydraulics Division, ASCE*, 98(HY8), 1427–1445.

Terada, K., Hirayama, K., and Sasamoto, M. (1997). "Field measurements of anchor and frazil ice." *Proc. IAHR Symposium on Ice*, International Association for Hydraulic Research, Delft, the Netherlands, 2, 697–702.

Tietze, W. (1961). "Uber die Erosion von unter Eis Fliessendem Wasser." *Mainzer Geographische Studien*, 125–141.

Tsai, W.-F., and Ettema, R. (1994). "Ice cover influence on transverse bed slopes in a curved alluvial channel." *Journal of Hydraulic Research*, 32(4), 561–581.

Tsang, G. (1982). *Frazil and anchor ice: A monograph*. National Committee on Hydraulics of Ice Covered Rivers, National Research Council of Canada, Ottawa, Ont., Canada.

Tuthill, A., and Mamone, A. C. (1997). "Selection of confluence sites with ice problems for structural solutions." *CRREL Special Report 97-4*, U.S. Army Corps of Engineers, Cold Regions Research and Engineering Laboratory, Hanover, N.H.

Tywonik, N., and Fowler, J. L. (1973). "Winter measurement of suspended sediments." *Proc. IAHS Conf. on the Role of Snow and Ice in Hydrology*, International Association for Hydraulic Science, Grenoble, Switzerland, 814–827.

U.S. Army Corps of Engineers (USACE). (1983). "Galena streambank protection." *Galena, Alaska Section 14 Reconnaissance Report*, U.S. Army Corps of Engineers, Alaska District, Anchorage, Ak.

Uunila, L. S. (1997). "Effects of river ice on bank morphology and riparian vegetation along the Peace River, Clayhurst to Fort Vermilion." *Proc. 9th Workshop on River Ice*, Natural Research Council of Canada, Ottawa, Ont., 315–334.

Wentworth, C. K. (1932). "The geologic work of ice jams in sub-Arctic river." *Contributions in geology and geography*, L. F., Thomas, ed., Washington University Studies, Science and Technology No. 7, Washington University, St Louis, Mo., 49–82.

Wigle, T. E. (1970). "Investigations into frazil, bottom ice, and surface ice formation in the Niagara River." *Proc. IAHR Symposium on Ice and Its Action*, International Association for Hydraulic Research, Delft, the Netherlands, Paper 2.8.

Wuebben, J. L. (1986). "A laboratory study of flow in an ice-covered sand bed channel." *Proc. 8th IAHR Symposium on Ice,* International Association for Hydraulic Research, Delft, the Netherlands, 1–8.

Wuebben, J. L. (1988a). "A preliminary study of scour under an ice jam." *Proc. 5th Workshop on Hydraulics of River Ice/Ice Jams*, National Research Council of Canada, Ottawa, Ont., 177–190.

Wuebben, J. L. (1988b). "Effects of an ice cover on flow in a movable bed channel." *Proc. 9th IAHR Symposium on Ice*, International Association for Hydraulic Research, Delft, the Netherlands, 137–146.

Wuebben, J. L. (1995). "Chapter 31: Ice effects on riprap." *River, Coastal and Shoreline Protection: Erosion Control Using Riprap and Armourstone*, C. R. Thorne, S. Abt, S. T. Barends, and K.W. Pilarczyk, eds., Wiley, New York, 513–530.

Wuebben, J. L., and Gagnon, J. J. (1995). "Ice jam flooding on the Missouri River near Williston, North Dakota." *CRREL Report 95-19*, U.S. Army Corps of Engineers, Cold Regions Research and Engineering Laboratory, Hanover, NH.

Yalin, M. S., (1992). *River Mechanics.* Pergamon Press, Oxford, Britain.

Zabilansky, L. (1998). "Scour measurements under ice." *Proc. ASCE Conf. Water Resources Engineering*, ASCE, Reston, Va., 1, 151–156.

Zabilansky, L., Ettema, R., Wuebben, J. L., and Yankielun, N. E. (2002). "Survey of river-ice influences on channel bathymetry along the Fort Peck reach of the Missouri River, winter 1998–1999." *CRREL Report* (in press), U.S. Army Corps of Engineers, Cold Regions Research and Engineering Laboratory, Hanover, N.H.

Copyrighted Materials
Copyright © 2008 American Society of Civil Engineers (ASCE)
Retrieved from www.knovel.com

CHAPTER 14

Computational Modeling of Sedimentation Processes

William A. Thomas and Howard Chang

14.1 INTRODUCTION

The notion that a river channel is stable is often accompanied by the mental image of a river channel whose bed profile, cross sections, and channel pattern do not change over time. However, dynamic equilibrium is a more appropriate concept for describing a stable alluvial channel. Dynamic equilibrium is the process by which an alluvial river transports its water-sediment mixture. Typical responses of a channel that is in dynamic equilibrium are deposition of sediment on the bed and erosion from it, channel widening and channel narrowing, bank failure and bank migration, smoother banks and rougher banks, the growth and removal of bank vegetation, and changes in the channel planform. Seldom do these processes occur singly. They are closely interrelated, and they seem to be delicately balanced to maintain a dynamic state of equilibrium. Experience has shown that changing or limiting one of these responses can impact the others (see Chapter 18).

The study of how a river develops is called river morphology by Leopold (1994) and Rosgen (1996) and fluvial geomorphology by Schumm (1971). River morphology studies correlate the dimensions, planform, and movement of a river channel with the historical loads imposed on it (see Chapter 6). The river can be described in terms of six variables:

channel width;
channel depth;
channel slope;
hydraulic roughness;
bank line migration;
channel pattern.

For example, the historical channel width is correlated with the historical water discharges and the type of materials that formed the banks of the channel. The channel depth and longitudinal slope are correlated with water discharge and the size of sediment particles. The meander pattern and changes in channel planform are correlated with channel width, slope, and water discharge. In each case these variables are correlated with the load imposed on the river. That load is composed of the water-sediment mixture conveyed by the river and the base-level energy control.

However, the correlations are empirical and do not describe the physics of the processes. Without physical theories one is not able to calculate the reaction of a channel to changes in the loads imposed upon it. Therefore, river morphology studies alone are not adequate for project design, but they do make valuable contributions to river engineering. First, they identify the variables that river engineers must analyze and change in the design of a new project or in the restoration of an existing river to a historical condition. Second, river morphology studies recognize that those variables are interrelated. Third, the variables are identified as the dependent variables in a river system and not the independent variables. Fourth, the river morphology approach recognizes that the materials through which a natural river flows are extremely diverse, and it allows nature to aggregate the microdistributions of force and resistance into average values for the six variables listed above. Finally, river morphology studies provide a framework for identifying and organizing the data that are essential for the computational modeling of river systems.

This chapter presents a systematic procedure for applying one-dimensional computational sedimentation models to the study of alluvial rivers. A computational sedimentation model includes the five basic processes of sedimentation: erosion, entrainment, transportation, and deposition of mixtures of sediment particles, and compaction of sediment deposits. Of paramount importance is the fact that computational sedimentation models may include only some of the equations that are needed to predict the morphology of a river channel. Therefore, the river morphology equations that are included in one-dimensional computational sedimentation models need to be identified, and the model should then be used in combination with river morphology principles to perform the desired sediment study.

The water-sediment mixture conveyed by a channel and the base-level control go together to determine the load on the river system. The load is the independent variable in the correlations discussed above. The six variables that are listed are the dependent variables. The significance of classifying these variables as either dependent or independent has to do with project stability. A design can change the value of an independent variable, but if a dependent variable is changed it will not remain changed. For example, a project in which the channel width is increased will not function as designed without continual maintenance because channel width is a dependent variable. Two- and three-dimensional models are discussed in Chapter 15.

14.2 LOCAL SCOUR AND DEPOSITION

This chapter does not address local scour or deposition. Local scour, as compared to channel degradation, refers to the scour hole that forms around a bridge pier, downstream from a hydraulic structure, along the outside of a bend, etc. The process involves fluid forces beyond local boundary shear. Such forces come from three-dimensional flow accelerations, pressure fluctuations, and gravity forces on the sediment particles. Three-dimensional computational models that make such calculations are in various stages of development, but at present the complexity of local scour processes relegates analysis to empirical equations or physical model studies.

Local deposition refers to deposits over a relatively small space, as opposed to channel aggradation, which raises the bed profile of the river over a substantial distance. Local deposition can be predicted with one-dimensional equations provided that adequate attention is given to the rate of expansion of the flow, both horizontally and vertically.

14.3 GENERAL EQUATIONS FOR FLOW IN MOBILE BOUNDARY CHANNELS

14.3.1 Energy and Continuity Equations

The one-dimensional differential equations of gradually varied unsteady flow in movable bed channels are extensions of the Saint-Venant equations for rigid boundary channels. They are the equation of continuity for sediment, the equation of continuity for water, and the equation of motion for the water-sediment mixture. The forms developed by Chen (1973) are as follows:

$$\frac{\partial(\rho Q)}{\partial t}+\frac{\partial(\rho QU)}{\partial x}+gA\frac{\partial(\rho y)}{\partial x} = \rho gA\,(S_o-S_f+\mathrm{D}_l) \tag{14-1}$$

$$\frac{\partial Q}{\partial x}+\frac{\partial A}{\partial t}+\frac{\partial A_d}{\partial t}q_w=0 \tag{14-2}$$

$$\frac{\partial G_s}{\partial x}+(1-P)\frac{\partial A_d}{\partial t}+\frac{\partial A_s}{\partial t}-g_s=0 \tag{14-3}$$

where

A = end area of channel cross section;
A_d = volume of sediment deposited on the bed per unit length of channel;
A_s = volume of sediment suspended in the water column per unit length of channel;
D_l = momentum loss due to lateral inflow;
g = acceleration of gravity;
G_s = sediment discharge;
g_s = lateral sediment inflow per unit length of channel, outflow (−), inflow (+);
P = porosity of the bed deposit (volume of voids divided by the total volume of sample);
Q = water discharge;
q_w = lateral water inflow per unit length of channel, outflow (−), inflow (+);
S_f = friction slope;
S_o = slope of channel bottom;
t = time;
U = flow velocity;
x = horizontal distance along the channel;
y = depth of flow;
ρ = density of the water.

The following assumptions were cited in deriving these equations:

1. The channel is sufficiently straight and uniform in the reach so that the flow characteristics may be physically represented by a one-dimensional mode.
2. The velocity is uniformly distributed over the cross section.
3. Hydrostatic pressure prevails at every point in the channel.
4. The water surface slope is small.
5. The density of the sediment-laden water is constant over the cross section.
6. The unsteady-flow resistance coefficient is assumed to be the same as for steady flow in alluvial channels and is approximated from resistance equations applicable to alluvial channels or from field survey.

14.3.2 Sediment Transport Equations

Sediment transport equations are so numerous and varied that only the most general functional form is selected to demonstrate the significant parameters,

$$G_s = f(\overline{U}, r, S_f, b, d_e, s, \mathrm{SF}, d_{si}, P_i, s_l, T, C_{fm}) \tag{14-4}$$

where

$\overline{U}$ = mean velocity at vertical;
r = hydraulic radius;

S_f = slope of energy gradient;
b = width;
d_e = effective grain size of the bed material mixture;
s_s = specific gravity of the particles;
SF = shape factor of the particles $_i$ in the bed mixture;
D_{si} = diameter of each size class, $_i$ in the bed mixture;
P_i = fraction of each size class, $_i$ in the bed mixture;
s_f = specific gravity of the fluid;
T = water temperature;
C_{fm} = concentration of fine sediment in the water column.

The variables U, r, S_f, and b are the hydraulic parameters. Sediment grain parameters are d_e, s_s, SF, D_{si}, and P_i. Fluid parameters are $S_p G_f$, T, and C_{fm}.

Computational modeling requires that sediment transport be calculated by size class. Therefore, if the transport function is a single-grain-size representation, the computational model must provide a separate bed-sorting algorithm to account for hiding and armoring processes. Even the multiple-grain-size functions require additional, sophisticated bed-sorting algorithms to accommodate the nonequilibrium conditions in the entrainment, transportation, and deposition processes being modeled (Copeland 1993).

To date most researchers in sedimentation have dealt with sand-bed streams (see Chapter 2). Less is known about gravel transport (see Chapter 3). Even less research has been conducted on cobble/boulder transport than has been conducted for gravels. Cohesive sediment transport is not understood as well as noncohesive sedimentation (see Chapter 4). The processes include electrochemical forces, and the presence of the sediment particles can change the properties of the water-sediment mixture. Transport capacity does not obey the equilibrium principle, which states that the number of particles being deposited must equal the number being eroded.

14.3.3 Diffusion and the Diffusion Equation

In mathematical modeling of sediment processes, the sediment discharge potential is computed at each discrete cross section. These potentials reflect the current hydrodynamic forces in the flow field. However, the actual suspended sediment concentration profiles do not adjust immediately to changes in hydrodynamic forces. Both advection and diffusion are significant processes in the physics of adjustment.

The concepts of diffusion in turbulent flow are presented in Chapter 2 of this volume. For nonequilibrium sediment transport, the transport potential must be corrected for the advection-diffusion processes to account for conditions where the development length for equilibrium sediment transport is longer than the grid size δx. The correction for deposition is different from the correction for entrainment.

One approach to accommodating the diffusion process is to include the advection-diffusion equation in the entrainment and deposition calculations for material moving between the bed and the water column. Another approach is to approximate the diffusion process with entrainment and deposition coefficients. In either case the objective is to distinguish between the actual transport rate C_s' and the transport capacity C_s for the equilibrium condition.

Generally,

$$C_s' < C_s \quad \text{for} \quad U/x > 0 \tag{14-5}$$

and

$$C_s' > C_s \quad \text{for} \quad U/x < 0 \tag{14-6}$$

In the diffusion theory of sediment transport, the concentration of suspended load C is described by the convection-diffusion equation,

$$\frac{\partial C}{\partial t} + u\frac{\partial C}{\partial x} + \frac{\partial}{\partial x}\epsilon_x \frac{\partial C}{\partial x} = -\alpha w_s (C - C_*) \tag{14-7}$$

The first term in Eq. (14-7) accounts for a nonsteady concentration of sediment with respect to time. The second term accounts for the nonuniform distribution of concentration in the direction of flow. Each of those two terms is zero for equilibrium sediment transport with no local inflows. The third term accounts for the diffusion process.

The right-hand side of the equation accounts for the mass transfer between the bed and the water column. Mass transfer is based on the sediment deposition and the entrainment rates, where C_* is the equilibrium concentration of sediment or the potential carrying capacity of a specific flow, and α is a dimensionless coefficient that characterizes the rate at which the new carrying capacity is attained. The term $-w_s C$ represents the actual flux; the second term, $w_s C_*$, is the transport capacity flux. In other words, the rate of deposition (or entrainment) by the flow is proportional to the difference between the actual suspended load and the sediment transport capacity of the flow.

The value of α must be determined separately for the cases of deposition and entrainment because of the different physical forces that dominate. The deposition case is the simpler of the two because it depends on the settling velocity of the sediment particles. Zhang et al. (1983) propose the expression

$$\alpha = 1 + \frac{\mathsf{P}}{2} \tag{14-8}$$

where P is the Peclet number, defined as $6w_s/\tau U_*$.

In the case of entrainment, they propose the following relationship for α':

$$\alpha' = \frac{2}{P} + \frac{P}{4} \tag{14-9}$$

In solving Eq. (14-7) appropriate boundary conditions and initial conditions are required. The upstream boundary condition is given by

$$C = C_o \text{ at } x = x_o \tag{14-10}$$

where the subscript o designates values at the upstream boundary.

Another approach to accommodating the diffusion process in sedimentation modeling is using entrainment and deposition coefficients. In the case of deposition the settling velocities of the individual sediment grain sizes can be used to calculate the deposition coefficients. However, the entrainment process is not associated as strongly with the settling velocity of the sediment particles as it is with the hydrodynamic forces in the flow field. A surrogate parameter for estimating the entrainment coefficient is flow distance. Flow distance refers to the distance that the water-sediment mixture has to travel before the velocity and sediment concentration profiles reach equilibrium. The concept comes from physical modeling in a flume. Some claim that, in a flume, the distance from the headgate that is required for the flow to attain the theoretical vertical velocity-distribution profile predicted by the log-velocity distribution law is 100 times the flow depth. By similitude, the travel distance in the flume can be used to approximate requirements in the river. For example, use flow depth as the scaling parameter. Therefore, the distance in the river that is needed for the sediment concentration to increase from a lower to a higher equilibrium value could be approximated as a coefficient times the flow depth.

14.3.4 Allocation of Scour and Fill

In one-dimensional modeling the solution of the sediment continuity equation provides a change in the cross-sectional area. That end area change must then be allocated to each coordinate point across the cross section. Different computational models approach the allocation calculation differently. In any case the computation of sedimentation processes is one-dimensional, which, at best, relegates the allocation calculation to an approximation. Consequently, the shape of the cross section is not a question to address with a one-dimensional sediment model. Perhaps some observations of different conditions will aid in understanding the different modeling approaches to this issue.

Emmett and Leopold (1963) investigated scour and fill of the bed profile and of the channel cross section in both ephemeral and perennial streams. They used scour chains, so conditions during the passage of the hydrograph were not measured. However, in a stable river channel on a perennial stream, sediment tends to deposit in the crossings and to erode from the bends during a flood event. After the flood passes, the deposition/erosion sequence will switch, so the crossings will tend to erode and sediment will deposit in the bends. The distribution of erosion and deposition across a cross section will be shaped by the same hydraulic forces that shaped the initial cross sections. Therefore, deposition will not be horizontal nor will it fill the deepest portion of the cross section first. The allocation can be made as a veneer over the surface of the original cross section. Similitude suggests that both deposition and erosion can be applied to the cross section using the veneer concept. Thomas utilized this concept in developing HEC-6 (HEC-6 1977; 1993; Thomas 2002).

In the ephemeral channels of the arid southwest, visual observation suggests that the surface of the channel cross section is usually horizontal at the beginning and at the end of a runoff event. However, during the flood runoff it is reasonable to suspect that the cross section will be reshaped by hydrodynamic forces and sedimentation processes appropriate for flow through a river bend. That is, the secondary flow cells will move the thalweg toward the outside of the bend and will form the classical point bar pattern on the inside of the bend. In ephemeral streams the veneer concept is probably a poor approximation to actual sedimentation processes in the cross section during the passage of an flood event. Chang utilized that observation in developing FLUVIAL12 (1985).

A horizontal deposit is more likely in reservoir deposition than it is in a river channel. In a reservoir the bed material load seems to deposit in the original channel section first. It fills the channel feature, and the water-sediment mixture spills out laterally. When the reservoir level falls the channel will cut through the delta deposit in, perhaps, some new location. However, unless there is a change in the runoff discharges, the width and depth of the new channel will be very similar to those of the original channel. Consequently, a one-dimensional model is able to predict the rate of delta growth and the resulting water surface elevations even though it does not mimic the channel avulsion process.

The physics of sedimentation processes are such that a natural levee tends to build along the top bank of the channel (James 1985). Those forces are also active in reservoir deposition. Sediment size and water velocity are the significant parameters in determining how far sediment particles move away from the channel. This is not a one-dimensional process, and one-dimensional models approximate the process differently.

Some sedimentation models are built around the concept that the width and depth of a river channel will be adjusted to effectively reduce the streamwise variation in stream power as the river seeks to establish a new equilibrium. In such models, the allocation of scour and fill across a section for a time step is assumed to be a power function of the effective tractive force $\tau_o - \tau_c$. Chang proposes the equations for allocating scour and fill

$$\Delta z = \frac{(\tau_o - \tau_c)^m}{\sum_B (\tau_o - \tau_c)^m} \frac{\Delta A_b}{\Delta Y} \tag{14-11}$$

where

Δz = the local correction in channel-bed elevation;
$\tau_o = \gamma DS$ = local tractive force;
τ_c = critical tractive force;
m = exponent;
y = horizontal coordinate; and
B = channel width.
The value of τ_c is zero in the case of fill.

The m value in Eq. (14-11) is generally between 0 and 1; it affects the pattern of scour-fill allocation. For the schematic cross section shown in Fig. 14-1, a small value of m, say 0.1, would mean a fairly uniform distribution of Δz across the section; a larger value, say 1, would give a less uniform distribution of Δz, and the local change will vary with the local tractive force or will vary roughly with the depth. The value of m is determined at each time step so the correction in channel bed profile will result in the most rapid movement toward uniformity in power expenditure, or linear water surface profile, along the channel.

Equation (14-11) can only be used in the absence of channel curvature. The change in bed area at a cross section in a curved reach is

$$\Delta A_b = \frac{1}{r_f} \int r \, dz dr \tag{14-12}$$

where r_f is the radius of curvature at the discharge centerline or thalweg. Because of the curvature, adjacent cross sections are not parallel and the spacing Δs between them varies across the width. Therefore, the distribution of Δz given in Eq. (14-11) needs to be weighted according to the r-coordinate with respect to the thalweg radius r_f/r (Chang, 1985). The equation is

$$\Delta z = \frac{(\tau_o - \tau_c)^{m/r}}{\sum_B (\tau_o - \tau_c)^{m/r}} \cdot \frac{\Delta A_b}{\Delta r} \tag{14-13}$$

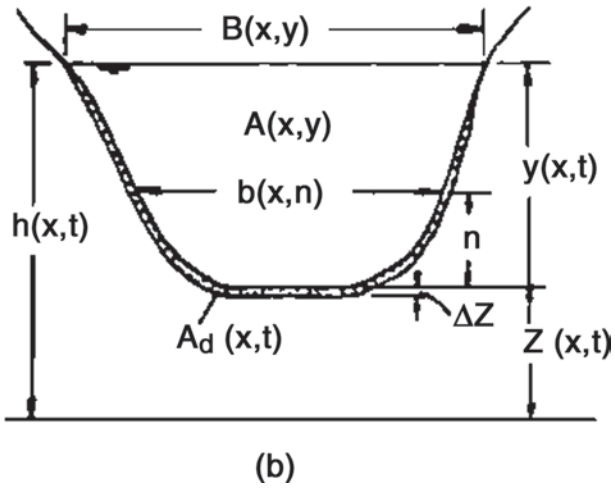

Fig. 14-1. Schematic cross-sectional change.

14.3.5 Channel Width

Channel width is one of the morphological variables listed previously. If the channel is too narrow for the runoff hydrology, the banks will erode, causing the channel width to increase. Likewise, in a channel experiencing bed erosion, banks will fail, resulting in channel widening. Modelers must accommodate changes to channel width, and the approach depends on the requirements of the model.

14.3.6 Planform and Bankline Migration

The natural alignment of an alluvial river channel is the result of hydrodynamic forces, sedimentation processes, and soil mechanics principles (see Chapter 8). The hydrodynamic forces are calculated from the conservation of energy, conservation of mass, and flow resistance. Sedimentation processes, as defined above, are the erosion, entrainment, transportation, and deposition of mixtures of sediment particles and the compaction of sediment deposits. Soil mechanics principles describe bank stability. However, channel-bed and bank materials are not homogeneous. The native materials range from inorganic and organic sediment particles to vegetation. The inorganic sediments range from cohesive clays to noncohesive boulders, and the organic sediments range from leaves to large woody debris. These different materials exhibit different strengths and weaknesses. They resist hydrodynamic forces via complex interactions that vary in time and space. For example, bank failure will remove trees and vegetation from the banks, resulting in a change of bank roughness. The effect of such a change in boundary roughness on energy dissipation is especially significant when the width/depth ratio is small.

For example, during the decade of the 1950s, creeks in northern Mississippi were converted into straight canals to improve drainage. The conversion changed the channel width and the slope. The first reaction of the creeks was erosion of the bed. Soon the bed had eroded so deeply that the banks became too high to remain stable, and bank failures occurred on a grand scale. As the channel became deeper, the bank-full water discharge increased, and that increased the amount of the total runoff energy that had to be dissipated on the channel bed and banks. The eroded banks not only were exposed to larger stresses from the larger channel discharges but also were exposed to erosive forces from raindrop impact.

At the same time that bank failure was increasing the channel capacity, it was reducing the hydraulic roughness. Two processes were involved. First, as the width/depth ratio increased, the effect of bank roughness on the composite hydraulic roughness of the channel cross section increased.

Second, the eroding banks removed the prevailing vegetation and prevented new growth. Consequently, the benefit of vegetation roughness on the banks was eliminated.

As the water and sediment mixture left the channelized reach at the downstream end, it entered the natural creek. However, the concentration of bed material load in the flow from the channelized reach was higher than could be transported in the natural creek. Transport capacity had returned to prechannelized conditions and was considerably less than in the channelized portion of the creek. Consequently, a deposition zone developed. The new deposits changed the current pattern, which initiated a new meander pattern. It is significant that where the channels were straightened during construction, they remained straight during the eroding phase of the channel evolution. However, when flow reached the deposition zone, channel meander intensified.

As time passed, all six channel parameters changed in the creeks of northern Mississippi. The amount of change showed significant variation from place to place. It is common to apply computational models to such problems and to use river morphology principles in developing the one-dimensional model. The channel evolution model proposed by Schumm et al. (1984) describes these processes.

The development of a river channel is often controlled by the microdistribution of its boundary materials along the stream corridor and not by the average of these distributions. Moreover, a single downed tree can realign an entire channel, change the channel pattern, and not change the channel width.

14.4 SIMILARITY BETWEEN COMPUTATIONAL MODEL STUDIES AND PHYSICAL MODEL STUDIES

A computational model study can be organized into ten tasks as follows:

1. Assemble available data from office files: maps, cross sections, suspended sediment measurements, bed load data, bed material measurements, soil types/sediment yield, hydrographs, water temperature, observed water surface profiles, reservoirs in the basin, construction activities.
2. Develop geometric data set and run a steady-state water discharge: run a 2-year peak discharge to identify trouble spots and data gaps.
3. Make a reconnaissance trip through the study area: identify locations of bank and bed instability; observe features that will aid in establishing n-values of the bed, banks, and overbanks; give particular attention to locations appearing to be trouble spots; prepare requests for additional/missing data.
4. Calibrate n-values: run the model in fixed-bed mode to compare calculated water surface elevations to observed values; add sediment and run the model in movable-bed mode; confirm that the calculated water surface approximates the observed value.
5. Develop the sedimentary data set: develop the bed gradation; develop the inflowing sediment concentration; select the transport function; develop the gradation of the inflowing sediment concentration.
6. Calibrate the model: estimate the channel-forming discharge in each segment; run a series of steady flows and confirm sediment delivery; run historical hydrographs and sediment concentrations and demonstrate that the model results will match specific gauge plots if data are available; confirm that model results match annual sediment yields.
7. Run base test: run the no-action condition using future conditions hydrology and sediment concentration.
8. Run plan test: define the conditions to be tested and organize into a series of model tests; install the conditions into the base test model, one at a time, and run.
9. Analyze results: compare the results of the plan test with those from the base test to evaluate how much impact sedimentation will have on the plan and how much impact the plan will have on stream system morphology.
10. Perform a sensitivity analysis: change the boundary condition values or the initial condition values by 25% and rerun; express model results as a comparison with those for the base test and the plans tested.

This list of tasks is not a recipe. It is suggested as tasks one can use to organize a model study. Exceptions to this organization are acceptable. However, it is desirable to document the reasons for exceptions.

The rational for these ten tasks comes from the similarity between computational model studies and physical model studies. That rationale is presented in more detail in the subsections that follow.

14.4.1 Model Limits

In physical model studies, the expression "model limits" refers to the limits of the prototype area that will be constructed in the model. The prototype refers to the actual project being studied. The space inside the model limits is the area that will be included in the model. Model construction is the process of molding the (x,y,z) dimensions of the prototype into the dimensions required for the scale model. Measurements of hydraulic parameters and the resulting sedimentation processes are made in the model area. The same concepts are followed in computational modeling. The process of converting the area of the prototype that is within the limits of the computational model into a digital representation of the prototype is called model development.

The location of model limits is not arbitrary. The inflow end of the model must be in a location where the inflowing water discharge and sediment concentration by particle size are known. The tailwater elevations at the outflow end

must be known. Moreover, these known values must not be changed by any changes that happen within the model area during the simulation period. The data assembled in Task 1 will be valuable in establishing model limits.

14.4.2 Headgate and Tailgate

In physical model studies the main water supply at the upstream end enters the model area through a headgate that regulates the inflowing water discharge rate and the flow pattern. Flow leaves the model area at a tailgate that regulates the tailwater elevation. These facilities provide the necessary boundary conditions for the model study. In this case, boundary conditions do not refer to the geometry or surface conditions within the model area.

14.4.3 Boundary Conditions for the Computational Model

Mathematically, computational sedimentation modeling is an initial-boundary value problem. That is, there are more unknowns to be solved than there are equations. Therefore, the problem is conditioned by prescribing the missing unknowns at the inflow and outflow boundaries of the model. There are four boundary conditions: the inflowing water discharge, the inflowing sediment concentration by particle size, the tailwater elevation, and the water temperature.

The need for inflowing water and sediment loads form a requirement in the computational model that is analogous to the headgate of a physical model. The need for a tailwater elevation (i.e., base-level control) in the computational model is analogous to the requirement for a tailgate in a physical model study.

14.4.4 Survey Data for Initial Conditions

The initial geometry of the prototype in the model area is needed to establish the starting conditions for the model study. Surveyed data must have sufficient resolution to establish hydraulic and sediment controls throughout the model area. These data are used for model design and construction. Tasks 2 and 3, cited above, pertain to model design and construction.

14.4.5 Survey Data for Final Conditions

A final geometry of the prototype in the model area is needed at the end of a sufficiently long period of time to verify the computational model.

14.4.6 Model Calibration

Model calibration is a process used in both physical and computational modeling. It is the process of demonstrating that the model is behaving like the prototype. Although the parameters being observed in a physical model are often more detailed than those in the computational model, the concept of demonstrating agreement with the prototype is the same in both. Tasks 4, 5, and 6 pertain to calibration of the computational model.

14.4.7 Base Test and Plan Tests

To minimize model biases, the usual procedure in physical model studies is to run a base test in which existing conditions are extended into the future. The project being studied is then inserted into the model and the test is rerun. The impact of the plan is measured by comparing the model results of the plan test with those from the base test. This same procedure is suggested for computational modeling. Tasks 7 through 10 pertain to running the model tests and analyzing the results.

14.4.8 Selection of Physical Model versus Computational Model

One of the most difficult tasks is deciding whether to use physical modeling or computational modeling in a sedimentation study. Dimensionality and scale are important technical parameters in the decision. Time and cost are important economic parameters. Each project has specific needs that must be factored into decisions as that project is moved through the formulation process. In the early planning phase, preliminary estimates of sedimentation are adequate most of the time. A key consideration is whether the impact of sediment on the project, or the impact of the project on the stream system morphology, could reverse decisions about project feasibility. In the engineering and design phase, sedimentation questions must be resolved in detail. It may be necessary to switch from computational models to physical models to achieve the necessary detail. These general concepts are discussed more specifically in the following examples.

For example, if the decision involves how to align and position a navigation channel within the river cross section, the problem needs a physical model. This is a three-dimensional hydrodynamic problem having a movable boundary. Computational modeling of such processes is evolving, but it is still largely experimental. Physical modeling is appropriate for such studies, provided the modeling approach recognizes what the significant sedimentation processes are and includes those processes in model calibration. The accuracy of physical modeling is affected by the scale distortion. In rigid-boundary hydraulics, the scale distortion may not be a serious problem, but in the case of erodible-boundary hydraulics,the scale distortion may not be totally overcome. Consequently, the selection of the modeling materials is very important.

On the other hand, if the decision requires prediction of maintenance dredging for a navigational channel located in the deepest part of the cross section, a one- or two-dimensional

model is adequate. The one-dimensional model will not predict where the deepest part of the cross section will be, but it will predict the size of cross section that is required to transport the inflowing sediment load.

Decisions involving flow in bends are three-dimensional. Also, when the decision requires predicting the concentration of sediment that would be diverted through an outflow structure, either a physical model or a three-dimensional computational model is required. Neither one- nor two-dimensional computational models account for the secondary flows that control the distribution of the bed material load.

Flow through an expansion or contraction can usually be treated as a two-dimensional process. Sedimentation processes can be analyzed with a two-dimensional model or, if conveyance limits that approximate the rate of expansion can be established, the calculation can be made with a one-dimensional model. Examples are a dike field or a sediment trap.

If the decision involves flood elevations, either in a reservoir or in an open river site, reliable predictions can be made without knowing exactly where the deepest part of the channel will form in the cross section. Such a problem can be evaluated using a one-dimensional computational model.

The performance of hydraulic structures is a three-dimensional problem. Decisions involving sedimentation processes should probably be analyzed with a physical model at this point in time. However, the utility of three-dimensional computational models is advancing at such a rate that one should consider that approach in the model selection phase of a study.

14.5 DATA TYPES AND RESOLUTION

14.5.1 Introduction

Generally, data requirements are grouped into two types. One type helps the engineer to understand the historical behavior of the prototype. The other data group is the data that are needed to develop and operate the computational model. The data used to understand the behavior of the prototype are summarized in the next paragraph.

14.5.1.1 History of Prototype The *project area and study area boundaries* should be marked on a project map to delineate the area needing data. Add the lateral limits of the study area and the tributaries to this study area map. *Bed profiles* from historical surveys in the project area are extremely valuable for determining the historical trends that which the model must reconstitute. Use *aerial photographs* and aerial mosaics of the project area to identify historical trends in channel width, meander wavelength, rate of bank line movement, and land use in the basin. Analyze *stream gauge records* to determine the annual water yield to the project area and the water yield from it. Obtain annual peak discharge frequency curves for the project. These are useful for assessing the historical stability of hydraulic parameters such as width, depth, velocity, slope, and channel pattern. Analyze the stage-discharge curves in and around the project reach for trends. It is important to work with measured data. Do not regard the extrapolated portion of a rating curve as measured data. An example of this is shown in Fig. 14-2 where the measured flows are less than 52.39 m^3/s (1,850 cfs) and the project formulation flows range up to 453.07 m^3/s (16,000 cfs). Hydraulic data such as measured water surface profiles, velocities, and flood limits in the project reach are extremely valuable. Local action agencies, newspapers, and residents along the stream are sources of information when field measurements are not available.

14.5.1.2 Model Development Developing the one-dimensional representation of a three-dimensional open channel flow problem is an art. It requires one to visualize the three-dimensional flow lines in the actual problem and translate that image into a one-dimensional model. This step will often require several iterations to arrive at an acceptable model. The concept is one of developing representative data. A successful approach is to creep up on a solution by first running an approximation of the problem using simplified geometry and hydrology and the best sediment data available. Next, a fixed bed model of the actual geometry should be developed and run using three steady-state water discharges: low-flow, median-flow, and high-flow. Sediment should be added to this model and run with the same three discharges. Finally, the actual hydrology should be run to verify model calculations, to run the base test, and to run the plan tests.

14.5.2 Geometric Data

Mobile-bed water surface profile models calculate the water surface elevation and the bed surface elevation as they change over time. It is necessary to prescribe the starting geometry. This is done using cross sections for one-dimensional models. After that, computations will either aggrade or degrade the cross sections in response to mobile-bed theory. The cross sections never change locations.

14.5.2.1 Cross-Sectional Layout and Spacing It is customary to view and lay out cross sections from left to right, facing downstream. As in fixed-bed calculations, it is important to locate the cross sections so that they model the channel contractions and expansions.

It is particularly important in mobile boundary modeling to recognize where conveyance limits are needed. That is, if it is not physically possible for flow to expand laterally to the full width of the prototype, then determine how much of the cross section will convey flow and set conveyance limits in the model. Conveyance limits can result from internal embankments or from the lateral rate of expansion of a flow jet.

There is no theory for spacing cross sections. Some studies have required distances as short as a fraction of the river width. Other studies have allowed cross sections to be

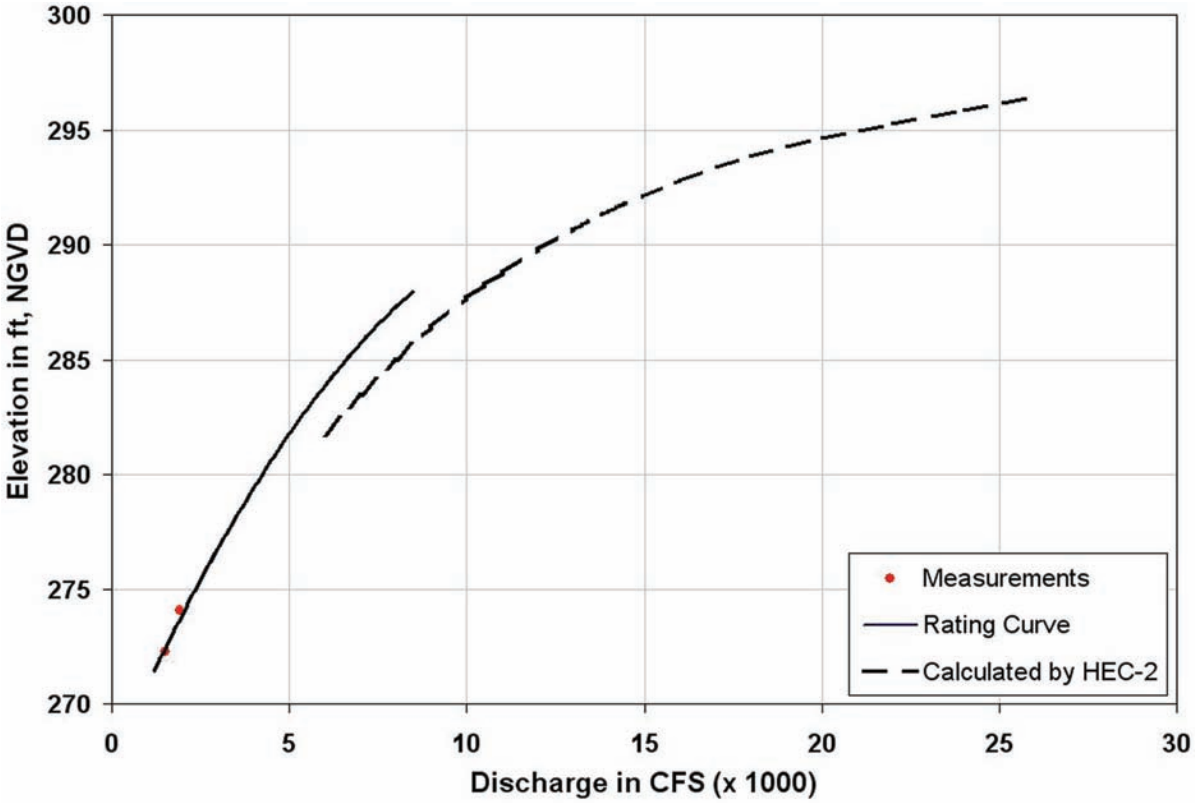

Fig. 14-2. Extrapolated discharge rating curve.

spaced from 16 to 32 km (10 to 20 mi) apart. The objective is to develop a model that will reconstitute the historical response of the streambed profile. The usual approach is to start with geometry that has already been developed for water surface profile calculations and transform it into geometry needed for sedimentation calculations.

There may be cases where cross sections must be eliminated from the data set to preserve model behavior. An example is a cross section in a bend or at a junction where the shape of the section is molded by three-dimensional hydraulic forces. It is not possible to reconstitute the shape of such sections with a one-dimensional hydraulic-sediment transport calculation. Those cases are the exception.

Document cross section locations for future reference using a layout map such as Fig. 14-3. River mile (or channel station) is suggested for the cross section identification number. It makes it much easier to use or modify an old data file if the cross sections are referenced by their position along the river rather than an arbitrary cross section number.

14.5.2.2 Hydraulic Roughness In a fixed-bed hydraulics study a range of *n*-values is typically chosen. The low end of that range provides velocities for riprap design, and the high end of the range provides the water-surface elevations for flood protection. In movable-bed studies such an approach is not satisfactory. The relationship between sediment transport and hydraulic roughness is too significant. Manning's *n*-values, which do not agree with that relationship, will either predict too much sand yield, too little sand yield, too much bed degradation, or too much bed aggradation. Analytical procedures that link *n*-values with hydraulic and sediment parameters are called bed roughness predictors. Models often provide bed roughness predictors. If so, modelers are encouraged to use these procedures in computational sedimentation. Brownlie (1983) developed a procedure for calculating the *n*-value in sand-bed streams. The procedure predicts the bed regime as well as the transition between upper and lower regimes.

Limerinos (1970) correlated field measurements to provide an equation for channel roughness in gravel-bed streams. Although not strictly a bed roughness equation, it was developed from data in which the channels were wide relative to their depth. Consequently, it can be used as a bed roughness predictor. The procedure does not predict bed regime.

Jarrett (1985) published a regression equation for composite channel roughness in Colorado streams. Although it may provide dependable results, it should be used as a composite channel roughness equation and not as a bed roughness equation.

Other methods for calculating *n*-values will surely become available as time passes, but the present bed roughness predictors are not substitutes for field measurements.

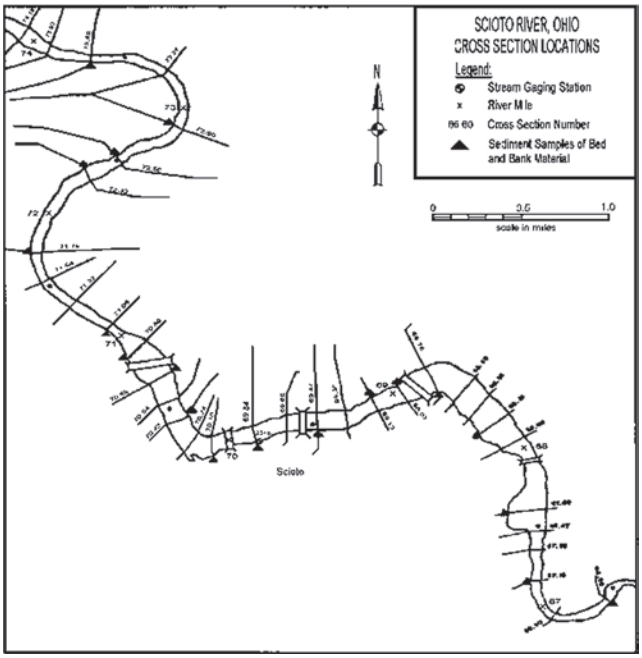

Fig. 14-3. Cross-sectional locations.

Measurements of water surface profiles and water discharges provide data that can be compared to model calculations. That is the most dependable technique for demonstrating hydraulic calibration. The second most dependable method is to reconstitute measured gauge records.

Regard data sets collected from a flood event as snapshots in time. When several of those snapshots are used along with the bed roughness predictors, the resulting calculation will account for variations in the hydraulic/sediment parameters during the entire runoff hydrograph. As a result, model performance will improve significantly.

In using bed roughness predictor equations, it is important to separate bed roughness from bank roughness. The equations do not include banks in the data set. Because bed roughness is completely tied to analytical equations, it cannot be used as the calibration parameter to match the calculated water surface elevation to historical flood profiles. That leaves bank roughness as the calibration parameter. There are no bank roughness equations, but the selection of n-values is not arbitrary. A systematic procedure for the selection of overbank n-values was developed by Arcement and Schneider (1989). They used Cowan's approach to associate n-value with surface grain, surface regularity, and surface vegetation materials. Their approach provides a systematic procedure for the selection of bank n-values, also. To apply this approach, document prototype conditions with photographs during the field reconnaissance.

The separation of bed from bank n-values requires that a composite channel n-value be calculated before the calculation of hydraulic parameters for the channel subsection. Compositing methods are described in Chow (1959).

Contraction and expansion losses, sometimes referred to as minor losses, are often included in sedimentation models. The information on contraction and expansion losses is more sparse than that for n-values. King and Brater (1963) give values of 0.5 and 1.0 for a sudden change in area accompanied by sharp corners and values of 0.05 and 0.10 for the best case. Design values of 0.10 and 0.20 are suggested. They cite Hinds (1928) as their reference. Values often cited by the U.S. Army Corps of Engineers are 0.1 and 0.3, contraction and expansion respectively, for gradual transitions. An acceptable alternative is to increase n-values to account for the effect of an irregular bank alignment.

14.5.3 Sediment Data

14.5.3.1 Size and Properties of Bed Sediment Reservoir

The bed sediment reservoir is the space in the bed of the stream from which sediment can be eroded or onto which it can be deposited. This reservoir occupies the entire width of the channel, and in some cases the width of the overbank also. However, it might have zero depth, as in a concrete channel, at a rock outcrop, or over an erosion-resistant clay layer.

14.5.3.1.1 Gradation of the Bed Sediment Reservoir

It is necessary to prescribe the gradation of sediment in the bed sediment reservoir. Section 14.5.3.1.2 gives insight into selecting sample locations for use in calculating an inflowing sand and gravel discharge rate. This section gives information to consider in selecting locations for sampling the bed. Studies need representative gradations for calculating sediment-transport capacity plus representative gradations for calculating streambed stability.

It is important to group bed samples according to geomorphological features and to select from the groups depending upon the purpose of the computation. For example, two samples were taken in the dry at 27 cross sections spaced over a 32 km (20-mi) reach of the creek in one study. One set of samples was near the water's edge and the other was from the point bar deposits about half the distance from the water's edge to the vegetated bank. These samples were considered as two populations, statistically, and sieved separately. The resulting gradations were plotted as bed gradation profiles, Fig. 14-4. The midbar samples were used to develop sediment transport rates for model calibration because they were taken from material deposited during high water. However, the results from the water-edge samples were used in the long-term simulations because the primary purpose of the study was to test for stream-bed erosion and these samples were coarser than the midbar population.

It is important to recognize that sampling the bed for a sedimentation study is an art. It is one of those activities that must result in providing representative data for a one-dimensional model. That means representative in the (x, y, z, t) coordinate system. It is common for one-dimensional models to develop a representative gradation for the bed surface at a cross section and to treat that bed as a homogeneous mixture

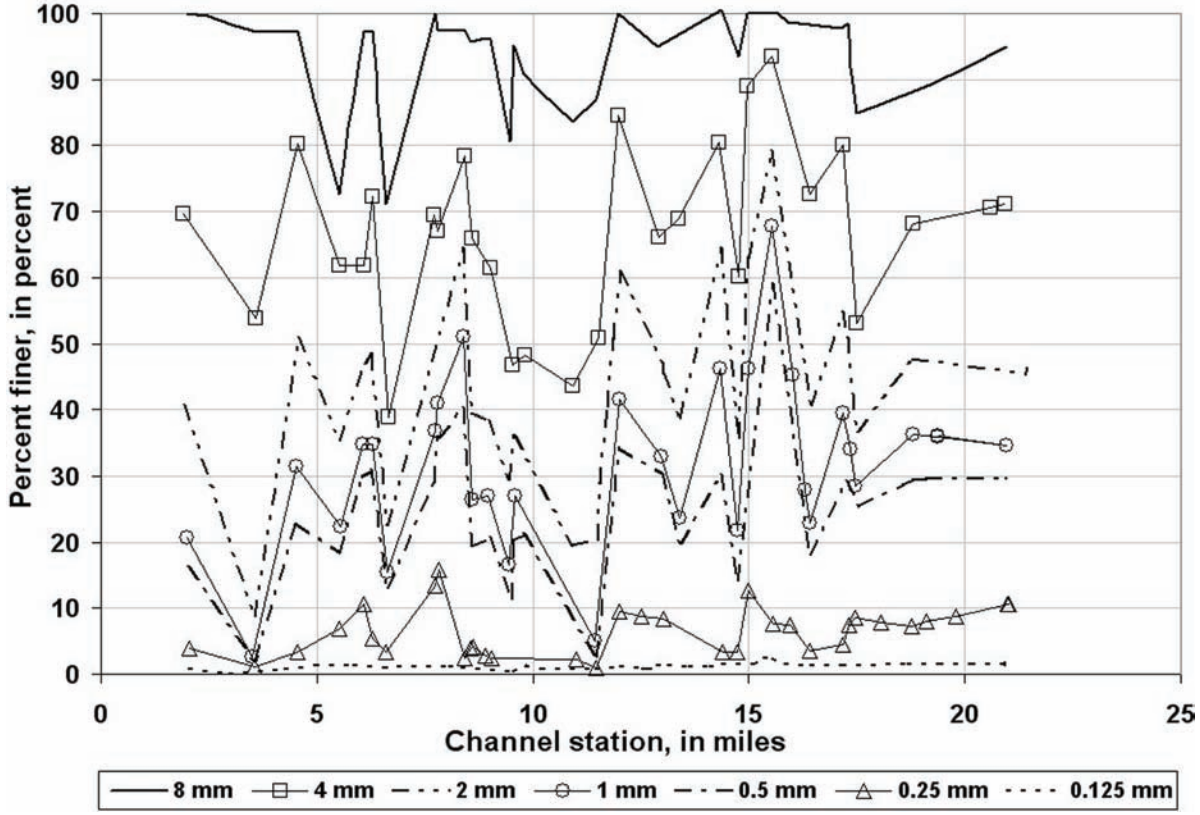

Fig. 14-4. Bed sediment profiles.

in the vertical. That is not adequate in cases where distinct layering is present in the bed-sediment reservoir. Bed layering is likely to be more of a problem on a coarse-bed stream than on a sand-bed stream. For example, bed layering is common at bridges because they are usually located at contractions. Pronounced bed layering can be created by a major flood runoff. In cases when layering is a problem, the model must be run in such a way as to approximate the effect of the change in bed gradation with respect to depth.

14.5.3.1.2 Sampling Concepts Sampling is largely a matter of experience. Sampling equipment and its operation have been standardized, but there are no standards for identifying the locations for collecting samples. The objective is to produce representative data. In this case "representative data" means a bed gradation curve that will produce the measured sediment concentrations in the flow field when used in concert with the representative channel hydraulics data.

In the absence of standards, the following general concepts are offered.

- The first choice of sample location is to sample in the dry. This allows the engineer to see the variability of the bed surface material and to collect samples that are representative of the active bed surface area.
- Use standard, calibrated sampling equipment and procedures. The Federal Interagency Sedimentation Project, located at the U.S. Army Engineer Waterways Experiment Station in Vicksburg, Miss., is responsible for standardizing sampling equipment.
- Organize sample sites into groups according to similar morphological features. Point or alternate bar samples probably provide the most representative gradations to use in calculating equilibrium sediment transport.
- In sand-bed streams, sample the depth of the active layer. If that is difficult to ascertain, favor about a 50 mm (2-in) depth, because that is the zone covered by the BM54 sampler.
- In gravel-bed streams, sample the surface layer and about 1 ft beneath the surface. Analyze the samples separately and composite the resulting gradations. Note the maximum size present on the bed surface, and include the larger sizes in bed gradation curves, because they will be necessary for bed stability calculations. Large sample volumes are recommended to avoid bias.
- Collect a sufficient number of bed and bank samples to provide a representative bed gradation for equilibrium sediment transport theory. The samples can be spatially weighted provided the distribution of sediment in the flow field is uniform over that same space. Otherwise, sample weighting should be adjusted in favor of the most active portion of the cross section for transporting bed material.

The sample locations cited for sediment transport calculations often miss the coarsest sizes in the stream bed. Therefore, also sample the stream bed in the geomorphological locations where coarser sediments are known to collect, such as deeper parts of the cross sections and the crossings. These samples will be important in bed profile stability calculations.

14.5.3.1.3 Variability of Samples There is often more variability from one side of the channel, or the point bar, to the other side than there is along the length of the sampled reach. Take a sufficient number of samples to be sure that this variability has been represented. A test of sufficiency is when the addition of one more sample does not change the composite bed gradation curve for the reach by a significant amount.

14.5.3.1.4 Test for Sufficiency The final test for sufficiency is to run the sampled gradations in the computational model using water discharges from the hydrograph prior to the time when samples were collected. The first event will entrain a high concentration from the new disturbed bed; subsequent iterations with that same water discharge should produce bed material load concentrations that match prototype measurements.

14.5.3.2 Size and Concentration of Inflowing Sediment Load

14.5.3.2.1 Inflowing Sediment Concentrations Occasionally suspended sediment concentration measurements, expressed as milligrams per liter, are available. These are usually plotted versus water discharge, Fig. 14-5. As in most cases, the concentrations in Fig. 14-5 show a great deal of scatter; however, such graphs are useful in developing or extrapolating the inflowing sediment data. It is desirable in most cases to develop the best estimate of the inflowing sediment concentration curve using the concentration graphs and then convert those values into sediment discharges in tons/day. That result is a sediment discharge rating curve, Fig. 14-6. The scatter is reduced from Fig. 14-5 but that is not because the correlation is better. It is because water discharge is being plotted on both axes. A scatter of about 1 log cycle is common in such graphs.

14.5.3.2.2 Grain Size Classes The total sediment discharge should then be partitioned into grain size classes. Table 14-1 shows the procedure that was developed for the Clearwater River at Lewiston, Id. Figure 14-7 is a graph of the sediment discharge by grain size class.

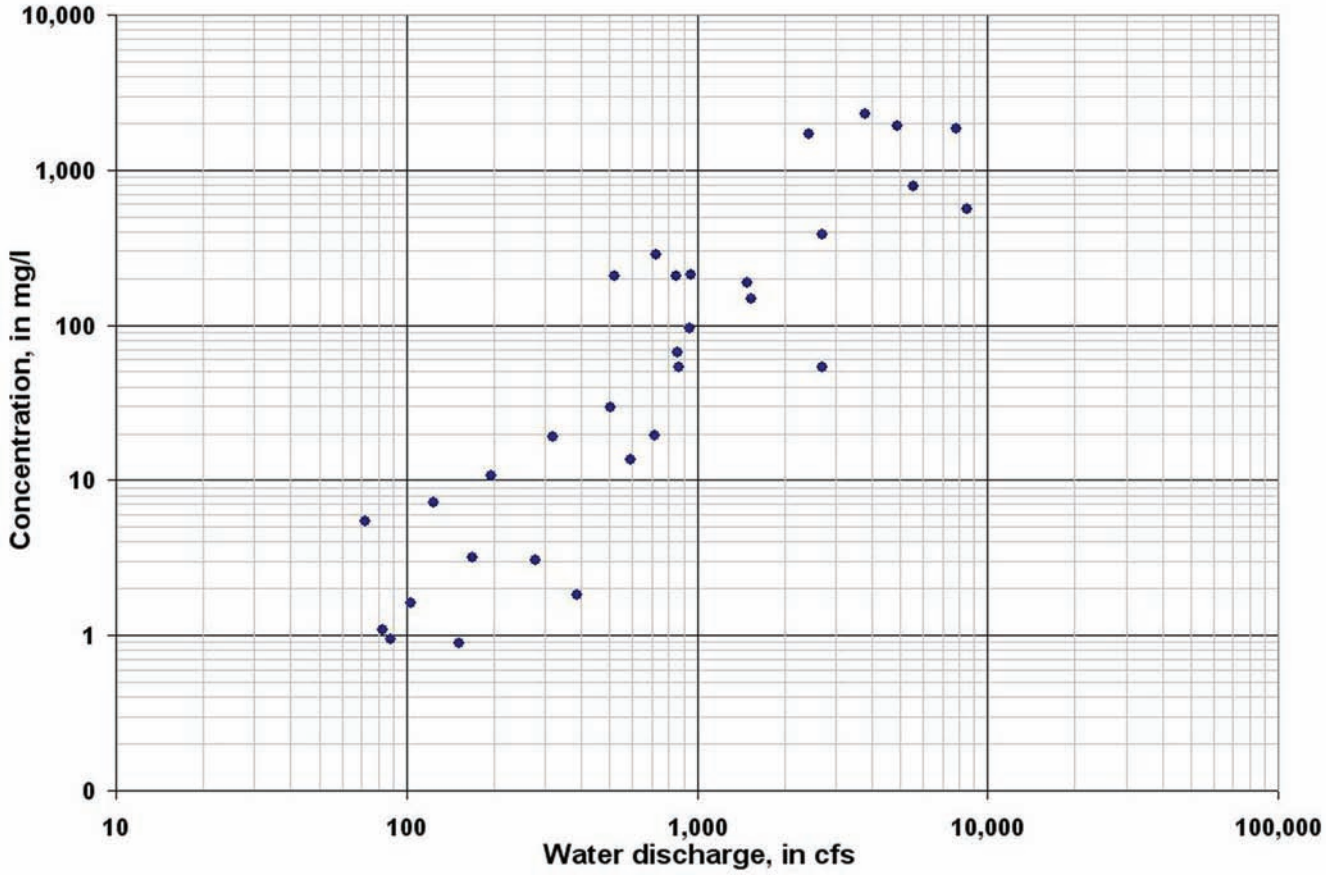

Fig. 14-5. Sediment concentration measurements.

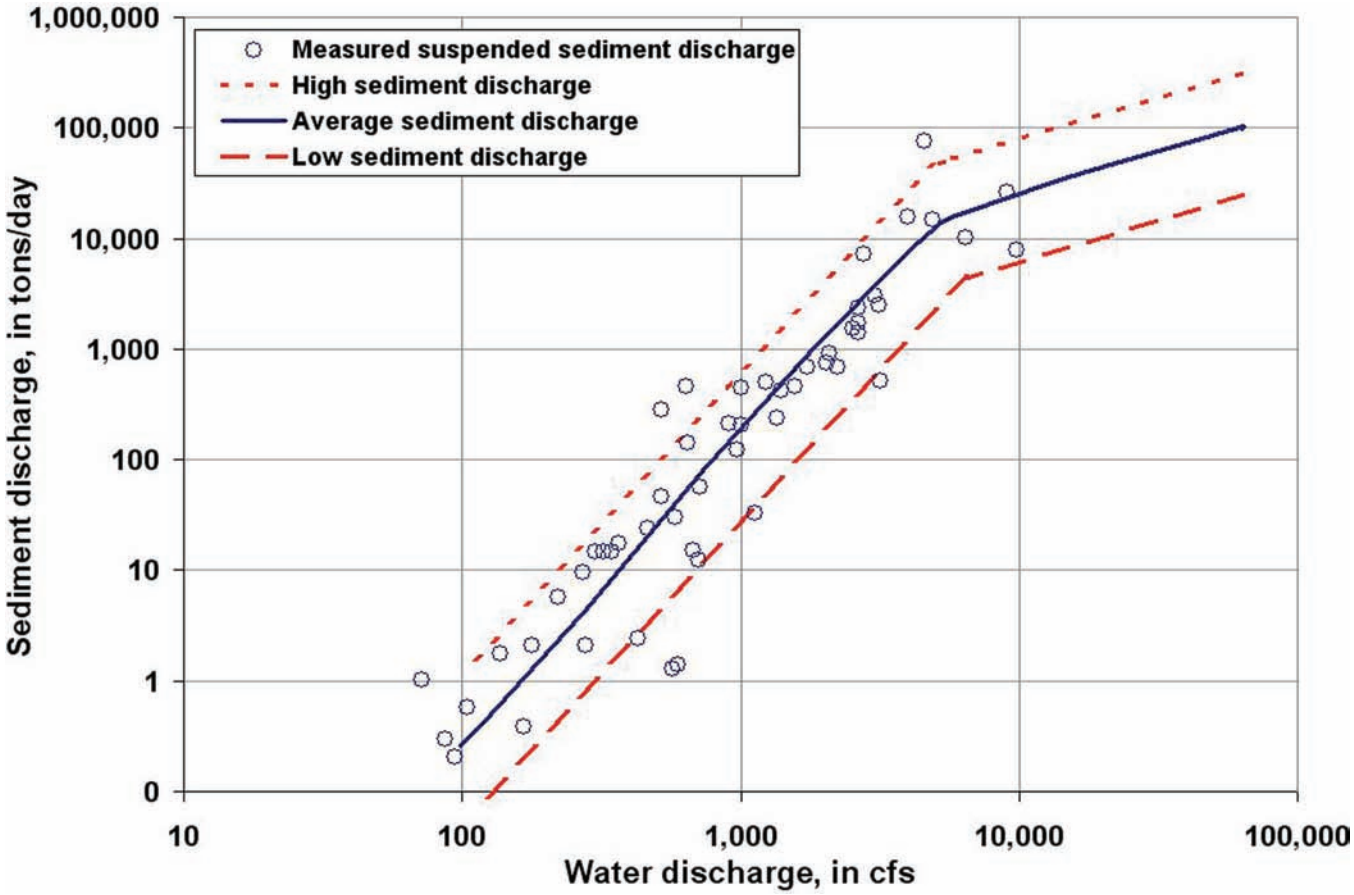

Fig. 14-6. Sediment discharge rating curve.

14.5.3.2.3 Calculating Sediment Inflow with Transport Theory When no suspended sediment measurements are available, the inflowing sediment boundary condition must be calculated with sediment transport theory. There is no theory for calculating the wash load concentration from sediment samples of the stream bed. This calculation can be made only for sand- and gravel-bed sediment using equilibrium sediment transport functions. The calculation should be made by particle size for the full range of water discharges in the study hydrograph.

Select the reach of channel very carefully for this calculation. The first choice is a reach approaching the project where the slope, velocity, width, and depth at one representative of the historical hydraulics. This reach should have a history of conveying the inflowing sediment load without aggradation or degradation. The selected reach should also have a bed surface that is in equilibrium with the sand and gravel discharge being transported by the flow. Finally, the selected reach should have locations where the bed gradation can be measured using standard procedures.

The second choice for calculating the inflowing sediment concentration is a reach within the project area. A location near the upstream end of the project is desirable. It is important that the selected location be a stable reach and have a history of conveying the inflowing sediment discharge without appreciable aggradation or degradation.

An example of an inappropriate location for calculating the inflowing sediment load is a reach within the project where dredging is performed.

Einstein made the following suggestions for choosing a river reach to apply his bed-load function. His suggestions are also appropriate for other equilibrium sediment-transport functions.

> In practical calculations of the bed-load function for a particular river reach, the length of the reach must be sufficient to permit adequate definition of the over-all slope of the channel. The channel itself should be sufficiently uniform in shape, sediment composition, slope and outside effects such as vegetation on the banks and

Table 14-1 Distribution of Sediment Load by Grain Size Class (Clearwater River at Lewiston, Idaho)

Grain size[a] diameter mm (1)	Classification (2)	Percent of total bed load[b] (3)	Bed load ton/day (4)	Percent of total suspended load[c] (5)	Suspended-load ton/day (6)	Total load Cols. (4) + (6) ton/day (7)
< 0.0625	silt & clay	0.04	1	54	216,000	216,001
0.0625–0.125	VFS	0.10	2	10	40,000	40,002
0.125–0.250	FS	2.75	52	13	52,000	52,052
0.250–0.500	MS	16.15	307	19	76,000	76,307
0.500–1.000	CS	13.28	252	4	16,000	16,252
1.000–2.000	VCS	1.19	23			23
2–4	VFG	1.00	19			19
4–8	FG	1.41	27			27
8–16	MG	2.34	44			44
16–32	CG	6.33	120			120
32–64	VCG	23.38	444			444
> 64	cobbles & larger	32.03	609			609
Total		100.00	1,900	100.00	400,000	401,900

[a]Values were read from the sediment load curve, 1972.74 measurements. (Total bed load, tons/day 1900.)

[b]These values were calculated by analyzing measured hydraulic parameters and measured bed loads using the computer program "Total River Sand Discharge and Detailed Distribution" by F. B. Toffaleti. (Total suspended load, tons/day 400,000.)

[c]These are representative values determined graphically by plotting the results of sieve analyses and developing a single percentage finer curve from all samples analyzed. (Total sediment load 401,900.)

Water discharge, cfs 200,000.

> overbanks, that it can be treated as a uniform channel characterized by an over-all slope and by an average representative cross section. (Einstein 1950, p. 45)

Having located a suitable reach, measure a sufficient number of cross sections to establish the width, depth, and slope of the channel in that reach. Composite the measured cross sections into a single cross section that is representative of the river just upstream from the project. Again, quoting from Einstein on the description of a river reach:

> One problem is that of determining how a number of cross sections can best be averaged. As the river reach is to be treated as a uniform channel with constant cross section and slope, in which only uniform flows are studied, a representative or average slope must be found, together with the average section. If a sufficiently long and regular profile exists for the river under consideration, the general slope of the reach should be taken from it. In the absence of such a profile, the slope must be derived from the cross sections themselves. Under all conditions, the cross sections must be tied together by a traverse which gives their relative elevations and the distance between them along the stream axis. Then the wetted perimeter and the wetted area are calculated for various water surface elevations. These are plotted in terms of the water surface elevation for each cross section.
>
> It is fairly common usage to construct the stream profile from the lowest points of the sections. This procedure is satisfactory for a long profile. If the reach is short, however, the use of a low-water surface is more satisfactory as the influence of insignificant local scour-holes is excluded. If such a low-water profile is not recorded when the sections are surveyed, a profile found from the area-curves may be substituted. A characteristic low-water discharge may be selected for the streams. The average velocity for such a flow can be estimated roughly. By division of the two one may find the corresponding low-water area of the cross sections. If the water-surface points which give this area at the different sections are connected, an approximate low-water surface is defined which represents a profile that is more regular and more representative than the profile of the low points of the bed.

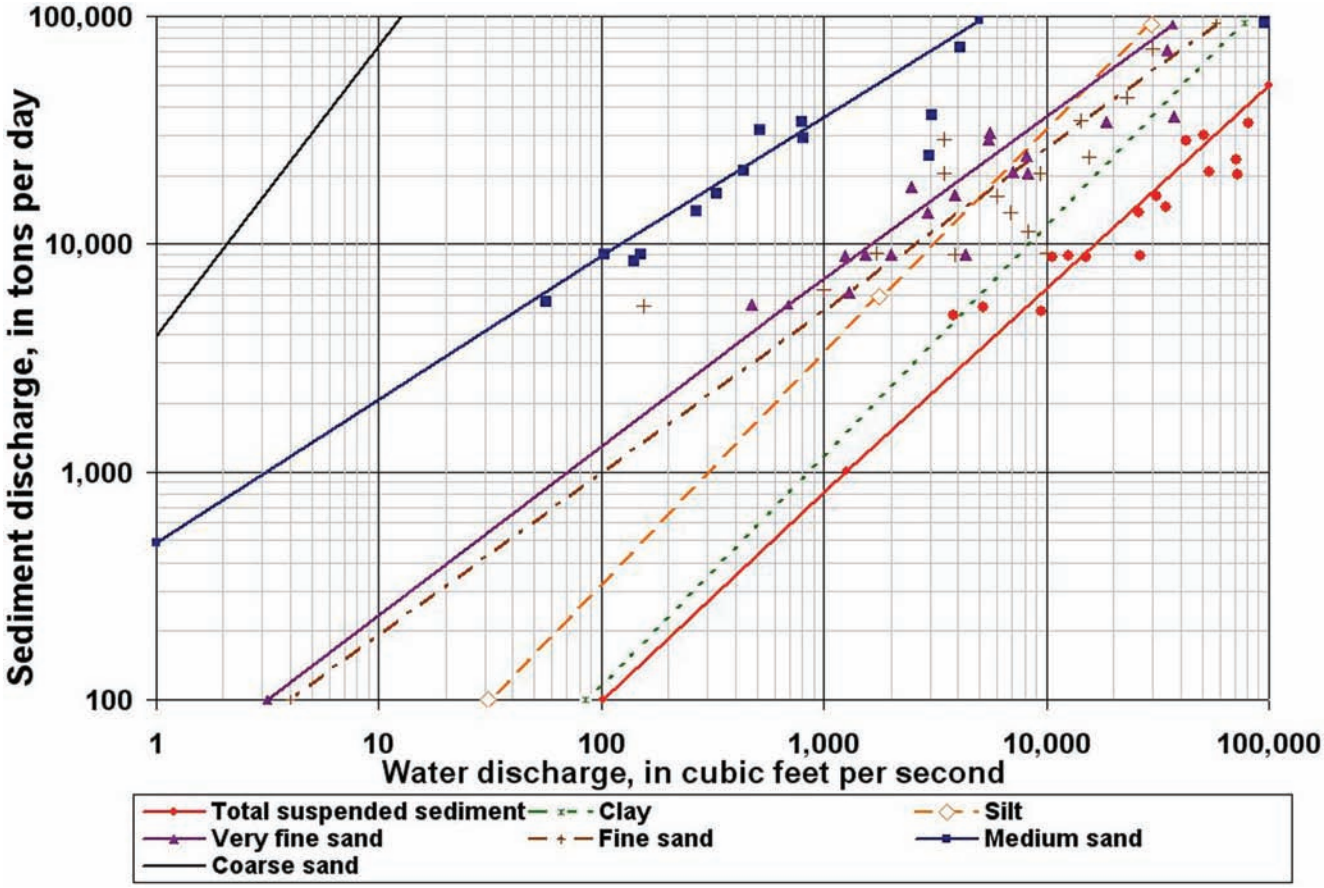

Fig. 14-7. Sediment discharge rating curve by particle size class.

After the representative slope is selected, by fitting a straight line through the profile points, this slope may be used in averaging the cross sections. This can be done by sliding all the sections along this average slope line together into, for instance, the lowest section. (Einstein 1950, pp. 45–46)

Einstein applied this procedure to Big Sandy Creek near Greenwood, Miss. Eleven cross sections were selected. They were spaced roughly at three times the channel width for a total distance of 5181.6 m (17,000 ft) along the channel. Both bend and crossing sections were included. Using a low-flow water discharge and low-flow water velocity, the low-flow wetted area was calculated to be 4.65 m^2 (50 sq ft). When the elevation for 4.65m^2 (50 sq ft) was read from the individual cross section area-elevation curves and plotted versus channel station, the least-squares regression line through the points provided the channel slope. The slope was 0.00105 ft/ft in this example.

It is also important to develop a representative sample of the bed gradation for the equilibrium sediment transport analysis. In the example application of his bed load function to Big Sandy Creek Einstein wrote:

> The grain-size composition of the bed is determined by sampling. A bed which appears to be very uniform, such as that of Big Sand Creek, may be described by three to five samples. Each of the four samples listed . . . was a composite of three or four cores, taken in the same cross section at evenly spaced points over the total width of the channel. The individual samples were obtained by means of an auger or a pipe-sampler and were taken down to a depth of about 2 feet, the estimated depth of scour or active bed movement (Einstein 1950, pp. 45–46).

Treat the calculation of the inflowing sediment load as if it were a calculation to verify a sediment transport function. That is, locate the sample reach so that the point where the concentration is needed is at the downstream end. To the maximum extent possible, collect samples of the bed sediment over the same reach covered by the cross sections.

However, avoid using average geometry and bed gradation over extended lengths of a river when calculating the equilibrium sediment transport entering a study area. Instead, focus attention on the river channel approaching the point of interest. Use the following rules of thumb:

- Sample the bed surface gradation at and upstream from the gauge.
- Sample for a distance of 50 to 100 times the depth of flow. The idea is to provide a sufficient distance to allow the vertical distribution of velocity and sediment concentration in the water column to approach equilibrium conditions as depicted by hydraulic forces that are reasonably close the average over the reach.

14.5.3.2.4 Typical Bed Gradation on a Point Bar Figure 14-8 illustrates a typical bed surface gradation pattern on a point bar. Use such information to determine where to sample for a sediment transport calculation. Note that the typical grain sizes found on the bar surface form a pattern from coarse to fine, but there is no one location that always captures the precise distribution that will represent the entire range of processes in the prototype. The bed gradation controls the sediment discharge calculation. For example, true, multiple grain size transport functions like Laursen and Toffaleti show that the rate of transport increases exponentially as the grain size decreases, Fig. 14-9. There is no simple rule for locating samples. The general rule is "always seek representative samples." That is, select sampling locations very carefully and avoid anomalies that would bias either the calculated sediment discharge or the calculated bed stability against erosion.

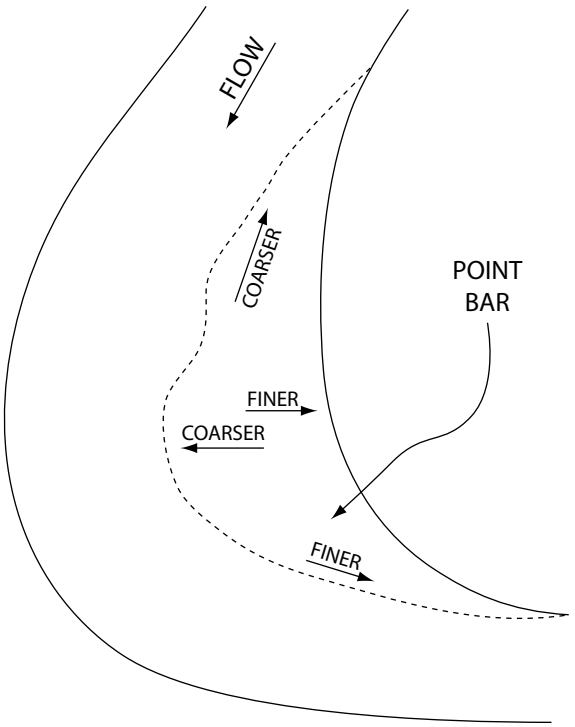

Fig. 14-8. Gradation pattern on a bar.

14.5.3.2.5 Sediment Inflow from Tributaries The sediment inflow from tributaries is usually more difficult to establish than it is for the main stem because there are usually fever data on the tributary. The recourse is to use the site reconnaissance to assess each tributary. For example, look for a delta at the mouths of the tributaries. Look for channel bed scour or deposition along the lower end of the tributary. Look for drop structures or other controls that would aid in stabilizing a tributary. Look for significant deposits if the tributaries have concrete linings. These observations guide the investigation of tributary sediment discharges.

14.5.4 Hydrologic Data

14.5.4.1 Main Stem Water Inflows Although a design water discharge is of interest, a single value is not adequate for a movable-bed computational model study. Simulating the change in channel behavior as the result of a flood requires the analysis of complete hydrographs. Consequently, the water discharge hydrograph must be developed. This step can involve manipulations of measured flows, or it can require a calculation of the runoff hydrograph.

Historical flows are needed for model calibration/verification because the model must reconstitute the historical behavior of the river, but future flows are needed to forecast the future stream-bed profile.

The length of the hydrograph period is important. Trends of a tenth of a foot per year becomes significant during a 50- or 100-year project life. On the other hand, a long-period hydrograph becomes a computation burden. Usually the bed profile changes are sufficiently slow to allow some aggregation of the forces involved. Therefore, aggregating the energy of a varying hydrograph into extended numbers of days is acceptable in most cases. For example, Fig. 14-10 shows the histogram for a year of mean daily flows.

In cases where measured flows are not available, the computational model still provides the framework for analyzing sedimentation in the project. Calculate hypothetical runoff hydrographs.

14.5.4.2 Tributaries Tributaries are a lateral boundary condition. They should be located, identified, and grouped as required to define the increase in water discharge as the drainage area increases along the project reach. The tributaries should be shown on the cross section location figure. Keep in mind that a 10% increase in water discharge will normally produce more than a 10% increase in bed material transport capacity. The transport relationship is nonlinear.

Often the tributaries are not gauged, and it is necessary to develop tributary inflows by analytical means. Table 14-2 illustrates such an approach in which six tributaries were grouped into three inflow points and their water discharges were calculated from the main stem discharge gage record.

Table 14-2 shows the 2-year flood peak at four locations along the project channel. These flood peaks were calculated

by a rainfall-runoff-routing program from subbasins. The peaks were then subtracted to determine the three lumped tributary inflow values, column 3. The ratio of *Q*-main at River Mile 7.903, 13,648/17,692, was calculated to determine *f*-main, column 4. The tributary discharge, 4,044, was divided by *Q*-main, 17,692, to determine the *f*-trib coefficient, 0.2296, in column 5. These tributary discharge coefficients were then applied to all flows in the long-term hydrograph of the study to calculate tributary inflows.

14.5.4.3 Tailwater Elevation The tailwater elevation specifies the water surface elevation at the downstream end of the project. It is referred to as a tailwater elevation (or base level) because it establishes the energy gradeline at the downstream end of the model. It can be a stage-discharge rating curve, such as Fig. 14-2, or it can be a stage hydrograph.

When a backwater condition exists, such as at the mouth of a tributary or in a reservoir, use a stage hydrograph as the boundary condition. Be sure it covers the same period of time as the inflow hydrographs.

14.5.4.4 Water Temperature The final boundary condition is the temperature of the inflowing water sediment mixture. Develop representative values by month or season if measurements are locking.

14.5.4.5 Boundary Condition Changes over Time The historical water inflows, sediment concentrations, particle sizes, tailwater elevations, and water temperatures may change in the future. That possibility should be evaluated for each project and the appropriate modifications made to the water sediment boundary condition values.

14.5.5 Operating Rules

The usual procedure for controlling the water surface elevation in a large reservoir is to follow a prescribed rule curve. Similarly, low-head dams may be operated to control the water surface at a gauge several miles upstream from the dam. Diversion structures are designed to pass a prescribed water discharge. In these cases the depth of flow is being controlled by manipulation of hydraulic structures and not by friction losses. This creates a modeling requirement called "operating rules." An operating rule is an internal boundary condition that will control the model.

14.5.6 Data Sources

14.5.6.1 General The data that will be needed to develop the model may come from office files, from other federal agencies, from state or local agencies, and from the team making the field reconnaissance of the project site.

14.5.6.2 U.S. Geological Survey (USGS) USGS topographic maps and mean daily discharges are used routinely in hydraulics and hydrology studies and are common

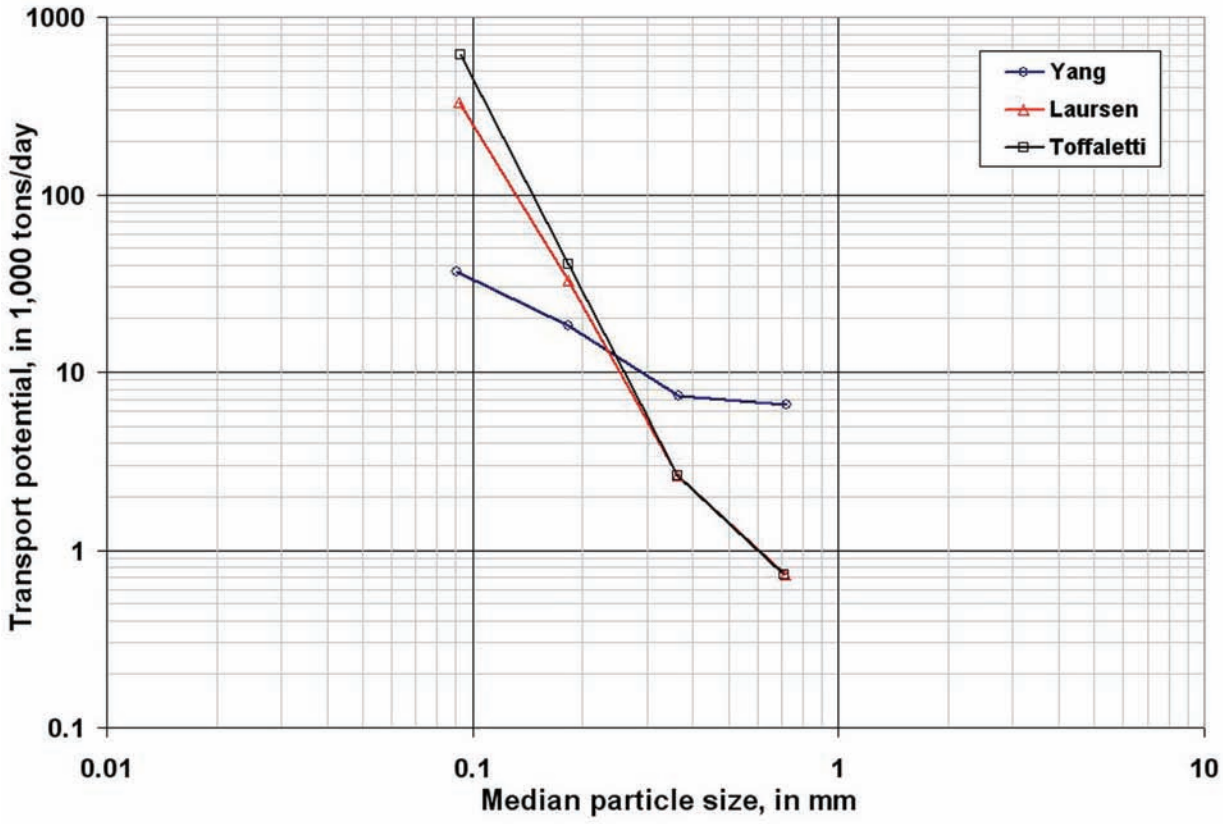

Fig. 14-9. Sensitivity of sediment transport potential to grain size.

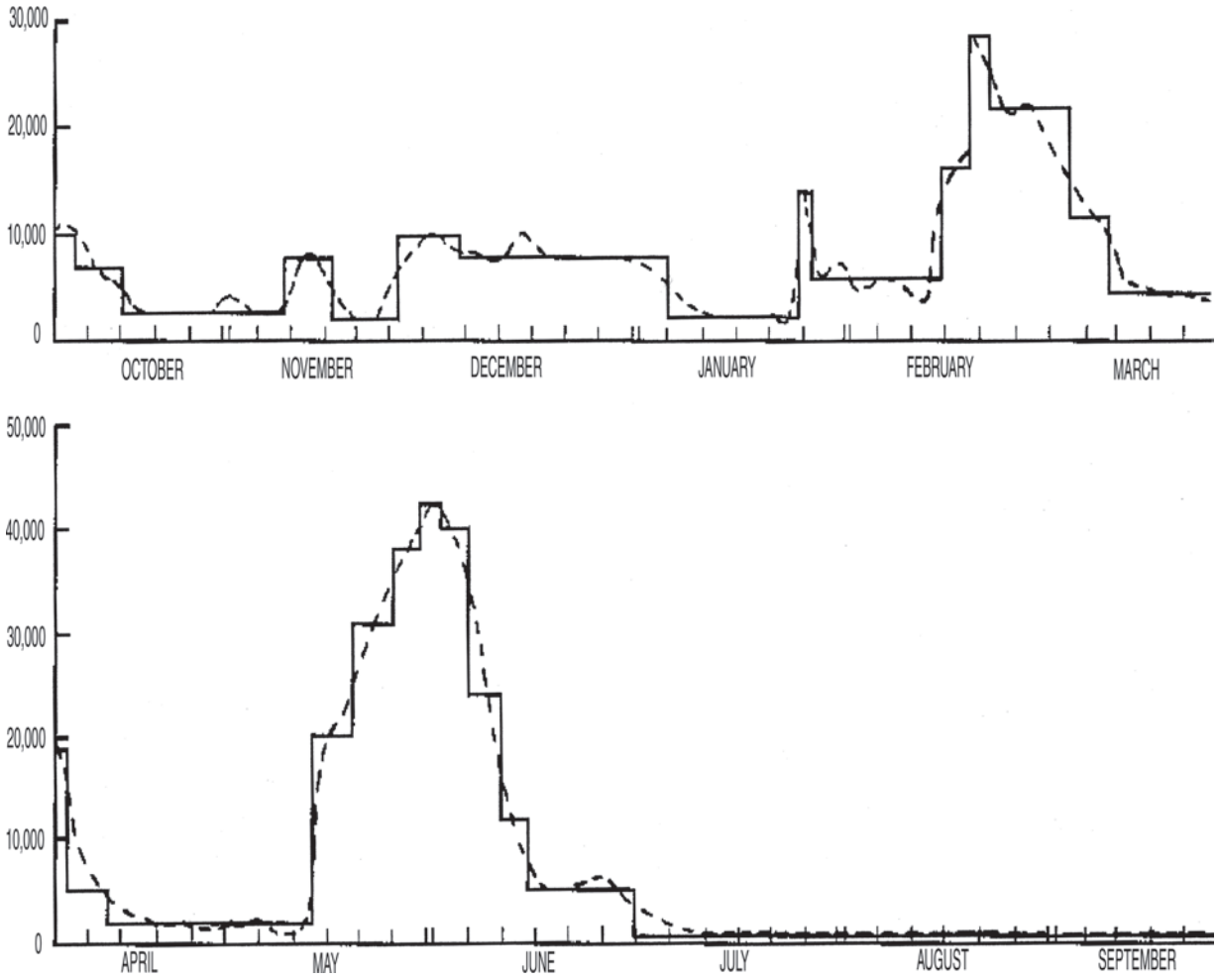

Fig. 14-10. Histogram for a year of mean daily

Table 14-2 Distribution of Runoff by Tributary, 2-Year Flood Peak

			Discharge coefficients	
River mile	*Q*-main cfs	*Q*-trib cfs	*f*-main	*f*-trib
0–7.903	17,692			
		4,044	0.7714	0.2286
7.903–11.942	13,648			
		4,777	0.6500	0.2699
11.942–17.346	8,871			
		1,696	0.8088	0.0959
17.346–21.005	7,175			

data sources for sediment studies, also. However, mean daily flows are often not adequate for sediment studies, and data for intervals less than 1 day or stage-hydrographs for specific events can be obtained, through strip-chart stage recordings, by special request. It may be preferable to use USGS discharge-duration tables rather developing such in house, and these are available from the state office of the USGS. Water quality data include suspended sediment concentrations and grain size distributions. Published daily maximum and minimum sediment discharges for the year and for the period of record are available, as are periodic measurements of particle size gradations for bed sediments.

14.5.6.3 National Weather Service (NWS) There are cases where mean daily runoff can be calculated directly from rainfall records and expressed as a flow-duration curve without detailed hydrologic routing. In those cases use the rainfall data published monthly by the National Weather Service for each state. Hourly and 1-day interval rainfall data, depending on the station, are readily accessible. Shorter interval or period-of-record rainfall data would require contact with the NWS National Climatic Center at Asheville, N.C.

14.5.6.4 Soil Conservation Service (SCS) The local SCS office is a good point of contact for historic and future estimates of land use, land surface erosion, and sediment yield. They have soil maps, ground cover maps, and aerial photos that can be used as an aid in estimating sediment yield. Input data for the universal soil loss equation one available for much of the United States. The SCS also updates reservoir sedimentation reports for hundreds of reservoirs throughout the country every 5 years, providing a valuable source of measured sediment data.

14.5.6.5 Agricultural Stabilization and Conservation Service (ASCS) This agency of the Department of Agriculture accumulates aerial photographs of crop lands for allotment purposes. However, those photographs will include the streams crossing those lands and are extremely valuable for establishing historical channel behavior, because overflights are made periodically.

14.5.6.6 U.S. Army Corps of Engineers Because the Corps gathers discharge data for operating projects and for those being studied for possible construction, considerable data from the study area may already exist. The Corps has acquired considerable survey data, aerial and ground photography, and channel cross sections in connection with flood plain information studies. Corps laboratories have expertise and methods to assist in development of digital models.

14.5.6.7 State Agencies A number of states have climatologic, hydrologic, and sediment data collection programs. Topographic data, drainage areas, stream lengths, slopes, ground covers, travel times, etc. are often available.

14.5.6.8 Local Agencies, Businesses and Residents Land use planning data are normally obtained through local planning agencies. Cross section and topographic mapping data are often available. Local agencies and local residents have some of the most valuable information to the engineer in their verbal and photographic descriptions of changes in the area over time, of channel changes from large flood events, of caving banks, of significant land use changes and when these changes occurred, of channel clearing/dredging operations, and other information. Newspapers and those who use the rivers and streams for their livelihood are valuable sources of data.

14.6 MODEL CALIBRATION

Computational studies fall into two general categories: (1) computational model studies and (2) computational analysis studies. Computational model studies are applications for which the model has been calibrated according to the formal procedures described in this chapter. Often the available field data are not sufficient to permit a formal calibration, but computational modeling is still the best method for analyzing the problem. In these cases model tests are devised so that engineering judgement can be used to assess the credibility of the calculated results. The resulting studies are called computational analysis studies.

Historically, there has not been a formal procedure for the calibration of computational models. Consequently, there has not been a formal definition of the word "calibration" It has been used to describe the initial work of adjusting a computational model until the calculated results matched whatever field data were available in the project area. This chapter proposes a formal calibration procedure. The word "calibration" will be reserved for those computational studies that have adequate field data to permit the implementation of the calibration procedure. Many studies will not have sufficient field data to calibrate models under this definition. Such studies will be beneficial because they will include the full computational capability of the model. Consequently, they will be called computational analysis studies rather than computational model studies.

Some believe that the word calibration should be reserved for instrumentation and have introduced the term "circumstantiation" to describe the process of demonstrating agreement between model and prototype. Their argument is based on the fact that model parameters are often adjusted using circumstantial evidence, whereas calibration is the result of scientific measurements. This chapter will continue the use of the term calibration.

14.6.1 Definitions

14.6.1.1 Calibration Calibration is the process of arriving at roughness coefficients, a sediment transport function, model parameters, and representative data on the study area that will allow the model to calculate values that agree with values measured in the prototype. For a one-dimensional model, the representative data are developed by transforming the three-dimensional (x, y, z) space of the

prototype into a one-dimensional digital representation. Variables of interest are water surface elevations, velocities, depths, widths, hydraulic roughness values, the concentrations of sediment in the water column, the gradation of the sediment in the water column, the gradation of sediment in the bed, the delivery of sediment along the study area, and aggradation/degradation of the channel.

A model cannot be calibrated using a data set that was also used by that model to calculate some of its boundary conditions.

The field data used for model calibration should contain measured values of parameters similar to those for which the model is being calibrated. For example, if the purpose of the model study is to calculate aggradation or degradation of the channel profile, the calibration data should contain field data that include some historical information on the channel profile. The model is expected to reconstitute those measurements when it is provided with the boundary conditions that existed when the measurements were made. On the other hand, if the purpose of the model study is to evaluate the change in a water surface elevation as sedimentation processes change the channel over time, the calibration criteria should contain some field measurements of historical water surface elevations in the study area.

The examples in this section are given to illustrate the concept of model calibration. They are only a starting point for deciding what is required for a model to be calibrated. They are necessary, but they may not be sufficient to provide complete calibration for the general case. In principle, the requirements for calibration are based on the questions to be answered by the model results, and it is the responsibility of the engineer to develop and justify the steps that are required.

14.6.1.2 Verification A calibrated model is not necessarily a verified model. Verification is sometimes called a split record test. It demonstrates that the calibrated model will match the prototype during a period of time that is not used in calibration. The calibration parameters cannot be adjusted during model verification. Only the boundary conditions can be changed to those for the verification period.

14.6.1.3 Computational Modeling Computational modeling is the formal process of assembling data that provide the geometry of a study reach at two points in time and that provide a continuous record of the inflowing water discharge, the inflowing sediment load, and the downstream stages between those two points in time. Geometric data are provided by hydrographic/topographic surveys. The initial model geometry is developed from the first survey. The model is then run using the recorded hydrological and sedimentary boundary conditions, and the calculated results at the end of the simulation are compared with prototype values in the second survey.

14.6.1.4 Computational Analysis An alternative to computational modeling is computational analysis. Computational analysis is the application of a computational model to a problem in which model calibration is not possible. Many sedimentation studies are made where there are not adequate prototype data to calibrate the model. Perhaps there is only one survey of the prototype. Perhaps there are two surveys, but boundary condition data are not available during the time period between the two. Perhaps the river is so highly disturbed that computational modeling is not possible. Whatever the case, computational analysis allows the engineer to use the latest technology in mobile boundary computations in decision making. Such studies are very useful because they recognize that we live in a movable-boundary world. How the study area responds to the systematic application of hydrodynamic and sedimentation theories illustrates how sensitive the area is to sedimentation processes. Often one can gain sufficient understanding to predict how reliable a plan will be by comparing the calculated results from the plan test with those from the base test.

In some cases, a computational analysis will demonstrate that the questions being asked are sufficiently sensitive to sedimentation processes so that prototype data must be collected before proceeding with a design.

14.6.2 Fixed-Bed, Steady-State Hydraulic Calibration

Model calibration is approached in phases. The first phase is to reconstitute the water surface profile that was measured at the time the hydrographic survey was made. When the channel was dry during that survey, choose a low flow from the testing hydrograph. The purpose is to check the model geometry for consistency in width, depth, and slope and to check n-values. The mean error between calculated and measured water surface elevations should normally be within ± 153 mm (0.5 ft), or 10% of the flow depth, whichever is smaller. Because most surveys are made during low-flow-periods, this first test will be the low-flow test.

The next fixed-bed test should use a water discharge that is approximately the channel-forming discharge. In any case, the flow should not be out of banks for this test. The purpose is to check the geometry for consistency with regime concepts in channel widths and depths and to confirm channel n-values while all flow is still confined to the channel cross section. This n-value may be different from that developed for the low-flow condition. If so, the n-value should vary in the vertical later when hydrographs are included in the calibration process.

The final fixed-bed test should use the maximum water discharge in the testing hydrographs. At this point the calibration of the movable-bed model becomes more exacting than is usually performed for a fixed-bed calculation. That is, not only must the water surface elevation match known elevations but also the flow distribution between the channel and the overbanks must match the true prototype values. The only parameters available to achieve such a match are geometry and n-values. Geometry is usually more reliable than n-values, but it has been reduced to a one-dimensional

approximation of the prototype. Therefore, ascertain that the cross sections and reach lengths are the best representation of the flow conditions in the prototype. Additional adjustments in both water surface elevation and the percentage of flow that is conveyed in the channel are made with the *n*-values. The process is neither random nor arbitrary. The resulting values must pass the test of "reasonableness." Keep the process of selecting *n*-values systematic. Base the estimates on physical conditions by using a procedure such as that of Arcement and Schneider (1989).

14.6.3 Fixed-Bed, Unsteady-State Hydraulic Calibration

When the hydraulic calculations include the unsteady-flow terms, as in the Saint-Venant equations, the calibration of the routing model involves storage in the geometric model. This is an important adjustment because the hydraulic results drive the sedimentation calculations. Calibration of an unsteady-flow model is such a formidable process that the reader is referred to unsteady-flow modeling procedures. The process will not be presented here. The same cautions apply as presented earlier for steady-state, fixed-bed calibration.

14.6.4 Movable-Bed, Steady-State Hydraulic/Sediment Calibration

Start with a steady-state discharge that approximates the channel-forming discharge. In the more arid regions where streams are ephemeral the 10-year flood peak is usually a reasonable value for these calculations. Elsewhere, a discharge about equal to the 2-year flood peak is usually a reasonable value. In a regime channel this calculation can be made with the channel full discharge. Ascertain that the model is producing acceptable hydraulic results by not only reconstituting the water surface profile but also plotting the water velocity, depth, width, and slope profiles. This test will often reveal width increases between cross sections that are greater than the expansion rate of the fluid and therefore require conveyance limits. Extremely deep bend sections will occasionally indicate velocities that are not representative of sediment transport around the bend, and the recourse is to eliminate them from the model. The results from running this discharge will also give some insight into how close the existing channel is to a regime condition. That is, if there is overbank flow, justify that it also occurs in the prototype and is not just a numerical condition.

It is useful to determine the model performance for the channel-forming discharge because, if the channel is near regime, this should cause very little aggradation or degradation. Before focusing on sediment transport, however, demonstrate that the Manning *n*-value for the channel is appropriate for the movable boundary. Make whatever adjustments are necessary to ensure that the *n*-value for the stream-bed portion of the cross section is in reasonable agreement with that from bed roughness predictors. Also, the sediment transport rate will usually be higher on the first computation event than it is on subsequent events because there is usually an abundance of fines in the bed samples that will be flushed out of the system as the bed layers are formed. The physical analogy is starting water flow down a newly constructed ditch. It is important to balance the sizes in the inflowing bed-material sediment load with transport potential and bed gradation. The scatter in measured data is usually sufficiently great to require smoothing, but the adopted curves should remain within that scatter.

It is useful to repeat this steady-state test for the maximum water discharge in the testing hydrograph. The key parameters to observe are water surface elevations, flow distribution between channel and overbanks, and velocities. However, each study is unique, and one should regard this paragraph as suggestions to illustrate thinking and not a list that is both necessary and sufficient.

14.6.4.1 n-Values The first approximation of *n*-values was coded into the original model. At this point refine those values using field observations of stage or velocity.

14.6.4.2 Water-Surface Profiles With movable-bed calculations active, it is important to recheck the model-to-prototype comparison for water surface elevations. Because prototype measurements are like snapshots in time, it is important to run prototype boundary conditions for a sufficiently long period for the bed surface profile to resemble that in the prototype when the data were surveyed.

14.6.4.3 Flow Distribution Reevaluate the calculated flow distribution, similar to that in the fixed-bed test, and adjust *n*-values or geometry if needed.

14.6.4.4 Coordination of Inflowing Gradation with Bed Sediment Gradation The bed gradation is prescribed as an initial condition for the bed sediment reservoir. The inflowing sediment discharge is prescribed as a boundary condition. These data sets are related. That is, if the prototype is in equilibrium, the inflowing sediment load will be transported by grain size class without excessive deposition or erosion. That requires confirmation because the calculation is sensitive to the transport function selected for the study. Observe model transport by grain size and adjust either the inflow or the bed gradations, depending on which is regarded as the weaker data set.

14.6.4.5 Sediment Yield One should confirm that the calculation sediment yields in the computational model match the annual yields for the watershed. Figure 14-11 is an example of such a comparison. It is important to develop consistent units before making such a comparison. That is, if the published sediment yields were calculated from suspended sediment measurements, then either convert the computational model results into the suspended sediment component of the total sediment load or add the load moving in the unmeasured zone in the prototype to the suspended measurements. The Toffaleti transport function will facilitate such an estimate by displaying the vertical distribution of sediment in the water column. Most other transport functions do not offer that feature.

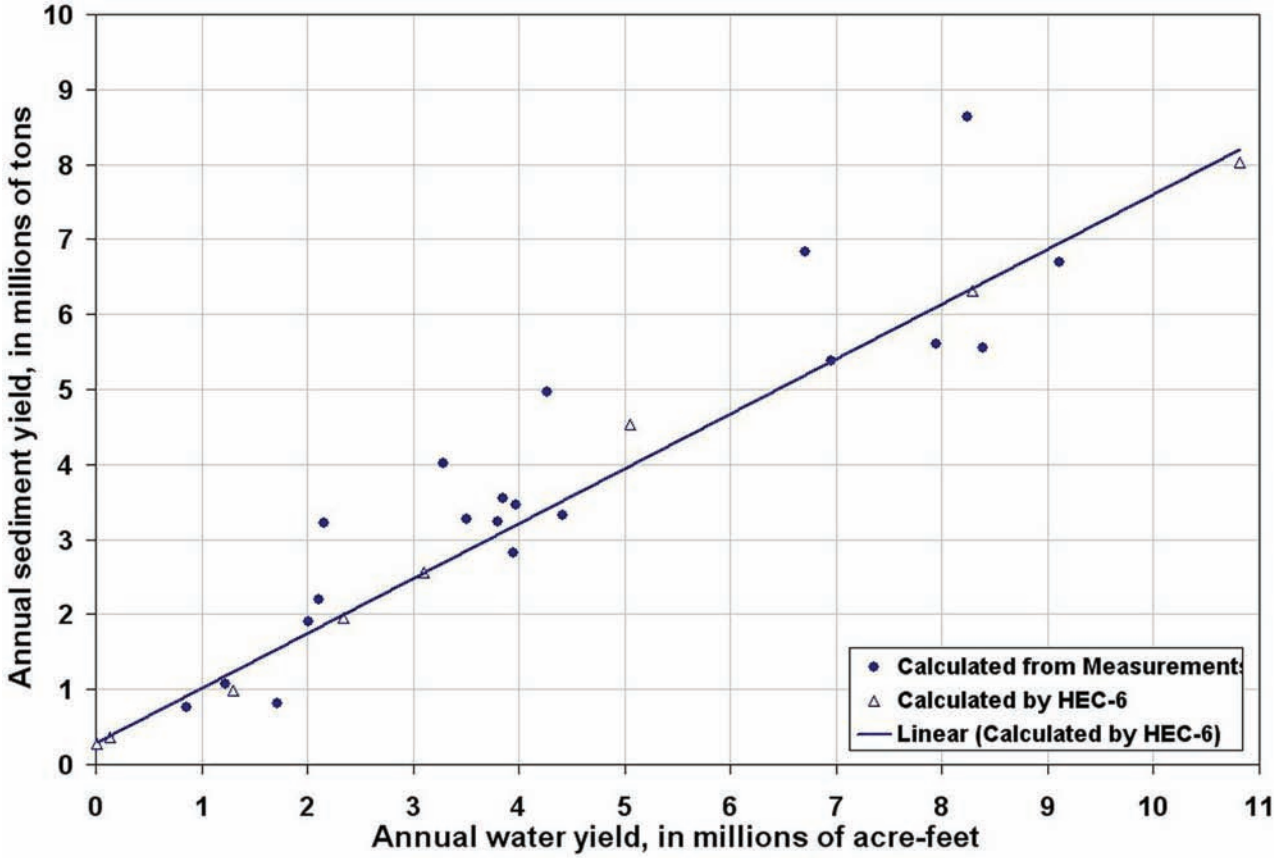

Fig. 14-11. Measured and calculated annual sediment yield.

14.6.4.6 Sediment Transport Profiles Another useful graphic is a plot of calculated sediment discharge versus river mile. It will show sources and sinks, which can then be one compared to the geometry data and to visual observations to test for reality. This will aid in improving the one-dimensional representation of the prototype to eliminate "numerical shadows" from the scour and deposition calculations.

14.6.4.7 Selection of Calibration Parameters Correlate model to prototype conditions in broad terms recognizing one dimensional approximations. For example, profiles of the bed elevation may exhibit little or no correlation with the prototype, but cross-sectional area changes should correlate with prototype behavior. Reconcile zones and amounts of aggradation and degradation by expressing accumulated volumes rather than depths. Reconcile accumulated weights passing each cross section.

14.6.5 Movable-Boundary, Unsteady-State Calibration

The final phase in model calibration is the movable-bed unsteady-state test. This is required for both unsteady-state and steady-state hydraulic calculations because the sedimentation equation is an unsteady-state equation. This phase utilizes both single-event and period-of-record hydrology. Of particular interest are the zones of deposition and erosion depicted during the passing of a hydrograph. When the stream is in a relatively equilibrium condition, these zones should cycle. When the graph of bed change versus time shows a trend to continue either deposition or erosion, investigate the cause. Resolve these issues starting with the most upstream location and continuing toward the downstream end of the model. Begin with the cross section showing the greatest change in bed elevation. Even if only one cross section is not responding properly, the model results downstream and sometimes upstream from it are not reliable.

14.7 BASE TEST

The most appropriate use of a movable-bed simulation is to compare an alternative plan of action with a base condition. In most cases the base condition is the predicted future behavior of the river in a "no-action future." In a reservoir study, for example, the base test would calculate the behavior of the reservoir reach of the river without the dam in place. In many cases, the base test simulation will show little or no net scour or deposition. These are the river reaches that

are near equilibrium (i.e., where scour approximately equals deposition) under existing conditions.

Two sets of boundary conditions are needed: one set is for model calibration and the other set is for analyzing the plan test. That is, model calibration is a task designed to demonstrate that the model calculations match historical prototype behavior. The calibration task begins with a survey of the model area, called initial conditions, and runs to a second survey of the model area. It is necessary to know the boundary conditions that existed between those two surveys. That requirement dictates the selection of boundary conditions for model calibration.

However, boundary conditions for the base test must represent the future conditions in the project. They will be the same as those for the plan tests unless the plan tests are designed to investigate a change in the boundary conditions. For example, if the purpose of the model study is to investigate a channel modification, the base test would be conducted with the same boundary conditions as the plan test. The length of the simulation hydrograph for the base test is usually selected by considering the economic life of the project.

It is likely that the hydrology and sediment boundary condition values for the calibration period will not be representative of the long-term future hydrology and sediment boundary condition values. However, if the purpose of the model study is to investigate what will happen in a river as the result of a change in the boundary conditions, the base test values will be different from the plan test values, but they should contain the same period of time.

14.8 PLAN TEST

The project alternatives can be simulated by modifying the base data set appropriately. In case of a reservoir, a dam can be simulated by inserting operating rule data into the base test model. For a channel improvement project, cross-sectional geometry and roughness can be changed. If a major change is required, make the evaluation in steps. That is, change one parameter at a time so that the model results will be easier to interpret.

For example, it is best to analyze a channel modification project in three steps. First, change the hydraulic roughness values and run future flows in the existing geometry. Second, insert the modified cross sections and complete the analysis by running the alternative to be tested. Finally, add the contraction and expansion coefficients for the modified channel design and run the plan test.

Use model results from each of the above steps as an aid in predicting future conditions. Rely heavily on engineering judgment when analyzing model results. Look for surprises in the calculated results. These surprises can be used by the experienced river engineer to locate data inadequacies and to better understand the behavior of the prototype system. Any unexpected response of the model should be analyzed and should be justified before the results are accepted.

14.9 INTERPRETATION OF RESULTS

14.9.1 Form of Study Results

Results from the plan tests should be expressed in terms of change from the base case. This will provide an assessment of the impacts of proposed projects on the stream behavior. The impact of sedimentation on the performance of the project should be presented in units appropriate to the decisions which need to be made. For example, a flood channel will require maintenance to remove sediment deposits. These units are usually cubic yards. However, the parameter to measure in arriving at a maintenance schedule will most likely be the water surface. The results of the sedimentation study should include the locations of deposits and their resulting impact on the water surface profile.

14.9.2 Sensitivity Tests

It is desirable during the course of a study to perform sensitivity tests. Quite often part of the input data (such as inflowing sediment load) will be missing or will contain measurement error. The impact of these uncertainties on model results can be studied by modifying the suspected input data by $\pm\, x\%$ and rerunning the simulation. If little change in the simulation results, the uncertainty in the data is of no consequence. If large changes occur, the input data need to be refined. Refinement should then proceed by using good judgment and by modifying only one parameter at a time. Sensitivity studies performed in this manner will increase the modeler's understanding of model behavior and that understanding will aid in predicting the behavior of the prototype.

14.10 EXAMPLES TO ILLUSTRATE MODEL APPLICABILITY

One-dimensional computational models of sedimentation have been used in a variety of studies over the past three decades. Examples are

- to confirm land acquisition for a run-of-river reservoir that required simulating sedimentation processes in that reservoir for a 50-year life;
- to calculate the stability of a hydraulic fill prior to placing it across the Mississippi River to arrest the upstream movement of salt water from the Gulf of Mexico during low water;
- to predict the water surface profile in setting a levee grade in a backwater area of a reservoir;

to reconstitute the degradation trend downstream from dams;
to design erodible bed channels with bank protection and grade control structures;
to predict general scour at a bridge crossing for bridge design or evaluation;
to evaluate the impacts of instream sand and gravel mining;
to predict maintenance dredging for existing and proposed navigation projects;
to study degradation and aggradation in the development of the Atchafalaya Basin and Delta;
to predict the stream-bed response of a river if water and sediment are diverted out;
to predict stream stability and maintenance dredging for a flood protection project;
to predict sedimentation processes following the removal of dams;
to predict aggradation and degradation in channel modification projects:
to design sediment traps; and
to predict the bed roughness and resulting water surface profile due to the transport of sand and gavel through concrete channels.

14.11 AN EXAMPLE APPLICATION

An example was provided by Chang (1984) to illustrate the general points in this chapter. The actual study encompassed the lower 3 miles of the San Dieguito River in California, Fig. 14-12. Because this is only an illustration, the entire study area is not reproduced in Fig. 14-12.

14.11.1 Model Data

Data for the fluvial processes during the January to March 1993 flood were used for calibration. Channel geometry is defined by 43 cross sections selected along the reach. A total of 17 cross sections were surveyed before the flood and resurveyed soon after the flood. Cross sections not included in the survey were developed from the 1992 topographic map of the river channel. The map has a contour interval of 304.8 mm (1 ft).

Sediment particle-size distributions for the stream bed material are based on samples taken along the study reach. The stream-bed sediment is sand.

The runoff hydrograph for the January to March 1993 flood is shown in Fig. 14-13. This runoff was measured by the county of San Diego at the Hodges Dam. The flood that occurred on January 14, January 16, and January 18, 1993

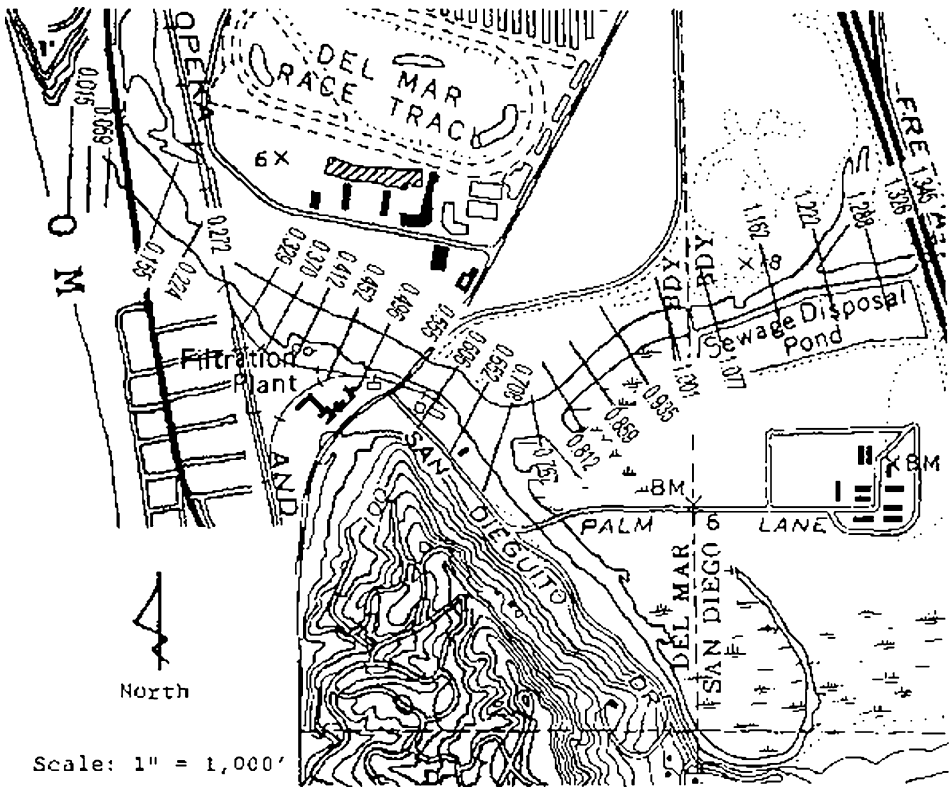

Fig. 14-12. Location of surveyed cross sections (multiply ft by 0.3048 to get m).

had three peaks. The discharges were 120.43 m^3/s (4,253 cfs), 188.39 m^3/s (6,653 cfs), and 120.43 m^3/s (4,253 cfs), respectively. The peak discharge of 188.39 m^3/s (6,653 cfs) has a return period of 14.7 years.

14.11.2 Selection of the Sediment Transport Formula

Numerous formulae have been developed for calculating sediment movement in sand-bed channels. Each one will predict a different sediment transport rate. The selection of the formula to use is best confirmed by comparing calculated results to measurements at the site. However, in an ephemeral stream such as the San Dieguito River, sediment discharge measurements can be made only during floods.

Consequently, data are scarce. Even when suspended sediment measurements are made, there is always the presence of the unmeasured zone near the bed. The substantial movement of the bed material in the unmeasured zone adds uncertainty to the measured data set.

Therefore, the approach to selecting the sediment transport function includes more than just a search for measured sediment concentrations. It also includes consideration of the physical conditions of the fluid, the hydraulic parameters of the flow, and the sediment characteristics of the stream bed. The engineer can start by comparing the hydraulic and sediment properties at the study site with those used in development of the transport function. The functions passing this test are then submitted to additional testing using measurements other than sediment concentrations.

Measured data include measured changes in channel dimensions. That is, the calculated rate and amount of erosion or deposition in a channel depend on the sediment transport formula used. If a formula overpredicts the sediment transport rate, it will calculate more deposition than the measured values. On the other hand, a formula that underpredicts the transport rate will show less deposition than the measured amount. At a cross section undergoing scour, the amount of scour is overpredicted by a sediment transport formula giving transport rates that are too high and vice versa. The use of calculated changes in bed elevation provides valuable information when the sediment transport function is being selected for a study. Stream channel changes in the lower San Dieguito River during the 1993 flood are characterized by channel-bed scour. The changes were significant.

In this study, the Ackers-White formula, the Engelund-Hanson formula, and the Yang formula (Vanoni 2006), were identified as possible choices. These functions were selected based on the extensive evaluation made by Brownlie (1983).

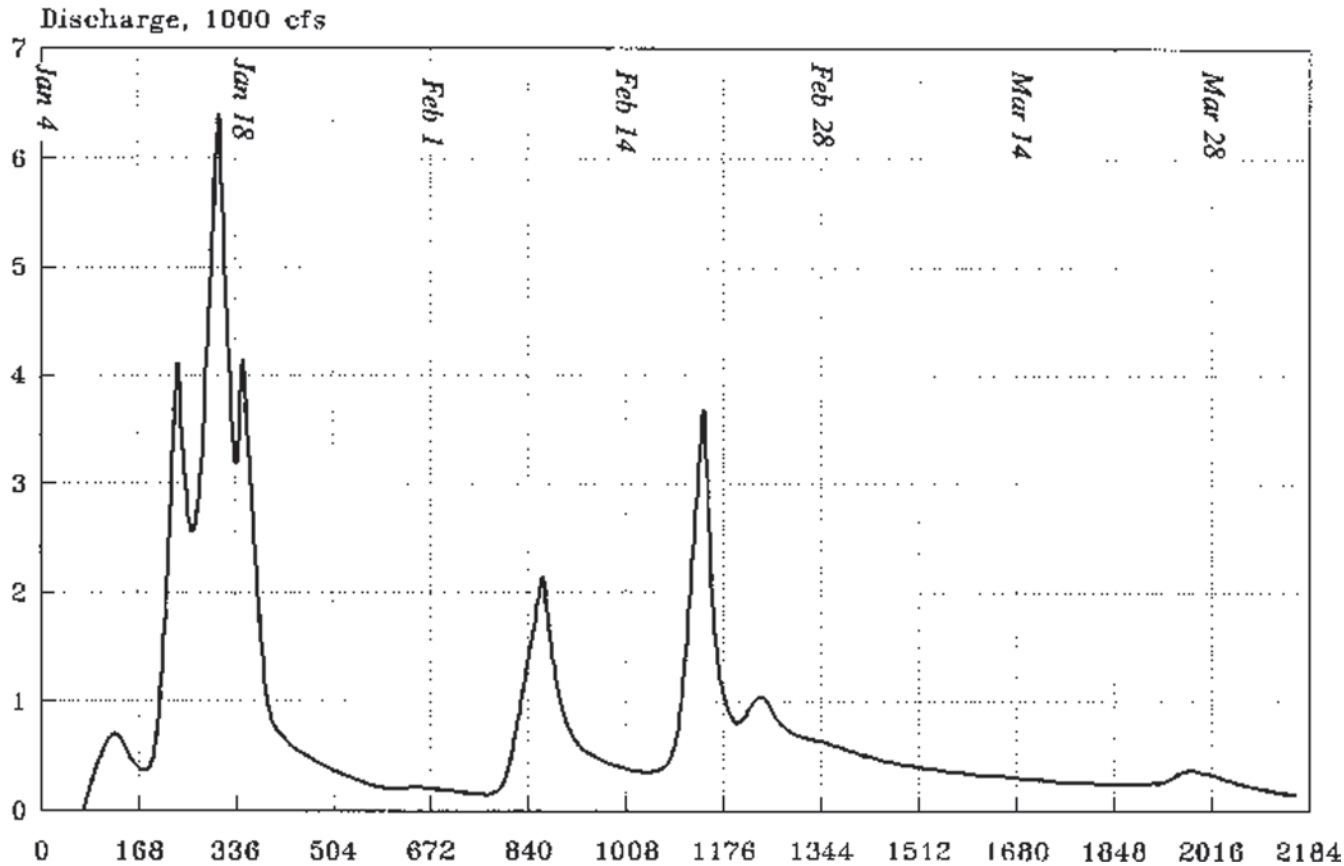

Fig. 14-13. Hydrograph for January to March 1993 floods (multiply cfs by 0.0283 to get m^3/s).

Each formula was tested to determine whether or not the computational model would simulate measured channel changes as described in the previous paragraph.

14.11.2.1 Calculated Sediment Delivery Sediment delivery is defined as the accumulated sediment load that passes a specified channel cross section. The equation is

$$Y_s = \int_T Q_s dt \tag{14-14}$$

where

Y_s = sediment delivery;
Q_s = sediment discharge;
t = time; and
T = the specified period of time.

Sediment delivery is widely employed by hydrologists working in watershed management. The quantity commonly used in their work is annual sediment yield. In computational modeling the accumulated sediment load is available, by particle size, at every cross section and for every computational time step. However, when the specified period of time for the sediment delivery calculation is a year, the sediment delivery becomes the annual sediment yield. Referring to the output from a computational model as sediment delivery preserves the historic definition of sediment yield.

The calculated sediment deliveries of bed material load based on the Ackers-White, Engelund-Hanson, and Yang formulas are shown in Fig. 14-14. These results were compared with the measured data in the final selection of the transport formula for this study.

In the general case the sediment discharge Q_s can be any part of the sediment load or it can be the total sediment load. In this case it pertains only to bed-material load. It was not necessary to include fine sediment, i.e., silt and clay, in this model because those particle sizes were not present in the samples of bed material. As a result, the conversion factor between volume and dry weight of sediment is 1633.9 kg/m^3 (102 lb/cu).

The shape of the sediment delivery graph identifies zones of erosion and deposition along a channel. The plot should be read in the direction of the water flow. A decreasing delivery in the downstream direction, i.e., a negative gradient for the delivery-distance curve, signifies that sediment is depositing into the channel bed and banks. On the other hand, an increase in the sediment delivery in the downstream direction indicates that sediment is being removed from the channel bed and banks. A horizontal sediment delivery plot indicates

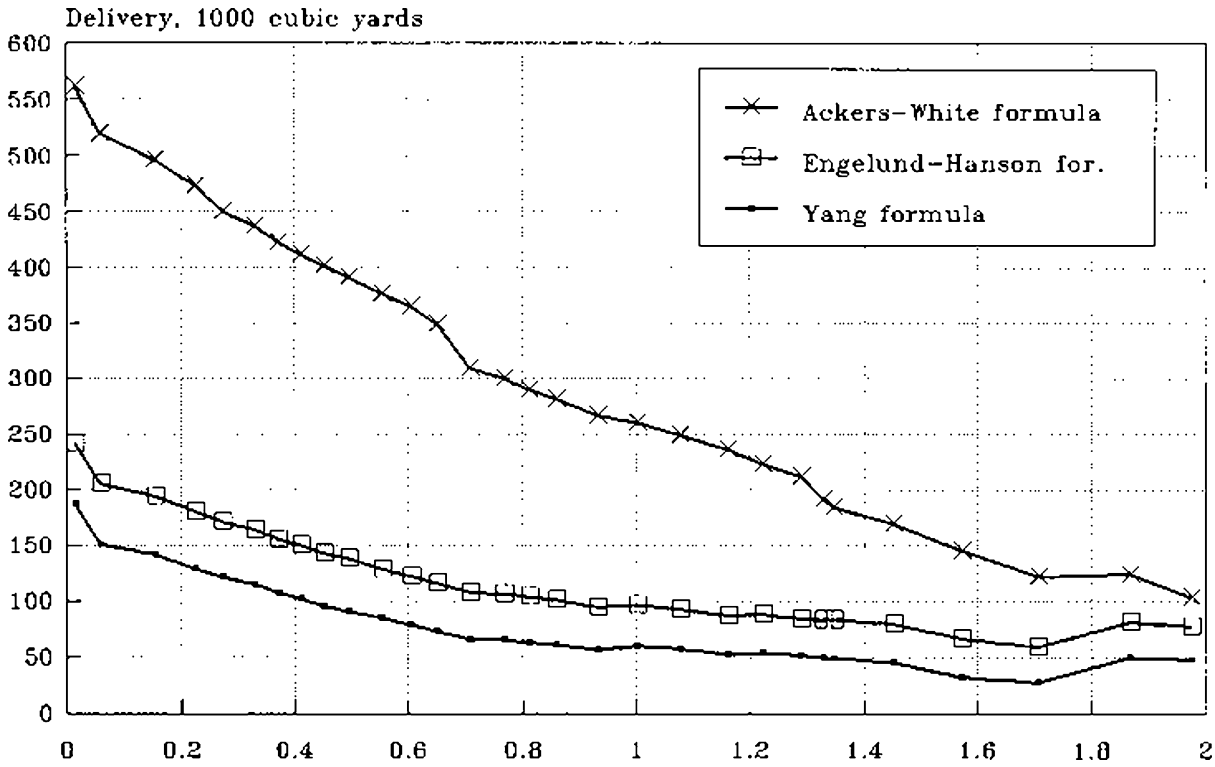

Fig. 14-14. Sediment delivery through the study reach (multiply cy by 0.7646 to get m^3).

zero deposition or erosion. Of course, the assumption in this illustration is that local sediment inflow or outflow is zero.

As depicted in Fig. 14-14, sediment delivery through the lower San Dieguito River during the 1993 flood was characterized by general erosion along most of the river reach. Although all three figures show the general trend of erosion, their quantities are nevertheless different. The total calculated erosion for the inlet channel and the west channel is shown in Table 14-3. The inlet channel is from the river mouth to river mile 0.713 and the west channel is from river mile 0.713 to Interstate 5 at river mile 1.345.

The delivery curves shown in Fig. 14-14 have different slopes for the inlet channel and the west channel, and the steeper slopes are in the inlet channel. The average slope for the delivery curve of a channel is the difference in delivery from one end of the reach to the other divided by the reach length. The average change in end area can also be calculated from measured cross sections and compared to the slope of the delivery curve as shown in Table 14-4. The row identified as "Measured" shows volumes calculated from measured cross-sectional changes integrated over the channel length.

Table 14-4 provides a direct comparison of the calculated channel changes with measurement. The amount of erosion is considerably overpredicted by the Ackers-White formula. It is slightly overpredicted by the Engelund-Hanson formula. The calculated results based on the Yang formula are similar to the measured values. For this reason, the Yang formula was selected for application on the lower San Dieguito River.

Both simulation and measurement show that the inlet channel underwent greater erosion than did the west channel. The modeler can use such information to understand the prototype. For example, a possible cause for this difference is that the inlet channel is replenished by beach sand after each episode of storm flow.

14.11.2.2 Reconstitution of the Measured Bed Profile Profiles of the calculated bed surface and water surface are shown in Fig. 14-15. The results based on the Yang formula are closer to prototype measurements than the results using the Ackers-White or the Engelund-Hanson formula. The differences are within 5%. For this reason, the Yang formula is selected for application on the lower San Dieguito River.

It should be noted that the version of Ackers-White formula used in this study is the earlier version. It was included in the Brownlie evaluation. Ackers and White have since modified this formula.

14.11.3 Calculated Changes in Channel Geometry

Calculated changes in river channel geometry are presented as changes in longitudinal channel-bed profiles and in channel cross sections. These changes reflect the spatial variations in sediment delivery described above.

14.11.3.1 Longitudinal Profiles Channel-bed profiles computed with the Engelund-Hanson and Yang formulae are generally similar (Fig. 14-15). The bed profiles at the peak flow are highly uneven, with the low points at channel bends and channel contractions. The channel-bed profiles become quite smooth toward the end of the flood. These results indicate that contraction scour is more pronounced during high flow and it becomes much less during low flow. The low point in bed profiles at a channel bend is related to deeper scour near the concave bank. This phenomenon will also be demonstrated by cross-sectional changes described in a later section. It can be seen from the relatively smooth channel-bed profiles at the end of the flood that channel-bed scour is at a maximum near the river mouth and it decreases gradually in the upstream direction.

For the simulated changes based on the Ackers-White formula, the extent of degradation is considerably greater than that based on the other two formulae. The deeper scour depths are related to the greater sediment delivery predicted by the Ackers-White formula.

14.11.3.2 Channel Cross Sections Calculated cross-sectional changes along the river reach are exemplified by those presented in Figs. 14-16 and 14-17. Each figure

Table 14-3 Simulated Sediment Deliveries (multiply cuyd by 0.7646 to get m^3)

	Simulated sediment delivery, cuyd		
Formula used	River mouth	Entrance of inlet channel	West channel
Ackers-White	520,000	309,000	184,000
Engelund-Hanson	205,000	107,000	83,100
Yang	151,000	65,800	48,800

Table 14-4 Calculated and Measured River Channel Erosion

	Total erosion, cuyd		Average change in cross section, sq ft	
Formula used or measured	Inlet channel	West channel	Inlet channel	West channel
Ackers-White	211,000	125,000	1,513	1,010
Engelund-Hanson	98,000	23,900	703	193
Yang	85,200	17,000	611	137
Measured	87,500	17,770	628	144

(multiply cuyd by 0.7646 to get m^3; multiply sq ft by 0.09290 to get m^2)

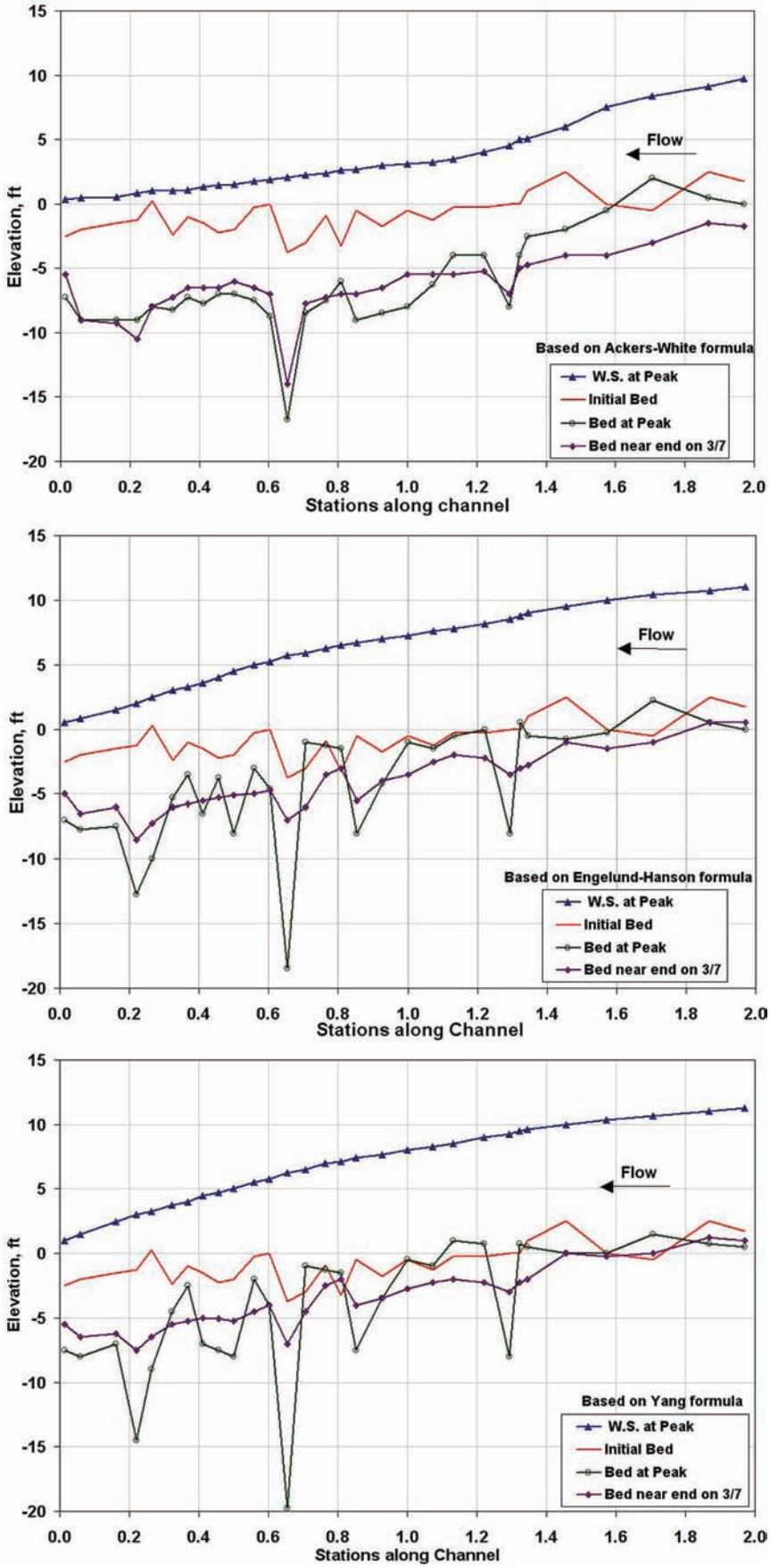

Fig. 14-15. Calculated bed and water surface profiles (multiply ft by 0.3048 to get m).

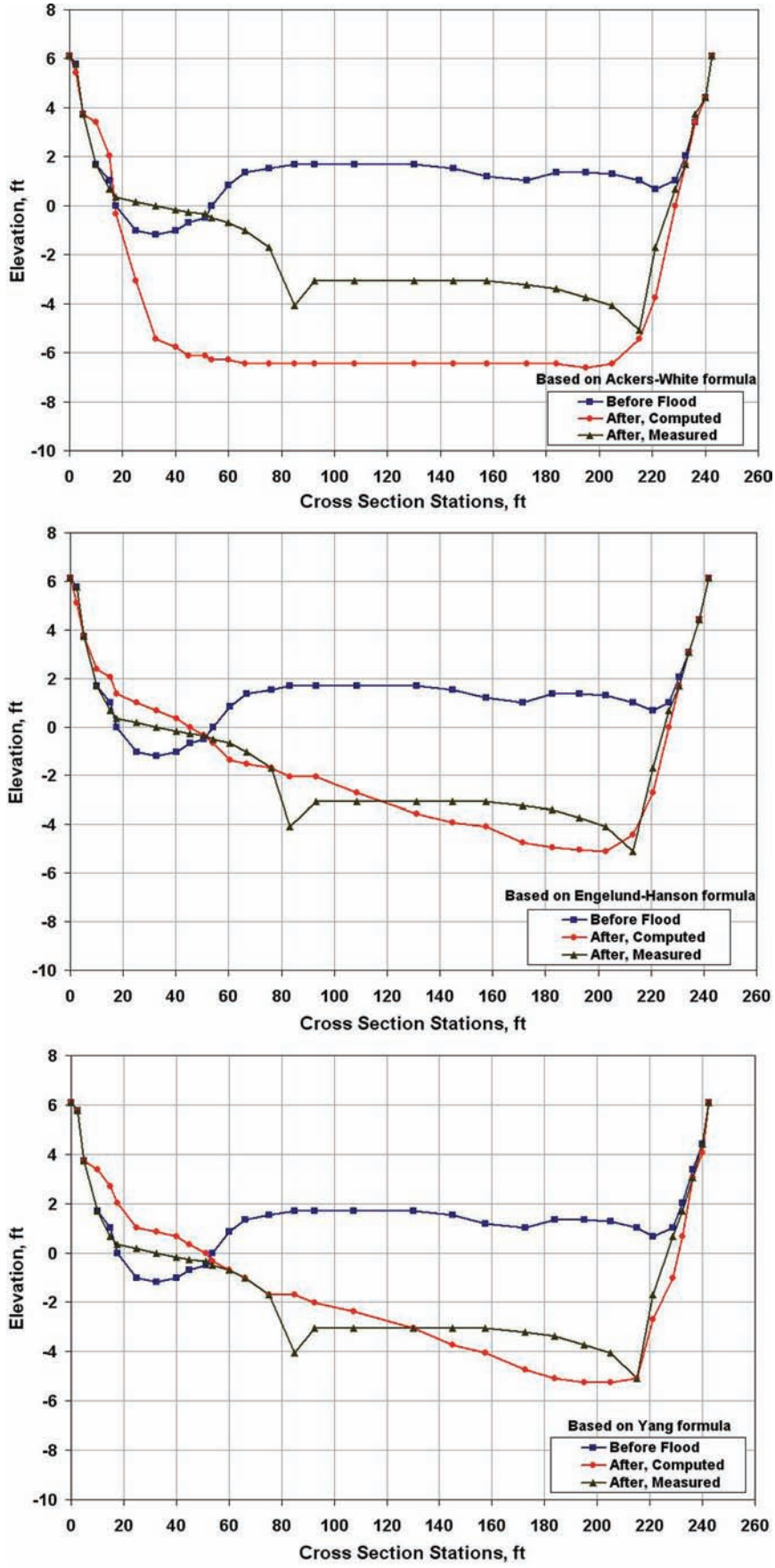

Fig. 14-16. Calculated and measured cross-sectional changes at Sect. 0.412 (multiply ft by 0.3048 to get m).

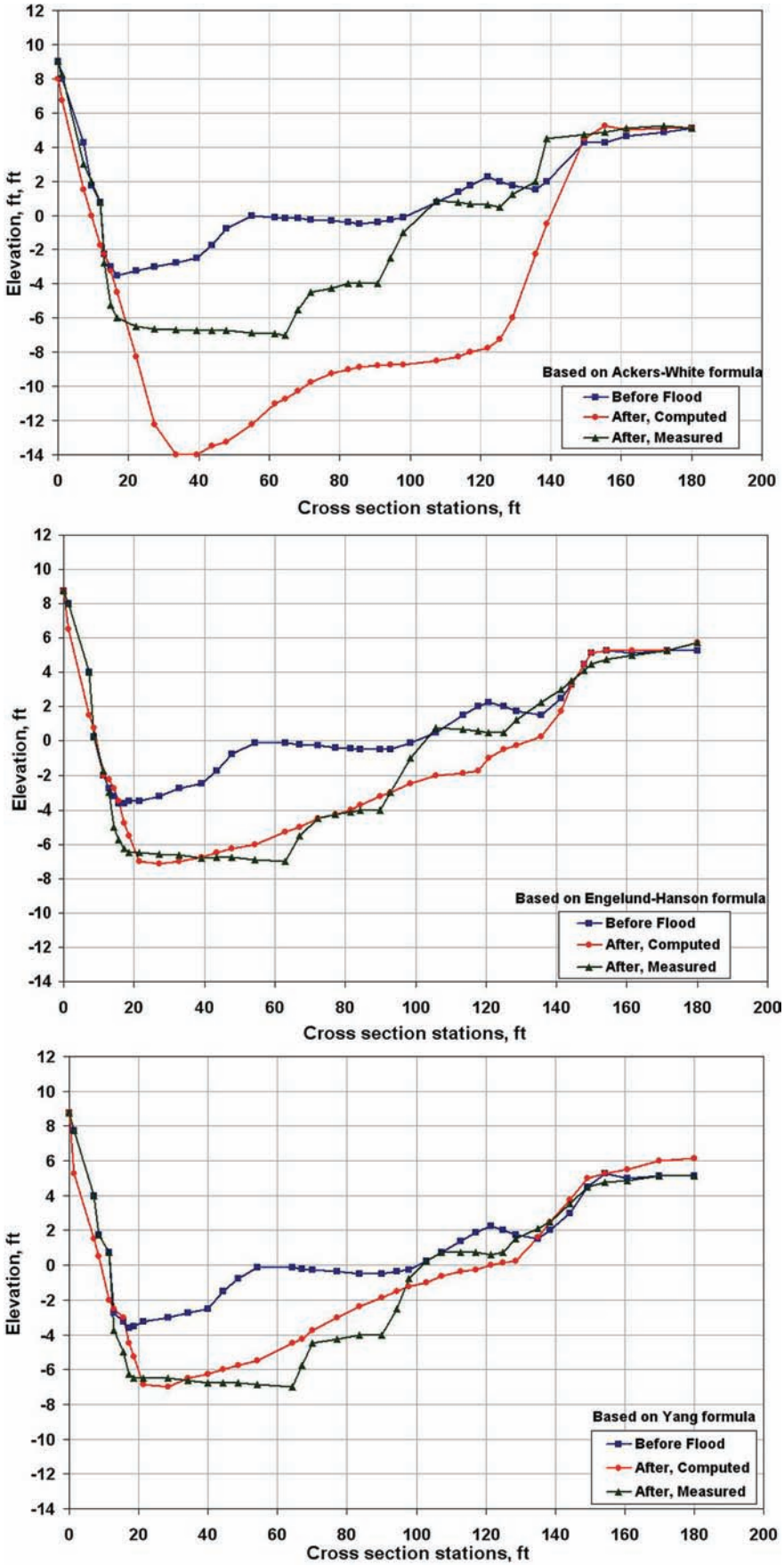

Fig. 14-17. Calculated and measured cross-sectional changes at Sect. 0.652 (multiply ft by 0.3048 to get m).

includes the following three channel-bed profiles: (1) The initial bed profile based on the preflood survey; (2) the calculated cross-sectional profile on the date of the postflood survey; and (3) the surveyed postflood cross-sectional geometry.

These figures provide comparisons of simulated and measured cross-sectional geometries. Cross-sectional changes simulated based on the Ackers-White formula far exceed the measured changes. It is therefore concluded that the results are unacceptable and that the Ackers-White formula cannot be used for this study.

Simulated cross-sectional changes based on the Engelund-Hanson formula are generally supported by the measurement. It can be seen that the net change in cross-sectional area as simulated tends to exceed the measured change. In other words, the scour is slightly overpredicted by the Engelund-Hanson formula. For the inlet channel, the overprediction is 12% averaged over the channel reach; the overprediction is 30% for the west channel, as summarized in Table 14-5.

Calculated cross-sectional changes based on the Yang formula are generally supported by the measurement. For the inlet channel, the scour is underpredicted by 2.7% averaged over the channel reach. For the west channel, the scour is overpredicted by 5%. It may therefore be concluded that the Yang formula is the most applicable to the lower San Dieguito River.

The simulated patterns of scour and fill are also used to demonstrate the complex channel geometry adjustments during floods. For the erosional changes, the scour pattern at a cross section is affected by the geometries of adjacent cross sections and channel curvature. Section 0.652 is located in a channel bend, and the shape of the cross section is influenced by the channel curvature. To approximate such morphological adjustments, the mathematical model must be able to calculate nonuniform patterns of deposition and erosion.

A general comparison of the calculated and surveyed cross-sectional profiles may be assessed as follows. The erosional changes as simulated by the Yang formula are clearly consistent with the survey. Any discrepancy between simulated and measured results may be attributed to the following factors.

1. A nonhomogenous horizontal distribution of the bed sediment (i.e., sediment particle sizes on and in the stream bed are not uniformly distributed at a cross section). The presence of coarse materials usually affects the pattern of channel changes, and a one-dimensional mathematical model does not account for such sediment distributions.
2. A horizontal distribution of the suspended sediment concentration in the inflowing water that is not in equilibrium with hydraulic forces at the current cross section. A one-dimensional mathematical model does not account for such sediment distributions.
3. Imprecision in measurements such as the size of the flood discharge, the river cross section, and the bed material composition.
4. Imprecision in computations related to the roughness coefficient, the sediment transport formula, etc.

Despite the differences between the calculated and measured cross-sectional changes, the calculated change in cross-sectional area and the pattern of erosion and deposition along the longitudinal profile are consistent with the survey. This validates the model for predicting longitudinal profiles and general cross-sectional end area changes along the lower San Dieguito River.

Table 14-5 Comparison of Calculated and Measured Scour

	Simulated scour/measured scour	
Formula used	Inlet channel	West channel
Ackers-White	241%	678%
Engelund-Hanson	112%	130%
Yang	97.3%	105%

14.12 AVAILABLE COMPUTATIONAL MODELS

The Subcommittee on Sedimentation, Interagency Advisory Committee on Water Data investigated available computational sedimentation models (Fan 1988). In 1986 they initiated a project on the "selection and proper use of computer models to estimate sediment transport." At the end of phase two of that three-phase effort they had selected 12 models for comparison and evaluation. These are presented in Table 14-6.

The field of computational modeling is continually changing. New models are being released and old ones are being improved. Even when originally printed, Table 14-6 was not an exhaustive list of sediment models. Fan writes,

> Beginning in the summer of 1987, the Work Group made a survey of the computer sedimentation models developed and implemented in the United States. Public responses to the survey were prompt and overwhelming. Within 2 months, the Work Group received approximately 48 sedimentation models which are available both in federal agencies and in the private sector in the United States. (Fan 1988, p. 3)

It was from this submission of models that the Work Group selected those listed in Table 14-6 for further investigation.

The purpose of this section is to illustrate what is meant by "computational model." It makes no endorsement of a specific model nor does it imply that all are equal in their performance and reliability. The list of available computational models will very likely be obsolete even before it is

Table 14-6 Currently Available Computer Models[a]

Model name	Background	Comments
HEC-6	Developed by William A. Thomas during the period 1968 through 1974 and released by the U.S. Army Corps of Engineers, Hydrologic Engineer Center, Davis, Calif. in 1976.	The model is designed to simulate one-dimensional, steady, gradually varied water and sediment flow problems.
TABS2	Developed by a team of researchers at the U.S. Army Waterways Experiment Station, Vicksburg, Miss. during the period 1977 through 1984 and released in 1984.	This is a fully two-dimensional, finite-element solution of the flow and sediment equations.
IALLUVIAL	Developed by F. W. Karim at the University of Iowa under contract with the U.S. Army Corps of Engineers, Omaha, Neb.	It is a one-dimensional, quasi-steady routing model.
STARS	This model is an outgrowth of a model originally developed by Albert Molinas at Colorado State University and was submitted under contract to the Bureau of Reclamation in 1983.	STARS has a unique feature of using a stream-tube concept to vary the hydraulic and sediment transport characteristics across a stream cross section.
GSTARS	Developed by Albert Molinas and Chih Ted Yang for the Bureau of Reclamation and released in 1986.	This is a generalized stream-tube model for alluvial river simulation.
ONED3X	Developed in 1987 by Vincent Lai, U.S. Geological Survey.	This is a coupled multimode method of characteristics.
CHARIMA and SEDICOUP	Developed from 1985 through 1987 by Forrest Holly, Jr., University of Iowa. Between 1986 and 1988, Dr. Holly developed SEDICOUP, a totally coupled program.	This represents the latest generation in a series of codes whose progenitor was IALLUVIAL The model is a partially coupled program for mobile bed simulation and can duplicate an IALLUVIAL computation. It is still under active development and modification.
FLUVIAL12	Developed in 1976 by Howard Chang of San Diego State University, Calif.	The model is intended for water and sediment routing in natural and man-made channels. The combined effects of flow hydraulics, sediment transport, and river channel changes are simulated for a given flow period.
HEC2SR	Developed in 1980 by Ruh-Ming Li of Simons, Li and Associates, Inc. (SLA).	This model is designed to simulate watershed sediment yield, aggradation, and degradation in a river basin. It incorporates a sediment-routine program into the HEC2 program developed by Bill S. Eichert, Hydrologic Engineering Center, U.S. Army Corps of Engineers
TWODSR	Developed in 1988 by Yung-Hai Chen.	This is a two-dimensional model based on an uncoupled, unsteady approach.
RESSED	Developed byYung-Hai Chen for the Canadian International Project Management (CIPM)-Yangtze Joint Venture.	Developed to study the Three Gorges Project on the Yangtze River in China. This is a simplified quasi-nonequilibrium model for reservoir and river erosion sedimentation related problems.

[a]The first six models are federally owned. The last five are privately owned (1986).

printed. However, the principles presented in this chapter will continue to be useful in evaluating and selecting a computational model.

REFERENCES

Arcement, G. J., Jr., and Schneider, V. R. (1989). "Guide for selecting Manning's roughness coefficients for natural channels and flood plains." *Water-Supply Paper 2339*, U.S. Geological Survey, Department of the Interior, Books and Open-File Reports Section, Federal Center, Box 25425, Denver, Colo.

Brownlie, W. R. (1983). "Flow depth in sand-bed channels." *Journal of Hydraulic Engineering, ASCE*, 109(7), 959–990.

Chang, H. H. 1982. "Mathematical model for erodible channels." *Journal of the Hydraulics Division*, *ASCE*, 108(HY5), 678–689.

Chang, H. H. (1984). "Modeling of river channel changes." *Journal of Hydraulic Engineering*, *ASCE*, 110(2), 157–172 and 113(2), 265–267 (1987).

Chang, H. H (1985). "Water and sediment routing through curved channels." *Journal of Hydraulic Engineering*, *ASCE*, 111(4), 644–658.

Chen, Y. H. (1973). "Mathematical modeling of water and sediment routing in natural channels." PhD dissertation, Department of Civil Engineering, Colorado State University, Fort Collins, Colo.

Chow, V. T. (1959). *Open-channel hydraulics*, McGraw-Hill, New York.

Copeland, R. R. (1993). "Numerical modeling of hydraulic sorting and armoring in alluvial rivers." PhD thesis, University of Iowa, Iowa City, Iowa.

Einstein, H. A. (1950). "The bed-load function for sediment transportation in open channel flows." U.S. Department of Agriculture Technical Bulletin No. 1026, Soil Conservation Service, Washington, D.C.

Emmett, W. W., and Leopold, L. B. (1963). "Downstream pattern of riverbed scour and fill." *Proc. Federal Inter-Agency Sedimentation Conference*, Miscellaneous Publication No. 970, Agricultural Research Service, Washington, D.C., 399–409.

Fan, S. ed. (1988). "Twelve selected computer stream sedimentation models developed in the United States." Subcommittee on Sedimentation, Interagency Advisory Committee on Water Data. Federal Energy Regulatory Commission, Washington, D.C.

Hinds, J. (1928). "The hydraulic design of flume and siphon transitions." *Transactions of the ASCE,* 92, 1423–1459.

HEC-6 Generalized Computer Program (1977, 1993). "Scour and deposition in rivers and reservoirs." *Users Manual*, the Hydrologic Engineering Center, U.S. Army Corps of Engineers, Davis, Calif.

James, C. S. (1985). "Sediment transfer to overbank sections." *Journal of Hydraulic Research*, 23(5), 435. IAHR (International Association for Hydraulic Engineering and Research Madrid, Spain).

Jarrett, R. D. (1985). "Determination of roughness coefficients for streams in Colorado." *Water-Resources Investigations Report 95-4004*, U.S. Geological Survey, Washington, D.C.

King H. W., and Brater. E. F. (1963). *Handbook of hydraulics.* McGraw-Hill, New York.

Leopold, L. B. (1994). *A view of the river*. Harvard University Press. Cambridge, Mass.

Limerinos, J. T. (1970). "Determination of the Manning coefficient from measured bed roughness in natural channels." *Geological Survey Water-Supply Paper 1898-B*, in cooperation with the California Department of Water Resources, U.S. Government Printing Office, Washington, D.C.

Rosgen, D. (1996). *Applied river morphology.* Wildland Hydrology, Pagosa Springs, Colo.

Schumm, S. A. (1971). "Fluvial geomorphology: Historical perspective." *River mechanics*. H. W. Shen, ed., Water Resources Publications, Littleton, Colo.

Schumm, S. A., Morrey, M. D., and Watson, C. C. (1984). *Incised channels: Morphology, dynamics and control*, Water Resources Publications, Littleton, Colo.

Thomas, W. A. (2002). "Sedimentation in stream networks." HEC-6T, *User Manual.* Mobile Boundary Hydraulics, Clinton, Miss.

Vanoni, V. (2006). "Sedimentation engineering." *Manual 54*, ASCE, Reston, Va.

Zhang, Q., Zhang, Z., Yue, J., and Dar, M. (1983). "A mathematical model for the prediction of the sedimentation process in rivers." *Proc. 2nd International Symposium on River Sedimentation*.

Copyrighted Materials
Copyright © 2008 American Society of Civil Engineers (ASCE)
Retrieved from www.knovel.com

CHAPTER 15

Two- and Three-Dimensional Numerical Simulation of Mobile-Bed Hydrodynamics and Sedimentation

Miodrag Spasojevic and Forrest M. Holly, Jr.

15.1 INTRODUCTION

15.1.1 When Is Multidimensional Mobile-Bed Modeling Necessary?

Although present understanding and conceptualization of mobile-bed processes are still far from complete, one-dimensional mobile-bed numerical models have been used with some success in engineering practice since the early 1980s. As described in Chapter 14 of this manual, such models are most often applied to situations involving extended river reaches and extended time periods, typically to determine the long-term response of a river to natural or man-made changes imposed upon its hydrologic and sediment regime. The mobile-bed and hydrodynamic processes in one-dimensional models must necessarily be expressed in terms of cross-sectional properties such as average velocity, average depth, hydraulic radius, and overall shear stress. Quantities such as bed scour and fill, bed-load transport, sediment-load concentration, and bed-material composition must also be expressed as total cross-sectional values. Although some modelers have developed means of extracting limited two-dimensional information from one-dimensional models, for example, through assumed transverse distributions of shear stress and depth-averaged velocity, the fundamental computation is one-dimensional. Demands on computational resources are generally not a significant factor or expense, and traditional field-data collection efforts are similar to those needed for steady- or unsteady-flow flood modeling.

Whatever their utility for studies of extended time periods and river reaches, one-dimensional models cannot resolve local details of flow and mobile-bed dynamics. Such local details might involve the plan-view distribution of deposition patterns in a reservoir; the scour and deposition patterns associated with flow around the ends of spur dikes or other river training works; or the scour and deposition provoked by bridge piers. For such problems, two- or three-dimensional models provide the possibility of resolving these kinds of local details, albeit at the cost of significantly increased program complexity and computational resources. In time, if computing power continues to increase at its current breathtaking pace, one may envisage use of two- or three-dimensional models even for large-scale problems such as those amenable only to one-dimensional models at the present time. At present, two- and three-dimensional use is limited to problems requiring resolution of local details over relatively short time periods, often as a complement to one-dimensional models of larger spatial and temporal scope.

15.1.2 Is the Additional Complexity of Multidimensional Mobile-Bed Modeling Justified?

It is often argued, and indeed has been argued since the advent of industrialized computational hydraulics in the 1970s, that the increased complexity and data needs of "the next level of modeling complexity" are not justified given our imperfect understanding of certain physical processes, the inadequacy of field data, and the uncertainty inherent in model results. The authors believe that this is a spurious argument. First, experience has shown that input data needs that may not seem justified at today's level of modeling capability will soon be justified by tomorrow's capabilities. Second, why should one compound the uncertainty in model results by adding inadequate field data to a simplified version of complex natural processes? Third, and perhaps most important, more complex models (in this case, two- and three-dimensional ones) obviate the need to describe all the complex and nonhomogeneous processes in a river cross section in terms of global cross-sectional average properties such as mean velocity, discharge, hydraulic radius, and average bed shear. In a two-dimensional

depth-averaged model, one still must relate near-bed processes to the depth-averaged properties in the water column, such as depth-averaged velocity and bed shear stress, but at least the heterogeneity of processes across the channel can be represented. In a three-dimensional model, near-bed processes can be related to the hydrodynamic properties at a computational grid point immediately adjacent to the bed and localized in a plan-view sense.

Therefore the authors believe that whether or not the particular features and requirements of a study mandate the use of multidimensional modeling, the model representation of physical processes can only be improved—or at least made more rational—by adopting a two- or three-dimensional approach. This may not be feasible for all studies because of computer-resource constraints, as described in the following section. But the authors believe it is time to begin planning for a study by asking, in the interest of better representation of physical processes, "Can this be done with a two- or three-dimensional model, or do we have to resort to a one-dimensional approach?" rather than "Can this be done with a one-dimensional model, or do we have to resort to a two- or three-dimensional approach?"

15.1.3 Limitations of Computer Resources

One obvious reason to answer the above question "we'll have to go one-dimensional" is the limitations of computer resources. Memory and disk space are not generally limiting, even for three-dimensional modeling. But the sheer central processing unit (CPU) time requirements of three-dimensional models, even in a parallel-processing environment, obviate any possibility of using them for extended spatial extents and simulation durations within the time frame of a study, at least as of this writing. For example, depending on the computing hardware in use, one-dimensional mobile-bed models covering the order of hundreds of kilometers can be used to perform simulations of the order of decades with a turnaround time on the order of several hours. By contrast, a fully three-dimensional mobile-bed model might require days of CPU time just to obtain a single steady-state solution over a river reach on the order of 20 kilometers. This three-dimensional demand is considerably less if the hydrostatic pressure assumption replaces the vertical momentum equation; and the CPU time per time step in a true unsteady calculation is generally less than that required to obtain a single accurate steady-state solution. Such CPU time requirements depend directly on the number of sediment size classes being transported, the number of subsurface bed strata considered, the type of computational grid (structured or unstructured), and other factors. Nonetheless, computer CPU time requirements can be a significant factor militating against the use of three-dimensional modeling given the calendar time constraints of a typical engineering study. The CPU time demands of two-dimensional modeling fall somewhere in between those of one-dimensional and three-dimensional, but turnaround time can still be a decisive issue depending on the temporal and spatial extent of the modeling effort.

15.1.4 Structure of This Chapter

The remainder of this chapter is structured to provide not only the model user and developer, but also the model "consumer" (i.e., the one paying the bill), with a framework for understanding the conceptual bases of multidimensional models, alternatives for mathematical representation of relevant physical processes, alternative computational grid representations and their associated approximate numerical solution methods, and a sense of what can go wrong. Within this chapter, the authors use the terms "mobile-bed modeling," "sediment modeling," and "sediment-process modeling" interchangeably.

Section 15.2 provides a brief overview of typical problem types and available techniques and modeling systems for each. Section 15.3 summarizes the mathematical and numerical bases of the two- and three-dimensional hydrodynamic models that underpin any mobile-bed modeling. Section 15.4 provides an overall conceptual framework for modeling sediment transport and bed evolution. The next three sections, 15.5, 15.6, and 15.7, go into detail in the treatment of sediment processes on or near the bed, those in suspension, and the exchange between the two domains. Section 15.8 deals with the need for empirical closure relations and their role in modeling systems, whereas Section 15.9 focuses on numerical-solution issues related to sediment processes. Section 15.10 provides some background on field data needs and the role of such data in model construction, calibration, and verification. Section 15.11 provides limited examples of two- and three-dimensional mobile-bed model studies. Finally, Section 15.12 provides the authors' view of the state of the art and future perspectives in multidimensional mobile-bed modeling.

The authors assume that the reader has a general familiarity with the vocabulary of numerical hydraulics, and also with some of its general techniques and support tools. Some of the relevant sections refer to the reader to background texts on computational hydraulics, computational fluid dynamics, and grid generation.

The authors do not pretend to have prepared this chapter from a purely objective framework. Most of the developments and examples build on the authors' own experiences with their particular conceptualization of the mobile-bed problem and simulation systems they have developed and used. It is hoped that this enables the reader to acquire solid depth and detail on at least one approach to the problem. The authors have tried to use their own frame of reference as a basis for less detailed description of conceptual, mathematical, and numerical approaches used by others.

15.2 PROBLEM TYPES AND AVAILABLE TECHNIQUES AND MODELING SYSTEMS—A SURVEY

15.2.1 Introduction

In preparation for the more detailed developments in subsequent sections, the authors present here a survey of typical problems for which two- or three-dimensional mobile-bed modeling may be required. The purpose is to draw attention to the features of each type of problem that may require corresponding features and techniques in a modeling system and to give an admittedly incomplete set of references to two- and three-dimensional modeling systems and applications currently available for each problem type. Table 15-1

Table 15-1 Summary of Model Capability Requirements

Section	Type of problem	Two-dimensional (depth-averaged)	Three-dimensional required?	Hydrostatic assumption in three dimensions?	Unsteady flow capability required?	Sediment mixture capability required?	Distinct treatment of bed-load/suspended-load processes?
15.2.2	Reservoir sedimentation	Often sufficient	If reentrainment into outlet structures is studied	OK if entrainment into outlet structures not studied	Sequence of steady flows usually OK	Required	Required unless inflow is fully bed load
15.2.3	Settling basins/tanks/clarifiers	Generally not relevant	Necessary for representation of interaction between geometry and sedimentation patterns	OK if flow is quiescent	Generally not necessary	Required unless sediment load is homogeneous	Not generally required
15.2.4	Riverbend dynamics and training works	Not applicable without special incorporation of secondary flow effects	Needed to capture secondary-flow effects	OK if detailed flow around structures is not an issue	Desirable for study of effects of hydrograph	Required unless sediments are entirely uniform	Required in most alluvial rivers
15.2.5	Mobile-bed dynamics around structures	Not applicable	Required	Generally not acceptable, because vertical accelerations are important	Generally not necessary	Required unless sediments are entirely uniform	Required in most alluvial rivers
15.2.6	Long-term bed evolution in response to imposed changes	Generally irrelevant	For focused local study within larger one-dimensional model	May be necessary for long-term simulation	Must accommodate series of annual hydrographs	If required for the overall one-dimensional model	If required for the overall one-dimensional model
15.2.7	Sorbed contaminant fate and transport	May be appropriate	May be required	OK if flow-structure-sediment interaction is not of primary interest	Likely necessary for studies of resuspension during floods	May not be required if focus is entirely on contaminated fine sediments	Suspension advection-diffusion required

summarizes this inventory. The authors limit their attention to subcritical flow, because supercritical flow capability is rarely needed for problems in which mobile-bed activity is of primary interest.

15.2.2 Reservoir Sedimentation

Chapter 12 of this manual is devoted to the issue of reservoir sedimentation, for which prediction and management simulation are best accomplished using two-dimensional (plan-view) models. The present chapter also includes an example application of a two-dimensional model to reservoir sedimentation (Section 15.11).

Although one-dimensional models have been, and indeed still are, used for reservoir sedimentation, by definition they can only resolve the longitudinal distribution of sedimentation, from the headwaters to the dam. Many reservoirs flood not only the incised river channel, but also adjacent floodplain areas; in addition, many have significant lateral embayments and islands. One-dimensional models can resolve such features only in terms of equivalent transverse cross sections, at best including distinct one-dimensional flow paths around islands (in models permitting looped channel structures) and one-dimensional segments extending into lateral embayments.

Of course three-dimensional modeling can also be used for reservoir sedimentation, and might be used if computational resources were available and especially if the local entrainment of sediment into outlet works was to be studied. The general absence of significant recirculation in reservoir flow, as well as the generally low velocities and lack of training structures, argues for a depth-averaged approach being sufficient. However, only a three-dimensional model can resolve and simulate the effects of reservoir density currents if these play a significant role in the sedimentation processes of a particular site. Vertically two-dimensional models have been used for the study of reservoir sedimentation in this case, but these are width-averaged and therefore can only approximately resolve the effects of lateral embayments.

Reservoir sedimentation simulation does not generally require full representation of unsteady-flow hydrodynamics. It is usually necessary only to simulate long-term hydrographs, and this can be done using a series of steady-state inflows and water-surface elevations if necessary. Similarly, sedimentation rates (by size fraction) can be determined for such a series of steady-flow situations and used to generate equivalent sedimentation quantities over time.

When three-dimensional models are employed for reservoir sedimentation, it is generally acceptable to use the vertically hydrostatic pressure assumption in lieu of the vertical momentum equation (see Section 15.3.3). Vertical accelerations are generally not strong in a typical reservoir, at least outside the vicinity of structures. The hydrostatic pressure assumption results in significant reduction in computational time compared to fully three-dimensional formulations. However, if the local entrainment of deposited sediment into outlet works is being studied, a fully three-dimensional treatment (i.e., with the vertical momentum equation included) may be required.

Reservoir sedimentation studies should be based on simulation models that accommodate sediment mixtures, through individual size classes or some other mechanism. The longitudinal (streamwise) differential sorting is intimately related to the differential transport modes of different sediment sizes (e.g., bed load for inflowing gravels or sands and suspended load for inflowing silts and washload) and to the variation of these transport modes from the upstream depositional delta to the downstream deep pool.

It is very important that both bed-load and suspended-load processes be represented in reservoir sedimentation models, unless there is no suspended load or washload in the inflowing streams. It is characteristic of a reservoir that suspended load or washload in the relatively steep, rapid, shallow inflow may transition through a bed-load mode of movement in the middle or downstream portions of the reservoir, where velocities are low, before being ultimately deposited on the bed. Similarly, fine material deposited during a previous event may become reentrained into bed load or suspended load during dynamic reservoir operations and/or extreme hydrologic inflow events, subsequently to be redeposited further downstream. A model must recognize these distinctly different mechanisms of transport and the associated differences in the time scale of sediment movement to capture the longitudinal sorting of deposited sediment.

A nonorthogonal curvilinear structured grid is usually needed for two- or three-dimensional reservoir modeling, especially to represent a sinuous flooded river channel within the overall embayment. Unstructured grid capability is not generally needed unless it is necessary to reproduce the detailed flow around structures as part of the study.

Reservoir sedimentation modeling is not highly demanding of sophisticated turbulence models, because most of the mobile-bed activity is deposition, and strong jet effects do not generally occur in reservoirs. However, if diffusion of a washload plume in the reservoir is an important factor in downstream deposition, or if sedimentation effects around structures within the reservoir (including intakes) are important in a three-dimensional model, then a simple turbulence model may not be adequate.

When deposited-material compaction and consolidation are included in a study, bed-layering capability is required in the two- or three-dimensional mobile-bed model. Consolidation calculations require knowledge of the age of deposits, and this in turn requires distinct accounting of deposited material, for example, in distinct layers.

Examples of two- and three-dimensional models that have been used for the study of reservoir sedimentation include those of Spasojevic and Holly (1990a; 1990b); Savic and Holly (1993); Olsen et al. (1999); and Fang and Rodi (2000).

15.2.3 Settling Basins

Simulation of deposition in engineered settling basins (including sedimentation tanks and clarifiers) is similar to that of reservoir sedimentation, but is somewhat less demanding, at least as long as the sediment is noncohesive, as assumed throughout this chapter. For purely volumetric analyses, one-dimensional modeling may be sufficient. It is difficult to imagine situations in which depth-averaged two-dimensional modeling is needed, though width-averaged two-dimensional approaches may be appropriate. These permit examination of the vertical structure of deposition. Generally, though, three-dimensional modeling is most likely needed. Indeed, the main purpose for performing a model study of a sedimentation basin is to analyze the interaction between the confined, engineered geometry of the basin and the deposition patterns, as input to the design process. Boundary effects are ubiquitous, and are naturally accommodated by three-dimensional modeling. Unless there are strong vertical accelerations near the inlet or the outlet, the hydrostatic pressure assumption may be adequate. Unsteady-flow dynamics is generally not relevant to continuous-flow sedimentation basins, so steady-flow models to determine sedimentation rates may be quite appropriate.

Unless the inflowing sediment is truly of uniform size, it is generally necessary that the modeling accommodate differential particle sizes, especially because this can have a direct bearing on the longitudinal deposition patterns in the sedimentation basin.

To the extent that reentrainment of deposited sediments in the basin is not an issue, it may not be necessary for the model to accommodate bed-load processes and their exchanges with the water column. However, if possible reentrainment near the outlet is under study, it may be necessary to include a full representation of bed-load dynamics and exchange with the water column.

Because settling basins tend to have regular geometric shapes, a simple Cartesian structured grid may be sufficient. Because the diffusive transport of suspended sediments entering the basin can be an important factor in its design, it is important for the model to include at least a one-equation model for turbulence in the horizontal plane. Bed layering is of importance only if sediment reentrainment in flushing operations is anticipated, and then only if significant stratification of sediment sizes is expected.

An example of a model study of sedimentation basins is that of Olsen and Skoglund (1994).

15.2.4 River-Bend Dynamics and Training Works

Three-dimensional modeling must be used for the study of mobile-bed processes in river bends and around their associated training works (bendway weirs, spur dikes, etc.). One-dimensional models simply cannot resolve the detailed interaction between flow and sediment within the cross section. Two-dimensional depth-averaged models cannot normally resolve the secondary currents that are an essential part of this process.

However, some investigators have implemented various special techniques that enable depth-averaged models to approximate secondary flow in bends. Flokstra (1977) substituted semi-empirical velocity distributions for helicoidal flow (obtained from a power law) into the dispersion terms of the depth-averaged equations. Jin and Steffler (1993) introduced the depth averaged moment-of-momentum equations to provide a measure of the intensity of the secondary flow. Duan et al. (2001) computed flow and bed-shear stress by using the depth-averaged model CCHE2D. Empirical functions of three-dimensional flow characteristics, formulated using the results of the three-dimensional model CCHE3D, were used to transform the flow and bed-shear stress into approximate three-dimensional distributions.

In three-dimensional bendway modeling, it is possible to adopt the hydrostatic pressure assumption if the details of water and sediment movement around training structures, or water intakes, are not of primary interest. Otherwise a full three-dimensional treatment is required.

Full unsteady-flow capability, as reflected in an unsteady-inflow hydrograph, is not of primary interest for this type of study, although the ability to simulate the effects of an annual hydrograph may be important, if only through a succession of steady flows. If, on the other hand, the dynamic flood effects of a rapidly varying hydrograph are important to mobile-bed response, full unsteady-flow capability is needed. As mentioned earlier, the combination of fully three-dimensional (nonhydrostatic) flow and full unsteadiness may require computational resources that preclude simulations of any meaningful length in prototype time. If the problem under study involves fairly rapid and/or substantial bed changes in response to some intervention, these changes may provoke corresponding changes in the free-surface elevations and slopes. This may then require either a series of steady-flow computations or truly unsteady simulation to capture the feedback from bed changes to the flow field.

In most alluvial rivers, bed topography and geomorphology are intimately related to the nonhomogeneity of transported sediments, whereby coarser material responds to near-bed currents and shear stresses quite differently from suspended material. Therefore bendway modeling invariably requires the capability to accommodate multiple sediment size classes, as well as the distinct differences between bed-load and suspended-load transport mechanisms.

Riverbend modeling requires a curvilinear grid. It may be orthogonal in regular channels such as the Missouri River, but generally must be nonorthogonal to permit correct representation of natural riverbank and island geometries. When local structure details must be represented (spur dikes, etc.), an unstructured-grid approach may be necessary.

A relatively high level of turbulence modeling (e.g., k–ε) is required, because strong jet diffusive effects around structures may be encountered and be decisive in determining the configuration of deposition zones in the wake of such structures.

Bed-layering capability may not be important for these studies, unless erosion into previously deposited layers of varying composition is foreseen. A particular situation might be erosion into strata provoked by river-training works successfully shifting the channel away from one bank.

Examples of river-bend mobile-bed modeling include those of Wang and Adeff (1986); Minh Duc et al. (1998); Gessler et al. (1999); Holly and Spasojevic (1999); Fang (2000); Wu et al. (2000); Spasojevic et al. (2001); and Spasojevic and Muste (2002). Section 15.11 of this chapter includes an example of a three-dimensional application.

15.2.5 Mobile-Bed Dynamics around Structures

This area and the previous one have considerable overlap; indeed, the details of mobile-bed response near training structures in river bends may well be of importance to relatively large-scale modeling of geomorphology in river bends. However, there is also a class of problems for which attention is focused on the structure itself, especially in habitat remediation studies. For example, V-notch weirs, wing dikes, and notched spur dikes may be configured to create low-velocity habitat, requiring a rather delicate balance between sediment through-flow and flow obstruction. Other applications of engineering importance are scour around bridge piers and abutments; scour/stability considerations for pipelines on the riverbed; and stability of structures associated with recreational facilities such as casino boat cofferdams, marinas, and beach-protection works.

Two-dimensional models cannot do justice to this problem. It is tempting to think that a depth-averaged approach may enable at least a plan-view analysis of the effect of the structure on currents and recirculation/deposition. But the flow around such structures and their associated scour holes can be strongly three-dimensional. In addition, such flow can be characterized by significant vertical accelerations, which cannot be captured using the hydrostatic pressure assumption in a three-dimensional model. Therefore this class of problems generally requires fully three-dimensional, i.e., nonhydrostatic modeling.

Full unsteady-flow dynamics is not normally required for this class of study. It may be necessary to run a series of studies of flows to study structure response throughout the expected hydrograph range of conditions, but the dynamic effects per se are generally not of great importance. It should be recognized, however, that insofar as the upstream boundary conditions to such a model, including both bed-load and suspended-load inflows, may reflect the hysteresis effects associated for flood dynamics, the true unsteadiness may have to be taken into account in the formulation of boundary conditions for the series of steady-state conditions.

Except in special circumstances of rivers having uniform sediment, it is generally necessary for the modeling system to accommodate multiple sediment sizes and recognition of the distinctly separate modes of sediment movement on the bed and in suspension. There can be considerable local sorting of sediments in the complex flows around structures, for example, when sediments in suspension are deposited in the recirculation zone behind a structure and then may undergo continued slow transport as bed load, perhaps back toward the structure in some cases.

It is very difficult to provide effective representation of near-field flow around structures with a structured grid. At the very least, this must be a nonorthogonal curvilinear grid, and an unstructured grid is highly desirable. Similarly, this modeling situation puts a premium on an effective high-order turbulence model (e.g., k–ε), because the diffusive exchange of momentum and sediment across zones of highly nonuniform velocity is the very essence of the problem.

Bed layering is generally not of great importance for near-field structure modeling, unless scour into antecedent nonuniform strata is an important issue.

Examples of model studies of mobile-bed dynamics around structures include those of Olsen and Melaaen (1993); Brors (1999); and Spasojevic and Muste (2002). Other examples of local-scour model predictions include those of Zaghloul and McCorquodale (1975) and Jia et al. (2001). Section 15.11 of this chapter includes an example of a three-dimensional application to a problem of structure configurations for habitat restoration.

15.2.6 Long-Term Bed Evolution in Response to Imposed Changes

One-dimensional models remain the method of choice for the study of long-term changes in river morphology over extended river reaches. Such changes include upstream regulation, changes in upstream sediment supply, water and sediment diversion/extraction, bank stabilization, and channelization. It can be necessary to focus on these long-term changes within a particular bend or short segment of river, often involving the presence of structures, within the larger context of the extended one-dimensional model. This focused interest is very likely to require three-dimensional modeling, especially if flow-structure-sediment interaction is an issue (e.g., sedimentation in water intakes, maintenance of navigation conditions). This triggers requirements for the same kinds of model capabilities as those described above in Sections 15.2.4 and 15.2.5, and in addition may well require the simulation of multiple annual hydrographs, either in a fully unsteady or a quasi-steady mode.

To the extent that this activity implies the embedding of a local three-dimensional model within a one-dimensional or two-dimensional one, the issue of deriving three-dimensional boundary conditions (e.g., upstream velocity and suspended-sediment concentration fields, bed-load distribution across

the section) from the one- or two-dimensional results, possibly within each time step, is a challenging one. It implies at the very least that the local three-dimensional model boundaries be taken at one-dimensional model cross sections that have relatively parallel and transversely uniform flow, if possible. It may also imply that there must be some feedback from the local three-dimensional model to the cross sections of the overall one- or two-dimensional model, though this may not be necessary.

If the local three-dimensional model is to be run in an unsteady mode, the hydrostatic pressure assumption is very likely to be necessary simply to keep computation time within reasonable limits (see Section 15.3.3). The three-dimensional model's need for treatment of nonuniform sediments, separation of bed load and suspended load, and other such factors is slaved to the comparable requirements for the overall one-dimensional model, depending on the sediment regime in the river.

The grid for an embedded three-dimensional model can generally be a structured curvilinear one, orthogonal in a fairly regular channel but nonorthogonal otherwise. Turbulence model demands are modest, because by definition this type of study is focused on identifying long-term changes rather than local and short-term details of flow and sediment movement; generally a one- or two-equation model should be sufficient—see Section 15.3.4. Bed layering may be quite important, if the long-term evolution of the river includes erosion into antecedent nonuniform strata, including strata that are laid down during the long-term simulation itself.

Although the authors are not aware of a specific application involving direct embedding of a two- or three-dimensional mobile-bed model in an overall one-dimensional extended model, there have been applications of two- and three-dimensional models to long-term bed evolution in specialized reservoir sedimentation contexts (Savic and Holly 1993; Fang and Rodi 2000). In addition, several models have been applied to long-term bed evolution in laboratory contexts.

15.2.7 Sorbed Contaminant Fate and Transport and Cohesive Sediment Problems

Modeling of sorbed contaminant fate and transport, be it one-, two-, or three-dimensional, is one of the most challenging activities in mobile-bed modeling. It combines the uncertainties of mobile-bed modeling with the uncertain description of sorption-desorption processes in the multiple transport modes of an alluvial system. In addition, these processes are most important for fine sediments, including cohesive sediments, for which the entrainment, transport, and deposition mechanics can be episodic rather than continuous and are poorly understood. Chapters 4 and 20 of this manual deal with the problems of transport of fine sediment and associated contaminants.

The particular problems associated with sorbed contaminant modeling are essentially the same whether the underlying mobile-bed modeling is one-, two-, or three-dimensional. The overall scope and focus of the study determines the level of dimensionality, whether unsteady capability is necessary, whether the hydrostatic pressure assumption is permissible, etc.

In sorbed contaminant modeling, contaminated fine material, once entrained or otherwise introduced into the system, is transported primarily as suspended load, i.e., essentially at the speed of the water velocity. Therefore it is mandatory that the modeling approach explicitly include advection-diffusion of suspension as a transport mechanism.

The source-sink term for advection-diffusion of suspension is particularly problematic when fine, especially cohesive, sediments are involved. Entrainment of cohesive sediments is understood to occur as episodic bursts of "mass entrainment" once a critical shear stress is exceeded, rather than as a progressive and continuous entrainment driven by the notion of an excess of shear stress over critical, as is generally accepted for noncohesive sediment. Cohesive sediment also tends to flocculate, or clump together once in suspension, and this behavior strongly influences its deposition tendencies and rates. Because salinity is an important parameter governing flocculation, a model must be capable of simulating transport (i.e., advection-diffusion) from a tidal boundary condition in parallel with fine-sediment and sorbed-contaminant transport in an estuary in many cases.

Given the episodic nature of cohesive-sediment dynamics, and the fact that studies of sorbed-contaminant fate and transport are likely to be focused on the risk of reentrainment of contaminants during flood events, this kind of modeling is likely to require unsteady-flow capability. But to the extent that flow-structure-sediment interaction is not an important feature of the study, it may be permissible to base modeling on the hydrostatic pressure assumption, thus enabling unsteady computations within reasonably computer time requirements.

Bed-layering capability is an important feature of models used for sorbed contaminant fate and transport, notably when alternate deposition-entrainment cycles are to be studied. During flood events, entrainment of contaminated sediments is generally from material laid down, and perhaps covered, during previous extended depositional periods. It is only through explicit representation of this layering process, with distinct differentiation of sediment and contaminant characteristics within layers, that this resuspension process can be faithfully represented.

Sorbed-contaminant modeling does not, in and of itself, invoke any special grid requirements; these follow from the physical situation as described in earlier sections. Turbulence modeling can be quite important, because diffusive transport of fine material in suspension can be an

important component of the contaminant fate and transport. Similarly, bed layering can be quite important, because contaminated sediments may lie in antecedent deposition strata that are disturbed through erosion during exceptional floods.

There do not appear to be recent examples of multidimensional sorbed-contaminant modeling in the literature. Earlier examples include those of Onishi and Trent (1982); Onishi and Thompson (1984); and Onishi and Trent (1985).

15.2.8 Summary

A common thread running through these discussions of typical modeling situations is that in mobile-bed modeling, there is a tradeoff between model complexity and computer (and human) resources. This is particularly true in the fully three-dimensional unsteady-flow domain (without the hydrostatic pressure assumption), in which, as of this writing, model complexity and fidelity are ultimately limited nearly by the calendar time available for the study. At the other extreme of one-dimensional modeling, computer resources are rarely a limiting factor; but the expert interpretation needed to draw meaningful results from a simplified one-dimensional schematization of reality may be as limiting as computer resources in the three-dimensional case. Two-dimensional modeling falls somewhere between these extremes. Ultimately the modeler must weigh the strengths, weaknesses, and costs of alternative modeling approaches against the objectives and resources of the particular study.

15.3 MATHEMATICAL BASIS FOR HYDRODYNAMICS IN TWO AND THREE DIMENSIONS

15.3.1 Introduction and Scope

Hydrodynamic and mobile-bed process modeling are intimately related. Although this chapter, and indeed this entire manual, are focused on sediment and mobile-bed processes, it is important for the reader to understand how the formulations and numerical solution of the hydrodynamic processes interact with those of the mobile-bed processes.

The purpose of this section is to provide a summary overview of the hydrodynamic-process formulations generally used in mobile-bed models. The general three-dimensional and two-dimensional equations are presented first, and then issues of simplification of the vertical momentum equation (hydrostatic assumption), solution techniques, coordinate transformations, and turbulence closure models are discussed in turn.

15.3.2 Summary of Basic Equations

Although the fields of direct Navier-Stokes and large-eddy simulation hydrodynamic modeling are receiving considerable attention in the field of computational fluid dynamics, the hydrodynamic formulations used in mobile-bed modeling, at least as of this writing, remain based on the Reynolds-averaged Navier-Stokes equations.

15.3.2.1 The Reynolds-Averaged Navier-Stokes Equations The Reynolds-averaged Navier-Stokes equations are derived from the incompressible-fluid Navier-Stokes equations through temporal averaging of instantaneous velocities over an appropriate time scale. This operation results in a shift of the stresses associated with the momentum exchange of correlated fluctuating velocities from the momentum-advection terms to Reynolds stress terms. These Reynolds stresses must then be resolved using an appropriate turbulence model, as discussed in detail in Chapter 16 of this manual.

Water mass conservation is expressed through the Reynolds-averaged mass conservation (continuity) equation

$$\frac{\partial u}{\partial x}+\frac{\partial v}{\partial y}+\frac{\partial w}{\partial z}=0 \tag{15-1}$$

in which

x, y, and z = Cartesian coordinate directions and $u(x, y, z, t)$, and $w(x, y, z, t)$ = time-dependent Reynolds-averaged velocities in the x, y, and z directions respectively, t being the time.

The Reynolds-averaged u-, v-, and w-momentum conservation equations are written

$$\begin{aligned}\frac{\partial u}{\partial t}+\frac{\partial (uu)}{\partial x}+\frac{\partial (vu)}{\partial y}+\frac{\partial (wu)}{\partial z}&=fv-\frac{1}{\rho_0}\rho g\frac{\partial z'}{\partial x}-\frac{1}{\rho_0}\frac{\partial p}{\partial x}\\&+\frac{1}{\rho_0}\left(\frac{\partial \tau_{xx}}{\partial x}+\frac{\partial \tau_{yx}}{\partial y}+\frac{\partial \tau_{zx}}{\partial z}\right)\end{aligned} \tag{15-2}$$

$$\begin{aligned}\frac{\partial v}{\partial t}+\frac{\partial (uv)}{\partial x}+\frac{\partial (vv)}{\partial y}+\frac{\partial (wv)}{\partial z}&=-fu-\frac{1}{\rho_0}\rho g\frac{\partial z'}{\partial y}-\frac{1}{\rho_0}\frac{\partial p}{\partial y}\\&+\frac{1}{\rho_0}\left(\frac{\partial \tau_{xy}}{\partial x}+\frac{\partial \tau_{yy}}{\partial y}+\frac{\partial \tau_{zy}}{\partial z}\right)\end{aligned} \tag{15-3}$$

$$\begin{aligned}\frac{\partial w}{\partial t}+\frac{\partial (uw)}{\partial x}+\frac{\partial (vw)}{\partial y}+\frac{\partial (ww)}{\partial z}&=-\frac{1}{\rho_0}\rho g\frac{\partial z'}{\partial z}-\frac{1}{\rho_0}\frac{\partial p}{\partial z}\\&+\frac{1}{\rho_0}\left(\frac{\partial \tau_{xz}}{\partial x}+\frac{\partial \tau_{yz}}{\partial y}+\frac{\partial \tau_{zz}}{\partial z}\right)\end{aligned} \tag{15-4}$$

in which

$f = 2\Omega\sin\phi$ is the Coriolis parameter, with Ω the angular rotational velocity of the earth and ϕ the latitude;
$\rho(x, y, z, t)$ = density of a mixture of water and suspended sediment;
ρ_0 = reference density;
g = acceleration due to gravity;
z' = the vertical direction;
$p(x, y, z, t)$ = pressure; and τ = fluid shear-stress tensor, here presumed to incorporate both molecular stresses and those resulting from the Reynolds averaging process.

Molecular stresses, being much smaller than Reynolds stresses, are often neglected. The Coriolis term, which describes the effect of the earth's rotation on the motion of fluid on the earth's surface, is important only when fairly large water bodies are modeled.

Equations (15-1) to (15-4) are considered the fully three-dimensional Reynolds-averaged set. They must be complemented with an appropriate turbulence closure model, possibly involving a parallel set of partial differential equations, before they can be used in a mobile-bed model, as is discussed below.

Equations (15-1) to (15-4) already evoke the Boussinesq approximation, which is valid for incompressible flows with variable density (the variation of gravity can be neglected in all flows considered in this chapter). According to this approximation, if the variation in density is relatively small, it may be assumed that the variation in density is negligible in all the terms in the equations except the gravitational term.

15.3.2.2 The Hydrostatic-Pressure Simplification In some applications, it is possible to bring considerable simplification to the fully three-dimensional set (Eqs. 15-1 to 15-4) by invoking the hydrostatic pressure assumption. This is tantamount to ignoring any vertical components of fluid acceleration, so that the pressure varies linearly from the surface to any point below it. If the z coordinate direction is taken as vertical ($z \equiv z'$), the assumption is formalized as

$$\frac{\partial}{\partial z}\left(z + \frac{p}{\rho g}\right) = 0 \tag{15-5}$$

in which

$$z + \frac{p}{\rho g} = \zeta(x, y, t)$$

is the free-surface elevation above datum.

Introduction of Eq. (15-5) into Eqs. (15-2 and 15-3), through a suitable rearrangement of the variable-density gravity term and the pressure term to include the free-surface elevation, yields

$$\frac{\partial u}{\partial t} + \frac{\partial(uu)}{\partial x} + \frac{\partial(uv)}{\partial y} + \frac{\partial(uw)}{\partial z} = fv - g\frac{\partial(z_b+h)}{\partial x} - \frac{g}{\rho_0}(\varsigma - z)\frac{\partial \rho}{\partial x} + \frac{1}{\rho_0}\left(\frac{\partial \tau_{xx}}{\partial x} + \frac{\partial \tau_{yx}}{\partial y} + \frac{\partial \tau_{zx}}{\partial z}\right) \tag{15-6}$$

and

$$\frac{\partial v}{\partial t} + \frac{\partial(vu)}{\partial x} + \frac{\partial(vv)}{\partial y} + \frac{\partial(vw)}{\partial z} = -fu - g\frac{\partial(z_b+h)}{\partial y} - \frac{g}{\rho_0}(\varsigma - z)\frac{\partial \rho}{\partial y} + \frac{1}{\rho_0}\left(\frac{\partial \tau_{xy}}{\partial x} + \frac{\partial \tau_{yy}}{\partial y} + \frac{\partial \tau_{zy}}{\partial z}\right) \tag{15-7}$$

in which

$z_b(x, y)$ = bed elevation above datum and
$h(x, y, t)$ = flow depth;

i.e., the free-surface elevation is expressed as $\zeta = z_b + h$. The free-surface elevation (or the flow depth) thus replaces the pressure as one of the four dependent variables, and this vastly simplifies the numerical solution of the set. In fully three-dimensional nonhydrostatic modeling, the solution for the pressure field is quite difficult and computationally demanding. The hydrostatic pressure assumption makes it possible to first obtain the free-surface elevation ς or the flow depth h, for example by solving the depth-averaged two-dimensional problem. The free-surface elevation then becomes a known variable in the second-step solution of the remaining three-dimensional equations.

Equations (15-6) and (15-7) retain the density-gradient terms to account for possible density changes due to changes in suspended-sediment concentration. The density-gradient terms, resulting from the rearrangement of gravity and pressure terms in Eqs. (15-2) and (15-3), are simplified by replacing $\frac{p}{\rho}$ with $g(\zeta - z)$, which amounts to combining the hydrostatic-pressure assumption and the Boussinesq approximation. Density, and therefore density-gradient terms, are evaluated from suspended-sediment concentrations through an appropriate empirical relation.

Equations (15-5), (15-6), and (15-7) make up the hydrostatic-pressure simplification of Eqs. (15-2), (15-3), and (15-4). The continuity equation, Eq. (15-1), remains the same in both systems.

15.3.2.3 The Depth-Averaged Equations The hydrodynamic equations for two-dimensional (depth-averaged) mobile-bed modeling are obtained through formal depth-averaging of the full three-dimensional set, Eqs. (15-1),

(15-6), and (15-7). Depth-averaged variables are defined as follows:

$$\tilde{f} = \frac{1}{h}\int_h f\, dz\,. \tag{15-8}$$

The depth-averaged mass conservation (continuity) equation then becomes

$$\frac{\partial h}{\partial t} + \frac{\partial (h\tilde{u})}{\partial y} + \frac{\partial (h\tilde{v})}{\partial z} = 0\,. \tag{15-9}$$

The depth-averaged $\tilde{u}$-momentum conservation equation is

$$\begin{aligned}
&\frac{\partial (\tilde{u}h)}{\partial t} + \frac{\partial (\tilde{u}\tilde{u}h)}{\partial x} + \frac{\partial (\tilde{v}\tilde{u}h)}{\partial y} \\
&\quad = f\,\tilde{v}h - gh\frac{\partial (z_b + h)}{\partial x} - \frac{g\,h^2}{2\,\rho_0}\frac{\partial \rho}{\partial x} \\
&\qquad + \frac{1}{\rho_0}\left[\frac{\partial}{\partial x}\left(\tilde{\tau}_{xx}\,h\right) + \frac{\partial}{\partial y}\left(\tilde{\tau}_{yx}\,h\right)\right] \\
&\qquad + \frac{\tau_{sx} - \tau_{bx}}{\rho_0} - \frac{1}{\rho_0}\left[\frac{\partial}{\partial x}\int_h \rho\,(u - \tilde{u})(u - \tilde{u})\,dz\right. \\
&\qquad \left. + \frac{\partial}{\partial y}\int_h \rho\,(u - \tilde{u})(v - \tilde{v})\,dz\right]
\end{aligned} \tag{15-10}$$

and the depth-averaged $\tilde{v}$-momentum conservation equation is

$$\begin{aligned}
&\frac{\partial (\tilde{v}h)}{\partial t} + \frac{\partial (\tilde{u}\tilde{v}h)}{\partial x} + \frac{\partial (\tilde{v}\tilde{v}h)}{\partial y} \\
&\quad = -f\,\tilde{u}h - gh\frac{\partial (z_b + h)}{\partial y} - \frac{g\,h^2}{2\,\rho_0}\frac{\partial \rho}{\partial y} \\
&\qquad + \frac{1}{\rho_0}\left[\frac{\partial}{\partial x}\left(\tilde{\tau}_{xy}\,h\right) + \frac{\partial}{\partial y}\left(\tilde{\tau}_{yy}\,h\right)\right] \\
&\qquad + \frac{\tau_{sy} - \tau_{by}}{\rho_0} - \frac{1}{\rho_0}\left[\frac{\partial}{\partial x}\int_h \rho\,(u - \tilde{u})(v - \tilde{v})\right. \\
&\qquad dz + \left.\frac{\partial}{\partial y}\int_h \rho\,(v - \tilde{v})(v - \tilde{v})dz\right]
\end{aligned} \tag{15-11}$$

In these equations, τ_{sx} and τ_{bx} are the x-direction shear stress at the water surface and bed, respectively, and similarly for τ_{sy} and τ_{by}. The terms containing the products, such as $(u-\tilde{u})(v-\tilde{v})$, represent effective stresses associated with the correlation in deviations of local velocities from their depth averages, and are commonly referred to as the dispersion terms.

15.3.2.4 Turbulence Closure One commonly used simplified approach to solve the "turbulence closure problem" is to express the Reynolds stresses through the Boussinesq eddy-viscosity model (for more detail see Chapter 16 of this manual). The Boussinesq eddy-viscosity model assumes that the Reynolds stress is related to the mean rate of strain (through the so-called eddy viscosity), and to the turbulent kinetic energy. The turbulent kinetic-energy term is usually absorbed into the pressure-gradient term, whereas the mean rate of strain is sometimes subject to further simplification. Thus the Reynolds stress τ_{xx} in Eq. (15-2), for example, can be replaced by $\nu_t(\partial u/\partial x)$, where ν_t is the eddy viscosity. This leads to a new set of equations that, when complemented by an appropriate turbulence model to estimate the eddy viscosities, are now ready to be discretized for numerical solution (possibly after additional coordinate transformation; see below), as follows for the hydrostatic case:

The Reynolds-averaged three-dimensional u-momentum conservation equation is

$$\begin{aligned}
\frac{\partial u}{\partial t} &= -\frac{\partial (uu)}{\partial x} - \frac{\partial (uv)}{\partial y} - \frac{\partial (uw)}{\partial z} \\
&\quad + f\,v - g\frac{\partial (z_b + h)}{\partial x} - \frac{g}{\rho_0}(\varsigma - z)\frac{\partial \rho}{\partial x} \\
&\quad + \frac{1}{\rho_0}\left[\frac{\partial}{\partial x}\left(\nu_t\frac{\partial u}{\partial x}\right) + \frac{\partial}{\partial y}\left(\nu_t\frac{\partial u}{\partial y}\right) + \frac{\partial}{\partial z}\left(\nu_t\frac{\partial u}{\partial z}\right)\right]
\end{aligned} \tag{15-12}$$

The Reynolds-averaged three-dimensional v-momentum conservation equation is

$$\begin{aligned}
\frac{\partial v}{\partial t} &= -\frac{\partial (vu)}{\partial x} - \frac{\partial (vv)}{\partial y} - \frac{\partial (vw)}{\partial z} \\
&\quad - f\,u - g\frac{\partial (z_b + h)}{\partial y} - \frac{g}{\rho_0}(\varsigma - z)\frac{\partial \rho}{\partial y} \\
&\quad + \frac{1}{\rho_0}\left[\frac{\partial}{\partial x}\left(\nu_t\frac{\partial v}{\partial x}\right) + \frac{\partial}{\partial y}\left(\nu_t\frac{\partial v}{\partial y}\right) + \frac{\partial}{\partial z}\left(\nu_t\frac{\partial v}{\partial z}\right)\right]
\end{aligned} \tag{15-13}$$

The depth-averaged two-dimensional $\tilde{u}$-momentum conservation equation is

$$\begin{aligned}
\frac{\partial \tilde{u}}{\partial t} &= -\frac{\partial (\tilde{u}\tilde{u})}{\partial x} - \frac{\partial (\tilde{u}\tilde{v})}{\partial y} \\
&\quad - f\,\tilde{v} - g\frac{\partial (z_b + h)}{\partial x} - \frac{g\,h}{2\,\rho_0}\frac{\partial \rho}{\partial x} \\
&\quad + \frac{1}{\rho_0 h}\left[\frac{\partial}{\partial x}\left(\nu_t\frac{\partial \tilde{u}}{\partial x}h\right) + \frac{\partial}{\partial y}\left(\nu_t\frac{\partial \tilde{u}}{\partial y}h\right)\right] \\
&\quad + \frac{\tau_{sx} - \tau_{bx}}{\rho_0 h}
\end{aligned} \tag{15-14}$$

The depth-averaged two-dimensional $\tilde{v}$-momentum conservation equation is

$$\frac{\partial \tilde{v}}{\partial t} = -\frac{\partial(\tilde{v}\tilde{u})}{\partial x} - \frac{\partial(\tilde{v}\tilde{v})}{\partial y} - f\tilde{u} - g\frac{\partial(z_b + h)}{\partial y} - \frac{gh}{2\rho_0}\frac{\partial \rho}{\partial y} + \frac{1}{\rho_0 h}\left[\frac{\partial}{\partial x}\left(\nu_t \frac{\partial \tilde{v}}{\partial x}h\right) + \frac{\partial}{\partial y}\left(\nu_t \frac{\partial \tilde{v}}{\partial y}h\right)\right] + \frac{\tau_{sy} - \tau_{by}}{\rho_0 h} \quad (15\text{-}15)$$

As in the case of similar derivations for constituent transport equations, the Boussinesq eddy viscosity coefficient υ_t is an artificial construct intended to capture the residual shear-stress effects of correlations in velocity deviations from temporal and/or depth averages. As such, the values of eddy viscosity appearing in the three-dimensional equations must be obtained from an appropriate three-dimensional eddy-viscosity model. Eddy-viscosity models vary from very simple, such as constant eddy-viscosity or zero-equation models, to more advanced, such as two-equation $k-\varepsilon$ or $k-\omega$ models (Chapter 16). The corresponding eddy viscosities appearing in the depth-averaged equations must be obtained from an appropriate depth-averaged eddy-viscosity model. The diffusion terms in depth-averaged hydrodynamic models, i.e., the effective stresses generated by the depth-averaging process, are typically modeled analogously to and combined with corresponding Reynolds stresses. The additional contribution to eddy viscosity arising from the depth averaging can be accounted for indirectly by adjusting one of the constants in the depth-averaged $k-\varepsilon$ model (see Rodi 1993).

Equations (15-12) and (15-13) and the continuity equation, Eq. (15-1), are the basis for the flow model built into the CH3D-SED code, used in Sections 15.11.2 and 15.11.3 of this chapter. The flow model built into the MOBED2 code, which is used in example 15.11.4 of this chapter, is based on Eqs. (15-14) and (15-15) and the continuity equation, Eq. (15-9).

15.3.3 Role of Hydrostatic Pressure Assumption

The previous section presented three-dimensional hydrodynamic equations both without and with the hydrostatic pressure assumption. Hydraulic engineers are quite accustomed to invoking hydrostatic pressure in the solution of most problems, without having to recall that it implicitly assumes that pressure differences associated with vertical fluid accelerations are unimportant for the problem under study.

As discussed in the previous section, invocation of the hydrostatic pressure assumption vastly simplifies the three-dimensional hydrodynamic problem. Indeed, as of this writing the computational time required to do a multiple-day unsteady simulation with the hydrostatic assumption is of the same order of magnitude as that required to obtain a single steady-state solution with the fully nonhydrostatic equations. Therefore it is important to consider the circumstances under which it is permissible to invoke the hydrostatic pressure assumption in three-dimensional mobile-bed modeling.

As a general rule, it is necessary to use fully three-dimensional, nonhydrostatic modeling whenever local details of mobile-bed dynamics around structures are of interest. Such structures include river training works such as dikes and bendway weirs, as well as habitat-restoration structures such as v-notched dikes, chevron weirs, or notched weirs. Experience has shown that calculated local velocity fields around structures, particularly near the bed, can be quite different for the hydrostatic and nonhydrostatic cases. This is of course due to the effects of vertical acceleration components near the intersection of the structure and the bed. Because the details of local scour and deposition in the immediate vicinity of such structures can depend quite strongly on the local velocity fields, the hydrostatic assumption can have an indirect but very important influence on mobile-bed behavior near the structure.

However, the overall mobile-bed response to using the hydrostatic-pressure assumption in the calculation of secondary currents has seldom been quantified. Therefore, it is difficult to give some general rule as to when the hydrostatic assumption is and is not acceptable. At the extreme limits, it is perhaps obvious that it is acceptable for studies of overall cross section response to changes in hydrologic or sediment regime, where local flow and sedimentation details are not of primary importance. By contrast, it is perhaps obvious that the hydrostatic assumption is not acceptable in studies focused uniquely on local sedimentation details around structures. In between these extremes, the acceptability of the assumption is a matter of judgment. Whenever it is possible to make preliminary comparative model runs with and without the hydrostatic assumption, in order to glean some insight into the apparent importance of vertical accelerations to the overall sedimentation pattern under study, this should by all means be done.

In the end, the ability to use the full nonhydrostatic equations on one hand, and the ability to perform truly unsteady calculations over some extended period of time on the other, appear as of this writing to be mutually exclusive. However, one would expect fully unsteady, nonhydrostatic modeling to become increasingly feasible as the exponential growth in computational power continues.

15.3.4 Solution Techniques and Their Applicability

Approximate numerical solution techniques for the two- and three-dimensional hydrodynamic equations generally fall into one of three categories: finite-difference methods (see, e.g., Shimizu et al 1990; Spasojevic and Holly

1990a; 1990b; 1993; and Lin and Falconer 1996); finite-element methods (see, e.g., Thomas and McAnally 1985; Wang and Adeff 1986; Brors 1999; Jia and Wang 1999; and the RMA-10 model at the Coastal and Hydraulics Lab, U.S. Army Corps of Engineers); or finite-volume methods (see, e.g., Olsen and Melaaen 1993; Minh Duc et al. 1998; Olsen et al. 1999; and Wu et al. 2000). Although there are important differences between finite-element and finite-volume approaches, both can be associated with unstructured grids and thus are grouped together here. It should be mentioned that the method of characteristics has been successfully applied to two-dimensional computation of rapidly varied flow, in particular for dam-break computation (see, e.g., Fennema and Chaudhry 1990), but generalization of codes based on this method to mobile-bed capability does not appear to be in the offing.

Finite-difference methods are based on approximation of partial derivatives by divided differences on a space-time grid. Such grids are called "structured," in that they comprise quadrilaterals (possibly curvilinear), all of which are defined by the same set of coordinate contours parallel (in transformed space) to the physical x, y, and z axes. Considerable computational economy can be achieved by structuring solution algorithms to proceed along single grid lines in each of the three directions, replacing the need to solve three-dimensional or two-dimensional problems with the solution of multiple one-dimensional problems, usually coupled through multiple iterations. However, this computational economy is obtained at the expense of grid inflexibility and/or excessive computer memory requirements. If the computational grid must be refined (i.e., more grid lines introduced) to provide high resolution in the vicinity of a structure or sharp natural feature, this grid refinement must extend throughout the computational domain, even though it may not be necessary far away from the local feature of interest. Nonetheless, the finite-difference method generally offers a simplicity of programming and intuitive conceptualization of the problem that are not so natural with finite-element methods.

Finite-element and finite-volume methods are integral-based approaches in the sense that they are derived not through approximations of partial derivatives, but rather through consideration of conservation laws applied to volumetric elements and careful evaluation of fluxes (mass, momentum) across nonparallel faces of the elements. The finite-element method is based on the notion of minimizing residuals in an average or integral sense over a volumetric (or surficial) element. The finite-volume method is more directly based on primitive conservation laws and can be interpreted as equivalent to a finite-difference method when quadrilateral or elements are selected as a special case (such an interpretation is not possible when tetrahedral, i.e., triangle-based, elements are used).

Application of the integral principles to one volumetric element is dependent only on the fluxes coming from or going to adjacent elements. This leads to the notion of an unstructured grid, where grid refinement around a local feature is accomplished through packing of small-scale volumetric elements around the feature. This packing or refinement is purely local, in that the local small scale does not propagate through the mesh of the entire solution domain. Thus local grid refinement can be accomplished without triggering the excessive memory requirements of structured grids. In addition, unstructured grids naturally accommodate dynamic (adaptive) grid refinement driven by spatially variable error detection.

The grid-refinement flexibility of finite-element/volume methods is obtained at the price of computational efficiency. Generally the multiple iterative one-dimensional computations that are possible on a structured (finite-difference) grid cannot be implemented on an unstructured one, because the very notion of continuous coordinate contours, along which partial derivatives are approximated, does not exist. Solution algorithms must generally be fully two- or three-dimensional, incurring the large computational time requirements of matrix inversion, often iterative. In practical terms, the flexibility of unstructured grids is obtained at the cost of practical limits to the duration of unsteady-flow simulations. Such practical limits may become less important as parallel processing becomes increasingly available.

The accurate computation of advection (of momentum or mass) is particularly challenging, and some hydrodynamic codes solve for advection in a separate, dedicated step using a numerical method best suited to the hyperbolic nature of the advective terms (examples include the CYTHERE-ES1 code of Benqué et al. 1982 and TELEMAC as reported by Jankowski et al. 1994). A mobile-bed code driven by a hydrodynamics solver having this feature for momentum advection should logically take advantage of it for the advection of sediment particles in suspension.

For detailed information on numerical-solution techniques for fluid flow equations, the reader may refer to numerous books in this area, such as Fletcher (1991); Hirsch (1991); or Ferziger and Peric (2002).

15.3.5 Coordinate Transformations for Finite-Difference Methods

The structured grids of finite-difference methods are, in their primitive form, inherently ill-suited to the representation of natural bank lines, submerged bars, etc. Early two-dimensional hydrodynamic models of the 1970s used "stair-stepping" to represent boundaries that were not aligned with one or the other orthogonal axes of a Cartesian grid (Benqué et al. 1982). The need to work with curvilinear grids quickly became apparent. However, orthogonal curvilinear grids (i.e., those for which coordinate lines intersect at right angles) still are quite inflexible for representation of local features. Further flexibility can be introduced by relaxing the orthogonality requirement to obtain a nonorthogonal curvilinear grid, in which computational cells can deform in an arbitrary manner to better fit the contour lines of natural features. Even then, it is important to maintain cell aspect

ratios within acceptable limits. Transformation of the governing partial differential equations into the coordinate system of the nonorthogonal curvilinear grid is quite tedious and generates many additional terms that must be discretized and evaluated, further increasing the complexity of the computational engine and required computational time. Most of the two- and three-dimensional codes referenced in Table 15-2 (Section 15.4.2) are based on some level of coordinate transformation.

In unsteady-flow simulation, various grid-adjustment schemes have been developed to cope with the time-dependent position of the free surface and the bed. Perhaps the most common approach is referred to as "sigma stretching," by which the vertical grid structure adapts to changes in the free surface (and changes in the mobile bed elevation) through stretching or compression, the number of grid intervals in the vertical remaining constant.

For detailed information on coordinate transformations, the reader may refer to basic tensor analysis books, such as Simmonds (1994).

15.3.6 Turbulence Closure Models

As mentioned earlier, the Reynolds averaging of the Navier-Stokes equations generates correlations between the fluctuating components of local velocities; these are the so-called Reynolds stress terms shown as effective shear stresses in Eqs. (15-2), (15-3), and (15-4). Evaluation of these terms requires some sort of empirical turbulence closure model. Chapter 16 provides a comprehensive overview of the turbulence-modeling problem in the context of mobile-bed hydraulics. In the simplest approach, the Boussinesq eddy-viscosity model is supplemented with a constant eddy viscosity, either simply assigned by the user based on macroscopic flow properties or derived from a zero-equation mixing-length model or equivalent.

More advanced approaches include the use of a one-equation eddy-viscosity model, or more commonly a two-equation eddy-viscosity model such as the $k-\varepsilon$ formulation (see for example Chapter 16 of this manual or Rodi 1993), in which the transport of the turbulence kinetic energy and its dissipation rate are solved in parallel with the flow solution, leading to eddy viscosity coefficients that reflect local shear and bed effects.

More advanced turbulence modeling techniques, such as direct Reynolds stress modeling and large eddy simulation, have been implemented for accurate calculation of internal flows and aerodynamic flows. However, the authors' arguments in Section 15.1.4 notwithstanding, the inherent uncertainties and imprecision of the mobile-bed problem would seem to obviate the need to require more than k–ε turbulence capability in the hydrodynamic computational engine of a mobile-bed model at the current stage of development, unless such advanced techniques are readily available and implementable in the mobile-bed model.

15.4 OVERVIEW OF MODELS OF SEDIMENT TRANSPORT AND BED EVOLUTION

15.4.1 Introduction

Although the Navier-Stokes equations, along with the continuity equation (usually Reynolds-averaged), represent a generally accepted mathematical description (model) of fluid flow, there is no comparable mathematical formulation for the complete processes of sediment-flow interaction. The most recent attempts to formulate a general mathematical model of sediment-flow interaction are based on the two-phase flow approach (Villaret and Davies 1995; Caoet al. 1995; Ni et al. 1996; Greimann et al. 1999; Liu et al., 1997). The attempts are inspired by the history of two-phase flow models in other fields (Ishii 1975; Drew 1983; Elghobashi 1994; Crowe et al. 1996). The basic idea behind the two-phase flow approach is to formulate governing conservation equations for both phases, which include terms defining interaction between phases such as the stress tensor due to phase interactions, or the interfacial momentum transfer term.

However, even though the two-phase flow approach seems promising, its use and even the formulation of the governing equations in flow-sediment problems are still in their infancy. Certain terms in the governing equations that are typically neglected in other fields may require quite a different treatment in the flow-sediment field. The stress between fluid and sediment particles is usually neglected under the assumption that it is much smaller than the turbulent stress between fluid particles. The stress coming from interactions among sediment particles is neglected under the assumption that sediment particles do not contact each other. Both of these assumptions are questionable in the case of high sediment concentrations, especially near the bed. This probably explains a lingering doubt about the use of the two-phase flow approach in the near-bed areas. Furthermore, certain terms in the two-phase flow governing equations, such as the interfacial momentum transfer, require additional modeling to achieve system closure. Such modeling has to be based on a detailed knowledge of turbulence and requires currently unavailable experimental data. Finally, the two-phase flow solution of practical sediment problems, which routinely require long-term simulations, is likely to be CPU-time-prohibitive even in the not-so-near future.

Therefore, virtually all two-dimensional and three-dimensional flow and sediment models used for solving practical problems are based on a simplified concept. The basic idea classifies sediment transport as either suspended load or bed load and defines a set of equations describing suspended-sediment transport, bed-load transport, and bed evolution. Thus, the concept requires artificially partitioning the otherwise single

Table 15-2 Typical Simplifications Used in Flow and Sediment Modeling

Model and/or references	Flow	Bed-load transport	Bed-elevation changes	Suspended-sediment transport	Sediment-exchange processes	Sediment mixtures	Base numerical method
SUTRENCH-2D, van Rijn (1987)	Quasi unsteady two-dimensional (width-averaged)	Bed-load-layer concept	Total-load concept	Quasi-unsteady two-dimensional (width-averaged)	Entrainment and deposition	No	Finite-volume with structured grid
Brors (1999)	Unsteady two-dimensional (vertical plane)	Yes	One-dimensional Exner equation	Unsteady two-dimensional (vertical plane)	Entrainment and deposition	No	Finite-element
Argos modeling system, Usseglio-Polatera and Cunge (1985)	Unsteady two-dimensional (depth-averaged)	No	Exner equation	Unsteady two-dimensional (depth-averaged)	Entrainment and deposition	No	Finite-difference with Lagrangian advection
TABS-2, Thomas and McAnally (1985)	Unsteady two-dimensional (depth-averaged)	No	Exner equation, empirical total-load formula	No	No	No	Finite-element
CCHE2D Jia and Wang (1999)	Unsteady two (depth-averaged)	Yes	Exner equation	No	No	No	Finite-element
Nagata et al. (2000)	Unsteady two (depth-averaged)	Yes	Exner equation with deposition and pickup terms	No	No	No	Finite-volume with structured grid
MOBED2, Spasojevic and Holly (1990a; 1990b)	Unsteady two (depth-averaged)	Active-layer concept	Active-layer and active-stratum concept	Unsteady two-dimensional depth-averaged)	Entrainment and deposition	Unlimited number of sediment size classes	Finite-difference with Lagrangian advection
FAST2D with sediment processes, Minh Duc et al. (1998)	Unsteady two-dimensional (depth-averaged)	Bed-load-layer concept	Total-load concept	Unsteady two-dimensional (depth-averaged)	Entrainment and deposition	No	Finite-volume with structured grid
Olsen (1999)	Unsteady two-dimensional (depth-averaged)	Yes	Discrepancy in sediment continuity for bed cells	Unsteady three-dimensional, near-bed concentration as boundary condition	No	A budget method for computing the change in bed grain size distribution	Finite-volume with structured grid

MIKE 21	Unsteady two-dimensional	Included in total load	No?	Sand and fine sediment	?	Yes?	Finite-difference
Shimizu et al. (1990)	Steady-state quasi-three-dimensional, hydrostatic pressure assumption, and an empirical longitudinal velocity component profile	Yes	Exner equation	Steady two-dimensional (depth-averaged)	Entrainment and deposition	No	Finite-difference
Demuren (1991)	Steady-state three-dimensional	Bed-load-layer concept	Algebraic equation and iterative procedure	Steady-state three-dimensional	Entrainment and deposition	No	Finite-difference/ volume on structured grid
Olsen et al. (1999)	Steady-state three-dimensional	No	No	Steady-state three-dimensional, near-bed concentration as boundary condition	No	No	Finite-volume with structured grid
Olsen and Melaaen (1993); Olsen and Skoglund (1994)	Steady-state three-dimensional	Yes	Discrepancy in sediment continuity for the bed cells	Steady-state three-dimensional, near-bed concentration as boundary condition	No	No	Finite-volume with structured grid
TELEMAC-3D with sediment processes, Jankowski et al. (1994); Hervouet and Bates (2000)	Unsteady three-dimensional, hydrostatic pressure assumption	No	No	Unsteady three-dimensional	Deposition	No	Finite-element
Sheng (1983)	Unsteady three-dimensional, hydrostatic pressure assumption	No	No	Unsteady three-dimensional, without the fall-velocity term	No	No	Finite-difference
FLESCOT, Onishi and Trent (1982), Onishi and Thompson (1984), Onishi and Trent (1985)	Unsteady three-dimensional, hydrostatic pressure assumption	No	Exner equation	Unsteady three-dimensional	Entrainment and deposition	Silt, clay, and sand	Finite-difference
SUTRENCH-3D, van Rijn (1987)	Quasi-unsteady two-dimensional (depth averaged) with a vertical logarithmic velocity profile	Yes	Layer-layer approach and total-load approach as alternatives	Unsteady three-dimensional	Entrainment and deposition	No	Finite-volume with structured grid

(Continued)

Table 15-2 Typical Simplifications Used in Flow and Sediment Modeling *(Continued)*

Model and/or references	Flow	Bed-load transport	Bed-elevation changes	Suspended-sediment transport	Sediment-exchange processes	Sediment mixtures	Base numerical method
Olsen and Kjellesvig (1998)	Unsteady three-dimensional	Yes	Discrepancy in sediment continuity for the bed cells	Unsteady three-dimensional, near-bed concentration as boundary condition	No	No	Finite-volume with structured grid
Lin and Falconer (1996)	Unsteady three-dimensional, hydrostatic pressure assumption	Yes	No	Unsteady three-dimensional	Entrainment and deposition	No	Finite-difference
Wang and Adeff (1986)	Unsteady three-dimensional, hydrostatic pressure assumption	Yes	Total load concept	Unsteady three-dimensional, near-bed concentration as boundary condition	No	No	Finite-element
CH3D-SED Spasojevic and Holly (1993); Gessler et al. (1999)	Unsteady three-dimensional, hydrostatic pressure assumption	Active-layer concept	Active-layer and active-stratum concept	Unsteady three-dimensional	Entrainment and deposition	Unlimited number of sediment size classes	Finite-volume with structured grid
RMA-10	Unsteady three-dimensional, hydrostatic pressure assumption?	No	?	Unsteady three-dimensional?	Entrainment and deposition of cohesive sediment	No?	Finite-element
MIKE 3	Unsteady three-dimensional, hydrostatic pressure assumption?	No	?	Unsteady three-dimensional, fine-sediment	Deposition of cohesive sediment	No?	Finite-difference
RMA-10	Unsteady three-dimensional, hydrostatic pressure assumption?	No	?	Unsteady three-dimensional?	Entrainment and deposition of cohesive sediment	No?	Finite-element
FAST3D with sediment processes Rodi (2000); Wu et al. (2000)	Unsteady three-dimensional	Layer-layer concept	Total load concept	Unsteady three-dimensional	Entrainment and deposition	No	Finite-volume with structured grid
Delft 3D	Unsteady two- and three-dimensional	No?	No	Unsteady two- and three-dimensional	Entrainment and deposition	Yes	?

and continuous domain of sediment processes into a bed and/or near-bed layer on the one hand, and the rest of the domain on the other. Then the governing equations for the bed and near-bed processes are associated with the bed and near-bed layer, whereas the governing equations for the suspended-material processes are associated with the rest of the domain.

15.4.2 Overview of Conceptual Models of Mobile-Bed Processes

There are several conceptualizations of the bed and near-bed layer, such as the mixing layer proposed by Karim and Kennedy (1982), the bed load layer proposed by van Rijn (1987), and the active layer proposed by Spasojevic and Holly (1990b). Similarly, there is no generally accepted set of governing equations for the bed and near-bed processes. The equations' formulations, even though not so different, may still vary depending on the bed and near-bed layer concept, or simply depending on the approach. More details on the governing equations for the bed and near-bed processes are presented in Section 15.5.

In contrast to the bed and near-bed processes, modeling of suspended-material processes is practically always based on the sediment-transport or advection-diffusion equation with an additional fall-velocity advection term. The suspended-sediment advection-diffusion equation can be derived either from the two-phase flow equations (Greimann et al. 1999) or directly, using the continuum approach. and the assumptions are that the sediment particles' horizontal velocity components are the same as the corresponding fluid velocities and that the sediment particles' vertical-velocity components are equal to those of the appropriate fluid velocity adjusted by the fall velocity. In either case, the result is the familiar suspended-sediment advection-diffusion equation with a special model for particle settling, characterized by a settling velocity. Details on suspended-material modeling are presented in Section 15.6.

The simplified model can only account for the sediment-flow interaction in an indirect way. The flow-sediment interaction in such models is achieved through the flow acting as the driving force for sediment processes and the associated sediment-process feedback to the flow. This sediment-process feedback comprises changes in bed elevation, changes in the flow and the suspended-sediment mixture density, and, possibly, changes in the bed friction coefficient.

This concept of sediment-process modeling based on separation of suspended-material and bed and near-bed processes inevitably requires formulation of sediment-exchange mechanisms. Sediment-exchange processes are commonly formulated as bed and near-bed material entrainment into suspension and suspended-material deposition onto the bed. The same exchange terms, with opposite signs, provide the coupling between equations for near-bed and suspended-material processes. Details on modeling of sediment-exchange processes are presented in Section 15.7.

Even when these simplifications are made, the development of two-dimensional and three-dimensional flow and sediment models is constrained by the available computing resources. Due to the complexity of the problem and the typical need for long-term simulations, flow and sediment modeling can be prohibitive in terms of CPU time. Therefore, many flow and sediment models adopt further simplification. Table 15-2 summarizes typical simplifications used in flow and sediment modeling. Although the list of models in the table is surely incomplete, the authors hope that the listed models reflect the general scope of current developments in two-dimensional and three-dimensional flow and sediment modeling.

15.4.3 Assessment of Conceptual Bases of Mobile-Bed Models

Because the bed-load flux is a vector parallel to the bed surface, the bed-load transport is essentially two-dimensional. But the flow and the suspended-sediment transport are fully three-dimensional processes. Therefore, two-dimensional flow and suspended-sediment transport models may have restricted applicability, as has been described earlier. On the other hand, use of the two-dimensional equations for flow and suspended-sediment transport is far less demanding of CPU time than use of three-dimensional models, as discussed earlier. The two-dimensional simplification was used extensively during the 1980s, when the available computing resources were typically insufficient for any practically meaningful three-dimensional flow and sediment modeling. The two-dimensional depth-averaged approach was used in the Argos Modeling System (as described by Usseglio-Polatera and Cunge 1985), and MOBED2 (Spasojevic and Holly 1990a; 1990b). TABS-2, as described by Thomas and McAnally (1985), is based on the depth-averaged flow equations, with the bed-load and suspended-sediment transport modeling replaced by the total load concept. Van Rijn (1987) developed the SUTRENCH-2D model in which the flow and suspended-sediment transport are modeled using the two-dimensional width-averaged equations. van Rijn (1987) also developed the SUTRENCH-3D model, in which the flow is modeled using the two-dimensional depth-averaged equations in combination with the assumption of a vertical logarithmic velocity profile, whereas the suspended-sediment transport is modeled using the three-dimensional equations. Shimizu et al. (1990) developed a model based on the depth-averaged suspended-sediment transport equations and quasi-three-dimensional flow equations, assuming a hydrostatic-pressure distribution and using an empirical longitudinal velocity component distribution along the depth.

After being neglected for a few years, during which time a number of three-dimensional flow and sediment

models have been developed and successfully applied, the two-dimensional approach seems to be enjoying renewed popularity. It appears that the price for the sophistication and generality of three-dimensional flow and sediment models is still the often-prohibitive CPU time. Thus, a number of two-dimensional models, often including corrections for three-dimensional effects, have recently been developed to be used for specific applications, perhaps even in combination with three-dimensional models. Minh Duc et al. (1998) presented the FAST2D model with sediment processes, based on the depth-averaged equations for the flow and the suspended-sediment transport, which can be used for relatively long simulations. The CCHE2D model (Jia and Wang 1999), including the depth-averaged flow equations, bed-load transport, and bed-elevation changes, has been developed for cost- and time-effective long-term simulations. Nagata et al. (2000) also developed a model based on the depth-averaged flow equations, bed-load transport, and bed-elevation changes, including the rarely modeled bank erosion. All three models include some kind of correction for three-dimensional flow effects. Brors (1999) reported a three-dimensional model of flow and sediment processes around a submerged pipeline, but its application was limited to consideration of conditions in a two-dimensional vertical plane. Olsen (1999) developed a model based on a combination of the depth-averaged flow equations and three-dimensional suspended-sediment transport, using an empirical expression for the vertical profile of eddy viscosity.

The development of three-dimensional flow and sediment models started in the early 1980s. The simplifications used in three-dimensional models involve both flow-modeling simplifications and the level of complexity included in the sediment equations. One of the typical three-dimensional flow modeling simplifications is the use of the steady-state equations for both flow and suspended-sediment transport (Demuren 1991; Olsen and Melaaen 1993; Olsen and Skoglund 1994; Olsen et al. 1999). Use of this simplification restricts the model's range of applicability, because the sediment processes are naturally unsteady and their effects accumulate in time, eventually affecting the flow computations. Another typical three-dimensional flow modeling simplification is the assumption of a hydrostatic-pressure distribution over the depth as described in Section 15.3.3 above (Sheng 1983; FLESCOT as reported by Onishi and Trent 1985; Wang and Adeff 1986; TELEMAC-3D with sediment processes as reported by Jankowski et al. 1994; Lin and Falconer 1996; CH3D-SED as reported by Gessler et al. 1999). The hydrostatic-pressure assumption is easily violated wherever streamline curvature is significant (e.g., in the vicinity of river-training structures, close to rapidly changing bed surface conditions, in river bends). However, this simplification is still commonly used because it provides for significant CPU time-saving and thus enables simulations over some significant period of prototype time.

In terms of complexity of sediment-processes modeling, both two- and three-dimensional models in use span quite a wide range. Some models concentrate on bed-load transport and associated bed elevation changes (e.g., the CCHE2D of Jia and Wang 1999 and two-dimensional models of Nagata et al. 2000). Others concentrate on suspended-sediment transport, some including the associated bed elevation changes (e.g., the two-dimensional Argos Modeling System as described by Usseglio-Polatera and Cunge 1985; the three-dimensional FLESCOT model of Onishi and Trent 1985), and some not including bed changes (e.g., the three-dimensional models of Sheng, 1983; Olsen et al. 1999; TELEMAC-3D with sediment processes as described by Jankowski et al. 1994). The three-dimensional model of Lin and Falconer (1996) includes both bed-load and suspended-sediment transport, but does not include bed elevation changes. Models concentrating only on certain aspects of sediment processes are obviously applicable to flow and sediment situations where the corresponding aspects dominate. Examples of such specific flow and sediment situations may include settling tanks or reservoir-sedimentation problems, where suspended-sediment transport and deposition are dominant processes.

More general models recognize that the same sediment particle can remain at the bed surface or move either in suspension or as bed load, all depending on local flow conditions, and attempt to include all relevant sediment processes. Examples of the more general approach among two-dimensional models include SUTRENCH-2D, van Rijn (1987); MOBED2 as reported by Spasojevic and Holly (1990a; 1990b); FAST2D with sediment processes, Minh Duc et al. (1998); and models of Shimizu et al. (1990); Brors (1999); Olsen (1999). Examples among three-dimensional models include SUTRENCH-3D, van Rijn (1987); models of Wang and Adeff (1986); Demuren (1991); Olsen and Melaaen (1993); Olsen and Skoglund (1994); Olsen and Kjellesvig (1998); CH3D-SED as reported by Spasojevic and Holly (1993) or Gessler et al. (1999); and FAST3D with sediment processes as reported by Rodi (2000) or Wu et al. (2000).

Finally, only a few models attempt to include the behavior of nonuniform sediment or sediment mixtures. Spasojevic and Holly (1990a; 1990b) introduced a relatively general approach to the treatment of sediment mixtures with an unlimited number of sediment size classes, as initially developed for the two-dimensional model MOBED2. The approach was subsequently generalized and built into the three-dimensional CH3D-SED model (Spasojevic and Holly 1993). The combined two-dimensional depth-averaged flow and three-dimensional suspended-sediment transport model reported by Olsen (1999) uses a budget method for computing the change in bed grain-size

distribution. The three-dimensional FLESCOT model, as reported by Onishi and Trent (1985), treats three distinct sediment components (clay, silt, sand). Modeling the behavior of sediment mixtures allows accounting for natural phenomena such as differential settling, hydraulic sorting, and armoring.

15.5 BED AND NEAR-BED PROCESSES

15.5.1 Introduction and Overview

One of the major differences among various two-dimensional or three-dimensional flow and sediment models is the treatment of bed and near-bed processes, including bed-load transport, bed elevation changes, and the exchange between the suspended material and the bed and near-bed material.

Demuren (1991) introduced a simplified model for bed-elevation changes in meandering channels using algebraic equations based on perturbations to equilibrium between bed elevations and beload transport. Olsen and Melaaen (1993), Olsen and Skoglund (1994), Olsen and Kjellesvig (1998), and Olsen (1999) presented models that solve the three-dimensional mass-conservation (advection-diffusion) equation for suspended sediment using an empirical near-bed concentration as a boundary condition. The near-bed concentration is assigned to computational cells next to the bed surface, but the mass-conservation equation for these cells is not solved. In a somewhat arbitrary manner, the discrepancy in the sediment continuity for computational cells next to the bed surface is used to compute bed-surface elevation changes.

Modeling bed-surface elevation changes is often based on an intuitive sediment mass-conservation equation, usually referred to as the Exner equation, written for the sediment resting on the bed or moving as a bed load. The full form of the Exner equation is

$$\rho_s \left(1-p_b\right)\frac{\partial z_b}{\partial t}+\nabla\cdot\vec{q}_b+E-D=0 \qquad (15\text{-}16)$$

where

ρ_s = density of sediment, assumed to be constant;
p_b = porosity of the bed material, assumed to be constant;
z_b = bed-surface elevation;
$\vec{q}_b$ = bed-load flux;
E = upward bed-sediment entrainment flux, representing the entrainment of sediment particles from the bed into suspension; and
D = downward suspended-sediment deposition flux, representing gravitational settling of suspended sediment particles onto the bed.

The Exner equation is essentially two-dimensional in the plane parallel to the bed surface.

The models of Shimizu et al. (1990) and Brors (1999) include both bed load and suspended-sediment transport and use a complete form of the Exner equation. The Argos Modeling System, as described by Usseglio-Polatera and Cunge (1985), and the FLESCOT model, as described by Onishi and Trent (1985), both of which include only suspended-sediment transport, use the Exner equation without the bed-load flux-divergence term. The CCHE2D model of Jia and Wang (1999) and the model of Nagata et al. (2000), both of which include only bed-load transport, use the Exner equation without entrainment and deposition sources. Nagata et al. (2000) also use the bed-load deposition and pickup functions instead of the bed-load flux-divergence term. TABS-2, as described by Thomas and McAnally (1985), which does not distinguish between the bed load and the suspended-sediment transport, uses the Exner equation with an empirical total load flux.

Van Rijn (1987) introduced the bed-load-layer concept and proposed two methods for computing the bed-surface elevation changes. One method is based on the sediment mass-conservation equation for the bed-load-layer control volume, and it is called here the bed-load-layer approach. The other is based on the sediment mass-conservation equation for the control volume spanning the entire flow depth and thus comprising the bed-load-layer control volume and the entire water column with suspended sediment above it. This second method requires combining the bed-load flux and the depth-integrated suspended-sediment flux into the total-load flux, so it is called here the total-load approach. The SUTRENCH-2D and SUTRENCH-3D models of van Rijn (1987) have both the bed-load-layer approach and the total-load approach built in as alternatives. The total-load approach was used in the model of Wang and Adeff (1986), in FAST2D with sediment processes (Minh Duc et al. 1998), and in FAST3D with sediment processes (Wu et al. 2000). Both FAST2D and FAST3D with sediment processes also adapted the bed-load-layer approach to compute the nonequilibrium bed-load flux.

Spasojevic and Holly (1990a; 1990b) introduced an active-layer and active-stratum concept and proposed a method to compute the bed-surface elevation and the active-layer size-class distribution changes in the case of nonuniform sediment, i.e., for natural sediment mixtures. The method, initially implemented in the two-dimensional (depth averaged) MOBED2 model (Spasojevic and Holly 1990a; 1990b), and subsequently generalized and built into the three-dimensional CH3D-SED model (Spasojevic and Holly 1993), is called here the active-layer and active-stratum approach.

15.5.2 The Bed-Load-Layer and the Total-Load Approach

Figure 15-1 shows a vertical schematization of the sediment-processes domain, as introduced by van Rijn (1987) and applied by Wu et al. (2000).

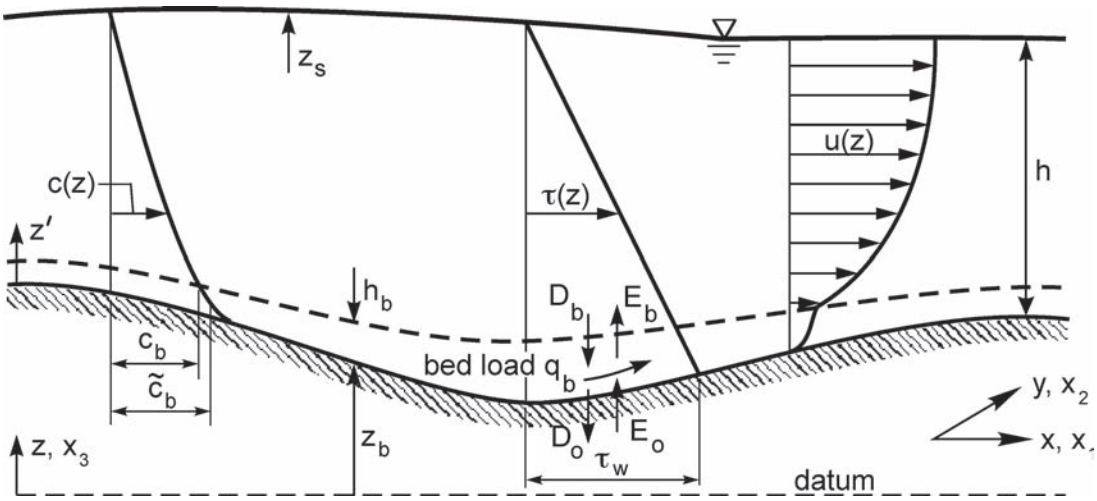

Fig. 15-1. Vertical schematization of the sediment-processes domain (van Rijn 1987; Wu et al. 2000).

According to van Rijn (1987), the mass-conservation equation for the bed-load-layer control volume reads

$$\frac{\partial}{\partial t}\left(h_b \tilde{c}_b\right) + \nabla \cdot \vec{q}_b + E_b - D_b - E_0 + D_0 = 0 \qquad (15\text{-}17)$$

where

h_b = bed-load-layer thickness;
$\tilde{c}_b$ = bed-load-layer sediment volumetric concentration averaged over the bed-load-layer thickness;
$\vec{q}_b$ = bed-load flux;
E_b = upward sediment entrainment flux at $z = z_b + h_b$;
D_b = downward sediment deposition flux at $z = z_b + h_b$;
E_0 = upward sediment entrainment flux at $z = z_b$; and
D_0 = a downward sediment deposition flux at $z = z_b$.

Entrainment and deposition fluxes E_b and D_b represent the exchange between the bed-load-layer sediment and the suspended sediment through the bed-load-layer control volume ceiling. Entrainment and deposition fluxes E_0 and D_0 represent the exchange between the bed-subsurface sediment and the bed-load-layer sediment through the bed-load-layer control volume floor.

Van Rijn also introduced a similar mass-conservation equation for the bed-subsurface sediment control volume,

$$\rho_s \left(1 - p_b\right)\frac{\partial z_b}{\partial t} + E_0 - D_0 = 0 \qquad (15\text{-}18)$$

where

z_b = the bed-surface elevation and is the bed-subsurface control volume ceiling.

Because the bed-subsurface control volume floor does not move, its location, i.e., the subsurface control volume thickness, is irrelevant.

Adding Eqs. (15-17) and (15-18) yields the mass-conservation equation for bed-load-layer and bed-subsurface sediment:

$$\rho_s \left(1 - p_b\right)\frac{\partial z_b}{\partial t} + \frac{\partial}{\partial t}\left(h_b \tilde{c}_b\right) + \nabla \cdot \vec{q}_b + E_b - D_b = 0 \qquad (15\text{-}19)$$

The mass-conservation equation for the control volume spanning the entire flow depth, including the bed-load layer and the entire water column with suspended sediment above it, reads (van Rijn, 1987)

$$\frac{\partial}{\partial t}\left(h\tilde{c}\right) + \nabla \cdot \vec{q}_T - E_0 + D_0 = 0 \qquad (15\text{-}20)$$

where

h = the entire flow depth;
$\tilde{c}$ = depth-averaged volumetric suspended-sediment concentration ;
$\vec{q}_T = \vec{q}_b + \vec{q}_s$ = total sediment load flux;
q_s = depth-integrated suspended-load flux (advection and diffusion).

Adding Eqs. (15-18) and (15-20) yields the mass-conservation equation for bed-subsurface sediment, bed-load-layer sediment, and suspended sediment in the entire water column above the bed load layer:

$$\rho_s \left(1 - p_b\right)\frac{\partial z_b}{\partial t} + \frac{\partial}{\partial t}\left(h\tilde{c}\right) + \nabla \cdot \vec{q}_T = 0 \qquad (15\text{-}21)$$

Van Rijn (1987) states that for steady-flow conditions the storage terms $\frac{\partial}{\partial t}(h_b \tilde{c}_b)$ in Eq. (15-19) and $\frac{\partial}{\partial t}(h\tilde{c})$ in Eq. (15-21)

can be neglected. This assumption may be inappropriate in cases of extensive deposition (such as settling in reservoirs) or extensive entrainment (e.g., erosion behind river-training structures such as chevron dikes). With van Rijn's assumption, Eq. (15-19) reduces to the specific form of the Exner equation (the location of entrainment and deposition fluxes E_b and D_b is well defined)

$$\rho_s(1-p_b)\frac{\partial z_b}{\partial t}+\nabla\cdot\vec{q}_b+E_b-D_b=0 \qquad (15\text{-}22)$$

whereas Eq. (15-21) becomes:

$$\rho_s(1-p_b)\frac{\partial z_b}{\partial t}+\nabla\cdot\vec{q}_T=0 \qquad (15\text{-}23)$$

Either Eq. (15-22) or Eq. (15-23) can be used to compute bed-surface elevation changes. Wu et al. (2000) state that Eq. (15-23) ensures better mass conservation in numerical procedures.

Equations (15-22) and (15-23) can be written in Cartesian coordinates as follows:

$$\rho_s(1-p_b)\frac{\partial z_b}{\partial t}+\frac{\partial q_{bx}}{\partial x}+\frac{\partial q_{by}}{\partial y}+E_b-D_b=0 \qquad (15\text{-}24)$$

and

$$\rho_s(1-p_b)\frac{\partial z_b}{\partial t}+\frac{\partial q_{Tx}}{\partial x}+\frac{\partial q_{Ty}}{\partial y}=0 \qquad (15\text{-}25)$$

where

q_{bx} and q_{by} = x- and y-direction components of the bed-load flux and
q_{Tx} and q_{Ty} = x- and y-direction components of the total sediment load flux.

Wu et al. (2000) further modified Eq. (15-24) to account for nonequilibrium effects on the bed-load transport by using the assumption

$$(1-p_b)\frac{\partial z_b}{\partial t}=\frac{1}{L_s}(q_b-q_{be}) \qquad (15\text{-}26)$$

where L_s is the nonequilibrium adaptation length for bed-load transport, and q_{be} is the bed-load flux under equilibrium conditions. The assumption expressed by Eq. (15-26) was introduced by Wellington (1978), Philips and Sutherland (1989), and Thuc (1991) for the case where the suspended load is negligible (i.e., $E_b - D_b = 0$). With the components of bed-load flux in x- and y-directions expressed as

$$q_{bx}=\alpha_{bx}q_b \quad , \quad q_{by}=\alpha_{by}q_b \qquad (15\text{-}27)$$

where

α_{bx} and α_{by} = direction cosines,

and with Eqs. (15-26) and (15-27) introduced into Eq. (15-24), one obtains

$$\frac{1}{L_s}(q_b-q_{be})+\frac{\partial(\alpha_{bx}q_b)}{\partial x}+\frac{\partial(\alpha_{by}q_b)}{\partial y}+E_b-D_b=0. \qquad (15\text{-}28)$$

15.5.3 The Active-Layer and Active-Stratum Approach—Sediment Mixtures

Inspired by the mixing-layer concept of Karim and Kennedy (1982), Spasojevic and Holly (1990a; 1990b) introduced the active-layer concept. The active layer (Fig. 15-2) is assumed to comprise sediment moving as a bed load, as well as bed-surface and subsurface sediment already agitated and ready to be set into motion. The active-layer concept is used in conjunction with a modeling approach designed for the treatment of sediment mixtures. Thus, the sediment mixture is represented though a suitable number of sediment size classes.

The active layer is assumed to have a uniform size-class distribution over its thickness h_a. It is assumed that all sediment particles of a given size class inside the active layer are equally exposed to the flow irrespective of their location in the layer. An active-layer control volume ΔV (Fig. 15-2) is defined as having dimension Δl not less than the maximum average saltation length, so that the bed-load flux represents bed-load exchange between two neighboring control volumes.

For a fixed active-layer floor elevation, the mass-conservation equation for size class ks of sediment in the active-layer control volume is written as follows:

$$\rho_s(1-p_b)\frac{\partial(\beta_{ks}h_a)}{\partial t}+\nabla\cdot\vec{q}_{bks}+E_{ks}-D_{ks}=0 \qquad (15\text{-}29)$$

where

β_{ks} = active-layer fraction of the size class ks, defined as a ratio of the mass of particles of the size class ks inside the active-layer control volume ΔV to the mass of all sediment particles contained in ΔV;
$\vec{q}_{bks}$ = bed-load flux for the size class ks;
E_{ks} = upward sediment entrainment flux for the size class ks;
D_{ks} = downward sediment deposition flux for the size class ks.

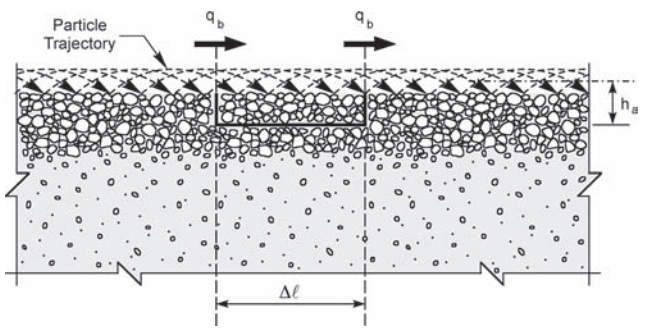

Fig. 15-2. Active-layer definition sketch.

The entrainment and deposition fluxes are evaluated at some distance above the bed surface, and that location is considered to be the near-bed boundary of the suspended material domain.

As Fig. 15-2 indicates, the only bed-load particles changing the mass balance inside the active-layer control volume are the ones entering and leaving the volume. Other bed-load particles start and end their trajectories inside the same active-layer control volume, remaining within the volume and not changing the mass balance within it. To make possible the use of a conventional bed-material porosity p_b, the active-layer thickness h_a in Eq. (15-29) is defined assuming that such bed-load particles are positioned at the bed surface.

Subsurface material below the active-layer control volume is discretized into a sequence of control volumes, one below the other, called here stratum control volumes (Fig. 15-3). Each stratum control volume has the same dimension Δl as the active-layer control volume above it. The bed material inside one stratum control volume is assumed to have uniform size distribution.

The stratum control volume immediately below the active-layer control volume is called the active-stratum control volume. It is possible, indeed likely, that the active-layer and active-stratum elemental volumes have different size distributions. The active-layer floor, which is at the same time an active-stratum ceiling, descends or rises whenever the bed elevation changes due to deposition or erosion occurring in the active-layer control volume. If, for example, the active-layer floor descends, some of the material that belonged to the active-stratum control volume becomes part of the active-layer control volume, whose homogeneous size distribution thus may change.

In order to represent the exchange of sediment particles between the active-layer and the active-stratum control volumes due to active-layer floor movement, another source term is introduced, called here the active-layer floor source F_{ks}, again specific to the size class *ks*. The mass-conservation equation for the size class *ks* of sediment particles in the active-layer control volume then reads

$$\rho_s (1-p_b)\frac{\partial(\beta_{ks}h_a)}{\partial t}+\nabla\cdot\vec{q}_{bks}+E_{ks}-D_{ks}-F_{ks}=0 \qquad (15\text{-}30)$$

The mass of a particular size class in the active-stratum control volume may change only due to active-layer floor movement, i.e., due to exchange of material between the active layer and active stratum, whereas the active-stratum floor elevation remains unchanged. This is expressed by a mass-conservation equation written for the size class *ks* in the active-stratum control volume,

$$\rho_s (1-p_b)\frac{\partial}{\partial t}\left[\beta_{sks}(z_b-h_a)\right]+F_{ks}=0 \qquad (15\text{-}31)$$

where

β_{sks} = active-stratum fraction of the size class *ks*; and
(z_b-h_a) = active-layer floor elevation, i.e., active-stratum ceiling.

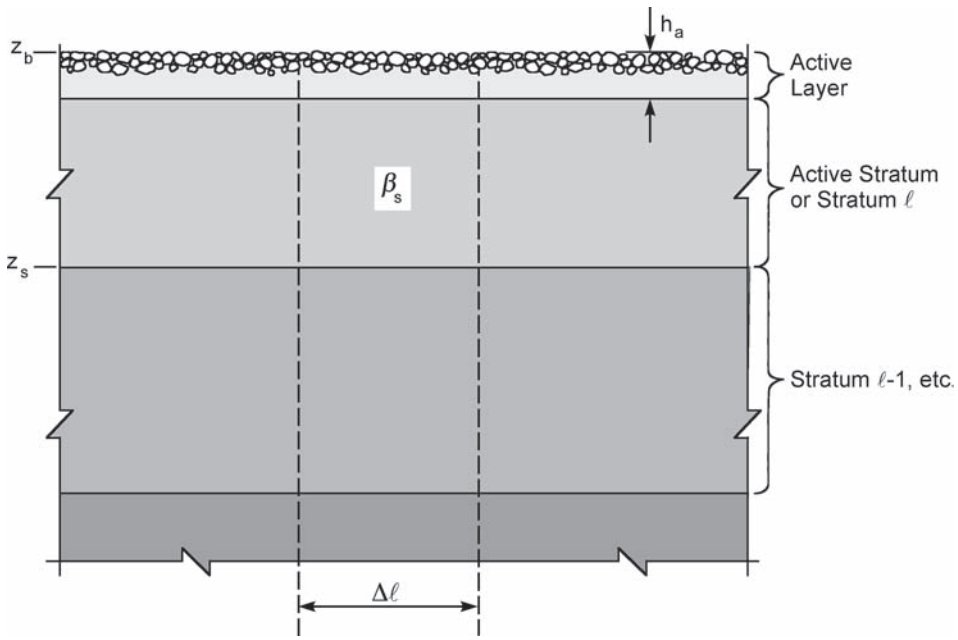

Fig. 15-3. Stratum control volumes below an active-layer control volume.

Summation of the mass-conservation equations for all size classes in the active-layer control volume and use of the basic constraint

$$\sum_{ks=1}^{KS}\beta_{ks}=1 \tag{15-32}$$

where

KS represents the total number of size classes,

leads to the global mass-conservation equation for the active-layer control volume:

$$\rho_s\left(1-p_b\right)\frac{\partial h_a}{\partial t}+\sum_{ks=1}^{KS}\left(\nabla\cdot\vec{q}_{bks}+E_{ks}-D_{ks}-F_{ks}\right)=0. \tag{15-33}$$

A similar equation can be obtained for the active-stratum control volume,

$$\rho_s\left(1-p_b\right)\frac{\partial\left(z_b-h_a\right)}{\partial t}+\sum_{ks=1}^{KS}F_{ks}=0 \tag{15-34}$$

where again Eq. (15-32) is invoked. Summation of Eqs. (15-33) and (15-34) gives the global mass-conservation equation for bed sediment,

$$\rho_s\left(1-p_b\right)\frac{\partial z_b}{\partial t}+\sum_{ks=1}^{KS}\left(\nabla\cdot\vec{q}_{bks}+E_{ks}-D_{ks}\right)=0 \tag{15-35}$$

which can be recognized as the form of the Exner equation written for the summation over all sediment size classes.

One global mass-conservation equation for bed sediment (Eq. (15-35)) written for the bed control volume (comprising active-layer and active-stratum control volumes), and *ks* mass-conservation equations for active-layer sediment (one Eq. (15-30) for each size class) written for the active-stratum control volume, are used to compute the bed-surface elevation and the active-layer size-class distribution changes. To satisfy the basic constraint (Eq. (15-32)), the equations must be solved simultaneously.

When the overall bed slope is small, the mass-conservation equation for the size class *ks* of active-layer sediment and the global mass-conservation equation for bed sediment, Eqs. (15-30) and (15-35), can be written in Cartesian coordinates as follows:

$$\rho_s\left(1-p_b\right)\frac{\partial\left(\beta_{ks}h_a\right)}{\partial t}+\frac{\partial q_{bxks}}{\partial x}+\frac{\partial q_{byks}}{\partial y}+E_{ks}-D_{ks}-F_{ks}=0 \tag{15-36}$$

and

$$\rho_s\left(1-p_b\right)\frac{\partial z_b}{\partial t}+\sum_{ks=1}^{KS}\left(\frac{\partial q_{bxks}}{\partial x}+\frac{\partial q_{byks}}{\partial y}+E_{ks}-D_{ks}\right)=0 \tag{15-37}$$

where

q_{bxks} and q_{byks} = *x*- and *y*-direction components of the bed-load flux for the size class *ks* of active-layer sediment.

15.6 SUSPENDED-MATERIAL PROCESSES

15.6.1 General Three-Dimensional Formulation

The majority of two-dimensional and three-dimensional flow and sediment models use the advection-diffusion equation with an additional fall-velocity term to describe the suspended-sediment transport. The three-dimensional mass conservation equation for suspended sediment reads

$$\begin{aligned}&\frac{\partial(\rho C)}{\partial t}+\frac{\partial}{\partial x}(u\rho C)+\frac{\partial}{\partial y}(v\rho C)\\&+\frac{\partial}{\partial z}(w\rho C)-\frac{\partial}{\partial z}\left(w_f\rho C\right)\\&=\frac{\partial}{\partial x}\left(\varepsilon_s\frac{\partial(\rho C)}{\partial x}\right)+\frac{\partial}{\partial y}\left(\varepsilon_s\frac{\partial(\rho C)}{\partial y}\right)\\&+\frac{\partial}{\partial z}\left(\varepsilon_s\frac{\partial(\rho C)}{\partial z}\right)\end{aligned} \tag{15-38}$$

where

ρ = density of a mixture of water and suspended sediment;
C = dimensionless concentration, i.e., ratio of the mass of the suspended-sediment particles contained in an elemental volume to the total mass of the elemental volume;
w_f = suspended-sediment particle fall or settling velocity;
u, v, and w = water-velocity components;
ε_s = turbulent mass-diffusivity coefficient, i.e., the eddy diffusivity for sediment-particle transport.

When the dimensional or so-called volumetric concentration $c=\rho C$ is used, Eq. (15-38) becomes

$$\begin{aligned}&\frac{\partial c}{\partial t}+\frac{\partial}{\partial x}(uc)+\frac{\partial}{\partial y}(vc)+\frac{\partial}{\partial z}(wc)-\frac{\partial}{\partial z}\left(w_f c\right)\\&=\frac{\partial}{\partial x}\left(\varepsilon_s\frac{\partial c}{\partial x}\right)+\frac{\partial}{\partial y}\left(\varepsilon_s\frac{\partial c}{\partial y}\right)+\frac{\partial}{\partial z}\left(\varepsilon_s\frac{\partial c}{\partial z}\right)\end{aligned} \tag{15-39}$$

where the volumetric concentration c = the ratio of the mass of the suspended-sediment particles contained in an elemental volume to the elemental volume.

The formulations of Eqs. (15-39) and (15-40), based on the dimensional and dimensionless concentrations, are fully equivalent. Most (but not all) model formulations are based on the dimensional concentration, and field and laboratory data are reported in both forms. There is no inherent advantage in using or the other of the two forms.

At the free surface, the vertical sediment flux is zero. Thus, the simplest free-surface boundary condition for Eqs. (15-38) or (15-39) is to set the vertical diffusion and the fall-velocity advection fluxes to zero at the free surface. The near-bed boundary condition for Eqs. (15-38) or (15-39) can be either the specified concentration, or the specified exchange between the suspended-sediment and the bed- and near-bed processes. The exchange is defined as the difference between the upward sediment entrainment flux E and the downward sediment deposition flux D, having signs opposite to the same terms in the governing equations for the bed- and near-bed processes. The sediment exchange condition is preferred if the model includes both suspended-sediment processes and the bed- and near-bed processes, because it provides the coupling between the two.

15.6.2 Two-Dimensional (Depth-Averaged) Formulation

The depth-averaged form of Eq. (15-39) is:

$$\frac{\partial(h\tilde{c})}{\partial t}+\frac{\partial}{\partial x}(\tilde{u}h\tilde{c})+\frac{\partial}{\partial y}(\tilde{v}h\tilde{c}) = \frac{\partial}{\partial x}\left(\tilde{\varepsilon}_s h\frac{\partial\tilde{c}}{\partial x}\right)+\frac{\partial}{\partial y}\left(\tilde{\varepsilon}_s h\frac{\partial\tilde{c}}{\partial y}\right)+E-D \tag{15-40}$$

where

h = depth;
$\tilde{c}$ = depth-averaged dimensional (volumetric) concentration;
$\tilde{u}$ and $\tilde{v}$ = depth-averaged water velocity components;
$\tilde{\varepsilon}_s$ = horizontal plane mass-diffusivity coefficient, usually only including the eddy diffusivity and neglecting the dispersion due to depth averaging.

As discussed in Section 15.3.2, model developers have tended to include neither this additional dispersion, nor a tensorial representation to account for the differential effective dispersion parallel and perpendicular to the local flow direction, as described by Holly and Usseglio-Polatera (1984).

15.6.3 Formulations for Sediment Mixtures

When the sediment mixture is considered, Eqs. (15-38) and (15-39) can be written for a particular size class. Equation (15-38) for the size class *KS* reads

$$\frac{\partial(\rho C_{ks})}{\partial t}+\frac{\partial}{\partial x}(u\rho C_{ks})+\frac{\partial}{\partial y}(v\rho C_{ks}) +\frac{\partial}{\partial z}(w\rho C_{ks})-\frac{\partial}{\partial z}(w_{fks}\rho C_{ks}) =\frac{\partial}{\partial x}\left(\varepsilon_s\frac{\partial(\rho C_{ks})}{\partial x}\right)+\frac{\partial}{\partial y}\left(\varepsilon_s\frac{\partial(\rho C_{ks})}{\partial y}\right) +\frac{\partial}{\partial z}\left(\varepsilon_s\frac{\partial(\rho C_{ks})}{\partial z}\right) \tag{15-41}$$

where the dimensionless concentration C_{ks} = the ratio of the mass of the size class *ks* suspended-sediment particles contained in an elemental volume to the total mass in the elemental volume; and w_{fks} = fall or settling velocity of the size class *ks* suspended-sediment particles.

Equation (15-39) for the size class reads

$$\frac{\partial c_{ks}}{\partial t}+\frac{\partial}{\partial x}(uc_{ks})+\frac{\partial}{\partial y}(vc_{ks}) +\frac{\partial}{\partial z}(wc_{ks})-\frac{\partial}{\partial z}(w_{fks}c_{ks}) =\frac{\partial}{\partial x}\left(\varepsilon_s\frac{\partial c_{ks}}{\partial x}\right)+\frac{\partial}{\partial y}\left(\varepsilon_s\frac{\partial c_{ks}}{\partial y}\right)+\frac{\partial}{\partial z}\left(\varepsilon_s\frac{\partial c_{ks}}{\partial z}\right) \tag{15-42}$$

where the volumetric concentration c_{ks} = the ratio of the mass of the size class *ks* suspended-sediment particles contained in an elemental volume to the elemental volume.

The depth-averaged Eq. (15-40) for size class *ks* reads

$$\frac{\partial(h\tilde{c}_{ks})}{\partial t}+\frac{\partial}{\partial x}(\tilde{u}h\tilde{c}_{ks})+\frac{\partial}{\partial y}(\tilde{v}h\tilde{c}_{ks}) =\frac{\partial}{\partial x}\left(\tilde{\varepsilon}_s h\frac{\partial\tilde{c}_{ks}}{\partial x}\right)+\frac{\partial}{\partial y}\left(\tilde{\varepsilon}_s h\frac{\partial\tilde{c}_{ks}}{\partial y}\right)+E_{ks}-D_{ks} \tag{15-43}$$

where

$\tilde{c}_{ks}$ = depth-averaged dimensional (volumetric) concentration of the size class *ks* particles;
E_{ks} and D_{ks} = the upward sediment entrainment flux and the downward sediment deposition flux for the size class *ks* particles, respectively.

15.7 SEDIMENT-EXCHANGE PROCESSES

15.7.1 Introduction

As stated in Section 15.6, the near-bed boundary condition for suspended-sediment computations can be either a specified concentration, or a specified exchange between suspended-sediment and bed and near-bed processes. Prescribing the near-bed boundary condition for suspended-sediment computations, i.e., defining the sediment-exchange processes, has proven to be one of the most challenging problems in mobile modeling.

15.7.2 Imposition of Near-Bed Concentration

A number of researchers use the near-bed concentration as a boundary condition for suspended-sediment computations. Examples include Wang and Adeff (1986); Olsen and Melaaen (1993); Olsen and Skoglund (1994); Olsen and Kjellesvig (1998); Brors (1999); Olsen (1999); or Olsen et al. (1999). The near-bed concentration is typically defined as an equilibrium concentration and evaluated using one of the available empirical relations (see Chapter 2 of this manual).

Celik and Rodi (1988) offer a comprehensive critique of using the equilibrium near-bed concentration in nonequilibrium situations. The two authors analyzed equilibrium and nonequilibrium situations based on two relatively simple experiments, both using a wide rectangular channel with a steady uniform flow. The Jobson and Sayre (1970) experiment had a suspended-sediment load, larger than the transport capacity, introduced at the upstream end of a flume with an initially sediment-starved bed. As a result, the upstream portion of the flume saw a nonequilibrium situation with net deposition and a gradual decrease of the suspended-sediment load along the flume, until the transport capacity was reached. The Ashida and Okabe (1982) experiment had clear water at the upstream end of the flume with a sand source on the fixed bed. As a result, the upstream portion of the flume reflected a nonequilibrium situation with net entrainment and a gradual increase of the suspended-sediment load along the flume, again until the transport capacity was reached. In both experiments, an equilibrium situation was achieved asymptotically in the downstream portion of the flume, characterized by an entrainment-deposition balance and no change in suspended-sediment load along that portion of the flume. Both experiments clearly show a significant difference between the actual near-bed concentration in nonequilibrium situations and the equilibrium near-bed concentration. Therefore, imposition of the exchange between the suspended-sediment and the bed and near-bed processes is a preferable boundary condition for suspended-sediment computations in nonequilibrium situations.

15.7.3 Imposition of Near-Bed Sediment Exchange

Exchange between the suspended-sediment and the bed and near-bed processes is defined as the difference between the near-bed upward sediment entrainment flux E and the corresponding downward sediment deposition flux D. The governing equations for the bed and near-bed processes contain identical exchange terms, but with opposite signs. Therefore, using sediment entrainment and deposition fluxes E and D as boundary condition for suspended-sediment computations also provides a proper coupling between suspended-sediment processes and bed and near-bed processes.

For an equilibrium situation in a wide rectangular channel with a steady uniform flow, eventually achieved in both the Jobson and Sayre (1970) and Ashida and Okabe (1982) experiments, the classical suspended-sediment transport Eq. (15-39) yields

$$w_f c_e + \varepsilon_s \frac{\partial c_e}{\partial z} = 0 \tag{15-44}$$

where

c_e = equilibrium concentration.

Equation (15-44), valid at any depth, describes an equilibrium between a downward advective flux due to fall velocity (gravity effects) and an upward diffusive flux due to turbulence.

At some near-bed location, Eq. (15-44) can be written as

$$w_f c_{be} + \varepsilon_s \left.\frac{\partial c_e}{\partial z}\right|_b = D - E = 0 \tag{15-45}$$

where

c_{be} = near-bed equilibrium concentration and

$\left.\frac{\partial c_e}{\partial z}\right|_b$ = near-bed equilibrium concentration gradient.

Equation (15-45) is the usual starting point in defining sediment entrainment and deposition fluxes E and D. Assuming that Eq. (15-39) offers an accurate enough description of sediment transport in near-bed regions, the relation can be thought of as representing a zero near-bed net sediment exchange for an equilibrium situation. By analogy, the near-bed net sediment exchange for a nonequilibrium situation is then represented as

$$w_f c_b + \varepsilon_s \left.\frac{\partial c}{\partial z}\right|_b = D - E \neq 0 \tag{15-46}$$

where

c_b = near-bed nonequilibrium concentration and

$\left.\frac{\partial c}{\partial z}\right|_b$ = near-bed nonequilibrium concentration gradient.

In most models that include sediment exchange processes, the near-bed sediment deposition flux D for nonequilibrium situations is defined as a downward advective flux due to the fall velocity, evaluated for the actual (nonequilibrium) near-bed concentration:

$$D = w_f c_b \tag{15-47}$$

The actual near-bed concentration c_b in Eq. (15-47) is derived from the suspended-sediment computations themselves. This approach was used in models described by Shimizu et al (1990); Spasojevic and Holly (1990a; 1990b); Spasojevic and Holly (1993); Jankowski et al. (1994); Minh Duc et al. (1998); Rodi (2000); and Wu et al. (2000). As an extension to this approach, some researchers (e.g., Jankowski et al. 1994) have proposed introduction of a probability factor into the deposition flux in Eq. (15-47) to account for the possibility that some near-bed sediment particles subjected to downward advection due to their fall velocity may be resuspended without reaching the bed.

Defining the near-bed entrainment flux E for nonequilibrium situations is a far more difficult task. Celik and Rodi (1984) and van Rijn (1986) proposed evaluating the entrainment flux using its equilibrium value. Thus, because the equilibrium entrainment flux is equal to the equilibrium deposition flux (Eq. 15-45), the entrainment flux becomes

$$E = w_f c_{be} \tag{15-48}$$

Equation (15-48) implies that the entrainment always occurs at its maximum rate (Celik and Rodi 1988). This approach was used in models described by Spasojevic and Holly (1990a; 1990b); Lin and Falconer (1996); Minh Duc et al. (1998); Rodi (2000); and Wu et al. (2000).

Brors (1999) specified the entrainment flux, as it appears in the Exner equation, in terms of the near-bed concentration and concentration gradient. Spasojevic and Holly (1993) introduced the entrainment flux evaluated as an upward near-bed mass diffusion flux,

$$E = -\varepsilon_s \left.\frac{\partial c}{\partial z}\right|_a \tag{15-49}$$

where subscript a denotes that the mass-diffusion flux is evaluated at a near-bed point some distance a above the bed surface. Following the basic definition of the derivative, the entrainment flux in Eq. (15-49) is further modeled as

$$E = -\varepsilon_s \frac{c_{a+\Delta a} - c_a}{\Delta a} \tag{15-50}$$

where

c_a = near-bed concentration reflecting the action of near-bed flow on the bed and bed-load particles, whereas

$c_{a+\Delta a}$ = near-bed concentration at distance $a + \Delta a$ above the bed surface, extrapolated from the suspended-sediment computations.

Equation (15-50) implies that the entrainment varies according to both the near-bed concentration of sediment present on the bed and the concentration of suspended sediment possibly carried by the flow from some upstream location. The concentration c_a is evaluated by using an empirical relation for the near-bed *equilibrium* concentration (see Chapter 2 for different empirical relations).

When applied in the context of sediment mixtures and the active-layer concept (Spasojevic and Holly 1993), the entrainment flux has to be modified by β_{ks} to reflect the availability of the size class *ks* in the active-layer control volume. Then Eqs. (15-49) and (15-50) become, respectively,

$$E_{ks} = -\beta_{ks}\varepsilon_s \left.\frac{\partial c_{ks}}{\partial z}\right|_a \tag{15-51}$$

and

$$E_{ks} = -\beta_{ks}\varepsilon_s \frac{(c_{ks})_{a+\Delta a} - (c_{ks})_a}{\Delta a} \tag{15-52}$$

In the same context, the corresponding deposition flux, defined as in Eq. (15-47), becomes

$$D_{ks} = w_{fks}(c_{ks})_{a+\Delta a} \tag{15-53}$$

More information can be found in Chapter 3.

15.8 SYSTEM CLOSURE AND AUXILIARY RELATIONS

15.8.1 Introduction

The mass-conservation principles on which the various governing equation sets described earlier are based do not, in themselves, compose a complete mathematical system. There is a further need for additional closure, or auxiliary, relations, often empirical. System closure for sediment processes is highly dependent on the adopted conceptual sediment model and number of sediment processes included in the model. Thus, these issues are presented here through several examples. For convenience, the governing sediment equations for each example are summarized again here.

Most three-dimensional models use Eq. (15-39) as the governing equation for suspended-sediment processes:

$$\frac{\partial c}{\partial t} + \frac{\partial}{\partial x}(uc) + \frac{\partial}{\partial y}(vc) + \frac{\partial}{\partial z}(wc) - \frac{\partial}{\partial z}(w_f c) = \frac{\partial}{\partial x}\left(\varepsilon_s \frac{\partial c}{\partial x}\right) + \frac{\partial}{\partial y}\left(\varepsilon_s \frac{\partial c}{\partial y}\right) + \frac{\partial}{\partial z}\left(\varepsilon_s \frac{\partial c}{\partial z}\right) \tag{15-54}$$

The sediment mass-diffusivity coefficient ε_s is typically related to the turbulent eddy viscosity ν_t (Brors 1999; Wu et al. 2000) through

$$\varepsilon_s = \frac{\nu_t}{\sigma_c} \tag{15-55}$$

where

σ_c = turbulent Schmidt number for sediment (often assumed to be unity).

Major differences among models arise from the treatment of bed and near-bed processes. Different approaches to the

treatment of bed and near-bed processes are classified in Section 15.5 into the bed-load-layer approach; the total-load approach; and the active-layer and active-stratum approach (designed for sediment mixtures).

15.8.2 The Bed-Load-Layer Approach

When the van Rijn bed-load-layer approach described earlier is used, the governing equation for bed and near-bed processes becomes Eq. (15-24) (models described by van Rijn 1987 and Brors 1999):

$$\rho_s (1-p_b)\frac{\partial z_b}{\partial t}+\frac{\partial q_{bx}}{\partial x}+\frac{\partial q_{by}}{\partial y}+E_b-D_b=0. \quad (15\text{-}56)$$

The deposition flux D_b is generally formulated through Eq. (15-47) (models described by Spasojevic and Holly 1993; Brors 1999; and Wu et al. 2000):

$$D_b = w_f c_b. \quad (15\text{-}57)$$

The entrainment flux E_b is usually formulated through Eq. (15-48) (models described by Lin and Falconer 1996 and Wu et al. 2000):

$$E_b = w_f c_{be}. \quad (15\text{-}58)$$

When the bed-load-layer approach is used, the governing equations for sediment processes are the mass-conservation equation for suspended sediment, Eq. (15-54), and the mass-conservation equation for bed-load-layer and bed-subsurface sediment, Eq. (15-56). Primary sediment unknowns are the volumetric suspended-sediment concentration and the bed-surface elevation z_b. Flow-velocity components *u, v,* and *w* are the result of flow computations. The actual near-bed nonequilibrium concentration c_b is the result of suspended-sediment computations. All other sediment-related terms in Eqs. (15-54) and (15-56), such as sediment mass-diffusivity coefficient ε_s (i.e., turbulent Schmidt number σ_c), bed-load flux q_b, fall velocity w_f, and the near-bed equilibrium concentration c_{be}, are in general functions of flow variables and primary sediment unknowns and are treated as auxiliary relations, often empirical. In addition, the near-bed equilibrium concentration c_{be} is evaluated at the top of the bed-load layer, so the bed-load-layer thickness h_b must also be specified on the basis of some empirical or other guidance.

15.8.3 The Total-Load Approach

When the total-load approach is used, the governing equation for computing bed-surface elevation becomes Eq. (15-25) (models described by Wang and Adeff 1986; van Rijn 1987; and Wu et al. 2000):

$$\rho_s (1-p_b)\frac{\partial z_b}{\partial t}+\frac{\partial q_{Tx}}{\partial x}+\frac{\partial q_{Ty}}{\partial y}=0 \quad (15\text{-}59)$$

where

$$q_{Tx} = q_{bx}+\int_{h_b}^{h}\left(uc-\varepsilon_s\frac{\partial c}{\partial x}\right)dz$$

and

$$q_{Ty} = q_{by}+\int_{h_b}^{h}\left(vc-\varepsilon_s\frac{\partial c}{\partial y}\right)dz \quad (15\text{-}60)$$

represent the total-load components combining the bed load with the suspended-load flux (advection and diffusion) integrated from the top of the bed-load layer h_b to the total depth *h*.

When the total-load approach is used, the governing equations for sediment processes are the mass-conservation equation for suspended sediment, Eq. (15-54), and the mass-conservation equation for bed-subsurface sediment, bed-load-layer sediment, and suspended sediment in the entire water column above the bed-load layer, Eq. (15-59). The primary sediment unknowns are volumetric suspended-sediment concentration *c* and bed-surface elevation z_b. The sediment mass-diffusivity coefficient ε_s (i.e., turbulent Schmidt number σ_c), bed-load flux q_b, and fall velocity w_f, are treated as auxiliary relations and evaluated through appropriate empirical relations; see for example Chapter 2.

Wu et al. (2000) introduced a modification to the total-load approach to account for nonequilibrium effects on the bed-load transport using Eq. (15-28):

$$\frac{1}{L_s}(q_b-q_{be})+\frac{\partial(\alpha_{bx}q_b)}{\partial x}+\frac{\partial(\alpha_{by}q_b)}{\partial x}+E_b-D_b=0 \quad (15\text{-}61)$$

where deposition and entrainment fluxes D_b and E_b are the same as in Eqs. (15-57) and (15-58), respectively. With this modification, nonequilibrium bed-load flux q_b also becomes the primary sediment unknown, computed from an additional governing sediment equation, Eq. (15-61). Because direction cosines α_{bx} and α_{by} are known parameters, additional auxiliary relations include equilibrium bed-load flux q_{be} and near-bed equilibrium concentration c_{be}.

15.8.4 The Active-Layer and Active-Stratum Approach—Sediment Mixtures

The active-layer and active-stratum approach (Spasojevic and Holly 1993) uses the following set of governing equations for sediment processes:

The mass-conservation equations for size class *ks* of suspended sediment (Eq. 15-42):

$$\frac{\partial c_{ks}}{\partial t}+\frac{\partial}{\partial x}(uc_{ks})+\frac{\partial}{\partial y}(vc_{ks})+\frac{\partial}{\partial z}(wc_{ks})-\frac{\partial}{\partial z}(w_{fks}c_{ks}) = \frac{\partial}{\partial x}\left(\varepsilon_s\frac{\partial c_{ks}}{\partial x}\right)+\frac{\partial}{\partial y}\left(\varepsilon_s\frac{\partial c_{ks}}{\partial y}\right)+\frac{\partial}{\partial z}\left(\varepsilon_s\frac{\partial c_{ks}}{\partial z}\right) \quad (15\text{-}62)$$

The mass-conservation equation for the size class *ks* of active-layer sediment (Eq. 15-36):

$$\rho_s (1-p_b)\frac{\partial(\beta_{ks} h_a)}{\partial t} + \frac{\partial q_{bxks}}{\partial x} + \frac{\partial q_{byks}}{\partial y} + E_{ks} - D_{ks} - F_{ks} = 0 \tag{15-63}$$

The global mass-conservation equation for bed sediment, comprising active-layer and active-stratum sediment (Eq. 15-37):

$$\rho_s (1-p_b)\frac{\partial z_b}{\partial t} + \sum_{ks=1}^{KS}\left(\frac{\partial q_{bxks}}{\partial x} + \frac{\partial q_{byks}}{\partial y} + E_{ks} - D_{ks}\right) = 0 \tag{15-64}$$

where

$$E_{ks} = -\beta_{ks}\varepsilon_s \frac{(c_{ks})_{a+\Delta a} - (c_{ks})_a}{\Delta a} \tag{15-65}$$

and

$$D_{ks} = {}^{w}f_{ks}(c_{ks})_{a+\Delta a} \tag{15-66}$$

are entrainment and deposition fluxes for size class *ks* sediment, respectively.

The active-layer floor source F_{ks}, again specific to the size class *ks*, can be expressed using Eq. (15-31). When the active-layer floor (active-stratum ceiling) descends, then

$$F_{ks} = -\rho_s (1-p_b)\frac{\partial}{\partial t}\left[\beta_{sks}(z_b - h_a)\right] \tag{15-67}$$

gives the mass of the size class *ks*, formerly comprising size fraction β_{sks} of the active-stratum control volume, which becomes part of the active-layer elemental volume. When the active-layer floor (active-stratum ceiling) rises, then

$$F_{ks} = -\rho_s (1-p_b)\frac{\partial}{\partial t}\left[\beta_{ks}(z_b - h_a)\right] \tag{15-68}$$

gives the mass of the particular size class, formerly comprising size fraction β_{ks} of the active-layer elemental volume, which becomes part of the active stratum control volume.

If the sediment mixture in a natural watercourse is represented by a total of *KS* sediment size classes, *KS* mass-conservation equations for suspended sediment (one Eq. (15-62) for each size class) can be written for each elemental volume in the suspension above the active layer. *KS* mass-conservation equations for active-layer sediment (one Eq. (15-63) for each size class) can be written for each active-stratum elemental volume, and one global mass-conservation equation for bed sediment, Eq. (15-64), can be written for each bed elemental volume (comprising the active-layer and active-stratum elemental volumes). The global set of sediment equations for all size classes, taken as a whole, describes the behavior of a nonuniform sediment, including natural phenomena such as differential settling, armoring, and hydraulic sorting. The following sediment variables are considered primary sediment unknowns: (1) *KS* suspended-sediment concentrations c_{ks} for each elemental volume containing a mixture of water and suspended sediment; (2) *KS* active-layer size fractions β_{ks} for each active-layer elemental volume; and (3) one bed-surface level z_b for each bed elemental volume.

The actual near-bed nonequilibrium concentration $(c_{ks})_{a+\Delta a}$ is extrapolated from the suspended-sediment computations. The equilibrium near-bed concentration $(c_{ks})_a$, bed-load flux q_b, active-layer thickness h_a, fall velocity w_f, and sediment mass-diffusivity coefficient ε_s are in general functions of flow variables and primary sediment unknowns and are treated as auxiliary relations. The location *a* may be evaluated on the basis of some empirical guidance. However, because the parameter Δa has no direct physical interpretation (being defined only for the purpose of estimating the concentration gradient near the bed), both *a* and Δa are perhaps best considered calibration parameters as discussed in Section 15.11.

The numerical procedure for solution of the sediment equations is formulated without reference to the specific empirical relations that ultimately must be invoked to evaluate the auxiliary relations. This allows use of any suitable empirical relation to evaluate a particular auxiliary relation and renders the formal numerical procedure independent of any specific empirical relation.

The equilibrium near-bed concentration $(c_{ks})_a$ (for size class *ks* sediment) generally depends on the near-bed flow characteristics. It is evaluated using an appropriate empirical relation, for example that of van Rijn (1984a).

The net bed-load flux is represented here as

$$q_{bks} = (1-\gamma)\zeta_h \beta_{ks} q_b^t \tag{15-69}$$

where

q_b^t = theoretical bed-load capacity for a bed containing only sediment of the size class *ks*, evaluated using an appropriate bed-load predictor such as proposed by van Rijn (1984a).

This load is adjusted by ζ_h, a so-called hiding factor accounting for the reduction or increase in a particular

size class transport rate when it is part of a mixture. Empirical relations such as those proposed by Karim and Kennedy (1982) or Shen and Lu (1983) can be used to evaluate ζ_h. The adjusted load is modified by β_{ks} to reflect the availability of the particular size class in the active-layer elemental volume. Finally, the load is modified by $(1-\gamma)$ to reflect the fact that some fraction γ of the particular size-class particles is expected to be transported only as suspended load, with γ typically related to quantities such as the ratio of fall velocity to shear velocity (Rouse number).

The active-layer thickness h_a is evaluated by an appropriate empirical concept of the depth of bed material that supplies material for bed-load transport and suspended-sediment entrainment. Examples are the concepts of Bennett and Nordin (1977); Borah et al. (1982); or Karim and Kennedy (1982).

Depending on the sediment-particle size, different experimental relations can be used to compute particle fall velocity, as described by van Rijn (1984b).

The sediment mass-diffusivity coefficient ε_s is obtained by modifying the turbulent eddy viscosity v_t coefficient to reflect the difference in the diffusion of a discrete sediment particle and the diffusion of a fluid "particle" (or small coherent fluid structure), and also to reflect possible damping of the fluid turbulence by sediment particles, as suggested by van Rijn (1984b).

The equations presented in this section are the basis for the sediment model incorporated in the CH3D-SED code, used in the examples of Sections 15.11.2 and 15.11.3.

15.8.5 Two-Dimensional Models

Because the governing equations for bed and near-bed processes are two-dimensional in plan parallel to the bed surface, the major difference between two-dimensional and three-dimensional models arises from the governing equation for suspended-sediment processes. For example, depth-averaged models use Eq. (15-40), i.e., the depth-averaged form of the mass-conservation equation for suspended sediment (model described by Minh Duc et al. 1998, etc.),

$$\frac{\partial(h\tilde{c})}{\partial t}+\frac{\partial}{\partial x}(\tilde{u}h\tilde{c})+\frac{\partial}{\partial y}(\tilde{v}h\tilde{c}) = \frac{\partial}{\partial x}\left(\tilde{\varepsilon}_s h\frac{\partial\tilde{c}}{\partial x}\right)+\frac{\partial}{\partial y}\left(\tilde{\varepsilon}_s h\frac{\partial\tilde{c}}{\partial y}\right)+E_b-D_b \quad (15\text{-}70)$$

or, in the case of sediment mixtures, Eq. (15-43), i.e., the depth-averaged form of the mass-conservation equation written for size class *ks* of suspended sediment (model described by Spasojevic and Holly (1990a; 1990b)),

$$\frac{\partial(h\tilde{c}_{ks})}{\partial t}+\frac{\partial}{\partial x}(\tilde{u}h\tilde{c}_{ks})+\frac{\partial}{\partial y}(\tilde{v}h\tilde{c}_{ks}) = \frac{\partial}{\partial x}\left(\tilde{\varepsilon}_s h\frac{\partial\tilde{c}_{ks}}{\partial x}\right)+\frac{\partial}{\partial y}\left(\tilde{\varepsilon}_s h\frac{\partial\tilde{c}_{ks}}{\partial y}\right)+E_{ks}-D_{ks} \quad (15\text{-}71)$$

Thus, instead of computing point concentrations, depth-averaged models compute depth-averaged concentrations. The near-bed concentration in deposition flux is typically evaluated through some kind of theoretical vertical concentration profile, e.g., the Rouse profile. Entrainment flux is usually evaluated as an equilibrium entrainment equal to the equilibrium deposition, which, in case of sediment mixtures, has to be modified by β_{ks} to reflect the availability of the size class in the active-layer control volume (Spasojevic and Holly (1990a; 1990b)):

$$E_{ks}=-\beta_{ks}(c_{ks})_a \quad (15\text{-}72)$$

All other system-closure considerations are basically the same as for three-dimensional models, of course depending on the bed and near-bed processes approach. Equations (15-71) and (15-72), together with the governing equations for bed and near-bed sediment processes and other closure auxiliary relations presented in Section 15.8.4, are the basis for the sediment model incorporated into the MOBED2 code, used in the example of Section 15.11.4.

An important issue that has achieved relatively little attention in multidimensional model development as of this writing is the inclusion of flow- and transport-dependent form roughness associated with mobile-bed bed forms such as dunes and ripples. As long as computer time and memory requirements restrict models to plan-view discretizations that are too coarse to resolve individual dune topography and movement, models should incorporate appropriate empirical formulations combining bed-material and bed-form roughness. The authors—always optimistic—expect that as computing resources and turbulence-model development gradually permit plan-view grid refinement that can capture bed-form activity in fully three-dimensional models, it will be necessary only to include bed-material roughness formulations, because the larger-scale bed form "roughness" will be captured within the model's own solution for momentum exchange in nonparallel flow.

15.8.6 Additional Considerations in Auxiliary Relations

Although the auxiliary relations described above are necessary for minimal closure, they do not, in themselves, account for many other possible subtle complexities in the physical processes. Considerable past and present research has been devoted to developing a better understanding, and conceptualizations, of these complex processes.

For example, Nakagawa and Tsujimoto (1980) studied bed instability due to lag system between bed-shear stress and velocity, which is composed of two elements: (1) the phase lag between sediment-transport rate and bed-shear stress; and (2) lag distance between sediment transport and flow field over a wavy bed. They evaluated the lag distance of bed-load transport for bed shear stress based on the model for bed-load transport that is applicable to such nonequilibrium situations as when sand waves are initially formed. In addition, the potential flow model of flow over a wavy bed was modified to take into account the effects of flow convergence and divergence. Using these models for flow and bed-load transport, the lag system in a perturbed sand bed was clarified, and the hydraulic conditions for unstable bed, which may correspond to the regimes for dunes or ripples and antidunes, was predicted. Kovacs and Parker (1994) derived a vectorial bed-load formulation for the transport of coarse sediment for up to the angle of repose both in the streamwise and transverse directions. They developed a mathematical model of the time evolution of straight river channels, focusing on the evolution processes due to the bank erosion in the presence of bed load only. Lau and Engel (1999) studied, using dimensional and theoretical analysis, together with available experimental data, how a combination of flow and stream bed slope affects the beginning of sediment transport. Damgaard et al. (1997) performed experiments on bed-load transport on steep longitudinal slopes and formulated a semiempirical relation that predicts the transport rate on horizontal as well mild and steep slopes. Kitamura et al. (1998) studied the influence of vegetation on sediment transport capability in channels.

These brief examples are intended only to give the reader a sense of the kinds of additional complexities that may need to be included in mobile-bed models.

15.9 MOBILE-BED NUMERICAL SOLUTION CONSIDERATIONS

15.9.1 Numerical Coupling of Flow and Mobile-Bed Processes

As of this writing, the simultaneous solution of all governing equations in three-dimensional or even two-dimensional flow and sediment models is not feasible, due to the prohibitive CPU time requirements. Thus, one of the important issues in flow and sediment modeling is how to provide adequate numerical coupling between and among water and sediment processes. In nature, this coupling is between flow and sediment processes in general, as well as between suspended-sediment and bed and near-bed processes. Numerical coupling or uncoupling of these different processes should reflect the nature and importance of the real physical coupling.

Although the flow is the driving force for sediment-transport and bed-evolution processes, the most important sediment feedback to the flow includes bathymetry changes, changes in the density of water and suspended-sediment mixture, possibly changes in the bed-surface roughness when sediment mixtures are considered, and flow-dependent form roughness associated with bed forms (dunes, ripples). The bathymetry and the bed-surface roughness changes during a time step appropriate for flow computations are usually too small to change the flow domain and flow field significantly. Only the suspended-sediment transport has the same time scale as fluid flow. In most cases, suspended-sediment concentrations in natural watercourses are relatively small and do not change abruptly with time, which suggests that changes in the density of the water and sediment mixture during a time step appropriate to flow computations are generally insufficient to influence the flow field significantly. Therefore, practically all existing two-dimensional and three-dimensional flow and sediment models uncouple water and sediment computations within one time step. Indeed, the same is true for most one-dimensional mobile-bed models. A notable exception is the SEDICOUP one-dimensional mobile-bed model (Holly and Rahuel 1990), which represented an experiment in complete coupling of all flow and sediment processes in an unsteady, multiple-size-class environment.

On the other hand, the nature of the real physical coupling between different sediment processes may preclude their complete numerical uncoupling, even at a scale of one time step. The entrainment and deposition fluxes (sediment-exchange processes) are the link relating suspended- and bed- and near-bed-sediment processes. It is generally agreed that the deposition flux depends on the actual near-bed concentration evaluated from suspended-sediment computations. The entrainment flux depends on the near-bed equilibrium concentration, associated with the bed surface, bed-load layer, or active layer, depending on the adopted conceptual model. Deposition and entrainment fluxes appearing in the governing equations for bed and near-bed processes are also commonly used as near-bed boundary conditions for suspended-sediment processes.

The active-layer and active-stratum approach associated with sediment mixtures (Spasojevic and Holly (1990a; 1990b; 1993)) emphasizes the need for some level of numerical coupling between suspended-sediment processes and bed and near-bed processes. Whereas the deposition flux in Eq. (15-66) depends on suspended-sediment concentration, the entrainment flux in Eqs. (15-65) and (15-72) depends on the size-class fraction of active-layer sediment. Therefore, models described by Spasojevic and Holly (1990a; 1990b; 1993) are structured to allow for iterative coupling between suspended-sediment and bed and near-bed sediment processes. The mass-conservation equations for bed and near-bed processes are solved by assuming the suspended-sediment concentration, and therefore the deposition flux, to be known from the previous iteration. An improved estimate of active-layer size fractions and the bed-surface elevation is thus obtained. The mass-conservation equations for

suspended-sediment processes are then resolved for the same computational time step, by assuming the active-layer size fractions, i.e., entrainment flux, to be known from the bed and near-bed processes computations. The whole procedure is repeated iteratively until a convergence criterion is satisfied.

Finally, in the case of active-layer and active-stratum concepts associated with sediment mixtures (Spasojevic and Holly 1990a; 1990b; 1993), the governing equations for bed and near-bed sediment processes require simultaneous solution to satisfy the basic requirement that the sum of all size-class fractions is equal to unity. Application of a chosen numerical method to discretize the global mass-conservation equation for bed sediment (Eq. (15-64)) and the mass-conservation equation for active-layer sediment (Eq. (15-63)) yields a system of nonlinear algebraic equations. The discretized (nonlinear algebraic) equations to be solved simultaneously for the same point at the bed are (1) one discretized global mass-conservation equation for bed sediment and (2) *KS* discretized mass-conservation equations for active-layer sediment. Solution using, e.g., a Newton-Raphson iterative procedure yields (1) one bed-surface elevation and (2) *KS* active-layer size fractions.

15.9.2 Choice of Numerical Method for Mobile-Bed Processes

Because a mobile-bed model is typically built into an already existing hydrodynamic model, the basic choice of numerical method for solving the sediment equations usually follows the choice of numerical method for solving flow equations. In certain cases, this is the only available possibility. For example, if the hydrodynamic model uses the finite-element method with an unstructured grid, it is impossible to use a finite-difference method to solve the sediment equations on the same grid. However, it would appear theoretically possible to allow the numerical method for solving the sediment equations to be different from the one used for solving the flow equations. For example, hybrid or split-operator approaches, which use different numerical methods to solve different parts of the same equation, have proven to yield satisfactory numerical solutions. To the extent that the numerical method for sediment equations can be independent of the method used for the flow equations, one can consider the possibility of developing an independent mobile-bed module, which could be used with different hydrodynamic modules. The numerical method for such an independent mobile-bed module would have to be able to support both structured and unstructured grids, which limits the basic choice to either the finite-element or the finite-volume method.

Existing two-dimensional and three-dimensional flow and sediment models use a variety of numerical methods. The finite-element method is used in models reported by Thomas and McAnally (1985); Wang and Adeff (1986); Brors (1999); Jia and Wang (1999); and the RMA-10 model at the Coastal and Hydraulics Lab, U.S. Army Corps of Engineers. Models reported by Shimizu et al. (1990), Spasojevic and Holly (1990a; 1990b), Spasojevic and Holly (1993), and Lin and Falconer (1996), use the finite-difference method. The model reported by Jankowski et al. (1994), i.e., that in Hervouet and Bates (2000), uses a split-operator approach with the method of characteristics used for advection processes and the finite-element method used for the remaining processes. Models reported by Olsen and Melaaen (1993), Minh Duc et al. (1998), Olsen et al (1999), and Wu et al. (2000) use the finite-volume method associated with a structured grid. As of this writing, no flow and sediment model has been known to use the finite-volume method with an unstructured grid. Advantages and disadvantages of methods associated with structured versus methods associated with unstructured grids have already been discussed in Section 15.3.

It should be noted that the finite-difference method is applied to the governing equations in Cartesian coordinates only in special cases with simple geometry. Models that use the finite-difference method typically require that the governing equations be transformed into curvilinear or body-fitted coordinates to accommodate complex geometries, usually associated with natural watercourses. Models that use the finite-volume method on a structured grid, and thus do not exploit the full potential of the method, also require that the governing equations be cast into in curvilinear coordinates.

Most numerical problems (instability, oscillations, etc.) in solving unsteady flow and sediment equations are caused by advection terms, especially in the case of sharp-front waves. Therefore, the advection terms in the governing flow and sediment equations may require special treatment, usually involving a numerical method that takes into account the hyperbolic nature of advection.

Existing two-dimensional and three-dimensional flow and sediment models typically do not anticipate the existence of bores or moving hydraulic jumps and have no special treatment for advection terms in flow equations. Exceptions include the TELEMAC-3D code, as described by Jankowski et al. (1994) or Hervouet and Bates (2000), which uses the method of characteristics for the momentum advection terms in the flow equations. The bed-load term in the governing equations for bed and near-bed processes, if one considers it as an equivalent advection term, is numerically benign due to the slow nature of the bed-load movement. However, suspended-sediment transport is likely to encounter a sharp-front wave situation. Examples include a postdredging resuspension in the form of a point source, extensive sediment entrainment behind a river-training structure such as a chevron dike, or simply extensive sediment entrainment due to incorrect initial and boundary conditions for sediment.

Several existing two-dimensional and three-dimensional flow and sediment models include special treatment of the advection terms in the suspended-sediment transport equation. For example, the TELEMAC-3D code, as described by

Jankowski et al. (1994), and the MOBED2 code (Spasojevic and Holly 1990a; 1990b), use a split-operator approach combined with the method of characteristics for the advection term in the suspended-sediment transport equation. The CH3D-SED code, as described by Spasojevic and Holly (1993), uses the QUICKEST scheme (Leonard 1979), whereas the model described by Lin and Falconer (1996) uses a modification, called ULTIMATE QUICKEST, of the same scheme, to discretize the suspended-sediment transport equation.

15.9.3 Grid-Generation and Adaptive-Grid Issues in a Mobile-Bed Environment

Grid generation was an important issue in the 1980s and early 1990s, when most two-dimensional and three-dimensional modelers had to develop their own grid-generation programs. Most two-dimensional and three-dimensional sediment modelers now use commercial grid-generation software. As of this writing, the grid-generation software associated with computational fluid dynamics applications (aerodynamics, auto industry, ship hydrodynamics, etc.) is quite sophisticated, but typically accepts geometry input files in specific formats, usually generated by design-support software. The grid-generation software associated with computational hydraulics applications, even though less sophisticated, is generally designed to accept the random geometry data associated with field-data collection for natural watercourses.

On the other hand, adaptive grid technology is currently quite an important issue in mobile-bed modeling. Because mobile-bed modeling typically assumes unsteadiness, both free-surface water elevation and bed-surface elevation are dynamically moving boundaries to which the three-dimensional grid has to adapt at each computational time step. The moving free-surface water elevation, usually being nearly horizontal, poses less of a problem than the moving bed-surface elevation, which presents a real challenge. To begin with, the bed surface has a naturally irregular shape, occasionally modified by man-made hydraulic structures such as river-training structures (weirs, lateral or L-shaped dikes, chevrons, bridge piers, etc.). Furthermore, bed-surface elevation changes may be quite uneven throughout a model domain. Newly installed hydraulic structures may cause extensive and rapid local bed-surface elevation changes, e.g., erosion behind the chevron dike followed by accompanying deposition further downstream. Long-term bed-surface elevation changes, such as river meandering, are slow but can accumulate significantly in time.

As of this writing, general treatment of the adaptive-grid problem in three-dimensional flow and sediment models is in the early stages of development. The most important adaptive grid issue in mobile-bed models arises from bed-elevation changes that require grid adaptation in the vertical direction. Most of the existing three-dimensional flow and sediment models keep the third coordinate direction straight and vertical, making it relatively easy to deal with bed-related adaptive-grid issues. For example, the CH3D-SED model, as described by Spasojevic and Holly (1993), uses a simple partial coordinate transformation, called σ-stretching, for the vertical coordinate direction. The vertical σ-stretching allows for simple redistribution of a fixed number of computational points along the depth at each time step. Grid adaptation in fully three-dimensional hydrodynamic models that do not rely on a straight vertical coordinate has not been fully addressed, either for hydrodynamic or for mobile-bed applications.

The roles of grid refinement and grid sensitivity in the quality of mobile-bed modeling have gotten rather short shrift, especially compared to the attention devoted to these considerations in computational fluid dynamics and fixed-bed computational hydraulics. D. A. Lyn (personal communication, 2002) has aptly posed a number of relevant questions, to wit,

- Should the grid simply be as fine as the budget allows?
- To what extent is it reasonable to accept a coarse grid in one direction, and a fine grid in the other directions?
- Is a coarse-grid high-dimensional (three-dimensional) model solution always better than a fine-grid low-dimensional (two-dimensional) model with more schematic empirical input?
- Can a coarse grid yield misleading results?
- Can a coarse (horizontal) grid be used for a nonhydrostatic problem where rapidly varied flow prevails?
- Are grid-independence tests necessary and practical?
- Does one just choose a grid and accept the fact that details finer than the grid simply cannot be resolved?
- Can/should one accept calibration as a means of working around a coarse-grid limitation?

The easy answer to all of these questions is "it depends." As mobile-bed modeling development and practice mature, these issues will surely attract more careful attention and hopefully lead to a body of literature and acquired wisdom that respond at least partly to the above questions.

15.10 FIELD DATA NEEDS FOR MODEL CONSTRUCTION, CALIBRATION, AND VERIFICATION

15.10.1 Field Data for Model Construction

Both two- and three-dimensional models require essentially the same type of bathymetric and geometric data to provide a basic description of the physical domain. An initial bed elevation must be assigned at every grid intersection, node, or spatial element of the plan-view computational mesh of a model, two-dimensional or three-dimensional.

It obviously would not be feasible first to lay out the computational mesh, identify the geographical coordinates of

every point requiring an initial bed elevation, and then visit each location in the field to determine the elevation. In reality, one first obtains the best available "mapping" of the bathymetry through spot elevations, generally taken from a moving vessel with GPS positioning technology, and describing the bed-surface bathymetry at a scale appropriate for the anticipated density of the computational mesh. For example, if it is expected that the mesh will resolve plan-view details at a scale on the order of 10 m, then the density of spot elevations taken in the field should be such that significant bed features of a scale of 10 ms or larger can be captured.

Once the actual computational mesh is laid out, the measured spot bed elevations are projected onto the required grid or nodal points. This is done through two-dimensional curve-fitting techniques, by which a two-dimensional curvilinear surface is appropriately fit to the data points, and then grid elevations are extracted from the fitted surface.

In a mobile-bed modeling context, these bed elevations so painstakingly and expensively obtained are nothing more than the initial conditions set for further evolution during the model simulation runs. In this sense, the initial bed elevations do not have the sacred, absolute character they are given in a fixed-bed model. Indeed, the initial bed-elevation data may reflect the movement of dunes several meters high, and an individual dune elevation is not necessarily representative of the bed area associated with a given computational mesh point. In some sense, the initial bed elevations can even be thought of as subject to calibration, and thus grid-dependent, if not model-dependent. If the bed elevation (and associated initial bed sediment size distribution; see further on) assigned to a grid point does not represent a quasi-equilibrium with the model's hydrodynamic and sediment equations, then the model will respond with rapid scouring (or deposition) in the first few time steps of the mobile-bed simulation, and the initial elevation may have to be adjusted accordingly. If it were feasible to obtain long-term time-averaged bed elevations on a network of points, thus averaging out the influence of dune movement, this would likely reduce, but probably not eliminate, the need for adjustment of initial elevations.

This approach to obtaining initial bathymetry is somewhat different from the traditional one used for one-dimensional river modeling. For backwater and flood-propagation river modeling, the general practice was to obtain transects, or cross sections, of the river channel, each associated with a single one-dimensional computational point. This historical practice was driven not only by its logical correspondence with one-dimensional model needs, but also by the practical pre-GPS need to identify position on a river with reference to distance along a well-defined transect anchored at surveyed points on the river banks. Multidimensional modeling, in contrast, makes good use of developments such as multibeam technology and GPS positioning for more general, off-transect bathymetric data acquisition.

Bed bathymetry must be complemented by geometric descriptions of any structures in the domain of interest. Such structures might include river-training works (submerged or emerged dikes, etc.), bridge pier bases, or hydraulic structures such as weirs, dams, or intake works. In two-dimensional modeling, a plan-view description of the boundaries of such structures may be sufficient. But for three-dimensional modeling, the complete three-dimensional description of the structural surfaces in contact with the flow domain must be obtained with precision at least consistent with the spatial scale of the computational mesh, especially in the vertical. For example, if the mesh is expected to have 10 vertical elements in the vicinity of the structure, then the details of the structure's wetted surfaces must be described geometrically in sufficient detail to be resolved at 10 points in the vertical.

15.10.2 Model Initialization

Initial conditions for water and sediment are far more important in mobile-bed modeling than in fixed-bed applications. In a fixed-bed environment, initial discharges and water-surface elevations must be assigned, but they quickly wash out of the model as boundary-condition influence takes over. Fixed-bed initial conditions can be quite arbitrary without affecting the simulations results of interest.

As is illustrated in the examples at the end of this chapter, mobile-bed models are usually started up in a fixed-bed mode. Somewhat arbitrary initial hydrodynamic conditions (water-surface elevations and velocities or unit discharges, often for horizontal, nil flow) are specified. Then the model is run with fixed bed for a sufficiently long period for the arbitrary initial condition to wash out or stabilize under fixed boundary conditions. At the end of this stabilization period the model should have nearly attained a viable steady-state hydrodynamic solution. Sudden imposition of the inflow boundary conditions on a zero-flow situation may cause unacceptable "sloshing," including bed uncovering, causing the computation to fail. Such a situation may require a more careful initial condition, or perhaps a progressive phasing in of the boundary inflows, as is the case in purely fixed-bed models.

The initial conditions for sediment must be handled with a great deal of care, because the bed elevations themselves are subject to change through interaction with the initial conditions. Initial sediment conditions fall into three categories: suspended-load concentrations, bed-material size distribution, and subsurface-material size distribution. It should be noted that the following guidelines, driven by the authors' experience with multiple-size-class models, reflect the special challenges of model initialization for nonuniform sediments. Initial-condition specification for a single-size-class model is considerably less challenging.

15.10.2.1 Suspended-Sediment Initial Conditions The initial conditions for suspended sediment comprise

concentration of each size class at each computational point of the two- or three-dimensional grid. These obviously are depth-averaged concentrations in a two-dimensional model, and point concentrations in a three-dimensional model. Because the time scale of movement of suspended sediment is relatively short (as is the time scale of movement of water through the model), a model is generally fairly forgiving of initial suspended-sediment conditions that may not be in equilibrium with the flow, bathymetry, bed-material size distribution, and inflow boundary conditions. The initial suspended-sediment mass advects out of the system fairly quickly, as boundary-condition suspended-sediment inflows progressively influence the model from upstream to downstream.

Of course the suspended sediment does interact with the bed during this washout process, so the initial concentrations must be assigned with reasonable care. For example, if the initial condition specified a grossly exaggerated suspended-sediment load for one or more size classes, that load will tend to be deposited quite quickly and influence the bed elevations in an unrealistic way during the sediment startup period. Similarly, an initial condition of clear water may provoke excessive entrainment from the bed in the sediment startup period as the model seeks to establish a local equilibrium between the water column and the bed material. A reasonable starting procedure is to consider inflow boundary and/or interior suspended-sediment size distributions, vertically and horizontally, and assign them to the model's interior vertical grid lines in a logical fashion. This might involve assigning some sort of average concentration values, based on all available measurements throughout the domain, as initial conditions. An alternative could be to assign average concentrations for subdomains, for example, if there are clear differences in concentration between the main channel and lateral channels. If the boundary inflow concentrations by size class are reasonable to begin with, then the initial suspended-sediment startup period should proceed smoothly, with minimal bed-elevation or bed-composition changes provoked by the suspended-sediment initial condition.

15.10.2.2 Bed-Surface Material Initial Conditions The initial conditions for bed-material composition comprise the size distribution (fractional representation of each size class in the model) at each computational grid point, or each computational cell, on the bed. It has been the authors' experience that this initial-condition assignment is quite delicate and unforgiving of casual treatment. Indeed, if the assigned initial bed-material size distribution does not reflect an approximate equilibrium condition given the initial hydrodynamics, bathymetry, and initial suspended-suspended concentrations, then the model will tend to adjust toward equilibrium (as defined by its own intrinsic sediment relations) quite rapidly, and this can cause excessive erosion or deposition in the first few time steps. For example, if the initial bed material distribution at a grid point contains a high fraction of fine silt, and yet there is no fine silt in suspension, but the initial water velocities and shear stresses are relatively large, the model may call for a large entrainment of fine silt into the water column in the first few time steps. Through the bed-sediment conservation laws, this may result in a large, and unrealistic, erosion of the bed at the particular grid point, essentially distorting the user's assigned initial condition for bed elevations and possibly causing subsequent model failure.

Because the initial bed-sediment size distribution is generally based on, if not taken directly from, actual field measurements, one is tempted to expect that as long as the truth as represented by the field data is assigned to the model, the above scenario of excessive bed adjustment should not occur. However, as is brought out in the examples of Section 15.11, field observations of bed-material size distribution are necessarily quite sparse. The bed-material size distribution assigned to a single computational grid point is implicitly assumed to be representative of the bed material on the entire portion of the bed associated with that grid point. On the other hand, an individual field sample may or may not be representative of an equivalent portion of bed surrounding it. The sample may have been taken from the top of a transient dune as it moved through, or from a briefly exposed lens of fine material, or from a local accumulation of gravel exposed only intermittently as dunes move across it. Whereas in nature the water-sediment response to the local bed-material size distribution remains local, in the model "local" is defined by the plan-view of the computational grid around that point, and therein lies the difficulty in assigning sparse field observations to computational grid points.

Field bed-material samples should be used to make an overall assessment of what appears to be the average bed-material composition in the computational domain, or subdomains, if there are clearly distinct geomorphological regions. Initial model response to average bed-material distributions will suggest the possible need to modify the initial bed-material distribution locally to achieve a nearly equilibrium situation in the initial condition. In this sense, one essentially needs to calibrate, or adjust, the initial bed-material distribution to achieve a benign model startup. This approach obviously presumes that the startup situation is not one of major dynamic change; if this were the case, an extremely detailed set of initial bed-material distributions, i.e., at subgrid scale, would be required.

15.10.2.3 Subsurface Strata Initial Conditions The initial conditions for subsurface bed material comprise specification of the thickness of each subsurface stratum and its sediment size distribution below each bed computational point or cell. This initial condition specification can obviously be quite onerous, and may or may not be important, depending on the problem under study and the nature of the bed material. For example, if it is anticipated that only persistent deposition will occur in the region under study, then

there is no need to specify the subsurface structure, because it will never be susceptible to entrainment through contact with the water column. Similarly, if the anticipated maximum depth of erosion in the region under study is such that the bed material is known to be essentially homogeneous to that depth, a single, infinitely deep subsurface stratum having the same size distribution as the initial bed-surface material may be sufficient. But in a general case in which there may be successive cycles of erosion and deposition, and/or the erosion is expected to progress through multiple strata of differing composition (e.g., historical lenses of deposition), the subsurface structure under each bed computational point or cell must be specified with care. Indeed, if erosion progresses into a layer having a size distribution that is markedly finer than that of the material initially above it, the model may display rapid erosion of this layer, and it is important that this be physically realistic and not the result of a careless assignment of excessively fine material to a subsurface layer. Similarly, a very coarse subsurface layer, physical or otherwise, will have a tendency to arrest further erosion.

15.10.3 Hydrodynamic and Sediment Boundary Conditions

The hydrodynamic boundary conditions for a mobile-bed model are the same as those required for a fixed-bed model, i.e., generally the water-surface elevation at model outflow boundaries, and unit discharges (two-dimensional model) or three velocity components (three-dimensional model) at all model inflow boundaries. Depending on the particular hydrodynamic model framework, additional combinations of levels, local velocities/unit discharges, or relations between them may be imposable.

Suspended-sediment boundary conditions comprise specifications of the suspended-sediment concentrations, by size class, at all model inflow points. For a two-dimensional model, these are depth-averaged concentrations; for a three-dimensional model, these are concentrations at every grid point in the plane of the inflow boundary.

A special consideration here is that in a model having strongly unsteady hydrodynamics, for example, a tidal model with a reversing flow boundary or even a riverine model with possible reversing flow during strong transients, a boundary may be outflow or inflow at different times during the simulation. Whenever inflow occurs at such a boundary, a corresponding suspended-sediment inflow condition must be assigned.

The inflow suspended-sediment concentrations for three-dimensional models, generally simulating a relatively short portion of a hydrograph, are taken from whatever suspended-sediment measurements are available for the discharges under study. For longer-term two-dimensional modeling, the time-varying suspended-sediment inflow concentrations must be generated from presumed suspended-sediment rating curves applied to a time-dependent inflow hydrograph. As increases in computing speed lead to the opportunity to make truly unsteady three-dimensional simulations (e.g., for one or more hydrographs), it will become important to acquire truly unsteady sediment-inflow boundary conditions.

As of this writing, few attempts have been made to measure the time history of suspended-sediment concentrations during an unsteady-flow event. However, current efforts by the U.S. Agricultural Research Service and others are leading to a better understanding of how suspended-sediment concentrations vary during a flood event, and such improved understanding should play an important role in setting unsteady inflow boundary conditions for suspended sediment.

The nature of bed-sediment boundary conditions depends on the model formulation. For example, in the authors' two- and three-dimensional models, the formulations are such that bed-sediment inflow boundary conditions comprise specification of the bed-material size distribution at each bed computational point or cell at an inflow boundary. In other formulations, the bed-material inflow condition may be bed-load flux by size class or other equivalent quantity. Inflow bed-material size distributions generally can only be deduced from existing field measurements of bed-material size, the same as used for initialization of the bed material as described above. Inflow bed-load fluxes are difficult to measure, and are more likely deduced from one or another empirical bed-load predictor known, or calibrated, to be applicable to the site under study.

Subsurface strata require no boundary conditions per se, because their interactions are limited to exchanges with the strata immediately above and below during deposition and erosion.

15.10.4 Hydrodynamic and Mobile-Bed Calibration and Verification

Mobile-bed model calibration and verification are considerably more challenging and elusive than their fixed-bed counterparts. The complex interactions between hydrodynamic and sediment processes, combined with the highly heterogeneous nature of field observations, make it extremely difficult to isolate, or target, the individual processes and associated empirical coefficients subject to adjustment. This is in contrast to fixed-bed modeling, in which the general reliability and accuracy of the Reynolds averaged-flow equations, combined with appropriate turbulence models, leave characterization of the bed roughness as the primary calibration target. Even the bed-roughness target becomes more elusive in a mobile-bed context, because the roughness comprises the bed composition itself, including flow-dependent bed forms, both intimately coupled with the flow hydrodynamics as well as sediment properties.

For sediment processes, three levels of calibration can be identified. One level is the very discretization of sediment into

appropriate size classes, because model response depends on the degree of resolution, i.e., the number of size classes and the representative particle diameter assigned to each. A second level, having no real counterpart in fixed-bed modeling, is the selection of auxiliary empirical relations most suited to the particular area under study. Such relations can include the bed-load predictor, the suspended-sediment entrainment predictor, the fall velocity predictor, and the bed-roughness characterization, as outlined in previous sections. The third level comprises adjustable parameters within the adopted auxiliary relation. For example, one might choose to use the van Rijn formulation for estimation of near-bed equilibrium concentration, and then be faced with the need to choose an appropriate value of the near-bed distance, which is a critical parameter in that formulation. How does one choose discretizations and relations and parameters at these three levels as part of the calibration process, especially in view of the fact that all three levels interact with each other?

There is no universal answer to this question. A particular size-class discretization and set of auxiliary relations and their associated parameters may not be unique; several different sets may produce equally viable mobile-bed response in a given problem. Ultimately one must simply rely on the not-so-tired notion of good engineering judgment.

The discretization of nonuniform sediment into size classes is driven by the need to achieve resolution as high as possible within the constraints of computational time, and judgment as to the role that the finest and coarsest sediment represented in the field may, or may not, play in the problem under study. Collapsing two or more traditional sediment types (e.g., silt and fine silt) into a single size class with a single representative particle diameter may need to be revisited during the calibration process to ensure that the collapsing and choice of representative diameter does not, in itself, influence the overall mobile-bed response being studied—it is in this sense that the size-class discretization is very much a calibration issue, as is the assignment of initial bed-material composition discussed earlier.

The choice of auxiliary relations should be guided first and foremost by an assessment of the likelihood that a given relation is valid for the particular area under study, based on previous studies and/or similarities between the study site and the conditions under which auxiliary relations were developed. For example, the bed-load predictor adopted for a particular model study ought to be one that might be adopted for general use at that site, based on published information and experience at that site and elsewhere. Still, during the calibration process, it may prove necessary to modify standard parameters in that predictor, or indeed adopt an alternative one based on model response in early trial runs.

Even if one accepts that there is no unique, or best, set of auxiliary relations and their parameters for a given discretization, how does one know that a given set is acceptable in the context of calibration? The situation is quite unlike fixed-bed modeling, in which, for example, measured water-surface slope, local or global, and perhaps measured local two- or three-dimensional velocities can be used as specific targets for adjusting bed roughness. It is far more difficult to identify individual response indicators in mobile-bed modeling. Imagine that a model's prediction of suspended concentration of a certain size class is an order of magnitude different from available field measurements at a particular location. Is this because of uncertainty arising from the chosen empirical auxiliary relations such as the fall-velocity predictor, suspended-load entrainment formulation, and bed-roughness predictor and their parameters? Or is it perhaps because of the sparseness and natural variability of available field data, which makes it difficult to assign an appropriate initial bed-material composition and/or choose a representative sediment size-class discretization?

Similarly, imagine that a model is showing what appears to be excessive scour at a certain location. What are the roles of the initial bed-material composition, the bed-load predictor, and the suspended entrainment function parameters in these predictors and functions, or the sediment discretization in causing this excessive scour?

These questions point to the need for sensitivity/uncertainty analyses to determine the range of influence of empirical relations on simulation results. They also point to the need for careful engineering judgment in dealing with sparse and stochastic field data, and/or the need for more comprehensive and detailed field data collection efforts.

Regarding calibration/verification of empirical auxiliary relations, it is generally impossible to associate a particular model response with a particular formulation or parameters within it. The only alternative appears to be one of seeking a self-consistent set of relations and parameters, guided by good judgment for the site under study, such that the overall model response conforms to reasonable expectations based on past experience. The overall response indicators most easily observed are bed-elevation changes, changes in bed-material composition, total suspended load concentrations, overall water-surface slopes, etc. A self-consistent set of relations and parameters, with the associated sediment and grid discretization and initial and boundary conditions, is one for which the model persists in a known flow-sediment quasi-equilibrium for some time into the future (if only a few days) with no major changes to bed elevation, total concentrations, bed-material composition, etc.

Another way of looking at this is to say that a self-consistent model, when run some time into the future, will continue to display the same range of variability of observable features (e.g., bed-material composition) that are characteristic of the site from previous observations. Then, when the model is used to study, e.g., structural modifications or long-term response to changes in the hydrologic and sediment-inflow imposed on the area under study, one can have some confidence that the model response is a valid one because it is a self-consistent (but perhaps not unique) representation of the physical site.

15.10.5 Special Considerations Regarding Acoustic-Doppler Current Profiling Velocity Data

Acoustic-Doppler current profiling (ADCP) techniques have become quite popular. They offer a combination of accuracy, ability to measure local velocities in three coordinate directions, and rapid field deployment and use.

However, the authors and their colleagues have found that use of ADCP measurements to provide boundary-condition and calibration/verification velocity fields for three-dimensional mobile-bed models must be cautious and mindful of the error that can be induced when the measurements are taken from a moving boat. The need for this caution is based on the experience and analyses reported by Morlock et al. (2002) and Muste et al. (2004a; 2004b).

15.10.6 Field Data—What Is the Truth?

In the field of computational hydraulics, both developers and users tacitly accept the notion that measured field data represent some sort of "truth" to which model results should aspire. As legitimate as this viewpoint may be in the abstract, in practice it has to be tempered by careful consideration of the temporal and spatial scales that a model is capable of resolving.

A numerical model cannot resolve hydrodynamic or mobile-bed processes at spatial or temporal scales finer than those of the computational grid. The computational grid resolution is constrained by computer memory and time limitations on one hand, and by numerical stability and convergence constraints on the other.

Because solvers of two-dimensional and three-dimensional mobile-bed models generally have both implicit and explicit features, numerical stability generally requires that the time step be constrained by a Courant-type criterion. In most applications a horizontal grid scale on the order of 10 m implies a maximum time step on the order of 10 s. Although one could, in principle, work with much smaller spatial and temporal scales, this is generally impractical due to computer memory and processor limitations.

Therefore mobile-bed codes do not generally resolve turbulent motions of scales smaller than the order of 10 m or 10 s or bed forms smaller than the order of 10 m, for reasons of grid resolution alone. Even if the grid scales were sufficiently small to resolve such features, it is doubtful that the mathematical formulations or numerical procedures of models available as of this writing could resolve the flow separation and turbulent moment exchange associated with such features.

Comparison of suspended-sediment data with model predictions is subject to similar problems of reconciliation of scales. Figure 15-4 shows a comparison of measured and computed fine-sand profiles across a river at a particular transect. Although the suspended-sediment samples necessarily represent a certain time-averaging (on the order of several seconds) at a well-defined stationary vertical profile, one can still observe the kind of nonmonotonic behavior in the measured data that suggests the existence of large-scale variability (probably associated with large eddies or possibly with dune migration) that cannot be resolved by the numerical model. Therefore one cannot conclude, from this comparison alone, that the model's suspended-sediment profiles are or are not correct in their detailed structure.

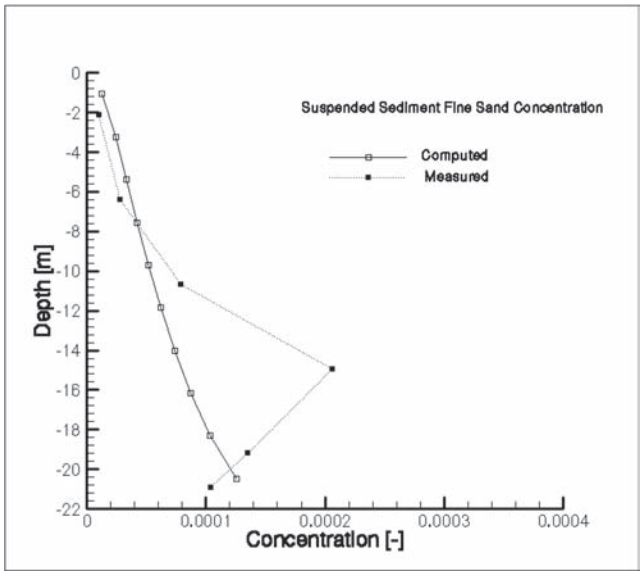

Fig. 15-4. Computed and measured suspended-sediment concentrations (fine sand).

Similar attention was focused on the issue of the appropriate initial bed-material size distribution in the model, as has been discussed earlier in Section 15.10.4. In this study, dozens of grab-samples of bed material were available in the study reach, and additional grab-sample thalweg data was available from a previous study.

Clearly several of the measured size distributions, although undoubtedly representative of "the truth" at the time and location they were taken, were not representative of the general area of the river at the spatial scale resolvable by the model. These samples may have been representative of the portion of a dune from which they were taken, or perhaps of lenses of finer material moving through the system, but were clearly not representative of a quasi-equilibrium bed condition representative of most of the width of the river over several hundred meters of length. This conclusion was driven by the fact that the mobile-bed model generates excessive and unrealistic scour in the first few time steps if the initially imposed bed-material distribution is unrealistic, or not nearly in equilibrium, with the hydraulic characteristics of the river in that vicinity.

Of course the "satisfactory" or "true" initial bed-material size distribution is also dependent on the particular bed-sediment entrainment algorithm in the model. Does this

suggest that the "truth" in field data must also be interpreted in light of the model's sediment-mechanics formulations?

The problem of reconciling the needs of field data collection with the needs of numerical models is not a new one. Even in one-dimensional modeling, the need for measurements of time-varying stages and discharges is still too seldom recognized when field data programs are designed and executed. Now that three-dimensional modeling has entered the realm of engineering practice, study managers and modelers must work together to ensure that data-collection efforts are aimed at collecting and/or processing data resolved at temporal and spatial scales that are meaningful to the model's grid resolution. Judgments as to the validity and accuracy of numerical predictions must be conditioned by a realistic view of the scales and processes that a model can and cannot be expected to resolve, given its mathematical formulation and grid constraints. The "truth" is relative in this context: relative to the model's framework, and to the accuracy of the field-data. With regard to the latter, it is important to keep in mind that just like model results, field data are also subject to errors in collection, analysis, and reporting, and thus must also be interpreted and assessed carefully in the context of their use in an overall modeling effort.

15.11 EXAMPLES

15.11.1 Introduction

The purpose of this section is to present a few examples of multidimensional mobile-bed modeling. These are necessarily based on the authors' own experiences and are intended to illustrate the scope, challenges, and possibilities of such modeling and to give the reader a sense of the kinds of problems to be anticipated. Section 15.11.2 describes application of the three-dimensional mobile bed model CH3D-SED to an analysis of sediment dynamics at the Old River Control Complex on the lower Mississippi River. Section 15.11.3 describes the application of CH3D-SED to the study of river habitat restoration measures on the Leavenworth Bend of the Missouri River. Section 15.11.4 describes application of the two-dimensional mobile-bed model MOBED2 to the prediction of reservoir sedimentation in three flood-control reservoirs in Iowa.

15.11.2 Old River Control Complex, Mississippi River

15.11.2.1 Background The Old River Control Complex is located on the lower Mississippi River about 300 km upstream of New Orleans, in the state of Louisiana and adjacent to the state of Mississippi. Figure 15-5 shows the general layout of the site, which has an interesting and complex history as described by Tuttle (unpublished manuscript, 1998).

Prior to the fifteenth century, the Red River flowed generally parallel to the Mississippi, continuing independently to the Gulf of Mexico. In the fifteenth century a westward meandering loop of the Mississippi broke into the basin of the Red River and captured it, also intersecting a south-flowing distributary of the Red currently known as the Atchafalaya River. Through time, and in response to both artificial cutoff construction and log-raft clearing, the Red came to flow directly into the Atchafalaya and henceforth to the Gulf of Mexico, but with a connecting channel to the Mississippi known as the Old River. Bidirectional flow occurred in the Old River according to hydrological and hydraulic conditions in the adjacent river systems.

After World War II, it became apparent that the increasing natural diversion of the Mississippi flow into the Atchafalaya channel through the Old River would begin to threaten the geomorphic viability of New Orleans as a deep-water port. Therefore, after extensive study and analysis involving Professor Hans Albert Einstein and others, it was agreed to seek a long-term flow distribution such that 30% of the "latitudinal" flow (i.e., the sum of the Red River and Mississippi River flows at the latitude of the Old River complex) would flow to the gulf through the Atchafalaya. This was to ensure the long-term geomorphic stability and navigational viability of both the Mississippi and Atchafalaya.

In 1959 the low sill structure and outflow channel (see Fig. 15-5) were constructed to achieve the 30 to 70% targeted flow split. However, during the Lower Mississippi flood of 1973, this structure was severely threatened and nearly failed due to scour and associated loss of a wing wall. Consequently, in 1986, the auxiliary structure (see Fig. 15-5) was constructed to obviate total reliance on the low sill structure to achieve the targeted flow diversion.

Recognizing the hydropower potential of the average 6-m head difference between the Mississippi and Atchafalaya, in 1977 a group of investors proposed construction of the Sidney A. Murray, Jr. Hydroelectric Station 2 km above the low sill structure (see Fig. 15-5). This 192-MW bulb-turbine facility was constructed in a New Orleans shipyard and towed up the Mississippi to the site, where it was sunk into place and completed in 1990. Since that time it has been operated successfully by the Louisiana Hydroelectric Corporation, in close coordination with the U.S. Army Corps of Engineers, to achieve the 30 to 70% target flow distribution in concert with the auxiliary and low sill structures. The facility passes an average discharge of about 2,800 m^3/s.

Although the turbines were designed to pass a significant sand and silt load, the hydroelectric facility is located on a relatively sediment-poor location of the right descending bank of the Mississippi. Because long-term geomorphic stability of the lower Atchafalaya River requires a continuing supply of sediment from upstream, Louisiana Hydroelectric and the U.S. Army Corps of Engineers have been exploring ways of increasing the diversion of sands and silts from the Mississippi to the Atchafalaya in and around the Old River Control complex. The purpose of the study was to develop an understanding of the short- and long-term sediment dynamics

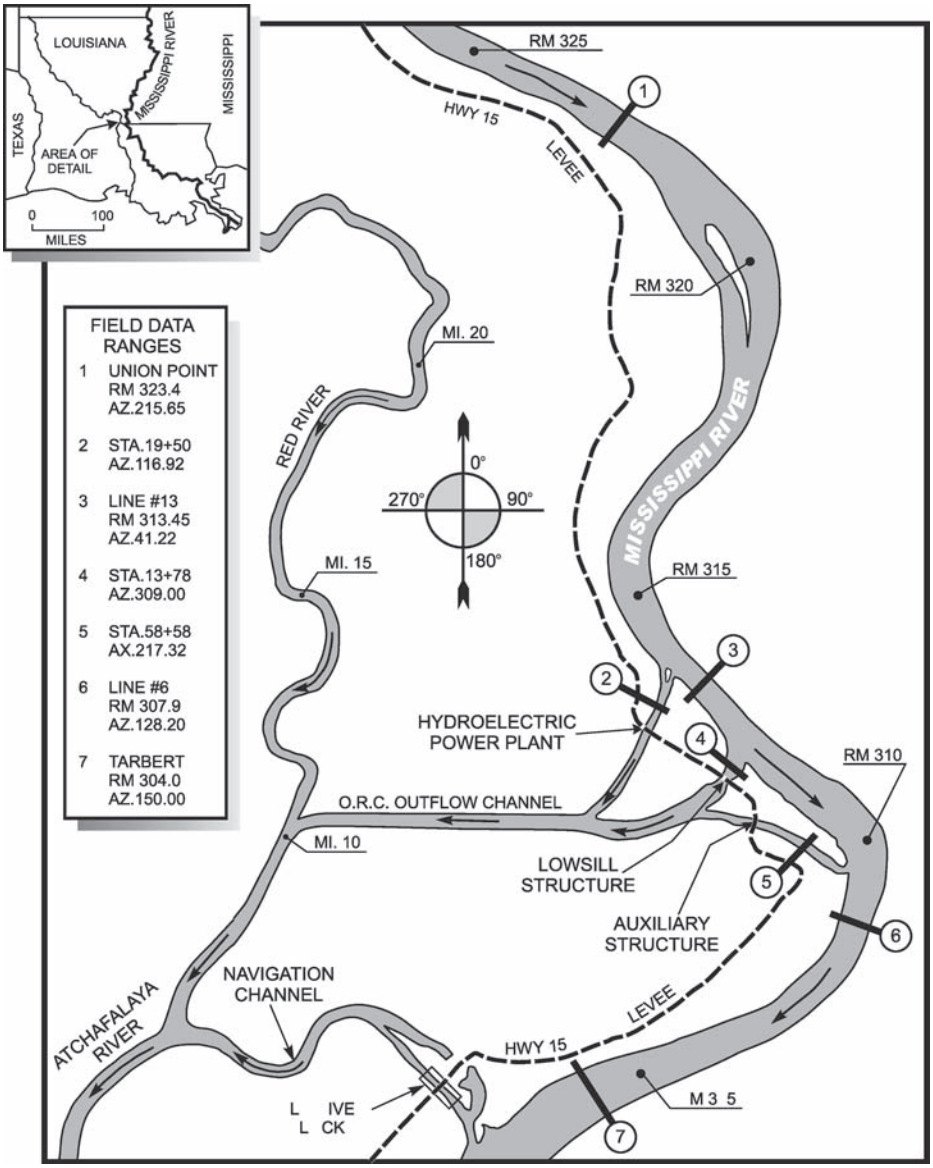

Fig. 15-5. Old River Control Complex, lower Mississippi River.

of the system, both locally and along extended downstream reaches of the Mississippi and Atchafalaya rivers.

Supported by extensive analysis of historical data and dedicated field campaigns to collect new hydraulic and sediment data, the project involved a detailed and comprehensive geomorphic study, the use of one-dimensional mobile-bed modeling for the study of long-term stability of the downstream reaches (see Chapter 14), and three-dimensional mobile modeling for the study of short-term sediment dynamics in the immediate vicinity of the complex. The overall objectives were to quantify the present diversion rate of Mississippi River sediment into the Atchafalaya River and identify possible structural or sediment-management strategies that could increase the diversion of suspended and bed-load sediments through the hydroelectric complex into the Atchafalaya. The overall study is the subject of a comprehensive report (Catalyst-Old River Hydroelectric Limited Partnership d.b.a. Louisiana Hydroelectric Limited Partnership 1999).

15.11.2.2 CH3D Modeling System The CH3D modeling system has been described in some detail by Gessler et al. (1999). The code simulates unsteady free-surface three-dimensional (hydrostatic) hydrodynamics, constituent and sediment transport, and mobile-bed dynamics in natural waterways. In one time step, the code sequentially solves the hydrodynamic, constituent, and mobile-bed equations.

In the hydrodynamic solution, CH3D first solves the depth-averaged Reynolds approximation of the momentum

equations (Eqs. (15-14) and (15-15)) coupled with the depth-averaged mass-conservation equation (Eq. (15-9)) to yield the depth-averaged velocity and water-surface elevation on a two-dimensional grid. This solution is based on finite-difference approximations applied to a boundary-fitted, nonorthogonal curvilinear grid in the horizontal plane. The deviations from the depth-averaged velocity are then computed for each computational cell through solution of the momentum-conservation equations (Eqs. (15-12) and (15-13)), whereas the vertical-velocity component is obtained by solving the mass-conservation equation (Eq. (15-1)), all coupled with a k–ε closure for vertical momentum diffusion on a sigma-stretched vertical grid. These procedures for the hydrodynamic solution are described in more detail by Chapman and Johnson (1996) and Sheng (1983).

The mobile-bed algorithms have been described in detail by Spasojevic and Holly (1993). In the mobile-bed solution within one time step, the computations are based on a two-dimensional solution of the mass conservation equations for the channel bed (Eqs. (15-63) and (15-64)) and the three-dimensional advection-diffusion equation for suspended-sediment transport (Eq. (15-62)), both for any number of distinct sediment size classes. Auxiliary relations used for the system closure are discussed in Section 15.8.4 of this chapter. The sediment transport algorithms autonomously account for the movement of multiple size classes as either bed load or suspended load, with the exchange between these modes of transport and the bed being governed by local hydrodynamic conditions interacting with sediment properties.

15.11.2.3 Field Data Campaign and Model Construction In the ORCC study, an initial CH3D model data was constructed to the prototype dimensions of an existing coal-bed 1:120 scale undistorted outdoor hydraulic model at the Waterways Experiment Station, Vicksburg, Miss. This preliminary study was used to verify the overall behavior of the CH3D model for a range of prototype discharges and support design of the actual ORCC model data set.

During the 1998 hydrologic cycle seven field-data collection campaigns were organized. A morphology survey was conducted during January 1998. Field sediment and flow data were collected on (1) February 27 (reported Mississippi River discharge at Union Point was Q = 1,059,000 cfs; 29,989 m^3/s); (2) March 23 (Q = 1,082,000 cfs; 30,640 m^3/s); (3) April 10 (Q = 1,224,000 cfs; 34,661 m^3/s); (4) April 17 (Q = 1,178,000 cfs; 33,358 m^3/s); (5) May 8 (Q = 1,445,000 cfs; 40,919 m^3/s); (6) June 9 (Q = 739,000 cfs; 20,927 m^3/s); and (7) August 3 (Q = 573,000 cfs; 16,226 m^3/s). The collected data were used in conjunction with data available from other sources, to formulate the initial and boundary conditions for the three-dimensional Old River Control Complex model, to calibrate the model, and to verify the model results.

Detailed calibration and verification of the three-dimensional Old River Control Complex model is presented here, as well as a critical assessment of the model's simulation results for the February 27, 1998, data set. Established calibration procedures and experience gained through simulations based on February 27 data were successfully used to make simulations of flow and sediment diversions for other data sets.

On February 27, 1998, field sediment and flow data were collected at six field-data ranges (Fig. 15-5): Range 1, the Mississippi River at Union Point; Range 2, the hydroelectric power plant (HPP) channel some distance upstream from the hydroelectric power plant; Range 3, the Mississippi River at Line 13; Range 5, the auxiliary structure channel some distance upstream from the auxiliary structure; Range 6, the Mississippi River at Line 6; and Range 7, the Mississippi River at Tarbert. The field data were not measured at Range 4, in the low sill structure channel, because the low sill structure was closed.

To obtain sediment data in a particular range, four verticals were chosen along the range. Twenty-four suspended-sediment samples were taken at the range, six point samples along each of the four chosen verticals. Also, four bed-sediment samples were collected at bed-surface locations corresponding to the same four chosen verticals. Suspended-sediment samples were processed to obtain vertical suspended-sediment concentration profiles by size class for each of the chosen verticals. Bed-sediment samples were processed to obtain bed-sediment size distribution at the bed-surface location of each vertical.

Flow data at a particular data range were obtained using an acoustic Doppler current profiler to measure the distribution of horizontal velocity vector intensities and directions across the range. The total water discharge at the range was obtained by integrating measured velocities across the range. To be consistent with sediment data, the distribution of horizontal velocity vector intensities and directions was reported only along the four chosen verticals, the same ones that were used for collecting suspended-sediment samples. Furthermore, reported vertical profiles of velocity vector intensities and directions were the result of ensemble averaging (Fagerburg 1998). Each velocity vector intensity and direction value, reported for a particular point on a particular vertical, is the average of the value at that particular point and five or eight surrounding points. Ensemble averaging, instead of time averaging, was introduced to eliminate significant randomness in measured velocities caused by ADCP high-frequency sampling (1–3 s per vertical).

All field sediment and flow data collected during the seven field data collection campaigns in 1998, including the February 27 data, can be found in the report of the Catalyst-Old River Hydroelectric Limited Partnership d.b.a. Louisiana wHydroelectric Limited Partnership (1999).

Certain data relevant to the Old River Control Complex model are available on a daily basis from sources other than the 1998 field-data collection effort. The Mississippi River discharges at Union Point and Tarbert, as well as the free-surface elevation at the Tarbert Landing gauge, are reported

daily. At the hydroelectric power plant, the low sill structure, and the auxiliary structure, free-surface elevations are measured and discharges computed on daily basis.

On February 27, 1998, the reported Mississippi River discharges at Union Point and Tarbert were 1,059,000 cfs (29,988 m^3/s) and 870,000 cfs (24,636 m^3/s), respectively. The calculated discharges at the hydroelectric power plant and the auxiliary structure were 162,000 cfs (4,587 m^3/s) and 27,000 cfs (765 m^3/s), respectively. The low sill structure was closed.

The three-dimensional model domain comprises (1) the Mississippi River between Union Point and Tarbert; (2) the channel between the Mississippi River and the hydroelectric power plant (HPP channel); (3) the channel between the Mississippi River and the low sill structure (low sill structure channel); and (4) the channel between the Mississippi River and the auxiliary structure (auxiliary structure channel) (Fig. 15-16).

The computational grid for the February 27 data has 344×49 points that lie in a horizontal plane and 10 points in a vertical direction, i.e., along the depth. However, for a complex domain such as the Old River Control Complex, the CH3D-SED computational grid covers an area larger than the actual model domain. In this case, the number of active computational points inside the model domain is 7,200 in the horizontal plane, with 10 points along the depth.

15.11.2.4 Hydrodynamic Boundary and Initial Conditions Hydrodynamic computations require either free-surface elevations or unit discharges as boundary conditions at all open boundaries. For the February 27 data, the open boundaries of the Old River Control Complex model are (1) the Mississippi River at Union Point as an upstream inflow boundary; (2) the Mississippi River at Tarbert as a downstream outflow boundary; (3) the hydroelectric power plant as an outflow boundary; and (4) the auxiliary structure as an outflow boundary. All other boundaries, including the closed low sill structure, are treated as impermeable boundaries.

It should be noted that available measured-velocity data did not support the imposition of measured unit discharges as a boundary condition at open boundaries, which would have been the ideal situation. For the Mississippi River at Union Point and Tarbert, measured velocities were reported only for four verticals along each of the respective data ranges, whereas there are 20 computational-grid verticals at each range. It was practically impossible to extrapolate data measured at four locations to 20 computational points, and still satisfy the total-discharge requirement, without using unfounded assumptions. Furthermore, in the HPP and auxiliary structure channels, velocities were not even measured at model boundaries, but rather at some distance upstream from the hydroelectric power plant and the auxiliary structure. Thus, when unit discharges were used as a boundary condition for the Mississippi River at Union, the total measured discharge was distributed across the flow so that the ratio between total discharge and the particular unit discharge through a computational-cell face was the same as the ratio between the total cross-section area and the appropriate cell-face unit area. This commonly used approximation amounts to assigning constant depth-averaged velocities across the flow. The measured free-surface elevation was assigned as a downstream boundary condition for the Mississippi River at Tarbert, horizontal across the section.

A measured free-surface elevation seemed to be the logical choice for the outflow boundary condition at the hydroelectric power plant and the auxiliary structure. The alternative, unit outflow discharges, required using the constant depth-averaged velocity approximation to distribute the total discharge across the channel. However, using the free-surface elevation as an outflow boundary condition at the hydroelectric power plant and the auxiliary structure would have made modeling the proper flow diversion at these two locations very difficult. It would have required almost perfect bed morphology and bed-surface friction data, as well as a very advanced flow model, to reproduce the complex flow pattern caused by the flow diversion through the HPP and the auxiliary structure channels. Assignment of unit discharges as boundary conditions at the hydroelectric power plant and the auxiliary structure automatically achieved the desired flow diversion, but the model still needed to be calibrated to reproduce the proper free-surface elevations in respective channels. This task was also difficult, because the free surface in the HPP and the auxiliary channels is dictated by specific rating curves at the hydroelectric power plant and the auxiliary structure. The CH3D hydrodynamic computations do not include a rating-curve boundary condition. Thus, final runs of the model, with calibrated parameters for the HPP channel, were made with unit discharges as the HPP boundary condition, ensuring the exact HPP discharge.

For the auxiliary structure, approximated unit discharges, providing the proper flow distribution, were assigned as a boundary condition. The discharge through the auxiliary structure on February 27 was small as compared to other discharges throughout the model. Thus, velocities and free-surface elevation slope at the auxiliary channel were small, leading to a relatively simple calibration of free-surface computations.

Zero-flow initial conditions (i.e., horizontal free-surface elevation and zero-velocity field) were used for the hydrodynamic computations. The chosen combination of initial and boundary conditions (realistic discharges and/or free-surface elevations imposed on initially still water) is known to produce a disturbance (wave) that propagates back and forth throughout the flow domain. A stabilization period is required to allow the disturbance to eventually die out. Avoidance of transient dry-bed conditions and high Courant numbers associated with the arbitrary initial condition required careful treatment, and is not discussed further here. At the end of the flow-stabilization period, the flow approached a steady-state condition.

15.11.2.5 Hydrodynamic Model Calibration and Verification For the purpose of model calibrationand verification, the results of the steady-state flow solution for the February 27 discharge were compared to available field data.

A flow-stabilization period of 10 h (2,400 15-s computational time steps) proved to be sufficient for the dissipation of the initially severe wave propagation in the domain. At the end of the flow-stabilization period, a steady-state flow solution was achieved.

The first series of calibration and verification runs was made with measured free-surface elevation as a boundary condition for the Mississippi River at Tarbert, and unit discharges (obtained by using the constant depth-averaged velocity assumption to distribute known total discharges across appropriate boundaries) as a boundary condition for the hydroelectric power plant, the auxiliary structure, and the Mississippi River at Union Point. The low sill structure was closed on February 27, 1998.

The goal of these runs was to achieve generally good agreement between the computed and measured data throughout the domain by globally calibrating the friction coefficient. The agreement between computed and known free-surface elevations was checked throughout the model domain (the Mississippi River at Union Point, the hydroelectric power plant, the low sill structure, and the auxiliary structure). Also, the agreement between computed and measured horizontal velocity vector intensities and directions was checked for all verticals at all data ranges.

The CH3D hydrodynamic-computations program module has two major physical parameters that can be determined through the calibration process: (1) the bed-surface friction coefficient and (2) the horizontal eddy-viscosity coefficient, used in conjunction with the boussinesq approximation for horizontal turbulent-diffusion terms. For both coefficients only an expected range of values can be estimated, because the exact values are unknown a priori.

Initially, a number of runs with different values for the eddy-viscosity coefficient were made. Changing the horizontal eddy-viscosity coefficient within the expected range of values, from 10 to 10,000 cm^2/s, did not significantly affect the computed hydrodynamic results. Thus, all subsequent hydrodynamic computations were made with an eddy-viscosity coefficient of 1,000 cm^2/s. Considerably more effort was devoted to the spatial variability of the absolute roughness and consequent friction and manning coefficients in the model. This is described in detail in Catalyst-Old River Hydroelectric Limited Partnership d.b.a. Louisiana Hydroelectric Limited Partnership (1999).

Through the calibration process, it became apparent that the present CH3D hydrodynamics model could not fully reproduce the complex flow pattern in the HPP channel, especially in the channel's upstream portion. In general, the existing CH3D hydrodynamic model cannot fully reproduce strong secondary currents, due to the simplified horizontal turbulence model, but even more to the vertical hydrostatic pressure assumption, which implies parallel streamlines in a vertical direction. Thus, even with carefully calibrated friction and a corrected cross-section area, the model could not reproduce the exact flow diversion through the HPP channel when the measured free-surface elevation was used as the HPP boundary. However, the calibrated friction and the corrected morphology could still be used to improve HPP free-surface computations in the case when unit discharges were used as a HPP boundary condition. HPP unit discharges were obtained by using the constant depth-averaged velocity assumption to distribute known total discharge across the HPP boundary. The described unit-discharge boundary condition amounts to assigning known total discharges at the hydroelectric power plant, thus forcing the correct HPP flow diversion. Using the previously calibrated friction coefficient and adjusted cross-section area in the HPP channel, resulted in a computed HPP surface elevation that was only 9 cm lower than the measured one.

Table 15-3 shows the final comparison between computed and known free-surface elevations throughout the model domain. This should be indicative of reasonable expectations for the water-surface elevation calibration in a three-dimensional hydrodynamic model of this type. As previously stated, after each calibration run the agreement between computed and measured horizontal velocity-vector

Table 15-3 Computed and Measured (or estimated) Free-Surface Elevations

	Measured (or estimated) free-surface elevations	Computed free-surface elevations
Mississippi River at Union Point	15.58 m asl (51.1 ft) (estimated)	15.60 m asl (51.18 ft)
Hydroelectric power plant	14.82 m asl (48.6 ft)	14.73 m asl (48.33 ft)
Low-sill structure	14.91 m asl (48.9 ft)	14.95 m asl (49.05 ft)
Auxiliary structure	14.69 m asl (48.2 ft)	14.66 m asl (48.10 ft)
Mississippi River at Tarbert	14.38 m asl (47.17 ft)	14.38 m asl (47.17 ft) assigned boundary condition

intensities and directions was checked for all data verticals in all data ranges. Fig. 15-6 shows a sample of computed (at the end of the calibration process) and measured horizontal velocity-vector intensities and directions for the Mississippi River at Line 13.

The computation of velocities at Line 13 (Fig. 15-6) required additional calibration of the local Mississippi River model area immediately downstream from the HPP channel. Specifically, the Mississippi River navigation charts show the presence of a clay shelf next to the Mississippi River's right bank immediately downstream from the HPP channel. In that location, the Mississippi River's main flow leaves the right bank and crosses toward the left bank. This is reflected in velocities measured at line 13. Evidently, the present CH3D hydrodynamic model cannot properly reproduce the flow over and around the clay shelf, due to an oversimplified horizontal turbulence model. Thus, an engineering approximation was used. At the clay shelf area, the wall-shear stress was significantly increased to compensate for the poorly modeled flow around the shelf and the associated drag. An absolute roughness of 3 cm, corresponding to a friction coefficient C_d of 0.02, i.e., a Manning coefficient n of 0.066, for $H = 10$ m, proved to be sufficient to achieve satisfactory agreement between computed and measured velocities at line 13 (Fig. 15-6).

Fagerburg (1998) reported the existence of a strong reverse flow area along the right bank of the auxiliary structure channel. Fig. 15-7 shows the computed mid-depth velocity vector intensities and streamlines at the auxiliary structure channel, featuring the predicted reverse flow. However, although it is known that the turbulence model based on constant eddy viscosity can predict the strong reverse flow, it cannot correctly predict the size of the reverse flow area. This was confirmed when computed and measured horizontal velocity-vector intensities and directions in the auxiliary structure channel were compared. Range 4 (Fig. 15-6) in the auxiliary structure channel is located slightly upstream from the predicted reverse flow area shown in Fig. 15-7. However, measured horizontal velocity-vector directions show that, whereas velocities at verticals 2, 3, and 4 are generally oriented toward the auxiliary structure, velocities at vertical 1 (next to the right bank) are still generally oriented away from the structure. Thus, the model underestimates the size of the reverse-flow area.

At locations other than the Mississippi River at line 13 and the auxiliary structure channel, similar calibration procedures

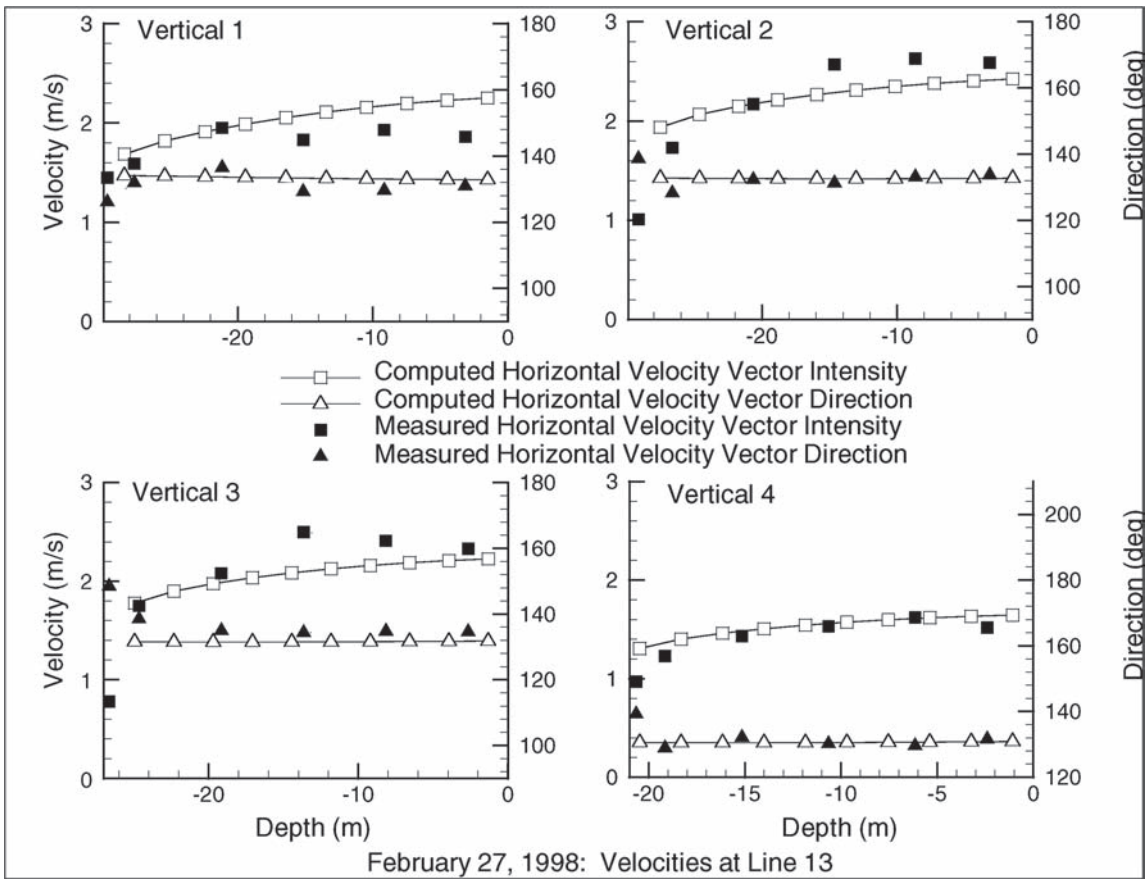

Fig. 15-6. A sample of computed and measured velocities at line 13.

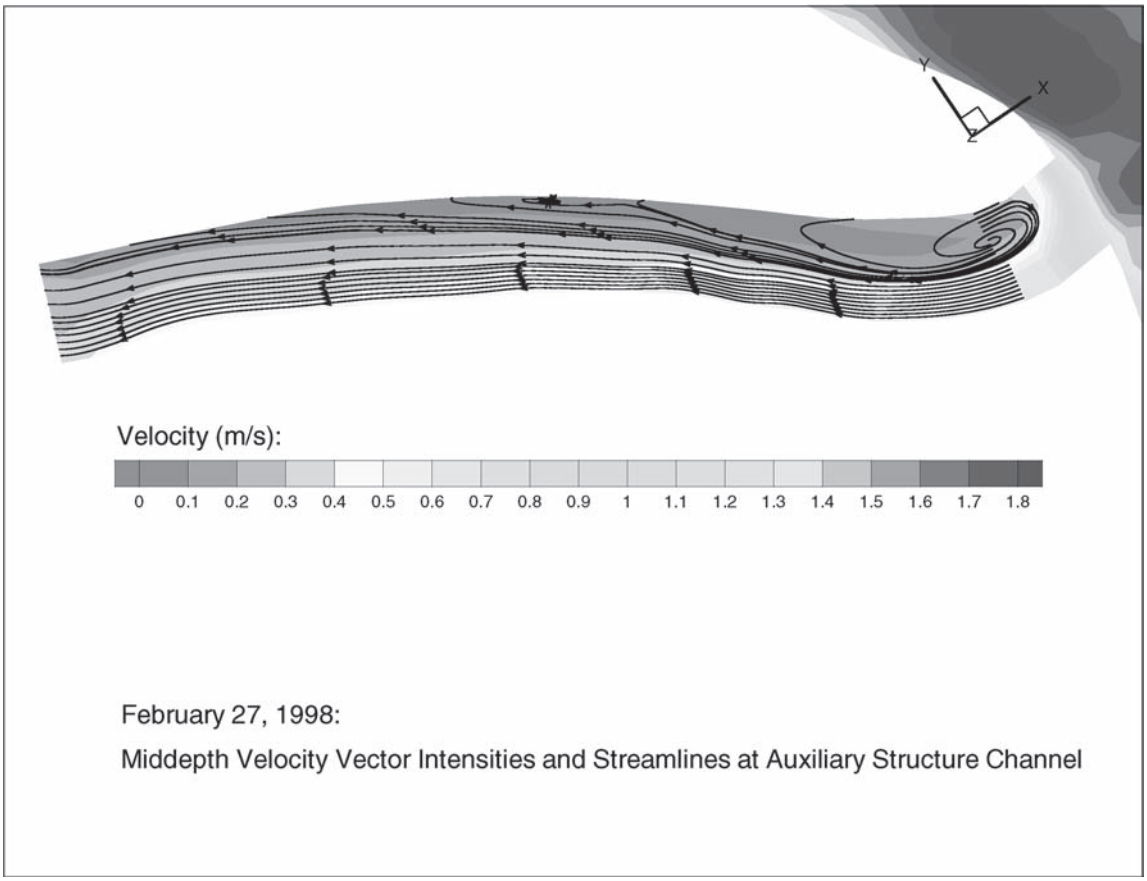

Fig. 15-7. Middepth velocity vector intensities and streamlines in the auxiliary structure channel.

produced generally good agreement between computed and measured horizontal velocity-vector intensities and directions.

It should be noted that the hydrodynamic-computations results were checked again after the sediment-model calibration and the sediment simulation runs. Results of the hydrodynamic computations at the end of the 10-h flow-stabilization period and at the end of the total flow and sediment simulation period of 34 h were virtually identical. The difference in free-surface elevations was 1 cm at Union Point and smaller everywhere else. The difference in velocity magnitudes at field-data verticals was less than 0.5%, and the difference in velocity angles at field-data verticals was around 0.1%.

15.11.2.6 Model Sediment Size Classes Suspended-sediment samples, collected on February 27, 1998, were processed to obtain suspended-sediment concentrations by size class. Grain-size analysis for suspended sediment showed the five size classes. These suspended-sediment samples generally contained a significant amount of silt and clay and fine sand (suspended-sediment size classes 1 and 2), some amount of very fine and medium sand (size classes 3 and 4), and very little coarse sand (size class 5).

Bed-sediment samples, collected on February 27, were also processed to obtain bed-sediment size distribution at the bed-surface. Grain-size analysis for bed sediment featured the 18 size classes. These bed-sediment samples generally contained a significant amount of sediment with diameter smaller than 1 mm (bed-sediment size classes 1 to 9), and only a small percentage of sediment with diameter larger than 1 mm.

In addition, it is known that the HPP channel bed is covered with very coarse material (essentially cobbles), and that revetments along the Mississippi River near the Old River Control Complex comprise very coarse material.

Based on the above observations, the six size classes in Table 15-4 were chosen to represent the totality of natural sediment mixtures relevant to the Old River Control Complex model.

Size class 6 (referred to as gravel) was used to model the coarse material found in small amounts at the bed surface, and also the coarse material at the HPP channel bed and the revetment material. The characteristic sizes for the silt and clay and the gravel were not known in advance, and were determined during the model calibration. Characteristic sizes for sand size classes were obtained as geometric means of the diameter-range limits.

15.11.2.7 Sediment Boundary Conditions Sediment computations in CH3D-SED recognize three boundary types: sediment-inflow, sediment-outflow, and impermeable

Table 15-4 Representative Size Classes for the Old River Control Complex Model

Model size class	Diameter range (mm)	Characteristic diameter (mm)(geometric mean of diameter-range limits)	Corresponds to suspended-sediment size class	Corresponds to bed-sediment size class
1(silt and clay)	$D < 0.062$		1	1
2(very fine sand)	$0.062 < D < 0.125$	0.088	2	2–4
3(fine sand)	$0.125 < D < 0.250$	0.177	3	5–6
4(medium sand)	$0.250 < D < 0.500$	0.326	4	7–8
5(coarse sand)	$0.500 < D < 1.00$	0.707	5	9
6(gravel)	$D > 1.00$			10–18

boundaries. Boundary conditions are required only along sediment-inflow boundaries.

Boundary conditions for suspended-sediment computations are known vertical suspended-sediment concentration profiles for all size classes, assigned at each vertical along all sediment-inflow boundaries. For bed load, the formulations of CH3D-SED require assignment of a size-fraction distribution (featuring size fractions for all size classes) to each bed point along all sediment inflow boundaries. The assigned size-fraction distribution at each particular bed point must satisfy the basic requirement that the sum of all fractions must be equal to unity. This requirement, in conjunction with other sediment boundary conditions, determines the proper total number of sediment boundary conditions, because the bed-surface elevation computations do not require a boundary condition in the formulation of CH3D-SED. Boundary conditions for both suspended- and bed-sediment computations can be either constant or time-dependent.

Sediment computations also require declaring a potential reverse-flow boundary (a boundary where the flow could potentially change direction during the simulation) as a sediment-inflow boundary, and assigning the appropriate boundary conditions along it. Assigned boundary conditions are used only when the potential reverse-flow boundary becomes an actual inflow boundary and are ignored otherwise.

The only real potential reverse-flow boundary is a tidal boundary. However, any flow boundary with an imposed free-surface elevation as a boundary condition can theoretically become a reverse-flow boundary, depending on the variations in the imposed water level. When CH3D-SED code is used to model river flow, transitory waves at the beginning of the flow-stabilization period may actually cause reverse flow for a short period of time at such boundaries.

For the Mississippi River at Union Point, initial suspended-sediment data, obtained as described later, were also used as the suspended-sediment inflow boundary condition. The Mississippi River at Union Point is the only real sediment inflow boundary. The Mississippi River at Tarbert and the hydroelectric power plant with free-surface elevation as a hydrodynamic boundary condition were identified as potential reverse-flow boundaries, and therefore declared as sediment-inflow boundaries. However, for the two potential reverse-flow boundaries, zero-concentration profiles were assigned as suspended-sediment boundary conditions, so that if momentary reverse flow occurred during the stabilization period, no suspended sediment would be advected into the domain through those normally outflow boundaries. The described suspended-sediment boundary conditions were kept constant for the duration of the simulation.

15.11.2.8 Suspended-Sediment Initial Conditions As an initial condition for suspended-sediment computations, vertical concentration profiles for all size classes must be defined for all verticals throughout the model domain, including outflow boundaries. Sediment data collected on February 27, 1998, were used to extract vertical suspended-sediment concentration profiles for all representative model size classes at all data-collection ranges and appropriate verticals.

Fig. 15-8(a) through 15-8(f) show a sample of measured suspended-sediment concentrations along four data verticals at Line 13. More specifically, Figs. 15-8(a) through 15-8(e) contain measured suspended silt and clay, very fine sand, fine sand, medium sand, and coarse sand concentrations, respectively. Fig. 15-8(f) contains measured total suspended-sediment concentrations.

Simultaneous inspection of measured suspended silt and clay concentrations for all data verticals in all data ranges shows a relatively modest variation in measured values. Similarly, measured vertical concentration profiles for suspended very fine sand do not show significant variation between different vertical locations. The same observations apply to measured vertical concentration profiles for suspended medium sand, as well as measured vertical concentration profiles for suspended coarse sand. Measured vertical concentration profiles for suspended fine sand are the only profiles showing relatively significant changes from one location to another.

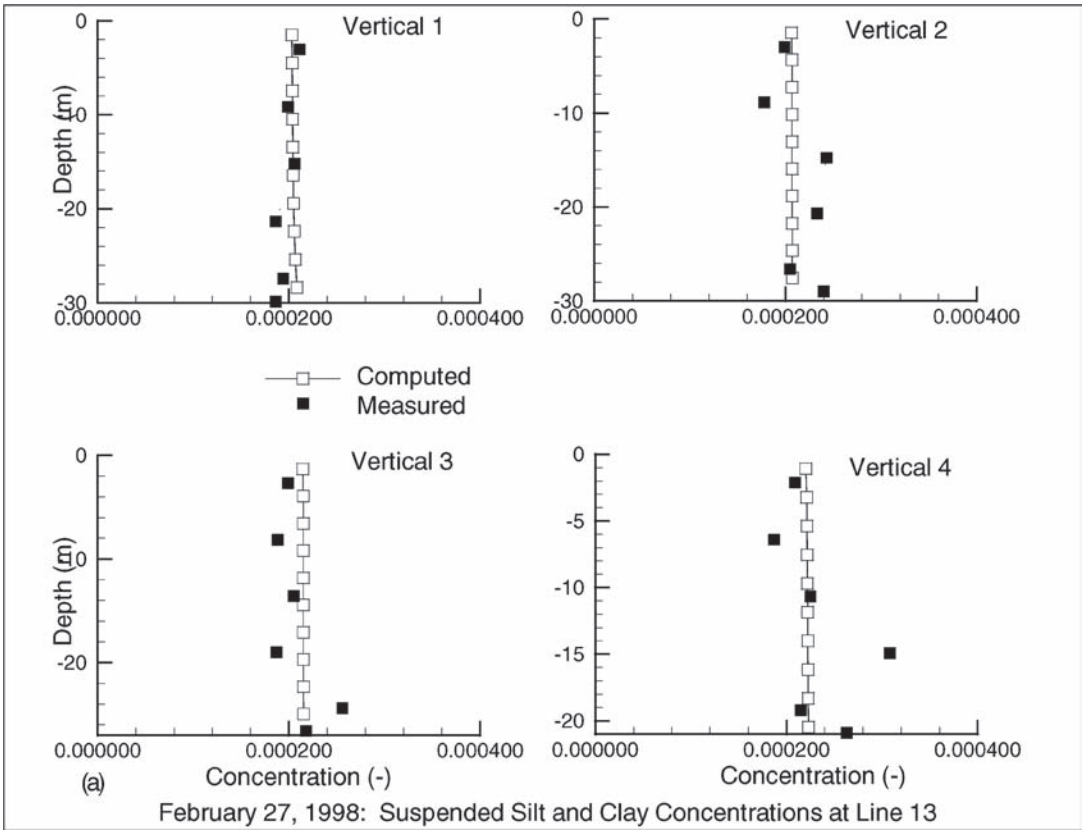

Fig. 15-8(a). Computed and measured suspended silt and clay.

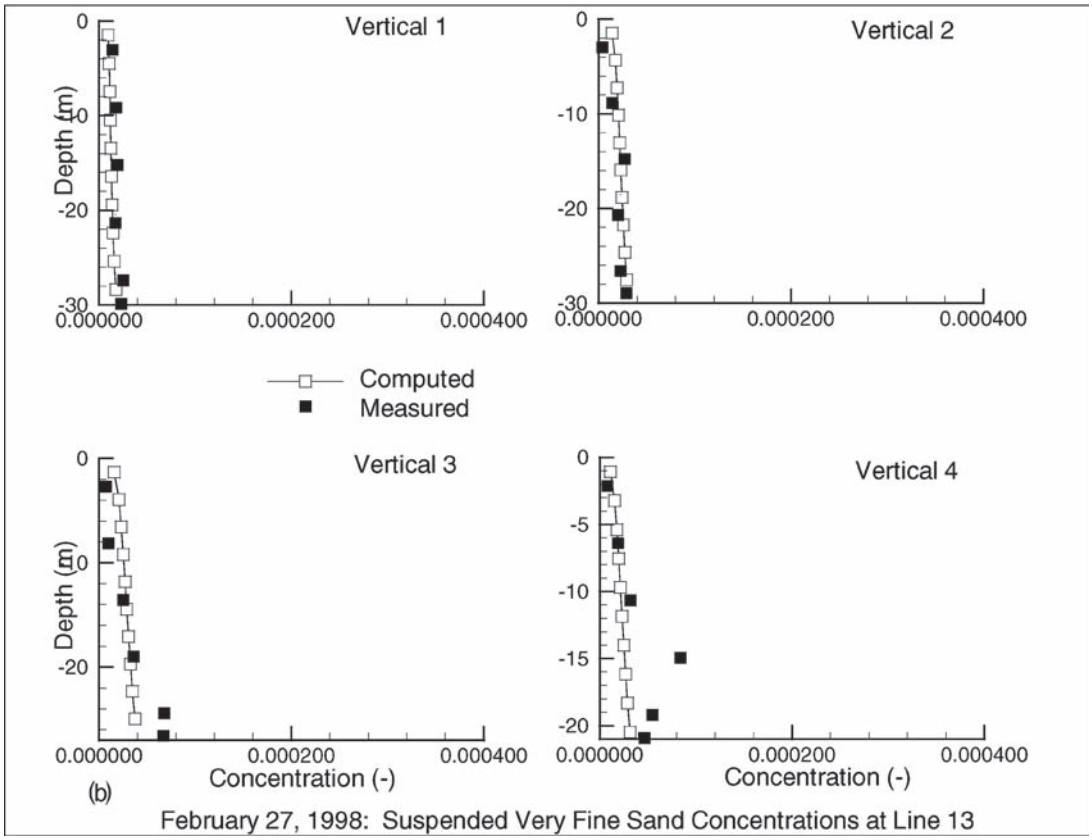

Fig. 15-8(b). Computed and measured suspended very fine sand.

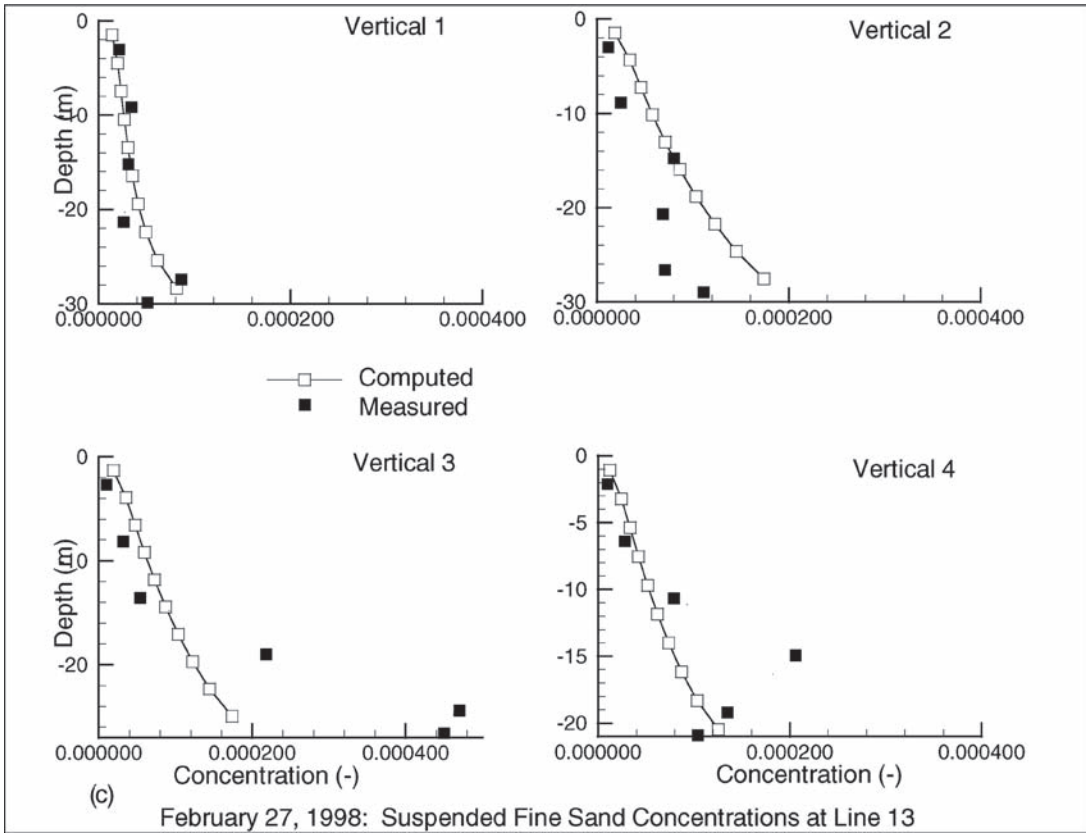

Fig. 15-8(c). Computed and measured suspended fine sand.

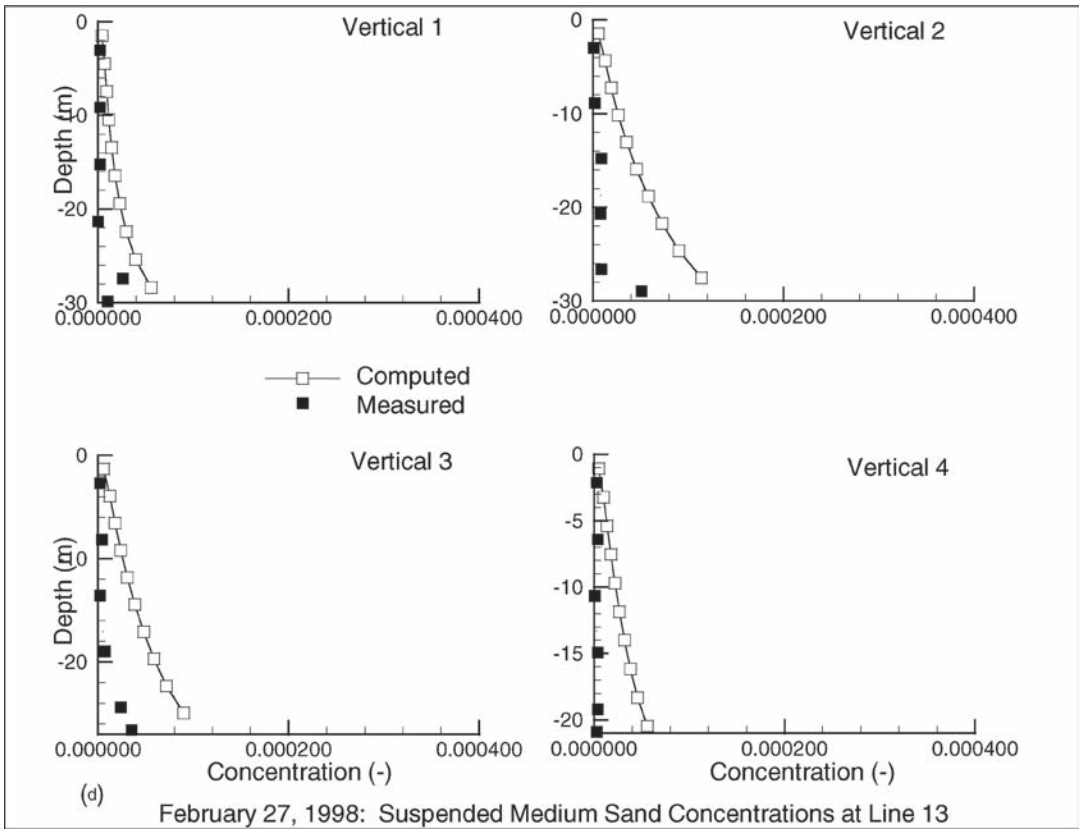

Fig. 15-8(d). Computed and measured suspended medium sand.

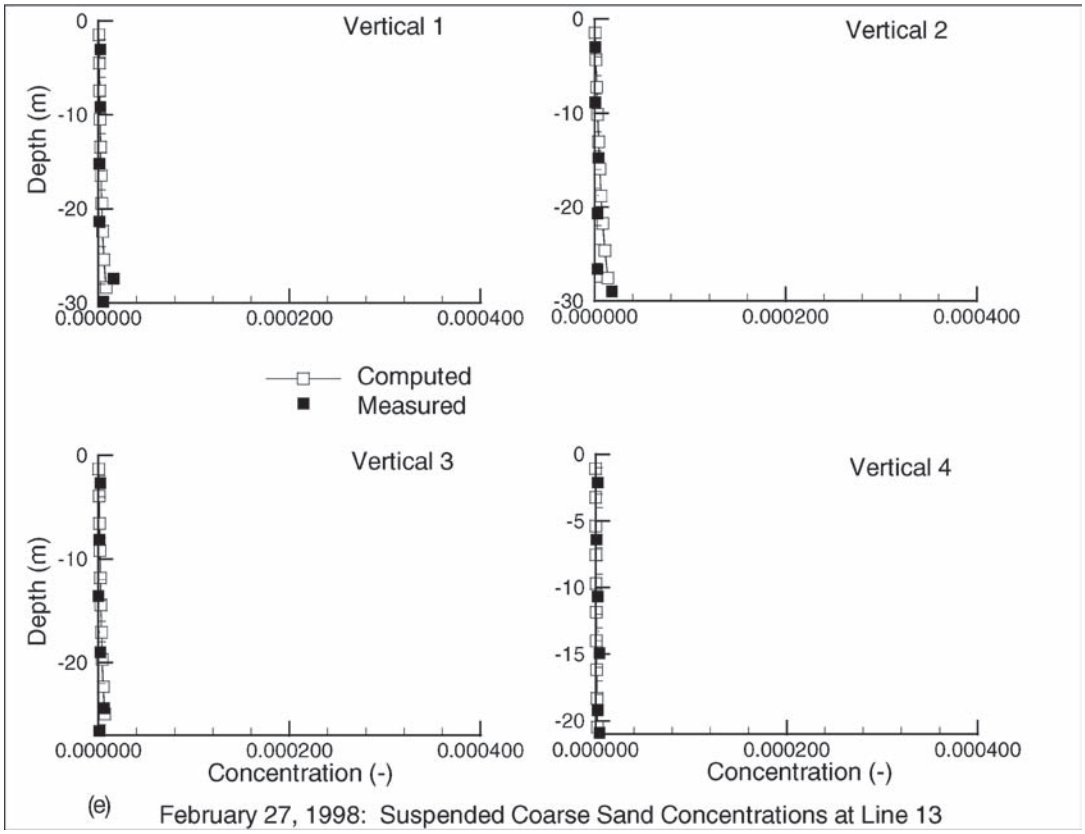

Fig. 15-8(e). Computed and measured suspended coarse sand.

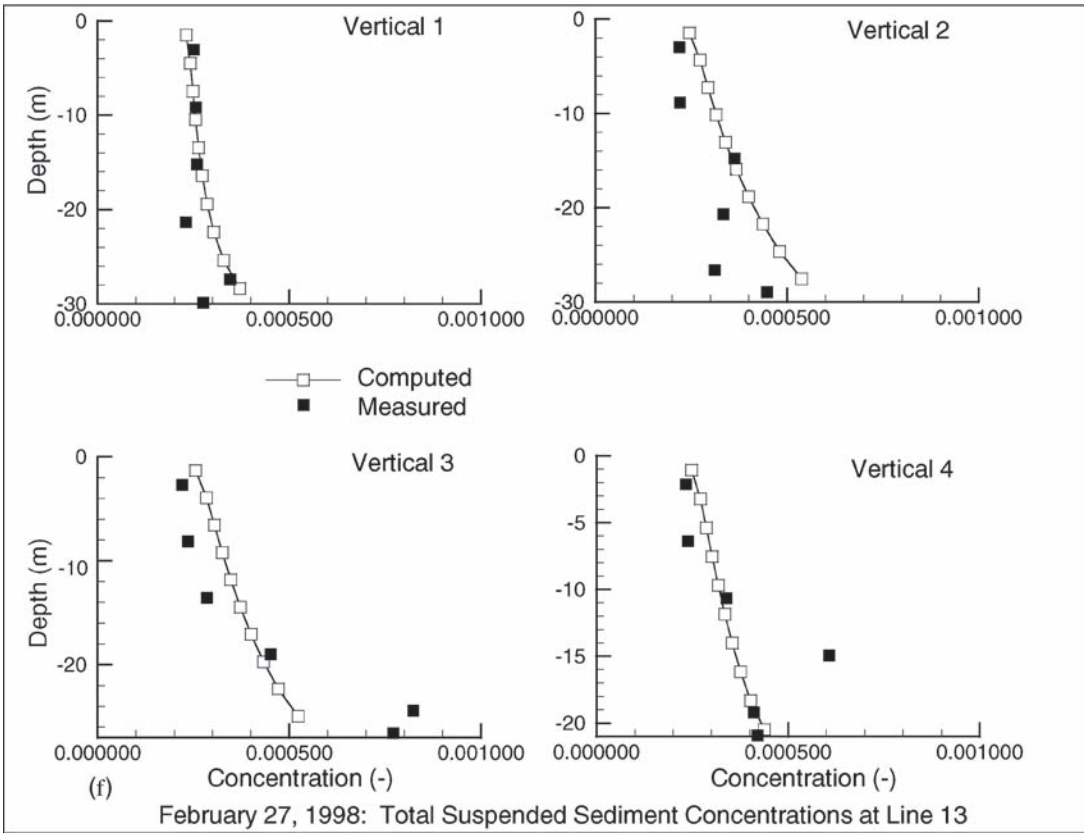

Fig. 15-8(f). Computed and measured suspended total concentrations at line 13.

The preceding observations supported the use of simple extrapolation to construct the initial condition for suspended-sediment computations. First, six suspended-sediment concentrations measured along a particular data vertical were used to construct a set of measured concentration profiles, one for each size class, corresponding to the appropriate computational grid vertical with ten computational points. Each constructed set of vertical concentration profiles was then assigned not only to the corresponding computational-grid vertical, but also to neighboring left and right grid verticals across the flow and grid verticals upstream and downstream from the corresponding grid vertical, until all computational verticals were assigned initial suspended-sediment data. The initial suspended-sediment distribution thus determined at the upstream model boundary, Union Point, was also assigned as a constant suspended-sediment boundary condition.

15.11.2.9 Bed-Sediment Initial Conditions As an initial condition for bed-sediment computations in CH3D-SED, initial size-fraction distributions and bed-surface elevations have to be defined for all bed-surface points throughout the domain, including outflow boundaries. In addition, bed-sediment computations in CH3D-SED require definition of initial bed-material characteristics below each bed-surface point in the model domain: (1) the initial active-layer (bed-surface layer) depth at a particular bed point; (2) the initial number of bed-sediment strata below a particular bed-surface point; and (3) the initial depth and size-fraction distribution for each stratum below a particular bed-surface point.

Flow-stabilization hydrodynamic computations, assuming a nonmovable bed, can successfully start up using exact but unrealistic zero-flow initial conditions (e.g., horizontal free-surface elevation and zero-velocity field). Fixed-bed hydrodynamic computations with simple zero-flow initial conditions and proper boundary conditions kept constant over a period of time yield an observed steady-state flow solution at the end of the flow-stabilization period.

Sediment computations, by contrast, initiated from the steady-flow hydrodynamic condition at the end of the flow-stabilization period, require initial conditions to be as close to reality as possible. With boundary conditions held constant over time, flow and sediment will eventually reach a balance, or state of equilibrium. But if the initial sediment conditions are unrealistic, then so will be the achieved solution. For example, if sediment computations are initiated in a flow with relatively high velocities (as observed on February 27, 1998), and if the assigned initial sediment condition assumes an unrealistically fine bed sediment for this flow rate, flow and sediment balance will still be achieved, but only after unrealistically excessive bed erosion (just as if one introduced a sudden large discharge into a channel with very fine material on the bed—the fine material would be removed very quickly). Thus determination of the appropriate initial bed-sediment size distribution comprises part of the model calibration process, as described below.

Sediment data collected on February 27, 1998, were initially used to extract size-fraction distributions at bed-surface points corresponding to locations of data-collection verticals at all data-collection ranges.

Bed-material samples were not collected in the HPP channel, where the bed is predominantly covered with large cobbles. Thus, the initial size-fraction distribution for the HPP channel was assumed to comprise 100% of the model size class 6 (gravel), and 0% of all other size classes.

Table 15-5 shows measured size-fraction distributions at bed-surface points corresponding to four data verticals in the auxiliary structure channel. Bed material in the auxiliary structure channel does not contain sediment coarser than fine sand. The reason is probably a combination of generally small velocities in the auxiliary structure channel (due to the relatively small average discharge through the auxiliary structure) and the reverse flow in the upstream portion of the auxiliary structure channel. Measured size-fraction distributions (Table 15-6) were extrapolated and assigned as an initial condition throughout the auxiliary structure channel area.

Table 15-6 shows measured size-fraction distributions at bed-surface points corresponding to all data verticals at four data ranges along the Mississippi River. Silt and clay were virtually nonexistent on the bed throughout the domain, except for the bed-surface point corresponding to Vertical 1 at Line 13, where silt and clay make up one-half of the bed-surface sediment mixture. Bed-material samples generally contain less than 5% of very fine sand, but again there are a few exceptions where very fine sand makes up one-third of the bed-surface sediment mixture (bed-material samples corresponding to Vertical 1 at Line 13 and Vertical 4 at Line 6). Fine sand and medium sand were found in virtually all bed-sediment samples, but their percentage in the bed-surface sediment mixture varies from 0% to 89% for the fine sand, and from 0% to 77% for medium sand. Coarse sand was not found in six bed-material samples, but for the remaining ten samples its percentage in the bed-surface sediment mixture varies from 0 to 43%. Gravel was found only in the bed-material sample corresponding to Vertical 1 at Union Point. Vertical 1 at Union Point is the vertical closest to the right bank, and it is also close to the island next to the upstream boundary.

Based on bed-material samples collected on February 27, 1998, it could be generally concluded that the bed-material composition varies significantly within the studied portion of the Mississippi River. Experience showed that the assumption that a particular measured size fraction distribution is representative of a large surrounding area (as was done successfully with measured suspended-sediment concentrations) lead to unrealistic initial conditions for bed-sediment computations. For example, the assignment of the measured size-fraction distribution corresponding to Vertical 1 at Line 13 (with a large silt and clay fraction) to a large model domain lead to excessive erosion in the first few hours of the mobile-bed simulation.

This conclusion is supported by consideration of the Nordin and Queen (1989) study, which presents particle size distributions for several hundred bed-sediment samples collected along the Mississippi River thalweg

Table 15-5 Measured Size-Fraction Distributions at the Auxiliary Structure Channel

		Size fractions					
Data range	Data verticals	Silt and clay	Very fine sand	Fine sand	Medium sand	Coarse sand	Gravel
Auxiliary structure channel	1	0.31	0.45	0.24	0.00	0.00	0.00
	2	0.34	0.41	0.25	0.00	0.00	0.00
	3	0.01	0.23	0.74	0.02	0.00	0.00
	4	0.42	0.31	0.27	0.00	0.00	0.00

Table 15-6 Measured Size-Fraction Distributions along the Mississippi River

		Size fractions					
Data ranges	Data verticals	Silt and clay	Very fine sand	Fine sand	Medium sand	Coarse sand	Gravel
Union Point	1	0.00	0.00	0.00	0.00	0.30	0.70
	2	0.00	0.00	0.34	0.55	0.11	0.00
	3	0.00	0.01	0.57	0.39	0.03	0.00
	4	0.00	0.01	0.78	0.21	0.00	0.00
Line 13	1	0.51	0.32	0.17	0.00	0.00	0.00
	2	0.00	0.00	0.15	0.64	0.21	0.00
	3	0.00	0.02	0.61	0.33	0.04	0.00
	4	0.00	0.01	0.73	0.26	0.00	0.00
Line 6	1	0.00	0.01	0.24	0.60	0.15	0.00
	2	0.00	0.01	0.44	0.41	0.14	0.00
	3	0.00	0.02	0.37	0.54	0.07	0.00
	4	0.04	0.30	0.65	0.01	0.00	0.00
Tarbert	1	0.00	0.04	0.89	0.07	0.00	0.00
	2	0.00	0.01	0.76	0.23	0.00	0.00
	3	0.00	0.00	0.19	0.77	0.04	0.00
	4	0.00	0.00	0.01	0.56	0.43	0.0

Table 15-7 Default Size-Fraction Distribution for the Mississippi River

Size fractions					
Silt and clay	Very fine sand	Fine sand	Medium sand	Coarse sand	Gravel
0.00	0.01	0.45	0.45	0.08	0.01

between Head of Passes and Cairo, Illinois. It includes 15 bed-material samples within the Old River Control Complex model domain. Relevant particle size distributions show similar variations in bed-material composition to those of the February 27, 1998, data. Samples containing a significant amount of silt and clay were also found, but seem to have been local phenomena, not representative of larger areas.

Thus, for the Old River Control Complex model, an average size-fraction distribution (Table 15-7), obtained by combining February 27, 1998, data and relevant Nordin and Queen (1989) data, was chosen to be representative of the default size-class distribution for the Mississippi River.

Initial size-fraction distributions for the Mississippi River were then obtained by assigning the default size-fraction distribution to all Mississippi River bed points, except for the local areas at and around the data-vertical locations, where measured (February 27, 1998) size-fraction distributions were assigned.

The initial thickness of the active (bed-surface) layer was assumed to be 5 cm throughout the model domain. Because no other information was available, a single very

thick stratum below the bed surface was initially assumed. The Mississippi River's default size-fraction distribution was initially assigned to all subsurface sediment below the Mississippi River's bed surface. The initial subsurface size-fraction distribution for the HPP and the auxiliary structure channels was assumed to be the same as the appropriate bed-surface size-class distribution.

Furthermore, measured size-fraction distributions at four union point verticals were extrapolated to neighboring points left and right across the flow and used as the bed-sediment boundary condition for the Mississippi River at Union Point. For the two potential reverse-flow boundaries (the Mississippi River at Tarbert and the hydroelectric power plant with free-surface elevation as the hydrodynamic boundary condition) the boundary size-fraction distribution was assumed to be 100% of the model size class 6 (gravel) and 0% of all other size classes. The described bed-sediment boundary conditions were held constant for the duration of the simulation.

15.11.2.10 Physical Calibration Parameters Calibration of the mobile-bed model comprised not only adjustment of the boundary and (especially) initial conditions, but also the adjustment of certain physical parameters associated with various terms in the auxiliary sediment equations used in CH3D-SED. For the sediment size classes that showed a significant presence in both suspension and at the bed surface (such as sand size classes), the bed-sediment erosion source and the near-bed concentration contain physical parameters that can be calibrated.

The sediment model uses an empirical relation to compute the concentration of near-bed sediment particles, detached from the bed and available either to be entrained into suspension, or to be moved near the bed (sliding, rolling, or saltating) as bed load. This near-bed concentration is evaluated at a certain distance a above the bed. The bed-sediment erosion source describes the entrainment of near-bed sediment particles into suspension. It is modeled as an upward mass-diffusion flux featuring a vertical-concentration gradient. The vertical-concentration gradient is computed using the difference between near-bed concentration, evaluated at distance a above the bed, and the suspended-sediment concentration, evaluated at distance $a+\Delta a$ above the bed. The suspended-sediment concentration at distance $a+\Delta a$ above the bed is obtained by extrapolating suspended-sediment concentrations computed at the two nearest computational points in suspension above the bed as described in Section 15.7.

Both near-bed distances a and $a+\Delta a$ are input data calibration parameters. Their proper assignment ensures proper values for the near-bed concentration and erosion source terms. The near-bed distances a and $a+\Delta a$ with assigned values of 8 and 2 cm, respectively, provided the most satisfactory computed concentrations for suspended very fine, fine, medium, and coarse sand.

For silt and clay (the size class that is present mainly in suspension as wash load and that has little contact with the bed surface) adjustment of the bed-sediment erosion source and the near-bed concentration term has virtually no effect on the sediment model. For this finest size class, the fall-velocity term decisively influences the final suspended-sediment model results. The fall velocity appears in the advection-diffusion equation governing suspended-sediment transport, but also in the bed-sediment governing equations throughout the suspended-sediment deposition source term. The calibration of the fall-velocity term was based on the proper choice of the previously unknown characteristic grain diameter for the silt and clay size class. A characteristic silt and clay diameter of 0.01 mm proved to provide satisfactory suspended silt and clay concentrations throughout the model domain, except in the auxiliary structure channel.

15.11.2.11 Model Calibration and Verification The three-dimensional model was used to simulate sediment fate and behavior at the Old River Control Complex on February 27, 1998. The sediment simulation period was 1 day. Sediment computations were initiated after a 10-h flow-stabilization period. Thus, the total flow and sediment simulation period was 34 h. Sediment computations were performed using a computational time step of 15 s.

Model calibration included choosing physical calibration parameters as well as choosing initial and boundary conditions as described earlier. To verify the model, computed suspended-sediment concentrations, at the end of the sediment simulation period, were compared to suspended-sediment concentrations measured on February 27. Also, computed bed-sediment size-fractions distributions, at the end of the sediment simulation period, were analyzed and compared to the February 27, 1998, data as well as to the Nordin and Queen (1989) data. Finally, computed changes in bed-surface elevations were analyzed to ensure that the January 1998 morphology data were not severely distorted during the sediment simulation period.

Figures 15-8(a–f) show the comparison between the computed (at the end of a 1-day simulation period) and the measured suspended-sediment concentrations along four data verticals at Line 13. More specifically, Figs. 15-8(a–e) contain computed and measured suspended silt and clay, very fine sand, fine sand, medium sand, and coarse sand concentrations, respectively, whereas Fig. 15-8(f) contains computed and measured total suspended-sediment concentrations. For silt and clay (Fig. 15-8(a)), the model correctly reproduces the total depth-averaged concentration. For very fine sand and coarse sand (Figs. 15-8(b and e)) the model correctly reproduces both total depth-integrated concentration and concentration-profile shape. For fine sand (Fig. 15-8(c)) the model slightly overestimates the total depth-integrated concentration along Vertical 2 and underestimates the total depth-integrated concentration along Verticals 3 and 4. Medium-sand concentrations (Fig. 15-8(d)) are generally overestimated, but small when compared to fine sand concentrations, and do not significantly influence the total suspended-sediment concentrations at Line 13. Thus, the computed total

suspended-sediment concentration (Fig. 15-8(f)) is mainly influenced by the computed fine-sand concentration. The model slightly overestimates the total depth-integrated concentration along vertical 2 and underestimates the total depth-integrated concentration along verticals 3 and 4 at line 13. At locations other than the Mississippi River at line 13, same calibration procedures produced similar agreement between computed and measured suspended-sediment concentrations.

Model calibration and verification consisted primarily of detailed analysis of changes that the bed-surface elevations and bed-sediment size-fraction distributions underwent during the 1-day sediment simulation period.

Except for a few local spots, the total deposition and erosion varied between +10 cm and −10 cm throughout the model domain. This relatively moderate bed-elevation change indicates that the assigned initial sediment conditions were appropriate. Somewhat higher erosion, up to −20 cm, is observed in the Mississippi River close to the HPP channel, and may be attributed either to the local flow pattern or to the fine material assigned to the bed surface next to the right bank at line 13. Large deposition values, up to +50 cm, were observed within the local area next to the upstream boundary at Union Point. This large amount of deposition can be attributed to the high fine-sand concentration assigned as a boundary condition at Union Point.

The silt and clay fraction was initially assigned a zero value everywhere throughout the domain, except for the small area next to the right bank at line 13, and the auxiliary structure channel. The computed silt and clay fraction at the end of the 1-day simulation period is below 0.05 (or 5%) throughout the domain. The initially assigned fine material at line 13 was eroded, whereas the initially assigned fine material at the auxiliary structure channel remained.

The very fine-sand fraction was initially assigned a value of 0.01 (1%) everywhere throughout the domain, except at the Mississippi River areas where collected bed-sediment samples dictate different values. The very fine-sand fraction at the auxiliary structure channel was also assigned according to the measured data. The computed very fine-sand fraction at the end of the 1-day simulation period shows almost no change as compared to initial data, except that the very fine-sand was eroded from the Mississippi River bed at those few spots where the initial very fine-sand fraction was assigned a larger value.

The fine-sand fraction was initially assigned a default value of 0.45 (45%) everywhere throughout the domain except at the Mississippi River data ranges, in the HPP and the auxiliary structure channels, and at the location of revetments along riverbanks. In the auxiliary structure channel and at the Mississippi River data ranges, the fine-sand fraction was initially assigned measured values. In the HPP channel and at the locations of revetments along the riverbanks, the fine-sand fraction was initially assigned a zero value. The computed fine-sand fraction after the 1-day simulation varied between 0 and 0.9 (90%) throughout the domain, depending on the location. A similar range of variation in the fine-sand fraction was also found in the February 27, 1998, data and the Nordin and Queen (1989) data. Small computed values of the fine-sand fraction generally coincide with the computed erosion areas. The largest computed values of the fine-sand fraction are found at and downstream of the Union Point area with the largest computed amount of deposition, and can be attributed to the high fine-sand concentration assigned as a boundary condition at Union Point. A slight computed increase of the initially zero fine-sand fraction in the HPP channel indicates a small computed amount of deposition of fine sand in the HPP channel. A computed increase in the fine-sand fraction along the left bank in the upstream portion of the auxiliary structure channel indicates the computed erosion of the initially assigned larger fractions of silt and clay and very fine sand.

The medium-sand fraction was initially assigned a default value of 0.45 (45%) everywhere throughout the domain except in the Mississippi River data ranges, in the HPP and the auxiliary structure channels, and at the location of revetments along riverbanks. In the auxiliary structure channel and in the Mississippi River data ranges, the medium-sand fraction was initially assigned measured values. In the HPP channel and at the locations of revetments along the riverbanks, the medium-sand fraction was initially assigned a zero value. The computed medium-sand fraction varies between 0 and 0.7 (70%) throughout the domain, depending on the location. A similar range of variation in the medium-sand fraction was also found in the February 27, 1998, data and the Nordin and Queen (1989) data. Small computed values of the medium-sand fraction coincide with the computed erosion areas. Small computed values of the medium-sand fraction are also found at and downstream of the Union Point area with largest amount of deposition, and can be attributed to the large amount of fine-sand deposition which is related to the high fine sand concentration values assigned as a boundary condition at Union Point. Large computed values of the medium-sand fraction at the mid- and downstream portions of the model domain are attributed to the fine-sand erosion in those areas. The slight increase of the initially zero medium-sand fraction in the HPP channel indicates a small amount of medium-sand deposition in the HPP channel.

The coarse-sand fraction was initially assigned a default value of 0.08 (8%) everywhere throughout the domain, except in the Mississippi River data ranges, in the HPP and the auxiliary structure channels, and at the location of revetments along riverbanks. In the auxiliary structure channel and at the Mississippi River data ranges, the coarse-sand fraction was initially assigned measured values. In the HPP channel and at the locations of revetments along the riverbanks, the coarse-sand fraction was initially assigned a zero value. The computed coarse-sand fraction varies between 0 and 0.4 (40%) throughout the domain, depending on the location. A similar range of variation in the coarse-sand fraction was also found in the February 27, 1998, data and the Nordin

and Queen (1989) data. Computed values of the coarse-sand fraction that are larger than the initially assigned values are generally attributed to the erosion of fine and medium sand.

Finally, the gravel fraction was initially assigned a default value of 0.01 (1%) everywhere throughout the domain, except in the Mississippi River data ranges, in the HPP and the auxiliary structure channels, and at the location of revetments along riverbanks. In the auxiliary structure channel and in the Mississippi River data ranges, the gravel fraction was initially assigned measured values. In the HPP channel and at the locations of revetments along the riverbanks, the gravel fraction was initially assigned a value of 1.0 (100%). The computed gravel fraction at the HPP channel is 10 to 15% below the initially assigned value, reflecting the small amount of fine and medium sand deposition in the HPP channel. The large computed gravel fraction (up to 80%) can also be found in the large-erosion areas. Evidently, in the large-erosion areas, all finer-than-gravel-size classes were gradually eroded, leading to the bed-surface armoring with gravel and preventing further erosion.

15.11.2.12 Use of Calibrated Model One of the primary objectives of the use of CH3D-SED in this study was to provide sediment rating curves, by size class, for flow in the ORCC structure channels and at Tarbert Landing. This was needed for study of the long-term stability of the Mississippi and Atchafalaya rivers below the ORCC with the hydropower facility in operation, using one-dimensional mobile-bed sediment transport simulation (HEC-6 model). An associated secondary objective was to determine the expected size distribution of sediment diverted from the Mississippi into the Atchafalaya through the various outlet structures.

For these purposes, the model as calibrated for the February 27 conditions as described above was first validated through application to three other flow events for which field data campaigns had been conducted; this resulted in no further adjustment of the bed roughness, eddy viscosity, or sediment parameters.

For each of these additional flows, which ranged from 573,000 to 1,178,000 cfs (16,226 to 33,358 m^3/s), the CH3D-SED model was run to a short-term water and sediment steady state, and the amount and size distribution of sediment transport, both bed load and suspended load, through the hydropower installation and auxiliary structure and downstream of Tarbert Landing were determined from model results. The limited number of discharges tested were marginally sufficient to establish rating curves for the one-dimensional models, yet the flows that were tested provided invaluable and heretofore unavailable information on sediment dynamics in the vicinity of the structures. In the end, the overall study, based on three-dimensional modeling, one-dimensional modeling, geomorphic analysis, and direct analysis of field data, concluded that operation of the hydropower installation did not have a detectable or measurable effect on the long-term stability of the Mississippi and Atchafalaya rivers downstream of the complex.

As is invariably the case in application of computational hydraulics to prototype situations, an extremely valuable secondary benefit of the three-dimensional modeling effort was the understanding of, and insight into, the interaction among flow, sediment, bathymetry, and structures in the Old River Control Complex. A detailed modeling effort such as this one can be thought of as a magnifying glass that draws the attention of the investigators to the fine details of mobile-bed hydraulics in the system, forcing them to reconcile model response with field data observations in a way that sharpens and deepens their overall understanding of the system.

15.11.3 Leavenworth Bend, Missouri River

15.11.3.1 Introduction As part of the Missouri River Mitigation Program, the U.S. Congress has mandated 48,000 acres of habitat mitigation in Iowa, Nebraska, Missouri, and Kansas. As of this writing, this mandate was being significantly expanded to well over 100,000 acres. The Omaha and Kansas City Districts of the U.S. Army Corps of Engineers are seeking guidance as to how to achieve bendway mitigation with minimal adverse affect on the stability and viability of the navigation channel. The study is presented in detail in Spasojevic et al. (2001).

The objective of this work was to perform a three-dimensional mathematical-model study of free-surface hydrodynamics, sediment transport, and bed evolution, in order to analyze the Missouri River habitat restoration measures. The chosen sample location was Leavenworth Bend on the Missouri River between Omaha and Kansas City. The CH3D-SED code was used as the basis of the mathematical model. The model's domain includes the Missouri River from river mile 399.4 to river mile 405. Fig. 15-9 shows the overall layout of Leavenworth Bend.

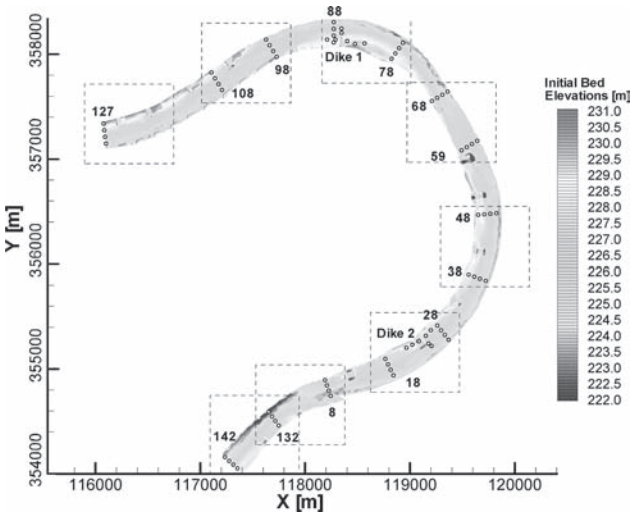

Fig. 15-9. General layout of Leavenworth Bend, Missouri River.

15.11.3.2 Field Data Campaigns Two field data sets were used for model calibration and verification to ensure that model results reproduce as closely as possible the available prototype data. One field sediment and flow data set was collected within the study area during October 5 to 7, 1999, the other during June 9 to 10, 2000. Both October 1999 and June 2000 data sets contained ADCP (Acoustic Doppler Current Profiler) discharge and velocity measurements, water free-surface elevation measurements, suspended- and bed-sediment data, and bathymetry survey data. However, the conventional techniques used during the October 1999 data set collection revealed a need for improvements, which were implemented during the June 2000 data collection effort (see Spasojevic et al. 2001). Therefore, the October 1999 data set was used for initial model calibration and verification, whereas the improved June 2000 data were used for the final model calibration and verification.

The upstream model domain boundary was chosen to approximately coincide with Line 127 (Fig. 15-9). The downstream model domain boundary was chosen to approximately coincide with Line 142. All other boundaries were treated as impermeable. Because sufficiently detailed bathymetry data around both perpendicular and L-shaped dikes were difficult to obtain, the exact dike shapes and crest elevations were recovered from the COE 1994 Hydrographic Survey maps.

15.11.3.3 Model Construction Once the exact location of model-domain boundaries and the dike geometry had been established, the computational grid was generated. Following experimentation with several levels of the grid refinement, a relatively uniform grid was constructed throughout the domain, with an average computational cell chosen to be about 10×10 m.

In the end, the computational grid had 22,947 so-called active points in a horizontal plane and 10 points in the vertical direction, i.e., along the depth. CH3D-SED uses a single-block computational grid, which, for a complex domain, covers an area larger than the actual model domain. The computational grid points inside the actual model domain are labeled "active," whereas the rest of the points are labeled "inactive." The size of the entire computational grid block was 823×33 points in the horizontal plane, again with 10 points along the depth.

The model construction, revisited as part of the calibration process, included choosing the proper representation of dikes within CH3D-SED limitations. The code offers two possibilities for dike modeling. One is to use an internal boundary condition called a thin barrier, which applies to the computational-cell face. The cell face is assumed to be a thin membrane with zero flow in the perpendicular direction. Because the thin barrier must extend all the way to the free surface, this condition can apply to nonsubmerged dikes or portions of dikes. For submerged dikes or portions of dikes, the dike crest elevation can be directly assigned as input data.

Eventually, a combination of the two possibilities for dike representation was used. For clearly submerged portions of dikes, the crest elevation was directly assigned, which also provided the dike-volume representation. For nonsubmerged portions of dikes, the thin-barrier condition was used in combination with an assigned crest elevation. To avoid the potential small-depth problem, the assigned crest elevation was chosen to be clearly submerged, although still providing a correct representation of the dike volume.

15.11.3.4 Boundary and Initial Conditions—October 1999 Event Hydrodynamic computations require either a free-surface elevation or an elemental-discharge distribution across the flow as a boundary condition at an open boundary. The elemental-discharge distribution across the flow can be extracted from the ADCP velocity measurements. However, the October 1999 velocity data, collected with the moving-vessel ADCP, are not fully reliable, as discussed by Spasojevic et al. (2001). The more reliable June 2000 velocity data were only collected at four verticals across the flow, which is insufficient for extraction of the elemental-discharge distribution across the width of the channel. Furthermore, measured velocities are generally not available for the model's prediction of future scenarios, such as the analysis of proposed habitat-restoration measures.

Thus, when an elemental-discharge distribution was used as a boundary condition, the total measured discharge was distributed across the flow using the assumption that the ratio between an elemental discharge and the maximum elemental discharge was the same as the ratio between the appropriate elemental area and the maximum elemental area, assuming that the maximum discharge corresponds to the maximum elemental area. This assumption amounts to forcing the depth-integrated velocities to be proportional to the corresponding flow depths. The assumption has been already tested elsewhere using ADCP velocity data and has proven to yield reasonable results.

The approximated elemental-discharge distribution was used as a boundary condition for the upstream inflow boundary at Line 127 (Fig. 15-9). The horizontal free-surface elevation was used as the boundary condition for the downstream outflow boundary at Line 142.

Suspended-sediment samples collected on October 5 to 7, 1999 were processed to obtain suspended-sediment concentrations by size class. Bed-sediment samples collected on October 5 to 7, 1999 were also processed to obtain bed-sediment size-class distributions at the bed surface.

Because of CPU time restrictions, it proved impractical to have more than three size classes in the model. Following considerable analysis, and based on early calibration runs, the three size classes in Table 15-8 were chosen to represent the natural sediment mixture in the model of the Missouri River at Leavenworth Bend.

Table 15-8 Representative Size Classes for the Model of the Missouri River at Leavenworth Bend

Model sediment size class	Diameter range (mm)	Characteristic diameter (mm)
Size class 1 (SC1)	D < 0.074	Determined in calibration
Size class 2 (SC2)	0.074 < D < 0.420	0.176
Size class 3 (SC3)	0.420 < D < 3.360	1.188

Even though it was obvious from field observation that there was appreciable sand content in suspension in Leavenworth Bend, the October 1999 suspended sediment data showed no sand size classes in suspension, even though the general shape of some of the fine-sediment vertical distributions bore a strong resemblance to the shape one would have expected for suspended sand. (Suspended fine-sediment concentrations are typically more or less constant over the flow depth. Suspended-sand concentration profiles typically resemble the theoretical profile (e.g., the Rouse profile), with highest concentrations close to the bed.)

After thorough analysis, it was concluded that the suspended-sediment sample measurements required double sampling, with one sample providing the proper total suspended-sediment concentration, and the other sample providing the proper size-class distribution. Double sampling was then used to collect the June 2000 suspended-sediment data.

Based on analysis of the field data, an approximate set of boundary and initial conditions for the October 1999 sediment computations was constructed. An average size class 1 concentration profile, with a concentration of 160 ppm constant over the flow depth, was assigned as the size class 1 initial condition throughout the domain. Zero-concentration profiles were assigned as an initial condition for size classes 2 and 3, again throughout the domain.

The measured suspended-sediment concentrations were also used to construct a set of vertical concentration profiles, one for each size class, at the location of each data vertical at the inflow sediment boundary (Line 127). Size class 1 profiles were constant over the depth, with average concentration values of 100, 175, 155, and 100 ppm, corresponding to verticals 1, 2, 3, and 4, respectively. Zero-concentration profiles were constructed for size classes 2 and 3. Each constructed set of vertical concentration profiles was then assigned not only to the corresponding computational-grid vertical, but also to neighboring grid verticals across the flow, until all computational verticals across the inflow sediment boundary were assigned a boundary suspended-sediment condition.

Because the free-surface elevation was used as a downstream boundary condition for flow computations, Line 142 was identified as a potential reverse-flow boundary and also defined as a sediment inflow boundary if the flow should reverse, which of course should not occur once initial-condition transients have settled down.

Bed-sediment data collected on October 5 to 7, 1999 were used to extract size-class percentage (or fraction) distributions at bed-surface points corresponding to locations of sediment data collection verticals at all sediment data collection lines (Fig. 15-9).

Size class 1 was seldom found at the bed surface. In addition, bed-sediment samples that contained size class 1 typically showed a very small amount of fine sediment (1–5%). Exceptions were a few samples with quite significant amounts (40–60%) of size class 1, such as Vertical 4 at Line 8, vertical 1 at Line 28, or Vertical 1 at Line 108. Such samples suggest the movement of fine-sediment lenses traveling through the system, typically close to the bank. The amount of size class 2 at the bed surface varied between 10 and 100%, whereas the amount of size class 3 at the bed surface varied between 0 and 90%. Except for its large variability, the bed-material data did not offer any specific clues on the spatial distribution of size classes 2 and 3, as related to different bathymetry or flow features.

Therefore, an average size-class fraction distribution, based on all the field data, was assigned as an initial condition for bed-sediment computations. This approach ensures the correct amount of bed material in the system, and allows for comparison between the computed and the measured spatial variation ranges for each size-class fraction. An average size-class fraction distribution, based on the data for four verticals at Line 127, was assigned as an inflow boundary condition for bed-sediment computations in CH3D-SED. The inflow bed-sediment boundary conditions were kept constant for the duration of the simulation.

The initial thickness of the active (bed-surface) layer was assumed to be 5 cm throughout the model domain. Because no other information was available, a single very thick stratum below the bed surface was initially assumed. The initial subsurface size-class percentage distribution was assumed to be the same as the appropriate bed-surface distribution.

15.11.3.5 Model Calibration—October 1999 Event The flow model was first built and calibrated without sediment. The computational time step for the flow computations was 5 s; this choice was dictated by the familiar Courant-number-related numerical stability criterion. Zero-flow initial conditions (i.e., horizontal free-surface elevation and zero-velocity field) were used to begin the flow computations. The chosen combination of initial and boundary conditions (realistic discharges and/or free-surface elevations imposed on initially still water) is known to produce a disturbance (wave) that propagates back and fourth throughout the flow domain. A stabilization period is required to allow the disturbance to eventually die out. At the end of the

flow-stabilization period, a steady-state flow solution was achieved. A flow-simulation period of 12 h (8,640 f5-s computational time steps) proved to be sufficient to achieve a steady-state flow solution for a given set of boundary and initial conditions.

The major physical parameter in the CH3D hydrodynamic computations, to be determined through the calibration process, is the bed-surface friction coefficient. The CH3D flow-computations program module requires the absolute roughness as input data. The absolute roughness k determined through calibration runs had a value of 0.7 cm throughout the model domain. The appropriate friction coefficient C_d varied from 0.0124 for depth $H = 5$ m to 0.0414 for $H = 1$ m. The high absolute roughness and corresponding friction coefficients probably compensated for the simplifications in the CH3D hydrodynamic computations module, most of all the hydrostatic-pressure assumption. This assumption is ill suited for the strong secondary currents associated with almost 180° bend flow at Leavenworth Bend. Furthermore, the hydrostatic-pressure assumption does not allow for a detailed simulation of the near-field flow around dikes, which is mainly responsible for the formation of large turbulent structures and associated energy losses.

Analysis of the computed discharges showed that the model was capable of reproducing the steady-state flow condition, as defined by the average ADCP discharge, to an accuracy of 0.5%. also, as shown in Table 15-9, the computed free-surface elevations showed good agreement with the measured ones.

Table 15-9 Measured and Computed Free-Surface Elevations for the October 1999 Event

	Free-surface elevation [m]	
River mile	Measured	Computed
399.4	230.50	230.50 (b/c)
400.6	230.80	230.83
402.1 (d/s)	231.22	231.20
402.1 (u/s)	231.26	231.25
404.0	231.81	231.82
405.0	232.09	232.05

However, computed velocities for the October 1999 event showed a fairly random pattern of agreement/disagreement with ADCP velocity measurements throughout the model domain. Fig. 15-10 presents a sample comparison of computed and measured velocities, in which significant data scattering is apparent.

The shift between measured and computed velocities in the figure appears randomly at other locations throughout the domain. As described in Spasojevic et al. (2001), the data scattering, associated with the moving-vessel ADCP velocity

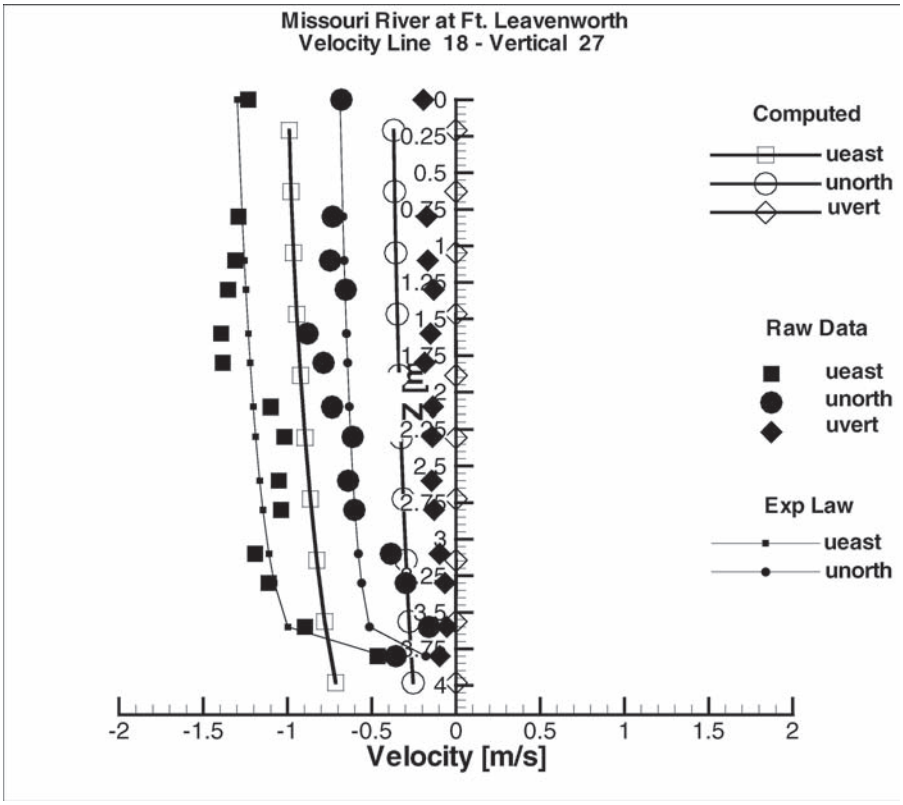

Fig. 15-10. Sample of computed and measured velocities for October 1999 event.

measurements, is caused by small-scale turbulence. Also, as shown in Spasojevic et al. (2001), the large-scale turbulence produces a random shift between the moving-vessel ADCP measurements and the proper mean-flow velocity profile. Thus, the disagreement between the computed and measured velocities in Fig. 15-10 can be attributed to the moving-vessel ADCP velocity measurements. This conclusion is further supported by the consistently fair agreement between computed and measured velocities for the June 2000 event as seen further on, when the stationary ADCP was used for collecting velocity data.

Sediment computations were initiated after a 12-h flow-stabilization period. A flow and sediment simulation period of one full day proved to be sufficient to achieve a quasi-equilibrium state between the flow and the sediment. The combined flow and sediment computations were made using a computational time step of 5 s, which was small enough to satisfy the stability condition associated with the suspended-sediment computations.

During the combined flow and sediment computations, the flow-model boundary conditions and physical parameters were kept the same as for the flow-only computations.

For the fine sediment of size class 1, the fall-velocity term had a decisive influence on the final suspended-sediment model results. The fall velocity appears in the advection-diffusion equation governing suspended-sediment transport, but also in the bed-sediment governing equations throughout the suspended-sediment deposition flux term. The calibration of the fall-velocity term was based on the proper choice of the previously unknown characteristic grain diameter for the fine sediment size class. A characteristic fine-sediment diameter of 0.015 mm proved to provide satisfactory suspended fine-sediment concentrations, but only for cases when the measured concentration profiles did not indicate the presence of sand in suspension.

Fig. 15-11 presents a sample of computed and measured suspended-sediment concentrations for the October 1999 event. Shown is a comparison between measured and computed suspended fine-sediment (size class 1) concentrations for all four sediment-data verticals at sediment data line 59. The measured size class 1 concentrations shown are also the total measured concentrations in suspension as described earlier.

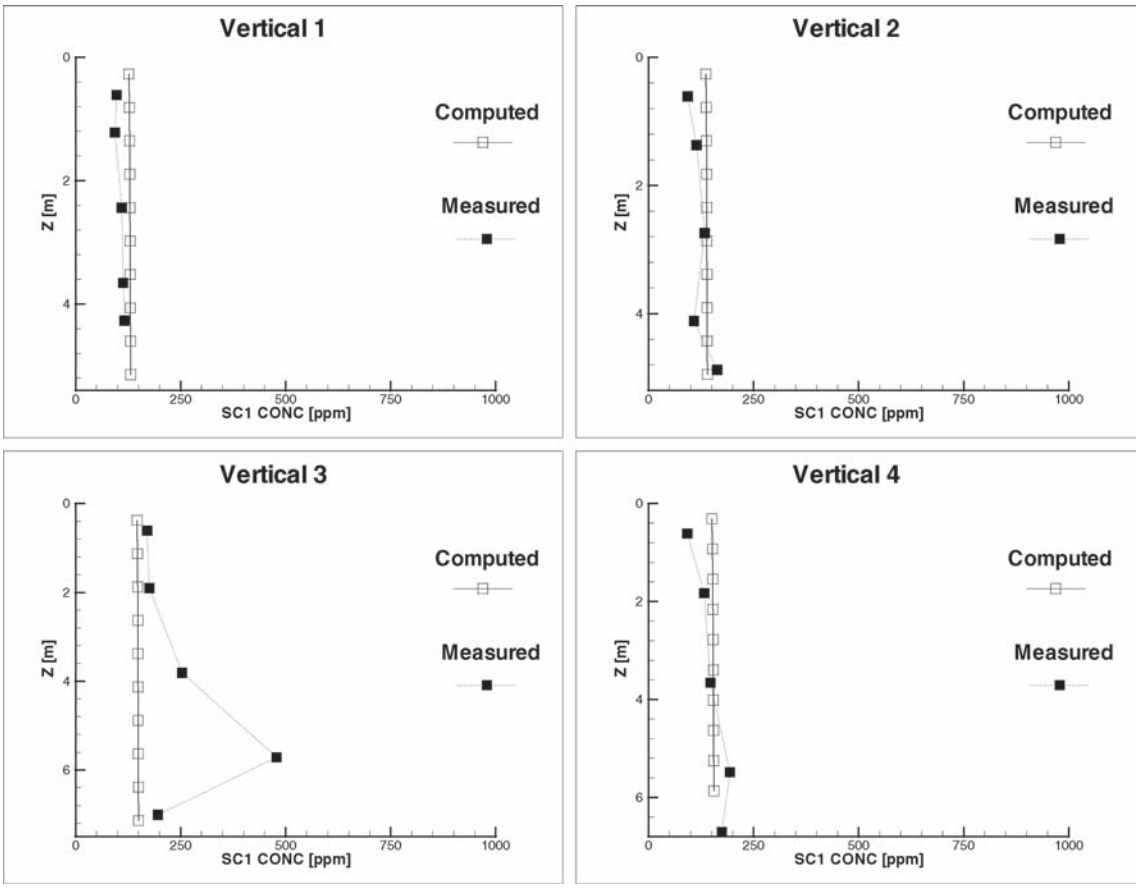

Fig. 15-11. Sample of computed and measured suspended-sediment concentrations for October 1999 event.

Copyrighted Materials
Copyright © 2008 American Society of Civil Engineers (ASCE)
Retrieved from www.knovel.com

CHAPTER 16

Turbulence Models for Sediment Transport Engineering

D. A. Lyn

16.1 INTRODUCTION

In problems of civil engineering interest, sediment transport invariably occurs under turbulent-flow conditions. Traditional discussions (*ASCE Manual 54*; see also Chapter 2) of turbulence models have, however, been mainly restricted to the problem of determining the vertical distribution of suspended sediment in the simplest case of uniform channel flow over a plane bed. Since the appearance of *ASCE Manual 54 in* 1975, there have been considerable advances in our understanding and hence modeling of complex turbulent flows, and these might be expected to have a positive impact on approaches to practical problems in sediment transport. In general, the scope of the problems that can be studied has been broadened substantially, and a larger range of engineering problems can be tackled with reasonable success. The more traditional basic questions have proven more refractory and progress in answering them has been correspondingly limited. Nevertheless, with ever-growing computational capabilities and the proliferation of commercial computational fluid dynamics (CFD) software packages, numerical modeling with turbulence models will in the foreseeable future become an increasingly important engineering tool in dealing with sediment transport problems. Hence, a basic familiarity with such models, their theoretical bases, and their limitations will be useful.

The present chapter describes the standard turbulence models currently being applied to problems involving sediment transport, focusing on so-called two-equation models, but also discussing more briefly simpler models that might be used judiciously for special problems, as well as more advanced models that may find more practical application in the future. In most applications thus far, the turbulence model has been taken without modification from fields where the use of these models is more solidly established, but where possibly important features unique to sediment transport are absent. The standard features, assumptions, and limitations of turbulence models are discussed in a number of monographs (Rodi 1993; Hallbäck et al. 1996; Chen and Jaw 1998; Wilcox 1998; Piquet 1999; Durbin and Petterson Reif 2001), as well as review articles (Launder 1984; Speziale 1991; Hanjalic 1994; Rodi 1995; Speziale 1996; Launder 1996; Spalart 2000), but, except for the review by the ASCE Task Committee on Turbulence Models in Hydraulic Computations (1988) and the works of Rodi, hydraulic or sedimentation engineering applications have not received much attention (see, however, the brief review by Lane 1998). General references on multiphase flows are also available (e.g., Crowe et al. 1998) that discuss aspects relevant to turbulent particulate flows, often, however, with gas-solid or bubbly flows in mind. Although the present chapter will necessarily rely heavily on these works, it will elaborate issues that may be of particular relevance to sediment-transport engineering applications. Turbulence modeling, especially for the very complicated problem involving sediment transport, is an extensive field undergoing continual development, and the present chapter can only serve as an introduction to the subject, targeted at a sedimentation engineering audience. For the most part, the discussion is restricted to classical problems in sediment-transport mechanics, emphasizing noncohesive uniform-sized sediment. The important case of depth-averaged models, in which complicating issues other than but closely related to turbulence modeling arise, is covered briefly in an appendix.

16.2 TURBULENCE, MODELS, AND PARTICULATE FLOWS

Before the mathematical models used to describe the behavior of turbulent flows in general and sediment-laden flows in particular are stated, a discussion of qualitative aspects introduces basic concepts, motivations, and terminology. Much use will be made of scaling arguments and dimensional analysis involving length scales and time scales (or velocity scales, because a combination of length and

time scales will define a velocity scale). These characteristic quantities associated with physical processes provide a measure of size and of duration. Turbulent flows exhibit a broad and continuous range of length (and time) scales corresponding loosely to the size of "eddying" motions or "eddies." The analogy between turbulent and molecular transport, although deficient in many respects, has been important in the development of turbulence models, and it will be helpful to consider the similarities and differences between the two types of transport.

16.2.1 Qualitative Features of Turbulent Flows and Modeling Implications

In attempting to define turbulence, Tennekes and Lumley (1972) list several essential features. The instantaneous flow quantities at a point of a turbulent flow, such as velocity and pressure, fluctuate irregularly in time in such a way as to preclude predictability, except possibly in a statistical "averaged" sense. Instead of attempting to solve the complete exact governing equation, which is not feasible for practical problems, the engineer resorts to describing the flow by suitably averaged equations involving at most second-order moments, such as variances. Because the influence of higher-order statistics is presumed to be weaker, the modeler is permitted greater flexibility in formulating models of correlations involving higher-order terms (Launder 1996).

As a consequence of the averaging operation, detailed flow information is lost that may still have important transport effects, for which models, preferably simple and of wide applicability, must be developed. This much-greater effectiveness in mixing or greater "diffusivity" compared to laminar flows is the feature of turbulent flows that is often of most practical interest. The ratio of turbulent diffusivity (viscosity in the context of momentum transfer) to molecular diffusivity may be several orders of magnitude, which can be qualitatively understood in terms of the much larger length scales involved in the former compared to the latter. As a result, turbulent diffusive transport may be of comparable importance to or, in some cases, may even dominate advective transport, and the effective modeling of turbulent transport becomes essential to reliable predictions of overall transport. Turbulence models have therefore focused on predicting the effects of the large-scale motions responsible for the enhanced diffusivity.

Even though the main flow features of engineering interest, and hence the (time-)averaged equations, may be well approximated as being one- or two-dimensional, instantaneous turbulent fluctuations are essentially three-dimensional in that they are nonzero in all spatial directions. Moreover, turbulence characteristics will vary in at least one, and possibly all spatial directions; i.e., the turbulence is inhomogeneous. The characteristics in each coordinate direction also may differ from one another; i.e., the turbulence is anisotropic. The modeling of strongly inhomogeneous and anisotropic features requires greater effort, both theoretically and computationally, and still is the subject of intensive research. The search for simpler models has often been based on assumptions of local homogeneity and isotropy, such that, in a sufficiently small volume in the flow region of interest, spatial variations and anisotropic effects may be neglected. The simple models, however, may not yield reliable results for flows far from the isotropic and homogeneous ideal.

A flow becomes turbulent at sufficiently high Reynolds number, $\mathsf{R} = UL/\nu$, where U and L are appropriate velocity and length scales, and ν is the fluid kinematic viscosity. In alluvial channel flows, R, based on an average velocity and the flow depth, h, can attain quite large values, because of the large length scale (h) involved. As a result, not only is the flow turbulent, but it is a high-R turbulent flow, a characteristic that has been exploited in turbulence modeling. Two aspects of high-R flows have been implicitly incorporated into most turbulence models (Launder 1996). The first is the empirical observation of high-R similarity, in which many practically important characteristics of high-R turbulent flows are largely insensitive to variations in R, or equivalently to the effects of molecular viscosity. This has implications for suspension flows, because it is known that the effective (molecular or small-scale) viscosity of a suspension may vary with the suspension concentration. For dilute suspensions, however, this effect is irrelevant as far as high-R turbulent flows are concerned, because viscous effects are unimportant in regions away from (smooth) solid boundaries. The second is that, at high R, turbulence at the smallest scales is considered locally isotropic, not being strongly influenced by the mean flow or the anisotropic large-scale turbulent motions. In smooth-channel flows, e.g., in the laboratory, however, viscous effects may be important in the near-bed region because the local R is low, and high-R model assumptions need to be reexamined. In sediment-transport applications with fine sands, viscous effects may also need to be considered in particular problems, such as the formation of ripples (Richards 1980).

In the shear flows of primary interest in hydraulic engineering, turbulent fluctuations or "kinetic energy," which is more precisely defined later (Eq. (16-5)), may be viewed as being produced or extracted from the mean flow by the interaction of the fluctuations with large-scale mean velocity gradients. On the other hand, the fluctuations are also seen as being dissipated at the smallest scales by the action of viscosity. The process by which the energy is produced and then eventually dissipated, essentially through the stretching of vortices, is often conceptually pictured as a cascade, in which large-scale eddying motions undergo continual transformation into motions on smaller and smaller scales. Fluctuating vorticity, which accompanies this cascade, is a defining feature of turbulence. In spite of the fact that dissipation is effected through fluid viscosity, the rate of dissipation of turbulent kinetic energy, denoted by ϵ, is controlled

by the largest scales. Changes in fluid viscosity influence the scale on which dissipation occurs, but do not affect ϵ, consistent with the high-R similarity already mentioned. The importance of the large scales in determining ϵ will be reiterated throughout this chapter. When production and dissipation are in approximate balance, i.e., a local equilibrium is established, this may permit model simplification. On the other hand, strongly nonequilibrium turbulence, like strongly anisotropic turbulence, will present problems for simple turbulence models.

16.2.2 Length and Time Scales in Turbulent Sediment-Transport Problems

A familiarity with the relevant length and time (or velocity) scales is important in the discussion of turbulent flows and models. Turbulence scales characteristic of the bulk flow are usually taken to be the average or maximum velocity and the flow depth or boundary layer thickness, with time and length scales on the order of at most minutes and tens of meters, respectively. For flows where the turbulence is primarily generated by boundary shear, the shear velocity, u_*, which characterizes the local boundary shear stress, $\overline{\tau}_b$, since $u_* \equiv \sqrt{\overline{\tau}_b/\rho}$, ($\rho$ is the fluid density), plays a particularly important role as a velocity scale. The smallest scales of turbulence are those associated with viscous dissipation of eddies, and hence are characterized by ν and ϵ (with dimensions of energy per unit mass per unit time, $[L^2/T^3]$). The Kolmogorov scales, the smallest length and time scales in turbulent flows, are determined from these variables as $\eta_K = (\nu^3/\epsilon)^{1/4}$ and $\tau_K = (\nu/\epsilon)^{1/2}$, respectively, with typical values of O(1 mm) and O(0.05 s).

A comparison of turbulence scales with scales of interest in sediment-transport engineering, which may span a very wide range, provides a preliminary assessment of the importance of effects on turbulence and serves as a guide to appropriate turbulence models. Morphological time scales over which changes of engineering significance in erodible boundaries occur may be on the order of months or even years. The migration speed of bed forms is much smaller than bulk-flow velocities, and so is associated with correspondingly much longer time scales. Flood hydrographs in rivers and the corresponding sedimentographs or flow reversals in estuaries occur on time scales of hours or days. Because of the large disparities in time scales, such "long"-time-scale unsteady phenomena should not interact strongly with "short"-time-scale turbulence-generating (or -dissipating) mechanisms, and hence turbulence models developed for steady-state problems should be adequate; i.e., deficiencies in predictive abilities are likely due to other than unsteady effects. The possibly different needs of sediment transport and flow predictions need to be pointed out. Because sediment transport may occur over relatively long time scales, detailed flow features may have important implications for sediment transport, and yet, from the narrow point of view of the gross flow, be unremarkable. Further, this does not address possible difficulties arising when problems involving large-scale unsteadiness are *deliberately* simplified and modeled as being steady. In problems involving shorter time (or length) scales, e.g., oscillatory waves with periods on the order of seconds, possible unsteady effects on turbulence may not be so easily dismissed. Because laboratory measurements play such an important role in verifying (and calibrating) turbulence models, it should also be emphasized that important length and time scales in the laboratory may differ from those in the field, and effects that may be small or negligible in the field may assume greater importance in small-scale laboratory experiments, and vice versa.

Particle length and time scales merit further discussion, because these may be comparable to turbulence scales, and so conducive to potentially strong interaction with turbulence. A characteristic length scale of a sedimenting particle is its size, d, and its time scale may be taken as the time required for it to respond to fluid velocity fluctuations, τ_p. A simple estimate of the latter is $\tau_p \sim w_s/[g(s-1)/s]$, where

w_s = terminal settling velocity;
g = the acceleration due to gravity, and
$s = \rho_s/\rho$ = relative density of the sediment.

The ratio of τ_p to a turbulence time scale is often termed a Stokes number, denoted as St; e.g., the Stokes number based on the Kolmogorov time scale is $\mathrm{St}_K \equiv \tau_p/\tau_K$. For fine to medium sands, $d/\eta_K = O(1)$ and $\mathrm{St}_K = O(10^{-1})$, suggesting that these sands will follow all but the highest frequency fluctuations. For noticeable effects on the bulk flow, it might be expected that a sufficiently large suspension volume concentration, c, is necessary. A length scale indicative of concentration would be an interparticle separation distance, $l_s \sim d/c^{1/3}$, which for moderate values of $c = O(10^{-3})$ would lie in a range, $\approx 10d$, comparable to smaller turbulence scales.

16.2.3 Turbulence in Particulate Flows

The qualitative features of suspension-free or clear-water turbulent flows should also apply to turbulent suspensions transporting solid particles, at least if the suspension is sufficiently dilute, i.e., for c sufficiently small. What level of c characterizes a dilute suspension? Lumley (1973) has argued on the basis of the neglect of particle-particle interaction that c should not exceed $O(10^{-3})$, which also has been suggested by Elghobashi (1994). For problems in sediment-transport engineering, this is often satisfied over much, though not necessarily all, of the flow region of interest. In particular, in the important near-bed region, the dilute assumption is suspect, and a dense-phase flow may need to be considered.

Particles in a suspension are discrete and dispersed throughout the flow. Because the trajectories of specific individual particles are generally of no interest to the sediment transport engineer, a continuum or two-fluid treatment

of a suspension flow is attractive. The discrete particles are considered to constitute a continuum like the carrier fluid, and hence to be governed by equations of motion very similar to the equations of fluid flow. This can be achieved (just as in the case of the carrier fluid) by averaging over a representative volume containing a sufficiently large number of particles, but it also requires that the length scale, $\mathcal{L}_\upsilon$, of the representative volume be sufficiently small compared to important flow length scales. When combined with the dilute-suspension assumption, this requirement places a rather severe restriction on such a modeling approach. For a fine sand, $d = 0.2$ mm; at $c = 10^{-3}$, this implies that $\mathcal{L}_\upsilon = O(1\text{ cm})$, which is certainly much larger than η_K, and, for laboratory flows, even becomes comparable to the largest scales. Thus, like much else in turbulence, the frequently used continuum models, though often effective for engineering purposes, can be difficult to justify with any semblance of rigor.

In the simplest models, encompassing the large majority of models, the particles or, in continuum models, the particulate phase is assumed to behave, like a dye, as a passive scalar, in that it does not influence the flow dynamics. At what level of c can this "one-way" coupling be justified? In a rough classification, Elghobashi (1994) suggests that $c < 10^{-6}$ for one-way coupling. This seems overly stringent, particularly in the parameter range more relevant to (aqueous) sediment transport, where density ratios are $O(1)$, but it does indicate that the usual neglect of the effects of the particulate phase on turbulence, sometimes termed turbulence modulation (or modification), should not be so casually assumed. The problem of modeling the two-way coupling, in which the particulate phase may significantly affect the flow, remains an active research topic, though mainly outside of the sediment-transport literature (e.g., Elghobashi and Abou-Arab 1983; Elghobashi and Truesdell 1993; Boivin et al. 1998). As will be discussed below, the main effect of sediment on the flow that has been considered within the sediment-transport literature is that analogous to density stratification stemming from vertical variation in particle concentration.

16.2.4 Aims and Scope of Modeling

Wilcox (1998) has defined an ideal turbulence model as one that "should introduce the minimum amount of complexity while capturing the essence of the relevant physics." For the sediment-transport engineer, this may be interpreted as implying that a useful prediction can be obtained reliably for a reasonable expenditure of effort. Much of the following will be concerned with describing relatively complex models requiring not only possibly lengthy numerical solution but also possibly extensive data collection to specify boundary/initial conditions and for model validation. It should not necessarily be assumed that the additional effort in formulating and setting up more complex models will always result in commensurate improvements in predictions. The incomplete understanding of turbulence without particles already sets an upper limit on what can be achieved in the modeling of the more complex problem of turbulence with particles. Similarly, limitations on our predictive ability may be set by our incomplete understanding of the most basic problems of sediment transport, such as the specification of bed load or an equilibrium bed concentration, which are needed in specifying boundary conditions.

16.3 THE REYNOLDS-AVERAGED EQUATIONS

The traditional modeling approach based on Reynolds averaging is likely to remain dominant for practical hydraulic problems. An instantaneous quantity of interest, $f(\mathbf{x},t)$, which may be a velocity component, u_i, or a sediment concentration, $c(\mathbf{x},t)$, is decomposed into an averaged, e.g., $\overline{f}$, and a random or at least unpredictable fluctuating component, f'. Here, $\mathbf{x} = x_i$, $i = 1, 2, 3$, denotes the position vector, and t denotes the time variable. Where convenient, the identifications $(x_1, x_2, x_3) = (x, y, z)$ and $(u_1, u_2, u_3) = (u, v, w)$ will be made, where x is taken to be in the streamwise direction, z in the vertical direction, opposite to the direction of gravity (or approximately in the direction away from the bed), and y in the horizontal direction perpendicular to x and z. For steady flows, the averaging can be performed over time,

$$\overline{f}(\mathbf{x}) = \lim_{T_{\text{avg}}\to\infty} \frac{1}{T_{\text{avg}}} \int_0^{T_{\text{avg}}} f(\mathbf{x},t)\, dt, \tag{16-1}$$

where T_{avg} denotes the time period over which the averaging is performed. In the case of unsteady flows, an ensemble average can be taken over different realizations of conceptually the same flow, such as experiments repeated under the same conditions. For steady flows, averaging over an ensemble and averaging over time may be assumed to be equivalent and to yield the same results. Though, in Eq. (16-1), T_{avg} is formally taken as going to infinity, in practice it is sufficient that T_{avg} be much longer than any relevant turbulence time scale, but much shorter than any time scale over which the flow might be considered unsteady (Lumley and Panofsky 1964; Wilcox 1998).

16.3.1 The General Flow Equations

With the averaged continuity equation, the general three-dimensional Reynolds-averaged Navier-Stokes (RANS) equations for an incompressible fluid may be conveniently written in Cartesian tensor notation (for those unfamiliar with this notation, a brief introduction is given in Appendix I to this chapter) as

$$\frac{\partial \overline{u}_j}{\partial x_j} = 0 \tag{16-2a}$$

$$\frac{D\overline{u}_i}{Dt} = \frac{\partial \overline{u}_i}{\partial t} + \frac{\partial\left(\overline{u}_i\,\overline{u}_j\right)}{\partial x_j}$$
$$= -\frac{1}{\rho_{\text{ref}}}\frac{\partial \overline{\rho}}{\partial x_i} + \frac{\partial}{\partial x_j}\left(-\overline{u_i' u_i'} + \frac{\mu}{\rho_{\text{ref}}}\frac{\partial \overline{u}_i}{\partial x_j}\right) + \overline{F}_i \tag{16-2b}$$

where

p = pressure;
ρ_{ref} = reference fluid density; and
μ = molecular dynamic viscosity.

The term $\overline{F}_i$ represents a force per unit mass, i.e., an acceleration. Here, the summation convention is followed, where repeated roman alphabetic subscripts indicate summation over all values of the subscript. For particle-free flows, $\overline{F}_i$ might be the gravitational body force, such as g_i, the component of gravitational acceleration in the i^{th} coordinate direction.

In the context of suspension flows, $\overline{F}_i$ would represent interaction forces exerted on the fluid by the particles. Frequently, the effect of sediment on the flow is modeled in a manner analogous to that of a variable-density fluid. A locally averaged density, ρ_m, for the suspension can be defined as

$$\rho_m(\mathbf{x}, t) = \rho_s c(\mathbf{x}, t) + \rho[1 - c(\mathbf{x}, t)]$$
$$= \rho[1 + (\mathbf{s} - 1)\, c\,(\mathbf{x}, t)]. \tag{16-3}$$

The Boussinesq approximation, which neglects inertial effects due to a variable (suspension) density, and includes only buoyancy effects, can then be invoked, with the result (using $\rho_{\text{ref}} = \rho$) that

$$\overline{F}_i = g_i \frac{(\overline{\rho}_m - \rho)}{\rho} = g_i (s - 1)\overline{c}. \tag{16-4}$$

To what extent the application of Eqs. (16-2) to suspensions can be justified is debatable, but if the suspension is sufficiently dilute, then Eqs. (16-2) should at least approximately hold. Whether the dominant interaction force between fluid and solid phases can be effectively modeled with a variable-density buoyancy term as in Eq. (16-4) is more controversial. Simplified forms of Eqs. (16-2) are often used; e.g., for primarily horizontal flows, the shallow-water-wave assumption of hydrostatic pressure distribution in the vertical direction is frequently invoked (see the discussion of spatially averaged flows in Appendix II).

The basic closure problem following from the adoption of the Reynolds averaging procedure arises because of the appearance, on the right-hand side of Eq. (16-2b), of the correlation terms, $-\overline{u_i' u_j'}$. These result from the averaging of the nonlinear advection term, $\overline{u_i' u_j'}$. As expressed in Eq. (16-2b), $-\overline{u_i' u_j'}$ is not known a priori and consequently, Eqs. (16-2) are not closed and cannot be solved as is. The

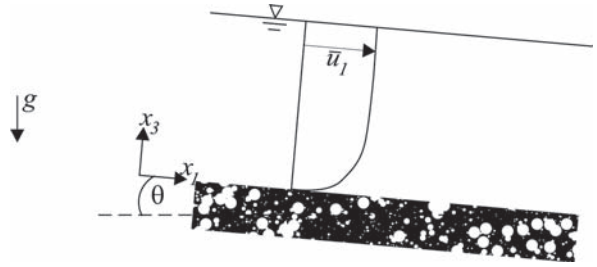

Fig. 16-1. Steady uniform flow without sediment in a wide channel on a slope θ.

nine elements of $-\overline{u_i' u_j'}$ may be interpreted as representing effective stresses and hence $-\overline{u_i' u_j'}$ is termed the (kinematic) Reynolds stress tensor. The three diagonal terms, $-\overline{u_1' u_1'}$, $-\overline{u_2' u_2'}$, $-\overline{u_3' u_3'}$, are interpreted as normal stresses, while the off-diagonal terms are interpreted as shear stresses. In general, the diagonal terms are all different in value, and hence turbulence is anisotropic. One of the most important parameters describing turbulence is obtained from the sum of the diagonal terms, namely, the turbulent kinetic energy,

$$k \equiv \frac{1}{2}\overline{u_i' u_i'} = \frac{1}{2}\left(\overline{u_1' u_1'} + \overline{u_2' u_2'} + \overline{u_3' u_3'}\right). \tag{16-5}$$

The Reynolds stress tensor is symmetric, so that only six of its nine terms (the diagonal terms and the three off-diagonal terms, $\overline{u_1' u_2'}$, $\overline{u_1' u_3'}$, $\overline{u_2' u_3'}$) are independent. Together with the four primary unknowns (the three mean velocity components, $\overline{u}_i'$ and the mean pressure, $\overline{p}$, the six independent Reynolds stresses form a total of ten unknown variables, whereas Eqs. (16-2) provides only four equations. Turbulence modeling provides closure of the system by formulating sufficient additional equations, algebraic or differential, that specify $-\overline{u_i' u_j'}$, in terms of already existing variables.

Example. In the following, the special case of a steady uniform plane-bed flow in an infinitely wide channel (Fig. 16-1) will be used recurringly as a simple illustration of the use of the model equations discussed. These illustrations will be set apart from the main text. In this special case, $\overline{u}_2 \equiv \overline{u}_3 \equiv 0$, $\partial/\partial t \equiv \partial/\partial x_1 \equiv \partial/\partial x_2 \equiv 0$. Equation (16-2a) is therefore satisfied automatically, and Eq. (16-2b) is reduced to

$$0 = \frac{\partial}{\partial x_3}\left(-\overline{u_k' u_3'} + \frac{\mu}{\rho_{\text{ref}}}\frac{\partial \overline{w}_1}{\partial x_3}\right) + g\sin\theta \tag{16-6a}$$

$$0 = \frac{\partial}{\partial x_3}\left(-\overline{u_2' u_3'}\right) \tag{16-6b}$$

$$0 = \frac{1}{\rho_{\text{ref}}} + \frac{\partial \overline{r}}{\partial z_3} + \frac{\partial}{\partial z_3}\left(-\overline{w_3' w_3'}\right) - g\cos\theta. \tag{16-6c}$$

This involves five unknowns ($\overline{u}_1$, $\overline{p}$, $\overline{u_1' u_3'}$, $\overline{u_2' u_3'}$, $\overline{u_3' u_3'}$) with only three equations. From Eq. (16-6b) and the boundary

condition at the bottom, $-\overline{u_2' u_3'}$ is found to be identically zero, and from Eq. (16-6c), the pressure distribution may be treated as hydrostatic because $\partial(\overline{u_3' u_3'})/\partial x_3$ is small. Interest is therefore focused on Eq. (16-6a), which still involves two unknowns, $\overline{u_1'}$ and $\overline{u_1' u_3'}$, and therefore is not closed.

16.3.2 Equation(s) for the Sediment Model

The basic flow equations, the continuity and Navier-Stokes equations describing (fluid) mass and momentum conservation, may be considered exact at least for a pure fluid, and very plausible for the fluid phase in a dilute suspension. In contrast, much remains unclear as far as the basic governing equations for sediment are concerned. Unlike "molecular" scalars like temperature or salinity, sediment constitutes a separate physical phase, the motion of which may not necessarily be the same as the motion of the fluid. The large bulk of the work on sediment transport modeling has been based on a continuum approach, similar to that taken with a molecular species. In analogy with the treatment of the latter, only a sediment mass conservation equation is taken, without mention of sediment momentum conservation equation. To further complicate the picture, the discrete nature of the solid phase permits an alternative (Lagrangian) modeling approach, in which the motion of individual particles is tracked. Thus, even before any attempt at the modeling of turbulent transport of sediment, the choice and justification of even the basic sediment equations must be addressed.

16.3.2.1 The Continuum Approach The continuum or two-fluid approach treats the discrete solid phase as a continuum, described by a possibly spatially and temporally varying local (either point or depth-averaged or cross-sectionally averaged) sediment concentration, $c(\mathbf{x},t)$. A differential conservation equation is then heuristically derived, which governs the temporal evolution and/or the change in spatial distribution of c. Most commonly, the sediment is treated in a manner analogous to a molecular species, assuming that the particulate phase moves with the fluid, with, however, a special model for particle settling, which is characterized solely by a constant settling velocity, w_s. In problems where sediment heterogeneity may play an important role, the problem may be attacked by modeling different size classes, such that the α^{th} size class would be characterized by its own settling velocity, $(w_s)_\alpha$. The standard Reynolds-averaged model equation describing the conservation of sediment in the α^{th} size class is thus written as

$$\frac{D\overline{c}_\alpha}{Dt} = \frac{\partial \overline{c}_\alpha}{\partial t} + \frac{\partial\left(\overline{u}_j \overline{c}_\alpha\right)}{\partial x_j} = \frac{\partial\left(-\overline{u_j' u_\alpha'}\right)}{\partial x_j} + \frac{\partial\left[\left(w_s\right)_\alpha \overline{c}_\alpha\right]}{\partial z} + \overline{R}_\alpha \cdot \qquad (16\text{-}7)$$

Here, the summation convention is not applied with repeated Greek subscripts (α). The source (sink) term, $\overline{R}_\alpha$, represents a reaction or transformation term, such as might be considered in cases involving particle coagulation, breakup, or entrainment from a heterogeneous bed, that may cause a change in the concentration of particles in any given size class. From Eq. (16-7), the settling term (the second term on the extreme right-hand side) might also be viewed as a somewhat special reaction term for a molecular species. The total solid-phase volume concentration, $\overline{c}$, can be obtained by summation as

$$\overline{c} = \sum_\alpha \overline{c}_\alpha \cdot \qquad (16\text{-}8)$$

In spite of its wide use and its intuitive physical interpretation and hence appeal, the theoretical basis of Eq. (16-7) deserves further examination. The questions surrounding the continuum approximation have already been discussed in Section 16.2.3. Even if a continuum model is adopted, the question remains of whether it suffices to formulate only a mass conservation equation for sediment, or whether a more consistent two-phase flow approach including not only sediment kinematics but also sediment dynamics is necessary. The latter would necessitate an equal treatment of the continuous solid phase with its own momentum conservation equation. In particulate flows, it is empirically observed that, even with the settling velocity taken into account, the mean particle velocity differs from the fluid velocity (e.g., Muste and Patel 1997), such that the implicit assumption of Eq. (16-7) of equal particle and fluid velocities is clearly violated. The velocity difference for aqueous suspensions of small sand particles is however generally small, $O(w_s)$, and so it is not clear if and when a detailed treatment of sediment dynamics would be required. A general discussion of the theoretical basis of two-phase flow models is given by Drew (1983) and Crowe et al. (1998). In practical sediment transport computations, the latter approach has rarely been taken, though two-phase flow models have been proposed (Drew 1975; McTigue 1981; Kobayashi and Seo 1985; Greimann et al. 1999; Hsu et al. 2003) and simple cases, such as uniform flow over a plane bed, have been analyzed. Subtle differences from the conventional approach can lead to confusion (see, e.g., the discussion between Celik 1982 and McTigue 1982); whereas Eq. (16-7) is conventionally interpreted as a *kinematic* sediment conservation equation, the two-phase modeler may view it (or at least its simplified form in the uniform-flow case) as resulting from a *dynamic* momentum balance. The main difficulty in the two-phase flow approach, however, is similar to that of turbulence closure, in that modeling assumptions regarding the interaction between phases must be made to close the governing system of equations, but these are often impossible to confirm experimentally in any detail.

16.3.2.2 The Settling Velocity in a Turbulent Suspension Even if Eq. (16-7) is accepted as an intuitively plausible model for describing sediment transport, it remains

to specify w_s. The simplest choice of w_s, which therefore has been the most popular, is that corresponding to the settling of an isolated equivalent-spherical particle in a stagnant fluid of infinite extent, and formulae for this are available (see Chapter 2, where other effects on w_s, such as those due to shape, are discussed). In a turbulent suspension, however, these assumptions are not strictly satisfied. For the present chapter, the effects due to concentration and turbulence (already discussed in *ASCE Manual 54*) are relevant. Presumably, if the dilute assumption implicit in the standard models is valid, then effects of concentration are likely negligible (though the effect of preferential particle clustering in a turbulent flow (Wang and Maxey 1993) might need to be considered). On the other hand, numerical simulations (Wang and Maxey 1993) have shown an effect of turbulence on w_s, with w_s *increasing* by as much as 40% over the fall velocity in a stagnant fluid. Unfortunately, these results have been obtained for small heavy particles ($d < \eta_K$, and $s \gg 1$) in homogeneous isotropic turbulence, which is not in the parameter range of greatest interest in sediment transport applications.

Since the publication of *ASCE Manual 54*, experimental studies of settling velocities of particles in water have been few. Boillat and Graf (1981; 1982) conducted experiments of spherical particle settling in stagnant water and in an approximately homogeneous turbulent flow for a range of particle Reynolds numbers, $200 \leqslant w_s d/\nu = \mathsf{R}_p \leqslant 20{,}000$, which for typical particle parameters would correspond to the size range of coarse sands and larger. The observed drag coefficients, C_D, which can be simply related to w_s, in the stagnant-water case were consistently larger than those given by the standard drag curve for spheres. Relative to the stagnant-water C_D, the turbulent-flow C_D was generally reduced, corresponding to a larger w_s, though an increased C_D, corresponding to a smaller w_s, was often observed when $\mathsf{R}_p \approx 2{,}000$. Although it was argued that both the intensity and the length scale of the turbulence influence C_D, a simple dimensionless correlation could not be found. In a similar study, Yang and Shy (2003) examined a range of smaller $\mathsf{R}_p < 40$, and observed increases in w_s (relative to still-water values) with increasing St_K with a maximum increase of up to 7% for $\mathsf{St}_K \approx 1$, but also found that decreases might occur for much larger St_K. The limited experimental evidence should be regarded with some caution, but does indicate that the use of a w_s based on stagnant-fluid condition may involve uncertainties of $O(10\%)$. Moreover, since most practical applications involve inhomogeneous turbulence, such that the settling particle is constantly adjusting to a changing turbulence environment, the practical implications of such results remain to be explored.

16.3.2.3 Lagrangian Models In this approach, the motion of individual particles is determined by writing a model equation of motion for an individual particle:

$$m_p \frac{d(u_i)_p}{dt_p} = (F_i)_p . \tag{16-9}$$

The subscript, p, refers to a particle quantity; hence, $(u_i)_p$ is the instantaneous velocity of a particle, m_p is mass, and $(F_i)_p$ denotes the sum of forces acting on the particle. In a popular variant of the Basset-Boussinesq-Oseen (BBO) equation for a spherical particle of radius a, the forces are modeled as

$$\begin{aligned}(F_i)_p = & \underbrace{m_p\left[\frac{3}{8}\frac{C_D}{a_s}\left\{(u_i)_f-(u_i)_p\right\}\left|(u_i)_f-(u_i)_p\right|\right]}_{I} \\ & + \underbrace{m_f\left[\frac{d(u_i)_f}{dt}\right]}_{II} + \underbrace{\frac{1}{2}m_f\left[\frac{d(u_i)_f}{dt}-\frac{d(u_i)_p}{dt_p}\right]}_{III} \\ & + \underbrace{6a^2(\pi\rho\mu)^{1/2}\int_{t_{p_o}}^{t_p}\frac{d\left[(u_i)_f-(u_i)_p\right]/d\tau}{\sqrt{t_p-\tau}}d\tau}_{IV} \\ & + \underbrace{\left(m_p-m_f\right)g_i}_{V}\end{aligned} \tag{16-10}$$

including (I) a drag force (i.e., in the direction of relative velocity), (II) forces due to fluid pressure gradient and viscous stresses, (III) virtual mass forces, (IV) the Basset force due to unsteady relative acceleration, and (V) gravitational forces (Hinze 1975; Elghobashi and Truesdell 1993; Frey et al. 1993). In Eq. (16-10), the subscript f refers to a fluid quantity, C_D is the drag coefficient, and $d(u_i)_f/dt$ is the total instantaneous acceleration of the fluid as seen by the particle at $(x_i)_p$. The BBO equation is intended for a single isolated particle, and cannot be rigorously justified outside of the Stokes regime (Clift et al. 1978). Lift forces, i.e., those acting in a direction normal to the relative velocity, may also be important, but are more difficult to model because they may arise from different mechanisms, such as shear and particle rotation (Clift et al. 1978; Stock 1996). Wiberg and Smith (1985; 1989) proposed a model for saltating particles, neglecting the Basset force and direct viscous forces but including an empirical expression for a lift force stemming only from shear. The possible importance of other lift mechanisms was also discussed. A similar study by Sekine and Kikkawa (1992) argued, however, that, at least for saltation, lift forces are negligible. For the case where $s \gg 1$, frequently encountered in the literature on two-phase flows, terms (II), (III), and (IV) are negligible, but for the conditions of interest in aqueous sediment transport, where $s = O(1)$, a priori neglecting any one of these terms is difficult to justify generally. Rigorous applications to turbulent flows require additional restrictions, including $d/\eta_K \ll 1$ (Maxey 1993; Elghobashi 1994; Stock 1996).

A solution of Eq. (16-9) can then be used to determine the trajectory, $(x_i)_p$, of the particle by integrating

$$\frac{d(x_i)_p}{dt_p} = (u_i)_p - (Z_{u_i'})_p, \tag{16-11}$$

where $(Z_{u_i'})_p$ is a random velocity-fluctuation term that models the stochastic motion of particle, if $(u_i)_p$ is assumed to be entirely deterministic.

In addition to the question of the settling velocity in turbulent flows dealt with in the preceding subsection, two other main classes of problems have been studied with the Lagrangian approach. The question of the diffusivity of solid particles in a turbulent flow relative to the diffusivity of fluid particles is a classical problem, discussed by Lumley (1973) and Hinze (1975), and more recently by Squires and Eaton (1991) and Mei and Adrian (1995). An early review in a more specifically sediment hydraulic context was given by Alonso (1981). These studies are of some relevance because they illuminate theoretically one of the empirical parameters in the transport models to be discussed later, namely the turbulent Schmidt number, $(\sigma_t)_s$, for turbulent diffusion of solid particles. The turbulent Schmidt number is defined and discussed in greater detail in Section 16.4.1.3. Under rather restrictive idealized assumptions, they predict that the particle diffusivity is less than or equal to the fluid diffusivity (i.e., $(\sigma_t)_s \geq 1$) for sedimenting particles. Unfortunately, the experimental evidence is somewhat equivocal regarding this prediction.

The other major class of problems that have been examined by means of Lagrangian models is the saltation of particles and the resulting bed load (e.g., van Rijn 1984b; Wiberg and Smith 1985). Typically, simplified versions of Eq. (16-10) were used. Rather more problematic, Eqs. (16-9) to (16-11) were integrated with time-averaged models of the fluid velocity instead of an instantaneous velocity, and did not include any stochastic component. It is not clear that the averaged, much less the instantaneous, trajectory of a particle in a turbulent flow can be predicted from such a procedure, but such a Lagrangian approach may provide an alternative more physically based starting point for developing bedload formulae. In a somewhat different application, Frey et al. (1993) computed the steady flow in a model sedimentation tank, and, based on this flow field, studied particle transport using Eqs. (16-9) to (16-11), including a stochastic component. Some of their results are given in Section 16.5.2.

16.3.3 Auxiliary Equations: Boundary Conditions—Introductory Discussion

The governing equations for the flow and the sediment (Eqs. (16-2) and (16-7)) form a system of partial differential equations that requires a specification of boundary conditions on the entire boundary of the domain being considered. Conditions at inlet and outlet boundaries are problem-dependent, and, for practical computations, are best based on laboratory or field measurements. If these are not available, then the problem of specifying these boundary conditions may be alleviated by choosing the boundaries of the computational domain sufficiently far from the region of greatest interest, such that the computational results in this region are not sensitive to exact details of the inlet and outlet conditions. For special problems, spatially periodic conditions in which inlet and outlet conditions are identical may be reasonable.

A boundary condition of special interest in sediment-transport problems is that at the bed, or at a solid boundary. The standard condition at a solid boundary, namely zero velocity, remains applicable to the instantaneous velocity, as well as to the mean and the fluctuating components. Because of the dominance of viscous effects, the elements of the Reynolds stress tensor tend to zero as the solid wall is approached. Although these wall conditions are undisputed, difficulties arise in its implementation in practical computations. For high-R problems, large gradients occur in the region adjacent to the solid boundary, and hence lead to difficulties in numerical resolution. For the rough-boundary flows of most interest in sediment transport, the detailed geometric representation of the rough wall is not feasible, and a fictitious boundary is used for modeling purposes, so that an exact bed boundary condition is not necessarily helpful. As might be expected from the preceding discussion of the uncertainties in the modeling of suspended sediment transport, an exact boundary condition on the sediment concentration at the bed is not available. The deformability of the bed/boundary due to an erodible bed introduces a further complication, such that if the details of the bed forms and their motion are of interest, then, just as in the case of the water surface, an additional boundary condition is required. In most applications, however, a simplified approach is taken in which bed details, whether small-scale sand-grain roughness or large-scale bed form, are ignored, and only their effect on the bulk flow is modeled.

The other boundary of special interest is the water surface. In most cases, a simplified approach is taken in which the water surface is treated as a rigid, i.e., nondeformable, shear-free plane lid, the location of which is known a priori. This is often implemented by treating the water surface as a plane of symmetry, with zero applied shear, analogous to the centerline of a pipe flow. In steady flows, this approximation can be justified when the appropriate Froude number is small and the direct effect of spatial variations in water surface elevations is negligible. If the water surface is treated more exactly as a free, i.e., deformable, surface, then the computational effort will be much more significant. In addition to a dynamic boundary condition, a kinematic boundary condition needs to be satisfied. These conditions per se are not unique to turbulent flows, and so are not discussed further here; the reader is referred to Liggett (1994) for details. Turbulence at a water surface, however, differs from that at a pipe centerline, so that if the effects of free-surface turbulence are of interest, then special models of free-surface turbulence may be required, even when a rigid-lid approximation is made.

In sediment transport applications, interest is usually focused on the near-bed region rather than on the free-surface region, and so detailed turbulence modeling of the latter is generally not necessary.

16.4 TURBULENCE CLOSURE MODELS

16.4.1 The Boussinesq Eddy-Viscosity Model

The turbulence closure problem arises because of the presence of the Reynolds stress tensor, $-\overline{u_i' u_j'}$, in the governing flow equations (Eq. (16-2)). Further, the effectiveness of turbulent transport relative to molecular transport has been remarked as perhaps the most important characteristic of turbulence for engineering purposes. The analogy between molecular and turbulent diffusivity has played a pervasive, some would say pernicious, role in turbulence modeling, but before this analogy is explicitly made, the basic features of molecular diffusive transport are recalled.

16.4.1.1 Molecular Transport of Momentum Consider a pure-shear steady laminar flow (Fig.16-2), in which only a single component of velocity is nonzero and varies only in one coordinate direction, $\mathbf{u} = (u_1(x_3), 0, 0)$. The only nonzero shear stress is

$$\tau_{13} = \tau_{31} = \mu \frac{du_1}{dx_3} = \nu \frac{d(\rho u_1)}{dx_3} \cdot \tag{16-12}$$

This constitutive equation (for a Newtonian fluid) relates the only nonzero shear stress *linearly* to the strain rate (here simply the velocity gradient) through the transport coefficient, μ, or its kinematic variant, $\nu = \mu/\rho$, which are *properties* of the *fluid*. Equation (16-12) is an example of a gradient-transport model, in which a flux, here the shear stress, which can be interpreted as a (negative) momentum flux, is related to a gradient of the quantity being transported, here the momentum per unit volume, i.e., ρu_1.

At the molecular level, this shear stress or momentum flux is effected by molecules in random motion. If the instantaneous fluctuating velocities of molecules in the x_1 and x_3 directions are denoted as u_1'' and u_3'', then the shear stress can also be written as $\tau_{12} = \rho \overline{u_1'' u_3''}$, exactly analogously to a Reynolds shear stress. Moreover, for ideal gases, a rigorous result can be obtained for ν using kinetic theory, namely,

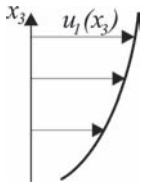

Fig. 16-2. Laminar shear flow.

$$\nu \alpha\, u_{th} \mathcal{L}_{mfp} \tag{16-13}$$

where

u_{th} = average molecular thermal velocity and
$\mathcal{L}_{mfp}$ = molecular mean free path, i.e., the average distance a molecule travels before a collision with another molecule.

This motivates an analogous treatment of turbulent transport, which is effected by random fluid motion rather than random molecular motion. Equation (16-13), however, can only be justified if the length scale over which u_1 varies is much larger than $\mathcal{L}_{mfp}$ and the time scale of the mean flow (measured by $(du_1/dx_2)^{-1}$) is much longer than molecular time scales (measured by $(u_{th}/\mathcal{L}_{mfp})^{-1}$). This is evidently satisfied for the case of molecular transport, but, as will be argued below, the equivalent condition is clearly not satisfied in the case of turbulent transport.

16.4.1.2 The Eddy Viscosity For multidimensional problems, the analogy between molecular and turbulent transport can be expressed in a general form as

$$\begin{aligned} -\overline{u_i' u_j'} &= \nu_t (2\bar{S}_{ij}) - \frac{2}{3} k \delta_{ij} \\ &= \nu_t \left(\frac{\partial \bar{u}_i}{\partial x_j} + \frac{\partial \bar{u}_j}{\partial x_i} \right) - \frac{2}{3} k \delta_{ij} \end{aligned} \tag{16-14}$$

which will be termed the Boussinesq eddy-viscosity model (BEVM), where ν_t denotes a (kinematic) turbulent eddy viscosity. An expanded version of Eq. (16-14) is given in Appendix I as Eq. (16-79). The mean strain-rate tensor

$$\bar{S}_{ij} = \frac{1}{2} \left(\frac{\partial \bar{u}_i}{\partial x_j} + \frac{\partial \bar{u}_j}{\partial x_i} \right) \tag{16-15}$$

and the Kronecker delta tensor $\delta_{ij} = 1$ for $i = j$ and $\delta_{ij} = 0$ for $i \neq j$. Eq. (16-14) specifies the Reynolds stress tensor in terms of gradients of the mean flow, and thus makes progress in closing the system, Eq. (16-2). It remains to specify ν_t, which is no longer a fluid property like its molecular counterpart, ν, but rather depends on the local flow state. Hence, ν_t will in general vary spatially within a flow and differ in different types of flows even with the same fluid.

The term, $(2/3)k\delta_{ij}$, is necessary for consistency with the definition of the turbulent kinetic energy (Eq. (16-5), since the sum $\overline{u_i' u_j'} = 2k$), and acts as an effective pressure. When Eq. (16-14) is substituted into Eqs. (16-2), this term can be absorbed into the pressure-gradient term. Hence, even though k appears explicitly in Eq. (16-14), it does not necessarily have to be determined independently.

Example. When Eq. (16-14) is applied to a steady plane uniform flow, the only relevant elements of $-\overline{u_i' u_j'}$ are obtained as

$$-\overline{u_1' u_3'} = \nu_t \frac{\partial \bar{u}_1}{\partial x_3} \tag{16-16a}$$

$$-\overline{u'_2u'_3} = \nu_t \frac{\partial \overline{u}_2}{\partial x_3} \tag{16-16b}$$

$$-\overline{u'_3u'_3} = 2\nu_t \frac{\partial \overline{u}_3}{\partial x_3} - \frac{2}{3}k \tag{16-16c}$$

thereby yielding for momentum conservation

$$0 = \frac{\partial}{\partial x_3}\left[(\nu_t + \nu)\frac{\partial \overline{u}_1}{\partial x_3}\right] + g\sin\theta$$

$$= \frac{\partial}{\partial x_3}\left(\frac{\overline{\tau}_{13}}{\rho_{\text{ref}}}\right) + g\sin\theta \tag{16-17a}$$

$$0 = -\frac{\partial}{\partial x_3}\left(\frac{\overline{P}}{\rho_{\text{ref}}}\right) - g\cos\theta \tag{16-17b}$$

In Eqs. (16-17), the conditions, $\overline{u}_2 = \overline{u}_3 = 0$, $\nu = \mu/\rho_{\text{ref}}$ have been used, an effective pressure has been redefined as $\overline{p} = \overline{p} + (2/3)\rho_{\text{ref}}k$, and $\overline{\tau}_{13} = \rho_{\text{ref}}(\nu_t + \nu)(\partial \overline{u}_1/\partial x_3)$. To solve for $\overline{u}_1$, a specification for ν_t is still needed. Equations (16-17) can be integrated over x_3, and, with the imposition of the condition that, at $x_3 = 0$, $\overline{\tau}_{13} = \rho_{\text{ref}}u_*^2$, where $u_* = \sqrt{gh\sin\theta}$ is the shear velocity, and at the free surface, $x_3 = h$, $\overline{\tau}_{13} = 0$, the following result is obtained:

$$\frac{\overline{\tau}_{13}}{\rho_{\text{ref}}} = u_*^2\left(1 - \frac{x_3}{h}\right) \tag{16-18a}$$

$$\approx -\overline{u'_1u'_3} \tag{16-18b}$$

where the second relation assumes a region sufficiently far from the bed that molecular viscous effects are negligible. Equations (16-18) already point to u_* as the appropriate scale for the turbulent velocity fluctuations in wall-bounded flows.

16.4.1.3 The Eddy Diffusivity and the Turbulent Schmidt Number A close analogy holds between the viscous transport of momentum and the diffusive (molecular) transport of heat or a solute species. In laminar flows, both momentum and mass diffusion are typically assumed to follow a gradient-transport law, with constant transport coefficients that are properties of the fluid and, in the case of mass transport, of the solute. The ratio of the molecular kinematic viscosity to the molecular diffusivity, termed the Schmidt number and denoted as σ, is necessarily constant, depending again only on the carrier fluid and the solute.

With the analogies between laminar and turbulent transport of momentum, and between mass and momentum transport, the extension of Eq. (16-14) to mass (sediment) transport applications in turbulent flows is naturally motivated. Unlike momentum, which is a vector, mass or concentration is a scalar. The turbulent mass fluxes are therefore assumed to follow a gradient-transport law of the form

$$\overline{u'_j c'} = -\epsilon_c \frac{\partial \overline{c}}{\partial x_j} = -\frac{\nu_t}{\sigma_t}\frac{\partial \overline{c}}{\partial x_j} \tag{16-19}$$

where the eddy diffusivity, ϵ_c, is specified as being proportional to the turbulent kinematic viscosity, ν_t. The turbulent Schmidt number, σ_t, is defined as the ratio of the turbulent eddy viscosity to the turbulent diffusivity of the relevant transported scalar,

$$\sigma_t = \frac{\nu_t}{\epsilon_c} \tag{16-20}$$

In traditional sediment transport hydraulics, the reciprocal of σ_t, denoted as β_s, is more often encountered; i.e., $\epsilon_s = \beta_s\nu_t = [1/(\sigma_t)_s]\nu_t$. Unlike its laminar counterpart, σ_t will not depend solely on fluid and species properties, but, like ν_t, may in general depend on local flow conditions. It is usually assumed to be constant spatially, though the justification for this is based more on convenience and ignorance than on theory. Another complication arises from the anisotropy of particle diffusivity for sedimenting particles, whereby vertical diffusivity differs from horizontal diffusivity (Lumley 1973). Further, because the large-scale transport and mixing effected by turbulent eddies is relatively insensitive to the transported quantity, whether momentum, heat, or mass, σ_t is $O(1)$ in contrast to σ, which may vary widely, e.g., for salt in water, $\sigma = O(10^3)$. A strict interpretation of the Reynolds analogy between momentum and mass turbulent transport would imply $\sigma_t = 1$.

The appropriate turbulent Schmidt number for sediment, $(\sigma_t)_s = 1/\beta_s$, has been much debated, and various prescriptions have been given (see the discussion in Davies 1995). Most studies (e.g., Li and Davies 1996; Olsen and Kjellesvig 1999; Wu et al. 2000) have simply chosen $(\sigma_t)_s = 1$, implicitly assuming the strict Reynolds analogy. Such a choice could plausibly be justified if d/η_K and w_s/u_* were sufficiently small. On the other hand, for a molecular scalar, e.g., an average value of $\sigma_t = 0.7$ is given by Launder (1978). For boundary-layer flows, which may be particularly relevant to the channel flows of sediment transport, the model of Rotta (1964) prescribes a σ_t varying from 0.9 in the near-wall region to a value of 0.5 toward the outer edge of the boundary layer.

The estimation of $(\sigma_t)_s$ from measurements is still problematic. Its basic definition (Eqs. 16-19) relies on local estimates of sediment and momentum fluxes that require estimation of gradients from noisy and often sparse point measurements. Consequently, these estimates can be erratic, but have the advantages that no additional model assumptions need to be made and a spatially variable $(\sigma_t)_s$ is allowed. Traditionally, β_s has been estimated by assuming specific velocity and concentration profiles for uniform sediment-laden flows over a plane bed and fitting these to measured profiles in uniform sediment-laden flow. Such an integral approach results in smoother estimates but rests on

dubious profile assumptions. Unfortunately, these different approaches may yield quite disparate estimates. An estimate of β_s based on fitting to a Rouse-type profile may be significantly *smaller* than an estimate based on local gradients.

Based on the flume studies of Coleman (1970), in which sediment diffusivity was estimated from local gradients, van Rijn (1984c) proposed that

$$(\beta_s)_{vR} = 1 + 2\,(w_s/u_*)^2,\ 0.1 < w_s/u_* < 1 \qquad (16\text{-}21)$$

Two aspects of the Coleman data deserve mention: (1) the relatively small width-to-depth ratio (< 3) raises questions regarding the effects of secondary currents, and (2) the lack of an equilibrium sand bed raises doubts regarding the extent to which the flows studied were actually "saturated," and therefore applicable to real equilibrium-bed cases. One version of the earlier model of Einstein and Chien (1954) related the fitted Rouse exponent, Z_R, to $(Z_R)_{\text{ref}} \equiv w_s/\kappa u_*$, and can be expressed as

$$(\beta_s)_{E-C} = \exp\left[\frac{(Z_R)_{\text{ref}}\, C_{E-C}}{\sqrt{\pi}}\right] + (Z_R)_{\text{ref}}\, C_{E-C}\, \text{erf}\left[\frac{(Z_R)_{\text{ref}}\, C_{E-C}}{\sqrt{\pi}}\right] \qquad (16\text{-}22)$$

with

$C_{E,C} = \ln 1.3$.

Both relations satisfy $(\sigma_t)_s \le 1$, and $(\sigma_t)_s \to 1$ as $w_s/u_* \to 0$.

Local estimates of $(\sigma_t)_s$ from uniform flows over a plane equilibrium beds are plotted in Fig. 16-3a; a large scatter is evident. The data of Cellino and Graf (1999) are interesting as an example of direct measurements of momentum and sediment fluxes using acoustic Doppler techniques. Their values, however, seem excessive (values in the region $z/h < 0.4$ consistently exceed 3, and so are not plotted) and remains to be independently supported. Experimental evidence for spatial variation in $(\sigma_t)_s$ is particularly strong in the Barton and Lin (1955) and Cellino and Graf (1999) data, with $(\sigma_t)_s$ decreasing toward the

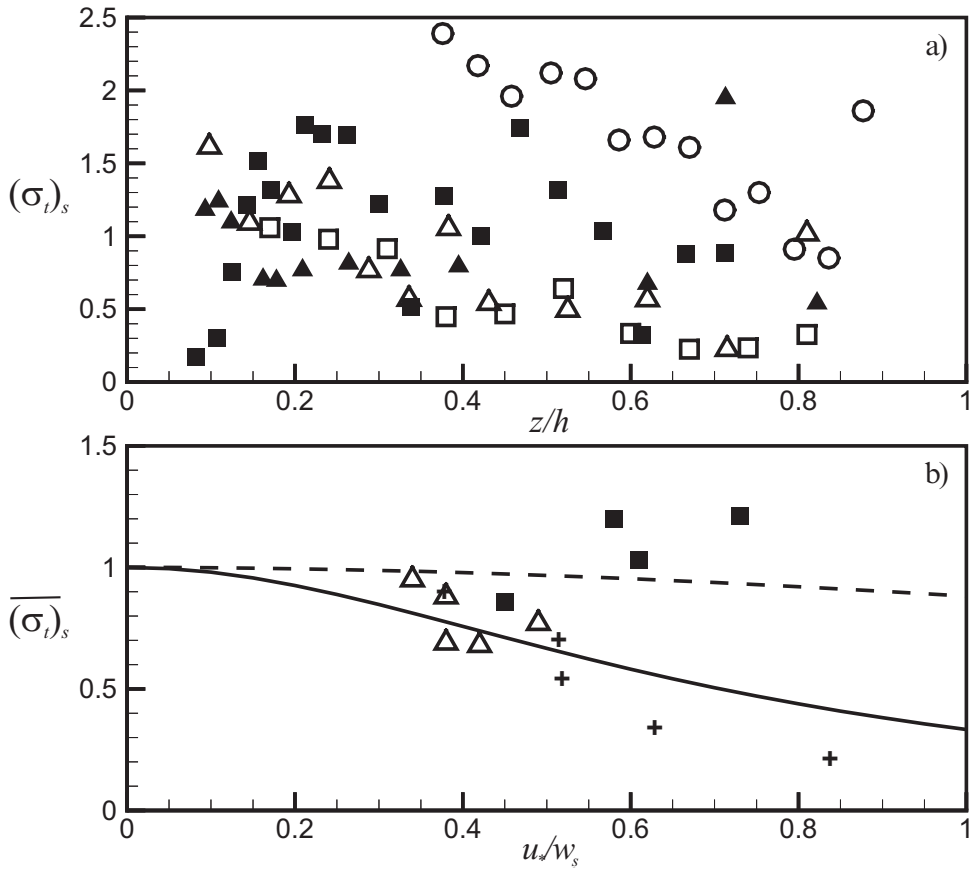

Fig. 16-3. (a) Local estimates of $(\sigma_t)_s$ for uniform flow over a plane equilibrium bed as a function of relative distance, z/h, from the bed: ○, Cellino and Graf (1999, $u_*/w_s = 0.27$, Run SAT S015); ■, Lyn (1988, $u_*/w_s = 0.73$, Run EQ2565); ▲, Lyn (1988, $u_*/w_s = 0.45$, Run EQ1665); □, Barton and Lin (1955, $u_*/w_s = 0.52$, Run 31); △, Barton and Lin (1955, $u_*/w_s = 0.36$, Run 36). (b) Averaged (over $0.1 < z/h < 0.5$) values of $(\sigma_t)_s$ as a function of u_*/w_s: △ Barton and Lin (1955); +, Coleman (1970), ■, Lyn (1988).

free surface, a variation consistent with the already-mentioned Rotta model for a flat-plate boundary-layer flow. Though scatter clouds the issue, the data, especially in the practically important near-bed region, point to the possibility of $(\sigma_t)_s > 1$, contrary to both Eqs. (16-21) and (16-22). For a spatially varying $(\sigma_t)_s$, the question of its dependence on u_*/w_s becomes complicated. The Lyn (1988) data generally indicate an increase in $(\sigma_t)_s$ with increasing u_*/w_s, whereas the Barton and Lin (1955) data exhibit the opposite tendency. The two studies, however, cover somewhat different ranges of u_*/w_s, and so the observed trends may not be entirely inconsistent.

As a simplification, the modeler may elect to use a constant averaged value of $(\sigma_t)_s$. Figure 16.3b shows values of $\overline{(\sigma_t)_s}$ (averaged over $0.1 \le y/h \le 0.5$, because this region carries the bulk of the suspended sediment) for different values of u_*/w_s. Also plotted are curves corresponding to Eqs. (16-21) and (16-22) (for the latter, a value of $\kappa = 0.4$ has been assumed).The different behavior of $(\sigma_t)_s$ with respect to u_*/w_s in the different studies discussed above can still be seen in the averaged quantities. The van Rijn model not surprisingly agrees well with the Coleman data on which it was based. The behavior of the Einstein–Chien model, which was based on traditional fitting to a Rouse profile, relative to the van Rijn model is also expected in that integral estimates of β_s based on the Rouse profile will generally yield values closer to unity than local estimates (assuming a clear-water value of $\kappa \approx 0.4$).

The preceding was concerned only with uniform flows homogeneous in the streamwise direction. In nonuniform flows, even more complications may be expected. That the appropriate value of $(\sigma_t)_s$ may vary not only with distance from the wall but also in the streamwise direction was observed by Celik and Rodi (1988), who simulated the experiments of Jobson and Sayre (1970) and found that better predictions were achieved with different values of $(\sigma_t)_s$ at different streamwise stations. Ouillon and le Guennec (1996), simulating the same experiment, showed that the $\overline{c}$–profiles nearer the inlet can even be well predicted by choosing $(\sigma_t)_s = \infty$, i.e., without any turbulent transport. They also found that agreement with measurements was improved by choosing different values of $(\sigma_t)_s$, ranging from 0.6 to 1, depending on the type of flow-bed interaction, i.e., on whether deposition to or entrainment from the bed was occurring. In practical computations with the k–ϵ model to be described, and where $(\sigma_t)_s$ is interpreted more as a model-tuning parameter that might compensate for model deficiencies and hence might be model-dependent, then experience indicates that $(\sigma_t)_s \le 1$ (or $\beta_s \ge 1$) will yield better results, though a definitive conclusion is still to be reached.

In view of the difficulties associated with specifying $(\sigma_t)_s$, alternative approaches that avoid it altogether or attempt to specify it more completely might be sought. The conceptual model of Lyn (1988) does not rely on an eddy-diffusivity model and hence does not require a $(\sigma_t)_s$, but makes quite restrictive similarity assumptions that apply only in simple flows such as uniform plane-bed flows. Two-phase-flow models, such as that of Greimann et al. (1999), may offer some guidance, because an explicit expression for $(\sigma_t)_s$ in terms of local flow and suspension parameters can be derived, though other constant(s) may need to be specified. A second-order model (a brief introductory discussion of second-order modeling is given in Section 16.4.7) for sediment concentration could also conceivably do without an eddy-diffusivity model. This would, however, not only likely require specifying *other* model "constants" but even in second-order turbulence models for singe-phase flows, isotropic-turbulent-viscosity models with turbulent Schmidt numbers remain popular for numerical reasons (see the discussion in Lien and Leschziner 1994).

Example. For the simple uniform-flow case, Eq. (16-7) with Eq. (16-19) reduces to

$$0 = \frac{\partial (w_s \bar{c})}{\partial z} + \frac{\partial \left(-\overline{w'c'}\right)}{\partial z} = \frac{\partial (w_s \bar{c})}{\partial z} + \frac{\partial}{\partial z}\left(\frac{\nu_t}{\sigma_c}\frac{\partial \bar{c}}{\partial z}\right) \tag{16-23}$$

where u'_3 and x_3 have been rewritten as w' and z, respectively. This can be integrated once, and, with the imposition of a no-flux condition at the water surface, yields the familiar

$$-\overline{w'c'} + w_s \bar{c} = \frac{\nu_t}{(\sigma_t)_s}\frac{d\bar{c}}{dz} + w_s \bar{c} = 0 \tag{16-24}$$

As with the momentum equations, a complete solution awaits a specification of ν_t (and $(\sigma_t)_s$).

16.4.2 The Specification of the Eddy Viscosity: Zero-Equation Models

A kinematic viscosity (or diffusivity) may be considered as a product of a velocity scale, u, and a length scale, $\mathcal{L}$. A prescription of ν_t will in general involve specifying these two scales in terms of quantities, either already known or for which equations are already available. The additional equations governing these scales may be formulated either as algebraic equations or as differential transport equations, and hence eddy-viscosity models have conventionally been classified as zero-, one-, or two-equation models depending on the number of differential transport equations used in specifying u and $\mathcal{L}$.

16.4.2.1 Constant-Eddy-Viscosity Models Not surprisingly, the oldest turbulence models are zero-equation models, because the computational requirements are least severe. The simplest of these assume that the turbulent velocity and length scales, and hence the eddy viscosity, are effectively constant over the entire flow region of interest. The main difficulty then is the choice of an appropriate value. Calibration with measurements, possibly combined with

dimensionally based scaling arguments to extend the range of application, is recommended. In fully developed wall-bounded wide channel flows, a common choice involves the product of the shear velocity and the depth, $\nu_t \propto u_* h$. For depth-averaged models (see Appendix II), this choice for a constant horizontal eddy viscosity is often justified as the result of integrating the classic parabolic mixing-length eddy-viscosity model, discussed below, which gives the proportionality constant as $\kappa/6$, where κ is the von Kármán constant. Observed horizontal diffusivities tend to indicate a larger proportionality constant (Fischer et al. 1979), and so, for practical computations, calibration is recommended. This simplest of models is unlikely to be successful where flow details strongly influenced by turbulence, e.g., separation and reattachment, are of primary interest; where turbulence plays a secondary role, this may prove to be an economical if limited model.

16.4.2.2 Mixing-Length Models The classic zero-equation model, which remains important in current discussions of turbulence in sediment-laden flows, is the mixing-length model. Originally introduced within the context of simple turbulent shear layers by Prandtl (1925), the mixing length, $\mathcal{L}_m$, may be motivated in a scaling of turbulent velocity fluctuations with mean velocity gradients as $u', w' \sim \mathcal{L}_m \partial\overline{u}/\partial z$, where u' is the velocity fluctuation in the dominant streamwise direction, w' the corresponding fluctuation in the (z) direction across the shear layer. In this way, with the only significant correlation term $\overline{u'w'} \sim [\mathcal{L}_m(\partial\overline{u}/\partial z)]^2 \sim \nu_t(\partial\overline{u}/\partial z)$, and with a choice of the velocity scale as $\mathcal{U} = \mathcal{L}_m \partial\overline{u}/\partial z$, the eddy viscosity can be specified as

$$\nu_t = \mathcal{L}_m \mathcal{U} = \mathcal{L}_m^2 \frac{\partial \overline{u}}{\partial z} \,. \tag{16-25}$$

To close the model, it remains only to specify $\mathcal{L}_m$. Physically, $\mathcal{L}_m$ may be thought of as the size of a typical turbulent eddy at any given location. In a simple shear flow with a single dominant velocity gradient, $\mathcal{L}_m$ can usually be related to a length scale across the shear layer (in the z-coordinate direction). In the important case of channel flows, this might be chosen as proportional to the distance z from the bed in the near-bed ("inner") region, i.e., $\mathcal{L}_m \propto z$, or the flow depth, h, in the "outer" bulk-flow region, i.e., $\mathcal{L}_m \propto h$.

For plane uniform flows, with $\mathcal{L}_m \propto z$ or $\mathcal{L}_m = \kappa z$, where the von Kármán constant, κ, is the proportionality constant, and also $\tau_{13} \approx \rho u_*^2$ (from Eq. 16-18 in the near-bed region and neglecting viscous effects), the momentum equation in the streamwise direction becomes

$$-\overline{u'w'} = \nu_t \frac{d\overline{u}}{dz} = \left(\kappa z \frac{d\overline{u}}{dz}\right)^2 = u_*^2 \,. \tag{16-26}$$

The specification of ν_t has thus closed the system of equations, permitting a solution for the velocity profile. Simplification and then integration of Eq. (16-26) yield the well-known logarithmic law for the velocity profile in the near-bed region (see Chapter 2). In spite of the apparent relation to molecular transport, a detailed mechanistic analogy between turbulent and molecular transport cannot be sustained. As previously noted, a key assumption of molecular momentum transport is that the relevant length scale for molecular viscosity, the mean free path, is much smaller than the length scale over which the strain rate or velocity gradient is defined. On the other hand, $\mathcal{L}_m$ is of the same order of magnitude as the length scale over which the velocity gradient is defined, and hence the mixing length model cannot be justified by analogy with molecular transport. As has been emphasized by Tennekes and Lumley (1972), the success of the mixing-length model results from the existence of a single dominant velocity and a single dominant length scale, from which an eddy viscosity can be unambiguously formulated from dimensional considerations. In this case, u_* and z are identified as the relevant velocity and length scales, and consequently, $\nu_t \propto u_* z$, which when substituted in to Eq. (16-26) also reproduces the logarithmic velocity profile.

The specification, $\nu_t = \kappa u_* z$, can only be justified for the near-bed region (but outside of the viscous region). This exemplifies the problem of defining the turbulent length scale in a mixing-length model. Multiple length scales are important in a channel flow; e.g., the viscous length scale, ν/u_*, in the viscous sublayer, and the flow depth, h, in addition to z, and the classic mixing-length model of $\mathcal{L}_m \propto z$ can be applied only in the intermediate layer, where the local length scale is dominant. To develop an expression for ν_t that may be extended to the outer region, a somewhat circular approach is conventionally taken. Equation (16-26) is first extended to $\nu_t(\partial\overline{u}/\partial z) = u_*^2(1-z/h)$. The logarithmic velocity profile is taken as an empirical observation, such that $\partial\overline{u}/\partial z = u_*/\kappa z$. It follows then that

$$\nu_t = u_*^2 \left(\frac{1-z/h}{d\overline{u}/dz}\right) = \kappa u_* z (1-z/h) \tag{16-27}$$

which is the classic parabolic eddy viscosity for open-channel flows, on which the traditional Ippen-Rouse suspended sediment concentration profile (see Chapter. 2) is based. The measurements of Nezu and Rodi (1986) agree reasonably well with this expression, though agreement could be improved with a more appropriate velocity model (Fig. 16-4(a)) through the addition of a wake component, characterized by a wake coefficient, II, to the logarithmic velocity profile. Equation (16-27) is also the basis of the constant-eddy-viscosity depth-averaged models, since depth-averaging of Eq. (16-27) yields $\kappa u_* h/6$. With similar reasoning, the following expression for the mixing length, $\mathcal{L}_m$, can be obtained:

$$\mathcal{L}_m = \kappa z[1-(z/h)]^{1/2} \tag{16-28}$$

Again, measurements show reasonable agreement with Eq. (16-28) (Fig. 16-4(b)). Equation (16-27) has also been applied to unsteady oscillating boundary flows under waves,

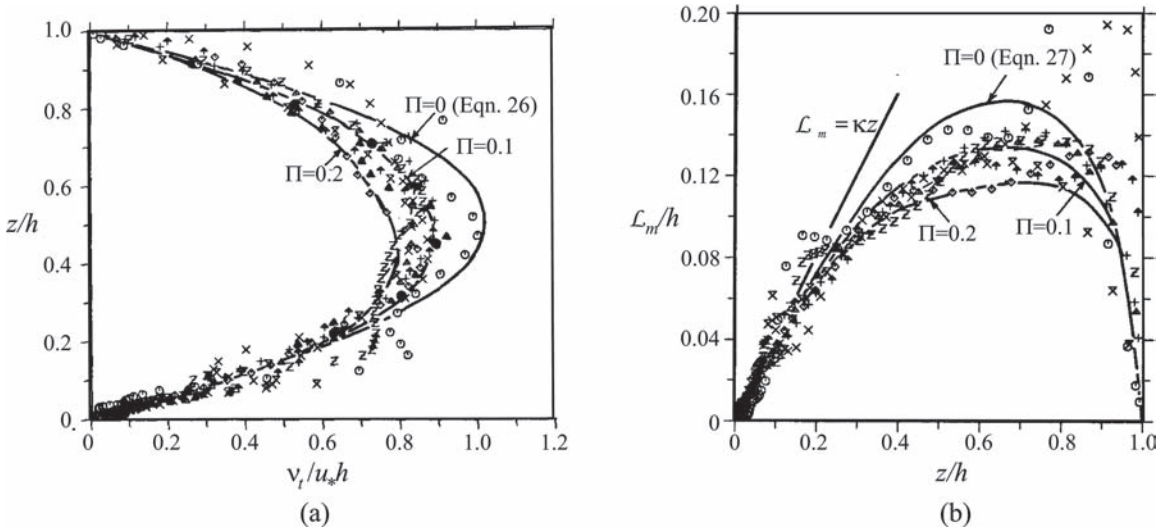

Fig. 16-4. (a) Nondimensional eddy viscosity, ν_t/u_*h, and (b) mixing length, $\mathcal{L}_m/h$, in a clear-water flow in a straight open channel (adapted from Nezu and Rodi 1986). Symbols are measurements; lines are theory based on a model mean velocity profile, incorporating a log-law and a wake component, with Π being the wake coefficient in the model velocity profile.

with u_* and $h = \delta_w$, where δ_w is the wave boundary layer thickness, both of which are allowed to vary in time (Fredsoe et al. 1985).

16.4.2.3 Turbulence Modulation and the Stably Stratified-Flow Analogy The effect of the suspension on the turbulent flow, sometimes termed turbulence modulation or modification, has been discussed extensively since the experimental work of Vanoni (1946), which showed a distinct steepening of the velocity profile in sediment-laden flows compared to profiles in clear-water flows. The traditional approach has been to model this effect by a reduced mixing length, via a reduced κ, and to develop a correlation for κ, e.g., as a function of a ratio of the energy required to suspend particles to the total energy dissipated by the flow (Einstein and Chien 1955). Figure 16-5 compares the eddy viscosity and mixing length for clear-water and suspension flows, plotted in semilogarithmic coordinates to emphasize the near-bed region. There is much scatter, but the evidence, if any, for a reduced eddy viscosity and mixing length

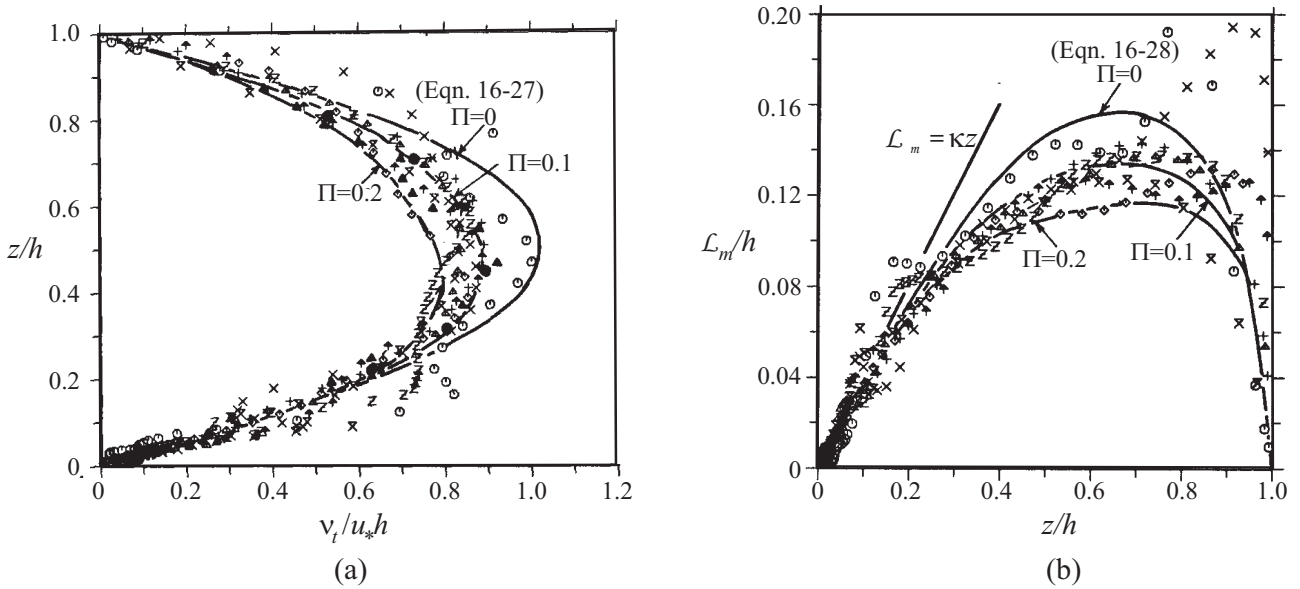

Fig. 16-5. (a) Nondimensional eddy viscosity, ν_t/u_*h, and (b) mixing length, $\mathcal{L}_m/h$, in a sediment-laden flow in a straight open channel (estimated from the data of Lyn 1988; open symbols: clear-water flow, filled symbols: sediment-laden flow).

is primarily in the inner region. The results of Cellino and Graf (1999) for a case with a smaller sand size and heavier load indicate a more substantial reduction in eddy viscosity over a more extensive region.

Only two models explicitly using the mixing-length approach are here discussed. Like the traditional model, both may be interpreted as resulting in a reduced mixing length, but whereas the traditional model assumes a constant proportional reduction over the entire depth, the two models propose a reduction dependent on local suspension conditions, either on the local concentration (van Rijn 1984c) or the local concentration gradient (Smith and McLean 1977). The van Rijn model modifies the standard eddy viscosity for flows without sediment, $(\nu_t)_0$, by a function, ϕ, dependent on the local mean suspended sediment concentration, $\bar{c}$, to obtain an eddy viscosity for a suspension, $(\nu_t)_s$, as follows:

$$(\nu_t)_s = \phi(\nu_t)_0 = \left[1 - 2\left(\frac{\bar{c}}{c_0}\right)^{0.4} + \left(\frac{\bar{c}}{c_0}\right)^{0.8}\right](\nu_t)_0 \quad (16\text{-}29)$$

where c_0 is the maximum possible volumetric sediment concentration, taken to be 0.65. The physical basis for Eq. (16-29) is obscure, and van Rijn (1984c) admitted that it "does not give optimal agreement for the entire profile," conjecturing that the expression for ϕ is "somewhat too simple."

Example. As has been noted, an analogy between a sediment-laden flow and the flow of a variable-density fluid has been drawn frequently by numerous researchers (e.g., Barenblatt 1953; Lumley 1973). For uniform flow, with variations only in the vertical, the effective density of the suspension, ρ_m (Eq. 16-3), decreases away from the bed as $\bar{c}$ decreases with increasing z. Vertical turbulent momentum transport is therefore inhibited relative to the nonstratified (neutral) case because fluid of vertically varying density displaced from its original elevation experiences a restoring buoyancy force acting to return it to its original elevation: i.e., the flow is stably stratified. The reduced vertical transport results in a velocity profile steeper than the neutral case, which, as noted above, is observed in sediment-laden flows. The analogy is attractive not only for its intuitive appeal, but also because it allows the application of results from a large literature on turbulent, stably (thermally or saline) density-stratified flows in atmospheric and oceanographic applications (Monin and Yaglom 1971; Turner 1973).

Smith and McLean (1977) proposed a density-stratified-flow model for sediment-laden flows, in which the effective mixing length is reduced, but, unlike the van Rijn model, the reduction is correlated with a suspension (gradient) Richardson number, Ri_s, defined as

$$\mathrm{Ri}_s = -\frac{g}{\rho_{\mathrm{ref}}}\frac{\partial\rho_m/\partial z}{(\partial\bar{u}/\partial z)^2} = -g(s-1)\frac{\partial\bar{c}/\partial z}{(\partial\bar{u}/\partial z)^2} \quad (16\text{-}30)$$

where ρ_{ref} has been taken to be ρ. Barenblatt (1996) has suggested that Ri_s be called the Kolmogorov number. As will become clearer below, for stable stratification, $\mathrm{Ri}_s > 0$ can be interpreted as being proportional to the ratio of the local rate of energy expenditure needed to overcome a stable stratification and the local rate of production of k (similar to the traditional Einstein–Chien (1955) model). In the Smith-McLean model,

$$(\nu_t)_s = \left[1 - \alpha_m\left\{\frac{\epsilon_s}{(\nu_t)_s}\right\}\mathrm{Ri}_s\right](\nu_t)_0 \quad (16\text{-}31)$$

where α_m is a model constant. Here, $\epsilon_s/(\nu_t)_s$ is seen as equivalent to $1/(\sigma_t)_s$, but, contrary to the usual practice where $(\sigma_t)_s$ is assumed constant in space (e.g., as in the van Rijn model), $\epsilon_s/(\nu_t)_s$ can be expressed as a spatially varying function in terms of other model parameters. Villaret and Trowbridge (1991) analyzed the performance of this model (actually a perturbation solution of this model, since, for most of the laboratory flows examined, $\mathrm{Ri}_s \ll 1$) in fitting an extensive series of laboratory measurements from various studies. They found some support for the stratified-flow model, but their results indicate that α_m might vary considerably, detracting from one of the main advantages of this model.

In contrast to the traditional approach, in which the solution for the velocity profile is effectively decoupled from the solution for the suspended sediment concentration profile, both the van Rijn and the Smith-McLean models require a fully coupled treatment, in which the relevant momentum and sediment equations are solved simultaneously. These two models may be expressed respectively as follows:

Van Rijn model:

$$[(\nu_t)_0\phi]\frac{d\bar{u}}{dz} = u_*^2\left(1 - \frac{z}{h}\right) \quad (16\text{-}32a)$$

$$[(\beta_s)_{\nu R}(\nu_t)_0\phi]\frac{d\bar{c}}{dz} = -w_s\bar{c} \quad (16\text{-}32b)$$

Smith-McLean model:

$$\begin{aligned}(\nu_t)_s\frac{d\bar{u}}{dz} &= (\nu_t)_0\left[1 - \alpha_m\left\{\frac{\varepsilon_s}{(\nu_t)_s}\right\}\mathrm{Ri}_s\right]\frac{d\bar{u}}{dz} \\ &= u_*^2\left(1 - \frac{z}{h}\right)\end{aligned} \quad (16\text{-}33a)$$

$$\varepsilon_s \frac{d\bar{c}}{dz} = (\nu_t)_0 \left[1 - \alpha_s \left\{ \frac{\varepsilon_s}{(\nu_t)_s} \right\} \mathrm{Ri}_s \right] \frac{d\bar{c}}{dz} = -w_s \bar{c} \tag{16-33b}$$

where α_s is another model constant.

A comparison of the predictions of the van Rijn and Smith-McLean models with two measured velocity and concentration profiles for flows under equilibrium-bed (capacity or saturated) conditions is given in Fig. 16-6. The experimental parameters are given in Table 16-1. In these computations, different models of $(\nu_t)_0$ were used. The $(\nu_t)_0$ of van Rijn (1984b) was used for the van Rijn model, whereas the $(\nu_t)_0$ of Villaret and Trowbridge (1991) was used for the Smith-McLean model. Bottom boundary conditions were based on measured velocity and concentration, and α_m and α_s were taken as 6.9 and 9.2, as specified in McLean (1992). According to the classification scheme of Soulsby and Wainwright (1987), based on u_* and d, both of the experiments should exhibit some stratification effects ($u_* \approx 4$ cm/s and $d_{50} \approx 0.18$–0.19 mm). Estimates of local flux Richardson numbers from the measurements indicate values exceeding $O(0.01)$ in both experiments. Both models perform reasonably well for both the velocity and concentration data of Barton and Lin, although slight systematic deviation of the data from predictions might be seen. The van Rijn model does somewhat better in predicting concentrations than the Smith-McLean model, which underestimates concentrations in the outer flow ($z/h = O(1)$), due to the reduced mixing caused by stable stratification. The Barton-Lin data were used in the calibration of the van Rijn model, and so good performance might be expected. Both models do comparatively poorly for the Lyn velocity data, which exhibit a much more pronounced deviation from the log-law profile that is, however, confined to the near-bed region. At the measured concentration values, both models predict profiles quite close to the classic log-law profile. Hence when the measured velocity at the lowest point is imposed as a boundary condition, there is notable disparity between measured and predicted profiles. Nevertheless, the Lyn concentration data are quite well reproduced by the Smith-McLean model, where as the van Rijn model predictions are substantially in error, attributable to the overly large β_s value given by Eq. (16-21) and the associated enhanced vertical sediment transport.

The problem of predicting the velocity and concentration profiles in a suspension flow over a nominally plane bed is still largely unresolved. Two other related aspects of uniform sediment-laden flows over plane beds shed light on appropriate models, namely flow resistance, e.g., parameterized by a friction factor, f_{DW}, and the root mean square of vertical velocity fluctuations, $\sqrt{\overline{w'^2}}$. In their purest (and simplest) form, the stably stratified-flow models predict

Table 16-1 Experimental Parameters for Equilibrium Plane-Bed Flows

Parameter	Barton and Lin (1955) Run 36	Lyn (1988) Run 1957EQ
Median sediment size, d_{50} (mm)	0.18	0.19
Depth, h (cm)	16.2	5.7
Shear velocity, u_* (cm/s)	5.6	3.95
$\bar{c}(z/h = 0.1)$ ($\times 10^{-3}$)	3.1	1.1
Slope, S ($\times 10^{-3}$)	2.10	2.95
$\mathsf{R}_\star = u^*h/\nu$ ($\times 10^3$)	9.1	2.3
$\mathsf{F} = U/\sqrt{gh_0}$	0.21	0.90

a decrease in f_{DW} (e.g., Itakura and Kishi 1980; McLean 1992) and a reduction in $\sqrt{\overline{w'^2}}$ in suspension flows. The choice of an appropriate benchmark or reference for comparison is important, because, unlike stratification due to temperature or salinity, density stratification in sediment-laden flows may be only one of several factors influencing flow characteristics. In the case of flow resistance, if the basis of comparison is a clear-water flow of the same depth and a roughness height equal to the *median grain size*, d_{50}, as is commonly done in clear-water flows, then the empirical evidence argues *against* this prediction of the stably stratified flow models (see the discussion below of boundary conditions for further details). In the case of $\sqrt{\overline{w'^2}}$, the laser-Doppler studies of Lyn (1993) and Bennett et al. (1998) indicate either no significant effect or indeed the opposite effect, namely, a slight increase in, contrary to that expected from stably stratified-flow analogies. On the other hand, Cellino and Graf (1999), using an acoustic Doppler technique, did observe a marked reduction in $\sqrt{\overline{w'^2}}/\mu_*$, and so the experimental evidence is at present inconclusive. Measurements of turbulence characteristics in the most interesting flow region, i.e., the near-wall region, in a sediment-laden flow over a plane sand bed in equilibrium with the suspension present very difficult challenges to all experimental techniques, and hence any such measurements should be considered with some caution.

The stably stratified flow analogy has been discussed here within the context of mixing-length models, but similar comments would also apply to the more sophisticated models discussed below, since they, as will be seen, may often be simplified to essentially mixing-length models for uniform-flow problems.

16.4.2.4 Limitations of Mixing-Length Models The success of the mixing-length model rests on the dominance of a single velocity and a single length scale, which also, as will be seen below, reflects a local equilibrium between production and dissipation of turbulent kinetic energy.

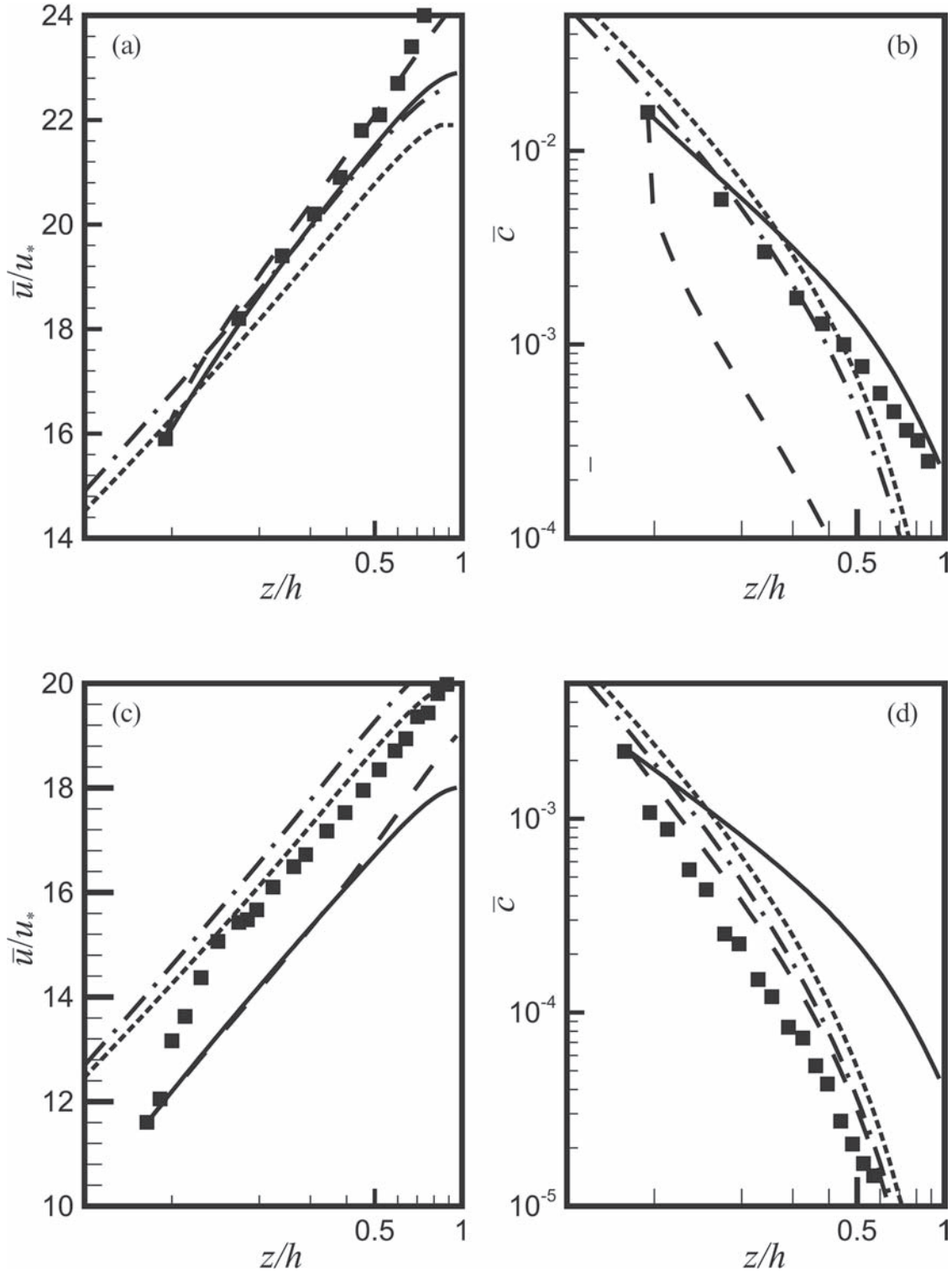

Fig. 16-6. Comparison of model predictions for steady uniform sediment-laden flows of (a) and (c) dimensionless velocity, $\bar{u}/u_*$, and (b) and (d) concentration, $\bar{c}$. Data (filled symbols) in (a) and (b) from Barton and Lin (1955), Run 36; data in (c) and (d) from Lyn (1988), Run 1957EQ. ——— : van Rijn model; — — : Smith-McLean model; … : standard $k-\epsilon$ model; –·–·– : $k-\epsilon$ model including buoyancy.

In multidimensional problems with strong spatial variation in more than one coordinate direction, the mixing-length model will likely perform poorly. Generalizations of Eq. (16-25) to multidimensional flows have been proposed, but the practical difficulty of specifying $\mathcal{L}_m$ for complicated flows remains. Nonequilibrium problems where history/transport effects are important will also present difficulties because of the time required to relax to an equilibrium state, which introduces another time (or velocity) scale into the problem. On the other hand, a great deal of practical experience has been accumulated with such models in a wide variety of problems, the computational demands are attractive, and reasonable predictions can be obtained with some degree of experience and judgment on the part of the modeler. The problem of turbulence modulation does illustrate the fundamental weakness of mixing-length models (as well as other more sophisticated models) in that the appropriate mixing length when the flow is sediment-laden is not clear, even for the simplest case of a fully developed uniform wall-bounded flow.

16.4.3 The Specification of the Eddy Viscosity: One-Equation Models

An algebraic specification of the eddy viscosity, as in zero-equation models, may be interpreted as implicitly assuming a local equilibrium where ν_t is determined entirely by local flow conditions. Nonequilibrium effects imply that the flow characteristics at a point may be significantly affected by the history of fluid parcels passing through that point. Zero-equation turbulence models are poorly suited to model such effects in any general way. An alternative approach seeks to include these effects in a differential rather than algebraic specification of the velocity scale, the length scale, or both. In one-equation models, a single differential equation for a turbulence quantity is formulated in addition to the momentum equations. Most frequently, the quantity chosen is the turbulent kinetic energy, k, the square root of which provides a velocity scale.

16.4.3.1 The Equation for Turbulent Kinetic Energy An exact equation for k can be derived from the Navier-Stokes equations (Hinze 1975; Kundu 1990):

$$\begin{aligned}\frac{Dk}{Dt} &= \frac{\partial k}{\partial t} + \frac{\partial\left(\overline{u}_j k\right)}{\partial x_j} \\ &= -\frac{\partial}{\partial x_j}\left(\frac{1}{2}\overline{u_i' u_i' u_j'} + \frac{1}{\rho_{\text{ref}}}\overline{u_j' p} - 2\nu\overline{u_i' s_{ij}'}\right) \\ &\quad + P_k - \epsilon + G_k \end{aligned} \tag{16-34}$$

where

$s_{ij}' = (\partial u_i'/\partial x_j + \partial u_j'/\partial x_i)/2$ fluctuating strain-rate tensor.

The rate of production, P_k, of k by the interaction of the Reynolds stresses with the mean strain rate is given by

$$\begin{aligned}P_k &= -\overline{u_i' u_j'}\, S_{ij} = -\overline{u_i' u_j'}\left[\frac{1}{2}\left(\frac{\partial \overline{u}_i}{\partial x_j} + \frac{\partial \overline{u}_j}{\partial x_i}\right)\right] \\ &= -\overline{u_i' u_j'}\frac{\partial \overline{u}_i}{\partial x_j}\end{aligned} \tag{16-35}$$

(see Appendix I, Eq. (16-82) for an expanded version of Eq. (16-35)). The rate of dissipation, ϵ, of k by viscosity can be expressed as

$$\begin{aligned}\epsilon &= 2\nu\,\overline{s_{ij}' s_{ij}'} \\ &= \frac{\nu}{2}\overline{\left(\frac{\partial u_i'}{\partial x_j} + \frac{\partial u_j'}{\partial x_i}\right)\left(\frac{\partial u_i'}{\partial x_j} + \frac{\partial u_j'}{\partial x_i}\right)} \\ &= \nu\overline{\left(\frac{\partial u_i'}{\partial x_j} + \frac{\partial u_j'}{\partial x_i}\right)\frac{\partial u_i'}{\partial x_j}}\,.\end{aligned} \tag{16-36}$$

The last term in Eq. (16-34), G_k, represents any other source or sink of k that may be due to additional forces, e.g., due to the presence of particles. If buoyancy effects are important, then

$$G_k = \left(G_k\right)_\rho = \frac{g_i}{\rho_{\text{ref}}}\overline{u_i' \rho'}\,. \tag{16-37}$$

The ratio $(G_k)_\rho/P$ is termed the flux Richardson number. If, as has been assumed in several models, the sole effect of particles in suspension on the k–budget is analogous to that caused by buoyancy, then

$$\frac{g_i}{\rho_{\text{ref}}}\overline{u_i' \rho'} = g_i\left(s-1\right)\overline{u_i' c'}\,. \tag{16-38}$$

Because Eq. (16-34) contains extra correlation terms (the triple velocity correlation, $\overline{u_i' u_i' u_j'}$, and the pressure-velocity correlation, $\overline{u_j' p'}$, as well as ϵ) that are not known, it is not immediately useful. For a one-equation model based on Eq. (16-34), the length scale, $\mathcal{L}$, is specified algebraically, and so the extra correlation terms must be expressed in terms of k and/or $\mathcal{L}$ for a closed system of equations. The terms involving the triple velocity and pressure-velocity correlations are interpreted as turbulent "diffusive" transport terms that do not increase or decrease the overall level of k but only redistribute k over the flow region of interest. A diffusion model for these terms together can be motivated, namely,

$$\frac{1}{2}\overline{u_i' u_i' u_j'} + \frac{1}{\rho_{\text{ref}}}\overline{u_j' p'} = -\frac{\nu_t}{\sigma_k}\frac{\partial k}{\partial x_j} \tag{16-39}$$

where the turbulent Schmidt number for k, σ_k, is defined by Eq. (16-39) and is usually assumed constant. The model for the rate of dissipation (sink) term, ϵ, is obtained from a dimensional scaling argument as

$$\epsilon = c_D \frac{k^{3/2}}{\mathcal{L}} \tag{16-40}$$

with c_D an empirically determined model constant. With these model choices, the inclusion of a buoyancy effect for suspensions, and the neglect of the viscous diffusive term (justifiable for high-R applications), the equation for k becomes

$$\begin{aligned}\frac{Dk}{Dt} &= \frac{\partial k}{\partial t} + \frac{\partial\left(\overline{u}_j k\right)}{\partial x_j} \\ &= \frac{\partial}{\partial x_j}\left(\frac{\nu_t}{\sigma_k}\frac{\partial k}{\partial x_j}\right) + \nu_t\left(\frac{\partial \overline{u}_i}{\partial x_j} + \frac{\partial \overline{u}_j}{\partial x_i}\right)\frac{\partial \overline{u}_i}{\partial x_j} \\ &\quad - g_i\left(s-1\right)\frac{\nu_t}{\left(\sigma_t\right)_s}\frac{\partial \overline{c}}{\partial x_i} - c_D\frac{k^{3/2}}{\mathcal{L}}\end{aligned} \tag{16-41}$$

where the standard eddy viscosity (Eq. (16-14)) or diffusivity (Eq. (16-19)) model has been applied to eliminate the Reynolds stress term, $-\overline{u'_i u'_j}$, and the buoyancy flux term, $\overline{u'_i c'}$. In this form, the ratio, $(G_k)_\rho/P$, becomes proportional to the gradient Richardson number, Ri_s, already introduced in the discussion of zero-equation models. The solution of Eq. (16-41) for k provides the required μ, and so ν_t is evaluated as

$$\nu_t = c'_\mu \sqrt{k}\mathcal{L} \tag{16-42}$$

where c'_μ is a model constant. The choice of c_D and c'_μ is constrained by the requirement for consistency in the case of local equilibrium, as will be elaborated below.

16.4.3.2 Local Equilibrium and Mixing-Length Models In Eq. (16-34) or (16-41), the left-hand side of the equation and the diffusive term (the first term on the right-hand side of the equation) represent the transport terms that become important in nonequilibrium problems. In cases where these effects may be neglected, i.e., those for which the mixing-length model might be appropriate, Eq. (16-41) reduces to

$$\begin{aligned}0 &= P_k + \left(G_k\right)_\rho - \epsilon \\ &= \nu_t\left(\frac{\partial \overline{u}_i}{\partial x_j} + \frac{\partial \overline{u}_j}{\partial x_i}\right)\frac{\partial \overline{u}_i}{\partial x_j} \\ &\quad + g\left(s-1\right)\frac{\nu_t}{\left(\sigma_t\right)_s}\frac{\partial \overline{c}}{\partial z} - c_D\frac{k^{3/2}}{\mathcal{L}}.\end{aligned} \tag{16-43}$$

Example. For the plane uniform-flow case, Eq. (16-43) becomes

$$\begin{aligned}P_k + \left(G_k\right)_\rho = \epsilon \quad \text{or} \quad & \nu_t\left(\frac{d\overline{u}}{dz}\right)^2 + g\left(s-1\right)\frac{\nu_t}{\left(\sigma_t\right)_s}\frac{\partial \overline{c}}{\partial z} \\ &= c_D\frac{k^{3/2}}{\mathcal{L}}\end{aligned} \tag{16-44}$$

which, together with Eq. (16-42), becomes

$$\begin{aligned}\nu_t &= \sqrt{\frac{\left(c'_\mu\right)^3}{c_D}}\mathcal{L}^2\frac{d\overline{u}}{dz}\left[1 - \frac{1}{\left(\sigma_t\right)_s}\mathsf{Ri}_s\right]^{1/2} \\ &= \left(\nu_t\right)_0\left[1 - \frac{1}{\left(\sigma_t\right)_s}\mathsf{Ri}_s\right]^{1/2}\end{aligned} \tag{16-45}$$

where

$(\nu_t)_0$ = eddy viscosity in the absence of buoyancy effects.

If $\mathsf{Ri}_s = 0$, then Eq. (16-45) reproduces the standard model. If $\mathcal{L}$ is taken as κz, then for consistency with the mixing-length model, the constants c'_μ and c_D must be chosen so that $(c'_\mu)^3/c_D = 1$, and cannot be chosen independently. For nonzero but small Ri_s, $[1 - \mathsf{Ri}_s/(\sigma_t)_s]^{1/2}$ can be expanded in a power series in Ri_s, and a relationship of the same form as Eq. (16-31) is obtained. The inclusion of buoyancy effects adds another relevant velocity (or length) scale, e.g., $\sqrt{g(s-1)\mathcal{L}^2(\partial\overline{c}/\partial z)}$, to the problem, and so introduces an ambiguity into the mixing-length model, which, as was argued above, relies on the dominance of a single velocity and a single length scale. An interesting alternative approach was taken by Barenblatt (1953; reported in Monin and Yaglom 1971 and in Barenblatt 1996), who sought similarity solutions to Eq. (16-44). With $k \sim u_*^2$, $\mathcal{L} \sim z$, and $\nu_t \sim \sqrt{k}\mathcal{L} \sim u_* z$, these could be found when $\overline{c} \sim 1/z$ and $\partial\overline{u}/\partial z \sim 1/z$, equivalent to a constant Ri_s, though the implications, practical or theoretical, of this result remain unclear.

16.4.3.3 Applications of a One-Equation Model Because of their intermediate nature between the simpler zero-equation model and the more complete two-equation model, one-equation models not making the local-equilibrium assumption have not been as commonly used in hydraulic or sediment-transport engineering as either of the other two model types. Two examples may, however, be cited. In a study of sand-wave evolution due to sediment transport, Johns et al. (1990) applied a quasi-two-dimensional model based on Eqs. (16-41) and (16-42) including buoyancy effects. Nonequilibrium transport effects might be expected because of the streamwise spatial variations in flow over bed

forms. All turbulent Schmidt numbers were assumed to be unity, whereas $c_D=(c'_\mu)^3= 0.15$, with $c'_\mu = 0.53$. The length scale was determined from a von Kármán type relationship (see the discussion in Rodi 1993),

$$\mathcal{L} = \frac{-\kappa\sqrt{k}/\mathcal{L}}{d\left(\sqrt{k}/\mathcal{L}\right)/dz} \tag{16-46}$$

which is not algebraic, but is not specified by means of a partial differential transport equation. Some of their numerical results are briefly mentioned in Section 16.5.1. The second example is due to Li and Davies (1996), who were interested in predicting sediment transport in combined wave-current flows. In this case, nonequilibrium effects might be expected because of the unsteadiness in problems with surface waves. The stratification analogy was also made, so that $(G_k)_\rho$ was included. The variable $(\sigma_t)_s$ was assumed to be unity, but $\sigma_k= 1.37$, while $c_D = (c'_\mu)^3 = 0.097$, corresponding to $c'_\mu = 0.46$. Wilcox (1998) reported on early one-equation models with values of c_D taken in the range from 0.07 to 0.09 and with $c'_\mu = 1$, where Rodi (1993) indicated that the product $c'_\mu c_D \approx 0.08$. The length scale, motivated by Eq. (16-28), was given by

$$\mathcal{L} = \left(1 - \frac{z}{h}\right)^{1/2} \kappa\sqrt{k}\left(z_0 k_0^{-1/2} + \int_{z0}^{z} k^{-1/2}\, d\eta\right) \tag{16-47}$$

where z_0 is a bottom roughness scale. Some results with this model will be given in Section 16.5.4. Further developments of this model are sketched in Villaret and Davies (1995) and tested on even simpler steady unidirectional flows, with still rather mixed results, as will be seen in Section 16.4.7. Both Eqs. (16-46) and (16-47) differ from classic mixing-length specifications and attempt to incorporate information obtained in the solution of k in the specification of $\mathcal{L}$, so that Λ can vary in both space and time depending on flow conditions, as characterized by the local value of k. In particular, buoyancy effects that affect k will therefore also affect $\mathcal{L}$.

16.4.3.4 Limitations of One-Equation Models The current verdict on one-equation models in comparison to mixing-length models remains rather negative in that the improvements in predictions tend to be rather marginal (Bradshaw 1997; Wilcox 1998). As with the mixing-length model, the main problem lies in the length-scale specification, which becomes increasingly difficult in complex flow problems. In both of the above examples, the length-scale specification was guided by results for a plane-bed uniform-flow case; in more complicated flows, the specification is more difficult to motivate. This problem can be circumvented by formulating a transport equation directly for the eddy viscosity, rather than for k, such that a second equation for the length scale is not necessary. The model of Spalart and Allmaras (1992; see also the discussion in Spalart 2000), following this logic, has revived interest in one-equation models for aeronautical problems, but does not seem to have been adopted so far in hydraulics or sediment transport, and so is not discussed further.

16.4.4 The Specification of the Eddy-Viscosity: Two-Equation Models

If the logic leading to the development of the k-equation is followed, then the problem of determining the relevant length scale can be resolved by formulating an additional transport equation for a quantity that would, possibly in combination with k, provide a length scale. Rodi (1993) has noted that any quantity of the form $k^m\mathcal{L}^n$, where m and n are arbitrary exponents, would lead to dimensionally consistent equations of the same form. The presence of ϵ in the k equation as an unknown variable leads naturally to its choice as the quantity for which a transport equation is developed. An exact equation for ϵ can be derived from the Navier-Stokes equations, but its dominant correlation terms are impossible to measure in the laboratory (though they could be evaluated from results of numerical simulations), so model proposals cannot rely on experimental observations for guidance (Launder 1984; Wilcox 1998). Further, because viscous dissipation occurs on the smallest scales, the relevance of the exact terms for specifying $\mathcal{L}$ is questionable, which is characteristic of the larger energy-carrying scales that determine the level of overall dissipation (recall the qualitative discussion of dissipation in Section 16.2.1). It has therefore been conventionally preferred to formulate a surrogate equation for ϵ along the lines of the k-equation, based primarily on dimensional analysis and appropriate asymptotic behavior, e.g., in the ideal case of homogeneous high-R turbulence (Launder 1984). The strict identification of ϵ with the rate of dissipation of k, however, becomes more tenuous.

16.4.4.1 The Equation for ϵ The standard model equation for ϵ, incorporating the eddy viscosity model and, as usual, neglecting viscous transport terms in high-R flows, is thus of the form

$$\begin{aligned}\frac{D\epsilon}{Dt} &= \frac{\partial\epsilon}{\partial t} + \frac{\partial\left(\overline{u}_j\,\epsilon\right)}{\partial x_j} \\ &= \frac{\partial}{\partial x_j}\left(\frac{\nu_t}{\sigma_\epsilon}\frac{\partial\epsilon}{\partial x_j}\right) + P_\epsilon - D_\epsilon + G_\epsilon\end{aligned} \tag{16-48}$$

where σ_ϵ is the turbulent Schmidt number for the diffusive transport of ϵ. The production-of-dissipation term, P_ϵ, is necessary because, if k is being produced and the level of k increases in time, then the level of ϵ must also increase in order ultimately to limit the level of k. A simple model of $P_\epsilon \propto P_k$ may therefore be motivated, but for dimensional consistency, a multiplicative factor of ϵ/k, which may be interpreted as a turbulence frequency, is needed, such that

$$P_\epsilon = c_{1\epsilon}\frac{\epsilon}{k}P_k = c_{1\epsilon}\left(\frac{\epsilon}{k}\right)\left[\nu_t\left(\frac{\partial \bar{u}_i}{\partial x_j}+\frac{\partial \bar{u}_j}{\partial x_i}\right)\right]\frac{\partial \bar{u}_i}{\partial x_j} \tag{16-49}$$

where

$c_{1\epsilon}$ = a model constant.

The destruction-of-dissipation term, D_ϵ, is similarly modeled as

$$D_\epsilon = c_{2\epsilon}\left(\frac{\epsilon}{k}\right)\epsilon = c_{2\epsilon}\frac{\epsilon^2}{k} \tag{16-50}$$

where

$c_{2\epsilon}$ = another model constant.

Like the corresponding term in the k-equation, the last term in Eq. (16-48), G_ϵ, reflects the effect on ϵ of other forces or strains. In the case of buoyancy effects, $G_\epsilon = (G_\epsilon)_\rho$, the modeling of which, however, still remains open. That a term similar to P_ϵ but proportional to $(G_\epsilon)_\rho$ is desirable is commonly accepted, particularly where buoyancy production is concerned, i.e., in *unstable* stratification. Rodi (1993) recommended that

$$(G_\epsilon)_\rho = c_{1\epsilon}\frac{\epsilon}{k}\left[(G_k)_\rho(1+c_{3\epsilon}\mathrm{R\,i}_s)+c_{3\epsilon}\mathrm{R\,i}_s P_k\right] \tag{16-51}$$

where

$c_{3\epsilon}$ = yet another model constant.

More often (Burchard and Baumert 1995; Chen and Jaw 1996), a simpler model for $(G_\epsilon)_\rho$, which can be viewed as a special case of Eq. (16-51) for horizontal flows, is applied:

$$(G_\epsilon)_\rho = c_{1\epsilon}c_{3\epsilon}\frac{\epsilon}{k}(G_k)_\rho \tag{16-52}$$

16.4.4.2 The Standard k–ϵ Model and the Closure Constants The buoyancy-extended k–ϵ model consists of Eq. (16-41) with the original ϵ rather than its model, $k^{3/2}/\mathcal{L}$, and Eq. (16-48). With $u = \sqrt{k}$ and $\mathcal{L} = k^{3/2}/\epsilon$, this yields

$$\nu_t = c_\mu\sqrt{k}\left(\frac{k^{3/2}}{\epsilon}\right) = c_\mu\frac{k^2}{\epsilon} \tag{16-53}$$

with c_μ, a further model constant. In total, the standard model without buoyancy extensions requires five model constants: the two coefficients in the source and sink terms of the ϵ equation, $c_{1\epsilon}$ and $c_{2\epsilon}$, the coefficient, c_μ, in the eddy viscosity specification, and the turbulent Schmidt numbers for k and ϵ, σ_k and σ_ϵ. The first three are chosen to agree with experimental observations in special (asymptotic) flow cases where the model equations simplify, such as equilibrium shear layers (where $P_k = \epsilon$), grid-generated wind-tunnel turbulence (where $P_k = 0$ and diffusive terms are zero), and the log-law region in wall-bounded flow (where $P_k \approx \epsilon$ and other terms are negligible). The remaining constants, σ_k and σ_ϵ, were tuned or calibrated to a variety of flows. The standard values for the k–ϵ model constants are given in Table 16-2, together with the value of the von Kármán constant, κ, resulting from the use of the standard constants. The range in values of κ may be surprising, though there have been some recent discussions on this topic (see, e.g., the review of Patel 1998). Other values of the closure constants have been suggested based on other considerations. From the case of homogeneous shear flows, Tennekes (1989) has offered an interesting scaling argument based on the special case of homogeneous shear flows for the choice, $c_{1\epsilon} = 3/2$, which is very close to the standard value for the various models in Table (16-2). Similarly, theoretical models for grid-generated turbulence at high R (Speziale and Bernard 1992) suggest, in spite of experimental evidence to the contrary, that $c_{2\epsilon} = 2$, which has been adopted in some models. Nevertheless, because the first three constants are generally tuned to the same types of flows, their values shown in Table 16-2 are quite similar. The values of the closure constants are *not* independent, and changes in one constant may for consistency require changes in other constants, similar to what was seen earlier for one-equation models.

Because of the prominence of the stratified-flow analogy in sediment-transport literature, the closure constant, $c_{3\epsilon}$, merits special discussion, which will be limited to the simpler model of Eq. (16-52). In the unstable case, where the density gradient is positive in the direction opposite to gravity, which might be assumed in models of sediment dumping or inflows, turbulence is generated by negative buoyancy, $(G_k)_\rho > 0$, and $c_{3\epsilon} > 0$. In this case, there seems to be general agreement with the value of $c_{3\epsilon} = 1$ (Rodi 1987; Burchard et al. 1998). For the more common case of stable stratification, which is of greater interest in sediment transport in alluvial channels, there is substantial variation in values used, with even the sign being in dispute. Baumert and Peters (2000) listed nine different choices ranging from −1.4 to 1.45, with the most common choice being $c_{3\epsilon} = 0$, but generally nonnegative. Chen and Jaw (1998), who give an extended discussion of turbulent buoyant flows, recommended values in the range from 1 to 1.33 (note that the notation for $c_{3\epsilon}$may vary; what is denoted here as $c_{1\epsilon}c_{3\epsilon}$ is denoted in Chen and Jaw as $c_{3\epsilon}$). A theoretical argument based again on the special case of strictly stationary ("full equilibrium") homogeneous stably stratified shear flows has been advanced by Burchard and Baumert (1995) for a negative value and the value of −1.4 was proposed (note that this value is given for a k–ϵ model with nonstandard choices of the other closure constants, so caution is advised in using this value with the standard model). Needless to say, a standard choice of $c_{3\epsilon}$

Table 16-2 Effective[a] Closure Constants for the Standard k–ϵ, the RNG k–ϵ, the k–ω, and the Mellor-Yamada (M–Y) Models, together with the Corresponding Value for the Von Kármán Constant, κ

Model	c_μ	$c_{1\epsilon}$	$c_{2\epsilon}$	σ_k	σ_ϵ	κ
Standard	0.09	1.44	1.92	1.0	1.3	0.43
RNG	0.085	1.42	1.68	0.72	0.72	0.39
k–ω	0.09	1.56	1.83	2 2	0.41	
M–Y[b]	0.095	1.6	2	2	2	0.40

[a]The k–ω and Mellor-Yamada models differ in formulation from the k–ϵ model, and hence the closure constants for the different models cannot be considered as exactly equivalent.

[b]This refers to the Mellor-Yamada level 2 ½ model for non-density-stratified flows, with the stability functions of Galperin et al. (1988).

has not as yet been established, and some sensitivity analysis with respect to its value is recommended.

That the closure coefficients satisfy constraints established in special asymptotic cases of homogeneous flows or flows in local equilibrium is certainly necessary; that they then should apply to flows far from the asymptotic conditions assumes, as Wilcox (1998) has remarked, that the model possess a degree of universality that may be grossly optimistic. The possibility that the closure constants may be functions of local dimensionless parameters reflecting the deviation of conditions from the asymptotic cases is naturally motivated (Hanjalic 1994; Bradshaw 1997). In near-wall models (Launder 1984, 1996; Patel et al. 1985; Wilcox 1998) that must deal with viscous effects, the closure constants are commonly assumed to vary with a local turbulent Reynolds number. For stratified flows, the Mellor-Yamada models discussed below propose what might be interpreted as a c_μ varying with Richardson flux numbers. For highly nonequilibrium flows, the closure constants might be taken to vary with $(P_k/\epsilon) - 1$ (or more simply, P_k/ϵ), which is a measure of the distance from local equilibrium (see also the discussion in Rodi 1993). A more systematic theoretical justification for the last two proposals can be based on algebraic stress models, which will also be dealt with below.

16.4.5 The Treatment of Boundary Conditions and Auxiliary Model Equations

The following is restricted to boundary conditions at the bed and at the free surface. The conventional approach to dealing with the condition at a solid surface, namely, through the use of so-called wall functions, is outlined. For sediment-transport problems, the difficulty of specifying a boundary condition for the sediment conservation equation, Eq. (16-7), must also be confronted. Because the boundary condition on Eq. (16-7) is conventionally not applied at the bed, Eq. (16.7) only treats suspended load (see Chapter 2 for a definition), and so if total load is of interest, then a bed-load relationship is also required. If further a mobile erodible bed is to be simulated, then an additional equation for the bed evolution, similar to a dynamic equation at a free surface, must be included.

16.4.5.1 The Treatment of the Near-Bed Region: Flow and Turbulence The problems of imposing an exact-flow boundary condition have been discussed previously. The solution most commonly applied is the so-called wall functions approach, based on an equilibrium model for the near-wall flow, and the wall boundary conditions are imposed, not at the wall, but at a level outside of the viscous region. The traditional local-equilibrium model, $P_k = \epsilon$ and $d\bar{u}/dz = u_*/\kappa z$, is assumed to apply in a constant-shear-stress layer, where the boundary conditions are to be imposed, with the result that the necessary boundary conditions for $\bar{u}_i$, k, and ϵ are expressed as

$$\frac{V_w}{u_*} = \frac{1}{\kappa}\ln\frac{z_w u_*}{\nu} + B(d_r^+),$$
$$k_w = \frac{u_*^2}{c_\mu^{1/2}}, \quad \epsilon_w = \frac{u_*^3}{\kappa z_w} \tag{16-54}$$

where the w-subscript refers to the level where the boundary conditions are imposed, V_w is the magnitude of the velocity, with direction opposite to that of the shear stress, and B, the integration constant in the log-law velocity profile, is a function of the roughness Reynolds number, $d_r^+ \equiv u_* d_r/\nu$ where d_r is an equivalent roughness height. Various specifications of B are available; one due to Cebeci and Bradshaw (1977) and used by Wu et al. (2000) can be expressed as

$$\frac{B_s - B}{B_s - B_r + (1/\kappa)\ln d_r^+} = \begin{cases} 0, & d_r^+ < 9/4, \text{ (smooth)}, \\ \sin\left[\dfrac{\pi}{2}\dfrac{\ln(4d_r^+/9)}{\ln 40}\right], & 9/4 \le d_r^+ < 90, \text{ (transitionally rough)}, \\ 1, & 90 \le d_r^+, \text{ (fully rough)} \end{cases} \tag{16-55}$$

Equation (16-55) is an interpolation formula for B, with B_s and B_r being the well-known integration constants in the log-law profile for hydraulically smooth and rough flows, taken to be 5.2 and 8.5. A slight inconsistency is noted in that Eq. (16-55) presumably is based on $\kappa = 0.41$, whereas the standard k–ϵ model constants are based on $\kappa = 0.43$.

This single-layer wall-function approach can be extended by the use of multilayer models, in which different functional forms for k, ϵ, and V_w are assumed in each layer (e.g., in Cheong and Xue 1997). In Eq. (16-54), u_* is to be determined as part of the solution, but this is accomplished via a momentum balance in the near-wall region. To be consistent with this equilibrium model, the nearest boundary point in the computational grid should be placed in a region where the log-law is presumed valid, e.g., $z_w u_*/\nu \gtrsim 40$ for a smooth wall or $z_w/d_r \gtrsim 2$ for a rough wall, though mild violations of these conditions do not seem to affect results significantly.

Several questions arise in the application of this traditional approach to treating the near-wall region. The log-law profile does not necessarily always hold in wall-bounded flows, e.g., in the recirculation region of separated flows of interest in flows over bed-forms. Measurements in smooth-walled backward-facing-step flows (Devenport and Sutton 1991; Jovic and Driver 1995), confirmed by direct numerical simulations (Le et al. 1997), also show that when the log-law profile first becomes reestablished, the associated constant is not necessarily the same as that (B_s) in an equilibrium wall-bounded flow. From the particular perspective of sediment-transport problems, z_w may be located in a high-concentration region, where particle-particle interactions are strong, and Eq. (16-54) can hardly be justified. Even if this is avoided by a judicious choice of z_w, the classic question of the appropriateness of the log law and/or the constancy of κ in a sediment-laden flow, discussed previously in Section 16-4.2.3, reappears. A related issue is the appropriate choice of wall roughness height, d_r. On a fixed (nonerodible) nominally plane bed characterized by homogeneous roughness in a flow without sediment, the choice of d_r is straightforward, namely, the equivalent median sand size, d_{50}. Experimental evidence indicates that, even on a nominally plane bed, flow resistance is *increased* in a sediment-transporting flow compared to an equivalent fixed-bed clear-water flow. While the deviation from the classic log-law profile may have contributed significantly to this increased flow resistance (Lyn 1991), an interpretation or parameterization in terms of an effective roughness height much larger than d_{50} is widely accepted in practice. Van Rijn (1982) listed six widely varying prescriptions for the effective roughness height for flow over plane alluvial beds, finally recommending an average value of $3d_{90}$ (see also Chapter 2). An alternative approach (Smith and McLean 1977; Dietrich 1982; Wiberg and Rubin 1989; see also Chapter 2), better known in coastal and oceanographical applications and in some respects more physically based, proposes a roughness height parameter that may be interpreted in terms of a saltation height, and hence may vary with both particle *and* flow parameters. The difficulties become more acute when bed forms are present and the details of the bed geometry are not simulated. In this case, not only must an effective roughness height *including* the form resistance of bed forms be given, the choice of the level at which the flow boundary conditions are to be imposed also becomes much more problematic. Although crude specifications, e.g., the van Rijn (1984c) proposal used by Wu et al. (2000), are available, these leave much to be desired.

In the turbulence-modeling literature, the development of low-Reynolds-number corrections to the standard k–ϵ model, primarily with the aim of obviating the use of wall functions, has attracted much attention (Launder 1984, 1996; Patel et al., 1985; Chen and Jaw 1998; Wilcox 1998). Here, low Reynolds number refers to the near-wall flow, where the local Reynolds number, based on the distance to a wall, becomes small, indicative of the increasing importance of viscous effects. Because of the complications noted above in sediment-transport problems, the advantages of such a more sophisticated treatment of the boundary becomes debatable.

16.4.5.2 Boundary Conditions for the Sediment Equation The condition on the suspended sediment concentration, $\bar{c}$, at the free surface is invariably a no-flux condition; in contrast, the condition at the bed or the near-bed region remains a vexing problem. In a manner similar to the wall-function approach to the flow boundary conditions, the bottom boundary condition for sediment is imposed at a level above the bed. This is already familiar from the traditional Ippen-Rouse profile, for which the boundary condition is usually applied at a reference level above the bed, $z = z_b$ (see Chapter 2). An "equilibrium" concentration condition,

$$\bar{c}\big|_{z=z_b} = \bar{c}_{\text{eq}} \tag{16-56}$$

has often been chosen (e.g., Li and Davies 1996; Olsen and Kjellesvig 1999), where an equation similar to that which might be traditionally used to close the Ippen-Rouse profile would be used for $\bar{c}_{\text{eq}}$. Alternatively, a net vertical sediment flux per unit area, $J_s|_b$, might be defined at $z = z_b$:

$$J_s|_b = w_s(E_s - \bar{c}_b) \tag{16-57}$$

where

E_s = entrainment concentration and
$\bar{c}_b$ = local concentration at $z = z_b$.

With w_s known and $\bar{c}_b$ part of the solution for $\bar{c}$, the only quantity to be externally specified is the entrainment concentration, E_s. Somewhat similarly to the treatment of flow quantities, a local-equilibrium hypothesis can be motivated in which the flow entrains as much as it possibly can (Celik and Rodi 1988), such that $E_s = \bar{c}_{\text{eq}}$, for which, as noted already, several prescriptions are available. A condition essentially equivalent to Eq. (16-57) can be expressed as a diffusive-flux condition (e.g., Murray et al. 1991) in which the combination $w_s E_s$, is termed a pickup function, which is then empirically obtained (e.g., van Rijn 1984a). Other variants of Eq. (16-57) and their practical implementation are discussed in Chapter 15. A somewhat different formulation has been adopted in unsteady sediment transport in coastal engineering applications (e.g., Hagatun and Eidsvik 1986; Davies et al. 1997; Savioli and Justesen 1997b) in which

$$\bar{c}\big|_{z=zb} = \max\left(\bar{c}_{\text{eq}}, \bar{c}_{ws}\right) \tag{16-58}$$

where

$\bar{c}_{\text{eq}}$ = equilibrium bed concentration associated with the time-varying ('instantaneous') bed shear stress, whereas

$\bar{c}_{ws}$ = concentration if only a settling flux (i.e., independent of the bed shear stress) is imposed.

Equation (16-58) aims to model a lag between settling and entrainment, such that the suspension is not always in equilibrium with the time-varying bed stress, e.g., during periods of small bed shear stress, when settling might dominate. This can also be modeled in Eq. (16-57), and so the advantage of Eq. (16-58) compared to Eq. (16-57) is not clear. Savioli and Justesen (1997b) suggested that $\bar{c}_{ws}$ is not only due to a settling flux, but also affected by turbulent diffusion; details were, however, not given, and some tuning was found necessary.

The question remains at what level this "bottom" boundary condition is to be imposed. As may also be said of the flow boundary conditions, this level should be located at or possibly above the lower limit of the applicability of the field equations (in this case, the advection-diffusion for sediment, Eq. (16-7)), but this remains controversial. The traditional bed-load formulae proposed in the sediment-transport literature, e.g., for a reference or equilibrium concentration, have been calibrated at specific levels, which have not necessarily been chosen with the needs of modern computational fluid dynamics or turbulence models in mind. For example, for flows over plane beds, the classic Einstein total-load model specifies the lower limit of the suspended load at $z_b = 2d_{50}$, with $\bar{c}|_{z=zb}$ taken from the Einstein bed-load model (see Chapter 2). On the other hand, $z_b = 2d_{50}$ may not be consistent with the local equilibrium model assumed in the flow boundary conditions, or even with the validity of the field equations. The reference level for the bottom concentration boundary condition need not be located at the same level as the flow boundary conditions (Wu et al. 2000), but the two types of boundary conditions must be formulated in a consistent manner, which may place constraints on the near-bottom grid.

Bed forms complicate the issue of boundary conditions. If individual bed forms are modeled, then conditions similar to Eq. (16-57) (or even Eq. (16-56)) could conceivably be imposed, though the local equilibrium assumption (and hence $\bar{c}_{\text{eq}}$) would be difficult to justify in the vicinity of the separated flow region. In all fairness, however, such an approach may be said to be equally justified (or unjustified) as the log-law velocity profile wall-function model imposed on the flow. If, as in most practical computations, individual bed forms are *not* modeled and hence details of the near-bed flow are sacrificed for simplicity, then, if Eq. (16-57) or Eq. (16-56) is imposed, then these conditions should be interpreted cautiously because, when a fictitious plane bed is assumed, they implicitly invoke spatial averaging. The application of equations for $\bar{c}_{\text{eq}}$ based on plane-bed flows is thus rather questionable, and alternative specifications of $\bar{c}_{\text{eq}}$ based on flows over bed forms, which might vary sensitively with bedform characteristics, should be considered. The fictitious level at which the sediment boundary condition is to be imposed becomes even more difficult to specify in this case.

16.4.5.3 Bed-Load Transport and Erodible-Bed Modeling If the total load is of interest, or if a mobile erodible bed is to be modeled, then a bed-load model is necessary. In the present context, the bed-load region may be defined as that below the level at which the bottom sediment boundary condition is imposed. The turbulence model and the flow and transport computations discussed above are directly concerned only with suspended load, and, in most if not all models, only indirectly affect bed-load transport through the estimate of the bed shear stress, $\bar{\tau}_b$. Conventional bed-load formulae in most models were developed for use in problems where only bulk quantities such as $\bar{\tau}_b$ were available. An interesting attempt to incorporate information about turbulence characteristics into bed-load models has been reported by Mendoza and Shen (1988). For flow models using wall functions (Eq. (16-54)), the turbulence quantities, k_w and ϵ_w, are defined in terms of $\bar{\tau}_b$, and so, unless z_b is chosen to be significantly higher than z_w, the turbulence model will still only affect bed load through $\bar{\tau}_b$.

For modeling of the erodible bed, a conservation equation for the overall bed-material load, including the effect of deformation and temporal evolution of the bed, is formulated, typically in the form of an Exner equation (see Chapter 2 and particularly Chapter 15 for an extensive discussion) relating changes in bed elevation to spatial variations in total load. Alternatively, because the suspended load is presumably already modeled (e.g., by Eq. (16-7)), a bed-load conservation equation can be formulated. A simple form of such an equation can be expressed as

$$\frac{\partial}{\partial t}[(1-p)z_{\text{bed}} + (\bar{c}|_{z=zb}\, zb)] + \frac{\partial Q_{sbx}}{\partial x} + \frac{\partial Q_{sby}}{\partial y} = -J_{s|b} \tag{16-59}$$

where

p = porosity of the bed;
z_{bed} = elevation of the bed;
z = height measured from the local bed elevation, such that z_b is the thickness of the bed-load layer; and
Q_{sbx} and Q_{sby} = volumetric sediment flux or discharge in the bed-load layer in the Cartesian coordinate directions x and y.

The sediment concentration in the bed-load layer has been assumed constant in Eq. (16-59) with a value equal to $\bar{c}|_{z=zb}$. This storage term involving $\bar{c}|_{z=zb}$ is often omitted as being negligible compared to the transport terms involving Q_{sbx} and Q_{sby}. Equation (16-59) can be considered an equation for the unknown z_{bed}, but involves Q_{sbx} and Q_{sby}, which need to be specified in terms of known quantities. A local-equilibrium assumption is usually made, wherein these are related to traditional bed-load transport functions, incorporating appropriate coordinate transformations (Wu et al. 2000). More sophisticated erodible-bed models, such as those that attempt to include nonequilibrium effects (Armanini and di Silvio 1998) have been proposed in the wider sediment-transport context. Similarly, the very practical problem of modeling the exchange of heterogeneous sediment between the bed and the flow is not addressed but receives extensive attention in Chapter 15. At the present stage of model development, these issues are only indirectly affected by the turbulence model and will not be dealt with further here.

Example. For the horizontally homogeneous unsteady case, the complete k–ϵ-model system of equations, including buoyancy effects only in the k–equation but neglecting viscous diffusion, may be written as

$$\frac{\partial \bar{u}}{\partial t} = \frac{1}{\rho}\frac{\partial \bar{p}}{\partial x} + \frac{\partial}{\partial z}\left(\nu_t \frac{\partial \bar{u}}{\partial z}\right) \tag{16-60a}$$

$$\frac{\partial k}{\partial t} = \frac{\partial}{\partial z}\left(\frac{\nu_t}{\sigma_k}\frac{\partial k}{\partial z}\right) + \nu_t\left(\frac{\partial \bar{u}}{\partial z}\right)^2 + g(s-1)\left[\frac{\nu_t}{(\sigma_t)_s}\frac{\partial \bar{c}}{\partial z}\right] - \epsilon \tag{16-60b}$$

$$\frac{\partial \epsilon}{\partial t} = \frac{\partial}{\partial z}\left(\frac{\nu_t}{\sigma_\epsilon}\frac{\partial \epsilon}{\partial z}\right) + c_{1\epsilon}\frac{\epsilon}{k}\left[\nu t\left(\frac{\partial \bar{u}}{\partial z}\right)^2\right] - c_{2\epsilon}\frac{\epsilon^2}{k} \tag{16-60c}$$

$$\frac{\partial \bar{c}}{\partial t} = \frac{\partial}{\partial z}\left[\frac{\nu_t}{(\sigma_t)_s}\frac{\partial \bar{c}}{\partial z}\right] + \frac{\partial (w_s \bar{c})}{\partial z}\,. \tag{16-60d}$$

Together with the relationship for ν_t, Eq. (16-53), and an equation for $\bar{p}$, the system is closed with four equations in four unknowns, $\bar{u}$, $\bar{c}$, k, and ϵ. For an oscillatory flow (further discussed in Section (16-5.4)), $\bar{p}$ would be related to an imposed free-stream velocity by a Bernoulli equation. For a steady mean flow down a plane inclined at an angle θ, the transient terms are zero and the pressure-gradient term can be replaced by a gravitational-force term, $g \sin \theta$.

The results of two k–ϵ computations, one with and one without buoyancy effects included in the k–equation (but $c_{3\epsilon} = 0$), for the same two steady laboratory flows previously examined with the van Rijn and Smith-McLean models are shown in Fig. (16-6). The boundary conditions imposed were standard (Eqs. (16-54) with the van Rijn value of $d_r = 3d_{90}$, Eq. (16-61), Eq. (16-56) imposed at $z_b = 3d_{90}$, and $(\sigma_t)_s = 1$) for the two computations. Thus, unlike the previous computations with the van Rijn and Smith-McLean models, which "benefited" from the measurements being used as boundary conditions, the present computations are complete predictions. The velocity predictions for the standard k–ϵ model agree well with measurements in both cases for the outer flow, but a tendency to overestimate velocities closer to the boundary is noted, very apparent for the Lyn data, but also seen in the Barton-Lin data. The flow boundary conditions are the same in the buoyancy-extended model, leading to predictions of larger velocities and smaller concentrations compared to the standard model because of a reduced eddy viscosity/diffusivity. In both cases, this leads to a deterioration in agreement with the velocity data, though the concentration predictions are improved. This does not necessarily imply a virtue or deficiency in the buoyancy-extended k–ϵ model as such. Much of the credit for the good agreement or blame for the discrepancies should not necessarily be attributed to the turbulence model as such but to the boundary conditions and the choice of model parameters (the choice of d_r and $\bar{c}_{\text{ref}}$ and $(\sigma_t)_s$). Viewed from this perspective, the differences between the predictions of the mixing-length models and the two-equation models are not as large as might at first be thought. As already pointed out, for the simple uniform-flow case, the k–ϵ model reduces to the mixing-length model because of local equilibrium. Thus, a comparison of the two types of models should focus on differences in predicted slopes rather than predicted values because the latter are

directly affected by boundary conditions. Not surprisingly, the predicted slopes of the two types of models are quite similar. The case of uniform flow over a flat bed is perhaps the simplest case of sediment-laden flow, and so is not a particularly stringent test of a turbulence model. Figure (16-6) shows what might be achieved with a k–ϵ model under the best of circumstances—in more complicated flows, larger discrepancies might be encountered.

16.4.5.4 Free-Surface Conditions The free surface is often treated as a symmetry plane, exactly analogous to the centerline of a pipe, such that, in the absence of wind shear, fluxes across the surface are set to zero. The turbulence in the vicinity of a free surface differs, however, from that in the vicinity of a pipe centerline due to a damping of vertical velocity fluctuations and a consequent flattening of turbulent eddies, somewhat similar to that occurring at a rigid wall. The resulting reduction in length scale has been modeled by imposing a condition on ϵ at the free surface, namely,

$$\epsilon_{fs} = \frac{k_{fs}^{3/2}}{c_{fsc} h}, \tag{16-61}$$

where k_{fs} is the turbulent kinetic energy at the free surface and $c_{fs\epsilon}$ is a constant, with a recommended value of 0.43 (Celik and Rodi 1988; Wu et al. 2000). Equation (16-61) which may be compared with the corresponding condition at the bed, reduces the length scale at the free surface relative to the situation when a simple symmetry condition is imposed. Celik and Rodi (1984, 1988) also proposed a direct reduction in ν_t through a reduction in c_μ by a factor depending on a surface damping function and the ratio ρ/ϵ.

16.4.6 Deficiences of the Boussinesq Eddy-Viscosity and k–ϵ Models and Some Alternatives

The weaknesses of the Boussinesq eddy-viscosity (BEVM) and k–ϵ models are discussed, and several alternative two-equation models developed to remedy some of these weaknesses are described. Because these have not yet been as widely adopted, only a select sample will be discussed here, and only rather briefly. The ϵ–equation, not surprisingly, has been the focus of modeling, either being entirely replaced or modified by additional terms. As noted above, an equation for any generic "length-scale" quantity of the form $k^m \mathcal{L}^n$, can form the basis for a two-equation model, and the two models discussed below that differ in form from the k–ϵ model may be interpreted in terms of particular choices of m and n. The k–equation is usually retained, with either no modification or only such modification as to make it consistent with the new or revised length-scale equation.

16.4.6.1 Weaknesses of the Boussinesq Eddy-Viscosity and k–ϵ Models It was noted in connection with mixing-length models that nonequilibrium and anisotropic turbulence would cause problems. To a perhaps distressingly large extent, this remains true even when the BEVM model is coupled with the more sophisticated k–ϵ model. Like the mixing-length model, the BEVM model was motivated primarily by thin shear flows, and the BEVM model usually performs well in predicting the important fluxes across shear-dominated flows. Fluxes in the other directions may not be so well predicted (Haroutunian and Engelman 1993). Flows in which differences in normal stresses are important, i.e., highly anisotropic flows, will pose difficulties for the standard models. These may include problems where turbulence-generated secondary currents play an important role, e.g., flows in compound channels. When extra strains, such as buoyancy forces, or when rapid changes in strain are imposed, model performance may also deteriorate (Wilcox 1998). As evident from the preceding sections, the effects of buoyancy may be relevant to suspension flows. Even if buoyancy is not accepted as the dominant mechanism for turbulence modification in sediment-laden flows, it may be argued on general physical grounds that the responsible mechanism is related to sedimentation in a gravitational field, and hence is expected to have an anisotropic effect on the flow field.

These deficiencies can be traced to the assumption of isotropy inherent in the BEVM, to the use of only scalar quantities, k and ϵ, to characterize the turbulence, and to the specification of the linear relationship between $\overline{u_i' u_j'}$ and only the mean strain rate. Because of the extent of model assumptions in the development of the ϵ–equation, it has been the subject of much criticism, with modifications or alternatives often being proposed. As noted previously, the use of wall-functions has also been criticized because they tend to be justified only under fairly limited conditions. From the specific sediment-transport point of view, whether the stratification model and the assumed log-law wall-function model are appropriate remains unclear. Although much has been said of the anisotropic nature of real turbulent flows, the possible anisotropy of diffusive transport of settling particles even in isotropic turbulence should also be mentioned.

16.4.6.2 The k–ω Model The k–ω model, associated with Wilcox (and discussed at length in his 1998 book), is perhaps the major alternative to the k–ϵ model as far as two-equation models for engineering applications are concerned. It is based on an equation for ω, which is interpreted as a frequency scale proportional to ϵ/k, the rate of dissipation per unit turbulent kinetic energy:

$$\frac{d\omega}{dt} = \frac{\partial \omega}{\partial t} + \frac{\partial \left(\overline{u}_j \, \omega \right)}{\partial x_j} = \frac{\partial}{\partial x_j} \left(\frac{\nu_t}{\sigma_\omega} \frac{\partial \omega}{\partial x_j} \right) + c_{1\omega} \frac{\omega}{k} P_k - c_{2\omega} \omega^2 \tag{16-62}$$

Whereas the ϵ–equation in the k–ϵ model may be interpreted as an equation for $k^{3/2} \mathcal{L}^{-1}$, i.e., $m = 3/2$ and $n = -1$, the

ω–equation corresponds to an equation for $k^{-1/2}\,\mathcal{L}$, or $m = -1/2$ and $n = 1$. With the additional model relations

$$\epsilon = c_{k\omega} k\omega \quad \text{and} \quad \nu_t = \frac{k}{\omega} \tag{16-63}$$

the k–ω model is completely specified. Like the k–ϵ model, there are five closure coefficients, $c_{k\omega} = 0.09$, $c_{1\omega} = 5/9$, $c_{2\omega} = 3/40$, and the two turbulent Schmidt numbers, $\sigma_k = 2 = \sigma_\omega$. A frequently cited advantage of the k–ω model for wall-bounded flow applications is that, without the need to use wall-functions, integration to the wall is feasible. For the transitionally rough-wall flows of most interest in sediment-transport applications, the boundary conditions to be applied at the bed are the no-slip conditions for the velocity components, together with

$$k = 0, \ \omega = u_*^2 S_r / \nu \tag{16-64}$$

where S_r is a parameter, analogous to E_r for the k–ϵ model (Eq. 16-55), that is correlated with the wall roughness, namely,

$$S_r = \begin{cases} \left(50/d_r^+\right)^2, & d_r^+ < 25 \\ 100/d_r^+, & d_r^+ \geq 25. \end{cases} \tag{16-65}$$

With the specification, Eq. (16-65) and boundary conditions, Eq. (16-64) the k–ω model reproduces the standard log-law for transitionally and fully rough flows for parallel or nearly parallel flows of a homogeneous fluid, such as clear-water boundary-layer or channel flows. Importantly, however, unlike the wall-functions approach, log-law behavior is *not* explicitly imposed on the flow. Yoon and Patel (1996) note that a fine grid close to the wall is necessary because of large spatial gradients. This does not imply that the flow very near the wall is being resolved, because individual roughness elements are not modeled; hence, the results very near the wall must be interpreted cautiously because the solution is only physically meaningful at some distance from the modeled wall. In addition to Wilcox (1998), Patel (1998) discusses the performance of the k–ω and k–ϵ models for wall-bounded flows in general, and, for rough walls in particular. Because it avoids explicitly assuming a log-law velocity profile at the wall, it may be advantageous in separated flows where it is known that the log-law profile does not hold in recirculating regions. Nevertheless, in a study of the backward-facing-step flow, Speziale and Thangam (1992) concluded that, at least for this flow, the use of wall functions does not entail major errors in spite of flow separation. The problems peculiar to sediment-transport applications discussed before, such as the appropriate roughness height in sediment-laden flows or dealing with bed forms, not to mention the question of turbulence modification, still need to be addressed. A well-known weakness of the k–ω model is its extreme sensitivity to free-stream boundary conditions, and so it should not be applied without modifications to flows with interfaces between turbulent and nonturbulent flows, e.g., boundary-layer flows, free shear flows. For alluvial-channel flows, this should be of little concern, but may require more consideration in the coastal or lacustrine context.

16.4.6.3 The RNG Model Since its introduction by Yakhot and Orszag (1986), the renormalization group (RNG or RG) approach to developing turbulence models has attracted much attention (Speziale and Thangam, 1992; Yahkot and Orszag 1992), as well as skepticism (McComb 1990; Hanjalic 1994; Bradshaw 1997). The standard k–ϵ model is apparently derived, with only changes in the values of the closure coefficients (see Table 16-2) and, in its latest version, the addition of a term involving the mean strain rate ϵ–equation, namely,

$$G = \left(G_\epsilon\right)_{RNG} = -\, c_\mu \frac{\epsilon^2}{k}\left[\frac{\eta^3\left(1 - \eta/\eta_0\right)}{1 + c_{RNG}\eta^3}\right] \tag{16-66}$$

where $\eta = S\,k/\epsilon$, and the two additional model constants, $\eta_0 = 4.38$, obtained from an analysis of homogeneous shear flow, and $c_{RNG} = 0.015$, the value of which was chosen to match a von Kármán constant, $\kappa = 0.39$ (a value of $c_{RNG} = 0.012$ would yield $\kappa = 0.4$).

A formidable, even impenetrable theory notwithstanding, the RNG results rely on an asymptotic perturbation argument for a small parameter, but the argument is then applied with a finite (not small) value of that parameter. On one hand, this is similar to the standard procedure of determining the closure constants from simple flows and applying the model to complex flows (see the discussion in Section 16-4-4); on the other hand, the claims to theoretical rigor and superiority vis-à-vis the standard procedure suffer accordingly. Although the RNG approach points to the necessity of an additional term in the ϵ-equation when S is large, the particular form of $(G_\epsilon)_{RNG}$ given in Eq. (16-66) is *not* directly derived from the RNG approach, and constitutes another possible weak point in the RNG model. Because $\eta \propto \sqrt{P_k/\epsilon}$, the additional term, $(G_\epsilon)_{RNG}$, can also be interpreted as $c_{2\epsilon}$ being a function varying with P_k/ϵ rather than being a constant as in the standard k–ϵ model. This recalls the earlier discussion concerning the possibility of the closure constants being made dependent on dimensionless parameters reflecting deviations from the conditions prevailing in the simple calibration flows. In practice, the RNG k–ϵ model has led to improved predictions in some flows, particularly those in which massive separation has occurred (Lien and Leschziner 1994; Kim and Patel 2000), but not in others (Hanjalic 1994; Lien and Leschziner 1994). Whether it represents a viable general alternative to the standard k–ϵ model (or the k–ω model) remains to be established.

In their usual implementation, both the k–ω and the RNG version of the k–ϵ models retain the BEVM assumption, so

that the deficiencies, notably the linear stress-strain rate relationship and the insensitivity to normal stresses and anisotropy stemming from it, still remain. Possible turbulence modulation effects from the presence of particles do not seem to have yet received much, if any, attention in the application of either the k–ω or the RNG models. Although neither model has been as extensively tested as the conventional k–ϵ model, their availability in commercial computational fluid dynamics codes will likely stimulate increased use in the future.

16.4.6.4 The Mellor-Yamada (or k–$k\mathcal{L}$ Model) Length-Scale Equation Mellor and Yamada (1982) describe a hierarchy of turbulence closure models ranging from a full second-moment model (level 4) to a local-equilibrium model (level 2). The intermediate level 2½ model is described in the next section. Unlike the k–ϵ model, Mellor-Yamada models eschew the ϵ–equation in favor of either a simple algebraic specification of the length scale, or more generally, an equation directly for the turbulence length scale, $\mathcal{L}$ or equivalently of a quantity $\mathsf{R} = 2k$. Although it can be written for more general flows (Mellor and Herring 1973; Rodi 1987), it is often expressed in a form aimed at boundary-layer applications (Mellor and Yamada 1982):

$$\begin{aligned}\frac{D\mathsf{R}}{Dt} &= \frac{\partial \mathsf{R}}{\partial t} + \frac{\partial\left(\overline{u}_j \mathsf{R}\right)}{\partial x_j} \\ &= \frac{\partial}{\partial z}\left[\frac{\left(\nu_t\right)_0}{\sigma_R}\frac{\partial \mathsf{R}}{\partial z}\right] + \mathcal{L} c_{1R}\left[P_k + \left(G_k\right)_\rho\right] \\ &\quad - \mathrm{c}_{2R}\left(2k\right)^{3/2}\left[1 + c_{3MY}\left(\frac{\mathcal{L}}{\kappa L_z}\right)\right] \end{aligned} \tag{16-67}$$

such that only diffusive transport in the vertical z direction is included. The basic eddy viscosity $(\nu_t)_0 = (2k)^{1/2}\Lambda$, whereas the length scale, L_z, is in general specified externally by an integral. For boundary-layer flow near a wall, the integral simplifies to $L_z = z$, the distance from the wall. The closure constants are $\sigma_R = 5$, $c_{1R} = 1.8$, $c_{2R} = 0.06$, $c_{3MY} = 1.33$. The last term, $\mathcal{L}/(\kappa L_z)$, is necessary for matching the von Kármán constant in the log-law velocity profile. The dissipation term in the k-equation is $\epsilon = c_{2R}(2k)^{3/2}/\mathcal{L}$. As usual, a wall-functions approach may be applied in imposing conditions at a solid boundary. An interesting feature of Eq. (16-67) is the choice of the coefficient of the buoyancy term, equivalent to $c_{3\epsilon}$ in the k–ϵ model. The choice of unity, tentatively made by Mellor and Yamada (1982), seems to have become the standard in subsequent work, and has not aroused any debate comparable to that surrounding $c_{3\epsilon}$.

Equation (16-67) falls within the class of models, sometimes termed k–$k\mathcal{L}$ (Wilcox 1998), that began with the work of Rotta (1951), who derived an equation for the integral of the two-point correlation function, which can serve to define a length-scale. Within the classification of length-scale equations in terms of $k^m\mathcal{L}^n$, Eq. (16-67) has $m = 1$, $n = 1$. Somewhat similar length-scale equations have been applied by Sheng and Villaret (1989) and Huynh Thanh and Temperville (1991) for sediment-transport application. Although widely used in geophysical applications, possibly because of its attention to stratification effects, the superiority of Eq. (16-67) to the ϵ–equation in practical engineering computations is controversial. Speziale (1991), for example, concludes that it does not offer any significant advantages over the standard ϵ–equation.

16.4.7 More Sophisticated Models

For the foreseeable future, practical computations of flows involving sediment transport will be dominated by the standard k–ϵ model, possibly including buoyancy extensions or other ad hoc corrections, or alternative two-equation models, coupled with the advection-diffusion equation for the sediment concentration, Eq. (16-7). Nevertheless, more advanced models continue to be developed, and some have already found or may eventually find their way into leading-edge practice. The two-phase approach to dealing with suspension flows and possible modifications to the k–ϵ model is very briefly discussed. Nonlinear k–ϵ models are examined as a possible solution to modelling effects of anisotropy and extra strains. The present state-of-the-art in turbulence modeling for practical computations lies in second-moment closure models, and so these are briefly outlined, though primarily with the aim of deriving simpler algebraic stress models.

16.4.7.1 Two-Phase Flow Turbulence Models The two-phase nature of a suspension flow presents special problems not only for the modeling of the turbulence, but also for the formulation of basic continuity and momentum equations, and the frequent appeal to the stratification analogy deserves greater scrutiny than it has received. Several two-phase flow descriptions of the sediment-transport problem have been given (Drew 1975; McTigue 1981; Kobayashi and Seo 1985; Lamberti et al. 1991; Greimann et al. 1999), but because they have only considered the simplest case of uniform flat-bed flow, they have typically resorted to simple mixing-length closures. Turbulence modification was either ignored or treated via a stratification analogy. The formulation of general numerical models for turbulent two-phase flows and the fundamental problems of averaging and turbulence closure have been reviewed by Crowe et al. (1996). The two-phase formulation starts with separate continuity and momentum equations for each phase, where correlations modeling the kinematic and dynamic interaction between phases already present closure problems (in addition to the turbulence closure problem), which may not be amenable to the standard BEVM approach (Elghobashi 1994). Elghobashi and Abou-Arab (1983) derived two-phase k–ϵ equations and proposed appropriate closures, with

applications to particulate jet flows. The exact k–equation is found to consist of 38 terms (this may be compared with the 8 terms in Eq. (16-34)), and rather drastic surgery is required to obtain closure. Interestingly, a buoyancy term does *not* explicitly appear in their formulation, though presumably the effect is implicitly captured in correlations involving the instantaneous slip between the two phases. Because of the abstract nature of the concept of interpenetrating continua, experimental determination of correlations or confirmation of detailed predictions is difficult or even impossible, except possibly in numerical simulations.

The near-bed bed-load region poses additional problems because particle-particle interactions become important or dominant, and a dense-phase (as opposed to a dispersed dilute-phase) flow model is necessary. In a single-phase flow approach based on Eq. (16-7), these problems are entirely avoided by using a bed-load transport model that bridges the immobile bed and the suspended-load region where Eq. (16-7) is applied. It is debatable to what extent the traditional views of turbulence can be applied to this region. The possibility of applying granular-fluid models to deal with this dense-phase region has been explored by a number of investigators (Hanes and Bowen 1985; Lamberti et al. 1991; Villaret and Davies 1995).

Example. Villaret and Davies (1995) reported simulations with a two-phase flow model, presumably a version of that described by Simonin (1991). The model incorporates granular-fluid concepts, suspension-induced buoyancy effects, and a low-R model for the near-wall flow, in a k–ϵ model framework. Figure 16-7 shows the results, including those from simulations with an enhanced version of the Li-Davies one-equation model discussed previously, including buoyancy effects. All of the cases studied did *not* involve an equilibrium bed. The predictions of both models with respect to the velocity profiles agree quite well with measurements, and are clearly superior to the clear-water velocity profiles (the basis of the standard k–ϵ wall-functions). The simpler one-equation model seems, however, to perform as well as or only marginally worse than the more sophisticated two-phase k–ϵ model, at least where experimental evidence is available. Larger discrepancies between concentration predictions and measurements can be seen, and the superiority of one or the other model is not clearly established. The simpler one-equation model did benefit from having a measured concentration as its bottom concentration boundary condition, whereas only the depth-averaged concentration was imposed on the two-phase flow model. The comparison suggests that, even for this simplest case of sediment-laden flows, even a very sophisticated model may not necessarily lead to significantly better predictions. Further, improved boundary conditions may play a more important role in better predictions than additional sophistication in turbulence modeling, at least at the present stage of model development.

Hsu et al. (2003) reported predictions using a dilute two-phase-flow k–ϵ model, which did not include either dense-phase or, at least explicitly, stratification effects, and so provides a contrast to the two-phase-flow model described in Villaret and Davies (1995). An approximate theoretical solution that agreed with a numerical solution of the resulting model near the bed suggested that effects on the velocity (and also the concentration) profile are $O(\bar{c})$. This seems too weak in general to explain observations, and may indicate that dense-phase and/or stratification effects need to be included.

16.4.7.2 Nonlinear k–ϵ Models The Boussinesq eddy viscosity model (Eq. (16-14)), relating the Reynolds stress *linearly* to the mean strain rate, analogously to that applied to a Newtonian fluid in laminar flows, is considered one of the major weaknesses of standard turbulence models. Nonlinear constitutive models, analogous to considering turbulent flow as a non-Newtonian fluid, have been proposed as a relatively simple remedy (Speziale 1987, 1996; Launder 1996; Wilcox 1998). An example is a model developed by Craft et al. (1993), which assumes that

$$
\begin{aligned}
-\overline{u_i' u_j'} = {} & \left(\nu_t S_{ij}^* - \frac{2}{3}\delta_{ij} k \right) \\
& - \nu_t \frac{k}{?} \Bigg[c_{1n} \left(S_{ik}^* S_{kj}^* - \frac{1}{3} S_{kl}^* S_{ij}^* \delta_{ij} \right) \\
& + c_{2n} \left(\Omega_{ik} S_{kj}^* + \Omega_{jk} S_{ki}^* \right) \\
& + c_{3n} \left(\Omega_{ik}\Omega_{jk} - \frac{1}{3}\Omega_{lk}\Omega_{lk}\delta_{ij} \right) \Bigg] \\
& - c_\mu \nu_t \frac{k^2}{?^2} \Big[c_{4n} \left(S_{kl}^* \Omega_{lj} + S_{kj}^* \Omega_{li} \right) S_{kl}^* + c_{5n} \\
& \times \left(\Omega_{il}\Omega_{lm} S_{mj}^* + S_{il}^* \Omega_{lm}\Omega_{mj} - \frac{2}{3} S_{lm}^* \Omega_{mn}\Omega_{nl}\delta_{ij} \right) \\
& + c_{6n} S_{ij}^* S_{kl}^* S_{kl}^* + c_{7n} S_{ij}^* \Omega_{kl}\Omega_{kl} \Big] .
\end{aligned}
\tag{16-68}
$$

The first bracketed group of terms is the standard BEVM, whereas the second and third bracketed groups are respectively quadratic and cubic terms in $S_{ij}^* = 2S_{ij}$ and a rotation tensor, $\Omega_{ij} = \partial \bar{u}_i / \partial x_j - \partial \bar{u}_j / \partial x_i$. There are seven additional closure coefficients, $c_{1n}, \ldots, c_{7n}$. Although the nonlinear constitutive relationship is much more complicated than the Boussinesq model, such a generalization is computationally attractive, because it still permits the use of two-equation models. Apsley et al. (1997) have argued that the early quadratic model of Speziale (1987), although sensitive to anisotropy, is insensitive to flow curvature, which requires at least a cubic model. They also point out that the physical interpretation of nonlinear models that are postulated solely on a formal basis is tenuous, and that the closure coefficient in the viscosity relationship, c_μ, will in general need to be made a function of the strain-rate and rotation tensors. An alternative, more physically based approach to developing nonlinear models simplifies second-moment closure models discussed below.

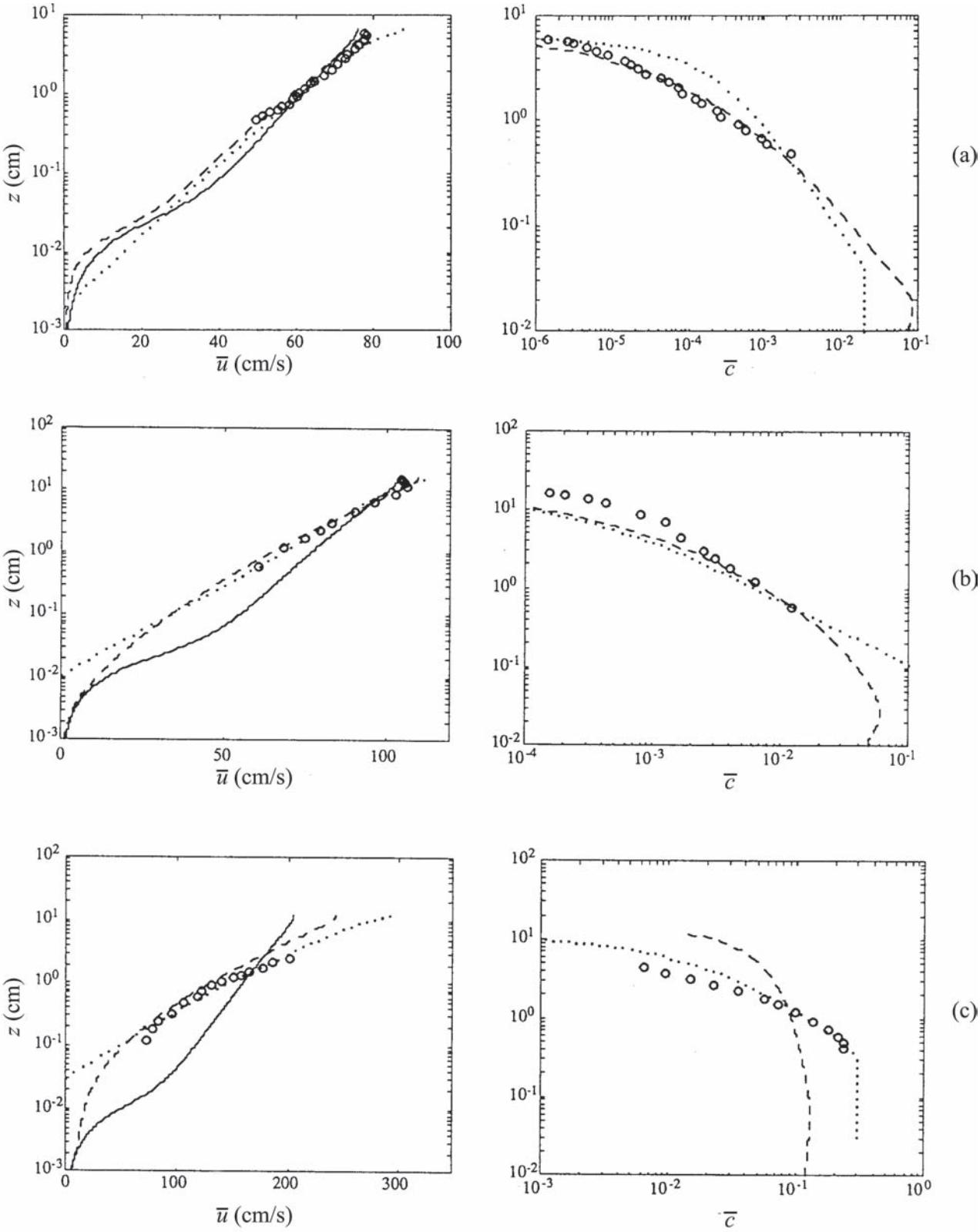

Fig. 16-7. Comparison of velocity ($\bar{u}$) and concentration ($\bar{c}$) predictions (Villaret and Davies 1995) and measurements of uniform-flow case: (a) data of Lyn (1988), (b) data of Coleman (1981), and (c) data of Einstein and Chien (1955). Symbols: measurements, ——— : clear-water prediction; — — : two-phase k–ϵ model prediction; . . . : one-equation model prediction.

16.4.7.3 Second-Moment Closure and Algebraic Stress Models The original problem posed by the Reynolds averaging of the Navier-Stokes equations is the appearance of unknown Reynolds stress terms. Whereas eddy-viscosity models attempt to relate these unknown terms to the mean fields via constitutive equations and thus resolve the turbulence closure problem, a more direct approach might be considered, namely directly deriving equations for the elements of the Reynolds stress tensor. This approach leads to higher-order correlation terms, which, however, could then be subjected to the type of modeling applied to the lower-order terms in eddy-viscosity models. This forms the theoretical basis of Reynolds stress (RS) or second-moment closure (SMC) models. The equation for $\overline{u_i'u_j'}$ can be written as

$$\frac{D(\overline{u_i'u_j'})}{Dt} = \frac{\partial(\overline{u_i'u_j'})}{\partial t} + \frac{\partial[\overline{u}_l(\overline{u_i'u_j'})]}{\partial x_l} = P_{ij} + G_{ij} + D_{ij} + \prod_{ij} - \epsilon_{ij} \qquad (16\text{-}69)$$

where D_{ij} denotes diffusive transport terms,

$$P_{ij} = -\overline{u_i'u_l'}\frac{\partial \overline{u}_j}{\partial x_l} - \overline{u_j'u_l'}\frac{\partial \overline{u}_i}{\partial x_l} \qquad (16\text{-}70)$$

represents the production of $\overline{u_i'u_j'}$ through interaction of the turbulence with the mean strain rate, G_{ij} the production of $\overline{u_i'u_j'}$ by other forces or strains, Π_{ij}, the pressure-strain term, and ϵ_{ij} the term representing the viscous dissipation of the Reynolds stresses. If the effects of buoyancy are modeled, then

$$(G_\rho)_{ij} = \frac{1}{\rho_{\text{ref}}}\left(g_i\overline{\rho' u_j'} + g_j\overline{\rho' u_i'}\right) = (s-1)\left(g_i\overline{c' u_j'} + g_j\overline{c' u_i'}\right) \qquad (16\text{-}71)$$

where the second equality invokes the suspension density relation. Besides the basic sediment conservation equation, transport equations for the second-moment quantities involving c' such as $\overline{u_i'c'}$ and $\overline{c'^2}$, are also formulated. The resemblance between Eq. (16-69) and the exact equation for k is not coincidental, since the latter can be derived from the former.

Because the RS model approach solves for each element of the Reynolds stress tensor, and not simply k, anisotropic flow features *should* be better handled. RS models also have the advantage that the production terms, both from shear and from extra strains, are exact, and so flow aspects strongly influenced by such extra strains should be more rationally modeled. This does not of course necessarily extend in a straightforward way to particulate flows, for which the basic models for the momentum equations are still being debated, though, if the stratification analogy is accepted, the effects of simple stratification should be better modeled. In practice, as will be seen in the next section, the promise of RS models has not yet been satisfactorily fulfilled (see also the general discussion of Bradshaw 1997 and that of Patel 1997 in the context of curvature effects). Apart from the difficulty of modeling the pressure-strain term, Π_{ij}, conventional RS models still use (1) the problematic ϵ–equation, (2) k^2/ϵ for the effective diffusion coefficient for diffusive transport terms, and (3) wall-functions at solid boundaries. Several computations using RS models will be reviewed in Section 16.5.

Although the full second-moment closure offers the promise of resolving some of the well-known problems of two-equation models, the computational demands are much more severe. If only the flow is considered, up to six additional partial differential equations must be solved for a three-dimensional simulation, and if the transport of a scalar, such as a sediment concentration, is also desired, then this may add up to four more partial differential equations, over and above what a two-equation model requires. A further practical problem, especially with sediment transport, is the specification of boundary conditions. The difficulties involved in specifying a bottom boundary condition for $\bar{c}$ have been discussed already; for an RS model, additional conditions on other second-moment quantities involving c must also be imposed. For such reasons, an intermediate approach may be sought in which Eq. (16-69) is simplified, such that $\overline{u_i'u_j'}$ may ultimately be specified algebraically without the need for solution of partial differential equations. Various algebraic stress (AS) models can be obtained depending on the simplifying assumptions made.

The simplest model makes a local equilibrium assumption in which transport terms in Eq. (16-69) are neglected, and $\overline{u_i'u_j'}$ is determined from the equation

$$P_{ij} + G_{ij} + \prod_{ij} - \epsilon_{ij} = 0 \cdot \qquad (16\text{-}72)$$

This is the basis of the well-known Mellor-Yamada level $2\frac{1}{2}$ model (Mellor and Yamada 1982), widely used in ocean modeling and more sporadically in hydraulic and coastal engineering (Blumberg et al. 1992; Davies et al. 1997). A feature of this model, absent in the standard or buoyancy-extended k–ϵ models, but common to AS models including AS k–ϵ models, is that the closure coefficients (such as c_μ in k–ϵ models and the stability functions S_M in Mellor-Yamada models) associated with the effective eddy diffusivities for momentum and for buoyancy depend on local dimensionless parameters, such as a gradient Richardson number. Comparisons of the predictions of the Mellor-Yamada level $2\frac{1}{2}$ model and other models have been made by Rodi (1987), and more recently by Burchard and Baumert (1995) and Baumert and Peters (2000), for stratified flows. A variant of the Mellor-Yamada level 2½ model was used by Sheng and Villaret (1989) to study the effect of sediment-induced stratification on erosion of cohesive sediments. Although

the results showed that such stratification could significantly affect erosion, detailed comparisons of flow predictions with experimental data were not given.

The AS model k–ϵ due to Rodi (1976; 1993) assumes that the sum of the history and transport terms for $\overline{u_i'u_j'}$ is proportional to the corresponding terms for k, with the proportionality factor being $\overline{u_i'u_j'}/k$, which is not constant. The resulting specification for $\overline{u_i'u_j'}$ can be written as

$$\overline{u_i'u_j'} = k\left[\frac{2}{3}\delta_{ij} + \frac{(1-c_{1A})\{P_{ij} - (2/3)\delta_{ij}P_k\} + (1-c_{2A})\{G_{ij} - (2/3)\delta_{ij}G_k\}}{P_k + G_k - (1-c_{3A})\epsilon}\right] \tag{16-73}$$

with the three additional closure coefficients c_{1A}, c_{2A}, c_{3A}. AS models share some similarities with nonlinear eddy viscosity models, and may be interpreted as a special class of nonlinear models for $\overline{u_i'u_j'}$. Lien and Leschinzer (1994) have argued that, being based on simplifications of the full RS models, they have a stronger physical basis than general nonlinear models in which the relationship between stress and stress is only formally postulated. Mendoza and Shen (1990) applied this model in a study of clear-water flow over nonerodible dunes, and some results are given in Section 16.5.1.

From a similar though rather more involved analysis, involving a number of additional approximations, an analogous specification for concentration flux term, $\overline{u_i'c'}$ can be given,

$$-\overline{u_i'c'} = \frac{k}{\epsilon}\left[\frac{\overline{u_i'u_l'}\left(\frac{\partial \bar{c}}{\partial x_l}\right) + (1-c_{2c})\,\overline{u_l'c'}\left\{\left(\frac{\partial \bar{u}_i}{\partial x_l}\right) - 2c_{3c}(k/\epsilon)\,g_i(s-1)\left(\frac{\partial \bar{c}}{\partial x_l}\right)\right\}}{c_{1c} + \{(P_k + G_k - \epsilon)/2\epsilon\}}\right] \tag{16-74}$$

with additional constants, c_{1c}, c_{2c}, and c_{3c}. Launder (1996) notes that, in wall-bounded flows where transport effects are not important, AS models yield results similar to RS models (which does not necessarily mean correct results) for $\approx 60\%$ of the computational effort, but warns that the performance in free turbulent flows is much less satisfactory. As with other aspects of stratified-flow models, the values proposed in the literature for c_{1c}, c_{2c}, and c_{3c} (e.g., Launder 1984; Rodi 1993; Chen and Jaw 1998) have been based on data from thermally stratified flows; to what extent, if at all, these are applicable to sediment-laden flows is still an open question. Velocity-sediment-concentration correlations are rather ill-defined experimentally, and, in any case, extremely difficult to measure.

Example. For a steady uniform plane flow, the algebraic stress model for the flow only (excluding buoyancy effects) can be expressed as

$$0 = g\sin\theta + \frac{\partial\left(-\overline{u'w'}\right)}{\partial z} \tag{16-75a}$$

$$0 = \frac{\partial}{\partial z}\left(\frac{\nu_t}{\sigma_k}\frac{\partial k}{\partial z}\right) - \overline{u'w'}\frac{\partial \bar{u}}{\partial z} - \epsilon \tag{16-75b}$$

$$0 = \frac{\partial}{\partial z}\left(\frac{\nu_t}{\sigma_\epsilon}\frac{\partial \epsilon}{\partial z}\right) + c_{1\epsilon}\frac{\epsilon}{k}\left(-\overline{u'w'}\frac{\partial \bar{u}}{\partial z}\right) - c_{2\epsilon}\frac{\epsilon^2}{k} \tag{16-75c}$$

$$\overline{u'^2} = \frac{2}{3}k\left[1 + \frac{2(1-c_{1A})\left\{-\overline{u'w'}\left(\partial\bar{u}/\partial z\right)\right\}}{-\overline{u'w'}\left(\partial\bar{u}/\partial z\right) - (1-c_{3A})\epsilon}\right] \tag{16-75d}$$

$$\overline{v'^2} = \frac{2}{3}k\left[1 - \frac{(1-c_{1A})\left\{-\overline{u'w'}\left(\partial\bar{u}/\partial z\right)\right\}}{-\overline{u'w'}\left(\partial\bar{u}/\partial z\right) - (1-c_{3A})\epsilon}\right] \tag{16-75e}$$

$$\overline{w'^2} = \frac{2}{3}k\left[1 - \frac{(1-c_{1A})\left\{-\overline{u'w'}\left(\partial\bar{u}/\partial z\right)\right\}}{-\overline{u'w'}\left(\partial\bar{u}/\partial z\right) - (1-c_{3A})\epsilon}\right] \tag{16-75f}$$

$$\overline{u'w'} = \frac{(1-c_{1A})k\left\{-\overline{w'^2}\left(\partial\bar{u}/\partial z\right)\right\}}{-\overline{u'w'}\left(\partial\bar{u}/\partial z\right) - (1-c_{3A})\epsilon} \tag{16-75g}$$

Again, with the ν_t–relationship, Eq. (16-53), the system is closed, with seven equations for the seven unknowns, $\bar{u}$, k, ϵ, and the four nonzero components of the Reynolds stress tensor, $\overline{u'^2}$, $\overline{v'^2}$, $\overline{w'^2}$, and $\overline{u'w'}$. That the algebraic stress model can reflect anisotropy is seen in the difference between the expression for $\overline{u^2}$ and $\overline{w'^2}$, with the latter being smaller, as is experimentally observed. Interestingly, $\overline{u^2}$ and $\overline{w'^2}$ are predicted to be equal, which does not agree with measurements, which indicate that $\overline{u^2} > \overline{w'^2}$. This incorrect behavior is also produced by the Mellor-Yamada level 2½ model (Mellor and Yamada 1982). The sum of the normal stresses is also seen to yield $2k$, as should be the case. Equation (16-75g) can also be expressed in a form consistent with a BEVM, i.e., $-\overline{u'w'} = c_\mu(k^2/\epsilon)(\partial\bar{u}/\partial z)$, with, however, c_μ being a function of P/ϵ (Rodi 1993), a characteristic of AS models wherein the model constants of the standard k–ϵ model are found to vary with local parameters, such as P/ϵ or Ri_f.

16.5 APPLICATIONS OF TURBULENCE MODELS TO PROBLEMS RELATED TO SEDIMENT TRANSPORT

In this section, six applications relevant to sediment transport are described in rather more detail. The limited number

of applications necessarily reflect the biases and interests of the author, though studies were chosen to illustrate the capabilities/limitations of turbulence models to simulate different flow features, and where available, to compare the performance of different models. In the following, unless otherwise specified, simulations were performed with the standard k–ϵ model without buoyancy, the free surface was not modeled (the rigid-lid approximation was invoked), and the turbulent Schmidt number for sediment, is $(\sigma_t)_s = 1/\beta_s = 1$. Four of the six problems involve the simulation of sediment transport, the cases without sediment being a study of flow over bedforms and a study of flow within model vegetation, both of which exhibit aspects of some relevance to sediment transport modeling. In four cases, the bed is assumed fixed. Even in those cases with sediment transport and with an erodible bed, it is helpful to examine simulations of the corresponding case without sediment and with a fixed bed to investigate possible model deficiencies in a simpler problem. Without the added complications of sediment and a movable bed, the results for the simpler problem of flow over fixed beds provide an upper bound on what can be achieved by turbulence models, as far as the flow is concerned. The first four involve two-dimensional (one-dimensional when horizontal homogeneity is assumed) simulations, whereas, in the last two, three-dimensional computations were undertaken. In both erodible-bed simulations, an Exner equation is applied to determine the temporal evolution of the bed. Experimental data for comparisons have mainly been obtained in laboratory studies, because these offer more detail and control than can usually be achieved in field studies. In two instances, however, field observations were used for comparison.

Cautionary notes must be sounded in comparing the results of numerical simulation with experimental measurements. This concerns, on the one hand, the effects due entirely to numerical choices, such as mesh resolution and treatment of advection, and those due to the turbulence model. The earliest studies and likely most field studies may be criticized for the use of overly coarse numerical grids, often combined with overly diffusive numerical techniques. By the same token, experimental observations may also be contaminated by extraneous features, such as those due to side walls. In the following, the discussion will not dwell on either numerical or experimental shortcomings, though these should be kept in mind.

16.5.1 Flow Over Bed Forms

Bed forms (a definition sketch is given in Fig. 16-8) are ubiquitous in alluvial channels and have posed some of the most challenging problems for those interested in predicting sediment transport. An understanding of flow over bed forms is a prerequisite for reliable transport predictions. The flow over fixed two-dimensional nonerodible bed forms has been studied experimentally (Raudkivi 1963; van Mierlo and de Ruiter 1988; Lyn 1993; McLean et al. 1994; Bennett and Best 1995; Cellino and Graf 2000). A comprehensive list of experimental work before 1995 is given in Bennett and Best (1995). Before the discussion of fixed-bed flows without sediment, however, the early work of Mendoza and Shen (1988) should be pointed out, in which not only flow but also sediment transport over dunes were simulated using an RS model, with however somewhat limited comparisons to measurements.

With separation, recirculation, and reattachment as prominent features, this flow shares similarities with the classic backward-facing step flow that has become a benchmark of turbulent flow simulation (for a recent study comparing the performance of various turbulence models, see Lien and Leschziner 1994). The quasi-periodic spatial pattern offers, however, simplifications as well as complications. On the one hand, a suitably defined outer flow may be less sensitive to details of bed geometry, somewhat analogously to the effective sand-grain roughness, which justifies to some extent the frequent approximation of treating the bed as being planer but with increased effective roughness (the main difficulty being that the flow region influenced by the bed forms may constitute a substantial fraction of the flow depth). On the other hand, the reattached flow will not have had sufficient time to approach an equilibrium state before separation occurs again, which contrasts with the typical backward facing-step flow, used in test cases, in which an equilibrium boundary-layer or fully developed channel flow separates.

The pioneering small-scale experiment of Raudkivi (1963) has been the subject of several studies, including those by Johns et al. (1990) using their one-equation model (see Section 16-4.3.3), by Mendoza and Shen (1990) with the AS model of Rodi (1976), by Sajjadi and Aldridge (1995) with one-equation, k–ϵ and RS models, and by Cheong and Xue (1997) with a k–ϵ model with a correction term for streamline curvature. The one-equation models have so far proved to be clearly inadequate, reproducing poorly the recirculation region in the mean velocity profile. The Sajjadi and Aldridge (1995) results with a one-equation model also largely overpredicted the magnitude of $\overline{u'w'}$. Some results of Mendoza and Shen (1990), in what seems to be the only study with an AS model (basically that of Rodi 1974), are shown in Fig. 16-9. Quite good agreement of predicted and measured velocity profiles is obtained, and even $\overline{u'w'}$, as well as bed shear

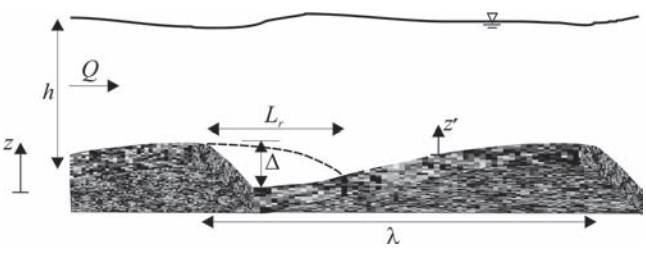

Fig. 16-8. Definition sketch for dune flow.

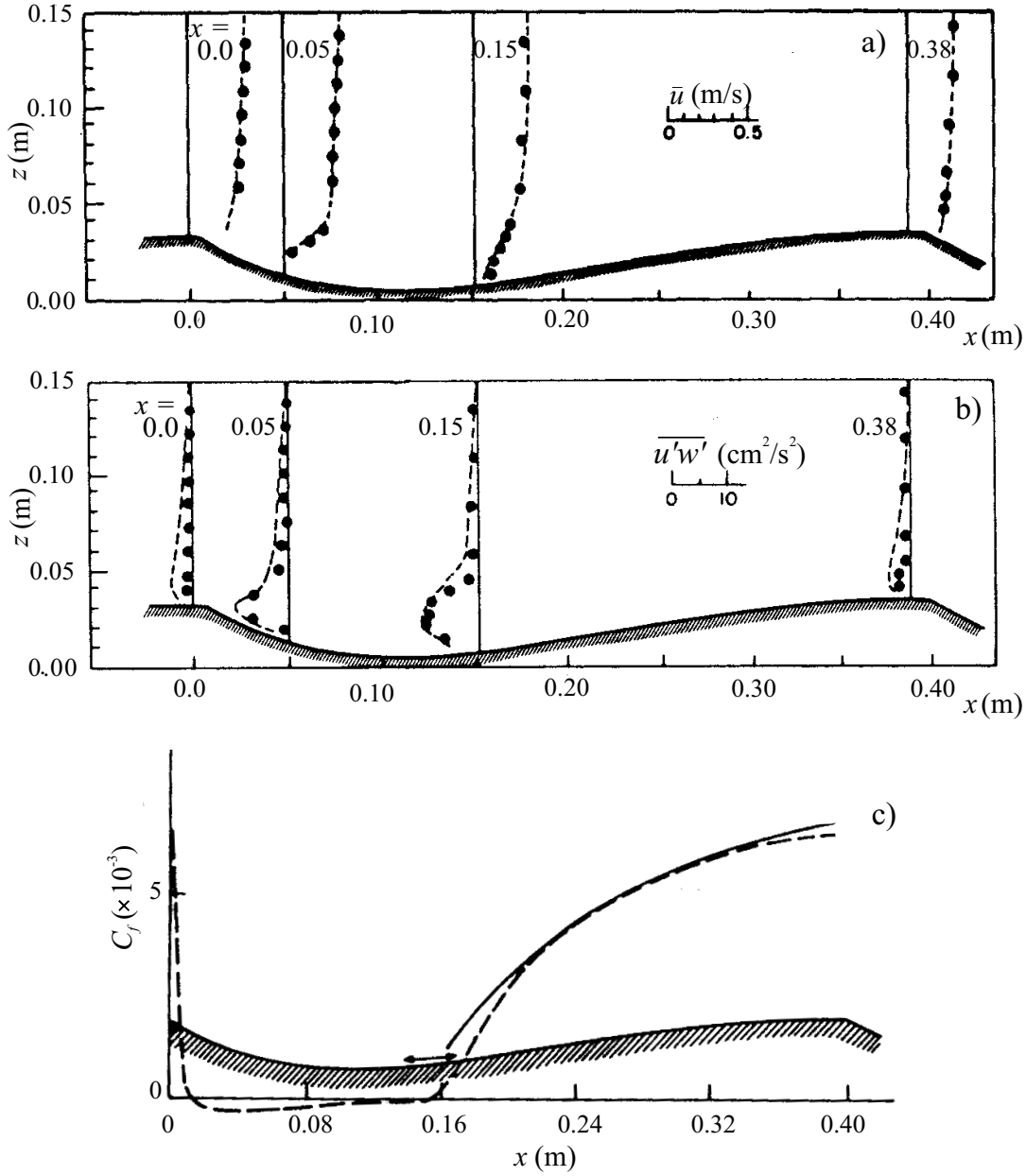

Fig. 16-9. Predictions of $\overline{u}$, $\overline{u'w'}$, and C_f with an AS k–ϵ model:—(Mendoza and Shen 1990); symbols and --- (measurements of Raudkivi 1963).

stresses, is quite well reproduced, though some deficiencies are seen, somewhat surprisingly, in regions away from the reattachment point. To a certain extent, this good performance is also found in the Sajjadi and Aldridge (1995) simulations of this case with k–ϵ and RS models, in contrast to results of more recent studies for other flows, as discussed below. This difference may be explained by the experimental parameters of this particular case, which, as seen in Table 16-3, are quite distinct from those of the other studies, but might also be due to the limitations of the experimental techniques.

Yoon and Patel (1996) simulated experiment T6 of van Mierlo and de Ruiter (1988) with a k–ω model, whereas Cheong and Xue (1997) computed the experiment T5 with a k–ϵ model (Johns et al. (1990) also studied T5 with their one-equation model, but its performance was similar to that already seen for the Raudkivi case). In spite of some

Table 16-3 Experimental Parameters for Flow over Bed Forms

Parameter	Raudkivi (1963; 1966)	van Mierlo de Ruiter (1988)		McLean et al. (Run 2, 1994)
		T5	T6	
λ/h	2.94	6.25	4.76	5
λ/Δ	12.8	20	20	20
Lr/Δ	n.r.	5	5	4.5
R (10^5)	0.39	0.99	1.71	0.6
F	0.27	0.25	0.28	0.30
d_r (mm)	0	1.6	1.6	1.5[a]
Measurement technique	Pitot tube, hot-film	LDV[b]	LDV	LDV

[a]Assumed (concrete specified).
[b]LDV: laser Doppler velocimetry.

differences between the two flows, T5 and T6, the two simulations are compared in Fig. 16-10. A three-layer wall-function approach at the bottom boundary was applied by Cheong and Xue, whereas the k–ω rough-wall model (Eq. 16-64) was used by Yoon and Patel. The latter report a reattachment length, L_r, in agreement with the measured value, compared to a smaller than measured value (about 20% in the case of the standard k–ϵ model and 10% in the case of the k–ϵ model with curvature correction) predicted by Cheong and Xue. The prediction of the bed shear stress, $\overline{\tau}_b$, by the k–ω model seems notably better, but Yoon and Patel reestimated $\overline{\tau}_b$ from the velocity profile data based on $d_r = 1.6$ mm rather than accepting the values provided by van Mierlo and de Ruiter, which assumed $d_r = 2.6$ mm based on plane-bed measurements. In spite of the good prediction of $\overline{\tau}_b$ and the fair agreement with regards to L_r, the results of Yoon and Patel *underestimated* overall flow resistance by 20%. This is likely associated with the poor performance of *both* models in predicting the peak Reynolds shear stress, $-\overline{u'w'}$, in the separated shear layer, which is markedly underpredicted. This differs from the experience in the backward-facing-step flow problem, where even the standard k–ϵ model predicts reasonably well the value if not the location of the peak $-\overline{u'w'}$ (Lien and Leschziner 1994), again pointing to subtle but important differences between this flow and the flow over periodic bed forms. An unfortunate characteristic of the van Mierlo and de Ruiter study is that, due to limitations of their optical system, measurements were taken at a location that was relatively far from the flume centerline, such that three-dimensional effects may have played some role.

Because these above studies examined different flows with various numerical grids and techniques, assessing the performance of turbulence models is made difficult. A comparison of four models for the same flow (Run 2 of McLean et al. 1994) with the same grid and numerical solver is given in Fig. 16-11. The computational domain and dune geometry are shown in Fig. 16-11(a). Periodic boundary conditions were imposed at the inlet and outlet, and the rigid-lid approximation was made. The commercial FLUENT (Version 6.0) code was used with second order upwind discretization on a 321 × 91 (x,y) grid. A roughness height of 1.5 mm was assumed, and an enhanced near-wall model, which, grid permitting and if appropriate, attempts to resolve through to the viscous sublayer by appropriate blending functions and/or a two-layer model, was chosen.

The largest differences in the predicted bed shear stresses (Fig. 16-11(b)) are seen in the region upstream and in the neighborhood of the reattachment point. As seen in other studies, the k–ϵ model significantly underpredicts L_r,with a slight improvement being achieved with the RNG modification. The L_r predicted by the k–ω model is approximately the same as that in the earlier Yoon and Patel (1996) study, which, in view of the similarity of the experimental parameters, is not surprising. This, however, exceeds the observed L_r by ≈10%. The RS model underpredicts L_r by a similar amount, and tends to yield a flatter variation for the reattached internal boundary layer. Because of uncertainties in the estimation of bed shear stress, only a single representative point relatively far from the reattachment point is shown in Fig. 16-11b. All model predictions agree reasonably well with the measurement point in this region.

The results on mean velocity and Reynolds shear stress (Figs. 16-11(c and d)) indicate that the relative performance of a model can be quite variable depending on the region. In general, the standard k–ϵ model fares the poorest, due in part to and consistent with its worst prediction of the reattachment point. In contrast, the k–ω and RS models, which

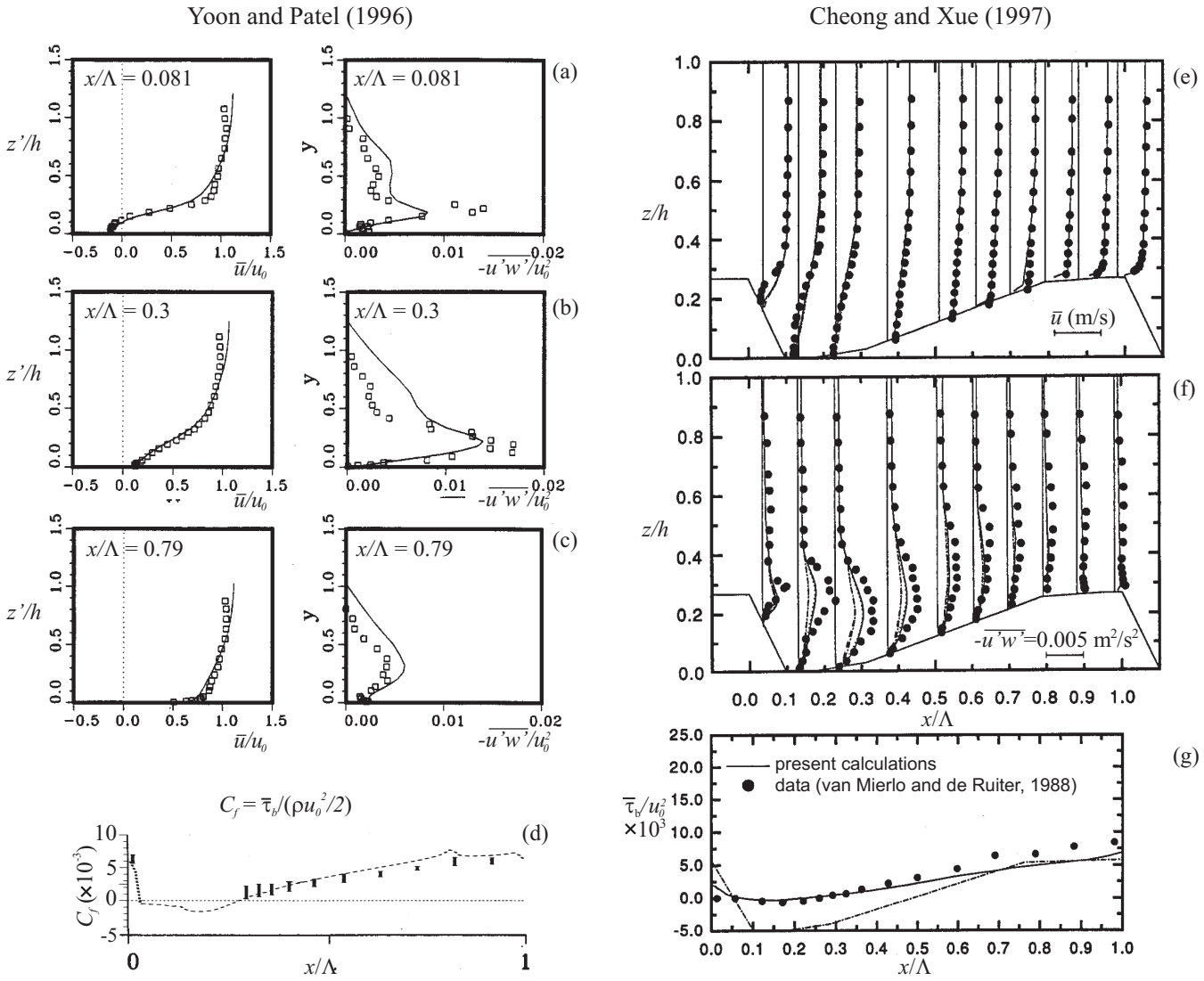

Fig. 16-10. Comparison of k–ω results (Yoon and Patel 1996; note that z' is measured from the bed) (a), (b), (c), (d) with k–ϵ model (Cheong and Xue 1997) (e), (f), (g) for van Mierlo and de Ruiter experiments, T6 and T5, respectively.

had best predicted the reattachment point, perform best, but only in the near-bed region. All models substantially underpredicted the peak $-\overline{u'w'}$ associated with the separated shear layer. The RS model consistently performed the best in this regard, but could be in error by more than 50%. This conclusion is consistent with that found in previous studies of the van Mierlo and de Ruiter cases. In the upper half of the flow, however, $-\overline{u'w'}$ was substantially underpredicted by all except the RNG k–ϵ model. Somewhat surprisingly, the RNG k–ϵ model did best in the upper half of the flow, particularly with respect to the prediction of $-\overline{u'w'}$. This behavior is rather at odds with previous studies, such as those shown in Fig. 16-10, where even an overprediction of $-\overline{u'w'}$ in this region is seen in the results of Yoon and Patel (1996).

16.5.2 Flow and Transport in Sedimentation Tanks

Sedimentation tanks are standard equipment in water-treatment plants for the removal of suspended solids. From a broader perspective, lakes and estuaries may be viewed as naturally occurring sedimentation tanks. Turbulent transport in sedimentation tanks or clarifiers may significantly influence their removal performance and hence their reliability. In the present context, this sediment-laden flow presents an example, like turbidity currents, where sediment-induced buoyancy effects may be most clear-cut, and hence where buoyancy extensions to flow and turbulence models may be required. On the other hand, a major simplification compared to the problem of flows in alluvial channels is the negligible

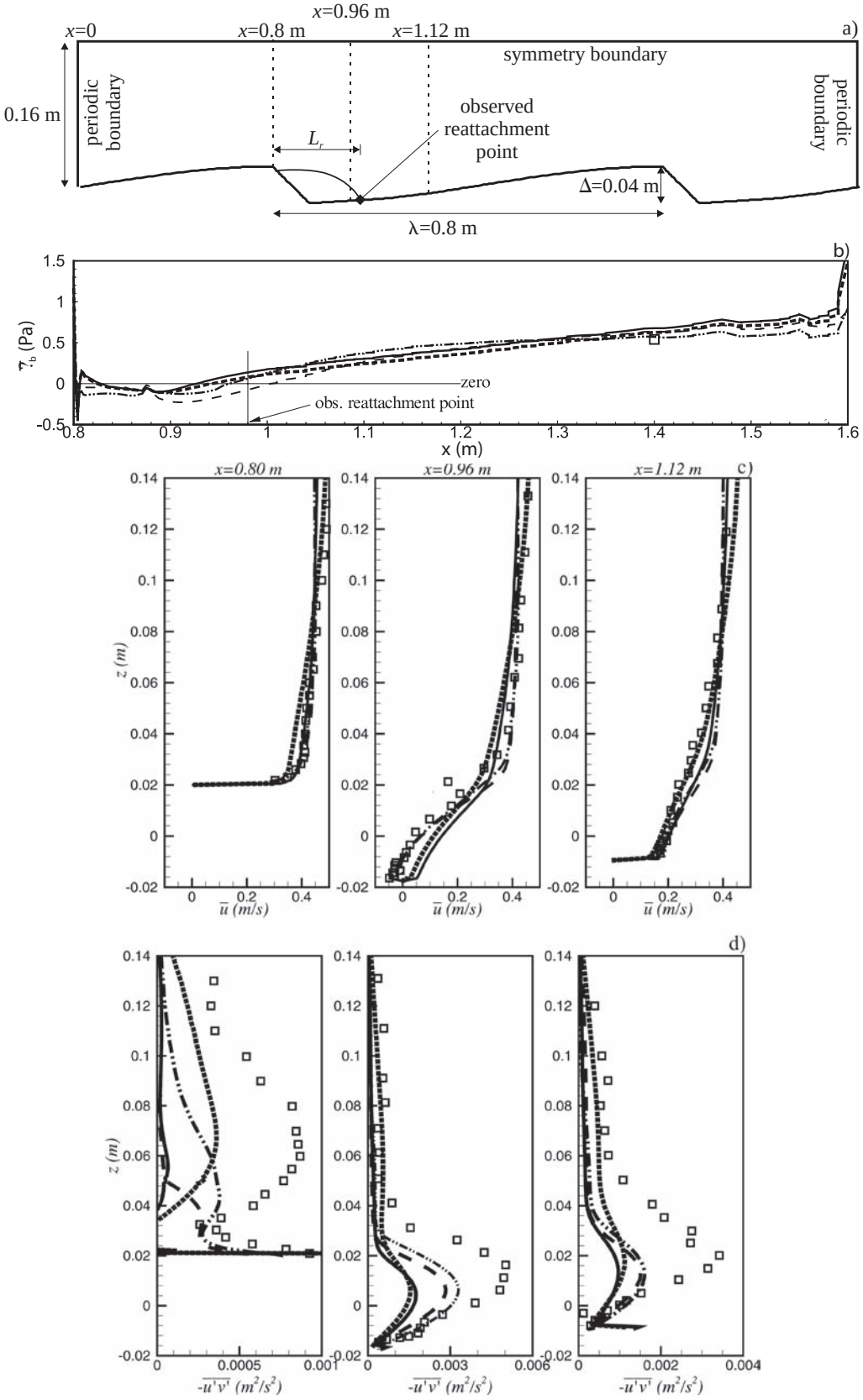

Fig. 16-11. Comparison of four model predictions for the same flow (Run 2 of McLean et al. 1994) using the same numerical grid and scheme: (a) definition sketch, computational domain, and flow geometry; (b) bed shear stress predictions; (c) velocity profiles; (d) Reynolds shear stress profiles; where —— is the $k-\epsilon$ model, --- is the $k-\omega$ model, . . . is the RNG $k-\epsilon$ model, and –·–·–·– is the Reynolds stress model. Symbols are measurements (or estimates from measurements).

role played by the near-bottom transport and hence the bottom boundary condition for the sediment equation. In this respect, the performance of the turbulence model is more precisely tested (in isolation from the other elements of the transport model) because only suspended load, which is directly related to the turbulence model, is of concern. Various computational studies have examined the flow and transport characteristics in clarifiers, ranging from the early constant eddy-viscosity models of Larsen (1977) and Imam et al. (1982) to the buoyancy-extended k–ϵ model of Devantier and Larock (1987) to an AS k–ϵ model in Zhou et al. (1994), with reviews of modeling issues by Krebs (1995) and Matko et al. (1996). Only two cases will be discussed in this section, those of Lyn et al. (1992) and Frey et al. (1993), who simulated the conditions listed in Table 16-4.

Lyn et al. (1992) applied a buoyancy-extended k–ϵ model with $c_{3\epsilon} = 0$ to predominantly stably stratified horizontal flows. Even at relatively low particle concentrations, suspension-induced buoyancy effects may be significant because of small velocities and hence low shear. The problem of non-uniform-sized particles was dealt with by considering different size classes and solving Eq. (16-7) for each size class. That a solution for ϵ is obtained in a k–ϵ model was exploited by developing a simple model for flocculation due to turbulent shear, such that the particle concentration in each size class may change not only by deposition but also by flocculation. A zero-diffusive-flux-concentration ($\partial c/\partial z = 0$) condition was imposed at the bottom, under the assumption that reentrainment of deposited sediment does not occur. Results from simulations including and not including sediment-induced buoyancy effects of an actual (tertiary) clarifier are shown in Fig. 16-12. The actual inlet configuration is a series of square jets at the same elevation, and hence the details of the three-dimensional inlet flow cannot be captured by the two-dimensional model. Nevertheless, significant difference in streamline pattern depending on whether buoyancy effects are or are not included in the model is clearly seen, and comparison with the velocity measurements lends support to the significance of buoyancy effects, though only fair agreement between predicted and observed mean horizontal velocities was achieved. The importance of simulating different sediment size classes when buoyancy effects are included is seen in the comparison with concentration measurements. Because of the presence of small size fractions in the influent, a notable suspended solids concentration is still observed even toward the end of the tank. Interestingly, the concentration predictions, including the effects of different size classes, but without the effects of buoyancy, are found to be, somewhat fortuitously, in reasonable agreement with measurements in spite of obvious discrepancies in the corresponding flow predictions.

When Frey et al. (1993) applied a k–ϵ model in determining the steady-state flow field, they evaluated the removal efficiency of the clarifier, i.e., the ratio of influent to effluent particle concentration, not by the conventional advection-diffusion equation for the sediment concentration (Eq. (16-7)), but by a Lagrangian model, along the lines of Eqs. (16-9) and (16-10). They also more consistently included a random velocity component to simulate the random motion of particles. In their flow model, the rigid-lid approximation, which could be justified from their very small Froude numbers (Table 16-4), was not made, but buoyancy effects were not included. Fig. 16-13 compares their predictions for the flow field and removal with measurements in a laboratory model experiments with non-uniform-sized particles. Although substantial discrepancies between predicted and measured flow profiles can be seen in the inlet region, surprisingly good agreement is obtained for the predicted particle deposition (Fig. 16-13, the area numbers referring to streamwise stations at which deposited sediment was measured) and the effluent concentration, rather similarly to the previous case. Reasonable prediction

Table 16-4 Experimental Parameters for Flows in Sedimentation Tanks

Parameter	Frey et al. (1993)	Larsen (1977)
Model type	Laboratory	Field
Suspended material	Fine sand	Waste solids
Inlet concentration, C_0 (g/l)	N.r	80
w_s (mm/s)	N.r	0.2–4
d_{50} (μm)	50–100	N.r
$\mathsf{R} = (Uh/\nu)$ (10^3)	4.4	9.5
$\mathsf{F} = U/\sqrt{gh}$ (10^{-3})	11.6	0.49
$\mathsf{Ri}_h = g(\Delta\rho_0/\rho)h/U^2$ [a]	N.r	105
Measurement technique	LDV	Ultrasonic current meter

[a]Bulk Richardson number, based on averaged downstream velocity, U, downstream depth, h, and inlet density difference, $\Delta\rho_0$.

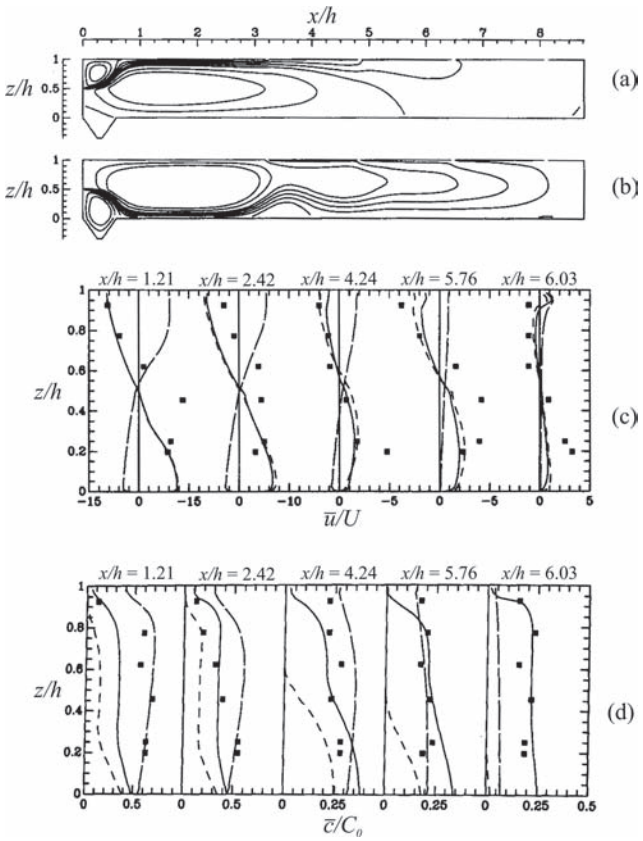

Fig. 16-12. Comparison of predictions (Lyn et al. 1992) of (a) simulated streamlines without (top) and (b) with (bottom) buoyancy effects included, (c) nondimensional horizontal velocity (U is the nominal velocity in the tank), and (d) suspended solids concentration normalized by the inlet concentration, C_0 (—: with buoyancy effects and particle size distribution modeled; ---: with buoyancy effects but monodisperse particles; — —: without buoyancy effects but with particle size distribution modeled, where symbols are data from Larsen 1977).

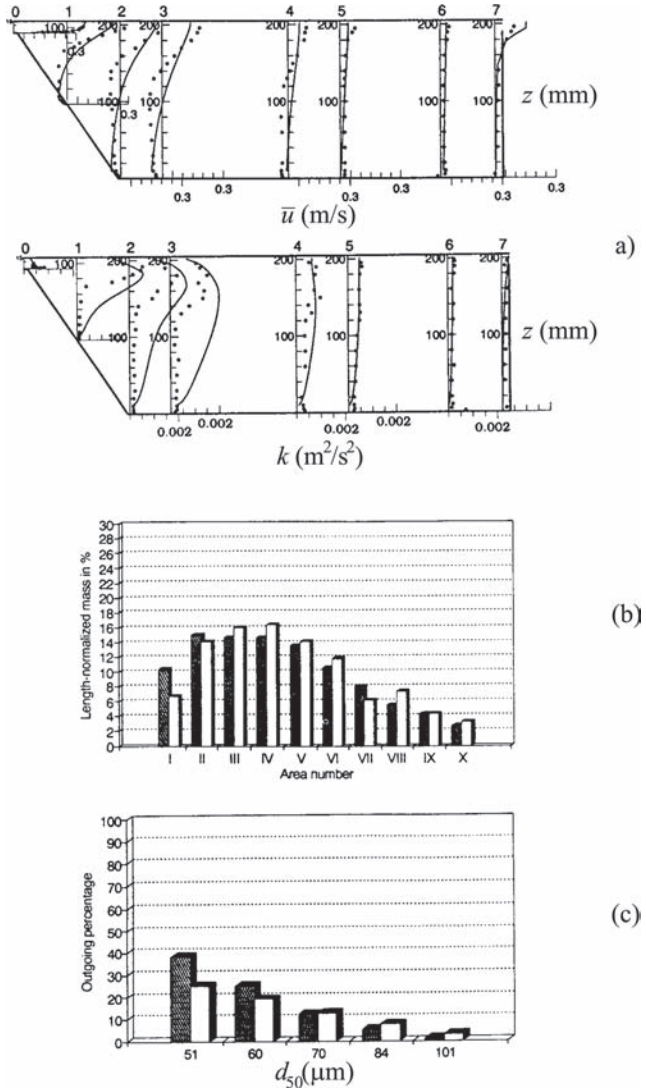

Fig. 16-13. Comparison of measurements in a model sedimentation tank with predictions of the k–ϵ model (Frey et al. 1993): (a) horizontal velocity, $\bar{\mu}$, and turbulent kinetic energy, k (symbols are measurements; — — — are predictions); (b) deposition of material at different streamwise stations (shaded bars are measurements; open bars are predictions); (c) effluent particle concentration relative to influent particle concentration as a function of particle diameter (shaded bars are measurements; open bars are predictions). Adapted with permission.

of derived overall quantities, such as sediment load, need not imply that detailed flow quantities are well reproduced, and caution is advised in evaluating numerical simulations based solely on derived quantities.

16.5.3 Flow in Vegetated Regions

With increased interest in the hydraulics of wetlands, interest in predicting flow and transport in vegetated areas has grown. Since it would be impractical to model the details of flows through vegetation (Fig. 16-14), questions regarding the appropriate averaging procedure may be raised. In this respect, the problem of predicting the average flow through vegetation resembles the two-phase flow problem in that, in addition to the modeling of turbulence, even the basic momentum balance as well as its effect on turbulence characteristics, must be modeled. The usual practice adds a suitably parameterized force term modeling averaged drag forces to the momentum equation (Tsujimoto et al. 1991; Naot et al. 1996), somewhat analogous to the buoyancy-force term if the stratification analogy is invoked for sediment-laden flows. Lopez and Garcia (2001) have pointed out that this approach does not directly deal with the effects of dispersion associated with the spatial averaging process (see the discussion of

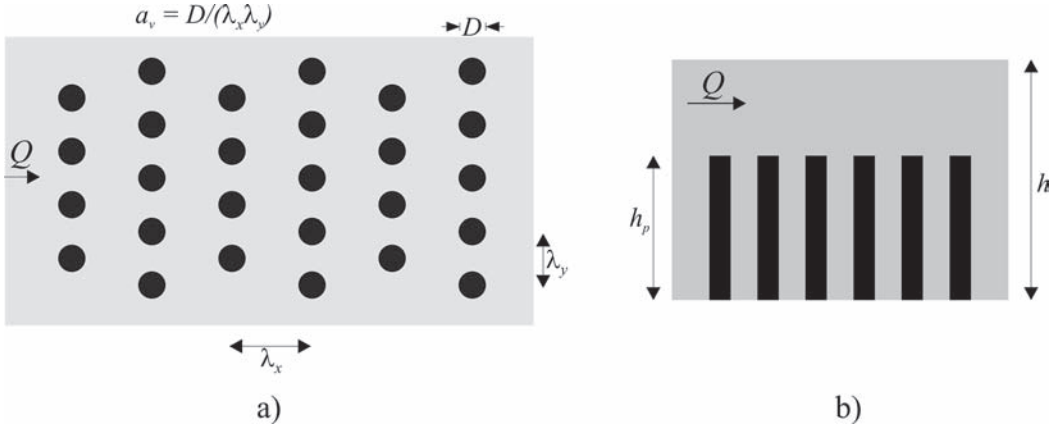

Fig. 16-14. Flow-through model (cylindrical) of nonemergent vegetation: (a) plan view, (b) profile view.

spatially averaged models in Appendix II to this chapter), but ultimately they resorted to the usual practice in their numerical modeling. In this subsection, for clarity, angle brackets will be used to denote variables that are spatially averaged over the horizontal plane.

Provided a model for the momentum equations has been chosen, the modeling of the effect of the vegetation on the turbulence follows essentially the same reasoning as in the development of the standard k–ϵ equations. If F_i denotes the additional force (per unit mass) term for modeling the effect of vegetation, then a production term, $G_v = c_{vk}F_i u_i$, is added as a source to the k–equation, and a balancing production term, $(G_v)_\epsilon = c_{v\epsilon}(\epsilon/k)G_v$, is added to the ϵ–equation (Tsujimoto et al. 1991; Naot et al. 1996; Lopez and Garcia 2001). As in previous discussions, c_{vk} and $c_{v\epsilon}$ denote model constants, and again, for consistency with the limit of local equilibrium, c_{vk} and $c_{v\epsilon}$ are related and cannot be chosen independently. There remains some debate as to the appropriate value of c_{vk}, which has been taken to be 0.07 by Tsujimoto et al. (1991) and Naot et al. (1996), and to be 1 by Burke and Stolzenbach (1983) and by Lopez and Garcia (2001). As noted by Lopez and Garcia, provided that c_{vk} and $c_{v\epsilon}$ are chosen to satisfy the local-equilibrium-limit constraint, the predictions of the eddy viscosity, v_t, may not be particularly sensitive to the particular value of c_{vk}.

Lopez and Garcia applied one-dimensional (horizontal homogeneity of the spatially averaged flow was assumed)

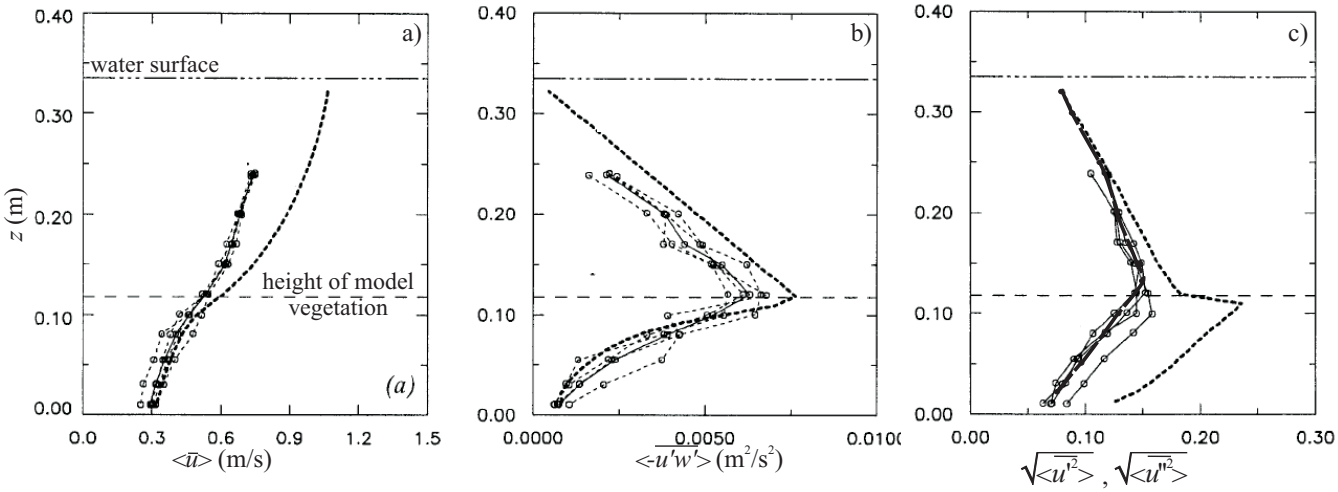

Fig. 16-15. Comparison of measurements (symbols; interpolated lines to aid visualization) and simulation (heavy lines) results for spatially averaged quantities in flow-through model of nonemergent (Lopez and Garcia 2001) (a) mean velocity (——) k–ϵ model, …. k–ω model, (b) Reynolds shear stress; (c) streamwise turbulence intensity (— k–ϵ model with $c_{vk} = c_{v\epsilon} = 1$, …. k–ϵ model with $c_{vk} = c_{v\epsilon} = 0$).

Copyrighted Materials
Copyright © 2008 American Society of Civil Engineers (ASCE)
Retrieved from www.knovel.com

CHAPTER 17

Watershed Sediment Yield

Deva K. Borah, Edward C. Krug, and Daniel Yoder

17.1 INTRODUCTION

17.1.1 General

Watershed sediment yield is the total amount of sediment generated within a watershed and delivered at its outlet during any given time. It starts with soil erosion, which is defined as the removal (detachment) of soil particles from the earth's surface. A portion or all of the eroded soil is then transported by flowing water as sediment. Sediment yield is defined as the amount of sediment that is delivered to a point remote from its origin. In a watershed, sediment yield includes erosion from land surface slopes, gullies, streams, and mass wasting, minus sediment that is deposited after it is eroded but before it reaches the point of interest.

Estimation of watershed sediment yield is critical in planning soil conservation and sustainable development of natural resources. Erosion is an important and pervasive watershed process that sculpts all aspects of watershed topography and affects all terrestrial and aquatic ecosystems. It reflects the interactive factors of climate, geology, biology, time, and topography and the influence that these exert on watersheds. Planners of human watershed activities must be cognizant of current erosion from all pristine and human-impacted watershed elements, as well as how the planned watershed activities themselves may influence erosion. Erosion can also affect those planned activities and can cause major damage to the environment. Sediment generated from erosion can pollute streams, rivers, and estuaries, fill reservoirs and navigation channels, and cover valuable floodplain lands and properties.

Agricultural, mining, forestry, and construction activities often involve clearing of vegetation and massive movement of soil, exposing it directly to the erosive actions of rain and flowing water. As a result, enormous amounts of soil can be lost from these sites, degrading the environmental quality and soil fertility of such highly eroded land surfaces. Sediment is also generated from streambeds, stream banks, and floodplains by the erosive actions of flowing water. As reported by Gianessi et al. (1986), the percentages of eroded soil in the United States attributable to various sources are as follows: cropland (37%), forests (16%), rangeland (11%), stream banks (11%), gullies (6%), pasture (4%), and other sources, including roads, construction sites, mines, and rural lands (15%).

In addition to its direct impact on waterways and aquatic ecosystems, sediment is a major contributor to non-point-source pollution. It can carry nutrients (particularly phosphates) to waterways, and it contributes to eutrophication of lakes and streams. This can severely affect aquatic habitat in streams, rivers, lakes, and wetlands. Adsorbed pesticides and toxic substances are also carried with sediment, and can adversely affect surface-water quality.

Proper land use and planning can greatly reduce the erosion potential during the periods of serious erosion hazard before the land is stabilized by vegetation growth or permanent structures. A good understanding of the complex processes of soil erosion, sediment transport, and sediment deposition (sedimentation or siltation) provides a sound basis for developing improved prediction and control methods. This chapter will discuss these processes and available methodologies for predicting the amount of sediment reaching a point collectively from different sources (sediment yield) and for evaluating the impacts of current or potential land-use changes and management practices. All of the erosion and sedimentation processes contributing to sediment yield take place within the boundary of a watershed. Therefore, watershed sediment yield from all watershed sources, managed and unmanaged, is the primary topic of interest.

This chapter deals only with sediment from rain and water erosion. In arid, semiarid, and some humid regions, wind causes considerable erosion of soil and damage to crops and infrastructure (fences, buildings, highways, etc.). The impact of wind erosion is generally not described or delimited by watershed boundaries, and although it does cause

significant soil degradation, whether it has any impact on aquatic systems depends on the specific situation. Wind erosion is therefore not covered here, though much information is available elsewhere in the literature (Schwab et al. 1993).

The remainder of this section discusses soil erosion, sedimentation processes, and physical factors affecting those processes. The remaining sections describe available methodologies, ranging from simple empirical equations to more comprehensive watershed models, for estimating soil erosion generated from different sources (upland slopes, gullies, and streambeds and banks) and finally computing sediment yield.

17.1.2 Soil Erosion and Sedimentation Processes

From a plan (bird's-eye) view, erosion begins on the relatively planar hillslopes that slope down from the watershed divides, and from ridges or other divides between subwatersheds. The runoff from these hillslopes concentrates in the lower portions of the local topography where the warped planar surfaces converge, defining the beginning of a concentrated-flow channel system. Though exceptions may exist—as when a steep channel empties onto a floodplain and forms an alluvial fan and poorly defined channel—most channels are ultimately linked together in a dendritic network. The smaller upland channels may be poorly defined broad swales, and generally have flow only when there is runoff from a storm event. Further down the watershed, larger drainage areas contribute flow, so channels generally become better defined and are more likely to have flow from subsurface baseflow even when there is no runoff. The channel system itself usually makes up a very small portion of the entire watershed area, with the planar hillslopes feeding runoff and any associated sediment into the channel system along most of its length.

Soil erosion and sedimentation by water include detachment from the soil mass, transport of some or all of the eroded soil as sediment downslope, and during its transit depositing some of the sediment or picking up more eroded soil. In following a droplet of runoff down the hillslope, three distinct forms of erosion are seen in the upland areas. These are sheet erosion, rill erosion, and gully erosion. Sheet erosion, also known as interrill erosion, takes place uniformly between rills or gullies and results primarily from raindrop impact. The erosive potential of this impact depends on raindrop size, fall velocity, and total mass at impact, but can be devastating. In the absence of vegetation, mulch, or other cover to absorb the impact, raindrops can detach tremendous quantities of soil. For that detachment to result in erosion, the detached particles must then be transported downslope. In sheet erosion areas, this is accomplished by the resulting shallow surface flow, which does not have enough power to detach particles but does have enough power to transport them.

In moving downslope, additional runoff water collects as the contributing area grows. The runoff soon (usually within 1-3 m of slope length) reaches a depth at which it has sufficient energy to begin detaching soil particles. This in turn lowers the soil surface at that point, causing even more runoff to flow in that direction. This ultimately forms a rill, which is defined as a small concentrated flow channel in the generally planar hillslope. Rills may be very shallow or very deep, but generally form parallel channels running downslope on the planar surface. Their location is controlled somewhat randomly by small irregularities in the microtopography, so if they are destroyed by tillage they will reform in different places.

Rill erosion is much more noticeable than interrill erosion. These small channels carry runoff and sediment from interrill areas, the rain that falls directly on them, and any sediment produced from erosion within the rill. Rill erosion increases rapidly as the slope steepens or lengthens and as the runoff rate increases.

Gully erosion is massive removal of soil by large concentrations of runoff. These occur in the low portions of the macrotopography where the planar hillslopes converge, so they are best thought of as the uppermost portions of the watershed channel system. When the gullies are small the erosion in them occurs primarily through the erosive action of the concentrated flow acting on the bottom and to a lesser extent the sides of the channel. Such gullies are referred to as ephemeral gullies, and are usually small enough so that they can be crossed by vehicles and can be erased by normal tillage operations. If precautionary measures are not taken, gullies will grow, and soon the erosive action of the flow is augmented by headcutting and sidewall sloughing, at which point the channels are defined as classical gullies. These may yield tremendous volumes of sediment. Timeliness of implementation and maintenance of erosion-control practices is all-important to keep this from occurring.

These processes take place primarily in the upland areas and upper channels of a watershed. Once the flow has reached the watershed channel system, sediment may also be generated from streams or channels as a result of streambed and bank erosion, in which case the channel is said to be degrading. On the other hand, if more sediment is added from the upland areas than the channel flow can transport, significant deposition and storage of upland sediment may occur within the channel system, in which case the channel is said to be aggrading. In a stable channel, very little net erosion occurs because of equilibrium between the sediment transported out of the channel system and that added by the upland erosion processes. When instability is introduced within the channel by removing vegetation along the banks, increasing the channel slope, or changing other channel characteristics, those influences on the channel can result in the production of significant amounts of sediment from erosion of streambed and/or bank.

The quantity and size of sediment material transported by channel flow are functions of runoff (or flow) velocity and turbulence, both of which increase as the slope steepens and

the flow increases. The larger the eroding material, the greater the flow velocity and turbulence must be to transport it. When velocity or turbulence decreases, some of the sediment may deposit. The largest and densest particles settle first, whereas the finer particles are carried farther downslope or downstream. The overall result depends on the balance between the flow's transport capacity and current sediment load. If the transport capacity is higher than the current sediment load, the potential exists for additional erosion. If the converse is true (sediment load > transport capacity), deposition will result. Though this is conceptually simple, both factors are constantly changing temporally and spatially as water and sediment are added to or removed from the flow and as the channel and flow characteristics change the flow velocity and degree of turbulence and therefore the transport capacity.

17.1.3 Factors Affecting Erosion by Water

The major factors affecting soil erosion are climate, soil, vegetation, topography, and time. Of these, vegetation—and to a lesser extent soil and topography—may be controlled through normal management. For our purposes, climatic factors are assumed to be beyond human control. The important climatic factors are precipitation, temperature, wind, humidity, and solar radiation. Temperature and wind are most evident through their effects on evaporation and transpiration, but wind also changes raindrop velocity and angle of impact. Humidity and solar radiation are recognized as being somewhat less directly involved, in that they are associated with temperature and rate of soil-water depletion, although humidity affects raindrops in that very dry conditions may prevent precipitation from ever reaching the ground.

Physical properties of the soil affect infiltration, detachment of soil particles, and transport of the sediment. In general, soil detachability increases as the size of soil particles and/or aggregates increases, and soil transportability increases with decrease in particle and/or aggregate size. For example, clay particles are more difficult to detach than sand, but clay is more easily transported. Other general soil properties that influence erosion include soil structure, texture, organic matter, water content, clay mineralogy, and density (or compactness), as well as chemical and biological characteristics of the soil. No single soil characteristic or index has been identified as a satisfactory means of predicting erodibility, so it is usually measured directly through field studies. However, it can generally be said that human activities that loosen and pulverize soil often promote accelerated erosion.

Vegetation has the major impact on resisting or reducing soil erosion. Vegetation intercepts rainfall and absorbs the raindrop energy, thus reducing soil detachment. It retards erosion by decreasing surface-water velocity and by physically restraining sediment movement. Vegetation improves soil aggregation and porosity through the impact of its roots and plant residues. These increase biological activity in the soil, and through transpiration decrease soil water, resulting in increased storage capacity and less runoff. Vegetation effects vary with season, crop, degree of maturity, and soil and climate interactions with the vegetation and with the nature of the vegetative material, i.e., roots, plant tops, and plant residues. Residues from vegetation protect the surface from raindrop impact and improve soil structure. Residue and tillage management practices used in growing the vegetation can have a dramatic effect on soil erosion.

Soil erosion is also controlled by topographic features, such as slope steepness, length, and shape, and the size and shape of the watershed. On steep slopes, runoff water is more erosive and can more easily transport detached soil downslope. On longer slopes, increased accumulation of overland flow tends to increase rill erosion and the potential for gully formation. Concave slopes, with lower slopes at the foot of the hill, are less erodible than are convex slopes.

17.2 UPLAND SOIL EROSION

Upland soil erosion consists mostly of sheet or interrill and rill erosion, the basic forms of erosion. Predictions of upland soil erosion and sediment yield are needed to guide the making of rational decisions in conservation planning. The prediction equations enable the planner to predict the average rate of soil erosion for alternative combinations of cropping systems, management techniques, and erosion-control practices on any particular site.

17.2.1 Soil Loss Tolerance

The term "soil loss tolerance" (T) denotes the maximum rate of soil erosion that can occur and still permit crop productivity to be sustained economically. A deep, medium-textured, moderately permeable soil that has subsoil characteristics favorable for plant growth has a greater tolerable soil loss rate than do soils with shallow root zones or high percentages of shale at the surface. For the soils of the United States, T values of 1 to 5 tn/acre/year were derived by soil scientists and conservationists, agronomists, engineers, geologists, and federal and state researchers at regional workshops around the country. These recommended T values may be obtained from the United States Department of Agriculture (USDA) Natural Resources Conservation Service (NRCS).

As part of the conservation planning process, if the predicted soil erosion rate exceeds the T value, various combinations of management practices, as discussed below, can be tested through application of a soil loss prediction equation until the predicted soil loss erosion rate is at or below the T value.

17.2.2 Soil Loss Equation

As discussed above, the rate of upland soil erosion depends on rainfall erosivity, soil erodibility, the length, steepness,

and shape of the slope, cultural practices used, stage of vegetation growth, and supporting conservation practices applied to the area. Factors representing these erosion-influencing characteristics have been combined in the Universal Soil Loss Equation (USLE), developed originally by Wischmeier and Smith (1965; 1978). Thousands of plot-years of data from runoff plots and small watersheds were used to develop the relationships in the USLE. This equation predicts soil loss from sheet (or interrill) erosion and rill erosion from the roughly planar hillslope areas. It enables land management planners to estimate average annual soil erosion rates from upland slopes for a wide range of rainfall, soil, slope, cover, and management conditions. It also enables planners to select from alternative cropping as cover and management combinations that would limit erosion rates to acceptable (*T*-value) levels.

A revised version of the USLE, called the Revised Universal Soil Loss Equation (RUSLE), was developed and documented by Renard et al. (1997) for computer applications, allowing more detailed consideration of farming practices and topography for erosion prediction. Both USLE and RUSLE use the following equation to compute average annual soil erosion expected on upland (field) slopes:

$$A = R \cdot K \cdot L \cdot S \cdot C \cdot P \qquad (17\text{-}1)$$

where

- A = spatial and temporal average soil loss (erosion) per unit area, expressed in the units selected for K and for the period selected for R. In practice, these are usually selected so that A is annual soil erosion rate expressed in tn/acre/year or t/ha/year.
- R = rainfall-runoff erosivity factor—the rainfall erosion index plus a factor for any significant runoff from snowmelt.
- K = soil erodibility factor—the soil-loss rate per erosion index unit for a specific soil as measured on a standard plot, which is defined as a 72.6-ft (22.1-m) length of uniform 9% slope in continuous clean-tilled fallow.
- L = slope length factor—the ratio of soil loss from the field slope length to soil loss from a 72.6-ft length under identical conditions.
- S = slope steepness factor—the ratio of soil loss from the field slope gradient to soil loss from a 9% slope under otherwise identical conditions.
- C = cover-management factor—the ratio of soil loss from an area with specified cover and management to soil loss from an identical area in tilled continuous fallow.
- P = support practice factor—the ratio of soil loss with a support practice such as contouring, stripcropping, or terracing to soil loss with straight-row farming up and down the slope.

These factors and their representative values for different geographic locations in the United States, and for different soils, topography, covers, and practices, are given and extensively described for the USLE by Wischmeier and Smith (1965; 1978), and more recently for RUSLE by Renard et al. (1997). Brief descriptions and recently updated values from Renard et al. (1997) are given here. Since the release of Renard et al. (1997), additional work has been done on RUSLE. A version released in 1998 (RUSLE1.06) includes features that allow the RUSLE hillslope to be carried all the way down to a concentrated flow channel (Toy et al. 1999). A new version, RUSLE2, is currently under testing and implementation by USDA-NRCS, but is based primarily on the science found in RUSLE1.06, with several enhancements.

Other significant differences exist between the USLE and the most recent version of this technology as found in RUSLE2. Perhaps the greatest of these is that in the USLE the factors could be considered relatively independent. This meant that simple comparison of the C factors could usually be used to compare management systems. This is no longer the case in the later version of RUSLE1 or in RUSLE2, because these recognize that many of the factors are interrelated. In RUSLE2, therefore, comparisons of management alternatives must be made on the basis of overall erosion estimates rather than on the basis of individual factors.

17.2.3 Rainfall-Runoff Erosivity Factor (*R*)

The rainfall-runoff erosivity factor R quantifies the effects of raindrop impact and reflects the amount and rate of runoff likely to be associated with rain. Field data indicate that when factors other than rainfall are held constant, soil losses from cultivated fields are directly proportional to the total storm energy (E) times the maximum 30-min intensity (I_{30}). The R factor used to estimate average annual soil loss A (Eq. (17-1)) must include the cumulative effects of the many moderate-sized storms as well as the effects of the occasional severe ones. The average annual total of the storm EI_{30} values in a particular locality is the R for that locality. Local values of R in the United States are calculated from rainfall data around the country and are plotted in isoerodent maps (Renard et al. 1997) as shown in Figs. 17-1 to 17-5 for the eastern United States, western United States, California, Oregon and Washington, and Hawaii, respectively. Isoerodents are lines of equal R values. R values for locations between the lines can be obtained by linear interpolation.

Although the R factor is assumed to be independent of slope, splash erosion is less on flatter slopes, where raindrops tend to be more buffered by water ponded on the soil surface. A correction factor (Renard et al. 1997) as shown in Fig. 17-6 may be used to adjust R values for various flatter slopes and 10-year-frequency EI_{30} values.

In the dry-farmed cropland areas of the northwestern U.S. wheat and range region (Washington, Oregon, and Idaho),

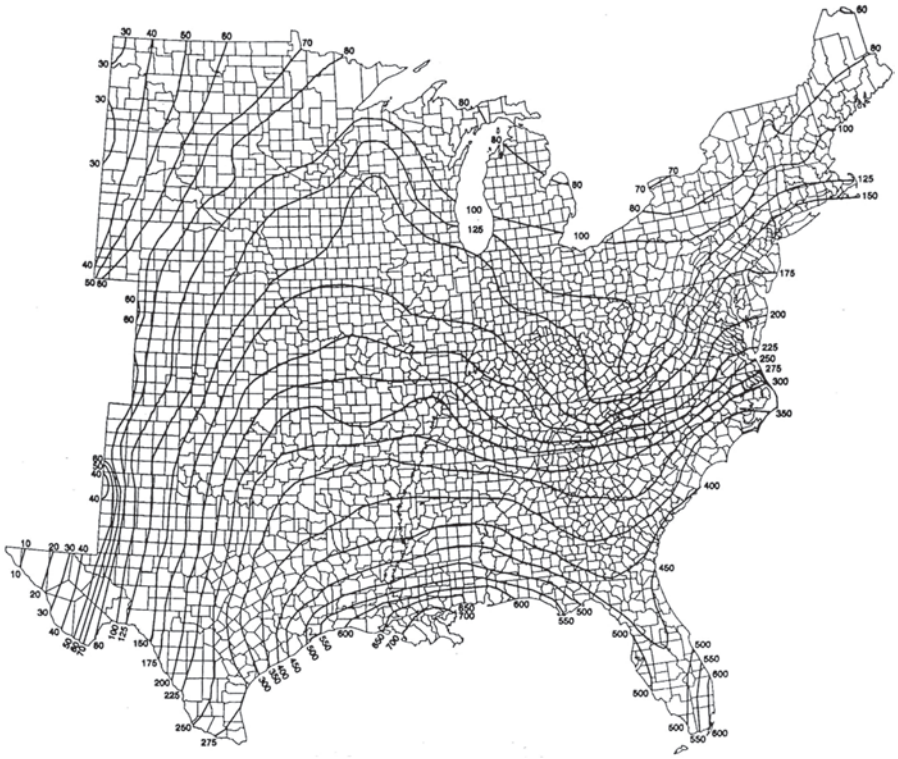

Fig. 17-1. Isoerodent map of eastern United States. Units are hundreds ft tnf in (ac h year)$^{-1}$. After Renard et al. (1997).

melting snow, rain on snow, and/or rain on thawing soil accelerate soil erosion resulting from higher R values. Renard et al. (1997) present a procedure to compute "R Equivalent (R_{eq}) for Cropland in the Northwestern Wheat and Range Region" and the R_{eq} isoerodent maps for estimating soil loss under these conditions.

17.2.4 Soil Erodibility Factor (K)

The soil erodibility factor (K) is the rate of soil loss per rainfall erosion index unit for a specific soil as measured on a unit plot, which is defined as being 72.6 ft (22.1 m) long, with a minimum width of 6 ft (1.83 m), 9% slope, and in a continuously clean-tilled fallow condition with tillage performed up and down slope (Wischmeier and Smith 1978). These factors are best obtained from direct measurements on natural-runoff plots. Guidelines for preparation and maintenance of natural-runoff plots in the United States were issued in 1961 by D. D. Smith (Romkens 1985). Renard et al. (1997) lists the soils and the locations in the United States on which natural-runoff plots for K-factor determinations were established, along with the resulting K-factor values. Rainfall simulation studies may also be used to determine K factors, but these short-term results are generally less accurate.

Soil erodibility is related to the integrated effect of rainfall, runoff, and infiltration on soil loss. The K factor accounts for the influence of soil properties on soil loss during storm events on upland areas. It is the average long-term soil and soil-profile response to the erosive powers of rainstorms and is a lumped parameter that represents an integrated average annual value of the total soil and soil profile reaction to a large number of erosion and hydrologic processes. These processes consist of soil detachment and transport by raindrop impact and surface flow, localized deposition due to topography and tillage-induced roughness, and rainwater infiltration into the soil profile. There is some interdependency of the K factor with the other USLE or RUSLE factors, specifically the topographic (LS), rainfall erosivity (R), and cover-management (C) factors.

The soil erodibility K can also be estimated by a variety of relationships. The most widely used relationship between the K factor and soil properties is the soil erodibility nomograph (Wischmeier et al. 1971; Wischmeier and Smith 1978; Renard et al. 1997). The nomograph comprises five soil and soil-profile parameters: percent modified silt (0.002–0.1 mm), percent modified sand (0.1–2.0 mm), percent organic matter (OM), and classes for structure (s) and permeability (p). The structure and permeability classes and groups of classes were taken from the *Soil Survey Manual* (USDA 1951). Structure (s) values are 1 for very fine granular, 2 for fine granular, 3 for medium or coarse granular, and 4 for blocky, platy, or massive structure. Permeability (p) values

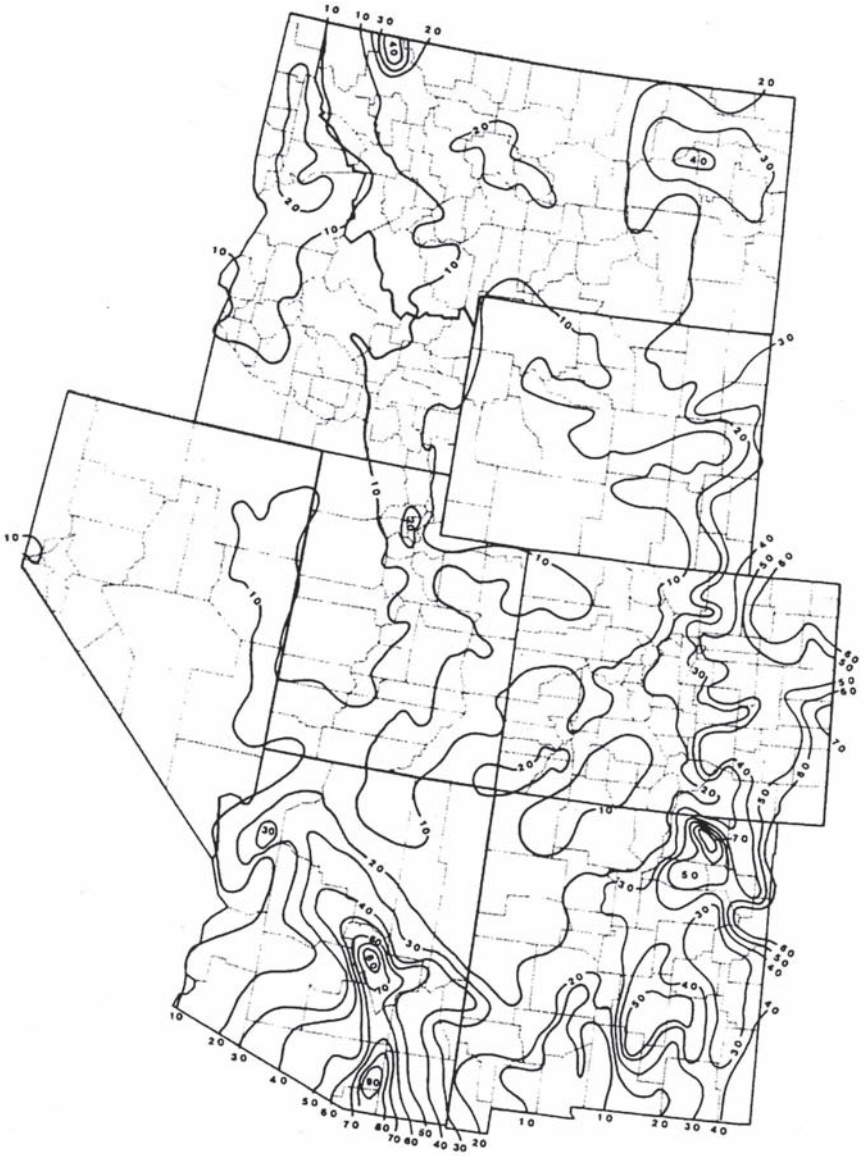

Fig. 17-2. Isoerodent map of western United States. Units are hundreds ft tnf in (ac h year)$^{-1}$. After Renard et al. (1997).

are 1 for rapid, 2 for moderate to rapid, 3 for moderate, 4 for slow to moderate, 5 for slow, and 6 for very slow. A useful algebraic approximation (Wischmeier and Smith 1978) of the nomograph for those cases where the silt fraction does not exceed 70% is

$$K = [2.1 \times 10^{-4}(12 - \mathrm{OM})\, M^{1.14} + 3.25(s-2) + 2.5(p-3)] / 100 \qquad (17\text{-}2)$$

where M is the product of the primary particle size fractions (% modified silt or the 0.002–0.1 mm size fraction) × (% silt + % sand) and K is expressed as tn/acre per erosion index unit. For example, a soil having 65% modified silt, 5% modified sand, 2.8% OM, fine granular structure ($s = 2$), and slow to moderate permeability ($p = 4$) will have a computed K value of 0.31.

The nomograph relationship was derived from rainfall-simulation data from 55 U.S. Midwest surface soils, mostly (81%) medium-textured surface soils. It is well suited for the less aggregated and medium-textured surface soils of the Midwest. Renard et al. (1997) present more relationships based on other soil types and soils from other locations, including Hawaiian volcanic soils (El-Swaify and Dangler 1976), soils from the upper Midwest (Young and Mutchler 1977), and Midwest clay subsoils (Romkens et al. 1977).

The presence of rock fragments in the soil may significantly affect soil detachment by rainfall. When present in a coarse-textured-soil profile (sands and loamy sands), the

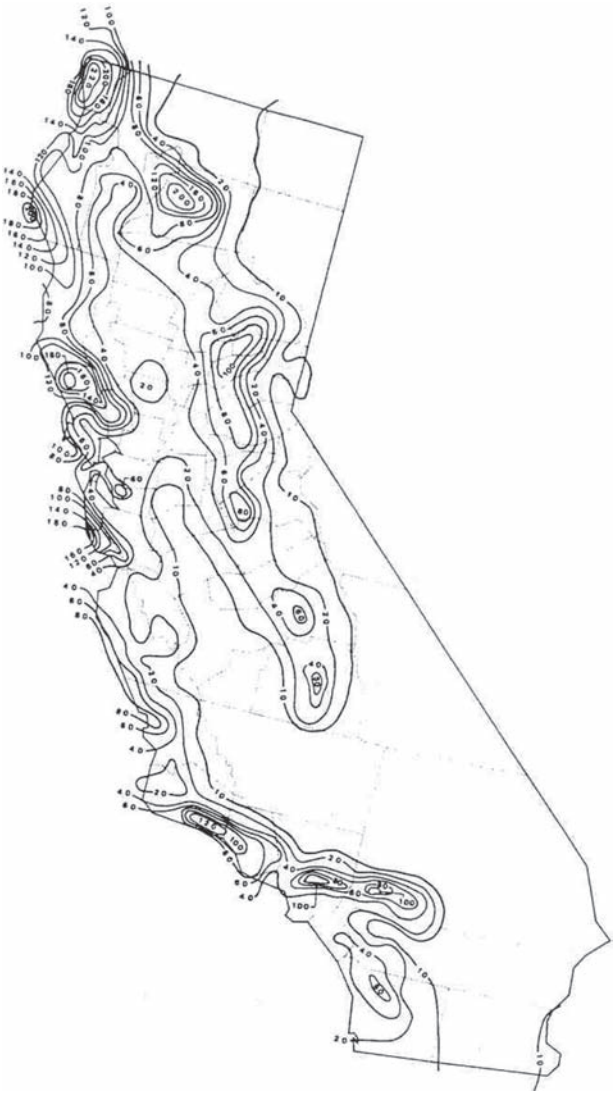

Fig. 17-3. Isoerodent map of California. Units are hundreds ft tnf in (ac h year)$^{-1}$. After Renard et al. (1997).

fragments can appreciably reduce infiltration, whereas in a fine-textured soil the fragments may actually increase infiltration. The effect of rock fragments on the soil surface is included in the *C* factor. However, the effect of rock fragments within the soil profile is included with the *K* factor insofar as it affects infiltration and runoff. These effects are discussed and quantified in Renard et al. (1997).

Seasonal variation of *K* values is also discussed and quantified in Renard et al. (1997). Soil freezing and thawing are major causes of these variations, because such processes change the effective soil texture and soil-water content, thereby increasing the *K* factor. The greater the number of freeze-thaw cycles, the longer the erosion resistance of a soil is at a minimum, resulting in higher erosion and *K* factor. In locations where frozen soil is not a problem, the *K* factor gradually decreases over the course of the growing season until it reaches a minimum near the end of growing season. Then it gradually increases until it reaches the maximum. For many locations this pattern follows rainfall patterns.

17.2.5 Slope Length and Steepness Factors *(LS)*

The slope length factor (*L*) and the steepness factor (*S*) account for the effects of topography on upland soil erosion. Erosion increases as slope length and/or steepness increases. Slope length for the USLE and early RUSLE versions was defined as the horizontal distance from the origin of overland flow to the point where either the slope gradient (steepness) decreases enough so that deposition begins or runoff becomes concentrated in a defined channel (Wischmeier and Smith 1978). In later versions, including RUSLE1.06 and all versions of RUSLE2, process-based deposition routines have been added, so the slope length extends down to a concentrated flow channel, which will normally be part of the watershed channel system. Surface runoff usually enters such a concentrated flow channel in less than 400 ft (122 m), which is a practical slope-length limit in many situations, although longer slope lengths of up to 1,000 ft (305 m) are occasionally found, most often when the surface has been carefully graded into ridges and furrows that maintain flow for long distances.

The factors *L* and *S* are usually evaluated together as the topographic factor *LS*, which represents the ratio of soil loss on a given slope length and steepness to soil loss from a slope that has a length of 72.6 ft (22.1 m) and steepness of 9%, where all other conditions are the same. The value of *LS* is 1.0 at the 72.6-ft slope length and 9% steepness. Values of *LS* for horizontal slope lengths from less than 3 ft (0.9 m) up to 1,000 ft (305 m), with steepness values ranging from 0.2% to 60%, and low, moderate, and high ratios of rill to interrill erosion are given in tabular form in Renard et al. (1997). These tables also present *LS* values for thawing soils where most of the erosion is caused by surface runoff. All of those values can also be computed using separate relations for *L* and *S* as given from Renard et al. (1997):

$$L = (\lambda/72.6)^{m} \tag{17-3}$$

where

λ = horizontal slope length (ft) and
m = a variable slope-length exponent (Wischmeier and Smith 1978).

The slope-length exponent *m* is related to the ratio of rill erosion (caused by flow) to interrill erosion (principally caused by raindrop impact), and is expressed (Foster et al. 1977) as

$$m = \beta/(1+\beta) \tag{17-4}$$

where

β = ratio of rill to interrill erosion.

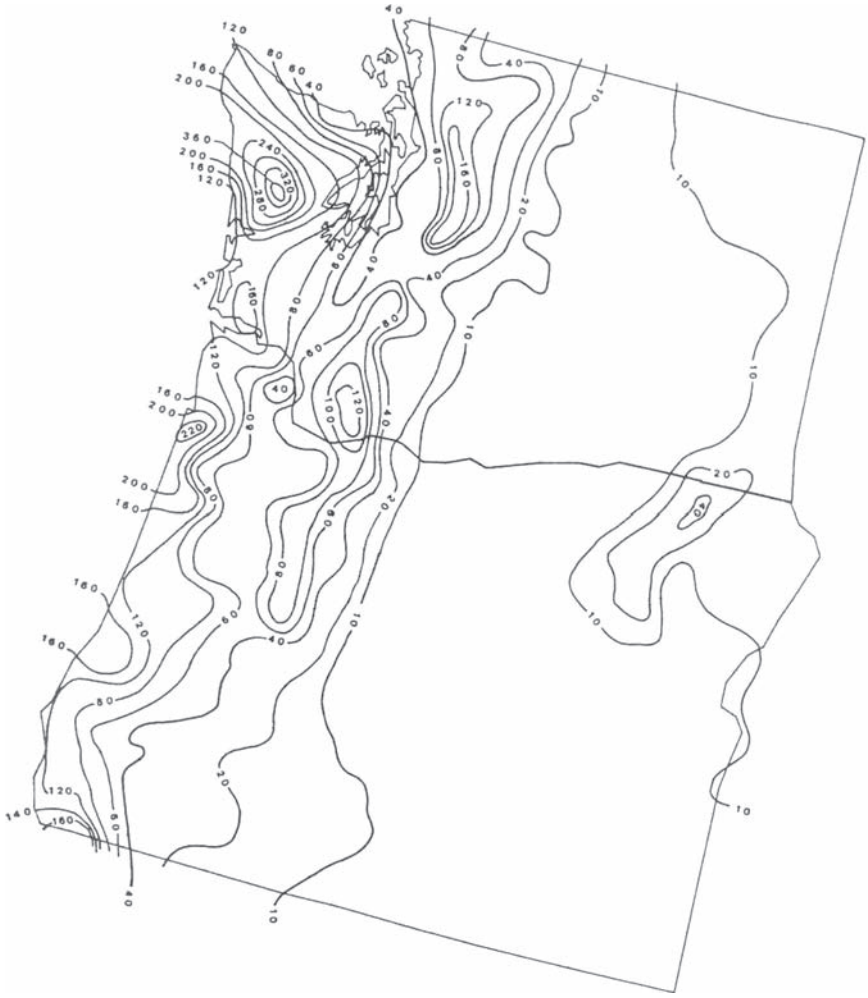

Fig. 17-4. Isoerodent map of Oregon and Washington. Units are hundreds ft tnf in (ac h year)$^{-1}$. After Renard et al. (1997).

For conditions where the soil is moderately susceptible to both rill and interrill erosion, β is expressed (McCool et al. 1989) as

$$\beta = (\sin\theta \ / 0.0896) / [3.0(\sin\theta)^{0.8} + 0.56] \qquad (17\text{-}5)$$

where

θ = slope angle.

Equation (17-5) gives β values for conditions that are typical of agricultural fields in seedbed condition, where the soil is moderately susceptible to both rill and interrill erosion.

When runoff, soil, cover, and management conditions indicate that the soil is highly susceptible to rill erosion, a condition most likely to occur on steep, freshly prepared construction slopes, the β value is doubled from that calculated by Eq. (17-5). Conversely, when the conditions favor less rill erosion than interrill erosion, a condition common to rangelands, β values are taken as half of those calculated from Eq. (17-5).

For the erosion of thawing, cultivated soil by surface flow, a condition common in the Northwest U.S. Wheat and Range Region, a constant value of 0.5 is used for the slope length exponent *m* (McCool et al. 1989; 1993). When runoff on thawing soil is accompanied by rainfall sufficient to cause significant interrill erosion, the β value is taken as half of that calculated from Eq. (17-5). To ease these calculations, RUSLE2 automatically calculates the β value based on the presumed soil, management, and climatic conditions.

Soil loss increases more rapidly with slope steepness than it does with slope length. The slope steepness factor *S* is computed using the following relations (McCool et al. 1987):

$$S = 10.8 \sin\theta + 0.03 \quad s < 9\% \qquad (17\text{-}6)$$

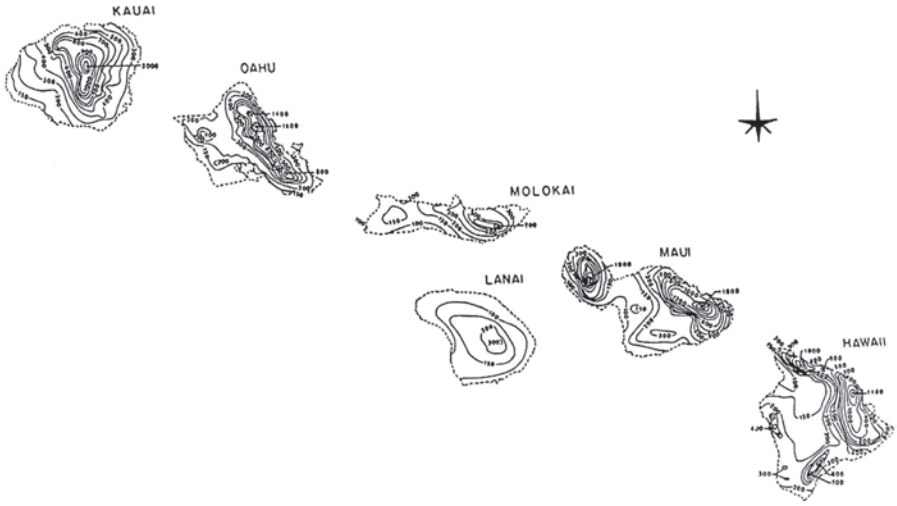

Fig. 17-5. Isoerodent map of Hawaii. Units are hundreds ft tnf in (ac h year)$^{-1}$. After Renard et al. (1997).

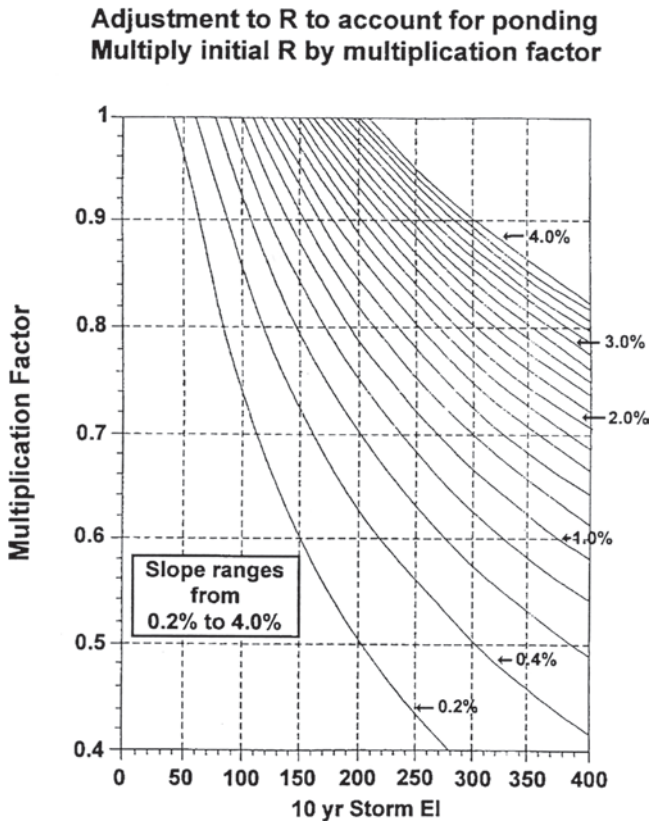

Fig. 17-6. Correction for R factor for flat slopes and large R values to reflect amount of rainfall on ponded water. After Renard et al. (1997).

$$S = 16.8 \sin\theta + 0.5 \qquad s \geq 9\% \quad \lambda \geq 15 \text{ ft} \qquad (17\text{-}7)$$

$$S = 3.0 (\sin\theta)^{0.8} + 0.56 \qquad s \geq 9\% \quad \lambda < 15 \text{ ft} \qquad (17\text{-}8)$$

where s = ground slope in percent. Equation (17-8) assumes that rill erosion is insignificant on slopes shorter than 15 ft (4.6 m), and therefore this equation should not be used on such slopes where rill erosion is expected to occur. Rill erosion usually begins with a slope length of 15 ft; however, it may take longer slope lengths on soils that are consolidated and resistant to detachment by flow.

For recently tilled soil under thawing, in a weakened state and subjected primarily to surface flow, Eq. (17-7) is rewritten as (McCool et al. 1993)

$$S = (\sin\theta / 0.0896)^{0.6} \qquad s \geq 9\% \quad \lambda \geq 15 \text{ ft} \qquad (17\text{-}9)$$

These relations are applicable to uniform slopes where steepness is the same over the entire length. Procedures of accounting for nonuniform or irregular concave, convex, or complex slopes in the erosion computations are outlined in Renard et al. (1997). They can also account for changing soil type along the slope. Within limits, they can be further extended to account for changes in the C and P values. These adjustments are all done automatically in RUSLE2. Renard et al. (1997) provides extensive guides for choosing slope lengths.

17.2.6 Cover-Management Factor (C)

The C factor is designed to reflect the effect of cropping and management practices on erosion rates, and is the factor used most often to compare the relative impacts of management options on conservation plans. The C factor is essentially a soil loss ratio (SLR), which is defined as the ratio of soil losses under actual conditions to losses

experienced under the clean-tilled continuous fallow reference conditions. The *C* factor depends on previous cropping and management, vegetative canopy, surface cover and roughness, and, in some cases, soil moisture, each of which is assigned a subfactor value. These subfactor values are multiplied together to yield an SLR (Laflen et al. 1985), expressed as

$$\text{SLR} = \text{PLU} \cdot \text{CC} \cdot \text{SC} \cdot \text{SR} \cdot \text{SM} \qquad (17\text{-}10)$$

where

SLR = soil-loss ratio for the given conditions;
PLU = prior-land-use subfactor;
CC = canopy-cover subfactor;
SC = surface-cover subfactor;
SR = surface-roughness subfactor; and
SM = soil-moisture subfactor.

PLU incorporates the influence of subsurface residue effects from previous crops and the effects of previous tillage practices on soil consolidation. PLU values range from 0 to 1. Renard et al. (1997) provide an extensive discussion and procedure to estimate PLU.

The CC subfactor value ranges from 0 to 1 and incorporates the effectiveness of vegetative canopy in reducing the energy of rainfall striking the soil surface. It is expressed as

$$\text{CC} = 1 - F_c \cdot \exp(-0.1 \cdot H) \qquad (17\text{-}11)$$

where

F_c = fraction of land surface covered by canopy, and
H = canopy height (ft), which is the distance that raindrops fall after striking the canopy.

The SC subfactor incorporates the effects of surface cover, including crop residues, rocks, cryptogams, and other nonerodible materials that are in direct contact with soil surface, on soil erosion. These affect erosion by reducing the transport capacity of runoff water, by causing deposition in ponded areas, and by decreasing the surface area susceptible to raindrop impact. It is perhaps the single most important factor in determining the SLR. The SC subfactor is expressed as

$$\text{SC} = \exp[-b \cdot S_p \cdot (0.24/R_u)^{0.08}] \qquad (17\text{-}12)$$

where

b = an empirical coefficient;
S_p = percentage of land area covered by surface cover; and
R_u = surface roughness (in.).

The b value in Eq. (17-12) ranges from 0.030 to 0.070 for row crops, and from 0.024 to 0.032 for small grains. In the Northwest U.S. Wheat and Range Region, b values may be greater than 0.050. For rangeland conditions with the impact of subsurface biomass removed, a b value of 0.039 is recommended. The b value can be also chosen based on the dominant erosion process. When rill erosion is the primary mechanism of soil loss (such as for irrigation or snowmelt or for highly disturbed soils), b values should be about 0.050. Fields dominated by interrill erosion have a b value of around 0.025. For typical cropland erosion conditions, a b value of 0.035 is suggested. Calculation of the b value is done automatically in RUSLE2, based again on the estimated soil and management conditions.

In RUSLE2 and recent versions of RUSLE1, the SC and CC subfactors are linked, so that canopy cover with a very low canopy height essentially becomes surface cover. In other words, a 50% canopy cover with a height of 0 will give combined SC and CC subfactors providing the same erosion reduction as 50% surface cover, not the CC = 0 value indicated by Eq. (17-11).

An R_u value of 0.24 in. (0.61 cm) is typical of a field in seedbed condition. An R_u value of 4 in. indicates more roughness than from most primary tillage operations. R_u values for various tillage operations in croplands, ranging from 0.30 to 1.9 in., and various conditions in rangelands, ranging from 0.25 to 1.30 in., are given in Renard et al. (1997).

Surface roughness directly affects soil erosion by reducing flow velocity and by decreasing transport capacity and runoff detachment. It also indirectly affects soil erosion by causing ponded water and reducing raindrop impact, as incorporated into Eq. (17-12). The direct impact of surface roughness on erosion is incorporated into the SR subfactor. Its baseline condition (SR = 1) is established in a unit plot of clean cultivated conditions smoothed by extended exposure to rainfall of moderate intensity. These conditions yield a random roughness of 0.24 in. The SR subfactor for random roughness greater than 0.24 in. is computed using the expression

$$\text{SR} = \exp[-0.66\,(R_u - 0.24)] \qquad (17\text{-}13)$$

The SM subfactor incorporates the influence of antecedent soil moisture on infiltration and runoff and hence on soil erosion. In general, antecedent moisture effects are an inherent component of continuously tilled fallow plots, which are reflected in variation in soil erodibility throughout the year, and are already taken into account in the derivation of soil erodibility factors. Therefore, the SM subfactor is kept at 1 without any adjustment for changes in soil moisture. However, it is recommended that SM subfactor in the Northwest U.S. Wheat and Range Region be adjusted between 1.0 on April 1, indicating response equivalent to that of a continuous fallow with soil moisture near field capacity,

and 0.0 from September 1 to October 1, indicating no runoff and erosion with soil moisture in soil profile near wilting point to a 6-ft (1.8-m) depth. SM values between these dates are linearly interpolated: 0.0 to 1.0 for October 1 to April 1, and 1.0 to 0.0 for April 1 to September 1.

For areas such as pasture or rangeland that have reached a relative equilibrium, the subfactors used in computing SLR values may change very slowly with time. In these cases, the PLU, CC, SC, and SR subfactor values are assumed to be annual averages, and are simply multiplied together to yield *C*-factor value (SM = 1.0), as

$$C = \text{PLU} \cdot \text{CC} \cdot \text{SC} \cdot \text{SR} \qquad (17\text{-}14)$$

In almost all cropland scenarios and in many cases where rangeland or pasture are being managed, the crop and soil characteristics change over time. This demands that the SLR values be calculated frequently enough over the course of a year or a crop rotation to provide an adequate measure of how they change. These values depend on tillage type, elapsed time since a tillage operation, canopy development, and date of harvest. An individual SLR value is calculated for each time period over which the subfactors can be assumed to remain constant. Each of the SLR values is then weighted by the fraction of rainfall and runoff erosivity (*EI*) associated with the corresponding time period, and these weighted values are combined into an overall *C*-factor value (Wischmeier and Smith 1978), expressed as:

$$C = (\text{SLR}_1 EI_1 + \text{SLR}_2 EI_2 + \ldots \text{SLR}_n EI_n)/EI_t \qquad (17\text{-}15)$$

where C = average annual or crop C factor value, SLR_i = soil-loss ratio for time period i, EI_i = percentage of the annual or crop EI occurring during that time period, n = number of periods used in the summation, and EI_t = sum of the EI percentages for the entire period. For RUSLE1 these calculations were performed for half-month periods; in RUSLE2 they are performed on a daily time-step.

17.2.7 Support Practice Factor (*P*)

The *P* factor represents support practice effects on soil erosion. These practices generally modify the amount, rate, flow pattern, or direction of surface runoff. For cultivated land, support practices include contouring (tillage and planting on or near the contour), stripcropping, terracing, and subsurface drainage. On dryland or rangeland areas, soil-disturbing practices oriented on or near the contour that result in storage of moisture and reduction of runoff are also used as support practices. For construction and mine reclamation areas, this includes such practices as contour plowing and diversions. Note, however, that improved tillage practices such as no-till and other conservation tillage systems, sod-based crop rotation, fertility treatments, and crop-residue management are not included in support practices, but rather are included in the *C* factor. The *P*-factor value is a product of *P* subfactors for individual support practices, some of which are used in combination. For example, contouring generally accompanies stripcropping and terraces.

The *P*-factor value for farming upslope and downslope is 1.0. Other *P*-factor values given in Renard et al. (1997) were obtained from experimental data, supplemented by analytical experiments involving scientific observation of known cause-and-effect relationships in physically based models such as CREAMS (Knisel 1980). Such an extensive discussion and procedure development are beyond the scope of this chapter, but the *P*-factor values for three major support practices in cultivated lands, as given earlier by Wischmeier and Smith (1978), are shown in Table 17-1. Within a practice type, the *P* factor is most effective for the 3 to 8% slope range, and effectiveness decreases as the slope increases. As the slope decreases below 2%, the *P*-factor value increases, due to the reduced effectiveness of the practice when compared to up-and-down-hill cultivation. The *P* factor for terracing in Table 17-1 is for prediction of total off-the-field soil loss. If within-terrace interval soil loss is desired, the terrace interval distance should be used for the slope length factor (*L*) and the contouring *P* value for the practice factor.

17.3 GULLY EROSION

Gully erosion is defined as the erosion process whereby runoff water accumulates and often recurs in narrow channels and, over short periods, removes soil from these narrow areas to considerable depths (Poesen et al. 2002). Gullies are often defined for agricultural land in terms of channels that occur in the low areas of the macrotopography and that are too deep to ameliorate easily with ordinary farm tillage equipment, typically ranging from 0.5 m to as much as 25 to 30 m (Soil Science Society of America 2001). In the 1980s, the term "ephemeral gully erosion" was introduced to include

Table 17-1 Support Practice Factor *P* for Cultivated Lands[a]

Land slope, %	Contouring	Contour, strip cropping, and irrigated furrows	Terracing[b]
1–2	0.60	0.30	0.12
3–8	0.50	0.25	0.10
9–12	0.60	0.30	0.12
13–16	0.70	0.35	0.14
17–20	0.80	0.40	0.16
21–25	0.90	0.45	0.18

[a]From Wischmeier and Smith (1978).
[b]For prediction of contribution to off-field sediment yield.

concentrated flow erosion larger than rill erosion but smaller than classical gully erosion. According to the Soil Science Society of America (2001), ephemeral gullies are small channels eroded by concentrated overland flow that can easily be filled by normal tillage, only to be reformed in the same location by additional runoff events. In the United States, the sediment contribution from ephemeral gullies has been estimated to average about 80% of that contributed by sheet and rill erosion (Bennett et al. 2000b). A study in Kenya (Wijdenes and Bryan 1994) reported that 50% of the eroded sediment in their study watershed was produced from gullies, with the other half resulting from sheet and rill erosion.

Numerous field and modeling studies on gully erosion are reported in the literature (Woodburn 1949; Beer and Johnson 1963; Thompson 1964; Piest et al. 1975; Bocco 1991; Wijdenes and Bryan 1994; Bennett et al. 2000a; 2000b; Nachtergaele et al. 2002; Poesen et al. 2002; 2003; Torri and Borselli 2003). Sources and references for many other studies may be found in these publications. However, there is still a lack of understanding of the processes that form gullies, including headcut migration. Understanding and quantification of gullies lag behind those for other forms of water erosion. One reason is scale. Gully erosion tends to operate on a larger scale than the runoff plot scale, where the vast majority of water erosion research has been conducted. Gully development also operates over longer time periods than is common for water erosion research studies. Finally, because of these scale and temporal issues it is very difficult to replicate scientific field studies of gullies, because no two gullies are found in exactly the same place in the landscape and because gullies are dependent on everything that happen upslope over long periods. In spite of these difficulties, there are some commonly used relationships describing gullies. A few of the key empirical relations discussed in Thompson (1964), United States Soil Conservation Service (1966), and Nachtergaele et al. (2002) are presented here.

Leopold and Maddock (1953) and Wolman (1955) described the hydraulic geometry of river channels by a set of empirical relations (as presented in Nachtergaele et al. 2002):

$$W = a\,Q^{b} \tag{17-16}$$

$$d_m = c\,Q^{f} \tag{17-17}$$

$$u_m = k\,Q^{l} \tag{17-18}$$

where

W = channel width (m);
Q = flow discharge ($m^3\ s^{-1}$);
d_m = mean flow depth (m);
u_m = mean flow velocity ($m\ s^{-1}$); and
a, b, c, f, k, and l = empirical constants.

The empirical constants are related as follows:

$$a \cdot c \cdot k = 1 \tag{17-19}$$

$$b + f + l = 1 \tag{17-20}$$

Wide variations of the empirical constants have been documented in the literature. From 20 investigators worldwide, the ranges of b, f, and l were found to be (Ming 1983)

$$0.39 < b < 0.60,\ 0.29 < f < 0.40,\ 0.09 < l < 0.28 \tag{17-21}$$

The coefficients a, c, and k depend on a number of variables, including the size of bed material and the type of channel bank. From an extensive study of rill development in seedbeds on 10 different soil types, Gilley et al. (1990) proposed $a = 1.13$ and $b = 0.303$ in the width-discharge relation (Eq. 17-16). From a limited number of data ($n = 7$), Lane and Foster (1980) obtained $a = 4.48$ and $b = 0.482$.

Sidorchuk (1996) analyzed extensive erosion data ($n = 617$) from the Yamal peninsula in the permafrost area of northwestern Siberia, which resulted in width-discharge constants of $a = 3.17$ and $b = 0.368$ (Nachtergaele et al. 2002), and which was recommended by Nachtergaele et al. (2002) for modeling ephemeral gully erosion. Based on rill and gully erosion data from laboratory and field experimental plots and field measurements in simulated cultivated topsoil and on cropland around the world, Nachtergaele et al. (2002) proposed the width-discharge constants of $a = 2.51$ and $b = 0.412$. Based on all these values, Nachtergaele et al. (2002) suggested different width-discharge exponent b values for the rill, gully, and river erosion domains of 0.3, 0.4, and 0.5, respectively.

An extensive equation for predicting ephemeral gully channel width has been used in the ephemeral gully erosion model (EGEM; Woodward 1999), and is expressed as (Watson et al. 1986)

$$W = 2.66\,Q_p^{0.396}\ n^{0.387}\ s^{-0.16}\ \tau_{cr}^{-0.024} \tag{17-22}$$

where

Q_p = peak flow discharge ($m^3\ s^{-1}$);
n = Manning's roughness coefficient;
s = soil surface slope ($m\ m^{-1}$); and
τ_{cr} = critical flow shear stress (Pa).

EGEM computes the critical flow shear stress as (Smerdon and Beasley 1961):

$$\tau_{cr} = 0.311 \cdot 10^{(0.0182\,P_c)} \tag{17-23}$$

where

P_c = percentage of clay content.

From an analysis of 409 data points obtained from slopes ranging from 0.035 to 0.45 m m^{-1} and soil materials ranging from stony sands over silt loams to vertisols, Govers (1992) found the coefficient and exponent of $k = 3.52$, $l = 0.294$ in flow velocity-discharge relationships (Eq. 17-18) for developing rills on loose nonlayered materials (e.g., seedbed conditions). Once a, b, k, and l are determined, the mean depth-discharge relation constants c and f may be computed from solving Eqs. (17-19) and (17-20).

The next major difficult variable in predicting gully erosion is the gully advancement rate. Thompson (1964) studied gully head advancement at locations in Minnesota, Iowa, Alabama, Texas, Oklahoma, and Colorado and developed the empirical equation

$$R = (7.13 \times 10^{-5})\, A^{0.49}\, S^{0.14}\, P^{0.74}\, E \qquad (17\text{-}24)$$

where

R = gully head advancement for the time period of interest (m);
A = drainage area above the gully head (m^2);
S = slope of the approach channel above the gully head (%);
P = summation of rainfall from 24-h rains equal to or greater than 12.7 mm for the time period of interest (mm); and
E = clay content of the eroding soil profile (%).

The United States Soil Conservation Service (1966) recommended a simplified form of this equation:

$$R = (5.25 \times 10^{-3})\, A^{0.46}\, P^{0.20} \qquad (17\text{-}25)$$

17.4 STREAMBED AND BANK EROSION

Streambed erosion mechanics and quantification are extensively discussed in Chapters 2 to 4. Local bridge scour is another form of streambed erosion; its processes and quantification are discussed in Chapter 10. Quantification of streambed erosion and bed elevation changes using one-, two-, or three-dimensional numerical models is discussed in Chapters 14 and 15. Quantification of streambed erosion, along with upland soil erosion (sediment yield), using watershed simulation models is discussed later in this chapter.

Mechanics of streambank erosion and river width adjustment and their quantification are extensively discussed in Chapter 7 and by the ASCE Task Committee on Hydraulics, Bank Mechanics, and Modeling of River Width Adjustment (1998a; 1998b). Twelve quantitative time-dependent models that may be used to quantify streambed and bank erosion were also reviewed and described there.

17.5 GROSS EROSION, DELIVERY RATIO, AND SEDIMENT YIELD

Gross erosion is the total soil eroded in a drainage area or watershed through interrill, rill, gully, and stream erosion processes. All the sediment generated from these processes (gross erosion) may not be delivered at the watershed outlet because some of it may be deposited at various locations in the watershed. Soil material eroded from a field slope may be deposited along field boundaries, in terrace channels, in depressional areas, or on flat or vegetated areas traversed by overland flow before it reaches a watercourse (stream). Sediment may be also deposited within the stream channel system itself, either in specific locations such as sand bars, or generally across the bottom of a long stream reach.

Sediment yield is the total sediment delivered past a point of interest or the watershed outlet during any given time. Sediment yield at a point may be computed simply by multiplying gross erosion in the watershed above that point by a delivery ratio. The sediment delivery ratio is the fraction of the gross erosion that is expected to be delivered to the point of the watershed under consideration.

The sediment delivery ratio is dependent upon drainage area size, watershed characteristics as described by relief and stream length, sediment source and its proximity to the stream, transport system, and texture of the eroded material. The United States Soil Conservation Service (1971) developed a general sediment delivery ratio versus drainage area relationship from data of earlier studies. The relationship shows that the sediment delivery ratio varies approximately inversely as the 0.2 power of the drainage area in acres (1 acre = 0.405 ha). The wide scatter of data used in the development of this relationship indicates that additional variables affect the relationship. Table 17-2 shows some estimates of the delivery ratios.

The use of the sediment delivery ratio estimates from Table 17-2 should be tempered by consideration of other factors that may affect the values at a particular location. A higher delivery ratio should be used when the eroding soil is fine-textured (high in silt or clay content) and a lower one if the eroding soil is coarse-textured (high in sand content). The conditions of the streams and the delivery system should also be evaluated to assess and alter, if need be, the general relationship of Table 17-2. Delivery ratio values from Table 17-2 should be used only if local or regional relationships are not established and time is not available to develop a sediment-yield relationship for the area of interest.

Note that the sediment delivery ratios listed in Table 17-2 all have values of less than 1.0. This implies that the channel system is aggrading, or accumulating deposited sediment. This will be the case in most watershed studies examining

Table 17-2 General Sediment Delivery Ratios[a]

Drainage area, km^2	Sediment delivery ratio
0.05	0.580
0.10	0.520
0.50	0.390
1.00	0.350
5.00	0.250
10.00	0.220
50.00	0.153
100.00	0.127
500.00	0.079
1000.00	0.059

[a]Based on United States Soil Conservation Service (1971).

the impacts of increased human activities, because such activities generally increase upland erosion and the delivery of sediment to the channel system. If things go the other way, and a watershed undergoing severe erosion is put under conservation management so that upland erosion is greatly reduced, the sediment delivery ratio may in fact become greater than 1.0, as little new sediment is delivered to the channel system but the sediment within the system is flushed out or new sediment is generated from streambed and/or bank erosion by continuing stream flows.

The most reliable sediment yield estimates come from direct measurements of suspended sediment and bed load at the point of interest. Sediment-yield calculations for the Illinois River Basin (Demissie et al. 2003) are an example. Reservoirs of known age and sedimentation history determined by surveys are also excellent data sources for determining sediment yields. The sediment accumulation over a known time span can be used to obtain the average annual sediment yield. However, reservoir deposition and sediment yield may not be the same, because the reservoir trap efficiency may not be 100%. The trap efficiency of a reservoir is the portion of the total sediment delivered to the reservoir that is retained in the reservoir. These methods and the associated data were presented and discussed extensively in Vanoni (1975). Recent advancements are discussed here in Chapters 5 and 12 and Appendix D.

More discussions and methods of computing delivery ratio and sediment yield may be found in Agricultural Research Service—U.S. Department of Agriculture (1975), Walling (1983), and Williams (1977). The first publication is a comprehensive compilation of research prior to 1972 and provides excellent background, data, analysis, and conceptual materials.

17.6 WATERSHED MODELS

Watershed models simulating hydrologic processes, upland soil and stream erosion, and transport and deposition of sediment are comprehensive tools in computing and predicting sediment yields from watersheds. In addition to simulating hydrologic, erosion, and sedimentation processes, some of the watershed models simulate chemical mixing with water and sediment and transport of these through watersheds. These models are also called non-point-source pollution models because they simulate surface-water pollutants, including sediment, nutrients, pesticides, and other chemicals, originated from nonpoint or diffused sources. Such models are useful analysis tools to understand some of environmental problems (flooding, upland soil and streambed-bank erosion, sedimentation, contamination of water, etc.) and to find solutions through land-use changes and best management practices (BMPs).

The models assist in the development of total maximum daily load (TMDL) estimates required by the United States Clean Water Act and in evaluating alternative land-use and BMP scenarios, implementation of which can help in meeting water-quality standards and reducing the damaging effects of storm-water runoff on water bodies and the landscape. The TMDL is the maximum amount of a pollutant from point (e.g., wastewater treatment plant) and nonpoint sources that a water body can receive and still meet water-quality standards. According to the U.S. Environmental Protection Agency report (USEPA 1998), agriculture is the leading contributor of non-point-source pollutants (sediment and nutrients) to streams and rivers in the United States. Other contributors include golf courses, urban development, streambank erosion, and mining operations.

Some of the commonly used watershed-scale hydrologic and non-point-source pollution models include the Areal Nonpoint Source Watershed Environment Response Simulation or ANSWERS (Beasley et al. 1980), the Precipitation-Runoff Modeling System or PRMS (Leavesley et al. 1983), the Agricultural NonPoint Source pollution model or AGNPS (Young et al. 1987), the KINematic runoff and EROSion model or KINEROS (Woolhiser et al. 1990), the Hydrological Simulation Program—Fortran or HSPF (Bicknell et al. 1993), the European Hydrological System model or MIKE SHE (Refsgaard and Storm 1995), the Soil and Water Assessment Tool or SWAT (Arnold et al. 1998), the Annualized Agricultural NonPoint Source model or AnnAGNPS (Bingner and Theurer 2001), the Dynamic Watershed Simulation Model or DWSM (Borah et al. 2002b), ANSWERS-Continuous (Bouraoui et al. 2002), and CASCade of planes in 2-Dimensions or CASC2D (Ogden and Julien 2002). Sources and descriptions of more models, including field-scale models, are available in the literature (e.g., Singh 1995; Singh and Frevert 2002a; 2002b).

Some of the models are based on simple empirical relations having robust algorithms, and others use physically

based governing equations having computationally intensive numerical schemes. The simple models are sometimes incapable of giving desirable detailed results, and the detailed models are inefficient and could be computationally prohibitive for large watersheds. Therefore, finding an appropriate model for an application and for a certain watershed is quite a challenging task. Borah and Bera (2003) reviewed the 11 models mentioned and compiled a report on their mathematical bases, computational techniques, and important features or structures. This report is useful for selecting the most suitable model for a specific application depending upon the problem, watershed size, desired spatial and temporal scales, expected accuracy, user's skills, computer resources, etc. The review is also helpful in determining the strengths, weaknesses, and directions for enhancements of the models. The following nine subsections are based on that review.

In addition to these 11 watershed-scale models, two other field-scale models are worth mentioning: Chemicals, Runoff, and Erosion from Agricultural Management System or CREAMS (Knisel 1980) and Water Erosion Prediction Project or WEPP (Foster and Lane 1987; Lane and Nearing 1989). These two models have been widely used in estimating sediment yields from field-scale catchments and hill slopes. WEPP is a detailed soil-erosion and sediment-transport model and can be considered as state-of-the-art in hill-slope simulations. There are many other models available in the literature. The Department of Defense (Doe et al. 1999) evaluated 24 soil-erosion models for use on military installations. Among those, the Simulated Water Erosion (SIMWE) model (Mitas and Mitasova 1998) was found to be one of the "best" erosion models.

17.6.1 Review of Watershed Models

AnnAGNPS, ANSWERS-Continuous, HSPF, and SWAT are long-term continuous simulation models useful for analyzing long-term effects of hydrological changes and watershed management practices, especially agricultural practices. AGNPS, ANSWERS, DWSM, and KINEROS are single-storm-event models useful for analyzing severe actual or design single-event storms and evaluating watershed management practices, especially structural practices. CASC2D, MIKE SHE, and PRMS have both long-term and storm-event simulation capabilities. The mathematical bases of different components of these models, the most important elements of these mathematical models, were identified and compiled by Borah and Bera (2003). A summary compilation is presented in Table 17-3 for the long-term continuous models and Table 17-4 for the storm-event models. PRMS has both long-term and storm-event modes. The long-term mode of PRMS is only a hydrological model. The storm mode of PRMS has a sediment component as well. Therefore, only the PRMS storm mode is reviewed and presented in Table 17-4. MIKE SHE and CASC2D are listed separately; MIKE SHE is presented in Table 17-3 with the continuous models, and CASC2D is listed in Table 17-4 with the storm-event models. In each of these tables, the summary includes model components or capabilities, temporal scale, watershed representation, procedures to compute rainfall excess or water balance on overland planes, overland runoff, subsurface flow, channel runoff, reservoir flow, overland sediment, channel sediment, reservoir sediment, chemicals, and BMP evaluations. Sources and brief backgrounds of the 11 models are given below.

AGNPS, the Agricultural NonPoint Source pollution model (Young et al. 1987; 1989), was developed at the USDA-ARS North Central Soil Conservation Research Laboratory in Morris, Minnesota. It is an event-based model simulating runoff, sediment, and transport of nitrogen (N), transport of phosphorus (P), and chemical oxygen demand (COD) resulting from single rainfall events. Version 4.03 of the model (Young et al. 1994) was widely distributed. The model is currently undergoing extensive revisions and upgrading at the USDA-ARS National Sedimentation Laboratory (NSL) in Oxford, Mississippi, and one of its upgrades is AnnAGNPS, the Annualized Agricultural NonPoint Source model (Bingner and Theurer 2001), for continuous simulations of hydrology, soil erosion, and transport of sediment, nutrients, and pesticides. It is designed to analyze the impact on the environment of non-point-source pollutants from predominantly agricultural watersheds.

ANSWERS, Areal Nonpoint Source Watershed Environment Response Simulation (Beasley et al. 1980), was developed at Purdue University in West Lafayette, Indiana, and uses a distributed parameter concept to model the spatially varying processes of runoff, infiltration, subsurface drainage, and erosion for single-event storms. The model has two major components: hydrology and upland erosion responses. The conceptual basis for the hydrologic model was taken from Huggins and Monke (1966) and for the erosion simulation from Foster and Meyer (1972). Similar to AnnAGNPS, ANSWERS-Continuous (Bouraoui and Dillaha 1996; Bouraoui et al. 2002) emerged from ANSWERS as a continuous model at the Virginia Polytechnic Institute and State University in Blacksburg, Virginia. The model was expanded with upland nutrient transport and losses based on GLEAMS (Leonard et al. 1987), EPIC (Williams et al. 1984), and others.

CASC2D, CASCade of planes in 2-Dimensions, initially developed at Colorado State University in Fort Collins, Colorado (Julien and Saghafian 1991; Julien et al. 1995), and further modified at the University of Connecticut in Storrs, Connecticut (Ogden 1998; Ogden and Julien 2002), is a physically based model. It simulates water and sediment in two-dimensional overland grids and one-dimensional channels and has both single-event and long-term continuous simulation capabilities. Similarly, MIKE SHE (Refsgaard and Storm 1995), based on SHE, the European Hydrological System (Abbott et al. 1986a; 1986b), is a comprehensive, distributed, and physically based model simulating water,

Table 17-3 Summary of Watershed-Scale Long-Term Continuous Models[a]

Description/ criteria	AnnAGNPS	ANSWERS-Continuous	HSPF	MIKE SHE	SWAT
Model components/ capabilities	Hydrology, transport of sediment, nutrients, and pesticides resulting from snowmelt, precipitation and irrigation, source accounting capability, and user interactive programs including TOPAGNPS (Bingner and Theurer 2001) generating cells and stream network from Digital Elevation Model.	Daily water balance, infiltration, runoff and surface-water routing, drainage, river routing, evapotranspiration, sediment detachment, sediment transport, nitrogen and phosphorus transformations, nutrient losses through uptake, runoff, and sediment.	Runoff and water-quality constituents on pervious and impervious land areas, movement of water and constituents in stream channels and mixed reservoirs, and part of the USEPA BASINS modeling system with user interface and ArcView Geographic Information System (GIS) platform.	Interception-ET, overland and channel flow, unsaturated zone, saturated zone, snowmelt, exchange between aquifer and rivers, advection and dispersion of solutes, geochemical processes, crop growth and nitrogen processes in the root zone, soil erosion, dual porosity, irrigation, and user interface with pre- and postprocessing, GIS, and UNIRAS (Refsgaard and Storm 1995) for graphical presentation.	Hydrology, weather, sedimentation, soil temperature, crop growth, nutrients, pesticides, agricultural management, channel and reservoir routing, water transfer, and part of the USEPA BASINS modeling system with user interface and ArcViewGIS platform.
Temporal scale	Long-term; daily or subdaily steps.	Long-term; dual time steps: daily for dry days and 30 s for days with precipitation.	Long-term; variable constant steps (hourly).	Long-term and storm event; variable steps depending on numerical stability.	Long-term; daily steps.
Watershed representation	Homogeneous land areas (cells), reaches, and impoundments.	Square grids with uniform hydrologic characteristics, some having companion channel elements; one-dimensional simulations.	Pervious and impervious land areas, stream channels, and mixed reservoirs; one-dimensional simulations.	Two-dimensional rectangular/square overland grids, one-dimensional channels, one-dimensional unsaturated and three-dimensional saturated flow layers.	Subbasins grouped based on climate, hydrologic response units (lumped areas with same cover, soil, and management), ponds, groundwater, and main channel.
Rainfall excess on overland/ water balance	Water balance for constant subdaily time steps and two soil layers (8-in. tillage depth and user-supplied second layer).	Daily water balance, rainfall excess using interception, Green-Ampt infiltration equation, and surface storage coefficients.	Water budget considering interception, ET, and infiltration with empirically based areal distribution.	Interception and ET loss and vertical flow solving Richards equation using implicit numerical method.	Daily water budget; precipitation, runoff, ET, percolation, and return flow from subsurface and groundwater flow.
Runoff on overland	Runoff curve number generating daily runoff following SWRRB and EPIC procedures and USSCS (1986) TR-55 method for peak flow.	Manning and continuity equations (temporally variable and spatially uniform) solved by explicit numerical scheme.	Empirical outflow depth to detention storage relation and flow using Chezy-Manning equation.	Two-dimensional diffusive wave equations solved by an implicit finite-difference scheme.	Runoff volume using curve number and flow peak using modified Rational formula or SCS TR-55 method.

(Continued)

Table 17-3 Summary of Watershed-Scale Long-Term Continuous Models[a] *(Continued)*

Description/ criteria	AnnAGNPS	ANSWERS-Continuous	HSPF	MIKE SHE	SWAT
Subsurface flow	Lateral subsurface flow using Darcy's (1856) equation or tile drain flow using Hooghoudt's (Smedema and Rycroft 1983) equation and parallel drain approximation.	Subsurface flow defined by tile drainage coefficient and groundwater or interflow release fraction; unsaturated zone drainage determined using Darcy's gravity flow.	Interflow outflow, percolation, and groundwater outflow using empirical relations.	Three-dimensional groundwater flow equations solved using a numerical finite-difference scheme and simulated river-groundwater exchange.	Lateral subsurface flow using kinematic storage model (Sloan et al. 1983), and groundwater flow using empirical relations.
Runoff in channel	Assuming trapezoidal and compound cross-sections, Manning's equation is numerically solved for hydraulic parameters and TR-55 for peak flow.	Manning and continuity equations (temporally variable and spatially uniform) solved by explicit numerical scheme.	All inflows assumed to enter one upstream point, and outflow is a function of reach volume or user-supplied demand.	One-dimensional diffusive wave equations solved by an implicit finite-difference scheme.	Routing based on variable storage coefficient method and flow using Manning's equation adjusted for transmission losses, evaporation, diversions, and return flow.
Flow in reservoir	Average outflow during runoff event is calculated based on permanent pool storage and stage, runoff volume, and coefficients derived from elevation-storage relation.	Not simulated.	Same as channel.	No information.	Water balance and user-provided outflow (measured or targeted).
Overland sediment	Uses RUSLE to generate sheet and rill erosion daily or user-defined runoff event, HUSLE (Theurer and Clarke 1991) for delivery ratio, and sediment deposition based on size distribution and particle fall velocity.	Raindrop detachment using rainfall intensity and USLE factors, flow erosion using unit-width flow and USLE factors, and transport and deposition of sediment sizes using modified Yalin equation.	Rainfall splash detachment and washing off of the detached sediment based on transport capacity as function of water storage and outflow plus scour from flow using power relation with water storage and flow.	No information.	Sediment yield based on Modified Universal Soil Loss Equation (MUSLE) (Williams and Berndt 1977) expressed in terms of runoff volume, peak flow, and USLE factors.
Channel sediment	Modified Einstein equation for sediment transport and Bagnold equation to determine transport capacity of flow (Theurer and Cronshey 1998).	Not simulated.	Noncohesive (sand) sediment transport using user-defined relation with flow velocity or Colby (1957) or Toffaleti (1969) method, and cohesive (silt, clay) sediment transport based on critical shear stress and settling velocity.	No information.	Bagnold's stream power concept for bed degradation and sediment transport, degradation adjusted with USLE soil erodibility and cover factors, and deposition based on particle fall velocity.

(Continued)

Table 17-3 Summary of Watershed-Scale Long-Term Continuous Models[a] *(Continued)*

Description/ criteria	AnnAGNPS	ANSWERS-Continuous	HSPF	MIKE SHE	SWAT
Reservoir sediment	Sediment deposition based on constant detention discharge, zero transport capacity, and dilution with pool water.	Not simulated.	Same as channel.	No information.	Outflow using simple continuity based on volumes and concentrations of inflow, outflow, and storage.
Chemical simulation	Soil moisture, nutrients, and pesticides in each cell are tracked using U.S. Natural Resource Conservation Service soil databases and crop information; reach routing includes fate and transport of nitrogen, phosphorus, individual pesticides, and organic carbon.	Nitrogen and phosphorus transport and transformations through mineralization, ammonification, nitrification, and denitrification, and losses through uptake, runoff, and sediment.	Soil and water temperatures, dissolved oxygen, carbon dioxide, nitrate, ammonia, organic N, phosphate, organic P, pesticides in dissolved, adsorbed, and crystallized forms, and tracer chemicals chloride or bromide to calibrate solute movement through soil profiles.	Dissolved conservative solutes in surface, soil, and ground waters by solving the advection-dispersion equation numerically for the respective regimes.	Nitrate N based on water volume and average concentration, runoff P based on partitioning factor, daily organic N and sediment-adsorbed P losses using loading functions, crop N and P use from supply and demand, and pesticides based on plant leaf-area index, application efficiency, wash-off fraction, organic carbon adsorption coefficient, and exponential decay according to half-lives.
BMP evaluation	Agricultural management.	Impact of watershed management practices on runoff and sediment losses.	Nutrient and pesticide management.	No information.	Agricultural management: tillage, irrigation, fertilization, pesticide applications, and grazing.

[a]After Borah and Bera (2003).

sediment, and water-quality parameters in two-dimensional overland grids, one-dimensional channels, and one-dimensional unsaturated and three-dimensional saturated flow layers. It also has both continuous long-term and single-event simulation capabilities. The model was developed by a consortium of the U.K. Institute of Hydrology, the French consulting firm SOGREAH, and the Danish Hydraulic Institute.

DWSM, the Dynamic Watershed Simulation Model (Borah et al. 2002b), was put together at the Illinois State Water Survey (ISWS) in Champaign, Illinois, based on research conducted over many years at several institutions (Borah 1989a; 1989b; Ashraf and Borah 1992; Borah et al. 1980; 1981; 2002b; 2002c; 2004). DWSM simulates distributed surface and subsurface storm-water runoff, propagation of flood waves, upland soil and streambed erosion, sediment transport, and agrochemical transport in agricultural and rural watersheds during rainfall events. Similarly, KINEROS, the KINematic runoff and EROSion model (Woolhiser et al. 1990; Smith et al. 1995), which evolved from the 1960s to the 1980s at the USDA-ARS in Fort Collins, Colorado, is a distributed rainfall-runoff and soil erosion-sediment transport model for single rainfall events.

Table 17-4 Summary of Watershed-Scale Storm-Event Models[a]

Description/ criteria	AGNPS	ANSWERS	CASC2D	DWSM	KINEROS	PRMS storm mode
Model components/ capabilities	Hydrology, soil erosion, and transport of sediment, nitrogen, phosphorus, and chemical oxygen demand from nonpoint and point sources, and user interface for data input and analysis of results.	Runoff, infiltration, subsurface drainage, soil erosion, and overland sediment transport.	Spatially varying rainfall inputs including radar estimates, rainfall excess and two-dimensional flow routing on cascading overland grids, continuous soil moisture accounting, diffusive wave or full-dynamic channel routing, upland erosion, sediment transport in channels, and part of U.S. Army Corps of Engineers' Watershed Modeling System (Ogden and Julien 2002) with graphical user interface and GIS data processing.	Spatially varying rainfall inputs; individual hyetograph for each overland, rainfall excess, surface and subsurface overland flow, surface erosion and sediment transport, agrochemical mixing and transport, channel erosion and deposition and routing of flow, sediment, and agrochemical and flow routing through reservoirs.	Distributed rainfall inputs; each catchment element assigned to a rain gauge from a maximum of 20, rainfall excess, overland flow, channel routing, surface erosion and sediment transport, channel erosion and sediment transport, flow and sediment routing through detention structures.	Hydrology and surface runoff, channel flow, channel reservoir flow, soil erosion, overland sediment transport, and linkage to USGS data-management program ANNIE for formatting input data and analyzing simulated results.
Temporal scale	Storm event; one step is the storm duration.	Storm event; variable constant steps depending on numerical stability.	Long-term and storm event; variable steps depending on numerical stability.	Storm event; variable constant steps.	Storm event; variable constant steps depending on numerical stability.	Storm event; variable constant steps depending on numerical stability.
Watershed representation	Uniform square areas (cells), some containing channels.	Square grids with uniform hydrologic characteristics, some having companion channel elements; one-dimensional simulations.	Two-dimensional square overland grids and one-dimensional channels.	Overland, channel, and reservoir segments defined by topographic-based natural boundaries; one-dimensional simulations.	Runoff surfaces or planes, channels or conduits, and ponds or detention storage; one-dimensional simulations.	Flow planes, channel segments, and channel reservoirs; one-dimensional simulations.
Rainfall excess on overland	Runoff curve number method.	Surface detention with empirical relations and infiltration with modified	Interception and ET loss, infiltration using Green-Ampt method, and overland	Two options: simple runoff curve number procedure for computing time varying rainfall	Interception loss and extensive infiltration procedure by Smith and Parlange (1978).	Interception and infiltration using an empirically based areal distribution of point infiltration

(Continued)

Table 17-4 Summary of Watershed-Scale Storm-Event Models[a] *(Continued)*

Description/ criteria	AGNPS	ANSWERS	CASC2D	DWSM	KINEROS	PRMS storm mode
		Holton-Overton relation.	flow retention.	intensities, or extensive interception and Smith-Parlange (1978) infiltration procedure.		(Green-Ampt equation), similar to HSPF.
Runoff on overland	Runoff volume using runoff curve number, and flow peak using an empirical relation similar to rational formula or SCS TR-55 method.	Manning and continuity equations (temporally variable and spatially uniform) solved using an explicit numerical scheme.	Two-dimensional diffusive wave equations solved by explicit finite-difference scheme.	Kinematic wave equations solved using analytical and approximate shock-fitting solutions.	Kinematic wave equations solved by an implicit numerical scheme.	Kinematic wave equations solved using a numerical scheme.
Subsurface flow	Not simulated.	Water moving from a control zone to tile drainage and groundwater release or interflow depending on infiltration rate, total porosity, and field capacity.	Not simulated.	Combined interflow, tile drain flow, and base flow using Sloan et al. (1983) kinematic storage equation and spatially uniform and temporally varying continuity equation.	Not simulated.	No subsurface simulation in the storm mode.
Runoff in channel	Included in the overland cells.	Same as overland.	Two options: one-dimensional diffusive wave equations solved by explicit finite-difference method mostly for head water channels, or implicit finite-difference solution of the one-dimensional full dynamic equations for limited subcritical flows.	Same as overland.	Same as overland.	Same as overland.
Flow in reservoir	Flow routing through impoundments associated with terrace systems having pipe outlets.	Not simulated.	Not simulated.	Modified Puls method solving analytically the temporally varying and spatially uniform continuity equation.	Finite difference solution of the temporally varying and spatially uniform continuity equation.	Modified Puls method solving the temporally varying and spatially uniform continuity equation.

(Continued)

Table 17-4 Summary of Watershed-Scale Storm-Event Models[a] *(Continued)*

Description/ criteria	AGNPS	ANSWERS	CASC2D	DWSM	KINEROS	PRMS storm mode
Overland sediment	Soil erosion using USLE and routing of clay, silt, sand, and small and large aggregates through cells based on steady-state continuity; effective transport capacity from a modification of the Bagnold stream power equation, fall velocity, and Manning's equation.	Raindrop detachment using USLE factors and flow erosion and transport of four sizes (0.01 to 0.30 mm) using modified Yalin's equation and an explicit numerical solution of the steady-state continuity equation.	Soil erosion and sediment deposition are computed using modified Kilinc-Richardson (1973) equation with USLE factors and conservation of mass.	Raindrop detachment and sediment transport, scour, and deposition of user-specified particle size groups based on sediment-transport capacity and approximate analytical solution of temporally and spatially varying continuity equation.	Raindrop detachment and sediment transport, scour, and deposition of one particle size based on sediment-transport capacity and explicit numerical solution of temporally and spatially varying continuity equation.	Raindrop detachment based on rainfall intensity, overland flow detachment based on transport capacity, and routing based on sediment continuity.
Channel sediment	Included in overland cells.	Assumed negligible and not simulated.	Sand-size total sediment load is computed using Yang's unit stream power method.	Streambed scour/ deposition and sediment transport of the same size groups based on sediment-transport capacity and approximate analytical solution of temporally and spatially varying continuity equation.	Streambed scour/ deposition and sediment transport of the same sediment size based on sediment-transport capacity and explicit numerical solution of temporally and spatially varying continuity equation.	Sediment delivered from flow planes is transported as conservative substance without detachment or deposition.
Reservoir sediment	Sediment routing through impoundments associated with terrace systems having pipe outlets.	Not simulated.	Not simulated.	Assumes all sediments are trapped and no downstream discharge.	For shallow ponds, erosion and deposition are simulated with a mean particle diameter; for reservoirs, deposition is simulated with a particle-size distribution.	Not simulated.
Chemical simulation	Nitrogen and phosphorus in runoff using extraction coefficients, and sediment using enrichment ratios and chemical oxygen demand in runoff water assuming accumulation without loss.	Not simulated.	Not simulated.	Nutrients and pesticides are simulated in dissolved and adsorbed phases with water and sediment, respectively, through mixing and exchange between rainfall, runoff, soil, and pore water, and routing through overland and channel segments using approximate analytical solutions of spatially and temporally varying continuity equations.	Not simulated.	Not simulated.

(Continued)

Table 17-4 Summary of Watershed-Scale Storm-Event Models[a] *(Continued)*

Description/ criteria	AGNPS	ANSWERS	CASC2D	DWSM	KINEROS	PRMS storm mode
BMP evaluation	Agricultural management.	Agricultural management.	No information.	Detention basins, alternative ground covers, and alterations to hydrologic and hydraulic conditions.	Detention basins and alterations to hydrologic and hydraulic conditions.	No information.

[a]After Borah and Bera (2003).

HSPF, the Hydrological Simulation Program—Fortran (Donigian et al. 1995), first publicly released in 1980, was put together by a group of consultants (Johanson et al. 1980) under contract with the USEPA. It is a continuous watershed simulation model that produces a time history of water quantity and quality at any point in a watershed. HSPF is an extension of several previously developed models: the Stanford Watershed Model (SWM) (Crawford and Linsley 1966); the Hydrologic Simulation Program (HSP) including HSP Quality (Hydrocomp 1977); the Agricultural Runoff Management (ARM) model (Donigian and Davis 1978); and the Nonpoint Source Runoff (NPS) model (A. S. Donigian, Jr., and N. H. Crawford, unpublished report, U.S. EPA Environmental Research Lab, 1979). HSPF uses many of the software tools developed by the U.S. Geological Survey (USGS) to providing interactive capabilities for model input, data storage, input-output analyses, and calibration. Several versions of the model have been released: Version 8 was released in 1984 (Johanson et al. 1984), and Version 10 was released in 1993 (Bicknell et al. 1993). HSPF has been promoted and marketed by these consultants worldwide. Its major application in the United States is the Chesapeake Bay basin model (Donigian et al. 1986). HSPF has been incorporated as a non-point-source model (NPSM) into the USEPA's Better Assessment Science Integrating Point and Nonpoint Sources (BASINS), which was developed by Tetra Tech, Inc. (Lahlou et al. 1998), under contract with the USEPA. The main purpose of BASINS is to analyze for and develop TMDLs nationwide.

PRMS, the Precipitation-Runoff Modeling System (Leavesley et al. 1983; Leavesley and Stannard 1995), developed at the USGS in Lakewood, Colorado, is a modular-design, distributed-parameter, physical-process watershed model that was developed to evaluate the effects of various combinations of precipitation, climate, and land use on watershed response. Watershed response to normal and extreme rainfall and snowmelt can be simulated to evaluate changes in water-balance relations, flow regimes, flood peaks and volumes, soil-water relations, sediment yields, and groundwater recharge. PRMS has been coupled with USGS's data management program ANNIE (Lumb et al. 1990) and the U.S. Weather Service's Extended Streamflow Prediction (ESP) program (Day 1985) to produce a watershed-modeling and data-management system for hydrologic simulation and data analysis. PRMS has both long-term and single-storm modes. The long-term mode of PRMS is only a hydrological model. The storm mode of PRMS has a sediment component as well. Therefore, only the PRMS Storm Mode is considered and discussed here.

SWAT, the Soil and Water Assessment Tool (Arnold et al. 1998; Neitsch et al. 2002), was developed at the USDA-ARS Grassland, Soil, and Water Research Laboratory in Temple, Texas. It emerged mainly from SWRRB (Arnold et al. 1990) and has features from CREAMS (Knisel 1980); EPIC (Williams et al. 1984); GLEAMS (Leonard et al. 1987); and ROTO (Arnold et al. 1995). It was developed to assist water resources managers in predicting and assessing the impact of management on water, sediment, and agricultural chemical yields in large ungauged watersheds or river basins. The model is intended for long-term yield predictions and is not capable of detailed single-event flood routing. It is an operational or conceptual model that operates on a daily time step. The model has eight major components: hydrology, weather, sedimentation, soil temperature, crop growth, nutrients, pesticides, and agricultural management. Although most of the applications of SWAT have been on a daily time step, recent additions to the model are the Green and Ampt (1911) infiltration equation using rainfall input at any time increment and channel routing at an hourly time step (Neitsch et al. 2002). Similarly to HSPF, SWAT is also incorporated into the USEPA's BASINS for non-point-source simulations on agricultural watersheds.

17.6.2 Basic Flow-Governing Equations

Flow routing is governed by flow equations basic to all of the hydrologic, soil erosion-sediment transport (sediment yield) and non-point-source pollution models. Performance,

efficiency, and applicability of a model depend greatly on these basic equations and how they are solved.

The basic flow-governing equations are the dynamic wave equations, often referred to as the St. Venant equations or shallow-water wave equations. These consist of the equations of continuity and momentum, respectively, for gradually varied unsteady flow, expressed as (Singh 1996)

$$\frac{\partial h}{\partial t}+\frac{\partial Q}{\partial x}=0 \tag{17-26}$$

$$\frac{\partial u}{\partial t}+u\frac{\partial u}{\partial x}+g\frac{\partial h}{\partial x}=g\left(S_0-S_f\right) \tag{17-27}$$

where

h = flow depth (m);
Q = flow per unit width ($m^3\ s^{-1}\ m^{-1}$);
u = water velocity ($m\ s^{-1}$);
g = acceleration due to gravity ($m\ s^{-2}$);
S_0 = bed slope ($m\ m^{-1}$);
S_f = energy gradient ($m\ m^{-1}$);
t = time (s);
x = longitudinal distance (m).

There is no analytical solution of Eqs. (17-26) and (17-27). Approximate numerical solutions of these two equations have been used in river flood routing models, such as the U.S. Army Corps of Engineers' Unsteady flow through a full NETwork of open channels (UNET) model (Barkau 1993); the National Weather Service's OPERational Dynamic Wave (DWOPER) model (Fread 1978); and models by Amein and Fang (1970), Strelkoff (1970), and Balloffet and Scheffler (1982), to name a few.

The dynamic wave equations have not been used in watershed models because of their computationally intensive numerical solutions. Only the CASC2D model uses these equations on a limited basis. Some of the models use approximations of these equations, ignoring certain terms in the momentum equation (Eq. (17-27)), as discussed below.

17.6.3 Diffusive Wave Equations Used by CASC2D and MIKE SHE

The diffusive wave equation consists of the continuity and simplified momentum equations, respectively expressed as (Singh 1996)

$$\frac{\partial h}{\partial t}+\frac{\partial Q}{\partial x}=q \tag{17-28}$$

$$\frac{\partial h}{\partial x}=S_0-S_f \tag{17-29}$$

where

q = lateral inflow per unit width and per unit length ($m^3\ s^{-1}\ m^{-1}\ m^{-1}$).

These equations are also known as "noninertia wave" equations (Yen and Tsai 2001).

The continuity equation (Eq. (17-28)) includes lateral inflow. The simplified momentum equation (Eq. (17-29)) expresses the pressure gradient as the difference between the bed slope and energy gradient, and is derived from Eq. (17-27) after ignoring the first two terms, representing, respectively, the local and convective accelerations.

As with the dynamic wave equations, there is no analytical solution of the diffusive wave equations (Eqs. (17-28) and (17-29)). Watershed models CASC2D and MIKE SHE use approximate numerical solutions of these equations for routing surface runoff over overland planes and through channel segments. CASC2D uses two numerical methods to solve Eqs. (17-28) and (17-29) for overland flow and channel flow (Ogden and Julien 2002). In solving these equations, Manning's formula is used to compute flow, and is expressed as

$$Q=\frac{1}{n}AR^{2/3}S_f^{1/2} \tag{17-30}$$

where

n = Manning's roughness coefficient;
A = flow cross-sectional area per unit width ($m^2\ m^{-1}$);
R = hydraulic radius (m).

17.6.4 Kinematic Wave Equations Used by DWSM, KINEROS, and PRMS

The kinematic wave equations are the simplest form of the dynamic wave equations. Lighthill and Whitham (1955) developed the kinematic wave theory and used it to describe the movement of flood waves in long rivers. Kinematic wave theory is now a well-accepted tool for modeling a variety of hydrological processes (Singh 1996). The governing equations consist of the continuity equation and the simplest form of the momentum equation, ignoring all the acceleration and pressure gradient terms of Eq. (17-27), respectively expressed as

$$\frac{\partial h}{\partial t}+\frac{\partial Q}{\partial x}=q \tag{17-31}$$

$$S_0=S_f \tag{17-32}$$

The momentum equation (Eq. (17-32)) expresses simply that the energy gradient is equal to the bed slope. Any suitable law of flow resistance can be used to express this equation as a parametric function of the stream hydraulic parameters. A widely used expression is

$$Q = \alpha h^m \tag{17-33}$$

where

α = the kinematic wave parameter;
m = the kinematic wave exponent;

and α and m are related to channel (or plane) roughness and geometry. Manning's formula (Eq. (17-30)) may be used to define α and m in terms of Manning's roughness coefficient (n) and channel or plane geometry (Borah 1989a).

Equations (17-31) and (17-33) constitute the kinematic wave equations. The advantage of these equations is that they have an analytical solution by the method of characteristics (Borah et al. 1980). The equations generate only one system of characteristics, which means that they cannot represent waves traveling upstream, as in the case of backwater flow. Research suggests that for most cases of hydrological significance, the kinematic wave solution gives accurate results (V. P. Singh, unpublished paper, "Kinematic wave modeling in hydrology," ASCE-EWRI Task Committee on Evolution of Computer Methods in Hydrology, Reston, Va., 2002). In open-channel flow, dynamic waves always occur. The friction and slope terms modify the wave amplitudes to such a degree that the dynamic waves rapidly become negligible and the kinematic wave assumes the dominant role.

The analytical solution of Eqs. (17-31) and (17-33) does not apply when two characteristics intersect, forming a shock wave and physically representing a larger and faster wave superseding a smaller and slower wave. Approximate numerical solutions of Eqs. (17-31) and (17-33), such as the ones presented by Li et al. (1975) and Smith et al. (1995), do not recognize shocks. The numerical solutions can be used for any situation but the numerical solutions smooth out the waves and the hydrographs (Borah et al. 1980), thus undermining the fundamental reason that Lighthill and Whitham (1955) introduced this simple theory. With the analytical and an approximate shock-fitting (closed-form) solution, the kinematic wave theory represents salient features of a hydrograph, including the sharp rising part under shock-forming conditions (Borah et al. 1980).

The DWSM, KINEROS, and PRMS watershed models are based on the kinematic wave equations. KINEROS (Smith et al. 1995) and PRMS (Leavesley and Stannard 1995) use approximate numerical solutions of Eqs. (17-31) and (17-33), whereas DWSM uses the analytical and shock-fitting solution (Borah 1989a; Borah et al. 1980).

17.6.5 Storage-Based Equations Used by ANSWERS, ANSWERS-Continuous, and HSPF

Many of the models, such as ANSWERS, ANSWERS-Continuous, and HSPF, use the simple storage-based (nonlinear reservoir) equations for flow routing. The equations consist of the spatially uniform and temporally variable continuity equation and a flow equation expressed in terms of channel (or plane) roughness and geometry, such as the Manning equation (Eq. (17-30)). The continuity equation is expressed as

$$\frac{ds}{dt} = I - O \tag{17-34}$$

where

s = storage volume of water (m^3);
I = inflow rate ($m^3\ s^{-1}$);
O = outflow rate ($m^3\ s^{-1}$).

Equation (17-34) assumes a level water surface throughout the overland plane or channel segment and does not represent any waveforms. This equation is more suitable for flood routing in lakes and reservoirs.

17.6.6 Curve Number and Empirical Equations Used by AGNPS, AnnAGNPS, and SWAT

Many of the models, such as SWAT, AGNPS, and AnnAGNPS, do not route water using mass-conservation-based continuity equations as described above. SWAT and AnnAGNPS maintain water balance through daily or subdaily water budgets. All three of them use the USDA Soil Conservation Service runoff curve number method (United States Soil Conservation Service 1972) to compute runoff volumes and other empirical relations similar to the rational formula (Kuichling 1889; Rosemiller 1982) to compute peak flows, which may be expressed as

$$Q_r = \frac{(P - 0.2S_r)^2}{P + 0.8S_r} \tag{17-35}$$

$$S_r = \frac{25400}{CN} - 254 \tag{17-36}$$

$$Q_p = 0.0028CiA \tag{17-37}$$

where

Q_r = direct runoff (millimeters or mm);
P = accumulated rainfall (mm);
S_r = potential difference between rainfall and direct runoff (mm);
CN = curve number representing runoff potential for a soil cover complex (values 2 to 100);
Q_p = peak runoff rate ($m^3\ s^{-1}$);
C = runoff coefficient (values 0.02 to 0.95);
i = rainfall intensity (mm h^{-1});
A = watershed area (ha).

In addition, SWAT uses an empirical procedure to route water through channels. The SCS runoff curve number

method (Eqs. (17-35) and (17-36)) is also used repeatedly by DWSM to compute rainfall excess rates at discrete time intervals in addition to an interception-infiltration alternative procedure (Table 17-4). Interception-infiltration routines are used by other models as well: ANSWERS, ANSWERS-Continuous, CASC2D, HSPF, KINEROS, MIKE SHE, and PRMS (Tables 17-3 and 17-4). The latest version of SWAT (Neitsch et al. 2002) has an option for using an infiltration equation for any time increment.

17.6.7 Model Algorithms and Efficiencies

CASC2D and MIKE SHE are both physically based models using multidimensional flow-governing equations with approximate numerical solution schemes, which make the models computationally intensive and subject to the numerical instabilities inherent in the numerical solutions. Both models use the diffusive (noninertia) wave equations (Eqs. (17-28) and (17-29)), and CASC2D uses the full dynamic wave equations (Eqs. (17-26) and (17-27)) on a limited basis, i.e., for stream channels less than 0.3% slope (Ogden and Julien 2002). Molnar and Julien (2000) examined the effects of grid size on the calculation of surface runoff using the CASC2D model. A sufficiently small time step is necessary to keep the model stable. The time step is on the order of 5 s for a 150-m grid size but decreases to about 1 s when standard 30-m GIS grid sizes are used. Calculation time can become prohibitive when the number of model grid cells exceeds 100,000 (Ogden and Julien 2002). MIKE SHE, using the same governing equations, has similar limitations. Although it uses a more stable numerical (implicit) scheme (Table 17-3), it is inefficient due to its iterative operation. Therefore, CASC2D and MIKE SHE would be suitable for small areas or watersheds for detailed studies of hydrology and non-point-source pollution under single rainfall events or for long-term periods in continuous mode.

Similar to CASC2D and MIKE SHE, the ANSWERS, KINEROS, and PRMS Storm Mode models (Table 17-4) are also physically based, using numerical solutions to solve the flow equations. ANSWERS uses the storage-based equations (Eqs. (17-34) and (17-30)), and KINEROS and PRMS use the kinematic wave equations (Eqs. (17-31) and (17-33)). These models were developed for single rainfall events using one-dimensional flow equations only, and therefore are less computationally intensive than CASC2D and MIKE SHE. However, potential problems inherent in the numerical solutions exist. Smith et al. (1995) suggested that KINEROS does a relatively good job of simulating runoff and sediment yield at watershed scales of up to approximately 1,000 ha. Therefore, applications of these models are limited to small watersheds and specific combinations of space and time increments for maintaining numerical solution stability. DWSM (Table 17-4), also a physically based model, uses analytical and approximate analytical solutions of the kinematic wave flow-governing equations (Eqs. (17-31) and (17-33)). Due to its robust closed-form solutions and algorithms, DWSM is not limited to any combinations of space and time increment sizes, and could potentially be used for large watersheds.

17.6.8 Long-Term Continuous Models

AnnAGNPS, ANSWERS-Continuous, CASC2D, HSPF, MIKE SHE, and SWAT are continuous simulation models and are useful for analyzing long-term effects of hydrological changes and watershed management practices. HSPF is capable of simulating urban and suburban land uses as well. Due to its use of daily time steps, SWAT does not simulate single-event storms adequately. HSPF can use time steps smaller than a day and, therefore, can simulate individual storm events. However, due to its conceptualization of the overland (subbasin) areas as leveled detention storage and use of the storage-based or nonlinear flow equations in routings, HSPF is not adequate for simulating intense single-event storms, especially for large subbasins and long channels. Reviews of applications of the HSPF and SWAT models (Borah and Bera 2004) revealed that these two models are not suitable for analyzing severe storm events. AnnAGNPS and ANSWERS-Continuous are also not adequately formulated to simulate intense single-event storms. Borah and Bera's (2004) reviews also confirmed that SWAT is applicable to predominantly agricultural watersheds and HSPF mixed agricultural and urban watersheds.

The long-term continuous models AnnAGNPS, ANSWERS-Continuous, HSPF, MIKE SHE, and SWAT have all three major components: hydrology, sediment, and chemicals (Table 17-3). Both HSPF and SWAT models are parts of the USEPA's BASINS for developing TMDL. With BASINS, both models have graphical user interfaces for data analysis, data processing, and graphical presentation of model outputs, which are useful for model calibration, validation, and analysis of BMPs and dissemination of model results. AnnAGNPS is a recent upgrade of the single-event AGNPS model. Similarly, ANSWERS-Continuous is a recent upgrade of the single-event ANSWERS model with extensive upland process simulations. However, ANSWERS-Continuous does not have channel erosion and sediment transport routines (Table 17-3), and, therefore, the sediment and chemical components are not applicable to watersheds. Due to its computationally intensive numerical schemes, MIKE SHE may become prohibitive for long-term continuous simulations in medium-to-large watersheds.

17.6.9 Storm-Event Models

Intense single-event storms cause flooding. These storms are especially critical when most of the yearly sediment and pollutant loads are carried through and out of a watershed (David et al. 1997; Borah et al. 2003). Certain BMPs, such as structural BMPs, must be designed to withstand certain single-event

design storms. The storm-event models AGNPS, ANSWERS, CASC2D, DWSM, KINEROS, MIKE SHE, and PRMS-storm mode analyze severe actual or design single-event storms and evaluate watershed management practices, especially structural practices. The conceptual design and mathematical formulations of these models are different. AGNPS is a single-event, empirically based, lumped-parameter model using one time step (storm duration) and generating a single value for each of the output variables: runoff volume, peak flow, sediment yield, and average concentrations of nutrients. It is used to study the overall response from a single severe or design storm, but it is not suitable for analyzing a storm when the flow and constituent concentrations and loads vary with time. Time-varying water, sediment, and chemical discharges are critical in certain analyses. For example, peak flow, peak constituent concentrations, and their timings are crucial information in flood warning, floodwater management, watershed assessment, and BMP evaluations. Use of AGNPS in studying impacts of BMPs is qualitative (Borah et al. 2002a). ANSWERS, CASC2D, DWSM, KINEROS, MIKE SHE, and PRMS in storm mode can generate time-varying hydrograph and constituent graphs.

The storm-event models AGNPS, DWSM, and MIKE SHE all have the three major components hydrology, sediment, and chemical (Table 17-4). Among these three models, DWSM provides a balance between the simple AGNPS and complicated MIKE SHE models. It is suitable for simulations of agricultural and suburban watersheds (Borah and Bera 2004). CASC2D and KINEROS have complete hydrology and sediment components, but no chemical component (Table 17-4). ANSWERS and PRMS in storm mode have hydrology and overland sediment, but no chemical component, and no sediment simulation in stream channels (Table 17-4). AGNPS, CASC2D, KINEROS, and PRMS in storm mode have no subsurface flow simulations (Table 17-4).

17.6.10 Sediment Yield Predictions Using Watershed Models

Watershed models can be used to predict sediment yields from a watershed through simulations of hydrologic, soil erosion, sediment transport, and sediment deposition processes (Tables 17-3 and 17-4). The models dynamically account for sediment delivery through their routing procedures, and therefore, delivery ratios are not required. As summarized in Tables 17-3 and 17-4, different models use different procedures and algorithms to simulate these processes. It is impossible to present here all those procedures beyond the summaries presented in Tables 17-3 and 17-4. However, the major steps taken in one of the models (DWSM) to simulate hydrology (the basic component), soil erosion, sediment transport, and sediment deposition and ultimately to compute sediment yield are outlined below to provide an understanding of a modeling approach.

To apply DWSM, the watershed is divided into one-dimensional overland planes, channel segments, and reservoir units (Borah et al. 2002b). These divisions take into account nonuniformities in topographic, soil, and land-use characteristics, which are treated as being uniform with representative characteristics within each of the divisions. An overland plane is represented as a rectangle, with width equal to the adjacent (receiving) channel length, and length equal to the overland plane area divided by the width. Representative slope, soil, land cover, and roughness are based on physical measurements and observations. A channel segment is represented with a straight channel having the same length as in the field and having a representative cross-sectional shape, slope, and roughness based on physical measurements and observations. A reservoir unit is represented with a stage-storage-discharge relation (table) developed based on topographic data and discharge calculations using outlet measurements and established relations.

The overland planes are the primary sources of runoff and sediment. Two overland planes contribute surface runoff, subsurface flow, and sediment to one channel segment laterally from each side. The excess rainfall and eroded soil are routed across an overland plane, resulting in variable flow and sediment discharge along its slope length. However, cross-slope flow and sediment discharge are assumed to be uniform. Thus flow and sediment routing are only necessary within a unit width of the plane. Tile drain flows are combined with lateral subsurface flow using an effective lateral saturated hydraulic conductivity concept (Borah et al. 2002b; 2004). As a result, each channel receives time-varying, but spatially uniform, lateral inflows of water and sediment from the adjacent overland planes.

The network of channel segments carries the receiving water and sediment from the overland planes toward the watershed outlet. Depending upon the sediment load and transport capacity of the flow, further erosion of soil materials from the channel bed or sediment deposition may take place. The model simulates erosion and deposition of the channel bed only, not the banks. Therefore, the model is applicable to fairly stable streambank channels only. Also, the model assumes that all the incoming sediment is settled (deposited) within a lake, reservoir, or detention pond. Therefore, the sediment component is applicable to large detention ponds, and perhaps most reservoirs and lakes, where sediment is largely trapped and sediment bypass is negligible. For routing water and sediment through the watershed, a computational sequence is determined starting from the uppermost overland plane and ending in a channel segment or reservoir unit at the watershed outlet.

Rainfall is the primary model input. Rainfall records either from single or multiple rain gauges may be used. With multiple rain gauges, rain gauges are assigned to the overland planes using the Thiessen polygon method (Thiessen 1911). Rainfall excess and infiltration rates on each overland plane are computed from the rainfall records using two alternative

procedures: the runoff curve number method (Eqs. (17-35) and (17-36)), as extended and described by Borah (1989a), and a detailed procedure involving computations of interception losses using a procedure of Simons et al. (1975) and infiltration rates using an algorithm developed by Smith and Parlange (1978), as described by Borah et al. (1981; 2002b). The first method computes rainfall excess rates, which are subtracted from rainfall rates (intensities) to compute infiltration rates assuming other losses, such as evapotranspiration are negligible during a storm event. The second method computes interception and infiltration rates, which are subtracted from rainfall intensities to compute rainfall excess rates. Losses in depression storage in the second method are indirectly accounted for in the interception as initial losses.

The excess rainfall over the overland planes and through the channel segments are routed using the kinematic wave equations (Eqs. (17-31) and (17-33)), as described in Borah (1989a). The routing scheme is based on analytical and approximate shock-fitting solutions (Borah et al. 1980) of Eqs. (17-31) and (17-33).

The sediment is divided into a number of particle size classes (groups). For agricultural watersheds, the sediment is divided into five size groups: sand, silt, clay, small aggregate, and large aggregate (Foster et al. 1985). Erosion, deposition, and transport of each size group are simulated individually, and total responses in the forms of sediment concentration and discharge and bed elevation change are obtained through integration of the responses from all the size groups.

The rate of soil detachment due to raindrop impact is computed using the relations (Meyer and Wischmeier 1969; Mutchler and Young 1975; Borah 1989b):

$$E_r = a_r I^2 (1-D_c)(1-D_g)\left(1-\frac{h+e}{3d_{50}}\right), \quad \text{if } (h+e) < 3d_{50} \tag{17-38a}$$

$$E_r = 0, \text{ if } (h+e) \geq 3d_{50} \tag{17-38b}$$

where

E_r = rate of soil detachment due to raindrop impact (m s^{-1});
a_r = raindrop detachment coefficient (RDC);
I = rainfall intensity (m s^{-1});
D_c = canopy cover density (m^{2}m^{-2});
D_g = ground cover density (m^{2}m^{-2});
h = water depth (m);
e = thickness of existing detached soil on the bed (m);
d_{50} = median raindrop diameter (m).

Equation (17-38a) can also be expressed similarly to the USLE or RUSLE (Eq. (17-1)), as shown by Van Liew and Saxton (1984) and Van Liew (1998) for interrill soil detachment rate. In that form, only the K and C factors are kept in the equation, the R factor is replaced with some power of rainfall intensity, and all multiplied by a coefficient (parameter). The L and S factors are dynamically accounted in the model algorithms, and the P factor is incorporated through changing all the model parameters affected by the support practice or appropriately subdividing the watershed to include the practice. These investigators use similar relationship for soil detachment rate by rill flow simply by replacing rainfall intensity with flow shear stress. In Eq. (17-38a), the K and C factors are lumped on the product $a_r(1-D_c)(1-D_g)$ in computing rate of soil detachment due to raindrop impact. In computing flow-induced erosion, the K and C factors are lumped into the FDC parameter discussed below.

Equations (17-38a) and (17-38b) give the detachment rate for the entire size distribution used in the simulation. The rate for each size group is calculated by multiplying this rate by the fraction of the corresponding size group in the distribution. The eroded (detached) soil is added to an existing detached (loose) soil depth, from which entrainment to runoff takes place during erosion if the sediment-transport capacity of the runoff water is sufficient. The model maintains a loose soil depth on the bed to keep track of loose soil accumulated from bed materials detached by raindrop impact and from deposited sediment.

Flow-induced erosion and sediment deposition depend on transport capacity of the flow and the sediment load (amount of sediment already carried by the flow). Sediment-transport capacity is computed using established formulas. Based on Alonso et al. (1981), the bed-load formula of Yalin (1963) is used to compute sediment-transport capacities in overland planes under any flow condition and for all size groups. In computing capacities in the channels, the total load formula of Yang (1973) is used for sediment sizes $\geq$0.1 mm (fine to coarse sands) and the total load formula of Laursen (1958) is used for sediment sizes $<$0.1 mm (very fine sands and silts). If the capacity is higher than the sediment load, erosion takes place and the flow picks up more materials from the bed. If the loose soil volume at the bed is sufficient, sediment entrainment takes place from the detached soil depth. Otherwise, the flow erodes additional soil from the parent bed material of the overland plane or channel segment. The potential erosion is the remaining transport capacity after partial fulfillment with the existing sediment load and the loose soil volume, if any. The actual erosion is computed simply by multiplying the potential erosion by a flow detachment coefficient (FDC). The FDC is a distributed calibration parameter, which may have different values for different overland planes and channel segments, depending on resistance to erosion.

If the sediment-transport capacity is lower than the sediment load, the flow is in a deposition mode and the potential rate of deposition is equal to the difference of the two. The actual rate of deposition is computed by taking into account particle fall velocities. Deposited sediment is added to the loose soil volume. If the sediment-transport capacity and the sediment load are equal, an equilibrium condition is

assumed where there is neither erosion nor deposition. From the actual erosion and deposition, change in bed elevation during a computational time interval is computed.

All these processes are interrelated and must satisfy locally the conservation principle of sediment mass expressed by the sediment continuity equation (Borah 1989b),

$$\frac{\partial Q_s}{\partial x} + \frac{\partial CA}{\partial t} = q_s + g \qquad (17\text{-}39)$$

where

Q_s = volumetric sediment discharge (m^3s^{-1});
C = volumetric concentration of sediment (m^3m^{-3});
A = cross-sectional area of flow (m^2);
q_s = volumetric rate of lateral sediment inflow per unit length of a channel segment ($q_s = 0$ for overland plane) ($m^3s^{-1}m^{-1}$);
g = volumetric rate of material exchange with the bed per unit length ($m^3s^{-1}m^{-1}$);
x = downslope distance (m);
t = time (s).

Assuming sediment moves with the same velocity of water V, and water discharge Q remains constant within time and space intervals, Equation (17-39) may be written as

$$\frac{\partial A_s}{\partial t} + V\frac{\partial A_s}{\partial x} = q_s + g \qquad (17\text{-}40)$$

where

A_s = sediment load, volume of sediment present in the flow per unit length ($A_s = CA = Q_s/V$) (m^3m^{-1});
V = average water velocity ($m\ s^{-1}$).

Equation (17-40) is a quasi-linear hyperbolic equation governing the propagation of sediment load wave and is solved by the method of characteristics (Borah et al. 1981; Borah 1989b). Equation (17-40) and its solution are used to keep track of erosion, deposition, sediment discharge, and bed elevation change along the unit width of an overland plane or a channel segment as described in Borah (1989b) and Borah et al. (2002b).

Time integration of sediment discharges at outlet of any channel segment gives sediment yield from all the upstream areas (overland planes, channel segments, and reservoir units) contributing to the channel. Such a value at the watershed outlet gives the watershed sediment yield.

REFERENCES

Abbott, M. B., Bathurst, J. C., Cunge, J. A., O'Connell, P. E., and Rasmussen, J. (1986a). "An introduction to the European Hydrological System—Système Hydrologique Européen, 'SHE.' 1: History and philosophy of a physically based distributed modeling system." *Journal of Hydrology* 87(1–2): 45–59.

Abbott, M. B., Bathurst, J. C., Cunge, J. A., O'Connell, P. E., and Rasmussen, J. (1986b). "An introduction to the European Hydrological System—Système Hydrologique Européen, 'SHE.' 2: Structure of a physically based distributed modeling system." *Journal of Hydrology* 87(1–2): 61–77.

Agricultural Research Service—U.S. Department of Agriculture. (1975). "Present and prospective technology for predicting sediment yields and sources." *Proceedings of the Sediment-Yield Workshop, USDA Sedimentation Laboratory, ARS-S-40*, Agricultural Research Service, U.S. Department of Agriculture, 1–285.

Alonso, C. V., Neibling, W. H., and Foster, G. R. (1981). "Estimating sediment transport capacity in watershed modeling." *Transactions of the ASAE* 24(5): 1211–1220, 1226.

Amein, M., and Fang, C. S. (1970). "Implicit flood routing in natural channels." *Journal of the Hydraulics Division, ASCE* 96(12): 2481–2500.

Arnold, J. G., Srinivasan, R., Muttiah, R. S., and Williams, J. R. (1998). "Large-area hydrologic modeling and assessment. I: Model development." *Journal of the American Water Resources Association* 34(1): 73–89.

Arnold, J. G., Williams, J. R., and Maidment, D. R. (1995). "Continuous-time water and sediment-routing model for large basins." *Journal of Hydraulic Engineering, ASCE* 121(2): 171–183.

Arnold, J. G., Williams, J. R., Nicks, A. D., and Sammons, N. B. (1990). *SWRRB—A basin-scale simulation model for soil and water resources management*, Texas A&M Press, College Station, Tex.

ASCE Task Committee on Hydraulics, Bank Mechanics, and Modeling of River Width Adjustment. (1998a). "River width adjustment. I: Processes and mechanisms." *Journal of Hydraulic Engineering, ASCE* 124(9): 881–902.

ASCE Task Committee on Hydraulics, Bank Mechanics, and Modeling of River Width Adjustment. (1998b). "River width adjustment. II: Modeling." *Journal of Hydraulic Engineering, ASCE* 124(9): 903–917.

Ashraf, M. S., and Borah, D. K. (1992). "Modeling pollutant transport in runoff and sediment." *Transactions of the ASAE* 35(6): 1789–1797.

Balloffet, A., and Scheffler, M. L. (1982). "Numerical analysis of the Teton dam failure flood." *Journal of Hydraulic Research* 20(4): 317–328.

Barkau, R. L. (1993). *UNET: One-dimensional unsteady flow through a full network of open channels: User's manual*. U.S. Army Corps of Engineers, Hydrologic Engineering Center, Davis, Calif.

Beasley, D. B., Huggins, L. F. and Monke, E. J. (1980). "ANSWERS: A model for watershed planning." *Transactions of the ASAE* 23(4): 938–944.

Beer, C. E., and Johnson, H. P. (1963). "Factors in gully growth in the deep loess area of western Iowa." *Transactions of the ASAE* 6: 237–240.

Bennett, S. J., Alonso, C. V., Prasad, S. N., and Romkens, M. J. M. (2000a). "An experimental study of headcut growth and migration in upland concentrated flows." *Water Resources Research* 36(7): 1911–1922.

Bennett, S. J., Casali, J., Robinson, K. M., and Kadavy, K. C. (2000b). "Characteristics of actively eroding ephemeral gullies in an experimental channel." *Transactions of the ASAE* 43(3): 641–649.

Bicknell, B. R., Imhoff, J. C., Kittle, J. L., Jr., Donigian, A. S., Jr., and Johanson, R. C. (1993). "Hydrologic Simulation Program—FORTRAN (HSPF): User's manual for Release 10." *Rep. EPA/600/R-93/174*, U.S. EPA Environmental Research Lab, Athens, Ga.

Bingner, R. L., and Theurer, F. D. (2001). *AnnAGNPS Technical Processes: Documentation Version 2*. <www.sedlab.olemiss.edu/AGNPS.html>. Accessed 3 October 2002.

Bocco, G. (1991). "Gully erosion: Processes and models." *Progress in Physical Geography* 15(4): 392–406.

Borah, D. K. (1989a). "Runoff simulation model for small watersheds." *Transactions of the ASAE* 32(3): 881–886.

Borah, D. K. (1989b). "Sediment discharge model for small watersheds." *Transactions of the ASAE* 32(3): 874–880.

Borah, D. K., Alonso, C. V., and Prasad, S. N. (1981). "Appendix 1: Single-event numerical model for routing water and sediment on small catchments." *Stream Channel Stability*, USDA Sedimentation Laboratory, Oxford, Miss.

Borah, D. K., and Bera, M. (2003). "Watershed-scale hydrologic and nonpoint-source pollution models: Review of mathematical bases." *Transactions of the ASAE* 46(6): 1553–1566.

Borah, D. K., and Bera, M. (2004). "Watershed-scale hydrologic and nonpoint-source pollution models: Review of applications." *Transactions of the ASAE* 47(3): 789–803.

Borah, D. K., Bera, M., and Shaw, S. (2003). "Water, sediment, nutrient, and pesticide measurements in an agricultural watershed in Illinois during storm events." *Transactions of the ASAE* 46(3): 657–674.

Borah, D. K., Bera, M., and Xia, R. (2004). "Storm event flow and sediment simulations in agricultural watersheds using DWSM." *Transactions of the ASAE* 47(5): 1539–1559.

Borah, D. K., Demissie, M., and Keefer, L. (2002a). "AGNPS-based assessment of the impact of BMPs on nitrate-nitrogen discharging into an Illinois water supply lake." *Water International* 27(2): 255–265.

Borah, D. K., Prasad, S. N., and Alonso, C. V. (1980). "Kinematic wave routing incorporating shock fitting." *Water Resources Research* 16(3): 529–541.

Borah, D. K., Xia, R., and Bera, M. (2002b). "Chapter 5: DWSM—A dynamic watershed simulation model." *Mathematical Models of Small Watershed Hydrology and Applications*, V. P. Singh and D. K. Frevert, eds., Water Resources Publications, Highlands Ranch, Colo., 113–166.

Borah, D. K., Xia, R., and Bera, M. (2002c). "Watershed model to study hydrology, sediment, and agricultural chemicals in rural watersheds." *Surface Water Hydrology*, V. P. Singh, M. Al-Rashed, and M. M. Sherif, eds., Vol. 1, Balkema, Lisse, The Netherlands, 343–358.

Bouraoui, F., Braud, I., and Dillaha, T. A. (2002). "Chapter 22: ANSWERS: A nonpoint-source pollution model for water, sediment, and nutrient losses." *Mathematical Models of Small Watershed Hydrology and Applications*, V. P. Singh and D. K. Frevert, eds., Water Resources Publications, Highlands Ranch, Colo., 833–882.

Bouraoui, F., and Dillaha, T. A. (1996). "ANSWERS-2000: Runoff and sediment transport model." *Journal of Environmental Engineering* 122(6): 493–502.

Colby, B. R. (1957). "Relationship of unmeasured sediment discharge to mean velocity." *Transactions, American Geophysical Union*, 38(5): 707–717.

Crawford, N. H., and Linsley, R. K. (1966). "Digital simulation on hydrology: Stanford Watershed Model IV." *Stanford University Tech. Rep. No. 39*, Stanford University, Palo Alto, Calif.

Darcy, H. (1856). *Les fontaines publiques de la ville de Dijon*. Victor Dalmont, Paris, France.

David, M. B., Gentry, L. E., Kovacic, D. A., and Smith, K. M. (1997). "Nitrogen balance in and export from an agricultural watershed." *Journal of Environmental Quality* 26(4): 1038–1048.

Day, G. N. (1985). "Extended streamflow forecasting using NWSRFS." *Journal of Water Resources Planning and Management* 111(2): 157–170.

Demissie, M., Xia, R., Keefer, L., and Bhowmik, N. G. (2003). "Sediment budget of the Illinois River." *International Journal of Sediment Research* 18(2): 305–313.

Doe, W. W., Jones, D. S., and Warren, S. D. (1999). "The soil erosion model guide for military land managers: Analysis of erosion models for natural and cultural resources applications." *Tri-Service CADD/GIS Technology Center Technical Report ITL 99-XX*, U.S. Army Engineer Waterways Experiment Station, Vicksburg, Miss.

Donigian, A. S., Jr., Bicknell, B. R., and Imhoff, J. C. (1995). "Chapter 12: Hydrological simulation program—Fortran (HSPF)." *Computer Models of Watershed Hydrology*, V. P. Singh, ed., Water Resources Publications, Highlands Ranch, Colo., 395–442.

Donigian, A. S., Jr., Bicknell, B. R., and Kittle, J. L., Jr. (1986). *Conversion of the Chesapeake Bay basin model to HSPF operation*. Prepared by AQUA TERRA Consultants for the Computer Sciences Corporation, Annapolis, Md., and U.S. EPA Chesapeake Bay Program, Annapolis, Md.

Donigian, A. S., Jr., and Davis, H. H. (1978). "User's manual for Agricultural Runoff Management (ARM) model." *Rep. EPA-600/3-78-080,* U.S. EPA Environmental Research Lab, Athens, Ga.

El-Swaify, S. A., and Dangler, E. W. (1976). "Erodibilities of selected tropical soils in relation to structural and hydrological parameters." *Soil erosion: Prediction and control*, Soil Conservation Society of America, Ankeny, Iowa, 105–114.

Foster, G. R., and Lane, L. J. (1987). "User requirements: USDA-Water Erosion Prediction Project (WEPP)." NSERL Rep. 1, USDA-ARS National Soil Erosion Research Laboratory, West Lafayette, Ind.

Foster, G. R., and Meyer, L. D. (1972). "Transport of soil particles by shallow flow." *Transactions of the ASAE* 15(1): 99–102.

Foster, G. R., Meyer, L. D. and Onstad, C. A. (1977). "A runoff erosivity factor and variable slope length exponent for soil loss estimate." *Transactions of the ASAE* 20: 683–687.

Foster, G. R., Young, R. A., and Neibling, W. H. (1985). "Sediment composition for nonpoint source pollution analyses." *Transactions of the ASAE* 28(1): 133–139, 146.

Fread, D. L. (1978). "National Weather Service operational dynamic wave model." *Proc., ASCE 26th Annual Hydraulics Division Conference on Verification of Mathematical and Physical Models*, ASCE, Reston, Va., 455–464.

Gianessi, L. P., Peskin, H. M., Crosson, P., and Puffer, C. (1986). "Nonpoint-source pollution: Are cropland controls the answer?" *Journal of Soil and Water Conservation* 41(4): 215–218.

Gilley, J. E., Kottwitz, E. R., and Simanton, J. R. (1990). "Hydraulic characteristics of rills." *Transactions of the ASAE* 33(6): 1900–1906.

Govers, G. (1992). "Relationship between discharge, velocity and flow area for rills eroding loose, non-layered materials." *Earth Surface Processes and Landforms* 17: 515–528.

Green, W. H., and Ampt, C. A. (1911). "Studies on soil physics. I: Flow of water and air through soils." *Journal of Agricultural Sciences* 4: 1–24.

Huggins, L. F., and Monke, E. J. (1966). "The mathematical simulation of the hydrology of small watersheds." *Technical Rep. 1*, Water Resources Research Center, Purdue University, West Lafayette, Ind.

Hydrocomp. (1977). *Hydrocomp water quality operations manual,* Hydrocomp, Inc., Palo Alto, Calif.

Johanson, R. C., Imhoff, J. C., and Davis, H. H. (1980). "User's manual for the Hydrologic Simulation Program—FORTRAN (HSPF)." *Rep. EPA-600/9-80-105*, U.S. EPA Environmental Research Lab, Athens, Ga.

Johanson, R. C., Imhoff, J. C., Kittle, J. L., Jr., and Donigian, A. S., Jr. (1984). "Hydrologic Simulation Program—FORTRAN (HSPF) user's manual for Release 8." *Rep. EPA-600/3-84-066*, U.S. EPA Environmental Research Lab, Athens, Ga.

Julien, P. Y., and Saghafian, B. (1991). CASC2D user's manual. Civil Engineering Report, Department of Civil Engineering, Colorado State University, Fort Collins, Colo.

Julien, P. Y., Saghafian, B., and Ogden, F. L. (1995). "Raster-based hydrological modeling of spatially varied surface runoff." *Water Resources Bulletin, AWRA* 31(3): 523–536.

Kilinc, M., and Richardson, E. V. (1973). "Mechanics of soil erosion from overland flow generated by simulated rainfall." *Hydrology Paper 63*, Colorado State University, Fort Collins, Colo.

Knisel, W. G., ed. (1980). "CREAMS: A field-scale model for chemicals, runoff, and erosion from agricultural management system." *Conservation Research Rep. 26*, USDA-SEA, Washington, D.C.

Kuichling, E. (1889). "The relation between the rainfall and the discharge of sewers in populous districts." *Transactions, ASCE* 20: 37–40.

Laflen, J. M., Foster, G. R., and Onstad, C. A. (1985). "Simulation of individual-storm soil loss for modeling the impact of soil erosion on crop productivity." Soil Erosion and Conservation, S.A. El-Swaify, W.C. Moldenhauer, and A. Lo, eds., Soil & Water Conservation Society of America, Ankeny, Iowa, pp. 285–295.

Lahlou, M., et al. (1998). "Better assessment science integrating point and nonpoint sources: BASINS Version 2.0." *EPA-823-B98-006, U.S. Environmental Protection Agency,* Washington, D.C. <www.epa.gov/OST/BASINS>. Accessed October 3, 2002.

Lane, L. J., and Foster, G. R. (1980). "Concentrated flow relationships." *CREAMS: A field scale model for chemicals, runoff, and erosion from agricultural management systems*, W. G. Knisel, ed., Conservation Research Report 26, U.S. Department of Agriculture, Washington, D.C., 474–485.

Lane, L. J., and Nearing, M. A., eds. (1989). "USDA—Water Erosion Prediction Project: Hillslope profile model documentation. *NSERL Rep. 2*, USDA-ARS National Soil Erosion Research Laboratory, West Lafayette, Ind.

Laursen, E. (1958). "The total sediment load of stream." *Journal of the Hydraulics Division, ASCE* 54(HY 1): 1–36.

Leavesley, G. H., Lichty, R. W., Troutman, B. M., and Saindon, L. G. (1983). "Precipitation-runoff modeling system—User's manual. *USGS Water Resources Investigative Rep. 83-4238,* U.S. Geological Survey, Washington, D.C.

Leavesley, G. H., and Stannard, L. G. (1995). "Chapter 9: The precipitation-runoff modeling system—PRMS." *Computer Models of Watershed Hydrology,* V. P. Singh, ed., Water Resources Publications, Highlands Ranch, Colo., 281–310.

Leonard, R. A., Knisel, W. G., and Still, D. A. (1987). "GLEAMS: Groundwater loading effects on agricultural management systems." *Transactions of the ASAE* 30(5): 1403–1428.

Leopold, L. B., and Maddock, T., Jr. (1953). "The hydraulic geometry of stream channels and some physiographic implications." *Professional Paper 252*, U.S. Geological Survey, Washington, D.C.

Li, R. M., Simons, D. B., and Stevens, M. A. (1975). "Nonlinear kinematic wave approximation for water routing." *Water Resources Research* 11(2): 245–252.

Lighthill, M. J., and Whitham, C. B. (1955). "On kinematic waves. 1: Flood movement in long rivers." *Proceedings of the Royal Society, Series A* (229): 281–316.

Lumb, A. M., Kittle, J. L., Jr., and Flynn, K. M. (1990). "User's manual for ANNIE, a computer program for interactive hydrologic analysis and data management. *USGS Water Resources Investigative Report No. 89-4080*, U.S. Geological Survey, Washington, D.C.

McCool, D. K., Brown, L. C., Foster, G. R., Mutchler, C. K., and Meyer, L. D. (1987). "Revised slope steepness factor for the Universal Soil Loss Equation." *Transactions of the ASAE* 30(5): 1387–1396.

McCool, D. K., Foster, G. R., Mutchler, C. K., and Meyer, L. D. (1989). "Revised slope length factor for the Universal Soil Loss Equation." *Transactions of the ASAE* 32: 1571–1576.

McCool, D. K., George, G. E., Freckleton, M., Douglas, C. L., Jr., and Papendick, R. I. (1993). "Topographic effect of erosion from cropland in the Northwestern Wheat Region." *Transactions of the ASAE* 36: 771–775.

Meyer, L. D., and Wischmeier, W. H. (1969). "Mathematical simulation of the process of soil erosion by water." *Transactions of the ASAE* 12(6): 754–758, 762.

Ming, Z. F. (1983). "Hydraulic geometry of alluvial channels." *Journal of Sedimentary Research* 4: 75–84.

Mitas, L., and Mitasova, H. (1998). "Distributed soil erosion simulation for effective erosion prevention." *Water Resources Research* 34(3): 505–516.

Molnar, D. K., and Julien, P. Y. (2000). "Grid size effects on surface runoff modeling." *Journal of Hydrologic Engineering* 5(1): 8–16.

Mutchler, C. K., and Young, R. A. (1975). "Soil detachments by raindrops." *Proc., Sediment Yield Workshop*, USDA-ARS-S-40, USDA-ARS Sedimentation Laboratory, Oxford, Miss., 113–117.

Nachtergaele, J., Poesen, J., Sidorchuk, A., and Torri, D. (2002). "Prediction of concentrated flow width in ephemeral gully channels." *Hydrological Processes* 16: 1935–1953.

Neitsch, S. L., Arnold, J. G., Kiniry, J. R., Srinivasan, R., and Williams, J. R. (2002). "Soil and Water Assessment Tool User's Manual Version 2000." *GSWRL Report 02-02; BRC Report 02-06; TR-192*, Texas Water Resources Institute, College Station, Tex.

Ogden, F. L. (1998). "CASC2D Version 1.18 Reference Manual." *U-37*, Department of Civil and Environmental Engineering, University of Connecticut, Storrs, Conn.

Ogden, F. L., and Julien, P. Y. (2002). "Chapter 4: CASC2D: A two-dimensional, physically based, Hortonian hydrologic

model." *Mathematical Models of Small Watershed Hydrology and Applications*, V. P. Singh and D. K. Frevert, eds., Water Resources Publications, Highlands Ranch, Colo., 69–112.

Piest, R. F., Bradford, J. M., and Wyatt, G. M. (1975). "Soil erosion and sediment transport from gullies." *Journal of the Hydraulics Division, ASCE* 101(1): 65–80.

Poesen, J., Nachtergaele, J., Verstraeten, G., and Valentin, C. (2003). "Gully erosion and environmental change: Importance and research needs." *Catena* 50: 91–133.

Poesen, J., Vanderkerckhove, L., Nachtergaele, J., Oostwould Wijdenes, D., Verstraeten, G., and van Wesemael, B. (2002). "Gully erosion in dryland environments." *Dryland rivers: Hydrology and geomorphology of semi-arid channels*, L. J. Bull and M. J. Kirkby, eds., Wiley, New York, 229–262.

Refsgaard, J. C., and Storm, B. (1995). "Chapter 23: MIKE SHE." *Computer Models of Watershed Hydrology*, V. P. Singh, ed., Water Resources Publications, Highlands Ranch, Colo., 809–846.

Renard, K. G., Foster, G. R., Weesies, G. A., McCool, D. K., and Yoder, D. C., coordinators. (1997). "Predicting soil erosion by water: A guide to conservation planning with the Revised Universal Soil Loss Equation (RUSLE)." *Agriculture Handbook No. 703*, U.S. Department of Agriculture—Agricultural Research Service, Washington, D.C.

Romkens, M. J. M. (1985). "The soil erodibility factor: A perspective." *Soil erosion and conservation*, S. A. El-Swaify, W. C. Moldenhauer, and A. Lo, eds., Soil & Water Conservation Society of America, Ankeny, Iowa, pp. 445–461.

Romkens, M. J. M., Roth, C. B., and Nelson, D. W. (1977). "Erodibility of selected clay subsoils in relation to physical and chemical properties." *Soil Science Society of America Journal* 41: 954–960.

Rosemiller, R. L. (1982). "Rational formula revisited." *Proc. of the Conference on Stormwater Detention Facilities: Planning, Design, Operation, and Maintenance*, W. de Groot, ed., ASCE, Reston, Va., 146–162.

Schwab, G. O., Fangmeier, D. D., Elliot, W. J., and Frevert, R. K. (1993). *Soil and water conservation engineering*, 4th Ed., Wiley, New York.

Sidorchuk, A. (1996). "Gully erosion and thermoerosion on the Yamal Peninsula." *Geomorphic hazards*, O. Slaymaker, ed., Wiley, Chichester, U.K., 153–168.

Simons, D. B., Li, R. M., and Stevens, M. A. (1975). "Development of models for predicting water and sediment routing and yield from storms on small watersheds." *Rep. CER 74-75DBS-RML-MAS-24,* Colorado State University, Fort Collins, Colo.

Singh, V. P., ed. (1995). *Computer models of watershed hydrology*. Water Resources Publications, Highlands Ranch, Colo.

Singh, V. P., ed. (1996). *Kinematic wave modeling in water resources: Surface-water hydrology*, Wiley, New York.

Singh, V. P., and Frevert, D. K., eds. (2002a). *Mathematical models of large watershed hydrology*, Water Resources Publications, Highlands Ranch, Colo.

Singh, V. P., and Frevert, D. K., eds. (2002b). *Mathematical models of small watershed hydrology and applications*, Water Resources Publications, Highlands Ranch, Colo.

Sloan, P. G., Moore, I. D., Coltharp, G. B., and Eigel, J. D. (1983). "Modeling surface and subsurface stormflow on steeply sloping forested watersheds." *Water Resources Institute Rep. 142*, University of Kentucky, Lexington, Ky.

Smedema, L. K., and Rycroft, D. W. (1983). *Land drainage*, Cornell University Press, Ithaca, N.Y.

Smerdon, E. T. and Beasley, R. P. (1961). "Critical tractive force in cohesive soils." *Agricultural Engineering* 42: 26–29.

Smith, R. E., Goodrich, D. C., Woolhiser, D. A., and Unkrich, C. L. (1995). "Chapter 20: KINEROS—A kinematic runoff and erosion model." *Computer Models of Watershed Hydrology*, V. P. Singh, ed., Water Resources Publications, Highlands Ranch, Colo., 697–732.

Smith, R. E., and Parlange, J. Y. (1978). "A parameter-efficient hydrologic infiltration model." *Water Resources Research* 14(3): 533–538.

Soil Science Society of America. (2001). "Glossary of soil science terms." Soil Science Society of America, Madison, Wisc. <www.soils.org/sssagloss/>. Accessed October 25, 2005.

Strelkoff, T. (1970). "Numerical solution of Saint-Venant equations." *Journal of the Hydraulics Division, ASCE* 96(1): 223–252.

Theurer, F. D., and Clarke, C. D. (1991). "Wash load component for sediment yield modeling." *Proc. of the Fifth Federal Interagency Sedimentation Conference*, Federal Energy Regulation Commission, Washington, D.C., 7-1–7-8.

Theurer, F. D., and Cronshey, R. G. (1998). "AnnAGNPS-reach routing processes." *Proc. of the First Federal Interagency Hydrologic Modeling Conference,* U.S. Interagency Advisory Committee on Water Data, Hydrology Subcommittee, Reston, Va.

Thiessen, A. H. (1911). "Precipitation averages for large areas." *Monthly Weather Review* 39: 1082–1084.

Thompson, J. R. (1964). "Quantitative effect of watershed variables on rate of gully-head advancement." *Transactions of the ASAE* 7: 54–55.

Toffaleti, F. B. (1969). "Definitive computations of sand discharge in rivers." *Journal of the Hydraulics Division, ASCE* 95(1): 225–248.

Torri, D., and Borselli, L. (2003). "Equation for high-rate gully erosion." *Catena* 50: 449–467.

Toy, T. J., Foster, G. R., and Renard, K. G. (1999). "RUSLE for mining, construction, and reclamation lands." *Journal of Soil and Water Conservation* 54(2): 462–467.

United States Department of Agriculture (USDA). (1951). "Soil survey manual." *Agricultural Handbook No. 18*. U.S. Department of Agriculture, Washington, D.C.

United States Environmental Protection Agency (USEPA). (1998). "National Water Quality Inventory—1996 report to Congress." *EPA 841/R-97/008*, Office of Water, Washington, D.C.

United States Soil Conservation Service (USSCS). (1966). "Procedures for determining rates of land damage, land depreciation, and volume of sediment produced by gully erosion." *Technical Release No. 32*, USDA Soil Conservation Service, Washington, D.C.

United States Soil Conservation Service (USSCS). (1971). "Section 3, Chapter 6: Sediment sources, yields and delivery ratios." *SCS national engineering handbook*, USDA Soil Conservation Service, Washington, D.C.

United States Soil Conservation Service (USSCS). (1972). "Section 4: Hydrology." *National engineering handbook*, USDA Soil Conservation Service, Washington, D.C.

United States Soil Conservation Service (USSCS). (1986). "Urban hydrology for small watersheds." *Technical Release 55,* USDA Soil Conservation Service, Washington, D.C.

Van Liew, M. W. (1998). "Prediction of sediment yield on a large watershed in North Central China." *Transactions of the ASAE* 41(3): 599–604.

Van Liew, M. W., and Saxton, K. E. (1984). "Dynamic simulation of sediment discharge from agricultural watersheds." *Transactions of the ASAE* 27(4):1087–1092.

Vanoni, V. A., ed. (1975). "Sedimentation engineering." *ASCE Manuals and Reports on Engineering Practice, No. 54*, ASCE, New York.

Walling, D. E. (1983). "The sediment delivery problem." *Journal of Hydrology* 65: 209–237.

Watson, D. A., Laflen, J. M., and Franti, T. G. (1986). "Estimating ephemeral gully erosion." *Paper 86-2020*, American Society of Agricultural Engineers, St. Joseph, Mich.

Wijdenes, D. J. O., and Bryan, R. B. (1994). "Gully headcuts as sediment sources on the Njemps Flats and initial low-cost gully control measures." *Advances in GeoEcology* 27: 205–229.

Williams, J. R. (1977). "Sediment delivery ratios determined with sediment and runoff models." *Erosion and solid matter transport in inland waters*, IAHS-AISH Publication No. 122, International Association of Hydrological Sciences, Wallingford, U.K., 168–179.

Williams, J. R., and Berndt, H. D. (1977). "Sediment yield prediction based on watershed hydrology." *Transactions of the ASAE* 20(6): 1100–1104.

Williams, J. R., Jones, C. A., and Dyke, P. T. (1984). "A modeling approach to determine the relationship between erosion and soil productivity." *Transactions of the ASAE* 27(1): 129–144.

Wischmeier, W. H., Johnson, C. B., and Cross, B. V. (1971). "A soil erodibility nomograph for farmland and construction sites." *Journal of Soil and Water Conservation* 26: 189–193.

Wischmeier, W. H., and Smith, D. D. (1965). "Predicting rainfall-erosion losses from cropland east of the Rocky Mountains: Guide for selection of practices for soil and water conservation." *Agriculture Handbook No. 282*, U.S. Department of Agriculture—Agricultural Research Service, Washington, D.C.

Wischmeier, W. H., and Smith, D. D. (1978). "Predicting rainfall-erosion losses: A guide to conservation planning. *Agriculture Handbook No. 537*, U.S. Department of Agriculture—Agricultural Research Service, Washington, D.C.

Wolman, M. G. (1955). "The natural channel of Brandywine Creek, Pennsylvania." *Professional Paper 282-C*, U.S. Geological Survey, Washington, D.C., C87–C109.

Woodburn, R. (1949). "Science studies a gully." *Soil Conservation* 15(1): 11–13.

Woodward, D. E. (1999). "Method to predict cropland ephemeral gully erosion." *Catena* 37: 393–399.

Woolhiser, D. A., Smith, R. E., and Goodrich, D. C. (1990). "KINEROS, A Kinematic Runoff and Erosion Model: Documentation and user manual." *ARS-77*, USDA Agricultural Research Service, Fort Collins, Colo.

Yalin, M. S. (1963). "An expression for bed-load transportation." *Journal of the Hydraulics Division*, *ASCE* 89(HY 3): 221–250.

Yang, C. T. (1973). "Incipient motion and sediment transport." *Journal of the Hydraulics Division, ASCE* 99(HY 10): 1679–1704.

Yen, B. C., and Tsai, C. W.-S. (2001). "On non-inertia wave vs. diffusion wave in flood routing." *Journal of Hydrology* 244: 97–104.

Young, R. A., and Mutchler, C. K. (1977). "Erodibility of some Minnesota soils." *Journal of Soil and Water Conservation* 32: 180–182.

Young, R. A., Onstad, C. A., Bosch, D. D., and Anderson, W. P. (1987). "AGNPS, Agricultural nonpoint-source pollution model: A watershed analytical tool." *Conservation Research Report No. 35,* U.S. Department of Agriculture, Washington, D.C.

Young, R. A., Onstad, C. A., Bosch, D. D., and Anderson, W. P. (1989). "AGNPS: A nonpoint-source pollution model for evaluating agricultural watersheds." *Journal of Soil and Water Conservation* 44(2): 168–173.

Young, R. A., Onstad, C. A., Bosch, D. D., and Anderson, W. P. (1994). *Agricultural Non-Point Source Pollution Model, Version 4.03: AGNPS User's Guide*, USDA-ARS North Central Soil Conservation Research Lab, Morris, Minn.

Copyrighted Materials
Copyright © 2008 American Society of Civil Engineers (ASCE)
Retrieved from www.knovel.com

CHAPTER 18

Engineering Geomorphology

S. A. Schumm and M. D. Harvey

18.1 INTRODUCTION

Geomorphology is the study of earth-surface forms and processes. It is "The science that treats the general configuration of the earth's surface; specifically the study of the classification, description, nature, origin and development of present landforms and their relationships to underlying structures, and of the history of geologic changes as recorded by these surface features" (Bates and Jackson 1987, p. 272). This rather involved definition stresses the origin and evolution of landforms, and such has been the traditional concern of geomorphologists. However, it is now acknowledged that a major contribution of geomorphology can be prediction, because an understanding of past landform changes can be a great aid in the recognition of problems and the future course of landform change. If, for example, we know how a river meander has changed through time, prediction of future change can be made with more confidence (Lagasse et al. 2004). Therefore, the historical perspective of most earth scientists is an aid in prediction for current and future conditions.

Engineering geology, a field in which geologists work closely with engineers to determine how earth materials will affect engineering structures, is a well-established field (Johnson and DeGraff 1988; Legget and Hatheway 1988; Kiersch 1991). However, the application of geomorphology to engineering and environmental problems has been a more recent phenomenon (Coates 1976; Fookes and Vaughn 1986). Coates (1976, p. 6) defines engineering geomorphology simply as the combining of the "talents of the geomorphology and engineering disciplines." Sometimes this is difficult because of the disparity between engineering and geomorphic training and experience. However, Chow (1964) included a chapter on geomorphology by Strahler (1964) in his *Handbook of Applied Hydrology*, and Chang (1988) has drawn heavily on the geomorphic literature in his book on river engineering. Therefore, engineering geomorphology is the application of landform science (geomorphology) to engineering problems (Schumm and Harvey 1993; Thorne et al. 1997; Anthony et al. 2001). The major objectives of this chapter are to bring to the attention of the engineering profession (1) the importance of landform history, (2) the need to view specific problems in a broad or system context, and (3) the importance of geologic and geomorphic controls and hazards to many engineering activities for which the nominal time scale is generally 50 to 100 yrs.

Landform history involves changes through time, which can lead to conditions that threaten engineering works. For example, the slow modification of landforms by erosion, deposition, and weathering can produce abrupt changes (gullying, channel avulsion, and slope failure) that can have significant effects on engineering activities. Hence, landform or geomorphic hazards need to be identified. In addition, it is important to realize that a specific engineering site or problem is part of an integrated geomorphic system. For example, a bridge site is a small part of a fluvial system, and the character of that system both up- and downstream can significantly affect future site stability and the stability of the structure itself (Mussetter et al. 1998). Therefore, a broader perspective on the situation is desirable, and one should back away from a specific site and view it in the context of the surrounding geomorphic setting. In addition, geologic and geomorphologic controls can be far more important than is generally supposed for an engineering time scale. For example, the world's great alluvial rivers (Mississippi, Nile, Indus), although presumably dominated by hydrologic, sediment, and hydraulic controls, are, in fact, significantly influenced by geologic variables (Schumm and Winkley 1994; Schumm et al. 2000). It is important to recognize that geomorphology and engineering can be combined to provide a rational approach to many engineering and environmental problems.

In this chapter, the measurements that can be used to describe landforms quantitatively and methods that are used to date landforms will not be introduced. The reader

can obtain information on specific techniques in Strahler (1964), Goudie (1981), Catt (1988), Thorne et al. (1997), and Kondolf and Piégay (2003). In addition, a discussion of the landforms and processes involved in their modification can be found in any geomorphology textbook (Ritter 1986; Bloom 1991; Scheidegger 1991; Summerfield 1991). These texts cover a wide range of topics including coastal, glacial, wind, and weathering processes, and they provide references to these topics. Fluvial geomorphology will be stressed in this chapter. Nevertheless, because engineering problems and projects are global, it is important to recognize the significance of climate and climate changes upon geomorphic processes and landforms (Bull 1991; Molnar and Ramirez 2001). Wilson (1968) has identified six morphogenetic regions where geomorphic processes differ (Table 18-1). Therefore, experience gained in one part of the world may not be directly applicable elsewhere.

The *Encyclopedia of Geomorphology* (Fairbridge 1968) and the *Glossary of Geology* (Bates and Jackson 1987) provide a ready entry to geomorphic terminology and basic literature. Because of the interdisciplinary nature of geomorphology, its literature is scattered through a variety of geologic, hydrologic, hydraulic, environmental, and geographic journals. In most of the world, with the exception of the United States, geomorphology is taught as a subject within the field of physical geography. Three journals that publish on only geomorphic topics are *Earth Surface Processes and Landforms, Geomorphology,* and *Zeitschrift für Geomorphologie*. Of considerable value is the geomorphic abstract journal *Geomorphological Abstracts*, which provides short abstracts arranged by topic of papers from the international literature.

Geomorphologists have also provided descriptions and erosional and depositional histories of identifiable regions (Thornbury 1965; Graf 1987, 1988). These provide useful background information. Goudie (1981) has provided a comprehensive review of techniques that have been used in the study of landforms and landscapes, and several volumes of collected "classic" papers deal with specific geomorphic topics (Schumm 1972; Schumm and Mosley 1973; Schumm 1977a).

Schuirman and Slosson (1992) provide examples of how geomorphic and geologic investigations can aid engineers and the courts in litigation resulting from landslides, flooding, and gravel mining. By citing examples, they indicate the type of information that is needed and the general approach that should be followed in such investigations. In a concluding chapter, they provide useful advice for engineers and geologists who become expert witnesses. It is essential to maintain objectivity and a high degree of professionalism. Similar advice to young scientists and consultants was proffered by Schumm (1988, 1991), who also stressed the need to maintain objectivity and to adhere to the standards of the profession if credibility is to be maintained and error is to be avoided.

Before the general field of engineering geomorphology is considered, especially as it pertains to the study of form, processes, and dynamics of rivers, it is necessary to consider the different types of rivers that exist and provide a brief discussion of river classification. Schumm (2005) has suggested that rivers and streams can be divided into two principal types, regime and nonregime (Table 18-2). The regime channels, defined as those that flow on and in sediments transported by the river during the present hydrologic regime, whose morphology is controlled primarily by the interactions of the flow regime and the sediment supply (Leopold et al. 1964; Schumm 1977b), can be further subdivided on the basis of patterns (straight, meandering, wandering, braided, anastomosing) and hydrology (ephemeral, intermittent, perennial, interrupted). Nonregime channels can be further subdivided into bedrock controlled or constrained, where the form of the channel is forced by nonalluvial factors such as bedrock, colluvium,

Table 18-1 Morphogenetic Regions

Region	Dominant geomorphic processes	Landscape characteristics
Glacial	Glaciation, nivation	Glacial scour and deposition, alpine topography
Periglacial	Frost action, solifluction, running water	Patterned ground, solifluction, lobes, terraces, outwash plains
Arid	Desiccation, wind action, running water	Dunes, salt pans (playas), deflation basins, angular slopes, arroyos
Semiarid (subhumid)	Running water, weathering (especially mechanical)	Pediment, fans, angular slopes with coarse debris, badlands
Humid temperate	Running water, weathering (especially chemical), creep (and other movements)	Smooth slopes, soil covered, stream deposits extensive
Selva	Chemical weathering, mass movements, running water	Steep slopes, knife-edge ridges, deep soils (laterites included)

After Wilson (1968).

glacial deposits, or extreme flood deposits (Montgomery and Buffington 1997; Tinker and Wohl 1998; O'Connor and Grant 2003) and unstable, which can include degrading (Schumm et al. 1984; Darby and Simon 1999), aggrading (Schumm 1977b), and avulsing (Schumm et al. 2000) channels.

There have been numerous attempts to classify rivers (Leopold and Wolman 1957; Schumm 1963, 1968; Mollard 1973; Kellerhals et al. 1976; Brice 1981; Mosley 1987; Rosgen 1994, 1996; Montgomery and Buffington 1997; Thorne 1997; Vandenberghe 2001), but no single classification has been developed that meets the needs of all investigators, and in fact Goodwin (1999) has even questioned the need for classification. Several factors have prevented the achievement of an ideal geomorphic stream classification, and foremost among these have been the variability and complexity of rivers and streams (Mosley 1987; Juracek and Fitzpatrick 2003). Extensive problems associated with the use of existing morphology as a basis for extrapolation (Schumm 1991) further complicate the development of a robust classification (Juracek and Fitzpatrick 2003).

However, notwithstanding the problems associated with classification in general, stream classification is widely used in the United States, with the Rosgen (1996) classification being the most commonly used. Numerous federal, state, and local agencies utilize the Rosgen (1996) classification for description of stream reaches and for guiding stream restoration or rehabilitation. Provided that the classification is used for descriptive or communicative purposes, it provides a useful tool. Unfortunately, given the widespread use of the classification, it is not appropriate in its present form for assessing stream stability, inferring geomorphic processes, predicting future geomorphic responses, or guiding stream restoration or rehabilitation activities (Miller and Ritter 1996; Wilcock 1997; Juracek and Fitzpatrick 2003). From a practical perspective, the geomorphologist's measurements of sinuosity, width-depth ratio, gradient, dimensions (width and depth), and sediment type (bed and banks), when combined with the engineer's measurements of discharge, flow velocity, shear stress, and stream power, provide the information necessary for understanding of a river and the knowledge required for prediction of future change (Schumm 2005). When quantitative information about a river is available, classifications are of less value in the design of stable stream channels and prediction of channel change.

Table 18-2 Channel Types

Regime channels
Patterns
straight
meandering (passive/active)
wandering
braided
anastomosing (can be any of above patterns)
Hydrology
ephemeral
intermittent
perennial
interrupted
Nonregime channels
Bedrock
confined
constrained
Unstable
aggrading (transport-limited)
degrading (supply-limited)
avulsing

After Schumm (2005).

18.2 HISTORY

The first objective of this chapter is to convince the reader that a combination of an understanding of present conditions (model of the present) with historical information (model of the past) is of great value for prediction of landform (drainage network, slope, river, alluvial fan, etc.) change, as a result of natural or human influences (model of the future). For the study of present conditions the collection of available topographic maps, aerial photographs, soil maps, and land-use maps, as well as hydrological and meteorological data and information on the geotechnical properties of bed and bank materials, bank vegetation, and the hydraulic character of flow, is necessary. These types of information permit description of the present situation, and this can be considered a *direct approach*, where existing information is assembled and utilized to provide present and recent historical information. However, such a short record often does not provide an adequate basis for prediction of future landform stability or change. This requires an *indirect approach*, which involves geomorphic evaluation of groups of landforms.

18.2.1 Direct Approach

A simple example of the need for recent historical information and of the direct approach is provided by a court case involving the Snake River in Jackson Hole, Wyoming (Schumm 1994). It was claimed that because the present banks of the river do not correspond with the banks as surveyed by the General Land Office (GLO) surveyors in the late 19th century, the surveys were either fraudulent or in gross error. This conclusion was supported by expert testimony that the river had not changed position for centuries. However, when the GLO surveys were compared with more recent maps and a series of aerial photographs, it became obvious that the Snake River was and is a very active river that continually erodes its banks, and therefore, the position of the banks changes through time. The historical evidence,

as well as dendrochronological and pedological data, convinced a federal judge that the GLO surveys were accurate.

The direct approach uses readily available historical information. For example, information that can be used to determine the stability of a bridge crossing can be obtained in at least five ways, as follows (Shen and Schumm, 1981):

1. The history of nearby bridges should be determined. If the new bridge is to replace an older one, considerable information should be available on the past morphology and behavior of the river at that site. For example, channel width and the distance from the crown of the highway to the streambed will be available. Any change can be readily determined by comparison of the present cross-sectional characteristics with those at the time of the construction of the old bridge.
2. Conversations with long-time residents of the valley can be useful in establishing the relative stability of the river channel. Recollections are sometimes suspect, but old photographs of the river obtained from private collections, family albums, and local historical societies can be invaluable. State archives and historical societies frequently contain photographs of old bridges and fords, and hence they are a source of valuable information.
3. In the midwestern and western United States, General Land Office surveys made in the nineteenth century frequently provide information on former river widths and patterns. The earliest maps can be compared with more recent topographic maps and aerial photographs. For example, there is a series of maps, the earliest being 1765, that can be used to document Mississippi River channel pattern changes. Aerial photographs may be available from the late 1930s.
4. Records such as newspaper reports, railroad company files, church records, court transcripts, and accounts of early travelers are all possible sources for identifying channel changes.
5. Gauging station records (specific stage analysis) can be used to assess channel stability and to detect long-term hydrologic trends or the occurrence of large morphologically significant floods.

According to Brice (1974), meander shift is one of the major problems at bridge crossings. Needless to say, this hazard should be one of the easiest to recognize if maps and aerial photographs for a period of years are available to provide historical background. An example of this problem and the procedure applied to the problems at the U.S. Highway 177 crossing of the Cimarron River near Perkins, Oklahoma is abstracted from Keeley (1971).

In 1953 a new bridge was constructed over the Cimarron River downstream from an old bridge, which in 1949 was judged to be in poor condition, with erosion concentrated on the south bank about 1,500 ft (457 m) above the bridge abutment (Fig. 18-1). In 1957, there was continued erosion of the south bank immediately upstream of the south abutment during a period of large floods. Following floods, 650 ft (198 m) of riprap was emplaced on the south bank between the piles and the bridge abutment.

The second highest flood of record occurred in 1959 and all five pile-dike diversions were damaged. There was some bank erosion on the northwest bank 1,500 ft (457 m) upstream of the north abutment. During a period of high discharges between 1959 and 1962, the point of attack shifted from the south bank to the north bank. There was up to 325 ft (99 m) of erosion of the north bank between the north abutment and 2,600 ft (793 m) upstream. Five pile-dike diversion structures were constructed on the north bank, and riprap was extended upstream from thenorth abutment. In 1965, there was further scour of the north bank.

The continuing problem at this crossing, especially the shift of erosion from the south to the north bank, could have been anticipated if an evaluation of the stability of the channel had been made prior to or after construction. For example, the 1938 aerial photographs show that the channel was straight and braided at the site at the time of bridge construction, but there was a large bend about one mile upstream (Fig. 18-1).

Relatively little effort would have been required to conclude that the Cimarron River was a relatively unstable channel at this site and that a major problem would be downstream bend shift. Examination of the 1938 aerial photographs with rapid field examination of the channel would have revealed the potential problem of bend shift. Hence, a minimum of historical information (the aerial photographs), combined with the perspective that a site is only a small part of a complex system, would have led to investigations of channel conditions both upstream and downstream of the bridge crossing. The major hazard was bend shift, but the accompanying shifting pattern of bank erosion and scour attracted the most attention. From the point of view of the engineer, the bridge site selected in 1958 was a reasonable one, because the channel was straight and it was near bedrock on the south side of the

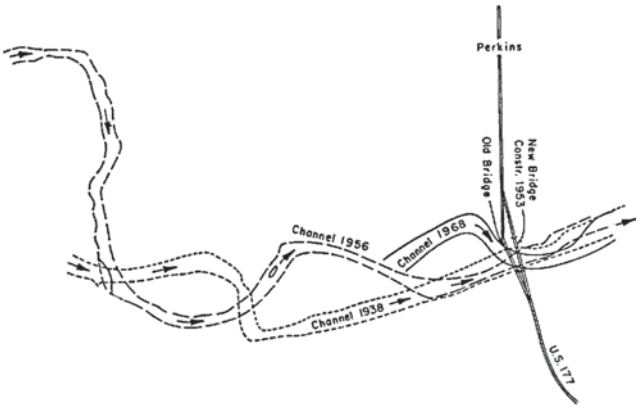

Fig. 18-1. Cimarron River meander shift as shown by 1938, 1956, and 1968 aerial photographs (from Keeley 1971).

channel. Only if the upstream changes in the channel position were recognized and the hazard identified could the engineer have anticipated the problems that developed at this site.

This example illustrates the utility of obtaining historical information as well as the need to consider a longer reach of a river rather than focusing entirely on the site of the bridge crossing. In this case, very little historical information was needed to identify the problem.

18.2.2 Indirect Approach

The indirect approach involves utilizing geomorphic information to develop a model of landform changes that in turn can be used to identify hazards and to predict change. A longer historical record can be developed using the *location for time substitution* (LTS) technique (Fig. 18-2). This has been used with great success to determine future changes of rapidly evolving landforms such as gullies, arroyos, and channelized streams, and it can be used to determine long-term evolutionary changes of landscapes (Schumm et al. 1984; Paine 1985; Schumm 1991).

If a series of cross-sections are surveyed along a channel (Fig. 18-2) that is incising as a result of natural or human-induced changes (e.g., channelization), an evolutionary model of channel adjustment can be developed (Fig. 18-3). In this way, location is substituted for time (LTS). The model presented in Fig. 18-3 was developed for incised channels in northern Mississippi using LTS, and it has both academic and practical value because it permits estimation of sediment production and agricultural land loss (Schumm et al. 1984; Darby and Simon 1999). The location-for-time substitution technique can be an effective means of developing a model of evolving landforms, which can aid the engineer in predicting change and developing a strategy for mitigation of or promotion of the change, depending upon his goals.

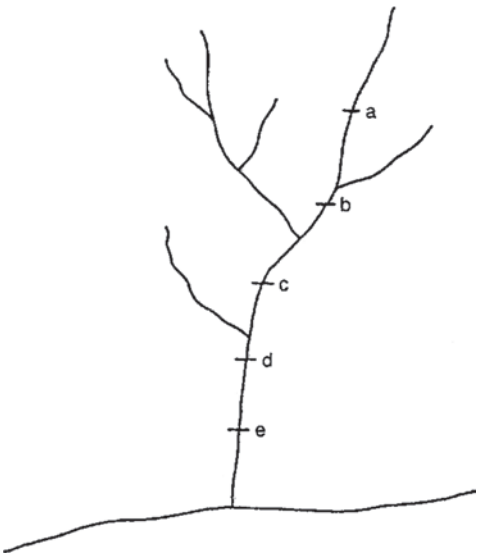

Fig. 18-2. Sketch shows method used to obtain data for location for time substitution (LTS) along an incised channel. Incision commences at mouth of channel and progresses upstream. Therefore cross sections a to e show channel evolution from original (a) to oldest (e); see Fig. 18-3.

In using LTS it is important to compare features produced by the same processes operating under the same physical conditions. For example, the evolution of an incised channel in alluvium can be determined by surveying cross-sections at several locations where the channel is in alluvium (Fig. 18-2), but one cannot combine data or compare channels in weak alluvium with channels in resistant alluvium or bedrock and expect to find meaningful results. LTS can be used to determine not only channel evolution, but also hillslope and drainage network change.

Time is an important variable in the development of an incised channel and therefore it should be an important variable in any scheme to curtail gully erosion and to reduce sediment loads. Fig. 18-4 is a conceptual diagram that shows the change in sediment yield and incised channel (gully) drainage density (length of gullies per unit area) with time. In a drainage basin that has been rejuvenated and in which gullies are developing, sediment production will increase as the length of incising channels increases (Fig. 18-4, times 1 to 4). However, at time 4 maximum headward growth of the channels has occurred, and they begin to stabilize between times 4 and 7, when there is an increase in the length of relatively stable reaches, and the length of active reaches decreases. By understanding this cycle of channel incision and gullying from initial stability (time 1) to renewed stability (time 8), it is possible to select spans of time in the cycle when land management and incised channel control practices will be most effective. For example, gullies just being initiated (time 1 or 2) and gullies almost stabilized (time 6, 7, or 8) will be the most easily controlled by structural means. Although the efforts at times 7 and 8 will have little effect, because the channels are stabilizing naturally. At time 4 control will be difficult and expensive. Obviously, consideration of such a complex evolving system for only short periods of record and short time spans can yield erroneous conclusions.

The sequence of events shown in Figs. 18-3 and 18-4 can also have wider applications. In the nineteenth century, throughout the arid and semiarid regions of the southwestern United States, channels incised to form the arroyos that were notorious suppliers of sediment to the Colorado, Green, Rio Grande, and San Juan rivers. Their incision also lowered water tables, and as a result, former grazing and farmlands were abandoned, as well as some small agricultural communities. Projections of the life of reservoirs on these rivers were based on the assumption that the high sedimentation rates generated by arroyo incision and widening (Fig. 18-3) would continue. However, if the sequence of incised-channel evolution as shown in Fig. 18-4 is generally applicable, then the arroyos will begin to stabilize, erosion will be less, and sediment will be stored in newly

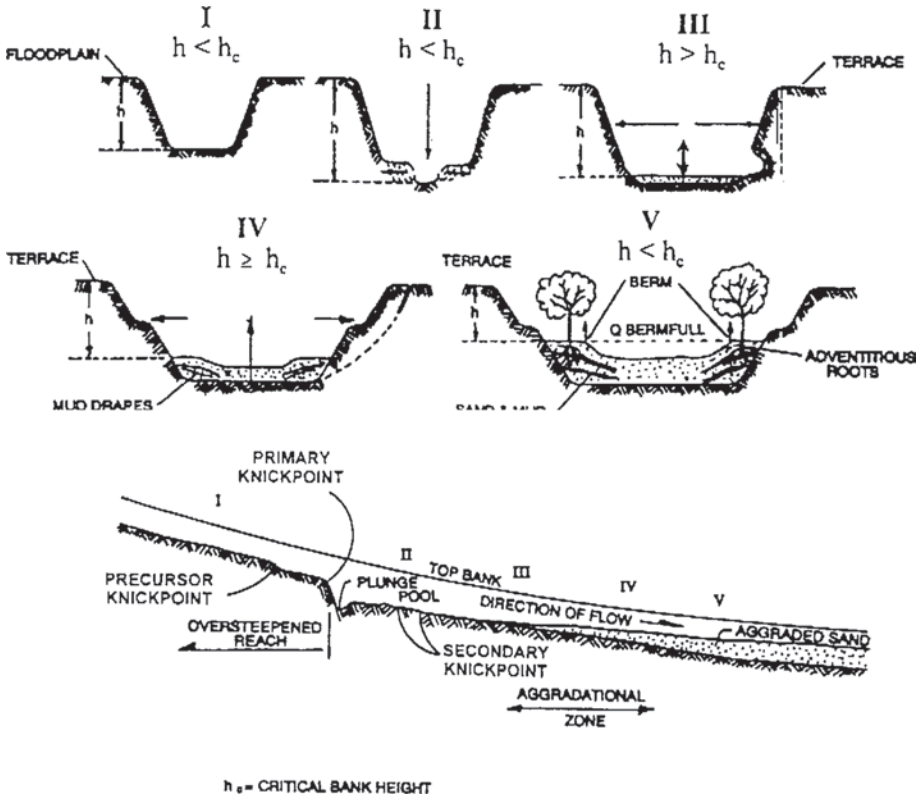

Fig. 18-3. Evolution of incised channel from original channel (I) to initial incision (II), widening (III), aggradation (IV), and eventual stability (V) (from Schumm et al. 1984).

forming floodplains. Indeed, sediment moving through the Grand Canyon of the Colorado River has decreased significantly since the later 1930s (Gellis et al. 1991), although discharge has not.

For example, based upon the average sediment delivery to Lake Powell from 1914 to 1957, it was estimated that 85,400 acre-feet (105,340,050 m^3) of sediment would be deposited in the reservoir each year. In 1963, the dam was closed, and 409 ranges were surveyed across the reservoir, which provided a means of measuring sediment accumulation in the reservoir. In 1986, the ranges were resurveyed and it was determined that only 36,946 acre-feet (45,554,420 m^3) of sediment was being deposited each year (Ferrari 1988), which is 43% of the previous calculation. During this time, flow into the reservoir was 91% of the 1914–1957 average. Hence, an understanding of the incised-channel cycle would have permitted a significant increase in the estimated reservoir life from 700 to 1,600 yrs. The same principle can be applied to other, smaller reservoirs and to sediment delivery to lakes and bays.

Location-for-time substitution is a valuable indirect tool that can be used to develop a qualitative incised channel evolution model (ICEM) that aids in understanding and prediction of landform change in both humid and semiarid regions of the United States. Harvey and Watson (1986), Watson et al. (1988, 1988b), Mussetter et al. (1994), Simon (1994), Bledsoe et al. (2002), and Watson et al. (2002) have taken this approach, and they have quantified and integrated four important facets of the ICEM process: (1) bank stability, (2) magnitude and frequency of the range of dominant

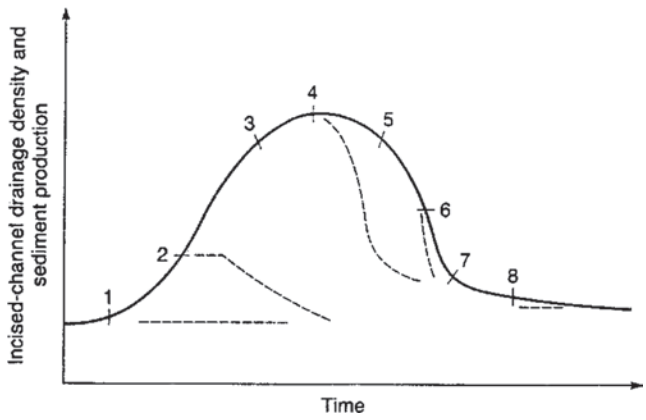

Fig. 18-4. Hypothetical change of sediment production and incised channel (gully) drainage density (ratio of channel length to drainage area) with time. Dashed lines indicate effect of gully-control structures at various times during channel evolution (from Schumm 1991).

discharges, (3) hydraulic energy of those discharges, and (4) morphological adjustments of the channel. These factors in the evolution of the incised channel can be further reduced to two dimensionless stability numbers, N_g, the geotechnical stability number, and N_h, the hydraulic stability number.

The geotechnical stability number N_g is defined as the ratio of the actual bank height (h) at a given bank angle to the critical bank height (h_c) (defined computationally or observationally):

$$N_g = \frac{h}{h_c}$$

When N_g is less than 1, the bank is geotechnically stable; when N_g is greater than 1, the bank is unstable and bank failure and channel widening are likely.

The hydraulic stability factor (N_h) is defined as the ratio of the sediment supply to the sediment transport capacity. N_h can be interpreted as a ratio of energy parameters. An example would be the ratio of shear stress or shear intensity at the effective or dominant discharge to the same parameter under conditions of equilibrium between sediment transport capacity and sediment supply. It is important to note that N_h includes sediment transport and supply. This is in contrast to most channel design procedures, which are generally based on fixed boundary approximations (Harvey and Watson 1986). N_h provides a rational basis for determining the equilibrium sediment transport–sediment supply relationship that will be required to achieve a state of dynamic equilibrium. Hydraulic stability in the channel is attained when $N_h = 1$. If $N_h > 1$, the channel will degrade, and if $N_h > 1$, the channel will aggrade.

When N_g and N_h are combined, they provide a set of design criteria that define both geotechnical and hydraulic stability in the channel. Channel stability is attained when $N_g < 1$ and $N_h = 1$. Because sediment supply to a channel fluctuates through time, it is prudent to aim for a hydraulic condition that is marginally aggradational; therefore, a more conservative approach is to allow for $N_h > 1$.

The relationship between the ICEM and the stability numbers can be seen in Fig. 18-5. The points labeled A through F can be viewed as individual locations along an incised channel (Fig. 18-3), or as a sequence of locations that are linked spatially or temporally, with point A being upstream and point F being downstream, or moving from point A counterclockwise to point F through time at a given location. These points generally correspond with the stages illustrated in Fig. 18-5. For example, if the geotechnical and hydraulic calculations place a reach of channel at point A on the diagram, the strategy should be to prevent the channel depth from increasing to the point where the critical bank height is exceeded. In contrast, if the reach is located at point E, there will be no need to treat the channel because it is in a condition of quasiequilibrium. If no action is taken when a reach is in a condition represented by point A, the sequence

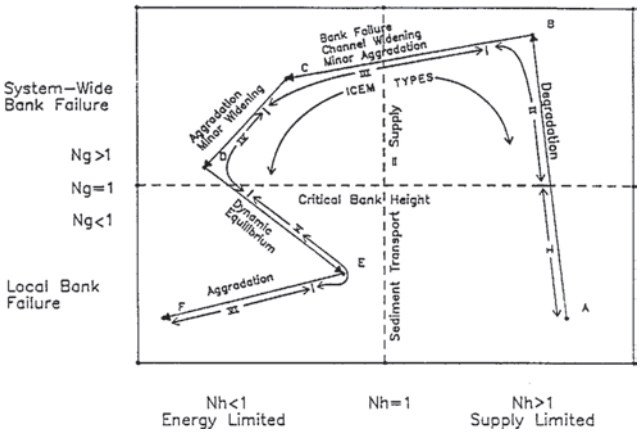

Fig. 18-5. Stability number (N_g/N_h) diagram showing the thresholds of bank stability and hydraulic stability for an incised channel. Also shown are the ICEM stages (Fig. 18-4). Note that the ICEM reach types form a continuum and the type boundaries are gradational (from Water Engineering & Technology 1989).

of channel incision and widening will move from point A to point F through time as the channel evolves.

As the channel evolves from a state of disequilibrium (A) to a state of dynamic equilibrium (E), the reach types move from the lower right to the lower left quadrant via the upper right and upper left quadrants (Fig. 18-5). Management of the channel should be aimed at keeping the channel in the lower right quadrant, or forcing it to move directly to the lower left quadrant, thereby eliminating the evolution cycle that is an inevitable consequence of bed degradation causing exceedence of the critical bank height. Forcing the channel to move directly into the lower left quadrant generally requires the use of grade-control structures and bank protection.

Utilization of ICEM and the dimensionless stability numbers N_g and N_h not only enables equilibrium reaches to be identified (i.e., $N_g < 1$: $N_h < 1$), but also permits reaches that are at risk to be identified, and provides a process-based rationale for selecting appropriate treatments. Further, this approach enables the effects of changed land use (runoff and sediment supply) to be evaluated in the context of a systems approach to watershed evaluation that is equally applicable in humid or arid regions as well as in rural or urbanizing situations (Mussetter et al. 1994; Watson et al. 2002).

18.3 SYSTEMS APPROACH

A systems approach simply means that one should not be fixated on site conditions. Rather, the site should be considered in the context of adjacent areas or landforms. Again, a court case provides a good example. Twenty-two landowners claimed that the erosion of their property along the Ohio River was caused by the raising of water levels behind navigation locks and dams. To maintain navigation on the

Ohio River during low water, a series of low dams with locks maintain a minimum navigation depth of 9 ft (2.7 m). The pool level behind the dam, therefore, never falls to the old low-water levels. It was alleged that the maintenance of the pools at a constant level caused bank erosion by wave action. Preliminary studies showed that, indeed, erosion was occurring on the litigants' lands, and their claims seemed valid. However, when the river as a whole was considered, rather than just 22 limited portions of the bank, it became clear that the river has eroding, stable, and healing banks, and the type and extent of erosion could be predicted (Schumm 1994). In fact, much of the erosion was due to the landowners' activities behind the bankline, which added water to the banks and caused slumping well above the pool level. In this case, the ability to consider a long reach of the river rather than a few specific locations permitted the development of a strong argument that the bank erosion was natural and that, in some cases, it was induced by the landowners themselves. The landowners lost the case because the judge found that the geomorphic arguments were convincing, but the landowners probably were not convinced because of their limited perspective.

18.3.1 Direct Approach

The direct approach here involves simply an evaluation of present conditions and recognition of anomalous conditions.

A major problem for the engineer is to anticipate changes of floodplain utilization and channel alterations. An excellent example is provided by the Salt River at Phoenix, Arizona, where the river and its floodplain are a convenient and abundant supply of sand and gravel. Human changes have significantly altered the Salt River in Phoenix, thereby causing changes of flow alignment, constriction of the channel, and degradation (Arizona Department of Transportation 1979).

The Interstate 10 bridge over the Salt River was constructed in 1962 (Fig. 18-6). The bridge was designed to accommodate a 50-yr flood with a peak discharge of 175,000 cfs (4,956 m^3/s). Discharges were relatively low or nonexistent for a number of years, but a large flood (67,000 cfs [1897 m^3/s]) occurred in January 1966, and a 22,000-cfs (632 m^3/s) flood in April 1973. The river was essentially dry until in March 1978 there was a 115,000-cfs (3,257-m^3/s) flood, and it was followed by a 120,000-cfs (3,398-m^3/s) flood in December 1978. In January 1979 there was an 80,000-cfs (2267-m^3/s) flood, and finally in March 1979 there was a 48,000-cfs (1,359 m^3/s) flood. During the latter flood, scour undermined the footing of Pier No. 11 (Fig. 18-7), which caused subsidence and tilting of one of the bridge spans. The footing was 20 ft (6 m) below the channel in 1962, and a low-water channel was dredged artificially to the north between Piers 5 and 10 (Fig. 18-7). The footings of these piers were 10 ft (3 m) deeper than for Piers 11 through 19.

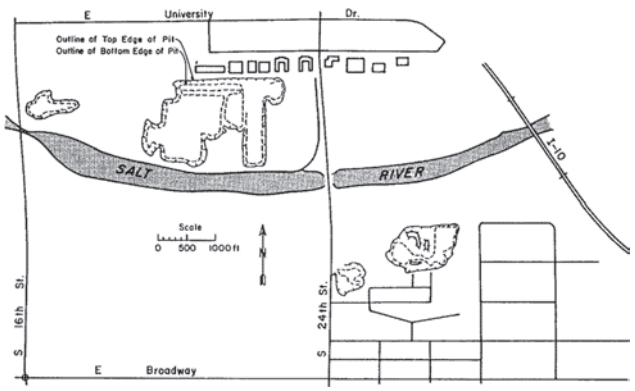

Fig. 18-6. Map showing 1-10 Bridge, Phoenix, Arizona, and downstream gravel pits (from Arizona Department of Transportation 1979).

When the bridge was designed, it was assumed that the low-water thalweg would remain fixed in position 5 ft (1.5 m) above the deepest pier. However, as the city of Phoenix grew during the period following bridge construction, gravel mining increased and gravel pits were opened near the bridge. For example, a 30-ft-(9.1-m-) deep gravel pit was dredged on the south side of the river about 2,000 ft (609 m) downstream and 750 ft (229 m) south of the low-water channel (Fig. 18-6).

Study of aerial photographs shows that during the large 1968 flood, another thalweg developed as the existing low-water channel was filled with sediment. Floodwaters flowed into the gravel pit (Fig. 18-6), and erosion of the head wall caused development of a new channel, which was centered on Pier 11 (Fig. 18-7). Scour and undermining of Pier 11 resulted, with serious damage to that span of the bridge. The rapidly developing Phoenix area ensured that this would be the case, as gravel was excavated for construction purposes. However, a cursory look downstream would have forewarned the engineer that a grade-control structure was needed to protect the bridge, because local base level had been lowered as a result of gravel mining.

Along a 5-mile-(8-km-) long reach of the San Benito River near Hollister, California, sand and gravel mining-induced channel degradation between 1952 and 1995 has resulted in the loss of one bridge and severe damage to two others, as well as loss and damage to utility crossings (Harvey and Smith 1998). Compilation and review of historical surveys of the channel and bridges showed the progression of the channel degradation through time, and could have been used to anticipate the occurrence of the infrastructure problems. Instead, each site of damage was considered singularly and repairs were conducted without consideration of further system changes. Ongoing channel adjustments caused many of the repairs to fail and ultimately led to failure and abandonment of the structures.

Another example of a systems approach is provided by the Nile River in Egypt (Schumm and Galay 1994). It was

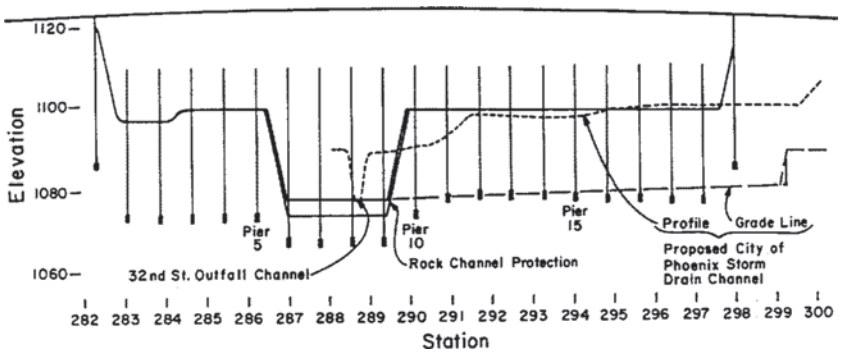

Fig. 18-7. Cross section at I-10 Bridge, Phoenix, Arizona, showing channel cross-section and location of low-water channel and bridge piers and footings (from Arizona Department of Transportation 1979).

assumed by many that following construction of the High Aswan Dam the sand-bed Nile River would be subjected to major degradation between Aswan and Cairo. However, degradation was minimal, although the bed material was mobile. Subsequent inspection of tributaries revealed that they contained coarse gravel and cobbles, which during infrequent floods and during past more humid periods were transported into the Nile valley. Available data from bores into the bed of the river reveal that gravel is encountered at shallow depths. A reasonable explanation for the lack of significant degradation is that below the sand bed of the river there is sufficient gravel to prevent degradation. Inspection of tributaries as well as of the main Nile channel would have provided information that might have led to a more complete sampling program and better estimates of potential degradation.

18.3.2 Indirect Approach

The indirect approach is similar to the location-for-time substitution, as described above, except that it is present conditions that need to be evaluated. The *location-for-condition* approach, which involves collecting data for a number of similar landforms in an area, is a means of determining the condition or relative sensitivity of a single landform or a site. A location-for-condition evaluation (LCE) has been used to identify sensitive valley floors (Fig. 18-8) that are likely to gully in Colorado and New Mexico (Patton and Schumm 1975; Begin and Schumm 1979; Wells et al. 1983a, 1983b); river reaches that are susceptible to a pattern change (Fig. 18-9) from meandering to braided (Schumm and Khan 1972; Schumm and Beathard 1976; Schumm et al. 1987); alluvial fans that are susceptible to fan-head incision (Schumm et al. 1987); and thresholds of hillslope stability (Carson 1975). Therefore, it is a means of identifying threshold conditions and the relative sensitivity of landforms (Schumm 1988).

In each of these cases data were collected at a number of locations, and a quantitative relation was developed, that could lead to the identification of threshold conditions of sensitive landforms. For example, the slope of the line in Fig. 18-8 identifies a valley floor slope in a given drainage area (a surrogate for discharge) at which erosion is likely to occur and gullies to form. The curve of Fig. 18-9, when developed for a specific river, can be used to identify river reaches that are susceptible to change from meandering to braided and vice versa. When a quantitative relation is developed between alluvial-fan slope and fan stability, alluvial fans that are susceptible to fanhead trenching can be identified (Fig. 18-10).

Both the location-for-time substitutions and the location-for-condition evaluation involve the collection of data at a number of locations and the utilization of the data

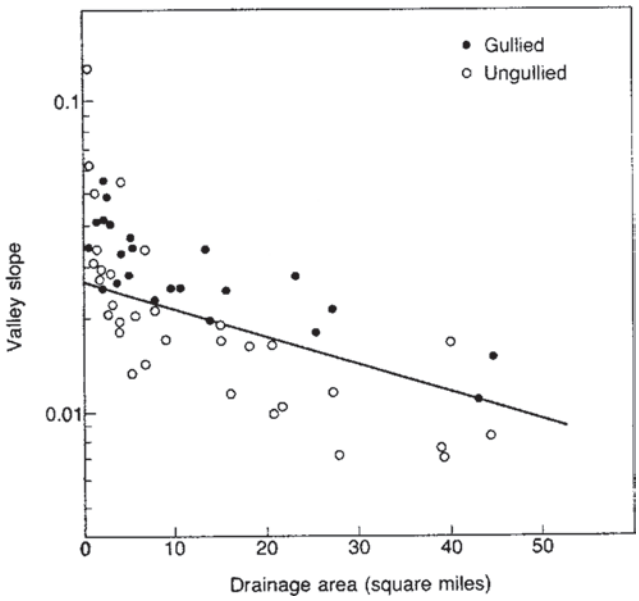

Fig. 18-8. Relation between valley slope and drainage area, Piceance Creek Basin, Colorado. The line defines the threshold slope that generally separates gullied from ungullied valley floor (from Patton and Schumm 1975).

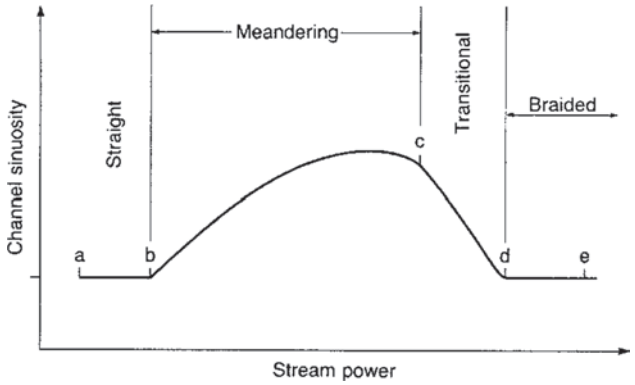

Fig. 18-9. Diagram showing how sinuosity (channel length divided by valley length) varies with stream power (tractive force times velocity of flow). With an increase of stream power or velocity, sinuosity remains constant at low values (a to b), increases with meandering (b to c), decreases through a transition from meandering to braided (c to d), and then remains braided (d to e) (from Schumm and Khan 1972).

to develop an evolutionary model (LTS) or to determine the sensitivity of a site (LCE). Both are valuable techniques that have been used primarily by geomorphologists for practical purposes of prediction, as well as for explanation of past events. Of even greater value is the fact that both techniques require that the investigator back away from a single site and look at many sites, which provides the big picture and a basis for identification of sensitive landforms.

A good example of how the system approach can put a local problem into perspective is that of Mississippi River variability. The lower river between Cairo, Illinois and Old River, Louisiana can be divided into 25 reaches based upon changes of valley slope, sinuosity, and sinuosity variability (Schumm et al. 1994). It becomes apparent immediately that this great alluvial river has significant variability, and it is not uniform for long distances. Clearly, any plan for river improvement should take these reach differences into consideration.

The number of severely eroded channelized streams in the Yazoo Basin of Mississippi precludes intensive study of all of them. Therefore, a lower-order reconnaissance-level approach to determining the status of the channel is required for planning purposes (Schumm et al. 1984; Harvey and Watson 1986). Historical and institutional data were obtained prior to the field investigation and aerial photographs and topographic maps were utilized for base maps. Aerial overflight of the watershed permitted the watershed problems to be identified in a general manner as watershed erosion, channel erosion, or flooding and sedimentation. Fieldwork involved walking (3 to 5 mi/day [5 to 8 km/day]) as much of the channel as was possible within the constraints of available time. Field mapping of ICEM reach types (Fig. 18-3) was done during the fieldwork. Thalweg slope measurements in relatively stable type reaches (Fig. 18-3) provide a minimal measurement for determining

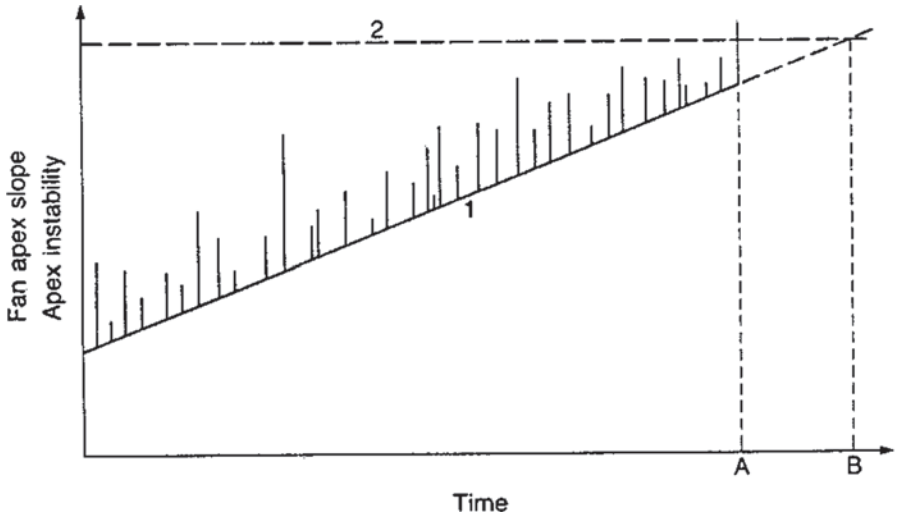

Fig. 18-10. Relation between gradient at a fanhead and alluvial fan apex instability through time. Line 1 portrays the gradually increasing slope of the fanhead. When the ascending line of fanhead slope intersects line 2, which represents the maximum slope at which the apex is stable, trenching will occur, at time B. Superimposed on line 1 are vertical lines representing changes in fanhead instability that are related to high-magnitude runoff events or longer-term climatic fluctuations. Normally, the operation of these processes has little significant morphological effect on the alluvial fan. However, when the fan slope and apex instability are high, trenching will occur sooner than expected (at time A) when a large-magnitude event exceeds the stability threshold (line 2). In reality, the event merely precipitated the eventual incision at time A rather than at time B (from Schumm and Hadley 1957).

hydraulic stability (N_h) for the channel. These values then can be compared with a regional relationship of equilibrium thalweg slope and drainage area (Fig. 18-11) that was developed from more intensive studies of other Yazoo Basin streams with similar characteristics (LCE) (Water Engineering & Technology 1989; Watson et al. 2002). For these Yazoo Basin streams, the amount of channel degradation that may occur can be estimated by plotting the hypothetical equilibrium stream slope profile of Fig. 18-11. Comparison of the existing channel profile with the hypothetical equilibrium slope profile provides information to determine possible grade control structure locations and reaches that may become geotechnically unstable ($N_g>1$) or hydraulically unstable ($N_h>1$). Within the range of drainage basin areas between about 5 and 250 square miles, equilibrium slopes range from 0.0025 to 0.0005. Bed-material samples should be obtained during the fieldwork because coarser sediments will result in higher equilibrium slopes. Most of the locations represented in Fig. 18-11 have bed material of approximately 0.15 to 0.3 mm sand.

The extent of channel erosion can also be mapped during the fieldwork. This mapping will include both bed and bank erosion, and a preliminary determination of the causes of the erosion can be made. The use of either generalized or channel-specific bank stability relations will provide an estimate of N_g.

Field mapping will provide an estimate of the number of small tributaries, field drains, and top-bank gullies that may have to be treated to prevent further erosion of these features. Further, the extent of threatened infrastructure features (bridges, culverts, and pipeline crossings) can be identified during the fieldwork. Measures previously installed to prevent erosion of the channel also can be mapped and an evaluation of their success or failure can be made. The

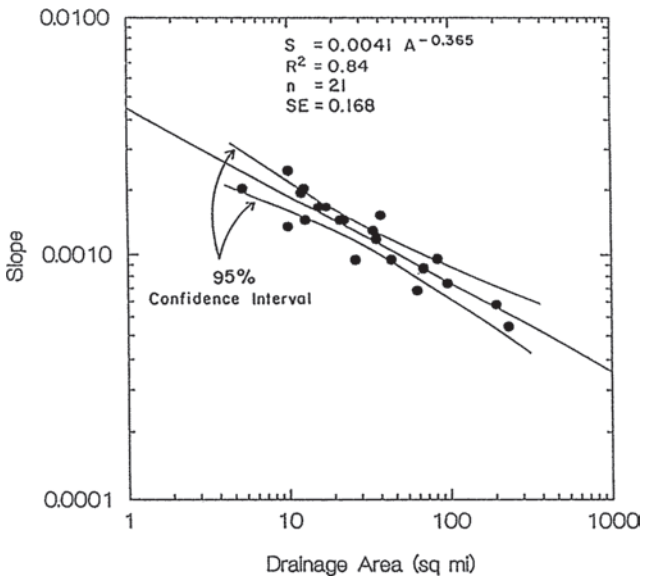

Fig. 18-11. Equilibrium channel slope plotted again drainage area for Hickahala, Batupan Bogue, and Hotopha Creeks, Mississippi (from Water Engineering & Technology 1989).

information derived from the reconnaissance geomorphic study can be used to provide a preliminary estimate of the requirements for watershed and channel rehabilitation.

In summary, the geomorphic investigation will permit the watershed problems to be quantified on a preliminary basis. The ability to define the ICEM types permits the equilibrium reaches to be identified. The equilibrium thalweg slope values (Fig. 18-11) provide a target slope for rehabilitation of reaches that are in a state of disequilibrium. A critical bank height can be estimated from a generalized relationship, or from a relationship that is specific to the channel under investigation. These data can then be used to develop a preliminary integrated watershed rehabilitation plan.

An example of how purely geomorphic observations can be of value to engineers concerned with highway and pipeline crossings of landforms and the identification of hazardous sites on landforms is provided by detailed geomorphic mapping of alluvial fans.

An alluvial fan is "a sedimentary deposit located at a topographic break, such as the base of a mountain front, escarpment, or valley side, that is composed of fluvial and/or debris flow sediments and which has the shape of a fan either fully or partly extended" (National Research Council 1996). Because fans can grow both vertically and longitudinally, highways and bridges on fans can be buried and culverts blocked either by vertical deposition on the fan or by fan enlargement (Fig. 18-12a). In addition, lateral channel shifting, avulsion, and bifurcation can direct flood flows against unprotected areas. Channel incision can lead to breaching of highways and bridge failure, and the instability of channels on fans can lead to abandonment of bridges as new channels form and as old channels fill. In addition, highways can redirect flow paths, causing property damage and even loss of life. Therefore, "an alluvial fan is an environment where the combination of sediment availability, slope and topography creates hazardous conditions . . ." (National Research Council 1996). In addition, urban development on fans requires a careful evaluation of alluvial fan topography to avoid construction in flood-prone areas.

Flood paths and the morphology of alluvial fans can differ greatly in space and time. For example, the sketches of Fig. 18-12 show examples from a continuum of alluvial fan types. Figure 18-12a shows a fan that has been trenched, and flow that is confined to a single deep channel from the topographic apex (T) to the hydrographic apex (H), where the flow expands. On this type of fan, a highway crossing the toe of the fan is subject to alluvial-fan flooding, whereas a highway crossing the middle or upper part of the fan is affected only by changes of the incised channel. The greater part of this fan lies above the effects of flooding. Figure 18-12b shows a fan with a fanhead trench. The hydrographic apex is closer to the topographic apex at the fanhead. Most of this fan below the hydrographic apex is subject to flooding. Figure 18-12c shows a fan that does not have a well-defined incised channel. The topographic and

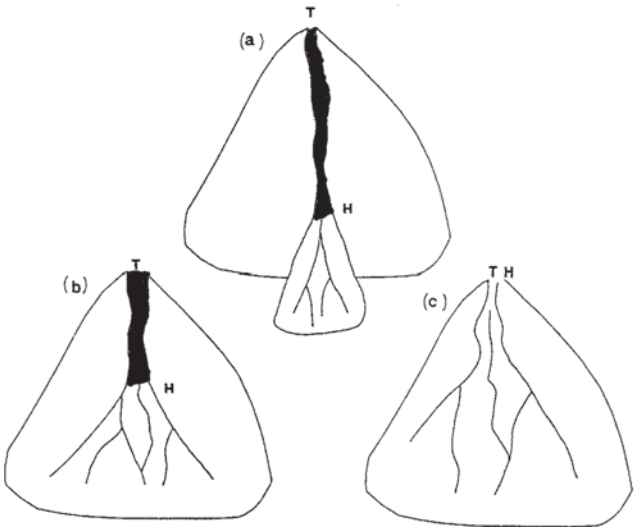

Fig. 18-12. Three examples of alluvial-fan morphology. The letter T identifies the topographic apex, which is the location where sediment and water from the upstream drainage basin enter the fan. The letter H identifies the location of the hydrographic apex, where channel flow becomes unconfined and produces alluvial-fan flooding. The shaded portions of the main channels of fans a and b are incised (from Schumm 2005).

hydrographic apex occupies the same location, and most of the fan surface is subject to flooding.

This range of fan types has been described by Hunt and Mabey (1966) in Death Valley and observed through time in experimental studies (Schumm et al. 1987). Therefore, within one area a range of fan types can occur, and during floods, fan morphology can change significantly.

A report prepared by the Committee of Alluvial Fan Flooding and published by the National Research Council (NRC) (1996) may provide engineers with useful information about these dynamic landforms. The purpose of the committee was to aid floodplain managers in determining the potential extent of flooding on alluvial fans.

Flooding on alluvial fans differs greatly from riverine flooding because it is characterized by (a) flow path uncertainty below the hydrographic apex, (b) abrupt deposition of sediment as a stream or debris flow loses its competence to carry material eroded from a steeper, upstream source area, and (c) channel incision, which reworks previously deposited sediment and shifts it down-fan (Fig. 18-12a). The potential for avulsion, deposition, and channel blockage and incision is important and some aspects of a three-stage procedure developed by the NRC committee can be of value to any engineer involved with alluvial fans.

The committee's procedure consisted of (1) identifying the fan and its extent, (2) identifying active areas on the fan, and (3) identifying areas subject to 100-yr flooding. Stages 1 and 2 involve the identification of active portions of a fan, where there is a probability of channel change, channel abandonment, and channel incision. For example, debris flows are effective in blocking existing channels. A drainage basin may produce stream flows for a very long time as sediment is stored in the valleys of the drainage basin above the topographic apex, but during major storms, flushing of the stored sediments may block channels on the fan and convert fan (a) of Fig. 18-12 to fan (b) or (c).

Surprisingly, identification of relatively recent debris flow deposits, which suggests very high sediment delivery from the drainage basin, may, in fact, be an indication of future stability. That is, stored sediment has been flushed from the drainage basin, and it may be a very long time before sufficient sediment accumulates again to produce debris flows, even under extreme rainfall.

Local aggradation in a channel can lead to avulsion because avulsion is likely to occur in places where deposition has raised the floor of the channel to a level that is nearly as high as the surrounding fan surface. This condition can be identified in the field by observation or by surveying cross-fan profiles.

To evaluate the relative stability of an alluvial fan or an alluvial-fan complex, the investigations should consist of three parts. The first part is an office study of aerial photographs and maps, which should identify the active zones of the fan that are subject to alluvial-fan flooding (Fig. 18-12) and the sites of potential channel change. If it is determined that the fan is deeply incised (Fig. 18-12a), then the hazards are restricted to incised-channel change (Fig. 18-3). Initial office procedures include the review of topographic maps and aerial photographs to determine the location and the morphology of the fan and its channels. Other data that can be gathered include historical maps and old photographs to document previous channel changes, changes in channel morphology, and the areas of the fan that may be classified as either active or inactive. Soil and geologic maps can be examined to confirm the relative geologic age of fan deposits. Climatologic data and appropriate hydrologic analyses will be needed to determine the magnitude and frequency of flooding to be expected.

The second part of the investigation consists of a field evaluation of sediment storage in the drainage basin above the topographic apex and the specific morphologic characteristics of the fan. Field investigations by a trained observer should include gathering information on elevation differences across the fan, if detailed topographic maps are not available. Vegetation types, soil characteristics, and other evidence of age (desert varnish, desert pavement) should be noted to confirm the location of active or inactive portions of the fan. Observations and measurements of channel conditions must be made. The results of the office and field investigations should provide sufficient information for the identification of potential problems. This is the third part of the investigation, which utilizes the results of Parts 1 and 2 of the investigation to provide sufficient information for an evaluation of the potential for debris flows and to

identify locations of potential channel deposition, incision, and avulsion on the fan. For example, on a fan like that of Fig. 18-12b, if two of the three unincised channels below the hydrographic index were to join, any bridge that was designed for present conditions would be inadequate, and it would probably fail. However, the field investigation should have determined if one of the channels would become dominant and capture the flow of other channels. If this would threaten the stability of the highway crossing, appropriate countermeasures could be undertaken.

The ideal result of any study of an alluvial fan is a geomorphic map delineating active and inactive portions of the fan and the identification of problem sites within the active portions of the fan. Figure 18-13 shows a hypothetical alluvial fan that has a variety of features of different ages. Careful investigation of the characteristics of the fan reveals areas that have not changed in perhaps thousands of years, whereas others are hazardous sites for construction. For example, the area designated as A is an old fan surface that has been entrenched and does not receive runoff or debris flows from the mountain source area. B is a surface that is entrenched (but stands at an elevation below that of A) and will not be flooded or eroded by the channel, but it can become subject to these hazards if the current channel becomes blocked by a debris-flow deposit. C and D are, respectively, bouldery lobes and levees indicating former deposition by debris flows within and along the channel. E denotes distributary channels that show no evidence of major scour, fill, migration, or avulsion during recent large floods and can convey all or most of a 1% (100-yr) flood. Areas indicated with F are subject to sheet flooding. G is a channel with signs of recent migration and for which future behavior is highly uncertain. H is a surface that is subject to overbank flooding, channel shifting, or invasion from a distributary channel that might avulse from G, and hence it is subject to alluvial fan flooding. A map such as Fig. 18-13 will be of great value to anyone concerned with the safety of structures on alluvial fans (highways, bridges, and urban development).

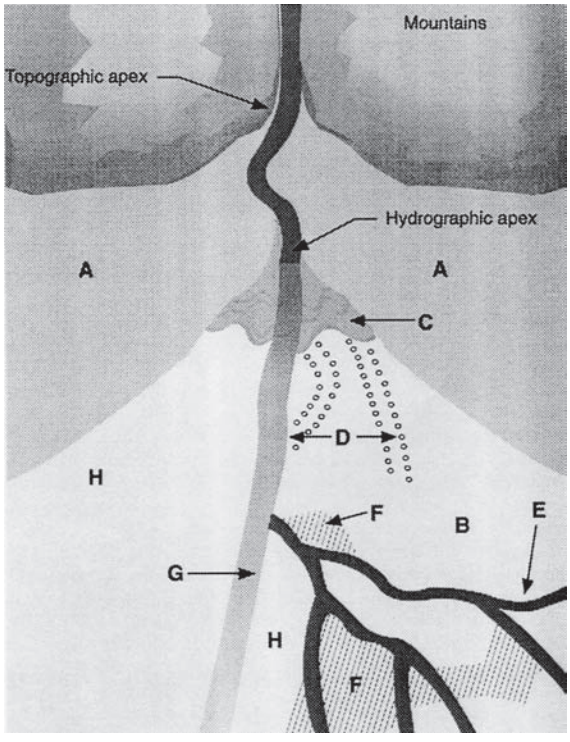

Fig. 18-13. Example of idealized geomorphic map of an alluvial fan. The areas with solid shading are recognizable channels; the darker ones have stable forms and positions; and the lighter ones have the capacity to change form or position. See text for discussion (from National Research Council 1996).

There are numerous ways that the landscape and individual landforms can change. An important issue in this regard is landform sensitivity. This involves the development of a condition at which a major change can be precipitated by a relatively minor perturbation. Examples are gullying in alluvial valleys or at the heads of alluvial fans as deposition progressively steepens these surfaces until incision occurs (Figs. 18-8, 18-9, 18-10). A further example is the growth of meander amplitude until a cutoff is inevitable as the gradient around a bend progressively decreases.

Point-bar development and concave bank erosion have been a principal concern of those studying the dynamics of meandering rivers. Figure 18-14 is a schematic diagram of a reach of a meandering river that defines the terms that are used in this discussion of the dynamics of the Sacramento River. Erosion along the concave bank occurs because of convective acceleration in downstream flow (Henderson 1966) and because of intensification of cross-stream flow. Both are caused by flow convergence, which implies that the shape of a meander bend significantly affects bank erosion (Nanson and Hickin 1986). As the radius of curvature of the bend decreases, the channel cross-section in the pool zone is constricted laterally because of vertical growth of the

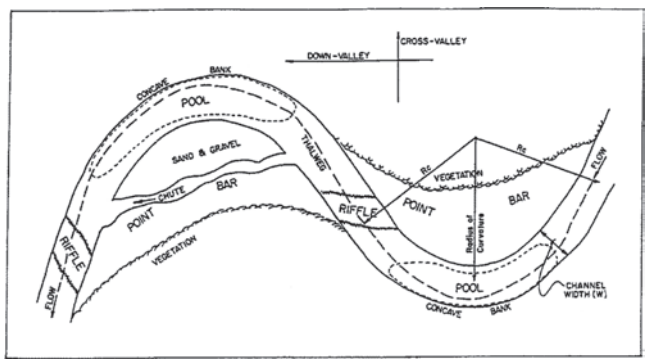

Fig. 18-14. Schematic diagram showing in planform the geomorphic surfaces and features that are associated with meander bends (from Harvey 1989).

point bar (Carson 1986). Therefore, lateral migration of the channel and concave bank erosion are dependent on the flow characteristics and the shape of the bend.

The rate of bank retreat is dependent on the resistance to erosion of the concave bank materials (Nanson and Hickin 1986), the duration and magnitude of the flows (Odgaard 1987), the radius of curvature of the bend (Nanson and Hickin 1986; Odgaard 1987), and the capacity of the flows to transport bed-material sediment (Neill 1984; Nanson and Hickin 1986). Channel migration is a discontinuous process because it is dependent on the occurrence of flood flows (Brice 1977). Initially bends migrate in a cross-valley direction (extension), but eventually bends advance in the down-valley direction (translation) (Leeder and Bridge 1975; Brice 1977; Nanson and Hickin 1986).

Meander bends eventually cut off when the radius of curvature decreases below a certain value, which is specific to each stream. Reduction of the radius of curvature of a bend causes backwater upstream of the bend, and this is expressed physically as a reduction in the slope of the water surface. Because the sediment transport capacity of the flows is proportional to the slope of the water surface squared, a reduction in slope reduces the sediment transport capacity of the flows. This causes deposition of sediment in the upstream limb of the bend between the pool and riffle (Fig. 18-14). Deposition of sediment reduces the flow capacity of the channel and this causes flows to be diverted over the point bar. These flows erode the point bar surface and form chutes (Carson 1986; Lisle 1986). However, cutoffs can occur as a result of either chute development (Brice 1977; Lewis and Lewin 1983) or neck closure (Fisk 1947).

Bagnold (1960), Leeder and Bridge (1975), and Nanson and Hickin (1986) have demonstrated that lateral migration rates of meandering rivers can be correlated with the radius of curvature (R_c) of bends. Migration rates are highest when the ratio of radius of curvature to channel width (W), R_c/W, is about 2.5. Radii of curvature and 1981–1986 migration rates (MR) for 11 Sacramento River bends were measured to obtain short-term data on river behavior (Harvey 1989). Radii of curvature ranged from 381 to 838 m and migration rates varied from 37 to 10 m/yr. A least-squares regression of the data is

$$\mathrm{MR} = 53.57 - 0.049R_c \quad (R^2 = 0.69) \tag{18-1}$$

To determine long-term behavior of the river, radii of curvature and migration rates of the Sacramento River for the period of record (1896–1986) were utilized. The radii of curvature were assigned to nine class intervals that varied by 76-m increments from 229 to 838 m. The average channel width in each bend was determined, and both the migration rate and radius of curvature were divided by the channel width. The average width of the river in the study reach was 150 m. The relationship between the ratio of radius of curvature to width (R_c/W) and the ratio of migration rate to width (MR/W) is shown in Fig. 18-15.

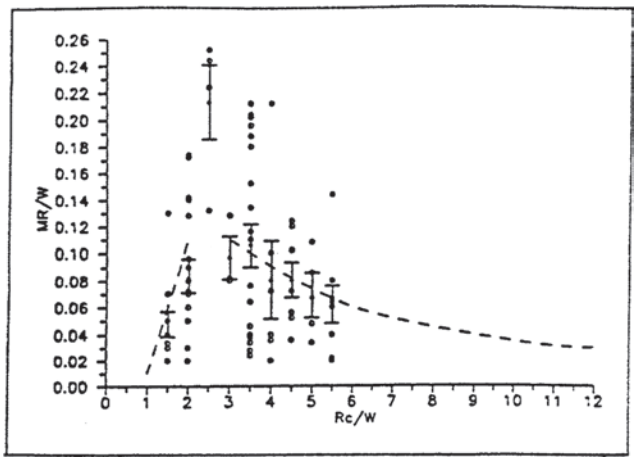

Fig. 18-15. The ratio of migration rate (MR) to channel width (W) plotted against the ratio of radius of curvature (R_c) to width. The asterisks and bars represent the means and standard errors, respectively. The curves are from Nanson and Hickin (1986) (from Harvey 1989).

For radii of curvature greater than 381 m ($R_c/W > 2.5$) the least-squares regression is

$$\mathrm{MR} = 6.98 \times 10^4 R_c^{-1.333} \quad (R^2 = 0.83) \tag{18-2}$$

and for radii of curvature less than 381 m ($R_c/W \geqslant 2.5$) the least-squares regression is

$$\mathrm{MR} = 2.2 \times 10^{-6} R_c^{2.875} \quad (R^2 = 0.94) \tag{18-3}$$

The reason for subdividing the data is provided by Fig. 18-15. Nanson and Hickin's (1986) curves show that for R_c/W values between 1 and 2.5 there is a direct relationship between MR/W and R_c/W. Conversely, for R_c/W values greater than 2.5 there is an inverse relationship between MR/W and R_c/W.

Brice (1977) assumed that most bends on the Sacramento River would cut off by the time the radius of curvature had decreased to 381 m. However, a number of low-radius-of-curvature bends (less than 381 m) are located in the lower part of the study reach near Colusa. This may be due to the fact that the sediments are finer, more cohesive, and therefore more resistant to erosion. The median radius of curvature for a cutoff is 380 m, but the range is from 305 to 610 m. Ninety percent of all cutoffs occur when the radius of curvature is less than 533 m. The radii of curvature of bends that had cut off since 1908 (10) and pre-1908 meander scars on the floodplain (22) were measured. The radii of curvature of four bends that had cut off following revetment were also measured.

A dimensionless cutoff index, defined as the ratio of the radius of curvature to the migration distance (R_c/MD), was developed to predict cutoff occurrence (Harvey 1989).

Equation (18.1) was used to determine the MD values for the cutoff index for both the recent (10) and floodplain (22) cutoffs. With the exception of two floodplain cutoffs, the R_c/MD values were less than 4. The mean and standard deviation for the recent cutoffs were 2.7 and 1.0, respectively, and the values for the floodplain cutoffs were 2.6 and 0.9, respectively. Therefore, cutoffs can be expected to occur when the value of the cutoff index (R_c/MD) lies between 1.7 and 3.7.

The cutoff indices for 14 bends between Glenn and Chico Landing were calculated using measured values of MD between 1981 and 1986. The data indicate that seven of the bends have R_c/MD values that lie within the range of values that were identified for cutoffs ($1.7 < R_c/\text{MD} < 3.7$). Associated with these R_c/MD values for these seven bends are two other characteristics that were identified on 1986 aerial photographs: (1) the presence of a midchannel bar in the upstream limb of the bend, and (2) the presence of chutes across the point bar. Therefore, it appears that cutoffs can be predicted on the basis of the value of the cutoff index and the presence of the two ancillary features. This was tested on the bend at river distance 278.4 km, which had cut off in 1986. This bend was revetted prior to 1981 and, therefore, no migration of the bend took place between 1981 and 1986. However, the radius of curvature of the bend decreased from 572 m in 1981 to 343 m in 1986. The MD value for a radius of curvature of 343 m (Eq. (18.1)) is 181 m and, therefore, the cutoff index (R_c/MD) is 1.9. The aerial photographs confirm the presence of both a midchannel bar in the upstream limb of the bend and chutes on the point bar.

The ability to predict changes in river planform is important for managing rivers for erosion and flood control. Prediction of future changes is dependent on understanding the past behavior of the river, but uncertainty in prediction is introduced because of the stochastic nature of flood events, which cause the change, and variability of floodplain sediments, which can either accelerate or retard erosion.

18.4 GEOMORPHIC HAZARDS

Objective 3 of this chapter is to consider the geomorphologic factors that influence landforms (engineering sites) and the hazards associated with them. This should aid the engineer in anticipating problems and avoiding hazardous situations, or at least, being aware of potential hazards.

Landform change can be considered to be a geomorphic hazard if it impacts on engineering plans or works. The word *hazard* refers to a potential danger or risk. The hazard may pose a relatively minor risk that will have a minimal impact, or it may be a potential catastrophe or disaster that involves great damage and loss of life. Most books on natural hazards concentrate on the spectacular events such as coastal erosion during hurricanes, volcanic eruptions, earthquakes, avalanches, landslides, and subsidence (White 1974; Bolt et al. 1975; Hewitt and Burton 1975; Asimov 1979; Blong and Johnson 1986).

There are at least three types of geomorphic hazards that involve different spans of time, different degrees of damage, and different energy expenditures: (1) an abrupt change that is a catastrophic event, e.g., a landslide that occurs rapidly as a result of an equally catastrophic meteorological event, earthquake, or human activity (removal of toe support); (2) a progressive change that leads to an abrupt change, e.g., weathering that leads to slope failure, gullying of a steepening alluvial fan, meander growth to cutoff, and channel avulsion; and (3) a progressive change that has slow but progressive results, e.g., bank erosion, hillslope erosion, channel incision, and channel enlargement. The difference between geomorphic hazards and others is that geomorphic hazards may involve a slow progressive change that, although in no sense catastrophic, can eventually involve costly preventive and corrective measures. Therefore, geomorphic hazards can be defined as any landform change, natural or otherwise, that adversely affects the geomorphic stability of a place.

As noted earlier (Figs. 18-8, 18-9, and 18-10), a major concern of the geomorphologist, which will be of value to the engineer, is the identification of sensitive landforms and the threshold conditions under which either failure or stability occurs. A failure threshold can be a meander cutoff, channel avulsion, channel incision, gullying, or slope failure. A stability threshold is the condition under which an unstable landform achieves a new condition of relative stability. Both conditions are important because the engineer would like to anticipate and plan for the first, and recognition of the second could result in less drastic reclamation or stabilization efforts (Fig. 18-4).

18.4.1 Hazard Identification

For purposes of discussion, the fluvial system can be divided into four landform types: (1) drainage networks, which consist of the stream channels and valleys that compose the sediment source area; (2) hillslopes, which fill the area between the channels of the drainage network; (3) main channels, which convey water and sediment from the drainage networks; and (4) piedmont and plain areas that include alluvial fans and deltas, the areas of sediment accumulation.

A list of 28 geomorphic hazards and the four major variables that influence them is summarized in Table 18-3, which can serve as a check list during site selection or evaluation, particularly if it is anticipated that human activity will alter hydrologic conditions or base level. Base level here is defined as the level to which a stream is graded, and a change, as a result of reservoir or lake draining or filling or any activity that causes a lowering of a stream channel such as channelization or gravel mining, will affect the stream. Time is included with the variables discharge (increase or decrease,) sediment load (increase or decrease), and base-level change (up or down), because landforms change naturally through time, and time is an index of energy expended or work done. The hazards are grouped according to the landforms affected

Table 18-3 Variables Affecting Geomorphic Hazards

	Variables						
		Discharge		Sediment load		Base level	
Geomorphic hazards	Time	+	−	+	−	Up	Down
A. Drainage networks							
(a) Erosion							
(1) rejuvenation		X			X		X
(2) extension		X			X		X
(b) Deposition							
(1) valley filling				X		X	
(c) Pattern change							
(1) capture	X	X		X		X	X
B. Slopes							
(a) Erosion							
(1) denudation-retreat	X	X			X		X
(2) dissection		X			X		X
(3) mass failure	X	X			X		X
C. Rivers							
(a) Erosion							
(1) degradation (incision)		X			X		X
(2) knickpoint formation and migration	X	X			X		X
(3) bank erosion	X	X		X	X	X	X
(b) Deposition							
(1) aggradation			X	X		X	
(2) back and downfilling			X	X		X	
(3) berming			X	X			
(c) Pattern change							
(1) meander growth and shift	X	X		X	X		X
(2) island and bar formation and shift	X			X		X	
(3) cutoffs	X	X		X		X	X
(4) avulsion	X	X		X		X	
(d) Metamorphosis							
(1) straight to meandering				X			X
(2) straight to braided		X	X	X		X	X
(3) braided to meandering					X		X
(4) braided to straight		X	X		X		X
(5) meandering to straight				X		X	X
(6) meandering to braided		X	X	X		X	

(Continued)

Table 18-3 Variables Affecting Geomorphic Hazards *(Continued)*

	Variables						
		Discharge		Sediment load		Base level	
Geomorphic hazards	Time	+	−	+	−	Up	Down
D. Piedmont and coastal plains							
(a) Erosion							
(1) dissection							
(b) Deposition							
(1) aggradation	X		X	X		X	
(2) progradation	X						X
(c) Pattern change							
(1) pattern development		X			X		X
(2) avulsion	X	X		X		X	

After Schumm (1988).

(drainage networks, slopes, channels, piedmont, and plains) and the results of the hazard (erosion, deposition, pattern change, metamorphosis). In Table 18-2, the hazards that will be affected by the passage of time or by a change of discharge, sediment load, or base level are indicated by an X. This provides a ready means of identifying potential geomorphic hazards that should be of concern at any site, and they are described in sequence below.

18.4.2 Drainage Network Hazards

Rejuvenation (Aa1) involves the deepening or incision of a drainage network. The deepening will also cause headward growth of tributaries and perhaps the addition of tributaries in formerly undissected areas. The depth of incision may only be minor if discharge is increased slightly or if sediment loads are decreased, but it can be major and deep with a major lowering of base level. In the latter situation any site may be in jeopardy, but in the former, only sites on floodplains or terraces will be affected. Rejuvenation of a drainage system and its headward extension can be halted by emplacement of grade-control structures (Schumm et al. 1984). If left unchecked, the impact can be very great over large areas, especially on fragile lands of the semiarid western United States (Cooke and Reeves 1976).

Extension (Aa2) is the headward growth of tributaries, and it involves the addition of tributaries in formerly undissected areas. It causes erosion closer to drainage divides, and surface sites can be significantly affected by gullying and the headward growth of channels (Schumm et al. 1984).

Valley filling (Ab1) involves major sediment deposition in channels and on floodplains. This is caused by a great influx of sediment or by base-level rise. Deposition may bury a site, or it may be inundated by floods, as flood levels increase. This type of major deposition can follow channel incision and rejuvenation (Aa) when large quantities of sediment are set in motion and eventually deposited on flatter slopes and wider reaches of valleys. Deforestation, urbanization, and agricultural and mining activities can have the same impact (Toy and Hadley 1987).

Capture (Ac1) is the change of a stream course by the natural diversion of water into a stream at a lower elevation. The diversion causes steepening of the stream gradient and rejuvenation and probably extension (Aa1, Aa2) of the captured drainage network. The progress can be induced by base-level lowering, which increases the energy of the lowland stream, or by base-level rise, which as a cause of deposition may induce a channel to shift to a steeper straighter route. It can occur naturally through time, and the process can be accelerated by an increase of discharge and sediment load. Capture is a type of channel avulsion (Cc4), but although evidence for it is common in the landscape, it will be a slow process and an unlikely event unless promoted by human activities that cause major flow diversions.

18.4.3 Slope Hazards

Denudation and retreat (Ba1) of both hillslopes and escarpments in a watershed can be accelerated by increased water flow over the slope, by reduced vegetation cover, and by increased flow in adjacent streams or decreased sediment loads that lead to channel degradation and undercutting of slopes (Ca1) or to drainage network rejuvenation (Aa1) by base-level lowering. However, slope erosion will occur inevitably, during the passage of time, which will threaten a site near the top, or near the edge of a slope (Carson and Kirkby 1972; Selby 1982; Brunsden and Prior 1984; Toy and Hadley 1987; Parsons and Abrahams 1992).

Slope dissection (Ba2) by channels will occur if there is network extension (Aa2) as a result of adjacent channel

incision or headward growth caused by discharge, sediment load, or base-level change.

Mass failure (Ba3) may occur (slumping, debris flow) owing to increased water content of the slope material or by an increase of slope height by channel incision or undercutting of the slope by fluvial or human action (Schuster and Krizek 1978).

18.4.4 River Hazards

Stream channels, wherever they are located in the fluvial system, change morphology and behavior with time, they respond to discharge, sediment load, and base-level changes, and they potentially pose a great hazard to the works of humans (Gregory 1977; Richards 1987; Brookes 1988; Petts et al. 1989).

Degradation (Ca1) is the lowering of a streambed by erosion. Degradation is a major adjustment of a river to external controls. The adjustment takes place over long reaches of channel. The deepening of the channel may also cause the undermining of banks and widening of the channel (Ca3).

Knickpoint migration (Ca2) is the upstream shift of an inflection in the longitudinal profile of the stream. This break in the smooth curve of the stream gradient results from rejuvenation of the stream or from the outcropping of more resistant materials in the bed. It is the former that is of concern here. A knickpoint in alluvium moves upstream, especially during floods. Above the profile break the river is stable; below the break there is erosion. As the knickpoint migrates past a point, a dramatic change in channel morphology and stability occurs (Schumm et al. 1987). Knickpoints are of two types: first is a sharp break in profile that forms an in-channel scarp called a headcut (Fig. 18-16a), and second is a steeper reach of the channel or knickzone over which elevation change is distributed (Fig. 18-16b). It is important to recognize that through time a stable reach of river may suddenly become very unstable as a result of passage of a knickpoint.

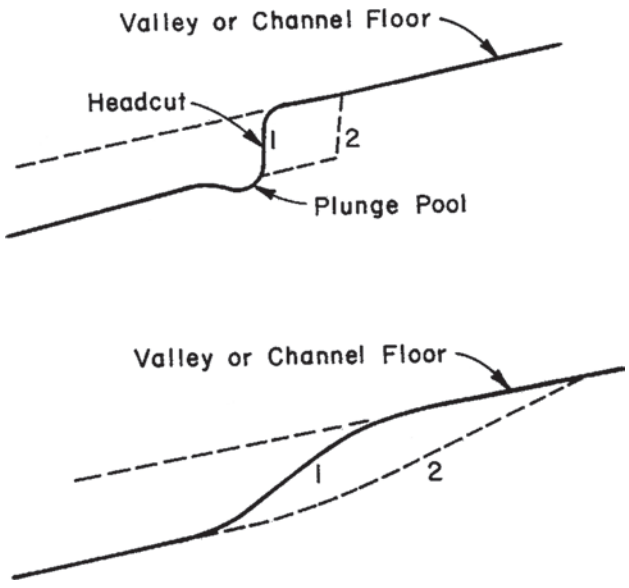

Fig. 18-16. Types of knickpoints. Dashed lines show former and future position of channel floor and knickpoint.

Bank erosion (Ca3) is the removal of bank materials either grain by grain or by mass failure. Erosion can occur by river action that undercuts a bank or by simple erosion of the bank sediments. In addition, bank erosion can occur by mass failure, as a result of surcharging the bank by construction or dumping, or by seepage forces and pore-water pressures that are related to increased water movement through bank sediment. In the latter case, the river is the transporting agent that removes the slumped bank materials rather than the primary erosive agent. The effect of bank erosion is a shift in the bankline of the river and the introduction of additional sediment into the channel. Erosion of both banks widens the channel, and may lead to aggradation (Cb1). Bank erosion is a major component of other hazards such as degradation and scour, meander shift, cutoffs, and various types of river metamorphosis.

Bank erosion is a natural consequence of normal river behavior through time, but it can be accelerated by changes of discharge, sediment load, and base level. Either an increase or decrease of sediment load or a rise or fall of base level can cause bank erosion. Channel incision increases bank height and the likelihood of bank failure.

Aggradation (Cb1) is defined simply as the raising of a streambed by deposition. Aggradation is not local; it is rather a major adjustment of a river to external controls. The main effect of aggradation is to raise the streambed. However, aggradation may continue to the extent that new hazards are generated. For example, it may cause avulsion, cut off meanders, and change channel pattern. In addition, aggradation may lead to bank erosion (Ca3) as flow paths are changed by bar formation, and decreased channel capacity will increase flooding.

Backfilling and downfilling (Cb2) are deposition or channel filling from downstream to upstream or vice versa. With backfilling, the channel is partly or entirely blocked and deposition begins at this point and then proceeds upstream (Schumm 1977, p. 150). Backfilling differs from aggradation as defined earlier because it starts at one location in the channel and then is propagated upstream. In contrast, downfilling (Cb2) occurs when deposition progresses in a downstream direction, and it is the reverse of backfilling. Both backfilling and downfilling are types of aggradation that influence long reaches of a channel, and they can affect a reach of river from either the upstream or downstream direction after it has been stable for a long time. Consequences of backfilling and downfilling are similar to those of aggradation (Cb1). The channel bed will rise as the wave of sediment passes. Increased flooding will result as the channel fills.

Berming (Cb3) refers to the deposition of primarily fine-grained sediments on the sides of the channel, and it is the opposite of bank erosion. Berming will reduce the area of the channel and cause increased flood stages. Berming reduces channel capacity, but the narrowing of the channel

may cause degradation and scour. This hazard is less serious than the other depositional hazards.

Pattern change (Cc) refers to the change of channel pattern and position that occurs naturally through time. The four types of pattern-change hazards occur in different ways. Meander growth and shift (Cc1) and bar and island formation and shift (Cc2) usually occur relatively slowly and at variable rates, but the change can be viewed as progressive, whereas cutoffs (Cc3) and avulsion (Cc4) occur relatively rapidly and episodically. Nevertheless, the conditions leading to cutoffs and avulsion can be observed, and these hazards should be predictable.

Meander growth and shift (Cc1) involve a change in the dimensions and position of a meander. Meander amplitude and width increase as a meander enlarges (Fig. 18-17). Meander shift involves the displacement of the meander in a downstream direction (Fig. 18-17). Usually the meander both grows and shifts downstream, although some parts of the bend can actually shift upstream. There is probably more information available on this hazard than on any other, with the exception of cutoffs. Meander growth and shift not only cause bank erosion at the crest and on the downstream side of the limbs of a meander, but also change the flow alignment. Further, increased meander amplitude results in local reduction of gradient, with possible aggradation in the bend. Meander growth and shift will be of greatest significance where discharge is great, bank sediments are weak, and bank vegetation is negligible due to aridity or to agricultural practices.

Island and bar formation and shift (Cc2) are within-channel phenomena. Unlike meander shift or meander cutoffs, which involve the entire channel pattern, bars and islands can evolve within the channel, and the bankline pattern itself may remain unchanged. Therefore, this hazard involves the development and migration of sediment accumulations (bars and islands) in alluvial channels, which can lead to increased bank erosion, local flooding, and threats to structures.

Popov (1964) has classified the types of island changes that he observed occurring in the River Ob in the Soviet Union. He found that there were five ways islands changed (Fig. 18-18). A sixth and seventh could be added, the formation of an island and the complete destruction of an island, but Fig. 18-18 does convey the important concept that bars and islands may be ephemeral as well as dynamic features of a channel (Osterkamp 1998; Osterkamp et al. 2001; Harvey et al. 2003). The result of bar and island formation in a channel is to deflect the flow and perhaps to increase erosion of the banks of the channel. This erosion will enlarge the channel and islands may form as a result of reduced water stage and increased channel width.

Cutoff (Cc3) produces a new and relatively short channel across the neck of a meander bend. This drastically reduces the length of the stream in that reach and significantly steepens its gradient. The neck cutoff has the greatest effect (Fig. 18-17e) on the channel. Another type of cutoff is the chute cutoff (Figs. 18-17f and 18-17g), which forms by cutting across a portion of the point bar. The chute cutoff generally forms in recently deposited alluvium, whereas the neck cutoff forms in recent alluvium as well as in older consolidated alluvium or even in weak bedrock.

The consequence of cutoffs of both types is that the river is steepened abruptly at the point of the cutoff. This can lead to scour at that location and propagation of the scour in an upstream direction. The results are similar to those described for degradation and knickpoint migration (hazards Ca1, Ca2).

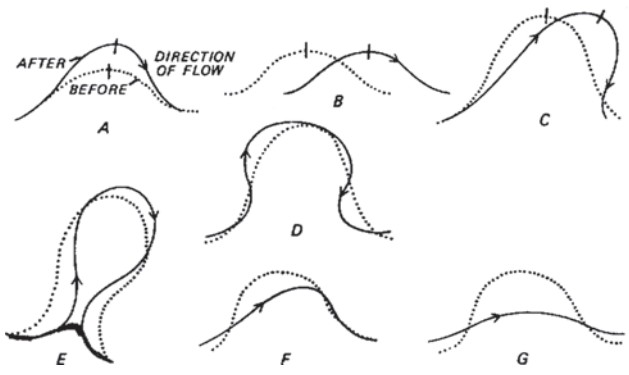

Fig. 18-17. Patterns of meander growth and shift: (a) extension, (b) translation, (c) rotation, (d) conversion to a compound meander, (e) neck cutoff, (f, g) chute cutoffs (from Brice 1974).

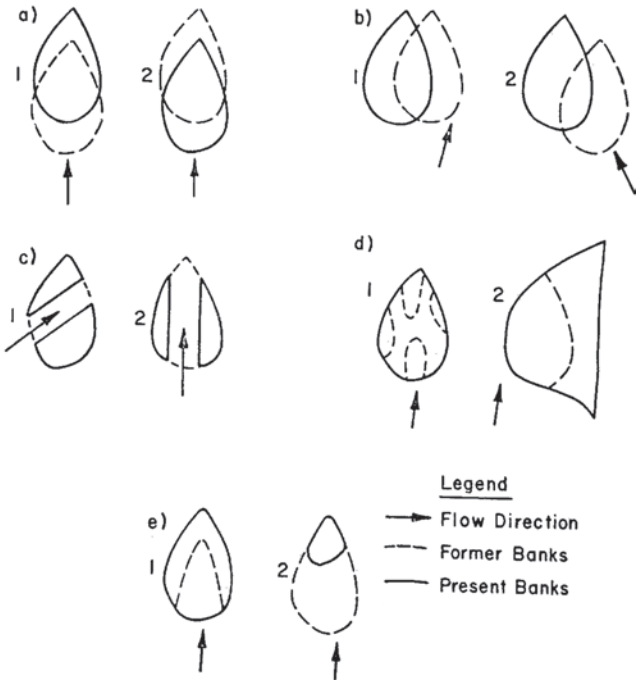

Fig. 18-18. Island change according to Popov (1964). Arrows show direction of flow. Solid lines are original locations of islands; dashed lines show changes. (a) Island shifts up or downstream. (b) Island shifts laterally. (c) Island divided by channel. (d) Small islands coalesce and island joins floodplain. (e) Islands increase or diminish in size.

In the downstream direction, the gradient of the channel is not changed below the site of the cutoff, and therefore, the increased sediment load caused by upstream scour will usually be deposited below the cutoff, forming a large bar, or it may trigger additional downstream cutoffs.

Avulsion (Cc4) is the abrupt change of the course of a river. A channel is abandoned and a new one formed as the water and sediment take a new course across the floodplain, alluvial fan, or alluvial plain (Figs. 18-12 and 18-13). A meander cutoff (Cc3) is a type of avulsion because it is a relatively rapid change in the course of the river during a short period of time, but avulsion, as defined here, involves a major change of channel position below the point of avulsion. If, through avulsion, the river takes a shorter course to the sea, it will have a steeper gradient, and erosion above the point of avulsion is likely unless a bedrock control prevents upstream degradation.

River metamorphosis (Cd) is a complete change of river morphology (Schumm 1977, p. 159). As the word indicates, this consists of significant changes not only in the dimensions of the river, but in its pattern and shape. Considering the types of channels identified, it is possible to consider six types of river metamorphosis as follows: a straight channel changes to (1) meandering or (2) braided, a braided channel changes to (3) meandering or (4) straight, and a meandering channel changes to (5) straight or (6) braided. It is not necessary to define each type of metamorphosis, because the change is obvious based on pattern alone. There is some similarity in the hazards posed by some types of metamorphosis, and they can be discussed as three pairs.

Straight and braided to meandering (Cd1 and Cd3). A straight channel may develop alternate bars and a sinuous thalweg if there is an increase of discharge and sediment load. If the straight channel begins to meander, meander growth, shift, cutoff, and avulsion (Hazards Cc1, Cc3, and Cc4) will also occur when the metamorphosis takes place.

In the case of a metamorphosis from braided to meandering, the change may actually result from a decrease of sediment load that produces increased channel stability. The decreased gradient will reduce the erosional forces acting on the channel, and although the development of meanders is a hazard itself (Hazard Cc1), they will probably form in the space occupied by the old braided channel. In both cases, the channel may degrade.

Meandering and braided to straight (Cd5 and Cd4). A bar-braided channel can become island-braided when the bars are colonized by vegetation, and then these islands are incorporated into a new floodplain to form a straight channel. The narrowed straight channel should degrade, but not appreciably. The narrower channel will probably represent a more stable condition, although the increased presence of vegetation may raise the stage of large floods.

The conversion of a meandering channel to a straight channel will be the result of a series of natural cutoffs. The steepened gradient will cause bank erosion and perhaps degradation. Unless there have been hydraulic changes, the channel will attempt to meander, and the channel will be very unstable. This is especially true when the channel has been straightened artificially.

Straight and meandering to braided (Cd2 and Cd6). A straight channel can braid if significant bank erosion occurs with aggradation (Cb1), a result of a major increase of sediment load. A meandering channel will braid for the same reasons. The result will be bank erosion and channel widening (Ca3) with bar and island formation (Cc2). Obviously the change from meandering to braided will be very dramatic.

18.4.5 Piedmont and Coastal Plain Hazards

On a coastal plain, piedmont plain, alluvial fan (Rachocki and Church 1990), or delta, the major hazards are associated with the channel changes discussed above. For example, an increase of discharge, a decrease of sediment load, or a fall of base level will cause channels to incise, dissecting (Da1) the alluvial or bedrock surface. Similar change may cause rejuvenation and extension of drainage networks (Aa1, Aa2) or the *development of a new drainage network* (Dc1). General *aggradation* (Db1) will eventually bury a site, but before the burial is complete, it will be subjected to increased flooding and potential erosion.

Progradation (Db2) is the growth of a delta or fan. It is characteristic of a dynamic landform that will be subjected to periods of erosion as it grows. *Avulsion* (4c2) will be common on an unconfined surface such as an alluvial plain, delta, or alluvial fan, especially if progradation or aggradation is occurring. This channel shifting will render any surface site hazardous. The avulsion can also occur on piedmont or alluvial plains by capture (1c1).

The identification of 28 geomorphic hazards provides a check list (Table 18-2) that can be used to review the potential geomorphic hazards that may exist at a site. For most sites, only a few hazards will be of concern. Although Table 18-2 provides a means of determining what hazards may occur in a landscape through time or with a change of discharge, sediment load, or base level, the most important aspect of hazard research is to determine where and when the hazard will occur.

18.5 THE ENGINEERING GEOMORPHIC APPROACH

An understanding of landform history, taking a broader view of the problem, and a recognition that geologic and geomorphic controls can exert a dominant influence on a river reach or construction site should provide the engineer with a valuable basis upon which to develop plans and to select sites that will not be exposed to geomorphic hazards, or at least to plan for the occurrence of particular hazards (Table 18-2).

Numerous problems must be considered in dealing with the complex surface of the planet. In particular, one should not extrapolate beyond the limits of available data. In fact, well-established relations developed in other areas may not always pertain, and therefore, field investigations are usually necessary. A good example of the need to understand the geomorphic setting is provided by litigation between the U.S. Forest Service and the State of Colorado regarding the need for channel maintenance flows. The Forest Service claimed that any diversion of streams in the National Forests would cause the streams to decrease in size, which was considered to be an unfavorable condition. This assumption was based upon hydraulic geometry relations that show close positive relations between channel width, depth, and discharge, which were developed for low-gradient alluvial streams (Leopold and Maddock 1953). However, these relations were not valid for mountain streams draining areas of less than 15 square miles with slopes greater than about 4% because other factors such as log jams, beaver dams, glacial deposits, colluvium, and bedrock become the dominant controls on channel morphology and adjustability (Montgomery and Buffington 1993, 1997; Schmidt and Potyondy 2004). Obviously, careful field study was necessary to determine the major influences on these streams. Additionally, even in locations where the form of the channel is not forced by nonfluvial factors, caution must be used with generalized hydraulic geometry relationships for design purposes (Rinaldi and Johnson 1997; Doll et al. 2002)

Examples have been provided of how a combined geomorphic engineering approach can result in better and cost-effective planning. The incised-channel model for channelized streams (Fig. 18-3), the evaluation of bridge sites (Figs. 18-1 and 18-6), and meander growth and shift (Fig. 18-17) are all examples of how consideration of change through time, taking a broader perspective, and recognition of geologic and geomorphic controls can aid the engineer. Thorne and Baghirathan (1994) have developed a scheme for morphological studies of large rivers using this approach.

The geomorphic-engineering approach to a problem or site evaluation should ideally consist of three phases or levels of sophistication, as follows: reconnaissance level, survey level, and design level. At the preliminary stage of a project the reconnaissance level would involve a system approach that brings together geologic and geomorphic data and observations, as well as available climatic and hydrologic data as needed. The survey level involves surveying, mapping, and perhaps geomorphic mapping (Fig. 18-13), to quantify the qualitative relations developed during the reconnaissance-level study. Both of these levels involve both geomorphologists and engineers. The final design-level work is carried out by the engineer, relying on the relations and data obtained during the previous two levels of study. This approach is described in some detail, with examples, in Schumm et al. (1984).

A final example reveals the problem of ignoring the cooperative approach (Keaton et al. 1988; Keaton 1995). In May and June 1983, significant damage occurred along the Wasatch Front, Utah, due to snowmelt-induced debris flows. The worst damage occurred in Farmington due to a debris slide, which mobilized into a debris flow, incorporating over 90% of its mass from the channel of Rudd Creek.

The 1983 debris flows were triggered by landslides caused by a heavy snow pack, an abnormally late rapid snowmelt, and an undrained bedrock aquifer. Geologic studies of the structural fabric and hydrogeology of the landslide source areas indicate that these landslide-induced debris flows were a rare geologic event, perhaps the first such event during the last few thousand years. Most of the earlier historical debris flows were generated by erosion during cloudburst storms that fell on watersheds depleted of vegetative cover by overgrazing and burning. Geologic studies of alluvial fans at the mouths of central Davis County canyons indicate that (1) the majority of alluvial-fan building occurred during the early Holocene (about 10,000 yrs ago) when much ice-age sediment was available for transport, (2) few if any debris flows occurred between the early Holocene and the 1920s, and (3) if historical debris-flow events were representative of the long-term rate of sediment deposition on alluvial fans, the fans would be major landforms instead of the minor features they actually are. The majority of sediment incorporated into debris flows triggered by either landslides or cloudburst storms was derived from the stream channel. Geologic studies of central Davis County stream channels indicate that (1) debris production and accumulation in channels is a slow, intermittent process, (2) stream channels that have produced debris-flow events during historical time have not yet been recharged with sediment, (3) future debris flows from drainages cleaned of sediment will likely be of less volume than initial historical events, until the drainages have been recharged with sediment, and (4) the most likely channels to produce large debris flows in the near future are those that have not produced historical debris flows.

Approximately $12 million was spent in Davis County to build or refurbish debris basins following the 1983 debris-flow events; less than $30,000 was spent on geologic research to understand the debris-flow processes. Had geologic studies been conducted prior to construction of the debris basins, more emphasis could have been placed on building debris basins at the mouths of canyons that have not produced historical debris flows, instead of canyons that had produced debris flows during historical time.

The results of the geologic investigation appear to be contrary to common sense, but the evidence is clear. The changing situation through time along the Wasatch Mountains front is expectable from a geomorphic point of view, and it is analogous to the declining sediment loads in the Colorado River as a result of decreased erosion in the incised arroyos of the Southwest (Fig. 18-4).

18.6 CONCLUSIONS

Geomorphology is the study of landforms, which involves their classification, description, origin, and evolutionary development. The traditional concern of geomorphologists has been the origin and evolution of landforms, but a more recent development is the prediction, based upon understanding of system dynamics, of landform response to natural and human influences.

The major objectives of this chapter were to bring to the attention of the engineering profession (1) the importance of system history, (2) the need to view a specific problem in a system context, and (3) the importance of geologic and geomorphic variables in engineering activities. For example, if a river meander has changed through time, prediction of future change can be made with more confidence. Therefore, the historical perspective can be a valuable aid in prediction. In addition, it is important to realize that a specific engineering project site is part of a larger geomorphic system. For example, a bridge site is a small part of a fluvial system and the character of that system both up- and downstream can significantly affect future site stability. Finally, geology and geomorphology can be far more important than is generally supposed within an engineering time scale. For example, the world's great alluvial rivers (Mississippi, Nile, Indus), although presumably dominated by hydrological, sediment, and hydraulic controls, are, in fact, significantly influenced by geologic variables. These principles were illustrated in the chapter by examples that were selected to demonstrate how geomorphology and engineering can be combined to provide a rational approach to engineering and environmental problems.

REFERENCES

Anthony, D. J., Harvey, M. D., Laronne, J. B., and Mosley, M. P., eds. (2001). *Applying geomorphology to environmental management.* Water Resources Pub., Highlands Ranch, Colo.

Arizona Department of Transportation. (1979). "Salt River Bed study report (Photogrammetry and mapping services)." Arizona Department of Transportation, Phoenix.

Asimov, I. (1979). *A choice of catastrophes.* Simon & Schuster, New York.

Bagnold, R. A. (1960). "Some aspects of the shape of river meanders." *Professional Paper 181E*, U.S. Geological Survey, Washington, D.C., 135–144.

Bates, R. L., and Jackson, J. A., eds. (1987). *Glossary of geology*. American Geological Institute, Alexandria, Va.

Begin, Z. B., and Schumm, S. A. (1979). "Instability of alluvial valley floors: A method for its assessment." *American Society of Agricultural Engineering* 22, 347–350.

Bledsoe, P. B., Watson, C. C., and Biedenharn, D. S. (2002). "Quantification of incised channel evolution and equilibrium." *American Water Resources Association Journal* 38, 861–870.

Blong, R. J., and Johnson, R. W. (1986). "Geological hazards in the Southwest Pacific and Southeast Asian regions: Identification, assessment and impact." *Australian Geology and Geophysics Journal* 10, 1–15.

Bloom, A. L. (1991). *Geomorphology*. Prentice Hall, Englewood Cliffs, N.J.

Bolt, B. A., Horn, W. L., MacDonald, G. A., and Scott, R. F. (1975). *Geological hazards.* Springer-Verlag, New York.

Brice, J. (1977). "Lateral migration of the middle Sacramento River, California." *Water Resources Investigation 77–43*, U.S. Geological Survey, Washington, D.C.

Brice, J. C. (1974). "Evolution of meander loop." *Geological Society of America Bulletin* 85, 581–586.

Brice, J. C. (1981). "Stability of relocated stream channels." *Report FHWA/RD-80/158*, Federal Highway Commission, Washington, D.C.

Brookes, A. (1988). *Channelized rivers, perspectives for environmental management.* Wiley, Chichester, U.K.

Brunsden, D., and Prior, D. B., eds. (1984). *Slope instability*. Wiley, Chichester, U.K.

Bull, W. B. (1991). *Geomorphic responses to climate change*. Oxford Univ. Press, Oxford, U.K.

Carson, M. A. (1975). "Threshold and characteristic angles of straight slopes." *Fourth Guelph Symposium on Geomorphology*, Geobooks, Norwich, U.K., 19–34.

Carson, M. A. (1986). "Characteristics of high-energy meandering rivers: The Canterbury Plains, New Zealand." *Bulletin Geological Society of America* 97, 886–895.

Carson, M. A., and Kirkby, M. J. (1972). *Hillslope form and process*. Cambridge Univ. Press, Cambridge, U.K.

Catt, J. A. (1988). *Quaternary geology for scientists and engineers*. George Allen & Unwin, London.

Chang, H. H. (1988). *Fluvial processes in river engineering*. Wiley, New York.

Chow, V. T., ed. (1964). *Handbook of applied hydrology.* McGraw-Hill, New York.

Coates, D. R. (1976). *Geomorphology and engineering*. Dowden, Hutchinson & Ross, Stroudsburg, Pa.

Cooke, R. V. and Reeves, R. W. (1976). *Arroyos and environmental change in the American Southwest*. Clarendon, Oxford, U.K.

Darby, S. E. and Simon, A., eds. (1999). *Incised river channels*. Wiley, Chichester, U.K.

Doll, B. A., Wise-Frederick, D. E., Buckner, C. M., Wilkerson, S. D., Harman, W. A., Smith, R. E., and Spooner, J. (2002). "Hydraulic geometry relationships for urban streams throughout the Piedmont of North Carolina." *Journal of American Water Resources Association* 38(3), 641–651.

Fairbridge, R. W., ed. (1968). *The encyclopedia of geomorphology*. Reinhold, N.Y.

Ferrari, R. L. (1988). "1986 Lake Powell survey." Bureau of Reclamation, Denver, Colo.

Fisk, H. N. (1947). "Fine-grained alluvial deposits and their effect on Mississippi River activity." *Waterways Experiment Station Report 2*, U.S. Army Corps of Engineers, Vicksburg, Miss.

Fookes, P. G., and Vaughn, P. R. (1986). *A handbook of engineering geomorphology*. Chapman & Hall, New York.

Gellis, A., Hereford, R., Schumm, S. A., and Hayes, B. R. (1991). "Channel evolution and hydrologic variations in the Colorado River basins." *Journal of Hydrology* 124, 318–344.

Goodwin, C. N. (1999). "Fluvial classification: Neanderthal necessity or needless normalcy." *Wildland Hydrology* 25, 229–236.

Graf, W. L., ed. (1987). *Geomorphic systems of North America*. Centennial Special Volume 2, Geological Society of America.

Graf, W. L. (1988). *Fluvial processes in dryland rivers*. Blackburn Press, Caldwell, N.J.

Gregory, K. J., ed. (1977). *River channel changes.* Wiley, Chichester, U.K.

Goudie, A. (1981). *Geomorphological techniques*. Allen & Unwin, London.

Harvey, M. D. (1989). "Meanderbelt dynamics of the Sacramento River, California." D. L. Abell, (ed), *Proceedings California Riparian Systems Conference*, D. L. Abell, ed., *General Technical Report PSW-110*, USDA Forest Service, Pacific Southwest Forest and Range Experiment Station, Berkeley, Calif., 54–61.

Harvey, M. D., Mussetter, R. A., and Anthony, D. J. (2003). "Abstract: Island aging and dynamics in the Snake River, Western Idaho, USA." *Proceedings of Hydrology Days 2003*, American Geophysical Union, Fort Collins, Colo.

Harvey, M. D., and Smith, T. W. (1998). *Gravel mining impacts on San Benito River, California*. "Proceedings of the 1998 International Water Resources Engineering Conference, Hydraulics Division," ASCE, New York.

Harvey, M. D. and Watson, C. C. (1986). "Fluvial processes and morphological thresholds in incised channel restoration." *Water Resources Bulletin* 3(3), 359–368.

Henderson, F. M. (1966). *Open channel flow*. Macmillan, New York.

Hewitt, K., and Burton, I. (1975). *The hazardousness of a place*. University of Toronto Press, Toronto.

Hunt, C. B., and Mabey, D. R. (1966). "The stratigraphy and structure, Death Valley, California." *Professional Paper 494-A*, U.S. Geological Survey, Washington, D.C.

Johnson, R. B., and DeGraff, J. V. (1988). *Principles of engineering geology*. Wiley, New York.

Juracek, K. E., and Fitzpatrick, F. A. (2003). "Limitation and implications of stream classification." *Journal of American Water Resources Association* 83(3), 659–670.

Keaton, J. R. (1995). "Dilemmas in regulating debris-flow hazards in Davis County, Utah." *Environmental and engineering geology of the Wasatch Front region*, W. R. Lund, ed., *Publication 24*, Utah Geological Association, Salt Lake City, 185–192.

Keaton, J. R., Anderson, L. R., and Mathewson, C. C. (1988). "Assessing debris flow hazards on alluvial fans in Davis County, Utah." *24th Symposium Engineering Geology and Soils Engineering, Proceedings*, Washington State University, Pullman, 89–108.

Keeley, J. W. (1971). *Bank protection and river control in Oklahoma*. Federal Highway Administration, Oklahoma Division, Oklahoma City.

Kellerhals, R., Church, M., and Bray, D. I. (1976). "Classification and analysis of river processes." *Journal of Hydraulic Division Proceedings* 102, 813–829.

Kiersch, G. A. (1991). "The heritage of engineering geology. The first hundred years." Centennial Special 3, Geological Society of America, Boulder, Colo.

Kondolf, G. M., and Piégay, H., eds. (2003). *Tools in fluvial geomorphology*. Wiley, Chichester, U.K.

Lagasse, P. F., Spitz, W. J., Zevenbergen, L. W., and Zachmann, D. W. (2004). "Handbook for predicting stream meander migration." *NCHRP Report 533*, Transportation Research Board, Washington, D.C.

Leeder, M. R., and Bridge, P. H. (1975). "Flow separation in meander bends." *Nature* 235, 338–339.

Legget, R. F., and Hatheway, A. W. (1988). *Geology and engineering*. McGraw-Hill, New York.

Leopold, L. B., and Maddock, T., Jr. (1953). "Hydraulic geometry of stream channel and some physiographic implications." *Professional Paper 252*, U.S. Geological Survey, Washington, D.C.

Leopold, L. B., and Wolman, M. G. (1957). "River channel patterns: Braided meandering and straight." *Professional Paper 282-B*, U.S. Geological Survey, Washington, D.C.

Leopold, L. B., Wolman, M. G., and Miller, J. P. (1964). *Fluvial processes in geomorphology*. Freeman, San Francisco.

Lewis, G. W., and Lewin, J. (1983). "Alluvial cutoffs in Wales and the Borderlands." *Special Publication No. 6*, International Association of Sedimentologists, Oxford, U.K., 145–154.

Lisle, T. E. (1986). "Stabilization of a gravel channel by large streamside obstructions and bedrock bends, Jacoby Creek, northwestern California." *Bulletin Geological Society of America* 97, 999–1011.

Miller, J. R., and Ritter, J. B. (1996). "An examination of the Rosgen classification of natural rivers." *Catena* 27, 295–299.

Mollard, J. D. (1973). "Airphoto interpretation of fluvial features: Fluvial processes and sedimentation." *Proceedings of Hydrology Symposium, University of Alberta*, Information Canada, Ottawa, Ont., 341–380.

Molnar, P., and Ramirez, J. A. (2001). "Recent trends in precipitation and streamflow in the Rio Puerco Basin." *Journal of Climate* 14, 2317–2328.

Montgomery, D. R., and Buffington, J. M. (1993). "Channel classification: Prediction of channel response and assessment of channel condition." *TFW-SH10-93-002*, Washington Department of Environmental Resources, Timber Fish & Wildlife, Seattle.

Montgomery, D. R., and Buffington, J. M. (1997). "Channel-reach morphology in mountain drainage basins." *Geological Survey of America Bulletin* 109, 596–611.

Mosley, M. P. (1987). "The classification and characterization of rivers." *River channels*, K. Richards, ed., Blackwell, Oxford, U.K., 295–320.

Mussetter, R. A., Harvey, M. D., Wolff, C. G., Peters, M. R., and Trabant, S. C. (1998). "Channel migration effects on bridge failure in South Fork Snake River, Idaho." *Proceedings of the ASCE 1998 Water Resources Engineering Conference,* ASCE, New York.

Mussetter, R. A., Lagasse, P. F., and Harvey, M. D. (1994). *Erosion and sediment design guide*. Prepared for Albuquerque Metropolitan Arroyo and Flood Control Authority.

Nanson, G. C. and Hickin, E. J. (1986). "A statistical analysis of bank erosion and channel migration in Western Canada." *Bulletin Geological Society of America* 97, 497–504.

National Research Council. (1996). *Alluvial fan flooding*. National Academy Press, Washington, D.C.

Neill, C. R. (1984). "Bank erosion versus bedload transport in a gravel river." *Proceedings of the River Meandering Conference*, ASCE, New York, 204–211.

O'Connor, J. E., and Grant, G. E., eds. (2003). "A peculiar river: Geology, geomorphology, and hydrology of the Deschutes

River, Oregon." *Water Science and Application 7,* American Geophysical Union, Washington, D.C.

Odgaard, A. J. (1987). "Stream bank erosion along two rivers in Iowa." *Water Resources Research* 23, 1225–1236.

Osterkamp, W. R. (1998). "Processes of fluvial island formation, with examples from Plum Creek, Colorado, and Snake River, Idaho." *Wetlands* (4), 530–545.

Osterkamp, W. R., Johnson, W. C., and Dixon, M. D. (2001). "Biophysical gradients related to channel islands, middle Snake River, Idaho." *Geomorphic processes and riverine habitat,* J. M. Dorava, D. R. Montgomery, B. B. Palcsak, and F. A. Fitzpatrick, eds., *Water Science and Application No. 4*, American Geophysical Union, Washington, D.C., 73–83.

Paine, A. D. M. (1985). "Ergodic reasoning in geomorphology: Time for a review of the term?" *Progress in Physical Geography* 9, 1–15.

Parsons, A. J., and Abrahams, A. D., eds. (1992). *Overland flow, hydraulics and erosion mechanisms*. Chapman & Hall, New York.

Patton, P. C., and Schumm, S. A. (1975). "Gully erosion, northern Colorado: A threshold phenomenon." *Geology* 3, 88–90.

Petts, G. E., Moller, H., and Roux, A. L., eds. (1989). *Historical change of large alluvial rivers: Western Europe*. Wiley, Chichester, U.K.

Popov, I. V. (1964). "Hydromorphological principles of the theory of channel processes and their use in hydrotechnical planning." *Soviet Hydrology*, 158–195.

Rachocki, A. H., and Church, M., eds. (1990). *Alluvial fans, a field approach*. Wiley, Chichester, U.K.

Richards, K., ed. (1987). *River channels*. Blackwell, Oxford, U.K.

Rinaldi, M., and Johnson, P. A. (1997). "Characterization of stream meanders for stream restoration." *ASCE, Journal of Hydraulic Engineering* 123, 567–570.

Ritter, D. F. (1986). *Process geomorphology*. Brown, Dubuque, Iowa.

Rosgen, D. L. (1994). "A classification of natural rivers." *Catena* 22, 169–199.

Rosgen, D. L. (1996). *Applied river morphology*. Wildland Hydrology, Pagosa Springs, Colo.

Scheidegger, A. E. (1991). *Theoretical geomorphology*, 3rd Ed., Springer-Verlag, New York.

Schmidt, L. J., and Potyondy, J. P. (2004). "Quantifying channel maintenance instream flows: An approach for gravel-bed streams in the western United States." *General Technical Report RMRS-GTR-128*, USDA, Forest Service, Rocky Mountain Research Station.

Schuirman, G., and Slosson, J. E. (1992). *Forensic engineering*. Academic Press, New York.

Schumm, S. A. (1963). "A tentative classification of alluvial river channels." *Circular 477*, U.S. Geological Survey, Washington, D.C.

Schumm, S. A. (1968). "River adjustment to altered hydrologic regimen, Murrumbidgee River and paleochannels, Australia." *Professional Paper 598*, U.S. Geological Survey, Washington, D.C.

Schumm, S. A., ed. (1972). *River morphology*. Dowden, Hutchinson & Ross, Stroudsburg, Pa.

Schumm, S. A., ed. (1977a). *Drainage basin morphology.* Dowden, Hutchinson & Ross, Stroudsburg, Pa.

Schumm, S. A. (1977b). *The fluvial system*. Wiley, New York.

Schumm, S. A. (1988). "Geomorphic hazards—Problems of predictions." *Zeit. Geomorph. Suppl.* 67, 17–24.

Schumm, S. A. (1991). *To interpret the Earth*. Cambridge University Press, Cambridge, U.K.

Schumm, S. A. (1993). "River response to baselevel change: Implications for sequence stratigraphy." *Journal of Geology* 101, 279–294.

Schumm, S. A. (1994). "Erroneous perceptions of fluvial hazards." *Geomorphology* 10, 129–138.

Schumm, S. A. (2005). *River variability and complexity*. Cambridge University Press, Cambridge, U.K.

Schumm, S. A., and Beathard, R. M. (1976). "Geomorphic thresholds: An approach to river management." *Rivers 76*, ASCE, New York, 1, 707–724.

Schumm, S. A., Dumont, J. F., and Holbrook, J. M. (2000). *Active tectonics and alluvial rivers.* Cambridge University Press, Cambridge, U.K.

Schumm, S. A., and Galay, V. J. (1994). "The River Nile in Egypt." *The variability of large alluvial rivers*, S. A. Schumm and B. R. Winkley, eds., ASCE, New York, 75–100.

Schumm, S. A., and Hadley, R. J. (1957). "Arroyos and the semiarid cycle of erosion." *American Journal of Science* 225, 161–174.

Schumm, S. A., Harvey, M. D., and Watson, C. C. (1984). *Incised channels. Initiation, evolution, dynamics, and control*. Water Resources, Littleton, Colo.

Schumm, S. A., and Khan, H. R. (1972). "Experimental study of channel patterns." *Geological Society of America Bulletin* 83, 1755–1770.

Schumm, S. A., and Mosley, M. P., eds. (1973). *Slope morphology*. Dowden, Hutchinson & Ross, Stroudsburg, Pa.

Schumm, S. A., Mosley, M. P., and Weaver, W. E. (1987). *Experimental fluvial geomorphology*. Wiley, New York.

Schumm, S. A., Rutherfurd, I., and Brooks, J. (1994). "Pre-cutoff morphology of the lower Mississippi River." *The variability of large alluvial rivers,* S. A. Schumm and B. R. Winkley, eds., ASCE, New York, 13–44.

Schumm, S. A., and Winkley, B. R. (1994). *The variability of large alluvial rivers.* ASCE, New York.

Schuster, R. L., and Krizek, R. J., eds. (1978). Landslides, analysis and control. *Transportation Research Board Special Report 176*, National Academy Sciences, Washington, D.C.

Selby, M. J. (1982). *Hillslope materials and processes.* Oxford University Press, Oxford, U.K.

Shen, H. W. and Schumm, S. A. (1981). "Methods for assessment of stream-related hazards to highways and bridges." *Report FHWA/RD-80/160*, Federal Highway Administration.

Simon, A. (1994). "Gradation processes and channel evolution in modified West Tennessee streams: Process, response and form." *Professional Paper 1470*, U.S. Geological Survey.

Strahler, A. N. (1964). "Quantitative geomorphology of drainage basins and channel networks." *Handbook of applied hydrology*, V. T. Chow, ed., McGraw-Hill, New York, 4-39–4-76.

Summerfield, M. A. (1991). *Global geomorphology*. Longmans, Harlow, U.K.

Thornbury, W. D. (1965). *Regional geomorphology of the United States*. Wiley, New York.

Thorne, C. R. (1997). "Channel types and morphological classification." *Applied fluvial geomorphology for river engineering and*

management, C. R. Thorne, R. D., Hey, and M. D. Newson, eds., Wiley, Chichester, U.K., 175–222.

Thorne, C. R., and Baghirathan, V. R. (1994). "Blueprint for morphologic studies." *The variability of large alluvial rivers*, S. A. Schumm and B. R. Winkley, eds., ASCE, New York, 441–453.

Thorne, C. R., Hey, R. D., and Newson, M. D., eds. (1997). *Applied fluvial geomorphology for river engineering and management*. Wiley, New York.

Tinker, K. J., and Wohl, E. E., eds. (1998). *Rivers over rock: fluvial processes in bedrock channels*. *Geophysical Monograph 17*, American Geophysical Union, Washington, D.C.

Toy, T. J., and Hadley, R. F. (1987). *Geomorphology and reclamation of disturbed lands*. Academic Press, New York.

Vandenberghe, J. (2001). "A typology of Pleistocene cold-based rivers." *Quaternary International* 79, 111–121.

Water Engineering & Technology, Inc. (1989). "Systems approach to watershed analysis." Prepared for U.S. Army Corps of Engineers, Vicksburg District, Contract No. DACW38-99-D-0099, Delivery Order 0004.

Watson, C. C., Biedenharn, D. S., and Bledsoe, B. P. (2002). "Use of incised channel evolution models in understanding rehabilitation alternatives." *American Water Resources Association Journal* 38, 151–160.

Watson, C. C., Harvey, M. D., Biedenharn, D. S., and Combs, P. G. (1988a). "Geotechnical and hydraulic stability numbers for channel rehabilitation. I: The approach." *ASCE Hydraulics Division 1988 National Conference Proceedings*, S. R. Abt and J. Gessler, eds., ASCE, New York, 120–125.

Watson, C. C., Harvey, M. D., Biedenharn, D. S., and Combs, P. G. (1988b). "Geotechnical and hydraulic stability numbers for channel rehabilitation. II: Application." *ASCE Hydraulics Division 1988 National Conference Proceedings*, S. R. Abt and J. Gessler, eds., ASCE, New York, 126–131.

Wells, S. G., Bullard, T. F., Smith, L. N., and Gardner, T. W. (1983a). "Chronology, rates, and magnitudes of late Quaternary landscape changes in the southeastern Colorado Plateau." *Chaco Canyon country, American Geomorphological Field Group, Guidebook*, S. G. Wells, D. W. Love, and T. W. Gardner, eds., Albuquerque, N.M., 177–185.

Wells, S. G., Bullard, T. F., Miller, J., and Gardner, T. W. (1983b). "Applications of geomorphology to uranium tailings siting and groundwater management." *Chaco Canyon country*, *American Geomorphological Field Group, Guidebook*, S. G. Wells, D. W. Love, and T. W. Gardner, eds., Albuquerque, N.M., 51–56.

White, G. F. (1974). *Natural hazards.* Oxford University Press, New York.

Wilcock, P. (1997). "Friction between science and practice: The case of river restoration." *EOS Forum* 78, October 14.

Wilson, L. (1968). "Morphogenetic classification." *The encyclopedia of geomorphology*, R. W. Fairbridge, ed., Reinhold, New York, 717–729.

Copyrighted Materials
Copyright © 2008 American Society of Civil Engineers (ASCE)
Retrieved from www.knovel.com

CHAPTER 19

Sedimentation Hazards

Marcelo H. García, Robert C. MacArthur, Richard French, Julianne Miller
with Appendix by Jeffrey Bradley, Tom Grindeland and Hans Hadley

19.1 INTRODUCTION

In May 1980 Mount St. Helens erupted, removing the upper 404 m (1,324 ft) of the mountain and depositing approximately 2.8B m^3 (3.7B cubic yd) of material over an area of 596 km^2 (230 square mi). The resultant debris avalanche buried the upper 27.2 km (17 mi) of the North Fork Toutle River to an average depth of 46 m (150 ft). Mudflows carried a significant amount of this material downstream into the Toutle, Cowlitz, and Columbia Rivers. It became clear at the time that knowledge about mass sediment movement was extremely limited. This geologic event of catastrophic proportions generated a substantial amount of interest on debris-flows and mudflows. Mount St. Helens is presented as a case study in an appendix to this chapter.

Hyperconcentrated flows had not received much attention in *ASCE Manual 54*, "Sedimentation Engineering", (Vanoni, 1975; 2006), which was originally published five years before the eruption of Mount St. Helens. In fact, one of the few references to hyperconcentrated flows was about the seminal work by Beverage and Culbertson (1964).

Since 1975, when *Manual 54* was first published, there have been several publications on the subjects of debris-flow (Takahashi, 1991; Lorenzini and Mazza 2004); hyperconcentrated flows (Wan and Wang 1994); mud flows (United Nations 1996; Coussot 1997); alluvial fans (French 1987; NRC 1996a); and landslides (NRC, 1996b). There have also been several international meetings devoted to debris-flows hazards and their mitigation (Walling et al. 1992; Chen, 1997a; Wieczorek and Naeser 2000; Rickenmann and Chen 2003). However, this is clearly an area where much interdisciplinary research is still needed, because there is quite a gap between theoretical analysis, numerical modeling, laboratory experiments and what is observed in the field.

In the past decade, a plethora of models for debris-flows and mud flows have appeared in the literature. Some of them are coupled to hydrologic models with GIS frameworks for hazard mapping. A recent international conference on debris-flows provides a good source of information on debris-flow modeling, laboratory experiments and field observations (Rickenmann and Chen 2003). Although computational modeling capabilities have increased substantially, it is also important to realize that physical experiments and field observations need to continue at a steady pace so that theoretical and numerical models can be tested and further improved. In this regard, many studies have been conducted at the USGS debris-flow facility located at H. J. Andrews Experimental Forest in Oregon (Iverson et al. 1992; Major and Iverson, 1999; Denlinger and Iverson 2001). Prototype-scale experiments such as these yield high-resolution data that help refine the interpretation of field observations as well the predictions of theoretical and numerical models.

The fact that current knowledge about sedimentation hazards is still rather limited, in particular for hazard assessment and mitigation, was made evident recently in Latin America. The torrential flows that took place in the north coastal range of Venezuela (state of Vargas) in December, 1999 were a unique event in Latin American history, and perhaps in the world. On that day simultaneous extreme debris-flows occurred in about 20 streams (Fig. 19-1) along 50 km of a narrow coastal strip (Lopez et al. 2003). The disaster caused losses of more than $2 billion and killed an estimated 20,000 people. In terms of human losses this was the worst natural disaster in Venezuelan history and one of the worst in South America (Wieczorek et al. 2001).

As shown in Fig. 19-2, most of the cities along the Venezuelan coastline that were devastated by sedimentation are located in alluvial fans (Lopez and Garcia, 2000). Obviously the people living at these locations were not aware of the potential dangers and the authorities were not aware of the need to have any evacuation or emergency plans. There is a clear need to create public awareness of mudflows and

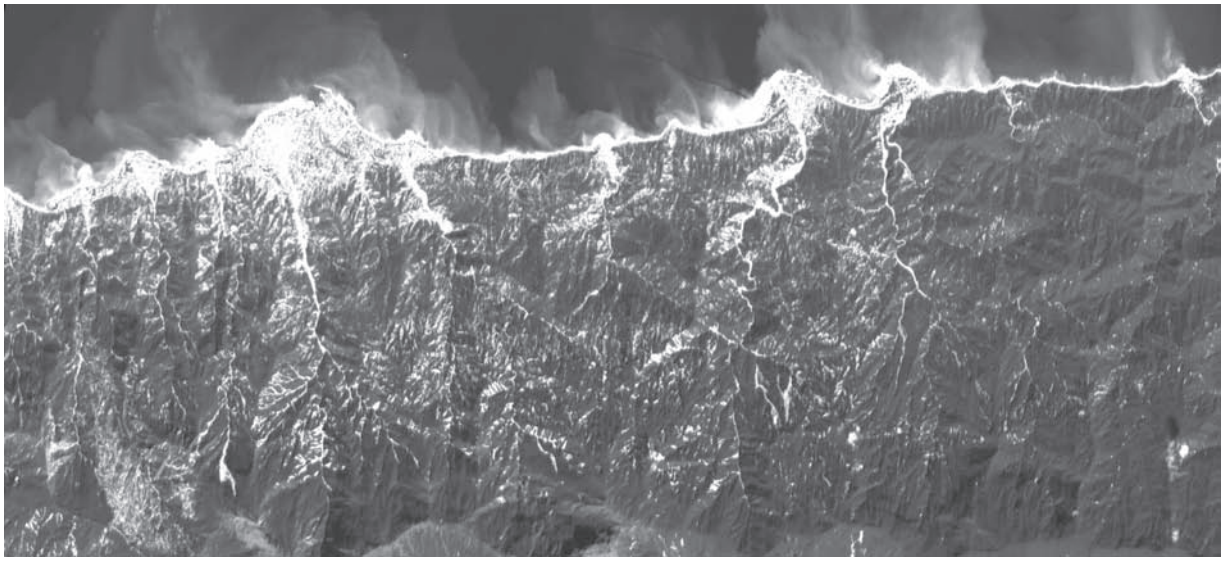

Fig. 19-1. Image of Venezuela northern coastline a few days after catastrophic sedimentation events of December 1999. (Source: SPOT Satellite)

Fig. 19-2. Town of Tanaguarena located in the alluvial fan of the Cerro Grande River in the aftermath of catastrophic sedimentation events, December 1999, Venezuela. (From López and García 2000 with permission).

sediment hazards in general. In a paper published in *Natural Disaster Science,* Takahashi (1981b) pioneered the estimation of potential debris-flow hazards, including the hydrologic and soil conditions leading to them, in Japan. His approach has great potential for the estimation of hazardous areas as well as countermeasures to prevent disasters in other debris-flow prone areas around the world. More recently, Rickenmann (1999) has advanced a series of useful empirical relationships that can be used by practicing engineers to assess debris flow hazard potential. Obviously the need to conduct field reconnaissance and to search for historic events wherever possible cannot be overemphasized.

In order to mitigate the damage caused by landslides, debris-flows and mudflows, it is necessary to introduce various structural and non-structural measures (United Nations 1996). For this purpose, policy makers, community leaders, and teachers in mudflow-prone regions have important roles to play. At the same time, most universities do not cover in their courses the mechanics of sediment transport during extreme hydrologic or geologic events, when the most destructive sedimentation events take place. Thus there is a need to summarize what is known about the subject of sedimentation hazards in this second volume *Manual 110* "Sedimentation Engineering."

This chapter attempts to summarize what is known about hyperconcentrated flows such as mud-floods, mudflows, and debris-flows, so that hydraulic and sedimentation engineers involved in the planning and design of mitigation measures as well as risk assessment have the best tools available for their use. However, the importance of public information and education to improve sediment hazard awareness and avoidance cannot be emphasized enough.

19.2 SEDIMENTATION HAZARDS—HISTORY AND MAGNITUDE

Throughout recorded history natural disasters have claimed lives and resulted in significant losses of property, income and social stability. Today there is far greater potential for worldwide catastrophic events, and there are far greater impacts from such events, because of a growing population in high-hazard areas, mounting investment and value of structures, dependency upon lines of communication, and the growing economic interdependence of businesses, communities and nations (NRC 1989). People's propensity to occupy areas subject to natural hazards, to alter natural watercourses, to alter land forms, and to engage in other activities that impact natural hydrologic and sedimentation processes creates a need to understand and forecast where and when such hazards may occur and to be able to avoid and mitigate for hazards. The first step for reducing natural sedimentation hazards is to become aware of their likely occurrence and their consequences. This awareness is necessary to motivate financial and scientific resources to prepare means for reducing and mitigating natural hazards.

Worldwide, nearly 3 million people died and approximately 820 million more were injured, displaced, or otherwise affected by natural disasters during the period from 1969 to 1989 (NRC 1989). Nearly 670,000 people were killed and approximately 211 million were adversely affected by natural disasters from 1991 to 2000 (IFRCRCS 2001). During the period from 1965 to 1985, floods and flood-related sedimentation processes were the greatest cause of deaths and property damage by natural disasters in the United States (Rubin, et al. 1986). Global flood disasters accounted for more than two-thirds of the people adversely affected by natural disasters from 1991 to 2000. Singh (1996) summarizes the historical occurrence of many of the largest worldwide natural and man-induced disasters since the turn of the century.

Singh (1996) also reports that flood damages, which exceeded $50 million per event in the United States from 1947 to 1964 (22 yrs.), accounted for approximately $5 billion in 1966 dollar equivalents. In 1968, the U.S. Water Resources Council (WRC) projected annual flood-related damages in the United States from the mid-1950's to 2020. The WRC forecast that during the period from 1966 to 2000, annual flood damages in the United States would double and by the year 2020, the annual damages would triple [from Singh (1996)]. According to the 1987 National Research Council, that forecast was low and the occurrence of significant flood-related damages in the United States and worldwide is growing because of increasing population, dramatic land use changes, and the propensity for people and valuable developments and infrastructure to locate in flood-prone zones.

Deaths and property losses from floods and fluvial processes exceeded those caused by other natural disasters such as earthquakes, hurricanes, tornadoes, tsunamis, landslides and volcanoes. These facts surprise many because floods are not usually thought to be significant causes of destruction and loss of life. This lack of public awareness of the increasing potential danger of floods and other fluvial processes, especially in the vicinity of rivers, channels, alluvial fans and coastal areas, is itself a problem. Rapidly urbanizing communities worldwide are especially susceptible to flooding problems because of the rate at which urbanization and land use are occurring. There is insufficient time to plan developments properly and they are commonly designed and constructed with a severe lack of long-term continuous rainfall and runoff records to document past flood occurrences and the capability of severe storm events to produce high-intensity, large-volume rainfall events in relatively isolated catchments. In regions where special sedimentation hazards occur (e.g., hyperconcentrated flows, flow bulking, and mud and debris-flows), traditional clear-water hydraulic design procedures for flood control works can lead to under sizing of debris retention facilities by 10 to 100 times and flood conveyance channels by 3 to 10 times depending on event sequencing, the severity of the storm event and geomorphic characteristics of the basin (MacArthur et al. 1992).

Landslide and debris-flow hazards often result from earthquakes, volcanic eruptions, and excessively wet rainy seasons, particularly those that immediately follow summer wildfires. Schuster and Flemming 1986 provide a historical review of large landslide and debris-flow events that have occurred in the western hemisphere, including the economic costs and loss of life associated with each event. The largest landslide in recorded history occurred during the May 1980 eruption of Mount St. Helens, a volcano in the state of Washington. The rock slide-debris avalanche contained

approximately 2.8 km^3 of material, which traveled as far as 22 km downslope along the North Fork Toutle River. The 1964 earthquake in Anchorage Alaska was one of the largest in recorded history (M9.2) and produced the most economically costly landslides of the 20th century, amounting to nearly $180 million ($1 billion in today's dollars) in damage to property and infrastructure in a series of landslides that moved an estimated 260,000 km^3 of material (Youd 1978). Earthquake-triggered landslides occurred in Whittier, California, causing property damages exceeding $350 million when a magnitude 5.9 earthquake struck the area for less than 5 s. In South America, the once prosperous Armero region of Colombia was devastated by mudflows spawned by the November 1985 eruption of Nevado del Ruiz, South America's northernmost active volcano. Though not a great eruption, a pyroclastic flow melted part of the mountain's snow and ice cap, generating mudflows called *lahars* that swept down the valleys flanking the summit (NRC 1989). "Two of the largest flows, augmented by scoured slope and valley debris and moving at more than 30 kph, swept from the mouth of Rio Lagunillas Canyon into the valley cradling the town of Armero. Successive waves of mud surged through the town, tearing homes from their foundations and burying sleeping residents to a depth of up to 3 meters. The peak discharge of the mudflow, estimated from the super-elevation left by the flood mark on a river bend immediately upstream from Armero, was 30,000 m^3/s (Takahashi, 1991). At least 22,000 perished, though the eruption had been predicted weeks in advance" (NRC, 1989). Similar eruption-induced mud and debris-flows, lahars and surge release debris torrents occurred at Mount St. Helens, Washington in 1980 and at Mount Pinatubo in the Philippines in 1991, killing many people and dramatically changing the landscape and rivers draining those mountains and floodplains (MacArthur et al.1993).

Massive landslides occurred in many California coastal communities during the heavy rainfall El Nino years of 1983, 1986 and 1995. Copious winter rains raise the local water level and pore pressures within hillslope soil materials, which increase the weight of hillslope materials while reducing the binding forces between layers of soil and bedrock. This often results in large slabs of weathered rock and earthen materials breaking free and sliding as a massive soil slip or rotational landslide or running out as a mud or debris-flow. Mechanisms for these types of rainfall-induced hazard are discussed by Varnes (1958), Campbell (1975), Krohn and Slosson (1976), Cannon and Ellen (1985), and Wilson and Wieczorek (1995). In 1987, California and Oregon experienced summer wildfires that lead to rainy-season fire-flood sequence-associated mud and debris-flows that damaged hundreds of homes and thousands of acres of urbanized area and dramatically affected the economies of many communities for years to come. Additional occurrences of fire-flood-associated landslides and mud and debris-flows have had dramatic effects in the states of Idaho, Wyoming, Montana, California, Arizona, New Mexico, Oregon, and Washington during the past decade (Bigio and Cannon 2001).

Death tolls and the collapse of homes or buildings often grab headlines after an earthquake or landslide. However, the effects of the quake and slides do not end there. Chassie and Goughnour (1976) of the Federal Highway Administration estimated that more than $100 million is a conservative total annual cost for landslide damage to highways and roads in the United States as of 1976. Water supply and sewer lines, reservoirs, pipelines, irrigation canals, flood-control channels, energy distribution and communication systems, and other transportation facilities—often referred to as *socio-economic lifelines*—are often directly impacted by landslide events as well.

Developments on alluvial fans may be at risk of severe periodic sedimentation and flooding hazards. During the spring of 1983, widespread flooding and mudflows caused an estimated $250 million in damages to Davis County communities located on numerous alluvial fans along the base of the Wasatch Mountains in Utah. The destruction was so extensive that 22 of Utah's 28 counties were declared national disaster areas (MacArthur and Hamilton 1988). Flash flooding and mudflows resulted from a rapidly melting snow pack that triggered over 1,000 landslides in the steep canyons above Farmington, Centerville, Bountiful and Salt Lake City. Detailed flood insurance studies had been completed for the communities in Davis County, Utah just prior to the events. Traditional steady-state, clear-water flood insurance study methods were used to delineate potential flood hazard zones. However, these studies did not account for the severe sedimentation processes (hyperconcentrated sediment loading and mud and debris-flows) associated with the events, so they grossly underestimated the magnitude and aerial extent of damage such an event could cause. The City of Rancho Mirage, located in Coachella Valley, California, experienced similar sedimentation hazards and debris-flow flood events on the Magnesia Spring Creek alluvial fan in 1976 and 1979. The occurrences of these destructive, high-velocity sedimentation-associated flood events led to the design and construction of a flood-control project by the U. S. Army Corps of Engineers. Unique to that project, however, was the recognition of the need to develop new methods for estimating severe-event hydrology (peak flows and event volumes) and for the design of mud—and debris-control facilities subject to such episodic, high-energy flood hazards.

Alluvial fan flooding and mud and debris-flow-hazards are often thought to occur in arid ephemeral locations of the world; however, similar hazards occur in warm tropical as well as cold polar regions of the world (Lecce, 1990; HEC, 1993). On New Year's Eve, 1987, severe flash floods and debris-flows occurred in Hawaii. The disaster happened unexpectedly, resulting in significant property loss, injuries, and economic impacts. The event was triggered by intense rainfall occurring in steep saturated basins above residential communities, resulting in several hillslope failures and

initiating significant mud and debris-flows that ran down valley for many miles, slamming into bedroom communities in the middle of the night (see MacArthur et al., 1992). As mentioned earlier, in December 1999 heavy rains in the mountains near Caraballeda, Venezuela caused landslides, debris-flows, and flash flooding on alluvial fans located along the densely populated coast. The community of Caraballeda, constructed on an alluvial fan, was partially buried by over 1.8 million tn of debris. Total damage caused by the storm was estimated at $1.9 billion with a loss of life exceeding 19,000 (Larsen et al., 2001; Wieczorek et al. 2001). Flash floods, debris-flows, and debris and boulder torrents are also common in steep cold-region catchments of Alaska and British Columbia. Neill, in *Hydrology of Floods in Canada* (Neill 1989), discusses special flood and sedimentation hazards associated with debris torrents and debris jam floods, phenomena typical of steep terrain. Neill (1989) also describes other unique sedimentation conditions associated with glacial outburst floods and ice jam flooding, typically found in cold regions of the world.

Other common types of sedimentation-related flood hazards include the following:

- Coastal flood and erosion hazards, including tsunami, hurricane surges, coastal bluff erosion and retreat, seasonal littoral sand transport, accelerated shoaling, sand dune and barrier island dynamics, and underwater debris-flows and turbidity currents resulting from seismic activity;
- Failure of natural debris dams formed by landslides in mountain areas;
- Collapse of mine-tailings dams. *In Tesero, Italy, a tailings dam collapsed in 1985 and the stored tailings together with the dam body material flowed down the Stava River as a mudflow, claiming the lives of 268 people and washing away 47 houses (Takahashi, 1991).*
- Gullying and hillslope instability due to deforestation, land use modification, road building, and urbanization;
- River and flood control channel instability due to local scour processes;
- Bridge pile, footing, and abutment instability due to local scour processes;
- Excessive accumulation of sediment and debris resulting in channel blockage and avulsion;
- Dam-break or glacial outburst-flood-induced debris-flows.

Even though much is yet to be learned about physical processes and consequences of sedimentation-related flood hazards, much has been learned on these esoteric topics since the first publication of *Manual 54* in 1975. During the past 30 yr, local, state, and federal researchers have advanced our abilities to identify hazard-prone zones and to estimate risks associated with sedimentation-related hazards. Since the passage of the Flood Control Act of 1936, the U. S. Corps of Engineers has been the leading federal agency responsible for regulating flood flows and building projects to reduce flooding damage. Beginning in the late 1970's and early 1980's, the U.S. Army Corps of Engineers, in cooperation with the Federal Emergency Management Agency (FEMA) and many private and state researchers, began to develop new study and design procedures to better account for sedimentation processes that affect fluvial systems during severe floods (MacArthur and Hamilton 1988; HEC 1993). Beginning in 1987, the United Nations General Assembly initiated the International Decade for Natural Disaster Reduction (IDNDR) to run from 1990 to 2000. Its aim was to reduce the loss of life, property damage, and social and economic disruption caused by natural disasters, including those attributed to sedimentation processes. The Decade concluded that floods cause about one-third of all deaths, one-third of all injuries and one third of all damage from natural disasters worldwide (Askew 1997). The IDNDR called for action by governments and international organizations to put greater emphasis and financial commitments to disaster prevention. Today, therefore, we see more awareness and understanding of flooding and special sedimentation hazards and improved study methods for forecasting their risk of occurrence and for designing mitigation measures are becoming available.

19.3 MECHANICS OF MUDFLOWS, DEBRIS-FLOWS, AND MUD-FLOODS

19.3.1 Definition of Hyperconcentrated Flow

Hyperconcentrated sediment flows can be initiated by numerous causes including intense rainfall, rapid snowmelt, and volcanic and man-made activities (Wan and Wang, 1994). The sediment load may also be increased by hillslope failure and bank collapse during flood events. The volume and properties of the fluid matrix, which is composed of the fluid and the sediment particles, govern flow hydraulics, flow cessation, and runout distances of hyperconcentrated sediment flows. The fluid matrix properties are usually dependent on sediment concentration, size fraction and clay content. A hyperconcentrated flow can be defined as a fluid in movement in which a high percentage of solid material is transported. The mean solid concentration by volume is defined as the ratio between the volume occupied by the solid fraction and the total mixture volume:

$C_V = \dfrac{V_{\text{solid}}}{V_{\text{solid}} + V_{\text{liquid}}}$, in which V_{solid} and V_{liquid} are the volume of the solid fraction and that of the liquid fraction of the mixture, respectively.

To avoid misinterpretation, the term *concentration* requires clarification, particularly for the case of hyperconcentrations. The units used in the measurement of sediment concentration vary with the range of concentrations and the standard measurement techniques utilized in different countries. The most common unit for sediment concentration is milligrams

per liter, which describes the ratio of the mass of sediment particles to the volume of the water-sediment mixture. Other units include kilograms per cubic meter (1 mg/l = 1 g/m^3), the volumetric sediment concentration C_V, the concentration in parts per million C_{ppm}, and the concentration by weight C_W, which are defined as follows:

$$C_V = \frac{\text{sediment volume}}{\text{total volume}} \tag{19-1a}$$

$$C_W = \frac{\text{sediment weight}}{\text{total weight}} = \frac{C_V G}{1+(G-1)C_V} \tag{19-1b}$$

in which $G = \gamma_s/\gamma$ is the specific gravity of the sediment and

$$C_{ppm} = 10^6 C_W \tag{19-1c}$$

Note that the percentage by weight C_{ppm} is given by 1,000,000 times the weight of sediment over the weight of the water-sediment mixture. The corresponding concentration in milligrams per liter is then calculated by the following formula:

$$C_{mg/l} = \frac{1\text{mg/l}\ GC_{ppm}}{G+(1-G)10^{-6}C_{ppm}} = 10^6\,\text{mg/l}\ GC_V \tag{19-1d}$$

The conversion factors in going from C_{ppm} to $C_{mg/l}$ are given in Table 19-1. Note that there is less than 10% difference between C_{ppm} and $C_{mg/l}$, at concentrations $C_{ppm} < 145{,}000$.

Table 19-1 Equivalent Concentrations for C_V, C_W, C_{ppm}, and $C_{mg/l}$

C_V	C_W	C_{ppm}	$C_{mg/l}$
Suspension			
0.001	0.00264	2,645	2,650
0.0025	0.00660	6,598	6,625
0.005	0.01314	13,141	13,250
0.0075	0.01963	19,632	19,875
0.01	0.02607	26,070	26,500
0.025	0.06363	63,625	66,250
Hyperconcentration			
0.05	0.12240	122,402	132,500
0.075	0.17686	176,863	198,750
0.1	0.22747	227,468	265,000
0.25	0.46903	469,027	662,500
0.5	0.72603	726,027	1,325,000
0.75	0.88827	888,268	1,987,500

Note: Calculations are based on mean density of water of 1g/ml and specific gravity of sediment G = 2.65.

Source: from Julien (1995) with permission.

In the laboratory, the sediment concentration $C_{mg/l}$ is measured as 1,000,000 times the ratio of the dry mass of sediment in grams to the volume of the water-sediment mixture in cubic centimeters (1 cm^3 = 1 ml). Two methods are commonly used: evaporation and filtration. The evaporation method is employed when the sediment concentration of samples exceeds 2,000 to 10,000 mg/l; the filtration method is preferred at lower concentrations. The lower limit applies when the sample consists mostly of fine material (silt and clay), and the upper limit when the sample is mostly sand. For samples having low sediment concentration, the evaporation method requires a correction if the dissolved solids content is high (Julien 1995).

Mud-floods are typically hyper concentrations of noncohesive particles (e.g., sand). They display very fluid behavior for a range of sediment concentrations by volume C_v as high as 40%. *Mud-floods* are turbulent and flow resistance depends on boundary roughness, as for turbulent flows with clear water. At volumetric sediment concentrations $C_v > 0.05$ the sediment concentration of small particles tends to become more uniform than described by the Rousean vertical concentration profiles for dilute suspensions presented in Chapter 2. Increased buoyancy and fluid viscosity reduce the settling velocity of sediment particles. A detailed analysis of hyperconcentrations of sands was presented by Woo et al. (1988). Turbulent diffusion and settling fluxes are dominant despite an increase in specific weight and viscosity of the mixture. An example of a *mud-flood* is shown in Fig. 19-3. Notice the instabilities in the free surface of the flow as predicted by Engelund and Wan (1984).

*Mudflows a*re characterized by a sufficiently high concentration of silts and clays (sediment size < 0.0625 mm) to change the properties of the fluid matrix and help support large clastic material. *Mudflows* behave as a highly viscous fluid mass, which at high concentrations is capable of rafting boulders near the flow surface. Based on laboratory results, the volumetric sediment concentration of a mudflow fluid matrix is in the approximate range $45\% < C_v < 55\%$ (O'Brien, 1986). *Mudflows* exhibit high viscosity and yield stress, can travel long distances on mild slopes at slow velocities, and leave lobate deposits on alluvial fans. A detailed analysis of *mud-flow* properties has been presented by O'Brien and Julien (1988); Major and Pierson (1992); and Coussot (1997). An example of a *mud-flow* deposit is shown in Fig. 19-4.

*Debris-flows a*re mixtures of clastic material, including boulders and woody debris, where lubricated interparticle collision is the dominant mechanism for energy dissipation. Knowledge of debris-flows is based largely on the contributions of Bagnold (1954) and Takahashi (1978). A recent review of debris-flows is given by Hutter et al. (1996). Granular flows (non-cohesive) flows without a lubricating fluid) constitute a sub class of debris-flows in which the exchange of momentum between the flow core and the boundary occurs exclusively through particle collision and friction.

Fig. 19-3. Example of mud flood (From Julien and Leon, 2000, with permission).

Fig. 19-4. Example of mudflow frontal deposit (from O'Brien et al, 1993, with permission).

Debris-flows involve the motion of large clastic material and debris characterized by destructive frontal impact surging and flow cessation on steep slopes (Fig. 19-5). Dispersive stresses arising from the collision of clastic particles control the exchange of flow momentum and energy dissipation. Debris-flows are much less fluid than mud-floods. The fluid matrix viscosity is comparatively small corresponding to the small concentration of fine sediments. The fluid matrix is essentially non-cohesive. The interstitial fluid does not significantly inhibit particle contact, permitting frequent collisions and impact between the solid clasts. Using a linear stability analysis, Lanzoni and Seminara (1993) have explored the conditions for the development of *debris waves* similar to the commonly observed *roll waves* in steep channels conveying clear water (Chow 1959).

19.3.2 Main Classification Criteria

In the past, the main classifications of hyperconcentrated flows were based on criteria obtained from direct observations, experimental process evaluations, and morphological analysis of deposits, physical models, and theoretical studies. Some investigators have focused on the classification of hyperconcentrated flows based on sediment concentration. Another group have categorized hyperconcentrated flows based on the triggering mechanism responsible for generation of these flows, and the third group of researchers have classified these flows according to the rheological and kinematic behavior. Classifications based on sediment concentration date back to the seminal study of Beverage and Culberson (1964). Motivated by the wide spectrum of sediment-laden flows observed in the aftermath of Mount St. Helens eruption, Bradley and McCutcheon (1987) were among the first to provide a comprehensive review on the classifications of hyperconcentrated flows. Their summary of commonly used classifications is shown in Table 19-2.

The first mass-wasting classifications concentrated in particular on landslides, a phenomenon that is of great interest to any new urban settlement (NRC 1996b). Sharpe (1938) considered two main parameters, relative velocity and sediment concentration and despite the fact that he did not specify transition boundaries, this classification has been widely used and refers to the following process categories: *debris avalanches, mudflows, earthflows, solifluction, soil creep* and *streamflows*.

Two decades after the Sharpe (1938) classification scheme first appeared in the literature, Varnes (1958) presented a classification that became a main reference point for the terminology of these processes. Varnes' classification is based on two main characteristics, the type of material and the type of movement involved, whereas velocity and mixture composition are used for subclassification purposes. Therefore, for coarser materials it identifies the phenomena as block streams, debris avalanches, debris-flows (mudflows if the coarser material content is lower than 50%), solifluction, and creep, and for finer materials: blends of dry sands and silt, blends of wet sands or silt, and *earthflows*. In the Chinese literature (Wan and Wang 1994), the term "hyperconcentrated" is generally used to indicate a material having measurable yield strength and therefore debris-flows

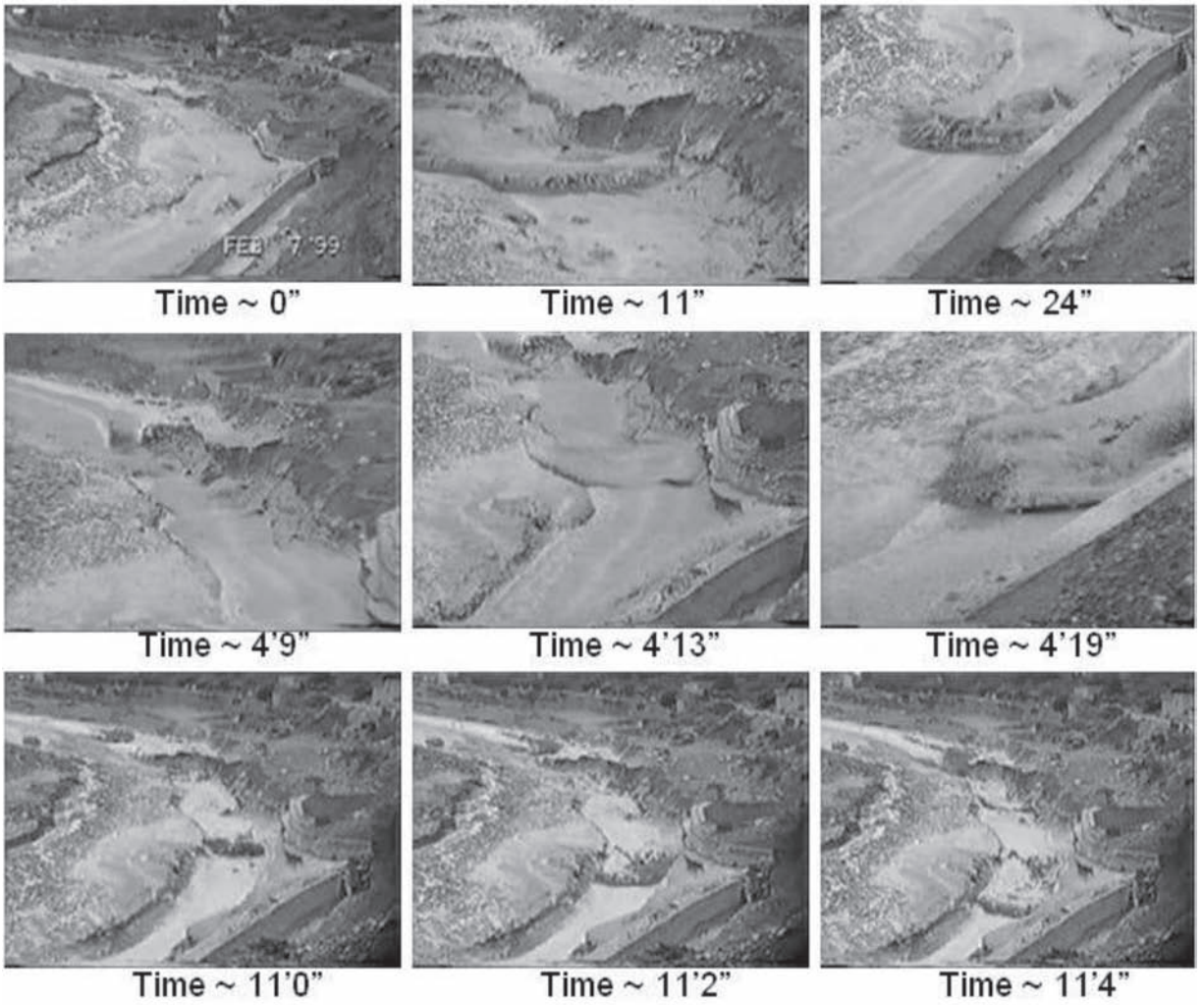

Fig. 19-5. Video images of debris flows passing by town of Iruya, Salta, Argentina, February 7, 1999 (courtesy of Daniel Brea and Pablo Spalletti).

are considered as hyperconcentrated flows. However, more recent classifications have attempted to systemize established terminology by introducing quantitative criteria.

Takahashi (1991) defines mass wasting as the fall, slide, or flow of a conglomerate or dispersed mixture of sediment in which gravity moves all the particles and the interstitial fluid, so that the relative velocity between the solid and fluid phases in the main direction of motion plays a minor role, whereas in a fluid flow the forces of lift and resistance caused by relative velocity are essential for the transport of each single particle. In this approach, the following four phenomena can be distinguished on the basis of the mechanism that supports the clasts, the properties of the interstitial liquid, velocity, and distance reached: *falls*, in which the single particles move separately with relatively small internal deformation; *sturzstroms*, particularly rapid and destructive events; *pyroclastic flows,* which are rapid and explosive events originated by volcanic eruptions, in which the suspension mechanism is linked to the expansion of the gas trapped within the flow; and, finally, *debris-flows,* in which the grains are dispersed in a water-clay interstitial fluid. These last three processes can be termed collectively *gravitational sediment flows* (Takahashi 1991) and constitute continuous processes that require a certain force for grain suspension.

In the case of debris-flows, the approach of Bagnold (1954) and Takahashi (1978) considers the dispersive pressure that results from the exchange of momentum between grains as predominant; if the interstitial fluid is particularly dense, large clasts can be suspended with relatively low dispersive pressures by floating in the fluid phase. Another approach, first advanced by Johnson (1970), considers that the viscous stress of the interstitial fluid is predominant and neglects interactions between grains.

Following a number of laboratory experiments with samples from Colorado, O'Brien and Julien (1985) classified hyperconcentrated flows according to the properties controlled by sediment concentrations, as *water floods, mud-floods, mudflows,* and *landslides* (Fig. 19-6). The characteristic

Table 19-2 Classification of High Sediment Concentration Flows (After Bradley and McCutcheon 1987).

	Concentration percent by weight (100% by WT = 1,000,000 ppm)									
	23	40	52	63	72	80	87	93	97	100
	Concentration percent by volume (G. = 2.65)									
Source	10	20	30	40	50	60	70	80	90	100
Beverage and Culbertson (1964)	High	Extreme	Hyperconcentrated			Mud Flow				
Costa (1984)	Water Flood		Hyperconcentrated			Debris Flow				
O'Brien and Julien (1985) using National Research Council (1982)	Water Flood		Mud Flood		Mud Flow		Landslide			
Takahashi (1981)	Fluid Flow			Debris or Grain Flow				Fall, Landslide, Creep, Sturzstrom, Pyroclastic Flow		
Chinese Investigators (Fan and Dou, 1980)	<---------- Debris or Mud Flow ---------->									
	<---------- Hyperconcentrated Flow ---------->									
	Sediment Laden									
Pierson and Costa (1984)	STREAMFLOW				SLURRY FLOW			GRANULAR FLOW		
	Normal: Hyperconcentrated				(Debris Torrent), Debris Mud Flow, Solifluction			Sturzstrom, Debris Avalanche, Earthflow, Soil Creep		

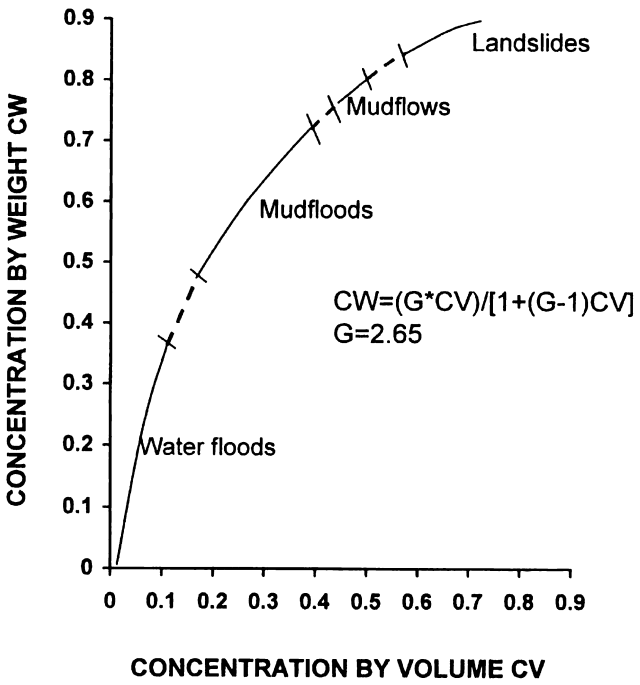

Fig. 19-6. Classification of hyperconcentrated flows after O'Brien and Julien (1985).

stresses of such processes are yield stress, viscous stress, turbulent stress in the fluid, and dispersive stress caused by the inertial impact of the coarser sediments. Which of these stresses dominates depends on the volumetric concentration of sediment and the percentage of the fine fraction. Despite the fact that the transition between the types of flow is difficult to determine, according to this approach they can be divided into three categories, which lie between conventional stream flooding on the one hand and landslides on the other end.

Mud-floods are hyperconcentrated flows of cohesionless particles (mainly sand) with limited quantities of cohesive particles, which show characteristics that are typical of fluids, with sediment concentrations by volume of 20 to 45% (Winterwerp et al. 1990). From a hydrodynamic point of view, *mud-floods* have characteristics that are typical of a conventional turbulent flow and resistance to motion depends on the roughness of the channel in which the flow occurs. Moreover, they are not able to support stress without deforming and show no yield stress. Sediment concentration tends to be uniformly distributed throughout the flow depth, because the viscosity of the interstitial fluid reduces the velocity of particle sedimentation.

Mudflows are hyperconcentrated flows composed, to a large extent, of cohesive silt and clay particles (smaller than 0.0625 mm), in which sediment concentration by volume varies between 45 and 55%. This composition alters the properties of the interstitial fluid, making it extremely viscous and giving it considerable yield strength. Consequentially, in the free surface area, *mudflows* can hold clasts of considerable size in suspension for long distances even on slight slopes, resulting in the formation of lobe-shaped deposits. Typical resistance to motion is a characteristic of pseudoplastic fluids that appears with high viscosity (Huang and Garcia 1998).

Debris-flows are mixtures of clastic material with high coarse particle contents, in which collisions between particles and therefore dispersive stresses are the dominant mechanisms in energy dissipation. Cohesionless granular debris-flows are a subcategory of debris-flows, in which momentum exchange takes place due to friction and collisions. These phenomena occur depending on the simultaneous occurrence of the following conditions:

- high volumetric concentration of sediments (>0.5);
- high shear rates (>100 s^{-1});
- large particle dimensions (>5% compared to streamflow depth).

Coussot (1992) considers two types of debris-flow: *granular* ones, which have a fine particle fraction quantity (dimension smaller than 40 μm) 10% lower than the entire solid mass, and *muddy* ones in which the fine fraction exceeds 10%. Coussot's classification is given in terms of dimensional grain distribution, as shown in Fig. 19-7.

When the rheological behavior of granular mixtures is used for classification purposes, two further studies must be considered. Savage (1984) identified three flow regimes for granular mixtures, each one characterized by a value of the solid fraction, interstitial viscosity, and deformation rate: the *macroviscous* regime, in which the viscous effects of the interstitial fluid and solid particle interactions cause the stresses; the *quasistatic* regime, in which dry friction and prolonged contacts between particles are important, whilst inertial effects are negligible; and last, the *inertial-granular* regime, in which the inertia associated to the individual particles prevails. Iverson (1985) developed a constitutive equation for the idealized behavior of mass wasting, based on linear and nonlinear rheological models, which range from the purely plastic case to the purely viscous one; this equation represents an important analytical relationship for differentiating between various types of flow.

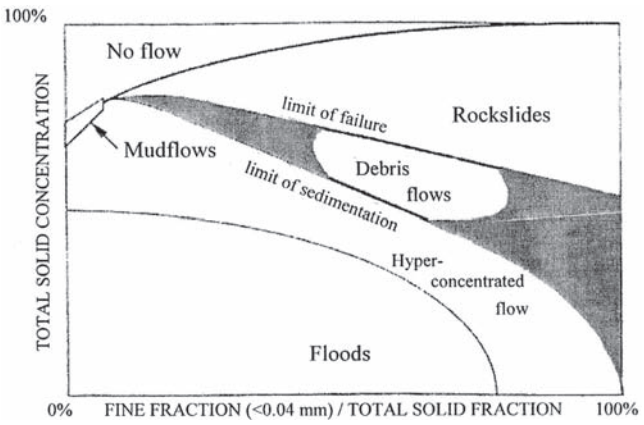

Fig. 19-7. Coussot's (1992) conceptual classification of hyperconcentrated streamflows.

A rheological classification of the various types of flow using a two-dimensional matrix (Fig. 19-8) that considers the mean flow velocity and sediment concentration was proposed by Pierson and Costa (1987). This classification makes it possible to distinguish each process from the others, if mean flow velocity is known or can be estimated and additional information is available on the existence of yield strength and stream capacity to suspend large clasts, characteristics that can be determined by an analysis of sediment deposits. This approach distinguishes between a dilute, ordinary streamflow and a hyperconcentrated streamflow according to whether the flow is Newtonian or non-Newtonian, and between a slurry and a granular flow, the limit being a function of sediment size and particle gradation. In the graph shown in Fig. 19-8, vertical rheological divisions A, B, and C depend on grain size and concentration. From left to right, boundary A represents the appearance of yield strength; boundary B marks sudden increase in yield strength rapid increase that enables the static suspension of granules and the onset of liquid behavior; boundary C marks the cessation of liquid behavior. The horizontal velocity limits, which are also functions of

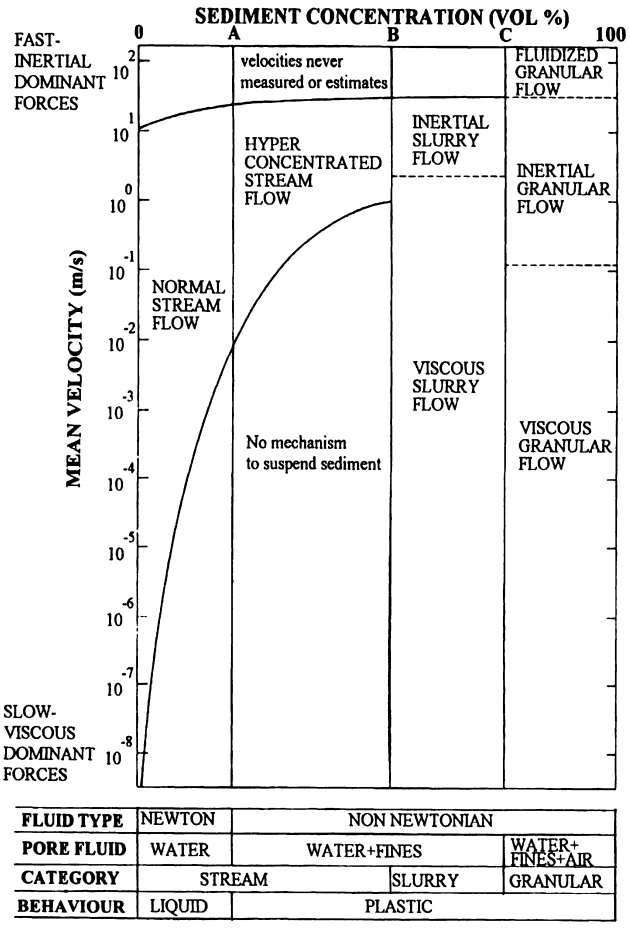

Fig. 19-8. Classification of water-sediment mixtures proposed by Pierson and Costa (1987).

grain-size distribution and sediment concentration as well as particle density, are determined by how shear stress is transmitted between particles during the flow. In the case of cohesive materials or those that contain a high proportion of fine materials, the vertical lines on the graph, that divide the various rheological behavior types, must be shifted to the left; the opposite is true if the mixture contains mainly well-sorted, coarse clasts. It is therefore possible to identify two large-flow categories: one that includes *ordinary streamflows* and *hyperconcentrated streamflows* and a second one that includes *slurry flows* and *granular flows.*

According to Davies (1986; 1988), who reviewed numerous debris-flow descriptions, basically three different debris-flow types can be distinguished:

Type 1: low-density, steadily moving turbulent flows, carrying coarse particles as bed load only and with the fluid made up of a slurry.

Type 2: high-density, laminar flows, carrying fine and coarse particles uniformly distributed over the depth, of unsteady nature with pulse-like motion.

Type 3: the same as Type 2 but consists of a single pulse or wave.

The latter two types have a higher viscosity than the first one, and selective deposition of the coarser particles does not seem possible. Due to their larger flow depths and velocities their destructive power is considerable. In order to distinguish between steady- and unsteady-type debris-flows, Davies (1997) proposed a density of 1.6 to 1.8 tn/m^3, corresponding to sediment concentrations of about 36 to 49% by volume. He pointed out that the transition seems to be rather abrupt if a particular flow changes from one type to another. This transition is also reflected in the sediment deposits of either a "water flood" or a debris-flow (Costa 1984).

One of the main problems in the development of a unifying classification scheme relates to the fact that the physical properties of debris-flows, and hyperconcentrated flows in general, vary over a wide range in the field (Iverson, 2003). A summary of physical properties of debris-flows prepared by Costa (1984) is reproduced in Table 19-3. It can be observed that the dynamic viscosity as well as the density of these flows can be much larger than in the case of dilute suspensions. Except for the fast-moving *mudflows and debris flows* observed in China, it is interesting to observe that most flows are laminar as pointed out by very low values of the estimated Reynolds number (Coussot, 1994).

An interesting graph showing a continuous spectrum of sediment concentrations from sediment-laden rivers to debris-flows first proposed by Hutchinson (1988) is shown in Fig. 19-9. What makes this graph particularly useful is that it includes information on conditions observed in the field (some of which are mentioned in Table 19-3), ranging from *streamflows* carrying modest amounts of sediment all the way to *landslides* having very low water content and very large solids concentrations (Bagnold 1956). This graph includes also the water content in the sediment-water mixture, a parameter that is relatively easy to measure in the field. This is important because soil saturation with water is an important factor in the triggering of *landslides* that might evolve into *debris* and *mud flows*. As shown therein, debris-flows are often of very high density, over 80% solids by weight, and may exceed the density of freshly-mixed concrete. They can therefore move boulders that are meters in diameter as shown in Fig. 19-10. The equation shown in Fig. 19-9 is given by the following expression,

$$\gamma_{sat} = G\gamma_w \left[\frac{1+W}{1+WG}\right]$$

where γ_{sat} is the specific or unit weight of a saturated soil (sediment plus water) sample, $G = \gamma_s/\gamma_w$ is the specific gravity of the sediment defined earlier as the ratio between the specific weight of the sediment and the specific weight of water. This parameter can have values between 2.6 and 2.75. The water content $W = M_w/M_s$ in the sample is defined as the ratio between the water mass M_w and the sediment mass M_s in the soil sample. It is clear that when the water content W is very large $\gamma_{sat} \rightarrow \gamma_w$ corresponding to a dilute open-channel suspension; and when the water content decreases and the sediment concentration increases $\gamma_{sat} \rightarrow \gamma_s$ corresponding to *hyperconcentrated flows* such as *mudflows and debris flows.*

As observed in Fig. 19-10, the impact of large boulders can cause substantial destruction of buildings so it can be useful to estimate potential impact loads resulting from *debris flows.* Impact loads result from objects entrained in the flow striking a structure surface with a velocity component perpendicular to the flow direction (Julien and O'Brien 1997). To compute the impact load, consideration should be given to the evidence of debris and boulders transported on the fan by recent flood events. To be conservative, the largest boulder transported by a flow should be used to determine the impact load. The impact loading P_I is given by:

$$P_I = \frac{wV}{(Ag\Delta t)}$$

where w is the weight of the object (largest boulder), g is the gravitational acceleration, V is the flow velocity, A is the area of impact assumed to be a percentage of the cross sectional area of the object and Δt is the duration of impact. It has been observed that the largest boulders in a given flow have a tendency to accumulate on the frontal area of debris flows (Suwa 1987), where they can be expected to have the largest effect when impacting a structure. Recently, the effect of particle segregation and its implications for debris flows have been studied experimentally by Zanutigh and Di Paolo

Table 19-3 Physical Properties of Observed Debris-Flows Compiled by Costa (1984)

Location	Velocity [m/s]	Slope [%]	Bulk density [g/cm^3]	μ [poise]	Clay [%]	Depth [m]	Solids [% wt.]	Reynolds No.
Rio Reventado, Costa Rica	2.9–10	4.6–17.4	1.13–1.98	–	1–10	8–12	20–79	–
Hunshui Gully, China	10–13	–	2–2.3	15–20	3.6	3–5	80–85	40,000
Bullock Creek, New Zealand	2.5–5.0	10.5	1.95–2.13	2.100–8,100	4	1.0	77–84	28.57
Pine Creek, Mount St. Helens	10–31.1	7–32	1.97–2.03	2.00–3,200	–	0.13–1.5	–	200
Wrightwood Canyon, California	1.2–4.4	9–31	2.4	2,100–6,000	<5	1.2	79–85	23.8
Wrightwood Canyon, California	0.6–3.8	9–31	1.62–2.13	100–60,000	–	1.0	59–86	1.33
Mayflower Gulch, Colorado	2.5	27	2.53	30,000	1.1 (<0.004 mm)	1.5	91	3.2
Dragon Creek, Arizona	7.0	5.9	2.0	27,800	–	5.8	80	29.2
Jian-jia Ravine, China	8.0	0.06	2.3	15.5–1,736	–	1.4	89	148–11,561

(2006). There is also a FEMA Manual (1994) that provides equations for the computation of the hydrostatic and hydrodynamic loads on structures.

19.3.3 Rheology of Hyperconcentrated Sediment Flows

The general flow behavior of hyperconcentrated sediment flows can be inferred from an examination of the physical processes triggering hyperconcentrations in a watershed, an assessment of sediment availability and sediment source, an investigation of historical flood events on the same or neighboring watershed, and a rheological and particle size analysis of deposits. Deposits from historical or recent events can be brought to the laboratory for a rheological investigation at various sediment concentrations. As discussed above, hyperconcentrated sediment flows can be classified, in general, as mud-floods, mudflows, and debris-flows. Distinct physical processes differentiate these types of hyperconcentrations based on the rheology of the water-sediment mixture.

Various researchers have developed and applied models of mud and debris-flow rheology. These models can be classified as Newtonian models (Johnson 1970; Hunt 1994; Aguirre-Pe et al. 1995); linear and nonlinear viscoplastic models (Johnson 1970; O'Brien and Julien 1988; Liu and Mei 1989; Huang and Garcia 1997a; 1997b; 1998; Imran et al. 2001); dilatant fluid models (Bagnold 1954; Takahashi 1978; Mainali and Rajaratnam 1994); dispersive or turbulent stress models (O'Brien et al. 1993); and frictional models (Iverson 1997).

Rheology is the science of describing the deformation and flow of matter. More specifically, the graphical measure of the shear stress applied at a given rate of deformation of a fluid defines a rheogram. In clear water flows, the shear stress increases linearly with the rate of deformation (i.e., velocity gradient) in the laminar flow regime and the fluid is said to be Newtonian (i.e., $\tau = \mu\, du/dz$). The dynamic viscosity of a sediment-water mixture μ is then defined as the slope of the rheogram.

There is substantial evidence indicating that mud at high enough concentrations shows non-Newtonian rheological behavior (e.g., Coussot 1994). Videos taken by Davies (1988) during his laboratory experiments show that there are both a thin shear layer near the bed and an upper plug-like layer in which the particles are nearly locked together. This upper plug-like layer is a property of non-Newtonian fluids, and is clearly associated with some yield stress. Rheological studies by Krone (1963), Migniot (1968), and Wan (1982) indicate that mud from different sources behaves approximately as a Bingham plastic fluid whose yield stress, τ_y, and viscosity, μ, increase monotonically with clay concentration. The ranges of values commonly observed for such parameters values are $10^{-6}\,m^2/s < \mu/\rho < 1.2 \times 10^{-3}\,m^2/s$ and $10^{-3}\,N/m^2 < \tau_y < 10^2\,N/m^2$, whereas sediment concentration varies in the

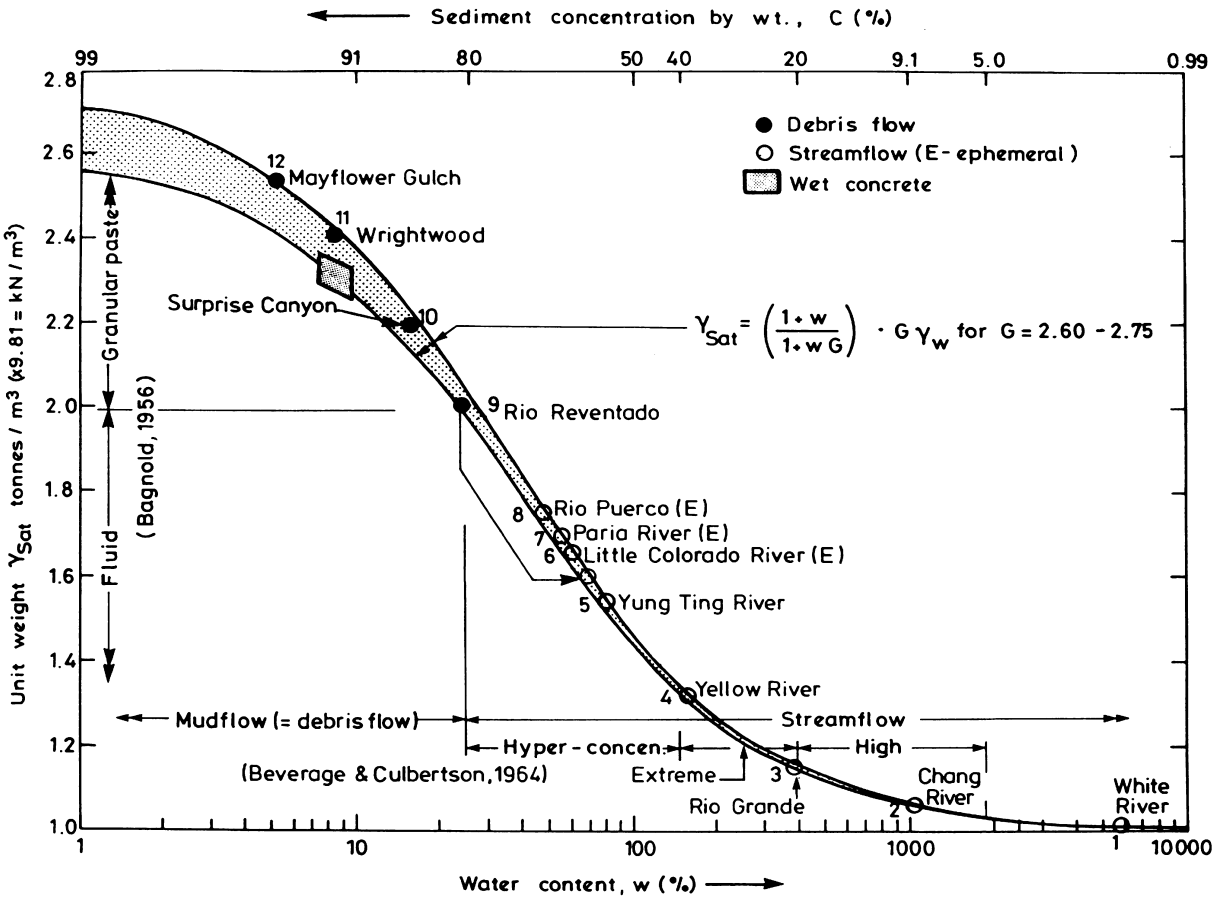

Fig. 19-9. Continuous spectrum of sediment concentrations and water content from sediment-laden rivers through ephemeral streams to mudflows and debris flows (Hutchinson 1988).

range from 2 to 700 kg/m^3. Such a fluid at rest is capable of resisting any shear stress less than the yield stress. When the yield stress is exceeded, the fluid structure changes and the material behaves like a Newtonian fluid driven by the excess of the shear stress beyond the yield stress. When the shear stress falls below the yield stress, the fluid structure changes again, and there is no fluid flow. There is also evidence that fine-grained debris-flows (Mainali and Rajaratnam 1991; 1994; Dominique and Coussot, 1997), liquefied mine tailings materials (Jeyapalan et al. 1983), molten lava (Johnson 1970), and snow avalanches (Dent and Lang, 1983) can be modeled as Bingham plastic fluid flows (Huang and García 1997b).

The Bingham rheological model is to some extent a limiting or idealized rheological model. Beyond a finite shear stress (i.e. *yield stress* τ_y) the rate of deformation, du/dz, is linearly proportional to the excess shear stress. The constitutive equation is

$$\tau = \tau_y + \mu \frac{du}{dz} \tag{19-2}$$

The Bingham plastic model is well suited to homogeneous suspensions of fine particles, particularly at low rates of deformation. Experimental laboratory results of Qian and Wan (1986) and others confirm that under rates of deformation observed in the field, fluids with large concentrations of fine particles behave like Bingham plastic fluids. Huang and Garcia (1997b) extended the perturbation-technique approach first proposed by Hunt (1994) for Newtonian flows and proposed a Bingham model to estimate the run-out distance of mudflows. However, it should be clear that rheological models can only provide a first-order approximation for the purpose of modeling hyperconcentrated flows in the field. A number of non-Newtonian rheological models have been proposed for debris-flows and mudflows, including Herschel-Bulkley's viscoplastic model (Chen 1988; Liu and Mei 1989; Huang and García 1998; Imran et al. 2001). It is difficult to say which constitutive equation best represents the behavior of a mud flow.

The analysis of coarse sediment mixtures as observed in debris-flows is somewhat more complex and involves an additional shear stress due to particle-particle interaction (MacTigue 1982; Shen and Ackermann 1982; Mih 1999).

Fig. 19-10. Boulders deposited by debris flows in the alluvial fan of the San Julian River, Venezuela, December 1999 (from López and García 2000 with permission).

Bagnold (1954) pioneered laboratory investigations on the impact of sediment particles. He defined the dispersive shear stress τ_d induced by the collision between sediment particles as

$$\tau_d = c_B \rho_s \left[\left(\frac{0.615}{C_v} \right)^{1/3} - 1 \right]^{-2} D_s^2 \left(\frac{du}{dz} \right)^2 \qquad (19\text{-}3)$$

where

C_v = volumetric sediment concentration;
D_s and ρ_s = sediment particle diameter and density, respectively; and
c_B = an empirical impact coefficient defined by Bagnold ($c_B \approx 0.01$).

Takahashi (1980) has found experimentally that the impact coefficient ranges between 0.35 and 0.5; an order of magnitude larger than the value suggested by Bagnold (1954).

The dispersive shear stress is shown to increase with three parameters: the second power of the particle size, the volumetric sediment concentration, and the second power of the rate of deformation. It is important to recognize that the dispersive stress is proportional to the product of these three parameters; therefore, high values of all parameters are required to induce a significant dispersive shear stress. An excellent analysis of constitutive equations for debris-flows and their applicability can be found in Egashira et al. (1997).

The non-Newtonian nature of hyperconcentrated sediment flows results from several physical processes and sediment-water mixture properties (Julien and O'Brien 1997): the cohesive yield strength τ_c, which accounts for the cohesive nature of fine sediment particles; the Mohr-Coulomb shear τ_{mc}, which accounts for the internal friction between grains; the viscous shear stress τ_v, which accounts for the fluid-particle viscosity; the turbulent shear stress τ_t; and finally,

the dispersive stress τ_d, which accounts for the collision of the largest particles or clasts. Then the total fluid shear stress τ in a hyperconcentrated sediment flow results from the sum (*assuming that all the shear stresses can be linearly added*) of the five shear stress components:

$$\tau = \tau_{mc} + \tau_c + \tau_v + \tau_t + \tau_d \tag{19-4}$$

A quadratic rheological model has been proposed by O'Brien and Julien (1985) and Julien and Lan (1991), which describes the flow continuum through the range of sediment concentrations for these shear stresses. When written in term of shear rates, or velocity gradient du/dz, τ_{mc} and τ_c are independent of velocity gradient, τ_v varies linearly with velocity gradient, and both τ_t and τ_d vary with the second power of the velocity gradient. The resulting quadratic constitutive equation is given by

$$\tau = \tau_y + \mu_m \frac{du}{dz} + \zeta\left(\frac{du}{dz}\right)^2 \tag{19-5}$$

where

$\tau_y = \tau_{mc} + \tau_c$ = yield stress;

μ_m = dynamic viscosity of the sediment-water mixture; and ζ= the turbulent-dispersive parameter. The last term of the quadratic model combines the effects of turbulence with the dispersive stress induced by the inertial impact of sediment particles. Combining the conventional expression for the turbulent stress in sediment-laden flows with Bagnold's dispersive stress gives

$$\zeta = \rho_m l_m^2 + c_B \rho_s \lambda_B^2 D_s^2 \tag{19-6}$$

where

ρ_m and l_m = the mass density and mixing length of the mixture, respectively; D_s and ρ_s = sediment particle diameter and density, respectively;

λ_B = Bagnold's linear sediment concentration (defined below);

and

c_B = Bagnold's empirical impact coefficient ($c_B \approx 0.01$). The mass density of the mixture, $\rho_{m,}$ is calculated from $\rho_m = \rho + (\rho_m - \rho)C_v$, where C_v is the volumetric sediment concentration and ρ is the density of water. Bagnold's (1954) linear sediment concentration is estimated as

$$\lambda_B = \frac{1}{\left(\frac{0.615}{C_v}\right)^{1/3} - 1} \tag{19-7}$$

Viscosity μ_m and yield stress τ_y have generally been explained through increasing exponential functions of the volumetric sediment concentration (Julien 1995; Lorenzini and Mazza 2004). O'Brien and Julien (1988) measured the rheological properties of natural silt and clay mudflow deposits from the Colorado Rocky Mountains. The yield stress and the viscosity increase by three orders of magnitude as the volumetric concentration increases from 0.10 to 0.40.

It is important to consider that the occurrence of granular debris-flows as prescribed by a dispersive stress relationship alone requires that the following three conditions be simultaneously satisfied: the flow has (1) very large sediment concentrations, typically $C_v > 0.5$; (2) large velocity gradients, typically exceeding 100 s^{-1}; and (3) very large sediment particles, typically coarser than 5% of the flow depth.

Yield stress is a factor that not only influences debris-flow mobilization, but also is indirectly connected to the resistance that causes stoppage in the final stages of movement. During experiments one can observe that yield stress is always higher for initiation of motion than the corresponding values in stoppage conditions. Thus the yield stress presents a certain form of hysteresis, which must be considered in forecasting the overall distance covered by a debris-flow (*runout*) for a given topography (Contreras and Davies 2000). In fact, by using the yield stress associated with initiation of motion in a runout-distance forecasting model, one is likely to seriously underestimate it.

19.3.4 Dimensionless Rheological Model

To establish a rheological classification for hyperconcentrated flows, Julien and Lan (1991) and Julien and O'Brien (1997) proposed a dimensionless formulation of the quadratic rheological model presented above (Eq. 19-5) in the form

$$\tau^* = 1 + (1 + T_d^*) c_B D_v^* \tag{19-8a}$$

in which the three dimensionless parameters τ^*, D_v^* and T_d^* are defined as follows:

1. Dimensionless excess shear stress

$$\tau^* = \frac{\tau - \tau_y}{\mu_m \frac{du}{dz}} \tag{19-8b}$$

When $\tau^* = 1$, the mixture behaves as a Bingham fluid.

2. Dimensionless dispersive—viscous ratio

$$D_v^* = \frac{\rho_s \lambda_B^2 D_s^2}{\mu_m}\left(\frac{du}{dz}\right) \tag{19-8c}$$

This is essentially the Bagnold number (Hanes and Bowen 1985). When D_v^* is large, the flow is dispersive; when D_v^* is small, it is viscous.

3. Dimensionless turbulent-dispersive ratio

$$T_d^* = \frac{\rho_m l_m^2}{c_B \rho_s \lambda_B^2 D_s^2} \qquad (19\text{-}8d)$$

When T_d^* is large, the flow is turbulent; when T_d^* is small, it is dispersive.

Julien and Lan (1991) tested the dimensionless model and the results are in agreement with the data sets from Bagnold (1954), Govier et al. (1957), and Savage and McKeown (1983), as shown in Fig. 19-11. The quadratic model is valid for all values of the parameter D_v^* and reduces to the Bingham model when $D_v^* < 30$ and to turbulent-dispersive formulations when $D_v^* > 400$.

The transition between grain-flow and fluid-mud is not easy to characterize, even in the realm of laboratory experiments (Parsons et al., 2001). Thus the limiting conditions should be used with caution in trying to distinguish between *mudflows* and *debris-flows*.

To relate the parametric delineation to the classification of hyperconcentrated sediment flows, the following guidelines are suggested (Julien and O'Brien 1997):

1. *Mud-floods* occur when the turbulent shear stress is dominant, as given by $D_v^* > 400$ and $T_d^* > 1$;
2. *Mudflows* occur when yield and viscous stresses are dominant, as given by $D_v^* < 30$;
3. *Debris-flows* or *granular flows* are expected when the dispersive stress is dominant, as given by $D_v^* > 400$ and $T_d^* < 1$.

A transition regime exists in the parameter range $30 < D_v^* < 400$, for which all the terms of the quadratic equation are not negligible. A series of examples showing the relative magnitudes of these terms can be found in Julien (1995).

Coussot et al. (1998) have proposed a laboratory test to obtain the rheological characteristics of a debris-flow that occurred on Moscardo Torrent, Italy. They added successively coarser particles obtained from the debris-flow deposits to clear water. At each addition different suspensions were obtained and tested with different rheometric techniques, such as a laboratory rheometer, inclined plane test, a large-scale rheometer, and field tests. The behavior was found to be viscoplastic and well represented by a Herschel-Bulkley model (Huang and Garcia, 1998). Schatzmann et al. (2003) have presented a new rheometer, the ball measuring system, to determine the behavior of fluids with large particles. In the absence of direct rheological measurements, Locat (1997) has shown that the liquidity index can provide a good first approximation for both mixture viscosity and yield stress of fine-grained mud flows. Bin and Huilin (2000) have advanced a methodology to determine the rheological properties of debris flows in the field which is similar to the one proposed earlier by Phillips and Davies (1991).

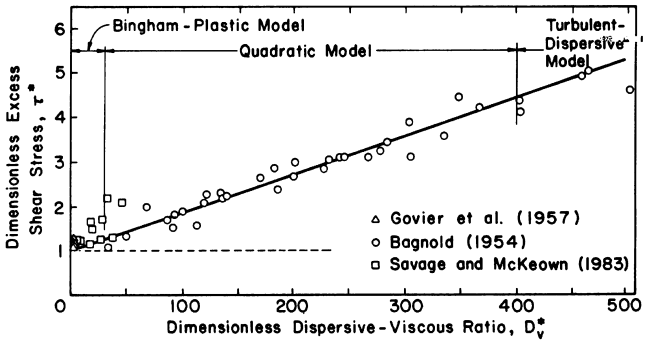

Fig. 19-11. Comparison of dimensionless model with Experimental Data (from Julien and Lan, 1991 with permission).

19.4 ALLUVIAL FAN FLOODING AND SEDIMENTATION

19.4.1 Introduction

It is generally acknowledged that the delineation of flood hazards and the design of flood mitigation structures in the semi—arid and arid western United States, and in similar environments throughout the world, is more difficult than in the humid areas of the country. The primary reason is that the southwestern United States remains sparsely settled, and most of the population and economic growth is concentrated in a few widely separated urban areas. Further, most of the development in the Southwest has taken place over the last five decades. Given this pattern of economic and population development and the episodic nature of precipitation and runoff events, few precipitation or flow gauges have records that could be characterized as either long-term or reliable; see, for example, French (1989). Also, flooding in the arid environment is less dependent on the magnitude of the event and more dependent on the ferocity, quickness, and sheer volume of materials moved. Compounding these challenges is that much of the development in arid environments has taken place on alluvial fans, which are complex landforms where ephemeral channels may be neither well-defined nor stable.

The classic definition of an alluvial fan (Doehring 1970) is

> "An alluvial fan is a relatively thick deposit of coarse, poorly sorted, unconsolidated, clastics found as a semiconical mass whose apex is adjacent to a mountain front. It has a relatively smooth subaerial surface which declines away from the mountain front."

From the viewpoint of hydraulic engineering, a more descriptive definition by the U.S. Federal Emergency Management Agency (FEMA) of an alluvial fan (Federal Register 1989) is

> Alluvial fans are geomorphic features characterized by cone- or fan-shaped deposits of boulders, gravel, sand,

and fine sediments that have been eroded from mountain watersheds, and then deposited on the adjacent valley floor. Flooding that occurs on an active alluvial fan is characterized by fast-moving debris and sediment laden shallow flows. The paths followed by these flows are prone to lateral migration and sudden relocation to other portions of the fan. In addition, these fast moving flows present hazards associated with erosion, debris-flow, and sediment transport.

The FEMA definition itemizes the hydraulic processes expected to occur on a generic alluvial fan from an engineering viewpoint, and this definition makes it clear that flood hazards on alluvial fans are due to a wide range of hydraulic processes that involve sediment movement and transport. Many of these processes are not yet well-quantified. Finally, Schumm et al. (1996), in a study of alluvial fan flooding for the National Research Council (NRC 1996a), proposed the following definition:

"Alluvial fan flooding is a type of flood hazard that occurs only on alluvial fans. It is characterized by flow path uncertainty so great that this uncertainty cannot be set aside in realistic assessments of flood risk or in the reliable mitigation of the hazard. An alluvial fan flooding hazard is indicated by three related criteria: (a) flow path uncertainty below the hydrographic apex, (b) abrupt deposition and ensuing erosion of sediment as a stream or debris-flow loses it competence to carry material eroded from a steeper, upstream source area, and (c) an environment where the combination of sediment availability, slope, and topography creates an ultra hazardous conditions for which elevation on fill will not reliably mitigate the risk."

An alluvial fan is a surface attempting to reach equilibrium with the long-term spectrum of precipitation and runoff events and will attempt to reach a new equilibrium in response to deviations from the existing surface. Engineers, primarily trained in temperate environments, often attempt a comprehensive control of the drainage—sediment transport problem without developing an appreciation of the geomorphologic viewpoint of the situation (Schick 1974; French and Keaton 1992; Keaton et al., 1990).

19.4.2 Background

Although the data on flow and precipitation in arid environments are generally sparse, the anecdotal record is replete with examples of the clear-water and sedimentation hazards associated with development on alluvial fans (McPhee 1989b). For example, in 1983, there was landslide-induced flooding at Ophir Creek, Nevada (Glancy and Bell 2000). Ophir Creek is a small, elongated watershed with an area of approximately 11.7 km^2 (4.5 mi^2) terminating in an alluvial fan. The total sediment deposited during this event was approximately 555,000 m^3 (450 ac-ft), and the flood surge was estimated to have a peak flow of approximately 1,400 m^3/s (50,000 ft^3/s). A wall of boulders, mud, trees, and water, 9 m (30 ft) high by 30 m (100 ft) wide destroyed structures outside of the estimated 100-yr regulatory floodplain; one life was lost.

Common sense, given the magnitude of these estimates, suggests that this was an extreme event; however, the historical record suggests a different answer. From the historical record, Glancy and Bell (2000) discovered that significant flooding had taken place on the Ophir Creek alluvial fan in 1874, 1875, 1890, 1907, 1937, 1943, 1950, and 1963. It would appear that this single event in 1983 confirms the old adages that those who fail to learn from history are destined to repeat it. This 1983 event was recorded because it took place along a major transportation alignment in the proximity of two major urban areas. It is unknown how many similar or larger events took place in the arid and semiarid areas of the world in 1983 and were not recorded or even noticed.

From the definitions of an alluvial fan presented previously, it is important to note that alluvial fans are not features unique to the arid environment. Rather, alluvial fans are ubiquitous to all climatic environments (see Fig. 19-12 of alluvial fans in Venezuela), which leads to the following observations:

1. The interest of engineers and geologists in alluvial fans in arid and semiarid environments may be due to their prominence in these environments given the lack of vegetation and state of preservation due to the episodic nature of precipitation and runoff. For example, Anstey (1965) estimated that alluvial fans constitute approximately 30% of the land area in the southwestern United States.
2. The current and anticipated rates of development on these landforms throughout the world demand that adequate and cost-effective flood mitigation be provided to residents and property owners.
3. There are significant differences between the FEMA and geological definitions of alluvial fans. As noted by French et al. (1993), the regulatory definition itemizes the hydraulic processes that may occur on an *engineering time scale,* whereas the geological definition focuses on the process that led to the shape and location of the landform on a *geological time scale*. This contradiction of definitions is appropriate given that the engineer is concerned with an analysis of structures on an engineering time scale, whereas the geologist is concerned with the geomorphic processes that resulted in the landform regardless of time scales.

The foregoing observation leads to the conclusion that when an analysis of flood flows on an alluvial fan is undertaken, the engineer must be sensitive to the processes that are active on the landform under current, engineering time scales, but also should be very aware of the geomorphic processes that continually form and reform the alluvial fan.

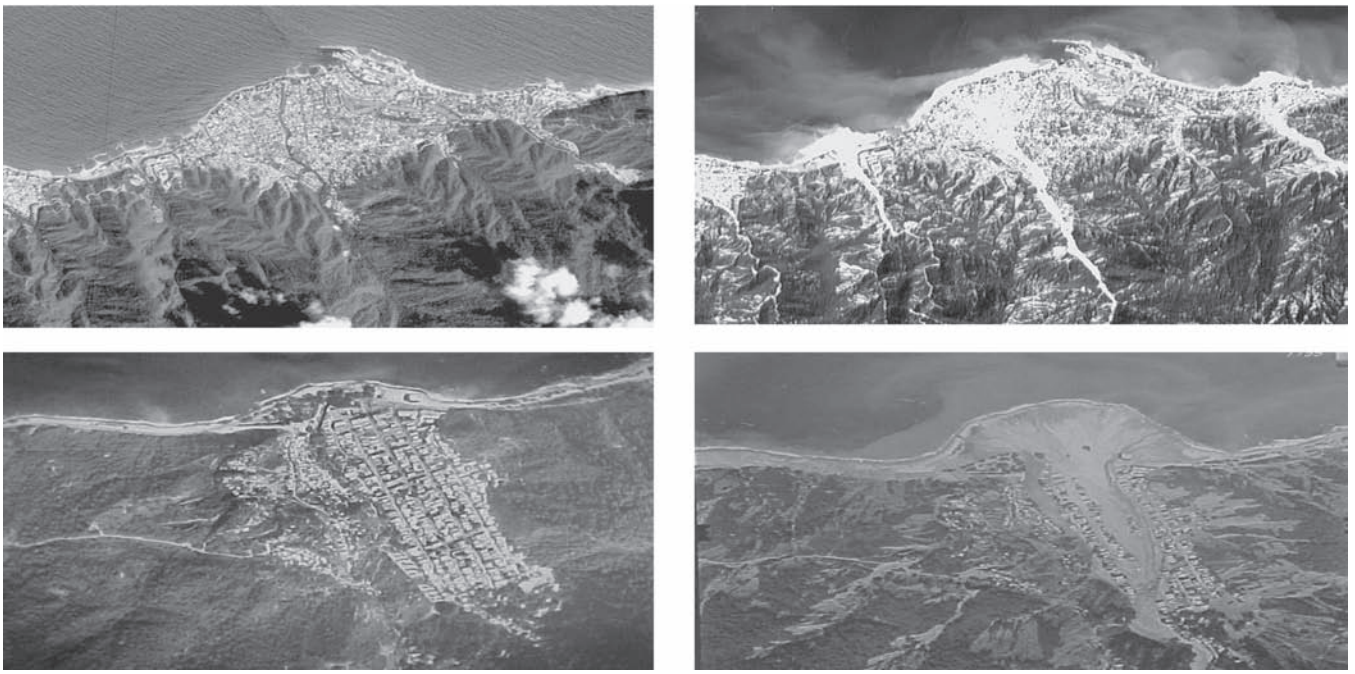

Fig. 19-12. SPOT Satellite images taken before and after the events of December 1999 of the alluvial fans in San Julián (above) and Carmen de Uria (below), Venezuela.

As Parker (1999) noted, the disparity between the engineering and geological time scales on alluvial fans can lead to significant misunderstandings regarding risk. For example, the fan-delta system on the Mississippi River south of Baton Rouge has avulsed several times to form multiple deltaic lobes over the past 5,000 years. However, over the lifetime of one engineer there was likely no change, which gives the illusion of stability (Parker 1999). It is pertinent to note that a lay discussion of this particular issue is provided in McPhee (1989a).

19.4.3 Early Developments

Attention to and focus on alluvial fan flooding and sedimentation issues in the engineering literature began with the publication of a probabilistic approach to identify regulatory flood hazard on alluvial fans (Dawdy 1979). The work by Dawdy was partially based on earlier results regarding channels formed by rare flood events on the surfaces of alluvial fans in the Albuquerque, New Mexico area, which were subsequently published (Magura and Wood 1980). These initial approaches to identifying flood hazard on alluvial fans were followed by others (*e.g.*, Edwards and Thielman 1984), and the establishment, by the regulators (*e.g.,* FEMA 1985), of guidance specifically for the evaluation of flood hazard on alluvial fans. These early papers dealt exclusively with the clear-water hazard on alluvial fans and did not incorporate the work and knowledge that the geoscience community had gained from decades of studying sediment processes on these landforms. Also, they did not acknowledge that not all alluvial fans are active alluvial fans and that sound engineering judgment and new technical approaches were required to properly evaluate the clear-water and sediment hazard issues on these landforms.

The original FEMA (1985) approach to delineating flood hazard on alluvial fans contained the following key assumptions: (1) alluvial fan flooding is conveyed at critical depth in flow-formed channels governed by regime equations of depth, velocity, and discharge at the apex; (2) the location of the flood channel is unpredictable; (3) topographic relief and urbanization on the fan are minimal; and (4) the hazard is due only to clear-water flows. These and other implied assumptions were discussed by French (1987). In the view of many competent professionals, this generic approach to alluvial fan flood hazard incorporated assumptions that were not valid on all alluvial fans and, in some cases, had been misapplied (*e.g.,*Fuller 1990; Pearthree 1991; and Pearthree et al. 1991). This controversy over the use of a generic model to identify alluvial fan flood hazards led the Flood Control District of Maricopa County, Arizona (FCDMC), to undertake a study of alluvial fans (FCDMC 1992). The results of this study were published in French et al. (1993). The measurable characteristics and expected hydraulic processes during flood events on the types of alluvial fans identified during the FCDMC study are shown in Tables 19-4 and 19-5.

The early studies neglected the need to address not only clear water but also water transporting a wide range of sediment loads. Dependent on the concentration of sediment relative to the water, flood flows on an alluvial fan can be

Table 19-4 Measurable Alluvial Fan Characteristics

Active alluvial fan	Distributary flow system	FEMA alluvial fan	Inactive alluvial fan
Abandoned discontinuous channels	Discontinuous channels	Continuous channels	Continuous channels
Channel capacity decreases downstream	No definite trend in channel capacity	Cummulative capacity constant downfan	Channel capacity increases downstream
Channel flow changes to sheetflow	Channel and sheetflow	Channelized flow (no overbank or sheetflow)	Channelized flow (overbank flow possible)
Debris-flow possible	Minor (or no) debris-flow	Debris-flow important	No debris-flow
Frequent channel movement	Rare channel movement	Unpredictable channel location	Stable channels
Low channel capacity	Variable channel capacity	Channel capacity equals flow rate	High channel capacity
No calcrete	Calcrete horizons possible	No calcrete	Calcrete horizons
No (or buried) desert varnish	Varnished surfaces possible	No (or buried) desert varnish	Varnished surfaces possible
No surface reddening of soils	Minor reddening of soils	No surface reddening of soils	Surface reddening of soils
Overall deposition	Local erosion and deposition	Overall deposition	Overall erosion
Radiating channel pattern changes to sheetflow area	Radiating channel pattern changes to tributary	Single or multiple channels	Tributary drainage pattern
Slope decrease downstream	Slope increase at apex	Slope not a factor above bifurcation point	Slope variable
Stream capture or avulsions?	Channel movement by stream capture	Channel movement by avulsions	No channel movement
Uniform topography (low crenulation index)	Medium to low topographic relief (medium to low crenulation idex)	Uniform topography (low crenulation index)	Topographic relief (high crenulation index)
Uniform vegetation in floodplain	Diverse vegetative community	Uniform vegetation in floodplain	Diverse vegetative community
Variable channel geometry	Variable channel geometry	Regular channel geometry	Regular channel geometry
Weak soil development	Variable soil development	Weak soil development	Strong soil development

Note: In a specific application not all of the characteristics noted may be present.

a fluvial flow, a hyper-concentrated flow, a mudflow, or a debris-flow; and in each of these situations a different modeling approach is required.

19.4.4 Current Developments

In response to the controversies raised over the use and misuse of the probabilistic method of identifying flood hazards promulgated in FEMA (1991), the National Research Council undertook a study of alluvial fan flooding (NRC 1996a). Although the report provides valuable data and insights, there are many issues that may be unresolved. In particular, the report relied mainly on the experience of the geosciences community but did not take full advantage of the valuable experience available in the engineering community. It is clear that cooperative input from both the geosciences and engineering fields is necessary to effectively study and analyze alluvial fan flooding. The NRC report did not consider also the alluvial fan development situation in what was then, and remains, one of the fastest growing, and most arid states in the United States—Nevada. It is in this state where alluvial fans are currently both primary engineering research and legal issues. The U.S. Department of Energy, Nevada Operations Office, has likely dedicated more resources to identifying and evaluating flood hazards on alluvial fans and arid region hydrology than most other Federal Agencies combined.

In addition, there are now two-dimensional models available for modeling flows on alluvial fans. FLO-2D (O'Brien 1999) is a two-dimensional hydrodynamic model designed for both clear water and sediment-laden flood flows on alluvial fans. An application of FLO-2D by Bello et al. (2003) is presented later in *section 19.6.3.6* of this chapter. Important new experimental-field scale advances regarding alluvial fans have also been recently published; for example by Parker et al. (1998a and 1998b) and Whipple et al. (1998). Progress has also been made with the linking of channel process with

Table 19-5 Expected Hydraulic Processes during Flood Events

Active alluvial fan	Distributary flow system	FEMA alluvial fan	Inactive alluvial fan
Channel movement possible	Channel movement rare	Unpredictable channel location	Channel location stable
Channel, overbank, and sheetflow	Channel, overbank, and sheetflow	All flow channelized	Channel, overbank, and sheetflow
Debris-flows important	Debris-flows not important	Debris-flows not considered	Debris-flows not important
Flows along existing and new channels	Flows along existing channels	Flow cuts new channel	Flow along existing channel
Flow attenuation	Flow attenuation	No flow attenuation	Flow attenuation likely
Net deposition on surface	Local deposition and erosion	Deposition not considered	Net erosion on surface
On-fan watershed flooding	On-fan watershed flooding	On-fan watersheds not considered	On-fan watershed flooding
Probable sediment bulking	Probable sediment bulking	No sediment bulking	Probable sediment bulking
Stream capture or avulsions?	Rare stream capture or avulsions	Channel movement by avulsions	No avulsions
Topography influences flow	Topography influences flow	Flow not affected by topography	Topography controls flow

Note: In a specific application not all of the characteristics noted may be present.

large-scale morphodynamic changes in fluvial fan-deltas such as the Mississippi delta (Sun et al., 2002) as well as in the use of physical models to assess flooding risks in alluvial fans (Cazanacli et al., 2002) and the limitations of such physical models (French and Miller, 2003). Physical modeling of sedimentation processes is addressed in *Appendix C-Sediment Transport Scaling for Physical Models* of this manual.

19.4.5 Conclusions

Although much has been done regarding the accurate and reliable definition of flood hazard on alluvial fans on an engineering time scale, still much remains to be accomplished. For example, even the basic definition of an engineering time scale remains to be defined. French et al. (1993) arbitrarily defined an engineering time scale to be 1,000 yr or less and a geologic time scale to be 10,000 yr or more. Although this definition provides a 9,000 yr difference, it is pertinent to observe that in the arid environment, engineers may be required to predict, given Federal requirements, the performance of flood mitigation structures for up to 10,000 yr. From the engineering viewpoint, predicting the performance of facilities 10,000 yr into the future involves pure speculation; however, under regulatory guidance specific to some types of waste management sites, this period is considered an engineering time scale. For example, by definition, an alluvial fan is an aggradational landscape feature on a geologic time scale; however, there are no guarantees that a channel could not be incised through a facility in response to a major event that occurs within an engineering time period, given that the facility design period (or likelihood of a rare event that has the same probability of occurring) may be up to 10,000 yr. That is, the Dawdy (1979) or random channel movement across an alluvial fan surface is correct on a geologic time scale, which accounts for the symmetrical depositional shape of the fan.

The challenge facing the research community is that of producing results that are useful to the regulators, the practitioners, and the public. Modern researchers in engineering and science have to understand the need to show how their results relate and pertain to a larger world. At the same time, regulators ought to become more flexible and use good engineering judgment rather than rigidly adhering to a single approach to defining flood hazard on alluvial fans. The need to move away from rigidity was one of the recommendations of Schumm et al. (1996) that struck a common cord in the professional community.

The engineering community has to remember that alluvial fan flooding is a cutting-edge technology. Hazard evaluations in this field require field investigations by engineers together with colleagues who have expertise in geosciences and risk analysis. As shown above, it is also very important to search for historical records that might help in conducting flood hazard risk analysis. The accurate identification of flood hazard and mitigation of flood hazard on alluvial fans must be a shared experience between the engineers, geologist and geomorphologists to ensure that the public will be afforded the best technologically feasible level of protection and to avoid potential litigation issues. Readers can find more material on alluvial fans in Chapter 18, *Engineering Geomorphology*, while legal issues associated with flood

and sedimentation hazards are addressed in Chapter 20—*Sedimentation Law*.

19.5 METHODS TO MITIGATE THE CONSEQUENCES OF SEDIMENTATION HAZARDS

19.5.1 Background

Reliable assessment and mitigation of hydraulic and sedimentation hazards depend on the engineers' ability to understand and describe in written and mathematical forms the physical processes that govern the fluvial system they are dealing with. As presented under 19.2, *Sedimentation Hazards—History and Magnitude*, significant hazardous conditions and natural disasters associated with sedimentation processes have occurred throughout recorded history. Today, however, engineers and scientists have greater access to data, information, and knowledge regarding where, when and how such events may occur. New procedures and mathematical modeling tools have evolved as aids to better assess present conditions and forecast future conditions. However, it must be recognized that the present state-of-the-science and our understanding of mobile boundary hydraulic processes related to different types of sedimentation hazards and mud and debris-flow processes are still limited. Exacerbated by our having few or no measured field data, these complex processes often evade theoretical attempts to characterize flow depth, location, orientation, velocity, sediment- and debris carrying capacity, and event predictability with a high degree of accuracy.

Methods for assessing and mitigating the consequences of severe sedimentation hazards, including mud and debris-flows, fall into three general approaches and levels of effort:

- *Hazard mapping and avoidance*—e.g., perform a hazard mapping study and have people not live there if it is mapped as a likely hazard zone; or if people already live there, help them to understand the risk and require that they buy hazard insurance. This approach focuses on avoidance of hazards, not mitigation.
- *Apply currently accepted hazard assessment and mitigation design procedures*; e.g., if you wish to develop in a hazard zone, apply currently accepted assessment procedures to define hazards and their levels of risk, and then apply appropriate design procedures to develop structural or nonstructural methods for mitigating the hazards.
- Apply new *state-of-the-science procedures*; e.g., if you wish to evaluate the risk of hazards or wish to develop in a hazard zone, you may elect to apply innovative methods including hazard forecasting, risk assessment, and process-simulation modeling and apply new design concepts to mitigate the hazards. New mitigation methods may include structural, nonstructural, or bio-technical procedures or a combination of these methods.

19.5.2 Hazard Mapping

Prior to the mid-1990's, there was very little guidance available for evaluating site-specific conditions or the mapping of flood hazards on alluvial fans or of hazards directly related to ultrahazardous sedimentation processes. As of the year 2000, however, hazard-mapping procedures predominantly follow those supported and documented by the Federal Emergency Management Agency (FEMA 1990; 1995; 2000), Federal Register (1989) guidelines and the National Research Council (NRC 1996a). FEMA prepares Flood Insurance Rate Maps (FIRMS) of flood hazard areas based on the results of Flood Insurance Studies (FIS). Those studies determine the areas with a 1% annual chance of being inundated (by water). The flood is called the *base* (100-year) *flood* by FEMA. The FIS must evaluate the existing flood conveyance system, including installed flood-control measures. Determination of the inundated area may depend on whether flood-control measures protect part of the floodplain. With increased development in the United States and other countries of the world, more people are being exposed to extreme flood hazards associated with flash floods, mud and debris-flows, high flow velocity, channel avulsion, severe erosion, and channel migration and episodic alluvial fan processes. FEMA (2000) recently expanded their guidance regarding the identification and mapping of traditional flood hazards to include procedures for flood hazards occurring on alluvial fans, *irrespective of the level of fan-forming activity* (see Section 19.4).

19.5.3 Currently Accepted Hazard Assessment and Mitigation Design Procedures

Most *accepted* assessment and design procedures depend on empiricism, experience, field observation, and the application of traditional clear-water assessment methods that have been modified to account for flow bulking, sediment dynamics, and the unpredictable and often episodic nature of sedimentation processes leading to hazardous flow conditions. These accepted practices have come into general usage because of their simplicity and relative accuracy. Accepted practices used primarily for the design of flood control channels are emphasized in this chapter. The most accepted and best documented sediment hazard assessment and design procedures are documented by the following federal agencies: the U.S. Army Corps of Engineers (USACE 1989; 1991; 1993; 1994), the HEC (1993), the Federal Highway Administration (FHWA, 2001), and the U.S. Department of Agriculture (1992; 1996). In the relatively new area of evaluating significant sedimentation hazards, and mud and debris-flows, sufficient time and proven testing has not yet occurred for accepted design practices to emerge.

19.5.4 State of the Science Procedures

New state-of-the-science procedures are often related to new computer simulation models or untested design concepts that may implement hybrid techniques, bio-technical flow diversion or stream stabilization measures. In such cases, the latest research has not yet been fully tested or documented sufficiently to become general practice. State-of-the-science procedures can be applied, but they, as well as the accepted practices, need to be thoroughly checked against real data and a reasonable range of possible hazard scenarios to cover all likely sedimentation and flow conditions the project area may experience during its lifetime. New procedures are most often presented in technical and trade journals or conference proceedings. For the most part these newly developed procedures are relatively untested and have not yet become general practice.

The following discussions are aimed at providing guidance to engineers and flood-hazard managers for planning and assessing the adequacy of flood-control measures exposed to significant sedimentation hazards and mud and debris-flows. This section is not intended to be a design manual for mitigation of sedimentation problems. It is intended to summarize general procedures for assessing flood hazards and for developing reasonable mitigation alternatives. A following section will list several accepted methods for hazard mitigation. Readers should also read Chapter 20—*Sedimentation Law*, for recent interpretations of pertinent court decisions regarding standards of practice and prudent levels of assessment and design.

19.5.5 General Approach

The following general approach is suggested to assess and develop sedimentation hazard mitigation alternatives. The approach consists of three phases of work:

Phase 1: Problem identification, preliminary assessment and design

- Perform site assessment and geomorphic analysis of project area
- Define hydrologic, hydraulic and sedimentation processes and hazards
- Perform surveys and hazard mapping if required
- Develop preliminary alternatives for hazard mitigation
- Perform preliminary engineering and environmental evaluation of alternatives for hazard mitigation
- Initiate the regulatory and environmental process
- Perform screening of preliminary alternatives to select a preferred alternative(s)
- Perform feasibility level design of preferred alternative(s)
- Prepare draft environmental documents (EIR and/or EIS)
- Seek public involvement and consensus

Phase 2: Prepare plans, specifications, and estimates (PS&E) along with CEQA/NEPA documentation and permitting

- Perform detailed design and environmental analyses
- Prepare final plans and specifications
- Prepare cost estimates
- Prepare final CEQA and NEPA documentation
- Respond to public comments
- Define project-related mitigation requirements
- Obtain regulatory permits
- Finalize project authorization and funding

Phase 3: Project construction, project mitigation, and monitoring

- Construct project
- Perform project-related mitigation
- Initiate project monitoring program

Phase 1 is perhaps the most important phase because it must identify the underlying physical processes affecting the site and properly define existing and potential hazards as well as other project constraints related to regulatory or environmental concerns if mitigation activities were to occur. It is essential that hazard mitigation alternatives not only reduce or eliminate identified hazards, but also not result in the initiation of other problems or impacts for areas upstream or downstream of the proposed project site (channel stability, scour, and significant changes in the hydrologic regime, environmental impacts, or significant project maintenance requirements). It is, therefore essential to perform a thorough regional assessment of the area's geomorphology, hydrology, hydraulics and sedimentation characteristics and compare those *existing* (baseline) *characteristics* to proposed *with-project conditions* to avoid project-induced impacts. MacArthur, et al., (1993) recommend that "reliance and single all-purpose model or computer program should be avoided," and they outline 14 elements of a multi-phased modeling and assessment approach for evaluating special sediment hazards. Environmental regulations require equal detail regarding the evaluation of potential impacts on the environment or endangered species.

19.5.6 Guidance

Detailed guidance on how to conduct planning and design studies for mitigation of flood hazards is found in many state and federal guidelines. Section 1–6 in the USACE (1991), manual *Hydraulic Design of Flood Control Channels (Engineering Manual 1110-2-1601)* outlines steps for conducting preliminary investigations for selection of type of improvement for mitigation of flooding hazards. The Corps emphasizes the need for careful consideration of the physical characteristics of the site, its history of flooding, and the nature of aggradation and degradation, debris transportation,

bank erosion, cutoffs, and bar formation. Other hydrologic, hydraulic, and economic aspects of the project are also important.

Engineering Manual 1110-2-1416, *River Hydraulics* (USACE 1993), states that "effective analysis of river problems requires recognition and understanding of the governing processes in the river system. There are two basic items that must always be considered in river hydraulics analyses: the characteristics of the flow in the river, and the geomorphic behavior of the river channel." These two components are sometimes treated separately, however, in alluvial channels and floodplains (zones with movable boundaries) the flow and the shape of the boundary are interrelated. This is especially true during severe events occurring on movable boundaries such as alluvial fans.

Engineering Manual 1110-2-4000, *Sedimentation Investigations of Rivers and Reservoirs* (USACE 1989) outlines procedures for conducting staged sedimentation studies, including (1) sediment impact assessments, (2) detailed sedimentation studies, and (3) feature design sedimentation studies for the final design and location of project features. *EM 1110-2-4000* discusses the approach, data requirements, analyses, validation requirements, and design procedures for conducting thorough sedimentation investigations and designs. The manual discusses the importance of and procedures for identifying potential river sedimentation problems, and associating those problems with project purposes and presents methods for analyzing them at various levels of detail.

Engineering Manual 1110-2-1418, Channel Stability Assessment for Flood Control Projects, provides guidance for determining potential channel instability and sedimentation effects (potential problems) in flood control projects. "It is intended to facilitate consideration of the type and severity of stability and sedimentation problems, the need for and scope of further hydraulic studies to address those problems, and design features to promote channel stability. The concept of channel stability implies that the plan, cross-section, and longitudinal profile of the channel are economically maintainable within tolerable limits over the life of the project" (USACE 1994). Principles of stability and the causes and forms of instability and sedimentation problems are discussed.

The HEC (1993) prepared a report for the Federal Emergency Management Agency on *Assessment of Structural Flood-Control Measures on Alluvial Fans*. The report summarizes key geomorphic aspects of alluvial fans and discusses their unique hydrologic and hydraulic characteristics. It also discusses the effects of channel avulsion, occurrence of mud and debris-flows, channel incision or entrenchment, and an alluvial fan's capacity to carry and deposit sediments during various flood events. The Flood Insurance Administration requires an assessment of the effectiveness of various structural approaches to flood control in alluvial fan special flood hazard areas (SFHAs), (HEC, 1993). This report documents how installed flood-control measures have performed during major floods and presents current methods for assessing the performance and adequacy of the measures. HEC did not investigate nonstructural measures or procedures for mapping of alluvial fans as part of their study. The report is not intended to be a design manual. It is aimed at providing guidance to floodplain managers and engineers in assessing the adequacy of structural flood-control measures on alluvial fans (primarily improved channels, flow diversions, bypasses, and detention storage facilities) to protect against the Base Flood (HEC, 1993).

19.5.7 Examples of Structural Flow, Sediment and Debris Management Measures

HEC (1993) presents several case studies of flooding problems and in some cases, failures of flood-control project features that were exposed to high flow, sedimentation, and/or mud- and debris-flow conditions. Types of bank protection, flow diversion, and debris and sediment management measures include the following:

Bank Protection Works:

- Works designed to stabilize erodible channel banks and protect them from high-energy flows
- Pipe-and-wire fences
- Riprap (dumped rock)
- Rock paving (hand-placed)
- Wire and rock mattresses
- Gunite slope paving
- Reinforced concrete open channels
- Reinforced concrete closed conduits
- Bio-technical bank stabilization and erosion control measures (see USDA 1996)

Debris Barriers:

- Structures, usually located in the watershed, that stop or reduce the movement of debris down the channel system
- Debris fences (typically vertical beams or rails anchored in a foundation, sometimes with wire or cable reinforcement, oriented perpendicular to expected debris-flows)
- Debris barrier walls, typically referred to as fire barriers in southern California and built across canyon mouths following fires to retard debris-flow induced by heavy rains on the burned watershed (LACFCD, 1979).

Crib Barriers:

- Series of check dams across a channel constructed from concrete, rock, or logs, which retard flows, capture sediment and debris, and may provide seasonal wetland areas, and help stabilize the toe of canyon side slopes (see LACFCD 1959 for sketches and designs).

Debris Basins:

- Facilities designed to capture, store and settle out coarse material and trash resulting from a major storm event
- Guidance for Debris Basin design may be found in (LACFD 1979)

Sediment Traps and Sediment Retention Structures:

- Sediment traps are constructed depressions in a channel, stream bed or floodway that encourage rapid accumulation of bed load sediments during high flows. The Corps of Engineers occasionally installs sediment traps in high bed load river systems in locations where sediment removal can be managed more effectively and with the least amount of impacts to the environment.
- Sediment retention structures (similar to debris barriers and basins) are designed to capture, store, and settle out sediment materials from major storm events. Perhaps the most documented large-scale sediment retention structure was designed and constructed by the Portland District Corps of Engineers on the Toutle River downstream of Mount St. Helens following its eruption in 1980 (HEC 1985). The structure was designed to retain annual sediment loads, as well as significant mud and debris-flows that could move down-valley from areas affected by the eruption of Mount St. Helens.

Other Sediment Control Structures:

- Constructed wetlands
- Vegetative filter strips and strategic planting of riparian vegetation
- Porous structures: small check dams, filter fences and straw bales

Retention Basins:

- Storage structures (usually uncontrolled) designed to reduce the peak flood flow from a drainage basin. Such structures can also (often by default) capture sediment and debris, which may affect their original design performance. A well-documented debris basin project with a spillway and concrete-lined flood control channel and energy dissipater is discussed by the Los Angeles District Corps of Engineers; see (USACE 1983; 1988).

Operation of Small Dams:

- Existing small dams also work as retention basins during large storm events unless they are operated to remain full for water supply, hydropower, or other reasons
- Outlet and storage capacity are typically reduced by sediment and debris accumulation

Flood Control Channels:

- Engineered works designed to pass flood flows more efficiently than natural, unimproved channels, thereby reducing flood stages.
- Unlined channels
- Lined channels
- Maintained and stabilized natural channels

Diversions and Bypasses:

- Constructed channels designed to provide additional flow capacity during floods, or designed to direct flows away from developed areas

Floodwalls:

- Vertical walls, usually constructed with reinforced concrete and typically oriented parallel to a stream or channel to prevent overtopping flows from leaving the channel and entering developed areas.

Levees:

- Usually constructed of earthen and rock materials, oriented parallel to the stream or channel; designed to prevent overflows into developed areas
- Single-levee projects (one side of channel only)
- Double-levee projects (both sides of channel)
- Set-back levees (levees set back on the floodplain a measurable distance from the main channel to allow controlled flows on the confined floodplain, although preventing overflows into developed areas)

Floodwalls and Dikes:

- Often used in conjunction with other flow or debris diversion structures
- May be placed across a channel, floodplain or alluvial fan to direct flow away from developed areas or direct flow into bypass or retention facilities

HEC (1993) discusses special problems related to sediment transport issues, including sediment accumulation, scour and debris. Evaluation and design procedures for these processes are documented in (USACE 1989; 1994). HEC (1993) also states:

> "Every factor affecting the nature of flood and debris problems, plus the development and its susceptibility to flooding, affect the feasibility of flood-reduction options. There is no cookbook approach to developing an effective flood reduction project. Planning and design of flood-control (*and sediment and debris control*) structures . . . must always consider **the effect of all possible flows on the structure as well as the effects the structure may have on the flow locally and downstream.** While FIA criteria are based on the 1-percent chance flood, the proper design of any flood-control project must consider project

Copyrighted Materials
Copyright © 2008 American Society of Civil Engineers (ASCE)
Retrieved from www.knovel.com

CHAPTER 20

American Sedimentation Law and Physical Processes

James E. Slosson, Douglas Hamilton, and Gerry Shuirman

20.1 INTRODUCTION

20.1.1 Recent Trends in American Sedimentation Law

This chapter, more than any other in the first edition of Manual 54, deserves to be updated and expanded. As the population of the United States grows, there is more demand for government to provide infrastructure, and to balance the pressure of urban expansion with regulatory objectives such as hazard mitigation and the environment. New theories of legal liability such as inverse condemnation have changed the way that government carries out this mission. In essence, the power we delegate to government and the decisions it makes on our behalf and with our participation add up to priorities that change society. This driving force is at least as great as the pursuit of science when it comes to breakthroughs in the application of sedimentation engineering concepts.

20.2 MANUAL 54: SEDIMENTATION ENGINEERING (VANONI 1975)

20.2.1 General Summary

After devising the problem, author C. E. Busby, when writing Chapter VII of Manual 54 entitled "American Sedimentation Law and Physical Processes" (1975), mapped out these physical processes of sedimentation, how they relate to supreme court case-law, and how engineering practice responded. He used the following concise yet well informed outline.

20.2.2 Legal Concepts Applied to Water, Air and Land

Erosion damage is part of the sedimentation process and possession or right to possession is the basis for rights in land and water. "In American jurisprudence, one cannot own the water as it runs in a stream or moves in the air, for one cannot legally possess it in these natural states. This has given rise to legal concepts as old as Roman Law; that these moving waters are the property of no one (res nullius) or of all people (res communes)."

20.2.3 Erosion and Sedimentation Processes Vary Geographically

The difference between natural rate and artificial rate produced by man is seen as significant in determining legal liability, and the concept of what is a public stream is changing as the needs of the public change.

20.2.4 Land Pattern Affects Process and Legal Consequences

As in common law, jurisdictions that shape land ownership tracts per settlements of the original states by metes and bounds or by sections and townships virtually ignore drainage lines for younger settlements. There are also public geographic boundaries such as counties, municipalities, states, and the nation, which include national forests, public parks, and wildlife refuges that may have ownership boundaries wherein governmental powers may be exercised over natural resources and people. This deals mainly with sovereign control of development and use.

20.2.5 Water Pattern Affects Process and Legal Consequences

Bearing in mind that the facts make the case, natural water patterns depend largely on slope, soil, bedrock, gullies, and stream channels and are superimposed by the invisible cultural pattern of water supply and rights of use, as defined and classified in law. Diffused surface waters, vagrant floodwaters, and watercourses defined as either navigable or non-navigable were originally based, per common law, on the ebb and flow of the tide. There is a need to bring law and science closer together in terms of reality and process.

20.2.6 Sources of Law

Water laws have been subject to local customs down through the ages, which has had a marked influence on such laws as they evolve. The old "cujus est solum" theory affects all water supplies because it affects every land ownership tract. Geographically, riparian laws are adapted according to the character of the land. Precipitation runoff plays a main part in common law, a partially unsound theory based on ownership per title to soil rights in turn expanding to ownership of all waters on and under titled soil, as well as the space above and the minerals below. Scientific fact brings into play other moving resources such as water, oil and gas, air and wildlife. Constitutional provisions within the broad scope of the law are veering away from older unscientific concepts and judicial administration toward more scientific concepts and executive administration. Due to this trend, the engineering and legal professions are increasing in importance due to development and application of basic scientific data within the broad framework of legal administrative processes and standards in the field of social engineering.

20.2.7 Rights in Land and Diffused Surface Waters

Busby's chapter includes a section on this topic.

20.2.7.1 Definitions of Supplies and Interests Applicable engineering principles are at the core of water cycles related to diffused and defined surface waters. "Engineers know that water is usually conveyed in some sort of 'channel' as soon as it starts to move over the land." Due to the law of streams, sediment deposits may be in one's "possession" during one year and in transit and out of possession during another.

20.2.7.2 Common Enemy Rule The so-called absolute property right in land is qualified by exceptions in several states in the interest of the rights or needs of neighbors. The rule of reason ableness incorporates more science into law due to sound reasoning with consideration of relevant scientific fact, method and technique when supported by local custom and practice.

20.2.7.3 Civil Law Rule Problems arising out of land improvement have led to the adoption of the reasonable use rule which states "that the upper landowner may not unduly collect, concentrate, and discharge diffused surface waters on the lower land in increased velocity and volume, so as to do substantial injury to the lower lands." This rule of reason law tends to balance the relative interests of upper, lower, and adjacent landowners as to damage resulting from harmful runoff. The task at hand for engineers is to define (for the courts) these rights and the interests thereof per scientific measure, evaluation and prediction of runoff and damage.

20.2.7.4 Reasonable Use Rule In effect, the reasonable use rule says that a landowner may use his own land as he pleases provided he does not unreasonably interfere with the like rights of others. Reasonableness and unreasonableness are questions of fact.

20.2.7.5 Rules Governing Pollution Damage by Sediments to Lower Lands and Diffused Surface Waters It has been upheld that the upper landowner is not liable for damage to lower lands caused by diffused surface waters carrying soil and rock when they constitute part of the "natural formation of the land." He is liable for resulting damage if he places other soil and rock where the natural drainage of such water will carry it to lower tracts of land or where it interferes with normal drainage, though there are exception.

20.2.7.6 Rules Governing Pollution Damage by Sediments to Navigable Waters and Adjacent Lands Works of improvement must adhere to the non-obstruction of navigable waters. It is of special interest to lawyers and engineers to interpret Section 10 of the Rivers and Harbors Act of 1899 that states, "That the creation of any obstruction not affirmatively authorized by Congress, to the navigable capacity of any of the waters of the United States is hereby prohibited" further to include industrial solids in suspension but not in solution. This applies to organic waste that reacts chemically on discharge into a stream, so as not to remain permanently as an obstruction in the form of a shoal deposit.

20.2.8 Rights in Land and Defined Surface Waters

The following excerpts outline Busby's findings on these subjects.

20.2.8.1 Definitions of Supplies and Interests Conditions under which riparian rights are acquired and lost are important to engineers and their clients due to the fact that engineers are called on to render services in measuring and appraising land and water resources and evaluating property damage from control and use.

20.2.8.2 Rights to Riparian Land as Deposited Sediment Sediments affect the position of a channel in the flood plain by changing channel capacity as well as the topography of the surrounding flood plain. Rights to deposited sediments in flood plains or stream channels may be gained or lost by changes in the position of the channel itself, due to the action caused by both water and sediment.

20.2.8.3 Riparian Rights Gained or Lost by Accretion This riparian right refers to permanent changes made to the land when a stream or river recedes below the watermark, exposing deposits recognized as accretions. For instance, an island "rising" in a river unconnected to the riverbank belongs to the owner of the bed at that particular place. In general the rule is that the State owns the bed of a navigable watercourse unless that State permits the adjacent riparian owner to own the bed subject to the navigation servitude.

20.2.8.4 Riparian Rights Gained or Lost by Avulsion Although the rule varies from state to state, generally speaking, when the tract of land is severed by sudden change in the channel of a given stream that does not indicate that the right to that tract has been lost. Basic riparian rights may be lost when the thread of the stream is no longer the natural boundary. The original owner may opt to ditch the stream back to its former

channel if done so within a reasonable amount of time and without trespassing on the land of another and without causing undue harm to another's land.

20.2.8.5 Rights to Be Free from Undue Damage Caused by Obstructions; Major Works of Improvement, Sediment Wedges, and Similar Causes; Definition of Influences Causing Undue Damages Environmental influences causing undue damage to lands, waters, and other resources are multiple in nature:

1. Construction of major works of improvement
2. Fluctuations in reservoir and other surface water levels
3. Severe erosion and high sediment yields of upstream watershed lands
4. Unwise use and treatment of upstream watershed lands
5. Backwater effects of dams, reservoirs, and sediment wedges
6. Combinations of environmental influences and their consequences

20.2.8.6 Rules Governing Recovery of Damages Caused by Obstructions and Sediment Wedges Discussion of sedimentation and other forms of related damage recognized in law due to court decisions related to taking of property by overflow, erosion, sediment deposition, and rise in groundwater table, with sediment depositions mapped out by date.

20.2.8.7 Other Rights Rights to be free from undue damage caused by obstructions such as major works of improvement, sediment wedges, and similar cases are outlined, with definitions of influences that cause undue damages; rules governing the recovery of damages caused by obstructions and sediment wedges.

20.2.9 Key Questions

The key questions the original Chapter VII addresses are:

1. Rights in and to sediments, as land (property), recognized in law as arising out of natural and artificial changes in the movement of water
2. Rights to legal damages recognized in law as arising out of artificial changes in the movement or effects of water and wind, with special reference to sedimentation; and
3. Powers of government recognized in law necessary to regulate land and water use to prevent undue change by sedimentation to resources and to the health, safety, and welfare of the community?[1]

20.2.10 Further Topics

In addition, the original chapter reiterates historical documentation that involves trends in sedimentation law due to legal consequences, as it relates to land development and land use, dating back to original settlements, colonies, Indian boundaries, water boundaries and their authorities at that time. Legal concepts are reviewed as they apply to the possession of water, air, and land, and how changes in erosion and the sedimentation process vary geographically. Busby concludes that resource management hinges on natural boundaries and cultural ownership. His well-referenced chapter deals with theories of property ownership and the use of legal boundaries, which ultimately leads to a definition of today's changing law as it pertains to water supplies, sedimentation, and saline processes.

20.3 RECENT TRENDS IN AMERICAN SEDIMENTATION LAW

Within the law pertaining to sediment engineering, recent trends involve riparian matters pertaining to the environment and conservation. Water law has evolved from water consumption to quality control, covering a wide spectrum of engineering—from dairy operations on creeks to mining techniques to building dams. As a result of these ecological concerns, unresolved legal issues materialize as they pertain to changes in physical boundaries due to consequences of natural hazards such as unexpected floods, unprecedented weather, and subsequent sediment transport.

Conservation systems and programs that are designed to reduce soil losses from erosion to acceptable levels are on the rise. Stringent guidelines, amending old laws, provide a mechanism for encouraging landowners to reduce erosion and siltation. For example, federal policy discourages conversion of wetlands to farmland, because the remaining wetlands have important ecological and hydrologic value (USEPA, 1998).

On 7 January, 1998, the U.S. Environmental Protection Agency released its first national report on the quality of sediments in the nation's rivers and streams. Although the report discovered that the majority of watersheds do not pose adverse risks, it cited that 7% of the surveyed watersheds have contaminated sediments. Every state in the union has some level of sediment contamination affecting its streams, lakes and harbors. This fact goes hand in hand with the trend toward laws supporting a watershed-wide consideration of environmental elements. Bearing in mind that impervious areas affect how water runs off the land, the development and maintenance of properly engineered drainage basins continues to play an important part in the future of water science.

20.4 KEY TREND-SETTING COURT DECISIONS

One of the most difficult problems in the field of sedimentation law is how to arrive at a final accounting of legal damage in the face of a physical process that changes over a span

[1] "Sedimentation Law" (Vanoni 1975).

of years, during which natural processes of control become established (Busby, 1975). In fact, sedimentation law evolves around the concept that legal components of a stream change as the needs of the public change. In the 1970s, public interest was already shifting to smaller watersheds. As a result, sedimentation law is connected to key trend-setting court decisions as they relate to individual cases.

20.5 PUBLIC LIABILITY AND NATURAL HAZARDS: COMMON LAW AND REGULATORY "TAKINGS"—FUTURE DIRECTIONS

Bearing in mind that the original chapter on this subject was written by an attorney, the authors of this revision, in order to maintain that same caliber of legal expertise, dedicate this portion of this chapter to the work of an expert in the field of law. In 1992, Jon A. Kusler, Executive Director for the Association of State Wetland Managers, Inc., in Berne, New York, an association dedicated to the protection and management of the nation's wetlands, prepared a book for the scientific community on the subject of natural hazards law. The draft entitled "Public Liability in Natural Hazards" was prepared for the National Science Foundation pursuant to Grant CES-8612277 and submitted to the foundation in 1992. The authors of Chapter 20 obtained permission from Kusler to quote portions of the draft for the purpose of documenting recent trends in sedimentation law.

Therefore, this portion of the revised chapter quotes extensively from the work of Kusler (1992). Kusler examined more than 1,000 flood and drainage-related cases. More generally, he addressed public liability, responsibility and defense. These hazard-related cases (both regulatory and nonregulatory) reveal that new legal issues, such as inverse condemnation, have come into existence.

Through Kusler's exhaustive research, it became apparent that tort-related hazard law has a rapidly changing nature. "Many state and federal statutory modifications in tort liability have been and are now being legislatively adopted. To some extent, the issue then becomes not simply the present status of law but: what should government liability be?"

Kusler's book is primarily a legal treatise designed to help public and private lawyers and agency employees understand when and where governments (federal, state, local) may be liable for actions or inactions with regard to natural hazard losses and avoidance of future losses. It was also designed for natural hazard policy-makers and managers, legislators, scientists, and others interested in the scope of government liability and possible techniques for limiting liability while, at the same time, reducing natural hazard losses.

To summarize his findings, we begin with an overview of public liability due to natural hazards including court cases addressing specific hazards. Although loss of life caused by natural hazards has been reduced in the United States from natural disasters, property losses continue to take heavy tolls, in the United States and abroad, due to both private and public developments in hazardous areas subject to floods, erosion, earthquakes, landslides and mudslides, hurricanes, tornadoes, wild-fires, and other natural disasters.

According to Kusler's findings

> when private individuals are damaged by natural hazards, they increasingly file liability suits against governments claiming that governments have caused the damages, contributed to the damages, or (in some instances) failed to prevent or provide adequate warnings of natural hazards. In determining the liability of governmental units for damages due to governmental activities which increase natural hazards or for damages due to mitigation measures, courts apply general common law and constitutional rules of liability. However, there are several aspects of theses cases which are somewhat unique to natural hazards: an emphasis upon the "duties" of landowners rather than simply "rights"; the highly technical nature of suits; strong public health and safety and nuisance issues; and the existence of a variety of government programs to economically or otherwise compensate those injured by natural hazards.

Kusler also pointed out that landowners may opt to sue governments for regulating their property through zoning, building codes, special codes, and so forth. However, the success rate of this type of lawsuit is very low. It is well to note that allegations against the government concerning cause or increased damages to property or individuals form the basis for both types of suits. However, natural hazard losses versus reduced property values and options in the use of private land vary.

There has been an increase in the last part of the 20th Century of successful lawsuits against governments for government activities that increased natural hazard losses, such as the increase of erosion and flood flows, resulting in damages to private individuals. However, there were few successful cases that dealt with nonstructural hazard mitigation measures such as mapping, warning systems, evacuation measures, government regulations and insurance programs.

It is important to point out that most successful suits involving liability have revolved around situations in which governments have been responsible for directly increased flood or drainage problems to private properties located adjacent to public lands or public works projects, such as bridges, and roads, or through hazard reduction measures. Again, a modest number of suits have addressed situations in which governments were responsible for increased damages from mudslides and landslides and sometimes from snow, weather prediction, modification, and erosion. Very few suits have addressed other natural hazards such as earthquakes and volcanoes.

In most tort-related cases, the courts have held private individuals and governments increasingly liable for

natural-hazard and nonnatural-hazard-related injuries caused by "unreasonable" conduct which causes injury to individuals or to private property. "This trend toward increased successful liability suits for unreasonable conduct (usually based upon a theory of negligence) is particularly pronounced for governmental units not because governmental units are now being treated more harshly than private individuals but because the defense of government sovereign immunity has been eroded during this period, and increasingly, courts hold governmental units to the same standard of reasonable care as private individuals. See *Shipp v. City of Alexandria*, 392 So. 2d 1078, 1079 (La., 1980) Court agreed with "the modern trend . . . for public bodies to be treated in the same manner as private individuals unless policy considerations suggest otherwise."

This trend is due to legislative policy rather than a willingness of courts to entertain suits against governments. Some expansion has been due to changes in standing which allow damaged individuals to bring suits under preexisting theories of action, which were formerly unable to be utilized. The Civil Rights Act of 1871 has been a standard for individuals claiming violation of their "civil rights" under Section 1983 of this original act. This is the result of U.S. Supreme Court decisions interpreting the Civil Rights Act of 1871 as applying to local government actions.

Liability litigation is a dynamic, evolving area of law. In its broader context, lawsuits against governments by private individuals based on natural hazard losses or based on government actions to reduce such hazards are broken into two principal forms.

First are suits by private individuals who suffer from natural hazard losses they claim were caused by governments. These suits are generally for damages and are based mostly upon common law tort or to a lesser extent on contract theories. Some suits are also based upon statutory or constitutional grounds.

Second are the less common cases by private individuals who are prevented by governments through the adoption of regulations from engaging in filling, construction of dams, houses roads or otherwise using, subdividing or selling hazard-prone lands. These cases are based on the 5th Amendment or the 14th Amendment of the U.S. Constitution, or similar provision in state constitutions. These cases are mostly to compel issuance of permits or they are filed for damages due to the partial or complete taking of private property without payment of just compensation.

There have been almost no successful lawsuits based upon regulatory takings in hazard area contexts despite a widespread perception among governmental units that regulatory "takings" are a significant problem.

Both case types require the proof of specific damages and they both require proof of causation. In addition, both types of cases have, at their core, the basic duties as well as rights of private landowners and individuals (both private and public) to other landowners and individuals.

Due to a lack of hard and fast rules for negligent or nonnegligent conduct, the site-specific nature of negligent actions encourages a large number of suits. However, negligence depends, to a considerable degree, upon the circumstances and negligence is also, to a considerable degree, what a judge or jury says it is in a specific circumstance.

Of course, advancements both in knowledge concerning hazards and in modelling techniques make it more difficult for landowners to prove that a particular activity on adjacent land substantially increases flooding, subsidence, erosion or other hazards on his or her land. "This was particularly true when the increase was due to multiple activities on many lands such as increased flooding due to development throughout a watershed. Today, sophisticated modelling techniques greatly facilitate proof of causation and allocation of fault." See, e.g., *Lea Company v. North Carolina Board of Transportation*, 304 S.E. 2d 164 (N.C., 1983).

The contexts in which government liability for hazard-related actions may arise can be summarized into four categories:

- Natural hazard injuries that occur on public lands or in public buildings.
- Offsite impacts of various government activities on public lands.
- Government actions not related to public ownership or management of lands which increase natural hazard losses.
- Tightly regulating private activities within hazard areas to prevent hazard area occupants from increasing hazards on adjacent lands or regulating to reduce onsite losses.

The federal government, states, and local governments can all be sued for negligence, nuisance, breach of contract, or the "taking" of private property without payment of just compensation.

1. Local governments are the most vulnerable to such liability suits based upon natural hazards due to the fact that they are the very units of government undertaking most activities resulting in increased natural hazards or "takings of private property" and are "least protected by defenses such as sovereign immunity and statutory exemptions from tort actions." It is at the local level that most hazardous lands are managed and occur (road construction and maintenance for example).
2. States may be sued for negligence, trespass, takings and contract theories. Limited land use controls limits cases against state governments.
3. Federal liability is much broader with regard to federal land use. Congress has specifically exempted federal agencies for liability for negligence with regard to flood control measures by the Flood Control Act of 1936. However, federal agencies may be sued for

uncompensated taking of private property under the 5th Amendment. For example, agencies may be held liable for permanently flooding private land or other activities of both a nonregulatory or regulatory nature that are a taking.

There are three phases of a natural disaster: predisaster, during-disaster, and postdisaster:

1. Prior to a disaster, inadequately designed, constructed, operated and maintained warning systems, emergency evacuation plans, and hazard reduction structures (such as groins, dams, and dikes), may result in damage and as a result cause public liability. A lawsuit might occur at this point if issuance of regulatory permits over a period of years without adequate consideration of natural hazards might in some jurisdictions result in liability.
2. During the time of an actual disaster, if government activities are undertaken without "reasonable care" a public liability may arise. Both loss of life and property loss during a disaster can impose huge demands upon government resources in a relatively short period of time. Actions with potential for liability include issuance of warnings, rescue, construction of emergency levees, emergency releases form dams, evacuation, fire-fighting, and destruction of buildings or other structures to prevent further damage.
3. Such post disaster activities such as clean-up, debris removal, repair of structures can put governments in a negligent position.

Rules of liability which apply to private landowners in their use of hazard areas is also relevant to the validity of government regulations which very tightly controls private actions in hazard areas (Kusler 1992). For example, the U.S. Supreme Court decision, Lucas v. South Carolina Coastal Council held that when a regulation denies all "economically viable use of land" such a regulation is not a taking only. In this case, constitutional and common law merge because the state background principles of nuisance and property law would not allow such uses.

Further proceedings on this case remanded a decision of the South Carolina Supreme Court holding that a Beachfront Management Act, designed to address flooding and erosion problems, prevented a landowner from erecting any permanently habitable structure on the barrier island parcels. This case was, therefore, not a taking of private property without first payment of just compensation.

Kusler's findings that pertain to flood hazard court cases are varied but all cases illustrate the fact that much of the landscape is subject to one natural hazard or another.

As a result of the broad incidence of flood and drainage problems and the foreseeability of the problems, most natural hazard-related liability suits against governments have been the result of flood or drainage damages. Cases illustrating various types of situations in which governments have been sued for flooding or drainage damages include the following:

- Pumpelly v. Green Bay Co., 80 U.S. (13 Wall) 166 (S. Ct., 1971). State is liable for taking of private property due to flooding private lands by state reservoir.
- Rodriques v. State, 472 P. 2d 509 (Haw., 1970). State is liable for damage due to inadequate maintenance of drainage culverts which were blocked by sandbars and tidal action.
- United States v. Kansas City Life Insurance Co., 70 S. Ct. 885 (S. Ct., 1950). Federal government is liable for maintaining the Mississippi River at an artificially high level that raised the low water table blocking drainage of properties and destroying the agricultural value of lands.
- Ducey v. United States, (713 F. 2d 504 9th Cir., 1983). Federal government is potentially liable for failure to provide warnings for flash flood areas for an area subject to severe flooding in Lake Mead National Recreation Area.
- Coates v. United States, 612 F. Supp. 592 (D.C. Ill., 1985). Federal government is liable for failure to give adequate flash flood warning to campers in Rocky Mountain National Park and to develop adequate emergency management plan.
- Barr v. Game, Fish and Parks Commission, 497 P. 2d 340 (Col., 1972). State agency is liable for negligent design of dam and spillway inadequate to convey maximum probable flood; "act of God" defense inapplicable because of the foreseeability of the hazard event.
- Masley v. City of Lorain, 358 N.E. 2d 596 (Oh., 1976). City is not liable for increased flooding due to urbanization including lots and streets but may be liable for inverse condemnation for damages due to storm sewer system.

It is well to note that a relatively large number of challenges have been made to floodplain regulations that restrict private development in flood hazard areas. For reference, see Kusler (1971, 1984).

- Linquist v. Omaha Realty, Inc. 247 N.W. 2d 684 (S.D., 1976). Court held that resolution of Rapid City city council of June 1972, prohibiting issuance of building permits for one block on each side of Rapid Creek after the devastating flood until a study was completed by the planning commission, was a valid exercise of police powers and not a taking.
- Cappture Realty corp. v. Board of Adjustment, 313 A. 2d 624 (N.J., 1973). Court upheld interim zoning ordinance declaring a 1-year moratorium (with a 1-year extension) on construction in flood-prone area unless special exception permit was obtained.
- Foreman v. State Department of Natural Resources, 387 N.E. 2d 455 (Ind., 1979). Court sustained an injunction

prohibiting defendants from making deposits on a floodway and requiring removal of deposits previously made as not a taking of property.

Although hurricanes are generally foreseeable they are difficult to predict in specific terms. Two examples of lawsuits filed against governments based upon claims that they have increased various types of hurricane damage are listed below:

- Alain-Lebreton, Co., v. Dept. of Army, etc., 670 F. 2d 43 (1982). No taking occurred in decision by local levee district and by Corps of Engineers not to locate hurricane protection levees on certain lands although levees were provided on other lands.
- Annicelli v. Town of South Kingstown, 463 A. 2d 133 (R.I., 1983). Court held that prohibition of construction on a heavily developed barrier island subject to hurricane damage was a taking of property where environmental values rather than hazards were heavily emphasized in regulation.

A modest number of lawsuits have been filed against governments for actions that increased erosion damages. The following court cases map out entitlements, limitations, and inverse condemnation decisions:

- Owen v. U.S., 851 F. 2d 1404 (Fed. Cir., 1988). Erosion allegedly caused by government dredging in river which caused collapse of house could constitute a compensable taking.
- Ballam v. U.S., 552 F. Supp. 390 (D. S.C., 1982). Erosion caused by wave wash along coastal water was a "continuous taking." Plaintiff was entitled to damages for valued land lost through erosion and for cost of protecting property from future erosion. However, recovery was limited to changes within 6-year statute of limitation period.
- Souza v. Silver Dev. Co., 164 Cal. App. 3d 165, 210 Cal. Rptr. 146 (Cal., 1985). City held not liable under a theory of inverse condemnation for city's use of creek as part of storm drainage system which caused stream bank erosion due to inadequate proof of causation.
- Baskett v. U.S., 8 Cl Ct. 201 (Cl. Ct., 1985). Government potentially liable for flooding and erosion but no liability due to lack of proof of causation.

Challenges made to erosion-related regulations sometimes prohibit removal of sand and gravel or prohibiting or setting minimum standards for development in erosion-prone areas, such as the following case:

- Rolleston v. State, 266 S.E. 2d 189 (Ga., 1980). Court held that Georgia's beach was constitutional and that denial of permit for landowner to construct a bulkhead while permitting others to build bulkheads, was not a taking.

In some instances there are special issues with regard to hazard-related litigation. We will discuss what this means in relation to flooding and subsequent sedimentation liability.

Unprecedented weather beyond scientific foreseeability can bring expensive lawsuits into play, imposing hefty liabilities upon the government. This makes reasonableness of actions difficult at best. Courts and juries must decide whether events are foreseeable, bearing in mind reasonable and unreasonable actions due to possibility of occurrence and hazard mitigation options available.

The issue in determining the reasonableness of government actions is not simply whether hazards are foreseeable (because they are becoming increasingly foreseeable) but under what degrees of risk individuals and governments must take actions to protect others. For example, there is always a mathematical possibility that a dam will be overtopped and destroyed by a truly extraordinary rainfall or an earthquake (e.g., once in 500 years, 1000 years) killing many. See, for example, Barr v. Game, Fish and Parks Commission, 497 p. 2d 340 (Col., 1972) in which the court held an agency responsible for a "maximum probable" flood.

Insofar as the "Good Samaritan" doctrine applies to governments in hazard contexts, courts and juries alike face difficult decisions even according to classic negligence theory, which is that governments are liable for lack of due care when they act as good Samaritans and undertake actions that they are not required to undertake such as, e.g., Indian Towing v. United States 765 S. Ct. 122 (S. Ct., 1955). Because issues of overall equity and public policy are considered by the courts, complication arises in the application of strict legal doctrines. For instance, if a landowner living in a floodplain sues the government over a faulty warning system, the landowner may collect twice from the government: once for the faulty warning system and a second time for alleged losses.

The almost total lack of successful landowner actions against the government due to inadequate maps, warning systems, flood insurance, disaster assistance and other nonstructural mitigation measures suggest that courts are reluctant to find governmental units liable in such contexts.

The trend in recent years at all levels is to shift government costs of occupancy of flood hazard areas to the landowner. In 1965, the Federal Task Force on Flood Control recommended "those who occupy the floodplain should be responsible for the results of their own actions." (A Unified National Program for Managing Flood Losses, H.R. Doc. No. 465, p. 3, 89th Congress 2d sess. 1966) (U.S. House of Representatives 1966). To date, cost-sharing requirements for federal flood loss reduction and reduced federal spending on flood damage issues support this philosophy. The interdependencies of liability suits with various hazard mitigation and disaster assistance programs such as FEMA's Project Impact suggest improved approaches for better coordination of liability and hazard mitigation and disaster assistance efforts across a broad spectrum (FEMA 2000b).

According to Kusler's findings, the relationship of court decisions to public policy support major hazard-related government programs that consist of laws and administrative guidelines that include the following key elements:

- A land planning and regulatory element preventing or controlling private and/or public development in high risk areas and establishment of a performance standard for development in low risk areas. Areas consistent with federal standards are given incentives on state and community levels of federally subsidized flood insurance. Federal agencies directly plan and control public/private activities on federal lands. Also, a limited measure of federal control is provided in some hazard areas such as flooding, subsidence and erosion through the Army Corps of Engineers Section 10 and Section 404 permit programs as well as by a variety of licensing statutes and federal permits. "The principal goal of these planning and regulatory efforts at all levels of government is to prevent private and public landowners from using their lands in a manner that will increase natural hazards on other lands, threaten public safety, or increase government natural hazard costs in other ways. Please note that these efforts are designed to prevent future problems while the common law tends to operate after-the-fact.
- Hazard prediction, mapping, warning and evacuation planning elements, not regulatory in nature tend to help inform the public and private sectors and other decision-makers just where hazards fall and the severity of risk per location. "Tort law and cases to date are, overall, consistent with government programs to encourage private and public actions to reduce potential losses since the overall trend in tort law is toward a reasonable use standard." Reasonable use standards require landowners to reasonably foresee hazards and take actions according and consistent to the foreseeable risk. "Tort law and contract-based actions such as the implied warranty of suitability for new residence help give teeth to and implement these non-regulatory efforts."
- Hazard reduction elements that include the construction of dikes, levees, reservoirs, beach nourishment, erosion control works, etc. Although smaller structures and projects have been accomplished at the state and local levels, most major hazard reduction measures in the case of flooding and erosion has been the responsibility of the federal government. "Tort law tends to discourage or add to the costs of such hazard reduction elements. As has been discussed, most successful tort cases to date have arisen with the design, operation, and maintenance of such structural measures. Most of the successful inverse condemnation cases have also arisen with these structures." In order to reduce potential liability suits, the government has been motivated to construct hazard reduction measures.
- A disaster-assistance element that includes assistance and rescue at the actual time of disasters such as emergency foods, medical care, temporary shelter, and post-disaster loans and grants also includes federally subsidized flood and erosion insurance. "Most of the funding for such disaster assistance efforts comes from the federal government while relief efforts are carried out on the state and local levels.

As a result of a Federal Task Force on Flood Control Policy in 1965 (Task Force on Federal Flood Control Policy, A unified National Program for Managing Flood Losses, H.R. Doc. No. 465, p. 3, 89th cong., 2d sess. 1966), a key policy for flood plain areas is, "Those who occupy the flood plain should be responsible for the results of their own actions." The upshot of this task force report serves as a blueprint for floodplain management at the national level over the past three decades. During the 1970s and 1980s, progress was made by reducing federal spending on hazard reduction measures by requiring that landowners in hazardous areas conduct their activities in a manner that keeps losses to a minimum:

- Flood loss reduction measures such as dams, dikes, and levees require a local cost share 25%.
- Emphasis upon nonstructural loss reduction measures such as flood plain regulations and warning systems funded privately.
- Cost-bearing by those in hazard areas directly related to potential losses.

But, rules evolve as the nation shifts from large national debts and growing budget deficits to a stronger economy. The rules, over a period of centuries, compensate one landowner for damages his or her actions may impose on other landowners (nuisance) or other individuals (negligence). As society continues to demand a high level of public and individual safety, the protection of this demand grows legislatively. Not only is the moral ethic ingrained in our national fiber to help those plighted by floods but America's high standard of protection for public health and safety is supported by tort and contract-related liability cases.

The nuisance suit in conjunction with broader regulations for land use when it comes to protection of the environment allows landowners to prevent industrial uses in a residential area. **Common law** practice enables private citizens who own land to prevent some types of potential water polluters through suits based upon riparian rights. However, due to limited abilities, common law suits are not able to allow governments or private sectors a broad planning objective.

Goals for the ***reasonable*** use of both private and public hazardous areas are both explicit and implicit in most government natural hazard programs. All hazard prevention and use measures tend to encourage or support "reasonable" use. "In general, both public and private landowners are responsible for 'unreasonable' conduct in light

of the conduct of others." Courts consistently uphold that landowners have no property right to use their land in situations where actions would not be permitted under ***common law***.

In general, disaster assistance and subsidized insurance are limited and, therefore, larger damage awards for specific damages and losses are available through *liability suits*, which are for the most part inefficient. In the situation where disaster insurance is not offered, governments may be sued for confirmed damages. But liability suits take an average of 4 to 10 yr to settle and most landowners are too poor to pursue this costly, hard-to-prove-fault type of legal action. Liability suits also may result in double-dipping, whereby lawyers and landowners get paid from policies and suits. In addition, this type of case adds to the cost of hazard measures themselves. The most successful liability suits have been the result of negligent design or badly operated hazard reduction measures such as a faulty dam or erosion control gone awry. Overall, the government views liability cases as a threat to its budget and hazard-reducing programs.

- For example, a community at risk might reduce that risk with the construction of a dike reducing flood elevations below natural levels, where the community has raised natural flood heights substantially over a period of years through bridge construction.
- Flood warning systems, evacuation plans, and other loss-reduction techniques can reduce liability potential if properly designed, operated, and maintained.
- Government insurance and disaster assistance programs can reduce the number of suits filed if customers are quickly compensated for their losses.
- Direct-pay compensation programs are relevant in some courts as a cause of action under the facts. See North Carolina Supreme Court, in ***Responsible Citizens v. City of Asheville***, 302 S.E. 2d 204 (N.C., 1983), which upheld floodplain regulations against constitutional due process and taking challenges and which noted that plaintiffs were "benefitted" by enactment of the regulations because they qualified the community and the plaintiff for federal flood insurance.
- Regulation may somewhat reduce lawsuits by provision of a general standard of care for governments, private architects, and the like rather than a nebulous unquantified standard of "reasonableness" in a given circumstance.

Loss reduction and mitigation programs enhance the potential for successful lawsuits in some contexts:

- Government subsidy policies for disaster victims in high-risk areas can increase liability awards.
- Regulations can increase potential liability for public and private individuals who fail to comply with government regulations.
- Various mapping and hazard prediction techniques as part of insurance parcels and zoning, warning, or other loss-reduction programs can increase foreseeability of hazards.
- New techniques improperly applied or failure of application when affordable and available and when not applied before a disaster, foreseen or not, thus causing high death rates, may be considered "unreasonable" and result in adverse liability decisions.

Disaster assistance and loss reduction measures such as flood control, avalanche control, and storm drains, when applied in a professional, timely, and expert fashion, tremendously reduce potential government losses in liability suits. This involves decision making for structural hazard reduction measures because of the high incidence of successful suits related to such measures; administrative measures; education on the local level; prevention of double-dipping; beefed-up government lawsuits against negligent private landowners who cause public liability; and recovery of government losses per legal rules to discourage hazard-related losses. See ***United States v. St. Bernard Parish*****,** 756 F. 2d 1116 (5th Cir. 1985).

Subrogation, a familiar insurance concept is defined in Black's Law Dictionary as follows:

> A legal fiction through which a person who, not as a volunteer or in his own wrong, pays the debt of another, is substituted to all rights and remedies of the other, and the debt is treated as still existing for his benefit.

The Standard Flood Insurance policy that is issued by the Federal Government specifically states that:

> In the event of any payment under this policy, the Insurer shall be subrogated to all the Insured's rights of recovery therefore against any party, and the Insurer may require from the Insured an assignment of all rights of recovery against any party for loss to the extent that payment therefore is made by the Insurer.

Government agencies that compensate landowners with disaster assistance, flood insurance and the like can potentially become the subrogees of rights of actions for flood, erosion, and other types of damage caused to the recipients of the disaster assistance, insurance, or payments by private individuals or any other public entities. See, e.g., ***United States v. Dold*****,** 462 F. Supp. 801 (D.C., S.D., 1978).

See also ***United States v. St. Bernard Parish***, 756 F. 2d 1116 (5th Cir., 1985) in which the U.S. government sought over $100 million from various Louisiana public and private defendants for flood damages which the federal government alleged were caused by failure to adopt and administer floodplain regulations that met the minimum standards of the N.F.I.P. "In this case, the U.S. Court of Appeals held that no 'contract' right existed between the federal government and the parishes which could serve as the basis for a subrogation

suit." It also held that the government could pursue damages under common law subrogation theories permitted by Louisiana law. Ultimately the federal government and the parishes settled this case.

Although by the 1990s there were few federal subrogation suits, the suits that were initiated in the 1980s attracted a great deal of attention across the nation and had an educational and enforcement value much greater than the actual recovery monies. They set a precedent for future suits, particularly if legislative changes provided an express contract basis for such suits.

The goal (in liability suits) should be not only to reduce government liability but also to promote responsible government and decision-making with natural hazards factored into the process. More specifically, administrative, legislative, and judicial approaches to achievement of these goals are paramount.

20.6 VARIOUS DEFENSES

Defenses based upon rules of law are decided by the courts, by judges. Defenses built on fact are decided either by juries or by judges in a trial without a jury. The general rule of thumb for cases based on the former defense (rules of law) is to raise questions/challenges during the preliminary pleadings stage through a process known as "demurrer's" or requests for "summary judgment" because at this stage, if successful results materialize, the case can be dismissed before trial. "From a government perspective, an early victory in a natural hazards liability-related case is especially desirable due to the high costs of expert witnesses and attorney's fees if the case goes to trial." The latter case based on questions of fact, such as "act of God" cases, must be proved during trial.

In any case, plaintiffs suing governments under all theories of action (common law, statutory, constitutional) must prove that:

- the government owed them a duty;
- the government breached said duty;
- the plaintiff suffered damages; and
- the breach of duty was the cause of the damages.

The burden of proof is on the plaintiff to "prove all of the essential facts that form the basis for his or her liability claim. This is true for all theories of action."

The most common successful challenges to a plaintiff's proof of essential facts in tort-based cases include the failure to establish "unreasonableness" when it comes to defendants actions in relation to negligence or to establish causation. On the other hand, the most common successful challenge to a plaintiff's proof of facts in a hazard-related regulatory takings case is the failure to show that regulations, as applied, deny all economic use of land.

The government cannot take private property in a hazard-prone area without just compensation. The hitch is that governments can reduce private land values through regulations adopted for proper goals when those regulations are adequately related to those goals. Courts are agreed that such land reductions labeled as "damages," often more severe than those serving as the basis for tort actions, are noncompensable as long as there is no physical interference with respect to the use of private land. So long as due process and equal protection have been a provision, and there is no taking of private property, courts are increasingly applying a "denial of all economic use test" in these cases. That being said, differences in allowable impacts as well as in the nature of these impacts; such as physical interference versus permissible uses, explain, in part, the great number of successful liability suits against governments operating as landowners, and on the other spectrum, the very small number of successful takings cases against governments acting as regulators of private property.

Governments claim that there is no breach of duty in tort-related, contract-related, or fact-driven cases. "Since most hazard-related cases are based upon claims of negligence, governments can rebut an allegation and attempted proof of breach of duty by establishing the reasonableness of government conduct in the circumstances taking into account the nature of the activity, the foreseeability of the hazard, the severity of the hazard, the possible impacts of government actions on landowners, and other factors." Constitutionally based suits in general are a judicial question, breach or no breach. See ***Belair v. Riverside County Flood Control District***, 253 Cal. Rptr. 693 (Cal., 1988), in which a determination of "negligence" in construction and maintenance of levees was necessary to establish an inverse condemnation claim.

Causation is straightforward in constitutionally based regulatory takings cases, as reductions in property values are caused by regulations but causation is hard to prove when the validity of basic regulations and impacts upon private lands is the issue.

Bearing in mind that no property will be taken if there is no damage, a plaintiff must prove damages in an inverse condemnation case. Exceptions exist when property is taken through public entry onto private land when no damages can be shown for such entry. See ***City of Austin v. Teague***, 570 S.W. 2d 389 (Tex., 1978) whereby the court held that regulations took property with no awards because plaintiff failed to prove specific damages.

20.7 SOVEREIGN IMMUNITY

There is no taking without proof that regulations deny all economic uses. Courts have quite often held that landowners cannot show a taking until they have exhausted all administrative remedies proving once and for all that they are "deprived" of all economic uses. This lies under the category of "Sovereign Immunity" which continues to be the most essential defense to tort suits against governments. See *Little v. City of Myrtle Beach*, 279 S.E. 2d 131 (S.C., 1981), whereby the city was not liable for alleged defects or negligent management of drainage facilities that caused flooding, due to sovereign immunity.

Sovereign immunity is a doctrine adopted by American courts from English common law after the American Revolution was won. It is based upon the concept that the "king can do no wrong," or at the very least, that the king is not responsible for his wrong. This concept has of course been broadly criticized as inappropriate for a nation without a king and particularly, a nation with strong egalitarian principles and strong restraints upon government action vis-à-vis the Constitution. Nonetheless, in the 19th century, the doctrine was applied to all levels of government and in 1834, the Supreme Court held that sovereign immunity applied to the federal government. See ***United States v. Clarke***, 33 U.S. (8 Pet.) 436 (S. Ct., 1834). At the state level, courts have held that states have nearly complete sovereign immunity and municipalities and counties less. See, e.g., ***Heffner v. Montgomery County***, 545 A.2d 67 (Md., 1968).

It is interesting to note that over time, the courts have provided a variety of explanations for adherence to this doctrine (Huffman, 1988, p. 449). For example, in 1868, the U.S. Supreme Court in the Siren, 74 U.S. (7 Wall.) 152, 154 (1868) observed that it was "obvious that the public service would be hindered and the public safety endangered" if the state could be sued and "consequently controlled" by its citizens. The Court also argued in another case that without sovereign immunity "government would be unable to perform the varied duties for which it was created." See ***Nicholos v. U.S.,*** 74 U.S. (7 Wall.) 122, 126 (1896).

During the last three decades of the 20th century, exceptions to the general rule involving sovereign immunity even at common law, have been rapidly expanded by judicial or legislative action or a combination of both. See ***Kind v. Johnson City***, 478 S.W.2d 63 (Tenn., 1971) where sovereign immunity defense does not apply to nuisances; and see ***Callaway v. City of Odessa***, 602 S.W.2d 330 (Tex., 1980) where the city may be liable when negligence becomes a nuisance although immune for negligence. "Sovereign immunity has also not been a defense to governmental violation of constitutional rights, including violation of due process and taking of private property." On the state and local levels, lawsuits involve the government when regarded in a proprietary role in connection with negligence.

See ***Enghauser Manufacturing Company v. Eriksson Engineering Ltd.,*** 451 N.E.2d 228 (Oh., 1983), for example of a judicial abrogation of sovereign immunity doctrine. In this case, the Ohio Supreme Court abolished municipal immunity and held that a municipality could held liable for negligently planning, designing and constructing a bridge and roadway that resulted in flooding of industrial property. Equally or even more important, Congress and state legislatures have adopted Tort Claim Acts and other legislation that restricts the defense of sovereign immunity with regard to tort claims. The trend is to duty to the individual versus public duty.

There are four situations in which governments are generally subject to a special duty of care to a particular plaintiff or class of plaintiffs:

- legislative intent: when the terms of a legislative enactment evidence an intent to identify and protect a particular and circumscribed class of persons;
- failure to enforce: where governmental agents responsible for enforcing statutory requirements possess actual knowledge of a statutory violation, fail to take corrective action despite a statutory duty to do so, and the plaintiff is within the class the statute intended to protect;
- rescue doctrine: when governmental agents fail to exercise reasonable care after assuming a duty to earn or come to the aid of a particular plaintiff;
- special relationship: where a relationship exists between the governmental agent and any reasonably foreseeable plaintiff, wetting the injured plaintiff from the general public and the plaintiff relies on explicit assurances given by the agent or assurances inherent in a duty vested in a governmental entity. (Id. at 1260)

See also Glannon (1982).

Statutory exceptions include acts and modifications:

- Federal Statutory Exceptions and the jurisdiction of the Court of Claims were expanded by the Tucker Act in 1887 and by later acts to follow, including claims based upon the Constitution, law of Congress, regulations of executive departments or contracts with the U.S., and patent infringements. 24 Stat. 505 (1887); 36 Stat. 85 (1910); 28 U.S.C.A. 1498 (1973); 28 U.S.C.A. 1346 (1976).
- In 1946, Congress adopted the Federal Tort Claims Act, which was a general waiver of sovereign immunity for "injury or loss of property or personal injury or death caused by the negligent or wrongful act or omission of any employee of the Government while acting within the scope of his office or employment, under circumstances where the United States, if a private citizen, would be liable to claimant in accordance with the law of the place where the act or omission occurred," 60 Stat. 812, title 4 (1946); 28 U.S.C.A. at 2672 (1965). This act is mentioned because it contains 13 exceptions, 2 of which are particularly relevant to claims that are a result of natural hazards. The first and more important is the "discretionary function" exception, which excepts from the act any claim based upon the failure to exercise or perform a discretionary function or duty, whether or not the discretion involved involves abuse (emphasis added), 28 U.S.C.A. 2680(a) (1965). The second exception excepts from the act any claim "arising out of misrepresentation, deceit, or interference with contract rights"(emphasis added), 28 U.S.CC.A. 2680(h) (1965).

U.S. courts are deciding if weather forecasts are the exercise of a discretionary function. The courts have consistently held that forecasts are, in themselves, discretionary. See, e.g. ***Brown v. United States***, 790 F. 2d 199 (1st Cir., 1986): N.O.A.A. could not be sued for failure to predict a hurricane. But, in ***Pierce v. United States***, 659 F. 2d 617, 621 (6th Cir.,

1982), the 6th Circuit held that "(s)ince the FAA has undertaken to advise requesting pilots of weather conditions, thus engendering reliance … it is under a duty to see that information which it furnishes is accurate and complete."

An extremely important statutory exemption for negligence is contained in section 702c of the Federal Flood Control Act of 1936, 33 U.S.C.A. 702c (1986). Section 702c exempts the federal government for liability for "negligence" associated with the design, operation, and maintenance of any given federal flood control facility.

When federal flood forecasts and federal floodplain mapping are characterized as "flood control" measures by lower federal courts, they are not subject to tort actions for negligence. Flooding is by far the most common basis for hazard-related liability suits against the government; therefore, the federal government has been principally responsible for the construction of all major flood control dams, dikes, levees, sea walls, and channelization projects. It is no surprise that this exception has acted to bar many lawsuits and has been challenged a number of times by claimants involved. See ***United States v. James***, 106 s. Ct. 3116 (S., Ct., 1986), where private tort actions for damages based upon federal negligence at a flood control facility was interpreted by the U.S. Supreme Court. The court held that the Corps of Engineers could not be held liable in situations where recreational water users were swept into dams when the Corps opened these structures in order to control flooding.

20.8 STATUTES OF LIMITATIONS

In general, statutes of limitations applying to architects and engineers now start to run from the time of construction rather than from an injury. See ***Klein v. Catalano,*** 437 N.E. 2d 514 (Mass., 1982).

Limitations that begin running at the time of design or construction provide a low probability of recourse for someone damaged by design errors or negligence during a severe but very infrequent flood, erosion event, or other natural disaster. The probability in these cases is only 1 in 20, according to Kusler, that a negligence action would arise for a 100-yr event within the time period allocated by a 5-yr statute of limitations where the statute begins to run from the initial design rather than from the time of injury.

20.9 HAZARD MITIGATION MEASURES BASED UPON TORT THEORIES

Courts have repeatedly held that governments at all levels must use reasonable care. Most successful cases against the government involve situations where mitigation measures increased natural hazards and damaged individuals not intended as the beneficiaries of such measures. A good example is a flood control measure that floods upstream properties (a nonbeneficiary).

Examples where courts have held that the basic decision to protect or not is not subject to liability, under theories of either no duty or discretionary function, include the following cases:

- ***Tri-Chem, Inc. v. Los Angeles County Flood Control District***, Los Angeles County, 132 Cal. Rptr. 142 (Cal. App., 1976), where the State has no duty to construct a flood control system for an area that acts as a natural sump.
- ***Deville v. Calcasieu Parish Gravity Drainage Dist.*** No. 5, 422 so. 2d 631 (La., 1982), where the city was not liable for a child falling into a storm drain where the drainage district normally maintained the drain and the city maintained it only during floods.
- ***Goldstein v. County of Monroe***, 432 N.Y. S. 2d 966(N. Y.A.D. 4th Dept., 1980), where a municipal corporation is not liable for failing to restrain waters between the banks of a creek or to keep a channel free from obstructions it did not cause.

A decision worth examining is the Supreme Court case ***Julius Rothschild and Co. v. State of Hawaii***, 655 p. 2d 877 (Haw., 1982) due to in-depth discussion of factors concerning reconstruction of a two-span bridge with the capacity to convey a 25-yr storm. A flash flood caused warehouse damage and the plaintiff argued that the replacement span was inadequate in light of a hydraulic design report prepared by a firm contracted by the state prior to the reconstruction. The report had recommended replacement of the bridge deck consistent with a 50-yr frequency design criterion.

In another case, ***PDTC Owners Ass'n v. Coachella Valley County Water Dist***., 443 F. Supp. 338 (D. Cal, 1978), the court held that owners of land damaged by flooding could not recover compensation from the water district under the Fifth and Fourteenth Amendments for failure to construct a levee large enough to protect landowners from a 50-yr flood. The levee in question had been constructed of sand and provided protection only from a 30-yr flood. The court held that the landowners might be able to recover any damages for negligent construction and maintenance. Also, in ***Vanguard Tours, Inc. v. Town of Yorktown***, 442 Y.Y.S. 2d 19 (N.Y., 1981) the city was not liable for failure to install a drainage system that adequately disposed of surface waters, but the city must rather use care in maintenance of such systems.

Such cases lead to the subject of adequacy of the design which all boils down to reasonableness of care and implied warranties. In cases where the actual construction of a government measure is faulty, nondiscretionary task and government forces may be held liable for negligence of government employees or contractors not properly supervised. See ***Price v. United States***, 530 F. Supp. 1010 (S.D. Miss., 1981), where the Corps of Engineers was liable for the negligence of

a contractor who dredged an area subject to hurricane damage, thus creating a deep hole, and subsequently failed to provide warnings. In general, operation or administration of a hazard mitigation measure is considered ministerial and governments are responsible for negligence.

By the same token, maintenance of a mitigation measure is considered ministerial and governmental units are responsible for negligence. See ***Carlotto Ltd. V. County of Ventura***, 121 Cal. Rptr. 171 (Cal., 1975), where a California court held a county liable for inadequate maintenance of a "debris basin." "The county had failed to maintain the debris basin behind the dam with the result that only 2.5 acre feet of its entire 12.7 acre feet of water storage remained and damages resulted."

20.10 MORE ON THE TAKINGS ISSUE: EXPANDED STATUS AND TRENDS IN TORT AND TAKINGS LAWS

Successful regulatory takings cases in connection with hazard-related regulations are outnumbered 500 to 1 by successful tort cases holding governmental units liable for increasing losses due to hazards. Lopsided fear of "taking" is out of proportion due to several factors:

First, takings cases are given inordinate attention by the press. Supreme Court decisions receive front-page press coverage across America. Unfortunately, it is a sign of the times, more often than not, that the press coverage is inaccurate, speculative, and paranoia-driven.

Second, there is a deep-seated belief that "taking" private property without just compensation is morally wrong. This ethic contrasts with negligence, breach of contract, or other typical torts that do not carry the same weight as a moral stigma. The U.S. Constitution prohibits "taking" without compensation.

Third, successful takings cases could have severe political repercussions for bureaucrats and legislators who authorize the very taking itself. These law abiders must answer to an electorate on this sensitive issue of "taking."

Fourth, a regulatory "taking" has its limits mainly due to the fact that governments are not positioned with established administrative procedures or funding for payment in conjunction with a regulatory taking. Usually, each case is handled individually through legislative appropriation. Unappropriated funds prove disruptive to government operations. However, a large unanticipated expense for a blizzard or even a large tort liability award due to highway construction, for example, is usually not an issue because eminent domain funds already exist.

Fifth, misunderstandings abound on government levels due to unclear concepts of what is or is not a taking. This inability to adjust measures to avoid "takings" is partly due to a lack of clear judicial guidance on the takings issue. The case-by-case approach to taking issues utilized by the court system involves a variety of tests to determine whether actions to "take" property are contributing factors.

Almost all hazard-related takings cases (regulatory and nonregulatory) deal with flood losses or floodplain regulations. This is due to the pervasiveness of flood and erosion problems throughout the United States as well as the many contexts in which government actions may increase flood damages on privately held lands.

Courts have traditionally held that governments may, in some instances, destroy private property during a disaster to prevent the spread of the disaster or may require the razing or raze private structures which are dangerous after a disaster.

See ***Boland v. City of Rapid City***, 315 N.W. 2d 496 (S.D., 1982) where the city had the power to destroy flood-damaged private houses after the Rapid City Flood of 1972 to alleviate public health problems but the city also had the burden to prove that houses created public health problems a nuisance. The city had not done this and was liable for a "taking."

In ***Oswalt v. County of Ramsey***, 371 N.W. 2d 241 (Minn., 1985) the court held that a landowner was entitled to compensation for the county's refusal of a permit to repair a flood-damaged house. The house was a valid nonconforming use under an ordinance, but the county had failed to consider the "useful life" of the proposed improvement for purposes of amortization and had instead, in effect, condemned the use by refusing to issue a building permit.

20.11 UPSTREAM VERSUS DOWNSTREAM LEGAL ISSUES

Unlike land, water is transient and moves.It recognizes no political boundaries. Therefore, water is legally and historically a public resource although water rights can be obtained. Private rights to water are often incomplete and subject to the public's common needs (CSI 1999). The transfer of water rights must go through the proper legal channels for the state; for example, ***Tyler v. Wilkinson*** is a case that adopted the reasonable use standard.

Other boundary disputes that went to the U.S. Supreme Court include the following:

- ***Georgia v. South Carolina***, 497 U.S. 376 (1990), a suit over the location of a boundary along the Savannah River, downstream from the city of Savannah and at the river's mouth, and the lateral seaward boundary. Historically, the treaty between these states declared

that "where there is no island in the river, the boundary is midway between the banks, and where there is an island, the boundary is midway between the island and the South Carolina shore (Georgia v. South Carolina)." The Special Master (above) submitted two Reports, making several boundary recommendations, but both states filed exceptions.

> Either state stands to lose riverbed as a result of natural erosion by the river; likewise, each state has the potential of acquiring additional riverbed as a result of accretion and erosion. For example, if an island existed in 1787 but was subsequently eliminated by gradual erosion, the boundary would be moved to the advantage of South Carolina, and the riverbed previously owned by Georgia would then be owned by South Carolina (Georgia Exceptions 56).

Part of Georgia's fourth exception included the small, unnamed islands upstream and downstream from Pennyworth Island. Georgia's exception was overruled and The Special Master's determination adopted a "forever after" boundary on behalf of South Carolina due to the theory that the South Carolina shore, over time, would create a regime of continually shifting jurisdiction, by creating a new "northern branch or stream" for even the smallest emerging island, thus frustrating the original state treaty [497 U.S. 376, 377]. The avoidance of sudden boundary changes and respect for settled expectations that generally attend the drawing of interstate boundaries, cf. ***Virginia v. Tennessee***, 148 U.S. 503, 522–525, pp. 394–398, was cited.

- ***Oklahoma v. New Mexico***, 501 U.S. 221 (1991), was concerned with an enlargement of the Ute Reservoir and a violation of the 200,000 acre-feet limitation law on New Mexico's constructed reservoir capacity available for conservation storage downstream from Conchas Dam, and with a so-called "desilting pool" exempt from the Article IV limitation, because it was not allocated solely to "sediment control." Floods from Canada affected the storage basin in the downstream states. The Court abandoned the literal text of the Compact and searched for a new interpretation of the "originating" due to the fact that the Compact would otherwise allow New Mexico to lay claim to any water originating above Conchas Dam, including tributaries that arose in boundary states.

20.12 ACT OF GOD DEFENSE

Since the sixteenth century, courts have recognized "act of God" as a common law defense to negligence, nuisance, trespass and even, in some instances, takings cases. The act of God defense has also been incorporated into some statures. See 33 U.S.C.A. 1321(a)(12)(1986), "an act occasioned by an unanticipated grave natural disaster."

The "act of God" defense is based upon the belief that one should not be held responsible for what cannot be reasonably anticipated or guarded against. It is a defense that must be affirmatively pleaded and proven by the defendant. It is a defense that was at one time much more broadly allowed by the courts. Today the defense is most often narrowly construed. See, e.g., ***Sabine Towing and Transp. Co., Inc. v. U.S.***, 666 F.2d 561 (Ct. Cl., 1981). (Spring runoff was not "act of God" which would excuse an oil spill.)

Cases dealing with "act of God" defenses focus on two important hazard issues that are common to all such cases: the predictability of various hazards, and the magnitude of events, such as destructive force and return frequency, which need to be addressed by public and private landowners.

Verifying "act of God" is another story. In order to prove such a case, the defendant must establish, to the satisfaction of the jury or court, that (1) the event falls within the legal definition of "act of God" and (2) the "act of God" and not the defendant's negligence was the proximate cause of the disaster.

Courts are in agreement that the defendant must more specifically prove that

- the event is an act of mother nature (hurricanes, storms, earthquakes, floods), not caused by human agency;
- the event is "extraordinary" in magnitude or size;
- the event and resulting damages could not reasonably have been anticipated or prevented; and
- the event was the proximate cause of the damage or injury.

The difficulty arises in the proof. Was the event an act of nature? An "act of God" is defined as an event that is due directly and exclusively to natural causes without human intervention. Kusler cites ***Northwestern Bell Tel. Co. v. Henry Carlson Co.***, 165 N.W. 2d 346, 349 (S.D., 1969). See also ***Dempsey v. City of Souris***, 279 N.W. 2d 418 (N.D., 1979), as another example of events that fall under the "act of God" category. Although meteorological events (hurricanes, storms, tornadoes, lightening) and geological/geomorphological events (erosion, landslides, earthquakes) continue to occur as they have throughout history, the actual causative elements of many events are no longer totally natural. Rains fall naturally but the height, velocity, and volume of floodwaters depend upon watershed uses, dams, dikes, levees, and many other alterations. Similarly, erosion has often been greatly impacted by human activities, as have landslides, mudslides, and wildfires.

Some courts have required that in order for an event to be classified as an "act of God" the event must be "unprecedented." An example cited is the Alabama Supreme Court decision in ***Bradford v. Stanley***, 355 So. 2d 328, 330 (Ala.,

1978) which observed that: "In its legal sense an act of God applies only to events in nature so extraordinary that the history of climatic variations and other conditions in the particular locality affords no reasonable warning of such events." However, with historical techniques now available, the occurrence of events over the last several thousand years is sometimes documented. In much of the world as we know it, there are historical written records of catastrophic floods, hurricanes, earthquakes, and other terrible storms that date back thousands of years. Paleo-flood studies combined with carbon dating and supplementary dating methods provide additional documentation. In addition, studies of tree rings, sediments, and soil science are providing quite specific documentation for large-scale hazard events at given locations.

If events are not unprecedented, courts have held that they must be at least extraordinary from a scientific and not simply a layman's perspective. One example is the U.S. Court of Appeals, District of Columbia Circuit in ***Shea-S&M Ball v. Massman-Kiewit-Early***, 606 F. 2d 1245 (1979), which rejected the "act of God" defense by a contractor where waters from his construction site overflowed during heavy rains resulting in damage on a second construction site. In this case, the court found insufficient evidence in the record to support a finding of an act of God and they noted that "The record is completely devoid of any evidence of the normal range of rainfall in Washington, D.C., and (they contended that) the amount of rain that actually fell during the time periods when the floods occurred" (Id. At 1248). The court, therefore, concluded that heavy rainfalls are not considered acts of God unless they are unusual and extraordinary and quoted with approval from an earlier case, *Garner v. Ritzenberg*, 167 A.2d 353, 354–65 (D.C., 1961):

> We take judicial notice that rains of heavy intensity and average duration are occurrences of common experience. This event was described as a flash flood. People often use that expression in describing accumulations of rainwater running off along natural or artificial contours of the ground; but that imports no particular legal significance. Such events, though infrequent, are to be expected. They do not create the widespread devastation commonly associated with earthquakes, tornadoes, hurricanes or extraordinary floods. The occasional filling of low-level or basement areas by rainwater is a probable and foreseeable result of a heavy rain. To classify it as an act of God is an unwarranted extension of that doctrine not supported by the authorities.

Due to the fact that predictability of events has become more accurate through modeling techniques for flooding, earthquakes, volcano eruption, hurricane tracking, etc., courts do not require that such events be specifically predictable with a "foreseeable" date and place; it is enough that such events could have been expected. Therefore, events with particular assigned recurrence intervals have persuaded a number of courts to consider the foreseeability of hazard events in a new light.

One such example resulted in a rejection. In ***Barr v. Game, Fish and Parks Commission***, 497 p. 2d 340 (Col., 1972) the Colorado Court of Appeals rejected an "act of God" defense for flooding, erosion, and silt deposition damage caused by construction of a dam with an adequate spillway by the Colorado Game, Fish and Parks Commission. The court held that a "maximum probable storm, by definition, is both maximum and probable." In the end, the court agreed (Id., at 344) with the lower court that had concluded,

> (W)ith modern meteorological techniques, a maximum probable storm is predictable and a maximum probable flood is foreseeable. Thus being both predictable and foreseeable to the defendant in the design and construction of the dam, the defense of an act of God is not available to them. In short, the flood that occurred in June of 1965 could not be classified as an act of God.

Therefore, the court concluded that the above dam should have been designed to meet the requirements of the maximum probable flood—200,000 cfs at this point of the stream. Proving that the event in and of itself was the proximate cause of the damage or injury is often difficult due to the fact that the defendant's actions (as in a negligence case) may also be part of the proximate cause. For example, storm waves from a hurricane may badly erode a beach, but the actual damage may also be caused, at least in part, by defendants' construction of a groin or seawall along another portion of the same beach.

There is a general rule in place that states that when a natural event concurs with acts of the defendant to produce the injury, the defendant is not liable if the event would have independently produced the damage without the defendant's transactions. Some well-documented cases include ***Fairbrother v. Wiley's, Inc.,*** 331 P. 2d 330 (Kan., 1958). The Maryland Court of Appeals in ***Mark Downs, Inc. v. McCormick Properties, Inc.,*** 441 A. 2d 1119, 1128–29 (Md., 1982) noted that an "act of God" will excuse mortal man from responsibility "only if God is the sole cause … where God and man collaborate in causing flood damage, man must pay at least for his share of the blame." Where the acts of man and the acts of God combine to cause damage, courts have generally held man responsible for the total damage. See also ***National Weeklies, Inc. v. Jensen***, 235 N.W. 905, 906 (Minn., 1931) in which the court stated:

> If the damage done was solely the result of an act of God, the city was not liable. If the negligence of the city approximately contributed and an act of God combined to produce the result, the city is liable.

"Act of God" has been a defense principally in tort cases. In some instances, however, it has been recognized as a defense in contract cases—for example, ***Firpine Prods. Co. v. Atchison, T. and S. F. Ry.***, 124 F. Supp. 906 (D.C. Mo., 1954). Other courts have disagreed with its application in contract contexts. For example, the Alabama Supreme

Court in ***Alpine Construction Company v. Water Works Bd. Of Birmingham***, 377 So. 2d 954, 956 (Ala., 1979) stated that

> Where one by his contract undertakes an obligation which is absolute, he is bound to perform within the terms of the contract or answer in damages, despite an act of God, unexpected difficulty, or hardship, because these contingencies could have been provided against by his contract.

20.13 FORENSIC GEOLOGY

Some turning points in forensic geology include the extensive use of aerial photography. According to *Forensic Geology,* by Raymond C. Murray and John C.F. Tedrow, the American Society of Photogrammetry has listed over 100 ways in which aerial photography serves a useful function from archaeological discoveries to finding modern burial sites. Altered soil conditions are key during court cases.

> During the course of an investigation, it is sometimes critical to establish the time of a certain activity, such as the filling in of wetlands, the digging of a borrow pit, the time a forest was cut, or when a structure was built or demolished. An aerial or ground photograph, with date, gives indisputable evidence as to the presence of physical features or landscape conditions at a specific time. (Murray, 1992)

Federal agencies such as the U.S. Geological Survey and the U.S. Department of Agriculture and military and commercial establishments take aerial photographs periodically. Aerial photographs are available through these various agencies, but the most comprehensive sets, including archives, may be obtained from the U.S. Department of Agriculture, ASCS, Aerial Photography Field Office, 2222 West 2300 South, Salt Lake City, Utah 84130.

20.14 FUTURE DIRECTIONS

The complex law of public liability for natural hazards is not easily summarized. According to Kusler, there are vast differences in the law of liability under tort, contract, and constitutional theories from state to state, particularly with regard to the sovereign immunity defense and the nuances of particular causes of action such as trespass. Although the precise theories and rules of law vary, overall theories of liability are identical, such as situations in which as government unit can be held liable for a particular act. A good example is found in local government, which in most states can be held liable for flooding private land by construction of public access. Of course, the law varies from state to state, but such an action could be based upon nuisance, violation of riparian rights, trespass, negligence, or inverse condemnation.

There is a general status of law throughout the nation, but particular attention should be rendered when it comes to jurisdiction. When it comes to reducing natural hazard losses through structural measures such as dams or nonstructural measures such as warning systems and regulations, officials, scholars and landowners are increasingly confused with regard to the liability potential of reducing natural hazards. It is a huge undertaking to reduce private losses from private use of public lands that are subject to flood, earthquake, or other hazards at the risk of damaging other private parcels. Flood control measures have a high potential for liability, while regulations are low-risk. However, a wide variety of low-cost measures are available to help reduce potential liability.

The majority of liability suits to date have involved governmental activities on public lands that cause damage to adjacent privately owned lands due to inadequate design, operation, or maintenance of roads, airports, utilities, reservoirs, dikes, dams, erosion-control structures, mudslide and landslide structures, or storm-water facilities. The lawsuits have been based upon nuisance, trespass, negligence, violation of riparian rights, strict liability, negligence or inverse condemnation theories of action.

> Although there is the potential for successful negligent suits based upon various nonstructural mitigation actions not related to government ownership and use of land such as inaccurate hazard maps, inadequate warning systems, inaccurate hazard predictions, inadequate dissemination of hazard information, inadequate emergency services, and inadequate administration or enforcement of regulations, few suits based upon such inadequacies have succeeded to date for several reasons. These actions are considered "discretionary" in nature by the courts and are also partially or wholly protected by sovereign immunity or statutory exemptions. (Kusler, unpublished work, 1992)

The *takings* issue is popular with the press because it is a strong political issue, but courts have overwhelmingly upheld hazard regulations against constitutional challenges. In the hundreds of appellate-level cases that involve constitutional challenges to regulations, courts have only held regulations unconstitutional as a taking of property in a few cases where regulations prevented all uses in relatively low-risk areas or an attempt was made to apply regulations retroactively to abolish hazard-prone structures without adequate documentation of the nuisance aspects. It is clear that natural hazard regulations can reduce property values without a taking and that performance-oriented hazard regulations do not, in general, pose a threat of "taking." Theories and cause of action for tort and inverse condemnation actions have been expanded to hold government liable for "unreasonable" conduct, much like a private citizen. Defenses such as sovereign immunity and "act of God" have been narrowed (see the *Act of God* section).

Advances in hazard-related technology and science deem hazard events more predictable and susceptible to various sorts of mitigation. As these options increase, the standard of care for "reasonable" conduct and also the potential for successful suits increases. Because of this fact, the "sovereign immunity" defense has been judicially or legislatively modified, particularly with regard to the actions of local governments. Therefore, it is possible to suggest trends in sedimentation law and possible future directions:

- Government actions that increase flooding, drainage, erosion, and landslide, problems that arise on private owned lands, will likely continue to pose inverse condemnation threat to governments.
- Government defenses will most likely narrow to engulf liability suits that relate to sovereign immunity, act of God, and inverse condemnation.
- The U.S. Supreme Court and lower courts will scrutinize land use regulations in terms of their impact on private landowners.

It is suggested, in Kusler's extensive work, that the best overall approach to reducing liability is through informed decision-making that considers the hazard-loss implications of government acts and takes actions based upon this analysis. The best way to avoid negligence-based liability is through "reasonable conduct in the circumstances."

From a scientific and engineering perspective, disasters equal moritoria to assess damages in greater detail. This includes probability of reoccurrence, and development of a mitigation plan. Speed in such studies is essential but the undertaking is often limited by availability of experts who are often in short supply after a major disaster. However, precise design and location of development must often be modified and re-modified to reduce impacts on other lands and to ensure the safety and structural integrity of the damaged area.

Examples of theories that have been modified on the judicial level and that apply to the reasonableness standard include the following:

- The "common enemy" doctrine for surface waters has been replaced by a reasonable use standard in most states;

  A recent case in Missouri, in fact, overturns the "common enemy rule": "Landowners who erect levees and otherwise back up DSW [downstream water] onto their neighbors can only do so with immunity if their actions are 'reasonable' (common law approaches to water rights 'invite' lawsuits if certainty is sought)." In addition, a cautionary as to DSW: common law includes a "line of cases" known as the Natural Drainage Rule which states that natural drainage patterns and flow rates cannot be altered unilaterally without consent of impacted neighbors (Missouri Water Law).

  For example, drainage decisions for the Illinois wetlands have been affected by the passage of the wetlands provisions of the Food Security Act of 1985 due to the fact that the remaining wetlands have important ecological and hydrologic value. Federal policy discourages conversion of wetlands to farmlands. The Illinois Drainage Law was revised in December 1997.

- Strict liability for dams has been replaced with a reasonable use standard in some states.
- The doctrine of caveat emptor ("let the buyer beware") has been replaced with one of implied warranty of suitability, incorporating a concept of reasonable anticipation of natural hazards on the part of sellers and protection of reasonable expectations of buyers.
- Reasonableness of activities has become a principal issue in many inverse condemnation suits.

The "reasonableness" standard is used more widely because it reduces each circumstance to a common denominator standard for liability assessment. It is flexible and fact-specific. In most cases, it incorporates basic concepts of fairness. In the context of natural hazards, it is consistent with the goal of responsible use of public or private lands.

In summary, Kusler recommends a status and certain trends prevalent in the courts at the time of his research (unpublished work, 1992). The bottom line, despite widespread concern about government liability for regulation of private activities in hazard contexts, is that virtually all successful liability cases to date (reported in thousands of decisions, some of which have been mentioned) have involved government activities that caused or increased natural hazard losses or failure of governments to remedy or warn of natural hazards on public lands.

Theories and grounds for tort and inverse condemnation actions have been expanded to hold government liable for "unreasonable" conduct, much like a private individual. Defenses such as sovereign immunity and "act of God" have been narrowed. Based on all factors considered, it is possible, according to Kusler, to suggest trends in law as well as a clear path for future of American sedimentation law and the physical processes thereof.

- The greatest tort liability or inverse condemnation threat to governments will continue to be liability suits; subsidence can also be predicted as mitigation measures improve causing more regulations to be adopted that will ultimately help establish a standard of "reasonable" care conduct.
- All other hazards fall under the same category (see recent developments in "Project Impact").
- The government and the individual will most likely fall into the same standard of care for nondiscretionary "unreasonable conduct."

- Governmental units will be expected to uphold an increasingly high standard of care for "reasonable" conduct.
- Foreseeability limits may occur along with counter legislative caps on government liability through "tort-claim acts."
- The U.S. Supreme Court as well as the lower courts, will more carefully examine land use regulations, not just related to hazard (again, see Project Impact in Recent Developments, next section).

In reducing potential government liability, there is a broad range of options available to maintain government responsibility, including administrative actions, legislative changes, and judicial responses.

Kusler concludes his survey with the theory that courts should continue to take a factually-specific, pragmatic approach to natural hazard cases and should tackle many unresolved legal issues with "the goal of encouraging responsible, equitable, and reasonable private and public conduct."

20.15 SUMMARY AND RECENT DEVELOPMENTS

In Arnold, Missouri, the total amount of Federal disaster assistance granted after the devastating floods of 1993 was well over $2 million. After the floods of 1995, the fourth largest flood in the history of Arnold, the damage was less that $40,000 due to the nonstructural mitigation, which culminated in the acquisition of flood-prone or flood-damaged properties (FEMA, 1995). The 1995 flood was much less severe due to the fact that most of the affected areas had been bought out by the government so the residents were no longer in harm's way. Therefore, the Arnold, Missouri case illustrates the value of acquisition and highlights the value of planning as a mitigation tool.

The unprecedented flood of 1993 offered a long-term solution that included the creation of land use plans that included changes to lessen the impacts of future disasters by following organizational plans implemented as land use strategies. This, along with capital improvement plans to obtain the necessary funds to accomplish the desired goals, in combination with the city's ability to facilitate a solution to sustaining flood damages, was documented in 1995 as part of an ongoing accomplishment.

FEMA's effort to reduce risk through mitigation culminates in a reduction in potential damages. The community of Darlington, Wisconsin experienced indirect benefits in connection with FEMA's mitigation efforts. Darlington's environment was rendered safer, its aesthetic quality was heightened, and the natural function of its floodplain was restored resulting in the city's economic development potential to increase.

The mitigation projects in the Midwest ranged in size and complexity from one to two home elevations to Valmeyer, Illinois which relocated a significant portion of the town to a new location, to Wakenda, Missouri which acquired and demolished all the town's structures, and disincorporated. What all these projects hold in common is that they reflect the communities' visions of themselves. Communities must be aware of their risks and plan accordingly, weighing mitigation alternatives with community needs (FEMA, 1995).

In May of 1995, the most expensive floods in the history of the National Flood Insurance Program (NFIP) took place in Louisiana, when $584 million was paid out in claims. The severe floods, which ravaged at least 14 states from Florida to Maine in mid-September 1999, culminated in claims averaging $21,237 per claim. At this writing, more than $310 million has been settled for 14, 614 flood damage claims. Although an unprecedented amount of claim money has been paid, the statistics report that the majority of Hurricane Floyd flood victims unfortunately did not have flood insurance; that, for example, in the state of North Carolina (the state hit hardest by Hurricane Floyd), only $1,000 policies were in force at the time of the disaster. "Nationwide, only about one-fourth of households in special flood hazard areas have flood insurance," then-Federal administrator Jo Ann Howard pointed out. She went on to say that the money paid out comes from premium income, and not tax dollars, and that the more that property owners take responsibility for their own protection against hazards by purchasing flood insurance, the fewer landowners will need to rely on disaster relief funded by U.S. taxpayers. She assured the public at large that flood insurance not only reduces government expenditures for disaster relief in great amounts, but provides victims of disasters with much greater compensation. She also said that while disaster grants are helpful, they are also very limited, and that disaster loans have to be repaid with interest. Therefore, it is a win-win situation when landowners take rainy day responsibility for future hazard damages by purchasing flood insurance. Howard noted that high-risk areas engulf properties currently located outside of known high-risk zones due to the fact that in recent years, floods (the most common type of natural disaster) have been reported in places that never experienced them in their histories.

Aside from the benefits of hazard insurance policies, Howard encouraged communities to get involved in further actions to reduce damage through FEMA's public awareness effort, ***Project Impact***—an effort devoted to building disaster resistant communities, its motto being "educating people to elevate, floodproof, or otherwise move structures out of harm's way" (FEMA 2000a).

20.15.1 Project Impact

The Federal Emergency Management Agency (FEMA) is changing the way America deals with disasters. Project Impact assists communities to protect themselves from the devastating effects of natural disasters by taking actions to dramatically reduce disruption and loss of properties and life. Project Impact

operates on a common-sense damage-reduction approach, basing its work and planning skills on three simple principles:

- Preventive actions decided at the local level;
- Private sector participation; and
- Long-term efforts and investments in prevention measures.

This unique experiment began with seven pilot communities across the country that partnered with FEMA for expertise and technical assistance on national and regional levels to include federal agencies and states in the equation. FEMA, using all available mechanisms to put the latest technology and mitigation practices into the hands of local communities (businesses, schools, private sectors) and governments, has expanded from the original seven pilot communities to 200 Project Impact communities. More than 1,100 businesses have joined FEMA's growing partnerships. The incentive for disaster-resistant communities across the land has been able to bounce back from a natural disaster with far less loss of property and consequently much less cost for repairs. The estimates are in that for every dollar spent in damage prevention, two are saved in repairs. (FEMA 2000b).

Former FEMA Director James Lee Witt outlined key provisions to Congress of the Fiscal Year 2001 budget. Besides asking Congress to authorize $971 million, FEMA also requested an additional $2.6 billion in emergency contingency funds for future disasters. Witt reminded Congress that with their support, Project Impact communities were established in every state in the union. He requested $30 million for the following fiscal year in order to continue expansion of this initiative for the express purpose of building a nation of disaster-resistant communities (FEMA 2000c).

As of February 15, 2000, Congress approved additional buyout funds from a separate emergency contingency fund for 13 states from Florida to Maine hit by Hurricanes Floyd, Irene and Dennis. FEMA announced that an additional $215 million was made available for buyouts and relocation of properties damaged by these floods. These funds must be matched by 25 percent of nonfederal funding and can be used only for primary residences that are deemed uninhabitable due to the disaster(s) (FEMA 2000d).

In addition to extra government fundings, projects related to the removal of structures from flood hazard areas were undertaken, such as the state of Iowa's case study, entitled The Benefit of Hazard Mitigation Projects in Iowa, which tracked 128 hazard mitigation projects or initiatives pursued by Iowa communities, counties, or the state, resulting in an anticipated overall government savings of $100 million. At this time, since 1993, Iowa has been impacted three times by floods. Many of the federally funded acquisition projects that removed properties avoided the subsequent impact of flooding, resulting in savings within a 2 to 3-yr period (FEMA 1999).

Successes in relation to reducing costs, overall costly court cases that result in taking of high-risk disaster prone lands, and unforeseen flood damages such as erosion and sedimentation problems due to unforeseeable natural disasters in unknown risk areas rests on sound public policy and strong support systems, such as FEMA's *Project Impact,* the NFIP insurance claims programs, and a demonstration of reasonable use of private and public lands by the citizens as well as by the government.

The Government Performance and Results Act (GPRA) requires that agencies submit annual performance plans to Congress along with fiscal year budget requests, and they must also prepare an annual performance report at the end of each fiscal year (FY) on how well their goals were met. The FY 1999 Annual Performance Plan was the Department of the Interior's first official plan submitted to Congress and Interior's first opportunity to report on their accomplishments. Further, their current plan and their proposal for their subsequent plan have been combined into a single presentation in order for trends in performance to be measured side by side with trends according to current results.

To make use of today's science for America's tomorrow, and science in general for a changing world, the strategic direction for the U.S. Geological Survey combined and enhanced diverse programs, capabilities, and talents, increased customer involvement in an effort to strengthen science leadership, and continued its reputation for contribution to the resolution of complex issues. As a world leader in the natural sciences with a vision of scientific excellence and responsiveness to society's needs, the USGS continues to have a mission to serve the nation by providing reliable scientific information. Its linkage to the bureau strategic plan, budget, and departmental goals is housed in its main mission objective: hazards, and environment and natural resources. Its most important product is quality science that is both relevant to a changing world and effectively communicated. Peer reviews and program evaluations will continue to measure its capabilities. The USGS sums up the future of hazard-related industry in general with its plans to meet the challenges of the 21st century with renewed vigor and a clarified sense of purpose and mission. "Understanding the delicate balance between the earth's natural resources and America's need for continued growth will enable us to make better decisions for future generations' enjoyment of this precious land," said Dr. Charles Groat, then-USGS Director, in defense of budget increases for science to provide reliable information and tools in order to accurately forecast a better tomorrow (USGS 2000).

20.15.2 Polluted Sediments and Sediments as Pollutants

Since the creation of nationwide regulations, such as the Federal Water Pollution Control Act Amendments of 1972, amended in 1977 and heretofore referred to as the Clean Water Act, legal liability has been assigned to situations where pollutants attach to sediment particles. However, the

legal framework for polluted sediments has emerged primarily from relatively recent environmental laws rather than from the body of law that examines the effects of sedimentation processes on changes in geography. For this reason, on the subject of polluted sediments, the authors recommend consulting reference materials that pertain to environmental law.

In addition to pollutants that attach to sediment, the individual particles can sometimes be recognized as pollutants by certain regulations. For example, introduction of high silt concentrations through surface erosion can affect fisheries, other aquatic species or habitats. This area of law and regulation is similarly beyond the scope of this chapter.

20.16 CONCLUSION

Sedimentation policy, in connection with the problems of property rights and damages due to flood disasters, stems from the changing tide of sedimentation engineering concepts and how those efforts must accommodate a constantly changing world that effects any given community subject to disasters. Engineering—the core of the vast field of water law and sedimentation—plays a vital role when it comes to recent trends in American sedimentation law and the physical processes it is based on. Key trend-setting court decisions serve to remind the powers that be of reasonable use standards and ethical practices. When it comes to public liability and natural hazards, hazard mitigation and awareness programs, insurance plans, and cooperation between government agencies and private citizens are key. Although Statutes of Limitation draw a line in the sand after certain disclosures, if reasonable use can be challenged, inverse condemnation can be considered. For the most part, "act of God" defenses occur when flood damage is unprecedented. Forensic geology is a valuable accuracy tool for technically proving physical changes. Overall, the new wave of sedimentation engineering demonstrates the benefits of reasonable use and cooperative awareness for both private and public lands that are interwoven with social controls, government regulations, and other legal agreements.

ACKNOWLEDGMENTS

We were fortunate to have knowledgeable references in the form of an unpublished draft book entitled *Public Liability and Natural Hazards: Common Law and Regulatory "Takings"; Future Directions,* compiled by legal expert Jon Kusler, who was generous enough to lend access to his extensive research to the world of civil engineering.

A portion of the research and the actual writing of this report was made possible through Grant No. CES-8612277 from the National Science Foundation. This funding and the help of Dr. William Anderson, project officer, is gratefully appreciated. In addition, a project advisory committee helped define the audience for the book and the level of analysis. Advisory committee members included, in addition to Dr. Anderson, James Wright, The Tennessee Valley Authority; Frank Thomas, the Federal Emergency Management Agency; Ross McKay, the Federal Emergency Management Agency; Larry Larson, the Association of State Floodplain Managers; and Gilbert White, the University of Colorado. Their assistance is much appreciated. Also, law student assistants at the Albany Law School who provided research assistance included Alan Baum, Robert McCann, Dan McCormick, Peggy Seilkin, and Peter Hickey. Their help and the use of law school library facilities are also much appreciated.

REFERENCES

Busby, C. E. (1957). "Chapter VII: American Sedimentation Law and Physical Process." *Sedimentation engineering,* Vito Vanoni, ed., *Manuals and Reports of Engineering Practice—No. 54,* ASCE, New York, pp. 629–685.

Central State University of Idaho (CSI). (1998). <http://www.csi.cc.id.us/ip/ag/water/chapter>.

Central State University of Idaho (CSI). (1999). (www.csi.cc.id.us), "Public rights." <http://www.csi.cc.id.us>.

Federal Emergency Management Agency (FEMA). (1995). "Out of Harm's Way: The Missouri Buyout Program." FEMA, Washington, D.C.

Federal Emergency Management Agency (FEMA). (1999). FEMA, Washington, D.C. <http://www.fema.gov/library/armstrong084> (Nov. 15, 1999).

Federal Emergency Management Agency (FEMA). (2000a). FEMA, Washington, D.C. <http://www.fema.gov/nwz00/nfipclai.htm> (March 1, 2000).

Federal Emergency Management Agency (FEMA). (2000b). FEMA, Washington, D.C. <http://www.fema.gov/impact/impact00> (Feb. 7, 2000).

Federal Emergency Management Agency (FEMA). (2000c). FEMA, Washington, D.C. <http://www.fema.gov/nwz00/2001budget> (Feb. 8, 2000).

Federal Emergency Management Agency (FEMA). (2000d). FEMA, Washington, D.C. <http://www.nara.gov; www.fema.gov/nwz00/add215m> (Feb. 15, 2000).

Georgia Exceptions 56. (1922). Georgia v. South Carolina, 259 U.S. 572. <http://www.caselaw.findlaw.com/scripts>.

Glannon. (1982). "Scope of public liability under the tort claims act: Beyond the public duty rule." *Massachusetts Law Review,* 67, 159.

Huffman, J. L. (1988). *Government liability and disaster mitigation: A comparative study,* Lewis and Clark Law School, Portland, Or.

Kusler, J. (1971). "Regulation of flood hazard areas to reduce flood losses," Vol. 1. *Prepared for the U.S. Water Resources Council,* U.S. Government Printing Office, Washington, D.C.

Kusler, J. (1972). "Regulation of flood hazard areas to reduce flood losses," Vol. 2. *Prepared for the U.S. Water Resources Council,* U.S. Government Printing Office, Washington, D.C.

Kusler, J. (1972). "Regulation of flood hazard areas to reduce flood losses," Vol. 3. *Prepared for the U.S. Water Resources Council,* U.S. Government Printing Office, Washington, D.C.

Missouri Water Law. <http://www.ssu.missouri.edu/courses/AgEc156/missouriwaterlaw>.

Murray, R. C. (1992). *Forensic geology*, Prentice-Hall, Englewood Cliffs, N. J., pp. 154–155.

U.S. Environmental Protection Agency (USEPA). (1998). *Water news: National inventory of contaminated sediments,* USEPA <http://www.epa.gov/ow/waternews/012098> (Jan. 20, 1998).

United States Geological Survey (USGS). (2000). *USGS News Release, February 7, 2000,* MS119 National Center, USGA, Reston, Va. <http://www.usgs.gov>.

COURT CITATIONS AND OTHER REFERENCES

References to legal literature within the text (**in bold**) are made in the following order from left to right: (1) Court Decision Name or Law Review Name; (2) volume number of the set of reports; (3) name of the set of reports, in abbreviated form; (4) page number or numbers of the volume; and (5) date of the decision or law review. If there are citations to two or more sets of reports, then repeat these items for (1) each such report, (2) set of abbreviations, and (3) page numbers. Finally comes the date of the decision or report in parentheses. The same applies to Law Reviews except that the volume number comes first, the full name of the Law Review, and then the page number and date, if any. Some Reviews are not quoted by date and page numbers because these are not always necessary.

Copyrighted Materials
Copyright © 2008 American Society of Civil Engineers (ASCE)
Retrieved from www.knovel.com

CHAPTER 21

Contaminant Processes in Sediments

Danny D. Reible

21.1 INTRODUCTION

Many of the most toxic and most persistent environmental contaminants in bodies of water are strongly associated with sediments, either suspended or settled to the bed. As a result, the transport and fate of sediments also often define the dynamics of associated contaminants. Contaminants are also influenced, however, by a variety of physical, chemical, and biological processes that involve no net movement of sediments. These processes include pore-water transport processes such as diffusion and advection and sediment mixing processes such as reworking by benthic organisms that involve no net downstream particle movement. Understanding these processes is critical to development of appropriate strategies for managing the risks these contaminants may pose to human health and the environment. Assessment of the processes that control contaminant migration and fate in a water body allows development of a conceptual model of the system and identification of intervention approaches that are most likely to succeed. Evaluation of these processes provides an assessment of the potential for natural attenuation of contaminants in a system. These processes are also critical to the evaluation of more active remedial approaches, such as dredging or capping, because the success of these approaches typically depends upon the fate of the residual contaminants in the water body. This paper will examine processes that influence the fate and transport characteristics of contaminants in sediments and interaction of these processes with common management or remedial approaches.

Any attempt to summarize and compare natural processes in sediments must recognize the different environments in which contaminated sediments are found. The relative importance of these processes differs significantly between lacustrine, riverine, estuarine, and coastal environments. The range and significance of natural processes are influenced heavily by site-specific characteristics. This paper attempts to identify all of the potentially important natural processes influencing contaminants and build a matrix relating sediment and waterbody characteristics to these processes. The individual processes are discussed, including a means of assessing the importance of each process in particular field situations.

The most important natural fate and transport processes at contaminated sediment sites are illustrated in Fig. 21-1 and include the following:

- In-bed fate processes, including irreversible adsorption and chemical or biological reactions;
- In-bed transport processes, including diffusion and advection as influenced by reversible sorption/desorption and colloidal transport;
- Interfacial transport processes (bed to water column or vice versa), including sediment deposition and resuspension, bioturbation, and water-side mass transfer.

Table 21-1 summarizes the relative importance of these processes in various sedimentary environments. These processes and their importance in the individual environments are discussed in more detail in subsequent sections. The most important factor in defining the fate and transport processes that influence contaminants in sediment beds is the energy of the overlying flow. In high-energy environments, bed sediment tends to be coarse-grained and noncohesive, with little sorptive capacity and low depositional rates. These sediments pose little barrier to advective transport and often allow oxygen transport deep within the sediment. In low-energy environments, significant deposits of fine-grained sediments exist, providing high sorptive capacity and significant slowing of advection and oxygen transport. Somewhat offsetting these differences is the fact that many organisms, especially head-down deposit feeders, prefer fine-grained sediments. Therefore, bioturbation (i.e., the mixing associated with the normal life-cycle activities of sediment-dwelling organisms) is often enhanced in areas of finer-grained sediments.

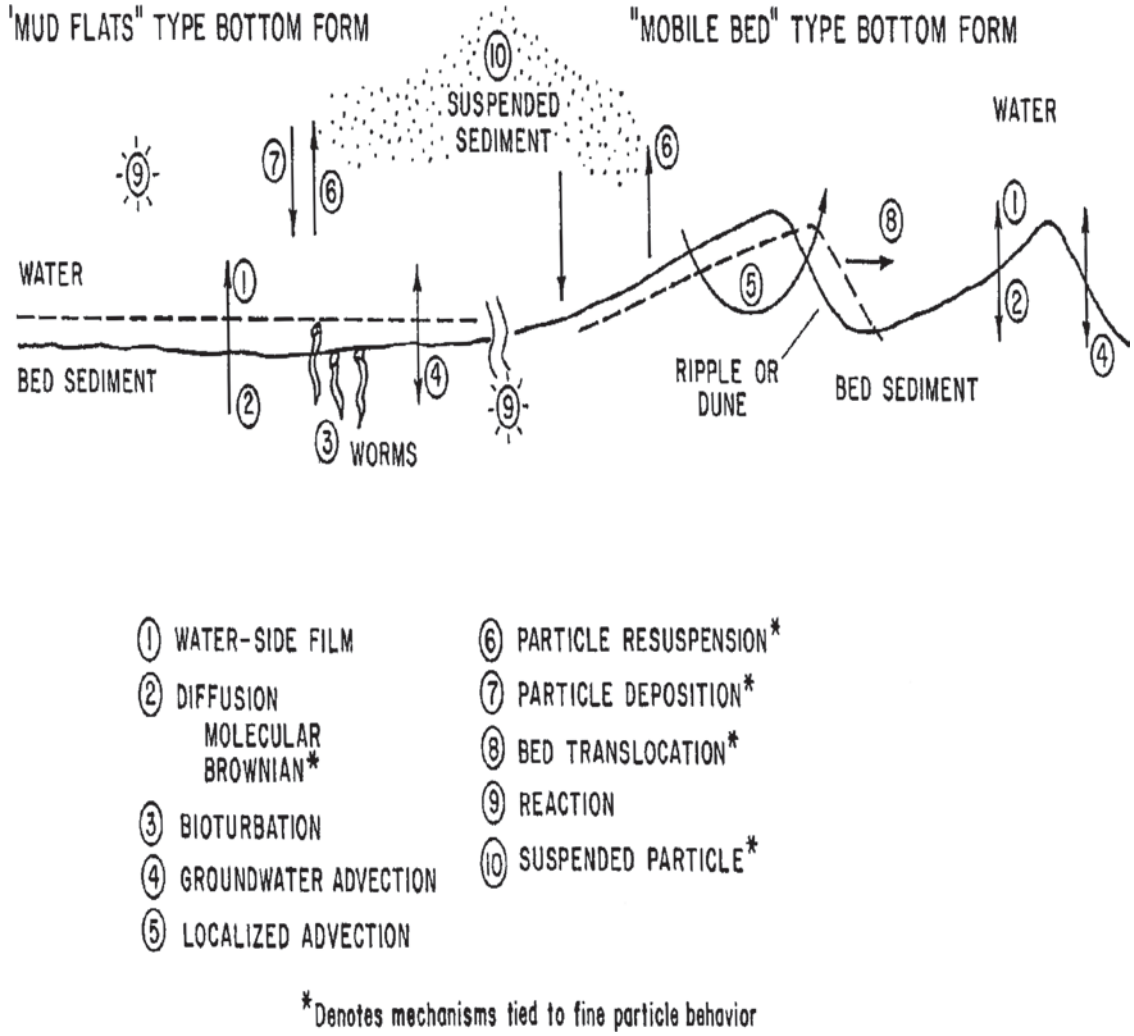

Fig. 21-1. Depiction of selected processes at the sediment-water interface.

21.2 CONTAMINANTS OF CONCERN

Relatively uncontrolled historical wastewater effluents often introduced priority pollutants and other contaminants of concern to the environment. Many of these compounds tended to accumulate in sediments because of persistence and hydrophobicity. Because wastewater effluents are now more controlled, the accumulation of contaminants in the sediments is reduced and other sources, such as atmospheric deposition and rural and urban runoff, may be equally or more important in contributing individual pollutants to the sediment. In addition, the sediments now often constitute a significant source controlling surficial water quality. Contaminants that do not strongly associate with solids, such as polar organic compounds or soluble metals, rarely accumulate in sediments, because these compounds are efficiently released to the overlying water. In this section we will examine some of the most important sediment contaminants and the physical and chemical characteristics that relate to fate and mobility in the environment. These contaminants include conventional pollutants such as nutrients and oxygen-demanding contaminants, heavy metals, pesticides, polycyclic aromatic hydrocarbons (PAHs), and chlorinated organic compounds such as polychlorinated biphenyls (PCBs) and multiply chlorinated benzenes.

21.2.1 Conventional Pollutants

Conventional pollutants include nutrients, oxygen demanding contaminants, and undifferentiated oil and grease. Sediments may harbor a significant inventory of nitrogen and phosphorus, release of which may dramatically change the biological characteristics of the overlying water. A variety of organic and inorganic compounds in sediments consume oxygen. The cumulative effect of these reactions is measured by sediment oxygen demand, a parameter similar

Table 21-1 Sediment Processes and Relationship to Various Sediment Environments

Environment	Environmental characteristics	Key fate and transport processes
Lacustrine	Low-energy environment Generally depositional environment Groundwater interaction decreasing away from shore Organic matter decreasing with distance from shore Often fine-grained sediment	Sediment deposition Water-side mass transfer limitations Groundwater advection in near-shore area Bioturbation (especially in near-shore area) Diffusion in quiescent settings Metal sorption Aerobic and anaerobic biotransformation Biotransformation of organic matter (e.g., gas formation)
Riverine	Low- to high-energy environment Depositional or erosional environment Potential for significant groundwater interaction Significant variability in flow and sediment characteristics within and between rivers	Local and generalized groundwater advection Sediment deposition and resuspension Aerobic biotransformation processes in surficial sediments (anaerobic at depth) Bioturbation
Estuarine	Generally low-energy environment Generally depositional environment Generally fine-grained sediment Grading to coarse sediment at ocean boundary	Bioturbation Sediment deposition Water-side mass transfer limitations Aerobic and anaerobic biotransformation of contaminants Biotransformation of organic matter (e.g., gas formation)
Coastal marine	Relatively high-energy environment, decreasing with depth and distance from shore Often coarse sediments	Bioturbation Sediment erosion and deposition Localized advection processes

in significance to oxygen-demanding measures in the overlying water. Sediment oxygen demand serves to reduce available oxygen and encourage anaerobic conditions within the sediment. This may affect the rate of fate processes, such as biological degradation of contaminants in the sediments, and the chemical state of metals, influencing mobility. The sediment oxygen demand can also impact oxygen levels in the overlying water. There are no specific levels of oxygen demanding constituents that are considered problematic. The impact of these contaminants depends upon the dynamics of the sediment, associated groundwaters, and overlying water column.

Long-chain nonpolar organic compounds, such as oil and grease, associate strongly with solids and sediments. Measures of these compounds include both oil and grease concentration and total petroleum hydrocarbon concentration. The source of these compounds is generally petroleum hydrocarbon production or processing facilities, or facilities that use or process significant amounts of these compounds. In addition, municipal and industrial wastewater-treatment effluents can lead to significant accumulation of hydrocarbons in sediments over time. Because many of these sources are much more carefully controlled than in times past, oil and grease or total petroleum hydrocarbons levels in sediments often represent excellent indicators of historical pollution.

21.2.2 Heavy Metals

The toxic metals and metalloids include antimony, arsenic, beryllium, cadmium, copper, lead, mercury, nickel, silver, thallium, and zinc. Importantly, these pollutants are nonbiodegradable, toxic in solution, and subject to biomagnification. The chemistry of many of these compounds is complex in sediments. A portion is generally chemically fixed and largely unavailable to fish and other organisms without significant chemical changes in the sediment. Often a portion is ion-exchangeable and may become available simply with the substitution of a more surface-active contaminant. Finally, a portion is soluble, mobile, and directly available for uptake by organisms.

Historically, the metals extraction and processing industries, as well as urban and rural runoff, provided the most significant sources of these elements. Lead was widely distributed in the environment as a result of the use of tetraethyllead in gasoline to control premature ignition (knocking). These sources have largely been controlled. Some sources of metals, however, are only poorly controlled and represent a continuing source of metals to sediments. These sources include leaching from abandoned mining sites and urban runoff. Unlike oxygen-demanding wastes, these pollutants are not easily neutralized or assimilated by natural processes.

21.2.3 Polycyclic Aromatics

The polycyclic aromatic hydrocarbon compounds are used as chemical intermediates and are present in fossil fuels. Polycyclic aromatics tend to be present in coal liquids and the heavier oil stocks as a result of lesser volatility. Many of the compounds have been found to be carcinogenic in animals and are assumed to be carcinogenic in humans. These tend to be intermediate in persistence and bioaccumulation potential compared with monocyclic aromatics/halogenated aliphatics and the PCBs. Production during combustion of industrial fuels and oils (diesel, coal liquids, heavy fuel oils) has resulted in the presence of PAHs at old industrial sites where contamination levels might be especially high. Sediment contaminant with PAHs is often associated with historical release of oils in wastewater but atmospheric deposition contributes to widespread contamination and specific locations may be influenced by oil seeps. Examples of PAHs include naphthalene, fluoranthene, pyrene, and chrysene. The compounds composed of two aromatic rings (naphthalene) tend to be the most volatile, soluble, and mobile, while solubility and volatility tend to decrease as the number of rings increases.

21.2.4 Pesticides

Priority pesticides are generally chlorinated hydrocarbons. These include such compounds as aldrin, dieldrin, DDT (dichlorodiphenyltrichoroethane), DDD (dichlorodiphenyldichoroethane), endosulfan, endrin, heptachlor, lindane, and chlordane. These organic compounds are readily assimilated by aquatic animals, and are subject to *bioaccumulation* and *biomagnification*. Bioaccumulation is the uptake and partitioning of contaminants by organisms, whereas biomagnification is the concentration of pollutants by natural processes such as the food chain. Greater amounts of pollutants may be accumulated higher in the food chain. These particular pesticides are also persistent contaminants. DDT, for example, remains an environmental contaminant many years after being banned in the United States.

DDT is an excellent example of the potential problems associated with these compounds. Although not considered extremely toxic and despite decreased usage during the 1960s, DDT use was banned in the United States in 1972 (although production and export continued after 1972) as a result of persistence and potential for biomagnfication. Hickey et al. (1966), for example, reported biomagnification of DDT by more than 170,000 times between Lake Michigan sediments and fish-eating birds. Bottom-feeding crustacea exhibited about 30 times sediment concentrations, where as the fish that fed off the crustacea exhibited concentrations about 10 times still higher than found in the crustacean. Finally, fish-eating birds exhibited concentrations of DDT 500 times higher than observed in the fish. The magnification at each level is dependent on the feeding habits and animal metabolism and, because the organochlorines tend to build up in the lipid or fat fraction of the body, the proportion of body fat.

21.2.5 Chlorinated Organic Compounds

Multiply chlorinated, high-molecular-weight organic compounds such as hexachlorbenzene and PCBs tend to be strongly hydrophobic and therefore partition into sediments. Due to low degradation rates, tendency to sorb, and high molecular weight, these compounds tend to exhibit low mobility in the environment and are persistent in sediments. PCBs are complex mixtures of organochlorines that are extremely stable. In addition, as with the organochlorine pesticides, PCBs are readily assimilated by aquatic animals and soluble in body fats and will biomagnify in the food chain. Although the toxicity of many of the individual PCBs is relatively low, specific isomers plus trace contamination with other chlorinated compounds give rise to significant health concerns. As a result, PCB production was banned in the United States in 1979. It should be emphasized that PCBs are a complex mixture of compounds and, in fact, are generally named only by the total percentage of chlorine in the mixture. Specific PCB mixtures are referred to as Aroclors, and Aroclor 1254 is 54% chlorine and Aroclor 1260 is 60% chlorine.

Again, as a result of persistence, significant quantities remain in the environment. Industrialized harbor areas in the Great Lakes and northeastern United States are often contaminated with PCBs. Fish advisories exist in many of the Great Lakes as a result of health concerns from eating PCB-contaminated fish. Because of the potential for PCBs to sorb onto organic materials in sediments and in fish lipids, such advisories are aimed primarily at fatty, bottom-feeding fish where PCB concentration is the highest, and will biomagnify in the food chain.

21.3 CONTAMINANT RELEASE AND EXPOSURE PATHWAYS

The risks of sediment contaminants to higher organisms such as fish and animals that feed off fish can arise via one of the following three pathways:

- Exposure by contaminant release due to erosion and resuspension of the sediment bed;
- Exposure by predation and harvesting of plants and animals living directly exposed at the contaminated sediment-water interface or by incidental ingestion of contaminated bed sediments;
- Exposure by contaminant release in dissolved or other form from a stable sediment bed by any of a variety of stable bed processes including advection, diffusion, and bioturbation.

Each of these pathways involves interaction of the higher organisms with the contaminants of and near the sediment-water interface. The absolute and relative importance of these pathways largely depends upon the rate of the various fate and transport processes that influence the pathway. Each of these will be examined in more detail.

These pathways are largely limited to the upper few cm of sediment, and thus exposure and risk due to sediment contaminants is largely related to surficial sediment concentrations. Due to significant erosion, it may be that the dynamics of the surface layer may result in exposure of previously buried contaminants, but at any given time, the surficial sediment concentrations largely define exposure and risk to organisms in the overlying water. In recognition of this fact, the surface-area-weighted average concentration ($<W_s>$) has come to be used as a good indicator of exposure and risk:

$$<W_s> = \frac{\int_A W_s(0)\,dA}{\int_A dA} \tag{21-1}$$

where

$W_s(0)$ = Surficial sediment-contaminant concentration (e.g., in μg/g), which may vary in space over the area A.

Similarly, the time-integrated $<W_s>$ is related to the time-integrated exposure, or dose,

$$\text{Integrated exposure} \sim \int_t <W_s>\, dt \tag{21-2}$$

The assessment of exposure is thus largely reduced to defining quantitatively the relationship between exposure and $<W_s>$ (or time-integrated $<W_s>$) for the different processes relevant to a particular environmental system. Especially challenging is the definition of future exposure associated with contaminants currently buried below the surface layer. The use of a relationship such as Eq. (21-1) does not imply that currently buried contaminants will not become a source of exposure and risk at some point in the future.

21.3.1 Exposure by Contaminant Release from Resuspended Sediment

The dominant characteristic that controls direct exposure of fish and other animals to contaminated sediment is resuspension and erosion of particles from the sediment bed. Since most persistent sediment contaminants are associated with the solid phase, any mobilization of this phase dramatically increases contaminant mobility. As a result, contaminants can be distributed over large areas, and significantly increased water-column concentrations can be observed relative to less active sediment-water transport. Erosion and resuspension conditions also hinder natural recovery that might occur in less active environments through deposition and burial of the contaminated sediment.

Under high-energy conditions in a stream, significant sediment transport occurs and individual sediment particles can be carried downstream either by bed-load or by suspended-load transport. This process normally results in the formation of dunes, ripples, and antidunes that progress downstream by erosion on the upstream face and deposition on the downstream face. During this overturning and migration process, sediment particles are exposed and either scoured and suspended in the stream or reburied by other sediment particles. During exposure to the stream water, contaminants sorbed to the sediment particles can desorb, and contaminants in the adjacent pore water can be released into the overlying water.

Should significant erosion and resuspension occur, the water-column concentration tends to approach the equilibrium defined by desorbable contaminants in the resuspended sediment. If K_{sw} is a distribution coefficient of the sorbed contaminant between the sediment and the water (units of volume per mass, e.g., cm^3/g), the aqueous phase concentration, C_w (mass/volume, e.g., $\mu g/cm^3$), is a function of the resuspended sediment concentration in the overlying water, C_S (mass/volume, e.g., g/cm^3). If the sediment carries an initial contaminant concentration, W_s (mass/mass, e.g., μg/g), the contaminant concentration in the overlying water is given by

$$C_w = \frac{C_s W_s}{1 + C_s K_{sw}} \tag{21-3}$$

For a hydrophobic organic compound, the distribution coefficient is often assumed to be given by the product of the organic carbon based partition coefficient, K_{oc}, a compound-specific parameter, and the fraction of organic carbon in the sediment, f_{oc}, a sediment-specific parameter. Theoretical predictions normally assume linearity, as indicated in Eq. (21-3), and complete reversibility, but deviations are often observed in practice. Equation (21-3) may still prove useful, however, if measured, rather than predicted, values of the effective partition coefficient are employed.

Equation (21-3) shows that for complete desorption (low suspended-sediment concentrations), the water concentration is simply the suspended-sediment concentration times the initial contaminant concentration in the sediment. At high suspended concentrations, however, the overlying water approaches equilibrium with the contaminated sediment bed as given by the equation

$$C_w = \frac{W_s}{K_{sw}} \tag{21-4}$$

For metals and other elemental species, the equilibrium state is much more complicated and depends on the chemical state of the water and sediment, particularly the pH and

oxidation-reduction conditions. The ratio of sediment loading to equilibrium water concentration is often very large for metals because only a small fraction of the metals is typically available for partitioning. Myers et al. (1996) indicate that the leachable fraction of metals is typically less than 10%, sometimes much less, and that the partition coefficient between the leachable fraction and the water is typically between 3 and 10 L/kg. For both organic and metal species, a site-specific measurement of the sediment-water partition coefficient is preferred.

As shown by Eq. (21-3), the concentration and exposure in the overlying water is a function of the concentration of sediment resuspended. The concentration of resuspended sediment is a function of the rate and depth of erosion. The ability to predict the rate of erosion based solely upon physical characteristics of the sediment such as grain size and density remains largely limited to cohesionless, coarse-grained particles. Site-specific measurements of sediment response to shear flows are needed to characterize erosion of cohesive, fine-grained sediment. Erosion of both cohesive and noncohesive sediments is discussed in detail in Chapters 2 and 4.

Because contaminants tend to be strongly associated with fine-grained sediments, the discussion of Chapter 4 is especially relevant. As discussed there, erosion of a sediment bed can occur via one of four processes: surface erosion, mass erosion, fluid mud generation, and fluid mud entrainment. Of these, surface erosion is likely to be the most important except in specific locations where mass erosion (erosion of clumps of bottom material) or fluid mud entrainment (mobilization of very soft sediments) may be important.

For cohesive sediments, the friction velocity required to produce particle motion is significantly larger for a given particular particle size than for noncohesive sediments. Offsetting this is the fact that cohesive sediments tend to be very fine-grained and thus may be subject to significantly more erosion than coarse-grained noncohesive sediments. The property of cohesiveness is a complicated function of particle size, bulk density, mineralogy, organic content, and salinity. These properties vary significantly with position and time. Often, due to the lack of sufficient data on the deposit properties with position and time, these variations are not fully incorporated in sediment transport models. Instead, the rate of erosion, E (i.e., the sediment erosion flux in $g \bullet cm^{-2} \bullet hr^{-1}$), is related to the local bed density, ρ_s, and the probability of a particle becoming resuspended, P_{ero}, which for a cohesive sediment is related to the bottom shear stress, τ_b, and the bed density,

$$E = P_{ero}\, \tau_b^N\, \rho_s = A\, \tau_b^n\, \rho_s^m \tag{21-5}$$

The exponent on the bottom shear stress depends on the bed properties but is typically between 2 and 3 for cohesive sediments. This implies that the erosion rate depends on the fourth to sixth power of stream velocity, because bottom shear stress typically depends on the square of velocity. The strong dependence on stream velocity emphasizes that a critical component of any effort to model sediment dynamics is knowledge of the stream hydrodynamics. Although it is not yet possible to predict the relationship between erosion rate and shear stress for cohesive sediments, it is possible to make measurements from which the values of A, n, and m can be determined (McNeill et al. 1996). The flux of contaminants returned to the sediment column, F_{ero} (e.g., in $\mu g \bullet cm^{-2} \bullet hr^{-1}$), as a result of erosion is then given by

$$F_{ero} = E\, W_s \tag{21-6}$$

where

W_s = sediment contaminant concentration (e.g., in µg/g).

When sediment is dredged, an artificial situation is created that is equivalent to high flow-related erosion of the sediment bed. Under such conditions, the water again tends to equilibrate with the sediment resuspended by the dredge head (DiGiano et al. 1993). Therefore, the approach outlined also can be used to assess exposure and risks due to dredging, at least for organic compounds, if an estimate or measurements of sediment resuspension are available. DiGiano et al. (1995) also developed an experimental protocol for estimating metals release and equilibration with a body of water during dredging.

Deposition may serve to isolate contaminants from the overlying water column and reduce the influence of erosion. The net sediment transport is the difference between the erosion rate, defined above, and the deposition rate. In general, the rate of deposition, D, can be modeled with relationships of the form

$$D = P_{dep}\, w_s\, C_s \tag{21-7}$$

where P_{dep} is the probability of capture of the depositing particle, w_s is the vertical settling velocity of the particles, and C_s is the suspended-sediment concentration. The probability of deposition tends to decrease as the bed shear stress increases. The local particle concentration can be modeled as a decreasing exponential function of height above the bed (Jones and Lick 2000). There are also significant differences between cohesive (flocculating) sediment and noncohesive (i.e., sandy) sediment. Sandy sediment deposition can be modeled employing the formulation of Cheng (1997). In cohesive sediments, deposition is affected by aggregation and/or disaggregation processes that are complex functions of sediment and stream conditions (Lick and Lick 1988). The flux of contaminants, F_{dep}, carried by deposition to the sediment bed is given by

$$F_{dep} = D\, K_{sw}\, C_w \tag{21-8}$$

Here the contaminant concentration on any depositing particles is assumed to be given by equilibrium with the overlying water concentration. The quantity $K_{sw}\, C_w$ is the sediment concentration that would be in equilibrium with the overlying water, W_s^*. The net contaminant flux from the

sediment bed due to erosion and deposition processes can thus be written by combining Eqs. (21-4) and (21-6) to give

$$F_{\text{net}} = E W_s - D W_s^* \tag{21-9}$$

For a sediment bed in a state of quasi-equilibrium where the average erosion and deposition rates are equal, the net contaminant flux can be written as proportional to the difference between the actual surficial sediment concentration and the surficial sediment concentration that would be in equilibrium with the overlying water.

21.3.2 Exposure by Ingestion of Sediments or Organisms at the Bed Surface

The evaluation of the ingestion exposure pathway involves two steps: (1) the assessment of the contaminant concentrations in plants and animals living at the sediment-water interface as a result of exposure to the sediments, and (2) the assessment of uptake of these organisms by fish and other higher animals. In this paper we are focused on the processes within sediments and so will largely limit our discussion to the first step, that is, defining the relationship between the sediments and the accumulation of contaminants in the sediment-dwelling organisms. Plants and animals living at the sediment-water interface are often assumed to be in equilibrium with the surficial sediments. Similarly, incidental ingestion of sediments by fish or higher animals involves direct exposure to the surficial contamination. Thus uptake into fish and higher animals by these mechanisms depends upon the rate of ingestion of sediments or benthic organisms and the sediment concentration that is bioavailable. The contaminant capable of partitioning into the adjacent pore water from the sediment solids is often assumed to define the portion that is available for uptake by the plants and animals (USEPA 1993b). In principle, therefore, partitioning measurements or predictions can largely define the quantity of contaminant available to sediment-dwelling organisms or to higher organisms coming into direct contact with or ingesting sediments. It is important to note, however, that the contaminant concentration in the surficial sediments may not be represented well by a depth-averaged composite concentration, even though that is what is typically measured. Freshwater benthos, for example, may only populate the upper 5 to 10 cm of sediments in significant quantities. In marine sediments, animals living at the sediment-water interface tend to be larger and influence a somewhat greater depth of sediment, although the bulk of the activity remains within 15 cm of the surface. More than 90% of the 240 observations of the layer depth effectively mixed by organisms reported by Thoms et al. (1995) were 15 cm or less and more than 80% were 10 cm or less. It is the sediment concentrations within this layer that are expected to control the body burden of sediment-dwelling organisms.

If the upper sediment layers are assumed in equilibrium with the adjacent pore water and if uptake is assumed to be defined by porewater concentrations, the contaminant concentration available to plants and animals living at the sediment-water interface is as given by Eq. (21-4). The rate of uptake to a benthic or higher organism depends upon the rate of uptake or ingestion but will ultimately approach a steady state defined by a balance between uptake and elimination mechanisms. The ratio of the concentration in the organism, W_b, to that in the sediment, W_s, is termed the biota-sediment accumulation factor (BSAF). For hydrophobic organic compounds, the partitioning of the contaminant is assumed to be controlled by the organic "solvent" fraction that exists within a particular phase. Thus, a more useful biota-sediment accumulation factor for such compounds is one that normalizes the concentration in each phase with the organic fraction in that phase. For the biota, this is the lipid fraction, f_{lipid}, and for the sediment, it is the organic carbon fraction, f_{oc}. Benthic organisms are in intimate contact with the sediment and pore water and often exhibit only slow metabolism or elimination of the contaminants of interest. Thus benthic organisms rapidly approach equilibrium with these phases. The BSAF then approaches the ratio of the organic-carbon-normalized partition coefficients,

$$\text{BSAF} = \frac{W_b / f_{\text{lipid}}}{W_s / f_{oc}} = \frac{K_{\text{lipid}} C_w}{K_{sw} / f_{oc}\ C_w} \approx \frac{K_{\text{lipid}}}{K_{oc}} \tag{21-10}$$

In the final relationship, K_{sw}/f_{oc} is equal to the commonly tabulated organic-carbon-based partition coefficient, K_{oc}, only if the desorption is governed by linear, reversible sorption to the sediment organic fraction. As indicated below, the effective partition coefficient, K_{sw}, may not be equal to $K_{oc} f_{oc}$ due to desorption resistance or nonlinear sorption-desorption equilibrium. The BSAFs for organic contaminants vary as a function of sediment, organism, and time of exposure, but the value for benthic organisms, especially those that ingest sediment as food, tends to approach unity (e.g., Ingersoll et al. 1997), suggesting that the organic-normalized partition coefficients in lipids and sediment are approximately equal ($K_{\text{lipid}} = K_{sw}$). It is important to note that BSAFs in organisms not intimately associated with the sediment may vary considerably from unity. In addition, no equivalent basis for the estimation or normalization of the accumulation of metals in organisms exists.

The normalization by organic carbon content assumes that essentially all of the hydrophobic organic contaminant in the sediment and organism is available for partitioning. A significant fraction of the contaminant, though, is often unavailable and is held in a desorption-resistant fraction. The results of many laboratory and field observations indicate, though, that a significant fraction of soil- and sediment-bound contaminants desorb slowly, if at all, are not biodegraded, and are difficult to remove by extraction with surfactants or cosolvents. For example, Pereira et al. (1988) found that the concentration of halogenated organic compounds in native

water, suspended sediments, and biota was far below the values predicted from concentrations in the contaminated bottom sediments collected from Bayou d'Inde, Louisiana. Similarly, McGroddy and Farrington (1995) and Readman and Montoura (1987) observed a fraction of PAHs in river sediments not available for desorption. For most of these sediments, the contamination source had ceased for many years, yet the sediment-bound contaminants persisted over tens of years without significant reduction in concentration or changes in the compound distribution.

The sorption of organic chemicals to soils and sediments is a complex process, given the diversity, magnitude, and activity of chemical species, phases, and interfaces commonly present in contaminated subsurface environments, which may also be quite variable in particle size and organic carbon content. The quantity sorbed is often found to be well represented by the combination of a compartment exhibiting linear, reversible sorption and a compartment that exhibits nonlinear and thermodynamic irreversibe sorption. Note that thermodynamically irreversibility simply means that the desorption process does not occur at the same rate or extent as sorption and does not imply that desorption does not occur. In addition to biphasic equilibrium behavior, the approach to equilibrium is controlled by different kinetics in the reversible and irreversible compartments. The kinetics of sorption and desorption in the reversible compartment are typically on the order of a day or less whereas desorption of the sequestered fraction may take weeks or months to approach completion (White et al. 1999).

Pignatello and Xing (1996) have presented a slow-sorption model in which sorption and desorption can be divided into a slow and a fast fraction. The quantity sorbed in each fraction can be described using a Freundlich isotherm or, if the fast release fraction is assumed linear and reversible and given by the organic-carbon-based partition coefficient, by

$$W_s = (W_s)_f + (W_s)_s = K_{oc}\ f_{oc}\ C_w + K_w\, C_w^{n_s} \qquad (21\text{-}11)$$

Here

W_s = sorbed quantity of solute;
C_w = adjacent porewater concentrations;
and the subscripts f and s represent fast and slow, respectively.

K_s and n_s are fitting parameters. Slow sorption may be strongly nonlinear and, combined with entrapment of contaminants in desorption-resistant compartments, is expected to be responsible for the effect of contaminant age on desorption and reduced bioavailability. Pignatello and Xing (1996) have related the different rates of sorption and desorption to the quality of the organic matter (i.e., soft and rubbery versus diagenetically aged hard and glassy).

Huang and Weber (1997) have presented the dual-reactive-domain model (DRDM), which is focused on this difference in sorbent character, to describe hysteresis in sorption-desorption. The soft, rubbery carbon that represents diagenetically young soils exhibits linear, reversible sorption, whereas aged, hard glassy carbon represents a nonlinear contribution to sorption-desorption. The degree of nonlinear desorption phenomena and contaminant sequestration is presumably related to the fraction of aged carbon. For many sediments, the fraction of diagenetically aged carbon is relatively small, although the capacity of that material for contaminant sorption may be large. Assuming Langmuir-type sorption in the nonlinear domain and that the linear reversible sorption is defined by the organic-carbon-based partition coefficient, the sorbed quantity for the dual-reactive domain-model can be written

$$W_s = (W_s)_\ell + (W_s)_s\ K_{oc}\ f_{oc}\ C_w + \frac{Q\,b\,C_w}{1+bC} \qquad (21\text{-}12)$$

where ℓ represents linear or labile fraction and s represents slow or sequestered fraction. Q and b represent the Langmuir fitting parameters of capacity factor and site energy, respectively. The model of Tomson and coworkers (Hunter et al. 1996; Kan et al. 1997; Kan et al. 1998) also assumes a biphasic sorption-desorption model that combines the linear and Langmuir sorption isotherms for the quantity sorbed.

Note that the net effect of a biphasic sorption model such as described by Eq. (21-11) or Eq. (12-12) is that the effective partition coefficient W_s/C_w increases:

$$K_{sw}\frac{W_s}{C_w} = K_{oc}\,f_{oc} + \frac{Q\,b}{1+bC_w} \qquad (21\text{-}13)$$

This can be used to estimate the steady-state accumulation in benthic organisms in which $K_{\text{lipid}} \sim K_{oc}$. The effect of the desorption-resistant fraction is an effective increase in the sediment-water partition coefficient and reduction in the pore-water concentration. Thus the effect of the desorption-resistant-related reduction on pore-water concentration is a decrease in the BSAF according to

$$\text{BSAF} = \frac{K_{\text{lipid}}}{K_{sw}/f_{oc}} \approx \frac{K_{oc}}{K_{oc} + \dfrac{Q\,b}{f_{oc}(1+bC_w)}} \qquad (21\text{-}14)$$

As noted by Pigantello and Xing (1996), the rate of release from the desorption-resistant contaminant fraction is significantly lower than that from the more labile fraction. Thus the normalized accumulation may be significantly lower than shown in Eq. (21-14) due to kinetic limitations in some plants or animals or under some environmental conditions.

The bioaccumulation behavior of metals and ionic species is significantly more complicated; however, the dissolved pore-water concentration in the sediment has been seen increasingly as the best indicator of metals and ionic species in both plants and animals. As indicated previously, the fraction that is ultimately leachable into the pore water is typically less than 10% of the total metal loading on the sediment, and the effective partition coefficient for this leachable fraction is typically 3 to

10 (Myers et al. 1996). Another indicator for specific metal contaminants is the ratio of the acid volatile sulfides (AVS) to the simultaneously extractable metals (SEM). A number of metals, including cadmium, copper, lead, nickel, and zinc, tend to form insoluble metal sulfides in reduced sediments. As long as the AVS exceeds the SEM, these metals are in reduced form and essentially unavailable in dissolved form to living organisms (SAB 1995). For some metals, however, such as arsenic, the reduced form may be of more environmental consequence than other forms. Considerably more complicated is mercury, which undergoes biologically mediated reduction reactions that may encourage the formation of methylmercury.

As a result of the complex and varied behavior of metal species and other chemicals, toxicity tests, rather than specific physicochemical tests, are often used to assess the potential for adverse sediment effects. The USEPA Assessment and Remediation of Contaminated Sediments (ARCS) Program performed a comparative evaluation of a number of toxicity tests for sensitivity and discriminatory power (USEPA 1994). Discussion of the individual tests and their ability to identify severely contaminated sediments is beyond the scope of the present discussion.

Thus, the assessment of the contaminant levels entering the food chain via uptake into plants and animals at the sediment-water interface is largely a question of contaminant availability. In the absence of site-specific toxicity information, measurements or predictions of pore-water concentrations or the AVS/SEM for some metals are useful indicators of availability under steady-state conditions, such as might apply for benthic animals that process large amounts of sediments. For organisms in the water column or for benthic plants and animals with only passive contact with sediments, the kinetics of release from the sediments and uptake and elimination from the organism significantly complicate assessment of exposure and risk.

21.3.3 Exposure by Release from Stable Bed Sediments

The rate of contaminant movement into the water column through either of the two previous pathways was controlled by processes that are largely unrelated to the presence of the contaminant (i.e., erosion of the sediment bed and the rate of ingestion of sediment or benthic organisms). The dominance of these external factors led to the usefulness of approximations based on local equilibrium between any resuspended sediment and the overlying water and between benthic organisms and surficial sediments. The direct exposure of fish and higher animals to contaminants in stable, noneroding beds, however, is a rate-limited process controlled by a variety of natural fate and transport processes, as depicted in Fig. 21-1. Among the most important of these in-bed fate and transport processes are biotransformation, sorption, diffusion, advection, and bioturbation. Under specific circumstances, a variety of other processes identified in Fig. 21-1 may be important.

The local flux from the sediment to the overlying water is related to the sediment concentration and an overall mass-transfer coefficient that lumps the effects of the individual processes. The relationship between sediment contamination and exposure in the overlying water by these processes is controlled by the surficial sediment concentrations. Deep in-bed processes may be responsible for transport of contaminants to the sediment-water interface, but release into the overlying water column is still controlled by the interfacial concentration. Thus, the surficial average sediment concentration remains a useful indicator of the potential release to the overlying water. The average flux from the sediment by stable bed-sediment processes, F_{bed} (e.g., in $\mu g \bullet cm^{-2} \bullet h^{-1}$) can then be estimated by

$$F_{bed} = K_s \, \rho_s \left(<W_s> - K_{sw} \, C_w \right) \qquad (21\text{-}15)$$

where

ρ_s = bulk (or dry) density of the sediments (g/cm^3) and
K_s = average sediment bed-mass transfer coefficient (e.g., in cm/h).

The concentration driving force in this equation is the deviation between the actual surficial sediment concentation ($<W_s>$) and that which would be in equilibrium with the overlying water ($K_{sw}C_w$). Alternatively, a water-based overall coefficient, K_w, can also be defined by $F_{bed}/(<W_s>/K_{sw} - C_w)$, where $K_w = K_s \, \rho_s \, K_{sw}$. In general, K_s is a combination of sediment- and water-side mass transfer resistances, as characterized by sediment- and water-side mass transfer coefficients k_s and k_w , defined by

$$k_s = \frac{F_{bed}}{\rho_s \left(< W_s > - W_i \right)} \quad k_w = \frac{F_{bed}}{C_i - C_w} \qquad (21\text{-}16)$$

where the subscript i defines the hypothetical interfacial concentrations at the sediment-water interface. Assuming that the resistances act in series and that the interfacial concentrations are in equilibrium, $W_i = K_{sw} \, C_i$, the overall mass transfer coefficient, K_s, can be written

$$K_s \, \rho_s = \frac{1}{1/k_s \, \rho_s + K_{sw}/k_w} \qquad (21\text{-}17)$$

Thibodeaux et al. (2001) showed that a range of both laboratory and field data were consistent with 12.5 cm/day $< k_w <$ 33.3 cm/day and 2 cm/yr $< k_s <$ 3.6 cm/yr.

It is perhaps easiest to characterize the effect of the various natural processes depicted in Fig. 21-1 that make up K_s by the time required to achieve specified reductions in contaminant concentration. Because the surficial sediments are typically mixed by the action of benthic organisms or other processes, the response of the surficial-area-averaged sediment concentration can be modeled as

$$\frac{d}{dt}\left(< W_s > \rho_s A\, h\right) = -\, K_s\, \rho_s < W_s > A \qquad (21\text{-}18)$$

assuming that there are no fate processes other than release by transport processes to the overlying water and the overlying water is always at zero concentration. Thus,

$$\frac{< W_s >}{< W_s > (0)} = e^{-\frac{K_s}{h} t} \qquad (21\text{-}19)$$

From the above equation, the concentration half-life (time to 50% reduction) and the time to 95% reduction (5% remaining) in the surficial area averaged sediment concentration is given by

$$\tau_{0.5} = 0.693 \frac{h}{K_s} \quad \tau_{0.05} = 3 \frac{h}{K_s} \qquad (21\text{-}20)$$

As indicated previously, the depth of the surficial sediment layer that is relatively well-mixed by the action of benthic organisms is typically 5 to 10 cm. The average value of K_s reported by Thibodeaux et al. (2001) in several laboratory experiments and in the Hudson River is approximately 1.3 cm/yr. Similarly, a surface area of 3,300 acres of the Lower Fox River, Wisconsin, containing an average surficial sediment concentration of 3.1 mg/kg PCBs accounts for the bulk of the approximately 125–280 kg/yr estimated to be transported into Green Bay (WDNR 2001). This is equivalent to a K_s of between 0.47 and 1.0 cm/yr. Employing $K_s \simeq$1cm/yr and a 10-cm surface layer, the contaminant half-life, assuming no exposure of freshly contaminated material and no resupply from upstream sources, is $\tau_{0.5}$= 6.9 yr and the time to 95% reduction in contaminant concentrations $\tau_{0.05}$= 30 yr. These estimates make no attempt to differentiate between the individual mechanisms that contribute to the average mass transfer coefficient. Estimates of the times required to achieve 50% and 95% recovery of the surficial sediment concentrations based upon individual mechanisms are provided in Section 21-5, and allow the mechanisms to be compared and ranked in their importance. The estimates of overall mass-transfer coefficients presented by Thibodeaux et al. (2001) and in the Fox River, however, incorporate mass-transfer resistances in both the sediment bed and in the benthic boundary layer of the water. Before the in-bed transport processes, are assessed, the water-side mass-transfer resistances should be examined in more detail.

21.4 WATER-SIDE MASS TRANSFER PROCESSES

The relative importance of water-side mass transfer resistances increases as the hydrophobicity and K_{sw} of the contaminants increase, as shown by Eq. (21-17). If the overlying water-transport processes control the rate of release from the sediment, measurements of in-bed processes are less important. It is often incorrectly assumed that the intrinsically slower sediment-side processes always control mass transfer to the overlying water. As shown by Thibodeaux et al. (2001), however, the effective coefficient mass transfer from the sediments approaches a limiting value defined by the water-side mass transfer resistances.

From Eq. (21-17), the water-side mass transfer resistances control overall mass transfer as long as

$$k_w < k_s\, \rho_s\, K_{sw} \qquad (21\text{-}21)$$

thus $k_w >> k_s$, which is normally true, does not necessarily mean that water-side resistances are negligible. Illustrative models of the water-side mass transfer coefficient under flowing and quiescent (generally wind-driven circulation) conditions are given by Thibodeaux (1996) as

$$k_w = \frac{\sqrt{\nu_w}\, v_*^{1/2}}{\mathrm{Sc}^{2/3}\, y_o^{1/2}} \quad \text{flowing, typically} \le 10 \text{ cm/h}$$

$$k_w = \left(0.031 \frac{\sec}{m^2}\right) \frac{\rho_a}{\rho_w} \frac{v_a^2 d^2}{M_w^{1/2} L} \quad \text{wind-driven, typically} \le 1\text{cm/h} \qquad (21\text{-}22)$$

where

ν_w is the kinematic viscosity of water (0.01 cm^2/s at 20 C);
Sc is the Schmidt number (typically O(1000) for hydrophobic contaminants);
y_0, v_* are the flow parameters surface roughness and friction velocity, respectively (m, m/s);
ρ_a, ρ_w are the density of air and water, respectively;
v_a is the wind velocity (m/s);
d is the water depth (m);
L is the fetch of the lake or water body in the direction of the wind (m);
M_w is the molecular weight of the contaminant of interest (g/mol).

As indicated previously, Thibodeaux et al. (2001) showed that a range of both laboratory and field data from streams were consistent with 12.5 cm/day $< k_w <$ 33.3 cm/day and 2 cm/yr $< k_s <$ 3.6 cm/yr. Using these estimates of magnitude for k_w, this suggests that the water-side mass transfer is of equal importance to the sediment side processes for a sediment-water partition coefficient of

$$K_{sw} = \frac{k_w}{k_s\, \rho_s} = \frac{12.5 - 33.3 \text{cm/h}}{(2 - 3.6 \text{cm/yr})(\sim 1 \text{ kg/L})} \approx 30{,}000 - 150{,}000 \text{ L/kg} \qquad (21\text{-}23)$$

Strongly sorbing compounds such as PCBs and heavy PAHs may exhibit partition coefficients in this range for moderate organic carbon content (4–6%). Water-side mass transfer

resistances may thus be important for strongly sorbing compounds even in relatively rapid flowing streams. In lakes and impoundments stirred by wind-driven circulations, the water-side mass transfer resistance may be important for less strongly sorbing compounds. The mobile fraction of most metals in sediments exhibits a partition coefficient much less than this, suggesting that their release from stable sediments is controlled by sediment-side processes.

21.5 ANALYSIS OF SEDIMENT BED FATE AND TRANSPORT MECHANISMS

Fate and transport processes are examined separately to determine the most important mechanisms influencing contamination mobility in sediment. Fate and transport mechanisms are separated into two categories: those operating in stable, immobile beds and those operating in an active bed. For this purpose, an active bed is one in which either the pore water or the sediment grains are in motion.

21.5.1 Passive Sediment Fate and Transport Processes

Sediment fate and transport involve the following passive processes:

21.5.1.1 Molecular Diffusion Molecular diffusion is a ubiquitous chemical transport process within a sediment bed. Molecules are in a constant state of motion, characterized by random molecular velocities (directions and magnitudes) and frequent collisions involving both the solvent (i.e., water) and contaminants. The net result is the movement of contaminant molecules from pore-water regions of high concentration to those of low concentration.

The existence of a concentration gradient within the pore water of a porous sediment bed is sufficient to initiate transport by this molecular process. The magnitude of the contaminant flux is

$$F^{\text{diff}} = - D_{sw} \frac{\partial C_w}{\partial z} \tag{21-24}$$

F^{diff} is quantified by Fick's first law and couples the concentration gradient to the diffusion coefficient.

The effective diffusion coefficient in the porous medium, D_{sw}, is less than the diffusion coefficient in water due to the porosity and tortuosity of the sediment. Often a constitutive relationship similar to that proposed by Millington and Quirk (1961) is used to relate the diffusion coefficient in the sediment to that in water, $D_{sw}=D_w\,\varepsilon^{4/3}$. Here ε represents the sediment porosity and D_w is the molecular diffusion coefficient of the contaminant in water, typically on the order of 10^{-5} cm^2/s.

Field investigations in sediment beds typically involve analytical measurements averaged over sediment depth and reflect a mixed sample from a few cm to 30 cm of core length. Profiles of concentration based on thin slices less than 1 cm in depth spanning the entire depth of contamination are rarely measured. Available concentration profile data usually are limited to a snapshot in time and seldom reflect trends over time. Typically, only single measurements for a particular year are available for hydrophobic organics and metals. These measurements are not very useful in assessing the influence of diffusion, which is manifested over long time periods and may only influence concentration profiles in thin layers. In addition, diffusion normally occurs at significant rates only within the pore-water phase, and bulk sediment concentrations may not reflect the mobile fraction of contaminants. For metals, in particular, total sediment concentration measurements are not very useful in defining the rates of passive transport processes.

A better approach to both conceptual and quantitative fate and transport model development is the use of high-resolution coring with both total and speciated measurements via phase and constituent. In this manner, the fraction of the available contaminant dissolved in the pore water is identified. By discriminaton between soluble and insoluble fractions of metals, a much better assessment of potential adverse effects can be made. High-resolution coring makes possible comparison to detailed mathematical models and can be very useful in identifying the most important transport processes. For example, diffusional processes give rise to concentration profiles that are quite different from those produced by advective transport.

21.5.1.2 Adsorption and Desorption Equilibrium between the Solid Surface and Pore Water Organic compounds that are hydrophobic by nature are capable of being adsorbed onto the organoclay fractions of the sediment. Thus, an adsorption-desorption equilibrium exists at the sediment and pore-water interface. In the case of transport into clean sediment, adsorption on the particles retards the movement of a concentration front due to transient accumulation of material in the sorbed phase. Adsorption slows transient pore-water processes (including diffusion) according to a retardation factor, R_f, that is essentially the ratio of the total concentration in the sediment to the concentration in the mobile pore-water phase:

$$R_f = \frac{\text{Total concentration}}{\text{Mobile phase concentration}} = \varepsilon + \rho_s K_{sw} \tag{21-25}$$

Here ε is the void fraction (porosity) of the sediment bed, ρ_s is the bulk (dry) sediment density, and K_{sw} is the effective sediment water-partition coefficient. Many authors define the retardation factor as R_f/ε, where R_f is as defined by Eq. (21-25). Care must be taken to define the retardation factors and the conservation equations in which they arise in a consistent manner.

A simple estimate of the time required for attenuation of a contaminant in the sediments as a result of retardation is the product of R_f and the time required for the attenuation to occur by diffusion assuming no retardation. The

effect of retardation can be quite large. For a compound such as pyrene ($K_{oc}=10^5$ L/kg), assuming 1% organic carbon, $\rho_s=1$ kg/L, and $K_{sw}=K_{oc}f_{oc}$, the retardation factor is about 1,000. As described earlier, a significant fraction of the contaminants may not readily desorb. Under such conditions the partition coefficients used in Eq. (21-25) must be measured via desorption experiments and not simply assumed to be given by $K_{oc}f_{oc}$. It is also important to recognize that retardation affects only transient processes. Under steady contaminant transport, there is no further accumulation of contaminants in the sorbed phase and, therefore, there is no retardation.

Diffusion is an extremely slow process if retarded by sorption. If diffusion is the primary transport process or can be made to be the primary process through elimination of active processes, contaminant release and exposure are generally negligible. The time for diffusion to reduce 50% and 95% of the contaminant within a layer, h, is defined by

$$\tau_{0.5}^{\text{diff}} = \frac{1.94}{\pi^2}\frac{h^2 R_f}{D_{sw}} \qquad \tau_{0.05}^{\text{diff}} = \frac{11.2}{\pi^2}\frac{h^2 R_f}{D_{sw}} \tag{21-26}$$

This assumes no migration of contaminants into the layer from below and assumes that the overlying water provides no resistance to mass transfer.

Although sorption onto an immobile phase can retard contaminant migration in the sediment, sorption onto a mobile particulate phase (e.g., fine particulate, colloidal matter) can enhance or facilitate transport. Natural organic colloids are fine particulate suspensions that are primarily decomposition products of plant and animal life. Colloids form in a marine sediment through fermentation reactions of degraded cellular material to form low-molecular-weight dissolved organic matter such as amino acids. Condensation reactions then give rise to higher-molecular-weight dissolved organic matter such as fulvic and humic acids. These higher-molecular-weight compounds generally constitute what is referred to as dissolved organic matter (DOM). DOM is generally operationally defined as the organic fraction that passes a 0.45-μm filter and consists of humic and fulvic acids, among other things. Colloidal matter is composed of groups of these fulvic and humic acid molecules that form large-diameter suspensions in water. The suspensions typically have a negative electrical surface charge and the stability is dependent on the structure of the electrical double layer formed, van der Waals forces, hydration phenomena, and the effects of adsorbed substances. Organic colloids represent a sink for hydrophobic organic contaminants in the water. They effectively increase the solubility by increasing the mass of contaminants that can partition into the mobile phase containing both water and colloidal material. In this manner, the mobility of organic contaminants can be enhanced. Colloids can enhance the effective solubility of metal and ionic contaminants. Various metals and metal complexes also form colloidal species.

The net effect of the increased effective solubility of a contaminant is a change in the retardation factor (Reible et al. 1991; Thoma et al. 1991),

$$R_f = \frac{\text{Total}}{\text{Mobile}} = \frac{\varepsilon + \rho_b K_{sw} + K_{cw}C_c}{1 + K_{cw}C_c} \tag{21-27}$$

Here

C_c = concentration of colloidal particles in the water and
K_{cw} = partition coefficient between the colloids and the water.

The effective retardation factor represented by Eq. (21-27) assumes that the colloidal particles are transported through the sediment pore water at the same rate as the water molecules themselves. This may not be a good assumption, due to filtration or preferential retention or exclusion of the polar colloidal molecules. A commonly used but approximate estimate of the partitioning of an organic contaminant to colloidal or dissolved organic carbon is that K_{cw} equals K_{oc}. The concentration of dissolved organic carbon in sediments is typically in the range of 10 to 100 mg/L. These values suggest that the effect of colloidal organic carbon, for example for pyrene, is to decrease the retardation factor by a factor of 2 to 10. Thus, the presence of colloidal matter can decrease the time for diffusion to result in recovery of a pyrene-contaminated sediment layer by a factor of 2 to 10.

21.5.1.3 Chemical Reaction and Biodegradation A stable sedimentary environment does not lend itself to rapid degradation dynamics. Many organic compounds of concern in sediments are persistent and not subject to rapid degradation by either abiotic or biological processes. Only the upper few cm of a fine-grained sediment may be aerobic; the remainder of the sediment column is generally anaerobic. Organic compounds that are subject to microbial degradation generally degrade more slowly under anaerobic conditions. Although degradation may be slow, the persistence of contaminants over decades or centuries may be of interest. Unfortunately, very little information exists about the persistence of sediment contaminants over these time-scales.

Hughes et al. (1997) have reviewed the potential for PAH degradation in sediments and identified some of the limitations in achieving significant degradation in the field. PAHs degrade most rapidly under aerobic conditions, but some degradation under anaerobic conditions has also been observed (Zhang and Young, 1997). Anaerobic conditions are important for biotransformation of chlorinated organic compounds. Chlorine can interfere with the action of oxygenating enzymes, meaning that reductive dechlorination is often necessary before aerobic transformation can proceed. For example, reductive dehalogenation under reducing conditions converts dichlorodiphenyltrichloroethane (DDT) to dichlorodiphenyldichloroethene (DDE) and lindane to benzene. Pesticides such as toxaphene have

been known to be anaerobically degraded in soils and salt marsh sediments. Anaerobic dechlorination of PCBs can also occur (Tiedge et al. 1993) and has been observed under field conditions (Brown et al. 1984). Dechlorination of highly chlorinated PCBs encourages subsequent aerobic degradation of the less chlorinated PCB or biphenyl (NRC 2001).

In the absence of site-specific quantitative information on the rates of these reactions, the conservative assumption of negligible degradation rates is normally applied. With no degradation, attenuation of contaminant concentrations can only result from transport processes.

21.5.2 Active Sediment-Transport Processes

Diffusion, sorption, and reactions were considered in the absence of sediment or bulk pore-water movement. If sediment or pore water is moving, an advective flux generally dominates any diffusive flux. Mechanisms resulting in advective transport in sediments and their implications for contaminant transport are discussed below. The focus of this discussion remains on stable sediments and slowly moving dunes and ripples (i.e., complete scouring of the sediment bed is not considered). The situation of high suspended-sediment loads was discussed previously while the influence of resuspended sediment on water-column concentrations and exposures was examined. Sediment-transport processes emphasized here are such that the basic character of the sediment bed remains largely intact and the resulting changes in contaminant concentration are slow. "Slow", in this case, implies that the dynamics of the overlying water concentration remains controlled by the sediment-bed processes and not simply the steady-state suspended-sediment load, as discussed previously.

21.5.2.1 Deposition or Erosion Sediment deposition or erosion rates are likely to vary significantly over space and time (see Chapters 2 and 4). On average, or in specific locations, however, it may be possible to characterize erosion or deposition by an average velocity $U=D/\rho_s$ or $U=E/\rho_s$, where E and D are the erosion and deposition rates defined by Eqs. (21-5) and (21-7), respectively. The growth of the sediment bed by deposition of clean sediment causes burial of contaminated sediment from the surficial mixed layer at a rate $<W_s>D/\rho_s$. Similarly, the process of erosion removes contaminated sediment from the surficial sediment layer at a rate $<W_s>E/\rho_s$. In either case, processes such as bioturbation mix the entire depth of the surface layer so that Eq. (21-19) applies as long as the rate of erosion or deposition is low compared to the rate of surficial layer mixing. If the contamination is initially limited to a uniformly mixed depth h, the times to 50% and 95% reduction in concentration in the layer for deposition or erosion at an average velocity U are given by

$$\tau_{0.5}^{\text{ero}} = 0.693\frac{h}{U} \quad \tau_{0.05}^{\text{ero}} = 3\frac{h}{U} \tag{21-28}$$

Deposition rates can sometimes be measured by sediment traps placed at the sediment-water interface, although these may not indicate net deposition rates, because they do not allow erosion. Thus sediment traps would track only the deposition portion of a deposition-and-erosion cycle driven, for example, by diurnal tidal variations. Deposition rates can also be estimated by the depth of burial of certain radionuclides, such as ^{210}Pb and ^{137}Cs: γ spectroscopy can be used to measure activities of excess ^{210}Pb (source: U-series, $t_{1/2}$ = 22 yrs, 46.5-KeV peak), and ^{137}Cs (source: nuclear fallout and reactors, $t_{1/2}$ = 31 yr, 661.6-KeV peak). The presence of a particular radionuclide can be used to date a layer in an undisturbed sediment core, and the location of this layer relative to the sediment surface defines the amount of deposition that has occurred. ^{137}Cs was introduced into the atmosphere as a result of above-ground nuclear testing in 1954 and peaked in 1964. ^{210}Pb decreases to background in surficial sediments, with the decrease indicating age since deposition. Changes in the geochemical character of depositing sediment and sediment erosion and mixing patterns, however, can greatly complicate the interpretation of profiles of these radionuclides.

21.5.2.2 Dune Formation and Transport by Bed Load In the previous section, deposition and erosion were assumed to occur at a uniform rate from an essentially flat surface. While this may be valid under low water velocity or in a low-energy environment in an estuary, this view of erosion and deposition does not hold under high-energy or high-velocity conditions. Under high-energy conditions, dunelike structures are formed that generally progress downstream by erosion on the upstream face and deposition on the downstream face, as shown in Fig. 21-2. During this overturn and migration process, sediment particles are exposed and either scoured or reburied by other sediment particles (see Chapter 2). During exposure to the stream water, contaminants sorbed to the sediment particles can be desorbed and contaminants in the adjacent pore water diluted mixed into the water column.

To quantify the rate of transport of sorbed and dissolved contaminants from the sediment bed, it is necessary to determine the spatial dynamics of the particle relocation process. The locations of particles as a function of time allow definition of the location of contamination as a function of time, the exposure time at the surface of the dune, and the total time required to overturn the dune. Savant-Malhiet and Reible (1993) developed a model of contaminant dynamics under these conditions that provides a means of estimating sediment recovery rates by bed-load transport of noncohesive sediment. The model is beyond the scope of the present paper, but results emphasize that bed turnover and contaminant release can be rapid (compared to processes such as diffusion) even under relatively low sediment-migration rates.

21.5.2.3 Advection Due to Groundwater Flow Streams, lakes, and estuaries are hydraulically connected to groundwater aquifer systems. These surface-water bodies can gain or lose water depending on the water level relative to the adjacent

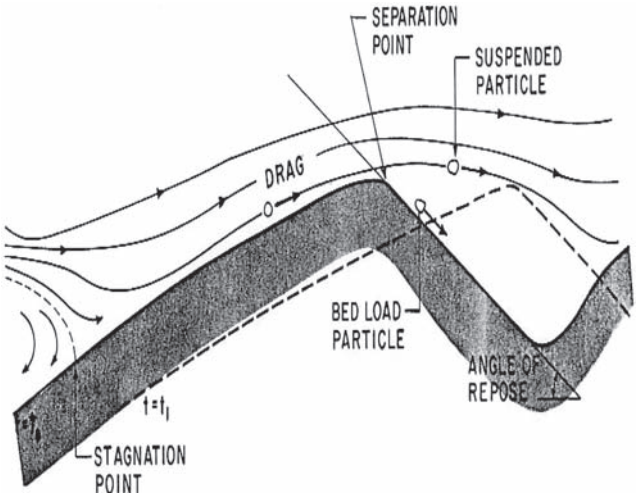

Fig. 21-2. Depiction of bed-load sediment flow over dunelike sediment structures.

water table. The bulk flow through the sediment can result in an advective flux of contaminant that complements the diffusive flux described above. The relative magnitudes of advective and diffusive transport can be quantified with a Peclet number,

$$\mathrm{P}_{pe} = \frac{V\,h}{D_{sw}} \tag{21-29}$$

Here V is the superficial, or Darcy, velocity perpendicular to the contaminated layer of height h. For low values of the Peclet number, the transport is dominated by diffusion and the previous discussion applies. For large values of the Peclet number, advection dominates and the characteristic times for reduction in concentration of a layer of sediment of height h are

$$\tau_{0.5}^{\mathrm{adv}} = 0.693\,\frac{hR_f}{V}\quad \tau_{0.05}^{\mathrm{adv}} = 3\,\frac{hR_f}{V} \tag{21-30}$$

Note that the advective processes are assumed to be sufficiently slow so that the upper layer remains mixed by bioturbation or other processes. It is also important to note that the retardation factor arises in Eq. (21-30). Advection is a pore-water process subject to retardation due to accumulation on the immobile solid particles and enhancement by sorption onto mobile fine and dissolved particulate matter.

The measurement of groundwater flow velocities and, in particular, stream-bed seepage velocities is difficult. Seepage meters (i.e., containers covering a portion of the sediment bed, which collect any water that seeps through the sediment) are commonly used. It is particularly important that such measurements reflect the seasonal nature of groundwater flow. Unfortunately, the wide variability in sediment characteristics (e.g., permeability) makes interpretation of such data difficult. In addition, it is difficult to measure seepage rates of less than about 0.1 $cm^3/cm^2/day$ with typically available meters. An alternative means of detecting slow vertical transport by groundwater flow is through tracers, such as described by Cornett (1989). The groundwater flow in the surrounding aquifer can also be a useful measure because it represents an average inflow or outflow from the water body. The general direction of the groundwater flow can be measured by piezometers placed at different elevations below the bed of the water body. If the underlying water head is greater than the head in the stream, inflow occurs; outflow occurs in the reverse situation. In addition to defining direction, this information is used to estimate flow rate if the permeability of the medium can be measured.

21.5.2.4 Advection due to Local Pressure Variations on the Sediment Surface Even in the absence of a mean hydraulic gradient, an advective flux may still be observed. Local pressure variations on the order of 100 to 1,000 N/m^2 can be observed between the upstream and downstream faces of the triangular-shaped dunelike sediment structures that typically form at the sediment-water interface. Figure 21-2 includes a depiction of the basic character of the flow over these dunes. The flow is a simple turbulent shearing flow on most of the upstream face and a recirculating wake on the downstream face which also influences a portion of the subsequent sediment dune. It is the weak and poorly organized flow in the wake that results in the leeward deposition of sediment grains under bed-load conditions. In addition to modifying the sediment dynamics, the formation of a separated recirculating wake on the downstream face results in an observed pressure difference. Thibodeaux and Boyle (1987) approximated the dunes as simple geometric shapes such as cylinders and showed that measured pressure data on those simple shapes are sufficient to generate a potentially significant in-bed advective flow.

Savant et al. (1987) used the pressure-profile data generated by Vittal et al. (1977) to predict head distributions and, through Darcy's law, velocity profiles in triangular sediment dunes in a laboratory flume. The relatively high pressure on the upstream face resulted in a flow down and into the dune, turning upward and out of the lower-pressure downstream face, as shown in Fig. 21-3. The experiments and modeling indicated that the induced in-bed flow could extend as much as four to five dune heights into the sediment. Elliot and Brooks (1997a, 1997b) also analyzed this mechanism and achieved similar results. This mechanism likely is important mostly in sediment beds subject to significant organism burrowing activity and in permeable, sandy sediments such as might be observed on the continental shelf of the coastal United States. Note that pressure differences in bends and under other flow irregularities may also cause advective flow in the adjacent sediments.

21.5.2.5 Bioturbation-Induced Transport The previous discussion largely considered sediment as a collection of particles separated by water-filled pore spaces. In reality, a variety of plants and animals reside in sediments. Root systems and animal burrows can provide channels for pref-

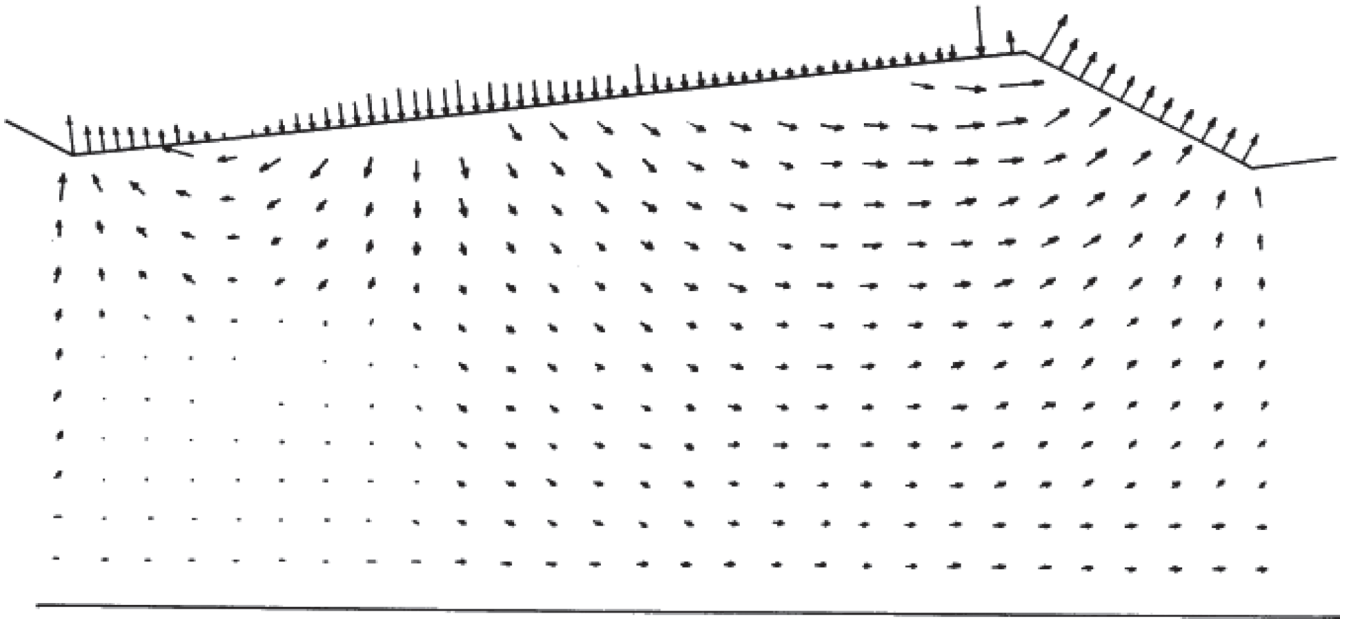

Fig. 21-3. Numeric simulation of the in-bed flow due to pressure variations on the surface of a dune (after Savant 1987).

erential xwater flow and contaminant transport. Even more important, the near-surface sediment is often continuously mixed by the activities of benthic organisms such as clams and worms. Sediment processing by animals residing in the upper layers includes burrowing, ingestion and defecation, tube building, and biodeposition. Taken together, these processes are termed bioturbation; a depiction of the type of animals that can be present and the interaction with sediments is provided in Fig. 21-4. The net result of bioturbation is the vertical and horizontal movement of sediment particles and pore water. Contaminants on the particles or in the pore spaces likewise are transported in the bioturbation process, which is especially important in the transport of hydrophobic contaminants that are heavily retarded by sorption in pore-water processes.

The possibility of bioturbation as a transport mechanism has long been recognized. Boudreaux (1986a) cites work on the effect of biological activity on sediment composition and properties as old as Davison (1891). A wide variety of animal organisms live on and in the upper sediment layer and interact with sediments in a variety of ways. If the scale of the individual organism mixing is very small compared to the depth and area of the sediment of interest (e.g., the depth and area of a box core sample of a sediment), then bioturbation has the appearance of a diffusive process. Boudreaux (1986a) examined the conditions under which a diffusive model of bioturbation is appropriate. Because of the decrease in organism density and activity with depth in sediment, some investigators have speculated that a

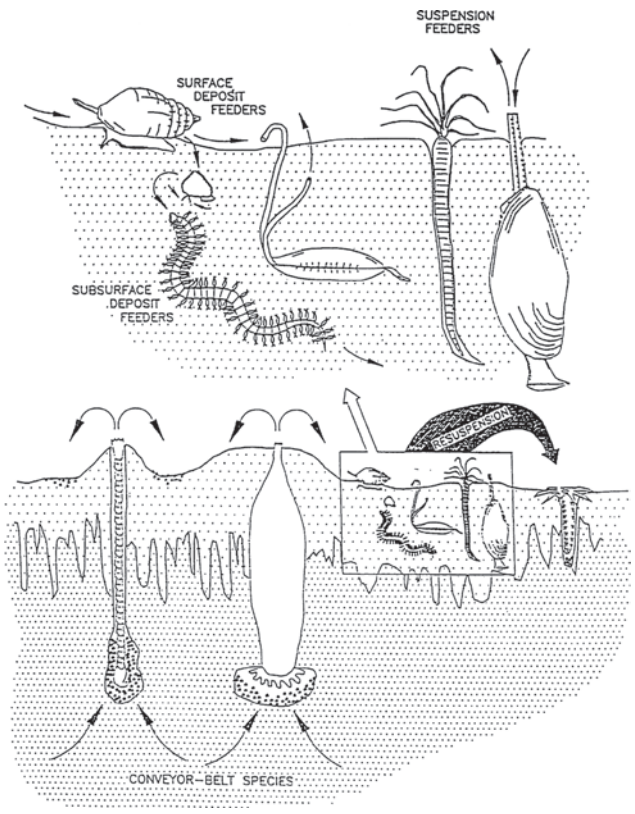

Fig. 21-4. Illustration of the variety of benthic organisms that interact with the sediments and solids associated contaminants (after Rhoads 1974).

depth-dependent biodiffusion coefficient is appropriate. However, as Boudreaux (1986b) noted, it is often difficult to differentiate between a constant and a depth-dependent biodiffusion coefficient on the basis of available data.

If the scale of the individual organism-related mixing is not sufficiently small so that the appearance of a random, diffusive process is achieved, other models must be postulated. For example, worm tubes and other macroscopic animal burrows can significantly enhance the contaminant transport rate across the sediment-water interface on larger scales. In addition, some marine and freshwater worms ingest sediment at depth and deposit the fecal matter at the surface, a process that has been called conveyor-belt feeding (Rhoads 1974). Neither of these processes can be described on a fundamental basis as a diffusive process. However, even nonlocal (i.e., macroscale) mixing events of this sort often give rise to contaminant profiles that have the appearance of a diffusive transport process.

Therefore, although diffusion characterized by a constant biodiffusion coefficient is not an adequate description of the actual physical processes that constitute bioturbation, it can be used to correlate the overall characteristics of the observed contaminant transport. The primary difficulty with such an approach is that due to the inadequacy of the assumption of a diffusive process, biodiffusion coefficients that adequately describe a particular sediment may not be applicable to another site, even a nearby site, if the density, distribution, and type of organisms are different.

Despite this, biodiffusion coefficients can show surprising similarity between different sites. For example, Aller (1982) estimated an effective biodiffusion coefficient of 5 to 32 cm^2/yr in Narragansett Bay, Brownawell (1986) estimated a biodiffusion coefficient of 9.4 cm^2/yr in Buzzards Bay, and, finally, Thibodeaux (1989), using the data of Spaulding (1987), observed an essentially identical biodiffusion coefficient of 9 to 13 cm^2/yr in the upper estuary of New Bedford Harbor. An analysis of the data of Matisoff (1982) suggests that more than 2/3 of the available measurements in both freshwater and saltwater conditions suggest an effective particle diffusion coefficient of 0.3 to 30 cm^2/yr. This can be restated as effective mass transfer coefficients of 0.03 to 3 cm/yr using an average effective layer depth h_{bio} of 10 cm. The vast majority of these measurements of effective bioturbation diffusivities were made by estimating particle-reworking rates using strongly sorbed radionuclides associated with nuclear testing. The times and amounts of the release of particular radionuclides and the current distribution within sediment allow estimation of the reworking rates in stable sediments.

The measurement range of 0.3 to 30 cm^2/yr is consistent with the measurements of Reible et al. (1996) of effective bioturbation mass transfer coefficients, $k_{bio} \sim D_{bio}/h$, equivalent to 1 to 10 cm^2/yr for tubificid worms at field densities in freshwater sediments. Tubificid worms are typically found at very high densities and often represent the bulk of the biomass in sediment bioassays (e.g., USEPA 1993a). These worms are head-down deposit feeders capable of processing 10 or more times their own weight in sediment every day. The high density of these organisms, along with the ability to process large amounts of sediment, leads to relatively high mass-transfer rates. Some organisms may also degrade certain contaminants, further speeding the attenuation of contaminant concentrations.

Focusing specifically on the transport effect of bioturbation, the diffusive models discussed previously can be applied. The time required for 50% and 95% reduction in concentration in a surface layer of depth h due solely to bioturbation at an effective particle reworking diffusion coefficient, D_{bio}, is given by

$$\tau_{0.5}^{bio} = \frac{1.94}{\pi^2}\frac{h^2}{D_{bio}} \quad \tau_{0.05}^{bio} = \frac{11.2}{\pi^2}\frac{h^2}{D_{bio}} \tag{21-31}$$

Because biodiffusion typically involves particle movement, there is no effect of retardation by sorption onto an immobile phase. Therefore, for a hydrophobic contaminant that is strongly sorbed to the sediment, bioturbation is a much more effective mixing process than molecular diffusion in the pore water.

As stated previously, effective molecular diffusion coefficients in sediments are on the order of 10^{-6} cm^2/s, which corresponds to approximately 30 cm^2/yr, or about the same as the largest of the typical effective bioturbation diffusion coefficients. For many elemental species, whose leachable fraction may partition only weakly into the solid phase, the enhancement by bioturbation is minimal. For a hydrophobic contaminant such as pyrene, however, bioturbation is expected to control contaminant migration in the upper layers of a stable sediment bed. In general, bioturbation is the primary migration mechanism of strongly sorbing contaminants in stable surficial sediments unless the physical character of the sediment or its level of contamination precludes significant colonization by benthic organisms.

21.6 ENGINEERING MANAGEMENT OF CONTAMINATED SEDIMENTS

The goal of remedial efforts at a contaminated sediment site is to manage the risks that they pose. The processes already described define the rate of natural attenuation of contaminants in the surficial sediment layer but also define the attenuation of any residual remaining from more active remediation.

Thus the above discussion of the fate and transport processes provides a basis for the assessment and implementation of natural attenuation. To ensure the effectiveness of natural attenuation as a management option, it is necessary to design a monitoring plan that tests and updates the conceptual model of contaminant release and exposure from the sediments and demonstrates the attenuation of concentration

and risk that is predicted by it. The design of such a monitoring plan is beyond the scope of this chapter, but the general approach must be consistent with the most important process or processes that influence contaminant behavior.

Engineered efforts to control exposure and risk beyond natural attenuation can be placed into two broad catergories:

1. Containment and/ or treatment in situ;
2. Removal and ex situ treatment or disposal.

The feasibility of sediment or dredged material treatment approaches is strongly dependent on the contaminants and the characteristics of the sediment and the environmental setting. Evaluation and the presentation of design approaches for treatment processes are beyond the scope of this work. The initial step in applying any treatment approach, however, is either containment by capping with clean sediments or removal by dredging. In some cases, the body of water can be diverted or contained, allowing removal by dry excavation. Dry excavation will not be considered here because of its similarity to conventional soil removal. Instead, the basic features and key design constraints of capping and wet dredging will be discussed.

21.6.1 Contaminated Sediment Containment by in Situ Capping

Capping is the placement of clean sediment or similar materials over contaminated sediment. For ease of placement, sand or other coarse media are normally used as capping material. Geomembrane material may be used beneath a cap in soft sediments to aid in the support of the cap, and stones or other large material may be employed as armoring on top of the cap to reduce cap resuspension and erosion. The purpose of a cap is to contain the contaminated sediment physically, separate the contaminants from organisms living at the sediment-water interface, or isolate the chemical contaminants from the overlying water by reducing flux. The design of a cap to meet each of these goals is discussed below.

21.6.1.1 Containment of Contaminated Sediment The goal of sediment containment is to armor the sediment bed and eliminate the resuspension and erosion that may control contaminant release. Contaminants tend to be associated with fine-grained sediments that are often cohesive and exhibit low shear strength or load-bearing capacity. A more coarse-grained cap can provide significant stabilization if placement can be achieved. In addition, since such a cap is generally composed of granular, noncohesive sediment, for which erosion properties are well known, uncertainties associated with the stability of the underlying cohesive sediment become irrelevant.

The ability to place a cap over a sediment with low load-bearing capacity can be estimated by considering local shear failure (Palermo et al. 1998). The thickness of a cap that can be supported for a certain strength sediment is given by

$$h_{\text{cap}} = (2+\pi)\frac{2}{3}\frac{C_\mu}{\gamma} \tag{21-32}$$

where

C_μ = the shear strength of the sediments and
γ = the specific weight of the cap materials.

If the cap is made of sand with a specific weight of 5 kN/m^3 and the sediments are at the liquid limit (C_μ ~2.5 kN/m^2 ; Das 1979), a load of almost 1.7 m or 5.6 ft may be placed without local shear failure of the sediment. A thinner cap may be required to ensure a factor of safety, or for weaker sediments. A thicker cap may be placed, if desired, by placement in multiple lifts to allow consolidation and strengthening of the sediment prior to placement of the entire cap.

The long-term stability of an armoring cap layer depends upon the erosion characteristics of the cap and the hydraulic forces to which it may be exposed. For simple preliminary design, the Transportation Research Board (1970) established a criterion for the onset of erosion of noncohesive granular media of particle size d_p that is dependent upon bed shear stress, τ_b:

$$\begin{aligned} \tau_b &= 4\, d_p \qquad (\tau_b \text{ in lbf/ft}^2, \quad d_p \text{ in ft}) \\ \tau_b &= 58.4\, d_p \quad (\tau_b \text{ in N/m}^2, \quad d_p \text{ in m}) \end{aligned} \tag{21-33}$$

Another approach, employing flow velocity rather than bed tractive force, may be found in Palermo et al. (1998). Use of Eq. (21-33) or the methods in Palermo et al. (1998) requires specification of a design flow condition. This is typically a major rare flood event such as a 100-yr flood or a maximum design flood. In addition, however, special care must be taken to ensure that such a flood event controls the potential for cap instability. Wind-driven seiche flows, wave action, or ice scouring of the sediments may challenge cap integrity more than a major flood event.

Simple relationships such as Eq. (21-33) do not recognize the spatial variability in shear stresses and the resulting cap erosion. Localized erosion of a cap, however, is unlikely to significantly affect overall cap effectiveness, which is proportional to the total area of sediment capped.

Palermo et al. (1998) also includes approaches to the evaluation of a stable grain size when a body of water is subjected to commercial or recreational navigation traffic. Regular exposure to high-powered traffic, especially in relatively shallow water, may limit the feasibility of capping as a management alternative. However, irregular recreational boat traffic outside of dock and marina areas, may not pose a significant challenge to cap integrity because any cap erosion may be localized.

Eq. (21-33) assumes that the cap grain size is uniform. Other criteria on cap materials may be required to ensure stability and eliminate the potential for fine-grained material to be lost through the cap, including (Palermo et al. 1998)

- A nonuniform particle-size distribution, e.g., $d_{85}/d_{15} \sim 4$;
- Angular shapes for coarse-grained particles such as gravel and cobbles;
- A maximum particle size of not more than 2 d_{50} (USBR 1973);
- A minimum particle size of not less than 0.05 d_{50} (USBR 1973);
- A minimum layer thickness of approximately 1.5 d_{50};
- Maintaining a ratio of particle sizes between upper and lower layers of a multilayered cap such that $d_{15}^{\text{upper}}/d_{85}^{\text{lower}} \leq 5$ (this criteria also defines an upper bound for the ratio of particle sizes in the cap layer immediately adjacent to the sediment layer desired to be contained); and
- Limiting placed cap slope to the stable angle of repose of the cap material (Palermo et al. 1998 suggested a vertical to horizontal slope of 1:1.88 for clean sand, although a factor of safety of 2 to 3 might be applied).

21.6.1.2 Separate Benthic Organisms from Contaminated Sediment The adequacy of a cap to physically separate organisms from contaminated sediment depends upon the thickness of the cap and the depth of penetration of the organisms. The depth and intensity of interaction of organisms with sediments is strongly dependent upon the type of organism and environmental characteristics such as sediment texture. Freshwater benthos, for example, may only populate the upper 5 to 10 cm of sediments in significant quantities. In marine sediments, animals living at the sediment-water interface tend to be larger and influence a larger sediment depth. Deposit feeders typically prefer fine-grained sediment high in organic carbon content, whereas burrowing filter feeders may prefer coarse-grained sandy sediment. More than 90% of the 240 observations of bioturbation mixing depths in both fresh and salt water reported by Thoms et al. (1995), however, were 15 cm or less and more than 80% were 10 cm or less. Almost all of these estimates were based upon measurements of the vertical distribution of various radionuclides, which have proven to be very useful tools in identifying the degree of mixing within the upper layers of sediment. Short-term mixing in this regard can be effectively assessed with beryllium (^{7}Be, cosmogenic source, $t_{1/2}$ = 52 days, 477 KeV peak), which is mixed downward from the water column by the benthic organisms.

Certain organisms may penetrate significantly deeper than 15 cm. The importance of these penetrations at the population level depends upon the density and intensity of organism behavior at the deeper levels. As indicated by the measurements reported by Thoms et al. (1995), however, 90% of the observations showed minimal mixing below 15 cm, leading to the conclusion that population-level impacts are generally limited to that depth. Deeper penetrations by individual organisms, however, may be important in particular environmental settings or when the organisms of concern are those that tend to penetrate more deeply.

If the depth of concern for organism penetration is h_{bio}, and the cap consolidation is given by Δh_{cap}, the depth of cap, h_{cap}, necessary for separation of benthic organisms and the contaminated sediments is given simply by

$$h_{\text{cap}} > h_{\text{bio}} + \Delta h_{\text{cap}} \tag{21-34}$$

Cap consolidation may be estimated by conventional consolidation measurements and models such as PCDDF (Stark 1991).

21.6.1.3 Reduce Contaminant Flux to the Overlying Water The final objective of a cap is reduction of chemical flux to the overlying water. If the criteron for cap stability is achieved, only pore-water processes are effective below the zone of bioturbation. Thus the pore-water concentration, C_{pw}, controls the driving force for flux to the overlying water. This flux is usually described by a combination of advective and diffusive processes,

$$F_{\text{cap}} = V C_w - D\frac{dC_w}{dz} \tag{21-35}$$

Here V is the superficial or Darcy velocity driven by local or mean hydraulic gradients and D is an effective coefficient including both diffusion (Eq. 21-24) and dispersion. Wang et al. (1991) and Thoma et al. (1993) demonstrated the applicability of flux models of the form of Eq. (21-35) and defined a modeling framework that was later extended by Palermo et al. (1998).

If it is assumed that the cap poses essentially the only mass transfer resistance and the pore-water concentration beneath the cap, C_0, remains constant, the flux at the top of the effective cap thickness, h_{cap}, is given by

$$F_{\text{cap}} = \frac{C_0\, V}{2}\,\text{erfc}\left\{\frac{R_f h_{\text{cap}} - V t}{2\sqrt{R_f D_{sw}\, t}}\right\} + C_0\sqrt{\frac{D_{sw} R_f}{\pi t}}\exp\left\{-\frac{\left(V t - R_f h_{\text{cap}}\right)^2}{4 R_f D_{sw} t}\right\} \tag{21-36}$$

where R_f is given by Eqs. (21-25) or (21-27) and defined by cap properties. The effective cap thickness is the cap thickness minus allowances for consolidation and bioturbation. The effective cap thickness is the thickness of the chemical isolation layer. For times long compared to $R_f h_{\text{cap}}/V$, the flux through the chemical isolation layer approaches VC_0. For $V << D_{sw}/h_{\text{cap}}$, however, the migration through the cap is diffusion controlled and the flux at the top of the chemical isolation layer is given by

$$F_{\text{cap}} = \frac{C_0 D_{sw}}{h_{\text{cap}}}\left[1 + 2\sum_{n\text{-}1}^{\infty}(-1)^n \exp\left(-\frac{D_{sw}\{n\pi\}^2 t}{R_f h_{\text{cap}}^2}\right)\right] \tag{21-37}$$

For times long compared to $R_f h_{\text{cap}}^2/(\pi^2 D_{sw})$, the flux through the cap approaches $C_0 D_{sw}/h_{\text{cap}}$.

Both Eqs. (21-36) and (21-37) predict minimal flux through the cap from the time of placement until times approaching

the characteristic time for the advective or diffusion-dominated process that controls migration through the cap. That is, the time until some contaminants have migrated over most of the cap can be estimated by

$$\tau_{\text{cap}}^{\text{adv}} \sim \frac{R_f\, h_{\text{cap}}}{V} \quad \text{advective conditions}$$
$$\tau_{\text{cap}}^{\text{diff}} \sim \frac{R_f\, h_{\text{cap}}^2}{\pi^2\, D_{sw}} \quad \text{diffusive conditions} \tag{21-38}$$

At times short compared to these characteristic times, the flux through the cap is effectively zero. Note that the flux through the cap, even after these times, may still be significantly less than the flux from the exposed sediment prior to cap placement. The uncapped sediment is typically subject to bioturbation and erosion that a well-designed cap will eliminate. Under diffusive conditions, the cap provides a longer diffusion path that effectively reduces flux even at steady state (long time).

The flux through the chemical isolation layer, defined by Eqs. (21-36) or (21-37), controls the flux through the bioturbation layer as well. This provides a basis for estimating the concentration in the bioturbation layer, which is defined by the balance of the flux in from the chemical isolation layer and out into the overlying water. If k_{bio} is the effective mass transfer coefficient in the bioturbation layer, k_w is the benthic water layer mass transfer coefficient, and V is the seepage velocity, assumed independent of either the bioturbation-layer or benthic-water-layer mass transfer processes, the water-phase concentration in the bioturbation layer is

$$C_{\text{bio}} = F_{\text{cap}}\left(\frac{1}{k_{\text{bio}}\, R_f + V} + \frac{1}{k_w}\right) \tag{21-39}$$

and the corresponding solid-phase concentration, which can be compared to sediment quality standards, is

$$W_{\text{bio}} = K_{sw} C_{\text{bio}} \tag{21-40}$$

Examination of Eqs. (21-36) and (21-37) shows that as the effective cap thickness increases, the flux decreases and the time required to achieve the steady state (maximum) flux increases. The cap thickness is initially defined by the placement thickness, h_0, which is reduced by consolidation of the cap, Δh_{cap}, mixing of the upper layers of the cap by bioturbation, h_{bio}, and consolidation of underlying sediment, Δh_{sed}, which expresses contaminated pore water over a portion of the cap. The contaminants expressed with the pore water due to underlying sediment consolidation, however, are subject to retardation. It is assumed that the time of consolidation and the time for bioturbative mixing of the upper layers of the cap are very small compared to the time required for contaminant transport through the cap. Thus the effective cap thickness for use in Eqs. (21-36) and (21-37) can be written

$$h_{\text{cap}} = h_0 - \Delta h_{\text{cap}} - h_{\text{bio}} - \frac{\Delta h_{\text{sed}}}{R_f} \tag{21-41}$$

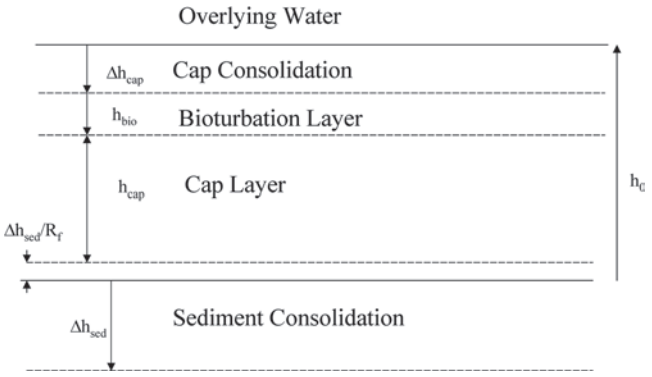

Fig. 21-5. Depiction of the different layers present in a cap as defined by the effective cap thickness.

The relationship of these terms within the cap is shown in Fig. 21-5.

In either the advection-dominated case or the diffusion-dominated case, it is possible to compare this flux to that estimated from the uncapped sediment-water interface to determine the effectiveness of the cap. Alternatively, it may be desired to design a cap by selecting the thickness necessary to achieve a desired reduction in flux or a time until significant migration through a cap might occur.

21.6.2 Dredging Contaminated Sediments

Options that involve removal of contaminated sediments from a water body are significantly more complicated than in situ approaches. Removal options require controls to minimize contaminant loss during sediment removal and transportation, pretreatment of produced dredged material for dewatering and equalization, treatment or transport and disposal of the dredged material, and management of the residual contamination in the sediment and treatment effluents. Thus removal options involve not only dredging but several other component technologies to manage the dredged material.

21.6.2.1 Dredging Technologies Dredges fall into one of two basic categories: hydraulic dredges that primarily use suction and hydraulic action to remove sediments, and mechanical dredges that remove sediments by direct, mechanical action. Hydraulic dredges are generally preferred for high production rates and to minimize sediment resuspension. Solids content of dredge material produced by hydraulic dredging, however, is typically less than 15% and in some environmental dredging operations has been as low as 1%. Hydraulic dredges with a rotating cutterhead or a horizontal auger are commonly used in contaminated-sediment removal. Mechanical dredges, such as a clamshell or cable-arm bucket dredges, are generally preferred for high solids content, low water production, improved performance in the presence of debris and obstructions, and greater accuracy. Close to in situ densities have been generated during mechanical dredging operations. Hybrid dredges have also been used that are predominantly mechanical in action but also withdraw water to control migration of a resuspension plume.

21.6.2.2 Resuspension of Contaminants One of the most significant factors in the selection of dredges for removal of contaminated sediments is the resuspension potential. Sediment characteristics such as grain size largely control resuspension. Fine-grained sediments settle the most slowly and result in the most resuspension in and around a dredgehead. Dredging effectiveness is also limited by residual sediment contamination not targeted or captured by the dredging operation, and by the influences of debris, sediment heterogeneity, and dredge type. In the presence of large debris, certain hydraulic dredges may be ineffective or lead to increased resuspension rates. Hard, consolidated sediment layers, or hardpan, may make dredging overlying contaminated sediments extremely difficult and of limited effectiveness. Sediments also tend to settle back into the cuts of mechanical dredges, leading to increased resuspension rates and residuals in the surface sediments.

Sediment resuspension and associated contaminant loss during dredging operations have been the focus of much attention. Limited data preclude reliable a priori predictions for all except conventional cutterhead and bucket dredges operating under near-normal conditions. Available data for conventional cutterhead and bucket dredges show resuspension rates generally less than 1% of the sediment dredged (Hayes et al. 2000), Whereas available data for smaller dredge types (USACE 1990; Foth and Van Dyke 2000; 2001) show resuspension and contaminant loss rates generally in excess of 1%.

If the contaminant is assumed to be largely associated with the sediment particles, a 1% sediment loss translates directly into a 1% contaminant loss. The mass of contaminant released per unit area of sediment dredged is given by

$$F_{\text{sus}} = f_{\text{sus}}\, h_{\text{dredge}} W_s\, \rho_s \tag{21-42}$$

where h_{dredge} is the depth of dredging, ρ_s is the sediment bulk density, W_s is the contaminant concentration, and f_{sus} is the fractional resuspension rate.

21.6.2.3 Residual Sediment Contamination The portion of sediments that remains as a residual contaminated layer may be a more significant source of long-term exposure and risk. Typically, removal of this contaminated residual is attempted by "overdredging," the process of removing an additional layer of less contaminated underlying sediment. Complete removal of the contaminated layer is not possible, however, due to the mixing of this layer with the less contaminated underlying sediment even during overdredging. Removal of the residuals is especially difficult where overdredging is hindered by debris or by "hardpan" or bedrock that limits the depth of the dredging cut.

It is not possible to predict with certainty either the depth or the concentration of the residual contaminated layer or its relationship to sediment and operational variables. Problems posed by residual contaminated sediment from dredging, however, have been demonstrated in a variety of dredging projects. The dredging of PCBs near a GM facility in Massena, New York required 15–18 dredge passes to reduce sediment concentrations below 500 mg/kg in areas where initial concentrations exceeded 500 mg/kg (BBL 1996). In some areas, a cap was ultimately placed over the residual contamination because repeated dredging passes could not reduce the sediment concentrations below 10 mg/kg. In an area of the Grasse River, also near Massena, removal of as much as 98% of the PCBs from the sediment column reduced the average PCB concentrations in surficial sediments (upper 8 in.) by only 53% (Thibodeaux et al. 1999). Both of these efforts were hindered by the presence of bedrock or hardpan, limiting the extent of overdredging, and by the fact that the highest PCB concentrations were observed at depth rather than at the sediment surface. Demonstration projects in the Lower Fox River of Wisconsin also indicate the potential for residual PCB contamination in the surficial sediments after cessation of dredging (BBL 2000).

Although no definitive approaches to estimating residual contaminant concentrations or residual sediment depths have been developed, mechanical mixing associated with dredging suggests that the residual layer would exhibit a concentration similar to the depth-averaged concentration in the layer being dredged,

$$\bar{W}_s \approx \frac{\int_0^{h_{\text{dredge}}} W_s(z)\, dz}{h_{\text{dredge}}} \tag{21-43}$$

The thickness of this residual layer is uncertain and dependent upon the presence of hardpan or debris but is likely to be at least 1–4 in. given the significant concentrations typically observed in 4- to 12-in. surficial sediment samples after dredging. Multiple passes can significantly reduce this residual concentration if the dredge is not limited by hardpan or debris.

The attenuation of concentrations in this thin surface layer may be very rapid in that the contaminants may be quickly removed by erosion, or bioturbation may rapidly mix the contaminants over at least the mixed layer of the sediments. A conservative estimate (i.e., an overestimate protective of human health) of the flux immediately after dredging is that the surficial sediment concentration is given by Eq. (21-43). That is, the flux to the overlying water due to the residual contamination immediately after dredging is then

$$F_{\text{res}} = K_s\, \bar{W}_s\, \rho_s \tag{21-44}$$

21.6.2.4 Dredged Material Handling In addition to management of resuspension losses and residuals from dredging, the dredged material requires significant handling. The additional required steps include pretreatment of produced dredged material for dewatering and equalization, treatment or transport and disposal of the dredged material,

and management of the residual and treatment effluents. Although it is beyond the scope of this paper to evaluate these steps, the cost and difficulty of onshore management of the contaminated sediments may exceed that in water and should be considered in any comparative analysis of in situ versus ex situ management options for contaminated sediments.

21.7 SUMMARY

Exposure and risk of sediments to higher trophic organisms (e.g., piscivorous birds and mammalian predators) are controlled by the type and extent of the contamination and the relative rates of the various natural fate and transport processes. Contaminants that are buried, sequestered, or degraded pose less risk, whereas contaminants that can be mobilized by natural physical, chemical, and biological processes can pose significant risks. This discussion quantitatively summarizes the most important fate and transport processes that attenuate contaminant levels and exposure in river, estuarine, lacustrine, and marine sediments. The key factors influencing contaminant release and exposure during the application of common remedial approaches, including in situ capping and dredging, were also summarized.

Exposure and risks to fish and higher animals were attributed to one of three contaminant pathways. The first pathway, direct exposure to resuspended sediment, can often be described by assuming chemical equilibrium between the suspended sediment load and water. The rate of resuspension of surficial sediments would then be needed to predict water-column concentrations. The second pathway, indirect exposure to contaminated sediment through the food chain, can often be described by chemical equilibrium between the bed sediment and the benthic organisms that inhabit the sediment-water interface. The rate of predation on these organisms would then indicate the rate of uptake by fish and higher organisms. The third pathway, direct exposure to contaminants released from stable sediments, requires analysis of the fate and transport processes in the sediment.

Although many of the fate and transport processes vary significantly in importance from site to site, it is possible to rank the potential importance of each mechanism depending upon the rate at which the process can influence contaminant concentrations. Relationships were presented for estimation of the time required to achieve 50 and 95% reductions in contaminant concentrations by the various mechanisms. Processes that exhibit a shorter characteristic time are likely to be the most important transport processes.

In general, active sediment processes in which contaminants are transported by bulk movement of pore water or particles exhibit the shortest characteristic transport times and, therefore, the shortest sediment-concentration attenuation times. These processes also exhibit the highest sediment-to-water fluxes and the potential for relatively high exposure and attendant risk to fish and higher animals. In high-energy environments, sediment resuspension and movement are likely to be dominant factors in particle transport; in low-energy environments, bioturbation is likely to dominate contaminant movement in the upper layer of sediments. It is important to note that each site is different and that only through detailed studies can the dominant process or processes at a particular site be identified and quantified, allowing the evaluation of the effect of these processes on natural attenuation and active remedial options. In all cases, the nature of the physical environment (e.g., sediment texture, water depth and flow velocities, temperature effects, and climatographic effects, as well as sediment chemistry and heterogeneity), the nature of the contaminants (e.g., hydrophilic versus hydrophobic, persistent versus ephemeral), and the biotic elements of the environmental setting all contribute to the fate of the contaminants in sediments.

There are few options for reducing exposure by active intervention rather than passive natural attenuation, largely removal or containment. There are limited in situ treatment options. Both removal and containment leave residual contamination and risks that must be assessed to appropriately select or design either option.

REFERENCES

Aller, R. C. (1982). "The effects of macrobenthos on chemical properties of marine sediments and overlying water." *Animal sediment relations*, R. L. McCall and M. I. S. Tevasz, eds., Plenum, New York.

Blasland, Bouck & Lee (BBL). (1996). "St. Lawrence River Sediment Removal Project Remedial Action Completion Report." *Prepared for General Motors Powertrain, Massena, New York*, Blasland, Bouck & Lee, Syracuse, N.Y.

Blasland, Bouck & Lee (BBL). (2000). "Fox River Dredging Demonstration Projects at Sediment Deposit N and Sediment Management Unit 56/57." *For River Group*, Blasland, Bouck & Lee, Syracuse, N. Y.

Boudreaux, B. P. (1986a). "Mathematics of tracer mixing in sediments. I: Spatially-dependent, diffusive mixing." *American Journal of Science* 286, 161.

Boudreaux, B. P. (1986b). "Mathematics of tracer mixing in sediments. II: Nonlocal mixing and conveyor belt phenomena." *American Journal of Science* 286,199.

Brown, J. F., et al. (1984). *Northeast environment science* 3, 167.

Brownawell, B. J.(1986). "*The role of colloidal organic matter in the marine geochemistry of PCB*." PhD dissertation. WHO1-8619-19, Woods Hole Oceanographic Institution, Woods Hole, Mass.

Cheng, N. S. (1997). "Simplified settling velocity formula for sediment particle." *Journal of Hydraulic Engineering, ASCE* 108(12), 1486–1503.

Cornett, R. J. (1989). "Measuring groundwater transport through lake sediments by advection and diffusion." *Water Resources Research* 25, 1815.

Das, B. M. (1979). *Introduction to soil mechanics.* Iowa State University Press, Ames, Iowa.

Davison, C. (1891). "On the amount of sand brought up by lob worms to the surface." *Geological magazine* 8, 489.

DiGiano, F. A., Miller; C. T., and Yoon, J. (1993). "Predicting release of PCBs at point of dredging." *Journal of Environmental Engineering, ASCE* 119(19), 72-89.

DiGiano, F. A., Miller, C. T., and Yoon, J. (1995). *Dredging elutriate test development.* U.S. Army Engineer Waterways Experiment Station, Vicksburg, Miss.

Elliot, A. H., and Brooks, N. H. (1997a). "Transfer of nonsorbing solutes to a streambed with bed forms: Theory." *Water Resources Research* 33(1), 123–136.

Elliot, A. H., and Brooks, N. H. (1997b). "Transfer of nonsorbing solutes to a streambed with bed forms: Laboratory experiments." *Water Resources Research* 33(1), 137–151.

Foth & Van Dyke (2000). "Summary Report: Fox River Deposit N." Wisconsin Department of Natural Resources Madison, N.J.

Foth & Van Dyke.(2001). "Final Report 2000 Sediment Management Unit 56/57 Project Lower Fox River, Green Bay, Wisconsin." *Prepared for United States Environmental Protection Agency*, Wisconsin Department of Natural Resources.

Hayes, D. F., Crockett, T. R., Ward, T. J., and Averett, D. (2000). "Sediment resuspension during cutterhead dredging operations." *Journal of Waterway, Port, Coastal, and Ocean Engineering* 126(3), 153–161.

Hickey, J. J., et al. (1966). "An exploration of pesticides in a Lake Michigan ecosystem." *Journal of Applied Ecology* 3, 141–154.

Huang, W., and Weber, W. J. Jr. (1997). "A distributed reactivity model for sorption by soils and sediments. 10: Relationships between desorption, hysteresis, the chemical characteristics of organic domains." *Environmental Science and Technology* 31(9), 2562–2569.

Hughes, J. B., Beckles, D. M., Chandra, S. D., and Ward, C. H. (1997). "Utilization of bioremediation processes for the treatment of PAH-contaminated sediments." *Journal of Industrial Microbiology and Biotechnology* 18, 152–160.

Hunter, M. A., Kan, A. T., and Tomson, M. B. (1996). "Development of a surrogate sediment to study the mechanisms responsible for adsorption/desorption hysteresis." *Environmental Science* 30, 1996.

Ingersoll, C. G., Dillon, T., and Biddinger, G. R. (1997). *Ecological risk assessment of contaminated sediments,* SETAC Press, Pensacola, Fla.

Jones, C., and Lick, W. (2000). "Effects of Bed Coarsening on Sediment Transport." Estuarine and Coastal Modeling, *Proceedings of the Sixth International Conference*, ASCE, Reston, Va., 915–993.

Kan, A. T., Fu, G., Hunter, M. A., Chen, W., Ward, C.H., and Tomson, M. B. (1998). "Irreversible sorption of neutral hydrocarbons to sediments: Experimental observations and model predictions." *Environmental Science and Technology* 32(7), 892–902.

Kan, A. T., Fu, G., Hunter, M. A., and Tomson, M. B. (1997). "Irreversible adsorption of naphthalene and tetraclorobiphenyl to lula and surrogate sediments." *Environmental Science and Technology* 31, 2176–2185.

Lick, W., and Lick, J. (1988). "Aggregation and disaggregation of fine-grained lake sediments." *Journal of Great Lakes Research* 14(4), 514–523.

Matisoff, G. (1982). "Chapter 7: Mathematical models of bioturbation." *Animal sediment relations*, R. L. McCall and M. I. S. Tevasz, eds., Plenum, New York.

McGroddy, S. E., and Farrington, J. W. (1995). "Sediment porewater partitioning of polycyclic aromatic hydrocarbons in three cores from Boston Harbor, Massachusetts." *Environmental Science and Technology* 29, 1542—1550.

McNeill, J., Taylor, C., and Lick, W. (1995). "Measurements of erosion of undisturbed bottom sediments with depth." *Journal of Hydraulic Research* 12(4), 361–369.

Millington, R. J., and Quirk, J. M. (1961). "Permeability of porous solids." *Transactions of the Society* 57, 1200–1207.

Myers, T. E., et al. (1996). "Estimating contaminant losses from components of remediation alternatives for contaminated sediments." *EPA 905-R96-001*, U.S. Environmental Protection Agency, Washington, D.C.

National Research Council (NRC). (2001). *A Risk-Based Framework for the Management of PCB Contaminated Sediments*, National Research Council, Washington, D.C.

Palermo, M. R., Maynord, S., Miller, J., and Reible, D. D. (1998). "Guidance for in situ subaqueous capping of contaminated sediments." *US EPA 905-B96-004,* Assessment and Remediation of Contaminated Sediments (ARCS) Program, Great Lakes National Program Office, U.S. Environmental Protection Agency, Chicago.

Pereira, W. E., Rostad, C. E., Chiou, C. T., Brinton, T. I., and Barbar, L. B., II. (1988). "Contamination of estuarine water, biota, and sediment by halogenated organic compounds: A field study." *Environmental Science and Technology* 22, 772–778.

Pignatello, J. J., and Xing, B. (1996). "Mechanisms of slow sorption of organic chemicals to natural particles." *Environmental Science and Technology* 30, 1–11.

Readman, J. W., and Mantoura, R. F. C. (1987). "A record of polycyclic aromatic hydrocarbon (PAH) pollution obtained form accreting sediments of the Tamar Estuary U.K.: Evidence for non-equilibrium behaviour of PAH." *Science of the Total Environment* 66, 73–94.

Reible, D. D., Valsaraj, K. T., and Thibodeaux, L. J. (1991). "Chemodynamic models for transport of contaminants from sediment beds." *Handbook of Environmental Chemistry*, O. Hutzinger, ed., Springer, Heidelberg, 187–228.

Reible, D. D., et al. (1996). "Contaminant fluxes from sediment due to tubificid oligachaete bioturbation." *Water Research* 30(3), 704.

Rhoads, D. C. (1974). "Organism sediment relations on the muddy sea floor." *Oceanography and Marine Biology Annual Review* 12, 263.

Savant, S. A., Reible, D. D., and Thibodeaux, L. J. (1987). "Modeling convective transport in stable river sediments." *Water Resources Research* 23, 1763.

Savant-Malhiet, S. A., and Reible, D. D. (1993). "Comparison of physical transport processes in river sediments." *Journal of Environmental Engineering*, *ASCE* 119(1), 90–102.

Science Advisory Board (SAB). (1995). "Review of the agency's approach for developing sediment criteria for five metals." *EPA-SAB-EPEC-95-020*, U.S. Environmental Protection Agency Science Advisory Board, Washington, D.C.

Spaulding, M. L. (1987). "Selected studies on PCB transport in New Bedford Harbor." *ASA 86-18*, Applied Science Associates, Narragansett, R.I.

Stark, T. D. (1991). "Program documentation and user's guide: PCDDF89, Primary consolidation and dessication of dredged fill." *Instruction Report D-91*-1, U.S. Army Engineers Waterways Experiment Station, Vicksburg, Miss.

Thibodeaux, L. J. (1989). "A theoretical evolution of the effectiveness of capping PCB contaminated New Bedford Harbor

sediment." *Project No. 629201*. Louisiana State University Report to Balsam Environmental Consultants.

Thibodeaux, L. J. (1996). *Environmental chemodynamics*. Wiley, New York.

Thibodeaux, L. J., and Boyle, J. O. (1987). "Bedform-generated convective transport in bottom sediment." *Nature* 325 (6102), 341.

Thibodeaux, L. J., Reible, D. D., and Valsaraj, K. T. (1999). Effectiveness of environmental dredging. *Final Report to Alcoa, Massena, NY*, Hazardous Substance Research Center/South and Southwest, Louisiana State University, Baton Rouge.

Thibodeaux, L. J., Valsaraj K. T., and Reible, D. D. (2001). "Bioturbation-driven transport of hydrophobic organic contaminants from bed sediment." *Environmental Engineering Science* 18(4), 215–223.

Thoma, G. J., Koulermos, A. C., Valsaraj, K.T., Reible, D. D., and Thibodeaux, L. J. (1991). "Chapter 13: The effects of pore water colloids on the transport of hydrophobic organic compounds from bed sediment." *Organic Substances in Soils and Sediments*, R.A. Baker, ed., Lewis, Boca Raton, Fla., 231–250.

Thoma, G. J., Reible, D. D., Valsaraj, K. T., and Thibodeaux, L. J. (1993). "Efficiency of capping contaminated sediments in situ. 2: Mathematics of diffusion-adsorption in the capping layer." *Environmental Science and Technology* 27(12), 2412–2419.

Thoms, S. R., Matisoff, G., McCall, P. L., and Wang, X. (1995). "Models for alteration of sediments by benthic organisms." *Final Report Project 92-NPS-2*, Water Environment Research Foundation, Alexandria, Va.

Tiedge, J. M., Quenson, J. F., Chee-Sanford, J., Schimel, J. P., and Boyd, S. A. (1993). "Microbial reductive dechlorination of PCBs." *Biodegradation* 4(4), 231–240.

Transportation Research Board. (1970). "Tentative design procedure for riprap-lined channels." *Report 108*, National Academy of Sciences, National Cooperative Highway Research Program, Washington, D.C.

U.S. Army Corps of Engineers (USACE). (1990). "New Bedford Harbor superfund pilot study: Evaluation of dredging and dredged material disposal." U.S. Army Corps of Engineers, New England Division, Concord, Mass.

U.S. Bureau of Reclamation (USBR). (1973). *Design of small dams*, 2nd Ed. U.S. Bureau of Reclamation, Washington, D.C.

U.S. Environment Protection Agency (USEPA). (1993a). "Biological and chemical assessment of contaminated Great Lakes sediment." *EPA 905-R93-006*, U.S. Environmental Protection Agency, Washington, D.C.

U.S. Environment Protection Agency (USEPA). (1993b). "Technical basis for deriving sediment quality criteria for nonionic organic contaminants for the protection of benthic organisms by using equilibrium partitioning." *EPA 822-R-93-011*, U.S. Environmental Protection Agency, Washington, D.C.

U.S. Environment Protection Agency (USEPA). (1994). "Assessment guidance document." *EPA 905-B94-002*, U.S. Environmental Protection Agency, Washington, D.C.

Valsaraj, K. T., Thibodeaux, L. J., and Reible, D. D. (1997). "A quasi-steady state pollutant flux methodology for determining sediment quality criteria." *Environment Toxicology and Chemistry* 16(3), 391.

Vittal, N., Rangu Raju, K. G., and Garde, R. J. (1977). "Resistance of two-dimensional triangular roughness." *Journal of Hydraulic Research, ASCE* 15(1), 19.

Wang, X. Q., Thibodeaux, L. J., Valsaraj, K. T., and Reible, D. D. (1991). "The efficiency of capping contaminated sediments in situ. I: Lab-scale experiments of diffusion/adsorption in the capping layer." *Environmental Science and Technology* 25(9), 1578–1584.

White, J. C., Hunter, M., Nam, K., Pignatello, J. J., and Alexander, M. (1999). *Environmental Toxicology and Chemistry* 18, 1720–1727.

Wisconin Department of Natural Resources (WDNR). (2001). "Draft feasibility study—Lower Fox River and Green Bay, Wisconsin." Wisconsin Department of Natural Resources, Madison.

Zhang, X. M., and Young, L. Y. (1997). "Carboxylation as an initial reaction in the anaerobic metabolism of naphthalene and phenanthrene by sufidogenic consortia." *Applied Environmental Microbiology* 63(12), 4759–4764.

Copyrighted Materials
Copyright © 2008 American Society of Civil Engineers (ASCE)
Retrieved from www.knovel.com

CHAPTER 22

Sediment Oxygen Demand (SOD) in Rivers, Lakes, and Estuaries

Miki Hondzo and Nancy Steinberger

22.1 INTRODUCTION

Sediment oxygen demand (SOD) is defined as the rate of oxygen consumption exerted by the bottom sediment on the overlying water (Lee et al. 2000b). The uptake of dissolved oxygen (DO) by sediment is usually attributed to the aerobic decomposition of organic material by microorganisms at the sediment surface and the reaction of oxygen with anaerobic respiration by-products (Sweerts et al. 1991). Because the sediments are a repository for decaying organic material, SOD is often a major contributor to DO depletion in rivers and lakes (Ellis and Stefan 1990; Sweerts et al. 1991; Nakamura and Stefan 1994; Seiki et al. 1994).

The amount of DO in a water body is an indication of the level of microbiological activity and the amount of decaying organic matter present, and often limits the amount of waste that a water body can safely assimilate from municipal and industrial discharges (Hatcher 1986; Lung and Sobeck 1999). In addition, DO is critical for the sustainability of fish habitat in temperate rivers and lakes. Low DO levels influence the composition of fish fauna, favoring species with tolerance for low oxygen levels, such as common carp (*Cyprinus carpio*), and can cause winterkill in ice-covered lakes (Moyle and Cech 2000). Because SOD is often a major component of the DO budget, accurate estimation of the flux of DO across the sediment-water interface is of paramount importance.

Davis and Lathrop-Davis (1986) have provided a brief history of the early investigations in SOD. Early reports relating water quality to sediments described the effects of wastewater sanitation practices and settled sludge deposits on surface-water quality in heavily populated areas (Hering et al. 1887; Stearns and Drown 1890; Forbes and Richardson 1913; Metcalf and Eddy 1916; Richardson 1928; Purdy 1930). Studies of oxygen dynamics in lakes considered the influence of bottom sediments on DO depletion (Birge 1906; Birge and Juday 1911; Alsterberg 1922; Welch 1935). Early models of DO dynamics include the work of Streeter and Phelps (1925), Wisely and Klassen (1938), Jansa and Akerlindh (1941), and Bouldin (1967).

Experimental investigations of SOD have considered chemical, biological, and hydrodynamic influences on the rate of DO consumption by sediments (Baity 1938; Fair et al. 1941; Lardieri 1954; Odum 1956; Hayes and MacAulay 1959; Teal and Kanwisher 1961; Isaac 1962; Edwards and Rolley 1965; O'Connel and Thomas 1965; Knowles et al. 1962; Lenard et al. 1962). More recently, the effect of velocity and boundary-layer interactions has become a major focus for SOD research (NCASI 1978; Jorgensen and Revsbech 1985; Whittemore 1986; Hall et al. 1989; Rahm and Svensson 1989; Sweerts et al. 1991; Dade 1993; Nakamura and Stefan 1994; Maran et al. 1995).

Current work related to DO dynamics and SOD is extensive and is being performed in many disciplines. Ecologists and aquatic biologists have recently published several studies on the effect of oxygen stress on the growth and survival of aquatic organisms (Matthews and Berg 1997; Sparks and Strayer 1998; Hale 1999; Harris et al. 1999; Lowell and Culp 1999; Rosas et al. 1999; Buentello et al. 2000; Ruggerone 2000), the effect of DO on habitat utilization and the distribution of organisms (McKinsey and Chapman 1998; Sellers et al. 1998; Elliott 2000), and the relationships between DO in nesting areas and mate selection and reproduction (Jones and Reynolds 1999a; 1999b; Takegaki and Nakazono 1999). In addition, biologists have been interested in the diurnal variation in DO as it relates to metabolism (Guasch et al. 1998; Marzolf et al. 1998; Young and Huryn 1998), the influence of benthic activity on DO consumption (Brekhovskikh et al. 1998; Moodley et al. 1998; Schallenberg and Burns 1999; Schol et al. 1999; Caraco et al. 2000), and relationships between ecosystem functioning and DO (Moore and Townsend 1998; Nishri et al. 1998).

Other recent work of biological importance includes studies of DO and SOD in estuaries, tidal rivers, and oceans (Bertuzzi et al. 1997; Borodkin and Makkaveev 1997; Najjar and Keeling 1997; Summers et al. 1997; Tishchenko et al. 1998; Boyer et al. 1999; Chen et al. 1999; Engle et al. 1999). Additional studies have recently been published on DO and SOD in large regulated rivers and ancient lakes (Martin et al. 1998; Bachmann and Usseglio-Polatera 1999).

Modeling DO dynamics and SOD for management and regulation of water quality continues to be an active area of research in environmental engineering (Chambers et al. 1997; Houck et al. 1997; Chaudhury et al. 1998; Leu et al. 1998; Neal et al. 1998; Sun and Wakeham 1998; Chapra and Runkel 1999; Park and Jaffe 1999; Lung and Sobeck 1999; Ansa-Asare et al. 2000; Kayombo et al. 2000). Thermal stratification in DO-limited systems also continues to be an important area of research, especially in relation to climate change (Fang and Stefan 1997; Jonas 1997; Chapman et al. 1998; Fang et al. 1999; Kelly and Doering 1999; Fang and Stefan 2000). Engineers are also concerned with the effect of velocity and turbulence on SOD as it relates to the physical mechanisms of DO mass transfer (Parkhill and Gulliver 1997; Guss 1998; Hondzo 1998; Mackenthun and Stefan 1998; Josiam and Stefan 1999; Steinberger and Hondzo 1999; Lee et al. 2000a; 2000b).

22.2 DIFFUSIVE SUBLAYER THICKNESS

The mechanisms of mass transfer at the sediment-water interfaces in rivers and lakes involve a combination of molecular diffusion and turbulent transport of DO from the overlying water to the sediment bed. Consider the physical effects occurring in the region adjacent to an interface (Fig. 22-1). In the near-bed region lies the diffusive sublayer, where molecular diffusional transport dominates over turbulent transport (Levich 1962; Dade 1993). The diffusive sublayer thickness has been reported as $\delta_c = 10\,\frac{\nu}{u_*}\mathrm{Sc}^{-1/3}$, where ν is the kinematic viscosity, u_* is the shear stress velocity, $\mathrm{Sc} = \nu/D$ is the Schmidt number, and D is the molecular diffusion coefficient. The dependence of the Schmidt number on water temperature is displayed in Fig. 22-2. According to this relationship, the Schmidt number decreases with increasing water temperature. A typical magnitude of the Schmidt number for DO in water is about 500 at 20°C (Fig. 22-2).

Therefore, the diffusive sublayer is on the order of one tenth the thickness of the viscous sublayer. The presence of this diffusive sublayer can act as a region of resistance to mass transport, and thus may limit chemical reactions occurring at the sediment-water interface (Jorgensen and Revsbech 1985; Hall et al. 1989; Rahm and Svensson 1989; Dade 1993; Steinberger and Hondzo 1999).

Consider a turbulent flow between two parallel plates as an example of shear dispersion (Fig. 22-3). The lower plate is a DO sink, whereas the upper plate constitutes a no-flux boundary condition. The boundary layer between the plates is considered to be either developed, or so slowly varying that the absence of variation in the streamwise direction can be assumed. For developed flow the mean velocity in the vertical direction, y, is zero (note that the turbulent velocity fluctuation v' is not zero), and streamwise velocity is a function only of y. As the fluid moves along the channel, DO diffuses from the fluid to the lower plate, causing the growth of the diffusive sublayer (Fig. 22-3). The bulk DO concentration at any distance x can be expressed as

$$C_B - C_w = \frac{\int_0^{2H} u\left(C - C_w\right) dy}{\int_0^{2H} u\, dy} \tag{22-1}$$

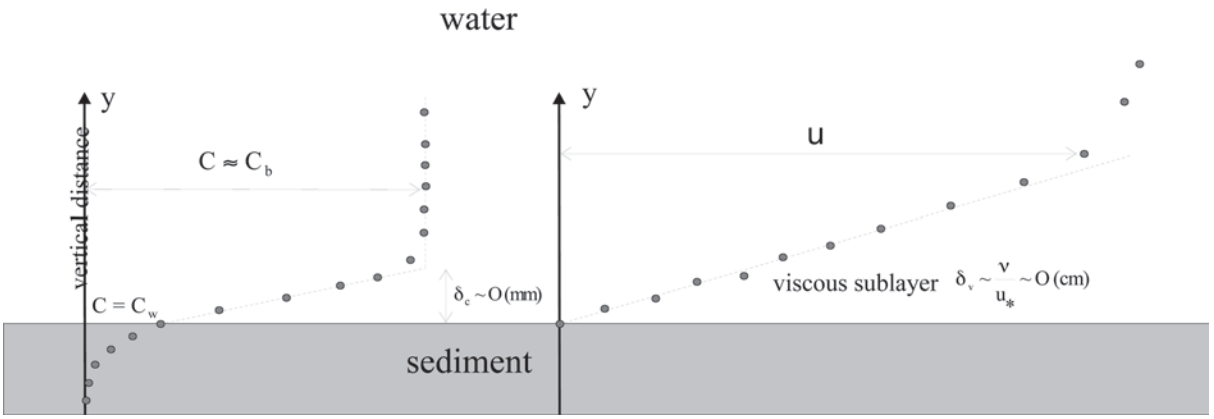

Fig. 22-1. Conceptual sketch for near-bed concentration and velocity distributions (δ_c is the diffusive sublayer; δ_v is the viscous sublayer).

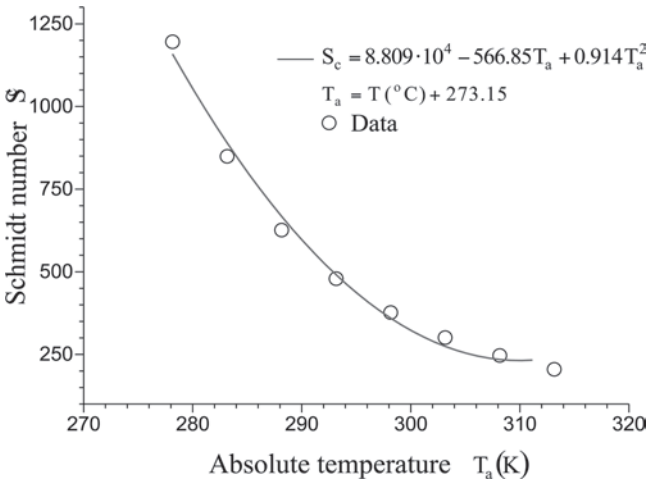

Fig. 22-2. Relationship of Schmidt number (Sc) for dissolved oxygen in water to temperature.

where

C = mean (time-averaged) DO concentration;
C_w = DO concentration at the sediment-water interface;
u = mean velocity in the x direction; and
H = the half-distance between the plates.

For developed flow the diffusive sublayer experiences no further growth in the streamwise direction. This suggests that the local mass-transfer coefficient is constant in the streamwise direction. The constant mass-transfer coefficient condition is equivalent to the condition that the concentration profiles at all x stations are mappable onto a single curve. This mapping is accomplished by the use of a concentration similarity group $\frac{C-C_w}{C_B-C_w}$. Note that C, C_w, C_B may vary with x, but not the group $\frac{C-C_w}{C_B-C_w}$. From the invariance condition

$$\frac{\partial}{\partial x}\left(\frac{C-C_w}{C_B-C_w}\right)=0, \tag{22-2}$$

it follows that

$$\frac{C-C_w}{C_B-C_w}=f(y) \tag{22-3}$$

Therefore, the concentration gradient follows from Eq. (22-3) as

$$\frac{\partial C}{\partial y}=\left(C_B-C_w\right)\frac{df}{dy} \tag{22-4}$$

The local mass flux per unit area from the fluid to the sediment-water interface can be evaluated as

$$\begin{aligned} M &= -D\frac{\partial C}{\partial y}\Big|_{y=0} = -D\left(C_B-C_w\right)\left(\frac{df}{dy}\right)\Big|_{y=0} \\ &= \frac{D}{\delta_c}\left(C_B-C_w\right) \end{aligned} \tag{22-5}$$

where M is the mass flux across the sediment-water interface, and δ_c is the diffusive-sublayer thickness or the "unstirred-layer" thickness. The diffusive-sublayer thickness is given by

$$\delta_c=\frac{1}{\left(\frac{df}{dy}\right)\Big|_{y=0}} \tag{22-6}$$

The first derivative of the DO concentration similarity variable profile $\frac{C-C_w}{C_B-C_w}$ is evaluated at the sediment-water interface. The derivative represents the slope of the similarity group in the diffusive sublayer region. The local mass-transfer coefficient is related to the diffusive sublayer thickness by

$$\mathrm{k}=\frac{D}{\delta_c} \tag{22-7}$$

The diffusive-sublayer thickness is constant in a developed flow. Therefore, for a given fluid temperature, the mass-

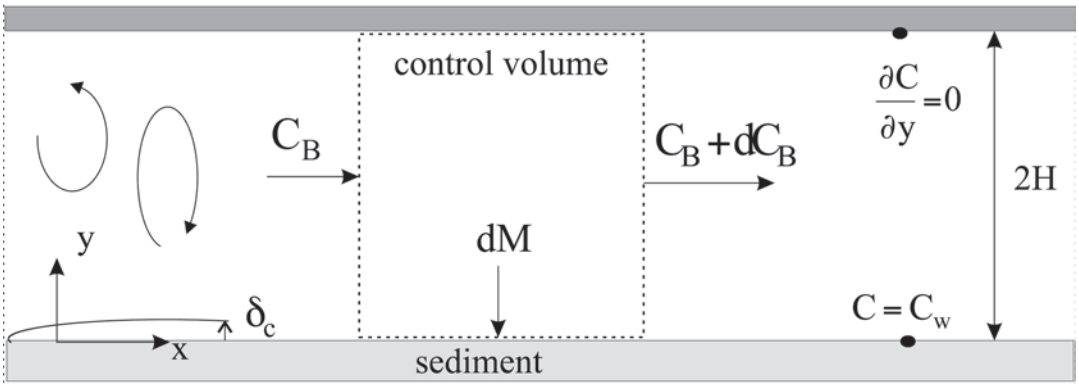

Fig. 22-3. Definition sketch for flow between two parallel plates.

transfer coefficient is constant as well. Once the diffusive-sublayer thickness is available the mass-transfer coefficient can be estimated from the above expression. The constant mass-transfer coefficient and concentration-profile similarity are important characteristics of the developed flow regime. Note that the DO flux across the sediment-water interface should always occur across the diffusive sublayer thickness. The thickness of this layer may be determined by turbulent activity, i.e., by mean frequency of large or small eddies in the fluid above the unstirred layer. The time-averaged micro-DO concentration profiles of natural sediments are shown for four experimental runs in Fig. 22-4 (Steinberger and Hondzo 1999). The data acquisition system, operating at 25 Hz, obtained a minimum of 200 readings at each vertical step. These readings were then averaged as represented by a single measurement point denoted by a circle in Fig. 22-4. The consistent shape of the microprofiles is an indication of the high level of repeatability of the experiments. As shown on the DO microprofiles, all DO arriving at the sediment bed was quickly utilized within the first few millimeters of the surface, indicating that the experiments were water-side-controlled as opposed to reaction-limited. The concentration-sublayer thickness near the sediment-water interface is the thin diffusive region within which the DO concentration changes rapidly. The diffusive-sublayer thickness ranged from 0.12 to 1.23 mm. In Fig. 22-4 it can be seen that δ_c decreased with higher Reynolds number. This smaller thickness corresponds to an increase in the flux of DO to the sediment bed.

Scaling arguments (Steinberger and Hondzo 1999) yield an expression for δ_c (Fig. 22-5) of the form

$$\delta_c = (19.4 \pm 5.5)\frac{\nu}{u_*} S_c^{-1/3} \tag{22-8}$$

where

δ_c = diffusive-sublayer thickness in mm

and ± 5.5 are the 90% confidence intervals for the mean slope. Prasad and Russell (2000) derived a similar expression, $\delta_c = 14.5\ \nu/u_* S_c^{-1/3}$, that falls within the 90% confidence limits of Eq. (22-8). This result is not in close agreement to

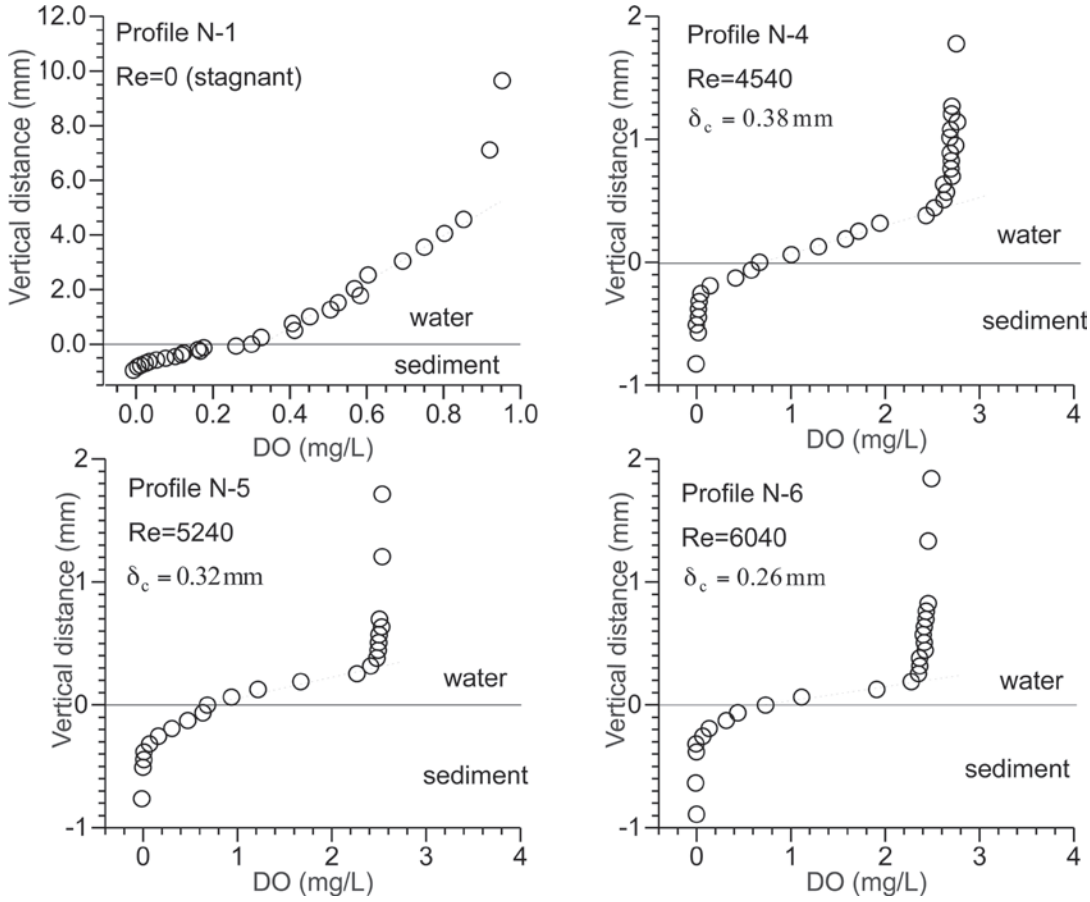

Fig. 22-4. Dissolved oxygen concentration profiles in near-bed region.

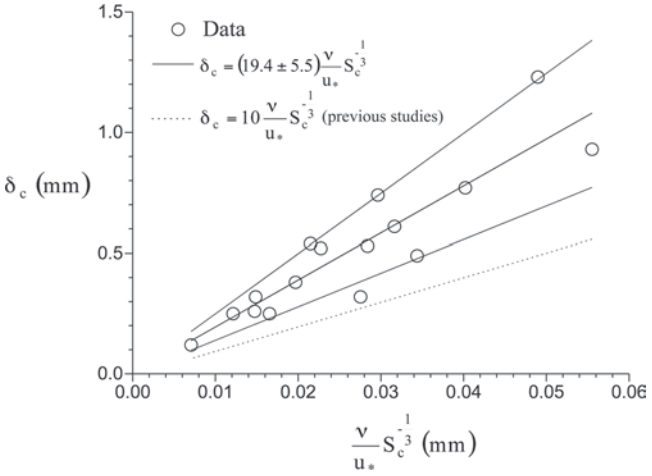

Fig. 22-5. Experimental data for diffusive sublayer thickness (δ_c) as function of viscous length scale (ν/u_*) and Schmidt number (Sc).

the theoretical formulation of previous studies (e.g., Levich 1962; Dade 1993), as presented by the dashed line in Figure 22-5. The cited studies provided useful scaling parameters and an order-of-magnitude estimate for the diffusive sublayer thickness; however, the nature of the function δ_c was not verified by experiment in the previous work. In Fig. 22-5 it can be seen that δ_c decreased with shear stress velocity. An increase in mean flow velocity produces a corresponding increase in the shear stress velocity, and therefore a decrease in the diffusive sublayer thickness.

22.3 MASS-TRANSFER COEFFICIENT

22.3.1 Dimensional Analysis: Bulk Flow

To relate the mass flux of DO to relevant system parameters, dimensional analysis was invoked. Let us consider the situation shown in Fig. 22-1, where a reaction at the sediment surface is causing a reduction in DO concentration of the turbulent water above it. It is assumed that the concentration at the sediment-water interface and the average bulk concentration are known. The remaining independent variables that influence the mass-transfer coefficient appear in the expression

$$k = f(D, H, U, \rho, \mu) \tag{22-9}$$

where

H = plate half-spacing (boundary layer thickness);
ρ = density; and
μ = dynamic viscosity.

The quantity of interest that is dependent upon these parameters is the mass-transfer coefficient. Using k as the dependent variable and D, H, and ρ as the repeating independent variables, π-theorem analysis can be used to obtain the following dimensionless variables, which are important to this system:

$$\mathsf{Sh} = \frac{kH}{F}; \quad \mathsf{R} = \frac{UH}{\nu}; \quad \mathsf{Sc} = \frac{\nu}{F} \tag{22-10}$$

where Sh is the Sherwood number, R is the Reynolds number based on H and U, and Sc is the Schmidt number. It therefore follows that the mass-transfer coefficient of oxygen to the sediment bed can be represented by an expression of the form

$$\mathsf{Sh} = f(\mathsf{R}, \mathsf{Sc}) \tag{22-11}$$

Investigators have reported mass-transfer data in terms of Sherwood-Reynolds-Schmidt number correlations of the form $\mathsf{Sh} = a\mathsf{R}^b\mathsf{Sc}^{1/3}$. The values for the constants a and b are typically determined from experimental measurements. In the next section, we will derive a Sherwood-Reynolds-Schmidt number correlation for DO transport in a turbulent flow between two parallel plates.

22.3.2 Mass-Transport Analysis

The mean DO concentration between two parallel plates (Fig. 22-3) is governed by the equation (Fischer et al. 1979)

$$\frac{\partial C}{\partial t} + \boldsymbol{u}\frac{\partial C}{\partial x} + \boldsymbol{v}\frac{\partial C}{\partial y} = \frac{\partial}{\partial x}\left[(\boldsymbol{D}_{cx} + \boldsymbol{D})\frac{\partial C}{\partial x}\right] + \frac{\partial}{\partial y}\left[(D_{ef} + D)\frac{\partial C}{\partial y}\right] \tag{22-12}$$

where t is time and D_{cx} and D_{cy} are the turbulent diffusion coefficients. Neither biological oxygen demand nor primary production-respiration is considered in the fluid between the plates. From the invariance condition $\frac{\partial}{\partial x}\left(\frac{C - C_w}{C_B - C_w}\right) = 0$, it follows that $\frac{\partial C}{\partial x} = \frac{\partial C_B}{\partial x} = \text{constant}$ (Appendix). Therefore, for steady developed flow Eq. (22-12) reduces to the form

$$u\frac{dC_B}{dx} = \frac{\partial}{\partial y}\left[(D_{cy} + D)\frac{\partial C}{\partial y}\right] \tag{22-13}$$

This two-process model implies a first-order balance between the advection and vertical diffusion in a developed flow. Equation (22-13) is subject to the boundary conditions

$$C = C_w \text{ at } y = 0 \text{ and } \frac{\partial C}{\partial y} = 0 \text{ at } y = 2H \tag{22-14}$$

Equation (22-13) may be integrated twice subject to the boundary conditions (22-14) so that

$$C - C_w = \frac{dC_B}{dx} U \int_0^{y'} \frac{y - 2H}{D_{cy} + D} dy \qquad (22\text{-}15)$$

where

U = discharge velocity.

To facilitate closed-form solution, we assumed that $u = U$.

The slope of the variation of the streamwise bulk concentration, dC_B/dx, is obtainable from the conservation-of-mass equation for the control volume shown in Fig. 22-3. The net mass flux into the control volume yields

$$\frac{dC_B}{dx} = -\frac{M}{2UH} \qquad (22\text{-}16)$$

Substituting Eq. (22-16) into Eq. (22-15) yields

$$C - C_w = -M \int_0^{y'} \frac{\frac{y}{2H} - 1}{D + D_{cy}} dy \qquad (22\text{-}17)$$

Introducing $\tilde{y} = yu_*/\nu$ into Eq. (22-17) as the independent variable yields

$$\tilde{C} = \frac{(C - C_w)u_*}{M} = -\int_0^{\tilde{y}'} \frac{\frac{\tilde{y}\nu}{u_*}\frac{1}{2H} - 1}{\frac{1}{S_c} + \frac{D_{cy}}{\nu}} d\tilde{y} \qquad (22\text{-}18)$$

The integral in Eq. (22-18) can be evaluated using different degrees of approximation. We will neglect the terms D_{cy}/ν and $\tilde{y}\nu/u_*$ in the diffusive sublayer and we will neglect $1/S_c$ in the region outside the sublayer. The diffusive sublayer extends to $\tilde{\delta}_c = 19.4 S_c^{-1/3}$ (Eq. 22-8). When these approximations are taken, the following equation for the concentration profile results:

$$\tilde{C} = \frac{(C - C_w)u_*}{M} = -\left(\int_0^{\tilde{\delta}_c} S_c \, d\tilde{y} + \int_{\tilde{\delta}_c}^{\tilde{y}'} \frac{\frac{\tilde{y}\nu}{u_*}\frac{1}{2H} - 1}{\frac{D_{cy}}{\nu}} d\tilde{y} \right) \qquad (22\text{-}19)$$

The turbulent diffusion of DO for the entire region outside the diffusive sublayer is expressed as (Hondzo 1998)

$$\frac{D_{cy}}{\nu} = \frac{\kappa \tilde{y}}{4\mathrm{Sc}_t}\left(2 - \frac{y}{H}\right)\left[1 + 2\left(1 - \frac{y}{H}\right)^2\right] \qquad (22\text{-}20)$$

where κ is the von Karman constant, taken as equal to 0.4, and Sc_t is the turbulent Schmidt number, taken as equal to 1.0. Substituting Eq. (22-20) into Eq. (22-19), integrating, evaluating the value of $\tilde{C}$ at the half distance between the plates ($y = H$), and defining $\mathrm{R}_* = u_* H/\nu = \mathrm{R}\sqrt{C_f}$ where, C_f is the friction coefficient, yields

$$\tilde{C}_c = 19.4 S_c^{2/3} + 10 S_{ct} \left\{ \frac{1}{6} \ln\left(\frac{19.4 S_c^{-1/3}}{\mathrm{R}\sqrt{C_f}} \right) + \frac{1}{2} \ln\left(\frac{4.5}{3 + 752 S_c^{-2/3} \frac{1}{\mathrm{R}^2 C_f} - 77 S_c^{-1/3} \frac{1}{\mathrm{R}\sqrt{C_f}}} \right) + \frac{\sqrt{2}}{6} \mathrm{atan}\left[\left(\frac{19.4 S_c^{-1/3}}{\mathrm{R}\sqrt{C_f}} - 1 \right)\sqrt{2} \right] \right\} \qquad (22\text{-}21)$$

The local mass-transfer coefficient can be represented by an expression of the form

$$\mathrm{Sh} = \frac{\mathrm{R}\sqrt{C_f}\,\mathrm{Sc}}{\tilde{C}_c} \frac{(C_c - C_w)}{(C_B - C_w)} \qquad (22\text{-}22)$$

The ratio $C - C_w/C_B - C_w \approx 1$; thus the nondimensional mass-transfer coefficient follows from Eq. (22-22) as

$$\mathrm{Sh} = \frac{\mathrm{R}\sqrt{C_f}\,\mathrm{Sc}}{\tilde{C}_c} \qquad (22\text{-}23)$$

where $\tilde{C}_c$ is given by Eq. (22-21) and C_f is the friction coefficient (e.g., $\mathrm{C}_f = 0.0791 \times \mathrm{R}^{-1/4}$; Dawson and Trass 1972).

A comparison of Eq. (22-23) with experimental data for DO transfer at the sediment-water interface (Steinberger and Hondzo 1999) is given in Fig. 22-6. Linear regression of the experimental data yields a mean exponent of 0.89 on R in the equation

$$\mathrm{Sh} = (0.012 \pm 0.001)\,\mathrm{R}^{0.89 \pm 0.05}\,\mathrm{Sc}^{0.33} \qquad (22\text{-}24)$$

where

± 0.001 and ± 0.05 = the 90% confidence intervals for the mean coefficient and the mean exponent, respectively.

The exponents of 0.89 closely match the reported values of: 0.87 (Probstein et al. 1972), 0.91 (Harriott and Hamilton 1965), and 0.80 (Colburn 1933; Incropera and DeWitt 1990).

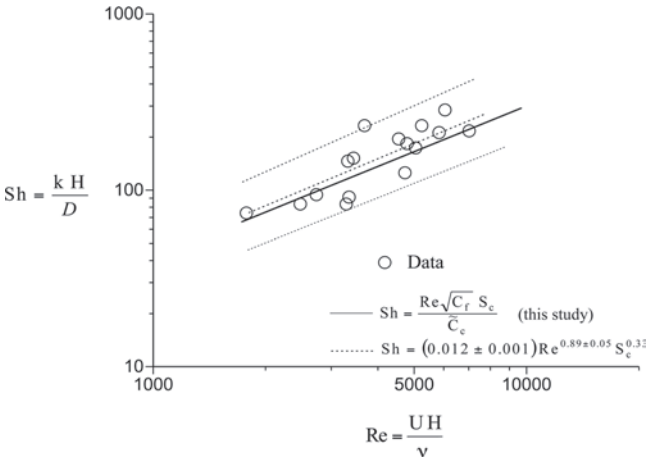

Fig. 22-6. Experimental data for Sherwood number (Sh) as function of Reynolds number (Re) with Sc = 500.

The results of the cited studies were not based specifically on diffusional DO transfer at the sediment-water interface. They were based on a semianalytical integral theory for electrodyalisis (Probstein et al. 1972), benzoic acid dissolution in glycerine-water solutions (Harriott and Hamilton 1965), and heat transfer data (Colburn 1933; Incropera and DeWitt 1990). The model developed in this study (Eq. (22-23)) compares very well with the data. The predicted values of the Sherwood number are within the 90% confidence intervals of the empirical relationships. Using Eq. (22-24) or Eq. (22-23), it is possible to estimate the mass-transfer coefficient, k, from the bulk measured quantities such as the mean flow velocity, the flow depth, and the mean water temperature.

Example: Consider a wide irrigation channel with a smooth channel bed. The channel has the following characteristics: mean depth $H = 0.5$ m, cross-section average velocity $U = 0.5$ m/s, and mean water temperature $T = 20^{\circ}$C. Using Eqs. (22-23) and (22-24) estimate the mass-transfer coefficient and DO flux at the sediment-water interface.

Solution: For water temperature at 20°C the kinematic viscosity is 1.005×10^{-6}m^2/s. The Schmidt number (Fig. 22-2) is $S_c = 8.809 \times 10^4 - 566.85 \times (20 + 273.15) + 0.914 \times (20 + 273.15)^2 = 464$. The DO diffusion coefficient in water is

$$D = \frac{\nu}{S_c} = \frac{1.005 \times 10^{-6}}{464} \approx 2.16 \times 10^{-9}\,\mathrm{m^2/s}.$$

The Reynolds number for the wide channel is

$$\mathsf{R} = \frac{UH}{\nu} = \frac{0.5 \times 0.5}{1.005 \times 10^{-6}} \approx 2.5 \times 10^5.$$

The mass-transfer coefficient can be estimated from Eq. (22-24) as

$$\begin{aligned} k_1 &= 0.012 \frac{D}{H} \mathsf{R}^{0.89} \mathsf{Sc}^{0.33} \\ &= 0.012 \frac{2.16 \times 10^{-9}}{0.5} \left(2.5 \times 10^5\right)^{0.89} 464^{0.33} \\ &= 2.5 \times 10^{-5}\,\mathrm{m/s}. \end{aligned}$$

With the mass-transfer coefficient, it is possible to estimate the DO flux using values for DO concentration at the bed and in the bulk flow. Assuming that $C_w = 0$ and $C_b = 6$ mg/L, and using Eq. (22-5), the DO flux is

$$\begin{aligned} M_1 &= k_1 \left(C_w - C_b\right) = 2.5 \times 10^{-5} \left(0 - 6\right) \times 10^3 \\ &= -0.15\ \mathrm{mg/m^2 s}. \end{aligned}$$

The minus sign designates DO flux from water toward the sediment (downward flux).

The nondimensional mass-transfer coefficient from Eq. (22-23) is

$$\begin{aligned} \mathsf{Sh} &= \frac{\mathsf{R}\sqrt{C_f}\, S_c}{\tilde{C}_c} \\ &= \frac{2.5 \times 10^5 \times \sqrt{(0.0791 \times (2.5 \times 10^5 \times 4)^{-1/4}} \times 464}{1151.03} \\ &= 5043.22. \end{aligned}$$

The mass-transfer coefficient is

$$k_2 = \frac{\mathsf{Sh} \times D}{H} = \frac{5043.22 \times 2.16 \times 10^{-9}}{0.5} = 2.18 \times 10^{-5}\ \mathrm{m/s}.$$

The DO flux is

$$\begin{aligned} M_2 &= k_2 \left(C_w - C_b\right) = 2.18 \times 10^{-5} \left(0 - 6\right) \times 10^3 \\ &= -0.13\ \mathrm{mg/m^2 s}. \end{aligned}$$

The relative difference between the DO flux and the corresponding mass-transfer coefficient is

$$\left(\frac{M_1 - M_2}{M_1}\right) = \left(\frac{-0.15 + 0.13}{-0.15}\right) \times 100 = 13\%.$$

APPENDIX: DEVELOPED FLOW CONCEPTS

The statement that the DO concentration similarity variable is invariant with x can be expressed as

$$\frac{\partial}{\partial x}\left(\frac{C - C_w}{C_B - C_w}\right) = 0. \qquad (22\text{-}25)$$

Differentiating and solving for $\frac{\partial C}{\partial x}$

$$\frac{\partial C}{\partial x} = \frac{dC_w}{dx} + \frac{C - C_w}{C_B - C_w}\frac{dC_B}{dx} - \frac{C - C_w}{C_B - C_w}\frac{dC_w}{dx}. \quad (22\text{-}26)$$

The constant DO flux and mass-transfer coefficient are characteristics of the developed regime.

$$M = k(C_B - C_w) = \text{const} \quad (22\text{-}27)$$

where M is the DO flux at the sediment water interface, and k is the mass-transfer coefficient. Therefore, if k is a constant, then $C_B - C_w$ = const. From this condition

$$\frac{dC_B}{dx} = \frac{dC_w}{dx}. \quad (22\text{-}28)$$

Thus, substituting Eq. (22-28) into Eq. (22-26),

$$\frac{\partial C}{\partial x} = \frac{\partial C_B}{\partial x} = \frac{\partial C_w}{\partial x}. \quad (22\text{-}29)$$

From Eq. (22-29), it follows that $\partial^2 C/\partial x^2 = 0$ in the developed regime.

REFERENCES

Alsterberg, G. (1922). "Die respiratorischen mechanismen der Tubificiden." *Kungl. Fysiografiska Sällskapets Handlingar,* 33(1), 1–175.

Ansa-Asare, O. D., Marr, I. L., and Cresser, M. S. (2000). "Evaluation of modelled and measured patterns of dissolved oxygen in a freshwater lake as an indicator of the presence of biodegradable organic pollution." *Water Research*, 34(4), 1079–1088.

Bachmann, V., and Usseglio-Polatera, P. (1999). "Contribution of the macrobenthic compartment to the oxygen budget of a large regulated river: The Mosel." *Hydrobiologia*, 410, 39–46.

Baity, H. G. (1938). "Some factors affecting the aerobic decomposition of sewage sludge deposits." *Sewage Works Journal*, 10(3), 539–568.

Bertuzzi, A., Faganeli, J., Welker, C., and Brambati, A. (1997). "Benthic fluxes of dissolved inorganic carbon, nutrients and oxygen in the Gulf of Trieste (Northern Adriatic)." *Water, Air and Soil Pollution*, 99, 305–314.

Birge, E. A. (1906). "The oxygen dissolved in the waters of Wisconsin lakes." *Transactions of the 35th Annual Meeting of the American Fisheries Society*, 142–163.

Birge, E. A., and Juday, C. (1911). "The inland lakes of Wisconsin: The dissolved gases of the water and their biological significance." *Wisconsin Geological and Natural History Survey Bulletin*, No. 22, Scientific Series No. 7, p. 259.

Borodkin, S. O., and Makkaveev, P. N. (1997). "The variability of the dissolved inorganic carbon and oxygen in the Gulf of Mexico's surface waters." *Oceanology*, 37(2), 201–205.

Bouldin, D. R. (1967). "Models for describing the diffusion of oxygen and other mobile constituents across the mud-water interface." *Journal of Ecology,* 56(1), 77–87.

Boyer, T., Conkright, M. E., and Levitus, S. (1999). "Seasonal variability of dissolved oxygen, percent oxygen saturation, and apparent oxygen utilization in the Atlantic and Pacific Oceans." *Deep-Sea Research I*, 46, 1593–1613.

Brekhovskikh, V. F., Vishnevskaya, G. N., Lomova, D. V., and Shakirova, E. R. (1998). "Contribution of the bottom sediment to the dissolved oxygen budget in the Mozhaiskoe reservoir." *Water Resources*, 25(1), 36–38.

Buentello, J. A., Gatlin, D. M., and Neill, W. H. (2000). "Effects of water temperature and dissolved oxygen on daily feed consumption, feed utilization and growth of channel catfish (*Ictalurus punctatus*)." *Aquaculture*, 182, 339–352.

Caraco, N. R., et al. (2000). "Dissolved oxygen declines in the Hudson River associated with the invasion of the zebra mussel (*Dreissena polymorpha*)." *Environmental Science and Technology*, 34, 1204–1210.

Chambers, P. A., Scrimgeour, G. J., and Pietroniro, A. (1997). "Winter oxygen conditions in ice-covered rivers: the impact of pulp mill and municipal effluents." *Canadian Journal of Aquatic Science*, 54, 2796–2806.

Chapman, L. J., Chapman, C. A., Crisman, T. L., and Nordlie, F. G. (1998). "Dissolved oxygen and thermal regimes of a Ugandan crater lake." *Hydrobiologia*, 385, 201–211.

Chapra, S. C., and Runkel, R. L. (1999). "Modeling impact of storage zones on stream dissolved oxygen." *Journal of Environmental Engineering, ASCE*, 125(5), 415–419.

Chaudhury, R. R., Sobrinho, J. A. H., Wright, R. M., and Sreenivas, M. (1998). "Dissolved oxygen modeling of the Blackstone River (northeastern United States)." *Water Research*, 32(8), 2400–2412.

Chen, G. H., Leong, I. M., Liu, J., and Huang, J. C. (1999). "Study of oxygen uptake by tidal river sediment." *Water Research*, 33(13), 2905–2912.

Colburn, A. P. (1933). "A method of correlating forced convection heat transfer data and a comparison with fluid friction." *Transactions of the American Institute of Chemical Engineers,* 29, 174–210.

Dade, W. B. (1993). "Near-bed turbulence and hydrodynamic control of diffusional mass transfer at the sea floor." *Limnology and Oceanography*, 38(1), 52–69.

Davis, W. S., and Lathrop-Davis, J. E. (1986). "Brief history of sediment oxygen demand investigation." *Sediment oxygen demand*, K. J. Hatcher, ed., Institute of Natural Resources, Athens, Ga.

Dawson, A. D., and Trass, O. (1972). "Mass transfer at rough surfaces." *International Journal of Heat and Mass Transfer*, 15, 1317–1336.

Edwards, R. W., and Rolley, H. L. J. (1965). "Oxygen consumption of river muds." *Journal of Ecology*, 53(1), 1–18.

Elliott, J. M. (2000). "Pools as refugia for brown trout during two summer droughts: Trout responses to thermal and oxygen stress." *Journal of Fish Biology*, 56, 938–948.

Ellis, C. R., and Stefan, H. G. (1990). "Oxygen demand in ice covered lakes as it pertains to winter aeration." *Water Research Bulletin*, 25(6), 1169–1176.

Engle, V. D., Summers, J. K., and MacAuley, J. M. (1999). "Dissolved oxygen conditions in northern Gulf of Mexico estuaries." *Environmental Monitoring and Assessment*, 57, 1–20.

Fair, G. M., Moore, E. W., and Thomas, H. A. (1941). "Stream pollution—The natural purification of river muds and pollutional sediments." *Sewage Works Journal*, 13(2), 270–307 and 13(4), 756–779.

Fang, X., and Stefan, H. G. (1997). "Simulated climate change effects on dissolved oxygen characteristics in ice-covered lakes." *Ecological Modelling*, 103, 209–229.

Fang, X, and Stefan, H. G. (2000). "Projected climate change effects on winterkill in shallow lakes in the Northern United States." *Environmental Management*, 25(3), 291–304.

Fang, X., Stefan, H. G., and Alam, S. R. (1999). "Simulation and validation of fish thermal DO habitat in north-central US lakes under different climate scenarios." *Ecological Modelling*, 118, 167–191.

Fischer, H. B., Imberger, J., List, E. J., Koh, R. Y. C., and Brooks, N. H. (1979). *Mixing in inland and coastal waters.* Academic Press, New York.

Forbs, S. A., and Richardson, R. E. (1913). "Studies on the biology of the Upper Illinois River." *Illinois Natural History Survey Bulletin*, 9, Art. 10, 95.

Guasch, H., Armengol, J., Mart, E., and Sabater, S. (1998). "Diurnal variation in dissolved oxygen and carbon dioxide in two low-order streams." *Water Research*, 32(4), 1067–1074.

Guss, S. (1998). "Oxygen uptake at the sediment-water interface simultaneously measured using a flux chamber method and microelectodes: Must a diffusive boundary layer exist?" *Estuarine, Coastal and Shelf Science*, 46, 143–156.

Hale, R. S. (1999). "Growth of white crappies in response to temperature and dissolved oxygen conditions in a Kentucky reservoir." *North American Journal of Fisheries Management*, 19, 591–598.

Hall, P. O. J., Anderson, L. G., van der Loeff, M. M. R., Sunby, B., and Westerlund, S. F. G. (1989). "Oxygen uptake kinetics in the benthic boundary layer." *Limnology and Oceanography*, 34(4), 734–746.

Harriott, P., and Hamilton, R. M. (1965). "Solid-liquid mass transport in a turbulent pipe flow." *Chemical Engineering Science,* 20, 1073–1078.

Harris, J. O., Maguire, G. B., Edwards, S. J., and Johns, D. R. (1999). "Low dissolved oxygen reduces growth rate and oxygen consumption rate of juvenile greenlip abalone, *Haliotis laevigata* Donovan." *Aquaculture*, 174, 265–278.

Hatcher, K. J. (1986). "Sediment oxygen demand processes." *Sediment oxygen demand*, K. J. Hatcher, ed., Institute of Natural Resources, Athens, Ga.

Hayes, F. R., and MacAulay, M. N. (1959). "Lake water and sediments. V: Oxygen consumed in water over sediment cores." *Limnology and Oceanography*, 4, 291–298.

Hering, R., Artingstall, S. G., and Williams, B. (1887). *Report by the Drainage and Water Supply Commission,* City of Chicago, Chicago.

Hondzo, M. (1998). "Dissolved oxygen transfer at the sediment-water interface in a turbulent flow." *Water Resources Research*, 34(12), 3525–3533.

Houck, C. P., Thornton, R. J., Brooks, J., and Saunders, J. F., III. (1997). "A model of alternative ways to meet dissolved oxygen standards." *Water Environmental Research*, 69(5), 948–954.

Incroprera, F. P., and DeWitt, D. P. (1990). *Fundamentals of heat and mass transport.* Wiley, New York.

Isaac, P. C. G. (1962). "The contribution of bottom muds to the depletion of oxygen in rivers, and suggested standards for suspended solids." *Biological Problems in Water Pollution*, U.S. Department of Health, Education and Welfare, Cincinnati, Ohio, 346–354.

Jansa, V., and Akerlindh, G. (1941). "A method for computing the oxygen curve in a polluted stream, with special reference to the oxygen consumption by sludge deposits." *Sewage Works Journal*, 13(3), 551–556.

Jonas, R. B. (1997). "Bacteria, dissolved organics and oxygen consumption in salinity stratified Chesapeake Bay, an anoxia paradigm." *American Zoologist*, 37, 612–620.

Jones, J. C., and Reynolds, J. D. (1999a). "Costs of egg ventilation for male common gobies breeding in conditions of low dissolved oxygen." *Animal Behavior*, 57, 181–188.

Jones, J. C., and Reynolds, J. D. (1999b). "The influence of oxygen stress on female choice for male nest structure in the common goby." *Animal Behavior*, 57, 189–196.

Jorgensen, B. B., and Revsbech, N. P. (1985). "Diffusive boundary layers and the oxygen uptake of sediments and detritus." *Limnology and Oceanography*, 30(1), 111–122.

Josiam, R. M., and Stefan, H. G. (1999). "Effect of flow velocity on sediment oxygen demand: Comparison of theory and experiments." *Journal of the American Water Resources Association*, 35(2), 433–439.

Kayombo, S., Mbwette, T. S. A., Mayo, A. W., Katima, J. H. Y., and Jorgensen, S. E. (2000). "Modelling diurnal variation of dissolved oxygen in water stabilization ponds." *Ecological Modelling*, 127, 21–31.

Kelly, J. R., and Doering, P. H. (1999). "Seasonal deepening of the pycnocline in a shallow shelf ecosystem and its influence on near-bottom dissolved oxygen." *Marine Ecology Program Series*, 178, 151–168.

Knowles, G., Edwards, R. W., and Briggs, R. (1962). "Polarographic measurement of the rate of respiration of natural sediments." *Limnology and Oceanography*, 7, 481–484.

Lardieri, N. J. (1954). "The aerobic and benthal oxygen demand of paper mill waste deposits." *TAPPI,* 37(12), 705–708.

Lee, J. H. W., Kuang, C. P., and Yung, K. S. (2000a). "Analysis of three-dimensional flow in a cylindrical sediment oxygen demand chamber." *Applied Mathematical Modelling*, 24, 263–278.

Lee, J. H. W., Kuang, C. P., and Yung, K. S. (2000b). "Fluid mechanics of triangular sediment oxygen demand chamber." *Journal of Environmental Engineering, ASCE*, 126(3), 208–217.

Lenard, G., Ross, W. R., and DuPlooy, A. (1962). "A study of methods for the classification of bottom deposits of natural water." *Hydrobiologia*, 20(3), 223–240.

Leu, H. G., Lee, C. D., Ouyang, C. F., and Pai, T. Y. (1998). "A modified water quality model for predicting BOD and DO variations in a shallow polluted channel." *Environmental Technology*, 19, 933–940.

Levich, V. G. (1962). *Physicochemical Hydrodynamics*. Prentice-Hall, Englewood Cliffs, N.J.

Lowell, R. B., and Culp, J. M. (1999). "Cumulative effects of multiple effluent and low dissolved oxygen stressors on mayflies at cold temperatures." *Canadian Journal of Fisheries and Aquatic Science,* 56, 1624–1630.

Lung, W. S., and Sobeck, R. G. (1999). "Renewed use of BOD/DO models in water quality management." *Journal of Water Research Planning and Management*, 125(4), 222–227.

Mackenthun, A. A., and Stefan, H. G. (1998). "Effect of flow velocity on sediment oxygen demand: Experiments." *Journal of Environmental Engineering, ASCE*, 124(3), 222–230.

Maran, S., Ciceri, G., and Martinotti, W. (1995). "Mathematical models for estimating fluxes at the sediment-water interface in benthic chamber experiments." *Hydrobiologia*, 297(1), 67–74 .

Martin, P., Granina, L., Martens, K., and Goddeeris, B. (1998). "Oxygen concentration profiles in sediments of two ancient lakes: Lake Baikal (Siberia, Russia) and Lake Malawi (East Africa)." *Hydrobiologia*, 367, 163–174.

Marzolf, E. R., Mulholland, P. J., and Steinman, A. D. (1998). "Reply: Improvements to the diurnal upstream-downstream dissolved oxygen change technique for determining whole-stream metabolism in small streams." *Canadian Journal of Fisheries and Aquatic Sci*ence, 55, 1786–1787.

Matthews, K. R., and Berg, N. H. (1997). "Rainbow trout responses to water temperature and dissolved oxygen stress in two southern California stream pools." *Journal of Fish Biology*, 50, 50–67.

McKinsey, D. M., and Chapman, L. J. (1998). "Dissolved oxygen and fish distribution in a Florida spring." *Environmental Biology of Fishes*, 53, 211–223.

Metcalf, L., and Eddy, H. P. (1916). *American sewerage practice. Vol. III: Disposal of sewage*. McGraw-Hill, New York.

Moodley, L., Heip, C. H. R., and Middelburg, J. J. (1998). "Benthic activity in sediments of the northwestern Adriatic Sea: Sediment oxygen consumption, macro- and meiofauna dynamics." *Journal of Sea Research*, 40, 263–280.

Moore, M. K., and Townsend, V. R., Jr. (1998). "The interaction of temperature, dissolved oxygen and predation pressure in an aquatic predator-prey system." *Oikos*, 81, 329–336.

Moyle, P. B., and Cech, J. J. (2000). *Fishes: An introduction to ichthyology*, 4th Ed., Prentice-Hall, Upper Saddle River, N.J.

Najjar, R. G., and Keeling, R. F. (1997). "Analysis of the mean annual cycle of the dissolved oxygen anomaly in the world ocean." *Journal of Marine Research*, 55, 117–151.

Nakamura, Y., and Stefan, H. G. (1994). "Effect of flow velocity on sediment oxygen demand: Theory." *Journal of Environmental Engineering, ASCE*, 120(5), 996–1016.

NCASI, Inc. (1978). "Interfacial velocity effects on the measurement of sediment oxygen demand." *Stream Improvement Technical Bulletin*, No. 317, National Council of the Paper Industry for Air and Stream Improvement, New York.

Neal, C., Harrow, M., and Williams, R. J. (1998). "Dissolved carbon dioxide and oxygen in the River Thames: Spring–summer 1997." *Science of the Total Environment*, 210/211, 205–217.

Nishri, A., Zohary, T., Gophen, M., and Wynne, D. (1998). "Lake Kinneret dissolved oxygen regime reflects long term changes in ecosystem functioning." *Biogeochemistry*, 42, 253–283.

O'Connel, R. L., and Thomas, N. A. (1965). "Effect of benthic algae on stream dissolved oxygen." *Journal of the Sanitary Engineering Division*, *Proceedings, ASCE*, 9(SA3), 1–16.

Odum, H. T. (1956). "Primary production in flowing water." *Limnology and Oceanography*, 1(2) 102–117.

Park, S. S., and Jaffe, P. R. (1999). "A numerical model to estimate sediment oxygen levels and demand." *Journal of Environmental Quality*, 28, 1219–1226.

Parkhill, K. L., and Gulliver, J. S. (1997). "Comparison of two sediment oxygen demand measurement techniques." *Journal of Environmental Engineering*, *ASCE*, 123(1), 97–98.

Prasad B.V. R., and Russell, M. J. (2000). "Diffusional mass transfer at sediment-water interface." *Journal of Environmental Engineering, ASCE*, 126(6), 576–577.

Probstein, R. F., Sonin, A. A., and Gur-Arie, E. (1972). "A turbulent flow theory of electrodialysis." *Desalination,* 11, 165–187.

Purdy, W. C. (1930). "A study of the pollution and natural purification of the Ohio River. II: The plankton and related organisms." *Public Health Bulletin*, No. 198, p. 212.

Rahm, L., and Svensson, U. (1989). "On the mass transfer properties of the benthic boundary layer with an application to oxygen fluxes." *Netherlands Journal of Sea Research*, 24, 27–35.

Richardson, R. E. (1928). "The bottom fauna of the Middle Illinois River, 1913–1925." *Bulletin of the Illinois Natural History Survey*, 17.

Rosas, C., Martinez, E., Gaxiola, G., Brito, R., Sanchez, A., and Soto, L. (1999). "The effect of dissolved oxygen and salinity on oxygen consumption, ammonia excertion and osmotic pressure of *Penaeus setiferus* (Linnaeus) juveniles." *Journal of Experimental Marine Biology and Ecology*, 234, 41–57.

Ruggerone, G. T. (2000). "Differential survival of juvenile sockeye and coho salmon exposed to low dissolved oxygen during winter." *Journal Fish Biology*, 56, 1013–1016.

Schallenberg, M., and Burns, C. W. (1999). "Does zooplankton grazing affect seston size-structure and areal hypolimnetic oxygen depletion in lakes?" *Archive of Hydrobiology*, 147(1), 1–24.

Schol, A., Kirchesch, V., Bergfeld, T., and Muller, D. (1999). "Model-based analysis of oxygen budget and biological processes in the regulated rivers Moselle and Saar: Modelling the influence of benthic filter feeders on phytoplankton." *Hydrobiologia*, 410, 167–176.

Seiki, D. A., Hirofumi, I., Etsuji, D., and Hiroshi, S. (1994). "Sediment oxygen demand in Hiroshima bay." *Water Research*, 28(2), 385–393.

Sellers, T. J., Parker, B. R., Schindler, D. W., and Tonn, W. M. (1998). "Pelagic distribution of lake trout (*Salvelinus namaycush*) in small Canadian Shield lakes with respect to temperature, dissolved oxygen, and light." *Canadian Journal of Aquatic Science* 55, 170–179.

Sparks, B., and Strayer, D. L. (1998). "Effects of low dissolved oxygen on juvenile *Elliptio complanata* (Bivalvia:Unionidae)." *Journal of the North American Benthological Society*, 17(1), 129–134.

Stearns, F. P., and Drown, T. M. (1890). "Special topics relating to the quality of public water supplies." *Examination by the State Board of Health of the inland waters of Massachusetts 1887–1890. Part I: Report on water supply and sewerage*. Wright and Potter Printing Co., Boston.

Steinberger, N., and Hondzo, M. (1999). "Diffusional mass transfer at sediment-water interface." *Journal of Environmental Engineering, ASCE*, 125(2), 192–200.

Streeter, H. W., and Phelps, E. B. (1925). "A study of the pollution and natural purification of the Ohio River. III: Factors concerned in the phenomena of oxidation and reaeration." *Public Health Bulletin,* 146, U.S. Public Health Service, Washington, D.C., 1–75.

Summers, J. K., et al. (1997). "Characterizing dissolved oxygen conditions in estuarine environments." *Environmental Monitoring and Assessment*, 45, 319–328.

Sun, M.-Y., and Wakeham, S. G. (1998). "A study of oxic/anoxic effects on degradation of sterols at the simulated sediment-water interface of coastal sediments." *Organic Geochemistry*, 28(12), 773–784.

Sweerts, J. P. R. A., Bar-Gilissen, M. J., Corneles, A. A., and Cappendberg, T. E. (1991). "Oxygen consuming processes at the profundal and littoral sediment-water interface of a small meso-eutrophic lake." *Limnology and Oceanography*, 36(6), 1124–1133.

Takegaki, T. and Nakazono, A. (1999). "Responses of the egg-tending gobiid fish *Valenciennea longipinnis* to the fluctuation of dissolved oxygen in the burrow." *Bulletin of Marine Science*, 65(3), 815–823.

Teal, J. M., and Kanwisher, J. (1961). "Gas exchange in a Georgia salt marsh." *Limnology and Oceanography*, 6, 388–393.

Tischenko, P. Y., Pavlova, G. Y., Salyuk, A. N., and Bychkov, A. S. (1998). "Carbonate system and dissolved oxygen in the Sea of Japan: An analysis of biological and thermal factors." *Oceanology*, 38(5), 614–619.

Welch, P. S. (1935). *Limnology*, 1st Ed., McGraw-Hill, New York.

Whittemore, R. C. (1986). "The significance of interfacial water velocity on the measurement of sediment oxygen demand." *Sediment oxygen demand*, K. J. Hatcher, ed., Institute of Natural Resources, Athens, Ga.

Wisely, W. H., and Klassen, C. W. (1938). "The pollution and natural purification of the Illinois River below Peoria." *Sewage Works Journal*, 10(3), 569–595.

Young, R. G., and Huryn, A. D. (1998). "Comment: Improvements to the diurnal upstream-downstream dissolved oxygen change technique for determining whole-stream metabolism in small streams." *Canadian Journal of Fisheries and Aquatic Science*, 55, 1784–1785.

Copyrighted Materials
Copyright © 2008 American Society of Civil Engineers (ASCE)
Retrieved from www.knovel.com

CHAPTER 23

Development and Application of Numerical Models of Sediment Transport Associated with Dam Removal

Yantao Cui and Andrew Wilcox

23.1 INTRODUCTION

Numerous dams have been removed in recent decades in the United States for reasons including economics, safety, and ecological restoration. For example, Edwards Dam, on the Kennebec River, Maine, was removed in 1999 to assist Atlantic salmon recovery efforts. In the Pacific Northwest, proposals to remove or breach dams on the Elwha River, Washington, and the Snake River, Idaho, to resuscitate declining stocks of anadromous salmonids have received national attention.

A key concern in many dam removal proposals is the routing of sediment stored behind reservoirs, including downstream channel response and release of contaminated sediments (e.g., Randle 2003). No studies have been completed to document and quantify channel response to the removal of large dams (Graf 1996), although field observations following the removal of small dams have intensified in recent years (e.g., Pizzuto 2002; Doyle et al. 2003). In addition, development of predictive models to estimate the effects of sediment release following dam removal has been limited until very recently. Decommissioning processes for dams, especially those with relatively large sediment deposits, have been hindered by shortcomings in our capacity to quantitatively predict sediment-transport dynamics following dam removal, and in the face of such uncertainties, costly dredging operations are often proposed before dam removal.

In this chapter we will discuss several issues in developing sediment-transport models following dam removal, including previous numerical modeling efforts relevant to dam removal, coupled modeling of reaches upstream and downstream of dams, reservoir sediment erosion, selection of sediment transport equations, and modeling of pre-dam-removal baseline conditions. We then present the development and application of numerical models for sediment transport following removal of Marmot Dam, a hydroelectric facility on the Sandy River, Oregon, that is scheduled for decommissioning. The Marmot Dam removal modeling example is used to demonstrate the development and application of numerical modeling of sediment transport following dam removal, thereby illustrating many of the general issues related to dam-removal modeling discussed in the following section.

23.2 DAM REMOVAL AND SEDIMENT-TRANSPORT MODELING

Many of the principles developed for modeling the transport of fluvial sediment are applicable to modeling sediment transport associated with dam removal. Effective numerical models of sediment transport following dam removal should have the capability to route both fine and coarse sediment downstream, account for abrasion of gravel, and simulate transient flows. In developing and applying sediment-transport models for dam removal, modelers must address several unique issues, including the difficulties of coupled modeling of reaches upstream and downstream of dam sites, uncertainties surrounding the channel morphology that will develop within the eroding reservoir sediments, selection of sediment-transport equations that account for the complex nature of reservoir sediment deposits, and the large spatial and temporal scales required for modeling the downstream transport of large volumes of reservoir sediment following dam removal. In the following section, we describe previous numerical modeling efforts relevant to dam removal and discuss special considerations in developing sediment-transport models for dam removal.

23.2.1 Previous Numerical Modeling Efforts Relevant to Dam Removal

Because reservoir sediment deposits behave as large sediment pulses once dams are removed, previous simulations of the evolution of sediment pulses in rivers have provided

a basis for modeling sediment transport associated with dam removal. In the sediment pulse model of Cui and Parker (2005), multiple lithology heterogeneous sediment pulses were routed downstream with full consideration of particle abrasion. The model has been applied successfully to simulate the evolution of a large landslide in the Navarro River, California (Hansler 1999; Sutherland et al. 2002). A simplified version of the Cui and Parker (2005) model has also been used to simulate evolution of gravel pulses in a laboratory flume (Cui et al. 2003).

The first adaptations of the Cui and Parker (2005) model to dam removal projects were applied to the potential removal of two dams in Oregon, Soda Springs Dam on the North Umpqua River and Marmot Dam on the Sandy River. This chapter presents the Marmot Dam removal modeling effort as a case study of the application of sediment-transport modeling to dam removal. Cui et al. (2006a; 2006b) further developed the Dam Removal Express Assessment Models (DREAM): DREAM-1 for simulation of dam removal with the reservoir sediment composed of primarily fine sediment, and DREAM-2 for simulation of dam removal with the top layer of the reservoir sediment composed of primarily coarse sediment (gravel and coarser).

Off-the-shelf sediment-transport models have also been applied to dam removal evaluations. For example, the U.S. Army Corps of Engineers' HEC-6 model was used to simulate sediment release associated with proposed dam removals on the Elwha River, Washington (Bureau of Reclamation 1996a; 1996b). Such models are usually not capable of simulating the upstream and downstream reaches of a dam simultaneously, however, because the models were not originally written for dam removal applications, and the code of the models may not be accessible to users for modification. Modelers may overcome these obstacles without access to and modification of the code in certain cases using two approaches: (1) modeling the upstream and downstream reaches of the dam separately, with the results of the upstream simulation providing input to the downstream reach; and (2) assuming that sediment-transport capacity is controlled at a critical cross section somewhere downstream of the dam, and assuming unlimited sediment supply to that location until all the reservoir sediment is exhausted. Simulating upstream and downstream reaches of the dam separately can be an effective solution in certain cases in which some physical separation between reaches upstream and downstream of the dam site is maintained during or after dam removal. Examples of such cases include dam removal methods in which sediment is metered out by an outlet structure with the dam still in place; early stages of a staged removal, where the remaining portion of the dam separates the two reaches; and a cohesive reservoir sediment deposit with limited potential for deposition immediately downstream of the dam. When the upstream and downstream reaches of the dam are connected and sediment is deposited downstream of the dam, as will normally be the case in dam removal modeling, such a technique will usually result in erroneous predictions, because the assumption that sediment transport upstream of the dam site is independent of that in the downstream reach becomes invalid. Using a critical cross section further downstream of the dam to meter out sediment may provide useful back-of-the-envelope estimates of suspended-sediment concentration in certain cases. Overall, however, this technique is problematic because sediment deposition following dam removal will inevitably alter the sediment-transport capacity, potentially by orders of magnitude.

Sediment-transport modeling following dam removal is as yet limited to one-dimensional models. One-dimensional models cannot simulate multidimensional effects such as lateral distribution of sediment deposition. This is true even if channel cross sections are used in simulations or if modeling rules are used to distribute sediment deposition and erosion across the cross section. One-dimensional models also cannot simulate local features such as topography generated by alternate bars and pool-riffle sequences and associated fine-scale effects on sediment deposition. As a result of the latter limitation, the best spatial resolution in the results of a one-dimensional model is on the order of several channel widths, i.e., the length of an alternate bar or pool-riffle sequence. Because of the coarse spatial resolution of one-dimensional models, professional judgment and general knowledge of sediment-transport dynamics should be applied to interpretation of one-dimensional model results in order to provide insight into finer-scale effects.

23.2.2 Coupled Modeling of Upstream and Downstream Reaches

A key challenge in any dam removal modeling exercise is the simultaneous modeling of sediment-transport processes upstream of the dam, in the reservoir-influenced reach from which sediment is eroded, and downstream of the dam, in the river reach to which the reservoir sediment is delivered. Simultaneous modeling of reaches upstream and downstream of the dam must address the difficulties in simulating flow over very steep bed slopes, such as would be expected, to characterize the downstream portion of the reservoir sediment wedge immediately following dam removal. In this important transition area between reaches upstream and downstream of the dam, very steep slopes can produce transient flow conditions (Fig. 23-1), potentially resulting in numerical instabilities.

Several techniques can be used in coupled modeling of upstream and downstream river reaches. For example, flow near the dam site can be simulated using a fully coupled model that retains the unsteady terms in the St. Venant shallow-water equations (Eq. (14-1)). Applying a fully coupled model to simulate the transient flow will involve the application of artificial viscosity terms in seeking a solution (e.g., Chaudhry 1993).

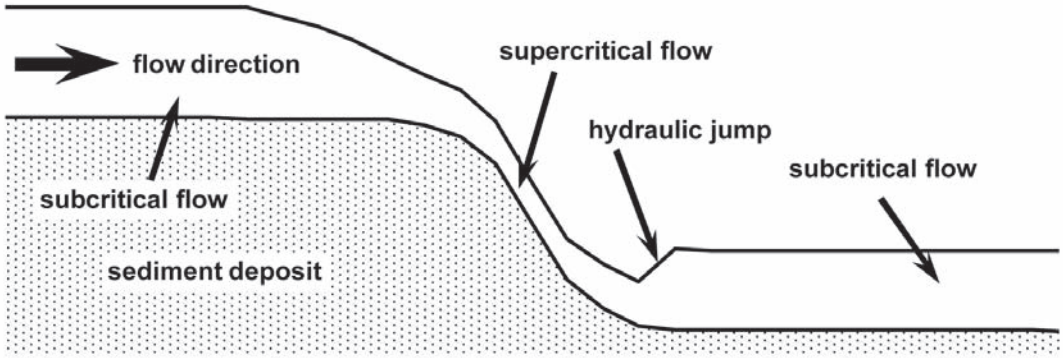

Fig. 23-1. Sketch demonstrating potential transient flow near a dam site following dam removal.

Even with the introduction of artificial viscosity terms, there will still be high-frequency oscillation in the solution for water depth and flow velocity, which, in turn, may result in instability in the solution for bed elevation. Thus, an artificial viscosity term will likely have to be introduced into the Exner equation as well. Cui et al. (2006b) found that applying a viscous term to the Exner equation may introduce artificial waves in bed elevation that can be on the same order of magnitude as the disturbance itself, resulting in an unacceptable solution. Model developers and users developing or applying fully coupled models for sediment-transport simulation following dam removal should therefore be cautious in the treatment of artificial viscosity terms and should be cognizant of the potential for artificial waves on the channel bed during model testing or application. Another method for modeling transient flow is a shock-fitting method, in which the program locates each hydraulic drop or jump and then solves different sections with different methods (e.g., Cui and Parker 1997). This method, however, is unlikely to be successful in application to dam removal simulation because of the complexity of natural rivers.

The U.S. Army Corps of Engineers HEC-6 model can simulate flow with transitions between subcritical and supercritical flow conditions. In the HEC-6 model, flow parameters are calculated with the standard energy conservation equation for subcritical flow conditions, and a quasi-normal assumption is applied for supercritical flow conditions (USACE 1993). The dam removal model presented in this chapter and those of Cui et al. (2006a; 2006b) applied similar principles as those used in HEC-6, whereby the standard backwater equation is applied for low Froude-number flow conditions and a quasi-normal flow assumption is applied for higher Froude-number flow conditions, as described further below in the Marmot Dam case study. In addition, Cui et al. (2006a; 2006b) applied a relatively coarse grid system so as to be compatible with the general resolution of one-dimensional sediment-transport modeling, although they applied an adaptive and much finer subgrid system for flow simulation whenever the channel bed is very steep. This method has been used successfully to simulate sediment-transport conditions in a laboratory experiment (Cui et al. 2006b).

23.2.3 Reservoir Sediment Erosion

In typical sediment-transport modeling applications, sediment and water discharge tend to be confined within a well-defined channel, whose characteristics can be quantified prior to model implementation. In dam removal modeling, the morphology of the channel that will develop within the reservoir following dam removal is unknown in advance, necessitating assumptions by modelers about how channel morphology will evolve within reservoir reaches. The dynamics of channel incision through a reservoir deposit following dam removal depends on how the dam will be removed, reservoir sediment characteristics (e.g., volume, grain-size distribution, and cohesion), the width of the reservoir sediment deposit relative to stable channel width, and water discharge during and after dam removal.

Dam removal methods will significantly affect subsequent patterns of reservoir erosion. Gradual lowering of the reservoir level (e.g., through notches or lower level outlets) prior to dam removal may produce a channel that is much wider than its stable channel form, as demonstrated in the Lake Mills drawdown experiment on the Elwha River, Washington (Childers et al. 2000). Complete dam removal within a short time span, however, may result in rapid incision into reservoir sediment and creation of a channel that is either similar to or slightly narrower than its stable channel form before the channel begins to migrate laterally when its gradient becomes relatively stable. In cases of cohesive sediment deposits or relatively small discharges, the erosion of reservoir sediment may be characterized by head-cutting or gully-like morphology (Fig. 23-2). In such cases, reservoir erosion is likely to be governed by the rate of head-cut retreat, as has been observed following removal of many small dams (e.g., Pizzuto 2002; Doyle et al. 2003). In contrast, head-cutting or gully-like morphology in reservoir sediment deposits is unlikely where these deposits are not cohesive

Fig. 23-2. Head cut developed following the removal of the Maple Gulch Dam, Evens Creek, Oregon, courtesy of Greg Stewart. The relatively small discharge before and at the time of the photograph after the dam was removed was probably responsible for the formation of the head cut. The strength from dense tree roots may also have contributed to the formation of the head cut.

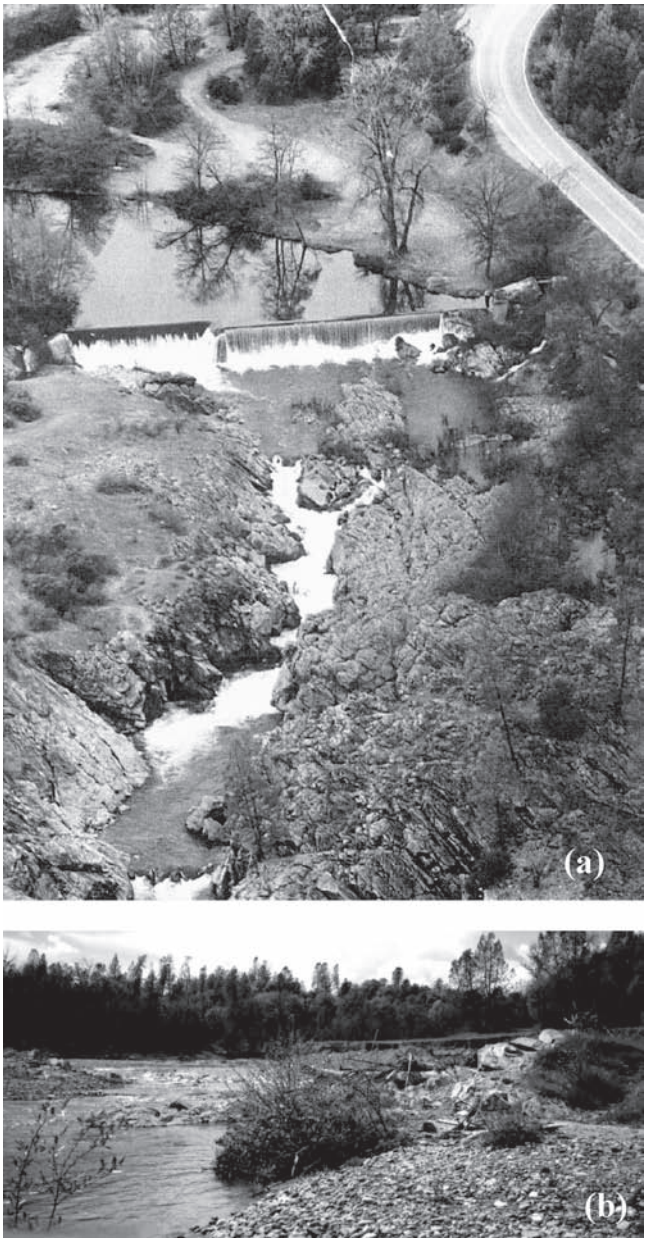

Fig. 23-3. (a) Saeltzer Dam on the Clear Creek, California, removed in 2000, courtesy of Geoff Fricker; and (b) former impoundment area of the Saeltzer Dam, photo taken in 2003, courtesy of Peter Miller. No head cut was observed in the reservoir deposit following the removal of the Saeltzer Dam (Matt Brown and Jess Newton, personal communication, 2003).

and where postremoval river discharges are adequate to transport reservoir sediment. For example, head cutting was not observed following removal of Saeltzer Dam on Clear Creek, California, where reservoir sediments were relatively coarse and river discharges were relatively large (Fig. 23-3). The implications of both reservoir-sediment and river-discharge characteristics for reservoir erosion dynamics must therefore be taken into account in modeling sediment transport following dam removal.

Modelers should also be conscious of the inadequacies of current sediment-transport theory for addressing certain reservoir erosion processes. For example, we know of no theory to address the head-cut process as a result of inadequate water discharge, and thus it may be difficult to build a numerical model to accurately simulate the downstream effect in such cases.

23.2.4 Selection of Appropriate Sediment-transport Equations

The complex nature of reservoir sediment deposits can complicate sediment-transport modeling. The size distribution of reservoir sediments is typically wide, ranging from boulders to clay, and reservoir deposits are often stratified, with a coarse top layer and fine bottom layer. Modelers must therefore select sediment-transport equations and

make other assumptions that are appropriate to the particular reservoir sediment characteristics of the case in question. Until recently, no sediment-transport equations were available to handle mixtures of coarse sediment (gravel and coarser) and fine sediment (sand and finer), such as are typical of reservoir sediment deposits; this complicates efforts to model transport of such sediments. The sediment-transport equation of Wilcock and Crowe (2003) provides the first attempt to calculate transport of coarse and fine sediment simultaneously while accounting for the grain-size distribution of the coarse sediment. The equation calculates gravel-transport rate by size fractions and sand transport rate based on known shear stress and surface grain-size distribution, including the fraction of sand on the bed surface. Development of a relation that links the grain-size distribution, including the fraction of fine sediment, in the subsurface to that on the channel surface and to the sediment load would facilitate incorporation of the Wilcock and Crowe (2003) equation into a sediment-transport model.

In lieu of using a sediment-transport equation that simultaneously calculates coarse- and fine-sediment transport, one approach to modeling a wide size range of sediments is to employ separate models of fine- and coarse-sediment transport that calculate coarse- and fine-sediment transport independently. This approach, which was adopted for the Marmot Dam removal study presented below, is based on the assumptions that (1) coarse sediment is transported primarily as bed load during high-flow events, when fine sediment is transported primarily as suspended load, and (2) most fine sediment is transported during the intermediate-flow events, when coarse sediment transport is limited. Observations that suggest that coarse- and fine-sediment transport may be only weakly correlated, and that modeling using independent equations for coarse- and fine-sediment transport is therefore defensible, are suggested by Cui et al. (2006b). These include the observations that (1) the fraction of fine sediment in gravel-bed sediment samples is relatively stable and insensitive to the amount of fine-sediment transport, and (2) the fraction of fine sediment in a clast-supported sediment deposit seems to be inversely correlated with the standard deviation of the particle grain-size distribution of the coarse sediment (Fig. 23-4), indicating that the fraction of fine sediment is dependent on the available space of the coarse-sediment deposit (Cui et al. 2006b). Although applying separate equations for coarse and fine sediment is not a perfect solution because gravel and sand transport likely affect each other, this approach may provide an acceptable approximation.

If the approach of using separate models of coarse- and fine-sediment transport is adopted, modelers must select from the array of published transport equations for sand and gravel. For example, in the modeling of the Marmot Dam removal, we used Parker's surface-based bed-load equation (Parker 1990) to model coarse-sediment transport and Brownlie's (1982) bed-material equation for modeling transport of fine sediment, as discussed further in Section 23.3.2.

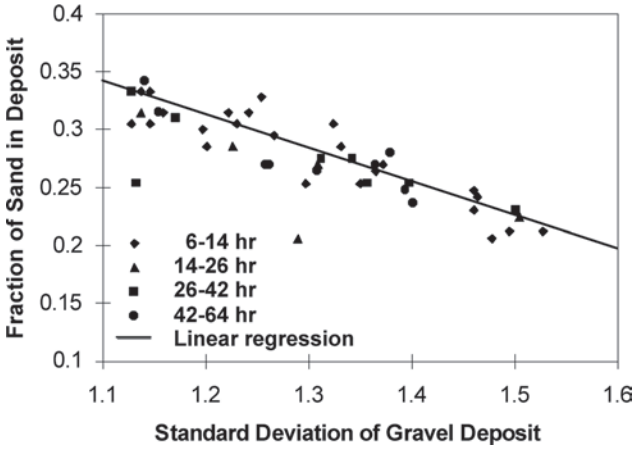

Fig. 23-4. Fraction of sand in gravel/sand deposit as a function of standard deviation of the gravel grain-size distribution in the sediment deposit. Data were derived from a large-scale flume experiment (SAFL downstream fining Run 3) by Toro-Escobar et al. (1996), and the diagram was presented in Cui and Parker (1998).

23.2.5 Reproducing the Pre-dam-removal Longitudinal Profile and Other Background Conditions

Because large volumes of sediment may be released downstream following dam removal, downstream sediment impacts may be spatially and temporally extensive. To predict the nature of these impacts, numerical models therefore must be capable of simulating long river reaches for multiple years, and modelers should be conscious of the potential for propagation of errors for such simulations. For example, the simulation of the Marmot Dam removal presented below was applied to a 50-km river reach for a 10-yr duration following dam removal.

Accurate simulation of a river reach over a long period of time requires that the model be capable of reproducing background conditions in the system of interest. Although reproduction of background conditions is a key task in sediment-transport modeling, this can be difficult to achieve because of a lack of sediment-transport theory, a lack of understanding of the system in question, and/or a lack of field data. In most cases the background condition can be treated as a quasi-equilibrium state, under which the channel bed experiences very limited amounts of aggradation and degradation over time. The process of trying to reproduce this quasi-equilibrium state, which we term the "zero process," provides a frame of reference from which subsequent changes predicted by modeling can be attributed to changes in input or boundary conditions, such as the removal of a dam. The zero process itself also provides model developers and users with an opportunity to test and adjust certain assumptions and input parameters used in modeling.

23.3 NUMERICAL SIMULATION OF SEDIMENT TRANSPORT FOLLOWING THE REMOVAL OF MARMOT DAM, SANDY RIVER, OREGON

The remainder of this chapter will present an application of one-dimensional numerical modeling simulation of sediment transport following dam removal. Our treatment of the issues detailed above, including selection of sediment-transport equations, modeling of reservoir erosion, and reproduction of background conditions (the zero process), will be described, and modeling results from the example application will be presented. The following sections provide background information on Marmot Dam and on the physical setting of the Sandy River basin, descriptions of the numerical models and their governing equations, discussion of the input data used in application of the models to the Sandy River, and results and discussion of the modeling.

Fig. 23-5. Marmot Dam, Sandy River, Oregon, scheduled for removal in 2007 (photo courtesy of Portland General Electric).

23.3.1 Project Background

Marmot Dam is located on the Sandy River approximately 48 km upstream of its confluence with the Columbia River. The dam was originally completed in 1913 as a wood crib rock-filled structure, and it was replaced in 1989 with a 14-m-high, 104-m-wide concrete dam (Fig. 23-5). Approximately 750,000 m^3 of sediment is stored behind Marmot Dam, about two-thirds of which is primarily gravel/pebble and one-third of which is primarily sand (Squier Associates 2000). The Sandy River originates from Mt. Hood on the western slopes of the Cascade Range and has a drainage area of 1,316 km^2, about half of which is upstream of Marmot Dam (Fig. 23-6). A detailed description of the geology, hydrology, and geomorphology of the Sandy River basin is provided in Stillwater Sciences (2000).

Marmot Dam is scheduled to be voluntarily removed by Portland General Electric (PGE), the holder of the Federal Energy Regulatory Commission (FERC) license for this project. Removal of Marmot Dam will provide unrestricted upstream and downstream passage for anadromous salmonids and other aquatic organisms, restore natural flows in the

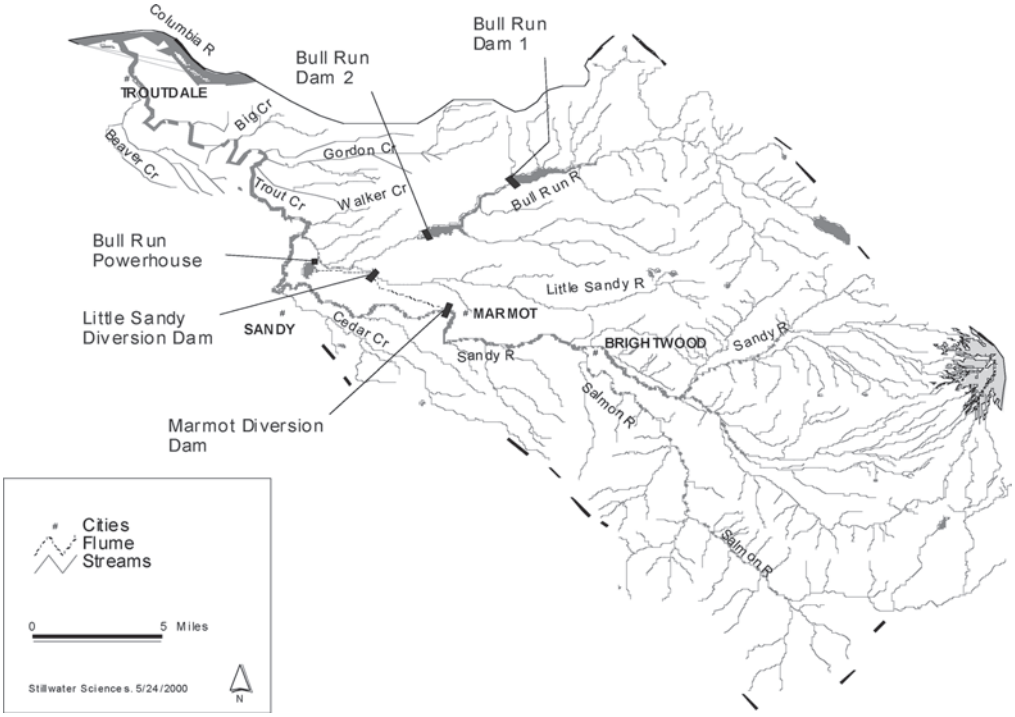

Fig. 23-6. Map of the Sandy River basin.

Sandy River from Marmot Dam to the Bull Run River confluence, and, under some removal alternatives, release sediment stored behind Marmot Dam. Several alternative methods for removal of Marmot Dam have been developed, which differ in the amount of sediment accumulated behind the dam that would be released downstream. These removal alternatives are described in detail in Portland General Electric (2000) and are summarized as follows:

- Single-season dam removal with minimal sediment removal;
- Removal of top of dam in year 1, followed by complete dam removal in year 2 with sand-layer excavation;
- Single-season dam removal after dredging of sediment to 830 m upstream of the dam;
- Single-season dam removal after dredging of 95,600 m^3 of sediment;
- Single-season dam removal after dredging of 229,400 m^3 of sediment.

The portion of the Sandy River likely to be affected by removal of Marmot Dam extends from the reservoir-influenced reach upstream of Marmot Dam downstream to the Sandy River's confluence with the Columbia River. For purposes of studying the potential geomorphic effects of removing Marmot Dam, the pertinent river reach was delineated into six subreaches (Fig. 23-7) according to their distinctive geomorphic characteristics, as described below and in Table 23-1:

- *Reach 0 (reservoir area):* The Sandy River upstream of the Marmot Dam is affected by the backwater effect of the dam for a distance of approximately 2 to 4 km. The impoundment formed by the dam has filled to the dam's crest with sediment and now functions as an alluvial river reach. Compared to upstream and downstream reaches, this reach currently has a lower gradient and finer bed substrates as a result of the grade control provided by the dam and the backwater effect of the dam's impoundment. The reservoir is believed to have filled with sediment in the early years following dam closure. Marmot Dam may continue to partially trap coarse sediment, although coarse- and fine-sediment transport over the dam do occur during high-flow events.
- *Reach 1:* Reach 1 extends from Marmot Dam to the mouth of the Sandy River gorge and has moderately pronounced forced pool-riffle morphology. This reach has an armored cobble/boulder bed surface with limited gravel, possibly due to supply reductions caused by Marmot Dam.
- *Reach 2:* Reach 2 is the Sandy River gorge, a steep (0.01 gradient) section of the river that is confined by 20- to 30-m-high bedrock strath terraces with steep hillslopes above. The steep gradient and high confinement in this reach create very high shear stresses, resulting in high sediment-transport capacity. Few deposition areas are therefore present in this reach, and bedrock exposure in the channel bed is common. The reach is characterized by long, deep bedrock pools that are separated by coarse-bedded riffles and boulder rapids, and large (house-sized) boulders are common in the channel.
- *Reach 3:* Reach 3 extends from the downstream end of the Sandy River gorge to the Bull Run River confluence. This reach is considerably wider and lower-gradient than Reaches 1 and 2, reducing sediment-transport capacity and increasing the potential for sediment deposition.

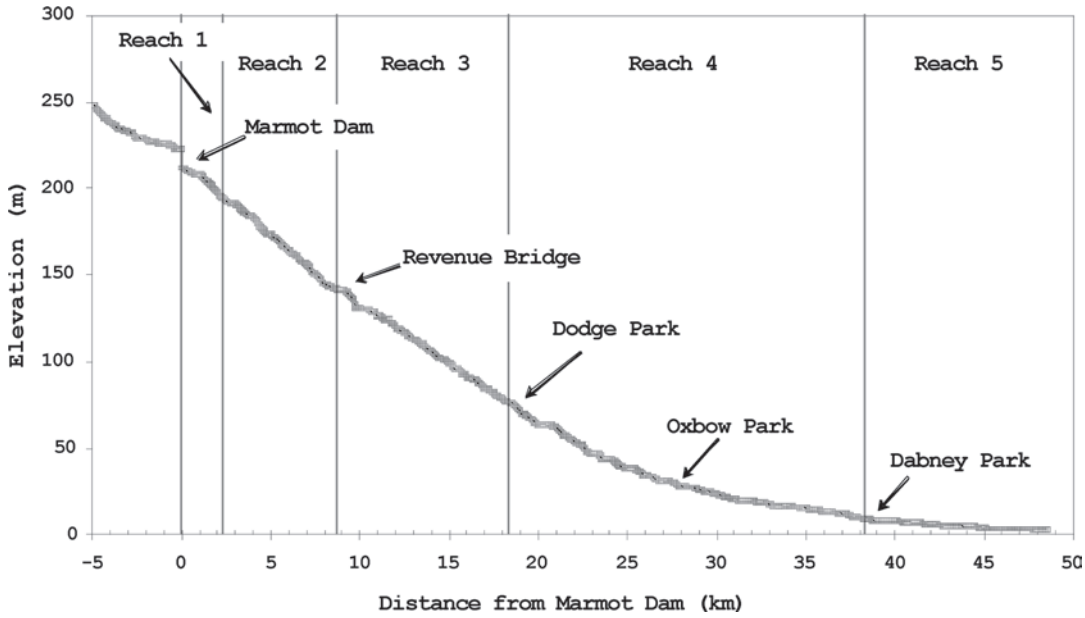

Fig. 23-7. Sandy River longitudinal profile, based on PGE 1999 photogrammetric data.

- *Reach 4:* Reach 4 extends from the Bull Run River confluence to Dabney State Park. In Reach 4, channel confinement, gradient, and bed particle size decrease further compared to upstream reaches, with these tendencies particularly evident in the lower half of the reach. Large cobble/gravel bars, side channels, and islands are common in Reach 4, which is bounded by high (mostly alluvial) terraces. Sand content in the bed subsurface, on the active bed, and on bars is high in the lower portion of the reach.
- *Reach 5:* Reach 5 extends from Dabney State Park to the confluence with the Columbia River. This reach is characterized by a highly mobile sand and gravel bed surface with large gravel/sand alternate and medial bars. In the Sandy River delta, which forms the downstream-most portion of Reach 5, the channel is sand-bedded and depositional dynamics are strongly influenced by the backwater effect of the Columbia River.

23.3.2 Numerical Model Development for Application to Marmot Dam Removal

One-dimensional numerical models of fine- and coarse-sediment transport were developed to predict the routing of sediment from behind Marmot Dam downstream through the Sandy River. Numerical models were completed to examine a variety of alternatives for removing Marmot Dam. Model results provide estimates of the time required for sediment to be cleared from the reservoir area, time required for sediment to travel out of the Sandy River (including various subreaches), thickness of downstream sediment deposits in various reaches (on a reach-averaged and cross-section-averaged basis), changes in deposition thickness through time, and total suspended-sediment concentrations through time along the river's longitudinal profile following dam removal. Questions explored with the numerical models for different dam removal alternatives include the following:

- Will substantial bed aggradation occur following dam removal, or is the sediment-transport capacity downstream of the Marmot Dam high enough to minimize aggradation? How long will any aggradational effect persist and in what reaches will it be most prominent?
- How much will suspended-sediment concentrations downstream of Marmot Dam increase following dam removal, and how long will any such increases persist?
- How does transport distance from the dam affect suspended-sediment concentration and coarse- and fine-sediment accumulations following dam removal? Is there a distance downstream of which no detectable changes are expected?
- How will dredging of varying amounts of sediment from Marmot Reservoir prior to dam removal affect downstream sediment deposition and suspended-sediment dynamics?
- How will discharge conditions during and following dam removal affect downstream sediment transport and deposition characteristics?

Because unified theory and transport equations for gravel/sand mixtures are still in a developing stage, as discussed above, two separate models were developed for application to the removal of Marmot Dam: a gravel model for simulation of

Table 23-1 Summary of Geomorphic Characteristics of Sandy River Reaches That Will Be Affected by Removal of Marmot Dam

Reach	Length (km)	Average width (m)	Average gradient	Confinement	Morphology	Dominant grain size
Upstream of Marmot dam (Reach 0)	2–4	50	0.0024	High	Pool-riffle	Gravel-sand
Marmot Dam to gorge (Reach 1)	2.4	45	0.008	Medium	Forced pool riffle/plane bed	Cobble-boulder
Sandy River gorge (Reach 2)	6.4	30	0.01	High	Step pool/ forced pool riffle	Bedrock-boulder
Downstream end of Sandy River gorge to Bull Run River (Reach 3)	9.6	50	0.006	Medium	Forced pool riffle/plane bed	Cobble-gravel
Bull Run River to Dabney Park (Reach 4)	20	70	0.0025	Medium/low	Pool riffle/ plane bed	Gravel-cobble-sand
Dabney Park to mouth (Reach 5)	9.6	100	0.0007	Medium/low	Pool riffle	Sand-gravel

the erosion of the reservoir deposit and downstream deposition of coarse sediment (diameter > 2 mm), and a sand model for simulation of suspended-sediment concentration and downstream deposition of fine sediment (diameter < 2 mm). The use of separate models assumes that (1) as the sediment is released from the reservoir deposit, gravel particles will be transported as bed load and sand will be transported mostly as suspended load because of the steep slope of the Sandy River, and (2) gravel and sand transport occur over different time scales (years versus days; i.e., a gravel particle may take years to travel the same distance that a sand particle travels in several days). In reality, use of separate models may create errors because transport of gravel and sand will each influence the transport rate of the other.

The gravel-transport model was developed based on Parker's surface-based bed load equation (Parker 1990) and is similar to the model of Cui and Parker (2005), with adjustments to accommodate the specific conditions of the Sandy River and Marmot Dam. The Parker equation calculates gravel-transport rate and bed-load grain-size distribution based on the grain-size distribution of the surface layer and the boundary shear stress. The Parker equation was developed to apply to gravel-bed streams (particles larger than 2 mm in diameter) and was not intended for application to sand or for suspended material of any size. Application of the Parker equation to a mixture with a relatively large amount of sand, such as the sediment accumulation behind Marmot Dam, may therefore create some error in predictions of the gravel-transport rate.

The one-dimensional model of sand transport was developed based on Brownlie's (1982) bed-material equation. Brownlie's equation was developed for sand-bedded rivers but is used here because no sediment-transport equations exist to calculate sand transport in a bedrock- or coarse-sediment-dominated river such as the Sandy River. In applying Brownlie's equation of sediment transport and friction, we modified the roughness height to account for the bedrock, boulders, and gravel present along the bed of the Sandy River. Calibration and validation of this approach are required, however, and the error associated with applying Brownlie's equation to a gravel-bed river, even with roughness adjustments, is not known. Our model of sand transport assumes the following: (1) sand transport can be represented as transport over a rough bedrock surface (i.e., the existing gravel bed of the Sandy River remains immobile with respect to sand transport); (2) silt is transported as throughput load that is carried in suspension and cannot be deposited in the channel bed; (3) reservoir sediment is not cohesive; and (4) sand transport is not affected by the amount of coarse-sediment aggradation and degradation downstream of the dam (i.e., the changes in channel gradient resulting from gravel deposition or scour are not accounted for in modeling sand transport). This last assumption may create some errors in reaches where significant coarse-sediment deposition occurs, such as immediately downstream of the dam.

As discussed in Section 23.2.3, simulation of reservoir erosion is a key challenge in dam removal modeling. In the Sandy River model, a number of simplifying assumptions were made to simulate sediment release from Marmot Reservoir. The model assumes laterally uniform sediment transport out of the reservoir, with sediment mobilization and transport derived by the gravel model from Parker's (1990) sediment-transport equation. In the reservoir area, the model assumes that erosion is exclusively dependent on the transport capacity of gravel and the amount of gravel that can be provided through erosion of reservoir sediment deposit. As the gravels within a layer are mobilized, the sand volume within that layer is also mobilized and transported downstream; it is assumed that sand is not available for transport until the gravel within the same layer as the sand is mobilized. Volumetric estimates of sand release from the reservoir deposit that are generated by the gravel model using this method are subsequently used as the upstream boundary condition for the sand model. The model further assumes that, because the reservoir-influenced reach upstream of Marmot Dam (Reach 0) is relatively narrow, all the sediment will be eroded downstream following dam removal (i.e., there will be no long-term storage of reservoir sediment in Reach 0 following dam removal). Sensitivity tests were performed to address uncertainties in modeling of sediment transport from the reservoir and to qualitatively assess the potential effects of incision, as described in Section 23.3.4 below.

The numerical models of fine- and coarse-sediment transport entail equations for calculating downstream changes in flow depth, Exner equations of sediment continuity for sand and gravel, transport-capacity equations, and flow-friction relations. The governing equations used in these models are introduced below; additional details are presented in Stillwater Sciences (2000; 2002).

To calculate downstream changes in flow depth, the standard backwater equation is used for low-Froude-number flows and a quasi-normal assumption is applied for high-Froude-number flows:

$$\frac{dh}{dx} = \frac{S_0 - S_f}{1 - \mathsf{F}^2}, \quad \mathsf{F} < F_c \tag{23-1a}$$

$$S_0 = S_f, \quad \mathsf{F} \geq F_c \tag{23-1b}$$

where

h = water depth;
x = downstream distance;
S_0 = slope of the channel bed;
S_f = friction slope;
F = local Froude number; and
F_c = a user-defined Froude number that is smaller than and close to unity and that is used to differentiate between low- and high-Froude-number conditions in the application of Eqs. (23-1a) and (23-1b) (see also Cui and Parker 2005).

In the Marmot Dam removal simulation, F_c was set equal to 0.75; below this value, Eq. (23-1a) is used; otherwise Eq. (23-1b) is applicable. The approach of alternating the backwater equation and the quasi-normal flow assumption based on a Froude number threshold has been used in the HEC models (USACE 1993) and in the models of Cui et al. (2003) and Cui and Parker (2005).

Local Froude number is calculated using the equation

$$\mathsf{F}^2 = \frac{Q_w^{\,2}}{gB^2h^3} \tag{23-2}$$

in which

Q_w = water discharge;
g = acceleration of gravity; and
B = local channel width.

The Exner equations of sediment continuity for gravel used here are variants of those in Parker (1991a; 1991b) and (Chapter 3, Eqs. (3-95a) to (3-95i)) and take the following form:

$$(1-\lambda_p) f_G B \frac{\partial \eta}{\partial t} + \frac{\partial Q_G}{\partial x} + \beta Q_G \left(2 + \frac{1}{3\ln(2)} \frac{p_1 + F_1^{'}}{\Delta\psi_1} \right) = 0 \tag{23-3a}$$

$$(1-\lambda_p) f_G B \left(\frac{\partial (L_a F_j)}{\partial t} + f_{Ij} \frac{\partial (\eta - L_a)}{\partial t} \right) + \frac{\partial \left(Q_G p_j \right)}{\partial x} + \beta Q_G \left(p_j + F_j^{'} \right) + \frac{1}{3\ln(2)} \beta Q_G \left(\frac{p_j + F_j^{'}}{\Delta\psi_j} - \frac{p_{j+1} + F_{j+1}^{'}}{\Delta\psi_{j+1}} \right) = 0 \tag{23-3b}$$

where

λ_p = porosity of the channel-bed deposit;
f_G = volumetric fraction of gravel in the channel-bed deposit;
η = deposition thickness above an arbitrary datum;
t = time;
Q_G = volumetric transport rate of gravel;
β = volumetric abrasion coefficient of gravel;
p_j = volumetric fraction of the j-th size range in bed load;
F_j = volumetric fraction of the j-th size range in the surface layer;
$F_j^{'}$ = an adjusted value of F_j providing an estimate of relative surface area exposure of gravel of the jth size range at the surface (Parker 1991a; 1991b);
f_{Ij} = volumetric fraction of the jth size range in the interface between bed load and the channel-bed deposit;
L_a = surface layer thickness; and
ψ = grain size in the ψ-scale, which is the negative of the ϕ scale (also see Chapter 3, Eqs. (3-1a) and (3-1b)).

Equation (23-3a) represents the mass conservation of total gravel, and Eq. (23-3b) represents the mass conservation of the gravel in the j-th size range.

The full grain-size distribution of coarse sediment (gravel and coarser) is discretized into a number of groups, represented by ψ and grain size D in such a way that grain size $\psi_j(D_j)$ and $\psi_{j+1}(D_{j+1})$, from finer to coarser, bound the j-th size group. The average grain size of the j-th range is then

$$\overline{\psi}_j = \frac{\psi_j + \psi_{j+1}}{2}, \quad \overline{D}_j = \sqrt{D_j D_{j+1}} \tag{23-4a,b}$$

and

$$\Delta\psi_j = \psi_{j+1} - \psi_j \tag{23-5}$$

The parameter $F_j^{'}$ in Eqs. (23-3a) and (23-3b) is estimated with the relation provided by Parker (1991a; 1991b):

$$F_j^{'} = \frac{F_j / \sqrt{\overline{D}_j}}{\Sigma \left(F_j / \sqrt{\overline{D}_j} \right)} \tag{23-6}$$

The Exner equations of sediment continuity for sand that were used in modeling of sand transport take the forms

$$\frac{1}{B} \frac{\partial \eta_s}{\partial t} + \frac{1}{(1-\lambda_s)\lambda_g} \frac{\partial Q_s}{\partial x} = 0, \ 0 < \eta_s \le k_{s0} \tag{23-7a}$$

$$\frac{1}{B} \frac{\partial \eta_s}{\partial t} + \frac{1}{1-\lambda_s} \frac{\partial Q_s}{\partial x} = 0, \ \eta_s > k_{s0} \tag{23-7b}$$

in which

η_s = thickness of the sand deposit;
λ_s = porosity of the sand deposit;
λ_g = porosity of the roughness elements;
Q_s = volumetric transport rate of sand; and
k_{s0} = height of roughness elements.

Equation (23-7a) applies to cases where the thickness of the sand deposit is less than the height of the roughness elements (in which case sand aggradation fills in the interstices of the roughness elements). Equation (23-7b) is applied when the thickness of the sand deposit is greater than the height of the roughness elements.

As discussed above, two sediment-transport equations were used for calculation of sediment-transport capacity: the surface-based bed-load equation of Parker (1990) for coarse sediment and the bed-material equation of Brownlie (1982) for sand. The surface-based bed-load relation of Parker (1990) is also described in Section 3.7.5 (Chapter 3), and minor adaptations of the bed-material equation of Brownlie (1982) can be found in Stillwater Sciences (2000) and Cui et al. (2006a; 2006b). It is important to note that both

equations are used to calculate sediment-transport capacities rather than sediment-transport rates. Actual sediment-transport rates at any location were evaluated based on upstream sediment supply, local sediment-transport capacity, erodibility of the channel bed, and sediment mass conservation. The application of the sediment-transport equations of Parker (1990), for gravel transport, and Brownlie (1982), for sand transport, requires the use of different friction relations. A Keulegan-type resistance relation (modified from Keulegan 1938) is used for gravel and Brownlie's (1982) friction formulation is used for sand, as detailed in Stillwater Sciences (2000) and Cui et al. (2006a; 2006b).

In addition to evaluating coarse and fine sediment-transport rates, this modeling effort includes estimates of total suspended-sediment (TSS) concentration following dam removal, to assist evaluation of biological impacts. The suspended-sediment concentration is calculated by combining the portion of sand that is transported in suspension with the entire silt and clay load (sediment finer than 62.5 μm) in transport. All of the silt and clay from the reservoir deposit is treated as throughput load that is carried in suspension once it has been mobilized from the reservoir. The criterion set for suspension of sand is given as follows (e.g., van Rijn 1984):

$$\frac{v_s}{\kappa u_*} < 1 \tag{23-8}$$

in which

v_s = particle settling velocity calculated with the procedure given by Dietrich (1982);
u_* = shear velocity; and
κ = von Karman constant, with a value of approximately 0.4.

TSS therefore is composed of all the particles finer than 62.5 μm from the reservoir deposit and those satisfying Eq. (23-8).

23.3.3 Input Data and Zero Process

The sediment-transport models developed for the simulation of the removal of Marmot Dam use input data on channel gradients, channel widths, water discharge at each section of the river for the duration of the simulation, grain-size distribution of the sediment deposit in the reservoir and in the downstream channel, and the sediment supply and associated grain-size distribution upstream of the Marmot reservoir. The modeling of total suspended sediment following dam removal also requires an order-of-magnitude estimate of the background average sediment concentration in the Sandy River. These input parameters and their sources are described in the following sections.

23.3.3.1 Channel Gradient and Width Data on channel gradients, and an associated longitudinal profile of the Sandy River from 4.8 km upstream of Marmot Dam downstream to the Columbia River, were derived from 1999 photogrammetric measurements of the Sandy River. The photogrammetric data measure water-surface elevation with an accuracy of ±0.6 m and were averaged over a 0.8-km distance to further smooth the longitudinal profile (Figs. 23-7 and 23-8).

Channel widths were measured from 1:6,000-scale aerial photographs of the Sandy River corridor. Field checking of randomly selected cross sections with a laser distance finder found that channel widths measured from aerial photographs were generally within 10% accuracy. One exception is in Reach 2 (the Sandy River gorge), where widths cannot be measured from aerial photographs due to the narrow channel and valley in this reach. A channel width of 30 m was applied to all of Reach 2 in the model, based on the average of field-measured widths in the Sandy River gorge. In all other reaches of the Sandy River, channel width was varied in the model according to the aerial photographic measurements.

23.3.3.2 Discharge Data and Hydrologic Scenarios Used in Numerical Modeling A daily discharge series spanning the length of model runs was also required as input. Daily discharge data used as input for the modeling are from the USGS Sandy River near the Marmot gauge (Station 1413700), which was assumed to represent the reach from Marmot Dam downstream to the Bull Run River confluence, and the Sandy River below the Bull Run River gauge (Station 14142500), which was assumed to represent discharge from the Bull Run River to the mouth (Fig. 23-6). The Bull Run River is the largest tributary that enters the Sandy River downstream of the Marmot Dam. Other tributaries have small drainage areas, and therefore are likely to create only small increases in water discharge in the Sandy River.

Numerical modeling was performed for three different hydrologic scenarios to evaluate the effects of various flow regimes following dam removal on sediment transport and deposition dynamics. The flows occurring following dam removal, particularly in the first year after removal, will have an important influence on the time required for downstream transport of reservoir sediment, on subsequent deposition patterns, and on the duration of impacts on aquatic organisms. Scenarios for wet, average, and dry hydrologic conditions were developed for input into the numerical modeling, with the flows in the first year after removal varying in each scenario (i.e., hydrologic scenarios were defined according to the discharge conditions in the first year of the model run). The hydrologic scenarios account for both peak flow magnitude and overall water yield, both of which influence sediment-transport dynamics. The peak and annual daily average discharges from the Marmot gauge were fit to a log Pearson III distribution and a normal distribution, respectively, to predict the return period of future discharges. Based on this analysis, daily discharge records were selected as input for Year 1 of model runs from three representative

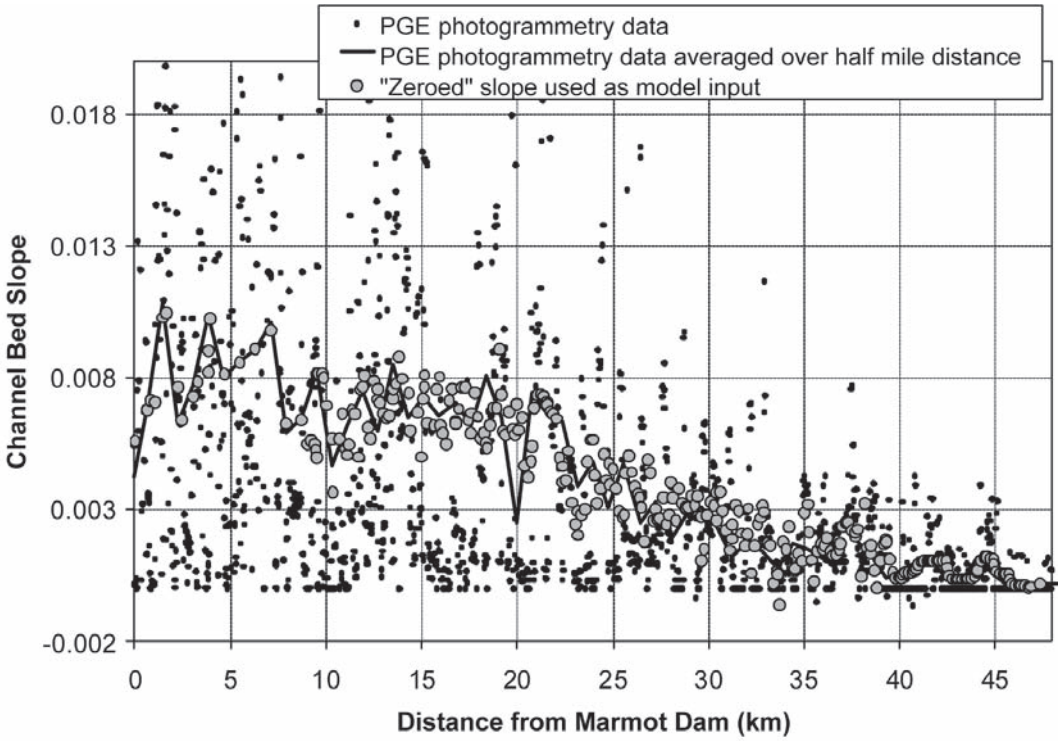

Fig. 23-8. Sandy River channel slope downstream of Marmot Dam.

water years, with exceedance probabilities for both annual peak discharge and average daily discharge corresponding to wet, average, and dry hydrologic conditions. In the scenarios for dry, average, and wet conditions, flows used as input for Year 1 had both peak flows and average annual discharges with exceedance probabilities of approximately 90% (1.1-yr return period), 50% (2-yr return period), and 10% (10-yr return period), respectively (Table 23-2). The years following the first year were selected randomly from all of the water years in the period of record using a numerical random generator, and the same water years for years 2 through 10 were used in the three different hydrologic scenarios (Table 23-2).

In each model run the simulation starts on the day of the water year (after 1 October) when discharge at the Marmot gauge first exceeds 48 m^3/s. This is because removal of Marmot Dam will be carried out with a cofferdam that can hold up to 48 m^3/s in place, and the cofferdam will be removed (allowing downstream sediment release) when flow reaches this threshold.

23.3.3.3 Surface Grain-Size Distribution of the Channel Bed and Abrasion of Coarse Sediment Estimates of the grain-size distribution of the channel-bed surface layer and of abrasion effects are necessary inputs to the gravel model. The surface grain-size distributions were collected at seven locations, shown in Fig. 23-9. The volumetric abrasion coefficient for gravel and coarser material is estimated to be on the order of 0.02/km based on abrasion values reported by Collins and Dunne (1989) from the Satsop River basin, Washington, for basaltic colluvium, which is geologically similar to river gravels in the Sandy River basin. Detailed input data on surface grain-size distribution are not important for this modeling effort, however, because the model quickly adjusts the grain-size distribution of the channel bed during model simulations.

Effects of abrasion on grain size can be characterized using a modification of Sternberg's (1875) law that can be derived from the Exner equations in Parker (1991a; 1991b), as follows:

$$D_x = D_0 \exp\left(-\frac{2}{3}\beta x\right) \tag{23-9}$$

where

D_0 = grain size (diameter) at an upstream section;
D_x = grain size at a downstream section;
β = volumetric abrasion coefficient (fraction of gravel volume lost due to abrasion per unit distance); and
x = distance between the two sections.

The abrasion coefficient used in the model dictates the rate of attrition of gravel released from the reservoir and therefore influences predicted deposition (i.e., if attrition is greater, less deposition will occur because fewer coarse particles will

Table 23-2 Water Year Series Selected for Use in Simulation

Year in model run	Water year	Peak flow (cms)	Exceedance probability of peak flow (%)	Annual average discharge (cms)	Exceedance probability of annual average discharge (%)
1a (Dry)	1987	230	83	28	91
1b (Average)	1991	371	55	37	59
1c (Wet)	1961	778	10	47	14
2	1932	365	56	40	43
3	1951	215	91	46	15
4	1991	371	55	37	59
5	1988	456	38	33	77
6	1949	334	67	43	25
7	1997	393	53	52	4
8	1992	425	48	29	83
9	1932	365	56	40	43
10	1948	546	29	46	15

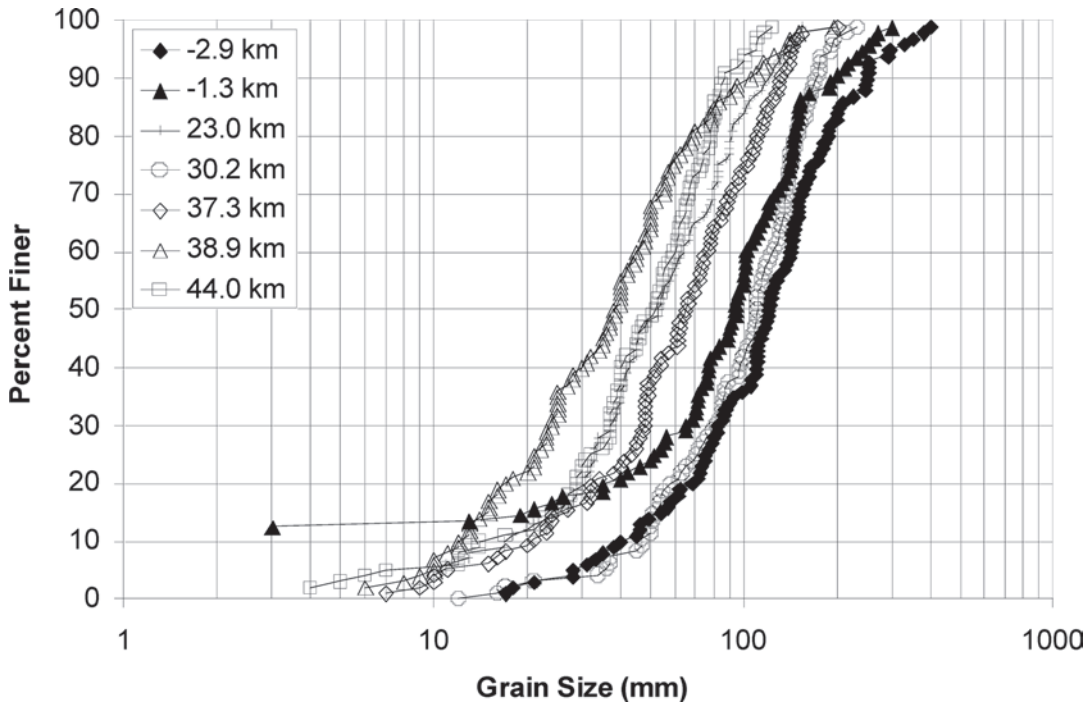

Fig. 23-9. Surface grain-size distributions in the Sandy River, based on selected pebble counts by stillwater sciences.

be available for deposition). Parker's (1991a; 1991b) modification of Sternberg's law considers the abrasion of both bed load and sediment on the channel surface. This modification is seen in Eqs. (23-3a) and (23-3b), which are the variants of the Exner equations of sediment-transport continuity for gravel suggested by Parker (1991a; 1991b). Integration of Eq. (23-3a) for the case of equilibrium conditions by ignoring the production of sand (the last term on the right-hand side of the equation) and then converting volume to diameter yield Eq. (23-9).

Because this modeling effort focuses on evaluation of channel aggradation following sediment release from the reservoir deposit (rather than degradation/incision in the downstream channel bed), results are not sensitive to subsurface grain-size distribution in the channel bed downstream of the dam. For simplicity, it is assumed that downstream of the reservoir area, the subsurface grain-size distribution is the same as that of the surface layer.

23.3.3.4 Grain-Size Distribution of the Reservoir Sediment The grain-size distribution of the sediment accumulation stored behind Marmot Dam, which will influence downstream sediment-transport and deposition patterns, was determined based on sampling conducted in October 1999. Sampling of the reservoir sediment consisted of drilling a series of cores within 1 km upstream of the dam and manual and mechanical excavation further upstream (Squier Associates 2000). A summary of the resulting interpretation of grain-size distribution in the reservoir deposit is given in Fig. 23-10. The reservoir sediment consists of two main units, with the predam channel bed representing a third distinct unit (Squier Associates 2000). The uppermost unit (Unit 1) ranges from approximately 2 to 5.5 m in thickness and is composed of sandy gravel with a small amount of cobbles and boulders, becoming thicker toward the dam. The next unit (Unit 2) is predominantly fine sediment (silty sand to sand with a small amount of gravel, ranging from 4 to 11 m thick). Unit 3, the predam channel, consists primarily of coarse sediment and is 0.8 to 3 m thick. Approximately 750,000 m^3 of sediment is stored behind the dam, of which 490,000 m^3 is primarily gravel/pebble and 260,000 m^3 is primarily sand (Squier Associates 2000).

The grain-size distribution of upstream sediment supply is also required as model input. The grain-size distribution of gravel in upstream sediment supply is assumed to be the same as that of the gravel portion of Unit 1 of the reservoir deposit. This assumption was based on the likelihood that as the reservoir filled in, all or most of the upstream bed load was captured in the reservoir. The grain-size distribution of the sand in sediment supply is assumed to be the same as that of the sand portion of Unit 2 of the reservoir deposit (Fig. 23-10).

The roughness height without sand coverage (k_{s0} in Eqs. (23-7a) and (23-7b)) is assumed to be 0.4 m at Marmot Dam and to decrease exponentially to 0.25 m at the Columbia River confluence. These values are estimates based on field observation and correspond to roughly 4 to 10 times the geometric mean grain size. A model run in which the roughness heights were doubled (i.e., 0.8 m at Marmot Dam and 0.5 m at the Columbia River confluence) was also performed to test the sensitivity of model results to the assumed roughness height. Doubling the roughness heights results in an increased likelihood that sand deposition will be initialized but has only a limited effect on the overall thickness of predicted sand deposition.

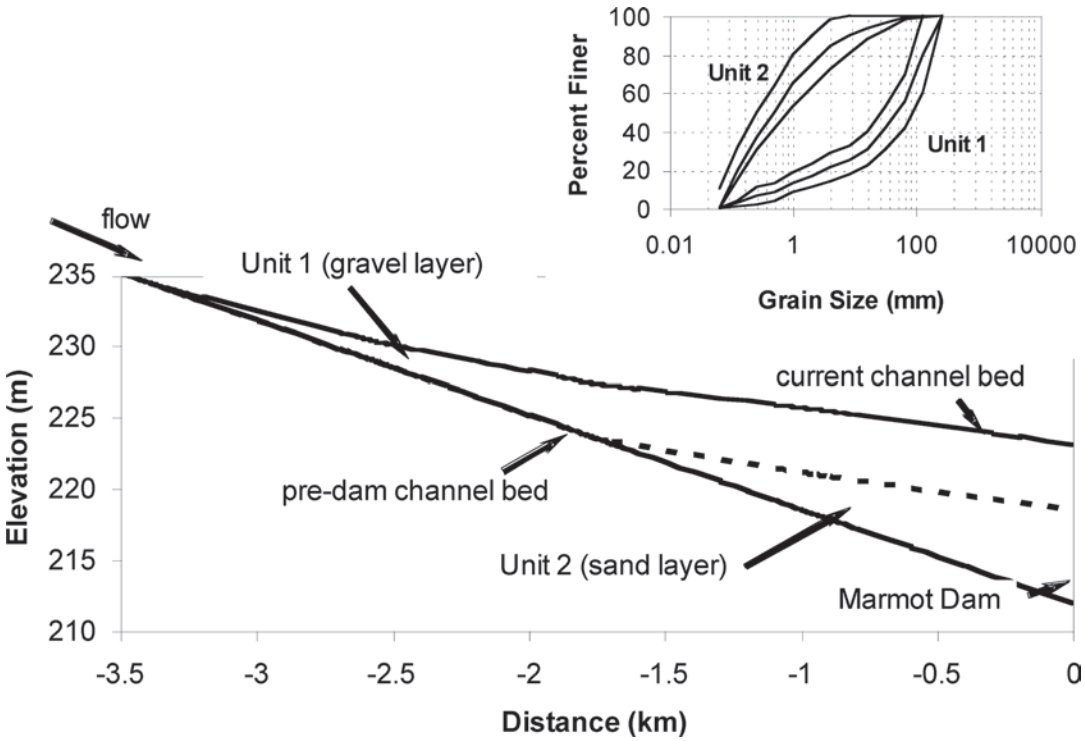

Fig. 23-10. Sediment deposit in Marmot Reservoir. Three grain-size distributions are shown for each unit, representing upper and lower bounds and their average values. Diagram developed based on information provided by Squier Associates (2000).

23.3.3.5 Background Gravel and Sand Transport Rates Background rates of gravel and sand transport in the Sandy River upstream of Marmot Dam are required inputs to the gravel and sand models, but no data are available for reference. To derive a gravel-transport rate, we assumed that the Sandy River's gravel-transport capacity upstream of Marmot Dam exceeds the supply, based on the abundance of bedrock outcrops and boulders in the channel. Thus it is possible to assume that the actual sediment-transport rate upstream of Marmot Dam is some fraction of the transport capacity. This fraction was determined by the model using trial and error as part of the "zero process," whereby various gravel-transport rates were plugged into reference-condition runs so that downstream aggradation and degradation are minimized over the entire river reach. This zero process is discussed in more detail below.

A rough estimate of background suspended-sediment concentration was developed based on an estimate of the long-term average sediment-transport rate and water discharge. For input to the model, the long-term average sediment-transport rate in the Sandy River at Marmot Dam is estimated to be about 250,000 tn/yr (roughly 350 tn/km^2/yr), of which the majority is fine sediment. This is a rough estimate based on review of sediment-yield data from other rivers in Oregon's western Cascade Range, which suggest average sediment yields that range from 100 to 500 tn/km^2/yr for undisturbed and disturbed basins (Curtiss 1975; Swanson and Dyrness 1975; Larsen and Sidle 1980; Swanson et al. 1982; McBain and Trush 1998). In the Sandy River basin, sediment yields may be substantially higher on average than elsewhere in the western Cascades due to Mt. Hood glaciers, the presence of semiconsolidated lahar deposits, steep topography, and land uses. The estimated sediment yield of 350 tn/km^2/yr translates to an average suspended-sediment concentration of about 200 mg/l, which was used as the background suspended-sediment concentration at Marmot Dam in this modeling effort. If the sediment flux from reservoir erosion following removal of Marmot Dam is much higher than the background value, as it is expected to be, model output is not sensitive to the accuracy of the background concentration assumed for model input.

23.3.3.6 Zero Process A "zero process" is generally required for long-term, large-scale sediment-transport simulation. The purpose of the zero process used in this modeling effort is to generate a starting point for the modeling and to evaluate certain input parameters. In the zero process, the model is run repeatedly under a reference condition, in which input data such as discharge are the same as for the simulation of dam removal, but neither Marmot Dam nor any sediment pulse from the reservoir deposit is considered. If the model is fed with raw input data (e.g., channel gradient, width) without modification, it typically will not produce quasi-equilibrium results under reference conditions. The goal of the zero process is to run the model, modifying certain input parameters if necessary, until the model produces quasi-equilibrium results, whereby the river experiences aggradation and degradation in different reaches over different periods of time and hydrological events, but overall, long-term aggradation or degradation is limited. If a quasi-equilibrium condition is established as the baseline for modeling, changes in the system can be interpreted as a direct result of the introduced disturbances, in this case the release of the sediment pulse from Marmot Dam. Boundary conditions in the model are given by (1) discharge at the upstream end of the modeled reach (4 km upstream of Marmot Dam) and along the Sandy River in a downstream direction, (2) background gravel transport at the upstream end (given as a fraction of the potential gravel-transport rate, as described above), (3) the assumed grain-size distribution of the background gravel load, and (4) a fixed bed elevation at the downstream end of the modeled reach (the confluence of the Sandy River with the Columbia River). The water-surface elevation at the downstream end is acquired by the normal flow assumption.

In the zero process for this modeling effort, channel width is modified in such a way that certain extremely wide sections are reduced to no less than 80% of the original value. The model is then run repeatedly, with the output of the channel bed elevation (slope) as the input of the subsequent run, until the channel bed reaches quasi-equilibrium. The zero process is also used to estimate the background gravel-transport rate upstream of Marmot Dam (which is needed as input to the model). Large-scale deposition (aggradation) will occur if the input sediment-transport rate is too high and large-scale erosion (incision/degradation) will occur if the input sediment-transport rate is too low. The input gravel-transport rates selected for modeling, based on trial and error in the zero process, vary with hydrology and, for the hydrologic conditions shown in Table 23-2, vary from about 7,000 to 72,000 tn/yr at Marmot Dam. These results suggest an average long-term gravel-transport rate of about 25,000 to 30,000 tn/yr (roughly 10% of the total sediment yield estimated above). Assuming a bulk sediment density of 1.7 tn/m^3, this average annual gravel-transport rate would have completely filled Marmot reservoir in about 30 yr following dam closure. The actual length of time required for the reservoir to fill is unknown but 30 yr appears to be a reasonable estimate, based on regional sediment-yield data and on the rapid sedimentation of an area of the reservoir that was excavated to facilitate reconstruction of the dam in 1989.

The "zeroed" bed slope is given in Fig. 23-8 along with the original photogrammetric data. This figure shows that the zero process retains the general overall channel slope but modifies local gradients to convey the background sediment load through all reaches of the Sandy River.

23.3.4 Model Results

Numerical modeling was used to simulate sediment-transport processes both for background conditions in the Sandy River and for the dam removal alternatives listed in Section 23.3.1. Results are presented for background conditions and for the

alternative entailing single-season dam removal with minimal sediment removal. Sensitivity tests to evaluate certain model assumptions and approaches are also summarized. Results for modeling of other removal alternatives, as well as additional details on sensitivity testing, are presented in Stillwater Sciences (2000; 2002).

23.3.4.1 Reference Runs of Numerical Models For both the gravel and sand models, model runs were performed for reference conditions assuming that no dam exists and downstream sediment transport is equivalent to estimated background (natural) conditions, with no release of reservoir sediment. Reference runs of the model are a component of the zero process described above and depict aggradation and degradation in the Sandy River in the absence of sediment release from Marmot Dam. Reference runs therefore provide a basis of comparison for interpretation of model predictions of deposition patterns following various dam removal alternatives.

For the gravel model, a 10-yr simulation was performed for reference conditions. In the reference run of the gravel model, a small amount of coarse sediment aggradation (and degradation) is indicated in Reaches 3 and 4, even without sediment release from Marmot reservoir (Figs. 23-11 and 23-12). The reference run indicates that up to about 1 m of aggradation would periodically occur in certain reaches.

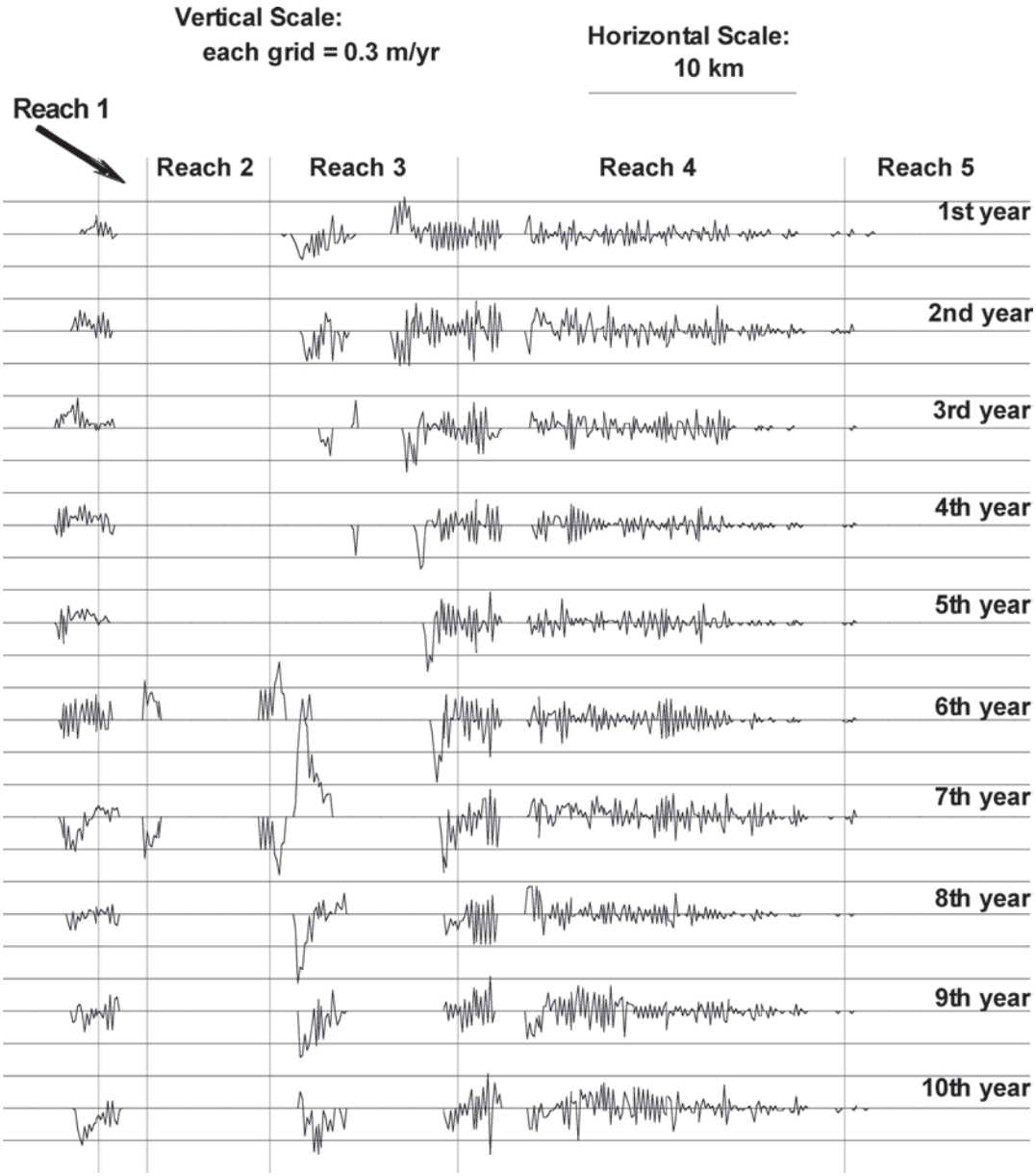

Fig. 23-11. Annual change in bed elevation from gravel erosion and deposition: reference run of the gravel model.

In particular, about 1 m of deposition is observed downstream of the gorge outlet in Year 6 of the model run (which uses water year 1949, a wet year with only moderate peak flow, as input flow data). This result indicates that under certain hydrological conditions, local aggradation or degradation could occur in certain reaches under reference conditions in the Sandy River.

Reference runs of the sand model indicate background suspended-sediment concentrations fluctuating between approximately 90 and 150 ppm at the site of Marmot Dam,

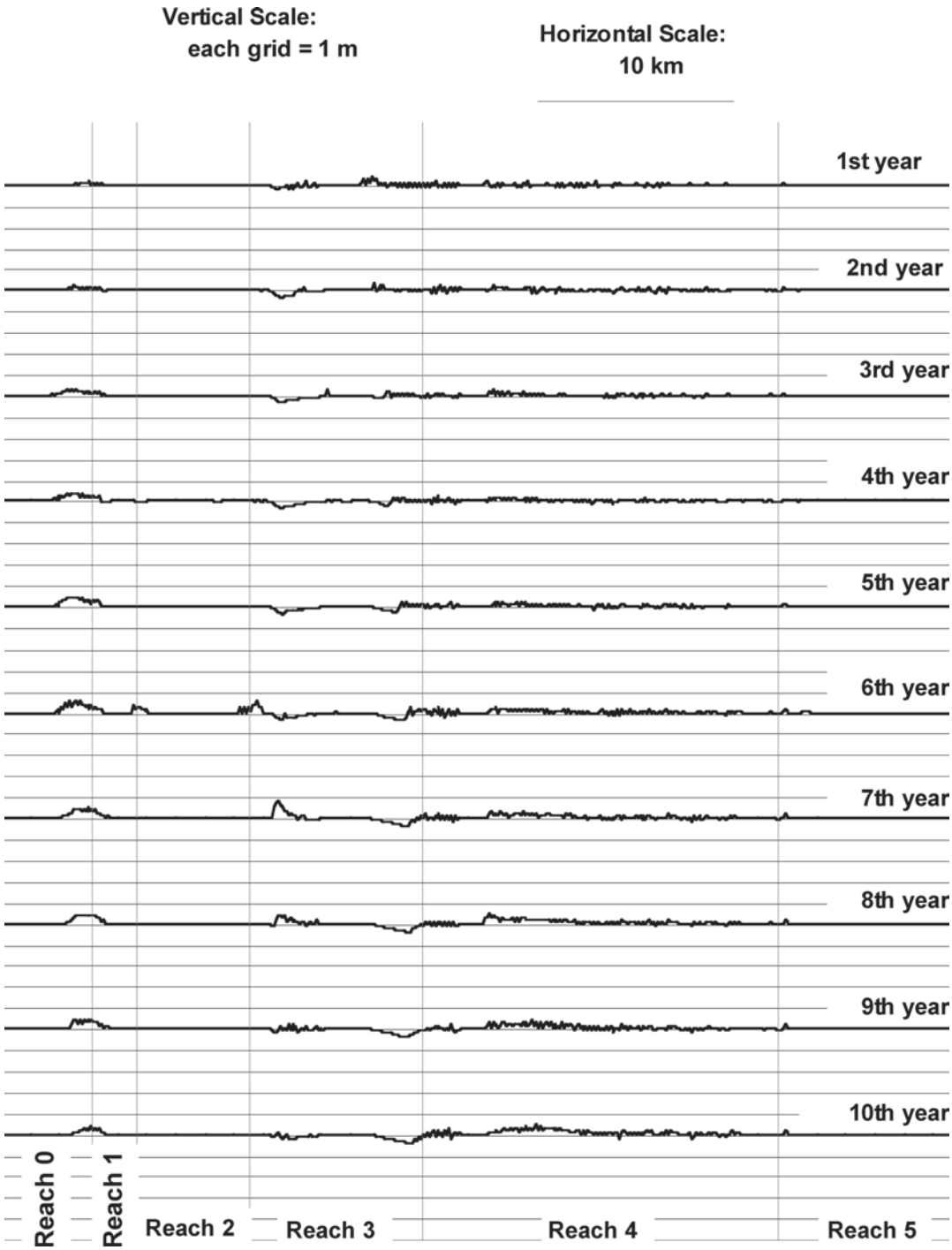

Fig. 23-12. Cumulative change in bed elevation from gravel erosion and deposition: reference run of the gravel model.

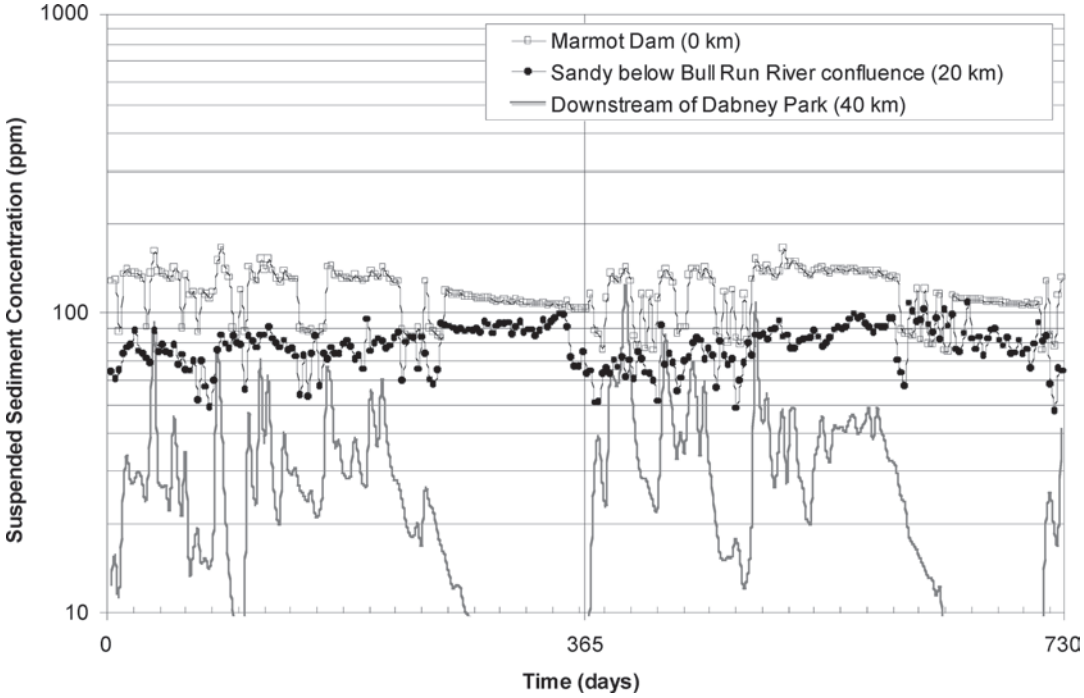

Fig. 23-13. Simulated suspended-sediment concentration downstream of Marmot Dam under reference conditions.

with lower concentrations further downstream (Fig. 23-13), based on the assumed background sediment concentration. Reference runs also show sand aggradation occurring in Reach 5, which is in agreement with field observations of the sand-bedded nature of this reach.

23.3.4.2 Modeling of Sediment Transport Associated with Single-Season Dam Removal and Minimal Sediment Excavation Under one of the alternatives being considered for removal of Marmot Dam, only a minimal amount of sediment (i.e., enough to facilitate dam removal activities) would be excavated from the reservoir prior to dam removal, which would be accomplished in one season. All of the remaining reservoir sediment would be released downstream following dam removal. Model runs for this alternative assumed that a slightly greater amount of sediment was in the reservoir and would be released downstream (800,000 m^3) than the sediment volume of 750,000 m^3 suggested by the Marmot reservoir coring study (Squier Associates 2000). This volume difference was arrived at based on review of PGE photogrammetric data (Fig. 23-7), which suggests that the reservoir deposit may extend further upstream than indicated by the coring study (Squier Associates 2000).

Figures 23-14 and 23-15 illustrate model predictions of the downstream movement of coarse sediment out of the reservoir and resulting increases in bed elevation (aggradation) downstream of Marmot Dam, under average hydrologic conditions and over a 10-yr period. These model results indicate that, in the first year following removal, coarse sediment would move downstream into the portion of Reach 1 immediately downstream of the dam, creating a depositional wedge up to a maximum of about 4 m thick, with small amounts of deposition predicted further downstream in Reach 1 and in Reach 3. In subsequent years, additional sediment would move out of the reservoir, resulting in a gradual increase in deposition thickness in the downstream portion of Reach 1, reaching a maximum of about 1 m on a reach-averaged basis. The aggradational wave is predicted to travel quickly through most of the gorge (Reach 2), with aggradation increasing at the downstream end of the gorge and the upstream end of Reach 3 from Years 1 through 10. Aggradation is predicted to gradually build to a maximum predicted thickness of about 1.5 to 2 m in the upper portion of Reach 3 (9–13 km downstream of the dam), where the channel widens and decreases in gradient (Fig. 23-15). In Reach 1, the greatest amount of aggradation would be expected in the early years following dam removal, whereas in Reach 3, aggradation would be expected to show gradual increases through the first 7 yr. After the first 7 yr, deposition thickness in Reach 3 would gradually decrease as the sediment wave is transported downstream. The model predicts small amounts of aggradation (typically <0.5 m) downstream of the Bull Run River confluence, although this aggradation is similar in magnitude to aggradation predicted in a reference run of the model and is not likely to be distinguishable from natural depositional processes.

Figure 23-16 shows the predicted change in bed elevation in a longitudinal profile view in the reservoir reach and in Reach 1 following dam removal. This figure shows how, following dam removal, the slope in the reservoir reach would gradually flatten out and return to that of the predam channel

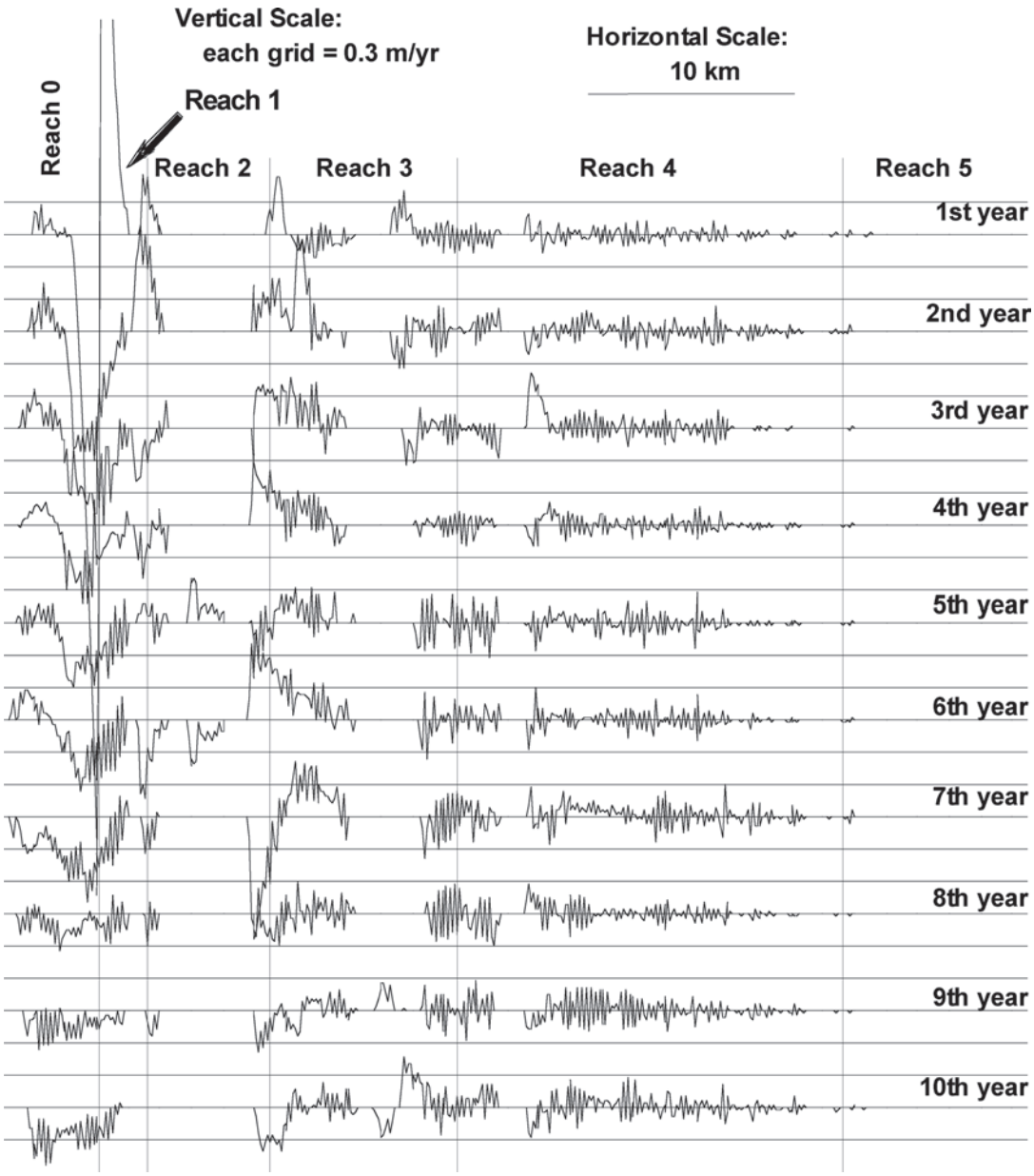

Fig. 23-14. Annual change in bed elevation following dam removal for single-season dam removal with minimal dredging.

bed. Model results show that under average hydrologic conditions, the depth of the sediment deposit in the reservoir would decrease from about 11 m at the time of dam removal to about 8 m after 30 days, 7 m after 60 days, 6 m after 1 yr, 3 m after 5 yr, and 1 m after 10 yr (Fig. 23-15).

After the dam is removed and the channel begins to incise into the reservoir deposit, sand and finer sediment will be mobilized from the reservoir deposit. The magnitude of sand transport out of the reservoir is predicted to be greatest in the first winter following dam removal, although sand transport out of the reservoir continues for the duration of the model runs. Modeling of sand transport indicates that sand aggradation is most likely to occur in the lower 10 km of the Sandy River (Reach 5) and that negligible aggradation would occur further upstream. Reach 5 has the lowest transport capacity of any reach in the Sandy River, reflecting its greater width and low gradient, and is currently sand-bedded in its lower portion. The model predicts deposition thicknesses of up to about 0.4 m in Reach 5 (Fig. 23-17), with the greatest aggradation expected to occur in the first year following removal of Marmot Dam. If stages are high enough in the Columbia River to create a backwater effect in the Sandy River during periods of sand transport in the Sandy River, however, the thickness of sand deposition in

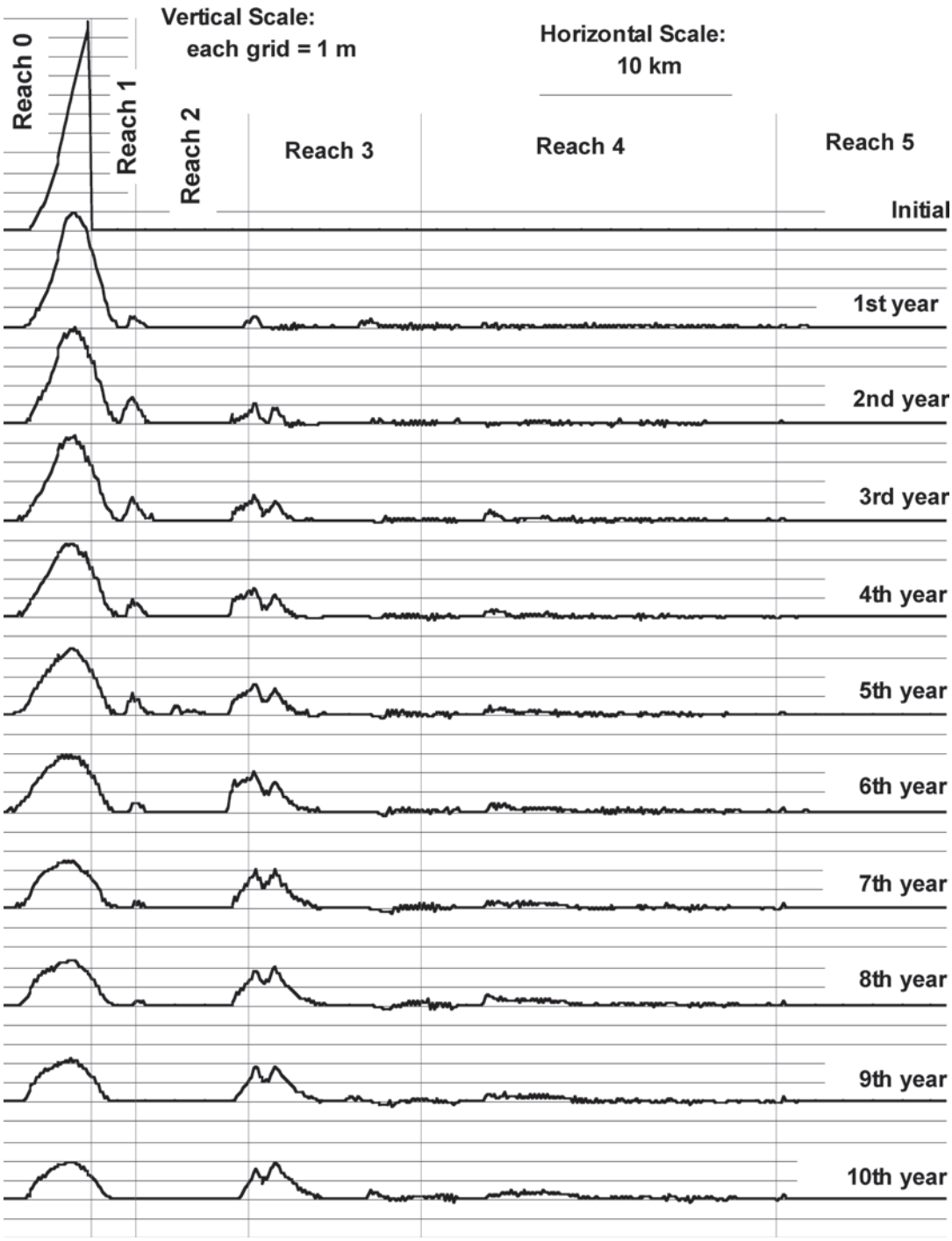

Fig. 23-15. Cumulative change in bed elevation following dam removal for single-season dam removal with minimal dredging.

the lower Sandy River could be much greater than predicted here. Because the model does not account for this backwater effect, there is considerable uncertainty in model predictions of deposition thickness in Reach 5.

Figures 23-17 and 23-18 show the pattern of sand deposition at selected locations in Reach 5 during the first 2 yr following removal of Marmot Dam and indicate that the magnitude of sand aggradation would fluctuate both seasonally and between years. Aggradation in Reach 5 is predicted to occur mainly in the lower 3 km of the Sandy River (with less aggradation in the upper part of the reach), which roughly corresponds to the location of the gravel/sand transition area

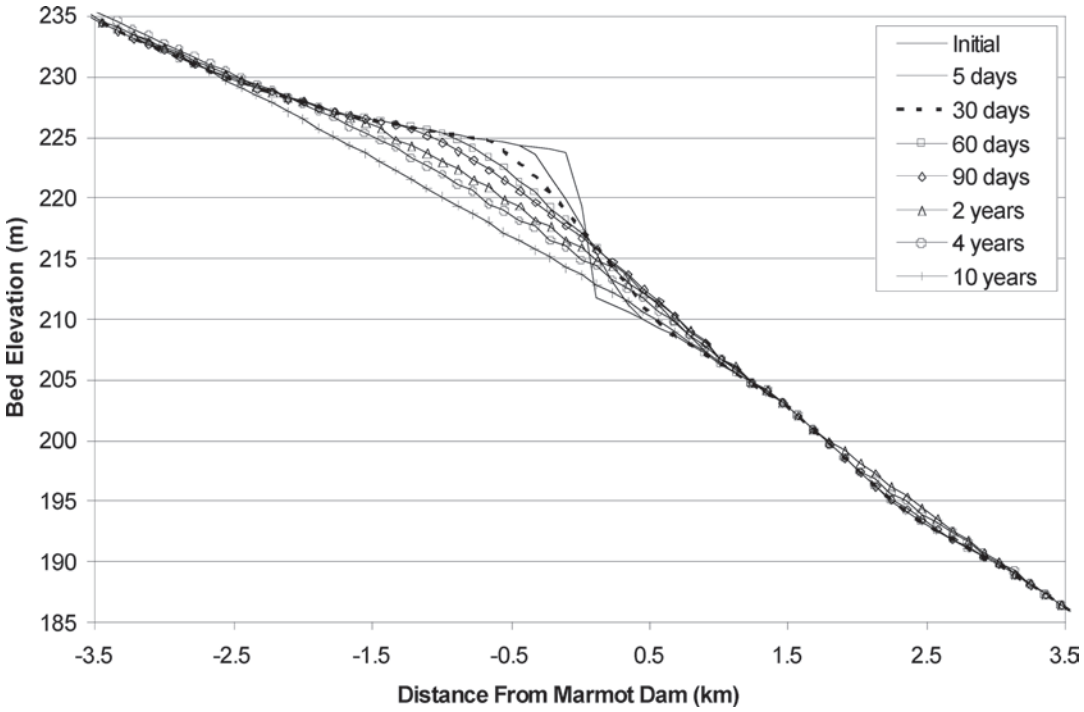

Fig. 23-16. Simulated bed elevation in the vicinity of the reservoir area following dam removal, for single-season dam removal with minimal dredging.

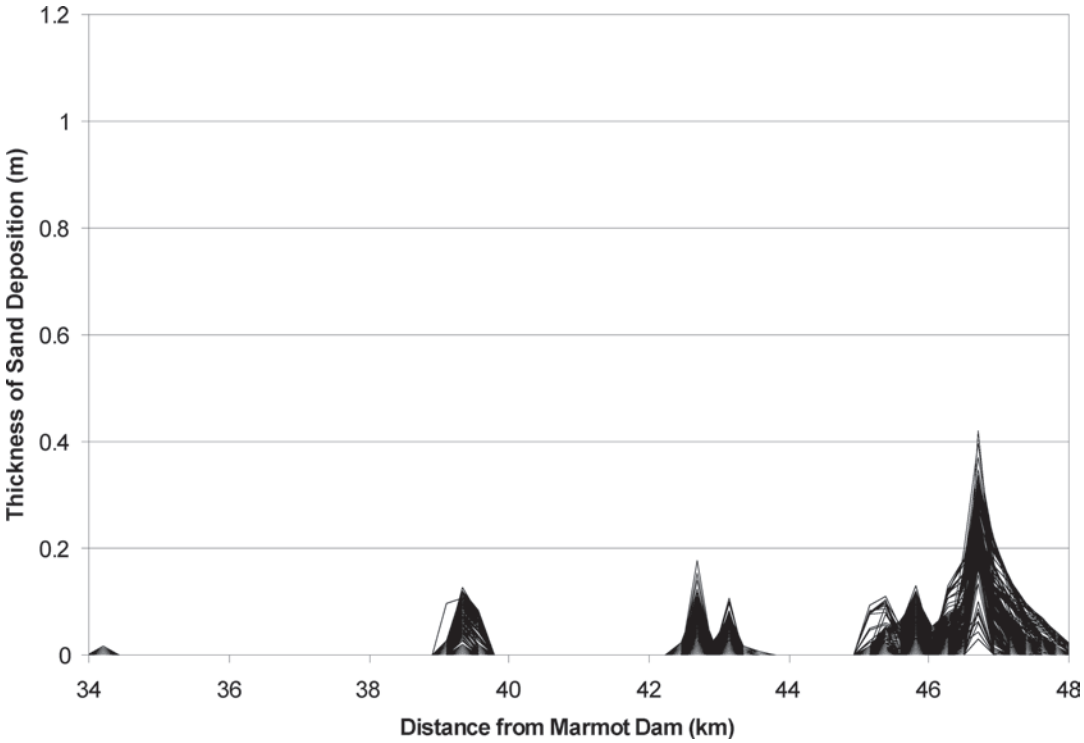

Fig. 23-17. Simulated thickness of sand deposit for single-season dam removal with minimal dredging. The diagram depicts the general areas and magnitudes of sand deposition. No attempt is made to identify individual lines on the diagram.

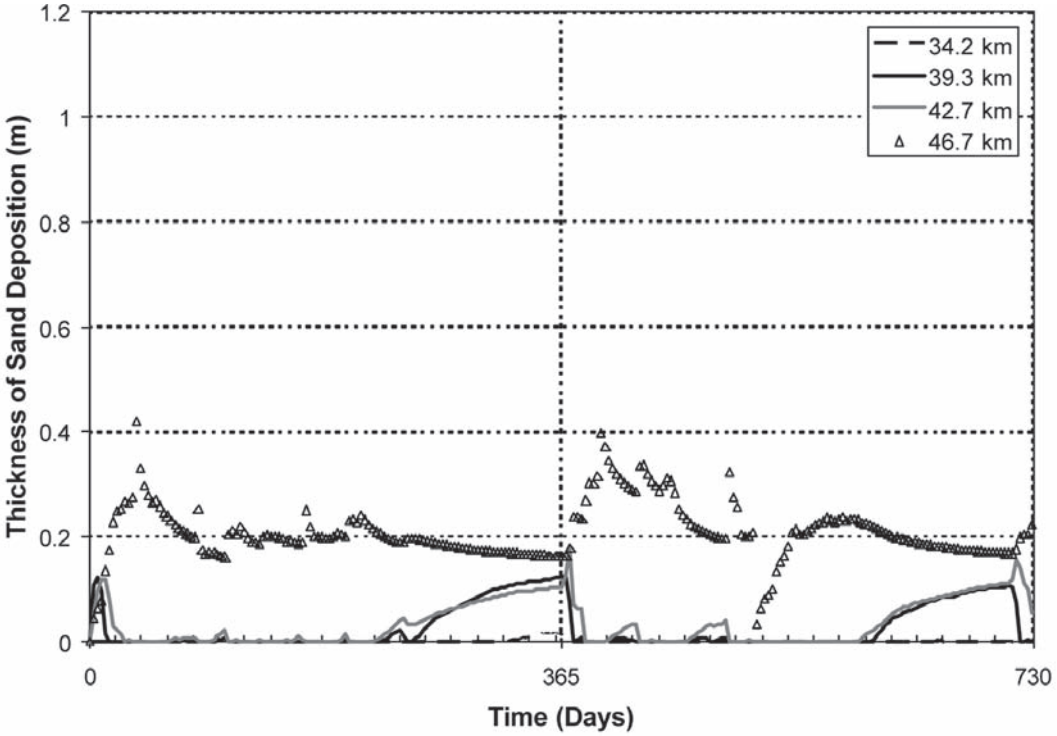

Fig. 23-18. Simulated thickness of sand deposit at four locations for the first two years following dam removal: single-season dam removal with minimum dredging.

in the Sandy River (i.e., very little gravel is found in the channel bed downstream of this portion, whereas upstream the bed contains both sand and gravel). Observations in other river systems suggest that the gravel/sand transition zone is typically an area of active deposition (Dietrich et al. 1999).

Model results also suggest that sand release from the reservoir would produce relatively small increases in total suspended-sediment (TSS) concentrations. Modeling indicates that, between Marmot Dam and the Bull Run River confluence, peak TSS of about 500 ppm would occur in the first winter following dam removal under average hydrologic conditions (Fig. 23-19). Suspended-sediment concentrations would generally remain between 100 and 200 ppm during the first 2 yr after removal, with periodic increases above this level during high flows. Downstream of the Bull Run River, suspended-sediment levels would be lower because of the dilution effect of flows from the Bull Run River. Suspended-sediment levels associated with dam removal are predicted to be relatively low because of the nature of the reservoir sediment deposit, in which fine sediment deposits are armored by a coarser surface layer (Fig. 23-10) and are therefore released gradually, rather than as one large pulse. Background suspended-sediment levels in the Sandy River are not known; modeled results should be considered indicative of potential increases in suspended-sediment concentration above background levels due to sediment release from Marmot Reservoir.

23.3.4.3 Sensitivity Tests Sensitivity tests were also performed to characterize the potential uncertainties in model results as a result of uncertainties either in model input data or in basic assumptions. Sensitivity tests were performed for the Marmot Dam removal simulation to evaluate uncertainties in (1) future hydrologic conditions, (2) grain-size distributions in the reservoir deposit, and (3) erosion rates from Marmot Reservoir. The results of these sensitivity tests are summarized below, and additional details are presented in Stillwater Sciences (2000; 2002). Cui et al. (2006a) present additional sensitivity tests for a hypothetical case study.

Modeling was completed to test the effects of "wet," "average," and "dry" hydrologic conditions in the first year following dam removal on sediment-transport dynamics; descriptions of the input data used for these scenarios are provided in Section 23.3.3. These model runs suggest that varying hydrology in the first year following dam removal strongly affects the rate of sediment transport out of the reservoir reach, with more rapid reservoir erosion under wetter conditions. For example, modeling indicates that after 1 yr, the thickness of the reservoir deposit would be about 3 m based on wet hydrologic conditions, compared to about 6 m based on average hydrology. Compared to average hydrologic conditions (results of which are described above), the more rapid movement of sediment out of the reservoir in Year 1 expected under wet conditions is predicted to slightly

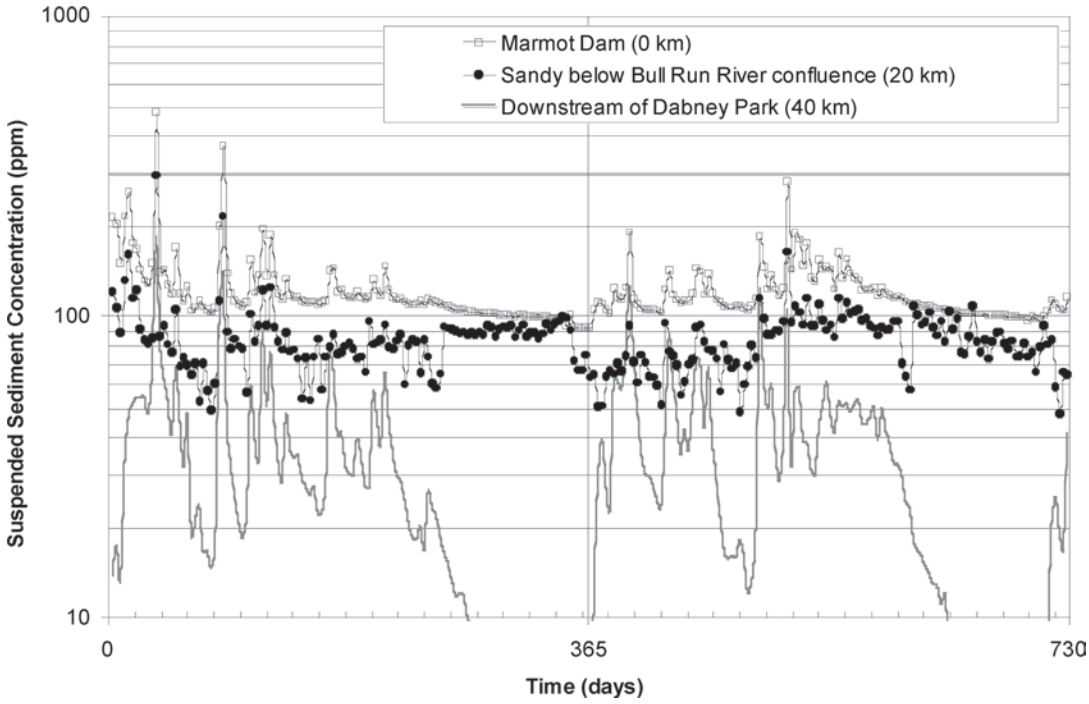

Fig. 23-19. Simulated suspended-sediment concentration at three locations for the first two years following dam removal: single-season dam removal with minimum dredging.

reduce overall gravel aggradation in Reach 1 in the years following removal, to alter the temporal pattern of aggradation in Reach 3 (with thicker deposition in the first several years after removal, but with similar magnitude of aggradation over a 10-yr scale), and to slightly increase aggradation in Reach 4. Model runs based on dry hydrologic conditions in Year 1 suggest that sediment would initially move more slowly out of the reservoir area compared to average hydrologic conditions, but that after 5 yr, the thickness of the deposit at the dam site would be the same as for average hydrologic conditions. Downstream patterns of predicted aggradation are similar for dry and average hydrologic scenarios, with aggradation concentrated in Reach 1 and Reach 3. The sensitivity of TSS levels to hydrologic conditions was also evaluated: predicted TSS levels are lowest for dry hydrologic conditions in Year 1, generally remaining below 200 ppm, and are similar in average and wet conditions.

In addition to varying the hydrologic input data, we also conducted model runs with different assumed grain-size distributions for the reservoir deposit. The model runs described above assumed an "average" grain-size distribution (Fig. 23-10). Using the "upper bound" (i.e., coarser) and "lower bound" (i.e., finer) grain-size distributions shown in Fig. 23-10 causes only very small changes in the predicted pattern of coarse sediment deposition. Predictions of TSS concentration are somewhat sensitive to the assumed grain-size distribution: TSS levels are highest for the assumed lower-bound distribution and lowest for the assumed upper-bound distribution.

Sensitivity tests were also used to evaluate simplifying assumptions used to simulate reservoir erosion, which is a key uncertainty in this modeling effort. As discussed in Section 23.3.2, basic model runs assume laterally uniform erosion of reservoir sediment from Marmot Reservoir. In reality, however, incision of a channel through the reservoir reach will likely occur to some extent following dam removal. A sensitivity analysis was performed to assess how an increase in the rate of gravel transport out of the reservoir resulting from channel incision could affect downstream deposition patterns. It was assumed that channel incision in the reservoir reach would be most likely when the local channel bed slope was high, as would be the case at the downstream end of the reservoir deposit immediately following dam removal, and that this could result in a gravel-transport rate that was greater than predicted by Parker's bed load transport equation. The increase in sediment-transport rate resulting from downcutting is therefore hypothesized to be an incremental function of bed slope. To simulate this, we applied a multiplier that varied with bed slope to the gravel-transport rate calculated by the Parker equation for channel bed slopes above 0.01. The transport rate out of the reservoir calculated by the Parker equation is thereby increased by a factor of up to 10 in this sensitivity test, depending on local bed slope. The results of this sensitivity test indicate that, if the down-cutting process affects the gravel-transport rate as is assumed in this sensitivity test, there will be only a short term effect on the pattern of gravel erosion from the reservoir and downstream deposition. This is because slopes

will be steepest immediately following dam removal at the downstream end of the sediment deposit, but downstream transport of this material would result in reduced bed slopes (and sediment-transport rates) within a short time, even if channel incision does occur. This sensitivity test does not fully simulate the effects of channel incision on sediment-transport patterns out of the reservoir reach, but it does capture one potential effect of incision (i.e., transport rates that are higher than calculated by the Parker equation when channel incision occurs).

The model also employs simplifying assumptions with respect to the mechanism of sand release from the reservoir, assuming that sand will be metered out of the reservoir in association with transport of gravel, as described in Section 23.3.2. To address the considerable uncertainties in this method, we completed sensitivity tests in which the rate of sand release from the reservoir was increased 5-fold and 10-fold over the rates of sand release predicted by the model based on predicted shear stresses and laterally uniform transport in the reservoir reach. Increasing the rate of sand release by a factor of 5 or 10 would result in complete sand evacuation from the reservoir in about 4 or 2 yr, respectively. The sensitivity analysis for the 10-fold increase indicates that sand release from the reservoir at 10 times the expected rate would result in a peak TSS concentration of approximately 4,000 ppm in the first winter following dam removal (compared with a maximum of about 500 ppm for basic model runs), with other spikes in TSS above 500 ppm during storm events. Otherwise TSS would generally remain between 100 and 400 ppm between Marmot Dam and the Bull Run River confluence, resembling assumed background conditions during late summer and early fall low-flow conditions. Increasing the rate of sand release 10-fold would also result in additional deposition downstream, including sand aggradation of approximately 0.2 to 0.4 m at the downstream end of Reach 4 (where no deposition is predicted for basic model runs), and aggradation predicted throughout Reach 5, with a maximum of about 1 m in this reach (compared to about 0.4 m in basic model runs).

23.3.5 Discussion

The case study presented in this chapter illustrates key considerations in the development of sediment-transport models for dam removal simulations. The model presented here and those of Cui et al. (2006a; 2006b) provide a framework for development of future models, either as a reference or as a starting point for modifications.

Numerical modeling of a process as complex as transport of a large volume of coarse and fine sediment following dam removal contains a number of uncertainties. The modeling approach presented here includes both uncertainties that are specific to the Marmot Dam removal application and those that would likely affect any dam removal modeling effort. Many hypotheses are incorporated in the models, in terms of both theoretical development (i.e., reflecting uncertainties in current scientific understanding about the mechanics of sediment transport) and input data. Key areas of uncertainty in this modeling effort, each of which is discussed further below, include modeling of reservoir erosion processes, selection of appropriate sediment-transport equations, uncertainty arising from the use of one-dimensional modeling, and uncertainty in input parameters.

A key source of uncertainty in this modeling approach arises from simplifying assumptions used to model reservoir erosion. Whereas the model assumes that transport out of the reservoir would be laterally uniform, erosion of reservoir sediment would in fact likely result in incision of a channel within the valley walls, potentially accelerating exposure of the underlying sand layer in the incised area and increasing the time (compared to model predictions) required for sediment on the margins of the reservoir deposit to be eroded downstream. Uncertainties also arise from the use of the Parker equation to model erosion of the mixed sand and gravel layers in the reservoir. The Parker equation is used to predict mobilization of the coarse fraction of various sediment layers in the reservoir, treating those layers as if fine sediments were not present. In fact, although the overall stratification of the reservoir results in a larger proportion of fine sediment in the lower layers of the reservoir and more coarse sediment in the upper layers, each layer in the deposit typically contains a range of grain sizes. The presence of a large amount of fines may create error in the use of the Parker equation because it is not intended for application to particles smaller than 2 mm. The model also assumes that fine sediments within each layer of the reservoir deposit are not transported out of the reservoir until shear stresses are sufficient to mobilize the gravel ($>$2-mm) component of the layer, as indicated by the Parker equation. Some fraction of the fine sediments in the reservoir, however, will likely be mobilized and transported at discharges lower than those that transport the coarse sediments found in the same layer as the fine sediments, resulting in more rapid transport of sand from a given layer in the reservoir deposit than of the gravel in that layer. In addition, sand following the gravel leaving the reservoir could smooth the bed and increase the mobility of the leading gravel front downstream (T. Lisle, personal communication, 2000). Sensitivity tests to address uncertainties related to reservoir erosion processes are described in Section 23.3.4.

Selection of appropriate sediment-transport equations is an important consideration in sediment-transport modeling of dam removal and, because of the complexities of dam removal modeling and incomplete knowledge of sediment-transport mechanics, the transport equations selected can be a potential source of uncertainty. The Marmot Dam removal case study involves simulation of transport of a mixture of coarse and fine sediment over a primarily coarse existing river bed. Because of the relatively undeveloped nature of transport equations for sand/gravel mixtures, we developed

separate transport models for sand and gravel components in the Marmot case study, rather than simultaneously modeling a sand/gravel mixture. Although sand and gravel transport are treated separately, they do likely affect each other, creating some uncertainty in model results. Moreover, the transport equation used here to model the downstream transport of fine sediment (Brownlie 1982) was developed for sand-bedded channels, and we know of no equations for sand transport over a coarse bed. Because most of the Sandy River has coarse bed materials downstream of Marmot Dam, use of the Brownlie equation (or of a comparable equation for sand transport) creates additional model uncertainty.

One-dimensional numerical modeling, such as the Marmot Dam removal model, provides results that are most applicable on a reach-scale and time-averaged basis, including estimates of sediment-transport rates and cross-section and reach-averaged depths of sediment deposits over the existing channel bed. Current state-of-the-art modeling, however, typically cannot predict complex three-dimensional geomorphic responses over long river reaches and time scales, such as depositional patterns in channel cross section, local changes in sediment particle size distribution, infiltration of sand into the channel bed, or changes in the mobility of the existing channel bed. The Marmot Dam removal model assumes a simplified, rectangular channel, and model predictions do not account for local variations in shear stress caused by features such as deep pools, bedrock outcrops, or large boulders. The modeling of fine sediment transport also does not account for the production of sand and silt from gravel abrasion (i.e., suspended load estimates do not include products of gravel abrasion). The amount of sediment actually deposited may therefore be substantially higher or lower than predicted by the model in localized areas of the channel. Because of the one-dimensional nature of modeling results, professional judgment and field observations of the system being evaluated should be used to interpret model results in terms of expected geomorphic effects.

Numerical models of dam removal, such as the model presented here for the Marmot Dam removal application, require input parameters on a range of physical characteristics that influence sediment transport. Modeling results typically will have varying levels of sensitivity to different types of input data, and input data typically contain varying levels of uncertainty. Modeling accuracy and efficiency will therefore be enhanced if the effort devoted to quantifying input parameters is commensurate with model sensitivity to these parameters. For the Marmot Dam removal application, data were collected specifically for this project or were already available for those input parameters to which the model is most sensitive (i.e., channel gradient, channel width, grain-size distribution of reservoir sediment, and water discharge). In addition, sensitivity analyses were performed to examine the effects of varying certain input data (hydrologic conditions, grain-size distribution of reservoir sediment) on model results, as described above. For other input parameters, such as background gravel- and sand-transport rates, size distribution of bed load, and abrasion rates in the Sandy River, existing data were not available and new data were not collected for this project. For many of these input parameters, only order-of-magnitude estimates are required for the models, and rough assumptions based on field observations of the Sandy River and on published data from elsewhere in the region were therefore used.

Despite the uncertainties in the modeling effort described here, this numerical modeling approach does provide predictions of sediment transport and deposition following dam removal over large temporal and spatial scales and can be used to compare sedimentation impacts associated with various dam-removal alternatives. Modeling efforts such as this one can be improved if field data describing the phenomena being modeled are collected and compared to modeling results. Monitoring of processes such as reservoir erosion, sand and gravel aggradation, and total suspended-sediment concentrations following dam removal is critical to improving upon nascent efforts to simulate sediment-transport dynamics following dam removal.

ACKNOWLEDGMENTS

We would like to thank the following reviewers for comments on this work: Jim Pizzuto (University of Delaware), Tom Lisle (U.S. Forest Service), Steve Wiele (U.S. Geological Survey), Bill Dietrich (University of California, Berkeley), and Marcelo Garcia (University of Illinois). Suggestions from Brian Cluer on this manuscript are gratefully appreciated. Discussions and helps from Stillwater Sciences employees, Christian Braudrick, Frank Ligon, Bruce Orr, Martin Trso, Jennifer Vick, and many others, too many to mention individually, are gratefully acknowledged. Funding for the Marmot Dam removal sediment-transport study was provided by Portland General Electric (PGE).

REFERENCES

Brownlie, W. R. (1982). "Prediction of flow depth and sediment discharge in open channels." PhD thesis, California Institute of Technology, Pasadena, Calif.

Bureau of Reclamation. (1996a). "Removal of Elwha and Glines Canyon Dams." *Elwha Technical Series PN-95-7,* Elwha River Ecosystem and Fisheries Restoration Project, Washington, Pacific Northwest Region, Boise, Idaho, <http://ww.nps.gov/olym/elwha/reclamation/removal.htm>(accessed on Sept. 26, 2005).

Bureau of Reclamation. (1996b). "Sediment analysis and modeling of the river erosion alternative." *Elwha Technical Series PN-95-9,* Elwha River Ecosystem and Fisheries Restoration Project, Washington, Pacific Northwest Region, Boise, Idaho, <http://ww.nps.gov/olym/elwha/reclamation/sediment.tm>(accessed on Sept. 26, 2005).

Chaudhry, M. H. (1993). *Open-channel flow.* Prentice-Hall, Englewood Cliffs, N.J.

Childers, D., Kresch, D. L., Gustafson, S. A., Randle, T. J., Melena, J. T., and Cluer, B. (2000). "Hydrologic data collected during the 1994 Lake Mills drawdown experiment, Elwha River, Washington." *Water-Resources Investigations Report 99-4215*, U.S. Geological Survey, Tacoma, Wash.

Collins, B. D., and Dunne, T. (1989). "Gravel transport, gravel harvesting, and channel-bed degradation in rivers draining the southern Olympic Mountains, Washington, USA." *Environmental Geology and Water Sciences*, 13, 213–224.

Cui, Y., Braudrick, C., Dietrich, W. E., Cluer, B., and Parker, G. (2006a). "Dam Removal Express Assessment Models (DREAM). 2: Sample runs / sensitivity tests." *Journal of Hydraulic Research*, 44(3), 291–307.

Cui, Y., and Parker, G. (1997). "A quasi-normal simulation of aggradation and downstream fining with shock fitting." *International Journal of Sediment Research*, 12(2), 68–82.

Cui, Y., and Parker, G. (1998). "The arrested gravel front: Stable gravel-sand transitions in rivers. II: General numerical solution." *Journal of Hydraulic Research* 36(2), 159–182.

Cui, Y., and Parker, G. (2005). "Numerical model of sediment pulses and sediment supply disturbances in mountain rivers." *Journal of Hydraulic Engineering,* 131(8), 646–656, doi: 10.1061/(ASCE)0733-9429(2005)131:8(646).

Cui, Y., Parker, G., Braudrick, C., Dietrich, W. E., and Cluer, B. (2006b). "Dam Removal Express Assessment Models (DREAM). 1: Model development and validation." *Journal of Hydraulic Research*, 44(3), 308–323.

Cui, Y., Parker, G., Pizzuto, J., and Lisle, T. E. (2003). "Sediment pulses in mountain rivers. 2: Comparison between experiments and numerical predictions." *Water Resources Research*, 39(9), 1240, doi: 10.1029/2002WR001805.

Curtiss, D. A. (1975). "Sediment yields of streams in the Umpqua River basin, Oregon." *Open-File Report*, U.S. Geological Survey, Portland, Ore.

Dietrich, W. E. (1982). "Settling velocities of natural particles." *Water Resources Research*, 18(6), 1615–1626.

Dietrich, W. E., Day, G., and Parker, G. (1999). "The Fly River, Papua New Guinea: Inferences about river dynamics, floodplain sedimentation and fate of sediment." *Varieties of fluvial form*, A. J. Miller and A. Gupta, eds., Wiley, New York.

Doyle, M. W., Stanley, E. H., and Harbor, J. M. (2003). "Channel adjustments following two dam removals in Wisconsin." *Water Resources Research*, 39(1), 1011, doi: 10.1029/2002WR001714.

Graf, W. L. (1996). "Geomorphology and policy for restoration of impounded American rivers: What is natural?" *The scientific nature of geomorphology: Proceedings of the 27th Binghamton symposium in geomorphology*, B. L. Rhoads and C. E. Thorn, eds., Wiley, New York, 443–473.

Hansler, M. E. (1999). "Sediment wave evolution and analysis of a one-dimensional sediment routing model, Navarro River, Northwestern California." MS thesis, Humboldt State University, Arcata, Calif.

Keulegan, G. H. (1938). "Laws of turbulent flow in open channels." *Journal of the National Bureau of Standards,* 21, Research Paper 1151, 707–741.

Larsen, K. R., and Sidle, R. C. (1980). "Erosion and sedimentation data catalog of the Pacific Northwest." *Rep. R6-WM-050-1981*, U.S. Forest Service, Pacific Northwest Region, Portland, Ore.

McBain and Trush. (1998). "Tuolumne River corridor restoration plan, Stanislaus County, CA." *Draft report prepared for Tuolumne River Technical Advisory Committee (Don Pedro Project, FERC License No. 2299)*, McBain and Trush, Arcata, Calif.

Parker, G. (1990). "Surface-based bedload transport relation for gravel rivers." *Journal of Hydraulic Research*, 28(4), 417–436.

Parker, G. (1991a). "Selective sorting and abrasion of river gravel. I: Theory." *Journal of Hydraulic Engineering*, 117(2), 131–149.

Parker, G. (1991b). "Selective sorting and abrasion of river gravel. II: Application." *Journal of Hydraulic Engineering,* 117(2), 150–171.

Pizzuto, J. (2002). "Effects of dam removal on river form and process." *BioScience*, 52(8), 683–691.

Randle, T. (2003). "Dam removal and sediment management." *Dam removal research: Status and prospects*, W. L. Graf, ed., H.J. Heinz III Center for Science, Economics and the Environment, pp. 81–104.

Squier Associates. (2000). "Sandy River sediment study, Bull Run Hydroelectric Project." *Draft report prepared for Portland General Electric*, Squier Associates, Lake Oswego, Ore.

Sternberg, H. (1875). Untersuchungen über Langen-und Querprofil geschiebeführende Flüsse. *Zietschrift für Bauwesen*, 25, 483–506.

Stillwater Sciences. (2000). "Evaluation of geomorphic effects of removal of Marmot and Little Sandy dams and potential impacts on anadromous salmonids." *Technical report prepared for Portland General Electric*, Stillwater Sciences, Portland, Ore., <http://www.stillwatersci.com/whatwedo/sedtranspubs>(accessed on Sept. 26, 2005).

Stillwater Sciences. (2002). "Sediment transport modeling following the removal of Marmot Dam with 125,000 and 300,000 cubic yards of dredging prior to dam removal." *Technical Memorandum to Portland General Electric*, Stillwater Science, Portland, Ore., <http://www.stillwatersci.com/whatwedo/sedtranspubs>(accessed on Sept. 26, 2005).

Swanson, F. J., and Dyrness, C. T. (1975). "Impact of clear-cutting and road construction on soil erosion by landslides in the western Cascade Range, Oregon." *Geology*, 1, 393–396.

Swanson, F. J., Janda, R. J., and Dunne, T. (1982). "Summary: sediment budget and routing studies." *Workshop on sediment budgets and routing in forested drainage basins: Proceedings,* F. J. Swanson, R. J. Janda, T. Dunne, and D. N. Swanston, eds., *General Technical Report PNW-141*, U.S. Forest Service, Pacific Northwest Forest and Range Experiment Station, Portland, Ore., pp. 157–165.

Toro-Escobar, C. M., Parker, G., and Paola, C. (1996). "Transfer function for the deposition of poorly sorted gravel in response to streambed aggradation." *Journal of Hydraulic Research,* 34(1), 35–54.

U.S. Army Corps of Engineers (USACE). (1993). "HEC-6: Scour and deposition in rivers and reservoirs." *User's Manual*, Hydrologic Engineering Center, <http://www.hec.usace.army.mil/software/legacysoftware/hec6/hec6-documentation.htm>(Sept. 26, 2005).

Van Rijn, L. C. (1984). "Sediment transport. II: Suspended load transport." *Journal of Hydraulic Engineering*, 110(11), 1613–1641.

Wilcock, P. R., and Crowe, J. C. (2003). "A surface-based transport model for sand and gravel." *Journal of Hydraulic Engineering*, 129(2), 120–128.

Copyrighted Materials
Copyright © 2008 American Society of Civil Engineers (ASCE)
Retrieved from www.knovel.com

VITO A. VANONI (1904–1999): LEADER IN SEDIMENTATION ENGINEERING

Norman H. Brooks, Honorary Member ASCE[1]

A LONG CAREER

Vito Vanoni, born on August 30, 1904 in Somis, Ventura County, California, attended Caltech, earning a B.S., M.S., and PhD in civil engineering. After ten years in a research position in hydraulics at Caltech, Dr. Vanoni was appointed assistant professor of hydraulics at the California Institute of Technology in 1942, promoted to associate professor in 1949, and served as professor from 1955 until becoming professor emeritus in 1974 (Fig. 1). He remained professionally active almost until age 90, and died at age 95 on December 27, 1999.

Professor Vanoni was a world-renowned authority on the mechanics of transport of sediments by streams and rivers. His teaching and research were not only in the area of mechanics of sediment transport, but also included advanced hydraulics, hydraulic structures, and coastal engineering. In his quiet determined way, he contributed greatly to the robust development of the field of sedimentation engineering, especially through his pioneering flume experiments of suspended sediment transport of fine sands in the late 1930s (Vanoni 1940, 1946), and the publication of the famous book *Sedimentation Engineering, ASCE Manual No. 54,* edited and written in part by Vanoni (1975).

He encouraged fundamental research on sediment transport using modern fluid mechanics, and recognized the need for much more graduate-level education to support the advances in research and applications of sedimentation engineering. In his later years he was the recognized distinguished patriarch of his field in the United States.

Youth on the Vanoni Farm

Vanoni was raised on the family farm developed by his unusually enterprising father, Battista Vanoni, an immigrant from Italy. They grew lima beans, then walnuts and citrus fruits. Early problems on the ranch included drainage of flood waters, erosion control, and sediment management. His father was the first in the area to bring the industrial revolution to the farm—during Vanoni's boyhood—first various horse-drawn machines, then trucks, tractors, and other motorized machines.

[1] W. M. Keck Laboratory of Hydraulics and Water Resources, Mail Code 138–78, California Institute of Technology, Pasadena, CA 91125. E-mail: brooksn@its.caltech.edu

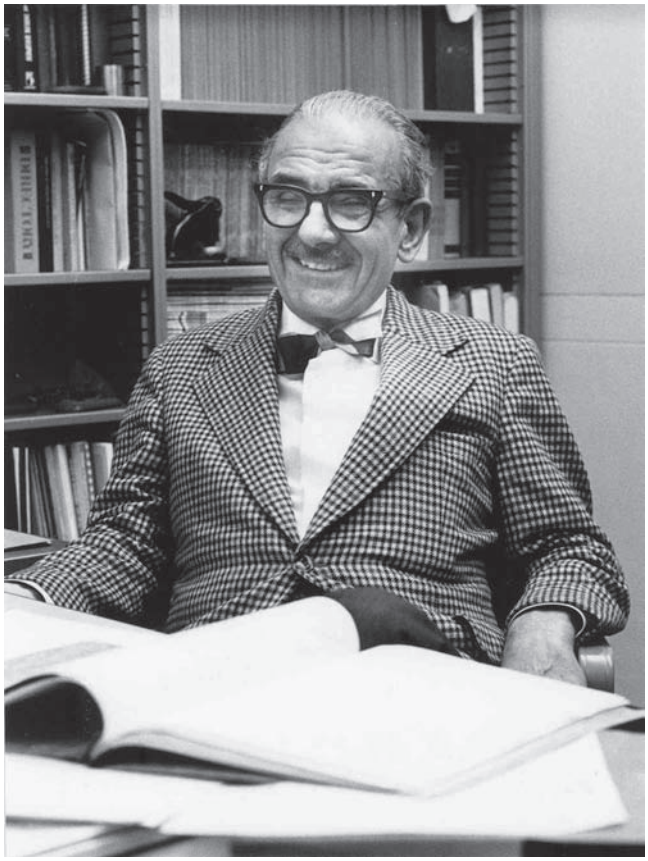

Fig. 1. Prof. Vito A. Vanoni in his office, 1974. (Photo credit: Caltech)

His father believed strongly in getting his many children the best education possible. After high school Vanoni enrolled in 1922 in the newly established California Institute of Technology, majoring in civil engineering, and graduated with a Bachelor of Science degree in 1926. His early experiences on the farm profoundly affected his attitudes and interests throughout his life. He loved the soil and had an active half-acre farm behind his large home lot in Pasadena for 50 years, right up to his final year. His future professional work in sedimentation must have had its common-sense intuitive roots in his early years on the family farm.

The Structural Engineer

As a new civil engineering graduate from Caltech, Vanoni worked five years for a consulting engineering firm doing structural steel design in Ohio, then returned to Caltech in 1931 to obtain a Master of Science degree in civil engineering in 1932, specializing in structural engineering. When he looked for a job in that depression year he got an offer from Professor Robert Knapp to work at the Hydraulic Structures Laboratory, then mostly outdoors. This was the starting point for his hydraulics career, first in hydraulic model studies of various proposed structures, often with sediment problems, and then into sedimentation research. At the same time he continued his graduate study toward his PhD.

The Hydraulic Researcher

From 1935 to 1947 Vanoni supervised the cooperative Sedimentation Laboratory of the Soil Conservation Service (SCS) and Caltech in a large one-story wooden building on the Caltech campus. The SCS sponsorship stopped in 1947, but research on sediment transport in open channel flumes and

turbulent diffusion in a low-speed water tunnel continued. In 1961 the new W. M. Keck Laboratories became the home for this program.

His meticulous experimental PhD research on transportation of suspended sediment in a 60-foot recirculating flume is still regarded as one of the classic contributions in his field, and was recognized by the American Society of Civil Engineers (ASCE) with the Hilgard Hydraulics Prize for the most outstanding paper in hydraulic engineering published by the ASCE in 1946.

During the war years, Vanoni did defense-related research for the National Defense Research Committee and the U.S. Navy, primarily related to the investigation and control of wave action in harbors using hydraulic models on the campus and later in a large off-campus facility in Azusa. He was also active in the design and testing of hydraulic structures such as drop structures for energy dissipation. When Lake Mead was being filled after the closure of Hoover Dam, he and his colleagues demonstrated qualitatively in the laboratory the newly recognized phenomena of inflowing density currents and selective withdrawal in density-stratified reservoirs.

Sediment research continued after the SCS sponsorship stopped in 1947, but at a reduced level. Five more doctoral students completed PhD research on sedimentation topics in the Sedimentation Laboratory up until 1960 (in chronological order): Hassan Ismail, myself, George Nomicos, Ronald McLaughlin, and John Kennedy. Vanoni was the thesis adviser for the first three of these.

In the late 1950s Vanoni and I planned the new Keck Hydraulics Laboratory, which opened in 1961. (Professors Fredric Raichlen and John List joined the laboratory group in 1962 and 1969 respectively.)

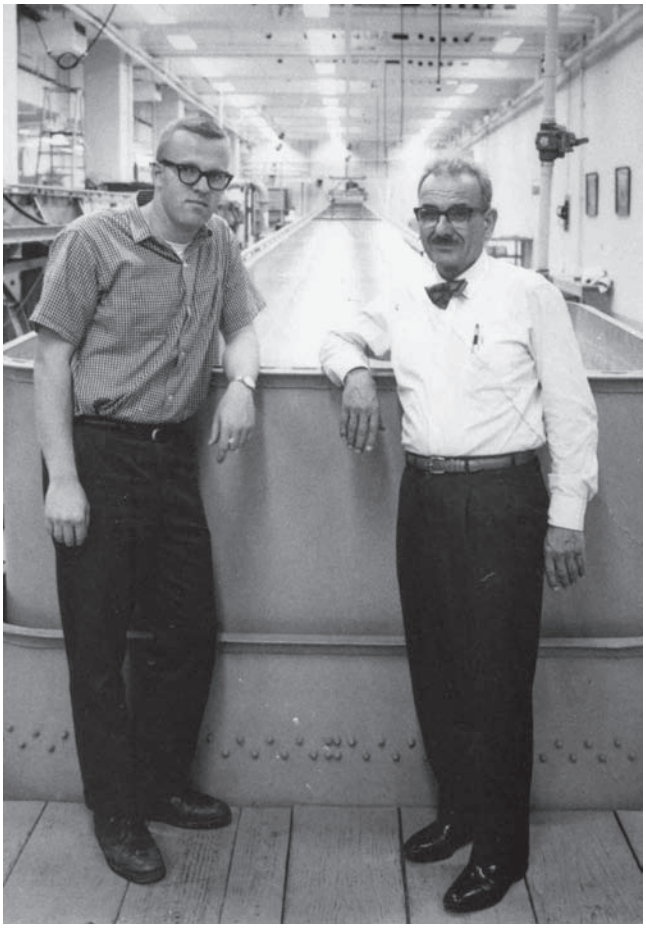

Fig. 2. Vanoni with Ph.D. student Richard Brock at the downstream end of the 40-meter tilting flume in the Keck Hydraulics Laboratory, approximately 1965. (Photo credit: Caltech)

Fig. 3. Members of the Missouri River Division Sediment Advisory Board (July 26, 1950). From left to right: H. A. Einstein, Univ. of California, Berkeley; T. H. Means, consulting engineer, San Francisco; E. W. Lane, Bureau of Reclamation, Denver; L. G. Straub, University of Minnesota, Minneapolis; G. A. Hathaway, Corps of Engineers, Washington, D.C.; and V. A. Vanoni, California Institute of Technology, Pasadena. Picture taken while on inspection trip of Missouri River below Fort Peck Dam. (Credit for photo and legend: Corps of Engineers, Fort Peck District, Photo No. 17920)

Under Vanoni's leadership, the program of the new Keck Hydraulics Lab focused on sediment transport, coastal engineering, and the emerging area of environmental hydraulics. Basic hydraulic structures and model studies became secondary. In the Keck Lab years, the PhD students he supervised were Alexander Sutherland, Li-San Hwang, Richard Brock (Fig. 2), and Brent Taylor.

One of Vanoni's fine attributes, starting from his earliest research work, was his extreme care in crediting other people's ideas and work, while claiming the minimum for himself.

The Sedimentation Engineering Manual

As a major contribution to the profession, he organized, partially wrote, and edited the 730-page definitive ASCE Manual 54, *Sedimentation Engineering* (Vanoni 1975). As chairman of the special Task Committee, established in 1954, charged with writing the manual, Vanoni worked very hard for two decades and set a high standard, persuading many contributors to do major rewrites as needed or doing them himself. In an unusual publication procedure, many of the sections of the original manuscript for the book were first published in the *Journal of the Hydraulics Division, ASCE;* they received consider-

able discussion, which was taken into account in the final manuscript. His effort was an example of strong multi-year persistence and unlimited patience with slow contributors.

The book has received worldwide recognition and widespread use in academia and practice, and was awarded the ASCE Hilgard Award for the best publication in hydraulics in 1976. The success of that book has inspired the current ASCE Sedimentation Committee, under the leadership of Professor Marcelo Garcia (University of Illinois), to write this second volume to document the progress of the past three decades.

The River Hydraulics Consultant

Dr. Vanoni served as an expert individual consultant on river channel and sedimentation problems for many government agencies and consulting firms, extending for almost twenty years into his retirement. Most notable were the several consulting boards he served on for the U.S. Army Corps of Engineers, dealing extensively with sediment problems on the Missouri, Mississippi, and Sacramento Rivers (Fig. 3). After the eruption of Mount Saint Helens in 1980, he served the Corps for several more years to advise on coping with the huge sediment inputs to the Toutle, Cowlitz, and Columbia Rivers.

More Honors in Retirement

In recognition of his outstanding lifetime work, Dr. Vanoni was elected to the National Academy of Engineering in 1977, and became an Honorary Member of the American Society of Civil Engineers in 1980.

In 1983 he was honored by his selection by ASCE to be the distinguished Hunter Rouse Hydraulic Engineering Lecturer (Vanoni 1984). In 1989 he was named the first recipient of the ASCE's Hans Albert Einstein Award. This prize is awarded annually for a "significant contribution to the engineering profession in the areas of erosion control, sedimentation and/or waterway development." It is interesting to note that both Rouse and Einstein had been Vanoni's colleagues at the Sedimentation Laboratory about 60 years ago. (Also Arthur Ippen and James Daily were among Vanoni's contemporaries at Caltech in the late 1930s.)

Personal Life

Vanoni and his wife, Edith, enjoyed many activities together, especially foreign travel to all the continents, and camping in the Sierra Nevada mountains in California. They often opened their home and wonderful patio and "farm" to colleagues, students, and visitors. They are remembered by many for their friendship and warm hospitality. After 61 years of marriage, Edith died in 1995. Although they had no children, Vanoni (or Uncle Vito) is survived by many relatives in his extended family in his native Ventura County and in Santa Barbara.

VANONI'S RESEARCH ON SUSPENDED SEDIMENT TRANSPORT IN FLOWING WATER

In the 1930s basic fluid mechanics was rapidly being infused into civil engineering hydraulics as well as all the other fields of engineering dealing with fluids. For his PhD research, Vanoni was the first to make definitive experiments to measure the transport of fine sand in suspension in turbulent flows of water in an open channel flume. He made his meticulous experiments using the new 60-foot-long steel recirculating laboratory flume, which he designed and built in the Sedimentation Laboratory. (He also designed the building.) His previous experience in structural steel design had proved to be very useful.

In his flume experiments Vanoni (1940, 1946) measured the vertical distribution of suspended sediment concentration along with velocity profiles for a number of experiments using fine, well-sorted sand. The flume bottom was artificially roughened to reduce the effect of the smooth sidewalls with a single layer of 0.88 mm-sand grains stuck to the steel bottom. He compared his measurements with the now well-known equation for the variation of the concentration of suspended sediment over the depth in an open-channel flow, first presented by Rouse (1937), who was also at the SCS Sedimentation Laboratory at Caltech at that time. The results confirmed this new equation derived from von Karman's logarithmic velocity distribution leading to a parabolic distribution of the diffusion coefficient—that is, for the upward diffusion of the sand grains to balance the gravitational

settling. In his PhD thesis he acknowledges both Professors Theodore von Karman and Robert Knapp for guidance in his research.

From the velocity distributions, Vanoni determined that the von Karman constant κ was decreased from its normal value of 0.40 by the presence of suspended sediment; the greater the concentration, the greater was the reduction in κ. This result has attracted the attention of numerous subsequent investigators.

To fit experimental results to theory, Vanoni had to determine the fall velocity of his carefully sorted sands by dropping hundreds of grains in water. Previous investigators had paid little attention to fall velocity of sands. He found that the sedimentation diameters are slightly larger than the sieve diameters for his sands (ranging from 0.10 to 0.16 mm mean diameter). He also observed longitudinal streaks of small sand deposits on the bed of the flume, indicating definite secondary circulations. This was probably one of the first observations of streaks in flumes and prompted much discussion of his ASCE paper (Vanoni 1946).

Another by-product of Vanoni's work was the acceptance of recirculating flumes for sediment transport experiments. Previous to his work the prevailing approach was to feed sediment at the upstream end of the flume and remove it at the downstream end. In Vanoni's experiments the water and sediment were collected at the downstream end in a hopper and pumped together through a return pipe to a well-designed diffuser and inlet section. The recirculation in a closed circuit allows control of the total volume of water in the system, thereby fixing the mean depth, while the flume slope remains adjustable (by a flume jacking system). With a discharge regulated by the speed of the pump, the velocity is also then predetermined in such experiments. This has interesting implications for transfer of results to the field in terms of which variables are independent or dependent.

It should be noted that in Vanoni's experiments the stream was really starved for sediment, namely there was not a sediment bed in the flume. This meant that no bedforms (ripples or dunes) were allowed to develop and there was no question about separating the resistance into skin friction and form drag.

With his students in the subsequent years, he continued to work on the effects of suspended sediment and bedforms on the flow resistance (friction factor) and the velocity profiles. In the 1950s the Sedimentation Laboratory had support from the Corps of Engineers and the Agriculture Research Service to continue flume studies of roughness and suspended load in alluvial channels. For example, in Vanoni and Brooks (1957), we showed clearly how greatly the friction factor changes in an alluvial stream as the bedforms change. Added form drag on the bed completely overwhelms any of the damping effects of sediment in suspension.

In the 1950s Vanoni was a collaborator with the Corps of Engineers in a large field study on the Missouri River, which again confirmed the basic equations for suspended sediment distribution at a much larger scale.

VANONI'S OVERVIEW OF PROGRESS IN SEDIMENTATION RESEARCH IN 1963

With the passage of so much time it is hard to get a good perspective on the developments that occurred during Vito Vanoni's prime years. This is also confounded by the burst of computer programs for solving lots of problems in alluvial channels in the last two decades. Vanoni had a time mismatch with the computer age because he was well into his 80s before the first user-friendly PC's came along. Nonetheless, he was a fan of the pocket calculators from Hewlett Packard and always bought the latest version as soon as it came out.

It is interesting to go back to see what the research progress in this field looked like before modern instrumentation and computers became available to process the data and run model simulations. An important conference held in 1963 in Jackson, Mississippi—the Federal Interagency Sedimentation Conference—provides this historical perspective. The 933-page proceedings volume is a very good summary of all the facets of U.S. sedimentation engineering work in progress at that time. Vanoni presented a paper titled "Review of Research Activities in Sedimentation" (Vanoni 1965) in which he summarized in six pages what he considered the significant advances in the previous 15 to 20 years. His paper is also a valuable source of 46 key references from the mid-1930s to the early 1960s. These will not appear in typical computer searches today.

Vanoni's remarks have relevance today. The following paragraph from the summary of his paper gives an example of his thinking in the early 1960s:

> I have pointed out three developments which in my opinion have keynoted the work of recent years. These are (1) the theory of turbulent suspension, (2) the clarification of the role of bed forms, and (3) the discovery of the great difference between flow in curved and straight channels. The first of these differs from the other two in that it is expressible theoretically in equations in concise and quantitative form. As such, it is readily understandable, and can be assimilated into textbooks and preserved permanently. The other two items are qualitative ideas, expressible only in words, and hence their true significance is appreciated only by those with some familiarity with sedimentation. Because of this they are more difficult to incorporate into textbooks and are in danger of being lost and then rediscovered, as was the work of river engineers of several generations ago.

Vanoni urged that information about peculiar behavior of streams be documented in the literature even if the investigator can't yet explain it. He was also a great promoter of more interaction between laboratory and field research, and believed that one of the reasons for good progress in the 1950s was increased collaboration on a personal level. He also encouraged university research as a way to increase the number of highly-qualified researchers and practitioners to handle the ongoing sedimentation problems, which he thought would be with us for many years.

His last significant research paper showed how to predict what type of bedforms occur (ripples, dunes, flat, antidunes) from dimensionless hydraulic parameters describing the characteristics of the flow and the bed sediment (Vanoni 1974). The paper presented graphs showing large quantities of sediment data which had been hand-calculated and hand-plotted, just before the advent of good computer-driven plotters.

In his retirement, Vanoni continued to publish excellent comprehensive review papers, most notably the monograph "River Dynamics" in *Advances in Applied Mechanics* (1975), and the ASCE Rouse Hydraulic Engineering Lecture, "Fifty Years of Sedimentation" (1984).

CLOSING REMARKS

It was a great privilege to have had Vito Vanoni as a mentor, faculty colleague, and friend—he had a tremendous impact on my career and life over 49 years. When I first came to Caltech in 1950, I was immediately attracted to work with him because of his knowledge and inspiring approach to hydraulics—and life in general. I was fascinated to learn the mechanics of rivers and how they were being disturbed by the works of man. He seemed especially enthusiastic when he took me out in the field to inspect local flood events and damage, which is a tradition I kept up with my students.

As a thesis adviser he showed me that careful observations trumped theories if they disagree. He turned me from being a young, idealistic theorist into a careful observer and pragmatist. I was trying to solve the problem of how to predict C_a, the sediment concentration at a small height "a" above the bed, which was needed to make the suspended load equation useful for applications. I worked out what I thought was a good theory first, then set out to "confirm" it with experiments. But when I started making flume experiments with a sand-covered bed, small sand dunes appeared, and I was distressed because they had no place at all in my theory. I consulted with him as to how I could get rid of the pesky dunes, so I could check my theory. Vanoni said, "Young man, that's the way it is, so that's what you should study." So right then and there my focus shifted to studying these bedforms and their impact on sediment transport and stream roughness.

After I became a faculty member in 1954, Vanoni never made me feel like a junior colleague. He shared many responsibilities of the lab with me and encouraged my initiatives. I had fun planning the new Keck Hydraulics Laboratory with him in the late 1950s. He sent me on a tour to visit other prominent hydraulics labs in the United States to pick up ideas of what to do or not do in designing a hydraulics lab. The visits also allowed me to meet numerous other hydraulics researchers around the country and find out what they were doing.

As Vanoni approached his mandatory retirement date at age 70, he was still impressing the students with his energy and enthusiasm. Vanoni was in a stage of life that I call "young old age," which lasts until you transition to "old old age." Vanoni made "young old age" last for about 20 more years, going

to the lab almost daily, writing papers, doing consulting work well into his 80s. He greatly enjoyed consulting with the Corps of Engineers after the Mount St. Helens eruption in the early 1980s about what to do with all that extra sediment.

Throughout his career and well into his retirement, he was always interested in visiting all the hydraulics research students in the lab (not just his own students); he wanted to hear and see what they were doing, make suggestions, and almost always offer words of encouragement. His comments were always quick and to the point. We miss his cheerful visits, as he seemed to represent the heart and soul of the Keck Hydraulics Laboratory at Caltech.

REFERENCES

Rouse, H. (1937). "Modern Conceptions of the Mechanics of Fluid Turbulence." *Trans., ASCE,* 102, 461–543. Reprinted with all discussions in *Classic Papers in Hydraulics, ASCE* (1982), 52–132.

Vanoni, V. A. (1940). "Experiments on the Transportation of Suspended Sediment by Water." Ph.D. Thesis, California Institute of Technology.

Vanoni, V. A. (1946). "Transportation of suspended sediment by water." *Trans. ASCE,* 111, 67–133. Reprinted with all discussions in *Classic Papers in Hydraulics, ASCE* (1982), 266–332.

Vanoni, V. A., and Brooks, N. H. (1957). "Laboratory studies of the roughness and suspended load of alluvial streams," *Report E-68,* Sedimentation Laboratory, California Institute of Technology.

Vanoni, V. A. (1965). "Review of research activities in sedimentation." *Proc., Federal Inter-Agency Sedimentation Conf.,* Jackson, Mississippi, January 1963, published as Agricultural Research Service Miscellaneous Publication No. 970, 8–13.

Vanoni, V. A. (1974). "Factors determining bed forms of alluvial streams." *J. of Hyd. Div., ASCE,* 100(HY3), 363–377. See also closing discussion, *J. of Hydrol. Div., ASCE,* 101(11), 1435–1440.

Vanoni, V. A., ed. (1975). *Sedimentation engineering, manuals and reports on engineering practice no. 54,* American Society of Civil Engineers.

Vanoni, V. A. (1975). "River dynamics." *Advances in Applied Mechanics, 15,* Academic Press, New York, 1–87.

Vanoni, V. A. (1984). "Fifty years of sedimentation." *Fourth Hunter Rouse Hydraulic Engineering Lecture,* presented at the August 1983 Hydraulics Division Specialty Conference held at Cambridge, Massachussets. *J. of Hydrol. Eng.*, *ASCE,* 110(8), 1022–1057.

Copyrighted Materials
Copyright © 2008 American Society of Civil Engineers (ASCE)
Retrieved from www.knovel.com

APPENDIX A

Rock Scour

George W. Annandale and Erik F. R. Bollaert

INTRODUCTION

Rock scour can occur when the erosive capacity of water exceeds the ability of rock to resist it. Typical environments where rock scour is a concern are downstream of overtopping dams, downstream of spillways, in plunge pools, around bridge piers, in unlined rock tunnels, and in channels and at other structures constructed in rivers and marine environments. Development of technology to predict scour of rock commenced in 1991 and has seen significant growth since then.

This appendix provides a summary of technology that can be used to determine the potential for and the extent and rate of rock scour. The latest technology in this field is explained in more detail in Schleiss & Bollaert (2002) and in Annandale (2006). Both works provide a detailed exposition of rock scour technology, explains methods for applying it, and provides a number of case studies validating the technology and demonstrating its application.

Two quantitative approaches, known as the Erodibility Index Method (EIM; Annandale 1995, 2006) and the Comprehensive Scour Model (Bollaert 2002, 2004; Bollaert & Schleiss 2005), can be used to predict the potential for and the extent of scour. While both approaches allow estimating the ultimate possible scour depth, only the latter model is capable of predicting scour evolution as a function of time. By following these approaches, the practitioner can cross-check results and identify failure modes leading to scour of rock.

The EIM is basically a semi-empirical model that is based on a scour threshold relating the relative magnitude of the erosive capacity of water to the relative ability of rock to resist it (Annandale 1995). When using this method, the relative ability of rock to resist erosion is quantified by a geomechanical index known as the erodibility index. The erosive capacity of water is determined by quantifying the stream power of the flowing water. The universality of the scour threshold relationship offered by the EIM and the use of stream power to quantify the relative magnitude of the erosive capacity of water provide practitioners with the ability to solve almost any scour problem in a global manner (Annandale 2006) for its ultimate depth. No rate of scour is available, however.

The Comprehensive Scour Model (CSM) developed by Bollaert (2002, 2004) is a completely physically based model that consists of two principal components: the comprehensive fracture mechanics (CFM) method and the dynamic impulsion (DI) method. Application of the CFM is focused mainly on fissured rock where brittle fracture or failure by fatigue dominates. Brittle fracture occurs instantaneously, while failure by fatigue is time dependent and thus allows estimating the time evolution of scour formation. The DI method is used principally to assess scour of intact blocks of rock formed by joints and fractures, but can also be used to predict sudden failure of concrete slab linings of stilling basins (Bollaert, 2004b). In some cases, large blocks of rock delineated by joints and fractures may also contain fissures within the principal mass of the rock and all three failure mechanisms; that is, brittle fracture, failure by fatigue, and removal by dynamic impulsion may be relevant. Application of both the CFM and the DI method requires quantification of the mean and fluctuating dynamic pressures acting within fissures, joints, and fractures. These pressures are caused by turbulence in flowing water. The method can in principle be applied to any type of turbulent flow situation and any type of fractured media, provided that turbulent pressure fluctuations and the strength of the fractured media can be reasonably estimated. The model not only provides the ultimate scour depth but also an estimate of the rate of scour during the lifetime of the structure in question.

OVERVIEW OF ROCK SCOUR

Rock scour occurs when the erosive capacity of water flowing over the rock exceeds its ability to resist scour. It is therefore

necessary to not only understand the characteristics of flowing water leading to scour of rock but also devise practical methods to quantify its erosive capacity. Similarly, it is necessary to investigate and understand the failure mechanisms in rock leading to scour and devise practical approaches for quantifying its ability to resist the erosive capacity of water. A relationship between the erosive capacity of water and the ability of rock to resist it at the threshold of motion is known as a scour or erosion threshold.

Erosive Capacity of Water

Most engineers interested in the interaction between flowing water and earth materials opine that the shear stress exerted by the flowing water on the material results in erosive action. Bollaert (2002) proves that the erosive capacity of turbulent flow on fractured rock is the result of fluctuating pressures and not shear stress, while Annandale (2006) demonstrates that use of shear stress is correct for laminar flow only. These are important observations, as application of a shear stress concept cannot explain how large blocks of rock can be removed from a rock formation or how turbulent flow can break rock blocks into smaller pieces.

To state this, Bollaert (2002) and Bollaert and Schleiss (2003; 2005) conducted detailed research into pressure fluctuations of turbulent plunging jets and determined how these pressure fluctuations interact with rock joints and fissures. They developed methods that can be used to quantify the relative magnitude of fluctuating pressures due to turbulent jet flows, which are very useful when investigating scour of rock in plunge pools or stilling basins downstream of hydraulic structures. They also showed that free air in the water can play a significant role in causing resonance of fluctuating pressures in close-ended rock fissures, increasing pressure magnitudes by up to 20 times. Such amplification plays an important role when rock scour occurs because of brittle fracture or fatigue failure. Bollaert (2002) also showed that block removal by dynamic impulsion occurs because of the transient effect of pressure waves introduced into rock joints and depends on the time persistency of the net uplift forces.

Pragmatic methods to quantify the relative magnitude of fluctuating pressures due to turbulent flow (Fig. A-1) are available for turbulent jets, hydraulic jumps and horizontal and vertical river constrictions, such as for example bridge abutments or bed sills (Hoffmans & Verheij, 1997). Other flow situations such as bridge piers are currently under investigation. For flow scenarios where the turbulence intensity of the flow cannot be readily estimated, indirect techniques can be used to quantify the relative magnitude of pressure fluctuations. Annandale (1995) used a direct relationship between stream power and the relative magnitude of turbulent pressure fluctuations. The other approach relies on findings by Hinze (1975), that is, that the magnitude of fluctuating pressures can be correlated to boundary shear stress caused by flowing water.

Stream power is equivalent to the rate of energy dissipation in flowing water, which is high when flow is very turbulent and decreases when flow is less turbulent. Turbulence in flowing water is the principal reason for energy dissipation.

A general expression for stream power is

$$SP = \int_{x2}^{x1} \rho\, g \cdot Q \cdot \Delta E(x) \cdot dx \tag{A-1}$$

SP = total stream power between locations x_1 and x_2;
t = time;
$\Delta E(x)$ = energy head loss of flow at location x;
Q = discharge;
ρ = mass density of water;
g = acceleration due to gravity.

Equation (A-1) is often of little use to most practitioners, who wish to have simple techniques to quantify the magnitude of stream power. Annandale (2006) has developed a suite of equations allowing practitioners to quantify stream power for varying flow conditions, including plunging jets, hydraulic jumps, flow around bends, flow around bridge piers, flow in tunnels and over knickpoints, as well as flow in channels.

Alternatively, should a practitioner be interested in estimating the relative magnitude of pressure fluctuations, and the shear stress exerted by the flowing water is already known, the following equations can be used. Hinze (1975) found that the root mean square of fluctuating pressures in turbulent flowing water can be correlated to the shear stress as

$$p' = 3 \cdot \tau \tag{A-2}$$

where p' = root mean square of the turbulent fluctuating pressures; τ = boundary shear stress.

In addition to this one also wishes to know the magnitude of the maximum pressure peaks that can result due to turbulence. Emmerling (1973) found that the maximum pressure peaks can be as high as $6 \cdot p'$; that is,

$$p_{max} = 18 \cdot \tau \tag{A-3}$$

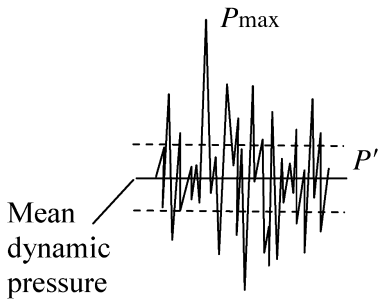

Fig. A-1. Mean dynamic pressure, root mean square of the fluctuating dynamic pressure, and maximum fluctuating dynamic pressure in turbulent flow.

An important observation when applying either of Equations (A-2) or (A-3) is that these are merely simple correlations relating pressure fluctuations to shear stress. It does not mean that scour is caused by shear but merely is a procedure to estimate the relative magnitude of pressure fluctuations if shear stress is known.

Rock Scour Mechanisms

Rock can scour by means of four mechanisms: block removal, brittle fracture, subcritical failure, and abrasion.

• Block Removal

Fluctuating pressure magnitudes resulting from turbulent flow vary as a function of space and time. The pressures introduced into rock joints due to turbulent flow can result in increased pressure directly underneath the rock. When upward pressure underneath the rock exceeds the weight of the rock block and the friction forces along its sides, the rock will start being removed from the rock formation (Fig. A-2). Depending on the time persistency of the uplift forces, this phenomenon can lead to imminent failure and occurs as soon as the upward forces exceed the downward forces for a minimum time duration (Bollaert 2002, 2004b). An example of uplift failure of concrete slabs has been observed at Gebidem Dam (Switzerland).

• Brittle Fracture

Brittle fracture of rock occurs when the stress intensity at the edges of close-ended fissures, resulting from the introduction of fluctuating pressures into the fissures, is greater than the fracture toughness of the rock (Bollaert, 2002, 2004a). When this occurs the rock fails in an explosive manner (Fig. A-3). Such failure typically results in the rock breaking up into smaller pieces. An example of rock scour by brittle fracture has been found at Santa Luzia Dam, Portugal (Annandale 2006). This failure type occurs instantaneously.

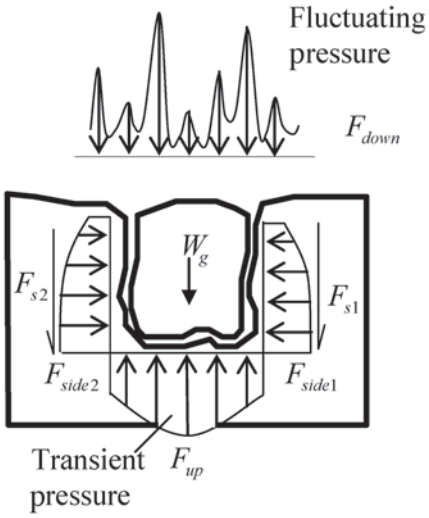

Fig. A-2. Rock scour by block removal (also known as dynamic impulsion) (based on Bollaert 2002).

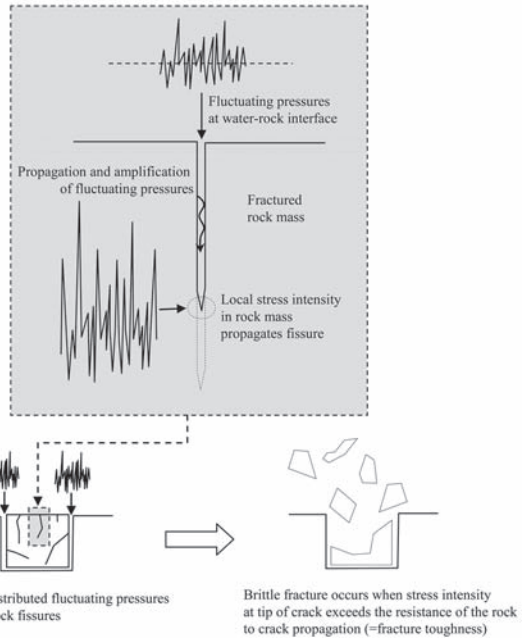

Fig. A-3. Scour of rock by brittle fracture (based on Bollaert 2002, 2004a).

• Subcritical Failure

Scour of rock by subcritical failure occurs when the stress intensities at the edges of close-ended fissures do not exceed the fracture toughness of the rock. Continued application of the fluctuating pressures in the close-ended rock fissures eventually results in breakup of the rock due to fatigue (Fig. A-4). This failure type is time dependent and both theory and practical implementations have been extensively described by Bollaert (2002, 2004a) and Bollaert and Schleiss (2005). An example of subcritical failure is the well-known scour at Kariba Dam in Zambia-Zimbabwe (Bollaert 2005).

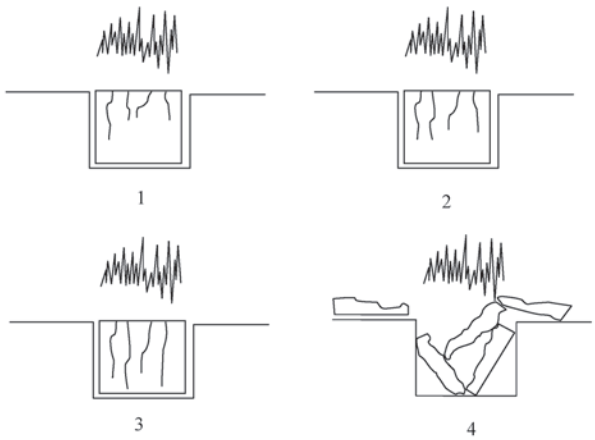

Fig. A-4. Rock scour by subcritical failure, also known as fatigue failure (based on Bollaert 2002, 2004a; Bollaert & Schleiss 2005).

• Abrasion

Scour by abrasion can occur if the fluid interacting with the rock is abrasive enough relative to the resistance offered by the rock to cause it to scour in a layer-by-layer fashion. An example of abrasion damage on concrete slabs has been observed at Gebidem Dam (Switzerland).

COMBINED APPLICATION OF METHODS

Rock scour by abrasion can currently only be analyzed by making use of laboratory testing. This type of scour is currently believed to be less prevalent than scour by sudden block removal (dynamic impulsion), brittle fracture, and fatigue failure (subcritical failure). The latter three scour mechanisms can be separately analyzed by making use of the CSM developed by Bollaert (2002, 2004), while the EIM only provides a global assessment of rock scour.

It has been found that scour analyses using the EIM and the CSM respectively provide comparable global results (Bollaert 2002; Bollaert and Annandale, 2004; George and Annandale, 2006). Comparison leads to the conclusion that the EIM predicts scour in a global manner, inherently accounting for all possible mechanisms of break-up but without any noticeable insight into which mechanism is most feasible. On the other hand, the CSM allows a much more detailed description of the type of scour as well as the scour rate.

Knowledge of how scour will occur is important for development of economical design solutions. For example, if a rock scour analysis concludes that scour will occur by brittle fracture and dynamic impulsion only, it is necessary to develop mitigation measures to protect against scour. If, in another case, an analysis indicates that scour will occur by subcritical failure (fatigue) only, it might not be necessary to design mitigation measures. This might be the case if it is found that the rock will only scour after, say, 30 days of continuous submission to fluctuating pressures. If the design flood would only submit the rock to, say, 10 hours of fluctuating pressures, the rock is unlikely to experience damage during such a flood, and protection against scour may not be warranted.

THE EIM

Hydraulic erodibility of natural and engineered earth materials can be evaluated in terms of a rational correlation between the stream power of flowing water and a geomechanical index. The relative ability of earth materials to resist scour can be characterized in terms of an erodibility index, *K*. The parameters of the index represent key material properties including mass strength, block/particle size, discontinuity/interparticle bond shear strength, and shape and orientation relative to flow. The relative magnitude of erosive power of flowing water as used in this method is represented by the stream power of flowing water.

Annandale (1995) developed a scour threshold relationship based on this approach by analyzing 137 field observations of spillway performance collected by the U.S. Department of Agriculture; observations at Bartlett Dam, Salt River Project, Arizona; and at four South African dams and published data related to initiation of sediment motion. This threshold relationship was established for a wide range of earth materials, ranging from noncohesive granular soils, cohesive soils, vegetated soils, and rock. The information presented in this appendix focuses on the erodibility of rock only. Application of this method to solve scour of other earth materials is discussed in Annandale (2006).

The observation that turbulence in flowing water is related to both energy loss and pressure fluctuations provides a convenient way to quantify the relative magnitude of the erosive capacity of water. This can be done by calculating the rate of energy dissipation (also referred to as stream power in this appendix), which has been shown to correlate to the relative magnitude of pressure fluctuations (Annandale 1995, 2006).

The correlation between rate of energy dissipation (P) and a material's resistance to erosion ($f(K)$) can be expressed by the function

$$P = f(K) \tag{A-4}$$

at the scour threshold. If $P > f(K)$, the scour threshold is exceeded, and the material is expected to erode. Conversely, if $P < f(K)$, the erodibility threshold is not exceeded, and erosion is not expected. The relationship between stream power and the Erodibility Index K is presented in Figure A-5. The data shown on the figure represent events that experience scour when subjected to flowing water and events that did not experience scour. The relationship between these values indicates a region that separates events that experienced scour from those that did not experience scour. The dashed line in this region indicates the possible location of the erosion threshold. When assessing rock scour potential, this graph is used to relate stream power to the relative ability of the rock to resist scour. If the relationship between stream power and the erodibility index for a case under consideration is located above the erosion threshold line, it is concluded that scour could occur. Alternatively, if it is located below the threshold line, it is concluded that scour is unlikely. Methods to quantify the relative magnitude of the erosive capacity of water and the relative ability of rock to resist scour are presented in the following sections.

Stream Power

A primary objective in the development of a method to calculate the relative magnitude of the erosive power of water associated with the EIM is to select parameters that reasonably represent the relative magnitude of the fluctuating pressures causing scour that can concurrently be calculated with ease. Rate of energy dissipation (or stream power) is such a parameter, and its selection can be justified per the following

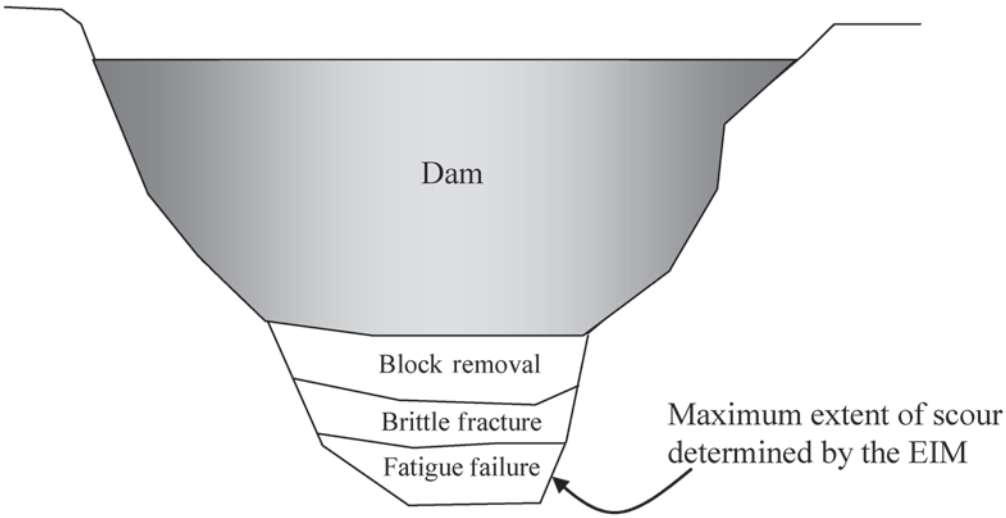

Fig. A-5. Example of scour estimation at a dam foundation resulting from overtopping by combined use of the EIM and CSM methods. Both methods are used to calculate the total scour extent. The CSM method moreover identifies the scour type (i.e., whether scour occurs by block removal, brittle fracture or fatigue failure) as well as the rate of scour.

reasoning. Turbulence causes both pressure fluctuations and energy loss, and increases in turbulence intensity concurrently result in increased rates of energy dissipation and increases in the magnitude of peak fluctuating pressures. Estimates of the rate of energy dissipation could therefore be expected to represent the relative magnitude of fluctuating pressure and thus the erosive power of the water.

Annandale (2006) presents a suite of equations to calculate the rate of energy dissipation for various flow conditions encountered in practice, including headcut formation, hydraulic jumps, channel grade change, and open channel flow. All these equations are based on a general equation that represents the rate of energy dissipation per unit area. If the energy loss is ΔE per unit length of flow (L), the unit discharge is q, average flow velocity is v, and flow depth is D, the rate of energy dissipation per unit area of the channel bed can be expressed as

$$P = \gamma \cdot q \cdot \Delta E / L = \gamma \cdot v \cdot D \cdot S_f = \tau \cdot v \qquad \text{(A-5)}$$

where τ = shear stress, S_f = energy slope.

The equations for particular flow conditions are not repeated in this appendix but can be found in the cited reference.

Erodibility Index

The erodibility index K (Eq. [A-6]) represents a measure of an earth material's resistance to erosion. The index is based on Kirsten's ripability index, for which a rational relationship was established between flywheel power of excavation equipment and the ripability of earth materials (Kirsten 1982, 1988). The primary geological parameters that are used to calculate the erodibility index are mass strength, rock block size, discontinuity/interparticle bond shear strength, and shape and orientation of rock blocks relative to the direction of flow. The index is calculated as

$$K = M_s \cdot K_b \cdot K_d \cdot J_s \qquad \text{(A-6)}$$

where M_s = mass strength number, K_b = block size number, K_d = discontinuity shear strength number, and J_s = relative ground structure number. All parameters can be assessed rapidly in the field by using simple identification tests and measurements. The paper by Kirsten (1982) provides standard tables quantifying these geological parameters that are also presented in Tables A-1 through A-5.

The value of M_s for rock can be determined by equating it to the unconfined compressive strength (UCS) in megapascal (MPa) if the strength is greater than 10 MPa and equal to $0.78 \times UCS^{1.05}$ when the strength is less than 10 MPa and then multiplying it with the coefficient of relative density. The latter is the ratio of a material's unit weight over 27.0 kN/m^3. Alternatively, if the unconfined compressive strength is unknown, field descriptions of the rock can be used to select values of M_s from Table A-1.

The block size number, K_b, is calculated as follows:

$$K_b = \frac{RQD}{J_n} \qquad \text{(A-4)}$$

where RQD = rock quality designation, a standard parameter in drill core logging (Deere and Deere 1988), and J_n = the joint set number, which is a function of the number of joint sets in a rock mass (Table A-2). K_b ranges between 1 and 100 for rock.

Table A-1 Mass Strength Number for Rock (M_s)

Hardness	Identification in profile	Unconfined compressive strength (MPa)	Mass strength number (M_s)
Very soft rock	Material crumbles under firm (moderate) blows with sharp end of geological pick and can be peeled off with a knife; is too hard to cut tri-axial sample by hand.	Less than 1.7 1.7–3.3	0.87 1.86
Soft rock	Can just be scraped and peeled with a knife; indentations 1 mm to 3 mm show in the specimen with firm (moderate) blows of the pick point.	3.3–6.6 6.6–13.2	3.95 8.39
Hard rock	Cannot be scraped or peeled with a knife; handheld specimen can be broken with hammer end of geological pick with a single firm (moderate) blow.	13.2–26.4	17.70
Very hard rock	Handheld specimen breaks with hammer end of pick under more than one blow.	26.4–53.0 53.0–106.0	35.0 70.0
Extremely hard rock	Specimen requires many blows with geological pick to break through intact material.	Larger than 212.0	280.0

Table A-2 Joint Set Number J_n

Number of joint sets	Joint set number (J_n)
Intact, no or few joints/fissures	1.00
One joint/fissure set	1.22
One joint/fissure set plus random	1.50
Two joint/fissure sets	1.83
Two joint/fissure sets plus random	2.24
Three joint/fissure sets	2.73
Three joint/fissure sets plus random	3.34
Four joint/fissure sets	4.09
Multiple joint/fissure sets	5.00

The discontinuity or interparticle shear strength number, K_d, is determined by the ratio J_r/J_a, where J_r = joint roughness number and J_a = joint alteration number. Joint roughness refers to the roughness condition of the facing walls of a discontinuity. The joint alteration number reflects the weathering condition of the joint face material. Shear strength of a discontinuity is directly proportional to the shear strength of the gouge and inversely proportional to the degree of alteration of the joint wall material. Values for the joint roughness and joint alteration numbers are found in Tables A-3 and A-4.

In addition to representing the effective dip of the least favorable discontinuity with respect to the flow, the relative ground structure number, J_s, accounts for the shape of the material units that affects the ease with which the stream can penetrate the ground and dislodge individual units. The effective dip is the apparent dip of a discontinuity adjusted for the slope of the stream channel relative to the direction of flow. Table A-5 contains values of the relative ground structure number for various ratios of joint spacing.

Scour Assessment

The extent (depth) of scour is determined by comparing the stream power that is *available* to cause scour with the stream power that is *required* to scour the earth material under consideration. The available stream power represents the erosive power of the water discharging over the earth material, whereas the required stream power is the stream power that is required by the earth material for scour to commence. If the available stream power is exactly equal to the required stream power, the material is at the threshold of erosion. In cases where the available stream power exceeds the required stream power, the material will scour. It the available stream power is less than the required stream power, the rock will remain intact.

Figure A-7 shows how the available and required stream power, both plotted as a function of elevation beneath the original ground surface, are compared to determine the extent of scour. Scour will occur when the available stream power exceeds the required stream power. Once the maximum scour elevation is reached the available stream power is less than the required stream power, and scour ceases.

The required stream power is determined by first indexing geologic core or borehole data. The values of the erodibility index thus determined will vary as a function of elevation, dependent on the variation in material properties. Once the index values at various elevations are known, the required stream power is determined from Figure A-6. The available stream power is calculated as a function of elevation by making use of methods presented in Annandale (2006).

THE CSM

Bollaert (2002, 2004) developed a physically based engineering model for prediction of the ultimate scour depth of fissured

Table A-3 Joint Roughness Number J_r

Joint separation	Condition of joint	Joint roughness number
Joints/fissures tight or closing during excavation	Discontinuous joints/fissures	4.0
	Rough or irregular, undulating	3.0
	Smooth undulating	2.0
	Slickensided undulating	1.5
	Rough or irregular, planar	1.5
	Smooth planar	1.0
	Slickensided planar	0.5
Joints/fissures open and remain open during excavation	Joints/fissures either open or containing relatively soft gouge of sufficient thickness to prevent joint/fissure wall contact on excavation	1.0
	Shattered or microshattered clays	1.0

Table A-4 Joint Alteration Number J_a

Description of gouge	Joint alteration number (J.) for joint separation (mm)		
	1.0[1]	1.0–5.0[2]	5.0[3]
Tightly healed, hard, nonsoftening impermeable filling	0.75	—	—
Unaltered joint walls, surface staining only	1.0	—	—
Slightly altered, nonsoftening, noncohesive rock mineral or crushed rock filling	2.0	2.0	4.0
Nonsoftening, slightly clayey noncohesive filling	3.0	6.0	10.0
Nonsoftening, strongly overconsolidated clay mineral filling, with or without crushed rock	3.0*	6.0**	10.0
Softening or low friction clay mineral coatings and small quantities of swelling clays	4.0	8.0	13.0
Softening moderately overconsolidated clay mineral filling, with or without crushed rock	4.0*	8.0**	13.0
Shattered or microshattered (swelling) clay gouge, with or without crushed rock	5.0*	10.0**	18.0

Notes:

[1] Joint walls effectively in contact.

[2] Joint walls come into contact after approximately 100-mm shear.

[3] Joint walls do not come into contact at all on shear.

[4] ** Also applies when crushed rock occurs in clay gouge without rock wall contact.

Table A-5 Relative Ground Structure Number J_s

Dip direction of closer spaced joint set (degrees)	Dip angle of closer spaced joint set (degrees)	Ratio of joint spacing, r			
		1:1	1:2	1:4	1:8
180/0	90	1.14	1.20	1.24	1.26
	89	0.78	0.71	0.65	0.61
	85	0.73	0.66	0.61	0.57
	80	0.67	0.60	0.55	0.52
	70	0.56	0.50	0.46	0.43
	60	0.50	0.46	0.42	0.40
In direction of stream flow	50	0.49	0.46	0.43	0.41
	40	0.53	0.49	0.46	0.45
	30	0.63	0.59	0.55	0.53
	20	0.84	0.77	0.71	0.67
	10	1.25	1.10	0.98	0.90
	5	1.39	1.23	1.09	1.01
	1	1.50	1.33	1.19	1.10
0/180	0	1.14	1.09	1.05	1.02
	-1	0.78	0.85	0.90	0.94
	-5	0.73	0.79	0.84	0.88
	-10	0.67	0.72	0.78	0.81
	-20	0.56	0.62	0.66	0.69
	-30	0.50	0.55	0.58	0.60
Against direction of stream flow	-40	0.49	0.52	0.55	0.57
	-50	0.53	0.56	0.59	0.61
	-60	0.63	0.68	0.71	0.73
	-70	0.84	0.91	0.97	1.01
	-80	1.26	1.41	1.53	1.61
	-85	1.39	1.55	1.69	1.77
	-89	1.50	1.68	1.82	1.91
180/0	-90	1.14	1.20	1.24	1.26

Notes:
[1] For intact material, take $J_s = 1.0$
[2] For values of r greater than 8, take J_s as for $r = 8$.

and jointed rock. The CSM incorporates two major failure modes of fissured and jointed rock. The first mode, described by the comprehensive fracture mechanics (CFM) method, determines the ultimate scour depth by expressing instantaneous or time-dependent crack propagation. The second mode, described by the dynamic impulsion (DI) method, determines ultimate scour depth by calculation of the ejection of rock blocks due to sudden net uplift impulsions. The CFM method is applied principally to fissured rock and the DI method to jointed rock. However, individual rock blocks in a jointed rock mass can contain fissures that can fail in brittle fracture or by fatigue, which can lead to formation of smaller rock blocks that can be removed by dynamic impulsion with less effort. Hence, both methods are strongly related to each other.

The structure of the CSM, specifically developed for predicting scour by plunging or submerged jets, distinguishes between three modules: the falling jet, the plunge pool, and the rock mass. The latter module allows simulation of the previously mentioned failure mechanisms, that is, brittle fracture, failure by fatigue, and dynamic impulsion. Emphasis is placed on the description of physical parameters that are necessary to accurately describe the different processes. This is presented in a way that allows practicing engineers to implement the concepts while still honoring the basic principles of physics.

The Module of the Falling Jet

This module describes how the hydraulic and geometric characteristics of the jet are transformed from its point of issuance from the dam down to the plunge pool (Figure A-8). Three main parameters characterize the jet at issuance: the velocity V_i, the diameter (or thickness) D_i, and the initial jet turbulence intensity Tu (Bollaert, 2004a).

The trajectory calculation for the jet through the atmosphere is based on ballistics and drag forces encountered by the jet as it plunges through the air and will not be further outlined herein. The basic output is the impingement

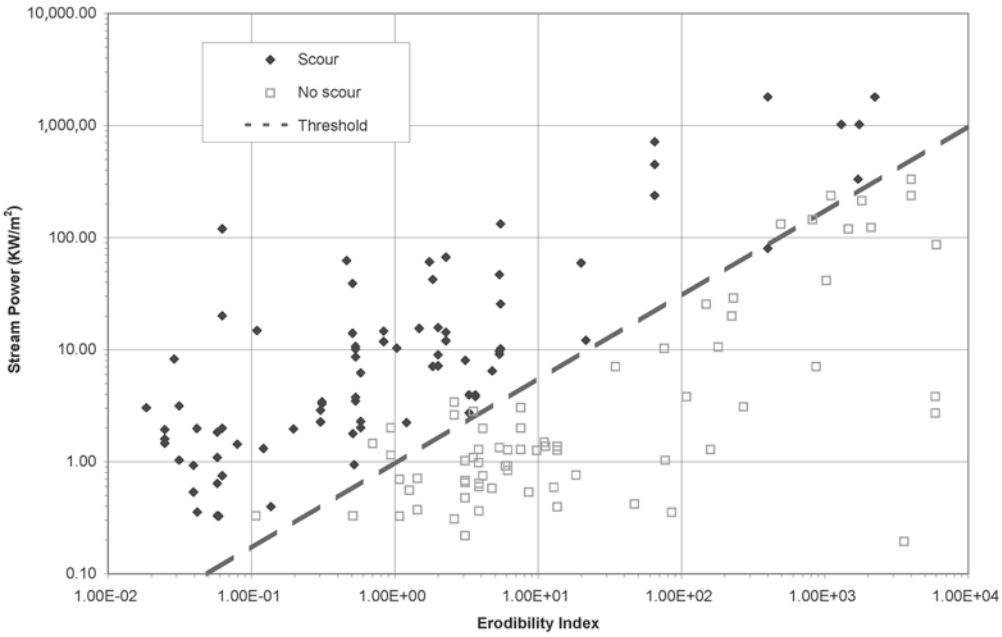

Fig. A-6. Scour threshold relating stream power and the Erodibility Index (Annandale 1995).

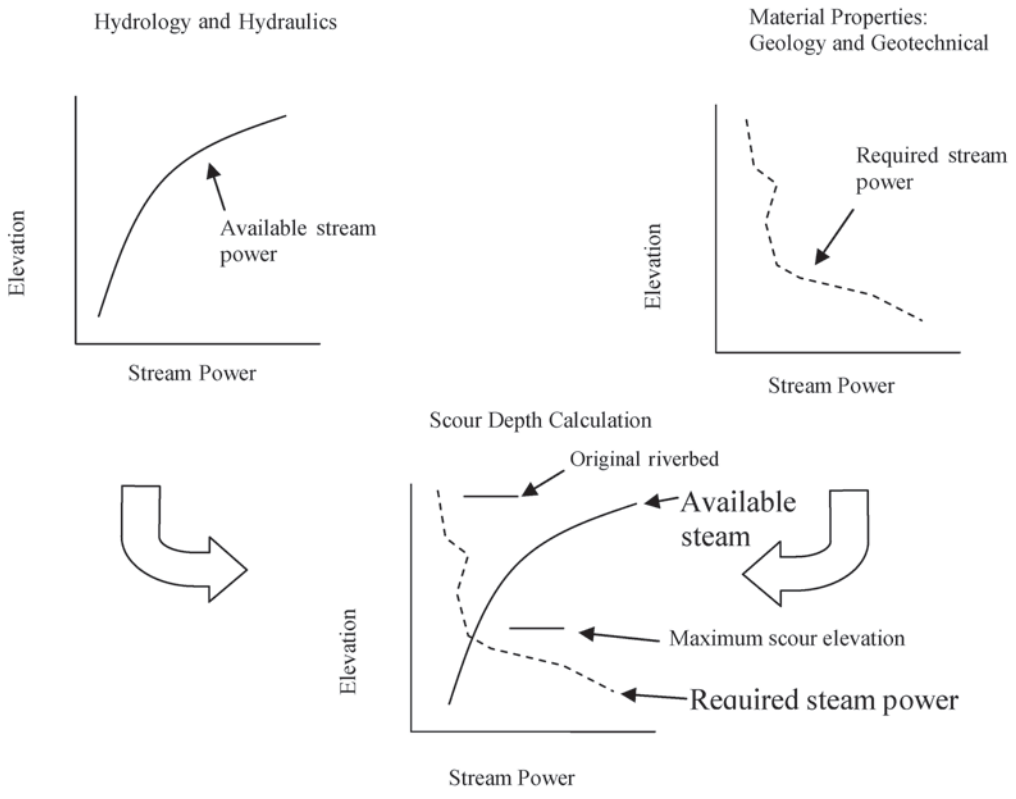

Fig. A-7. Determination of the extent of scour by comparing available and required stream power.

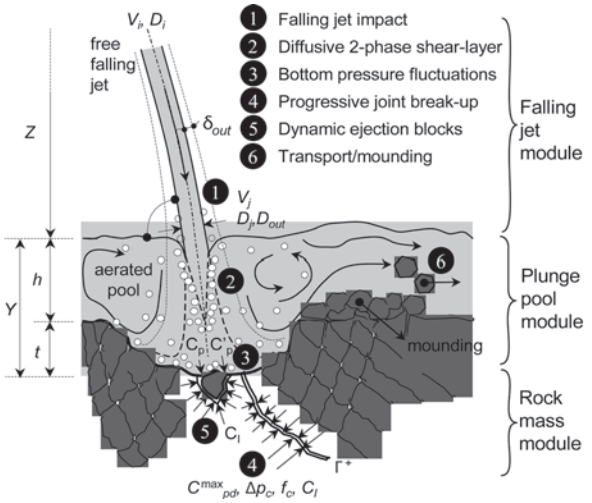

Fig. A-8. Definition sketch of the main parameters of a free overfall jet plunging into a pool and breaking up the rock mass (Bollaert 2004a).

location of the jet at impact, the jet trajectory length L, and the jet velocity at impact V_j. Knowledge of the jet trajectory length L is used to determine the contraction of the jet due to gravitational acceleration. This allows calculation of the jet diameter or thickness at impact D_j. This diameter is essential to determine the Y/D_j ratio in the plunge pool.

Second, the turbulence intensity Tu defines the lateral spread of the jet δ_{out} (Eq. [7]; Ervine et al. 1997). Superposition of the outer spread to the initial jet diameter D_i results in the outer jet diameter D_{out}, which is used to determine the extent of the zone at the water–rock interface where severe pressure damage may occur. The corresponding expressions are

$$\frac{\delta_{out}}{X} = 0.38 \cdot \mathrm{Tu} \tag{A-7}$$

$$D_j = D_i \cdot \sqrt{\frac{V_i}{V_j}} \tag{A-8}$$

$$V_j = \sqrt{V_i^2 + 2gZ} \tag{A-9}$$

$$D_{out} = D_i + 2 \cdot \delta_{out} \cdot L \tag{A-10}$$

in which δ_{out} is the half angle of outer spread, X the longitudinal distance from the point of issuance, and Z the vertical fall distance of the jet. When using Equation (A-7), it is important to note that the angle δ_{out} is in degrees and X in meters.

The turbulence intensity Tu is dimensionless, expressed as a decimal. Typical outer angles of jet spread are 3% to 4% for rough turbulent jets (Ervine and Falvey 1987). The corresponding inner angles of jet spread are 0.5% to 1%. When investigating scour in practice, Tu is usually unknown. Under such circumstances, an estimation can be made based on the type of outlet structure (Table A-6, Bollaert 2002, 2004a).

This classification constitutes a simplification of reality. Tu may depend largely on specific geometric characteristics of the outlet, the flow pattern immediately upstream of the outlet, and so on. Whenever possible, all these aspects should be accounted for, and appropriate engineering judgment is necessary.

Furthermore, the angle of the jet at its point of impact is neglected in the present analysis, which is reasonable for impingement angles that are close to the vertical (70–90°). For smaller impingement angles, it is proposed to use the same hydrodynamic parameters as for vertical impingement but to redefine the water depth in the pool Y as the exact trajectory length of the jet through the water cushion and not as the vertical difference between water level and pool bottom.

Calculation of the other relevant variable when analyzing the plunging jet can be accomplished with Equations (A-8) to (A-10).

It is obvious that this module can be replaced by any type of turbulent flow structure that allows determining its main hydraulic and geometric characteristics (diameter, width, velocity, turbulence intensity). Types of flow already applicable are hydraulic jumps, vertical and horizontal river constrictions (abutments, sills, etc.), horizontal jet flows, etc. The module is actually being updated to account for bridge pier scour situations.

Plunge Pool Module

The second module refers to the hydraulic and geometric characteristics of the plunge pool downstream of the dam and defines the statistical characteristics of the hydrodynamic loading at the water–rock interface. The water depth Y in the plunge pool is an essential parameter of the scour model, because it defines the diffusion length of the impacting turbulent flow. During scour formation, the water depth Y has to be increased with the depth of the already formed scour h. Prototype observations indicate possible mounding at the downstream end of the pool. The mounding of rock results when the detached rock blocks are swept away and deposited immediately downstream. This can raise

Table A-6 Estimation of the Initial Jet Turbulence Intensity Tu Based on the Type of Outlet Structure (Bollaert 2002b)

Type of outlet	Tu
1. Free overfall	0–3 %
2. Ski-jump outlet	3–5 %
3. Intermediate outlet	3–8 %
4. Bottom outlet	3–8 %

the tailwater level. The effect is not described in the present model but can easily be added to the computations.

Knowledge of the water depth Y and the jet diameter at impact D_j (defined in the falling jet module) determines the ratio of water depth to jet diameter at impact Y/D_j. This ratio is directly related to diffusion characteristics of the jet.

The root-mean-square values of the pressure fluctuations at the water–rock interface, expressed by the C'_{pa} pressure coefficient, depend on the Y/D_j ratio and on the initial turbulence intensity Tu. Experimental data measured at near-prototype jet velocities (Bollaert 2002b) have been approximated by a polynomial regression (Eq. [12]) and are presented in Table A-7 for different turbulence intensity levels. Each curve corresponds to a degree of jet stability. The key issue is that Tu is considered to be fully representative of low-frequency instabilities of the jet. The curves are valid up to a Y/D_j ratio of 18 to 20. For higher ratios, the C'_{pa} value that corresponds to a ratio of 18 to 20 should be used. The range of values in Table A-7 is representative of the range of jet characteristics encountered in practice. Compact jets are smooth as they fall through the atmosphere, with no significant source of turbulence leading to low-frequency instability. Very turbulent jets are characterized by Tu values greater than 5%. In between these two outer bounds, other curves have been defined. They are applicable to low and moderately turbulent jets:

$$C_{pa} = 38.4 \cdot (1-\alpha_i) \cdot \left(\frac{D_j}{Y}\right)^2 \quad \text{for } Y/D_j > 4\text{–}6 \quad \text{(A-11)}$$

$$C_{pa} = 0.85 \quad \text{for } Y/D_j < 4\text{–}6 \quad \text{(A-12)}$$

$$\alpha_i = \frac{\beta}{1+\beta} \quad \text{(A-13)}$$

$$C'_{pa} = a_1 \cdot \left(\frac{Y}{D_j}\right) + a_2 \cdot \left(\frac{Y}{D_j}\right) + a_3 \cdot \left(\frac{Y}{D_j}\right) + a_4 \quad \text{(A-14)}$$

Table A-7 Polynomial Coefficients and Regression Coefficient for Different Turbulence Intensities of Jets (Bollaert 2002b; Bollaert & Schleiss 2005)

Tu [%]	a_1	a_2	a_3	a_4	Type of Jet
<1	0.000220	-0.0079	0.0716	0.000	Compact
1–3	0.000215	-0.0079	0.0716	0.050	Low turbulence
3–5	0.000215	-0.0079	0.0716	0.100	Moderate turbulence
>5	0.000215	-0.0079	0.0716	0.150	High turbulence

The nondimensional mean dynamic pressure coefficient C_{pa}, defined by Equations (A-11) to (A-13), decreases with increasing air content in the plunge pool and with increasing root-mean-square values of pressure fluctuation. The fluctuating dynamic pressure coefficient is calculated with Equation (A-14).

Similar to the falling jet module, any other type of turbulent flow impacting the water-rock interface can be used as input to the model, provided that the statistical parameters of the pressure fluctuations can be reasonably described (mean, RMS, extreme values).

Rock Mass Module

The plunge pool module defines the principal parameters of the hydrodynamic loading at the water-rock interface. This is used as input for determination of the hydrodynamic loading inside open- and closed-ended rock joints. The governing parameters are defined as (Fig. A-4, Bollaert 2002, 2004a)

1. maximum dynamic pressure coefficient $C_p^{\max}$
2. characteristic amplitude of pressure cycles Δp_c
3. characteristic frequency of pressure cycles f_c
4. maximum dynamic impulsion coefficient $C_I^{\max}$

The first parameter is relevant to brittle propagation (immediate failure) of closed-ended rock joints. The second and third parameters are used to calculate time-dependent failure (failure by fatigue) of closed-ended rock joints. The fourth parameter is used to define dynamic uplift of rock blocks formed by open-ended rock joints.

The maximum dynamic pressure coefficient $C_p^{\max}$ is obtained through multiplication of the root-mean-square pressure coefficient C'_{pa} with the amplification factor Γ^+ and by superposition with the mean dynamic pressure coefficient C_{pa}. The product of C'_{pa} times Γ^+ results in a pressure coefficient C^+_{pd}. The distinction between C_{pa} and C^+_{pd} is necessary because the amplification of the root-mean-square pressures influences only the fluctuating part of the dynamic pressures. As such, the maximum pressure value is written (Bollaert 2002) as

$$P_{\max}[\text{Pa}] = \gamma \cdot C_p^{\max} \cdot \frac{\phi \cdot V_j^2}{2g} = \gamma \cdot (C_{pa} + \Gamma^+ \cdot C'_{pa}) \cdot \frac{\phi \cdot V_j^2}{2g} \quad \text{(A-15)}$$

As a first approximation, the ϕ value for nonuniform velocity profiles is chosen equal to one. The main uncertainty of Equation (A-15) lies in the amplification factor Γ^+. Near-prototype scaled experiments resulted in the relationship for the amplification factors shown in Figure A-9.

The characteristic amplitude Δp_c of the pressure cycles is determined by the characteristic maximum and minimum pressures of the cycles. The minimum pressures are relatively constant and always close to standard atmospheric pressure. The maximum pressures are chosen equal to the $C_p^{\max}$ value.

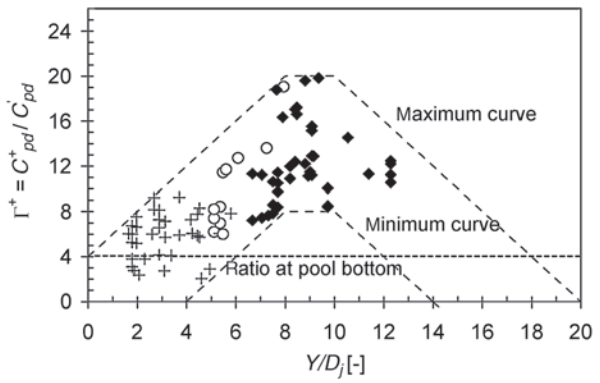

Fig. A-9. Amplification factor Γ^+ as a function of Y/D_j. The measured data are circumscribed by a maximum curve and a minimum curve, and represent core (+) and developed jet impact (♦) (Bollaert 2002).

The characteristic frequency of the pressure cycles f_c follows the assumption of a perfect open-closed resonator system and, thus, depends on the air concentration in the joint α_i and on the length of the joint L_f. The air content inside the joints can be directly related to the air content in the plunge pool (Bollaert and Schleiss 2003). This air content depends on the velocity of the jet at impact and on the plunge pool depth. The joint length depends on the distance between the different joint sets. For practice, a preliminary estimate of f_c can be made by assuming a mean celerity of 100 to 200 m/second (depending on the concentration of free air in the water) and joint lengths of typically 0.5 to 1 m. This results in frequencies of 25 to 100 Hz.

Besides the pressure loading inside the rock joints, the resistance of the rock to failure also has to be determined. The cyclic character of the pressure loading generated by the impact of a high-velocity jet on a closed-ended rock joint makes it possible to describe joint propagation by fatigue stresses occurring at the tip of the joint. This can be defined by linear elastic fracture mechanics (LEFM), assuming a perfectly linear elastic, homogeneous, and isotropic rock mass (Bollaert and Schleiss 2005). Despite these simplifying assumptions, its application to fractured rock becomes quite complicated when accounting for all the relevant parameters (Atkinson 1987; Whittaker et al. 1992; Andreev 1995).

Bollaert (2002, 2004a) developed a simplified methodology known as the comprehensive fracture mechanics (CFM) method for investigating rock scour that honors the underlying theory. Using this approach, pure tensile hydrodynamic loading inside rock joints is described by a stress intensity factor K_I. This parameter represents the amplitude of the rock mass stresses that are induced by the water pressures at the tip of the joint. The corresponding resistance to crack propagation offered by the rock mass is expressed by its fracture toughness K_{Ic}.

The challenge is to develop a comprehensive and physically representative implementation of the complex and dynamic conditions encountered in scour of fractured rock. Crack propagation distinguishes between brittle (or instantaneous) crack propagation and time-dependent crack propagation, subject to failure by fatigue. The former occurs when the stress intensity factor is equal to or greater than the fracture toughness of the material. The latter occurs when the maximum possible water pressure results in a stress intensity that is less than the material's resistance. Cracks can then be propagated by fatigue. Failure by fatigue depends on the frequency and the amplitude of the load cycles. The implementation of the fracture mechanics approach as it relates to hydrodynamic loading consists of a transformation of the water pressures σ_{water} in the joints into rock mass stresses at the joint end. The approach that was followed is based on the following simplifying assumptions: 1) the dynamic character of the loading has no influence, 2) the water pressure distribution inside the joints is constant, 3) only simple geometrical joint configurations are considered, and 4) joint surfaces are planar.

These stresses are characterized by the stress intensity factor K_I as follows:

$$K_I = P_{max} \cdot F \cdot \sqrt{\pi \cdot L_f} \tag{A-16}$$

in which K_I is in MPa$\sqrt{m}$ and P_{max} in MPa. The boundary correction factor F depends on the type of crack and on its persistency, that is, its degree of cracking defined as a/B or b/W in Figure A-9. This figure presents three basic configurations for partially jointed rock, and simplifying assumptions are that the water pressure in the joints are assumed to be applied from outside, and no geometries with multiple joints are considered.

The choice of the most relevant geometry depends on the type and the degree of jointing of the rock. The first type of crack shown in Figure A-9 is of semielliptical or semicircular shape and, pertaining to the laterally applied water pressure P_{max}, partially sustained by the surrounding rock mass in the two horizontal directions. As such, it is the geometry with the highest possible support of surrounding rock. Appropriate stress intensity factors should be used in case of low to moderately jointed rock. The second type of crack is a single-edged notch that is of a two-dimensional nature. Support from the surrounding rock mass is exerted only perpendicular to the plane of the notch, and, as a result, stress intensity factors will be substantially higher than for the first case. Thus, this crack type is relevant to significantly to highly jointed rock. The third geometry type is center cracked throughout the rock. Similar to the single-edge notch, only one-sided rock support can be accounted for. This support, however, should be slightly higher than that of the single-edged notch. The second and third configurations correspond to a partial destruction of the first one. They are more sensitive to stresses and have to be used for significant to highly jointed rock.

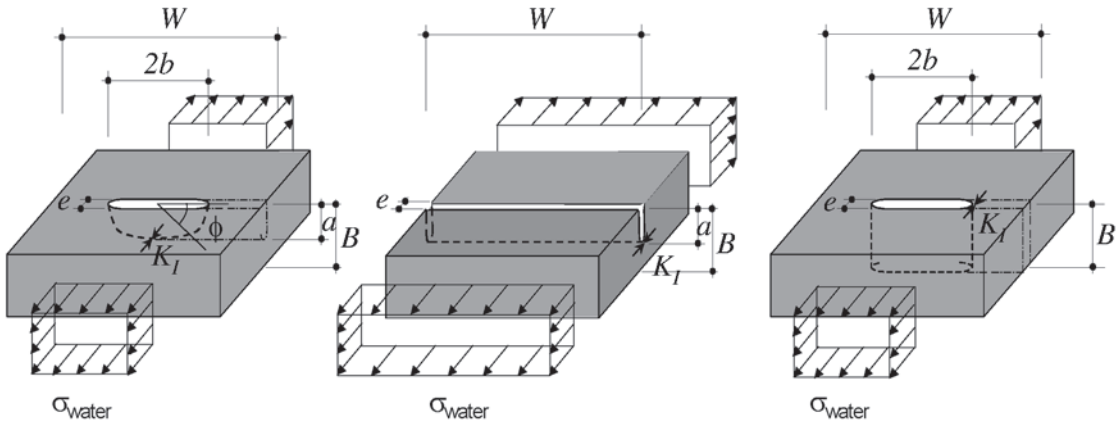

Fig. A-10. Main geometrical configurations of jointed rock: (a) semi-elliptical (EL) joint; (b) single edge (SE) joint; (c) center-cracked (CC) joint (Bollaert 2004a).

A summary of F values is presented in Figure A-10. For practical purposes, values of a/B of b/W greater than or equal to 0.5 are considered to correspond to completely broken-up rock; that is, the DI method is considered to be more applicable than the CFM method. For values of 0.1 or less, it is considered that a pure tensile strength approach is more plausible than a fracture mechanics approach. The F values for fissured rock where the CFM is assumed relevant are those associated with the range of a/B or b/W values between 0.20 and 0.40. This determination also depends on the type and number of joint sets, the degree of weathering, joint spacing, and so on.

The fracture toughness K_{Ic} depends on a wide range of parameters. Its determination has been simplified below by relating it to tensile strength T or unconfined compressive strength UCS and the in-situ stress field of the rock mass (σ_c). Based on a regression of data available in the literature,

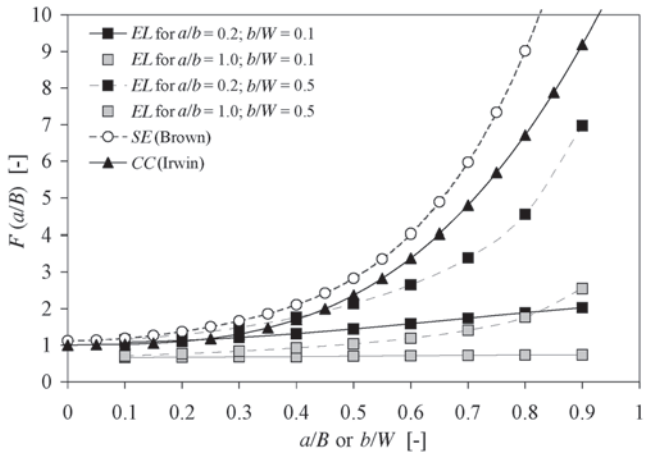

Fig. A-11. Comparison of different boundary correction factors F for the computation of the stress intensity at the tip of a rock joint (Bollaert 2004a).

the in-situ fracture toughness K_{Iins} can be defined as (Bollaert 2002):

$$K_{Iins,\,T} = (0.105 \text{ to } 0.132)\cdot T + (0.054\cdot\sigma_c) + 0.5276 \quad \text{(A-17)}$$

$$K_{Iins,\,UCS} = (0.008 \text{ to } 0.010)\cdot UCS + (0.054\cdot\sigma_c) + 0.42 \quad \text{(A-18)}$$

The units of T, UCS, and σ_c are expressed in MPa.

Instantaneous or brittle crack propagation will occur if

$$K_I \geq K_{I,ins} \quad \text{(A-19)}$$

If this is not the case, crack propagation is time dependent. This is expressed by an equation of the type originally proposed to describe fatigue crack growth in metals (Bollaert 2002, 2004a):

$$\frac{dL_f}{dN} = C_r \cdot (\Delta K_I / K_{Ic})^{m_r} \quad \text{(A-20)}$$

in which L_f is the joint length and N the number of pressure cycles. C_r and m_r are rock material parameters that can be determined by fatigue tests and, ΔK_I is the difference of maximum and minimum stress intensity factors at the joint tip. To implement time-dependent crack propagation into a comprehensive engineering model, the parameters m_r and C_r are summarized at Table A-8 for different rock types. First-hand calibration of these parameters resulted in an m_r value of 10 to 12 and a C_r value of 1E-07 for granite rock. Hence, while the m_r values can reasonably be used for practical purposes, the value of the C_r coefficients appears to be not as well defined. It could be one to two orders of magnitude higher than the theoretically proposed values in Table A-8.

The fourth hydrodynamic parameter is the maximum dynamic impulsion $C_I^{\max}$ in an open-end rock joint (underneath a rock block). This parameter is obtained by a time integration of the net forces on the rock block (Bollaert 2002, 2004a):

$$I_{\Delta tpulse} = \int_0^{\Delta tpulse} (F_u - F_o - G_b - F_{sh})\cdot dt = m\cdot V_{\Delta tpulse} \quad \text{(A-21)}$$

Table A-8 Fatigue Exponent m_r and Fatigue Coefficient C_r for Different Rock Types (Bollaert 2002b)

Type of Rock	Exponent m_r	Coefficient C_r
Arkansas novaculite	0.5	1.0E-8
Mojave quartzite	10.2–12.9	3.0E-10
Tennessee sandstone	4.8	4.0E-7
Solenhofen limestone	8.8–9.5	1.1E-8
Falerans micrite	8.8	1.1E-8
Tennessee marble	3.1	2.0E-6
Westerley granite	11.8–11.9	8.0E-10
Yugawara andesite	8.8	1.1E-8
Black gabbro	9.9–12.2	4.0E-9 to 5.0E-10
Ralston basalt	8.2	1.8E-8
Whin Sill dolerite	9.9	4.0E-9

in which F_u and F_o are the dynamic forces under and over the block, G_b is the immersed weight of the rock block, and F_{sh} represents the shear and interlocking forces. The shape of a block and the type of rock define the immersed weight of the block. The shear and interlocking forces depend on the joint pattern and the in-situ stresses. As a first approximation, they can be neglected by assuming that progressive dislodgment and opening of the joints occurred during the breakup phase of the rock mass. The pressure field over the block is governed by the turbulent shear layer of the jet. The pressure field under the block corresponds to transient pressure waves inside open-ended rock joints.

The pressures and forces are considered independent of block movement, which is a simplification of reality because shear and interlocking forces can vary considerably, depending on changes in block position and orientation. These forces depend on the points of contact between the blocks and on the in-situ horizontal stress field and are difficult to assess. Also, the pressure forces under the block may decrease because of the cavity that is formed once the latter starts moving. This, however, is difficult to formulate. As a firsthand approximation, the transient pressures under the block are assumed to be independent of the movement of the block. This seems plausible for a high peak pressure value during a small time interval but is less evident for lower pressures during a relatively long time period.

The first step is to define the instantaneous differences in forces over and under the block. By integrating the net uplift forces over a small time period Δt, the net impulsions I and a maximum net impulsion I^{max} can be obtained.

Second, I^{max} is made nondimensional by defining the impulsion as the product of a net force and a time period. For this, the net force is firstly transformed into a pressure. This means that the problem is solved for a unit surface area of the block (1 m^2 depending on the units). This pressure can then be made nondimensional by dividing it by the incoming kinetic energy $\phi \cdot V^2/2g$ as was done for the surface pressures. This results in a net uplift pressure coefficient C_{up}. The time period is made nondimensional by the travel period characteristic for pressure waves inside open-ended rock joints, that is, $T = 2 \cdot L_f/c$, in which L_f stands for the total joint length and c for the mean wave celerity. This results in a time coefficient T_{up}. Following this line of reasoning, a nondimensional impulsion coefficient C_I can be defined by the product $C_{up} \cdot T_{up} = V^2 \cdot L/g \cdot c$ [$m \cdot s$], presented in Figure A-12 as a function of Y/D_j.

The maximum net impulsion I^{max} is then obtained by multiplication of the value for C_I by $V^2 \cdot L/g \cdot c$. For jet velocities V_j greater than 20 m/second, a relatively constant value for C_I of 0.35 was observed during experiments (Bollaert 2002b). When expressed as a function of the Y/D_j ratio, the observable scatter is quite low. For core jets, a value of 0.6 to 0.8 seems plausible. For developed jets, the values are between 0.2 and 0.5. For practice, it is proposed to use the following polynomial expression:

$$C_I = 0.0035 \cdot \left(\frac{Y}{D_j}\right)^2 - 0.119 \cdot \left(\frac{Y}{D_j}\right) + 1.22 \qquad \text{(A-22)}$$

Failure of a rock block is then expressed by the displacement it undergoes due to the net impulsion (Eq. [A-21]). This kinetic energy is transformed into a net uplift displacement h_{up}. The displacement that is necessary to eject a rock block from its matrix is difficult to define. It depends on the degree of interlocking of the blocks, which depends on the in-situ stress field of the rock mass. A very tightly jointed rock mass will need a displacement that is equal to or higher than the height of the block. Less tightly jointed rock will probably be uplifted more easily. The necessary displacement is a model parameter that needs to be calibrated. Firsthand calibrations performed on the well-known Cabora-Bassa scour

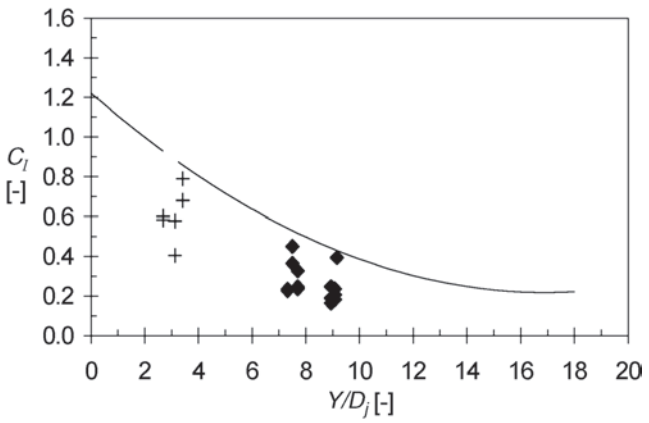

Fig. A-12. Non-dimensional impulsion for pressures inside open-end rock joints: CI as a function of Y/D_j; (Bollaert 2002).

case in Mozambique (Bollaert 2002) resulted in a necessary displacement equal to 0.20 times the block height.

SUMMARY

The current state-of-the-art in rock scour technology is represented by the EIM (Annandale 1995, 2006) and the CSM (Bollaert 2002, 2004a; Bollaert and Schleiss 2005). Both these methods can be used to determine scour thresholds and extent. However, the CSM offers the additional ability to calculate rate of scour, which is particularly relevant in the case of fissured media, such as rock, concrete of stilling basins or strongly cohesive soils. Also, the DI method incorporated into the CSM allows describing sudden failure of anchored concrete slabs of stilling basins (Bollaert 2004b).

Comprehensive descriptions, examples, and case studies demonstrating application of these methods to assess scour of rock and other earth and engineered earth materials are presented in Bollaert (2004b) for dynamic uplift of stilling basin concrete slabs, in Bollaert (2005), (2006), Bollaert et al. (2006) and Bollaert and Mason (2006) for time-dependent scour of rock in plunge pools, and in Annandale (2006) for applications of the EIM.

Theory and applications of most other existing methods to predict rock scour can be found in Schleiss and Bollaert (2002).

The EIM is based on an erosion threshold that is defined by relating the relative magnitude of the erosive capacity of water (expressed in terms of steam power) to the relative ability of rock to resist scour (expressed in terms of a geomechanical index known as the erodibility index). The scour threshold relationship can be used concurrently with estimates of the rate of change of stream power in scour holes, as they develop, to calculate the extent of scour.

The CSM addresses two failure modes of rock scour: scour of fissured rock and scour of jointed and fractured rock. In both cases, the erosive power of water is represented by pressure fluctuations that can easily be calculated in practice for plunging jets using methods proposed by Bollaert (2002, 2004a) and for any other type of turbulent flow whenever mean and fluctuating pressure values can be readily estimated. As an example, the method has already been applied to hydraulic jumps and is actually being extended towards scour of bridge piers founded in rock. The ability of rock to resist scour when using the CSM is determined by making use of LEFM approaches in the case of fissured rock and a force balance in the case of jointed and fractured rock. Fissured rock can fail by brittle fracture or in a time-dependent fashion in subcritical failure mode. In the case of brittle fracture, the stress intensity within a fissure exceeds its fracture toughness. Time-dependent failure is subject to the amplitude of pressure fluctuations and its frequency and the ability of the rock to withstand these forces to prevent fatigue failure. Dynamic impulsion of rock blocks occurs when net uplift pressures occur during a certain time interval. This impulsion method is also applicable to uplift of concrete slab linings.

Joint application of the EIM and CSM provides improved understanding of rock scour potential and extent. The geomechanical index used by the EIM provides a means to represent varying rock properties in an empirical manner using borehole and core data. It can be used to calculate scour potential and scour extent for varying flow conditions. The CSM uses basic fracture mechanics approaches and basic principles of physics to assess rock scour potential. In addition to providing the ability to assess scour threshold and extent, it can also be used to calculate the rate of rock scour. As such, it provides a much more detailed assessment of the phenomenon. A sound and complete parametric comparison of both models has been developed, allowing combined application in a fully consistent manner (Bollaert and Annandale 2004; Annandale and George 2006).

REFERENCES

Andreev, G. E. (1995). *Brittle failure of rock materials,* Balkema, Rotterdam, Brookfield.

Annandale, G. W. (1995). "Erodibility." *J. Hydr. Res.,* 33(4), 471–494.

Annandale, G. W. (2006). *Scour technology*, McGraw-Hill, New York.

Atkinson, B. K. (1987). *Fracture mechanics of rock,* Academic Press, London.

Bollaert, E.F.R. (2002). "The influence of plunge pool air entrainment on the presence of free air in rock joints." *Proc. of the Int. Workshop on Rock Scour,* EPFL, Lausanne, Switzerland, 137–149.

Bollaert, E.F.R. (2004a). A comprehensive model to evaluate scour formation in plunge pools. *Int. J. Hydropower & Dams*, 2004, 2004(1), pp. 94–101.

Bollaert, E.F.R. (2004b). A new procedure to evaluate dynamic uplift of concrete linings or rock blocks in plunge pools, *International Conference on Hydraulics of Dams and River Structures*, Teheran, Iran.

Bollaert, E.F.R. (2005). The Influence of Geomechanic and Hydrological Uncertainties on Scour at Large Dams: Case Study of Kariba Dam (Zambia-Zimbabwe). *73rd Annual ICOLD Meeting*, Tehran, Iran.

Bollaert, E.F.R. (2006). Physics Based Model Applied to Tucurui Dam (Brazil). *3rd Intl. Conference on Scour and Erosion*, Amsterdam, The Netherlands.

Bollaert, E. F. R., and Annandale, G. W. (2004, April). "Parametric comparison of erodibility index method and comprehensive scour model." *Int. Conference on Hydraulics of Dams and River Structures,* Tehran, Iran.

Bollaert, E.F.R. and Schleiss, A. (2003). Scour of rock due to the impact of plunging high velocity jets Part II: Experimental results of dynamic pressures at pool bottoms and in one-and two-dimensional closed end rock joints. *Journal of Hydraulic Research*, 41(5), 465–480.

Bollaert, E.F.R., and Schleiss, A. (2005). Physically based model for evaluation of rock scour due to high-velocity jet impact. *Journal of Hydraulic Engineering*, 131(3), 153–165.

Bollaert, E.F.R. and Mason, P.J. (2006). A Physically Based Model for Scour Prediction at Srisailam Dam. *Intl. Journal on Hydropower & Dams*, Issue 4, 96–103.

Bollaert, E.F.R., Vrchoticky, B. and Falvey, H.T. (2006). Extreme Scour Prediction at High-Head Concrete Dam and Stilling Basin (United States). *3rd Intl. Conf. on Scour and Erosion*, Amsterdam, The Netherlands.

Deere, D. U., and Deere, D. W. (1988). "The rock quality designation (RQD) index in practice." *Rock classification systems for engineering purposes: ASTM STP-984,* L. Kirkaldie, ed., American Society for Testing and Materials, Philadelphia, 91–101.

Emmerling, R. (1973). "The instantaneous structure of the wall pressure under a turbulent boundary layer flow," Report 56/1973, Gottingen, Germany, Max Planck Institute for Flow Research.

Ervine, D. A., and Falvey, H. R. (1987). "Behavior of turbulent jets in the atmosphere and in plunge pools." *Proc. of the Institution of Civil Engineers,* pt. 2, vol. 83, 295–314.

Ervine, D. A., Falvey, H. R., and Withers, W. (1997). "Pressure fluctuations on plunge pool floors." *J. Hydr. Res.,* 35(2), 257–279.

George, M., and Annandale, G. W. (2006). "Case study: Kariba Dam plunge pool scour." *Proc. Third Int. Conference on Scour,* Amsterdam.

Hinze, J. O. (1975). *Turbulence*, 2nd ed., New York, McGraw-Hill.

Kirsten, H. A. D. (1988). "Case histories of groundmass characterization for excavatability." *Rock classification systems for engineering purposes: ASTM, STP 984,* L Kirkaldie, ed., American Society for Testing and Materials, Philadelphia, 102–120.

Kirsten, H. A. D. (1982). "A classification system for excavation in natural materials." *The Civil Engineer in South Africa,* July, 292–308 (discussion in vol. 25, no. 5, May 1983).

Schleiss, A.J. and Bollaert, E.F.R. (2002). *Rock Scour due to Falling High-Velocity Jets*, A.A. Balkema Publishers, The Netherlands.

Whittaker, B. N., Singh, R. N., and Sun, G. (1992). *Rock fracture mechanics,* Elsevier, The Netherlands.

Copyrighted Materials
Copyright © 2008 American Society of Civil Engineers (ASCE)
Retrieved from www.knovel.com

INDEX

Index Terms	Links		
Page numbers with (f) refer to figures: those with (t) refer to tables			
A			
abrasion	210		
bank	643	645	
coefficients	212(f)		
quantification	211		
rivers, application to	212		
selective sorting	223		
abutment protection. *see also* riprap protection for abutments			
scour at abutments: alternatives for failure	573		
mechanisms	568		
guide banks	569	569(f)	570(f)
shape of abutment	569		
accelerated (human-induced) deposition	11		
accelerated erosion: agricultural activities	5		
causes	7		
dams and river regulation	6		
forest activities	5		
mining activities	6		
roads, railways, bridges, levees	5	6(f)	
urbanization	5		
warfare and population migration	7		
accuracy, defined	719	1089	
Ackers-White extended with Proffitt-Sutherland relation	201		
Ackers-White relation	126		
active-bed channels: example	490(t)		
slope and depth	489		
width determination	488		
active-layer composition	1090(f)		

This page has been reformatted by Knovel to provide easier navigation.

Index Terms	Links			
active-layer concept: bed and near bed processes	703	703(f)		
bed elevation during transport	183			
diagram	184(f)	703(f)		
entrainment formulation	185			
generalizations	185			
Hirano formulation	183			
system closure for sediment processes	709			
thickness and interfacial exchange fractions	184			
active sediment-transport processes: advection	971			
bioturbation-induced transport	972			
deposition or erosion	971			
dune formation	971			
active-stratum approach	704	704(f)	709	
ADCP (Acoustic Doppler Current Profiler): flow velocities				
measured with	293	295	722	
Leavenworth Bend, Missouri River	736	738		
special considerations regarding	719			
adjustment factor	387	522(f)	1089	
advection	971			
aggradation: bridge site selection	548	556		
defined	876	1085		
induced by dams	172			
long-term, total scour	506			
aggregation: concentration	264			
fine-grained sediment transport	261			
floc strength	263			
floc transport	261	261(f)		
fractal depression	263			
order	262	263(t)		
settling velocity	266			
shear stress	264			
transport modes	265			
turbulence	264			
AGNPS (Agricultural NonPoint Source pollution model)	840	841	850	852
agricultural activities	5			
Agricultural Runoff Management (ARM) model	848			
Agricultural Stabilization and Conservation Service (ASCS)	667			

This page has been reformatted by Knovel to provide easier navigation.

Index Terms	Links			
air temperatures	614(f)	615	617	618
	624			
algebraic stress models	793			
algorithm	591	910	1089	
alluvial-channels. *see also* alluvial streams: classification	377(t)			
hydraulic and geomechanical impacts, combined	645			
hydraulic impacts	635			
ice effects	635	640		
alluvial deposit, defined	1089			
alluvial fan flooding	900			
before and after comparison	914(f)			
background	901			
boulder deposit	898(f)			
characteristics	903(t)			
current developments	903			
early developments	902			
hydraulic processes	904(t)			
alluvial fans	12			
bridge site selection	549			
characteristics	903(t)			
examples	870(f)			
geomorphic map	871(f)			
inundation	917(f)			
alluvial reach	470	635	1089	
alluvial streams	33(f)	367	476	1089
	1096			
alluvium	58	220	402	863
	877	1089		
alternate bars	81	82(f)	84	362(f)
	1089	1090(f)		
American sedimentation law: “act of God” defense	950			
court decisions, trend-setting	937	939		
defenses	946			
forensic geology	952			
future directions	952			
Manual	54	937		
natural hazards	940			
Project Impact	954			

This page has been reformatted by Knovel to provide easier navigation.

Index Terms	Links			
American sedimentation law: "act of God"				
defense (*Cont.*)				
public liability	940			
recent developments	954			
sovereign immunity	946			
statutes of limitations	948			
stream *vs.* downstream legal issues	949			
taking laws	940	949		
tort laws	949			
tort theories, hazard mitigation				
measures based on	948			
trends in, recent	939			
anabranching	636			
Anaconda copper mine	235(f)			
analytical model, defined	1089			
analytical methods	489			
Annualized Agricultural NonPoint Source				
model (AnnAGNPS)	840	841	842(t)	850
anomaly, defined	1089			
ANSWERS	840	850	851	852
ANSWERS-continuous	840	841	850	
antidunes	81	82(f)	83	
arbitrarily sloping bed	59			
Argos Modeling System	699			
armor (dark grains): coarse static	169(f)			
layer	165	216	551	1089
armoring measures	165(f)	216	550	550(f)
	552(t)	1089		
Ashida-Michiue relation	195			
Assessment of Structural Flood-Control				
Measures on Alluvial Fans (HEC)	907			
auxiliary relations	711			
see also system closure				
avalanches	9	22	891	897
average end concept	1090			
avulsion: defined	878	1090		
hydraulic impacts of river ice	632			
riparian rights gained or lost by	938			

This page has been reformatted by Knovel to provide easier navigation.

Index Terms	Links			
B				
backfilling	876			
backwater curve	125	135	1090	
backwater profile	1090			
Bagnoldean formulation	66			
bag samplers	328			
bank erosion: conceptual models	408			
defined	876			
empirical methods	415			
equilibrium approaches	411			
bankfast-ice: frazil-ice	616(f)			
loading	615	615(f)	642	642(f)
bank-full discharge	364			
vs. bank-full depth	180(f)			
frequencies	365(t)			
stage-discharge diagram	178(f)			
bank-full flow	121	122(f)		
bank mechanics: advance	406			
basal endpoint control	404			
erosion	400			
erosion, resistance to	401			
extremal hypotheses	422			
geofluvial approaches	422			
retreat *vs.* near-bank velocity	415(f)			
seepage effects	406			
stability, mass failure	401			
vegetation effects	405			
bank migration	443	649	1090	
bank protection	549			
armoring measures	550	550(f)	552(t)	
artificial riprap	550			
bendway weirs	553			
broken concrete	550			
cable-tied blocks	550			
concrete-grouted riprap	551			
concrete pavement	551			
flow-retarding measures	553			

This page has been reformatted by Knovel to provide easier navigation.

Index Terms	Links		
bank protection (*Cont.*)			
gabions	551		
groins	553	553(f)	554(t)
grout-filled bags	550		
grout-filled mats	551		
hardpoints	553		
Iowa vanes	553		
overview	549		
precast blocks	550		
Reno mattresses	551		
rock riprap and broken concrete	550		
used tires	550		
vegetation	551	553	
bank sediment reservoir	1090		
basaltic rocks	34		
base test	655		
BASINS	848	851	
bathymetric survey	591		
bay, defined	533		
bechevnik	643	644(f)	
bed and near-bed processes: active-layer and active-stratum			
approach	703		
bed load-layer and total-load approach	701		
overview	701		
bed-elevation changes	696(t)	698(t)	700
bed forms	77	1090	
see also flow resistance; alternate bars	81	82(f)	84
antidunes	81	82(f)	83
characteristics	96(f)		
charts	89(f)		
classification	88(f)	93(f)	
criteria diagram	87(f)		
dimensionless characterization	85		
discriminators	86(f)		
dunes	81	82(f)	
equilibrium			

This page has been reformatted by Knovel to provide easier navigation.

Index Terms	Links			
bed forms (*Cont.*)				
predictions	94			
geometry types	93			
knowledge in	78			
progression	85			
ripples	81	83		
river stage effects	97			
transition zone	93(f)			
types	82(f)			
undermining	558			
bed-layer	178	238	629	1090
bed load: be-material-load equations	1079(t)			
box-and-whisker plots	1076(f)			
defined	8	1090		
discharge	121	308	344	1090
	1099			
field data on	633			
functions	74(f)			
bed load-layer approach	701	709		
bed load material equations	1079(t)			
data issues	1074	1074(f)	1075(f)	
overview	1073			
sediment supply issues	1076			
summary	1083(t)			
technical issues	1077	1083		
bed load samplers	338			
calibrations	341			
discharge measurements	344			
Helley-Smith	1074(f)			
manually operated portable	339	341(f)		
pit and trough	342			
summary	343			
types	339			
vortex tube	343			
bed load transport	66			
see also bed-material load in sand-bed				
streams, dimensionless relations for; analysis	67			
defined	68			

This page has been reformatted by Knovel to provide easier navigation.

Index Terms	Links		
bed load transport (*Cont.*)			
rate and flow changes	339(f)		
rates measurements	1074(f)		
relations	70		
sediment mass (Exner equation)	69		
two-dimensional	74		
bed load transport in mixtures,			
relations for hiding: Ackers-White extended			
with Proffitt-Sutherland	201		
Ashida-Michiue	195		
Einstein	195		
Parker, surface-based	196		
Parker-Klingeman-McLean	195		
Powell-Reid-Laronne	200		
Tsujimoto	197		
Wilcock-Crowe	199		
Wilcock-Kenworthy	198		
Wu-Wang-Jia	200		
bed load transport of mixtures: analysis	186		
equal-threshold limiting cases, size independence and	190		
field data comparisons	208		
hiding functions	189		
mobile armor	219		
sample applications	202		
shear stress and flow			
parameters calculation	193		
significant, onset	187		
similarity hypothesis	188		
substrate-based formulation	190		
surface-based formulation	186	191	196
surface-based *vs.* substrate-based	208		
threshold of motion and hiding	191		
variability, patchiness, and partial transport	204		
bed-material load	8		
estimating	1073		
predictors, grain-size-specific bulk	232		
sediment transport loads	8	60	

This page has been reformatted by Knovel to provide easier navigation.

Index Terms	Links			
bed-material load in sand-bed streams,				
dimensionless relations for.				
see also Brownlie relation;				
Engelund-Hansen relation:				
Ackers-White	126			
form	123			
Karim-Kennedy	127			
Molinas-Wu	128			
other	129			
Yang	127			
bed-material measurement techniques: bias				
sampling methods	311			
sample collection and analysis	310			
sample size and accuracy	313			
sediment-sampling issues	309			
bedrock	476	860	1001	1090
bed-sediment transport: control volume	1090			
field data	633			
laboratory data	632			
bed-slope, incipient motion and:				
arbitrarily sloping bed	59			
granular sediment	55			
side slopes	57			
bed-sorting, defined	1100			
bendway weirs (stream barbs)	451	523	553	1038
	1101			
berming	876			
best management practices (BMPs)	840	851		
bias	204	1091		
bioaccumulation	962			
biomagnification	962			
Boguchwal-Southard diagram	86	86(f)		
Bonnefille-Pernecker diagram	88	88(f)	89(f)	
bottomset evolution	133			
linked-one dimensional model	139			
boundary conditions	108	655	668	717
	1091			
boundary effect	1091			

This page has been reformatted by Knovel to provide easier navigation.

Index Terms	Links			
boundary roughness	468	620	653	1049
	1091			
Boussinesq approximation	691	724	767	
Boussinesq Eddy-viscosity model.				
See Eddy-viscosity model				
box-and-whisker plots	1076(f)			
braided meandering	441(f)	877	878	
braided river deposits	12	12(f)		
Brandywine Creek	415			
Bridge-Bennett model	55			
bridge-scour evaluation	505			
see also HEC-18 pier scour				
equation; pier foundations (complex), scour				
for; scour at abutments; analysis	534			
bed material movement, critical	510			
clear-water scour	507			
computer models	530			
general scour	508			
hydraulic variables	536			
Jain-Fisher's scour	511			
long-term changes	507			
Melville's equation	524			
pier debris	523			
pier scour equations	525			
pier scour holes	525			
stream instability	530			
tidal processes	533			
tidal waterways	531			
total scour	506			
bridge-scour prevention	543			
abutment protection	568			
countermeasures	544(t)			
distribution	546(t)			
environmental considerations	574			
general scour and				
contraction scour	549			
(*see also* bridge site selection);				
piers	557			

This page has been reformatted by Knovel to provide easier navigation.

Index Terms	Links		
bridge-scour processes: abutments	546		
piers	543	546	
river morphology and channel contraction	547		
bridge site selection.			
see also bank protection: aggradation	548	556	
alluvial fans	549		
bank protection	549		
bend scour	556		
catchment influences	549		
channel curvature	549		
channel lining	555		
channel widening	555		
check dams	555		
confluence scour	556		
contraction scour	553	555	
debris	557		
degradation	553	555	
ice jams	557		
relief bridges	555		
river training works	549		
sediment-wave effects	553	555	
submerged Iowa vanes	553		
thalweg effects	553	555	
waterway areas	549		
BRI-STARS model	417		
broad-level classification criteria	378(t)		
Brownlie relation: gradually varied flow	126		
hydraulic resistance	126		
normal flow	126		
sediment transport	125		
bulking factor	605		

C

cable-and-reel samplers	325		
cable-tied blocks	550	563	564(t)
Cache Creek	6		
calibration	667		
see also hydraulic calibration; parameters	670	733	

This page has been reformatted by Knovel to provide easier navigation.

Index Terms	Links			
California, isoerodent map	833(f)			
California Bank and Shore Protection (CBSP) Manual	1050			
Canadian River	587			
cantilever failure	405(f)			
Canton Dam	587			
capture	875			
Cartesian tensor notation	815			
CASC2D	840	841	849	851
	852			
Castle Creek channel profile	929(f)			
Catalyst-Old River Hydroelectric Limited Partnership d.b.a. Louisiana Hydroelectric Limited Partnership	722			
catchment influences on bridge site selection	549			
CCHEBank model	417			
CCHE3D	417			
CCHE2D	700			
central processing unit (CPU)	684	699		
Cerro Grande River	886(f)	914(f)		
channel morphological response	915			
conclusions	916			
flood description	913			
mudflow and debris-flow modeling	915			
1999 flood hydrograph	913			
rainfall analysis	913			
simulation results	916			
Chang-Davis abutment scour	527			
Chang-Davis abutment scour equation	527			
channel(s): anabranching	636			
avulsions	636			
bed slope-drainage area	480(f)			
bed slope *vs.* bank-full discharge	180(f)			
classifications	376(f)			
confluences	638			
curvature	549			
cutoffs	636			

This page has been reformatted by Knovel to provide easier navigation.

Index Terms	Links
channel(s): anabranching (*Cont.*)	
degradation	172(f)
erosion	675(t)
geometry	362(f)
morphology	6(f)
narrowing by floodplainequation	523
live-bed scour	507
local formation	389(f)
parameters	124(f)
pattern classifications	376(f)
simulation	809(f)
types	861(t)
widening	555
channel design: active-bed	487
alignment and geometric detail	490
for restoration projects	485
threshold	486
channel evolution and processes:	
channel stability diagram	410
incised	408
sequence *vs.* channel stability parameters	410(f)
channel-floodplain connectivity,	
river restoration design:	
confinement, longitudinal variation in	490
reconnection issues	490
channel-forming discharge: bank-full discharge	364
effective discharge	365
overview	367
representations	470(t)
channel lining (paving)	555
channel stability	445
see also meander/meandering; dominant	
wavelength	447
finite-amplitude meanders	448
flow and stability relations	449
perturbation stability analyses	446
prediction uncertainties	448
regime theories	446

This page has been reformatted by Knovel to provide easier navigation.

Index Terms	Links			
channel stability (*Cont.*)				
strategy	451			
submerged vanes	452			
technologies	451			
Channel Stability Assessment for Flood Control Projects (Engineering Manual 1110-2-1418)	907			
Chaubert-Chauvin diagram	87	88(f)	89(f)	
check dams	555			
Cheng formula	73			
Chezy coefficient	28	33		
ch3d hydrodynamic module	721	723	738	740
CH3D-SED	700	701	723	726
	733	735		
Churchill's curve	595	596(f)		
Churchill's sedimentation index				
civil law rule	938			
Civil Rights Act of 1871	941			
clay	728(f)	1091(t)		
Clear Creek	998(f)			
clear-water abutment scour	528			
coastal processes, defined	533			
colloids	970			
Colorado River	2	2(f)	138	173
	1071(f)			
Colorado State University (CSU) equations	512	513	515	
comprehensive fracture mechanics (CFM)	1028			
Comprehensive Scour Model (CSM)	1026	1028		
computational analysis	668			
computational hydrograph	1092			
computational modeling	668			
see also sedimentation processes, computational modeling;				
channel cross sections	675	679	679(t)	
channel geometry	675			
defined	668			
longitudinal profiles	675			
measured bed profile	675			
model data	672			

This page has been reformatted by Knovel to provide easier navigation.

Index Terms	Links		
computational modeling (*Cont.*)			
sediment delivery	674	675(t)	
sediment transport formula	673		
conceptual model	408	1092	
concrete: bridge site selection	550		
broken	550		
check dam	555(f)		
grouted riprap	551	563	566
pavement	551		
confirmation, defined	1092		
confluence scour	556		
Conservation Technology Information Center	599		
consistency, defined	1092		
consolidation	272	1092	
contaminant processes in sediments	959		
active sediment-transport	967		
chlorinated organic compounds	962		
conventional pollutants	960		
dredging	452	977	
engineering management	974		
heavy metals	961		
passive sediment fate	965		
pesticides	962		
polycyclic aromatics	962		
release and exposure pathways	962		
sediment bed fate and transport mechanics	969		
sediment processes in sediment environments	961(t)		
in situ capping	975		
water-side mass transfer process	968		
contour surveying	591	592(f)	
contraction scour. *see also* bank protection: aggradation	556		
bend and confluence scour	556		
bridge waterway area	549		
debris and ice jams	557		
degradation, contraction scour, thalweg effects, or sediment-wave effects	554		
equations	508		
river training works	549		

This page has been reformatted by Knovel to provide easier navigation.

Index Terms	Links			
contraction scour (*Cont.*)				
site selection	549			
control point	1092	1092(f)		
convergence	106	712	815	1092
conversion of units	1103			
conveyance	361	1092		
Coralville Reservoir	746	748	749(f)	750(f)
	751(f)	751(f)		
Corps of Engineers CTH	295			
Coulcomb friction	45	47		
cover layer, defined	1092			
cover-management factor	835			
CREAMS	841	848		
critical depth	902	1092		
critical flow	1092			
critical shear velocity: grain diameter	53(f)			
streamwise bed slope effects	57(f)			
crossing	360			
cross-section, defined	1093			
Cruickshank-Maza Flow Resistance				
Predictor diagram	97	98(f)		
CUR Manual	1050			
cutoffs	636	877		

D

dam removal	607			
see also Marmot Dam, removal of (simulation); modeling				
efforts, numerical	995			
pre-dam-removal longitudinal profile	999			
reservoir sediment erosion	997			
sediment-transport equations	998			
sediment transport following	1000			
upstream and downstream reaches, coupled modeling of	996			
Danish Hydraulic Institute	844			
Darcy-Weisbach friction factor	85	85(f)		

This page has been reformatted by Knovel to provide easier navigation.

Index Terms	Links			
data types and resolution: definitions	667			
equilibrium and nonequilibrium channels	429			
field	719			
fluvial	593	1083		
geometric	656			
hydraulic calibration	668			
hydrologic	664			
model development	656			
movable-bed unsteady-state test	669			
operating rules	665			
prototype history	656			
sediment	658			
sources of data	665	667		
DDD (dichlorodiphenyldichoroethane)	962			
DDT (dichlorodiphenyltrichloroethane)	962			
debris-flows. *see also* mudflows, debris-flows and				
mud-floods, mechanics of; mudflows and debris-flows,				
mathematical modeling of: bridge site selection	556			
defined	890	894		
physical properties of	986(t)			
default size-fraction distribution	732(t)			
degradation	506	553	556	875
	1093			
bridge site selection	549	555		
channel	172(f)			
defined	876			
long-term	505	531		
riprap				
protection at piers	562			
river corridor	464(t)			
delivery ratios, sediment	839	840(t)		
delta progradation	136	137(f)	226	
deltas	133	404	595	1093
density. *see also* turbid density currents				
(turbid currents): current	603	1093		
profile, instantaneous	273(f)			
of reservoir sediment deposition	597	597(t)	598(t)	
size distribution				

This page has been reformatted by Knovel to provide easier navigation.

Index Terms	Links		
density (*Cont.*)			
and size density scale	37(f)		
stone, riprap design and	1039		
denudation and retreat	875		
deposition. *See* sediment deposition			
deposits. *See* sediment deposits			
depth-averaged equations	691		
depth-averaged model	817(f)		
depth-discharge computation: bad load	121		
bank-full	121		
overview	119	121	
sediment	121		
depth of flow, defined	1093		
design discharge: bank-full	472		
channel-forming	473		
drainage area-flow duration curve	473		
effective	470		
range of	473		
regional duration curve	473		
specific return intervals	473		
ungauged sites	473		
Des Moines River	755		
deterministic model, defined	1093		
diffusion	291		
diffusivity and the turbulent			
Schmidt number	772		
digitize/digitization	1093		
dikes	451		
dimensionless number, defined	1093		
discretization	177	815	1093
dissolved organic matter (DOM)	970		
dissolved oxygen concentration profiles	986(f)		
distorted model, defined	1093		
distortion, defined	1093		
distributaries, defined	1093		
dominant discharge	364	1093	
downfilling	876		
Down's channel classifications	379(f)		

This page has been reformatted by Knovel to provide easier navigation.

Index Terms	Links			
downstream fining: *vs.* abrasion	223			
in laboratory channel	225(f)			
laboratory studies	224			
numerical models	226			
tectonics and base level variation	226			
draft depth	1093			
drainage basin	172	355	869	870
	1093			
drainage network development	878			
drawdown: characteristics of	601	601(f)		
rule curve	603			
seasonal	602			
dredging: contaminated sediments	452	977		
hydraulic	604			
material handling	978			
overdredging	978	1097		
residual sediment contamination	978			
resuspension of contaminants	978			
vs. sediment-pass through	583(f)			
technologies	977			
drop	1093			
dune flow	795(f)			
dunes	81	82(f)		
dynamic impulsion (DI)	1028			
dynamic model	1094			
defined				
Dynamic Watershed Simulation Model (DWSM)	840	844	849	
dynamism	463	482		

E

earthflows	891			
ebb/ebb tide	533			
echosound bottom profile	78(f)			
ecological disaster, man-induced	13(f)			
Eddy-viscosity model: constant	774			
deficiencies of	788			
diffusivity and the turbulent Schmidt number	772			

This page has been reformatted by Knovel to provide easier navigation.

Index Terms	Links	
Eddy-viscosity model: constant (*Cont.*)		
equilibrium and mixing-length models	781	
k–ω model	788	
Mellor-Yamada length-scale equation	790	
mixing-length models	775	778
momentum molecular transport of	771	
one-equation model	780	
RNG model	789	
sophisticated models	790	
specifications	774	
stably stratified-flow analogy	776	
turbulent kinetic energy, equation for	780	
two-equation		
model	782	787
edge failure	558	
effective discharge	365	470(f)
effective (grain) size	1040	1094
Einstein, Hans Albert	66	70
Einstein integrals	115(f)	
Einstein partition	100	
Einstein relation	195	
empirical equations	368(t)	
empirical models	1021	1094
Engelund-Fredsøe partition	73	102
Engelund-Hansen relation: gradually varied flow	125	
hydraulic resistance	125	
normal flow	125	
sediment transport	125	
engineering geomorphology, approaches to.		
see also geomorphic		
hazards: direct	861	
indirect	863	
systems	865	
engineering geomorphology,		
systems approach to	865	
direct approach	866	
indirect approach	869	
engineering treatment projects	16	

This page has been reformatted by Knovel to provide easier navigation.

Index Terms	Links			
entrainment: active-layer concept	183			
bank materials	419			
defined	1094			
fluid mud	283	289		
formulation	185			
rate against Richardson number	282(f)			
relation of Tsujimoto surface-based	197			
sand-bed rivers, suspension-dominated	229			
suspended bed-material load	116			
Environmental Protection Agency (EPA)	599	848	851	
equal-discharge-increment (EDI)	330	332		
equal-width-increment (EWI)	331			
equations. *see also* bed load material equations; flow in mobile boundary channels, equations for; HEC-18 pier scour equation; Reynolds-averaged equations; scour equations: basic	690			
Chang-Davis abutment scour	527			
depth-averaged	691	909		
empirical	368(t)			
Exner equation	69			
governing, in meandering flow bed topography	443			
Mellor-Yamada length-scale	790			
morphodynamics of rivers	129			
one-equation model	780			
Reynolds-averaged Navier-Stokes equations	690			
rheological	909			
St. Venant	10	213	391	650
	669			
sediment-transport	998			
summary of	1083(t)			
turbulent kinetic energy	780			
two-equation model	782	787		
equilibrium: bank erosion	408			
bed forms	94			
depth	1085	1090		

This page has been reformatted by Knovel to provide easier navigation.

Index Terms	Links		
Eddy-viscosity model	780		
load	1090		
near-bed sediment concentration	116		
nonequilibrium channels	429		
passive sediment fate and transport processes	969		
river width adjustment	428		
in wide channel	109		
Erodibility Index Method (EIM): erodibility index	1025	1026(t)	
scour assessment	1026	1027(t)	1028(t)
stream power	1024		
erosion. *see also* accelerated erosion; wave-induced erosion:			
defined	1094		
engineering works	8		
fluid mud entrainment	283		
geologic or natural	4		
mass	282		
modes	275		
overview	4		
rate constant	281		
rates and quantities	7		
sedimentation delivery	587		
shear strength	276		
streambank	387		
(*see also* river width adjustment); surface	275		
EROSion model	840		
erosion rate: *vs.* bed shear stress for mixtures	276(f)		
constant *vs.* bed shear strength	281(f)		
vs. excess shear stress	276(f)		
vs. meander bends	363(f)		
surf zone functions	288(f)		
estuary	533		
Exner equation	10	69	
explicit scheme	1094	1095	
extension	875		

F

falling jet module	1028		
fall velocity	41	42(f)	1094

This page has been reformatted by Knovel to provide easier navigation.

Index Terms	Links			
fan-delta	143(f)			
FAST2D	700	701		
FAST3D	700	701		
Federal Emergency Management Agency (FEMA)	889	900	905	954
Federal Highway Administration	512			
Federal Interagency Sedimentation Project BL-84	341(f)			
feldspar	34			
Fernandez-Luque-van Beek formula	73			
FHWA manual design of riprap revetment	1051			
final conditions, survey data for	655			
fine-grained sediment transport	253			
see also erosion; aggregation	261			
applications	293			
deposition under flow	270			
diffusion	291			
gelling	274			
sediment characterization	254			
sediment transport processes	259			
settling and consolidation	272			
settling velocity	266			
finite-difference methods	694			
finite element method, defined	1094			
fixed-bed model, defined	1094			
FLESCOT	700	701		
floating material	61	62		
flocculation	254(t)	272(f)	278(f)	
floc strength, aggregation and	263			
floc transport, aggregation and	261	261(f)		
floes	617			
flood/flood tide	533			
floodplain	232	233(f)	234(f)	
flood protection levees	7			
flood routing, defined	1094			
floods	892			
flow: aligned with piles	518(f)			
around a circular bridge pier	811(f)	812(t)		
in a bend	806(t)			
in a channel reach and fixed ice cover	636(f)			

This page has been reformatted by Knovel to provide easier navigation.

Index Terms	Links	
flow: aligned with piles (*Cont.*)		
competence	51	
discharge rating curve	122(f)	
distribution	669	
duration curve	473	1094
field, around consecutive vanes	453(f)	
measurements and predictions of	809(f)	
open-water	638(f)	
over bed forms	797(t)	
retarding measures	553	
routing models	416(t)	
in sedimentation tanks	800(t)	
sediment modeling	676(f)	
stability relations	449	449(f)
structures at a rectangular pier	547(f)	
through non-emergent vegetation	802(f)	
between two parallel plates	985(f)	
flow and bed topography in meanders: governing		
equations and sample solution	443	
simulation of	445	
flow in mobile boundary		
channels, equations for:		
allocation of scour and fill	652	
bankline migration	653	
channel width	653	
continuity	650	
diffusion	651	
energy	650	
planform migration	653	
sediment transport	650	
flow resistance. *see also* shear stress		
partitions; stage-discharge		
relations: channel	27	
diagrams	103(f)	
equivalent roughness of bed forms	33	
fixed-bed (skin or grain) roughness	29	
form drag and skin friction	99	
movable flat-bed roughness	32	

This page has been reformatted by Knovel to provide easier navigation.

Index Terms	Links	
flow velocity: concentration profiles	284(f)	
law of the wall	24	
velocity-defect and log-wake laws	25	
fluidization	261	
fluid mud generation experiments in flumes	290(t)	
FLUVIAL-12 model	415	422
fluvial data: sediment	1083	
sediment rating curves	593	
turbidity measurements	594	
fluvial geomorphology: channel classification	375	
channel evolution models	379	
channel-forming discharge	364	
channel instability	371	372
channel morphology	359	
channel narrowing	389(f)	
channel stability	371	
channel widening	388(f)	
closure	382	
complexity of	357	
defined	355	
dynamic system	356	
fluvial system	355	
geomorphic assessment	381	
local instability	372	
relationships in rivers	367	
scale and	358	
sediment transport	363	
system stability and instability	373	
thresholds of	357	
time	358	
fluvial hydraulics in bank mechanics:		
cross-sectional shape	392	
hydrodynamics	415	
interactions	422	
longitudinal changes	398	
near-bank zones	399	
Food and Agricultural		
Organization (FAO)	5	

This page has been reformatted by Knovel to provide easier navigation.

Index Terms	Links			
foreset evolution	133			
linked-one dimensional model of	139			
forest activities	5			
fractal depression	261			
frazil ice	616	617(f)	618(f)	
free overfall jet plunging	1030(f)			
free-surface elevations	724(t)	738(t)	740(t)	
freeze-up jam	618(f)			
frequency, defined	1094			
Froude number	92	182(f)	1094	
full sediment balance	581			
fuse plug: core	1059	1059(f)		
lateral erosion process	1060(f)			
prototype gradation curves	1063(f)			
test	1062	1063(f)	1065(f)	
G				
gabions	551	563	565(t)	
García-Parker sediment entrainment function	118	118(f)		
gauging station	334	748	862	1094
gelling	274			
General Land Office (GLO)	861			
general scour	508	549		
geological control, defined	1094			
geological erosion	3(f)			
geologic (natural) deposition	11			
geology, defined	1094			
geometric data: cross-sectional layout and spacing	656			
hydraulic roughness	657			
geometric similarity	1057			
geomorphic hazards: drainage network	875			
identification of	873	874		
piedmont and coastal plains	878			
river	876			
slope	875			
variables affecting	874(t)			
geomorphology. *see also* fluvial geomorphology: defined	355			
glacial till profile plot	296(f)			

This page has been reformatted by Knovel to provide easier navigation.

Index Terms	Links			
GLEAMS	841	848		
glossary	1089			
gouging of banks	643	644(f)		
Government Performance and Results Act (GPRA)	955			
gradation: of bed sediment reservoir	658			
curves	1040(f)	1063(f)	1095(f)	
defined	1094			
model calibration	668			
on point bar	664	664(f)		
of riprap	559	561(f)	1040	1040(t)
types	1040(t)			
grade scale, sediment	36(t)			
grain shape factor, defined	1097			
grain-size distributions: annual bed load	222(f)			
bed samples	177			
definitions and continuous formulations	175			
densities	45(f)	171(f)	176(f)	
discretization	177			
fifty-stone grid samples	319(f)			
grain mobility number and grain size	46	94(f)		
numerical modeling	213	216		
reaches plot, range and number of	178(f)			
scale	37(f)	37		
sediment deposits	1008(f)			
sediment load	662(t)			
sediment transport sensitivity	665(f)			
granite	34			
granular flows	895			
graphical user interfaces (GUIs)	10			
gravel, defined	1091(t)	1095		
gravel and sediment mixtures, transport of. *see also* active-layer concept; bed load transport of mixtures: abrasion	210			
in bed loads, fraction of	203(f)			
distributions	203(f)			
downstream fining	223			

This page has been reformatted by Knovel to provide easier navigation.

Index Terms	Links			
gravel and sediment mixtures, transport of (*Cont.*)				
engineering relevance	171			
equal				
mobility, hypothesis of	221			
field data	209			
fluvial phenomena associated with	165			
geometric mean size and	203(f)			
gravel-bed and sand-bed streams, dimensionless				
bank-full relations	178			
mobile armor	219			
numerical modeling	213			
planform sorting	227			
static armor	216			
suspension-dominated sand-bed rivers	229			
tracers	237			
vertical sorting	238			
gravel-bed streams	63			
gravelometer	310	310(f)	311	313
gravitational sediment flows	892			
gravity	35(t)			
grid	714	1095		
groins/groin fields	553	553(f)	554(t)	
gross erosion	839			
grout-filled bags	550	563	566(t)	
grout-filled mats	551	563		
GSTARS model	417	419	422	
gauge stations	588(t)			
guide banks	555	569(f)		
gullies: erosion	2(f)	837		
in floodplains	374(f)			

H

habitat structures: design of	491	492(t)		
migratory barrier				
removal (fish passage)	491	493		
river restoration design	491			
spawning gravel	491	493		
handheld and hand-line samplers	323	325	326(f)	

This page has been reformatted by Knovel to provide easier navigation.

Index Terms	Links			
hardpoints	553			
Hawaii, isoerodent map of	835(f)			
headcutting: development	997	998(f)		
severe erosion	7	7(f)		
headgate	655			
HEC-1 hydrologic model	914	915(f)	916	
HEC-6	294	508	602	652
	680(t)	758	996	997
HEC-18 pier scour equation	513			
see also pier foundations (complex), scour for; correction factor for very large piers	514			
Mueller (1996) K_4 correction coefficient	514			
multiple columns skewed to flow	521			
pressure flow scour	523			
Helley-Smith bed load samplers	1074(f)			
heuristic model	1095			
hexachlorbenzene	962			
hiding function plot	192(f)	202(f)		
high sediment: concentration flows	893(t)			
concentration turbidity currents	13(f)			
Hirano formulation	183			
historic flows, defined	1095			
horizontal collars	568	568(f)		
hybrid model	1095			
hydraulic calibration: fixed bed steady and unsteady-state	668			
hydraulic and sediment calibration	669			
movable-bed, steady-state	669			
movable-boundary, unsteady-state	669			
hydraulic depth	1095			
Hydraulic Design of Flood Control Channels (Engineering Manual 1110-2-1601)	906	1051		
hydraulic dredging	604			
hydraulic flushing	605	606(f)		
hydraulic geometry formulas	370(t)			
hydraulic impacts and geomechanic impacts	644(f)			

This page has been reformatted by Knovel to provide easier navigation.

Index Terms	Links		
hydraulic impacts of river ice	635		
avulsions	636		
channel anabranching	636		
channel confluences	638		
cover influence on thalweg alignment	638	638(f)	639(f)
cutoffs	636		
ice-cover influence	636		
jam-collapse surges	639		
hydraulic loading: for bank protection	1042		
below energy dissipators	1043		
classifications of	1042(t)		
descriptors of channel type and bend severity	1041		
parameters	1041	1042(t)	
from propeller jets	1043		
for steep slopes and river closures	1043		
from waves	1043		
hydraulic model	722	1095	
hydraulic radius	126	1095	
hydraulics, defined	1095		
hydraulic sorting, defined	1100		
hydraulic variables, determination of: computer programs for	539		
for constricted waterways	538		
design flows	536		
for unconstricted waterways	537		
hydrodynamic boundary conditions	749(f)		
hydrodynamic modeling	488	690	756
coordinate transformations for finite-difference methods	694		
depth-averaged equations	691		
hydrostatic pressure assumption	691	693	
introduction and scope	690		
Reynolds-averaged Navier-Stokes equations	690		
solution techniques and applicability	693		
turbulence closure models	692	695	
hydrodynamic-process formulations: basic equations	690		
depth-averaged equations	691		
hydrostatic-pressure simplification	691		
Reynolds-averaged Navier-Stokes			

This page has been reformatted by Knovel to provide easier navigation.

Index Terms	Links			
hydrodynamic-process formulations (*Cont.*)				
equations	690			
turbulence closure problem	692			
hydrograph: computational	1092(f)			
defined	1095			
1999 flood				
estimated	913			
prediction	602	603(f)		
hydrographic track lines	592(f)			
Hydrological Simulation				
Program—Fortran (HSPF)	848	850		
hydrologic data: boundary condition				
changes over time	665			
main stream water inflows	664			
trailwater elevation	665			
tributaries	664			
water temperature	665			
Hydrologic Engineering Center				
(HEC). *see also* HEC-18 pier				
scour equation: *Assessment of*				
Structural Flood-Control				
Measures on Alluvial Fans	907			
HEC-1 hydrologic model	914	915(f)	916	
HEC-6 numerical model	294	508	602	652
	680(t)	758	996	997
numerical models	495			
Hydrologic Simulation Program (HSP)	848			
hydrology, defined	1095			
hydrostatic pressure assumption:				
ch3d hydrodynamic				
module	738	740		
role of	693			
streamline curvature	700			
three-dimensional models for				
reservoir sedimentation	686	755	756	
hyperconcentrated flow: defined	885	891		
rheology of	892			
streamflows	894	895		

This page has been reformatted by Knovel to provide easier navigation.

Index Terms	Links			
hypothetical stability assessment	484(t)			
I				
ice-cover effects	613	614(f)		
see also hydraulic impacts of river ice; river-ice effects on alluvial channel				
morphology; effects on secondary currents	623(f)			
flow distribution	619			
ice-cover breakup	623			
ice-cover effects on sediment transport by flow	627			
on a meandering channel	640(f)			
open-water proportions	621(f)			
sediment transport by ice	627			
sinuous-braided channel	637(f)			
transverse bed slope	624(f)			
ice-cover effects on sediment transport by flow: bed-sediment transport	632			
constriction scour and local scour at bridge piers	634			
flow resistance	630			
local scour beneath ice jams	634			
overview	627			
parameters	628			
sediment movement and bed forms	629			
water-temperature effects	629			
ice formation: bankfast ice	616	616(f)		
frazil ice	616(f)	617(f)	618(f)	
skim ice	616			
ice jams	557	625(f)	634	
ice model, defined	1095			
Ikeda-Coleman-Iwagaki analysis	46	48	48(f)	53
Illinois State Water Survey (ISWS)	844			
impeded removal	404			
implicit scheme	851	1094		
impoundment	1001	1095		
inactive layer	1095			

This page has been reformatted by Knovel to provide easier navigation.

Index Terms	Links			
in-bed flow pressure variations	973(f)			
in-channel and overbank flow diagram	214(f)			
in-channel habitat structures	492(t)			
incipient motion	480	483	1052	1095
stability checks	481(t)			
incised channel evolution model (ICEM)	380(f)	409(f)	864	864(f)
ineffective flow	1095			
inflowing sediment, size and concentration				
of: bed gradation on point bar	664			
concentrations	660			
grain size classes	660			
transport theory	661			
from tributaries	660	664		
initialization, model	655	715		
in situ capping of contaminated sediment	975			
instantaneous samplers	321			
Institute of Hydrology (U.K.)	844			
International Erosion Control Association	600			
Iowa vanes: installation of	453(f)			
as a pier-scour countermeasure	567	567(f)		
submerged	553			
island and bar formation and shift	877			
isoerodent maps	830			
of California	833(f)			
of Hawaii	835(f)			
of Oregon	834(f)			
of U.S. (western)	832(f)			
of Washington	834(f)			
isokinetic samplers	322	324(t)		

J

Jacalitos Creek	6
Jain-Fisher's equation	523
jam-collapse surges	639
jet turbulence intensity: based on outlet structure	1030(t)
polynomial coefficients and	1031(t)
joint alternate number	1027(t)
jointed rock	1033(f)

This page has been reformatted by Knovel to provide easier navigation.

Index Terms	Links			
joint roughness number	1027(t)			
joint set number	1022(t)			
June 2000 event.				
See Leavenworth Bend, Missouri River				
K				
Kankakee River	43	43(f)	44	
kaolinite	78	254		
Karim-Kennedy relation	127			
KINematic runoff	840			
kinematic similarity	1057			
kinematic-wave approach to debris-flow routing:				
depth-averaged equations of motion	909			
kinematic wave approximation	910			
model application	911			
rheological equations	909			
KINEROS model	840	844	849	
Knapp-Vlugter criterion	62			
knickpoints	876	876(f)		
k–ω model	788			
L				
Lagrangian models	71	769		
Laguna Dam	2			
lake and reservoir sedimentation, morphodynamics of: delta				
formation	133	133(f)		
detrainment and sediment trap efficiency, muddy				
pond formation in reservoir	144	144(f)	145(f)	146(f)
linked one-dimensional model of topset, foreset,				
bottomset evolution	139	141(f)		
linked quasi-dimensional model of topset,				
foreset, bottomset evolution	141	143	143(f)	144(f)
numerical modeling of, parameters used in	136(t)			
plunging of muddy turbidity current	138	138(f)		
topset and foreset, fluvial deposition				
of formation	134	135(f)	136(f)	136(t)
	137(f)			

This page has been reformatted by Knovel to provide easier navigation.

Index Terms	Links			
Lake Erie	288			
Lake Francis Case	582(f)			
Lake Mead	133	133(f)		
Lake Ontario	288			
landslides	170(f)	887	892	893(f)
	895			
Lane's balance	372(f)			
Lara-Pemberton method	598(t)			
lateral turbulence intensity	809(f)			
lateral velocity	807(f)			
Leavenworth Bend, Missouri River: background	735			
boundary and initial conditions, October 1999 event	736	737(t)		
field data campaigns	736			
flow computations	738(t)	740		
layout of	735(f)			
measured and computed free-surface elevations, June 2000 event	740(t)			
measured and computed free-surface elevations, October 1999 event	738(t)			
model calibration, June 2000 event	740			
model calibration, October 1999 event	737	738(t)	739(f)	
model construction	736			
model to study proposed habitat restoration measures	743	744(f)	745(f)	746(f)
sediment computations	740	742(f)	743(f)	
left overbank. *see* overbank				
Leopold scour chains	237(f)			
limestone	34			
equation	523			
linear elastic fracture mechanics (LEFM)	1032			
linear model	1069	1095		
linear scale	37(f)			
linked-one dimensional model of topset, foreset, bottomset evolution	139			
liquefaction	261			
Lischtvan-Levediev diagram	55	56(f)		
Little Salmon Creek	17			

This page has been reformatted by Knovel to provide easier navigation.

Index Terms	Links		
littoral drift	532		
live-bed abutment scour	527		
local agencies	667		
local inflow and outflow point	1095		
local scour.			
see also piers, local scour			
at: bridge-scour			
evaluation	511		
ice jams	634		
sedimentation processes,			
computational modeling of	646		
tidal waterways, calculations for	529		
total scour and	503		
location-for-condition evaluation (LCE)	867		
location for time			
substitution (LTS) technique	863	867	
logarithmic law: critical stress for			
flow over a granular bed	46		
vs. power laws for velocity	27(f)		
velocity distribution	775		
log scale	37(f)		
Loíza reservoir	603(f)		
longitudinal staggered discharges	751(f)	753(f)	
Loowit Creek channel profiles	928(f)		

M

Mad River	172		
Madsen-Jimenez formula	41	73	106
magnetite	34		
Mahatta River	16(f)		
main stem: defined	1096	1096(f)	
downstream fining	172		
water inflows	664		
Manning's *n:* with flow discharge	98(f)	489(f)	1096
Manning-Strickler form of	28	29	
Manual	54	937	
Maple Gulch Dam	998(f)		
Mapocho River	28		

This page has been reformatted by Knovel to provide easier navigation.

Index Terms	Links			
Marmot Dam, removal of (simulation):				
background gravel and				
sand transport rates	1009			
channel gradient and width	1005			
discharge data and hydrologic scenarios	1005			
discussion	1018			
grain-size distribution of reservoir sediment	1008	1008(f)		
grain-size distribution of the channel-bed surface layer	1006	1007(f)		
input data	1005			
model results	1009			
project background	1000	1000(f)	1001(f)	
reference runs of numerical models	1010	1011(f)		
Sandy River, effects on	1001	1002(t)		
Sandy River channel slope	1006			
sediment-transport models developed for	1002			
sensitivity tests	1016			
single-season				
dam removal and minimal sediment excavation	1012	1013(f)	1017(f)	
water year series selected for use in	1007(t)			
zero process	1009			
Marmot Reservoir	1003	1008	1008(f)	1010(f)
	1016			
mass failure	876			
mass strength number for rock	1026(t)			
mass-transfer coefficient	987			
mathematical modeling: Bridge-Bennett model				
for entrainment and transport	55			
defined	1096			
of mudflows and debris-flows	909			
Matilija dam	608(f)			
mean annual discharge	412	413(f)		
mean channel velocities	483(t)			
meander bend	361			
active surface-layer thickness	184			
average annual erosion rate *versus r/w*	363(f)			
bank erosion	87(f)	871		
competing transverse effects	75			

This page has been reformatted by Knovel to provide easier navigation.

Index Terms	Links			
meander bend (*Cont.*)				
flow and transport processes, numerical				
models for computing	399	400(f)		
radius-of-curvature-to-width ratio	362			
meander/meandering.				
see also channel stability: amplitude	361			
braided	441(f)	877	878	
criteria	441			
evolution, simulation of	450			
finite-amplitude	448			
flow and bed topography	443			
growth and shift	877	877(f)		
migration	442			
path length	361			
planform	441			
point bar	361	361(f)	406	871
process	439	441(f)		
river	13(f)	871		
straight and braided to meandering (Cd1 and Cd3)	878			
straight and meandering to braided (Cd2 and Cd6)	878			
stream	359	361	406	530
	1096			
wavelength	361			
mean velocity, defined	1096			
Mellor-Yamada length-scale equation	790			
Melville's equation	524			
mesh	36	551		
Meyer-Peter-Muller formula	72			
middle bar	361	361(f)		
migration: meander	442			
planform and bankline	653			
rates, lateral and down-valley	449(t)			
MIKE SHE (European Hydrological System model)	840	841	849	851
	852	857		
mining activities	12	13(f)		
accelerated erosion	6	6(f)		
sedimentation due to	12	13(f)		
undermining bed forms	558			

This page has been reformatted by Knovel to provide easier navigation.

Index Terms	Links			
mining activities (*Cont.*)				
wash load of river systems	61			
Minnesota River	35	235(f)		
Mississippi River	95	732(t)	1068(f)	1070(f)
see also Old River Control Complex (ORCC), Mississippi River				
Missouri River	79	95	99	582(f)
	616(f)	735(f)	737(t)	1069(f)
see also Leavenworth Bend, Missouri River				
mitigation. *See* sedimentation hazards				
mixing-layer concept	703			
mixing-length models	775	778	782	
limitations of	778			
MOBED2 two-dimensional mobile-bed program				
mobile-bed modeling, multidimensional. *see also*				
Leavenworth Bend, Missouri River:				
bed-sediment initial condition	731	732(t)		
calibrated model, use of	735			
calibration parameters	733			
CH3D modeling system	721			
complexity of	683			
computer resources, limitations of	684			
Coralville Reservoir	746	749(f)	751(f)	
field data campaign and model construction	722	736		
flow computations	737	737(t)		
habitat restoration measures	743			
hydrodynamic boundary and initial conditions	723			
hydrodynamic model calibration and verification	724	724(t)		
June 2000 event	740	742(t)		
mobile-bed program	746			
model calibration and verification	733	737		
model construction	736			
model sediment size classes	726	727(t)		
necessity of	683			

This page has been reformatted by Knovel to provide easier navigation.

Index Terms	Links			
mobile-bed modeling, multidimensional (*Cont.*)				
October 1999 event	737	738(f)	738(t)	739(f)
Old River Control Complex (ORCC)	720	721(f)		
Red Rock Reservoir	755	757(f)		
Saylorville Reservoir	755	756(f)		
sediment boundary conditions	726			
sediment computations	740	742(f)		
suspended-sediment conditions	727	728(f)		
mobile-bed numerical solution				
considerations: choice of				
numerical method	713			
grid-generation and adaptive-grid				
issues	714			
numerical coupling and uncoupling	712			
mobile-bed processes, conceptual models of	699			
model calibration: defined	655			
definitions	667			
fixed				
bed, steady-state hydraulic calibration	668			
fixed bed unsteady-state hydraulic calibration	669			
movable-bed, steady-state hydraulic and sediment				
calibration	669	670(f)		
movable-boundary, unsteady-state sediment				
calibration	670			
model capability requirements	685(t)			
modeling systems	10			
see also hydrodynamic-process				
formulations; mobile-bed modeling, multidimensional;				
ADCP techniques	719			
for bed and near-bed processes	701			
bed-surface material initial conditions	716			
capability requirements	685	685(t)		
critical assessment of, art and future perspectives and	755			
field data for construction of	714			
finite-difference methods	694			
hydrodynamic boundary conditions	717			
hydrostatic pressure assumption	693			
initialization of model	715			

This page has been reformatted by Knovel to provide easier navigation.

Index Terms	Links		
modeling systems (*Cont.*)			
limits of	654		
long-term bed evolution in response to changes	688		
mobile-bed numerical solution considerations	712		
mobile-bed processes	699		
mobile-bed dynamics aroundequation	524		
structures	688		
mobile-bed model calibration and verification	716		
overview	695	699	
reservoir sedimentation	685		
reviewed models, list of	416(f)	418(t)	420(f)
river-bend dynamics and training works	687		
sediment-exchange processes	707		
settling basins	687		
simplifications used in	700		
solution techniques and applicability of	693		
sorbed contaminant fate and transport	689		
subsurface strata initial conditions	716		
suspended-material processes	705		
suspended-sediment initial conditions	715		
system closure and auxiliary relations	708		
turbulence closure models	695		
Molinas-Wu relation	128		
momentum, molecular transport of	771		
momentum-diffusion model	413(f)		
M1 curve	134		
morphodynamics. *see also* lake and reservoir			
sedimentation, morphodynamics of; sediment			
transport: defined	70		
of rivers,			
equations governing	129		
Mount Fubilian	13(f)		
Mount St. Helens	23		
chronology of	923		
conclusions	934		
eruption, after effects of	925(f)	926(f)	
sediment sources	930		
sediment yield	933		

This page has been reformatted by Knovel to provide easier navigation.

Index Terms	Links			
Mount St. Helens (*Cont.*)				
watershed recovery	927			
moveable bed, defined	1096			
M2 curve	134			
mud balls, armored	8	9(f)		
mud definition and rheology: coefficient values	259(t)			
fine-grained sediment transport	255(t)			
parameters	259(t)			
properties	258(t)			
muddy pond: detrainment and sediment trap efficiency	144	144(f)	145(f)	146(f)
reservoir set up	144(f)			
mud-floods. *see also* mudflows, debris-flows				
and mud-floods, mechanics of: defined	890	893		
examples	891(f)			
mudflows, debris-flows and mud-floods, mechanics of:				
dimensionless rheological model	899			
hyperconcentrated flow, defined	885			
hyperconcentrated sediment flows,				
rheology of	892			
main classification criteria	887	893(t)		
mudflows, defined	890	893		
mudflows and debris-flows, mathematical modeling of:				
Cerro Grande River, simulation of mudflows				
and debris-flows in	913			
kinematic-wave approach	909			
mathematical modeling of				
muds, coefficient values	259(t)			
multivertical sampling	330			

N

National Weather Service (NWS)	667			
DWOPER model	849			
naturalization, defined	462(t)			
Natural Resources Conservation Service	595			
Navier-Stokes Equations	690			
near-bank zones	393	400	419	
Nelson-Smith partition	101			
neural network models	594			

This page has been reformatted by Knovel to provide easier navigation.

Index Terms	Links			
Newton-Raphson method	747			
Nielsen formula	73			
Niger River	60	61(f)	226	233
Nikuradse sand-roughened pipe experiments	29	30(f)	31(t)	
	53	119		
Nile River	61	344	866	
Ningerum Flats	171(f)			
Niño- García formula	66	71		
node, defined	1096			
nonengineering treatment techniques	16	16(f)		
nonequilibrium channels	429	429(t)		
nonlinear κ-ε models	399	791	792(f)	
non-point-source model (NPSM)	848			
Nonpoint Source Runoff (NPS) model	848			
numerical experiments	66	295		
numerical modeling. *see also* numerical width adjustment models; one-dimensional models; three-dimensional models: of lake and reservoir sedimentation, parameters used in	136(t)			
one-dimensional	1000	1019		
overview	10			
sediment transport mechanics and dune morphology research	97			
two-dimensional	903	909	915	
numerical modeling of bed level variation with sorting: elements of	213			
examples using grain-size distributions	215			
field applications to engineering problems	214	214(f)		
numerical scheme	841	851		
numerical stability	719	737		
numerical width adjustment models: cohesive and noncohesive-bank stability analyses	419	420(t)	421	
equilibrium and nonequilibrium channels	429	429(t)		
extremal hypotheses	422			
field testing	424	426(f)		
fluvial entrainment of bank materials	419			
fluvial hydraulics and bank mechanics	422			

This page has been reformatted by Knovel to provide easier navigation.

Index Terms	Links			
numerical modeling (*Cont.*)				
fluvial hydraulics and hydrodynamics	415	416(t)	417	
geofluvial	422	429(t)		
homogenous and heterogeneous bank structures	421			
laboratory data, tests with	423	425(f)		
longitudinal extent of mass failure	421			
numerical models, testing and application of	419			
overview	415	416(t)		
retreat and advance processes	419			
riverbank mechanics	419			
sediment transport and continuity	417	418(t)	419	
summary of	424(t)			
testing and application of	423			
width adjustment problems, approaching	426			
n-values	654	669	916	
O				
Oak Creek: bed material samples, size distribution of	43	44	44(f)	193(t)
	195	207	207(f)	
ratio of unit bed load transport rate q_i / F_i *versus* grain size D_i,	207			
substrate-based relation of Parker et al.	195			
total bed load transport rate q_T* *versus* Shields stress τ*	50	207	207(f)	
Values of γ	193(t)			
Oaklimiter Creek	408	409(f)	410(f)	
observed debris flows, physical properties of	896(t)			
October 1999 event. *See* Leavenworth Bend, Missouri River Ohio River	405	865	1044	1044(f)
OK Tedi Mine	13(f)	171(f)	174(f)	
Old River Control Complex (ORCC), Mississippi River: background	720	721(f)		
bed-sediment initial conditions	731			
calibrated model, use of	735			
Ch3D modeling system	721	723		
field data campaign and model construction	722			
free-surface elevations, computed and measured	724(t)			
hydrodynamic boundary and initial conditions	723			

This page has been reformatted by Knovel to provide easier navigation.

Index Terms	Links			
Old River Control Complex (ORCC), Mississippi River: background (*Cont.*) hydrodynamic model calibration and verification	723	725(f)		
hydroelectric power plant (HPP)	723	726	733	
model calibration and verification	733			
model sediment size classes	726			
physical calibration parameters	733			
sediment boundary conditions	726			
size classes for	727(t)			
size-fraction distributions	732(t)			
García suspended-sediment initial conditions	727	728(f)	731	
ormula	66	71		
Tarbert Landing	722	724	727	733
	735			
Union Point	722	724	726	727
	731	733	734	
1D flow-routing methods	415	417		
one-dimensional models. *see also* Marmot Dam, removal of (simulation): allocation of scour and fill channel	652			
cross sections, locating	758			
flow through an expansion or contraction	656			
limitations of	996			
linked, of topset, fireset, bottomset evolution	139			
long-term bed evolution in response to changes	688			
measurements of time-varying stages and discharges	720			
reservoir sedimentation	686			
settling basins	687			
volumetric analyses	687			
one-equation model *see also* Eddy-viscosity model	780			
open-channel flow diagram	81	118	146	321
	1111			
operating rule (policy)	665	1097		
ordinary stream flows	894	895		
Oreti River	555	555(f)		

This page has been reformatted by Knovel to provide easier navigation.

Index Terms	Links			
organic-rich sediments, shear strength parameters for	279	279(t)		
Orinoco River	62			
oscillatory flow	803	803(f)	804(t)	
overbank	234	637	643	1097
overdredging	978	1097		
oxygen concentration profiles	464	465	986(f)	
P				
Padma River	97	98(f)		
Paintal formula	72			
Palo Verde Dam	2			
pans	616	617(f)	618(f)	
Paraguay River	83			
parameters: calibration	670	733		
channel	124(f)			
defined	1097			
hydraulic loading	1041	1042(t)		
ice-cover effects	628			
lake and reservoir sedimentation, numerical modeling	136(t)			
sequence *vs.* channel stability	410(f)			
shear stress and flow, bed load transport in mixtures	193			
Paraná River	77	77(f)	78(f)	83
	95	96(f)	99	
Parker formula	73			
see also Shields-Parker's River sedimentation diagram				
Parker-Klingeman-McLean relation	195			
Parker relation, surface-based	196			
partial sediment balance	581			
particle shape factor, defined	1097			
particle size, defined	1097			
passive sediment fate and transport processes: adsorption and desorption equilibrium	969			
chemical reaction and biodegradation	970			
molecular diffusion	969			

This page has been reformatted by Knovel to provide easier navigation.

Index Terms	Links			
pass-through: characteristics of	601			
hydrograph prediction	602	603(f)		
rule curve	603			
seasonal drawdown	602			
turbid density currents, routing of	603	604(f)		
pattern change	877			
PCBs (polychlorinated biphenyls)	960	962	968	971
	978			
peak shear stress	405	1042(f)		
permeability, defined	1097			
perturbation stability analyses	446			
phasing, defined	1097			
physical models. *See* sediment transport scaling for physical models				
pier foundations (complex), scour for. *see also* HEC-18				
pier scour equation: components method of analysis				
and, superposition of	516	516(f)		
depth scour, determining	515			
overview	514			
pier stem scour depth, determination of	516	517(f)		
pile cap (footing) scour depth				
component, determination of	517	518(f)	519(f)	
pile group scour depth component, determination of	519	520(f)	521(f)	
piers, local scour at. *see also* bridge-scour				
evaluation; pier				
foundations (complex), scour for: countermeasures				
for local scour at	557			
(*see also* bridge-scour prevention; riprap				
protection at piers); debris on, scour depths with	523			
local scour at	512	512(f)		
nose shape	515(t)			
scour depth in a sand-bed stream	507(f)			
scour equations, other	525			
scour holes, top width of	525			
scour ratio	517	517(f)	521	
shapes	514(f)			
pit and trough samplers	342			
plane slip failure, Culmann analysis for	402	403(f)		

This page has been reformatted by Knovel to provide easier navigation.

Index Terms	Links			
planform: bankline migration	653			
channel	375			
defined	1097			
meander	441	442(f)		
metamorphosis	373			
sorting	227	228(f)		
plan test	671			
plunge point	138(f)			
plunge pool module	1030	1031(t)		
plunging: free overfall jet	1030(f)			
of turbid density currents	138	138(f)		
point bar: bed gradation on	664	664(f)		
defined	1097			
in meandering river, development	871			
in meandering stream	361	406		
point-integrated sampling	333			
polycyclic aromatic hydrocarbon (PAHs) compounds	960	962	966	968
	970			
pool-riffle sequences	360	360(f)		
population migrations	7			
pore pressure: channel widening	548			
determining	256			
fluidization	261			
landslides	888			
loose riprap, drainage				
advantages of	551			
positive	401	404		
slaking	401			
Powder River	390	407	412	413(f)
Powell-Reid-Laronne relation	200			
precast blocks	550			
Precipitation-Runoff Modeling System (PRMS)	840	848	849	
preservation, defined	461	462		
probabilistic models and methods	70	1052	1077	1097
prototype, defined	1097			
pumping samplers, automatic. *See* sampling				
methods, automatic pyroclastic flows	892			

This page has been reformatted by Knovel to provide easier navigation.

Index Terms	Links			
Q				
$Q_{1.5}$ discharge	588	588(t)		
quartz	34	35		
quasi-2D method	417	419		
quasi-steady flow	144(f)	145		
quasi-steady-state model, defined	1097			
quasi-three-dimensional model	699	755		
R				
radius of curvature	362			
rainfall-runoff erosivity factor	830			
rating curves	122(f)	593		
reasonable use rule	938			
Red Lake River, evolution of	450	451(f)		
Red Rock Reservoir	755	757(f)		
regime formulas	369(t)			
regression analysis	116(t)			
rehabilitation: activities	494			
defined	462(t)			
planning	357			
rejuvenation	875			
relative ground structure number	1025	1026	1028(t)	
relative shearwave velocity	258(f)			
relief bridges	555			
Reno mattresses	550	551	563	565(t)
REServoir CONservation (RESCON) approach	584			
reservoirs, sedimentation delivery to. *See* sediment yield; sediment yield, quantifying				
reservoir sedimentation: numerical modeling, parameters used in	136(t)			
one dimensional model	686			
sediment transport	133			
three-dimensional models and hydrostatic pressure assumption	686	755	756	
reservoir sedimentation rates: capacity-history curves	582			
reservoir half-life	581			
reservoir life	581	582(f)		

This page has been reformatted by Knovel to provide easier navigation.

Index Terms	Links		
reservoir sedimentation rates (*Cont.*)			
worldwide	580	581(t)	
reservoir sediment deposition. *see also* lake and reservoir sedimentation, morphodynamics of: bulk density of	597	597(t)	598(t)
Churchill's curve	595	596(f)	
Churchill's sedimentation index	596		
sedimentation index	596		
consolidation of sediment over time	598	598(t)	
depositional geometry	596		
patterns of sedimentation, prediction of	598		
trapping and releasing efficiency	595		
turbid density currents	597		
reservoir sediment management. *see also* reservoir sediment deposition; reservoir sediment management; sediment-routing strategies: control strategies	598		
dam removal	607		
delivery of sediment	587		
hydraulic dredging	604		
hydraulic flushing	605	606(f)	
impacts	585	585(t)	586(f)
large storage volume, provision of	600		
rates	580		
sediment focusing	607		
sustainability and economic analysis	582		
yield reduction	599		
reservoir survey, estimating sediment yield by: bathymetric survey	591	592(f)	
deposit thickness over event horizons	592		
overview	590		
resistance ratio for an ice-covered flow	632(f)		
restoration: activities	463		
channel design	485		
defined	462		
objectives	464	465	
problems	466	466(t)	

This page has been reformatted by Knovel to provide easier navigation.

Index Terms	Links			
restoration: activities (*Cont.*)				
vegetation				
used in	495			
restoration of function movement	17			
revetments	451			
see also riprap revetments				
Reynolds-averaged equations: auxiliary				
(boundary conditions)	770			
general flow equations	766			
Navier-Stokes equations	690			
overview	766			
for sediment model	768			
Reynolds number, defined	1098			
rheology. *see also* mud definition and rheology:				
dimensionless rheological model	899			
equations	909			
of hyperconcentrated flow	892			
Rhine River	95	340		
Richardson et al. abutment scour equation	530			
Richardson-Trivino abutment scour equation	529			
right overbank	234	637	643	1097
rigid-bottle samplers	323			
Rio Calicanto plateaus	2(f)			
Rio Grande	97	98(f)	99	105
	320	586	863	1072
Rio Maule	12(f)			
Rio Paraná dunes	77			
RIPA model	417			
riparian rights	938			
ripples	82(f)	83		
riprap, environmental requirements for:				
ecological impacts	1046			
overview	1045			
reduced riprap protection, lower bank only	1046			
vegetation in revetments	1046			
riprap, geotechnical requirements for: filter objectives	1044			
geotextile filters	1045			

This page has been reformatted by Knovel to provide easier navigation.

Index Terms	Links			
riprap, geotechnical requirements for: filter objectives (*Cont.*)				
mineral filters	1045			
seepage effects	1044	1045(f)		
riprap design. *see also* riprap structure types:				
advantages and disadvantages of	1037			
factors	1037			
objective and scope of	1037			
riprap protection at piers: construction and maintenance	1053			
degradation, tolerance to	562			
design of riprap and	554			
failure mechanisms	557	558(f)		
filters	562			
gradation	559	561(f)		
lateral extent	559	561		
layer thickness	651			
overview	557			
placement level	561	562(f)		
size	558	559(t)		
riprap protection at piers, alternatives to: cable-tied blocks	563	564(t)		
concrete apron and grouted riprap	563	566		
design	558	559(f)		
gabions	563	565(t)		
grout-filled bags and mats	563	566(t)		
horizontal collars	568	568(f)		
Iowa vanes,curve	595	596(f)	567	567(f)
overview	557	558(f)		
Reno mattresses	563	565(t)		
sacrificial riprap	566	567(f)		
riprap protection for abutments: filter requirements	573			
overview	570			
rock protection, extent of	572	573(f)		
size of riprap	571	572(t)		
thickness of riprap	573			
riprap revetments: adjacent to hydraulic structures	1038			
bank	1037			
protection on lower bank	1038(f)			
scour and protection at ends and tops	1048			
thickness	1040			

This page has been reformatted by Knovel to provide easier navigation.

Index Terms	Links	
riprap revetments: adjacent to hydraulic structures (*Cont.*)		
toe scour along bank revetments	1046	1047(f)
toe scour protection requirements	1047	1048(f)
vegetation in	1046	
riprap size requirements: characteristic size		
and gradation effects	1050	
forces on riprap	1048	1049(f)
maximum force, design for	1049	
stability, velocity profile and turbulence	1049	
riprap sizing methods: California Bank and Shore		
Protection (CBSP) Manual	1050	
Corps of Engineers Manual—Hydraulic		
Design of Flood Control Channels	1051	
CUR Manual	1050	
FHWA manual-design	1051	
field data-based	1052	
flow competence and	51	
hydraulic structures (riprap around)	1053	
overview	1050	
probabilistic methods	1052	
propeller jets	1053	
river closures	1053	
safety factor methods	1051	
stability of, ice and debris effects on	1053	
for steep slopes	1052	
Wallingford Design Manual for River and		
Channel Revetments	1051	
waves	1053	
waves and currents combined	1053	
riprap stone, physical		
characteristics of: durability	1039	
gradation	1040	1040(f)
revetment thickness	1040	
rock-type sources	1039	
roughness	1041	
shape and porosity	1039	
stone density	1039	
testing and sampling	1039	

This page has been reformatted by Knovel to provide easier navigation.

Index Terms	Links		
riprap structure types.			
see also hydraulic loading: adjacent to			
hydraulic structures	1038		
bank revetments	1037		
bed protection	1039		
bendway weirs	1038		
dikes	1038		
factors	1037		
river closure structures	1039		
steep chutes and channels	1038		
toe protection and launchable stone	1038		
wave protection	1038		
riverbank mechanics. *see also* fluvial hydraulics in bank			
mechanics: cohesive and noncohesive-bank			
stability analyses	419	420(t)	
fluvial entrainment of bank materials	419		
homogenous and heterogeneous bank structures	421		
dunes	77		
longitudinal extent of mass failure	421		
retreat and advance processes	419		
river corridor degradation	464(t)		
River Hydraulics (Engineering Manual 1110-2-1416)	907		
river-ice effects on alluvial channel morphology. *see also*			
hydraulic impacts of river ice: bankfast-ice			
loading of banks	642	642(f)	
combined hydraulic and geomechanical			
impacts	645		
freeze-thaw influences on riverbank strength	640		
gouging and abrasion of banks	643	644(f)	
overview	635	640	641(f)
riverbanks, impacts on	640		
strength, reduction of	642		
thalweg sinuosity	639(f)		
river metamorphosis	878		
river restoration design. *see also* channel design:			
of backwater protection	494		
of channel bottom habitats	493	494(t)	
of channel-floodplain connectivity	493		

This page has been reformatted by Knovel to provide easier navigation.

Index Terms	Links			
river restoration design (*Cont.*)				
of habitat structures	491	492(t)		
overview	485			
river training works	549			
river width adjustment	422			
see also bank erosion; bank mechanics; fluvial hydraulics in bank mechanics; numerical width adjustment models; cause and effect, influence of scale and	391			
channel evolution, conceptual models of	408	410(f)	427	
empirical methods based on field observations	415	415(f)		
engineering or river management solution	428			
equilibrium approaches	411	412(f)	413(f)	
equilibrium morphology, assessment of	427			
field data collection	426			
geomorphic context of	387	388(f)	389(f)	
model prediction	428			
model validation	427			
numerical models	415	416(t)	418(t)	
problem identification	426	427(f)		
retreat and advance processes	419			
RNG model	789			
rock joints: closed-ended	1031			
open-ended	1031	1034	1034(f)	
pressure fluctuations	1022	1022(f)		
rock mass module	1031	1032(f)	1033(f)	1034(f)
	1034(t)			
rock scour: combined application methods	1024			
Comprehensive Scour Model (CSM)	1026	1028		
Erodibility Index Method (EIM)	1024			
falling jet module	1028	1030(f)		
mechanisms	1023	1023(f)		
overview of	1021			
plunge pool module	1030	1031(t)		
rock mass module	1031	1032(f)	1033(f)	1034(t)
water, erosive capacity of	1022	1022(f)		
roundoff error, defined	1098			

This page has been reformatted by Knovel to provide easier navigation.

Index Terms	Links			
Rouse-Vanoni-Ippen suspended sediment distribution, flow stratification effects, inclusion of	111	112(f)		
routing, defined	1098			
runoff, defined	1098			
Russian River	16(f)			
S				
sacrificial riprap	566	567(f)		
Saeltzer Dam	998	998(f)		
St. Anthony Falls Laboratory (SAFL)	64	71		
St. Venant equations	10	213	391	650
	669			
saltation	66			
sampling methods, automatic: activation	336			
installation and use criteria	334			
overview	333	334		
placement and orientation	335	335	336(f)	536(f)
sampling methods, manual: bag	328			
cable-and-reel	325			
EDI method	330	332		
EWI method	331			
handheld and handline	323	325		
instantaneous	321			
isokinetic	322	324(f)		
multivertical	330			
overview	328			
point-integrated	333			
rigid-bottle	323			
single-vertical	328			
transit rates	332			
transit rates for suspended-sediment	332			
sand: size classification scale	1091(t)			
transport rates	1009			
sand-bed rivers, suspension-dominated:				
downstream fining	233	234(f)		
entrainment and near-bed concentration,				

This page has been reformatted by Knovel to provide easier navigation.

Index Terms	Links	
sand-bed rivers, suspension-dominated (*Cont.*)		
grain-size specific relations	231	
fine sediment deposition, flushing from gravel	236	
floodplain deposition, grain-size-specific formulations	234	235(f)
grain-size-specific bulk predictors	232	
Rouse-Vanoni approach for grain-size-specific suspended load	229	
sorting in	229	
sand-bed streams. *see also* bed-material		
load in sand-bed streams, dimensionless relations for: flow resistance	99	103
vs. gravel-bed streams	65	
Sandy River. *see* Marmot Dam, removal of (simulation)		
San Francisco sediment, orders of	261(t)	
saturation: defined	1098	
landslides	895	
Saylorville Reservoir	755	756(f)
scale: defined	1098	
effect	1096	
fluvial geomorphology	358	
influence of	391	
laws	1096	
sediment grade	36(t)	
size classification of sediment particles	1091(f)	
time (in turbulent sediment transport)	765	
watershed	842(t)	
scale effect	1098	
Schmidt number	772	
Schumm and Rosgen channel classifications	376	
scour. *see also* local scour, total scour, bridge-scour: bend	556	
confluence	556	
general	508	
local	511(f)	511
(*see also* pier foundations (complex), scour for; piers, local scour at); total	506	
scour at abutments: Chang-Davis abutment scour equation	527	
design for scour	526	
overview	525	526(f)

This page has been reformatted by Knovel to provide easier navigation.

Index Terms	Links			
scour at abutments (*Cont.*)				
Richardson et al. abutment scour equation	530			
Richardson-Trivino abutment scour equation	529			
shape	526	527(f)		
site conditions	526			
skew adjustment of	526	527(f)		
Sturm abutment scour equation	528			
scour equations: Colorado State University (CSU)	512	513	515	
contraction	508			
Jain-Fisher's equation	523			
Melville's equation	524			
other	525			
Richardson et al. abutment scour equation	530			
Richardson-Trivino abutment scour equation	529			
Sturm abutment scour equation	528			
secondary currents (flow): defined	1098			
ice-cover influence on	623			
second-moment closure	793			
sediment, defined	8	1098		
sedimentation, defined	1098			
Sedimentation Committee of the Hydraulics Division of ASCE	1			
sedimentation engineering: global aspects and changing roles in	1			
scope of	3			
state of, general observations on	3			
Sedimentation Engineering Manuals	1	21	907	1051
	1110			
sedimentation hazards	881			
see also alluvial fan flooding				
geomorphic hazards; mud flows and debris-flows, mathematical modeling of; bank protection works	907			
crib barriers	907			
debris barriers	908			
debris basins	908			
dikes	908			
diversions and bypasses	908			
flood control channels	908			
floodwalls	908			

This page has been reformatted by Knovel to provide easier navigation.

Index Terms	Links		
sedimentation hazards (*Cont.*)			
general approach to	906		
guidance	906		
hazard assessment and mitigation design procedures, currently accepted	905		
hazard mapping and avoidance	905		
history and magnitude of	887		
levees	908		
overview	885	886(f)	
retention basins	908		
sediment control structures	908		
sediment retention structures	908		
sediment traps	908		
small dam operations	908		
state-of-the-science procedures	905		
Sedimentation Investigations of Rivers and Reservoirs (Engineering Manual 1110-2-4000)	907		
sedimentation problems, management and treatment of:			
engineering treatment and	15		
fish habitat and environmental issues	17		
identification and definition of	15		
nonengineering treatment and	16		
sedimentation processes, computational modeling. *see also*			
data types and resolution; flow in mobile boundary channels, equations for: base test	670		
boundary conditions for	655		
computational and physical model studies, similarity between	654		
example application	672	675(t)	676(f)
local scour and deposition	650		
model applicability, examples to illustrate	671		
overview of	649		
vs. physical model	654		
plan test	671		
results, interpretation of	671		
sediment characterization tests	254	255(t)	
see also mud definition and rheology			
sediment cycle	22		

This page has been reformatted by Knovel to provide easier navigation.

Index Terms	Links			
sediment data: bed gradation on a point bar	664	664(f)		
gradation of bed sediment reservoir	658	659(f)		
grain size classes	660	662(t)		
inflowing sediment concentrations	660	660(f)	661(f)	
sampling concepts	659			
sediment data set, criteria for	320			
sediment inflow from tributaries	664			
size and properties of bed sediment reservoir	658			
test for sufficiency	660			
transport theory, calculating with	661			
variability of samples	660			
sediment delivery ratios	839	840(t)		
sediment deposition.				
see also reservoir sediment deposition:				
accelerated (human-induced)	11			
causes of	11			
environmental and habitat effects of	14			
geologic (natural)	11			
rates and quantities, estimation of	7	14		
sediment deposits: debris flow	11			
intermediate and lowland				
river deposits	12	12(f)		
in lakes and reservoirs	12			
river	11	12(f)		
sand, for single season dam removal	1012(f)			
thickness over event horizons	592			
sediment-discharge, defined	1097			
see also sediment load				
sediment discharge, estimating	1063			
see also bed load material				
equations; fluvial-sediment data, collection of	1083			
suspended-sediment concentration interpolation method	1067	1068(f)		
transport-curve method	1069(f)	1069	1071(f)	1072(f)
	1073(t)			
sediment-exchange processes: introduction	707			
near-bed concentration, imposition of	707			
near-bed sediment exchange, imposition of	707			
sediment finer, defined	12			

This page has been reformatted by Knovel to provide easier navigation.

Index Terms	Links			
sediment focusing	599	607		
sediment grade scale	36(t)			
sediment-laden open-channel flow	61	62(f)		
sediment load. *see also* depth-discharge				
computation; suspended				
bed-material load: classification	60	60(t)	61(f)	
field data on bed-sediment load	633			
rating curves	593			
Rouse-Vanoni approach for grain-size-specific				
suspended load		229		
spatial modeling	595			
suspended	601			
turbidity measurements	594			
sedimentological scale	37(f)			
sediment oxygen demand (SOD):				
developed flow concepts	989			
diffusive sublayer thickness	984	984(f)	985(f)	986(f)
	987(f)			
mass-transfer coefficient	987	989(f)		
overview	983			
sediment properties: fall velocity	41	42(f)		
model laboratory sediments	35			
porosity	39	40(f)		
rock types	34			
shape	40	40(f)		
size	35	36(t)		
size distribution	37(f)	37		
size distribution *vs.* stream morphology	43	43(f)	45(f)	
specific gravity	34	35(t)		
sediment-routing models	418(t)			
sediment-routing strategies.				
see also pass-through: offstream				
reservoir for sediment bypass	600	600(f)		
onstream reservoir for sediment bypass	601			
turbidity density currents, routing of	603	604(f)		
sediment studies plan, preparation of: data collection	468			
data inventory	468			
other elements	468	469(t)		

This page has been reformatted by Knovel to provide easier navigation.

Index Terms	Links			
sediment studies plan, preparation of: data collection (*Cont.*)				
overview	466	467(f)		
problem areas, identification of potential	468			
tability assessment	468			
study area, boundary of	468			
sediment transport. *see also* bed forms; bed load transport				
gravel and sediment mixtures, transport of; suspended				
bed-material load; threshold conditions for sediment				
transport: bed material load and wash load, modes of	60	64(f)		
continuity and	417	418(t)	419	
Engelund-Hansen relation for bed-material				
load in sand-bed streams	125			
equations, summary of	1083(t)			
by ice	625	626(f)		
(*see also* ice-cover effects on sediment transport				
by flow); modeling and	10			
modes of	8	60		
sediment load classification	60	60(t)	61(f)	
Shields-Parker river sedimentation diagram	63	64(f)	65(f)	
sediment transport, fluid mechanics and hydraulics				
for: bed forms, equivalent roughness of	33	33(f)	34(f)	
channel flow resistance, relations for	27			
fixed-bed (skin or grain) roughness	29	30(f)	31(t)	
flow velocity distribution, law of the wall	24			
flow velocity distribution, velocity-defect and				
log-wake laws	25	26(f)		
movable flat-bed roughness	32			
sediment transport and hydraulic variables, relationships				
between: incipient motion	480	481(t)	482(f)	483(t)
sediment budgets	484			
silt and clay beds	483	483(f)		
slope-drainage area relations	479			
stream power	480	480(f)		
sediment transport measurements. *see also* bed load samplers				
bed-material measurement techniques; suspended-sediment				
samplers: overview	307			
sediment-sampling equipment, history				
of development of	308			

This page has been reformatted by Knovel to provide easier navigation.

Index Terms	Links			
sediment transport measurements (*Cont.*)				
techniques	9			
terminology	307	308(f)		
sediment-transport mechanics	9			
dune morphology and	97			
related phenomena	9	21		
sediment-transport processes. *see also* active sediment-transport processes; passive sediment fate and transport processes: concentration profile	259	259(f)		
unit transport processes	260			
sediment transport scaling for physical models: cohesive sediment, structural modeling of	1059(f)			
dimensionless unit sediment discharge	1059	1061		
model-prototype comparison	1062	1063(f)	1064(f)	1065(f)
nomenclature	1064			
overview	1057			
settling velocity adjustment	1061	1062(f)		
similitude	1057			
similitude deficiency of Froude scaling	1058			
tractive stress	1058	1058(f)		
sediment trapping: continuous	581	582(f)		
trap efficiency	144(f)	595	1101	
sediment-water interface	955(f)			
sediment-wave effects	553	555		
sediment yield. *see also* model calibration; watershed sediment yield: *vs.* drainage area	589	589(f)	590(f)	
erosion	587			
$Q_{1.5}$ discharge	588	588(t)		
reduction	599			
spatial variation	587	588(f)		
temporal variation	588	589(f)	590(f)	
sediment yield, quantifying: from fluvial data	593			
neural network models for	594			
reservoir survey for	590			
spatial modeling for	595			
SEDIMONT	587			
settling and consolidation	272			

This page has been reformatted by Knovel to provide easier navigation.

Index Terms	Links			
settling basins	687			
settling velocity. *see also* fall velocity: aggregation	266			
concentration and	267			
other effects on	270			
settling flux variation and	267(f)			
shallow-water (long-wave) model	82			
shape factor, defined	1097			
shear failure	558			
shear force	820			
shear intensity	865			
shear strength to solid volume fraction	277(t)			
shear stress	194	1099		
aggregation, fine-grained sediment transport	264			
boundary, calculation of	193			
for cohesive materials	454(f)			
diagram	264(f)			
distribution	397(f)			
distribution sketch and bed slope	398(f)			
shear stress partitions: Einstein partition	100			
Engelund-Fredsøe partition	102			
Nelson-Smith partition	101			
shear velocity	776(t)	1099		
Shields curve, defined	1099			
Shields diagram	48	49(f)	50(f)	
Shields parameter	48	414	485	
Shields-Parker's sedimentation diagram	63	64(f)	65(f)	
Shields velocity, defined	1099			
shock-capturing formulation	135(f)			
shock-fitting formulation	136	137(f)	140(f)	144(f)
	145(f)			
shorefast ice erosion	642(f)			
shoreline recession	297(f)			
side slopes, threshold condition on	57			
sieve diameter	42	311	1099	
silt	483	728(f)	1091(f)	
siltation	13(f)	309	827	939
Silver Bow Creek	235(f)			
similarity plots	189(f)			

This page has been reformatted by Knovel to provide easier navigation.

Index Terms	Links			
similarity (similitude)	652	1057	1099	
Simons and Richardson diagram	86	86(f)	87(f)	
simulate, defined	1099			
Simulated Water Erosion (SIMWE) model	841			
simulation	445	687	913	1099
simulation model	844			
single-stage samplers	336			
single-vertical sampling	328			
sinking material	61	62		
sinuosity	361			
size-class fraction distribution	742(t)			
size distribution and size density scale	37(f)			
skewed flow	520(f)			
skim ice	615			
slaking	401			
slope bed, granular sediment on a	55			
slope-discharge relationships	441(f)			
slope dissection	875			
slope length and steepness factor	833			
slope slide, particle located on a	58(f)			
slurry flows	893			
slush	616			
socioeconomic lifelines	888			
SOGREAH	844			
Soil and Water Assessment Tool (SWAT)	840	848	850	
Soil and Water Conservation Society	599			
Soil Conservation Service (SCS)	667			
soil creep	891			
soil erodibility factor	831			
soil loss equation	829			
soil loss tolerance	829			
solifluction	891			
sophisticated models	786	790		
nonlinear κ-ε models	791			
second-moment closure and algebraic stress models	792			
two-phase	790			
Soquel Creek	16(f)			
sorbed contaminant fate and transport	689			

This page has been reformatted by Knovel to provide easier navigation.

Index Terms	Links		
sorting, defined	1100		
specific recurrence interval discharge	365		
specific weight computation by Lara-Pemberton method	598(t)		
split flow	1100(f)		
stability analysis	448(f)		
stability assessment for stream restoration	474		
bank stability	484		
channel classification	477		
hydraulic geometry relationship	479		
lane relations	476		
qualitative	475		
sediment transport and hydraulic variables, relationships between	479		
selection of	484		
stability checks for stream restoration: of bed and bank stability	494		
sediment budget analysis	495		
River diagram	63	64(f)	65(f)
stability numbers *vs.* observed shore stability	287(t)		
stable channel	1100		
stable channel design chart	489(f)		
stably stratified-flow analogy	776	778	
stage, defined	1100		
stage-discharge relations	103		
Brownlie & Cruickshank-Maza method	106		
Einstein-Barbarossa method	103		
Engelund-Hansen method	104		
Karim-Kennedy method	107		
other	107		
Wright-Parker method	105		
standard solid viscoelastic model	257(f)		
standard step method	415	417	1100
Stanford Watershed Model (SWM)	848		
state agencies	667		
static armour: from equilibrium bed conditions	218(f)		
vs. experimental data	217(f)		
steady state model, defined	1097	1100	
steady uniform sediment-laden flows	779(f)		

This page has been reformatted by Knovel to provide easier navigation.

Index Terms	Links			
steep chutes and channels	1038			
step-pool topography, side view of	167(f)	228(f)		
stochastic model	70	1052	1077	1097
stone, launched	1048(f)			
stone cells on bed surfaces	216(f)			
storm surge	533			
straight meandering	878			
straight trapezoidal cross section	396(f)			
strain rate	256(f)			
stratification and sorting	239(f)			
stratification correction	291(t)			
stratum control volumes	704	704(f)	709	
streambank erosion, defined	1098			
see also river width adjustment				
stream discharge	366	593	1100	
streamflows	891			
stream gauge	656	1100		
stream gauge, defined	1100			
stream power: sinuosity variations and	868(f)			
stability criteria	480(f)			
stream profile, defined	1100			
stream reach classifications	494(t)			
stream restoration: definitions	461			
discharge	469			
implementation and construction	496			
monitoring and postconstruction adjustment	496			
projects	17	17(f)	467(f)	
river dynamism	463			
sediment studies plan, preparation of	466			
stability assessment	474			
stability checks	494			
stream restoration, role of sedimentation				
engineering in. *see also* river restoration design:				
bed material size distribution	474			
engineer and, as part of a team	463			
habitat assessment, setting objectives and	464			
habitat restoration objectives, specific	465			
large scale projects, opportunities offered by	465			

This page has been reformatted by Knovel to provide easier navigation.

Index Terms	Links			
stream restoration, role of sedimentation				
engineering in (*Cont.*)				
monitoring and postconstruction adjustment	496			
objectives, setting	464			
project scale and, effects of objectives on	465			
risk evaluation	466			
sedimentation analysis, scope of	465			
stream segment, defined	1100			
streamwise velocity profiles	114(f)			
structure channel	732(t)			
Sturm abutment scour equation	528			
sturzstroms	892			
subcritical flow	1100			
submerged Iowa vanes	453	553		
submodel domain	744(f)			
subsampling equipment	338			
sub-surface layer	1090			
summation convention	816			
supercritical flow	83	140	1100	
supplies and interests, definitions	938			
support practice factor	837	837(t)		
surface armoring, contrasts in	165(f)			
surface-based relation of Parker plot	196	197(f)		
surface grain-size distribution: pebble counts				
by stillwater sciences and	1007(f)			
in the Sandy River	1006(f)			
suspended bed-material load: depth-discharge				
and sediment load computation, example of	119			
(*see also* depth-discharge computation); eddy				
diffusivity (Prandtl analogy), form of	110			
equilibrium, in wide channel	109			
equilibrium near-bed sediment concentration	116			
mass conservation of	107			
Rouse-Vanoni-Ippen suspended sediment				
distribution	111			
sediment advection-diffusion equation,				
boundary conditions for	108			
sediment entrainment, functions for	116			

This page has been reformatted by Knovel to provide easier navigation.

Index Terms	Links			
suspended bed-material load: depth-discharge				
and sediment load computation, example of (*Cont.*)				
vertically averaged concentrations	114			
suspended-material processes: sediment				
mixtures, formulations for	706			
three-dimensional formulation	705			
two-dimensional (depth-averaged) formulation	706			
suspended medium sand, computed and measured	728(f)			
suspended-sediment samplers	326(f)	327(f)		
see also suspended bed-material				
load; boundary				
conditions	749(f)			
concentrations	739(f)	742(f)	749(f)	751(f)
concentrations following dam				
removal, simulated	1015(f)			
distribution	112(f)			
fluxes	296(f)			
loads, estimations of annual	1073(t)			
suspended silt and clay concentration	481(f)			
suspended very fine sand	728(f)	729(f)		
suspension concentration during a neap tide	269(f)			
sustainability: economic analysis and	582	583(f)		
regulatory and legal aspects	584			
RESCON approach	584			
SUTRENCH-2D	699	700	701	
SUTRENCH-3D	699	700	701	
SWRRB	848			
system closure: active-layer and				
active-stratum approach	709			
auxiliary relations, considerations	711			
bed load-layer approach	709			
introduction	708			
total-load approach	709			
two-dimensional models	711			
system instability: basin-wide factors	375			
downstream factors	373			
upstream factors	374			

This page has been reformatted by Knovel to provide easier navigation.

T

TABS-2	699		
tactical dredging	604		
tailgate	655		
tailwater elevation	665		
Taiwanese River	555(f)		
Tanaguarena	913		
Tanaguarena (f)	886		
Tanana River	622(f)		
Tarawera River	78		
TELEMAC-3D	700		
tensors	815		
thalweg: alignment	639	640(f)	641(f)
defined	1100		
effects	553	555	
sinuosity and channel variations	640(f)		
thalweg alignment	638	638(f)	639(f)
thalweg effects	553	555	
thalweg sinuosity	639(f)		
theoretical model	48		
3D hydrodynamic model	417		
three-dimensional models: computer resources,			
limitations of	684	686	
contaminant-sediment capability	758		
field data for model construction	715		
long-term bed evolution in response to changes	688		
river-bend dynamics and training works	687		
settling basins	687		
structured *vs.* unstructured grids.	755		
Three Gorges Reservoir profile	601(f)		
three-point bars	1098(f)		
threshold channel, river restoration design of: example of	487		
refinements	487		
step-by-step approach	487		
velocity and tractive force, allowable	487		
when to use	486		

This page has been reformatted by Knovel to provide easier navigation.

Index Terms	Links	
threshold conditions for sediment transport. *see also*		
bed-slope, incipient motion and: critical stress for flow over granular bed	46	
Lischtvan-Lebediev diagram for sediments for maximum permissible flow velocity	55	
Shields diagram	48	
submerged angle of response	45	
Wiberg-Smith diagram for heterogeneous sediments	52	
Yalin-Karahan diagram	51	
tidal amplitude	533	
tidal cycle	533	
tidal inlets	533	536(f)
tidal model	717	
tidal passage	533	
tidal period	533	
tidal prism	533	
tidal processes: defined	533	
tidal range	533	
tidal terms, principle	535(f)	
tidal waterways: crossings, types of	534(f)	
definition	533	
tidal waterways, scour calculations for: contraction scour	532	
design discharge	532	
local scour	533	
long-term degradation	532	
tides	533	
Tinau River	11	11(f)
topographic variability	206(f)	
topset evolution: fluvial deposition	134	
linked-one dimensional model of	139	
linked-quasi-two-dimensional model of	141	
top width, defined	525	1101
total-load approach	709	
total maximum daily load (TMDL)	840	
total scour: aggradation and degradation, long-term	506	
general scour (bridge-scour evaluation)	506	
lateral shifting of a stream	507	

This page has been reformatted by Knovel to provide easier navigation.

Index Terms	Links		
total scour: aggradation and degradation, long-term (*Cont.*)			
local scour	503	507	
total sediment load	8	61(f)	308(f)
Toutle River channel profiles	926(f)		
toxic sediments on a floodplain	235(f)		
tracers as function relative to grain size	237(f)		
tractive force	413	428	
transect, defined	1101		
transient flow and dam site following dam removal	997(f)		
transport capacity	651	654	1101
transport modes, aggregation and	265		
transverse bed slopes	445(f)		
trap efficiency	595	1101	
of a reservoir	144(f)		
trapezoidal channels	393(f)	394(f)	395(f)
tributaries: defined	1100		
hydrologic data	664		
sediment inflow from	660	664	
uncontaminated, healthy	235(f)		
truncation error, defined	1101		
Tsujimoto relation	197		
tsunami	533		
turbid density currents (turbid currents): morphodynamics of,			
equations governing	131		
overview	597		
plunging of	137		
rivers and	129		
routing of	603	606(f)	
turbulence, aggregation and	264		
turbulence models. *see also* Eddy-viscosity model: aim and			
scope of modeling	766		
applications of	794		
auxiliary, boundary conditions and	770	784	
Cartesian tensor notation	815		
choice models, considerations in assessment of	812		
closure	695		
defined	1101		

This page has been reformatted by Knovel to provide easier navigation.

Index Terms	Links			
turbulence models (*Cont.*)				
erodible-bed modeling, bed load transport and	786			
free-surface conditions	788			
other types of	815			
particulate flows, turbulence in	763			
problems in sediment transport, length and time scales in	765			
Reynolds-averaged equations	766			
sediment equation, boundary conditions and	785			
spatially averaged models	817			
turbulent flows, qualitative features of	764			
turbulent kinetic energy, equation for	780			
two-dimensional bed load transport	75(f)			
two-dimensional fan-delta	143(f)			
two-dimensional model	141	711		
two-equation model: equation for ε	782			
κ–ε model and closure constants	783	788		
two-phase models	790			

U

U.K. Institute of Hydrology	844			
uniform flow, general resistance diagram for	1058(f)			
unimpeded removal	404			
U.S. Army Corps of Engineers: Unsteady flow through a full NETwork of open channels (UNET) model	849			
U.S. Geological Survey (USGS)	665	667	848	955
U.S. Water Resources Council (WRC)	887			
U.S. Weather Service, Extended Streamflow Prediction (ESP) program	848			
U.S. Environmental Protection Agency (USEPA), Better Assessment Science Integrating Point and Nonpoint Sources (BASINS)	848	851		
unit longitudinal staggered discharges	751(f)			
units of measurement	321			
unit transport processes	260	261(f)		
Universal Soil Loss Equation (USLE)	587			
unsteady-state model	1101			
upland river deposits	11			

This page has been reformatted by Knovel to provide easier navigation.

Index Terms	Links		
upland soil erosion: cover-management factor	835		
rainfall-runoff erosivity factor	830		
slope length and steepness factor	833		
soil erodibility factor	831		
soil loss equation	829		
soil loss tolerance	829		
support practice factor	837	837(t)	
urbanization and accelerated erosion	5		
U.S. Army Corps of Engineers	667		
HEC-6 model	996	997	
Hydraulic Design of Flood Control Channels	1051		
USDA allowable-velocity charts	481(f)		
USDA-ARS National Sedimentation Laboratory (NSL)	841		
USDA-ARS North Central Soil Conservation Research Laboratory	841		
used tires	550		
V			
valley filling	875		
vane shear strength and soil consistency	277(t)		
Vanoni, Vito A.	1108(f)	1109(f)	1110(f)
career of	1107		
as hydraulic researcher	1108		
personal life	1111		
retirement honors	1111		
as river hydraulics consultant	1111		
Sedimentation Engineering Manuals	1	21	1110
sedimentation research, overview of	1112		
as structural engineer	1108		
suspended sediment transport research	1111		
youth of, on farm	1107		
Van Rijn formula	73		
Varnes' classification	891		
vectors	815		
vegetation: bank mechanic effects	405		
bridge site selection	551	553	
restoration	495		

This page has been reformatted by Knovel to provide easier navigation.

Index Terms	Links			
vegetation: bank mechanic effects (*Cont.*)				
in revetments	1046			
velocity: boundary sheer stress and	392(f)			
depth on exposed footing and	519(f)			
for movement of bed material, critical	510			
Venezuela	886(f)			
verification	668	714	1101	
vertical mass diffusive flux	292(f)			
vertical momentum equation	684	686	690	756
	818			
viscous length scale	987(f)			
Voigt viscoelastic model	257(f)			
volumetric samples and clay samples	312(f)			
vortex tube bed load samplers	343	343(f)		
W				
Walker River	13(f)			
warfare	7			
wash load	8	60	1077	1101
water column, defined	1101			
Water Erosion Prediction Project (WEPP)	587	841		
water floods	892			
watershed management, literature on	599			
watershed models: algorithms and efficiencies	851			
curve number and empirical equations	850			
defined	1100			
diffusive wave equation used by CASC2D and MIKE SHE	849			
flow-governing equations, basic	848			
kinematic wave equations used by DWSM, KINEROS, and PRMS	849			
long-term continuous	842(t)	851		
review of	841	848		
sediment yield predictions using storage-based equations	852	850		
storm-event	845(t)	851		

This page has been reformatted by Knovel to provide easier navigation.

Index Terms	Links			
watershed sediment yield.				
see also upland soil				
erosion: gross erosion	839			
gully erosion	837			
sediment delivery ratios	839	840(t)		
soil erosion and sedimentation processes	828			
stream bed and bank erosion	839			
water erosion, factors affecting	829			
water-surface profiles	669			
water temperature	665			
waterway areas	549			
waterway openings	533			
Waterways Experiment Station,				
Vicksburg, Miss	722			
water year series selected				
for use in simulation	1007(t)	1008(t)		
wave-induced erosion: by breaking waves	288	288(t)		
concave and convex				
profile configurations	286	286(t)		
fluid mud entrainment by waves	289	290(t)		
nearshore zone	284	284(f)		
by nonbreaking waves	288	289(t)		
profile stability factor	286	287(t)		
wavelets	81			
wave model	909	912		
wave period	533			
weir	451	523	553	1038
	1101			
wetted perimeter	361			
width adjustment models.				
See numerical width				
adjustment models width-depth ratio	361			
Wilcock-Crowe relation	199			
Wilcock-Kenworthy relation	198			
Wilson formula	72			
winnowing failure	558			
Wu-Wang-Jia relation	200			

This page has been reformatted by Knovel to provide easier navigation.

Index Terms	Links	
Y		
Yalin formula	72	
Yang relation	127	
Yangtze River profile	601(f)	
Z		
Zingg classification scale	40	40(f)

This page has been reformatted by Knovel to provide easier navigation.